PROCEEDINGS OF ELEVENTH CONFERENCE

ON

COASTAL ENGINEERING

LONDON, ENGLAND

SEPTEMBER 1968

Volume I: Parts 1 and 2

Volume II: Parts 3 and 4

Published by

American Society of Civil Engineers
United Engineering Center
345 East 47th Street
New York, New York 10017

$12.00

ACKNOWLEDGMENTS

This conference was held at the Institution of Civil Engineers in London. It was sponsored jointly by the Institution of Civil Engineers and the Coastal Engineering Research Council of the American Society of Civil Engineers. Cooperation in planning and conducting the conference was provided by the Hydraulics Research Station, Wallingford, England, and the International Association for Hydraulic Research.

CONTENTS

VOLUME I: PARTS 1 and 2

FOREWORD

The Council on Wave Research of the Engineering Foundation was the sponsor of the first nine conferences on Coastal Engineering. This Council was abolished and was replaced in 1964 by the Coastal Engineering Research Council of the American Society of Civil Engineers. However, in spite of the change of name and affiliation there has been no discontinuity in either the activity of the Council or its management, which continues to function under the able guidance of the Secretary, Professor J. W. Johnson of the University of California, Berkeley.

When the Council was formed eighteen years ago, many possible activities were considered. The field is international but small; coastal engineering works are predominantly under the jurisdiction of public agencies; research is conducted almost exclusively with governmental support; and specialists in many fields of engineering and science are active. It became clear that a major contribution towards advancing this branch of engineering practice could be made by sponsoring conferences and publishing the proceedings. Other activities have been considered by the Council from time to time, but none have been judged to meet a real need of the profession not already met by other organizations.

Each field of engineering practice is related to a body of knowledge in basic and applied science. The degree to which this scientific base provides quantitative means of analyzing real problems differs greatly from one field of practice to another. Judgment based on experience plays an important role in all branches of engineering practice. In coastal engineering practice, judgment still plays the major role in spite of the large, and growing, volume of experimental and theoretical results available. The gap between reliable predictions from analyses and the needs of the engineer engaged in the design of coastal works is still very wide. As an indication of the nature of this gap, a few of the deficiencies are as follows:

1) The wave environment is important in design. Measurements of height and period are being made, but wave direction is not included routinely in the measurements.

2) The surf actually produced by waves measured at sea has not been adequately explored by observing both concurrently.

3) Littoral transport is a major factor in many coastal problems. Field data are almost entirely the integrated net

transport caused by wave action over a long period. A means of measuring the rate of littoral transport is needed so as to relate the rate to the concurrent wave conditions.

4) Records of the life of structures, and more particularly case histories of failures are very limited. Records of the design and history of structures, and of the complete environment to which they were exposed, are needed.

5) Methods of appraising the probability of damage to structures are needed as the basis for insurance, not now generally available against damage by the sea.

6) Scale models of coastal problem areas offer many advantages, in cost, in range of conditions represented, in elapsed time required. Many models have been employed successfully but the choice of scale ratios seemed still to be more a matter of intuition than a quantitative analysis. These remarks are positively pertinent to movable bed models.

This list could be greatly extended. Work has been done, and more is in progress. An overall impression gained on reviewing the pre-prints of this conference and the previous proceedings is that coastal engineering research requires more comprehensive and powerful methods of attack on these problems than has been possible in the past. Much of the work done has been in the category of "half an experiment;" "whole" experiments are needed to relate effects uniquely to their causes.

An applied science should be not only scientific but should be applied. To be applied, the research results must be put in a form understandable by the practicing engineer and should be related back quantitatively to the primary variables of waves, tides, local winds, bottom configuration, and materials. Another impression is that there exists today a vast amount of field and laboratory data and of analytical results which should be sifted, analyzed, compared and generally shaken down to be useful in practice.

Morrough P. O'Brien, Chairman
Coastal Engineering Research Council
American Society of Civil Engineers

PART 1

WAVE THEORY AND MEASUREMENTS

CHAPTER 1

WAVES AT CAMP PENDLETON, CALIFORNIA

William H Powers, Jnr., Institute of Geophysics and Planetary Physics, La Jolla, California

Laurence Draper and Patricia M Briggs, National Institute of Oceanography, Great Britain

ABSTRACT

Waves were recorded for nine years at Camp Pendleton, California, and the results of an analysis of records over two years are presented in this paper.

INTRODUCTION

From 1953 to 1961, waves have been recorded at an exposed point 3000 feet west of the boat basin of Camp Pendleton, between San Diego and Los Angeles, by means of a Snodgrass Mk IX wave recorder (Snodgrass 1955) situated in a mean depth of 32ft Records were taken at six-hourly intervals and were of 20-minutes' duration The instrument also recorded continuously, but with a very much reduced chart speed. The distribution of wave heights for each year has been determined, and, from the nine years, two have been selected for a fuller analysis and the results have been combined to represent a typical year One of these years, 1954, was relatively calm and the other, 1958, was relatively rough. By using this method of selection it seems unlikely that these results represent unusual conditions The recording and analysis were done at Camp Pendleton, and the interpretation and presentation of the results were done at the National Institute of Oceanography. (The analysis does not follow the pattern recently suggested by one of the authors (Draper, 1966) as it was undertaken soon after the instrument was removed, but the interpretation and presentation are in accordance with that paper)

PARAMETERS DERIVED FROM THE RECORDS

The methods of analysis used yield the following parameters

T_s The significant wave period This was determined from visual inspection of the 20-minute record by selecting groups of four or more consecutive waves. The groups are selected by using two conditions:-

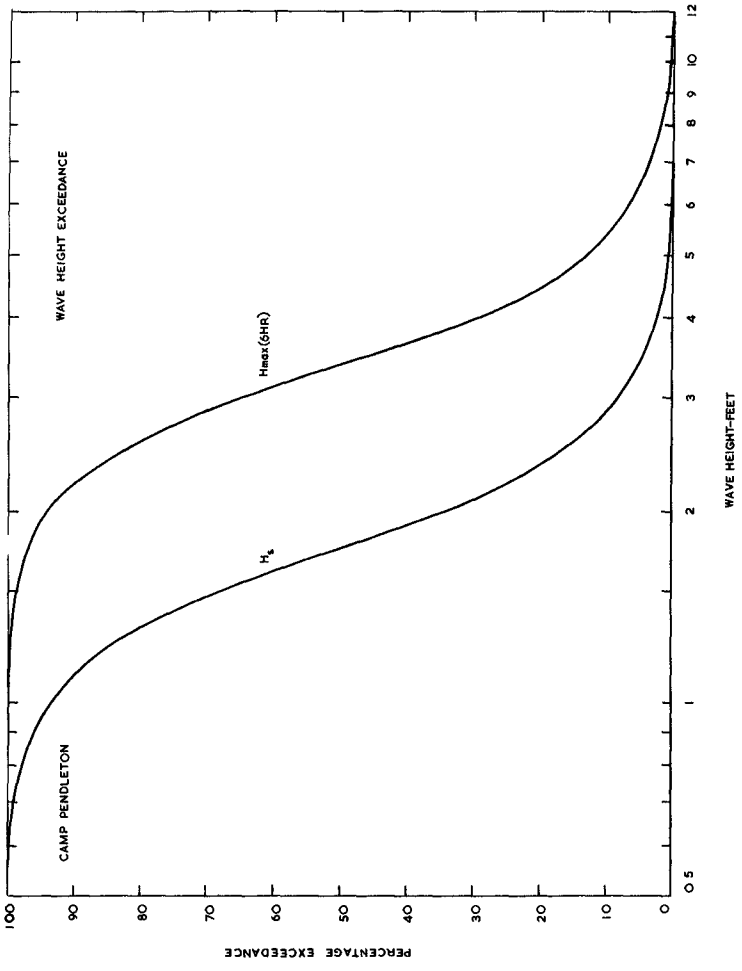

Figure 1 The cumulative distribution of significant wave height, H_S and of the most probable value of the height of the highest wave in the recording interval, H_{max} (6 hours).

1 The waves should be well formed.

2 The period within each group should appear to be consistent The periods of the groups do not have to be consistent from one group to the other but in most cases they vary by only one or two seconds

The total number of waves in all the selected groups is then divided into the total duration, in seconds, of those groups, to yield T_s.

$H_{max\ (20\text{-minutes})}$ The height of the highest individual wave in the record.

H_s The significant wave height, the average height of the highest one third of all the waves on the record

This is calculated in the following manner. the length of record, in seconds, is divided by the significant period to yield the effective number of waves in the record. The effective number of waves is divided by three, and this latter number of the higher waves (starting with the highest) is averaged to yield the significant wave height

These heights have been corrected for instrumental response and the attenuation of wave motion with depth, this latter correction is the theoretical hydrodynamic one, unmodified by any experimental technique

$H_{max\ (6\ hours)}$ The most probable value of the height of the highest wave in the recording interval (Draper, 1963)

PRESENTATION OF RESULTS

There appeared to be no consistent seasonal distribution of wave heights or periods, so the results are presented on a yearly basis, and are as follows:

Fig I The cumulative distribution of significant wave height, H_s and of the most probable value of the height of the highest wave in the recording interval, H_{max} (6 hours)

Fig II The distribution of wave periods.

Fig. III A scatter diagram relating significant wave height to significant wave period

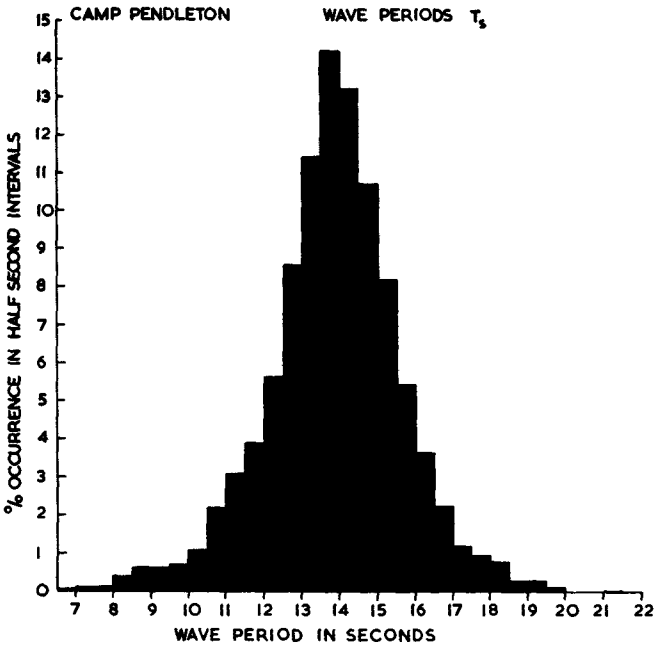

Figure II The distribution of significant wave periods

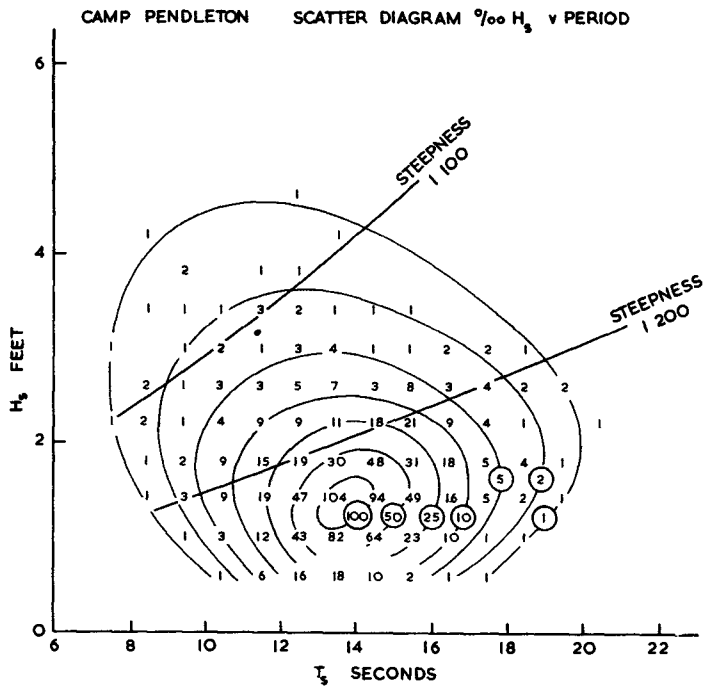

Figure III A scatter diagram relating significant wave height to significant wave period

Fig IV A cumulative persistence diagram for waves of various significant heights

Fig V 'Lifetime' wave prediction

Discussion of results

From Fig I may be determined the proportion of time for which H_S or Hmax (6 hours) exceeded any given height For example, the significant height exceeded two feet for 34 per cent of the time

Because of the difficulty of differentiating on the low-speed record between waves and any spurious electrical pulse, H_{max} (6 hours) has been calculated from H_{max} (20 minutes) However, although the calculated 6-hour maximum waves are, on average, 28 per cent higher than the 20-minutes maximum, the average measured value of H_{max} (6 hours) is only 2.3 per cent higher than the calculated value

The highest wave of all which occurred during a 20-minute record in the two years which were studied was 11 5 feet high The calculated height of the highest wave of all during the nine years was 14 5 feet (in 1955)

The scatter diagram of Fig 111 relates the significant wave height to significant wave period The numbers of occurrences are expressed in parts per thousand. For example, the most common situation with a significant wave height of about 1 5 feet and a period of between 13 and 14 seconds, occurred for 104 thousandths, or 10 4 per cent, of the time.

A parameter which is sometimes of interest is the wave steepness, defined as the ratio of wave height to wavelength, it may also be expressed as a decimal number It should be noted that the steepness of a wave is not the same as the maximum slope of the water surface during the passage of a wave Lines of constant steepness of 1·100 and 1·200 are drawn on Fig 111 (in this case, steepness relates to the significant wave height:significant wave length). Because the waves are predominantly swell, the steepness is much lower than can occur in an area where waves are generated, where the significant-height steepness can exceed 1:20 There is a theoretical limit to steepness of an individual wave of 1·7, and such a steepness is known to be approached occasionally during storms in an area such as the North Atlantic, (Draper and Squire, 1967) and is almost certainly approached on any ocean during a severe storm

Because of the depth of installation of the instrument, waves of periods shorter than about five seconds are not recorded adequately. It seems unlikely that this is the primary cause of the cut-off in measured

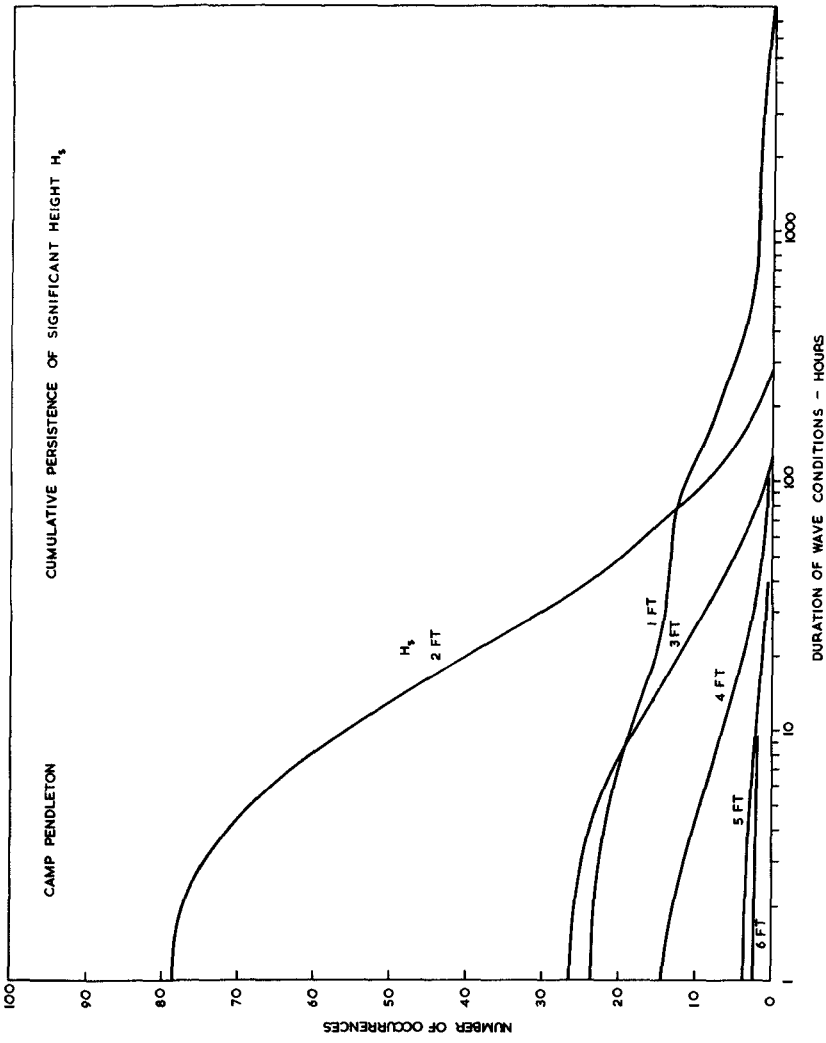

Figure IV A cumulative persistence diagram for waves of various significant heights.

wave period below about seven seconds, so that it is therefore reasonable to conclude that locally generated waves rarely predominate over the swell

Fig. IV From this diagram may be deduced the number and duration of the occasions in one year on which waves will be likely to persist at or above a given height. For example, if the limit for a particular operation of a vessel is a significant height of three feet, it will be unable to operate for spells in excess of ten hours on 18 occasions or spells in excess of 60 hours on four occasions.

Fig. V From this diagram it can be inferred that the most probable value of the height of the highest wave in, say, 50 years, is likely to be about 19 feet 'Draper 1963) The parameter used in the preparation of this figure is H_{max} (6 hours).

It is hoped that an analysis of the variability of wave conditions from year to year will be published later.

Other publications on waves in this area are given in the references.

Acknowledgment

The help given by Frank E. Snodgrass at all stages of the project is greatly appreciated.

REFERENCES

SNODGRASS, F. E (1955) Mark IX Shore Wave Recorder Proc. of First Conference on Coastal Engin. Instr , Council on Wave Research The Engineering Foundation Chapter 6.

DRAPER, L. (1963) The derivation of a design wave from instrumental records of sea waves. Proc Inst. civ. Engrs. (London) 26, pp 291-304

DRAPER, L (1966) The Analysis and Presentation of Wave data - a plea for uniformity. Proc. 10th Conference on Coastal Engineering, Tokyo 1966, Vol 1, Chapter 1 pp 1-11

DRAPER, L and SQUIRE, EILEEN M (1967) Waves at Ocean Weather Ship Station 'India' Trans roy Inst. nav. Archit. (Lond) 109, pp 85-93

WIEGEL, R. L. An analysis of data from wave recorders on the Pacific Coast of the United States. T. A. G. U. 30, 5, pp. 700-704.

WIEGEL, R. L. and KUKK, J. (1957) Wave measurements along the Californian coast. T. A. G. U. 38, 5, pp. 667-674

S. I. O. University of California, Wave Report No. 68, 1947 A Statistical Study of Wave Conditions at five open-sea locations along the Californian coast.

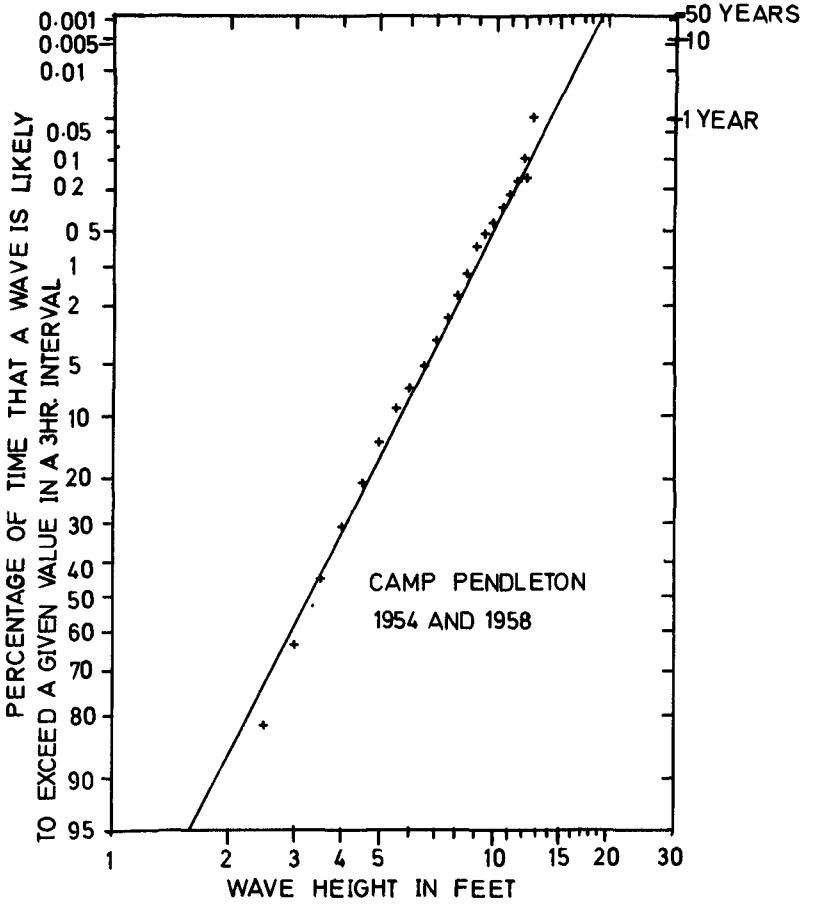

Figure V Prediction of a 'Lifetime' Wave

CHAPTER 2

WAVES OFF BENGHAZI HARBOUR - LIBYA

K. Y. Singh

Senior Engineer - Sir William Halcrow & Partners - Great Britain

and

L. Draper

National Institute of Oceanography - Great Britain

ABSTRACT

This paper gives details of the wave studies associated with the reconstruction of Benghazi Harbour, from the early forecasts, the installation of a recording instrument, its failures and repairs, to forecasts based on more recent techniques and subsequent analysis and presentation of results of records taken from 1961 to 1965. Conclusions have been drawn and some suggestions for future consideration have been given.

INTRODUCTION

At the time of preparing the designs for the Reconstruction of Benghazi Harbour, there was hardly any information available on the observed or measured waves. Recourse had therefore to be made to wave forecasting techniques using whatever wind records that were available. It was decided to include this information in this paper as a record of historical development of forecasting techniques.

In order to obtain more reliable information it was decided to install a wave recorder. Wave records have been analysed in accordance with Draper's[1] and Tucker's[2] methods except that H_{max} instead of $H_{\frac{1}{3}}$ was abstracted from every 10min. record because it was found that for all practical purposes H_{max} was equal to $H_{\frac{1}{3}}$. The results of the analysis have been presented in accordance with the proposals made by Draper[3] at the 10th Coastal Engineering Conference.

It was considered important to give in some detail the damages and breakdown sustained by the wave recorder installation in order to emphasize the hazards which are liable to affect almost any wave recording enterprise.

It was also felt important to compare the maximum waves predicted by using the actual wave records with those obtained by the latest forecasting techniques in order to ascertain how much reliance could be placed on these techniques which have to be used on many occasions to predict "design waves" in the absence of information on actual wave records.

WAVE FORECASTS (OR HINDCASTS)

In 1955, Sir William Halcrow & Partners asked Neyrpic, Laboratoire Dauphinios d'Hydraulique, Grenoble, to undertake hydraulic model tests for breakwater designs and for various layouts of the harbour. As the information on waves at that time was very scarce and unreliable, Neyrpio decided to resort to forecasting methods based on the knowledge of winds in order to augment the available data on waves. Various National meteorological records were consulted for information on winds. Two values of wind velocities; 40 knots which was the maximum observed value, and 28 knots corresponding to Beaufort 7, were used in making the forecasts. It was assumed, although no positive evidence was available, that these wind velocities were constant for the directions and fetches under consideration for relatively long periods. Methods of Suthons and Sverdrup as well as empirical formulae of Stevenson and Iribarren were used. Four directions were considered but Neyrpic's results for N.W. and N. only, which have the maximum fetch of 350 nautical miles, are given below.

	Wind velocity - 40 knots		Wind velocity - 28 knots	
	Suthons	Sverdrup	Suthons	Sverdrup
Wave Height	25'	30'	15'	16'
Period	12 sec.	10.2 sec.	9.7 sec.	8.7 sec.
Min. Duration	24 hrs.	31 hrs.	28 hrs.	36 hrs.

Stevenson's formula: $H(ft) = 1.5\sqrt{\text{fetch (nautical miles)}} = 28'$

Iribarren's formula: $H(m.) = 1.2\sqrt[4]{\text{fetch (km.)}} = 20'$

It was assumed that Suthon's method gave maximum wave height and Sverdrup's method gave significant height. It was also assumed that maximum wave heights were obtained from the formulae of Stevenson and Iribarren. Neyrpic recommended that for directions N.W. and N. a wave height of 23' of 10 sec. period should be used for wave agitation tests in the harbour but that to allow for exceptional storms higher waves of 25' to 30' height and 12 sec. period should be used for breakwater stability tests. Further meteorological data based on actual storms upto January, 1968 has been examined and it is now conoluded that a wind speed of 40 knots for a duration of 24 hours is possible for the most severe storms. Using the latest methods the following forecasts are now made for deeper water off the harbour.

Darbyshire - Draper graphical method (oceanic)[4]:

$H_s = 20'$, $H_{max.\ (storm)} = 44'$ and $Ts = 11.5$ secs.

Bretschneider's method[5]:

$H_s = 26'$, $H_{max.\ (storm)} = 52'$ and $Ts = 13.5$ secs.

Fig. 1. Underwater Unit, Wave Recorder.

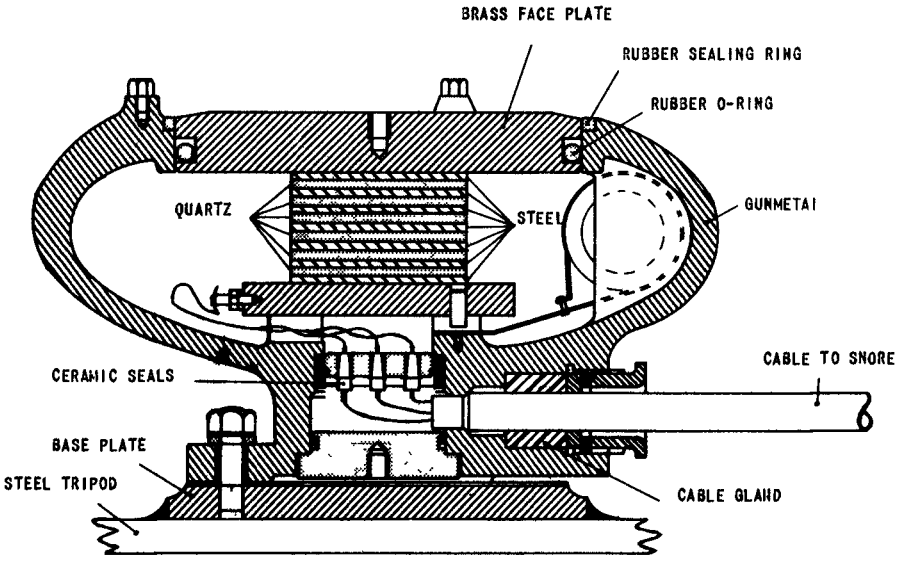

Fig. 2. Section through the Underwater Unit.

Wave Spectrum (P-N-J) method[5]:

H_s = 25', $H_{max.(storm)}$ = 50' and T_s = 12 secs.

It should be noted that $H_{max.(storm)}$ given above is the maximum wave height which is likely to occur in a storm of 24 hours duration. In the case of Darbyshire - Draper method the appropriate height factors given in their paper[4] were used. For Bretschneider and Wave Spectrum methods the height factor was obtained from the formula: $H_{max.} = 0.707\ H_s\sqrt{\log_e N}$ where N = number of waves in the duration under consideration.

WAVE RECORDER INSTALLATION

The instrument is an N.I.O. piezo-electric wave recorder which measures fluctuations in pressure. These are transmitted as voltages through a seven core cable to the amplifier and recording instrument located on shore. An outside view of the sea unit is given in Fig. 1 and a cross-section through it is given in Fig. 2. The underwater unit is mounted on top of a steel tripod 6' high. The wave traces are recorded on two separate charts, a continuous record being taken at a chart speed of 6"/hour and an intermittent record of 12 min. duration taken every four hours at a speed of 2"/min.

The instrument was first installed in 1956 and functioned until early 1958 when the submarine cable was damaged by tanker moorings. The meter head was lifted up, re-assembled and re-placed in August 1960. During a severe storm on 5th/6th February 1961, the power supply to the recorder failed and records at the peak of the storm were not obtained. In 1962 a standby generating set was provided which automatically came into operation in the event of mains failure. Wave records obtained during the storm of 15th/16th March 1962, showed unusual features suggesting that the cable was damaged. Subsequent inspection showed that the cable was stretched to breaking point by tanker moorings. It was then decided to re-locate the sea unit where the cable would be clear of moorings. This opportunity was taken to obtain a more streamlined meter head as the old one was suspected of suffering from eddies and turbulence. The recording instrument was also moved close to the Chief Resident Engineer's Office where it could be kept under close supervision. The new unit and the cable were installed in December 1962. The instrument functioned reasonably satisfactorily until July 1965, when the cable was broken in a storm. A completely new cable had to be provided and was connected up in November 1967.

WAVE RECORDS AND ANALYSIS

The first and second sitings of the sea unit were in depths of water of 42' and 48' respectively. Some of the deep sea waves were, therefore, not measured as they had already broken before reaching the recorder. Intermittent wave records covering the period from 1961 to 1965 have been analysed in accordance with the methods described by Draper and Tucker. The results are presented in Figs. 3, 4 and 5.

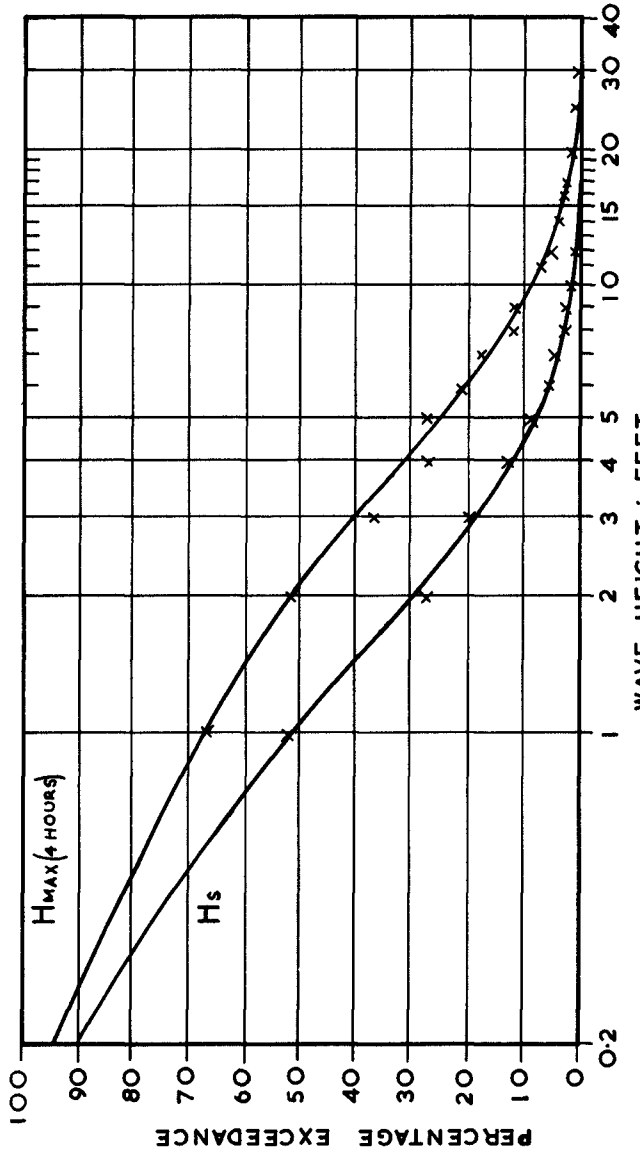

Fig. 3. The cumulative distribution of significant wave height and the most probable highest wave in the recording interval.

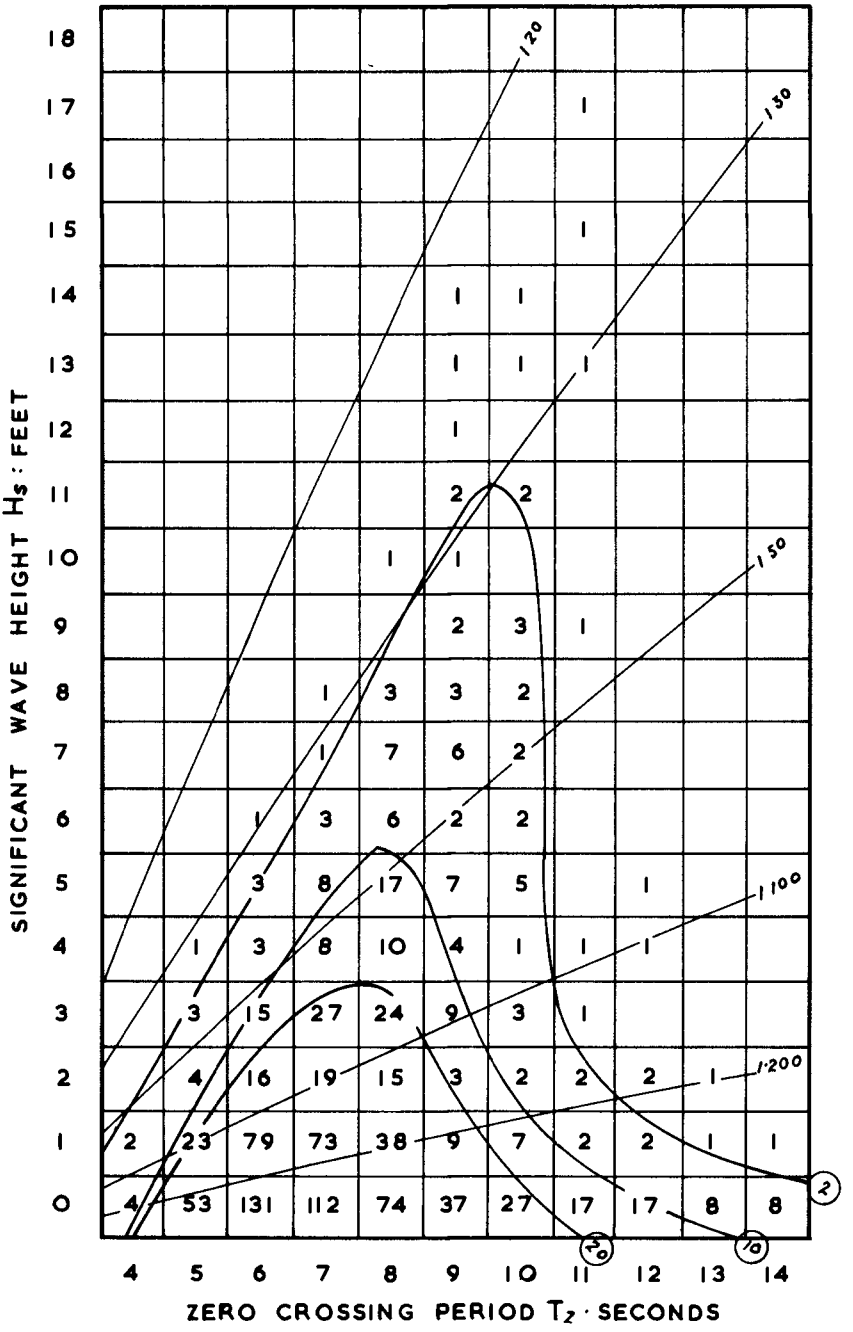

Fig. 4. A scatter diagram.

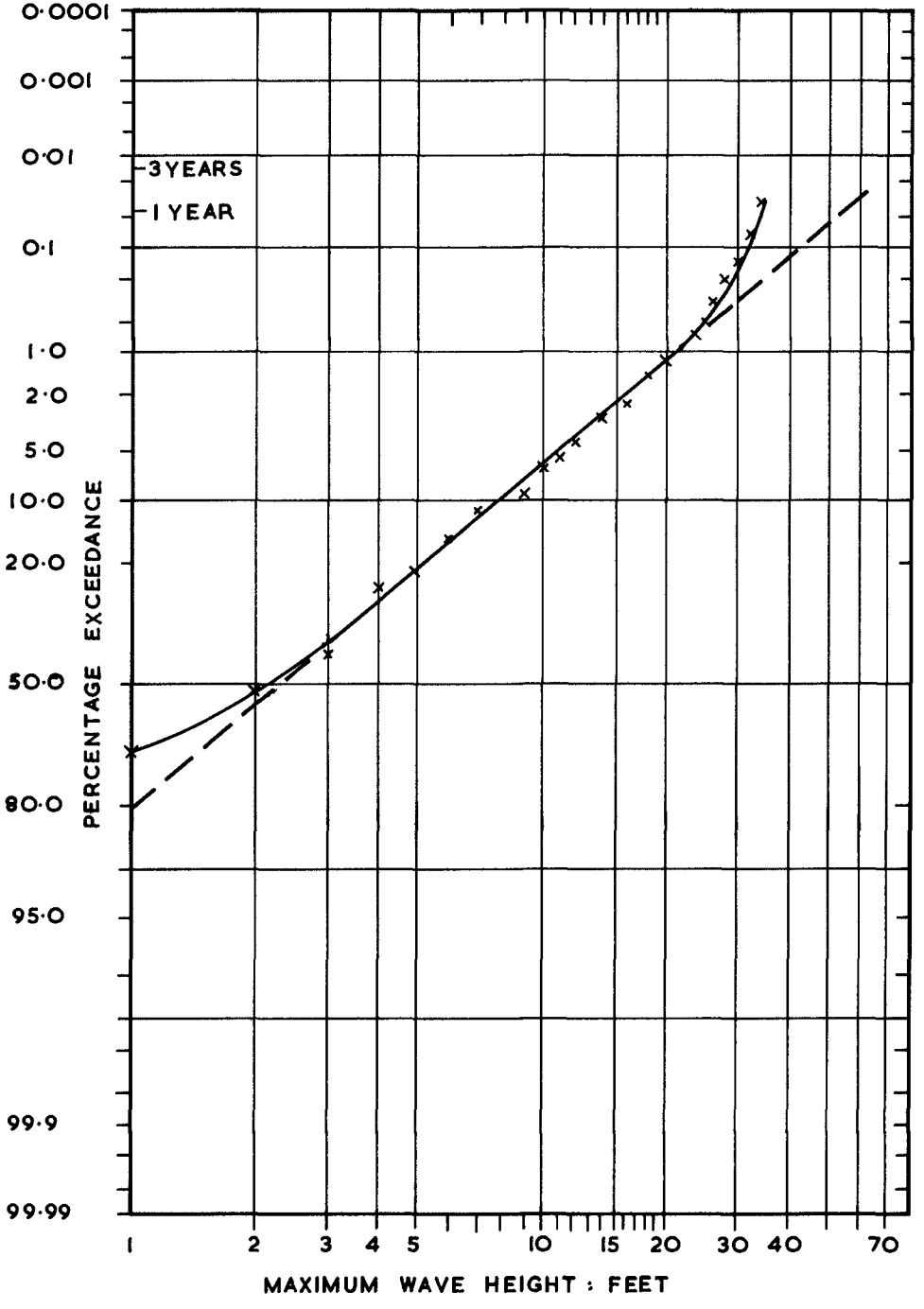

Fig. 5. Prediction curve.

Fig.3. This diagram shows the proportion of time for which H_s and $H_{max.}$ (4 hours) exceeded any given height. For example, H_s exceeded 5 feet for 20% of the time.

Fig.4. This is the scatter diagram relating the significant wave height to the zero crossing period. The wave records are presented as parts per thousand. The wave steepness lines are drawn using the wave length at the recorder location and from these it can be seen that most of the waves lie between steepnesses of 1:200 to 1:20. Contours have been drawn from which the frequency of occurrence of certain combinations of wave height and period can be obtained. The most common zero crossing period appears to be 7 seconds.

Fig.5. The calculated values of H_{max} (4 hours) have been plotted against percentage exceedance. The graph is a straight line between wave heights of 3' and 25' and breakaways below and above these heights. The non-linearity above about 25' is due in part to the shallow water, as depths of 42' and 48' cannot sustain waves of a height greater than about 32' to 37' respectively. Low wave heights are often associated with short periods resulting in large depth attenuation which prevents such waves appearing on the record. This results in a lower apparent percentage of waves of one and two feet in height and may explain some of the non-linearity at low heights. Using the straight dotted extension of the graph it can be predicted that a wave height of 52' (maximum) can be expected to occur once every year in deeper water. This compares well with the waves forecast by the Bretschneider and P-N-J methods. Non-linearities are almost certain to occur at these wave heights, yielding extremes somewhat less than those predicted by the straight line, but until the behaviour of waves at these heights is better understood the linear extrapolation must be used. This should give a slight error on the "safe" side.

CONCLUSIONS AND SUGGESTIONS

Although reasonable agreement has been obtained between the waves forecast using the latest techniques and the actual measured records, it is obvious that there is still considerable room for improvement in both the forecasting and recording techniques. Forecasting would be more accurate if wind speed and its duration over the fetch could be determined with greater accuracy. It is suggested that if wind data is available in a form suitable for extrapolation to long intervals of time it might included in the paper to enable the user to make his own forecasts at a later date if more accurate wave forecasting techniques become available.

There is still a great need for a simple but reliable wave recording instrument which would be less subject to breakdowns. There are instruments available now which reduce the manual task of analysis but their use in remote locations devoid of servicing facilities probably causes more problems than it solves. It is also suggested that every encouragement be given to the development of instruments which would record wave heights and directions simultaneously.

ACKNOWLEDGEMENTS

The authors wish to express their gratitude to their collegues and in particular to Mr. R. K. Hayward, Chief Resident Engineer, and to his staff at Benghazi without whose unfailing efforts the recorder could not have been

kept in operation for so long. Acknowledgements are also due to many engineers who assisted in the analysis of the wave data.

REFERENCES

1. L. Draper. Derivation of a "design wave" from instrumental records of sea waves. Proc.Instn.Civ.Engrs., 1963, 26, pp. 291 - 304.

2. M. J. Tucker. Analysis of records of sea waves. Proc.Instn. Civ.Engrs., 1963, 26, pp. 305 - 316.

3. L. Draper. The analysis and presentation of wave data - a plea for uniformity. 1966. Proc.Xth Conf. Coastal Eng. pp. 1 - 11.

4. M. Darbyshire and L. Draper. Wind-Generated Sea Waves. Engineering. 1963, April, pp. 482 - 484.

5. Shore Protection Planning & Design. Technical Report No.4. U.S. Beach Erosion Board.

CHAPTER 3

WAVE MEASUREMENTS BY A PRESSURE TYPE WAVE GAUGE

P.O. Bergan, A. Tørum and A. Trætteberg

Research Engineers, River and Harbour Laboratory,
Technical University of Norway, Trondheim
NORWAY

ABSTRACT

The paper deals with comparative measurements of irregular model waves by a pressure type wave gauge and a continuous wire wave gauge. For the depth and wave conditions used in the study it is concluded that the height of individual waves obtained by a pressure type gauge and using the first order wave theory may be in considerable error, while wave height distributions and wave spectra are fairly good estimated.

INTRODUCTION

Pressure type wave gauges have been extensively used in many locations throughout the world. Along the Norwegian coast wave measurements with such gauges have been carried out at four exposed locations since 1959 by the Norwegian State Harbour Authorities. The data from these gauges are collected by and analysed at the Technical University of Norway.

The Norwegian gauges are placed close to the bottom at depths 17-20 m.

When using pressure type wave gauges, the wave height is usually obtained by using the first order wave theory, sometimes modified by an emperical factor which often is a function of the wave frequency.

According to the first order wave theory the relation between the wave height and the recorded differential pressure is the following

$$\Delta p = \gamma \cdot \frac{H}{2} \frac{\cosh k\,(d-z)}{\cosh kd}$$

where:

γ = specific weight of water. H = wave height
$k = 2\pi/L$. L = wave length. d = water depth
z = vertical distance from the still water level to the pressure gauge

A record of pressure variations due to waves is more or less similar to what has been sketched in Fig. 1. The apparent wave period may be obtained by some method like the zero-up-crossing method which has been used in this paper as shown in Fig. 1.

First order wave theory leads to errors in the wave height estimates, (1), (2) and (3). Higher order wave theories have not usually been used because of the excessive computing work involved to obtain wave heights from the pressure records. It should also be pointed out that really no reliable wave theory exists for short crested irregular waves. For practical reasons it has therefore been usual to modify the wave heights obtained by first order wave theory by some empirical factor.

The work reported in this paper were carried out to investigate in a wave flume the accuracy of pressure wave gauges with particular reference to the conditions of the gauges along the Norwegian coast. All the data in this paper are presented as model data. However, if a linear scale of 1:20 is applied the water depth used in the wave flume corresponds to 20 m, the significant wave periods to 9 seconds and the significant wave heights to 3 to 5 metres.

WAVE MEASUREMENTS

The measurements of wave heights by a pressure wave gauge and a continuous resistance wire gauge were made in a wave channel, 78 metres long, 3,8 m wide and with a water depth of 1 m.

The wave channel is equipped with a wave generator which can generate unidirectional regular or irregular waves. The unidirectional spectra of the irregular waves can be of any reasonable shape and the significant waves up to 25 cm high.

The pressure wave gauge was a pressure transducer from a Swedish company: SWEMA. The transducer was mounted outside the channel and connected by a plastic tube to a pressure tap in the channel wall. As shown in Fig. 2 the continuous wire gauge was located in the same cross-section as the pressure gauge.

Recordings of pressures from regular waves were analysed using both first and fifth order wave theory. Fig. 3 shows comparisons of pressures measured by the pressure gauge and pressures calculated from wave heights obtained by the wire gauge using the first order wave theory. Fig. 4 shows a similar comparison between measured pressures and pressures obtained by the fifth order wave theory. There is a fair agreement

between measured pressures and pressures calculated according to the fifth order wave theory, indicating that the testing arrangement was working satisfactorily.

It should be pointed out that the pressure transducer and the set up in the model is an ideal pressure gauge with a full pressure response for all frequencies. Prototype gauges may, due to hydraulic, mechanical and electronical conditions respond to the pressures differently than the transducer used in the present investigation.

Fig. 5 shows a sample of simultaneous recordings of irregular waves from the continuous wire gauge and the pressure gauge. This sample shows a characteristic feature of the pressure wave gauge, namely that it does not record as many waves as the wire gauge.

The zero upcrossing method was first applied to the recording from the wire gauge, and the waves were numbered consecutively. Then the same procedure was applied to the pressure gauge record. Waves that could more or less be traced to be the same on the two records were given the same numbers while waves on the pressure gauge that could not be traced on the continuous wire gauge were given a combined number corresponding to the waves on the wire gauge recording during the same time interval.

Fig. 6 shows a comparison of waves measured by the wire gauge and waves obtained from the pressure gauge using first and fifth order wave theory respectively. Only waves which are comparable according to Fig. 5 have been used in Fig. 6. The agreement is not very good, and it is probably not to be expected to be better. The usual concept of irregular waves is that the irregular surface configuration is generated by regular waves travelling at their own individual speed. It is then understandable that a poor result is obtained when applying a theory that is valid to only the individual waves to a phenomenon that is an interference of many waves.

Some calculations have been made to compare wave power-spectra and wave height distributions from the wire gauge and the pressure gauge.

The calculations of the wave power spectra and the wave height distributions were based on records of 100-200 consecutive waves, varying somewhat from sample to sample. The power spectras were calculated through the autocorrelation function and the raw spectra smoothed according to the Hanning method. The time lag used in the calculations was 1/4 seconds, and eighty points were calculated of the autocorrelations function.

The power spectra of the waves measured by the pressure gauge were obtained by calculating the power spectra of the pressures and applying a transfer function according to the first order wave theory.

The wave heights used in obtaining the wave height distribution are those obtained by applying the zero upcrossing method. The wave heights from the pressure gauge were obtained by using the apparent wave period when calculating the pressure response factor.

Fig. 7 and 8 show spectra and wave height distributions from the two gauges. The agreement is rather good. Several similar analysis have been made. The agreement was not always as good as shown in Figs. 7 and 8, but the agreement between significant wave heights obtained from the pressure and continuous wire gauge was in general within 10% of the wave height.

In view of the poor accuracy on the individual waves obtained by the pressure gauge, it is quite surprising that the accuracy is so good when dealing with the waves in a statistical manner.

CONCLUSION

The present investigations have shown that wave heights of individual waves obtained from pressure records of irregular unidirectional waves may have considerable errors, irrespective of whether first or fifth order wave theory is used.

However, using first order wave theory when analysing pressure gauge records of unidirectional irregular waves may give reasonably accurate wave spectra and wave height distributions. In particular a fair estimate of the significant wave height is obtained.

REFERENCES

1. Masashi Hom-ma, Kiyoshi Horikawa and Shuzo Komori: Response Characteristics of underwater wave gauge. Proc. of Tenth Conference on Coastal Engineering, Tokyo, Japan 1966.

2. Hiromoto Fumiyasu
A note on a Correction factor for the Pressure of Progressive waves. Report No. 13 of Port and Harbour Research Institute, Ministry of Transport, Japan, April 1967.

3. Gerhard, Jehn and Katz:
"A Comparison of step-pressure - and continuous - wire - gauge wave recordings in the Golden Gate Channel".
Trans. American Geophysical Union, Volume 36, No. 2, April 1965.

4. Skjelbreia and Hendrickson:
Fifth order gravity wave theory. Proc. of the Seventh Conference on Coastal Engineering, The Hague 1960.

5. Røslie, A. and Skauerud, S:
An investigation on the accuracy of pressure wave gauges.
Unpublished thesis, Technical University of Norway, Trondheim, Norway, 1966 (In Norwegian).

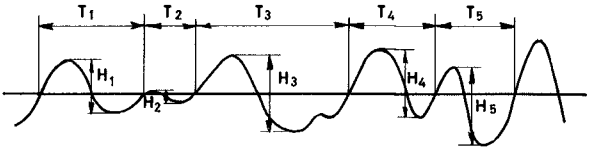

FIG. 1 ZERO UPCROSSING

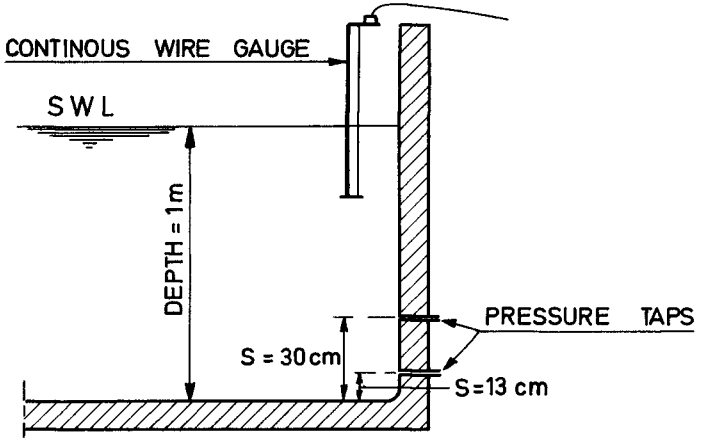

FIG. 2. SETUP LOCATION OF PRESSURE TAPS AND CONTINUOUS WIRE GAUGE

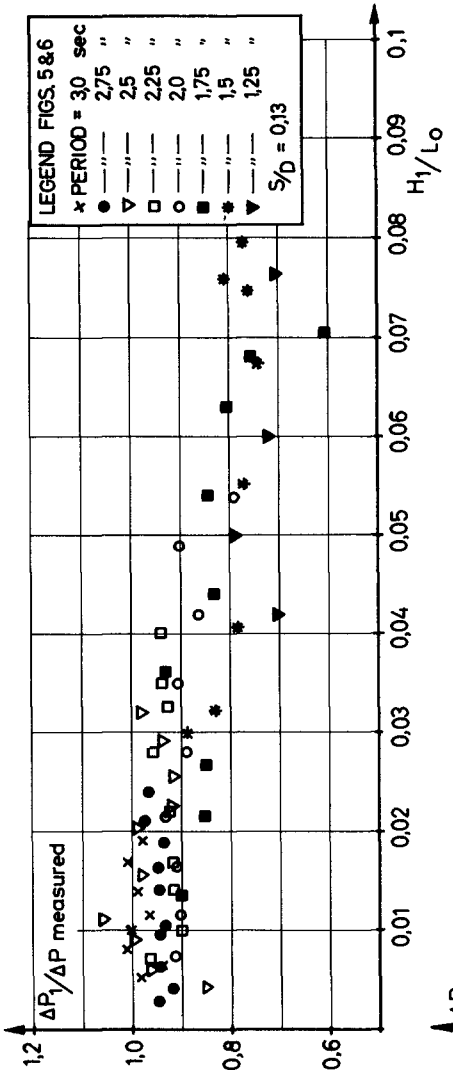

FIG. 3

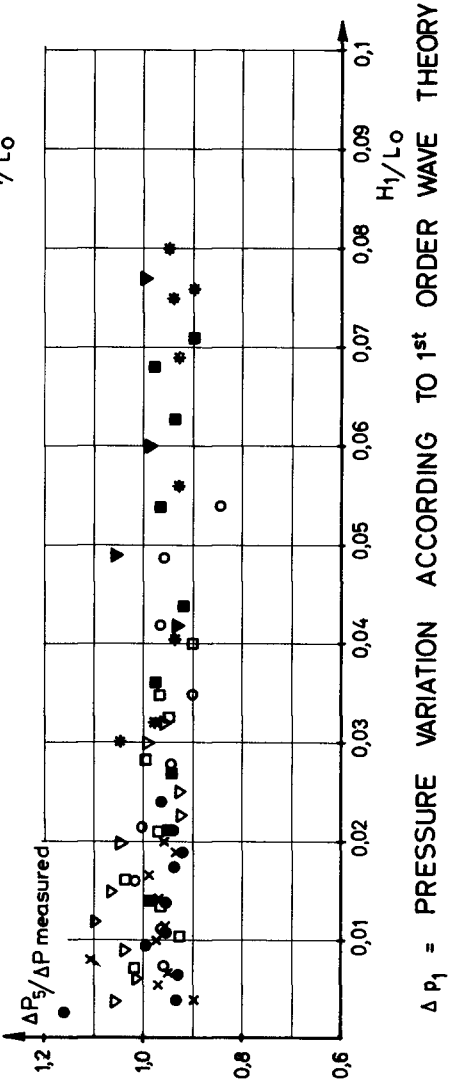

FIG. 4

Δp_1 = PRESSURE VARIATION ACCORDING TO 1st ORDER WAVE THEORY

Δp_5 = " " " " 5th " "

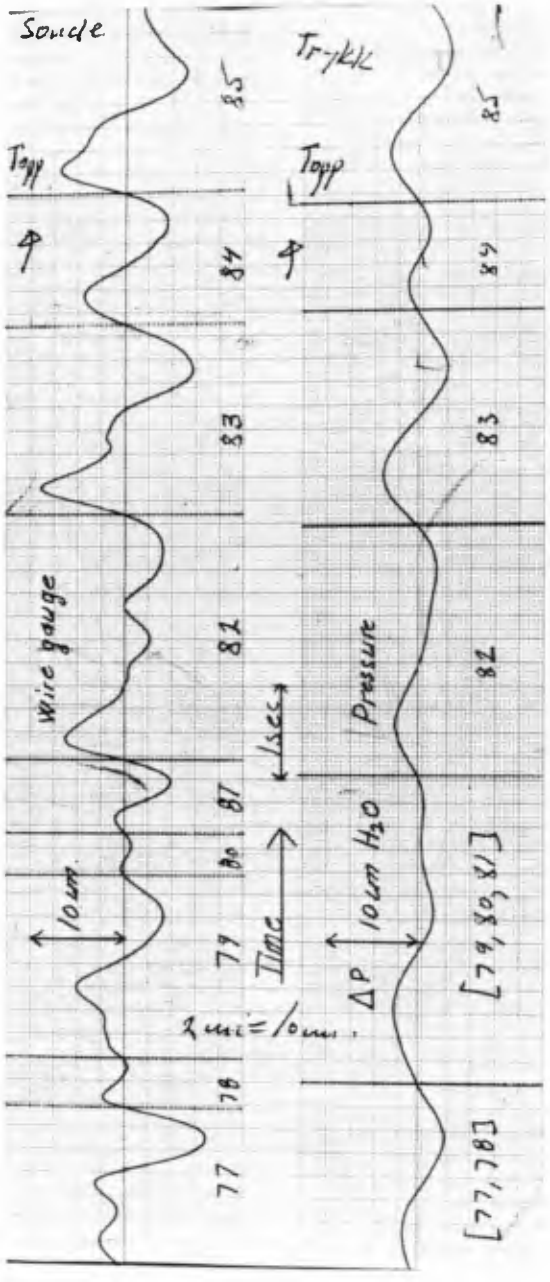

FIG. 5 SIMULTANEOUS RECORDINGS FROM THE CONTINOUS WIRE GAUGE AND THE PRESSURE GAUGE

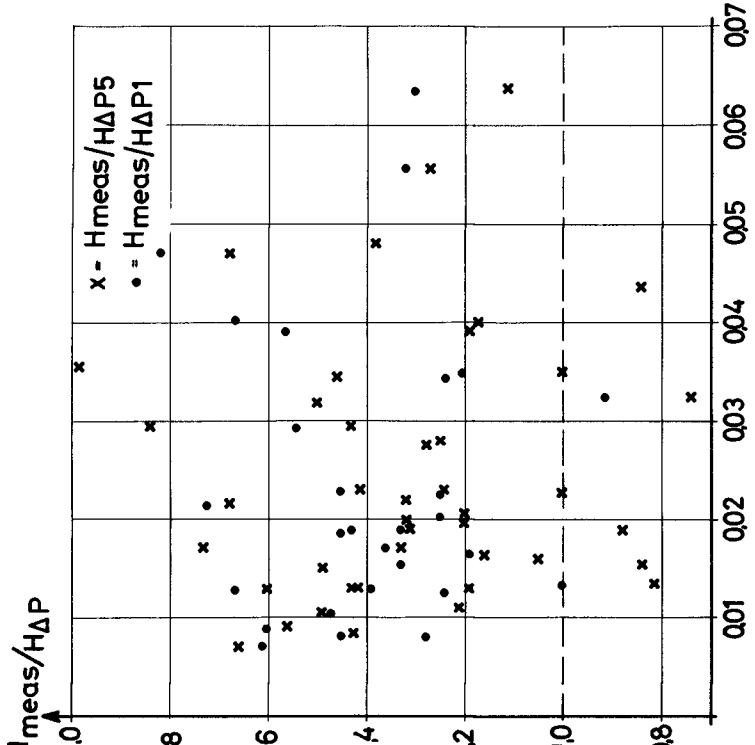

FIG. 6 COMPARISON OF WAVEHEIGHTS OBTAINED BY A CONTINOUS WIRE GAUGE, (H means), AND A PRESSURE GAUGE, ($H_{\Delta p}$)
$H_{\Delta p1}$ = ACCORDING TO 1st ORDER WAVE THEORY
$H_{\Delta p5}$ = " " 5th " " "

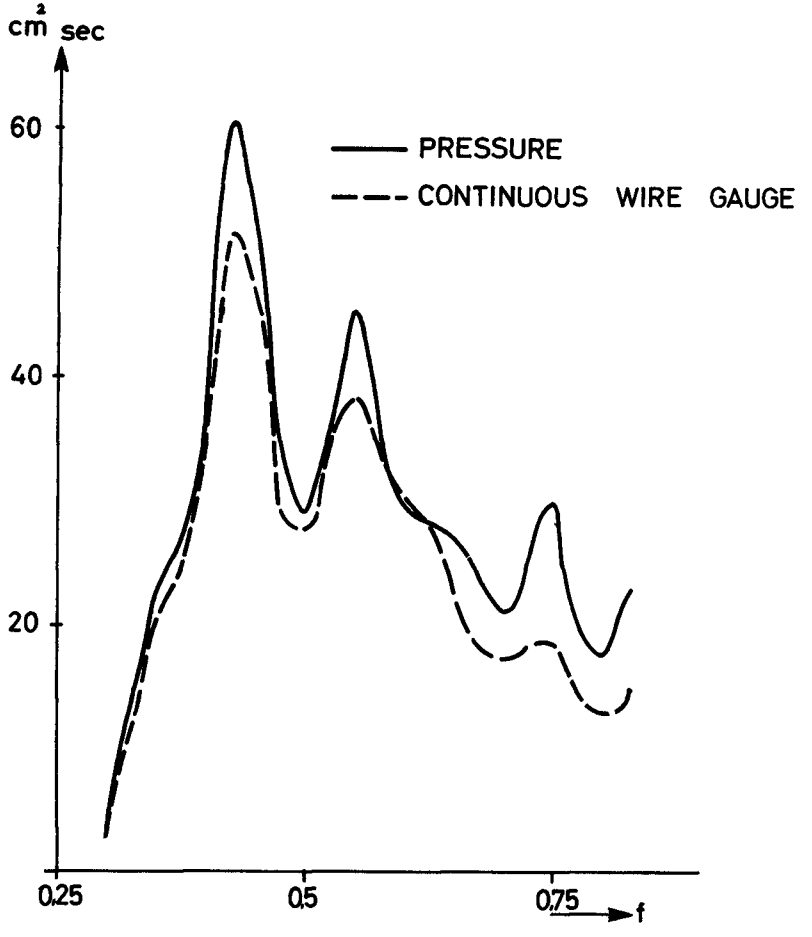

FIG. 7 WAVE SPECTRA

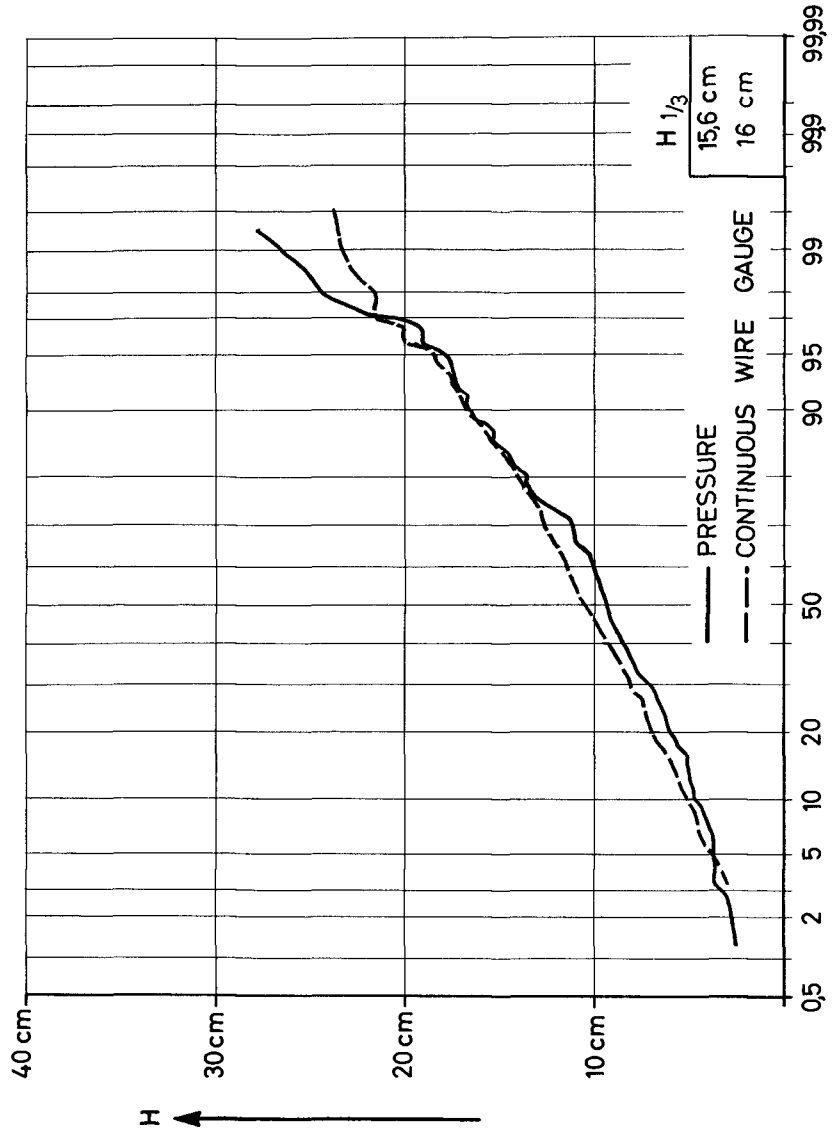

FIG. 8 WAVE HEIGHT DISTRIBUTION

CHAPTER 4

THE CHARACTERISTICS OF WIND-WAVES GENERATED IN THE LABORATORY

by

Theodore T Lee
Associate Researcher
Look Laboratory of Oceanographic Engineering
University of Hawaii
Honolulu, Hawaii
U.S.A.

A B S T R A C T

Wind-wave characteristics were recorded in the laboratory for the primary purposes of (a) analysis of the probability distribution of wave height and wave period with wind speed, water depth, and fetch length as major parameters, and (b) comparison of the test results with existing theory and empirical formulae.

An important aspect of this study was to test the validity of the Tucker and Draper method (Draper, 1966) for the presentation of ocean wave data as applicable to wave-data analysis for simulated wind waves. It was interesting to note that some corrections were necessary when the method proposed by Draper at the 10th Coastal Engineering Conference was used for analyzing waves generated in the laboratory. Approximately a positive 20% correction was necessary for this study in which the wave spectra distribution is of very narrow range, the wave width parameter $\varepsilon = \sqrt{1-(T_c/T_z)^2}$ varies from 0.25 to 0.50, where T_c and T_z represent crest wave period and zero-crossing wave period, respectively. However, only a negative 5% correction was necessary when the method was used to analyze sea waves (ε = 0 73 to 0 76) measured off the shoreline near Look Laboratory Therefore, it was concluded that the Tucker and Draper Method is quite feasible for engineering purposes in analyzing wind-waves having a spectral width parameter of 0.60 to 0.75

The experimental data were compared with those wave heights predicted by the Darbyshire formulas (Francis, 1959) developed for ocean waves. A significant correction factor was necessary for laboratory waves produced by low-speed winds.

The "fetch graph" was prepared and compared with those developed theoretically by Hino (1966) and empirically by Ijima and Tang (1966) at the 10th Conference on Coastal Engineering, Tokyo, Japan Comparison was also made with the previous empirical formulae by Bretschneider (1951, 1957), Sverdrup and Munk (1947), and Wilson (1961,1962). The experimental results compared well with the Hino theory for both wave heights and wave periods, and fairly well with Bretschneider's fetch graph for wave heights The difference in the comparison of wave data with other investigators is illustrated in this paper.

It is recommended that further study be made with emphasis on (a) theoretical and experimental studies of wind-wave characteristics on pre-existing waves, particularly moving storms, (b) wave-energy spectra involving stochastic characteristics and extreme values of wind waves

INTRODUCTION

Wind-generated water waves are considered the most significant phenomenon confronted by ocean engineers in the design of protective shoreline structures and the prediction of response of offshore floating structures moored in the open sea This type of wave is distributed in random form compared to the long-period waves generated from an artificial disturbance, such as earthquakes and underwater explosions. The spectrum of the wind-waves varies with wind speed, wind duration, and fetch over which the wind blows. The topography of the local ocean bottom is often the governing factor in the modification of wave spectra in shallow water.

One of the problems is how to present the wave data in forms which can be used by ocean engineers for design purposes. The most widely accepted method is the use of the significant wave (i e., the average of the highest one-third of the waves) as the design wave. The significant wave may be determined from field measurements during several storms, or it can be predicted by wave forecasting or hindcasting techniques, such as those suggested by Sverdrup-Munk-Bretschneider (1951, 1957), Pierson-Neumann-James (1955) and Darbyshire (1963). Based on the significant wave, many shore structures have been designed with certain safety factors. In recent years, some questions have been raised as to whether or not a structure should be designed for maximum wave height (extreme values), allowing due consideration for the frequency distribution. The distribution of wave periods becomes more important when resonance is of major concern Therefore, the method of presenting wave data requires further investigation in order to provide ocean engineers not only with significant wave data, but with extreme values and frequency distribution as well.

At the 10th International Conference on Coastal Engineering in Japan, L. Draper (1966) presented a method of analyzing and presenting sea-wave data as a plea for uniformity. The method is simple and meritorious in sea-wave applications, but its validity as applied to simulated wind waves generated in the laboratory needed to be determined. This paper describes the experimental results of wind-wave characteristics obtained by this author who has applied this method for both laboratory and sea waves. The data have also been compared with existing theoretical and empirical formulae which are commonly used in coastal engineering

The primary objectives of the experimental investigation are to· (a) analyze the frequency distribution of wind-waves simulated in the laboratory and/or measured in the Pacific Ocean; and (b) compare the test results with existing methods of wave prediction by theoretical or semi-empirical approaches, (c) evaluate the applicability of the simplified Tucker and Draper method for analyzing wind-waves generated in the laboratory and/or ocean; (d) calibrate the pilot wind-wave flume and establish criteria for the wave-generating mechanism of the large wind-wave flume.

EXPERIMENTAL EQUIPMENT

The laboratory experiments were conducted in a wind-wave flume (9 inches wide, 13 inches high, and 48 feet long) with a blower-generator capable of simulating wind speeds from 9 to 44 feet/second (Fig. 1). The flume is a pilot model of a large wind-wave flume (4 feet wide, 6.25 feet high, and 180 feet

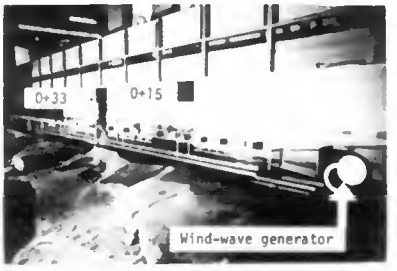

(a) View from wind-wave generator end

(b) View from absorbing-beach end

Fig. 1 - The pilot wind-wave flume

long) being constructed at the Look Laboratory of Oceanographic Engineering. The wind speed depends on the blowing opening; water depth, and fetch length in the flume.

A plexiglas absorbing-beach of 1:12 slope is located at the leeward end of the flume. Wave height and wave period pick-ups were installed at two stations having a fetch length of 15 feet (0 + 15) and of 33 feet (0 + 33), respectively, from the wind-generator. Two wave gages of submerged electrode type and a direct-writing oscillograph were used to sense and record the waves. A pitot-tube was used to measure wind velocity pressure, which in turn determines the wind speed. The pressure was read from a portable manometer. The effects of temperature and barometric pressure were insignificant. Wind velocities were measured at both fetch stations with a number of measurements sufficient to define the profiles along three vertical sections.

EXPERIMENT PROCEDURE AND TEST RESULTS

The preliminary tests included the measurements of wind speeds, wave heights, and wave periods as a function of blower opening, water depth, and fetch distance along the flume A relationship between the wind speed and blower opening was established. Twenty-two test conditions were formulated with four water depths and six wind speeds for each depth. A thorough analysis of wave characteristics in a water depth of 4 inches was made and compared with the values computed by the Tucker and Draper method (Draper, 1966) developed for analyzing ocean waves at the National Institute of Oceanography, England.

Since the wind-waves generated in the pilot flume are of narrow spectral distribution, no attempt has been made to conduct a power-spectral analysis of the wave data collected Instead, only a spectral width parameter based on the reproducibility of wind-waves in the flume is presented. It was found that the reproductivity of wind-waves is valid with relation to the significant wave heights and periods. However, there are some discrepancies in the wave spectral width parameters. It is planned to collect more wave data to facilitate the analysis of extreme values and to study the dependence of wind-wave characteristics on pre-existing waves, includeing the effect of moving storms

The test results showing the relationship between average wind speeds and blower openings are presented in Fig 2. It should be noted that the average wind speeds at Station 0+33 (33 feet along the flume from the wind-wave generator) are generally higher than those measured at Station 0+15 because the cross section of the air stream at Station 0+33 was decreased as higher waves were presented, thus increasing the wind speed above water surface for a given discharge of air flow During the tests, the wind speed for each run was gradually brought up to the desired level in order to avoid undesirable surges in the flume. This procedure was also necessary in order to have the wind-wave system developed in a reasonably short time

The average magnitudes of wave heights equal to or greater than 10 percent, 33 percent, 50 percent and 100 percent of all waves measured are compared in Fig. 3.

The significant wave heights as a function of wind speed, fetch location, and water depth are compared in Fig. 4. The maximum significant wave height measured under various test conditions varied from 0 9 to 1.9 inches at the fetch Station 0+33, and from 0 55 to 1.4 inches at Station 0+15. Similarly, the relationship between wave period and wind speed for the different fetch locations and water depths is compared in Figs. 5 and 6. The average wave period varies from 0.43 to 0.66 seconds at Station 0+33 and from 0.26 to 0.52 seconds at Station 0+15 It is shown that wave period increases with wind speed and fetch. Generally, the measured wave heights and wave periods increase with wind speed. However, they tend to decrease when wind speed reacher certain values, as shown in Figs 4 and 6. This is perhaps because of the turbulance of the water surface for higher wind speeds. The relationship between significant wave heights and mean wave periods is shown in Fig. 7. The experimental

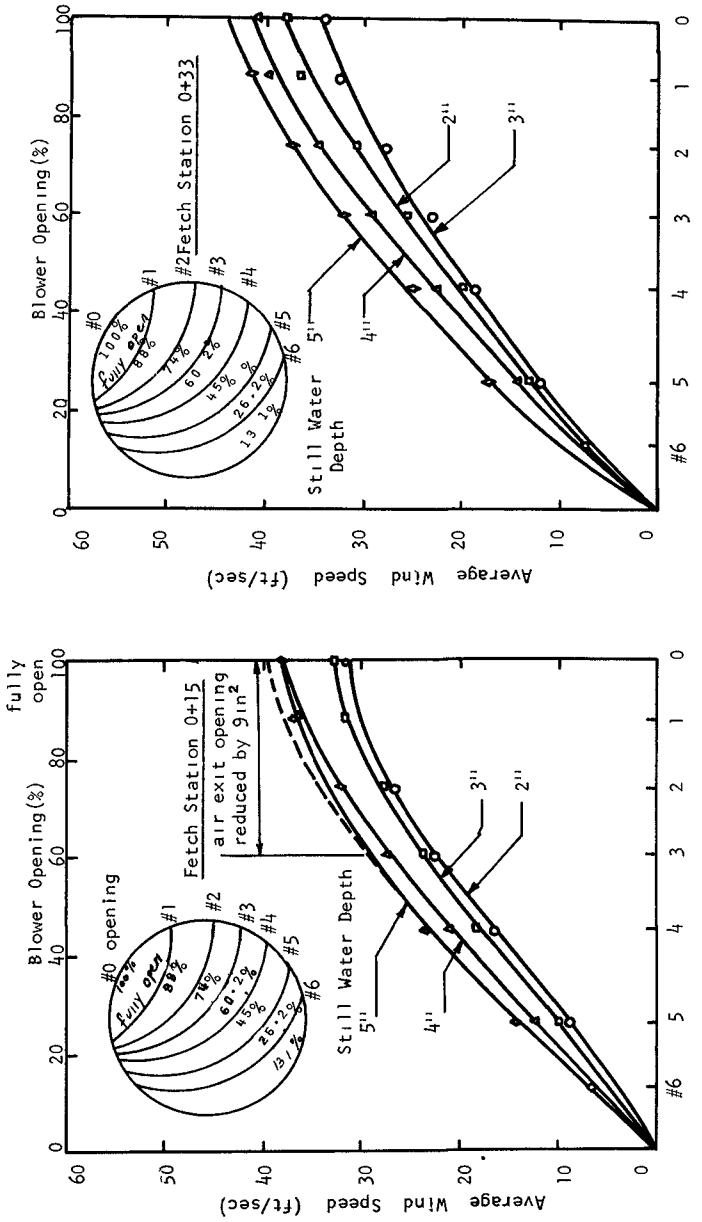

Fig. 2. Wind speed versus blower opening at the fetch Stations 0+15 and 0+33

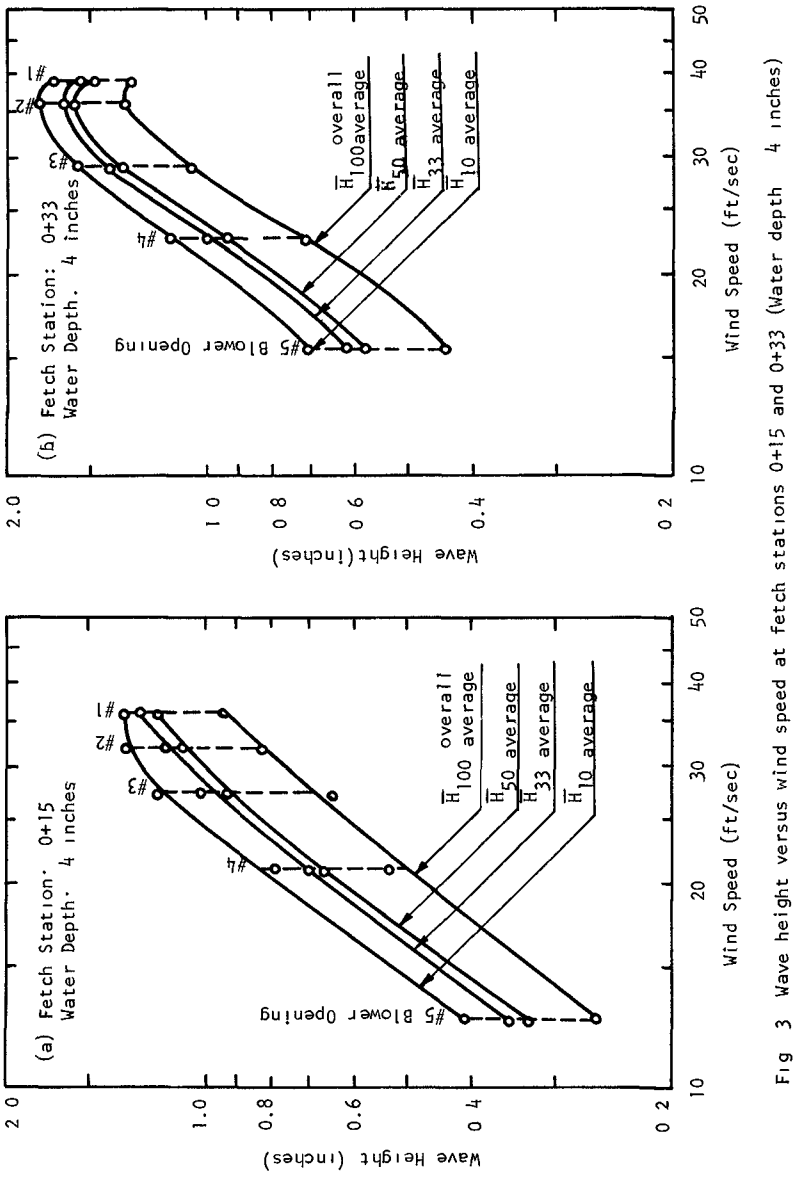

Fig 3 Wave height versus wind speed at fetch stations 0+15 and 0+33 (Water depth 4 inches)

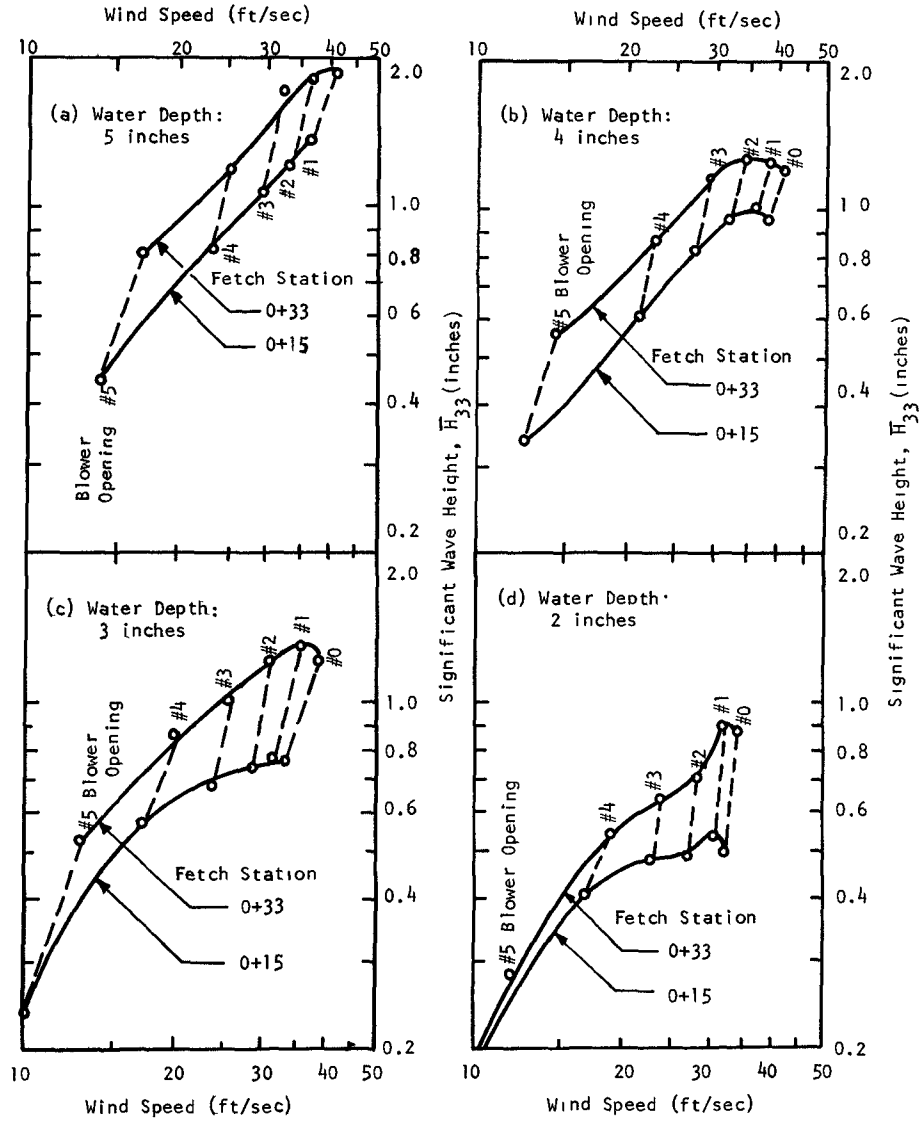

Fig. 4 Comparison of significant wave heights between the fetch stations 0+15 and 0+33

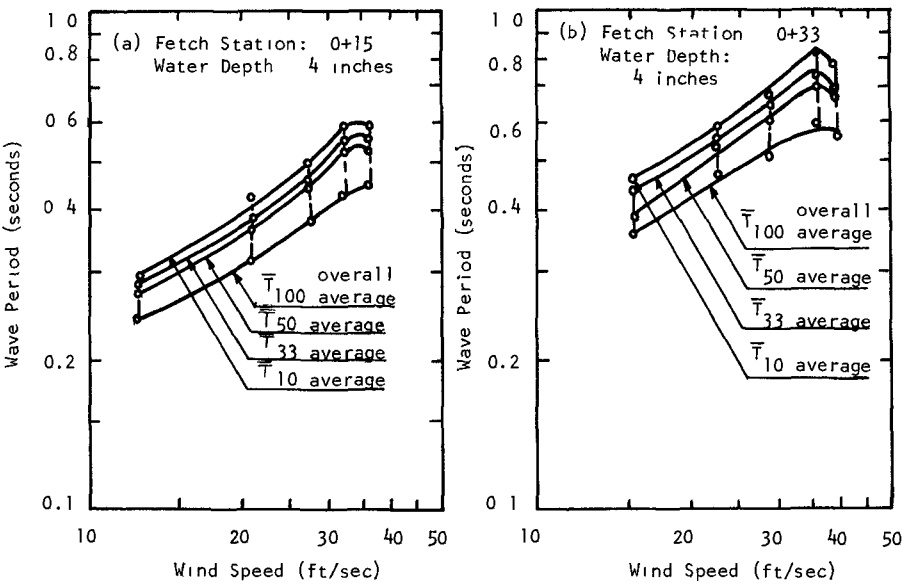

Fig. 5 Wave period versus wind speed at the fetch stations 0+15 and 0+33 (Water depth· 4 inches)

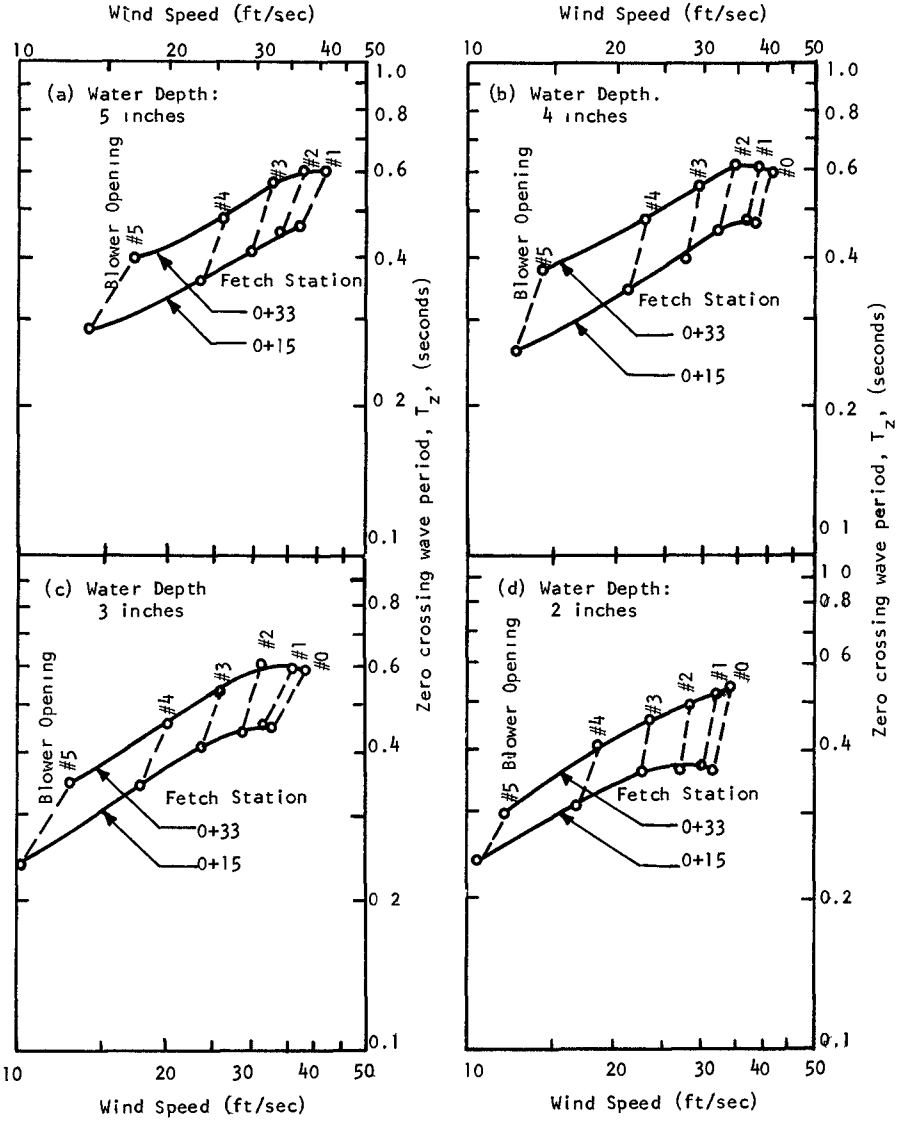

Fig. 6 Comparison of zero-crossing wave periods between the fetch stations 0+15 and 0+33

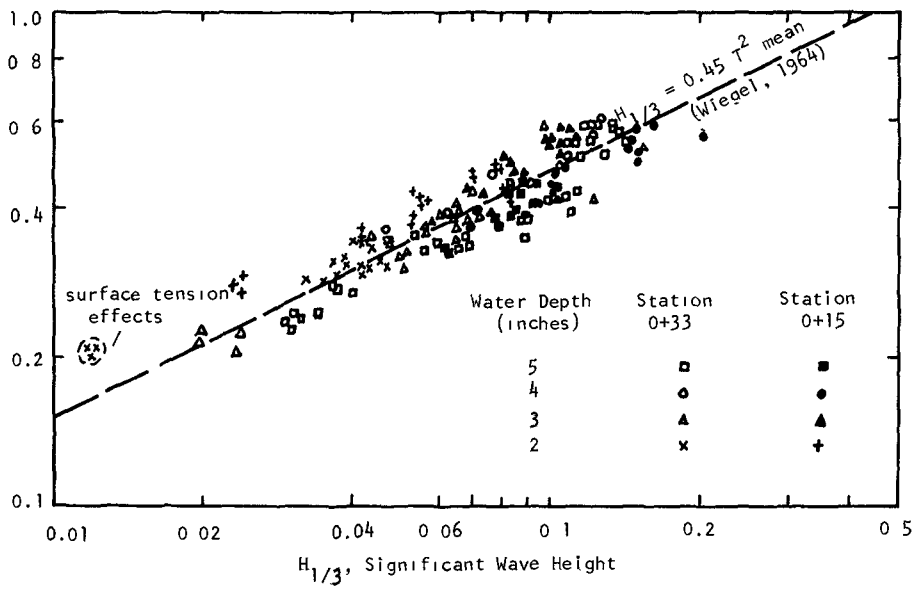

NOTE The relationship of $H_{1/3} = 0.45\ T^2_{mean}$ was established by Weigel (1964) and based on Sibul (1955) experimental data collected in the wind-wave flume of the University of California, Berkeley, Calif.

Fig. 7 Relationship between significant wave height and average wave period.

data coincided very well with the empirical formula ($H_{1/3} = 0.45\ T^2_{mean}$) proposed by Wiegel (1964) and depicted in the figure as a dashed line.

FREQUENCY ANALYSIS OF WAVE HEIGHT AND WAVE PERIOD

A thorough analysis was made of the frequency of occurrence of wave heights and wave periods for run No. 6, during which time the still water depth was maintained at 4 inches and tests were conducted for five wind conditions. The frequency of occurrence or percentage of excess for the two fetch locations was compared to the significant wave heights and wave periods (Figs. 8 and 9). On the average, the wave height and wave period measured at Station 0+33 were 14 percent greater than at Station 0+15

ANALYSIS OF WAVE DATA BY TUCKER AND DRAPER METHOD

The experimental wave data were further analyzed by a method developed by the National Institute of Oceanography, England (Tucker, 1961; Draper, 1966). According to Draper, this method of analysis is the result of theoretical studies of the statistical properties of sea waves and the analysis of numerous wave data collected in the sea, with due consideration of the results of many users. Because of the simplicity of the method, which is of merit in field applications, it is considered advisable to analyze the wave data collected in the laboratory in order to determine the validity of the technique, i e , to determine whether or not it is equally applicable to both sea waves and wind-waves generated in the laboratory The general procedure of analysis is given in Appendix A.

Comparing the significant wave heights as determined from the Tucker and Draper method and from normal frequency analysis, it was found that a positive correction of approximately 21% was necessary for wind-waves generated in the Look Laboratory, of which the wave-spectra distribution was of very narrow range; $H_{max} = 1.3\ H_s$ against $H_{max} = 1.6\ H_s$ for sea waves The wave spectral width parameter, $\varepsilon = \sqrt{1 - (T_e/T_z)^2}$ varied from 0.25 to 0.50, where T_c is crest wave period, and T_z is zero-crossing period. This means that the significant wave heights were approximately 21% underestimated by the Tucker and Draper method. However, the significant heights of sea-waves off the Look Laboratory as computed by this method were very close to the actual values needed; this is within engineering accuracy. In this case, the sea-waves have a larger wave spectral width parameter of 0.73 to 0.76 than the wind-waves simulated in the laboratory ($\varepsilon = 0.25$ to 0.50). Based on the above test results, the corrected significant wave height factors for data analysis by Tucker and Draper method is applicable to the laboratory and sea-waves measured at the Look Laboratory are shown in Fig 10. It may be concluded that analysis of sea-waves by the Tucker and Draper method is feasible for engineering purposes but certain corrections are necessary to analyze laboratory wind-waves, particularly of narrow wave spectra distribution. The prediction is quite satisfactory when the wave spectral width parameter is between 0.60 and 0.75.

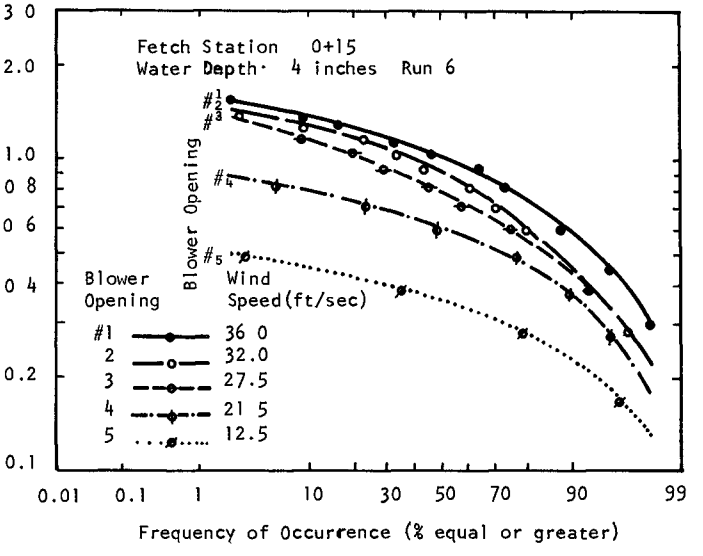

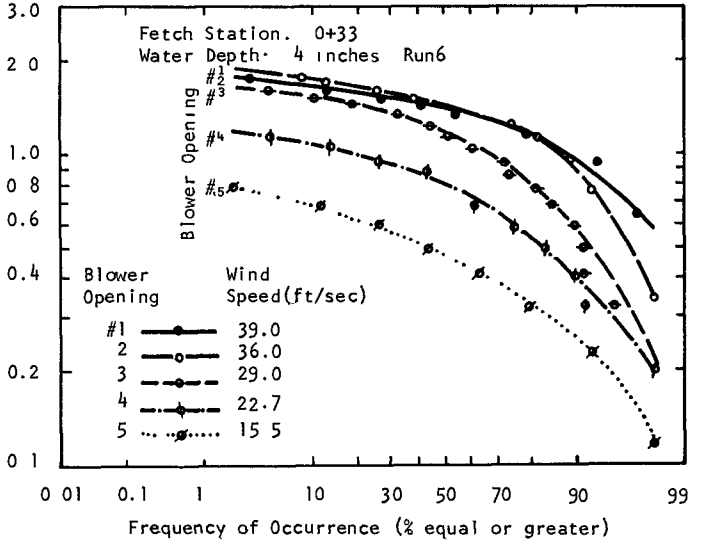

Fig 8 Frequency analysis of wave height at the fetch stations 0+15 and 0+33 (water depth: 4 inches)

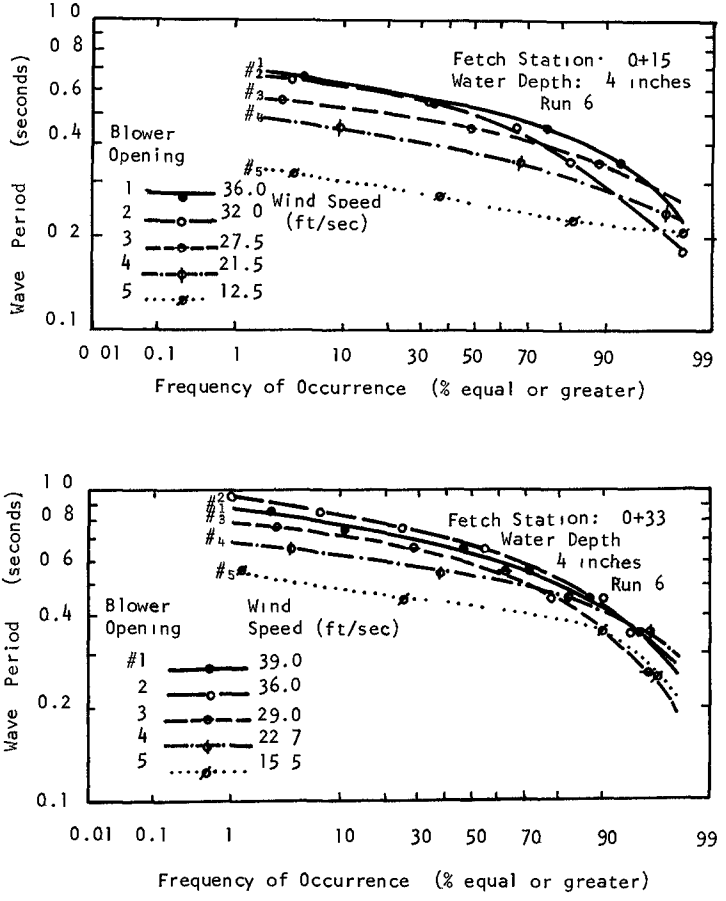

Fig 9 Frequency analysis of wave period at the fetch stations 0+15 and 0+33 (water depth. 4 inches)

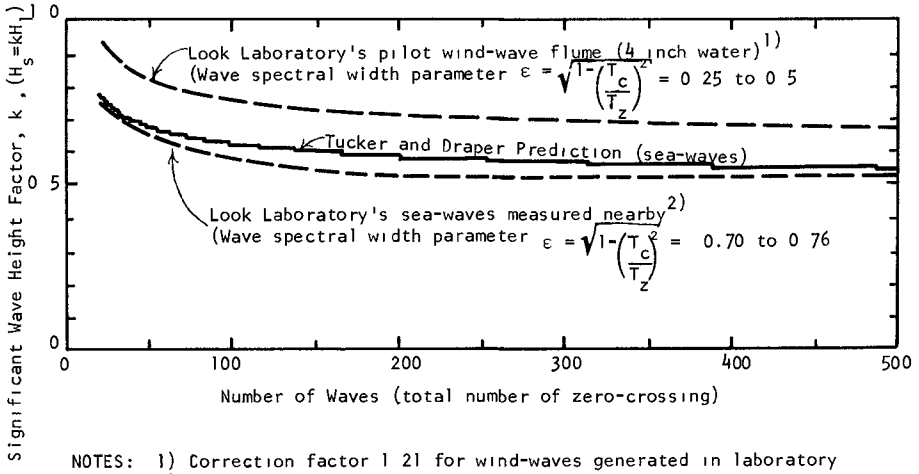

NOTES: 1) Correction factor 1 21 for wind-waves generated in laboratory
2) Correction factor 0.92 for sea-waves in shallow water near Look Laboratory.

Fig 10 Significant wave height factor for data analysis by Tucker and Draper method

It must be pointed out that, according to Draper (1966), the wave heights must be corrected for: a) response of the recording instrument, and b) attenuation of waves with water depth if the wave height is measured as a function of pressure fluctuation of the sea bottom.

During this study, the response of the recording instrument was investigated by comparing the recorded wave heights at different periodic oscillations The experimental apparatus is shown in Fig 11. It consists of a mechanical drive connected to a wire-resistant wave probe excited to oscillatory motion. The amplitude of oscillation was kept constant, but the frequency of oscillation was varied in order to determine the effect of frequency response on the recorded wave amplitudes As shown in Fig 12, the recorded wave height is slightly higher for waves of high frequency (greater than 4 cps) than for waves of low frequency There was a maximum 9 percent error observed in the interval of frequencies from 1 to 10 cps However, there was no significant effect of frequency of wave heights for wave periods between 0 20 and 1.0 seconds, which covers the majority of wave periods measured under this study Therefore, it is concluded that the effect of the response of the recording instrument can be ignored, although the wave height at any frequency from 5 cps up to 10 cps could be over-estimated by 3 to 9 percent

The water level variations in the tests were sensed by wire resistance techniques. Therefore, it was not necessary to make any corrections for the attenuation of waves with water depth

A comparison of the mean zero-crossing period (T_z) and mean crest period (T_c) with average wave period was made and there proved to be no significant difference (less than 6 percent among these parameters) Therefore, it is considered advisable to use the mean zero-crossing period as the relevant average wave period for civil engineering purposes, as recommended by Draper

For engineering applications, the significant wave height and a spectral-width parameter, ε, may be used to describe the statistical distribution of wave heights. The significant wave height may be determined by the analysis of statistical distribution of waves. The spectral-width parameter, $\varepsilon = 1\sqrt{-\left(\frac{T_c}{T_z}\right)^2}$, may vary from zero to unit. When ε approaches unity, the waves would cover a wide range of frequencies. For waves having a narrow range of frequencies, such as swells and tsunami waves, ε would be nearly zero

In the selection of design waves, it is customary to use maximum wave height or the average of the highest 1/10 of waves, in lieu of the significant wave height, for designing important fixed structures It is interesting to note that the ratio of the maximum wave height to the significant wave height varies from 1.2 to 1 3, as compared with 1.60 for wind-waves in the ocean, as estimated by Darbyshire and Draper (1963) This is because the laboratory-generated wind-waves have a much narrower wave spectrum than ocean waves.

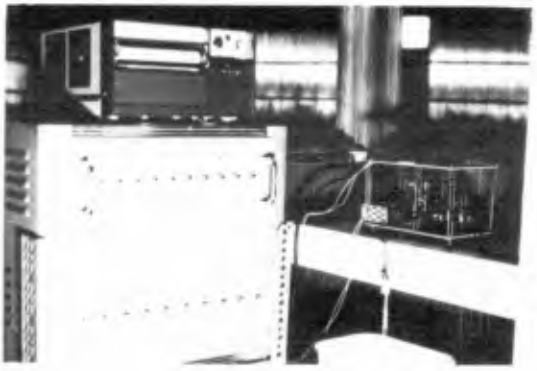

Fig. 11 Experimental apparatus for evaluation of frequency response of the wire-resistance wave gage.

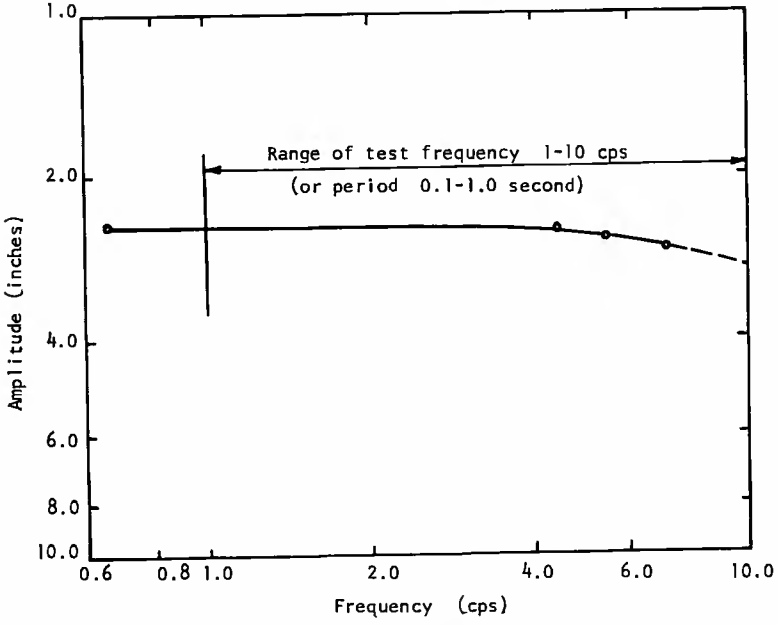

Fig. 12 Frequency response of the wire-resistance wave gage

ANALYSIS OF WAVE DATA BY THE DARBYSHIRE METHOD

The Darbyshire formula (Francis, 1959) suggested the relationship between wave height, wind speed, and fetch as follows.

$$H_{max} = 0.0076\ (1 - e^{-0.23F^{1/2}})\ U^2 \qquad (1) \quad F^{1/2}$$

or $$H_{max} = 0.0060\ (1 - e^{-0.003F_1^{1/2}})\ V^2 \qquad (2) \quad F_1^{1/2}$$

where

H = maximum wave height of 100 waves in feet
F = fetch length in nautical miles, F_1 = fetch length in feet
U = gradient wind speed in knots estimated to be 1 5 times the wind speed at 30 feet above the mean sea level
V = average wind velocity in ft/sec measured over water surface in the wind-wave flume.

As shown in Fig 13, the use of the Darbyshire formula to predict the maximum height of wind-waves generated in the laboratory is feasible for high wind speeds but a significant correction factor may have to be applied for the cases of low wind speeds. Therefore, the discrepancy may have resulted from the use of 1.5 times the average wind speed at 30 feet above mean water level in the ocean. Further investigation of these aspects is necessary. Due consideration should be given the use of gradient wind speed which needs to be defined for laboratory wind waves.

In summary, the application of experimental results to field conditions should be done carefully to avoid any significant error in maximum wave prediction

FETCH GRAPH COMPARISON

The dimensionless relationships gF/U^2, gH/U^2, and $gT/2\pi U$ determined from the fetch (F), wind speed (U), and wave period (T) are referred to as "Fetch Graph." This is considered the most effective means for correlating the above variables The non-dimensional representation has facilitated the comparison of various wave data collected either in the field or in the laboratory.

The experimental results were compared with those developed theoretically by Hino (1966), and Ijima and Tang (1966) as presented at the 10th Conference on Coastal Engineering, Tokyo, Japan. Comparison was also made with the previous empirical formulae by Bretschneider (1951, 1957), Sverdrup and Munk (1947) and Wilson (1961, 1962). The data compared well with the Hino theory for both wave heights and wave periods, and fairly well with Bretschneider's fetch graph for wave heights The difference in the comparison of wave data with other investigators is shown in Figs. 14, 15, 16 and 17. The discrepancies

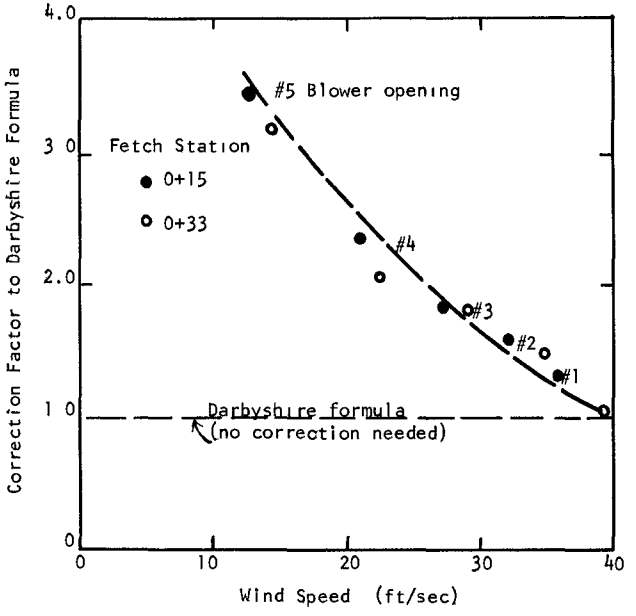

Fig. 13 Correction factor to the maximum wave height computed by Darbyshire's formula as a function of wind speed for simulated wind-waves

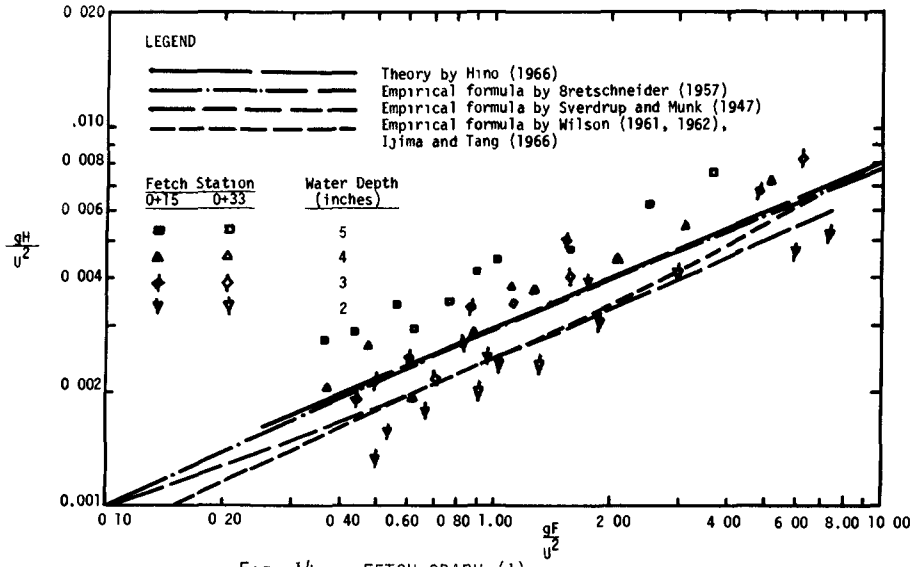

Fig. 14 FETCH GRAPH (1)

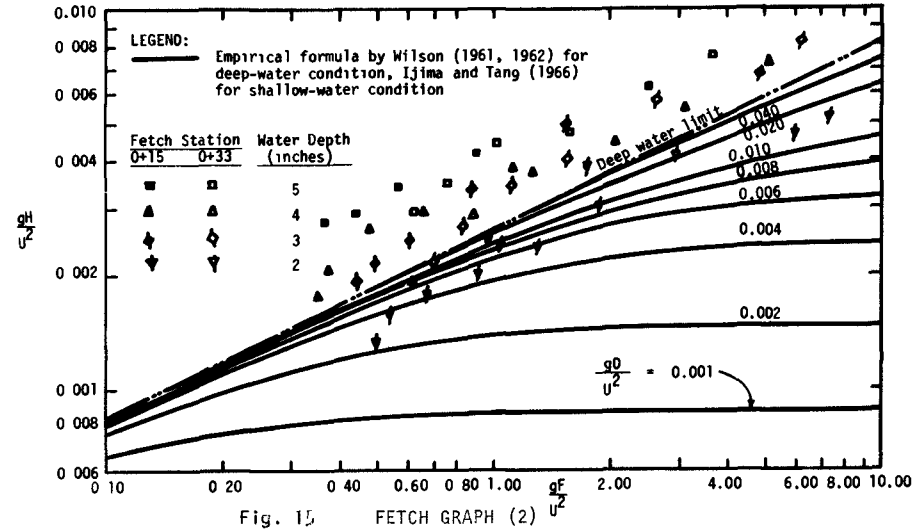

Fig. 15 FETCH GRAPH (2)

Deep Water Condition, Wilson (1961, 1962)

$$\frac{gH}{U^2} = \alpha \tanh\left[K_1\left(\frac{gF}{U^2}\right)^{1/2}\right]$$

where
$\alpha = 0.26$
$K_1 = 0.01$

Shallow Water Condition, Ijima and Tang (1966)

$$\frac{gH}{U^2} = \alpha \tanh\left[K_3\left(\frac{gd}{U^2}\right)^{3/4}\right] \tanh\left[\frac{K_1\left(\frac{gF}{U^2}\right)^{1/2}}{\tanh K_3\left(\frac{gd}{U^2}\right)^{3/4}}\right]$$

where
$K_1 = 0.578$
$K_3 = 0.01$
$\alpha = 0.26$

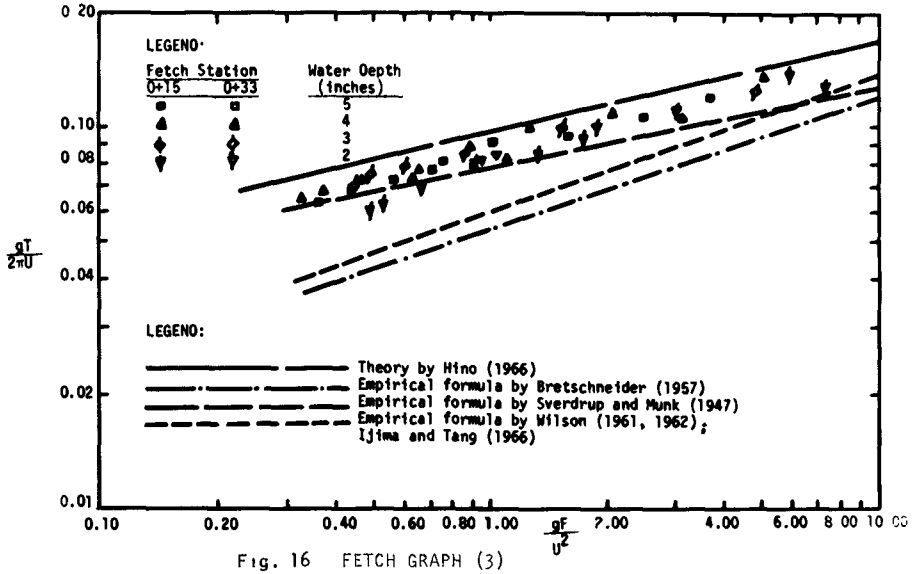

Fig. 16 FETCH GRAPH (3)

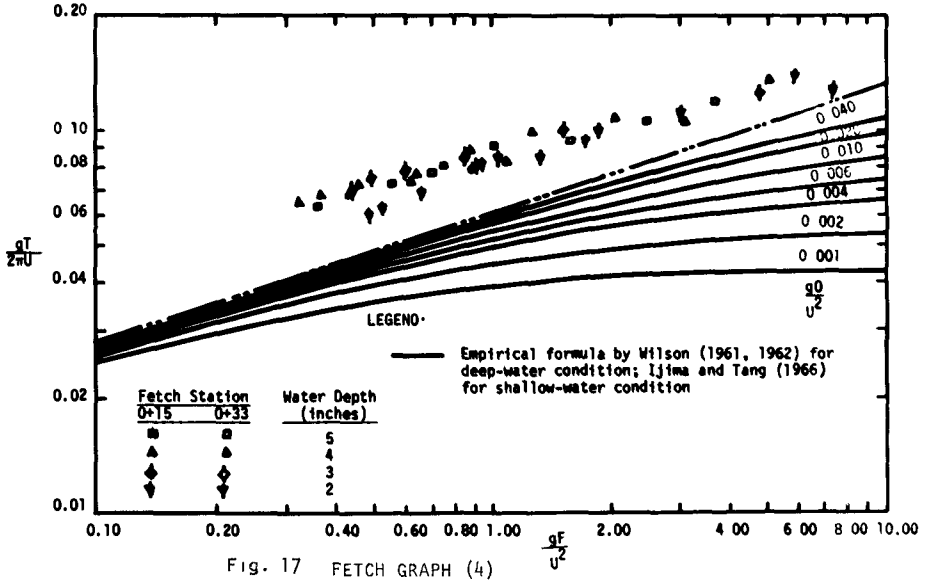

Fig. 17 FETCH GRAPH (4)

Deep Water Condition, Wilson (1961, 1962)

$$\frac{gT}{2\pi U} = \beta \tanh\left[K_2\left(\frac{gF}{U^2}\right)\right]^{1/3}$$

where:
$\beta = 1.40$
$K_2 = 0.0436$

Shallow Water Condtion, Ijima and Tang (1966)

$$\frac{gT}{2\pi U} = \beta \tanh\left[K_4\left(\frac{gd}{U^2}\right)^{3/8}\right] \tanh\left[\frac{K_2\left(\frac{gF}{U^2}\right)^{1/3}}{\tanh K_4\left(\frac{gd}{U^2}\right)^{1/8}}\right]$$

where
$K_2 = 0.436$
$K_4 = 0.520$
$\beta = 1.4$

are perhaps due to the fact that the wind waves generated in the laboratory were of narrow wave spectra distribution. Furthermore, the empirical coefficients as shown in Figs. 16 and 17 are being adjusted in the 1968 revision of wave forecasting (Bretschneider, 1968).

APPENDIX A

ANALYSIS OF WAVE DATA BY TUCKER AND DRAPER METHOD

The basic procedure of analysis is as follows (Draper, 1966)·

1. Select a section of wave record which covers at least 100 waves or more for the short fetch Station 0+15 during which period the waves are fully developed. The same period of time is used to analyze waves measured at the long fetch Station 0+33.

2. Wave height parameters are calculated from the sum of amplitudes measured from the mean water level to the highest crest (A) and to the lowest trough (C), regardless of whether or not the amplitudes are part of the same wave. The sum of (A) and (C) is defined as H_1. The mean water level is drawn by eye, although it could be determined more accurately by other methods such as the use of a planimeter However, experience indicated that the error introduced by determining wave periods from zero-crossing by eye is rather minor, and there will be no significant errors in the determination of wave heights and crest periods.

3 Count the number of zero crossings of the waves over the record period, (t), selected and then divide by two (2) to get N_z.

4. Compute the mean zero-crossing wave period, T_z, i.e., $T_z = \frac{t}{N_z}$.

5. Count the number of wave crests, N_c, including both those above and below mean water level.

6. Compute the mean wave period of the crests, T_c, i.e., $T_c = \frac{t}{N_c}$.

7. Compute the spectral width parameter, which is an indicator of the statistical distribution of wave periods This parameter shows that when the waves cover a wide range of frequencies or periods, the long waves will carry short waves on top of them and there will be many more wave crests, N_c, than zero-crossings N_z. Then, T_c will be much smaller than T_z and approaches unity, which indicates that the wave train has a wide wave-spectral distribution. On the other hand, if the range of frequencies is narrow, each wave crest will be associated with a zero crossing, then T_c and T_z will be approximately equal and will be close to zero (Draper, 1966).

8 Compute the significant wave height from the following relationship $H'_s = H_1$ factor The factor is determined from Fig 1D, as plotted from Draper's data

9 Compare the values of significant wave heights obtained from item No 8 above with those determined from the frequency analysis described in the preceding section Fig. 17 shows the deviations; it is apparent that a correction factor of 1.21 should be entered According to Draper (1966), H_1 should be corrected for the response of the recording instrument and for the attenuation of waves with depth In this case, $H_s = H'_1$ • factor and $H_s = (H_s$ • factor) 1.21

1D Similarly, the zero-crossing and crest periods were compared with the average wave periods obtained from the frequency analysis described in the preceding section.

11 Based on the new relationship of $H_s = (H_1$ • factor) 1 21, the significant wave heights were computed for the other runs under test conditions other than the 4-inch water depth in the flume

ACKNDWLEDGEMENTS

Permission of the Center for Engineering Research, University of Hawaii, to publish this paper is acknowledged

REFERENCES

1 Bretschneider, C L (1951), "Revised Wave Forecasting Relationships," Proceedings of Second Conference on Coastal Engineering (Houston, Texas, November 1951), Council of Wave Research, 1952, pp 1-5

2. Bretschneider, C. L (1957), "Revision in Wave Forecasting Deep and Shallow Water," Proceedings of Sixth Conference on Coastal Engineering (Florida, 1957), Council on Wave Research, 1958, pp. 3D-67.

3 Bretschneider, C L (1958), "Significant Waves and Wave Spectrum," Ocean Industry, Vol 3, No 2, February (1968), pp. 44-46.

4 Darbyshire, M., and L Draper (1963), "Forecasting Wind-Generated Sea Waves," National Institute of Oceanography, Wormley, Surrey, England, published in Engineering, April 5, 1963, pp 482-484

5 Draper, L (1966), "The Analysis and Presentation of Wave Data - a Plea for Uniformity," Proceedings of Tenth Conference on Coastal Engineering (Tokyo, Japan, September 1966), American Society of Civil Engineers, New York, N Y., 1967

6 Francis (1959), "Wind Action on Water Surface," Proceedings of Institution of Civil Engineers (England), Vol 12, February 1959, p 211.

7 Hino, M. (1966), "A Theory on the Fetch Graph of the Sea and the Energy Transfer Between Wind and Wave," Proceedings of Tenth Conference on Coastal Engineering, (Tokyo, Japan, September 1966) American Society of Civil Engineers, New York, N Y , 1967

8 Ijima, T., and F L. W. Tang (1966), "Numerical Calculation of Wind Waves in Shallow Water," Proceedings of Tenth Conference on Coastal Engineering (Tokyo, Japan, September 1966), American Society of Civil Engineers, New York, N Y 1967

9 Lee, T. T. (1968), "Characteristics of Wind-Waves Generated in Laboratory," Technical Report No. 3, Look Laboratory of Oceanographic Engineering, University of Hawaii, February 1968

10 Pierson, W. J , Jr , G. Newmann and R W. James (1955), "Practical Methods for Observing and Forecasting Ocean Waves by Means of Wave Spectra and Statistics," U. S Naval Oceanographic Office, Pub. No. 603, 1955.

11. Sibul, O. (1955), "Laboratory Study of the Generation of Wind Waves in Shallow Water," U S. Army Corps of Engineers, Coastal Engineering Research Center, Technical Memorandum No. 72, March 1955

12. Sverdrup, H. U., and W. H. Munk (1947), "Wind, Sea and Swell Theory of Relations for Forecasting," U S. Naval Oceanographic Office, Pub No 601, 1947.

13. Tucker, M J (1961), "Simple Measurement of Wave Records," Proceedings of Conference on Wave Recording for Civil Engineers, National Institute of Oceanography, Great Britain Also published in Dock and Harbor Authority, Vol. 42, p 231, 1961.

14. Wiegel, R L. (1964), "Oceanographic Engineering," Prentice Hall, Inc , Englewood Cliffs, New Jersey, 1964.

15. Wilson, B W (1961), "Deep Water Wave Generation by Moving Wind Systems," Journal of the Waterways and Harbor Division, Proceedings of American Society of Civil Engineers, paper 2821, Vol 87, No. WW2, May 1961.

16. Wilson, B. W. (1962), "Closure Discussion on 'Deep Water Wave Generation by Moving Wind Systems,' by B. W Wilson," Journal of the Waterways and Harbors Division, Proceedings of American Society of Civil Engineers, Vol. 88, No. WW3, WW4, August 1962 and November 1962, respectively.

CHAPTER 5

WIND VELOCITY PROFILE ABOVE PROGRESSIVE WATER WAVES

Omar H. Shemdin

Department of Coastal and Oceanographic Engineering,
University of Florida, Gainesville, Florida

ABSTRACT

An investigation of the air velocity profile above progressive, mechanically-generated waves was made in the wind and wave facility at Stanford University. The influence of propagating waves on the mean velocity profile was sought especially.

Both the instantaneous and mean velocity profiles were obtained with the use of high response total head and static pressure probes, in conjunction with a wave height gage. Experimental evidence is presented which suggests that the air velocity field responds to the wave motion.

The dependence of the mean velocity profile on wave frequency was investigated experimentally over mechanically generated waves having a constant amplitude. Also, the dependence of the mean velocity profile on wave amplitude was investigated over mechanically-generated waves with a specified frequency.

The theoretical results suggest that the wave influence is threefold. The first is due to the fact that a velocity-measuring instrument continuously shifts streamlines when measuring the air velocity above a perturbed water surface. The second is due to the wave-induced perturbation in the air velocity. The third is due to the interaction between the two effects just described. The results contribute towards explaining the lack of consistency in the existing data.

INTRODUCTION

In the study of the aerodynamic drag on the water surface, the method of attack was to relate the properties of the wind to the slope of the mean water level, the surface currents, and the waves generated. The total drag coefficient is usually defined

$$C_n = \frac{D}{\rho U_n^2} , \qquad (1)$$

where D is the total drag per unit area at the water surface and U_n is a velocity at height y above the water surface. Keulegan found that C_n increases linearly with U_n in wind channel experiments (ref. 1). Results similar to Keulegan's were found by Fitzgerald in another wind channel and by Van Dorn in a pond (ref. 2 and 3). The increase in the total drag coefficient was also observed by Francis, Sibul, and Hidy and Plate under laboratory conditions, and by Sheppard and Omar in the ocean (ref. 4, 5, 6, and 7). Large scatter in the total drag coefficient was reported by Keulegan and by Johnson and Rice under laboratory conditions, and by Hellström in the field with little evidence that it followed any stress law (ref. 8, 9, and 10). More recently, Kato and Takemura have reported a decrease in the drag coefficient with increasing U_n (ref. 11).

Munk derived an analytical expression for the total drag at the water surface based on the Jeffreys sheltering hypothesis and predicted an increase in the total drag coefficient with increasing U_n (ref. 12). A similar theoretical result was reported recently by Hino (ref. 13). An expression by Neumann, however, predicts a decrease in the total drag coefficient with increasing U_n (ref. 14). Roll, in a review of the studies related to the aerodynamic drag on the water surface, concluded that the state of knowledge is far from satisfactory (ref. 15).

The air velocity profile with respect to the mean water level has been approximated, most commonly, by a logarithmic velocity distribution given by

$$U = \frac{U_*}{\kappa} \ln \frac{y}{z_0} \qquad (2)$$

where $U_* = [\tau_0/\rho]^{1/2}$, τ_0 is the surface shearing stress, κ is the Kármán universal constant, z_0 is the roughness height. The uncertainty in determining the mean water level accurately leaves room to adjust the velocity data so that it can be approximated by a logarithmic distribution, whence values of U_* and z_0 are obtained. If the assumption is made that $\tau_0 = D$, then

$$C_n = \left| \kappa / \ln \left(\frac{y_n}{z_0} \right) \right| , \qquad (3)$$

which implies that C_n depends on z_0 and the height y_n at which the reference velocity U_n is taken. It is natural to expect that z_0 be related to the characteristics of the propagating waves at the air-water surface. Evidence of such dependence was given by Kunishi for very small amplitude waves (ref. 16). Holmes, however, found no correlation between z_0 and wave characteristics (ref. 17).

The results of previous investigators do not agree on a common relationship between U_* and z_0 as shown in Fig. 1. The disagreement leaves room to question the validity of applying a logarithmic velocity distribution to a shear flow over the water surface. A logarithmic fit was observed by some authors to be reasonable over a portion of the velocity data only. Thus, the

conclusions of Kato and Takemura were based on fitting a logarithmic distribution to the measured velocities close to the water surface, while the conclusions of Francis were based on fitting a logarithmic distribution to the measured velocities away from the water surface (ref. 11 and 18). The aim of the present study is to investigate both experimentally and theoretically the effect of propagating water waves on the measured mean velocity profile in the air stream above the water surface.

EXPERIMENTAL APPARATUS AND PROCEDURE

The 115-foot-long, 74-1/2-inch-high, and 35-1/2 inch-wide wind and wave facility at the Stanford University Hydraulics Laboratory was used for this study. A description of this facility was given by Shemdin and Hsu (ref. 19). The facility wave generator is equipped with an electrohydraulic control system which is capable of generating simple waves ranging in frequency from 0.2 to 4.0 cps. The air intake is located 17 feet downstream of the wave generator plate so that the mechanically generated waves become fully established before exposure to wind. A suction fan is provided at the downstream end of the channel. The fan is driven by a motor capable of creating a maximum wind speed of 80 fps when the water level is at a nominal depth of 3 feet. The channel has a steel plate floor, glass walls in the test section, and is closed by 3-foot by 5-foot interchangeable roof plates. The instruments are mounted on a special 3-foot by 5-foot plate which can be placed at any station along the channel.

The velocity in the air was measured with total head and static-pressure probes, in conjunction with a Pace differential pressure transducer (Model P90D) and a Sanborn 650-1100 series optical-type recorder. Two types of velocity probes were used:

1. a 1/32-inch O.D. pitot-static probe to obtain time-average velocities at a point. The probe is a standard shelf item manufactured by United Sensors and Control Corporation, and has a low cut-off frequency in its response characteristics;
2. a 3/32-inch O.D. total head and static-pressure probe to measure the instantaneous fluctuations of air velocities due to the perturbed water surface. The frequency response was flat up to about 3 cps, which is beyond the frequency range in the present investigation.

The Pace differential pressure transducer was calibrated with a Harrison micromanometer. The effect of both temperature and humidity were taken into account in converting the dynamic head signal into velocity.

The instantaneous velocities above simple mechanically generated waves were obtained by simultaneously recording the dynamic head signal and the water surface elevation. At each fixed position above the mean water level, a recording was obtained. Recordings were obtained at different preselected elevations above the mean water level to adequately describe the instantaneous boundary layer. The water surface elevation was measured by a capacitance-type wave height gage. A Nyclad insulated wire, No. 36 HNC, with

0.006-inch O.D. was used as a sensor. Adequate linearity was obtained in the relationship between the change in the water surface elevation and the voltage change due to wetting the sensor.

The instantaneous velocity at a fixed position above the crest of a mechanically-generated wave was obtained by averaging instantaneous dynamic head values which correspond in time to the wave crest. The crest velocity was typically obtained from an average over ten waves (*i.e.*, an average of ten crest dynamic head values). The position of the velocity probe above the wave crest was obtained from the initial position of the probe above the mean water level and the instantaneous water surface elevation. The crest velocity profile was obtained by simply graphing the crest velocities at different elevations above the mean water level with respect to the wave crest. A velocity profile over the trough was obtained by a similar procedure.

The mean velocity at any elevation above the mean water level was obtained by averaging the dynamic head signal at that level. The mean velocity profile was obtained by graphing the velocity at different elevations above the mean water level with respect to the mean water level. The change in the mean water level due to wind (set-up) was taken into account. The latter was found to be small.

EXPERIMENTAL RESULTS

The influence of surface waves on the mean air velocity profile can be evidenced by comparing: (1) a mean velocity profile over wind-generated waves to (2) one over a rigid flat plate under otherwise identical conditions. The wind-and-wave facility offers a unique possibility for such a comparison since the facility is enclosed by smooth roof plates. At any station the velocity profile vertically upward from the mean water level (profile above water surface) can be compared to the velocity profile vertically downward from the roof (profile over a rigid flat plate). Such a comparison at Station 32.5 (32.5 feet from air intake to test section) is shown in Fig. 2. The intake conditions were shown by Shemdin and Hsu (ref. 19).

Instantaneous velocity profiles were obtained over both the crest and trough of a mechanically-generated wave having a wave height of 3.4 inches and a wave frequency of 0.6 cps. Three trough and three crest profiles were obtained at three different fan speeds at Station 17.5. The instantaneous profiles are shown in Fig. 3. The corresponding mean velocity profiles are shown in Fig. 4. The mean velocity profiles are approximated by logarithmic distributions by the method of least squares.

Further evidence indicating the influence of waves on the mean air velocity profile is given by comparing: (1) the mean velocity profiles over wind-generated waves to (2) those over wind-and-mechanically-generated waves, under otherwise identical conditions. The velocity profiles over wind waves only are shown in Fig. 5 for three fan speeds at Station 57.5. The velocity profiles over wind-and-mechanically-generated waves are shown in Fig. 6 for the same fan speeds and at the same station. The velocity profiles in Figs. 5 and 6 are approximated by logarithmic distributions by the

method of least squares. The logarithmic distribution is seen reasonable for the velocity profiles in Fig. 6 but not for those in Fig. 5.

The influence of the waves on the air velocity profile shown above suggests a more detailed study of the dependence of the air velocity profile on the amplitude and frequency of waves. For this purpose a comprehensive study was made of the mean velocity profile at Station 47.5 so that the geometrical effects of the air entrance and exit of the wind-wave facility can be minimized. Two sets of mean velocity profiles were obtained. The first was over mechanically-generated waves with a constant amplitude and varying frequency. The second was over mechanically-generated waves with a constant frequency and varying amplitude. The frequencies used for the first set were 0.6, 0.75, 1.0, and 1.20 cps. The amplitude used for the first set was 2.00 inches. For each frequency five distinct velocity profiles were obtained at different fan settings with maximum velocity ranging from 13.0 to 40.0 fps.

The frequency used for the second set of velocity profiles was 0.75 cps. The corresponding amplitudes were 1.1, 2.0, and 3.0 inches. For each amplitude, five distinct velocity profiles were obtained at different fan settings with the maximum velocities ranging from 13.0 to 40.0 fps. The velocity profiles of the second set for amplitudes 1.1 and 3.0 inches are shown in Figs. 7 and 8 respectively.

From the velocity profiles of the first set the customary relationship between U_* and z_0 was investigated for each frequency. The results are shown in Fig. 9. The dependence of z_0 on wave frequency was also investigated and the results are shown in Fig. 10. More details on the dependence of U_* and z_0 on both wave amplitude and frequency were given by Shemdin (ref. 20). Previous investigators have attempted to find a relationship between z_0 and U_* as suggested by the data in Fig. 1. A dimensionless graph of gz_0/U_*^2 vs. C/U_* is a convenient artifice to investigate the influence of waves on z_0 and U_*. A dimensionless graph which includes all the acquired data in this study is given in Fig. 11. The graph indicates that C/U_* is an important parameter which influences the relationship between U_* and z_0. The relationship suggested by Charnock (on purely dimensional grounds) is also shown for comparison (ref. 21).

THEORETICAL ANALYSIS

A standard method for measuring the velocity above a perturbed water surface is to measure the time average dynamic head (*i.e.*, the average difference between the total head and static pressure) at a fixed position of the probe above the mean water level. The measured dynamic head p at any point in the flow field can be expressed

$$p = \frac{\rho}{2} \frac{1}{T} \int_0^T u^2(x,\zeta,t)dt \qquad (4)$$

where ζ is the elevation of the probe above the instantaneous water

surface and is consequently a function of time t, u is the air velocity at elevation ζ and station x along the direction of flow, T is the length of time over which the averaging process is considered, and ρ is the air density. The aim of the present analysis is to investigate the variation of p above the mean water level when the water surface is disturbed by a simple, small-amplitude, progressive water wave and the undisturbed mean velocity has a logarithmic profile. The turbulent fluctuation is considered only insofar as they affect the unperturbed mean velocity profile.

The velocity $u(\zeta,t)$ at a station x_0 can be expressed in terms of a mean velocity $U(\zeta)$ and a wave-induced perturbation velocity $u'(\zeta,t)$

$$U(\zeta,t) = U(\zeta) + u'(\zeta,t). \tag{5}$$

The behavior of $u'(\zeta,t)$ was predicted by Miles for a mean velocity profile given by Eq. (2) (ref. 22). Turbulent fluctuations were neglected in the flow field above perturbed water surface. The water surface η was described by

$$\eta = a \exp ik(x - ct), \tag{6}$$

where a is the wave amplitude, k is the wave number, and x is the axis along which the wave propagates with a phase speed c. The real part of η is taken as the actual perturbed surface. The unperturbed mean velocity profile $U(\zeta)$ was described

$$U(\zeta) = U_1 \ln \frac{\zeta}{z_0}, \tag{7}$$

where U_1 is U_*/κ. The flow field considered by Miles has no upper bound, and the perturbation velocity was defined (ref. 22).

$$u'(\zeta,t) = - k\eta U_1 \frac{\partial \phi}{\partial \zeta}, \tag{8}$$

where ϕ is a complex function which satisfies the inviscid Orr-Sommerfeld equation and the surface condition, and decays as $y \to \infty$. A numerical solution of the boundary value problem governing ϕ was given by Conte and Miles and their results will be used in this investigation to predict the dynamic head above the mean water level (ref. 23).

At an arbitrary station x = 0, the position of a probe fixed in space at a specified distance y above the mean water surface, can be expressed in terms of its distance to the instantaneous water surface. The water surface motion is periodic at x = 0

$$\eta = a \cos kct, \tag{9}$$

so that

$$\zeta = y - a \cos kct, \tag{10}$$

as shown schematically in Fig. 12.

The dynamic pressure p at any elevation y above the mean water level can be obtained by expressing ζ in terms of y and t in Eq. (4) and integrating with respect to time. The wave-induced perturbation velocity may be expressed at x = 0

$$u'(\zeta,t) = kaU_1 g(\zeta) \cos (kct - \theta) , \tag{11}$$

where

$$g(\zeta) = \left| \frac{\partial \phi(\zeta)}{\partial \zeta} \right| , \tag{12}$$

and

$$\theta = \tan^{-1} \frac{I_m(\partial\phi/\partial\zeta)}{R_e(\partial\phi/\partial\zeta)} + \pi . \tag{13}$$

The dynamic pressure may then be expressed (it is recognized that the angle between the pitot-static probe and the resultant velocity vector is small above small-amplitude waves)

$$p(y) = \frac{\rho}{2} \frac{1}{T} \int_0^T \left| U(y - a \cos kct) + kaU_1 g(y - a \cos kct) \cos (kct - \theta) \right|^2 dt , \tag{14}$$

where $g(\zeta)$ and θ are obtained from the numerical solution given by Conte and Miles (ref. 23). The function g is shown typically in Fig. 13 for a wave number k equal to 0.5 ft^{-1}, and an air velocity profile specified by U_1 equal to 3.4 fps and z_0 equal to 0.05 in. Conveniently, the function g may be approximated by an exponential function

$$g(\zeta) = C_1 e^{-h\zeta} , \quad \zeta \leq \zeta_0 \tag{15}$$

and

$$g(\zeta) = C_2 , \quad \zeta > \zeta_0 \tag{16}$$

where C_1, C_2, and h are constants. The above approximation is also shown graphically in Fig. 13.

The dynamic pressure p, given by Eq. (14), may be expanded into three integrals

$$p(y) = \frac{\rho}{2}(I + II + III) . \tag{17}$$

The integral expression I represents the effect of a probe crossing streamlines above a perturbed surface and is given by

$$I = \frac{1}{T} \int_0^T U_1^2 \left| \ell n \frac{(y - a \cos kct)}{z_0} \right|^2 dt. \tag{18}$$

The integral expression II represents the interaction effect between crossing streamlines and wave-induced velocity perturbation and is given by

$$II = \frac{2kaU_1^2}{T} \int_0^T \ell n \left(\frac{y - a \cos kct}{z_0} \right) g(y - a \cos kct) \cos (kct - \theta) dt. \tag{19}$$

The integral expression III represents the effect of wave-induced perturbation on the velocity measurement and is given by

$$III = \frac{(kaU_1)^2}{T} \int_0^T g^2(y - a\cos kct)\cos^2(kct - \theta)dt \ . \qquad (20)$$

The logarithmic mean velocity may be expressed in a series to $O[(a/y)^4]$

$$U(\zeta) = U_1 \ln \frac{y}{z_0} - U_1 \left| \left(\frac{a}{y}\right)\cos kct + \frac{1}{2}\left(\frac{a}{y}\right)^2\cos^2 kct + \frac{1}{3}\left(\frac{a}{y}\right)^3\cos^3 kct + \frac{1}{4}\left(\frac{a}{y}\right)^4\cos^4 kct + \ldots \right| , \ -1 \leq \frac{a}{y} < 1. \qquad (21)$$

The dynamic pressure p in the region $\zeta \leq \zeta_0$ may be evaluated by substituting Eqs. (15 and 21) into Eq. (14). The dynamic pressure p in the region $\zeta \leq \zeta_0$ becomes for a < y to $O[(a/y)^4]$

$$\begin{aligned} p = \frac{\rho}{2}\{ & \left| \left(U_1 \ln \frac{y}{z_0}\right)^2 - \frac{1}{2}[U_1^2 \ln \frac{y}{z_0} - U_1^2] \left(\frac{a}{y}\right)^2 \right. \\ & \left. - \frac{3}{8}[\frac{1}{2} U_1^2 \ln \frac{y}{z_0} - \frac{11}{12} U_1^2] \left(\frac{a}{y}\right)^4 \right| \\ & + \{2C_1 kaU_1^2 \exp(-2hky) \cos\theta \left| \frac{1}{2}[hka \ln \frac{y}{z_0} - \left(\frac{a}{y}\right)] \right. \\ & + \frac{3}{8}\left(\frac{hka)^3}{6}\right) \ln \frac{y}{z_0} - \frac{1}{3}\left(\frac{a}{y}\right)^3 - \frac{1}{2}(hka)^2\left(\frac{a}{y}\right) \\ & \left. - \frac{1}{2}(hka)\left(\frac{a}{y}\right)^2) + \ldots \right| \} \\ & + \left| C_1^2 (ka)^2 U_1^2 \exp(-2hky)[\frac{1}{2} + \frac{(hka)^2}{4} (2 + \cos\theta) \right. \\ & \left. + \frac{(hka)^4}{24} (3 + 2\cos 2\theta)] \right| \} \ . \end{aligned} \qquad (22)$$

In the region $\zeta > \zeta_0$ the dynamic pressure p becomes for a < y to $O[(a/y)^4]$

$$p = \frac{\rho}{2}\{ \left| \left(U_1 \ln \frac{y}{z_0}\right)^2 - \frac{1}{2}[U_1^2 \ln \frac{y}{z_0} - U_1^2]\left(\frac{a}{y}\right)^2 - \frac{3}{8}[\frac{U_1^2}{2} \ln \frac{y}{z_0} - \frac{11}{12} U_1^2]\left(\frac{a}{y}\right)^4 + \ldots \right|$$

$$- \left| ka\, U_1^2\, C^2 \left[\left(\frac{a}{y}\right) + \frac{1}{4}\left(\frac{a}{y}\right)^3 + \ldots \right] \right| \cos\theta$$

$$+ \frac{1}{2}(ka)^2 U_1^2\, C_1^2 \} \quad . \tag{23}$$

The apparent velocity which is extracted from the dynamic pressure is

$$U_{app} = [2p/\rho]^{1/2} \quad . \tag{24}$$

The effects of shifting streamlines and wave-induced perturbation are shown typically in Fig. 14 for the case of an undisturbed logarithmic distribution with U_1 equal to 3.4 fps and z_0 equal to 0.05 inches and a propagating wavy surface with an amplitude of 1.70 inches and a wave number of 0.5 ft^{-1}. It is suggested that the two effects may be compensating. The interaction effect is appreciable, as shown also in Fig. 14.

The above analysis suggests that the measurements of the mean velocity profile above a perturbed water surface depend upon the properties of the propagating waves at the surface. Such an effect has been discounted in the past and thus may constitute the reason for the existing disagreement between the results of previous experimental investigators. The expressions developed for the apparent velocity profile lend themselves readily to numerical evaluation on the computer. The IBM 7090 was used in the present investigation.

DISCUSSION OF RESULTS

The theoretical and experimental results arrived at in this investigation can be viewed as two independent sets of results both aimed at investigating the influence of surface waves on the mean velocity profile above the surface. Conveniently, the theoretical results are discussed first and then the experimental results are explained in light of the theoretical results.

The theoretical results suggest that when a truly logarithmic velocity profile exists over an undisturbed surface, the measurement of such a profile by a pitot-static probe over a surface disturbed by a propagating wave may give a velocity profile which is significantly different from the original profile. The difference between the two profiles is seen to be due to three effects. These are conveniently referred to as the effect of shifting streamlines, the wave-induced perturbation effect, and the interaction between these two effects.

The effect of shifting streamlines is due to the fact that a probe fixed in space above a perturbed surface intercepts different streamlines when the probe is over the wave crest, than when it is over the wave trough. This is shown schematically in Fig. 12. This effect is analogous to that caused by a probe oscillating in a boundary layer above a fixed flat plate. In a turbulent velocity profile, the effect of shifting streamlines gives a velocity which

is less than the true velocity. The effect depends strictly on the shape of the original velocity profile and the ratio of the amplitude of the wave to the height of the probe above the mean water level. The effect is independent of the wave frequency. A numerical computation of this effect is shown in Fig. 14 for the case of an undisturbed logarithmic velocity profile with U_1 equal to 3.4 fps and z_0 equal to 0.05 inch and a propagating wavy surface with an amplitude of 1.7 inches and a wave number of 0.5 ft^{-1}.

The wave-induced perturbation effect is due to the fact that the instantaneous velocity profile over the crest is different from that over the trough of a perturbed water surface as shown in Fig. 3. According to Miles this effect depends on $g(\zeta)$, θ, ka, and U_1. This effect decays rapidly with increasing distance from the mean water level when compared to the effect of shifting streamlines.

The interaction between the effect of shifting streamlines and the wave-induced effect may either increase or decreased the measured velocity, depending on the coupling between the wave-induced effect and the effect of shifting streamlines. Thus a velocity probe, for example, may gauge a higher velocity over the crest of a wave due to the wave-induced perturbation effect, even though the probe is at a velocity region closer to the boundary.

The predicted influence of wave amplitude on the measured velocity profile is shown in Fig. 15 for the same undisturbed velocity profile and wave frequency discussed above. The wave-induced effect appears to be relatively significant for small-amplitude waves and is consistent with the rapidly decaying property of this effect with height above the perturbed surface. The effect of shifting streamlines becomes dominant for large-amplitude waves. The results of Fig. 15 suggest that high values of both U_1 and z_0 will be measured when compared to the corresponding values of U_1 and z_0 of the undisturbed profile. The overestimate increases with increasing amplitude.

The predicted influence of wave frequency on the measured velocity profile is shown in Fig. 16 for waves having the same amplitude and the same undisturbed velocity profile discussed above. The wave-induced effect decays exponentially upwards from the mean water level. The decay factor depends directly on the wave number k. Consequently, the wave-induced effect in a high-frequency wave (large wave number) is expected to be smaller than that for a relatively lower-frequency wave. The effect of shifting streamlines, however, is independent of the wave frequency as it has already been noted. The interaction effect depends on both wave amplitude and frequency. For the 0.4 and 0.6 cps waves in Fig. 16, the interaction effect is of the same order of magnitude as the effect of shifting streamlines. The interaction effect in these cases is also in the same direction as that due to the shifting of streamlines. The two effects add up to a significant deviation from the undisturbed velocity profile. Contrary to the above, the interaction effect is small compared to the effect of shifting streamlines for the 1.0 and 1.4 cps waves in Fig. 16. The wave-induced effect is also relatively

small, so that most of the deviation indicated is due to the effect of shifting streamlines. The results shown in Fig. 16 suggest that at certain frequencies the velocity profile may deviate significantly from a velocity profile over an undisturbed water surface.

In conclusion it is emphasized that the present theoretical analysis is valid only insofar as the water surface is perturbed by a simple propagating wave, and only insofar as the Miles inviscid Reynolds stress mechanism remains valid. Recent work by Bryant suggests that the inviscid Reynolds stress mechanism underestimates the transfer of energy to waves (ref. 24). No analytic solution of the wind field was proposed, however, to replace Miles's solution. The present theoretical analysis can be extended to any wind flow field if it can be described analytically. Within the above restrictions the results of Figs. 15 and 16 suggest, as a rule of thumb, that the influence of waves on the measured velocity profile becomes small at an approximate distance of three amplitudes above the mean water level.

It is to be noted again that the theoretical predictions shown in Figs. 15 and 16 are for an undisturbed logarithmic profile which corresponds to a fan speed of 240 rpm. At different fan speeds, the theoretically predicted wave-influenced velocity profiles are expected to be different. The different behaviors indicated in Figs. 10 and 11 for different wind speeds may be explained in light of the two competing influences and their interaction, all of which are induced by the presence of waves.

The present investigation in no way gives an answer to the question of whether the actual velocity profile over a disturbed surface is truly logarithmic. It only suggests that if it is logarithmic, then the measured profile by a velocity probe would deviate from the true velocity profile. The fact that the velocity profiles over wind-generated waves, shown in Fig. 5, deviate from a logarithmic distribution still remains to be explained. The theoretical results presented in this investigation predict a deviation from the logarithmic distribution in the opposite direction from that shown in Fig. 5. The fact that the measured velocity profiles over mechanically-generated waves shown in Fig. 6 come closer to the logarithmic distribution, is consistent with the theoretical results of this investigation. Stewart suggested that the velocity profile over a wavy surface may deviate from a logarithmic distribution in a manner similar to the profiles shown in Fig. 5 (ref. 25). More recently, however, Phillips has discounted such a behavior (ref. 26).

REFERENCES

1. Keulegan, G. H. Wind Tides in Small Closed Channels, 1951, *J. Res. Natl. Bureau of Standards*, **46**, 258-381.

2. Fitzgerald, L. M. Wind-Induced Stresses on Water Surfaces: A Wind Tunnel Study, 1963, *Austr. J. Phys.*, **16**, 475-489.

3. Van Dorn, W. G. Wind Stress on an Artificial Pond, 1953, *J. Mar. Res.*, **12**, 249-276.

4. Francis, J. R. D. Wind Stresses on a Water Surface, 1954, *Quart. J. Roy. Met. Soc.*, 80, 438-443.

5. Sibul, O. Laboratory Study of the Generation of Wind Waves in Shallow Water, 1955, *Beach Erosion Board T. M.* 72, Washington.

6. Hidy, G., and Plate, E. Wind Action on Water Standing in a Laboratory Channel, 1966, *J. Fluid Mech.*, **26**, 651-687.

7. Sheppard, P. A., and Omar, M. H. The Wind Stresses over the Ocean from Observations in the Trades, 1952, *Quart. J. Roy. Met. Soc.*, **78**, 583-589.

8. Keulegan, G. H. Hydrodynamic Effects of Gales on Lake Erie, 1953, *J. Res. Natl. Bureau of Standards*, 50, 99-109.

9. Johnson, J. W., and Rice, E. K. A Laboratory Investigation of Wind Generated Waves, 1952, *Trans. A. G. U.*, 33, 845-854.

10. Hellström, B. Wind Effect on Rinköbing Fjord, 1953, *Trans. A. B. U.*, **34**, 194-198.

11. Kato, H., and Takemura, K. Wind Profiles over the Shallow Water (1st Report), 1966, *Port and Harbor Tech. Res. Inst.*, **5**, No. 1.

12. Munk, W. H. Wind Stresses on Water: A Hypothesis, 1955, *Quart. J. Roy. Met. Soc.*, **81**, 320-332.

13. Hino, M. A Theory on the Fetch Graph, the Roughness of the Sea and the Energy Transfer between Wind and Wave, 1966, *Proc. 10th Conf. Coastal Engrg.*, 1, Tokyo, 18-30.

14. Neumann, G. Über den Tangential druck des Windes und die Ranigkeit der Meeresoberfläche, 1948, *Z. Met.*, 2, 193.

15. Roll, H. U. On the Present State of Knowledge in Air-Sea Boundary Layer Problems, 1965, *Proc. Sea-Air Interaction Conf.* (Tallahassee, Florida, Feb., 1965), Tech. Note 9-SAIL, ESSA, Washington 30-58.

16. Kunishi, H. An Experimental Study on the Generation and Growth of Wind Waves, 1963, *Diss. Prev. Res. Inst.*, **Bull. 61**, Kyoto.

17. Holmes, P. Wind Generation by Waves, 1963, Ph.D. Thesis, College of Swansea, Univ. of Wales.

18. Francis, J. R. D. The Aerodynamic Drag of a Free Water Surface, 1951, *Proc. Roy. Soc.*, Ser. A, 206, 387-408.

19. Shemdin, O. H., and Hsu, E. Y. The Dynamics of Wind in the Vicinity of Progressive Water Waves, 1966, *Proc. 10th Conf. on Coastal Engineering*, Tokyo, 396-317.

20. Shemdin, O. H. Experimental and Analytical Investigation of the Air Velocity Profile Above Progressive Waves, 1967, *Dept. of Civil Eng. Tech. Rept.*, 82, Stanford Univ., Stanford.

21. Charnock, H. Wind-Stress on a Water Surface, 1955, *Quart. J. Roy. Met. Soc.*, 81, 639.

22. Miles, J. W. On the Generation of Surface Waves by Shear Flows, 1957, *J. Fluid Mech.*, 3, 185-204.

23. Conte, S. D., and Miles, J. W. On the Numerical Integration of the Orr-Sommerfeld Equation, 1959, *J. Soc. Indust. Appl. Math.*, 7, 361-366.

24. Bryant, P. J. Wind Generation of Water Waves, 1966, Ph.D. Dissertation, Univ. of Cambridge.

25. Stewart, R. W. The Drag of Wind over Water, 1961, *J. Fluid Mech.*, 10, 189-194.

26. Phillips, O. M. The Dynamics of the Upper Ocean, 1966, Cambridge Univ. Press.

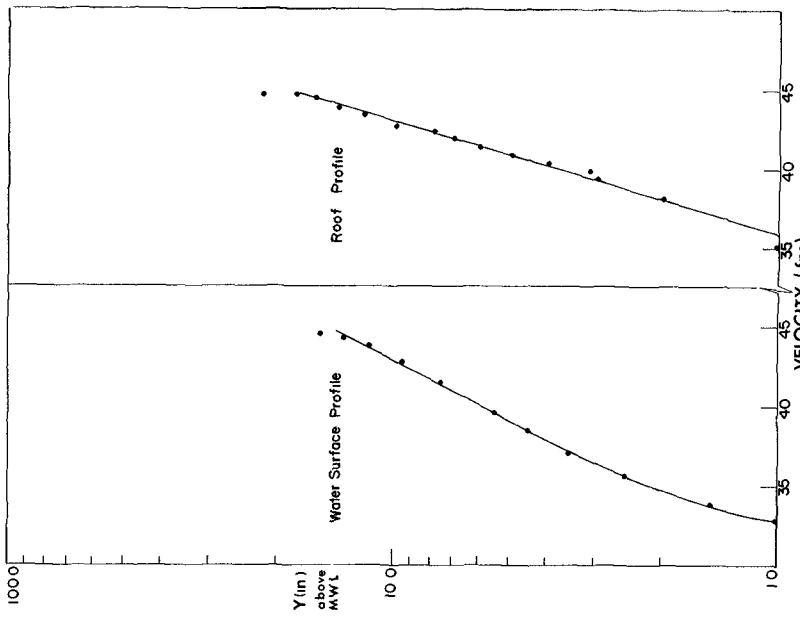

Fig. 2. Comparison between the water surface and flat plate velocity profiles, at Sta. 32.5.

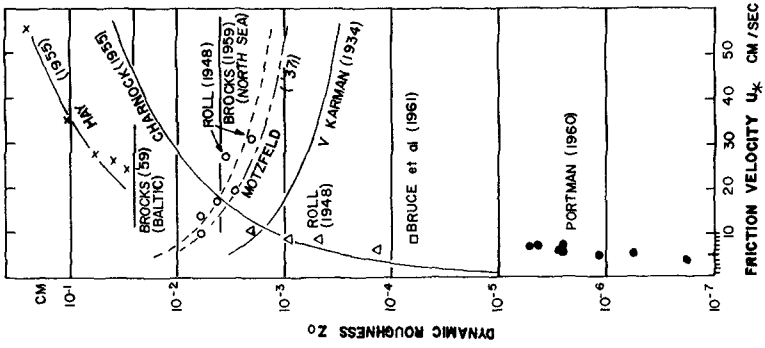

Fig. 1. U* vs. z_0 after Roll (1965).

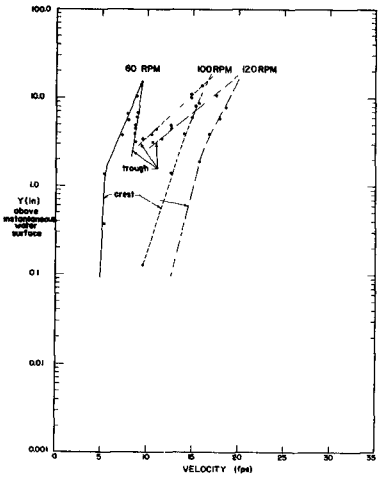

Fig. 3. Instantaneous crest and trough profiles over a mechanically generated wave (a=1.7 in., f=0.6 cps).

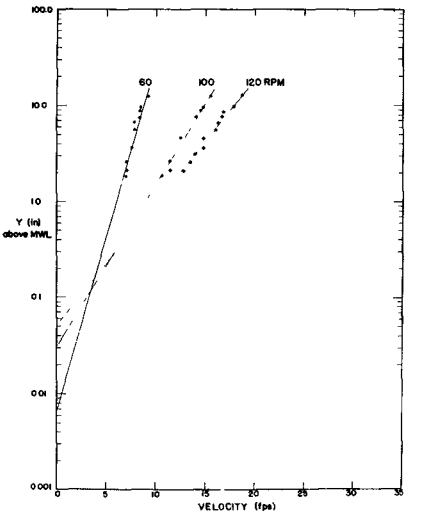

Fig. 4. Mean profiles over a mechanically generated wave (a=1.7 in, f=0.6 cps).

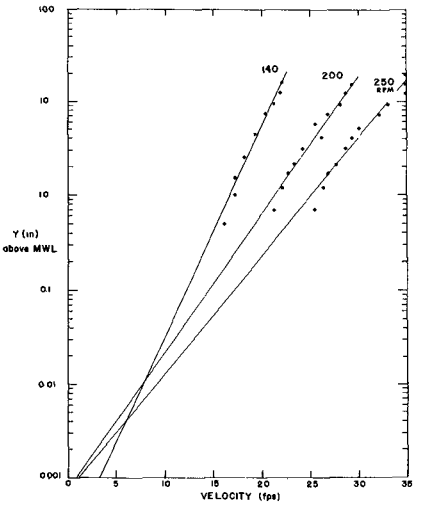

Fig. 5. Mean profiles over water surface perturbed by wind waves only.

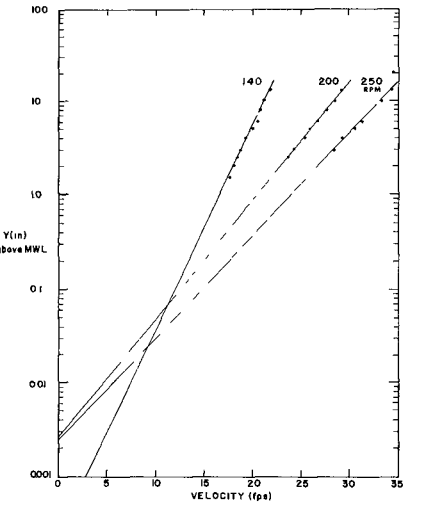

Fig. 6. Mean velocity profiles over water surface perturbed by wind and mechanical waves.

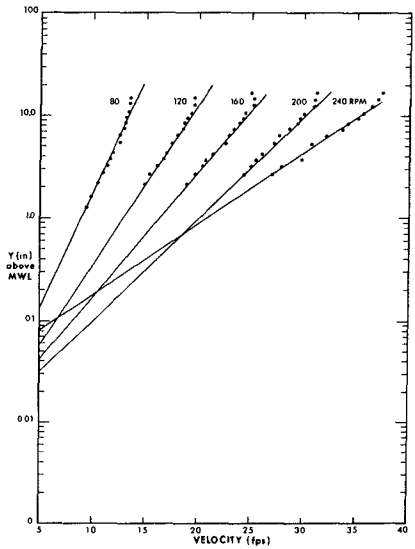

Fig. 7. Mean profiles over a mechanically generated wave (a=1.10 in., f=0.75 cps).

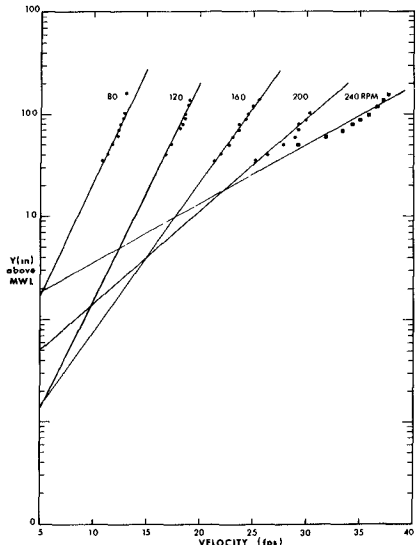

Fig. 8. Mean profiles over a mechanically generated wave (a=3.00 in, f=0.75 cps).

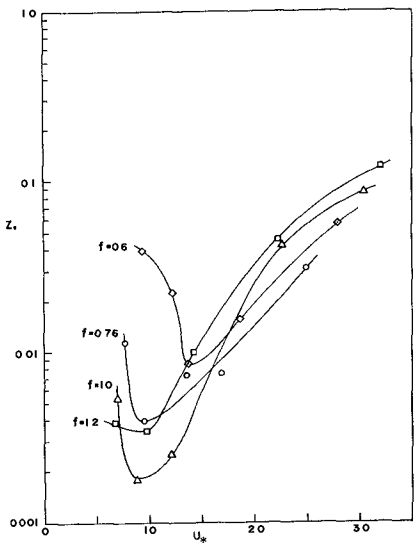

Fig. 9. z_0 vs. U_* at preselected frequencies (a=2.00 in.).

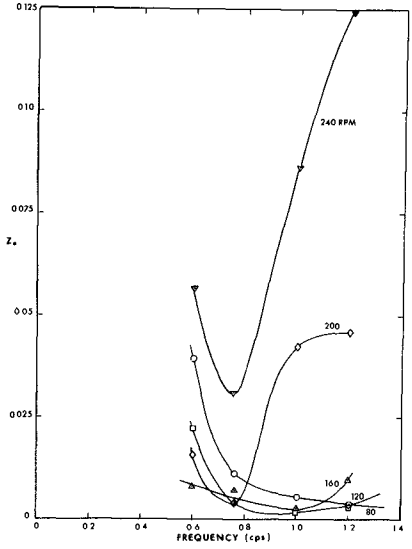

Fig. 10. z_0 vs. f for mechanically generated waves (a=2.00 in.).

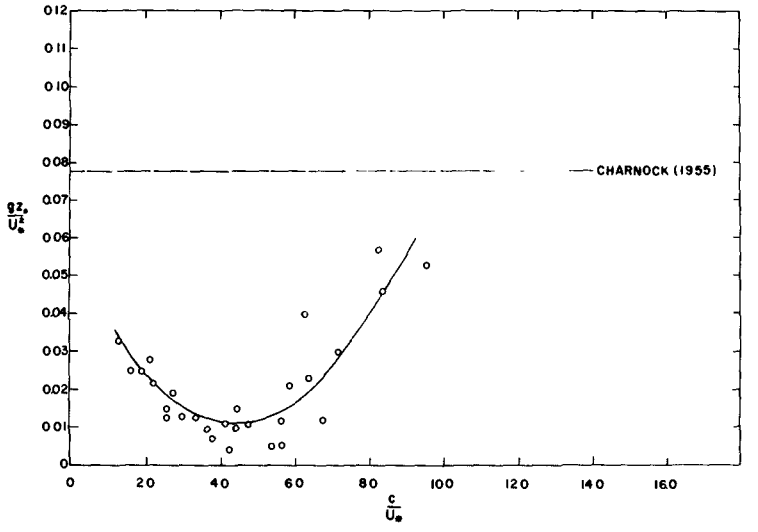

Fig. 11. Dimensionless relationship of all acquired data.

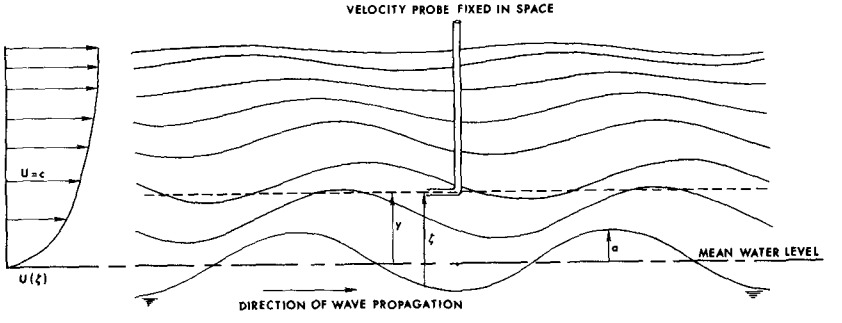

Fig. 12. Schematic diagram of streamlines over a perturbed surface.

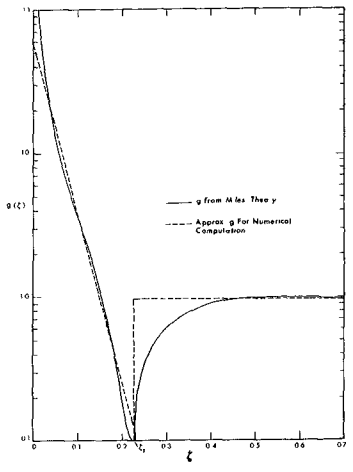

Fig. 13. g(ζ) vs. kζ from Conte and Miles (1959).

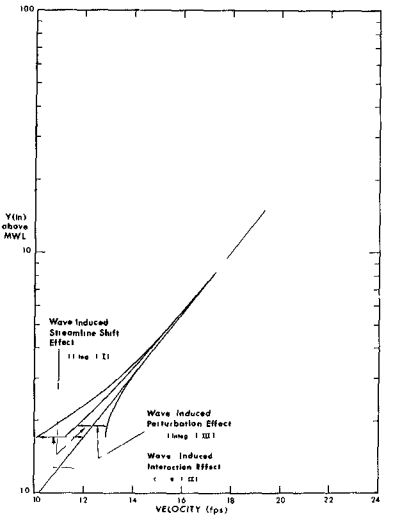

Fig. 14. Theoretically predicted effects of shifting streamlines, velocity perturbation, and interaction of two effects.

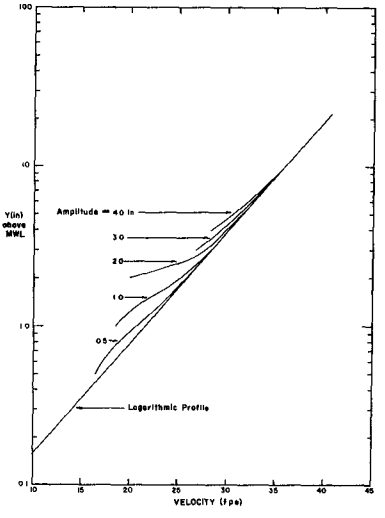

Fig. 15. Predicted wave-influenced mean profiles at different wave amplitudes (f=0.75 cps).

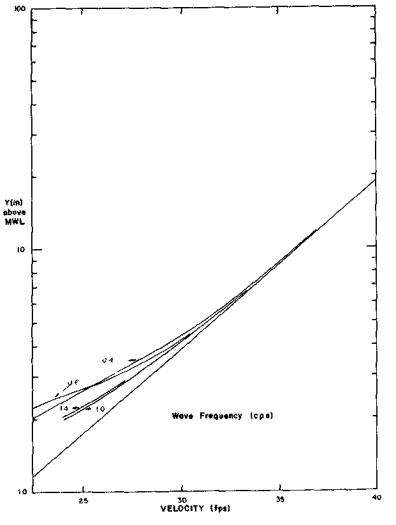

Fig. 16. Predicted wave-influenced mean profiles at different wave frequencies (a=2.00 in.).

CHAPTER 6

PRESSURE DISTRIBUTION OVER A MOVING WAVY BOUNDARY

Konstantín Zagustin, Ph.D.

Agregate Professor and Head Hydraulic Laboratory
Central University of Venezuela
Caracas - Venezuela

ABSTRACT.-

Experimental data on pressure distribution over a sinusoidal wavy boundary with a fixed and a moving condition, measured in a water tunnel, are presented for a number of flow - velocities. The model with the moving boundary condition is related to the situation prevailing in the steady state flow picture of a small amplitude wind-generated gravity wave in - which the water flow represents the air flow in nature, while the "fixed in space" moving wavy boundary corresponds to the nearly constant water particle velocity at the surface of the wave.

The results show that the normal stress distribution - over a moving boundary differs from that over a fixed one by a phase-lag with respect to the wave shape, which varies with the ratio of flow velocity to the boundary velocity (wave celerity), as predicted by the recent theories of Miles and Benjamin.

These results provide an explanation for the energy - transfer from wind to wave due to normal stresses and show that those experiments performed on fixed boundary models can not be associated with the phenomena of water wave genera - tion.

INTRODUCTION.-

Most of the experimental data available on the pressure distribution over wavy boundaries such as those of Stanton, - Marshall and Houghton (1932). Motzfeld (1937), Thijsse (1952) Bonchkovskaya (1955) and Larras and Claria (1960), were obtained from tests performed in wind tunnels or water flumes, -- using fixed boundary models built from wood or wax. (See ref. 1 or 2, for a complete experimental survey). When these pre - ssure distributions are used to compute the energy transfer - from the wind to a gravity water wave the result is too small to explain the growth of such waves. This lack of agreement is a result of the erroneous boundary condition that prevails in the fixed boundary experiments. The flow configuration of an air flow, with velocity U blowing in the same direction of the wave train moving at a celerity c, is an unsteady one and is represented in Fig. 1. To reduce it to a steady case, a coordinate system which moves at the same speed as the wave is introduced. When viewed from the moving coordinate system the wave profile is stationary and the water flows upstream at the wave propagation velocity. The water velocity at the surface of the wave varies from a maximum at the trough to a minimum at the crest, but for small amplitudes the speed is nearly constant and equal to the same celerity c. In this steady flow picture (Fig. 2), the zero velocity point (critical level) is located at a certain height over the wave surface (critical layer), while, in a fixed boundary model this critical level is at the boundary.

Mathematical theories presented by Miles (ref. 3, 4 - and 5) and Benjamin (ref. 6) and explained from the physical point of view by Ligh thill (ref. 7), had proven that the - thickness of the critical layer plays a crucial role on the

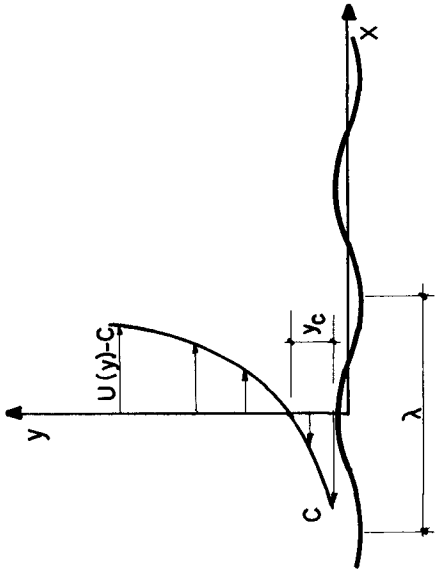

FIG. 2 STEADY FLOW

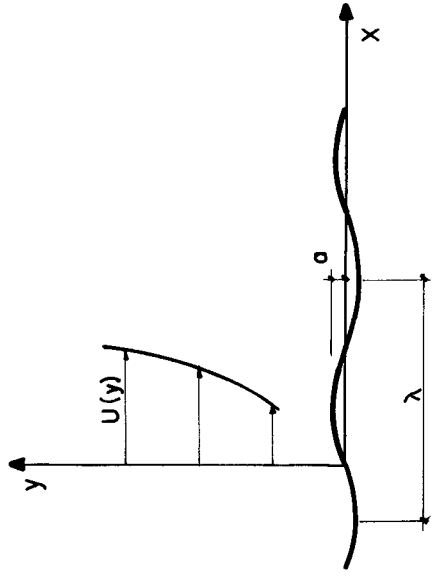

FIG 1 UNSTEADY FLOW

stress distribution over a wavy boundary. Previous experiments performed by the author in (ref. 1 and 2) using a model in which the moving boundary conditions were reproduced by a a belt located vertically in a flume in which water was used as a working fluid, and moving at a constant speed following the shape of the wave, have proven that the pressure distribution differs radically from that prevailing in a fixed boundary. While, the pressure distribution over a fixed boundary was almost in phase with the wave's shape, in the case of a moving boundary these exists a noticable phase lag, in agreement with Miles's theoretical results. However, since the experimental data were obtained in an open flume the range of flow velocities was very small due to the appearance of surface disturbances which affected the already small magnitudes of the pressure (the boundary has moved at a fixed speed, which corresponds to the celerity of a gravity wave with the same wave length). In order to increase the range of flow velocities and improve the precision of the measurements, a different experimental set-up had been designed.

EXPERIMENTAL SET-UP.-

The moving boundary conditions were reproduced by a cold rolled stainless steel band 10 cm. wide and 3 mt. long located in a water tunnel with a test section 2 mt. long and 10 cm. x 50 cm. cross section. The wavy boundary was formed by 3 waves with 40 cm. wave length, and the mechanism was such that the amplitude could be changed easily, starting from a flat surface and increasing to a large ratio of amplitude to wavelength. To produce the wavy form the stainless steel band had a fixed support at the trough and a movable support at the crest. The thickness of the band and the diameter of the supports was selected in such a way that the wave's shape approximates a sinusoidal one. The speed of the moving boundary was set to be equal to a celerity of a gravity wave with 40 cm. wavelength -

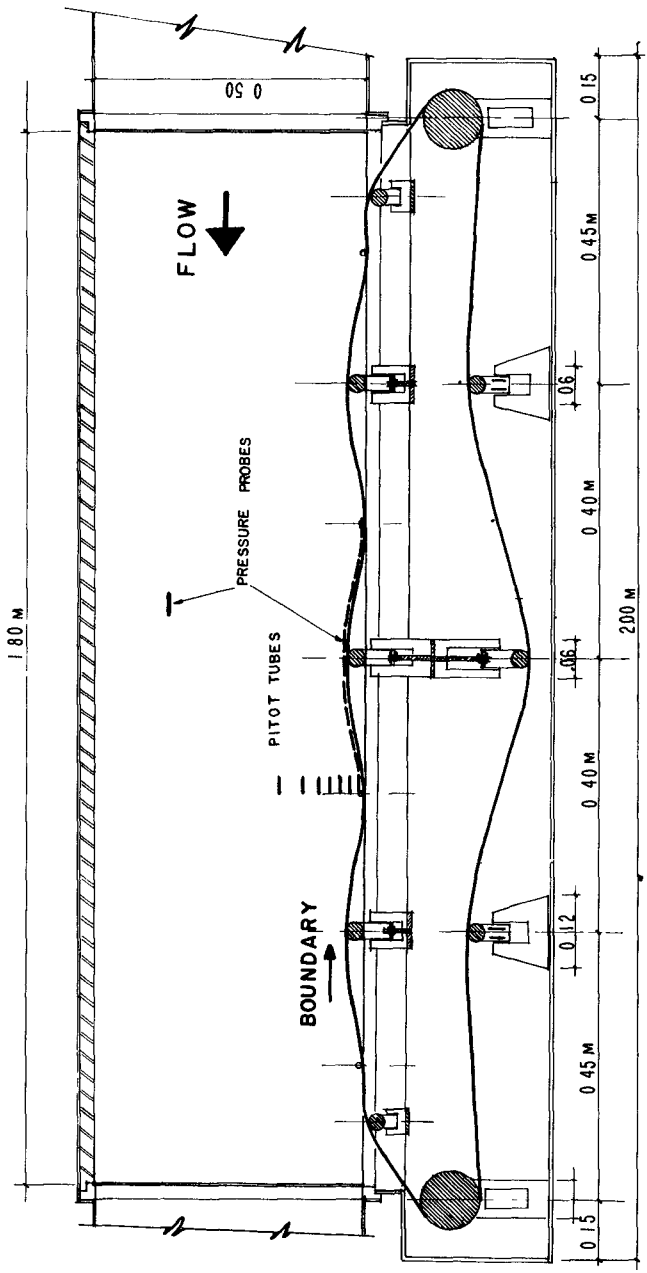

TEST SECTION

FIG. 3

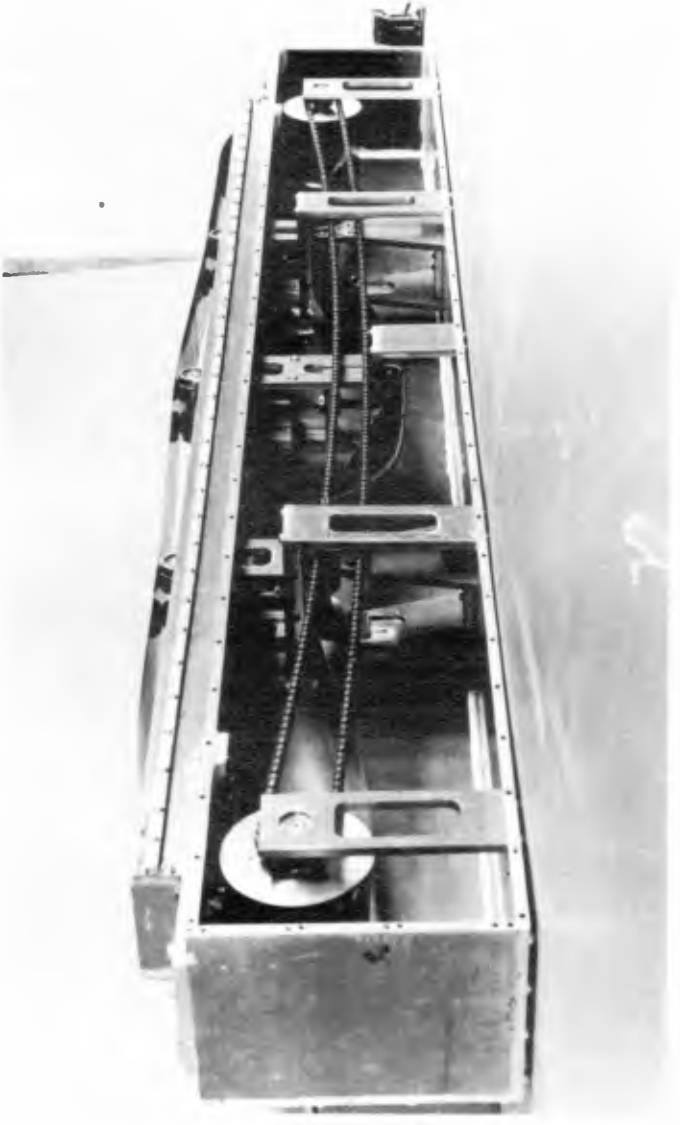

Fig. 4 View of the moving boundary mechanism.

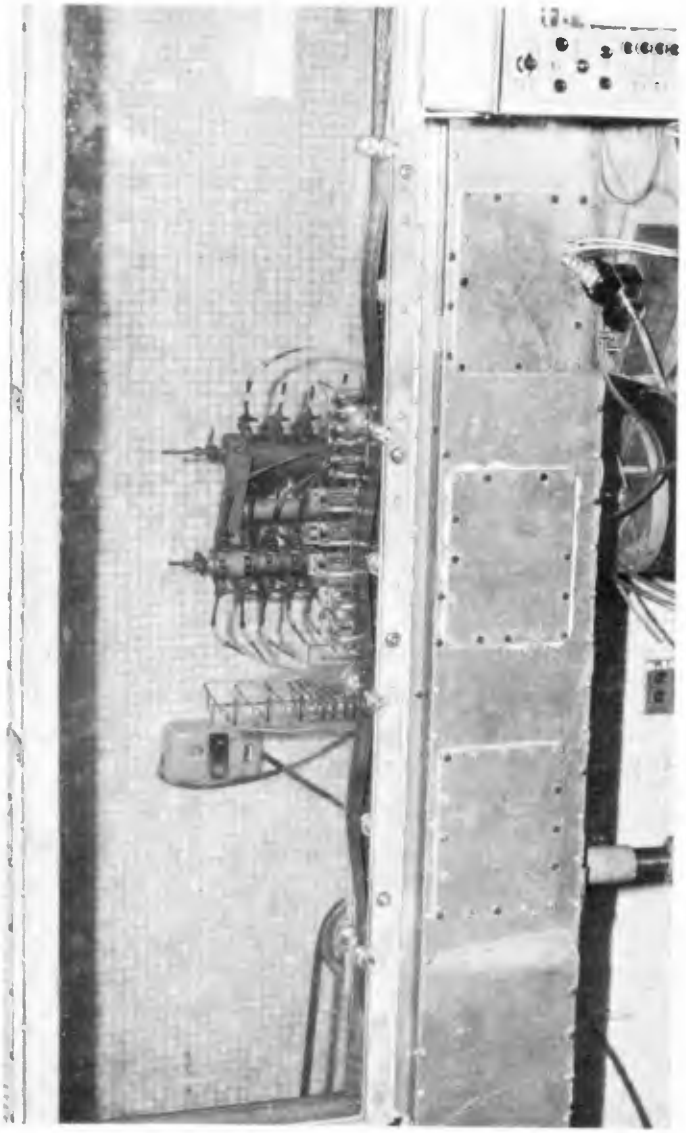

Fig. 5 General view of the test section.

(0,79 m/seg), althoagh it could be changed to any other value through a system of pulleys connected to an electric motor with a speed reductor. Water could flow at a maximum speed of 3 mt/sec. and the velocity could be controled by a valve loca - ted downstream of the test section. Care was taken to obtain a well developed turbulent flow at the upsteam part of the test section, and for that reason a series of honey combs were pla - ced in several sections of the apparatus. The sketch of the test section is shown in Fig. 3, and the photographs of Fig. 4 and 5 shows the detail of the moving boundary mechanism and the general view of the aparatus.

Velocity measurements were made at the trough of the cen tral wave using a number of small pitot tubes (1/8" O. D.) pla - ced in the back side of the test section. In the inmediate vici nity of the boundary some of the pitot tubes were placed in the opposite direction so as to measure velocities in the critical layer. Pressure distribution was obtained with static pressure probes (1/8" O.D.) located parallel to the moving boundary at a 1/4" from it. These probes were placed every 1/8 of the wave length and were mounted at the back side of the test section in such a way that it was possible to adjust the height, the depth, and the inclination of the probe. Preliminary experiments showed that the pressure variation accross the test section was very small at the central part, and that the selected height of the probe was the most adequate one.

All the measurements were performed at the mid section of the central wave, using differential pressure transducers model PACE P90 (range $\pm$ 1 in of water) with a Sanborn two cha - nnel thermal recorder model 320.

EXPERIMENTAL RESULTS.-

Pressure and velocity distribution measurements were performed for stationary and moving boundaries with three di - fferent wave amplitudes and several flow velocities. The wave

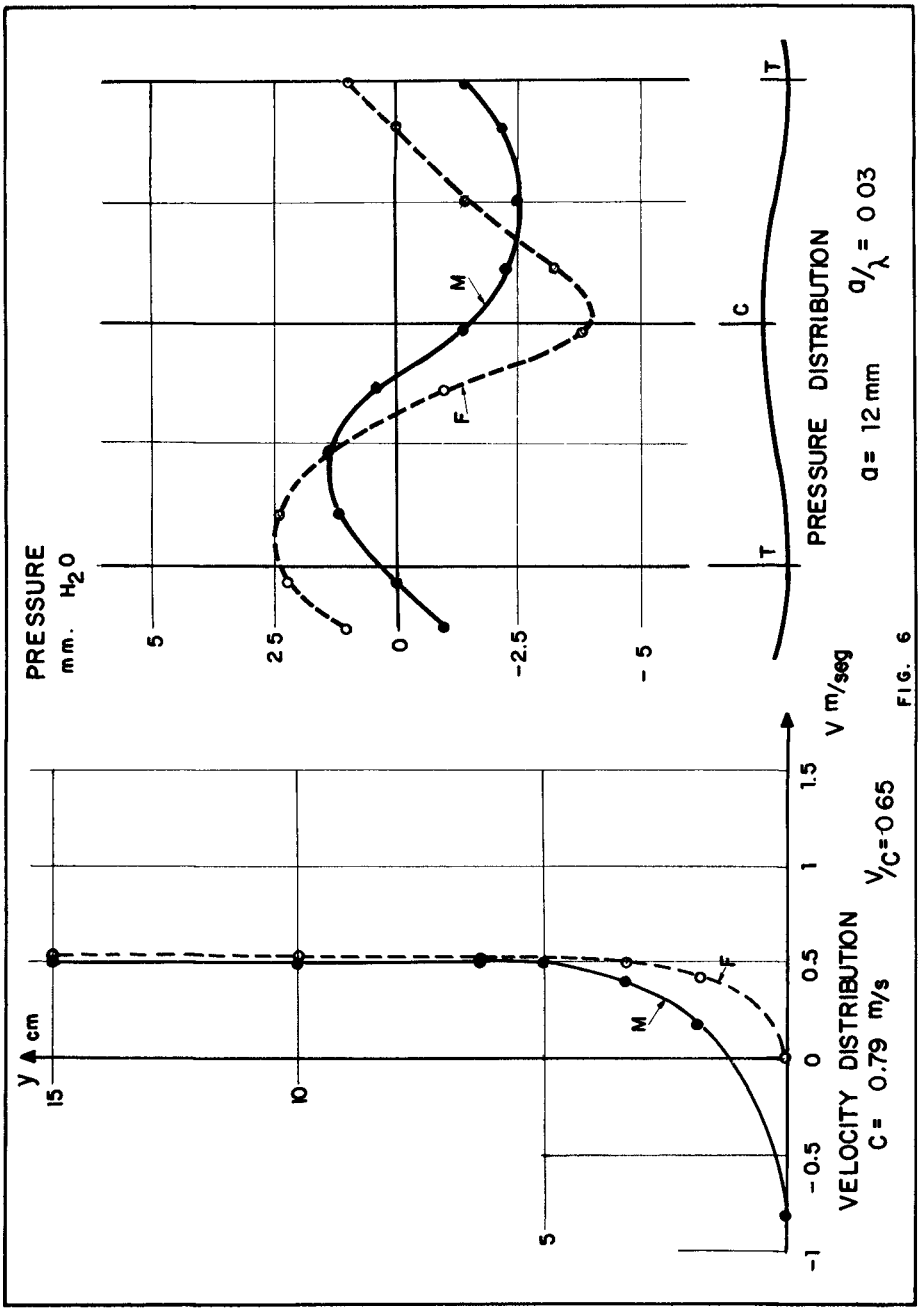
PRESSURE
mm. H_2O
5
2.5
0
-2.5
-5
M
F
T
C
T
PRESSURE DISTRIBUTION
a= 12 mm
a/λ = 0.03
y cm
15
10
5
M
F
-1
-0.5
0
0.5
1
1.5
V m/seg
VELOCITY DISTRIBUTION
C= 0.79 m/s
V/C=0.65

FIG. 6

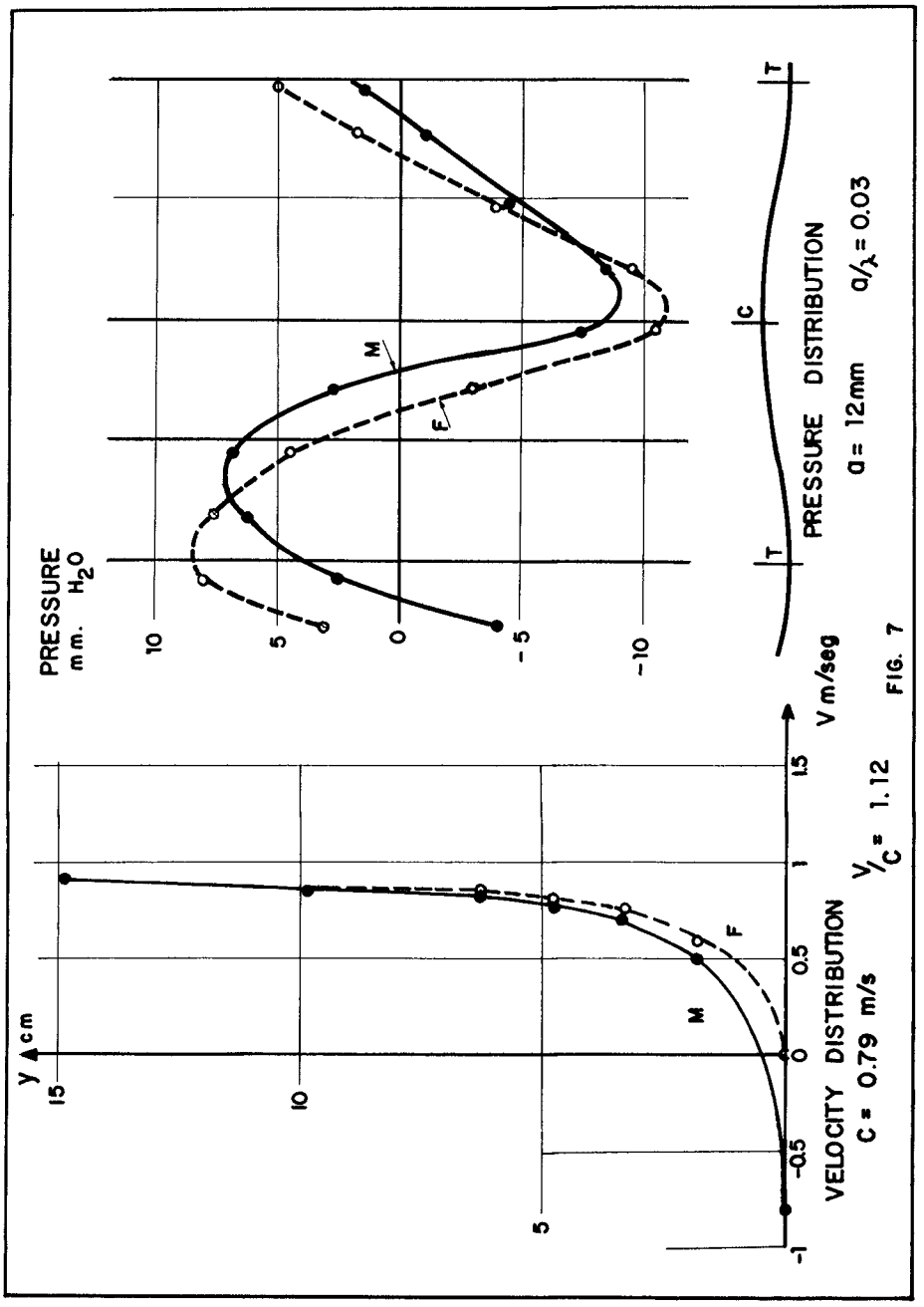
PRESSURE
mm. H_2O
10
5
0
-5
-10
M
F
T
C
T
PRESSURE DISTRIBUTION
a = 12mm
a/λ = 0.03
y cm
15
10
5
0
-0.5
-1
0.5
1
1.5
V m/seg
M
F
VELOCITY DISTRIBUTION
C = 0.79 m/s
V/C = 1.12

FIG. 7

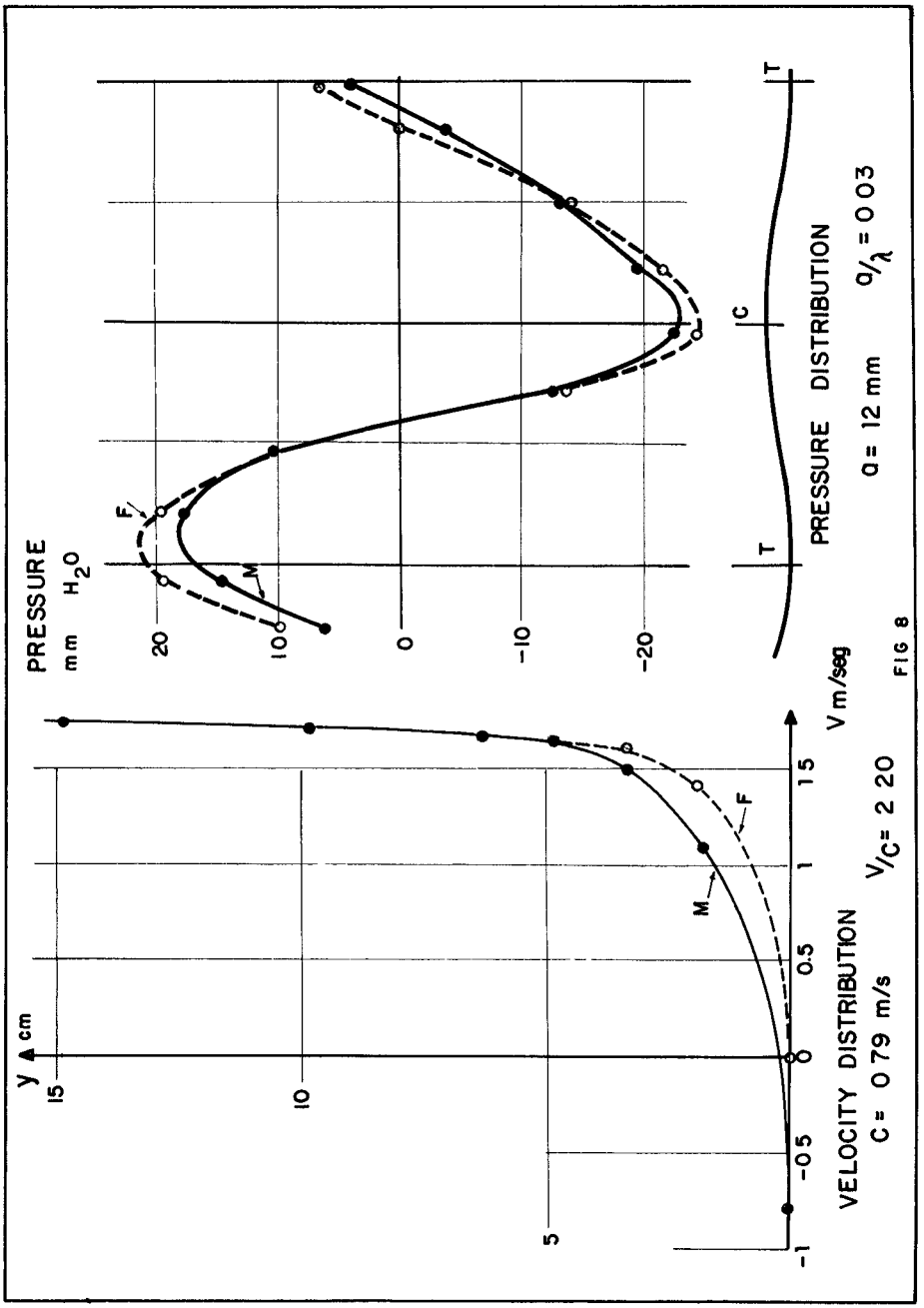
PRESSURE
mm H_2O
20
10
0
-10
-20
F
M
T
C
T
PRESSURE DISTRIBUTION
a = 12 mm
a/λ = 0 03
y cm
15
10
5
-1
-0 5
0
0.5
1
1 5
V m/seg
M
F
VELOCITY DISTRIBUTION
C = 0 79 m/s
V/C = 2 20
FIG 8

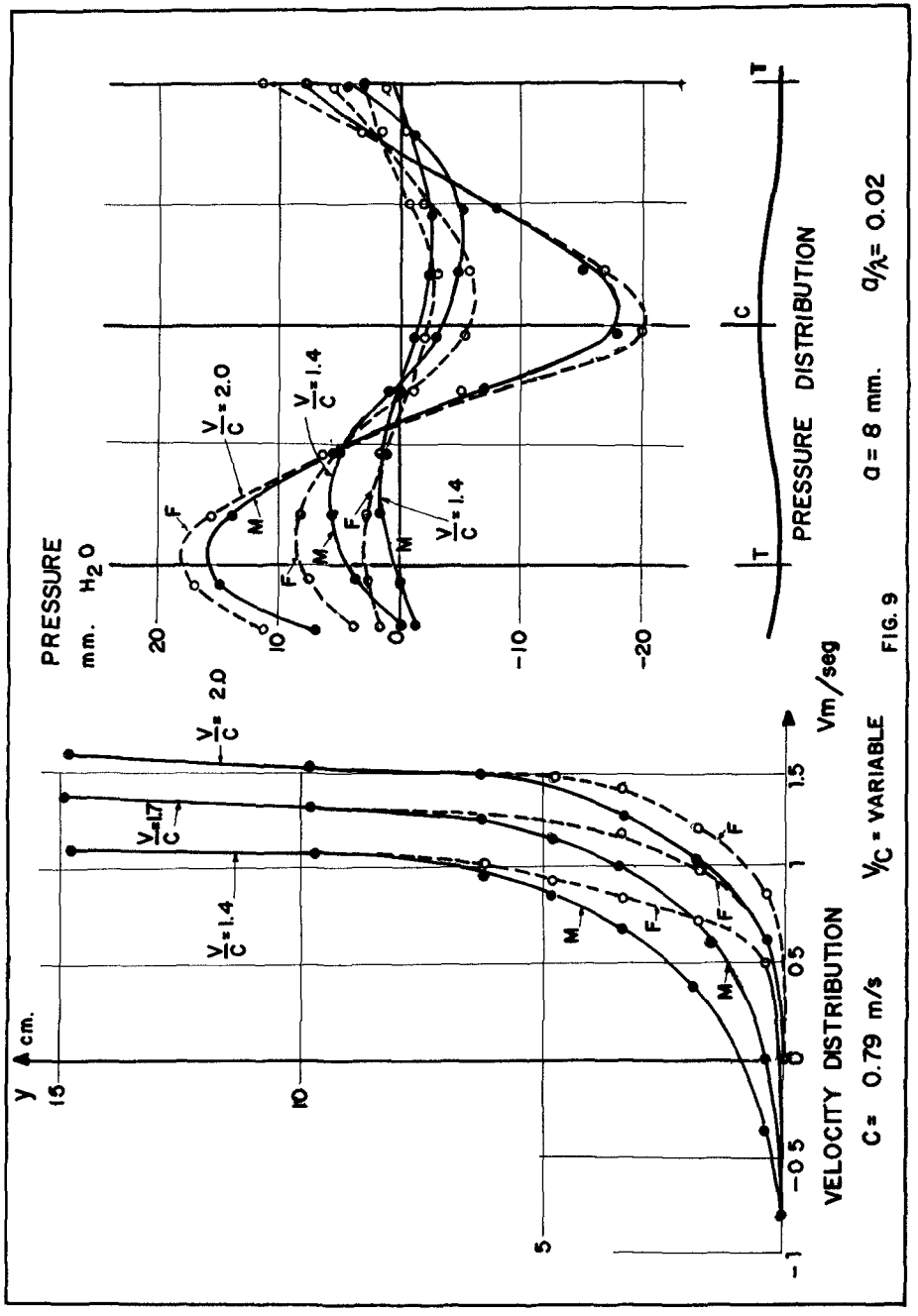
PRESSURE
mm. H_2O
20
10
0
-10
-20
$\frac{V}{C}$= 2.0
$\frac{V}{C}$= 1.4
$\frac{V}{C}$= 1.4
F
M
T
C
T
PRESSURE DISTRIBUTION
a = 8 mm.
a/λ= 0.02
y cm.
15
10
5
$\frac{V}{C}$= 2.0
$\frac{V}{C}$=1.7
$\frac{V}{C}$= 1.4
Vm/seg
1.5
1
0.5
0
-0.5
-1
VELOCITY DISTRIBUTION
C= 0.79 m/s
V/C = VARIABLE
FIG. 9

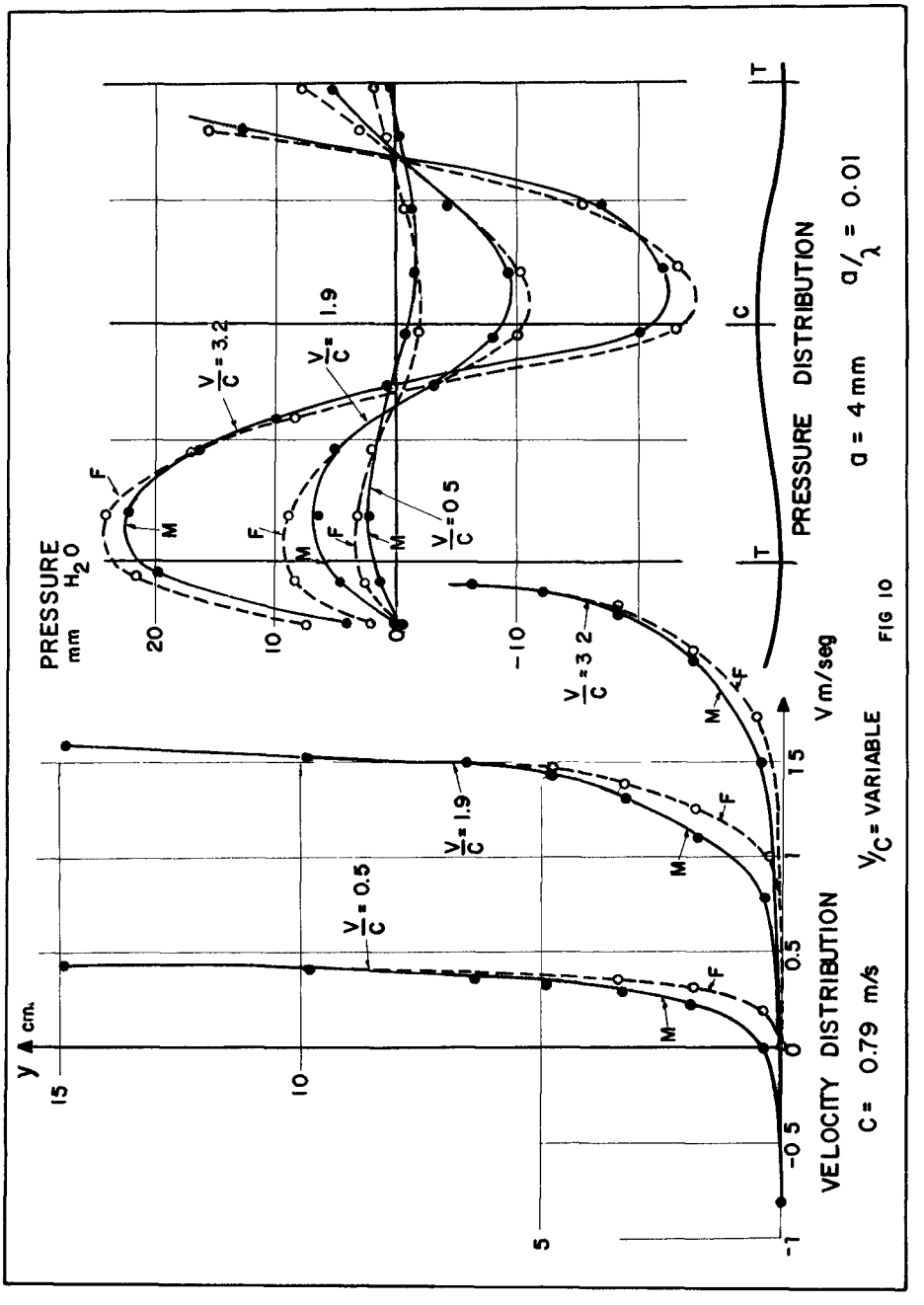
PRESSURE
mm H2O
20
10
0
-10
V/C = 3.2
V/C = 1.9
V/C = 0.5
F
M
T
C
PRESSURE DISTRIBUTION
a = 4 mm
a/λ = 0.01
y cm.
15
10
5
V/C = 0.5
V/C = 1.9
V/C = 3.2
-1
-0.5
0
0.5
1
1.5
V m/seg
VELOCITY DISTRIBUTION
C = 0.79 m/s
V/C = VARIABLE

FIG 10

amplitude varied from 4 mm. (a/ = 0.01) up to 12 mm. (a/ = 0.03) and the flow velocities changed from aproximately 0,5 m/seg. up to 3 m/sec. No higher wave amplitude were tested because the boundary conditions at the wave surface would differ considerable from the constant velocity prevailing in the model. The series of graphs given in Fig. 6, 7 and 8 show the corres - ponding velocity and pressure distribution curves for both boun dary conditions when the wave amplitude is 12 mm. and the ratio of maximum flow velocity to wave celerety is 0,65, 1,12 and 2,20 respectively. From this figures it is possible to observe the phase-lag existing in the moving boundary as compared with the fixed boundary condition. This difference is largest when the ratio of flow and boundary velocities is small, and diminishes when the flow velocity increases, as it is expected from the theory.

In Fig. 9 and Fig. 10 the results for several ratio of flow and boundary velocities are presented, for wave amplitu - des of 8 and 4 mm. respectively. In these graphs the same trend can be observed for the pressure distribution curves with the moving boundary condition.

CONCLUSIONS.-

The experimental pressure distribution curves obtained for the moving boundary conditions confirm the theoretical pre diction of the phase-lag existing in the pressure curve, and explain the phenomena of energy transfer from wind to a water wave due to the normal stresses. This phase-lag become smaller as the flow velocity increases and at very high flow speeds the fixed and moving boundary pressure distribution become almost identical.

This results prove the importance of representing the right boundary conditions when dealing with a model of wind generated waves and show that the previos experiment performen in wind tunnel or water flumes using a fixed wavy boundary can

not be directly related to wind generated water waves.

ACKNOWLEDMENTS.-

Financial support for this research was provided by the Consejo de Desarrollo Científico y Humanístico of the Central University of Venezuela through the research project Nº 99. - The author is grateful for the assistance of R. Lozano in the design,construction and maintenance of the apparatus.

REFERENCES.-

Ref. 1 Zagustin K., "Flow over a moving boundary in rela - tion to wind - generated waves", Ph.D. thesis Stanford University, 1966. pp 1-167.

Ref. 2 Zagustin K., Hsu E.Y., Street R.L., Perry B. "Flow over a moving boundary in relation to wind-generated waves". Tech. report No. 60 Office Naval Research, March 1966.

Ref. 3 Miles, J.W., "On the Generation of Surface Waves by Shear Flows", J. Fluid Mech., Vol. 3, Part 3, (1957), pp. 185-204.

Ref. 4 Miles, J.W. "On the Generation of Surface Waves by Shear Flows", J. Fluid Mech., Vol. 6, (1959), pp. 568-582.

Ref. 5 Miles, J.W., "On the Generation of Surface Waves by Shear Flows", J. Fluid Mech, Vol. 13, (1962), pp. 433-448.

Ref. 6 Benjamín, T.B., "Shearing Flow Over a Wavy Boundary", J. Fluid Mech, Vol. 6, Part. 2 (1959) pp. 161-205.

Ref. 7 Lighthill, M.J., "Physical Interpretation of the Mathematical Theory of Wave Generation by Wind", J. Fluid Mech. Vol 14, (1962), pp. 385-398.

CHAPTER 7

SHALLOW WATER WAVES A COMPARISON OF THEORIES AND EXPERIMENTS

by

Bernard Le Méhauté*
David Divoky**
Albert Lin**

ABSTRACT

A series of experiments were performed to determine the velocity field and other characteristics of large amplitude shallow water waves. The experimental results were compared with the predictions of a variety of wave theories including those commonly used in engineering practice. While no theory was found exceptionally accurate, the cnoidal wave theory of Keulegan and Patterson appears most adequate for the range of wavelengths and water depths studied.

1. INTRODUCTION

This paper presents the results of an experimental program performed to establish the major characteristics of waves in shallow water and to determine by detailed comparisons which of the many wave theories commonly used in engineering practice best describes them. Knowledge of the features of these waves is essential to the engineer interested, for example, in the forces on submerged structures, such as pilings. For this purpose, he needs reliable expressions for the velocity field within the wave Upon choosing a suitable design wave (that is, mean water depth, wave height, and wave period) he then proceeds to select a theory to describe that wave. This choice is not easily made. He must evaluate the applicability of at least a dozen theories. It may be hoped, for example, that a theory developed to a fifth order of approximation is more accurate than its lower order counterparts which may or may not actually be the case. We have, therefore, conducted an extensive series of experiments to measure the characteristics of large shallow water waves and have, further, compared these results with a large number of theories in order to suggest one as most applicable for practical use. In this comparison and selection, we have settled upon the horizontal particle velocity under the crest as the single most important feature, since, in applications, velocity is generally most critical and the velocity under the crest is the greatest attained at any

---

* Vice President, Tetra Tech, Inc , Pasadena, California
**Technical Staff, Tetra Tech, Inc., Pasadena, California

depth. Other factors are of lesser importance; for example, the surface profile in all theories must be roughly similar since the wave height is imposed. Furthermore, a theory which prescribes the velocity field well is constrained to be good for other features, such as accelerations and pressures, a priori

The range of waves considered included relative depths, D/T^2, from 0.05 to 0.8 ft sec^{-2} with heights near the breaking limit. The maximum horizontal particle velocity in these waves has been compared with the predictions of twelve theories not all of which are expected to apply. Nevertheless, it is possible that a theory may, fortuitously, describe waves outside its range of analytical validity better than one developed for those waves. Therefore, our selection of theories has been rather broad, including all those commonly used in engineering practice.

Prior to presenting our experimental results and a comparison of these results with various theories, a general discussion on the arbitrariness which prevails in the development of these theories is presented. Even though it is realized that it is a difficult task to be fully aware of all of the mathematical intricacies leading sometimes to small differences, it is assumed that the reader is familiar with the subject. It is not a critical analysis of the shallow water wave theories, but rather it is attempted to call attention to some known facts which are pertinent prior to presenting our experimental results.

2. ARBITRARINESS OF WAVE THEORIES

In an Eulerian system of coordinates a surface wave problem generally involves three unknowns the free surface elevation η (or total water depth), the pressure p (generally known at the free surface), and the particle velocity $\vec{V}$, expressed as a function of space and time.

Since a general method of solution does not exist, a number of simplifying assumptions are generally made which apply to a succession of particular cases with varying accuracy.

First of all, it is assumed that a periodic progressive wave travelling over a horizontal bottom is characterized by a steady state profile, i.e.,

$$\eta, \vec{V}, p = f(x - Ct)$$

where C is a constant equal to the wave velocity or phase velocity (In fact, it has been observed that under certain conditions the wave profile in shallow water becomes unstable, asymmetric, and even degenerates into a succession of smaller undulations)

The problem now consists essentially of solving a system satisfying continuity, momentum and boundary conditions. However, these are not sufficient for solving the nonlinear problem and two more considerations are necessary.

This leads us to a discussion of the problem of rotationality and mass transport (since they are related).

It is first pointed out that a steady flow of arbitrary velocity distribution can always be superimposed on a given wave motion, so leading to any arbitrary mass transport velocity distribution (Dubreuil-Jacotin 1934) The arbitrariness in the calculation of wave motion is inherent in the arbitrariness which prevails in the assumptions which are used in the calculation of the mass transport.

The wave motion can be determined by assuming that there is no mass transport at all. These are the closed orbit theories, such as the exact solution of Gerstner (1809) in deep water, and the power series solution of Boussinesq and Kravtchenko and Daubert (1957) for shallow water. As a result of this assumption, the motion is found to be rotational and the vorticity is in the opposite direction to the particle rotation, i.e., in the opposite direction to what should be expected physically under the influence of a shearing stress due to wind blowing in the wave direction.

The wave motion can also be assumed to be irrotational, in which case a mass transport distribution is found as a result of nonlinearity (Wehausen and Laitone, 1960). These are the Stokesian wave theories which include Stokes (1847), Levi-Civita (1925), Struik (1926), and Nekrassov (1951).

Even though there is a given mass transport distribution which is a function of the vertical coordinate, the integrating constant is often determined by assuming that the average mass transport is nil for the sake of continuity, i.e., a steady flow is superimposed such that the average mass transport velocity is zero (Miche, 1944).

Let

$$U(z) = (\mu + 1)\, U_{\zeta=0}(z)$$

where $U(z)$ is the mass transport velocity as a function of vertical distance z and $U_{\zeta=0}$ is the mass transport in an irrotational wave ($\zeta=0$) of the same family and approximation.

The case where $\mu = -1$ corresponds to the Boussinesq (closed orbit) solution. $\mu = 0$ corresponds to the irrotational theory of Stokes If $\mu > 0$, the average vorticity is in the same direction as the orbit direction, such as due to a strong wind blowing in the wave direction. The case where $\mu < -1$ gives a negative vorticity and a negative mass transport at the free surface which can be due to a wind blowing locally in the opposite direction to the wave propagation (a frequent nearshore occurrence) In the case where $-1 < \mu < 0$, the vorticity is in the opposite direction and the mass transport is smaller than in the irrotational case.

It is recalled that Longuet-Higgins (1953) has demonstrated the importance of the viscous force at the bottom to explain the well-observed

fact that mass transport at the bottom is always in the wave direction.

In addition to the first assumption regarding rotationality or mass transport, another condition is required. For example, for progressive monochromatic waves, it is attempted to establish a steady state solution such that the potential function $\varphi = f(x - Ct)$ where C is a constant equal to the wave velocity in which case the solution is unique. Although the steady state solutions are of the same form, C is undetermined, and for the determination of C, another condition is required. For example, the average horizontal velocity over a wave period at a given location may be taken to be zero, but the mass transport is then imposed to be minimum. Another condition is generally preferred. This condition consists of assuming that the average momentum over a wave length is zero by addition of a uniform motion, in this case, another expression for C is found which results in a different mass transport. Thus, it is realized that the calculation of wave theories is subject to some arbitrariness because different assumptions can lead to different values of C. (Le Méhauté, 1968)

Consider further the case of irrotational waves. The values of the wave characteristics depend upon the number of terms chosen for the power series expansion, either in terms of wave steepness H/L (Stokesian solution) or in terms of relative height H/D (cnoidal type solution). The deficiency of the calculation of mass transport is inherent in the deficiency of the power series solution. It has been pointed out (Koh and Le Méhauté, 1965) that the Stokesian power series solution is not uniformly convergent, and the validity of the solution is lost when the relative depth D/L tends to a small value (say, $D/L < 0.1$ for a fifth order solution) since the coefficient functions of D/L tend to infinity. The same occurs in the case of the cnoidal wave solution. There is no unique cnoidal theory, rather, the literature contains several theories which may not be identical. As in Stokesian theories, since all cnoidal representations are truncated series, the order of approximation is important because certain factors are zero in low order theory

There are two types of cnoidal theories. The oldest is intuitive in nature and the newer theories are straightforward and more rigorous. All are irrotational. The primary intuitive theory is that of Korteweg and de Vries (1895). The first and second terms of the series are deduced but no scheme is presented for extension to higher order terms. The terms which are found are unique. The rigorous theories are those of Keller (1948), Laitone (1960, 1962) and Chappelear (1962) which are all based on a perturbation expansion developed by Friedrichs (1948). The work of Keller confirms the results of Korteweg and de Vries, whereas that of Laitone and Chappelear gives a higher order term.

Unfortunately, even though rigor prevails, the newer theories diverge after the third term. According to a personal communication with L. Webb, the fourth terms exceed the third by factors of 10 to 25. The

cnoidal wave theory of Keulegan and Patterson is not consistent mathematically as some second order terms are neglected while third order terms are included, but it may be the most appealing physically.

There are questions which can be raised as to the legitimacy of truncating these series, either Stokesian or cnoidal, just because the coefficients blow up. For true rigor it must be shown that the series are asymptotic in the pure mathematical sense. This has not been done and indeed it would be a difficult task.

As it would have been a tremendous task to consider all wave theories, a selection has been made for convenience. The following wave theories were chosen for comparison with our experiments (listed with the sources of equations and tables used in this study)

1. Linear Airy theory in Eulerian coordinates (Wiegel, 1964)
2. Linear Airy theory in Lagrangian coordinates (Biesel, 1952)
3. Linear long wave theory (Wiegel, 1964)
4. Stokes' waves, 2nd order of approximation (Wiegel, 1964)
5. Stokes' waves, 3rd order of approximation (Skjelbreia, 1959)
6. Stokes' waves, 5th order of approximation (Skjelbreia and Hendrickson, 1962)
7. Cnoidal theory of Keulegan and Patterson (Masch and Wiegel, 1961)
8. Cnoidal theory of Laitone, 1st order of approximation (Laitone, 1961)
9. Cnoidal theory of Laitone, 2nd order of approximation (Laitone, 1961)
10. Solitary wave theory of Boussinesq (Munk, 1949)
11. Solitary wave theory of McCowan (Munk, 1949)
12. Empirical modification of linear Airy theory by Goda (Goda, 1964)

While our experiments involved only periodic waves, solitary wave theory has been included in the comparisons, this is so since for the waves studied, the phenomenon of short high crests and long flat

troughs is observed. It is possible, then, that solitary wave theory might describe these waves in the vicinity of their crests.

While not an analytical theory, the twelfth referenced empirical modification of Airy theory was included to determine the validity of its extension to waves of the type studied here.

It should also be noted that the source utilized for 3rd order Stokes' theory contains some small errors in its mathematical development. Nevertheless, it is a standard reference and was utilized without modification.

The theories chosen involving nonlinearity are irrotational and have mass transport in the wave direction. Since mass transport velocity is always small compared with particle velocity, this effect has not been measured as it is not judged to be a significant factor in the validity of these theories at this stage. For this reason, the comparison of experiment with 2nd order Stokes' theory is also valid for the theory of Miche (1944).

3. EXPERIMENTAL PROCEDURES AND RESULTS

The current experimental program was performed in the Tetra Tech wave tank which is illustrated in Figure 1. The tank is 105 feet long with an approximately four-foot square cross-section. The wave generator is of the versatile plunger type. The period of the waves can be varied by the motor speed control through a range of approximately one to twelve seconds.

In order to produce large amplitude shallow water waves in the test section, a convergence was combined with a sloping bottom prior to the constant depth and width region. This arrangement concentrates the wave energy in the test section and easily permits the generation of high amplitude shallow water waves. The wave is thus generated as a deep water "linear" wave and is transformed into a "nonlinear cnoidal type" shallow water wave through the transitional section.

The wave channel was entirely sealed nullifying mass transport. Provision for a return flow under the test station would result in a difficult to specify mass transport through the channel due to unknown head-loss Hence, a sealed channel was preferred, giving zero net mass transport, in the interest of well-defined conditions.

Water particle motions were determined photographically through observation of neutrally buoyant particles suspended in the water. Nitrile rubber, especially compounded to a specific gravity of unity, was used for this purpose, cut into one-eighth inch cubes, it was found

to follow the water motion quite well and reflect sufficient light to photograph easily.

Lighting was provided by a stroboscope of accurately controllable flash rate allowing, with open camera shutter, the recording of several successive particle positions on a single negative

To provide a spatial scale, a rectangular grid of wires with one inch spacing was placed at the observation window and is visible, with the channel bottom, on each negative. In order to minimize parallax problems, a 200 mm telephoto lens was used in conjunction with a 35 mm camera. Data processing is then easily accomplished, particle image spacing and flash rate giving local velocity vectors, and position within the wave being known by reference to the bottom

The data scatter was found to be gratifyingly small and systematic errors (predominately due to wave reflection) are judged to be at most ± 5 %

Two sets of non-breaking waves were studied, one set with heights just below breaking and another with heights considerably lower Figures 2 through 5 show the measured horizontal particle velocities under the crest for the lower waves while Figures 6 through 9 give the same results for the limit waves. The experimental conditions (wave height and period and water depth) are indicated on the figures

It is noted from these figures that no theory is uniformly valid However, some general observations can be made. Firstly, Airy theory (the same in both Eulerian and Lagrangian coordinates) is surprisingly good for the shorter waves but departs significantly from the data as the period increases. Even for these longer waves, however, Airy theory provides a reasonable approximation to the velocity at the bottom The higher order Stokes' theories are never as good as simple Airy theory and, considering their much greater complexity, are not to be preferred

The Boussinesq, 1st order cnoidal (Laitone) and linear long wave theories all show a constant velocity profile. The Boussinesq and cnoidal values are most suitable near the surface while (like Airy theory) the linear long wave result is in best agreement with the data near the bottom.

While no theory appears best in all cases, the cnoidal theory of Keulegan and Patterson (K & P) is seen from the figures to be the best compromise. This may be somewhat surprising considering, for example, the greater rigor of the Laitone cnoidal formulations which are uniformly worse in this confrontation with data. The question of analytical niceties aside, the Keulegan and Patterson cnoidal theory is seen to find practical justification for the long, high waves considered here.

Figure 10 shows a typical comparison between measured (photographically) and computed surface profiles. As stated earlier, the variation

between theories regarding profile is not as great as that for particle velocity since the most significant feature, the wave height, is imposed by experiment.

The solitary wave theories of Boussinesq and McCowan are seen to match the experimental shape near the crest quite well, but are, of course, displaced upward. Better is the Keulegan and Patterson cnoidal profile which not only matches the shape adequately but also is accurately placed with respect to the still water level.

The appearance of humps within the troughs of the Stokes' waves at all orders is an indication that they are being applied here beyond their range of validity. Still, the 3rd and 5th orders appear preferable in gross characteristics to the simpler Airy theory. The formulation in Lagrangian coordinates is seen to improve Airy theory, even at the first order, since the profile is a trochoid with the crest somewhat narrower than the trough, however, the amount of correction is insufficient to produce adequate agreement with the data.

Again, one is led to select the cnoidal formulation of Keulegan and Patterson although the solitary wave theories may also be useful if only the shape of the crest is of interest

Determination of the maximum horizontal velocity, presented previously, is relatively simple since it always corresponds to the top of the particle orbit, which is readily located on the photographs, and occurs at $x = 0$ (at the crest) in all theories so that computations, too, are straightforward. Figure 11 is an example of data obtained when the particle motion is purely vertical (that is, at the sides of the particle orbit). In contrast to the horizontal case just described, comparison with theory is not straightforward. In particular, the phase position at which purely vertical motion occurs is not (except for Airy theory) immediately known, but must be found from the equation for horizontal velocity with $u = 0$. For this reason, and since vertical velocity is generally of less practical significance than horizontal velocity, we have not made a complete comparison with all the theories. Instead, we show in Figure 11 Airy theory, because of its simplicity, Keulegan and Patterson cnoidal theory, because of its success in the previous comparisons, and McCowan theory, in order to assess the applicability of the solitary wave approximation (Since the water particle motion is never purely vertical under a solitary wave, the theoretical curve is that of maximum vertical velocity.) It is seen that the McCowan theory is best with Keulegan and Patterson next and Airy theory least satisfactory

It was found in the course of the experiments that an increase in period beyond about four seconds, in water depths on the order of one-half foot, was accompanied by the development of a wave instability. That is, the high, narrow wave crest split into several smaller undulations upon entering the test section, as many as five

being distinctly visible under some circumstances. The appearance of this instability precluded extension of the experiments to longer waves. The limit of stability, while not investigated in detail, was approximately $D/T^2 \approx 0.04$ ft sec^{-2}.

4. CONCLUSION

It has been found that for the range of relative depths, D/T^2, and relative heights, H/T^2, studied here, none of the commonly used wave theories are in exceptional agreement with data. However, for these large amplitude shallow water waves, the cnoidal theory of Keulegan and Patterson is perhaps the most generally acceptable description.

This conclusion may be compared with many previous classifications of wave theories (for example, Druet, 1965). Dean (1965) has compared the closeness of fit of several theories to the free surface boundary conditions as a criterion of relative validity. He found that this method is particularly valid for deep water waves, but may not be sufficient for shallow water waves.

For applications requiring information only near the surface or involving only the crest shape, the solitary wave theory of McCowan is an adequate approximation, while simple Airy theory may be applied at the bottom

These results should ease the problem of choice for the engineer concerned with the effects of large amplitude shallow water waves; perhaps, too, some assistance will be found by analysts in development of improved theories for those waves.

It should be recalled that the value of the vorticity has to be determined from the viscous effect which is particularly strong at the bottom and at the free surface under the influence of wind. A rotational theory at a second order of approximation, with an arbitrary vorticity distribution (and, consequently, mass transport) remains to be established. This theory should take into account not only the viscous effect due to the bottom boundary layer, but also the effect of wind shearing stresses at the free surface. This can be achieved as a solution of the vorticity transport equation with an approach similar to that proposed by Longuet-Higgins. One can only hope at this stage that the mathematical model for the distribution of vorticity can be empirically correlated with wind characteristics by making quantitative observations on mass transport.

Such an approach, combined with the application of stochastic processes, will provide the engineer with a much more realistic model of water waves than any high order Stokesian or cnoidal wave theory Further mathematical refinements of such theories would appear to be of little practical interest.

ACKNOWLEDGEMENTS

This work was perfomed under the sponsorship of the Defense Atomic Support Agency, Contract Number DASA 01-67-C-0099 Numerous discussions with Drs. I. Collins, Li-San Hwang and R.C.Y. Koh have been very fruitful.

REFERENCES

Biesel, F., "Equations Generales au Second Ordre de la Houle Irregulier," La Houille Blanche, May 1952.

Chappelear, J.E , "Shallow Water Waves," Journal of Geophysical Research, Vol. 67, 1962.

Dean, R.G., "Stream Function Wave Theory, Validity and Application," Specialty Conference on Coastal Engineering, ASCE, 1965.

Druet, C., "Nomographic Chart for Determination of the Monochromatic Wave Type in the Region of Foundation of a Designed Hydrotechnical Structure," Paper S,II-1, pp. 183-201, XXIst International Navigation Congress, Stockholm, 1965.

Dubreuil-Jacotin, L., "Sur le Determination Rigoureuse des Ondes Permanentes Periodiques d'ampleur Finie," J. Math., Vol. 13, 1934.

Friedrichs, K. O., "On the Derivation of the Shallow Water Theory," Communications on Pure and Applied Mathematics, Vol. 1, 1948.

Gerstner, F., "Theorie der Wellen," Annalen der Physik, Vol. 32, 1809.

Goda, Y., "Wave Forces on a Vertical Circular Cylinder," Report No. 8, Port and Harbor Technical Research Inst., Japan, 1964.

Keller, J.B., "The Solitary Wave and Periodic Waves in Shallow Water," Comm. Applied Math., December 1948.

Koh, R.C.Y., and Le Méhauté, B., "Wave Shoaling," Journal of Geophysical Research, April 1966

Korteweg, D.J., and de Vries, G., "On the Change of Form of Long Waves Advancing in a Rectangular Canal and on a New Type of Long Stationary Waves," Philosophical Magazine, Series 5, Vol. 39, 1895.

Kravtchenko, J., and Daubert, A., "La Houle a Trajectoires Fermees en Profondeur Finie," La Houille Blanche, Vol. 12, 1957.

Laitone, E.V., "The Second Approximation to Cnoidal and Solitary Waves," J. Fluid Mech., Vol. 9, 1960.

Laitone, E.V., "Higher Approximation to Nonlinear Water Waves and the Limiting Heights of Cnoidal, Solitary, and Stokes' Waves," Inst. of Eng. Res., Tech. Rept. Series 89, Issue 6, University of California, 1961

Laitone, E.V., "Limiting Conditions for Cnoidal and Stokes' Waves," J. Geophysical Research, Vol. 67, 1962.

Le Méhauté, B., "Mass Transport in Cnoidal Waves," J. Geophysical Research, September, 1968.

Levi-Civita, T., "Determination Rigoureuse des Ondes Permanentes d'ampleur Finie," Mathematische Annalen, Vol. 93, 1925.

Longuet-Higgins, M.S., "Mass Transport in Water Waves," Philosophical Transactions, Series A, Vol 245, 1953.

Masch, F.D., and Wiegel, R.L., "Cnoidal Waves, Tables of Functions," University of California, 1961.

Miche, R., "Mouvements Ondulatoires des Mers en Profondeur Constante ou Decroissante," Annales des Ponts et Chaussees, 1944.

Munk, W.H., "The Solitary Wave Theory and its Application to Surf Problems," in "Ocean Surface Waves," Annals of the N.Y. Academy of Sciences, Vol. 51, Art. 3, 1949.

Nekrassov, A.I., "The Exact Theory of Steady Waves on the Surface of a Heavy Fluid," Izdat. Akad. Nauk, SSSR, Moscow, 1951.

Skjelbreia, L., "Gravity Waves, Stokes' Third Order Approximation Tables of Functions", Council on Wave Research, The Engineering Foundation, 1959.

Skjelbreia, L., and Hendrickson, J.A., "Fifth Order Gravity Wave Theory," National Engineering Science Company, 1962.

Stokes, G.G., "On the Theory of Oscillatory Waves," Transactions of the Cambridge Philosophical Society, Vol. 8, 1847.

Struik, D.J., "Determination Rigoureuse des Ondes Irrotationelles Periodiques dans un Canal a Profondeur Finie," Mathematische Annalen, Vol 95, 1926.

Wehausen, J.V., and Laitone, E.V., "Surface Waves," Handbuch der Physik, 1960.

Wiegel, R.L., Oceanographical Engineering, Prentice-Hall, 1964.

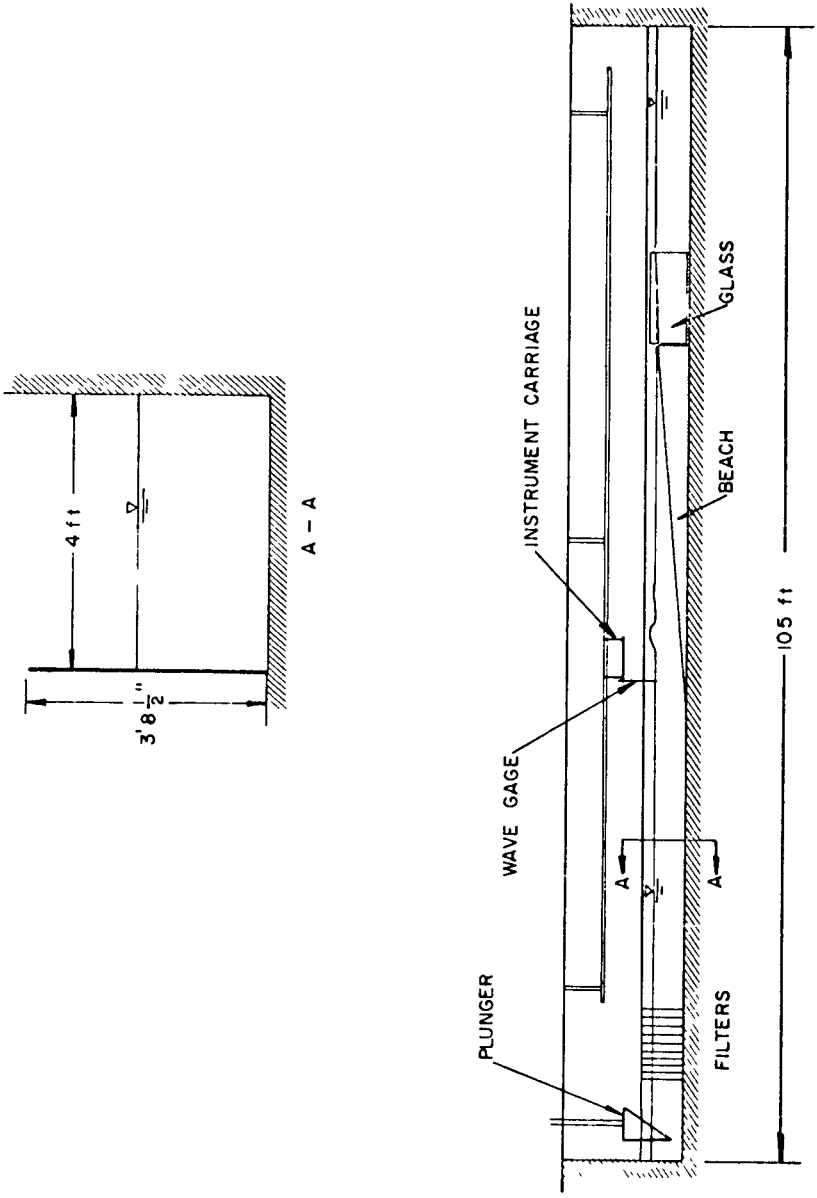

Figure 1. Diagram of the Tetra Tech wave tank.

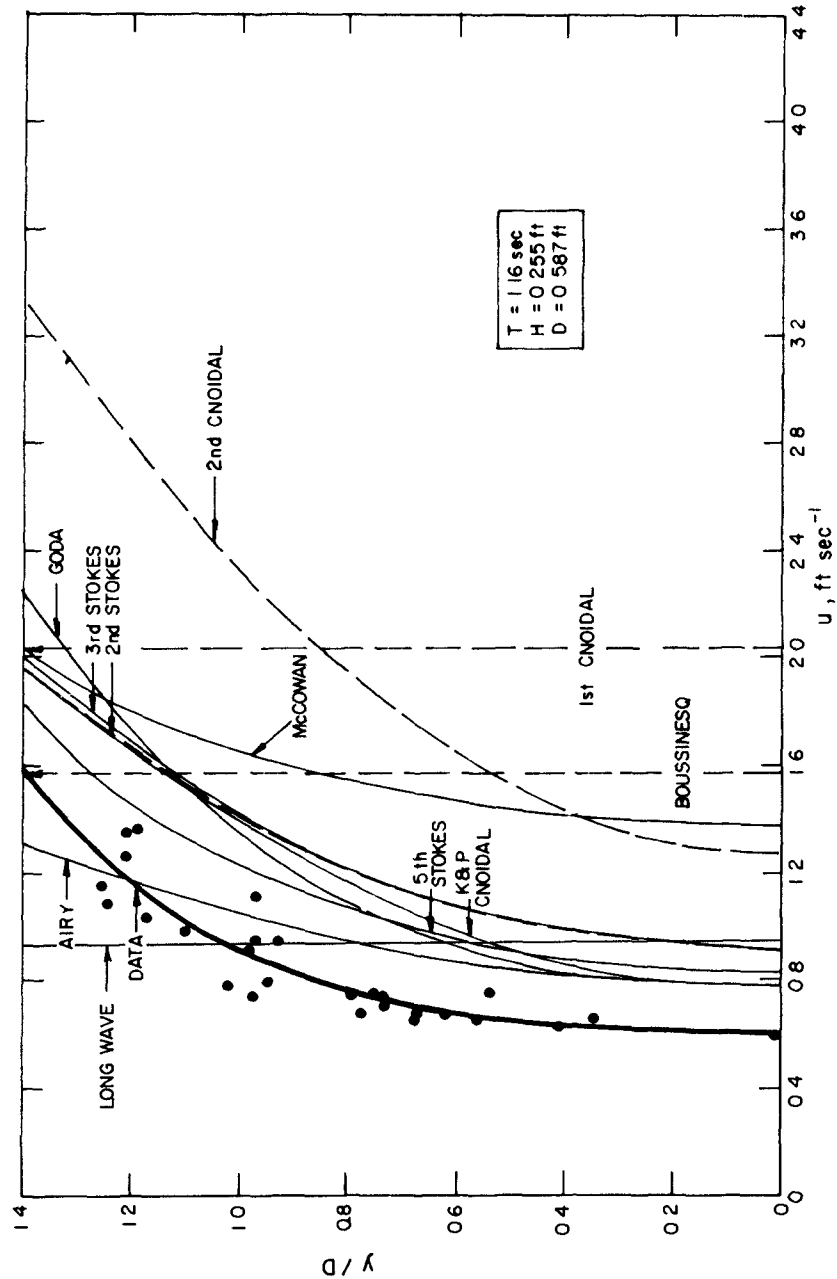

Figure 2. Horizontal Particle Velocity under the Crest - NON-BREAKING WAVE

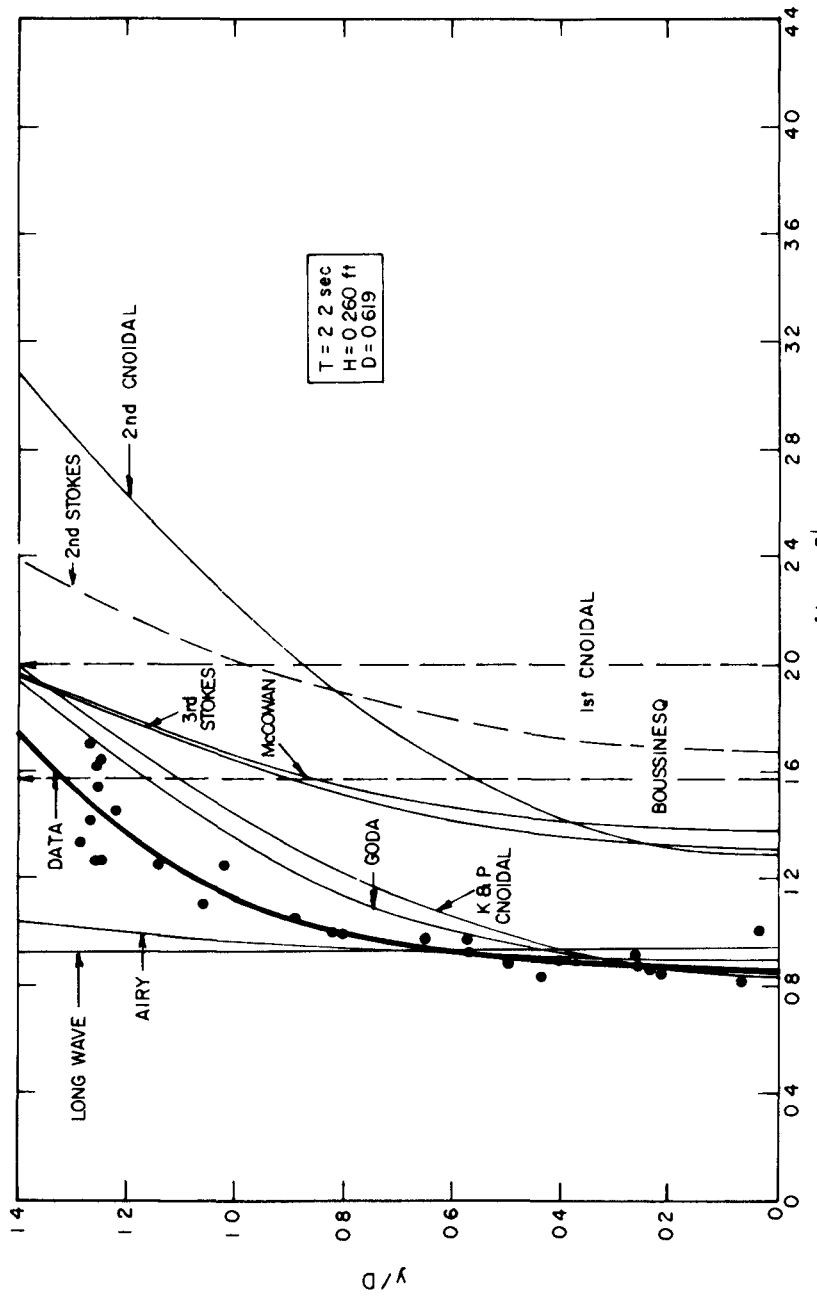

Figure 3. Horizontal Particle Velocity under the Crest - NON-BREAKING WAVE.

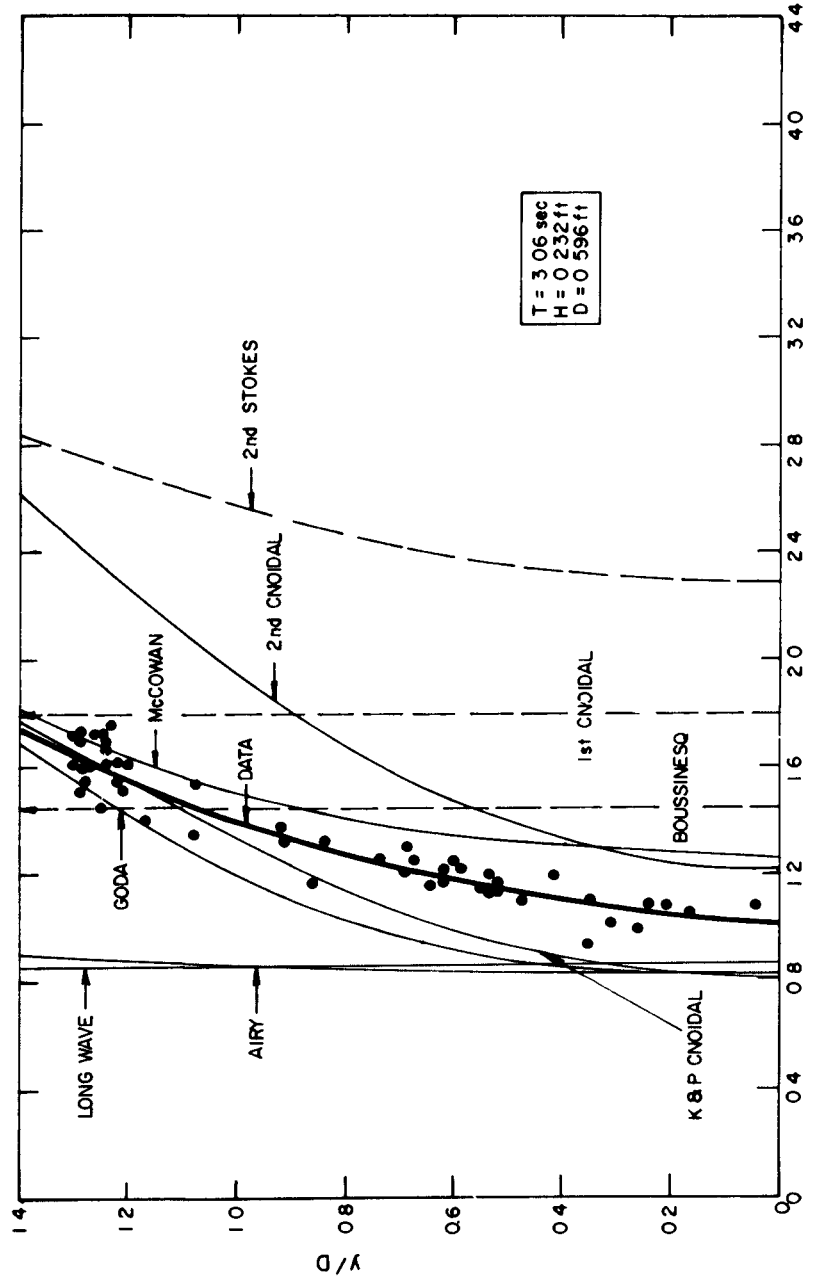

Figure 4. Horizontal Particle Velocity under the Crest - NON-BREAKING WAVE.

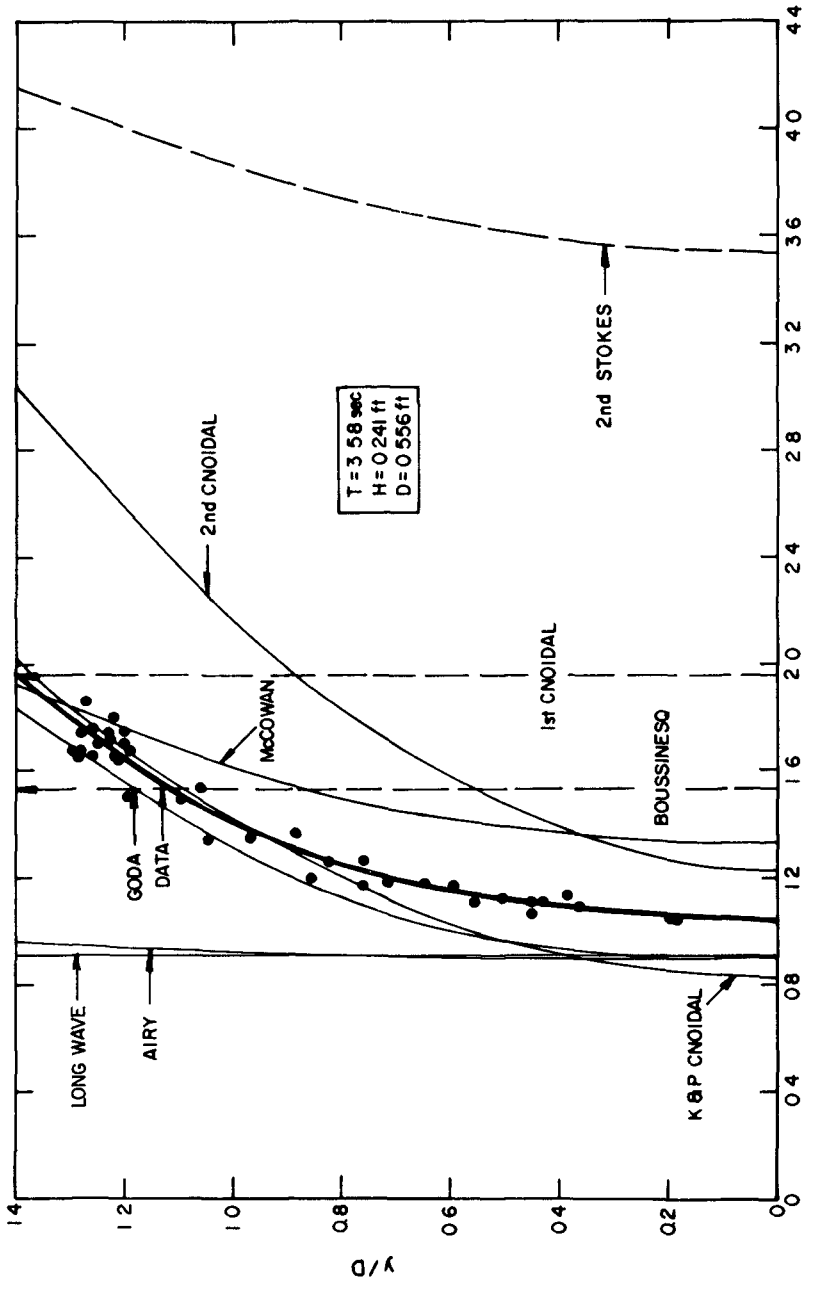

Figure 5. Horizontal Particle Velocity under the Crest - NON-BREAKING WAVE.

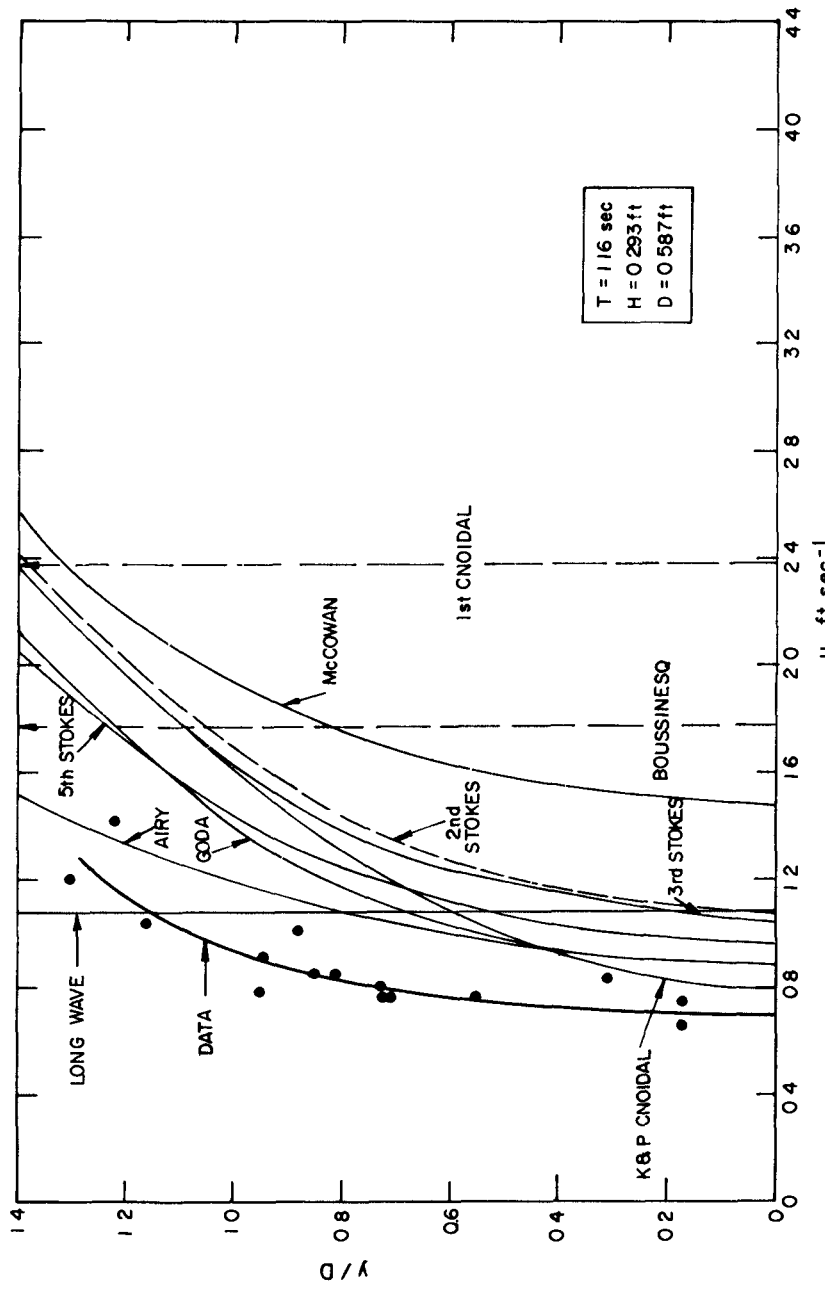

Figure 6. Horizontal Particle Velocity under the Crest - NEAR-BREAKING WAVE.

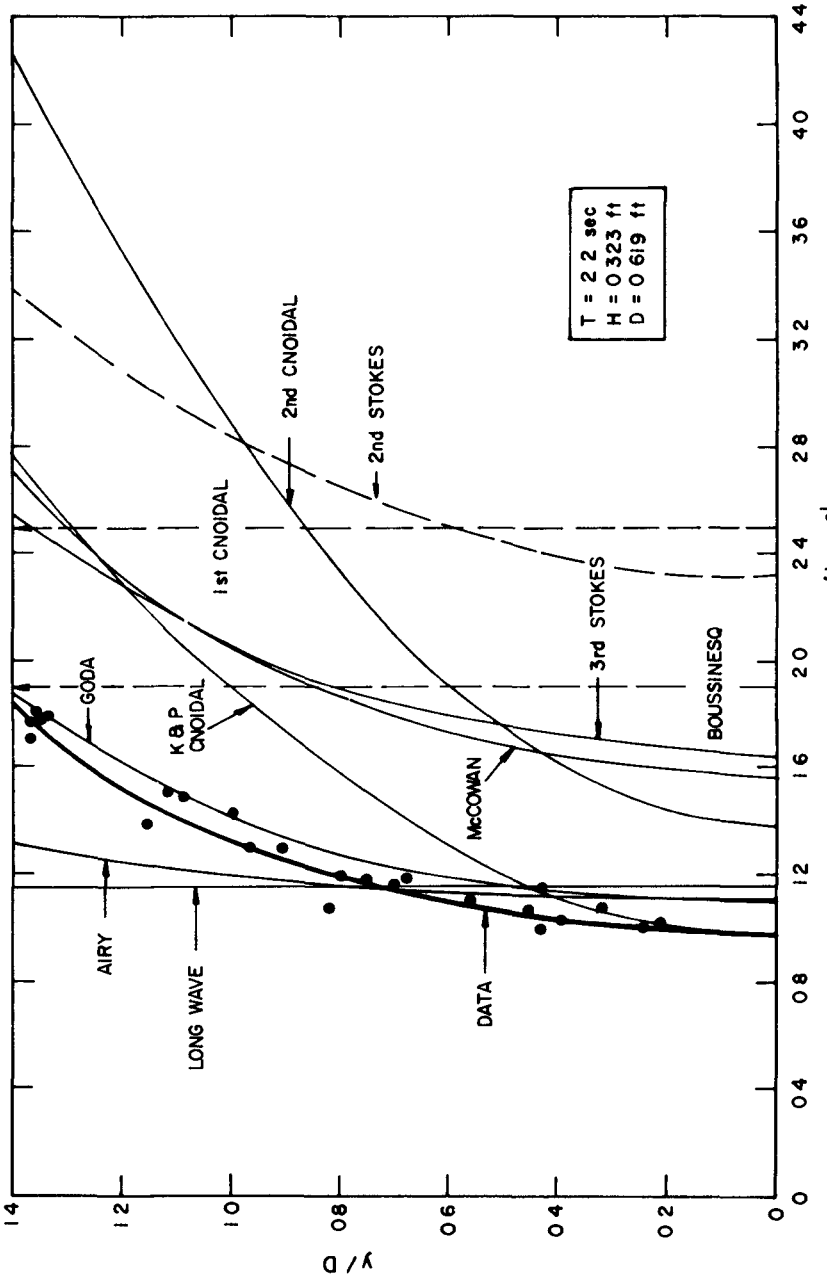

Figure 7. Horizontal Particle Velocity under the Great - NEAR-BREAKING WAVE.

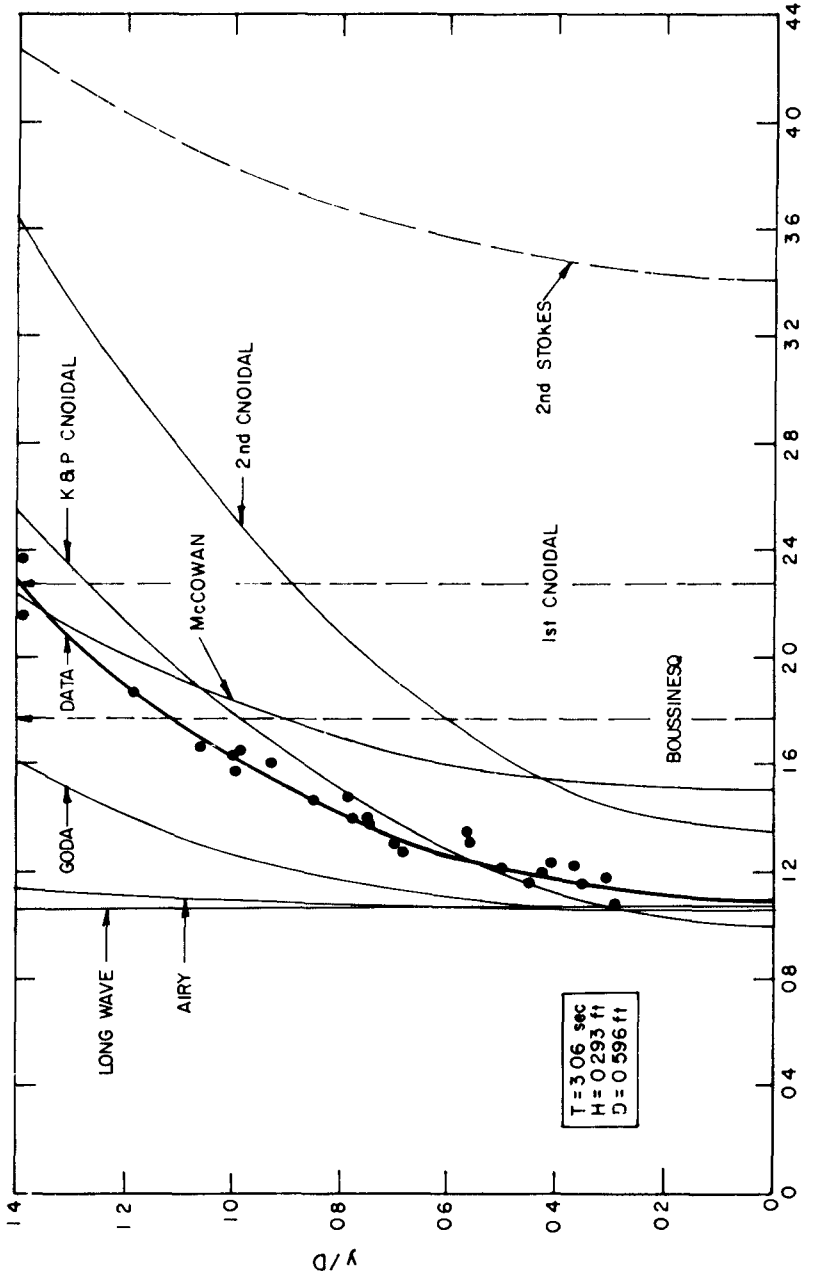

Figure 8. Horizontal Particle Velocity under the Crest - NEAR-BREAKING WAVE.

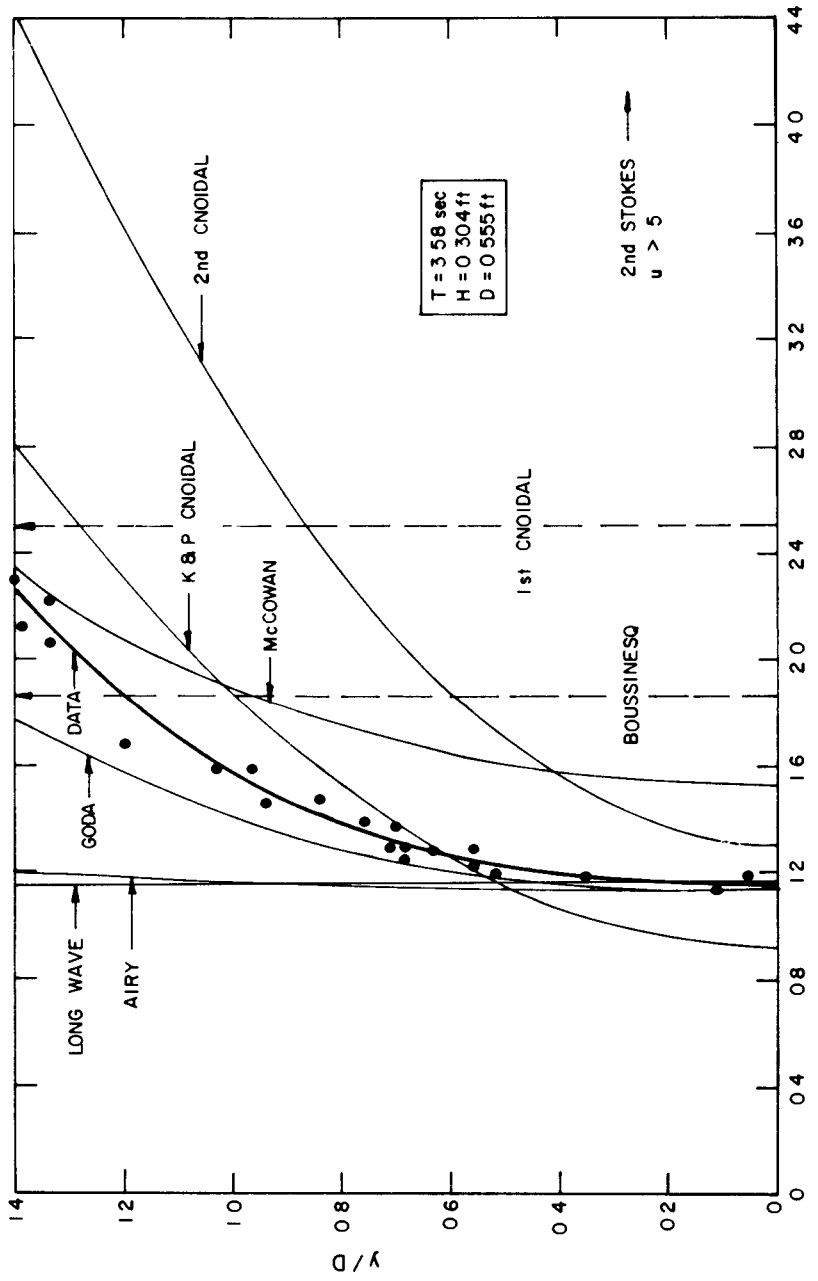

Figure 9. Horizontal Particle Velocity under the Crest - NEAR-BREAKING WAVE.

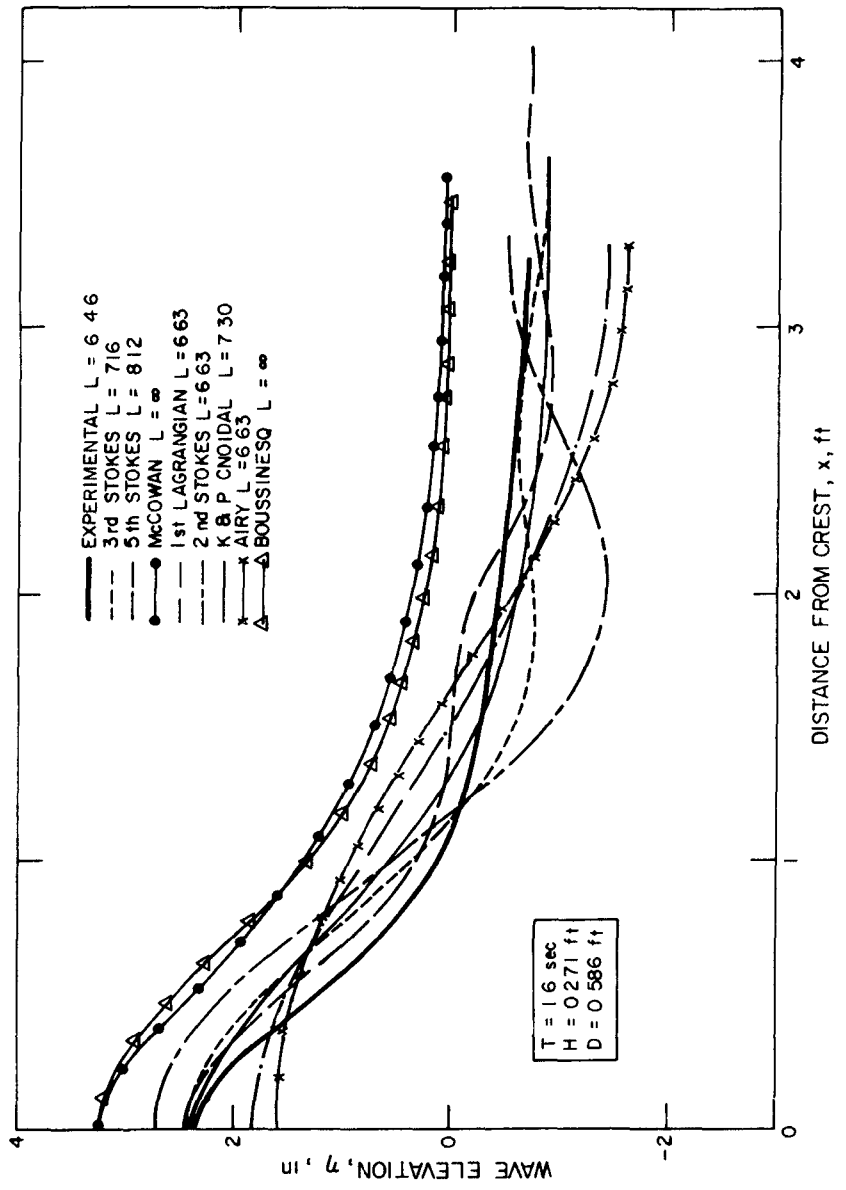

Figure 10. Free Surface Elevation.

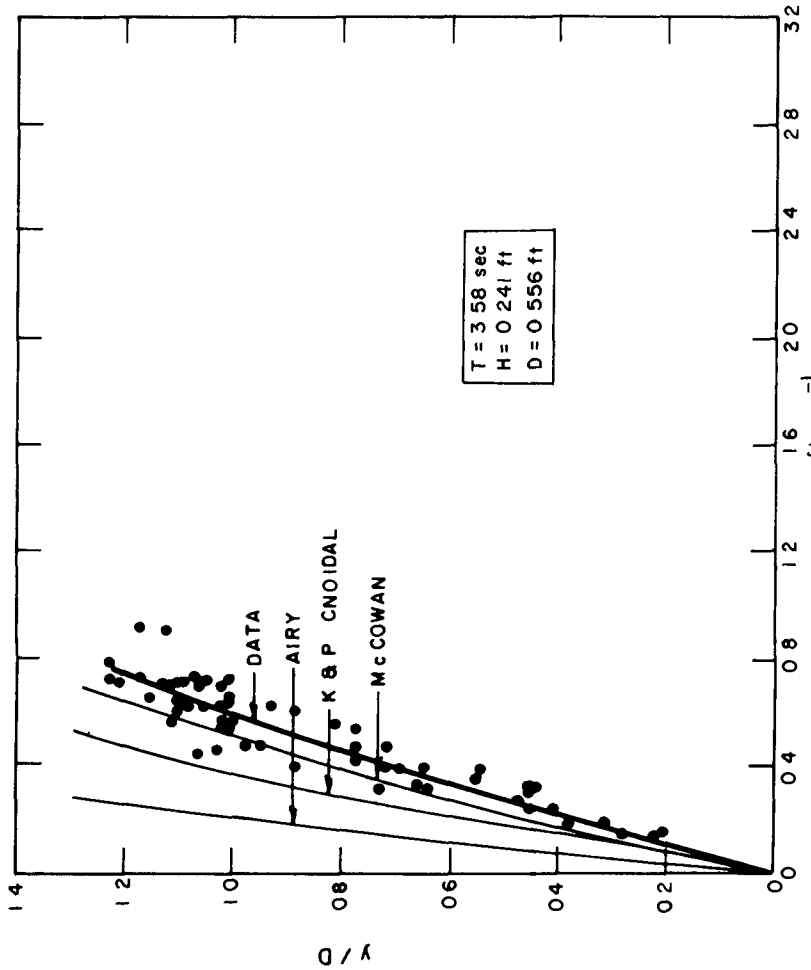

Figure 11 Vertical Particle Velocity (see text).

CHAPTER 8

BREAKING WAVE CRITERIA; A STUDY EMPLOYING A NUMERICAL WAVE THEORY

Robert G. Dean

Chairman, Department of Coastal and Oceanographic Engineering
University of Florida, Gainesville, Florida

INTRODUCTION

Although it is well recognized that wave systems in nature are irregular, comprising a spectrum of fundamental periods, there is still a need for improving our understanding of near-breaking nonlinear wave systems which contain a single fundamental period. For example, most of the shallow water design situations and other cases including forces on small diameter structures in which drag forces predominate are more directly treated in terms of a "design wave" rather than a wave spectrum. This situation is contrasted to many important engineering design problems in which the dynamics of the system are paramount; for example, in the case of a moored drilling vessel. Finally, one may reasonably expect that accurate solutions to the problem of nonlinear wave systems with a single fundamental period will lend insight regarding productive approaches to the more realistic problem of a spectrum of nonlinear waves.

This paper investigates the applicability of the stream function wave theory[1] for the representation of breaking and near-breaking waves. This particular problem has received little attention, although considerable progress has occurred on two related problems:

1. The development of wave theories covering a wide range of relative water depths and wave heights, and

2. The development of wave theories which apply <u>at</u> breaking conditions. In general, although these theories may be applicable for the limiting wave conditions, their basis of derivation is such that they cannot be extended to non-breaking waves.

The purpose of the present investigation, then, is to establish whether or not the stream function wave theory can be applied to span the range extending up to breaking conditions.

BACKGROUND

A great deal of effort[2,3,4,5,6,7] has been devoted to development of non-breaking wave theories based on mathematical approaches selected to

cover various ranges of relative water depths and wave heights. Recently, Dean[8] has compared the relative validities of eight wave theories based on the agreement of these theories to the boundary conditions included in their formulation. This comparison showed that the stream function wave theory provided a best fit to the boundary conditions over the range $0.05 < h/T^2 < 10.0$ ft/sec^2 and a range of wave heights encompassing most conditions encountered in engineering design problems.

A second problem area, that of conditions at wave breaking, has also received considerable attention[9,10,11,12,13,14]. These investigations generally predict an upper limit for wave stability, and, although the various results differ somewhat in numerical values, they are in approximate agreement. These results will be discussed in greater detail later. Aspects of these limiting wave theories that are important to the goals of the present investigation include:

1. The limiting wave theories cannot be applied to highly nonlinear, but non-breaking conditions.

2. No results are available to compare the results of existing non-breaking theories with the limiting wave theories for conditions at or near breaking.

3. All of the limiting wave theories require an a priori assumption concerning the shape of the wave crest. This assumption raises questions of the validity of the stability limit and of the wave kinematics and dynamics at breaking.

ANALYTICAL CONSIDERATIONS OF PRESENT INVESTIGATION

In the present investigation, two stability parameters will be defined as possible mechanisms limiting the heights that waves can attain without breaking. These parameters are defined to equal unity if their respective breaking mechanisms are fulfilled. Employing the stream function wave theory, the variations of these parameters are then investigated as the wave height is increased. The calculations are continued with increasing wave height until one of the stability parameters equals unity. The wave conditions and the values of the stability parameters at breaking are compared with previous results.

Formulation of Water Wave Problem

The system considered here will be that of a two-dimensional periodic water wave propagating over a horizontal bottom. Since the basis of the formulation includes the inherent assumption that the wave travels without change of form, it is possible to select a coordinate system moving with the wave celerity, C, thereby reducing the problem viewed in this reference system to one of steady motion. The formulation for this problem and the inherent assumptions have been presented and discussed thoroughly elsewhere[1]. Therefore, the governing equations will be simply set forth below without detailed discussion.

The Laplace differential equation expressed in terms of the velocity potential, ϕ, or stream function, ψ, must be satisfied throughout the region formed by the wave system. (See Figure 1 for a description of the wave system and notation employed.)

Formulating the problem in terms of a stream function, the associated differential equation is

$$\nabla^2\psi = 0 \tag{1}$$

The kinematic boundary conditions on the bottom and free surfaces ensure that no flow occurs normal to these surfaces, that is, on the bottom,

$$w = \frac{\partial\psi}{\partial x} = 0 \ , \ z = -h \tag{2}$$

and on the free surface,

$$\frac{\partial\eta}{\partial x} = \frac{w}{u-C} \ , \ z = \eta \tag{3}$$

The remaining (dynamic) boundary condition on the free surface ensures that the pressure on the free surface is uniform

$$\eta + \frac{1}{2g}\left[(u-C)^2 + w^2\right] = Q \ , \ z = \eta \tag{4}$$

where Q is a constant. The problem formulation is completed by requiring that all of the variables be periodic in the horizontal space coordinate, x.

If an analytical representation could be found that would satisfy the differential equation and boundary conditions, the representation would be exact within the limitations of the formulation.

The Stream Function Solution

The stream function representation for highly nonlinear waves has been explored in previous papers; hence, it will be presented here only in outline form. The stream function solution is written as

$$\psi(x,z) = \frac{L}{T}z + \sum_{n=1}^{N} A(n) \sinh\left[\frac{2\pi n}{L}(h+z)\right] \cos\frac{2\pi n}{L}x \tag{5}$$

and an expression for the free surface displacement, $\eta(x)$, is determined in implicit form by setting $z = \eta$ in Eq. (5), that is,

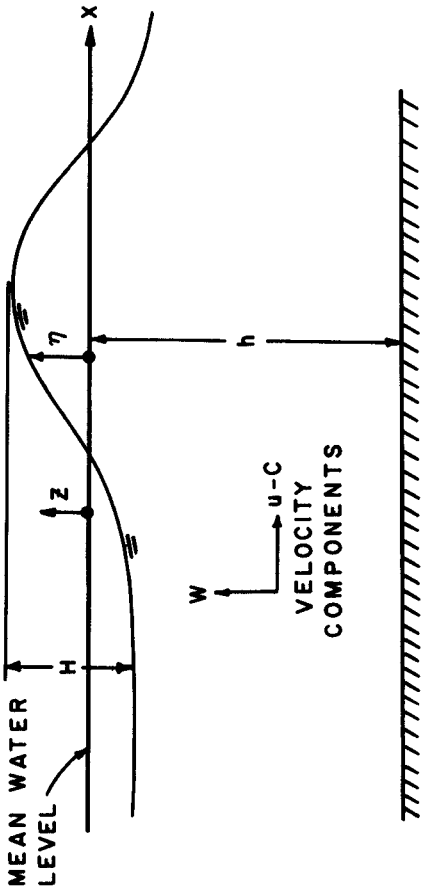

FIGURE 1. DEFINITION SKETCH, STATIONARY WAVE SYSTEM

$$\eta = \frac{\psi_\eta}{C} - \frac{T}{L} \sum_{n=1}^{N} A(n) \sinh \left[\frac{2\pi n}{L}(h+\eta)\right] \cos \frac{2\pi n}{L} x \qquad (6)$$

where ψ_η is the (constant) value of the stream function on the free surface.

It can be shown that, for arbitrary A(n) and L values, the stream function solution expressed in Eqs. (5) and (6) satisfies the formulation exactly except for the dynamic free surface boundary condition, Eq. (4). The problem is now posed, for given values of wave height, H, wave period, T, and water depth, h, of determining the wave length, L, and stream function coefficients, A(n) such that the dynamic free surface boundary condition is best satisfied. (It should be noted that the stream function value at the free surface is determined by requiring that the mean of the water surface displacement, η, be zero.) A numerical iterative procedure has been established to successively improve on the values of A(n) and L in accordance with the requirement of uniform Bernoulli constant, see reference 1 for details. During the present investigation, a property of the A(n) coefficients was found which appears to be general and which facilitates their determination.

STABILITY CRITERIA

In previous investigations of limiting forms of progressive and standing waves, two possible mechanisms for wave breaking have been proposed.

Kinematic Stability Parameter (KSP)

The KSP is a measure of the maximum horizontal water particle velocity, u_m, (which occurs at the crest) relative to the wave phase speed, C,

$$\text{KSP:} \quad \frac{u_m}{C} \qquad (7)$$

This criterion is proposed to be limiting if the water particle velocity equals the celerity, that is, $u_m/C = 1$. For conditions of the KSP equal to unity, it is sometimes argued that the crest particles will travel faster than the wave form, and the wave will become asymmetric and topple over. The soundness of this argument is not clear to this author.

Dynamic Stability Parameter (DSP)

The DSP is a measure of the total maximum vertical acceleration, Dw/Dt, relative to the acceleration of gravity, g, and is defined as

$$\text{DSP:} \quad -\frac{1}{g}\frac{Dw}{Dt} \qquad (8)$$

The physical interpretation of this limiting condition is evident; if this parameter exceeds unity, it can be shown that the pressure gradient at the

crest is zero and further increases in the wave height would cause water particles to leave the crest of the wave in a vertical direction. It is clear that this must be the breaking mechanism in standing waves. The KSP is generally regarded to be limiting for progressive waves. The pertinence of the DSP to limiting progressive waves is believed to be unresolved by published accounts, although Laitone[13] and Kinsman[15] have indicated that the DSP is governing for progressive waves.

Finally, it is emphasized that both the KSP and DSP are defined such that a value of unity of either of these quantities would indicate breaking due to their respective mechanisms.

RESULTS

Three wave conditions, spanning the range from relatively shallow to deep water, were chosen for further examination. The wave periods and water depths of these three cases are shown in Table I.

TABLE I

WAVE CHARACTERISTICS SELECTED FOR BREAKING STUDY

Case	Relative Depth	Water Depth (ft)	Period (sec)
A	Shallow	20.0	20.0
B	Intermediate	100.0	10.0
C	Deep	1000.0	10.0

In the initial calculations, the numerical stream function approach described earlier[1] was applied to determine the stream function coefficients, A(n), individually. It was found, by examination, that these coefficients vary in a semi-logarithmic manner with the index, n,

$$A(n) = A(1)\ e^{-bn} \tag{9}$$

An example is shown in Figure 2 for a 17th order Case A wave. It is emphasized that these coefficients were not constrained to a semi-logarithmic variation, but this form of variation appears to provide the best fit to the dynamic free surface boundary condition (DFSBC). Although the last few coefficients shown in Figure 2 deviate from the semi-logarithmic form, it was found that repeated iterations of the numerical procedure would improve this distribution. Calculations for Cases B and C and other relative depths

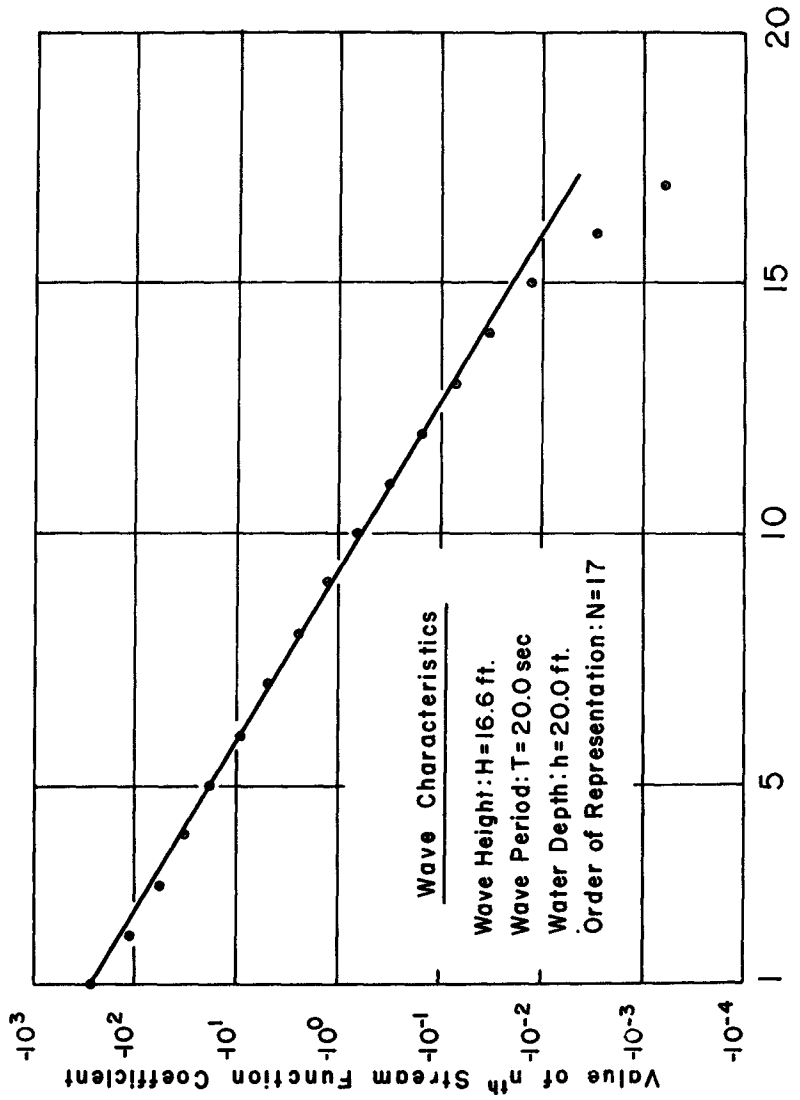

FIGURE 2. SEMI-LOGARITHMIC VARIATION OF STREAM FUNCTION COEFFICIENTS

indicated that the observed semi-logarithmic variation could be regarded as a property of these coefficients when a good fit to the DFSBC was attained, the reason for the semi-logarithmic variation is not known. The simplifications associated with the semi-logarithmic variation are substantial; for example, the number of independent wave parameters is 3 for a 20th order wave assuming a semi-logarithmic variation as compared to 21 if no a priori relationship is recognized for the A(n) coefficients. This feature was accounted for in the numerical scheme, thereby greatly reducing the computational time required, especially for near-breaking conditions, which require a high order representation.

Case A - Shallow Water Wave ($h/T^2 = 0.05$ ft/sec^2)

The kinematic and dynamic stability criteria for this case are plotted as a function of H/h in Figure 3. Note that breaking is predicted at a ratio H/h = 1.0 while the usually referenced breaking limit is H/h = 0.78; the range reported by previous investigators is $0.73 < H/h < 0.87$. For the results obtained here, it is clear that the kinematic criterion governs breaking, and it is surprising at first that the dynamic parameter is zero when breaking occurs. This point will be discussed later in greater detail.

The wave forms for a near-breaking Case A wave are presented in Figure 4. Note that the enclosed angle of the wave form is in approximate agreement with the previously determined value of 120 degrees.

The amplitude spectrum, determined by a harmonic analysis of the wave form, is also shown in Figure 4. As expected, the higher order terms are quite significant for the case of a near-breaking shallow water wave for which the crests are high and peaked and the troughs low and broad. As a reference for later comparison, the 10th order term (9th harmonic) is about 25 per cent of the fundamental.

Case B - Intermediate Depth Water Wave ($h/T^2 = 1.0$ ft/sec^2)

For the sake of brevity, the graphical results pertaining to this case are not shown here. The stability parameter results were the same as for Case A, that is, the KSP governed breaking and the DSP equals zero at breaking. The ratio H/T^2 at breaking was determined to be 0.69 ft/sec^2 which, as will be shown later, is in good agreement with previously referenced results.

Case C - Deep Water Wave ($h/T^2 = 10.0$ ft/sec^2)

The kinematic and dynamic stability parameters are shown in Figure 5 and indicate, as in Cases A and B, that the KSP governs and the DSP equals zero at breaking. The value of H/T^2 at breaking is 1.06 ft/sec^2 compared with the usually referenced value of 0.873 ft/sec^2. The wave form and amplitude spectrum for a near-breaking Case C wave are shown in Figure 6. Of interest is the rapid decrease in amplitude coefficients for large n. The ratio B(10)/B(1) equals 0.02 for Case C, whereas for Case A the corresponding ratio is 0.25. The angle enclosed by the wave in the vicinity of the crest is approximately 120 degrees for Case C.

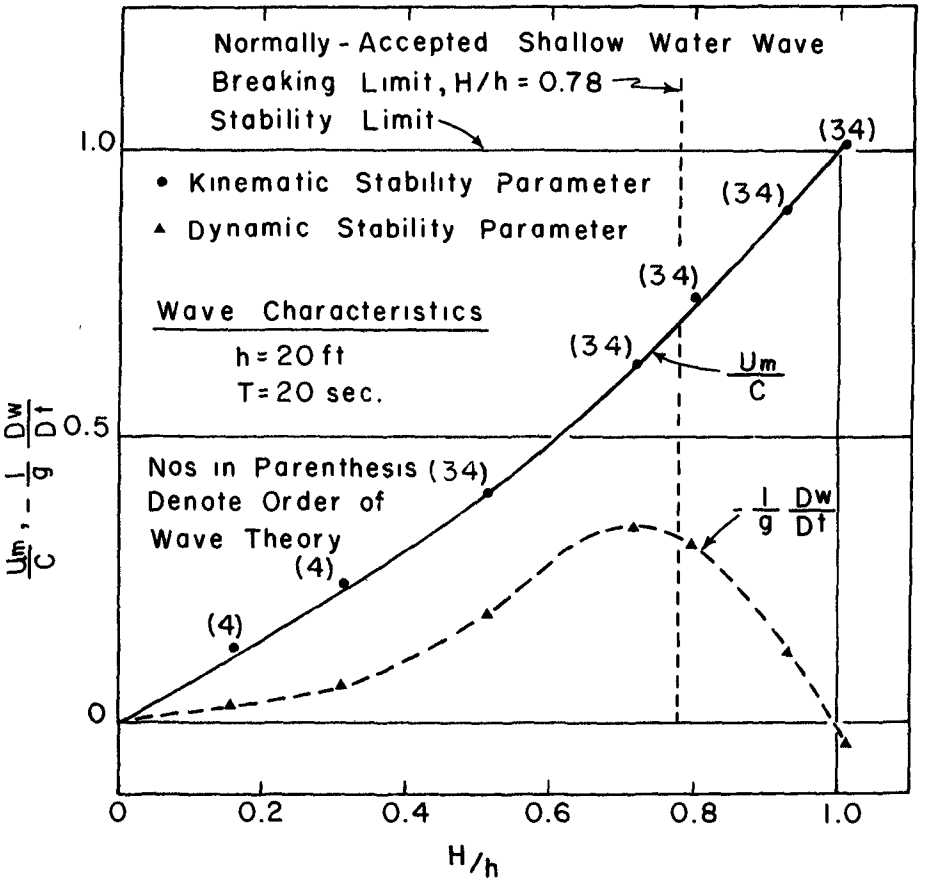

FIGURE 3. VARIATION OF STABILITY PARAMETERS WITH H/h; SHALLOW WATER WAVE

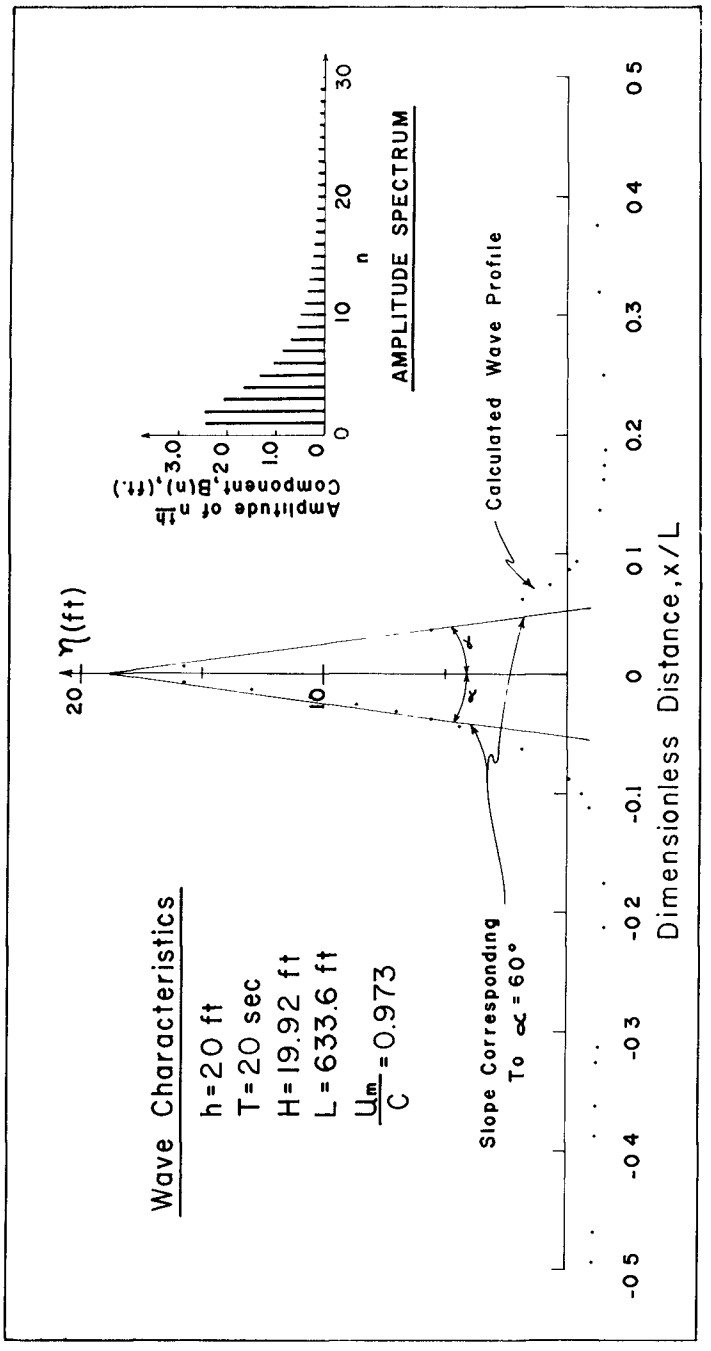

FIGURE 4 CALCULATED PROFILE AND AMPLITUDE SPECTRUM FOR NEAR-BREAKING SHALLOW WATER WAVE

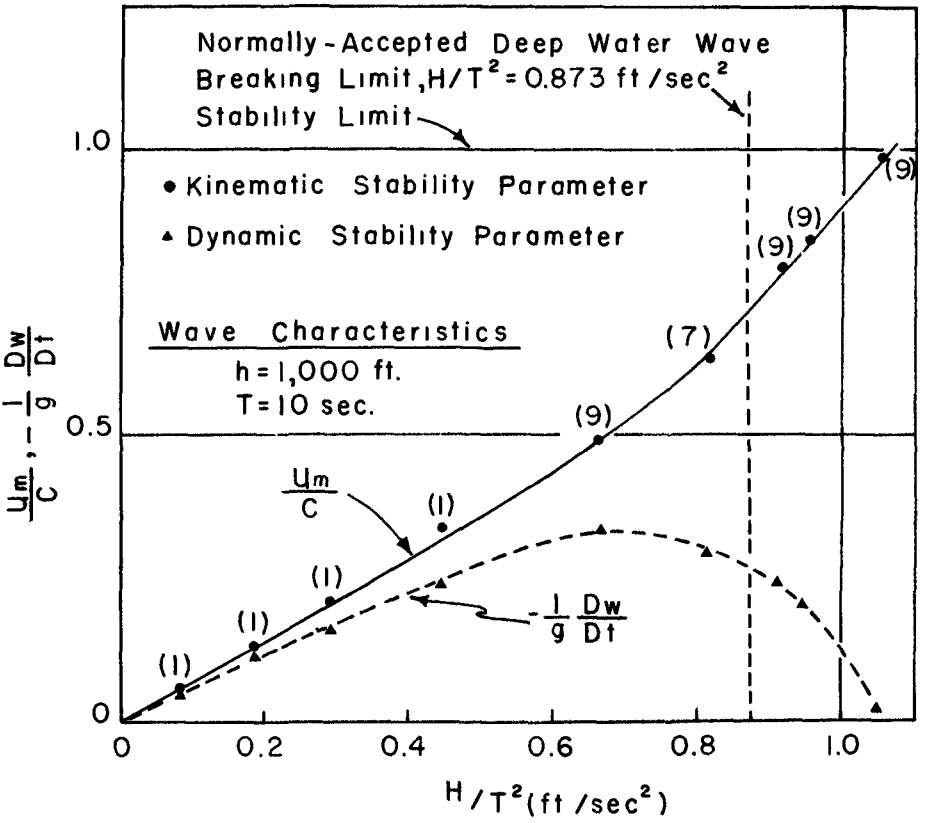

FIGURE 5. VARIATION OF STABILITY PARAMETERS WITH H/T^2; DEEP WATER WAVE

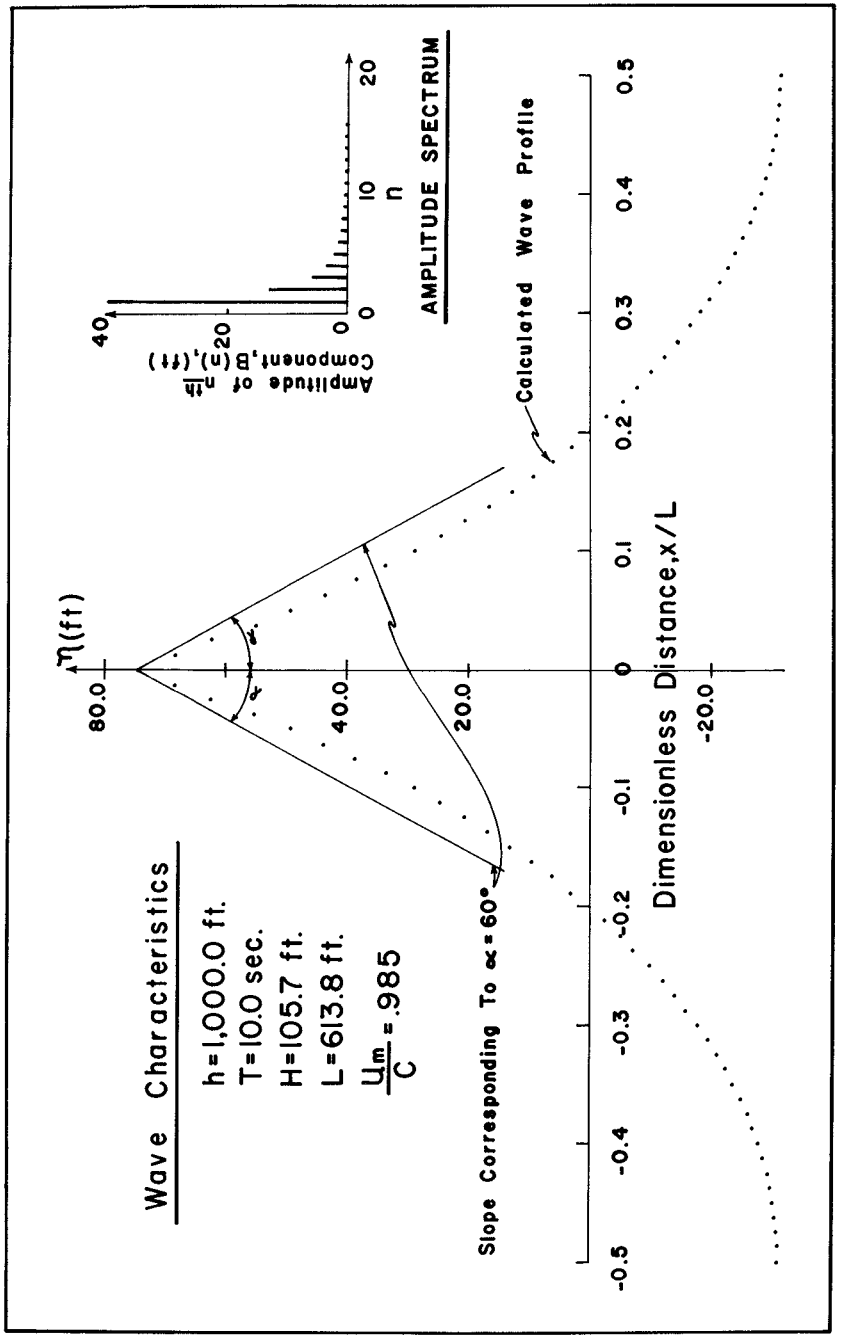

FIGURE 6. CALCULATED PROFILE AND AMPLITUDE SPECTRUM FOR NEAR-BREAKING DEEP WATER WAVE

Breaking Index

The breaking wave parameters for the three cases examined here are compared with the usually referenced breaking index in Figure 7. It is seen that the results obtained in the present investigation for Cases A, B, and C are 28 per cent higher, 0 per cent higher, and 21 per cent higher, respectively, than the index shown. Possible reasons for this difference are discussed in the next section.

CONCLUSIONS AND DISCUSSION

Conclusions

The results of this investigation indicate that:

1. For progressive waves, the kinematic stability parameter, $\frac{u_m}{C}$ rather than the dynamic parameter, $-\frac{1}{g}\frac{Dw}{Dt}$, governs breaking. The dynamic criterion was found to equal zero at breaking; this implies that immediately under the crest, hydrostatic conditions prevail.
2. The enclosed crest angle associated with the limiting wave is approximately equal to 120 degrees, a value determined by previous investigators. Earlier investigators, however, required the a priori assumption that the crest form be an angle which is a submultiple of 360 degrees.
3. The breaking wave heights determined here are somewhat higher (0 to 28 per cent) than those usually referenced.
4. The stream function wave theory appears well suited for representing the geometry, kinematics, and dynamics of periodic water wave systems up to breaking conditions.

Discussion

Probably the most significant results of this study are that: (1) the dynamic parameter, as defined, is zero at breaking rather than one-half as usually referenced, and (2) the breaking wave heights determined in this study are somewhat larger than those determined in earlier investigations. It is important, when considering these differences, to recall that all but one of the previous studies has required the a priori assumption that the limiting wave crest at breaking be a sharp angle which is a submultiple of 360 degrees. The present investigation required no a priori assumptions, but was based on determining the representation which best satisfies all of the defining equations.

With regard to the question of the value of the dynamic stability parameter at breaking, it is instructive to expand the expression for this parameter at breaking for the case of a stationary wave system

$$\text{DSP:}\quad -\frac{1}{g}\frac{Dw}{Dt} = -\frac{1}{g}\left[(u-C)\frac{\partial w}{\partial x} + \frac{1}{2}\frac{\partial w^2}{\partial z}\right]_{\text{crest}} \qquad (10)$$

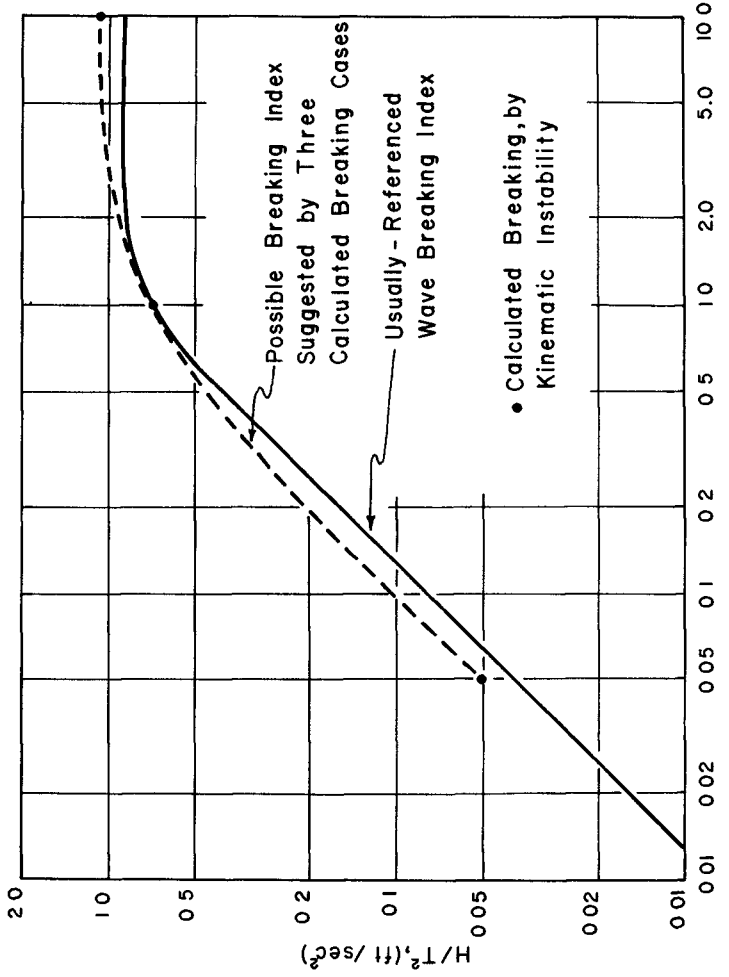

FIGURE 7. COMPARISON OF CALCULATED BREAKING WAVE CHARACTERISTICS WITH USUALLY-REFERENCED INDEX

Consider the two terms enclosed by the brackets. The second term is identically zero at the crest phase position where instability would be initiated. The first term contains the kinematic stability parameter; and since this is zero at breaking, therefore, it is seen that the dynamic stability parameter must be zero at breaking unless $\partial w/\partial x = \infty$. This will only occur if $\partial n/\partial x = \infty$ at the crest which is precisely the feature embodied in other investigations with the a priori assumption that the crest form a sharp angle. The interpretation here is that the DSP is zero at breaking and that the term $\partial w/\partial x$ is finite up to breaking. There is always the possibility that the term $\partial w/\partial x$ would approach infinity as the number of terms in the stream function expression increases without limit. To test this possibility, higher order representations were checked to see whether the additional terms contributed substantially to the wave form or to $\partial w/\partial x$. The conclusion reached from these calculations was that the observed result was not an artifice of the finite number of terms in the series representation. Other possible extraneous causes, that could be associated with the numerical procedure employed, are being examined.

The final question to be considered is whether the breaking values determined here or those in previous investigations are more nearly correct. Although this question cannot be absolutely resolved, the writer concludes that because the approach presented here requires no a priori assumption concerning the wave form (as discussed above) the results of the present investigation may be more valid. Further work, including breaking computations for a greater number of relative depths, is warranted to provide additional results on this facet of the problem.

ACKNOWLEDGMENTS

The investigation presented in this paper was sponsored by the Coastal Engineering Research Center under Contract #DACW72-67-C-0009.

REFERENCES

1. Dean, R. G., "Stream Function Representation of Nonlinear Ocean Waves," Journal of Geophysical Research, 70(18), pp. 4561-4576, September, 1965.

2. Stokes, G. G., "On the Theory of Oscillatory Waves," Transactions, Cambridge Philosophical Society, Vol. 8, and Supplement, Scientific Papers, VII, 1847.

3. McCowan, J., "On the Solitary Wave," London, Edinburgh and Dublin Philosophical Magazine and Journal of Science, Vol. 32(5), 1891.

4. Gerstner, F., "Theorie der Wellen," Abhandlung en der Koniglichen Bohmischen Gesellschaft der Wissenschaften, Prague, 1802; also, Gilberts Annalen der Physik XXXII, pp. 412-445, 1809 (in English as Technical Report Series 3, Issue 339, University of California Institute of Engineering Research, Wave Research Laboratory, 1952, Translated by R. M. Kay).

5. Borgman, L. E. and J. E. Chappelear, "The Use of the Stokes-Struik Approximation for Waves of Finite Height," Proceedings, Sixth Conference on Coastal Engineering, Chap. 16, 1958.

6. Laitone, E. V., "The Second Approximation to Cnoidal and Solitary Waves," Journal of Fluid Mechanics, Vol. 9, Part 3, pp. 430-444, November, 1960.

7. Skjelbreia, L. and J. A. Hendrickson, "Fifth Order Gravity Wave Theory," Proceedings, Seventh Conference on Coastal Engineering, Chap. 10, pp. 184-196, 1961.

8. Dean, R. G., "Relative Validities of Water Wave Theories," Proceedings, ASCE Specialty Conference on Civil Engineering in the Oceans, San Francisco, pp. 1-30, 1968.

9. Michell, J. H., "On the Highest Waves in Water," Philosophical Magazine, 36(5), pp. 430-435, 1893.

10. McCowan, J., "On the Highest Wave of Permanent Type," London, Edinburgh and Dublin Philosophical Magazine and Journal of Science, Vol. 38, 1894.

11. Yamada, H., "Highest Waves of Permanent Type on the Surface of Deep Water," Reports Research Institute of Applied Mechanics, Vol. 5, No. 18, pp. 37-52, 1957.

12. Chappelear, J. E., "On the Theory of the Highest Waves," Beach Erosion Board, TM No. 116, July, 1959.

13. Laitone, E. V., "Limiting Conditions for Cnoidal and Stokes Waves," Journal of Geophysical Research, 67(4), pp. 1555-1564, April, 1962.

14. Lenau, C. W., "The Solitary Wave of Maximum Amplitude," Journal of Fluid Mechanics, Vol. 26, Part 2, pp. 309-320, 1966.

15. Kinsman, B., "Wind Waves," Prentice Hall, Inc., Englewood Cliffs, New Jersey, p. 273, 1965.

CHAPTER 9

HYPERBOLIC WAVES AND THEIR SHOALING

Yuichi Iwagaki
Professor, Department of Civil Engineering
Kyoto University, Kyoto, Japan

ABSTRACT

Is is very difficult for engineers to deal with the cnoidal wave theory for practical application, since this theory contains the Jacobian elliptic functions, their modulus k, and the complete elliptic integrals of the first and second kinds, K and E respectively.

This paper firstly proposes formulae for various wave characteristics of new waves named "hyperbolic waves", which are derived from the cnoidal wave theory under the condition that k = 1 and E = 1 but K is not infinite and are a function of $T\sqrt{g/h}$ and H/h, so that cnoidal waves can be approximately expressed as hyperbolic waves by primary functions only, in which T is the wave period, h the water depth and H the wave height.

Secondly, as an application of the hyperbolic wave theory, the present paper deals with wave shoaling, that is, changes in the wave height, the wave crest height above still water level, and the wave velocity, when the waves proceed into shallow water from deep water.

INTRODUCTION

Cnoidal waves, which were discovered by Korteweg and de Vries (1895), are not familiar to engineers, despite a long history, because of mathematical treatments including the Jacobian elliptic function and the complete elliptic integrals of the first and second kinds. Since, however, it has been noticed that the theory of Stokes waves is not appropriate to periodic waves progressing in shallow water in cases where $h/L < 1/10$ (Keulegan, 1950), $h/L < 1/8$ (Laitone, 1962) or $h/L < (\eta_0/L)^{1/3}$ (Wilson, Webb and Hendrickson, 1952), and that the theory of cnoidal waves should be applied to those waves, it is necessary to modify the theoretical results of cnoidal waves and provide graphs to easily find the wave characteristics, where L is the wave length and η_0 the wave crest height above the still water level. For this purpose, graphs were presented by Wiegel (1960) and tables published by Masch and Wiegel (1961) to obtain the profile and velocity of cnoidal waves from a given wave height, water depth, wave length or wave period. These graphs and tables, however, were based on the theoretical results of the first approximation by Keller (1948) and Keulegan and Patterson (1940), and furthermore the mean water depth was replaced by the water depth below the wave trough, so that they seem to be unsatisfactory compared with those of Stokes waves of the third order approximation presented by Skjelbreia (1959).

For this reason, the author tried to provide graphs to easily obtain the wave profile, wave velocity, wave length and wave steepness from a given wave period, still water depth and wave height for practical use based on Laitone's cnoidal wave theory of the second approximation (Laitone, 1961, 1962), and confirmed the validity of the cnoidal wave theory by making a comparison with the results of an experiment conducted for a case where $T\sqrt{g/h} \geq 15$ (Iwagaki, 1964, 1965; Iwagaki and Hosomi, 1966a, 1966b).

Theoretical curves of the wave height change in shoaling water for a large depth to wave length ratio were presented by Le Méhauté and Webb (1964) based on the Stokes wave theory of the third order approximation and by Koh and Le Méhauté (1966) based on that of the fifth order approximation. On the other hand, the computation of wave height change in shoaling water for a small depth to wave length ratio using the cnoidal wave theory was attempted by Masch (1964), but it was not successful because of the difficulty of numerical computation for complicated expressions including the Jacobian elliptic functions.

In this paper, after firstly defining the new waves named "hyperbolic waves" (Iwagaki, 1967), which are derived from the cnoidal wave theory, formulae for various wave characteristics of hyperbolic waves are presented, which are expressed by primary functions only. Secondly, changes in the wave height, the wave crest height above still water level and the wave velocity in shoaling water are computed based on the hyperbolic wave theory and compared with experimental results to confirm the validity of the hyperbolic wave theory.

DEFINITION OF HYPERBOLIC WAVES

Wave characteristics of cnoidal waves in dimensionless form ϕ are generally expressed as follows:

$$\phi = f\left(\frac{h_t}{H}, \frac{z}{h_t}, K, \frac{E}{K}, k, \mathrm{cn}(v,k), \mathrm{sn}(v,k), \mathrm{dn}(v,k)\right) \quad \cdots\cdots\cdots (1)$$

in which $v = 2K(x-ct)/L$, h_t is the water depth below the wave trough, cn, sn and dn are the Jacobian elliptic functions, c the wave velocity, t the time, x the distance in the direction of wave propagation, and z the distance taken upwards from the wave trough as shown in Fig. 1.

Since the solitary wave theory can be derived with the limitation that $k = 1$ or $K \to \infty$, $E = 1$ and $L \to \infty$, and in this case $\mathrm{cn}(v,k)$ and $\mathrm{dn}(v,k)$ are written as $\mathrm{sech}v$ and $\mathrm{sn}(v,k)$ as $\tanh v$, wave characteristics of a solitary wave in dimensionless form ϕ_s are expressed as

$$\phi_s = f_s\left(\frac{h_t}{H}, \frac{z}{h_t}, \mathrm{sech}v, \tanh v\right) \quad \cdots\cdots\cdots (2)$$

and

$$v = 2\alpha(x-ct)/h_t \quad \cdots\cdots\cdots (3)$$

in which α is a function of h_t/H.

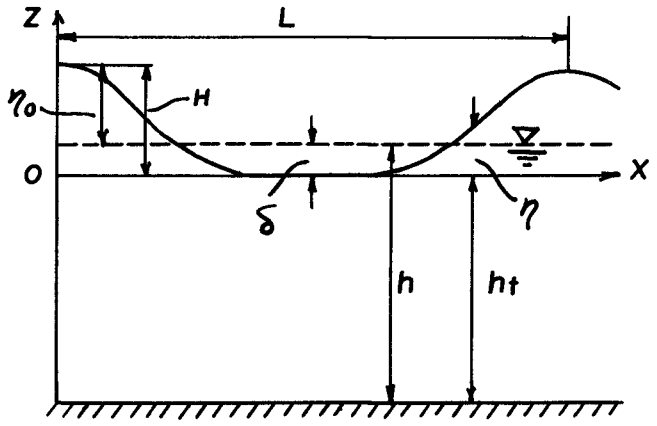

Fig. 1 Coordinate system.

Now, let us consider a case where k can be approximately put as unity, which is not the limiting case k = 1 as in the solitary wave theory. The value of K does not become as large as infinity even if the values of k and E tend to unity and can be put approximately as unity, as seen in Fig. 2. In other words, when K = 3, k = 0.98 and E = 1.05, then k and E can be put approximately as unity. Therefore, if k and E are put as unity on condition that

$$K \geq 3 \quad \cdots\cdots(4)$$

the following expression for wave characteristics of new waves in dimensionless form Φ_h can be derived corresponding to Eq. (1):

$$\Phi_h = f_h\left(\frac{h_t}{H}, \frac{z}{h_t}, K, \operatorname{sech} v, \tanh v\right) \quad \cdots\cdots(5)$$

The waves are not periodic because they are expressed by hyperbolic functions. However, if the wave troughs are connected with each other for every wave, they can be treated as periodic waves, since the wave length is not infinite. The author has named the new waves "hyperbolic waves", because the characteristics of the waves can be expressed by hyperbolic functions with finite wave lengths (Iwagaki, 1967).

Since the dimensionless quantity for wave characteristics of hyperbolic waves Φ_h contains the complete elliptic integral of the first kind K as shown in Eq. (5), it is necessary to obtain the relationship between the wave period, wave height, water depth and K. The relationship was already presented graphically by the author (Iwagaki, 1965) based on Laitone's cnoidal wave theory of the second approximation (Fig. 3). Then, the relationship between K, $T\sqrt{g/h}$ and h/H is formulated using Fig. 3. Fortunately in the range of $K \geq 3$, the curves for each value of a parameter h/H can be expressed approximately by parallel straight lines, which are shown by a solid line in Fig. 4. The formula to fit this solid line was proposed as follows (Iwagaki, 1967; Iwagaki and Sakai, 1968);

$$\frac{K}{T\sqrt{g/h}} = \frac{\sqrt{3}}{4}\left(\frac{H}{h}\right)^{1/2}\left\{1 - a\left(\frac{H}{h}\right)^{n}\right\}^{m} \quad \cdots\cdots(6)$$

in which

$$a = 1.3,\ n = 2 \text{ and } m = 1/2 \text{ for } H/h = 0.55 \quad \cdots\cdots(7a)$$

and

$$a = 0.54,\ n = 3/2 \text{ and } m = 1 \text{ for } H/h > 0.55 \quad \cdots\cdots(7b)$$

The plotted points are values computed by Eq. (6), which are in good agreement with the solid line.

The limit condition for application of the hyperbolic wave theory can be obtained from Eqs. (4) and (6). Fig. 5 shows a graphical expression of the limit.

CHARACTERISTICS OF HYPERBOLIC WAVES

Formulae for various characteristics of hyperbolic waves can be derived by putting k and E as unity and replacing the Jacobian elliptic functions with hyperbolic functions in the cnoidal wave theory as mentioned previously.

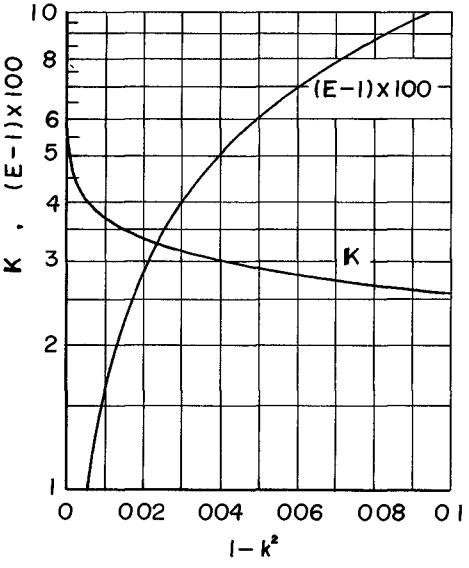

Fig. 2 Relationships between the complete elliptic integrals of the first and second kinds and the modulus of the Jacobian elliptic function.

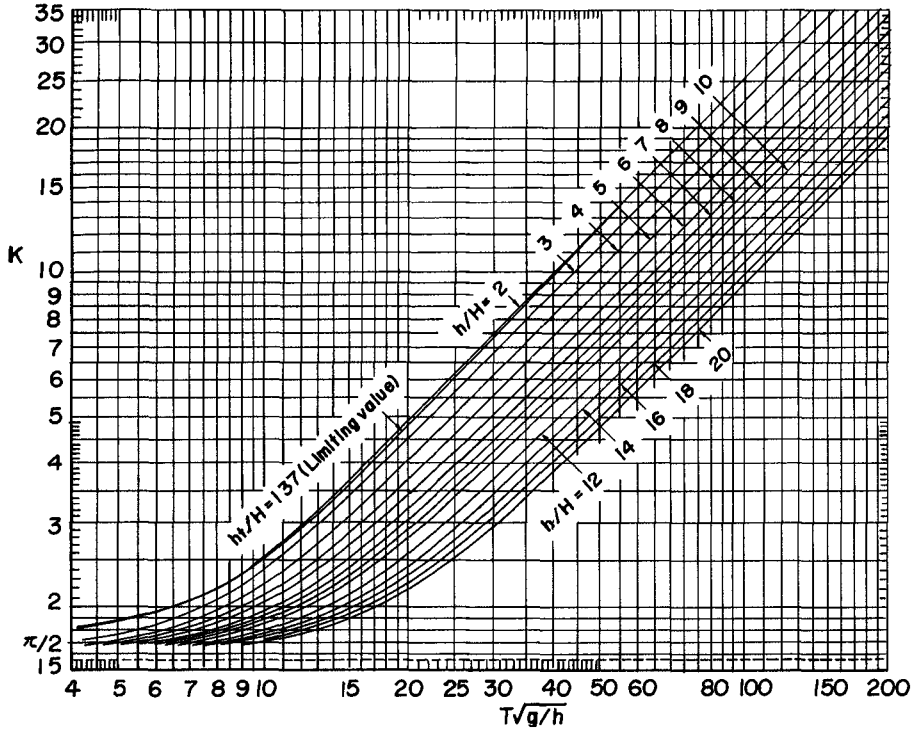

Fig. 3 Relationship between K and $T\sqrt{g/h}$ with a parameter of h/H.

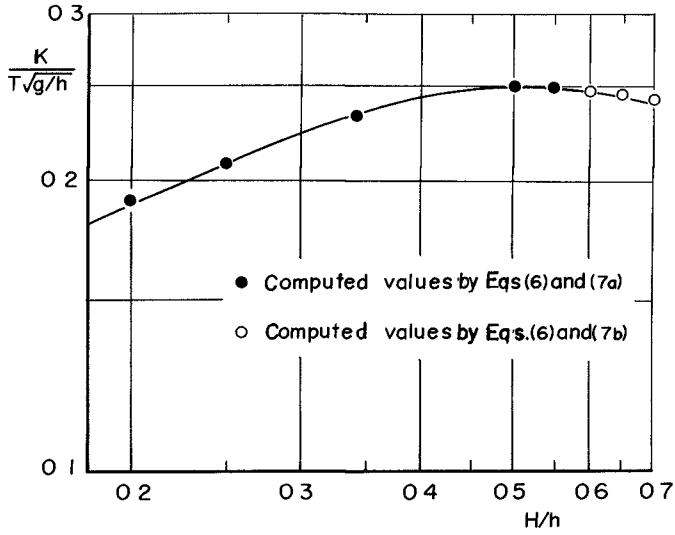

Fig. 4 Relationship between $K/T\sqrt{g/h}$ and H/h.

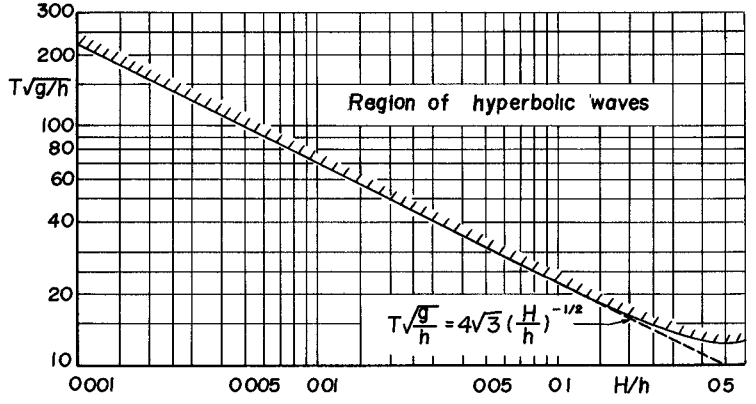

Fig. 5 Limit for application of hyperbolic wave theory.

HEIGHT OF STILL WATER LEVEL ABOVE WAVE TROUGH

$$\frac{\delta}{H}=\frac{1}{K}\left\{1-\frac{1}{12}\frac{H}{h}-\frac{1}{12}\frac{1}{K}\left(\frac{H}{h}\right)^2\right\} \quad \cdots\cdots(8)$$

WAVE PROFILE

$$\frac{\eta}{H}=\operatorname{sech}^2\left(\frac{2K}{L}X\right)-\frac{3}{4}\frac{H}{h}\operatorname{sech}^2\left(\frac{2K}{L}X\right)\left(1+\frac{1}{K}\frac{H}{h}\right)\left\{1-\operatorname{sech}^2\left(\frac{2K}{L}X\right)\right\} \quad \cdots\cdots(9)$$

in which $X=x-ct$ $\cdots\cdots(10)$

WAVE VELOCITY

$$\frac{c}{\sqrt{gh}}=\left(1-\frac{1}{2}\frac{1}{K}\frac{H}{h}\right)\left[1+\left(1+\frac{1}{K}\frac{H}{h}\right)\frac{H}{h}\left(\frac{1}{2}-\frac{1}{K}\right)+\left(1+\frac{2}{K}\frac{H}{h}\right)\left(\frac{H}{h}\right)^2 \times\left\{\frac{1}{K}\left(\frac{1}{K}-\frac{1}{4}\right)-\frac{3}{20}\right\}\right] \quad \cdots\cdots(11)$$

WAVE LENGTH

$$\frac{L}{h}=\left(1-\frac{3}{2}\frac{1}{K}\frac{H}{h}\right)\frac{4K}{\sqrt{3}}\left(\frac{H}{h}\right)^{-1/2}\left\{1-\left(1+\frac{1}{K}\frac{H}{h}\right)\frac{5}{8}\frac{H}{h}\right\}^{-1} \quad \cdots\cdots(12)$$

PRESSURE

$$\frac{p}{\rho gH}=\operatorname{sech}^2\left(\frac{2K}{L}X\right)-\frac{3}{4}\frac{H}{h}\operatorname{sech}^2\left(\frac{2K}{L}X\right)\left(1+\frac{1}{K}\frac{H}{h}\right)\left\{1-\operatorname{sech}^2\left(\frac{2K}{L}X\right)\right\} -\frac{3}{4}\frac{H}{h}\operatorname{sech}^2\left(\frac{2K}{L}X\right)\left\{2\frac{z}{h_t}+\left(\frac{z}{h_t}\right)^2\right\}\left(1+\frac{1}{K}\frac{H}{h}\right)\left\{2-3\operatorname{sech}^2\left(\frac{2K}{L}X\right)\right\} -\frac{z}{H} \quad \cdots\cdots(13)$$

PARTICLE VELOCITIES

Horizontal velocity

$$\left.\begin{aligned}&\frac{u}{\sqrt{gh}}=A_1\operatorname{sech}^2\left(\frac{2K}{L}X\right)+A_2\operatorname{sech}^4\left(\frac{2K}{L}X\right)-A_3,\\&A_1=\left(1+\frac{1}{2}\frac{1}{K}\frac{H}{h}\right)\frac{H}{h}\left[1-\frac{5}{4}\left(1+\frac{1}{K}\frac{H}{h}\right)\frac{H}{h}-\frac{3}{2}\left(1+\frac{1}{K}\frac{H}{h}\right)\frac{H}{h}\left\{2\frac{z}{h_t}+\left(\frac{z}{h_t}\right)^2\right\}\right]\\&A_2=\left(1+\frac{3}{2}\frac{1}{K}\frac{H}{h}\right)\left(\frac{H}{h}\right)^2\left[\frac{5}{4}+\frac{9}{4}\left\{2\frac{z}{h_t}+\left(\frac{z}{h_t}\right)^2\right\}\right]\\&A_3=\left(1+\frac{1}{2}\frac{1}{K}\frac{H}{h}\right)\frac{H}{h}\frac{1}{K}\left\{1-\left(1+\frac{1}{K}\frac{H}{h}\right)\frac{H}{h}\left(\frac{1}{K}-\frac{1}{4}\right)\right\}\end{aligned}\right\} \quad \cdots\cdots(14)$$

Vertical velocity

$$\frac{w}{\sqrt{gh}}=\left(1+\frac{1}{K}\frac{H}{h}\right)\left(1+\frac{z}{h_t}\right)\sqrt{3}\left(\frac{H}{h}\right)^{3/2}\operatorname{sech}^2\left(\frac{2K}{L}X\right)\tanh\left(\frac{2K}{L}X\right) \times\left[1-\frac{7}{8}\left(1+\frac{1}{K}\frac{H}{h}\right)\frac{H}{h}-\frac{1}{2}\left(1+\frac{1}{K}\frac{H}{h}\right)\frac{H}{h}\left\{2\frac{z}{h_t}+\left(\frac{z}{h_t}\right)^2\right\} -\frac{1}{2}\left(1+\frac{1}{K}\frac{H}{h}\right)\frac{H}{h}\operatorname{sech}^2\left(\frac{2K}{L}X\right)\left\{1-6\frac{z}{h_t}-3\left(\frac{z}{h_t}\right)^2\right\}\right] \quad \cdots\cdots(15)$$

WAVE ENERGIES

Potential energy per unit area

$$E_p=\frac{1}{2}\rho g\frac{1}{L}\int_{-L/2}^{L/2}(\eta-\delta)^2dx$$

$$= \frac{1}{3}\rho g H^2 \frac{1}{K}\left\{1-\frac{3}{2}\frac{1}{K}+\frac{H}{h_t}\left(-\frac{3}{10}+\frac{3}{4}\frac{1}{K}\right)+\left(\frac{H}{h_t}\right)^2\left(\frac{27}{560}-\frac{15}{288}\frac{1}{K}\right)\right\} \quad \cdots\cdots\cdots (16)$$

Kinetic energy per unit area

$$E_k = \frac{1}{2}\rho\frac{1}{L}\int_{-L/2}^{L/2}\int_{-h_t}^{\eta}(u^2+w^2)\,dx\cdot dz$$

$$= \frac{1}{3}\rho g H^2 \frac{1}{K}\left\{1-\frac{3}{2}\frac{1}{K}+\frac{H}{h_t}\left(\frac{1}{10}-\frac{3}{4}\frac{1}{K}+\frac{3}{2}\frac{1}{K^2}\right)\right.$$

$$\left.+\left(\frac{H}{h_t}\right)^2\left(\frac{23}{560}+\frac{113}{160}\frac{1}{K}+\frac{3}{8}\frac{1}{K^2}\right)\right\} \quad \cdots\cdots\cdots (17)$$

Total energy per unit area

$$E = E_p + E_k$$

$$= \frac{2}{3}\rho g H^2 \frac{1}{K}\left\{1-\frac{3}{2}\frac{1}{K}+\frac{H}{h_t}\left(-\frac{1}{10}+\frac{3}{4}\frac{1}{K^2}\right)+\left(\frac{H}{h_t}\right)^2\left(\frac{5}{112}+\frac{157}{480}\frac{1}{K}+\frac{3}{16}\frac{1}{K^2}\right)\right\} \quad \cdots\cdots (18)$$

RATE OF WAVE ENERGY TRANSMISSION

$$W = \frac{\rho}{T}\int_{-T/2}^{T/2}\int_{-h_t}^{\eta}\left\{\frac{1}{2}(u^2+w^2)+\frac{p}{\rho}+gz\right\}u\,dz\,dt$$

$$= \frac{2}{3}\rho g H^2\sqrt{g h_t}\cdot\frac{1}{K}\left\{1-\frac{3}{2}\frac{1}{K}+\frac{H}{h_t}\left(\frac{2}{5}-\frac{5}{2}\frac{1}{K}+\frac{3}{K^2}\right)\right.$$

$$\left.+\left(\frac{H}{h_t}\right)^2\left(-\frac{31}{112}-\frac{29}{160}\frac{1}{K}+\frac{13}{4}\frac{1}{K^2}\right)\right\} \quad \cdots\cdots\cdots (19)$$

CHANGE IN WAVE HEIGHT ON SLOPING BEACH

The change in the wave height on a sloping beach can be calculated from the condition that the rate of wave energy transmission is constant at each section if the wave motion on a sloping beach is assumed to be the same as that on a horizontal sea bottom having the corresponding water depth. If wave energy dissipation due to bottom friction and wave refraction and reflection due to variable water depths are neglected, the relationship described above is expressed as follows;

$$\overline{W} = \overline{W}_0 \quad \cdots\cdots\cdots (20)$$

Eq. (19) is applied to $\overline{W}$ at the left side of Eq. (20) and the following relationships derived by Le Méhauté and Webb (1964) based on Stokes wave theory of the third order approximation by Skjelbreia (1959) is used for $\overline{W}_0$ at the right side of Eq. (20), in which the suffix o denotes the quantity in deep water:

$$W_0 = \frac{\rho T^3}{32\pi}\left(\frac{L_0}{T^2}\right)^4\lambda_0^2\left\{4\left(1+\frac{3}{4}\lambda_0^2\right)\right\} \quad \cdots\cdots\cdots (21)$$

$$\frac{3}{8}\lambda_0^3+\lambda_0 = \pi\frac{H_0}{L_0} \quad \cdots\cdots\cdots (22)$$

$$\frac{L_0}{T^2} = \frac{g}{2\pi}(1+\lambda_0^2) \quad \cdots\cdots\cdots (23)$$

Finally the following equation of H/H_0 is derived as a function of H_0/L_0 and h/L_0:

$$\frac{H}{H_0} = \frac{3}{16}\left(\frac{1}{4}\right)^{1/3}\left(\frac{h}{L_0}\right)^{-1}\left(\frac{H_0}{L_0}\right)^{1/3}\left\{1-\pi^2\left(\frac{H_0}{L_0}\right)^2\right\}\left\{1-\frac{1}{K}\frac{H}{h}+\frac{1}{12}\frac{1}{K}\left(\frac{H}{h}\right)^2\right\}^{-1/3}$$

$$\times\left\{1-a\left(\frac{H}{h}\right)^{n}\right\}^{2m/3}\left\{1-\frac{3}{2}\frac{1}{K}+\frac{H}{h_t}\left(\frac{2}{5}-\frac{5}{2}\frac{1}{K}+\frac{3}{K^2}\right)\right.$$
$$\left.+\left(\frac{H}{h_t}\right)^{2}\left(-\frac{31}{112}-\frac{29}{160}\frac{1}{K}+\frac{13}{4}\frac{1}{K^2}\right)\right\}^{-2/3} \quad \cdots\cdots\cdots\cdots\cdots\cdots (24)$$

because

$$\frac{h_t}{H}=\frac{h}{H}-\frac{\delta}{H}=\frac{h}{H}\left\{1-\frac{1}{K}\frac{H}{h}+\frac{1}{12}\frac{1}{K}\left(\frac{H}{h}\right)^{2}\right\} \quad \cdots\cdots\cdots\cdots\cdots\cdots (25)$$

$$\frac{H}{h}=\frac{H}{H_0}\frac{H_0}{L_0}\left(\frac{h}{L_0}\right)^{-1} \quad \cdots\cdots\cdots\cdots\cdots\cdots\cdots\cdots (26)$$

and $T\sqrt{g/h}$ in Eq. (6) is a function of h/L_0 and H_0/L_0 from Eqs. (22) and (23).

Since the right side of Eq. (24) contains H/H_0, successive approximate computation using a digital computer has been adopted. A group of curves on the left side of Fig. 6 shows the result of computation by Eq. (24). In addition, a group of curves on the right side of the figure is that by Le Méhauté and Webb (1964) for the third order approximation of Stokes waves. As a condition of breaking inception for hyperbolic waves,

$$\frac{H_b}{h_t}=0.73 \quad \cdots\cdots\cdots\cdots\cdots\cdots\cdots\cdots\cdots\cdots (27)$$

has been used, which was proposed by Laitone (1961) for cnoidal waves.

CHANGE IN WAVE CREST HEIGHT ABOVE STILL WATER LEVEL

From Eq. (8), the wave crest height above still water level of hyperbolic waves η_0 is expressed as

$$\frac{\eta_0}{H}=\frac{H-\delta}{H}=1-\frac{\delta}{H}=1-\frac{1}{K}\left(1-\frac{1}{12}\frac{H}{h}\right) \quad \cdots\cdots\cdots\cdots\cdots\cdots (28)$$

which is a function of H_0/L_0 and h/L_0 as seen from Eq. (26) and Fig. 6. Fig. 7 shows the relationship between η_0/H and h/L_0 with a parameter of H_0/L_0 besides the curves for Stokes waves.

CHANGE IN WAVE LENGTH AND WAVE VELOCITY

From Eqs. (6), (12), (22) and (23), the expression for the wave length ratio L/L_0 is derived as follows:

$$\frac{L}{L_0}=\sqrt{2\pi}\left(\frac{h}{L_0}\right)^{1/2}\left\{1-\frac{\pi^2}{2}\left(\frac{H_0}{L_0}\right)^{2}\right\}\left(1-\frac{3}{2}\frac{1}{K}\frac{H}{h}\right)$$
$$\times\left\{1-a\left(\frac{H}{h}\right)^{n}\right\}^{m}\left\{1-\left(1+\frac{1}{K}\frac{H}{h}\right)\frac{5}{8}\frac{H}{h}\right\}^{-1} \quad \cdots\cdots\cdots\cdots\cdots\cdots (29)$$

Since L/L_0 is also a function of H_0/L_0 and h/L_0 and Fig. 8 is a result of numerical calculation. Of course, the wave velocity ratio c/c_0 is equal to L/L_0.

EXPERIMENT

EQUIPMENT AND PROCEDURE

The wave tank used for the experiment of wave shoaling on a beach was 63 m long, 50 cm wide and 65 cm deep, with a wave

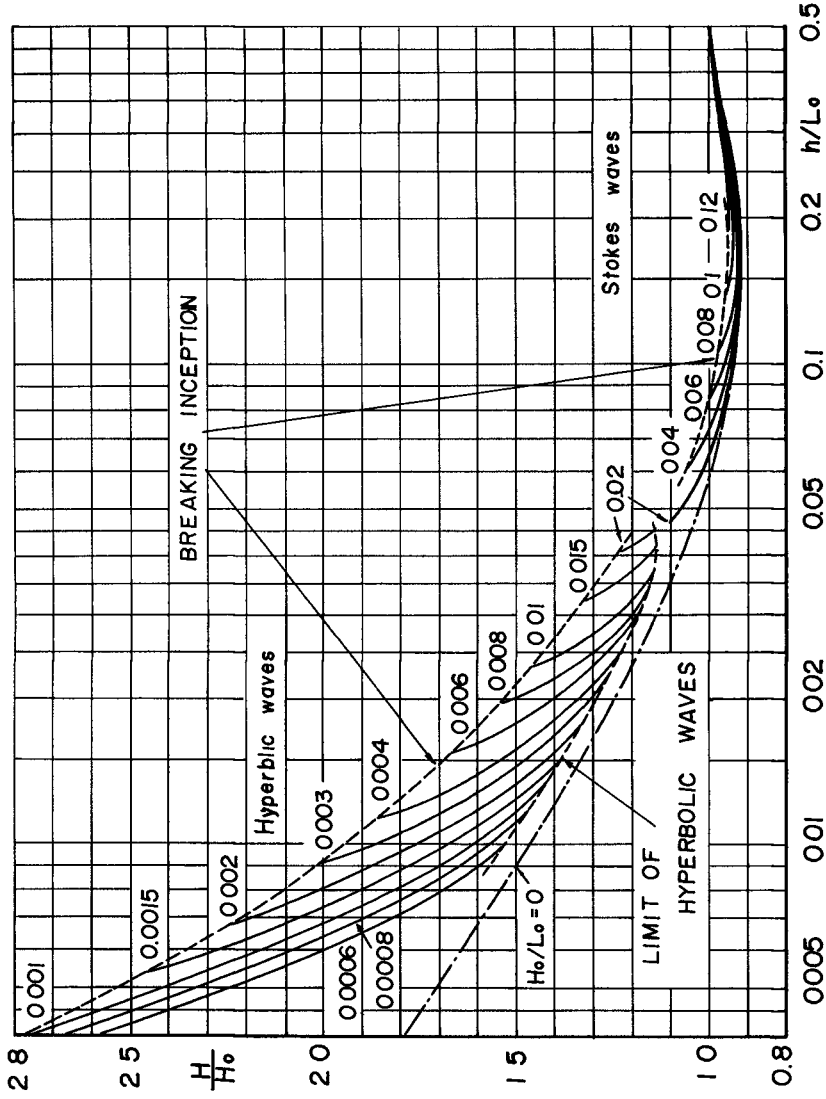

Fig. 6 Wave height change in shoaling water based on hyperbolic wave and Stokes wave theories.

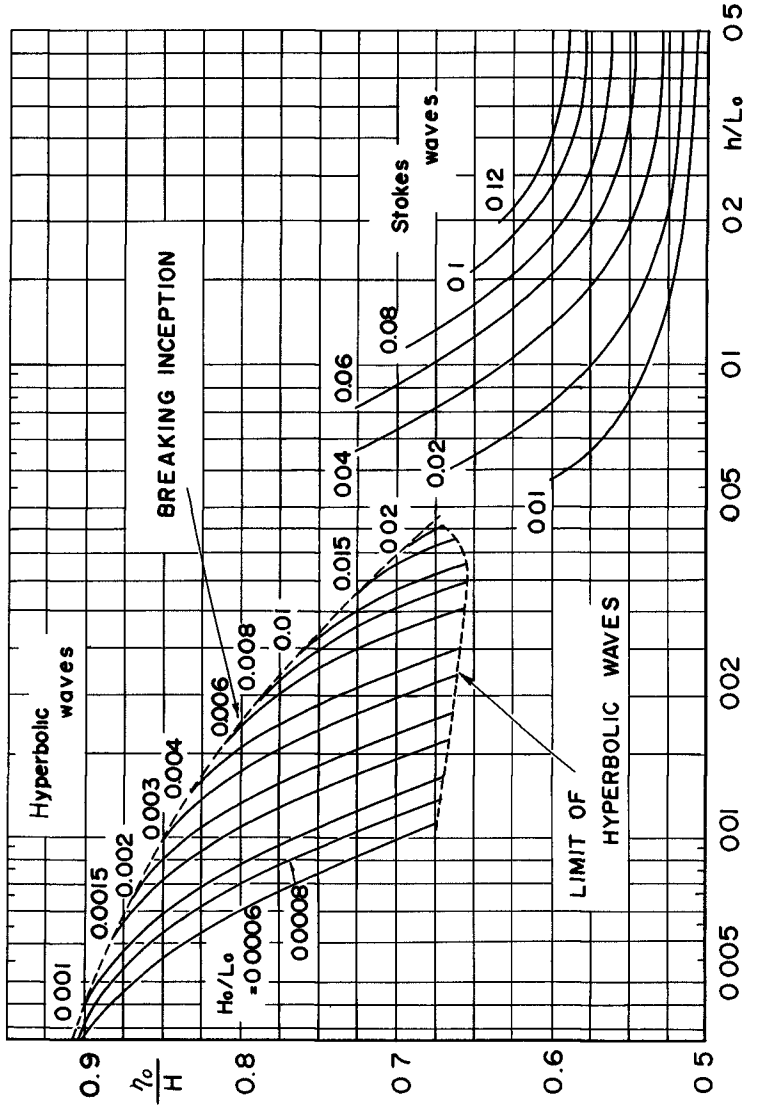

Fig. 7 Wave crest height change in shoaling water based on hyperbolic wave and Stokes wave theories.

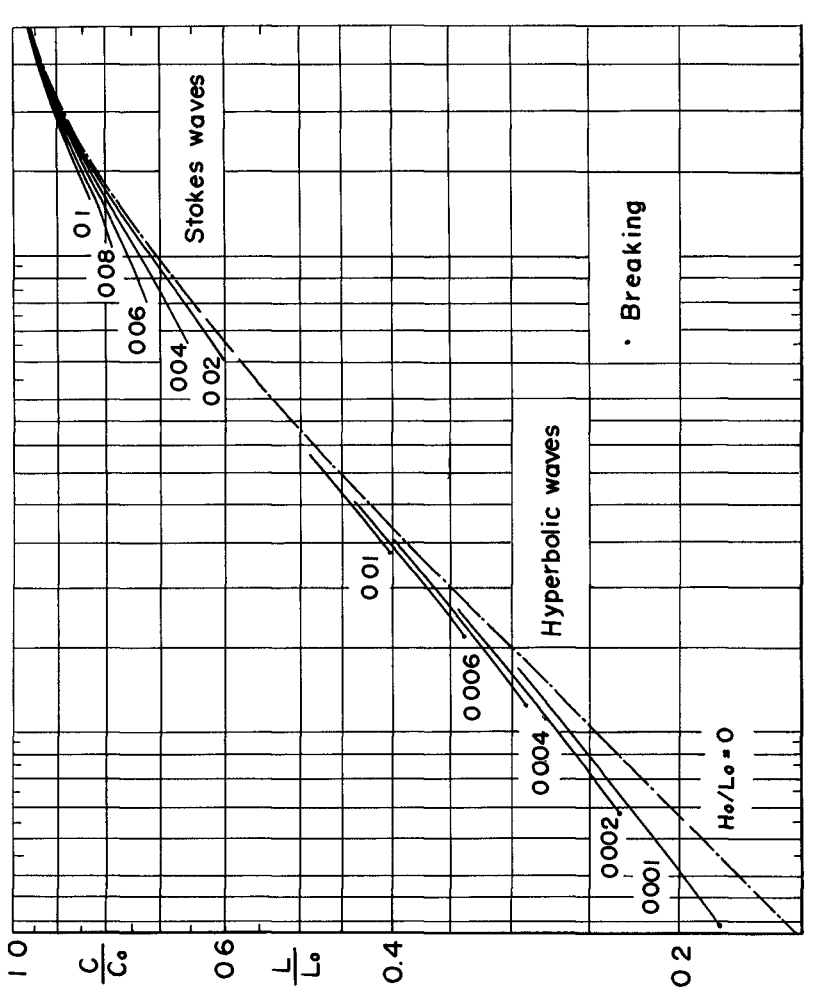

Fig. 8 Wave velocity change in shoaling water based on hyperbolic wave and Stokes wave theories.

generator of piston type. A model beach of uniform slope 1/20, which was made of steel plate, was set 8 m long about in the middle of the wave tank. The top of the slope was just 40 cm high from the bottom, and the water depth above the horizontal bottom was always controlled at 40.5 cm, so that breaking waves overtopped on the upper edge of the slope and reflected waves were reduced as much as possible. Periods of waves used were 1, 1.2, 1.5 and 2 sec, and wave heights at uniform depth were from 1.5 to 12.0 cm. Wave records were taken instantaneously by six wave meters of electric resistance type set at uniform depth and on the slope. The wave height in deep water H_0 was obtained from the water depth and the wave height at uniform depth using theoretical curves of wave height change based on the third order approximation of Stokes waves by Le Méhauté and Webb (1964). The wave length L_0 and wave velocity c_0 in deep water were computed approximately using $gT^2/2\pi$ and $gT/2\pi$ respectively. Wave velocity data were taken by measuring the time necessary for each wave crest to pass between two adjacent wave meters, as the wave velocity in the middle of the wave meters. Several waves were adopted as data, which were recorded until waves reflected by the beach returned again from the wave generator after the wave height became constant.

EXPERIMENTAL RESULTS AND CONSIDERATIONS

Fig. 9 shows a comparison between experimental values and the theoretical curves on wave height change in shoaling water. It is found that the experimental data in the figure agree well with both theoretical curves based on the hyperbolic and Stokes wave theories. According to the plots of experimental data taken by Wiegel (1950), Iversen (1952) and Eagleson (1956), their experimental results are not in agreement with the theoretical curves except Eagleson's data in the case of $H_0/L_0 = 0.02$ (Iwagaki and Sakai, 1967). This fact can not be explained even if the effect of bottom friction is taken into account. As far as the present experiment by the author is concerned, the effect of bottom friction is estimated as approximately 1 % when the wave period is equal to two seconds.

Experimental data of the wave crest height are plotted in Fig. 10 with the theoretical curves of hyperbolic and Stokes waves for comparison. Agreement between them is very poor. The reason will be due to asymmetric deformation of the wave profile in shoaling water. This fact suggests that it is necessary to study not only wave height change but also wave profile deformation in shoaling water including breaking of waves over a sloping beach.

Fig. 11 shows experimental results of wave velocity change in shoaling water compared with the theoretical curves. Agreement of the experimental data with the theoretical curves is as poor as in the case of the wave crest height. The reason may also be due to asymmetric deformation of the wave profile in progress.

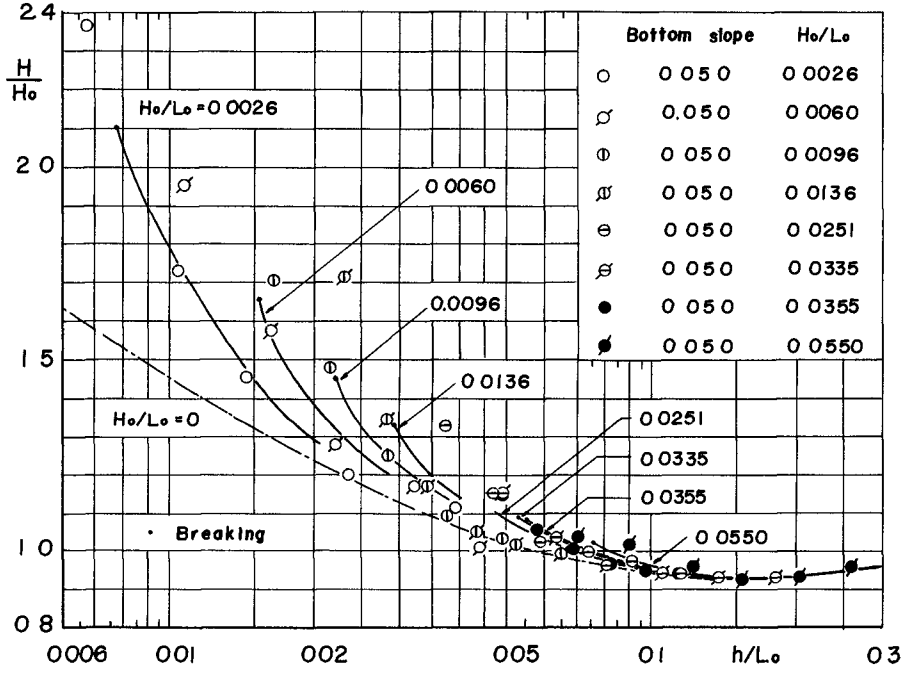

Fig. 9 Comparison of experimental data of wave height change with theoretical curves.

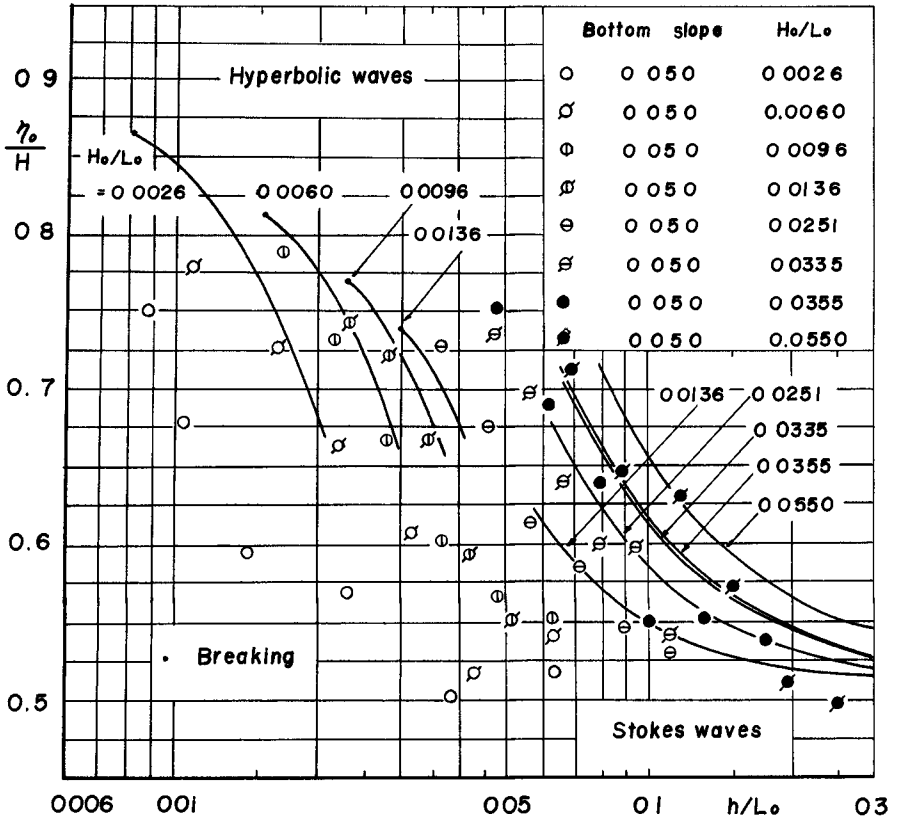

Fig. 10 Comparison of experimental data of wave crest height change with theoretical curves.

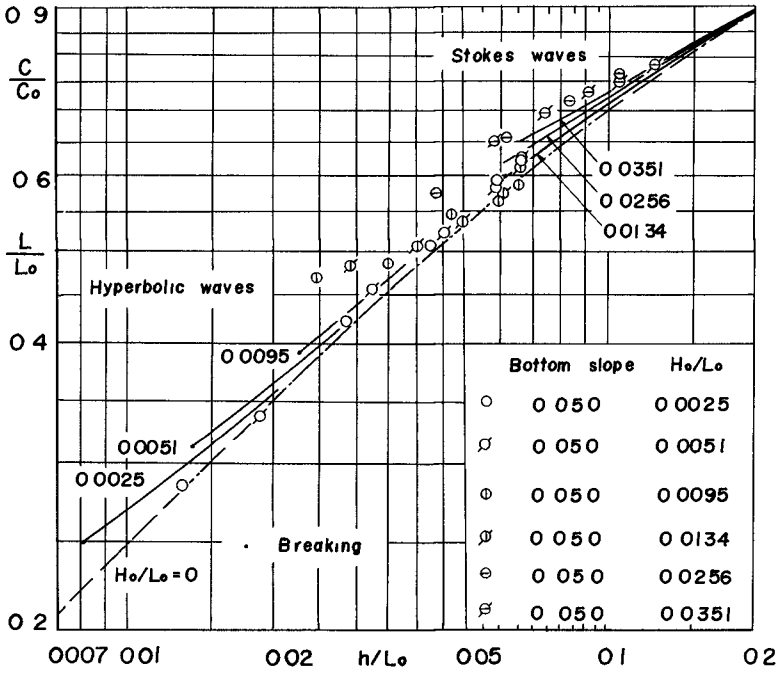

Fig. 11 Comparison of experimental data of wave velocity change with theoretical curves.

CONCLUSIONS

The author proposed new waves named "hyperbolic waves", which are derived from the cnoidal wave theory under the condition that $k = 1$ and $E = 1$ but $K \neq \infty$. Since the theory of the waves does not contain the Jacobian elliptic functions but primary functions only, it is possible to easily compute various wave characteristics of finite amplitude long waves. The computation of wave shoaling presented here is an application of the hyperbolic wave theory to coastal engineering problems. A combination of the hyperbolic wave theory and Stokes wave theory now makes it possible to give a qualitative description of finite amplitude wave characteristics all over the region of shallow water before breaking, subject to the limitation that the waves are of permanent type.

ACKNOWLEDGEMENT

Part of this investigation was accomplished with the support of the Science Research Fund of the Ministry of Education, for which the author expresses his appreciation. Thanks are due to Mr. Sakai for his help during this investigation and Professor Tsuchiya for his help in preparing the paper.

REFERENCES

Eagleson, P. S. (1956). Properties of shoaling waves by theory and experiments: Trans. AGU, Vol. 37, pp. 568 -572.

Iversen, H. W. (1952). Waves and breakers in shoaling water: Proc. 3rd Conf. on Coastal Eng., pp. 1 - 12.

Iwagaki, Y. (1964). Studies on cnoidal waves (First report) -- On the wave steepness and profile --: Dis. Pre. Res. Inst. Annuals, No. 7, Kyoto University, pp. 373 - 386 (in Japanese).

Iwagaki, Y. (1965). Studies on cnoidal waves (Second report) -- On the wave velocity and wave length --: Dis. Pre. Inst. Annuals, No. 8, Kyoto University, pp. 343 - 351 (in Japanese).

Iwagaki, Y. (1967). Studies on cnoidal waves (Fourth report) -- On hyperbolic waves (1) --: Dis. Pre. Res. Inst. Annuals, No. 10B, Kyoto University, pp. 283 - 294 (in Japanese).

Iwagaki, Y. and Hosomi, M. (1966a). Studies on cnoidal waves (Third report) -- Experiments on the wave profile, wave velocity and wave length --: Dis. Pre. Res. Inst. Annuals, No. 9, Kyoto University, pp. 637 -645 (in Japanese).

Iwagaki, Y. and Hosomi, M. (1966b). Some experiments on cnoidal waves: Proc. 13th Conf. on Coastal Eng. in Japan, pp.

1 - 8 (in Japanese).

Iwagaki, Y. and Sakai, T. (1967). On the shoaling of finite amplitude waves: Proc. 14th Conf. on Coastal Eng. in Japan, pp. 1 - 7 (in Japanese).

Iwagaki, Y. and Sakai, T. (1968). Studies on cnoidal waves (Fifth report) -- on hyperbolic waves (2) --: Dis. Pre. Res. Inst. Annuals, No. 11B, Kyoto University, pp. 463 - 476 (in Japanese).

Keller, J. B. (1948). The solitary wave and periodic waves in shallow water: Communication on Pure and Applied Math., Vol. 1, pp. 323 - 339.

Keulegan, G. H. (1950). Wave motion: Engineering Hydraulics; Wiley, New York, ed by H. Rouse, Chapt. 11, pp. 711 - 768.

Keulegan, G. H. and Patterson, G. W. (1940). Mathematical theory of irrotational translation waves: Jour. of Res. of N. B. S., U. S. Dept. Commerce, Vol. 24, pp. 47 - 101.

Koh, R. C. Y. and Le Méhauté, B. (1966). Wave shoaling: Jour. of Geophy. Res., Vol. 71, pp. 2005 - 2012.

Korteweg, D. L. and de Vries, G. (1895). On the change of form of long waves advancing in a rectangular canal and on a new type of long stationary waves: Phil. Mag., Ser. 5, Vol. 39, pp. 422 - 443.

Laitone, E. V. (1961). The second approximation to cnoidal and solitary waves: Jour. of Fluid Mechanics, Vol. 9, pp. 430 - 444.

Laitone, E. V. (1962). Limiting conditions for cnoidal and Stokes waves: Jour. of Geophy. Res., Vol. 67, pp. 1555 - 1564.

Le Méhauté, B. and Webb, L. M. (1964). Periodic gravity waves over a gentle slope at a third order approximation: Proc. 9th Conf. on Coastal Eng., pp. 23 - 40.

Masch, F. D. (1964). Cnoidal waves in shallow water: Proc. 9th Conf. on Coastal Eng., pp. 1 - 21.

Masch, F. D. and Wiegel, R. L. (1961). Cnoidal waves, tables of functions: Council on Wave Research, The Engineering Foundation, pp. 1 - 129.

Skjelbreia, L. (1959). Gravity waves, Stokes' third order approximation, tables of functions: Council on Wave Research, The Engineering Foundation, pp. 1 - 337.

Wiegel, R. L. (1950). Experimental study of surface waves in

shoaling water: Trans. AGU, Vol. 31, pp. 377 - 385.

Wiegel, R. L. (1960). A presentation of cnoidal wave theory for practical application: Jour. of Fluid Mechanics, Vol. 7, pp. 273 - 286.

Wilson, B. W., Webb, L. M. and Hendrickson, J. A. (1952). The nature of tsunamis, their generation and dispersion in water of finite depth: National Science Co., Tech. Rep. No. SN57 - 2, pp. 1 - 150.

CHAPTER 10

EFFECT OF BEACH SLOPE AND SHOALING ON WAVE ASYMMETRY

M. D. ADEYEMO, B.So. (Eng) Lond. Ph.D. (Lond)
Engineer, Western Nigeria Water Corporation.

SYNOPSIS

This paper is concerned with the quantitative study of the geometrical asymmetry associated with shallow water oscillatory waves in the breaker zone. Three descriptions of wave asymmetry are defined and examined :

(1) Wave vertical asymmetry
(2) Wave slope asymmetry
and (3) Wave horizontal asymmetry

The effects of shoaling, produced by beaches of different slope, on the wave asymmetry are examined. Six beach slopes in the range 1:4 to 1:18 were employed, and a quantitative correlation was found to exist between the wave slope asymmetry, wave horizontal asymmetry and the wave vertical asymmetry.

An expression is given for the wave horizontal asymmetry based on the expression for the wave vertical asymmetry from the cnoidal wave theory. The theoretical study of wave slope asymmetry made by Biesel (1) and the results of the experimental work on the wave slope asymmetry in the present work are compared and gave a good agreement.

INTRODUCTION

The asymmetry of the wave in shallow water induces the asymmetrical forces which influence the near shore sediments and coastal structures to a very great extent. Thus the understanding of the shallow water wave processes is of extreme importance in the design of coastal engineering projects.

As waves approach shallow water over bed slopes similar to those reproduced in the model, they change from the deep water to the shallow water category and become markedly asymmetric before breaking. The shoreward side of the wave becomes nearly vertical whilst the seaward face is appreciably inclined. The actual configuration is affected by the bed slope.

Owing to the continually varying geometry of waves in shallow water and in order to have a detailed understanding of wave transformation in shoaling water, three main types of wave asymmetry are defined in the present work. Their quantitative definitions being as follows :-

$$\text{Wave vertical asymmetry} = \frac{\text{Vertical distance from crest to S.W.L.}}{\text{Total wave height}}$$

$$\text{Wave slope asymmetry} = \tfrac{1}{2}(\text{Front face slope at S.W.L.} + \text{Back face slope at S.W.L.})$$

Both the front face slope and the back face slope were measured in radians. The front face slope was taken as negative and the back face slope as positive. Thus, a negative mean slope would indicate that the wave front is steeper than the rear face slope.

Two types of wave horizontal asymmetry are defined and given the symbols H_A and HA'.

$$H_A = \frac{\text{Horizontal dist. from crest to front face at S.W.L.}}{\text{Horizontal dist. from crest to back face at S.W.L.}}$$

$$H_A' = \frac{\text{Horizontal dist. from crest to preceding wave trough}}{\text{Horizontal dist. from crest to following wave trough}}$$

Diagrams showing the definitions of the wave asymmetry are shown in the appropriate graphs discussed later in the paper.

Some mention of the wave vertical asymmetry has been made in the literature. For instance, the trochoidal wave theory gives the positions of the wave crest and trough relative to the still water level in the shallow water as :-

$$\text{Height of crest} = \frac{H}{2} + \frac{\pi H^2}{4L} \coth \frac{2\pi d}{L} \qquad \text{---------(1)}$$

$$\text{and depth of trough} = \frac{H}{2} - \frac{\pi H^2}{4L} \coth \frac{2\pi d}{L} \qquad \text{---------(2)}$$

Stokes' finite amplitude wave theory shows that the wave crest lies above the still water level by the amount

$$\frac{\pi H^2}{4L} \left\{ 1 + \frac{3}{2 \sinh^2 \frac{2\pi d}{L}} \right\} \coth \frac{2\pi d}{L}$$

which is more than the value given by the trochoidal wave theory by the factor

$$\left(1 + \frac{3}{2 \sinh^2 \frac{2\pi d}{L}} \right)$$

The experimental results of the wave vertical asymmetry in this work were compared with the expression from the cnoidal wave theory corresponding to the wave vertical asymmetry, and a good agreement was obtained.

It is important to note that whereas the cnoidal wave theory predicts wave vertical asymmetry, it does not predict wave horizontal asymmetry and wave slope asymmetry.

An expression for the wave horizontal asymmetry is provided later in the work reported in this paper based on the expression for the wave vertical asymmetry from the cnoidal wave theory.

A brief summary of both the cnoidal wave theory and the theory of Biesel are presented below :

SUMMARY OF THE CNOIDAL WAVE THEORY

Korteweg and De Vries (10) developed the cnoidal wave theory which is generally considered very useful for describing the propagation of periodic waves in shallow water where the depth is less than one-tenth of the wave length. The cnoidal theory also provides a link between sinusoidal waves and solitary waves.

Korteweg and De Vries, (10) Keulegan and Patterson (9) and Keller (7) used different symbols, but the formulae obtained by them are essentially the same. The equations below are obtained by Wiegel (17) based mainly on the theory of Korteweg and De Vries.

The notations used in the equations below are as follows :

L	Wave length
d	still water depth
K(k)	complete elliptic integral of the first kind
E(k)	complete elliptic integral of the second kind
k	modulus of elliptic integral
H	Wave height (trough to crest)
T	wave period
$\bar{u}$	incomplete elliptic integral of the first kind
$cn\bar{u}, sn\ \bar{u}$	elliptic functions
x	horizontal co-ordinate
Y	vertical co-ordinate measured from the ocean bottom
Ys	vertical distance from ocean bottom to wave surface
Yt	vertical distance from bottom to wave trough
Yc	vertical distance from bottom to wave crest
S.W.L.	still water level

The wave length is given by

$$\frac{L}{d} = \frac{4}{\sqrt{3}} K(k) \left(2\bar{L} + 1 - \frac{Yt}{d}\right)^{-\frac{1}{2}} \qquad \text{---------(3)}$$

where L and k are defined by the following two equations

$$k^2 = \frac{\frac{Yc}{d} - \frac{Yt}{d}}{2\bar{L} + 1 - \frac{Yt}{d}} \qquad \text{---------(4)}$$

$$\left(2\bar{L} + 1 - \frac{Yt}{d}\right) E(k) = \left(2\bar{L} + 2 - \frac{Yc}{d} - \frac{Yt}{d}\right) K(k) \qquad \text{---------(5)}$$

For k to be real in equation (4), the following equations must also hold

$$2\bar{L} + 1 \;>\; \frac{Yc}{d} \;>\; \frac{Yt}{d} \quad \text{and } o < k^2 \leq 1 \qquad \text{----------(6)}$$

Equation (4) can be re-arranged in the form

$$\left(2L + 1 - \frac{Yt}{d}\right) = \frac{\frac{Yc}{d} - \frac{Yt}{d}}{k^2} = \frac{\frac{H}{d}}{k^2} \qquad \text{----------(7)}$$

Substituting eq. (7) into equation (3) and squaring gives

$$\frac{HL^2}{d^3} = \frac{16}{3}\left[k\,K(k)\right]^2 \qquad \text{----------(8)}$$

i.e. $$L = \sqrt{\frac{16d^3}{3H}}\; k\,K(k) \qquad \text{----------(9)}$$

Equation (5) can be re-arranged to give

$$E(k) - K(k) = \frac{\left[1 - \frac{Yc}{d}\right] K(k)}{2\bar{L} + 1 - \frac{Yt}{d}} \qquad \text{---------(10)}$$

Substituting equation (3) into equation (10) and re-arranging terms we have

$$\frac{Yc}{d} = \frac{16d^2}{3L^2}\left[K(k)\left((K(k) - E(k)\right)\right] + 1 \qquad \text{--------(11)}$$

multiplying equation (11) by $\frac{d}{H}$ we get

$$\frac{Yc - d}{H} = \frac{16d^3}{3L^2H}\left[K(k)\left(K(k) - E(k)\right)\right] \qquad \text{--------(12)}$$

Equation (12) is important as it expresses the WAVE VERTICAL ASYMMETRY.

The elliptic function cn is in general doubly periodic, it will be singly period (period 4K) providing k is a real number and $o \leq k \leq 1$. It is important to note that when k = o; $sn\bar{u} = \sin \bar{u}$, $cn\bar{u} = \cos \bar{u}$ and $K = \pi/2$ i.e. the period $4K = 2\pi$, thus when k = o the elliptic cosine reduces to the circular cosine and the wave profile is given by the trigonometric functions. On the other hand when k = 1, $cn\bar{u} = \operatorname{sech} \bar{u}$, and we have the hyperbolic function with $K(k) = \infty$ hence the period becomes infinite and we have the solitary wave expression. Thus the cnoidal wave theory gives the solitary wave and the sinusoidal wave as its two limiting cases.

The properties of the cnoidal waves are given in terms of the complete elliptic integrals of the first and second kind, and the Jacobian elliptic functions hence the term 'cnoidal' analogous to sinusoidal.

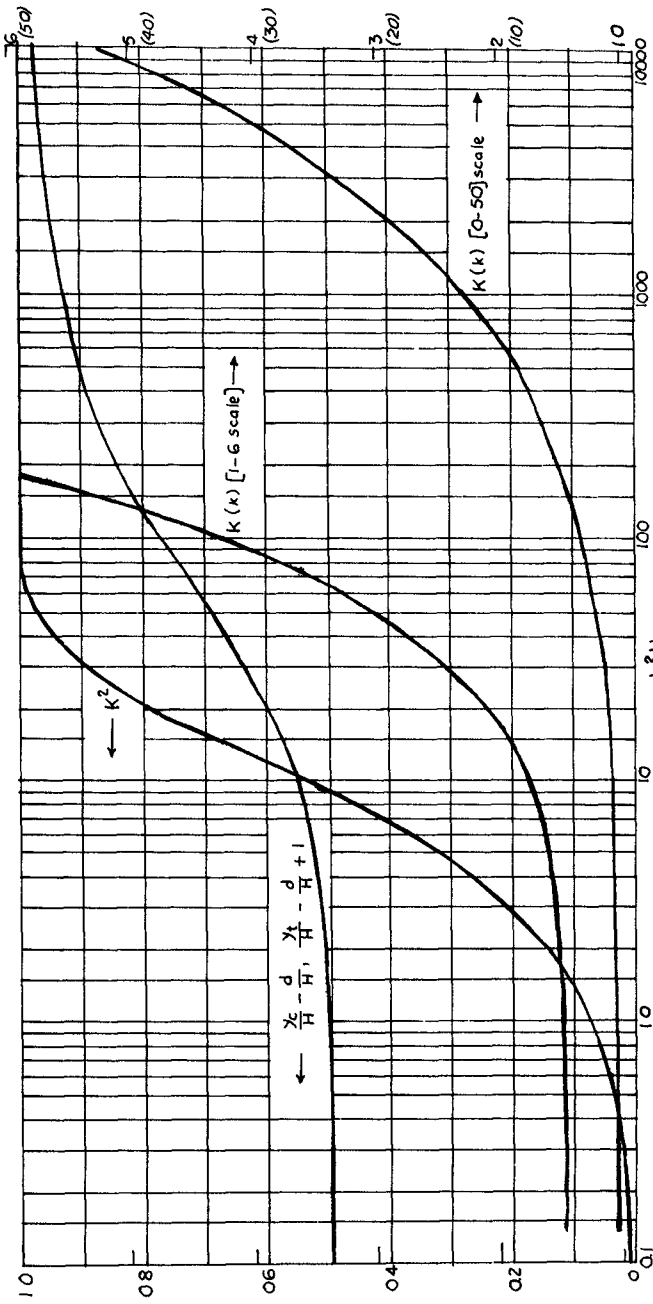

$$\frac{L^2H}{d^3} = \frac{16}{3}k^2 \quad K^2(k) \qquad \frac{y_c}{H} - \frac{d}{H} = \frac{y_t}{H} - \frac{d}{H} + 1 = \frac{16d^3}{3L^2H}\left\{K(k)\left[K(k) - E(k)\right]\right\}$$

Fig. 1 Relationship among $\frac{L^2H}{d^3}$ and the square of the elliptic modulus (k^2), $\frac{Yc}{H}$, $\frac{Yt}{H}$, and K(k)
(after Wiegel, [17] 1960)

Masch and Wiegel (11) computed several of the cnoidal wave characteristics from the equations obtained by Wiegel (17) based on the work of Korteweg and De Vries and they presented the results together with the elliptic integrals and the Jacobian elliptic funotions in tabular form. The graph of equation (12) is shown in fig. 1.

WAVE SLOPE ASYMMETRY

In studying the progression of periodic waves in water of variable depth Biesel (1) produced a second-order theory for the wave slope asymmetry at still water level. Let OX and OY be rectangular co-ordinate axes located at mean sea level, with x positive in the direction of wave propagation and OY being directed vertically upward.

The other notations are defined as follows :-

T Wave period
ω angular frequency
L wave length
u, v OX and OY velocity components
m $2\pi/L$
a wave amplitude
d water depth
$\gamma = -\left(\frac{\partial d}{\partial x}\right)$ = slope of the bed
suffix 0 denotes deep water conditions
ϕ velocity potential

Under conditions of irrotational and incompressible flow, the continuity equation gives

$$\frac{\partial^2\phi}{\partial x^2} + \frac{\partial^2\phi}{\partial y^2} = 0 \qquad \text{----------(13)}$$

The velocity components are given by

$$u = \frac{\partial\phi}{\partial x}, \quad v = \frac{\partial\phi}{\partial y} \qquad \text{----------(14)}$$

In order to satisfy the boundary condition at the bed we have

$$\frac{\partial\phi}{\partial y} - \gamma\frac{\partial\phi}{\partial x} = 0 \quad \text{for } y = -d \qquad \text{----------(15)}$$

Assuming constant surface pressure we have

$$\frac{1}{g}\frac{\partial^2\phi}{\partial t^2} + \frac{\partial\phi}{\partial y} = 0 \quad \text{for } y = 0 \qquad \text{----------(16)}$$

From Biesel the above four conditions are satisfied by the function.

$$\phi(x,y,t) = -\frac{a\omega}{m}\frac{1}{\sinh md}\left[\cosh m(y+d)\sin\left(\omega t - \int m\,dx\right) + \gamma\left\{\frac{m(y+d)\sinh m(y+d)}{D^2\tanh md} - m(y+d)\cosh m(y+d) + \frac{m^2(y+d)^2\cosh m(y+d)}{D\sinh md\cosh md}\right\}\cos\left(\omega t - \int m\,dx\right)\right] \qquad \text{. . . . (17)}$$

where $D = 1 + \frac{md}{\sinh md \cosh md}$ ----------(18)

m, ω and d are related by

$$gm \tanh md = \omega^2 \quad \text{----------(19)}$$

and

$$a = \frac{ao}{(D \tanh md)^{\frac{1}{2}}} \quad \text{----------(20}$$

The free surface equation can be expressed parametrically by the equations

$$\eta = x + a_o A \sin\left(\omega t - \int m dx\right) + a_o \gamma A_1 \cos\left(\omega t - \int m dx\right) \quad \text{----------(21)}$$

$$\lambda = a_o B \cos\left(\omega t - \int m dx\right) + a_o \gamma B_1 \sin\left(\omega t - \int m dx\right) \quad \text{----------(22)}$$

where A, A_1, B and B_1 are functions of md with η and λ being the co-ordinate of a point on the free surface.
The free surface slope of the wave is given by

$$S = \frac{\frac{\partial \lambda}{\partial x}}{\frac{\partial \eta}{\partial x}} = \frac{m a_o B \sin\left(\omega t - \int m dx\right) + \left(-m\gamma a_o B_1 + a_o B\right) \cos\left(\omega t - \int m dx\right)}{1 - m a_o A \cos\left(\omega t - \int m dx\right) + \left(m\gamma a_o A_1 + a_o A\right) \sin\left(\omega t - \int m dx\right)} \quad \text{----------(23)}$$

For the wave slope in the neighbourhood of a particle with the initial co-ordinates (x, o) at the instant when the particle crosses the plane y = 0 we then have

$$y = 0 \quad \text{or}$$

$$B \cos(\omega t - mdx) + \gamma B_1 \sin(\omega t - mdx) = 0$$

Hence there are two sets of possible values for $\cos(\omega t - mdx)$ and $\sin(\omega t - mdx)$

i.e.

$$\cos(\omega t - mdx) = \frac{\gamma B_1}{B}; \quad \sin(\omega t - mdx) = -1 \quad \text{----------(24)}$$

or

$$\cos(\omega t - mdx) = -\frac{\gamma B_1}{B}; \quad \sin(\omega t - mdx) = 1 \quad \text{----------(25)}$$

Equation (24) corresponds to the passage of the front face of the wave, and equation (25) to the passage of the back face of the wave.

Combining equations (24) and (25) with (23) and noting that terms of γ^2 have been neglected we have :-

$$S_F = -ma_0B - m^2a_0^2\gamma(AB_1 + A_1B) - ma_0^2AB \quad \text{--------(26)}$$

and for the back of the wave :

$$S_B = ma_0B - m^2a_0^2\gamma(AB_1 + A_1B) - ma_0^2AB \quad \text{---------(27)}$$

The mean slope $S = \frac{1}{2}(S_F + S_B)$ is a measure of asymmetry of the wave. Thus from equations (26) and (27)

$$S = -m^2a_0^2\gamma(AB_1 + A_1B) - ma_0^2AB \quad \text{---------(28)}$$

Replacing A, B, A_1 and B_1 by their values we have

$$S = m^2a_0^2\gamma\left\{\frac{3 + \frac{md}{\tanh md} - 3md\tanh md}{D^2(\sinh md)^2\tanh md}\right\} \quad \text{---------(29)}$$

where $D = 1 + \frac{md}{\sinh md \cosh md}$ ---------(18)

As pointed out by Biesel (1) the analysis above assumes that the slope of the bottom is small.

This theory had not previously been tested experimentally, and its verification formed part of the present work. A satisfactory agreement was obtained.

WAVE HORIZONTAL ASYMMETRY

In order to completely define the asymmetry of the wave in shoaling water, note has to be taken of the asymmetry of the wave in the horizontal sense too. For this purpose, two types of wave horizontal asymmetry are noted and are given the symbols H_A and HA'. They are already defined above.

As far as the author is aware, there is no theory describing wave horizontal asymmetry for shoaling waves. As will be shown later in this work it was found that the two types of wave horizontal asymmetry i.e. HA and HA' follow the same trend. It was found possible therefore, to produce an empirical relationship expressing one in terms of the other.

Later in this work an expression is given for the wave horizontal asymmetry HA based on the theoretical expression for the wave vertical asymmetry from the cnoidal wave theory.

APPARATUS

The study described in this paper involved the use of an hydraulic model with an impermeable beach. The impermeable beach was chosen to permit beach slope variation and to enable a detailed study of the effect of the backwash to be made. The study on the effect of backwash is reported in another paper in this same journal (ref.4).

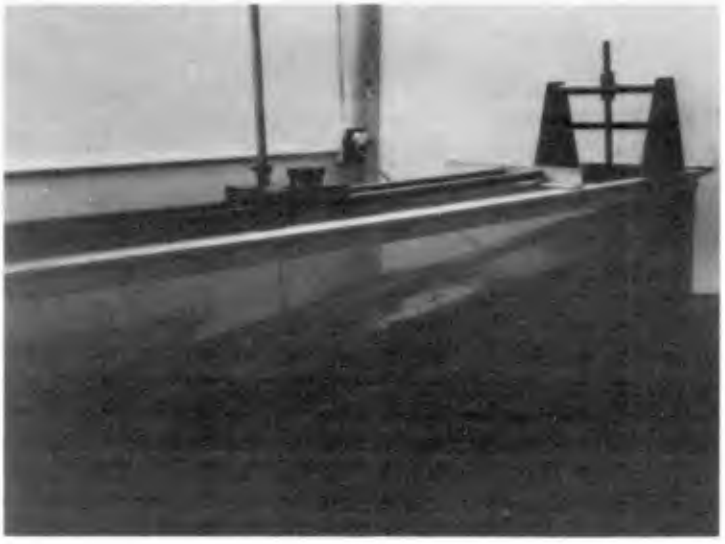

Plate 1

Plate 2

The Beach arrangement and the Wave Generator

In order to overcome the scale limitations imposed by the model size, the measurements were based on parameters used in certain aspects of wave theory, so that the behaviour of the model could be assessed.

The choice of variables was made in the light of pilot experiment conducted by the author and recent experiments by Plinston (14) and Kemp (8) of wave action on granular beaches. These examined amongst other things the variation of beach slope with wave characteristics, and the phase relationship between two successive waves breaking on the beach. The change of beach slope using a plane beach and constant wave characteristics is equivalent to a change in beach material size, although the effect of permeability is not allowed for. Nevertheless, the reduction in phase relationship between uprush and backwash with increasing beach slope, and higher backwash velocities are both produced and are important factors in the movement of beach material.

The overall size of the apparatus was limited by the space available. The wave flume was 24 feet long, 9 inches wide and 15 inches deep. At the wave generator end, the bed of the channel sloped down to a depth of 21 inches. The channel was made of marine plywood, with the exception of long perspex windows which formed the sides of the channel at the beach end.

A satisfactory convex shaped slatted wave absorber was built behind the paddle to damp out reflections from the generator end. The beach was made of marine plywood and stiffened at the back with an I section to prevent vibration of the beach. The toe of the beach was hinged to the beach plate. A false toe was used for the feat beach slope in order to contain the beach in the tank. The upper end of the artificial beach was supported by a vertical screwed rod by which the beach slope was raised. Plate 1 shows the beach arrangement and plate 2 the wave generator.

A special feature of the design was that the motor and reduction gears were mounted on a very strong support, and were quite separate from the channel . Thus there would not be any vibration of the flume arising from the machinery.

Several sets of waves were generated by varying the wave period and the deep water wave height with the intention of selecting suitable wave characteristics, and also finding the position on the horizontal portion of the channel at which the wave had become steady. This enabled a wave measuring station to be chosen in the horizontal section of the channel.

The wave characteristics selected were :- Period T = 0.8 secs Ho = 1.45 ins and horizontal section still water depth = 9.5 ins. These wave characteristics were held constant. The beach slopes used were $\frac{1}{4}$, 1/6, 1/9, 1/12, 1/15 and 1/18.

The filters used consisted of $\frac{1}{2}$ ins. chicken mesh folded many times so as to suitably occupy the width of the channel for a length of $6\frac{1}{2}$ feet. The filters were placed at a suitable distance in front of the paddle. An experiment was conducted to determine the amount of wave reflection in the wave tank for the six beach slopes.

The lowest value of the coefficient of reflection was found to be about 3% for the flattest beach slopes and the highest value was about 8% for the steepest slopes of $\frac{1}{4}$ and 1/6. These values correspond with typical values from Miche (12).

MEASURING TECHNIQUES

General Procedure

The wave lengths were measured by using two capacitance - wire probes suspended separately on a carriage with the ends inserted in water in the tank to the mean operating depth. The output wave form from the wave meter was displayed on a D.C. oscillosoope. The arrangement allowed visual observations to be made on D.C. oscilloscope.

The wave height and the wave shape at the different positions along the beach were found by using the capacitance - wire probe system in conjunction with a 'visicorder' - ultra violet type instrument giving a parmanent trace on paper. This recorder offers 8 paper speeds (6 to 800 mm/sec) and also 0.1 and 1 second timing intervals.

Two graduated scales were made on the side of the wave channel for the purpose of reading the still water depth. The scales were graduated in 1/10 of an inch divisions.

The first step for every beach slope was to locate the wave break-point by placing the probe at several marked places very close to each other in the neighbourhood of the position where the wave was visually observed to be breaking and noting the deflection registered on the oscilloscope. The position at which the wave height was a maximum and shoreward of which the wave lost its wave form was selected as the wave break-point.

The location of the break-point was followed by the marking out of the several positions along the beach where the detailed study of the wave asymmetry was to be made. The capacitance-wire probe was positioned at each of the places marked out, and while the wave generator was switched off a line corresponding to the S.W.L. was defined on the recording paper. This was done at the start and end of every reading.

After marking out the S.W.L. line the wave generator was then switched on, with the probe still in position the visicorder was then also switched on, and the wave profile for the particular position of the wire probe was recorded. The probe position was then changed and by repeating the processes again for each probe position the wave trace and wave length measurements were obtained for the different positions marked out along the beach, up to the break-point. At the end of such a series of experiments a calibration test was carried out for the particular setting of the visicorder.

EVALUATION OF WAVE VERTICAL ASYMMETRY

The S.W.L. mark lines on the wave trace paper, one at the start and the other at the end of every reading for every position of the probe were joined, thus providing the S.W.L. line from which measurements were made. Both the measurements of the vertical distance from the wave crest to the S.W.L. and the total wave height were scaled off.

EVALUATION OF WAVE HORIZONTAL ASYMMETRY

Two alternative definitions of wave horizontal asymmetry are made. The evaluation of these two values HA and HA' required the measurements of the horizontal distances from crest to the front and rear faces of the wave at S.W.L. and the horizontal distances from crest to the preceding and the following wave trough. The two types of wave horizontal asymmetry HA and HA' have already been defined earlier in this paper.

EVALUATION OF WAVE SLOPE ASYMMETRY

In the evaluation of the wave vertical asymmetry and the wave horizontal asymmetry any scale exaggeration of the output wave trace from the visicorder would be of no importance, as the wave vertical asymmetry and the wave horizontal asymmetry are dimensionless ratios, of which the terms involved are either both horizontal measurements or both vertical measurements, in which case any scale exaggeration of the output wave trace would cancel out.

On the other hand, the wave slope asymmetry is measured in radians, and because of the scale exaggeration of the wave trace, the profile has to be reproduced to the natural scale from the wave trace.

To evaluate the wave slope asymmetry, the angles made by the front and rear faces of the wave with the still water level line were measured in degrees and then converted into radians. The wave slope asymmetry is defined as :

$\frac{1}{2}$ (Front face slope at S.W.L. + Back face slope at S.W.L.) radians

The front face slope was taken as negative and the back face slope as positive.

REVIEW OF PREVIOUS WORK

Wiegel (16) conducted a series of experiments to compare the wave profile with the trochoidal wave theory. He commented that the surface profiles were similar to that given by the trochoidal wave theory when the wave was not in relatively shallow water (say $d/L > 0.15$) but that near the breakers the experimental results were considerably higher than those given by the theory.

In a study of breakers and beach erosion Hamada (5) remarked that at breaking, the displacement of the orbital centre above the still water level was 0.204Hb on a 1/10 slope and 0.228 Hb on a slope of 1/15. He noted the observation that when a wave is about to break on a shallow sloping beach the trough becomes wide and flat; and the crest narrow and steep. He considered that the forward leaning of the wave crest might be an important factor in wave breaking.

Eagleson (2) compared experimental values of wave height steepness and wave length with stokes' theory. The commented that stokes' third order theory applied only in the early stages of transformation, the divergencies being too large as the wave begins to deform.

Ursell (15) theoretically predicted in a qualitative sense the effect of shoaling on wave asymmetry by consideration of parameter., $\frac{HL^2}{d^3}$. He concluded that large values of the parameter $\frac{HL^2}{d^3}$ would predict an increased tendency towards wave asymmetry.

Ippen and Kulin (6) studied the shoaling and breaking of the solitary wave. They classified breakers as "symmetric," "asymmetric" and "intermediate." They described waves which retained much of their original symmetry during shoaling and which deformed by what they termed "peaking up" of the crest, as symmetric breakers. On the other hand, they classified as asymmetric breakers, waves which showed a marked steepening of the front face. They did not define what they termed as the intermediate breaker, but presumably they intended something between what they called the symmetric and the asymmetric breakers. When they tried to translate their results into a graph, they found that there was some scatter and they rightly noted that their classification depended very much on personal judgement. From the studies made in the work reported in this paper, and within the experimental limits, it is evident that nothing like a symmetric breaker was observed.

Miller and Zeigler (13) selected about 200 breaker traces from the very many recorded, and plotted each breaker on a dimensionless graph. By comparing the breaker profiles, Miller and Zeigler considered that the breaker forms fell into three major categories, which they referred to as "symmetric", 'asymmetric' and very 'asymmetric' breakers. They then averaged the individual breaker traces for each class to obtain a single trace. Comparing the breaker they classed as asymmetric breaker with the "near breaking wave" i.e. the mean profile just seaward of the break-point they commented that the profile of the asymmetric breaker was more peaked.

The author would like to comment that from the study made in the work reported in this paper, the breaker Miller and Zeigler referred to as a symmetric breaker in fact possessed a distinct vertical asymmetry and some wave horizontal and wave slope asymmetry. Miller and Zeigler themselves remarked that the transition from the profile of the "near breaking wave" which already possessed asymmetry to the symmetric breaker, was difficult to appreciate. On the whole their classification seems to be based on visual judgement of the wave trace with a bias towards what is referred to in the present work as wave slope asymmetry. It was however, very surprising that Miller and Zeigler considered that the breaker type they referred to as the symmetric breaker was possibly analogous to the plunging type and the very asymmetric breaker was similar to the spilling type; the author considers that, if anything, a plunging breaker ought to correspond to a very asymmetric breaker.

EXPERIMENTAL RESULTS ON WAVE VERTICAL ASYMMETRY

On all the beach slopes it was found that as the wave progressed shoreward, the wave vertical asymmetry was continuously increasing and was maximum at the break-point. On the beach slope of $\frac{1}{4}$ it was found that the experimental results gave values very slightly higher than the theory for $d/L > 0.18$. Shoreward of this the experimental results were lower than the theory. The maximum divergence was about 18% of the theoretical value, and that was the greatest divergence found throughout the work including the other beach slopes.

The maximum divergence between the experimental results and the theory for the beach slope of 1/6 was 10% of the theoretical prediction. The experimental result of the wave vertical asymmetry at the wave break-point on the beach slope of 1/6 was found to be 0.707 which was higher than the corresponding value of 0.62 at the break point on the beach slope of $\frac{1}{4}$ but lower than the value of 0.725 at the wave break point on the slope of1/9.

It was found that whereas the graphs of wave vertical asymmetry against d/L were non-linear for the steeper beach slopes, they became linear for slopes $< 1/12$. The experimental results of the wave vertical asymmetry on the beach slope of 1/15 were quite close to the theoretical predictions. However, the theoretical curve was non-linear.

The graph of wave vertical asymmetry against d/L on the beach slope of 1/18 (see fig. 2) showed the same trend on shoaling as on the slope of 1/15. The maximum divergence between the value of the experimental results and the theory was 5% of the theoretical prediction. The value of the wave vertical asymmetry at the break point on the beach slope of 1/18 was 0.74 which was considerably higher than the corresponding value of 0.62 at the breaker position on the beach slope of $\frac{1}{4}$.

Whereas on the beach slopes of $\frac{1}{4}$, 1/6 and 1/9 the breakers formed were plunging breakers, on the beach slope of 1/12 and for the flatter slopes of 1/15 and 1/18 the breaker in each case was spilling.

The effect of beach slopes on wave vertical asymmetry is shown in figure 3, and it indicated that the wave vertical asymmetry is greater for flat slopes when the wave is in very shallow water of about $d/L < 0.10$.

EXPERIMENTAL RESULTS ON WAVE HORIZONTAL ASYMMETRY

The graph of HA and HA' against d/L on the beach slope of $\frac{1}{4}$ is shown in figure 4. The value of HA at the break point was about 0.2 which meant that at the breaker position, the horizontal distance from the wave crest to the wave front face at still water level, was 1/5 of the horizontal distance from the crest to the rear face. At a d/L value of 0.15, the value of HA was 0.80, and so the wave was not really very asymmetric at that stage. The most rapid change in HA and HA' was found to take place at $d/L < 0.15$. The graph of HA' against d/L was quite similar to that of HA against d/L. This was, however, in line with expectation as both HA and HA' are measures of wave horizontal asymmetry.

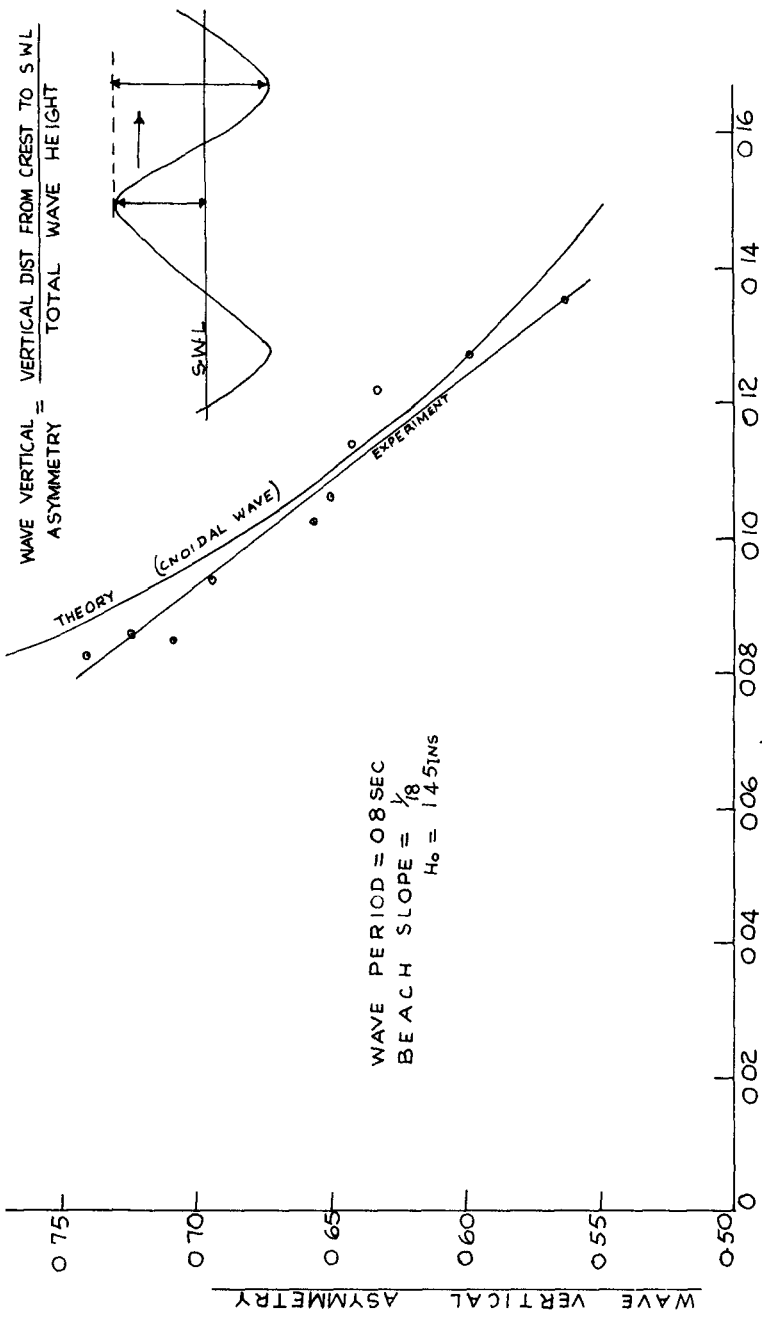

Fig 2. Wave Vertical Asymmetry Experimental and Theoretical Results

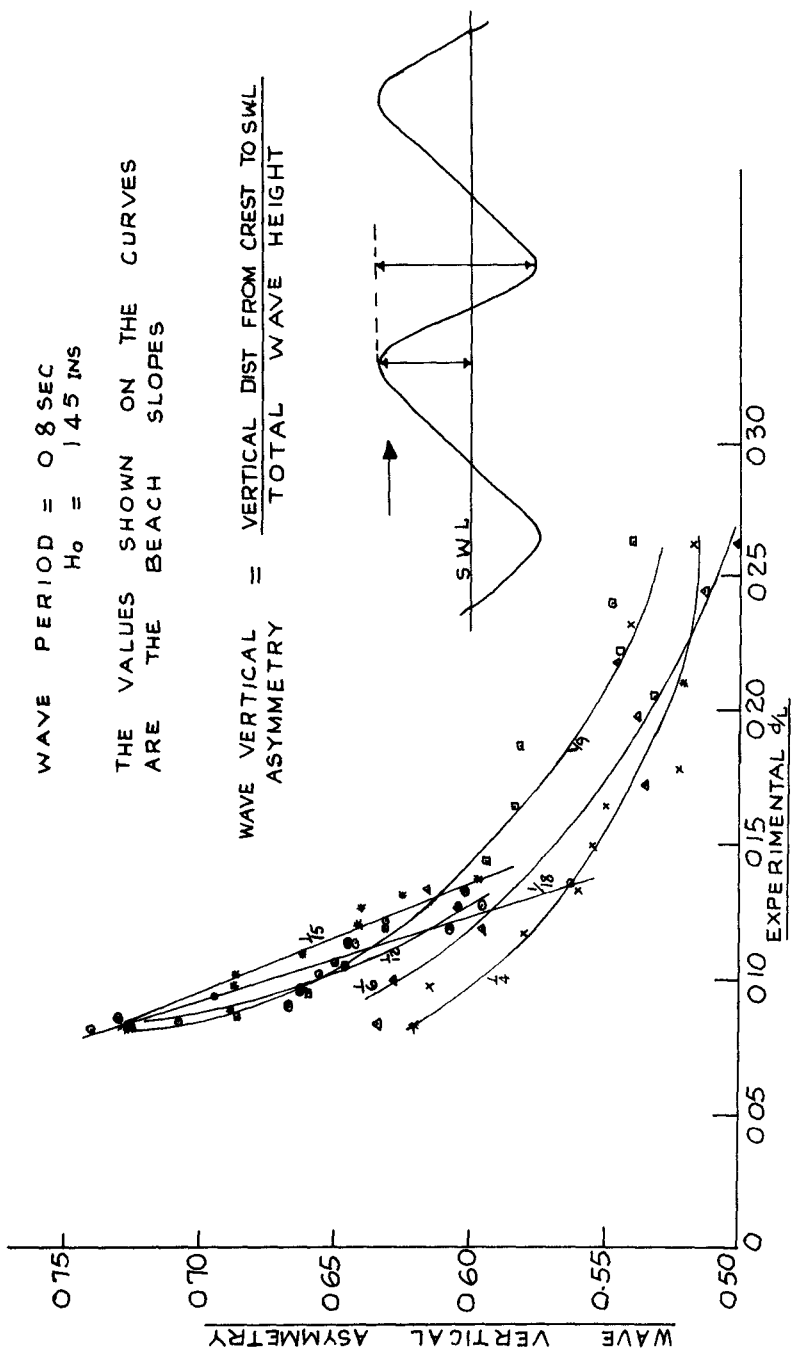

Fig 3 Effect of Beach slope on Wave Vertical Asymmetry

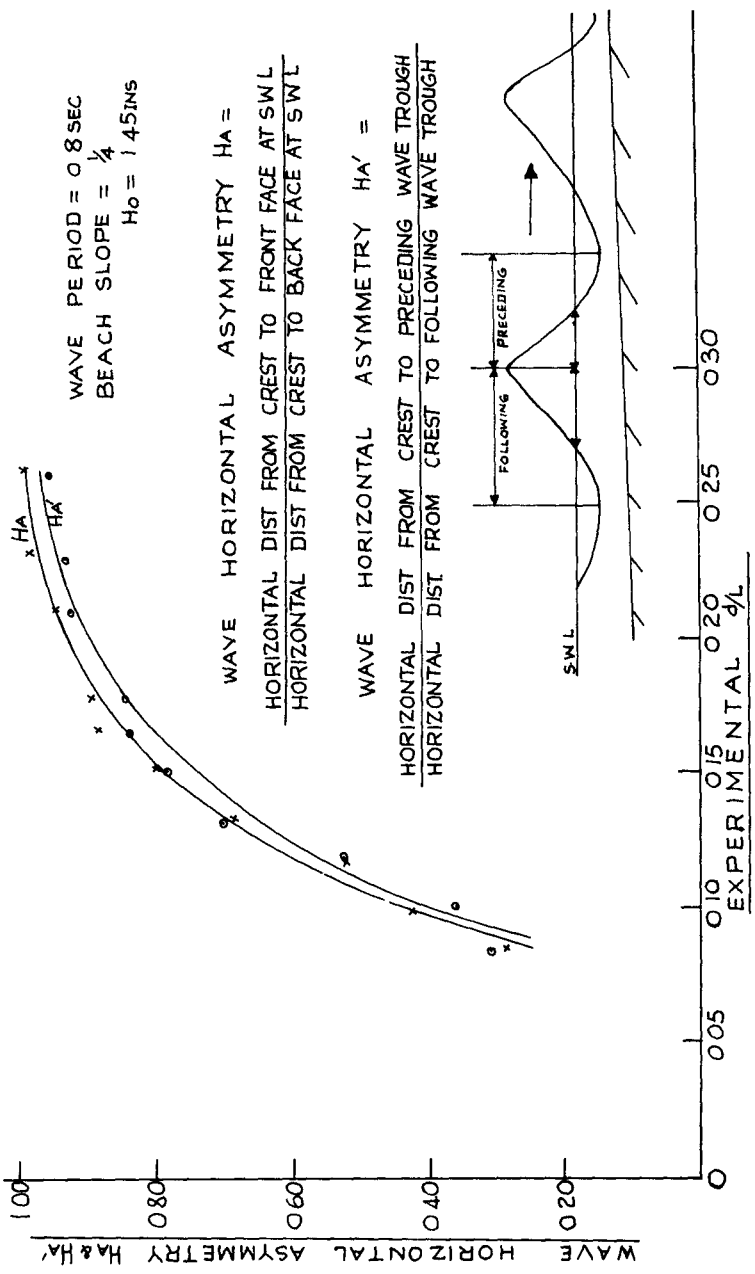

Fig 4. Graph of Wave Horizontal Asymmetry H_A and H_A'

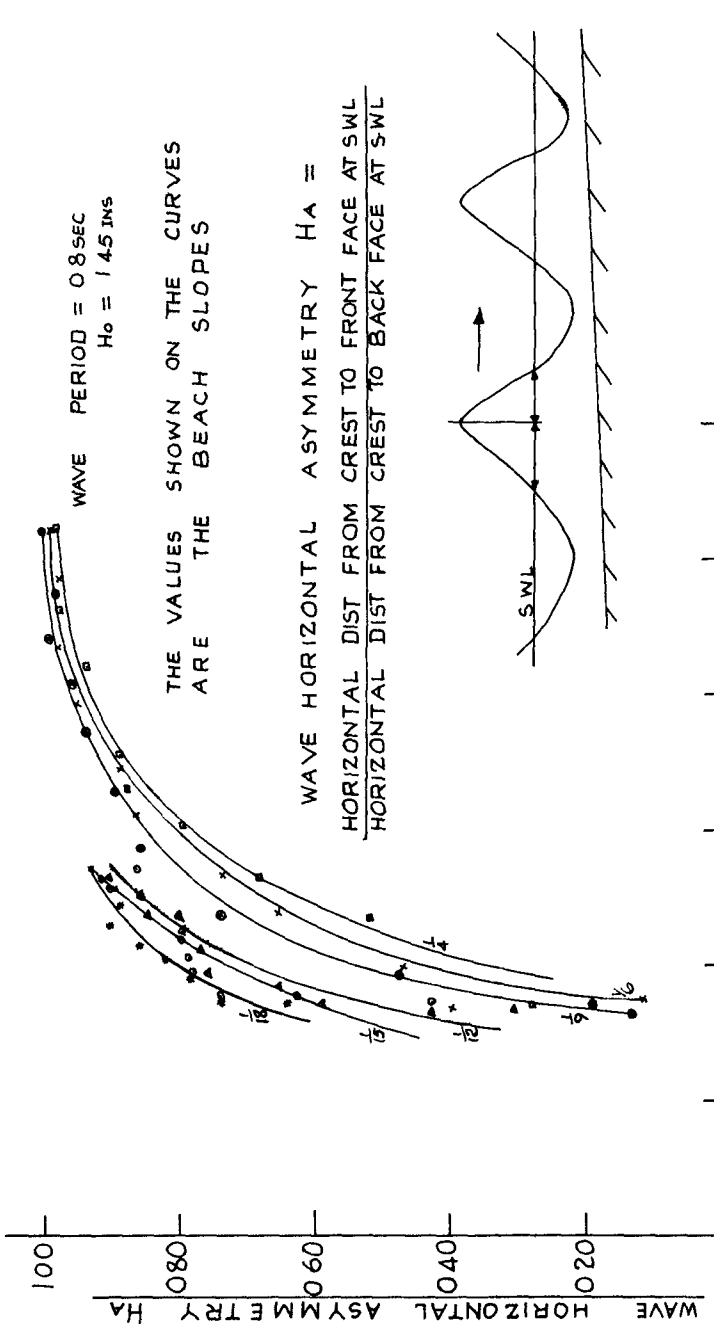

Fig. 5 Effect of Beach slope on Wave Horizontal Asymmetry H_A

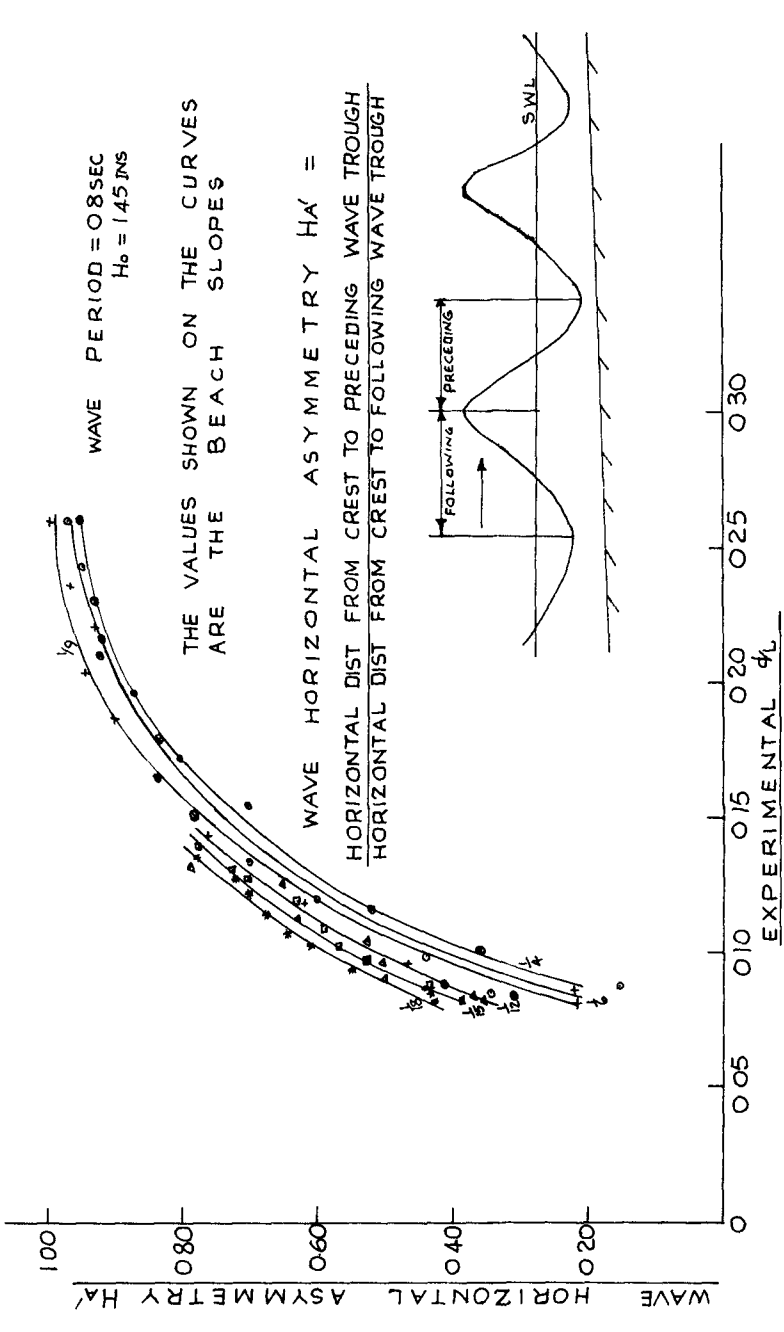

Fig 6 Effect of Beach slope on Wave Horizontal 'Asymmetry H_A'

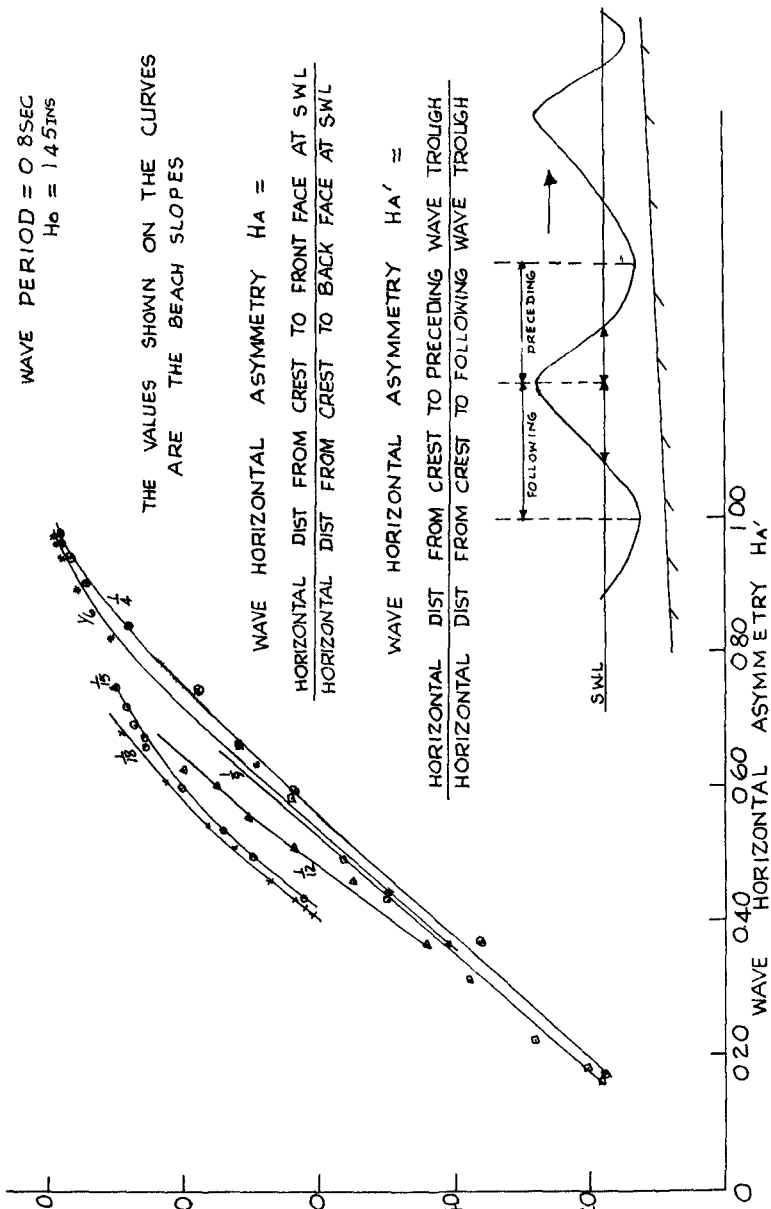

Fig. 7 Graph of Wave Horizontal Asymmetry H_A against H_A'

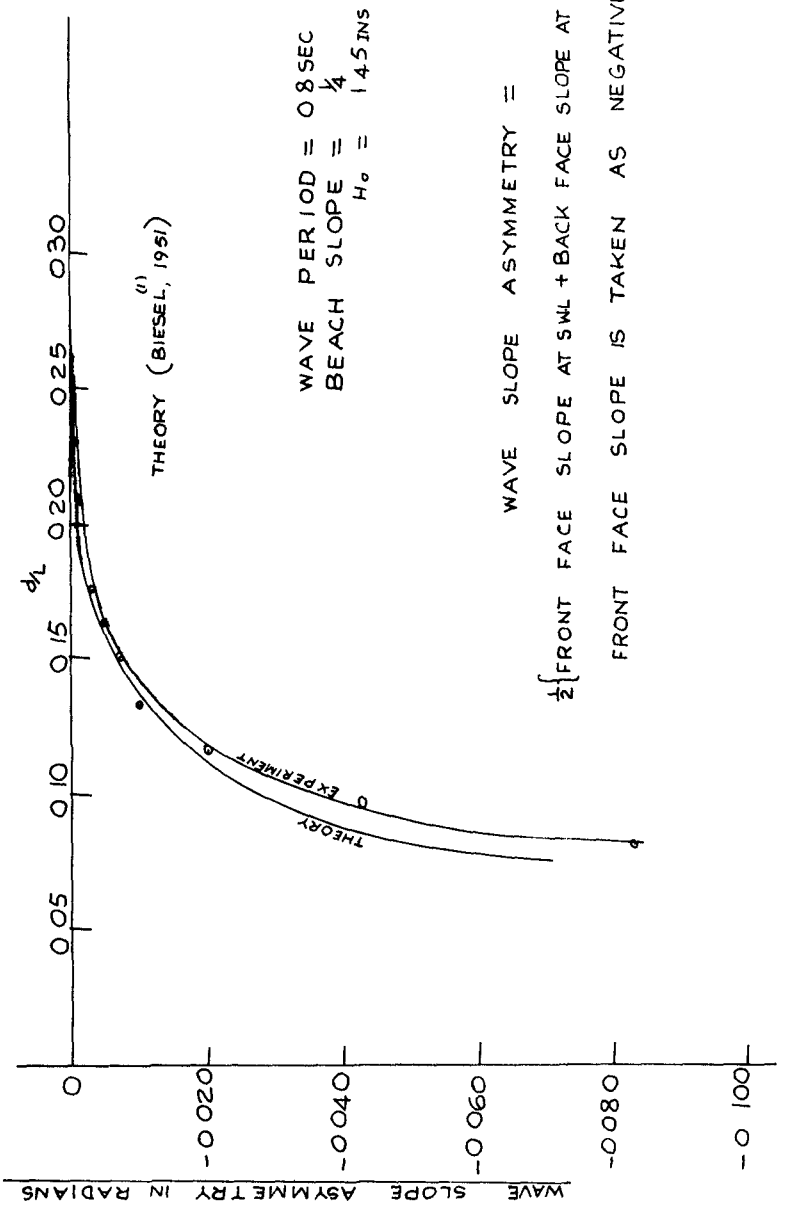

Fig 8. Wave slope Asymmetry Experimental and Theoretical Results

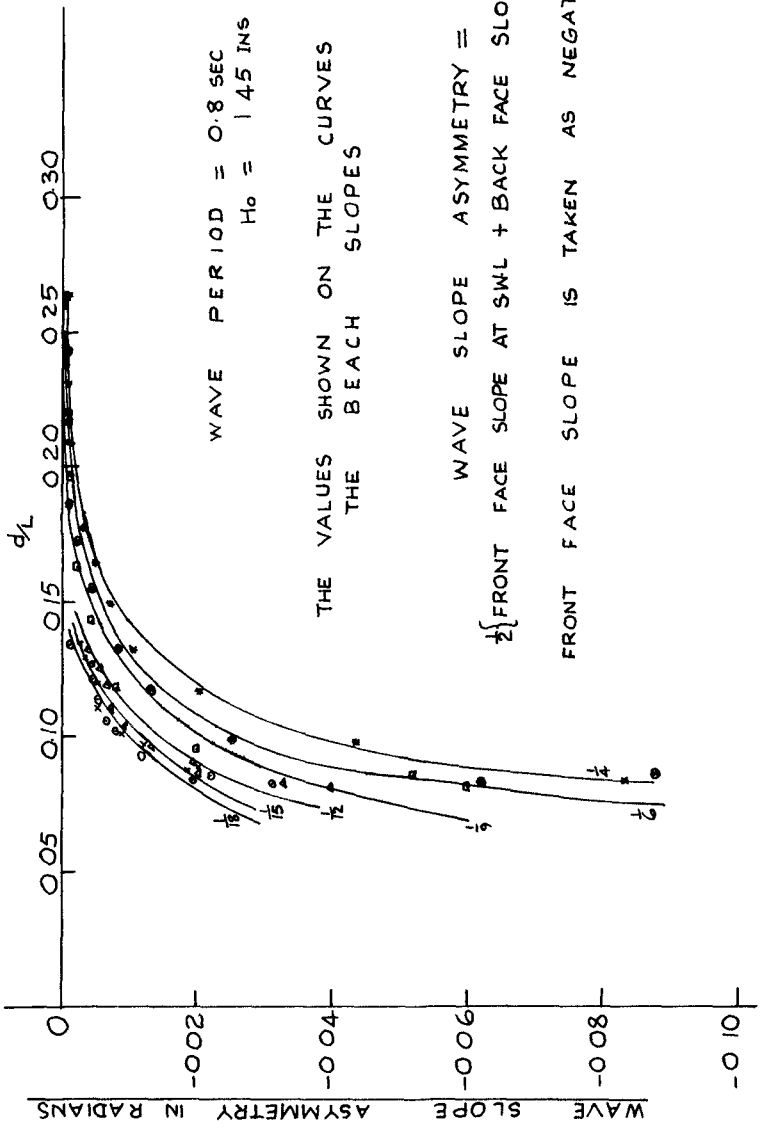

Fig. 9 Effect of Beach slope on Wave Slope Asymmetry

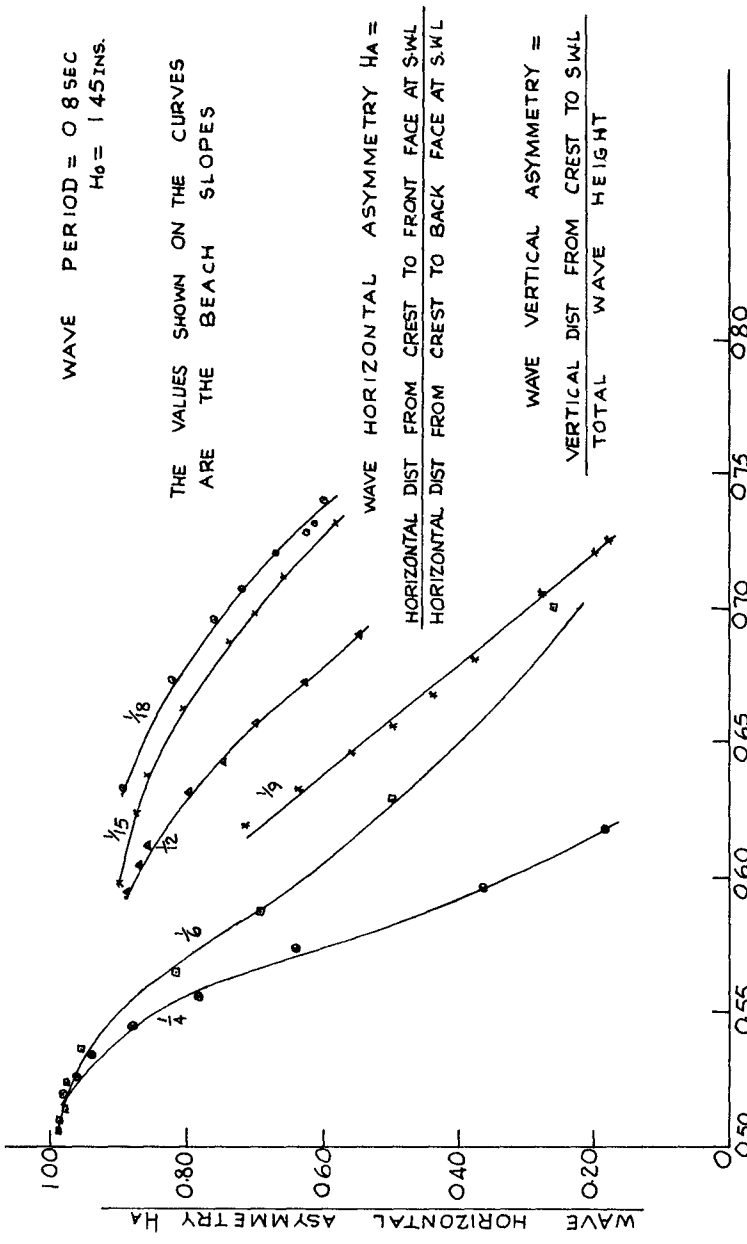

Fig. 10. Graph of Wave Horizontal Asymmetry H_A against Wave Vertical Asymmetry

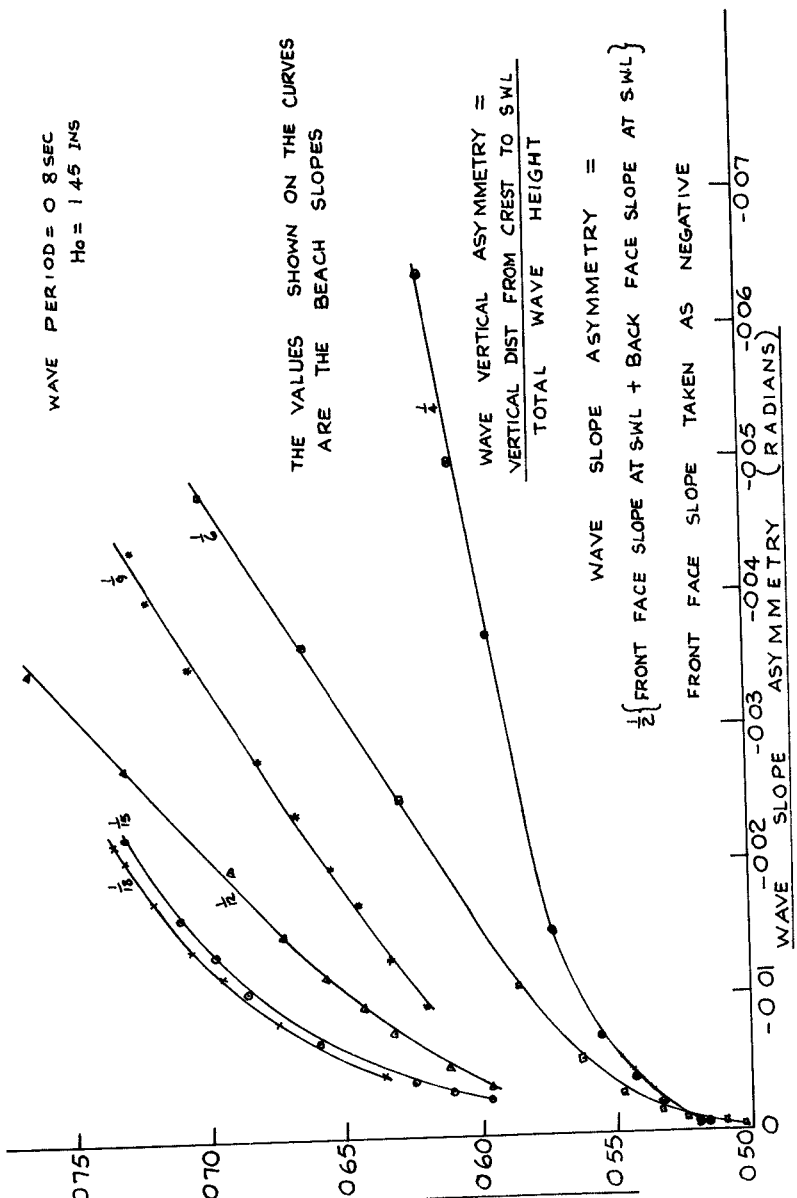

Fig 11 Graph of Wave Vertical Asymmetry against Wave Slope Asymmetry

It was found however that HA' indicated a higher asymmetry than HA.

The graphs of HA and HA' against d/L for the beach slopes of 1/6, 1/9, 1/12, 1/15 and 1/18 follow the same trend as that on the beach slope of $\frac{1}{4}$ discussed above.

Figures 5 and 6 show the effect of beach slope on the wave horizontal asymmetry HA and HA'. It is evident from the figures that the horizontal asymmetry of the wave increases as the beach slope gets steeper, whereas it will be remembered that in very shallow water in the case of wave vertical asymmetry, the vertical asymmetry decreases as the beach slope gets steeper.

As can be seen that figure 7 which shows the graph of HA and HA' for the different beach slopes, establishes a correlation between the two types of wave horizontal asymmetry HA and HA'. This is not unexpected, but it is quite useful, in that it does mean that observations or calculations in wave studies can be made in terms of either parameter.

EXPERIMENTAL RESULTS ON WAVE SLOPE ASYMMETRY

On the beach slope of $\frac{1}{4}$, the graph of wave slope asymmetry against d/L (see figure 8) showed that the wave slope asymmetry increased as the wave advanced into shallower water. The wave slope asymmetry was negligible at d/L value of 0.26 whereas at d/L value of 0.15 the value of the wave slope asymmetry was - 0.007. The most rapid change in wave slope asymmetry took place at d/L $<$ 0.15. For instance, at d/L value of 0.10 the value of the wave slope asymmetry became - 0.037. At the breaker position where the wave was most asymmetric the value of the wave slope asymmetry was - 0.083. The theoretical curve gave results rather lower than the experimental results. On the beach slope of 1/6, it was again found that the most rapid change in wave slope asymmetry took place in the region d/L $<$ 0.15. The maximum divergence between the theory and the experimental results was about 7% of the theoretical prediction. The results for beach slopes of 1/9, 1/12, 1/15 and 1/18 indicated a similar trend to those discussed above.

As can be seen from fig. 9 showing the effect of beach slope on wave slope asymmetry, the wave slope asymmetry increases as the beach slope gets steeper. This is in marked contrast with the wave vertical asymmetry which decreases as the beach slope gets steeper. On the other hand the wave horizontal asymmetry increases with increasing beach slope.

Figures 10 and 11 show, however, that all of the asymmetries, 'slope', 'vertical', and 'horizontal', are correlated. As a result of the studies, the following relationships were obtained :

Let Av = wave vertical asymmetry
S = wave slope asymmetry
$|s|$ = modulus of s
γ = beach slope

HA & HA' = wave horizontal asymmetry

$$HA = \frac{\text{Horizontal distance from crest to front face at S.W.L}}{\text{Horizontal distance from crest to back face at S.W.L.}}$$

$$HA' = \frac{\text{Horizontal distance from crest to preceding wave trough}}{\text{Horizontal distance from crest to following wave trough}}$$

The empirical relationships between Av, S, γ, HA and HA' are:

$$HA = \frac{1.31}{e^{\gamma}} \tanh HA' \qquad \text{--------(30)}$$

$$HA = \frac{1.52}{e^{\gamma}} (1.18 - \sinh Av) \qquad \text{--------(31)}$$

$$Av = \frac{8.8}{e^{\gamma}} \tanh |s| + 0.5 \qquad \text{--------(32)}$$

From the cnoidal wave theory as developed by Korteweg and de Vries (10), the wave vertical asymmetry Av is given by

$$Av = \frac{Y_c - d}{H} = \frac{16 d^3}{3L^2 H}\left\{K(k)\left[K(k) - E(k)\right]\right\} \qquad \text{--------(12)}$$

where Yc = distance from the ocean bottom to the wave crest
d = still water depth
H = wave height (trough to crest)
L = wave length
K(k) = complete elliptic integral of the first kind
E (k) = complete elliptic integral of the second kind
k = modulus of the elliptic integral.

From equations (31) and (12)

$$HA = \frac{1.52}{e^{\gamma}}\left\{1.18 - \sinh\left(\frac{16 d^3}{3L^2 H}\left[K(k)\left\{K(k) - E(k)\right\}\right]\right)\right\} \qquad \text{-------(33)}$$

Thus equation (33) gives a general expression for wave horizontal asymetrry HA. Values of K(k) and E(k) are tabulated in Masch and Wiegel (11) (1961).

CONCLUSIONS

The wave asymmetry defined in all of the three ways increases as the wave advances into shallower water and the wave is most asymmetric at the wave break point. The most rapid change in wave asymmetry takes place in the region $d/L < 0.15$.

The cnoidal wave theory is adequate for predicting wave vertical asymmetry. However, whereas, the cnoidal theory indicates a non-linear curve throughout, the experimental curves of the wave vertical asymmetry against d/L became linear for slopes $< 1/12$. The studies on the effect of backwash showed that the linearity was due to the backwash and the flat beach slope.

The work on the wave slope asymmetry showed good agreement with the theory of Biesel (1). The results of the experiments for the beach slopes $\frac{1}{4}$, 1/6 and 1/9 indicated that the wave slope asymmetry ceases at d/L = 0.26. The theory of Biesel (1) predicted that the wave slope asymmetry ceases at d/L = 0.27. This would appear to be a valuable verification of a theory which had not previously been checked experimentally.

The wave horizontal asymmetry (both HA and HA') and the wave slope asymmetry increase as the beach slope gets steeper, whereas the wave vertical asymmetry is greater for flat slopes when the wave is in very shallow water. The rule of thumb that the trough is a quarter of the breaker height below the undisturbed water level, whatever the beach slope is not quite correct.

A correlation was found to exist between the two types of wave horizontal asymmetry HA and HA'. Further they both show the same trend, thus any studies connected with the wave horizontal asymmetry could be made using either HA or HA'. As shallow water waves tend towards the characteristics of long waves, it is evident that measurement of HA would be more precise than HA'.

Apart from the correlation between the two types of wave horizontal asymmetry HA and HA' a correlation was also found to exist between the wave slope asymmetry, wave horizontal asymmetry and wave vertical asymmetry, this thus make it possible to obtain a general expression for the wave horizontal asymmetry HA.

REFERENCES

(1) Biesel, F :- Study of wave propagation in water of gradually varying depth. Gravity waves circular No. 521. Nat. Bureau of Standards Washington D. C. 1951.

(2) Eagleson P.S. :- Properties of shoaling waves by theory and experiment. Trans. Amer. Geophys. Un. 37 No. 5 1956.
PP 565 - 572 and 38 (5) 1957 PP 760 - 763

(3) Adeyemo, M.D. :- Wave transformation and velocity fields in the breaker zone, Ph.D. thesis Univ. of London, 1967.

(4) Kemp, P.H. and Adeyemo, M.D. :- Effect of backwash on wave asymmetry close to breakers. Proc. XI conf. coastal Eng. London, 1968 September.

(5) Hamada, T. :- Breakers and beach erosions. Rept. Transportation Tech. Res. Inst. Tokyo, Report No. 1 December, 1951.

(6) Ippen, A.T. and Kulin, G. :- The shoaling and breaking of the solitary wave. Proc. Fifth Conf. Coastal Engineering. September, 1954. Published 1955.
PP 27 - 47.

(7) Keller, J.B. :- The solitary wave and periodic waves in shallow water, Commun. Appl. Math. 1, 1948.

(8) Kemp, P.H. :- The relationship between wave action and beach profiles Proc. Seventh Conf. coastal Engineering 1960 PP 262 - 277.

(9) Keulegan, G.H. and Patterson, G.W. :- Mathematical theory of irrotational translation waves. J. Res. National Bur. standards, 24, 1. Jan. 1940. PP 47 - 101.

(10) Korteweg, D.J. and De Vries, G. :- On the change of form of long waves advancing in a rectangular canal, and on a new type of long stationary waves. Phil. Mag. 5th Series 39, 1895: PP 422 - 43.

(11) Masch, F.D. and Wiegel, R.L. :- Cnoidal waves - Tables of Functions. Council on wave research. The Engineering Foundation, Richmond, Calif 1961 129 pp.

(12) Miche, R. :- The reflecting power of maritime works exposed to action of the waves. Bulletin of the Beach Erosion Board. Corps of Engrs. U.S. Army 7. 2 (April, 1953).

(13) Miller, R.L. and Zeigler, J.M. :- The internal velocity field in breaking waves. Proc. Ninth Conf. coastal Engineering 1964. PP 103 - 122.

(14) Plinston, D.T. :- The effect of waves breaking on beaches. Ph.D. thesis Univ. of London, 1966.

(15) Ursell, F. :- The long wave paradox in the theory of gravity waves. Proc. Camb. Phil. Soc. V 49 (4) 1953.

(16) Wiegel, R.L. :- Experimental study of surface waves in shoaling water. Trans. Amer. Geophys. Union Vol. 31, 1950: PP 377 - 85

(17) Wiegel, R.L. :- A presentation of cnoidal wave theory for practical application. Jour. Fluid Mech. 7, Part 2, 1960. PP 273 - 86.

CHAPTER 11

THE EFFECTS OF BOTTOM CONFIGURATION ON THE DEFORMATION, BREAKING AND RUN-UP OF SOLITARY WAVES

Frederick E. Camfield

Research Associate, Department of Civil Engineering
Oregon State University, Corvallis, Oregon
(formerly of Stanford University)

and

Robert L. Street

Associate Professor, Department of Civil Engineering,
Stanford University, Stanford, California

ABSTRACT

Experiments were conducted to determine the various effects on the shoaling, breaking and run-up of solitary waves resulting from the bottom configuration. An initial set of experiments investigated the effect of the initial bottom slope on the breaking and run-up of a wave on a second, higher slope. A second set of experiments considered the effect of a continental shelf configuration on the transmissibility of waves in the shoreward direction, and the decomposition of the waves due to the shallower water depth on the continental shelf. It was found that, in order to make predictions at or near the shoreline for waves generated in deep water, it is necessary to consider the total configuration of the bottom leading to the shoreline.

INTRODUCTION

Large, long ocean waves moving shoreward are influenced by the bottom topography while still at a great distance from the shoreline. Two major changes occur in the bottom topography: a relatively steep continental slope which flattens out into the continental shelf, and a steepening of the bottom slope in the area of the shoreline. To the latter one must add the slope change created by man on structures placed at or near the shoreline. The primary objectives of the experiments described herein were, therefore, to establish bounds on the fluid volume delivery onto a shelf resulting from long wave encroachment, and to study the behavior of waves on a sloping bottom as a function of a previous incident slope.

While large ocean waves are most commonly described in terms of periodic wave trains or impulsively generated wave groups, our experience has shown that solitary wave studies provide valuable information on the complex bottom-wave interaction processes because of the ultimate simplicity

of the solitary wave and its description (Camfield and Street, 1967). Accordingly, solitary waves have been used in the present study. As the solitary wave is the limiting case for finite amplitude periodic waves as length becomes large relative to other parameters, this study of the limiting case is very instructive and should provide a basis for future investigations.

THE EXPERIMENTS

FACILITIES AND EQUIPMENT

The present experiments were run in the Stanford Wind, Water-Wave Research Facility (Hsu, 1965) located in the Hydraulics Laboratory at Stanford University. The facility consists of a 115 foot long by 3 foot wide wave channel (Fig. 1). A glass-walled test section, 85 feet long, is located downstream from the wave generator, and waves from the generator travel 15 feet through the channel forebay before entering the test section. The inside width of the test section is 35½ inches.

Waves are generated by a vertical piston-type wave plate with a total available forward motion of 18 inches. The motion and position of the wave plate are controlled through a hydraulic-servo-electronic system by an externally applied voltage from an electronic function generator. For the present experiments a small, self-contained, electronic function generator was used. This generator produces a voltage signal in the form of a hyperbolic tangent function, has a continuously adjustable signal amplitude with a range of 0 to 5 volts, and also has an adjustable time base with a range from 0.5 to 10.5 seconds (Camfield and Street, 1967). The position of the wave plate is registered electronically by means of a gear-rack and potentiometer, and the control system matches the plate position with the input signal through a feedback circuit. The distance through which the wave plate moves is linearly related to the change in applied voltage. A change of 5 volts produces the full 18-inch motion of the plate. To produce a solitary wave a single, unidirectional, forwsrd motion of the wave plate is used.

The beach for the continental shelf configuration is shown schematically in Fig. 2. The beach is composed of three sections: the beach slope, the horizontal beach shelf, and the vertical reflecting barrier. Clearly, the objective of the beach slope and horizontal shelf was to simulate the continental slope and shelf. The vertical reflecting barrier was installed with the idea in mind that the barrier, by perfectly reflecting the waves, would provide a virtual doubling of the shelf length as the reflected waves ran back over still water.

The second beach configuration consists of a long, low slope, 45 feet in length, followed by a short, steep slope, varying in length from 5 to 10 feet. This allowed the simulation of waves in a shoreline region, impinging on a higher slope such as a man-made structure.

The initial beach slope for the continental shelf configuration is a single 10 foot long aluminum plate. This plate is 35 inches wide

and 0.125 inch thick. It is rigidly supported on a welded frame composed of 2 inch by 2 inch aluminum angles. The beach slope plate was anchored to the wave tank bottom at the toe of the slope (see Fig. 2) and connected by hinges to the first plate in the horizontal beach shelf, this plate was also specially stiffened with 2 inch by 2 inch angles. In spite of the firm support, some minor flexing of the beach slope under the action of the waves was observed. The flexing had no apparent effect on the results.

The remaining beach sections were constructed from series of aluminum plates interconnected to form long, flat surfaces. The individual aluminum plates are 30 inches long by 35 inches wide and are made of 0.125 inch thick plate. Stiffening members were added to the underside of each plate. The interconnection of the individual plates is accomplished with 0.188 inch thick by 4 inch wide aluminum plates placed under the joint and connected to the plate on either side by eight machine screws. The plate assembly is suspended from above by steel rods; there are two 0.5 inch rods attached to each plate at a distance of 1.5 inches from the walls of the wave tank.

The vertical reflecting barrier is composed of two plates identical to those used in the sections above. The barrier is attached by hinges to the final plate in the shelf. When the slope and shelf were in proper position the reflecting barrier was blocked firmly in place with 2 inch by 4 inch wood studs to which the barrier was clamped after the assembly was plumbed to vertical. This barrier was also used to study wave run-up on a vertical wall, and was later adjusted to a 45° slope for studies of wave run-up.

Wave heights were recorded by means of capacitance-type wave height gages (Camfield and Street, 1967; Colonell, 1966). The output from the gages was recorded by means of a Sanborn recording oscillograph system, series 950, equipped with carrier preamplifiers. The gages were suspended on long steel tubes from 2 inch by 6 inch aluminum channels mounted atop the wave tank. The gage calibrations were linear and were obtained by raising and lowering the gage (and mounting tube) in still water. Motion pictures were taken of the breaking and run-up detail, using a 16 mm Bolex movie camera with a 10 mm wide-angle lens and Tri-X film.

THE SOLITARY WAVE

The solitary wave has a form lying entirely above the still water line and consisting of a single swell that propagates without change of form and at a constant celerity in water of uniform depth (Ippen, 1966, Camfield and Street, 1967). Figure 3 shows a solitary wave of height H, in water of depth D, and traveling with celerity c in the positive x-direction. On the basis of considerable analysis and many experiments, it has been determined that the following equations quite adequately describe the wave on a horizontal bottom. The surface profile η is given by

$$\eta = H \operatorname{sech}^2 \left[\left(\frac{3H}{4D^3} \right)^{\frac{1}{2}} (x - ct) \right] \qquad (1)$$

where t is time. The celerity c is

$$c = [g(H + D)]^{\frac{1}{2}} \tag{2}$$

where g is the acceleration due to gravity.

From Equation (1), the volume above the still water line in the wave is

$$V = \int_{-\infty}^{\infty} \eta \, dx = \left[\frac{16}{3} D^3 H \right]^{\frac{1}{2}} \tag{3}$$

per unit of crest length. It follows that

$$\frac{H}{D} = \frac{3}{16} \left(\frac{V}{D^2} \right)^2 \tag{4}$$

Hence, V/D^2 is a useful measure of the volume in a given wave and simultaneously is directly related to the relative wave height H/D. As we are concerned here with the volume delivery over a beach slope and onto a shelf, the ratio V/D^2 is taken as the primary non-dimensional parameter of the study.

HYDRAULIC JUMPS AND BORES

If a solitary wave moves up a plane beach into ever shallower water, the wave will eventually break. If the beach slope is small (say less than 8°, cf., Camfield and Street, 1967), the breaking wave will propagate shoreward and maintain a relatively steep, turbulent face. Such a progressing wave with a steep front is called a bore (Stoker, 1957). This bore is the direct analog of the hydraulic jump, i.e., the bore is a moving hydraulic jump. In the shelf experiments, it was observed that the appearance and behavior of the experimental solitary waves after passage over the slope onto the shelf was not unlike that of hydraulic jumps.

Consider a moving hydraulic jump. View this jump with respect to a set of coordinates fixed in the face of the jump and traveling at the speed C_S of the jump. The classical results of stationary jump analysis (Henderson, 1966) are easily adapted to the moving system. Figure 4 shows the two common types of hydraulic jump expected for the Froude number range of the present experiments and the notation to be employed here.

If the depth in front of the jump is $y_1 = D_S$ and that behind the jump is y_2, application of the momentum and continuity principles in the moving coordinates yields the sequent depth relationship

$$\frac{y_2}{y_1} = \frac{1}{2} \left[(1 + 8F_1^2)^{\frac{1}{2}} - 1 \right] \tag{5}$$

where the Froude number F_1 is given by

$$F_1 = \frac{C_S}{(gD_S)^{\frac{1}{2}}} \tag{6}$$

Recall that C_S is the speed of the jump over the fixed bottom of the shelf, while $D_S = y_1$ is the still water depth ahead of the moving jump.

The rationale behind the existence of the undular and broken jumps has been examined by Benjamin and Lighthill (1954). Their comments on the work of Favre (1935) and Lemoine (1948) are summarized below.

The classical jump analysis shows that, across the jump, the rate of energy loss $\dot{e}$ per unit of jump crest length per unit time is

$$\dot{e} = \frac{1}{4} g \frac{(y_2 - y_1)^3}{y_2 y_1} \rho q \tag{7}$$

where ρ is the fluid density and q is the flow rate. The point of basic interest here is that the energy loss need not necessarily be dissipated into heat and lost; part (even most in some cases) may be radiated downstream behind the jump through the trailing wave train of the undular jump.

Thus Favre found that, for $F_1 < 1.21$, none of the waves of the jump exhibited any breaking. Lemoine concluded that under these circumstances the required loss of energy may occur not by friction, but by radiation through the trailing wave train. Favre found further that the trailing waves form behind the bore one by one after it is first created. The number of waves present at any instant may then be regarded as an indicator of the period of existence of the bore. This is in accord with Lemoine's view that the trailing wave group carries the energy away as it is liberated at the bore.

An essential contribution to this concept by Benjamin and Lighthill (1954) was the extension of the analysis of Lemoine to finite amplitude waves. They show that the behavior of a supercritical stream (or, as in the present case, a disturbance moving over still water at a speed such that $F_1 > 1$) is describable as follows: for a bore with no frictional effects at all the only form of disturbance that can arise is the solitary wave; for a bore in which the classical value of energy is dissipated in friction at the bore, no trailing wave train can arise; the undular jump or bore with trailing wave train exists when the frictional losses lie between these extremes. Thus, the formation of a train of waves behind the bore front requires some frictional dissipation, but not too much.

EXPERIMENTAL RESULTS

THE CONTINENTAL SHELF PROBLEM

The experimental configuration is shown schematically in Fig. 2. The independent variables of the study were:

D_T = the "deep water" depth at the toe of the beach slope

D_S = the water depth on the horizontal beach shelf

α = the angle of inclination of the beach slope

H = the solitary wave height

Accordingly, the test parameters were:

H/D_T = relative deepwater wave height

D_T/D_S = water depth ratio

α

For the present tests, water depth ratios of D_T/D_S = 2.0, 3.0, 6.6, 9.2 and 12.1 and beach slopes of α = 4, 6, and 8 degrees were used. The range of the volume parameter was $0.10 \leq V/D_T^2 \leq 1.25$. This corresponds to a range of relative, deepwater wave heights of $0.002 \leq H/D_T \leq 0.30$. Under the given conditions and with the present facility and equipment, the lower limit on H/D_T was imposed by the resolution of the wave gages and the limited ability of the wave plate to generate pure solitary waves of extremely small heights, while the upper limit on H/D_T was imposed by the limited motion of the plate (18 inches maximum).

Wave volume data were obtained from capacitance wave height gages located at stations 17, 28.15 feet to the right of the toe; 18, 30.85 feet to the right of the toe; and 19, 33.20 feet to the right of the toe (Fig. 2). The area beneath the oscillograph wave height trace was planimetered, and the wave volume on the shelf was obtained from the product of this area and the wave celerity C_S (Street, Burges, and Whitford, 1968).

The volume of the initial, solitary wave in deep water (depth D_T) was determined directly from the displacement of the wave generating plate through use of the following argument. First, the leakage between the wave plate and the channel walls is assumed to be negligible. Then, if the sole effect of the single, unidirectional forward motion of the wave plate is to produce a solitary wave form, given by Eq. (1), lying entirely above the still water line, it can be assumed that all the water displaced by the motion of the plate has gone into the region above the still water line. That this should be the case is intuitively obvious. In addition, we have made the necessary experimental observations to verify the assumptions for waves with a proper time base.

Shelf wave height data were taken at station 17. This has been designated H_{17} . The adjoining station 18 was used in a few cases, but on the average the data from the two stations appear to be essentially the same.

The results are defined using the parameters:

K_T = the fraction of the initial wave volume that reaches station 17; V_S/V , where V_S is the wave volume on the shelf.

$1 + \frac{H_{17}}{D_S}$ = the relative total water depth beneath the crest of the leading wave or bore on the horizontal beach shelf.

C_S = celerity of the leading wave or bore front on the shelf.

These results will be interpreted in terms of their relationships to the volume V of the incident solitary wave, the ratio of water depths and the beach slope angle α. Data have been plotted for K_T and $1 + (H_{17}/D_S)$ versus V/D_T^2 for the various ratios of D_T/D_S. These results are summarized in Figs. 5 and 6.

The significance of the various parameters is now summarized. First, the relationships between K_T and V/D_T^2 depicted in Fig. 5 describe the fraction of fluid volume delivered onto a shelf by the encroachment of a long wave. Fig. 6 gives the equivalent results in terms of the relative total water depth, $1 + (H_{17}/D_S)$, at the bore front, the crest of the leading wave of a system or the crest of a single wave on the shelf. Recall that the incident wave height $H/D_T = (3/16)(V/D_T^2)$.

Fig. 7 depicts the relationship between the actual sequent depth ratio of a wave system, $(D_S + H_{17})/D_S$, and the sequent depth ratio, y_2/y_1, of an equivalent hydraulic jump, i.e., a jump with Froude number F_1.

The summary plots (Figs. 5 and 6) show the deepwater to shallow water depth ratio D_T/D_S as a parameter. It is clear that a change in D_T/D_S has a pronounced effect on the shelf wave heights and on the fraction of volume transmitted. The linear relationships proposed in Fig. 5 were chosen because no consistent results could be obtained with curves of a more sophisticated nature. For $D_T/D_S = 12.1$ data were available only for $\alpha = 8^\circ$. The linear fit to these data was not consistent with that for other D_T/D_S values. Because of the absence of other data for $D_T/D_S > 12.1$ (not possible in the present facility) or other α, the 12.1 data for K_T are not included on Fig. 5.

As little as 40 percent of the initial wave volume appeared on the horizontal beach shelf in some cases. However, a significant or coherent reflected wave moving to the left away from the beach slope was never observed. It is thought that the reflected volume moved away as a low solitary wave.

It is noted that the wave system on the shelf continued to evolve as it propagated. In particular, it was observed that wave crests continued to appear after the initial deformation on the beach slope, that after the wave system reflected from the vertical barrier the waves in the system began to appear to take on equal heights, and finally that the deformation to an undular bore occurred in many cases without breaking. If these observations are coupled with those above that establish that the wave system on the shelf moves like a moving hydraulic jump, then it is clear that the precise situation described by Benjamin and Lighthill (1954) and Lemoine (1948) has been observed. Thus, the wave system is continually radiating energy downstream (or to the rear). Finally, a check of the data confirms the Favre (1935) result that the transition of a supercritical stream can take place for $F_1 < 1.25$ without any breaking.

THE TWO-SLOPE PROBLEM

When a submerged, symmetrical hump was placed on a horizontal channel bottom, and solitary waves were generated in the channel, waves of a proper height were observed to break downstream from the hump. This breaking occurred in relatively the same location for a fairly wide range of wave heights. From this the following conclusions were drawn·

(1) Waves which reach a critical ratio of wave height to water depth, H/D, will not necessarily immediately break, as the breaking process depends upon particle motion within the wave and is time dependent.

(2) Waves which reach some critical state, as yet not well defined, will always break, even if the wave has passed into a region where the ratio H/D no longer exceeds a critical value.

From these conclusions it is possible to say that the breaking process is not dependent on the bottom configuration immediately below the wave, but instead is dependent on the slope which the wave has passed over preceding its arrival at the breaking position. Also, it may be concluded that the bottom slope affects the shape of the wave, and that sufficient loss of wave symmetry precipitates breaking.

The above leads to a question concerning the validity of previous results for wave breaking and run-up on a slope, where the generated waves passed over a horizontal bottom before impinging on the slope. The bottom slope in the region of a shoreline would not normally be expected to be horizontal. This created the necessity for investigating waves passing over initial low slopes before running up on a second, higher slope.

Extensive experiments have been conducted (Camfield and Street, 1967) for solitary waves shoaling for long distancea over low slopes. From these an empirical solution was obtained for the limiting height of waves on low slopes. The ratio H_B/D_B, where H_B ia the wave height at breaking and D_B is the still water depth at that point, was found to be represented by the expression

$$H_B/D_B = 0.75 + 25\,S - 112\,S^2 + 3870\,S^3 \qquad (8)$$

This expression was found for $0.000 \leq S \leq 0.045$.

Experiments were then performed for waves traveling long distances over low slopes and then onto higher slopes. If the initial low slope is S_1, the second alope S_2, the water depth at the intersection of the two alopes D_o and the wave height at that point H_o, the maximum value of the ratio H_o/D_o is given by Eq. (8) as

$$(H_o/D_o)_{max} = 0.75 + 25\,S_1 - 112\,S_1^2 + 3870\,S_1^3 \qquad (9)$$

Values of H_B/D_B were recorded for waves which broke on the second slope. Fig. 8 shows a summary of results for $0.01 < S_1 < 0.03$ and $S_2 = 4^\circ$. The solid lines terminate at the point where the waves break at the toe of the second slope and $H_B/D_B = H_o/D_o$. It can be seen that H_B/D_B increases with

increasing S_1 for given values of H_o/D_o . Limited experiments were run for $S_2 = 8^\circ$ and $S_2 = 12^\circ$ and the same trend was seen to exist. However, the number of data points was insufficient to plot due to the experimental errors inherent in obtaining this type of data.

In addition to measuring H_B/D_B , values were obtained for the vertical rise of water, R , on the second slope. Fig. 9 shows a summary of data for $0.01 < S_1 < 0.03$ and $S_2 = 4^\circ$ and 8° . Again, limited data obtained for $S_2 = 12^\circ$ showed the same general trend, but data on this slope is insufficient to include in the plots. It is readily noted that the run-up factor R/H_o increases for fixed values of H_o/D_o and S_2 as the initial slope S_1 increases. It is also evident that R/H_o increases as H_o/D_o decreases and S_2 increases.

Additional experiments were carried out with the initial slope set at values of $S_2 = 45^\circ$ and 90° . This allowed a comparison with previous results on wave run-up obtained for waves impinging on 45° and 90° slopes after passing over a horizontal bottom (Camfield and Street, 1967). Results for a 45° slope are shown in Fig. 10 in comparison with the empirical line of Hall and Watts (1953). Results for $S_2 = 45^\circ$ show that the run-up was increased by the non-zero initial slope. For a second slope of 90° (Fig. 11) results of considerably more interest were obtained. Previously, for waves passing over a horizontal bottom and onto a vertical wall, the equation

$$R/H_o = 2.0 + H_o/D_o \qquad (10)$$

was obtained. For waves passing over a slope of $S = 0.01$ and when H_o/D_o was small, values of R/H_o were still somewhat within the range of the above equation as the waves remained fairly symmetrical. However, as H_o/D_o increased, the waves became very steep fronted and came into contact with the vertical wall with explosive impact. Visual observations of waves having high values of H_o/D_o indicated values of $R/H_o \approx 5.0$ with spray reaching approximately twice this height. As the higher portion of the run-up became a thin film, it was difficult to accurately measure the exact height of run-up. Therefore the values shown in Fig. 11 are somewhat conservative.

It can be noted that the trend of data on the higher slopes is the opposite of the trend on the lower slopes, i.e., the run-up increases with increasing H_o/D_o and decreases with increasing S_2 . This can be explained by noting that the waves broke where the second slope had a low value. As waves having lower values of H_o/D_o and/or traveling over higher values of S_2 tended to break relatively closer to the shoreline, less energy was dissipated and the run-up increased where the second slope was small. On the other hand, as the second slope reaches a high value the wave does not break but the effect of gravity becomes more predominant.

Attention is called to the one point on Fig. 11 for a wave which broke on the initial slope before reaching the vertical wall. When a wave breaks there is a rapid decrease in wave height (Camfield and Street, 1967), much more rapid in fact than the decrease in energy. Therefore, for waves which break in front of the wall, the value of R/H_o can be expected to be higher than the value of R/H_o for a nonbreaking wave with the same value of H_o/D_o ,

where H_o/D_o is measured at a point the equivalent of one-half of the effective wave length in front of the vertical wall in each case.

Limited observations were made for a case where the first slope was set at $S = 0.03$ and 0.045, the second slope was set at $1/5$, and the wave was allowed to break on the first slope, forming a bore. It was found that the bore would reflect from the second slope. This reflected bore was superimposed on the increased water level caused by the incident bore and the resulting water level was higher than the incident bore.

CONCLUSIONS

By use of solitary waves propagated over a stepped slope it has been shown that long waves can deliver a significant portion of their initial volume to an arbitrary point on a shelf beyond the slope. In addition, the wave system, formed on the shelf by shoaling of a solitary wave, was shown to behave essentially as a moving hydraulic jump or bore when the ratio of water depths before and after the slope is, at least, greater than or equal to 2.0.

The restricted travel distance of the present wave generator plate limited the range of these exploratory tests. It is believed that it would be instructive, for example, to run tests for $D_T/D_B < 2.0$ and > 12.1 to ascertain if the indicated trends persist in these domains. In addition, it would be instructive to use larger values of α or a longer beach slope (hence, greater D_T/D_B) to see if the solitary wave could be forced to break on the beach slope. This did not occur herein. Accordingly as the wave size (volume) increased, K_T increased. It is believed that K_T will reach a maximum value when either the initial wave exceeds its limit height in deep water or when it breaks on the beach slope. Thus, one of the original questions posed at the start of this investigation, to wit: "Is there an optimum combination of parameters for the maximum volume delivery to a shelf?" remains unanswered, while on the other hand much has been gained in terms of our understanding of wave behavior on a stepped slope.

The results for a low initial slope followed by a second higher slope show that the initial slope has a significant effect on both the breaking height and the run-up of the waves. It is therefore necessary to consider the bottom slope at some distance from the shoreline when analyzing waves approaching the shoreline, and when predicting the breaking and run-up of the waves on the shoreline or on structures near the shoreline. The present experiments showed qualitative trends which could be used to predict the effects of various slope combinations. However, it is suggested that further data should be obtained for any quantitative analysis for design purposes.

ACKNOWLEDGEMENT

This work was supported by the Defense Atomic Support Agency and the Office of Naval Research (Field Projects Branch) under contract Nonr 225(85), NR 089-041.

REFERENCES

Benjamin, T. B. and Lighthill, M. J. (1954). On cnoidal waves and bores: Proc. Roy. Soc., London, Series A, V. 224, pp. 448-460.

Camfield, F. E. and Street, R. L. (1967). An investigation of the deformation and breaking of solitary waves: Dept. of Civil Engineering Technical Report No. 81, Stanford Univ., Stanford, Calif., December, DDC AD 664 249.

Colonell, J. M. (1966). Laboratory simulation of sea waves: Dept. of Civil Engineering Technical Report No. 65, Stanford Univ., Stanford, Calif., July, DDC AD 488 372.

Favre, H. (1935). Etude théorique et experimental des ondes de translation dans les canaux découverts: Dunod, Paris.

Hall, J. V., Jr. and Watts, G. M. (1953). Laboratory investigation of the vertical rise of solitary waves on impermeable slopes: Beach Erosion Board Technical Memo No. 33, U.S. Army Corps of Engineers.

Henderson, F. M. (1966). Open Channel Flow: The Macmillan Co., New York.

Hsu, E. Y. (1965). A wind, water-wave research facility: Dept. of Civil Engineering Technical Report No. 57, Stanford Univ., Stanford, Calif., October.

Ippen, A. T., ed. (1966). Estuary and Coastline Hydrodynamics: McGraw-Hill Book Co., Inc., New York.

Lemoine, R. (1948). Sur les ondes positives de translation dans les canaux et sur le ressaut ondule de faible amplitude: La Houille Blanche, V. 2, pp. 183-185, March-April.

Stoker, J. J. (1957). Water Waves: Interscience Publishers, Inc., New York.

Street, R. L., Burges, S. J. and Whitford, P. W (1968). The behavior of solitary waves on a stepped slope: Dept. of Civil Engineering Technical Report No. 93, Stanford Univ., Stanford, Calif., August.

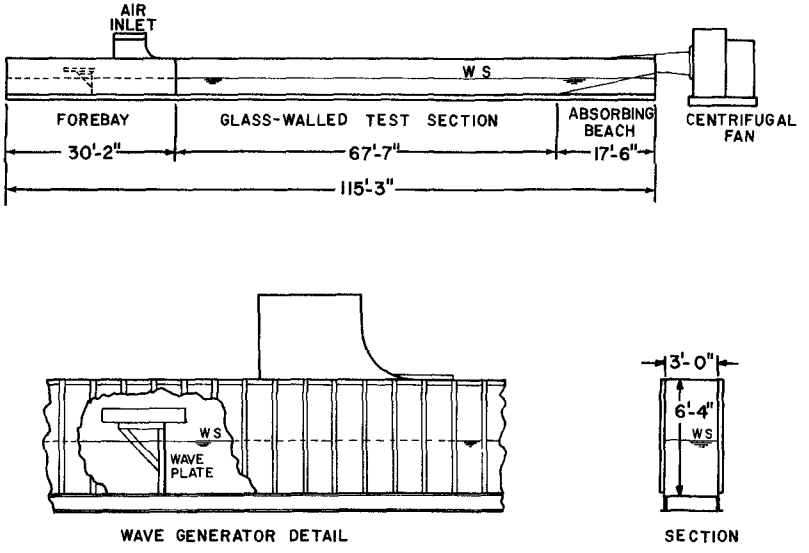

Fig. 1. The Research Facility.

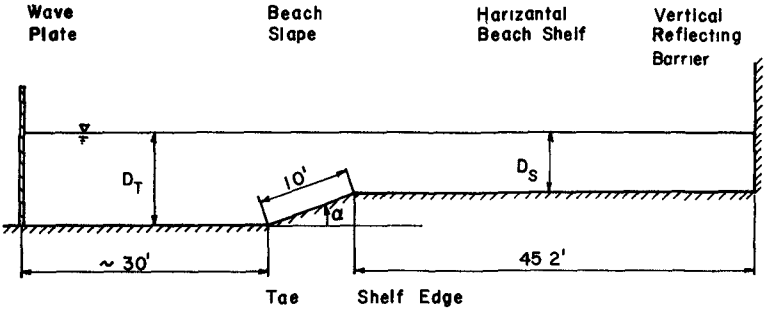

Fig. 2. The Continental Shelf Configuration.

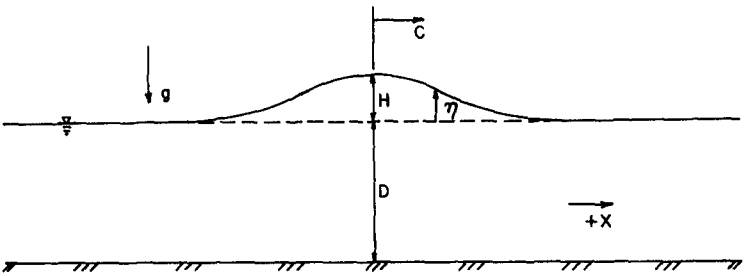

Fig. 3. Schematic of a Solitary Wave.

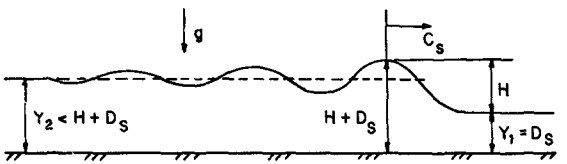

Moving Undular Jump (at fixed time)

$$F_1 = C_S / (g D_S)^{1/2}$$

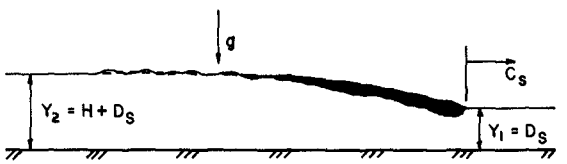

Moving Broken Jump (at fixed time)

Fig. 4. Schematic of Hydraulic Jumps.

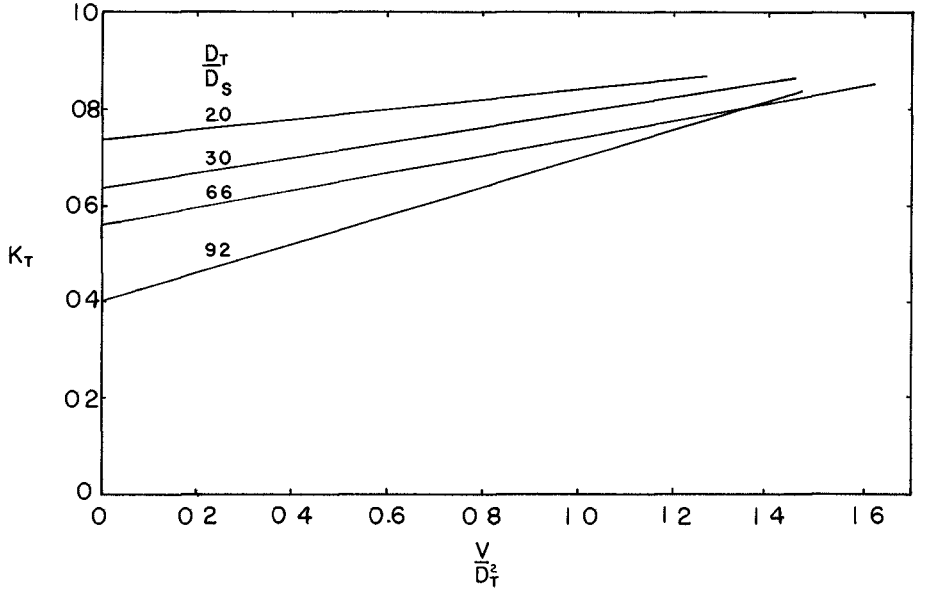

Fig. 5. K_T versus V/D_T^2 .

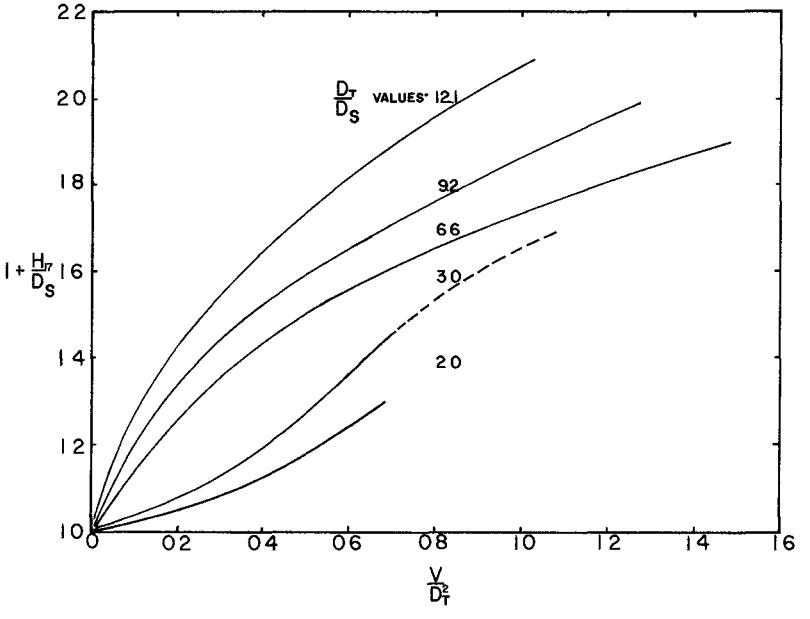

Fig. 6. $1 + (H_{17}/D_S)$ versus V/D_T^2 .

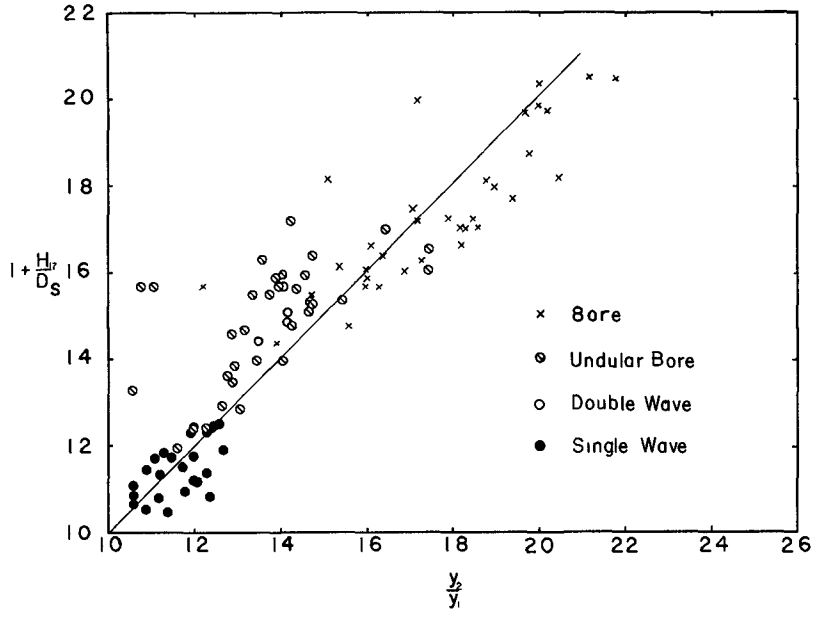

Fig. 7. $1 + (H_{17}/D_S)$ versus y_2/y_1 .

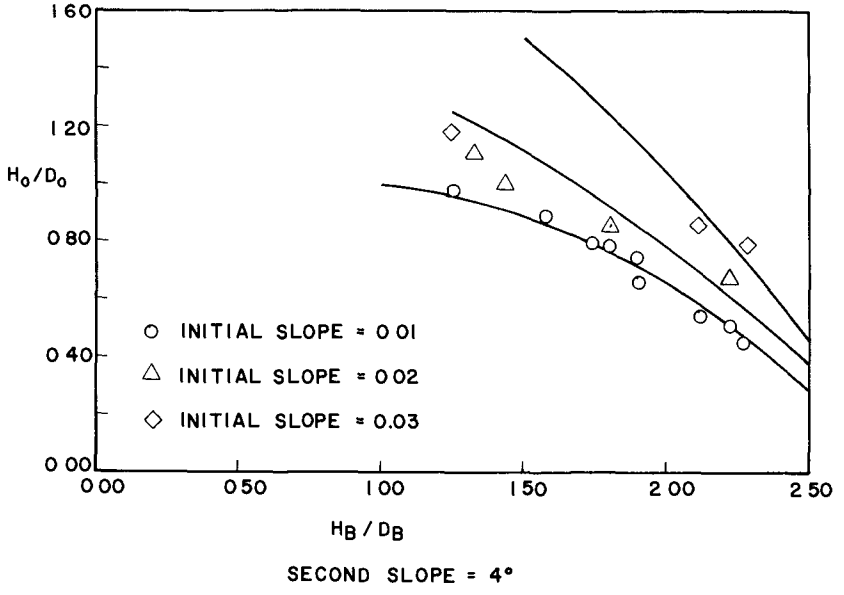

Fig. 8. Breaking Characteristics on Broken Slopes

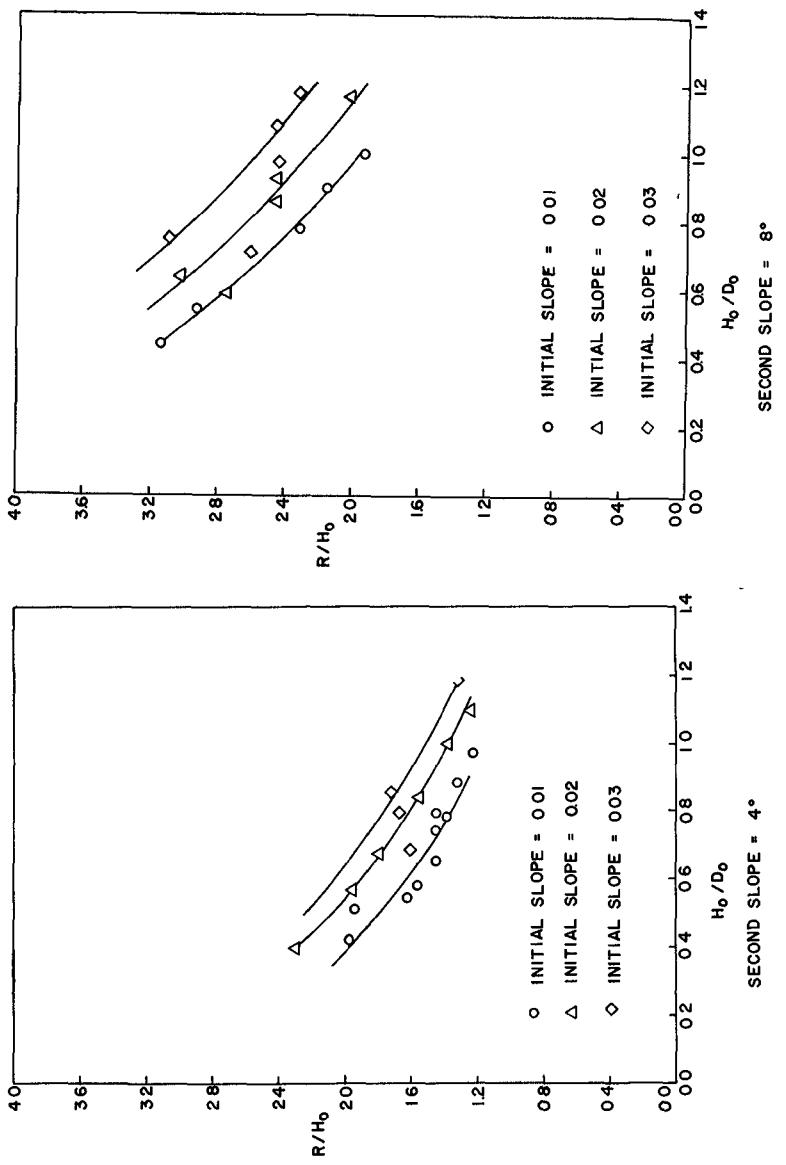

Fig. 9. Wave Run-up on Broken Slopes

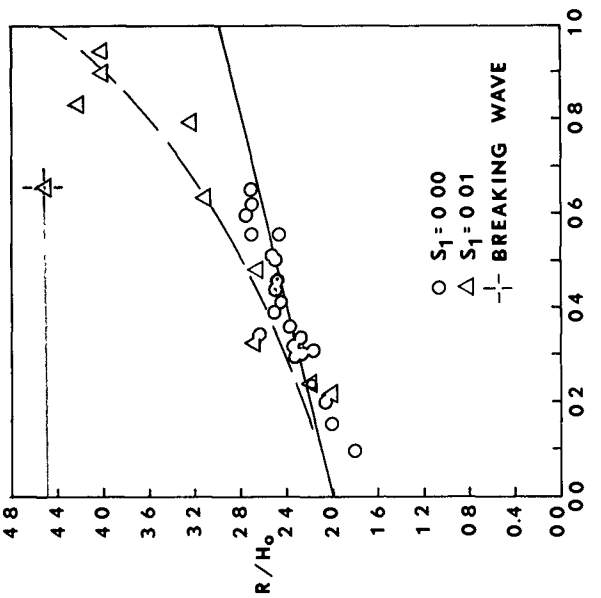

Fig. 11. Wave Run-up on a Vertical Wall.

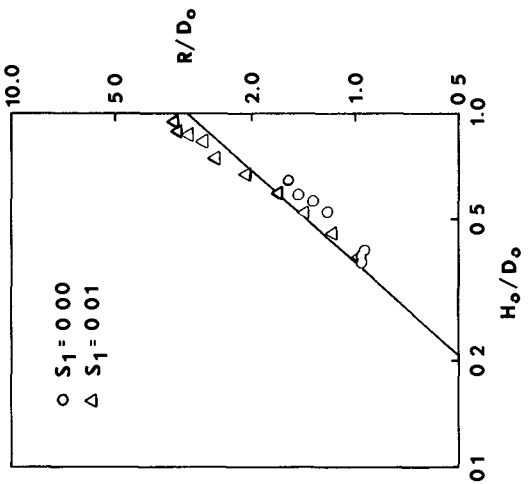

Fig. 10. Wave Run-up on a 45-Degree Slope.

CHAPTER 12

LONG WAVES IN CHANNELS OF ARBITRARY CROSS-SECTION

D. H. Peregrine

Lecturer in Applied Mathematics
Department of Mathematics
University of Bristol
England

This paper summarises some recent work on long gravity waves on still water in channels of arbitrary constant cross-section. Theoretical results have been obtained for both straight and curved channels. Some experimental work has been performed in straight trapezoidal channels and shows reasonable agreement with theory. For straight channels some details of the second approximation are given, and the cases where the approximation breaks down are indicated. For curved channels it is found that the effect of channel curvature is more pronounced when the cross-sectional shape of the channel is not symmetric with respect to its centre-line.

The waves considered are long gravity waves on the surface of water contained in a channel. If the waves are very long compared with both the breadth and depth of the channel, then it is reasonable to assume uniform conditions across the whole cross-sectional area of the channel. That is, a uniform height of water and a uniform velocity of water along the channel. If, further, it is assumed that the amplitude of the wave is very small compared with the depth of water, it is simple to show that the pressure is hydrostatic, and the wave motion in a straight channel is governed by the equations,

$$\frac{\partial u}{\partial t} + g\frac{\partial \zeta}{\partial x} = 0, \qquad B_0\frac{\partial \zeta}{\partial t} + \frac{\partial}{\partial x}(A_0 u) = 0, \tag{1}$$

where u is the velocity of water along the channel which is taken to be in the x direction, ζ is the height of the water surface above its undisturbed level, A_0 is the cross-sectional area of the channel and B_0 is the width of the free surface of the channel, where both A_0 and B_0 are evaluated for the undisturbed water surface. If attention is now confined to straight channels of uniform cross-section, A_0 and B_0 are constant and the wave velocity c_0 is given by

$$c_0^2 = g\frac{A_0}{B_0} = gh_0$$

where h_0 is the mean depth.

For the linearized equations (1) to be useful it is necessary for waves to have exceedingly small amplitudes, so it is desirable to find a better approximation. This can be done by retaining the assumption of uniform conditions over a cross-section, but such an approach leads to equations which are not uniformly valid. That is, the assumption of long waves breaks down, since the equations predict that the front of waves of elevation continually steepens. However, for two-dimensional motion it is known that this only happens for relatively large amplitudes, and that the appropriate uniformly valid approximation is that leading to solutions such as the solitary wave. This includes the effect of the vertical acceleration of the water on the pressure, as well as the next approximation in the amplitude. In addition to these we therefore also include here the effect of transverse water motions in channels which are not rectangular in section. This has been done and mathematical details may be consulted in a recently published paper (ref. 1).

It is found that the transverse and vertical velocities (v,w) are given by

$$\frac{\partial u}{\partial x}\frac{\partial \psi}{\partial y}, \quad -\frac{\partial u}{\partial x}\frac{\partial \psi}{\partial z},$$

where $\psi(y,z)$ satisfies

$$\frac{\partial^2 \psi}{\partial y^2} + \frac{\partial^2 \psi}{\partial z^2} = 1 \tag{2}$$

within the area A_o, with boundary conditions $\frac{\partial \psi}{\partial x} = 0$ on the channel walls and $\frac{\partial \psi}{\partial z} = h_o$ on the free surface. The variations of longitudinal velocity and amplitude across the channel are also in terms of ψ. In particular, the variation of amplitude across the channel is

$$-\frac{\partial^2 \zeta}{\partial x^2}\,\psi(y,0),$$

where $z = 0$ is the undisturbed water level. As may be expected ψ also appears in the equations of motion, which are

$$\frac{\partial u}{\partial t} + u\frac{\partial u}{\partial x} + g\frac{\partial \zeta}{\partial x} = 0, \tag{3}$$

$$\frac{\partial}{\partial t}\left(\zeta + \tfrac{1}{2}b\zeta^2\right) + \frac{\partial}{\partial x}\left[(h_o + \zeta)u\right] + \frac{\psi_B - \psi_A}{g}\frac{\partial^3 u}{\partial x \partial t^2} = 0, \tag{4}$$

where $b = B'(0)/B_o$, if $B(z)$ is the width of the channel at height z, and

$$\psi_B - \psi_A = \frac{1}{B_o}\int_{B_o} \psi(y,0)\,dy - \frac{1}{A_o}\iint_{A_o} \psi(y,z)\,dy\,dz.$$

These equations are no more difficult to deal with than the corresponding two-dimensional equations, and in many cases of interest it is simple to transform these equations into the two-dimensional ones. There is, for example, a solitary wave solution, and it is interesting to note that its velocity c is independent of $\psi(y,z)$ and depends only on the geometry of the channel:

$$c^2 = g[h_0 + (1 - \tfrac{1}{3}bh_0)a]$$

where a is the amplitude of the wave.

This theory is of most interest where it departs from the two-dimensional theory and from the first approximation, in particular in the variation of surface level across the channel. One general result can be found fairly easily by considering the boundary conditions on ψ at the shore line. If the shore line is at an angle α to the vertical, measured in the y direction, then the slope of the water surface at the shore,

$$\frac{\partial \zeta}{\partial y} = - \frac{\partial^2 \zeta}{\partial x^2} h_0 \tan \alpha .$$

This result shows that the crest of a wave ($\frac{\partial^2 \zeta}{\partial x^2} < 0$) will slope up towards the shore if $\alpha > 0$ and thus reach a higher level than at points away from the shore. Conversely if the banks are over-hanging, i.e. $\alpha < 0$, then the level of the crest will be depressed near the shore. Similarly the depth of a wave trough is increased or decreased near the shore if α is greater than or less than zero respectively.

It is possible to solve equation (2) analytically in a number of simple cases; but for most channels a numerical solution is needed. One particularly simple solution is for any triangular channel where

$$\psi(y,z) = \frac{1}{4}(y^2 + z^2)$$

when the origin of the coordinates is taken at the bottom of the channel. In this case the transverse surface profile is always part of a parabola.

Attempts to solve equation (2) analytically for trapezoidal channels led to an interesting result concerning wide channels. That is, as such a channel gets wider so the difference in crest height between the centre and the shore increases like the width of the channel. Thus, an essential part of the derivation of the solution, that such variations be small, no longer holds. It seems likely that long waves travelling along wide channels will usually break at the shore line.

Figure 1 shows how the function $\psi(v,0)$ varies for a sequence of three channels of different widths. For wider channels the value of ψ at the shore line increases linearly with L.

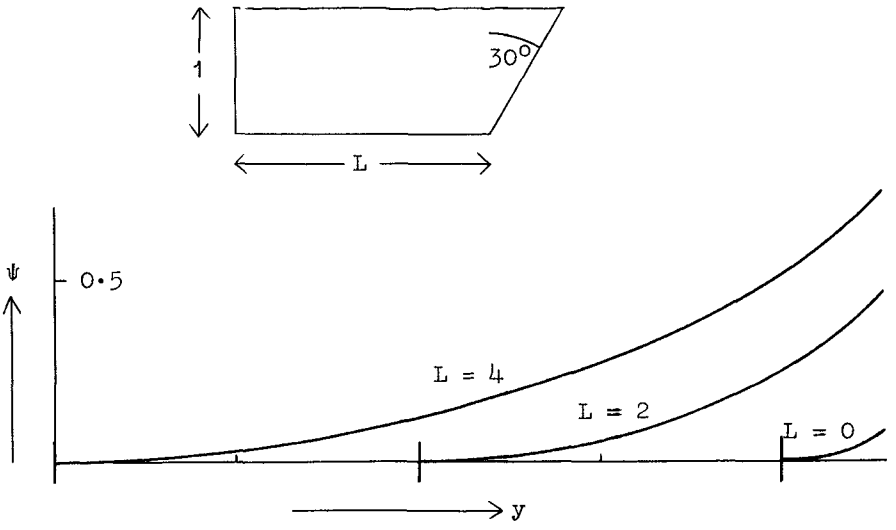

Figure 1 : Values of $\psi(v,0)$ for channels of the cross-sectional form shown at the top of the figure.

Some simple experiments measuring the variation in surface height along the crests of solitary waves have been conducted in three different channels. Two were trapezoidal, with one vertical side and the other side at 30^0 or 45^0 to the vertical. The measurements from these channels were in reasonable agreement with the theoretical results. The third channel was triangular, with one side vertical and the other at 60^0 to the vertical. The results from this latter channel were not very consistent and usually differed substantially from the theoretical values. It is clear from the theory that it is not applicable for shore lines sloping at small angles to the horizontal and it may be that, for waves of the amplitude used, 30^0 is too small an angle. Further details are given in reference 2.

This theory has been extended to curved channels (Towers, unpublished thesis, University of Bristol 1968). The equations corresponding to equations (1) are

$$\frac{\partial f}{\partial t} + g\frac{\partial \zeta}{\partial x} = 0, \qquad B_0\frac{\partial \zeta}{\partial t} + \frac{\partial}{\partial x}(Q_0 f) = 0, \tag{5}$$

where $f = (1 + \kappa y)u$, $Q_0 = \iint_{A_0} \frac{dydz}{1 + \kappa y}$, and κ is the radius of curvature of the centre-line of the channel. Note that

even in the first approximation the velocity is not uniform across the channel, u is the velocity at y = 0. As before, x is measured along the channel, y in the horizontal transverse direction and z vertically upwards: however, this now defines curvilinear coordinates which is why $(1 + \kappa y)$ appears in some terms. The surface y = 0 is chosen to be midway between the two shore lines. The form of the equations and the values of f, u, κ, Q and x are all slightly different if a different zero is used, but ζ is unchanged, so that it is preferable to look on equations (5) as equations for $\zeta(x,t)$. In this, the first, approximation ζ is constant across the channel.

If f(x,t) is eliminated from equations (5) it is clear that the effect of channel curvature only appears in Q_0. If κ is assumed to be small, which it must be if this long wave approximation is to be consistent, then we may write

$$Q_0 = A_0 - \kappa \iint_{A_0} y \, dy \, dz + \kappa^2 \iint_{A_0} y^2 \, dy \, dz + \ldots \qquad (6)$$

If the cross-sectional area is symmetrical about the centreline the second term in (6) is zero, otherwise it may be non-zero. Hence it appears that the curvature of the channel may have a stronger influence when the channel cross-section is aysymmetrical.

By comparing equations (1) and (5) it may be seen that the effect on wave amplitude of varying curvature along a channel is the same as would occur if the cross-sectional area A_0 varied in a straight channel while B_0 was constant, for example a rectangular channel with varying depth.

The next approximation, which gives the variation of wave amplitude across the channel has been worked out, and solutions obtained for channels of three different cross-sections. The results indicate that these second-order effects are quite small in those circumstances where the theory is most likely to be applicable. For example, in a channel of square cross-section of unit depth with $\kappa = \frac{1}{3}$ and a solitary wave of amplitude of 0·3 the wave crest is only 0·028 higher at the outer edge of the channel than at the inner edge.

References

1. Peregrine, D. H. 1968 Long waves in a uniform channel of arbitrary cross-section. Jour. Fluid Mechanics 32, 353 - 365.

2. Peregrine, D. H. (to be published) Solitary waves in trapezoidal channels. Jour. Fluid Mechanics.

CHAPTER 13

WAVE REFLECTION AND TRANSMISSION IN CHANNELS OF VARIABLE SECTION

E. L. Bourodimos*

A. T. Ippen **

SUMMARY

Reflection and transmission phenomena were investigated in a laboratory channel for transitions of linearly varying depth and/or width terminating in channels of reduced cross-section. Upstream wave characteristics were varied from deep to shallow water waves by changing wave frequencies, amplitudes and channel depths over a wide spectrum of conditions. Experimental values were corrected to correspond to transmission in an endless channel. The reflection and transmission coefficients are given as functions of the pertinent dimensionless parameters such as: group velocity ratio, channel depth ratio and wave steepness. Associated wave energies were also evaluated.

THE PROBLEM

Ocean waves arriving on beaches and in estuaries undergo a process of shoaling, i.e., they are transformed by the variation in the bottom topography of these areas. Changes in wave length, amplitude and phase angle are produced, and the transmission of wave energy is affected; part of the energy is transmitted, a part is reflected, and in addition processes of dispersion and of dissipation are active. Detailed knowledge concerning these phenomena is important in the design of maritime structures and harbors.

This study deals with an experimental program on reflection and transmission of waves in channel transitions of linearly varying bottom elevations and/or width for three geometries of the channel transition as given in Figure 1. labelled A, B and C. The depth in the approach channel was varied to give ratios of h_1/h_2 between 1.80 and 3 to 5. The periods of the incoming waves could be varied from .8 to 12.0 seconds resulting in a range of characteristics from deep water to shallow water waves. Wave steepness also was considered as a significant parameter and varied accordingly from 1/1000 to 1/20.

---

* Assistant Professor of Civil Engineering, Rutgers, The State University, New Brunswick, New Jersey

** Ford Professor of Engineering, Hydrodynamics Laboratory, Department of Civil Engineering, M.I.T., Cambridge, Massachusetts

The limits of the theory for such transitions are well established. On the one end of the spectrum is Green's Theorem which gives the amplitude of the transmitted wave on the basis of frictionless flow for shallow water waves in long, gradual transitions while reflection is zero. On the other end we find the theoretical transmission and reflection coefficients for abrupt transitions in width and/or depth given by Lamb (2) for linearized shallow water waves. There have been a number of attempts to generalize the theory for transitions between these limits by various investigators such as Rayleigh (3), Carrier (4), Takano (5), Kajiura (6) and Dean (7). An extensive review of this literature is given in references (8) and (9). The theory for the amplitude and phase changes for a wave of discrete frequency encountering a gradual transition is rather complex.

The mass flux varies with position and time over the transition length, such that the net storage within this length is variable and is zero only over a full wave period.

THE EXPERIMENTAL STUDY

In view of the rather limited scope of the theoretical results available so far, the present study adopted for the experimental program a systematic variation of the basic wave parameters within the possibilities of the available laboratory wave channel. These parameters are in dimensionless form: the group velocity ratio C_{G3}/C_{G1}, the reflection coefficient $K_r = a_2'/a_1'$ the transmission coefficient $K_t = a_3'/a_1'$, the depth ratio h_3/h_1 and the incoming wave steepness H_1/L_1.

The experimental wave channel is 100 feet long and is of rectangular cross-section, 2.5 feet wide and 3.0 feet deep as shown in Figure 2. The sides and 40 feet of the bottom consist of plate glass. Both a piston-type and a flap-type wave maker are available at one end followed by an expanded aluminum wave filter. At the other end energy absorbers of several types were utilized. Data were obtained by means of resistance wire wave gages mounted on carriages travelling over the channel sections upstream and downstream of the transition. The wave envelopes were recorded on Sanborn oscillographs.

Several transitions with linearly varying depth were tested during the overall program, the first attempts being made with relatively steep transition of 1:0.58 ($\alpha = 60°$) and 1:2.75 ($\alpha = 20°$). The depth ratios h_1/h_3 employed varied from 2.5 to 7.0. The short and intermediate waves were kept to small amplitudes. The channel following the transition section terminated abruptly. The results obtained for this initial study for reflection and transmission are reported in reference (8) and are employed for the present study primarily for comparison. This is true also for the second study with a transition of 1:16 ($\alpha = 3.57°$), however, wave steepness was varied in this program as an important parameter. Depth variations extended over a more

limited range of h_1/h_3 = 2.0 to 3.0. The wave periods corresponding to the range of short waves to shallow water waves were T = .67 seconds to 7.25 seconds. The wave steepness varied correspondingly from a maximum of .058 for short waves to a minimum of .00072 for long waves (8).

The test program to be emphasized here is the one specified for the three transitions A, B and C, indicated in Figure 1. As for the transition 1:16 these transitions were also exposed to the full range of waves from short to shallow water waves with depth ratios and wave steepnesses as given before.

EXPERIMENTAL RESULTS

Although the channel following the transition terminated in wave absorbers at the end of the wave channel some reflection remained as determined from the wave amplitude envelope. This necessitated the reduction of the data again as originally developed by Ursell and Dean (10) for an endless channel. This was done by a computer program for the wave systems S_1 and S_3 shown in Figure 3. The corrected emplitudes a'_1, a'_2 and a'_3 are related to the measured wave amplitudes a_1, a_2, a_3 and a_4 for the linearized waves assumed as follows:

$$a_1' = a_1 \sqrt{1 + \left(\frac{a_2}{a_1}\right)^2 \left(\frac{a_4}{a_3}\right)^2 - 2 \left(\frac{a_2}{a_1}\right) \left(\frac{a_4}{a_3}\right) \cos\left(\delta_1 - \delta_2 + \delta_4\right)} \qquad (1)$$

$$a_2' = a_2 \sqrt{1 + \left(\frac{a_1}{a_2}\right)^2 \left(\frac{a_4}{a_3}\right)^2 - 2 \left(\frac{a_1}{a_2}\right) \left(\frac{a_4}{a_3}\right) \cos\left(\delta_1 - \delta_2 + \delta_4\right)} \qquad (2)$$

$$a_3' = a_3 \left[1 - \left(\frac{a_4}{a_3}\right)\right]^2 \qquad (3)$$

Hence, the experimental reflection and transmission coefficients are defined by:

$$K_r = \frac{a_2'}{a_1'} \qquad (4) \qquad K_t = \frac{a_3'}{a_1'} \qquad (5)$$

These coefficients derived from experimental data are compared in the graphical presentations of results with those given by Lamb for abrupt transitions for long waves (2). Since in the short and intermediate wave range Lamb's analysis is not applicable the coefficients of reflection and transmission were restated from the energy balance quite generally for a channel of constant width:

$$\left(1 - K_r^2\right) C_{G1} = K_t^2 \, C_{G3} \qquad (6)$$

and
$$K_r = \left[1 - K_t^2 \left(\frac{C_{G3}}{C_{G1}}\right)\right]^{1/2} \tag{7}$$

wherein
$$C_G = nC = \frac{1}{2} C \left[\frac{2\,kh + \sinh 2kh}{\sin 2\,kh}\right] \tag{8}$$

Values for the group velocity ratios are readily obtained from wave tables (11).

Lamb has derived the reflection and transmission coefficients for abrupt transitions and shallow water waves as:

$$K_r = \frac{1 - \left(\frac{B_3}{B_1}\right)\sqrt{\frac{h_3}{h_1}}}{1 + \left(\frac{B_3}{B_1}\right)\sqrt{\frac{h_3}{h_1}}} \tag{9}$$

$$K_t = \frac{2}{1 + \left(\frac{B_3}{B_1}\right)\sqrt{\frac{h_3}{h_1}}} \tag{10}$$

Noting that the terms $\sqrt{h_3/h_1}$ represent group velocity ratios for shallow water waves and since $C = L/T$ these coefficients may be stated for our purposes as:

$$K_r = \frac{1 - \left(\frac{B_3}{B_1}\right)\left(\frac{C_{G3}}{C_{G1}}\right)}{1 + \left(\frac{B_3}{B_1}\right)\left(\frac{C_{G3}}{C_{G1}}\right)} \tag{11}$$

and
$$K_t = 1 + K_r = \frac{2}{1 + \left(\frac{B_3}{B_1}\right)\left(\frac{C_{G3}}{C_{G1}}\right)} \tag{12}$$

Values of the coefficients computed from equations (11) and (12) were used for comparison with the experimental results defined by equations (4) and (5).

Figure 4 gives these experimental values for transition A and short and intermediate waves versus the group velocity ratio. Previous experimental investigations for linearly varying bottom transitions 1:2.75 and 1:16 are shown by respective average lines. As in the previous studies the scatter for this transition of slope 1:8 is very large and a good physical explanation is difficult. A possible reason is the restricted length of channel, within which only a few waves can be generated ahead of

the transition. Damping effects also make an accurate evaluation of amplitude changes difficult, since wave envelopes extend over a considerable portion of the channel. Generally, reflection coefficients for gradual transitions are considerably higher than those established for Lamb's case. The most abrupt transition 1:2.75 is closest to this case, the transition 1:8 giving the highest values of K_r. The transition 1:16 shows the reflection coefficient lower again as one would expect for decreasing bottom slopes, the reflection eventually becoming negligible.

The trend for both the reflection and transmission coefficients is a decreasing one with an increase in the group velocity ratio. Differences in the transmission coefficients for the various transitions are relatively small in the significant range of group velocity ratios near unity and all K_t values are close to unity. Maximum values of $K_t = 1.25$ were reached for the lowest group velocity ratios. To be noted in connection with the scatter of the results in Figure 4 is the fact that they are not differentiated with regard to wave steepness, which was found however, to have relatively little effect on reflection and transmission for the short and intermediate wave range.

Figure 5 gives the experimental data for transition B for short and intermediate waves. Within the scatter the average experimental trend shows surprising agreement with the equivalent curves computed from Lamb's theory for shallow water waves. No previous results are available for this type of transition.

Figures 6 and 7 show a comparison of the reflection and transmission coefficients for transitions A and B for shallow water waves with Lamb's theory for abrupt changes in section as a function of group velocity ratio. The reflection coefficients for transition A are again higher than Lamb's values and the transmission coefficients are lower, but the change is not great. Transition B gives higher values than transition A, as expected, in view of the additional side contraction. However, it is seen that Lamb's theory overcompensates for this effect and the reflection and transmission coefficients are now lower and higher respectively than those from this theory.

Reflection and transmission coefficients both decrease with increasing group velocity ratio. The scattering for shallow water waves for each change in the depth ratio is more distinctly attributable to wave steepness as is seen from the following figures 8 and 9. In view of the absence of any theory including wave steepness as a parameter results for the reflection and transmission coefficients are compared to the mean curve of the transition 1:16 for shallow water waves for transition A and show higher values for A than obtained for the transition 1:16 (8). Transitions A and B both show a considerable decrease in the K_r values with increasing wave steepness. Some of this effect is undoubtedly associated with the markedly increased energy dissipation in the transition process as the wave steepness increases. This, although subject to extensive experimental error, was

verified from energy balance considerations in reference (9). Energy losses for the range of wave steepnesses tested on transitions A and B show increasing dissipation rates for shallow water waves to maxima of 5 and 8% respectively. For the intermediate wave range these dissipation rates are somewhat higher, increasing from 2% for the lowest steepnesses of H_1/L_1 = 1/1000 to 6% and 12% for transitions A and B for the highest steepnesses of 6/100.

Transmission coefficients seem very little affected by wave steepness changes for both transitions. This trend is confirmed by the previous study on transition 1:16.

Figure 10 shows the effect of wave steepness on the K_r and K_t values for transition C of constant depth, hence of constant group velocity ratio. While again the scatter is sizeable a generally decreasing value of K_r with rising wave steepness is noticeable, while the value of K_t is constant.

CONCLUSIONS

An extensive experimental program was conducted in a rectangular wave channel to determine the reflection and transmission coefficients for transitions of linearly varying depth and/or width. Experimental results were obtained for three transitions: a transition A of constant width and linearly sloping bottom (1:8), a transition B with a linear reduction in width to one half (1:12.8) and a linearly sloping bottom (1:8), a transition C with a linear reduction in width to one half (1:25).

The variables were: the wave frequency, which could be adjusted from deep water to shallow water waves in the approach channel, the wave amplitude, to give a maximum possible range of wave steepness, the channel depth resulting in different depth ratios for the upstream and downstream channels. The experimental results obtained in this program were compared to results of previous experiments on transitions of constant width with linearly varying depth of 1:2.75 and 1:16 where applicable.

Data reduction was on the basis of linearized, small amplitude theory with systematic reference to the theory for abrupt transitions by H. Lamb for shallow water waves. Generally, the coefficients of reflection and transmission were related to the resulting dimensionless parameters: group velocity ratio, wave steepness and channel depth ratio. Only very general conclusions are possible due to the relatively large scatter of the data in spite of considerable care exercised in the measurements.

1. For transitions of constant width and linearly rising bottom experimental reflection coefficients for all slopes are materially above the values predictable from Lamb's theory for abrupt transitions. This holds for waves from deep water to shallow water in the approach channel.

2. For these transitions transmission coefficients are somewhat lower than predicted from Lamb's equations, but generally quite close.

3. For the case of the transition of linearly decreasing width and depth Lamb's theory seems to predict the transmission and reflection coefficients quite well in the shorter wave range. For shallow water waves the reflection coefficient was found to drop lower and the transmission coefficient to rise above the values computed from Lamb's relations.

4. All values of reflection and transmission coefficients tend to decrease with increasing group velocity ratios as is predicted from Lamb's expressions.

5. Wave steepness was confirmed to have a material effect on reflection coefficients for all transitions tested, as had been established in a previous study. It does not seem probable that viscous effects alone are responsible for this. Non-linear wave characteristics may account for part of this effect. Transmission coefficients were found essentially constant with wave steepness within experimental accuracy.

ACKNOWLEDGMENTS

It is a privilege to acknowledge the support of the Fluid Dynamics Branch of the Office of Naval Research, U. S. Department of the Navy, for this study carried out at the Hydrodynamics Laboratory of M.I.T. in its program of graduate research.

REFERENCES

1. Green, G., (1837), "On the Motion of the Waves in a Variable Canal of Small Depth and Width", Cambr. Trans. Vol. VI, p. 225.

2. Lamb, H., "Hydrodynamics", 6th edition, Dover Publ., New York, 1932, pp. 260 - 273.

3. Rayleigh, Baron (Strutt, John William), (a) "On Progressive Waves", Proc. Lond. Math. Soc., (1) 9, 21-26 (1877), (b) "Hydrodynamical Notes", Phil. Mag. (6) 21, 177-195 (1911), (c) "On the Theory of Long Waves and Bores", Proc. Roy. Soc. London Ser. A90, 324-328 (1914), (d) "On Waves", Phil. Mag. (5) Vol. 1, 257-279 (1876).

4. Carrier, G. F., (a) "Gravity Waves on Water of Non-Uniform Depth", (b) "Gravity Waves on Water of Variable Depth", U. S. - Japan Cooperative Scientific Res. Sem. on Tsunami Run-Up, April 18-24, 1965, Sapporo, Japan.

5. Takano, K., "Effets d'un Obstacle Parallépipédique sur la Propagation de la Houle", La Houille Blanche, Vol. 3, 1960, pp. 247 - 267.

6. Kajiura, K., "On the partial Reflection of Water Waves Passing over a Bottom of Variable Depth", Earthquake Research Institute, Univ. of Tokyo, Japan, 1961.

7. Dean, R. G., "Long Wave Modification by Linear Transitions", Journal of Waterways and Harbors Div., Proc. A.S.C.E., Vol. 90, No. WWI, p. 1-29, Feb. 1964.

8. Ippen, A. T., Alam, A. M. Z., and Bourodimos, E. L., "Wave Reflection and Transmission in Channels of Gradually Varying Depth", M.I.T. Hydrodynamics Lab. Technical Report No. 72, July 1964.

9. Bourodimos, E. L., and Ippen, A. T., "Wave Reflection and Transmission in Open Channel Transitions", M.I.T. Hydrodynamics Lab. Technical Report No. 98, August 1966.

10. Ursell, F., and Dean, R. G., "Interaction of a Fixed Semi-Immersed Circular Cylinder with a Train of Surface Waves", M.I.T. Hydrodynamics Lab. Technical Report No. 37, September 1959.

11. Wiegel, R. L., "Gravity Waves - Tables of Functions", Council of Wave Research, The Engineering Foundation, University of California, February 1954.

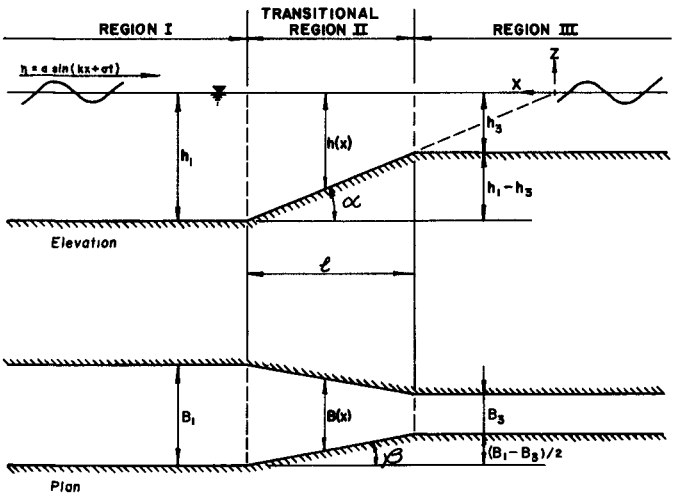

TRANSITION	VARIATION OF DEPTH	VARIATION OF WIDTH
A	$(h_1-h_3)/\ell = 1/8$ ($\alpha = 7\,16°$)	$B_1 = B_3 = \text{const}$
B	$(h_1-h_3)/\ell = 1/8$	$B_3/B_1 = 1/2$ $\frac{B_1-B_3}{2\ell} = 1/12.8$ ($\beta = 4\,46°$)
C	$h_1 = h_3 = \text{const}$	$B_1/B_3 = 1/2$ $\frac{B_1-B_3}{2\ell} = 1/25$ ($\beta = 2\,29°$)

Figure 1

Schematic of Channel Transitions Tested

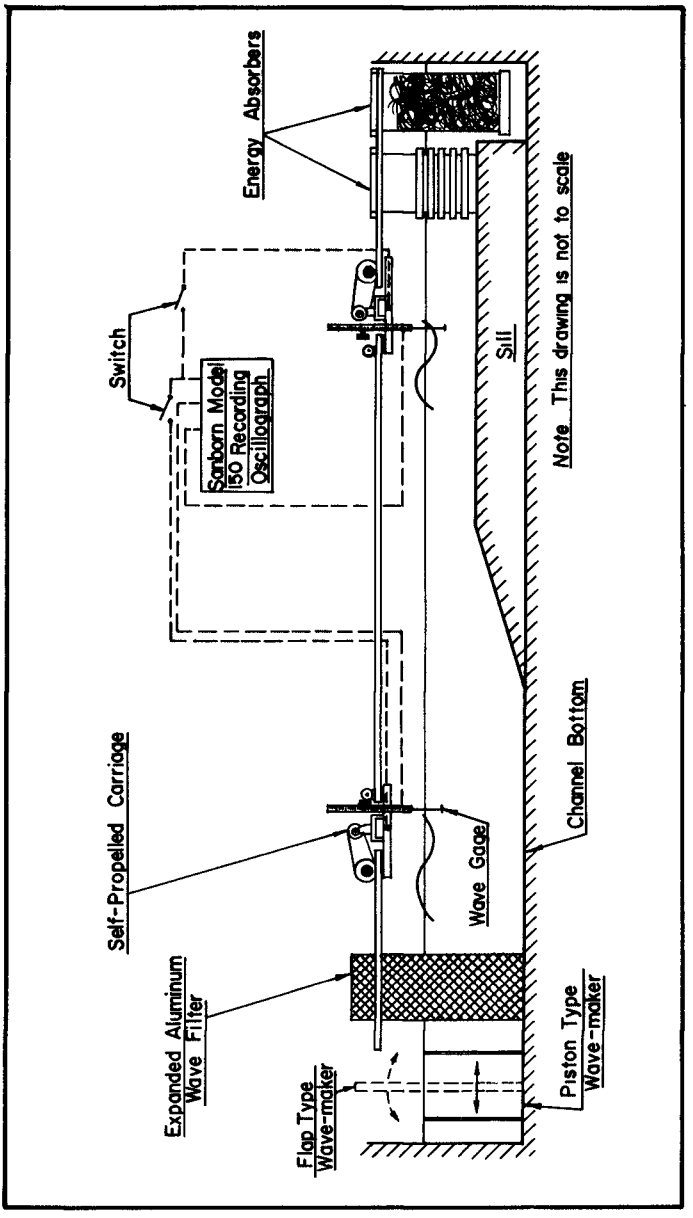

Figure 2
Schematic Diagram of Experimental Equipment

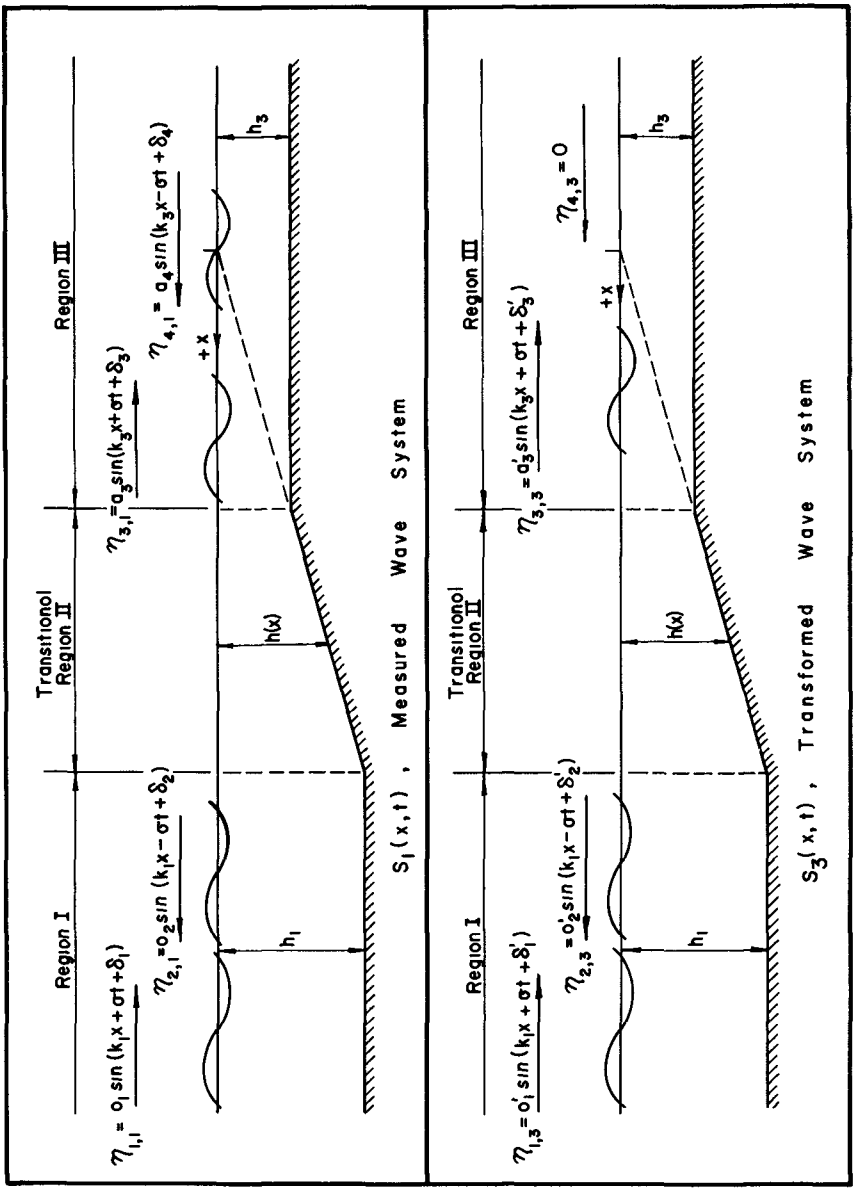

Figure 3
Measured and Transformed Wave System

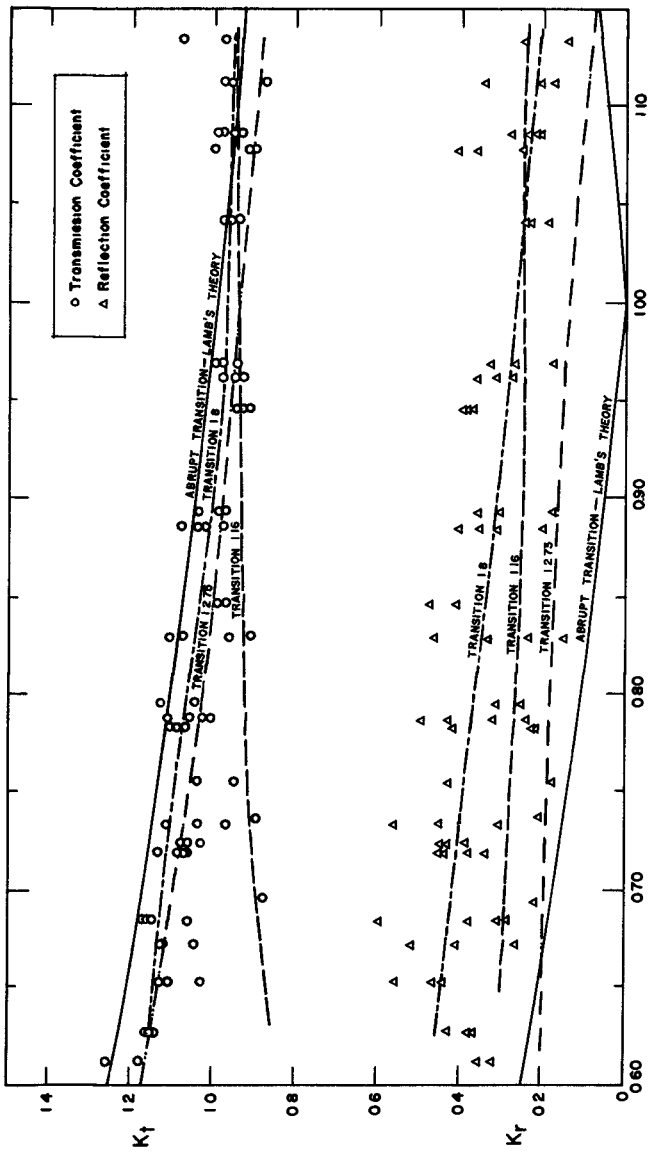

Figure 4

Reflection and Transmission Coefficients vs Group Velocity Ratio – Short and Intermediate Waves – Transition A

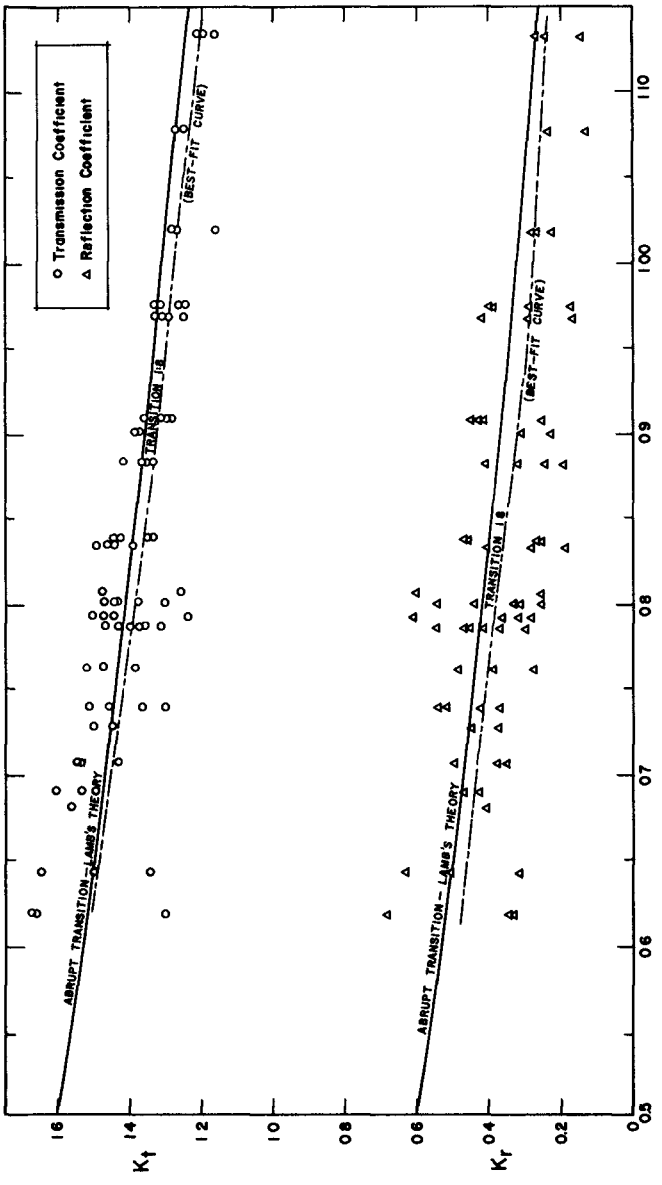

Figure 5.

Reflection and Transmission Coefficients vs Group Velocity Ratio — Short and Intermediate Waves — Transition B

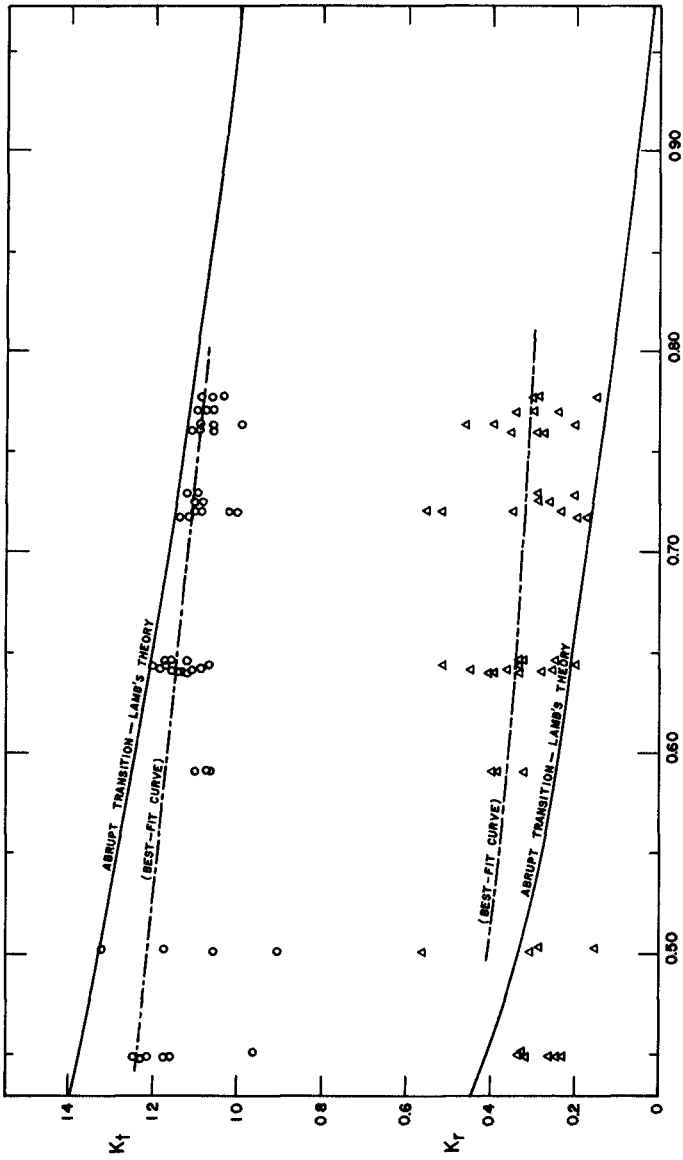

Figure 6.

Reflection and Transmission Coefficients vs Group Velocity Ratio – Shallow Waves – Transition A

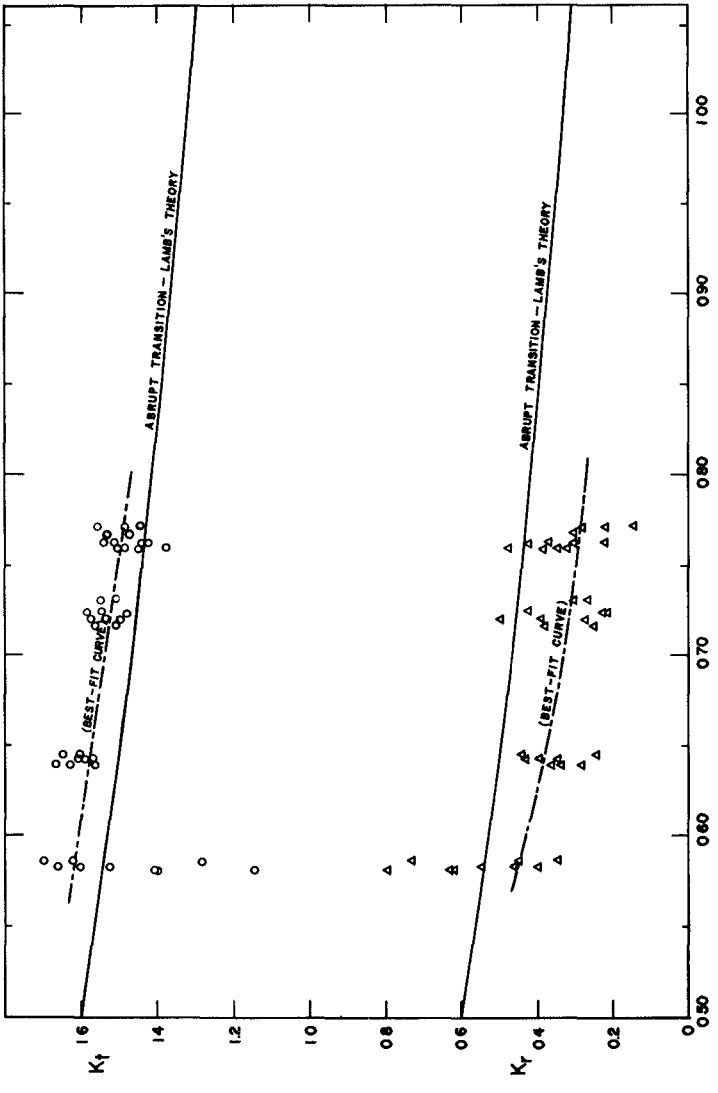

Figure 7.

Reflection and Transmission Coefficients vs Group Velocity Ratio—Shallow Waves—Transition B

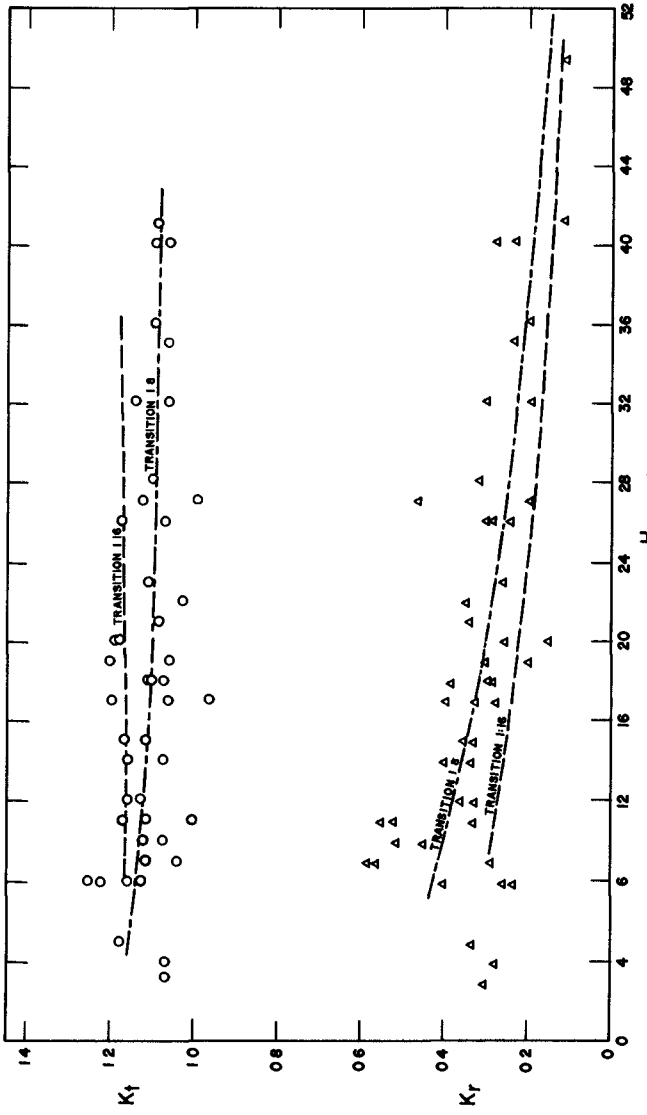

Figure 8

Reflection and Transmission Coefficients vs Wave Steepness – Shallow Waves – Transition A.

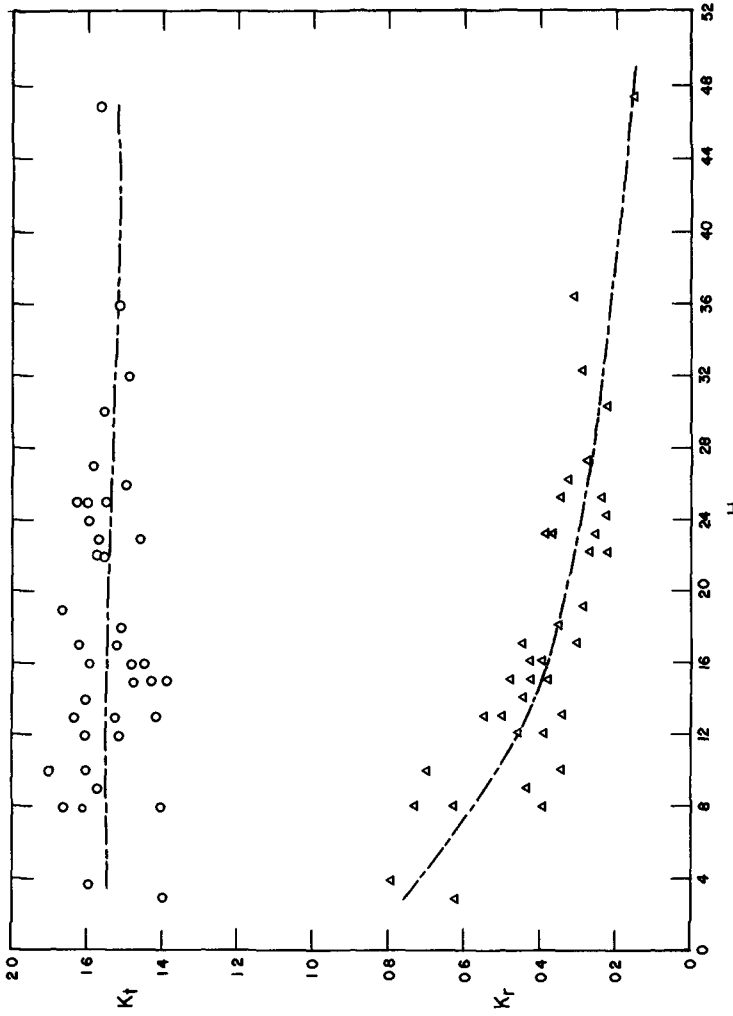

Figure 9

Reflection and Transmission Coefficients vs Wave Steepness—Shallow Waves—Transition B

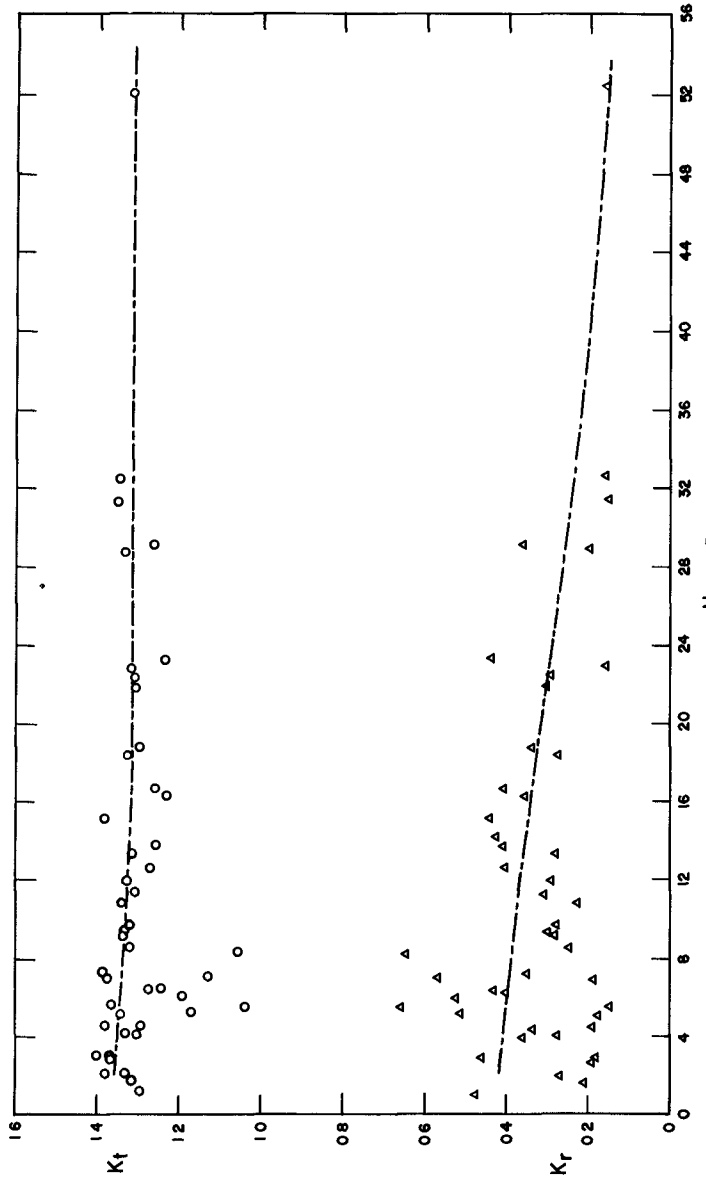

Figure 10.

Reflection and Transmission Coefficients vs Wave Steepness—Short and Intermediate Waves—Transition C

CHAPTER 14

UPWIND TRAVEL OF REFLECTED WAVES

by E. P. Richey[1]

ABSTRACT

Wind waves in a lake have been observed to reflect from a barrier and to travel upwind for considerable distances. A model has been devised which provides a means of predicting the decay of these waves as a function of wind speed and direction with respect to the barrier. Two floating bridges across a deep lake have formed a convenient, full-scale test basin for the formation and observation of the reflected waves under a range of wind speeds and directions. Wave characteristics have been measured to a limited extent by photographic means, a portable wave probe and visually to provide some verification of the results computed from the model. The measured and the predicted wave heights and the zones influenced by the waves were found to be in general qualitative agreement.

INTRODUCTION

Reflected waves will be assuming a more important role in the design of marine structures. The objective of many of these structures is to provide shelter or shielding from wave energy, so transmission characteristics receive most attention, with reflected energy usually being a residual of only secondary interest. However, the pressures of the modern society are leading to a rapidly increased use of our space on and in the water. In addition to the more conventional structures, there are proposals out for floating airports, stadiums, marinas and the like. There are a few large floating bridges in operation and others in the design stages. In some circumstances waves reflecting from structures like these could cause undesirable interactions with those nearby and the general environment. A reconnaissance study was undertaken to put limits on "nearby" and "general" by assessing the parameters of upwind decay rate and areal extent of reflected waves as dependent upon wind speed, frequency and direction. A convenient field site for observing the reflection problems in full-scale was provided by a floating bridge installed recently across a deep lake.

SITE DESCRIPTION

Geography - A convenient field observation basin is formed by two floating bridges across Lake Washington. As shown on Figure 1, this lake forms the easterly boundary of the City of Seattle, in the State of Washington at the northwestern corner of the United States. The lake is about twenty miles long and mile and half wide, with its long axis in the north-south orientation. It is quite deep, especially through its midsection, where the bottom shelves off to a depth of 70 feet within 100 feet of shore and then to nearly a constant 200 feet within about a thousand feet of either

1. Associate Professor of Civil Engineering, University of Washington, Seattle, Washington 98105.

shore. The lake level is controlled within a range of about one and one-half feet by a set of locks which separates the lake from the tidal waters of Puget Sound. Hills from one to two hundred feet high ring most of the lake on the east and west shores; Mercer Island, rising about 400 feet above the lake, divides the southern third into two channels.

Structures - Until recently, cross-lake traffic demands were met by a ferry system. The width and depth of lake and the absence of suitable foundation sites made conventional bridge or tunnel crossings impractical. However, a floating pontoon concrete structure 6400 feet long reaching from the west shore to Mercer Island near the southern end of lake (see Figure 2) was completed in 1940. Continued urban expansion led to a second, similar bridge completed in 1963 about three miles north of the first crossing. This one, the Evergreen Point Bridge, has a floating section 7,578 feet long. A typical pontoon has vertical side walls, a width of 60 feet and a draft of about eight feet. The two bridges, therefore, form clean-cut end boundaries on a deep-water basin about 19,000 feet in length and a mile and half in width.

Meteorology - The cyclonic weather systems typical of a mid-latitude (47°N) west coast climate generally dominate the area from late fall to early spring with winds mostly in the sector from the southeasterly to southwesterly direction. Important northerly winds occur during the summer season when the Pacific anticyclone is suitably situated, and in conjunction with the cold frontal systems that pass occasionally during the winter months. The main axis of the lake parallels the common wind directions, and the topography surrounding the lake exerts a marked steering effect on the winds at ground level. Neither the general meteorological conditions nor the site topography is conducive to the formation of winds from either the due westerly or easterly direction.

There are four weather stations in the vicinity of Lake Washington. The annual wind rose for one of these, the Seattle-Tacoma Airport, which lies about 6 miles from the south end of the lake is given as Figure 3 to show a measure of the speed, direction and frequency of concern in the wave generation within the basin between the two bridges. A wind gage installed on the Evergreen Point Bridge provides data for the wind effective over the basin, but has not been in operation long enough to allow compilation of any statistical information. Cross-correlation of readings concurrent with those at the airport station shows that the speed group of 8 - 12 miles per hour from the southerly sector as appearing on hourly weather reports, is the best index of minimum speed needed for the generation of waves of interest to this study. These waves are primarily fetch limited.

DECAY OF REFLECTED WAVES

Model for Analysis - A prediction equation for the decrease in the height of waves as they move upwind may be obtained through an adaptation of the work by Jeffreys (1925, 1926) who formulated that the power P per unit area transmitted from the wind to waves could be expressed as

$$P = B(U-C)^2HC \qquad (1)$$

in which B includes a numerical constant, the mass density of air, the wave number and a sheltering coefficient. The wind speed is denoted by U, and H and C represent the wave height and phase speed. Equation (1) is basically an application of the standard hydrodynamical drag equation to a moving, deformable boundary. In the definition sketch of Figure 4, points 1 and 3 along the incident and reflected wave rays, are equally distant from the reflecting surface or barrier at 2.

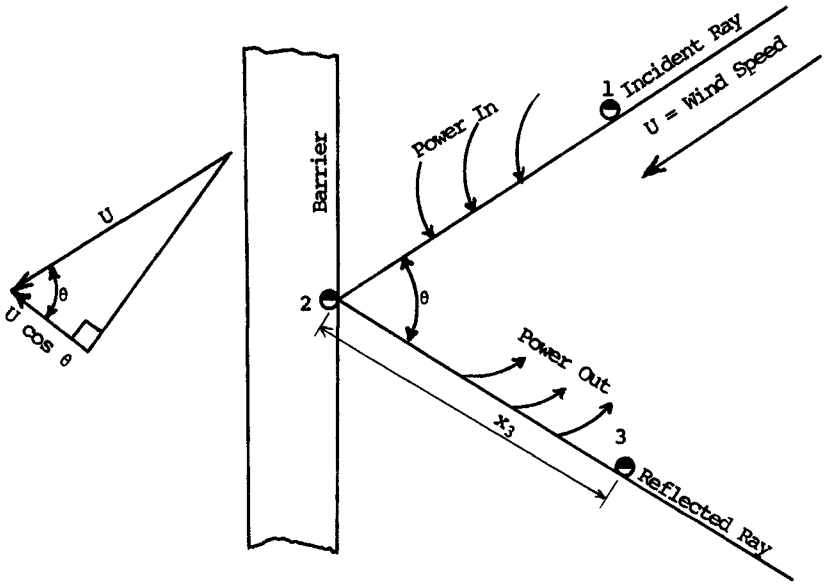

Figure 4. Definition Sketch

The energy flux of a wave system having a characteristic height H, entering the boundary at 1, plus the power added to it by the wind is equal to the energy flux at the downwind position 2, i.e.,

$$\frac{\gamma H_1^2 C_{G_1}}{8} + 1/2 C_d \rho A V^2 C_{1,2} = \frac{\gamma H_2^2 C_{G_2}}{8} \qquad (2)$$

wherein γ is the specific weight of water, C_G is a group velocity, C_d is a drag coefficient, V is the wind velocity relative to the wave, and $C_{1,2}$ is $1/2(C_1+C_2)$, the average phase speed. For a wave moving with the wind (from 1 to 2), the relative velocity is

$$V = U - C_{1,2} \qquad (3)$$

and the projected area normal to the wind is

$$A = 1/2(H_1+H_2) \tag{4}$$

All waves encountered in the test basin are in the "deep water" class so that the group speed is equal to one-half the phase speed, and then Eq. (2) may be written as

$$C_d\rho(H_1+H_2)(U-C_{1,2})^2C_{1,2} = 1/4\gamma(H_2^2C_2-H_1^2C_1) \tag{5}$$

It is assumed here that the reflection coefficient at the barrier is unity, so that the reflected "H_2" is equal to the incident "H_2". The analysis could be adapted to any other known reflection characteristics.

Waves moving against the wind from 2 to 3 must do work on the surroundings so now

$$V = U\cos\theta + C_{2,3} \tag{6}$$

$$A = 1/2(H_2+H_3) \tag{7}$$

and Eq. (2) applied to this reach becomes

$$C_d\rho(H_2+H_3)(U\cos\theta+C_{2,3})^2C_{2,3} = 1/4\gamma(H_2^2C_2-H_3^2C_3) \tag{8}$$

The division of Eq. (5) by Eq. (8) yields

$$\frac{(H_1+H_2)(U-C_{1,2})^2C_{1,2}}{(H_2+H_3)(U\cos\theta+C_{2,3})^2C_{2,3}} = \frac{H_2^2C_2 - H_1^2C_1}{H_2^2C_2 - H_3^2C_3} \tag{9}$$

in which the approximations surrounding the drag coefficient and some of the averaged terms have been minimized in this dimensionless form. The wave heights implied thus far have been any characteristic of the systems; hereafter the "H_i's" shall be regarded as the significant heights.

The distance or fetch, F_2, to the barrier is an implied known quantity in Figure 4; for a given wind speed and direction, the unknowns in Eq. (9) are the values of height and phase speed at points 1 and 3. One might assume a value for the fetch distance to point 1 and thereby reduce the unknowns to two, the height and speed at 3. However, the more convenient solution follows from selecting a value of H_3, then solving for where it occurs relative to the barrier, which is by formulation a distance equal to that to point 1. The equations additional to Eq. (9) needed for a solution may be obtained from published relationships among fetch, wind speed, and wave height and speed. Thus an

additional but desirable unknown, the fetch F, is introduced. From the results given by Bretschneider (1958) the familiar parameters of gH/U^2 and C/U vs. gF/U^2 may be represented very closely by the equational forms

$$gH/U^2 = 0.0044(gF/U^2)^{0.38} \tag{10}$$

$$C/U = 0.082(gF/U^2)^{0.26} \tag{11}$$

in the range of $10^2 < gF/U^2 < 10^4$, which brackets all conditions of interest in the test basin.

For a given wind speed U and fetches F_1 and F_2, the ratio of Eq. (11) to (10) reduces to

$$(C_1/H_1)/(C_2/H_2) = (F_2/F_1)^{0.12} \tag{12}$$

The right hand side of the above equation is not far (14%) from unity for fetch ratios up to 3, so it is assumed that the linear relationship may be applied between 2 and 3 to obtain

$$C_3 = H_3/H_2C_2 \tag{13}$$

$$C_{2,3} = 1/2C_2(1+H_3/H_2) \tag{14}$$

The substitution of these two equations into Eq. (9) brings it to the final form:

$$\frac{(H_1+H_2)(U-C_{1,2})^2C_{1,2}}{(H_1+H_3)[U\cos\theta+1/2C_2(1+H_3/H_2)]^2[C_2(1+H_3/H_2)]} = \frac{H_2^2C_2-H_1^2C_1}{H_2^2C_2-H_3^2(H_3/H_2)C_2} \tag{15}$$

Equation (15) can be solved by a computer in the following outline form:

1. Select U, θ, F_2 as fixed for one condition
2. Compute H_2, C_2 from Eqs. (10) and (11)
3. Select a value for H_3
4. By iteration solve Eqs. (10), (11) and (15) for F_1
5. The distance from the barrier to the point where the reflected wave decreases to the selected value for H_3 is

$$x_3 = F_2 - F_1 \tag{16}$$

The mapping of the reflected waves on the test basin as predicted for the wind of U=20 mph, θ= 15° (S20W) is shown on Figure 2. Heights versus distance for three wind speeds and two values of θ as computed from Eq. 15 are given on Figure 5. Values of distance from this plot need to be referred to Figure 2 with the appropriate value of θ to determine where the rays of the reflected waves may intersect a shoreline, which determines the limiting value of "x_3". The ensuing discussions of the observations and measurements on the lake will bring out where these predictions agree and disagree with field conditions.

OBSERVATIONS AND MEASUREMENTS

Scope - The extent of the observations and measurements of field conditions was matched to the initial objective of the study, i.e., to make a reconnaissance of the limits to which waves reflecting from a barrier in deep water might extend under a range of natural conditions. Therefore, the field investigation was limited to the simpler techniques of photography, visual observations, and a sampling of wave heights using a portable wave gage and recorder.

Photography - A series of areal photographs for four occasions, and a motion picture sequence for one wind-wave condition were taken to ascertain wave lengths and zones where reflected waves could be identified. Although none of these is reproduced herein, the results do enter indirectly in support of other observations. A near-shore condition resulting from a steady southerly wind of about 20 mph is shown on Figure 6. The stepped breakwater in the foreground is about 3000 feet from the bridge. Groups of reflected waves with heights of nearly a foot are discernible over much of the picture, which was taken from a high building that shields the bay from southerly winds. A common network pattern of incident and reflected waves appears in the foreground. Figure 7 shows the source of the reflected waves for a somewhat slower wind speed. Figures 8 and 9* show the near-bridge and traffic conditions under an infrequent wind speed of 40 mph with higher gusts. Note the plumed waves moving out against the wind. Even here, the lee (north) side of the barrier shows no energy transmission. Some breaking of waves in the vicinity of the bridge begins at a speed of about 25 mph, and under the higher speeds like those in the last two photographs, considerable energy is expended in the reflection process.

Wave Height Measurements - A parallel-wire resistance gage and strip recorder were teamed as a portable unit to sample waves for a few different wind conditions. Four sites on the lake were chosen where accessible piers extended to water depths of about 15 feet. Since the bottom shelves off quite rapidly and few waves had lengths longer than 30 feet, shoaling effects at these sites was not important. The wave gage was not directionally sensitive so the reflected waves, when present, had to be sorted out visually by their orientation and direction of travel and suitably marked on the oscillograph record. Very commonly a group of reflected waves would dominate a site for a time, then would

*Figures 8 and 9. Courtesy Seattle Times, photographer J. Scaylea.

give way to an incident pattern. As distance upwind of the barrier increased, the number of reflected waves identifiable decreased, as well as their heights; components at the higher frequencies also tended to disappear due to the filtration process. A brief summary of the wave gage measurements appears in Table 1, with site locations A, B, C and D spotted on Figure 2, where the wave pattern forecast for U-20 mph θ=15° is shown. The sampling serves to give a good measure of period and height; no attempt was made to prepare comparative energy spectra. The maximum excursion of the reflected waves was traced visually

Table 1
Summary of Wave Gage Measurements

No.	Site	x_3 ft.	U mph	Dir.	θ deg.	i or r	T sec	L* ft	H ft	Sample
1	B		20	S	25	i	1.5	12	0.66	181
						r	2.0		0.84	145
2	A		10	SSE	45	i	1.7	15	0.54	58
						r	2.0		0.71	24
3	C		9	SSE	45	i	1.3	10	0.29	93
						r	1.2		0.40	38
	A		12	SE	65	i	1.4	10	0.87	71
						r	1.5		0.85	53
4	A	900	30	SSW	5	i	2.2	25	1.02	222
						r	2.5		1.17	78
	B	1800				i	2.1	23	1.17	132
						r	2.6		1.60	44
	C	4000				i	2.0	20	1.11	205
						r	2.2		1.00	12
5	D	2200	16	SSW	5	i	2.3	27	1.61	274
						r	2.5		1.83	143
6	B		10	SW	15	i	2.2	23	1.10	306
							2.2		1.39	105

i=incident r=reflected * $L=5.12T^2$

from the shoreline and from examination of the aerial photographs. The frequency with which reflected waves are discernible on the east side of the basin is markedly less than on the opposite shore, and none have been identified more than about 3000 feet from the bridge. However, on the west shore under favorable conditions reflected waves, usually in groups, can be detected as far as Denny Blaine (see Figure 2) which is about 8000 feet from the source. This distance would match H_3=0.4 feet on Figure 2.

Comparison of Analysis with Observations - The analysis assumes the winds to be constant in magnitude and direction, that the incident wave crests are normal to the wind vector, and that no energy (a known reflection coefficient could be accommodated) is lost in the reflection process at the barrier. None of these stipulations is strictly true, of course. Observations show that the waves do not grow uni-directionally as implied

in the analysis and as illustrated on Figure 2, but tend to develop in a sector about 20° or so to either side of the mean wind direction. The steering effect of the lake valley does not seem to allow the angular spread up to 45° as referred to by Wiegel (1964, p. 230). Wave systems were difficult to categorize visually when the wind was especially gusty; no measure of turbulence levels was available.

The predicted heights of the reflected waves with distance from the barrier were in qualitative agreement with the observations up to the stage when breaking at the barrier became significant. The distance to the "zero-height" also agrees with the comments from observant sailors of small boats who notice the effect of the extra wave system on the trimming of their craft for optimum performance. When the analysis is matched to the wind speed, frequency and directional data, it does substantiate quite properly the observations concerning the relative frequencies of occurrence and upwind travel of reflected waves on the two sides of the lake. The heights and periods of the reflected waves were sampled under several different wind conditions, but the data needed to evaluate the energy spectra of these waves could not be acquired with the equipment available. Therefore, the change in the energy of the reflected system with distance from the source has not been evaluated.

CONCLUSIONS

The prediction analysis foretold quite well the general limits of travel of the reflected waves and the regions they influence as a function of wind speed and direction so long as the reflection process did not entail significant loss of energy in the reflection process. The analysis could be modified to correct for a known reflection coefficient. Both the analysis and observations indicate that the reflected waves in deep water can be identified for a considerable distance from their source; in some situations these waves could be an undersirable component and designs should be sought to minimize their effect on the environment. A more extensive and detailed set of field observations is needed to answer some questions raised by the study concerning (1) the reflection characteristics of the barrier as dependent upon incident wave height and direction, and (2) the energy spectrum in the reflected wave system at various distances from the source.

REFERENCES

1. Jeffreys, Harold, "On the Formation of Water Waves by Wind," Proc. Royal Society, Series A, 107, 1925, pp. 189-206, and Series A, 110, 1926, pp. 241-247.

2. Bretschneider, C. L., "Revisions in Wave Forecasting; Deep and Shallow Water," Proc. Sixth Conference on Coastal Engineering, 1958.

3. Wiegel, Robert L., Oceanographical Engineering, Prentice-Hall, Inc. Englewood Cliffs, New Jersey, 1964.

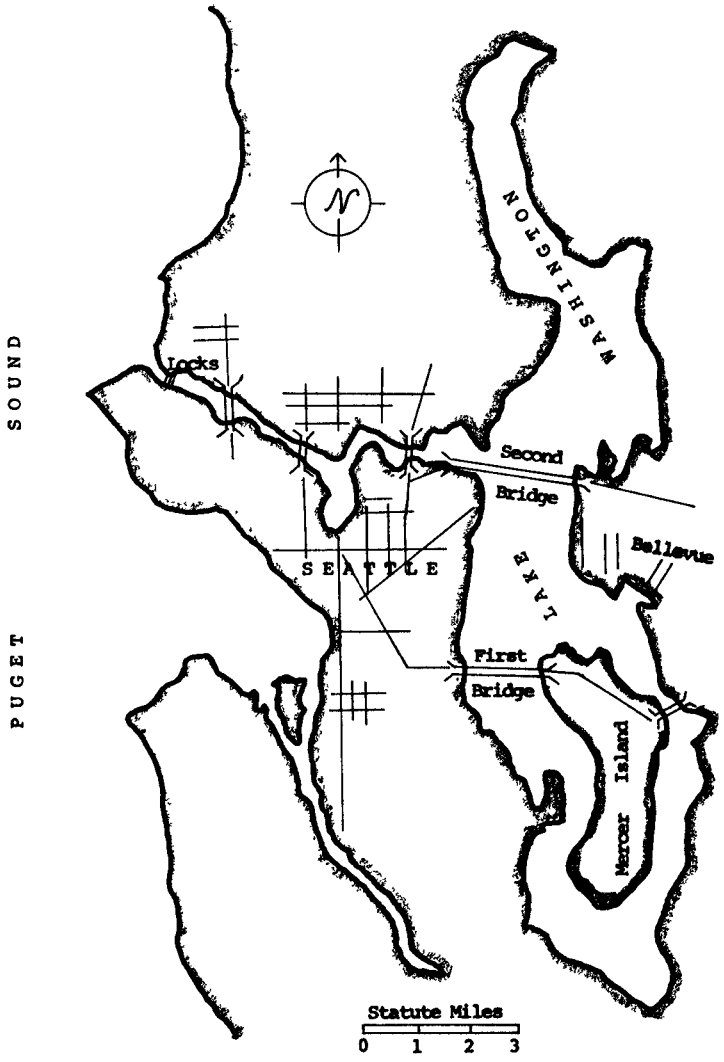

Figure 1. Location Map

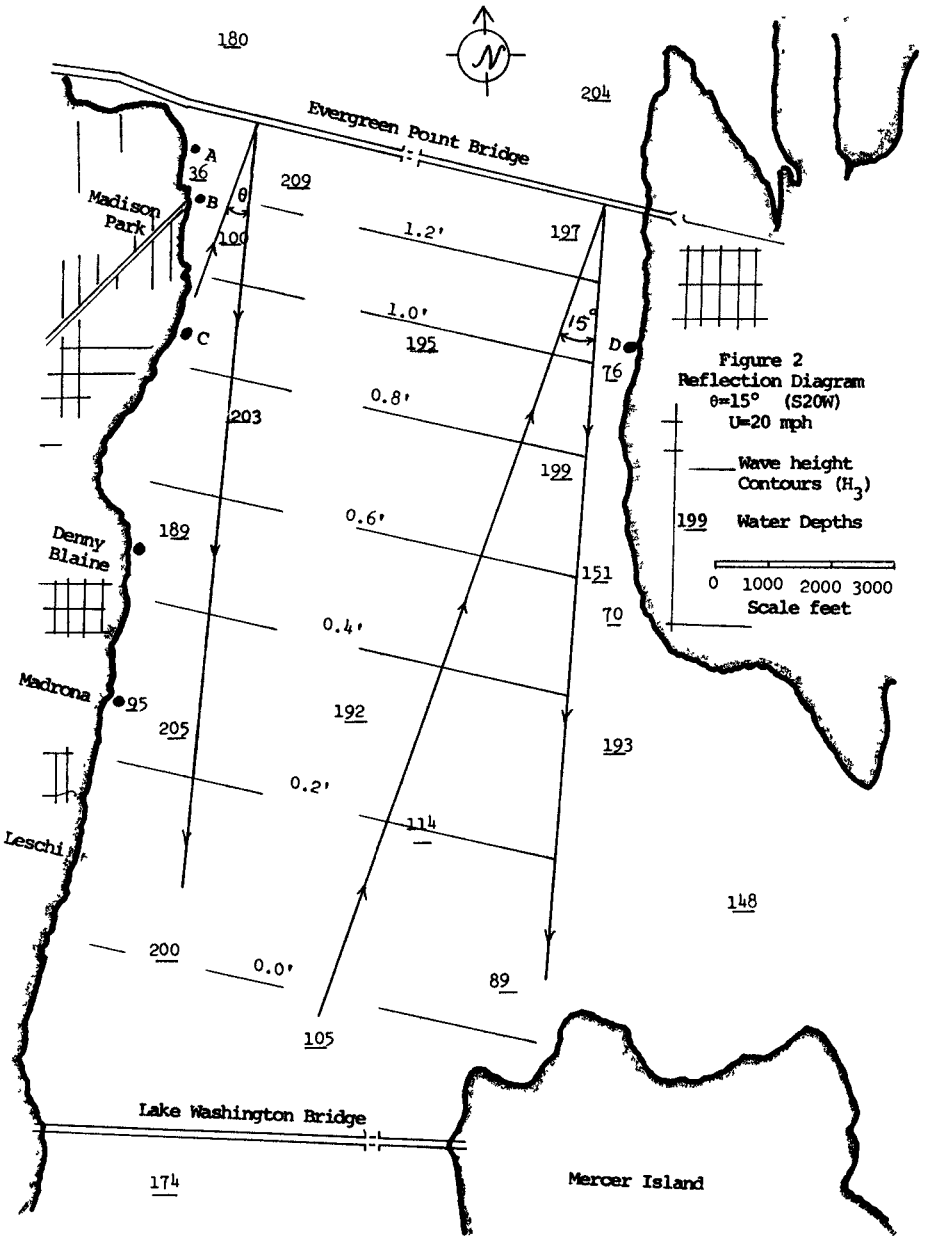
180
204
Evergreen Point Bridge
A
36
B
θ
209
Madison Park
100
1.2'
197
1.0'
15°
C
195
D
76
0.8'
203
199
0.6'
189
Denny Blaine
151
0.4'
70
Madrona
95
205
192
193
0.2'
114
Leschi
148
200
0.0'
89
105
Lake Washington Bridge
174
Mercer Island
Figure 2
Reflection Diagram
θ=15° (S20W)
U=20 mph
Wave height Contours (H_3)
199 Water Depths
0 1000 2000 3000
Scale feet

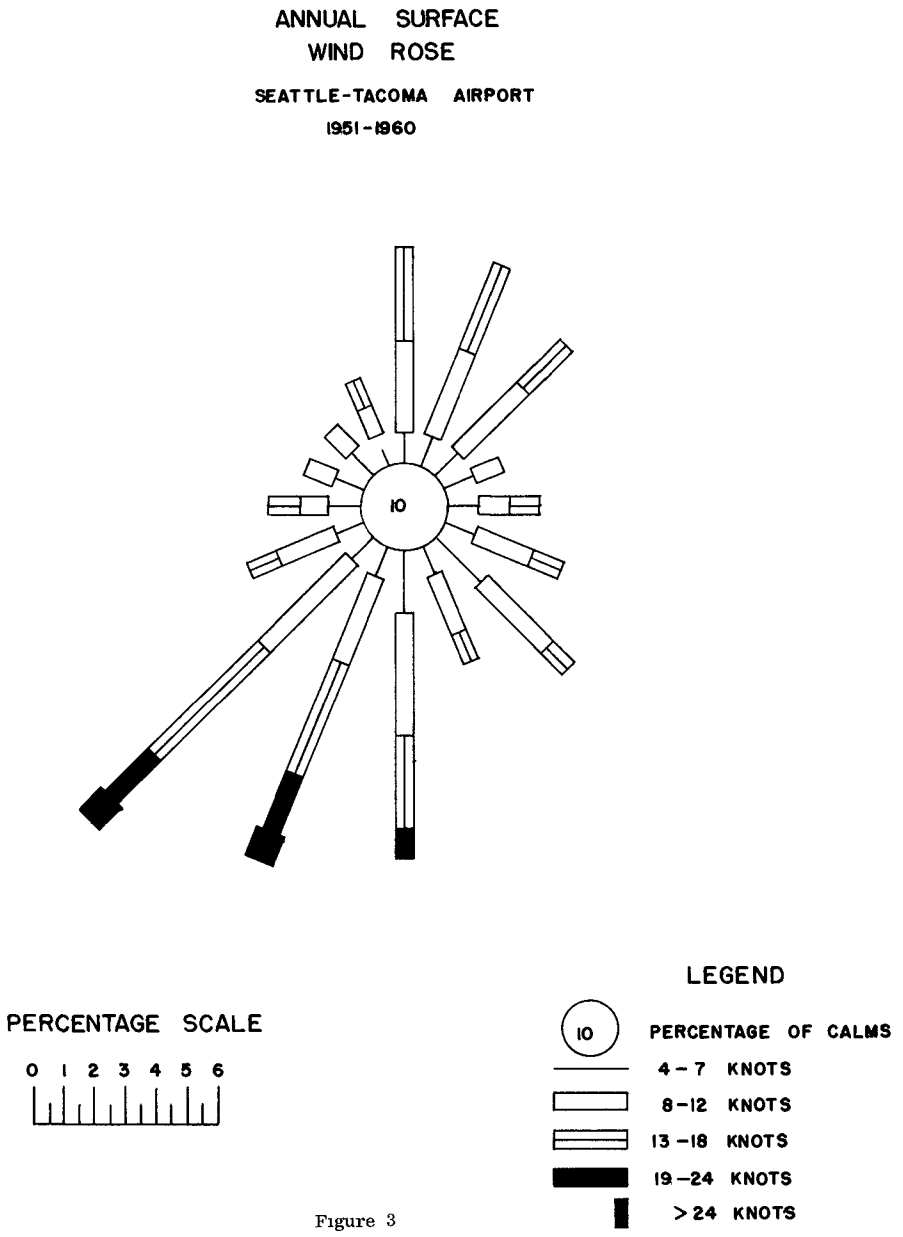
ANNUAL SURFACE
WIND ROSE
SEATTLE-TACOMA AIRPORT
1951-1960
10
PERCENTAGE SCALE
0 1 2 3 4 5 6
LEGEND
10
PERCENTAGE OF CALMS
4-7 KNOTS
8-12 KNOTS
13-18 KNOTS
19-24 KNOTS
>24 KNOTS

Figure 3

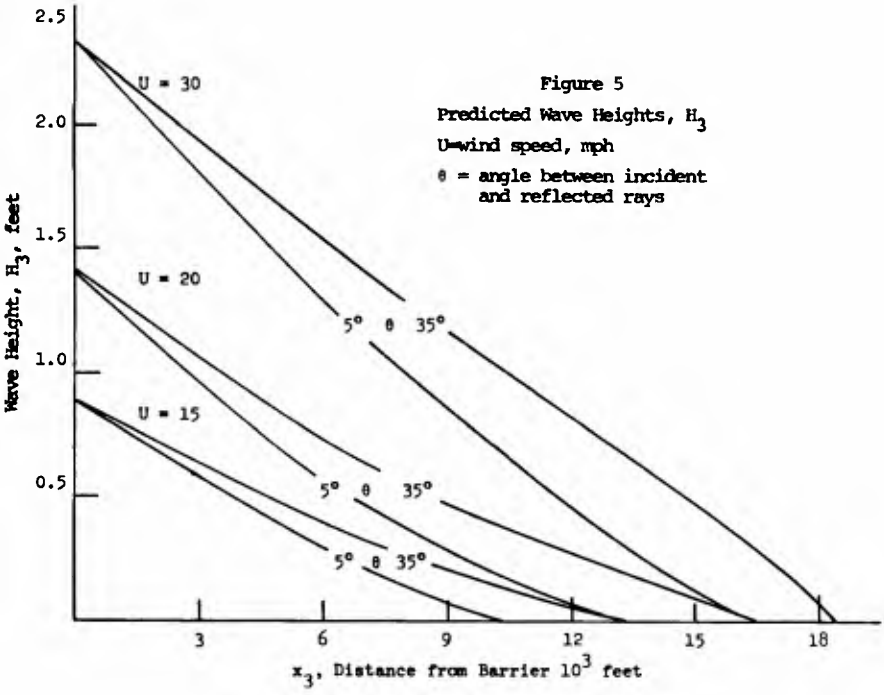

Figure 5
Predicted Wave Heights, H_3
U=wind speed, mph
θ = angle between incident and reflected rays

Figure 6. Waves at Madison Beach

Figure 7. Evergreen Point Bridge, U=20 mph

Figure 8. Evergreen Point Bridge U=40+mph

Figure 9. Evergreen Point Bridge U=40+mph

CHAPTER 15

A STUDY ON MASS TRANSPORT IN BOUNDARY LAYERS IN STANDING WAVES

Hideaki Noda

Assistant Professor of Hydraulics
Disaster Prevention Research Institute
Kyoto University, Kyoto, Japan

ABSTRACT

This paper deals with the mass transport in the boundary layers developed on smooth and horizontal bottoms by standing waves in shallow water. In a theoretical approach, the basic equations of laminar boundary layers are applied to solving the oscillatory motion in the boundary layers caused by the standing waves. The mass transport velocities are derived on the basis of solutions of the second approximation which describe the flow velocity near the bottom, and the effects of convective terms involved in the basic equations are investigated.

Experimental measurements in standing waves of mass transport velocity in the bottom boundary layer were carried out using dye-streak and solid-particle methods. The experimental data are compared with the theoretical prediction.

INTRODUCTION

The depositional behaviour of sediments is an important factor in the control of shoaling in harbor basins and the maintenance of the harbor function for navigation. The considerations developed in this paper began with some of the problems of the Gumizaki Fishery Harbor being filled up by drifting sands.

It has been shown in the previous paper, presented at the Tenth Conference on Coastal Engineering, that sand bars are formed at definite locations in a harbor basin, and that the standing waves induced in the harbor basin play an important role in the formation of these bars. Lettau (Ref.1) has theoretically shown that sand bars are formed at the anti-node positions of standing waves by the deposition of suspended sediments. On the other hand, Nomitsu (Ref. 2) has described bar formation at both the node and anti-node positions of standing waves by the movement of bed loads. Hayami (Ref. 3) has also shown that the filling-up of the basin by drifting sands in Tomari Harbor can be explained by Nomitsu's theory. Nevertheless, the author's experimental results differ from his prediction: these bars are formed only at the anti-node of standing waves.

The movement of sediments is caused by the fluid motion near the bed. Therefore, the resolution of this question is necessary in order to give an adequate description of the character-

istics of the oscillatory motion near the bottom due to standing waves. The mechanism of such bar formation must then be found on the basis of the above description. Therefore, an attempt has been made to study the fluid motion in the boundary layers developed on smooth bottoms in the case of standing waves in shallow water of uniform depth, especially the velocity profile and the mass transport velocity in the boundary layers.

Longuet-Higgins (Ref. 4) derived an appropriate field equation for the stream function of the mass transport, and described a general method for determining the mass transport velocity in the boundary layers. In general, it is well known that in the irrotational standing waves the mass transport velocity vanishes everywhere. However, Longuet-Higgins showed the existence of the mass transport in the boundary layers by taking into account the viscous action of the fluid, even in standing waves.

On the other hand, Iwagaki and Tuchiya (Ref. 5) described the perturbation method for determining the velocity profile in the boundary layers developed on the bottom of a wave tank by progressive waves, when they treated the problem of wave damping due to bottom friction.

In this paper, the latter method is applied to the case of standing waves. By this method, an approximate solution of non-linear, laminar boundary layer equations is applied to deriving the mass transport velocities of this layer in standing waves. The author's result for the mass transport velocity is in agreement with that predicted by Longuet-Higgins.

Experimental measurements of mass transport velocity in the boundary layer near the bottom under standing waves are then compared with theoretical results.

THEORY OF LAMINAR BOUNDARY LAYER DUE TO STANDING WAVES

For two-dimensional case, the laminar boundary layer equations on the assumption of incompressible fluid are given by:

$$\left.\begin{aligned} &\frac{\partial u}{\partial t} + u\frac{\partial u}{\partial x} + w\frac{\partial u}{\partial z} = -\frac{1}{\rho}\frac{\partial p}{\partial x} + \nu\frac{\partial^2 u}{\partial z^2} \\ &\frac{\partial u}{\partial x} + \frac{\partial w}{\partial z} = 0 \\ &-\frac{1}{\rho}\frac{\partial p}{\partial x} = \frac{\partial u_\infty}{\partial t} + u_\infty\frac{\partial u_\infty}{\partial x} \end{aligned}\right\} \quad (1)$$

in which x is the horizontal distance from the vertical wall of one end of a wave tank, z the vertical distance from the bottom, t the time, p the pressure, ρ the density, ν the kinematic viscosity, u and w the velocity components in the boundary layer in the direction of x and z, respectively and u_∞ the velocity just outside the boundary layer due to the finite amplitude wave theory.

Selecting the wave length of standing waves L and the boundary layers thickness parameter $\delta = (\nu T/2\pi)^{1/2}$ as the representative length, and using the dimensionless quantities defined as follows:

$$\left.\begin{aligned} &u = Cu^*,\ w = \omega\delta w^*,\ p = \rho C^2 p^*,\ u_\infty = C u_\infty^* \\ &x^* = kx,\ t^* = \omega t,\ z^* = z/\delta,\ h^* = kh \end{aligned}\right\} \qquad (2)$$

the non-dimensional form of Eq.(1) can be expressed by:

$$\left.\begin{aligned} &\frac{\partial u^*}{\partial t^*} + u^*\frac{\partial u^*}{\partial x^*} + w^*\frac{\partial u^*}{\partial z^*} = \frac{\partial u_\infty^*}{\partial t^*} + u_\infty^*\frac{\partial u_\infty^*}{\partial x^*} + \frac{\partial^2 u^*}{\partial z^{*2}} \\ &\frac{\partial u^*}{\partial x^*} + \frac{\partial w^*}{\partial z^*} = 0 \end{aligned}\right\} \qquad (3)$$

in which T is the wave period, h the water depth, $C = L/T$, $\omega = 2\pi/T$, and $k = 2\pi/L$. The boundary conditions for Eq.(3) can be written as

$$\left.\begin{aligned} &u^* = 0 \text{ and } w^* = 0 \text{ at } z^* = 0, \\ &u^* = u_\infty^* \text{ at } z^* \to \infty. \end{aligned}\right\} \qquad (4)$$

The velocity just outside the boundary layers u_∞^* on the basis of the finite amplitude wave theory is given by:

$$u_\infty^* = -\left(\frac{H}{L}\right)\frac{\pi}{\sinh h^*}\sin x^*\cos t^* - \left(\frac{H}{L}\right)^2\frac{3\pi^2}{8\sinh^4 h^*}\cos 2x^*\sin 2t^* - \cdots\cdots \qquad (5)$$

for the case of standing waves, in which H is the wave height.

The solution of Eq.(3) can be obtained by the perturbation method which expresses the solution of u^* and w^*, respectively as follows:

$$\left.\begin{aligned} u^* &= \varepsilon u_1^* + \varepsilon^2 u_2^* + \cdots\cdots \\ w^* &= \varepsilon w_1^* + \varepsilon^2 w_2^* + \cdots\cdots \end{aligned}\right\} \qquad (6)$$

in which a small quantity ε is equal to H/L .

From Eq.(5), the velocity just outside the boundary layers can be rewritten by:

$$u_\infty^* = \varepsilon u_{\infty 1}^* + \varepsilon^2 u_{\infty 2}^* + \cdots\cdots\cdots \tag{7}$$

in which

$$\left.\begin{aligned} u_{\infty 1}^* &= -\frac{\pi}{\sinh h^*} \sin x^* \cos t^* , \\ u_{\infty 2}^* &= -\frac{3\pi^2}{8\sinh^4 h^*} \cos 2x^* \sin 2t^* \end{aligned}\right\} \tag{8}$$

Substituting these expressions into Eq.(3) gives the differential equations of the first approximation for u_1^* and w_1^*:

$$\left.\begin{aligned} \frac{\partial u_1^*}{\partial t^*} - \frac{\partial^2 u_1^*}{\partial z^{*2}} &= \frac{\partial u_{\infty 1}^*}{\partial t^*} \\ \frac{\partial u_1^*}{\partial x^*} + \frac{\partial w_1^*}{\partial z^*} &= 0 \end{aligned}\right\} \tag{9}$$

with the boundary conditions $u_1^* = w_1^* = 0$ at $z^* = 0$ and $u_1^* = u_{\infty 1}^*$ at $z^* \to \infty$. Eq.(9) indicates the linearized theory and its solutions are given by:

$$\begin{aligned} u_1^* &= -\hat{u}_{\infty 1}^* \sin x^* \{\cos t^* - e^{-\eta^*} \cos(t^* - \eta^*)\}, \\ w_1^* &= -\hat{u}_{\infty 1}^* \cos x^* \{\sqrt{2}\,\eta^* \cos t^* + e^{-\eta^*} \cos(t^* - \eta^* - \pi/4) - \cos(t^* - \pi/4)\} \end{aligned} \tag{10}$$

in which $\eta^* = z^*/2$ and $\hat{u}_{\infty 1}^* = \pi/\sinh h^*$.

For u_2^* , the equation of the second approximation can be written by:

$$\begin{aligned} \frac{\partial u_2^*}{\partial t^*} - \frac{1}{4}\frac{\partial^2 u_2^*}{\partial \eta^{*2}} = {} & \frac{1}{4}\hat{u}_{\infty 1}^{*2} \sin 2x^* \{(1+\sqrt{2}\,\eta^*)e^{-\sqrt{2}\eta^*} \cos(2t^* - \sqrt{2}\,\eta^*) \\ & - \sqrt{2}\,\eta^* e^{-\sqrt{2}\eta^*} \sin(2t^* - \sqrt{2}\,\eta^*) \\ & - 8\,(\hat{u}_{\infty 2}^*/\hat{u}_{\infty 1}^{*2}) \cot 2x^* \cos 2t^*\} \\ & + \frac{1}{8}\hat{u}_{\infty 1}^{*2} \sin 2x^* \{2(2+\sqrt{2}\,\eta^*)e^{-\sqrt{2}\eta^*} \cos\sqrt{2}\,\eta^* - 2e^{-2\sqrt{2}\eta^*} \\ & - 2(1-\sqrt{2}\,\eta^*)e^{-\sqrt{2}\eta^*} \sin\sqrt{2}\,\eta^*\} \end{aligned} \tag{11}$$

in which $\hat{u}_{\infty 2}^* = 3\pi^2/8\sinh^4 h^*$. The approximate solution for u_2^* , which must satisfy the boundary conditions, $u_2^* = 0$ at $\eta^* = 0$ and $u_{2p}^* = u_{\infty 2}^*$, $\partial u_{2s}^*/\partial \eta^* = 0$ as $\eta^* \to \infty$, as shown by Schlichting (Ref. 6) taking into account $u_2^* = u_{2p}^* + u_{2s}^*$ where u_{2p}^* denote the periodic and u_{2s}^* the steady contribution of the second approximation, respectively, is given by:

$$u_2^* = -\hat{u}_{\omega 2}^* \cos 2x^* \left\{ \sin 2t^* - e^{-\sqrt{2}\eta^*} \sin(2t^* - \sqrt{2}\eta^*) \right\}$$
$$+ \left(\frac{\pi}{2 \sinh h^*} \right)^2 \sin 2x^* \sin 2t^* \left\{ e^{-\sqrt{2}\eta^*} \cos \sqrt{2}\eta^* - e^{-\eta^*} \cos \eta^* + \sqrt{2}\eta^* e^{-\eta^*} \sin(\eta^* + \pi/4) \right\}$$
$$+ \left(\frac{\pi}{2 \sinh h^*} \right)^2 \sin 2x^* \cos 2t^* \left\{ - e^{-\sqrt{2}\eta^*} \sin \sqrt{2}\eta^* + e^{-\eta^*} \sin \eta^* + \sqrt{2}\eta^* e^{-\eta^*} \cos(\eta^* + \pi/4) \right\}$$
$$+ \frac{\pi}{8 \sinh^2 h^*} \sin 2x^* \left\{ -3 + e^{-2\eta^*} + 8e^{-\eta^*} \sin \eta^* + 2e^{-\eta^*} \cos \eta^* - 2\sqrt{2}\eta^* \cos(\eta^* + \pi/4) \right\} \quad \ldots\ldots\ldots\ldots \quad (12)$$

Therefore, the approximate solution for the velocity u^* is obtained by substituting Eq.(11) and (12) into Eq.(6). Fig.1-(a) and (b) show the velocity profiles calculated for the case of $\varepsilon = 0.04$ and $\sinh h^* = 1.18$ at $x^* = \pi/2$ and $\pi/4$, respectively, in which $u_{\omega 1} = C \varepsilon \hat{u}_{\omega 1}^* = \pi H / T \sinh kh$. These figures positively demonstrate that at $x^* = \pi/2$, the positive, maximum velocity of a water particle in the boundary layers is identical with the negative one, but that at $x^* = \pi/4$, the positive motion is less than the reverse movement. Seemingly, these results are important, since the direction of sediment movement may be determined by the larger of the two maximum values of the velocity.

Fig. 2 shows the relationship between $u/u_{\omega 1}$ and η^* for the various values of ε ; that is, the effects of convective terms in the boundary layer equations on the velocity profile. This figure indicates that the maximum velocity in non-dimensional form slightly increases with the increasing of the values of ε.

MASS TRANSPORT VELOCITY IN BOUNDARY LAYERS UNDER STANDING WAVES

Longuet-Higgins gives the mass transport velocity in the boundary layers in non-dimensional form, $\overline{U}^*$ as

$$\overline{U}^* = \varepsilon \overline{U}_1^* + \varepsilon^2 \overline{U}_2^* + \cdots\cdots \quad (13)$$

in which $\overline{U}^* = \overline{U}/C$, $\overline{U}_1^* = 0$ and

$$\overline{U}^* = \frac{1}{2\pi} \left\{ \int_0^{2\pi} u_2^* \, dt^* + \overline{\int^{t^*} u_1^* dt^* \frac{\partial u_1^*}{\partial x^*}} + \overline{\int^{t^*} w_1^* dt^* \frac{\partial u_1^*}{\partial z^*}} \right\} \quad (14)$$

Substituting Eqs.(10), (12) and (14) into Eq.(13), the mass transport velocity in the boundary layers developed on the smooth bottom is given by:

$$\overline{U}^* = \frac{1}{8} \left(\frac{\varepsilon \pi}{\sinh h^*} \right)^2 \sin 2x^* \, K(\eta^*) \quad (15)$$

in which

$$K(\eta^*) = -3 + 8e^{-\eta^*} \sin \eta^* + 3e^{-2\eta^*} \quad (16)$$

This equation can be rewritten in the form:

$$\overline{U} = \frac{\pi^2}{8} \frac{H^2}{LT \sinh kh} \sin 2kx \; K(\eta^*) \qquad (17)$$

which is identical with that obtained by Longuet-Higgins.

Fig.3 shows the result calculated of the vertical profile of the mass transport velocity in the boundary layer to the case of standing waves. An outstanding feature which this figure shows is that the transport near the bottom, that is the lower layer, for the range of $\eta^* < 0.9$, is always in the direction from the anti-node to the node of the standing waves, but the transport in the upper layer for the range of $\eta^* > 0.9$ is contrary to the lower one.

In any discussion of bar formation, this result is important, since the direction of sediment movement may be determined by the ratio of sediment diameter d with the boundary layer thickness parameter δ .

EXPERIMENTS ON MASS TRANSPORT VELOCITY IN BOUNDARY LAYERS

EXPERIMENTAL EQUIPMENT - Experimental apparatus consists of a glass side wave tank 3.0 m long, 30 cm wide and 70 cm deep, as shown in Fig.4. The walls are vertical and the glass bed is horizontal. Standing waves were produced by a flutter type wave genarator installed at one end of the tank. Wave heights were measured by an electric resistance type wave gage placed at the anti-node position.

METHODS OF MEASUREMENT - The first method of observing the mass transport velocity involved photographing dye streaks obtained by dropping small grains of potassium permanganate, which sank to the bottom with negligible solution enroute, into water. This method proved advantageous in that a series of water particle displacements could be recorded in a single exposure as shown in Photo. 1, since a conspicuous dye streak was produced in the boundary layer every cycle. The maximum displacement of water particles and its vertical profiles per cycle were measured from similar photographs.

The second method was to examine the transport in the opposite direction near the bottom as predicted by theory. The method involved photographing the movement of vinyl pellets (median diameter 0.13 mm, specific gravity 1.15) which were spread in a thin, uniform layer on the bottom before beginning the tests.

The third method of recording the mass transport velocity involved photographing displacements of a small nylon particle that had the same density as water every 5 cycles of waves using a strobo-scope. When the wave period and water depth are maintained constant, and wave heights are gradually in-

creased, flows in bottom boundary layers undergo a transition from the laminar to the turbulent regime. Therefore, the dye-streak method mentioned above cannot be used because of the dispersion of dye. Then, measurement of the mass transport velocity in the turbulent boundary layers was made using nylon particles (diameter 3 mm). Photo. 2 shows an example of a series of displacement of a nylon particle.

SUMMARY OF EXPERIMENTAL RESULTS - Fig. 5 and 6 show the results of the maximum displacements observed by the dye-streak method for the h/L values of 0.16 and 0.08, respectively. The experiments were carried out by measuring the maximum displacement $\bar{U}_{max}T$ for varying wave heights and for a wave period and water depth that were kept constant. In these figures, the theoretical curve which describes the non-dimensional, maximum displacement of a water particle in the boundary layer, λ^*, can be given by putting $\eta^* = 3.94$ in Eq.(17):

$$\lambda^* = -\sin 2k\alpha \tag{18}$$

in which

$$\lambda^* = \bar{U}_{max}T/(3.12\,\pi^2 H^2/8L\,\sinh^2 kh) \tag{19}$$

and $\bar{U}_{max}$ is the maximum mass transport velocity in the boundary layer. Although the scatter of points can be seen, these figures show that the results of the experiments are in agreement with theory except when the wave height is as small as 4 cm. Russell and Osorio(Ref.7) showed in their experiments in the case of progressive waves, that low waves result in faster transport values than high waves when plotted non-dimensionally. It seems that their results are identical with those of the authors in the case of standing waves.

Fig.7 shows the observed mass transport velocity profiles in the boundary layer for the h/L values of 0.16 and 0.08. It is found that the results are in good agreement with the theoretical curve shown by a full line for the range of $\eta^* > 3.0$.

But it was not possible to measure accurately the mass transport velocity in the lower layer for the range of $\eta^* < 0.9$ by this method. Therefore, the different method mentioned above was used to examine the transport in the opposite direction near the bottom as predicted by the theory.

Photos.3 and 4 show the results of the experiments in the h/L value of 0.16 for wave heights 3.3 cm and 8.0 cm, respectively. Both ends of the photographs correspond to the anti-node positions and the center to the node position of the standing waves. In addition, the white and black parts of the photographs show the vinyl pellets and the bottom of the wave tank, respectively. The photographs demonstrate that the transport of the vinyl pellets is in the direction of the node position, and that high waves result in faster transport of vinyl pellets than low waves. Thus, the experimental evidence

is in qualitative agreement with the theory.

Fig.8-(a), (b) and (c) show the results of the experiments in $h/L = 0.08$ for wave heights of 12 cm, 16 cm and 19 cm, respectively. These figures indicate that the experimental values of λ^* are less than those predicted by the theory. Collins (Ref.8) and Brebner (Ref.9) found that in the experiments in the case of progressive waves, the observed mass transport velocity near bottoms is less than that predicted by laminar theory as the bottom boundary layer becomes turbulent. The results for standing waves also indicate that at the inception of turbulence there is a break from the laminar theory in which $\overline{U}_{max}$ is proportional to H^2.

Fig. 9 shows the relationship between $|\overline{U}_{max}|L$ and $H^2(T \sinh^2 kh)^{-1} \times |\sin 2kx|$ for laminar and turbulent ranges. In addition, the limiting value indicated by Brebner and Collins is also shown in this figure. In the case of progressive waves, Brebner and Collins proposed a critical Reynolds number defined by $V_0\delta/\nu$ and obtained the value of 160, in which V_0 is the maximum velocity at the bottom on the basis of the linearized wave theory. Therefore, replacing V_0 by $\pi H(T \sinh^2 kh)^{-1}|\sin 2kx|$ gives the critical Reynolds number in the case of standing waves.

CONCLUSION

The following conclusions may be derived from the results of this study:

1) The mass transport in a laminar boundary layer is in agreement with the theoretical value except for the low waves and the direction of the mass transport in the upper layer is contrary to that of the lower one.

2) In the case of standing waves, boundary layers are turbulent at higher Reynolds number than 160, which is a critical one, and the mass transport is less than the theoretical value for laminar boundary layers.

ACKNOWLEDGEMENTS

The author wishes to express his great appreciation to Prof. Y. Iwagaki for his encouragement in carrying out this study and to Messrs. T. Shibano, Y. Kawashima and A. Kimura for their co-operation in the experiments.

REFERENCES

(1) Lettau, H. (1932). Stehende Wellen als Ursache und Gestaltender Vorgange in Seen; Ann. d. Hydrogr. u. Mar. Met. 60, Jahrg, p. 385.

(2) Nomitsu, R. (1943). Generation of Sand Bar and Sand Ripple due to Stationary Waves: The Geophysics, Vol. 7, No. 1, pp. 61-79. (in Japanese).

(3) Hayami, S. (1950). On the Buried Tomari Harbor: Proc. of JSCE, Vol. 35, No. 4, pp. 167-171. (in Japanese).

(4) Longuet-Higgins, M.S. (1953). Mass Transport in Water Waves: Phil. Trans. Royal Soci., London, Series A. No. 903, pp. 535-581.

(5) Iwagaki, Y. and Tsuchiya, Y. (1966). Laminar Damping of Oscillatory Waves due to Bottom Friction: Proc. 10th Conf. on Coastal Eng.,pp 149-174.

(6) Schlichting, H. (1960). Boundary Layer Theory, translated by J. Kestin:McGraw-Hill, Series in Mechanical Eng., pp. 207-229.

(7) Russell, R.C.H. and Osorio, J.D.C. (1958). An Experimental Investigation of Drift Profiles in a Closed Channel: Proc. 6th Conf. on Coastal Eng., pp. 171-183.

(8) Collins, J.I.(1963). Inception of Turbulence at the Bed under Periodic Gravity Waves: Jour. Geophs. Res., Vol. 68, pp. 6007-6014.

(9) Brebner, A., Askew, J.A. and Law, S.W. (1966). The Effect of Roughness on the Mass-Transport of Progressive Gravity Waves; Proc. 10th Conf. on Coastal Eng., pp. 175-184.

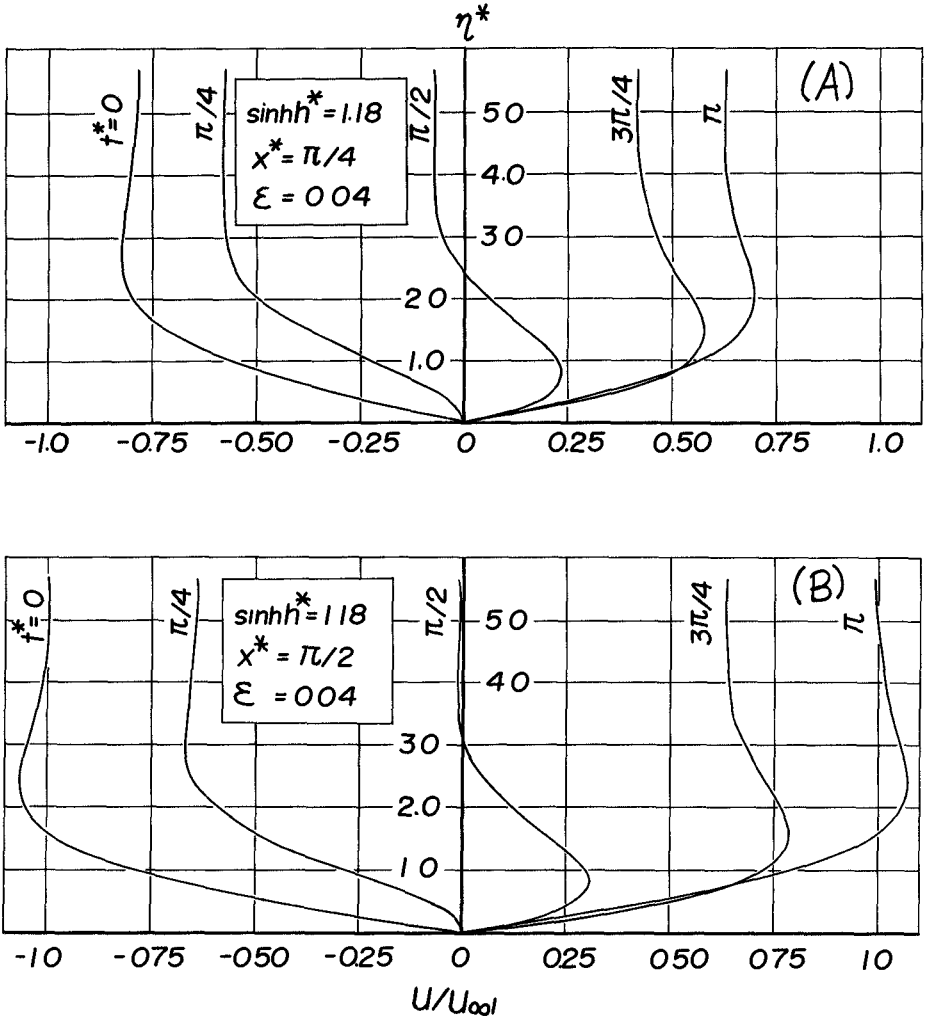

Fig. 1 Velocity profiles in the boundary layer.

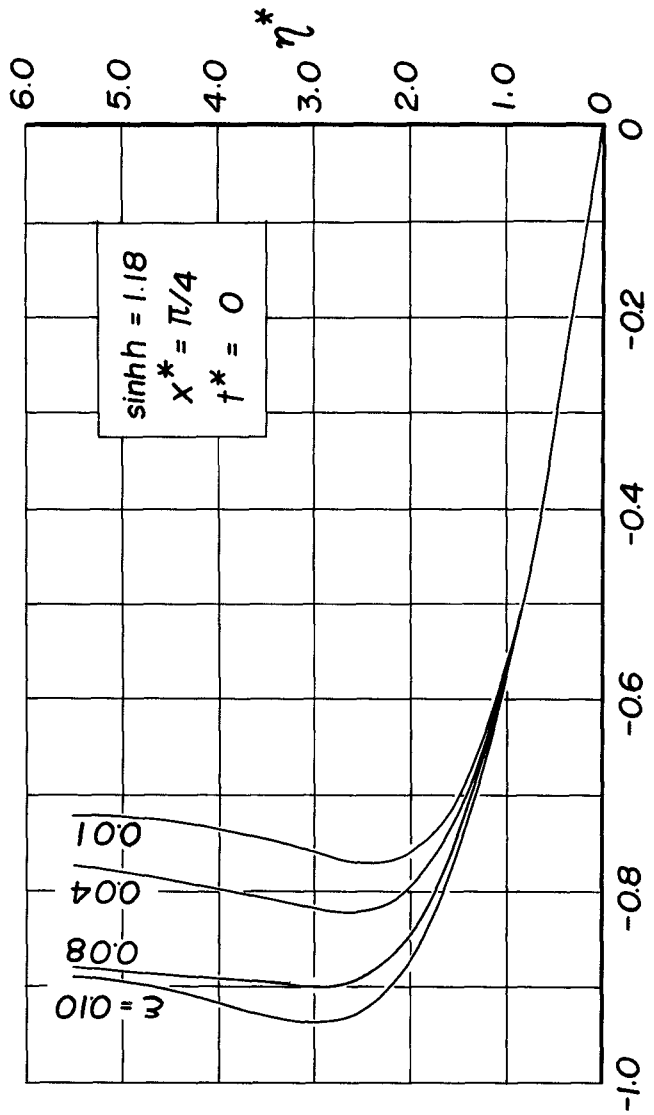

Fig. 2 Effects of H/L value on velocity profile.

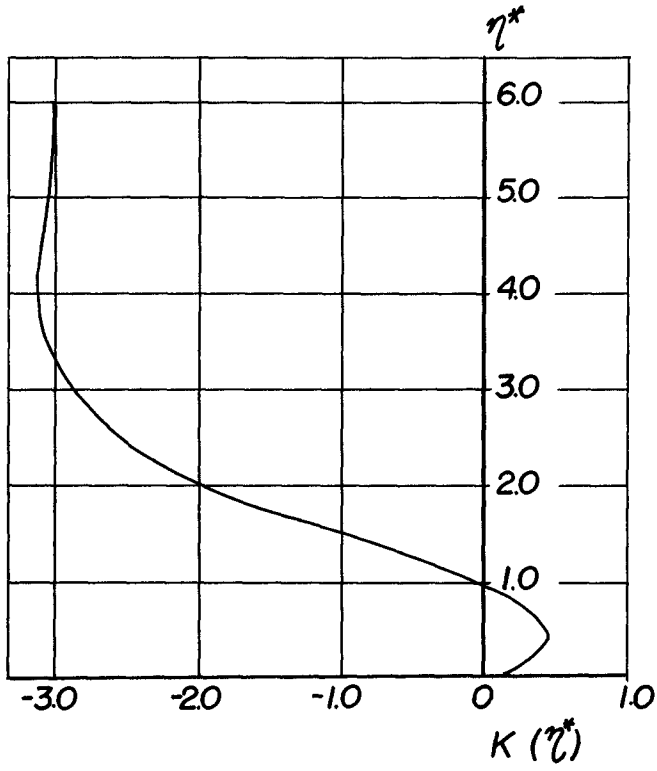

Fig. 3 Distribution of non-dimensional mass transport velocity.

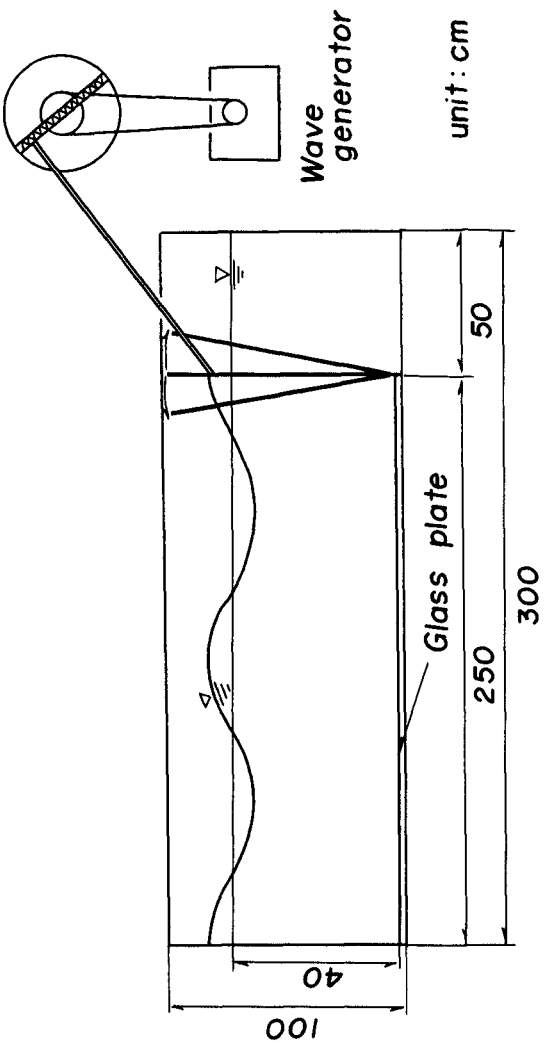

Fig. 4 Schematic view of wave tank.

Photo. 1 An example of dye streaks.

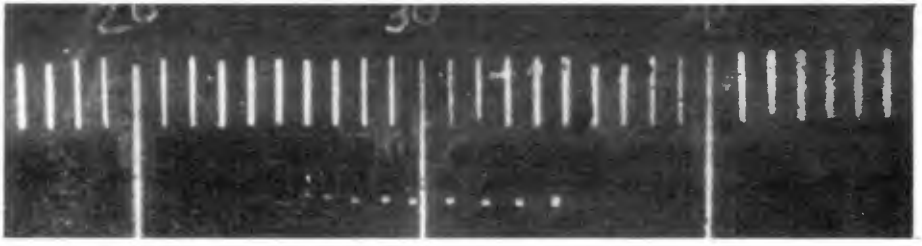

Photo. 2 An example of movement of a nylon particle.

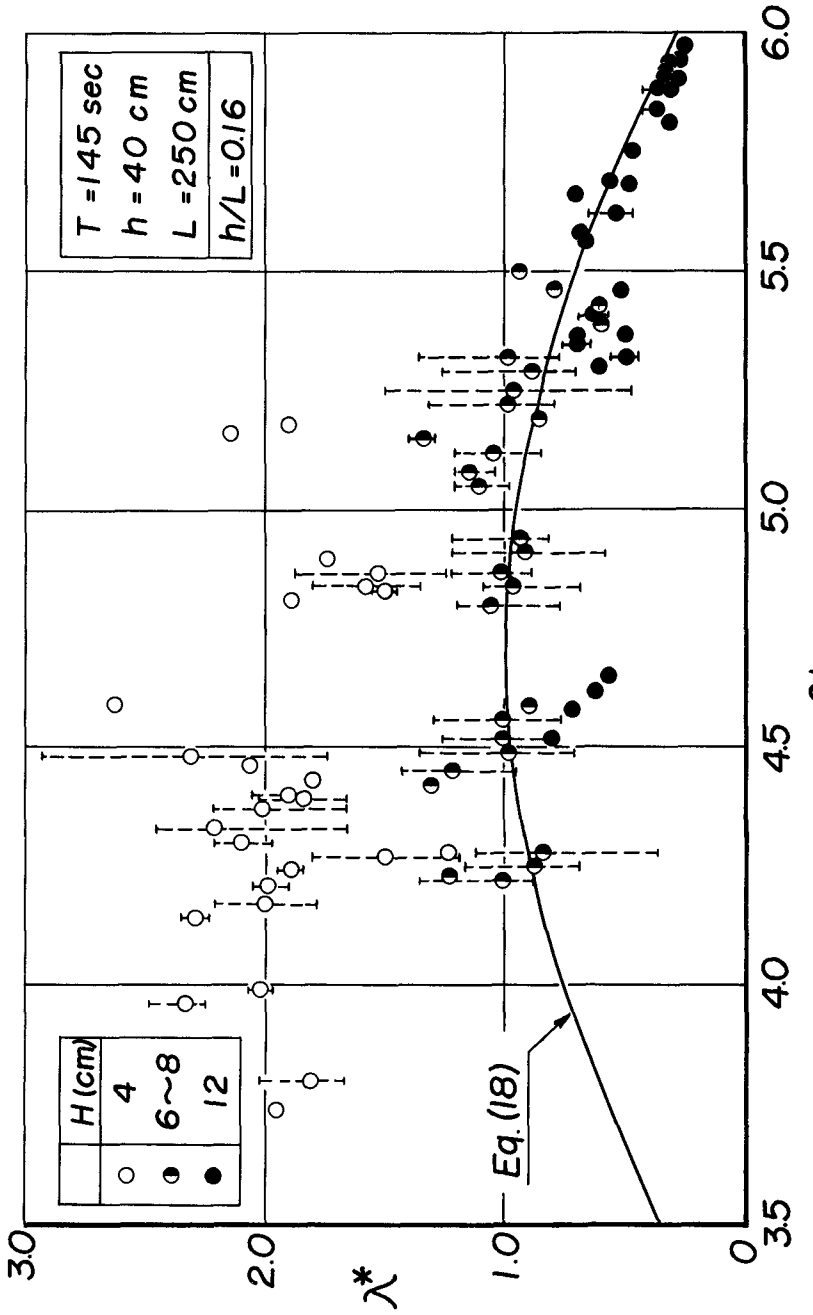

Fig. 5 Comparison between theoretical and experimental non-dimensional mass transport velocity by dye-streak method. (T = 1.45 sec., h/L = 0.16)

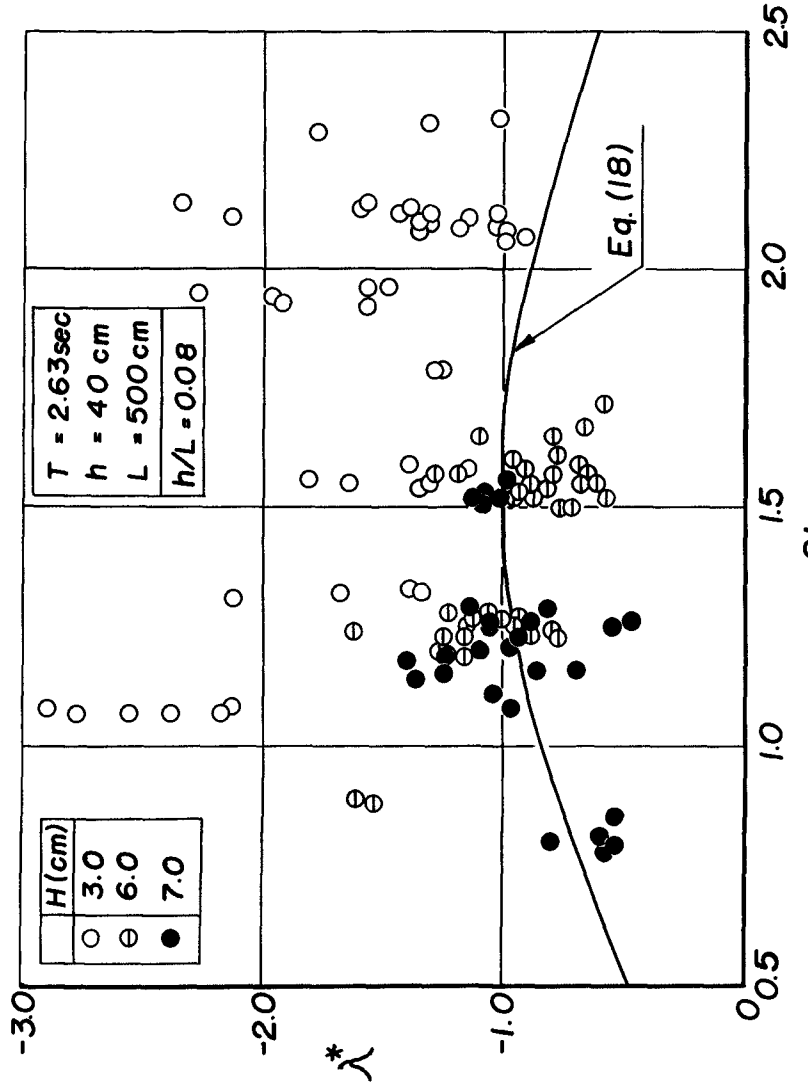

Fig. 6 Like Fig. 5 but (T = 2.63 sec., h/L = 0.08).

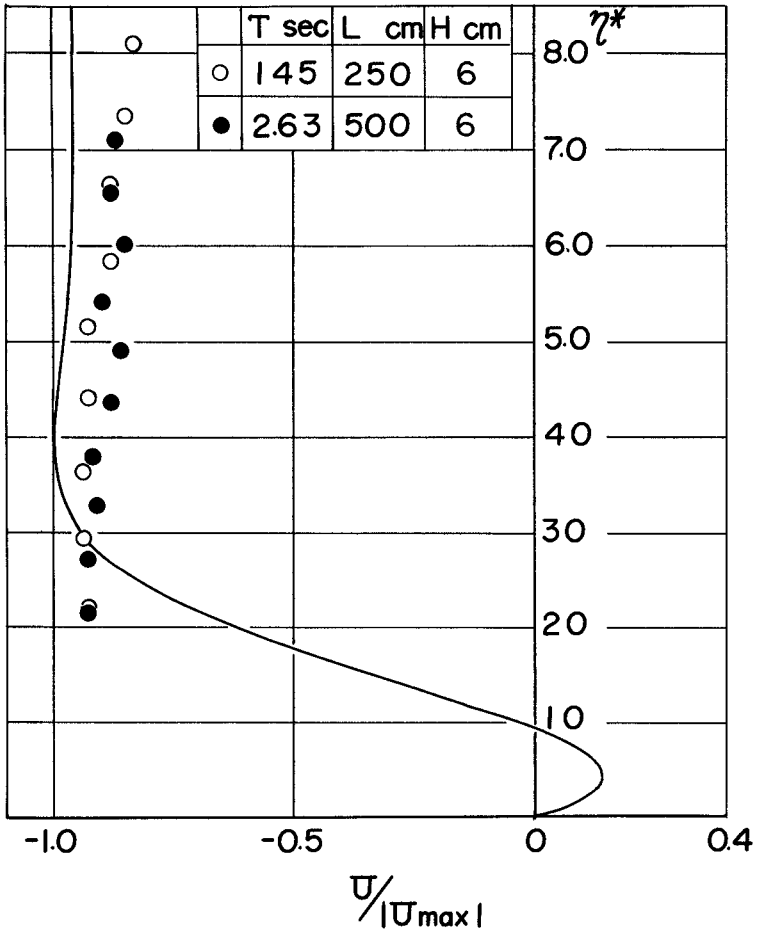

Fig. 7 Comparison between theoretical and experimental non-dimensional mass transport velocity profile.

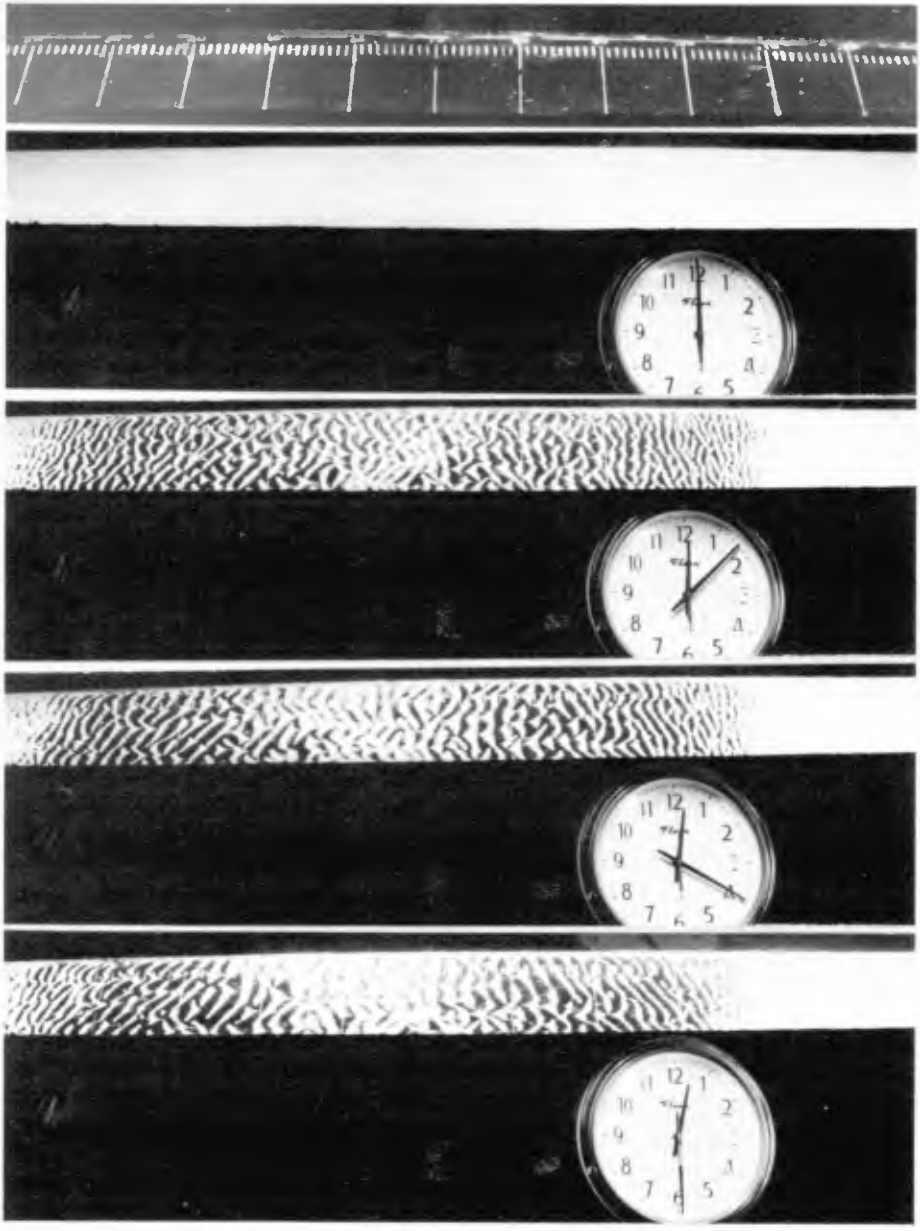

Photo. 3 Movement of vinyl pellets near bottom with time (H = 3.3 cm).

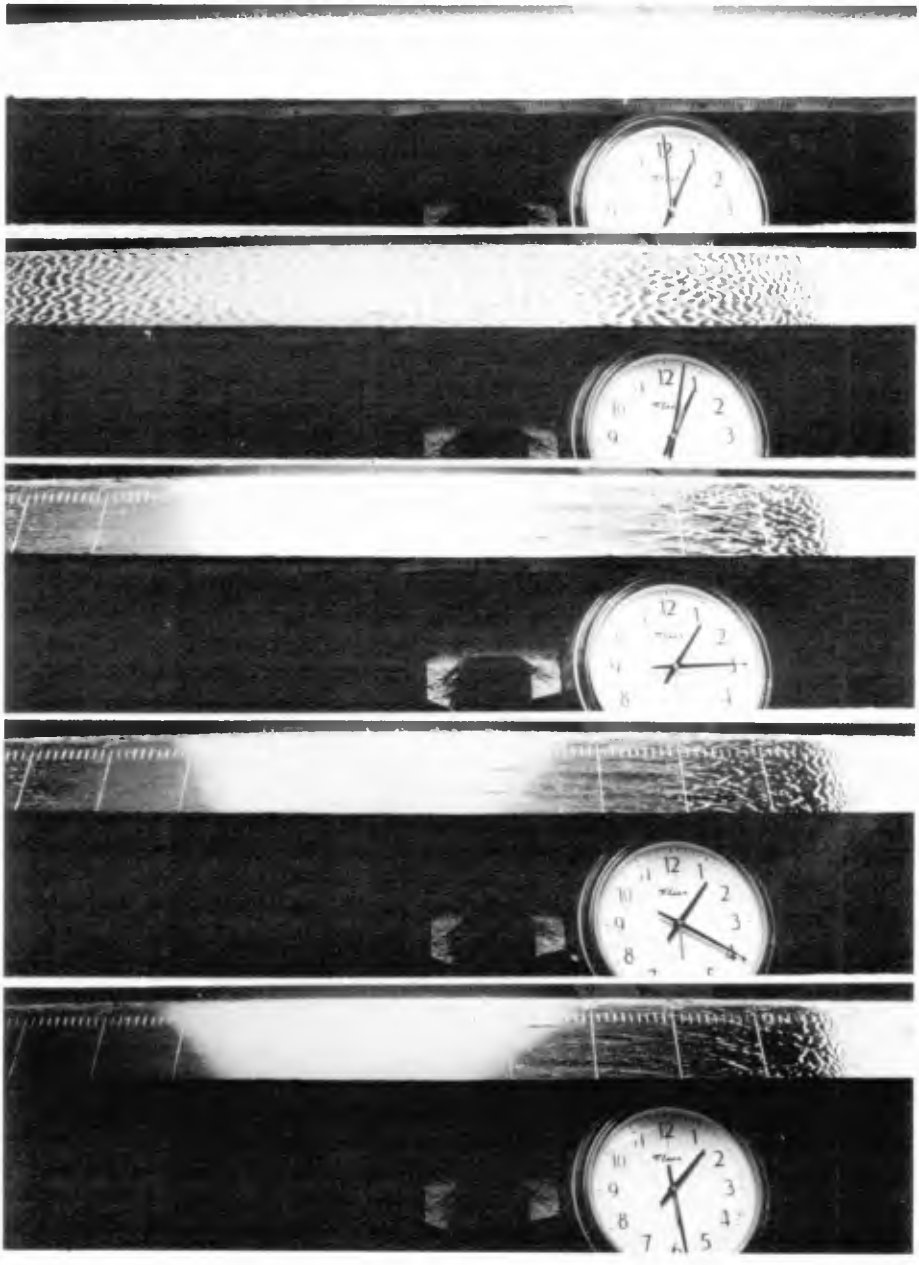

Photo. 4 Movement of vinyl pellets near bottom with time (H = 8.0 cm).

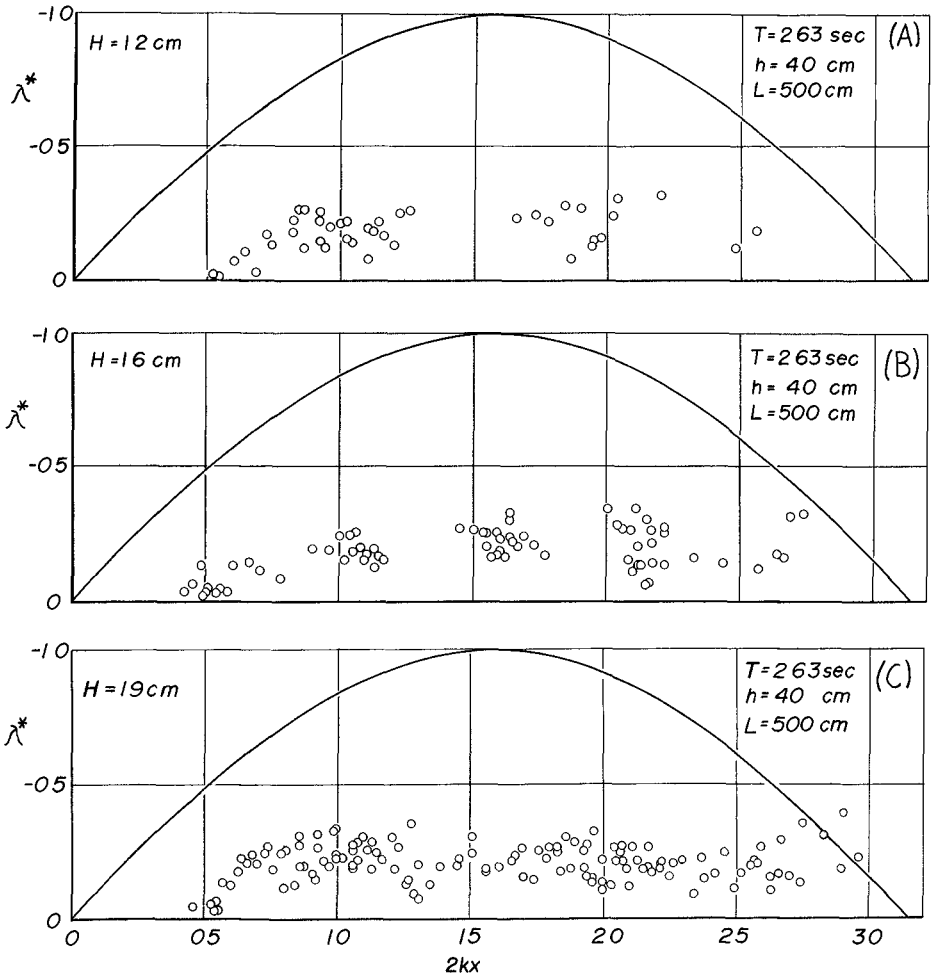

Fig. 8 Comparison between theoretical and experimental non-dimensional mass transport velocity by solid-particle method.

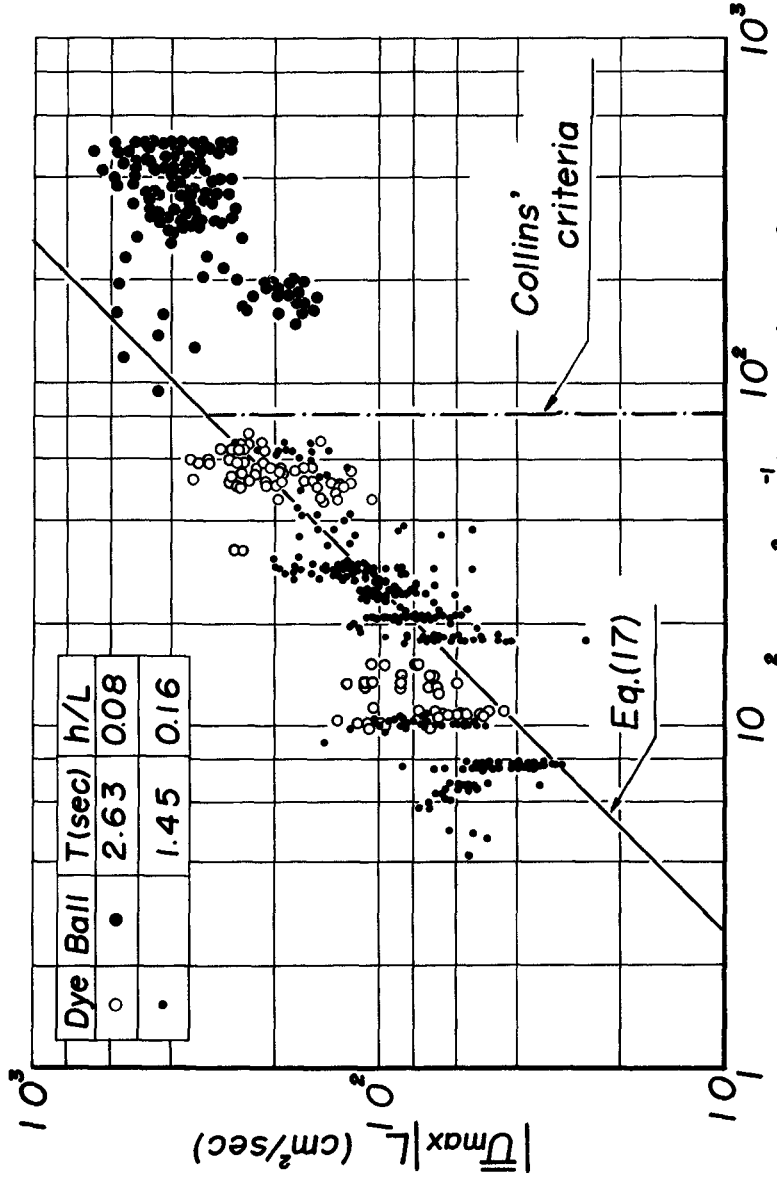

Fig. 9 Relationship between $|\overline{U}_{max}|L$ and $H^2(T\sinh^2 kh)^{-1}\times|\sin 2kx|$ for the smooth bottom.

CHAPTER 16

APPLICATION OF WAVE DIFFRACTION DATA

Richard Silvester[1] and Teck-Kong Lim[2]

ABSTRACT

By considering separately the two termsof the Sommerfeld solution of wave diffraction behind a semi-infinite breakwater, the influence of the wave reflection from the structure can be evaluated The diffraction coefficient at any point can be obtained from a graph or table for full, partial or no reflection by the simple addition of two coefficients From the similarity of the energy-spreading process to the dam-burst problem, it was found that wave heights decreased consistently along the near circular crests for all distances from the breakwater tip For a workable range of incident angle and distance from the breakwater, wave heights could be defined by this arc distance from the shadow line expressed in wave lengths These relationships have been verified experimentally for all but the smallest incident angle in proximity to the breakwater This can be likened to the dam model in which the dam is moving too slowly to permit normal spreading.

The several theoretical solutions for the breakwater gap, when graphed on the same basis, are shown to be very similar, diverging only for small incident angles New parameters are provided which greatly simplify the presentation of information The scatter of past experimental data precludes the verification of this theory and indicates the need for further tests

INTRODUCTION

Theoretical solutions have been available over many years for computing wave heights behind breakwaters These are based upon the diffraction process in optics and hence have given rise to the term "shadow zone" for the area behind the structure The relevant equations can be solved by computer and thus results, to apparent high degrees of precision, are becoming available. This tendency perhaps is not commensurate with the inaccuracies inherent in the wave data of coastal engineering problems.

This paper attempts to simplify the presentation of information by an averaging process, thus reducing the number of variables. The modest error so introduced should not influence the accuracy of general design procedures.

---

[1]Professor of Coastal Engineering, Asian Institute of Technology, Bangkok, Thailand.

[2]Graduate Student, AIT, Bangkok, Thailand

Diffraction of ocean waves can be divided to three main topics, namely: (a) the semi-infinite breakwater, in which the water zone beyond the breakwater is considered to be unlimited as far as wave energy supply is concerned

(b) the breakwater gap, in which two structures extend to less than five wave lengths apart, so limiting the wave energy available for spreading into the one or two shadow zones so formed

(c) the island or offshore breakwater, in which waves diffract to leeward of the structure from either end

Only cases (a) & (b) are discussed in this paper, with the following assumptions applying: (i) uniform depth of water throughout, inferring a constant wave length for any specific wave period

(ii) breakwaters which have a width that can be considered thin in respect to the wave length If the structure or land mass has a sizable width the diffraction solution should be applied from the leeward or shadow-zone face.

(iii) small amplitude waves in keeping with the linear theory, although experimental verification is available for relatively steep waves

SEMI-INFINITE BREAKWATER

The general case is illustrated in Figure 1 in which it is seen that a train of waves is approaching at an angle θ to the breakwater Thus the orthogonals of the incident waves are angled θ to the structure and the one passing through the breakwater tip will be considered the limit of the shadow zone and will be termed the "shadow line". Wave heights only in the shadow zone are considered in this paper. The location of any point P will be defined by either the polar coordinate system (α, R/L) or the circular arc system (S/L, R/L) As will be seen later, this latter system can be reduced to S/L alone, with little loss of accuracy.

It can also be observed in Figure 1 that the waves reflected from the breakwater also diffract whilst they proceed seawards Before entering the shadow zone they must spread through an angle of $360^{o}-2\theta$, so that to supply energy at point P they have a diffraction angle of $360^{o}-2\theta+\alpha$ Outside the shadow zone the interaction of the reflected waves with the incident waves creates a short-crested system, the detailed characteristics of which are available[1] Immediately outside the shadow zone the two waves are practically aligned and, although a slight phase difference may be present between the incident and the reflected waves, heights in excess of those of the incident wave are theoretically possible As noted already, this zone is not treated herein

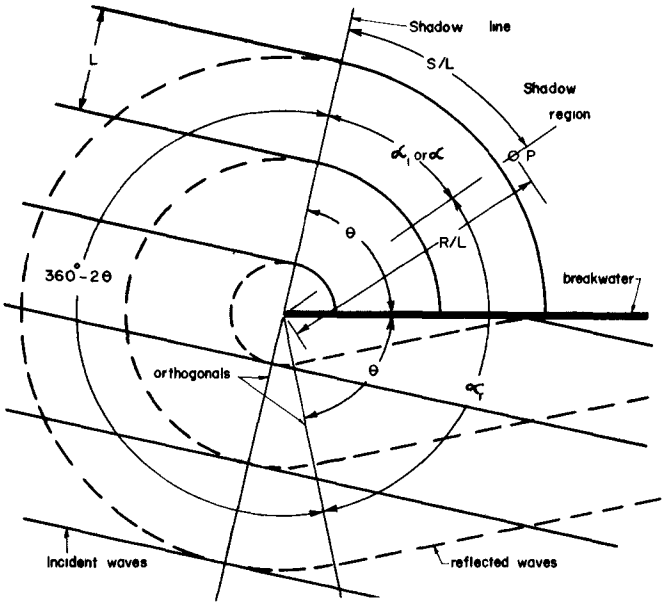

FIG 1
DEFINITION
SKETCH

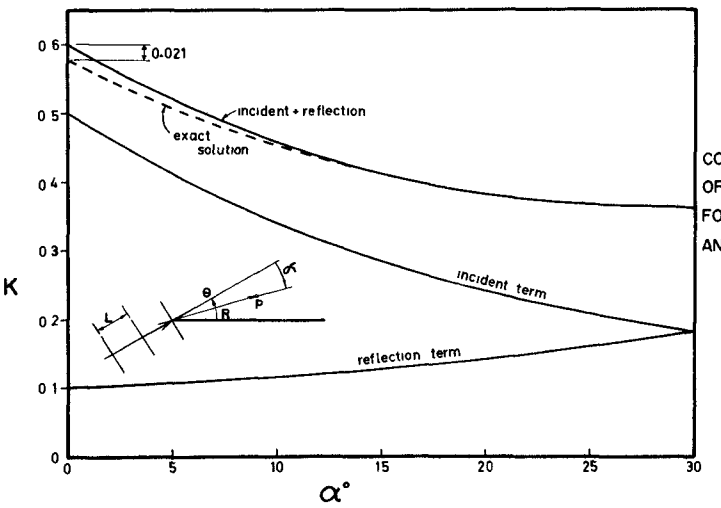

FIG 2
COMPARISION
OF METHODS
FOR R/L=2.5
AND θ = 30°

It can be readily accepted that the influence of the reflected wave in the shadow zone is small, but no insignificant for the case of 100% reflection. Inspite of the tendency to design breakwaters for the fullest dissipation of waves, diffraction theory in current use is based upon 100% reflection In proximity to the breakwater tip, where the reflection component is greatest its correct assessment could result in worthwhile economies of design

THEORETICAL SOLUTION

The Sommerfeld[2] solution of optical diffraction was applied to water waves by Penney and Price[3][4]. The basic equation with the definition of α_1 and α_r as in Figure 1, can be written as follows:

$$F(R,\alpha) = f(u1).\exp(-ikR\cos\alpha_1) + f(u2)\exp(-ikR\cos\alpha_r) \quad \ldots\ldots (1)$$

where $$u1 = -\sqrt{8R/L}\,\sin(\alpha_1/2) \quad \ldots\ldots (2)$$

$$u2 = -\sqrt{8R/L}\,\sin(\alpha_r/2) \quad \ldots\ldots (3)$$

$$k = 2\pi/L \quad \ldots\ldots (4)$$

$$f(u) = \frac{1+i}{2}\int_{-\infty}^{u} \exp(-i\pi u^2)\,du \quad \ldots\ldots (5)$$

$$f(-u) = \frac{1+i}{2}\int_{-\infty}^{-u} \exp(-i\pi u^2).du \quad \ldots\ldots (6)$$

$$f(u) + f(-u) = 1 \quad \ldots\ldots (7)$$

The diffraction coefficient K is defined as

$$K = \frac{\text{diffracted wave height}}{\text{incident wave height}} \quad \ldots\ldots (8)$$

The numerical value of K is equal to the modulus of equation (1) so that $$K = \left|F(R.\alpha)\right| \quad \ldots\ldots (9)$$

In this event the second term of the RHS in equation (1) can be written $$f(u2)\exp(-i\,k\,R\cos\overline{360^\circ - \alpha_r}) \quad \ldots\ldots (10)$$ which represents the diffraction of the reflected wave, from its orthogonal through the breakwater tip around to the polar direction of point P. The first term of equation (1) represents the fraction of the wave height resulting from diffraction of the incident wave from the shadow line. Thus

$$K = \left|F(R.\alpha)\right| = \text{incident term} + \text{reflected term.}$$

The generalised form for equation (9) is thus

$$K = \left|f(u)\exp(-i\,k\,R\cos\alpha)\right| \quad \ldots\ldots (11)$$

in which α can be measured from the shadow line to give the diffraction coefficient for the incident wave, and from the tip orthogonal of the reflected wave ($360 - 2\theta + \alpha$) to give the coefficient for the reflection component. The two values are added to give K for the case of 100% reflection. For partial reflection a proportion of the second component should be used.

Separating the components in the above manner introduces a slight error for incident angles $\theta \leq 45^{o}$, but this is on the conservative side and it occurs only near the shadow line and for small radial distances as indicated in Figure 2.

Larras[5] has recently made a similar approach to the problem, by solving the sine and Fresnel functions from the geometry of the point P in terms of orthogonal axes and the use of Cornu spirals. In this case also the diffraction coefficient is the addition of an incident and reflected term, the latter being modified according to the degree of reflection.

POLAR CO-ORDINATE SYSTEM

Equation (11) can be graphed as in Figure 3, or tabulated as in Table I. The values of K representing incident and reflected components are read from the angle α as previously indicated and then added. For example, with $\theta = 60^{o}$, $\alpha = 30^{o}$ and R/L = 10 we have from Figure 3: $360 - 2(60) + 30 = 270^{o}$, so that K(incident) = 0.10 and K(reflected) = 0.03, giving K(100% reflection) = 0.13, K(zero reflection)= 0.10 and K(50% reflection) = 0 115.

The respective values as obtained from Table I are as follows:

$$K(\alpha = 30^{o}) = 0.096$$

$$K(360^{o} - 2\theta + \alpha = 270^{o}) = K(360^{o}-270^{o} = 90^{o}) = 0.036$$

$$K(100\% \text{ reflection}) = 0.132$$

In reading table I it is sufficient for the reflection term to use $2\theta - \alpha$, which in this case = $120^{o}-30 = 90^{o}$.

It is noteworthy that with no reflection the wave height along the shadow line ($\alpha = 0^{o}$) remains static at 0.5. Also, on the lee-side of the breakwater, where $\alpha = \theta$, it is found that the incident and reflection components are each 50% of the total. This is significant when the latter might not exist at all due to adequate dissipation on the breakwater.

CIRCULAR ARC SYSTEM

Consider the wave at the shadow line just after it has reached the the breakwater. At the crest alignment two distinct water levels attempt to exist simultaneously, that of the wave crest and that of the still-water level inside the shadow zone. This instantaneous

TABLE 1 - $K' = \left|f(u)\ \exp(-2\pi i(R/L)\cos(\alpha))\right|$

R/L / α degrees	K x 1/1000									
	1	2	3	4	5	6	8	10	15	20
0	500	500	500	500	500	500	500	500	500	500
2	476	466	459	453	448	443	435	428	413	402
4	453	435	422	411	402	393	379	367	344	325
6	431	406	388	373	361	350	332	317	288	266
8	411	379	357	340	325	313	292	275	244	222
10	392	355	329	310	294	280	258	241	210	188
12	373	332	304	283	267	253	230	213	182	162
14	356	311	282	260	243	229	207	190	161	141
16	340	292	262	240	222	208	187	170	143	125
18	325	275	244	221	204	191	170	154	128	112
20	310	259	228	205	189	175	155	140	116	101
25	278	225	194	173	157	145	127	115	94	82
30	251	197	168	148	134	123	107	96	79	69
35	228	175	147	129	116	107	93	83	68	59
40	208	157	131	115	103	94	82	73	60	52
45	191	142	118	103	92	84	73	66	54	46
50	176	130	107	93	84	77	66	59	49	42
55	164	120	99	86	77	70	61	54	44	39
60	153	111	91	79	71	65	56	50	41	36
65	143	104	85	74	66	60	52	47	38	33
70	135	97	80	69	62	57	49	44	36	31
75	128	92	75	65	58	53	46	41	34	29
80	122	87	71	62	55	51	44	39	32	28
85	116	83	68	59	53	48	42	37	30	26
90	111	79	65	56	50	46	40	36	29	25
95	107	76	62	54	48	44	38	34	28	24
100	103	73	60	52	46	42	37	33	27	23
105	99	71	58	50	45	41	35	32	26	22
110	96	69	56	49	43	40	34	31	25	22
115	94	67	54	47	42	39	33	30	24	21
120	91	65	53	46	41	38	32	29	24	21
125	89	63	52	45	40	37	32	28	23	20
130	87	62	51	44	39	36	31	28	23	20
135	86	61	50	43	39	35	30	27	22	19
140	84	60	49	42	38	35	30	27	22	19
145	83	59	48	42	37	34	29	26	22	19
150	82	58	48	41	37	34	29	26	21	18
160	80	57	47	40	36	33	29	26	21	18
170	80	56	46	40	36	33	28	25	21	18
180	79	56	46	40	36	32	28	25	21	18

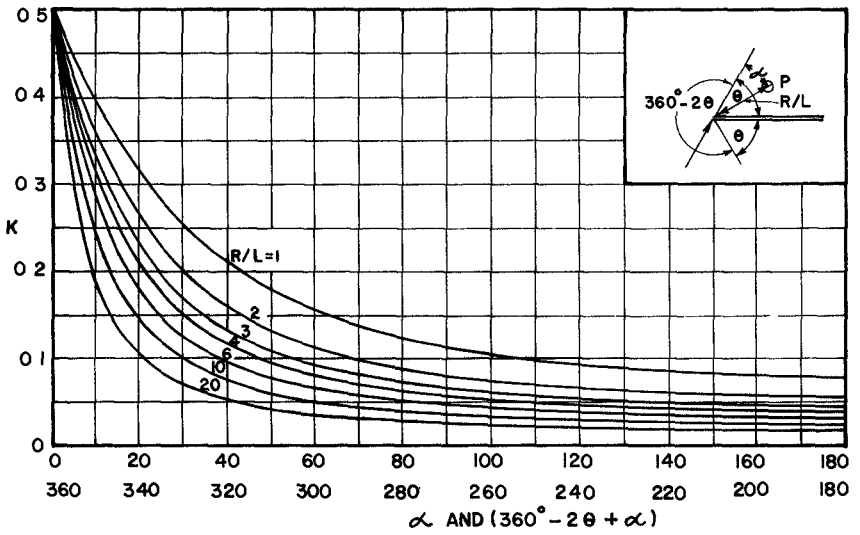

FIG. 3 K FOR ALL θ WITH OR WITHOUT REFLECTION

differential can be likened to the dam-break problem, in which the vertical wall of water gives way to a sloping surface which flattens swiftly with time

The major differences in these two phenomena are the element of time and the supply of energy In the case of the dam-burst the slope at the channel alignment varies with time, whereas in diffraction the wave crest is changing position and would appear to maintain a fixed profile In respect to energy supply, this is limited in the dam case by the volume of water available in the resevoir, but appears unlimited for the semi-infinite length of the wave crests outside the shadow zone of the breakwater. This comparison suffers many disabilities, but it is felt significant that the water at the dam site remains constant at 4/9 of the original depth, whilst the energy level remains constant In an apparaently similar manner the energy transfer in diffraction, for the incident wave alone, maintains a constant depth along the shadow line. The order of the depth changes are vastly different and crest to trough measurements are involved rather than SWL, so that strict equality cannot be expected

From the above generalisations it was surmised that along a wave crest, which in the shadow zone could be accepted as circular in plan, a constant wave-height profile should exist for all its positions from the breakwater. This distance measurement from the shadow line is designated an arc length (S/L) which could thus replace the (R/L, α) coordinate system previously used for defining positions in the shadow zone. (See Figure 1).

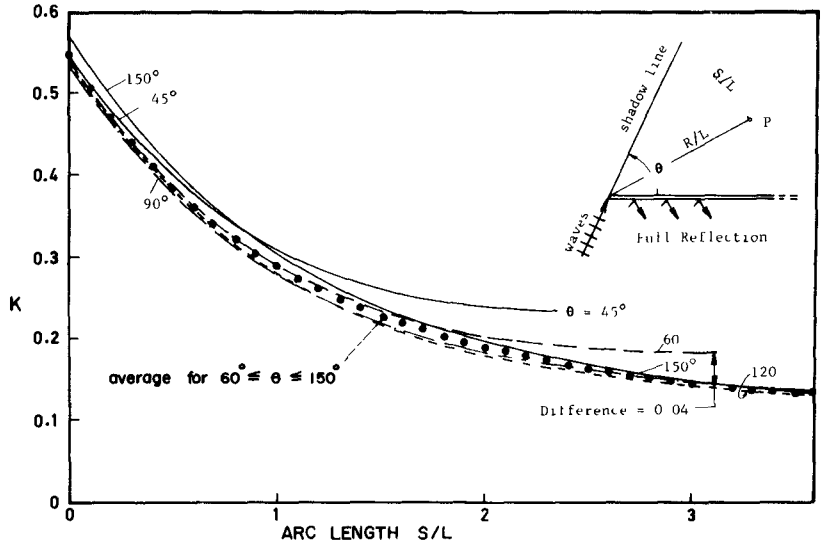

FIG 4 K VALUES FOR R/L = 3 AND FULL REFLECTION.

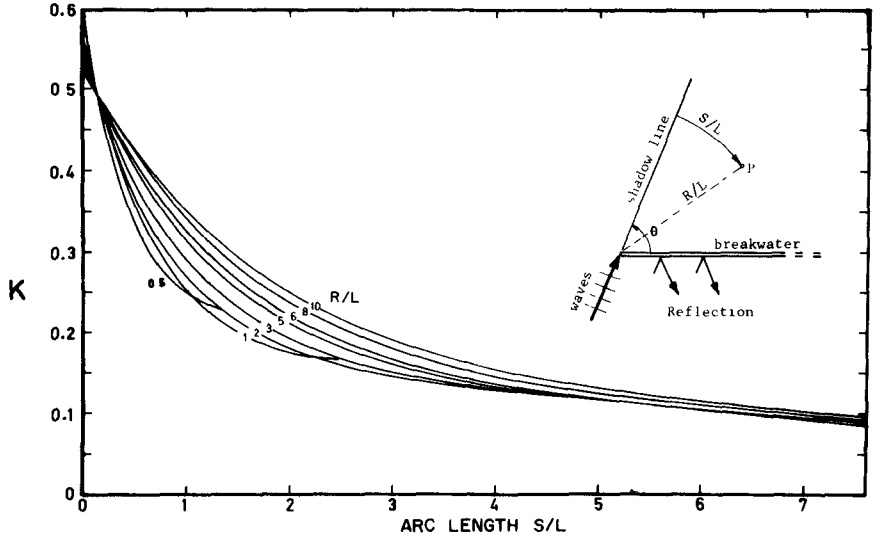

FIG 5 K AVERAGED FOR 60° ≤ θ ≤ 150° AND FULL REFLECTION

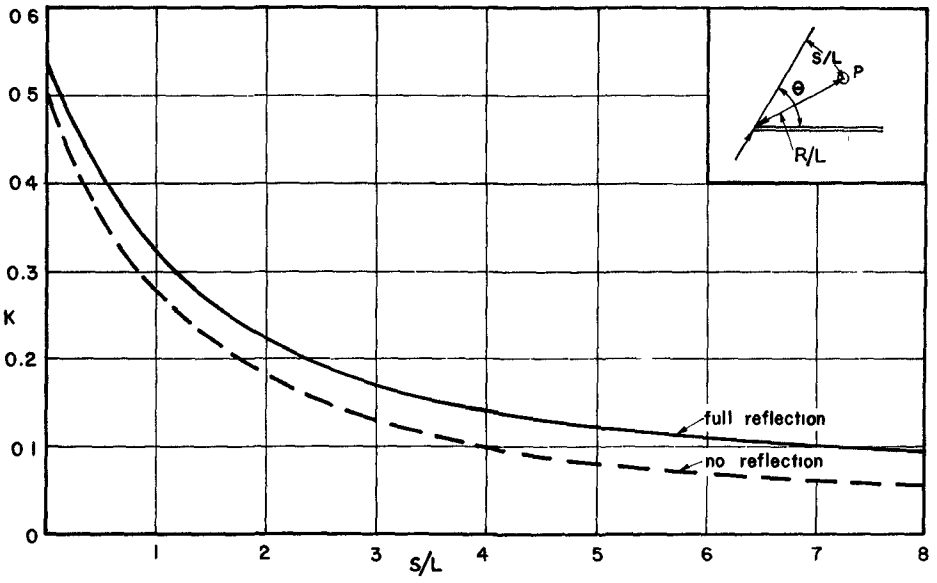

FIG 6 K ALONG CREST FOR $60^\circ \leq \theta \leq 150^\circ$ AND $3 \leq R/L \leq 10$

Curves were drawn from the Sommerfeld solution in the circular arc system for values of R/L = 0.5 to 10 and $\theta = 45^\circ$ to 180° A typical set of results is displayed in Figure 4, which shows the curves for the various angles θ and the specific value of R/L = 3. An average curve was drawn for $\theta = 60^\circ$ to 150°, as indicated, for each R/L value and then collected in a single diagram (as Figure 5). From this a single curve appeared acceptable to represent R/L values from 3 to 10.

The errors so introduced by this averaging procedure can be ascertained from the two figures. As seen in Figure 4, that due to averaging θ occurs mainly in the smaller θ values, for example a maimum of K = +0.04 for $\theta = 60^\circ$ at S/L = 3 for the case of R/L = 3.0. In Figure 5 an average line (not drawn) involves a maximum error of about $\pm$ 0.035 at S/L = 2.0, or 3 5% of the incident wave. These error values are not strictly cumulative since they occur at different S/L values and the first one quoted is for the 60° incident angle only The average error for θ larger than this was in the order of $\pm$ 0.01.

Figures 4 and 5 represent full reflection conditions. Similar graphs can be obtained for zero reflection, resulting in the curves of Figure 6 This figure can be used instead of Figure 3 or Table I with

the slight loss of accuracy indicated To find the relevant S/L value an arc should be drawn through the point of interest P, centered on the breakwater tip, and the length along it from the shadow line measured in wave lengths. This can be accomplished on any harbour layout where constant depths can be assumed

EXPERIMENTAL VERIFICATION

Putman and Arthur[6] conducted experiments which avoided reflection from the breakwater Their results, which were presented in x-y coordinates, were transformed to the arc length system and are displayed in Figure 7 Agreement is clearly shown with the zero reflection curve.

Tests conducted by Lim[7] at the Asian Institute of Technology were concentrated on the region within three wave lengths of the breakwater tip Incident angles of 45°, 60°, 90°, 120° and 180° were examined and measurements were made for R/L = 1, 2 and 3 at intervals of either 7½° or 15° from the shadow line The main elements of the equipment are shown in Figure 8, where it is seen that the incident angles were varied by changing the position of the breakwater. Reflection from the exposed side of the breakwater is obviously excluded.

Waves were measured by a step wave probe to an accuracy of $\pm$ 1.0 mm. The range of wave heights and wave periods for all tests are listed in Table II where it can be noted that periods ranged from 0 5 to 0.7 seconds and incident wave heights from 19 to 36 mm This latter measurement was an average of values taken at 3 points in the approach channel (See Figure 8) to obviate the resonant cross-waves established there.

Results from runs with similar waves presented some scatter, as exemplified in Figures 9 and 10 and observed in Table II. This would have arisen from the probe error, incomplete dissipation of the waves at the basin boundary, and long period surge of the basin Averages of the several runs are listed in Table II for each α and R/L value (probe location), and graphed for each θ in Figures (11 to 15). For angles of 60° and 90° the experimental data agree very well with the theory for zero reflection. For angles 120° and 180° the experimental points are a little low, but for 45° are high, in all cases increasing with distance inside the shadow zone. This difference decreased as R/L approached 3. The maximum error was in the order of 4% of the incident wave height. Since the theory is conservative for $\theta \geq 60°$, based upon this experimental evidence, it is suggested that Figures 3 and 6 or Table I can be used with confidence, by computing an appropriate allowance for reflection.

For the special conditions of $\theta < 60°$ and R/L < 3, an addition of 0.1 should be made to the K evaluated above The previous comparison of wave diffraction to the dam-burst problem may help explain this deviation from the theory. When θ is small the wave has insufficient room to spread properly. This situation is similar to a moving dam whose velocity does not permit the formation of the water surface profile commensurate with a sudden dam collapse

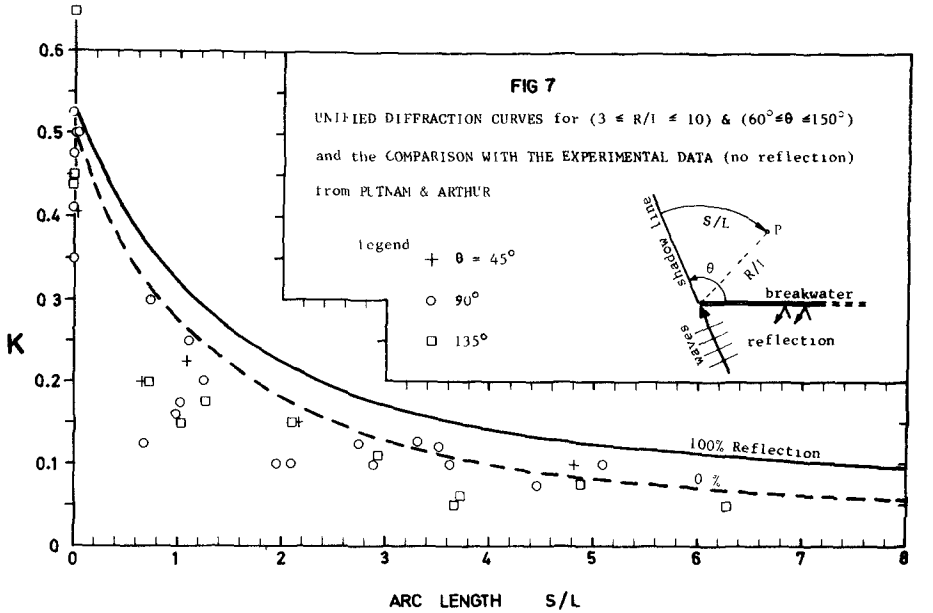

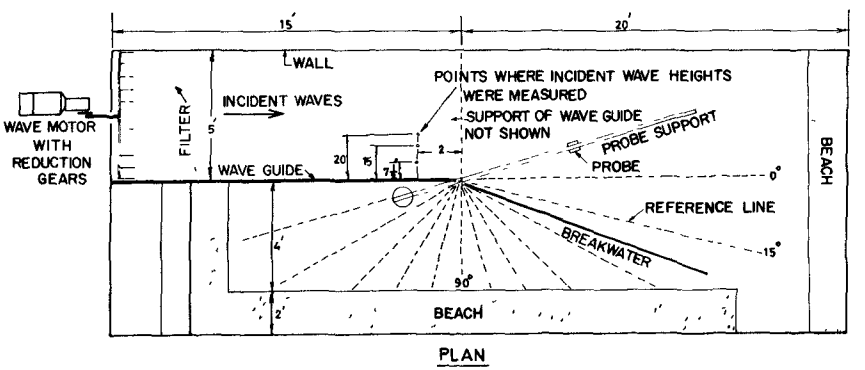

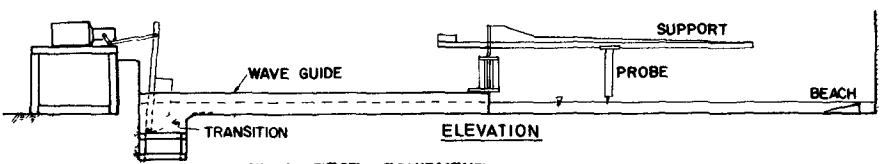

FIG 8 TEST EQUIPMENT

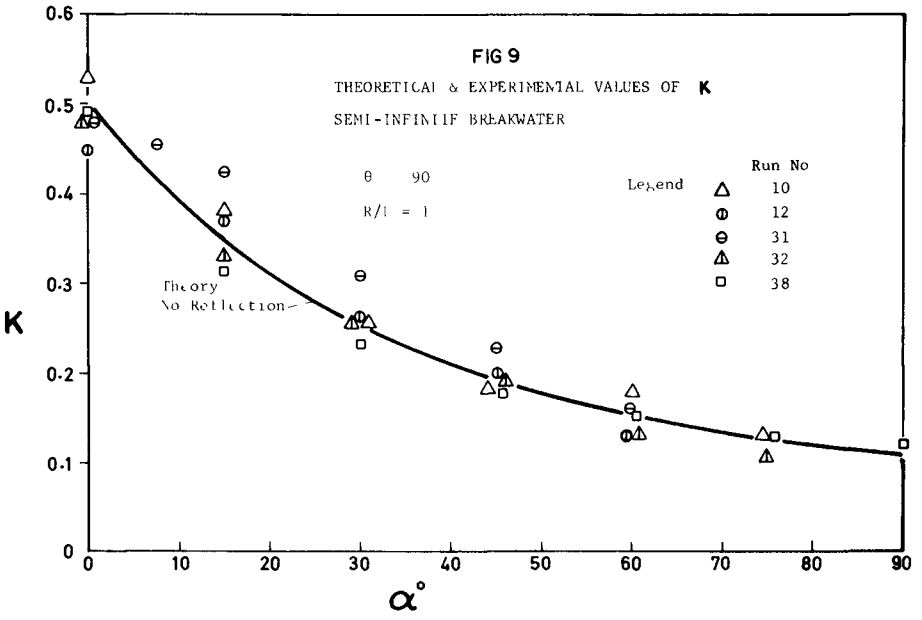
FIG 9
THEORETICAL & EXPERIMENTAL VALUES OF K
SEMI-INFINITE BREAKWATER
θ 90
R/L = 1
Legend
Run No
10
12
31
32
38
Theory
No Reflection
K
α°
0.6
0.5
0.4
0.3
0.2
0.1
0
0 10 20 30 40 50 60 70 80 90

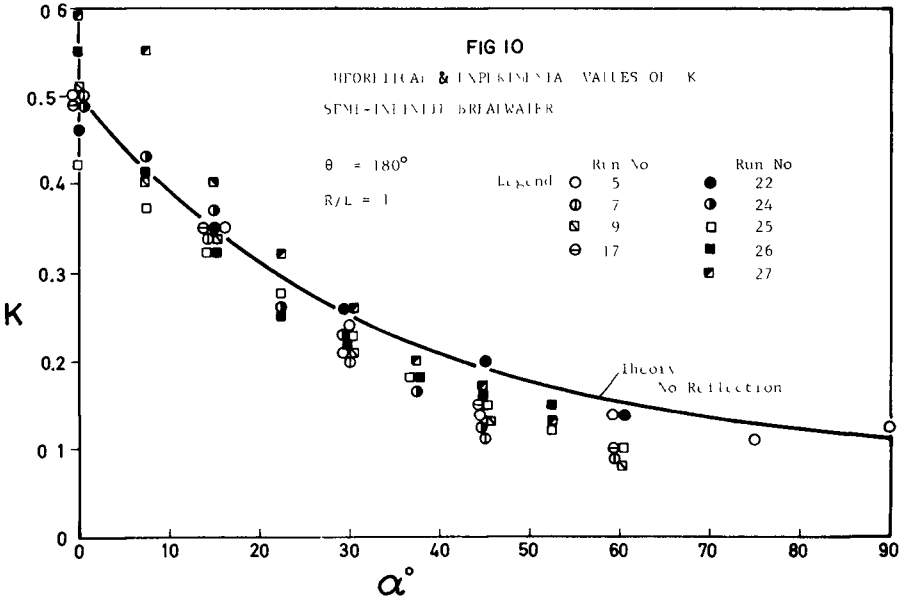
FIG 10
THEORETICAL & EXPERIMENTAL VALUES OF K
SEMI-INFINITE BREAKWATER
θ = 180°
R/L = 1
Legend
Run No
5
7
9
17
Run No
22
24
25
26
27
Theory
No Reflection
K
α°
0.6
0.5
0.4
0.3
0.2
0.1
0
0 10 20 30 40 50 60 70 80 90

Table II Results of Experiments in Semi – infinite Breakwater With No Reflection

θ = 45°

R/L	Run No / α°	EXPERIMENTAL K 18	19	20	37	Average	THEORETICAL K Full Reflection	No Reflection
1	0	56	52	64	49	55	589	500
	7 5	45	45	55	49	48		
	15	45	40	44	47	44	469	348
	22 5	43	30	42	41	39		
	30	39	27	39	38	36	402	251
	37 5	40	24	34		33		
2	0	53	57	58	67	56	561	500
	7 5	42	35	39	46	40		
	15	34	30	40	39	36	289	302
	22 5	26	30	40	31	32		
	30	25	27	37	28	29	308	197
	37 5	30	15	28	23	24		
3	0	48	59	61		56	549	500
	7 5	28	47	56		44		
	15	30	30	31		30	344	272
	22 5	25	21	26		27		
	30	24		22		23	259	168
	37 5	28						
Depth (in)		4 5	4 5	6 0	5 0			
Period (sec)		557	657	628	517			
L_t (in)		17 5	22 4	22 5	15 8			
H_I' (mm)		19 0	19 3	23 7	19 7			

θ = 60°

R/L	Run No / α°	EXPERIMENTAL K 29	33	34	35	36	39	Average	THEORETICAL K Full Reflection	No Reflection
1	0	54	46	56	40	49	51	49	571	500
	7 5	49		46	37	42	42	43		
	15	43	36	35	32	36	35	36	440	348
	22 5	41		27	30	31	32	32		
	30	37	29	19	26	27	26	27	380	251
	37 5	26		13	25	25	25	22		
	45	26	19	13	19	21	22	19	318	191
	52 5	27		15	13	18		18		
	60						21		305	153
2	0	60	52	49	30	43	42	47	549	500
	7 5	41		37	38	33	39	37		
	15	36	28	27	25	27	32	28	369	302
	22 5	33		23	20	28	30	24		
	30	35	19	19	18	24	21	20	276	197
	37 5	28		17	16	21	19	18		
	45	20	14	10	15	15	16	14	234	142
	52 5	16		08	05	15	18	13		
	60						16		222	111
3	0			40	41	50		44	539	500
	7 5			31	40	36		36		
	15			28	26	25		27	327	272
	22 5			25	15	18		19		
	30			23	15	16		15	232	168
	37 5				10	13		12		
	45					14			193	118
Depth (in)		6 0	6 0	6 0	5 0	5 0	5 0			
Period (sec)		626	590	392	599	533	515			
L_t (in)		22 4	20 3	19 8	20 1	18 6	15 7			
H_I' (mm)		23 2	24 8	26 5	20 0	16 8	21 6			

θ = 90°

R/L	Run No / α°	EXPERIMENTAL K 10	12	17	31	32	38	Average	K_t No Reflection
1	0	53	45		48	48	49	49	500
	7 5	38	37		42	33	31	36	368
	15	30	25	26		31	28	28	251
	22 5	18	20		23	19	18	20	191
	30	18	13		16	18	15	14	153
	45	13				11	13	12	120
	60						13		111
2	0	49	55		44	46	48	49	500
	7 5				44				
	15	27	31		30	31	34	38	302
	22 5				24				
	30	21	28		19	22	18	20	197
	37 5				15				
	45	12	19		11	17	15	15	142
	60	09	08			11	13	10	111
	75	10					10	10	092
	90						09		079
3	0	49	43	68			51	48	500
	7 5		39				31		
	15	27	33	31			26	29	272
	22 5		23	24			22		
	30	15	16	13			13	16	168
	37 5		12						
	45	13	11					11	118
	60						10		091
	75						07		075
	90						07		065
Depth (in)		4 5	4 5	4 5	6 0	6 0	5 0		
Period (sec)		500	630	607	381	590	510		
L_t (in)		14 6	20 5	20 0	19 8	28 2	13.4		
H_I' (mm)		23 5	24 5	27 2	28 2	24 0	19 5		

θ = 120°

R/L	Run No / α°	Experimental K 20	21	Average	Theoretical K No Reflection
1	0	50	48	49	500
	7 5	41	42	41	
	15	31	32	32	368
	22 5	25	29	27	
	30	22	21	22	251
	37 5	20	16	18	
	45	16	16	16	191
	52 5	15	15	15	
	60				153
2	0	45	46	46	500
	7 5	32	31	32	
	15	26	28	27	302
	22 5	24	27	25	
	30	19	25	22	192
	37 5	14	18	16	
	45		13	13	142
	52 5		10	10	
3	0	38	39	49	500
	7 5	44	35	40	
	15	28	25	23	272
	22 5	14	19	17	
	30	16	18	17	168
	37 5	14	15	15	
	45				118
Depth (in)		4 5	4 5		
Period (sec)		651	536		
L_t (in)		22 1	16 5		
H_I' (mm)		21 6	19 5		

θ = 180°

R/L	Run No / α°	EXPERIMENTAL K 3	7	9	17	22	24	25	26	27	Average	K_t No Reflection
1	0	50	50	51	49	46	49	42	55	59	50	500
	7 5			40			43	37	46	55	44	
	15	35	34	34	35	33	37	32	32	40	35	348
	22 5						26	27	25	32	28	
	30	21	20	21	24	27	23	23	22	26	23	251
	37 5						16	18	18	28	18	
	45	14	11	13	15	20	12	15	16	17	15	191
	52 5							12	15	13	13	
	60	14	09	08	10	14		10			11	153
	75	11										128
	90	13										111
2	0	53	51	49	52	53	50	47		46	50	500
	7 5			34	35		36	31		42	36	
	15	31	21	16	21	39	23	25		32	26	302
	22 5				19		23	23		32	28	
	30		16		21	16	19	19		23	19	197
	37 5				18		13	15		15	15	
	45				13	14		14		08	12	142
	52 5							08				
	60					10						111
3	0			49	49	48	55	45		63	51	500
	7 5			37	31	37	39	39		45	39	
	15			17	26	27	28	16		25	23	272
	22 5					16	23	09		21	17	
	30					11	14			19	15	168
	37 5									15		
	45											118
Depth (in)		4 6	4.4	4 5	4 5	4 5	6.0	6 0	6 0	6 0		
Period (sec)		370	604	691	607	517	637	585	630	622		
L_t (in)		18 1	19 8	24 1	20 0	15 5	23 1	20 0	22 6	22 2		
H_I' (mm)		36	32	30 5	27 2	25 3	23 7	25 7	34 2	30 0		

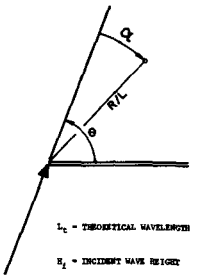

L_t = THEORETICAL WAVELENGTH

H_I = INCIDENT WAVE HEIGHT

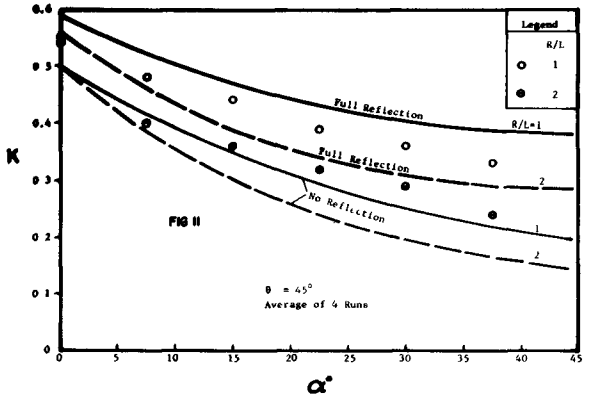

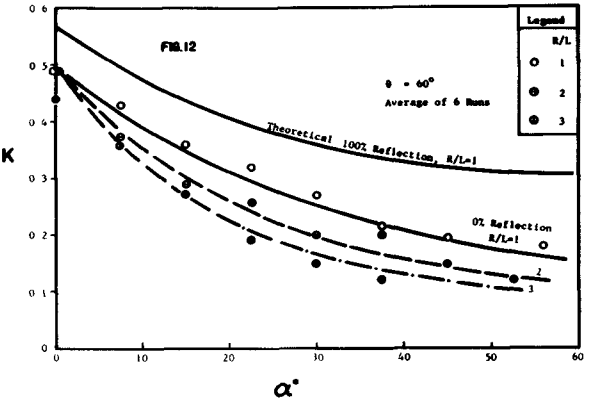

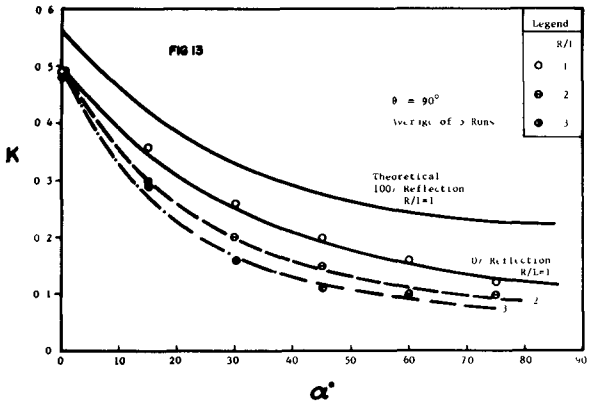

FIGS 11, 12, 13 THEORETICAL AND EXPERIMENTAL VALUES OF DIFFRACTION COEFFICIENT (K), SEMI-INFINITE BREAKWATER, NO REFLECTION

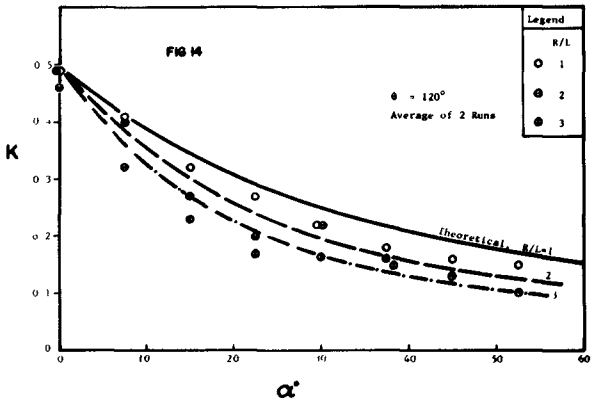

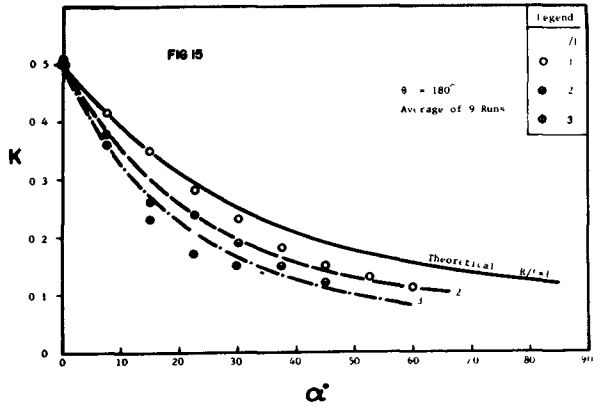

FIGS 14, 15 THEORETICAL AND EXPERIMENTAL VALUES OF DIFFRACTION COEFFICIENT (K), SEMI-INFINITE BREAKWATER, NO REFLECTION

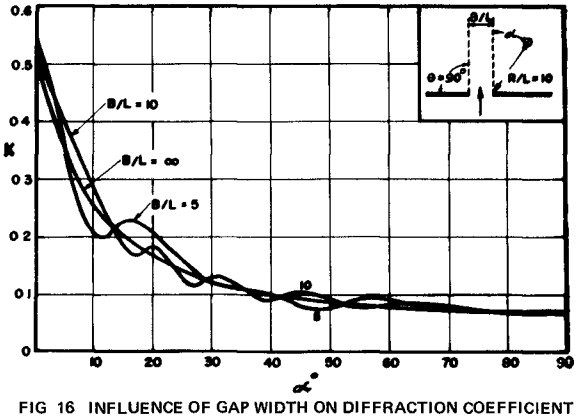

FIG 16 INFLUENCE OF GAP WIDTH ON DIFFRACTION COEFFICIENT

BREAKWATER GAP

Where two breakwaters are aligned and full reflection is realised from each, the waves in each shadow zone are comprised of the incident wave and the two reflected waves Since the crest curvature of one of these is not centered on the breakwater tip of the incident and other reflected wave, the resultant wave height measured along the arc length fluctuates about the smooth curve of the semi-infinite breakwater solution. This is illustrated in Figure 16, where it can be observed that the deviations increase as the gap width decreases. Down to the value of B/L = 5 the semi-infinite breakwater solution can be used without great loss of accuracy. Where no reflection occurs such undulations are not present as noted in the experiments reported herein, which are essentially half a breakwater gap without the reflection component.

APPLICATION OF SOMMERFELD'S SOLUTION[4]

It can be shown, by graphing values of K and R/L in Table I, that the wave height is reduced in proportion to $(R/L)^{\frac{1}{2}}$. This suggests a parameter $K\sqrt{R/L}$ for combining radial and arc distance influences. It is also convenient to centre the polar coordinate at the mid-point of the breakwater gap. In the knowledge that for R > 5B the value of $K\sqrt{R/L}$ is essentially constant for any α a simple series of graphs can represent conditions anywhere in the protected basin. An example of this is Figure 17, which is drawn for R/L = 20, the largest probable radius to be encompassed In the absence of reflection, the fluctuations exhibited in Figure 17 will not be present, so that averaging them should not involve undue error in a prototype situation Figure 18 results for $\theta = 90^{o}$ and $B/L \leq R/L \leq 20$, in which curves are grouped into two categories· R/B = 1 and R/B > 1. For gaps smaller than 2L the single curve (full line) represents both cases of R/B

The above simplifications lead to a maximum error in $K\sqrt{R/L}$ of $\pm$ 0.3 at the maxima and minima of the undulations (See Figure 17). The average deviation is in the order of $\pm$ 0.2. Since reflection is likely to be much smaller than 100% these errors appear acceptable. Although Figure 18 applies only to $\theta = 90^{o}$, other angles can be treated by the method suggested by Blue and Johnson[8][9], in which the equivalent width B′ is used for the angle θ (See inset of figure).

MORSE-RUBENSTEIN SOLUTION

For gap widths of 3L and less an exact solution in optics has been derived by Morse and Rubenstein[10], and applied to water waves by Carr and Stelzriede[11], to which the reader is referred for the relevant equations. The computation procedure is tedious, but a graphical solution is provided in Reference No (11)

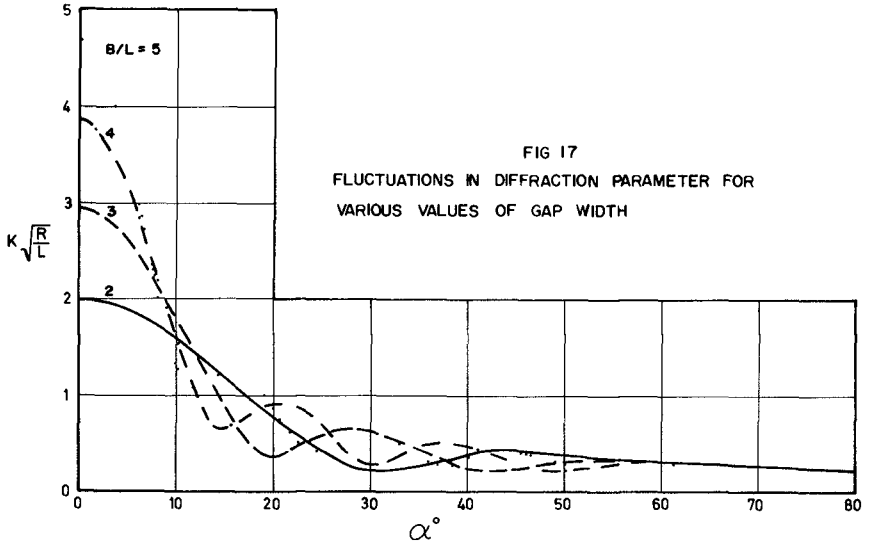

FIG 17
FLUCTUATIONS IN DIFFRACTION PARAMETER FOR VARIOUS VALUES OF GAP WIDTH

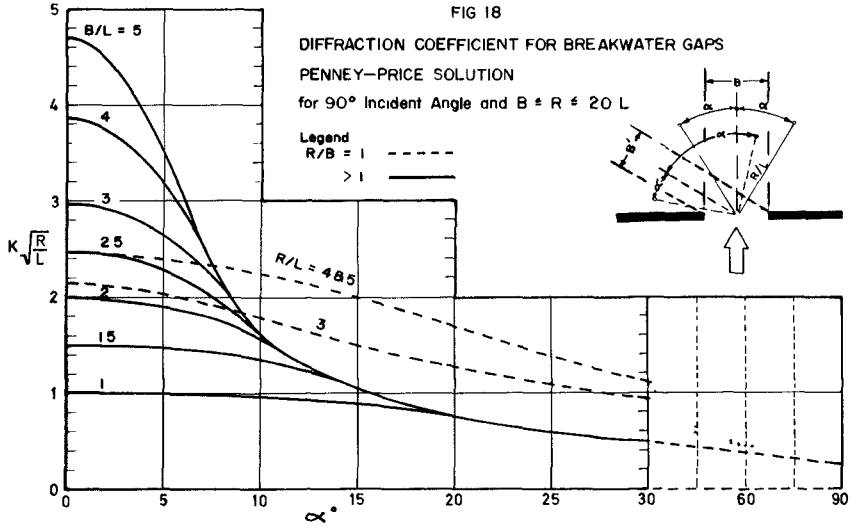

FIG 18
DIFFRACTION COEFFICIENT FOR BREAKWATER GAPS
PENNEY–PRICE SOLUTION
for 90° Incident Angle and B ≤ R ≤ 20 L

Using the previously derived parameter $K\sqrt{R/L}$, graphs for $B/L_o = 0.5$, 1 0 and 2 0 are presented in Figure 19 for incident angles of 30^o, 60^o and 90^o These are applicable to zones where $R > B$

LACOMBE'S SOLUTION

Lacombe[12] has derived an approximate solution which is based upon a polar coordinate system centered on the mid-gap point It applies to $R > B$ and is best used to determine the maxima values in the fluctuations previously discussed For $B \geq 2L$ the solution is close to that of Morse-Rubenstein.

COMPARISON OF SOLUTIONS

For the smaller gap widths ($B \leq 2L$) a direct comparison of the above mentioned solutions is possible As seen in Figures 20 and 21 the solution of Penney and Price[4] is extremely close to that of Morse and Rubenstein, for the incident angle of 90^o and to the limit of α to which the latter is carried For this same normal incidence the Lacombe approximation is sensibly the same It is not until $\theta = 30^o$ that major deviations occur between the Lacombe and Morse-Rubenstein solutions. The latter should be preferred for design purposes because of its conservative tendencies

EXPERIMENTAL EVIDENCE

Blue[13] carried out extensive model tests on diffraction behind a breakwater gap His measurements were made on a square grid system, which had to be converted to the polar coordinate system. Only those results could be used, therefore, which approximated the B/L value for the theory. The points plotted in Figures 22 and 23 suffer extreme scatter, which is probably due in part to the variety of depth/wavelength and height/length ratios used, both of which would have influenced the degree of reflection from the vertical walls of the model breakwaters The results as presented cannot be accepted as verification of the theoretical curves, so that further practical work appears necessary. In order to exclude the reflect on component, tests similar to those reported herein are indicated, the only difference being the width of the approach channel in respect to the wave length. No drastic differences in wave attenuation should be expected, since the only change is the limited crest length from which the diffraction energy is supplied

CONCLUSIONS

SEMI-INFINITE BREAKWATER

1. The theoretical value of diffraction coefficient for a semi-infinite breakwater can be divided for engineering purposes into two components, arising respectively from the incident and reflected waves.

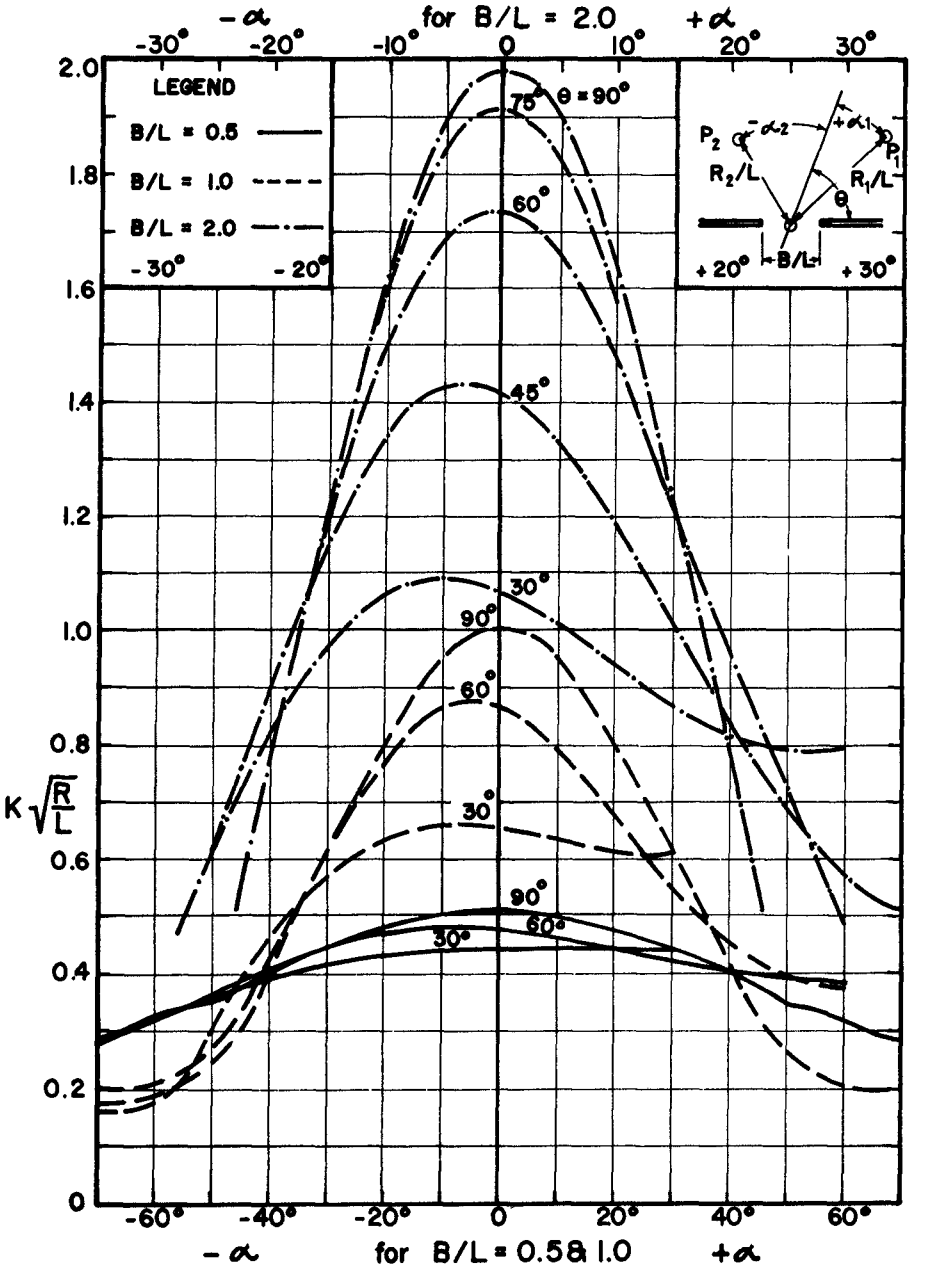

FIG. 19 K FOR B/L = 0.5, 1 & 2 AND θ = 30°, 60° & 90°

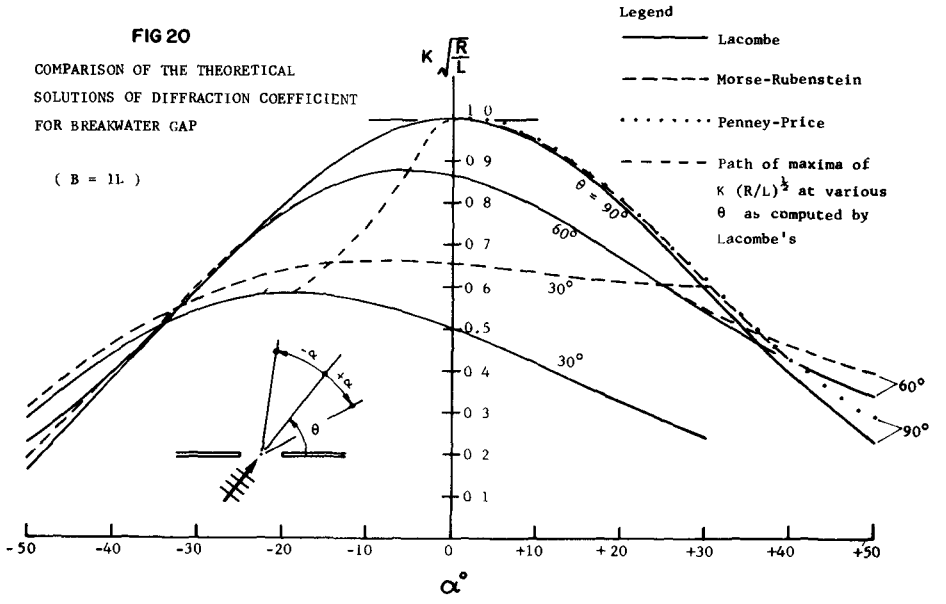
FIG 20
COMPARISON OF THE THEORETICAL
SOLUTIONS OF DIFFRACTION COEFFICIENT
FOR BREAKWATER GAP
(B = 1L)
Legend
Lacombe
Morse-Rubenstein
Penney-Price
Path of maxima of
K (R/L)^½ at various
θ as computed by
Lacombe's
K √(R/L)
1 0
0 9
0 8
0 7
0 6
0.5
0 4
0 3
0 2
0 1
θ = 90°
60°
30°
30°
60°
90°
-α
+α
θ
- 50
-40
-30
-20
-10
0
+10
+ 20
+30
+40
+50
α°

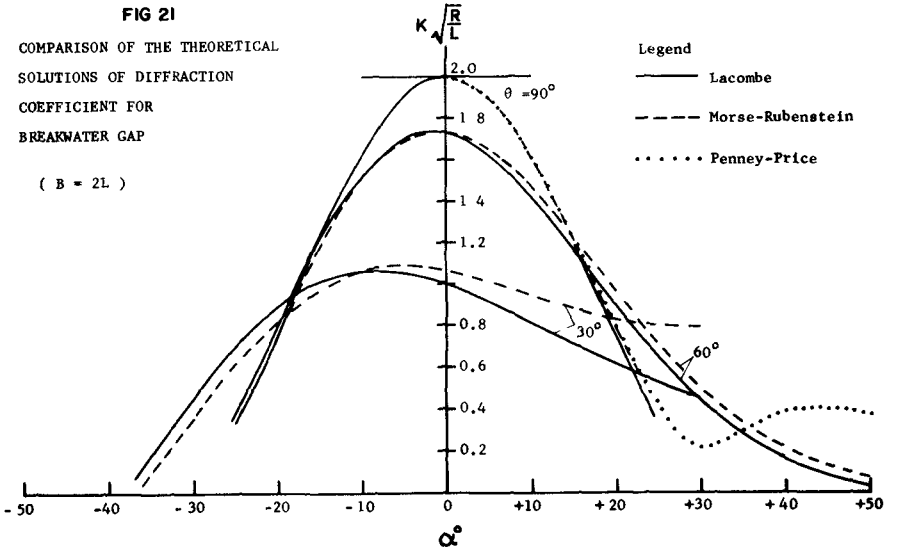
FIG 21
COMPARISON OF THE THEORETICAL
SOLUTIONS OF DIFFRACTION
COEFFICIENT FOR
BREAKWATER GAP
(B = 2L)
K √(R/L)
Legend
Lacombe
Morse-Rubenstein
Penney-Price
2.0
1 8
1 4
1.2
0.8
0.6
0.4
0.2
θ =90°
30°
60°
- 50
-40
- 30
-20
- 10
0
+10
+ 20
+30
+ 40
+50
α°

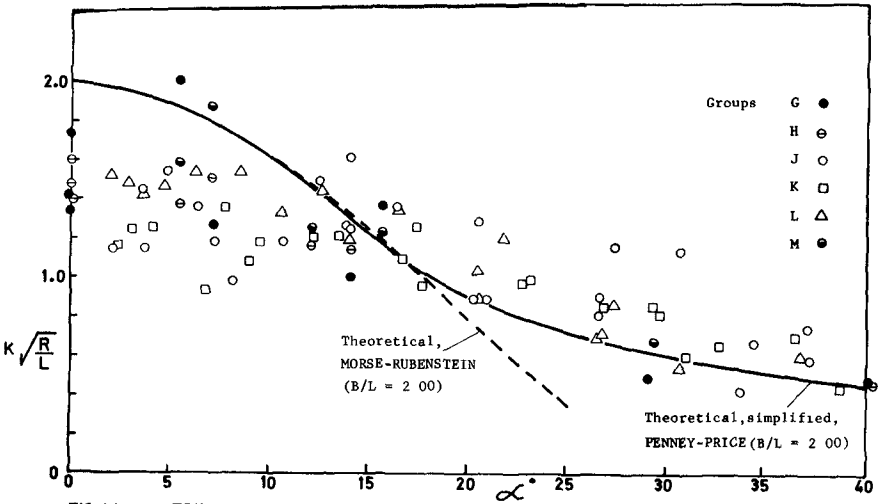

FIG 22 EXPERIMENTAL RESULTS FROM BLUE (13) FOR B/L = 1 95 AND R/L = 4 TO 10 (GROUPS REFER TO ORIGINAL REFERENCE)

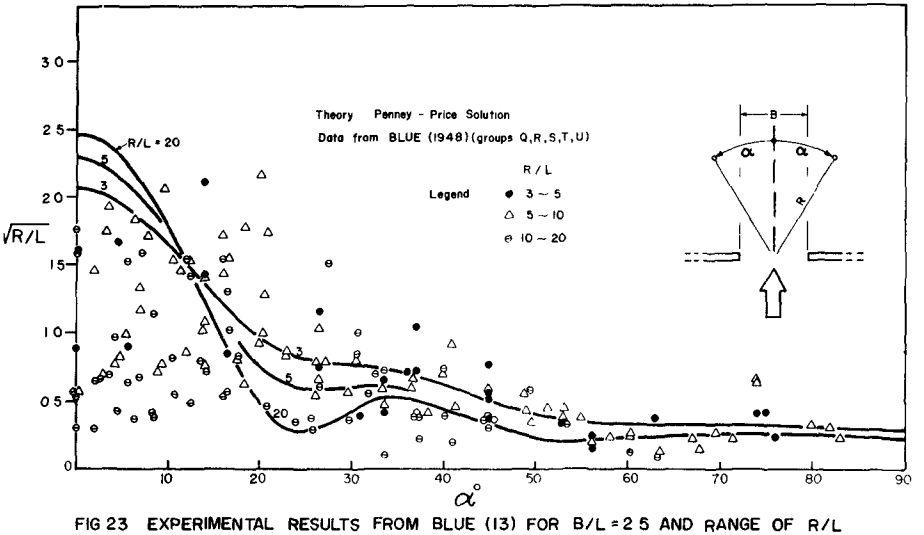

FIG 23 EXPERIMENTAL RESULTS FROM BLUE (13) FOR B/L = 2 5 AND RANGE OF R/L

2. The diffraction coefficient from (1) above can be presented in a simple table or graph which involves an angular measure and distance from the breakwater tip. The incident and reflection components determined from the angle through which diffraction takes place, are additive.

3. The sensibly constant profile along the nearly circular crests of the diffracting waves permits a simplified presentation of diffraction coefficient for arc distances from the shadow line, which covers a wide range of incidence angle and radial distance Various degrees of reflection from the breakwater can be incorporated into the diffracted wave height

4. Experimental evidence confirms the reflection component approach. It also verifies the zero reflection solution for incident angles from 60^{o} to 150^{o} inclusive. For lesser angles an addition of 0.1 in the diffraction coefficient is recommended.

BREAKWATER GAP

5 The various theoretical solutions for wave diffraction behind a breakwater gap give very similar results for incident angles approaching 90^{o} Only when the angle is less than 45^{o} do deviations become pronounced.

6. The simplest presentation of data results from the use of the parameter $K\sqrt{R/L}$, together with a polar coordinate system based upon the incident orthogonal passing through the mid-point of the gap.

7 Results from past experiments on the breakwater gap contain too much scatter to verify the theory, indicating the need for further work in this direction.

ACKNOWLEDGEMENTS

During the course of this research the junior author was in receipt of a scholarship at the Asian Institute of Technology, formerly the SEATO Graduate School of Engineering. The wave probe was kindly lent by the University of Western Australia, where it was developed by the senior author.

REFERENCES

(1) Fan S.H., J.E. Cumming and R.L. Wiegel "Computed Solution of Wave Diffraction by Semi-Infinite Breakwater" University of California, Berkeley, Tech. Rep. HEL-1-8, 1967.

(2) Sommerfeld A. "Mathematische Theorie der Diffraction" Math. Ann. No.47, 1896, 317-374.

(3) Penney W.G and Price A.T. "Diffraction of Sea Waves by Breakwaters" Directorate of Miscellaneous Weapons Development. Technical History No.26, Artificial Harbour, Sec.3D.

(4) Penney W.G and Price A.T. "The Diffraction Theory of Sea Waves by Breakwaters" Phil. Trans. Roy. Soc. (London) A244, 1952, 236-253.

(5) Larras J. "Diffraction de la Houle par les Obstacles Rectilignes Semi-indefinis sous Incidence Oblique" Cahiers Océanographiques 18, 1966, 661-667.

(6) Putman J.A. and R.S. Arthur "Diffraction of Water Waves by Breakwaters" Trans Am. Geoph. Un 29, 1948, 481-490.

(7) Lim T.K. "Wave Diffraction" M.Eng. Thesis, Asian Institute of Technology, Bangkok, Thailand, 1968.

(8) Blue F.L. and J.W. Johnson "Diffraction of Water Waves Passing Through a Breakwater Gap" Trans. Am Geoph. Un. 30, 1949, 705-718.

(9) Johnson J.W. "Generalised Wave Diffraction Diagrams" Proc. 2nd Conf. Coastal Eng., 1952, 6-23.

(10) Morse P.M. and P.J. Rubenstein "The Diffraction of Waves by Ribbons and Slits" Physical Review No.54, 1938, 895-898.

(11) Carr J.H. and M.E. Stelzriede "Diffraction of Water Waves by Breakwaters" Gravity Waves, U.S. Natl Bur. Stds., Circ. No.521, 1952, 109-125.

(12) Lacombe H. "The Diffraction of a Swell. A Practical Approximate Solution and its Justification" Gravity Waves, U.S. Natl. Bur. Stds., Circ. No.521, 1952, 129-140.

(13) Blue F.L. "Diffraction of Water Waves Passing Through a Breakwater Gap" Ph. D. Thesis in Civil Engineering, University of California, Berkeley, 1948

PART 2

COASTAL SEDIMENT PROBLEMS

CHAPTER 17

SYSTEMATIC COLLECTION OF BEACH DATA

Dennis W. Berg
Coastal Engineering Research Center
Washington, D. C

ABSTRACT

Theoretical considerations of beach behavior are often hampered by a lack of systematically obtained data sets which reflect the beach environment. For specific studies, lack of time and money often prevent the collection of such data sets. Thus, any opportunity for the collection of such data, on a routine basis, should be fully exploited [1]

In 1967, the U S Army Corps of Engineers and the State of California initiated a cooperative program to collect empirical data at selected locations along the California coast. The objective was to establish a reservoir of repetitive, systematic observations, by qualified personnel, with the hope of securing a better understanding of the physical characteristics of the California shore and the littoral processes occurring there.

Once a sufficient volume of data has been collected, analysis of the data will begin with the aim of determining meaningful correlations between the various recorded parameters.

The number of distinct observations and sites dictated standardized observational procedures and recording methods amenable to automatic processing Observational methods and a recording form were designed to provide a base of comparison and an efficient means of processing the expected large volume of data Investigation of various methods of recording data led to the design of a suitable optical scanning form. This form, completed in the field by individual observers, can automatically be converted to punched cards for further processing Experience in collecting similar data in connection with other studies of the Coastal Engineering Research Center influenced the selection of comparatively inexpensive instruments for data collection.

Approximately 50 observation sites, extending from the Oregon-California boundary to the United States-Mexican border are presently contributing data. These sites represent a wide variety of shore types, beach sediments, geographic orientations, and morphology It is anticipated that future expansion of this program will include sites other than those directly controlled by State agencies and will allow a more detailed description of the California shore Although not presently programmed, the extension of this study to other coastal areas of the United States where little or no information is presently available would be desirable, and could provide the necessary background for more comprehensive description of the overall behavior of the littoral zone

INTRODUCTION

BACKGROUND

Although increasing emphasis is being placed on investigative study of the deep oceans, the boundary zones of the lands and seas remain generally unknown areas and of concern to relatively few investigators. In some respects, this classically forsaken zone should invite greater concern, for it is here that man leaves one environment

[1] The field collection of data, laboratory procedures and consequent study here reported are being carried out in connection with the general research program of the U S Army Corps of Engineers, Coastal Engineering Research Center However, the interpretations expressed are those of the author and are not necessarily concurred in by the Corps of Engineers. Permission granted by the Chief of Engineers to publish the information contained herein is appreciated

to enter another This general lack of active interest can certainly be partially attributed to the complex problems that confront those investigators intrepid enough to evince an interest, this boundary or littoral zone has all these forces and problems associated individually with land or sea occurring here in strange and unwonted interfusion.

However, despite this somewhat bleak prognosis, knowledge of the littoral zone and its many interacting forces has increased markedly in recent times, although a great deal is still to be learned Theoretical studies of shorelines, designed to increase our understanding of the environment are often hampered by a lack of systematically obtained data sets which adequately reflect the dynamic character of the littoral zone. For specific, project-oriented studies, a lack of time and money generally prevents the collection of statistically significant data sets, this expediency often imposes misleading conclusions, resulting in projects that fail from the outset or are of only limited success. Thus, whenever an opportunity for the collection of environmental data on the littoral zone occurs, the occasion should be fully exploited and supported.

In late 1966, such an opportunity occurred when the State of California proposed the collection of empirical data at selected sites along the California Coast, utilizing available State Park employees in order to document beach configurations. Due to the large volume of information that would ultimately be developed in a program of this type, the U. S. Army Corps of Engineers was asked to cooperatively participate in the study and act as custodian of all collected data with a possible overview toward compiling the data so obtained to eventually prepare a suitable summary report. The Coastal Engineering Research Center (CERC), the primary representative of the Corps in this field, accepted the proposal, provided that the data would be obtained and furnished in reasonably complete sets on a regular and systematic basis

The ultimate aim of the proposed data collection program was to establish a reservoir of repetitive, systematic observations which would be compiled and made available to the scientific community for applicable analytic study. The results of such studies would hopefully result in an increased understanding of the littoral environment and more particularly, greater knowledge of the physical characteristics of the California shore and the littoral processes taking place.

STUDY CONCEPT

Early in 1967, after a series of meetings between representatives of all interested parties, the State of California began a test collection of field data at New Brighton State Beach located at the north end of Monterey Bay, primarily for the purpose of evaluating the extent of effort required by individuals to make a specified number of observations. Since the proposed study would utilize the employees of California as the observers, the collection of any data would necessarily be in addition to their regular duties, and could not unduly interfere with their normal routine. This initial test satisfactorily confirmed the feasibility of using such employees as observers. During the test, twice daily observations were made of surf characteristics, i.e , wave height and period, as well as direction of wave

origin, tide level, and measurements of the location and elevation of the beach berm crest with respect to a reference point and an arbitrary datum Additionally, panoramic photographs of the beach were taken weekly.

At the outset of planning and coordination of this study, it was readily apparent that the intended scope of the study would yield a large volume of data, of the order of 30,000 bits of information per month, which if improperly recorded and processed would negate the value of the data collected It was envisioned that approximately 70 observation sites would be included in the study in order to yield data on a variety of shore conditions. The number of distinct observations and sites dictated standardized observational procedures for logical compatibility of data and recording methods amenable to automatic processing of the data Experience in collecting similar data in connection with other studies of the Coastal Engineering Research Center influenced the selection of the particular observations and a limited number of comparatively inexpensive instruments for making the observations. The experiences of the Center and of others in various methods of recording data was investigated, and this led to the design of a specialized form employing optical scanning techniques to facilitate automatic processing of data

Based on the results of the test at New Brighton State Beach and of other similar studies, the parameters selected for observation include

1 Surf observation (twice daily)

   a. Wave period
   b. Wave height
   c. Wave direction
   d. Type of breaking wave

2. Wind observations (twice daily)

   a. Velocity
   b. Direction

3 Beach observations (once daily)

   a. Beach berm crest elevation referred to some specific datum
   b. Beach berm crest distance from an established reference station
   c. Foreshore slope angle

4 Littoral current observations (once daily)

   a. Velocity
   b. Direction

5 Tide level (twice daily)

6. Presence of rip currents (twice daily)

7. Presence of beach cusps (twice daily)

8. Panoramic photographs of the observation site (monthly)

9. Collection of representative beach materials (monthly)

10. Water temperature (twice daily, this factor is observed only if it is obtained for other purposes as a normal procedure at a particular site).

11. Reports of any unusual occurrences.

Additionally, periodic visits by Corps of Engineers personnel to each observation site will be made to ensure that correct observational procedures are being consistently practiced and to emphasize and explain the importance to the study of doing so.

PROCEDURES

SITE SELECTION

As originally proposed by the State of California, observation sites would be established at selected beaches and shoreline parks, operated and staffed on a full year basis by the Department of Natural Resources, Division of Beaches and Parks. In the final selection of the observation sites, consideration beyond personnel availability was given to the need for data to assist in the planning, design, construction or maintenance of coastal works in an area, correlation of the observed data with existing or planned basic data collection programs, general shore conditions, i.e., a variety of shore exposures, orientations and beach configurations, and spacing of sites to give the greatest coverage with the fewest locations Within those shoreline segments where there are no State operated beaches but where the collection of data is desirable, locally operated beaches and parks have been included.

Of over 80 beaches operated under State direction, 39 observation sites have been established and are submitting data Additional sites will be added as the State expands its recreational program, and stations personnel at more beaches. Further, there are approximately 20 observation sites operated by local agencies which are being added to the study. A map of California with the locations of the active observation sites is shown in Figure 1. As previusly noted, the shoreline conditions vary at each site and typical illustrations of these conditions are shown in Figure 2. Conditions vary from pocket beaches to long, uninterrupted shores, and from heavily populated areas to remote, uninhabited shores.

INSTRUCTIONS, RECORDING FORMS AND INSTRUMENTS

To minimize variance in data collection methods by the large number of individuals involved, a set of instructions describing the preferred methods of observation was prepared and distributed to each site The instructions for each item, arranged in the same sequence as these items appear on the actual recording form, consist of short,

concise statements relative to each individual parameter and the manner in which each observation is to be made. These instructions, illustrated in Figure 3, have been laminated with plastic to facilitate their use in the field as a ready reference at the actual site In addition to these instructions, brief statements concerning individual observations have also been printed on the data recording form to facilitate the observational procedures.

The form on which the observations are recorded has been designed for automatic processing through an IBM 1231/1232, optical mark page reader, which converts the data to acceptable computer language[4]*. Once the value of an individual observation has been determined, the data is recorded on the form shown in Figure 4 by filling in the appropriate blanks with an ordinary lead pencil.

Two comparatively inexpensive instruments have been selected for measurement of the three parameters, wind velocity, elevation of the beach berm crest and the angle of the foreshore slope. A Dwyer Wind Meter, shown in Figure 5, is used to measure the wind velocity rather than using visual estimates such as Beaufort Wind Scales. The instrument's simplicity of construction and use, as well as its comparative accuracy assures compatibility of data between observation sites An Abney Topographic Hand Level allows the measurement of the beach berm crest elevation in the normal manner, the angle of the foreshore slope is measured by using the level as an inclinometer. Use of the Abney Level in the latter fashion is shown in Figure 6.

Each site has also been supplied with a measuring tape, a supply of plastic bags for collecting samples of the beach materials, a supply of fluorescein or rhodamine B dye for use in observing the littoral current patterns, cameras, film and sturdy envelopes for mailing the data to the Coastal Engineering Research Center.

METHODS OF OBSERVATION

At each observation site, a permanent reference point with a known elevation has been established near the shoreline. Observations are referred to this station so that all subsequent data sets can be used to reflect variations of the littoral environment from a fixed reference. The observations are made during a normal inspection of the shoreline by personnel assigned to the area. These inspection tours usually occur twice a day so that two sets of observations are possible each day at each site. The various instruments, instructions and recording forms require no special handling and can easily be carried by the observer during his normal tour. Once on station, observation of the desired parameters by following the procedures outlined in the instructions and on the data-recording form is a simple task requiring approximately 20 minutes.

Observed data is forwarded to the Coastal Engineering Research Center on a weekly basis, samples of the beach materials and photographs (obtained monthly) are mailed as taken

OFFICE PROCEDURES

At CERC, the data is processed through an optical mark page reader and converted

*Numbers in parentheses refer to References at end of report.

to standard punched data cards which are stored for analysis in future studies The only data reduction now planned is the compilation and data printout of the observations. However, once a statistically significant volume of data has been accumulated, detailed studies of data will be started to seek meaningful correlations between the various parameters.

Granulometric analysis of beach materials is accomplished on a routine basis by the Geology Branch of the Coastal Engineering Research Center as the samples are received. Utilizing a rapid sediment analyzer similar to that described by Schlee[5], size distributional characteristics of the samples are calculated by computer techniques and include cumulative size-frequency distribution, median and mean diameters, standard deviation, skewness and kurtosis of each sample. Presently, this is the only analysis being made of the beach material samples, however, the samples are being retained so that other types of analysis (compositional, heavy mineral, etc.) can be made by investigators in the future if deemed desirable.

EXAMPLES OF USE FOR COLLECTED DATA

Although no detailed studies of the submitted data have yet been accomplished, several possible methods of investigation are discernible when scanning the observation forms and the results of beach material analysis and photographs. Examples of these methods of investigation are illustrated, but are not intended as a complete catalogue of possible uses. Illustrative examples represent only minimum analysis. It is believed that the information will have many more uses beyond those suggested by the author

SURF AND BEACH OBSERVATIONS

Data from an observation site has been randomly selected to illustrate the possible correlations of the surf and beach observations. Approximately 60 days of record for Seacliff State Beach on Monterey Bay, collected during the spring of 1968, are shown in Figure 7 Although there are lapses of several days each in the record, apparently caused by lack of manpower at these times to collect the data, the record is essentially complete and is open to several qualitative interpretations.

For example, the data in Figure 7 shows for the recorded period that the waves were small, varying from 1 to 4 feet in height, had rather long periods, averaging slightly higher than 10 seconds and they originated from a distant generating area in the southwest quadrant. Generally, the waves broke on the shore as spilling waves. The overall response of the shore to these waves resulted in an accreting beach characterized by a lowering berm crest with a gentle foreshore slope.

Qualitatively, it can be stated that the predominant wave climate during this period was conducive to movement of available littoral materials toward the observation site and allowed it to remain in the area. Additional data will, in all probability, record varying responses during other periods of the year. Studies by Shepard[6] and Trask[7] have shown that California beaches undergo annual cycles with general erosion of the beaches occurring during the winter months when large, steep waves accompanying storms out of the northwest predominate, and accretion during the summer months of southwesterly sea swells which return sand to the upper portion of the beach profile.

This type of data, once more of it has been accumulated and processed, will assist various individuals and agencies in project oriented studies of the California shores. A case in point is a recent report of the Corps of Engineers Los Angeles District on Newport Beach, California[8], using data on beach sidths observed since 1954 by Mr. Robert E. Reed, Chief Lifeguard of that city This information, in conjunction with studies of a more conventional nature was used to predict the time when the beach would erode to a dangerous position, and require restoration by placing sand fill on the shore. A summary of Reed's data as used by the Los Angeles District is shown in Figure 8 This dat is similar to that being obtained in the cooperative program reported on, as indicated in the instructions and observation form and Figure 7.

Surf observations at locations on parts of the U. S. Coast other than those shown on Figure 1 are presently being analyzed at CERC under a different study[2] (cooperation with USCG), but data collected under any of these studies will be correlated with any that may be available from any of the other study programs Observations of the surf are intended to supplement more detailed study of waves using recording wave gages installed at various locations on the coastline of the United States[1]

Compilations of the observed data on surf characteristics and beach response should also prove useful in studies directed primarily toward the recreational aspects of the shore The ability to predict the overall characteristics of a beach for such uses as swimming and surfing will allow the appropriate agencies to assign various classifications for safety and use to the beaches.

BEACH MATERIALS ANALYSIS

As previously mentioned, analysis of sample beach materials received at CERC under this program is made by the Geology Branch The results of the analysis from the rapid sand analyzer are processed by computer methods yielding the size-frequency distributions of the individual samples as well as the computation of the statistical parameters which are descriptive of size distributions. Several typical examples of this process are shown in Table 1. The samples listed were all obtained on 1 July of this year and are representative of the type of analyses presently being made

Availability for comparison of the various parameters of the beach materials for many beach locations should result in additional understanding of the geomorphology of the California shore, and when correlated with all the other observed data, should enhance the understanding of shore characteristics in relation to the materials composing the beach. An example of such a comparison is shown in Table 2 where mean diameters and standard deviations of the beach samples have been listed for a number of observation sites. The data listed in Table 2 is based on analyses of samples taken during the spring of 1968. The locations are listed in a north to south direction as shown on Figure 1 and the variance in the physical characteristics of beach materials at different locations is indicated.

As directed in the study instructions shown in Figure 3, the samples of beach material are obtained from the wetted zone of the beach and although sampling is small compared to the whole beach area, hopefully the results of the sample analysis will bear some significant relationship to the physical characteristics of the materials forming the entire beach. It is already clear that there is substantial variation in

TABLE 1 - Typical Results of Computer Analysis of Beach Material Samples
Littoral Environment Observations

PHI Size	MM. Size	Frequency Percent	Cumulative Percent
Wright's Beach No 05021			
-1.00	2.000	.00	00
- .50	1.414	87.55	87.55
.00	1.000	10.98	98.52
.50	.707	1.48	100.00
1.00	.500	.00	100 00
1.50	.354	.00	100.00
2.00	.250	.00	100 00
2.50	.177	.00	100.00
3 00	125	.00	100 00
3 50	.088	.00	100.00
4.00	.062	.00	100.00
San Simeon Beach No 05009			
.50	.707	.00	.00
1.00	.500	23.17	23.17
1.50	.354	35.56	58 73
2.00	.250	29.18	87 91
2.50	.177	9.92	97 84
3.00	.125	2.16	100.00
3.50	.088	.00	100 00
4.00	.062	00	100.00
Carpinteria Beach No. 05014			
1.00	.500	.00	00
1.50	.354	11 25	11.25
2.00	.250	29.71	40.96
2.50	.177	37.91	78.88
3.00	.125	19.67	98.55
3.50	.088	1.45	100.00
4.00	.062	.00	100.00
Huntington Beach No. 05027			
.50	.707	.00	.00
1.00	.500	11.79	11 79
1.50	354	16.61	28.40
2.00	.250	22.21	50.61
2.50	.177	31.59	82.20
3.00	.125	16.34	98.54
3.50	.088	1.46	100.00
4.00	.062	.00	100.00

Sample taken 1 July 1968

STATISTICAL PARAMETERS

	PHI	MM
Median	- 64	1.562
Mean	-.63	1.552
Stand Dev.	18	1 136
Skewness	1 38	
Kurtosis	6.85	

Sample taken 1 July 1968

STATISTICAL PARAMETERS

	PHI	MM
Median	1.40	380
Mean	1 42	372
Stand Dev.	47	1 383
Skewness	46	
Kurtosis	2 62	

Sample taken 1 July 1968

STATISTICAL PARAMETERS

	PHI	MM
Median	2.13	.229
Mean	2 11	.232
Stand. Dev	.45	1.365
Skewness	.03	
Kurtosis	2.13	

Sample taken 1 July 1968

STATISTICAL PARAMETERS

	PHI	MM.
Median	1.99	.252
Mean	1.90	269
Stand. Dev.	.64	1.553
Skewness	-.36	
Kurtosis	2.28	

TABLE 2 - Comparison of Computer Derived Statistical Parameters for Beach Material Samples - Littoral Environment Observations

Location	Date of Sample	Mean Diameter φ Units	mm	Standard Deviation φ Units	mm.
Mackerricher	1 Apr 68	-0.05	1 04	+0 30	0.82
Russian Gulch	25 Apr 68	+1 70	0 31	+0.53	0.69
Van Damme	8 Apr 68	+0 10	0 93	+1 02	0 49
Manchester	11 May 68	+0.80	0.57	+0 80	0.57
Goat Rock	15 Apr 68	+0 10	0.93	+0.80	0.57
Wright's	15 Apr 68	+0.70	0 62	+0 87	0 55
Stinson	17 Apr 68	+2.15	0 23	+0.39	0 76
Thornton	15 Apr 68	+1 85	0 28	+0.39	0.76
Half Moon Bay	15 Apr 68	+0 50	0.71	+0.45	0.73
Natural Bridges	1 Apr 68	+1 60	0.33	+0.57	0.67
Twin Lakes	8 Apr 68	+1.25	0 42	+0.48	0 72
New Brighton	24 Mar 68	+2 10	0.23	+0 50	0.71
Seacliff	6 Apr 68	+2 00	0 25	+0 48	0.72
Sunset	5 Apr 68	+1 90	0.27	+0.42	0.75
Carmel River	6 Feb 68	+0.25	0 84	+0 57	0 67
San Simeon	9 Apr 68	+1.40	0.38	+0 45	0.73
Montana de Oro	1 Nov 67	+1 00	0.50	+0.63	0.65
Pismo	1 Apr 68	+2.40	0 19	+0.30	0.81
El Capitan	1 Apr 68	+2.10	0 23	+0 36	0.78
Carpinteria	1 Feb 68	+1.90	0 27	+0.42	0.75
San Buenaventura	1 Apr 68	+2.10	0.23	+0 42	0 75
McGrath	1 Apr 68	+0.70	0 62	+0.33	0 80
Point Mugu	1 May 68	+2 00	0.25	+0.36	0.78
Leo Carrillo	3 Jan 68	+1.35	0 39	+0.50	0 71
Bolsa Chica	6 Apr 68	+0 75	0.59	+0.60	0 66
Huntington	1 May 68	+1.75	0 30	+0.50	0.71
Newport	1 Apr 68	+1.40	0.38	+0.45	0.73
Doheny	26 Apr 68	+0.90	0 54	+0.70	0.62
San Clemente	19 Apr 68	+1 45	0 37	+0.50	0.71
Torrey Pines	18 Apr 68	+1.75	0 30	+0.42	0.75

TABLE 3 - Comparison of Variations in Mean Diameters of Beach Materials
Littoral Environment Observations

	Locations of Beaches							
	Thornton		San Simeon		San Buenaventura		Bolsa Chica	
Date	ϕ Units	mm.	ϕ Units	mm.	ϕ Units	mm	ϕ Units	mm
Oct 67	1 60	0 33	1.05	0.48	2 15	0 22	2 20	0 22
Nov 67	2 00	0 25	1 25	0.42	2 10	0 23	1 30	0.41
Dec 67	2 05	0.24	1 45	0.37	2 00	0 25	0 95	0 52
Jan 68	1 95	0.26	1 45	0 37	2 10	0.23	1 10	0 47
Feb 68	1 95	0.26	0.80	0.57	2.10	0 23	0.50	0.71
Mar 68	1 90	0 27	0 60	0 66	1.60	0 33	0.70	0 62
Apr 68	1.85	0 28	1 40	0.38	2 30	0 20	0.75	0 59
May 68	1 55	0.34	0 75	0 59	1.20	0 44	1.50	0 35
Jun 68			1 20	0 44	1.80	0 29	1 40	0 38

the composition of samples at different points in time from the same locations Table 3 lists the results of part of the beach material analyses for four observations sites for a 9-month period. It can be seen that the mean diameter of the materials varies considerably, especially for the observation sites at San Simeon and Bolsa Chica State Beaches. This variation may be a result of resorting and redistributing by increased storm action that is typical along the California Coast during the winter months but it cannot be directly attributed to any one factor until sufficient data has been collected and interpreted.

PHOTOGRAPHS OF OBSERVATION SITES

Photography has long been an accepted method of documenting the condition of beaches and shoreline structures and in many cases has been the only evidence gathered. The use of such photography in a number of studies has revealed changes which would otherwise have been impossible to describe without having resorted to difficult, expensive and time-consuming surveying techniques. A historical record of the New Jersey shoreline by Vesper and Essick[9] is an example of the judicious use of photography, a capsule commentary on the variations of a large segment of the coastline of the United States is placed in one brief, easy-to-comprehend, volume. However, ground photographs by themselves do not allow quantitative descriptions of the shoreline variations which occur, and therefore can only complement data of a more conventional nature For this reason, panoramic photographs of each observation site are taken monthly. The photographs reveal the general conditions at each site which cannot be recorded on the observation form It is felt that the photographs will allow an investigator studying the data to form impressions of the observation sites which would not be otherwise possible unless he actually visited each site, and will hopefully assist in the interpretations of the data.

A series of photographs, acquired under this study, are shown in Figures 9 and 10. Three overall views of El Capitan State Beach, plus three views to the south of the actual observation point at this beach are shown in Figure 9. Several recognizable landmarks are clearly discernible in all six photographs, such as the small grove of trees and the stone groin in the background, and these assist in the evaluation of the general beach condition. It can be seen that in November 1967 the beach was generally broad, with a gentle foreshore slope, and had at least two berms, in January 1968 the beach was slightly narrower, having been recently affected by storm waves as indicated by the cuspate tonal difference of the sand above the waterline in the left photograph and the beach scarp in the right photograph. An added inference is that wave conditions were conducive to the formation of beach cusps at the time the photographs were taken By March 1968, the beach is still narrower and again shows recent effects of storms as denoted by seaweed and debris on the shore in the left photograph and the beach scarp, considerably larger than that shown in the photograph for January 1968, on the right.

Figure 10 is a series of six photographs taken at Natural Bridges State Beach over the period November 1967 through April 1968 The variation in the condition of the beach which is easily noted in these photographs reflects a seasonal cycle at this observation site.

Detailed analysis of other observed data should be concurrently considered in order to confirm these conclusions but the photographs do allow rather quick analysis of overall beach conditions. All of the photographs taken at each observation site are being filed at the Coastal Engineering Research Center and will become a part of the data bank for future analytic studies.

STUDY SUPPORT

As stated, this study is a cooperative effort of the State of California and the U. S. Army Corps of Engineers. The State, acting through the Department of Natural Resources Division of Beaches and Parks provides the necessary manpower for the collection of data. The cost of this manpower contribution at present far exceeds the other efforts in a monetary sense. A typical observation site can be initially equipped for under $100 and requires sustaining funds of approximately $30 per year. The funds for this support are budgeted under the general research program of the Coastal Engineering Research Center. It should be noted, however, that without the cooperation of the State of California, the collection of this type of data could not be unilaterally carried out by the Center.

The distant location of the Coastal Engineering Research Center from California makes assistance from other branches of the Corps of Engineers a requirement, the South Pacific Division and the Los Angeles and San Francisco District Engineer offices have been instrumental in the coordination and implementation of this study by providing the necessary technical liaison between the Center and local park employees at each observation site. Personnel of these offices, by their knowledge and experience, have contributed immeasurably in the selection of individual observation sites, in obtaining the excellent cooperation experienced to date from a large number of individual observers located at many distant points.

The initial compilation and reduction of the collected data will be made by CERC as part of a much broader program of data collection and analysis, seeking full understanding of littoral environment around the United States.

It is presently contemplated that this study will continue for three years, however, the value of the data could conceivably extend the life of the program well beyond this period. Specific analysis of the data will ultimately be made by scientists and engineers of the Center, but all data will be available to any interested investigator who desires to make use of it.

CLOSURE

This study of the California shoreline is in no way unique or original. The Netherlands[3] has long led the world in documenting coastal variations, and the Coastal Engineering Research Center itself has conducted or supported similar studies of the shores of the United States, including those of California in more limited scope. However, it is felt that the frequency and number of observations, and the number of observation sites, place this study in a novel status. It is expected that future analysis of collected data will enhance understanding of the littoral environment and allow greater utilization of this zone by man.

ACKNOWLEDGEMENTS

This study, entitled Littoral Environment Observations, is being carried out in connection with the general research program of the U. S. Army Corps of Engineers, Coastal Engineering Research Center in cooperation with the State of California, Department of Natural Resources. The success of the study will be primarily the result of the efforts of those many individuals who have shown an unbounded interest in observing the California shoreline and faithfully recording their observations for the future use of scientists and engineers Without these individuals, a study of this scope could not exist

NOTE Use of trade names or manufacturers in this report does not constitute an official indorsement or approval of the use of such commercial hardware or software.

REFERENCES

1. Darling, J M., The Wave Record Program at CERC, U S Army Coastal Engineering Research Center Miscellaneous Paper 1-67 January 1967.

2. Darling, J M., Surf Observations Along the United States Coasts, Journal of Waterways and Harbors Division, Proceedings of the American Society of Civil Engineers, WW1, Feb 1968, pp 11-21.

3 Edelman, T.; Systematic Measurements Along the Dutch Coast, Proc., Coastal Engineering Conference, September 1966, Vol. 1, Part 2, pp 483-501.

4. IBM Corp , IBM 1231,1232 Optical Mark Page Readers, IBM Systems Reference Library, 1963, File No. 1231-03.

5. Schlee, J A., A Modified Woods Hole Rapid Sand Analyzer, Journal of Sedimentary Petrology, Vol. 36, No 2, June 1966, pp. 403-413.

6 Shepard, F P ; Beach Cycles in Southern California, U S. Army Beach Erosion Board Technical Memorandum 20, July 1950

7. Trask, P D , Changes in Configuration of Point Reyes Beach, California, U. S Army Beach Erosion Board Technical Memorandum 91, September 1956

8, U, S. Army Corps of Engineers, Los Angeles District, Design Memorandum for Beach Stabilization, Stage 2, Construction in the Segment from Santa Ana River to Newport Pier, Orange County, California, August 1967, Plate 6

9 Vesper, W H and Essick, M G., A Pictoral History of Selected Structures Along the New Jersey Coast, U. S Army Coastal Engineering Research Center Miscellaneous Paper 5-64, October 1964

Fig. 1. Map of California showing the locations of Littoral Environment Observation Sites.

a. Goat Rock State Beach, Sonoma Coast.

b. San Buenaventura State Beach and McGrath State Beach.

c. Stinson State Beach.

d. Newport Beach, City of Newport Beach.

Fig. 2. Aerial photographs of typical California Littoral Environment Observation sites.

LITTORAL ENVIRONMENT OBSERVATIONS

Instructions for filling out CERC form No 32

CERC form No 32 has been designed for processing by optical scanning equipment This equipment automatically reads the observation forms and converts the recorded data to punched cards which will then allow analysis of the data by computer methods It is therefore recommended that a number 2 black lead pencil be used to mark the forms When data positions are marked the mark should be made the full length of the mark positions and should fill at least two-thirds of the space between the top and bottom of the guide lines The marks should not extend more than 1/16 beyond the ends of the guide lines and in no case should they be extended beyond the margin on the right hand side of the form Marks beyond the margin will result in erroneous reading of the data form If an error is made in recording data erasures should always be made carefully and completely An incomplete erasure will be read as a mark

STATION IDENTIFICATION

Each site in the Littoral Environment Observation study has been assigned a numerical code consisting of 5 digits The first two digits define the state or territory in which the sate is located and the remaining 3 digits define the particular beach or park within the state or territory A space has also been provided to write in the name of the particular beach or park at which the observation is taking place

DATE

Indicate in the spaces provided the year month and day on which an observation is made

TIME

Indicate the time to the nearest quarter hour at which the observations are being made The 24 hour system of recording time has been selected in order to eliminate any confusion between AM and PM The hour 00 refers to midnight 07 to 7 00 AM 13 to 1 00 PM etc

SURF OBSERVATIONS

a Wave Period - Record the time in seconds for eleven (11) wave crests to pass some stationary point Eleven "crests" will include ten complete waves (crests and troughs) The first (1) crest selected for observation is recorded as time zero and the eleventh (11) crest will be the stop or cut time Record this time in seconds in the spaces provided

b Wave Height - This observation is based solely on the judgement of the observer Natural or manmade features on the shoreline or in the surf zone whose dimensions are known may aid in judging the height of a wave Otherwise the observer s best estimate will be sufficient Record the wave height to the nearest foot

c Wave Direction - To indicate the direction of the approaching waves the observer must know the approximate orientation of the beach with respect to north The observer can then determine the direction from which the waves are approaching the beach

d Type of Breaking Wave

Spilling - Spilling occurs when the wave crests becomes unstable at the top and the crest flows down the front face of the wave producing an irregular foamy water surface (see figure 1 on reverse side)

Plunging - Plunging occurs when the wave crest curls over the front face of the wave and falls into the base of the wave producing a high splash and much foam (see figure 2 on reverse side)

Surging - Surging occurs when the wave crests remains unbroken while the base of the front face of the wave advances up the beach (see figure 3 on reverse side)

WIND OBSERVATIONS

a Wind Velocity - A wind meter is provided to each observer and it is recommended that the instructions provided with the meter be followed to obtain wind velocity measurements

b Wind Direction - After the approximate orientation of the beach with respect to north has been defined the observer can determine the direction from which the wind is coming

BEACH OBSERVATIONS

a Elevation of most seaward beach berm crest To obtain this measurement a graduated reference pole has been installed on the beach and the observer has been provided with a hand level The hand level will be used as a surveying level therefore it is suggested that the observer provide himself with a vertical support such as a 2 by 4 or a pipe to rest the instrument on This support must be of a known length say 4 or 5 feet After locating the position of the most seaward beach berm crest the observer standing on the berm crest and using his level will take a reading of the graduated reference pole This reading minus the known length of the level support shall be indicated on the form in the spaces provided Space is also provided on the form to indicate whether the elevation is plus or minus

b Distance of most seaward beach berm crest from reference pole The observer will measure the distance from the installed graduated reference pole to where he takes his level reading

c Angle of the foreshore slope For this measurement it is suggested that the observer have with him a clip board Lay the clip board on the foreshore slope and place the hand level on the board with the long axis perpendicular to the shoreline Next loosen the arc set screw, center the bubble on the crosshair in the bubble tube tighten the arc set screw and note the reading on the DEGREE scale

LITTORAL CURRENT OBSERVATIONS

a Current Velocity For this measurement the observer has been provided with dye The dye should be thrown into or just forward of the breaker zone The observer will note the position of the dye at entry into the br aker zone and the position of the dye after an elapsed time of one (1) minute Measure the distance between these two positions and enter the value in the spaces provided on the form

b Current direction Having already established the approximate orientation of the beach the observer can readily determine the direction in which the dye or current is moving

TIDE LEVEL

The times of low and high tide for a particular area can be obtained from local newspapers or from tide tables published by various agencies The relative state of the tide at the time of observation can readily be deducted from this information

ARE RIP CURRENTS PRESENT?

Rip currents are defined as seaward moving channels of water which return the water that has been piled up along the shore by incoming waves Rip currents are fed by feeder currents, water moving along the shore (see figure at right) Two currents join and extend out in what is known as the neck Where the water rushes through the breaker zone in a narrow lane Beyond the breaker zone the current spreads out in what is called the head and dissipates If such rip currents are present indicate so and if multiple currents exist record the distance between such rip currents

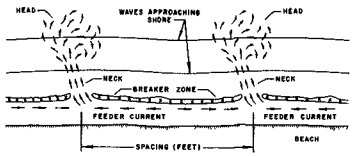

Fig. 3.a. Obverse side of Littoral Environment Observations instructions.

ARE BEACH CUSPS PRESENT?

Cusps are semicircular or crescent shaped cutouts in the beach face (see figure 4 below). If such shapes are observed on the beach face, the distance between the "horns" of the cusps, as shown in figure 4 should be recorded in the space provided.

WHEN PHOTOGRAPHS TAKEN?

Photographs are to be taken once a month, preferably early each month and at low tide. General panoramic views of the beach in the up and down coast direction are desired. Photographs each month should be taken from the same location and showing the same area with a recognizable landmark in the background if possible. At least 3 photos should be taken each month, however the observer is not limited to this number and photos of unusual features on the beach are desirable. It is suggested that the 3 photos taken be as follows:

1. Overall view of the beach looking toward the ocean with the reference pole in the background.
2. View upcoast from the reference pole. (Reference pole may be in the scene).
3. View downcoast from the reference pole. (Reference pole may be in the scene).

It is requested that each observer note the following information on the back of the photos:

1. Name of park or beach.
2. Date and time when photograph was taken.
3. Direction of scene (general, up/down coast).
4. Remarks, if any.

WAS SAND SAMPLE OBTAINED?

Sand samples are to be taken once a month from the same general location on the beach. Special plastic bags are provided to collect the sand in. The bags should be filled full and the sample should be obtained from the foreshore slope of the beach, preferably in the zone wetted by the wave up-rush (see for example figure 3 below). All samples obtained should be identified with the following information: a) name of park or beach, b) date and time sample was taken.

WATER TEMPERATURE:

If water temperature is presently being obtained it is desired that this information be recorded.

REMARKS:

Give any information which you may think may be helpful in this study. Reasons as to why some observations could not be made would also be appreciated.

FIGURE 1. SPILLING WAVE

FIGURE 2. PLUNGING WAVE

FIGURE 3 SURGING WAVE

FIGURE 4 CUSPS

Fig. 3.b. Reverse side of Littoral Environment Observations instructions.

LITTORAL ENVIRONMENT OBSERVATIONS — **COASTAL ENGINEERING RESEARCH CENTER**

5201 Little Falls Road N W , Washington, D C 20016

STATION IDENTIFICATION

State or Territory

Beach or Park

Name of beach or park

DATE — Year: 68 69 70 71 Month: Jan Feb Mar Apr May Jun Jul Aug Sep Oct Nov Dec

Day: 01 02 03 04 05 06 07 08 09 10 11 12 13 14 15 16 17 18 19 20 21 22 23 24 25 26 27 28 29 30 31

TIME — Hour: 00 01 02 03 04 05 06 07 08 09 10 11 12 13 14 15 16 17 18 19 20 21 22 23

Nearest quarter hour: 00 15 30 45

1 SURF OBSERVATIONS These observations are to be made twice (2) daily once in the morning and once in the afternoon

a Wave Period Give the time in seconds for eleven breaker crests to pass a point Eleven crests will include ten complete breakers (crests plus troughs) Crest 1 is zero time, crest 11 is cut time — 0 1 2 3 4 (100s) 5 6 7 8 9 / 0 1 2 3 4 (10s) 5 6 7 8 9 / 0 1 2 3 4 (1s) 5 6 7 8 9

b Wave Height Give the average wave height from crest to trough in feet for the highest third of the observed breakers. If less than one half (1/2) foot record 0 — 0 1 2 3 4 (10s) 5 6 7 8 9 / 0 1 2 3 4 (1s) 5 6 7 8 9

c Wave Direction Note the direction from which the waves are coming See instructions for illustration. — Calm N NE E SE S SW W NW

d Type of Breaking Wave See instructions for illustration of types — Spilling Plunging Surging

2 WIND OBSERVATIONS These observations are to be made twice (2) daily at the same time that the surf observations are made

a Wind Velocity To be measured to the nearest mile per hour (mph) — 0 1 2 3 4 (10s) 5 6 7 8 9 / 0 1 2 3 4 (1s) 5 6 7 8 9

b Wind Direction Note the direction from which the wind is coming — Onshore: Calm N NE E — Offshore: SE S SW W NW

3 BEACH OBSERVATIONS The beach measurements are to be once (1) a day preferably at the same time each day between 1300 and 1900

a Measure the elevation of the most seaward Beach Berm crest above or below a reference point to the nearest tenth of a foot — 0 1 2 3 4 (10s) 5 6 7 8 9 / 0 1 2 3 4 (1s) 5 6 7 8 9 / 0 1 2 3 4 (0 1s) 5 6 7 8 9 — Plus Minus

b Measure the distance of the most seaward Beach Berm crest from a reference point to the nearest foot — 0 1 2 3 4 (100s) 5 6 7 8 9 / 0 1 2 3 4 (10s) 5 6 7 8 9 / 0 1 2 3 4 (1s) 5 6 7 8 9 — Plus Minus

c Angle of the Foreshore Slope measured in the area of the wave uprush to the nearest degree See instructions for illustration — 0 1 2 3 4 (10s) 5 6 7 8 9 / 0 1 2 3 4 (1s) 5 6 7 8 9

4 LITTORAL CURRENT OBSERVATIONS To be made once (1) a day preferably at the same time each day between 0700 and 1200

a Current Velocity Measure in feet the distance that the dye patch is observed to move during a one (1) minute period — 0 1 2 3 4 (100s) 5 6 7 8 9 / 0 1 2 3 4 (10s) 5 6 7 8 9 / 0 1 2 3 4 (1s) 5 6 7 8 9

b Current Direction Observe direction in which current is moving toward — Calm N NE E SE S SW W NW

5 TIDE LEVEL If known indicate the relative state of the tide — Rising Falling — Low to 1/4 to 1/2 to 3/4 to High

6 ARE RIP CURRENTS PRESENT? (See inst for illustration) — Yes No If yes indicate spacing in feet _____

7 ARE BEACH CUSPS PRESENT? (See inst for illustration) — Yes No If yes indicate spacing in feet _____

8 WERE PHOTOGRAPHS TAKEN? Yes No

9 WAS SAND SAMPLE OBTAINED? Yes No

10 WATER TEMPERATURE To the nearest degree if available — 0 1 2 3 4 (10s) 5 6 7 8 9 / 0 1 2 3 4 (1s) 5 6 7 8 9

REMARKS Yes No If yes use reverse side of form as necessary

CERC Form No 32 (16 Oct 67)

Observer s Signature

MAKE ALL MARKS WITH A NUMBER 2 BLACK LEAD PENCIL — ERASE COMPLETELY ALL MARKS YOU WISH TO CHANGE

Fig. 4 Copy of Littoral Environment Observations form, CERC Form No. 32 (16 Oct. 67).

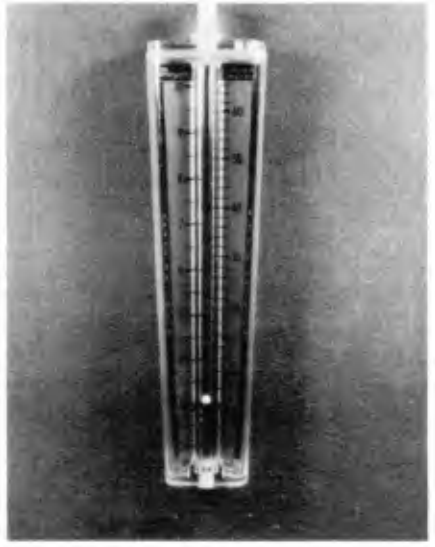

Fig. 5. Photograph of Dwyer Wind Meter used in measuring predominate wind velocities.

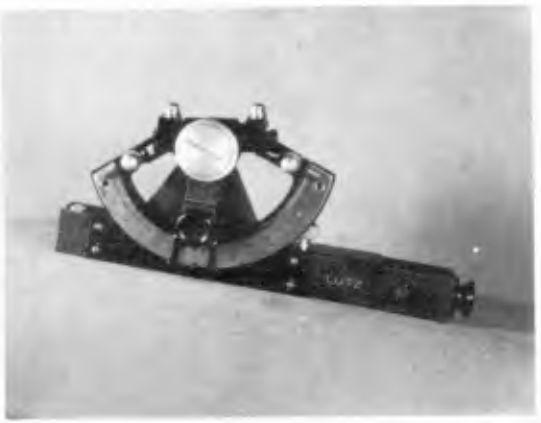

Fig. 6. Photograph of Abney Tapagraphic Hand Level being used as an inclinameter ta measure the angle af the foreshare slope.

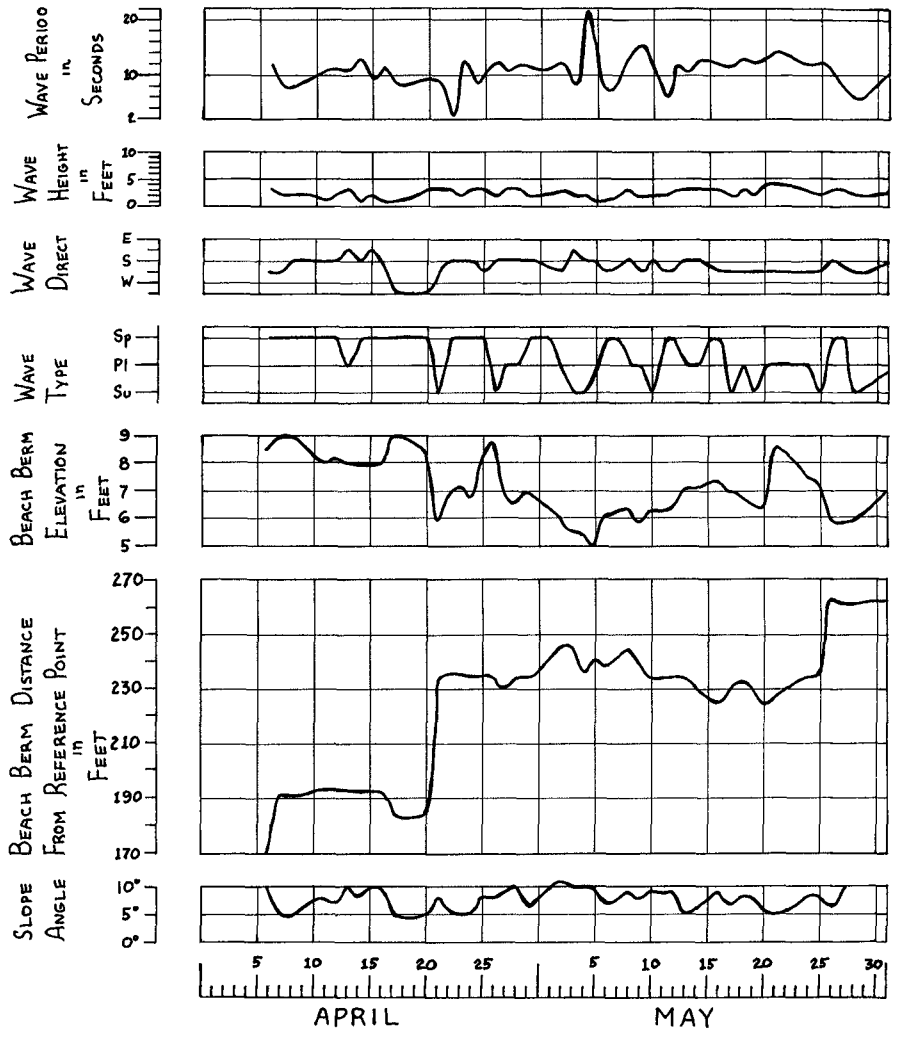

Fig. 7 Graphical presentation of Surf and Beach Observations, Seacliff State Beach, April - May, 1968

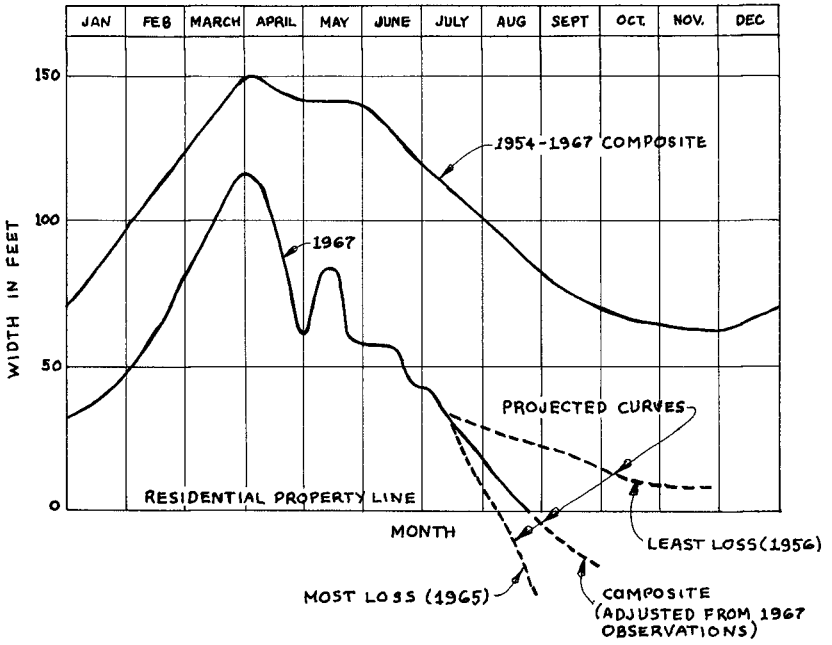

NOTE
1 WIDTH FIGURE SHOWN IS WIDTH OF LEVEL BEACH FROM SOUTHERLY LINE OF PRIVATE PROPERTY LOCATION FROM 1954 TO 1964 IS 36th ST, FROM 1965 ON IS 41st ST
2. PLOTTED FROM DATA FURNISHED BY CITY OF NEWPORT BEACH, PUBLIC WORKS DEPARTMENT DATA OBSERVED BY MR ROBERT E REED, CHIEF LIFEGUARD

Fig 8. Graphical presentation of observed beach widths, Newport Beach.

Fig. 9. Panoramic photographs of El Capitan State Beach, California taken during Nov. 1967, Jan. and March 1968.

Fig. 10. Panaramic photagraphs of Natural Bridges State Beach, Califarnia taken during the periad Nav. 1967 thraugh April 1968.

CHAPTER 18

LONGSHORE TRANSPORT OF SAND

by

Douglas L. Inman, Paul D. Komar
Scripps Institution of Oceanography, University of California
La Jolla, California 92037

and

Anthony J. Bowen
Tidal Institute, University of Liverpool
Birkenhead, Cheshire, England

ABSTRACT

Simultaneous field measurements of the energy flux of breaking waves and the resulting longshore transport of sand in the surf zone have been made along three beaches and for a variety of wave conditions. The measurements indicate that the longshore transport rate of sand is directly proportional to the longshore component of wave power.

INTRODUCTION

The importance of waves in transporting sand along the shore has been recognized for many years, but quantitative measurements of transport rate as a function of wave energy flux have only been possible during the last two decades and then only in model wave basins. The study of the longshore transport phenomena in the real surf zone requires synoptic measurements of the flux of wave energy and the transport rate of sand.

This is a preliminary report of a continuing study that is being conducted along three natural beaches. El Moreno Beach, Mexico, on the northern Gulf of California; Silver Strand Beach, Coronado, California, and, Scripps Beach, La Jolla, California. The sands on these beaches range in median diameter from 180 to 600 microns, and the waves incident to the beaches varied from one-third to one meter high wind waves from the Gulf of California, to one to two meter high swell from the Pacific Ocean.

Contribution from the Scripps Institution of Oceanography, University of California, La Jolla, California. This study was supported by the Coastal Engineering Research Center, U. S. Army, and the Office of Naval Research, under contract with the University of California.

PROCEDURE

The direction and flux of wave energy is measured from an array of digital wave sensors placed in and near the surf zone. The wave staffs and their installation is described in Koontz and Inman (1967) and a schematic diagram of the array is shown in Figure 1. The array has both on-offshore and longshore components with spacings between staffs of about one-quarter of the wave length of the prevailing waves.

The output from the array is entered on magnetic tape, and later programmed on a computer to obtain the wave spectra and cross-spectral analysis for the various members of the array. The wave spectrum is obtained by Fourier analysis of the time series of water level fluctuations at each sensor, using a rapid procedure (Fast Four) modified from Cooley and Tukey (1965). The spectrum consists of the squares of the absolute values of the complex Fourier coefficients, which serve as estimates (having dimensions of length squared) of the energy density in each elemental frequency band (Figure 2). The sum of the energy densities under the spectral peak of the incident waves is the mean-square elevation $\langle \eta^2 \rangle$ of the water surface described by the time series. The mean wave energy per unit area of the water surface is given by the product of $\langle \eta^2 \rangle$ and the weight per unit volume ρg of the water

$$E = \rho g \langle \eta^2 \rangle = \frac{1}{8} \rho g H_{rms}^2 \qquad (1)$$

where H_{rms} is the root-mean-square wave height. The flux of energy, or power transmitted per unit of wave crest length is given by the product of E and the group velocity G of the waves, $P = EG$. The direction of energy flux is interpreted from the phase difference between the various sensors. Sensors at or near the breakpoint of the waves are used to obtain the angle α that the breaking wave makes with the beach. The longshore component of wave power per unit length of beach is then given by

$$P_l = P \sin\alpha \cos\alpha \qquad (2)$$

Quantitative measurements of the longshore transport rate of sand are obtained from the time history of the position of the center of gravity of tracer injected onto the beach. The sand tracer is native sand colored with a thin coating of fluorescent dye. The tracer is introduced onto the beach face in single injections of between 45 and 90 kilograms. The movement of the sand is indicated by the subsequent distribution of the tracer as determined from approximately 200 volume samples taken from the beach face at various times after injection. Figure 3 shows an example of a tracer distribution obtained from such a sampling. The mean distance of transport is taken as the distance between the injection point and the new center of gravity of the tracer

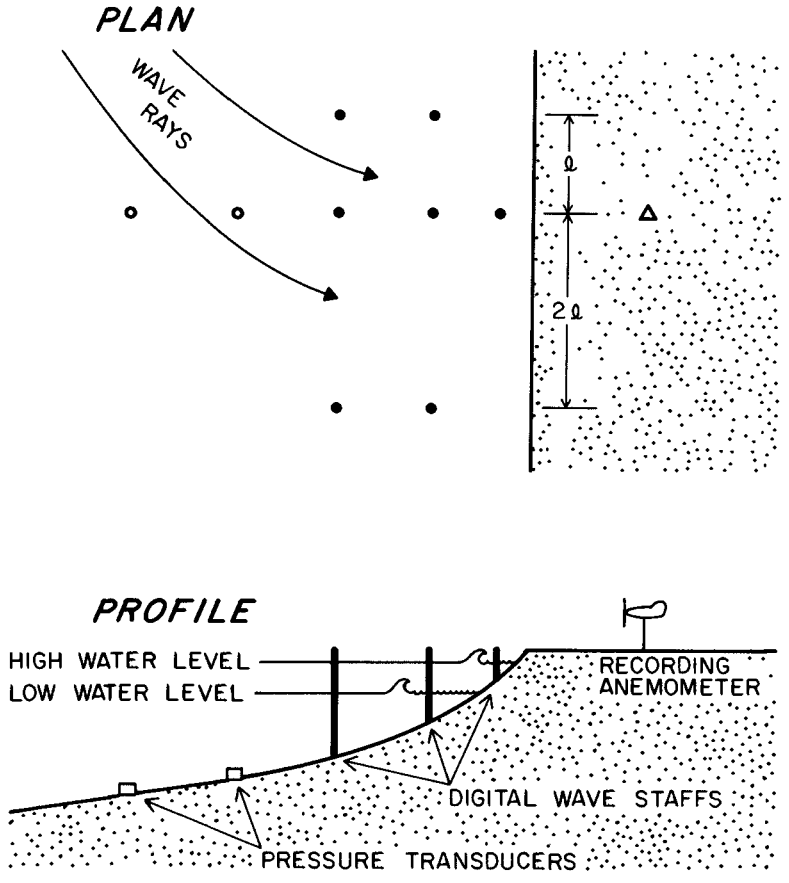

Figure 1. Schematic diagram of sensor array used for measuring direction and flux of wave energy (after Koontz and Inman, 1967, Fig. 16) Cross-spectral analysis shown in Figure 2 is from a longshore pair of such an array.

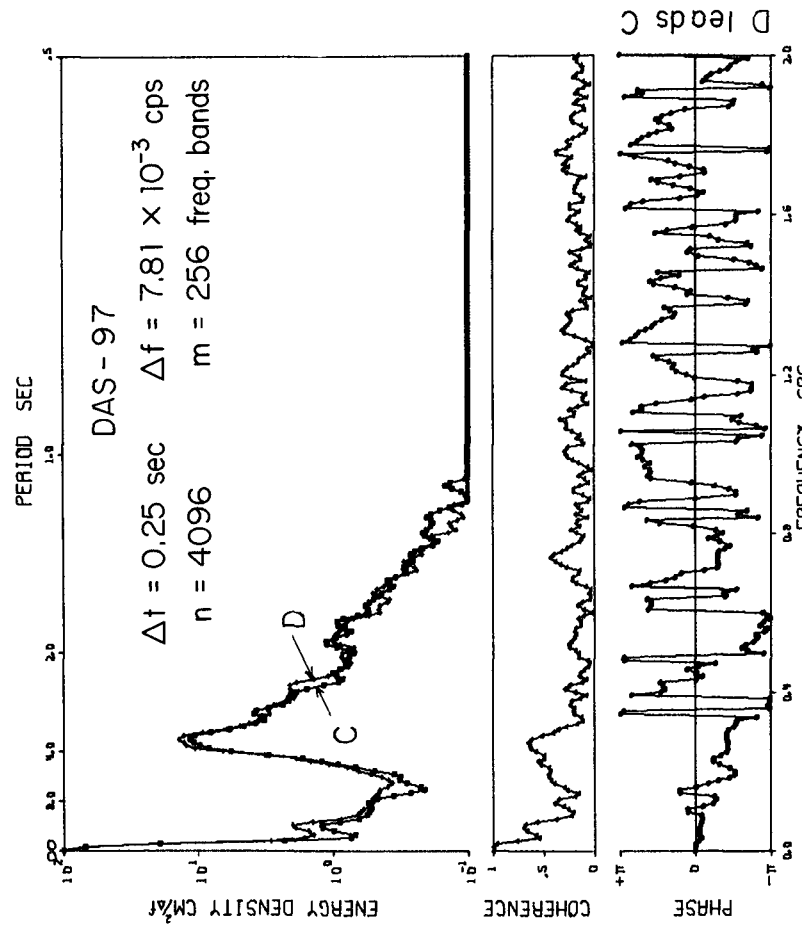

Figure 2. Wave spectra and cross-spectral analysis for two members of an array of digital wave staffs. Staffs were parallel to and just outside of the break point of the waves. The analysis shows that the spectral peak for the incident waves occurs at a frequency of 0.28 cps (period of 3.6 sec), and that the rms wave height was about 34 cm.

distribution, while the thickness of the sand layer involved in the transport is determined from the depth of burial of tracer in cores taken from the beach. The bulk volume of sand transported per unit time, S, is the product of the mean longshore distance of transport, the width of the beach, and the thickness of the layer of motion, all divided by the time between injection and sampling.

The accuracy of the measured transport rate is dependent upon the portion of the original tracer that can be accounted for by the sampling program. Most of the tracer should be accounted for by an initial sampling soon after injection of the tracer. The rate of decrease in the accountable tracer budget with successive sampling intervals should be commensurate with the estimated loss by lateral diffusion to concentration levels below the threshold of sampling sensitivity. If more than one-quarter of the injected tracer cannot be accounted for in the sampling program, the data are considered unsatisfactory and not used.

DISCUSSION

Simultaneous measurements of the longshore transport rate of sand and the flux of wave energy have been made on three beaches and under six different wave conditions with breaker heights up to two meters. The new data is plotted together with previous field and laboratory data in Figure 4. The longshore transport rate, I_l, is expressed as immersed weight transport per unit time so that the transport is defined in terms of the difference in densities of the sand, ρ_s, and of the fluid, ρ. The relation between the immersed weight transport and the volume transport per unit time, S, is given by

$$I_l = (\rho_s - \rho)\, g\, a_1\, S \qquad (3)$$

where g is the acceleration of gravity and a_1 is the correction for porespace. a_1 was assumed equal to 0.6 in transforming the data of other workers into immersed weight.

The best fit curve for the new data agrees generally with the relation

$$I_l = K\, P_l \qquad (4)$$

suggested by Inman and Bagnold (1963), with a value of K equal to about 0.7. Figure 4 shows that the longshore power of the new measurements is about one-half that for previous field data, for a given transport rate. This discrepancy appears to result from the erroneous use of the significant wave height in computing wave power for the earlier field observations (Inman and Frautschy, 1966). The expressions for wave power are based on the root-mean-square wave height, H_{rms}, which is also the wave parameter measured in the laboratory for simple waves of steady

amplitude. For real waves having a single narrow band of frequencies, the use of the significant wave height gives a wave power that is erroneously high by a factor of two (Longuet-Higgins, 1952).

The results of this study indicate that the rate of longshore transport of sand is: (1) directly proportional to the longshore component of wave power for fully developed transport conditions; and, (2) independent of sand size within the range of about 180 to 600 microns studied here.

The new field data indicate that the longshore transport of sand is directly proportional to the longshore component of wave power. However, it appears that the transport conditions are not fully developed for all laboratory experiments and that the transport mechanism is therefore less efficient than for conditions that prevail in the field. This difference in efficiency must be considered in any attempts to extrapolate laboratory measurements to field conditions.

The size of the sand on the beach appears to have little effect on the transport rate. In suspended load transport, the size of the sediment, because of the dependence of settling velocity on size, is an important variable. This suggests that suspended load transport of sand in the surf zone is less important than bed load transport.

REFERENCES

Caldwell, J. M., 1956, "Wave action and sand movement near Anaheim Bay, California:" Beach Erosion Board, Tech. Memo. 68, U. S. Army Corps of Engrs., 21 pp.

Cooley, J. W. and J. W. Tukey, 1965, "An algorithm for the machine calculation of complex Fourier series", Mathematics of Computation, Washington, D. C., Vol. 19, No. 90, pp 297-301.

Inman, D. L. and R. A. Bagnold, 1963, "Littoral processes", The Sea. Ideas and Observations, vol 3 The Earth Beneath the Sea (M. N. Hill, ed) Interscience Publ., pp 529-553.

Inman, D. L., and J. D. Frautschy, 1966, "Littoral processes and the development of shorelines", Coastal Engineering, Amer. Soc. Civ. Engrs., pp 511-536.

Koontz, W. A. and D. L. Inman, 1967, "A multi-purpose data acquisition system for field and laboratory instrumentation of the nearshore environment", Coastal Engr. Res. Center, Tech Memo 21, U. S. Army, Corps of Engrs., 38 pp.

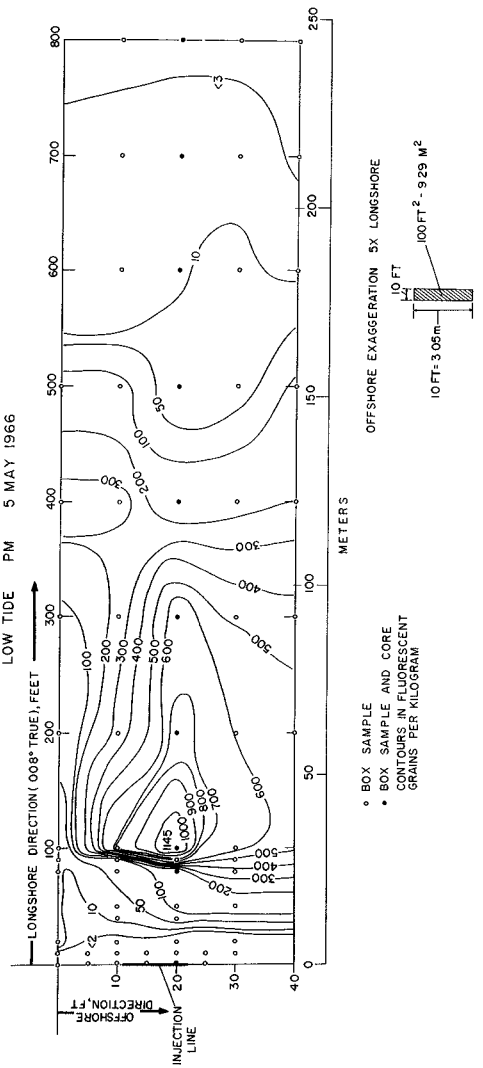

Figure 3. Distribution of tracer along El Moreno beach after approximately 200 minutes of wave action. Injection was 45.9 kilograms of El Moreno beach sand treated with fluorescent dye. The center of gravity of the new distribution is 75 meters from the injection line and the depth of motion was found to be 10.5 cm. The transport rate for this run was 6.2×10^6 dynes/sec and the longshore component of wave power was 1.0×10^7 ergs/cm sec.

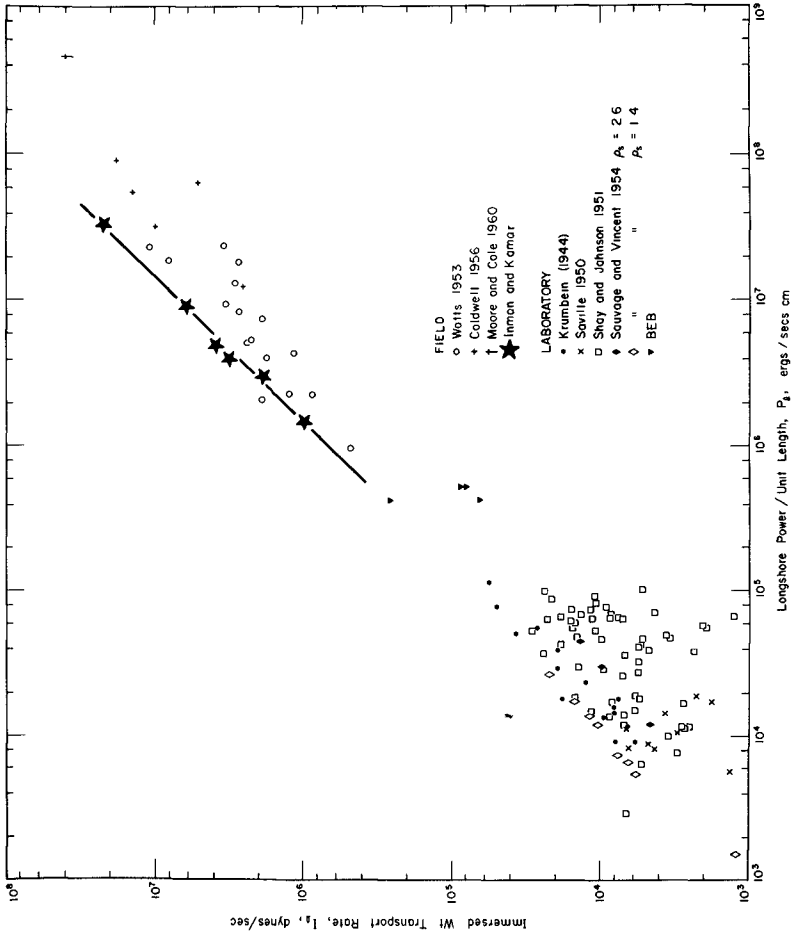

Figure 4. Relation between the immersed weight longshore transport rate and the longshore component of wave power per unit length of beach. The various sources of plotted data are listed in the references, the "BEB" data is given in Savage (1962).

Krumbein, W. C., 1944, "Shore currents and sand movement on a model beach", Beach Erosion Board, Tech. Memo. 7, U. S. Army Corps of Engrs., 44 pp.

Longuet-Higgins, M. S., 1953, "Mass transport in water waves", Phil. Trans. Royal Soc. London, ser. A, no. 903, vol. 245, pp 535-581.

Moore, G. W. and J. Y. Cole, 1960, "Coastal processes in the vicinity of Cape Thompson, Alaska", (in R. Kachadoorian et al, Geological investigations in support of Project Chariot in the vicinity of Cape Thompson), U. S. Geol. Survey Trace Elements Investigations Report 753, pp. 41-54.

Savage, R. P., 1962, "Laboratory determination of littoral transport rates", Proc. Amer. Soc. Civ. Engr., Journal Waterways and Harbors Div. WW2, no. 3128, pp 69-92 and discussion by T. Saville and M. Manohar, WW4, no. 3335, pp. 141-147.

Saville, Thorndyke, Jr., 1950, "Model study of sand transport along an infinitely long, straight beach", Amer. Geophy. Union, Transactions vol. 31, p. 555-565.

Sauvage, G., de St. Marc, and G. Vincent, 1954, "Transport littoral formation de fleches et de tombolos", Proc. Fifth Conference Coastal Engin., Council on Wave Research, Univ of Calif., pp. 296-328.

Shay, E. A. and J. W. Johnson, 1951, "Model studies on the movement of sand transported by wave action along a straight beach", Univ. of California, Berkeley, Inst. Engrs. Res. Issue 7 Series 14 (unpublished).

Watts, G. M., 1953, "Study of sand movement at South Lake Worth Inlet, Florida", Beach Erosion Board, Corps of Engrs., Tech Memo. 42, 24 pp.

CHAPTER 19

APPLICATION OF FLUORESCENT COATED SAND IN LITTORAL DRIFT AND INLET STUDIES

Minze Stuiver and J. A. Purpura

Department of Coastal and Oceanographic Engineering,
University of Florida, Gainesville, Florida

ABSTRACT

The use of fluorescent coated sand in tracing the sand movement along beaches and around inlets is an important tool in the field of Coastal Engineering. As a part of an extensive beach erosion study along the shore of West Palm Beach, Florida, four areas were subjected to such a "tracer study." Each area represented a particular beach configuration either with or without erosion protective structures. In this paper the procedure and results for one area is described.

As a second application of sand tracers, the results of a study concerned with the sand migration in and around South Lake Worth Inlet is discussed.

LITTORAL DRIFT STUDY ALONG A BEACH

Injection

Figure 1 shows the methods of injection and sampling of the fluorescent tracers. The tracer sand, whose properties have to be exactly the same as the properties of the sand of the test beach, is injected during low water. It is spread out on the dry beach from approximately the high water line to the low water line over a width of 50 feet and is mixed with the beach sand by raking. In this way the tracer material is wet before it is subjected to the wave action. Experience has shown that this is a particularly important step in the injection procedure for if the tracer material is not "wetted" it will float on top of the water due to surface tension and may result in misleading information. Water soluble bags were used for tracer injection from the low water line to approximately the MSL -3 foot line. These bags often being placed under water dissolve within ten to fifteen seconds releasing the tracer material.

Sampling Procedure

The sampling of beach material is started at the first low tide after injection. The tides along Florida's east coast are semi-diurnal. The time intervals between sampling are generally taken as the period between

two low tides. The low tide during the daytime is most convenient for working on the beach. The distances between sampling points generally depend on the nature of the study. If only a small area is to be studied in detail, the distances between sampling points may be as small as 100 feet; whereas a littoral drift study along a relatively uniform beach does not require such small distances. In the discussed littoral drift study, the distances between sampling points was chosen at 500 feet. In the offshore direction, three samples were taken, at the high water line, the low water line, and the MSL -3 foot line, respectively. Although, in general, there exists no rule for the number of samples to be taken, the accuracy of information obtained by the sand tracing method improves proportionally to the number of samples taken. However, the time required for analysis of each sample sets a practical limit to the total number of samples to be collected during each survey.

Sample Analysis

The sand samples are collected in small labeled bags, dried, and examined for tracer content. For reasons of comparison, one-hundred grams of the well-mixed sample are analyzed. This analysis is carried out for all of the samples taken.

The results for a particular set of sampling give a concentration distribution of tracer as a function of distance from the injection point. The least square method was applied to fit a third-degree polynomial curve to the "raw" field data (Figure 2). If this is done for each consecutive survey, a family of concentration curves as a function of time can be formed as shown in Figure 3. Since samples have been taken at three water lines, three sets of curves are obtained.

From Figure 3 it can be seen that, in general, the concentration decreases for each subsequent survey and that the maximum of the concentration curve shifts. The decrease of tracer concentration is due to dispersion as well as burial of part of the tracer material. If one assumed uniform erosion or accretion, the absolute maximum of the concentration would be affected; but the location of the tracer concentration maximum would remain the same. If the distance, Δs, between two successive concentration maxima is divided by the according time interval, Δt, the average migration speed, $\bar{v}$, of the tracer material is obtained. Since the tracer material is identically the same as the beach material, the speed of the littoral drift is known for the time, Δt, between two surveys. Figure 4 shows $\bar{v}$ as a function of time for the high water line, low water line, and MSL -3 foot line. Since the test beach has a north-south orientation, the drift is found to change from north to south.

As a next step, it has been tried to correlate the speed of littoral drift with the longshore component of the wave energy. The Coastal Engineering Research Center, U.S. Army Corps of Engineers kindly allowed the Department of Coastal and Oceanographic Engineering to obtain the daily records of a step-gauge wave recorder located at the end of the 1,000 foot long public pier at Lake Worth, Florida. The analysis of the records showed that 85 per cent of the wave periods ranged from 3 to 6 seconds and that the remaining 15 per cent of the waves were in the range of 6 to 11 seconds. Accepting an average period of 5 and 9 seconds for the two categories,

respectively, refraction diagrams were calculated for these two periods and for wave directions from the northeast, east, and southeast. Diagrams were calculated for each study area in addition to a small area around the wave recorder. Knowing the wave energy E_R and the width between adjacent rays b_R at the recorder, the energy E_s in each consecutive ray in the study area could be extrapolated from

$$E_s = \frac{b_R}{b_s} E_R$$

The longshore component of the wave energy is represented by

$$E_L = E_s \cos \alpha = \frac{b_R}{b_s} E_R \cos \alpha$$

where α is the angle between the normal to the beach and the wave crest.

Discussion of Results

The result of a long and tedious analysis is comprised in Figure 4. The figure shows the speed of sand migration as a function of time in one study area and is correlated with the longshore wave energy of that area. The figure shows the change in direction of the longshore energy component to agree fairly well with the change in direction of littoral drift. It also indicates an increase in speed of littoral drift with an increase in longshore energy. There seems to be a tendency for the littoral drift to slightly lag the longshore energy component. A very significant feature of the figure is the sensitivity of the high water area to the wave energy, indicated by the maximum amplitudes of the solid line. A remarkable fact is that the transport in the MSL -3 foot area is also very pronounced. Less movement is observed in the low water region. This generally has been observed in the analysis of the other three areas. The latter results are not shown to avoid repetition.

It has to be stated that the accuracy and the correlation are not perfect. Particularly, the representation of the speed of sand movement as a function of time does not generate the desired confidence; although, a pattern of similarity in the modes of transport for the high water line, low water line and MSL -3 foot line can be unmistakably defined. It is believed that the indicated approach for obtaining information concerning littoral drift can be made very useful especially for calculating and comparing the speed of littoral drift for a wide variety of beach configurations found in nature.

From the results of this study it is evident that the sampling methods need to be improved. As a first step, it seems to be necessary to take more than one sample at each sampling point and to determine the tracer concentration at this point from the analysis of three or four samples. Another step could be to reduce the distance between the sampling points.

As stated before, this may not be possible from a practical point of view.

SOUTH LAKE WORTH SAND TRACING STUDY

General

A very effective use of sand tracers can be made in the study of sand migration in-and-around inlets. Figure 5 shows the South Lake Worth Inlet connecting the Intracoastal Waterway with the Atlantic Ocean. The width of the inlet channel is 130 feet, and the length measured from the easternmost jetty tip to the Intracoastal Waterway is 1900 feet. The average depth is 14 feet below MSL. The channel bottom has a rocky composition with some patches of sand, particularly in the bridge area. The channel is confined between vertical steel sheet piling over its entire length. A serious problem, dating back to the time the inlet was dredged in 1927, is the sand drain into the inlet. This results in a substantial loss of sand from the surrounding Atlantic beaches. This problem has been partially solved by installing a permanent dredge on the north side of the inlet to artificially transfer sand by a 10-inch pipeline to the south side of the inlet. Qualitative determinations of natural and artificial bypassing as well as the transport of sand into the inlet have been made by using four different colors of tracer material.

Locations of Injection and Sampling

Green tracer in the amount of 2000 pounds was placed on the beach 600 feet north of the inlet; 2000 pounds of red tracer material was injected at the same location on a bar at a distance of approximately 100 feet offshore. This bar extended southward and terminated due east of the inlet entrance. Another 2000 pounds of yellow tracer material was injected 500 feet to the south of the inlet between the high water line and the MSL -3 foot line. Finally, 2000 pounds of rose-violet tracer material was injected in the inlet on the Intracoastal Waterway side. Figure 6 shows all the locations of injections.

The samples on the north side of the inlet were taken at 100 foot intervals from Station 0 + 00N through Station 5 + 00N. The sampling points on the south side of the inlet also had a spacing of 100 feet between each station from Station 0 + 00S through 10 + 00S and were spaced 500 feet apart from here on through Stations 25 + 00S.

In the inlet channel, bedload and suspended load samplers were installed from which samples could be remotely drawn (See Figures 5 and 6). A small hand dredge was used to obtain samples from the Intracoastal Waterway bottom in the immediate vicinity of the inlet and the area adjacent to the jetty.

Current and Wave Measurements

Current measurements employing a Price current meter were made in the inlet channel in order to obtain a correlation of the mode and speed of sediment transport to the prevailing currents during the test. The velocities were measured in the middle of the channel and 40 feet to the north

and south of the middle at a distance of approximately 150 feet east of the bridge crossing the inlet (See Figure 5). This location coincides with the location of the samplers. Table I shows the current velocities during the peak of the flood tide.

TABLE I

CURRENT VELOCITIES IN INLET CHANNEL

Average Current Velocity (ft/sec)			
Date of Measurement	North of Middle	Middle	South of Middle
12-6-1967	5.8	5.2	2.8
12-7-1967	5.6	5.0	2.7

The current velocity distribution is highly asymmetric about the channel centerline. Figure 5 shows how the current even reverses direction in a region south of the middle. The location of the trap was such that it was not affected by this negative current. In addition to the skewed current pattern, the flow was highly turbulent. To record the current pattern, use was made of dye packages attached to anchored floats. The dissolved dye created clearly distinguishable streaks in the water which were recorded by aerial photography.

The wave heights and wave periods were measured visually. Table II shows that during the test the direction of wave approach was at about 15 degrees north of the normal to the beach with wave heights of 3 to 5 feet and periods of 4 to 5 seconds. This produced a relatively strong longshore current flowing south.

Discussion of the Results

Natural and artificial bypassing

Figure 5 shows the concentration curves for the green tracer material between the north jetty and Station 5 + 00N for eleven consecutive surveys. The migration of the maxima of the curves to the south indicates the speed of sediment movement which appears to be slow. Of particular interest is the zero concentration for survey 1 through 5. This most likely was caused by stagnancy of the water in a strip directly north of the jetty. This feature is evidenced by the fact that during the first and second day the samples taken from the artificially bypassed sand show almost negligible amounts of green tracer material. (P indicates location of permanent dredge, and the arrow at Station 10 + 00S indicates discharge of bypassed effluent.)

TABLE II

WAVE HEIGHT, WAVE PERIOD AND WAVE DIRECTION DURING TESTING PERIOD

Date	Survey No.	Wave Height in Ft.	Wave Period in Seconds	Wave Direction
12-5-67	1	6.10	5.06	ENE
12-6-67	2	5.00	3.83	NE
12-7-67	3	3.88	3.60	NE
12-8-67	4	2.51	3.40	NE
12-9-67	5	2.15	3.48	ESE
12-10-67		4.10	3.73	SE
12-11-67	6	3.58	3.71	SE
12-12-67		1.66	3.13	E
12-13-67		1.65	2.95	E
12-14-67		2.18	4.48	E
12-15-67	7	No Waves		
12-16-67		No Waves		
12-17-67		1.80	6.00	E
12-18-67		2.08	4.20	E
12-19-67	8	2.56	5.20	E
12-20-67		3.78	4.75	SE
12-21-67		2.48	3.93	ENE
12-22-67	9	4.50	5.30	NE
12-23-67		4.15	4.26	NE
12-24-67		4.73	5.76	NE
12-25-67		2.35	4.73	NE
12-26-67	10	1.30	4.76	E
12-27-67		1.85	3.46	E
12-28-67	11	3.80	3.66	E
12-29-67		0.96	4.14	E
12-30-67		1.18	3.63	E
12-31-67		2.05	3.56	SE

The notation "green 1/100" refers to the presence of one green tracer grain in a sample of 100 grams. Only at the point where waves rushed up on the beach and then hit the jetty was a substantial amount of green tracer observed.

Due to the prevailing rough weather only a few samples could be collected from the bar. However, the few bar samples taken show high amounts of red tracer indicating a considerable sediment transport along the bar. The high concentrations of red tracer sampled from the artificial bypassed effluent show that the feeding of the bypassing plant occurred predominantly by the sediment migrating along the bar. Evidence of considerable natural bypassing is given by the relatively high concentration of red tracer found on the beach to the south of the inlet (See Figure 5, curves in the right top corner).

Looking at the concentration curves for the yellow tracer, which initially had been injected on the south side of the inlet, it appears that for survey Nos. 2, 3, and 4 there is substantial transport to the south. This is in agreement with the wave information of Table II. For the next three days, the waves were from the southeast shifting the maxima of the concentration curves Nos. 5 and 6 back, indicating a transport to the north. For the remaining surveys, Nos. 7 through 11, the waves were from the east or northeast which, in combination with the orientation of the shoreline, should result in a littoral transport to the south. This is substantiated in the curves between Station 10 + 00S and Station 20 + 00S by the drop in tracer concentration. However, north of Station 10 + 00S there is a tendency for the tracer concentration to increase, indicating that sand is transported toward the inlet from the south and, as will be shown later, moves into the inlet. This tendency also appears in the concentration curves of the naturally bypassed red tracer material.

The explanation for this behavior can be found in the analysis of the dye patterns. They showed that, for waves approaching from southeasterly directions, the longshore current was directed toward the north and transported the sand into the inlet. For wave conditions from the northeast, as prevailed during the two days of measurements on which Figure 6 has been based, there existed a large eddy on the leeside of the north jetty rotating in a clockwise direction (See Figure 5). Dye packages released in the surf zone at various locations between Stations 0 + 00S and 10 + 00S produced south oriented streaks which reversed direction around Station 5 + 00S. The streaks north of Station 5 + 00S advanced to the easternmost tip of the south jetty giving rise to the idea that even under these conditions sand from an area extending approximately 500 feet to the south of the inlet is transported into the inlet.

Sediment transport into the inlet during flood

Bedload and suspended load samples were collected in the inlet channel. The suspended load was sampled for fifteen minutes by pumping the water-sand mixture through a fine sieve in a sample bag. The rate of pumping was such that continuity existed at the intake nozzle. The bedload was collected by means of bedload traps for thirty minute cycles. (Bedload traps are of the type described by Thornton (1968) in these Proceedings.) The qualitative results of this part of the test program are shown in Figure 6, I R, II R, I L, II L, III L, respectively. The figures represent the unsmoothed tracer

concentration curves for three consecutive days. The legend at the bottom of the figure only applies to these concentration curves.

The curves in I R and I L, representing the tracer concentrations two days after injection in the south and north bedload and suspended load sampler respectively, show that in the south side of the inlet the yellow tracer predominates, and the green tracer concentration is minor. On the north side of the inlet, green is dominant, and yellow is present in smaller quantities. II R and II L show the same tendency three days after injection. The yellow suspended tracer material is dominating on the south side, and the yellow bedload, green suspended load and green bedload occur in decreasing quantities. On the north side of the inlet, the appearance of red tracer in the bedload, as well as in the suspended load, indicates that the travel distance for the green tracer has been smaller than it was for the red tracer. This suggests a leakage in the north jetty. The tracer concentration of the red material also far exceeded the concentration in the bedload.

Figure 7 shows the grain size distribution curves for the beach samples north of the inlet and the samples taken north of the centerline in the inlet. Figure 8 shows the same set of curves for the south side. It is important to note that the difference between the grain size of the suspended sediment and the bedload material in the channel is insignificant. This can be explained by the high degree of turbulence in the inlet, causing intensive mixing of the sediment vertically. However, there is a substantial difference between the grain sizes of the sediment carried through the inlet on the north side and the sediment carried through the inlet on the south side, which is evidenced by the curves for the channel on Figures 7 and 8.

In general, there is always wave action on the north side of the north jetty entraining relatively coarse and heavy sediment. On the leeside of the north jetty, where there is little wave action, the only means of transporting the sediment towards the inlet is the eddy current generated in the lee of the north jetty. The current is so slow that only the light material is entrained. This explains the difference in coarseness of the material transported through the inlet.

Sediment Transport Outward During Ebb

Very small amounts of organic matter were collected in the suspended load trap as well as in the bedload trap during the outgoing tide. Of the rose-violet tracer, nothing was collected in the samplers either. Visual inspection of the injection area showed that the patches of rose-violet tracer material were still present indicating that no movement takes place in a region approximately 75 feet away from the inlet (See location of rose-violet injection in Figure 6). Both observations seem to imply that the transport out to the ocean is negligible.

Conclusions

The sharp decline in concentration of the green tracer in the immediate vicinity of the jetty very likely is caused by stagnancy of water next to the jetty. The lack of green tracer in the bypassed effluent and the presence of the same color tracer in the channel trap indicates a drain of sand through the north jetty occurring in the wave uprush zone, rather than being transported around the jetty. This has been confirmed by detailed tests at a later date. There appeared to be a rather pronounced transport along the

bar which even results in substantial natural bypassing of the inlet. This was evidenced by red tracer material collected on the south side of the inlet.

Concerning the artificial bypassing for the given situation, it can be concluded that most of the bypassed material originated from the bar region and not from the beach. This means that sediment not only is transported along the bar but also in substantial quantities across the bar.

Of great importance are the observations made in the inlet channel. They show that the sediment carried into the inlet is predominantly a suspended load. Of even more significance is the observed transport through the inlet from sediment originating from the south side (lee side) of the inlet for waves approaching from a northeasterly direction. Figure 6 shows that the order of magnitude of concentrations north and south of the channel center are approximately the same. This implies that, considering the low current velocity on the south side, the sand drain from the south is relatively high compared to the contributions from the north side.

The negligible amount of sediment transported outward to the ocean makes this inlet an extreme example of a sand drain causing a considerable loss of sand from the surrounding beaches as evidenced by these tracer studies.

Acknowledgements

This investigation was sponsored by the Florida Board of Conservation, Division of Beaches and Shores. The authors wish to express their appreciation for the permission granted by the Florida Board of Conservation to publish this paper. They are also indebted to the U.S. Army Corps of Engineers for the support received while collecting the necessary wave information.

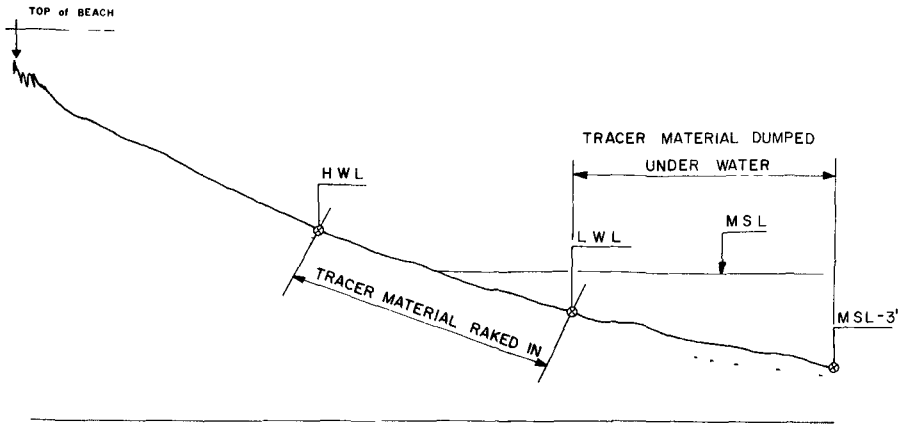

BEACH CROSS SECTION

FIG 1

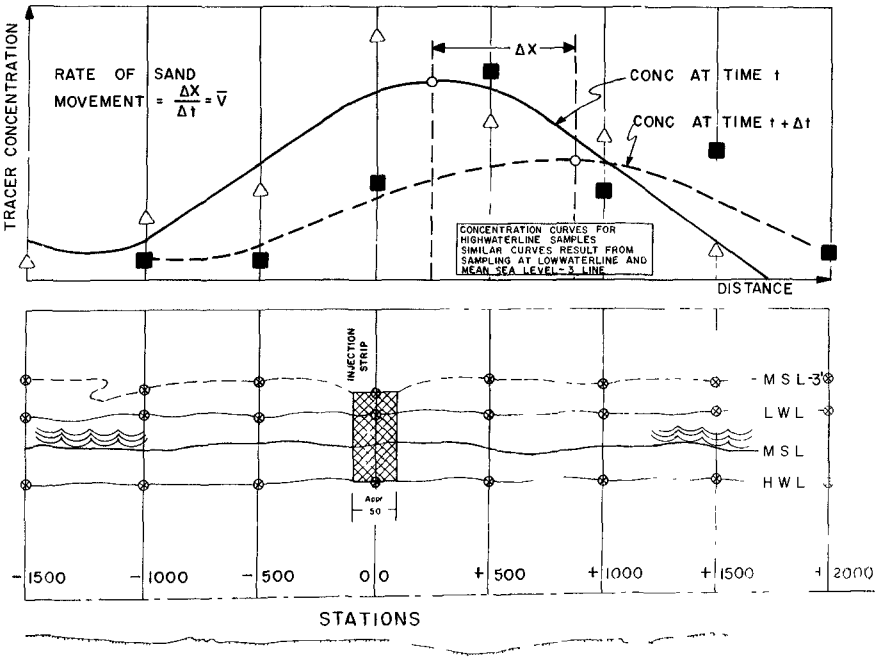

INJECTION AND SAMPLING LOCATIONS

FIG 2

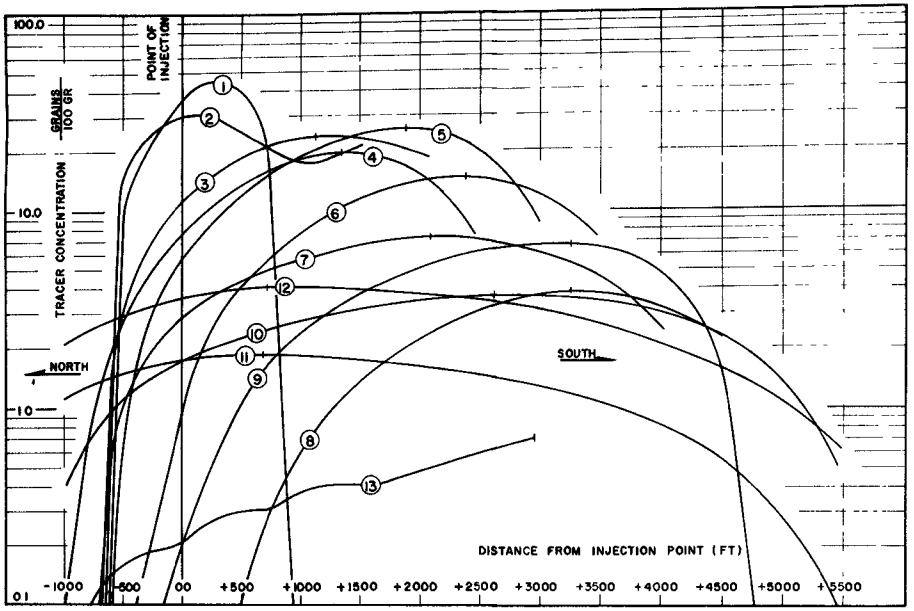

FIG 3 TRACER CONCENTRATION AS A FUNCTION OF DISTANCE FROM POINT OF INJECTION

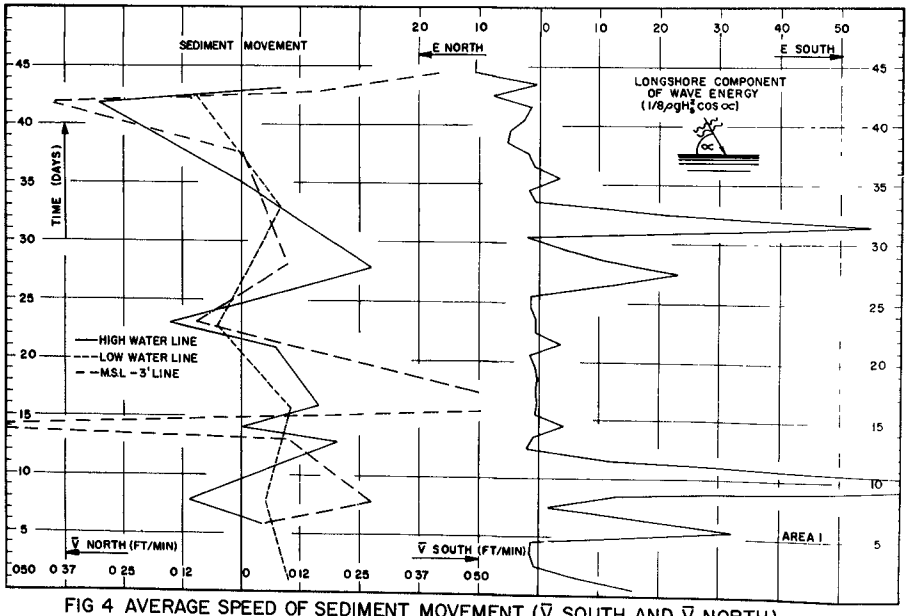

FIG 4 AVERAGE SPEED OF SEDIMENT MOVEMENT ($\bar{V}$ SOUTH AND $\bar{V}$ NORTH) COMPARED WITH THE LONGSHORE COMPONENT OF WAVE ENERGY

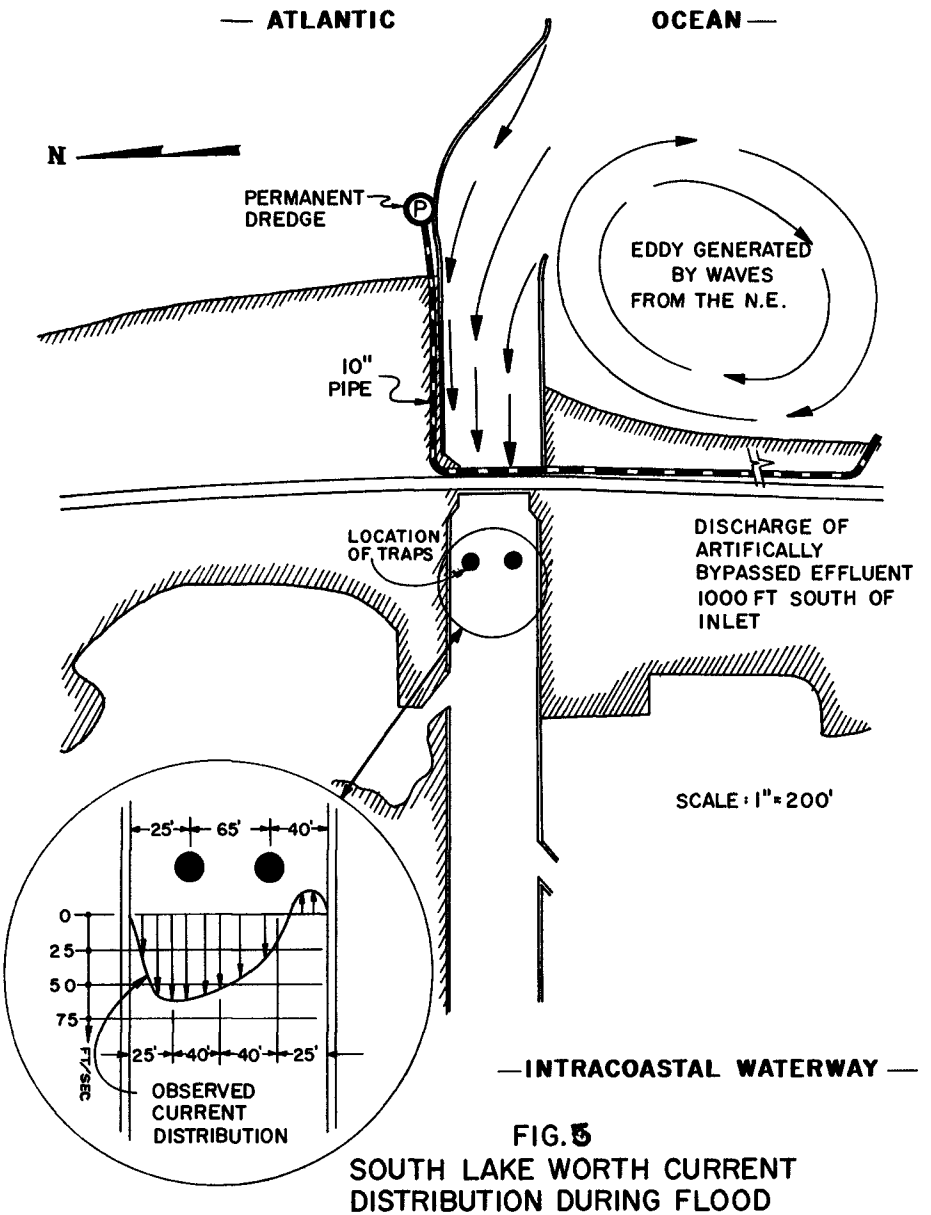

FIG. 5
SOUTH LAKE WORTH CURRENT DISTRIBUTION DURING FLOOD

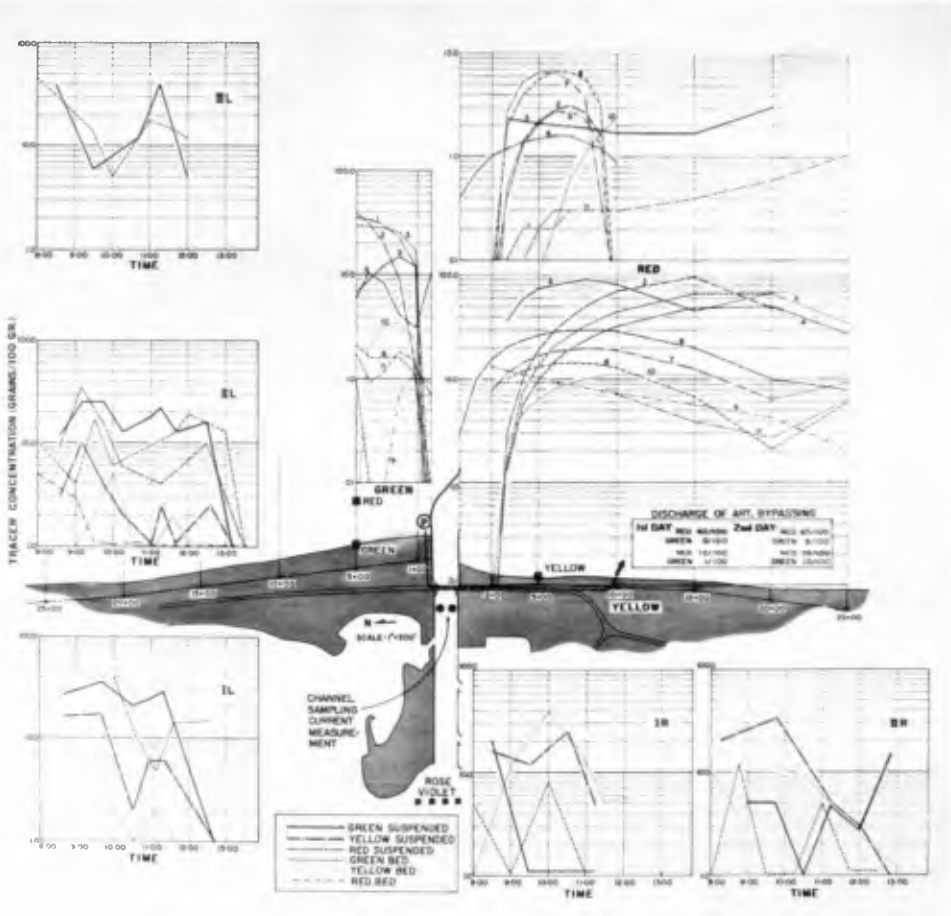

SOUTH LAKE WORTH SAND TRACING STUDY
FIG. 6

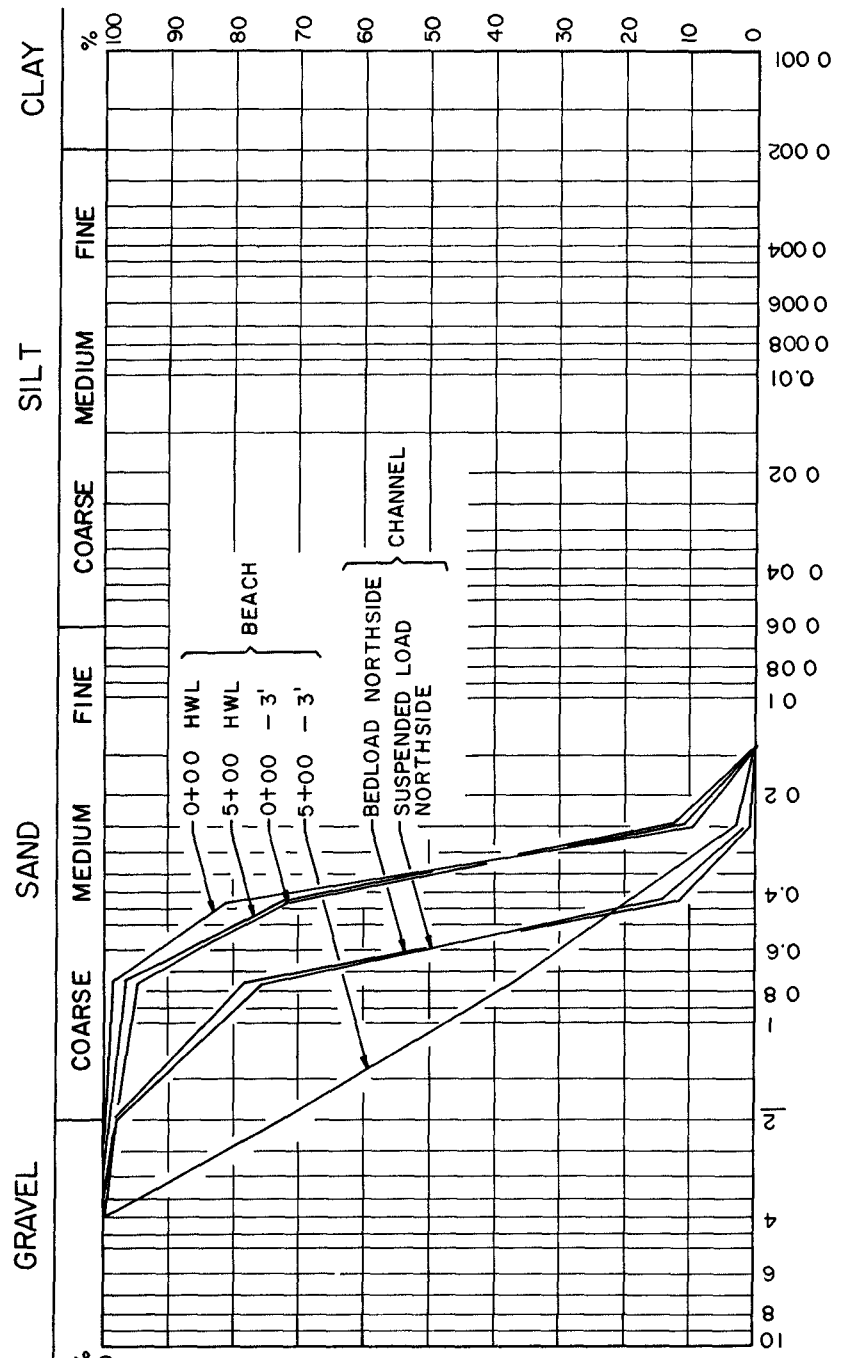

FIG 7 GRAINSIZE DISTRIBUTION OF THE BEACHSAND NORTH OF THE INLET AND OF THE SUSPENDED LOAD AND BEDLOAD NORTH OF THE CENTERLINE IN THE CHANNEL

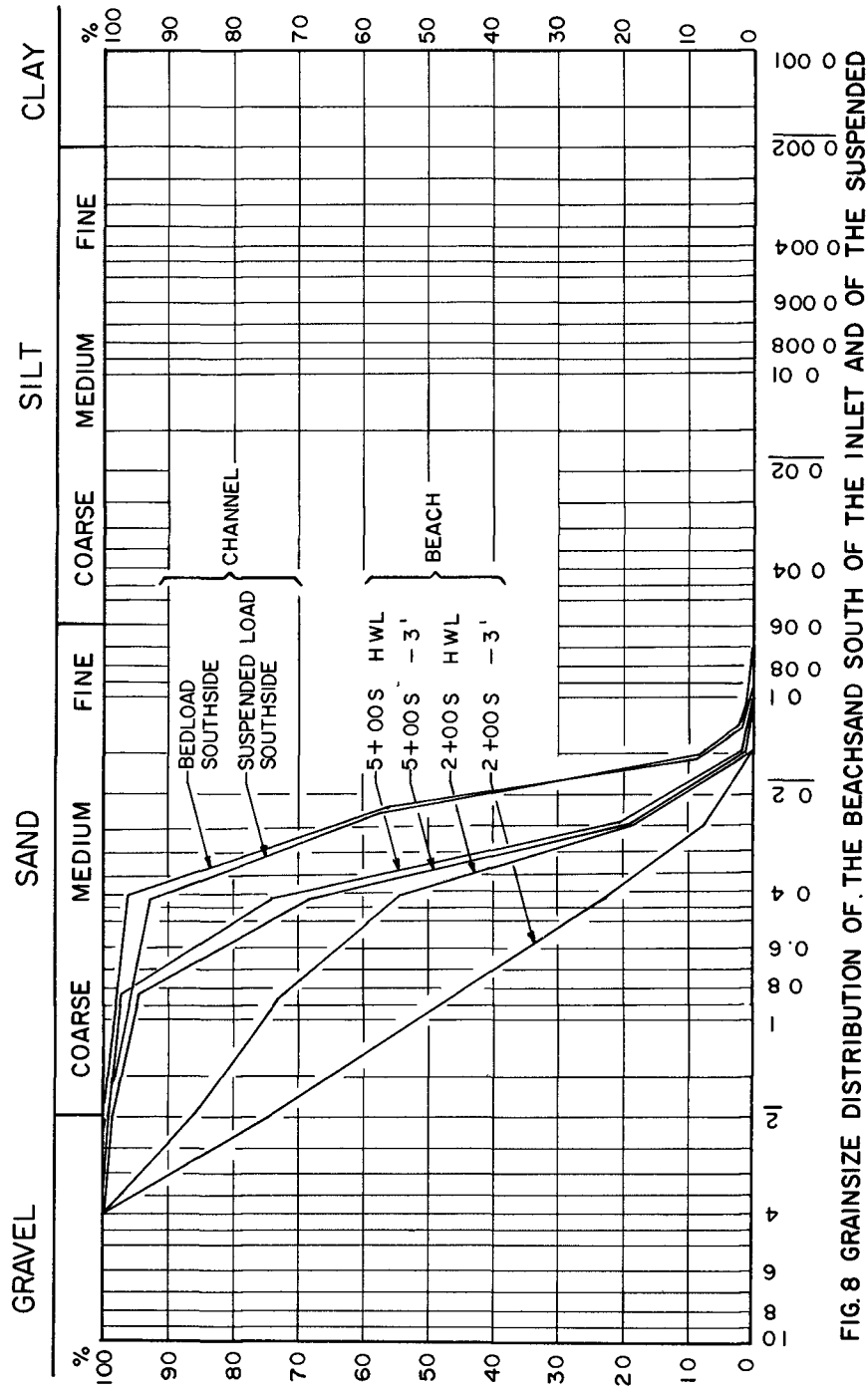

FIG. 8 GRAINSIZE DISTRIBUTION OF THE BEACHSAND SOUTH OF THE INLET AND OF THE SUSPENDED LOAD AND BEDLOAD SOUTH OF THE CENTERLINE IN THE CHANNEL

CHAPTER 20

QUANTITATIVE TRACING OF LITTORAL DRIFT

Dr. Per Bruun

Professor of Harbour Engineering,
Technical University of Norway, Trondheim
NORWAY.

ABSTRACT

Tests were run at Fernandina Beach, Florida, using fluorescent tracers and bed load traps with automatic doors and hydraulic lift to determine the thickness of the bed load transport layer on the bottom ("bottom creep") (ref.1). Four special bed load traps with hydraulic remote controlled doors were installed on an ab. 800 ft. long pier. Fig. 1. Tracers of various colours were dumped at various distances from the pier. Two types of bottom profiles, Fig. 2, "berm profile" and Fig. 3, "bar-profile" were tested. As an example Fig. 4 shows test arrangement and wave action for test No. 17 (berm profile). Longshore wave power for this particular test was 1,5 Watts per ft of wave (one Watt is ab. 0,1 kg m/sec or ab. 0,0014 Horse Power), $H_{1/3}$ was 0,45 m, $T_{1/3}$ was 4-5 sec.

Fig. 4 shows average velocities of grains up to the point of maximum concentration as well as average velocities during the test of 1,3 to 1,5 hours (in paranthesis). Thickness of the moving bed load sheet layer based on the average velocities found during the testing period (ref.1) and the migrating quantities per meter of bottom were as indicated in Table 1.

Table 1. Sheet layer thickness, ave. grain velocity and quantities per meter per hour. Longshore wave power ab. 1,5 Watts)ft or ab. 5 Watts/meter.

	Station 2	Station 3
Layer thickness in cm	0,00064	0,00073
Number of grains of 0,2 mm	1/35	1/30
Average velocity of grains meters/min.	1,3	0,95
Quantity in liters per hour/m	0,48	0,42
Quantity in kilograms per hour/m	0,28	0,25

It is interesting to note from this and other tests that quantities of drift seemed to be related to the longshore wave energy. Fig. 5 shows longshore drift per ft as function of longshore wave energy per ft for a number of tests which include berm as well as bar profiles and wave energy input ranging from a few Watts to ab. 50 Watts per ft of wave crest. Tidal currents could not be eliminated. Results seem to bear some witness hereof.

From Fig:5 it may be seen that:

a) Longshore transport as bed load seems to increase with longshore wave energy. Not enough results are available however to draw any conclusions, and it should be noted that all results refer to bed-load in narrow areas only. Most littoral drift formulas assumes a linear relationship between longshore drift and longshore wave energy.

b) The importance of a longshore (tidal) current superimposed on the wave-energy current may be noted for the low-energy section.

c) The importance of the longshore incl. tidal currents combined with the stir-up may be seen from the results for the higher energy levels. The perpendicular-to-shore component of the wave energy is twice as high for the 44 Watt/ft longshore wave energy case as for the 32 Watt/ft.

d) The importance of the longshore current is also evident from the trough transports predominance over bar transport for the energy levels under consideration. This is undoubtedly going to change for higher inputs of wave energy accompanied by frequent wave breaking and stir-up activity on the bar.

e) The results mentioned above are of preliminary and indicative nature only. Larger equipment and continuous recording is necessary in order to draw conclusions of more general value. Such test should if possible be carried out on a shore without longshore tidal currents. Two piers a few thousand feet apart on a straight shore would be a great advantage for the tracer tests and for comparison between quantities.

Other results from this testing program are mentioned in paper by E. Thornton at this conference.

Bruun, P. and J. Purpura (1964): "Quantitative Research on Littoral Drift in Field and Laboratory", Proc. IXth Conference on Coastal Engineering, Lisbon, Portugal, pp. 267-288.

This paper will be published in the Proceedings of the 22nd Congress of the Permanent International Association of Navigation Congresses, Paris, 1969.

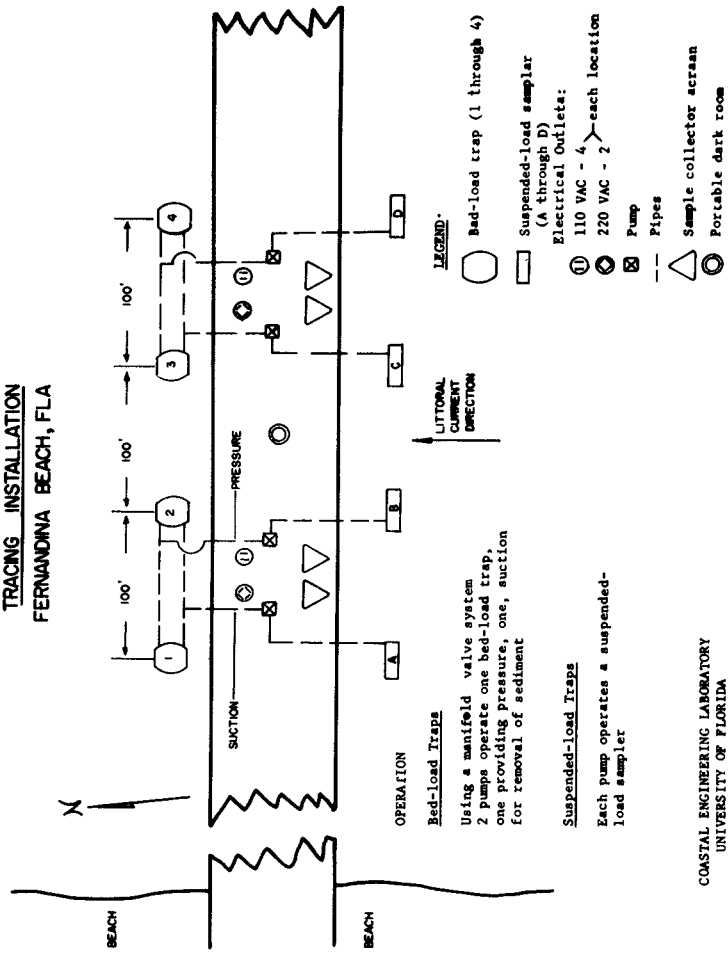

FIGURE 1 FERNANDINA BEACH PIER WITH SAMPLING STATION

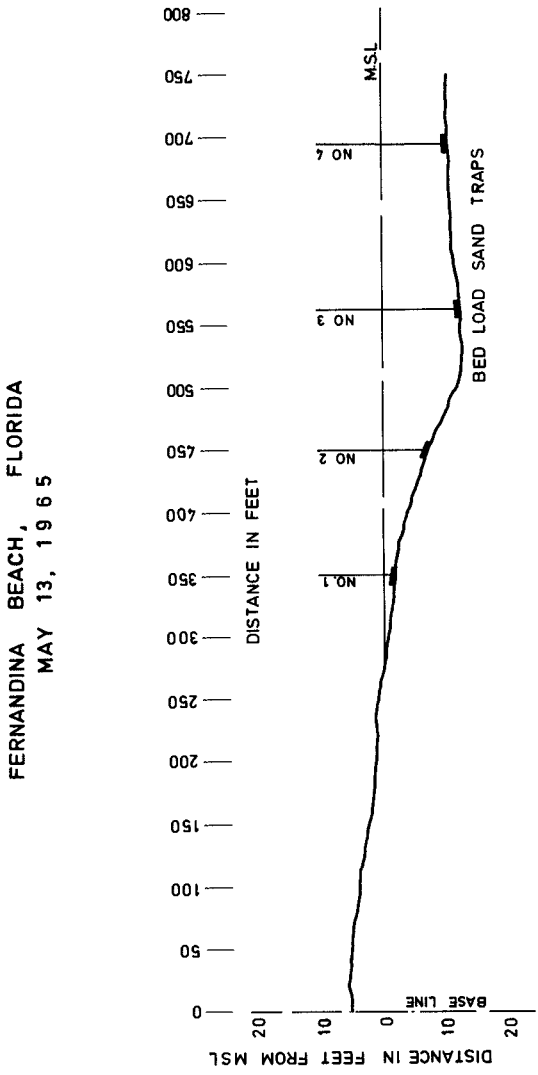

FIGURE 2 BOTTOM PROFILE, TEST NO 17 (berm)

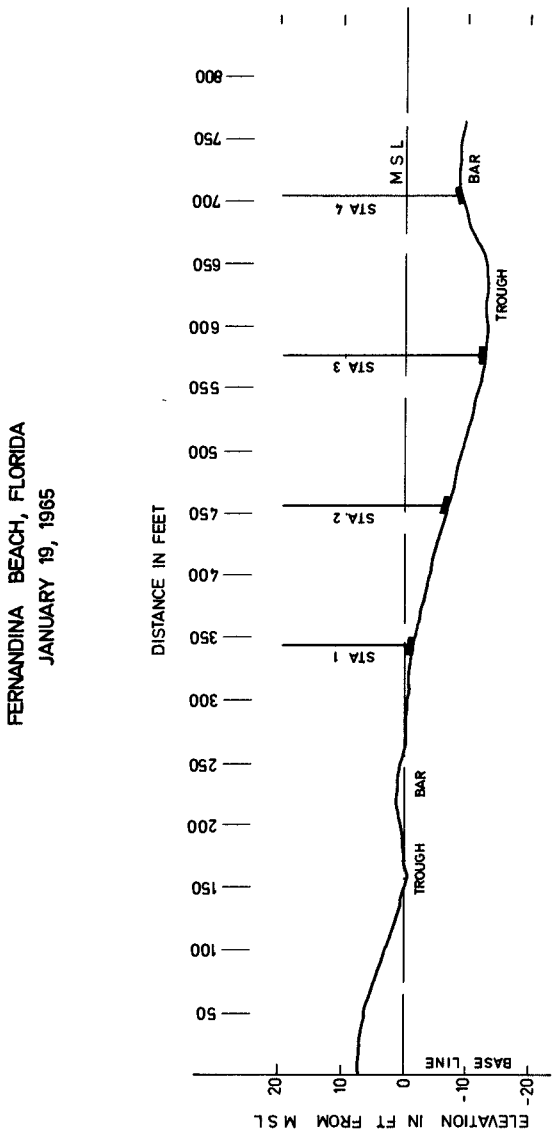

FIGURE 3 BOTTOM PROFILE FOR TEST NO 14 (bar)

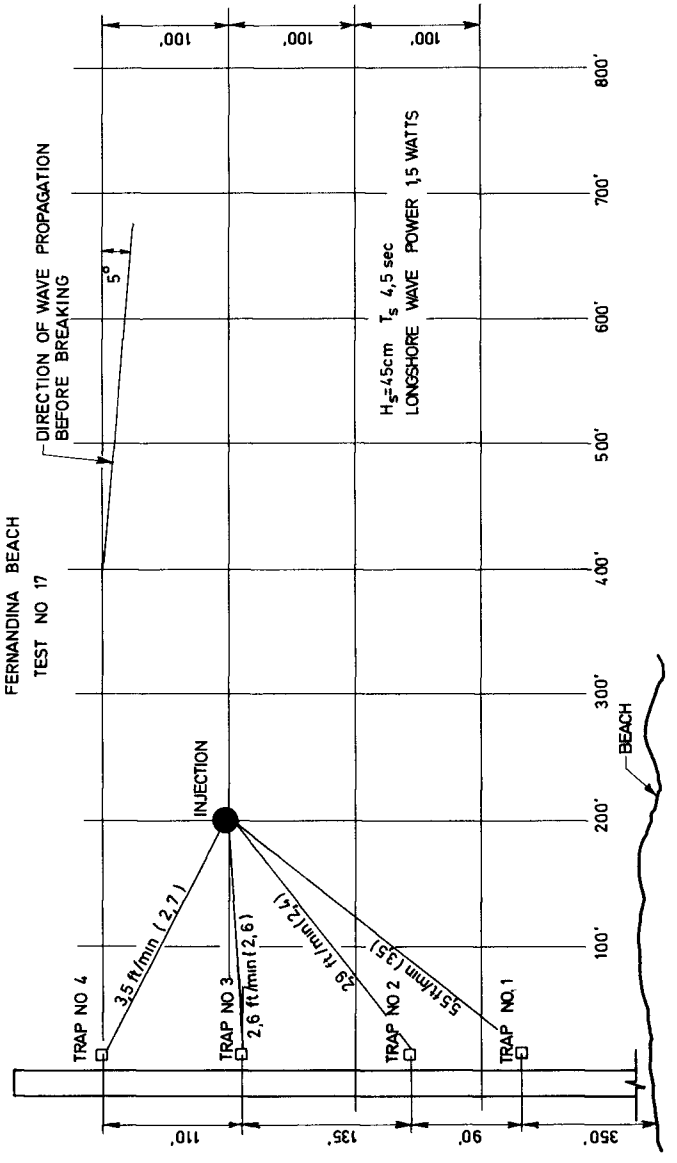

FIGURE 4 TRACER INJECTION PLAN, TEST NO 17 (berm)

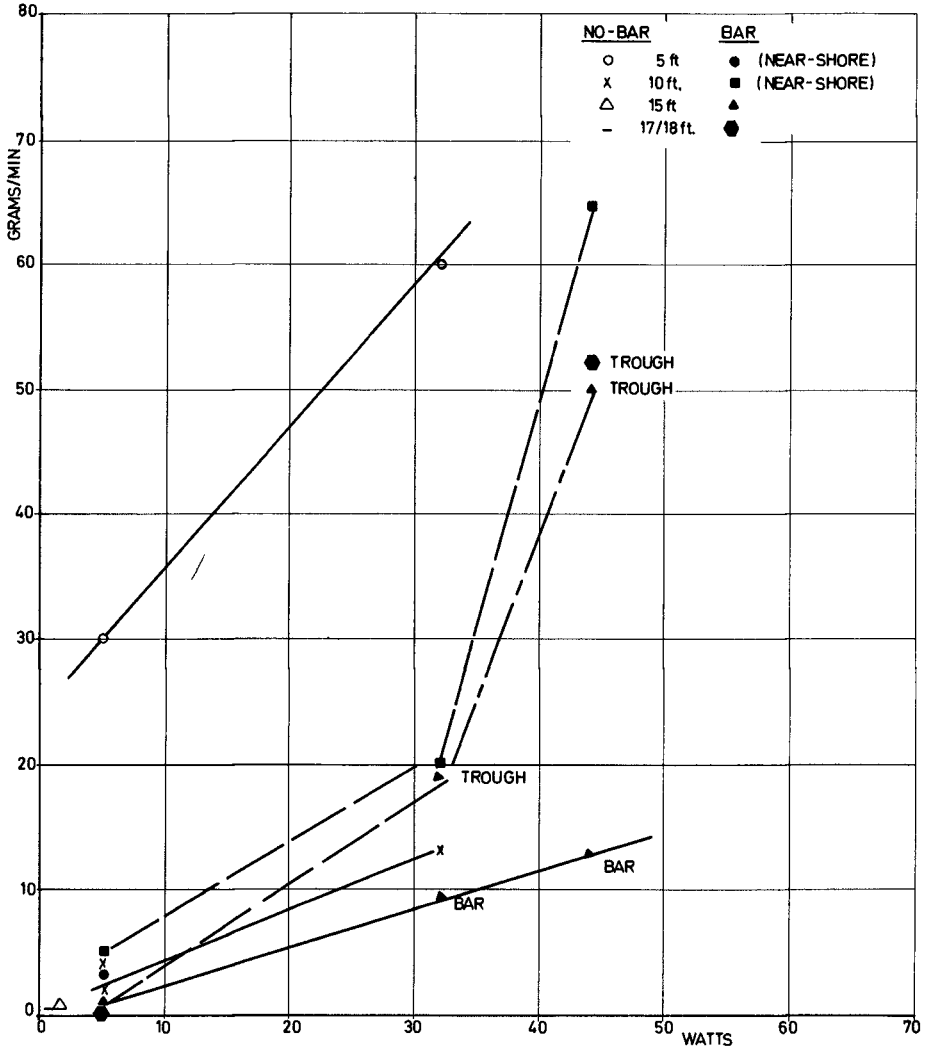

FIGURE 5 LONGSHORE DRIFT AS FUNCTION OF LONGSHORE WAVE ENERGY PER ft

CHAPTER 21

VARIABLE DISPERSION AND ITS EFFECTS ON THE MOVEMENTS OF TRACERS ON BEACHES

W. A. Price, Senior Principal Scientific Officer
Hydraulics Research Station, Wallingford, Great Britain

SUMMARY

To arrive at a quantitative assessment of sediment transport using tracers it is usual to analyse the results using the "centroid method". It is quite satisfactory to apply such a method when the dispersion from any cause is constant over the area under study. However, when tracers are used in a variable dispersive field, as on a beach, the interpretation of the results by normal methods can give misleading results. A simple arithmetical model is used to illustrate the ideas put forward in the paper.

INTRODUCTION

It is the author's contention that the results of many fluorescent tracer experiments carried out on beaches, particularly with respect to the movement of tracer in an onshore/offshore direction, have been misinterpreted. The purpose of this note is to show that when tracers are used on or near beaches in a variable dispersive field even the net direction of sediment transport, as indicated by the trace elements, can be misleading if interpreted by normal methods. Although the author and his colleagues have questioned for some time the validity of some of the conclusions drawn from the results of tracer movements on beaches the main stimulus towards the formulation of the idea presented in this note came from reading the excellent book by J. C. Ingle. Jr. - "Developments in Sedimentology - The movement of beach sand". (Ref. 1). Ingle describes field tests carried out on beaches in Southern California where fluorescent tracers were used to track the movement of beach sand. One of the conclusions was that the tracer invariably moved offshore towards the breaker zone. Quoting from Page 54. (Ref. 1).

> "Since offshore tracer transport was dominant under all surf conditions (i.e. long-period low amplitude waves to short-period high-amplitude waves) an incongruity is presented as monthly beach profiles indicate that alternating periods of accretion and erosion occurred at all five test beaches over the period of the investigation".

The present author believes that the results are not as incongruous as they appear. When the beaches were building up (net onshore transport of material) or eroding (net offshore

transport of material) the tracer placed on the foreshore might well be expected to move in an offshore direction. Unless there is a large sediment transport in one direction tracers will move towards the area of maximum dispersion - in this case towards the breaker zone. Tracer placed seawards of this point will move onshore while tracer placed shorewards of this point will move offshore.

Arithmetical Model

An attempt will be made to explain this concept by means of a simple arithmetical model. For simplicity take the case of a beach subjected to regular waves in a laboratory wave tank. After some time stability will be reached and an equilibrium beach profile established. (Fig. 1).

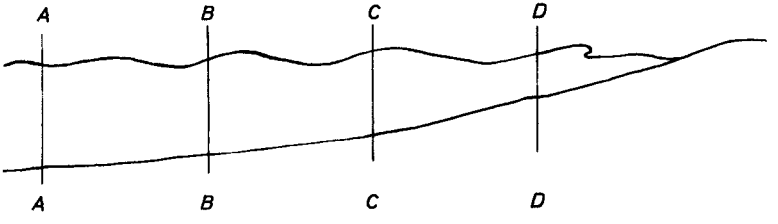

FIG. 1. A Stable beach

If the profile is stable a number of statements can be made.

1. There is no net transport of material past any section AA, BB, CC, DD.

2. The movement in a backwards and forewards direction will be greater at D than at C, greater at C than at B ..... etc. This follows from the fact that the wave orbits and the general level of turbulence are greater at D than at C etc.

3. Proceeding offshore, a point will be reached where even the maximum wave-orbital velocities are not large enough to move material and such a point could be at A.

Any arithmetical model, describing the way material moves on a stable beach, must satisfy the conditions in 1, 2 and 3.

At the Hydraulics Research Station, Wallingford, quite a lot of work is carried out in wave flumes on model beaches. What do we see? With relatively low waves the bed ripples and within a ripple the material moves back and fore. The activity of this movement varies with the position on the beach and the degree

of this activity will control the number of particles exchanged between adjacent ripples during one wave cycle.

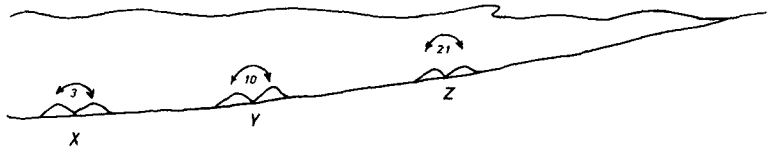

FIG. 2. Exchange of particles

For example, in one wave stroke, 3 particles might be exchanged between ripples in the vicinity of X, 10 particles between ripples in the vicinity of Y and 21 particles between ripples in the vicinity of Z (Fig. 2). Proceeding through the breaker zone the exchange will then decrease to zero. If this is the case then at a point on the bed in the area seawards of the breaker zone more material will be exchanged between this point and points right than this point and points left. An arithmetical model of a stable beach might, therefore be described as shown on (Fig. 3).

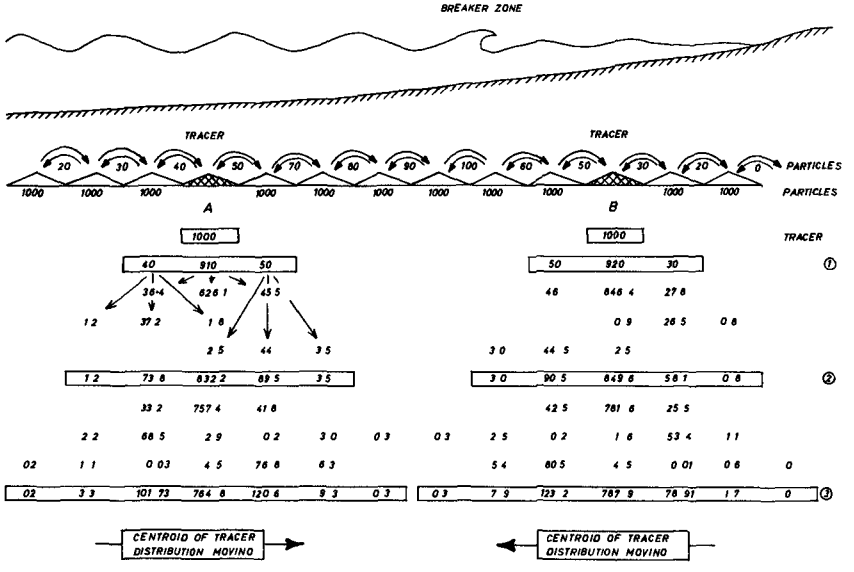

FIG. 3. Model of Tracer movement on a stable beach.

Although it is not necessary to interpret the model in terms of the exchange of particles between ripples the ideas are easier to put across on this basis. Consequently the triangular shapes in the diagram are meant to represent ripples and the figures between the ripples the number of particles exchanged in one wave stroke. The variation in the exchange of material between ripples has been exaggerated for illustrative purposes and it has been assumed that each ripple contains the same number of particles - in this case 1000. Also, any material entering a ripple is assumed to be uniformly mixed with that which was already present at the end of each wave stroke.

Suppose the ripples at A and B are now replaced by tracer. Its distribution can be calculated at the end of every wave stroke as shown in the diagram. Even by inspection it can be seen that the centroid of tracer distribution is moving onshore from A and offshore from B. If the normal "centroid" method is used to interpret the results then unreal directions of sediment transport will be indicated - the initial premise for a stable beach being no net movement of sediment. (The model can be extended to include net sediment movement in one direction and to demonstrate the anomolous situation of an apparent tracer movement in the opposite direction.)

Tracer distributions measured in one of our laboratory wave tanks confirm that qualitatively the arithmetical model describes the movement of tracers quite well. It was hoped that when we came to write the full paper we might have been able to describe the process quantitatively. Pressures of work from other sources, however, have prevented us proceeding any further. A number of problems have to be solved in the quantitative case. For example, what controls the number of particles exchanged between adjacent parts of the bed? Perhaps the exchange rate is proportional to the maximum wave orbital velocities, the orbit length, or the net movement of water close to the bed. Tests in a wave tank are now planned to resolve some of these questions.

THE EFFECT OF TIDAL VARIATION

So far the ideas have been explained in terms of a beach subjected to waves with a constant water level. However, the dominating influence of variable dispersion is perhaps more marked when the water level on the beach is subject to changes brought about by tides. Here the periods of time that the water stands on the beach varies from place to place and, therefore, the phenomenon for the part of the beach between L.W. level and H.W. level is now time dependent.

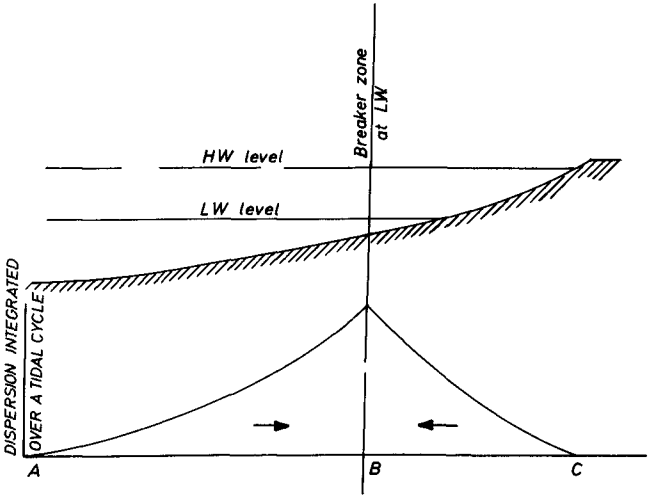

FIG. 4. Diagrammatic sketch showing dispersion with tides

Let us describe qualitatively the cumulative effect of dispersion over a tidal cycle. On the part of the beach below L.W. level the dispersive agencies integrated over a tidal cycle will increase towards the breaker zone (A B) in Fig. 4. Shorewards of point B the cumulative effect of dispersion will decrease because the time at which water stands at the various levels decreases when moving from L.W. to H.W. level (B C) in Fig. 4. On this basis, as shown earlier, tracer placed shorewards of L.W. level will tend to move seawards while tracer placed seawards of L.W. level will move shorewards.

SUMMARY AND CONCLUSIONS

It is realised that such a simple model, at least in its present form cannot represent the movement of beach material completely. For example, when violent movements of the bed material take place under large waves particles can be displaced many ripple lengths in one wave stroke. Nevertheless, it is hoped that the model demonstrates that it could be misleading to interpret the movements of tracers injected into a variable dispersive field, on and near a beach, by the normal methods.

It would be instructive in the field for a variety of reasons to measure the quantity of material travelling as littoral drift, not so much in total, but at various levels on the beach. The author and his colleagues have thought about this problem and have come up against the obvious difficulties of using tracers for this purpose. If, however, the present arithmetical model could be made to work quantitatively (that is values could be ascribed to the dispersion coefficients at all points on the bed) then tracer distributions measured in nature could be corrected for the apparent mass transport effect in the onshore/offshore

direction so that lateral distributions of tracer could then be used to establish the quantity of drift at various levels.

Finally, I would like to thank Mary Kendrick, George Lean and Maurice Crickmore for the many enjoyable arguments we have had on this subject.

This paper is published by permission of the Director of Hydraulics Research, Wallingford, England.

Ref. 1. Developments in Sedimentology 5. The movement of beach sand. James C. Ingle Jr. Elsevere Publishing Company, Amsterdam. London, New York 1966.

CHAPTER 22

A FIELD INVESTIGATION OF SAND TRANSPORT IN THE SURF ZONE

Edward B. Thornton

Department of Coastal and Oceanographic Engineering,
University of Florida, Gainesville, Florida

ABSTRACT

The distribution of bed-load sand transport normal to the beach has been measured in a series of field experiments conducted in the surf zone at Fernandina Beach, Florida. Simultaneous measurements were made of the waves and water particle motion at various locations in the surf zone. The energy flux of the waves was resolved into its longshore component from the measured directional and energy spectra. It is found that the bed-load transport is related to the depth of water and longshore energy flux. Insight into the mechanics of sediment transport is obtained by comparing the wave and water particle motion energy spectra, which give a direct measure of the kinetic and potential energy, at various locations in the surf zone.

INTRODUCTION

A meaningful field investigation of the sand transport processes in the surf zone requires the synoptic measurement of a number of hydrodynamic and sediment variables. Fairly complete and extensive data are required to evaluate the validity of various proposed sand transport relationships and the formulations of new relationships where necessary.

This paper describes field experiments conducted in the surf zone at Fernandina Beach, located on the northeastern coast of Florida. The emphasis of this study was to obtain information concerning the distribution of bed-load transport perpendicular to shore and the physical processes causing such movement. Sediment transport in the surf zone can be considered as being caused by a combination of shear stresses due to wave and current action. An attempt to correlate sediment transport with physical parameters then must include good wave and current measurements.

The experiments were conducted from October, 1966 to May, 1967, a period that encompasses the more intense wave activity along this coast. The beach and nearshore bottom profile is typically a one or two bar system with a gentle slope of two to three per cent. The sand has a mean grain size of approximately 0.2 millimeters. The mean tidal range is 1.7 meters.

The physical parameters measured during the experiments were the time history of the wave height, wave direction, instantaneous water particle velocities, tides, wind direction and speed, quantity of sediment transport, bottom contour profiles, and sediment characteristics.

The measurements were conducted from a pier traversing the surf zone seaward to the outer bar, that is to the first breaker line. A plan of the pier and location of the instrumentation is shown in Figure 1. A typical bottom profile taken adjacent to the pier is also shown in this figure. During the course of the experiments the waves "peaked" or spilled on the outer bar, crossed the bar, and carried on into the inner bar where they broke. The experiments were limited to the study of the bed-load transport in the area bounded by the outer and inner bar.

Since this is not the area of intense turbulence, the mode of transport is primarily due to bed-load which includes saltation. It should be pointed out that this area represents only a portion of the surf zone, and the quantity of sand measured was not the total littoral drift, but represents a significant contribution to the total.

EXPERIMENT

The experiments were conducted over approximately half a tidal cycle, usually four to six hours. The tide recorder, anemometer, and sand traps operated continuously during the experiment. Current measurements were taken at various locations for durations of at least five minutes and up to twenty minutes. Waves were measured simultaneously and at the same location as the current measurements. Also during the test, wave measurements at two locations at the end of the pier were taken simultaneously for a period of twenty minutes. The instrumentation and details of measurements are described below.

Taking measurements in the surf zone is very difficult due to the tremendous forces exerted by the waves. It is almost essential for synoptic measurements to have a stable platform from which to work. This platform, a fishing pier in this case, exerts some local influence on the environment being measured and care must be taken to minimize this effect. Thus, all measurements were made as far from the pier and its piling as possible, and the measurements were taken on the updrift side of the pier on which the incident waves impinge first.

A pier or similar structure extending out from the beach can also exert an influence on the general circulation patterns of the surf zone. The pier can act as a perturbation on the longshore current system, and one often observes a rip current generated near the tip of such structures. Care was taken to note the occurrence of rip currents being generated at the pier, and such occurrences have been treated as being anamolous. Data taken during such experiments have been excluded.

Another effect of the pier was noted from the bathymetry of the area adjacent to the pier. It is found that there was considerable scour about the seaward end of the pier which certainly influences the sediment transport

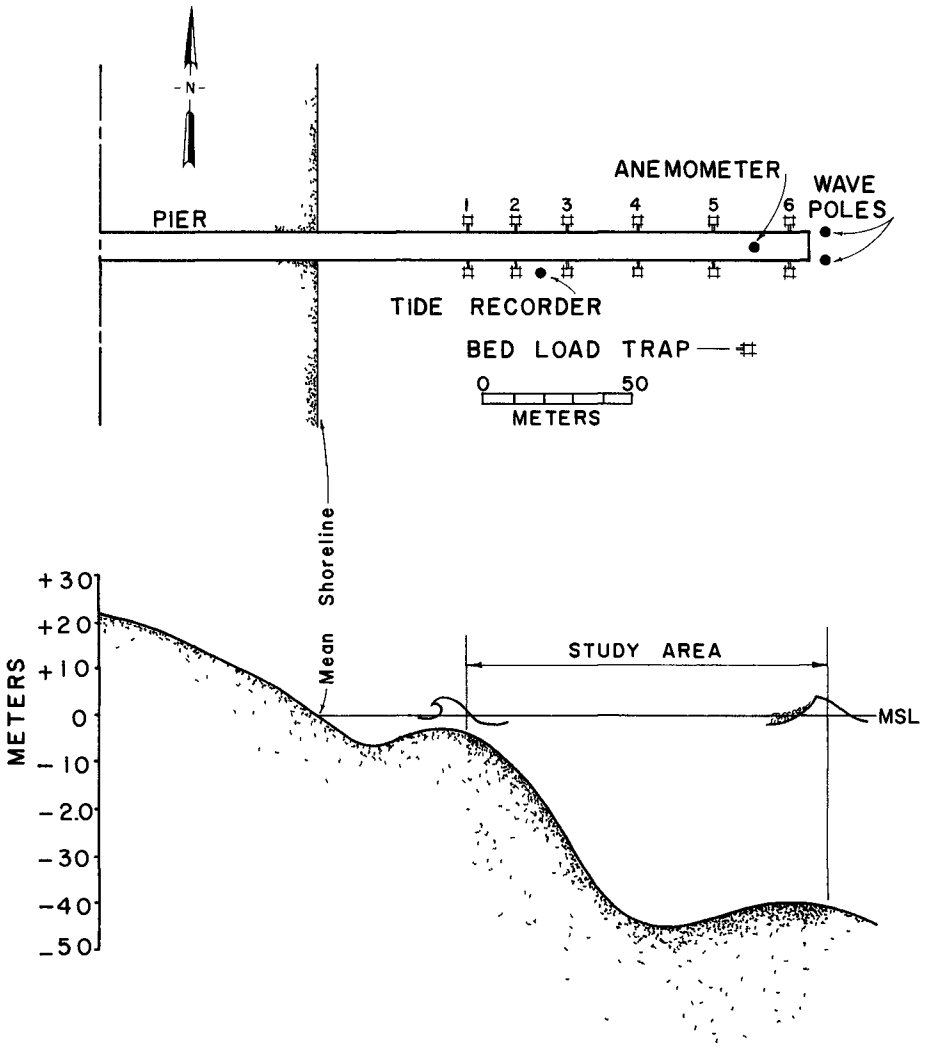

FIGURE I. INSTRUMENTATION AND BOTTOM PROFILE AT FERNANDINA BEACH PIER

in this vicinity. Similar scour about the ends of other piers has also been found elsewhere. It was also noted that there was some slight accretion of sand at the shoreward end of the pier in the swash-zone area.

Current measurements

The measuring of accurate current velocities in the presence of a wave field, such as the surf zone, has long been a problem. This has greatly limited the quantitative nature of results collected pertaining to sediment transport in the ocean. An electromagnetic flowmeter was used during these experiments and proved applicable for use in the surf zone. This instrument was used essentially as a turbulence meter. With this instrument, not only the mean, but the fluctuations about the mean, or the turbulent velocities, are measured.

Problems encountered in the surf zone with conventional current meters are due to the suspended sediments and rapid water particle accelerations. The suspended sediments tend to wear out bearings or moving parts. Propeller or rotor-type meters have a poor response to rapid accelerations due to the inertia of the blades. Since the electromagnetic current meter utilizes no moving parts, these problems have been eliminated.

The current meter mounted on a tripod is shown in Figure 2. Its overall length is 15 centimeters with an inside bore diameter of 1 centimeter. Calibration of the instrument showed it to have very linear characteristics over the velocity range of less than 0.03 meter per second to more than 5 meters per second, which was the range of the calibrating facilities. The tests also showed the instrument to have a fairly flat response up to frequencies of one cycle per second. For a complete description of the current meter and other instrumentation the reader is referred to Thornton (1968).

It was found necessary to mount the current meter on a tripod rather than on the pier in order to have the desired rigid mounting. The pier, although a stable platform to work off, responds to the wave motion with a frequency approximately the same as the frequency of the waves. The motion of the pier is mostly lateral. This motion has negligible effect on the wave measurements but introduces a serious impressed motion on the current meter record. The natural frequency of the tripod is much higher than frequencies of interest for the measured water particle velocities and has proven to be an excellent mounting.

Wave measurements

Waves, as they appear in nature, are essentially aperiodic or random in nature and as such have to be treated as a statistical phenomenon. The studies were conducted over a relatively short duration of time, half tidal cycle or less, and, as such the physical environment may be assumed quasi-stationary. Since a stationary system can be assumed, spectral analysis was employed in treating this aperiodic phenomenon.

Both energy-density spectra and directional spectra of the waves were measured by means of two resistance wire wave poles located at the end of the pier. The outer bar delineates the seaward edge of the surf zone, and,

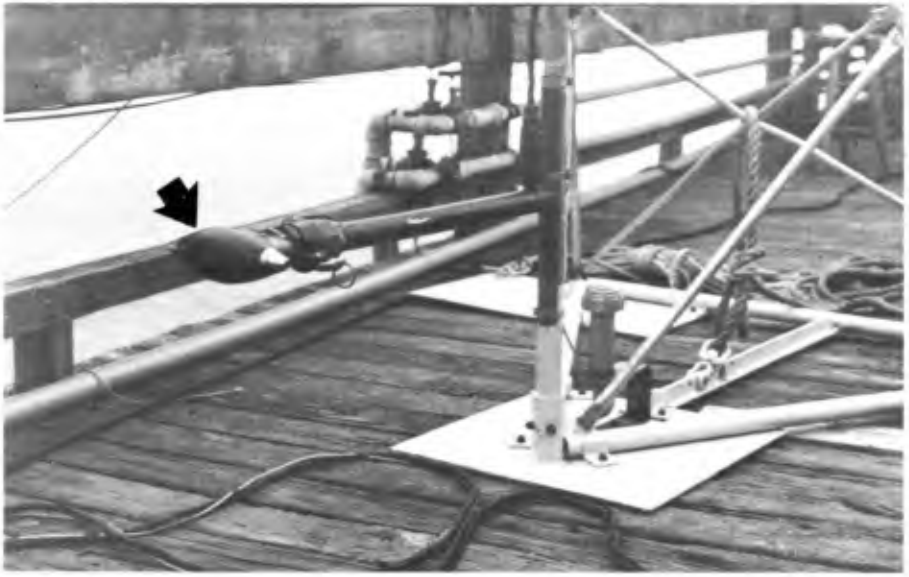

FIGURE 2
ELECTROMAGNETIC FLOW METER

FIGURE 3
BED-LOAD TRAP

since the waves were recorded here, the energy input into the surf zone was measured directly. By computing the Fourier transform of the cross-correlation function of the two wave records, a single directional spectrum is obtained. This analysis associates a direction with each frequency component and is essentially a measure of the phase difference between the two measuring locations for each Fourier component.

A pressure transducer to measure wave heights was mounted on the same tripod as the current meter so that a direct correlation of the water particle velocity and wave height could be obtained at the same location in the surf zone.

Bed-load traps

The quantity of sand transport was measured by means of bed-load traps which are aligned in the direction of the longshore current. These traps, shown in Figure 3, rest on the bottom and sample an area 20 centimeters high by 40 centimeters wide. The bed-load movement here is defined by the height of the traps and, as such, includes saltation. Up to six traps were used simultaneously.

The unique design of these traps has evolved over several years of use, and they have proven to be very rugged and dependable for the severe conditions under which they are subjected. For a more complete description of the traps and attendant system, see P. Bruun and J. Purpura (1964).

Analysis

Meaningful information from the wave and current meter records can be obtained by computing the individual energy-density spectra. A time series record of finite duration, extending from t_1 to t_2 can be represented in the form of a Fourier integral

$$\eta(t) = \frac{1}{\sqrt{2\pi}} \int_{-\infty}^{\infty} A(\sigma)\, e^{i\sigma t}\, d\sigma \qquad (1)$$

where the $A(\sigma)$ is the complex amplitude spectrum and is a continuous function of the frequency, σ. $A(\sigma)$ can be determined by the Fourier transform of the time series representation of the wave record given by

$$A(\sigma) = \frac{1}{\sqrt{2\pi}} \int_{-\infty}^{\infty} \eta(t)\, e^{-i\sigma t}\, dt = |A(\sigma)|\, e^{i\varepsilon} \qquad (2)$$

where ε is the argument, or phase angle, of $A(\sigma)$.

The energy-density spectrum, $\Phi(\sigma)$, is proportional to the square of the modulus of the amplitude spectrum

$$\Phi(\sigma) = |A(\sigma)|^2 \qquad (3)$$

The amplitude spectrum can be determined via either the mean-lagged product as presented in Blackman and Tuckey (1958) or directly by the computationally faster Fast-Fourier-transform method that is outlined in Bingham, et al. (1967).

The potential and kinetic energy of the waves and water particle motion, respectively, can be obtained by integrating the energy-density components over all frequencies where

$$\frac{1}{16}\rho g\overline{H^2} = \frac{1}{2}\rho g \int_0^\infty |A_H(\sigma)|^2 \, d\sigma = \text{average potential energy of waves/unit area}$$

$$\frac{1}{2}\rho\overline{u^2} = \frac{1}{2}\rho \int_0^\infty |A_u(\sigma)|^2 \, d\sigma = \text{average kinetic energy of water particle motion/unit volume}$$

A measure of the directional characteristics of the waves can be obtained from the simultaneous time records of the two wave poles at the end of the pier. This method of analysis was suggested to the author by Dr. R. G. Dean and is fully described by Thornton (1968). A single directional spectrum of the waves is obtained by computing the Fourier transform of the cross-correlation function of the two wave records. The analysis associates a direction with each frequency component and is essentially a measure of the phase difference between the two measuring locations for each Fourier component.

Let us consider for the moment monochromatic waves having an infinitely long-wave train approaching under asimuth β, with amplitude a, frequency $\sigma = 2\pi/T$, and wave number $k = 2\pi/L$, where T and L are wave period and length, respectively. We will assume the frequency and wave number can be related with sufficient accuracy by the small amplitude wave theory relation

$$\sigma^2 = gk \tanh kh$$

The wave displacement is represented as

$$\eta(x,y,t) = A(\sigma)\, e^{(\sigma t - k\cos\beta\cdot x - k\sin\beta\cdot y - \varepsilon)}$$

Using a coordinate system (x,y) with the origin at the reference wave sensor (1) and the x-axis through the secondary wave sensor (2) (see Fig. 7), the measured water surface displacement due to this single component can be represented in complex notation

$$\eta_1(o,o,t) = |A_1(\sigma)|\ e^{i(\sigma t-\varepsilon_1)} \tag{4a}$$

$$\eta_2(o,s,t) = |A_2(\sigma)|\ e^{i(\sigma t-ks\sin\beta\cdot s-\varepsilon_2)} \tag{4b}$$

where s is the separation distance between the wave sensors. For monochromatic waves, the phase angles are equal $\varepsilon(\sigma) = \varepsilon_1 = \varepsilon_2$.

The cross-spectrum $\Phi_{12}(\sigma)$ for a particular frequency can be obtained from the complex amplitude spectra of the two individual wave records as computed in Equation (2).

$$\begin{aligned}\Phi_{12}(\sigma) &= C_{12} + iQ_{12} = |\Phi_{12}|\ e^{i\delta} \\ &= |A_1(\sigma)|\ |A_2(\sigma)|\ e^{iks\sin\beta\cdot s}\end{aligned} \tag{5}$$

where C_{12} is the co-spectrum, and Q_{12} is the quadrative spectrum, and

$$|\Phi_{12}| = [C_{12}^2 + Q_{12}^2]^{\frac{1}{2}} = |A_1(\sigma)|\ |A_2(\sigma)|$$

$$\delta = \tan^{-1}\frac{Q_{12}}{C_{12}}$$

Equating arguments in Equation (5), we find

$$\beta(\sigma) = \sin^{-1}\left[\frac{\delta(\sigma)}{k(\sigma)s}\right] \tag{6}$$

where β is the asimuth of the approaching wave for a particular frequency. Thus, from the record of two wave sensors it is possible to infer a single wave direction for each frequency. The assumed wave system is, therefore, equivalent to an infinite number of wave frequencies composing the spectrum, with the directional characteristics of each component described by a single value.

The separation distance, s, of the wave meters must be short enough so that the criterion of long-crested waves is realized, and it is also required that they be separated by sufficient distance to obtain good resolution. It should be noted that for the case of two sensors, there is a direction ambiguity for each frequency of 180 degrees. In our application, the measurement of waves is close enough to the shore so that, except for possibly very high frequencies which are of minor importance, the direction is uniquely determined. It also should be cautioned that the interpretation of the determined direction for a frequency component with broad directional or multi-directional characteristics would certainly be questionable.

Past sediment transport studies have indicated the longshore component of wave energy flux to be an important parameter in determining the littoral drift. We can easily calculate the total longshore energy flux, P_l, from the information obtained from the energy and directional spectra of the waves. Assuming the linear wave theory approximation for the group velocity of the individual energy components

$$C_G(\sigma) = \frac{\sigma}{2k}\left[1 + \frac{2kh}{\sinh 2kh}\right]$$

and equal partitioning of kinetic and potential energy in the wave, P_ℓ is given by

$$P_\ell = 2 \sum_0^\infty C_G(\sigma)\, \rho g \Phi(\sigma)\, \sin 2\beta \qquad (7)$$

RESULTS

Insight into the mechanics of sediment transport in the surf zone can be gained by examining the waves and currents. The results of the experiment conducted on May 24, 1967, are used as typical of the results to illustrate the fluid-sediment mechanics of the system measured. The weather on this date was very good with maximum winds of less than eight knots. A predominant swell which was quite regular was from the north quadrant which originated from a distant storm system located off the northeastern part of the United States. The wind and swell conditions were quite constant throughout the test.

The quantity of bed-load sand transport as a function of time is shown in Figure 4. Each point of the curve represents a twenty minute average for the longshore bed-load transport at a particular location in the surf zone. The four curves indicate the sand caught at traps 1 through 4. (See Figure 1 for location of traps.) The tidal curve is represented below to show the changes in the mean water depth during the experiment. The changes in water depth were minimized by working over the peak of the tidal curve.

One of the most striking features of the diagram is the variability of the sand transport with time, even though the waves were quite constant during this time. This is indicative of the very complex nature of the sediment transport problem in the surf zone. Generally, it is noted that the sediment transport is related to the depth, that is, the sand transport increases with decreasing depth.

The results of the spectral analysis of the wave and current records is given in Figures 5-7 showing a comparison of measurements taken at various locations in the surf zone. Generally, it can be seen from the figures that the kinetic energy of the fluid particles increased in a shoreward direction while the potential energy decreased which is indicative of a system dissipating energy. In this case, the waves were "spilling" between the two

measuring locations. In an "ideal" wave system (non-dissipative), for which potential theory would be valid, we would expect the potential energy to increase since the energy flux would be constant and the group velocity would be decreasing due to decreasing depth.

A comparison of the energy spectra of the waves at the breaker's edge and at a location 70 meters inshore in Figure 6 shows the potential energy of the waves to be decreasing in a shoreward direction. The shape of the spectra is attributed to the nonlinear character of the waves in the surf zone wherein several harmonics of the fundamental peak can be seen. It will be noticed in the comparison of the two wave spectra that there is a decrease in the fundamental peak of the inshore spectra but an increase in the higher frequency peak. This might indicate the loss in energy in the lower frequencies due to spilling and nonlinear transfer of energy to higher frequencies. The spectra of the water particle velocities demonstrated a similar shift in energy-density to higher frequencies.

Figure 6 shows the measurement of the kinetic energy measured 55 centimeters from the bottom at two locations in the surf zone. It can be seen that there is an increase in the kinetic energy from the offshore station (150 meters) to onshore (120 meters). This can be attributed to the transfer of potential energy to kinetic and turbulent energy in the shoaling and spilling process. The increase in kinetic energy would be indicative of an increase in shear stress at the bottom due to wave and turbulent action. This increase in shear stress would result in more sediment being placed in motion for transport by the longshore current. Assuming a uniform longshore current (the shear stress for the current alone being essentially uniform), one would expect longshore drift to increase in the shoreward direction. This was generally substantiated by the sampling of the bed-load traps.

Also shown in Figure 6 is the kinetic energy spectrum of the parallel to shore component. The energy of this spectrum was approximately one-tenth that of the component aligned with the waves. It should be pointed out that the directional response of an orifice-type current meter is not fully determined for angles of incidence approaching 90 degrees. Therefore, the spectrum of this component should be viewed with reservations although it is felt that the measure of the mean current of 0.23 meters per second is fairly accurate. This spectrum does show relatively more energy content in the low frequencies as one would expect.

The calculated directional spectrum from the two wave sensors is given in Figure 7. From this spectrum and the wave energy spectrum the longshore energy flux can be resolved as given in Equation (7).

An empirical correlation of the wave and sediment transport quantities by dimensionless grouping of the pertinent variables was attempted in order to determine the relative importance of the various parameters. These can be represented in terms of dimensionless parameters in the following functional form

$$\frac{QH_s}{P_\ell} = f(H_s/d) \qquad (8)$$

where

Q = quantity of sand transport (gm/min/m)

H_s = significant wave height (m)

P_ℓ = longshore wave component of energy flux (gm-m^2/sec/m^2)

d = depth of water (m)

The results of these and earlier experiments are summarized in Figure 8. The figure indicates that generally the sand transport increases as the depth decreases. Since a bar-trough profile was usually present, this relationship indicates higher transport rates on the bars than in the troughs. The greater transport of sand on the bar and other shoal areas in comparison with the trough was also demonstrated in earlier experiments using fluorescent tracers.

These results were limited to experiments where the significant wave height at the edge of the surf zone was generally less than one meter. For larger wave heights, the sediment transport data greatly deviated, falling under the curve shown. This may be due to the fact that for higher waves the mode of sand transport is changed; a significant portion of the transport may be due to suspended load and was not measured by the bed-load traps.

The results of these experiments were compared to the littoral drift formula used by the Coastal Engineering Research Center (ref. 5) which relates longshore wave energy flux to total littoral drift. The total bed-load during the tests between the outer and inner bar can be determined approximately by integrating the empirical curve shown in Figure 8 over the limits from deep water to the inner breaker line for a particular set of wave conditions. The comparison of the two relations showed the bed-load measurements to be ten to forty per cent of the total littoral drift as given by the CERC formula. This is within the range of expected values and appears to give good comparison of the two sets of information.

ACKNOWLEDGMENTS

The author wishes to express his appreciation to Dr. R. G. Dean for his helpful discussions and to Dr. P. Bruun who initiated the studies at Fernandina Beach and was responsible for some of the earlier experiments.

This research was sponsored by the Department of the Interior, Water Pollution Control Administration under contract WP-00889 with the University of Florida.

REFERNCES

1. Blackman, R. B. and J. W. Tukey, The Measurement of Power Spectra, Dover Publications, Inc., New York, 1959.

2. Bruun, P. and J. Purpura, "Quantitative Research on Littoral Drift in Field and Laboratory," Proceedings, Ninth Coastal Engineering Conference 1964, pp. 267-288.

3. Bingham, C., M. D. Godfrey and J. W. Tukey, "Modern Techniques of Power Spectrum Estimation," IEEE Trans. Audio and Electroacoustics, Vol. AU-15, No. 2, June, 1967, pp. 56-66.

4. Thornton, E. B., "Quantitative Measurements in the Surf Zone," Dept. of Coastal and Oceanographic Engineering, University of Florida, Tech. Report No. 2, 1968.

5. "Shore Protection Planning and Design," U.S. Army Beach Erosion Board, Tech. Report No. 4, 1961, p. 83.

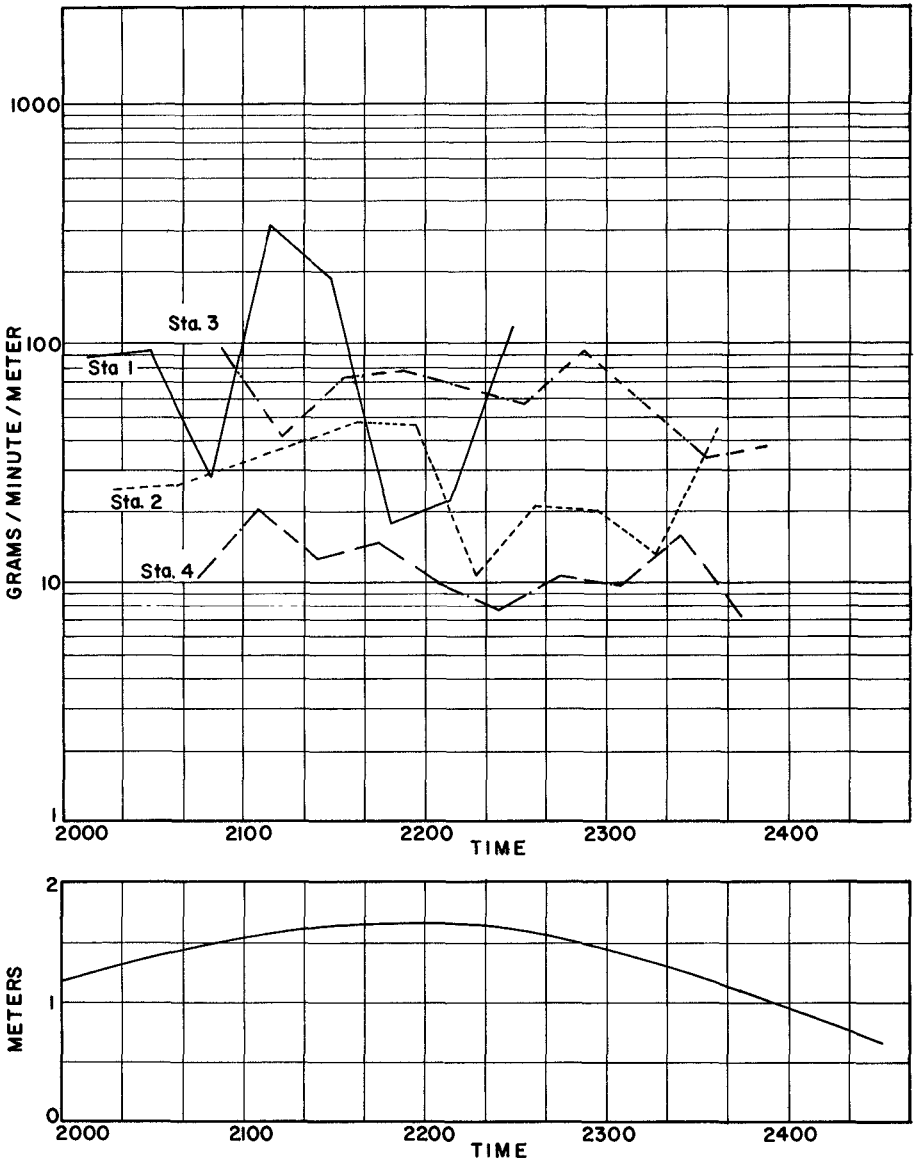

FIGURE 4. SAND TRANSPORT, 24 MAY 1967

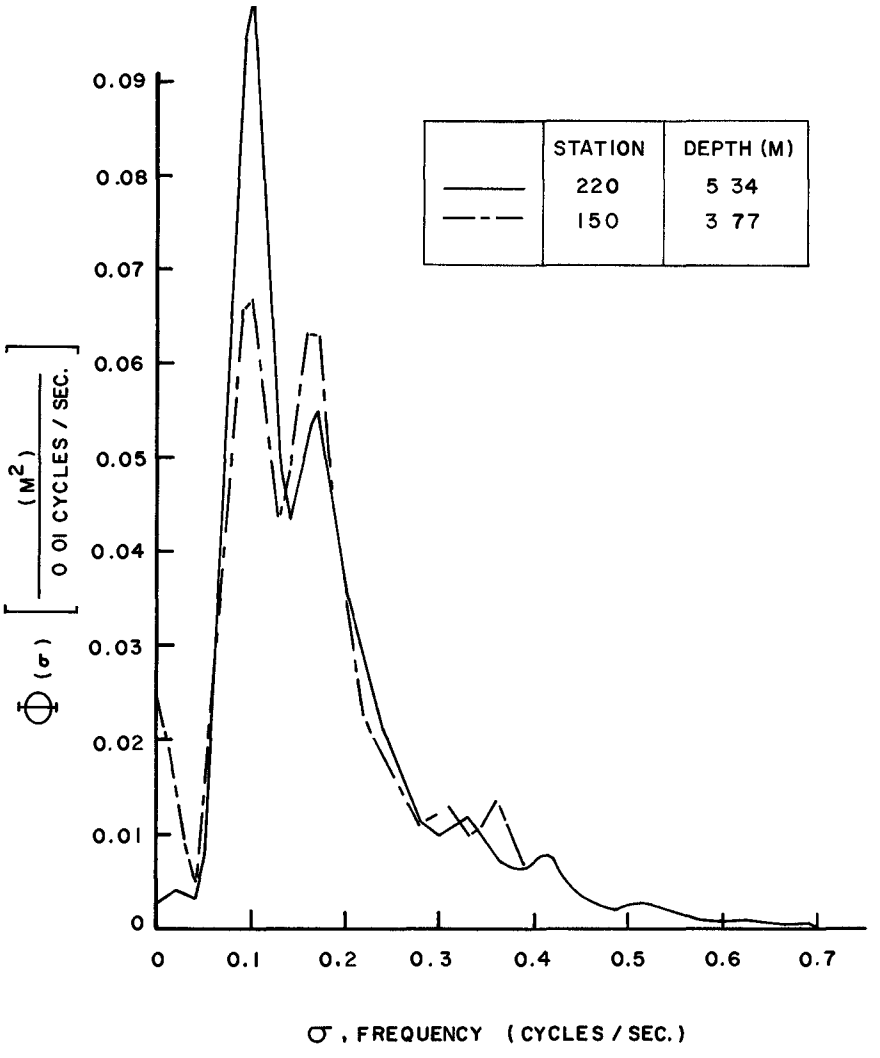

FIGURE 5. WAVE SPECTRA, 24 MAY 1967

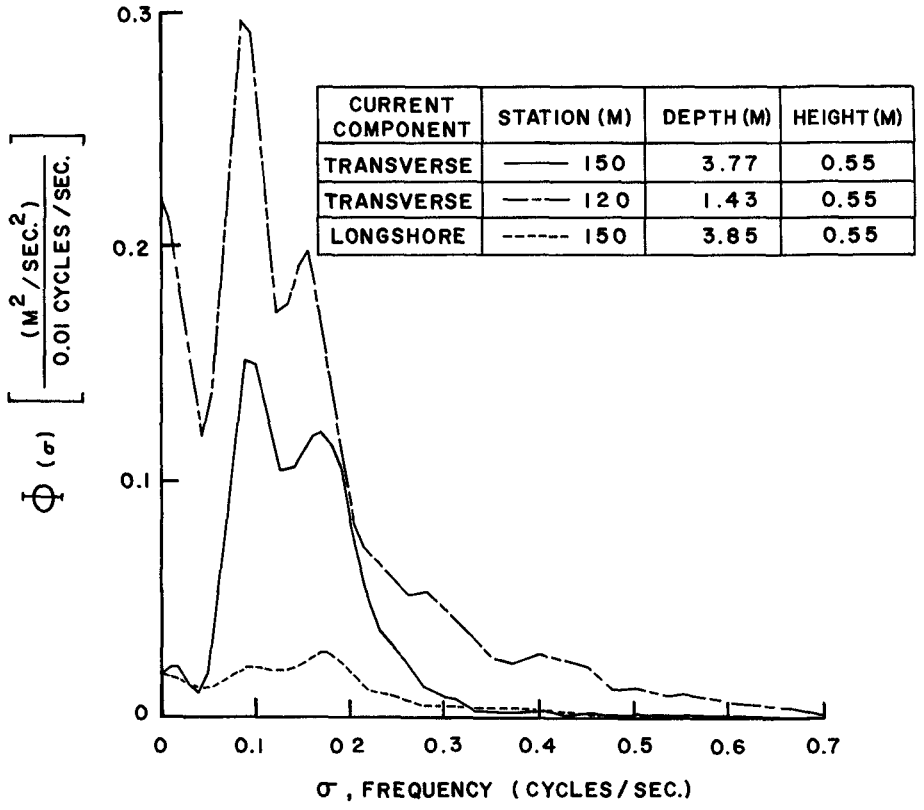

FIGURE 6. WATER PARTICLE VELOCITY SPECTRA
24 MAY 1967

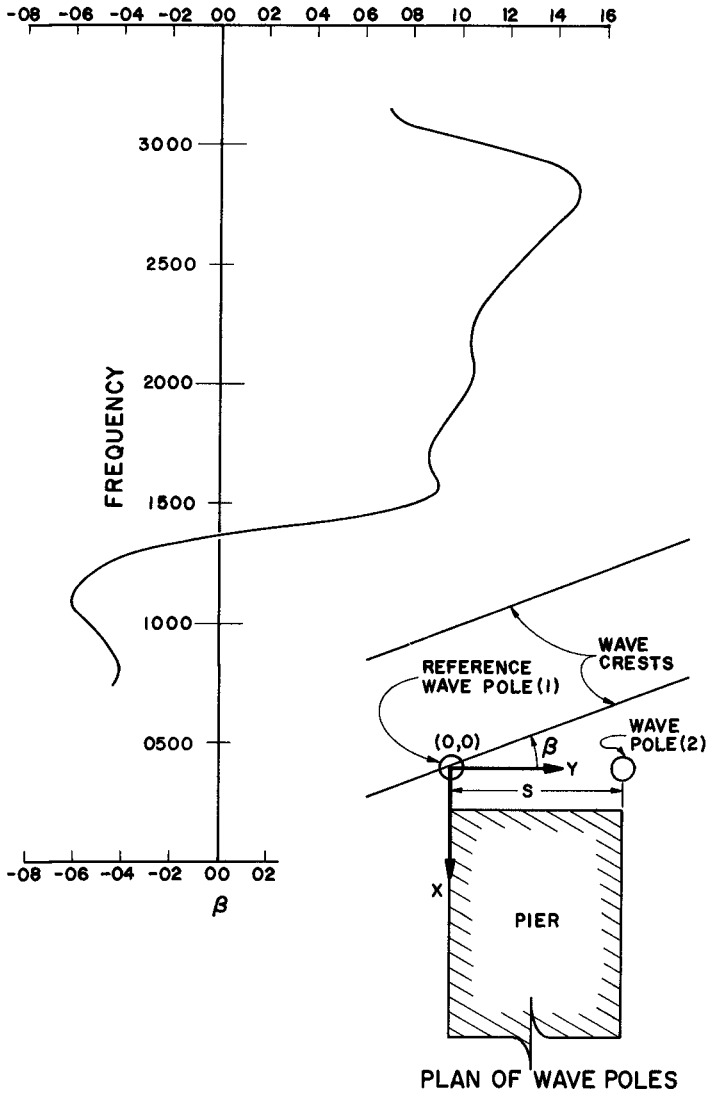

FIGURE 7. DIRECTIONAL SPECTRUM OF WAVES

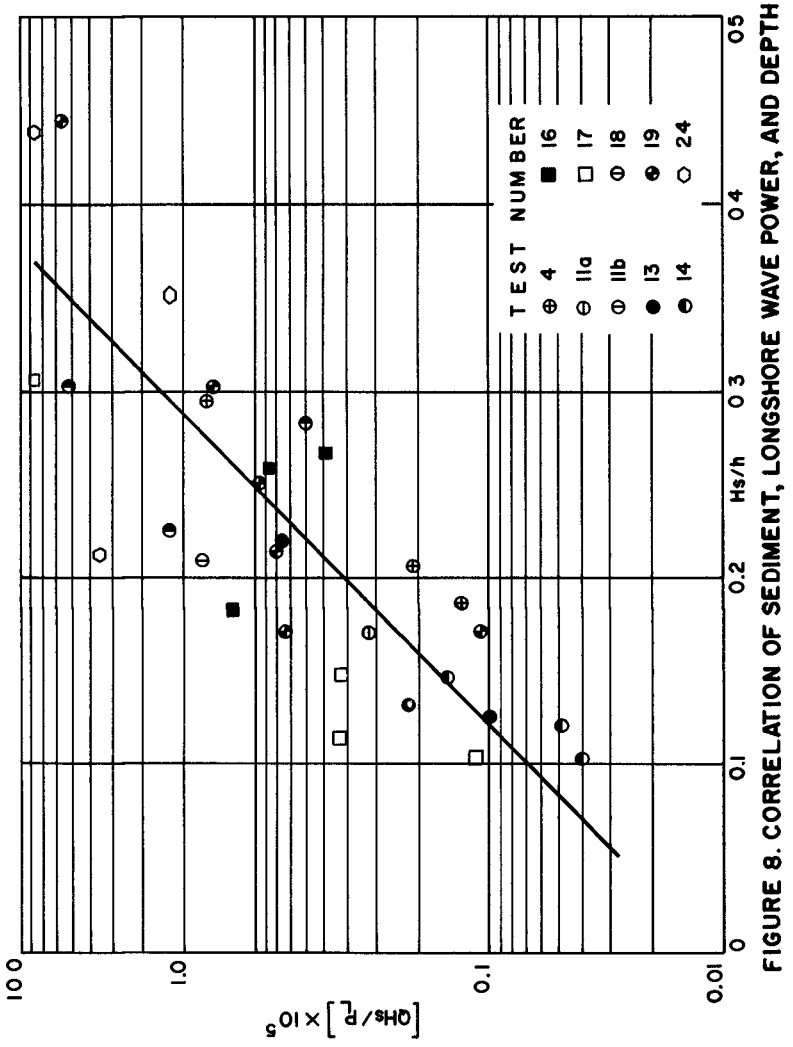

FIGURE 8. CORRELATION OF SEDIMENT, LONGSHORE WAVE POWER, AND DEPTH

CHAPTER 23

THE EFFECT OF WAVES ON THE PROFILE OF A NATURAL BEACH

Warren C. Thompson, Professor of Oceanography
and
John C. Harlett, Lieutenant, United States Navy

U. S. Naval Postgraduate School
Monterey, California

ABSTRACT

A 60-day field study was conducted on a selected natural beach in which the beach profile was measured daily and the waves incident upon the profile were recorded continuously. Beach and wave parameters derived from the field data were empirically combined to yield: (a) quantitative relationships between the change in the profile and the average deep-water wave steepness and wave power over a lunar day (24.8 hours) given the profile at the beginning of the period, (b) equilibrium profiles for different values of wave steepness, (c) an empirical relationship between wave steepness and wave power which agrees well with theory, and (d) rates at which the beach profile approached equilibrium for given initial conditions of non-equilibrium. Using the relationship developed between beach change and wave steepness, hindcasts were made of the day-to-day sand elevation at a selected location near the middle of the profile and were found to agree fairly well with the observed sand level.

INTRODUCTION

Observations made daily or on a shorter term basis show that natural sand beaches change sensitively in evident response to changing wave conditions, but in a complex way. This paper reports on a successful attempt to establish a quantitative relationship between daily changes in the profile and the waves incident upon a selected beach. The development of this relationship is a very preliminary step toward the ultimate development of methods for making daily synoptic forecasts of the behavior of natural beaches given predicted or observed wave conditions and knowledge of the tides and the sand properties.

The beach where this field study was conducted is a long, gently curving strand named Del Monte Beach, which is located in the southern end of Monterey Bay, California. A brief review of its environmental characteristics is given here before proceeding.

Del Monte Beach is a stable beach and has remained in very nearly the same location since the earliest hydrographic survey of 1851. The

profile across the beach and through the surf zone characteristically lacks a well-defined berm and offshore bars, and is fairly simple most of the time. Seaward of the surf zone the bottom slopes evenly across the continental shelf. The beach in the vicinity of the profile studied is uniform laterally for some distance, except for subdued cusps that frequently occur on the upper beach. The material composing the beach is well-sorted medium to fine siliceous sand having a mean grain diameter of 2 ϕ (0.25 mm).

The predominant waves on the beach are moderate to long period swell usually having narrow frequency spectra. The beach is partially sheltered from the Pacific Ocean in such a manner that waves entering the bay from all open ocean directions refract so as to arrive with their crests parallel or nearly parallel to shore. Littoral drift is negligible most of the time, and beach profile changes involve essentially offshore-onshore transport of sand. The tides are of the mixed type and have a diurnal range of 5.3 feet. Meteorologically induced water-level variations are negligible.

It may be seen from this description that the beach selected for study is a natural laboratory where beach response to changing wave conditions may be investigated under relatively simple environmental conditions.

BEACH OBSERVATIONS

The beach and wave information used in this study were collected over a 60-day period in February and March 1967 by Harlett (1967) along a permanently established profile. The profile, shown in Figure 1, consists of a line of 20 railroad rails driven into the sand at approximately 10-foot intervals extending from the rear of the beach to the lowest tide level.

Beach profiles for every day of the study were constructed from measurements of the sand level against the rails. The latter were made at the time of lowest tide each day when the beach exposure was greatest, and accordingly at a sampling interval of one lunar day or 24.8 hours. The observation times during the study are marked by dots on the tide curve in Figure 2.

Synchronization of the observation times with the diurnal lunar tidal cycle may be seen in Figure 2 to result in a very nearly repetitive tidal sequence between successive observations as well as tide levels that differ only slightly from one sampling time to the next. It thus appears probable that this choice of sampling interval tends to filter out the effect of the tides and thereby to amplify the effect of changing wave conditions in producing the observed profile changes.

Waves were recorded continuously during the field study, except

Figure 1: PERMANENT PROFILE ON DEL MONTE BEACH
The front edge of the foam line is at Rail 8.

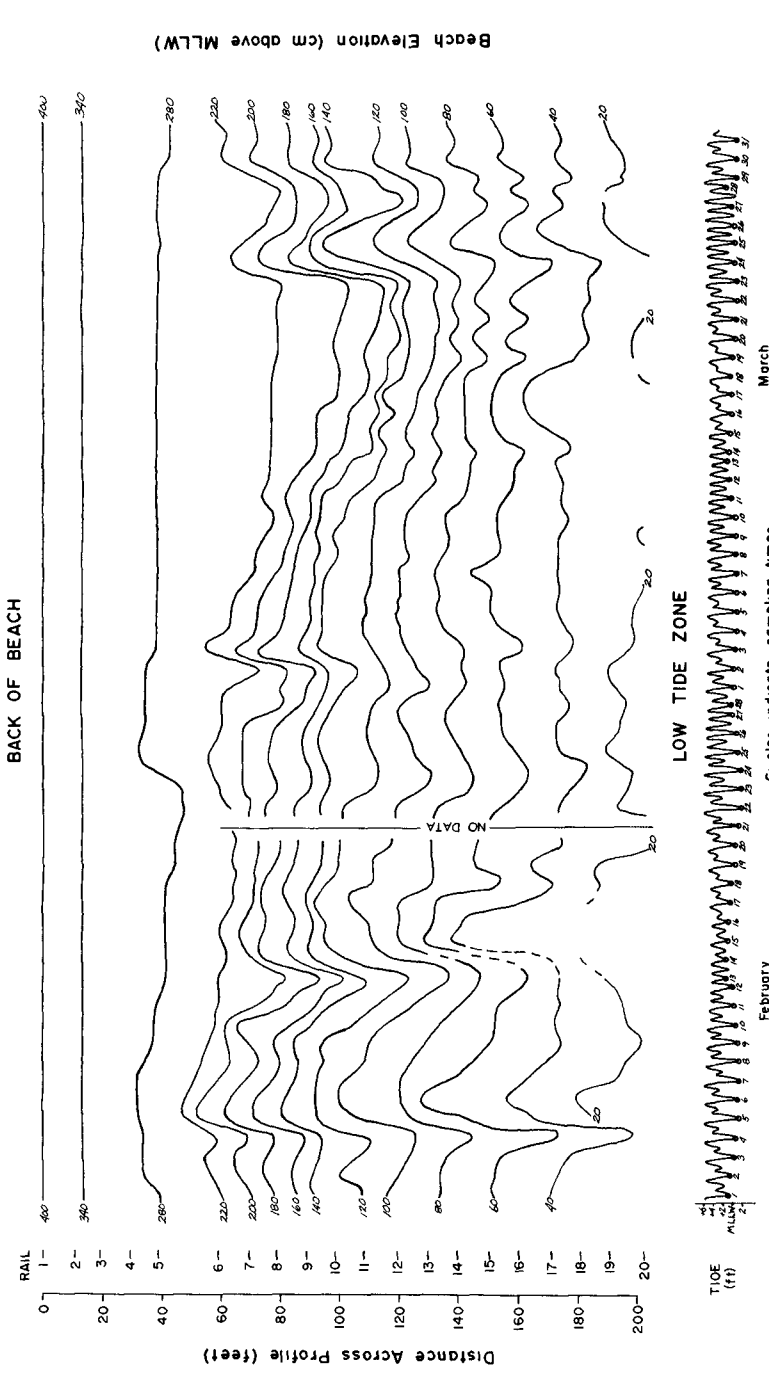

Figure 2 BEACH PROFILE TIME SERIES

for the first five days, using a pressure sensor located 600 feet directly seaward of the rails. The analog records were analyzed manually for significant height and dominant period. The waves observed during most of the study were low swell with periods in the range from 8 to 20 seconds. The wave height exceeded three feet on only one occasion, and most of the time was under one foot.

Deep-water wave height, which was used to calculate deep-water wave steepness and wave power, was computed from the recorded height in shoal water using linear wave theory. Application of the linear theory appears valid in view of the relatively narrow frequency spectrum evident in the swell most of the time.

Sand samples collected from the uppermost thin skin of the beach surface were also obtained daily across the profile along with the measurements of the sand level. Information on the textural properties of the sand are not presented in this paper but may be found in Harlett (1967). It is of interest to record here only that the phi mean grain diameter during the field study ranged between extreme values of 1.6 and 2.3 ϕ.

The field study was limited to the exposed intertidal portion of the beach above the lowest daily tide level because of the practical difficulty of making measurements in the surf zone. A wave-tank study by Rector (1954) and a field study by Eubanks (1968), who extended his profile measurements through the surf zone on this beach, show that the intertidal section of the profile behaves very differently from the section that lies seaward of the approximate low tide level and that it should be studied as a separate beach unit.

OBSERVED BEACH PROFILES

The daily profiles for the 60-day period are presented in Figure 2 in the form of a time series. The curves in the figure represent contours of beach elevation above MLLW. The contour interval is 20 cm except near the rear of the beach where it is 60 cm. Seaward movement of the contours with time represents accretion and shoreward movement denotes erosion. Spacing of the contours is inversely proportional to the beach slope. For reference to the tides, the elevations of the principal tidal datum planes are: MLLW = 0.0 cm, MSL = 83 cm, and MHHW = 159 cm.

Perhaps the most obvious feature to strike the eye in this figure is the constant change that occurs in the profile. During the two-month period the change in sand level from one day to the next amounted to 6 cm or more somewhere on the profile. This was the case even during extended periods when the incident wave heights recorded did not exceed 0.5 feet

(10-13 February, and 5-10, 12-23, 26-28 March). The rear portion of the beach where the contours remain stationary with time was not reached by waves during the study.

To the observer walking on this beach, the profile on most days is quite smooth to the eye. Examination of the figure shows, however, that the beach does not usually erode or accrete in a simple way. At times the entire profile in the intertidal zone changed fairly uniformly, particularly when the change was large (as from 4 to 5 February), but most of the time the change tended to be localized along the profile. On several occasions there were as many as five separate zones of minor cut and fill across the profile.

Changes in the profile are by no means random, however, as evidenced by the patterns of cut and fill that may be seen. Focusing attention on the five prominant sequences of cut and fill, it may be noted that erosion rates were ordinarily greater than accretion rates. The extreme values measured were 61 cm and 44 cm per 24.8 hours, respectively. On the other hand, significant cutting usually lasted only one day and never more than two, whereas accretion ordinarily occurred more or less continuously over a series of days. These prominant cycles of erosion and accretion were found to occur in response to the arrival of prominant wave trains propagated from individual wind areas. Another feature of interest, which was observed in an earlier field study of this beach (Rohrbough, Koehr, and Thompson, 1964), is that cutting sometimes begins on the upper beach with fill on the lower beach (as from 23 to 24 March), but ordinarily within a day a reversal occurs and the upper beach accretes while the lower beach erodes.

It is evident that this beach reacts sensitively to the waves arriving upon it. It appears that the reaction is in the form of constant profile readjustments to continuously changing wave properties, which in turn are superimposed in an endless variety of combinations on the regularly changing tide levels.

PROFILE CHANGES RELATED TO WAVE PARAMETERS

In the belief that it should be possible, in view of the comparatively simple beach and wave conditions normally prevailing on Del Monte Beach, to quantitatively relate the observed daily profile changes to the incident waves, a systematic effort was made to find representative parameters that incorporate time changes in the beach and the waves and to combine these successfully.

Two waves parameters of several that were investigated proved to show a good correlation with the profile changes, namely deep-water wave

steepness, γ, and wave power, P. The selection of steepness as a parameter is of interest particularly because of its demonstrated relationship to various wave characteristics such as wave mass transport, breaker height, breaker type, and wave runup. Wave power was adopted as a parameter upon the suggestion of D. L. Inman in the discussion of this paper following its presentation at the London conference. With respect to beach profile changes and the offshore-onshore sand transport that is implied, wave power has obvious dynamic significance whereas wave steepness does not. Steepness on the other hand conveys a sense of wave age which power does not.

It is of interest to observe that both of these parameters incorporate the two fundamental wave properties, height and period, and that steepness tends to stress the influence of wave period ($\gamma \propto HT^{-2}$) whereas power stresses wave height ($P \propto H^2T$). It may be noted that neither parameter has a discrete value for every H-T combination since a range of H-T pairs can yield the same value. Finally, it will be recognized that wave steepness has a definite upper limiting value which is determined by wave stability whereas the value of wave power has no such upper limit.

The relationship found between beach changes and wave steepness will be considered first.

Wave Steepness

The relationship to be presented between beach parameters and wave steepness was arrived at on the basis of assumptions derived from the results of wave-tank studies conducted by others and from subjective examination of the field data collected in this study. These assumptions are (a) that real ocean waves (wave spectra) having a specific set of properties would produce a characteristic equilibrium profile on this beach if the waves were to remain constant with time (note the laboratory studies by Watts, 1954), (b) that this beach tends constantly to readjust its profile so as always to approach the equilibrium profile associated with the wave conditions prevailing at the moment, and (c) that the response of the profile to changing wave conditions is sufficiently rapid that the profile assumes the hypothetical equilibrium profile at all times to a first approximation.

It was concluded from these assumptions that if, at a given point on the beach, the sand elevation at a given time is higher than the equilibrium elevation associated with the wave conditions prevailing during the

interval immediately following, the beach should cut in order to approach the equilibrium profile for those waves. Conversely, if the elevation is initially too low the beach should fill. From this reasoning an empirical relationship was established between the following beach and wave parameters.

h_i the initial beach elevation at a given point on the profile (elevation above MLLW at the beginning of a 24.8-hour sampling interval)

Δh change in the beach elevation over the 24.8-hour sampling interval at that point

$\overline{H'_o/L_o}$ the average unrefracted deep-water wave steepness during the 24.8-hour sampling interval ($\overline{\gamma_o}$).

H'_o is the deep-water significant wave height computed from the recorded waves and uncorrected for refraction, and L_o is the deep-water wave length. Both quantities were calculated from linear wave theory using the observed dominant period. The average steepness for a given sampling interval was obtained by averaging the values of H'_o/L_o at the two consecutive observation times. This method of integrating the wave characteristics over a sampling interval is obviously gross but yielded good results. No wave data were used for periods of very low waves because of difficulty of analyzing the records.

The relationship established between the selected beach and wave parameters is illustrated in Figure 3 for the arbitrarily chosen location on the beach occupied by Rail No. 10, which is near the mid-point of the daily swash zone. In the graph the negative the positive values of Δh represent cut and fill in centimeters. The curve of $\Delta h = 0$ cm is of particular interest because it can be considered to represent the equilibrium elevation of the beach over the range of wave steepnesses shown. Application of the graph is best indicated by means of an example. If the sand level at Rail 10 is observed to be 160 cm above MLLW and the wave steepness averaged over the following 24.8-hour interval is 0.001, then a drop in the sand level of 20 cm may be expected over the interval.

Figure 3 indicates that when wave properties are averaged over a suitable time interval, the beach can be shown to cut with an increase in wave steepness and to build with a decrease. The figure thus confirms empirically the often made statement to this effect. The figure also reveals that very high sand levels are produced only by swell of very low steepness, and suggests that the lowest sand level possible is that given by the equilibrium elevation associated with storm waves of limiting steepness.

Graphs similar to that in Figure 3 have been constructed for other rail locations, and the information contained in each for the equilibrium condition has been extracted and combined to produce Figure 4 in which is shown a family of equilibrium profiles for the range of wave steepnesses observed. The equilibrium profiles are seen to have a gentle upward curvature. The profile is not completed on the upper part of the beach between Rails 1 and 7 because of the sparsity of beach change observations due to less frequent wetting.

Wave Power

The wave power arriving at the surf zone per unit length of beach for the case of simple waves having a zero breaker angle can be shown to be

$$P = \frac{\rho g}{16} \frac{g}{2\pi} (H_o')^2 T \qquad (1)$$

where ρ is the density of sea water, g is the acceleration of gravity, and H_o' and T are as defined above. As pointed out earlier refraction is such that waves arrive on the beach most of the time with little or no wave angle.

Wave power, when computed using this equation and averaged over the 24.8-hour observation interval in the same manner as the deep-water wave steepness, was found to display a similar relationship to the beach parameters as that shown in Figure 3. Similar conclusions regarding cut and fill as related to wave-power can also be drawn. The wave-power relationship is presented in Figure 5. Wave-power graphs for other rail locations along the profile have not been constructed.

Relationship Between Wave Steepness and Wave Power

An empirical relationship between the average values of wave steepness and power was obtained for the condition of equilibrium at Rail 10 by combining data from Figures 3 and 5, and is shown in Figure 6.

The trend of the beach elevation values (h) on the curve indicates that the maximum height to which waves can build the beach at this location is limited by a building rate that approaches zero as the wave power approaches zero, and also by the length of time over which waves of very low steepness can prevail. Thus, the highest beach levels are evidently constructed during long intervals in which only very low swell arrive on the beach. This explains the general observation that the longest intervals of low swell on this and other beaches on the Pacific Coast of the United States normally occur in the summer and that

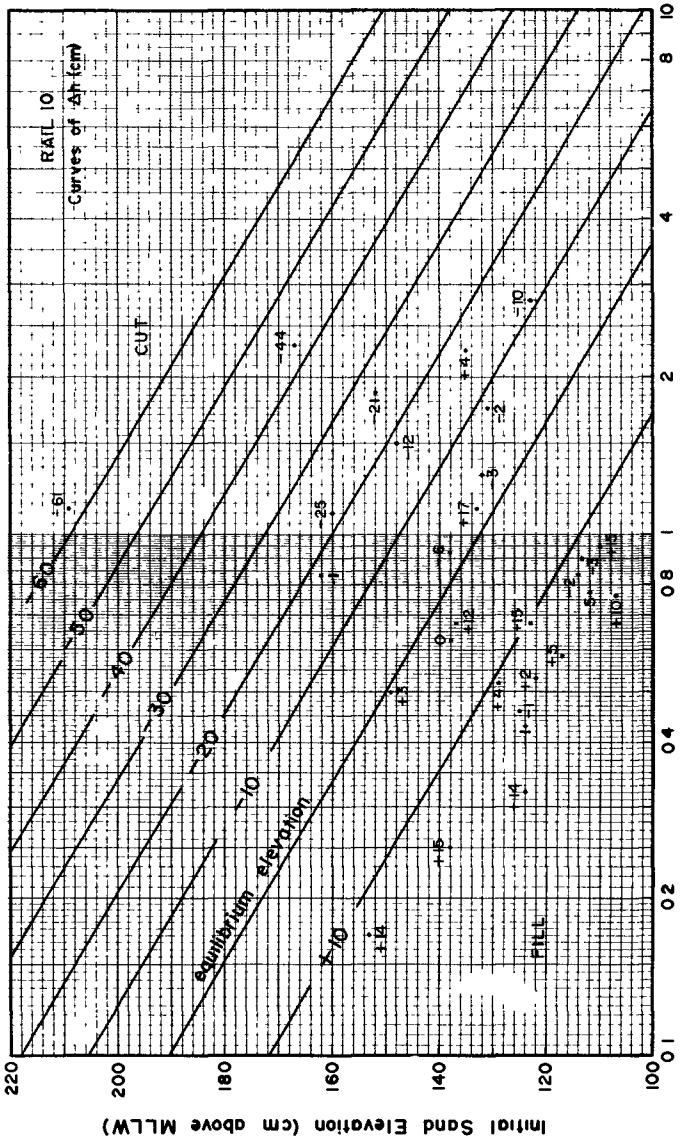

Figure 3: SAND LEVEL CHANGE RELATED TO WAVE STEEPNESS

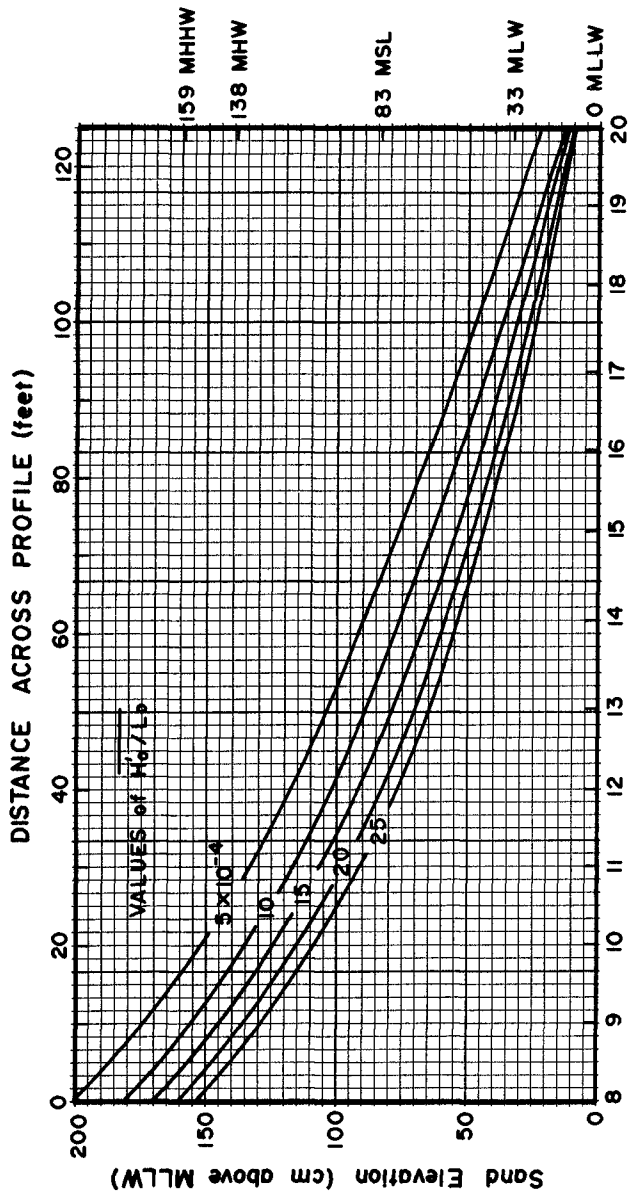

Figure 4: EQUILIBRIUM PROFILES FOR WAVE STEEPNESSES OBSERVED

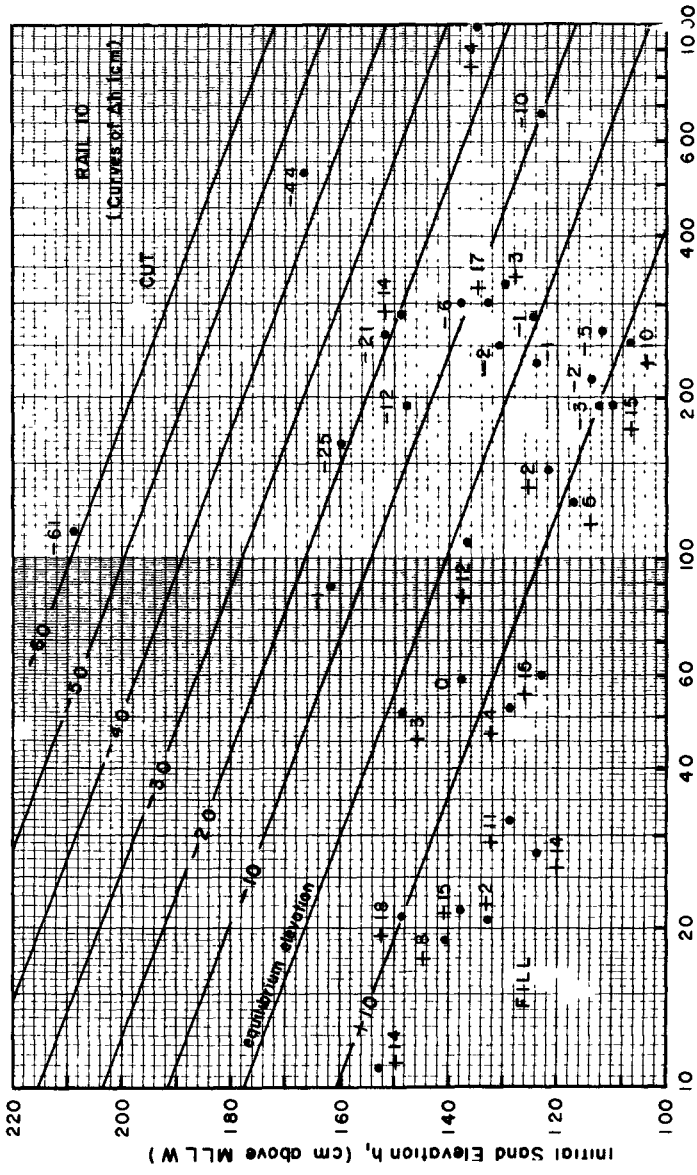

FIGURE 5: SAND LEVEL CHANGE RELATED TO WALL POWER

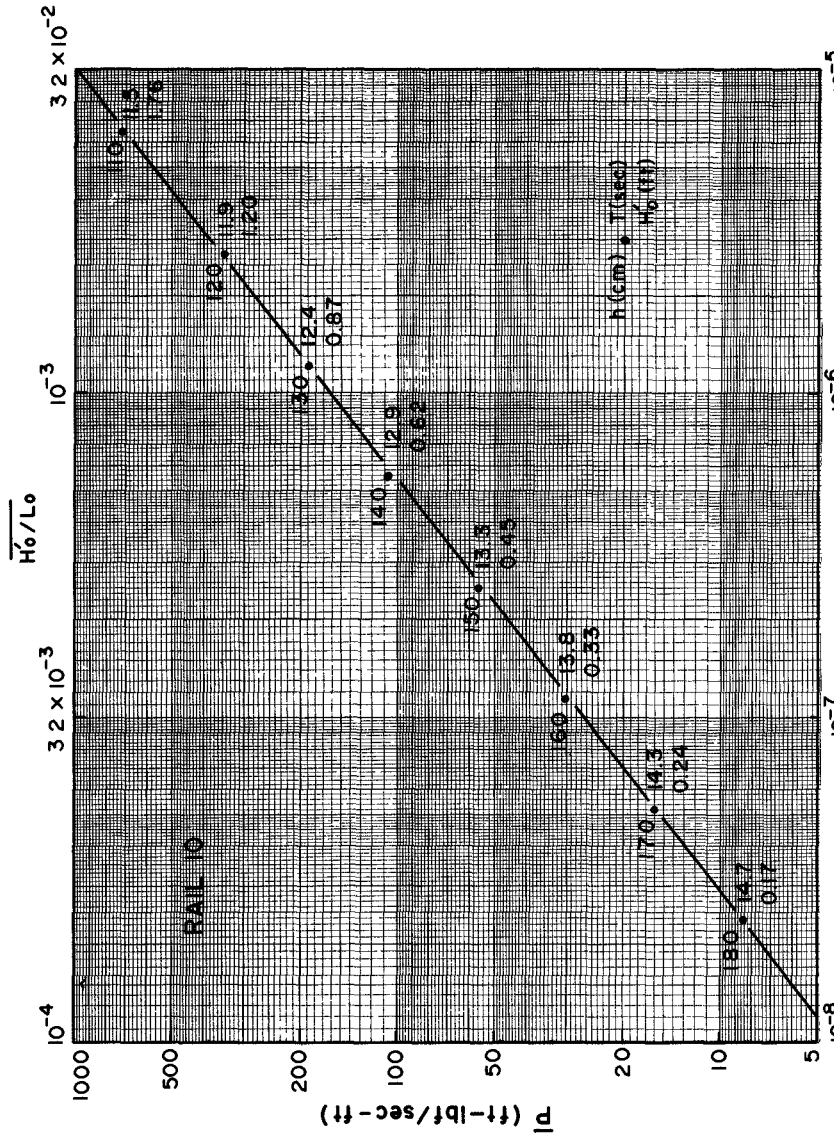

Figure 6: WAVE STEEPNESS vs WAVE POWER for the EQUILIBRIUM CONDITION

it is in this season that the beach usually acquires the most sand. The period of prolonged beach building that may be seen in Figure 2 in the month of March coincided with an interval of very low swell generally under 1/2 foot in height.

The lowest beach levels, on the other hand, are seen to occur with large waves of maximum steepness. The minimum elevation to which waves can be expected to lower the beach is clearly determined by the wave power available since exponentially increasing amounts of power are required according to Figure 6 to produce the incremental lowerings of the profile shown by the beach elevation values on the curve. The minimum elevation is also determined by the length of time that waves of exceptional height can persist.

An independent relationship between wave power and wave steepness can be derived mathematically through multiplication of Equation (1) by $(L_o'/L_o)^2$, where $L_o = \frac{g}{2\pi} T^2$:

$$P = \frac{\rho g}{16} \left(\frac{g}{2\pi}\right)^3 \left[\frac{H_o'}{L_o}\right]^2 T^5 = 537 \left[\frac{H_o'}{L_o}\right]^2 T^5 \left(\frac{\text{ft-lbf}}{\text{sec-ft}}\right) \quad (2)$$

If T is solved for in this equation by inserting the associated values of $\overline{P}$ and $\overline{H_o'/L_o}$ from Figure 6, values of the period are obtained which are plotted in the figure. The values of H_o' shown in the figure were obtained by introducing these T values and the associated values of $\overline{P}$ into Equation (1). The pairs of H_o' - T values presented in the figure evidently represent average wave conditions that would maintain the beach in equilibrium at Rail 10 for different values of average wave steepness and power.

The form of Equation (2) indicates that the empirically derived curve in Figure 6 is not a straight line but obeys the 5th power of T. If the curve is treated as a straight line, however, and is equated with Equation (2) a value of T = 11.8 sec is found. The reasonableness of this value, which is characteristic of the wave periods measured during this study, indicates unexpectedly good agreement between the empirical and theoretical relationships between $\overline{H_o'/L_o}$ and $\overline{P}$.

Equilibrium Condition for Limiting Wave Steepness

The condition of limiting wave steepness at which the dominant waves become unstable in the real ocean is assumed here to occur when $H_o'/L_o = 0.10$. For this steepness value the lowest equilibrium elevation

of the beach that can be expected at Rail 10, and the extreme wave conditions required to produce this level, are estimated as follows:

$\overline{P} = 2.4 \times 10^5$ ft-lbf/sec-ft
$T = 8.5$ sec
$H_o' = 37.2$ feet
$h = 15$ cm above MLLW

$\overline{P}$ was derived from Figure 6 by extrapolation to the limiting steepness, T was obtained from Equation (2) using the limiting values of $\overline{P}$ and $\overline{H_o'/L_o}$, and H_o' was obtained from Equation (1) using $\overline{P}$ and T. The beach elevation obtained by extrapolation of Figures 3 and 5 to the limiting values of power and steepness were 16.7 cm and 13.5 cm, respectively, giving an average of 15 cm.

The value obtained for the deep-water wave height is particularly interesting because it is identical to that hindcasted by Bixby (1962) for the most severe storm occurring over a 50-year period off Monterey. A wind speed of 40 knots or greater blowing for a sufficient length of time would be needed to produce waves of this height. In order to lower the beach level approximately to the equilibrium elevation would require that these or equivalent wave conditions have a duration on the order of two days or more according to considerations presented in the next section, which appears to be a possible but exceedingly rare event off Monterey.

TIME TO REACH EQUILIBRIUM

The rate at which the beach at Rail 10 would approach equilibrium if the wave conditions remained constant with time can be derived from Figure 3. Examination of this figure shows that the beach profile, if initially out of adjustment, does not reach the equilibrium state in one observation interval but approaches it rapidly during the first interval and increasingly more slowly during successive intervals.

If, for example, the sand level was measured at Rail 10 and found to be 210 cm and the wave steepness during the succeeding 24.8 hours averaged 0.001, then the beach should cut 60 cm during the interval and come to a new level of 150 cm. If the same wave conditions prevailed the beach should cut 12 cm, 3 cm, 1cm, and 1/2 cm during successive observation intervals and finally stabilize at an elevation of 133 cm, or 77 cm below the initial elevation. Thus, 78% of the total cut would be accomplished during the first interval. By the end of the second, third, and fourth intervals the cut would amount to 91%, 97%, and 99% of the total. Of course ocean waves do not remain constant over such lengths of time except in limited geographical areas.

It may be noted from Figure 3 that the rate of adjustment of the sand level for a given value of Δh is independent of the wave steepness. Thus if $\Delta h = -60$ cm the graph indicates that the sand level should fall 78% of the total drop expected for equilibrium regardless of the wave steepness during the interval.

The time required for the beach to approach equilibrium under uniform conditions at Rail 10 may be seen in Figure 7. The figure, constructed from the information in Figure 3, shows the rate of change of the sand level toward the equilibrium elevation for different initial relative beach elevations at Rail 10. It indicates, for example, that if the beach elevation at time zero is 40 cm above the equilibrium level then the elevation expected after 10 hours would be 21 cm above the equilibrium elevation. It also shows that the beach should approach equilibrium 50% of the way after 11 hours, 75% after 25 hours, and 90% after 42 hours. The percentage rates of cutting may be seen to be significantly more rapid than the rates of upbuilding. It is interesting to note here that in wave tank studies Watts (1954) found an essentially stable profile to be formed after 40 hours of test time.

These high response rates, when coupled with the observation that individual swell trains arriving during this study had durations of commonly 2 to 4 days, indicate that every train of swell should induce a beach-change sequence of the same duration. Whether or not this was the case is difficult to tell because of the coarseness of the sampling interval used.

The rate at which the beach approaches equilibrium at other points along the profile has not been determined.

BEACH PROFILE HINDCAST

Figure 3 can be used as a profile forecasting graph by virture of the fact that if the sand elevation at Rail 10 is measured and the wave conditions during the following 24.8-hour interval are forecasted or observed, the expected change in sand level is obtained.

Accordingly, a test was performed in which the sand elevation was hindcasted daily from this graph using the beach and wave data collected during the 60-day study. In this test each day's forecast was based on the observed sand level of the day before. The hindcasted beach heights are shown in Figure 8 along with the observed heights. It may be seen that the hindcast is best when significant cut occurs and poorest when the profile is near equilibrium or the beach is building. The agreement between the hindcasted and the observed beach elevation, of course, gives a measure of

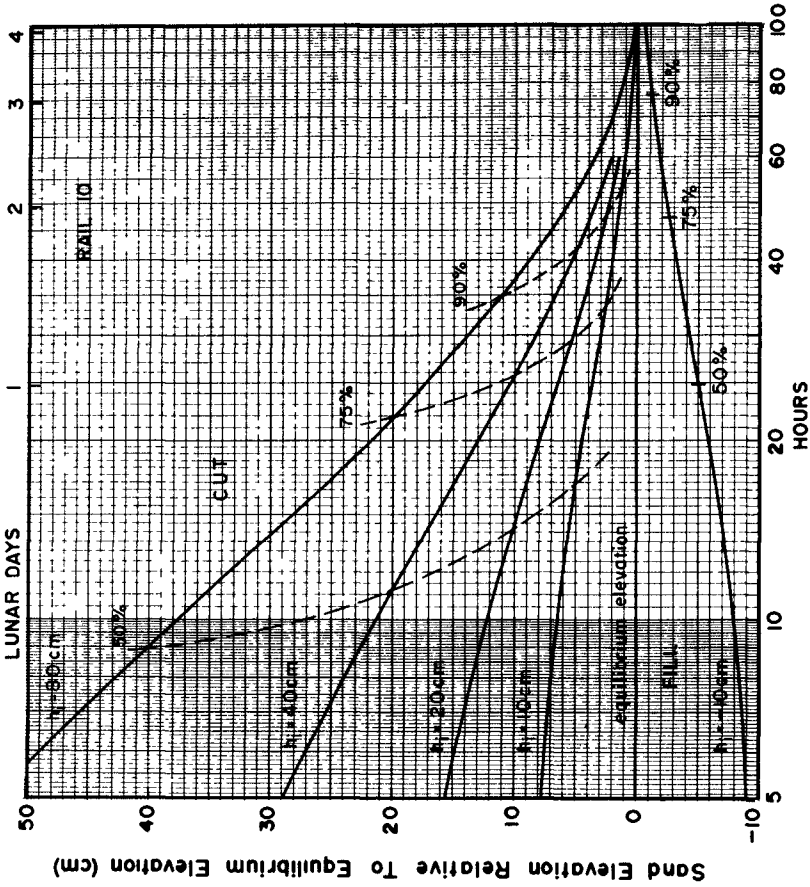

Figure 7: TIME TO REACH EQUILIBRIUM

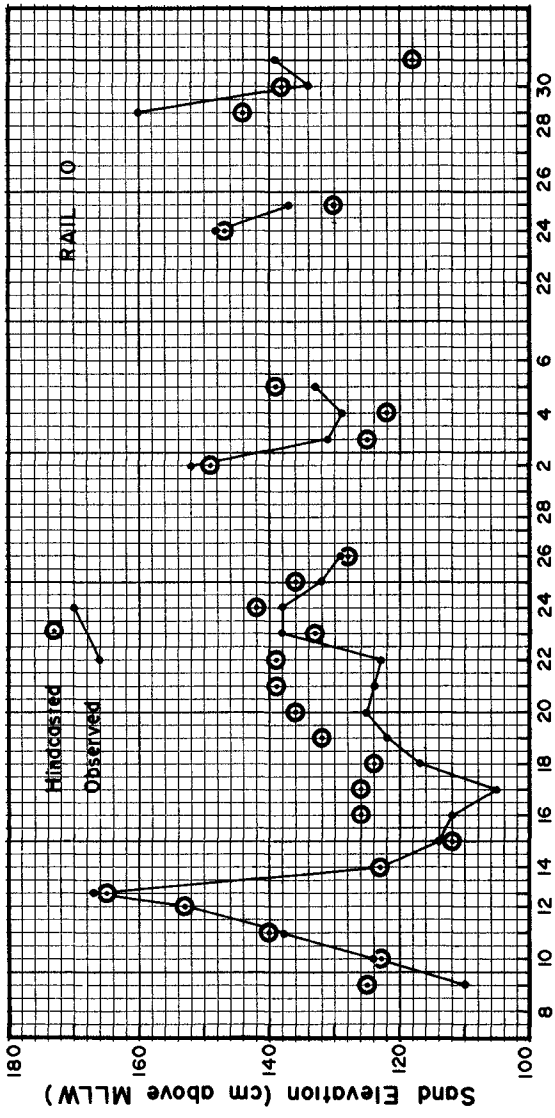

Figure 8: SAND LEVEL HINDCAST

the closeness of fit of the curves in Figure 3 to the basic data. The agreement is in general reasonably good.

A second test was also performed in which, beginning with an initial beach elevation on a given day, each day's sand level was hindcasted from the previous day's hindcasted sand level. This running hindcast, the results of which are not shown, proved somewhat less satisfactory than the first forecast. It was found that if a fictitious sand level falling within the working area of the graph is used as an initial value and each successive hindcast is based on the previous day's hindcast, the sand level immediately begins to approach the hindcast produced by the second test and after several days becomes identical with it.

It is evident that the accuracy of a beach forecast depends critically upon the accuracy of the wave information used. Fortunately, because of the rapid response of the beach profile to changing wave conditions, a poor forecast of the sand level caused by an error in the wave data would not be propagated long and would largely die out after one day.

DISCUSSION

The wave records were analyzed at intervals of 1/2 to 3 hours and therefore provided essentially continuous information on height and period with time. These data reveal a series of wave trains which arrived one after another and sometimes simultaneously. In view of the short-term variations exhibited, the use of wave steepness values at a one day interval gave unexpectedly good results. Inspection of the wave data shows, however, that a once daily sample represents the trend of the wave properties reasonably well most of the time. It appears that the sampling interval for both wave and beach data should not be much longer than one day, otherwise resolution of the information becomes poor rapidly.

The equilibrium profiles shown in Figure 4 were developed for swell having heights of mainly one foot or less. Consideration of the shape of the profiles leads to the conclusion that waves of the same steepness but different height must produce equilibrium profiles of different absolute configuration. In this regard Saville (1957) concluded from laboratory experiments that the deformation of a beach under wave attack is as much a function of absolute wave size as of wave steepness.

The present study is also limited to swell having a moderate to narrow frequency range, and the response of the beach to waves having wide frequency spectra has not been examined. It should be remarked, in this regard, that wave tank experiments described by Watts (1954) revealed no significant difference in the equilibrium profiles produced by waves of

variable period compared with constant period, except for a certain sand size used in the tests.

The equilibrium profiles of Figure 4 integrate the effects of the wave conditions that prevailed during the 60-day field study and are therefore composite profiles. The profiles are also presented in the figure as being rigidly fixed in space relative to the rails. It is probable, however that they migrate landward and seaward with the seasons and through the years due to net changes in the volume of sand on the beach with time. Additional field measurements will be required to determine how the shape and position of equilibrium profiles vary over a winder range of wave and beach conditions than was encountered in this short field study.

The daily range of the tide was several times larger than the wave height and runup during most of the study. Accordingly, it appears that the general shape of the profiles in Figure 4 significantly reflects the local tidal characteristics. On the other hand, the day-to-day changes observed in the profile, as stated earlier, are presumed to show little tidal influence because the profile measurements were made in phase with the tides. For a pertinent laboratory study dealing with the effect of tide on the formation of equilibrium profiles the reader is referred to Watts and Dearduff (1954)

No attention has been directed here to possible effects on the profile of variations in the textural parameters of the sand, but it appears from the obvious reaction of the profile to the incident waves that grain-size variations have a very minor influence by comparison.

ACKNOWLEDGMENT

This research was supported by a grant from the Coastal Engineering Research Center of the U.S. Army Corps of Engineers and by the Office of Naval Research Foundation Grant to the Naval Postgraduate School, and is a contribution from the beach research program being conducted at the school.

REFERENCES

1. Bixby, H. L., 1962. Storms Causing Harbor and Shoreline Damage Through Wind and Waves near Monterey, California. Naval Postgraduate School, M. S. Thesis, 179 pp.

2. Eubanks, G. E., 1968. A Field Study of Tide-Induced Sand Movement on Del Monte Beach, California. Naval Postgraduate School, M.S. Thesis, 102 pp.

3. Harlett, J. C., 1967. Daily Changes in Beach Profile and Sand Texture on Del Monte Beach, California. Naval Postgraduate School, M.S. Thesis, 116 pp.

4. Rector, R. L., 1954. Laboratory Study of Equilibrium Profiles of Beaches. Corps of Engrs., Beach Erosion Board, Tech. Memo. No. 41, 38 pp.

5. Rohrbough, J. D., J. E. Koehr, and W. C. Thompson, 1964. Quasi-Weekly and Daily Profile Changes on a Distinctive Sand Beach. Amer. Soc. Civil Engr., Proc. 9th Conf. on Coastal Engr., 10 pp.

6. Saville, T., 1957. Scale Effects in Two Dimensional Beach Studies. Proc. IAHR Meeting, 10 pp.

7. Watts, G. M., 1954. Laboratory Study of Effect of Varying Wave Periods on Beach Profiles. Corps of Engrs., Beach Erosion Board Tech. Memo. No. 53, 19 pp.

8. Watts, G. M. and R. F. Dearduff, 1954. Laboratory Study of Effect of Tidal Action on Wave-Formed Beach Profiles. Corps of Engrs, Beach Erosion Board, Tech. Memo. No. 52, 21 pp.

CHAPTER 24

COLLECTIVE MOVEMENT OF SEDIMENT IN LITTORAL ENVIRONMENT

By Choule J. Sonu
Coastal Studies Institute
Louisiana State University
Baton Rouge, Louisiana

ABSTRACT

Collective movements of sediment occur in the form of sand waves in the nearshore zone and affect beach topography to a significant extent. Bar-type sand waves move only in the onshore direction and account for various accretive profiles on the subaerial beach. When the beach is eroded, these sand waves are simply disintegrated on the subaerial beach, instead of migrating back in the form of sand waves. These characteristics of bar-type sand waves help explain dynamic behavior of beach profiles with respect to profile configuration, sediment storage, and beach width. Cusp-type sand waves are considered to be a product of interaction between longshore currents and an erodible bed. Their presence causes variability in beach profiles along the shore between those containing a prominent bar and those without a bar. Migration of these sand waves may well produce pulsational transfer of material along the shore.

INTRODUCTION

In spite of a large number of studies in the past, the mechanism governing dynamic changes in beach topography has not been generally explained. The basic difficulty may be attributed to the fact that the contribution of the behavior of individual sediment particles to modification of the bottom boundary is not sufficiently understood.

Investigations by the writer indicate that the interaction between sediments and topography in the nearshore zone may involve the role of sand wave activity. Although the detailed mechanism of the formation of sand waves in the presence of both wave and current actions is not yet known, the effects of these sand waves on beach topography are significant enough to warrant attention.

Sand waves of nearshore origin display characteristics which are essentially similar to those of the so-called "dunes" which occur in a sand bed acted upon by wind (Bagnold, 1941) or by unidirectional current (Simons and Richardson, 1960). It appears that in the nearshore zone, particularly inshore of the breaker line, where sediments are moved in large quantities, dynamics of beach topography are better explained in terms of collective behavior of sediments associated with sand waves, rather than of discrete movements of individual particles such as suggested by the null-point concept (see, for instance, Eagleson et al., 1963).

Sand waves occurring in the nearshore bed are distinguished into two groups: those attributed mainly to wave orbital motion and those to longshore currents. In the absence of accepted terminology, they are called, respectively, "bar-type" and "cusp-type" sand waves.

BAR-TYPE SAND WAVES

Formation of Bar-type Sand Waves

Bagnold (1947) was probably the first to describe in detail the properties of bar-type sand waves. In a wave-tank experiment using sand of low density, he observed a series of "bars" forming on the bed and migrating in the onshore direction. They were clearly distinguished from the so-called "plunge-line bars" which are formed by and remain stationary near breaking waves. He stated:

> ..as the bars developed, the sand on their down-wave sides was first seen to halt, and then to begin to drift backwards towards the bars. The sand on their up-wave sides continued to drift forward onto them, so that the bars were fed from both sides at the expense of the sand in the hollows. There was also a general forward drift up and over the bars which made them advance.... Regarded from a viewpoint moving with the slowly advancing bar, the sand composing it must move over and backwards through it in just the same way as that of a wind-blown barchan dune which was described by the Author in 1941.

A field investigation conducted by the Coastal Studies Institute on a beach at Nags Head, North Carolina, disclosed evidence of bar-type sand waves. This beach is situated on a long, gently curved coast of the Outer Banks and is exposed to the Atlantic Ocean on the east. Details of field technique were published previously (Sonu and Russell, 1965).

It was generally observed that the bar-type sand waves were formed during a period of wave decay immediately following storm activity. Figure 1A shows an actual example of the formation of a bar-type sand wave observed on the Nags Head beach. Between February 27 through 29, wind waves with relatively large steepness persisted (Fig. 1B), and the beach was generally eroded on both its subaerial and subaqueous beds (profiles 1 through 3). As soon as the wind waves began to decay, a sand wave emerged on the foreshore bed (profile 4), then migrated steadily onshore (profile 5) and seemed to climb onto the subaerial slope (profile 6). Eventually it moved upward as far as the run-up limit of existing swashes, then remained stabilized there until it was destroyed by the next storm.

As seen in Figure 1, the bar-type sand wave had the appearance of a dune, its cross section consisting of a steep front slope and a gentle rear slope. The depth/height ratio varied considerably, between 1 and a maximum of 2.85, which is far less than the maximum of 5.0 reported in a fluvial bed (Simons and Richardson, 1960). There was a tendency for the depth/height ratio to decrease as the sand-wave crest approached the shoreline. Although the reason for this phenomenon is not evident, it seems to corrobo-

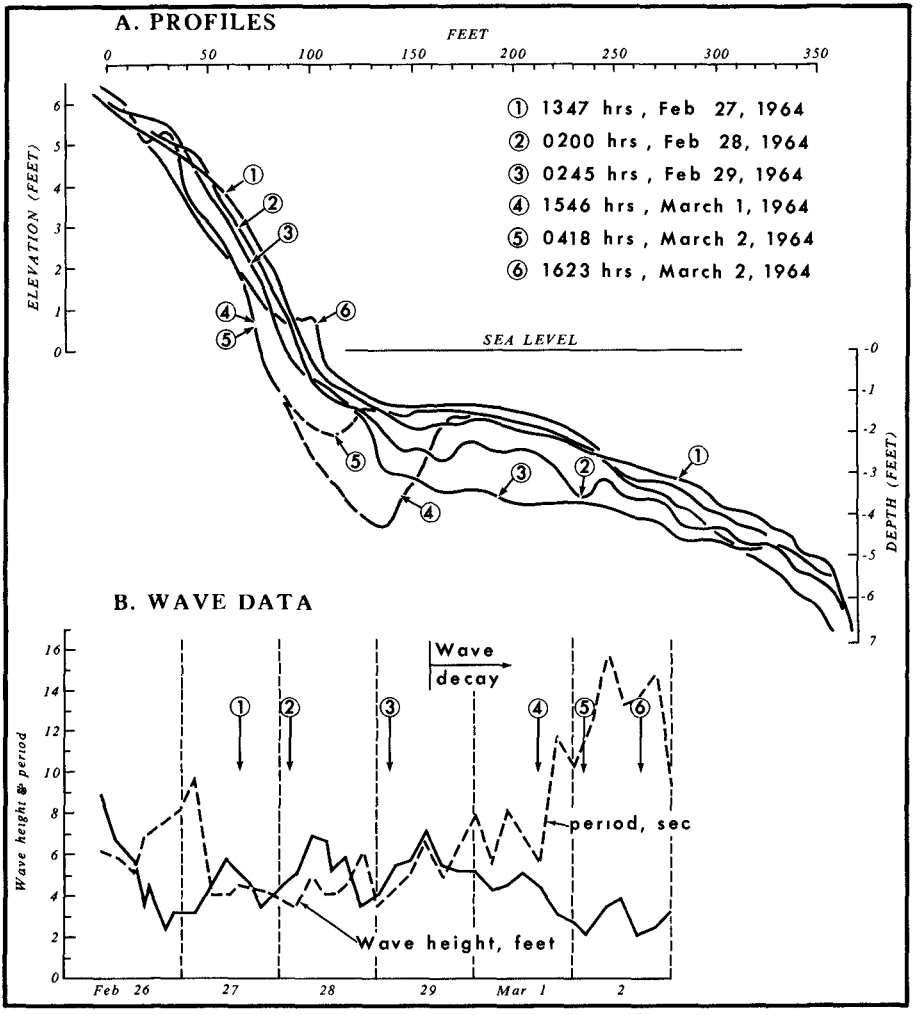

Figure 1. Formation of bar-type sand wave during decay of storm waves, Nags Head, North Carolina

rate the observation in a fluvial model that "the dune will only grow until its crest is within a certain distance from the water surface, unless three-dimensional flow exists" (Simons and Richardson, 1960).

The length/height ratio of the bar-type sand wave was not determined, since this type of sand wave usually occurred as a single pair of trough and crest, the former preceding the latter. The speed of migration was less variable than other parameters, usually remaining on the order of 4 ft/hour.

Generally, the greater the storm waves, the more prominent were the subsequent activities of sand waves. However, available data are not sufficient to determine quantitative relationship between characteristics of sand waves and those of incident waves.

Effects of Bar-type Sand Waves on Beach Profile

Figures 2 and 3 show two distinct behaviors of sand waves observed on the Nags Head beach. The one shown in Figure 2 consisted of a prominent trough and a dune-shaped crest following it As this wave approached the shore, the trough first landed on the subaerial beach. As a result, the subaerial beach was eroded, while the ensuing crest caused a steady accretion on the foreshore bed. Bagnold (1947) reported a similar phenomenon in the experiment already quoted. He stated:

> Whenever the sand of foremost approaching bar reached the beach, or, in other words, whenever the nearest distinguishable bar was one bar pitch from the beach, the beach suddenly began to build up and the waterline advanced quickly up-wave. But, thereafter, it began to erode, the sand moving outward down the slope towards the next oncoming bar. The maximum recession of the waterline occurred when the oncoming bar was half a bar-pitch from the beach, so that the beach behaved as if it were an imaginary fixed cross-section of the bed through which the bars are advancing. As a result, the beach profile was never mature, but was constantly changing in a periodic manner.

According to Bagnold, observations by Zenkovich off the Crimea corroborated his observation on the model "that the movement of the sand coastline is closely linked with that of the bar series out at sea, and that beach erosion or beach building depends on the position of the bar series relative to the beach." On the Nags Head beach, a wave crest preceded by a prominent trough such as seen in Figure 2 disappeared completely upon arrival at the shoreline, therefore failing to produce alternate erosion and accretion of the beach.

The sand wave shown in Figure 3 had a relatively obscure trough and a prominent crest, therefore bore resemblence to a solitary wave. Although there was a slight tendency for the crest to attenuate as it approached the shore (profiles 2 and 3), it eventually forced its way onto the subaerial slope. Thereafter, it continued the movement upward while steadily growing in size (profiles 4 through 6). This wave had a characteristic

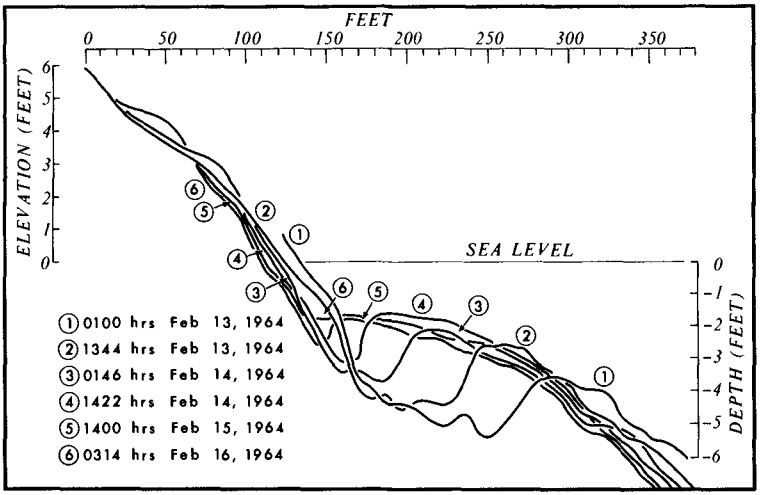

Figure 2. Bar-type sand wave with a prominent trough, Nags Head, North Carolina.

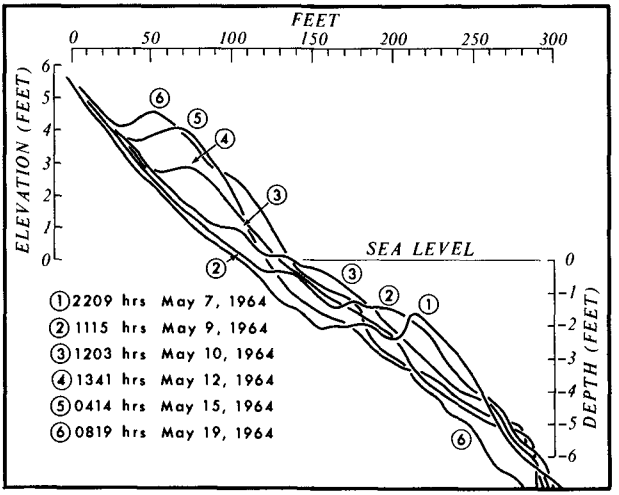

Figure 3. Bar-type sand wave with a prominent crest, Nags Head, North Carolina.

similar to the translatory property of a solitary wave in that it transported in its crest a large amount of material, which produced a "berm" on the subaerial slope

Analysis of beach profiles observed at Nags Head indicated that the translatory sand waves such as are shown in Figure 3 were most typical and were most important with respect to their effects on beach profiles. The major activities of the translatory sand waves which were of particular importance were (1) migration upward on the subaerial slope, (2) fluctuation in the size of crest, and (3) disintegration. Migration placed the wave crest--or a berm--at various elevations on the beach. It was found that, depending on the location of a berm on the lower, intermediate, and upper elevations, beach configurations of concave, linear, and convex appearances were produced, respectively. Fluctuation of the wave crest affected the prominence of these curvatures. Disintegration of the wave crest resulted in the formation of a smooth, concave profile. Consequently, as shown in Figure 4, six major categories of profile configuration were distinguished. Alphabetical notations A, B, and C represent, correspondingly, concave, linear, and convex profiles, and those letters with prime, the prominence of a berm in these profiles. Practically all the 291 observed beach profiles could be classified into these categories of distinctive configuration.

The beach profiles displayed characteristic patterns of transition which were associated with the described behaviors of bar-type sand waves. The direction in which the transitions of a beach profile occurred are shown by arrows in Figure 4, the solid arrows denoting accretive transition and the broken arrows, erosional transition.

The changes initiating from A', B', and C' occurred either as accretive changes directed from A' to B' or from B' to C', or as erosional changes from A' to A, from B' to B, or from C' to C. Transitions from C' to B' or from B' to A', which might imply backward migration of a wave crest, failed to take place. In other words, as the profiles A', B', and C' were eroded, the material composing their berms was simply dispersed seaward, without taking the form of a receding sand wave. Consequently, erosion initiating at profiles A', B', and C' led to attenuation of a berm at each respective elevation and eventually to the formation of profiles A, B, and C, respectively.

On the other hand, the changes initiating at A, B, and C occurred either as accretive changes directed to A', B', and C', respectively, or as erosional changes directed from B to A or from C to B. Transitions such as from A to B or from B to C failed to occur.

In general, erosion of the subaerial beach occurred during a period of growth of incident waves, and accretion, during a period of wave decay This is shown in Figure 5, which compares changes in the subaerial topography with those in incident wave heights. The beach topography is represented in terms of the volume of sediment existing between the shoreline and the limit of swash run-up above datum level. Wave heights were recorded with a step-resistance gage of the Coastal Engineering Research Center, installed approximately 150 m from the shoreline. The curves in Figure 5 suggest a negative correlation between the subaerial sediment and wave heights.

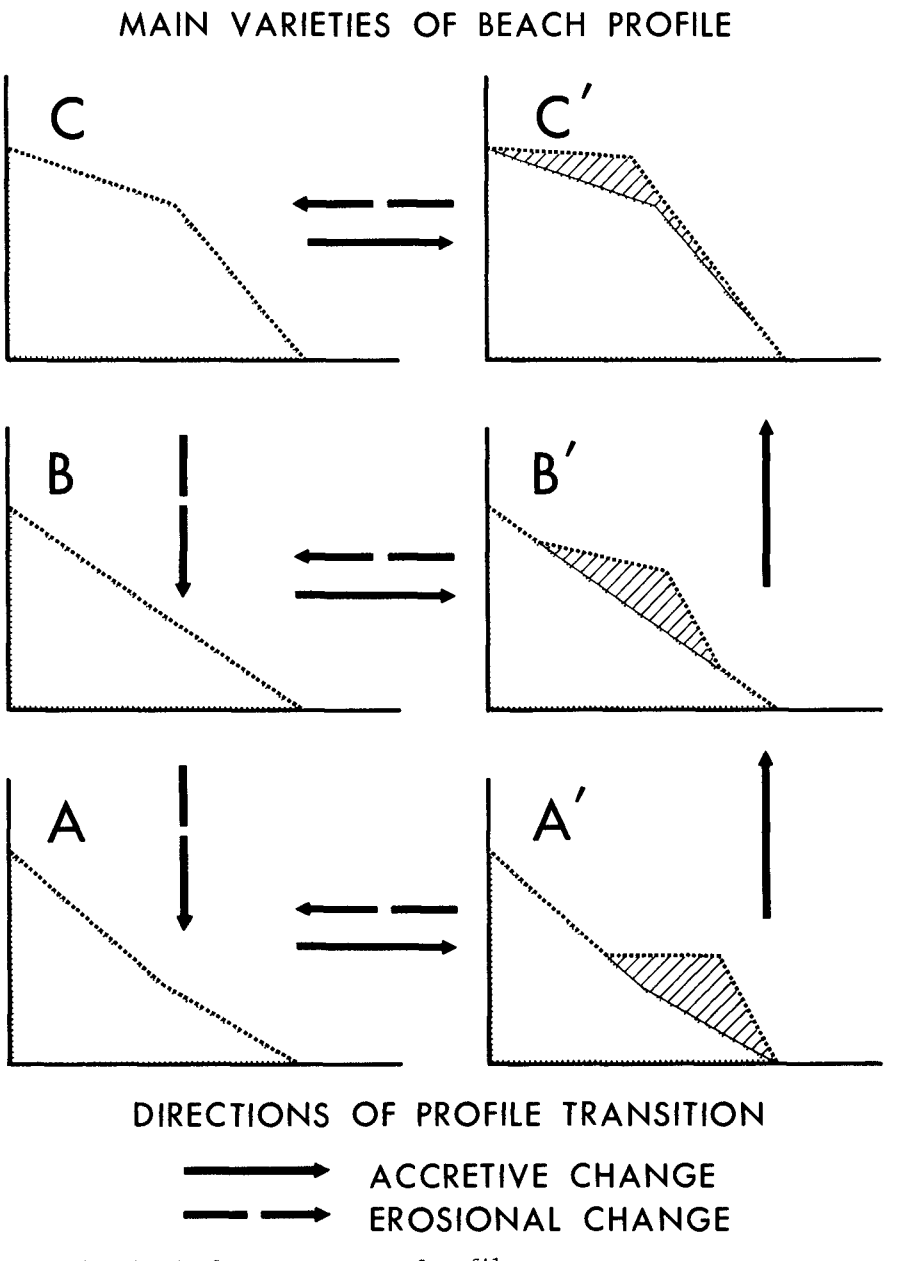

Figure 4. Sketch of six major types of profile.

However, when this correlation was measured statistically, it proved to be too low to be of significant value. It was found that the response of a beach profile to wave action depended not only upon wave heights but also upon the characteristics of an existing profile, particularly the profile configuration. This relationship is shown in Figure 6. The ordinate represents the sediment storage in the subaerial profile (as already defined), denoted by Q. The abscissa represents the beach width, a horizontal distance measured between the datum-level shoreline and the limit of swash run-up, denoted X. When plotted in the Q - X plane, the profile data at Nags Head were found to fall into groups which were identified with the six major configurations previously classified (see also Fig. 4). The numerals in Figures 5 and 6 denote transitions of profile configuration in the order of occurrence.

Short-period fluctuations of beach topography seen in Figure 5, which were repeated at an average interval of 14 days, are found in Figure 6 as consisting of cyclic transitions in terms of profile configuration. Especially, the beach changes associated with severe storms tended to produce closed cycles. For instance, a series of beach responses which occurred during a storm from January 10 through 20 (Fig. 5) is traced in the Q - X plane along transitions 4 through 8, which formed a closed cycle B'→B→A→A'→B', followed by upward migration of a berm, which finally led to C'. The storm of February 10 through 20 also produced transitions 11 through 14, which formed a cycle C'→C→B→B'→C'.

According to Figure 5, long-term beach changes also displayed a cyclic feature. For instance, a cycle with a period of approximately 90 days occurred between the end of December, 1963, and the end of March, 1964 (see Fig. 5). There is an indication that this cycle was probably repeated, since it is seen that following a trend of erosion between the end of January and the end of March there occurred a trend of accretion until the end of the field investigation in April and May. This feature is attributed to the characteristics of transition vectors in Figure 6, in which those involving pairs of A', B', and C' are directed upward only and those involving pairs of A, B, and C, downward only. Given a series of wave excitations causing alternate erosion and accretion over a sufficient length of time, long-term beach changes to be traced in the Q - X plane are bound to produce a counterclockwise cycle through A→A'→B'→C'→C→B→A. The period of this long-term cycle is thought to depend upon wave heights and intervals between successive storms.

Sediment Properties Related to Bar-type Sand Waves

The size characteristics of sediments sampled on the beach surface demonstrated close relationships with the bar-type sand waves thus far described. Figure 7 compares the grain size histograms of these sediments with profile configurations. The numerals represent sampling positions. In descending order, the profiles indicate a sequence of upward migration of a wave crest (profiles I through III), followed by its disintegration (profile IV) and final disappearance from the profile (profile V). Corresponding to this sequence, the grain size histograms changed from a unimodal shape with coarse diameters, through a bimodal shape with intermediate diameters, and finally to a unimodal shape with fine diameters. The shaded areas in the profiles indicate a zone where deposition of coarse material took place. It is seen that this area initially expanded onshore, accompanying the sand wave migra-

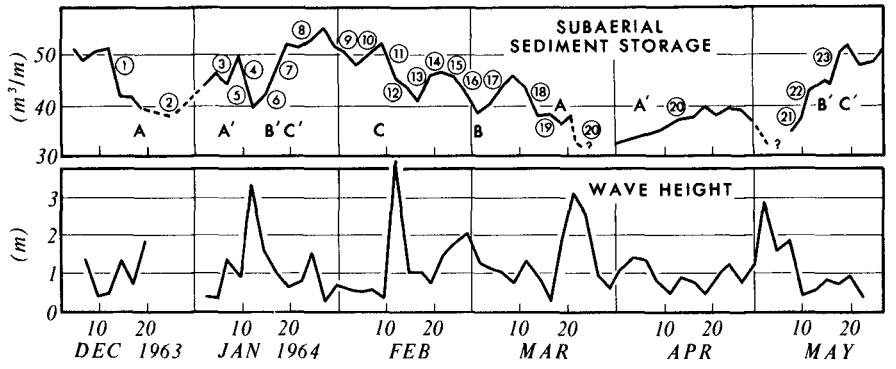

Figure 5. Time series of subaerial sediment storage and wave heights, Nags Head, North Carolina (see also Figures 4 and 6).

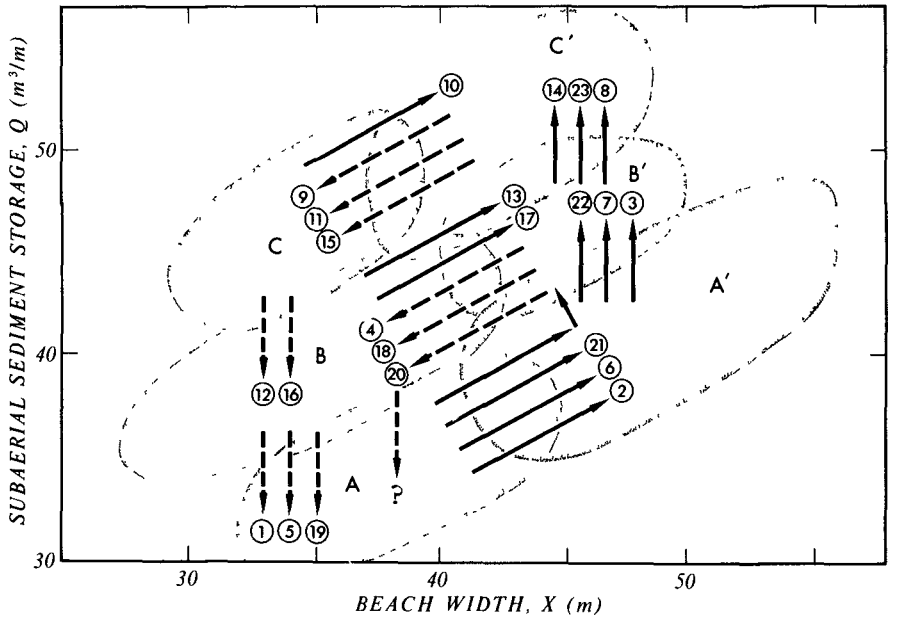

Figure 6. Profile data as a function of sediment storage, beach width, and configuration, Nags Head, North Carolina.

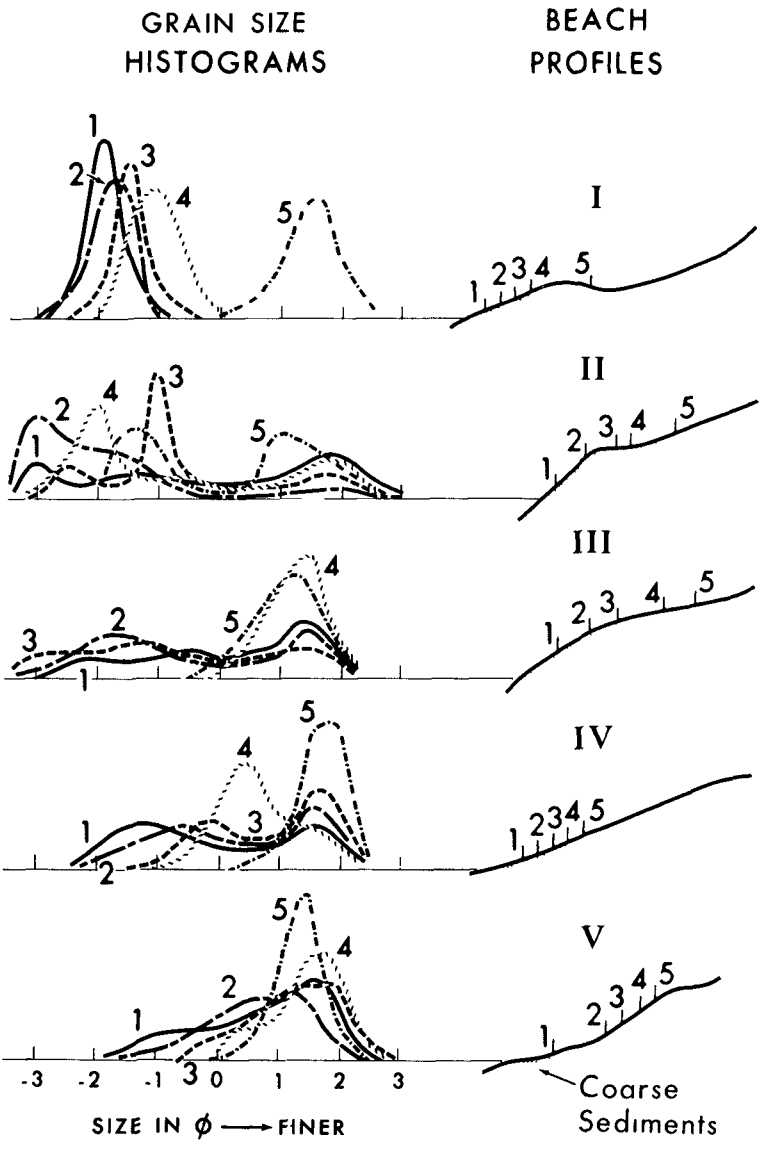

Figure 7. Comparison between grain-size histograms and their corresponding profiles, Nags Head, North Carolina.

tion, and later withdrew seaward as the sand wave was obliterated. Finally, in the concave profile (profile V), deposition of coarse sediment was essentially missing on the subaerial beach.

There is no doubt that the coarse material was of subaqueous origin and arrived on the subaerial beach with a sand wave. These coarse materials do not seem to have mixed with fine materials to produce a homogeneous mixture. The bimodality of sediment samples which contained both coarse and fine materials suggests that these materials may have existed as separate layers in the subaerial bed.

It seems unlikely that the presence of coarse materials is essential for the initial formation of the bar-type sand wave. However, it may well be that it is a factor which favors growth and movement of a wave crest once it has arrived on the subaerial beach. Since the water carried by swash over a layer of coarse sediments in part will seep through it in its return seaward, the drag exerted by swash oscillation will produce a net onshore transport of material on the subaerial slope. Consequently, growth and onshore propagation of the wave crest may be facilitated. This inference is supported by the result of a field experiment conducted by Longuet-Higgins and Parkin (1962), in which permeability of the subaerial surface was varied artificially by means of a tar-coated sheet inserted in the sand layers. They found that the waves quickly eroded the material overlying this sheet while disturbing the material on either side to a lesser extent.

CUSP-TYPE SAND WAVES

Formation of Cusp-type Sand Waves

In contrast to the bar-type sand waves, which are attributed to wave orbital motion, there exist sand waves which are believed to be associated with longshore currents. These sand waves develop periodic crests and troughs in a series along the shore and tend to migrate in the direction of existing longshore currents. Unlike bar-type sand waves, the crests of cusp-type sand waves are oriented obliquely to the shoreline, and often extend across the entire width of the surf zone between the shore and the longshore bar.

Because of its interference with an existing beach topography, the presence of cusp-type sand waves is manifest in the form of sinuous shorelines and crescentic bars. An example is shown in Figure 8. A cuspate projection of the shore and a shoal in front of it, both representing an accretive feature, correspond to the wave crest, and an embayment and a depression on the foreshore bed, representing an erosional feature, correspond to the wave trough. These features were studied previously by Hom-ma and Sonu (1962) and were designated "rhythmic beach topography."

Evans (1939) was probably the first to describe the formation of cusp-type sand waves in detail. His observations on the east shore of Lake Michigan indicated that the formation was "particularly noticeable when the wind blows at an angle to the shore." At such times, unequal

Figure 8. An example of cusp-type sand wave, Akita, Japan (courtesy of Japan Geographical Institute).

erosion on the shore first formed separate indentations and the material taken out of them was "carried and deposited in ridges along the course of currents which leave the shore, forming cusps and ridges." Eventually, topography such as shown in Figure 9 was formed, in which the spacings between successive projections ranged between 100 and 400 feet. Evans stated:

> At first, deposition off the points C_1 and C_2 is not very great, but as erosion continues the irregularity of shoreline thereby produced causes a more rapid growth. As the process goes on subaqueous deposition of sand continues at the ends of the cuspate forms. They are thus lengthened, and submerged ridges are formed which increase in length to the northwest. As soon as the formation of a ridge starts, the incoming waves begin driving it toward the shore. As a result it becomes dune-shaped with the steeper face at B where the sand lies at the angle of repose....The water brought over the ridge by the incoming waves caused a current at A, which was in some cases strong enough to superimpose current ripples in the troughs of the oscillating ripples. This water in finding its way out again to deeper water produced an undertow at D....It is evident that some of the sediment carried by this current enters into the building of the next subaqueous ridge extending out from C_2.

A general picture of material movement to be inferred from the Evans observation is illustrated in Figure 10. The material leaving an embayment and being carried to a submerged shoal is further moved across the crest of the shoal and deposited on the leeward slope. Thus, a zonation of alternate erosion and accretion may occur along the sand wave train, erosion characterizing the up-current slope of the shoal, and accretion, the leeward slope. The result will be a migration of this system in the direction of longshore currents, similar to the propagation of a sand wave train which takes place in a fluvial bed.

Alongshore displacement of sinuous shorelines and crescentic bars has been reported by various investigators, although it has not necessarily been recognized as a sand wave mechanism. Rates of migration (U) derived from various published sources are plotted in Figure 11 against intervals between successive projections, i.e., wave lengths (L). The distribution of these data suggests a relationship:

$$U \propto L^{-4/5} \tag{1}$$

or, approximately

$$U \propto L^{-1} \tag{2}$$

Thus, the rate of migration is found to be inversely proportional to the wave length, i.e., the larger a sand wave, the slower its movement. Essentially the same finding is recognized with respect to the dunes associated with a unidirectional flow (for instance, see Simons and Richardson, 1960).

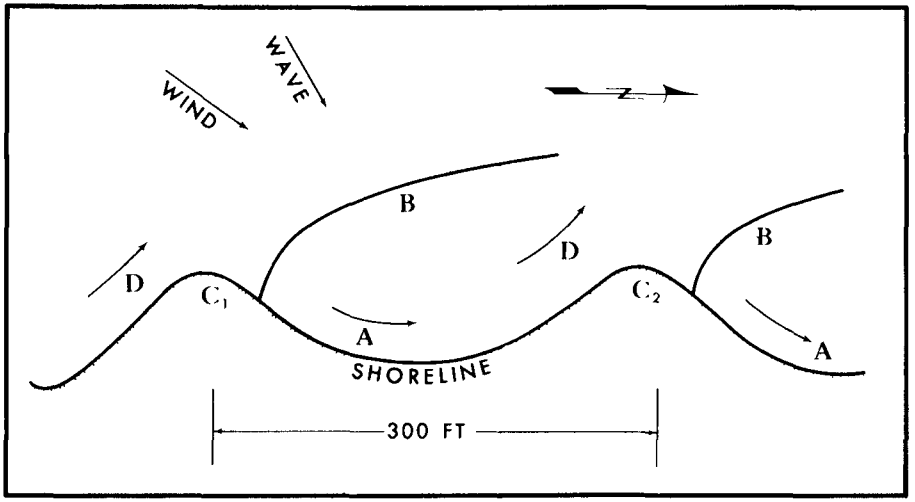

Figure 9. Formation of cusp-type sand wave on Lake Michigan shore (after Evans, 1939).

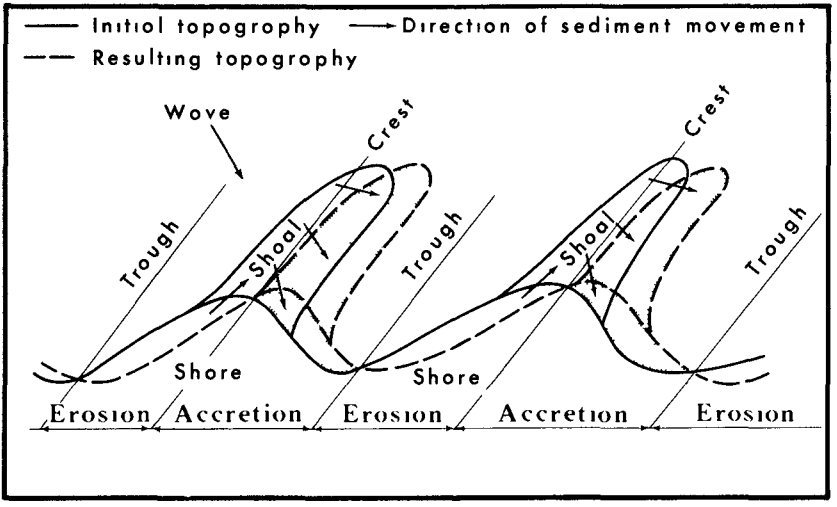

Figure 10. Alongshore migration of cusp-type sand wave.

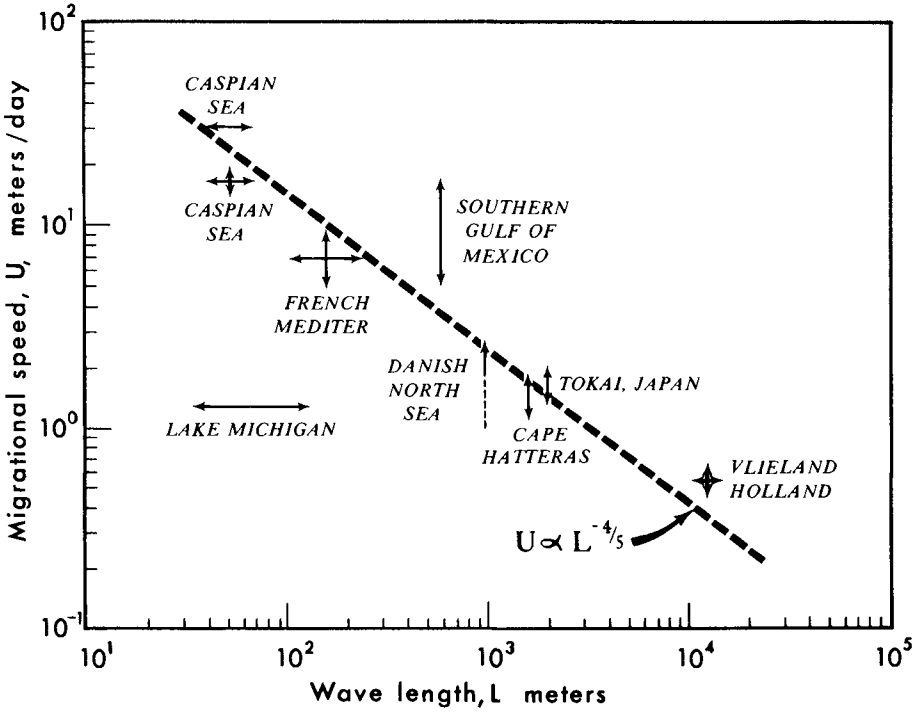

Figure 11. Rates of migration of cusp-type sand wave versus wave length.

It is recalled that sand waves forming in a fluvial bed are represented uniquely as a function of Froude number F_r, i.e.,

$$F_r = V/\sqrt{gh} \qquad (3)$$

in which V is the mean flow velocity, g the acceleration caused by gravity, and h the mean water depth. Simons and Richardson (1960) determined in a flume experiment various ranges of Froude numbers associated with a variety of bed forms for a median grain diameter of 0.45 mm. Following their result, Figure 12 shows current velocities and water depths necessary to create different bed forms in a unidirectional flow.

It appears that an analogy may be drawn between the cusp-type sand waves and the dunes associated with unidirectional flow. According to Figure 12, the deeper the water depth, the greater the velocity required for the formation of dunes. It then follows that for a given velocity, the gentler the foreshore slope, the longer the wave crest and the more prominent the formation of sand waves. In the experience of the writer, a gentle foreshore slope is an essential condition for the formation of cusp-type sand waves, along with sustained activity of longshore currents.

According to Figure 12, the current velocity required for dune formation in the nearshore zone--say, up to a depth of 5 feet--ranges up to approximately 4 ft/sec. This velocity may appear too high for ordinary longshore currents to attain, therefore incompatible with the common observation of cusp-type sand waves. A partial explanation is that whereas the longshore current of high velocity may take place only briefly, the sand waves thus produced would remain for some time. Furthermore, it appears that high velocities in longshore currents could occur more frequently than generally thought possible. Statistics based on actual measurements of currents at Nags Head are shown in Figure 12. A total of 350 individual measurements were made under various wave conditions for 6 months between December, 1963, through May, 1964 (see Sonu et al., 1965). It is found that a velocity equal to or in excess of 4 ft/sec could occur at a frequency of 8 per cent, i.e., 28 times during a 6-month period. Similarly, frequencies of occurrence of current velocities required for the formation of sand waves down to depths of 4 feet, 3 feet, and 2 feet are estimated at 12, 18, and 26 per cent, respectively. A study by Sonu and Russell (1965) disclosed indications of cusp-type sand waves on the Nags Head beach.

The foregoing discussion may apply mainly to sand waves having asymmetrical crests. These sand waves have relatively short wave lengths--say, up to several hundred meters. The wave lengths and amplitudes are presumably functions of size and movement of bed material, and perturbations and intensity, of turbulence in the flow. However, no quantitative criteria of general validity are known.

Sand waves with wave lengths of several kilometers have been reported to occur in depths between 3 and 10 meters (Hom-ma and Sonu, 1962). Whereas sand waves of shorter lengths would move rather rapidly and change readily in response to waves and currents, these large sand waves are relatively

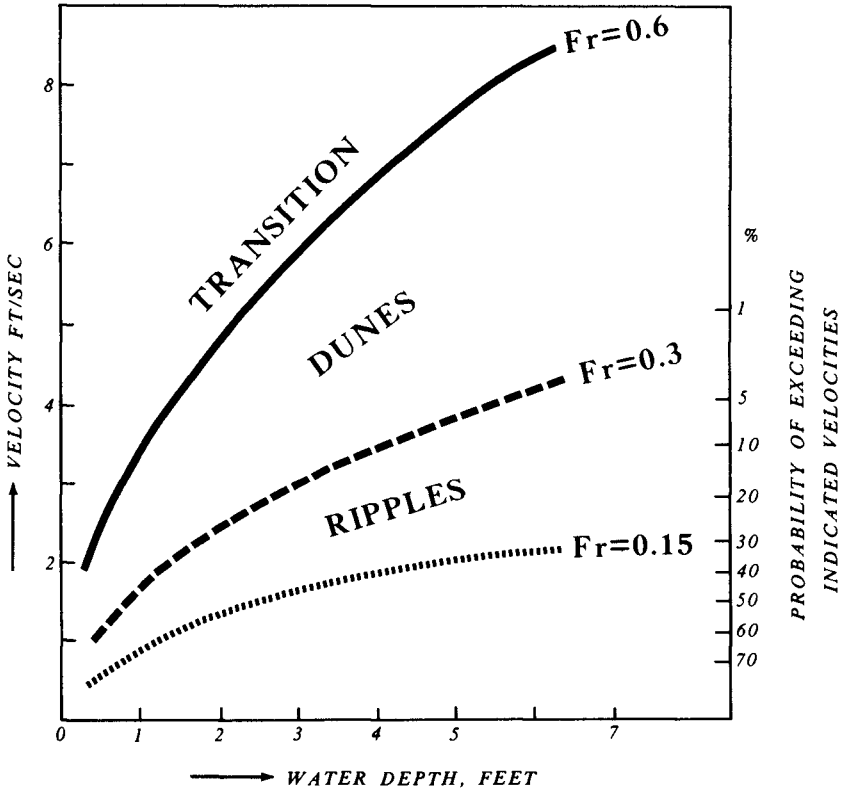

Figure 12. Water velocities, depths, and Froude numbers required for development of bed forms (after Simons and Richardson, 1960).

stable both in position and form. They also feature symmetrical crests.

When both long and short sand waves take place in the nearshore bed, they may produce dual rhythms in the shoreline. Figure 13 shows an example from the Tokai beach, Japan (Mogi, 1960), where two separate rhythms were found to be superimposed on one another. One was approximately 250 meters long and the other, approximately 2.5 km long. Usually, the crescentic pattern of the outer bar reflects the effect of long waves, and that of the inner bar, the effect of short waves.

Stride (1963) reported that the long sand waves of symmetrical crests occur in depths to about 200 m, where the corresponding Froude number is much below that required in flumes. Cartwright (1959) suggested that these sand waves may be formed in response to internal waves which develop in the presence of vertical density stratification in the water layer. The possibility was mentioned that a sufficient stratification may occur because of sediment suspension by wave action. According to Cartwright, this mechanism requires the following criterion:

$$h_2 \, (2 \, q\mu / \, U_1^{\,2})^{1/2} > \frac{\pi}{2} \tag{4}$$

in which h_2 is the thickness of the upper layer, g the acceleration caused by gravity, μ the vertical density gradient defined as

$$\mu = - \frac{1}{2} \rho'(y)/\rho(y) \tag{5}$$

in which $\rho(y)$ is the specific gravity of the fluid at elevation y, $\rho'(y)$ is the vertical density gradient, and U_1 is the fluid velocity. According to Hom-ma (1960), measurements of suspended sediment at an average depth of 3 meters off the coast of Niigata, Japan, yielded an average concentration of 176 ppm in the 1-meter layer above the bed and 108 ppm beyond this layer. Assuming a linear density gradient between the center of the 1-meter layer below and that of the 2-meter layer above, the density gradient μ is calculated from equation (5)

$$\mu = \; 2.3 \times 10^{-2} \; (m^{-1}).$$

From equation (4) we get:

$$\mu > \; (\frac{\pi}{2})^2 \, \frac{U_1^{\,2}}{2 \, g \, h_2^{\,2}} \tag{6}$$

Substituting h_2 = 2 m, g = 9.82 m/sec^2, and U_1 = 0.3 m/sec, the right hand side yields

$$2.8 \times 10^{-3} \; \; (m^{-1})$$

Thus, it is possible, at least theoretically, that conditions favorable for

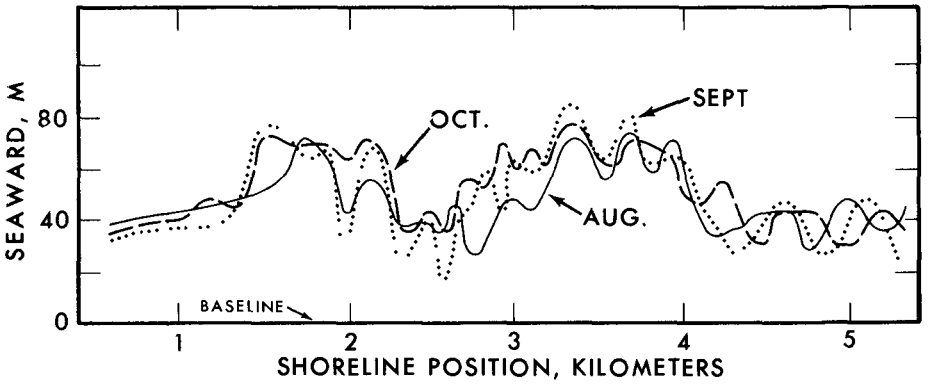

Figure 13. Dual rhythms in shoreline at Tokai, Japan (after Mogi, 1960).

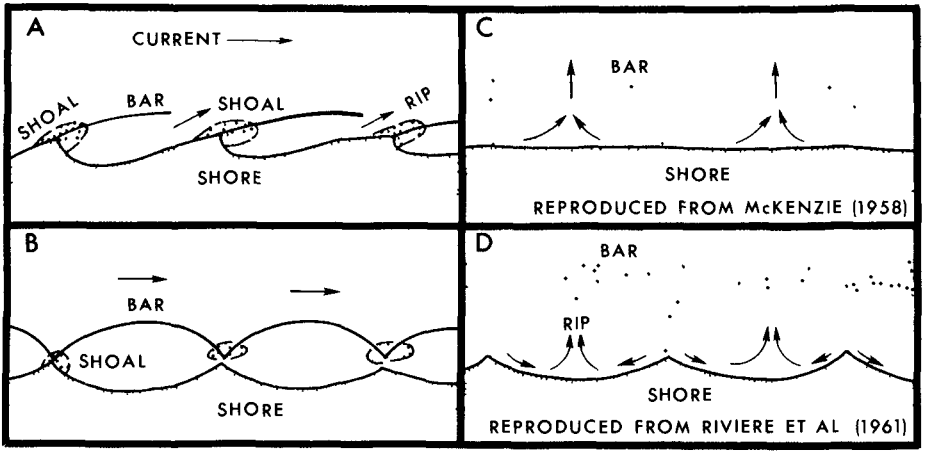

Figure 14. Typical effects of cusp-type sand wave on beach topography.

the formation of symmetrical sand waves arise in the nearshore zone. Because of the need for internal stratification, such sand waves may develop initially away from the shore and extend their influence shoreward. However, verification of this mechanism will require further studies.

Effects of Cusp-type Sand Waves on Beach Topography

Beach topography is affected by cusp-type sand waves in a variety of ways. Figure 14 shows typical examples.

One of the most remarkable effects occurs on the bar. The wave crest which extends out from a cuspate projection reaches the bar, and at the same time the bar is breached by a rip current immediately upstream of this junction. As a result, the bar is deformed into separate crescentic units such as shown in Figure 14 A. Usually, this type of topography indicates the existence of sustained activities of longshore currents in a single direction. The acute curve of the shoreline indentation faces downstream. The wave lengths are relatively small, ranging between approximately 40 meters (Black Sea, Egorov, 1951; Lake Michigan, Evans, 1939) and 600 meters (Tobasco, Mexico, Thom, 1966).

Mode B in Figure 14 features a series of crescentic bars linked with each other along the shore. The points of the bar usually form a broad shoal which may connect with a cuspate projection or remain away from the shore. The shape of the cross section across a shoal is symmetrical. Wave lengths may range up to approximately 3 km (Niigata and Tokai, Japan, Hom-ma and Sonu, 1962).

Mode C in Figure 14, reported by McKenzie (1958) on the New South Wales coast, Australia, may well be a slight modification of mode A, probably caused by additional activities of swells which arrived normal to the shore. A rip flowing in the breach across the bar is known to be so strong as to induce a sliding action of the sides of the channel. Mode D, reported by Riviere et al. (1961) on the French Mediterranean coast, again may be a modification of mode A or C, probably associated with a weak rip activity which caused deposition on the bar crest.

In general, the basic structure of a beach topography affected by cusp-type sand waves may be summarized as shown in Figure 15 (see also Hom-ma and Sonu, 1962). A major characteristic of such topography is that a remarkable distinction exists between profiles across a cuspate projection and those across an embayment. The former (profiles A-A') displays a well developed berm on the subaerial beach and a shallow shoal on the foreshore bed, where a bar may be absent. The latter (profile C-C') displays a narrow berm, a concave subaerial profile, and a relatively deep subaqueous bed. Occasionally, in this profile, a berm may be completely absent and, instead, an escarpment may be found. A step is usually more prominent in this profile than near a cuspate projection. Consequently, the profile across a cuspate projection bears accretive features similar to those of the so-called summer profile, and that across an embayment, erosional features similar to those of the so-called winter or storm profiles.

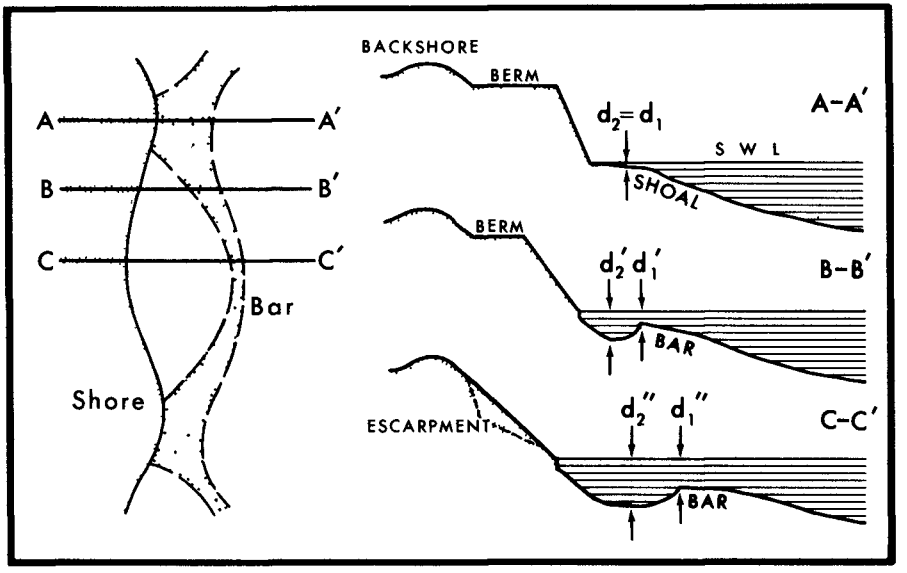

Figure 15. Structure of beach topography affected by cusp-type sand wave.

Of further interest is the distinction in the properties of bar in these profiles. The bar displays most prominent relief in the profile across embayment. With distance away from this profile, the prominence of bar relief decreases steadily, so that the depths over the crest (d_1) and the trough (d_2), as well as the depth difference between them ($d_2 - d_1$), show the following relationship (see Fig. 15):

$$d_1'' > d_1' > d_1$$

$$d_2'' > d_2' > d_2$$

$$(d_2'' - d_1'') > (d_2' - d_1') > (d_2 - d_1)$$

Finally, in front of a cuspate projection, the relief disappears, i.e.,

$$(d_2 - d_1) \to 0.$$

Consequently, in the presence of cusp-type sand waves, the beach topography will contain both profiles having a bar and those without a bar.

There exist relatively few studies regarding the effects of sand wave migration on beach changes. In a study dealing with behaviors of subaqueous beach profiles at Nags Head, North Carolina, Sonu and Russell (1965) suggested that abrupt changes in profile configuration observed in a stationary traverse could be attributed to migration of sand waves across this traverse during wind waves of oblique incidence. They reported that when this effect was suspected the beach change observed in the traverse was many times more pronounced than the changes associated with higher waves arriving normal to the shore.

Figure 16 shows a remarkable example of sand wave migration reported by van Bendegom (1949) on the Vlieland coast, the Netherlands. Continuous beach surveys since 1865 revealed the presence of two gigantic shoreline projections which steadily migrated toward the east. The amplitude of the curved shoreline was as great as 200 meters, and the rate of migration averaged 200 meters per year. As this wave moved along the shore, the beach was steadily eroded for about 40 years, then was accreted for more than 10 years.

DISCUSSION

It is not known how bar-type and cusp-type sand waves may interfere with each other. According to Evans (1939), subaqueous ridges originally formed by oblique storm waves could approach the shore and finally reach it, filling the embayments between cuspate projections. When observed in a single traverse normal to the shoreline, this movement of subaqueous ridges may appear to be similar to the onshore migration of bar-type sand waves already described. However, it is also evident, as shown in the Bagnold experiment, that in a purely two-dimensional situation a bar-type sand wave could be formed. According to Evans, as the wind direction is

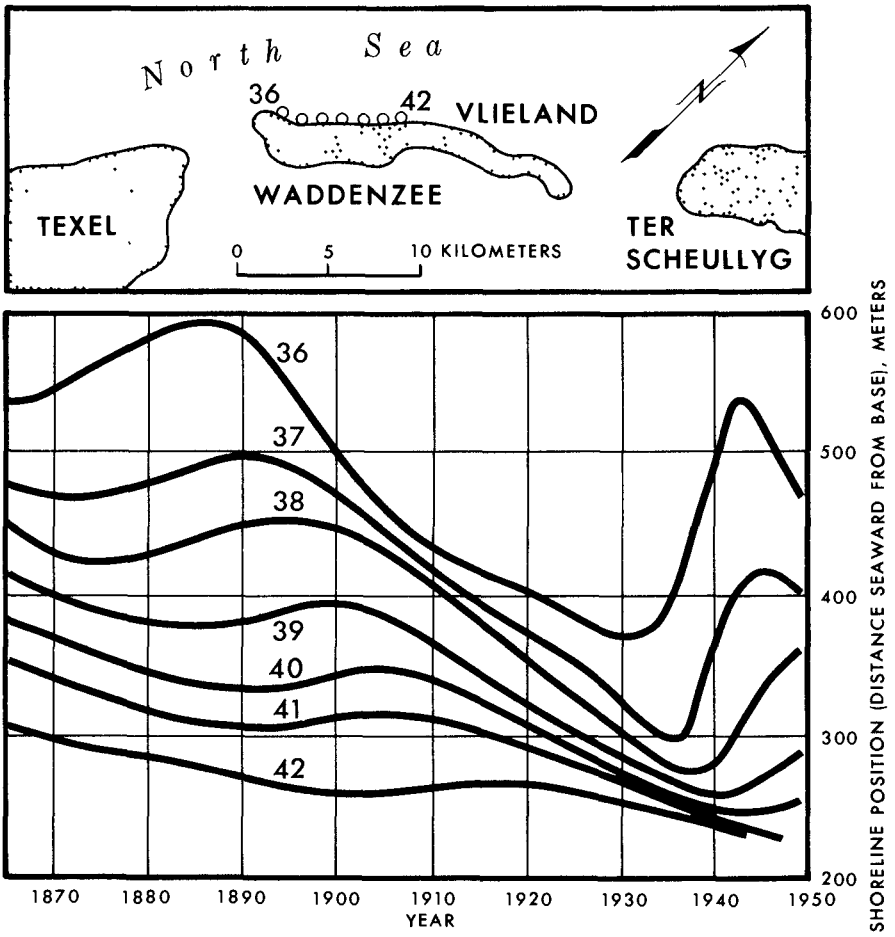

Figure 16. Migration of a gigantic sand wave along the Vlieland coast, the Netherlands (after van Bendegom, 1949).

reversed, "the new system of waves and currents guided by the trough between the subaqueous dune and the shore may succeed in cutting off the ridge at the tip of the cusp, thus forming an isolated shallows some distance out from shore." It is possible that these independent shoals generate activities of bar-type sand waves and, in the event of their progress up the subaerial beach, create convex profiles periodically along the shore.

One of the major implications of littoral sand waves is that the beach processes affected by them are non-uniform and often periodic. Suppose that the cusp-type sand waves migrate along the shore continuously. Since the wave crest contains a large mass of sediment, the littoral drifts may be pulsational when observed across a stationary cross section. A pulsational transport of sediment along the shore was reported by Taney (1962) in a laboratory experiment using radioisotopic tracer on a movable bed. Hom-ma and Sonu (1962) reported that the grain size of sediments sampled along the step exhibited periodic fluctuations consisting of coarse diameters near cuspate projections and fine diameters near embayments. A study by Trask and Johnson (1955) on the Point Reyes beach and that by Miller and Zeigler (1964) on the Cape Cod beach also indicated grain size fluctuations of the subaerial and nearshore sediments along the shore, in which coarse sediments were found near embayments and fine sediments, near projections. The alongshore distribution of longshore current velocities can also be non-uniform in the presence of cusp-type sand waves. This problem was previously dealt with by Sonu et al. (1965). A phenomenon of particular interest is the periodic occurrence of a series of rip currents along the beach. A field investigation currently underway at the Coastal Studies Institute disclosed close relationships between cusp-type sand waves and rip currents. One interesting result was that the rips originate at embayments formed by cusp-type sand waves. They discharge seaward the water which has been brought in predominantly through the crests of these sand waves. A similar model of longshore current system has been previously proposed by Inman and Bagnold (1962), although the role of periodic bottom topography is not emphasized.

It may be argued that the cusp-type sand wave is not found in many beaches, therefore is a special feature. King (1959) and Shepard (1963) suggest that it is typical of a tideless coast. However, it has been shown to occur where the tidal range is as much as 1 meter (namely, Tokai, Japan, Hom-ma and Sonu, 1962; Nags Head, North Carolina, Sonu and Russell, 1965). The periodicity caused by cusp-type sand waves is not always obvious to casual observers. On coasts exposed to an outer ocean, it tends to be obscured by swells which arrive normal to shore. Also, a large tidal range is thought to affect adversely its prominence. The literature reveals indications of cusp-type sand waves in many areas of the world. To the knowledge of the writer, these areas include the following: the Mediterranean coast (King and Williams, 1940; Vernhet, 1953; Riviere et al., 1961), the Dutch coast (van Bendegom, 1949), the Danish North Sea coast (Bruun, 1954), the Black Sea, Caspian Sea, and Azov Sea coasts (Egorov, 1951; Zenkovich, 1967; Shadrin, 1961), the Baltic Sea coast (Seibold, 1963; Aibulatov et al., 1966), the Japan Sea coasts (Hom-ma and Sonu, 1962), the New South Wales coast, Australia (McKenzie, 1958; Thom, 1966), the

Guiana coast (Diephuis, 1966), the Tobasco coast, Mexico (Thom, 1966), and various regions of the United States (namely, Point Reyes Beach, California, Trask, 1956; Cape Cod beaches, Zeigler et al., 1959; Virginia Beach, Harrison and Wagner, 1964; Nags Head, North Carolina, Sonu and Russell, 1965; Lake Michigan, Evans, 1939). Aerial photography is particularly useful in detecting the presence of rhythmic features on the coast. Inspection of U.S. Coast and Geodetic Survey aerial photographs indicates signs of rhythmic beach topography in numerous localities along U.S. coastlines, including a stretch on the Atlantic seaboard from Long Island, New York, to Cape Hatteras, along the Gulf of Mexico coasts of Florida (especially between Panama City and Pensacola), Alabama, Mississippi, Louisiana, and Texas, and along the Pacific coast from Portland, Oregon, to San Francisco, California.

ACKNOWLEDGMENTS

This study was conducted under contract Nonr 1575(03), NR 388 002, with the Office of Naval Research, Geography Branch. Field data relating to Nags Head, North Carolina, were collected by the personnel of the Coastal Studies Institute, Louisiana State University, particularly Dr. Robert Dolan, presently with the University of Virginia. Mr. J. L. van Beek cooperated ably in the analysis of subaerial beach profiles associated with bar-type sand waves, and should be given partial credit for that part of the paper. A grateful acknowledgment is due these people.

REFERENCES

Aibulatov, N., Y. Dolotov, G. Orlova, and M. Yurkevitch, 1966, Some features of shore dynamics. In Development of sea shores in the environments of transient earth surfaces. Tallin, U.S.S.R. (in Russian), 66-74.

Bagnold, B. R. A., 1941, Physics of wind-blown sand and desert dunes. London (Methuen).

Bagnold, B. R. A., 1947, Sand movement by waves: some small-scale experiments with sand of very low density. Journ. of Inst. of Civil Engineers, Paper 5554:447-469.

Bruun, P. M., 1954, Migrating sand waves and sand humps, with special reference to investigations carried out on the Danish North Sea coast. Proc., Vth Conf. on Coastal Engineering, Council on Wave Research, Grenoble, 269-295.

Cartwright, D. E., 1959, On submarine sand waves and tidal leewaves. Proc., Royal Society of London, A, 253:218-241.

Diephuis, J. G. H. R., April 1966, The Guiana coast. Tijdschrift van het Koninklijk Nederlandsch Aurdrijkskundig Genootschap, Tweede Reeks, Deel LXXXIII:145-152.

Eagleson, P. S., B. Glenne, and J. A. Dracup, 1963, Equilibrium characteristics of sand beaches. Journ. Hydraulics Div., Proc. A.S.C.E., HY1, 35-57.

Egorov, E. M., 1951, On some forms of accretive beach related to continuous sediment movement. Doklady Akademii Nauk, Tom LXXX(5) (in Russian).

Evans, O. F., 1939, Mass transport of sediments on subaqueous terraces. Journal of Geology, 47:324-334.

Harrison, W., and K. A. Wagner, 1964, Beach changes at Virginia Beach. U. S. Army Coastal Engineering Research Center, Misc. Paper No. 6-64.

Hom-ma, M. (ed.), 1960, Beach erosion studies in Niigata, Japan. Niigata Prefecture Public Works Department (in Japanese).

Hom-ma, M., and C. J. Sonu, 1962, Rhythmic pattern of longshore bars related with sediment characteristics. Proc., VIIIth Conf. on Coastal Engineering, Council on Wave Research, Mexico City, 248-278.

Inman, D. L., and R. A. Bagnold, 1962, Beach and nearshore processes: littoral processes. In The Sea, New York (John Wiley and Sons, Ltd.), 2:540-553.

King, C. A. M., and W. W. Williams, 1949, The formation and movement of sand bars by wave action. Geographical Journal, CXII:70-84.

King, C. A. M., 1959, Beaches and coasts. London (Edward Arnold, Ltd.).

Longuet-Higgins, M. S., and D. W. Parkin, 1962, Sea waves and beach cusps. Geog. Journ., 128.194-201.

McKenzie, P., 1958, Rip-current systems. Journal of Geology, 66(2):103-113.

Miller, R. L., and J. M. Zeigler, 1964, A study of sediment distribution in the zone of shoaling waves over complicated bottom topography. In (R. L. Miller, ed.) Papers in marine geology, Shepard Commemorative Volume, New York (MacMillan Co.), 133-153.

Mogi, A., 1960, On the topographical change of the beach of Tokai, Japan. Japan Geographical Review (in Japanese with English abstract), 398-411.

Riviere, A., F. Arbey, and S. Vernhet, Jan. 1961, Remarque sur l'evolution et l'origine des structures de plage a caractere periodique. Comptes rendus des seances de l'Academie des Sciences, No. 252.

Seibold, E., 1963, Geological investigation of nearshore sand-transport--examples of methods and problems from the Baltic and North seas. In (M. Sears, ed.) Progress in oceanography, New York (MacMillan Co.), 1:3-70.

Shadrin, I. F., 1961, Longshore currents and compensating currents on the shallow accretive beach. Trudy, Oceanographic Committee, Akademii Nauk, U.S.S.R. (in Russian), 158-169.

Shepard, F. P., 1963, Submarine geology. New York (Harper and Row), second edition.

Simons, D. B., and F. V. Richardson, 1960, Resistance to flow in alluvial channels. Proc., A.S.C.E., 87, No. HY5.

Sonu, C. J., J. M. McCloy, and D. S. McArthur, 1965, Longshore currents and nearshore topographies. Proc., Xth Conf. on Coastal Engineering, Council on Wave Research, Tokyo, 525-549.

Sonu, C. J., and R. J. Russell, 1965, Topographic changes in the surf zone profile. Proc., Xth Conf. on Coastal Engineering, Council on Wave Research, Tokyo, 502-524.

Stride, A. H., 1963, Current-swept sea floors near the southern half of Great Britain. Geol. Soc. of London, Quarterly Journal, 119:175-199.

Taney, N. E., 1962, Laboratory applications of radioisotopic tracers to follow beach sediments. Proc., VIIIth Conf. on Coastal Engineering, Council on Wave Research, 278-303.

Thom, B., 1966, Personal communication.

Trask, P. D., and C. A. Johnson, 1955, Sand variation at Point Reyes beach, California. Beach Erosion Board Tech. Memo. No. 65, Corps of Engineers, U. S. Army.

Trask, P. D., 1956, Changes in configuration of Point Reyes beach, California, 1955-1956. Beach Erosion Board, Tech. Memo. No. 91, Corps of Engineers, U. S. Army.

van Bendegom, L., 1949, Consideration of the fundamentals of coastal protection. Mimeographed thesis, the Netherlands (in Dutch).

Vernhet, S., Nov. 1953, Sur un mode de cheminement littoral par migration lente de rides obliques ou perpendiculaires. Comptes rendus de l'Academie des Sciences, No. 237.

Zeigler, J. M., C. R. Hayes, and S. D. Tuttle, 1959, Beach changes during storms on outer Cape Cod, Massachusetts. Journ. Geology, 67(3):318-336.

Zenkovich, V. P., 1967, Submarine sand bars and related formations. In (J. A. Steers, ed.) Processes of coastal development, New York (John Wiley and Sons, Inc.), pp. 219-236.

CHAPTER 25

WAVE PERIOD AND THE SWASH ZONE ENERGY BALANCE

Graham S. Giese
Department of Marine Sciences
University of Puerto Rico
Mayaguez

ABSTRACT

The shape sorting of pebbles in the swash zone was studied in an effort to determine the effect of the amount of foreshore infiltration per wave on the swash zone energy balance. Measurements were made of pebbles collected from the swash limit and from the step of selected sandy beaches. The pebbles were sampled on occasions when, and at locations where, the conditions of breaker height, breaker approach angle and foreshore slope fell within predetermined limits. The wave period and the foreshore infiltration rate varied among the beaches and were measured. The results of these measurements indicate that the mean shape of swash limit pebbles, and presumably, therefore, the swash zone energy balance depends upon the amount of foreshore infiltration per wave. This finding leads to the conclusion that in the study of the dynamics of the swash zone the effect of wave period and the effect of foreshore permeability must be considered together.

INTRODUCTION

The response of a beach to a particular set of sea conditions depends upon both its composition and its configuration. However, at the present time, the mechanics of beach processes are not sufficiently well understood to permit a quantitative prediction of the response of a given beach to a given set of conditions, despite the rapidly increasing need for such predictions. The following discussion is intended to contribute toward the eventual development of this predictive capacity.

Bagnold has discussed the ratio of backwash energy to swash energy as an important parameter in the study of the dynamics of the swash zone of beaches (Ref. 1). Backwash energy is less than swash energy by the amount of energy lost above a given potential level due to friction and infiltration into the foreshore. In the upper swash zone where velocities and turbulence are relatively low, the energy lost is mostly in the form of potential energy and depends primarily upon the amount of water which infiltrates the foreshore during the swash-backwash cycle. Thus Bagnold was able to demonstrate that foreshore slope, as a function of the energy ratio depends upon the permeability of the foreshore.

More recently, Kemp has reported on intensive studies of swash zone processes in which he emphasizes the role played by foreshore permeability in the control of wave energy absorption, beach slope, and the phase difference between swash duration and wave period (Ref. 2,3).

The purpose of the present paper is to report the results of field experiments which indicate that the amount of energy lost due to infiltration into the foreshore, and therefore the swash zone energy ratio, depends

upon both the foreshore permeability and the incident wave period. The experimental techniques make use of the readily observed movements and shape sorting of beach pebbles as external indices of the physically complicated swash zone mechanics. All of the studies and observations herein reported were made on the predominantly sandy beaches of Cape Cod, Massachusetts, which contain pebbles as a minor constituent (Fig. 1). The tides in the study area are semi-diurnal with mean annual ranges varying from 6.7 to 9.5 feet, depending on location.

BACKGROUND

It has often been reported that beach pebbles are sorted according to shape such that those deposited at the swash limit are flatter than those deposited at the step (Ref. 4). (As used in this paper, "swash limit" refers to the zone of deposition at the uppermost part of the swash zone, while "step" refers to the coarse deposit located at the final breaking point of the waves.) It has also been reported that swash limit pebbles are flatter on beaches of low permeability than on beaches of high permeability (Ref. 5). In addition, however, I have noticed over a number of years of field studies on Cape Cod beaches, that swash limit pebbles deposited under the action of short period storm waves are flatter than the swash limit pebbles deposited on the same beach when the wave period is longer. It occurred to me that the two effects may be due to the same cause. Both a decrease in permeability and a decrease in wave period act to increase the saturation of the foreshore and therefore decrease the amount of water which is lost from the swash due to infiltration into the foreshore. This suggested that the degree of flatness of swash limit pebbles is controlled by the ratio of the force exerted on the pebbles by the swash to the force exerted on the same pebbles by the backwash.

Preliminary field experiments designed to reveal the movements of beach pebbles provided information critical to the problem of pebble shape sorting (Ref. 6). In these experiments, painted pebbles were embedded in a chiefly sandy beach at 5-foot intervals and in a line normal to the shoreline between high tide and low tide lines. The pebbles were placed such that their top surfaces were visible, and the movements of each pebble were observed and recorded for 6-hour, half-tidal periods. The full results of these experiments will be published separately and this paper will include only those results immediately applicable to its subject.

The movements of the painted pebbles in the swash zone confirmed the existence of the continuous processes of erosion in the mid-swash zone and deposition in the upper swash zone and at the step as first described by Strahler (Ref. 7). Once exposed to wave action as a result of mid-swash zone erosion, the pebbles were moved by successive flows of the swash and the backwash until they were carried either to the step or the swash limit. Any pebble deposited at the swash limit had its immediate origin in the mid-swash erosion zone. No pebbles were carried directly from the step to the swash limit. If carried to the swash limit on the falling tide, the pebble was simply deposited there with no further movement. Although pebble shape was not considered during these experiments, later trials with matched pairs of similarly shaped pebbles clearly

demonstrated that the flatter the pebble, the more likely it was to be carried to the swash limit.

Another set of observations which bears upon the present discussion concerns the effect of pebble weight upon the shape sorting of beach pebbles. It was observed that when waves were large and steep, the sandy foreshore at low tide was commonly left "clean" with very few pebbles. Those which remained varied greatly in size, but all were extremely flat. On one such occasion, at Nauset Coast Guard Beach, an attempt was made to collect all foreshore pebbles large enough to be easily visible when walking for a distance of 350 feet. Eighteen pebbles were collected ranging in weight from 0.15 g. to 611.30 g. Despite the wide range of weight, the pebbles were all quite flat. Pebble shape was determined according to the coefficient $c/\sqrt{ab}$, where a, b, and c represent the lengths of the major, intermediate, and minor axes respectively. The values of the coefficient for the eighteen pebbles ranged from 0.09 to 0.37, even the largest of which describes a quite "flat" pebble.

PEBBLE SHAPE AS AN ENERGY RATIO INDEX

The observations of the movements of marked pebbles over half-tidal cycles indicated that the pebbles active in the swash zone on the falling tide have their immediate origin in the mid-swash erosion zone of the foreshore. These pebbles are in a condition of unstable equilibrium because the ratio of the force exerted by the backwash to the force exerted by the swash decreases going up the foreshore. Once exposed to the alternate action of the swash and backwash, they are eventually deposited either at the step or at the swash limit. If a pebble, such as a very flat pebble, is moved by the swash but not the backwash, it is deposited at the swash limit. If another, say a nearly spherical pebble, is easily moved by both the swash and the backwash, it is deposited at the step due to the downslope component of gravity. If, however, there were no backwash, that is to say, the ratio of the force exerted by the backwash to the force exerted by the swash equaled zero, even a sphere would be deposited at the swash limit; and if the ratio equaled one, even the flattest pebble would be taken to the step. Since the forces exerted on pebbles are proportional to the kinetic energies of the flows, and since the sorting action is considered to take place at a single potential level, the mean shapes of the pebbles which are left scattered on the foreshore by the falling tide were taken as an index of the ratios of the backwash energy to the swash energy which existed in the mid-swash zone at the time of their deposition.

DESIGN OF FIELD EXPERIMENTS

In the field experiments to be described, the intermediate axes of the pebbles sampled ranged from 0.5 inches to 2.0 inches. Pebbles of this size were found to be readily movable by the swash of the beaches selected. It was assumed that the pebbles would be sorted according to their shape independent of their weight. This assumption was confirmed by the analysis of the data.

The experiments were performed at mid-tide on the falling tide on beaches which were selected such that the foreshore slopes were $7^{\circ} \pm 30'$,

the breaker heights were 1.5 feet $\pm$ 0.5 feet, and the breaker approach angles were $0^{o} \pm 10^{o}$. This permitted the assumption that the value of the swash energy was constant in all experiments, and therefore that the value of the energy ratio in the mid-swash zone depended only upon the energy lost, in the form of potential energy, due to infiltration into the foreshore in the upper swash zone. It was further assumed that the volume of water which infiltrated the upper foreshore per wave was a function of the foreshore infiltration rate, Q , ($cm^3/ cm^2/ sec$), and the incident wave period, T , (sec). The product, QT , will be referred to as the "infiltration-per-wave" index. QT has the dimensions of length, and it may be thought of either as an index of the volume of water which infiltrates a unit area of foreshore per wave or as an index of the vertical displacement of the foreshore water table between successive swashes.

In brief, the field experiments to be described were designed to test the hypothesis that on beaches of a given slope, acted upon by breakers of a given height and approach angle, the energy balance of the swash zone, as indicated by the mean shape of the pebbles deposited at the swash limit on the falling tide, is a function of both the foreshore infiltration rate and the incident wave period, as indicated by the infiltration-per-wave index.

EXPERIMENTAL PROCEDURE

On a given day a site was sought within the study area where breaker height, breaker approach angle and foreshore slope all fell within the given limits. Breaker height and approach angle were estimated visually. Foreshore slope was determined by means of an inclinometer (Brunton compass) resting on a timber. The $7^{o} \pm 30'$ limits were chosen because foreshore slopes in the study area were frequently within that range and because experience indicated that this was sufficiently steep to produce backwash accelerations such that pebbles were moved before the commencement of scour which, as has been reported by Johnson (Ref. 8) and Smith (Ref. 9), can lead to burial. It was also required that the wave form be simple, that is, that practically speaking, only a single wave train be running. Finally, it was required that variations along the shore at the site be minimal. If these basic requirements were satisfied, and pebbles were in evidence, an experiment was conducted. Each experiment was designed so that the foreshore pebbles sampled were those which had been deposited at approximately mid-tide on the falling tide in order to minimize the variations in the relative position of the beach water table due to the propagation of the tidal wave through the beach (Ref.10).

Each experiment began shortly before mid-tide. First, general wave and beach characteristics were noted, and then a determination of wave period was made by measuring with a stop watch the time interval between breakers. This done, iron rods were placed along shore at the swash limit marking the top of the foreshore area to be sampled. The length of the sample area varied with the pebble concentration from a minimum of 27 feet to a maximum of 300 feet. After placing the top foreshore sample area boundary rods, the step pebbles were sampled with a fine mesh dip net

from a position seaward of the step and along the entire length of the step seaward of the foreshore sample area. Brought back to the dry beach, the step pebbles were size-sorted using an aluminum template with hole 0.5 inches and 2 inches in diameter. Only those pebbles were retained which would pass through the larger hole but not the smaller one. The others, with an intermediate (b) axis less than 0.5 inches or greater than 2 inches were discarded. This method of size-sorting, which was used for both the step and foreshore pebble collections, was the source of a sampling error which was later detected and corrected, as is later discussed in this section. The step pebble collection was completed when 100 pebbles had been gathered.

Sampling Foreshore Pebbles

When the tide had dropped far enough, the iron rods marking the bottom of the foreshore sample area were placed at the swash limit in a line along shore, downslope from the top rods. On the foreshore sample area, between the two rows of rods lay the pebbles which had been deposited at the swash limit while the step pebbles were being sampled. The foreshore sample area was always narrow (9 to 15 feet in width) as compared to its length, because foreshore variations are generally more extreme up and downshore than along shore. After the setting of the bottom foreshore sample area rods, the wave characteristics were determined again in the same manner as before, thus giving a reading at both the beginning and the end of the period during which the sample pebbles were deposited. All of the collections and measurements which then remained to be made concerned the rectangular foreshore sample area. In most of the experiments this area measured 9 feet by 27 feet, and a method was devised to take a random sample of approximately 100 pebbles from within the area. If, however, the foreshore pebble concentration was such that there were fewer than 100 pebbles within the standard 9- by 27-foot area, the sample area was increased so that it contained approximately 100 pebbles, and in such cases all pebbles (0.5 inches $< b <$ 2 inches) within the area were taken for the foreshore sample. A maximum permissable size for the foreshore sample area was set at 15 feet by 300 feet. If it so happened, as it did once, that there were fewer than 100 pebbles in an area of this size, the foreshore pebble sample consisted of the total number of proper sized pebbles found within the area, regardless of how few they might be. This limit was set because it was felt that the variations inherent within an area larger than this would necessarily be too great to justify the assumption that the mean value of the variables measured within the sample area were characteristic of the entire area.

The following describes the methods of sampling within the 9- by 27-foot areas. Adaptations of the sampling techniques necessary for the larger areas will be self-evident. The 9- by 27-foot rectangle was divided into three 9-foot squares, the corner of each square being marked by an iron rod. The center of each square was marked by an upside-down sample bucket. These would later be the locations for the three samples to be taken for the determination of the foreshore infiltration rate. At two locations halfway between buckets, the foreshore slope was determined by the methods previously described. Next, the foreshore pebbles were collected. For this purpose each square was visually divided into quadrants. If there were less than about 14 pebbles of the proper size per quadrant, all pebbles in the 12 quadrants were collected after

being checked for size, using the template previously described. If there were more than about 14 pebbles per quadrant, use was made of one of four aluminum hoops which had diameters of 3, 2, 1.5 feet and 1 foot. The hoop was chosen which would encircle approximately 5 to 10 pebbles of the proper size. This hoop was then tossed successively in each of the 12 quadrants, and all pebbles encircled, after being checked for size, were kept.

Infiltration Rate Determination

The infiltration rate of the foreshore sand was determined by a system basically similar to one described by Emery and Foster (Ref. 10). The core tube made of lucite plastic was 6.58 cm. in diameter and 50 cm. in length. The cores were taken by inserting the tube vertically into the sand at the three locations previously described within the foreshore sample area. The length of each core was kept constant at 15 cm. Disturbance to the core in sampling was minimized by digging a moat of depth equal to the core length around the region to be sampled, leaving a sand column with a diameter only slightly larger than that of the core tube. After the core tube had been inserted to a depth of 15 cm., a thin aluminum plate was slid across the bottom of the tube,thus preventing core disturbance in removal. Once removed, the plate and upright core tube were placed upon a square of cloth resting on a board. The aluminum plate was then carefully slid out and the cloth pulled up and around the tube and secured in place with a stainless steel hose clamp. The core was then slowly immersed in a tall bucket of sea water taken only a short while previously in order to minimize temperature change and thus to take into account the local temperature effect on viscosity. It was found that if a pressure head of about 3 cm. was maintained during the saturation of the core, there was virtually no disturbance to the sample. The water level was allowed to continue rising in the core tube until it stood somewhat above a mark 30 cm. from the bottom (and 15 cm. above the top of the sample). The tube was then capped at the bottom and taken to a nearby stand to which it was attached in a position below a reservoir containing one liter of sea water. The cap was then removed and when the water level within the tube fell to the 30 cm. mark, water was allowed to flow into the core tube from the reservoir. At this instant a stop watch was started. During the entire test the water was kept at the 30 cm. mark. When the reservoir was exhausted, the stop watch was stopped. In this manner, a measurement was made of the time required for one liter of sea water with a head of 30 cm. to flow through a 15 cm. length of relatively undisturbed beach sand with a known surface area. This test was made three times during the experiment and the results averaged to give a measurement of the infiltration rate per unit area of local sea water through the sand of the foreshore sample area.

Laboratory Analyses

Ten such experiments were performed, not including two preliminary experiments which were performed prior to the initiation of the standardized procedure. The pebble samples were analyzed in the laboratory. First, each pebble was weighed: to the nearest gram for five samples and to the nearest 0.1 gram for the others. Next, a determination was

made of the lengths of the major axis, "a", the intermediate axis, "b", and the minor axis, "c". Specifically, "c" was taken as the vertical extent of the pebble above a horizontal plane when the pebble lay in its preferred stable position. Axis "a" was assumed to be the greatest dimension of the pebble in a plane perpendicular to "c", while axis "b" was the maximum distance covered by the pebble in a direction perpendicular to both "a" and "c". The axial lengths were each measured to the nearest millimeter: the "a" and "b" axes by laying the pebble in the corner of a specially designed box having orthogonal graph paper graduated in millimeters affixed to the surface of the bottom. The "c" axis was measured by means of vernier calipers.

Following the axial measurements, the shape of each pebble was determined by calculating the value of the coefficient $c/\sqrt{ab}$. It was then noted that there was a certain correlation between pebble weight and pebble shape in the respect that for each sample the pebbles which weighed less than 3 grams had a mean $c/\sqrt{ab}$ value which was lower than that of the remainder of the sample. This correlation was discovered to be a fallacious one — the result of a bias introduced by the sampling method. By rejecting all pebbles with a "b" axis length less than 0.5 inches, the lightest weight classes were in fact "enriched" with flatter pebbles. Similarly, the rejection of all pebbles with a "b" axis length greater than 2 inches would tend to decrease the percentage of flat pebbles in the highest weight classes. However, as is commonly the case of pebbles in all natural environments, the sampled pebbles were approximately log normally distributed by number with respect to weight. Light pebbles were much more numerous than heavy ones, and therefore the bias did not show up in the heavier weight classes.

An analysis of the distribution of pebble shapes within the samples revealed that the heaviest pebble likely to pass through the 0.5 inch hole would weigh less than 3 grams, while the lightest pebble likely to be too large for the 2 inch hole would weigh more than 80 grams. Therefore, all pebbles which weighed less than 3 grams or more than 80 grams were rejected. This left a total of 1,609 pebbles in the twenty samples. Plots of pebble shape frequency within randomly selected samples on normal probability paper indicated that the pebbles in each sample were normally distributed with respect to shape.

The sample statistics, sample mean and standard deviation, were computed by means of a General Electric 225 computer making use of the preliminary portion of a factor analysis program written and published by Derek W. Spencer (Ref. 11). This program also permitted the computation of various transforms of the original variables (a, b, c, and weight) for each pebble. Finally, a correlation matrix was provided of the original and transformed variables for each sample.

RESULTS

The results of the field and laboratory measurements are summarized in Table 1. Column 1 gives an abbreviation of the name of the beach from which the samples were taken (Fig. 1) and a notation of the zone

sampled: foreshore (F) and step (S). Column 2 gives the mean shape, $\overline{c/\sqrt{ab}}$, of the pebbles in each sample; column 3 the standard deviation, σ, of the distribution; and column 4 the number of individuals, n, in each sample. Column 5 records the mean value of the infiltration rate, Q, measured at each foreshore sample area. Column 6 gives the mean value of the wave period, T, measured at the time the samples were taken. Column 7 shows the value of the infiltration-per-wave index, QT, calculated for each site. It is the product of the values in columns 5 and 6. Column 8 gives $(QT)^{-1}$, the inverse of the values in column 7, and column 9 shows the symbol used to represent each sample location on Figure 2.

Foreshore Pebble Samples

In Figure 2 the x's and dots represent the values of the mean shapes of the foreshore pebble samples, $\overline{c/\sqrt{ab}}$, plotted against the mean values of the corresponding infiltration-per-wave index, QT. The dots represent the results of two preliminary experiments as explained in the footnote to Table 1. Seeking a transformation which would produce a linear relationship between $\overline{c/\sqrt{ab}}$ and some function of QT, it was found that a suitable transformation was $(QT)^{-1}$, the values of which are given in column 8 of Table 1. The least square regression line of $\overline{c/\sqrt{ab}}$ on $(QT)^{-1}$ was found to be:

$$\overline{c/\sqrt{ab}} = -0.55\ (QT)^{-1} + 0.66. \qquad (1)$$

The correlation coefficient between the two sets of variables was found to be -0.92. The 95 per cent confidence limits for the correlation coefficient are -0.69 and -0.99. The standard error of estimate of $c/\sqrt{ab}$ on $(QT)^{-1}$ is 0.046. The standard error of the regression coefficient was found to be 0.08. The 95 per cent confidence limits of the regression coefficient are -0.55 ± 0.19, and the 99 per cent confidence limits of the regression coefficient are -0.55 ± 0.28.

Making use of Student's "t" test to test the hypothesis that the regression coefficient is equal to 0 at a significance level of 0.01, we find that we must reject the hypothesis. That is to say, at the 0.01 level of significance, the shape of the foreshore pebbles is a function of the infiltration-per-wave index.

The least square regression line of $\overline{c/\sqrt{ab}}$ for foreshore pebbles on Q^{-1} alone was found to be:

$$\overline{c/\sqrt{ab}} = -0.052\ Q^{-1} + 0.56. \qquad (2)$$

The correlation coefficient between the variables is -0.77, while the standard error of estimate of $\overline{c/\sqrt{ab}}$ on Q^{-1} is 0.076. A comparison of these statistics with the corresponding statistics for the regression line of $\overline{c/\sqrt{ab}}$ on $(QT)^{-1}$ indicates the importance of the incident wave period, T, in the regression of $\overline{c/\sqrt{ab}}$ of the foreshore pebbles.

The lower solid line in Figure 2 shows the regression equation, rewritten in terms of QT, plotted on the scatter diagram of the data points. This equation has the form:

$$QT(0.66 - \overline{c/\sqrt{ab}}) = 0.55. \qquad (3)$$

TABLE 1

REDUCED DATA FROM FIELD EXPERIMENTS

1 Location		2 $c/\sqrt{ab}$	3 σ	4 n	5 Q cm/sec	6 T sec	7 QT cm	8 $(QT)^{-1}_{cm^{-1}}$	9 Symbol
RP	F	0.60	0.12	93	1.00	5.0	5.0	0.20	x
	S	0.54	0.13	95					+
HM	F	0.49	0.13	73	0.69	7.0	4.8	0.21	x
	S	0.58	0.12	88					+
GH	F	0.46	0.15	70	0.86	4.5	3.9	0.26	x
	S	0.65	0.12	97					+
FB	F	0.46	0.13	76	0.81	4.3	3.5	0.29	x
	S	0.59	0.14	93					+
HH	F	0.56	0.13	86	0.85	3.8	3.2	0.31	x
	S	0.58	0.14	93					+
P3	F	0.45	0.13	61	0.32	9.2	2.9	0.34	x
	S	0.58	0.12	89					+
HC	F	0.48	0.14	84	0.82	3.3	2.7	0.37	x
	S	0.59	0.13	89					+
BP	F	0.45	0.13	71	1.14	2.3	2.6	0.38	x
	S	0.52	0.17	89					+
P2	F	0.40	0.14	79	0.20	10.6	2.1	0.48	x
	S	0.51	0.12	88					+
N3	F	0.18	0.03	2	0.20	6.0	1.2	0.83	x
	S	0.54	0.15	93					+
N2*	F	0.27	0.11	13	0.17	10.0	1.7	0.59	●
	S	0.67	0.12	14					◆
N1*	F	0.22	0.08	18	0.16	6.0	1.0	1.00	●
	S	0.55	0.14	14					◆

*The beaches N1 and N2 were sampled prior to the initiation of a standardized procedure. Beach slope varied considerably from the experimental $7^{\circ} \pm 30'$ and the values for the wave period were obtained from another source. The data from N1 and N2 are not included in the following calculations and are presented only for the sake of completeness.

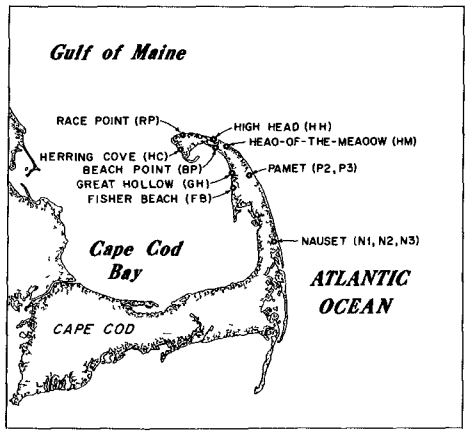

Fig. 1. Location of field experiment sites on Cape Cod, Massachusetts.

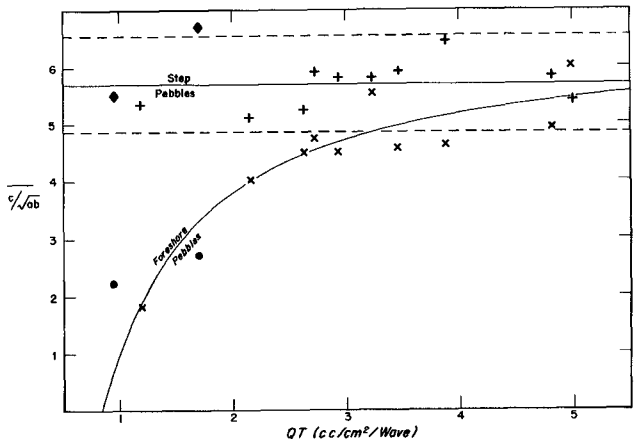

Fig. 2. Distributions of mean shapes of foreshore and step pebble samples with respect to mean values of infiltration-per-wave index of foreshore at time of sampling. Upper solid line and two dashed lines represent the mean of means and 95% confidence interval of means of step pebble samples. Lower solid line is least square regression line of best fit for foreshore pebble samples. Symbols explained in Table 1.

Step Pebble Samples

In Figure 2 the crosses and diamonds represent the values of the mean shapes of the step pebble samples, $\overline{c/\sqrt{ab}}$, plotted against the mean values of the corresponding infiltration-per-wave index, QT . The least square regression line of $\overline{c/\sqrt{ab}}$ on QT was found to be:

$$\overline{c/\sqrt{ab}} = 0.014\ QT + 0.52. \quad (4)$$

The correlation coefficient between the two sets of variables is 0.46, while the 95 per cent confidence limits for the correlation coefficient are -0.23 and 0.82. The standard error of the regression coefficient was found to be 0.011. The 95 per cent confidence limits of the regression coefficient are 0.014 ± 0.024, and the 99 per cent confidence limits of the regression coefficient are 0.014 ± 0.036. An application of Student's "t" test indicates that we cannot reject the hypothesis that the regression coefficient is equal to 0 at the 0.01 significance level.

Due to the lack of a significant correlation between the mean shapes of the step pebble samples and the values of the infiltration-per-wave index, the upper solid line of Figure 2 represents the mean shape of the total step pebble population, which is given by the mean of the means of the individual step pebble samples:

$$\overline{\overline{c/\sqrt{ab}}} = 0.57. \quad (5)$$

The dashed lines indicate the 95 per cent confidence interval of the step pebble means. Since the lower solid line represents the best estimate of the variation of the mean shape of the foreshore pebbles with respect to the beach infiltration-per-wave index, the figure indicates that the degree of shape sorting of pebbles on the foreshore of the sampled sandy, tidal beaches is dependent upon the period of the waves and the infiltration rate of the foreshore as expressed by the infiltration-per-wave index.

DISCUSSION

Table 2 gives the values of the correlation coefficients (r) calculated between pebble weight and pebble shape ($c/\sqrt{ab}$) for each of the twenty samples used in the foregoing analysis. The size of each sample (n) is also indicated. The low values of the correlation coefficients indicate that there is no relationship between the shape and the weight of the step pebbles. This is to be expected since the step pebbles represent the total, non-sorted pebble population. The correlation coefficients for the foreshore pebbles are also low (except for N3 which, since it consists of only two individuals, must give a value of 1.000). An application of Student's "t" test indicates that at the 5 per cent significance level the hypothesis that the population correlation coefficient is equal to zero, for any of the populations from which these samples were selected, cannot be rejected. On the other hand, the fact that the correlation is negative in every case suggests that in fact there is a slight decrease in the value of the shape factor with an increase in weight. However, since even in the case of the highest correlation, FB foreshore, the variation of the weight

explains less than 5 percent of total variation in shape, the relationship between the infiltration-per-wave index and the mean shape of the foreshore pebbles would not be appreciably affected by any variation in the proportion of pebble weights which might have occurred between the samples.

TABLE 2

COEFFICIENTS OF CORRELATION BETWEEN PEBBLE WEIGHT AND PEBBLE SHAPE

Sample		r	n	Sample		r	n
BP	F	-0.080	71	GH	F	-0.202	70
	S	0.232	89		S	0.282	97
HH	F	-0.001	86	HM	F	-0.186	73
	S	-0.051	93		S	-0.001	88
HC	F	-0.162	84	RP	F	-0.075	93
	S	-0.032	89		S	0.213	95
P2	F	-0.164	79	FB	F	-0.223	76
	S	0.019	88		S	0.117	93
N3	F	-1.000	2	P3	F	-0.152	61
	S	-0.012	93		S	-0.089	89

The shape of foreshore pebbles and therefore the ratio of backwash energy to swash energy, both dimensionless quantities, have been related to the inverse of the infiltration-per-wave index which has the dimension (L^{-1}) with the result that the constant, 0.55, of equations (1) and (3) must have the dimension (L). Recalling that the experiments were performed on beaches chosen with constant values for breaker height, breaker approach angle,and foreshore slope, let us now generalize this concept and consider the dynamics of the swash zone to depend upon the ratio of infiltration rate of water into the foreshore to the rate of supply of water by breakers. Consider: the infiltration rate to be proportional to the infiltration rate per unit area, Q , times the foreshore swash area; the foreshore swash area per unit length of shoreline to be given by the distance of the swash run-up; the swash run-up to be proportional to $H/\sin\theta$, where H is the breaker height and θ is forshore slope; and the breaker angle to reduce the expression by the amount, $\cos\phi$, where ϕ is the angle between the breaker crest and the shoreline. Thus:

$$\text{infiltration rate} \sim Q(H/\sin\theta)\cos\phi. \tag{6}$$

Assuming that the breaker volume per unit distance of shoreline is proportional to H^2 and again multiplying by $\cos\phi$ to account for breaker angle:

$$\text{supply rate} \sim H^2\cos\phi/T. \tag{7}$$

Dividing (6) by (7) and simplifying yields:

$$\frac{\text{infiltration rate}}{\text{supply rate}} \sim \frac{QT}{H\sin\theta} \tag{8}$$

It is interesting to note that the breaker angle, ϕ , does not appear in the final expression.

Such a ratio may be thought of as a coefficient of similarity for the swash zone, and variations in its value could possibly be related to

variations in beach stability. By maintaining constant values of H and Θ, and by making an estimate of Q from infiltrameter measurements, the results of the study of shape sorting of foreshore pebbles yield partial support for the validity of this coefficient. This is not to underestimate the gross simplifications implied by the above formulation, in particular, the difficulties of obtaining an accurate measure of Q and the unlikelihood in nature of constant values for T, H, and Θ; rather it is to suggest a possible relationship between some of the more important factors involved in the dynamics of the swash zone of beaches.

SUMMARY

Field experiments performed on predominantly sandy, tidal beaches indicate that the mean shape of the pebbles deposited on the foreshore during the falling tide depends upon both the foreshore infiltration rate and the incident wave period. If the mean shape of the foreshore pebbles is taken as an index of the ratio of the backwash energy to the swash energy, the results suggest that in the study of swash zone mechanics the amount of foreshore infiltration per wave be considered rather than the rate of foreshore infiltration alone.

ACKNOWLEDGMENTS

The studies described in this paper benefited from the use of the facilities of the University of Chicago and the Woods Hole Oceanographic Institution. The assistance of Professor Robert L. Miller of the University of Chicago and Professor John M. Zeigler of the University of Puerto Rico is gratefully acknowledged. Support was furnished in the form of a traineeship by the National Aeronautics and Space Administration.

REFERENCES

1. Bagnold, R.A., 1940, Beach formation by waves; some model-experiments in a wave tank: Jour. Inst. Civ. Eng., v. 15, n. 1, p. 27-52.

2. Kemp, P.H., 1963, A model study of the behaviour of beaches and groynes: Proc. Inst. Civ. Eng., v. 25, June, p. 207-217.

3. Kemp, P.H., and Adeyemo, M.D., 1968, Effect of backwash on wave asymmetry close to breakers: Proc. Eleventh Conf. Coastal Eng., London.

4, Flemming, N.C., 1964, Tank experiments on the sorting of beach material during cusp formation: Jour. Sed. Pet., v. 34, n. 1, p. 112-122.

5. Blenk, M. ,1960, Ein Beitrag zur morphometrischen Scotteranalyse: Z. Geomorphol., Band 4, p. 202-242.

6. Giese, G.S., 1966, Beach pebble movements and shape sorting: indices of swash zone mechanics: Unpub. Ph.D. Dissertation, Univ. of Chicago.

7. Strahler, A.N., 1966, Tidal cycle of changes in an equilibrium beach, Sandy Hook, New Jersey; Jour. Geol., v. 74, n. 3, p. 247-268.

8. Johnson, R.G., 1957, Experiments on the burial of shells: Jour. Geol., v. 65, n. 5, p. 527-535.

9. Smith, J.D., Unpublished manuscript, The orientations of Mya arenaria shells by tidal currents.

10. Emery, K.O., and Foster, J.F., 1948, Water tables in marine beaches: Jour. Marine Res., v. 7, n. 3, p. 644-654.

11. Spencer, D.W., 1966, Factor Analysis: Woods Hole Oceanographic Institution Ref. No. 66-39, 80 p. Unpublished manuscript.

CHAPTER 26

LITTORAL DRIFT AS FUNCTION OF WAVES AND CURRENT

E.W. BIJKER
Delft Hydraulic Laboratory, Delft, Netherlands

1. SYNOPSIS

For the computation of littoral drift due to waves hitting a coast obliquely, most formulae are based upon the assumption that this longshore transport is some function of the energy flux of the waves towards the coast. For the actual computation the component of this flux parallel to the coast is introduced. Most of the available prototype data are incorporated in the formula of the U.S. Army Coastal Engineering Research Center (ref. 4 and 1). In this formula no reference is made to the grain size and the slopes of beach and foreshore. The explanation for the fact that nevertheless reasonable results are obtained is probably owing to the fact that variation of grain size and beach slope for sandy beaches is not so very great. A more serious disadvantage is, however, that it is not possible to take into account the influence of a possible longshore current which is not generated by the wave motion, such as for instance tidal currents.

In this paper an attempt is made to compute the littoral drift, starting from the longshore current velocity as it is generated by the waves or as it may originate from other causes (ref. 4). For the actual computation of the bed load transport a normal bed load transport formula is used, in which, however, according to the method developed by the author in earlier studies, the bed shear is increased as a result of the wave motion (ref. 2). From the tests briefly described in the present paper it becomes clear that the transport may be treated indeed as a function of the longshore current, even when this current has a direction opposite to that of the component of the wave propagation parallel to the coast.

Finally, a computation procedure for littoral drift is presented in which also the transport of suspended load is taken into account, and an example is given of the computation of the littoral drift along Ivory Coast near Abidjan. The result of this computation corresponds rather well to the data known from the prototype.

2. DERIVATION OF BED LOAD TRANSPORTATION FORMULAE AND DESCRIPTION OF TESTS

Most bed load formulae may be written in the form

$$\frac{S}{f(D^{3/2}g^{1/2}\Delta)} = f\left(\frac{\Delta D}{\mu h I}\right) \qquad (1)$$

where Δ = relative apparent density, D = grain size, h = waterdepth, I = energy gradient, μ = ripple coefficient and g = acceleration of gravity.

Frijlink (ref. 6) suggested, starting from the formula of Kalinske, to write formula (1) in the following way:

$$\frac{S}{D(\mu\tau/\rho)^{1/2}} = b\, e^{a\frac{\Delta D\rho g}{\mu\tau}} \qquad (2)$$

where C = resistance coefficient, and τ = bed shear = $\rho g h I = \rho g\, v^2/C^2$ (ref. 6).

In an earlier paper the present author called the first term the transport parameter and the exponent of e in the second term the stirring parameter (ref. 2). For the bed shear in the stirring parameter, the mean resultant bed shear of the combination of waves and current will be introduced. This shear is denoted by τ_r in figure 1. This resultant bed shear is hold responsible for the stirring up of the material. Once the material is stirred up it will be transported by the normal current. Hence, in the transport parameter, the value of the bed shear τ_c, resulting from the current only, is introduced. As demonstrated by the present author in ref. 2,

$$\tau_r = \left[1 + \frac{1}{2}\left(\xi \frac{u_o}{v}\right)^2\right] \tau_c \quad , \qquad (3)$$

in which u_o = amplitude of orbital velocity near the bed, v = mean current velocity, and ξ is a coefficient which has been determined theoretically and emperically and which has a value $\xi = 0.45\kappa C/g^{1/2} = 0.0575\, C$.

In figure 2 all data are represented, viz.: data for current only, for current and waves combined with wave crests parallel to the current, and for current and ditto, with wave crests making an angle of 15° with the current.

The regression line for all data with regression of $\log S/D(\tau_c/\rho)^{1/2}$ on $\Delta D\rho g/\mu\tau_r$ is

$$S = 0.22\, D(\tau_c/\rho)^{1/2}\, e^{-0.19\,\frac{\Delta D\rho g}{\mu\tau_r}} \qquad (4)$$

and the regression line for all data with regression of $\Delta D\rho g/\mu\tau_r$ on $\log S/D(\tau_c/\rho)^{1/2}$ is:

$$S = 1.95\, D(\tau_c/\rho)^{1/2}\, e^{-0.33\,\frac{\Delta D\rho g}{\mu\tau_r}} \qquad (5)$$

In the original formula of Frijlink the coefficient in the exponent of e was 0.27 (ref. 6). With this exponent the formula becomes

$$S = 0.74\, D(\tau_c/\rho)^{1/2}\, e^{-0.27\,\frac{\Delta D\rho g}{\mu\tau_r}} \qquad (6)$$

The fact that the coefficient 0.74 is much lower that the coefficient in Frijlink's formula, which was 5, has most likely to be attributed to the fact that Frijlink discussed prototype data, whilst the data used in the present paper are obtained from a relatively narrow sand trap, which does not catch the whole transport (ref. 2).

After the completion of these tests, further tests were performed, viz. with waves the crests of which make in still water an angle of 25° with the direction of the current, having a component in the direction of the current and having a component against the direction of the current (ref. 2). Due to streamrefraction, the angle becomes in these two cases respectively 27° to 28° and 22° to 23°.

Using the coefficient 0.27 in the exponent of e, the value of b has been calculated for the various cases. The sand has been captured in a sand trap which has been divided in several compartiments. The sand trap had a total length of 0.93 m measured in the direction of the current. The computations have been carried out for the material captured in the complete trap (wide trap) and in the foremost 0.15 m (narrow trap). The results are represented in table I.

Table I Values of b

	current ←	current ← and waves ↙ $\varphi = 28^{\circ}$	current →	current → and waves ↙ $\varphi = 22^{\circ}$
Narrow trap	0.4 ± 0.2	0.4 ± 0.2	0.2 ± 0.1	0.2 ± 0.1
Wide trap	1.3 ± 1.0	1.1 ± 0.8	1.0 ± 0.6	0.6 ± 0.2

The following test results were obtained.

(i) The scatter in the results with the wide trap is very great. The reason is most likely that, in the lower layers of the flow, part of the material is moved in suspension (saltation). It is quite to be expected that a great variation will occur in the quantities of this portion of the material caught in the trap. This is supported by the fact that the values of b, computed with the quantities measured in the wide trap with waves and current combined, are slightly smaller than for current only. This may be explained by the fact that the turbulence for the combination of waves and current is greater than for current only, so that a smaller part of the total quantity of material transported will be trapped.

(ii) The quantities transported in the two different directions for current only, differ significantly, assuming that the values of b, as calculated by this procedure, are distributed like stochastic variables around their mean values. The reason may attributed to the

fact that, although sand of the same diameter was applied, the packing of the sand at both sides of the sand trap was different. A different explanation may be that, although the mean velocity was equal, the upstream conditions for the two current directions were unequal. This results in a different vertical velocity distribution and hence, in a different bed shear. Although from visual judgement, the ripple patterns and heights for both situations were equal, a slight change in ripple coefficient might also cause this difference in the values of b. Since it was not possible to predict the difference in the ripple coefficient beforehand, it has not been introduced in the calculations.

(iii) For both wide and narrow sand traps the values of b for current only and for the combination of current and waves, are not significantly different. Since b is computed with formula (6) which takes into account the increased bed shear by the wave motion, the conclusion may be drawn, that the transport of material is increased by the waves, independently of the fact whether the waves are propagating obliquely with the current, or against the current.

The main conclusions, drawn from the tests described above and discussed in full in the author's paper "Some considerations about scales of coastal models with movable bed" (ref. 2) are the following:

(1) The transport of a combination of waves and current may be written as:

$$S = b.D \frac{v}{C} g^{1/2} e^{-0.27 \frac{\Delta D C^2}{\mu v^2 (1 + \frac{1}{2}(\xi \frac{u_o}{v})^2)}} \qquad (7)$$

where $\xi = 0.45 \sqrt{\kappa}\, C/g^{1/2} = 0.0575\, C$, or:

$$S = b.D(\tau_c/\rho)^{1/2} e^{-0.27 \frac{\Delta D \rho g}{\mu \tau_r}} \qquad (8)$$

(ii) The principal difference of this equation with the original one of Kalinske-Frijlink is, that the ripple factor is operative only in the stirring parameter, and not in the transport parameter. Keeping in mind the definition of the ripple factor, as defining that part of the bed shear which is not used to overcome bedform resistance, it is physically more justified to introduce this factor only in the stirring parameter. Once the material is stirred up, it is moved with the current velocity. Hence, a ripple factor seems here to have less sense.

(iii) A rather important variation may occur in the factor b. For the time being, the value of 5 seems the most appropriate.

(iv) Another source of uncertainties is the value of the resistance coefficient C. The advantage of the described procedure is, however, that the origin of the uncertainties becomes visible.

3. COMPUTATION OF LITTORAL DRIFT

Using the formula derived in paragraph 2 in combination with a formula for the longshore current, it should be possible to compute the littoral drift generated by a wave motion approaching the coast obliquely.

For the longshore current the equation as given by Eagleson is applied:

$$v_L^2 = \frac{3}{8}\left(\frac{g\, H_b^2\, m_b}{h_b}\right) \frac{\sin \alpha \sin \varphi_b \sin 2\varphi_b}{f} - \qquad (9)$$

where v_L = the value of the longshore current velocity, H_b = the breaker height, h_b = the breaker depth, m_b = ratio of group velocity c_g to wave celerity $= \frac{1}{2}\left[1 + \frac{4\pi h/L}{\sin h(4\pi h/L)}\right]$, α = beach slope, φ_b = angle between breaker crests and coast line and f = Darcy Weisbach resistance coefficient $= 8g/C^2$ (ref. 4).

The study of Eagleson does not give values for the distance from the coast over which this current occurs, particularly not outside the breakerzone. For a first approximation the current will be assumed invariable with the distance from the coast. Due to the increasing depth, the transport will presumably drop at some distance from the coast to a negligible value.

Since the bed load transport should be calculated with formula (7) and (8), using the ratio between orbital velocity and main current velocity, the values of the orbital velocity in the breaker region have to be evaluated. From tests by Iversen, which are summarized in table II, it becomes evident that orbital velocities computed with the first-order theory from waves breaking according to the solitary wave theory, are in reasonable agreement with actual measured orbital velocities at the point of breaking (ref. 7). According to the solitary wave theory $h_b = 0.45\ (H_o\ T)^{2/3}$, and with these values and the tables of Tech. Rep. 4 of C.E.R.C. the data of table II have been obtained (ref. 1).

Table II

				breaker depth calculated from solitary wave theory		normal theory			tests
Beach slope	T_o sec	L_o m	H_o m	$H_o T$ m s	h_b m	$\frac{h_b}{L_o}$	H_b m	u_o m/s	u_o m/s
1/10	1.51	3.56	.073	.11	.103	.0290	.082	.38	.30
1/10	1.98	6.10	.043	.085	.087	.0142	.057	.29	.39
1/50	1.74	4.72	.061	.106	.101	.0214	.074	.35	.33
1/50	2.65	10.95	.071	.188	.148	.0135	.095	.38	.32

The above figures show a mean deviation between calculated and observed values of 20% to both sides. In view of the inevitable inaccuracy of the tests of Iversen, the author accepted to use the calculated values of the orbital velocity for the computation of u_o/v, for the calculation of ξ.

Since expecially in the breaker zone the transport of suspended load will be considerable, this transport will also be calculated. For this calculation the procedure of Einstein will be applied (ref. 5). One of the difficult points in this computation procedure is the determination of the concentration of suspended load immediately above the bed. The best procedure seems to be to take this concentration equal to that of the bed load transport, assuming an even distribution of this transport over half the ripple height. According to unpublished work of van Breugel, the fictitious bed may be assumed to be at half the ripple height (ref. 3). Since the fictitious roughness is equal to half the ripple height, the suspended load concentration is derived from the bed load by assuming that this bed load will be transported in a layer immediately above the bed with a thickness equal to that of the fictitious bed roughness.

The mean velocity in this layer is, with the well-known assumption that $v(y) = (v_* / \kappa) \ln 33\, y/r$;

$$\bar{v}_{o-r} = \frac{\int_0^{er/33} v(y)dy + 1/2\, v_{er/33}\, er/33}{r} = \frac{2.54\, v_*}{\kappa} = 6.35\, v_* \qquad (10)$$

The expression for the suspended load transport is,

$$S_s = \int_a^h c(y)\, \bar{v}(y)\, dy \qquad (11)$$

The concentration c(y) may be written as:

$$\frac{c(y)}{c_a} = \left(\frac{h - y}{y} \cdot \frac{a}{h - a}\right)^z \qquad (12)$$

in which

$$z = w/\kappa v_* \qquad (13)$$

in which w = fall velocity of the grains. In the case of a combination of current with waves for v_* the increased v_*' due to the wave motion should be introduced, which has the value $v_*' = \left[1 + \frac{1}{2}(\xi \frac{u_o}{v})^2\right] v_*$.

In this equation c_a is the concentration of suspended load immediately above the bed and this may be written according to the reasoning given above as

$$c_a = S_b / 6.35\, v_*\, r\ , \qquad (14)$$

under the assumption that the suspended load is transported with the velocity of the fluid.

The formula for the total transport of suspended load according to Einstein may be written now as follows:

$$S_s = 1.83\, S_b \left[I_1 \ln 33\, h/r + I_2 \right] \qquad (15)$$

with: $$I_1 = 0.216 \frac{(a/h)^{z-1}}{(1 - a/h)^z} \int_{a/h}^{1} \left(\frac{1 - y}{y}\right)^z \, dz \qquad (16)$$

and $$I_2 = 0.216 \frac{(a/h)^{z-1}}{(1 - a/h)^z} \int_{a/h}^{1} \left(\frac{1 - y}{y}\right)^z \ln y \, dy \qquad (17)$$

In his paper, Einstein suggests that $S_b = 11.6\, v_* \, c_a \, a$, where "a" is a layer of 2 grain diameters. Since, according to the author's opinion, this set up is not in complete agreement with the physical phenomenon of bed load transport over a bed with ripples or dunes and moreover, the factor 11.6 is based upon one limited series of measurements only, he suggests the approach discussed on page 9 leading to formula (14).

4. COMPUTATION OF LITTORAL DRIFT ALONG THE COAST OF IVORY COAST

According to the available estimates, the littoral drift along Ivory Coast is 10^6 m^3/year = 0.032 m^3/s. If the wave period is assumed to be 12 s and, the wave height in deep water H_o is assumed to be 1.6 m, with the angle φ_o between wave crests in deep water and the coastline equal to 13^o, the littoral drift as calculated by the formula of the C.E.R.C. is just about 0.032 m^3/s (ref. 1). For this computation the version of this formula as presented by the author is used, viz.:

$$S = 1.4\ 10^{-2}\ H_o\ c_o\ K^2\ \sin\varphi_b\ \cos\varphi_b \qquad (18)$$

in which c_o = wave velocity in deep water, K = refraction coefficient = square root of ratio of distances between wave orthogonals in deep water and at the breaker region (ref. 2).

The longshore current velocity according to Eagleson has an equilibrium value as given by equation (9) (ref. 4).

For the coast of Ivory Coast the following data hold:

$$\alpha = 1/14 = 4^o, \quad \varphi_b = 4\tfrac{1}{2}^o \quad (\varphi_o = 13^o).$$

$$D_{50} = 0.5 \text{ mm}, \quad D_{90} = 0.9 \text{ mm} \quad \Delta D = 1.65\ \ 5\ 10^{-4} = 8.25\ 10^{-4} \text{ m}$$

$$w = 0.08 \text{ m/s}, \quad v_*^{\ 1} = v_* \sqrt{1 + 1\tfrac{1}{2}(\xi \frac{u_o}{v})^2}$$

The resistance coefficient of Chezy C = 42 m$^{1/2}$/s, which corresponds to a fictitious apparent bottom roughness of 0.17 m at the breaker depth of 3.2 m. This results in $f = 8g/C^2 = 0.045$.

$$m_b = \tfrac{1}{2}\left(1 + \frac{4\pi h_b/L_b}{\sinh 4\pi h_b/L_b}\right) = 0.97 \qquad (19)$$

From this follows:

$$v_L^2 = \frac{3}{8}\left(\frac{g\ 2.5^2\ 0.97}{3.2}\right)\frac{0.07\ \ 0.078\ \ 0.156}{0.045} = 13.2\ 10^{-2}\ m^2/s^2 -$$

$$v_L = 0.36\ m/s.$$

With these data the following computations will be performed in the tables III through VII.

Table III $v_e = 0.36$ m/s

h	C	ξ	$C_{d_{90}}$	μ	C^2	$\frac{v}{C}\sqrt{g} = v_*$	$5\ Dv_*$ / $5\ D\frac{v}{C}\sqrt{g}$
1	42	2.42	74	0.43	1760	$2.7\ 10^{-2}$	$67\ 10^{-6}$
3	42	2.42	83	0.36	1760	$2.7\ 10^{-2}$	$67\ 10^{-6}$
5	46	2.65	87	0.38	2110	$2.45\ 10^{-2}$	$61\ 10^{-6}$
7	49	2.82	90	0.40	2400	$2.3\ 10^{-2}$	$57.5\ 10^{-6}$
9	51	2.94	92	0.41	2600	$2.2\ 10^{-2}$	$55\ 10^{-6}$
11	52	3.00	93	0.42	2700	$2.15\ 10^{-2}$	$54\ 10^{-6}$
13	54	3.11	95	0.43	2910	$2.1\ 10^{-2}$	$52\ 10^{-6}$
15	55	3.17	96	0.43	3020	$2.05\ 10^{-2}$	$51\ 10^{-6}$
17	56	3.22	97	0.44	3120	$2.0\ 10^{-2}$	$50\ 10^{-6}$

For different values of the depth, h, the resistance coefficient C, the coefficient ξ, the ripple coefficient and the parameter $5\ Dv_* = 5\ D\ \sqrt{g}\ v/C$ are computed.

For the above mentioned depths, the ratios of wave heights at this depth to deep water wave height, if not influence by refraction, H'/H_o are computed and, via the refraction coefficient, the actually occurring wave height H. From this value the amplitude of the orbital velocity at the bottom u_o and the ratio u_o/v is computed.

Table IV

h	$\frac{h}{L_o}$	$\frac{H'}{H_o}$	K	$K\frac{H'}{H_o}$	H	$\sinh \frac{2\pi h}{L}$	u_o	$\frac{u_o}{v}$
1	.0045	1.74	.99	1.72	0.78	.170	1.20	3.33
3	.0134	1.34	.99	1.33	2.13	.30	1.86	5.15
5	.0222	1.20	.99	1.19	1.90	.395	1.26	3.5
7	.0312	1.12	.99	1.11	1.77	.473	0.98	2.72
9	.040	1.06	.99	1.05	1.68	.55	0.80	2.22
11	.049	1.02	.99	1.01	1.62	.62	0.68	1.89
13	.058	1.00	.99	0.99	1.58	.69	0.60	1.67
15	.067	0.98	.99	0.97	1.55	.76	0.54	1.50
17	.076	0.96	.99	0.95	1.52	.82	0.49	1.36

Table V

h	$(\xi \frac{u_o}{v})^2$	$1 + \frac{1}{2}(\xi \frac{u_o}{v})^2$	v^2	$1 + \frac{1}{2}(\xi \frac{u_o}{v})^2$	$\frac{0.27\ \Delta DC^2}{\mu v^2 \left[1+\frac{1}{2}(\xi\frac{u_o}{v})^2\right]}$	$e^{-\frac{}{}}$	S_b · 10^{-6} m^2/s
1	65	33	1.84	0.21	0.81		54
3	156	79	3.69	0.11	0.90		60
5	86	44	2.17	0.22	0.80		49
7	74	38	1.97	0.27	0.76		44
9	49	26	1.38	0.42	0.66		36
11	36	19	1.03	0.58	0.56		30
13	27	14	0.78	0.83	0.44		23
15	22	12	0.61	1.10	0.33		17
17	19	11	0.63	1.10	0.33		16

From the results of tables III and IV the factor $1 + \frac{1}{2}(\xi\ u_o/v)^2$, by which the bed shear of the current is increased due to the wave motion, is computed and with these results the stirring factor, and finally the total bed load transport S_b. These transports are computed for belts, parallel to the coast, ranging in width from 0-2, 2-4, 4-6 m etc, the mean depths of these belts, viz.: 1, 3, 5 m, etc. respectively.

The values of the transports, as given in this table, are the transports per unit of width. The total transport in each belt can be obtained by multiplying the transport per unit of width with the width of the belt, that is 2 . 14 = 28 m, since the beach slope is 1:14.

Table VI

h	$v_* = v_* \left[1+\frac{1}{2}(\xi\frac{u_o}{v})^2\right]$	$\frac{w}{0.4\, v_*}$	$v_{0.17} = 8.75\, v_*$	$c_a = \frac{S_b}{0.17\, \bar{v}_{0-0.17}}$		$\bar{v}_{0-0.17} = \frac{2.54}{\kappa} v_* = 6.35\, v_*$
1	0.155	1.30	0.235	1.9	10^{-3}	0.17
3	0.24	0.84	0.235	2.1	10^{-3}	0.17
5	0.16	1.25	0.215	1.9	10^{-3}	0.155
7	0.14	1.43	0.20	1.8	10^{-3}	0.145
9	0.11	1.82	0.19	1.5	10^{-3}	0.14
11	0.095	2.10	0.19	1.3	10^{-3}	0.135
13	0.08	2.5	0.185	1.0	10^{-3}	0.13
15	0.07	2.86	0.18	0.8	10^{-3}	0.13
17	0.065	3.07	0.175	0.8	10^{-3}	0.125

The necessary values for the computation of the suspended load transport are calculated.

Table VII

h	A = a/h	$\ln \frac{33h}{r}$	I_1	$I_1 \ln \frac{33h}{r}$	$-I_2$	$I_1 \ln \frac{33h}{r} + I_2$	$1+1.83(I_1 \ln \frac{33h}{r} + I_2)$	$S_{b+s}\ 10^{-6}$ m^2/s	$S_{tot}\ 10^{-3}$ m^3/s
1	.17	5.26	.18	0.95	0.23	0.72	2.32	125	3.5
3	.057	6.36	.55	3.50	0.90	2.60	5.75	345	13.2
5	.034	6.87	.38	2.61	0.84	1.77	4.05	198	19.1
7	.024	7.21	.33	2.38	0.83	1.55	3.85	169	22.4
9	.019	7.46	.22	1.64	0.68	0.96	2.77	100	26.3
11	.016	7.67	.18	1.38	0.60	0.78	2.43	73	28.3
13	.013	7.84	.14	1.10	0.51	0.59	2.08	48	29.5
15	.011	7.98	.11	0.88	0.45	0.43	1.79	30	30.5
17	.010	8.1	.10	0.81	0.42	0.39	1.71	27	31.3

Table VIIa a = 0.1 m

h	A = a/h	$\ln \frac{33h}{r}$	I_1	$I_1 \ln \frac{33h}{r}$	$-I_2$	$I_1 \ln \frac{33h}{r} + I_2$	$1+1.83(I_1 \ln \frac{33h}{r} + I_2)$	$S_{b+s}\ 10^{-6}$ m^2/s	$S_{tot}\ 10^{-3}$ m^3/s
1	0.1	5.80	.24	1.39	.38	1.01	2.84	170	4.7
3	0.033	7.53	.69	5.20	1.30	3.90	8.12	511	19.1
5	0.02	7.46	.44	3.28	1.10	2.18	5.0	290	27.3
7	0.014	7.75	.32	2.48	.96	1.52	3.77	196	33.9
9	0.011	8.00	.22	1.76	.80	0.96	2.76	127	36.1
11	0.009	8.20	.17	1.39	.67	0.72	2.32	93	39
13	0.008	8.37	.13	1.09	.54	0.55	2.0	68	40.6
15	0.007	8.50	.12	1.02	.53	0.49	1.9	61	42.5
17	0.006	8.63	.11	0.95	.51	0.44	1.8	52	44.0

Table IIIa $v_L^2 = \frac{3}{8}\left(\frac{g\ 2.5^2\ 0.97}{3.2}\right)\left(\frac{0.07\quad 0.078\quad 0.156}{0.019}\right) = 31{,}2\ \ 10^{-2}\ m^2/s^2$

$f = 8g/C^2 = 0.019$ $\qquad v_L = 0.56$ m/s

h	C	ξ	$C_{d_{90}}$	μ	C^2	$v_* = (v/C)\sqrt{g}$	$5\ D\ V_*\ 10^{-6}$
1	64	3.68	74	0.81	4100	$2.7\ 10^{-2}$	67
3	64	3.68	83	0.68	4100	$2.7\ 10^{-2}$	67
5	68	3.91	87	0.69	4630	$2.6\ 10^{-2}$	65
7	71	4.08	90	0.70	5020	$2.5\ 10^{-2}$	63
9	73	4.20	92	0.71	5310	$2.4\ 10^{-2}$	60
11	74	4.25	93	0.71	5490	$2.35\ 10^{-2}$	59
13	76	4.36	95	0.72	5790	$2.3\ 10^{-2}$	58
15	77	4.43	96	0.72	5920	$2.3\ 10^{-2}$	57
17	78	4.49	97	0.72	6080	$2.25\ 10^{-2}$	56

Table IVa

h	$\frac{h}{L_o}$	$\frac{H'}{H_o}$	K	$K\frac{H'}{H_o}$	H	$\sinh\frac{2\pi h}{L}$	u_o	$\frac{u_o}{v}$
1	.0045	1.74	.99	1.72	0.78	.170	1.20	2.15
3	.0134	1.34	.99	1.33	2.13	.30	1.86	3.31
5	.0222	1.20	.99	1.19	1.90	.395	1.26	2.25
7	.0312	1.12	.99	1.11	1.77	.473	0.98	1.75
9	.040	1.06	.99	1.05	1.68	.55	0.80	1.43
11	.049	1.02	.99	1.01	1.62	.62	0.68	1.22
13	.058	1.00	.99	0.99	1.58	.69	0.60	1.06
15	.067	0.98	.99	0.97	1.55	.76	0.54	0.96
17	.076	0.96	.99	0.95	1.52	.82	0.49	0.87

Table Va

h	$(\xi \frac{u_o}{v})^2$	$1+\frac{1}{2}(\xi \frac{u_o}{v})^2$	$\mu v^2 \left[1+\frac{1}{2}(\xi \frac{u_o}{v})^2\right]$	$\frac{0.27\ \Delta DC^2}{\mu v^2 \left[1+\frac{1}{2}(\xi \frac{u_o}{v})^2\right]}$	$e^{-\gamma}$	$S_b\ 10^{-6}$ m^2/s
1	63	32	8.15	0.11	0.90	60
3	149	75	16.00	0.06	0.94	63
5	77	39	8.49	0.12	0.89	58
7	51	26	5.73	0.20	0.82	52
9	36	19	4.25	0.28	0.76	46
11	27	14	3.13	0.39	0.68	40
13	21	11	2.49	0.52	0.59	34
15	18	10	2.26	0.58	0.56	32
17	15	9	2.04	0.66	0.52	29

Table VIa

h	v_*'	$\frac{w}{0.4\ v_*'}$	$v_{0.17} = 8.75\ v_*$	$c_a = S_b/0.17\ \bar{v}_{0-0.17}$	$\bar{v}_{0-0.17} = \frac{2.54}{\kappa} v_* = 6.35\ v_*$
1	0.15	1.33	0.235	$2.1\ 10^{-3}$	0.17
3	0.23	0.87	0.235	$2.2\ 10^{-3}$	0.17
5	0.16	1.25	0.230	$2.1\ 10^{-3}$	0.165
7	0.13	1.54	0.22	$1.9\ 10^{-3}$	0.16
9	0.105	1.90	0.24	$1.8\ 10^{-3}$	0.15
11	0.09	2.22	0.205	$1.6\ 10^{-3}$	0.15
13	0.076	2.64	0.20	$1.4\ 10^{-3}$	0.145
15	0.073	2.74	0.20	$1.3\ 10^{-3}$	0.145
17	0.0675	2.95	0.195	$1.2\ 10^{-3}$	0.14

Following the procedure described in ref. 5 the total transport, being the sum of suspended load and bed load transport, is computed, using the slightly modified formula (15), viz.:

$$S_{b+s} = S_b(1 + 1.83\left[I_1 \ln 33h/r + I_2\right]) \qquad (20)$$

These transports are computed for the various belts. Finally, also the integrated total transport for belts from 0-2, 0-4, 0-6, etc. indicated by S_{tot}, are given. From these data it is clear indeed that the total littoral drift does not increase very much when the depth to be taken into consideration is greater than some 11 m. If it is assumed that the longshore current velocity outside the breaker zone decreases rapidly, the total transport could be obtained by taking into account only the values upto the 6 m depth contour. The total transport is in this case 0,019m^3/s.

In order to study the influence of the assumed bed roughness on the results, the same computations have also been executed for a roughness of 0.1 m. The resistance coefficient C at the breaker depth of 3 m is in this case 64 $m^{1/2}/s$. From this follows for the longshore velocity, according to Eagleson, the value v_L = 0.56 m/s. The results are given in tables IIIa through VIIa. The total littoral drift is in this case 0.044 m^2/s which does not differ very much from the value of 0.032 obtained with a bed roughness of 0.17 m. The total transport within the 6 m depth contour is in this case 0.027 m^3/s.

From this result the conclusion may be drawn that, although the total transport is of course influenced by the assumed bed roughness, uncertainties in this value do not invoke too great complications.

DISCUSSION

The method of computation of littoral drift discussed in this paper is based upon two basic assumptions, viz.:

(i) The longshore current velocity, resulting from the waves approaching coast obliquely, should be calculated. For the time being the formula of Eagleson is used. In this formula no velocity gradient perpendicular on the coast line is given, nor a width of the belt over which this current does occur. From the results it appears that this is perhaps not a very serious drawback since the transport of material decreases rather quickly with increasing depth, hence with the distance from the shore. It may be expected, however, that for these reasons the values of the transports are too high. The approach of Svasek, who relates the littoral drift to the energy loss of the waves approaching the coast, may be useful also for determining the longshore current.

(ii) Starting from the longshore current, and taking into account the effect of the wave motion on the bed shear due to this current, the littoral drift is calculated. For this calculation it is necessary to take also the suspended load into account, since this will be normally rather high under these conditions. This introduces another point of inaccuracy into the results as the relationship between suspended load and bed load is still rather vague.

The possible advantage of the present procedure over the existing littoral drift formulae is, however, that this approach shows more clearly the origins of possible inaccuracies in the results. Further study may, moreover, solve the unknown points.

A second advantage is the fact that with this procedure it is also possible to take into account a longshore current that is not generated by the waves.

REFERENCES

1. ANONYMUS
Shore protection planning and design.
U.S. Army Coastal Engg. Res. Center, Tech. Rep. 4.

2. BIJKER, E.W.
Some considerations about scales for coastal models with movable bed.
Publ. no 50 of the Delft Hydraulics Laboratory, 1967.

3. van BREUGEL, J.W.
Metingen in de grenslaagstroming langs een geribbelde wand.
Technological Univ. Delft. April 1963.

4. EAGLESON, P.
Theoretical study of longshore currents on a plane beach.
M.I.T., Dep. of Civ. Engg. Hydr. Lab., Rep. no 82, 1965.

5. EINSTEIN, H.A.
The bed load function for sediment transportation in open channel flow.
U.S. Dep. of Agr., Tech. Bull. no 1026, 1950.

6. FRIJLINK, H.C.
Discussion des formules de debit solide de Kalinske, Einstein et Meyer-Peter et Mueller compte tenue des mesures recentes de transport dans les rivieres Neerlandaises.

7. IVERSEN, H.W.
Laboratory study of breakers. Syposium on gravity waves.
Nat. Bur. of Standards, circ 521 nov. 1952, pp 9 - 32.

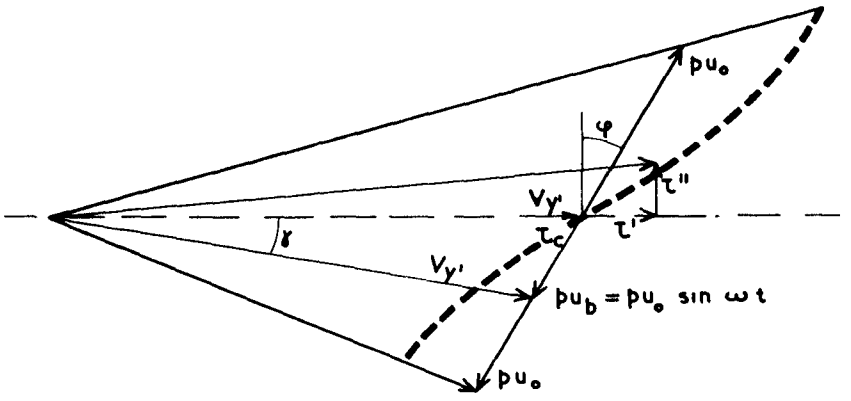
ρu_o
φ
τ''
$V_{y'}$
τ'
τ_c
γ
$V_{y'}$
$\rho u_b = \rho u_o \sin \omega t$
ρu_o

FIG. 1

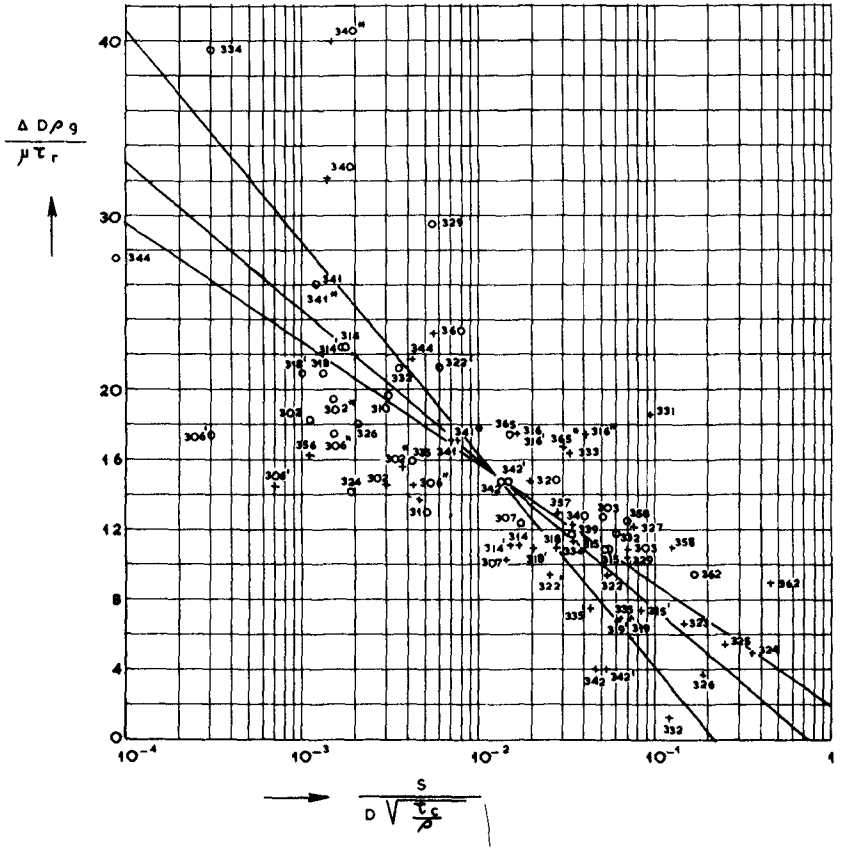
$\frac{\Delta D \rho g}{\mu \tau_r}$
40
30
20
16
12
8
4
0
10^{-4}
10^{-3}
10^{-2}
10^{-1}
1
$\frac{S}{D\sqrt{\frac{\tau_c}{\rho}}}$

FIG. 2

CHAPTER 27

MEASUREMENT OF COASTAL CURRENTS

J. M. Zeigler
Department of Marine Sciences
University of Puerto Rico
Mayagüez, Puerto Rico

and

H. J. Tasha
Provincetown, Massachusetts

Abstract

Getting a drift buoy into and over the surf zone in rough weather has always been a problem. A cheap, cold-propellant rocket launcher using either compressed air from aqua-lung bottles or liquid carbon dioxide is admirably suited for hurling drift bottles to ranges of over 1,000 feet. This launcher weighs less than one hundred pounds and can be easily transported to places of difficult access such as cliffed or reefy coasts. The float package can be modified to include mid-depth drogues if that is desired. An example of work done by a single field operator illustrates the versatility of this technique.

Naval Mark II flares are useful for current tracing because they are easily obtained and can be set in arrays from aircraft. As they burn, however, they change their freeboard and are therefore more subject to wind drift than when they are lower in the water. Mark II flares were calibrated for wind drift with results given.

A wind velocity profile between 5/8 inches and 5 inches above the water surface was obtained from floating arrays of flares with the results given.

In their search for better ways to measure currents in or near the surf zone, the writers have developed improvements in some old methods, namely, methods which measure the rate of drift of floating objects.

The present work reports on a new technique which was developed wherein drift bottles were fired into the sea

from a cold-propellant rocket launcher. The bottles, properly trimmed to float with less than an inch of neck exposed, were then tracked for a known time by theodolite. By this means one could measure the velocity of surface currents over a spectrum of sea states which otherwise would be too rough to work in.

Furthermore, the technique can be used especially well on rugged, cliffed or remote coasts which are awkward to reach. The writers consider this technique especially well-suited for reconnaissance.

The launcher

The rocket launcher is manufactured by Texaco Research Corp.; the system is named the Cricket. The launcher consists of an aluminum barrel 8 feet long that fits into a console in which a series of valves controls the pressure of carbon dioxide to be released into the base of the tube. This blast of carbon dioxide, up to 400 p.s.i., is in reality a booster charge used to hurl the rocket clear of the tube. The writers used compressed air from aqua-lung bottles instead of carbon dioxide because it was cheaper and more readily available at our field site. In this work we did not use the rockets but only the launcher and its booster much like a mortar or muzzle-loading cannon. A newspaper stuffed down the muzzle acted as wadding; the drift bottle rammed on top of it completed the charge. After some practice an operator could drop his bottle quite accurately at ranges up to 1300 or 1400 feet, which probably could be increased. The process of loading and firing took only two or three minutes.

There is no reason why the package fired cannot be modified to hold a mid-depth drogue as well as a surface drifter, thereby making it possible to take measurements of the current profile.

The launcher is portable, weighing only 90 pounds, easily set up, safe to use, store and transport, and cheap to operate. We have on one occasion had three drifters operational simultaneously. The number can be whatever the field party can handle without confusion. Weak points in the operation are loss of visibility in fog and rain, loss of range in strong winds, increasing loss of drifters as sea state becomes more frothy, and the requirement that the theodolite be of sufficient elevation above the sea that vertical angles can be measured easily.

The writers used this system as part of a program designed to separate wind-driven, wave-driven and tidal-driven components of the nearshore currents. Figure 1

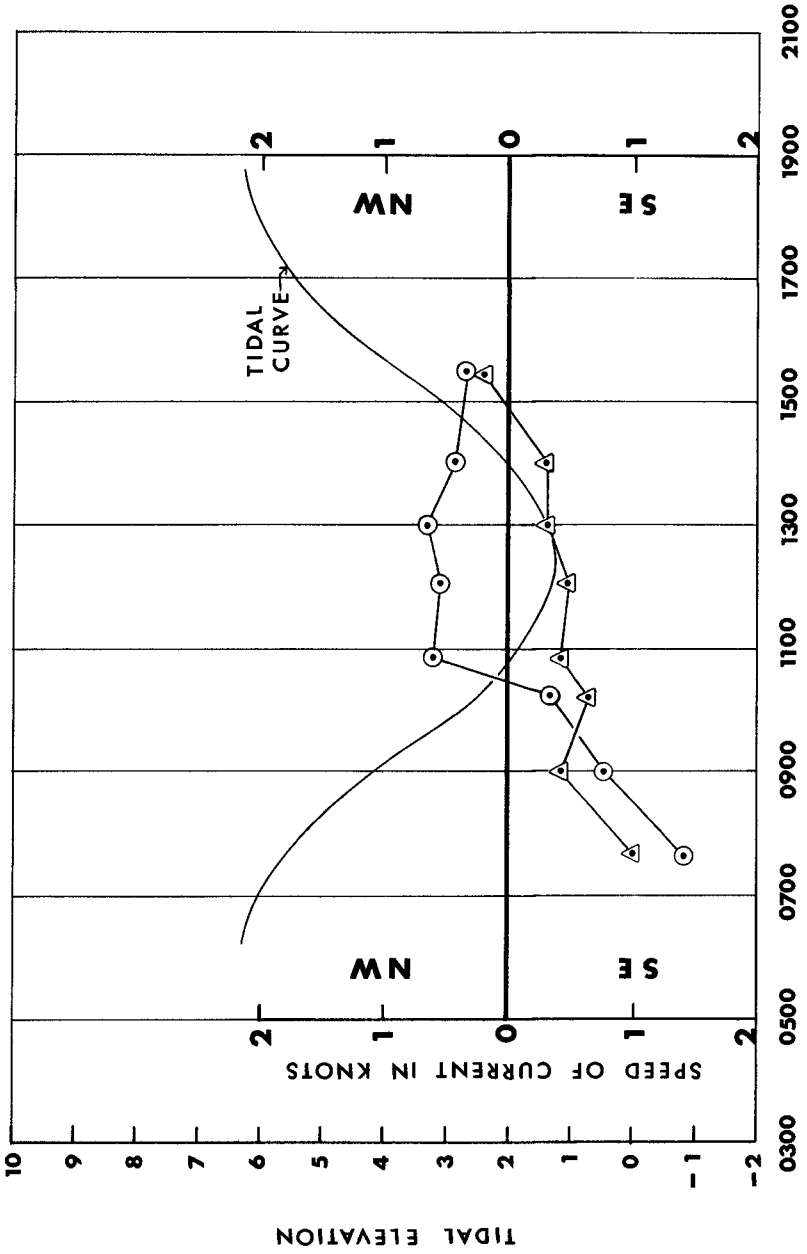

Figure 1. Measurements of coastal currents from drift bottles set by rocket launcher.

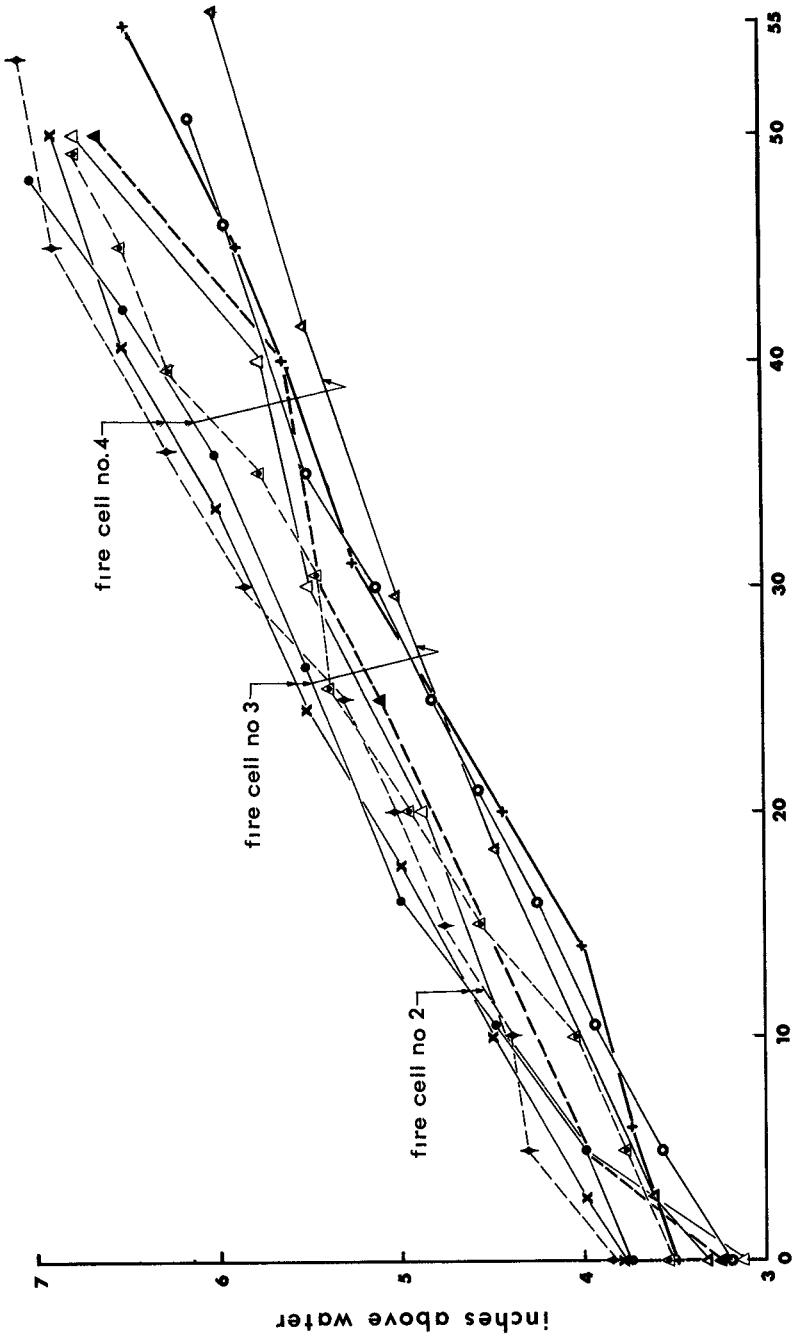

Figure 2. Change of freeboard of Mark II flares as they burn.

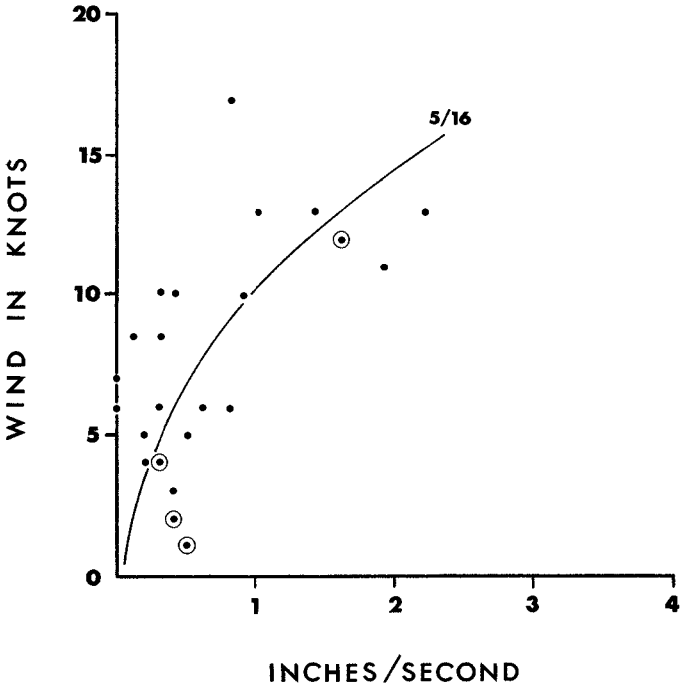

Figure 3. Drift of a flare with 5/8 inch freeboard for various wind velocities.

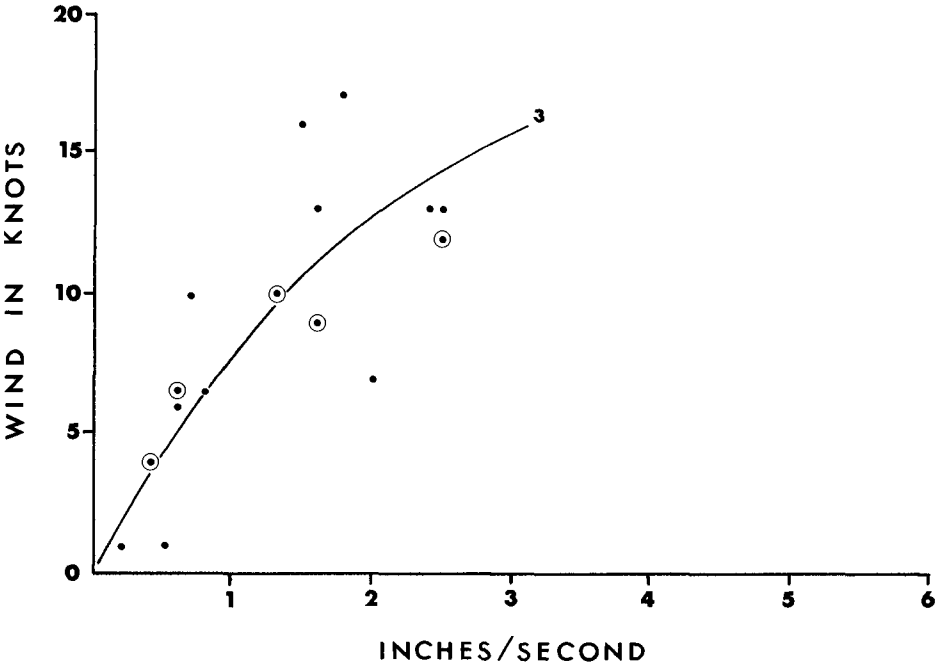

Figure 4. Drift of a flare with 3 inch freeboard for various wind velocities.

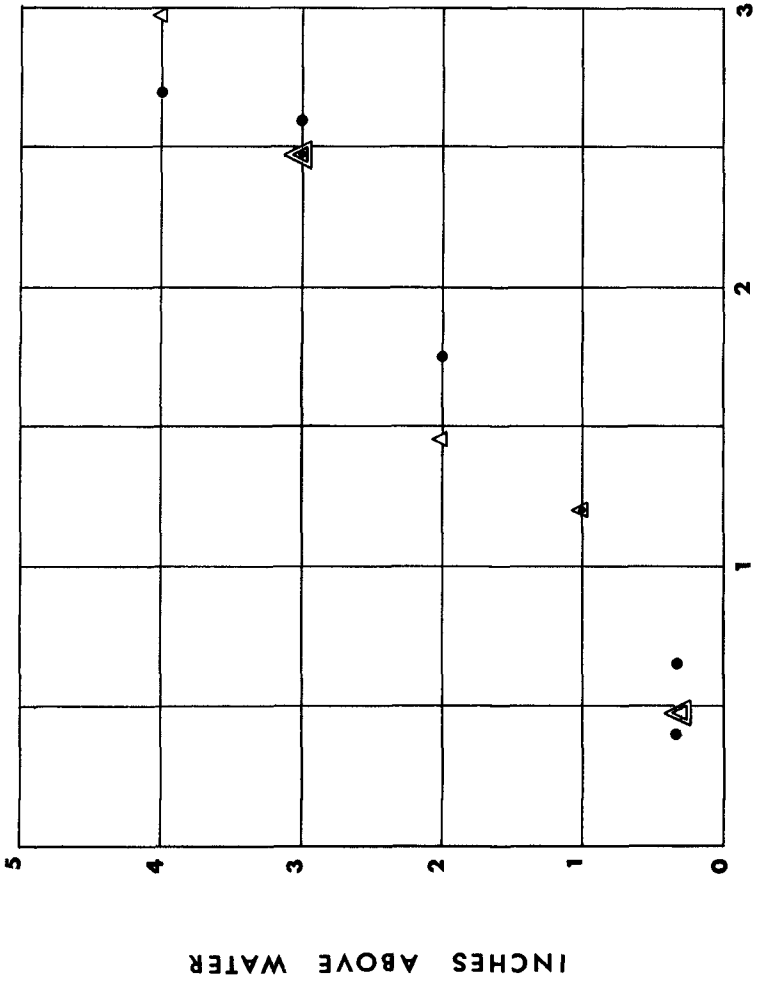

Figure 5. Wind velocity profile calculated from wind stress on flares of different freeboard.

shows data taken on a single day by this technique; they are representative of all the rest. Considering that it is the work of a single observer who operated both launcher and theodolite, the cost per day is low. Yet, the observations obtained are not easy to get using a crew, and they are literally impossible when the sea is up.

Measurements

Measurements were taken at Highland Light beach, Cape Cod, Massachusetts, a location used by us for a variety of studies. The beach is about 200 feet wide separated from the nearshore bar by a low approximately 150 feet wide. The offshore bar lies 900 to 1300 feet from the low tide line.

Figure 1 shows the velocity and direction of currents inside and outside the bar as the tide changed. No attempt will be made in this paper to draw conclusions from these data because they represent part of another study. Our objective is simply to illustrate a use for this technique as an efficient tool in hard-to-reach waters.

Use of flares as drogues

Navy Mark II aerial flares are generally available to holders of naval contracts. These flares burn for approximately 53 minutes with a plume of white smoke. Because of their availability and ease in setting, the writers have used them in arrays to measure currents. We discovered that as the flare burns it rises higher into the air and wind drag on it becomes greater. Therefore, we calibrated these flares for wind drag. Figure 2 shows the change of freeboard as the flare burns. One can see that the flares initially have a freeboard between 3 and 4 inches and that they change their freeboard linearly as they burn. In practice we pre-trim our flares to an initial freeboard of 5/8 inch before using them.

Flares were calibrated in a coastal lagoon four feet deep with essentially no tidal currents. A post driven into the bottom marked the origin; floats pre-trimmed to have almost no scope were dropped to mark terminal points. Distance was measured by surveyor's chain, time with a stop watch, angle by an azimuth circle mounted on top of the pipe, and wind velocity by a Weston hand-held anemometer at two and five feet above the water surface. Groups of flares carefully trimmed to float with freeboards of 5/8, 1, 2, 3, 4, and 5 inches were started at the origin and allowed to drift. A mid-depth drogue was used to determine the direction and velocity of the current. The ratio of the surface area of the drogue to its float was approximately 1:100. These measurements were continued

over a period of weeks until a sampling of drift caused by wind velocities between 2 and 20 knots was measured. Figures 3 and 4 show the drift due to wind blowing on naval aerial flares with freeboards of 5/8 and 3 inches respectively.

The flares followed paths which for the most part indicated movement to the right of the observed wind rather than directly downwind. It was noted that this angle between wind and flare path was lowest when wind velocities were greater than nine miles per hour, and that the angle between flare path and wind direction was high when wind velocities were low. For example, the angle between flare drift path and wind direction was between zero and fourteen degrees (average 6 degrees) for winds greater than nine miles per hour, and the angle was between twenty-two and forty-eight degrees (average 36 degrees) for winds whose velocities were less than nine miles per hour. Out of fifty trials, the flares moved to the left of the wind direction only six times, and all of these were at times of very light winds. The results of our measurements coincided with the visual observations that wind direction and velocity were most difficult to obtain when winds were light. Observation of cat's-paws on the water showed much variation in wind direction when winds were light.

We concluded, in spite of the scatter in the data and the uncertainty of wind direction, that by using the results given in figures four and five and the angles stated we can make meaningful corrections to the flare paths and velocities when we use them in the field.

Wind velocity profile calculated from flare drifting

As stated, the wind was measured at an elevation of five feet and two feet above the water with no observed reduction in velocity. Since several flares of different freeboards were drifted simultaneously in the same wind field, the wind velocity required to push a given flare of known area through the water at a measured velocity can be computed from the relationship of balanced forces of wind being opposed by water, assuming no acceleration is taking place after a short interval of time.

$$F_{wind} = F_{water}$$

$$\text{(wind)}\ \frac{C_D \rho_A V^2 A_A}{2} = \frac{C_D \rho_W V_W^2 A_W}{2}\ \text{(water)}$$

$$V^2_{wind} = \frac{\rho_W V_W^2 A}{\rho_A A}$$

V Velocity of wind acting at a point 0.793 of the freeboard measured upward from the water

V_W Wind drift component of the flare through the water

C_D Drag coefficient for flare of given dimensions

A_A Cross-sectional area of flare exposed to wind

A_W Cross-sectional area of the part of flare exposed to water

ϱ_A Density of air

ϱ_W Density of water

The factor 0.793 is calculated as the point on the flare, measured upward from the water, at which the moments of force due to wind are balanced. These calculations were made for experiments done under the same wind velocity, thirteen miles per hour, where several flares were drifted at the same time. Figure 5 gives the wind velocity profiles caloulated from these measurements.

It is difficult to assess the exact meaning of the profile obtained because too many unknowns are involved. For example, we have no idea what forces were exerted by the orbital motions of waves, nor do we know the vertical motions of the flares and their upward and downward penetrations into the wind field. Gustiness was clearly observed at the water surface. On the other hand, the data were taken carefully and repeated runs plotted with remarkably little scatter. In spite of the unsteady conditions, one gets a uniform result.

Acknowledgements The writers wish to thank their colleagues, Dr. Robert Byrne, Dr. Graham Giese and Mr. William D. Athearn, for their assistance in this work both in the field and in the discussions which followed.

CHAPTER 28

SIMULATION OF HORIZONTAL TURBULENT DIFFUSION OF PARTICLES UNDER WAVES

By Stephen P. Murray
Coastal Studies Institute
Louisiana State University
Baton Rouge, Louisiana

ABSTRACT

By oscillation of an array of turbulence-generating grids in still water, the turbulent fluid velocity field in shoaling waves near the bottom is simulated in a laboratory channel. Solid particles with fall velocities varying between 1 and 40 mm/sec are introduced into the test volume from above. Multiple-image photography using ultraviolet lighting techniques and a suitably placed mirror allow recording of the grain trajectories as functions of time and three space dimensions simultaneously. The Lagrangian intensities of turbulence and diffusion coefficients are then directly measured from the photographic data. The scale times, scale lengths, and the frequencies of the power spectra modes can then be calculated. Properties of the fluid turbulence are inferred from the quasi-neutral particles. The analysis, which is restricted to the component of diffusion in the horizontal direction normal to the grid motion, shows that the turbulent velocity distributions of both fluid and heavy particles are Gaussian, and that their standard deviations (intensities of turbulence) increase regularly with increasing grid Reynolds numbers (grid speeds). Diffusion coefficients likewise generally increase with increasing grid Reynolds numbers. Diffusivities of the heavy particles relative to the fluid are a function of both particle fall velocity and the structure of the fluid turbulence itself.

I. INTRODUCTION

With the advent of fluorescent sand tracers in the marine environment, much attention has recently been focused on the dispersion of solid particles by waves. In this regard, studies by Bowen and Inman (1966) and Murray (1967) suggest that the role of turbulent diffusion must be investigated. The basic aims of this study, therefore, are (1) to determine the effect of increasing terminal fall velocity on the turbulent diffusion of solid particles inside shallow-water waves, (2) to investigate the applicability of the statistical theory of turbulence to heavy particles, and (3) to compare the internal properties of the fluid and particle turbulence.

In unidirectional flow the mean velocity in any direction k is generally defined by

$$\bar{u}_k \equiv \frac{1}{T} \int_{t_o-1/2T}^{t_o+1/2\ T} u_k \, dt, \qquad (1)$$

where u_k is the velocity at any instant and T is taken sufficiently long to yield a stable average. The difference between u_k and $\bar{u}_k$

$$u_k' = u_k - \bar{u}_k \tag{2}$$

is referred to as the turbulent velocity. In the case of the periodically varying velocities within waves it is less evident how to define mathematically the average and turbulent terms. Knowledge of turbulence in waves is scant. Stewart and Grant (1962) measured the turbulent energy spectra in the presence of surface waves and illustrated a low-frequency peak attributed to orbital motions. Perhaps turbulence in waves can be defined in terms of such deviations in the energy spectra. In any case, the flow in nature is clearly not laminar, and a turbulence term must exist which in turn gives rise to the diffusion effects which are the basic aim of this study.

The complexities of the problem demand an experimental approach, and, since the available wave tank was not of sufficient size to generate fully turbulent waves, a simulation technique was devised. This technique consists essentially of oscillating an array of grids through still water in a sinusoidal manner. Variation of the grid oscillation speed allows the generation of several turbulent-flow fields. Fluorescent lighting techniques, combined with multiple-image photography, provide records of the coordinates of individual particles in time and three-dimensional space for further analysis. The experimental work, which was conducted in the Fluid Mechanics Laboratory of the Delft Technological University, the Netherlands, has direct implications on the dynamics of suspended sediment in the surf zone.

II. THEORETICAL CONSIDERATIONS

Of the several theories describing and predicting the turbulent spreading of a collection of particles, the "single particle" theory of G. I. Taylor (1921, 1935) offers the best framework for the present study. Taylor expressed particle displacement caused by turbulence x_k' as a time-integrated effect of the turbulent velocity u_k'

$$x_k' = \int_o^t u_k'(t)\, dt. \tag{3}$$

Considering a collection of many particles and taking the mean square of all such net displacements as the appropriate statistical measure of the particle dispersion yields the Taylor diffusion equation

$$\sigma_k^2(T) = 2\,\overline{u_k'^2} \int_o^T \int_o^t R_k(\xi)\, d\xi\, dt. \tag{4}$$

Here σ_k^2 is the variance of the displacements of the particles from their initial position, $\overline{u_k'^2}$ is the square of the turbulence intensity--alternatively known as the root mean square turbulent velocity--which should be approximately constant in a given flow field, R_k is the Lagrangian autocorrelation function of the velocity, and ξ is the autocorrelation lag time. The subscript k refers

to any direction and (4) applies equally to the x, y, or z direction when only turbulent motions are present with the corresponding velocities u', v', and w'. For a detailed derivation of (4) see Haltiner and Martin (1957, p. 276).

For large values of the lag time ξ the velocity autocorrelation $R_k(\xi)$ approaches zero and the area c under the autocorrelation function versus time curve--that is, the inner integral of (4)--becomes constant

$$\int_0^\infty R_k(\xi)\, d\xi = c_k. \tag{5}$$

Henceforth all equations will be written in the y direction. Performing the second integration of (4) leads to

$$\sigma_y^2(T) = 2\,\overline{v'^2}\, c_y T. \tag{6}$$

Taking the first derivative of (6)

$$\frac{d\sigma_y^2}{dT} = 2\,\overline{v'^2}\, c_y, \tag{7}$$

which shows that, for long elapsed diffusion times, the slope of the $\sigma^2 - T$ curve is a constant, a result we shall use later. For very short diffusion times the autocorrelation is unity and (4) reduces to

$$\sigma_y^2 = \overline{v'^2}\, T^2. \tag{8}$$

This equation applies only up to about .04 seconds, as deduced from Frenzen's results (1963) under conditions similar to ours. The resolution of our data is insufficient for (8) to be of any use. The area under the Lagrangian autocorrelation coefficient is generally referred to as the scale time of the turbulence, denoted by t_y^* (9),

$$t_y^* \equiv c_y, \tag{9}$$

$$\ell_y^* = \left(\overline{v'^2}\right)_y^{1/2} t_y^*, \tag{10}$$

$$K_y^* = 1/2\left(\frac{d\sigma_y^2}{dT}\right) = \left(\overline{v'^2}\right)_y t_y^* = \left(\overline{v'^2}\right)^{1/2} \ell_y^*. \tag{11}$$

The scale time t_y^* can be considered to measure the lifetime of the largest turbulent cell (Inoue, 1960). The Lagrangian scale length ℓ_y^* (10) is usually interpreted as a measure of the average turbulent eddy size. It is analogous to the "mixing length" of Prandtl's earlier theory. The Lagrangian diffusion coefficient K_y^* is equal to one half the ultimate rate of particle spread (11), and using (7) and (10) it can be expressed in terms of the turbulence intensity, the scale time, and the scale length. In addition, t_y^* can be interpreted in terms of the distribution of energy in the Lagrangian power spectrum

through a Fourier cosine transform (Taylor, 1938). Frenzen (1963, p. 67) shows that the mode of the power spectrum n in cycles per second can be closely approximated by

$$n_y = 1/2\ (\pi t_y^*)^{-1}. \tag{12}$$

The complete integral solution of (4) requires knowledge of the form of the autocorrelation function $R_y(\xi)$. Inoue's theoretical analysis (1951) predicts the autocorrelation function to approximate the form

$$R_y(\xi) = \exp\ (-\xi/c_y), \tag{13}$$

which was verified experimentally by Kalinske and Pien (1944) and Frenzen (1963) for unstratified flows. Substituting (13) into (4) and integrating yields a general diffusion equation

$$\sigma_y^2 = 2\ \overline{v'^2}\ c_y\ T - 2\ \overline{v'^2}\ \ c_y^2 + 2\ \overline{v'^2}\ c_y^2\ \exp\ (-T/c_y), \tag{14}$$

showing that in a fluid velocity field composed only of turbulent motions the dispersion of a collection of particles is a function of the turbulence intensity, the elapsed diffusion time, and the scale time of the turbulence.

III. EXPERIMENTAL PROCEDURES

The use of turbulence-generating grids has yielded great advances in the knowledge of turbulence in air streams, but they have been used only rarely in hydrodynamics. The disturbances generated in the lee of a grid (with either the fluid or the grid in motion) has been shown by Taylor (1935) to transform rapidly into a quasi-isotropic turbulent field. For an excellent photograph of this phenomenon showing the initial vortices degenerating into a homogeneous turbulent field, see Prandtl (1939). Although it is well recognized that quasi-isotropic grid-produced turbulence only crudely resembles the turbulent shear flows of nature, its study has precipitated great progress in the understanding of the mechanics of turbulence itself. Frenzen (1963) describes detailed experiments in which a single grid is towed through a water channel so that the turbulent trajectories of particles may be studied without the disadvantage of a mean flow moving the particles rapidly out of the field of view. As a variation of Frenzen's technique, in this study a series of grids is oscillated in simple harmonic motion in still water.

To rationalize the analogy between turbulence in shallow-water waves and grid-produced turbulence, consider Figure 1. Diagram A of this figure shows the well known result that in idealized water waves to the first approximation the orbital velocity varies sinusoidally in time. If the wave flow were turbulent, the velocity trace would presumably resemble Figure 1 B, since the "turbulent fluctuations are approximately proportional to the mean velocity" (Sutton, 1953, p. 251). The elimination of the sinusoid from Figure 1 B represents a turbulence field (Fig. 1 C) without the

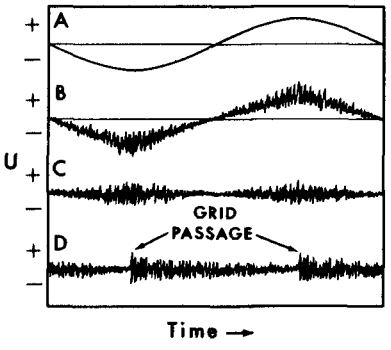

Fig. 1. Sketch to illustrate similarity of oscillating grid-produced turbulence to turbulent wave flow.

disturbance of orbital motions. The present experiments attempt to simulate Figure 1 C by sinusoidally oscillating a grid in still water. In Eulerian coordinates the turbulent velocity so produced (see Figure 1 D) will abruptly peak as the grid passes; this will be followed by a gradual decay until the next grid passage, and a crude approximation to the turbulence shown in diagram C will ensue. However, as will be shown later, the observed frequency distributions of the turbulent velocity are Gaussian in nature, so perhaps the results concerning the particle diffusion apply equally as well to turbulent fields in general. The laboratory flow is a simulation or model of turbulent wave flow in nature only in the sense of this paragraph.

The grids which fill the 50 cm wide channel are composed of steel rods 1 cm in diameter and 5 cm apart. The array, consisting of three grids, each 30 cm apart, has a stroke length kept constant at 40 cm. For the experiments average grid velocities of 16, 30, and 45 cm/sec are determined by variation of the oscillation period. The grid Reynolds number Re_g is defined by the mean fluid velocity $\bar{U}$, the grid mesh length M, and the kinematic viscosity of the fluid ν

$$Re_g = \frac{\bar{U}\, M}{\nu} \,. \tag{15}$$

With $\bar{U}$ considered as the average grid speed, (15) defines three grid Reynolds numbers: 0.66×10^4, 1.2×10^4, and 1.9×10^4. Water depth is kept constant at 40 cm. The elimination of data taken (a) within 5 cm of the walls because of boundary effects and (b) within the 10 cm section at each end of the grid stroke leaves an experimental volume inside the tank 80 cm long, 30 cm high, and 40 cm across.

In conventional studies of grid-produced turbulence a correction for the time decay of the turbulence is generally made. In this study a new burst of turbulence, associated with the oscillating grids, reinforces the velocity field every few seconds (cf. Fig. 1 D). The particle trajectories from which the data are taken encompass the entire volume and time duration of an experiment. Thus the trajectories are a direct result of several turbulent bursts, and their sampling (at 1-second intervals) is considered to produce an average which represents an effective turbulence field, no decay corrections being required.

As a means of observing particle diffusion, solid, wax-like particles

2 mm in diameter d are impregnated with a fluorescent powder and injected into the test volume from above. The density of such particles (diameter remains constant) can be varied to evaluate changes in the diffusion brought on by the terminal fall velocities. Repeated timing of the duration of fall through a column of water determines terminal fall velocities w_p of 0.2, 1.0, 2.0, 3.0, and 4.0 cm/sec. Table 1 lists the corresponding particle Reynolds numbers ($Re_p = w_p\, d/\nu$) and sedimentation diameters d_s--that is, the size of spherical quartz grains having the same fall velocities as our test particles (Brown, 1950). The 0.2 cm/sec particle is referred to as the fluid or quasi-neutral particle and is used to infer the statistics of the fluid turbulence.

Table 1

Properties of the Test Particles					
w_p cm/sec	0.2	1.0	2.0	3.0	4.0
Re_p	2.4	16.6	33.3	50.0	66.6
d_s (mm)	0.03	0.12	0.18	0.24	0.38

Two 500-watt mercury vapor lamps are directed diagonally down into the test volume to provide illumination of the fluorescent particles and several centimeter scales. The camera is situated 3 m in front of the water channel and aimed at the center of the front glass experimental area. A red filter on the lens insures that the only light to strike the 10 cm x 12 cm negative comes from the red-emitting objects treated with the fluorescent powder--that is, the particles and the centimeter scales. To achieve the multiple-image effect, a metal disc pierced with six holes along its periphery rotates in front of the camera lens. The holes act as a rapidly repeating camera shutter. In order to see both a front and a top view of the experimental volume simultaneously in the same photograph--that is, all three dimensions at once--a high-quality glass mirror is rigidly suspended over the channel. One essential feature of this photographic technique is that the grids are invisible to the camera.

Rouse (1939) describes a device used in a study of vertical particle diffusion which is mechanically similar to the one discussed above. Rouse calculated diffusion coefficients from the concentration statistics of a collection of particles.

IV. ANALYSIS AND RESULTS

Fifteen photographs (2 grain trajectories per photograph) were taken of each fall velocity at each grid Reynolds number. After development of the film 50 cm x 60 cm enlargements were made in the photographic laboratories of both the Delft Tecbnological University and the Coastal Studies Institute. Figure 2 is an example of one data-bearing photograph. The lower half is the front view, giving the x and z coordinates, z being the vertical direction; the upper half is the image in the mirror, giving the x and y coordinates, the y direction being across the channel width. In this photograph there are eighteen particle images per second, a fall

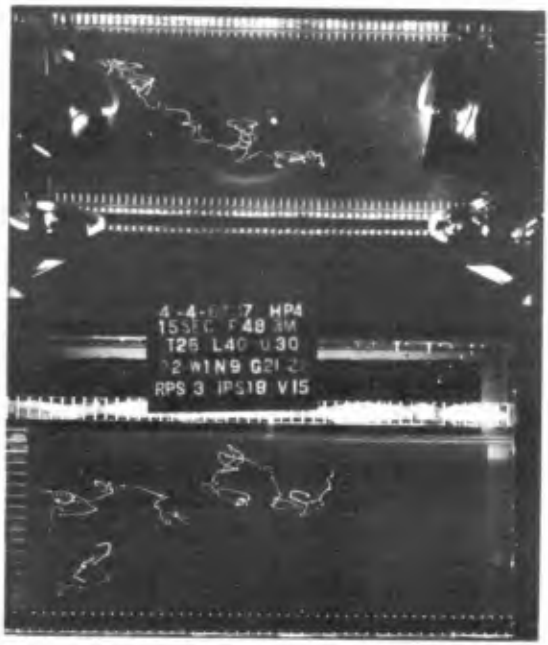

Fig. 2. Example of a data-bearing photograph; grid speed of 30 cm/sec, 18 images per second.

velocity of 0.2 cm/sec, and an average grid speed of 30 cm/sec. Four fall velocities are examined at the lowest value of Re_g and five, at the two higher. Thus there are fourteen data sets, each composed of thirty grain trajectories. The grains are followed in the x, y, and z directions for about 10 seconds.

Scale overlays are constructed to facilitate the reading of the particle coordinates from the photographs, and by counting the number of images we can tell the duration of elapsed time from the start of the trajectory. As a means of distinguishing the end of the trajectory from the beginning, the last few seconds of the photograph are made with the disc stopped and a hole directly in front of the lens so that the particle makes an easily distinguished continuous streak on the negative.

The x coordinate is common to both halves of the photograph, which helps in correlating the front and top views. With practice the paths of the particles can be followed in all three dimensions and time quite well. The particle coordinate is read each second up to 10 seconds for the data analysis. This sampling procedure controls the frequency band within which we are viewing the particle movements. For N observations taken ΔT seconds apart the spectral band we are viewing is given approximately by

$$\frac{1}{2N\Delta T} < f < \frac{1}{2\Delta T}, \tag{16}$$

where f is the frequency in cycles per second. In the present experiments $\Delta T = 1$ second and $N = 10$, so our observations are restricted to the range between 0.05 and 0.5 cps.

Because of the proximity of the camera to the experimental tank there is a significant parallax error. A centered difference correction technique

is employed which reduces this error to at most 4 percent.

In the remainder of the paper discussion will be restricted to the component of diffusion in the y direction; that is, horizontal diffusion laterally across the channel, normal to the grid motion. The component of particle motion in the y direction is obtained simply by projecting the particle onto the y axis. In a sense we are then observing the particle moving back and forth along a single line--the y axis.

The particle motion along the x axis is difficult to interpret because of dragging effects of the grids. This is not a serious drawback, however, as the turbulence characteristics in any horizontal direction should be approximately the same in our simplified flow field; i.e., the x-direction data should approximate that of the y direction. The data on diffusion in the vertical (z) direction, including the interaction of turbulence and fall velocities, will be presented elsewhere. The three-dimensional value of any of the turbulence parameters can be obtained, if desired, by calculation of the resultant vector.

Particle Spread

We now have the particle coordinates as a function of time. In order to utilize equation (6), we calculate the variance (σ_y^2) of particle displacements from the initial position for each 1-second time increment using

$$\sigma_y^2 (T) = \sum_1^n \frac{(y_i - y_o)^2}{n} , \tag{17}$$

where n refers to the number of particles, y_o to the initial and y_i to the subsequent coordinates. Unlike the more conventional mean, y_o will vary with each particle, but in a field of homogeneous turbulence this is inconsequential. A plot of σ_y^2 against time T should then, from (7), become linear after a few seconds, with the slope equal to twice the product of the turbulence intensity (squared) and the scale time; or, alternatively, the diffusion coefficient is equal to one half of this slope (see equation 11). In practice we calculate the slope of the least squares regression line passing through the points for $t \geq 2$ sec. These slopes, together with the corresponding correlation coefficients r, are presented in Table 2.

The uniformly high values of the correlation coefficients indicate the linear spread law holds valid after 2 seconds in our experiments for both the fluid and the heavy particles at all values of Re_g.

Turbulent Velocities

The data on the time change of the particle coordinates also allow measurement of the turbulent velocities v' from

$$v' = \frac{y(t) - y(\Delta t)}{\Delta t} . \tag{18}$$

Table 2
Ultimate Slope of Dispersion Curves

Re_g	0.66×10^4			
w_p (cm/sec)	0.2	1.0	2.0	3.0
$\frac{d\sigma^2}{dT} = 2K^*$ (cm^2/sec)	8.8	4.8	5.0	4.4
r	.98	.96	.99	.98

Re_g	1.2×10^4				
w_p (cm/sec)	.2	1.0	2.0	3.0	4.0
$\frac{d\sigma^2}{dT} = 2K^*$ (cm^2/sec)	7.6	18	16	7.4	9.5
r	.89	.99	.98	.93	.94

Re_g	1.9×10^4				
w_p (cm/sec)	.2	1.0	2.0	3.0	4.0
$\frac{d\sigma^2}{dT} = 2K^*$ (cm^2/sec)	25	22	18	14	22
r	.96	.98	.99	.97	.97

Since Δt = 1 second the difference in successive particle coordinates is a direct measurement of the turbulent velocity. In a given data set there are thirty particles followed for 5 to 10 seconds, resulting in about 200 measurements of the turbulent velocity per data set. Percent distribution (histograms) of turbulent velocities and corresponding Gaussian curves of best fit are plotted in Figure 3, where N is the number of observations. At this point there are three notation changes:

1. We shall use the notation $\underline{v}'$ for the intensity of turbulence; that is, $\underline{v}' \equiv (v'^2)^{1/2}$;

2. The subscript o, e.g., $\underline{v}'_o$, refers to a property of the fluid, the subscript p refers to a property of a heavy particle, e.g., $\underline{v}'_p$, lack of a subscript refers to both phases;

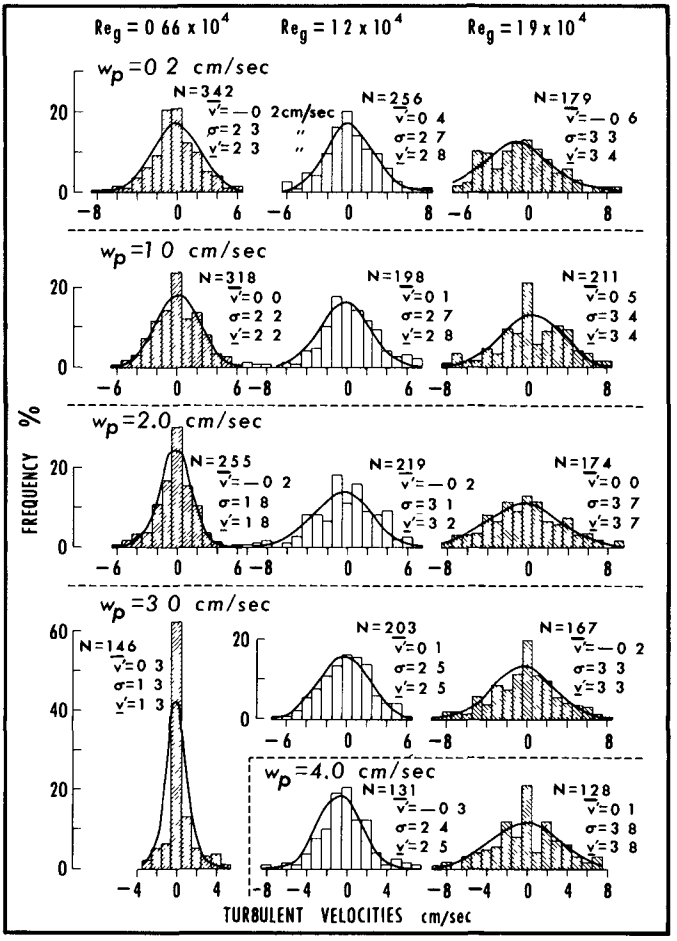

Fig. 3. Distributions of turbulent velocities v' as functions of grid Reynolds number Re_g, and particle fall velocity w_p.

3. The subscript y will hereafter be omitted and understood unless otherwise noted.

Much previous work suggests that the distribution of the fluid turbulence

should be Gaussian, and our data (w_p = 0.2 cm/sec) agree quite well. Liu (1956) states that the heavy particle turbulent velocities should also be Gaussian in distribution, which our present data likewise corroborate. Since the observations that make up any single velocity frequency distribution are scattered in time and space from many flow realizations, they lend strong support to the assumptions of long-term stationarity and homogeneity of the flow.

From elementary statistics we know the variance σ^2 of a quantity v'

$$\sigma^2(v') = \overline{(v'^2)} - \overline{(v')}^2, \tag{19}$$

or, transposing and taking roots,

$$\underline{v}' = \left[\sigma^2(v') + \overline{(v')}^2\right]^{1/2}. \tag{20}$$

Thus the intensity of turbulence $\underline{v}'$ may be evaluated directly from the variance and mean of our velocity frequency distributions. For a zero mean the intensity of turbulence is by definition equal to the standard deviation. Values of the mean $\overline{(v')}$, the standard deviation (σ), and intensity of turbulence ($\underline{v}'$) are given in Figure 3. Velocity means as anticipated are close to zero and show no preferential direction, supporting the absence of a mean flow.

Values of $\underline{v}'$ are presented in Figure 4 as a function of Re_g and w_p. For all values of w_p, higher grid Reynolds numbers produce higher intensities of turbulence. If $w_p >> 0$ then $v' \to 0$, since a particle with sufficient mass will not respond to even the highest fluid velocity fluctuations. At $Re_g = 0.66 \times 10^4$, $\underline{v}'$ apparently decreases monotonically with increasing values of w_p, but at higher grid Reynolds numbers a tendency is evident for an initial increase in $\underline{v}'$ before the descent to zero begins. These enhanced velocities are perhaps the result of centripetal accelerations; that is, the heavy particles are unable to maintain the rate of curvature of the fluid eddy and so are thrown from the eddy. This tendency decreases as the relative inertia increases, as postulated by Singamsetti (1966).

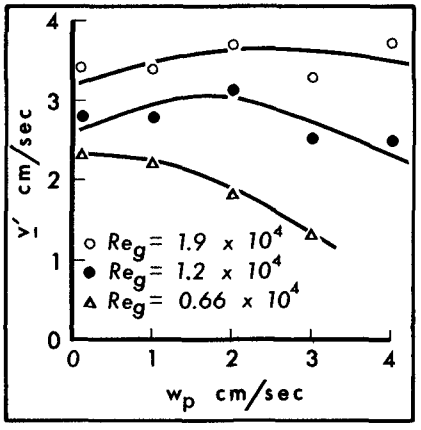

Fig. 4. The effect of the particle fall velocity w_p on the turbulence intensity $\underline{v}'$ for the three grid Reynolds numbers Re_g.

The ratio $w_p/\underline{w}_o$ was suggested by Rouse (1939) as a possible control on the mixing coefficient. Figure 5 is a nondimensional plot of $\underline{v}'/w_p$ against $w_p/\underline{w}'_o$ where $\underline{w}'_o$ is the fluid intensity of turbulence in the direction of fall.

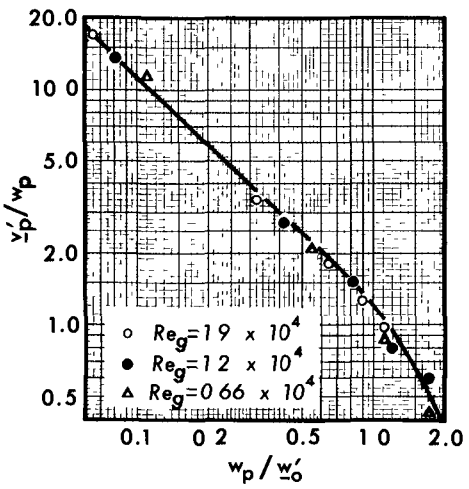

Fig. 5. Nondimensional representation of the effect of the particle fall velocity on the turbulence intensity.

The points of Figure 4 now fall on a single smooth curve. This curve can predict the horizontal turbulence intensity of the particle phase from that of the vertical fluid phase for a given particle fall velocity. This curve suggests that the initial increase in v'_p with increasing w_p is now present to some degree for all values of v'_o. The critical value of w_p/w'_o, computed from Figure 5, where v'_p begins to decrease (that is, where gravitational forces become dominant over inertial forces), varies $.7 < w_p/w'_o < .9$ as a function of w'_o. The onset of dominant particle gravitational effects is therefore not controlled by a critical particle Reynolds number as suggested for investigation by Rouse (1939).

In our quasi-isotropic flow field there is, of course, an intimate relation between w'_o and v'_o. Substitution of v'_o for w'_o in the abscissa variable of Figure 5 gives a very similar curve but with a little more scatter. Future work in a non-isotropic fluid must decide which of the two turbulence intensity components is the real controlling factor.

Other Fluid Turbulence Characteristics

Using our measured values of the time change of variance $d\sigma_o^2/dt$ (Table 2) and fluid turbulence intensity v'_o (Table 3) we can calculate other fluid properties such as scale time ($c \equiv t_o^*$) from (6), scale length ℓ_o^* from (9), diffusion coefficient K_o^* from (10), and the location of the mode of the Lagrangian power spectrum n_o from (11). These four quantities, together with the fluid turbulence intensity and energy per unit volume, are presented as a function of grid Reynolds number Re_g in Figure 6. As shown in (12), the scale time t^* can be interpreted in terms of the location of the mode of the Lagrangian power spectrum. In this regard it is generally found (see, e.g., Taylor, 1939) that the turbulence generated by grids at low values of Re_g is deficient in small-scale eddies; that is, the energy is concentrated at low frequencies. Increase of the grid Reynolds number should result in the production of relatively more high-frequency energy, producing a corresponding shift of the spectral mode toward high frequencies. This effect is seen both in the present study (Figure 6 C, D) and in that of Frenzen (1963) for the initial increase in grid Reynolds number. Our increase in the frequency of the spectral mode is evidently so severe as to force a slight increase in the diffusion coefficient K_o^* since, combining (10) and (11),

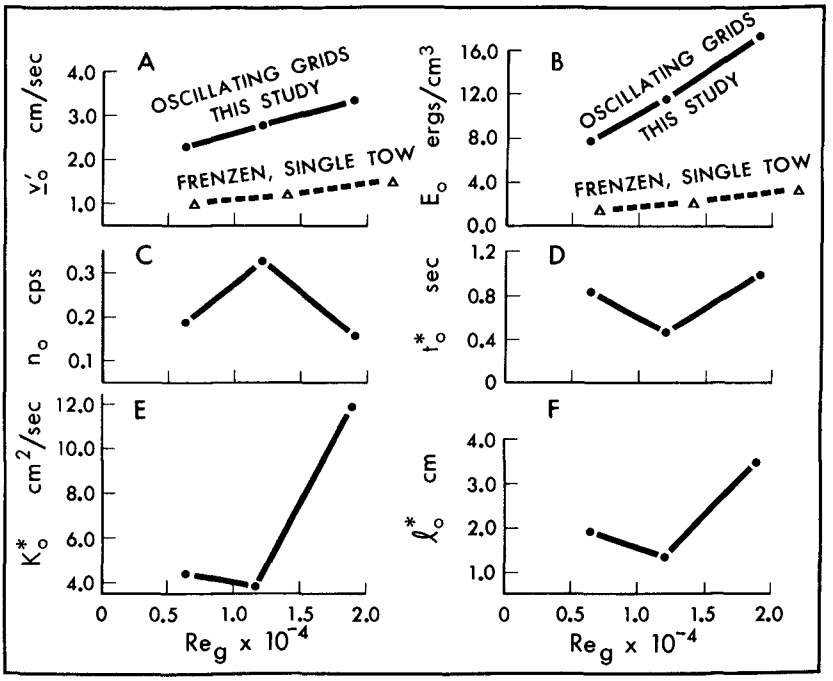

Fig. 6. Properties of the fluid turbulence produced by moving grids.

$$K^*_o = (\underline{v}')^2/2\pi n_o. \tag{21}$$

Taylor (1935) showed the energy of turbulence E_o per unit volume of fluid to be

$$E_o = \frac{\rho}{2}(3\underline{v}'^2_o). \tag{22}$$

Figure 6 B demonstrates that there is considerably more energy produced by the oscillating grids (this study) than by the single pass of a solitary grid (Frenzen). If the first increase in Re_g has excited considerable high-frequency energy, a further increase in the grid Reynolds number could conceivably be unable to shift the spectral mode any higher. In fact, owing to the overall increase in energy over the entire spectrum, the peak could shift back again toward lower frequencies, as suggested by Frenzen (1963) in a slightly different context. This did not, as a rule, occur in Frenzen's experiments but, as seen in Figure 6 B, at the highest grid Reynolds number we have considerably

Table 3
Characteristics of Fluid and Particle Turbulence

Re_g	0.66×10^4			
w_p cm/sec	0.2	1.0	2.0	3.0
$\underline{v}'$ cm/sec	2.3	2.2	1.8	1.3
t^* sec	.83	.49	0.77	1.3
ℓ^* cm	1.91	1.1	1.4	1.7
K^* cm^2/sec	4.4	2.4	2.5	2.2
n cps	.19	.32	.21	.12

Re_g	1.2×10^4				
w_p cm/sec	0.2	1.0	2.0	3.0	4.0
$\underline{v}'$ cm/sec	2.8	2.8	3.2	2.5	2.5
t^* sec	0.48	1.1	.78	0.59	.77
ℓ^* cm	1.4	3.2	2.5	1.5	1.9
K^* cm^2/sec	3.8	9.0	8.0	3.7	4.8
n cps	.33	.14	.20	.27	.21

Re_g	1.9×10^4				
w_p cm/sec	0.2	1.0	2.0	3.0	4.0
$\underline{v}'$ cm/sec	3.4	3.4	3.7	3.3	3.8
t^* sec	1.0	.95	.66	.64	.76
ℓ^* cm	3.5	3.2	2.4	2.1	2.9
K^* cm^2/sec	12	11	9.0	7.0	11
n cps	.16	.17	.24	.25	.21

more energy than he did--17 ergs/cm^3 as against 3.4 ergs/cm^3. This is likely the cause of the decrease in the frequency of the spectral mode n_o, the increase in the scale time t_o^*, and the corresponding sharp increase in the

diffusion coefficient K_o^* at the high value of Re_g. The scale length ℓ_o^* follows the same trend as the scale time t_o^*.

The relative particle diffusivity--that is, the ratio of the particle diffusion coefficient to that of the fluid K_p^*/K_o^*--is presented in Figure 7 as a function of particle fall velocity and grid Reynolds number. For the lowest and highest values of Re_g the relative diffusivity decreases fairly regularly with increasing particle fall velocity. For the middle value of Re_g there is a sharp increase in the relative diffusion, three out of four heavy particles diffusing at a higher rate than the fluid (quasi-neutral) particles. As can be seen in Table 3, this relative diffusion peak is entirely the result of the unexpectedly low value of the fluid diffusion coefficient (w_p = 0.2 cm/sec) at the intermediate grid Reynolds number $Re_g = 1.2 \times 10^4$. To add to our suspicion of this value, the heavy particle diffusion coefficients at this grid Reynolds number have values which are fairly consistent with the two other data sets.

Nonetheless, a detailed recheck of the raw data revealed no errors in the analysis. In its support it should be noted that the diffusion coefficient is directly measured (not computed) from the time change of particle displacement; as such it is based on approximately 150 points. Furthermore, the turbulent velocity frequency distribution of w_p = 0.2 cm/sec at $Re_g = 1.2 \times 10^4$, which is based on the same raw data as the diffusion coefficient in question, is very well behaved. This distribution (cf. Fig. 3) fits a Gaussian curve extremely well and has a standard deviation (intensity of turbulence) falling midway between those of neighboring Reynolds numbers. Thus the relative diffusion anomaly is apparently quite real and must be related to shifts in the power spectra along the frequency axis, as discussed earlier (cf. equation 21). The unresolved question is why at the intermediate Re_g there is a lack of coupling between the fluid and the heavy particles with respect to diffusion, but coupling with respect to particle velocity.

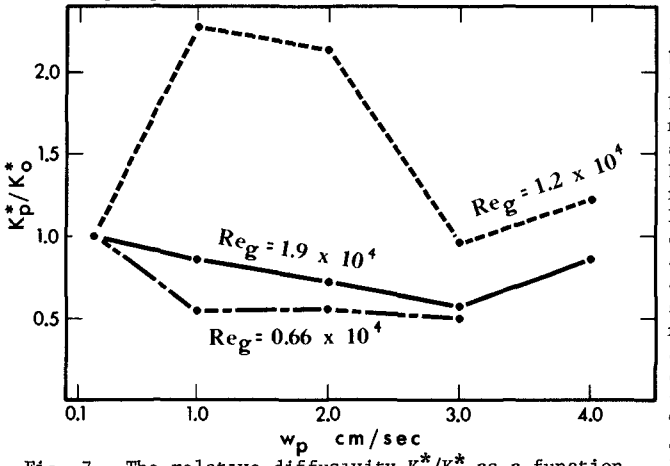

Fig. 7. The relative diffusivity K_p^*/K_o^* as a function of the particle fall velocity w_p.

It is generally believed that the more turbulent the flow the higher the degree of mixing (diffusion) of such properties as heat, momentum, sediment, aerosols, etc. Despite the relative diffusion anomaly in our data, this tendency is still clearly shown for our experiments in Figure 8, even allowing for scatter caused by varying particle fall velocity. There is also some evidence for a correlation (see Figure 9) between relative

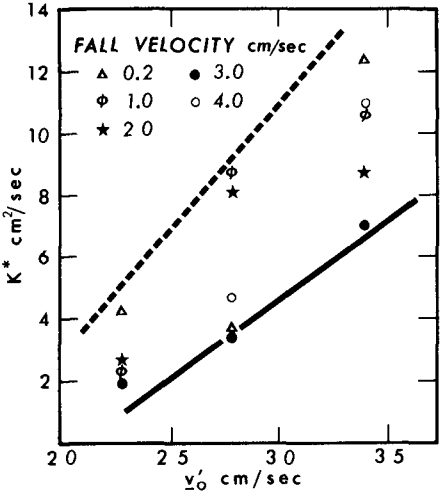

Fig. 8. The effect of the fluid turbulence intensity on the diffusion coefficients.

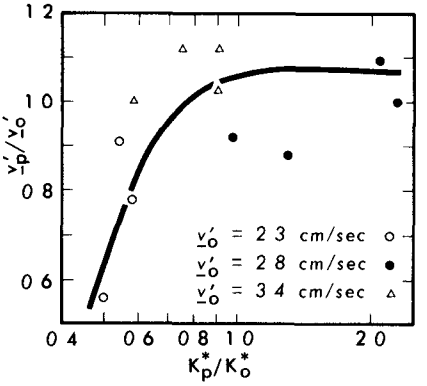

Fig. 9. The relative diffusion coefficient as a function of relative particle velocity.

particle velocity $\underline{v}_p'/\underline{v}_o'$ and relative particle diffusivity K_p^*/K_o^*. The rate of increase of the relative particle diffusivity accelerates greatly after the ratio $\underline{v}_p'/\underline{v}_o'$ exceeds approximately unity.

The particle turbulence intensity $\underline{v}_p'$ is equal to the ratio of the scale length ℓ_p^* and the scale time t_p^*

$$\underline{v}_p' = \ell_p^*/t_p^*. \tag{23}$$

It is of interest to investigate the interrelation of these three quantities. Figure 10 shows that the particle scale length (average eddy size) increases with increasing particle turbulence intensity, but with appreciable scatter because of fall velocities and frequency shifts in the power spectra. With this constraint as particle turbulence intensity increases, the scale time may then either be a constant or increase at various rates. A plot of our data is inconclusive as to the behavior of t_p^* with $\underline{v}_p$, except that t_p^* is not a constant. Apparently, fall velocity effects, power spectra shifts, and other unknown interactions control the particle scale time. This conclusion applies also to the frequency of the peak of the particle power spectrum n_p.

The frequency of the power spectral modes, both fluid and particle phases, do, however, fall in the range predicted by (16) as available to our observation.

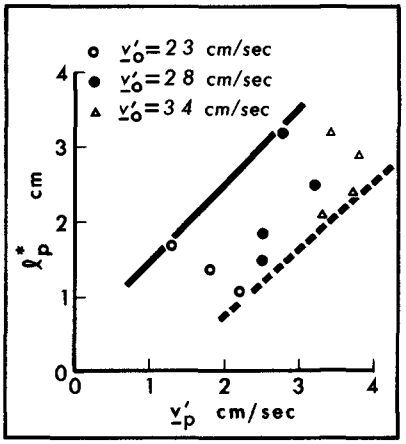

Fig. 10. The Lagrangian heavy particle length scale ℓ^*_p as a function of the turbulence intensity.

Further Discussion

All of the results up to this point have been independent of any assumption concerning the nature of the Lagrangian autocorrelation function. If we assume the often observed negative exponential shape for this function the general diffusion equation (14) results. Through (11) this equation could be written directly in terms of our measured quantities v' and K^*. Figure 11 shows a selection of the theoretical relations predicted by (14)--using our measured values of v' and K^*--compared to the experimentally observed values of particle variance σ^2 at a given time t. In general, the agreement is good. Part of the agreement is forced, of course, since the linear slope of the solid lines is computed from the observed points, but the line itself is free to wander in the σ^2-t plane. Certain systematic deviations of the observed values from the theoretical predictions (such as $Re_g = 1.2 \times 10^4$, $w_p = 2.0$ cm/sec in Figure 11) are perhaps caused by the fact that the heavy particle autocorrelation functions do not follow the exponential decay rule. This general agreement, however, supports the application of the Taylor diffusion theory to heavy particles.

A further check on the suitability of the Taylor theory can be made starting from (13). The exponential term is negligible after 2 seconds. By rearranging the remaining terms on the right hand side into the slope-abscissa intercept form of the linear equation, it is seen that the abscissa intercept of the linear portion of the σ^2-t curve is equal to the scale time t^*. Using (11) and the measured values of K^*, it is now possible to calculate values of the turbulence intensity. These are compared to the experimentally observed values in Table 4.

Table 4
Value of Turbulence Intensity cm/sec

$Re_g \times 10^{-4}$	0.66				1.2					1.9				
w_p *	.2	1	2	3	.2	1.0	2.0	3.0	4.0	.2	1	2	3	4
v' Obs. *	2.3	2.2	1.8	1.3	2.8	2.8	3.2	2.5	2.5	3.4	3.4	3.7	3.3	3.8
v' Calcu.*	2.5	2.8	3.6	1.5	3.4	2.6	2.7	1.8	3.2	2.9	2.8	6.1	11	4.0

* cm/sec

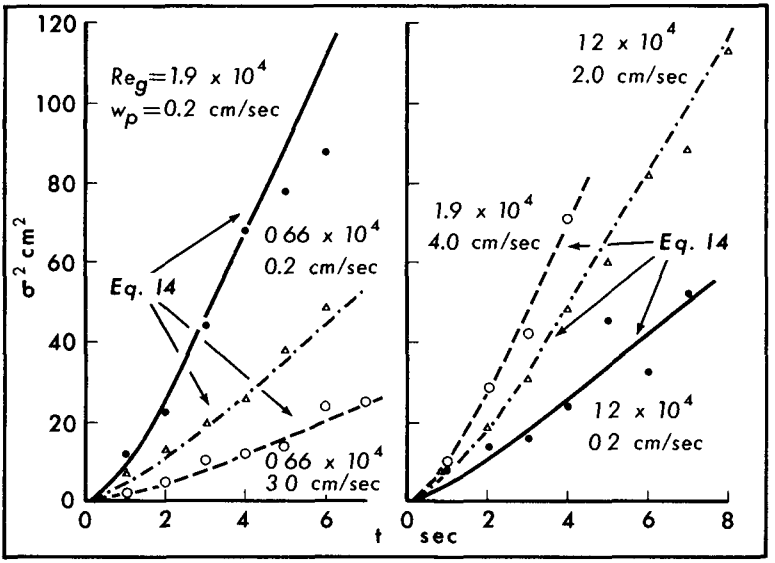

Fig. 11. A selection of experimental data on the time change of the variance of particle displacements σ^2 compared to a form of the Taylor diffusion equation.

The average error for the fourteen observations is $\pm$23 percent, which is not unreasonable considering the large error in t^* and $\underline{v}'$ produced by a relatively small error in the linear slope of the σ^2-t curve. Orlob (1959) describes yet another method of calculating diffusion parameters from particle spread.

V. SUMMARY AND CONCLUSIONS

The turbulent diffusion of quasi-neutral and heavy particles is studied in a turbulence field generated by an array of oscillating grids. Particle displacements caused by turbulence are measured by means of multiple-image photography. Diffusion coefficients and intensities of turbulence are directly measured from the photographic data. Other turbulence parameters can then be calculated.

The principal conclusions concerning the horizontal component of the turbulence are as follows:

(1) The simple experimental technique of oscillating an array of grids at various speeds produces turbulent fields with suffi-

cient homogeneity and stationarity to permit accurate study of heavy particle diffusion.

(2) The turbulent velocity distributions of both the fluid (quasi-neutral particles) and the heavy particles are Gaussian, with no evidence of a mean flow.

(3) The turbulent intensity of the heavy particle phase is closely controlled by the particle fall velocity and the fluid turbulent intensity in the vertical direction. Gravitational effects begin to dominate the heavy particle turbulence intensity after $w_p/\underline{w}_o'$ exceeds approximately 0.8.

(4) Taylor's statistical theory of turbulence effectively describes the horizontal diffusion of heavy particles suspended in a fluid.

(5) In general, the heavy particle diffusion coefficients and the scale length of the particle eddies increase with increasing fluid turbulent intensity.

(6) Relative diffusion (ratio of heavy particle diffusivity to fluid diffusivity) is a function of particle fall velocity and internal characteristics of the turbulence such as frequency shifts in the power spectra. This suggests that the turbulence spectrum as well as the orbital velocities may exert control on grain diffusion by waves.

ACKNOWLEDGMENTS

The experimental portion of this study was conducted in the Fluid Mechanics Laboratory of the Delft Technological University under a National Science Foundation Postdoctoral Fellowship.

Further support enabling the detailed data analysis and manuscript preparation was provided by the Coastal Studies Institute under the sponsorship of the Office of Naval Research, Geography Branch, Contract No. Nonr 1575(03), NR 388 002. Hyuck J. Kwon of the Institute was especially valuable in the data analysis.

NOTATION

c	the area under the autocorrelation curve
d	the diameter of the test particles (2mm)
d_s	the sedimentation diameter
E	the energy of the turbulence
K^*	the diffusion coefficient
ℓ^*	the scale length of the turbulence
M	the grid mesh length
n	the frequency of the power spectrum mode or the number of observations
N	the number of observations
Re_g	the grid Reynolds number
Re_p	the particle Reynolds number
t, T	time
t^*	the scale time of the turbulence
$\bar{U}$	the mean horizontal velocity, or its experimental equivalent the average speed of the sinusoidal grid motion
u', v', w'	turbulent velocity in the x, y, or z direction
$\overline{(v'^2)}^{1/2}$, $\underline{v'}$	the turbulence intensity in the y direction
w_p	the terminal fall velocity of a particle in still water
$\underline{w'_o}$	the fluid turbulence intensity in the vertical direction
x, y, z	the direction, respectively, of the grid motion, horizontal across the grid motion, in the vertical
ν	the kinematic viscosity
ξ	the autocorrelation lag time
ρ	the fluid density
σ^2	the statistical variance of a quantity
$( )_o$	the subscript refers to fluid or quasi-neutral particle or to initial particle position
$( )_p$	the subscript refers to a heavy particle

References

Bowen, A. J. and D. L. Inman, 1966, Budget of littoral sands in the vicinity of Point Arguello, California. Tech. Memo. No. 19, Coast. Eng. Res. Center, Corps of Eng., 41 pp.

Brown, C. B., 1950, Sediment transportation. In (H. Rouse, ed.) Engineering hydraulics. New York (J. Wiley & Sons), pp. 769-855.

Frenzen, P., 1963, A laboratory investigation of the Lagrangian autocorrelation function in a stratified fluid. Argonne National Lab. Rept. 6794, 168 pp.

Haltiner, G. J. and F. L. Martin, 1957, Dynamical and physical meteorology. New York (McGraw-Hill Book Co., Inc.), 470 pp.

Inoue, E., 1951, On the Lagrangian correlation coefficient for turbulent diffusion and its application to atmospheric diffusion phenomena. In Geophys. Res. Pap. No. 19, Geophys. Res. Dir., A.F.C.R.C., Cambridge, Mass., 530 pp.

Inoue, E., 1960, On the shape of stack plumes. Mem. on Meteor. Res., Jap. Met. Soc., 11:332-339.

Kalinske, A. A. and C. L. Pien, 1944, Eddy diffusion. Ind. Eng. Chem., 36:220-223.

Liu, V. C., 1956, Turbulent dispersion of dynamic particles. Jour. of Meteorology, 13, No. 4, pp. 399-405.

Murray, S. P., 1967, Control of grain dispersion by particle size and wave state. Jour. Geol., 75, No. 5, pp. 612-634.

Orlob, G. T., 1959, Eddy diffusion in homogeneous turbulence. Proc. A.S.C.E., 85, No. HY 9, pp. 75-101.

Prandtl, L., 1939, Beitrag zum turbulenz symposium. Proc. 5th Inter. Cong. App. Mech., pp. 340-346.

Rouse, H., 1939, Experiments on the mechanics of sediment suspension. Proc., 5th Inter. Cong. App. Mech., pp. 550-554.

Singamsetti, S. R., 1966, Diffusion of sediment in a submerged jet. Jour. of the Hydraulics Div., A.S.C.E., No. HY 2, pp. 153-168.

Stewart, R. W. and H. L. Grant, 1962, Determination of the rate of dissipation of turbulent energy near the sea surface in the presence of waves. Jour. Geophys. Res., v. 67, no. 8, pp. 3177-3180.

Sutton, O. G., 1953, Micrometeorology. New York (McGraw-Hill Book Co., Inc.), 333 pp.

Taylor, G. I., 1921, Diffusion by continuous movements. Proc. Lon. Math. Soc., 20:196 -212.

Taylor, G. I., 1935, Statistical theory of turbulence. Parts I-IV, Proc. Roy. Soc. Lon., A151, pp. 421-478.

Taylor, G. I., 1938, The spectrum of turbulence. Proc. Roy. Soc. Lon., A164, pp. 476-490.

Taylor, G. I., 1939, Some recent developments in the study of turbulence. Proc. 5th Inter. Cong. App. Mech., pp. 294-310.

CHAPTER 29

LABORATORY STUDY ON OSCILLATORY BOUNDARY LAYER FLOW

Kiyoshi Horikawa
Professor
and
Akira Watanabe
Postgraduate

Department of Civil Engineering
University of Tokyo
Tokyo, Japan

ABSTRACT

The characteristics of oscillatory boundary layer flow have been treated with keen interest during the last decade from the various aspects. Among the previous results the theoretical treatment by K. Kajiura must be the most important and fruitful one to advance in our knowledge on the present phenomena. On the other hand the senior author has had a real interest in the behaviour of sediment particles due to oscillatory fluid motion, and has conducted his systematic investigations on the sediment movement in nearshore area.

The aim of this paper is to introduce some results of the recent investigations conducted at the Coastal Engineering Laboratory, University of Tokyo, with the intention of investigating the applicability of Kajiura's theory to the oscillatory flow in the vicinity of bottom with sand ripples.

In order to accomplish the above purpose, the authors applied the hydrogen bubble technique to measure accurately as much as possible the time history of velocity distribution especially in the very thin layer above the bottom boundary associated with the progressive waves. The above measuring technique was verified to be enormously powerful even in the case of unsteady flow. The bottom conditions tested in the present investigation were of 1) hydrodynamically smooth bottom, and 2) rough bottom with artificial ripples. The pictures of hydrogen bubble lines released successively from a fine platinum wire were taken by using a 16mm cinecamera specially equiped, and were analyzed flame by flame to take the digitalized data of horizontal velocity of fluid. The data were analyzed in Fourier series and the first mode of the series was only taken to compare with the numerical curves obtained through the Kajiura's theory. The horizontal velocity amplitude and its phase, the eddy viscosity

and the shear stress at each elevation above bottom were calculated by using not only the experimental data of present investigation, but also the laboratory data obtained by I. G. Jonsson.

The agreement between the analysed data and the theoretical curves is basically consistant; this fact verifies the usefulness of the Kajiura's theory. Even though, there are some questions in the theoretical treatment which are arising out of the present investigations. The accumulation of more accurate data is basically requested to clarify these problems. Lastly the comparative study on eddy viscosity averaged over wave cycles in the neighbourhood of sand ripples was established by using the laboratory data of suspended sediment concentration.

INTRODUCTION

The characteristics of oscillatory boundary layer flow induced by surface waves seem to take a primarily important role on the generation, growth and decay of shallow water waves and on the behaviour of coastal sediment in nearshore area. Up to now some prominent treatments on this subject have been made mainly from the theoretical point of view by M. S. Longuet-Higgins,[1] K. Kajiura[2] and others, while from the experimental point of view by I. G. Jonsson,[3] getting a great deal of advanced insight into the characteristics of oscillatory boundary layer flow. But still numerous questions have been remained unsolved due to mainly the profound difficulty in observation and measurement of actual state as well as to the complexity of questioned phenomena.

The aim of this paper is to introduce the main results of the laboratory studies on the above subject carried out at the Coastal Engineering Laboratory, University of Tokyo, during the last few years. The authors have been applying the hydrogen bubble techniques to measure the time history of vertical distribution of horizontal velocity component, especially in the vicinity of bottom, associated with the propagation of surface waves. The laboratory measurements have been repeated under the various conditions of wave and bottom surface. After the laborious improvement of measuring procedures, it was finally successful to visualize the instantaneous velocity distribution and/or the intensity of turbulent fluctuation and to measure the velocity within a really thin boundary layer developed along the flume bottom. In this paper will be presented the data of horizontal velocity distribution in the oscillatory boundary layer which were measured under the conditions of 1) hydrodynamically smooth bottom and 2) roughened bottom with artificial ripples. In the following the comparison of the Kajiura's theory for the bottom boundary layer in water waves with the laboratory data will be conducted by use of the present data mentioned above and the one reported by I. G. Jonsson in 1963. Finally the values of eddy viscosity evaluated by using the measuring data of vertical distribution of suspended sediment concentration will be given and compared with the calculated ones on the basis of the Kajiura's assumption.

BASIC THEORIES ON OSCILLATORY BOUNDARY LAYER FLOW

Equation (1) was introduced by M. S. Longuet-Higgins[1] as an expression for the horizontal velocity component u in a laminar boundary layer induced by progressive waves:

$$u = \hat{U}[\cos(\sigma t - kx) - e^{-z/\delta_L}\cos(\sigma t - kx - z/\delta_L)] \tag{1}$$

where $\hat{U} = \pi H/(T \sinh kh)$, $k = 2\pi/L$, $\sigma = 2\pi/T$, $\delta_L = (2\nu/\sigma)^{1/2}$, ν kinematic viscosity of fluid, H:wave height, T:wave period, L:wave length, h:water depth, t:time, x:horizontal axis, and z:vertical axis taking upward positive from channel bottom.

On the other hand, K. Kajiura[2] presented a model of the bottom boundary layer in water waves and obtained quite important results. He introduced and/or defined such relationships as shown in the following:

$$\frac{\tau}{\rho} = \hat{u}_B^* u^* = K_z \frac{\partial u}{\partial z} \tag{2}$$

$$\delta^* = \mathrm{Amp}\int_0^\infty (U-u)\,dz \,/\hat{U} \tag{3}$$

where τ:friction stress, ρ:density of fluid, u^*:friction velocity, u_B^*:friction velocity at bottom, u:horizontal velocity component in a boundary layer, U:horizontal velocity component at the outeredge of frictional layer, K_z:vertical eddy viscosity, δ^*:wave displacement thickness, and $\hat{}$ denotes the amplitude of physical property.

Following the hypothetical concept of the wall and the defect layers established for the case of a steady turbulent boundary layer, K. Kajiura assumed the frictional layer of the oscillatory flow to consist of three layers: the inner layer, the overlap layer, and the outer layer. He also introduced three numbers such as $N(=12)$, $\kappa(=0.4)$ and $K(=0.02)$ corresponding to the above three layers, and defined the value of K_z as follows:

For the case of hydrodynamically smooth bottom:

$$K_z = \begin{cases} \nu & 0 \leqq z \leqq D_L \quad \text{(inner layer)} & (4a) \\ \kappa \hat{u}_B^* z & D_L < z \leqq d \quad \text{(overlap layer)} & (4b) \\ \kappa \hat{u}_B^* d & d < z \quad \text{(outer layer)} & (4c) \end{cases}$$

where D_L, the thickness of laminar sublayer (or inner layer), is determined by $\hat{u}_B^* D_L/\nu = N$, while d, the upper limit height of the overlap layer above bottom, is by $\kappa u_B^* d = K\hat{U}\delta^*$.

For the case of hydrodynamically rough bottom:

$$K_z = \begin{cases} \alpha\kappa \hat{u}_B^* D_R & 0 \leqq z \leqq D_R \quad \text{(inner layer)} & (5a) \\ \kappa \hat{u}_B^* z & D_R < z \leqq d \quad \text{(overlap layer)} & (5b) \\ \kappa \hat{u}_B^* d & d < z \quad \text{(outer layer)} & (5c) \end{cases}$$

where z_0:roughness length, D:Nikuradse's equivalent roughness, and D_R:thickness of inner layer. The following relations are also assumed:

$$\left.\begin{aligned} D&=30\ z_o \\ D_R&=(1/2)D=15z_o \\ \alpha&=\ln(D_R/z_o)=2\ 708 \end{aligned}\right\} \tag{6}$$

If the total thickness of the bottom frictional layer is assumed to be very small compared with the wave length, and the nonlinear effect is also assumed to be negligible (except turbulence), the equation of oscillatory motion in the boundary layer is given by

$$\frac{\partial}{\partial t}(u-U)=\frac{\partial}{\partial z}\left(\frac{\tau}{\rho}\right) \tag{7}$$

Combination of Eqs. (2) and (7) gives the following basic equation:

$$\frac{\partial^2 u^*}{\partial z^2}-\frac{i\sigma}{K_z}u^*=0 \tag{8}$$

where τ/ρ is replaced by u^* with the aid of Eq. (2). Substituting the hypothetical expression of K_z, Eq. (4) or Eq. (5) corresponding to the bottom condition, into Eq. (8), K. Kajiura solved the basic equation to obtain the generalized equations for u and u^*. He also defined the friction coefficient C by $\tau_B/\rho=C\hat{U}U$ and found that the amplitude $\hat{C}$ and phase θ of friction coefficient were expressed as functions of $R=\hat{U}\delta_L/\nu$ (where $\delta_L=(\nu/\sigma)^{1/2}=\delta_L/\sqrt{2}$) for smooth bottom or $\hat{U}/(\sigma z_o)$ for rough bottom.

He took tentatively the following criterions to classify the bottom conditions in the hydraulic sense and the flow regimes.

For the transitional region from smooth to rough:

$$0.4\leq D/D_L\leq 5 \tag{9}$$

For the transitional region from laminar to turbulent:

$$0.4\leq \overset{*}{\delta}/D_L\leq 5 \tag{10}$$

Rewriting Eqs. (9) and (10), the transitional region from laminar to turbulent for smooth bottom is expressed by

$$25\leq R\leq 650 \tag{11}$$

while that rough bottom is given by

$$10^2\leq M\leq 10^3 \tag{12}$$

where $M=\hat{U}D/\nu$.

The description mentioned above is the outline of Kajiura's

theory, in which thereare several questions to be clarified. These are:

(1) Whether the assumption for K_z is appropriate to the present problem or not?

(2) Whether the basic equation (7) is adequate to express the flow characteristics in the vicinity of bottom with ripples or not? The question of this kind arises from the fact that a relatively large vortex exists behind a ripple.

(3) How should we determine the origin of z axis when the bottom is rough?

(4) Is the assumption for the estimate of D_R and z_0 as shown in Eq. (6) reasonable?

In order to clarify the above questions the systematic and careful measurements of the flow characteristics in a boundary layer are basically required.

In addition to the above discussion we will consider the critical condition for the disappearance of overlap layer. For the smooth bottom the criterion is given by $D_L > d$. According to K. Kajiura, the height of the outeredge of overlap layer is expressed by

$$d = 0.05\hat{C}^{\varkappa}\hat{U}/\sigma \tag{13}$$

Considering the relations of $D_L = \nu N/\hat{u}_B^*$ and $R^2 = (\hat{U}\delta_L'/\nu)^2 = \hat{U}^2/(\sigma\nu)$, we will obtain the following inequality as the critical condition for the disappearance of overlap layer:

$$\hat{C} < 240/R \tag{14}$$

Taking into consideration the given relationship between $\hat{C}$ and R, the criterion of Eq. (14) is rewritten as

$$R < 217 \tag{15}$$

Comparing Eq. (15) with Eq. (11), we may conclude that the overlap layer for the smooth bottom exists always in the range of turbulent flow, but not in the range of laminar flow.

On the other hand, the criterion for rough bottom is expressed by $D_R > d$, which is equivalent to Eq. (16) or Eq. (17).

$$\hat{C} < 9.0\times10^4(\hat{U}/\sigma z_0)^2 \tag{16}$$

$$\hat{U}/(\sigma z_0) < 3.5\times10^3 \tag{17}$$

The above criterion is again rewritten as follows by using the total excursion distance of horizontal particle motion just outside of boundary layer d_0:

$$d_0/D < 230 \tag{18}$$

As a result of the above discussion it is known that when the roughness elements with relatively large size exist along the bottom, the overlap layer may always disappear.

LABORATORY APPARATUS AND MEASURING TECHNIQUES

The present authors have recognized that the hydrogen bubble technique is quite powerful to visualize the stream line and velocity distribution in a laboratory flume even in the case of oscillatory flow.[4] The principle of this instrument is to take moving pictures of hydrogen bubble line which is generated from a cathode of a fine platinum wire (50μ in diameter). The schematic diagram of the instrumentation system is shown in Fig. 1. The voltage charged between the cathode and anode is as high as about 1 KV, and the input pulse is discharged at intervals of about 50 cps. An iodine lamp (200 V and 1 KW) is used as a light source for illuminating the hydrogen bubble lines, and a 16mm camera (Canon Scoopic-16) is used for taking clear and accurate pictures with negligible aberration of camera lens.

The wave flume used for the present investigation is 50m long, 60cm wide and 90cm high. The bottom conditions tested are two; one is smooth bottom made of hard vinyl plate and the other is rough bottom made of plastic wavy board as shown in Fig. 2. The rise and pitch of the artificial ripple are 0.8cm and 3.2cm respectively. The test waves for the rough bottom are adjusted as much as possible to have the combination of wave height and period which suits to the size of the ripple. In order to adjust the wave conditions the generalized diagrams among wave characteristics, water depth, ripple size and grain diameter are applied under the assumption of $M_d=200\mu$, where M_d is the medium grain diameter of sediment.

The test waves are generated by a flap type wave generator which is installed at the end of wave flume. The 5th to 7th waves are selected for the measurement of velocity by the reason that these waves are almost in a steady state and that the waves reflected from the other end of flume have not arrived at the measuring section yet. The hydraulic conditions of the present investigations are given in Table 1 together with that of Jonsson's experiment.

In order to compare the laboratory data with the theory, the time histories of surface profile and of velocity at each elevation are analyzed in Fourier series and the first mode of corresponding data is only, in general, taken into consideration. Therefore in Table 1, H is the wave height corresponding to the fundamental period T, and $\hat{U}$ is calculated by the relation of $\hat{U}=\pi H/(T \sinh kh)$. The Reynolds number $R=\hat{U}\delta/\nu$ or $M=\hat{U}D/\nu$ is also given in Table 1 as an index of flow regions such as laminar, transitional and turbulent. The computation of M is based on the assumption of $D=4\eta$, where η is the rise of ripple.

The close-up of hydrogen bubble rows is taken by the 16mm cine camera with the speed of 48 flames per second. Analysis of each flame of film gives the time history of horizontal velocity component at each elevation. In the case of rough bottom with artificial ripples, the measuring section is fixed at the trough of a certain ripple.

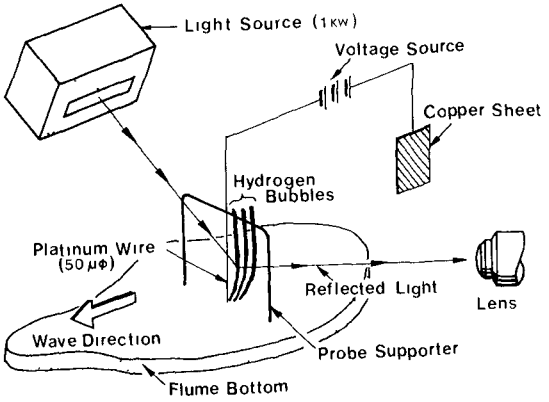

Fig. 1. Instrumentation system.

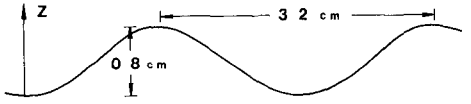

Fig. 2. Artificial ripple.

Table 1. Experimental conditions.

Investigators	Experimental Method	Bottom Condition	No	T (sec)	h (cm)	H (cm)	ν (cm²/sec)	$\hat{U}$ (cm/sec)	$R = \hat{U}\delta_s/\nu$	$M = \hat{U}0/\nu$
Authors	Progressive Waves	Smooth	—	1 50	41 0	3 71	$9\,23\times10^{-3}$	6 82	35	—
		Artificially Roughened with Ripples	1	1 07	39 4	8 16	$1\,00\times10^{-2}$	10 9	—	$3\,5\times10^{3}$
			2	1 60	34 6	11 8	$1\,37\times10^{-2}$	25 6	—	$6\,0\times10^{3}$
Jonsson	Oscillatory Tank	Artificially Roughened	—	8 39	—	—	$9\,33\times10^{-3}$	213 1	—	$3\,4\times10^{4}$

ANALYSIS OF DATA AND DISCUSSION

SMOOTH BOTTOM

1) Velocity Distribution

The horizontal velocity at each elevation read from film as well as the surface profile recorded by a parallel wire resistance gauge is, as mentioned in the previous chapter, analyzed in Fourier series, and the data corresponding to the fundamental period T are plotted as shown in Fig. 3. Figure 3(a) is for the amplitude ratio between u and U, $\hat{u}/\hat{U}$, and Fig. 3(b) is for the phase difference ϵ between u and U. The reader should notice that the velocity at the elevation of z=0.018cm is measurable. In the same figures the theoretical curves calculated through the Kajiura's theory are also shown by solid line for the comparison between the theory and the experimental results. In this particular case the Reynolds number R is equal to 35; this fact indicates that the flow is in the transition between laminar and turbulent (see Eq. (11)). Under such condition the rate of discrepancy in $\hat{u}/\hat{U}$ and ϵ between Eq. (1) for laminar flow and the Kajiura's theory is at the most 1% respectively.

The comparison of the experimental data with the theoretical curves indicates that:

(1) The rate of discrepancy in velocity amplitude between them is in the order of 1 to 5%, but increases up to about 10% in the very vicinity of bottom (z=0.018cm).

(2) The agreement of velocity phase difference is very good in the region of $z \geq 0.09$cm, but is not satisfactory at the elevation of z=0.018cm. The phase of experimental data at the latter elevation is about 12° smaller than the theoretical one. It is still uncertain whether such systematic differences mentioned above are caused by the nonlinear effect of higher harmonics or by the inaccuracy of the measuring techniques and of the data analysis.

2) Eddy Viscosity

Combining Eqs. (2) and (7), we obtain the following expression for the vertical eddy viscosity K_z:

$$K_z = -\int_{\delta}^{z} \frac{\partial}{\partial t}(u-U)\,dz \Big/ \frac{\partial u}{\partial z} \tag{19}$$

where δ is the thickness of frictional layer.

By using the analyzed data of velocity distribution, the value of K_z at each elevation for each phase is calculated numerically on the basis of Eq. (19) and plotted in Fig. 4. In the same figure the vertical distribution of K_z assumed by K. Kajiura is also shown by solid lines. The reader should be mentioned that the overlap layer disappears in this case because of R=35 (see Eq. (15)). The data of K_z estimated from the experimental values are distributed in the vicinity of solid lines

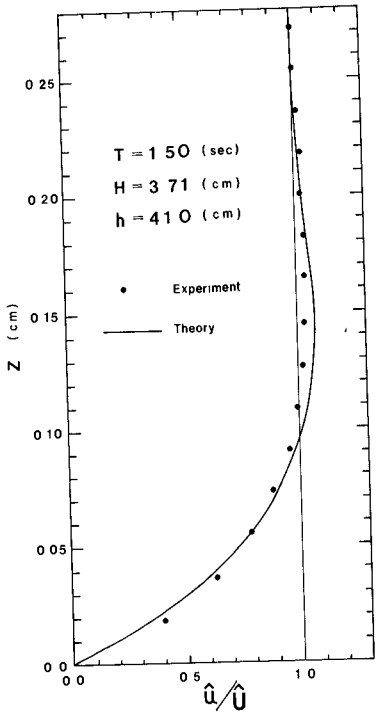

Fig. 3(a). Amplitude ratio of u to U. (Smooth bottom)

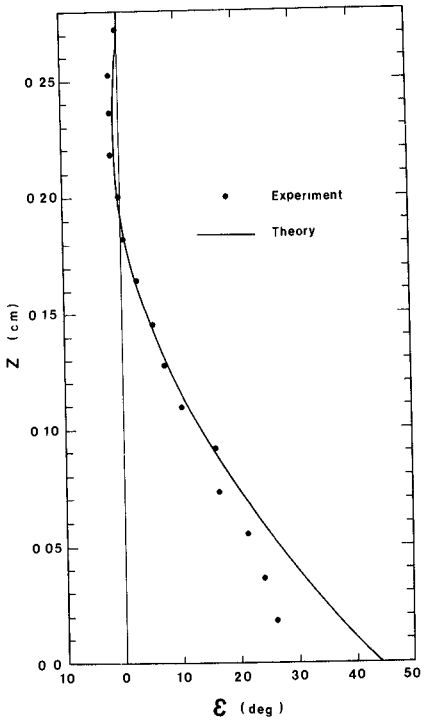

Fig. 3(b). Phase difference between u and U. (Smooth bottom)

with great scattering especially at the level of $z \gtrsim 0.05$cm. As an example the variation of K_z at $z=0.091$cm with the wave phase φ is shown in Fig. 5. The origin of abscissa φ in this figure is taken at the moment when the corresponding crest of surface wave arrives at the measuring station. According to the assumption taken in the Kajiura's theory, $K_z=\nu$ in the inner layer ($z \leq D_L$), and $K_z=\kappa \hat{u}_* d$ in the outer layer ($z>D_L$), therefore there is a discontinuity of K_z at the boundary between the inner and outer layers in the present case. On the other hand, the estimated values of K_z at each elevation indicate a periodic fluctuation and also the mean of K_z averaged over one wave cycle seems to be expressed quite naturally by a certain continuous function of z.

3) Shear Stress

Figure 6 gives the value of τ/ρ estimated through Eq. (7) by using the analyzed data of velocity distribution. Figure 6(a) is for the amplitude of τ/ρ and Fig. 6(b) is for the phase difference γ between τ/ρ and U. In these figures the solid circle indicates the data calculated from the fundamental mode of velocity u_1, while the open circle indicates the first mode data of τ/ρ calculated from the combined velocity $u_{1\sim6}$. Where $u_{1\sim6}$ is the combined velocity which includes 1st to 6th modes. The mode higher than 6th is practically negligible. The good agreement between the open circle and closed circle suggests us the applicability of superposition of shear stresses as a simple approximation. In Fig. 6 the theoretical curves of $\hat{\tau}/\rho$ and γ are also shown for the comparison. The agreement between the estimated values and the theory is satisfactory.

ROUGH BOTTOM

1) Velocity Distribution

Figures 7 and 8 give the amplitude $\hat{u}/\hat{U}$ and phase ϵ of u/U corresponding to the fundamental mode of different waves. As stated in the previous chapter the velocity was measured at the section of ripple trough. The flow characteristics in both cases are in a fully turbulent region judging from the values of M given in Table 1 (see Eq. (12)). The overlap layer is also disappeared in both cases. In order to compare the above data with the Kajiura's theory, we have to consider the following two questions: One is how to determine the origin of z axis (apparent bottom level) and the other is how to assume the thickness of inner layer $D_R (=15z_0)$. H. Motzfeld[5] conducted his laboratory experiments by using a ripple model, which had the shape of crest angle being 120° and of the trough with circular arc, under the condition of steady turbulent flow, and determined the Nikuradse's equivalent roughness D as 4 times the rise of ripple η. Supposing that the Motzfeld's result is applicable to the present unsteady flow also, we determined the thickness D_R as follows:

$$D_R = D/2 = 2\eta = 1.6cm$$

In Figs. 7 and 8 are shown the theoretical curves calculated on

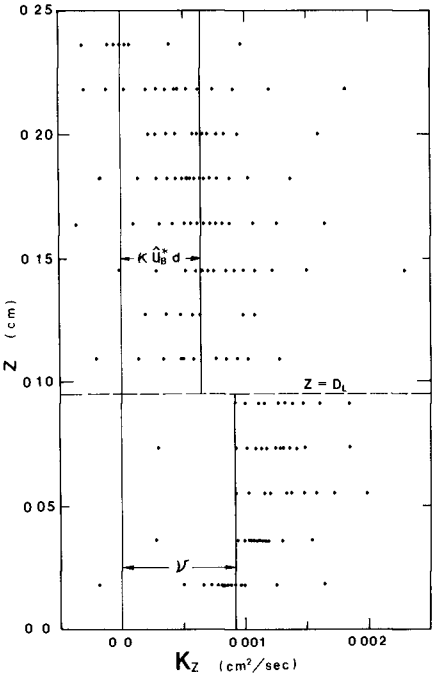

Fig. 4. Vertical distribution of eddy viscosity. (Smooth bottom)

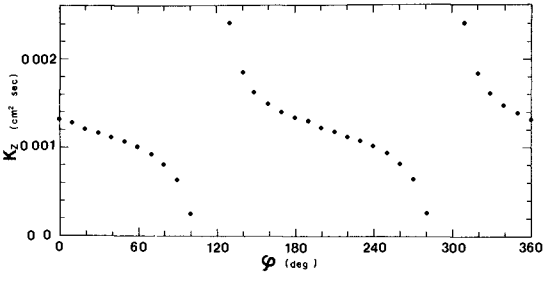

Fig. 5. Variation of eddy viscosity with wave phase. (Smooth bottom, z = 0.191cm)

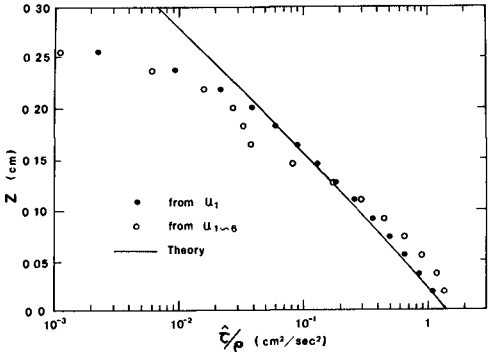

Fig. 6(a). Amplitude of shear stress. (Smooth bottom)

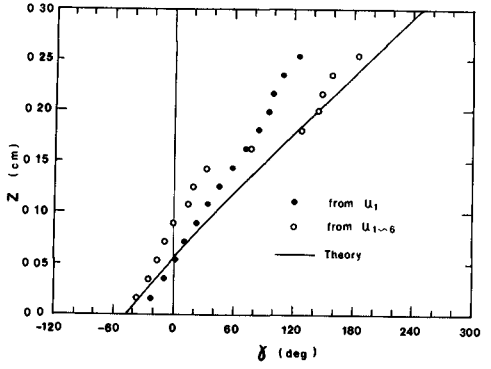

Fig. 6(b). Phase difference between shear stress and U. (Smooth bottom)

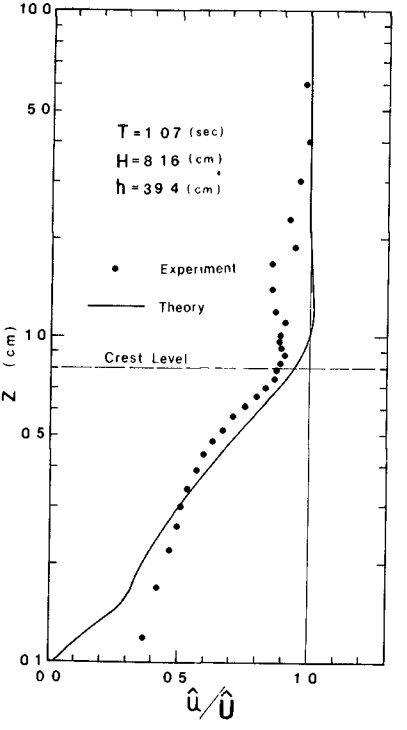

Fig. 7(a). Amplitude ratio of u to U. (Rippled rough bottom, Test series No. 1)

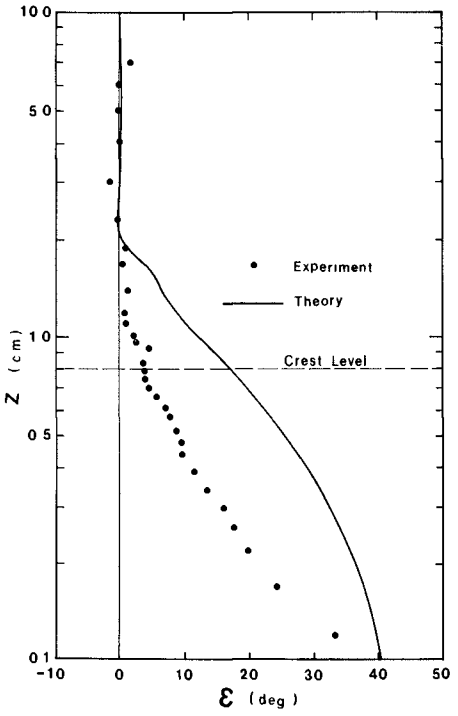

Fig. 7(b). Phase difference between u and U. (Rippled rough bottom, Test series No. 1)

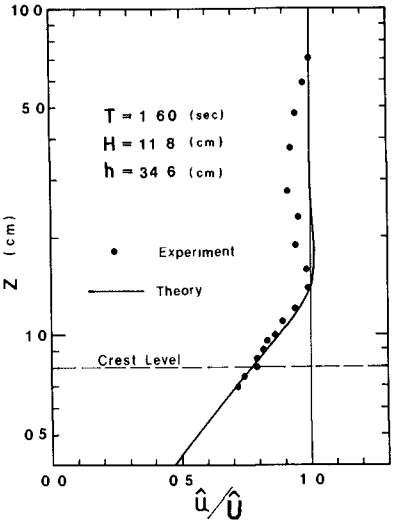

Fig. 8(a). Amplitude ratio of u to U. (Rippled rough bottom, Test series No. 2)

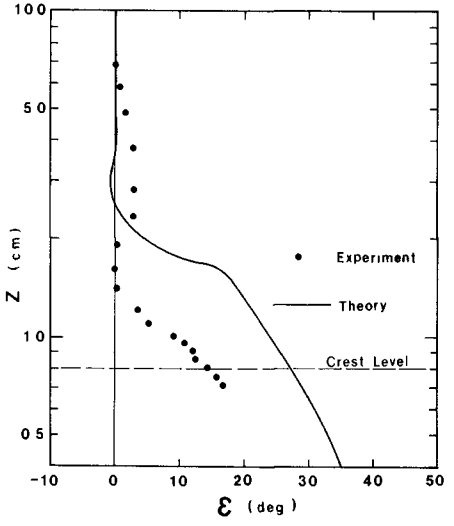

Fig. 8(b). Phase difference between u and U. (Rippled rough bottom, Test series No. 2)

the basis of the above assumption and also by taking the zero level of z at the trough of artificial ripple. The agreement between the laboratory data of $\hat{u}/\hat{U}$ and the theoretical curve is fairly good in general. But the data at the elevation a little higher than the ripple crest (z=0.8cm) have a consistent tendency of taking smaller values compared with the theoretical ones. This tendency may be caused by the influence of vortex appeared behind a ripple. On the other hand the laboratory data of ϵ are about 10° to 20° smaller than the theoretical ones.

It is well known that I. G. Jonsson conducted his valuable experiment on oscillatory flow by using the ingenious apparatus of oscillatory tank. He installed artificial roughness elements as shown in Fig. 9 on the bottom of oscillatory tank and measured the velocity distribution by means of a miniature current meter of propeller type. Figures 10(a) and 10(b) were taken from the figures appeared in the Kajiura's paper. In this case K. Kajiura took z=0 at the height of 0.35cm above the trough of roughness elements and also assumed as z_0=0.05cm , which was equivalent to the condition of $D=30z_0=2.5\eta$, η being the height of artificial roughness. In this experiment the total excursion length d_0 was fairly large compared with the scale of roughness elements, hence the value of d_0/D=380 was large enough to maintain the overlap layer. The agreement between the theoretical curves and the experimental data for the first mode is quite satisfactory.

The agreement in the authors' cases (T=1.07sec and 1.60sec) is not so good as in Jonsson's case (T=8.39sec). The above fact may be explained by the following reason: The artificial roughness elements of the authors' experiment are relatively large compared with the scale of oscillatory motion, hence the turbulence induced by vortex is predominate. As a result of this situation Eq. (17), in which the vertical component of velocity is neglected, is incomplete to represent the flow characteristics of the present case.

3) Eddy Viscosity

Figure 11 gives the distribution of K_z determined through Eq. (19) as for the case of smooth bottom by using the velocity distribution of the first mode oscillation. The scattering of data indicates the time variation of K_z as in the case of smooth bottom. There happens a curious result such as negative value of K_z. This may be caused partly by the error of numerical computation for K_z, but mainly by the following fundamental reason. That is, Eq. (7) is inadequate to express the present phenomena due to the existance of vortex with relatively large scale. The vortex induces the vertical velocity component which is comparative to the horizontal one.

Figure 12 shows the vertical distribution of K_z estimated from the Jonsson's data. The fluctuation of K_z in the vicinity of bottom is small compared with that in Fig. 11, but it seems relatively large in the range of $z \gtrsim 2$cm. The agreement between

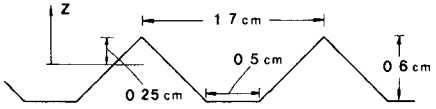

Fig. 9. Artificial roughness in Jonsson's experiment.

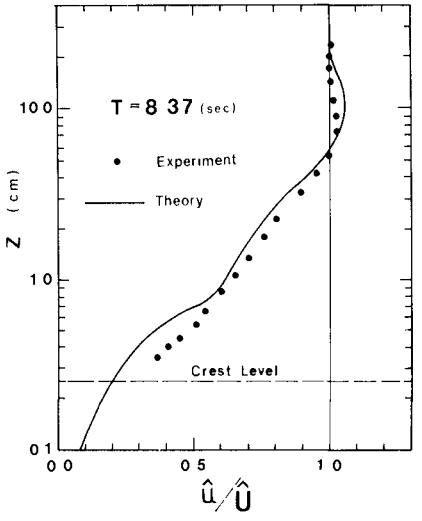

Fig. 10(a). Amplitude ratio of u to U based on Jonsson's data. (After K. Kajiura[2])

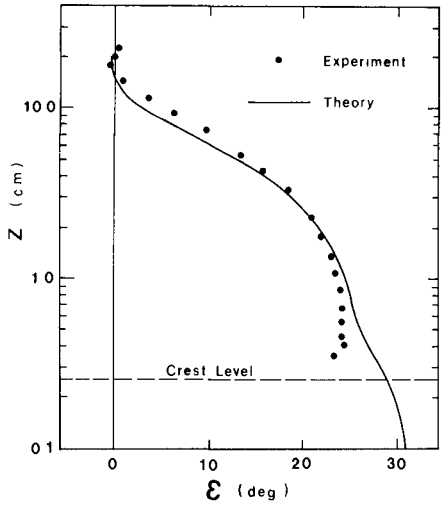

Fig. 10(b). Phase difference between u and U based on Jonsson's data. (After K. Kajiura[2])

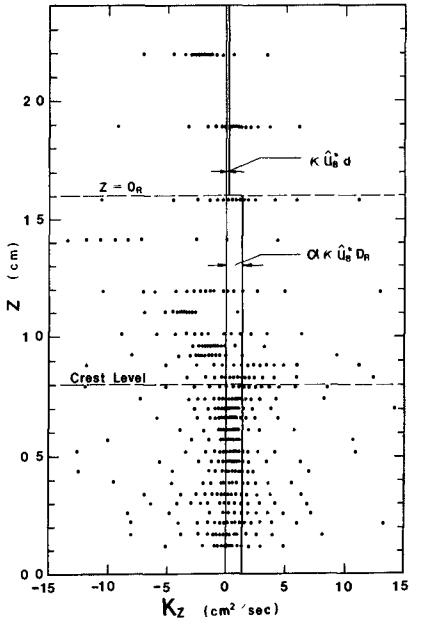

Fig. 11. Vertical distribution of eddy viscosity. (Rippled rough bottom, Test series No. 2)

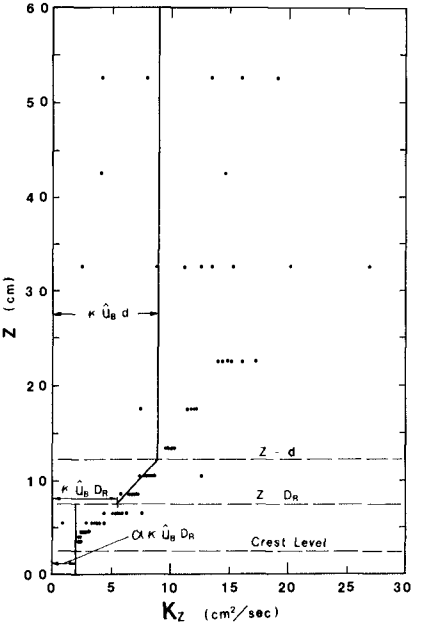

Fig. 12. Vertical distribution of eddy viscosity based on Jonsson's data.

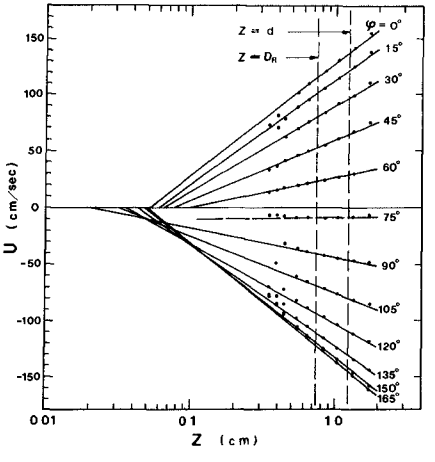

Fig. 13. Velocity distribution for each wave phase based on Jonsson's data.

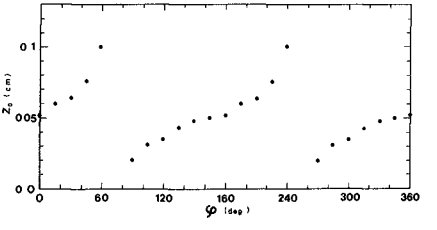

Fig. 14. Variation of roughness length with wave phase based on Jonsson's data.

the theoretical assumption (Eq. (5)) and the estimated value is fairly well, but the expression of $K_z=\kappa\hat{u}_R^* z$ for $D_R<z<d$ and $0\leq z\leq D_R$ too seems better than that of Eq. (5) at least in the questioned case.

4) Roughness Length

The horizontal velocity distribution in the overlap layer is well approximated by the logarithmic distribution curve. From this point of view in Fig. 13 the analyzed data of Jonsson are plotted in each phase. The roughness length z_o is determined as an intersection between the axis of $u=0$ and the extended straight line of velocity distribution curve in the overlap layer on a semilog paper. The value of z_o thus determined fluctuates with the phase of surface wave motion as shown in Fig. 14. But it can not be determined at the phases near 75° and 255°, where shear stress becomes zero.

5) Shear Stress

Similar to the case of smooth bottom, the vertical distribution of shear stress τ/ρ is calculated numerically by using the Jonsson's data and is shown in Fig. 15. Figure 15(a) is for $\hat{\tau}/\rho$ and Fig. 15(b) is for the phase difference γ between τ/ρ and U. The definition of open and closed circles is the same as in the smooth bottom case. The agreement between the two results is fairly well for $\hat{\tau}/\rho$, but is not well for γ. The discrepancy of γ is about 5°~6° between the two cases. At any rate the superposition of shear stress seems to be a good approximation in the rough bottom case as well as in the smooth bottom case.

SUSPENDED SEDIMENT CONCENTRATION

During the last decade the senior author has devoted his continuous efforts to study the suspended sediment concentration and reported a part elsewhere.[6] In the following a further study will be described briefly.

The suspended particle is actually heavier than the fluid, hence the following will be given as the fundamental equation of the suspended sediment concentration.[7]

$$\frac{d}{dz}\left(K_z\frac{d\bar{c}}{dz}\right)+(\beta w_o)\frac{d\bar{c}}{dz}=0 \tag{20}$$

where $\bar{c}$: sediment concentration averaged over one wave cycle, w_o: fall velocity of sediment particle, and β: a coefficient usually taken as unity.

The senior author has analyzed the suspended sediment phenomena due to surface waves and proposed a method to determine the vertical distribution of suspended sediment concentration.[6] The basic assumption of the above treatment was that the diffusion process was governed by the turbulence associated with the orbital motion of water particle, and that the potential theory of surface waves was applicable as a first approximation to

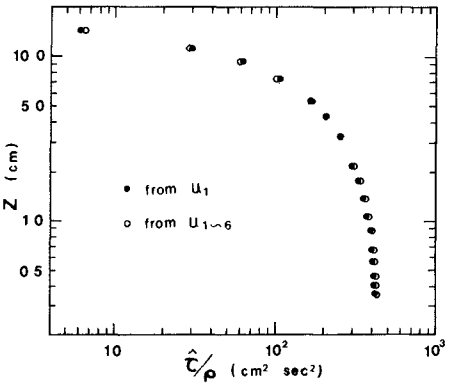

Fig. 15(a). Amplitude of shear stress based on Jonsson's data.

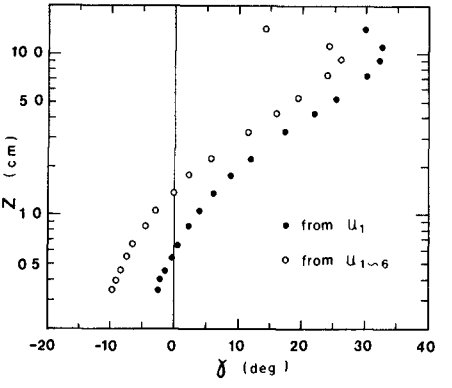

Fig. 15(b). Phase difference between shear stress and U based on Jonsson's data.

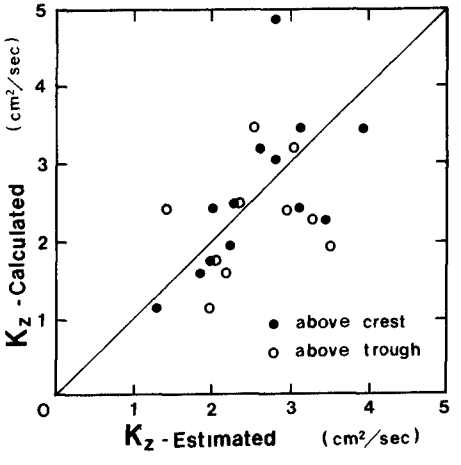

Fig. 16. Comparison between estimated and calculated eddy viscosity.

estimate the eddy viscosity K_z. Therefore the above treatment may be applicable only to the suspended sediment phenomena in the upper layer of water beyond the outer layer.

While Kishi et al.[8] applied the expression of eddy viscosity such as $K_z=\alpha' \kappa u_B^* (z+z_0)$ to the suspended sediment problem, where α' is a coefficient. The above expression of eddy viscosity was originally proposed by K. Kajiura[9] in his early paper. Considering the assumption of K_z, we may recognize that their result on the vertical distribution of suspended sediment concentration is applicable to a certain limited layer near the bottom. Here the authors will concentrate their attention on the effect of ripples on the sediment motion.

According to Eq. (5a) the eddy viscosity for the inner layer is expressed by $K_z=\alpha\kappa\hat{u}_B^* D_R$, hence the integration of Eq. (20) gives the following solution:

$$\bar{c}=\bar{c}_0 \exp[(\beta w_0/K_z)z] \tag{21}$$

where $\bar{c}_0$ is the concentration at the level of $z=0$. Under the assumption of $\beta=1.0$ the value of K_z for each run of experiment reported previously was estimated,[10] while the theoretical one was calculated under the assumption of $D_R=2\eta$, η being the rise of sand ripple. Figure 16 shows the comparison between K_z (estimated) and K_z (calculated), where the laboratory data are grouped into two; one is the data measured above ripple crest and the other above ripple trough. Even a large scattering of data, the majority of them falls near the 45° straight line. From the above fact, the dimensionless number β, which was introduced to express the influence of relative scale between grain size and the scale of turbulence, may be taken as unity at least in the very vicinity of sand bottom.

CONCLUSIONS

The characteristics of oscillatory boundary layer flow have been investigated from many aspects on the basis of laboratory data of velocity distribution in a boundary layer. The hydrogen bubble technique is surprisingly powerful to measure the velocity in the very vicinity of bottom or in the space behind ripple. In order to increase the accuracy of measurement and of data processing, it is still required to improve more the present instrumentation system.

The Kajiura's theory is a very important treatment to clarify the characteristics of oscillatory boundary layer flow, but involves some questionaries to be solved in future. These are as follows:

1) According to the present investigation, the eddy viscosity seems to be a time dependent function with the same period as the surface wave, and also a continuous function of z. Based on the above fact, the Kajiura's assumption is not always satisfactory to the present phenomena.

2) There is no rule how to determine the zero level of z axis

in the case of rough bottom.

3) It is still uncertain whether the estimation of D_R, D and z_0 introduced into the Kajiura's theory is appropriate to the present phenomena.

More accurate data are required to make the above problems clear. Besides, it is necessary to introduce another basic equation which is applicable to the phenomena in the very vicinity of sand ripple. The flow is very complicative owing to the existence of a large vortex. Further studies are truely needed to advance our knowledge on the oscillatory flow phenomena.

ACKNOWLEDGEMENTS

The work reported herein is a part of investigations carried out under the support of the Scientific Research Fund of the Ministry of Education in Japan. The authors wish to acknowledge with appreciation Dr. Kinjiro Kajiura, Professor at the Earthquake Research Institute, University of Tokyo, who gave the authors valuable suggestions and discussions on this work.

REFERENCES

1) Longuet-Higgins, M. S.: The Mechanics of the Boundary Layer near the Bottom in a Progressive Wave, Proc. 6th Conf. on Coastal Eng., 1957.
2) Kajiura, K.: A Model of the Bottom Boundary Layer in Water Waves, Bull. Earthquake Res. Inst., Univ. of Tokyo, Vol. 46, 1968.
3) Jonsson, I. G.: Measurements in the Turbulent Wave Boundary Layer, 10th Congress, I.A.H.R., London, Vol. 1, 1963.
4) Horikawa, K., A. Watanabe and H. Maoka: On a New Device to Measure the Water Particle Velocity due to Surface Waves, Memoir 22nd Annual Conv., J.S.C.E., 1967. (in Japanese)
5) Motzfeld, H.: Die Turbulente Strömung an Welligen Wanden, Z. angew. Math. u. Mech., 17, 1937.
6) Hom-ma, M. and K. Horikawa: Suspended Sediment due to Wave Action, Proc. 8th Conf. on Coastal Eng., 1962.
7) Batchelor, G. K.: The Motion of Small Particles in Turbulent Flow, Proc. 2nd Australasian Conf. on Hydraulics and Fluid Mechanics, 1965.
8) Kishi, T., S. Yamazaki and K. Enoki: Suspension of Sediment due to Surface Waves, Memoir 21st Annual Conv., J.S.C.E., 1966. (in Japanese)
9) Kajiura, K.: On the Bottom Friction in an Oscillatory Current, Bull. Earthquake Res. Inst., Univ. of Tokyo, Vol. 42, 1964.
10) Hom-ma, M., K. Horikawa and R. Kajima: A Study on Suspended Sediment due to Wave Action, Proc. 11th Conf. on Coastal Eng. in Japan, 1964, (in Japanese) and Coastal Engineering in Japan, Vol. 8, 1965.

CHAPTER 30

THE THRESHOLD OF MOVEMENT OF COARSE MATERIAL IN OSCILLATORY FLOW

P. J. Rance, Principal Scientific Officer
N. F. Warren, Assistant Experimental Officer
Hydraulics Research Station, Wallingford, Great Britain

ABSTRACT

Experimental results are presented from which it is now possible to predict the threshold of movement of shingle.

Introduction

The experiments were conducted in an Oscillating Water Tunnel, (Ref. 1), on the threshold of movement of shingle size material. The Tunnel simulates the oscillatory water motion at the sea bed due to wave action with a semi-orbit range of 0-4.5 metres and a period range of 5-15 seconds. Additionally, a uni-directional current of up to 0.6 m/sec can also be superposed upon the oscillatory motion.

Although limestone chips of between 0.32 cm and 2.5 cm diameters were the basic material tested, other materials such as coal and sand were examined in order to observe the effects of the various parameters over a wider range.

The Experiments

The various materials were placed in a bed 2.44 m. long and 45 cm, wide, with smooth wooden ramps at each end and in all cases was made at least 3 or 4 particles deep with a minimum depth of 5 cm. In some cases, for reasons of economy, a smaller bed 30 cm. long by 45 cm, wide was used: for example when glass spheres and concrete cubes were studied. To generate the appropriate boundary layer conditions within such a short bed, limestone chips of appropriate sizes were set into bitumen, on boards either side of the test material.

At the beginning of the study, it was thought to be desirable to define the initiation of movement in some precise way rather than rely upon a purely visual assessment. A method, analagous to the zero transport approach, was carried out for a number of test runs by initially marking a band across the bed and subsequently noting the number and position of particles which had moved out of the marked area. This type of test was carried out for various amplitudes, at set periods for a common number of oscillations.

From the distribution curves, the probability of a particle moving from its initial position to a position within the range x to $(x + \delta x)$ was determined. The standard deviations of the probability curves thus found were plotted against amplitude and the intercept of the curve, passing through these points, with

the axis taken to be the threshold condition. Simply plotting the number of particles moved against amplitude yields an ill-conditioned curve for the determination of the point of intersection.

Obviously a great deal of work was entailed in the determination of a single value of threshold. However, observation showed three distinct phases in bed movement. Firstly, a broad band of conditions existed in which particles rocked to and fro without actually moving position. Secondly, one or two particles would be dislodged and move a few places downstream and finally, with a small increase in velocity and acceleration many particles moved. It was the second condition that was found to equate with the deduced limit of threshold. After a few tests the observer was able to decide upon the limiting conditions which were consistently in agreement with the calculated values. Thus having 'calibrated' the observer, all subsequent determinations were carried out visually: only at the extremes with relatively small and relatively large particles was it considered difficult to assess the limiting conditions with reasonable accuracy.

Since the period of oscillation may be varied while the machinery is running it was found expedient for visual determinations, to fix the amplitude and gradually decrease the cycle period until the threshold was reached.

The Results

The independent variables describing the purely oscillatory motion are

a, the semi-orbit length,

T, the period

ρ, the density of the fluid (water)

μ, the viscosity of the fluid (water)

ρ_s, the density of the grains,

d, the equivalent sphere diameter of the grains

and g.

Apart from the sands, all materials were classified by their average equivalent sphere diameters, i.e. the diameter of the sphere of equivalent volume. This was considered to avoid the introduction of spurious shape factors and give a more direct representation of gravitational force when combined with the specific weights.

An acceptable grouping of the variables into dimensionless parameters is

$$\frac{a^2}{g'T^2d}, \quad \frac{ad}{T\nu}, \quad \frac{a}{d} \quad \text{and} \quad \frac{\rho_s}{\rho},$$

where $g' = \frac{\rho_s - \rho}{\rho}.g$ and $\nu = \frac{\mu}{\rho}$ the Kinematic viscosity. The first and second parameters are the grain Froude number and the grain

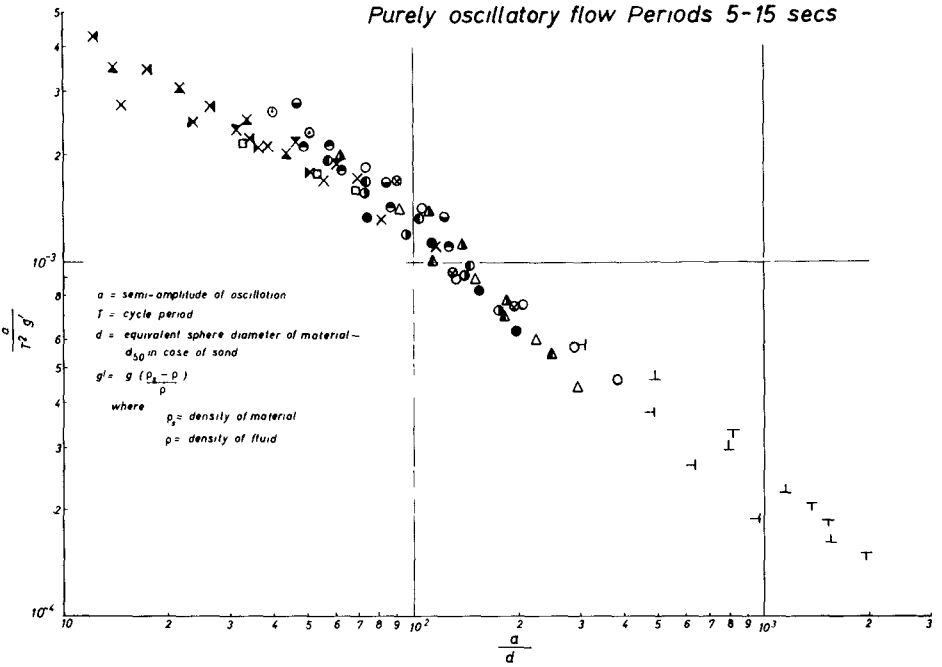

FIG. 1. THRESHOLD OF MOVEMENT OF COARSE MATERIAL IN OSCILLATORY FLOW

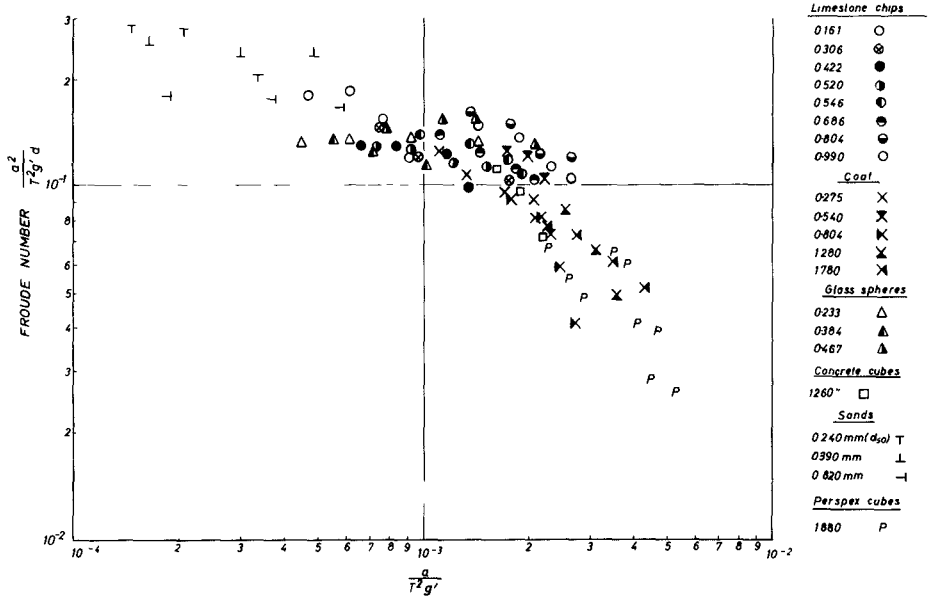

FIG. 2. PLOT OF FROUDE NUMBER v ACCELERATION NUMBER

Reynolds number respectively and one is tempted to plot one of these parameters against the other; analagous to the work in uni-directional flow. The remaining two parameters would then be expected to give rise to families of curves at constant values of $\frac{a}{g}$ and $\frac{\rho_s}{\rho}$. However, such a plot unnecessarily exaggerates the experimental error and the influence of the other parameters becomes indiscernible.

An alternative is to replace the Fr. No. by an acceleration number a/T^2g': this represents the ratio of the acceleration forces to the gravity forces. A plot of this parameter against a/d is shown in Fig. 1. The influence of viscosity appears as an increase in the scatter on the right hand side of the plot in the region where drag forces predominate. So far, insufficient data has been collected to enable lines of constant Re. No. to be drawn in with any degree of certainty. It is only in the other extreme of high acceleration numbers and low a/d numbers that one might expect the fourth parameter, ρ_s/ρ to exert any influence. Again no conclusive evidence on this effect has been observed so far.

The particular plot given in Fig. 1 does not illustrate the relative importance of drag forces and acceleration forces although the parameter a/d may be considered to be the ratio of the two. The comparison is best made by plotting the Fr. No. against the acceleration number as shown in Fig. 2. This plot shows clearly, despite the scatter, that neither drag force not acceleration force can be considered insignificant in any part of the range: even with sand where Manohar (Ref. 2) considered it safe to account for drag forces only.

The foregoing discussion has assumed that the effects of acceleration are the result of an acceleration force. This is not necessarily so since the rate at which work is done on the grain is possibly more important. If insufficient work is done in each cycle the grain will fall back into its original position. Thus the significance of the acceleration number is possibly an expression of the time variation of velocity rather than an expression of acceleration force.

Although it would appear that drag forces cannot be completely ignored within the range of conditions tested, it was surprising that the superposition of uni-directional flow did not markedly change the oscillatory conditions necessary for the initiation of movement. Unfortunately the introduction of yet another variable makes the analysis of results extremely difficult and impossible to present in a simple plot as in Fig. 1.

A few experiments with graded materials showed that the threshold value was appropriate to the d_{50} size.

Acknowledgements

This work was carried out as part of the research programme of the Hydraulics Research Station, Ministry of Technology and

and is published with the permission of the Director of Hydraulic Research. The painstaking work of J.E. Philpott is acknowledged with thanks.

References

1. Dedow H.R.S. A Pulsating Water Tunnel for research in reversing flow. La Houille Blanche No. 7-1966.

2. Manohar M. Mechanics of bottom sediment movement due to wave action. June 1955, Technical Memorandum No. 75. U.S. Beach Erosion Board.

CHAPTER 31

THE DYNAMICS OF A COAST WITH A GROYNE SYSTEM

Bakker, W.T.
Senior Engineer
Coastal Research Department, Rijkewaterstaat
The Hague, Netherlande

ABSTRACT

A mathematical theory will be given about the phenomena, which occur if on a coastal area groynee are constructed.

In former similar theories ([1] , [2], [3], [4], [5]) the coast was schematised by one coastline. In the following theory it is presented by two lines, one line repreeenting the beach and the other one the inshore.

The theory is based upon the following assumptions·

1° the littoral drift along beach and inshore is linear dependent of the angle of wave incidence and therefore of the direction of the line of beach and inshore respectively;

2° the transport perpendicular to the coast depends on the eteepness of the profile.
If the distance between the line of the beach and the line of the inehore is less than a certain equilibrium distance, the profile is too steep and there is an offshore transport. In the opposite case there is an onshore transport. The relation between offshore transport and dietance between the mentioned lines is linearised.

Some results are shown in fig. 8, 9 and 13.

It is found, dat the influence of a groyne system is threefold: they reflect short-period beach processes on the adjacent areae, they retard erosion and they give a lee-side scour.
But the theory only gives one aspect: influence of diffraction and of currents is not yet taken into account.

INTRODUCTION

In order to know what will happen with a coast after the building of coastal structures, one can make use of several approaches.

If one should know the wave spectra during a long time at the site, if a reliable sand transport formula wae available, if one would know the interaction between waves and currente on the eand transport and if the rulee for the onshore- and offshore transport were known, one would probably be able to predict the changemente. Unfortunately, the state of knowledge is not so far just now.

Another approach, which we will use here ie more or less morphological. With the aid of the continuity equation and a simplified dynamical equation with some unknown constants one can find formulae for the coastline in couree of time. With the aid of curve fitting one can find the unknown

conetants, which are only valid for the considered area. Furthermore one can find the constants from theories, following the first-mentioned approach, which gives a quick check of these theories.

The firet one, who published a paper about the second approach was PELNARD-CONSIDÈRE [1]. The original idea was of BOSSEN.

PELNARD-CONSIDÈRE assumes, that the profile of the coast always remains the equilibrium profile, so that he only needs to consider one coastline, being one of the contourlines. He assumee no currents, constant wave direction, small angle of wave incidence and a linear relation between angle of wavee incidence and littoral drift. Ae the angle of wave incidence at A is larger than at B, the littoral drift at A ie larger than at B; this means that there is accretion between. A convex coast erodes, a concave coast accretes.

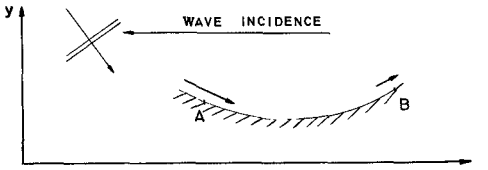

Fig 1 Accretion on a concave coast

He finds (cf "Appendix"), that the accretion is linear dependent of the curvature of the coast and inveree proportional with the depth D, up to where accretion takes place:

$$\frac{\partial y}{\partial t} = \frac{q}{D} \frac{\partial^2 y}{\partial x^2} \qquad \ldots\ldots\ldots (1)$$

in which the x-direction is the main coastal direction, the y-axis points in seaward direction and in which

$$q = \frac{dQ}{d\alpha} ,$$

the derivative of the littoral drift Q to the angle of wave incidence α.

From thie differential equation the coastline y as a function of x and t can be found for many boundary conditions. PELNARD-CONSIDÈRE finds solutions for the coastline of river deltas, the coastline in the vicinity of harbour moles and so on. His experiments confirm the theory.

GRIJM [2], [3] extends the theory by using a better formula for the littoral drift:

$$Q = \bar{Q} \sin 2\alpha ,$$

in which α is the wave direction. He computee the shape of river deltas and finde fundamentally two possible solutione for these deltae: one in which the angle of wave incidence is everywhere less than 45° (fig. 2a) and the other one, in which this angle is everywhere more than 45°(fig. 2b). Aleo combinations are possible (fig. 2c).

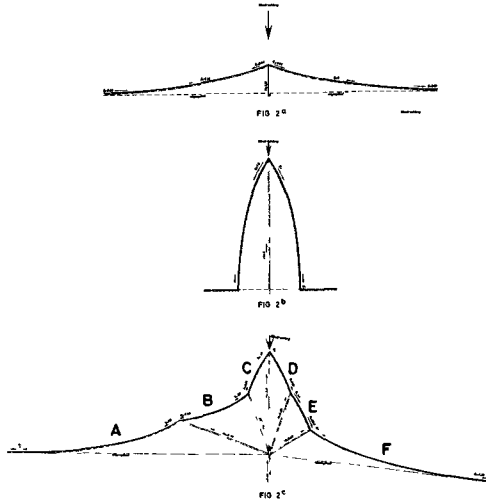

In figure 2c the angle of wave incidence is less than 45^{o} at the parts A, B, F and more than 45^{o} at the parts C. D, E. As one never knows which combination one has to choose, the problem seems to be indefinite. BAKKER and EDELMAN [4] treat the same problem with the linear Pelnard-Considère approach. They investigate also the case of negative $q(= \frac{dQ}{d\alpha})$, which occurs if the angle of wave incidence is large. Their solutions are more or less similar to GRIJM, but opposite to GRIJM, they also find a periodical solution:

$$y = e^{-\frac{q}{D}K^{2}t} \cos Kx \quad . . \quad (2)$$

This is a sinusoidal shaped coastline of which the amplitude decreases in course of time if q is positive (small angle of wave incidence), but increases if q is negative (large angle of wave incidence). Therefore, solutions of the shape of fig. 2b are unstable and will be destroyed, because slight deviations trigger large deviations according to (2).

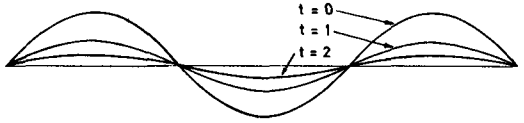

Fig 3 Decay of sinussoidal shaped coastline

This solves the problem of the indefiniteness: nature will prefer solutions of category I. GRIJM did not find this solutions, because he confined himself to solutions growing with $\sqrt{t}$ in all directions.

PELNARD-CONSIDÈRE [1] considered river deltas and coastal structures, GRIJM [2], [3] and BAKKER and EDELMAN [4] merely treat river deltas. BAKKER [5] investigates the periodical solutions of eq.(1). Besides the

"standing" and attenuating wave of fig. 3, also propagating and attenuating waves are possible. The propagating sandwave found in the prototype on Vlieland could be explained with theory. BAKKER also examines the influence of coastal structures on these sandwaves. The sandwave appears to be reflected by the structure: the amplitude at the site of the structure is enlarged. One can sense this, because there is an analogy between these moving sandwaves and tidal waves. The coastline is analogous to the vertical tide and the littoral drift to the horizontal tide. If one stops the littoral drift (current) by a dam, one increases the variations of the coastline (vertical tide).

One of the beauty failures of the solutions of PELNARD-CONSIDÈRE [1] and BAKKER [5] is the assumption of parallel depth contours. Near coastal structures the deviations of the prototype can be considerable. For instance, the solution near a breakwater is sketched in fig. 4a. PELNARD-CONSIDÈRE finds, that the coast on the left-hand side builds up to the head of the breakwater and that the coastline on the right-hand side erodes the same amount. This might be true for constructions, extending to large depths. But in the case of groynes only the littoral drift on the beach is prevented: at the beach there will be sedimentation of material on one side of the groyne and erosion on the other side. But in deeper regions this disturbance does not take place, so on the left-hand side the profile becomes steeper than the equilibrium profile and the sand drops down, and on the right-hand side the profile is flatter than the equilibrium profile and the sand is pushed by the waves in upward direction.

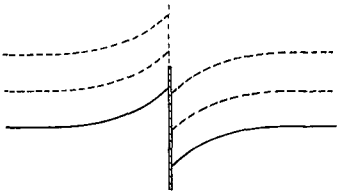

Fig 4a Coastline with parallel contour-lines

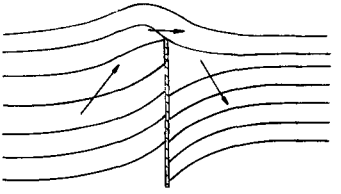

Fig 4b More reasonable approximation
The arrows give the direction of the sanddrift

In order to reproduce this feature in a mathematical model it is necessary to schematise the coast by two lines instead of one. This will be done in this article. The difference with former theories is, that thus off- and onshore transport are taken into account.

Definitions and assumptions.

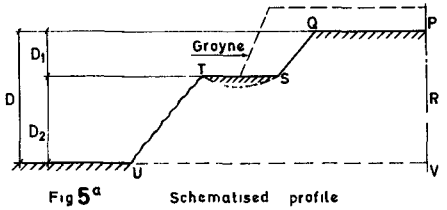

Fig 5a Schematised profile

Fig. 5a denotes a schematized profile. The profile is under-d vided into two parts, one part consisting of the profile between 0 and D_1 below sea level (beach), the second one between D_1 and $D_1 + D_2$ (inshore). Between beach and inshore is a horizontal shelf at depth D_1, the total depth D being $D_1 + D_2$.

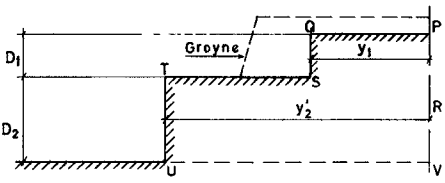

Fig 5b Two-line theory

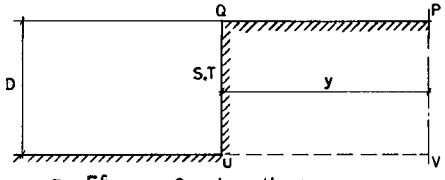

Fig 5c One-line theory
the area PQSTUV
is always the same

The depth D is aesumed to be so large, that no littoral drift takes place here.

In reality one can imagine, that a breaker ridge occurs at depth D_1 and that a trough links the two parts of the coast (dotted line), fig. 5a.

It is assumed, that a groyne reachee up to the horizontal ehelf at depth D_1 and prevente all littoral drift along the beach, but of course not along the inshore.

In the theory the profile is still more schematized, according to fig. 5b. A stepwiee profile remains. The areas PQSR and RTUV in fig. 5a are equal to the corresponding areas in fig. 5b.

In top view one sees two lines at a dietance y_1 and y_2' from the x-axis, which will be called "the line of the beach" and "the line of the inshore" respectively.

The "equilibrium distance" W is the dietance $y_2' - y_1$ between beach and inshore, when the profile is an equilibrium profile.

The following dynamic equations are aesumed.
If the distance $y_2' - y_1$ is equal to the equilibrium distance W, no interaction is assumed. If the distance $y_2' - y_1$ is less than W, the profile is too steep and an offshore transport will be the result. An onshore traneport will occur in the oppoeite case.

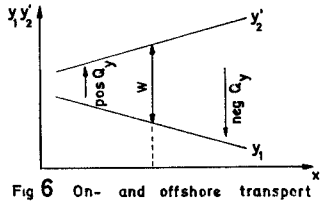

Fig 6 On- and offshore transport

We linearize this relation and take for the offshore transport Q_y per unit length:

$$Q_y = q_y \left\{ y_1 - (y_2' - W) \right\} \quad . . . . \quad (3a)$$

in which q_y is a proportionality constant. The dimeneion of q_y ie $[1/t]$. For a simpler notation, we denote:

$$y_2 = y_2' - W \quad . . . . . \quad (4)$$

Then (3a) becomee

$$Q_y = q_y (y_1 - y_2) \quad . . . . . \quad (3)$$

With respect to the littoral drift, the assumption of PELNARD-CONSIDÈRE [1] is applied, bothfor beach and inshore: the transport in linearized:

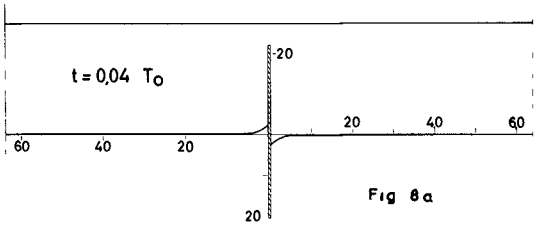

Fig 8a

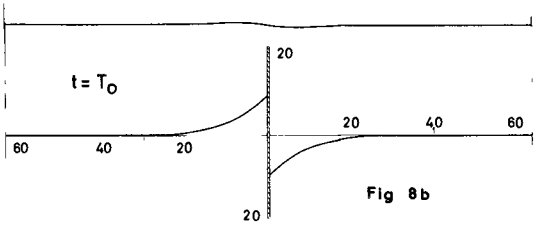

Fig 8b

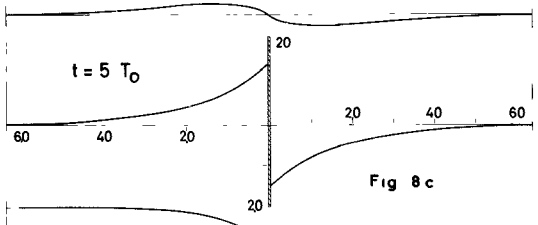

Fig 8c

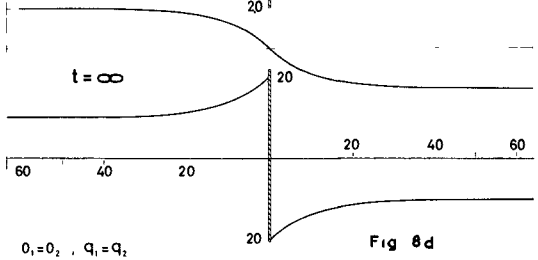

Fig 8d

$O_1 = O_2$, $q_1 = q_2$

Scales

Horizontal $1 \triangleq L_o = \sqrt{\frac{1}{q_y(\frac{1}{q_1}+\frac{1}{q_2})}}$

Vertical $1 \triangleq L_o \tan \alpha = \frac{q_1}{q_1}\sqrt{\frac{1}{q_y(\frac{1}{q_1}+\frac{1}{q_2})}}$

Time $T_o = L_o^2 \frac{D_1}{q_1} = \frac{1}{2}\frac{D_1}{q_y}$

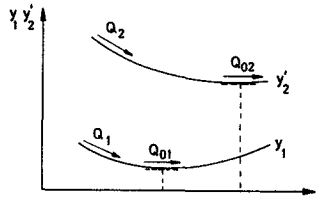

Fig 7 Littoral drift along beach and inshore

$$\left.\begin{aligned} Q_1 &= Q_{o1} - q_1 \frac{\partial y_1}{\partial x} \\ Q_2 &= Q_{o2} - q_2 \frac{\partial y_2}{\partial x} \end{aligned}\right\} \quad \ldots\ldots\ldots \quad (5)$$

in which Q_{o1} and Q_{o2} are respectively the "stationary transport" (littoral drift where $\frac{\partial y_1}{\partial x} = 0$, resp. $\frac{\partial y_2}{\partial x} = 0$, fig. 7) on beach and inshore and in which q_1 and q_2 are proportionality constants. The dimension of q_1 and q_2 is $[l^3/t]$.

RESULTS

By making use of the continuity equation and the above-mentioned dynamical equations one can compute many stationary and instationary cases (cf. "Appendix").
Of importance appears to be a reference length:

$$L_o = \sqrt{\frac{1}{q_y \left(\frac{1}{q_1} + \frac{1}{q_2}\right)}} \quad \ldots\ldots\ldots\ldots \quad (6)$$

Fig. 8 shows the result in the case of accretion and erosion near one groyne when $q_1 = q_2$ and $D_1 = D_2$. (cf Appendix, 3).

In the initial situation the lines of beach and inshore are parallel. Fig. 8a shows the situation immediately after the construction of the groyne. Only the beach shows some build-up on the right-hand side and eroeion on the left-hand side. It must be streesed, that the influence of diffraction is not taksn into account.

In fig. 8b and 8c the profile on the left-hand side becomes too eteep and eand drops down to the inshore. Here the littoral drift was originally everywhere the same. The supply of sand from the beach overcharges the transport capacibility of the inshore and therefore eand sedimentatss here.

Now the littoral drift Q_2 along the groyne at the inshore becomee larger ($\frac{\partial y_2}{\partial x}$ becomes negative, cf (5)). In the final stage (fig. 8d) beach and inshore on the left-hand side and on the right-hand side are shiftsd with respect to each other. This is in correspondence with the results of PELNARD-CONSIDÈRE [1], but he finds, that ths coaet builds up to the top of the groyne, and here it is found, that it builds up to a distance, only dependent of q_1, q_2, q_y and the angle α of wave incidence, where $\tan \alpha = \frac{Q_{o1}}{q_1}$

Fig. 9 shows sevsral etationary cases.
Fig. 9d gives again the final state of fig. 8d. The transport is the sams ae without a groyne, because the transport at a long distance of the groyne does not change. If more groynes are constructed, the littoral drift along the beach is stopped more and more, because the beach turns in the direction

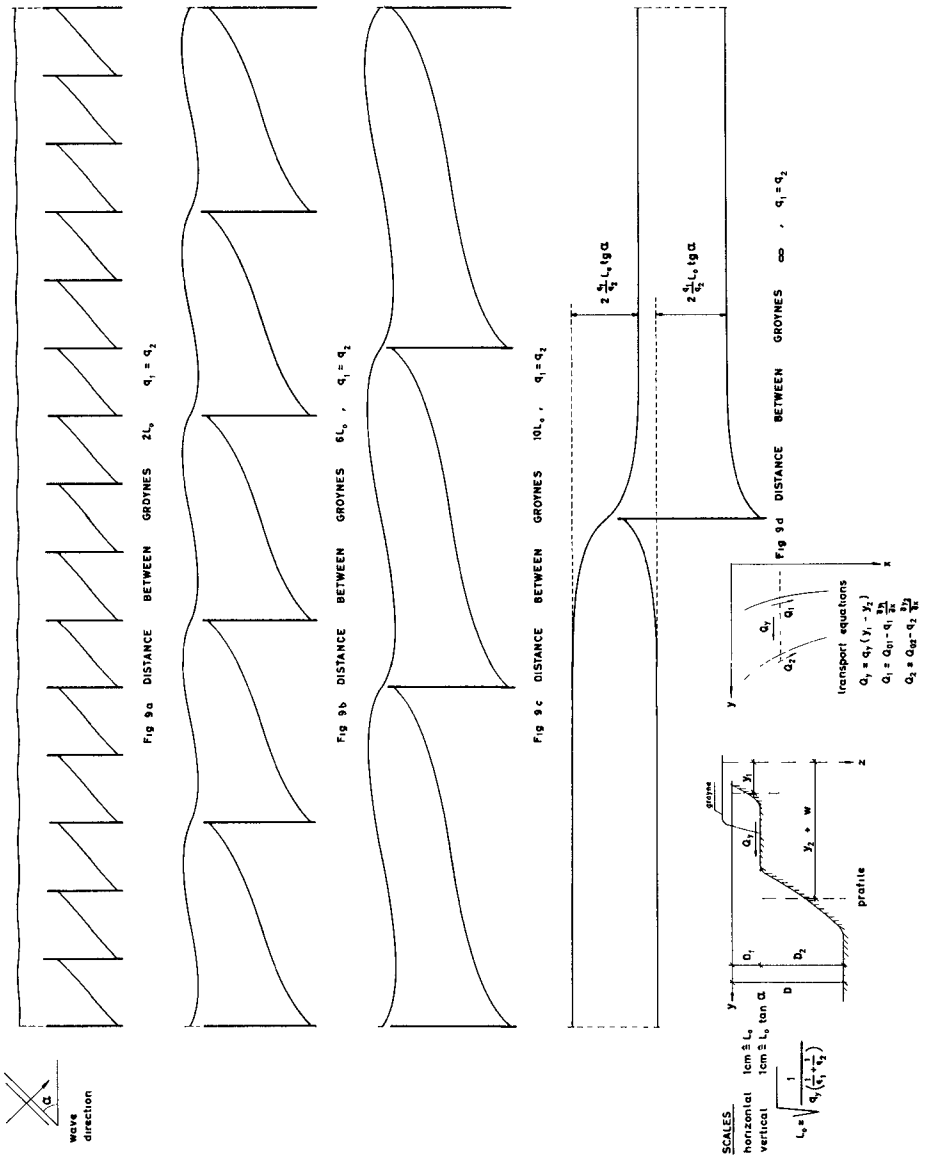
α
wave direction
Fig 9a DISTANCE BETWEEN GROYNES 2L₀ q₁ = q₂
Fig 9b DISTANCE BETWEEN GROYNES 6L₀ , q₁ = q₂
Fig 9c DISTANCE BETWEEN GROYNES 10L₀ , q₁ = q₂
Fig 9d DISTANCE BETWEEN GROYNES ∞ , q₁ = q₂
SCALES
horizontal 1cm ≙ L₀
vertical 1cm ≙ L₀ tan α
groyne
profile
transport equations

of the wave crest (fig. 9c,b,a).

We now consider the case, that the groynes are so near to each other, that they prevent all the transport along the beach (fig. 9a). In this case the total littoral drift is the drift along the inshore:

$$Q = Q_2 = Q_{o2} - q_2 \frac{\partial y_2}{\partial x}$$

Before the construction of the groynes this transport was:

$$Q = Q_1 + Q_2 = Q_{o1} + Q_{o2} - q_1 \frac{\partial y_1}{\partial x} - q_2 \frac{\partial y_2}{\partial x}$$

Following the conception of PELNARD-CONSIDÈRE (cf Appendix, 1), and assuming that the sedimentation takes place equable on beach and inshore (q_y sufficiently large), the coastal equation for a protected area would be:

$$\frac{\partial y}{\partial t} = \frac{q_2}{D} \frac{\partial^2 y}{\partial x^2}$$

The coastal constant q/D is changed in q_2/D. The assumption, that the sedimentation takes place equable on beach and inshore, is about correct for long-term coastal processes (long with respect to T_o, cf Appendix 2,(19),7.

We considered the case, that the groynes were so near to each other, that they prevent all the transport along the beach. If the distance between the groynes is larger, the coastal constant will not diminish with a factor q_2/q, but less:

$$\frac{\partial y}{\partial t} = \frac{q'}{D} \frac{\partial^2 y}{\partial x^2}, \text{ in which } q_2 < q' < q_1 + q_2 \quad . . (7)$$

This factor can be computed (cf Appendix, 4) and will be called $\frac{1}{p^2}$:

$$\frac{1}{p^2} = \frac{q'}{q_1 + q_2} \longrightarrow p = \sqrt{\frac{q_1 + q_2}{q'}} \quad . . . . . (8)$$

We now have returned to the one-line theory of PELNARD-CONSIDÈRE a protected area can be considered as an area with another coastal constant ($\frac{q'}{D}$) than the neighbouring unprotected area, and this constant can be computed with the two-line theory.

In the following section we shall give first some rough statements, making use of the one-line theory, considering a protected area as an area with another coastal constant, and afterwards we shall illustrate it with more accurate computations with the two-line theory. The advantage of the one-line theory is, that it gives a quick insight in the essence of the matter.

LAWS OF SCALE

One can make the coastal equation (1) dimensionlees by substituting: $x = n_x \cdot \chi$, $y = n_y \cdot \eta$, $t = n_t \cdot \tau$, $q/D = n_{cc} \cdot C$, in which χ , η , τ

and C are dimensionless and n_x, n_y, n_t, n_{cc} give the scale factor of x, y, t and the coastal constant q/D.

One finds the following relation:

$$n_{cc} \frac{n_t}{n_x^2} = \text{constant} \quad \ldots\ldots\ldots (9)$$

The scale n_y of y can be chosen arbitrary, because y occurs on both sides of eq. (1). We shall give some examples:

Consider two half-infinite coastal areas with different coastal constants, which are in rest at infinity. Suppose that the ends of both areas carry out the same movements in course of time. The shape of the coastline will be the same in both cases, but the x-scale will be equal to the square root of the coastal constants (fig. 10a).

Consider now two areas with different coastal constants, which are identical at time t = 0 and of which the ends of the areas are in rest. Now the x-scale is the same and therefore the timescale of the changements will be inverse proportional to the coastal constants (fig. 10b).

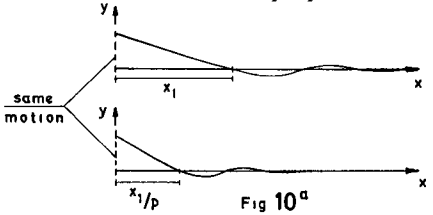

Fig 10a

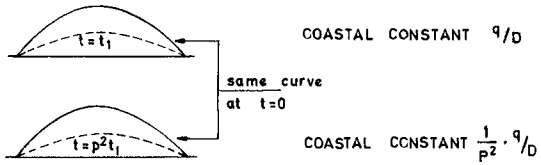

Fig 10b

INFLUENCE OF A ROW OF GROYNES

We consider a coast, where over a long stretch groynes are constructed at time t = 0.

What is the influence of the groynes on the coast?

We will consider three influences, which can be superponed, because all equations are linear.

1° the influence of external causes (boundary conditions);

2° the influence of the oblique incidence of the waves (stationary transport);

3° the influence of the shape of the coast.

1° Influence of external causes.

Assume a wave direction, perpendicular to the coast and a straight coastline at time t = 0.

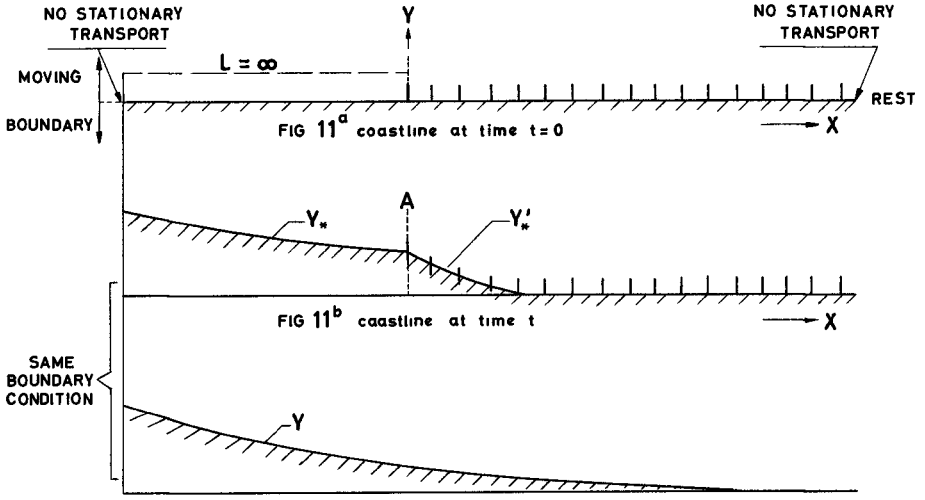

FIG 11[a] coastline at time t = 0

FIG 11[b] coastline at time t

FIG 11[c] coastline at time t, if no groynes would have been constructed

Assume, that by one or another external cause (for instance, a river or tidal canal, which embouches left of the left boundary, fig. 11) the coastline at time t, would have been according to fig. 11c, if no groynes would have been constructed.

What is the coastline if groynes are constructed at time t = 0 ?

This coastline can be constructed with the following method.

The coastline y_*' of the protected area can be found by reducing the x-scale of y by a factor 1/p (p defined by (8)) and by multiplying the y-scale with a factor 1 + r, in which:

$$r = \frac{p - 1}{p + 1}, \quad \text{so} \quad 1 + r = \frac{2p}{p + 1} \qquad \ldots\ldots\ldots (10)$$

In formula: $$y_*'(x) = (1 + r)\, y\,(px) \qquad \ldots\ldots\ldots (11a)$$

The coastline of the unprotected part y_* can be found as the sum of the original y plus a "reflected y"; the latter one being the reflection of the original y (for $x > 0$) with respect to the y-axis and multiplied with the reflection factor r, given in eq. (10):

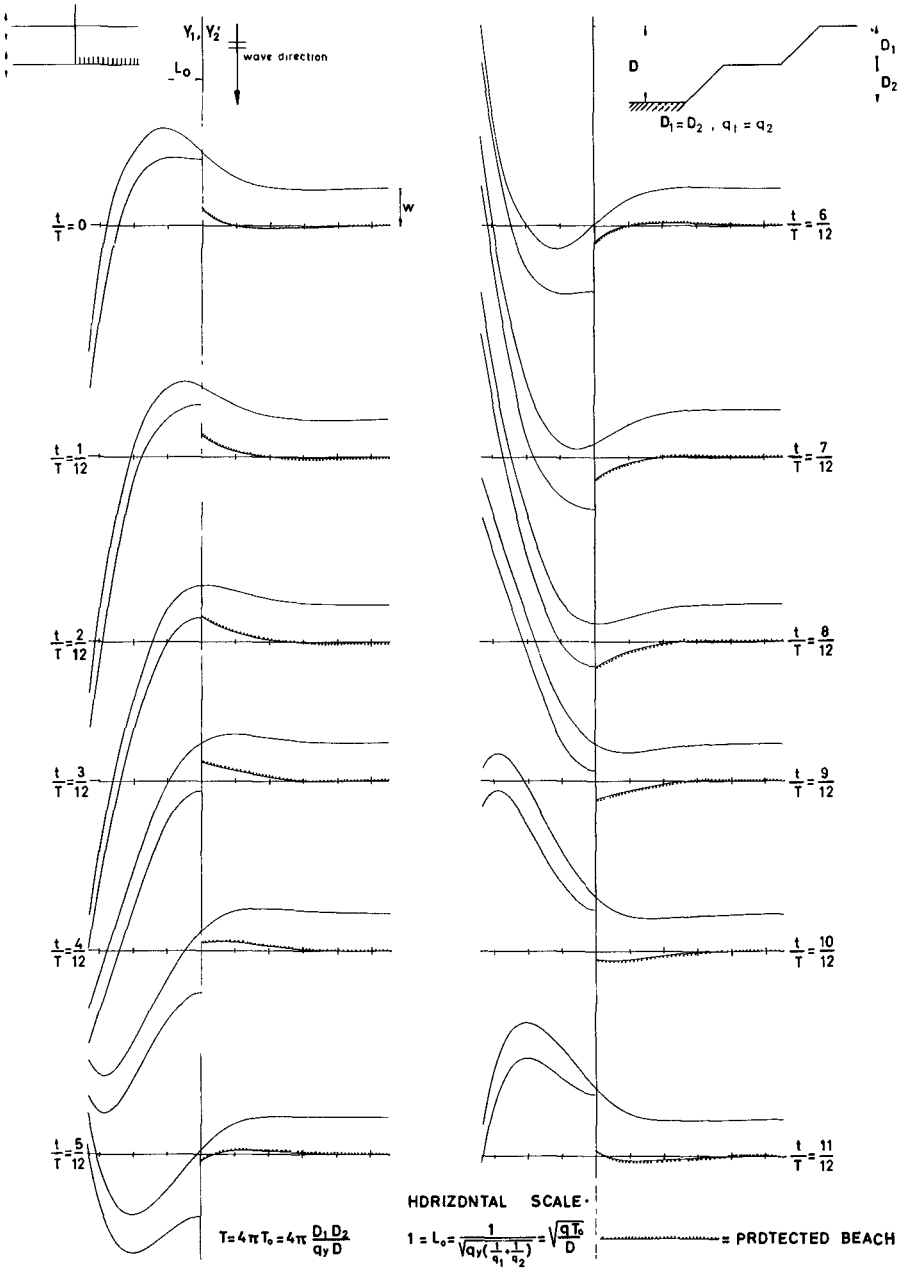

FIG 13 PRDPAGATING SANDWAVE ACCDRDING TD TWD-LINE SYSTEM

if $x < 0$, then $y_* (x) = y(x) + r \cdot y(-x)$ . . . . (11b)

In fig. 12 the method of construction is visualissd.

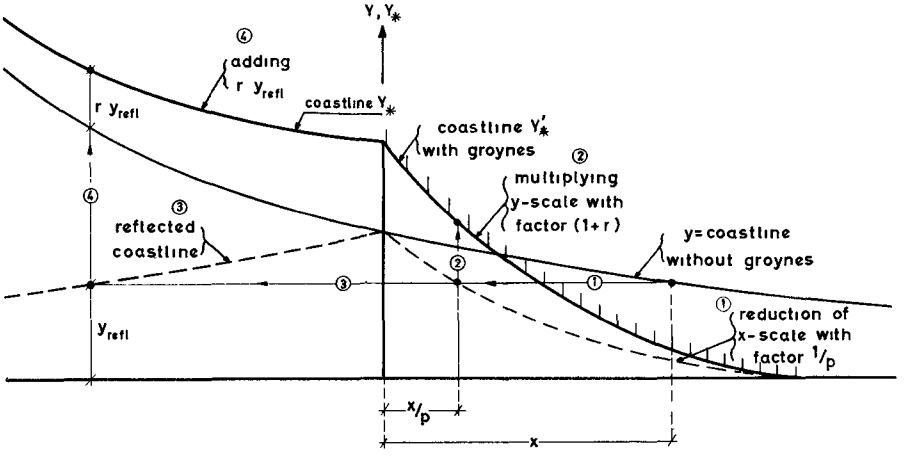

FIG 12

One can proof sasily, that:

a. the new coastline of the unprotected part y_* sufficss the coastal equation (1) for an unprotected area: it consists of the sum of two functions, both obeying this linear equation.

b. the nsw coastline of the protected part y_* suffices the coastal equation (7) for a protscted area. For the timescale of the changemsnts at A is the sams in fig. 11b and 11c and the x-scale is proportional to ths square root of the coastal constants (fig. 10a).

c. ths transport a littls bit on the left of A in fig. 11b is equal to the transport a littls bit on the right of A.

d. the y-coordinates at A of the protected and unprotected area are the same.

As an example of the influence of external causes in the case of the two-line system, fig. 13 shows the influencs of groynes on a harmonical, propagating sandwave. Thess sandwaves occur, if the left-hand boundary erodss and accrstes harmonically (by an external cause), if the right-hand boundary (protected coast) is in rest, and if the profile at ths boundariss is an squilibrium profile [4], [5]. In the case of fig. 13, it is assumed, that the distance betwesn the groynes is so small, that no littoral drift takss place on the beach. The protscted bsach just rsacts as a store. The formulae are given in the Appendix, 7.

As fig. 13 shows, for short-period processss[1], the motion of the

[1] defined in the appendix

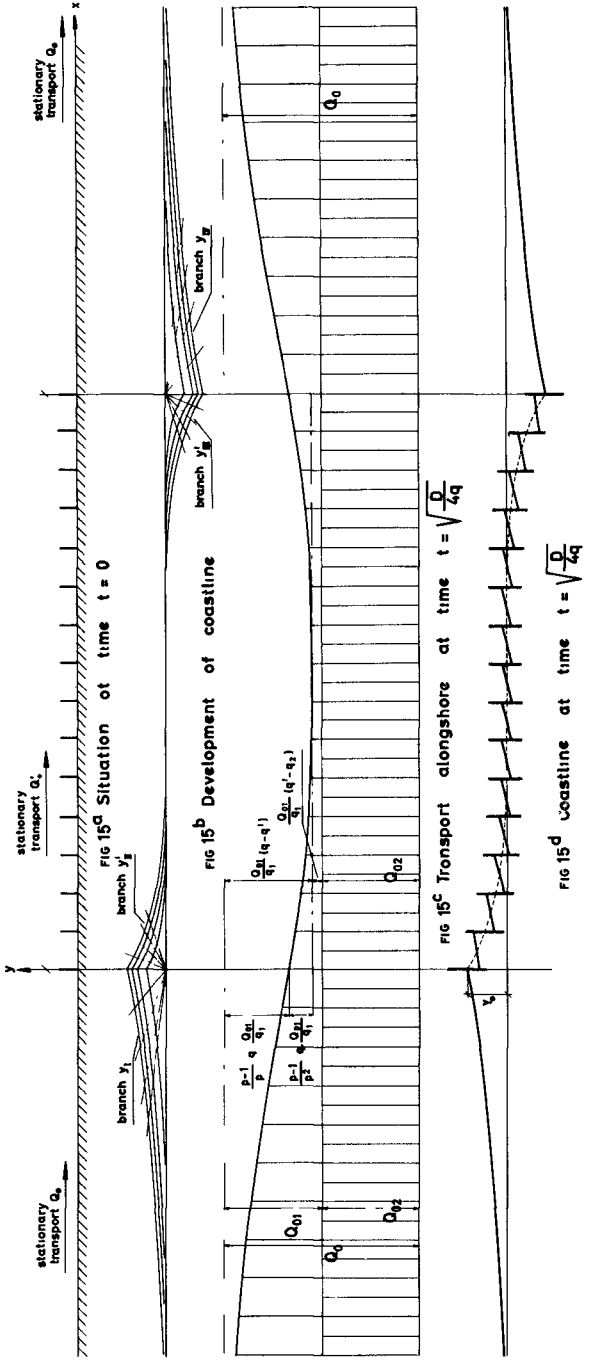

FIG 15[a] Situation at time t = 0

FIG 15[b] Development of coastline

FIG 15[c] Transport alongshore at time $t = \sqrt{\frac{D}{4q}}$

FIG 15[d] Coastline at time $t = \sqrt{\frac{D}{4q}}$

inehore is practically the same either if groynee are constructed, either if they are not. Then the motion of the protected beach is small, but there is a large edge effect on the unprotected beach, near the beginning of the groyne eyetem.

For long-period proceeeee[1] the reeults of the one-line theory are confirmed: the wave-length along the protected beach and inshore is a factor 1/p timee the wave-length along the unprotected beach and the amplitude ie enlarged by a factor 1 + r, according to (10).

2° Influence of oblique incidence of waves

According to the one-line system, the traneport along an unprotected coast y and along a protected coast y' are respectively:

$$Q = Q_o - q \frac{\partial y}{\partial x}$$

$$Q' = Q_o' - q' \frac{\partial y'}{\partial x}$$

In this formula Q_o' and q' are smaller than Q_o and q. If the transport along the beach is prevented totally, Q_o' and q' are respectively Q_{o2} and q_2, the conetante of the inshore.

Consider an area, partly protected with groynes, which is at t = 0 parallel to the x-axie (fig. 15a). On the unprotected beach the traneport will be Q_o and on the protected beach Q_o' and therefore the eedimentation per unit time will be $Q_o - Q_o'$. With the eame conaideratione ae in the chapter "influence of external cauees" it can be shown, that a kind of delta will be formed, which will increase with a velocity proportional to $\sqrt{t}$ (fig. 15b). Thie delta is not symmetrical: the same y-coordinate at the point (-x) of the unprotected coaet occure in the point x/p of the protected coast (fig. 14). The inveree will occur on the lee-eide of the groyne eyetem. Here a similar ehape ecour-hole will be formed. Fig. 15 shows the ehape and the traneport, the formulae are given in appendix, 8.

The corresponding two-line eyetem is rather intricate and still in study.

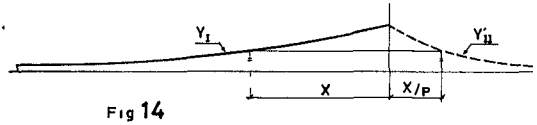

Fig 14

3° The influence of ehape

Even if the coastline would not change because of external causes and even if the influence of stationary transport is not taken into account, a convex coast would erode and a concave coaet accrete according to eq. (1):

$$\frac{\partial y}{\partial t} = \frac{q}{D} \frac{\partial^2 y}{\partial x^2}$$

In the one-line system the difference between a protected coast and an unprotected coaet is a difference in the constant q/D, which differe a factor p^2, according to (8). Thie means, that a protected coaet accretee

[1] defined in the appendix

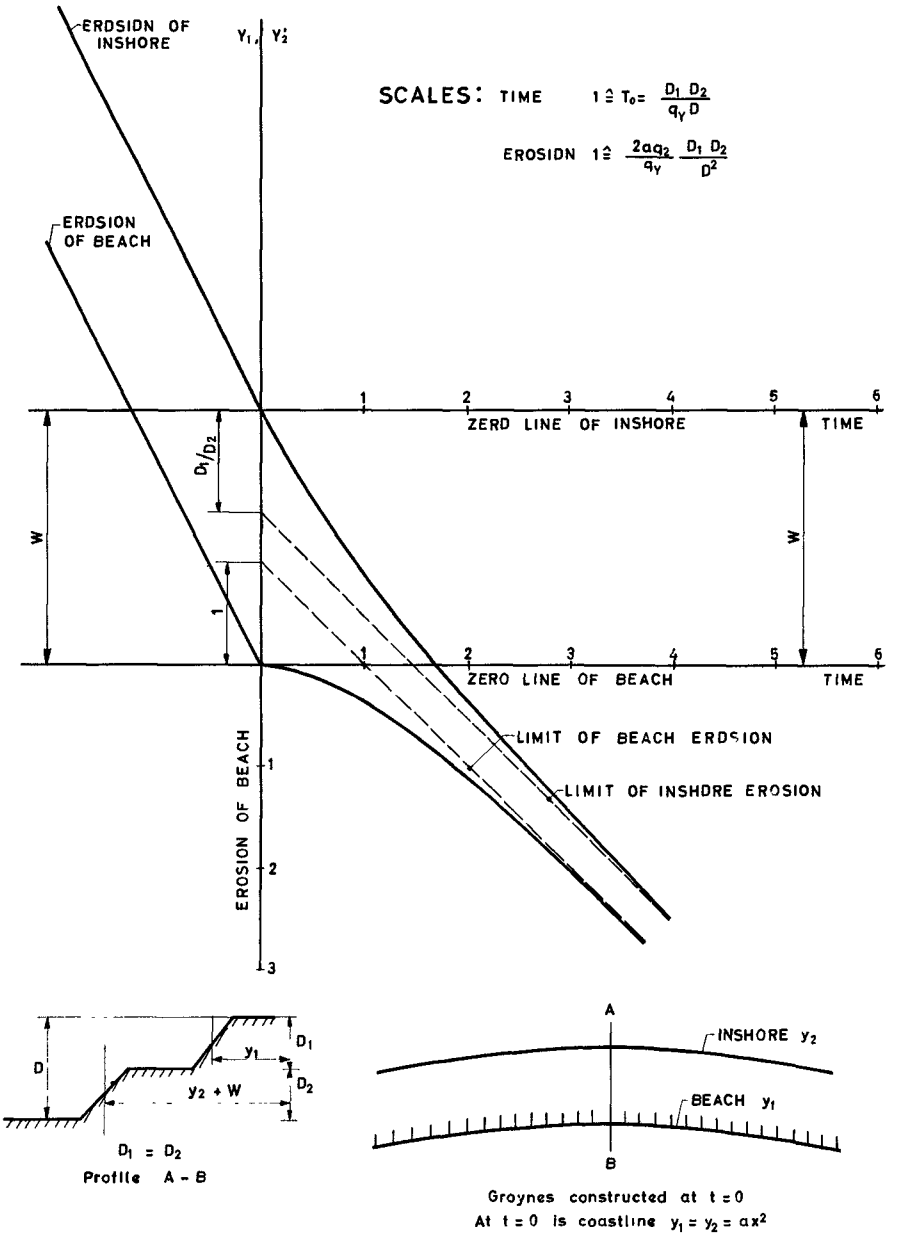

Fig 16 ERDSIDN DF BEACH AND INSHORE ACCDRDING TO THE TWO - LINE SYSTEM

(erodes) slower than an unprotected coast with the same curvature. The timescale is p^2 times as large, according to (9) and fig. 10b.

At the boundary between a protected part and an unprotected part edge effects arise, which can be computed graphically with the method of Schmidt [5].

Fig. 16 shows the erosion of a convex coast, according to the two-line system. The formulae are given in appendix, 9.

It is assumed, that before t = 0 beach and inshore have the same parabolic shape and an equilibrium profile. They erode with the same velocity. At time t = 0 groynes are constructed at the beach, so near to each other, that they prevent all transport along the beach. The erosion along the inshore is not stopped, however, the profile becomes too steep and sand moves from beach to inshore.

The erosion of the inshore diminishes and the erosion of the beach begins again. Finally, beach and inshore erode together again, but the profile remains steeper than the equilibrium profile, and the total rate of erosion is less than before, according to the one-line theory.

DISCUSSION

The theory only deals with one aspect.

Other aspects are:

1° the influence of rip-currents near the groynes.
This influence is two-fold: rip-currents transport material from beach to inshore and they cause stream-refraction. These two influences work against each other. The transport of material from the beach causes a scour-hole on the beach and the stream-refraction causes a spit on the beach.
At the moment experiments with dyed water in the prototype are carried out to get an impression of the order of magnitude of these rip-currents. Rip-currents flatten the profile and lower the rate of effect of a groyne-system. Therefore it is very important, that they give the correct transport in models, because otherwise one can find the inverse effect of groynes as in practice.

2° the influence of diffraction on the lee-side of groynes.
The author has the feeling that diffraction does not really change the effect of a groyne system, but only has minor effects in the immediate vicinity.

3° variable wave direction
This causes changing boundary conditions near the groynes.
Most influence will be found near the first groyne of a groyne system, where this will generate short-period moving sandwaves on the beach. These sandwaves have a short wavelength and will decay at a short distance of the groyne. At a long distance of the groynes one only finds the effect of mean wave conditions and no influence of variations. Therefore, also with varying wave conditions, most of what has been said, especially about long-period processes, remains its validity with changing wave conditions.

4° non-linearity in the transport equation.
According to the author, this is mostly of minor importance, except if anywhere the angle of wave incidence along beach or inshore becomes

about 45° or more. In this case the matter of instability, mentioned in the introduction becomes important. A point where this can occur is in fig. 8 on the inshore, right in front of the groyne.

Of course everyone will be interested in the values of the coastal constants.

The following is not more than a reasonable guess, because serious investigations have not yet been done.

For some parts of the Dutch coast, $q/D \approx 0{,}4 \times 10^6$ m^3/m depth/year/radian and q_y might be 1 to 10 m/year at a depth D_1 of 3 m.

REFERENCES

[1] R. Pelnard-Considère, Essai de théorie de l'évolution des formes de rivages en plages de sable et de galets.
Quatrième Journées de l'Hydraulique, Paris 13-15 Juin 1954.
Les Énergies de la Mer, Question III.

[2] W. Grijm, Theoretical Forms of Shorelines.
Proc. 7th Conf. on Coastal Engng., The Hague 1960.

[3] W. Grijm, Theoretical Forms of Shorelines.
Proc. 9th Conf. on Coastal Engng., Lisbon 1964.

[4] W.T.J.N.P. Bakker and T. Edelman. The Coastline of River Deltae.
Proc. 9th Conf. on Coastal Engng., Lisbon 1964.

[5] W.T.J.N.P. Bakker, A mathematical theory about sandwaves and its applications on the Dutch Wadden Isle of Vlieland.
Shore and Beach (unpublished yet).

[6] U.S. Department of Commerce, National Bureau of Standards,
Handbook of Mathematical Functions (ed. M. Abramowitz and I.A. Stegun).

APPENDIX

1. THE DERIVATION OF PELNARD-CONSIDÈRE

If x is the main coastal direction and y is in seaward direction, the angle of wave incidence is nearly (taking

$$\text{arctg}\,\frac{\partial y}{\partial x} \approx \frac{\partial y}{\partial x}): \alpha = \alpha_o - \frac{\partial y}{\partial x}$$

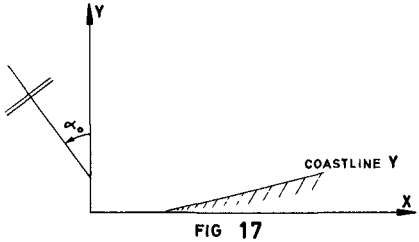

FIG 17

The littoral drift Q is a function of the angle of wave incidence and can be put into a Taylor series:

$$Q = Q_o + \frac{dQ}{d\alpha}(\alpha - \alpha_o) + \ldots.$$

in which Q_o denotes the traneport Q if the angle of wave incidence is α_o This gives in linear approximation:

$$Q = Q_o - q\frac{\partial y}{\partial x}$$

in which $q = \frac{dQ}{d\alpha}$ for $\alpha = \alpha_o$.

The equation of continuity says that the sedimentation is equal to the decrease of littoral drift:

$$\frac{dQ}{dx} + D \frac{\partial y}{\partial t} = 0.$$

Substituting Q gives the equation of Pelnard-Considère:

$$\frac{\partial y}{\partial t} = \frac{q}{D} \frac{\partial^2 y}{\partial x^2} .$$

It will be seen, that this derivation remains its validity when Q denotes the mean yearly transport along a coast.

In practice, the transport is zero if the angle of wave incidence is zero. In order to get this correct in the mathematical model, it has sense to choose Q_o less than the transport when the angle of wave incidence is α_o (fig. 18)

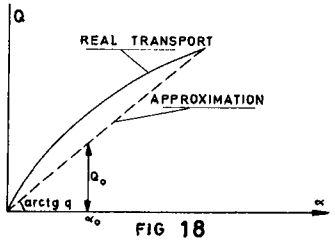

FIG 18

2. DERIVATION OF THE FORMULAE FOR THE TWO LINE SYSTEM

The equations of continuity are:

$$\left.\begin{aligned} -\frac{dQ_1}{dx} - Q_y &= D_1 \frac{\partial y_1}{\partial t} \\ -\frac{dQ_2}{dx} + Q_y &= D_2 \frac{\partial y_2}{\partial t} \end{aligned}\right\} \quad \ldots\ldots\ldots\ldots (12)$$

Substituting the dynamical equations (3) and (5) for Q_1, Q_2 and Q_y gives:

$$\left.\begin{aligned} q_1 \frac{\partial^2 y_1}{\partial x^2} - q_y (y_1 - y_2) &= D_1 \frac{\partial y_1}{\partial t} \\ q_2 \frac{\partial^2 y_2}{\partial x^2} - q_y (y_2 - y_1) &= D_2 \frac{\partial y_2}{\partial t} \end{aligned}\right\} \quad \ldots\ldots\ldots (13)$$

Adding both equations gives:

$$\frac{\partial^2 (q_1 y_1 + q_2 y_2)}{\partial x^2} = \frac{\partial (D_1 y_1 + D_2 y_2)}{\partial t}$$

which can be written as:

$$\frac{q}{D}\frac{\partial^2 y}{\partial x^2} + \frac{D_1 D_2}{D^2}\left(\frac{q_1}{D_1} - \frac{q_2}{D_2}\right)\frac{\partial^2 (y_1 - y_2)}{\partial x^2} = \frac{\partial y}{\partial t} \quad \ldots\ldots (14),$$

in which $\frac{q}{D} = \frac{q_1 + q_2}{D_1 + D_2}$ and $y = \frac{1}{D}(D_1 y_1 + D_2 y_2)$.

y is the "coastline" of Pelnard-Considère. We will confine ourselves to to cases where $\frac{q_1}{D_1} = \frac{q_2}{D_2}$, which means, that if beach and inshore have the same curvature, they fill up equable and the profile does not change. In this case the second left-hand term of (14) is zero and we have back eq. (1) of Pelnard-Considère.

By dividing the equations (13) by D_1 and D_2 respectively and subtracting one finds:

$$\frac{q}{D}\frac{\partial^2 y_-}{\partial x^2} - \frac{q_y D}{D_1 D_2} y_- = \frac{\partial y_-}{\partial t} \quad \ldots\ldots (15)$$

in which $y_- = y_1 - y_2$ $\ldots\ldots (16)$

Eq. (15) is the equation for the offshore transport, which equals $q_y y_-$. By using the auxiliary variable y_e, equal to:

$$y_e = y_- e^{\frac{q_y D}{D_1 D_2} t} \quad \ldots\ldots (17)$$

this can be written as:

$$\frac{q}{D}\frac{\partial^2 y_e}{\partial x^2} = \frac{\partial y_e}{\partial t} \quad \ldots\ldots (18)$$

(1) and (18) both represent the diffusion-, warmth-, or conductivity equation, for which many numerical or graphical integration processes are available, for instance the method of Schmidt [5].
By substituting the appropriate boundary conditions for y and y_s, one can find y and y_s at every time and place, from which y_1 and y_2.

Some problems can be solved analytically, of which some examples will be given.

From (17) it will be seen, that the time scale of this kind of processes is highly dependent of a reference time T_o:

$$T_o = \frac{D_1 D_2}{q_y D} \quad \ldots\ldots (19)$$

3. THE PROBLEM OF FIG. 8. $D_1 = D_2$, $q_1 = q_2$.

Boundary conditions: a $y_1 = y_2 = 0$ for $x = \infty$ and $0 < t < \infty$
b $y_2 = 0$ for $x = 0$ and $0 < t < \infty$

$$\underline{c} \quad \frac{\partial y_1}{\partial x} = \tan\alpha = \frac{Q_{o1}}{q_1} \quad \text{for } x = 0 \text{ and } 0 < t < \infty$$

$$\underline{d} \quad y_1 = y_2 = 0 \qquad \text{for } 0 < x < \infty \text{ and } t = 0$$

First the equations (1) and (15) are made dimensionless by substituting $x' = x/L_o$, $t' = t/T_o$ and $y_{1,2}' = y_{1,2} \cot\alpha$, in which L_o and T_o are defined in (6) and (19) respectively. In the following the accents will be omitted. Denoting the Laplace transform of y' with $\bar{y}$, the Laplace transforms of the new equations are for the given boundary conditions:

$$\frac{\partial^2 \bar{y}}{\partial x^2} = s\,\bar{y} \qquad \ldots\ldots\ldots\ldots (20)$$

$$\frac{\partial^2 \bar{y}_-}{\partial x^2} - \bar{y}_- = s\,\bar{y}_-$$

Solving eq. (20) and substituting the boundary conditions give:

$$\left.\begin{aligned} \bar{y} &= \frac{-e^{-x\sqrt{s}}}{s(\sqrt{s} + \sqrt{s+1})} \\ \bar{y}_- &= \frac{-2e^{-x\sqrt{s+1}}}{s(\sqrt{s} + \sqrt{s+1})} \end{aligned}\right\} \qquad \ldots\ldots (21)$$

The functions of (21) can be splitted up into fractions. Then terms arise as $\dfrac{e^{-x\sqrt{s+1}}}{\sqrt{s}}$, which can be developed into series of the kind

$$s^{-n+\frac{1}{2}}\, s^{-x\sqrt{s}},$$

of which the inverse are integrals of the error function. From this, one finds the final solution. In the following, the coordinates ars given for $x > 0$ (the eroded part). For $x < 0$, there is antisymmetry. The solution is:

$$y_{1,2} = \frac{1}{2\sqrt{\kappa t}} \sum_{n=1}^{\infty} \frac{(-1)^{n-1}}{n-\frac{1}{2}} \cdot \frac{t^n}{n!}\, Y_{2n-1}\left(\frac{x}{2\sqrt{t}}\right) \mp \frac{e^{-t}}{\sqrt{\kappa t}} \sum_{n=1}^{\infty} \frac{t^n}{n'}\, Y_{2n-1}$$

$$\left(\frac{x}{2\sqrt{t}}\right) \pm \tfrac{1}{2}\, s^{-x}\, \mathrm{erfc}\left(-\sqrt{t} + \frac{x}{2\sqrt{t}}\right) \mp \tfrac{1}{2}\, e^{x}\, \mathrm{erfc}\left(\sqrt{t} + \frac{x}{2\sqrt{t}}\right) \quad \ldots\ldots (22)$$

(22) is in abridged notation: $x = x/L_o$ (cf (6)), $t = t/T_o$ (cf (19)) and $y_{1,2} = y_{1,2} \cot\alpha$.
The upper sign gives y_1, the lower sign y_2.
In (22), the meaning of Y_n is: $Y_n(x) = 2^n\, \Gamma(\frac{n}{2} + 1)\, i^n\, \mathrm{srfc}\, x$.

i^n erfc x has nothing to do with complex numbers, but denotes the n^{th} integral of the complementary error function.

Thus $y_{-1}(x) = e^{-x^2}$. The functions y_n are shown in fig. 19. We refer to [6], also for tabels and recurrence formulae (page 300 till 318).

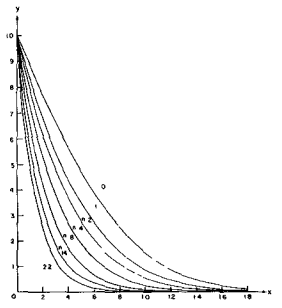

Fig. 19 Repeated Integrals of the Error Function

The erosion of the coast at x = 0 is:

$$[y_1]_{x=0} = 2 \tan\alpha \left(\frac{1 - e^{-t/T_o}}{\sqrt{\pi t/T_o}} - \operatorname{erf}\sqrt{\frac{t}{T_o}}\right) \quad . . (23)$$

in which $\operatorname{erf} x = \frac{2}{\sqrt{\pi}} \int_o^{\infty} e^{-x^2} dx$ and $\operatorname{erfc} x = 1 - \operatorname{erf} x$.

4. STATIONARY CASE WITH GROYNES: FIG. 9.

In the stationary case $\frac{\partial y_1}{\partial t}$ and $\frac{\partial y_2}{\partial t}$ in (13) are zero.

This gives the general solution:

$$\left.\begin{aligned} y_1 &= Ae^{x/L_o} + Be^{-x/L_o} + Cx + E \\ y_2 &= -\frac{q_1}{q_2}(Ae^{x/L_o} + Be^{-x/L_o}) + Cx + E \end{aligned}\right\} \quad . . . . . (24)$$

Boundary conditions for fig. 9.

a antisymmetry A = -B

b $y_1 = y_2 = 0$ for x = 0: E = 0

c $Q_1 = 0$ for $x = L$. $\left(\frac{\partial y_1}{\partial x}\right)_{x=L} = \frac{Q_{o1}}{q_1} = \tan\alpha$

d $y_2 = 0$ for $x = L$

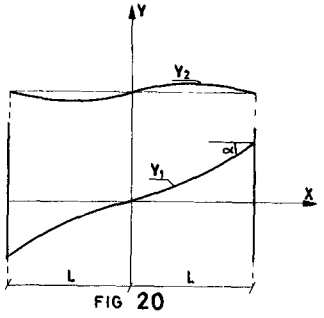

FIG 20

Result.

$$\left.\begin{aligned} y_1 &= \tan\alpha \frac{x + \frac{q_2}{q_1} L \frac{\sinh x/L_o}{\sinh L/L_o}}{1 + \frac{q_2}{q_1} \frac{L/L_o}{\operatorname{tgh} L/L_o}} \\ y_2 &= \tan\alpha \frac{x - L \frac{\sinh x/L_o}{\sinh L/L_o}}{1 + \frac{q_2}{q_1} \frac{L/L_o}{\operatorname{tgh} L/L_o}} \end{aligned}\right\} \quad . . (25)$$

5. STATIONARY CASE WITH ONE GROYNE: FIG. 8d AND FIG. 9.

This case can be found from the former by taking $L = \infty$ and $x' = L + x$. The coordinates of the eroded part are:

$$\left.\begin{aligned} y_1 &= -L_o \tan\alpha \left(\frac{q_1}{q_2} + e^{-x/L_o}\right) \\ y_2 &= -L_o \tan\alpha \frac{q_1}{q_2}\left(1 - e^{-x/L_o}\right) \end{aligned}\right\} \quad \ldots\ldots\ldots \quad (26)$$

6. LITTORAL DRIFT ON A PROTECTED AREA.

In order to return from the two-line system to the one-line system, we look for a transport formula for a protected area of the kind:

$$Q = Q_o' - q' \frac{\partial y'}{\partial x} \qquad \ldots\ldots\ldots \quad (27)$$

in which y' gives the overall coastal direction of a protected area (fig. 21) and Q_o' denotes the transport if the overall coastal direction is parallel to the x-axis, as in fig. 9. By applying the transport formula (5) to (25) we find ($\tan\alpha = \frac{Q_{o1}}{q_1}$):

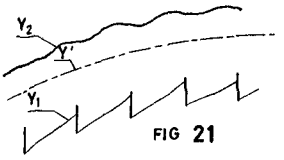

FIG 21

$$Q_o' = Q_{o2} + Q_{o1} \frac{1 - \dfrac{\operatorname{tgh} L/L_o}{L/L_o}}{1 + \dfrac{q_1}{q_2}\dfrac{\operatorname{tgh} L/L_o}{L/L_o}} \qquad \ldots \quad (28)$$

If the overall coastal direction $\frac{\partial y'}{\partial x}$ hae a certain value, the transport changes because Q_{o1} and Q_{o2} in (28) have to be replaced by

$$Q_{o1} - q_1 \frac{\partial y'}{\partial x} \quad \text{and} \quad Q_{o2} - q_2 \frac{\partial y'}{\partial x}.$$

From this one can find q' and p^2:

$$p^2 = \frac{q_1 + q_2}{q'} = 1 + \frac{q_1}{q_2}\frac{\operatorname{tgh} L/L_o}{L/L_o} \qquad \ldots\ldots \quad (29)$$

7. THE SANDWAVES OF FIG. 13.

Differential equations: for the unprotected part (1) and (15), for the protected part (13) with $q_1 = 0$. Assumed is no littoral drift along the protected beach.

In this harmonical case, the derivates to t like $\frac{\partial y}{\partial t}$ can be replaced by $i\omega y$, by example

Boundary conditions:

a $y_1 = y_2 = 0$ at $x = \infty$

b $y_1 = y_2 = e^{-K_+'x} \cos(\omega t - K_+'x)$ at $x = -\infty$, in which

$K_+' = \sqrt{\frac{\omega D}{2q}}$

c $\frac{\partial y_1}{\partial x} = 0$ for $x = -0$

d y_2 continuous and differentiable at $x = 0$

Solution:

See adjacent page. The "offshore transport wave" is the solution of the equation (15) for y_-, the incoming and reflected wave are solutions of (1). The solution is highly dependent of the value of ωT_o. This value defines the short-period waves ($\omega T_o << 1$) and large-period waves ($\omega T_o >> 1$).

8. INFLUENCE OF OBLIQUE WAVES INCIDENCE (FIG. 15). FORMULAE.

Accretion at unprotected coast (branch y_I in fig. 15b):

$$y_I = \frac{1}{\sqrt{\pi}} \frac{p-1}{p} \frac{Q_{o1}}{q_1} \left\{ \sqrt{\frac{4qt}{D}}\, e^{-x^2 D/4qt} + x\sqrt{\pi} + x\sqrt{\pi}\ \mathrm{erf}\left(x\sqrt{\frac{D}{4qt}}\right) \right\}$$

Littoral drift Q at unprotected coast (branch y_I)

$$Q = Q_o - \frac{p-1}{p} \cdot q \frac{Q_{o1}}{q_1} \left\{ 1 + \mathrm{erf}\left(x\sqrt{\frac{D}{4qt}}\right) \right\}$$

Accretion at protected coast (branch y'_{II} in fig. 15b):

$$y'_{II} = y_I(-px)$$

Littoral drift Q at protected coast (branch y'_{II} in fig. 15b)

$$Q = Q_o - \frac{p-1}{p} q \cdot \frac{Q_{o1}}{q_1} \left\{ 1 + \frac{1}{p} \mathrm{erf}\left(px\sqrt{\frac{D}{4qt}}\right) \right\}$$

in which: $\mathrm{erf}\, x = \frac{2}{\sqrt{\pi}} \int_o^x e^{-t^2} dt$.

For the scour hole (branch y'_{III} and y_{IV}), the formulae are similar.

UNPROTECTED COAST

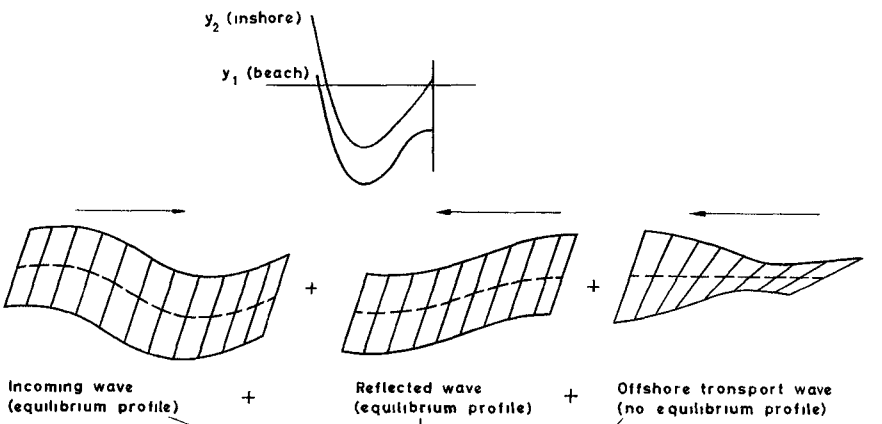

$$y_1 = Re\left[\left(e^{-k_+x} + \frac{C_2}{C_1}\, e^{+k_+x} + \frac{D_2}{D}\,\frac{C_3}{C_1}\, e^{k_-x}\right)e^{i\omega t}\right]$$

$$y_2 = Re\left[\left(e^{-k_+x} + \frac{C_2}{C_1}\, e^{+k_+x} - \frac{D_1}{D}\,\frac{C_3}{C_1}\, e^{k_-x}\right)e^{i\omega t}\right]$$

PROTECTED COAST

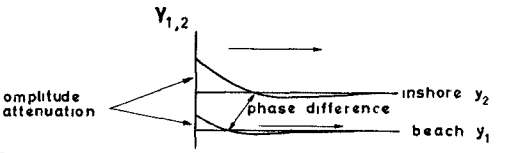

$$y_1 = Re\left[\frac{e^{-kx + i\omega t}}{C_1\left(1 + \frac{D_1}{q_y}\, i\omega\right)}\right]$$

$$y_2 = Re\left[\frac{1}{C_1}\, e^{-kx + i\omega t}\right]$$

IN WHICH

$$k_+ = \sqrt{\frac{D}{q}\, i\omega} = \sqrt{\frac{\omega D}{2q} + i\frac{\omega D}{2q}} = \frac{1}{L_o}\sqrt{i\omega T_o}$$

$$k_- = \sqrt{\frac{D}{q}\left(\frac{1}{T_o} + i\omega\right)} = \frac{1}{L_o}\sqrt{1 + i\omega T_o}$$

$$k = \sqrt{i\omega\,\frac{D}{q_2}\left(\frac{1 + i\omega T_o}{1 + \frac{D_1}{q_y}\, i\omega}\right)} = \frac{1}{L_o}\sqrt{\frac{1 + i\omega T_o}{1 + \frac{D_2}{i\omega D}}}$$

$$C_1 = \frac{1}{2} + \frac{D_1}{2D}\,\frac{k}{k_-} + \frac{D_2}{2D}\,\frac{k}{k_+}$$

$$C_2 = \frac{1}{2} + \frac{D_1}{2D}\,\frac{k}{k_-} - \frac{D_2}{2D}\,\frac{k}{k_+}$$

$$C_3 = \frac{k}{k_-}$$

9. EROSION OF BEACH AND INSHORE ACCORDING TO TWO-LINE SYSTEM (fig. 16). FORMULAE.

Differential equations for $t > 0$: (13) with $q_1 = 0$.

Results·

$t < 0$ (groynes not yet constructed)·

$$y_{1,2} = ax^2 + \frac{2aq_2}{q_y} \cdot \frac{D_1 D_2}{D^2} \cdot \frac{D}{D_2} \cdot \frac{t}{T_o}$$

$t > 0$ (groynes constructed):

$$y_1 = ax^2 + \frac{2aq_2}{q_y} \cdot \frac{D_1 D_2}{D^2} \cdot \left(e^{-t/T_o} - 1 + \frac{t}{T_o} \right)$$

$$y_2 = ax^2 + \frac{2aq_2}{q_y} \cdot \frac{D_1 D_2}{D^2} \left\{ e^{-t/T_o} - 1 + \frac{t}{T_o} + \frac{D}{D_2} \left(1 - e^{-t/T_o}\right) \right\}$$

CHAPTER 32

THE EFFECT OF GROYNES ON STABLE BEACHES

W. A. Price, Senior Principal Scientific Officer
K. W. Tomlinson, Senior Scientific Officer
Hydraulics Research Station, Wallingford, Great Britain

ABSTRACT

The paper describes tests carried out in a wave basin to study the effect of groynes on a beach that was stable for a particular wave climate and a given supply of littoral material. The main conclusion was that on the part of the beach between H.W. and L.W. level the groynes produced no build up. The only build-up that occurred took place seaward of the impermeable groynes. Permeable groynes had little effect either inshore or offshore.

Introduction

The Hydraulics Research Station is undertaking a research programme to study the effect of groynes on beaches. The work is carried out in a wave basin 190 ft long and 75 ft wide fitted with a serpent type wave maker and equipped with tide and tidal current generators. (Plate 1).

Plate 1. Wave Basin

Description of Tests

In the absence of groynes, waves and tides were generated until the beach was in equilibrium. A check was kept on stability by surveying the beach from time to time and measuring the

littoral transport in traps placed at right angles to the beach at the down drift end of the wave tank. A stable beach was normally achieved after 25 tides which amounted to approximately 31 hours continuous operation - a surprisingly long time considering the mobility of the bed material. The particular groyne installation under study was then placed on the foreshore. Again, the same waves and tides were generated and the littoral drift was measured tide by tide. During the tests with groynes the quantity of material fed to the updrift beach was the average quantity of littoral transport measured on the stable beach without groynes. This will be referred to as the "open beach drift". Surveys were carried out after 5, 10, 20, 30, 40 and 50 tides. They were used to compute the volume of coal (a) in each groyne compartment and (b) in the seaward continuation of each groyne compartment between the ends of the groynes and a level 11 in below H.W. mark. (See Fig. 1). The slope of the beach without groynes was 1:17, at mean tide level.

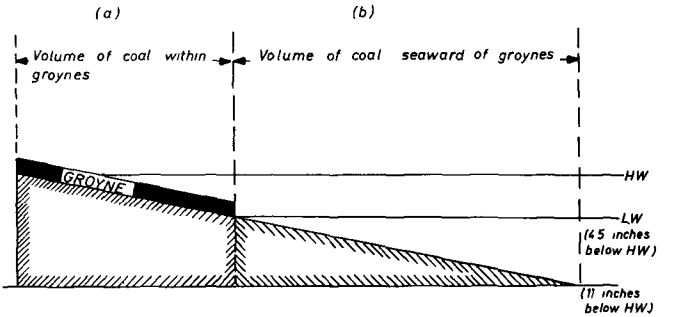

Fig. 1. Beach zones referred to in computations

In all tests the waves had a height of 2.5 in at mean tide level, a period of 1.15 secs and an angle of approach in deep water of 5 degrees. The tides had a range of 4.5 in and a period of 75 minutes. The bed material was a granulated coal which had a mean grain size of 0.8 m'm and a specific gravity of 1.35.

The following groyne installations were tested (See Fig. 2):

(i) Permeable groynes (Plate 2). These were of the Mobbs type used extensively in Norfolk - they were modelled from $\frac{1}{8}$ in diameter rod at $\frac{1}{4}$ in centres. Arranged zig-zag in plan, and at right angles to the beach, their length and spacing = 6 ft 6 in - the horizontal distance from H.W. to L.W. on the stable model beach without groynes. This dimension will be referred to as L.

(ii) Impermeable groynes (Plate 3). 1 in high and of length L they were placed at right angles to the beach and tested at 3 spacings L, $1\frac{1}{2}$L and 2L.

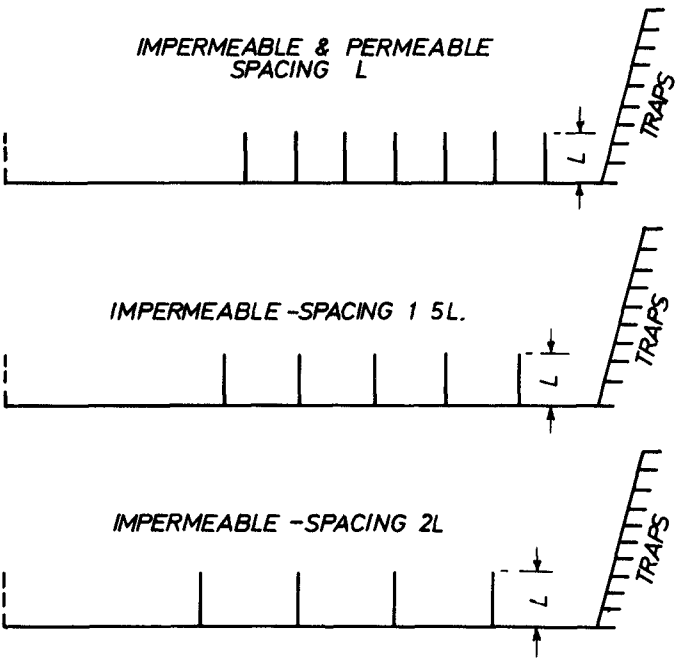

Fig. 2. Groyne installations tested

Plate 2. Permeable Groynes

Plate 3. Impermeable Groynes

Summary and Interpretation of Results

On the part of the beach within the groynes and between H.W. and L.W. marks none of the groynes produced a significant increase in beach levels. The only build-up that occurred took place seaward of the impermeable groynes. This increase not only took place in front of the groynes, but was also apparent, and even more marked in some cases, along the stretch without groynes. (See Fig. 3).

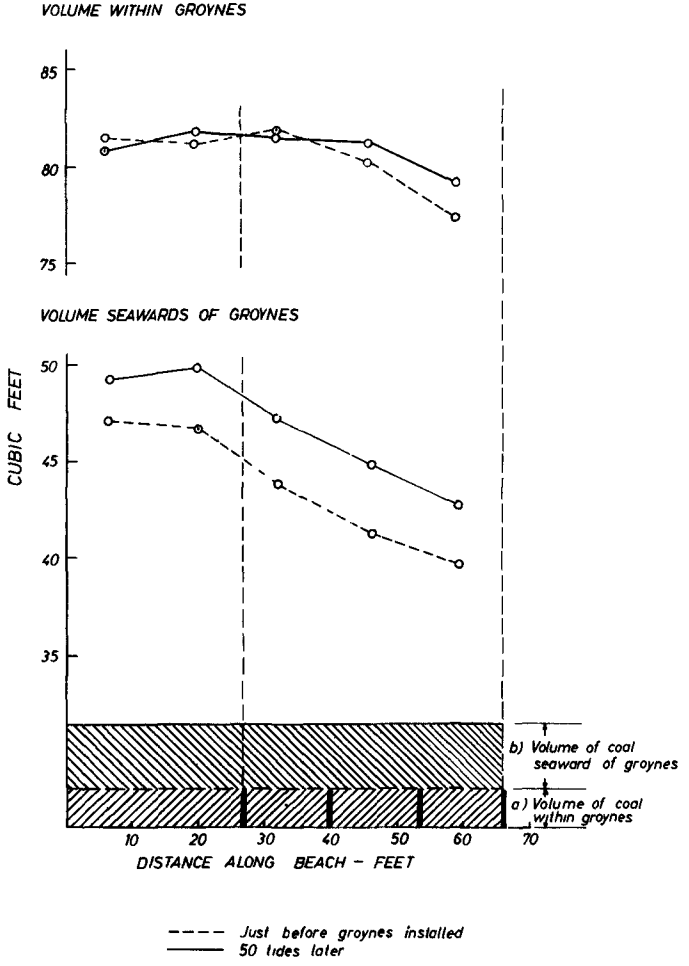

Fig. 3. Volume changes after installation of groynes.

The permeable groynes had little effect either inshore or offshore. The total drift varied considerably during the experiments. Fig. 4 demonstrates the variation that took place after the installation of groynes. Permeable and impermeable groynes at the smallest spacing L affected the total drift the least. However, up to 20 tides after installation the drift increased, indicating that erosion was taking place during this period. Subsequently the total drift dropped below the "open beach" value.

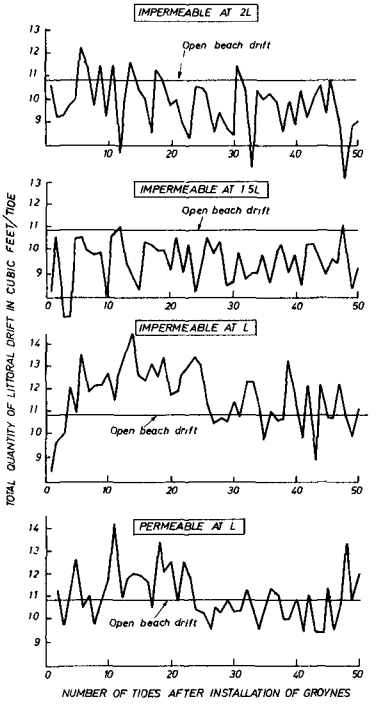

Fig. 4. Changes in littoral drift.

Impermeable groynes at a spacing of 1½L and 2L considerably reduced the total drift; the "open beach" drift was never re-established even after continuing the run for 50 tides. The area seawards of the groynes was still building up at the end of these runs.

In Fig. 3 the graph shows a reduction in the volume and cross sectional area with distance along the beach, the effect is particularly marked seaward of the groynes. This would have the effect of changing the angle of wave approach to the beach and therefore the rate of littoral drift with distance along the beach.

The intensity of littoral drift was measured at various points on the beach without groynes is shown on Fig. 5. The major part of the drift took place between mean water level and just seawards of low water. This distribution is very similar to the one put forward for sandy beaches by Knaps in 1952 (Ref. 1). In the vicinity of a groyne intensity of drift has increased in the area seawards of the end of the groyne although the total drift has been reduced.

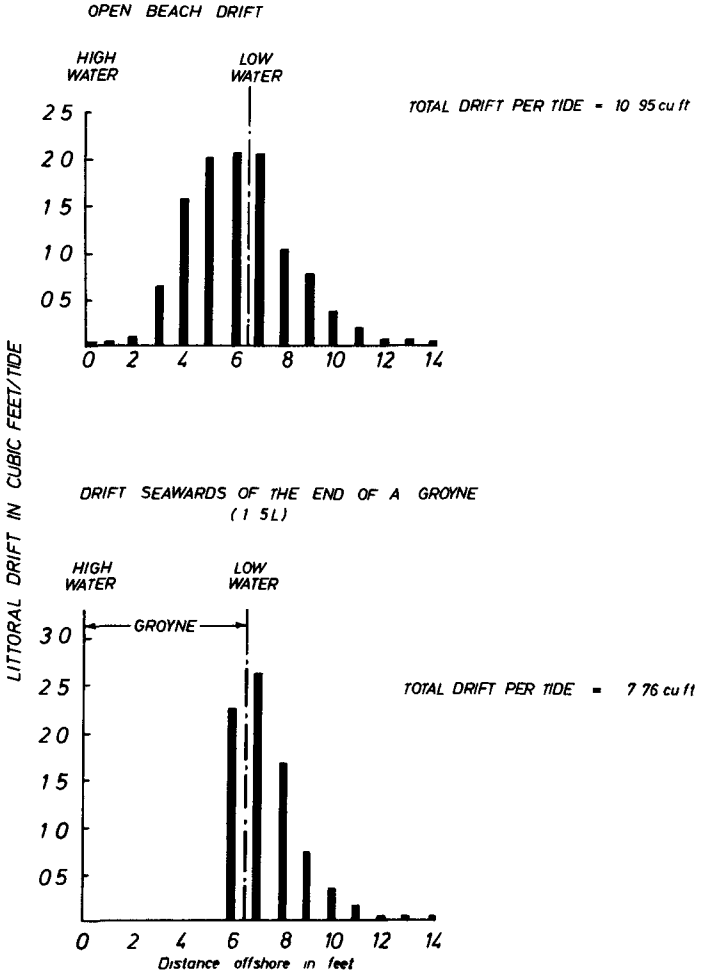

Fig. 5. Drift with and without groynes

In interpreting the results of these tests two comments are relevant. Firstly, they show the effects of groynes on a stable beach - a situation not normally met with in practice. Coastal engineers mainly use groynes on beaches that for one reason or another are eroding, though they may once have been satisfactory; a satisfactory beach, in this context, meaning one that is stable and in equilibrium with the prevailing wave climate and littoral drift. The main cause of erosion is usually that the beach has been starved of its supply of material and the groynes are used in an attempt to catch what drift there is. This is not the case under discussion; the updrift beach in the present series of tests was fed with the "open beach" drift.

A further series of tests were carried out with a deep water angle of wave approach equal to 20°, and a groyne spacing of $1\frac{1}{2}L$. The effect of the groynes on the beach was similar to that with waves from 5°, i.e. no build-up of the beach between groyne compartments was observed but the offshore sea bed levels increased significantly. The total rate of littoral drift decreased, which corresponded with the accretion on the offshore sea bed.

It might be concluded from the results of the present series of tests that when a beach is in equilibrium with the wave climate and the littoral drift, groynes are unlikely to increase beach levels. There is of course the possibility that groynes are more successful in building up or at least preventing further erosion of eroding beaches.

The build-up in the area seaward of the groynes is perhaps the most significant fact that has emerged from the present series of tests. If some time after the installation of groynes a stable topography is ever achieved the same littoral drift must pass every section as it did previously. Assuming then that the groynes inhibit the drift along the upper beach, the drift along the lower beach must be correspondingly increased. The shallower depths offshore permit the increased littoral drift along these contours.

Future research will be directed to establishing the best type of groyne installation to improve an eroding beach. There is the possibility that in this context groynes will increase foreshore levels.

References

1. Knaps R. Ya. Protective structures of breakwater type, and the movement of material on sandy shores. Izv. Akad, Nauk, Latv. SSR 7(36).

This paper is published with the permission of the Director of Hydraulics Research, Wallingford.

The authors wish to acknowledge the careful and painstaking work of A. H. Vallance who carried out the experiments and analysed the results.

CHAPTER 33

EXPERIMENTAL STUDY OF THE HYDRAULIC BEHAVIOUR OF GROYNE SYSTEMS

Júlio Patrıarca Barceló
Research Officer. Department of Hydraulics
Laboratório Nacional de Engenharia Civil. Lisboa. Portugal

SYNOPSIS

Results of an experimental study of the hydraulic behaviour of groyne systems, a very widespread coast erosion protection structure, are described. The characteristics of the evolution of beach stretches between groynes under the action of waves with different obliquity, heights and periods are defined. The results obtained are intended for design of systems of functional groynes which secure an adequate partition of the beach in satisfactory hydraulic conditions, and also meeting use requirements, notably from the architectural and recreation standpoints. Additionally the author briefly discusses longshore drift and presents some experimental conclusions on the relations between longshore drift and the characteristics of the waves.

1 - INTRODUCTION

Coast erosion and the creation of artificial beaches are two of the main problems which arise concerning the development of coastal areas. Both the problems can, in many instances, be solved using groyne systems, (see fig.1). This type of protection is also currently used to solve accretion problems in certain coastal zones or control shoal progression. Generally, hidraulic and architectural standpoints make the design of this type of works difficult, especially the determination of the length, spacing and crown elevation of the groynes, taking into account that the groyne structure itself is ruled by hydraulic characteristics and by its required utilization which, often, involves landscaping problems. The importance of designing efficient groyne which can be applied to a large number of extensive coastal areas (see fig.2) led to the present study, the purpose of which is to contribute towards the solution of the problems presented by such systems.

Systematical tests of fixed, high and impermeable groynes was carried out, (see figs.3 and 4). The groyne slopes had different structures and they were put perpendicularly to the shoreline, corresponding to rockfill prototypes with the purpose of studying the most usual type of groynes. The pattern beaches selected for study were those which can be classified as independent physiographical units, i.e stretches of beach located between groynes long enough to prevent the transposition of mobile material at their edge. The main purpose was the determination of the evolution characteristics

Fig.1 - Groyna. Cova do Vapor beach.

Fig.2 - Coast erosion. Caparica baach. February 1964.

Fig.3 - Laboratory test. Wave action. 1st sarias of tests.

Fig.4 - Laboratory test.Final situation(wava with maximum height).

Fig.5 - Tank.

of the beach stretches under the action of cycles of waves with different characteristics, setting the spacing and the length of the groynes in order to obtain stable beaches. Secondarily, taking advantage of the groynes as a way of measuring the littoral drift, it was tried to establish a relation of dependence between the littoral drift and the characteristics of the acting waves.

As fundamental parameters of the hydraulic behaviour of the groynes it was considered: the slope of the beach, the specific weight and the granulometrical characteristics of the mobile material; the height, period and obliquity of the acting waves; the length, spacing, crown elevation and slope structure of the groynes and also the orientation of groyne directrix.

The basis of this work were established as a contribute to the study of long groynes use at parcelling coastal areas, as it was referred in {1}.

2 - EXPERIMENTAL TECHNOLOGY

This study was carried out almost in its whole in a 20 m x 10 m tank (see figs. 5 and 6) equipped with a snake type wave generator and a tide reproducing system. This generator allowed the reproduction of single sinusoidal waves, the only ones which were taken into account in this study, although a generator able of reproducing wave trains is already available but not yet operative; tests under the action of wave trains will be soon carried out. The characteristics and limitations of the wave generator can be evaluated from figs. 7, 8 and 9. The graph in fig.7 shows, as ordinates, the wave heights and, as abscissas, the eccentricities to be introduced into the generator. The wave range to be reproduced covers heights between 1.0 and 7.0 cm, periods of 1.0 to 1.8 sec and three obliquities: 20°, 10° and 5° (although the generator allows for obliquities in the 60° range). The thick lines in fig.7 refer to situations where regular sinusoidal waves are generated while the interrupted lines correspond to irregular waves reproduced under deficient conditions. The histogram in fig.8, plotted on the basis of 232 readings, shows the occurrences of certain deviations regarding a mean value of wave heights recorded by 12 resistance probes; the distribution of these deviations follows rather closely Gauss's normal law; it must be said that deviations from the mean values ranging from 15 to 18% have a rate of occurrence of 4%. Wave period was determined by chronometry with errors of 1%. The obliquities of the generated waves, obtained through calculated de-phasing of the paddles, were checked against photographic plans. The tidal records were made through limnographs.

Beach cross sections were considered and readings taken of the distances between the water line and a reference line; the error in the determination of such distances was of ± 0.5 cm. A complete survey of the bottoms was made at the end of each test through direct measurement of successive water lines obtained by lowering the level inside the tank. An automatic probe for direct recording of the bottom profiles was studied by LNEC's Instru-

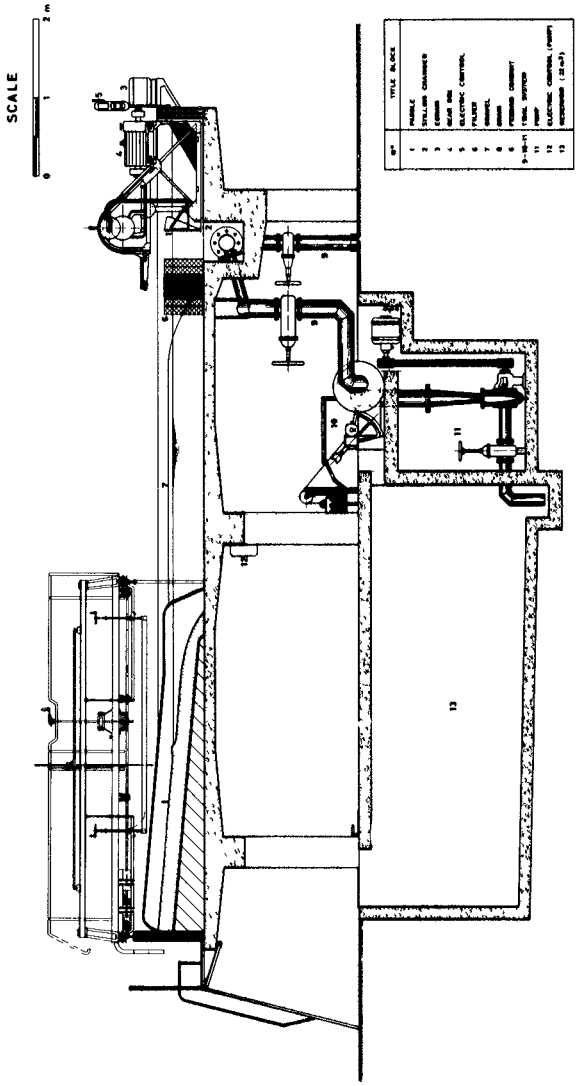

Fig.6 - Tank. Cross section.

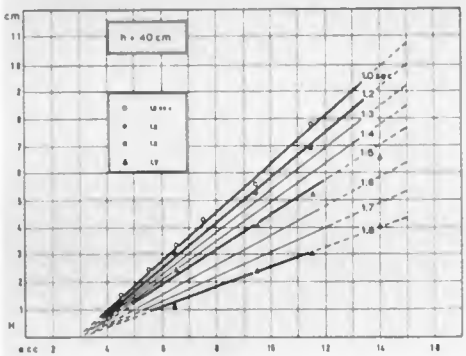

Fig.7 - Calibration curve of the wave-ganerator

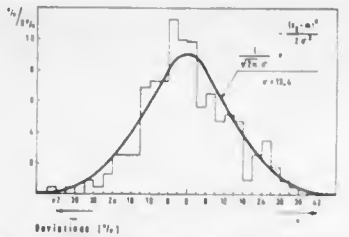

Fig.8 - Distribution of deviations of weve heights.

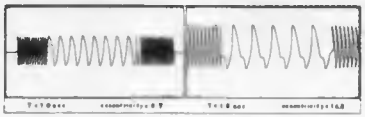

Fig.9 - Wave records (model).

Fig.10 - Servo-coordinograph. Experimentel sat-up.

Fig.11 - Servo-coordinograph.Deteil of the probe.

Fig.12 - Servo-coordinograph.Deteil of the record.

Fig.13 - Pumice-stone. γ_s = 1,67 gf/cm^3.

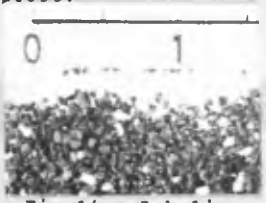

Fig.14 - Bakelite. γ_s = 1,38 gf/cm^3.

Fig.15 - Send (modal). γ_s = 2,61 gf/cm^3.

Fig.16 - Sewdust.

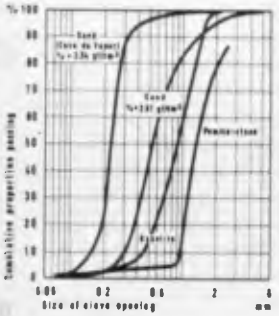

Fig.17-Mobile materials. Granulometric curves.

ment Design and Construction Division. This probe was studied and mounted at its experimental stage with excellent results (see figs. 10, 11 and 12); the need to make a few corrections and the difficulties of constructing the equipment in its final design made impossible the use of this recording method, which would have allowed a much more detailed study of the cross section evolution characteristics.

The technological characteristics of another tank where a few tests were made are identical to those described above.

The mobile materials used were pumice-stone, bakelite, sand and saw-dust. The specific weight of the satured grains and the granulometrical characteristics can be seen in figs. 13 to 17 (figs. 13, 14, 15 and 16 are photographs of microscope observations).

Fresh water was used for all the tests. The Reynolds' number has values over 3000, calculated according to Miche's formula, $R=\frac{L}{T}\frac{H}{2\nu}$ with $\nu=1.01\times10^{-6}m^2s^{-1}$ thus justifying the classification of the movement as turbulent. As the testing set-up does not correspont to any specific case, but is only a schematic situation for systematic testing, there is no scale.

3 - EXPERIMENTAL RESULTS

A first series of tests was made by using the set-up described in fig.18. It was taken as a pattern a pumice-stone beach with an 8% slope in cross section and a depth of 40 cm at the base of the slope, (see fig.6). Groyne E1 was studied in different positions, in order to change the distances between groynes. E1 and E3 groynes were formed by loose rockfill with a 2/1 absorvent slope; E2 groyne, this non-absorvent, had a 1/5 slope. This set-up made possible the investigation of the differences of behaviour in groynes with different structures in the two stretches of beach. The initial water line is defined in fig.18 (t = 0).

The action of oblique waves on the stretches of the beach arises generally a longitudinal drift characterized by zigzag movements of the grains, which result from the combination of the oblique jet from the run-up of the wave after breaking, with the return flow following the highest slanting line of the beach (see fig. 3). A zone of erosion is thus created seaward while leeward, under the action of the groyne, there will be a zone of retention. The typical evolution can be observed in fig.18 and, after a period of time referred to as stabilization time, there will be a situation of equilibrium (see fig.19) with an adjustment between the water line and the acting wave, the incidence of which will become frontal along the whole stretch of beach. Littoral drift will consequently disappear. This situation is due to the evolution of the beach as well as to the refraction of the acting wave resulting from the alterations on the bottoms which happen during evolution. The wave action on stretch 1 is conditioned by the influence of the absorvent slopes of E1 groyne which, being a long groyne, originates, besides the wave difraction, an energy dissipation on the side slopes; thus, the final configuration of equilibrium (see fig.19) shows the point of highest

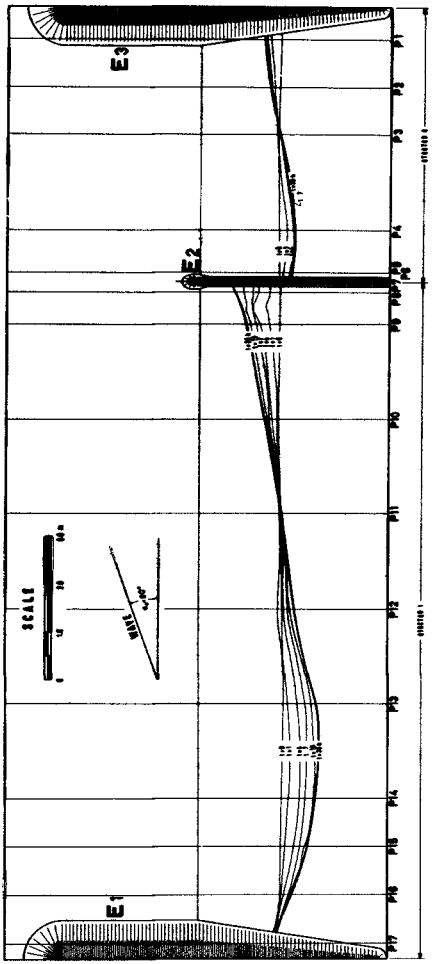

Fig.18 - Typical plan of evolution. 1st series of tests.

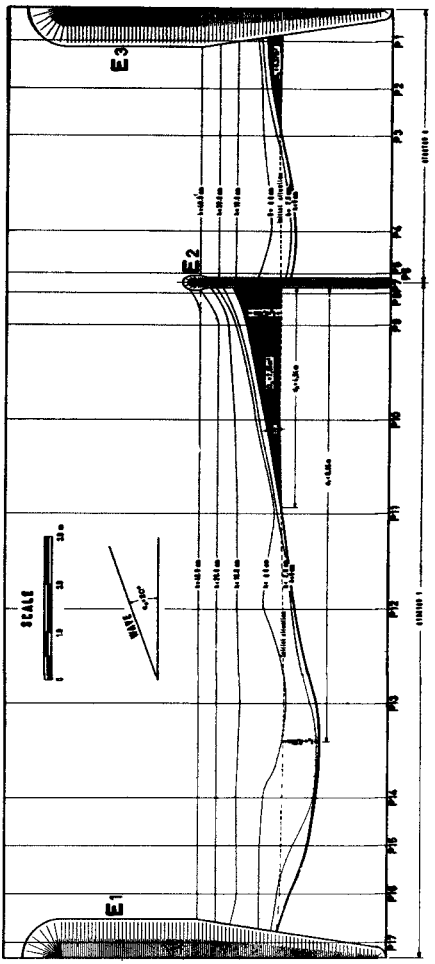

Fig.19 - Typical plan of final equilibrium situation. 1st series of tests.

erosion far away from the groyne E1, contrary to what happens in stretch 2 where that point is nearer to the groyne on account of the latter being non-absorvent.

In view of the importance of wave refraction on groyne behaviour it might be assumed that beach evolution would only be dependent on the wave obliquity and period and that the wave height would be a less important parameter. Actually, the influence of height is very much important, seeing that it restrains the location of the breaking line and the run-up. Thus, two waves with the same obliquity α_o the same period but different heights will present different incidences on breaking for the highest wave will break at greater depths and its slope base obliquity will thus suffer a minor variation through refraction. One can actually obtain bigger accretion with higher waves provided the material will not go into suspension. It was found that for the same obliquity at the slope base and the same period, the value of the ω angle for lower waves was about $\alpha_o/2$ while for higher waves the ω angle increased until it reached values around α_o. The accretion zone located next to the groyne generally presents certain singularities due to the action of the jet formed under the action of the oblique wave on the groyne slope (see fig.22). As significant data on beach evolution it was presented the graph on fig.20 referring to P9 and P5 profiles defined in fig.18. A rather accentuated beach evolution was recorded during the first few hours of tests. This evolution decreases progressively until it reaches, for each wave, a final situation of equilibrium. Advances on profile P9 increase, for the same obliquity and period, whenever wave height increases but after a certain value is reached, which for pumice-stone may be set at 6.0 cm, mobile material goes openly into suspension and beach behaviour acquires different characteristics as in the case of the 7.0 cm high wave; the diagram in fig.20 shows a backward movement of the beach at the starting near the centre groyne and final values lower than those obtained with waves 5.0 cm high. As the other hand when the material is carried in suspension it goes through the end of the groynes and there is a recovery of the initially eroded beach in profile P5. Beach evolution is very regular for major obliquities; for 5° obliquity its behaviour is more irregular and there are some cases where transversal movements predominate over the longitudinal ones. It can be seen from profile P5 that for 5° obliquity waves with greater wave-steepness led to erosions while those with lesser wave-steepness originated accretion.

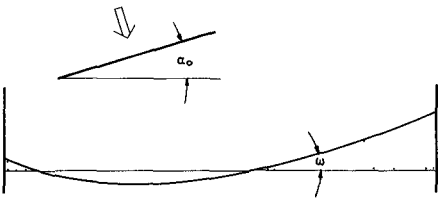

The pumice-stone used for testing is a heterogeneous material. As it can be seen from fig.4 there are two distinctive zones in the final situation of equilibrium: one of dark coloured material and the other of light coloured one which correspond, respectively,

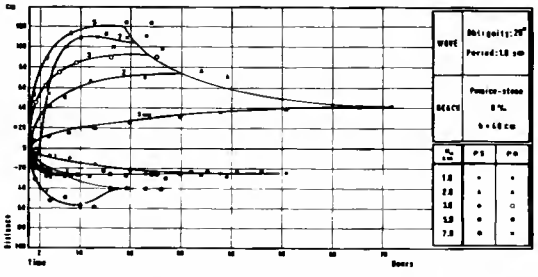

Fig.20 - Typical curva of profile evolution. 1st series of tests.

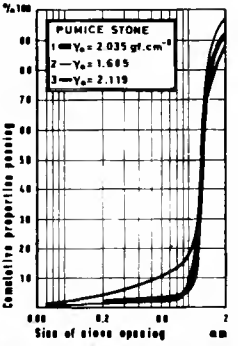

Fig.21 - Pumice-stone. Granulometric curvas.

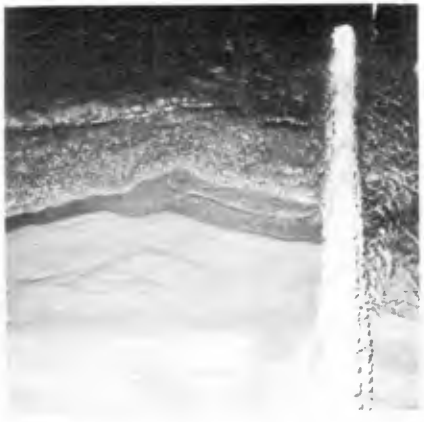

Fig.22 - Wave action naar the groyna.

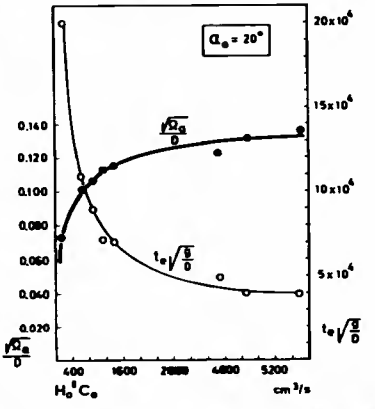

Fig.23 - Typical curva of dimensionless paramstars variation.

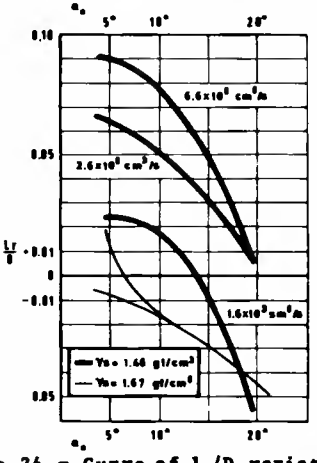

Fig.24 - Curva of l_r/D variation. Laeward

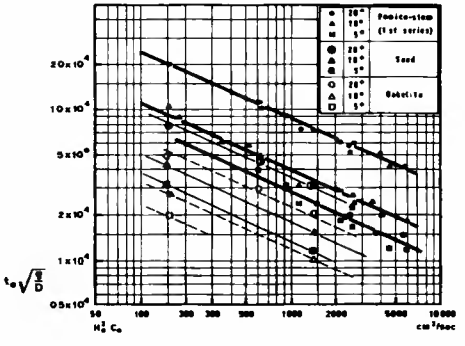

Fig.25 - Curva of $t_a\sqrt{g/D}$ variation.

to higher specific weights and a larger percentage of fine components, and lower specific weights with larger diameters. The material initially found on the beach is a mixture of both (see fig. 21). The zone of retention is formed by the lighter material, while the heavier material remained on the eroded zone. However, the tests carried out with sand, a more homogeneous material, showed that behaviour characteristics were identical to those obtained with pumice-stone. It should be noted that although the darker pumice-stone, with higher specific weight, has a large percentage of fine components, its mean diameter is the same as that of the lighter pumice-stone.

To define the evolution characteristics of the beach stretches it was considered values expressing quantitatively the forward and backward movements, accretion areas, stabilization times, length of groynes and the distances defining the area of erosion. These values, whenever no indication on the contrary is to be given, refer to the final situation of equilibrium. Thus, designating as D the distance between the groynes which limit a stretch of beach, it is to be consider the following dimensionaless parameters:

l_a/D - defining the maximum advance, l_a, of the water line near the groyne (on a cross section close to the groyne not affected by the singularities described).

l_r/D - defining the maximum erosion, l_r, found on the beach stretch.

$\sqrt{\Omega}_a/D$ - defining the emersed area of accretion, Ω_a, near the groyne.

c/D - defining the effective length, c, of the groyne.

$t_e\sqrt{g/D}$ - defining the stabilization time, t_e, for the beach stretch.

d_A/D - defining the distance, d_A, measured from the retention groyne, to the point where evolution is null, (intersection of the final situation of equilibrium with the initial situation).

d_r/D - defining the distance, d_r, measured from the retention groyne to the point of highest erosion.

Values l_a, l_r and Ω_a were measured between the water lines corresponding to the initial and final situations. Value Ω_a was considered to be representative of the groyne capacity of retention instead of the volume of the material retained, owing to the difficulty of measuring accurately the volumes retained (these calculations were only made in connection with the volumes retained during the 1st hour of the tests with a view to the determination of littoral drift). Value c was measured between the line corresponding to the initial situation and the limit of the underwater deposits at the final situation, next to the retention groyne. The c value defined in this way takes only into account the beach evolution seaward, since the consideration of possible erosions leeward close to the groyne, would make necessary to determine, for each case, the length of the rooting portion which will be added to c value. t_e represents the number of test hours until the stretch of beach reaches the equilibrium.

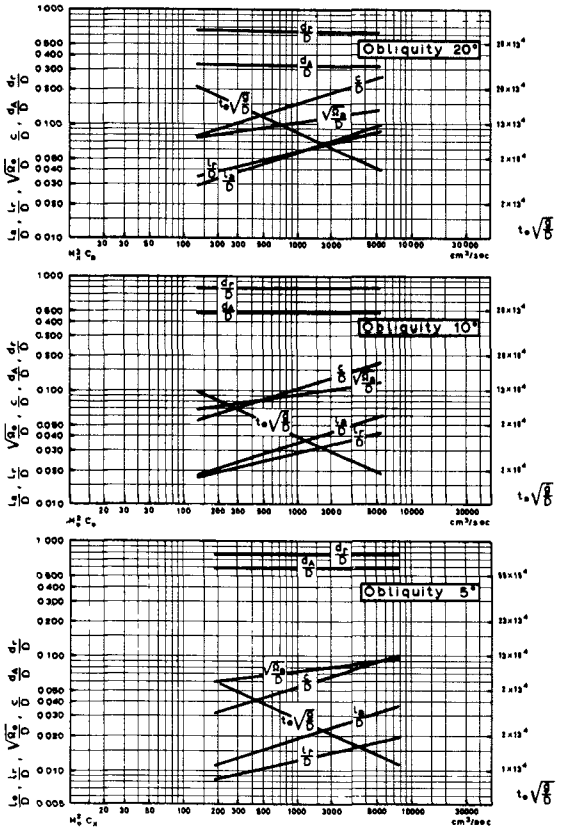

Fig.26 - Results of 1st series of tests.

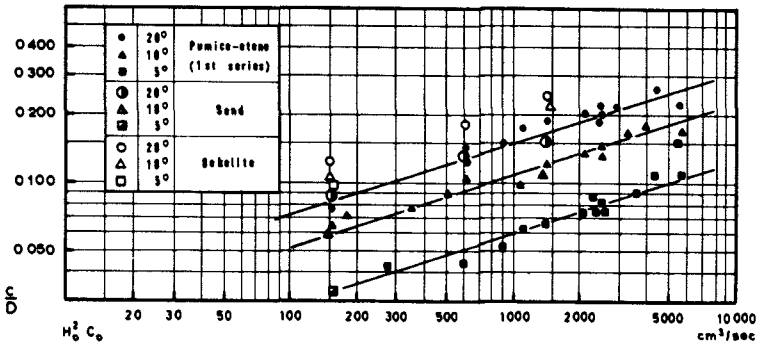

Fig.27 - Curve of results obtained with different mobile materials.

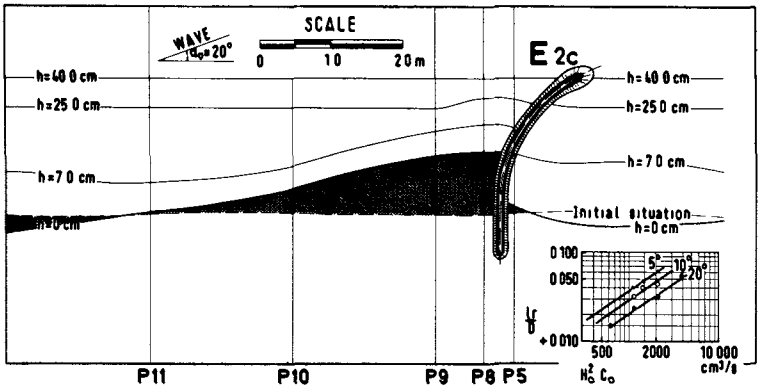

Fig.28 - Partial plan of curved groyne.Curve of the avolution leaward of the groyne.

The value $H_o^2 C_o$ was considered as typical parameter of the acting wave, proportional to the power transmitted by the wave, conjugated with a function of α_o angle, obliquity at the base of the beach slope. Values H_o and C_o are, respectively, the deep water wave height and celerity. The results now presented refer to the evolution of beaches where bed-load transport is predominant. The extrapolation to $H_o^2 C_o$ values higher or lower than these tested is not valid, as the conditions of evolution where transport by suspension is predominant and the critical conditions at the starting of transport will have to be the object of detailed studies.

The results obtained in stretch 1 of the set-up for the 1st series of tests are represented on the diagrams in fig.26. It was found that the dependence of the parameters characterizing the evolution of the beach stretch as related to the power transmitted by the wave is represented, for each obliquity and within the limit values tested, by straight lines in logarithmic graphs. There is a minimum dispersion of the experimental points as it can be seen from the typical diagram, in linear scale, in fig.23. The values of l_a/D, l_r/D, $\sqrt{\Omega_a}/D$ and c/D increase, for the same obliquity, whenever the $H_o^2 C_o$ value increases and present maximum values resulting from the mobile material going into suspension. The value of $t_e\sqrt{g/D}$ decreases as $H_o^2 C_o$ increases for the same obliquity. d_A/D and d_r/D values remain constant for the same obliquity when $H_o^2 C_o$ increases. For the same amount of power transmitted, the values of l_a/D, l_r/D, $\sqrt{\Omega_a}/D$, c/D and $t_e\sqrt{g/D}$ increase whenever the wave obliquity increases, while the values of d_A/D and d_r/D increase with decreased obliquity, i.e. the accretion area covers a larger part of the beach for lower obliquities, although the accretion surface is smaller, while the erosion area gets closer to the seaward groyne (E1). As an example, and in order of importance to the values of these parameters, admitting an extrapolation into nature, there will be, for a distance between groynes D = 200 m and an obliquity of 20°, the following maximum values. l_a = 20 m, l_r = 18 m, Ω_a = 730 m^2, d_A = = 68 m, d_r = 134 m, c = 52 m and t_e = 250 h. One should take notice that an actual length of the groyne including the rooting portion, which depends upon the characteristics and possible erosions of stretch 2, must correspond to c value. On the other hand, c length was determined from the initial water line, corresponding to the mean level at rest which was constant during testing; however as due to tides there are actually variations of the level at rest, it becomes necessary, for practical purposes, to set a level wherefrom to measure the c length which presents, for each case, particular conditions either due to the dimensions rize of tides, or to wave breaking conditions and intensity of littoral drift. As regards t_e value, it must be put in evidence that it corresponds to a period of constant action of a certain wave which, in the case under consideration, would correspond to a wave of minimum power from a transport capacity standpoint, and would equal, in an extrapolation into reality, to a continuous action over a period of approximately 10 days. However, in the case of t_e the minimum value, correspond

ing to the more powerful wave, might be of interest from a point of view of the movement into suspension of the material which would result, for 20° obliquity and D = 200 m, a value t_e = 50 h, approximately 2 days of continuous wave action.

In stretch 2 of the set-up for the 1st series of tests identical results were obtained, with the exception of the erosion areas characteristics, defined by l_r and d_r values. The area of greatest erosion is located nearer to the seaward groyne (E2), due to the structural characteristics of its slopes (lesser degree of wave power dissipation). It can be said, in practical terms, that the ratio d_r/D becomes equal to 1.00. Relatively to the l_r/D value it can be seen from the diagram in fig.24 that with a 20° obliquity a practically constant value in the order of 0.044 can be obtained when $H_o^2C_o$ varies. For this obliquity and for D = 200 m there would be a backward movement of about 9.0 m near the seaward groyne. It is found that for lesser obliquities erosion is smaller and that for a 5° obliquity there is a reduced erosion for greater wave steepness and accretion along the whole stretch for smaller wave steepness.

The tests made with sand on stretch 1 of the set-up for the 1st series of tests produced results identical to those obtained with pumice-stone. The diagrams in fig.26 remain unaltered to the exception of the one corresponding to $t_e\sqrt{g/D}$, as these values are lower to those obtained with pumice-stone (see fig.25). As this material goes easily into suspension due to the low diameter values of the particles, the straight lines in fig.26 are limited as it regards the value of $H_o^2C_o$ = 1000 cm^3/s. The only few significant differences were obtained with 5° obliquities where the prevailing influence of the transversal movements is reinforced by the facility with which the material goes into suspension.

With bakelite and a similar set-up, identical results were also obtained. Bakelite, with low mean diameter value and a specific weight lower than the former, goes into suspension even more easily and the limit value of $H_o^2C_o$ is approximately equal to 600 cm^3/s. There was consequently a tendency to higher accretion as compared to pumice-stone. However, although the parameters defining the accretion areas, advancement and effective length of the groyne are higher the maximum values remain the same taking into account that the limit $H_o^2C_o$ is lower than for pumice-stone (see fig.27). The $t_e\sqrt{g/D}$ values are even lower than those obtained with sand (see fig.25).

When using sawdust with the same set-up of the previous tests no satisfactory results were obtained regarding the extreme facility which made sawdust go into suspension together with the very high heterogeneousness of the particles (see fig.16) which present an exceedingly irregular shape. This causes the material look like a paste when submerged.

All the previous tests were carried out with an 8% slope for the initial cross section of the beach. The tests made with 5% and 11% slopes did not show any significant changes in comparison with the previous tests. Actually the cross section of the beach varies according to the acting wave, and for the range of slopes tested,

the initial slope of the beach lead to no alterations in the characteristics of the equilibrium situation.

As a variant of the set-up used for the 1st series of tests a central and curved groyne was adopted and its positioning oriented in order to avoid the erosions which take place leeward of the groyne. (see fig.28). For the range of values tested there was an advancement near the groyne slope leeward, the value of which increases, for the same obliquity, as the $H_o^2C_o$ values increases. For the same $H_o^2C_o$ value the rate of advancement is higher when the wave obliquity decreases as the diffraction originated by the groyne forms a shadowed area where the decrease in power is greater for waves of higher obliquity. For the range of values tested, reduced advancement values are obtained (maximum 12 m for D = 200 m), but the roots are no longer subject to erosions. The hydraulic behaviour of the curved groyne tested presents on stretch 1 characteristics identical to those of straight groynes. There is only a slight increase in the c length of the groyne for the higher obliquities tested.

Tests with tide reproduction were also made using the 1st series set-up and pumice-stone. The water level was made to alter gradually, without the reproduction of tidal currents. This is a very interesting aspect in certain cases (see [2]). Tests of tides with amplitudes equalling 4.30 to 6.40 cm and cycle periods equivalent to 20 and 30 minutes were made. In all the cases the mean level corresponded to a depth of 40 cm and the maximum level variations were calculated not to introduce significant changes in the generated waves. It is found that the characteristics of groyne behaviour are maintained without significant differences; there was only a slight increase - maximum 30% - in the values for the accretion area, due to the retention effects which are originated by the underwater deposit. This is higher along its whole length owing to the depositions occuring in the low tide. There were, however, for the values tested, no alterations concerning the values of the c length of the groynes.

A 2nd series of tests was made using the set-up shown in figs.29 and 31 with pumice-stone and an 8% slope for the initial beach cross section. The pumice-stone used for this series had a specific weight of 1.46 gf/cm^3 (lower than that of the pumice-stone of the 1st series) and mean diameter approximately equal to that of the pumice-stone weighing 1.67 gf/cm^3. The groynes, shorter than those previously used, are of the non-absorvent type. The results obtained can be seen in fig.30. Regarding the 1st series results, there were the following changes:

- In a general way, there was an accretion along the whole stretch of beach between groynes due to the influence of the transversal movements which became easier by the granulometrical characteristics of the mobile material as well as by the wave action which, in this case, have not the retarding and dissipation action of the absorvent slopes of the groynes. Bigger areas of accretion were achieved on the beach stretch due to the combined effects of the transversal and longitudinal movements, the latter being also more

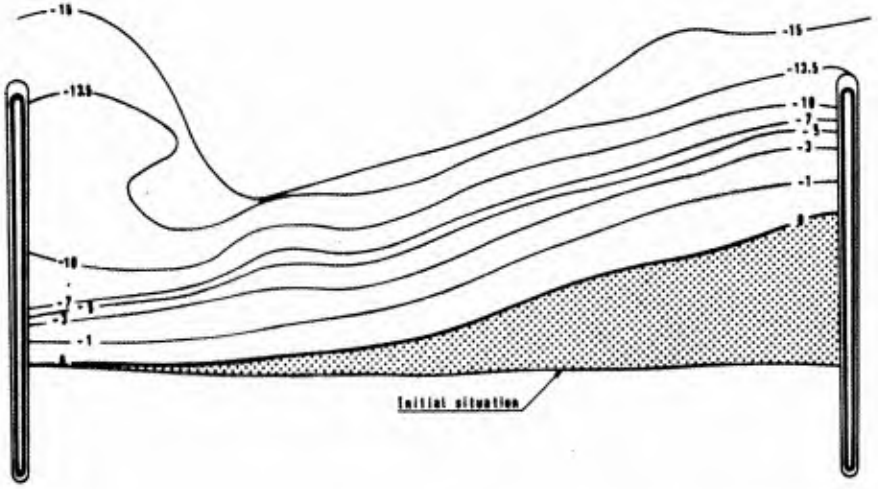

Fig.29 - Plan of test setting for 2nd series of tests.

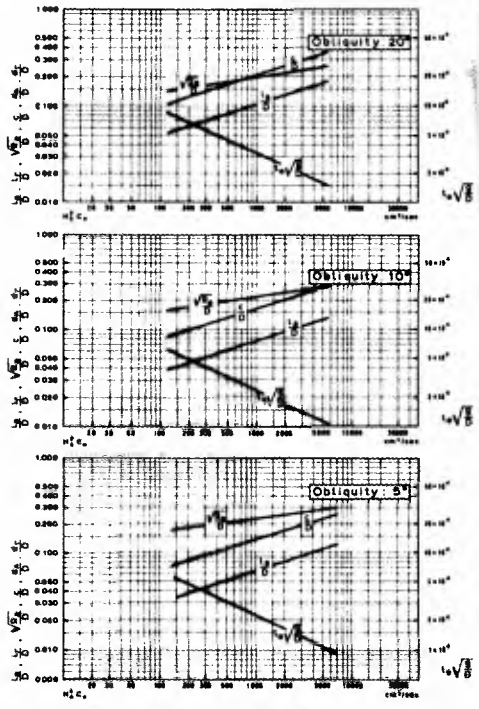

Fig.30 - Results of 2nd series of tests.

Fig.31 - Test setting for 2nd series of tests.

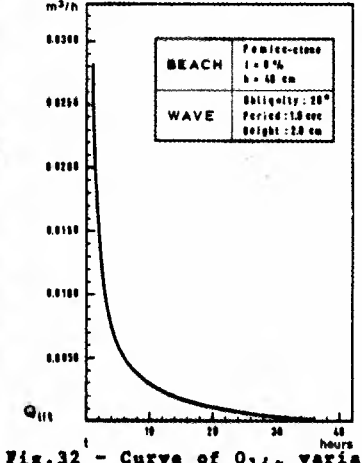

Fig.32 - Curve of $Q_{lit.}$ variation. 1st series of tests.

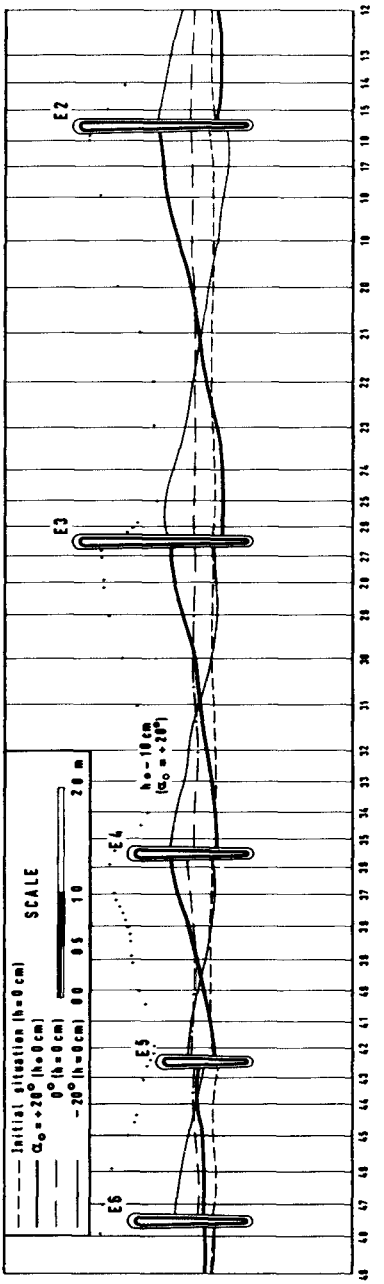

Fig.33 - Plan of groyne system. 3rd series of tests.

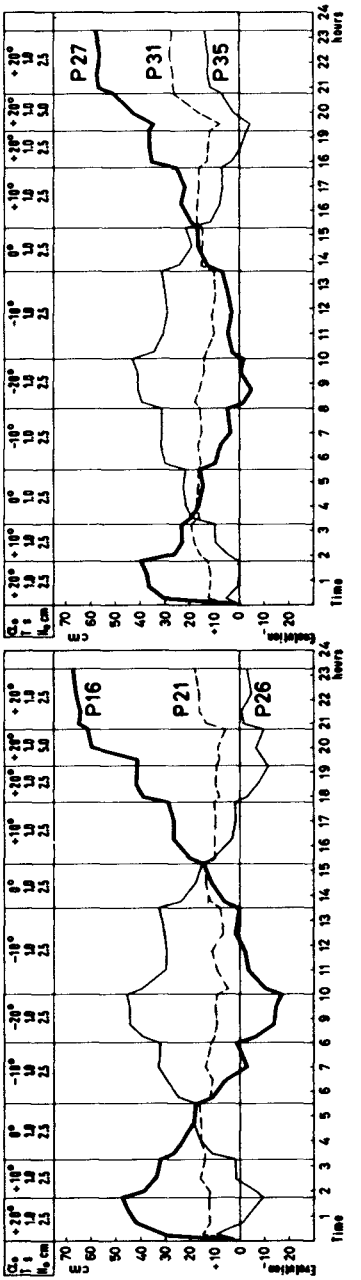

Fig.34 - Curves of profile evolution. 3rd series of tests.

intensive as the wave action took place with higher obliquities in the seaward area. As it can be seen on fig.24 there was one erosion near the leeward slope of the groyne only for the lowest value of transmitted power, this erosion being of the same importance as the one which occurred in stretch 2 of the 1st series set-up. In all the other cases it was found that the higher the transmitted power was, the higher were the accretion values for the 10° and 5° obliquities leeward of the groyne. For the same $H_o^2 C_o$ value, the accretion value increases when obliquity diminishes due to transversal movement influence.

- An increase of $\sqrt{\Omega_a}/D$, l_a/D and c/D values was observed due to the reasons set forth in the previous paragraph. The d_A/D value is close or equal to the unit. The $t_e\sqrt{g/D}$ values are near those obtained with bakelite in stretch 1 of the 1st series set-up. The operating conditions of this set-up are the most unfavourable from the point of view of establishing the c length. For this reason the c/D values of this series will be the ones proposed for the design of groyne systems.

At last a 3rd series of tests was made with wave cycles acting on the groyne system defined in fig.33. Pumice-stone, similar to the one used for the 1st series, and an 8% slope for the initial beach cross section were adopted. Obliquities of +20°, +10°, 0°, -10° and -20°, a period of 1.0 sec, a mean height of 2.5 cm and a maximum height of 5.0 cm were tested. Results are shown in fig. 34. The evolution is not perfectly symmetrical as the underwater deposits formed for the +20° obliquity are kept during the action of the wave with a -20° obliquity. It was however observed the reversibility of the equilibrium situation for the extreme symmetrical obliquities of the acting wave. With the frontal attack, $\alpha_o = 0°$, the stretch of beach goes forward in a practically uniform way owing to the transversal movements, the cross section being dependent upon the characteristics of the acting wave. Beach oscillations were noticed around the line corresponding to the frontal wave action. The action of very high waves, after an equilibrium situation corresponding to a wave of average height had been reached, led to a new evolution, by increasing the accretion area. With short groynes, allowing for transposition, final equilibrium situations are also obtained for each obliquity. After the action of waves with great obliquity a shoal is formed around the transposed groyne. This shoal facilitates the reversibility of movements for the extreme symmetrical obliquity. On the stretch of beach lying next to the transposed groyne it was formed during the frontal attack an accretion bigger that the one found in stretches where no transposition was observed. With short groynes it was found that for the highest wave there was an erosion concerning the average wave equilibrium situation due to the greater intensity of movements. That erosion was only compensated after the average wave had acted again with the same obliquity.

4 - CONSIDERATIONS ON LITTORAL DRIFT

The movement of mobile materials on sandy beaches is fun-

damentally characterized by longitudinal transport due to the oblique action of the waves. Quantitatively it may be considered as an amount of sands carried through one section in one period of time. This value is known as littoral drift. Groynes being elements of retention of mobile materials, make possible to establish the accumulated volume in a certain section and for a certain period of time, and consequently estimate the littoral drift.

It is considered in this study that, owing to transport by bed load, the littoral drift is directly related to the power transmitted by the wave. Assuming that $(\gamma s-\gamma)$ is the specific weight of the submerged solid matter, β the friction coefficient of movement by dragging of the grains, and $d\omega$ an element of volume, with a v velocity, the power needed to carry such a volume at such a velocity will be $\beta.(\gamma s-\gamma).d\omega.v$. Assuming further that the power used for the transport of the grains is a η fraction of the power transmitted by the wave, P_{tr}, it will be found that $\int_V \beta.(\gamma s-\gamma).d\omega.v=\eta P_{tr}$, where V is the volume of material crossing a given section for the time unit. If $d\Omega$ were the cross section of the grains, perpendicular to the course, and dl the dimension in the movement direction, there will be then, for a Ω cross section:

$$\int_V \beta.(\gamma s-\gamma).d\omega.v=\int_\Omega \{\beta(\gamma s-\gamma).dl.v\}d\Omega=\beta.(\gamma s-\gamma).dl.\int_\Omega v.d\Omega=$$
$$=\beta.(\gamma s-\gamma).dl.Q_{lit}$$

The Ω cross section will be directly related to the wave and beach characteristics, namely the location of the wave breaking line, wave

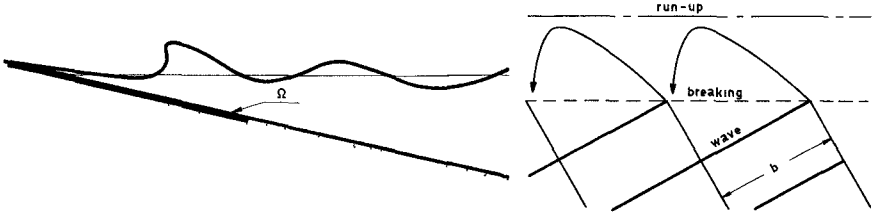

run-up and beach slope. It could then be said that $\beta.(\gamma s-\gamma).dl.Q_{lit}=\eta.P_{tr}=\eta.\frac{1}{8}.\rho g.H^2\frac{L}{T}.b$ in which b is the wave crest width occurring to the zigzag movement seen on the diagram and which, since a beginning, will depend both upon the wave characteristics, especially upon its obliquity, and the beach characteristics. It will then be $Q_{lit}=\frac{\eta.\frac{1}{8}.\gamma.H^2C.b}{\beta.(\gamma s-\gamma).dl}$, i.e. $Q_{lit}=kH^2C$, in which k is related to the characteristics of the mobile material and to wave obliquities. So it can be seen that, at a first approach, the littoral drift for a certain obliquity and a certain beach is proportional to the power transmitted by the wave and that the coefficient k depends on the characteristics of the mobile material, as far as its specific weight, dimensions and friction coefficient are concerned, as well as to the fraction of transmitted power that originates transport. This fraction will depend fundamentally upon the obliquity of the wave action. On the other hand, the application of dimensional analysis, consider

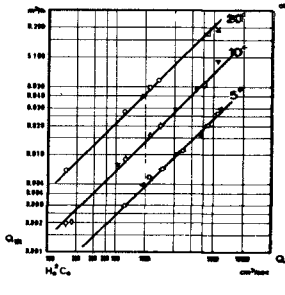

Fig.35-Log curve of the $Q_{lit.}$ variation.

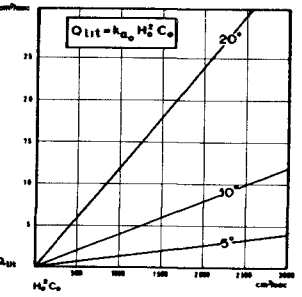

Fig.36-Lineer curve of the $Q_{lit.}$ veriation.

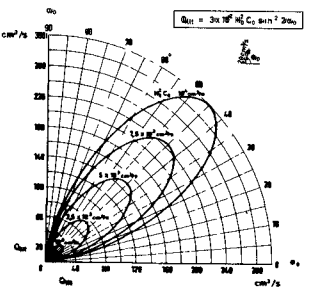

Fig.37-Polar curva of the $Q_{lit.}$ variation.

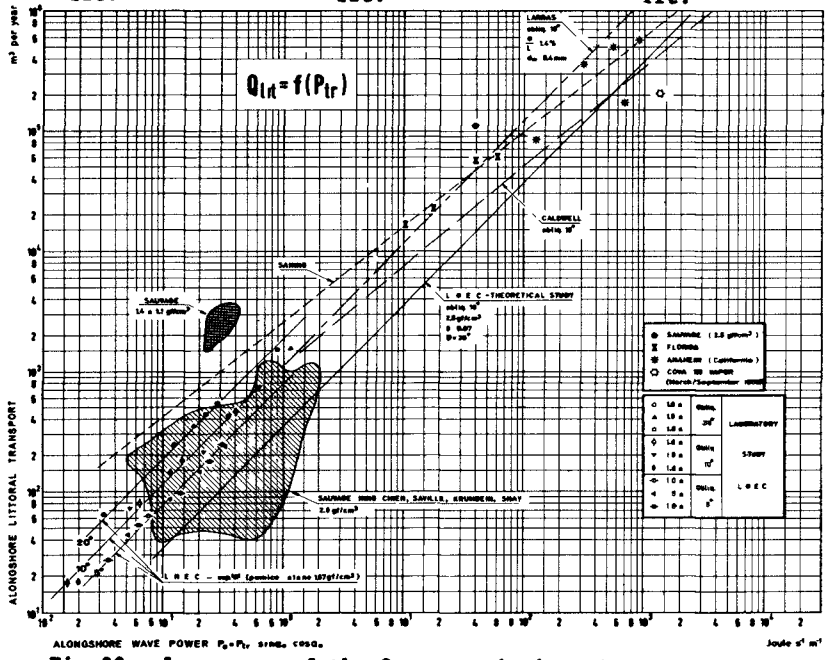

Fig.38 - Log curva of the $Q_{lit.}$ variation with wave powar.

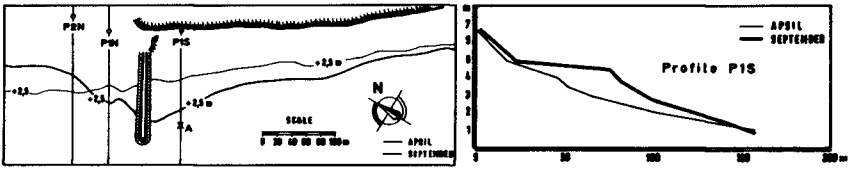

Fig.39 - Cove do Vapor groyns. Plan and cross-section.

ing the littoral drift which is depending on the wave height and its celerity, makes possible the conclusion that the ratio of dependence, for a certain beach and a certain obliquity, will be of the type $Q_{lit} = kH^2C$, i.e. the littoral drift will be proportional to the power transmitted by the wave.

The determination of littoral drift values, for the various waves tested, was made by measuring the areas of accretion near E2 groyne in the 1st series set-up, during the 1st hour of each test. This value, multiplied by the mean height of accretion in cross section, allowed to the calculation of an hour mean volume of accretion. In the tested set-up, the Q_{lit} value decreases during testing until it becomes null (see fig.32). The readings taken at test starting may thus be considered approximately equal to the wave carrying capacity, which value has to be determined. It was found that it is possible to establish a ratio of dependence of the type theoretically deduced, in which Q_{lit} is proportional to the power transmitted by the wave as well as to a trigonometrical function of α_o obliquity. The tests with 20°, 10° and 5° obliquities, the results of which are shown on the diagram in fig.35, allows the deduction of the following ratio:

$$Q_{lit} = 0.03.H_o^2C_o.\sin^2 2\alpha_o \quad cm^3/s$$

These results are represented on the diagrams in fig.36 and 37. In reference to the first one it must be said that although the straight lines concur to the origin, which means that littoral drift is annulled whenever the power transmitted by the wave is annuled too, actually the conditions of annulment of littoral drift will be a function of the critical conditions under which the material is dragged which were not included in this study. The diagram in fig.38 shows the experimental results obtained, as they were compared to the results obtained through other studies (see [3]). It was found that the values referring to readings taken with the pumice-stone model fit in pretty well with those obtained in other studies with different materials and that the extrapolation of results from actual cases leads to acceptable values. The diagram shows a point referring to readings taken at an experimental groyne built at Cova do Vapor, a beach situated near the mouth of Lisbon harbour (see figs. 39 and 40); the value which was given, 200 000 m^3/year for the period which goes from April till September 1959, in which T = 9 sec, $\alpha_o \approx 10°$ and $H_o = 1.0$ m may be considered, is very low but its determination offers several difficulties. On the one hand, the groyne is too short (see fig.40) and its efficiency very much reduced. A correction had to be made to the values obtained through previous calculations due to the fact that, for low tidal levels, there was no retention of sand by the groyne. On the other hand, there was no accurate data available on the wave regimen which could make possible calculation with accuracy the mean value of the transmitted power susceptible of association with the value considered as littoral drift. A sand spit formed by the sands which passed over the above mentioned groyne, can be seen in fig.40.

Fig.40 - Aerial view of Cova do Vapor beach.

5 - CONCLUSIONS

- The hydraulic behaviour of groynes in the case of physiographically independent units, subject to the obligue action of sinusoidal waves of constant characteristics, is marked by an evolution of the beach stretches which are in process until they reach a final equilibrium situation conditioned by the obliquity and the power transmitted by the acting wave. That evolution is fundamentally due to the littoral drift originated by the longitudinal currents which are caused by the oblique breaking of waves. In the case of reduced obliquities there is also a significative influence from the transversal movements. The groyne accretion areas increase, for the same obliquity, whenever there is an increase of the power transmitted by the wave, but they present a maximum which is determined by the suspension transport of the mobile material. The stabilization times become smaller, for the same obliquity, as the value of transmitted power grows higher, which leads to very swift evolution during the storms acting upon the beach. There is, generally, a possibility of erosions in the seaward area of the beach stretch near the groyne slopes but its characteristics are mainly governed by the transversal movements on the beach. The design of the groyne infrastructure is also depending upon the erosion characteristics which occur in the leeward of the groyne. For the same value of power transmitted by the wave, the accretion areas and the stabilization times increase as much as the wave obliquity increases.

- Groyne efficiency is conditioned by the suspension transport. Even for wave regimes with very variable directions, a groyne systems can be efficient provided that it has been dimensioned taking into account the above principles, since there is no intensive transport in suspension. This conclusion is of particular interest in the case of groyne systems where the artificial accretion of sands has to be done. When applying the results of this study to real cases, the maximum values of the dimensionaless parameters present, for the 1st series of tests, the same values for pumice-stone and for bakelite, although corresponding to different amounts of transmitted power; it is assumed that the maximum values taken into consideration will be kept in the prototype, corresponding to extreme power values conditioned by the prevalent transport in suspension. The results of the tests using sand (see fig.27) show that there will be no correct reproduction of the phenomena, from a similarity standpoint, as the final maximum values obtained with this material would be lower than the former. It is evident that only a thorough knowledge of similarity ratios, allied to the observation take into account the behaviour of a prototype with an identical set-up to the one used for tests, would make correctly possible to estimate the extrapolation which had been considered.

- The evolution characteristics of the beach stretches depend on the structure, implantation and length of the groynes. It might be interesting, in certain cases, to adopte an asymmetrical structure for the cross section of the groynes with softer absorvent slopes in the leeward. In the case of non-absorvent groynes

the use of curved groynes, creating a difraction area in the leeward, is recommended.

- The D/c ratio (the reverse of the dimensionaless parameter previously considered), the relation of the distance between groynes and their effective length presents, for the obliquities tested, maximum values conditioned by the entering into suspension of mobile material, which are, for the most unfavourable case: 2.5 for $\alpha_o = 20^o$; 3.5 for $\alpha_o = 10^o$ and 4.0 for $\alpha_o = 5^o$. To apply these values it must be taken into account the tide level in each case, depending on the characteristics of the tide itself, the intensity of transport during the several tidal stages, and the transversal limits of the beach stretch under consideration. The total length of the groyne will have to include its rooting portion, conditioned by wave run-up and by eventual erosions near the leeward slope.

- The reversibility of equilibrium situations for extreme symmetrical obliquities is found in groyne systems acted upon wave cycles with variable directions.

- Short groynes, adopted in emergency works of temporary nature due to the very high costs of maritime works and the lack of knowledge of the coastal physiographic regimes, have been found to be of extremely reduced efficiency. Nowadays techniques, taking advantage of an increasingly through knowledge of coastal phenomena, especially as it regards wave regimes, allow for the designing of efficient groyne systems. Amongst these, long groynes - for the design of which this study will have contributed - occupy an outstanding position concerning the interest they offer in solving many coastal engineering problems.

- The consideration of a dependence ratio between littoral drift and wave characteristics, based on the proportionality between the littoral drift and the transmitted power, was accepted in view of the experimental results of several studies and the readings taken from actual cases.

BIBLIOGRAPHY

{1}- Council on Wave Research - "Deficiencies in research on gravity surface waves". Engineering Foundation, Berkeley, California, 1961.

{2}- Kemp, P. Hubert - "A model study of the behaviour of beaches and groynes" - Proceedings, The Institution of Civil Engineers. vol.22. 1962.

{3}- Beach Erosion Board - "Laboratory study of the effect of groins on the rate of littoral transport". Technical memorandum nº 114. Department of the Army. Corps of Engineers. Washington. 1959.

CHAPTER 34

THE TERMINAL PROBLEM IN COAST PROTECTION

by

N. Pallett, C.Eng., M.I.C.E.
Senior Engineer, C.H. Dobbie and Partners

ABSTRACT

This paper introduces the terminal erosion problem which usually occurs down drift of coast protection works, an important aspect of coast protection which is often overlooked.

To provide the background to this problem, the formation, replenishment and function of a natural shingle beach is discussed in relation to coast protection. The value of groynes in stabilising the foreshore, the use of artificial beach replenishment, and the effect on the long shore regime following the introduction of a sea wall, are discussed in outline with typical examples.

Terminal erosion is described in more detail, with reference to its cause, and illustrated by examples taken around the coast of the British Isles. Suggestions are made for the investigation of the terminal problem, design considerations are discussed, and terminal groynes and various types of terminal works described. Particular reference is made to the permeable type of terminal section.

Finally the paper is illustrated by examples of terminal works which have been constructed at two sites in this country. The foreshore conditions and exposure are described, together with the details of the sea wall and groynes, and the details of the terminal works at each site.

NATURAL COAST PROTECTION

Along many hundreds of miles of the coastline of the British Isles the adjoining low ground is protected entirely by natural ridges of sand and shingle. The formation and replenishment of these natural ridges depends on the supply of material available, the tidal levels, and the characteristics of the waves reaching the foreshore.

During calm weather the swash from the long, low, constructive waves breaking on the foreshore carries the beach material up the slope, and then, depending on the permeability of the slope, the backwash returns seaward beneath the surface leaving the suspended material higher on the slope. The profile of the foreshore and the height of the ridges or fulls varies from tide to tide, as the beach material is redistributed both across and along the foreshore. During storms the beach material absorbs the greater energy of the higher, steeper, storm waves, and becomes redistributed across the foreshore. Some is thrown into ridges well above the normal level by the destructive waves, but much is raked down the foreshore and deposited further seaward to await the next calm period. The beach material thus provides a continuous natural mantle of protection as it moves along the coast. A good example of this on the South Coast of England is the Chesil Bank, a shingle bank which extends for a distance of 30 kilometres and rises to a height of 15 metres above the mean sea level at the Eastern end.

However, where a natural headland or an artificial obstruction retains part of the drift material, there is a reduction in the volume of littoral drift passing that point, and the coast beyond is starved of beach material.

GROYNES TO ASSIST A NATURAL BEACH

If there is still a sufficient supply of littoral drift along the foreshore, groynes can be constructed to reduce the rate and retain an adequate beach along the frontage concerned. The formation and retention of an adequate, stable foreshore in front of the works is an essential part of any coast protection scheme. We have used groynes in many places around the coast and have successfully stabilised the foreshore.

Some authors have doubted the effectiveness of groynes, based upon tests carried out with models in the laboratory. This is most likely due to the difficulties arising from the scale effects, and also in attempting to reproduce the variations in wave height and direction in combination with changes in level due to tides. At the Coast Protection Conference held in Santa Barbara in 1965 it was stated that "Competence in appraisal may be the key to successful groyne installation" (ref. 1). This proves to be very true in practice. After installation long-term maintenance and adjustment to level is most essential.

A very good example of the effects of groyning a foreshore can be seen at West Wittering in Sussex (Fig.1). Prior to 1902 erosion was taking place at the rate of 5 metres per annum, but following the construction of groynes, the foreshore has been more or less stabilised.

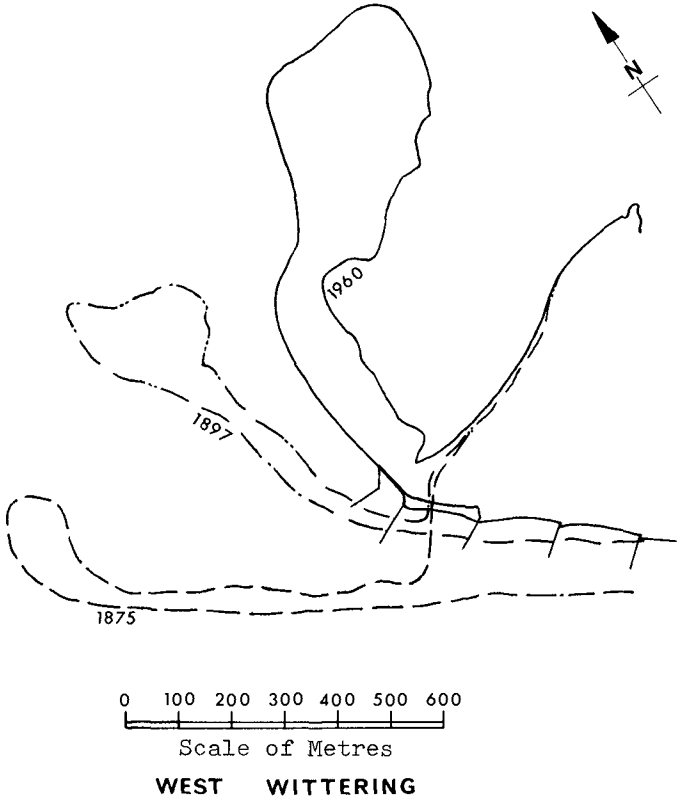

Fig.1: Movements of High Water Mark

In another case at Aberdeen on the North East coast of Scotland, the face of the sand dunes had been eroding at the rate of 2 metres per annum from 1868 up to 1962, and the foreshore was becoming steeper. Since a system of groynes was constructed in 1962, accretion has taken place between high and low water marks, and a considerable volume of sand has accumulated below low water.

There are many other examples where groynes have been used to provide an effective and economic form of coast protection and in some without the need for a sea wall.

ARTIFICIAL REPLENISHMENT

A system of groynes can only be successful where there is a sufficient supply of beach material available. In some cases where the volume of littoral drift passing along the foreshore is inadequate, it is economic to replenish artificially the foreshore from other sources.

Artificial replenishment was used on the Pett foreshore of Rye Bay on the South Coast in the nineteen thirties, and in recent years has been carried out on this and other frontages by the Kent River Authority. At Pett 30,000 cubic metres of shingle is taken annually from the natural deposits at Rye Harbour, and redistributed back along the foreshore to the west from whence it came (fig.2).

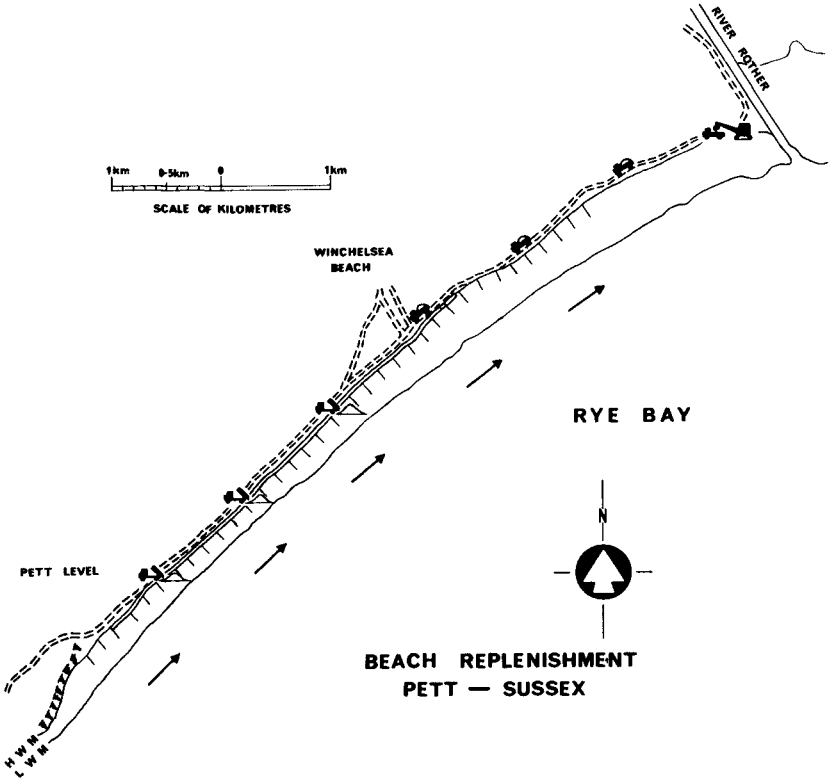

Fig. 2

A recent scheme, which includes new groynes and artificial replenishment at Clacton on the East Coast, is described in a paper presented to this Conference by W.T. Fryde (ref.2).

Replenishment can only be carried out economically where there is a nearby source of suitable material, good access to the foreshore, and where the rate of longshore drift is not high. In the future it could well become economic to replenish the foreshore in many places with material taken from offshore deposits of sand and shingle.

SEA WALLS

In many places along the coast it becomes necessary to construct a sea wall to resist further erosion, and these can be divided into two basic types:

The first of these is the vertical, mass or reinforced concrete walls, which rely on their mass to resist the violent impact caused by waves breaking against them. However, the vertical face causes considerable disturbance and the reflected waves scour the foreshore in front of the wall.

The second type is the sloping revetment, which is usually surfaced with concrete blockwork, light reinforced concrete or stone pitching, and with sheet piling to protect the toe, and a wave coping to reduce over-topping by waves. A sloping revetment enables the waves to dissipate much of their energy in running up the slope, and thus causes much less disturbance to the foreshore.

TERMINAL WORKS

Where an impermeable sea wall is introduced into a foreshore, it interferes with the natural regime, and under certain wave conditions tends to increase the erosion of the foreshore in front of the wall. To retain the natural protection which an adequate beach affords, a system of groynes can be provided to slow down the littoral drift, and retain the beach material in front of the wall. The sea wall itself in many cases, causes erosion of the unprotected coastline immediately adjoining the down drift end of the wall, while the groynes further aggravate the erosion by retaining the drift material and starving the adjoining coastline of its natural protection.

A good example of terminal erosion can be seen at Hastings, Sussex, where three miles of sea wall and groynes and a massive terminal groyne provided by the abandoned harbour arm, is causing erosion of the cliffs beyond. Over 1,000,000 cubic metres of shingle has been accumulated by the harbour arm over the last 60 years, while the rate of erosion down drift is limited by the material supplied from the 100 metre cliffs.

The terminal works should be considered in detail when the design of the main sea wall is undertaken, not added piecemeal later as the problem develops and erosion becomes serious. As with the main wall, the geophysical features of the coastline should be examined for a distance beyond both ends of the frontage being protected, especially at the end down drift from the proposed works. An adequate transitional length is essential between the section of the main sea wall and the terminal works, as an abrupt change in profile produces scour which aggravates the problem.

It is the permeability of the shingle which encourages ridges to form and build up. We can aim at producing a similar condition by providing a permeable slope which will allow the material on the foreshore to build up over the slope, but which will also retain its profile during storms. It is impracticable to give the permeable slope the freedom of movement which a natural shingle beach enjoys, so a permeable toe is provided to stabilise the bottom of the slope. The permeable slope can be constructed from many materials, but flexibility to take up movement without damage is desirable.

Gabions with suitable rock filling are highly permeable and are also flexible enough to take up settlement without damage. Where suitable fill is available locally a gabion mattress provides an effective and economic slope protection.

A steel mesh bearing onto a steel grillage, supported on light piles has also been used successfully, a layer of hard-core being placed beneath the mesh to trap the beach material.

Various types of precast concrete interlocking units have been used to protect the slope but their cost is high. These units, which can be placed in various patterns, become interlocked, and can take up settlement. The units have a high voids ratio when placed but due to their large mass, tend to create local scour which does not assist the build up of the finer beach material. At a holiday resort they can also present a danger to children who climb amongst them.

In many parts of this country wartime anti-tank blocks weighing up to six tons each are still awaiting disposal, and seem at first sight to be ideal for coast protection works of this type. Experience has shown however, that they are most unsuitable as they do not lock together, and despite their weight tend to roll in rough seas.

Special care is needed in determining the length and top levels of the terminal groynes, and provision should be made to allow the height of the groynes to be adjusted. Permeable groynes of timber, steel or concrete have been used, but not

extensively in the British Isles. Gabion groynes can settle to take up the beach profile but can become expensive to maintain over a long period. Timber groynes have proved most effective and economic, allowing flexibility in design and enabling the height of the planks to be readily adjusted.

EXAMPLES OF TERMINAL WORKS

Pett Level, Sussex.

This wall was constructed between 1946-50 to protect the marshes adjoining Rye Bay, and terminated in a narrow shingle ridge at the east end. The foreshore was predominantly shingle with sand towards low water, and with the littoral drift towards the east. The sea wall consisted of a sloping revetment of bitumen-jointed concrete blockwork with steel sheet toe piling, a berm, and upper blockwork with coping.

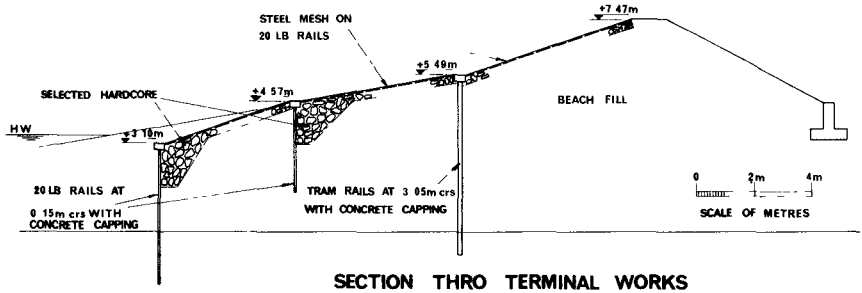

SECTION THRO TERMINAL WORKS
PETT SEA WALL SUSSEX

Fig. 3

When the terminal works were constructed all materials were in short supply, especially new mild steel sections. Old rails were used to form a permeable toe, and to support a steel grillage which was covered by war-surplus steel mesh. A layer of broken concrete was used beneath the mesh to trap

and retain the beach material (fig.3). This form of construction worked very well but in recent years has been covered by beach tipped by the Kent River Authority.

Aberdeen

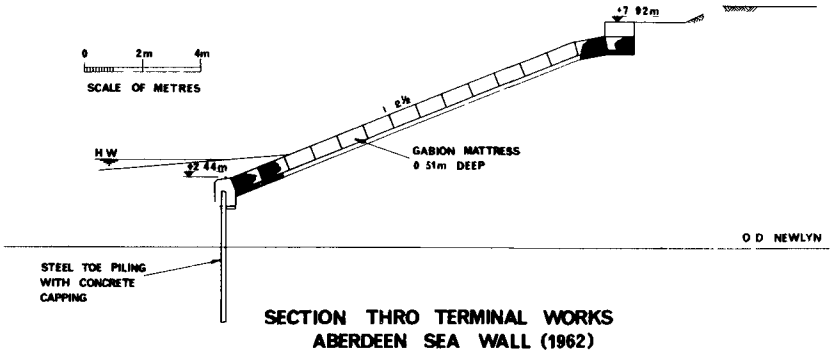

SECTION THRO TERMINAL WORKS
ABERDEEN SEA WALL (1962)

Fig. 4

This wall was constructed in 1962-63 to protect the rapidly eroding face of the sand dunes which protected the low ground behind. The foreshore was predominantly sand, and the wall terminated at the north end in the sand dunes at the River Don. With the introduction of groynes along a frontage of 2,500 metres, a terminal erosion problem was anticipated at the north end, down drift of the works. The sea wall consisted of a sloping revetment of blockwork, with steel sheet toe piling and a coping at the top of the slope.

This coast is exposed to the prevailing winds and waves from the South East, with a fetch of 600 kilometres, and waves of up to 5 metres in height have been reported. The terminal section comprises a sloping gabion mattress with steel sheet toe piling and bulkheads (fig.4). At the extreme end the toe piling is replaced by a low gabion apron.

These works allow a very satisfactory accretion of sand on the slope under most conditions, but during on-shore gales the sand is carried seaward and deposited in banks, in a similar manner to the natural foreshore to the north of the river.

References:

1. Lillevang, Omar J. "Groins and Effects - Minimizing Liabilities". Proceedings of the Santa Barbara Specialty Conference on Coastal Engineering, October 1965.

2. Fryde, W.T. "Cliff Drainage and Beach Distribution". Conference on Coastal Engineering, London, September 1968.

CHAPTER 35

THE CREATION OF AN ARTIFICIAL BEACH
IN LARVOTTO BAY - MONTE CARLO
PRINCIPALITY OF MONACO

by

Louis Tourmen
Sogreah
Grenoble - France

1. INTRODUCTION

One of the features of a recent big Monaco Government modernisation scheme was an artificial beach in Larvotto Bay at Monte Carlo, which was to offer first-class bathing and amenities matching the very high standard of urban development planned for the area. Most of the Monaco coast is rocky and very steep, and the only places with a gradual slope down to the sea were a few very inferior beaches the waves had formed with widely varied materials from local builders' rubble dumps.

2. THE LARVOTTO SHORE BEFORE DEVELOPMENT

In some of the small bays between rocky headlands such as the Rock of Monaco, Pointe Faucignane and Pointe la Vigie, sediment deposits cover the rock to varying degrees. Most of them are not yet fully stable and have either been formed by local erosion or have built up from rubble The old Larvotto beach was one of these (Fig. 1).

The developed part of the Larvotto shore is between the reclaimed areas of the Sporting Club and Le Portier. It is about 500 metres long. As figure 2 shows, the slope of the old beach was about 10 per cent out to a depth of about 4 metres, and was fairly even all along this stretch of coast. A kind of shelf with a much flatter slope then followed out to about 8 metre depth, varying in width from about 120 metres at the Le Portier end to 230 metres at the Sporting Club (these being the distances from the datum level water line to the 8 metre depth contour) Beyond the 8 metre line the sea bed slope is about 10 per cent.

Old Larvotto beach was divided into compartments by short groynes reaching down to the waterline. The beach materials included lumps of rock up to several kilogrammes in weight, shingle and sand. Beyond the waterline the bed consisted almost uniformly of shingle over a wide size range, followed further out mainly by sand of locally varying coarseness and patches of seaweed beyond depths of 7 or 8 metres.

The local sea bed features confirmed the assumption that Larvotto beach had formed from materials dumped on the shore year after year over a very long period of time, for very little inshore sediment drift occurs in the area, and certainly not enough to have had any appreciable effect on the configuration of the sea shore. Most of Princess Grace Avenue is built on a backfill embankment for example, and the occasional damage it has suffered due to collapsing confirms that this stretch of shore has not always been absolutely stable. Before development, the Larvotto shore had been substantially built up by massive dumping of material, especially at the Portier end, and this had increased its stability accordingly.

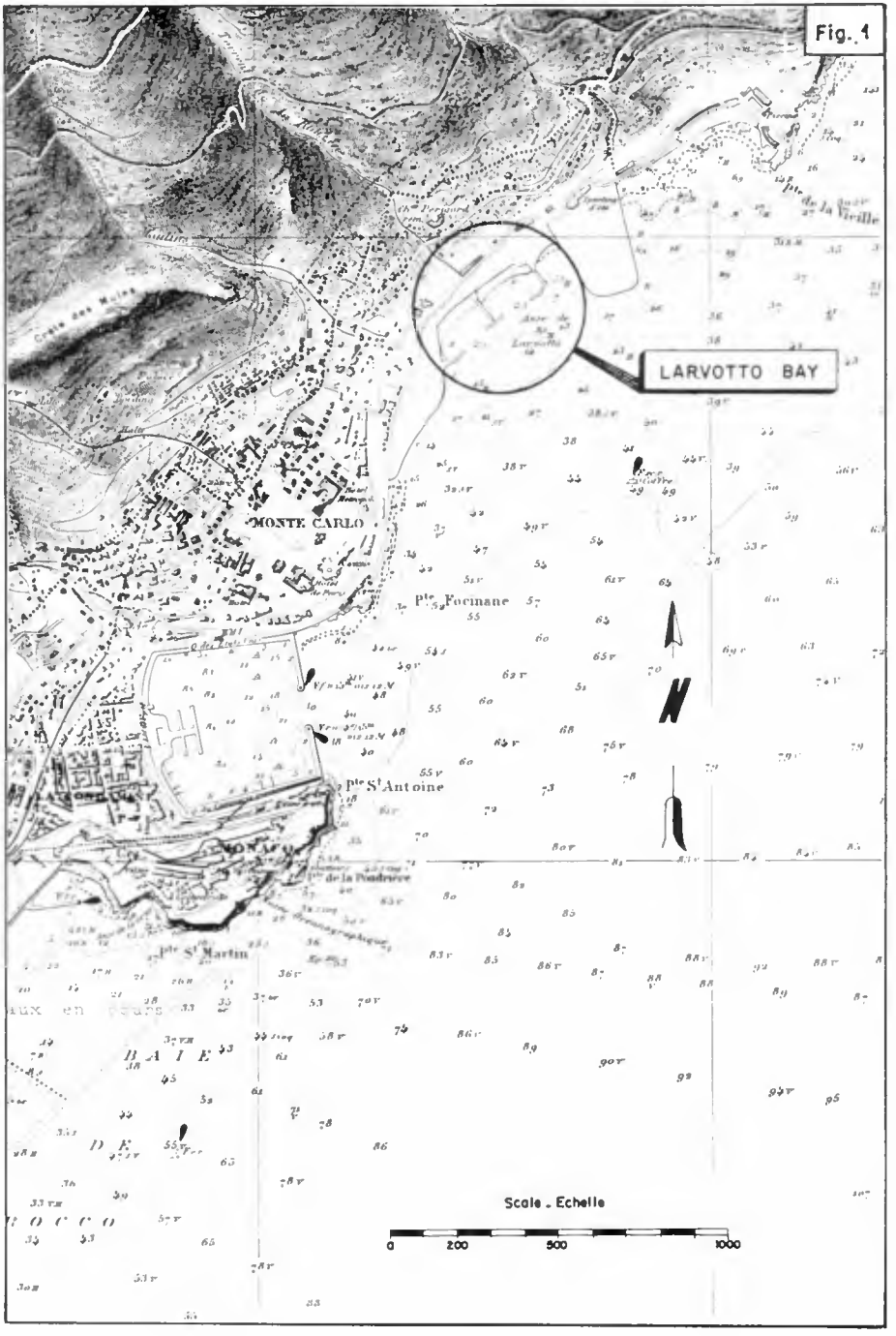
Fig. 1
LARVOTTO BAY
MONTE CARLO
Pte Focinane
Pte St Antoine
Pte St Martin
Scale - Echelle
0
200
500
1000

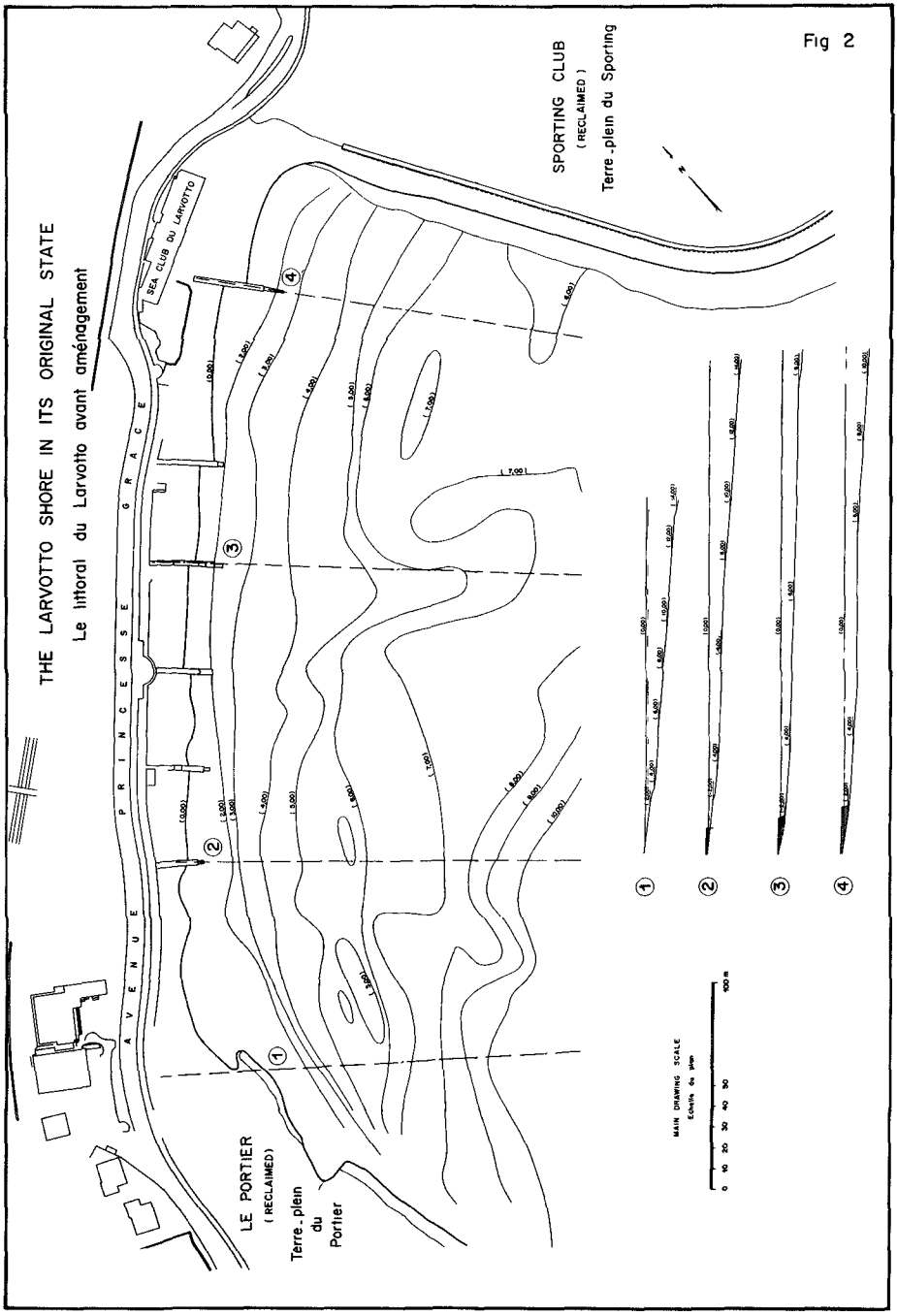
THE LARVOTTO SHORE IN ITS ORIGINAL STATE
Le littoral du Larvotto avant aménagement
Fig 2
AVENUE PRINCESSE GRACE
SEL CLUB DU LARVOTTO
SPORTING CLUB
(REGLAIMED)
Terre - plein du Sporting
LE PORTIER
(REGLAIMED)
Terre - plein du Portier
MAIN DRAWING SCALE
0 10 20 30 40 50 100 m

3. SEA LEVEL AND WAVES

The French Mediterranean coast has a tide range which is so small that it is insignificant for practical purposes Atmospheric conditions sometimes cause an abnormal rise or fall in level (though more seldom the latter). For example, a strong east wind can cause rises of up to 50 centimetres, but in relatively calm weather the water level can be considered to generally lie around 40 centimetres above datum.

From information supplied by the Principality of Monaco Public Works Department, wave conditions in the vicinity of Monaco harbour (Fig. 3) can be described as follows :

The prevailing wave frequency direction is from the east-south-east sector, with comparatively short-period waves (5 to 7 seconds) and maximum heights around 3 metres.

The prevailing wave height direction is from the southerly sector (south-south-easterly to south-south-westerly at sea), with longer periods (7 to 10 seconds) and maximum heights around 4 or 5 metres.

Propagation diagrams have been plotted for these various prevailing wave directions in order to show how the sea bed affects the wave crest directions in the immediate vicinity of Larvotto Beach. These diagrams are shown in figure 3, from which it is seen that although the effect of the sea bed tends to close the angle between the prevailing wave frequency and height directions, this angle is still quite large near the Larvotto Bay shore. In other words, waves must be reaching this shore from many very different directions, and this assumption is borne out by local beach evolution near the groynes, where the sediment is seen to drift to and fro depending on the incoming wave direction. It is considered that wave heights and periods off Larvotto Beach do not differ very much from those off Monaco harbour, except perhaps for the south-south-westerly waves. The refraction diagram for these in figure 3 shows that their orthogonals spread out a little, denoting some loss of wave height.

4 THE AIMS OF THE PROJECT - These were as follows :

a. Widening of the shore seawards

The planning scheme for the Larvotto urban district provided for the reclamation of an appreciable area from the sea. A platform was to be built up to 5 metres above datum level on the seaward side of Princess Grace Avenue, ending in a vertical step designed to accommodate a row of shops along the beach front. The beach itself was to be about 30 metres wide to the water's edge. The whole project was based on this feature.

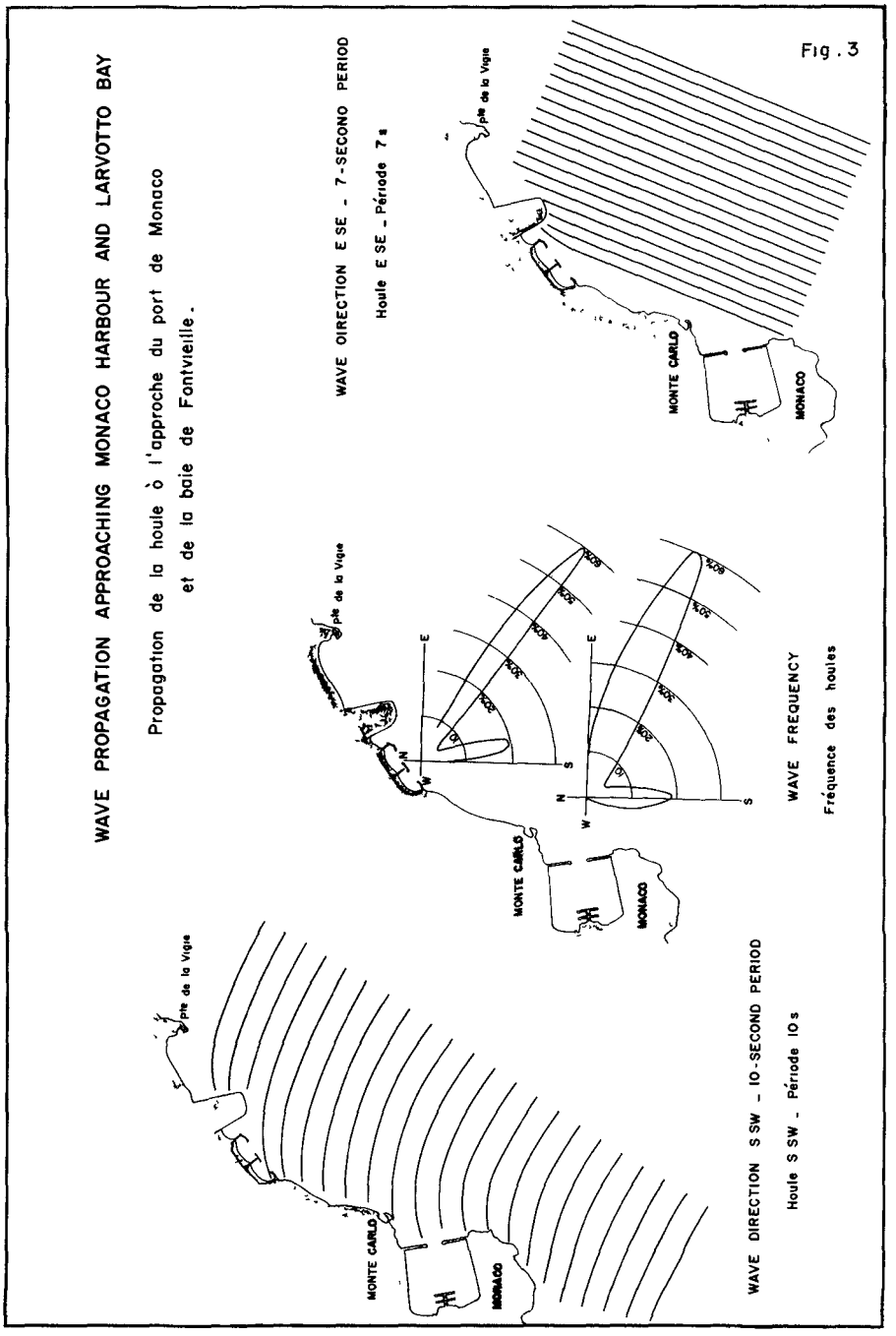
WAVE PROPAGATION APPROACHING MONACO HARBOUR AND LARVOTTO BAY
Propagation de la houle à l'approche du port de Monaco et de la baie de Fontvieille.
Pte de la Vigie
MONTE CARLO
MONACO
WAVE DIRECTION S SW - 10-SECOND PERIOD
Houle S SW - Période 10 s
WAVE DIRECTION E SE - 7-SECOND PERIOD
Houle E SE - Période 7 s
WAVE FREQUENCY
Fréquence des houles
Fig. 3

b. Sea Club Landing facilities

The Public Works Department had asked for a groyne to be built at the north-east end of the beach so as to provide a sheltered embarkation and landing area for the passengers of small craft.

c. Maximum beach extension

The project was to provide for the maximum possible beach area consistent with its general framework.

5. DESIGN PRINCIPLES - These were as follows :

a. The need to build up the sea bed

As mentioned in paragraph 2 the slope of the sea bed out to a depth of about 4 metres off Larvotto Beach was about 10 per cent, as consistent with the submerged beach material consisting of various sizes of shingle. The comparatively fine new beach materials provided for in the project could only be expected to remain stable under attack by the comparatively strong local waves, if placed so as to form an average slope consistent with their grain size and generally flatter than 10 per cent. In other words, it was necessary to correct the slope of the natural bed in order to ensure the stability of a new beach of fine material , this meant building up an underwater shelf on the sea bed with backfill, with a containment structure at its seaward end designed to withstand wave attack and sloping steeply down to the natural sea bed beyond. The effect of this structure on the incoming waves was expected to be quite considerable, especially in making them break.

The purposes of the shelf and its containment structure were thus as follows :

(i) To ensure that the beach settled down with a cross-sectional shape consistent with the size of its materials.

(ii) To make the biggest waves break and thus to reduce wave energy dissipation on the beach.

b. The need for groynes divlding the beach into compartments

As we have seen, the waves reach Larvotto Beach from a wide range of directions. The artificial beach material will tend to drift along the shore, therefore, and without special precautions this could modify the width of the beach to the point of affecting its amenities and possibly also

causing a permanent loss of beach material. Groynes dividing a beach up into compartments are an effective way of preventing longshore sediment drift by containing the beach materials, and it was considered that at least two such groynes were required for a beach the size of Larvotto. Thus, the new Larvotto Beach consists of three self-contained compartments which are considered adequately safe from waves for normal practical purposes.

c. The need for wave-diffracting structures

It was considered that wave diffraction by separate offshore breakwaters running roughly parallel to Larvotto Beach would be most effective in stabilizing the artificial beach material for the following reasons :

(i) They would substantially reduce wave energy dissipation on the beach by stopping some of the incident wave energy.

(ii) By diffracting the waves, they would also substantially reduce the effects of changes in incident wave direction on the beach configuration.

Incidentally, a point to note in this connection is that the finer a beach material the stronger the case for incident wave diffraction.

A further effect of these breakwaters was that they would enable the length of beach at datum level to be increased by an appreciable amount, which was one of the aims of the project, and in fact this is precisely what has happened in practice for the beach has stabilized with a more or less marked curved outline.

6. THE BEACH-BUILDING MATERIAL

The problem of finding a suitable material for Larvotto Beach was a very stricky one indeed. A systematic exploration was made for prospective borrow areas - some a considerable distance from Monaco - but in the end, economic considerations led to the choice of local dolomite chippings ranging from 3 to 8 millimetres in size. This rather unusual material for a beach had sharp edges, but tumbling wear tests on a 'Los Angeles' machine had shown that they would soon wear smooth and produce a material with an attractive appearance and not at all uncomfortable underfoot. Figure 4 shows the results of these attrition tests for 3 to 8 millimetre and 5 to 15 millimetre chippings.

It was hoped that the waves would fairly soon wear the sharp edges of the chippings smooth. It was realized that it would be necessary to periodically 'turn the beach over' so as to ensure that all the material went

through this process in time, but this was not expected to be difficult as the beach would have to be levelled with earthmoving equipment before each summer season anyway, and this would be a good time to do the job.

From the wear test results in figure 4, it can also be hoped that normal permanent wear of the beach material - that is to say more than just the wearing-down of the sharp edges - will be slow and that it will not be necessary to add fresh material to the beach too often.

7. INFRASTRUCTURE (Fig. 5)

The three offshore breakwaters running parallel to the beach vary between 80 and 100 metres in length with gaps of about 80 metres between them, which are filled in under water by a containment structure topping at 2.5 metres below datum level.

Behind these works, which are set in 6 to 10 metres of water, the sea bed has been built up with quarry run levelled off at 2.5 m below datum level, and the beach has been subdivided into three compartments by groynes built of concrete blocks.

8. PLACING THE BEACH MATERIAL

When the beach compartments were ready the beach material was gradually added, being tipped on the shore and spread roughly by bulldozers. The beach was then left to settle down naturally under wave action.

80,000 cubic metres of chippings were placed on the beach, including 34,000 cubic metres in the middle compartment and 46,000 cubic metres in the west compartment.

Very little material was added to the east compartment as it was mainly intended to provide landing facilities for small craft.

9. RESULTS OBTAINED

Work on the beach started early in 1965. Part of the beach was opened in 1966 and the whole job was completed in 1967, and the beach has since proved very popular with bathers. The improvement clearly shows up in the photographs in figure 6 of Larvotto Bay 'before' and 'after'.

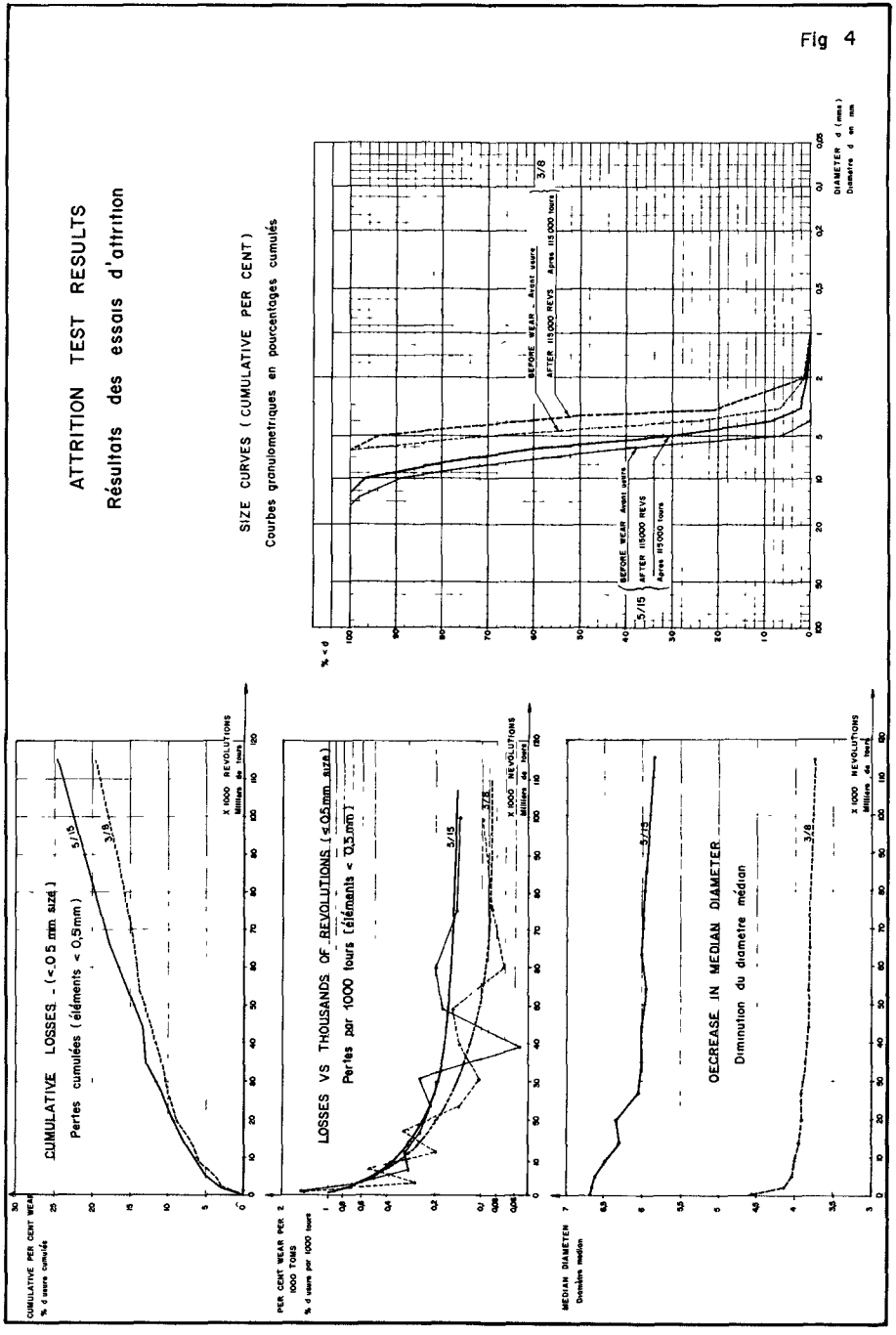
Fig 4
ATTRITION TEST RESULTS
Résultats des essais d'attrition
SIZE CURVES (CUMULATIVE PER CENT)
Courbes granulométriques en pourcentages cumulés
% < d
DIAMETER d (mm)
Diamètre d en mm
BEFORE WEAR Avant usure
AFTER 115000 REVS
Après 115000 tours
3/8
5/15
CUMULATIVE LOSSES (<0.5 mm size)
Pertes cumulées (éléments < 0,5mm)
CUMULATIVE PER CENT WEAR
% d'usure cumulée
X 1000 REVOLUTIONS
Milliers de tours
LOSSES VS THOUSANDS OF REVOLUTIONS (≤0.5mm size)
Pertes par 1000 tours (éléments < 0,5mm)
PER CENT WEAR PER 1000 TONS
% d'usure par 1000 tours
DECREASE IN MEDIAN DIAMETER
Diminution du diamètre médian
MEDIAN DIAMETER
Diamètre médian

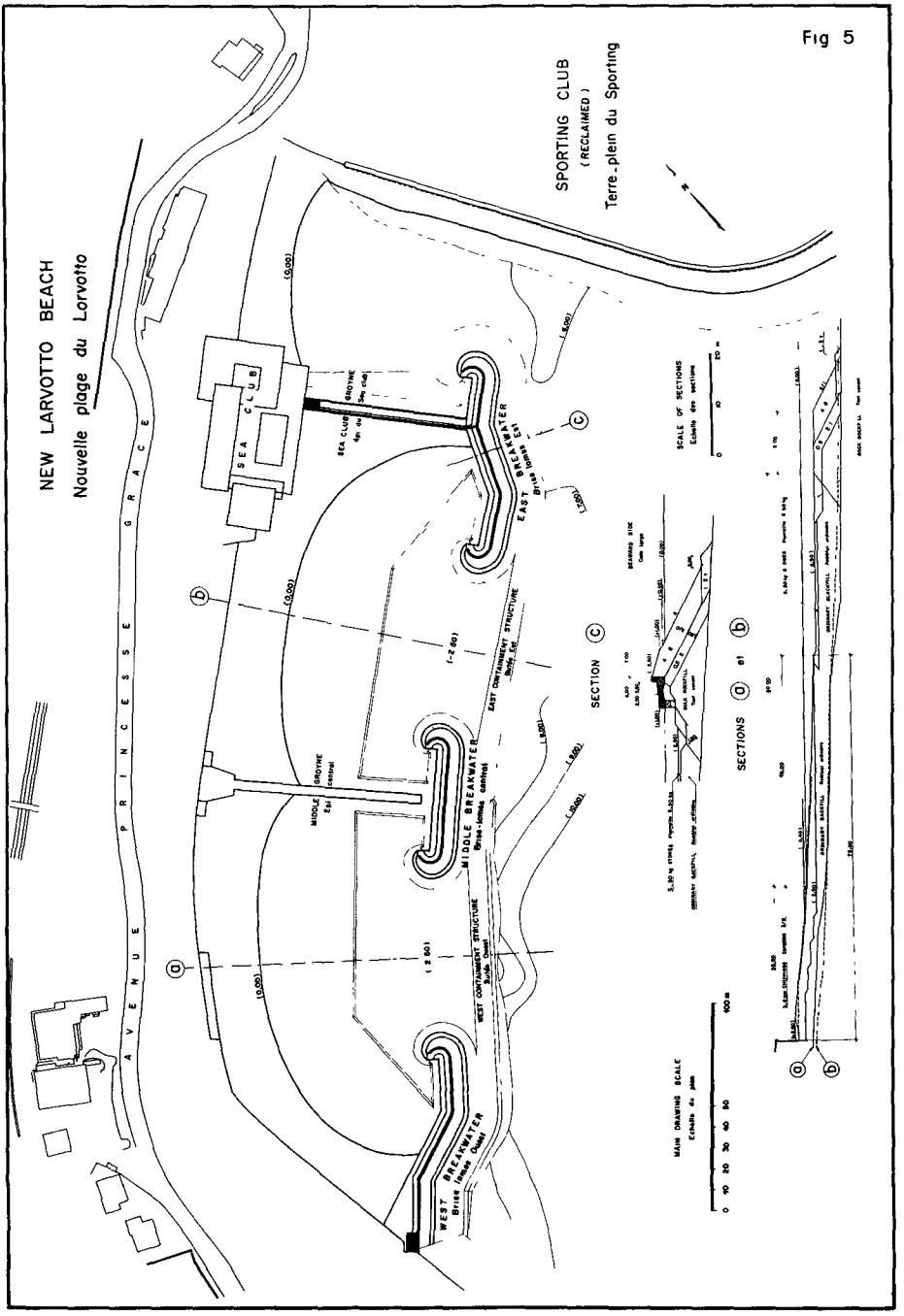
NEW LARVOTTO BEACH
Nouvelle plage du Larvotto
AVENUE PRINCESSE GRACE
SPORTING CLUB
(RECLAIMED)
Terre-plein du Sporting
SEA CLUB
SEA CLUB GROYNE
MIDDLE GROYNE
MIDDLE BREAKWATER
EAST BREAKWATER
WEST BREAKWATER
EAST CONTAINMENT STRUCTURE
WEST CONTAINMENT STRUCTURE
SECTION
SECTIONS
SCALE OF SECTIONS
MAIN DRAWING SCALE

Fig 5

Fig. 6

Artificial beach of Larvotto _ Plage artificielle du Larvotto
MONACO

Now, two years later, close inspection has shown that the materials washed by the waves are gradually wearing smooth as expected. The beach is turned over once a year to make sure that all its materials are gradually exposed to this natural process of attrition.

In addition, the plan outline of the beach has developed into something very similar to the theoretical one predicted from the wave diagrams. At its narrowest, the new beach represents some 50 metres won from the sea. Its slope is about 10 per cent near datum level, which is still quite steep, but as it is directly due to the angular shape of the chippings it should flatten off in time as their edges wear smooth and they move more freely under wave action.

With regard to the lose of material due to permanent wear, that is to say beyond the initial stage of the corners wearing smooth, it is still too soon to say exactly how this will develop. From observations so far it seems unlikely that over-frequent additions of make-up material will be required, and beach upkeep costs may therefore be expected to remain low.

In conclusion, the Larvotto Beach Project shows how crushed chippings can provide an attractive solution to the beach material problem where sand of a suitable grain size is not economically available.

CHAPTER 36

THE EFFECT OF ARTIFICIAL SEAWEED IN PROMOTING THE BUILD-UP OF BEACHES

W. A. Price, Senior Principal Scientific Officer
K. W. Tomlinson, Senior Scientific Officer
Hydraulics Research Station, Wallingford, Great Britain

J. N. Hunt, Professor of Applied Mathematics,
University of Reading, Great Britain

ABSTRACT

The paper describes tests carried out in the laboratory and in the field in an attempt to discover whether a field of artificial seaweed placed offshore can promote an onshore transport of bed material and hence a build-up of beach levels. Tests in a wave tank showed that beach levels could be built up in this way - the effect of the seaweed being to increase the net drift of bed water in the direction of wave propagation i.e. towards the shore. The field trials were not as conclusive as was hoped, but nevertheless some build-up of beach levels did take place at a time when erosion of the beach due to many storms might have been anticipated.

A simple hydrodynamic model is proposed to represent the effect of artificial seaweed on gravity waves. The model predicts increased wave attenuation and increased shoreward mass-transport consistent with the experimental results.

Introduction

Considerable interest has been shown in recent years in the use of artificial sea-weed as a means of building up beaches by promoting an on-shore transport of sand. The Hydraulics Research Station at Wallingford, in co-operation with Imperial Chemical Industries (Fibres) Ltd., have been investigating the idea in the laboratory and in the field.

Tests in a Wave Tank

A model beach was subjected to regular waves until surveys showed that stability had been achieved. A field of polypropylene "pony tails" were then placed in an off-shore position and again the model beach was subjected to the same waves until it was established that no changes were taking place. (See Plate 1, Fig. 1)

Plate 1. Artificial Seaweed.

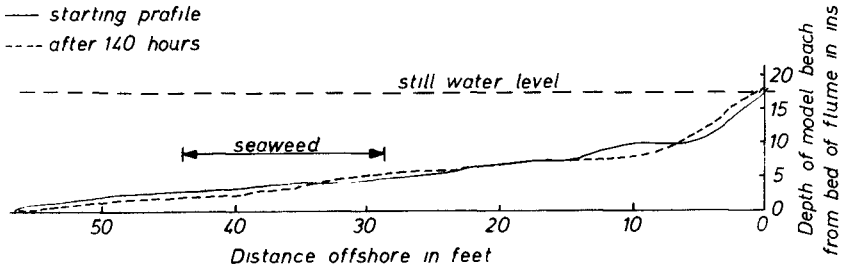

Fig. 1. Model beach with and without seaweed.

Many arrangements and spacing of "pony tails" were tried; the results shown in Figs. 1 and 2 were for the following test conditions. The "pony tails" consisted of 0.5 grammes of fibre having a specific gravity of 0.9 and a strand diameter of 0.055 mm. The strands, which were 3 in long, were spaced on a 3.6 in grid in the area shown in Fig. 1. The waves were 3 in high and had a period of 1.33 seconds.

The stable beach cross-sections, with and without the presence of sea-weed, are shown in Fig. 1. The result is typical of many experiments that were carried out; the effect of the sea-weed was to transfer material from the off-shore sea bed towards the shore causing an increase in beach levels.

The Effect on Wave Orbital Velocities

It was necessary to establish why an offshore field of artificial sea-weed promotes an onshore transport of sediment. To this end the change in the wave orbital motion at various cross-sections in the wave tank was established using a miniature propeller current meter having a high rate of response. The pulses from the meter were applied to a high speed pen recorder and the distances between pulses were measured by an electronic trace reader which automatically transferred the information on to punched cards suitable for processing on an IBM 1620 Digital Computer. This calculated the mean velocity between pulses and the time at which it was deemed to occur. One such record, for 10 consecutive wave periods, is shown in Fig. 2. (To speed up this time consuming process H.R.S. has recently developed a true instantaneous rate meter which produces a velocity plot directly on a high speed pen recorder.)

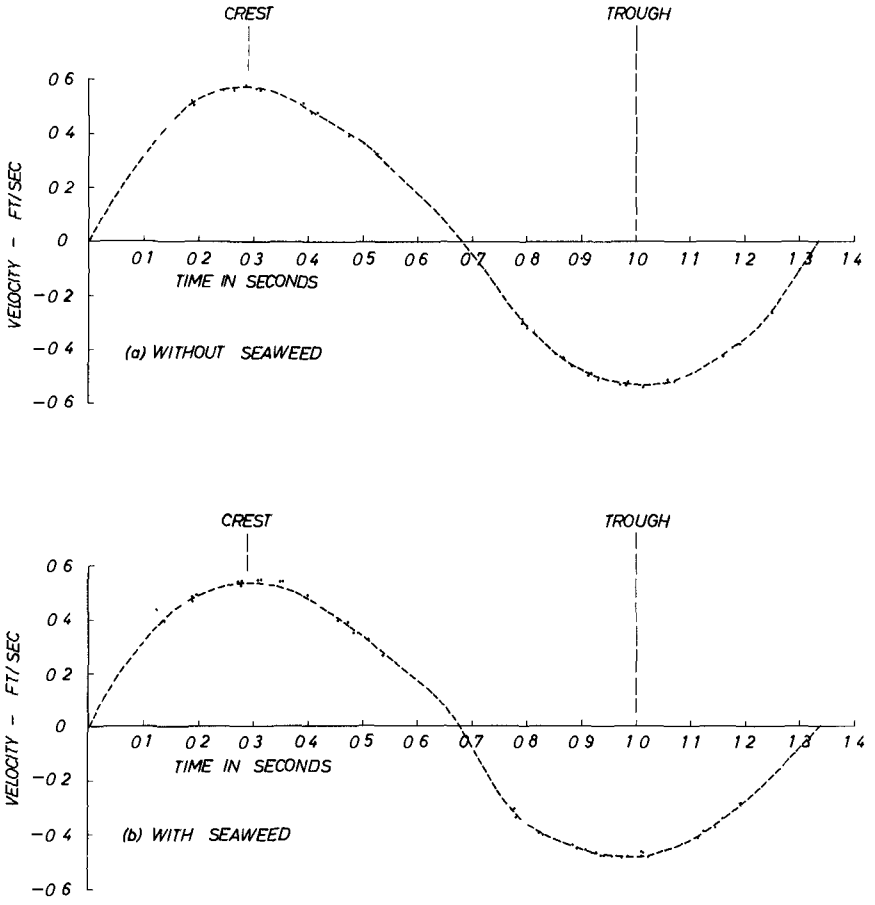

Fig. 2. Wave orbital velocities.

The area under the velocity/time curve is a measure of the length of water passing the observation point. The difference between the lengths of the forward and backward motion is a measure of the net drift. Carrying out such observations at many depths and sections it was established that the sea-weed increased the net drift near the bed in the direction of wave propagation, i.e. towards the shore. One result for a section situated in the centre of the sea-weed array is shown on Fig. 3.

The Effect on Wave Heights

The effect of the sea-weed was to reduce the wave height shoreward of the installation by approximately 4 per cent.

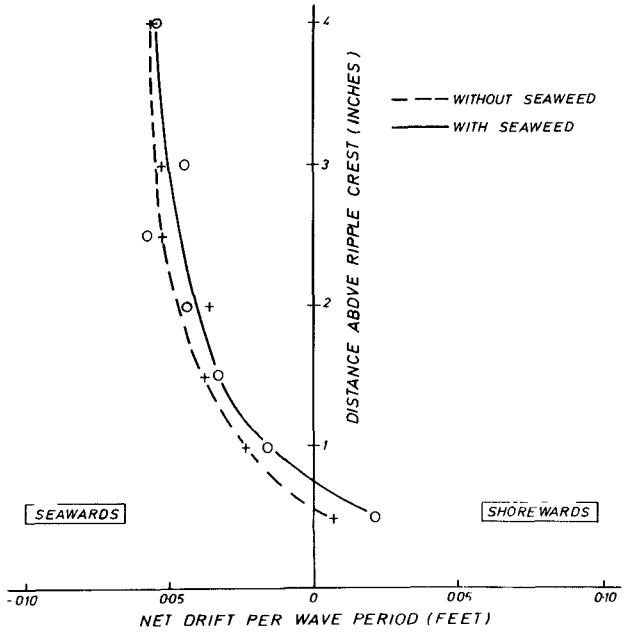

Fig. 3. Net wave induced drift.

A Theoretical Model

A simple hydrodynamic model is proposed to represent the effect of artificial sea-weed on gravity waves. The model predicts increased wave attenuation and increased shoreward mass-transport consistent with the experimental results. The introduction of regularly spaced tufts of polypropylene fibres at the sea bed creates a layer which possesses unusual rheological properties. This layer of water and fibres, adjacent to the sea bed, is to a small extent visco-elastic, but for the purpose of assessing its effect on gravity waves, it appears to be an adequate approximation to regard the layer as consisting of a fluid of somewhat higher viscosity than water. This simplification is suggested by the manner in which the slightly buoyant fibres remain near-vertical close to the bed, and thereby offer resistance to the shearing in horizontal planes caused by waves. This "stiffening" of the water is not isotropic, but since wave attenuation arises principally from viscous shearing stresses in a horizontal plane at the bed, suggests the use of an "effective viscosity" for the water-seaweed layer.

The modulus for wave attenuation with distance in a homogeneous fluid, due to dissipation of energy at the bed, is given to a first approximation by

$$K = \left(\frac{2\nu}{\sigma}\right)^{\frac{1}{2}} \frac{k^2}{2kH + \sinh 2kH} \qquad (1)$$

where k is the wave number $2\pi/\lambda$, σ the wave frequency and H the depth. The wave amplitude is then given by

$$y = A_o\, e^{-Kx} \cos(kx - \sigma t). \qquad (2)$$

Unpublished results on multi-layer systems by Dr. B. D. Dore, and Mr. M. J. Cross, show that in the case of two superimposed fluids, the upper of viscosity ν_1 and depth h_1, and the lower of viscosity ν_2 and depth $h_2 = H_1 - h_1$, the leading term in the decay modulus is given by

$$K = \left(\frac{2\nu_2}{\sigma}\right)^{\frac{1}{2}} \frac{k^2}{2kH + \sinh 2kH} \qquad (3)$$

Thus when we assume the densities of the two layers to be virtually the same, then the wave attenuation due to the bed depends only on the viscosity of the lower layer.

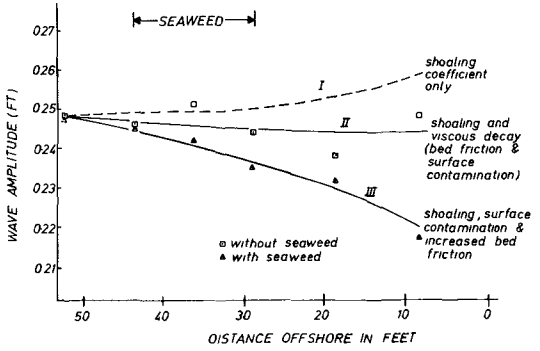

Fig. 4. Wave amplitudes.

In Fig. 4 the observed wave heights are plotted both with and without sea-weed in place. Curve I shows the variation in wave height to be expected without friction, that is, due to shoaling only. Curve II shows the theoretically expected variation of wave height with distance along the beach taking into account (i) the shoaling coefficient, as tabulated by Wiegel (1964) and (ii) bed dissipation based on equation (1) and surface contamination as calculated by Van Dorn (1966). The scatter of

the observations about the theoretical curve could be almost entirely due to rather less than 2 per cent wave energy reflected from the beach. Curve III represents the best theoretical curve through the observations made with sea-weed present, and includes shoaling, surface contamination and increased viscosity near the bed according to equation (3). Again, a component of reflected wave energy may be detected. The effective viscosity of the lower layer suggested by Curve III is $\nu_2 \approx 15\nu_1$, which corresponds to an increase in the laminar boundary layer thickness by a factor of 4.

Earlier theoretical work, Hunt (1961), showed the existence of an increased mass-transport near the bed in the presence of a layer of high viscosity. The observations of wave orbital velocity reported in the present paper, of which Fig. 3 is an example, showed the shoreward mass transport at the outer edge of the boundary layer to be increased by a factor of three in the presence of artificial sea-weed. With the viscosity ratio $\nu_2/\nu_1 = 15$ given by the wave attenuation data, the results of the 1961 paper suggests that the more viscous layer is of order $10(\nu_1/\sigma)^{\frac{1}{2}}$ thick. This is about twice the laminar boundary layer thickness $4(\nu_1/\sigma)^{\frac{1}{2}}$ but is still extremely thin.

In summary, the wave attenuation and mass transport observations are both consistent with a model in which the effect of the sea-weed is simulated by a very thin, but highly viscous, layer adjacent to the bed. If the model is applicable over a reasonably wide range of conditions, then it could be inferred that thicker, shorter fibres would produce similar effects in building up a beach, and that an increase in the number of fibres per unit area of the bed would further "stiffen" the boundary layer and enhance the build up process. Experiments to confirm or refute these suggestions would be very desirable, and would enable the model to be used to choose the optimum length and fibre spacing for any specified wave conditions.

Field Trials

These were carried out at Bournemouth by I.C.I. (Fibres) Ltd. in conjunction with H.R.S. Here the tidal range at springs is 8 ft, the beach sand has a mean diameter of 0.2 mm and there is an adequate supply of sand off-shore. Waves produced by local storms in the English Channel and those generated in the Atlantic produce a net littoral current from West to East. The beach had been eroding over the last few years.

The installation consisted of 1 lb hanks of fibre, (Specific Gravity 0.95) 8 ft long at 3 ft centres, layed over an area of sea bed 400 ft long and 150 ft wide. The landward edge of the installation was 480 ft from high water mark.

A series of beach and offshore cross-sections were surveyed prior to installing the sea-weed in October 1965. The intention was to re-survey these sections six times a year for a number of

years but unfortunately, due to an exceptional number of severe storms in the first winter, it was impossible to examine the site until March 1966. However, a comparison of the October 1965 and March 1966 surveys was very interesting, because whereas it might have been expected that general erosion of the beaches would have taken place during the long periods of destructive wave attack, a small increase in sand levels was found in the lee of the installation. Again, unfortunately, the story is not as simple as this because an inspection of the sea-weed array showed that it had been severely damaged and it was left to conjecture when this took place. A particularly severe storm occurred in February 1966 and it has been assumed that the installation was working satisfactorily up to this time.

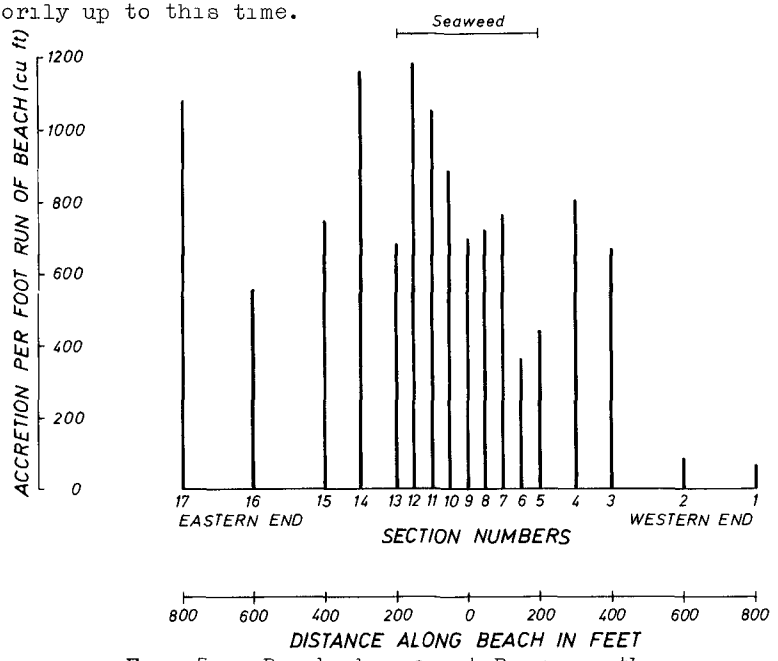

Fig. 5. Beach changes at Bournemouth.

Figure 5 shows the change in cross-sectional area of 17 cross-sections measured between the level of high water of mean spring tides and 5 ft below low water mark for the period October 1965 to March 1966. Accretion of the inshore zone was accompanied by erosion of the offshore sea bed; a result which might have been anticipated from the wave tank experiments.

Summary of results and future work

Enough has been done theoretically, in the laboratory, and in the field to suggest that artificial sea-weed can build up beaches by promoting an onshore transport of material. Plans are now being made to carry out a larger trial on the East coast

of England in the near future.

Acknowledgments

The authors would like to record their thanks to Mr. Bert Vallance whose careful experimental work, (carried out well before any theories were proposed) made the comparison with theory so satisfactory.

This report is published by permission of the Director of Hydraulics Research, Wallingford, England.

References

Wiegel, R. L., (1964) "Oceanographical Engineering", Prentice-Hall.

Van Dorn, W. G., (1966) "Boundary dissipation of oscillatory waves", J. Fluid Mech. 24, 769-779 and Corrigendum.

Hunt, J. N., (1961) "Oscillations in a viscous liquid with an application to tidal motion", Tellus XIII, 79-84.

CHAPTER 37

STUDY ON SCOURING AT THE FOOT OF COASTAL STRUCTURES

by

Shoji Sato, Norio Tanaka and Isao Irie
Hydraulic Division, Port and Harbor Research Institute
Ministry of Transport
3-chome, Nagase, Yokosuka, Japan

ABSTRACT

This paper presents the results of two-dimensional model experiments conducted in order to clarify the basic characteristics and to find out some preventive measures against scouring around coastal structures. The applicability of these results to the field are discussed on the basis of some results of field investigations.

The results of two-dimensional experiments presented herein show that the characteristics of waves just in front of structures and their reflection by structures are most important factors of scouring. The results of field investigations, however, indicate that in addition to those two factors, the currents caused due to waves around structures play important roles in scouring.

INTRODUCTION

Scouring around structures is one of the important factors to be considered in the design and construction of coastal structures. So far as authors know, however, there are few reports on scouring, because of the complexity of the phenomenon and the difficulty of the field observations under storm condition. Some of them are; experiments introduced the variation of the water level due to the tide by R. C. Russel & Sir C. Inglis (1953), study on the submerged breakwater by M. Homma & K. Horikawa (1961), study on scouring at the foot of an inclined sea wall by J. B. Herbich, H. D. Murphy & B. V. Welle (1965), study on scouring at the toe of permeable structures by T. Sawaragi (1966) and so on.

Therefore, authors have conducted several model experiments on the scouring around coastal structures. In this paper, are mentioned the results on the following four kinds of experiments conducted in the two-dimensional wave-tanks using natural sand.

a. Scouring at the foot of a vertical sea wall.
b. Scouring at the foot of an inclined sea wall.
c. The effectiveness of plastic filters for the prevention of scouring.
d. Scouring at the foot of a composite breakwater.

SCOURING AT THE FOOT OF A VERTICAL SEA WALL

In this experiment, the basic characteristics were investigated on scouring at the foot of a vertical sea wall installed at several points along two types of beach profile; the normal and storm beaches.

EQUIPMENT AND PROCEDURES

Equipment

Experiments were conducted in the two wave-tanks of different size shown

in Fig.-1. The medium size wave-tank shown in the upper side of this figure is 40 m long, 0.5 m wide and 0.9 m deep and the large size wave-tank in the lower side is 105 m long, 3.0 m wide and 2.5 m deep. As shown in this figure, these both tanks were divided longitudinally into two or three parts with partition-walls and the two parts of 17 cm in width for the medium size wave-tank and the part of 80 cm in width for the large size wave-tank were used for the experiments.

Procedures

In these wave-tanks, at first, a model beach with the slope of one to ten was exposed to the action of test waves until the model beach reached the equilibrium state. Then, a vertical wall was installed and the same waves were acted again. Through a test-run, the beach profile and the shape of scour were measured with a point-gauge at intervals of several minutes near the beginning of the test-run and one hour near the end, until the steady state of the scouring was established after 6 to 10 hours of wave-run. Wave heights were measured with an electric-resistance wave-gauge and recorded on a pen-writing oscillograph.

For some cases, radio-active tracers which were made by adhering the radioisotope of Au-198 on the surface of sand, were used in order to know the movement of bed materials. Distributions of radio-active tracers were measured with a scintillation-type detector.

Test cases

Table-1 shows the cases of the experiments. For each case in Table-1, the vertical wall was installed at various points of the equilibrium beach, therefore, the number of test-run was fourty-two. The test waves could be classified into two ranges of wave steepness as shown in the first column of this table, one is flat waves which make the normal beach and the other is steep waves which make the storm beach.

Table-1

Equilibrium profile	Ho/Lo	Ho (cm)	T (sec)	d (mm)	Ho/d	d/Ho	Wave tank
Normal beach	0.0062	8.7	3.0	0.69	1.3×10^2	0.0079	Medium
	0.0062	8.7	3.0	0.38	2.3×10^2	0.0044	Medium
	0.0065	26.0	5.1	0.21	1.2×10^3	0.0008	Large
Storm beach	0.033	8.7	1.3	0.69	1.3×10^2	0.0079	Medium
	0.033	8.7	1.3	0.38	2.3×10^2	0.0044	Medium
	0.051	42.4	2.3	0.21	2.0×10^3	0.0005	Large

RESULTS OF THE EXPERIMENTS

Process of scouring and distributions of the scouring depth

Variation of the scouring depth with the lapse of time was different with the position of the vertical wall and could be classified into following four types. Types of scouring;

Type-I Scouring progresses rapidly for several minutes in the beginning, then the scouring stops, and accretion occurs.

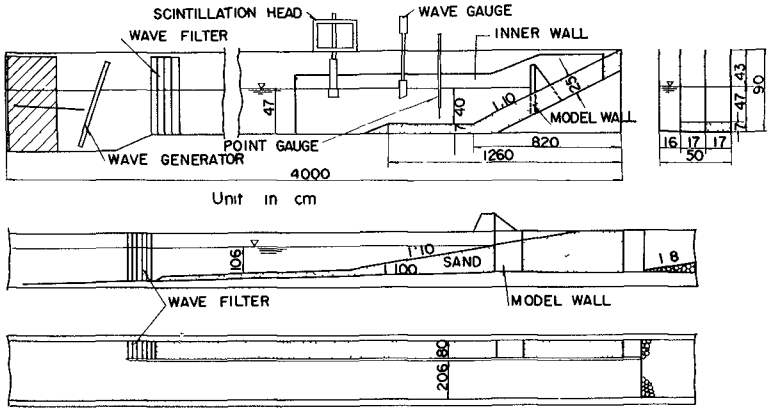

Fig. 1. wave-tanks

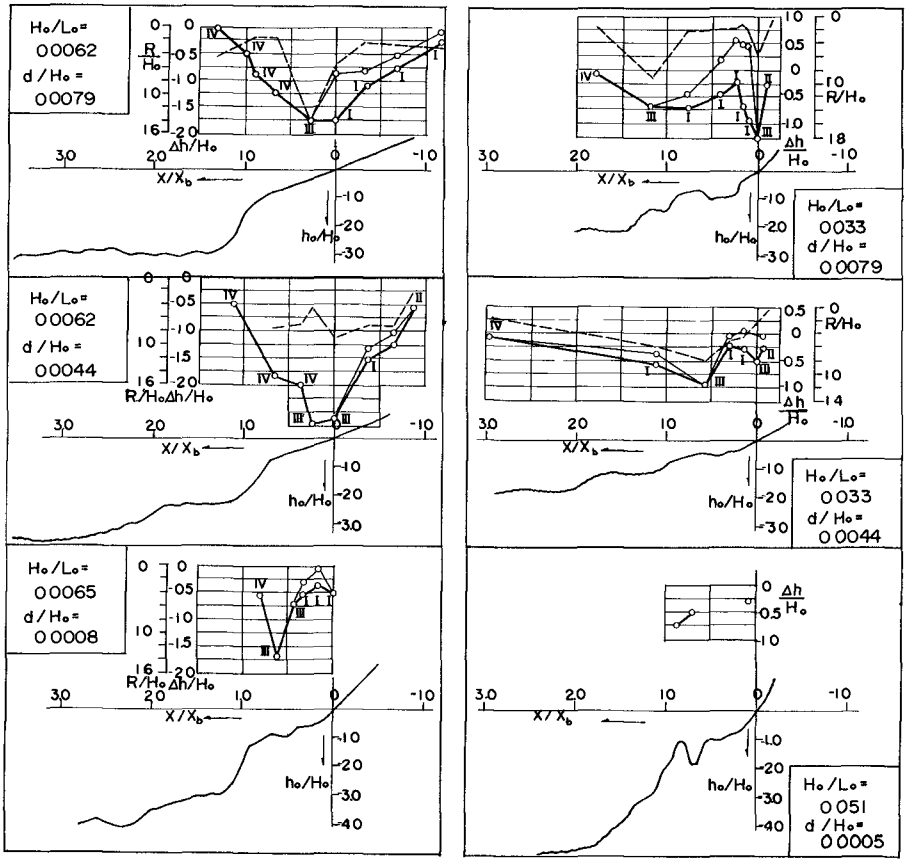

Fig. 2. The distributions of the maximum and the final scouring depth along the beach profiles.

Type-II The stable condition is achieved after the initial rapid scouring.

Type-III The additional slow scouring occurs following the initial rapid scouring.

Type-IV Slow scouring continues from the beginning of the test-run.

Fig.-2 shows the distributions of the non-dimensional scouring depth ($\Delta h/Ho$), and the wave run-up height (R/Ho) along the beach profile; the left figures are for the normal beach and the right figures are for the storm beach. In these figures, the broken lines show the wave run-up height on the vertical wall, the thick lines indicate the maximum scouring depth during each test-run and the thin lines represent the final scouring depth. Therefore, the difference between the latter two lines corresponds to the amount of refilling. The abscissas of these figures are the distance from the shore-line (X) non-dimensionalized with the distance between the shore-line and the breaking point of waves (Xb). These factors such as R, Δh, Xb, X and so on are defined in Fig.-3 and Ho indicates the height of deep water waves. The breaking point of wave was defined as the point at which the front of wave crest became vertical.

Fig.-2 shows that;

i) For the normal beach, the maximum scouring depth appears to be the largest at the point a little shoreward of the final wave breaking point and the distributions along the beach profile are of V shape.

ii) For the storm beach, the distributions of the maximum scouring depth have two peaks and are of W shape; the one peak near the first breaking point and the other near the final breaking point.

iii) The largest maximum scouring depth for both the normal and storm beaches appears in type-III of scouring. For the normal beach, type-IV of scouring is found in the region seaward of type-III of scouring and type-I of scouring in the region shoreward of type-III. On the other hand, for the storm beach, type-IV of scouring appears in the region seaward of the offshore-side peak of the maximum scouring depth, type-II of scouring in the region shoreward of the shore-side peak and type-I of scouring in the region between the two peaks.

Mechanism of the four types of scouring.

Fig.-4 shows variations of the beach profiles for the typical examples of the above mentioned four types of scouring. In this figures, the dash-dot lines show the mean elevations of wave crests or troughs. Variation of the scouring depth with lapse of time for these examples are as shown in Fig.-5.

In the example of type-I of scouring shown in the top of Fig.-4, the vertical wall was installed at the shore-line and radio-active tracers were injected at the toe of the wall.

Since waves after breaking act directly on the wall in the beginning of the test-run, the foot of the vertical wall was scoured rapidly in the same mechanism as scouring by water jet, and the region just seaward of the step was accreted remarkably. Because the amount of this accretion on the seaward

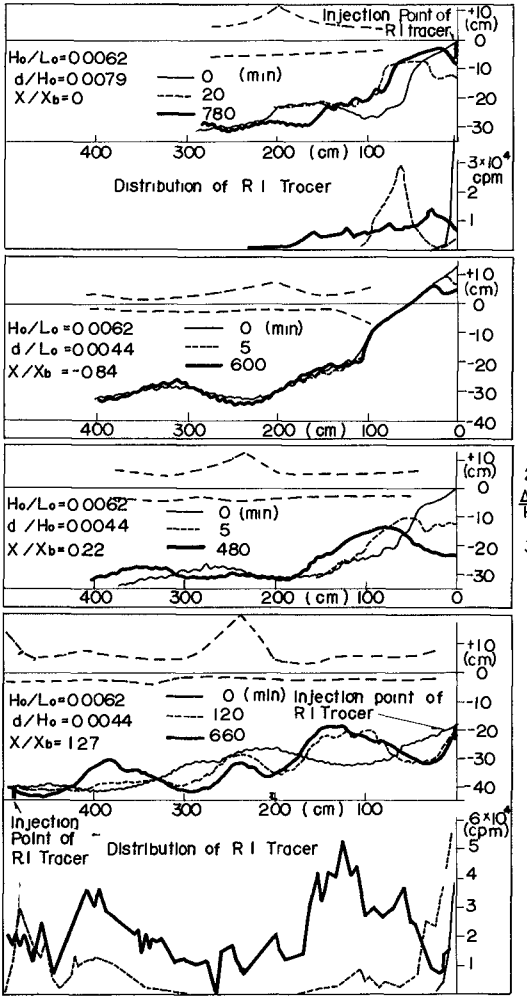

Fig. 4. Variations of the beach profiles of the typical examples of the four types of scouring, and distribution of R. I. tracers.

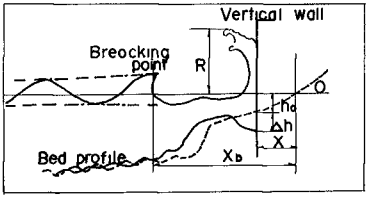

Fig. 3

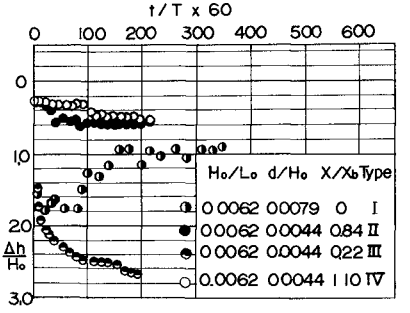

Fig. 5. Variations of the scouring depth with lapse of time for the examples shown in Fig.-4.

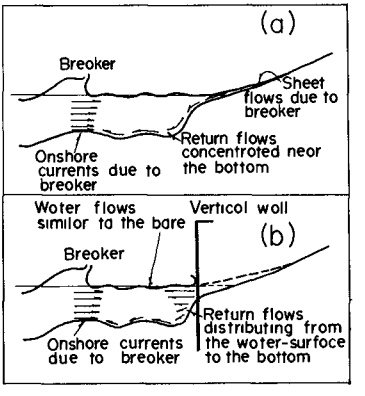

Fig. 6.

slope of the step is more than the amount of scour at the foot of the vertical wall, it is clear that sand was also supplied to this region from the offshore-zone due to the shoreward sand transport.

As illustrated in Fig.-6(a), in the equilibrium beach without the vertical wall, waves after breaking rush up on the shore to form the sheet flow, which cause return flows concentrated near the bottom. And this return flows may balance with the onshore currents near the bottom due to waves. When a vertical wall is installed as shown in Fig.-6(b), the water currents after wave breaking reflect from the vertical wall to bring out return-flows distributing from the water-surface to the bottom, because this water currents in the zone near to the breaking-point is similar to the bore. As the result, the return flows near the bottom decrease as compared with the case without the sea-wall; this decrease of return flows near the bottom results in the increase of the net onshore currents. Therefore, at the portion seaward of the step in front of the vertical wall, bed materials are transported shoreward to accumulate in front of the step from the beginning of test-run. This accumulation of sand extends toward the toe of the vertical wall gradually and refills the scouring hole. The distribution of radio-active tracers shown in Fig.-4 shows clearly the above mentioned process of refilling.

In the cases where a vertical wall was installed near the shoreward end of the foreshore, the decrease of the return flow near the bottom did not occur so much, since the sheet flow acted on the vertical wall. Therefore, the steady state was attained without the refilling. This type of scouring is type-II.

Since waves break at the two points such as near the longshore-bar and the shoreline, the energy of the water flow after breaking may be small in the cases of the storm beach. Therefore, type-II of scouring appears near the shoreline as shown in Fig.-3.

When a vertical wall is installed in the offshore zone, type-IV of scouring appears. The lowest figure of Fig.-4 shows an example of this type. In this case, the vertical wall was installed at the point of 20 cm in water depth and radio-active tracers were injected at the two points; one at the toe of the wall and the other at 500 cm seaward from the wall. As known from the variation of beach profiles and the distribution of R. I. tracers, sand seaward and shoreward of the loop of the standing wave are transported to seaward and shoreward respectively to accumulate near the node of the standing waves. Since the surface of the vertical wall corresponds to a loop of standing waves, sand at the foot of the wall are transported seaward and scouring proceed gradually.

Type-III of scouring occures in the location between type-I and type-IV of scouring, and the mechanism of scouring in this type is composed of two steps of scouring, that is, in the first step, the foot of the vertical wall is scoured rapidly by the waves after breaking in the mechanism similar to scouring by water jet and in the second step, the foot of the wall is scoured gradually due to the standing waves which are formed due to the increase of the water depth in front of the vertical wall by scouring.

Maximum scouring depth

Fig.-7 shows the relation between the largest maximum scouring depth non-dimensionalized with the height of the deep water waves $(\frac{\Delta h_m}{H_o})$ and the

steepness of the deep water waves. In this figure, it is clear that the values of $\Delta h_M/H_o$ are larger for the flatter wave and for the steepness of 0.02 to 0.04, $\Delta h_M/Ho$ takes the value of nearly 1.0, that is, the largest maximum scouring depth is approximately equal to the height of the deep water waves.

On the other hand, in Fig.-8, the value of $\Delta h_M/Ho$ decreases with the ratio of the relative median diameter of the bed materials (d/Ho).

Since, wave steepness is the value of 0.02 to 0.04 under ordinary storms and the value of d/Ho is smaller than that in present experiments, the maximum scouring depth under the actual storm condition may be considered not to exceed the height of the deep water waves.

SCOURING AT THE FOOT OF AN INCLINED SEA WALL

EQUIPMENT AND PROCEDURES

Equipment and procedures

Experiments were conducted in the medium size wave-tank shown in Fig.-1 and their procedures were the same as the experiments on the vertical wall mentioned above.

Experimental conditions and test cases

Wave conditions and bed materials of this experiment were the same as the matters listed in the fifth line of the Table-1, and the model beach was of storm beach. Inclination of the wall surface was varied at three values of 90, 60 and 30 degrees from the horizontal line. The model wall was made of wooden plates and was driven into the sea-bed.

RESULTS OF THE EXPERIMENTS

Fig.-9 indicates the distribution of the maximum and the final scouring depth along the beach profile. Except a few cases, the process of scouring could be classified into the before mentioned four types of scouring. For example, in the case of $X/Xb = 0.96$, no scouring appear, but accretion occurs from the beginning of test-run. This new type of scouring was defined as type-V of scouring. Those types of scouring are shown with Greek figures in Fig.-9.

The graphs shown in the upper side of Fig.-9 represent the relation between the scouring depth and the angle of inclination of the wall. The thick lines indicate the maximum scouring depth and the thin lines the final scouring depth.

From the lower figure, it is clear that although the distribution of the maximum scouring depth for 90^o sea wall is of W shape as the above mentioned experiments on the vertical wall, the distribution for 30^o sea wall is of V shape having a peak near the longshore-bar. And the different types of scouring appear at the same point due to the difference of the inclination of the wall.

In the graphs in the upper side of this figure, the scouring depth

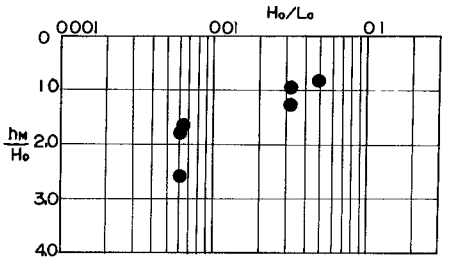

Fig. 7. Relation between the largest maximum scouring depth and the wave steepness.

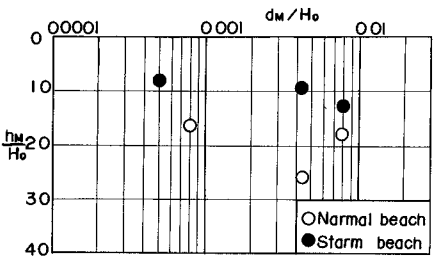

Fig. 8. Relation between the largest maximum scouring depth and the median diameter of sand.

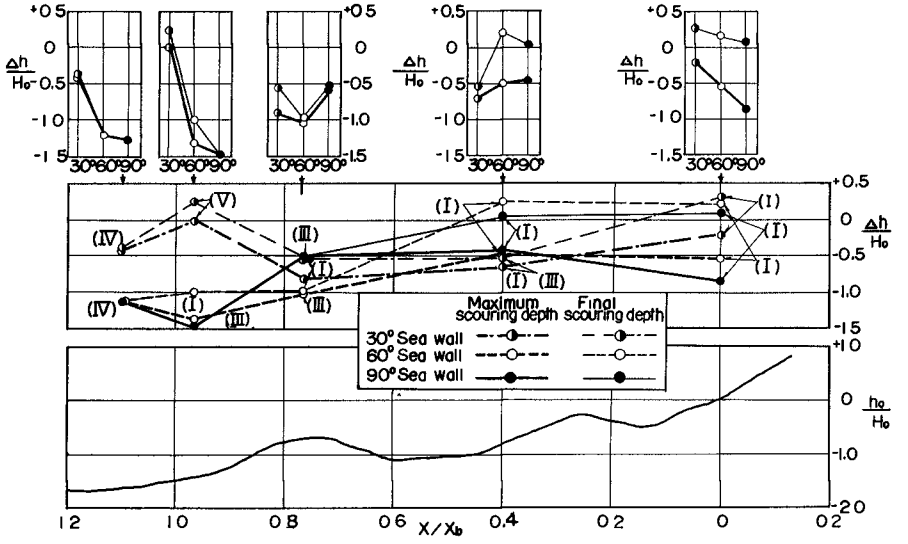

Fig. 9. Distribution of the scouring depth along the beach profile and the relation between the scouring depth and the inclination of the wall.

decreases with the angle of inclination of the wall in the regions around the shoreline and seaward of the longshore-bar, although the difference are small between the scouring depth of 90° sea wall and 60° sea wall in the region seaward of the longshore-bar. The tendency, however, can not be found at the crest and trough of the longshore-bar.

As known from this figure, the amount of refilling decreased with the angle of the inclination of the wall at the point of X/Xb = 0 and X/Xb = 0.4. The reason of this fact may be similar to the matter mentioned about Fig.-6. That is, in the case of the inclined wall, the decrease of the return-flow near the bottom would be little in comparison with the case of the vertical wall, because the water-flow after wave-breaking rushed up on the surface of the wall having the characteristics of the sheet flow.

In the seaward region of the longshore-bar, the standing waves due to the reflection of wave from the surface of the wall was formed. As seen in Fig.-10 showing the distributions of the mean elevations of the wave crest or trough in front of the sea wall installed at the point of X/Xb = 0.96, the positions of the nodes and loops of the standing waves are shifted remarkably in the case of 30° sea wall. When the distance of this shifting was close to a quarter of the wave length, the foot of the wall was accreted from the beginning of test-run without scouring. This type is type-V.

By the results of these experiments it may be concluded that the inclined sea-wall is effective for the prevention of the scouring except the region near the longshore-bar, while the effectiveness of 60° sea wall is small in the offshore zone.

THE EFFECTIVENESS OF PLASTIC FILTERS FOR THE PREVENTION OF SCOURING

Use of plastic fiber cloths as filters for prevention of scouring at the feet of coastal structures was reported by R. J. Barrent and others in the 10th Conf. on Coastal Engineering in Tokyo. Authors examined experimentally the effect of these plastic filters for the prevention of scour taking the two cases of the armor-stone revetment and the wave-absorbing structure.

EQUIPMENT AND PROCEDURES

Equipment and procedures

The experiments were conducted in the medium size wave-tank without partition-walls shown in Fig.-1. The cross sections of modeles of the armor-stone revetment and the wave-absorbing structure are shown in Fig.-11 and Fig.-12. The models shown in these figures correspond to 1/20 in scale of the structures in the field.

In the experiment on the armor-stone revetment, the models were built on the flat bed of sand having the median diameter of 0.2 mm and for the wave-absorbing structure, models were built on the equilibrium beach which was formed by acting test-waves on the initial beach of sand of 0.14 mm in median diameter having the slope of 1/10.

The permeability of plastic filters tested in these experiments is shown in Table-2.

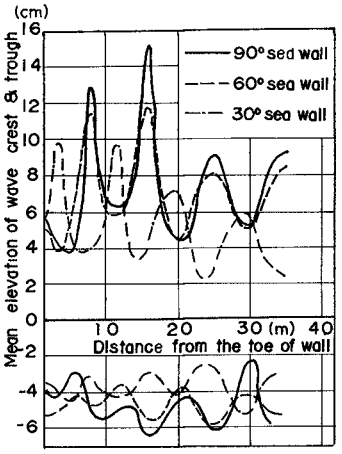

Fig. 10. Distributions of the mean elevation of the wave crest or trough.

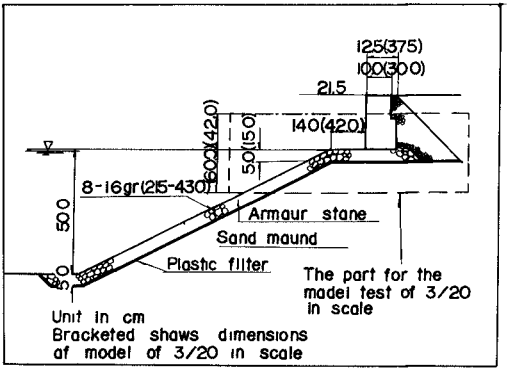

Fig. 11. Cross section of the model of the armour-stone revetment.

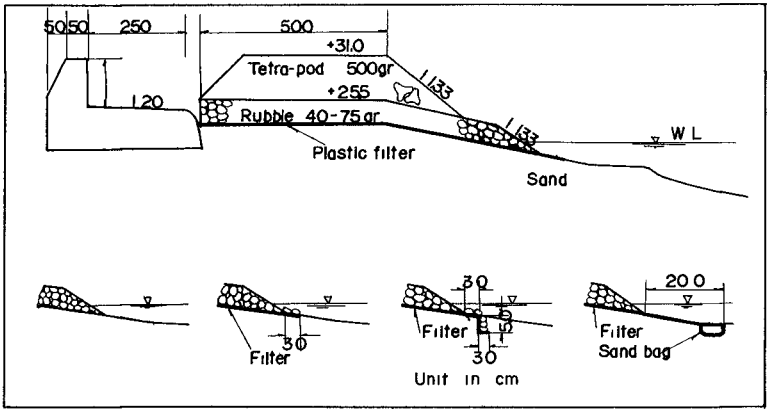

Fig. 12. Cross section of the model of the wave-absorbing structure.

Table-2. Permeability of plastic filters

Experiment	Armor-stone revetment	Wave-absorber
Mesh of filter	a-14 mesh	a-16 mesh
Permeability (m/sec)	1.1×10^{-2}	5.72×10^{-3}

EXPERIMENTAL CONDITIONS AND TEST CASES

In the experiments on the armor-stone revetment, the three types of sublayers; sand mound only, sand mound covered with rubbles only and sand mound covered with rubbles and plastic filters were tested. The test cases and the conditions are shown in Table-3.

Table-3

Case No.	Scale	Wave height	Wave period	Type of sublayer
a	1/20	5 cm	0.9 sec	Sand mound only
b	1/20	5	0.9	Sand mound covered with rubbles
c	1/20	5	0.9	With plastic filters
A	3/20	15	2.2	Sand mound only
B	3/20	15	2.2	Sand mound covered with rubbles
C	3/20	15	2.2	With plastic filters

In case-A, B and C listed in Table-3 the part enclosed by dash-dot line in Fig.-11 was tested in the scale of 3/20 in order to examine the scale effect of experiments.

RESULTS OF EXPERIMENTS

On the armor-stone revetment

Fig.-13 shows the variation of the front surface of the mound of revetment for case-A, B and C. In case-A the foot of the upper structures was scoured very remarkably and the upper structure was on the point of falling. In the case-B where sand mound covered with rubbles, the shoulder of the mound was scoured and the upper structure was inclined remarkably. And in the case-C with plastic filters the scouring was hardly seen except a slight scouring at the shoulder of the mound.

Fig.-14 shows the variation of the scouring depth, non-dimensionalized by the height of the deep water wave, at the foot of the upper structure with the lapse of time. In this figure, it is clear that the case-C with plastic filters is very effective for the prevention of the scouring.

On the wave-absorbing structure

Fig.-15 shows the variation of the front surface of the wave-absorbing structure and the sea bed. The thin and thick lines represent the initial state and the state after 240 minutes of wave-run respectively. And the thickest solid lines indicate the filters.

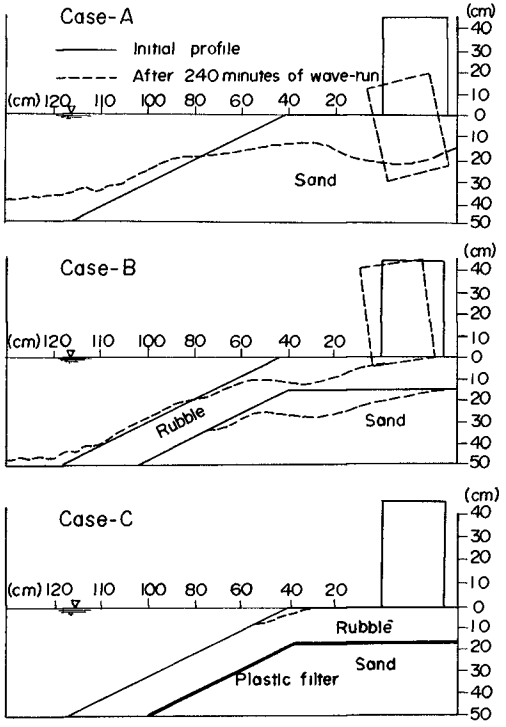

Fig. 13. Variations of the cross-section of the armour stone revetment.

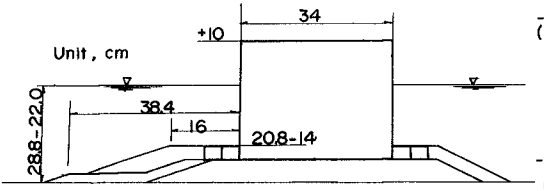

Fig. 16. Cross-section of the model of the composite breakwater.

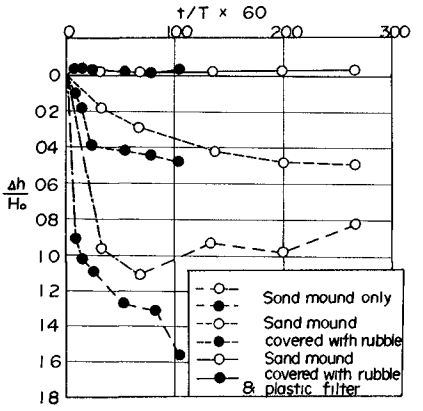

Fig. 14. Variation of the scouring depth at the foot of the upper structure of the revetment.

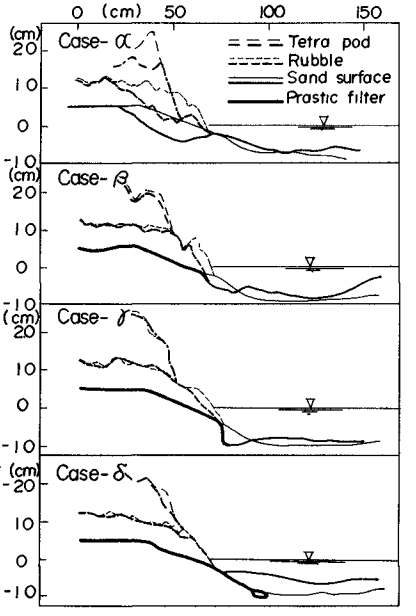

Fig. 15. Variation of the cross-section of the wave absorbing structure.

In the case (α) without filters, the sand base of rubbles was washed away and the structure sank remarkably. In the other case with filters, those sinking of structure due to scouring of the base did not occur, but the toe of the rubbles was scoured in the case (β) and (γ). In the case (δ) which produced the best result, filters were protruded seaward long enough until the water depth at the edge of filters became deep. But this device tested in the case (δ) might have a problem of the difficulty of construction and the durability of filters at the part protruded. Therefore, further studies would be performed on the scouring at the toe of the rubble mound.

SCOURING AT THE FOOT OF A COMPOSITE BREAKWATER

EQUIPMENT AND PROCEDURES

Equipment and procedures

The experiments were conducted in the medium size wave-tank without the partition-walls shown in Fig.-1. The cross section of the model breakwater is shown in Fig.-16. The models were made on the flat bed of sand of 0.2 mm in median diameter.

During the tests, test-waves were acted on the model intermittently every 30 seconds, that is, the wave generator was operated for 30 seconds and stopped for 2 minutes until waves entirely decayed out, in order to prevent reflected-waves from attacking the structure.

Experimental conditions and test cases

The test cases and conditions are shown in Table-4, where only the water depth was different among case-1 to 3.

Table-4

Case No.	Wave height	Wave period	Water depth
1	11.5 cm	1.98 sec	28.8 cm
2	11.5	1.98	26.0
3	11.5	1.98	22.0
4	7.7	1.41	22.0

RESULTS OF THE EXPERIMENT

Fig.-17 shows final bed profiles after three hours of wave action and distributions of the wave height. The vertical dash-dot lines shown in this figure indicate the position of loops of standing waves formed by the reflection of waves from the breakwater. As known from this figure, the sea beds were erroded under the loops of standing waves and were accreted under the nods as mentioned concerning to type-IV of scouring in the preceding experiments on the vertical wall. As the result, the sea beds formed sinusoidal patterns roughly having the wave length of a half length of the incident waves.

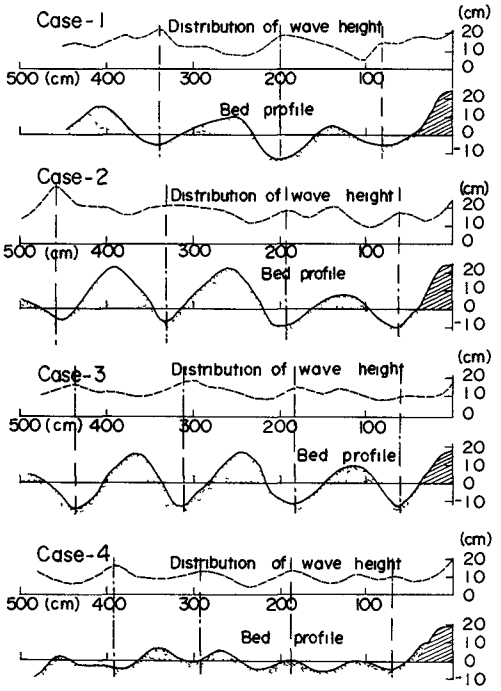

Fig. 17. The equilibrium profile of bed in front of the composite breakwater.

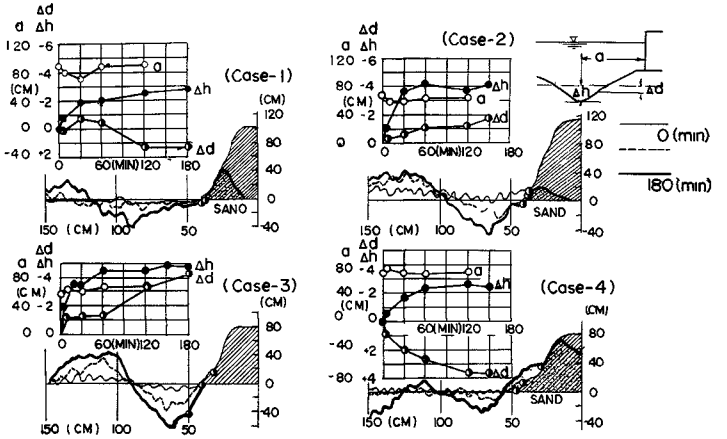

Fig. 18. Variation of the shape of the scouring hole at the toe of the composite breakwater.

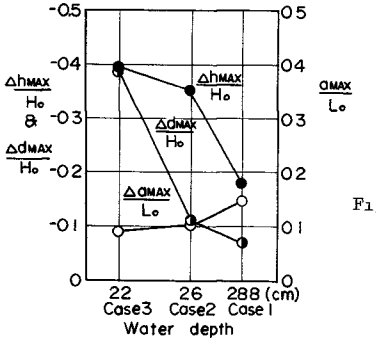

Fig. 19. Relation among $\Delta h_{max}/H_o$, $\Delta d_{max}/H_o$, $\bar{d}/L_o$ and the water depth

While the distance between the vertical surface of the breakwater and the vertical dash-dot lines nearest to the breakwater is less than the interval distance among each loop. Therefore, the patterns of distribution of the wave height and of sea bed profile are seen as if the hypothetical surfaces of reflection located at the position of the vertical dash-dot lines nearest to the breakwater.

The hypothetical surface of wave reflection approaches toward the breakwater with the decrease of the water depth in case-1 to 3.

Fig.-18 shows the variation of profiles of scouring holes at the foot of the breakwater. In this figure, the black dots indicate the toe of the rubble mound. And the final profile of sand intruding among rubbles is also represented in this figure. The graphs shown in this figure show the time variation of the scouring depth (Δh), the amount of the sliding of rubble due to scouring (Δd) and the distance (ℓ) between the deepest point of the scouring hole and the vertical surface of the breakwater.

For case-1 to 3, the maximum values of Δh, Δd and ℓ (Δh_{MAX}, Δd_{MAX} and ℓ_{MAX}) non-dimensionalized with the height (Ho) and the length (Lo) of the deep water wave are represented against the water depth in Fig.-19.

According to these figures, the maximum scouring depth and the amount of the sliding of rubbles increase with the decrease of the water depth. But, on the other hand, the position of the deepest point of the scouring hole approaches to the breakwater and the amount of sand accumulated among rubbles decreases with the decrease of the water depth.

These facts may be considered to indicate that the position of the hypothetical surface of wave reflection acts the important roles on scouring in addition to the effect of the water depth itself. That is, when this hypothetical surface approaches to the toe of the rubble mound, damage of the rubble mound due to scouring would become more intensitive.

THE COMPARISON BETWEEN MODEL EXPERIMENTS AND THE FIELD INVESTIGATION

In this section, the preceding results of model experiments will be compared with some data obtained from field investigation.

ON THE MAXIMUM SCOURING DEPTH

Fig.-20 shows the relation between the scouring depth and the wave height obtained in the port of Kashima. The port of Kashima is a new port being under construction on the sandy beach facing to the Pacific Ocean. The general characteristics of sand drift in this coast was reported in the 10th Conf. on Coastal Engineering in Tokyo. The scouring depth was defined as the difference between the water depth at the deepest point of the scouring hole surveyed at the tips of the rubble mound breakwater stretched perpendicularly to the shoreline and the water depth before construction at the same point. The wave height is the maximum significant wave height measured at the point of -12 m deep for two weeks before the surveying date of each scouring depth.

In this figure, almost all data distribute below the line of $\Delta h = Ho$.

Since the scouring depths were surveyed in calm days after a storm, some of them plotted in this figure would be one which had been refilled by small waves after a storm. Therefore, the maximum scouring depth under the stormy condition may be considered to be nearly equal to the maximum significant wave height during the storm. This result coincides with the characteristics of the largest maximum scouring depth obtained by the experiments on the vertical wall.

ON THE LOCATION OF INTENSITIVE SCOURING

Fig.-21 presents the relation between the scouring depth at the both sides of the breakwater and the water depth obtained in the port of Kashima. As shown in the small figure, the scouring depth was defined as the vertical distance between the deepest point and the outside of this scouring hole. And the abscissa is the water depth at the outside of the scouring hole.

In this figure, the distribution of the scouring depth has a peak at the water depth of -2 to -3 m. On the other hand, on the Kashima Coast, the longshore-bars are found around the water depth of -2.5 to -3.0 m. Therefore, although there are no data around the shoreline, the results presented in this figure may be considered to coincide with the distribution of the maximum scouring depth for the storm beach shown in preceding Fig.-4.

Fig.-22 shows examples of the sounding maps of three new ports in Japan, the port of Kashima mentioned above, the east port of Niigata and the port of Kanazawa. The latter two ports have been under construction on the coast of fine sand of 0.15-0.20 mm in median diameter facing to the Japan Sea and are attacked by large waves of 3 to 5 m in height from the north-west direction in winter, but it is very calm in summer. In these both ports, two raws of the large longshore-bars are found usually.

In these maps, some common characteristics are seen from the view point of scouring. That is, the feet of the breakwaters are scoured remarkably in the part crossing the longshore-bar and in the vicinity of the projected corner and the head of breakwaters.

Remarkable scour near the longshore-bar was also seen in the above mentioned experiments on the vertical and inclined walls. But, in the field, in addition to the agitation by wave breakers, the scouring would be accelerated by the seaward return flow along the breakwater.

Scouring around the projected corner and the tip of breakwaters would be considered to be brought by the sudden change of currents and waves in the vicinity of them. That is, sharp gradient of the energy of the turbulence may be an important factor causing the intensitive scouring around the projected corner, in addition to the intensitive turbulence itself.

From such considerations on the field data, it would be revealed that the transport of suspended materials due to the currents along the structures plays important roles for the scouring at the feet of structures, in addition to the agitation of bed materials by waves. Therefore, the further studies should be conducted about the effect of the currents for scouring.

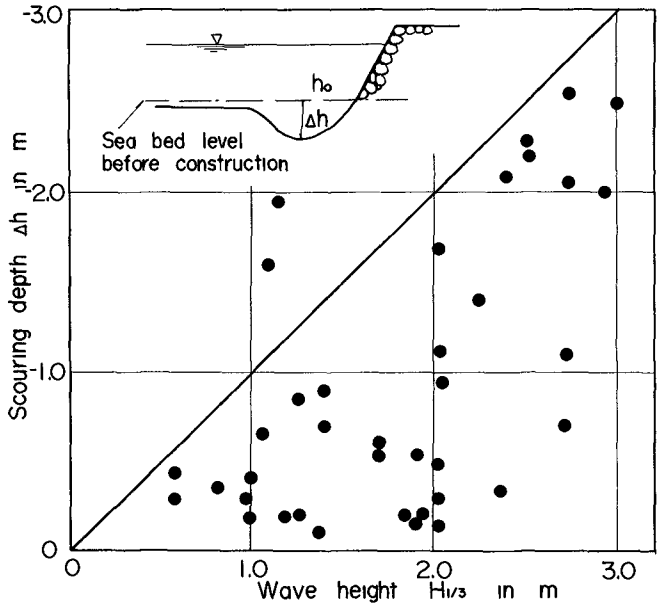

Fig. 20. Relation between the scouring depth and the wave height obtained in the port of Kashima.

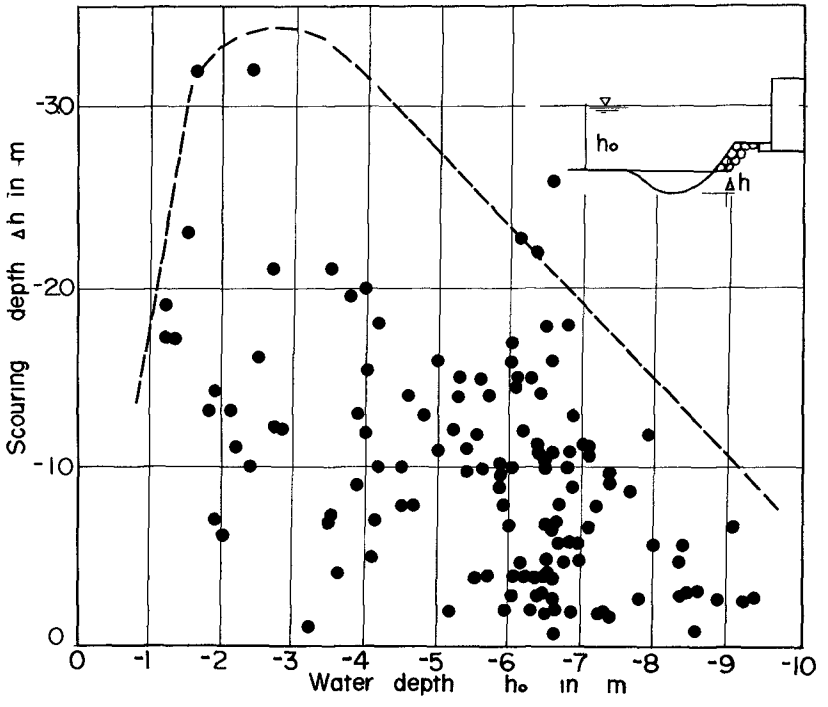

Fig. 21. Relation between the scouring depth and the water depth obtained in the port of Kashima

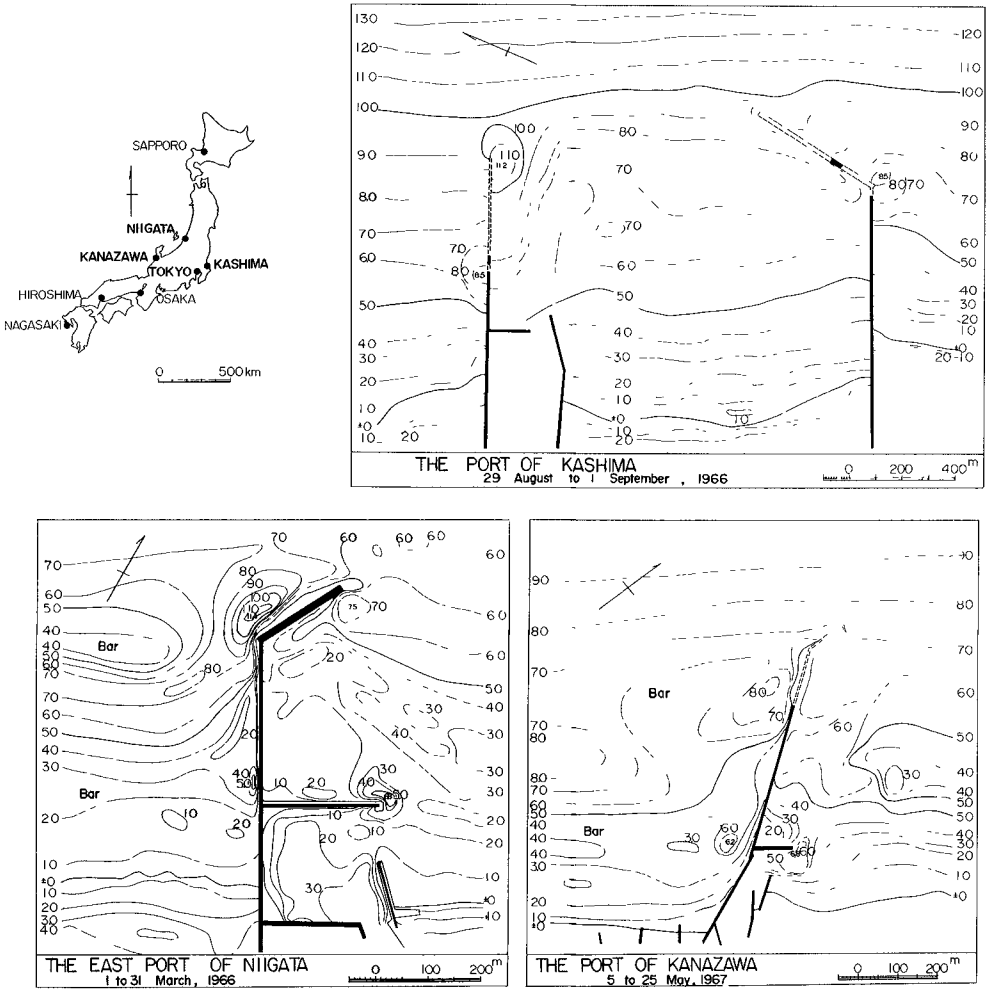

Fig. 22. Examples of sounding maps of the port of Kashima, the east port of Niigata and the port of Kanazawa.

CONCLUSION

The results mentioned above may be concluded as follows.

1) The process of scouring is classified into the following four types.

Type-I	After rapid scouring, the refilling occurs.
Type-II	The stable condition is achieved after rapid scouring.
Type-III	The additional slow scouring occurs following the initial rapid scouring.
Type-IV	The slow scouring continues from the beginning of the test-run.

2) Intensitive scouring occurs in type-III of scouring when a vertical wall installed near the plunging point of the breaker.

3) The relative largest maximum scouring depth tends to decrease with the increase of wave steepness, but it is nearly equal to the deep water wave height in case that steepness is 0.02 to 0.04, which is for ordinal storm condition.

4) An inclined wall is effective for the prevention of scouring in the region except the vicinity of the longshore-bar, although the effectiveness of 60° sea wall is small in the offshore zone.

5) Plastic filter was very effective for the prevention of scouring, but further studies would be necessary on its durability.

6) The position of the hypothetical surface of wave reflection is an important factor of scouring, in addition to the water depth itself. Damage of the rubble mound is more indtensitive when this hypothetical surface approaches to the toe of the mound.

7) The comparison of the experimental results with the data obtained in the port of Kashima shows that the matters mentioned in the second and third conclusions would be applied to the field.

8) Around breakwaters, the feet of the breakwaters are scoured remarkably in the part crossing the longshore-bar, the vicinity of the projected corner and the tip of breakwater.

9) In the field, in addition to the agitation of sea water due to wave itself, currents around the structures play important roles in scouring.

REFERENCES

1) Russel R.C. and Sir, C. Ingles, The Influence of Vertical Wall on a Beach in front of It, Proc. of Minesota International Hydraulics Convention, 1953.

2) M. Honma and K. Horikawa; A Study of Submerged Breakwater, Coastal Eng. in Japan, Vol. 4, 1961.

3) J.B. Herbich, H D. Murphy and B.V. Weele; Scour of Flat Sand Beaches due to Wave Action in front of Sea Walls, Conf. on Coastal Eng. in Santa Barbara, 1965.

4) T. Sawaragi; Scouring due to Wave Action at the Toe of Permeable Coastal Structure, 10th Conf. on Coastal Eng. in Tokyo, 1966.

5) S. Sato, N. Tanaka and I. Irie; On the Utilization of Radio-Active Tracers for the Sand Drift Experiments, Tech. Note of P.H.R.I., No.13, 1964. (in Japanese).

6) Shore Protection Planning and Design, Tech. Report No.4, B.E.B.

7) R.J. Barrett, Use of Plastic Filters in Coastal Structures, 10th Conf. on Coastal Eng. in Tokyo, 1966.

8) S. Tato and N. Tanaka; Field Investigation on Sand Drift at Kashima Facing to the Pacific Ocean, 10th Conf. on Coastal Eng. in Tokyo, 1966.

CHAPTER 38

PATTERN OF WAVE-INDUCED EROSION UNDER CAISSON-TYPE BREAKWATER

P. Donnelly, Head, Marine Structures Section, Department of Public Works, Ottawa, Canada

and

Richard Boivin, Senior Hydraulic Engineer, Lasalle Hydraulic Laboratory Limited, Montreal, Canada

ABSTRACT

When caisson-type breakwaters or wharves are built in areas exposed to severe wave attack, adequate precautions must be taken to ensure that all parts of the foundations are protected from erosion The joint between abutting caissons is a particularly vulnerable location

This paper describes patterns of erosion which may be expected at joints between caissons resting on sand or gravel foundations for a number of joint configurations The results are based on model studies Criteria are given for estimating scouring velocities through joints and sizes of particles moved Suggestions are made for minimizing the risk of erosion An example of erosion under a prototype structure is given

INTRODUCTION

One of the advantages of the rubble or similar type of breakwater is its relative immunity against suddenly disastrous damage under wave attack For these types of structure, the choice of design criteria are not quite so critical as in the case of wave reflecting, gravity structures such as reinforced concrete caissons or cribs which are to be founded on a sea bed which is not resistant to scour

A foundation failure beneath a gravity type structure can result in either complete collapse or excessive settlements The causes of foundation failure are usually inadequate bearing capacity of the underlying soil strata or scour of foundation material by waves or currents Even if the structure does not collapse, the excessive settlements which may occur reduce the effectiveness of the breakwater because

- overtopping is likely to be increased
- joints in the structure are opened up
- movements of deck traffic may be adversely affected
- appearance of the structure suffers

Repairs to such a structure tend to be expensive. Hence a relatively conservative approach to the design of caisson-type breakwaters is warranted and extra attention should be paid to the foundations

PROTOTYPE FOUNDATION PROBLEMS

This investigation was initiated to clarify the mechanism by which extensive foundation damage was caused to a recently installed prototype installation. Fig 1 illustrates the settlement of the prototype which occurred during the first year after complete construction

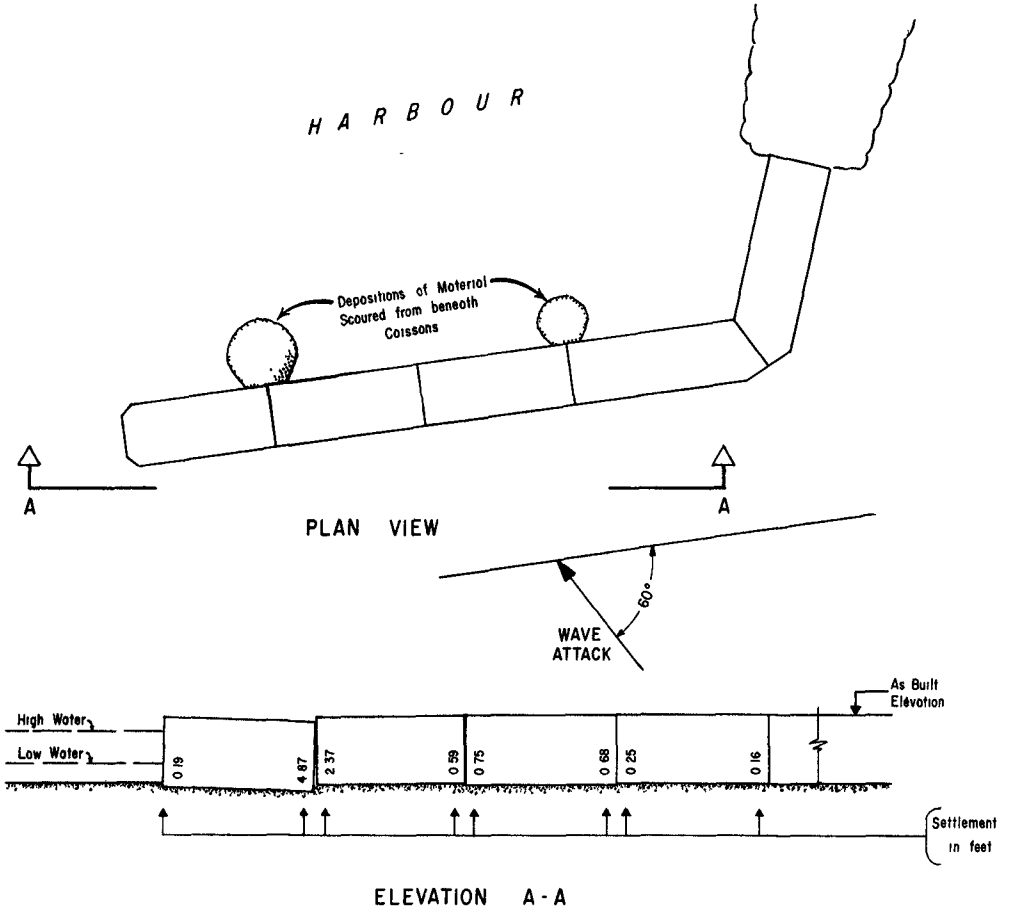

FIG. 1 SETTLEMENT OF PROTOTYPE DURING FIRST YEAR AFTER CONSTRUCTION.

It was suspected that the problem was caused by erosion by wave action of the foundations which began at an inadequately closed joint between abutting caissons and extended progressively under the caissons A laboratory study was undertaken to

(a) Obtain a better insight into the erosion phenomenon,

(b) Devise the most effective way to prevent this problem in future installations,

(c) Assist in the design of an appropriate repair method for the damaged structure.

EXPERIMENTAL STUDY OF EROSION PATTERNS

Some of the tests were carried out in a 2 ft wide wave flume where erosion patterns were studied at a joint between abutting caissons under perpendicular wave attack Additional tests were performed in a 16 ft wide wave flume on a partial model of the prototype structure where erosion patterns were studied under wave attack inclined at an angle of 60° from the face of the structure, which corresponded to the direction of predominant wave attack in the prototype

For all tests, the wave period was kept constant at 9 0 seconds The depth of water at the structure was 30 feet, although a few tests were run in the 16 ft wide flume for water depths of 12 feet (prototype dimensions, based on the Froude law, are used throughout this paper)

A sample of the test results are shown in Fig 2

The scour patterns shown in Fig 2(a) were obtained in the 2 ft flume with 4 foot incident waves acting 2½ hours, the bed material had the same critical speed of erosion as coarse sand (0 5 mm) does in the prototype Quite similar patterns resulted from tests carried out at a 6¼ foot incident wave height and with a bed material which behaved the same from the point of view of critical speed of erosion as 2 inch gravel in the prototype

Although the period of time of 2½ hours corresponded in no way to an "equilibrium state" in the erosion process, widespread damage had resulted even from a relatively light wave action The erosion was not confined to the joint itself, but extended several feet away from it, underneath the caissons

The tests conducted in the 16 ft wide flume, under oblique wave attack, led to similar scour patterns, as evidenced in Fig 2 (b)

The fluid motions in the joints between caissons was observed visually in the 2 ft wave flume A complex wave motion prevailed, made up of an incident wave component coming from the seaward face, which combined with a reflected component from the harbour side, the phase lag between the two wave components depending on the incident wave period and on the width of the caisson In each of the two tests series carried out in the 2 ft flume it was noted that if the incident wave which initiates erosion at the node of the clapotis ia H, the eroaion in the joint commences for an incident wave of approximately 0 75H Since the nodal velocity varies linearly with the wave height the velocity through an open joint may be estimated at approximately 25% higher than the nodal velocity in the clapotis existing in front of the structure. Thus as a first approximation for perpandicular wave attack·

$$V = 1.25 \left(\frac{2\pi H}{T}\right) \left(\frac{1}{\sinh 2\pi d/L}\right) \qquad (1)$$

No success was achieved with tentative mathods of sealing the jointa, such as a single key placed eithar at the seaward or at the harbour faca of the joint, or a double key arrangement (one at aach face of the caisson). Evan when tha keya were drivan into the foundation soils, piping daveloped around the edge of the keys and lad progressively to the erosion patterns shown in Fig. 2.

Howaver, a double key arrangament with fill placed in tha apaca batween tha keys, as shown in Fig. 4 (insert) performed succesafully, both in the 2 ft. and 16 ft. wave flumea. When granular material is employed as fill a minimum height is needed in order to prevant piping. Piping affects are proportional to the affactive differential head, ΔZ, at tha bottom of tha clapotia.

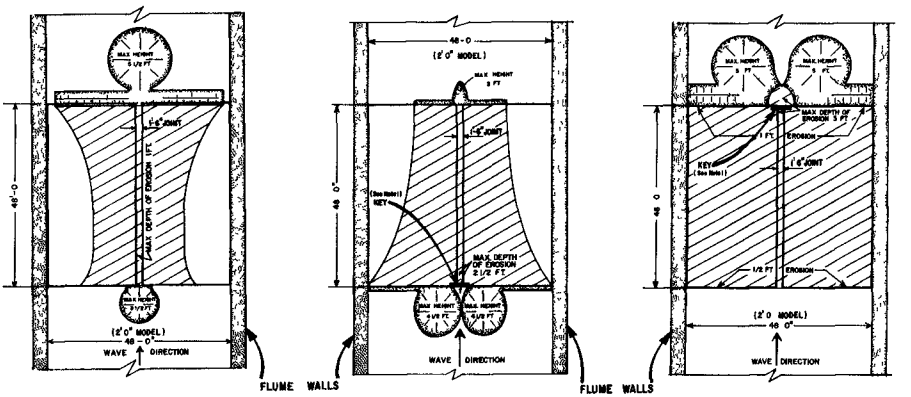

(a) TESTS IN 2FT WIDE WAVE FLUME

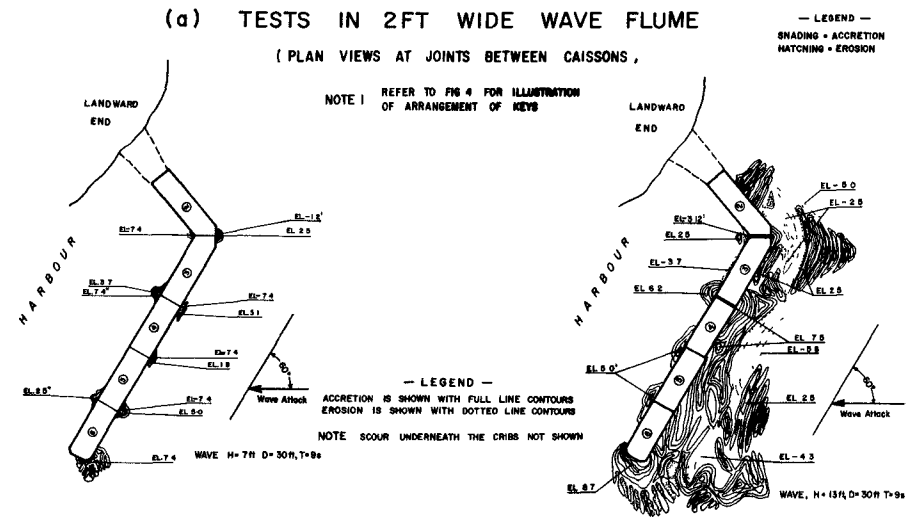

(b) TEST IN 16FT WIDE WAVE FLUME

(PLAN VIEWS OF PARTIAL MODEL OF PROTOTYPE)

Fig. 2 SAMPLE OF TEST RESULTS SHOWING EROSION PATTERNS

Using

$$\Delta Z = H/\cosh 2^{\pi} d/L \qquad (2)$$

it was found that the height, h, of granular fill required to prevent piping could be estimated with sufficient accuracy from the expression

$$h = 2H/\cosh 2^{\pi} d/L \qquad (3)$$

For coarser types of gravel fill with suitable filters, this height could safely be reduced by 30% - 40%

Figures 3 and 4 are graphical representations of equations (1) and (3) respectively Figure 4 also shows the critical speed of erosion of various sizes of foundation materials based on a typical equation (Ref 1) for critical speed of erosion of particles of diameter, D, larger than the laminar boundary layer

$$Vc = 1\ 75\sqrt{(S-1)\ g\ D} \qquad (4a)$$

$$\text{or } Vc = 3\ 68\sqrt{D} \qquad (4b)$$

where Vc = velocity in feet per second

D = diameter in inches of a spherical stone whose unit weight is 165 lbs per cubic foot

Figure 3 provides a convenient means of making a quick preliminary check to determine if an erosion problem can be anticipated

The investigation did not include study of the effect of variation of the gap width between caissons The tests are considered representative of the gaps which might be expected in normal construction practice i e in the range of 6 inches to 3 feet For wider gaps between caissons, lower velocities, on the average, could be expected

CONCLUSIONS

1. For caisson-type structures exposed to wave action, the most vulnerable part, as far as erosion of the foundations is concerned, is at joints between abutting caissons For direct wave attack, the velocity through an open joint may be estimated approximately by equation (1) Unless the material in the joint is coarse enough to resist this scouring velocity, erosion problems will occur Fig. 3 can be used to make a quick preliminary check to determine if an erosion problem can be anticipated

2 In practice, joints between abutting caissons should be effectively sealed if erosion problems are to be avoided To seal the joint, two keys are necessary one on the seaward side and one on the harbour side, with a suitable fill material placed in the space between the keys If a granular fill is used, it should be placed to a minimum height given by equation (3) to prevent piping underneath and around the sides of the individual keys For coarser types of gravel fill with suitable filters, the height given by equation (3) could safely be reduced by 30% - 40%

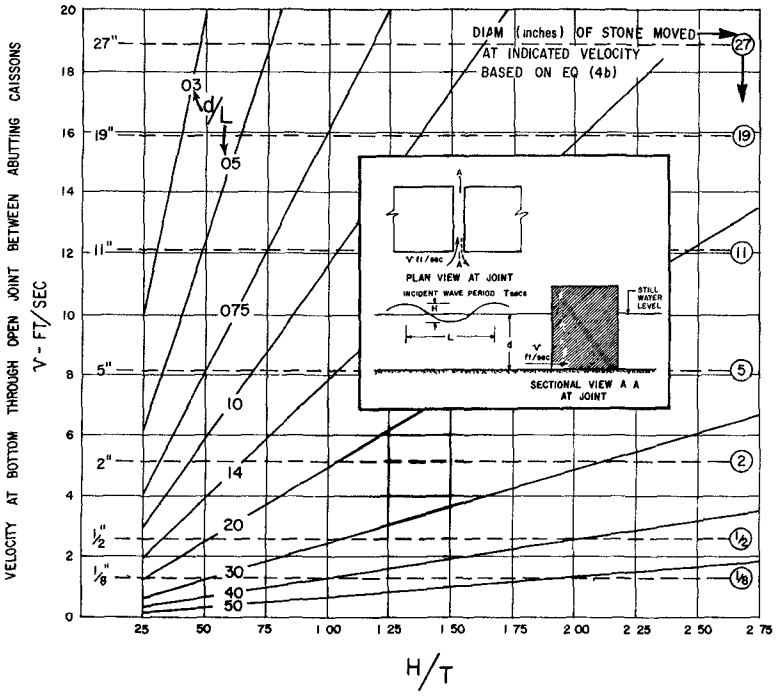

FIG 3 BOTTOM VELOCITY THROUGH OPEN JOINT BETWEEN ABUTTING CAISSONS, AND SIZES OF STONE ERODED, AS A FUNCTION OF WAVE CONDITIONS

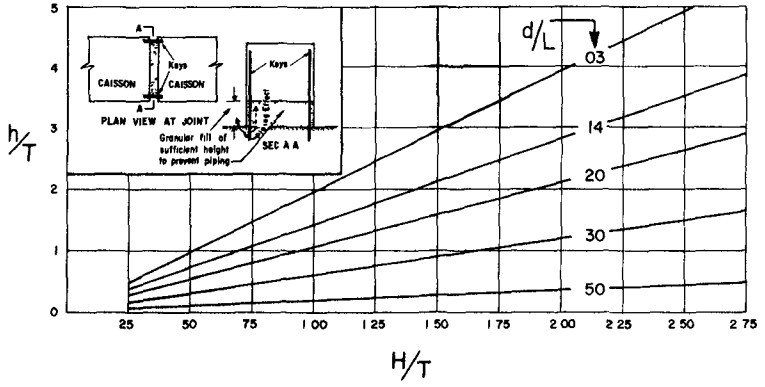

FIG 4 HEIGHT OF GRANULAR FILL IN JOINT BETWEEN ABUTTING CAISSONS TO PREVENT EROSION AND PIPING

REFERENCES

GODDET, J and JAFFRY, P – *La Similitude des transports de sédiments sous l'action simultanée de la houle et des courants* – *LA HOUILLE BLANCHE* NO 2, 1960 p p 136-147

APPENDIX – NOTATION

LIST OF SYMBOLS AS USED IN THIS PAPER

Symbol	Definition	Units
d	depth of water below the still water surface	ft
D	Diameter of rock particle	ft or ins
g	gravitational acceleration (– 32 2 ft/sec ^{2})	ft/sec ^{2}
h	height of granular fill in joint between abutting caissons	ft
H	wave height, amplitude, height of incident wave	ft
L	wave length	ft
S	Specific gravity of a rock particle	
V	wave induced bottom velocity in an open joing between abutting caissons	ft/sec
Vc	velocity which initiates motion of a particle of diameter, D, larger than the laminar boundary layer	ft/sec
ΔZ	differential pressure on the bottom cause by a totally reflected incident wave (clapotis)	ft

CHAPTER 39

CLOSELY SPACED PILE BREAKWATER AS A PROTECTION STRUCTURE AGAINST BEACH EROSION

Taizo HAYASHI, Professor
Masataro HATTORI, Associate Professor
Department of Civil Engineering
Chuo University, Tokyo

and

Masujiro SHIRAI, Research Engineer
Taisei Construction Company, Ltd., Tokyo

ABSTRACT

The theory for the transmission and reflection of the waves at the closely spaced pile breakwater has been developed by the use of shallow water wave theory of small amplitude. Experiment on the hydraulic characteristics of the breakwater has been performed in a two dimensional wave flume. The agreement between the theory and the experiment is pretty good with respect to the coefficients of transmission and reflection of waves, and also to the shoreward velocity of the jet discharged from a space between any two adjacent piles.

Experiment was also made on the local scouring at the foot of the clocely spaced pile breakwater. The maximum scouring depth at the foot of the breakwater relates closely to the ratio of the velocity of the jet to the mean fall velocity of bed material. The relation between the maximum scouring depth and the power of the jet is discussed.

INTRODUCTION

Closely spaced pile breakwater is a type of offshore breakwater which consists of a row of steel or concrete piles driven into the sea bottom. In a previous paper the authors presented the theory on the hydraulic characteristics of the breakwater [1]. The present paper deals with the following two subjects:

1. Modification of the authors' previous theory of the coefficients of transmission and reflection of waves on the assumption that the waves near the breakwater are shallow water waves of small amplitude.
2 Experimental study on the local scouring at the foot of the breakwater and on the function of the breakwater against beach erosion.

THE COEFFICIENTS OF TRANSMISSION AND REFLECTION OF WAVES

Theoretical Consideration

The problem under consideration is in the two dimensional case when waves approach normally to a breakwater. The coordinate system and notations used are shown in Fig. 1. Denoting the coefficients of transmission and reflection of waves by r_T and r_R, respectively, they can be determined as follows (see Appendix):

$$r_T=4\frac{h}{H_I}\varepsilon\frac{a^2kh}{\alpha\tanh kh}\left[-\varepsilon+\sqrt{\varepsilon^2+\frac{H_I}{2h}\frac{\alpha\tanh kh}{a^2kh}}\right] \qquad \cdots\cdots\cdots\cdots(1)$$

$$r_R=1-r_T \qquad \cdots\cdots\cdots\cdots(2)$$

Here,

$$\varepsilon=\frac{Cb}{D+b}\Big/\sqrt{1-\left(\frac{b}{D+b}\right)^2} \qquad \cdots\cdots\cdots\cdots(3)$$

$$\alpha=4\int_0^{\frac{1}{4}}\sqrt{\sin 2\pi\xi}\,\sin 2\pi\xi\,d\xi=1.1139\approx 1.1 \qquad \cdots\cdots\cdots\cdots(4)$$

$$\alpha=\int_{-h}^{0}\left(\frac{v}{\bar{v}}\right)^3\frac{dz}{h}=\left(\frac{kh}{\sinh kh}\right)^2\left(1+\frac{\sinh^2 kh}{3}\right) \qquad \cdots\cdots\cdots\cdots(5)$$

C is the coefficient of discharge of each space of the breakwater, V is the water particle velocity in the x-direction, and $\bar{V}$ is the averaged value of V with respet to water depth.

The velocity of the jet discharged from a space between any two adjacent piles at the instant of collision of the crest of an incident wave against the breakwater can also be determined as follows (see Appendix):

$$V=C_v\sqrt{\frac{2g}{\alpha}H_I(1-r_T)\Big/\left\{1-\left(\frac{b}{D+b}\right)^2\right\}}\,\frac{kh}{\tanh kh}\,\frac{\cosh k(h+z)}{\cosh kh} \qquad \cdots\cdots\cdots\cdots(6)$$

in which C_V is the coefficient of velocity of the jet. In the special case when h/L tends to zero, i. e., in the case of long waves, Eqs. (1) and (6) reduce to the following equations:

$$r_T=4\frac{h}{H_I}\varepsilon a^2\left[-\varepsilon+\sqrt{\varepsilon^2+\frac{H_I}{2h}\frac{1}{a^2}}\right] \qquad \cdots\cdots\cdots\cdots(7)$$

and

$$V=C_v\sqrt{\frac{2g}{\alpha}H_I(1-r_T)\Big/\left\{1-\left(\frac{b}{D+b}\right)^2\right\}} \qquad \cdots\cdots\cdots\cdots(8)$$

These two equations are the same to those given in the authors' previous paper [1].

The coefficients of transmission and reflection computed for various values of b/D, h/L and H_I/L are illustrated in Figs. 2 through 10.

Experiments

Experiments were made, like in the authors' previous paper, in a two dimensional wave flume, 30m long, 0.80m wide and 0.70m deep. The model breakwater consisted of 60.5mm diameter steel pipes

The heights of incident waves and transmitted waves were measured by conventional resistance-type wave height gauges and were recorded with an oscillograph. The coefficient of reflection of waves was calculated by the use of the formula, $r_R=(H_{max}-H_{min})/(H_{max}+H_{min})$, in which H_{max} and H_{min} are the amplitudes of standing waves at the antinode and at the node, respectively. These maximum and minimum amplitudes of standing waves were read on the oscillograph records of the vertical movement detected by a wave height gauge moving along the flume axis at a constant speed.

The comparison between the theory and the experiment with respect to the coefficients of transmission and reflection are shown in Figs. 11 and 12. It is seen from these figures that the agreement between the theory and the experiment is pretty good.

Figure 13 illustrates the vertical distribution of velocity of the jet discharged from a space of piles, together with the theoretical value calculated by Eq. (6). It is seen from this figure that the experimental value for the shoreward jet velocity agrees fairly well with the theory.

The difference between the shoreward and the seaward jet velocities may be attributed to the nonlinear effect of the partial clapotis generated on the seaside of the breakwater. This velocity difference plays an important role in the transport of suspended sediment. The bed material is suspended by the action of the partial clapotis at the breakwater and is carried into the nearshore zone through the spaces of piles by the prevailing current caused by this velocity difference. This phenomenon gives the closely spaced pile breakwater the function of a protection work against beach erosion.

Russell made a series of experiments on the effect of an offshore permeable screen erected on a two dimensional model beach [2]. The screen consisted of either single row or double rows of 1/2 in pipes, their space ratio having been 0.21 and 0.25, respectively. His experiments showed that, although the erection of a permeable screen did reduce the rate at which any erosion proceeded, it did not cause either a beach that was eroding, or even a beach that was substantially stable, to build up. This result, however, may be attributed to the large space ratios of the screens in his case, the coefficient of transmission of waves for these space ratio being read from Fig. 2-10 to be 0.6-0.8.

LOCAL SCOURING AT THE FOOT OF THE CLOSELY SPACED PILE BREAKWATER

The sea bed in the vicinity of offshore structures tends to be scoured by the action of waves and wave induced currents. The slumping of offshore struc-

tures caused by the effect of local scouring lowers their function as shore protection works. An essential question on the closely spaced pile breakwater is how to protect the breakwater from the local scouring at its foot and how to predict the depth of local scouring. Experimental study was made from this point of view on the local scouring at the foot of the closely spaced pile breakwater.

Experimental Equipment

The wave flume and the model breakwater used for this experiment were the same to those described in the previous section.

The bed material used was either amberlite or expanded shale, a kind of artificial light weight fine aggregate. The properties of these two kinds of bed material are shown in Table 1. The bed material was placed in a uniform thickness of about 22cm above the wave flume bottom, of a range of 2.5m long seaward and 1.5m shoreward from the model breakwater.

The water depth and the period of incident waves, in all runs, were 29.1cm and 1.7sec, respectively. The bed configuration in the vicinity of the breakwater, which configuration was induced by wave action, was observed and measured visually through a side wall of the wave flume.

During a test run, the period of the continuous driving of the wave generator was limited within 20 - 30 sec in order to eliminate the effect of the rise of the water level in the inshore zone to the breakwater. This operation procedure of the wave generator was repeated until the variation of the bed configuration reached a condition of equilibrium.

Experimental Results and Discussions

By dimensional consideration the maximum scouring depth at the foot of the closely spaced pile breakwater can be expressed by the following equation:

$$\Delta_m/D=f(H_I/L,\ h/L,\ b/D,\ \bar{V}/\sqrt{(s-1)gd}) \qquad \text{.....(9)}$$

in which Δ_m is the maximum scouring depth at the foot of the breakwater, $\bar{V}$ is the value averaged with respect to water depth, of the velocity of the jet discharged shorewards from a space of piles, and s and d are respectively the specific weight and the mean diameter, of bed material.

According to the previous researches [3] [4] on the bed scouring by jet flows, $\bar{V}/\sqrt{(s-1)gd}$ is the most important parameter in equation (9).

Figure 14 illustrates the experimental results of the relation between the relative maximum scouring depth and $\bar{V}/\sqrt{(s-1)gd}$. It is seen from this figure that the relative maximum scouring depth can approximately be expressed by a linear function of $\bar{V}/\sqrt{(s-1)gd}$. Within the range of this experiment, the maximum scouring depth at the foot of the closely spaced pile breakwater seems to reach 1.5 - 2.0 times of the diameter of piles.

Figure 15 illustrates the relation between the relative maximum scouring

depth and the wave steepness of incident waves. In this figure, the maximum scouring depth for the space ratio of 0.075 is larger than those for 0.041 and 0.200.

The power of the jet velocity per unit length of the breakwater is expressed by

$$P=w\overline{V}\frac{C_c b}{D+b}h\left\{\frac{H_I}{2}+\frac{H_R}{2}-\frac{H_T}{2}\right\}=w\overline{V}\frac{C_c b}{D+b}h\,H_I\,r_R \qquad \cdots\cdots\cdots(10)$$

Substituting Eq. (8) into Eq. (10) and taking account of Eq. (3), we obtain the following equation:

$$P=w\,\epsilon(1-r_r)^{3/2}h\sqrt{2gH_I^3/\alpha} \qquad \cdots\cdots\cdots(11)$$

From this equation, the value of the space ratio of piles for which the power of the jet becomes maximum is determined as

$$\epsilon=\frac{1}{4\alpha}\sqrt{\alpha\frac{\tanh kh}{kh}\frac{L}{h}\frac{H_I}{L}} \qquad \cdots\cdots\cdots(12)$$

Figure 16 illustrates this relation in the case of h/L = 0.109. It is read from this figure that, when H_I/L = 0.01~0.035, the range of the space ratio b/D for which the power of the jet attains maximum is 0.07~0.13. This fact gives physical interpretation why the relative maximum scouring depth for the space ratio of 0.075 is larger than the relative maximum scouring depths in the other two cases shown in Fig. 15.

CONCLUSION

The theory on the transmission and reflection of waves at the breakwater has been developed by the use of shallow water wave theory of small amplitude. The coefficients of transmission and reflection of waves have been obtained as Eqs. (1) and (2), which are illustrated in Figs. 2 through 10.

As to the velocity of the jet discharged from a space between any two adjacent piles, experiment shows that shoreward velocity is larger than seaward velocity. This phenomenon gives the closely spaced pile breakwater the function as a protection work against beach erosion.

The maximum scouring depth at the foot of the breakwater is closely related to the ratio of jet velocity to the mean fall velocity of the bed material, this relation being shown in Fig. 14. The maximum scouring depth seems to attain 1.5~2.0 times of the diameter of piles.

The relation between the maximum scouring depth and the wave steepness of incident waves is shown in Fig. 15. The space ratio of piles for which the maximum scouring is theoretically supposed to occur has been obtained as Eq. (12).

LITERATURE REFERENCES

[1] Hayashi, T., M. Hattori, T. Kano and M. Shirai, Hydraulic Research on the Closely Spaced Pile Breakwater, Proc. of 10th Conference on Coastal Engineering, 1961, Chapter 50, pp. 873-884.
[2] Russell, R.C. H., The Influence of An Offshore Permeable Screen on A Two-Dimensional Model Beach, Proc. of 6th General Meeting of I.A.H.R., Vol. 1, 1955, pp. A 5-1 - A 5-6.
[3] Rouse, H., Criteria for Similarity in the Transportation of Sediment, Proc. of Hydraulic Conference, University of Iowa Studies in Engineering, Bulletin 20, 1940, pp. 33-49.
[4] Kurihara, M. and T. Tsubaki, On the Bed Scouring by Horizontal Jet, Report of Research Institute for Applied Mechanics, 1954, No. 4.

APPENDIX. DERIVATION OF EQS. (1), (2) AND (6)

The problem under consideration is in a two dimensional case when waves approach normaly to a breakwater. The coordinate system and the notations are shown in Fig. 1. We assume that the waves near the breakwater are shallow water waves of small amplitude. Then, the mean horizontal velocities of water particles induced by an incident wave, a reflected wave and a transmitted wave are respectively given as follows.

$$\bar{v}_I=\frac{H_I}{2}\frac{g}{\sigma_I h}\tanh k_I h \sin(\sigma_I t-k_I x) \qquad \cdots\cdots\cdots(A\cdot1)$$

$$\bar{v}_R=-\frac{H_R}{2}\frac{g}{\sigma_R h}\tanh k_R h \sin(\sigma_R t+k_R x) \qquad \cdots\cdots\cdots(A\cdot2)$$

and

$$\bar{v}_T=\frac{H_T}{2}\frac{g}{\sigma_T h}\tanh k_T h \sin(\sigma_T t-k_T x) \qquad \cdots\cdots\cdots(A\cdot3)$$

in which H is the wave height, $k = 2\pi/L$ is the wave number, $\sigma = 2\pi/T$ is the wave angular frequency, L is the wave length, T is the wave period, g is the acceleration of gravity, I,R and T are the suffixes referring respectively to an incident wave, a reflected wave and a transmitted wave, and an overscore means the averaged value with respect to water depth.

Neglecting the effect of the wave height at the breakwater, the equation of continuity becomes

$$\bar{v}_I h+\bar{v}_R h=\bar{v}_T h \qquad \text{at} \quad x = 0 \qquad \cdots\cdots\cdots(A\cdot4)$$

The mean velocity of the jet discharged from a space between any two adjacent piles is given by the Bernoulli's theorem as

$$\bar{V}=\pm C_v\sqrt{\frac{2g}{\alpha}(\eta_I+\eta_R-\eta_T)}\Big/\sqrt{1-\left(\frac{b}{D+b}\right)^2} \qquad \cdots\cdots\cdots(A\cdot5)$$

where V is the jet velocity, η is the vertical displacement of water surface from still water level ($z = 0$), C_V the coefficient of velocity of jet and α is the correction factor to compensate for use of mean velocity, α being given as

$$\alpha=\int_{-h}^{0}\left(\frac{v}{\bar{v}}\right)^2\frac{dz}{h}=\left(\frac{kh}{\sinh kh}\right)^2\left(1+\frac{\sinh^2 kh}{3}\right) \qquad \cdots\cdots\cdots(5)$$

On the other hand, the equation of continuity to be satisfied just at the back of the breakwater is written as follows:

$$C_c bh\overline{V}=(D+b)h\bar{v}_T \qquad \cdots\cdots\cdots(A\cdot 6)$$

in which C_C is the coefficient of contraction of a jet.

From Eqs. (A 1) through (A 6) and by the use of the assumption that $k_I = k_R = k_T = k$ and $\omega_I = \omega_R = \omega_T = \omega$ we can obtain the following equations.

$$r_T=\frac{H_T}{H_I}=4\frac{h}{H_I}\epsilon\frac{a^2kh}{a\tanh kh}\left[-\epsilon+\sqrt{\epsilon^2+\frac{H_I}{2h}\frac{a\tanh kh}{a^2kh}}\right] \qquad \cdots\cdots\cdots(1)$$

$$r_R=\frac{H_R}{H_I}=1-r_T \qquad \cdots\cdots\cdots(2)$$

and

$$V=C_v\sqrt{\frac{2g}{a}H_I(1-r_T)\Big/\left\{1-\left(\frac{b}{D+b}\right)^2\right\}}\,\frac{kh}{\tanh kh}\frac{\cosh k(h+z)}{\cosh kh} \qquad \cdots\cdots\cdots(6)$$

where

$$\epsilon=\frac{cb}{D+b}\Big/\sqrt{1-\left(\frac{b}{D+b}\right)^2} \qquad \cdots\cdots\cdots(3)$$

$$a=4\int_0^{\frac{1}{8}}\sqrt{\sin 2\pi\zeta}\,\sin 2\pi\zeta\,d\zeta=1\,1139=1\,1 \qquad \cdots\cdots\cdots(4)$$

and C is the coefficient of discharge of a jet.

Table 1. Properties of bed material.

Bed material	specific wt. in air	mean dia. of grains (mm)	mean fall velocity (cm/s)	angle of repose (tan θ)	
				In water	in air
Expanded shale	2.24	0.76	10.50	0 705	0.772
Amberlite	1 46	0.34	1.89	0 499	0 539

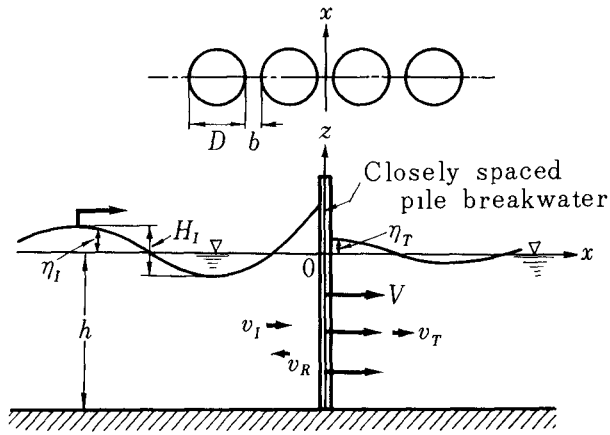

Fig. 1. Notations.

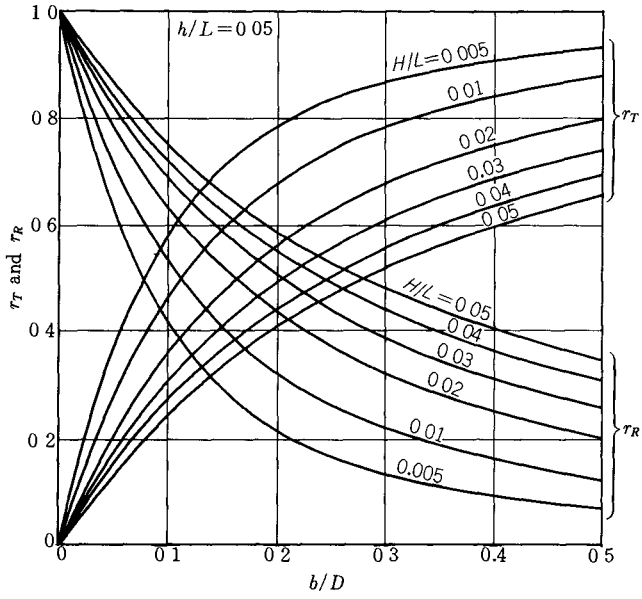

Fig. 2. Coefficients of wave transmission and wave reflection in the case of C = 1.

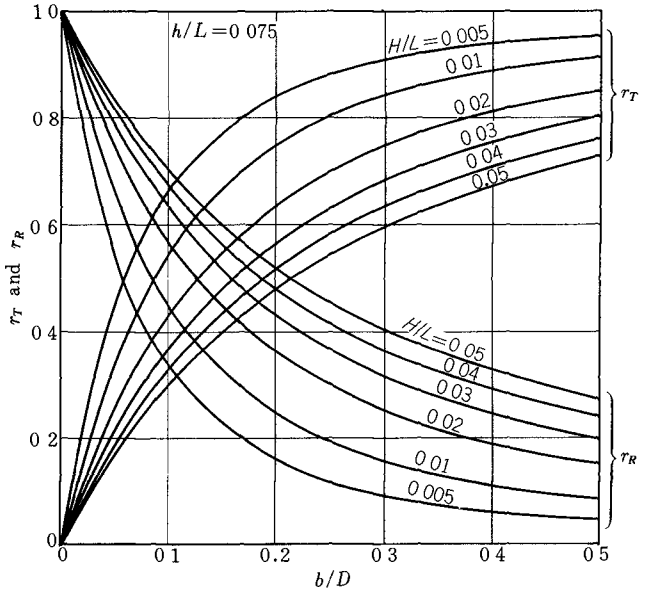

Fig. 3. Coefficients of wave transmission and wave reflection in the case of C = 1.

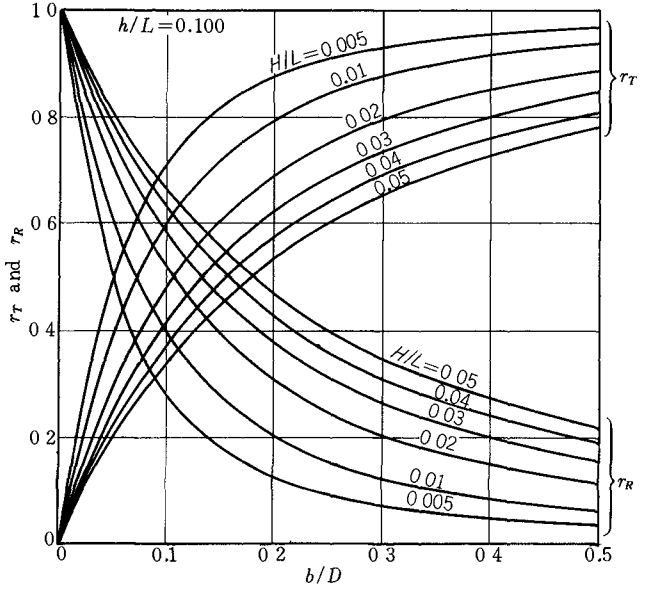

Fig 4. Coefficients of wave transmission and wave reflection in the case of C = 1.

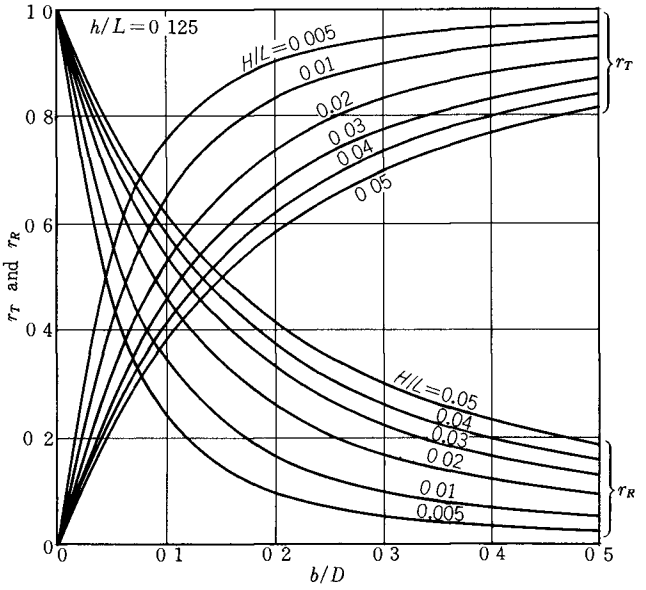

Fig. 5. Coefficients of wave transmission and wave reflection in the case of C = 1.

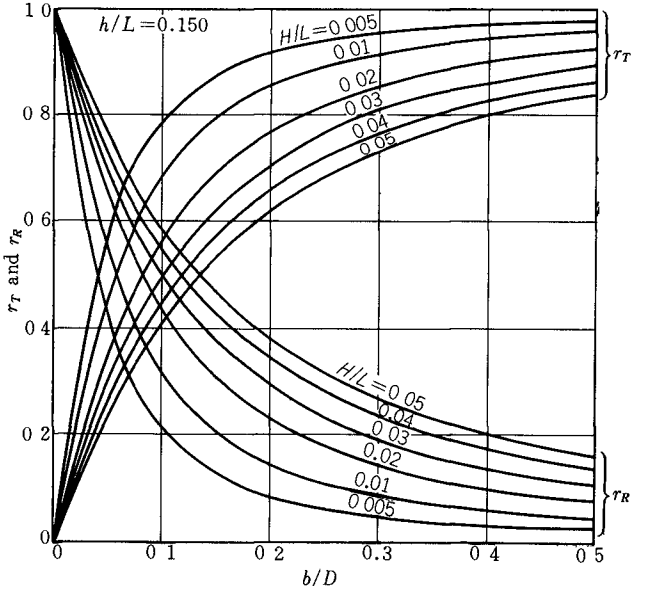

Fig. 6. Coefficients of wave transmission and wave reflection in the case of C = 1

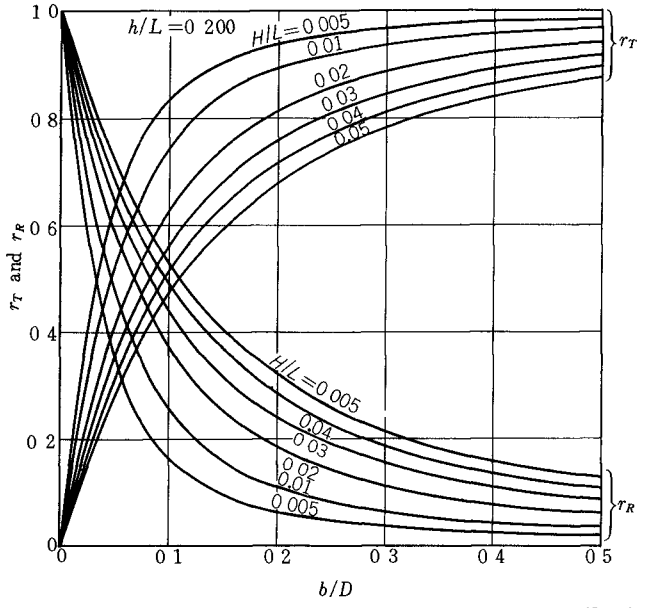

Fig. 7. Coefficients of wave transmission and wave reflection in the case of C = 1.

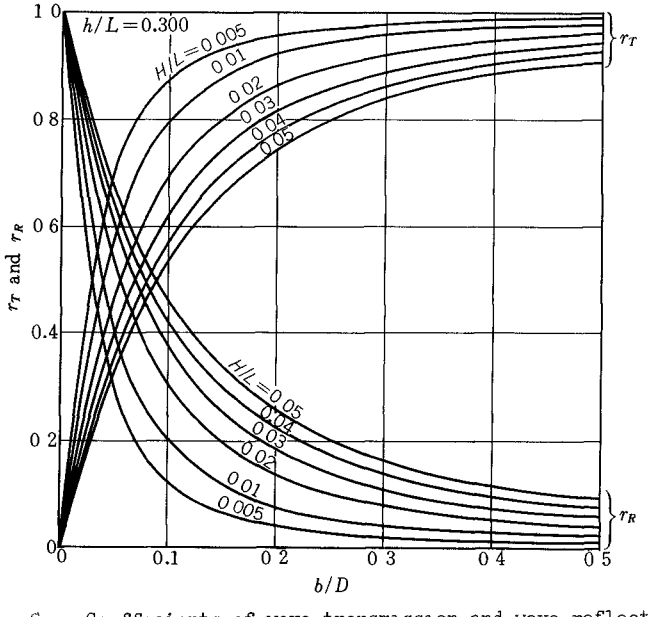

Fig 8. Coefficients of wave transmission and wave reflection in the case of C = 1.

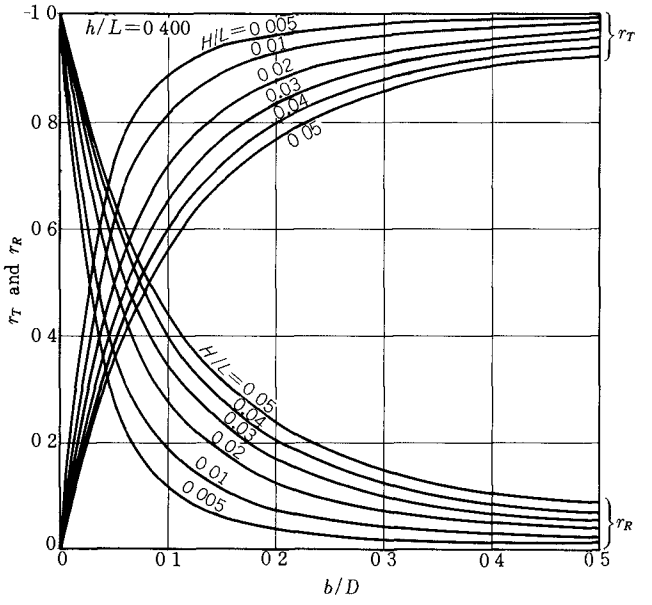

Fig. 9. Coefficients of wave transmission and wave reflection in the case of C = 1.

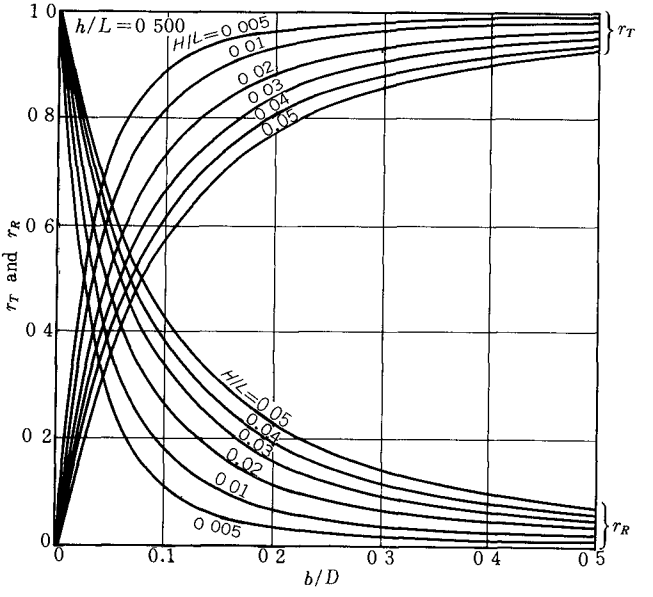

Fig. 10. Coefficients of wave transmission and wave reflection in the case of C = 1.

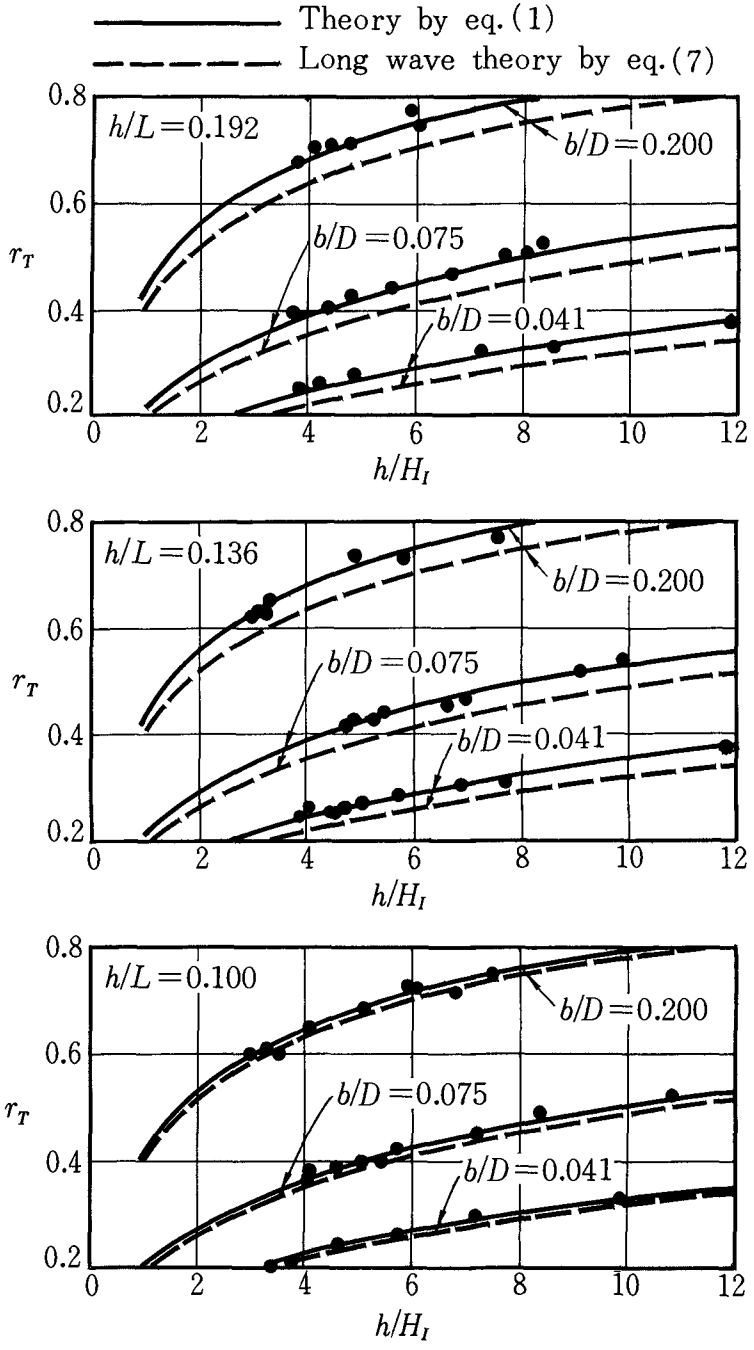

Fig. 11. Coefficients of wave transmission.

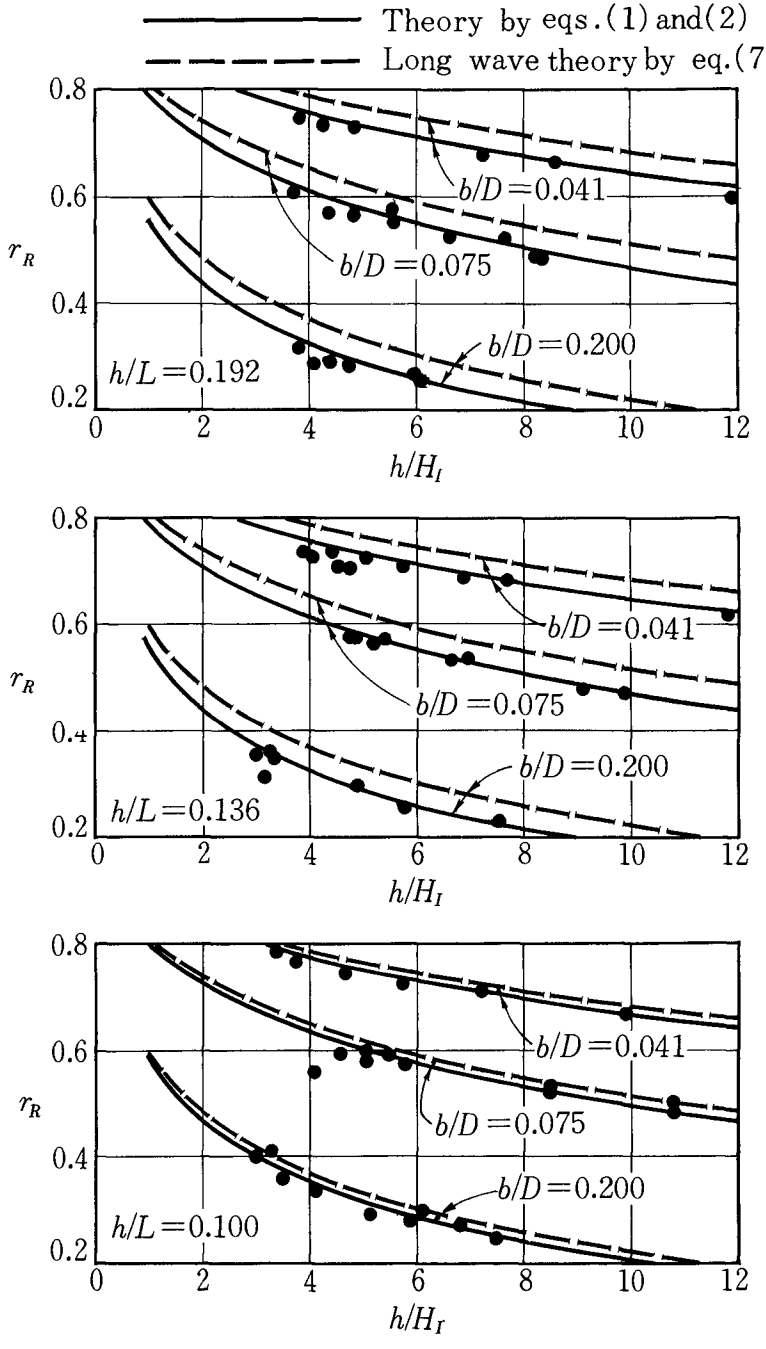

Fig 12. Coefficients of wave reflection.

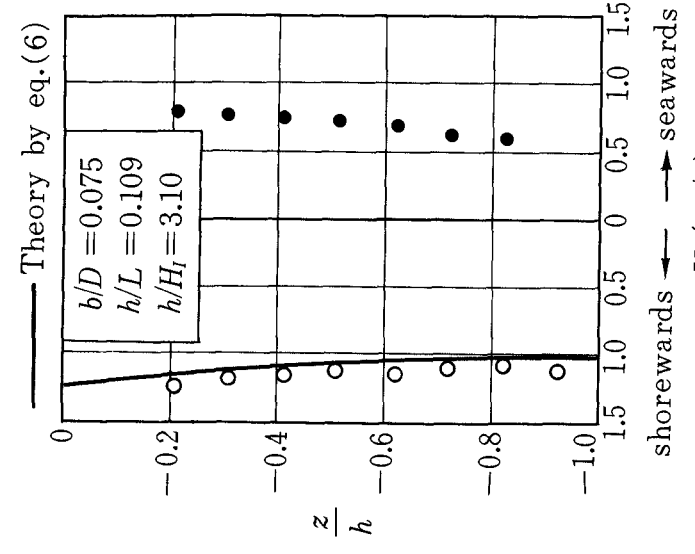

Fig. 13. The vertical distribution of jet velocity.

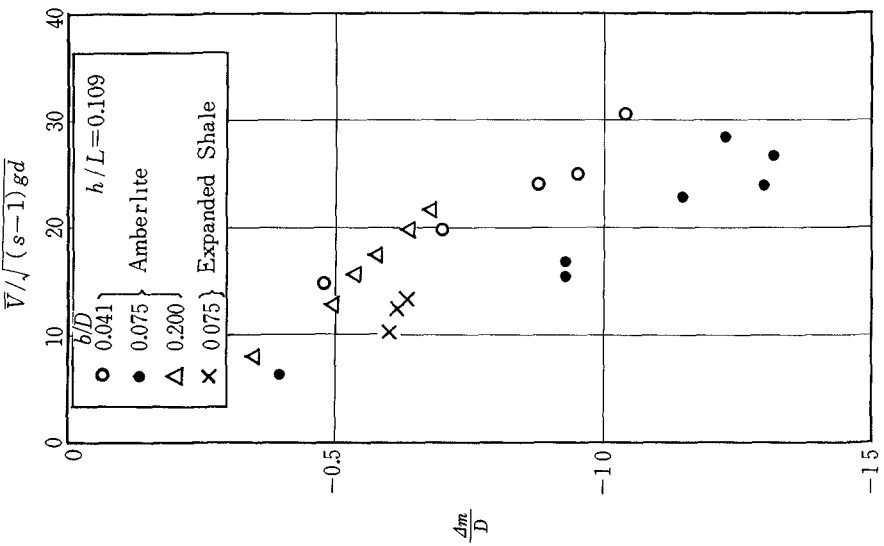

Fig 14 The jet velocity and the maximum scouring depth

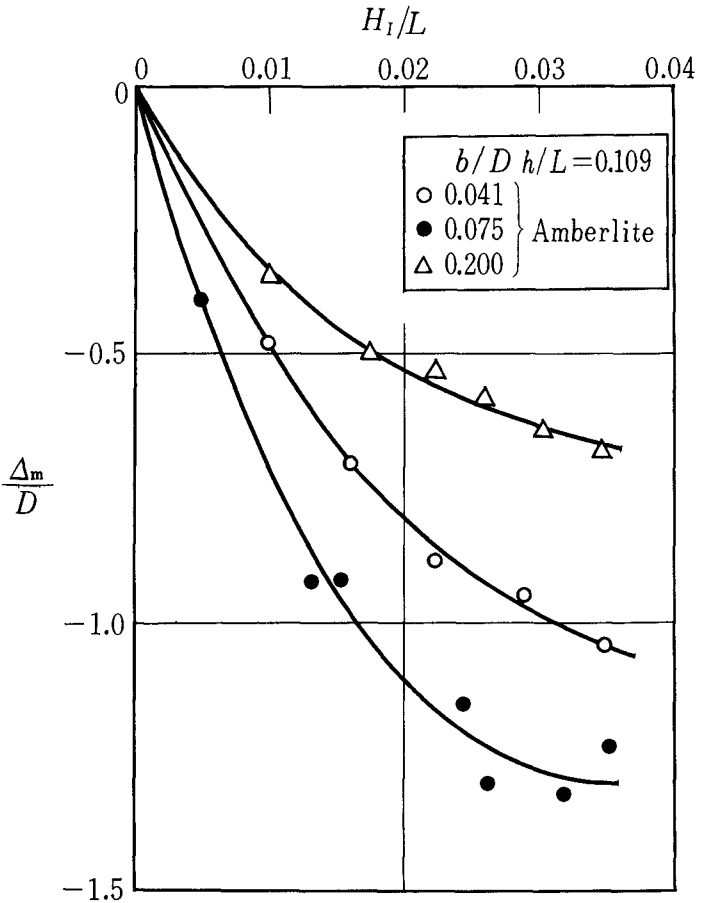

Fig. 15. The scouring depth and the wave steepness.

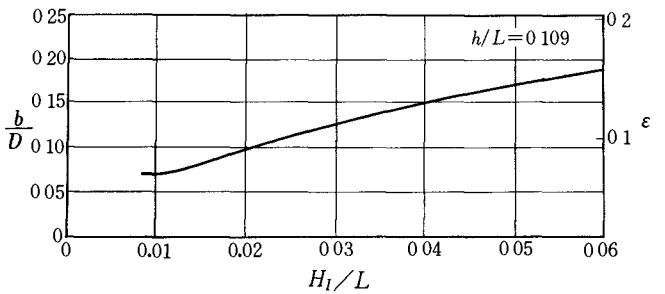

Fig. 16. The space ratio of piles making the scouring depth maximum.

CHAPTER 40

SCOUR OF SAND BEACHES
IN FRONT OF SEAWALLS

by
John B. Herbich, Ph.D., P.E.
Professor of Civil Engineering
Texas A&M University
College Station, Texas
and
Stephen C. Ko, M. S.
Research Instructor
Lehigh University
Bethlehem, Pennsylvania

ABSTRACT

Many previous studies were confined to problem of beach erosion due to waves breaking on the structure. The investigation reported here involved regular non-breaking, shallow water waves progressing toward a seawall. An analytical solution was developed and compared with laboratory-scale experiments.

The shallow-water wave theory and boundary layer equations were used in theoretical development, which resulted in a mathematical model for the ultimate scour depth in front of a seawall.

The theoretical equation for scour is as follows:

$$S = (D-1/2A)\left[(1-C_r)\ u^*\ (3/4\ C_D\ \rho\ \frac{\cot\theta}{d\ (\gamma_s-\gamma)})^{1/2} - 1\right]$$

where D = still water depth, $A = H_I + H_R$, H_I = incident wave height, H_R = reflected wave height, and $C_r = \frac{H_R}{H_I}$ = coefficient of reflection

also u^* = horizontal velocity within boundary layer, C_D = coefficient of drag, ρ = fluid density, θ = seawall slope angle, d = effective sand diameter, 50% finer, γ_s = specific weight of sand, and γ = specific weight of water.

The comparison between theoretically calculated values and experimental results indicates fairly good agreement. The model experiments also indicate that depth of scour depends to a large extend on wave characteristics and that scour length (distance between scour trough or crests) is independent of time, but is a function of incident wave length.

INTRODUCTION

Most of the studies in the past were confined to problems of beach erosion due to "breaking waves."

The investigation discussed here involved regular, water waves progressing toward a seawall. In such a case, waves may or may not break on the seawall, and the objective of the study was to investigate the nature of scour of a flat sand beach in front of a simple seawall. (Figure 1) Earlier part of the study was reported elsewhere(1)*.

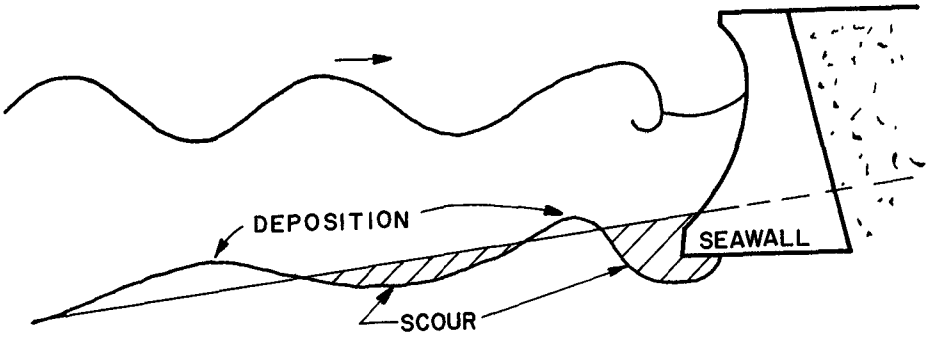

FIG. 1 DEFINITION SKETCH

When a system of oscillatory, incident waves progresses toward the seawall and hits the seawall, another system of waves if formed due to the reflection from the seawall. These two wave systems form a third wave system as the reflected wave is superimposed on the incident wave. The velocity components of the new wave system are given by the summation of the velocity component vectors of the incident and reflected waves. (Figure 2)

The theoretical development is based on the continuity equation and on boundary layer equations. The development resulted in a mathematical model which predicts the "ultimate" scour depth.

An experimental physical laboratory model was constructed and data on the "ultimate" scour depth were obtained.

---

* Numbers in parenthesis refer to references on page 20.

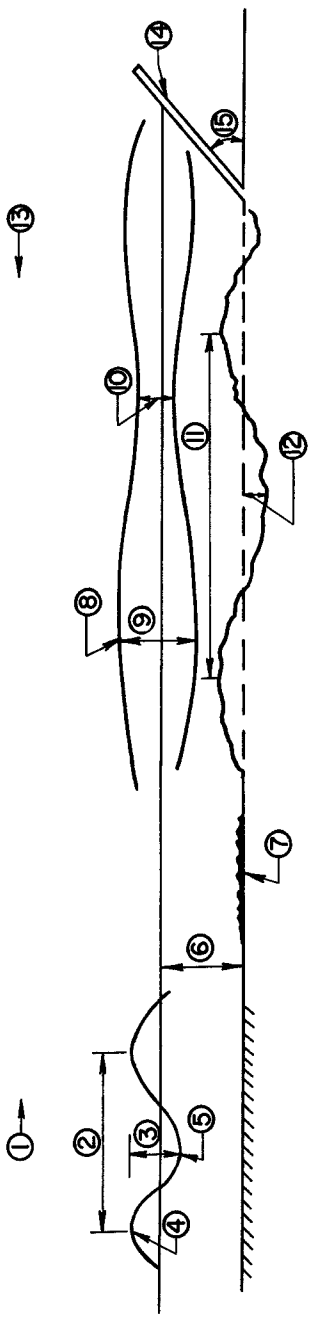

① Incident Wave
② Wave Length
③ Wave Height
④ Wave Crest
⑤ Wave Trough
⑥ Water Depth
⑦ Ripples
⑧ Envelope
⑨ Loop of Envelope
⑩ Node of Envelope
⑪ Sand Scour Length
⑫ Sand Scour Depth
⑬ Reflected Wave
⑭ Seawall
⑮ Angle of Seawall

FIGURE 2. SCHEMATIC EXPLANATION OF TERMINOLOGY

Reasonably good agreement was obtained between the mathematical and physical model.

THEORETICAL CONSIDERATIONS

Equation of Motion and Equation of Continuity - Assume that water wave motion is generated from rest by a horizontal force, and that the fluid pattern is irrotational and satisfies the velocity potential requirements. Under these assumptions two equations must be satisfied, namely, Euler's equation of motion and Laplace's equation of continuity.

Euler's equation of motion may be stated as follows:

$$-\frac{1}{\rho}\,\text{grad}\,p + \bar{F} = \frac{\overline{DV}}{Dt} \tag{1}$$

and the Laplace Equation may be written as:

$$\nabla^2 \bar{\psi} = \bar{\psi}_x^2 + \bar{\psi}_y^2 + \bar{\psi}_z^2 \tag{2}$$

or in two-dimensional cartesian coordinate form:

$$\frac{\partial^2 \psi}{\partial x^2} + \frac{\partial^2 \psi}{\partial y^2} = 0 \tag{3}$$

In addition, the following boundary conditions must be satisfied:

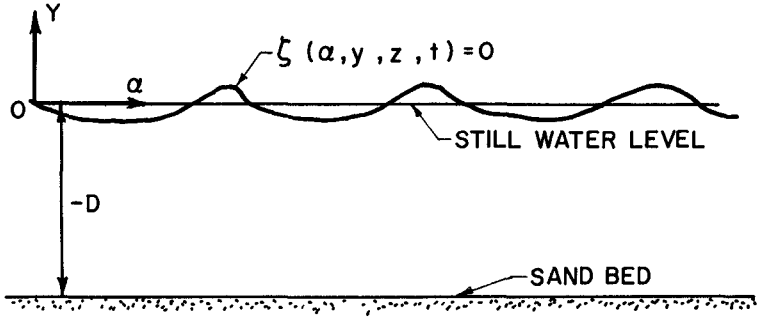

FIG. 3 GEOMETRY OF WAVE MOTION

The free surface of the water in contact with air can be defined by:

$$\xi\,(x,y,z,t) = 0 \tag{4}$$

Along the surface the pressure must be zero, so that,

$$-\frac{1}{\rho}\nabla p = 0 \tag{5}$$

Along the bottom, where y = -D, the water particles must remain in contact with it,

$$\frac{\partial \Phi}{\partial y} = -\frac{\partial \Phi}{\partial x} = 0 \text{ at } y = -D \tag{6}$$

In two-dimensions, Equation (1) can be written as:

$$\frac{du}{dt} = \frac{\partial u}{\partial t} + u\frac{\partial u}{\partial x} + v\frac{\partial u}{\partial y} = F_x - \frac{1}{\rho}\frac{\partial p}{\partial x} \tag{7}$$

or

$$\frac{1}{\rho}\frac{\partial p}{\partial x} = -\frac{\partial \Omega}{\partial x} - \frac{\partial u}{\partial t} - u\frac{\partial u}{\partial x} - v\frac{\partial u}{\partial y}$$

$$= -\frac{\partial \Omega}{\partial x} - \frac{\partial^2 \Phi}{\partial t \partial x} - \frac{1}{2}\left[\frac{\partial}{\partial x}\left(\frac{\partial \Phi}{\partial x}\right)^2\right] - \frac{\partial \Phi}{\partial y}\frac{\partial^2 \Phi}{\partial x \partial y}$$

$$= -\frac{\partial \Omega}{\partial x} - \frac{\partial^2 \Phi}{\partial t \partial x} - \frac{1}{2}\left[\frac{\partial}{\partial x}\left(\frac{\partial \Phi}{\partial x}\right)^2 + \frac{\partial}{\partial x}\left(\frac{\partial \Phi}{\partial y}\right)^2\right] \tag{8}$$

where Ω = gy positive for upward direction. Integrating Equation (8), we have,

$$\frac{P}{\rho} = -gh - \frac{\partial \Phi}{\partial t} - \frac{1}{2}\left[\left(\frac{\partial \Phi}{\partial x}\right)^2 + \left(\frac{\partial \Phi}{\partial y}\right)^2\right] \tag{9}$$

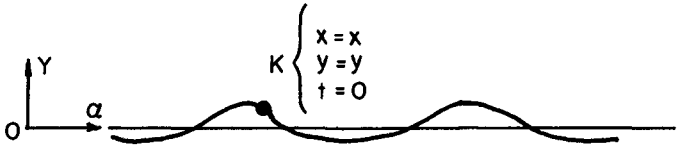

FIG. 4 FREE SURFACE OF WAVE MOTION

From Figure 4, consider a particle K on the surface. After an infinitesimal time δt, the particle will move to $x + \delta x$.

$$u\ \delta t = \delta x$$

$$\frac{\partial \Phi}{\partial x} = \frac{\delta x}{\delta t} \tag{10}$$

The corresponding pressure change will be,

$$\delta P = \frac{\partial p}{\partial t}\ \delta t + \frac{\partial p}{\partial x}\ \delta x + \frac{\partial p}{\partial y}\ \delta y \tag{11}$$

From Equation (10) and (11), we will have the condition of,

$$\frac{\delta p}{\delta t} = \frac{\partial p}{\partial t} + \frac{\partial \Phi}{\partial x}\frac{\partial p}{\partial x} + \frac{\partial p}{\partial y}\frac{\partial y}{\partial t} = 0, \text{ along free surface} \tag{12}$$

From Equation (9) and Equation (12), neglecting the second order of small values, we have,

$$g\frac{\partial \Phi}{\partial y} + \frac{\partial^2 \Phi}{\partial t^2} = 0, \text{ when } y = 0 \tag{13}$$

Equation (5), (6), (9), or (13) represent the boundary conditions for the wave motion.

Stokes' Wave With Finite Amplitude

Shallow water waves were first studies by Stokes (1880), he obtained the solution by expanding the velocity potential about the still water level. In this theory, it is not necessary to assume that amplitude and steepness are small. The final results are presented as nonlinear equations.

From Equation (4), the hydrostatic pressure of any water particle is,

$$P = \rho g\ (\xi - y) \tag{14}$$

where ρ is the density of water, g is the gravitational acceleration.

The differentiation of Equation (14) is,

$$\frac{\partial P}{\partial x} = \rho g \frac{\partial \xi}{\partial x} \tag{15}$$

From Equation (15), it is obvious that u, horizontal component of velocity, is independent of y.

The second order differentiation of Equation (15) will yield the horizontal component of acceleration which, again, is independent of y.

Up to this point in using the theoretical hydrodynamic concepts, no approximations have been made. It is obvious, that the important question is how to define the stream function Φ and free surface ξ.

Fourier's theorem, Jacobian elliptical function and complete elliptic integral have been used by many investigators as approximative approaches. In 1952, Biesel developed a second order approximation of potential function as

$$\Phi = \frac{HL}{2T}\frac{\cosh 2\pi(y + D)/L}{\sinh (2\pi D/L)} \sin 2\pi\left(\frac{x}{L} - \frac{t}{T}\right) + \frac{3}{16}\frac{H^2}{T}\frac{\cosh 4(y + D)/L}{\sinh^4 (\frac{2\pi D}{L})} \sin 4\pi\left(\frac{x}{L} - \frac{t}{T}\right) \qquad (16)$$

By differentiating Equation (16) with respect to x and Y, the velocity components of any particle are obtained

$$u = \frac{\partial \Phi}{\partial x}$$

$$u = \frac{\pi H}{T}\frac{\cosh \frac{2\pi(y + D)}{L}}{\sinh (2\pi D/L)} \cos 2\pi\left(\frac{x}{L} - \frac{t}{T}\right) + 3/4\left(\frac{\pi^2 H^2}{TL}\right)\frac{\cosh 4\pi(y + D)/L}{\sinh^4 (2\pi D/L)} \cos 4\pi\left(\frac{x}{L} - \frac{t}{T}\right) \qquad (17)$$

and, $$v = \frac{\partial \Phi}{\partial y}$$

$$v = \frac{\pi H}{T}\frac{\sinh 2\pi(y + D)/L}{\sinh 2\pi D/L} \sin 2\pi\left(\frac{x}{L} - \frac{t}{T}\right) + 3/4\left(\frac{\pi^2 H^2}{TL}\right)\frac{\sinh 4\pi(y + D)/L}{\sinh^4 (2\pi D/L)} \sin 4\pi\left(\frac{x}{L} - \frac{t}{T}\right) \qquad (18)$$

The free surface is

$$\xi = \frac{H}{2} \cos 2\pi \left(\frac{x}{L} - \frac{t}{T}\right) \frac{\pi H^2}{4L} + \frac{\pi H^2}{4L}$$

$$\frac{H^2}{4L} \left(1 + \frac{3}{2 \sinh^2 (2\pi D/L)}\right) \coth \frac{2\pi D}{L} \cos 4\pi \left(\frac{x}{L} - \frac{t}{T}\right) \tag{19}$$

Cnoidal Theory

In 1844, Russell described a different kind of wave called the "solitary wave", which represents a single disturbance, propagated essentially unaltered in form over long distance at a constant velocity. A few years later, Boussinesq (1871), (9) and Rayleigh (1876), (9) developed mathematical equations for its profile and velocity. In 1895, Korteweg and deVries modified Rayleigh's theory in such a way as to obtain waves that are periodic in profile and which tend to the solitary wave in the limiting case of long wave length. (The cnoidal theory).

The velocity components of any water particle in the water can be determined from

$$u = (\sqrt{gd}) \left[\frac{h}{D} - \frac{h^2}{4D^2} + \left(\frac{D}{3} - \frac{y^2}{2D}\right) \frac{\partial^2 h}{\partial x^2}\right] \tag{20}$$

$$v = (\sqrt{gd})\, y \left[\left(\frac{1}{D} - \frac{h}{2D^2}\right) \frac{\partial h}{\partial x} + \frac{1}{3} \left(D - \frac{y^2}{2D}\right) \frac{\partial^3 h}{\partial x^3}\right] \tag{21}$$

where

$$h = -D + y_t + H\, cn^2 \left[2K(k) \left(\frac{x}{L} - \frac{t}{T}\right), k\right] \tag{22}$$

where K(k) is the first kind of complete elliptical integral, defined as

$$K(k) = \int_0^{\pi/2} \frac{d\Phi}{(1 - k^2 \sin^2 \Phi)^{\frac{1}{2}}} \qquad 0 \leq k \leq 1$$

The free surface profile is

$$\xi = y_t + H\, cn^2 \left[2K(k)\ \left(\frac{x}{L} - \frac{t}{T}\right),\ k\right] \qquad (23)$$

A comparison of horizontal velocity components of water particles among the Linear Theory, Stokes Second Order Theory and Cnoidal Theory had been made by Wiegel (1960). (9)

The Mechanics of Sediment Movement

If the mean diameter of a sediment particle (50 per cent finer by weight) is d, and u_* is the local fluid velocity parallel to the bottom, then the drag force just sufficient to initiate movement of a particle in the bed is

$$F_D = C_D\ \rho \frac{u_*^2}{2}\ \frac{\pi d^2}{4} \qquad (24)$$

where C_D is the coefficient of drag, ρ is the density of the fluid.

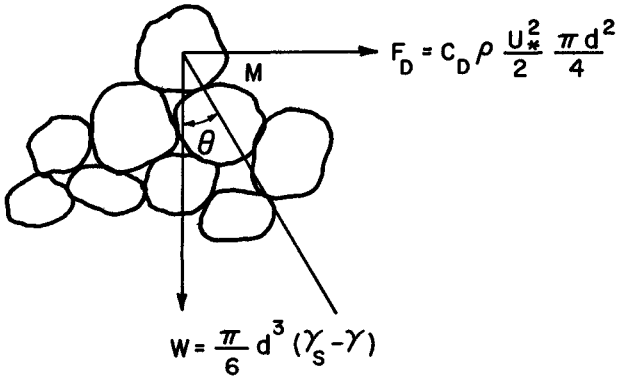

FIG. 5 INITIAL MOVEMENT OF A SAND PARTICLE

Consider a particle P as shown in Figure 5; θ is the angle of repose. The moment which is just sufficient to initiate movement of the particle about M must equal the moment of its own weight about point M.

$$F_D = C_D \rho \frac{u_*^2}{2} \frac{\pi d^2}{4} = \frac{\pi}{6} d^3 (\gamma_s - \gamma) \tan \theta \qquad (25)$$

where γ_s is the specific weight of the sediment, γ is the specific weight of the fluid, and C_D is the coefficient of drag, which is a function of Reynolds Number. (Re)

Boundary Layer Along a Flat Sand Bed

The mechanics of sediment movement were discussed in the previous section and u* was defined as the local horizontal velocity parallel to the bottom. However, the sand particle is so small that the boundary layer effect must be taken into consideration. Fortunately the boundary layer along a flat plate is the simplest case of the application of Prandtl's Boundary Layer Theory.

Based upon the cnoidal wave theory and laboratory observations (Figure 4), it is reasonable to assume that the fluid flow pattern between the sand bed and water surface (within the scour wave length) is uniform and steady, or that $\frac{\partial v}{\partial y}$ = constant. Following Prandtl's development the thickness of boundary layer may be expressed as:

$$\delta \approx \left(\frac{\nu x}{U} \right)^{\frac{1}{2}} \qquad (26)$$

or $$\eta = y \left(\frac{U}{\nu x} \right)^{\frac{1}{2}} \qquad (27)$$

where $\eta = y/\delta$ is defined as a dimensionless term.

From the definition of stream function, we have

$$u_* = \frac{\partial \Psi}{\partial y} = \frac{\partial \Psi}{\partial \eta} \cdot \frac{\partial \eta}{\partial y} = U f'(\eta) \text{ or} \qquad (28)$$

$$\frac{u*}{U} = f'(\eta) \qquad (29)$$

The solution of this equation was obtained by Howarth. (10)

A Theoretical Equation For Wave Scour

Wave reflection from a simple seawall (or a flat plate) is a function of its angle of inclination, (i.e. for a vertical wall the reflection is 100 per cent and for sloping beaches partial reflections will occur) (2). The incident and superimposed waves will form an envelope as shown in Figure 6.

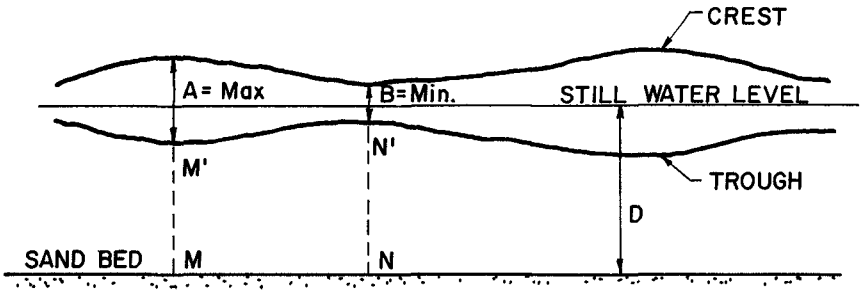

FIG. 6 ENVELOPE OF WAVE MOTION

It was observed that the surface of the sand bed first becomes rippled under the nodes of the envelope. (Point N in Figure 6). A few minutes later the rippled surface extends to cover the entire sand bed. Soon after the formation of these ripples the actual scour formations appear. The crests and troughs of the sand formations correspond to the loops and nodes of the envelope.

The mechanics of the scouring process may be explained as follows: When the experiment is started with a flat sand bed, the horizontal velocity component under the node is affected more than the horizontal velocity component under the loop, so that the primary scour occurs under the nodes of the envelope. A few hours later (usually 1 to 3 hours) the crests of the sand formation move under the nodes of the envelope. This relative position will normally last throughout the duration of the experiment.

From equation (25), for a particular grain size of sand, the most important is u_*. In other words, u_w, the local velocity parallel to the bottom, is the main factor determining the depth of scour. Since the wave is generated from rest, the equation of continuity is valid in this case. It is then logical to say, that when scour depth increases,

the local velocity must decrease until a certain point when the ultimate scour depth is reached. This does not imply that scour and sediment transfer come to a halt, it is only a limit which is approached asymptotically.

Figure 7 shows a side elevation of sand bed. Section "a" represents the initial condition (before the scour) and section "b" represents the condition when the ultimate scour is reached.

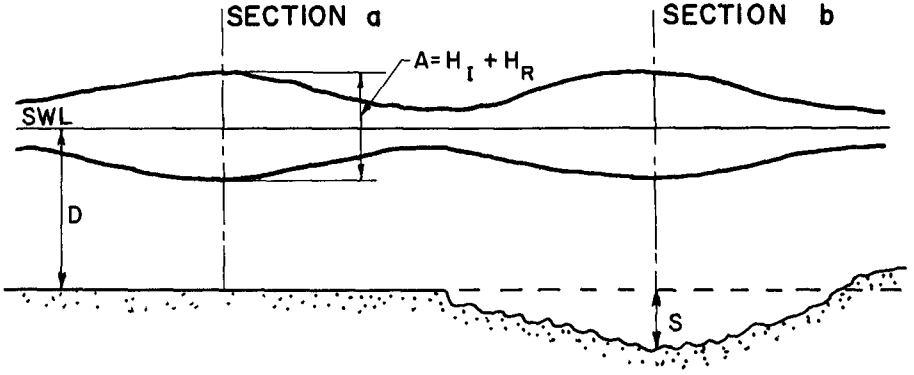

FIG. 7 GEOMETRY OF SAND SCOUR

Continuity equation may be written between section "a" and "b".

$$U_a \ (D - \tfrac{1}{2}A) = U_b \ (D - \tfrac{1}{2}A + S) \qquad (30)$$

$$\text{or} \quad U_b = U_a \ \frac{D-\frac{1}{2}A}{D-\frac{1}{2}A + S} \qquad (31)$$

This equation must be modified to take account of reflection which is a function of the slope of the seawall. When the two wave systems approach from opposite directions and are superimposed, the velocity components may be added vectorially. Introducing equation (28), we have

$$f'(\eta)\ (1 - C_r)\ U_b = (1-C_r)\ f'(\eta)\ U_a \left(\frac{D - \frac{1}{2} A}{D - \frac{1}{2} A + S}\right) \quad (32)$$

where C_r is reflection coefficient, defined as:

$$C_r = \frac{A - B}{A + B} = \frac{H_R}{H_I} \quad (33)$$

Substituting Equation (32) into Equation (25) and simplifying, the following expression is obtained:

$$S = (D - \tfrac{1}{2} A) \left[(1 - C_r)\ u_* \left(3/4 C_D \rho \frac{\cot \theta}{d\,(\gamma_s - \gamma)}\right)^{\frac{1}{2}} - 1\right] \quad (34)$$

where $A = H_I + H_R$

Dimensional Analysis

The following dimensionless terms may be obtained from the dimensional analysis:

$$\frac{S}{K},\ \frac{\lambda}{L},\ \frac{T}{t},\ R_e,\ \frac{v^2 \rho}{d(\gamma_s - \gamma)},\ F_r,\ C_r$$

where the following functional equation may be written:

$$f\left(\frac{S}{K}, \frac{\lambda}{L}, \frac{T}{t}, \frac{1}{R_e}, \frac{v^2 \rho}{d(\gamma_s - \gamma)}, \frac{1}{F_r}, \theta, \alpha, C_r\right) = 0 \quad (35)$$

$$\text{or} \quad \frac{S}{K} = f'\left(\frac{\lambda}{L}, \frac{T}{t}, \frac{1}{R_e}, \frac{v^2 \rho}{d(\gamma_s - \gamma)}, \frac{1}{F_r}, \theta, \alpha, C_r\right) \quad (36)$$

For the sake of comparison Equation (34) may be re-written in the following form:

$$\frac{S}{K} = (1 - C_r)\ (3/4\ C_D)^{\frac{1}{2}} \left(\frac{v^2 \rho}{d(\gamma_s - \gamma)}\right)^{\frac{1}{2}} (\cot \theta)^{\frac{1}{2}} - 1 \quad (37)$$

It is obvious that equations (36) and (37) are very similar. However, it must be pointed out that equation (34) should be used only for the "ultimate" scour depth.

EXPERIMENTAL STUDY

Facility

The wave channel employed was two feet wide, two feet deep, and sixty seven feet long, glass walled, with absorbers at both ends.

Pendulum-type wave generator was used, its frequency could vary from zero to 2.1 cycles per second. The stroke, period and movement of oscillating plate of the generator were all adjustable. The capacitance-type probe and wave recorder were used to collect the data.

Geometric Configuration

A false bottom of five inches deep and a bulk-head of plywood were placed under the generator and extended toward seawall of a distance of about 15 feet. Sand bed five inches deep extended throughout the remainder of the tank. The seawalls, also made of plywood, were placed in front of the downstream absorber. Wire-mesh filter (about 5 feet thick and 2 feet wide) was placed about 5 feet in front of the generator in an attempt to reduce the reflected-waves hitting the paddle and causing re-reflected waves. Unfortunately, it was very difficult (if not impossible) to eliminate the reflected-waves completely. Grain size distribution curve for the sand is shown in Figure 8.

Procedure

The experimental program was as follows:

Experiment No.	H/L	H/D	L/D	T (sec)	Remarks
A1	0.03314	0.38400	10.500	1.265	15 Degree Seawall
A2	0.04012	0.42125	10.500	1.600	" " "
A3	0.03291	0.34556	10.500	1.695	" " "
A4	0.02343	0.24600	10.500	1.790	" " "
B5	0.03621	0.34625	9.563	1.410	" " "
B6	0.02680	0.33500	12.500	2.080	" " "
B7	0.02741	0.38375	14.000	2.100	" " "
B8	0.01732	0.35959	17.466	1.620	" " "
C9	0.02609	0.33552	12.656	2.000	No Seawall
C10	0.02609	0.33552	12.656	2.000	45 Degree Seawall
C11	0.04057	0.44000	10.844	1.500	" " "
C12	0.03852	0.49000	10.600	1.500	" " "

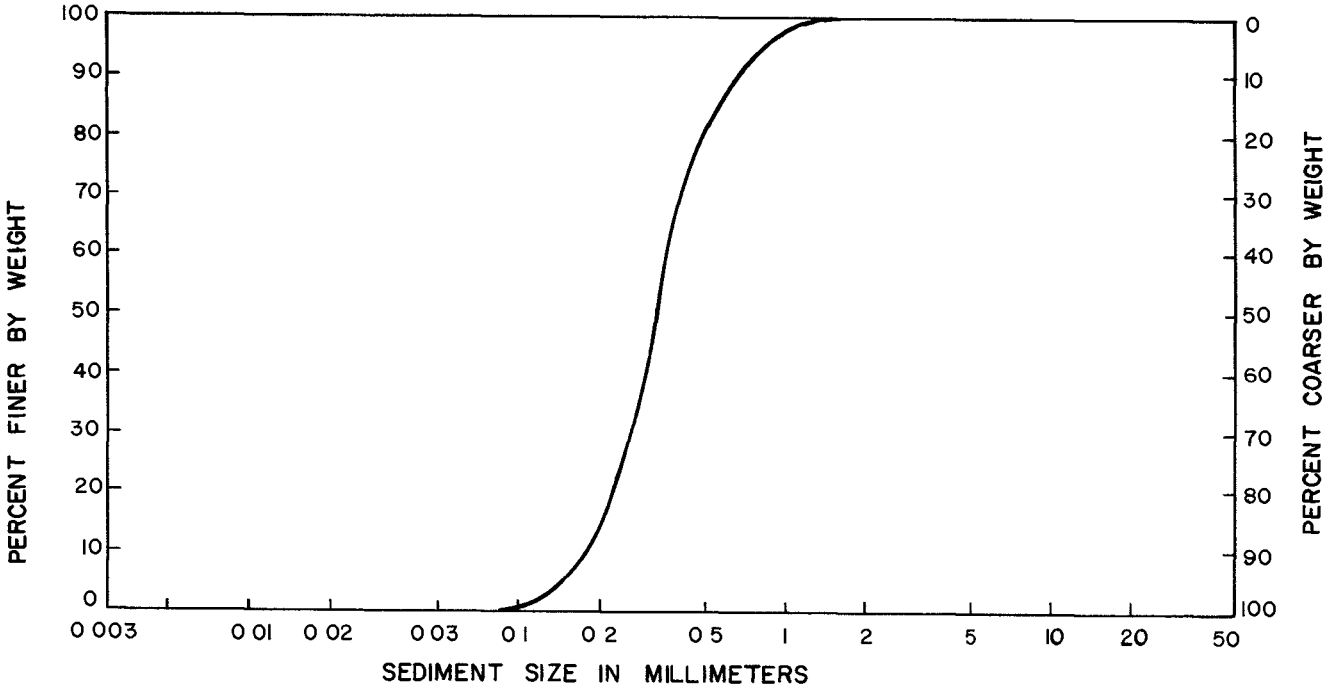

CLAY	SILT				SAND					GRAVEL				
Coarse	Very Fine	Fine	Medium	Coarse	Very Fine	Fine	Medium	Coarse	Very Coarse	Very Fine	Fine	Medium	Coarse	Very Coarse

AMERICAN GEOPHYSICAL UNION CLASSIFICATION

FIG. 8 GRAIN SIZE DISTRIBUTION

Before each experiment, the sand bed was carefully leveled, wave recorder calibrated, water depth checked, and wave period and wave length adjusted. The reflection coefficients and wave heights were taken at a location between 10 to 20 feet away from the seawall. The scour depths were taken upstream of the seawall over a distance of 20 feet. All experiments were conducted until the scour depths became fairly constant with time.

Results

All experiments performed indicate that there may be a limit of scour depth which is approached asymptotically. The scour depth increases very rapidly during the first few hours and then the erosive process slows down and reaches a state of what other investigators called "ultimate" scour depth. Figure 9 is a plot of $\frac{\bar{S}}{K}$ as a function of $\frac{T}{t}$, where $\bar{S}$ is the average scour depth taken within a range of 15 feet in front of the seawall. The term T/t is actually the number of waves generated.

Figure 10 is a plot of $\frac{\bar{S}}{K}$ as a function of the coefficient of reflection, C_r, for a 15 degree seawall. It appears that the scour depth is only a random function of the reflection coefficient. This is probably due to the fact that the reflection coefficient depends on the wave characteristics, seawall slope and the kinematic behavior upon hitting the seawall. There is a great deal of difference between the reflection coefficients of a non-breaking and breaking wave on the seawall for the same wave characteristics.

Fluctuations in values of measured wave height and wave reflection were observed throughout the test, these are shown in Figure 11. It should be noted that the average wave height was used in all calculations.

Herbich and Murphy (1) concluded previously that the scour length is not influenced by wave height, water depth, seawall slope or the reflection coefficient. The same was observed in the current study and the scour length was approximately equal half the wave length.

The following comparison was made between theoretically calculated values and experimental results.

Experiment	Calculated Value from Equation 34 (inches)		Average Scour Depth $\bar{S}$ (inches)	Maximum Scour Depth S max (inches)
	$y = \frac{1}{2}\delta$	$y = 5d$		
A1	-1.13	0.585	0.457	0.50
A2	1.56	1.664	1.103	1.50
A3	1.22	1.950	1.170	1.55
A5	1.35	1.272	1.300	1.80
A6	1.09	1.170	1.420	1.80
A7	1.21	2.380	1.373	1.45

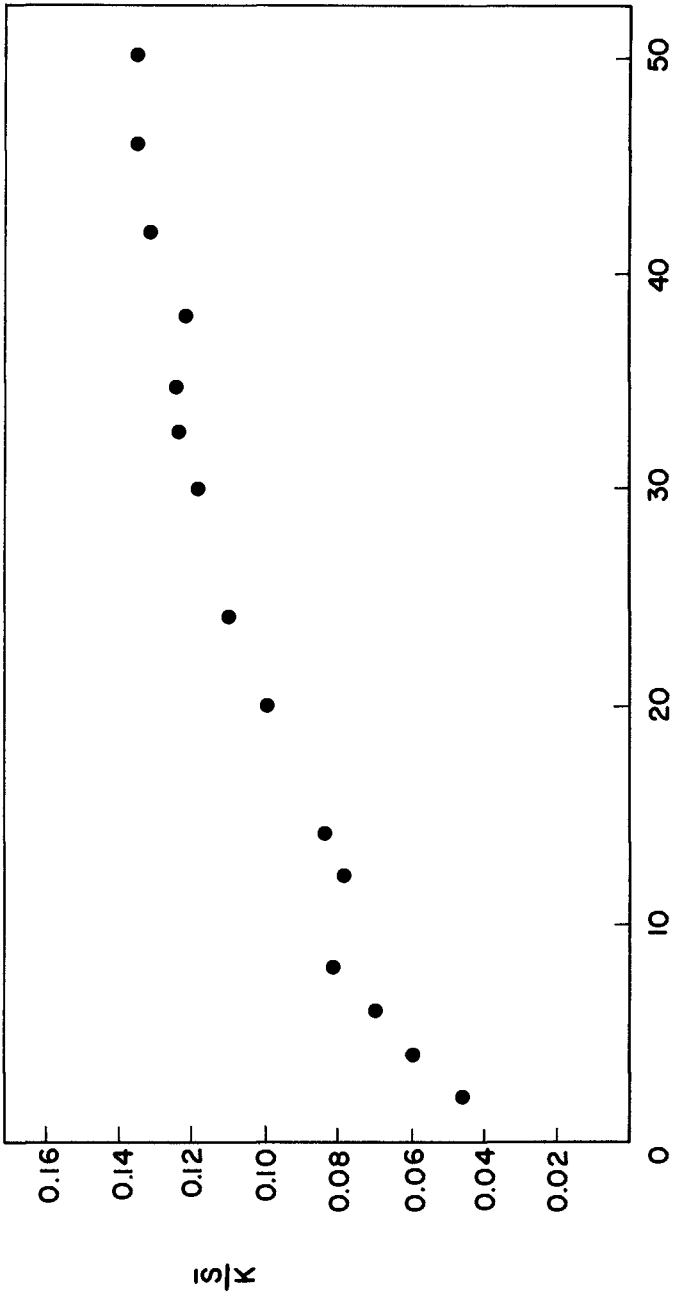

FIGURE 9 RELATIONSHIP BETWEEN $\frac{\bar{S}}{K}$ AND $\frac{T}{t}$

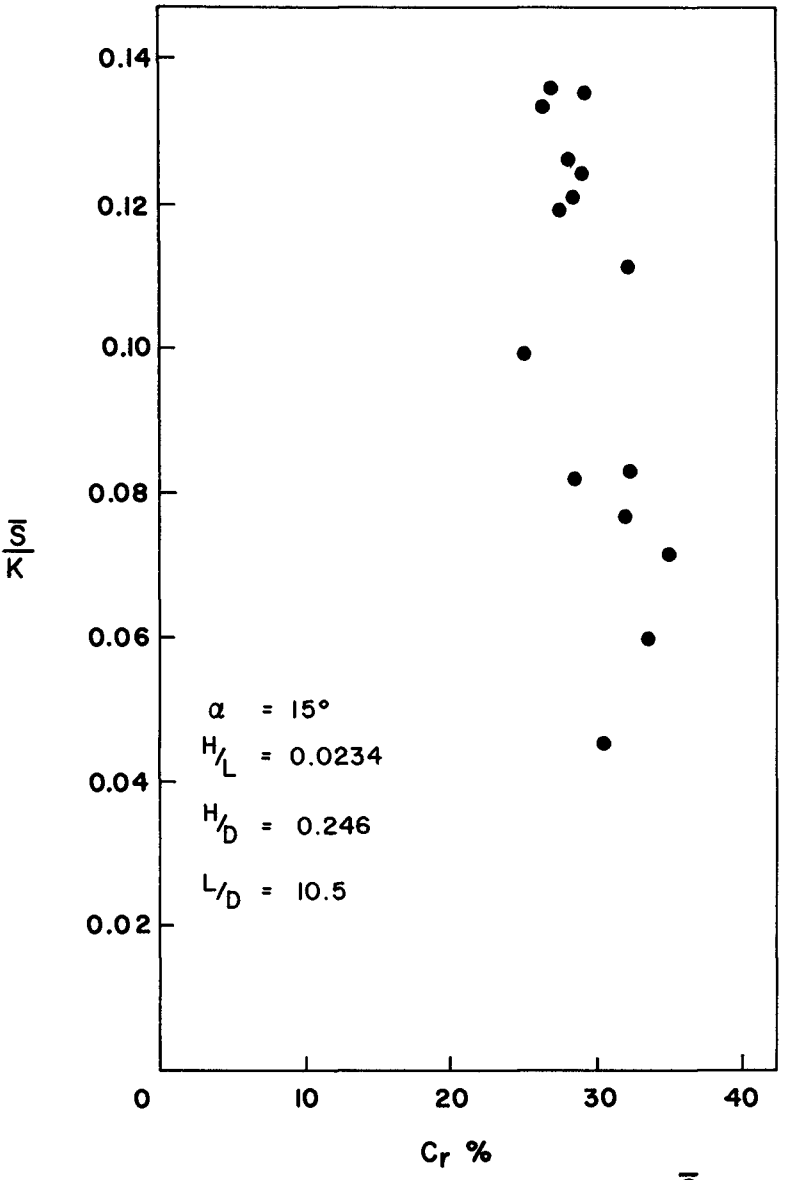

FIG. 10 RELATIONSHIP BETWEEN $\frac{\bar{S}}{K}$ AND C_r

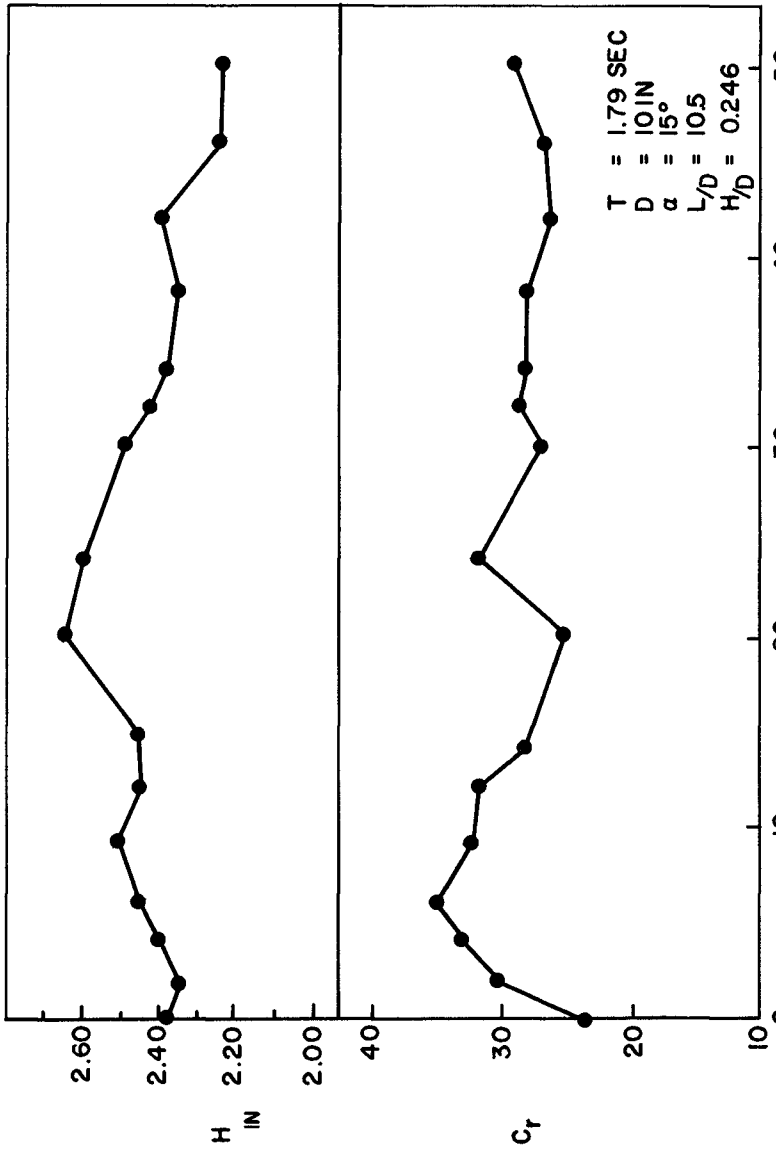

FIG. 11 FLUCTUATION OF H, C_r AS A FUNCTION OF $\frac{T}{t}$

The calculated values were based on two assumptions (a) that $y = \frac{1}{2}$ and that $\delta = 1.72 \left(\frac{ux}{U}\right)^{\frac{1}{2}}$ and $\eta = y \left(\frac{U}{L/2}\right)^{\frac{1}{2}}$ (column 2) and (b) that $y = 5d$ (column 3).

The agreement between theoretically predicted values and experimentally obtained values is considered good.

CONCLUSIONS

1. A mathematical model to describe scour in front of seawalls was developed. In considering the model the most important factors affecting ripple formation are water velocity and sand diameter.
2. The scour length is independent of time and only a function of wave length.
3. The "ultimate" scour limit is approached asymptotically.
4. Agreement between proposed theoretical equation and experimental data is reasonably good.

REFERENCES

1. Herbich, J. B., Murphy, H. D., and Van Weele, B., "Scour Flat Sand Beaches Due to Wave Action In Front of Seawalls", Coastal Engineering, Santa Barbara Specialty Conference, ASCE, 1965.

2. Straub, L. G., Herbich, J. B., Bowers, C. E., "An Experimental Study of Wave Absorbers", Project Report No. 54, St. Anthony Falls Hydraulic Laboratory, University of Minnesota, 1957.

3. Straub, L. G., Herbich, J. B., Bowers, C. E., "Laboratory Tests of Permeable Wave Absorbers", Coastal Engineering, Chapter 44, 1958.

4. Milne-Thomson, L. M., "Theoretical Hydrodynamics", Macmillan, New York, 1960.

5. Rouse, H., "Fluid Mechanics for Hydraulic Engineers",Dover Publication, New York, 1961.

6. Schlichting, H., "Boundary Layer Theory", 4th Edition, McGraw-Hill Book Co.

7. Stoker, J. J., "Water Waves", Interscience Publisher, Inc., New York, 1957.

8. Vallentine, H. R., "Applied Hydrodynamics", Butterworths, London, 1959.

9. Wiegel, R. L., "Oceanographical Engineering", Prentice-Hall, 1964.

10. Howarth, L., "The Solution of the Laminar Boundary Layer Equations", Proceedings of the Royal Society (London), A 164, 547, 1938.

DISCUSSION

Mr. J. A. Zwamborn, of Pretoria, South Africa, asked a question regarding the slope of the beach and said that it was not clear to him whether the slope was one of the variables investigated. He also indicated that Sato, Tanaka and Irie have done some work on scour of beaches as reported in paper 116 at this Conference. He also inquired whether similar vertical scour patterns may be found in front of natural coastal structures, such as sand dunes.

Mr. A. Paape, of Delft, The Netherlands, stressed the fact that the study was conducted in the laboratory and that difficulties may arise in predicting the behavior in the prototype due to possible scale effect. He also mentioned that nothing was said about the possible scale effect.

Mr. Thorndike Saville of Coastal Engineering Research Center, Washington D. C., U.S.A., concurred with Mr. Paape and indicated that more field studies are needed.

In closing the author said the following:

(A) In answer to Mr. Zwamborn: The first phase of the study was conducted with a horizontal beach. The next step in this investigation will be to vary the slope of the beach and study the effect of the slope on scour patterns and scour depth. The author was not aware of the study by Sato and others and will be looking forward to reading their complete paper. It is assumed that similar scour patterns will occur in front of other obsticles such as natural dunes.

(B) In answer to Mr. Paape and Mr. Saville: The question of scale effect between the model and prototype has not yet been solved for sediment movement in the rivers and no attempt has been made to predict the depth of scour on beaches under prototype conditions.

Two sizes of sand were used in this investigation and the results were found to be comparable. It is planned to make measurements in the field, some time in the future, along the beaches of the Gulf of Mexico.

Originally it was thought that scour would occur at the toe of the seawall - this however proved not to be the case as the first scour hole developed some distance seaward from the structure.

LIST OF SYMBOLS

A	$H_I + H_R$	L
B	$H_I - H_R$	L
C_D	Drag Coefficient	—
cn	Jacobian Function	—
C_r	Reflection Coefficient	—
D	Still Water Depth	L
$\underline{d}$	Effective Sand Diameter 50 per cent finer	L
F	Drag force, vector	F
F_x, F_y, F_z	Force Component	F
g	Acceleration due to gravity	L/T^2
h	ξ - D, Water particle under free surface	L
H	Wave Height	L
H_I	Incident Wave Height	L
H_R	Reflected Wave Height	L
K	D - ½ A, refer to Figure 2	L
K(k)	Elliptical Integral, first kind	—
L	Wave Length	L
P	Pressure	F/L^2
S	Scour Depth	L
$\bar{S}$	Average scour depth in front of a seawall	L
t	Wave Period	T
T	Time Elapsed	T
u_*	Horizontal velocity within boundary layer	L/T
U	Horizontal velocity of wave motion	L/T
V	Velocity Vector	L/T
ρ	Water Density	F/L^3
ρ_s	Sand Density	F/L^3
θ	Angle of repose	degrees
Φ	Velocity potential function	—
γ	Specific weight of water	F/L^3
γ_s	Specific weight of sand	F/L^3
μ	Dynamic viscosity	FT/L^2
ν	Kinematic viscosity	$\frac{L^2}{T}$
R_e	Reynolds Number = $\frac{KV}{\nu}$	—
F_r	Froude Number = $\frac{V^2}{gK}$	—
α	Slope of seawall	degrees
λ	Scour wave length	L
ξ	Free water surface	—
η	Dimensionless co-ordinate of boundary layer	—

CHAPTER 41

CLIFF DRAINAGE AND BEACH DISTRIBUTION

by

W.T. Fryde, Dip.Ing., C.Eng., M.I.C.E.
Senior Engineer, C.H. Dobbie and Partners

ABSTRACT

The works described in this paper are part of a large Coast Protection scheme recently completed at Clacton-on-Sea, Essex, England. The paper is in two parts, the first describing cliff drainage and the second dealing with beach distribution.

The method of drainage departs from the usual one of surface rubble drains and comprises a system of auger bored vertical and inclined drains. This method of drainage does not depend on the slope of the cliff face, its most important feature being that it makes it possible to drain the water away from within the cliffs.

The second section describes the effect of large impermeable groynes on beach distribution as experienced at Clacton and the remedial works carried out, including tipping of imported material to improve the beach levels, and the results achieved.

Both sections of the paper refer to the specific problems encountered on the Clacton frontage and the methods adopted to deal with them. The solutions found could be applied to other frontages but thorough investigations would be necessary beforehand due to the very varying nature between one frontage and another.

INTRODUCTION

At Clacton-on-Sea, a holiday resort on the East Coast of England, there have been coastal problems and construction works ever since the first organised attempt to stop the recession of the cliff line was undertaken in 1881. At first, only a comparatively short length of frontage was protected by a sea wall, but gradually with the urban development this was extended and today Clacton Urban District Council are

responsible for 5.9 kilometres of coastline. The cliffs, which comprise the entire length of the Clacton frontage, were always a source of problems which originated from small slips usually well above the promenade level. In 1963, however, as the result of a large slip 46 metres of promenade and sea wall were destroyed and emergency works had to be implemented. It was then that the author's firm was called in to make comprehensive recommendations, which were subsequently carried out, including among other things cliff drainage and works to improve the beach, both of which are described in this paper.

The drainage system comprises vertical and inclined auger-bored drains (Fig.1) and the beach nourishment includes a groynage system and beach tipping (Fig.3).

CLIFF DRAINAGE

Following the slip of 1963 an intensive investigation into the stability of the Clacton cliffs was carried out. First, two 15.2 m. deep boreholes were sunk from the top of the cliffs, one opposite the slip, the other some distance away, both at about 6.0 m. from the cliff edge. At each borehole core samples were taken throughout for laboratory analysis. These two boreholes established that the cliffs are of London clay, known locally as 'Platimore', capped with sand and gravel, and also that there is a ground water table about 0.6 m. above the clay and a perched water table above a thing layer of clay some 0.9 m. to 1.5 m. below ground level at the top of the cliffs. The clay was found to be fissured and containing clay stones. Laboratory tests showed among other rhings that the sand is finer at the top becoming coarser with depth and ending in a highly permeable layer of 38 mm. gravel on top of the clay.

From the geological map it was clear that the London clay extends far beyond the area concerned at Clacton and well below the foreshore level. It remained then to establish the top of the clay and for this purpose 30 boreholes at 91.4 m. centres were taken on a line more or less parallel to, and about 5.0 m. from the edge of the cliffs. The clay was found to be 3 m. to 7.6 m. below cliff top level, sloping uniformly from west to east and was capped by sand and gravel throughout. The ground water table was uniform at approximately 0.6 m. above the clay all along the line of investigation. Two further boreholes taken 61.0 m. from the cliff edge indicated that the clay top also slopes gently landwards. The level at the top of the cliffs is approximately 14.0 above Newlyn Datum throughout their length.

In addition to the boreholes the cliffs were inspected thoroughly for slips, wet spots, springs and any revetment works which had been carried out previously.

From the information available it was not difficult to arrive at the conclusion that the main cause of the cliffs' instability was water within, and therefore to stabilise the cliffs drainage was of the first importance. To substantiate this conclusion it is worth describing the special physical properties of the London Clay.

London clay (Platimore) is of the overconsolidated type of clay, which means that at one time it was subjected to a load very much greater than it is today. It is known that as a result of the great reduction in the load upon it this type of clay expands and becomes vulnerable to attack by water or atmosphere on its surface. If the clay is fissured, as it is at Clacton, the process of expansion and consequential deterioration takes place also within the fissures, which could themselves be the result of the expansion. The process is very slow, but it is continuous and progressive and this is usually the cause of sudden slips. If water is in contact with the clay the deterioration on the surface or within the fissures is very much accelerated although still comparatively slow. Because of this continuous and progressive deterioration taking place in the overconsolidated type of clay, drainage is of the utmost importance, or complete disintegration will result and the clay turns into a mud slurry. It should be stressed again that although the process of deterioration is slow it is the most important factor to be considered in a long term stabilisation of the cliffs of the overconsolidated type of clay. Scarping or laying back the cliff face alone without drainage would require a slope of not less than 1 in 6.

At Clacton the normally accepted method of laying back the cliff face to a slope of 1 in 3, and providing surface rubble drains was not possible due to the proximity of the main roadway and the urban development. The method adopted, therefore, was a combination of limited scarping of the cliff face and a system of auger-bored drains. The scarping was confined mainly to laying back the cliff face in places to a slope of 1 in 1½ and where possible 1 in 2, and general tidying up. The drainage system on the other hand is quite extensive and covers nearly 1.6 Kilometres of frontage.

Generally, the drainage system comprises vertical and inclined auger-bored drains, a toe collecting drain and sea outfalls (Fig.1). Vertical drains were constructed first in order to determine accurately at their locations the top of the clay and also to deal with the perched water table by perforating any impermeable layers within the sand and gravel. Next, from suitably located pits in the promenade, inclined holes were augered through the clay to meet the bottom of the vertical drains. The method of auger boring was specially devised by the sub-contractor using a hydraulic pack. After the auger had been withdrawn perforated pitch fibre pipes were inserted into the hole to provide a permanent drain

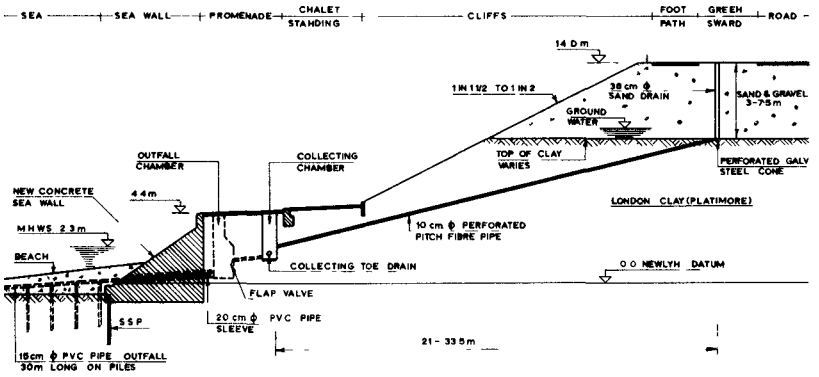

FIG 1 SECTION THROUGH THE CLIFF SHOWING THE DRAINAGE SYSTEM

within the clay and also to drain away water from the top of the clay. A perforated, galvanised metal cone was fitted to the leading pipe to prevent gravel entering the drain.

The number of vertical drains was determined from a visual survey of the condition of the cliff face, and accordingly these are at 7.6 m., 10.1 m. or 12.2 m. centres. To reduce the number of pits, which can be quite expensive, three inclined drains usually radiate from one pit towards three corresponding vertical drains. In each pit a collecting chamber is provided and this is connected with others by a collecting toe drain which discharges finally into the outfall chamber and from there the drainage water is carried by a P.V.C. pipe to the sea.

For the construction of the inclined drains a newly-developed machine called a "Traveller" was used. With this machine, using a continuous auger, up to two 24.4 m. long drains were completed per shift. Mass and reinforced concrete and brickwork can be drilled through with reasonable ease using a diamond auger bit. Non-cohesive materials on the line of the auger, however, constituted a considerable obstruction and required steel casing which can increase the cost of augering to as much as four times that of working in sound clay.

The augering as such, with or without casing, is no longer a problem, but there is still no reliable method of assessing the true line, level or position of the leading end of the drain either in the course of augering or when completed. At Clacton a "U" tube was used to determine the level of the drain at any point and the only guide as to the line was the comparison of the calculated length with the length of the completed drain.

When the auger entered the gravel strata usually a flush of water came down the augered hole bringing with it some of the material, which gave a good indication of whether the vertical drain had been met, although this is not essential since the gravel on top of the clay is quite permeable being much coarser than that higher up.

Fig.2: Auger-bored inclined drains lined with pitch fibre pipes ready for connection to the collecting toe drain.

The discharge from the drains varied. Some of the drains ran for a few days only after completion, which indicated that the extent of the water table at that location was small. Others have not ceased running indicating that a large catchment area is being drained. A number of drains did not discharge and from this it was deduced that a local high spot or ridge on top of the clay had been struck. On the whole the drainage can be considered a success since the discharge measured weekly for the past year at three of the five outfalls was almost constant at a total rate of 181,840 litres per day.

In conclusion, there is no doubt that the drainage system as described above can be used efficiently in dealing with many similar problems where normal drainage methods are neither

possible nor practical. Site investigations prior to implementation of such a scheme are of great importance and highly skilled supervision during construction is necessary.

BEACH DISTRIBUTION

The main supply of material to the Clacton beaches was cut off following the construction of a sea wall at the toe of the cliffs along the entire frontage. The supply from littoral drift is very small and therefore the only hope of preserving the beaches lies in a good system of groynes and the occasional tipping of imported material.

The previous groyne system (Fig.3) comprised large mass concrete groynes with smaller groynes of reinforced concrete or timber construction. The large groynes (Nos.34 to 43) were constructed in the years 1912 to 1927. These were 125 m. long with the top level 1.0 m. above and sloping to 2.4 m. below M.H.W.S. (2.3 m. above Newlyn Datum) from the landward to the seaward ends. These groynes were spaced at approximately 305 m. At the same time intermediate timber groynes 76 m. long at 100 m. centres were constructed. The frontage with the groynes was protected by a concrete gravity wall built at the end of the last century. In 1942-43 reinforced concrete groynes were added along the almost unprotected cliffs from groyne 34 to the eastern end of the frontage, a distance of 3.4 km. These groynes, 46 m. long and at 100 m. centres comprised reinforced concrete king piles and planks. A number of similar intermediate groynes, each 30.5 m. long, were added later along part of the distance. The cliffs remained unprotected until 1948 when works on a major sea defence scheme commenced. This scheme comprised the construction of the last two (Nos. 22 and 10) mass concrete groynes, a length of 201 m. of concrete gravity sea wall just west of groyne 22, and also a continuous reinforced concrete sheet pile wall east of groyne 10 and in the gaps between various lengths of old sea walls to the west. The mass concrete groynes were each 94.5 m. long with the top level 1.5 m. above M.H.W.S. at the landward end.

The erosion of the cliffs continued caused by the action of the waves breaking over the sheet pile wall. As a result of the damage to the cliffs that occurred during the 1953 flood an apron (promenade) behind the sheet pile sea wall was added, and with this the last gap in the cliff protection was sealed, and with it a major source of beach supply cut off. From then on gradual denudation of the beach was apparent along the greater part of the frontage and by 1963 a section of sea wall west of groyne No. 10 had collapsed and other sections were in danger. The lowering of the beach was most drastic to the leeward of the mass groynes, Nos. 10 and 22. These high groynes, completely impermeable and without any provision for adjustment, formed a barrier to the meagre littoral drift and consequently a situation similar to the

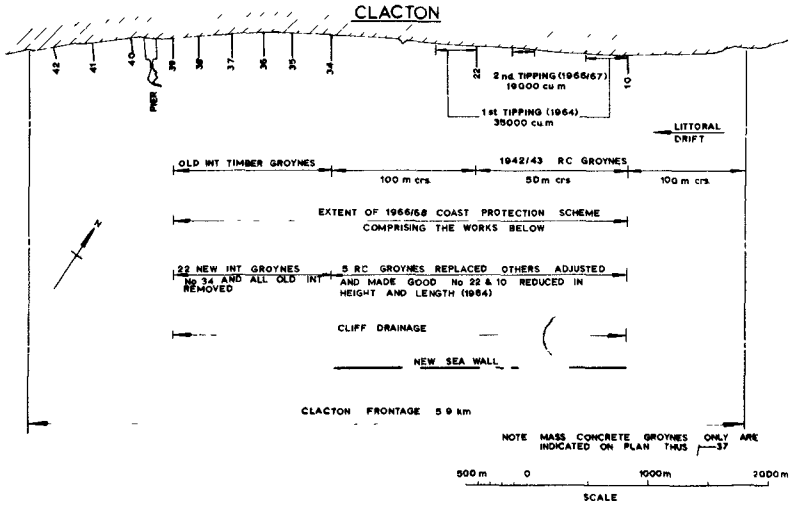

FIG 3 PLAN OF CLACTON FRONTAGE

terminal groyne problem developed (Fig. 4 and 5). This also applied to the other large groynes (nos. 34-39) near the Pier, but to a lesser degree. The problem did not arise to the west of the Pier, the conditions there being somewhat different.

To safeguard the sea wall Emergency works were carried out in 1964. These comprised shortening of groynes Nos. 22 and 10 by 30.5 m. and reducing the height by as much as 2.0 m., adjusting planks and making good as necessary the intermediate groynes. This was followed by tipping on to the beach 35,000 cubic metres of imported material.

The imported material was tipped along a distance of approximately 350 m. on the leeward side of each of the two large groynes at an average rate of 40 to 50 cubic metres per metre of frontage. At first the material was spread on the beach by a bulldozer but this was soon abandoned and the job of spreading was left to the tides with good results. Usually it took four to six tides, depending on the rate of tipping, to spread and consolidate the material over the beach sufficiently to be walked on. It is important that the beach is inspected after tipping for any soft areas, but these disappear usually after a few days but in the meantime can be a nuisance or even dangerous.

Fig. 4: Part of the frontage with large groyne No. 10 (Distance between numbered groynes 100 m.)

Fig. 5: Part of the frontage with groyne No. 22

The improvement in the beach after the completion of the Emergency Works could be seen far beyond the area of tipping and was better than had been anticipated.

The imported material matched that on the existing beach very well since it came from the cliffs that had been the main source of beach supply before the sea wall was constructed.

In 1966 a further 19,600 cubic metres of suitable material became available from cliff scarping and this was one of the works included under the Main Coast Protection Scheme along the frontage started in that year. This time there was an access problem and the material was tipped at one point only for a length of approximately 100 m. halfway between groynes Nos. 22 and 10 (Fig.3). This did not, however, affect its distribution and further improvement in beach levels were apparent almost everywhere.

Under the same scheme the groyne system was reshaped by removing old ineffective timber and some of the reinforced concrete groynes, the latter having been severely damaged by abrasion, and constructing 29 new timber groynes, each 30.5 m. long. The reinforced concrete groynes which were retained were made good and their planks adjusted to suit the beach levels. Of the large groynes only No. 34, which was already in a dilapidated condition, was replaced by a timber groyne and the others were left for the present since the cost of replacement would be considerable.

The scheme also included 1.4 kilometres of new sea wall and drainage of 3.2 km. of cliffs.

Today, four years after the first imported material was tipped there is no doubt that there is a considerable improvement in the beach levels and there is every reason to expect that the beach can be maintained in the future with occasional tipping of imported material.

For long-term action the recommendation was that a beach nourishment be implemented in conjunction with the neighbouring authorities, that is Frinton and Walton Urban District Council and the Essex River Authority. The River Authority have started investigations into possible sources of supply but nearly all the inland deposits have been purchased by commercial interests. There are extensive deposits on the sea bed but at present there appears to be no reasonable method of moving them on to the shore.

CHAPTER 42

RECESSION OF MARINE TERRACES - WITH SPECIAL REFERENCE TO THE COASTAL AREA NORTH OF SANTA CRUZ, CALIFORNIA

Robert M. Sorensen
Assistant Professor of Civil Engineering
Coastal and Ocean Engineering Division
Texas A&M University

ABSTRACT

The concept "wave base" (or "surf base"), i.e. the maximum depth below mean sea level at which shoaling waves will effectively erode the ocean bottom leading to the recession of a shoreline, is discussed. Also, past and present opinions as to the magnitude of wave base in general and specifically in the area near Santa Cruz, California, and the variables controlling this phenomenon are presented.

Then, an account of the author's successful and unsuccessful attempts to determine average rates of cliff retreat in the study area is presented along with the specific cliff recession rates obtained. These compare favorably with the recession rates measured by the U. S. Army Corps of Engineers for nearby areas of similar geology and topography and with rates determined for similar coastal areas in various parts of the world. A brief discussion of the spectrum of cliff recession rates found in areas of varying geology and wave climate is also presented.

The accepted history of sea level since the last glacial maximum, particularly during the last 7,000 years, is reviewed as well as pertinent information on the geology, topography and wave climate of the study area.

It is then shown that average recession rates estimated by relating extrapolated bedrock profiles of the lowest marine terraces with the accepted history of the latest sea level rise compare favorably with the recently measured recession rates. However, a conflict exists between the present wave-cut terrace profiles, the accepted history of sea level and the accepted value of wave base.

INTRODUCTION

The objective of this study was to measure, wherever possible, the average rate of marine terrace cliff recession at points along the Pacific Coast around and north of Santa Cruz, California. The seaward slopes of the coastal range in the study area are occupied at many locations by one or several elevated marine terraces and the sea floor at many of these locations is a modern wave-cut platform being extended shoreward by wave erosion.

Recession rates were to be determined by comparing cliff locations shown on old dated maps, photographs, etc., with the present location of the cliffs in the same areas. If any recession rates could be determined, they were to be compared to average historic recession rates roughly estimated by a com-

parison of the seaward extrapolation of the lowest marine terrace and the generally known late Quaternary (20,000 years Before Present, to date) history of sea level.

Average historic recession rates generally agree with rates of cliff recession now taking place. However, a comparison of the modern wave-cut platform profiles with the profiles to be expected considering the accepted sea level history of the last 7,000 years, the recent rates of cliff retreat and the concept of wave or surf base indicates that the existing and expected profiles are in disagreement.

THE STUDY AREA

The specific areas of interest in this study are located along the California coast at 36°55'N to 37°40'N and 122°00'W to 122°30'W; that is, from south of San Francisco to Santa Cruz (see Figure 1). Of special concern are the areas around Rockaway Beach, Montara, Halfmoon Bay, Davenport and just to the west of Santa Cruz.

Topography

The sea coast along the entire study area borders on the steep seaward slopes of a section of the tectonically active California coastal range that is historically uplifting and tilting seaward. At many locations the seaward slopes are interrupted by steep cliffs over 100 feet high, while in other areas there is a single marine terrace or many step-like marine terraces mantled by deposits that are marine and nonmarine in origin.

The lowest marine terraces at Montara and Santa Cruz vary in elevation between 100 feet or less at the base of the old sea cliff and 40 to 50 feet at the top of the modern sea cliff. These elevations include a mantle of marine sands deposited on the old wave-cut platform as the ancient beach that covered these terraces prograded seaward during a period of relative emergence as sea level lowered (Bradley, 1957). The terrace mantle deposits are generally 5 to 15 feet thick but at some places they exceed 20 feet in thickness. Figure 2 is a photograph of the interface between the old wave-cut platform (lowest marine terrace) and the prograded beach sediments at Montara. Boulders deposited on the old wave-cut platform can be seen at the interface. Figure 3 is a photograph of the lowest marine terrace with its beach deposits, taken near Santa Cruz. Carbon 14 dating of mollusk shells found in bore holes in the old wave-cut platform near the area shown in Figure 3 (Bradley, 1956) show dates of around 39,000 years. This indicates that the terrace was carved prior to 39,000 B.P. (Before Present), beach sands were then deposited, and sea level has been lower than the elevation of this terrace since that time. At Santa Cruz there are five distinct raised terraces between sea level and an elevation of 850 feet (see Alexander, 1953 for example).

The continental shelf varies in width from approximately 25 miles at San Francisco to 7 miles at Santa Cruz. The nearshore sea floor over most of this area is a modern wave-cut platform of varying width.

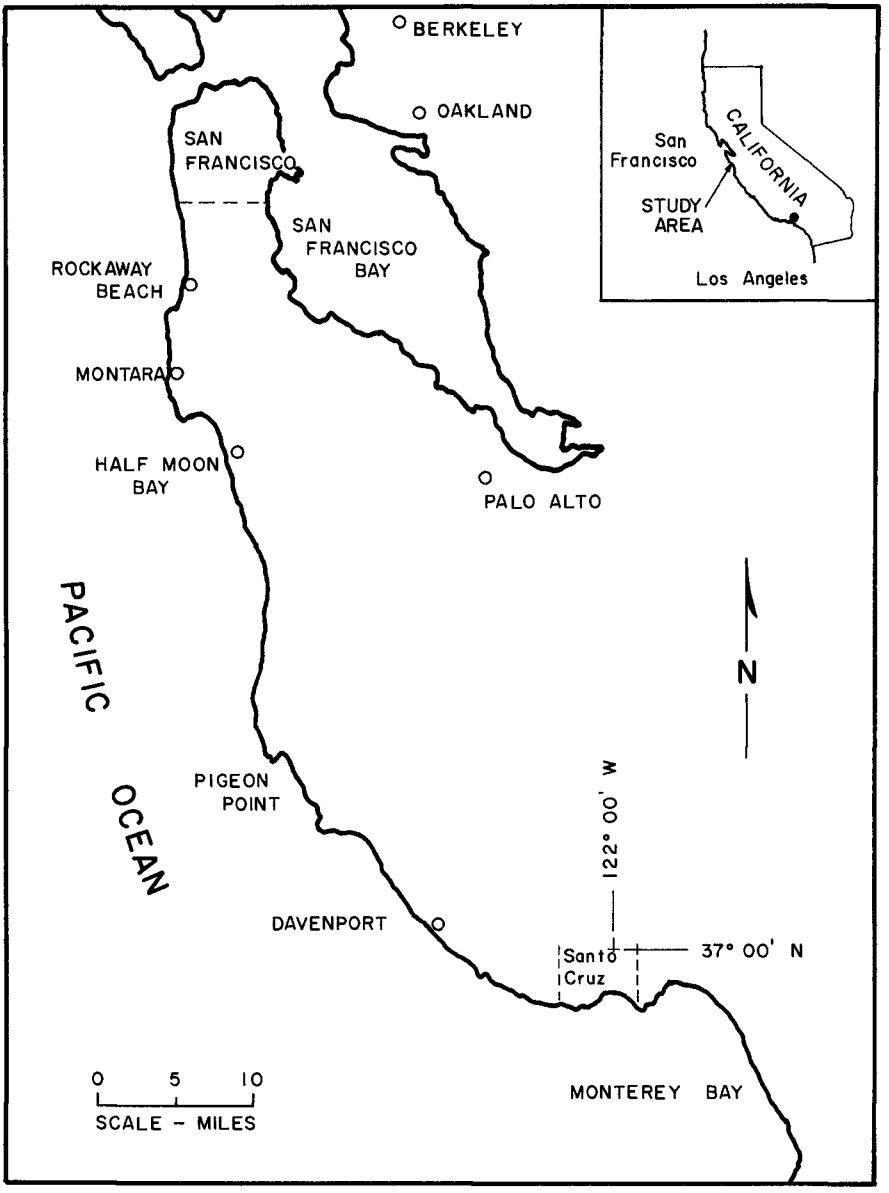

FIGURE 1- LOCATION MAP

FIGURE 2 - INTERFACE BETWEEN OLD WAVE-CUT PLATFORM AND PROGRADED BEACH SEDIMENT, AT MONTARA

FIGURE 3 - LOWEST MARINE TERRACE AT SANTA CRUZ

Figure 4 shows a schematic profile of the wave-cut platform and lowest marine terrace at the City of Santa Cruz. Small undulations in the profile have been "smoothed out". Profiles in the areas near Davenport and Montara are somewhat similar in nature but the wave-cut platform reaches to a slightly greater depth at the same distances offshore. The wave-cut platform is continuous for at least the inner half mile (Hyde and Howe, 1925-26) and is thought to be so for at least the first 1.5 miles or to a depth of 75 feet (Bradley, 1957). Over this distance the platform is covered by a layer of sand generally 2 to 4 feet thick but reaching 10 feet in thickness at some locations as the natural relief of the platform varies by as much as 7 feet. Sand grain sizes on the platform are typically smaller than those found on the beach and decrease seaward.

The platform slope is in the order of 1° near the shore becoming uniform seaward at about 0.5° as the inshore upward concavity evens out in the seaward direction. Except for a slight tectonic warping the lower marine terrace is similar in slope and profile to the modern wave-cut platform.

Along the coast, north of Santa Cruz to Davenport, the shoreline remains irregular with the 30 foot depth contour being located about 0.25 miles seaward and the 75 foot depth contour lying about 0.8 miles seaward of the cliffs. At Montara, these contours are approximately 0.2 miles and one mile from the cliffs, respectively.

Geology

Near Santa Cruz and Davenport the marine terraces and the modern wave-cut platform are carved into the southwest tilting seaward slopes of Ben Lomond Mountain. Willis (1925) believed the mountain to be a block that has been faulted along the northeast resulting in tilting toward the southwest while Rode (1930) stated that faulting is of minor significance and that the mountain is an asymmetric elongated dome. In either case, active lifting and tilting have occurred in the geologic past.

The core of Ben Lomond Mountain consists of Mesozoic granitic rocks exposed at higher elevations (California Division of Mines, 1961). The core is flanked by outward dipping Miocene marine sedimentary rocks that dip at angles of 3° to 15°. In the area of interest near the northwest city limit of Santa Cruz the Miocene sedimentary rock is from the Monterey formation (see Bramlelte, 1946 for a thorough description) and consists principally of mudstone with some closely jointed, thin bedded, shales which are dark gray or brown if fresh and white if weathered. When the mudstone is eroded it breaks into particles that are too fine to make a significant contribution to local beaches.

In the Montara area Mesozoic granitic rocks that are a continuation of Ben Lomond Mountain, known as Montara Mountain, predominate. However, at the exact study site at Montara the wave-cut platform and terraces are carved into sedimentary rock that is essentially a marine conglomerate with a fine-grained base.

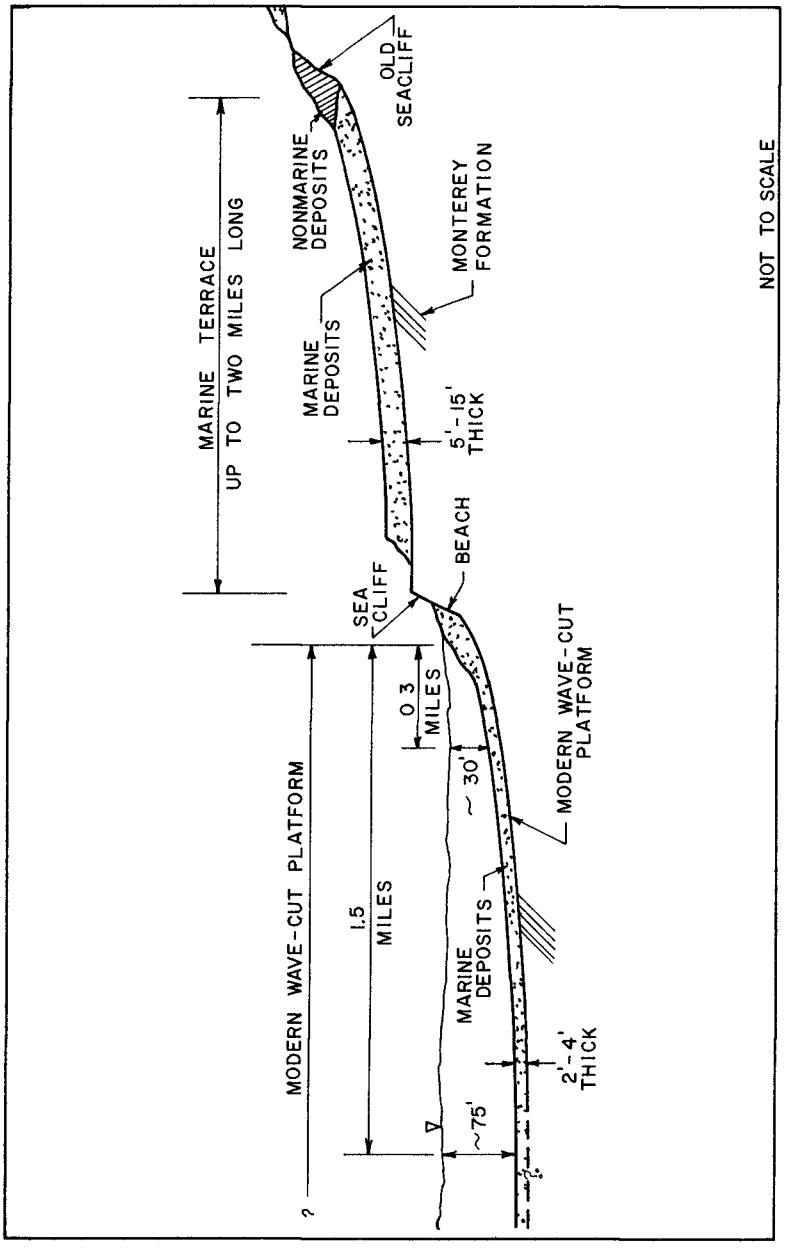

FIGURE 4 - TYPICAL SCHEMATIC PROFILE NORMAL TO THE COASTLINE NEAR SANTA CRUZ, CALIFORNIA

Marine terrace deposits near Santa Cruz and Montara are generally a fine sand with a small gravel fraction. They offer little resistance to erosion as they can generally be scraped away by hand. Thus, the terrace deposits will retreat with the sedimentary bedrock as it yields to the erosive action of waves.

Wave Climate

An indication of the deep water wave climate offshore of the study area is available from wave recordings taken at Point Sur, California (45 miles to the south of Santa Cruz) from April, 1947 to April, 1950 (U. S. Corps of Engineers, 1956) and from sea and swell hind casts for a ten year period at a point off the California coast at 37.6° N and 123.5° W (National Marine Consultants, 1960a, 1960b).

Waves will approach the study area over a sector between due south and north-northwest with periods ranging from 5 to 20 seconds. A large majority of the waves come from the west to northwest and have significant heights of 5 to 7 feet or less. However, local and distant storm waves with significant wave heights of 15 to 20 feet and higher do occur a small percentage of the time mostly from the west and southwest. Estimates (U. S. Corps of Engineers, 1956) indicate that waves with deep water heights of 15 feet may be expected on the average of 5 times a year while 20 foot waves may be expected every 8 to 10 years.

Refraction diagrams indicate that northwesterly swell are strongly refracted and suffer a large decrease in height before breaking on the shore in the study area. However, waves from the southwest are generally unaffected by refraction.

As waves from the west to northwest greatly predominate, net littoral drift is to the south and southeast. However, recent studies (Sayles, 1965; Moore, 1965; and Johnson, 1965) have indicated that little beach-size sediment is contributed to the coast between San Francisco and Santa Cruz so that quantities of littoral drift in this area are small and beaches are not well developed.

WAVE BASE CONCEPT

Definition

The term "wave base" has occurred in the literature since the early part of this century. Certain writers (Dietz and Menard, 1951; Rich, 1951; Dietz, 1963) define wave base as the depth above which sediment particles will not come to rest because of being stirred by wave action. Others (Fairbridge, 1952; Bradley, 1958) including the author define wave base as the maximum depth below sea level at which significant erosion (platform cutting) due to wave action will occur. Dietz (1963) uses the term "surf base" or "surge base" for this depth of erosion as significant erosion is believed to be limited to the surf zone.

Johnson (1919), Davis (1909) and others believed that, given a static sea level, significant erosion extends to depths in the order of 600 feet as fine sediment could be moved by waves at this depth and would act as an abrasive causing marine planation. At present, however, most authors (Dietz and Menard, 1951; Fairbridge, 1952; Longwell and Flint, 1955; Bradley, 1958) feel that, except in rare situations, vigorous wave agitation and erosion are limited to the surf zone or a maximum water depth ranging from 25 to 35 feet.

Local Wave Base

Bradley (1957, 1958) studied platform and terrace deposits between Davenport and Santa Cruz and concluded that wave base near Santa Cruz is limited to a distinct depth of about 30 feet. Twenhofel (1945) reported that sand must be of a certain size (0.5 mm for quartz grains) before it can act as an abrasive. At Santa Cruz, Bradley (1958) found that sand grains larger than 0.5 mm are found only at depths of 30 feet or less while beyond this depth deposits tend to be finer grained than 0.2 mm. Also, he found that a large percentage of pyroxene grains were finely etched at depths greater than 30 feet but at water depths of 30 feet or less nearly all the pyroxene grains sampled were blunted, and indication of vigorous abrasion.

The well known study of breaking waves conducted by Iverson (1952) demonstrated that on a beach slope of 1:50 (or 1.15°) the ratio of water depth to wave height at breaking varies between 1.1 and 1.3 for a deep water wave steepness between .005 and 0.04 (this includes all storm waves to be expected at Santa Cruz). Shoaling waves will increase in height as they move shoreward. As an example (see Wiegel, 1964, p. 17) we can expect unrefracted shoaling storm waves to increase in height by 15 to 30 percent depending upon their period. So, storm waves 20 feet high which occur at Santa Cruz and undergo little refraction when arriving from the southwest would break in water 26 to 34 feet deep. Thus, as nearly all shoreline recession occurs during storms (see discussion in next section) and within the surf zone we would expect a wave base of about 30 feet at Santa Cruz.

Platform Cutting and Cliff Retreat

The general mechanism of cliff retreat involves a relatively long period between major storms in which preparation of the cliff takes place, followed by spectacular retreat during a storm in which the beach in front of the cliff is often removed and waves strike directly upon the cliff. The amount of retreat during a particular storm depends upon the cliff geometry; bedrock material; tide and surge levels during the storm; height, period and duration of storm waves; and, to some extent, the time interval since the last major storm during which weathering, biological action, jointing, etc., prepared the cliffs for further erosion. Williams (1960) reports a case history of the easily eroded cliffs (30 feet high) at Clovehithe, England, in which little erosion occurred over a 17 month period and then, in one evening during a two-hour period, 35 feet of cliff retreat occurred due

to wave attack superimposed upon a storm surge. Photographs taken in 1860 and 1960, and reported by Johnson (1961), showed that along the north coast of California where highly resistant rock outcrops total retreat was small but often retreat again involved slow preparation followed by total removal of a large block of material.

Bradley (1958) studied profiles of the wave-cut platform and five marine terraces (corrected for subsequent deformation) at Santa Cruz and found that the 30 foot depth contour consistently occured at a distance of 0.30 to 0.33 miles seaward of the cliff line. He concluded that for the rocks and wave conditions at Santa Cruz, a platform up to one-third of a mile wide can be carved by the sea at a static sea level and wider platforms, therefore, necessitate submergence, i.e. a rise in sea level and/or tectonic lowering of the land.

CLIFF RECESSION RATES

Study Area Recession Rates

As mentioned in the introduction to this paper, an objective of this study was to measure average cliff recession rates around, and north of Santa Cruz. Due to the sporadic nature of cliff retreat average recession rates can be estimated only by comparing the location of the cliff at various times over an interval of many years or decades.

The usual procedure involves the study of old maps, photographs, book descriptions, etc., that are dated and give a reasonably accurate location of the cliff. This cliff location must cover a good distance along the cliff (several hundred feet, if possible) as recession is variable with location as well as with time.

A search was conducted in the Bancroft Library of the University of California which is devoted to the history of California. Some old photographs taken in the study area were found but they were not very clear and no satisfactory reference points or scale could be determined.

During the period between 1851 and 1860 the U. S. Coast and Geodetic Survey mapped the coastline from a point 30 miles northwest of Santa Cruz to a point 10 miles to the east. They resurveyed this area in 1932 and 1933 and the U. S. Army Corps of Engineers conducted surveys in this area in 1948. In a beach erosion control report for the Santa Cruz area the Corps of Engineers (1956) reported the following erosion rates, based upon the surveys mentioned, local maps and comments from local authorities.

1. Over a 2400 foot stretch of cliffs that face to the southwest and lie along the eastern portion of the City of Santa Cruz (see Figure 1) a total average recession of 103 feet occurred in 80 years for an average rate of 1.3 feet per year. These cliffs have a general profile as shown in Figure 4 and are carved in the Monterey formation.

2. Critical areas along the western edge of the city of Santa Cruz have been receding at an average rate of one foot per year while the overall average recession rate for a section about two miles long is one-half foot per year.

The report concluded that rip-rap protection was needed to halt this rapid destruction of valuable coastal property. This protective seawall has since been constructed (Figure 5).

Shortly after the turn of the century the Ocean Shore Railroad Company (now defunct) began construction of a railroad along the coast from San Francisco to Santa Cruz. From the original plans of the railroad (dated 1912) it was possible to determine the amount of shoreline recession that has occurred in a few locations.

Figure 6 shows the cliff line for a section of the coast just north of Montara as measured in 1912 and 1965. The cliffs, including the bedrock and terrace deposits are nearly vertical along this entire section. Point recession varies from 10 to 80 feet over the fifty-three year period, with the average recession rate for this period being in the order of 0.85 to 0.95 feet per year.

Six miles north of Montara, at Rockaway Beach, a road was constructed in the early 1930's out around a point on the abandoned road bed of the Ocean Shore Railroad. The bedrock is Franciscan volcanic and metavolcanic rocks that are somewhat more resistant than the conglomerate at Santa Cruz. Comparison of the road construction date, road width and present cliff profile indicates a recession rate of one-half foot per year.

The shoreline in Half Moon Bay is presently at the same location as indicated by the 1921 survey. This is due to the wide beaches developed along the coast and to the refraction and resulting wave height decrease that storm and regular waves undergo in reaching the shore.

World Wide Shoreline Recession Rates

It is of interest, at this point, to mention some of the cliff recession rates reported throughout the world as an indication of recession rates possible for shorelines with various topographic and geologic characteristics.

The cliff height, bedrock material and size of protective beach are usually more important than wave exposure in establishing a rate of recession.

Johnson (1919) reported observing glacial striations down the face of granitic shoreline cliffs indicating no retreat of the cliffs since at least the last glacial period i.e. for over 10,000 years.

In incoherent materials such as unconsolidated sand, loess, recent alluvium, volcanic ash, etc. cliff recession rates can be extremely large. For the previously mentioned 30 feet high sand cliffs at Clovehithe, England,

FIGURE 5 - CLIFFS AND PROTECTIVE RIP-RAP SEAWALL AT SANTA CRUZ.

Williams (1960) reported a total recession of 86 feet in 2 years and 7 months or about 30 feet per year. In his recent book, Guilcher (1958) reports that at Krakatoa, Indonesia, volcanic ash cliffs produced by an eruption in 1883 retreated 1,500 meters between 1883 and 1928 for an average recession rate of 99 feet per year. No cliff elevations were reported. Guilcher (1958) presents an interesting discussion of cliff retreat in his chapter on "Coastal Features Related to Sea Action".

Contribution to Littoral Drift

The bedrock being eroded at Montara and Santa Cruz breaks into grains that are too fine to remain on local beaches. Some of the sand from the terrace deposits probably does remain on the beach. It is interesting to consider what contribution eroding sandstone cliffs, say 50 feet high and eroding at a rate of one or two feet per year, might make to local littoral drift. A one mile section of such cliffs would provide about 15,000 cubic yards of material per year so, a long section of rapidly eroding unconsolidated sand cliffs would make a major contribution to littoral drift provided most of the sand grains were large enough to remain on the beach and not be carried offshore into deeper water.

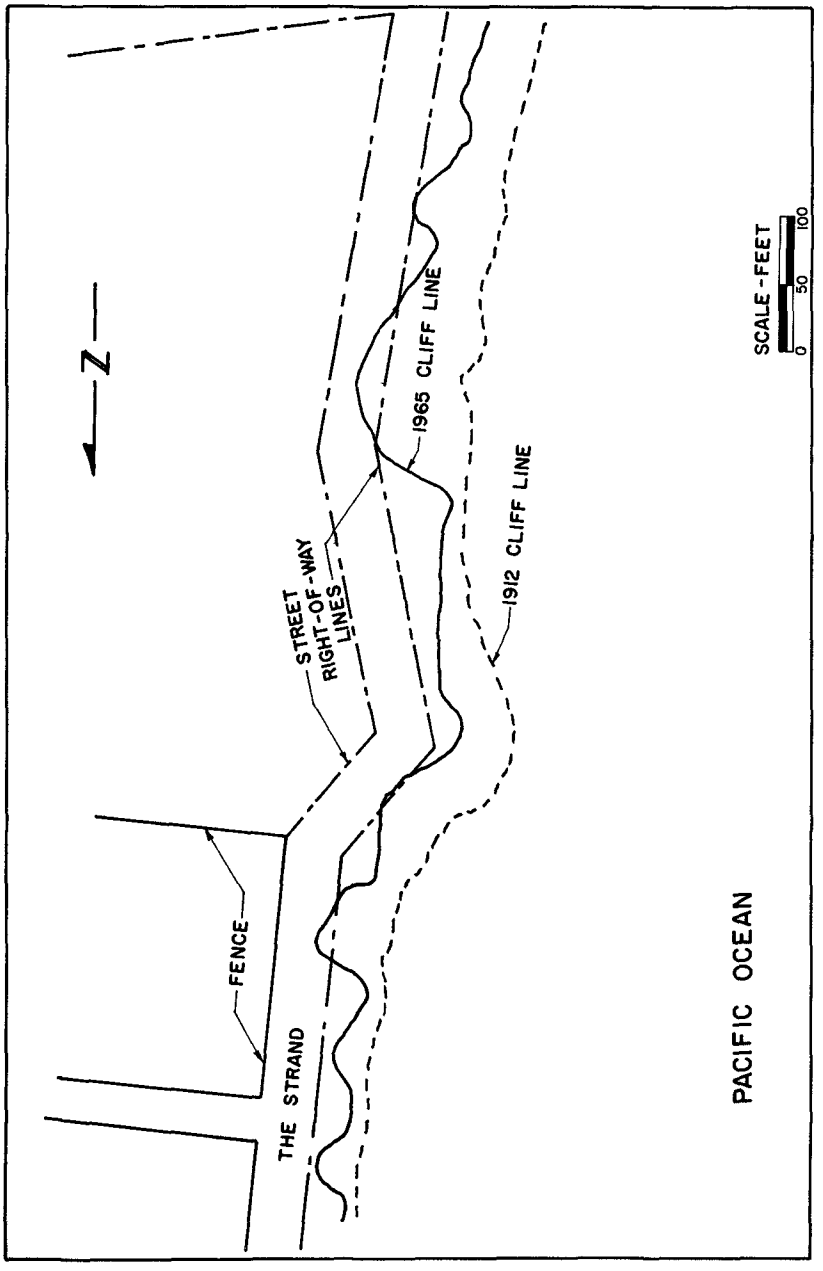

FIGURE 6 - SHORE SECTION NEAR MONTARA SHOWING CLIFF LINE IN 1912 AND 1965

RECENT SEA LEVEL HISTORY

The Quaternary history of sea level, particularly since the last or Lake Wisconsin glacial period must be considered so that the present offshore sea bottom profile can be compared with this sea level history to obtain approximate average historic marine terrace recession rates. It is not possible to perfectly define historic sea levels due to certain difficulties such as recent tectonic activity and isostatic adjustment along the coast; sparsity of data; inaccuracies in carbon-14 dating, etc. However, it is possible to present a first approximation of sea level history for the last 15,000 to 20,000 years that is adequate for our purposes. Fortunately we are most interested in the past 5,000 to 7,000 years and dating accuracy generally increases as the time span decreases.

Fairbridge (1961) has presented a thorough discussion of past attempts at defining historic sea levels, techniques used and problems encountered; and a consensus summary of Quaternary sea level fluctuations. Further data of interest are presented by Curray (1965), Shepard (1964) and others. It is generally believed that the maximum low stand of sea level during the last glacial maximum occurred 17,000 to 20,000 B.P. at 300 to 360 feet below the present sea level. This was followed by the Holocene Transgression during which sea level rose in a rapid irregular fashion to within 30 feet of its present level 6,000 to 7,000 years B.P.

There is some disagreement on the finer details of sea level fluctuations during the last 7,000 years with three basic opinions being offered: (1) Sea level has risen slowly during this time from around-30 feet to its present position asymptotically (see Shepard, 1964). (2) Sea level has been stable at its present position for the past 5,000 years (see Gould and McFarlan, 1959). (3) Sea level reached its present position at 6,000 B.P. and has fluctuated above and below this level ($\pm$ 10 to 15 feet) since that time (see Fairbridge, 1961). For our purposes we can place sea level no lower than about 15 or 20 feet below its present level for at least the last 5,000 years.

DISCUSSION

As glaciers advanced and sea level lowered during the last glacial period the old wave-cut platform and sea cliffs were abandoned and a layer of beach sands was deposited over the exposed sea bottom. It is probable that no major cliffs were carved but small notches may have been carved if there were major still stands of sea level during the overall period of sea level retreat. It is of interest to try to reconstruct events as sea level returned; especially, with regard to tieing together the accepted history of sea level, offshore bottom profiles, and current average cliff recession rates.

Offshore at Montara, the bottom profile is relatively steep for the first mile but it then flattens considerably as the continental shelf is

quite wide. Bottom depths in excess of 300 feet are first reached at a distance of 20 miles from shore. Seaward extrapolation of the lowest marine terrace bedrock surface (assuming a slope similar to that at Santa Cruz) indicates that the surface would intersect the present sea bottom at a distance of four to five miles from the present cliffs. Beyond this point of intersection it is unlikely that platform cutting occurred during the last or Halocene Transgression. Thus, when this rise in sea level occurred it is probable that no sea cliff developed beyond four or five miles from the present shoreline as the sea just drowned a flat beach. The point of intersection between the present sea bottom and the extrapolated terrace bedrock surface lies at a depth of 130 to 150 feet below the present sea level. This was the sea level elevation approximately 10,000 to 12,000 years ago. Cliff recession of four to five miles in 10,000 to 12,000 years gives an average recession rate of 2.0 to 2.3 feet per year. This rate is in reasonable agreement with the present rate of 0.85 to 0.95 feet per year considering our technique of estimating average historic recession rates and since recession rates would initially be higher than average as a cliff line was just developing (so cliffs were low) and sea level was actively rising. Also, we would expect the recession rate to be considerably below average when sea level remains constant, larger cliffs have developed, and waves have a longer shallow water distance to travel and dissipate energy before reaching the shore as has been the case for the last several thousand years.

Just north of Santa Cruz the offshore bottom profile reaches a depth in excess of 300 feet about six miles from shore. Extrapolation of the old marine terrace bedrock surface indicates that the bed was at approximately 260 feet below the present sea level at a distance of six miles from the present shoreline; so, a sea cliff has probably always existed in the Santa Cruz area during the Halocene Transgression. Six miles of recession in 17,000 to 20,000 years gives an average rate of 1.6 to 1.85 feet per year. As at Montara, the recession rate was probably greater than average initially and then less than average and decreasing as sea level stabilized and the wave-cut platform increased in size. Again, average historic recession rates are in reasonable agreement with current recession rates.

Bradley (1958) stated that at Santa Cruz, for a wave base of 30 feet, a wave-cut platform up to one-third mile wide can be carved with sea level remaining constant. A wider platform requires continuous submergence during cutting. This would suggest that, as the 30 foot depth contour is approximately one-third mile from shore where recession rates were measured, no cliff recession should now be occurring nor should the cliffs have undergone recession for the last 5,000 years or so as sea level has remained essentially constant. Thus, Bradley's conclusion is in disagreement with conditions at Santa Cruz and the history of sea level.

Figure 7 shows typical near shore ocean bottom profiles at points near Santa Cruz and Montara where recession rates were measured. These profiles are inconsistent with the local wave base of 30 feet, the history of sea level that states that sea level has been constant or within $\pm$ 10

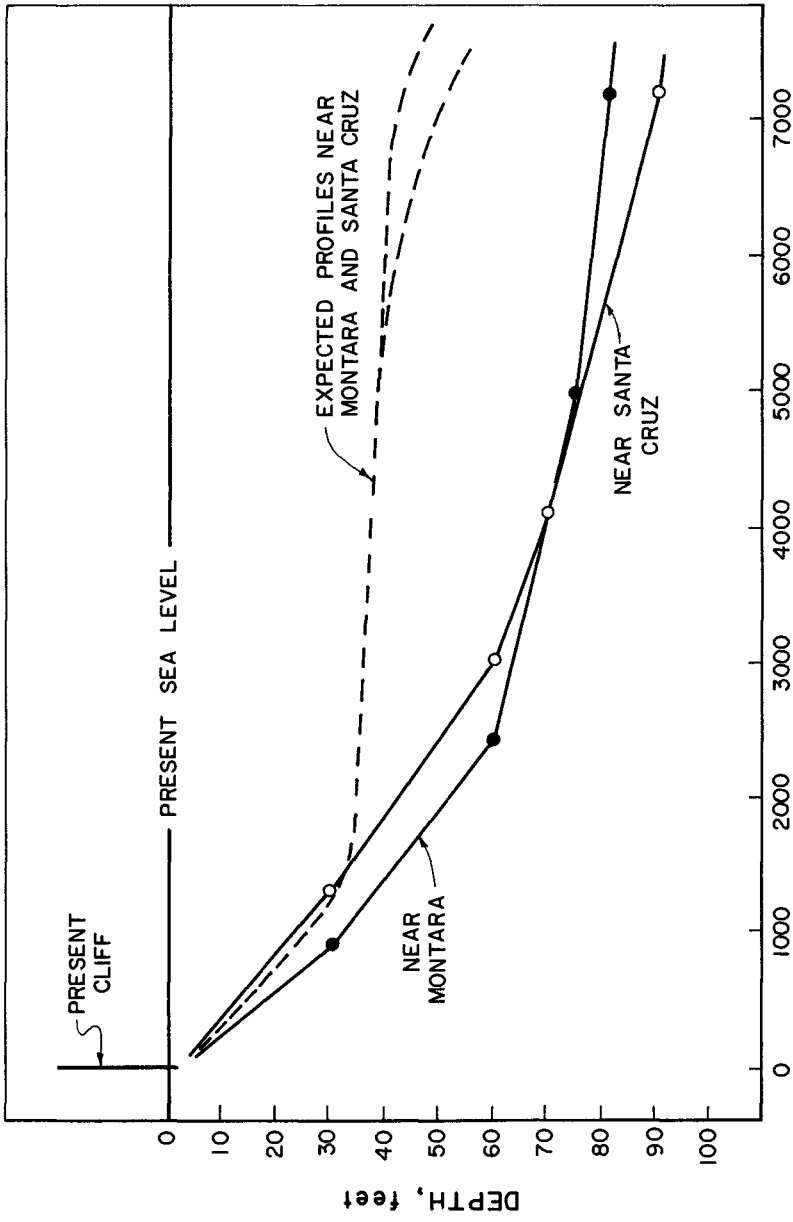

FIGURE 7 EXISTING AND EXPECTED OFFSHORE PROFILES NEAR SANTA CRUZ AND MONTARA

to 15 feet of its present location for 5,000 to 7,000 years, and the observed recession rates at Santa Cruz and Montara. With average recession rates of 0.5 and 0.85 to 0.95 feet per year (or higher) respectively over a period of 5,000 to 7,000 years and a maximum possible erosion depth of 45 feet (30 $\pm$ 15 feet), we would expect profiles similar to those shown by the broken line in Figure 7. From this, it appears that the concept and numerical value of wave base as defined herein requires further consideration.

ACKNOWLEDGEMENT

Dr. Clyde Wahrhaftig, Department of Geology, University of California at Berkeley, suggested that the author conduct this study as part of a graduate seminar course in geomorphology. Professor Wahrhaftig also provided guidance and encouragement during the study.

The author appreciates the assistance provided by employees of the California Public Utilities Commission in helping to locate the Ocean Shore Railroad route survey plans and their patience while the plans were being used.

REFERENCES

Alexander, C. S. (1953). The Marine and Stream Terraces of the Capitola-Watsonville Area. University of California Publications in Geography, Vol. 10, pp. 1-44.

Bradley, W. C. (1956). Carbon-14 Date for a Marine Terrace at Santa Cruz, California. Bulletin, Geological Society of America, Vol. 67, pp. 675-678.

Bradley, W. C. (1957). Origin of Marine-Terrace Deposits in the Santa Cruz Area, California. Bulletin, Geological Society of America, Vol. 68, pp. 421-444.

Bradley, W. C. (1958). Submarine Abrasion and Wave-Cut Platforms. Bulletin, Geological Society of America, Vol. 69, pp. 967-974.

Bramlette, M. N. (1946). The Monterey Formation of California and the Origin of its Siliceous Rocks. U. S. Geological Survey Prof. Paper 212, 57ppp.

Curray, J. R. (1965). Late Quaternary History, Continental Shelves of the United States. The Quaternary of the United States, Princeton University Press, pp. 723-735.

California Division of Mines (1961). San Francisco Sheet: Geologic Map of California.

Davis, W. M. (1909). The Outline of Cape Cod. Geographical Essays, Boston, Ginn and Co., pp. 690-724.

Dietz, R. S. and Menard, H. W. (1951). Origin of Abrupt Change in Slope at Continental Shelf Margin. Bulletin, Amer. Assoc. of Petroleum Geologists, Vol. 35, pp. 1995-2016.

Dietz, R. S. (1963). Wave-Base, Marine Profile of Equilibrium, and Wave Built Terraces: A Critical Appraisal. Bulletin, Geological Society of America, Vol. 74, pp. 971-990.

Fairbridge, R.W.(1952). Marine Erosion. Seventh Pacific Science Congress, Proceedings, Pacific Science Association, Vol. 3, pp. 347-358.

Fairbridge, R. W. (1961). Eustatic Changes in Sea Level. Physics and Chemistry of the Earth, Pergamon Press, Vol. 4, pp. 99-185.

Gould, H. R. and McFarlan, E. (1959). Geologic History of the Chenier Plain, Southwestern Louisiana. Transactions, Gulf Coast Association of Geologists, Vol. 9, pp. 261-270.

Guilcher, A. (1958). Coastal and Submarine Morphology. John Wiley and Sons, Inc., New York.

Hyde, C. G. and Howe, W. C. (1925-1926). Report Upon Improved Sewerage and Sewage Disposal for the City of Santa Cruz, California. Office of the City Engineer, Santa Cruz, pp. 259-260.

Iverson, H. W. (1952). Laboratory Study of Breakers. U. S. National Bureau of Standards Circular 521, pp. 9-32.

Johnson, D. W. (1919). Shore Processes and Shoreline Development. John Wiley and Sons, Inc., New York, 584 pp.

Johnson, J. W. (1961). Historical Photographs and the Coastal Engineer. Shore and Beach, April, 1961.

Johnson, J. W. (1965). Nearshore Sediment Movement-Central California Coast. Santa Barbara Specialty Conference in Coastal Engineering, Chapter 23.

Longwell, C. R. and Flint, R. F. (1955). Physical Geology. John Wiley and Sons, New York, 432 pp.

Moore D. (1965). Recent Coastal Sediments, Double Point to Point San Pedro, California M. A. Thesis, University of California, Berkeley, 86 pp.

National Marine Consultants (1960a). Wave statistics for seven deep water stations along the California coast. For Los Angeles and San Francisco Districts, U. S. Army Corps of Engineers.

National Marine Consultants (1960b). Wave statistics for ten most severe storms affecting three selected stations off the coast of Northern California during the period, 1951-1960. For San Francisco District, U. S. Army Corps of Engineers.

Rich, J. L. (1951). Three Critical Environments of Deposition and Criteria for Recognition of Rocks Deposited in Each of Them. Bulletin, Geological Society of America, Vol. 62, pp. 1-20.

Rode, K. (1930). Geomorphogenie des Ben Lomond (Kalifornien) eine Studie uber Terrassenbildung durch marine Abrasion. Zeitschrift Geomorph., Vol. 5, pp. 16-78.

Sayles, F. L. (1965). Coastal Sedimentation: Point San Pedro Miramontes Point. M. A. Thesis, University of California, Berkeley, 103 pp.

Shepard, R. P. (1964). Sea Level Changes in the Past 6,000 Years: Possible Archeological Significance. Science, Vol. 143, pp. 574-576.

U. S. Corps of Engineers (1956). Beach Erosion Control Report on Cooperative Study of Santa Cruz Area, Pacific Coast of California. U. S. Army Engineers, San Francisco District.

Wiegel, R. L. (1964). Oceanographical Engineering. Prentice Hall, Inc., New York, 527 pp.

Williams, W. W. (1960). Coastal Changes. Routledge and Kegan Paul Ltd., London, p. 84.

Willis, R. (1925). Physiography of the California Coast Ranges. Bulletin, Geological Society of America, Vol. 36, pp. 641-678.

CHAPTER 43

CREATION AND STABILIZATION OF COASTAL BARRIER DUNES

By R. P. Savage[1] and W. W. Woodhouse, Jr.[2]

ABSTRACT

Experiments are underway along the coast of North Carolina using sand fences and dune grasses to create and stabilize a barrier dune line parallel to and behind the existing beaches of low lying barrier islands. Several miles of experimental sections have been established, and their effectiveness in trapping wind-blown sand has been analyzed. Results to date (1968) show that sand fences and dune grasses will trap wind-blown sand and create a barrier dune. A vigorous, rapidly-growing strip of American beachgrass, 90 feet wide, will trap and retain all of the sand being transported by the wind in the area. Thus, a stabilized dune can be "grown" in the area using American beachgrass.

Sand fences have been shown to be effective sand traps and can be used where satisfactory plants are not available or where it may not be feasible to await the establishment of vegetation. Two methods of using sand fences to create large dunes have been investigated; both are workable.

The use of fabrics as sand fences has been investigated; their effectiveness varies with the porosity of the fabric.

INTRODUCTION

Barrier dunes (the line of dunes sometimes found just landward of the beach) can be effective protective structures if they are high enough and wide enough to withstand the onslaught of storm waves. Dunes can provide the land elevation necessary to prevent the wave overtopping and storm tide overwash which often devastates low-lying land forms (barrier islands) during coastal storms. Even in their destruction, dunes provide material (sand) that enables the beach to better adjust to storm conditions and continue to perform its function as a wave energy absorber.

Many examples of protective barrier dunes could be cited, but none are so striking as those of the Netherland Coast where a significant portion of the system that holds back the sea is a massive dune system. These dunes have, understandably, been preserved and strengthened. In other countries, however, the barrier dune system has been neglected and removed or destroyed by man. As a result, many low-lying areas have little or no protection from coastal storms. Property is vulnerable and islands are often breached by inlets that must be closed at considerable expense or allowed to close over long time periods, often at considerable inconvenience.

---

[1]Assistant Chief, Research Division, U. S. Army Coastal Engineering Research Center

[2]Professor of Soil Science, North Carolina State University at Raleigh

This paper presents the results of field experiments to create and stabilize barrier dunes along the North Carolina Coast during the past decade. All of the experimental work has been carried out on low-lying barrier islands, a geographical environment typical of most of the Atlantic and Gulf Coasts of the United States. The experimentation has been directed toward the use of sand fences and dune grasses to catch and hold wind-blown sand and thus create and maintain a barrier dune.

LOCALE OF THE EXPERIMENTS

The barrier islands on which most of the work was done are that part of the barrier-island system of the east coast of the United States that extends from Cape Hatteras to Cape Lookout, North Carolina. (See Figure 1.) One study area is on the southern end of Ocracoke Island just northeast of Ocracoke Inlet; the other is on Portsmouth Island just northeast of Drum Inlet. These areas are characterized by low island profiles, generally rising from the ocean to an ordinary storm berm 4 to 6 feet above mean sea level, and then gently sloping to the sound behind the islands. The islands vary from 1/4 to 1 mile in width and are composed of medium-to-fine sands (approximately 0.2 mm in median diameter) mixed with shell. The tide is diurnal and has a mean range of about 4 feet. The relative transporting capacity of sand-moving winds (those with speeds greater than 12 miles per hour) at Cape Hatteras for a 5-year period is shown in Figure 2.

During late summer and fall the area is often subjected to waves from offshore hurricanes; occasionally, hurricanes move onshore over the area. In winter and spring, the area is affected by northeasters - extra-tropical storms that either move offshore in the area or form along this part of the coast. The low elevation and narrow width of these islands, plus the high waves along this coast, tend to produce a harsh environment for plant growth, as compared with other regions where stabilization work has been done. The salt problem here can be particularly acute. The experimental sites, covered in this paper, receive salt spray from both sea and sound, and have been flooded by both sea and sound. Under these conditions, variability of experimental data tends to be high since storm damage is extremely erratic and unpredictable.

EXPERIMENTAL PROCEDURE

General

The experimental procedure has consisted of establishing experimental sections of either dune grasses or sand fences parallel to the beach and from 200 to 700 feet from the shoreline. These sections vary in length from 200 to 1000 feet, but are generally 500 feet long. Profiles are taken by surveying along at least two ranges across (perpendicular to the beach) the experimental section before the fence or grass is put in place; periodic surveys of the same ranges are made to follow the sand accumulation of the section. The performance of the section is measured by the volume of sand trapped per foot of section length.

Description of Experiments

Vegetation - Three general categories of trials are reported herein:

1) Small exploratory plantings at several locations designed to obtain information on the ability of American beachgrass (Ammophila breviligulata Fern.) to become established under critical conditions and to get estimates of the ability of such plantings to trap and hold sand. These were made at 15 locations distributed along about 200 miles of the North Carolina Coast in March 1964. Plants were spaced 18" x 18" in plantings roughly 100' x 100'. Sand accumulation was measured on three of these in 1964-65.

2) Two series of plots long enough (400-500 feet) to grow frontal dunes and to provide estimates on rate of sand accumulation, dune shape, and grass survival. These were planted during the winter of 1964-65, one on Ocracoke Island and the other on Portsmouth Island (see Figure 3) Variables included presence or absence of sand fence, width of planting, and plant density. In addition, sand fence sections were included so that their sand-trapping effect could be compared with that of the grasses. Comparisons available at Ocracoke are shown in Table 1. The Portsmouth experiment was similar, but not identical.

3) Intermediate size plots (200 feet long) utilizing a non-uniform spacing pattern and comparing four selections of American beachgrass with each other, with nursery-run beachgrass, with sea oats (Uniola paniculata L), and with sea oats interplanted with American beachgrass in growing stabilized dunes.

These treatments were in duplicate making a total of 16 sections and were established on Ocracoke Island in November 1966 beginning a few hundred feet southwest of the 1965 experiment.

The same spacing plan was used on all planted sections, starting with a thick spacing in the center, thinning step-wise to a very wide spacing on the outer edges with 4 rows each as follows:

4 rows 48" x 48"
4 rows 36" x 36"
4 rows 24" x 24"
4 rows 15" x 21"
4 rows 24" x 24"
4 rows 36" x 36"
4 rows 48" x 48"

Total width, front to back, was 78 feet. The fence-alone sections were 500 feet in length, but in order to conserve planting stock, the planted sections were shortened to 200 feet, except those adjacent to fence sections and the end section which were 300 feet long.

All plants used in these studies were nursery-produced. The first exploratory trials were hand-planted, but all planting thereafter was by machine, placing 3-5 culms per hill. Fertilization consisted of three to four applications of 125 pounds per acre of 30-10-0 the first growing season, followed by two such applications the second year, and one application annually thereafter. (For details on planting and fertilization see Reference 3.)

Sand Fences - Two general sets of sand fence experiments were conducted.

The first set was designed to determine if either of two methods proposed earlier (Reference 1) for use in constructing coastal barrier dunes with sand fences was feasible. If both methods proved feasible, this set would determine which method is more economical. Since previous experiments (Reference 1) had shown that straight slat-type fences 4 feet high (see Figure 4) were satisfactory sand traps, straight slat-type fences were used in these tests. The second set of experiments was designed to test the effectiveness of fabric fences 4 feet high. The primary variable tested was the percent porosity (100 times the ratio of the open area of the fence to the total area of the fence). Slat-type fencing (50% porosity) was used in these tests as the standard to which the various fabric fences could be compared.

The two methods of barrier dune construction tested in the first set of experiments are illustrated in Figure 5. Using method (A) of this Figure, fences 1 and 2 would be installed, and allowed to fill by installing either fence first and installing the other after the first had filled, or by installing them both at the same time and allowing them to fill together. Fence 3 would then be installed atop the accumulation of fences 1 and 2. Fence 4 would be installed concurrently with fence 3 or after fence 3 had filled. Fence 5 would be installed after fence 4 had filled and then fences 6 and 7 would be added. This process would be followed, using the fences in numerical order, to achieve the desired dune profile.

Using method (B), fence 1 would be installed and allowed to fill. Fence 2 would be constructed two-thirds of the distance up the front slope of the accumulation of fence 1 and allowed to fill. Fence 3 would then be constructed two-thirds of the distance up the front of the accumulation of fences 1 and 2 and allowed to fill. This process would be continued until the desired dune profile had been created.

The two test sections used to test methods A & B were sections 2 and A of the study sections. Section 2 was 500 feet in length and the first two fences of this section were installed in March of 1964. Section A was 1000 feet in length and the first fence was installed in December of 1962. Surveys of the sand accumulation of both sections were made periodically, and later fences were added as the existing fences filled. In all cases a survey was obtained just before each new fence was added.

In the fabric-fence tests, 16 test sections (sections 32-47), each 500 feet in length, were installed end-to-end parallel to and about 500 feet from the ocean mean-waterline. The sections at each end of the test area (sections 32 and 47) were slat-type fencing as was each fourth section within the test area. The remainder of the test sections were fences of the 6 fabrics to be tested. Two test sections of each fabric were used and these were randomly distributed within the test area. All test sections were installed in December 1965 and periodic surveys were made to follow the sand accumulation of the sections (two profiles across each section). By July 1968 the slat-type fencing was essentially filled, and the experiment was considered complete.

The fabrics used as sand fences are made from plastics or artificial fibers (see Figures 6-a through 6-f). Their porosity (see Figure 6) was determined by covering a field of 200 randomly placed points (dots on an 8 1/2 by 11-inch sheet of paper) with a sample of each fabric and counting the visible points. The number of visible points divided by the total number of points (200) determined the porosity. Five counts were made for each fabric and the average was used in computing the porosity.

Fabric fences were mounted on 2 by 4-inch posts 6 feet apart and 4 feet high. A 4-foot strip of the fabric was stretched between the posts and fastened by nailing a 4-foot lath to each post in such a way that the width of the fabric was clamped between the lath and the post. In addition, a galvanized steel wire of about 1/8-inch diameter was stretched along the top of the posts. The fabric was fastened to this wire with nylon electrical fasteners (cable ties) at 1-foot intervals to prevent sagging of the fabric between posts.

RESULTS

Vegetation

Capacity of vegetation to trap sand - Portsmouth.

This estimate was obtained from cross section surveys taken on the 100 x 100 foot plantings north of Drum Inlet in July 1965, 15 months after planting. At that time, sand accumulation of some profiles was as great as 16 cubic yards per foot of beach (an average accumulation depth of 4.3 feet over the area of the planting). Since these small plantings were exposed on all four sides, they trapped wind-blown sand from all directions. Therefore, the volume of sand trapped greatly exaggerates the amount of sand available in this area for barrier dune construction over large lengths of beach. However, there is no reason to question this figure as an estimate of the capacity of grass plantings to trap sand.

Dune Sections, 1964-65, Ocracoke and Portsmouth Islands.

The most meaningful observations on these plantings came from the Ocracoke trial. The Portsmouth site became rather heavily armored with shell by early 1966, resulting in greatly reduced sand movement at that

location. Fortunately, sand movement on the Ocracoke site has continued at a moderate, though somewhat variable, rate through the experimental period. Sand accumulation for these experiments is shown in Tables 1 and 2.

Planting Width - The 100-foot sections definitely trapped more sand than the narrower plots during the first few months (February 7-August 10). However, by the following June the narrower plots (25 and 50-foot) had caught up, and later differences appeared to be due to variations in sand supply.

Plant Spacing - The only spacing comparison is between sections 13 (plants on 24-inch centers) and 14 (plants 16 inches apart in 20-inch rows) both without sand fence. The 24" x 24" spacing trapped noticeably less sand during the period of early growth (February-June 1965) with little or no difference after that date.

Sand Fence in Combination with Grass - Trapping of sand appeared to be increased in the early stages by putting a sand fence in the narrower plantings (section 16 vs section 18 and section 14 vs section 15) with no consistent difference in the 100-foot sections. This effect tended to disappear after the first growing season. The fences on the 25-foot sections were essentially full by that time, and apparently the mass of vegetation on the wider plantings trapped most of the sand before it could penetrate to the fences.

Dune Shape - Cross section profiles are presented in Figures 7 and 8 to show the development of grass-grown dunes in dense, uniformly spaced plantings under two conditions. Figure 7 is from the site on Portsmouth Island where sand movement was very limited during the period of observation. Figure 8 is from Ocracoke Island where a fairly large volume of wind-blown sand was available.

Dune shape at this planting density is greatly affected by the volume of sand available. With a low volume (Figure 7), there was never enough sand to satisfy the trapping capacity of more than a few feet of the planting. This resulted in a narrow, rather steep, dune along the seaward edge which tended to move seaward in succeeding years as the grass spread into the bare sand in front of the planting. Very little sand succeeded in penetrating to the interior. A similar pattern developed on the landward side of the planting, but involved a much smaller volume of sand.

Under the condition represented in Figure 8, the same principle was operating, but the much larger volume of sand available, particularly from the seaward side, changed the pattern of development somewhat. More sand penetrated to the interior of the planting during the early part of the first growing season, and during the winter and early spring of each succeeding year. This resulted in a dune consisting of two ridges separated by a low area about 20 feet wide. During the approximately three-year period from planting until the March 1968 survey, the total width of the grassed area and the resulting dune had increased from the original 50 feet to around 100 feet, and the top of the seaward ridge was more than 5 feet above the starting level.

Table 1. Ocracoke Island - Sand accumulation by section (in yards^3 per foot of beach) on plots established February 7, 1965.

	25-foot sections			
	Section 17 Sand fence alone	Section 16 Planted 16 x 20 No fence	Section 18 Planted 16 x 20 With fence	Section 19 Planted 16 x 20 With fence
To June 21, 1965	1.12	0.72	1.68	1.35
To Aug. 10, 1965	2.09	1.66	1.94	2.09
To June 1966	4.46	4.46	4.90	5.05
To Jan. 1967	6.09	8.01	7.03	6.34
To Mar. 1968	7.87	10.13	9.87	10.86

	50-foot sections		
	Section 13 Planted 24 x 24 No fence	Section 14 Planted 16 x 20 No fence	Section 15 Planted 16 x 20 With fence
To June 21, 1965	0.62	1.05	1.32
To Aug. 10, 1965	1.78	2.30	2.18
To June 1966	3.46	4 04	5.30
To Jan. 1967	4.65	5.11	7.13
To Mar. 1968	10.07	10.98	10.73

	100-foot sections			
	Section 8 Sand fence alone	Section 12 Planted 16 x 20 No fence	Section 10 Planted 16 x 20 With Fence	Section 9 Planted 16 x 20 With fence
To June 21, 1965	1.02	1.81	2.52	1.40
To Aug. 10, 1965	1.93	2.36	2.74	2.61
To June 1966	3.05	4.61	5.04	4.67
To Jan. 1967	3.69	6.14	6.37	5.17
To Mar. 1968	4.72	9.78	11.35	9.25

Table 2. Ocracoke Island - Average sand accumulation of similar sections (in yards^3 per foot of beach) by periods.

	Av. of 3-25 foot plots	Av of 3-50 foot plots	Av. of 3-100 foot plots	Av. of 2 Sand Fence sections
Feb. 7 - June 21, 1965	1.25	1.00	1.91	1.07
June 21-Aug. 10, 1965	0.65	1.09	0.66	0.94
Aug. 10,1965-June 1966	1.90	2.18	2.20	1.75
June 1966 - Jan. 1967	3.33	1.36	1.12	1.14
Jan. 1967 - Mar. 1968	3.16	4.93	3.23	1.41
Total	10.29	10.56	9.12	6.31

Effect of plant species and strains and planting pattern on dune development - Ocracoke, November 1966.

These sections were located on a very low sand flat (average elevation above MSL of 4 feet or less) which is subject to overtopping by only moderately high storm tides. However, no serious damage occurred to these plantings until April 27, 1967, when they were overtopped by a succession of tides for the next three days. Very few plants were washed out, but salt damage on all sections was severe, with the nursery-run plants being almost completely eliminated and sea oats severely decimated as shown in Table 3.

Table 3. Stand Estimates and Sand Accumulation, Ocracoke Island.

Treatment No.	Species	Selection	Estimated survival - %* Oct. 17, 1967	Sand Accumulation yards^3* March 1968
1	Amer. beachgrass	N.C. Selection A	70	4.52
2	Amer. beachgrass	N.C. Selection B	78	5.01
3	Amer. beachgrass	N.C. Selection 1	77	5.71
4	Amer. beachgrass	N.C. Selection 3	75	5.59
5	Amer. beachgrass	Nursery-run	5	trace
6	Sea oats		30	trace
7	Sea oats**		32)	3.01
	Amer. beachgrass**	N.C. Selection A	68)	
8	(Sand fence alone)		--	7.15

* Average of 2 replications.
**Alternate rows.

The severity of salt damage at this stage is believed to be due to the fact that this was a dry storm occurring during an extended dry period.* Consequently, there was maximum opportunity for sea water to penetrate the root zone during and immediately following the storm, and little opportunity for dilution or removal of salt for some time afterward. In addition, this occurred after spring growth had begun, at a time when the metabolic rate of the plants would be expected to be high. Consequently, many plants were killed and all were obviously damaged with their regrowth drastically delayed.

Differential survival between species and strains can be explained on the basis of the work of Berenyi (Reference 2) who showed that where even a small patch of these grasses is able to survive long enough to trap a few inches of sand, a blister of less saline water begins to develop, under the resulting hummock, enabling the plants to better tolerate later additions of salt.

*Precipitation (in inches) recorded at Ocracoke Village, about two miles from the experimental site, was 0.73 in March, 1.26 in April (0.76 after April 12), with a total of 0.70 occurring as light showers in the period between May 5 and May 21. Fortunately, 4.67 inches fell in the May 22-31 period.

The survey made on this experiment in March 1968 (see Table 3) showed sand accumulations roughly in line with the stand estimates. All four beachgrass selections had collected substantial amounts of sand, the mixed sea oats-beachgrass planting about half as much, while the sea oats-alone and nursery-run beachgrass plots showed only a trace. In this instance, the sand fence sections were superior to the best vegetative plots, accumulating 7 cubic yards per foot against 5 cubic yards per foot for the beachgrass selections.

The spacing pattern followed in this experiment was successful in developing a dune having a much more desirable shape than those in previous trials as shown in Figure 9. The typical beachgrass-selection dune was highest slightly behind the center with an average seaward slope of about 5%. The dune formed by the mixed planting which, due to thinner stand and slower growth, had developed more slowly, had an average slope of about 3% on the seaward side.

The more rapidly growing dunes produced by the beachgrass selections exhibited a definite break in slope about two-thirds of the way down the seaward side (see Figure 9). This appears to have been caused by the large drop in plants/unit area between the 24" and 36" spacings.

Sand Fences

Results of the tests to determine the feasibility of constructing a barrier dune with sand fences are shown in Table 4 and Figures 10 and 11. Table 4 shows the volume of sand accumulated by the existing fences of the test sections just before new fences were added and the volume of sand accumulated by all of the existing fences to July 1968. The sand accumulations of both measured profiles of each section are shown in this Table. However, Figures 10 and 11 show only one of the two profiles of each of the two test sections at the beginning of the tests, just before new fences were added, and in July 1968. While the profiles shown in Figures 10 and 11 are of the area of the test section which trapped more sand than the other profile area, the shape of the dune is representative of the entire test section.

In general, the results shown in Table 4 and Figures 10 and 11 indicate that either method A or B of Figure 3 can be used in constructing a barrier dune. However, method B appears to be superior because it trapped more sand per fence used (3.8 cubic yards per foot of fence) than does method A (2.4 cubic yards per foot per fence)*. In this respect, the comparison is biased because the third set of fences of section 2 were installed before the second set had completely filled. However, it is clear that the results of section 2 would not have been commensurate with those of section A if the third set of fences had been installed at the proper time.

Further improvement in the performance of section 2 might have been realized by increasing the space between fences (20 feet apart instead of 15 feet). Previously (Reference 1) fence spacings of 25 and 50 feet were

*Profile 2-C not used in this computation. See Footnote to Table 4.

Table 4. Sand Accumulation of Multiple Fence Sections - yd^3/ft

SECTION A First fence installed December 1962			SECTION 2 First fence installed March 1964		
Survey date	Profile number	Volume trapped	Survey date	Profile number	Volume trapped
Jan. 1963	A-1	4.9	March 1965	2-A	6.0
	A-3	2.7		2-C*	3.6
		Avg 3.8			Avg 4.8
March 1964	A-1	8.2	June 1966	2-A	8.8
	A-3	5.8		2-C*	7.5
		Avg 7.0			Avg 8.2
March 1966	A-1	13.2	July 1968	2-A	14.3
	A-3	10.0		2-C*	10.4
		Avg 11.6			Avg 12.4
July 1968	A-1	19.0			
	A-3	11.7			
		Avg 15.4			

*Sand accumulation in vicinity of this profile washed out by overtopping water in November of 1964. Fences were replaced, but later sand accumulation not comparable with that of profile 2-A.

tested in this area. In both cases, the two fences accumulated separate dunes (no sand accumulated in the center between the fences) and method A could not be pursued. Therefore, the 15-foot spacing was used in the present test and proved to be a workable spacing. A 20-foot spacing may also prove workable, but study of Figures 10 and 11 leads to the conclusion that one of the fences in such an arrangement would be partially in the area of effect of the other fence installed at the same time and, therefore, would be less efficient than each fence of the configuration of method B.

The results of the fabric fence tests are shown in Figures 12 and 13. Figure 12 shows the volume of sand trapped by each of the test sections, which are shown in the order of installation. The volumes shown were computed from the average of 2 profiles across each test section (at the 1/3 points along the length of the test section) with the exception of sections 35 and 41. A field inspection of the test sections just before the July 1968 survey revealed that one of the profiles of each of these sections was not representative of the sand accumulation of the section. Therefore, only the representative profile of each of these sections was used in the volumetric computations.

The results shown in Figure 12 are quite variable. In at least 4 cases (Fabrics 2, 4, 5, and 6) the volume of sand trapped by a fabric in one location is half that of the same fabric in another location. There is also considerable variation in the performance of the control (slat) fences - a range of from 2.6 cubic yards per foot to 3.1 cubic yards per foot. However, the results of sections made from the same fabrics vary generally with the variation of the control sections (compare slope of line between like fabrics with the slope of the lines between the control sections). Therefore, in using the data of Figure 12, the results were normalized by dividing the volume of sand trapped by the fabric section by the volume of sand indicated by the line between the control sections at that fabric section. Figure 13 shows the normalized volume data as a function of the fabric porosity.

Though the volumetric data is quite variable, there is a marked relationship between fabric porosity and the volume of sand trapped; less porous fabrics trapping more sand. Unfortunately the range of fabric porosities used did not include fabrics dense enough to indicate the fabric porosity beyond which increasing density would not increase the effectiveness of the fabric. However, the results do show that the effectiveness of the fabrics increases with decreasing fabric porosity down to a fabric porosity of 40 percent.

CONCLUSIONS

Vegetation

Vigorous, rapidly-growing stands of dune grasses, such as American beachgrass, have a capacity to trap and retain wind-blown sand which is greatly in excess (up to 16 yd^3 per foot of beach) of the amounts usually

available. This ability to trap wind-blown sand within fairly short distances (12-20 feet), and to renew this capacity by growth and spreading during the growing season tends to minimize the importance of width of planting. For example, from our present data and observations, it appears that where annual sand movement is from 1-3 cubic yards per foot of beach and plants (3 culms per hill) are spaced 18 to 24 inches apart, a planting width of 35' to 40' will trap essentially all of the sand moving. However, where storm damage is likely to occur early in dune development, wider strips are needed to retain sand that becomes dislodged by overtopping of the frontal ridge.

There does appear to be a certain critical mass as well as spacing of vegetation required to effectively halt sand movement. On the North Carolina Coast this can be obtained with American beachgrass, under good growing conditions, by early July of the first year with plants spaced 18" x 18", 3 to 5 culms per hill. Reducing planting density to 24" x 24" reduces cost considerably and may delay attainment of full cover by no more than a month to as much as a year, depending on growing conditions and storm sequences. Good plant survival is, of course, essential, and effectiveness appears to decline rapidly when survival at these densities drops below 75% (see Table 3).

A minimum of 3 culms per hill appears to be a practical compromise between cost and effectiveness. First-year growth has been found to be roughly proportional to the amount of vegetation planted (Reference 3), and single culm hills seldom develop sufficient growth to be effective the first year, unless spaced 12" x 12" or closer.

No evidence has been found to indicate that "staggered" planting patterns have any real merit over plantings in rows containing sufficient optimum size plants/unit area.

Uniformly-spaced plantings of American beachgrass have been the rule in the past. This appears to be an acceptable, although perhaps not ideal, practice where the primary purpose is that of stabilizing a previously constructed dune. However, in the use of this vegetation as a dune-building device, uniform spacing, dense enough to become effective the first year, results in a multi-humped dune cross section. The very characteristic which makes beachgrass useful in building and protecting dunes, the pronounced ability to trap and hold sand, works against the development of a dune which is highest near the center with a long, gentle fore-slope, resulting instead in cross sections such as those depicted in Figures 7 and 8. However, some pattern of non-uniform plant spacing, wide spacings on the outer edges of the grass strip and dense spacing in the center, would seem to offer a fairly simple and inexpensive solution to this problem.

Our preliminary trials along this line are quite encouraging. The planting pattern chosen for the 1966 Ocracoke trial appears to be very close to optimum, producing a dune at the end of two years with an average

slope on the seaward side of 5% or less (Figure 9). We feel that this type of dune should be considerably more resistant to storm action than those produced in the earlier trials and that this is at least approaching the desired cross section. It appears that this pattern could be improved by widening the close-spaced core by 2 or 4 rows, adding a 30" spacing between the 24" and 36" plantings and perhaps omitting the outer 2 rows of 48" on each edge.

This pattern would be about 90 feet wide and require less than 8500 hills per acre, around 80% of that required for a strip of the same width, uniformly spaced 24", and less than half that needed for an 18" planting. Since planting costs are almost directly proportional to the number of hills planted, the variable spaced pattern would be more economical*. In the absence of storm damage, it would probably not trap more sand than the other two, but would build a dune which would have, from the beginning, a more stable cross section. Also, in the event that it was overtopped by one or more storm tides during the first year or two, it would be less vulnerable to damage than the uniform 24" planting.

The addition of a sand fence to such plantings has little effect beyond the first few months since after the first flush of growth, essentially all sand is intercepted by the vegetation before it can reach the fence. A fence can, in some situations, however, play a very vital role by trapping sand during the several months between planting (in winter or early spring), and the development of sufficient new growth to begin to effectively halt sand movement (early summer). If there is sufficient sand movement during this period, the fence will trap a significant amount of sand before the grass becomes effective.

The distinct advantage of early vigor in American beachgrass was clearly demonstrated by all 4 N.C. selections in the 1966 experiment on Ocracoke. Under these critical conditions, the superior ability of these selections to grow off early in the spring enabled them to survive where ordinary nursery-run material failed completely.

These selections were also vastly superior to sea oats in survival, rapidity of establishment, and sand trapping ability during the first two years of the 1966 Ocracoke experiment. Even so, the latter is the dominant species on unplanted foredunes along the Atlantic Coast from the Virginia-North Carolina line southward, and tends with time to replace American beachgrass on planted foredunes in this region (Reference 4).

---

*Estimated cost of large scale machine planting and maintenance through the third year for strips 90 feet wide following a variable planting pattern, similar to that adopted for the Ocracoke-1966 experiment, runs less than $0.50 per foot. This estimate is based on:
American Beachgrass at $15 per thousand 3-stem plants; labor at $2.50 per hour; machine time at $5.00 per hour; 30-10-0 fertilizer at $90 per ton; fertilizer application by helicopter at $2.50 per acre per application.

This is the reason for the interest in interplanting the two to help insure an orderly succession. Our limited experience with this point suggests that this may well be the way to insure continued long-term protection of dunes. However, due to the rapidity with which the beachgrass becomes effective, the planted mixture might better consist of a 5 or 10 to 1 ratio of beachgrass to sea oats rather than the 1 to 1 mixture tried on Ocracoke Island.

Sand Fences

Where a satisfactory beachgrass is not available, sand fences can be used to construct a barrier dune. Either method A or B of Figure 5 can be used, but some experimentation would be required in the area in which the dune is to be constructed to determine the best distance between fences if method A is to be used. Method B appears to make more efficient use of each sand fence used and, for the conditions existing on the North Carolina Coast, is the preferred method.

Fabrics can be used as sand fences and fabric porosity is an important factor in the effectiveness of fabrics as sand traps. Under the conditions existing along the North Carolina Coast during these tests, the volume of sand trapped by fabrics varied essentially linearly with fabric porosity. Fabrics with more than 80% porosity trapped very little sand (an average of 0.6 cubic yards per foot) while a fabric with 40% porosity trapped an average of 2.7 cubic yards per foot. Slat-type fencing used as a control in the tests, trapped an average of 2.8 cubic yards per foot. If the fabric-fence data is normalized, using the slat fence results as the reference, fabrics trapped from 20 percent to 84 percent as much sand as did slat fencing.

Though the range of fabric fence porosities included the porosity of the slat fencing, slat fencing trapped on the average more sand than any of the fabrics. This is an anomaly which cannot be explained by the authors.

ACKNOWLEDGMENTS

This paper is number 2710 of the Journal Series of North Carolina State University Agricultural Experiment Station, Raleigh, N.C., in cooperation with the Coastal Engineering Research Center, Department of the Army, Washington, D.C. The authors appreciate the support and cooperation furnished by the Cape Hatteras National Seashore of the National Park Service, the Wilmington District of the U. S. Army Corps of Engineers, the North Carolina State Department of Water Resources, and the North Carolina Forestry Division. Much of the work described herein is a portion of the research program of the U. S. Army Corps of Engineers and the permission granted by the Chief of Engineers to publish this information is appreciated.

REFERENCES

1. Savage, R. P. (1963). Experimental Study of Dune Building with Sand Fences. Proceedings. Eighth Conference on Coastal Engineering, Mexico City. p. 380.

2. Berenyi, N. M. (1966). Soil productivity factors on the Outer Banks of North Carolina. Unpublished PhD Thesis, N. C. State University at Raleigh.

3. Woodhouse, W. W., Jr. and R. E. Hanes. (1967). Dune stabilization with vegetation on the Outer Banks of North Carolina. Technical Memorandum No. 22. U. S. Army Coastal Engineering Research Center, Washington, D.C.

4. Woodhouse, W. W., Jr., E. D. Seneca and A. W. Cooper. (1968). The use of Sea Oats for dune stabilization in the Southeast. Shore and Beach. Vol. 36, n. 2, (In Press).

5. Zak, J. M. and E. Bredakis. (1963). Dune stabilization at Provincetown, Mass. Shore and Beach. Vol. 31, n. 2. pp. 19-24.

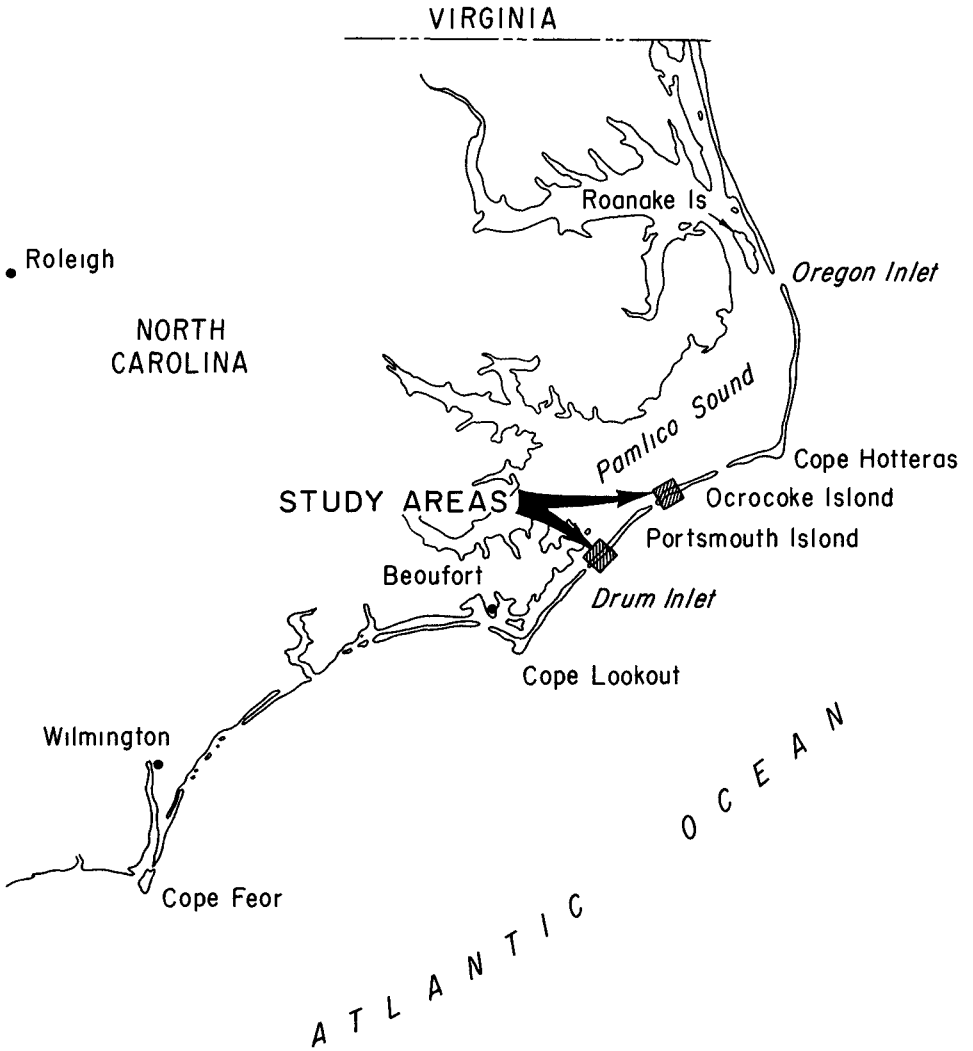

FIGURE I. LOCATION MAP

Compiled from data furnished by the U.S Weather Bureau at Hatteras, N.C. for the period from Jan., 1953 to Dec., 1957

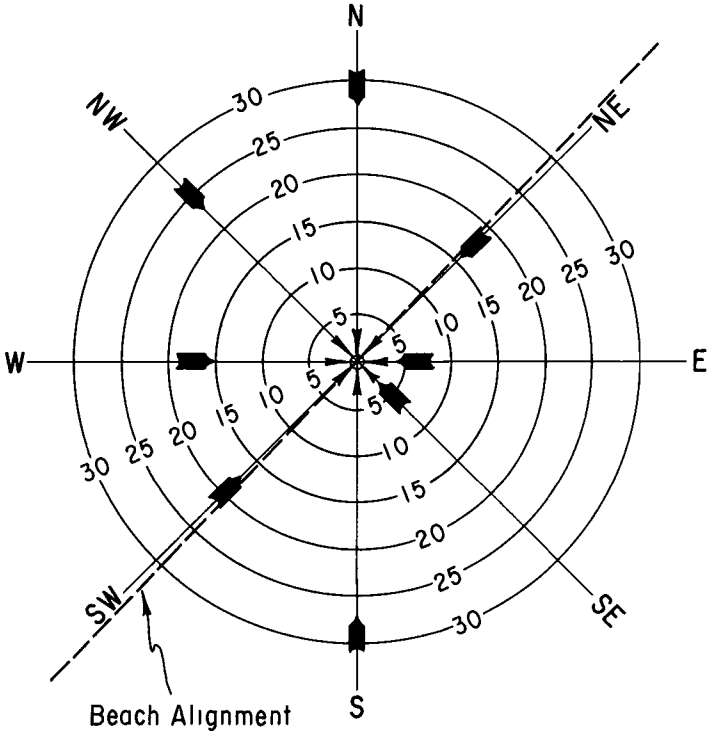

Capacity of the wind to transport sand assumed to be proportional to the wind velocity cubed

FIGURE 2. RELATIVE TRANSPORTING CAPACITY OF THE SAND MOVING WINDS IN THE STUDY AREA

FIGURE 3. EXPERIMENTAL PLOT OF AMERICAN BEACHGRASS (OCEAN TO RIGHT)

FIGURE 4. SLAT-TYPE SAND FENCING

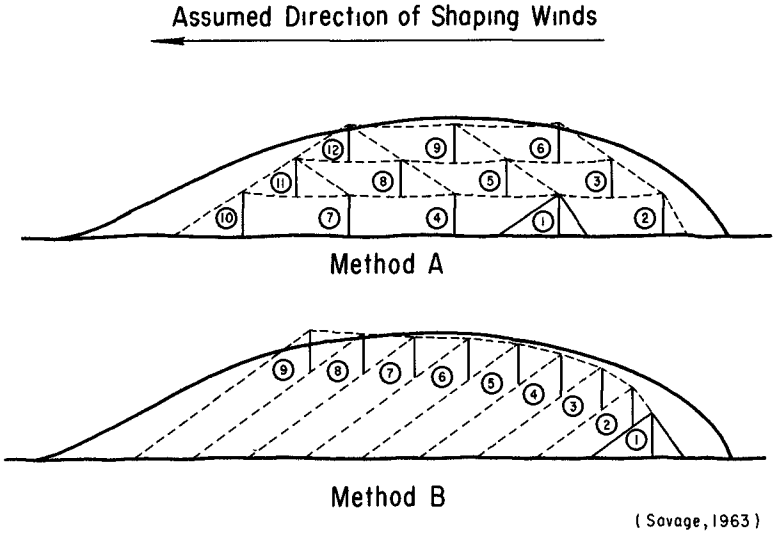

FIGURE 5 PROPOSED PROGRAMS FOR BUILDING A BARRIER DUNE

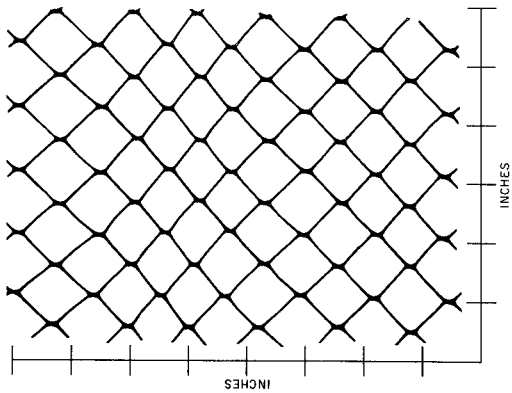

Figure 6b Fabric No 2 (Polyethylene) 86% Porosity

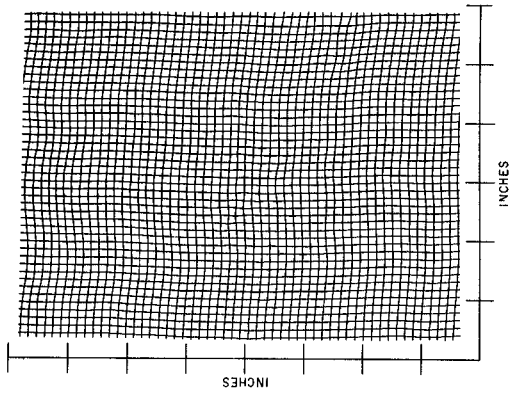

Figure 6a Fabric No 1 (Saran) 55% Porosity

FIGURE 6. FABRICS USED AS FENCING

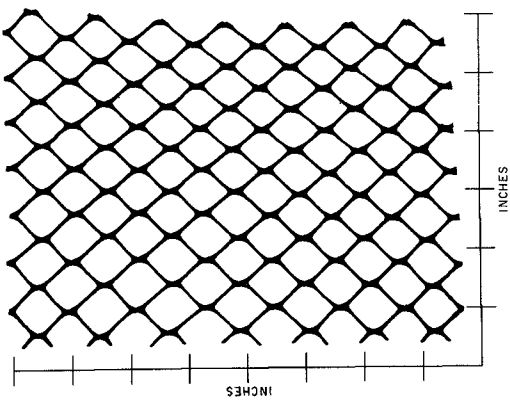

Figure 6d Fabric No 4 (Polyethylene) 82% Porosity

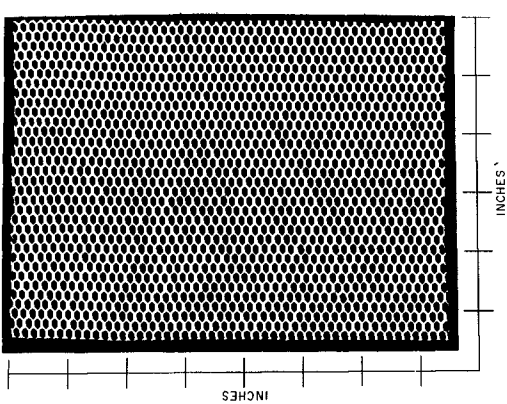

Figure 6c Fabric No 3 (Nylon) 48% Porosity

FIGURE 6 FABRICS USED AS FENCING (Cont'd)

Figure 6e Fabric No 5 (Polyethylene) 68% Porosity

Figure 6f Fabric No 6 (Nylon) 40% Porosity

FIGURE 6 FABRICS USED AS FENCING (Cont'd)

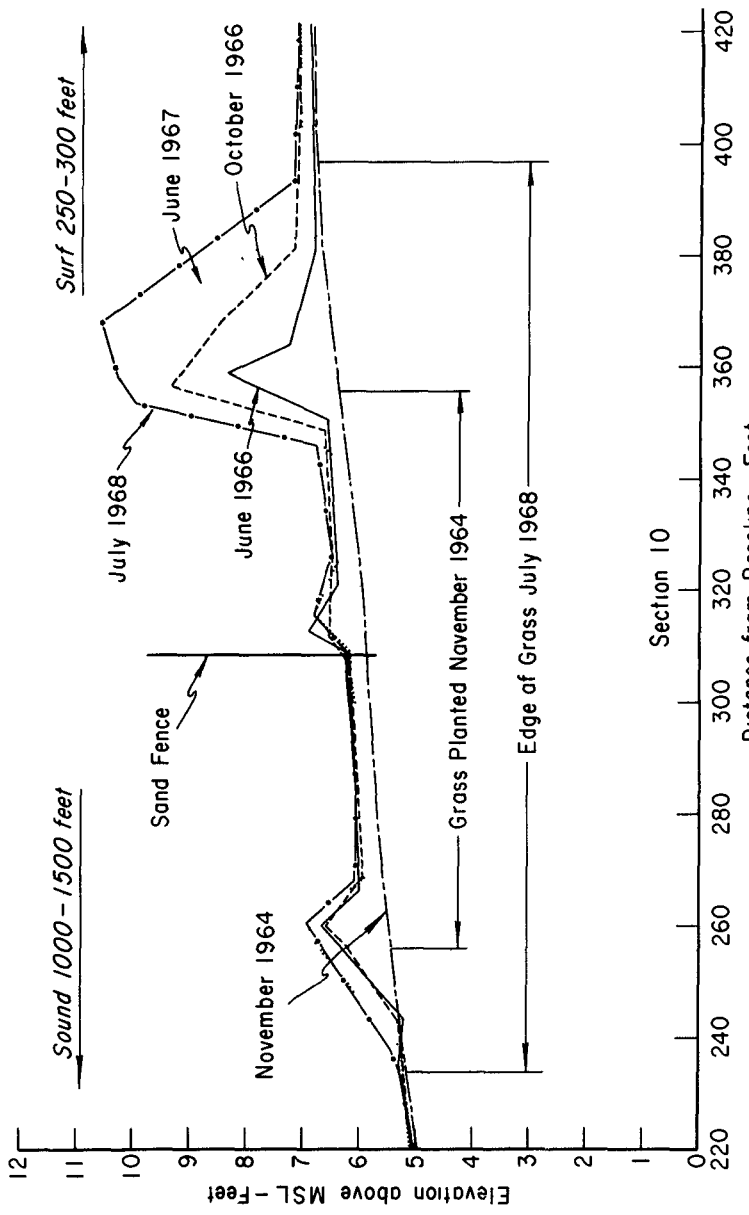

FIGURE 7. DUNE GROWTH – PORTSMOUTH ISLAND

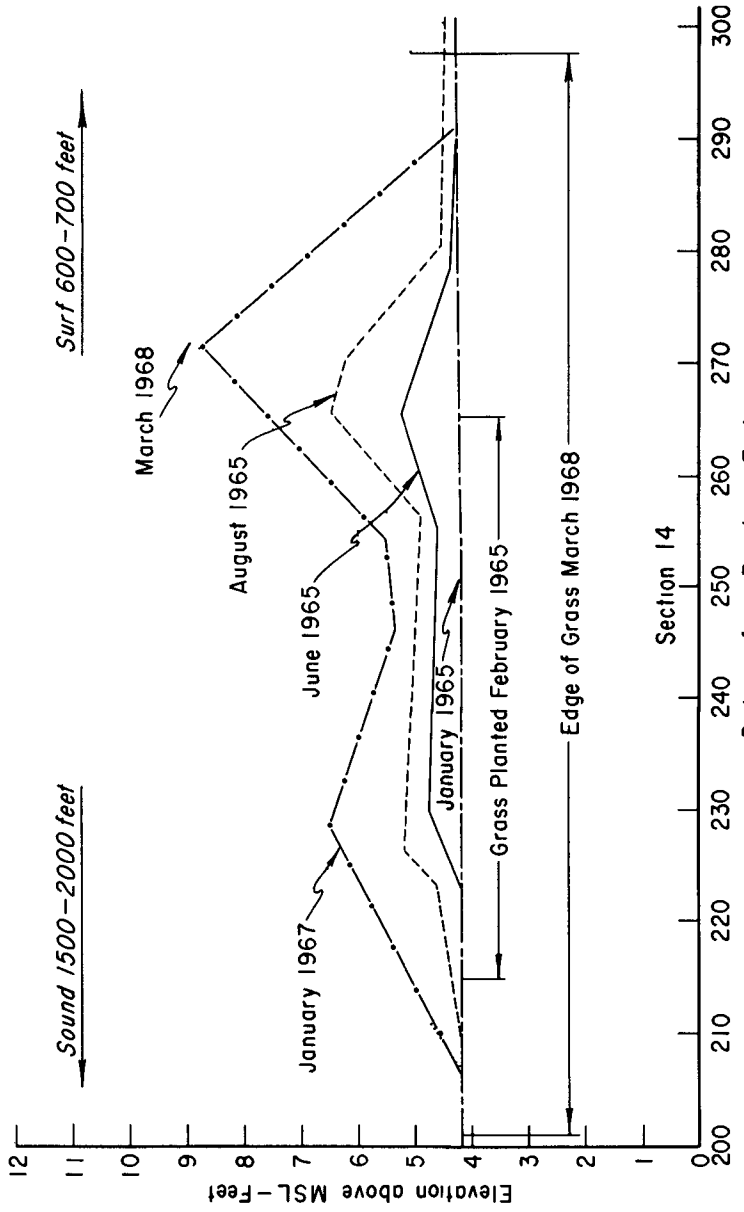

FIGURE 8. DUNE GROWTH – OCRACOKE ISLAND

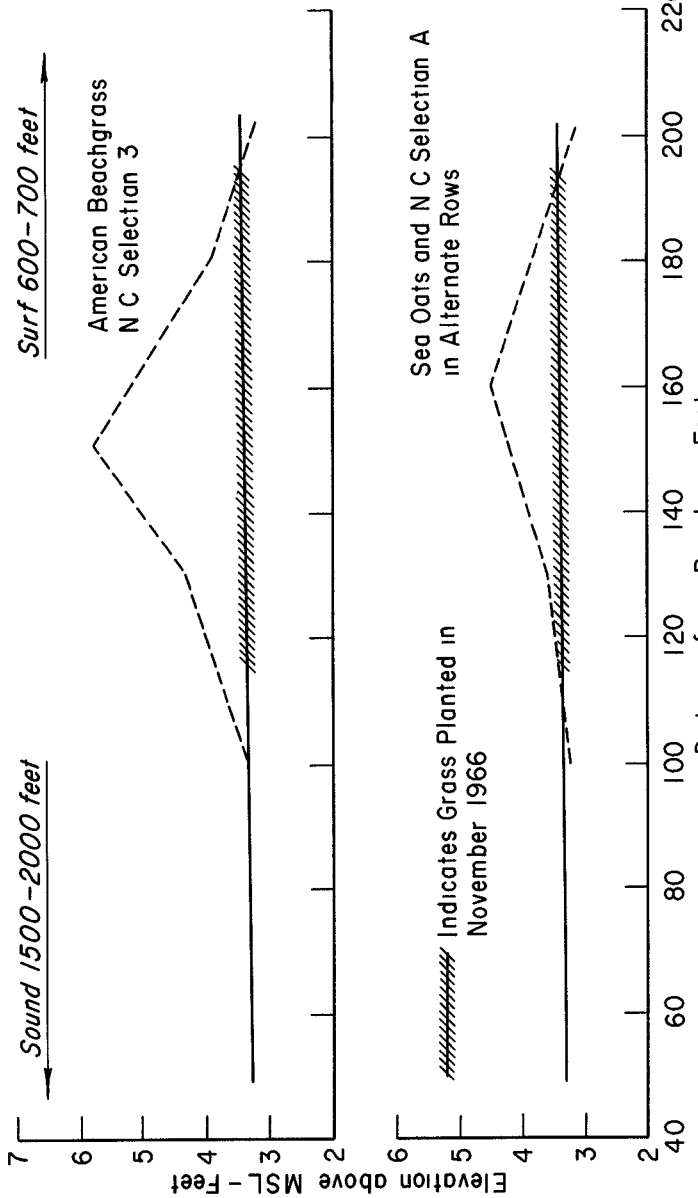

FIGURE 9 DUNE GROWTH BETWEEN NOVEMBER 1966 AND MARCH 1968 - OCRACOKE ISLAND

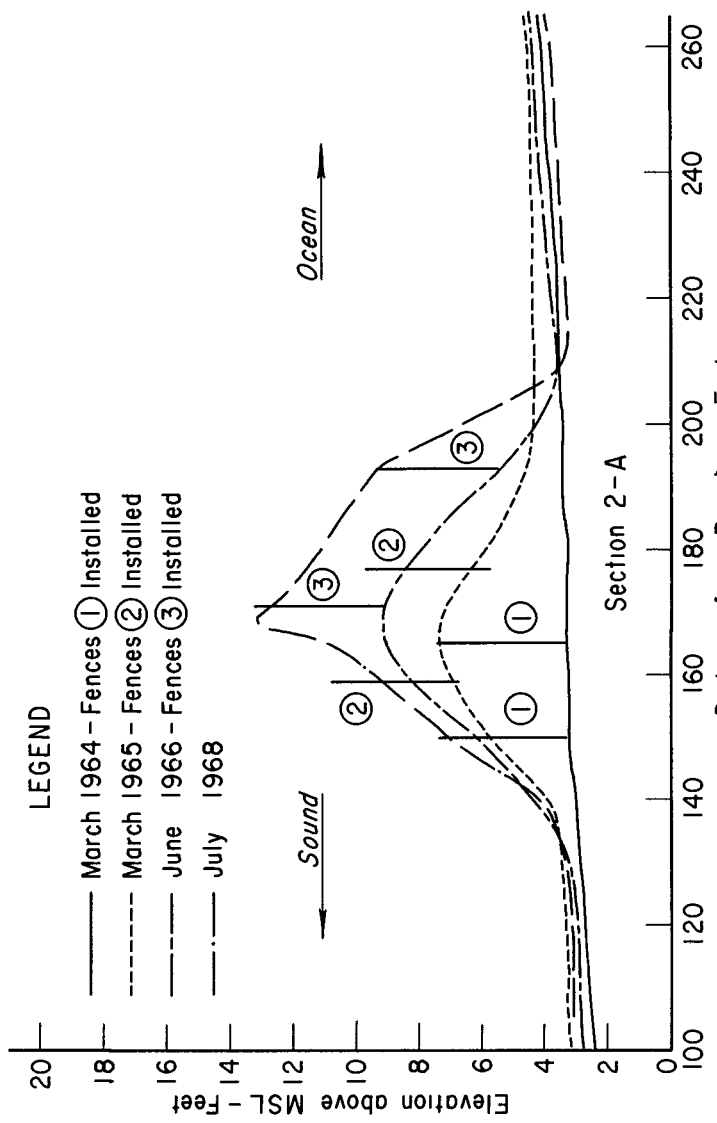

FIGURE 10. SAND ACCUMULATION OF MULTIPLE FENCES – METHOD A

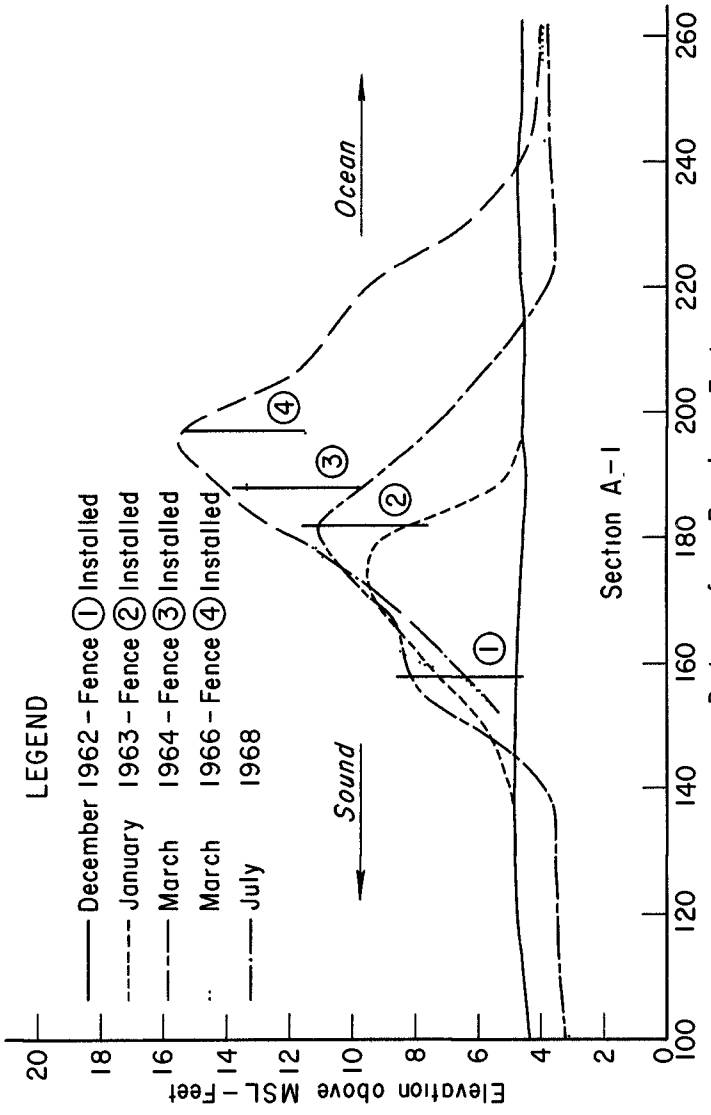

FIGURE 11. SAND ACCUMULATION OF MULTIPLE FENCES—METHOD B

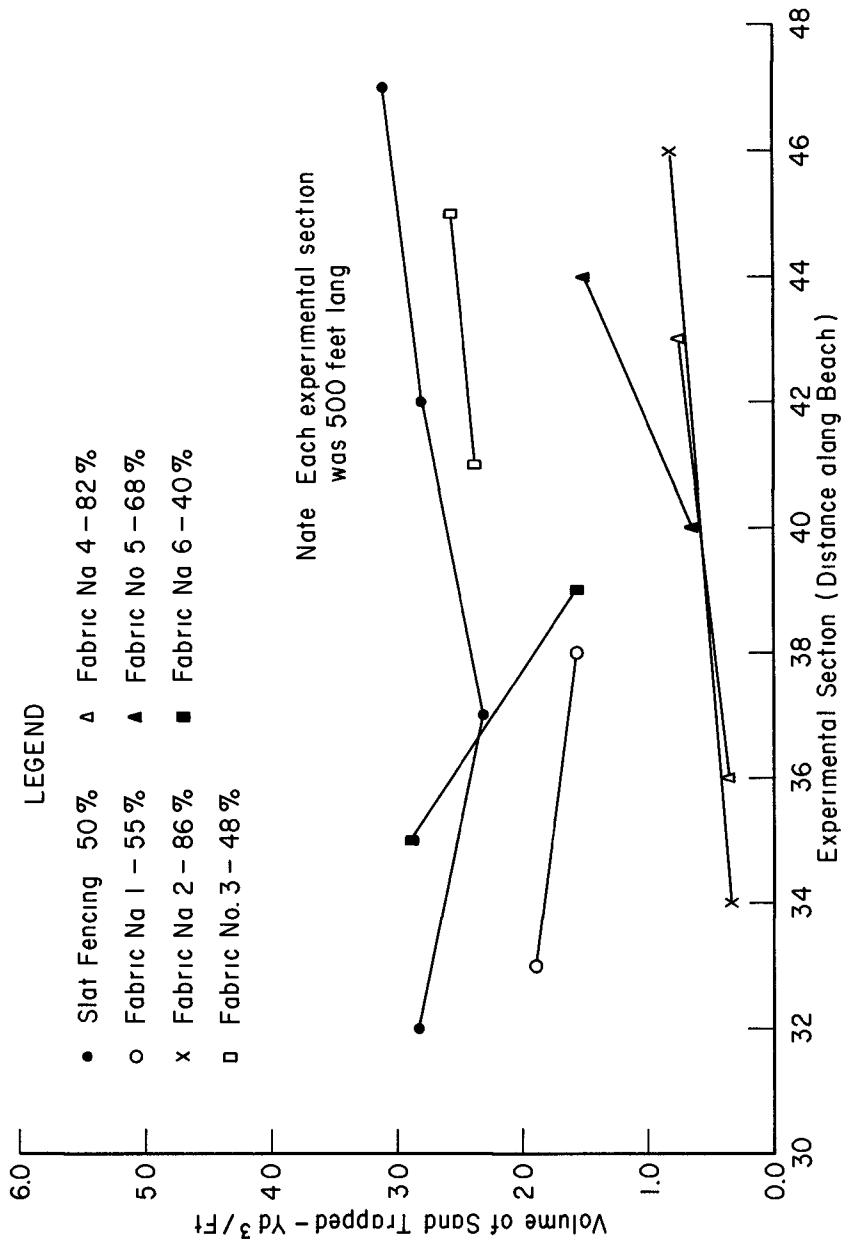

FIGURE 12 VOLUME OF SAND TRAPPED BY FABRIC FENCE TEST SECTIONS

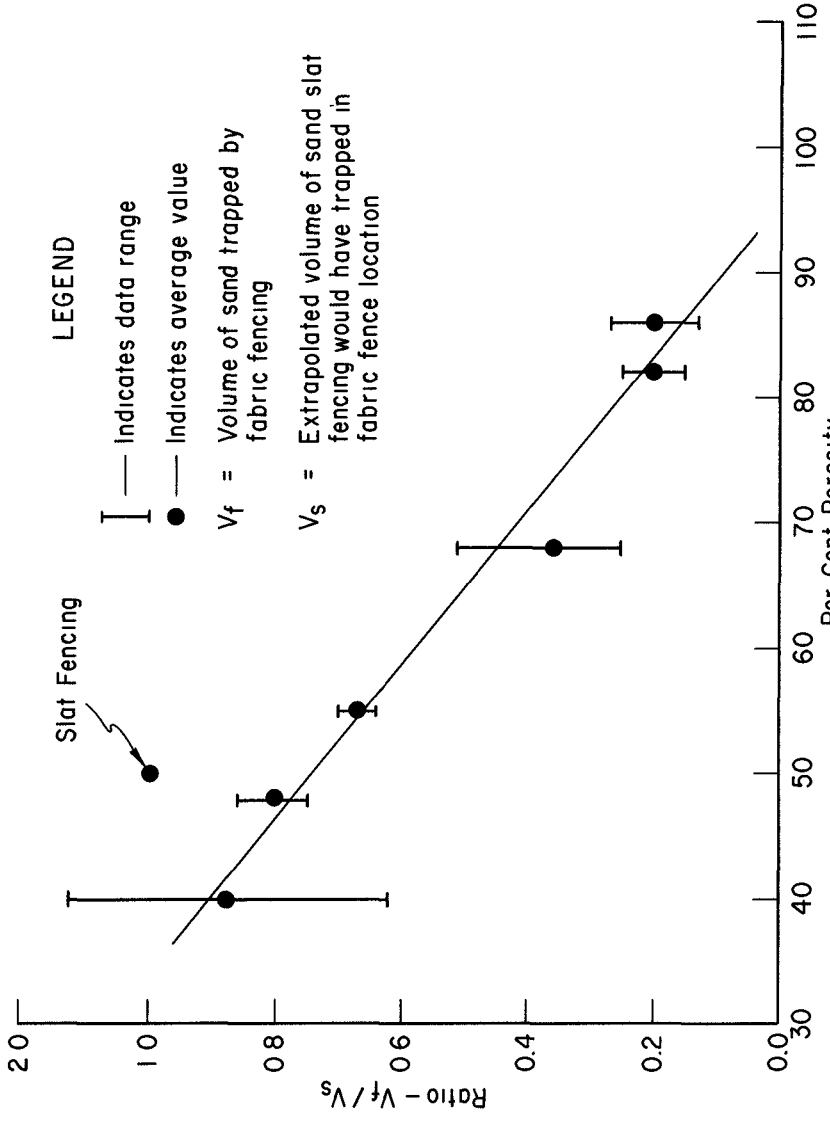

FIGURE 13 EFFECT OF FABRIC FENCE POROSITY ON VOLUME OF SAND TRAPPED

CHAPTER 44

BEACH AND DUNE EROSION TESTS

T. van der Meulen, Delft Hydraulics Laboratory, Netherlands

M.R. Gourlay, Delft Hydraulics Laboratory,
on leave from the University of Queensland, Australia.

INTRODUCTION

In the Netherlands a large part of the country lying below sea level is protected by sand dunes. The erosion of sand dunes during storms at the North Sea, by which the strong wave action is attended with a high sea level, is therefore of extreme importance in the Netherlands.

It is almost impossible to do adequate measurements along the coast during storms. Accordingly the Delft Hydraulics Laboratory was requested by the Public Works Department of the Dutch government to investigate in a model a number of matters related to both the maintenance of existing dunes and the design of artificial sand dunes as sea defence works.

The investigations reported in this paper are concerned with the following problems

a) the influence of the height of sand dunes upon the amount of coastal recession during storm conditions.

b) the influence of the wave characteristics upon the amount of coastal recession.

c) the differences in coastal recession and profiles obtained with regular waves and those obtained with wind waves.

The reproduction on scale of the phenomena in the surf zone is a difficult matter. Many investigators have come to the conclusion that there are several scale effects. Till now our knowledge is not sufficient to determine the magnitude of the scale effects. Owing to this the described tests can give only qualitative information.

DESCRIPTION OF THE TESTS

A synopsis of the tests is shown in table 1. The tests have been carried out in different wave basins, which dimensions are given in table 1. In all tests the wave direction was perpendicular to the beach. The bed of the model and the dune were composed of fine sand (d_m = 0.22 x 10^{-3} m). A wave filter has been placed in front of the wave machines to reduce the effect of innatural reflection from the wave paddle.

The starting profile was the same for all the tests and was obtained by regular waves T = 1.56 secs and H_o = 0.155 m with normal water level (N.W.L.). The slope of the upper beach obtained with this wave condition was produced till 0.12 m above normal water level. From this point a sand dune was placed with a slope and a height as marked in table 1.

For the erosion tests the still water level was heightened till 0.12 m above normal water level and this water level was marked as storm surge water level (S.S.W.L.).

The test T_1 - T_5 give information about the influence of the dune height, T_6 - T_{12} give information about the influence of the wave steepness and the period, while T_{10} - T_{15} give some information about the influence of wind waves in regard to regular waves.

The basis of comparison between the wind waves and the regular waves was:
1) The period of the regular waves is equal to the central spectral period of the wind waves.
2) The root mean square wave height of the wind waves (calculated from the energy density spectrum) is equal to the root mean square wave height of the regular wave (sine wave: $H_{rms} = 0.707\ H$).

The wind velocity in the wind flume was 10.5 m/s, 16.2 m/s and 21.7 m/s, respectively for T_{13}, T_{14} and T_{15}.

test	dune height in m	slope	period in sec	H_o in m	model dimension in m	type of wave
T1	0.10	1:1.75	1.56	0.197	16x15	regular wave
T2	0.20	1:1.75	1.56	0.197	16x15	regular wave
T3	0.30	1:1.75	1.56	0.197	16x15	regular wave
T4	0.40	1:1.75	1.56	0.200	16x15	regular waves
T5	0.80	1:1	1.56	0.207	16x15	regular waves
T6	0.40	1:1.75	1.63	0.176	100x4	rsgular waves
T7	0.40	1:1.75	1.63	0.195	100x4	regular waves
T8	0.40	1:1.75	1.56	0.107	16x4	rsgular waves
T9	0.40	1:1.75	1.56	0.154	16x4	rsgular wavss
T10	0.40	1:1.75	1.04	0.098	16x4	regular waves
T11	0.40	1:1.75	1.16	0.134	16x4	regular wave
T12	0.40	1:1.75	1.29	0.182	16x4	regular waves
T13	0.40	1:1.75	1.00	0.134 *	100x4	wind waves
T14	0.40	1:1.75	1.11	0.190 *	100x4	wind waves
T15	0.40	1:1.75	1.29	0.210 *	100x4	wind waves

table 1 * H_{15}

MEASUREMENTS

The beach profiles were measured from the crest of the sand dune seawards through the surf zone to the 16 metres distance mark (i.e. just in front of the wave filter for the basins of 16x15 m and 16x4 m). The measurements were made by ordinary level and staff at 10 cm intervals up to the 5 metres distance mark and at 20 cm there after along each profile. The distance between the profiles was 1.5 m for the basin with a width of 15 m and 0.75 m for the flumes with a width of 4 m. The measurements were made at 0, 1/2, 1, 2, 3 1/2, 5 1/2, 8, 11, 14 1/2 and 19 hours after the commencement of the test.

The wave heights were measured using the Laboratory's own design of temperature compensated parallel resistance wave height meter.

The regular waves were measured at 13 points spaced over a distance of one wave length in the direction of wave propagation and located on the deeper part of the beach profile (i.e. at a depth of roughly 0.5 m). With this information it was possible to distinguish the incident wave and the reflected wave from the beach. During a test large variations of the reflection coefficient were observed, which can be related with the changes in the beach profiles. The wave heights in table 1 are the wave heights of the incident wave.

The wind waves were measured at a fixed point (at a depth of roughly 0.5 m) over a period of at least 500 waves, mostly every half hour during a test. Records were made upon both Sanborn recorder and magnetic tape. The latter were used to produce a punched paper tape from which the energy density spectrum was calculated using a digital computer. An anoloque root mean square analyser was also used in the wind wave tests to obtain a rapid evaluation of the root mean square wave height, which values generally compared favourably with those calculated from the wave spectra.

RESULTS OF THE TESTS

Results of the tests T_1 - T_5

At the beginning of all the tests the sand eroded from the dune is deposited largely inshore of the 5 metres distance mark and rapidly builds up an inshore breakpoint bar. Visual observations on the model indicated that a definite plinging breaker occurred in this vicinity. Spilling breakers however occur at the initial breakpoint near the 7.5 metres distance mark. After a maximum building up of the inshore bar the slope of the seaward face of this bar flattens as an increasing part of the eroded sand moves seawards into the outer bar, which builds up steadily during the test and at which the initial breakpoint finally stabilises. In the latter part of the test plunging breakers occur in the initial breakpoint.

The profiles after a long time for different dune heights are basically the same except that they has been displaced in position along the horizontal axis (fig. 1 for T_1 and T_5). The represented profiles are average profiles of ten individual profiles. Especially in the surf zone 3-dimensional effects such as rip currents occur. In T_1 the inner bar is shifted away by taking an average profile. The difference in the seaward slope of the outer bar between T_1 and T_5 can be caused by a too short time of testing.

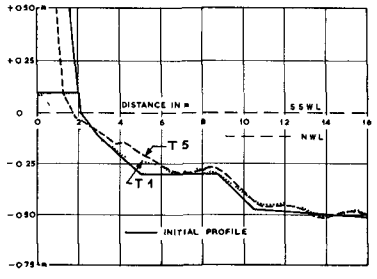

Fig. 1 Average profiles after 19 hours T_1 and T_5.

In figure 2 the recession of the dune foot for several dune heights is represented as function of time. The recession is measured as the horizontal displacement from the initial storm surge waterline. The dune foot corresponds in the tests to the limit of wave run up, so the dune foot is the limit of the wave formed profile.

The recession of the storm surge waterline shows the same tendence as the recession of the dune foot, but of course with a smaller amount of recession. Figure 2 shows a very definite influence of the dune height upon the recession of the dune.

In figure 3 the eroded volume from dune and beach is represented as a function of the time. From the two figures one can make the statement that with an increasing dune height the recession of the dune decreases, but the sand volume eroded from the dune and the upper beach increases.

Dune erosion is very rapid in the early stages of the test. Almost 50% of the erosion expressed in eroded volume occurs in the first 1/8 of the time required to reach more or less equilibrium.

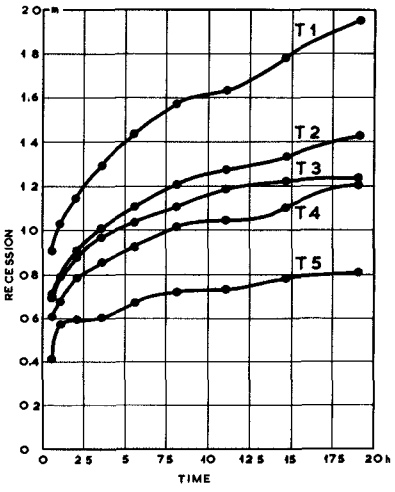

Fig. 2 Dune foot recession $T_1 - T_5$.

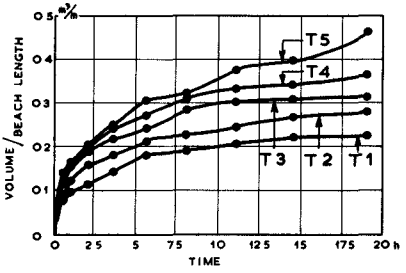

Fig. 3 Total volume eroded from beach and dune $T_1 - T_5$.

The recession of the dune foot is much more rapid. After 1/40 of the time required to reach more or less equilibrium almost 50% of the obtained maximum dune foot recession is reached.

For the given wave conditions, storm surge water level and sediment the profiles seem to be independent of the dune shape. The obtained profiles after 19 hours can be practically considered as equilibrium profiles. Their general shape can be represented by a parabola similar to that given by the empirical formula of Larras (reference 1). However bars occur in the profiles in the model and therefore this formula is not adequate for calculation purposes mentioned here after.

Maximum dune recession can be determined by moving the initial and the final (equilibrium) profile relative to one another until the eroded and deposited volumes are equal. This means that the dune recession is influenced by the initial profile.

Of course the above mentioned method is only valid if the eroded material from the dune and the upper beach is deposited in the cross section perpendicular to the coast, which we can expect with waves perpendicular to the coast and with no resulting currents along the coast.

Results of tests $T_6 - T_{12}$

In figure 4 the dune foot recession has been plotted as a function of time for $T_6 - T_{12}$. From this figure it is apparent that the recession of the dune foot at a given time is greater when the wave height is greater while the period is the same or almost the same.

For waves with wave heights of the same order but different periods the recession of the dune foot is smaller for the waves with the smaller period.

So we can conclude that the recession is not alone a function of the wave steepness, but also a function of the wave length. This is in agreement with the investigations of Saville (reference 2) and Iwagaki and Noda (reference 3) for initial profiles with one straight slope.

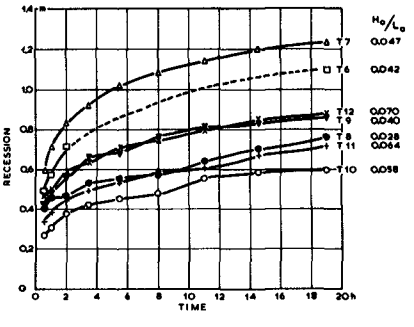

Fig. 4 Dune foot recession $T_6 - T_{12}$.

The number of tests is too small to determine a functional relationship between dune foot recession, wave steepness, wave length and time for a given sediment, water level, shape of sand dune and initial profile.

Results of tests $T_{10} - T_{15}$

There is no consistent difference in the recession of the storm surge waterline for wind waves as compared with regular waves. The recession of the dune foot however is consistently greater for wind waves than for comparable regular waves (fig. 5, 6 and 7).

The beach slope near the storm surge waterline is not much different for wind waves, but the dune foot is laying higher than for regular waves (fig. 8).

This can have several causes:

1° The greater wave run up height due to
   a) a certain percentage of the wind waves is higher than the wave height of the regular waves.
   b) the direct action of the wind as the uprush moves up the beach.
   c) the smoother profiles which are obtained with the wind waves.

2° The wind is moist from spray blown off the wave crest, which fact probably results in a dune face having a higher moisture content than with regular waves. The extra weight of this increased water content of the sand will increase the rate of collapse of the dune face due to instability.

By the above mentioned causes extra sand is placed within the reach of the waves and probably the bottom return current may assist in the removal of this sand in the seaward direction.

Looking to the figures 5, 6 and 7 it appears that the effect of the wind velocity (and model effects) are more important than those of wave irregularity. In order to separate the influence of the irregularity and the wind velocity it would be valuable to have a third serie of tests with waves generated by a programmed wave paddle.

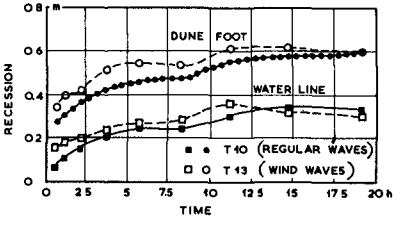

Fig. 5 Dune foot and waterline (S.S.W.L.) recession T_{10} and T_{13}.

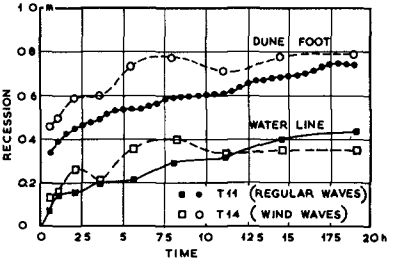

Fig. 6 Dune foot and waterline (S.S.W.L.) recession T_{11} and T_{14}.

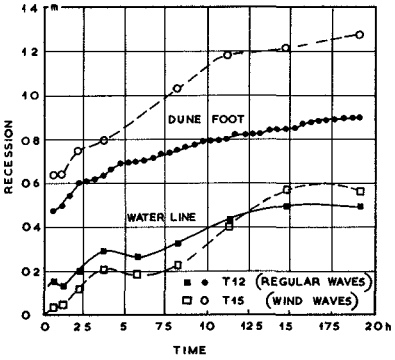

Fig. 7 Dune foot and waterline (S.S.W.L.) recession T_{12} and T_{15}.

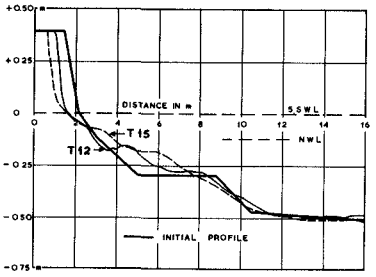

Fig. 8 Average profiles after 19 hours T_{12} and T_{15}.

CONCLUSIONS

1)The recession of a sand dune at a given time when measured by either the change in position of the storm surge waterline or the dune foot position increases as the height of the sand dune decreases. The eroded volume from the dune and the upper beach decreases as the height of the dune decreases.
2)For given wave conditions, storm surge water level and sediment the equilibrium profiles seem to be independent of the dune shape.
3)The dune erosion at a given time is a function of the wave steepness and also of the wave length for a given sediment, storm surge water level, shape of sand dune and initial profile.
4)The dune foot recession at a given time is greater for wind waves than for regular waves with the same energy (or H_{rms}) and a period equal to the central spectral period of the wind waves.
5)With wind waves the bars in the final profiles are not so prominent as with regular waves.
6)Dune erosion is very rapid in the early stages of the tests.
7)For circumstances where the eroded material is deposited in a cross section perpendicular to the coast maximum dune erosion can be determined by moving the initial profile and the equilibrium profile relative to one another until the eroded and deposited volumes are equal. This requires knowledge of:

a) the initial profile
b) wave conditions
c) storm surge water level
d) equilibtium profile for b and c
e) wave run up
f) slope of the eroded dune face

REFERENCES

1. Larras, J. - Les profils d'équilibre des fonds de sable sous la mer. Ann. des Ponts et Chaussées, vol 129, no. 4, 1959, pp. 391 - 404.

2. Saville, T. - Scale effects in two dimensional beach studies.
Procs. 7th I.A.H.R. Congress Lisbon, vol 1, paper A_3, 1957.

3. Iwagaki and Noda - Laboratory study of scale effects in two dimensional beach processes.
Procs. 8th Coastal Engineering Conference, Mexico City, Nov. 1962, pp. 194 - 210.

CHAPTER 45

DUNE EROSION AND PROTECTIVE WORKS AT PENDINE, CARMARTHENSHIRE, 1961-68

R.S. COLQUHOUN, Senior Civil Engineer, Ministry of Public Building and Works, LONDON

ABSTRACT

The paper describes the application of a novel method of protecting parts of the sand dunes at Pendine, S.W. Wales. These dunes are subject to erosion under conditions when high tides are combined with south-westerly gales.

A series of random rock-fill mounds were sited 20 feet away from the toe of the dunes in certain areas where structures erected on the dune crest were liable to damage through erosion at the toe of the dunes. The object of the mounds is to trap wind-borne sand in the area enclosed between the mounds and the dunes, and also to check wind-driven waves before they can reach the dune face.

Over seven years the mounds and sand traps have operated in accordance with their design concept. Not only have the traps filled with sand but further sand accretion has occurred on the protected dunes, resulting in a flatter slope and a strong growth of self-sown pioneer vegetation on the protected face and on the sand trap surface.

INTRODUCTION

This paper describes an empirical solution to the problem of combatting erosion on parts of the dunes at Pendine sands, and records the results achieved over a period of seven years. Pendine has a place in the history of mechanical engineering, since it was on Pendine sands that the world's land speed record was raised by Sir Malcolm Campbell from 146.16 m.p.h. in 1924 to 174.88 m.p.h. in 1927. It was at Pendine also that Parry Thomas, seeking to break Sir Malcolm's record, met his death.

GENERAL DESCRIPTION OF THE SITE

Topography and Geology

The site of the works lies at the head of Carmarthen Bay, S.W.Wales. It consists of a wide, flat, sandy beach - Pendine Sands and Laugharne Sands - backing on to a range of dunes, 6 miles long, which vary in width between 400 and 700 yards. Behind the dunes is an extensive area of reclaimed alluvial marshes, which extend northwards to the foot of steeply sloping hills of old red sandstone. At the west end, the site is bounded by limestone cliffs, and there is a limestone peninsula, worked as a quarry, jutting into the central marsh area. The eastern end is bounded by the river Taf.

The sand composing the dunes, both in the old-established and recent growth areas, is of a very uniform character, 100% passing B.S.52 and being retained on B.S. 200. Similar grading results

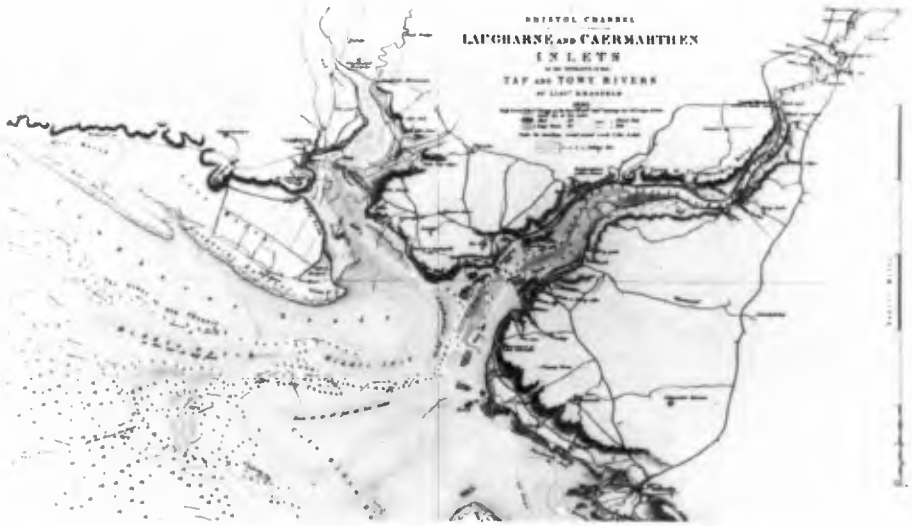

Fig.1. Pendine and the Taf estuary in 1830

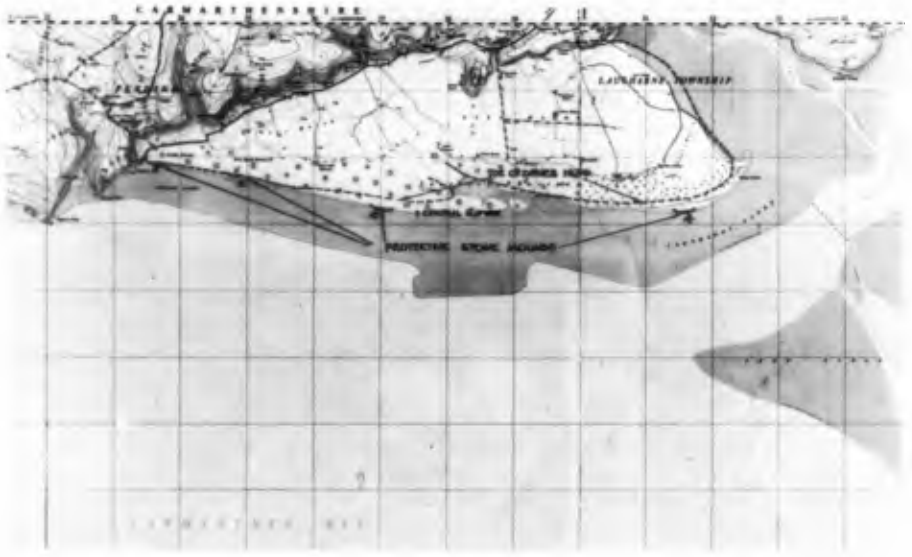

Fig. 2. Pendine and the Taf estuary in 1950

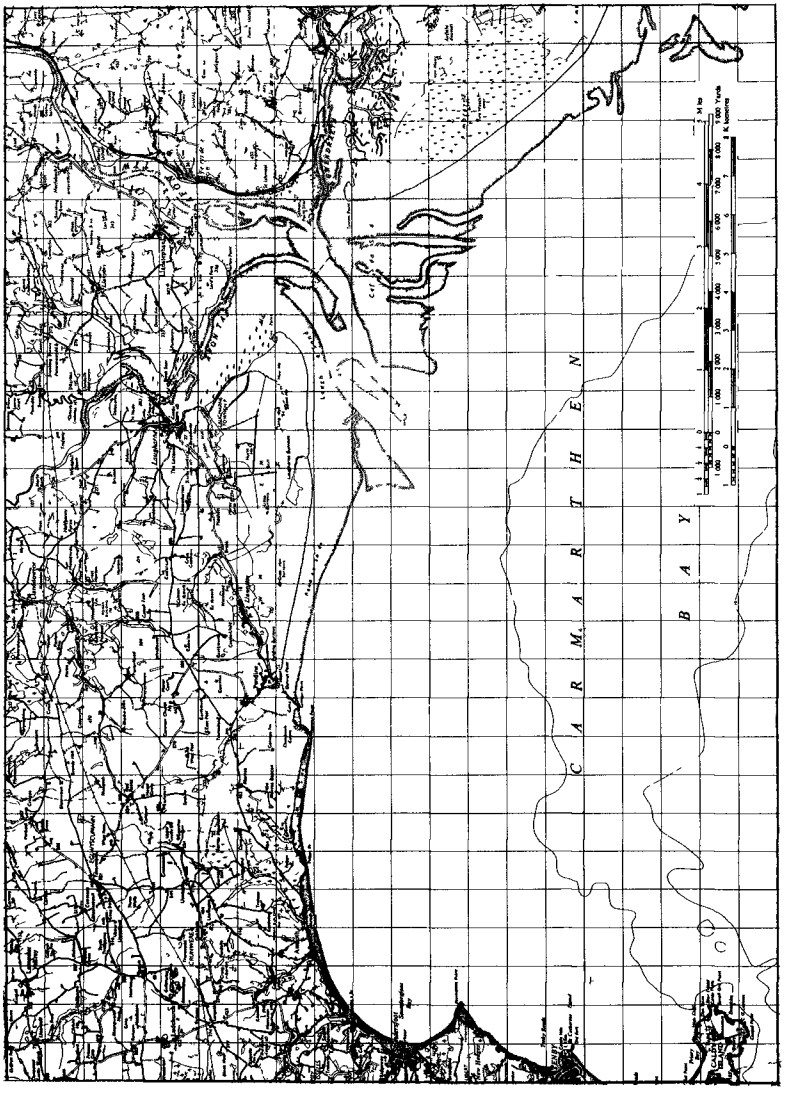

Fig. 3. Carmarthen Bay

were obtained from 10 out of 12 boreholes, situated at intervals over a 3,000 foot length behind the first ridge of the dunes and taken to depths of up to 60 feet. In two boreholes only, the typical grading was varied by the presence of shell fragments at depths of 25 to 30 feet.

Saxton's map of Carmarthen and Pembroke (1578) shows the area, but with insufficient accuracy for scaled measurement. Morris's chart of "Carmarthen, Laugharn and Cydwely" (1800) locates certain fixed points with sufficient accuracy for comparisons to be made with the Admiralty charts of 1830, 1856, 1888 and 1952, and these, together with the Ordnance Survey maps, enable major changes in the Pendine dunes to be assessed with some accuracy. In 120 years the average depth of the dunes has increased by approximately 100 yards.

The outlet of the Watchett Pill onto the beach has moved approximately 1300 yards eastward, due to the eastward growth of the dunes. During the same period the channels of the rivers Taf and Towy have tended to move eastward, the Gwendraeth inlet has largely silted up, and there has been a general accretion on the west side of the Towyn Burrows sand dunes, between Kidwelly and Burry Port.

Between 1800 and 1830 the Pendine Marshes were reclaimed for agriculture by installing drainage and by the construction of earth banks on the Taf estuary. In 1940 the marsh area was acquired by the Government for an Experimental Establishment, and the site is now controlled by the Ministry of Defence.

Morphology

Fig. 1 reproduces the Admiralty chart of 1830. Fig. 2 shows the 1830 dune line transferred to the 1950 Ordnance Survey 2½" to 1 mile map, together with the location of four protective stone mounds at intervals along the six mile dune front. Fig. 3 shows Pendine sands in relation to the whole of Carmarthen Bay.

The half-heart shape of Saundersfoot Bay is a text-book example of a stable sedimentary coastline shape, as described by Silvester[1] in a paper published in 1962. At present Saundersfoot Bay (sand) and Marros Bay (shingle) appear to be relatively stable, while parts of Pendine sands, Laugharne sands, the Gwendraeth estuary and Pembrey sands all show evidence of accretion. There is insufficient data at present to establish whether there are three (or four) half-heart shapes evolving or whether Carmarthen Bay will eventually stabilise on a single macro-half-heart system. The research carried out by Yasso[2], published in 1965, suggests that the mathematical form of such a coast when in equilibrium is a logarithmic spiral. He obtained reasonably accurate fitting, using an IBM 7000 computer programmed to generate a best-fitting log-spiral to each shoreline curve surveyed. With all log-spiral fits, however, there comes a point where the spiral deviates away from the coast and into the ocean. It seems possible that a cubic parabola may hold the key to this problem, but this hypothesis has yet to be tested.

Present Conditions

The prevailing wind is from the S.W., and there is considerable movement of sand, both sea- and air-borne. High water spring tide mark is normally about 20 to 30 feet seaward from the toe of the dunes. Records of beach levels are few, and insufficient data are available to establish whether there is any seasonal pattern of beach movement. While most of the Establishment's buildings are sited inland from the dunes, certain installations are built on the dune edge. In the autumn of 1961, a combination of high tides and S.W. gales caused some erosion at the toe of the dunes, which was sufficient to endanger the stability of these installations. At one site a stepped mass concrete wall was built on the dune face as a protective measure. Completed in March 1962, this work in fact aggravated the problem. Some undercutting of the beach in the centre of the wall resulted, together with further dune erosion at the ends, thus endangering both the wall and the installation behind it. An alternative method of protection was urgently required. A novel system, using a pervious random rock-fill mound and sand trap, was designed in order to make the best use of local materials and physical conditions.

THEORETICAL OPERATION OF THE MOUND AND SAND TRAP

Hypothesis

Under normal conditions, high spring tides do not reach the toe of the dunes. If, therefore, a pervious rock-fill mound was set up 20 feet from the toe of the dunes, such tides would reach the edge of the seaward face of the mound. Wave action would be checked, and this would result in sand deposition in the voids of the mound and subsequently on the beach in front, thus raising the beach and steepening its gradient. At the same time wind-blown sand would be checked at the returned ends of the mound, and this sand would be trapped in the area enclosed between the mound and the toe of the dunes. A combination of S.W. gales and high tides might result in some overtopping of the mound, but the mound would have to be breached before any damage could be inflicted on dunes so protected.

Application

The foregoing was applied in the protection of the mass concrete wall, and also of sections of unprotected dune. The rock-fill mounds were of triangular cross-section 4' 6" high, with the seaward face sloped at 1 : 5 and the inner face at 1 : 1 (Fig. 4). The mounds were built of random limestone "as blown", varying in size from 2 feet down to 6 inches. The rock was placed on a base of Somerfelt Track (a temporary airfield surfacing of galvanized wire and steel flats), the mounds being sited with the inner toe of the mound 20 feet from the toe of the dunes. The ends of the mounds were returned back at 45° to join the dunes. Three sites were protected in this way during the summer of 1962, and an additional

Fig.4. Stone mound, August 1962

Fig.5. Ice/Sand barrier, March 1963

site in 1966. (Sites 1, 2, 3 and 4 in Fig. 2).

Confirmation of the Mound Theory

From January to March 1963 there was continuous snow and frost at Pendine. This produced a build-up of an ice and sand barrier, 12 inches to 15 inches thick and of varying width, sited at mean high water mark (Fig. 5). The effect of this barrier was to cause sand to accrete between it and the toe of the dunes along the whole length of the beach, thus providing a reasonable confirmation of the theory of mound design. With the melting of the ice, this sand accretion was dispersed.

Operational Experience

Over the past seven years the mounds and sand traps have operated in accordance with their design concept. The voids have filled with sand, as also have the sand traps between the mounds and the dunes. The mounds have proved exceptionally stable. The slopes of the dunes so protected have flattened to between 20^{o} and 30^{o}, compared with the 35^{o} to 37^{o} slopes of the unprotected dunes. Natural growth of vegetation is much stronger on the surface of the protected dunes than on the unprotected, and this, in its turn facilitates further sand accretion. (Fig. 6). No planting has been carried out. The pioneer self-sown vegetation consists mainly of Sand Couch (Agropyron Junceiforme), Marram Grass (Ammophila Arenaria) and Sea Spurge (Euphorbia Poralias).

Some local erosion occurs at the junctions of the returned ends of the mounds with the dunes (Fig. 7) and similar erosion occurs at places where vehicle slipways cut through the dunes and join the beach. In May 1968 work was carried out to try the effect of lower mounds, of similar construction and shape, but 18 inches high only. These were sited so as to extend the ends of existing mounds by 50 feet, parallel to the dunes. The ends of these extensions were not returned back at 45^{o} into the dunes, but were gradually reduced in height.

It is too early to predict how these low mounds will behave under a combination of gales and high tides. However, four months after their construction, there was already an appreciable build-up of sand between the mound and the toe of the dunes. Terminal erosion appears to have been halted, and, in fact, reversed.

Fig. 8 shows the application of a short low mound at Site No. 3.

Immediately behind the crest of the dunes between the east end of Site 3 and the Central Slipway there is a roadway, the stability of which was becoming endangered by dune erosion. Placing additional stone on the dune face and at the junction of the slipway with the dunes did not remedy the condition. Erosion has now been checked and the accretion of sand facilitated by the construction of a low stone mound, 20 feet from the toe of the dunes and running from the Site 3 mound to the Central Slipway (Figs. 9 and 10).

Fig.6. Sand accretion in sand trap, October 1967

Fig.7. Erosion of dune at returned end of mound

Fig.8. Short low mound extension, Site 3, September 1968

Fig.9. Low mound between Site 3 and Central Slipway, September 1968

Fig.10. Low mound looking eastward to Central Slipway, September 1968

Fig.11. Low mound extended beyond slipway, September 1968

The effect of continuing the low mound for 50 feet on the east side of the Central Slipway is shown in Fig. 11, when the beach has started to build up on the seaward face of the mound and also between the mound and the dune face.

Over the 7-year period since the original mounds were constructed, they have shown no tendency to settle into the sand or to disperse when over-topping has taken place. Where over-topping has occurred, some sand has been washed out of the sand traps, leaving behind a swallow-hole formation. However this has subsequently filled up with additional trapped sand.

So far, the works described have required no maintenance whatsoever, and, as regards the effects of overtopping, can be said to be self-maintaining. While the efficacy of the low mounds has yet to be proved over an extended period, the high mounds and sand traps have adequately fulfilled their local purpose of "controlling one of the great sources of power in Nature for the use and convenience of Man".

References:-

1. Silvester R.; "Sediment Movement Around the Coastlines of the World", Inst.C.E. Civil Engineering Problems Overseas Proceedings, Paper No. 14, 1962.

2. Yasso W.E.; "Plan Geometry of Headland - Bay Beaches", Jl. of Geology 73, 1965, 702-714.

CHAPTER 46

DUNE EROSION DURING STORM CONDITIONS

Edelman, T. Ir., Coastal Research Department of Rijkswaterstaat,
The Hague, Netherlands

INTRODUCTION

Since in the Netherlands large areas of low lands are protected against the sea by coastal dunes only, it is very important to know how far, during a storm surge, the erosion of these dunes will proceed. In order to obtain an answer to this question, the cross-section of the coast has been studied.

The shape of the cross-section of a sandy coast is mainly caused by displacements of sand perpendicular to the coast-line. Obviously this transport is mainly caused by waves. Since our knowledge of the very intricate physical processes, governing the sand transport by waves is, even now, still very incomplete, we can, perhaps, obtain an insight into the behaviour of a sandy coast, if we start from some rather simplified basic assumptions which are roughly in accordance with observations in nature.

SIMPLIFYING ASSUMPTIONS

a) The quantity of sand: q_w, transported by waves may be:

$$q_w = - K \left(\frac{2\pi h}{L}\right)^2 \frac{1}{\left(\text{Sinh } \frac{2\pi z}{L}\right)^2}$$

in which K is a constant, depending on the nature of the transported material only, h is the wave-height, L is the wave-length and z is the water-depth. In the neighbourhood of the coast the value of the quotient $\frac{2\pi z}{L}$ will mostly be rather small; thus it is allowed to replace $\text{Sinh } \frac{2\pi z}{L}$ by: $\frac{2\pi z}{L}$, from which the formula takes the simple form:

$$q_w = - K \frac{h^2}{z^2} \qquad \ldots\ldots\ldots\ldots (1)$$

b) It is further assumed, that h and L are independent of z and that q_w does not include the sand transported in suspension; the latter will be neglected in this paper.

c) The waves try to bring the sand up against the slope of the shore; gravity tries to move it slope-downward. This counteracting influence of the slope is put into account as a slope-transport: q_s that is assumed to be proportional to the steepness of the slope:

$$q_s = \gamma \frac{dz}{dx} \quad \ldots\ldots\ldots\ldots (2)$$

d) Within the breaker-zone the wave-height will never surpass the value: 0,78 z; thus $h_b \leq 0{,}78\ x$ $\ldots\ldots\ldots\ldots (3)$

OBSERVATIONS IN NATURE UNDER NORMAL WEATHER CONDITIONS

a) Along the dutch coast it has been observed, that under normal weather conditions the cross-section of the beach is a straight line from the highwater-level to some distance below the lowwater-level. Nearly always the slope of this straight line has the same main value, depending, as it seems, only on the nature of the sand. This steepness varies along the dutch coast from 1:40 in the South, to 1:60 in the North-East.

b) Under normal weather conditions the waves within the breaker-zone are propagating through this zone in the shape of a spilling breaker. The breaker comes into being at a depth z = 1,3 h and runs as a foaming wall through the whole breaker-zone towards the water-line, decreasing gradually in height.

If we assume, that in a spilling breaker <u>everywhere</u> $h_b = 0{,}78\ z$, it follows from equation (1), that in the breaker-zone q_w has everywhere the same value. The straight line indicates, that also $\frac{dz}{dx}$ is a constant; thus q_s has, everywhere in this part of the breaker-zone, the same value. Therefore, this straight line must be an equilibrium profile. The length of this straight line depends on the wave height; its steepness is undependent of the wave height off-shore.

OBSERVATIONS DURING AND AFTER STORMS

a) During a heavy storm we observe that the breaker-zone is much broader than under normal weather conditions. At the seaward end of the breaker-zone we observe plunging breakers, while in the region nearer to the beach spilling breakers are dominant.

b) If the storm surge level is higher than the existing dune-foot, we observe that the outer parts of the dunes erode and that whole quantities of sand disappear into the boiling sea.

c) After the storm, we see that a new dune-foot has established itself on a level, which lies a little bit lower than the highest level reached by the sea. Between this new dune-foot and the normal lowwater-line the cross-section of the beach is a straight line under the same slope as originates under normal weather conditions on the wet beach (equilibrium profile).

CONCLUSIONS

If we consider the fact, that at the seaward end of the breaker-zone the quantity of sand, transported by the waves from off-shore reaches its maximum, and that in this region the transport capacity of the waves will strongly decrease in the, even there occurring plunging breakers, (which means that the greater part of the landward transported sand will precipitate here) it seems to be obvious, that a seaward transport of the

eroded dune-sand beyond the breaker-zone is not likely to occur. We may assume, therefore, that the whole quantity of sand, eroded from the dunes, will precipitate within the breaker-zone proper. If we assume, further, that this sand is spread-out equally over the whole breaker-zone, we are able to estimate rather exactly the spot where the new dune-foot after a storm will come into existence. We have to know, however: 1) the profile of beach and dunes before the storm; 2) the equilibrium slope of the wet beach in the considered coastal area; 3) the highest storm-surge-level; 4) the wave height during the storm. A determination of the place of the new dune foot is very easily done by a graphical construction (fig. 1); we have only to shift the straight line AB so long till both the hatched surfaces are equal.

However, if we want to investigate in a more general way the influence of the height of the dunes (H), or the influence of the wave height (h), on the erosion of the dunes (the distance "d" in fig. 1), we can better start from a simplified original profile (fig. 2) and make a real calculation. The results of such a calculation have been plotted in fig. 3 which shows how "d" depends on H in the case that the storm-surge-level lies 5.20 m above mean sea level, the original dune-foot lies 3.80 m above mean sea level, the waveheight off-shore h = 10 m and the equilibrium slope is 1:50. In fig. 4 has been plotted how the dune erosion depends on the height p of the storm-surge-level and the dune height H, assuming that the wave height h = 1.5 p.

It can easily be seen, that high dunes give a certain amount of safety; this trend has been found in nature as well as in laboratory tests. It must be pointed out, however, that such a prediction holds good only if we are dealing with a "normal" beach. If, for instance, a channel exists in the fore-shore, that can swallow up the whole quantity of sand eroded from the dunes, a high dune produces no extra safety at all.

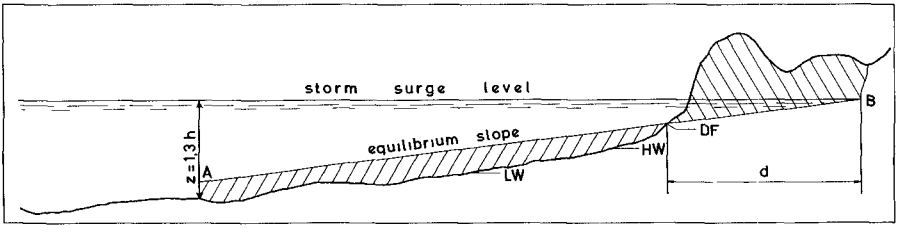

Fig. 1 Graphical construction

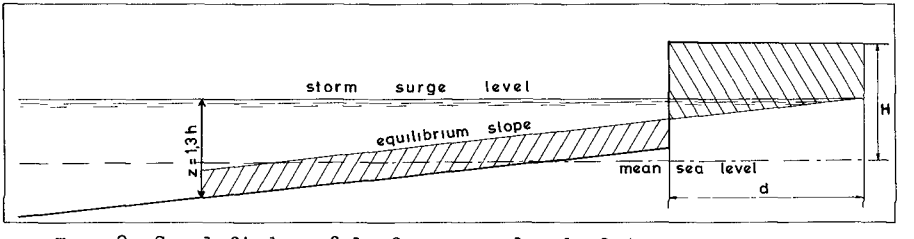

Fig. 2 Simplified profile for general calculation

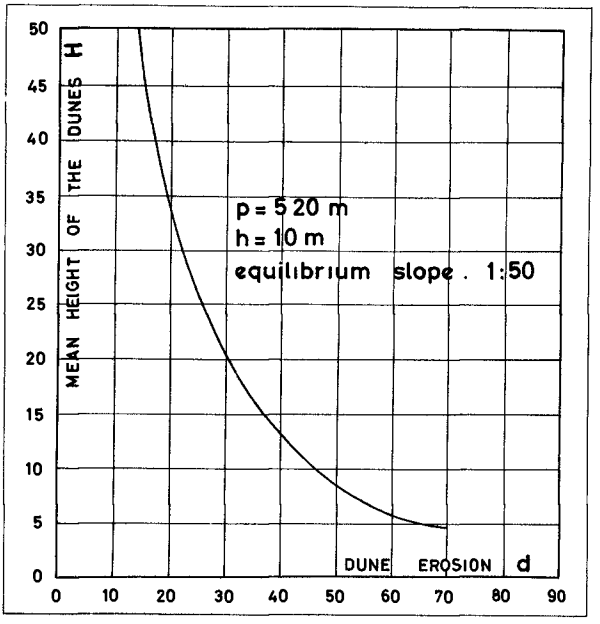

Fig. 3 Dune erosion with different dune height

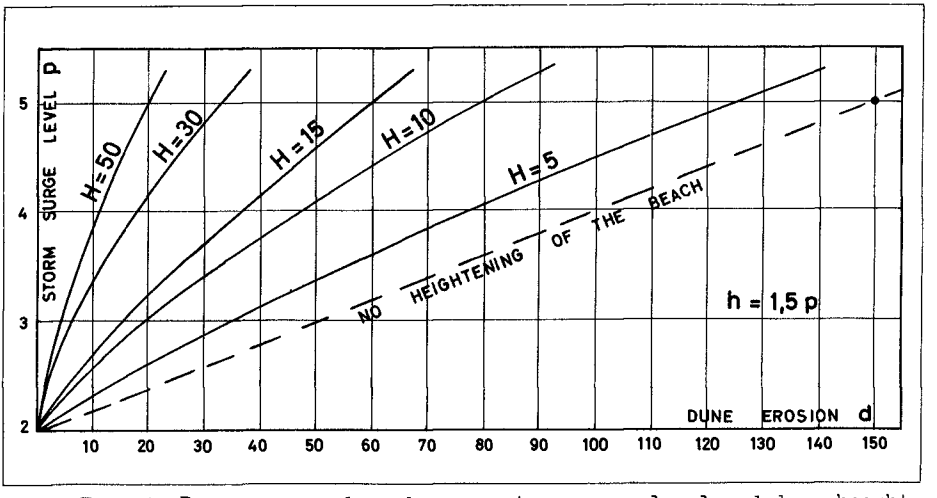

Fig. 4 Dune erosion depending on storm surge level and dune height

CHAPTER 47

FURTHER RESULTS ON THE DEPOSITION OF COHESIVE SEDIMENTS

Emmanuel Partheniades
Associate Professor of Engineering and Applied Sciences
State University of New York at Buffalo, Buffalo, New York

Ralph H. Cross, III
Assistant Professor of Civil Engineering
Massachusetts Institute of Technology, Cambridge, Massachusetts

and

Alfredo Ayora
Formerly Research Assistant, Hydrodynamics Laboratory
Massachusetts Institute of Technology, Cambridge, Massachusetts

Abstract

Experimental investigations on the depositional behavior of suspensions of fine cohesive sediments in turbulent flows have been conducted in a special laboratory apparatus. This apparatus consists essentially of an annular channel containing the water-sediment mixture, and an annular ring positioned within the channel and in contact with the water surface. A turbulent shear flow is generated by a simultaneous rotation of the channel and ring in opposite directions at the proper relative speeds to minimize secondary currents in the bottom of the channel, so that the sediment deposits uniformly.

The first reported results indicated that after a short period of rapid deposition the suspended sediment concentration approaches a constant value, known as the "equilibrium" concentration, C_{eq}. The ratio $\frac{C_{eq}}{C_o}$, where C_o is the initial concentration, is constant for constant flow conditions, and independent of C_o. It was found to depend very strongly on the average shear stress τ_{ch} over the channel perimeter.

The following are the more recent results of the continuing investigations.

The shear stress τ_b on the channel bottom has been found to be approximately uniform for flows for which the sediment deposits uniformly. This stress was also found to be a power function of τ_{ch}. This suggests that τ_b controls $\frac{C_{eq}}{C_o}$, i.e., the percentage of the initial sediment which eventually deposits. There exists a well-defined minimum bottom shear stress, $\tau_{b_{min}}$, below which essentially no sediment stays in suspension. The ratio $\frac{C_{eq}}{C_o}$ is related to the difference $\tau_b - \tau_{b_{min}}$ by a logarithmic-

normal law, whose geometric standard deviation and geometric mean are expected to be functions of the physical and chemical properties of the sediment and the water quality.

Limited time-deposition data indicated that the relative concentration $C' = \frac{C_o - C(t)}{C_o - C_{eq}}$, where $C(t)$ is the instantaneous concentration, varies in proportion to the logarithm of time t, and to the logarithm of the C_o. The rate of deposition, there, $\frac{dC}{dt}$ varies in inverse proportion to t, and in proportion to C_o. These conclusions are valid within limited time and concentration intervals.

INTRODUCTION

The depositional behavior of fine cohesive sediments in turbulent flows controls the shoaling process in estuarial channels. These sediments are predominently composed of silt and clay ranging in size from a small fraction of one micron up to 50 microns. Although they may be abundant in rivers as suspended sediment, they are not normally encountered in the bed of alluvial channels, but are transported as wash load (2), and generally deposit in areas of very low velocities such as estuaries and reservoirs. Because of their small size and their large specific area (surface area per unit volume), the behavior of these particles in a flow field is controlled by a variety of interparticle forces. Some of these forces are attractive, such as the van der Waals atomic forces, and, others are repulsive, such as the surface ionic forces due to charge deficiency of either surface molecules or adsorbed ions. The net effect of these interparticle forces may be repulsion or attraction. In the first case the smaller particles (smaller than about one micron) may stay in suspension even in quiescent water for an extremely long period of time, due to Brownian motion. In fact, even very slight agitations can be adequate to prevent settling of the heavier particles. In the second case particles tend to cling together and form agglomerations known as flocs. Their size and settling velocities may become several orders of magnitude higher than those of the individual particles. This phenomenon, greatly enhanced by dissolved salts, is known as flocculation and is the cause, under proper hydraulic conditions, of rapid deposition of fine suspended sediment in estuaries.

A rational approach to the control of shoaling in estuarial waters, generally due to predominantly fine sediments (2), requires a good understanding of the behavior of this type of sediment in a flow field. More specifically, the important flow parameters and soil properties which control the initiation and rates of deposition need to be investigated, and quantitative functional relationships between these variables need to be determined.

The present phase of the investigation described here is concerned with the role of flow parameters.

SUMMARY OF THE FIRST RESULTS

Fig. 1 shows a picture of the experimental apparatus used. It consists of an annular channel with external and internal diameters of 28-3/8 and 36 inches respectively and with a depth of 12 inches. An annular ring of slightly smaller width than that of the channel is positioned within the channel and can be adjusted vertically to contact the water surface in the channel. A turbulent flow field is generated by rotating the channel and ring in opposite directions. The ring supports are instrumented so that the total tangential shear stress on the ring (and thus on the water surface) can be measured. The relative speeds of channel and ring have been adjusted to minimize the effects of secondary currents on the bottom, so that the sediment deposits almost uniformly across the channel. The details of the equipment are described in (3,6). For depths between 8 cm and 16 cm the average shear stress in the ring varies in proportion to $(\Delta\omega)^2$, where $\Delta\omega$ is relative angular velocity between the channel and ring, and is independent of the depth. This shear stress, τ_r, is given by the equation

$$\tau_r = 4.65 \times 10^{-5} (\Delta\omega)^2 \qquad (1)$$

where τ_r is given in psf and $\Delta\omega$ in rpm. The first experiments with kaolinite clay-silt suspensions (1,3,6) revealed the following important depositional characteristics:

1. For given geometry, sediment, and flow conditions, the suspended sediment concentration eventually reaches a constant value, herein called "equilibrium concentration", C_{eq}.
2. The ratio of the equilibrium concentration to the initial concentration C_o, i.e., $\frac{C_{eq}}{C_o}$, is independent of C_o, but depends strongly on flow conditions, sediment properties, water chemistry and channel geometry. Hence each flow can maintain in suspension a constant fraction of a particular sediment.
3. For the three different depths used the ratio $\frac{C_{eq}}{C_o}$ appears to be very strongly controlled by the average shear stress, τ_{ch}, around the channel boundary, provided that the speed of the channel and ring are so adjusted that the sediment deposits uniformly. τ_{ch} was determined by considering the torque of all the shear stress about the axis of rotation and using eq. 1. It is given by the following expression

$$\tau_{ch} = 4.65 \times 10^{-5} \frac{(\Delta\omega)^2}{1 + 2\frac{d}{b}} \qquad (2)$$

where d is the depth and b the width of the channel.

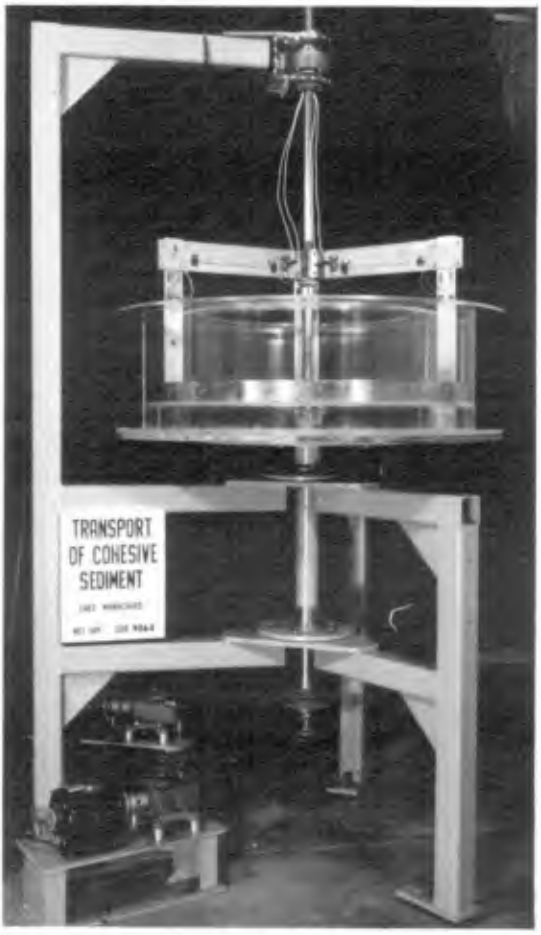

Fig. 1 Experimental Apparatus

4. $\frac{C_{eq}}{C_o}$ varies for different combinations of speeds other than those corresponding to uniform deposition even if $\Delta\omega$ remains constant. Hence the secondary currents generated by the rotational motion have a significant effect on the equilibrium concentrations and the rate of deposition.

5. A size analysis of a sample of suspended material obtained at equilibrium concentration showed that the sediment contained the entire grain size range of the original material although in the average it was somewhat finer. This confirms the fact that the interparticle physico-chemical forces are far more important as a settling agent than the individual particle size and it suggests that there is no strong correlation between these forces and particle size.

RECENT EXPERIMENTAL RESULTS

I. Equilibrium Concentrations

The shear stress at the bottom of the channel measured by a Preston tube (in clear water) was found to be almost uniform across the channel as long as the deposition was uniform. Therefore the shear stress τ_o at the centerline of the channel was considered as a good measure of the average bottom shear stress τ_b.

The quantity $P_\omega = \frac{(\Delta\omega)^2}{1 + 2\frac{d}{b}}$, called "shear stress parameter", was shown to be proportional to the average shear stress, τ_{ch}, over the channel boundary, and therefore, according to the earlier results, controls the relative equilibrium concentration $\frac{C_{eq}}{C_o}$.

The shear stress at the centerline of the channel, $\tau_o \approx \tau_b$, was plotted versus the shear stress parameter on logarithmic paper, as shown in Fig. 2. The plot may be approximated by a straight line corresponding to the empirical expression

$$\tau_b = \left[4.20 \times 10^{-5} \frac{(\Delta\omega)^2}{1 + 2\frac{d}{b}} \right]^{1.20} \qquad (3)$$

or, combining eqs. 2 and 3,

$$\tau_b = (.903\ \tau_{ch})^{1.20} \qquad (4)$$

All shear stresses are in psf and $\Delta\omega$ is in rpm.

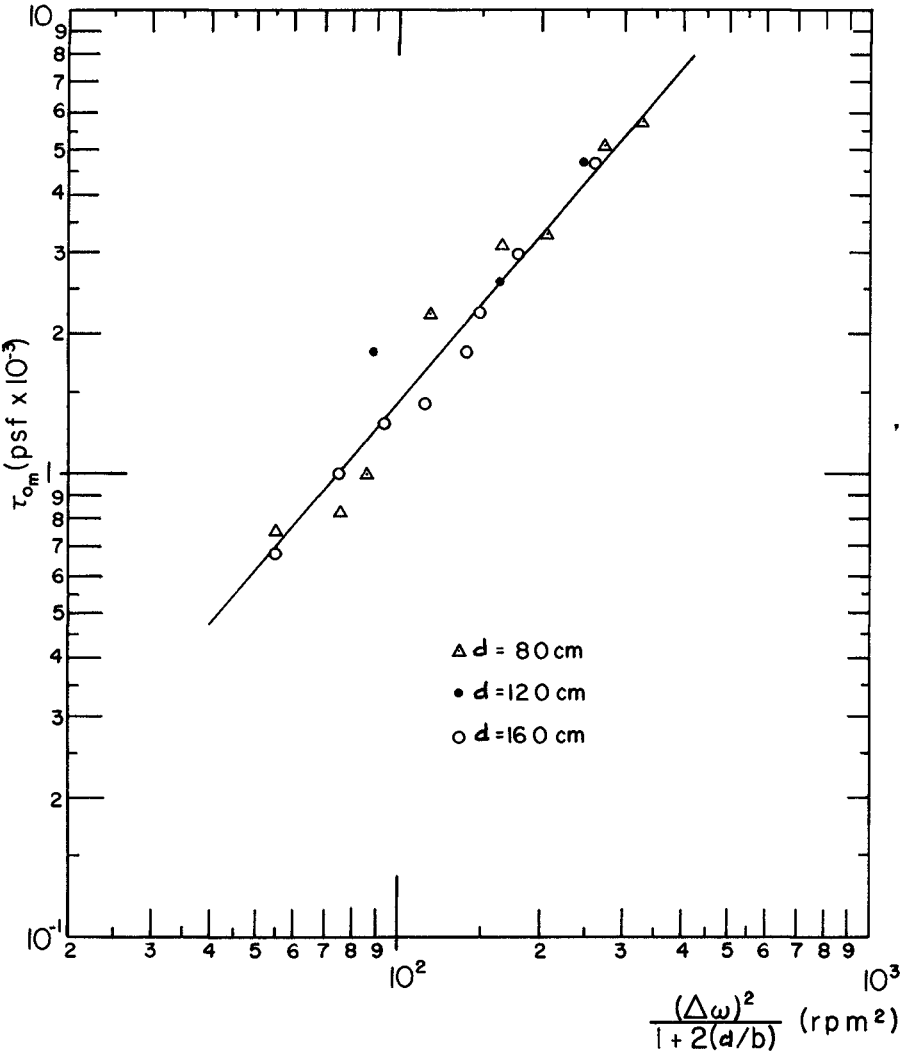

Fig. 2 LOGARITHMIC CORRELATION BETWEEN MEASURED SHEAR STRESS AND SHEAR STRESS PARAMETER

Hence it can be said that the bottom shear stress appears to be the important flow variable which controls deposition. There exists a minimum value of the shear stress parameter, $P_{\omega_{min}}$, below which $C_{eq} = 0$. The ratio $\frac{C_{eq}}{C_o}$ is shown plotted in Fig. 3 versus the difference $\Delta P_\omega = P_\omega - P_{\omega_{min}}$ in a logarithmic normal graph. It is seen that over a wide range of ΔP_ω and $\frac{C_{eq}}{C_o}$ the points can be fitted very closely by a straight line described by the equation

$$\frac{C_{eq}}{C_o} = \frac{1}{3.085\sqrt{\pi}} \exp\left\{-\frac{1}{2}\left[\frac{\log \Delta P_\omega - \log M}{\sigma_g}\right]^2\right\} \tag{5}$$

where M is the geometric mean and σ_g is the geometric standard deviation of ΔP_ω. M and σ_g are expected to be functions of the physico-chemical properties of the sediment and of the water. For the kaolinite clay used and distilled water, $P_{\omega_{min}} = 65(\text{rpm})^2$, $M = 58(\text{rpm})^2$ and $\sigma_g = 3.085$. Therefore eq. 5 becomes

$$\frac{C_{eq}}{C_o} = \frac{1}{3.085\sqrt{\pi}} \exp\left\{-\frac{1}{2}\left[\frac{\log^2\left(\frac{(\Delta\omega)^2}{.58(1 + 2\frac{d}{b})} - 1.120\right)}{9.52}\right]\right\} \tag{6}$$

or combining eq. 3 and 6

$$\frac{C_{eq}}{C_o} = \frac{1}{3.085\sqrt{2\pi}} \exp\left\{-\frac{1}{19.04} \log^2\left(410\, \tau_b^{0.834} - 1.120\right)\right\} \tag{7}$$

The dependence of the relative equilibrium concentration can be explained in the following way.

As stated in the introduction, under certain conditions there exist net attractive forces between the particles. As a result, particles may cling to each other, forming flocs. When the flocs grow large enough they start settling towards the bottom of the channel, a region of high velocity gradients. In that region the flocs are subjected to the highest disruptive stresses. These stresses are generated by the velocity difference at two extreme points of the floc, and by the collision with other particles.

The net interparticle attractive forces vary in intensity. In the process of particle collision and flocculation some particles will be attracted to each other with stronger bonds than others. Hence, the average shear strength of the flocs, or their resistance to the high boundary disruptive stresses, will vary over a wide range. The flocs with high enough bonds will eventually reach the bed and will become part of it. The flocs with

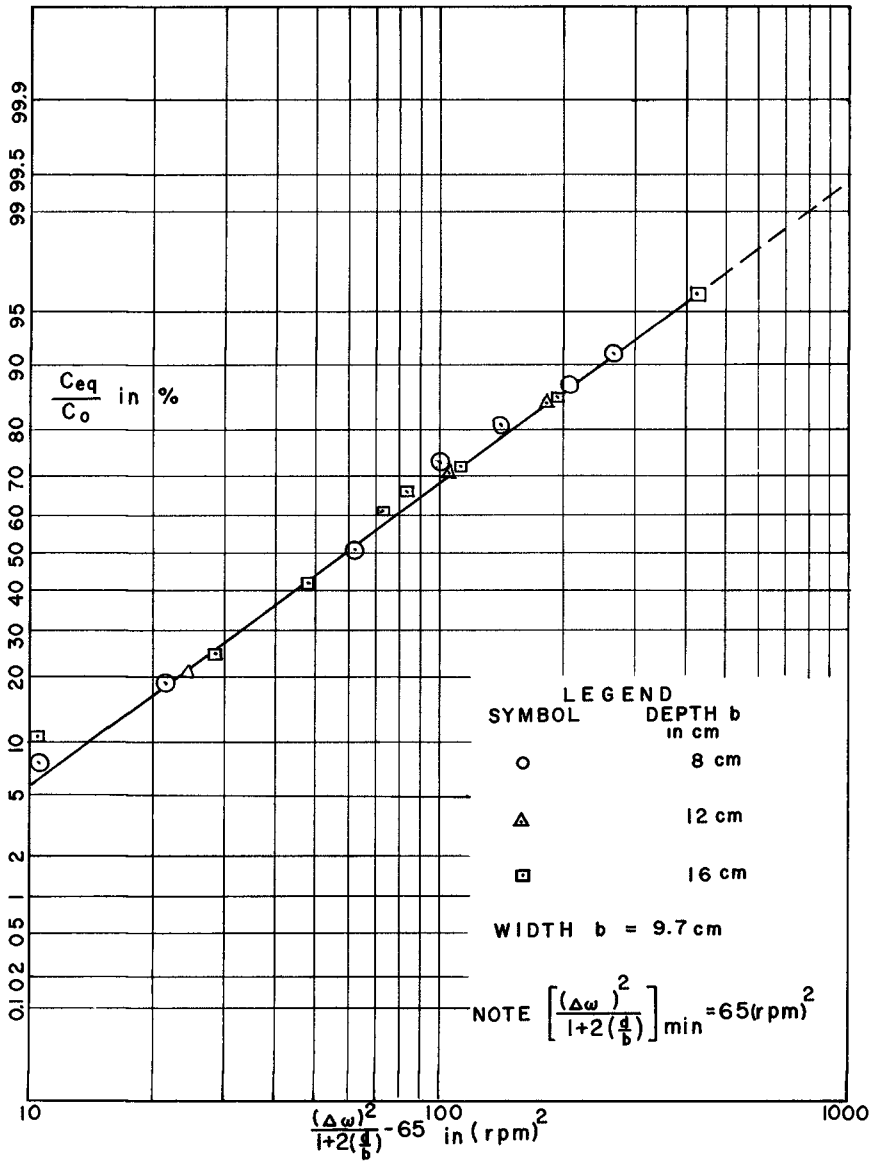

Fig 3 Relation between Relative Equilibrium Concentration and Shear Stress Parameter

weaker bonds will be disrupted and reentrained without reaching the stage of developing permanent bonds with the bed. This study and previous investigations (5,8) have clearly shown that the bed shear stresses for the initiation of erosion of deposited flocs are considerably higher than the shear stresses for which the same type of sediment deposits. The reason, or at least one of the reasons, for this phenomenon is the property of thixotropy, i.e., the gradual increase of the interparticle bonds with time. Hence, the bonds of a deposited floc, as well as its bonds with the bed will increase after deposition considerably above the flow induced shear stresses.

Therefore, the relative equilibrium concentration, $\frac{C_{eq}}{C_o}$ represents in fact the percentage of fine particles which can form flocs with sufficiently strong bonds to resist the flow induced disruptive shear stress near the bed. The remaining particles in suspension will never be able to form such flocs.

At this point a note seems appropriate about the nature of the equilibrium concentration of fine sediment suspensions in contrast to that of coarse sediment. In the latter case and as long as the sediment falls in the category of bed material load (2), a simultaneous entrainment and deposition of particles of a given size occurs. The concentration of such particles in suspension reaches a constant value when the number of particles eroded per unit bed area and unit time is equal to the number of particles deposited per unit area and unit time. At this point it is said that the sediment transport capacity of a given flow for a particular sediment size is saturated.

In the case of fine sediments no such flow saturation exists. If deposited fine particles and flocs could be simultaneously deposited and resuspended, then the rate of their reentrainment should be constant for given flow. However, the rate of deposition does increase with concentration. Hence increasing the overall initial concentration C_o would result in an increase of the deposition rate without increasing the erosion rate. As a result the suspended sediment concentration would reduce to the point when the deposition rate would be made equal to the constant erosion rate; that is the C_{eq} should then be independent of the initial concentration C_o.

Another series of experiments was performed to test the validity of the hypothesis that no exchange between the bed and the suspension occurs after the equilibrium concentration has been reached. A suspension of 1835 gm/liter was allowed to deposit to an equilibrium concentration of 983 ppm, giving $\frac{C_{eq}}{C_o} = 0.535$. After equilibrium, the channel was slowly flushed, by simultaneously (and slowly, as not to disturb the bed) draining the suspension and replenishing the tank with clear water at the same rate, while maintaining the channel and ring speeds. If no resuspension occurs, the concentration in the channel should decrease according to $C(t) = C_{eq}\, e^{-(Q/V)t}$, where Q is the flushing rate and V is the volume

of water in the tank. Measurements of suspended sediment concentration during the flushing process, given in Table I, show this to be the case.

Table I

Suspended Sediment Concentrations vs. Time

t min	Calculated C(t) ppm	Measured C(t) ppm
0	983	983
10	796	800
20	644	650
30	520	500
40	420	400
50	341	300
60	275	300

The flushing was continued until a concentration of 200 ppm in suspension was reached, when flushing ceased. The channel was still rotating at the same speed, and samples of suspension taken some time later showed no further change in concentration, indicating that the bed was not eroding.

Next, the channel was stopped, and the water agitated with an electric mixer to resuspend the bed, yielding a "second initial concentration", C'_o, of 945 ppm. After sampling, the channel was set running at the same speed as before, until again equilibrium was reached, at a "second equilibrium concentration", C'_{eq} of 340 ppm, for a ratio of $\frac{C'_{eq}}{C'_o}$ of 0.36.

It is instructive to account for the quantities of sediment involved in the processes outlined above. Based on a tank volume of 19.9 liters, the weights can be calculated from the concentrations as follows: The initial dose was 36.5 g of clay. At the first equilibrium, 19.6 g was still in suspension; thus 16.9 g had deposited. After flushing to 200 ppm, 4.0 g was left in suspension. When the bed was resuspended, however, only 18.8 g was in the tank, compared with 16.9 + 4.0 = 20.9 g; this indicates that 2.1 g of bed material was eroded during the flushing process. The fact that the concentration didn't change after the flushing stopped, however, suggests that this erosion may have been due to the disturbance of the flushing process. After the second settling period, 6.8 g was left in suspension, with 12.0 g deposited.

The difference between $\frac{C_{eq}}{C_o}$ (0.535) and $\frac{C'_{eq}}{C'_o}$ (0.36) suggest that in the flushing process, much of the clay unable to settle was removed; however, some must have been entrained in the bed, or the bed-forming flocs, since if all the material that had settled initially (16.9 g), (less that eroded during flushing, 2.1 g) had settled again, the value of

$\frac{C'_{eq}}{C'_o}$ would have been $\frac{18.8 - 14.8}{18.8} = 0.21$ instead of 0.36. Alternately, the intense agitation used in the resuspension of the bed may have disrupted the flocs sufficiently to alter their ability to settle.

II. Deposition Rates

The deposition rates were also studied on the basis of limited time-concentration data. Therefore the presented conclusions should be considered as tentative. Two approaches were used: In the first approach the instantaneous suspended sediment concentration, $C(t)$, was plotted versus the time, t, in minutes, on logarithmic paper. Fig. 4 shows the plot for the 8 cm. depth. It is seen that the data falls on straight lines of various slopes. These lines become abruptly horizontal when the point of equilibrium concentration is reached. The data for the 12 cm. and 16 cm. cases give similar plots (1). The equation describing the time deposition relation is of the form:

$$C(t) = K_1 t^{\alpha} \tag{8}$$

where α is the slope of the lines in Fig. 4 and K_1 is a reference concentration value which may be obtained for any arbitrary reference time, t_r. Since eq. 8 is dimensional, it is valid for C in ppm and t in minutes. Moreover, all the curves were obtained for an initial concentration $C_o = 8{,}020$ ppm.

Fig. 5 shows a plot of concentration-time data for constant speed, 16 cm. depth and variable initial concentration C_o. The points again plot very nearly on straight and parallel lines. So do similar data for the 8 cm. depth case. It may be concluded, therefore, that the exponent α is constant for constant flow conditions and independent for the suspended sediment concentration.

The various values of α were next plotted versus the shear stress parameter, $P_\omega = \frac{(\Delta\omega)^2}{1 + 2\frac{d}{b}}$ on a logarithmic paper (Fig. 6). It is seen that the points are concentrated near a straight line which indicates a strong correlation of α with P_ω and, therefore, with the bed shear stress, τ_b. This relation has the form

$$\alpha = K_2 \left[\frac{(\Delta\omega)^2}{1 + 2\frac{d}{b}} \right]^{\beta} \tag{9}$$

From Fig. 6 it was found that $\beta = -2.21$ and $K_2 = -9{,}760$.

Introducing the value of P_ω from equation (3) we obtain:

$$\alpha = -2.14 \times 10^{-4} \tau_b^{-1.84} \tag{10}$$

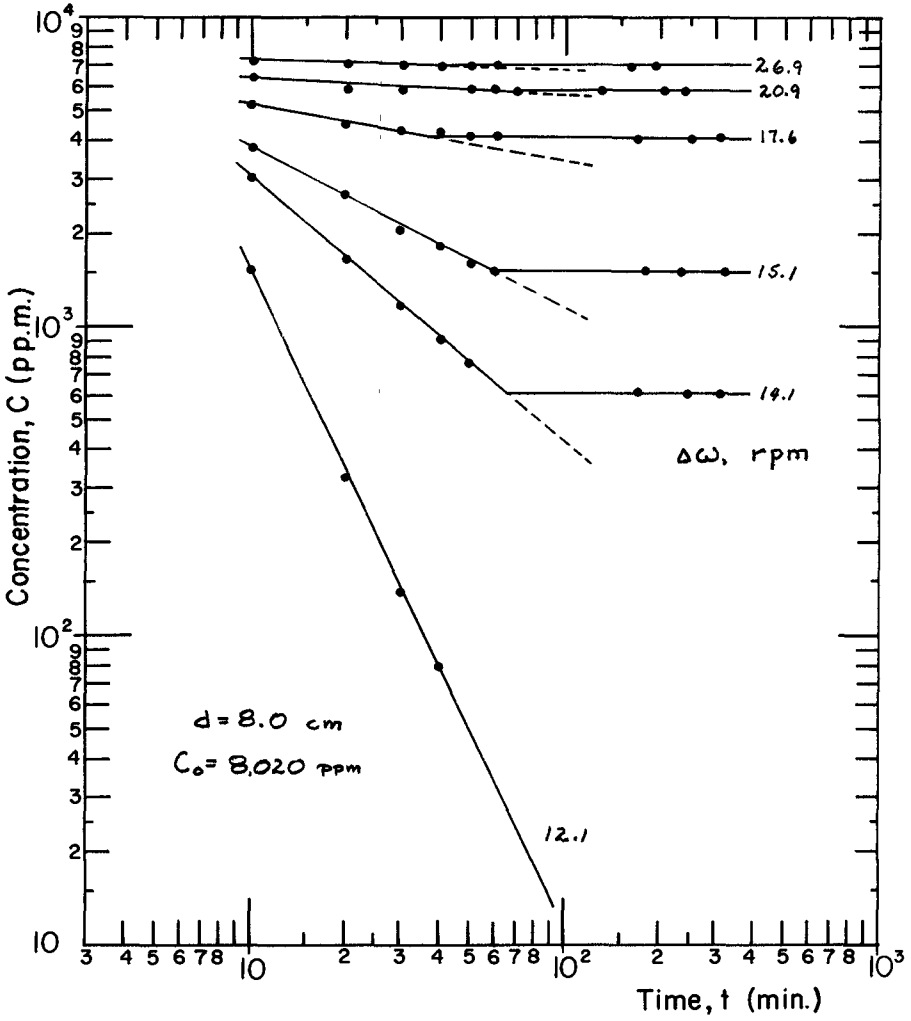

Fig. 4 Concentration-Time Relationships

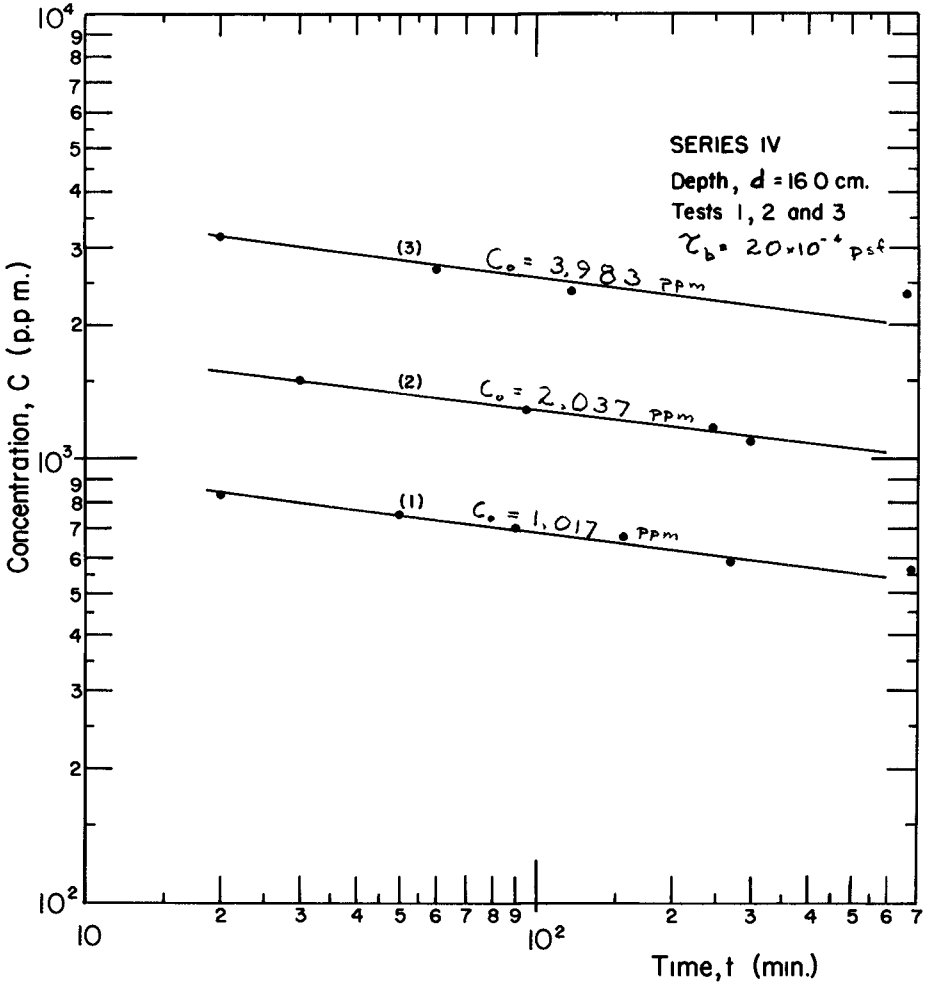

Fig 5 Concentration-Time Relationships

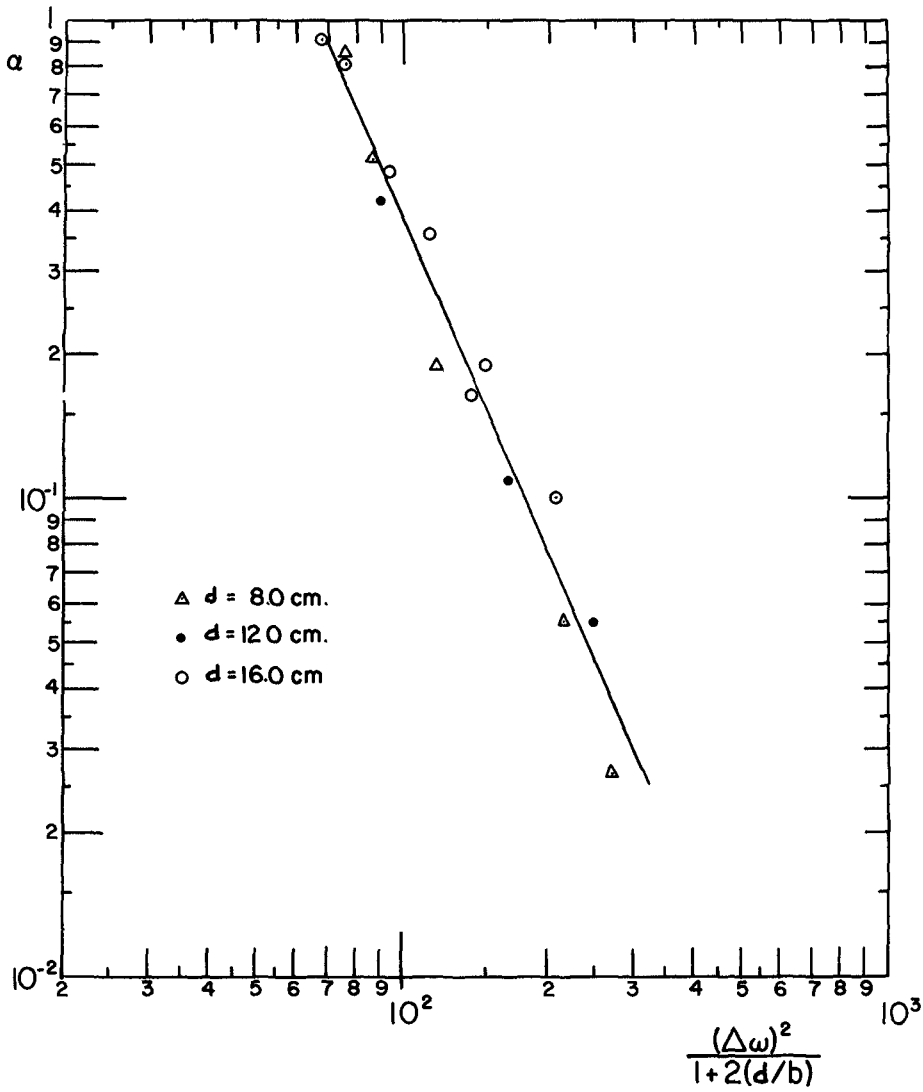

Fig. 6 Variation of Exponent α with Shear Stress Parameter

The coefficient K_1 can be expressed in terms of the concentration at 10 minutes, the time at which the first concentration sample was taken i.e., $K_1 = \frac{C_{10}}{(10)^{\alpha}}$. A close correlation esixts between $\frac{K_1}{C_o}$ and the shear stress parameter as shown in Fig. 7. Hence equation (8) becomes

$$C(t) = C_o\, f(\tau_b)\, t^{-2.14 \times 10^{-6}\, \tau_b^{-1.84}} \qquad (11)$$

That is at any time t , the instantaneous concentration $C(t)$ is proportional to the initial concentration C_o and a function of time and the bed shear stress τ_b .

In the second approach the relative instantaneous concentration $C = \frac{C_o - C(t)}{C_o - C_{eq}}$, that is the fraction of $C_o - C_{eq}$, deposited at time t after the beginning of deposition, was plotted versus log t (Fig. 8) for a depth of 16 cm. and $\tau_b = 0.0020$ psf. The plot gives a set of almost parallel straight lines corresponding to various initial concentrations. The extrapolated values of C' at $t = 10$ min. plotted versus log C_o give another straight line (Fig. 9). From Figs. 8 and 9 the following equation is obtained:

$$C' = \frac{C_o - C(t)}{C_o - C_{eq}} = -0.592 + 0.135 \log C_o + 0.455 \log t \qquad (12)$$

The same plot of data for constant C_o but varying speeds for depths 8 cm. and 16 cm. indicated a rather wide scattering but no correlation with τ_b . The average lines through these points are shown in Fig. 8. They also have a slope of 0.455. However, the other constants, which depend also on the water chemistry, differ. These last data were from experiments with tap water, whereas the ones eq. 12 are based upon, were from tests with distilled water.

The rate of deposition is given by:

$$\frac{dC(t)}{dt} = -\frac{0.198}{t}\, C_o \left(1 - \frac{C_{eq}}{C_o}\right) \qquad (13)$$

where $\frac{C_{eq}}{C_o}$ is a function of the bed shear stress according eq. 7.

Hence both approaches give a deposition rate proportional to the initial concentration, C_o and to a function of time and the bed shear stress.

All time-deposition equations are based on data between $t = 10$ and 300 minutes. The lowest measured values of C' were of the order of 0.5. More detailed investigations are needed in this direction.

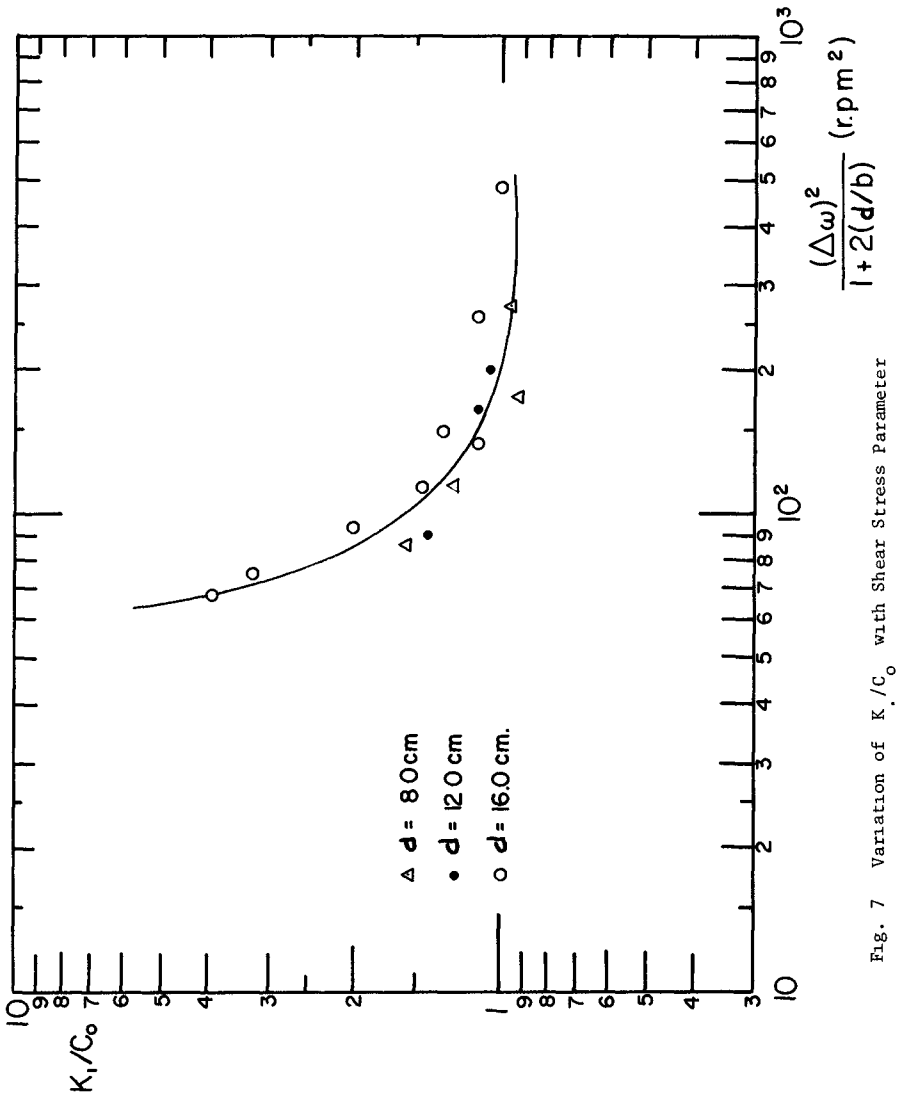

Fig. 7 Variation of K_1/C_o with Shear Stress Parameter

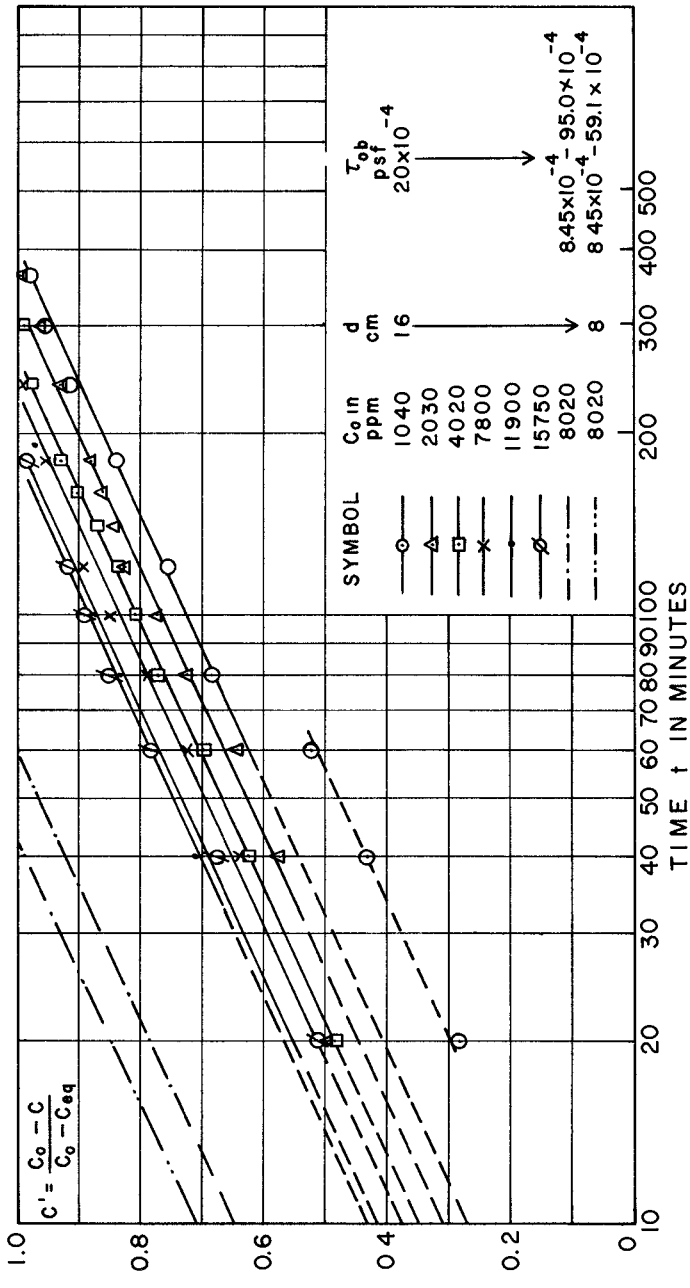

Fig. 8 Variation of Relative Concentration $\frac{C_o - C(t)}{C_o - C_{eq}}$ with Time

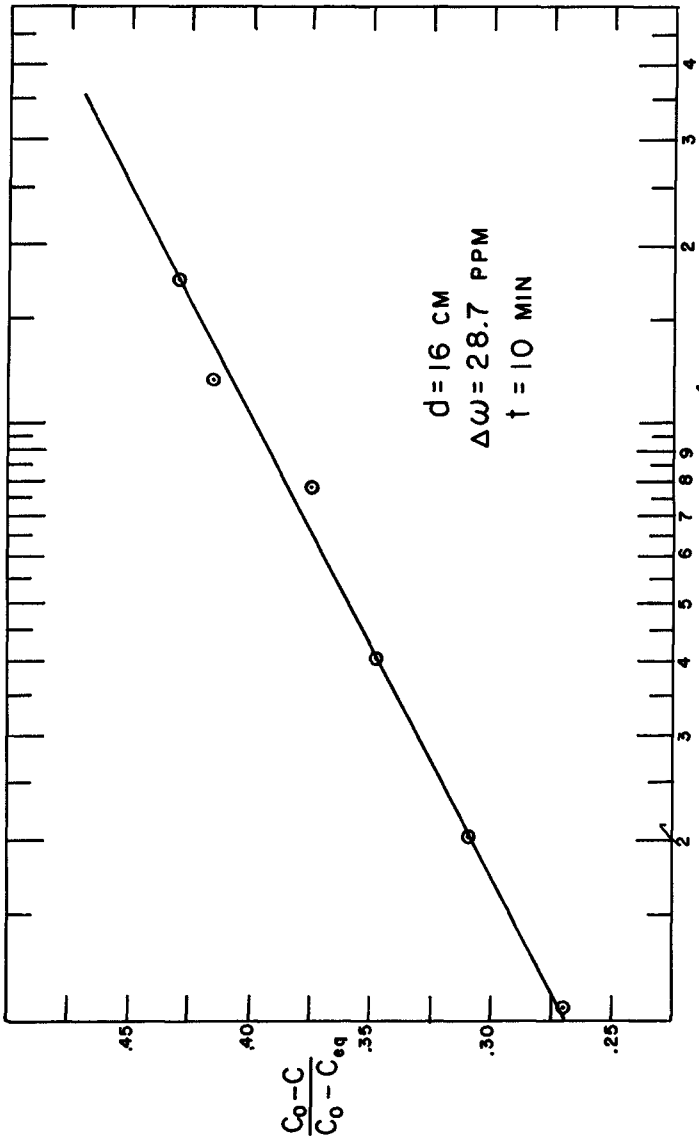

Fig. 9 Variation of Relative Concentration $\frac{C_o - C(t)}{C_o - C_{eq}}$ at 10 Minutes with Initial Concentration C_o

SUMMARY AND CONCLUSIONS

The recent experiments with kaolinite clay suspensions in the rotating annular channel revealed the following new important depositional characteristics of fine sediments in turbulent flows.

1. The shear stress at the bottom of the channel was found to be almost uniform across the channel as long as the deposition was uniform. Hence by a proper regulation of the speeds of the channel and the ring a two-dimensional flow can be well approximated.

2. For the experimental range of the channel depth, the average bed shear stress τ_b is very nearly proportional to the $\tau_{ch}^{1.20}$. It may be concluded, therefore, that this bottom shear stress is the variable controlling the relative equilibrium concentration, $\frac{C_{eq}}{C_o}$.

3. The relative equilibrium concentration is related to the shear stress parameter $\frac{(\Delta\omega)^2}{1 + 2\frac{d}{b}}$ and to the bed shear stress τ_b by log-normal relations given by equations (5) and (7). A qualitative argument as to why the bed shear stress is the controlling variable has been discussed.

4. Slow and gradual flushing of the suspended sediment at equilibrium confirmed the earlier deduced fact that after equilibrium has been achieved erosions and deposition of fine sediment cannot take place simultaneously. The nature of the equilibrium concentration of fine material in relation to that for coarse sediment has been discussed.

5. Limited time-concentration data revealed that the instantaneous suspended sediment concentration and the deposition rates depend on the initial concentration and the bed shear stress.

REFERENCES

1. Ayora, A., "Deposition of Cohesive Sediments", M.S. Thesis, Department of Civil Engineering, M.I.T., 1967.

2. Einstein, H. A., "The Bed-Load Function for Sediment Transportation in Open Channel Flows", Tech. Bull. No. 1026, U.S. Department of Agriculture, 1950.

3. Etter, R. J. and Hoyer, R. P., "A Laboratory Apparatus for the Study of Transport of Cohesive Sediment in a Flow Field", M.S. Thesis, M.I.T., Department of Civil Engineering, 1965.

4. Partheniades, E., "A Summary of the Present Knowledge of the Behavior of Cohesive Sediments in Estuaries", Tech. Note, No. 8, Hydrodynamics Lab., M.I.T., Cambridge, Massachusetts, 1964.

5. Partheniades, E., "Erosion and Deposition of Cohesive Soils", Proc., ASCE, Vol. 91, No. HY1, pp. 105-138, January 1965.

6. Partheniades, E., Kennedy, J., Etter, R. J., and Hoyer, R. P., "Investigations of the Depositional Behavior of Fine Cohesive Sediments in an Annular Rotating Channel", Tech. Report No. 96, Hydrodynamics Lab., M.I.T., Cambridge, Massachusetts, 1966.

7. Partheniades, E., and Kennedy, J. F., "Depositional Behavior of Fine Sediment in a Turbulent Fluid Motion", Proc., 10th Conference on Coastal Engineering, Tokyo, Japan, Vol. 1, pp. 707-729, September 1966.

8. Partheniades, E., and Paaswell, R. E., "The Present State of Knowledge on Erosion of Cohesive Sediments and its Practical Applications", Tech. Report (under preparation), Department of Civil Engineering, State University of New York at Buffalo, Buffalo, New York.

PART 3

COASTAL STRUCTURES

CHAPTER 48

MODELING OF STRUCTURES SUBJECTED TO WIND GENERATED WAVES

by

Erich J Plate* and John H Nath*

ABSTRACT

The difficulties inherent in the direct determination of loads on off-shore structures which are exposed simultaneously to wind and waves make it desirable to model each situation in the laboratory It is shown here that scaling of the loads and the waves is possible by using waves which are generated by blowing air over the surface of a laboratory channel, and by choosing a model material with an appropriate modulus of elasticity Wind-generated waves such as those measured in the wind water tunnel of Colorado State University have a dimensionless spectrum (Hidy and Plate (1965)) that is identical in shape to that found off the coast of Florida under hurricane conditions (Collins (1966)) Furthermore, it has been shown that hydro-elastic modeling is quite feasible (LeMehaute (1966)) These two results are combined to give modeling criteria for off-shore structures if direct wind forces are disregarded

INTRODUCTION

The increased use of off-shore structures for the exploration and exploitation of the oceans has created a demand for accurate design information on the load conditions to which the structures are subjected. In contrast to most land based structures, the critical load conditions for an off-shore structure may be dynamic in nature and induced by the water surface waves, so that analytical design procedures may become very complicated except for simply shaped structural elements

Present analytical procedures for determining the response even of simple structures to periodic waves are not exact For example, it is customary to use the Morrison equation to determine the wave forces acting on a vertical cylinder. In the Morrison equation, the inertia and drag coefficients must be determined experimentally In some cases these coefficients can only be described statistically Furthermore, they may vary with depth, as has recently been demonstrated by Pierson and Holmes (1965)

Under these circumstances it becomes desirable to study the dynamic behavior of a structure on a laboratory scale, which is quite feasible as will be shown in this paper. LeMehaute (1966) has shown that hydro-elastic modeling can be accomplished conveniently by using modern plastics for model construction If it can be ascertained that the response of the structure is linear, then the modeling problem consists of requiring identical shapes of transfer functions in model and prototype obtained by the modeling transformation The transfer function is then the quantity which needs to be determined from the experiment, and it can be found conveniently by exciting the model structure with a sequence of sine waves, and finding the response to each of them

CER67-68EJP-JN68

*Civil Engineering Department, Colorado State University

Most structural responses are nonlinear (although many are nearly linear), so that their transfer functions cannot be constructed by superposition. In such cases laboratory experiments are the only alternatives to potentially extremely complex calculations, for which the model structure must be excited with a forcing function which is dynamically similar to the prototype forcing function. In particular, for structures excited by wind generated waves, the model wave spectrum must be dynamically similar to that of the prototype Dynamic similarity of the spectrum does imply similarity of the shape of the spectra, as well as similarity of the energy contained in the spectra.

The need for similarity in spectral shape has been realized for some time Thus, Nath and Harleman (1967) produced a spectrum whose shape was similar to that of spectra found in parts of the Atlantic Ocean by Pierson and Moskowitz (1964). They used a wave generator for exciting model structures which was programmed to generate a quasi-random wave train with a spectrum of the desired shape.

Wave trains produced by a wave generator have several features which differ from that of a wind generated wave pattern. A wave generator can only produce wave components which agree with the free modes of the water surface. That is, each of the wave components is sinusoidal in shape and travels independently of all other wave components Thus, when a large wave is formed by the superposition of component sinusoidal waves that are momentarily in phase, although of different wave lengths, one finds that the life of the wave is fairly short. The large wave forms when the components are in phase, and then disappears as the components become out of phase due to the different component celerities. In contrast to this, one finds that large wind generated waves at high wind speed are quite long-lived and are, therefore, not composed of independently traveling sinusoidal waves. Nor is their total shape sinusoidal In Fig. 1 an example is shown of a significant wave which is found at a wind speed of approximately 10 m/sec This wave has been obtained by averaging the highest 20 waves from a record of about 300 waves measured in a laboratory channel. The waves were superimposed in such a way that their highest points coincided on the time axis and the ordinate values were averaged. A confidence band given by the local standard deviations of the coordinate values about the mean is also shown. It is apparent that even though the wave travels as a whole, its shape is definitely not sinusoidal Consequently, even though the spectrum of generator produced random waves might match that of wind generated waves, the shapes of the resulting individual waves are not exactly the same. Results obtained by this procedure are therefore subject to question, particularly if the dynamic response of the structure is nonlinear.

A second, and possibly more important difference between a generator produced spectrum and a fully developed wind wave spectrum lies in the inability of the former to properly model the magnitudes of the spectral densities. Complete dynamic modeling requires that both wave lengths and amplitudes are modeled by the same scale factor As shall be shown later, this condition requires that the dominant wave, which corresponds to the frequency at the peak in the spectrum for fully developed conditions, reaches its maximum possible amplitude. It is doubtful that this condition can be met while maintaining the required spectral shape, because the variance of a wave spectrum driven by strong winds increases with fetch, while that of the paddle generated wave spectrum decreases, partly due to viscosity, and partly due to breaking when superposition of component waves increases wave amplitudes beyond their stability limit

More suitable test conditions are obtained when wave trains are used, whose spectra, as well as shape and amplitudes of individual waves, resemble those of wind generated waves, but on a smaller scale. Such wave trains are found in the laboratory

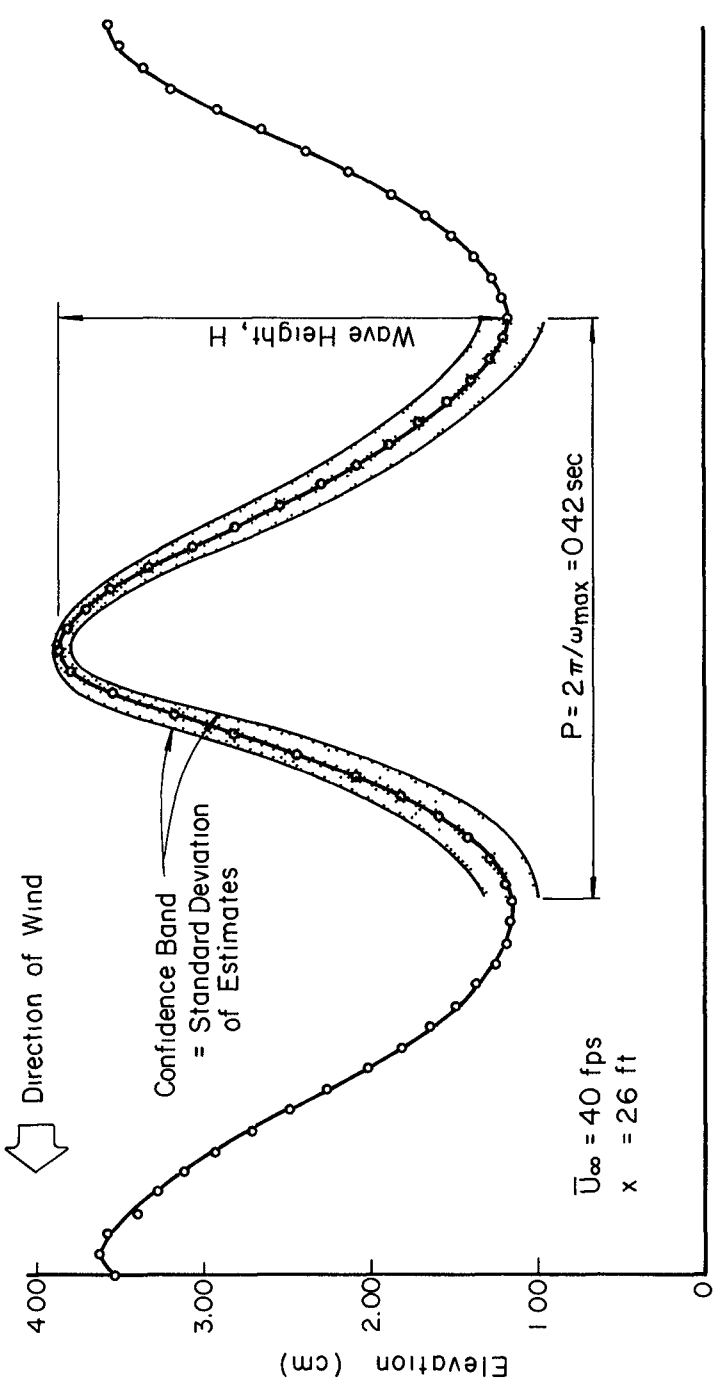

Fig. 1 Average Wave Form of wave at high wind velocity (from Po-Chang).

if air is blown over the surface of water standing in a channel. In this paper, the application of wind generated waves to modeling of wave forces is discussed. Since the wind generated laboratory waves have fewer drawbacks than paddle generated waves, it would be advisable to use them to obtain the load conditions on model structures By this method one also obtains a means to evaluate the wind loads on the part of the structure above the water surface

As shall be discussed in the first part of this paper, the spectrum of fully developed wind generated waves in a laboratory is similar in shape to that found for ocean waves, and it also yields a relationship between peak frequency and variance of the spectrum which is scaled by the Froude number in such a way that no change in scale between vertical and horizontal dimensions becomes necessary In the second part, considerations will be given to the modeling requirements of the structure This will be discussed on the basis of simple linear structures, and it is shown that Cauchy number similarity is feasible together with Froude number similarity.

The Similarity Spectrum of Wind Generated Waves

The driving forces acting on the submerged portion of a dynamically loaded offshore structure result from the wave field generated by the wind. They act in addition to the wind force on the superstructure Even though this wave field usually appears random both in space and time, it is nevertheless possible to distinguish, especially in the neighborhood of coasts, crests of waves which give the wave field an appearance of local two-dimensionality, with a predominant direction of progression perpendicular, or almost perpendicular, to the crest For such a wave pattern, a laboratory analogue exists in the wind generated waves which are obtained when air is blown over the surface of the channel in which water is standing It seems possible that the majority of all wind driven ocean waves outside of a storm center consists basically of a dominant pattern of this kind This would offer a logical explanation for the observation that one-dimensional wave spectra both in the laboratory and in oceans have an approximately equal shape. An illustration of this phenomenon is given in Fig 2a where a typical laboratory spectrum, obtained by Hidy and Plate (1965), is compared with a set of ocean wave spectra generated by strong off shore winds off the coast of Florida shortly after the passage of Hurricane Dora, in September 1964. The spectra were calculated by Collins (1966) The peak density of the larger ocean wave spectrum is 10,000 times larger than the peak density of the laboratory spectrum Yet, the shapes do not differ significantly.

The identical shape of the dimensionless spectra shall be explored here A non-dimensional form of the spectral shape that is suitable for the purpose of this paper has been suggested by Hidy and Plate (1965) Hidy and Plate (1965) recommended to non-dimensionalize the spectra by dividing the frequency axis by ω_{max}, which is the angular frequency at which the spectral peak $\phi(\omega_{max})$ is observed The spectral density $\phi(\omega)$ was reduced so that the area under the non-dimensional spectrum $S(\omega/\omega_{max})$ is equal to 1 This leads immediately to the requirement

$$S\left(\frac{\omega}{\omega_{max}}\right) = \frac{\omega_{max}}{\sigma^2}\ \phi(\omega) \qquad (1)$$

where σ^2 is the variance of the water surface elevation. This non-dimensionalizing procedure is equally valid for ocean wave data, as was shown by Colonell (1966). In Fig. 2b, the average curve of Hidy and Plate (1965) is given, which is representative for many different laboratory spectra. The similarity of this shape with that of Fig. 2a is noted Also, it is seen that the high frequency end of the spectrum follows

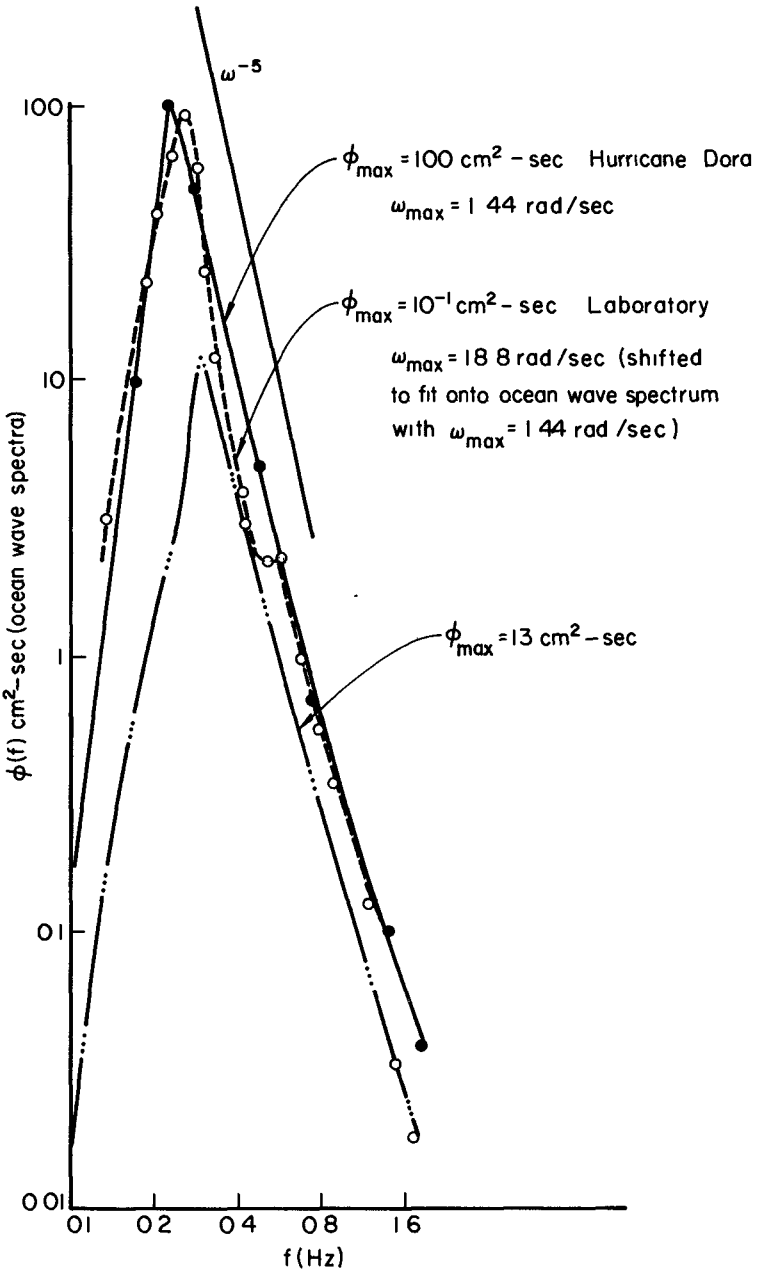

Fig 2a Examples of Ocean and Laboratory Spectra

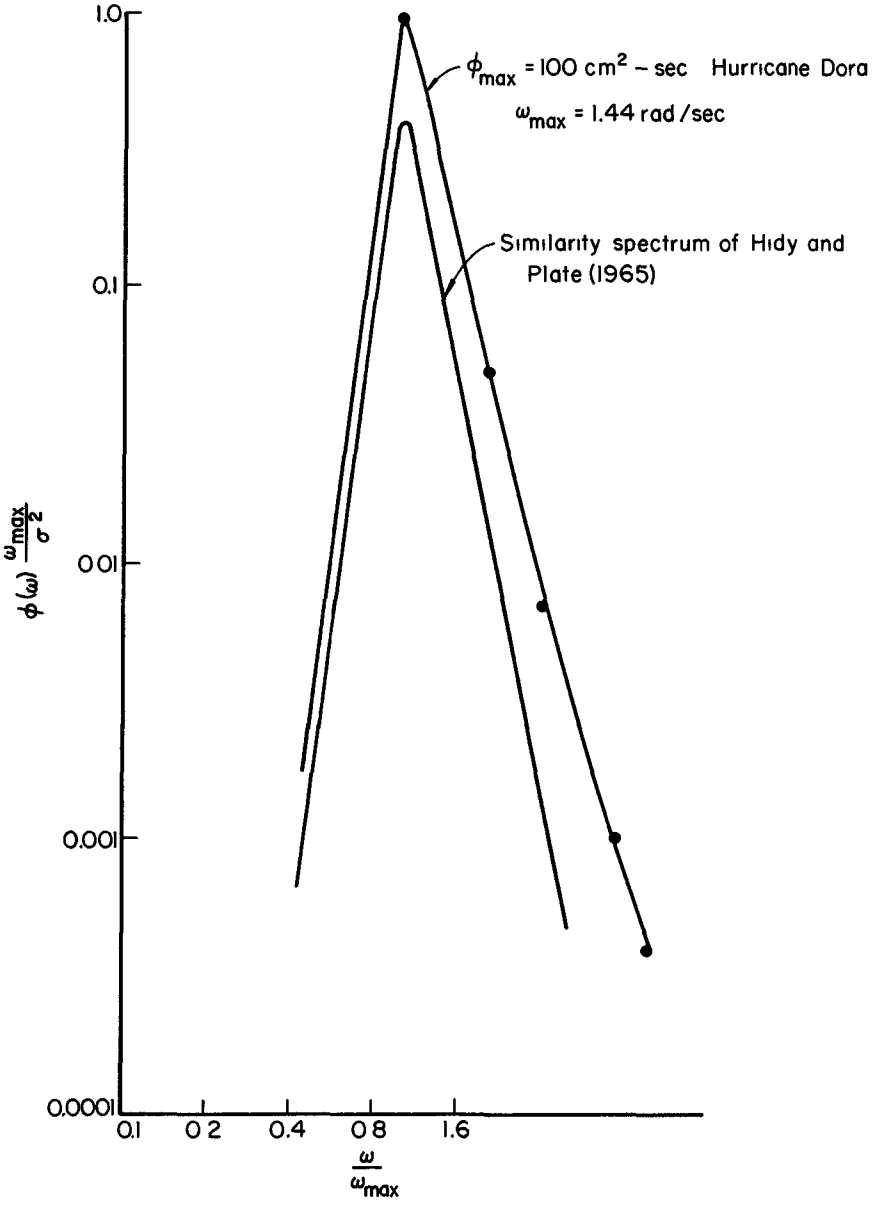

Fig 2b Examples of Ocean and Laboratory Spectra

approximately a ω^{-5} law, as predicted by Phillips (1958) However, the -5 law seems to be only an approximation to the spectra at high frequencies There is evidence that the exponent in the power law varies from about -7 near the spectral peak to -4 at higher frequencies.

More significant than the high frequency behavior of the individual spectrum is the fact that all spectra obtained from ocean or laboratory are bounded at the high frequency end by a universal curve given by the equation of Phillips

$$\phi(\omega \geq \omega_{max}) = 1\ 05\ \ 10^{-2} g^{+2} \omega^{-5} \tag{2}$$

where g is the constant of gravity This is shown in Fig. 3, which has been reproduced from Hess (1968). Phillips (1958) derived Eq. 2 by using dimensional analysis. Recently Plate, Chang and Hidy (1968) have provided arguments which deduce the -5 power law as an upper limit of spectral growth, independent of the shape of the individual spectrum, provided only that all spectra are similar The -5 power law then becomes a law which relates peak spectral density $\phi(\omega_{max})$ to ω_{max} Since this law plays a key role in the modeling criteria to be developed, the derivation shall be outlined here

The basic assumptions are

a. The spectrum has a sharp peak near ω_{max} , and can be described by the similarity shape of Fig 2b. According to Longuet-Higgins (1952) this implies that the water surface undulations consist mainly of a train of waves of frequency ω_{max} whose amplitudes are subject to a random modulation. This model agrees well with observations both of water surface elevation recordings and of wave spectra The wave of frequency ω_{max} shall be called the dominant wave, whose height is denoted by H .

b The maximum growth of the dominant wave component is limited by the acceleration of gravity such that

$$a_{max} = \alpha g \tag{3}$$

where a_{max} is the maximum acceleration of the surface of the dominant wave, and α is a number which is smaller than 1 It will be shown that $\alpha \approx 0.3$ leads to an estimate which is consistent with the numerical factor of 0.0105 in Eq. 2.

Longuet-Higgins (1952) has shown that a Gaussian wave record which satisfies condition (a) above has wave heights H which are Rayleigh distributed. Consequently, the mean value, $H^{(p)}$, of the pN highest of N waves is a constant multiple of the mean wave height $\bar{H}$, or

$$\frac{H^{(p)}}{\bar{H}} = m \tag{4}$$

where m is a constant. Typical values of m are m = 1 42 for p = 1/3 and m = 1.26 for p = 1/2. Thus, if each wave is basically sinusoidal, then the average vertical acceleration of the water particles at the peak of the highest pN dominant waves is found to be equal to

$$a_m = \frac{1}{2}\ \omega^2_{max}\ \ H^{(p)} \quad . \tag{5}$$

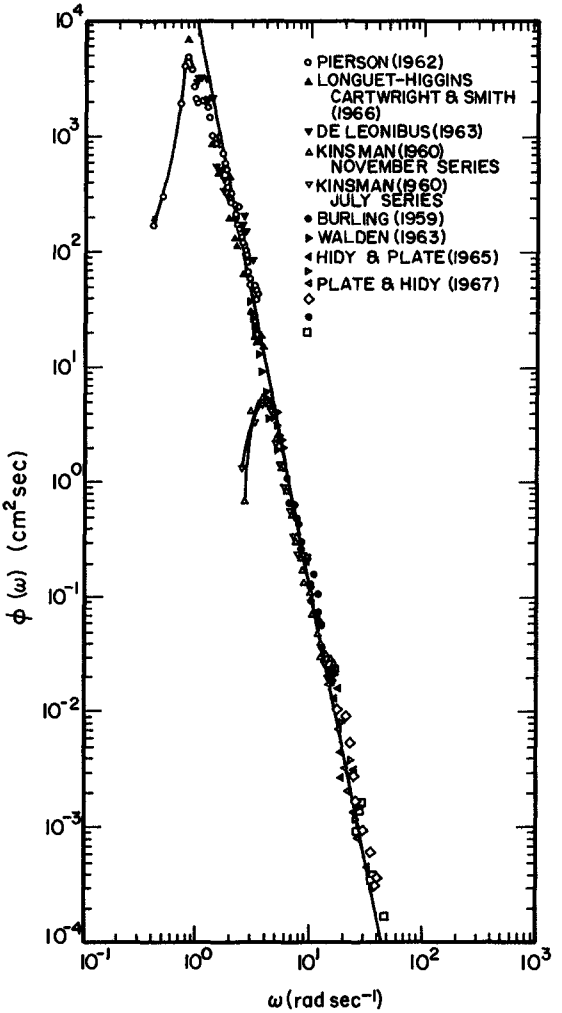

Fig. 3 A Comparison of Observed Wave Spectra with Geophysical Wave Spectra (from Hess, 1968)

Somewhat arbitrarily, it is assumed that the significant acceleration is that of the significant wave $H^{(1/3)}$. For a wave record whose water surface elevation is Gaussian (which is approximately true both for the laboratory and the field), there exists the following relation between mean wave height and variance of the water surface elevation (Collins, 1966)

$$8\,\sigma^2 = \overline{H}^2 \tag{6}$$

with $m = 1.42$, the relationship between the acceleration of the significant wave $H^{(1/3)}$ and the variance σ^2 of the wave record is found as

$$a_m^2 = 4\,\omega_{max}^4\,\sigma^2 \tag{7}$$

But according to assumption Eq. 3, this is also equal to $\alpha^2 g^2$, so that

$$\sigma^2 = \frac{\alpha^2 g^2}{4\,\omega_{max}^4} \quad . \tag{8}$$

We can eliminate σ^2 in Eq. 1 and let $\omega = \omega_{max}$. It is then seen from Fig 2 that $S(\omega_{max}/\omega_{max}) = S(1) \approx 0\,5$ for a fully developed sea, and consequently

$$\phi(\omega_{max}) = \frac{\sigma^2}{\omega_{max}}\,0\,5 = \frac{\alpha^2 g^2}{8\,\omega_{max}^5} \tag{9}$$

which is independent of the spectral shape except for the requirement of similarity. This result is now compared with Eq 2 where ω is replaced with ω_{max}. One obtains

$$\phi(\omega_{max}) = 1\,05\,10^{-2}\,g^2\,\omega_{max}^{-5} \tag{10}$$

Consequently, one finds

$$\alpha = 0\,29 \tag{11}$$

which is somewhat lower than the limiting vertical acceleration of the Stokes wave, where $\alpha = 0.5$.

The reasoning leading to Eq. 10 is of consequence for the purpose of modeling. When conducting a model study, it is naturally desirable to model the maximum forces that can occur Waves with amplitudes exceeding that of the significant wave would presumably break, because their accelerations exceed the critical value αg Therefore, waves at frequencies $\omega > \omega_{max}$ of larger amplitudes than that at ω_{max}, cannot occur in an equilibrium spectrum described by the similarity shape and by the relation between peak spectral density and the corresponding frequency expressed through Eq 10 If larger waves are to occur they must therefore be of lower frequencies.

Equation 10 also implies that the waves that reach the limit of growth are subjected to continuous addition of energy through work done by the wind, so that the dominant wave remains at its maximum height. A spectrum of waves with a dominant wave consisting of swell from a far away, and perhaps long subsided storm, might still have the similarity shape of wind generated waves, but its maximum spectral density will be below that of Eq. 10. Consequently, the maximum possible spectral density for waves of frequency ω_{max} is given by Eq. 10, which therefore describes the envelope for all fully developed wave spectra.

Fully developed wave spectra are found in particular when wind of long duration is blowing, such as during hurricanes An example is given by results of Collins (1966) which were obtained at two different times at two different off-shore fetches during an off-shore blowing wind. In Table 1 the peaks of the spectra calculated from Eq. 10 are compared with the peaks obtained by Collins. It is remarkable that the long fetch spectra are in exact agreement with Eq 10, while the lower fetch data are below the saturation value given by Eq 10 Many other data show the same behavior, as is evident from the data of Fig 3.

TABLE 1. PEAK AMPLITUDES OF HURRICANE DORA DATA
(from Collins, 1966)

Case	f_{max}(Hz)	$\phi(f_{max})$ (observed) m^2-sec	$\phi(f_{max}) = 2\pi\phi(\omega_{max})$ (from Eq 10) m^2-sec	Remarks
AI	0.35	0.130	0 124	Sept. 9, 64 Fetch 11 miles
AII	0 45	0 018	0 034	Sept. 9, 64 Fetch 1.7 "
BI	0.23	1 05	1.00	Sept 10, 64 Fetch 11 "
BII	0 27	0.2	0 45	Sept.10, 64 Fetch 1.7 "

We notice that the results of Eqs 9 and 11 yield the important relationship between variance, σ^2 , and ω_{max}

$$\sigma^2 = 2.1 \quad 10^{-2} \; g^2 \; \omega_{max}^{-4} \quad . \tag{12}$$

Equation 12 shows that the scale of the amplitudes of the wave which must also scale the square root of the variance of the spectrum fixes the scale of the frequencies, so that it is not possible to adjust the two scales independently. If it is desired to model wave heights so that

$$(\sigma/L)_m = (\sigma/L)_p \tag{13}$$

then it follows that the frequencies must be related like

$$\frac{\sigma_m}{\sigma_p} = \frac{L_m}{L_p} = \frac{\omega^2_{max\ p}}{\omega^2_{max\ m}} \tag{14}$$

Here, L is any characteristic length, the subscript m refers to the model, and the subscript p to the prototype. This condition is in accord with the requirements imposed on the wave length λ . If it is desired to have identical non-dimensional wave lengths, λ/L , for model and prototype, then it would be necessary to set

$$\frac{L_m}{L_p} = \frac{k_p}{k_m} = \frac{\lambda_m}{\lambda_p} \quad . \tag{15}$$

However, for gravity water waves, the frequency is related to the wave number, $k = 2\pi/\lambda$, by.

$$\omega^2 = g\, k \tanh kh \tag{16}$$

where h is the depth, as defined in Fig 4, and thus

$$\frac{\omega_p^2}{\omega_m^2} = \frac{k_p}{k_m} = \frac{L_m}{L_p} = \frac{h_m}{h_p} \tag{17}$$

in agreement with Eq 14. Consequently, the use of a fully developed wave spectrum in the laboratory for simulating a fully developed wave spectrum for prototype conditions results in identical scale ratios of both wave heights and wave lengths, if the spectra are related by Eq 14. The use of Eq. 14 thus leads to an undistorted geometrical scaling of the whole wave field This result establishes the advantage of using wind generated waves in the laboratory for modeling wind generated waves in the field

It is interesting to note that modeling according to Eq. 14 implies Froude number scaling, i.e.,

$$Fr = \frac{u_{wave}}{\sqrt{gL}_m} = \frac{u_{wave}}{\sqrt{gL}_p} \tag{18a}$$

where u_{wave} is a wave related velocity such as c_o, or the wave induced at some reference depth. For the latter, u_{wave} is proportional to $\sigma\omega$ for any frequency component and one obtains

$$\frac{\omega_m \sigma_m}{\sqrt{gL}_m} = \frac{\omega_p \sigma_p}{\sqrt{gL}_p} \,. \tag{19}$$

If σ is eliminated through Eq. 14, then Eq 17 follows Consequently, Froude number modeling according to Eq 19, in conjunction with Eqs. 9 and 10, results in fully developed wind generated wave spectra in model and prototype which are geometrically similar with equal vertical and horizontal scales Therefore, the model structures can be built to scale, and the complications which arise from distorted scales can be avoided. It should be mentioned that the definition of a modeling Froude number according to Eq 19 is somewhat more stringent than is required for linear response of structures under the effect of a wave force. For such a system, the amplitude appears only in the load function and therefore need not be scaled properly because its effect can be included into the conversion factor which is used for calculating prototype response data from model data. Then the Froude number is more suitably defined by

$$Fr = \frac{c_o}{\sqrt{gL}} \tag{20}$$

Since c_o is independent of the vertical scale of the wave motion, this modeling criterion only suffices to satisfy Eq 15, but not Eq. 13.

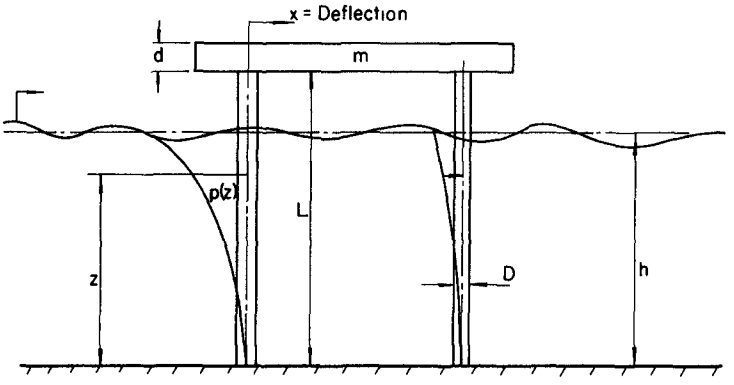

Fig 4 Definition Sketch for Off-Shore Structure

In applying Eq. 10 to laboratory modeling, it is required that some value of the height of the significant wave is known which can be expected under prototype conditions at the position where the structure is to be constructed. How this wave height can be found shall not be discussed here If it is known, then the variance of the water surface follows from Eqs. 4 and 6, the peak frequency, ω_{max}, from Eqs. 8 and 11, and the spectral peak from Eqs 9 and 11. The spectrum can then be constructed with variance σ^2, ω_{max}, and the similarity spectrum of Fig. 2. After choosing a suitable length scale, the model spectrum can be obtained by reducing the variances of the water surface and the frequencies according to Eq. 14. It remains to show under what conditions it will be possible to obtain a scaled dynamic response of the structure.

Modeling of Structures Subjected to Wave Forces

When a linear structure is excited by a random dynamic load whose stationary spectrum is $\phi_L(\omega)$, it is well known that the deflection spectrum $\phi_x(\omega)$ of a characteristic point on the structure can be expressed by

$$K^2 \phi_x(\omega) = | H(\omega) |^2 \phi_L(\omega) \quad . \tag{21}$$

where K is the spring constant of the support legs and H is a transfer function. Multiplication of the deflection spectrum by the square of the spring constant K of the support legs signifies that we assume the structure to be so stiff that deflections are within the range of validity of Hooke's law. Then the spring constant is a multiplier whose magnitude must be known. It is to be chosen according to dynamic similarity of the structural response

The function $H(\omega)$ of Eq. 20 is the transfer function of the structure which establishes the dynamic response of the structure under the effect of the load spectrum. In our notation, it is a dimensionless function whose value at zero

frequency must be one, to correspond to the case of static loading. The simplest structure, such as shown in Fig 4, consists of one or more cylindrical supports which are clamped to some degree into the ground and into the working platform. The transfer function of each of these cylinders is then given by that of a simple second order system

$$|H(\omega)|^2 = \frac{1}{\left(1 - \frac{\omega^2}{\omega_n^2}\right)^2 + \left(2\zeta \frac{\omega}{\omega_n}\right)^2} \tag{22}$$

which is valid for the dominant first vibrational mode, whose natural frequency is equal to ω_n. The coefficient ζ is the relative damping factor. It is determined almost completely by the internal structural damping, while the natural frequency is given to

$$\omega_n = \sqrt{\frac{K}{m}} \tag{23}$$

where m is the mass of the load on the single cylinder, and K is the spring constant

$$K = \gamma \frac{3\,EI}{L^3} (1-\beta) \tag{24}$$

In this equation, E is the modulus of elasticity, I the moment of inertia, and L the length of the cylinders, as indicated in Fig 4. The clamping coefficient γ corrects for the possibility of rotation of cylinder top and bottom. When the cylinder is clamped into the ground, and into the platform (i.e., the cylinder is one leg of a multilegged structure) so that the joints cannot rotate then $\gamma = 1$. A more flexible structure, resulting from only partial clamping in the ground or at the platform yields a smaller γ, while increased stiffness, as obtained for example by braces across the legs results in a larger value of γ. Evidently, for more complex structures a simple correction of the single cylinder spring constant does not suffice, and a suitable elastic model may be the only feasible alternative. The coefficient β is the reduction factor due to vertical loads, i.e.,

$$\beta = \frac{4WL^2}{\pi^2 EI} \tag{25}$$

where W is the vertical load applied to the cylinder top. As long as β is significantly smaller than 1, a vertical load can be used to tune the structure, so that its natural frequency assumes the desired value.

For the multilegged structure as a whole, the transfer function is the same as that for the individual legs except for a modification factor which results from the time lag between the forces on different cylindrical legs. The phase shift may either lead to adding total forces on the structure or subtracting, and might even cancel depending on the distance between legs as related to wave length, and on the orientation of the structure. This effect has been discussed by Nath and Harleman (1968).

In a model study, the effects of structural complications and intramodal coupling on the transfer function may possibly be determined experimentally We notice that for the transfer function to be modeled in the laboratory, it shall have to meet the following requirements

1 Model and prototype must be geometrically similar, and must be scaled such that the length scales of the wave motion are identical to the scale of the geometry of the structure. In this manner, interference effects due to loads on different individual legs and other structural elements are accounted for.

2. Dimensionless (or relative) damping coefficients of model and prototype associated with each mode must be identical. This requirement is not met easily. It is probably suitable to use a damping coefficient based on experience and correct the damping of the model structure by an external arrangement of dashpots

3. The natural frequencies of model and prototype must be chosen such that ω/ω_n is identical in model and prototype This must be interpreted as requiring that the ratio of the ω_{max} of the peak of the load spectrum to the natural frequency of the structure, ω_n, is the same, or

$$\left(\frac{\omega_{max}}{\omega_n}\right)_{model} = \left(\frac{\omega_{max}}{\omega_n}\right)_{prototype} \tag{26}$$

Evidently, the preceding requirements imply that the output spectrum, as well as the input spectrum, is similar in model and prototype. The modeling requirement expressed by Eq. 26 implies simultaneous equality of both Froude number and Cauchy number in model and prototype. Generally speaking, the Cauchy number is defined as

$$C_a = \frac{u_W}{u_E} \tag{27}$$

where a wave reference velocity might be $u_W = \sigma\omega_{max}$, while the reference elastic velocity u_E usually is the speed of sound E/ρ However, in the case of bending deformation of the structure, it appears to be more rational to use an elastic velocity $u_E = L\omega_n$, so that

$$C_a = \frac{\omega_{max}\,\sigma}{\omega_n\,L} \tag{28}$$

for similar geometrics, Cauchy number similarity for model and prototype requires that Eq. 26 be satisfied This equality together with Froude number equality can be met, however, only if the elastic properties are suitably adjusted By using the definition of the natural frequency, Eq 23, in conjunction with Eqs. 24, 14 and 27, it is seen that

$$\alpha\ \frac{E_m\,\rho_p}{E_p\,\rho_m} = \frac{L_m}{L_p} \tag{29}$$

when ρ_p and ρ_m are the bulk densities of the loads on the cylinder for prototype and model, respectively. The factor α, given by

$$\alpha = \frac{\gamma_m (1 - \beta_m) I_m L_p^4}{\gamma_p (1 - \beta_p) I_p L_m^4} \tag{30}$$

reduces to one if exact geometric similarity of the model and prototype support structures exist, and if the damping conditions are identical. A factor $\alpha = 1$ is, of course, not necessary. For example, instead of the thin-walled cylinders used for the legs of prototype structures, we might prefer to use solid legs in the model.

The result given by Eq 28 can be derived more formally by the methods of inspectional analysis, as was evidently done by LeMehaute (1966) It gives a means of obtaining, by suitably adjusting α, E_m and ρ_m, the dynamically correct response of the structure to wave forces, provided that the load spectrum is also modeled properly.

Acknowledgments

Financial support for this study has been provided by the National Science Foundation under Grant No. GK 188. P C Chang kindly made Fig. 1 available, which will appear in his Ph.D Dissertation at Colorado State University.

REFERENCES

Collins, J., (1966), "Wave statistics from Hurricane Dora near Panama City, Florida," Proc. ASCE Conference on Coastal Engineering, Santa Barbara, p. 461.

Hurty, W. C and M. F Rubinstein, (1965), "Dynamics of Structures," Prentice-Hall, Englewood Cliffs, New Jersey

Hess, G. D , (1968), "Turbulent air flow over small water waves," Ph D Dissertation, Department of Meteorology, University of Washington, Seattle, Washington.

Hidy, G. M., and E. J. Plate, (1965), "The frequency spectra of wind generated waves," Physics of Fluids, p. 1387

LeMehaute, B., (1965), "On Cauchy-Froude similitude," Proc. ASCE Conference on Coastal Engineering, Santa Barbara, p. 327.

Longuet-Higgins, (1952), "On the statistical distribution of the heights of sea waves," Journal of Marine Research, Vol 11, p. 245.

Nath, J. H., and D. R F Harleman, (1967), "The dynamics of fixed towers in deep water random waves," Proc. of the Conference, "Civil Engineering in the Oceans," ASCE, San Francisco, California, p 99

Phillips, O. M., (1958), "The frequency spectra of wind generated waves," Journal of Fluid Mechanics, Vol. 4, p. 426.

Pierson, W. J., and Moskowitz, L., (1964), "A proposed spectral form for fully developed wind seas based on the similarity theory of Kitaigorodskii," Journal of Geophysical Research, Vol. 69, No. 24, p. 5181.

Plate, E. J., P. Chang and G. M. Hidy, (1968), "Experiments on the generation of small water waves by wind," Journal of Fluid Mechanics, (to be published).

CHAPTER 49

DESTRUCTION CRITERIA FOR RUBBLE-MOUND BREAKWATERS

By Adelkis J. Rogan, Docteur Ingénieur
Laboratoire National d'Hydraulique, Chatou, FRANCE.

ABSTRACT

The general purpose of the author's research undertaken in the "Laboratoire National d'Hydraulique" was to study wave action on rubble-mound breakwaters with regular (periodic) waves on the one hand and irregular (random) wind generated waves on the other, and to compare the effects of these two types of waves by use of the storm duration t. With a first series of periodic waves experiments we have obtained the destruction of the breakwater's cover-layer for different storm durations t, by varying H and T. The mass of armor units remained constant. The angle of the slope, according to the seaward equilibrium profile could be considered as constant.

For the destruction cases we obtained a risk criterion:

$$\frac{t}{T} = - A.\log\left(\frac{H^2}{\nu T}\right) + B$$

which provides the storm duration t, knowing H, T and ν.

Then for a second series of random wind generated waves experiments we eliminated t and found that the constant periodic wave height ($H_{dest.}$) is equal to the "significant wave height" ($H_{1/3}$) for the random waves. This is an experimental demonstration of the justifiable use of $H_{1/3}$ as "project wave height".

1. INTRODUCTION

1.1. Analysis of Classical stability formulas.

First of all an analysis of classical empirical and semi-empirical stability formulas was necessary to show the importance of some variables and the absence of others. Thus formulas of CASTRO, IRIBARREN, MATHEWS, EPSTEIN and TYRELL, IRIBARREN and NOGALES, RODOLF, LARRAS, IRIBARREN (modified by HUDSON), HEDAR, HENNES and LEONOFF, BEAUDEVIN, HUDSON (or W.E.S. formula) have been analysed and were adapted to "L.N.H." commonly used notation. Afterwards, they were transformed to show common parameters and to verify their dimensional homogeneity (1). Only two of them are homogeneous: IRIBARREN's (modified by HUDSON) and HUDSON's formulas. Stability formulas have the following general aspect:

$$M = H^3.F$$

where $F = k.f_1(\delta).f_2(\alpha)$ ....

Two of them (the formulas of MATHEWS and RODOLF) have the aspect $M = H^2.T.F$, but they are not used in practice.

The stochastic character of waves and the time of action, or otherwise storm duration, do not appear in the previous formulas. On the other hand, engineers use more and more the "significant wave height" $H_{1/3}$ as "project wave height" for maritime structures.

1.2. Main purpose.

The main purpose was to introduce the "time of action" t (or storm duration) into the consideration of rubble-mound breakwater's stability and to verify experimentally the empirical and theoretical (2,3) assumption that $H_{1/3}$ is really the representative and afterwards destructive mean wave height value of a random sea.

The reasoning below was followed prior to laboratory experimentation on multi-layered breakwaters:

(a) Cover-layer's profile can be modified till stabilization. When second layer is reached then destruction is imminent. Smaller armor units of the second cover-layer can no longer resist wave attack.

(b) It is easier to observe the complete destruction of the cover-layer than to measure the number of displaced armor units.

(c) Wave height or period of random waves are not known a priori. Duration of wave action on the breakwater is the only parameter for comparison between periodic and random waves.

Therefore we have chosen as a criterion of comparison the complete destruction of the cover-layer in the same time, obtained one time from periodic waves (H and T constant) and another time from random waves (H_i and T_i random values). Thus, eliminating the parameter t, H and H_i can be compared as well as T and T_i.

Figure 1 shows the general configuation of "L.N.H." research facilities as well as pertinent dimensions in meters.

1.3. Similitude.

The assumption was made that the inertia forces are very much larger than viscous forces. In general, similitude of the two flows with free surface requires two conditions:

$$F_1 = F_2$$

$R_1 = R_2$ (or in default of: $R_1 \geq R_c$ and $R_2 \geq R_c$).

For our investigation we used the FROUDE-REECH condition, which is essential for model studies in open channels with strongly turbulent flows. Nevertheless, we did not throw aside the assumption of the importance of the condition of REYNOLDS. The dimensions of the model were sufficiently small that infiltration or percolation flows accompany the wave attack on armor units.

The scale 1:40, has been chosen according to the dimensions of "L.N.H." research facilities. Specific gravity of water used during experimentation was assumed to be equal to 1.00. Difference of specific gravity between model water (1.00) and sea water (1.026 - 1.029, according to salinity) is big enough to be important if model investigation is related to field construction (4). Our study was theoretical; therefore we did not take the difference into account. The mass per unit-volume of armor units was

$$\rho_6 = 2.6 \text{ t/m}^3$$

2. PERIODIC WAVES

2.1. Introduction.

The variables H and T were constant during each experiment and the following values were chosen for these variables:

H = 0.05, 0.075, 0.10, 0.125 m. (i.e. 2, 3, 4, 5 m. in nature) approximately.

T = 0.948, 1.265, 1.581, 1.897 sec. (i.e. 6, 8, 10, 12 sec. in nature).

It was easy to set the wave generator at the period desired with the channel empty. Afterwards, the model was constructed, the channel filled with water to the level 0.35 m. (corresponding to 14 m. in nature), the resistance type wave gauges calibrated and, then the generator started. The wave height was increased from zero to the desired value and then remained constant during the whole experiment.

2.2. Model.

Figure 2 shows one of the breakwater profiles studied. It is a type commonly employed with three cover-layers. The same armor units of specific gravity 2.6, weighed one by one and arranged always in the same way, have been used throughout all experiments.

Particle size distributions used for each layer were:

A = 50 - 80 g. (i.e. 3 - 5 t in nature) with $A_m \simeq 63$ g. (i.e. 4t).

B = 20 - 50 g. (i.e. 1.5 - 3 t in nature) with $B_m \simeq 37$ g. (i.e. 2.36 t).

C = 5 - 25 g. (i.e. 0.32 - 1.6 t in nature) with $C_m \simeq 11$ g. (i.e. 0.7 t).

Where A_m is the median of A, B_m of B and C_m of C.

The middle-layer armor units were coloured blue. The colouring made it easier to know the moment at which the middle-layer was reached in the process of destruction.

Water depth on the sea side was always constant and equal to 0.35 m. (i.e. 14 m. in nature). The angle of breakwater slope varied from 30 to 36 degrees in steps of 2 degrees.

2.3. Experiments with periodic waves.

Every experiment lasted, as a rule, 3 hours 45 minutes (i.e. 24 hrs. in nature) if the cover-layer was stabilised. If the destruction of the cover-layer was achieved before 3 hrs. 45 min., we stopped the experiment. If the destruction was imminent around 3 hrs. 45 min., we prolonged the experiment until complete destruction was obtained. Sixteen experiments were made for every angle of breakwater slope: 4 for every wave period (0.948, 1.265, 1.581, 1.897 sec.) for each wave height,(0.05, 0.075, 0.10, 0.125 m. approximately).

Some experiments were omitted when no influence of the breakwater slope was obtained (for instance for H = 0.05 m. and T = 0.948 sec.). At the end of the experiment we drew the new profile on the glass-wall and we photographed it. The destruction of the cover-layer was obtained in 13 cases.

Ten minutes after the waves were fully developed, a record of the clapotis between the model and the wave generator was made. From this record we obtained the value of H, which we will later compare with the destructive mean value of the irregular wave height.

2.4. Seaward equilibrium profile.

During the first minutes of every experiment we observed the tendency of attacking waves to move armor units from the upper portion of the slope to the lower portion. After some minutes a new profile was "carried" on the seaward face of the breakwater (Figure 3, profile DA BC). The new discontinuous slope was composed of three different slopes, one of which (the slope AB) was flatter than the initial one.

From this moment onwards, the destruction of cover-layer progressed, with a good approximation, parallel to the new slopes. Comparison between corresponding slopes for various tests (1, section 4.33) shows no big differences between them. Their mean values were:

$$\tan\alpha_1 = 1/1.059, \quad \tan\alpha_2 = 1/2.627, \quad \tan\alpha_4 = 1/1.278$$

$$\alpha_1 \simeq 43 \qquad \alpha_2 \simeq 21 \qquad \alpha_4 \simeq 38$$

Therefore profiles with different slopes of 30, 32, 34, and 36 degrees were transformed, after a few minutes, to an identical discontinuous seaward profile; i.e. to an identical reflection slope for

incident waves. Thus, values measured during all these experiments have been used together for calculations.

2.5. Characterization of the risk of cover-layer destruction.

a) Study of parameters: $Y = \log\left(\frac{H^2}{\nu T}\right)$ and $X = \frac{t}{T}.10^{-3}$

We first specify r as the sample coefficient of correlation and as the value for the true bivariate distribution of Y and X.

We obtained destruction of the cover-layer in 13 cases (n = 13). Thus we have studied the coefficient r for the bivariate distribution of dimensionless functions Y and X, of parameters measured during the above experiments (5). Pursuing the calculation of Table 1, we obtained:

$$\sigma_x^2 = \frac{D_x}{n^2} = 7.297 \qquad \sigma_x = 2.701$$

$$\sigma_y^2 = \frac{D_y}{n^2} \qquad \sigma_y = 0.063$$

$$C = n \cdot \Sigma XY - \Sigma X \cdot \Sigma Y = -23.008$$

and $$r = \frac{C}{\sqrt{D_x D_y}} = -0.796 \qquad = -0.796$$

We will now test its significance with the Z - Transformation of FISHER:

$$Z = {}^1/_2 \log\left(\frac{1 + r}{1 - r}\right)$$

which is distributed approximately according to a GAUSS law of expectation:

$$\xi = {}^1/_2 \log\left(\frac{1 + \rho}{1 - \rho}\right)$$

and standard deviation:

$$\sigma = \frac{1}{\sqrt{n-3}}$$

For r = - 0.796 we obtained Z = - 1.088 and for
n = 13 : $1/\sqrt{n-3} = 0.3164$

If no real correlation exists for the true bivariate distribution of Y, X (i.e. $\rho = 0$), the variable $u = Z/\sigma$ is distributed according to a unit normal distribution, then u = - 3.44.

The probability of finding a value less than or equal to u = - 3.44, if $\rho = 0$, is equal to 0.0003, i.e. Pr ($u \leq -3.44 \;/\; \rho = 0$) = 0.0003. Thus the correlation observed in our sample corresponds to a strong one for the true bivariate distribution of Y and X.

TABLE 1

	T (sec.)	H (m)	H^2	$\frac{H^2}{\nu T}$	t (sec.)	$X=\frac{t}{T}.10^{-3}$	$Y=\log\frac{H^2}{\nu T}$	X^2	Y^2	X.Y
F510	10	4,37	19,0969	$1,90969.10^6$	$86,4.10^3$	8,64	6,280942	74,649589	39,450233	54,267333
F412	12	4,38	20,9764	$1,7480.10^6$	$86,4.10^3$	7,2	6,242541	51,840003	38,969314	44,946296
F512	12	5,095	25,9590	$2,1632.10^6$	$7,2.10^3$	0,6	6,335096	0,36	40,133438	3,801057
G510	10	5,365	28,7832	$2,87832.10^6$	$14,4.10^3$	1,44	6,459136	2,073599	41,720436	9,301155
G412	12	4,60	21,1600	$1,7633.10^6$	$50,4.10^3$	4,2	6,246326	17,640003	39,016586	26,234571
G512	12	5,05	25,5025	$2,1252.10^6$	$10,8.10^3$	0,9	6,327699	0,81	40,035976	5,694659
H58	8	4,31	18,5761	$2,3220.10^6$	$64,8.10^3$	8,1	6,365862	65,610008	40,524196	51,563484
H510	10	4,315	18,6192	$1,86192.10^6$	$10,8.10^3$	1,08	6,269956	1,166399	39,312351	6,771552
H412	12	5,095	25,9590	$2,1632.10^6$	$43,2.10^3$	3,6	6,335096	12,960000	40,133438	22,806346
H512	12	5,025	25,2506	$2,1042.10^6$	$25,2.10^3$	2,1	6,323086	4,410000	39,981414	13,278481
158	8	4,55	20,7025	$2,5878.10^6$	$21,6.10^3$	2,7	6,412930	7,29000	41,125671	60,602188
I510	10	4,53	20,5209	$2,05209.10^6$	$54,0.10^3$	5,4	6,312177	29,16000	39,843582	34,085758
I512	12	4,585	21,0222	$1,7518.10^6$	$19,8.10^3$	1,65	6,243484	2,722499	38,981094	10,301748
$\nu = 10^{-6}$ m^2/sec.		n = 13		n^2 = 169		ΣX = 47,81	ΣY = 82,154031	ΣX^2 = 270,6921	ΣY^2 = 519,227729	$\Sigma X.Y$ = 300.367350

$\overline{X} = \frac{\Sigma X}{n} = 3,677692$ $\quad (\Sigma X)^2 = 2285,795898$ $\quad n\Sigma X^2 = 3518,997313$ $\quad n.\Sigma XY = 3904,775390$

$\overline{Y} = \frac{\Sigma Y}{n} = 6,319540$ $\quad (\Sigma Y)^2 = 519,227729$ $\quad n\Sigma Y^2 = 6749,960449$ $\quad \Sigma X.\Sigma Y = 3927,783691$

$D_x = n\Sigma X^2 - (\Sigma X)^2 = 1233,201415$; $\quad D_y = n\Sigma Y^2 - (\Sigma Y)^2 = 0,677246$; $\quad D_x D_y = 835,180725 \sqrt{D_x D_y} = 28,899494$

The linear regression of X on Y is:

$$X = b.Y + a$$

with approximately : $$b = \frac{C}{D_y} = -34$$

and $$a = \bar{X} - b\bar{Y} = 218$$

so that (Fig. 4) : $$\frac{t}{\bar{T}} = -34.10^{-3} \log\left(\frac{H^2}{v\bar{T}}\right) + 218.10^{-3} \qquad (1)$$

Equation (1) allows the theoretical prediction of a mean value of X for a given value of Y. But this value depends on the particular sample to which the regression curve was fitted. The values of the sample are subject to random fluctuations, so that we must estimate the variance of random fluctuation resulting for X, in order to ultimately estimate the confidence interval (6):

$$S_x^2 = \left[\frac{1}{n} + \frac{(Y-\bar{Y})^2}{\Sigma(Y_i-\bar{Y})}\right] S_2^2$$

where n is the number of variables of our sample and

$$S_2^2 = \frac{1-r^2}{n-2}\Sigma(X_i-\bar{X})^2$$ is the estimate of the conditional variance.

But if we are willing to consider X, not as a mean value for Y, but as a forecast of the particular value which X obtains, we have to add the proper variance of X (conditional variance S_2^2) to this variance of the linear regression curve:

$$S_x^2 = \frac{1-r^2}{n-2}\Sigma(X_i-\bar{X})\left[\frac{1}{n} + \frac{(Y-\bar{Y})^2}{\Sigma(Y_i-\bar{Y})^2} + 1\right]$$

or: $$S_x^2 = (1-r^2)\frac{n-1}{n-2}\sigma_x^2\left[\frac{1}{n} + \frac{(Y-\bar{Y})^2}{(n-1)\sigma_y^2} - 1\right]$$

The predicted value of X for a given Y is approximately distributed according to a GAUSS law; its standard deviation we have given above. The tables of the GAUSS law give the reduced limits of intervals, which cover the true value with a given probability. Limits of a confidence interval for a probability P = 0.95 are: $\pm$ 1.96 S_x. It is easy to plot the two curves of limits:

$$F(Y) = \pm 1.96.\ \sigma_x\sqrt{(1-r^2)\frac{n-1}{n-2}\left[\frac{1}{n} + \frac{(Y-\bar{Y})^2}{(n-1)\sigma_y^2} + 1\right]}$$

$$= \pm 3.35\sqrt{1.077 + \frac{(Y-6.319)^2}{0.048}}$$

b) Study of parameters: $Y = \log\left(\frac{H}{gT^2}\right)$, $X = \frac{t}{\bar{T}}.10^{-3}$

According to the same argument we obtained:

$$r = 0.336$$

r is too small, therefore we cannot have any conclusion about the real coefficient of correlation of the true bivariate distribution of Y and X.

c) Conclusion

The equation: $\frac{t}{T} = - A.\log \frac{H^2}{\nu T} + B$ permits us to determine the time t needed for the destruction of the cover-layer, knowing H, T and ν. The parameter t/T can also be considered as an index of fatigue of the structure: period T is constant for periodic waves, therefore t/T represents the number of shocks received by the structure till its destruction. We ascertained also that the parameter $H^2/\nu T$ is strongly correlated with t/T, whereas H/gT^2 is not.

Further analysis of the strong correlation between $H^2/\nu T$ and t/T, recalling at the same time that H^2 is an energy factor, we conclude from this equation that we can relate wave energy to wave period and storm duration.

3. RANDOM WIND GENERATED WAVES

3.1. Production of wind waves.

Random waves were induced by an air flow over a fetch of 30 m - maximal length. Water depth was, as for the periodic waves, 0.35 m. and wind speeds up to 9.4 m/sec. were obtained. We observed during the first tests, that a constant wind flow over the water surface generated quite periodic waves. After some investigations (1, section 5.31) we connected to the blower's motor an electro-mechanical system, which produced different cycles of start-off and stops. With this system and the variation of wind velocity and fetch we obtained a sufficient variety of wave heights and periods. Surface elevations were measured, with the help of a sonar, every 0.1 sec. and punched on a paper tape. A resistance type wave gauge placed at the same location gave an immediate picture of the waves.

3.2. Experiments with wind generated waves.

The purpose of this series of experiments was to destroy the total thickness of the cover-layer along the model in approximately the same time as in experiments with periodic waves. Several experiments, with variations of wind velocity, fetch and motor cycles, were necessary to obtain this.

Every experiment involved the following operations:

(a) Construction of the model and the filling of the channel with

water to a depth of 0.35 m.

(b) Choice of a motor-cycle, a fetch and a wind velocity.

(c) Calibration of the resistance wave gauge.

(d) Regulating of wind deflector.

(e) Starting of blower.

(f) Ten minutes afterwards (time necessary to obtain fully developed waves) the first record with the sonar and at the same time with the resistance wave gauge. Duration of records: 4 minutes.

(g) Continuous observation of the profile's transformation, especially approaching any time in which we obtained the destruction with periodic waves. If the maximal time of periodic waves destruction was exceeded we stopped the experiment. If we observed that we were near to a "same time destruction" a second wave record was obtained.

(h) At the end of the experiment we drew the new profile on the glass-wall and photographed the profile.

3.3. Seaward equilibrium profile.

During the random waves experiment series we observed the same evolution of the equilibrium profile as in the periodic waves experiment series. We generally distinguished 3 new slopes with mean values:

$$\tan \alpha_1 = 1/0.96 \ , \ \tan \alpha_2 = 1/2.78 \ , \ \tan \alpha_4 = 1/1.37$$

$$\alpha_1 \simeq 46 \qquad \alpha_2 \simeq 19 \qquad \alpha_4 \simeq 36$$

The comparison with the values obtained from the periodic waves series shows no big difference between corresponding slopes.

4. - COMPUTER ANALYSIS OF THE RECORDS

Every tape record contained 2,400 values. It was converted in an I.B.M. 47 machine to punched cards. The "Service E.R.C.A." of "Electricité de France" is equipped with a C.D.C. 6600 digital computer. Another facility, the System D.D. 280 made graphical output possible.

The process of surface elevation was assumed stationary and ergodic, the frequency distribution similar to a GAUSSIAN process.

4.1. Autocorrelation function, Spectral density and relative width E.

The purpose of this computer calculation was to investigate the randomness of the wind waves produced in our channel. Our records have been discreetized into observations $X_i(t)$. We have obtained

the autocorrariance function from the following equation (7):

$$W(J) = \frac{1}{N-J} \sum_{I=1}^{N-J} X(I) \cdot X(I+J)$$

and then the autocorrelation function:

$$R(J) = \frac{W(J)}{\frac{1}{N-J} \sum_{I=1}^{N-J} X(I)^2}$$

Thus the first approximation of the spectral density was:

$$LP(J) = W(0) + 2 \sum_{K=1}^{199} W(K) \cdot \cos\left(\frac{K \cdot J \pi}{200}\right) + W(200) \cos(J \cdot \pi)$$

and finally after smoothing by HAMMING:

$$SP(J) = 0.23 \cdot LP(J) + 0.54\ LP(J+1) + 0.23\ LP(J+2).$$

An example of graphical presentation is given on Figure 5. Values of ε have varied from 0,70 to 0,97.

4.2. Joint distributions of H and T (Fig. 6).

With the help of zero up-crossings of the sea level we have obtained the wave heights and periods for every sample. The principal difficulty was the determination of the mean level.

The different cycles of start-off and stops of the blower provoked seiches. As the waves were random this was not of importance from an energy point of view, but was very important for the definition of wave heights and periods; nevertheless the method utilized was the zero-up-crossings one. Therefore we have eliminated the seiches with the help of a moving-mean over 75 points. H and T values have been classed in increasing order, to evaluate the mean values $H_{n/m}$, $T_{n/m}$ (where n = 1,2,3 and m = 1,2,.....,10).

Recalling that $H_{dest.}$ has been defined as the constant periodic wave height for the experiments during which we obtained the destruction of the cover-layer, we have calculated the ratios:

$$H_{dest.} / H_{1/3} \quad \text{and} \quad H_{1/3} / \bar{H}$$

a) for $H_{dest.}/H_{1/3}$ we have obtained values going from 0.87 to 1.10, with a mean of 1.00 (Ex. Fig. 6). This is an experimental demonstration of the empirical and theoretical assumption that $H_{1/3}$ is the representative wave height and thus good to be used as a project wave height.

b) for $H_{1/3} / \bar{H}$ we have obtained values going from 1.33 to 1.48. Through the use of LONGUET-HIGGIN'S formula, we can obtain the value of 1.598 for the same parameter.

Ocean observations (8) have given values going from 1.37 to 1.85.

c) The comparison between constant periods of periodic waves and random periods of wind generated waves did not give a significant relationship between them because of the different ranges; i.e. periodic waves period varied from 0.948 to 1.897 sec., but the random wind generated wave period varied from 0.7 to 1.5 sec. Nevertheless in some cases, where constant and random periods belonged to the same range, we obtained $T_{dest.} = T_{1/3}$, though from a statistical point of view it is impossible to correlate $H_{1/3}$ and $T_{1/3}$. Definite results do not exist in this domain, we would suggest correlating $\overline{T}$ with $H_{1/3}$.

4.3. Conclusion.

With a first series of periodic waves experiments we have obtained the destruction of the breakwater's cover-layer for different storm duration t, by varying H and T. The mass of armor units remained constant. The angle of the slope, according to the seaward equilibrium profile could be considered as constant. For the destruction cases we obtained a risk criterion:

$$\frac{t}{T} = - A.\log \left(\frac{H^2}{\nu T}\right) + B$$

which provides the storm duration t, knowing H, T and ν.

Then for a second series of random wind generated waves experiments we eliminated t and obtained that the constant periodic wave height ($H_{dest.}$) is equal to the significant wave height $H_{1/3}$ of random waves. This is an experimental demonstration of the justifiable use of $H_{1/3}$ as "project wave height".

5. SUGGESTIONS FOR FURTHER RESEARCH

The restricted research time as well as some problems with laboratory facilities did not permit us to study every aspect of the regular and wind generated action on rubble-mound breakwaters. The flow is two-dimensional. Our investigations have been strictly limited to the effects of these two types of wave action on the structure. It was technically impossible to study the production of waves by the wind, at the same time.

There is certainly more to do, and we would suggest the following:

(a) The seaward face of rubble-mound breakwaters, as we have seen in sections 2.4 and 3.3., is "carved" by wave attack, during the first minutes of the experiment. Therefore variations of the angle of slope every two degrees do not influence the results. Figure 7 illustrates this point. The experimental destruction border line is nearly horizontal for varying from 30 to 36 (every 2). Thus, there are two, more efficient, ways to experiment with breakwaters: either to

retain a constant slope during all experiments, or to vary the angle every 5 or 6 degrees.

(b) We have to choose random values for H and T during experiments with periodic waves. The statistical study could be then generalised.

(c) It would be also desirable to measure exactly the stabilization time for the cover-layer, when wave attack did not destroy it.

(d) A relationship between $H/H_{1/3}$ and other characteristics of the power spectrum would permit a reduction in the scatter of the results concerning the comparison between periodic and random waves.

REFERENCES

1. ROGAN, A. J. (1968): "Comportement des jetées en enrochements vis-a-vis de la houle". Laboratoire National d'Hydraulique, Chatou, FRANCE. (Thèse presentée a l'Université de PARIS).

2. LONGUET-HIGGINS, M. S. (1952): "On the statistical distribution of the heights of sea waves". Journ. Mar. Res. 11 (3).

3. CARTWRIGHT, D. E. and LONGUET-HIGGINS, M. S. (1956): "The statistical distribution of the maxima of a random function". Proc. Roy. Soc., A 237 (1209).

4. VALEMBOIS, J. (1962): "Similitude dans les essais de stabilite de digues". Note DR L.N.H. - Chatou.

5. BERNIER, J. (1963): "Cours sur les applications des methodes statistiques aux travaux de recherche experimentale". Rapport interne, L.N.H. Chatou.

6. MORICE, F. et CHARTIER, F. (1954): "Methodes statistiques". 2me partie. Imprimerie Nationale, PARIS.

7. BLACKMAN, R. B. and TUKEY, J. W. (1959): "The measurement of power spectra from the point of view of communications engineering". Dover Publ. Inc. NEW YORK.

8. WIEGEL, R. (1965): "Oceanographical Engineering". Prentice Hall Int. Series in Theor. and Appl. Mech.

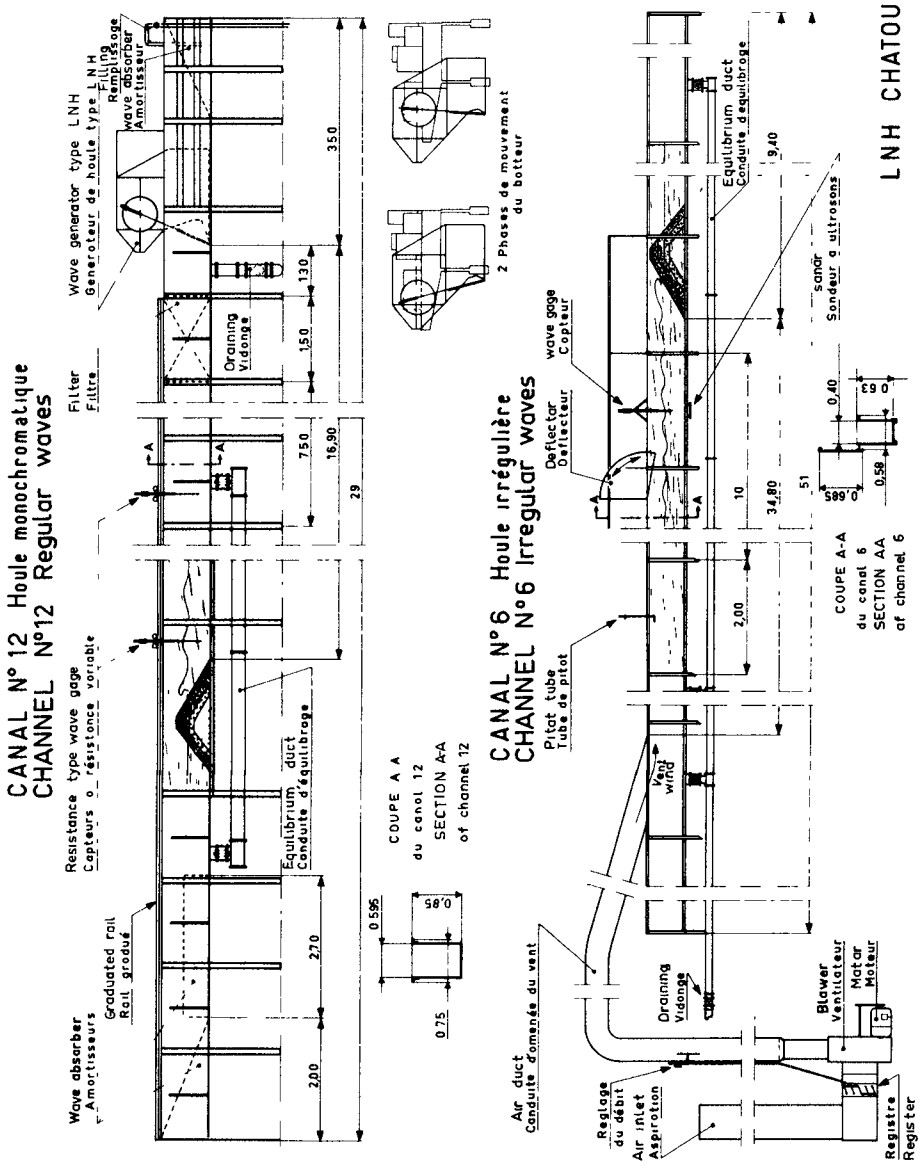
CANAL N° 12 Houle monochromatique
CHANNEL N°12 Regular waves
Wave generator type LNH
Generateur de houle type LNH
Filling
Remplissage
wave absorber
Amortisseur
Filter
Filtre
Draining
Vidange
Resistance type wave gage
Capteurs a résistance variable
Equilibrium duct
Conduite d'équilibrage
Graduated rail
Rail gradué
Wave absorber
Amortisseurs
COUPE A A
du canal 12
SECTION A-A
of channel 12
2 Phases de mouvement
du batteur
CANAL N°6 Houle irrégulière
CHANNEL N°6 Irregular waves
wave gage
Capteur
Deflector
Deflecteur
Pitot tube
Tube de pitot
Wind
vent
Air duct
Conduite d'amenée du vent
Reglage
du débit
Air inlet
Aspiration
Blower
Ventilateur
Motor
Moteur
Register
Registre
sonar
Sondeur a ultrasons
COUPE A-A
du canal 6
SECTION AA
of channel 6
LNH CHATOU

Figure 1

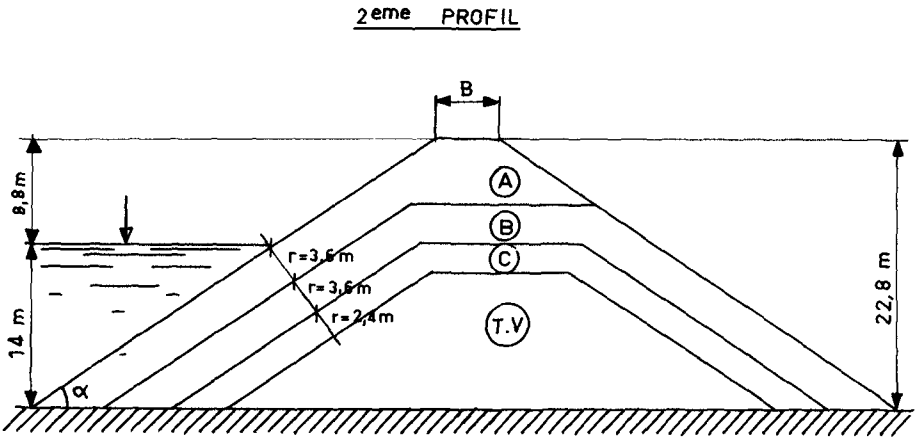

Figure 2

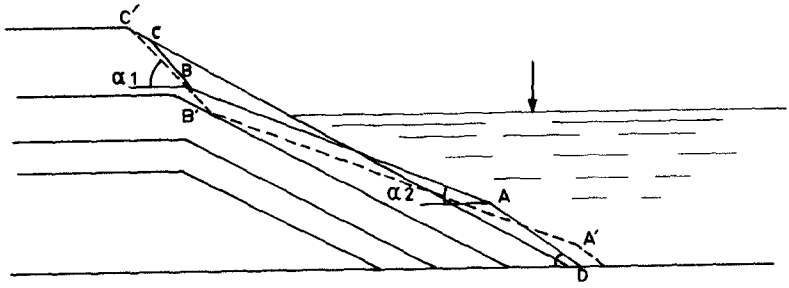

Figure 3

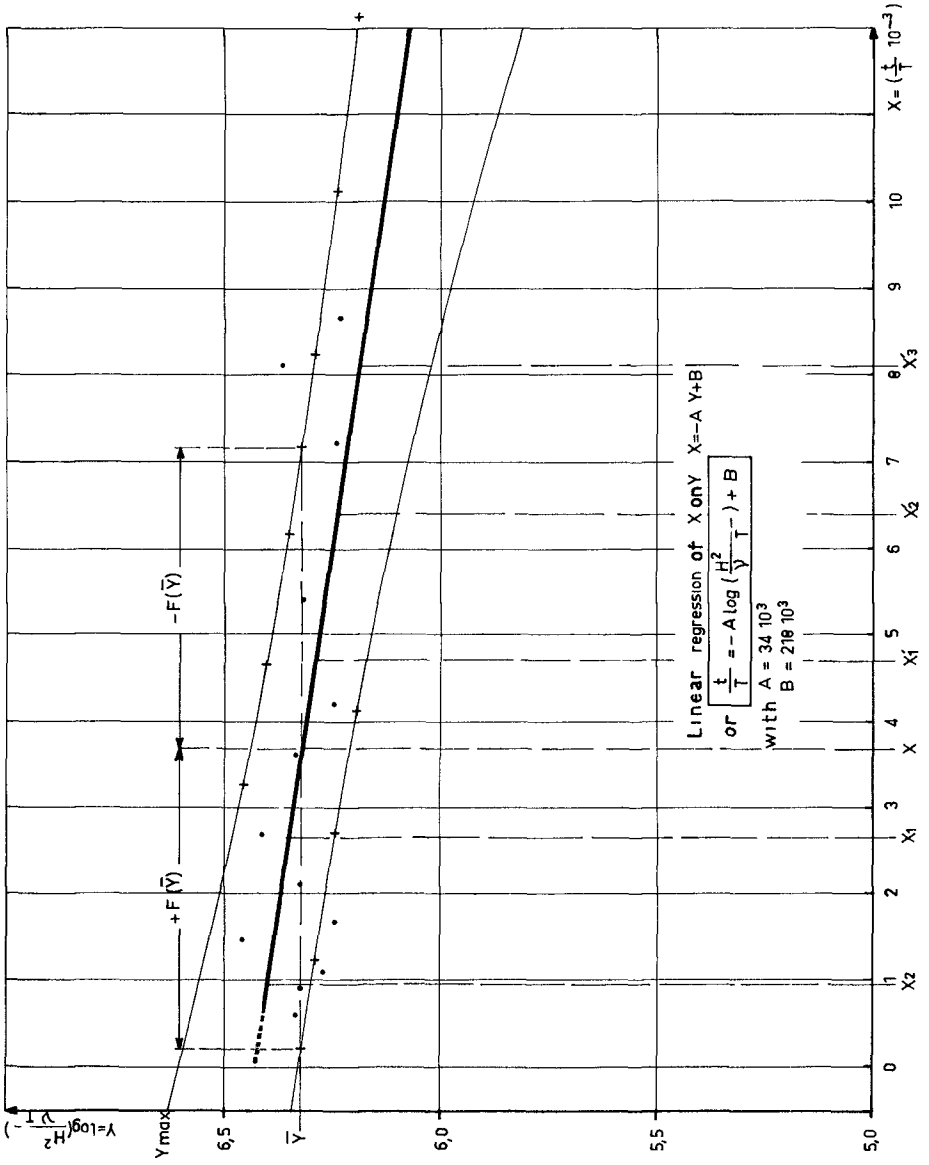
Linear regression of X on Y X=-A Y+B
or $\frac{t}{T} = -A \log\left(\frac{H^2}{\sqrt{T}}\right) + B$
with A = 34 10³
B = 218 10³
$X = \left(\frac{t}{T}\, 10^{-3}\right)$
$Y = \log\left(\frac{H^2}{\sqrt{T}}\right)$
Ymax
$\bar{Y}$
+F($\bar{Y}$)
-F($\bar{Y}$)
X1
X2
X3
X
6,5
6,0
5,5
5,0

Figure 4

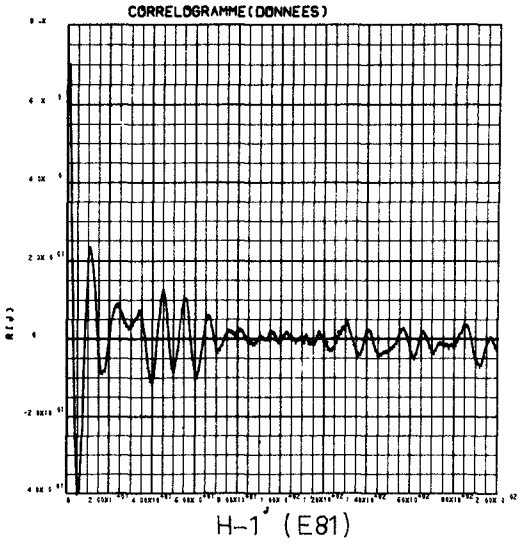
CORRELOGRAMME(DONNEES)
H-1 (E81)

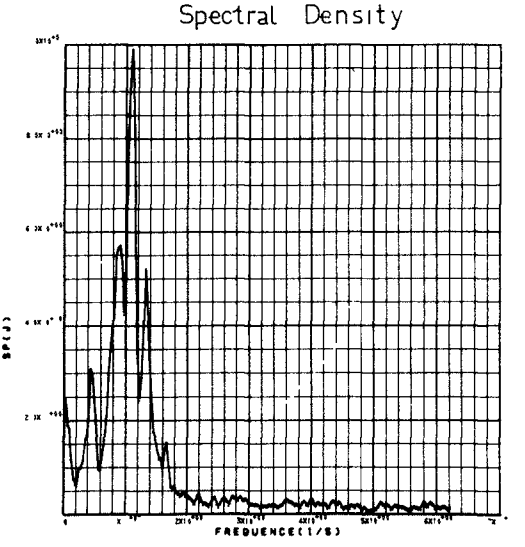
Spectral Density
FREQUENCE(1/S)

Figure 5

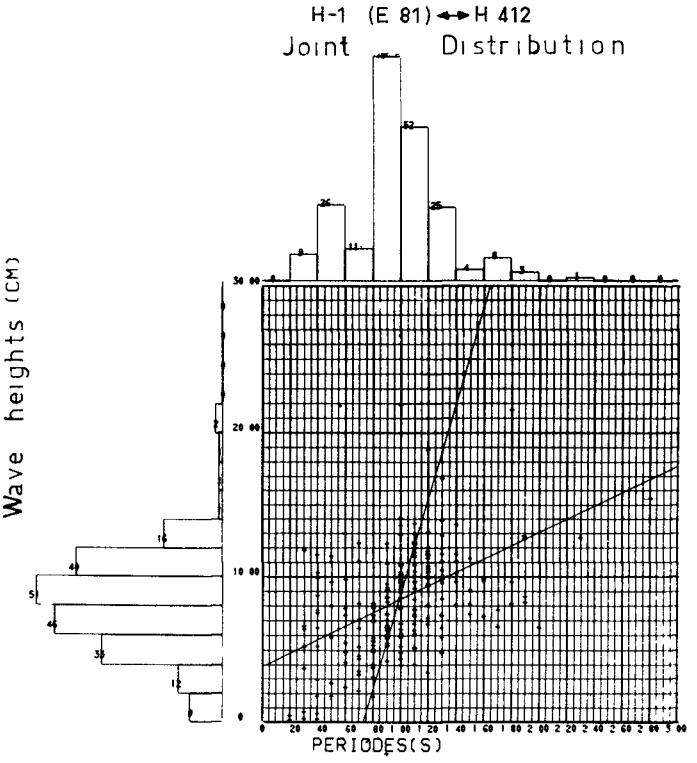

Figure 6

$\bar{H}$	= 8,47 cm	t = $43,210^3$ s		$\bar{T}$	= 0,99 s
H_{dest}	= 12,74 "	r = 0,37		T_{dest}	= 1,90 s
$H_{\frac{1}{10}}$	= 16,577 "	$H_{dest}/H_{\frac{1}{3}}$	= 1,02	$T_{\frac{1}{10}}$	= 1,652 s
$H_{\frac{1}{3}}$	= 12,536 "	$H_{dest}/\bar{H}$	= 1,50	$T_{\frac{1}{3}}$	= 1,356 s
$H_{\frac{1}{2}}$	= 11,374 "	$H_{\frac{1}{3}}/\bar{H}$	= 1,48	$T_{\frac{1}{2}}$	= 1,257 s

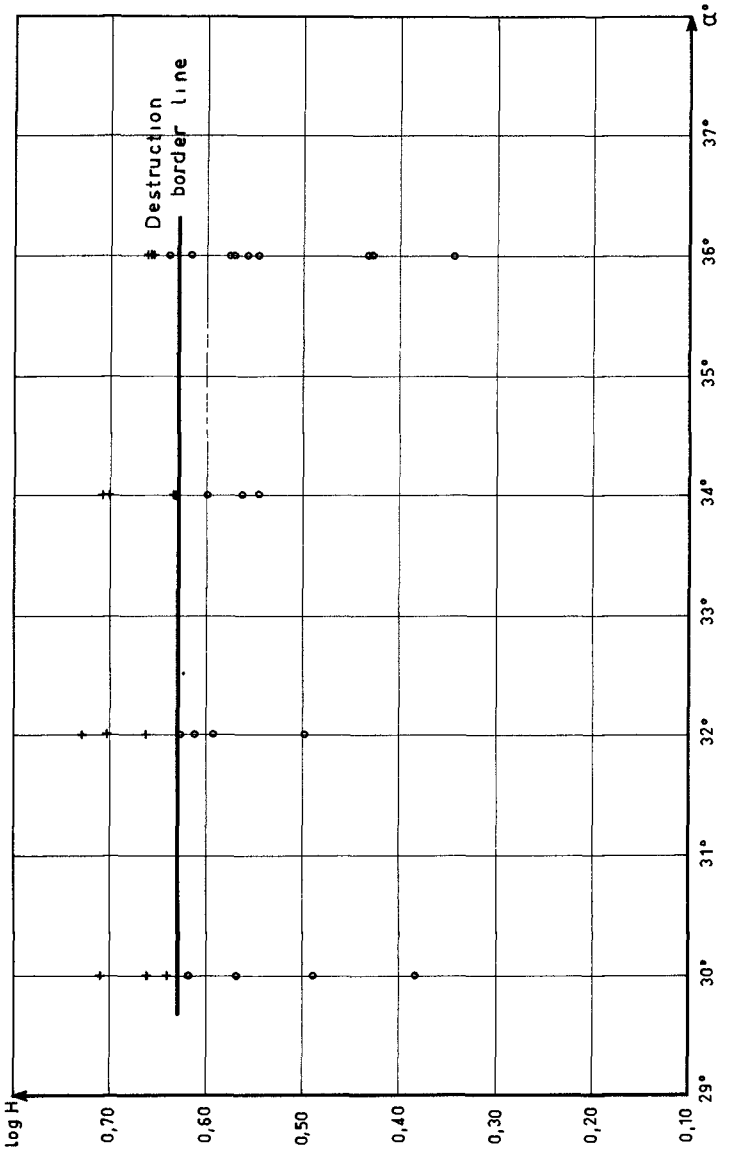
Destruction
border line
log H
0,70
0,60
0,50
0,40
0,30
0,20
0,10
29°
30°
31°
32°
33°
34°
35°
36°
37°
α°

Figure 7

F1

CHAPTER 50

THE EFFECT OF STORM DURATION ON RUBBLE MOUND BREAKWATER STABILITY

Juan B. Font
Assistant Professor, Faculty of Engineering
Central University, Caracas, Venezuela

ABSTRACT

Experimental data are given to aid in the selection of the wave height for the design of a rubble mound breakwater as a function of the type and duration of the wave storm, and the allowed percentage of damage in the armour layers.

In these experiments the model breakwater was subjected to the attack of periodic waves of height and in number according with the known statistical distribution for actual swells.

Some noteworthy differences were found in the effects of different duration storms.

Observation of the destruction process of the breakwater with double layer of armour rocks, showed that the filter layers uncovering occurred always for armour damage percentages above 5% and thus this last value is suggested as the maximum permissible in case of a storm of very high recurrence period.

INTRODUCTION

Very often the engineer has to face the design of a rubble mound structure taking into account the strongest possible storm. Such a storm may have a peak lasting a few hours with very high waves. It may prove very costly to design a breakwater for that situation on the basis of no damage as defined by Hudson (1959).

If some damage is allowed, then the storm type and duration become important.

THE DESIGN WAVE HEIGHT

Considering the experiments of Hudson (1959), Iribarren (1965) and those reported in the present paper, it may be concluded that the total breakwater failure occurs for wave heights from 1.5 to 1.8 times the design wave heights. All of these experiments were conducted with periodic waves breaking on the face of the structure. On the other hand the experiments of Rogan (1968) and Carstens, Torum and Traetteberg (1966) show that the effect of a locally wind generated wave storm is similar to that of a periodic wave with height equal to the significant wave height ($H_{1/3}$) of the storm.

A real storm may have waves with height up to 2.4 times the significant wave height and thus it is obvious that in the design wave selection the duration and the wave period spectrum of the storm must play an important rol. If a storm is such that some waves break before hitting the breakwater, then the wave period is determinant of the action of the waves on the structure. Very valuable are in this concern the experiments made by Carstens, Torum and Traetteberg (1966). They showed the remarkable difference between storms of the same significant wave height but of different kind of spectrum. As it is already known by experience swell waves are more deletereous to breakwaters than locally generated waves.

DESCRIPTION OF THE EXPERIMENTAL WORK

THE MODEL STORM.

The model storm was considered to be of the swell type and to have a wave height distribution as given by Putz (1954), with all waves breaking on the breakwater face. In this case the wave period may be considered irrelevant and thus it was held constant throughout the experiments.

It was also assumed that the effect of waves of different height may be added linearly and thus that there is no influence of the time secuence. This difference between the actual and the model storms will probably make a little conservative the experiments since in the model the largest waves act when the breakwater has been already weakened by the rest of the waves.

THE EXPERIMENTAL SET-UP.

See Fig. 1 for the description of the experimental set-up.

THE TESTS.

Waves and trains were calibrated before placing the model sections in the wave channel in order to select the needed height and duration. The model breakwater was subjected to the attack of regular waves of height and in number according with the statistical distribution above mentioned. The wave height was increased by steps of about one centimeter. The data were taken in terms of percentage of damage of the armour layers. The period was held constant for all of the experiments as well as the water depth. The period was 1.58 sec. and the depth 0.55 m.

CORRELATION OF DATA.

In Fig. 2 are summarized the results of the tests.

The symbol H_D refers to the wave height as computed from Hudson's formula for a given size of rock and breakwater slope. Thus:

$$H_D = \sqrt[3]{\frac{W \cdot K_D \cdot \cot \alpha}{\gamma_r}} \left(\frac{\gamma_r}{\gamma_f} - 1 \right)$$

W being the weight of the rocks and K_D the Hudson's formula coefficient taken equal to 3.2 and 2.8, depending on different techniques for placing the rocks as determined in previous tests.

The symbol n is equal to $t/T_{H_{1/3}}$ where t is the storm duration and $T_{H_{1/3}}$ is the mean period of the highest 33 per cent of the waves and, according to Sibul (1955), the most common period for the largest waves.

CONCLUSIONS

1. The experimental data show a scatter inherent to this kind of tests.

2. For the initial movement of the rocks it seems that the duration of the storm is not important. The duration becomes relevant for advanced damage.

3. In the experiments it was observed that the incipient destruction occurred in the way of sliding of isolated rocks. Eventually, for grater damage, several rows of rocks slide at the same time. Also, the filter layers uncovering occurred usually for damage in the range of 10% and always over 5%, therefore this last value is suggested as the maximum design damage allowable for a storm of recurrence period high enough as to assure that the breakwater will be repaired before it is affected by the next major storm.

4. The use of the wave breaking criteria combined with Fig. 4 of this paper may help to select the design wave for a critical storm. It is suggested that in future experimentation, related with the non-uniform waves effect on breakwaters, the relation between the significant wave height and the breaker height for the mean wave period at the depth of the structure be considered as a significant parameter. In the present experiments this relation was:

$$\frac{H_{1/3}}{H_b} = 0.3$$

H_b being the breaker height corresponding to the wave period and water depth of the tests as computed after the experiments of Danel (1952).

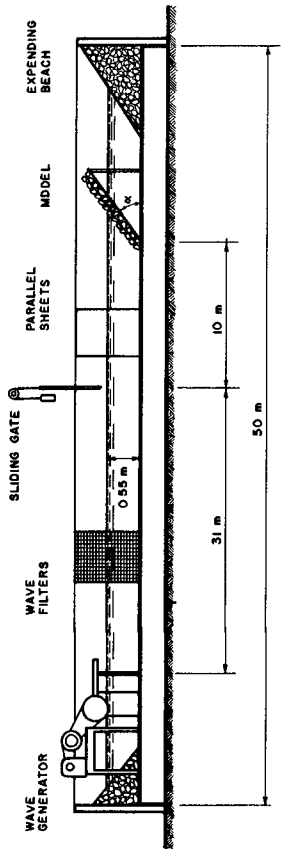

Fig. 1. Wave channel and experimental set-up

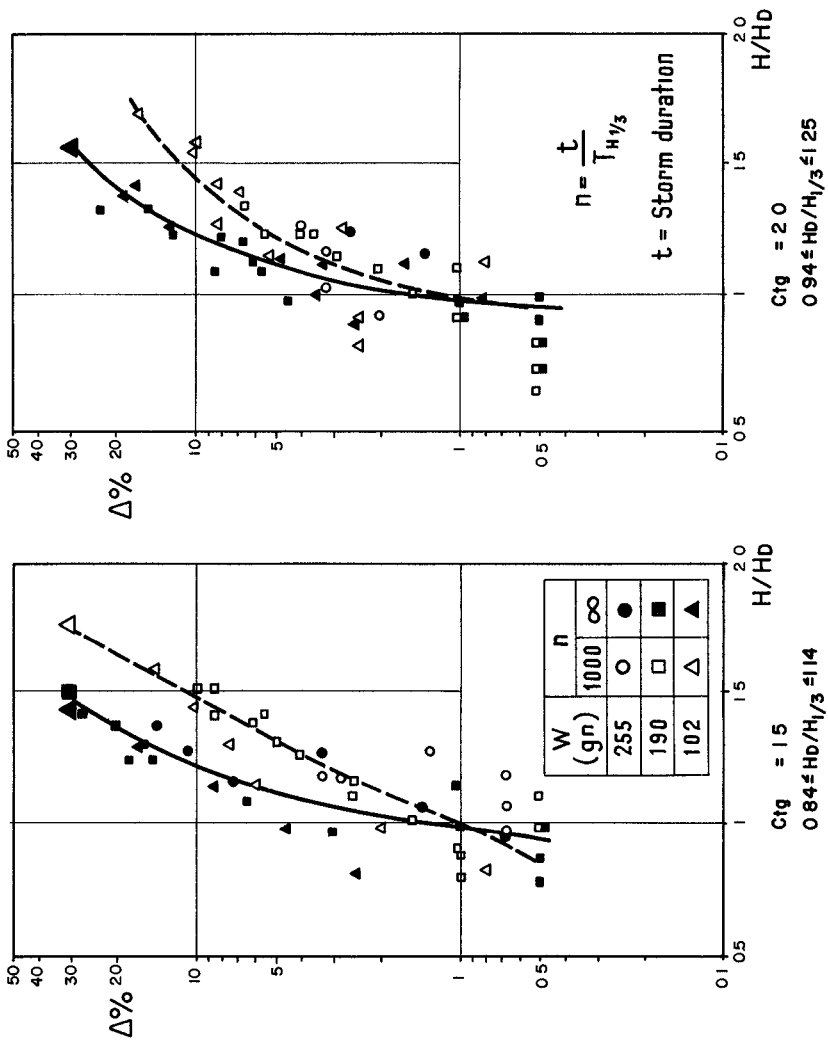

Fig. 2. Damage curves for different storm durations

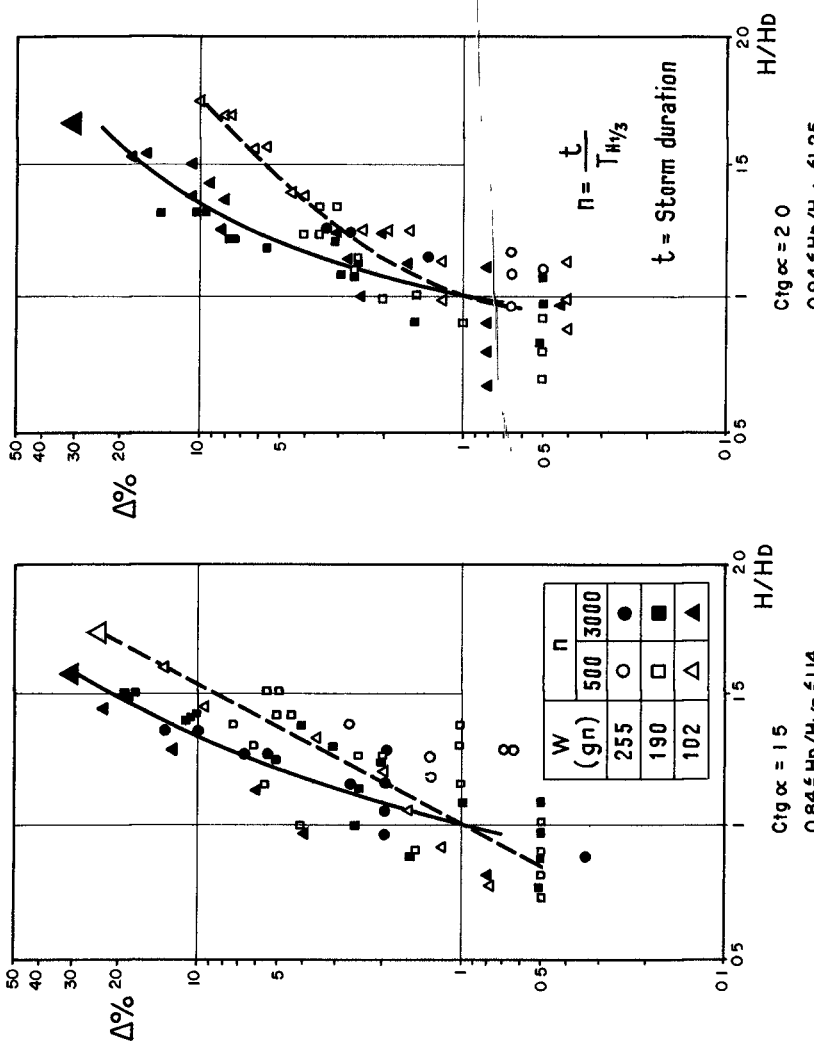

Fig. 3. Damage curves for different storm durations

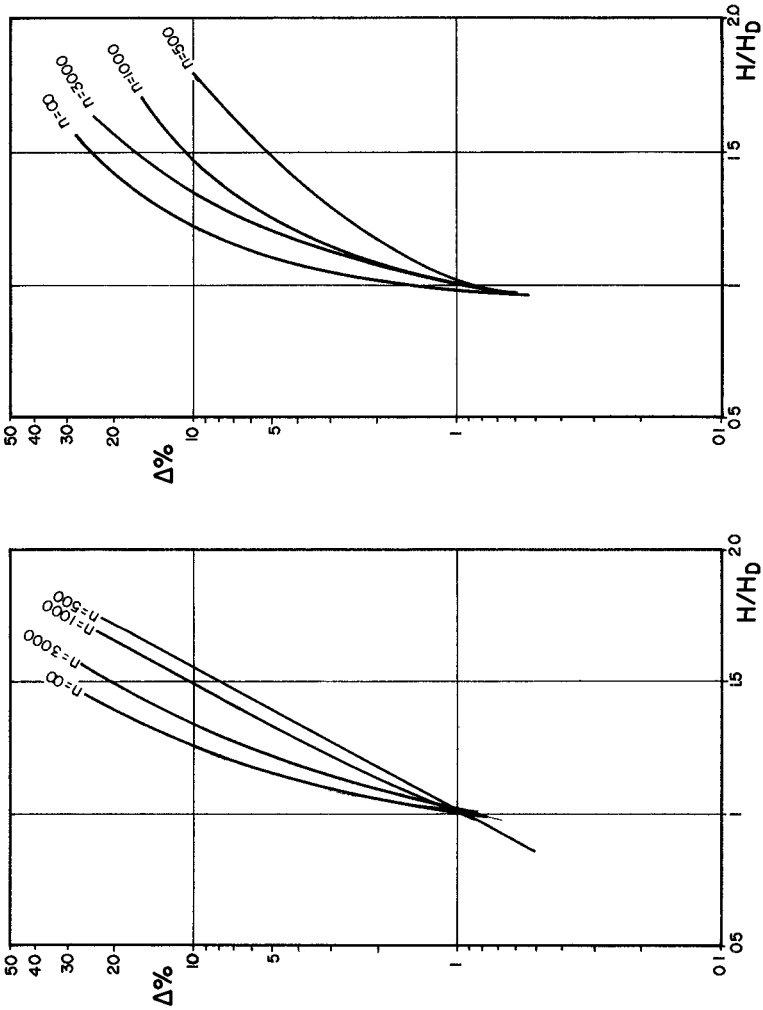

Fig. 4. Synthesis of experimental curves

REFERENCES

Carstens, T., A. Torum and A. Traetteberg; "The stability of rubble mound breakwaters against irregular waves", Proc. Tenth Conference on Coastal Engineering, A.S.C.E., 1966, Volume II; pp. 958-971.

Danel, Pierre, "On the limiting clapotis", Gravity Waves, National Bureau of Standards Circular No. 521 (November, 1952), 35-38.

Hudson, Robert Y., "Laboratory investigation of rubble-mound breakwaters", J. Waterways Harbors Div., ASCE, 85, WW3, Paper No. 2171 (September, 1959) 93-121.

Iribarren, R., "Formule pour le calcul des diques en enrochements Naturels ou cle ments artificiels". XXIst International Navigation Congress - Stokholm, - 1965, P.I.A.N.C.

Putz, R.R., "Statistical analysis of wave records"Proc. Fourth Conference on Coastal Engineering, Berkeley, Calif., The Eng. Foundation Council on Wave Res,; 1954 pp. 13-24.

Rogan, A.J., "A Comparison of regular and wind generated wave action on rubble mound breakwaters". Abstract submitted to the XIth Conference on Coastal Engineering, London, 1968, The Institution of Civil Engineers, London; paper 9, pp. 17-18.

Sibul, O., "Laboratory study of the generation of wind waves in shallow water". - U.S. Army Corps of Engineers - B.E.B. Tech. Memo. No. 72, March, 1955.

CHAPTER 51

STABILITY OF QUADRIPOD COVER LAYERS *

by

Olin F. Weymouth
Chief, Coastal Engineering Branch
U. S. Army Engineer Division, South Pacific
Corps of Engineers
San Francisco, California, U.S A.

and

Orville T. Magoon
Coastal Engineering Branch
U. S. Army Engineer Division, South Pacific
Corps of Engineers
San Francisco, California, U.S.A.

ABSTRACT

The purpose of this paper is to present the results of a four-year study of the stability of a prototype breakwater armor layer composed of 28-ton concrete quadripods The study was conducted by measuring the incident wave height and the quadripod movements during this period. The ultimate goal of this study is the verification of empirical breakwater design equations.

INTRODUCTION

In the past decade considerable effort has been expended to derive rational methods for the design of cover layers for rubble-mound structures. Generally, these methods have been reduced to formulas based on dimensional or theoretical analysis, but contain experimentally determined coefficients for each armor shape. Due to the relatively large size of prototype breakwater armor units, model tests under carefully controlled conditions are generally used to determine these coefficients. In order to verify the results of model tests, the seaward end of the Santa Cruz Harbor West Jetty, which contains 28-ton concrete quadripods, was instrumented so that the incident wave heights and quadripod displacements could be measured. This paper provides information on the design and construction of the jetty, the instrumentation, and the results of measurements taken over the past four years. The quadripod armor unit is protected by patents owned by Etablissements Neyrpic and Societe d'Exploitation de Brevets Pour Travaux a la Mer, Grenoble, France.

* Title of paper as presented at conference was PROTOTYPE INVESTIGATION OF STABILITY OF QUADRIPOD COVER LAYER, SANTA CRUZ HARBOR WEST JETTY, CALIFORNIA

BASIS FOR DESIGN

Santa Cruz Harbor is located at the northerly end of Monterey Bay about 65 miles south of the entrance to San Francisco Bay. A location map and a plan of the harbor are shown on Plate 1. The harbor was formed by development of Woods Lagoon, a shallow fresh water pond near the eastern boundary of the City of Santa Cruz. The shoreline in the immediate vicinity consists of sandy beaches backed with a relatively high marine terrace. Harbor elements include an entrance channel, protected by jetties, 100 feet wide and 20 feet deep; an interior access channel 150 feet wide and 15 feet deep reducing to 10 feet within the principal harbor area; a turning basin 250 feet by 300 feet and 10 feet deep; and mooring basins with an initial capacity of almost 400 recreational craft. Wave approach from the ocean is limited to the south to southwest sector by Point Cypress, a projecting headland south of Monterey Bay and by Point Santa Cruz, which is about one and one-half miles to the southwest. Accordingly, the jetties are aligned slightly east of south, the east jetty about 800 feet in length and the west jetty 1,200 feet in length with the outer 250 feet turned 50 degrees easterly to protect the entrance channel and harbor from all storm waves.

Wave Analysis

Based on deep water wave studies, relatively large (25 feet or greater) deep water waves from the south through southwest direction have been produced during storms in the past decade. A refraction analysis was made for waves of various periods and directions which may approach the harbor. The analysis consisted of the construction of refraction-fan diagrams diverging from the head of the jetties. With deep water directions determined, companion orthogonals were projected shoreward to determine the refraction coefficients. The maximum theoretical height of wave that would reach the jetties was then determined taking into account the refraction coefficient, the depth of water, the shoaling coefficient, and the seaward slope of the bottom. The maximum breaker height at the jetties was determined to be 21.2 feet and could be produced by a 16 second wave from the SSW with deepwater significant heights of 24.8 feet. This value was rounded to 21 feet and selected as the design wave.

Jetty Design

Design of the structure was based on available criteria published by the Corps of Engineers, principally "Shore Protection Planning and Design, Technical Report No. 4." Based on comparative costs of a number of alternatives, quadripod-rubble-mound construction was determined to be the most economical. The quadripod armor layer was limited to the outer 400 feet of the west jetty.

Armor Layer

Determination of the weight of the armor unit was based on the Hudson or WES equation. The equation is:

$$W_r = \frac{\gamma_r H^3}{K_\Delta \, (Sr-1)^3 \, \cot \alpha}$$

where W_r = the weight of armor unit in primary cover layer, lbs, γ_r = specific weight of armor unit, lbs/ft^3; H = design wave height ft., K_Δ = experimentally determined coefficient, S_r = specific gravity of the armor unit relative to the water in which it is immersed, and α = angle of breakwater slope measured from the horizontal.

For the quadripod sections, the selected design called for two layers of 25-ton quadripods (pell mell) placed on a 1 on 2 slope along the trunk and on a 1 on 3 slope around the conical head section. The quadripods were backed by a concrete cap, essentially 18 feet wide and 10 feet thick to prevent displacement of armor units from the cap by overtopping waves. The quadripods were underlaid by a 6 foot B stone layer (50% greater than 6,000 lbs., minimum 4,000 lbs) and a C stone core 4,000 lbs to 4" (50% greater than 500 lbs.). Crest height was established at +16.0 M.L.L.W. datum. Typical quadripod dimensions are shown in Plate 2. A typical cross section is shown in Plate 3

Substituting actual constructed values (e.g., 28 ton quadripods) and currently accepted K_Δ values in the foregoing stability equation indicates that the structure would be stable for a design wave of 25 feet.

QUADRIPOD CONSTRUCTION

Construction of the jetties, employing standard equipment and methods, was noteworthy principally for the ease and simplicity of quadripod construction and placement Steel forms, comprising 8 top sections and 48 bottom sections were utilized in the casting of the quadripods. A 6-man crew, working a 9-hour day, cast the required 900 quadripods in 114 working days extending from 27 July 1962 to 5 February 1963. One quadripod was cast the first day, three the third day, and eight on all other days. The average time to strip eight top forms and connect to bottom forms was 1.77 hours; casting eight quadripods required approximately 5.0 hours, and average time for stripping bottom forms and storing was 2.12 hours. The daily operation provided for removal of top forms with a minimum time lapse of 18 hours after casting and removal of the quadripods from the bottom forms after a minimum 5-day cure period. A special lifting sling was used at the casting yard to keep all legs in compression. Transit-mix concrete (6-1/2 cubic yards truck capacity) was employed with placement utilizing one Link Belt crawler crane and two 3-1/2 cubic yards concrete buckets. Each quadripod was numbered in the order cast.

Hauling and placing started 2 November 1962 and was completed 5 March 1963, with a total of 122 working days. Quadripods were not placed continuously throughout the job. On days when quadripods were placed, daily placement ranges from a maximum of 69, with an overall daily average of 41. The quadripods were loaded at the storage yard by a crane onto a tractor drawn (40-ton capacity) low-boy trailer At the jetty, a Lima Crawler crane, Series 2400, with a 100-foot boom, using a double cable sling with a quick release hook attachment lifted the quadripods from the trailer and placed them on the seaward slope of the west jetty.

INSTRUMENTATION AND MEASUREMENTS

Upon completion of the structure, detailed surveys were conducted to serve as a basis for measurement of future displacements. These surveys consisted of establishment (horizontally and vertically) of 5 standard brass disks in the concrete cap. Steel pins were set in each corner of concrete cap pours and in 44 numbered quadripods throughout the upper layer. Repeat measurements of all monuments and pins have been taken annually and of selected quadripod pins after stormy periods. Horizontal and vertical distances are measured from the cap by standard surveying techniques. Vertical displacements recorded during the 4-year period to April 1967 are summarized in the table following. All quadripods above water are also identified in aerial photographs of the seaward portion of the jetty.

QUADRIPOD VERTICAL DISPLACEMENT

Vertical Displacement (feet)			Number of Quadripods			
			June 63 to June 64	June 64 to June 65	June 65 to May 66	May 66 to April 67
0	-	0.05	21	21	21	22
0.06	-	0.10	8	5	12	5
0.11	-	0.20	6	6	5	2
0.21	-	0.40	5	2	3	2
0.41	-	0.60	1		1	1
0.61	-	0.80				1
0.81	-	1.00				1
>	-	1.00	2		1	1
			43	34	43	33

With the exception of a few quadripods near the jetty head, no significant movements have occurred. The maximum cap settlement is about 0.1 foot, near the seaward end. Quadripods on the head section are also moving, however, the largest displacements occurred during the initial measurements and with but few exceptions the displacements are extremely small. The armor units appear to be consolidating in predicted manner in that, with settlement, the individual units tend to interlock thus providing for maximum stability. In general, movement of a few units is not indicative of failure in the structure. Horizontal and vertical displacements are shown on Plates 4 and 5, respectively.

Design waves for coastal structures are calculated for the condition before the structure has been built. Thus in any attempt to verify the design formulas a wave for a similar condition must be obtained. In order to measure the waves at the structure as they would be without the structure in place, a wave gage was located 400 feet seaward off the end of the west jetty in an area of low reflected waves. In this location it was impractical to construct a platform at the desired gauging location so it was necessary to use a subsurface pressure transducer connected with a cable to a wave gage on shore. The wave sensor installed initially was one which

permitted detection of pressure fluctuations such as sea and swell waves, but canceled out long period pressure fluctuations such as those resulting from tides One advantage of this system is that the sea and swell waves are clearly shown without the effect of the tides and additionally results in better utilization of chart paper. After the first year's operation a check of the overall accuracy of the system, independent of the theoretical and electrical calibration built into the wave recorder, was developed through bypassing the filter. Thus the sensor responds to absolute pressure less the static head including the tides. On days when the sea is essentially calm, the recorder trace is due to the tides alone and may be quickly checked by comparison with predicted values In addition, a portable tide recorder occasionally placed in operation inside the harbor permits comparison of records. This comparison is considered to be an independent check. Atmospheric pressure fluctuations are neglected in this study.

The shore based equipment consists of a strip chart type recorder and a "Beach Erosion Board" magnetic tape recorder. Normally, the significant wave height is read from the strip chart every six hours at the U. S. Weather Bureau synoptic interval. During periods of high waves, detailed spectral analyses are made by the U. S. Army Coastal Engineering Research Center from the magnetic tapes

The maximum monthly significant wave heights recorded to date are given in the table following. The highest wave recorded during the study was recorded on 12 December 1967 when the significant wave height reached 12.7 feet It is obvious that these values are well below that expected to cause displacement or failure.

MAXIMUM SIGNIFICANT WAVE HEIGHTS
RECORDED AT SANTA CRUZ

Months	Years						
	1963	1964	1965	1966	1967	1968	Average
January		5.9	10.3	6.7	-	4.0	6.7
February		3.5	2.8	6 0	-		4.1
March		3.4	2.1	4.5	-		3.3
April		3.8	1.4	1 0	-		2.1
May		3.5	1.5	-	-		2.5
June		4.2	1.3	-	8.4		4.6
July		3.0	-	3.4	3.1		3.2
Auguat		2.6	-	-	3.8		3.2
September		4.1	-	-	4.2		4 1
October	5.0	-	-	-	6.8		5.9
November	5.3	7.8	-	-	5.2		6.1
December	4.2	8.7	-	-	12.7		8.5

CONCLUSIONS

Based on repeated measurements of selected points in the seaward portion of the Santa Cruz West Jetty, it is concluded that no displacements have occurred that approach those to be expected from failure, thus no verification of the breakwater stability equation is possible at this time. The measurements taken to date, however, provide a record of progressive reaction of the structure to storm waves.

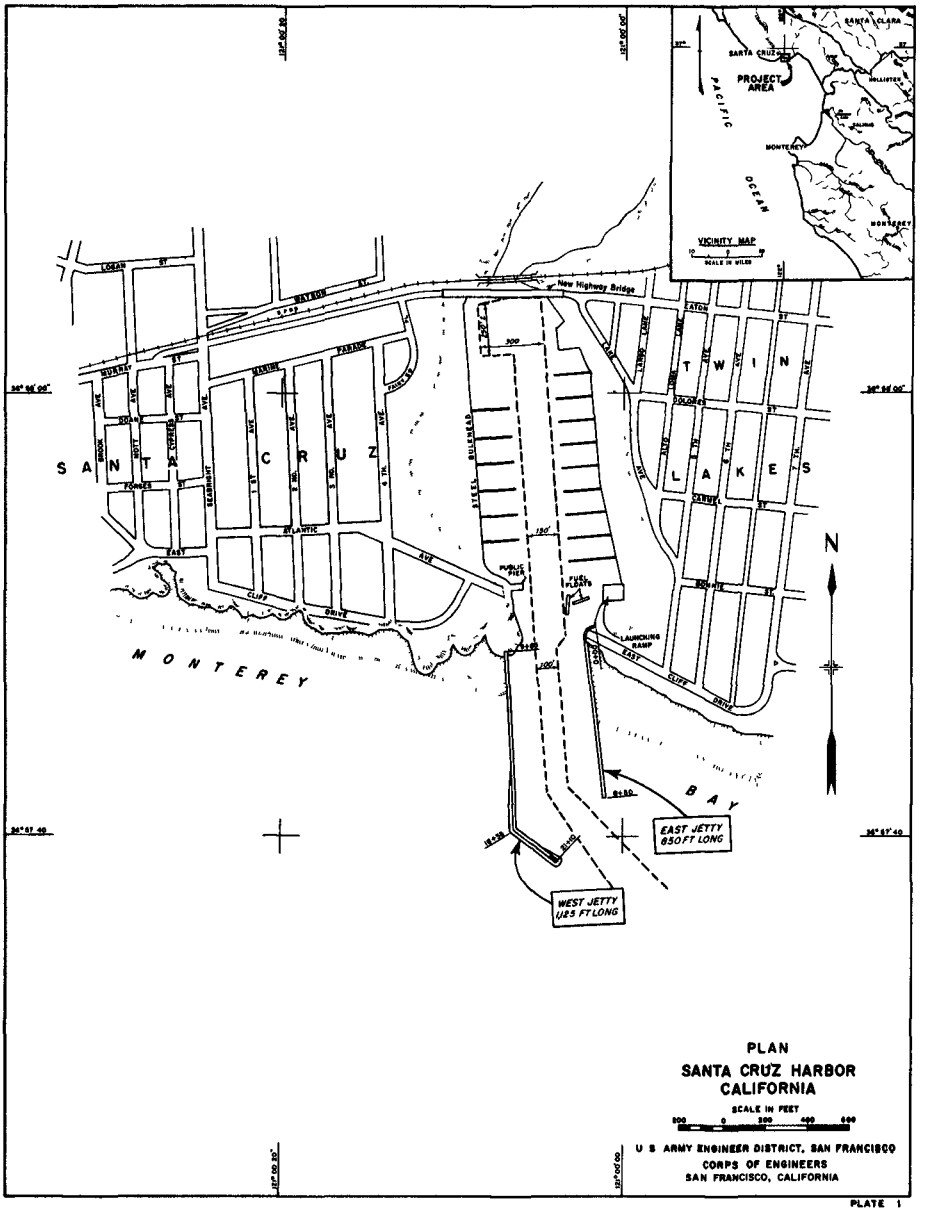
VICINITY MAP
PROJECT AREA
PACIFIC OCEAN
SANTA CRUZ
MONTEREY
SALINAS
SANTA CLARA
HOLLISTER
SAN JOSE
SAN FRANCISCO
MONTEREY
SCALE IN MILES
New Highway Bridge
SANTA CRUZ
TWIN LAKES
MONTEREY BAY
EAST JETTY 850 FT LONG
WEST JETTY 1125 FT LONG
PUBLIC PIER
FUEL PLANT
LAUNCHING RAMP
EAST CLIFF DRIVE
BEACH ST
WATSON ST
LOGAN ST
MURRAY ST
BROOK ST
SEABRIGHT AVE
ATLANTIC AVE
PACIFIC AVE
BULKHEAD
N
PLAN
SANTA CRUZ HARBOR
CALIFORNIA
SCALE IN FEET
U S ARMY ENGINEER DISTRICT, SAN FRANCISCO
CORPS OF ENGINEERS
SAN FRANCISCO, CALIFORNIA
PLATE 1

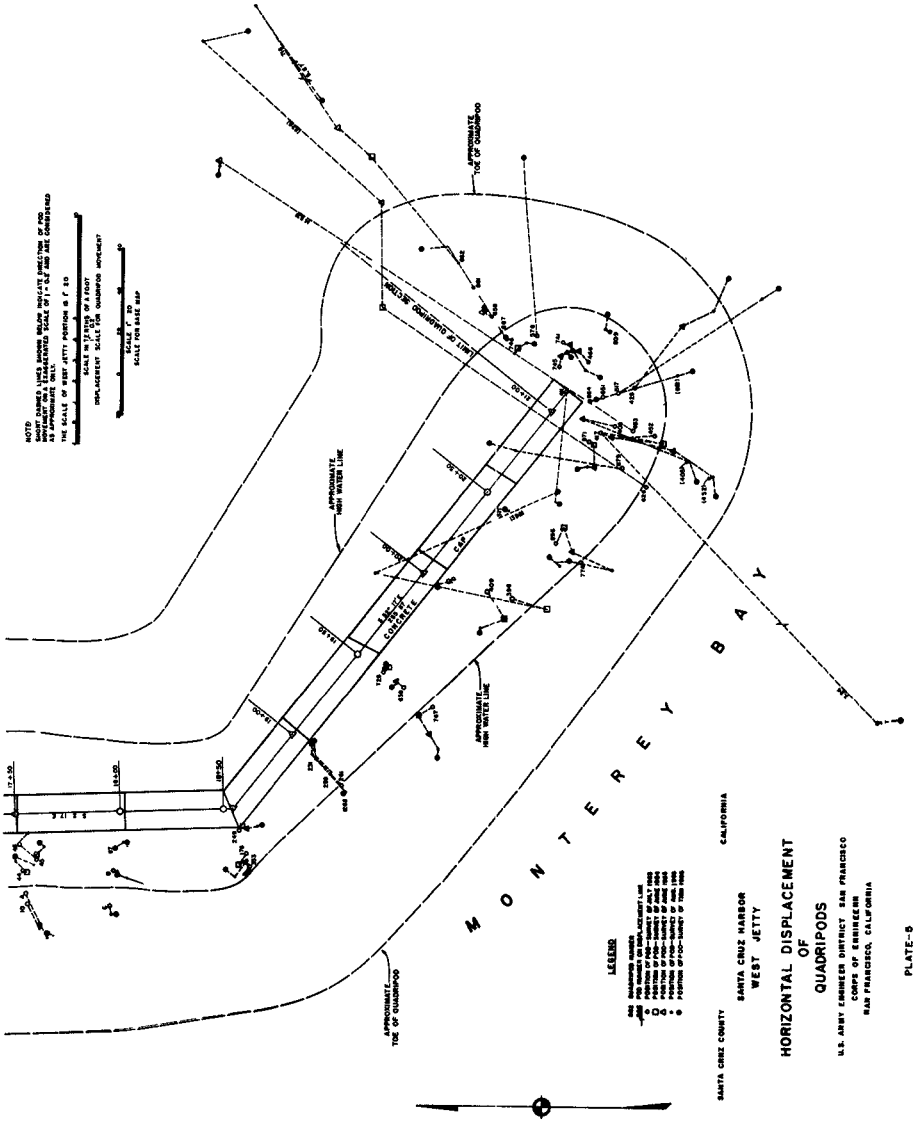
MONTEREY BAY
APPROXIMATE TOE OF REVETMENT
APPROXIMATE HIGH WATER LINE
APPROXIMATE TOE OF QUADRIPOD
LEGEND
SANTA CRUZ COUNTY
CALIFORNIA
SANTA CRUZ HARBOR
WEST JETTY
HORIZONTAL DISPLACEMENT
OF
QUADRIPODS
U.S. ARMY ENGINEER DISTRICT SAN FRANCISCO
CORPS OF ENGINEERS
SAN FRANCISCO, CALIFORNIA
PLATE-5

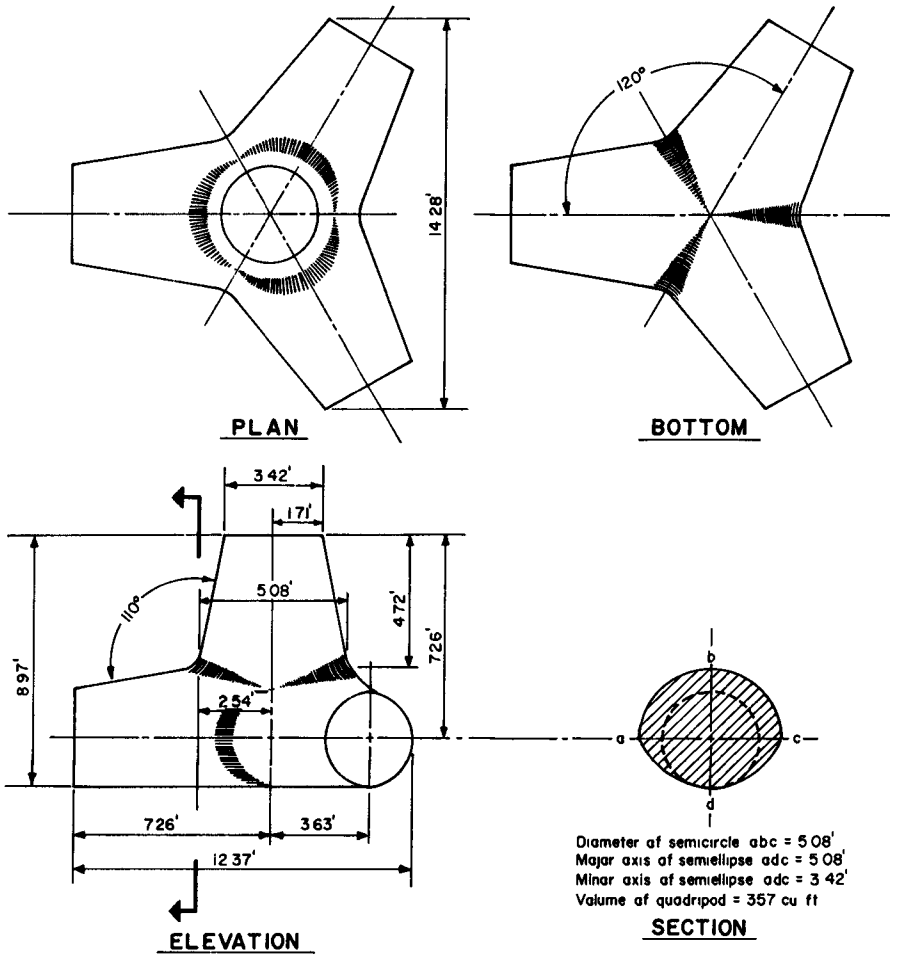

PLATE 2

SANTA CRUZ HARBOR
CALIFORNIA
QUADRIPOD DIMENSIONS

U.S ARMY ENGINEER DISTRICT, SAN FRANCISCO
CORPS OF ENGINEERS
SAN FRANCISCO, CALIFORNIA

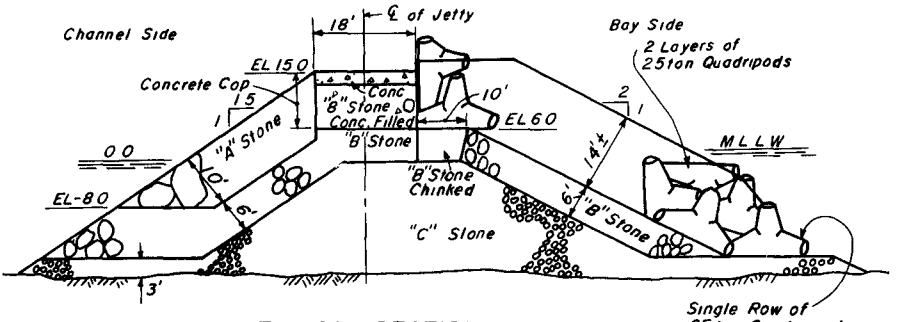

TYPICAL SECTION

PLATE 3

SANTA CRUZ HARBOR
CALIFORNIA

TYPICAL
JETTY CROSS-SECTION

U S ARMY ENGINEER DISTRICT, SAN FRANCISCO
CORPS OF ENGINEERS
SAN FRANCISCO, CALIFORNIA

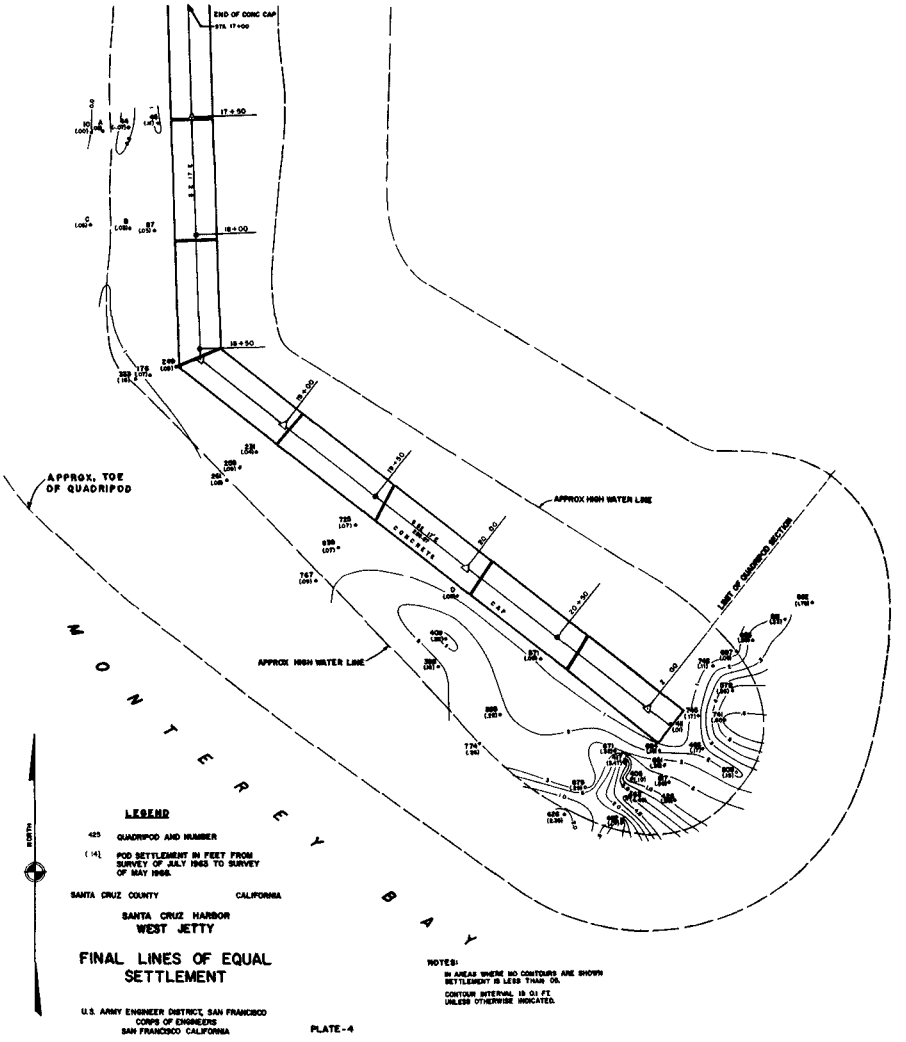
END OF CONC CAP
STA. 17+00
17+50
18+00
18+50
19+00
19+50
20+00
20+50
APPROX. TOE OF QUADRIPOD
APPROX HIGH WATER LINE
LIMIT OF QUADRIPOD SECTION
MONTEREY BAY
LEGEND
425 QUADRIPOD AND NUMBER
(.14) POD SETTLEMENT IN FEET FROM SURVEY OF JULY 1965 TO SURVEY OF MAY 1966.
SANTA CRUZ COUNTY CALIFORNIA
SANTA CRUZ HARBOR
WEST JETTY
FINAL LINES OF EQUAL SETTLEMENT
U.S. ARMY ENGINEER DISTRICT, SAN FRANCISCO
CORPS OF ENGINEERS
SAN FRANCISCO CALIFORNIA
PLATE-4
NOTES:
IN AREAS WHERE NO CONTOURS ARE SHOWN SETTLEMENT IS LESS THAN 0.0.
CONTOUR INTERVAL IS 0.1 FT. UNLESS OTHERWISE INDICATED.

CHAPTER 52

'STABIT' - A NEW ARMOUR BLOCK

by

K. Y. Singh

Senior Engineer, Sir William Halcrow & Partners,
Great Britain

ABSTRACT

There are a number of specially shaped concrete armour units in use today. The Stabit is one of them and was first developed in 1961 for use on the reconstruction of breakwaters at Benghazi Harbour, Libya. This paper describes the development of Stabits and gives the technical details relating to their use. The subjects covered include full scale and model tests, stability coefficients, wave run-up, coverage, placing patterns, moulds, casting, handling and placing.

INTRODUCTION

The first Stabits were experimental and 7 ton in weight of Mark I variety used at Benghazi Harbour, Libya, early in 1961. These were placed at the end of one of the existing protective moles where they were exposed to open sea waves. This experiment proved that Stabits had excellent wave energy dissipation properties and were worthy of development. However, load testing to destruction indicated that Mark I Stabits did not possess an adequate reserve of structural strength and Mark IT Stabits of increased strength were introduced.

In order to decide whether Stabits would be satisfactory for full scale breakwater armouring, hydraulic model tests were instituted at the National Hydraulics Research Laboratory in 1961. These tests were carried out using models of Mark II Stabits and demonstrated that Stabits offered a satisfactory solution. In consequence it was decided to use 29 ton Stabits in the reconstruction and extension of existing moles at Benghazi Harbour.

During the course of construction when some 2,000 Mark II Stabits had been cast and placed on the Outer Mole it became increasingly evident that undue care had to be exercised to prevent breakages during placing. In consequence a still more robust Mark III unit was devised.

The Mark III design supersedes all the previous designs and is currently in use. A 29 ton Mark III Stabit is illustrated in Fig. 1.

The number of 29 ton Stabits which have been used on the reconstructed moles at Benghazi is about 10,000 and about 900 of the smaller 7 ton units are being used as absorbent facing to reduce wave effects in certain parts of the harbour. An aerial view of the harbour with the completed moles is given in Fig.2.

In England, about 600 of the 7 ton units were used to stabilise the beach at the root of the East Breakwater at Shoreham in 1962. Fig.3 illustrates these Stabits in position.

Fig.1 - 29 ton Mark III Stabit

Fig.2 - Aerial view of Stabits at Benghazi

Construction commenced in 1968 on Port Rashid, Dubai, Arabian Gulf, where 13,000 of 15 ton and 12,000 of 7 ton Stabits will be used as armouring for breakwaters. In addition about 2000 of 7 ton Stabits may have to be used at the root of breakwaters to stabilise the beach if further investigations and observations show that erosion is likely to occur in these areas.

TESTS

Hydraulic Models

The first hydraulic model tests were carried out in 1961 by the National Hydraulic Research Station, Wallingford, England. The purpose of these tests has been explained in the previous section.

Model Stabits were made representing prototype 29 ton Stabits to a linear scale of 1/47 and tested in a flume. Prototype wave periods of 10 and 12 secs. with a tidal range of 3 ft. and a storm duration of 7 and 12 hours simulating 32 feet maximum waves were used. The breakwater armouring of Stabits was found to be stable for waves of this height and the tests confirmed that for stability under such wave attack, Stabits of 29 ton weight with concrete density of 145lb/cu.ft. were a satisfactory alternative to any other form of artificial armour.

Stabits of Mark II variety were used in these tests.

In September, 1963 further hydraulic model tests were undertaken from which formulae were derived for use in the preparation of preliminary designs and estimates.

Models of Mark III Stabits made from concrete of 145lb/cu.ft. density were used. Design coefficients were established and wave run-up, porosity and the thickness of armour layer were measured for various breakwater slopes and wave periods. The data obtained from these tests are reproduced in the following pages.

It should be noted that in the original tests a conventional method of placing known as the "double layer" method was used whereas in the subsequent tests a new method called the "brickwall pattern" was adopted.

The brickwall pattern was evolved during the course of construction of the breakwaters at Benghazi and confirmed by model tests as providing maximum efficiency and economy on slopes of 1 in 2 and steeper.

The two methods of placing have been described in detail in the section dealing with design.

Full Scale

As mentioned in a previous section, full scale tests were carried out using the experimental 7 ton Mark I Stabits at Benghazi Harbour, structurally expected to resist waves 8-10 feet in height.

The armoured test face received open sea waves of 11 to 12 ft. in height over a period of about four months and sustained very little damage.

Fig.3 - 7 ton Stabits at Shoreham

Fig.10 - Stripping Moulds from 29 ton Stabit

The performance of the experimental Stabits in disrupting and destroying the assaulting waves was particularly striking when compared to that of the adjacent pell mell blockwork. Waves collapsed almost completely and run-up was small by comparison.

Static and dynamic load tests were also carried out on Stabits from time to time. In the final tests a Mark III unit was dropped through a height of 15 feet onto rock armour without destruction.

DESIGN DATA

Dimensions

The Stabit is basically a hollow tetrahedron. Its proportions are related to the basic dimension 'T' and are shown in Fig.4. Once the required weight of a unit and thus its volume are known the basic dimension 'T' can be calculated from the following simple formula:-

$$V(\text{volume}) = 11.34\ T^3$$

Stability

The results of hydraulic model tests were used in the evaluation of the experimental coefficient K_Δ in the stability formula developed by Mr. R. Y. Hudson[1] of Waterways Experiment Station, Vicksburg, Mississipi, U.S.A. The Research work of Mr. R. Y. Hudson which led to the evolution of his stability formula has been published in various technical articles and will not be described here.

This formula is generally stated as follows:-

$$W_r = \frac{\gamma_r H^3}{K_\Delta (S_r - 1)^3 \cot \alpha}$$

where W_r = Weight of armour unit (lbs)
H = Wave Height (feet) (significant)
γ_r = Specific weight of armour unit (lbs/cu.ft.)
S_r = Specific gravity of armour unit (should be related to the density of water in which the structure is located).
α = Angle of slope of the armour layer.
K_Δ = Experimentally derived coefficient.

The experimentally derived K_Δ values of Stabit armouring for no damage condition are as follows:-

K_Δ = 25.4 - Use with discretion and only where good supervision and control over placing available.
K_Δ = 19.04- Normal usage and where average supervision and control over placing available.

The wave flume used for this investigation was 78 ft. long, 4 ft. wide and 4 ft. deep. The depth of water was kept constant at 17 inches at the breakwater test section and therefore the effect of tidal variation was excluded. Three breakwater slopes of 1 in 2, 1 in 1.5 and 1 in 1.3 were used. Four wave periods of 1.2, 1.4, 1.6 and 1.8 sec. were used for each

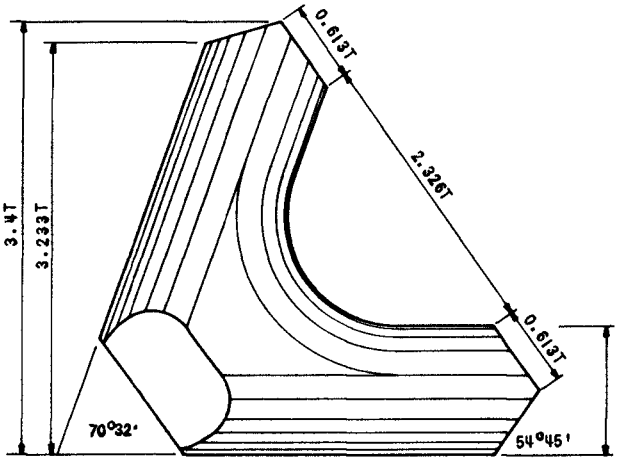

SIDE ELEVATION OF STABIT SITTING ON TWO LIMBS

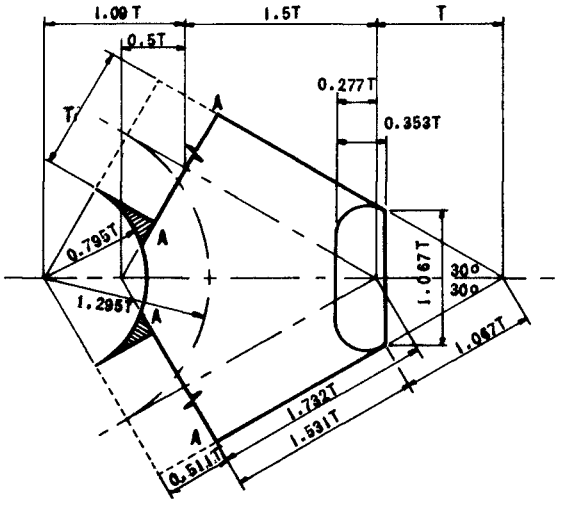

PART PLAN OF STABIT SHOWING CORNER

FIG 4 - STABIT PROPORTIONAL DIMENSIONS

NOTE.

The Stabit comprises, in effect, four identical corners joined along section AA The area shown shaded overlaps the adjoining corner An overlap (not shown) also occurs where the inner radius of the adjacent corner extends a corresponding distance beyond this section

breakwater slope. For any particular wave period, every cross-section was tested with waves, the height of which was decreased from test to test until a wave height was found which would result in less than 1% damage. Tests using higher waves causing over 1% damage were terminated after about 30 minutes continuous running. Tests using lesser wave heights to establish the no damage condition were continued for up to two hours. If the applicability of these general tests can be considered to hold good for Stabits ranging between 5 to 30 tons, then two hours in the tests would represent prototype storm conditions over a period of 12 to 14 hours.

The Stability Number, $N_s = \frac{\gamma_r^{1/3} H}{W_r^{1/3}(s_r - 1)}$,was

calculated using a Stabit weight of 0.6381bs., a specific weight of the armour unit of 145lbs/ft^3, a specific weight of fresh water of 62.4lbs/ft^3 and the significant wave height causing damage of 1% or less. The calculated values of the Stability Number were plotted as the ordinate with the reciprocal of the breakwater slope ($\cot \alpha$) as the abscissa as illustrated in Fig.5. It can be seen that there is a wide scatter of results the cause of which can be attributed primarily to the difficulty of repeating exactly the way in which the Stabits were placed on the breakwater face between tests. It should be noted that every effort was made to simulate prototype placing and no attempt was made to force Stabits to interlock one with another. It was felt that variations in standards of control over placing might also occur in practice and therefore it was decided to draw two lines representing two standards. Line AB represents good standard of supervision and control whereas line CD represents average to poor standard.

It can be shown that $N_s = a(\cot \alpha)^{\frac{1}{3}}$

For line AB, a = 2.94

& For line CD, a = 2.67

It can also be shown that $K_\Delta = a^3$

$\therefore$ For line AB, $K_\Delta = (2.94)^3 = 25.4$

& For line CD, $K_\Delta = (2.67)^3 = 19.04$

It should be noted that the "no damage" condition was defined as the removal and/or excessive oscillation of Stabits of up to 1% of the total number of units on the test face.

It is interesting to mention that completely independent model tests were carried out in New Zealand where a value of 19.9 was obtained for K_Δ. However, it should be noted that these tests were for a particular design and a particular site and damage of 2.5 to 3% was accepted. The details of these tests have been published by Mr. P. D. L. Holmes[2] in New Zealand Engineering of November, 1965 and reproduced in the Dock & Harbour Authority[3] of June, 1966.

It must be emphasized that the above formula and the experimentally derived values of K_Δ should be used with discretion and preferably only for the purpose of preliminary designs and estimates for the following reasons:-

1) Only a limited number of variables could be taken into account in the model tests and, in particular, wind was not produced. It is believed that wind waves have a different shape and are generally steeper than

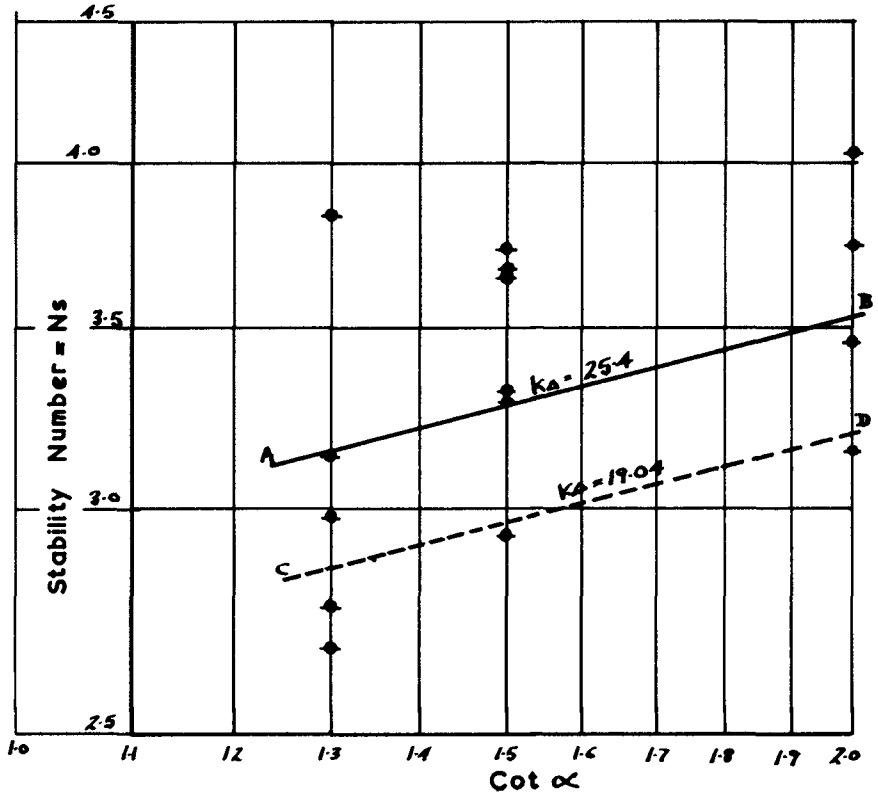

$$\text{Stability Number (Ns)} = \frac{\gamma_r^{1/3} H}{W_r^{1/3} (S_r - 1)}$$

Fig. 5.

STABILITY NUMBER AS A FUNCTION OF BREAKWATER SLOPE FOR NO DAMAGE CRITERIA

those generated by the normal paddle type mechanism.

2) Waves attacking the breakwater obliquely were not reproduced in the tests nor was the special case of a roundhead tested.

3) In nature, storm-waves contain a large proportion of waves which are higher than the significant whereas in the model tests it was not possible to reproduce a similar proportion, nor the same ratio of maximum to significant wave height. Therefore, some doubt remains as to which of the various wave heights present in storm-waves occurring in nature should be selected as the "design" wave.

It is strongly recommended that for final design, specific conditions pertaining to the particular site in question should be examined and, if necessary, hydraulic model tests should be undertaken to confirm the adopted design.

Prototype Results

The breakwaters at Benghazi, a typical cross-section of which is illustrated in Fig.6, were completed in 1962. Wave records for the period 1961 to 1965 were analysed and have been presented in another paper[4] to this conference. A careful record of damage has also been kept and which has been found to be about $\frac{1}{4}\%$ per annum taken as an average over the period of 5 years up to January, 1968. From an examination of the wave records it has been confirmed that the breakwaters have been subjected to the "design wave" several times. The experimentally derived stability coefficients have, therefore, been amply verified in practice.

Placing Patterns

There are two methods of placing Stabits; the "double layer" and the "brickwall". Both the methods were tried at Benghazi where it was found that the latter method resulted in good interlocking on slopes steeper than 1 in 2. Thus, on breakwaters, Stabits would be placed using the "double layer" method on the soleplate on the sea bed at the toe of the slope whilst the "brickwall" method would be adopted for armouring the side slopes of the breakwater itself.

Double Layer In this method Stabits are placed to a predetermined grid in two layers; the top layer being displaced from the bottom layer by half the grid spacing in both the directions. The upper Stabits thus sit in cradles formed by lower Stabits. The grid dimension is approximately equal to $\frac{3}{4}T$.

Brickwall This method closely follows the principle of bonded brickwork construction and hence the name. Stabits in the first row are placed side by side. In the next row up the slope, Stabits are placed staggered from those in the first row. Each succeeding row partly overlaps the lower row so that every Stabit penetrates into it but at the same time rests against the slope. The brickwall method was developed during the course of construction at Benghazi where a trial length of breakwater was constructed using this method and was found to be very successful. For work above water and also for under-water where visibility is good, placing is carried out by eye but where under-water visibility is poor a predetermined grid for placing can be defined. Placing by eye and by means of a grid have been tried and both result in equally well interlocked armour layers. Fig.7 shows a photograph of 29 ton Stabits placed with this method.

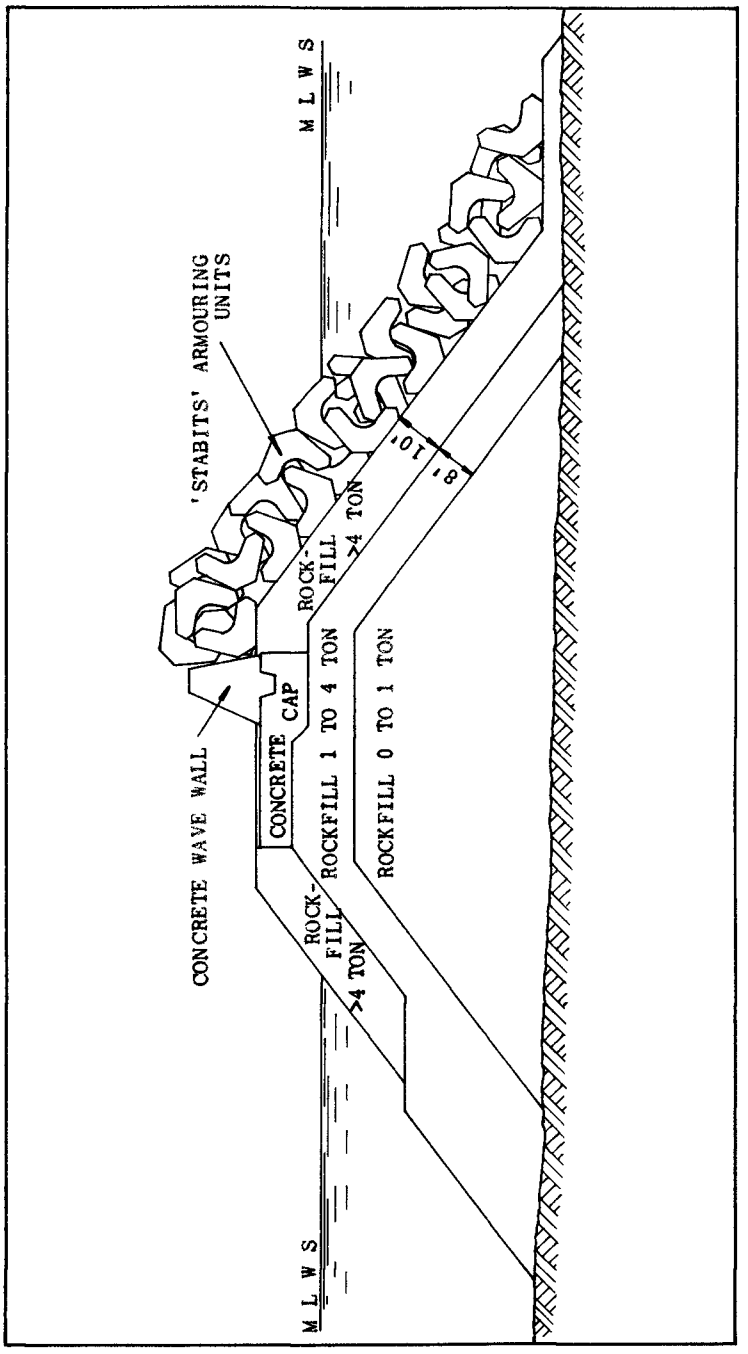

FIG 6 - TYPICAL BREAKWATER CROSS-SECTION AT BENGHAZI

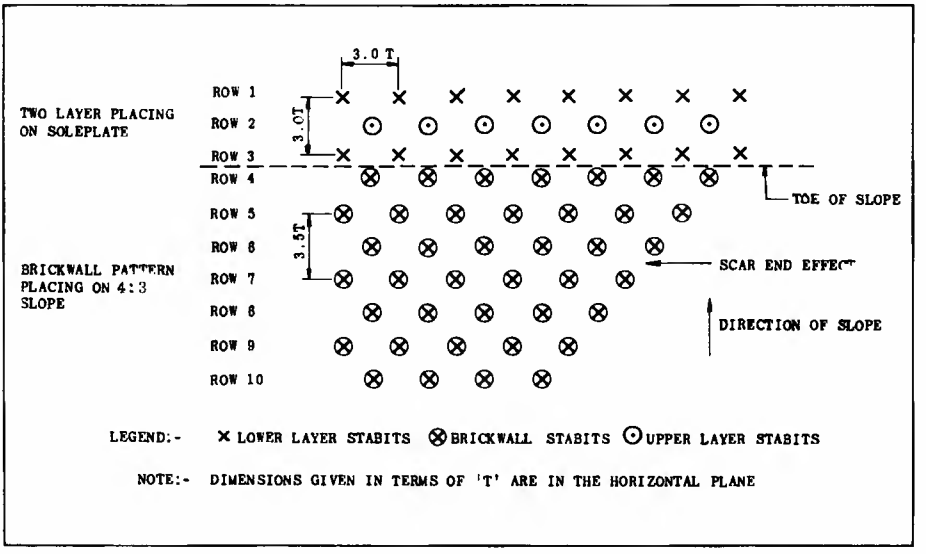

FIG 8 - DIAGRAMMATIC PATTERN FOR BRICKWALL PLACING

Fig.7 - Stabits placed "brickwall" method

Fig.8 shows a diagrammatic illustration of the sequence of placing operations on a typical breakwater.

Thickness and Porosity

The thickness of armour layer placed brickwall fashion is approximately equal to 4T, and the porosity is about 55%. The corresponding values for double layer armouring are 5T and 52%. These values were obtained in model tests and have been verified in practice.

Coverage

The breakwater surface area per Stabit in an armour layer placed brickwall fashion is given approximately by the following simple relationship which has been verified in practice:-

$$\text{Area/Stabit} = 6.3T^2 \text{ sq.ft.}$$

Some typical brickwall coverages are given in the table below:-

SIZE Long tons	COVERAGE/100 sq.yd.
4	47 No.
5	40
7	32
12	22
15	19
18	17
23	14.5
29	12

The coverage for the double layer method can be calculated from the grid spacing which is approximately equal to 3T.

Wave Run-Up

Hydraulic model tests have indicated that the wave run-up on a Stabit armoured slope is governed by the following simple relationship:-

$$R = 1.3\ H$$

Where, R = Run-up measured vertically above S.W.L. (Feet)
H = Wave height (Feet)

The above formula should only be used as an approximate guide since it is not possible to generalise to cover an extensive variety of waves nor is it possible to measure accurately the run-up on a rough and porous sloping surface. Moreover, it should be noted that no wind was present in the tests, which is also believed to have an effect on the run-up.

The results of the wave run-up tests are given in Fig.9.

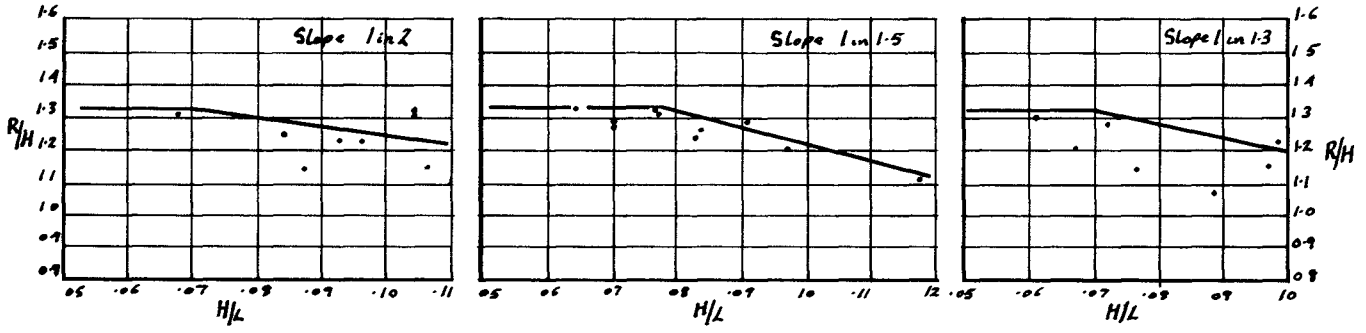

Fig 9. Results of Wave Run up Tests

	T secs	d/L	H	H/L	R	R/H
Slope 1 in 2	1 8	0 126	9 2"	0 067	12"	1 31
	1 8	0 123	7 75"	0 056	–	–
	1 8	0 126	9·00"	0 067	–	–
	1 8	0 125	8 25"	0 060	–	–
	1 6	0 139	10 75"	0 088	12"	1 12
	1 6	0 144	11 50"	0 097	14"	1 22
	1 6	0 149	9 75"	0 085	12"	1 23
	1 4	0 177	9 00"	0 093	11"	1 22
	1 4	0 171	10 50"	0 107	12"	1 14
	1 2	0 166	10 75"	0 105	14"	1 30
	1 2	0 20	9 00"	0 105	12"	1 33

	T secs	d/L	H	H/L	R	R/H
Slope 1 in 1·5	1 8	0 125	9 5"	0 070	+12"	1 26
	1 8	0 123	11 4"	0 083	+14"	1 23
	1 8	0 125	8 66"	0 064	+11 5"	1 32
	1 6	0 137	10 45"	0 084	+13"	1 24
	1 6	0 137	8 68"	0 070	+11"	1 27
	1 4	0 173	9 58"	0·097	+11 5"	1 20
	1 4	0 173	7 58"	0 088	+10"	1 32
	1 4	0 180	8 57"	0 071	+11"	1 28
	1 4	0 175	7 64"	0 078	+10"	1 31
	1 2	0 209	9 71"	0 119	+11"	1 13

	T secs	d/L	H	H/L	R	R/H
Slope 1 in 1·3	1 8	0 127	9·0"	0 067	+11"	1 22
	1 6	0 149	8 7"	0 076	+10"	1 15
	1 6	0 149	7 26"	0 061	+9 5"	1 31
	1 4	0 177	7 0"	0 072	+9"	1 28
	1 4	0 177	8 6"	0 089	+9"	1 05
	1 2	0 210	7 75'	0 096	+9"	1 16
	1 2	0 205	8 2"	0 098	+10"	1 22

MOULDS

Description

The mould consists basically of eight elements as follows:-

2 lower side supporting elements on props and castors

2 upper side elements

2 inner lower segments

2 inner upper segments

All the elements are inter-connected by means of bolts. Tapered pins are used in some of the bolt holes for drawing elements together during assembly. The supporting elements are provided with props on castors with screw jacks for ease of erection and stripping. On larger sizes opening hatches are usually provided at the gussets for concreting purposes. On smaller sizes small opening lids are provided for vibration purposes only. The top end plates are hinged to the supporting elements and can be used as working platforms but, depending on the method of working, the hinge can be eliminated with some economy. In addition to the above mentioned elements, each mould is provided with two baseplates which are mounted on plinths on which moulds are erected in the casting yard.

Erection and Stripping

Raised concrete plinths are constructed in the casting yard to which the baseplates are bolted and on which the moulds are erected. A small crane is required for handling the mould elements for the larger sizes of Stabits during erection and stripping operations. The complete operation of striking, cleaning, oiling and erection of a mould generally takes $\frac{3}{4}$ to 1 hour. Each mould may be stripped completely 24 hours after casting depending upon the quality of concrete and the climatic conditions. Fig. 10 shows the stripping operation in progress.

CASTING AND HANDLING

CONCRETE

Ordinary portland cement concrete is generally used in making Stabits. The maximum size of aggregate is generally $1\frac{1}{2}$in. but larger sizes up to 3in. may be used with care in mix design. The concrete should have a cube crushing strength of 3,500lb/sq.in. at 28 days or flexural strengths can be specified, if required, as a supplementary or an alternative method of concrete quality control. No reinforcement is required in making Stabits.

Mixing and Placing Concrete

The size of the mixer should be such as to enable each mould to be filled completely in a single operation without any horizontal construction joints. Concrete can be transported to the casting yard by any convenient means where each shutter opening is fed alternatively. Thorough compaction is ensured by internal vibrators. In the case of large Stabits, vibration of the lower parts is carried out by a man standing on the 'saddle' and/or through the inspection hatches. For smaller Stabits, vibration is carried out from the top openings as well as from the small hatches especially provided for this purpose. As the concrete reaches the level of gussets,

Fig.11 - Stabit being lifted by double sling method

Fig.12 - Low loader transporting Stabit

the surplus concrete is skimmed off and the hatches are closed. Average casting times for 29 ton and 7 ton Stabits were found to be 35 mins. and 20 mins. respectively. However, these figures depend very much on the plant used on site.

Handling to Storage

Normally Stabits can be moved to storage 3 days after casting using a simple double sling arrangement which keeps all members in compression. This method of slinging is extremely simple and is illustrated in Fig.11. Mobile cranes, Tournacranes or gantries can be used for handling Stabits to storage.

PLACING

Time of Placing

Generally Stabits are placed in their final position not earlier than 28 days from casting but this period may be reduced to as little as ten days depending upon the quality of concrete, prevailing temperature and other conditions at a particular site.

Transport

The type of transport required for moving Stabits from storage to the site depends on the site and size of units. In most cases, however, ordinary lorries or low-loaders should suffice. Fig.12 shows a 29 ton Stabit being transported by a low-loader.

Cranage

The types of cranes required for placing Stabits in the works depend upon the size of unit and the working radius; Figs.13 and 14 show a Lima 2400 and a floating crane in action.

Slinging

Lifting hooks cast into Stabits are not recommended as they can result in corrosion and bursting of concrete. A simple sling method, illustrated in Fig.13 has been found to be very successful in practice. It will be seen that the sling consists simply of a rope passed through the centre of the Stabit with both ends attached to the crane hook. After the Stabit has been placed in position, the crane hook is lowered and one end of the sling is unhooked by hand or auxiliary wire. The crane hook is then raised thus withdrawing the sling clear of the Stabit.

Method of Placing

Stabits should be placed in such a manner as to achieve fully interlocked armour using the placing patterns described in another section. The method of placing is quite simple. A crane lifts the Stabit using the method of slinging described above and lowers it into the position directed. Sometimes it is found that the best interlocking position is not obtained at the first placing operation. In that event all that is required is to

Fig.13 - Lima crane placing Stabit

Fig.14 - Floating crane placing Stabit

raise and lower the Stabit until it adopts a stable attitude.

Where underwater visibility is good, instructions to the crane driver are given by a man in a boat observing through a glass box projecting into the water. Where underwater visibility is poor, placing has to be carried out to defined grid spacing in relation to a fixed base or wire. For work above water, all placing is carried out by eye to achieve maximum interlock. With a little experience placing can proceed at rates varying from 6 per hour,one mile from the store yard for 29 ton Stabits,to 10 per hour,for 7 ton Stabits in close proximity to the yard.

It must be appreciated that a certain degree of consolidation of the Stabit armouring is likely to occur during wave action after construction. This is quite normal as Stabits settle into their final interlocked positions.

ACKNOWLEDGEMENTS

The author wishes to express his gratitude to Mr. Ridehalgh, a partner in his firm and the inventor of the Stabit, for his permission to publish this paper. He would also like to thank his colleagues and in particular Mr. R. J. Daniels and Mr. R. K. Hayward for their considerable contribution in the development of the Stabit. Acknowledgements are also due to the National Hydraulics Research Station, Wallingford, and the Central Laboratory of George Wimpey & Company Limited who carried out the hydraulic model tests.

REFERENCES

1. R. Y. Hudson, Laboratory Investigation of Rubble-Mound Breakwaters. Proc. Am.Soc. Civil Eng. September 1959, Vol.85 No.WW3, pp.93-119.

2. P. D. L. Holmes and A. G. Park, Design of a Mound Type Breakwater for Port Taranaki. New Zealand Engineering, November 15, 1965.

3. P. D. L. Holmes and A. G. Park, Hydraulic Model Studies for a Mound Type Breakwater. Dock and Harbour Authority, June 1966.

4. K. Y. Singh and L. Draper, Waves off Benghazi Harbour, Libya. Proc. XIth Conf. Coastal Eng. 1968.

CHAPTER 53

VELOCITIES IN DOWNRUSH ON RUBBLE MOUND BREAKWATERS

A. Brandtzæg, Professor of Construction and Harbour Engineering, (retired)
A. Tørum, First Laboratory Engineer,
O. R. Østby, Scientific Assistant.

Technical University of Norway, Trondheim, Norway.

ABSTRACT

This paper is a sequence to two papers, (1) and (2), previously read at Coastal Engineering Conferences. They presented a mathematical model for estimating displacements, velocities and accelerations in a downrushing wave on a rubble mound breakwater slope. Verification by photographic recording of displacements involved some uncertainties. In the present paper are reported measurements of velocities, which gave much more definite data. The correlation with velocities calculated from the model is shown to be good.

INTRODUCTION

At the VIIIth Conference on Coastal Engineering Brandtzæg (1) presented a mathematical model intended for estimating roughly the displacements, velocities and accelerations in the downrushing water on a rubble mound breakwater slope. A very few experiments indicated fair agreement between observed values and those calculated from the model.

At the Xth Conference Brandtzæg and Tørum (2) presented data from a greater number of waves of different heights and periods on slopes of 1:1,25, 1:1,5 and 1:2,0. Displacements calculated from the model were found to agree reasonably well with the observed ones, although the scatter was quite considerable. This was to be expected, since displacements had to be deduced from photographs of the wave surface profiles. As these were often rather irregular, the deduction became difficult and involved some uncertainty.

Therefore it was highly desirable to measure velocities directly, and the more so because in application of the model, velocities and accelerations are the interesting quantities. However, getting reliable readings of velocities in the rapidly accelerated downrushing water is difficult. But recently such measurements have been made, and the results are presented here. They are compared with velocities calculated from the model, partly by use of the particular values of z and β (Fig. 3) found for each wave dimension and slope, as in reference (1) (Calculation 1)and partly by use of more general

values of z and β, permitting calculation without previous knowledge of specific experimental data, as in reference (2) (Calculation 2).

VELOCITY MEASUREMENTS

The tests were made in the wave channel shown in Fig. 1. The wave generator has an ordinary piston type paddle adjustable as to wave height and wave period. The wave gage was placed about 11 m in front of the model. Vertical surface displacement at this point was recorded on a Sanborn paper recorder.

The model itself was a wooden platform with a sloping front on which the cover blocks were placed on top of a layer of smaller stones, about 5 cm thick. As the stability of the armour was not at issue in these tests, the blocks were held in place with a few nails, none of which protuded above the top of the blocks.

In the tests of ref. (1) and (2) the cover blocks were arbitrarily placed with regard to orientation as well as location. In the present tests, however, it was found necessary to have a slightly smoother breakwater front (Fig. 2), so as to avoid too much air bubbles in the downrushing water, as this tended to blur the photographic recording described below.

As stated in ref. (1) the mathematical model applies to the downrushing wave only as far down as the stream is not influenced by the incoming next wave. From the wave profiles (Fig. 8) and also from the direction of velocities indicated by confetti in the water (see ref. 1, Fig. 5) it is seen that this condition holds good also somewhat below the SWL. In order to extend as far as possible the time interval during which velocity readings could be obtained, the limiting line at which velocities were measured (point A) and calculated, was shifted from the line M - N, as used in ref. (1) and (2), to the line P - Q, Fig. 3 and Fig. 8.

An Armstrong-Whitworth Miniature Current Flowmeter, Type 176/1 was placed 10 cm from the glass wall of the channel. It had a very light plastic propeller with outer diameter 1,5 cm. The range of reliable registration in a steady current covered velocities from 2 to 150 cm/sec. The instrument apparently worked satisfactorily also in unsteady currents. The propeller movements were recorded by means of a motion picture camera making some 800 - 900 exposures pro second, while a time mark was made on the film every 1/100 second.

The test programme included three slopes of the breakwater face, and with each slope three wave periods, each with

two wave heights, in total 18 waves (Table 1). Due to difficulty with the camera one wave, No. 6, dropped out.

Velocities were measured during downrush of one of the first waves arriving at the model front after the generator had been started and a reasonably stable wave height had been attained. First a trial wave train was run. From the registration diagram (Example in Fig. 4a) was picked out the wave to use, and its number (n) from the front of the wave train was noted. After rest the wave generator was started again and when the nth wave arrived at the model, the fast motion camera was started. Mostly the third or fourth wave was used (Fig. 4 b).

Beside the fast camera film, giving the velocities, another motion picture film was needed to give the wave surface profiles required for determination of β and z (Fig. 3 and 8). As the two exposures could not be made simultaneously, a third wave train was run for this purpose (Fig. 4 c), and photographs taken with a camera making about 24 exposures a second. As in earlier tests, the time between exposures could be read off on the clock shown in Fig. 2. The surface profiles were drawn up, β and z determined as described in ref. (1) page 456, and the values plotted against time, t, after start of downrush, in diagrams of which examples are shown in Fig. 5, 6 and 7. Smooth curves for β and z were drawn for each wave.

From the fast film strips the number of revolutions pro second of the propeller could be ascertained. From calibration curves the corresponding velocities were taken off and plotted against t, time from start of downrush. Examples are shown in Fig. 9 to 17.

Velocities measured in this way will be roughly average values. An effort was also made to register velocities by means of confetti in the water. Only a few data were obtained. They showed great variations, as was to be expected, but seemed to group themselves fairly well around the propeller-observed values.

CALCULATION 1.

Velocities calculated with β- and z-values as observed in the tests.

The definition of the mathematical model here employed and the underlying assumptions and simplifications have been set out in detail in ref. (1) and briefly summarized in ref. (2). For ease of reference the basic consept of motion is restated here (Fig. 3):

1) The body of downrushing water is considered as a triangle. That is, the surface profile is assumed to be a straight

line forming an angle β, with the breakwater front and an angle, δ, with the horizontal.

2) The triangular body is divided into individual slices, "s_u". Each slice is defined by its original distance, u, from the top, 0, of the triangle.

3) Each individual slice is taken to move integrally and independently, without regard to continuity of the fluid, but otherwise in accordance with the gravity, the pressures and the boundary resistance, frictional and inertial, acting in the fluid.

As shown in (1) and (2), the assumption that the "slices" move independently of each other should not be expected to cause significant error in the calculations, because restoring the continuity need not to any considerable degree alter the general picture of the motion.

The model leads to the following equations for the displacements, x, velocities, v, and accelerations, a, as functions of the time, t, from the start of downrush:

$$x = B^2 \ln \left(\cosh \left(\frac{A}{B} t\right)\right) \tag{1}$$

$$v = AB \cdot \tanh \left(\frac{A}{B} t\right) \tag{2}$$

$$a = \frac{A^2}{\cosh^2\left(\frac{A}{B} t\right)} \tag{3}$$

$$A^2 = \frac{g(\sin\alpha - \tan\beta \cdot \cos\alpha)}{1 + 0{,}5 C_{MP} \frac{k}{z}} \tag{4}$$

$$B^2 = \left(1 + 0{,}5 C_{MP} \frac{k}{z}\right) \cdot 32 \cdot z \cdot \left(\log_{10} \frac{5z}{k}\right)^2 \tag{5}$$

Figures for C_{MP}, cover block dimension, k, and β and z (Fig. 1) are required for the calculation. Like in ref. (2) $C_{MP} = 1{,}0$ has been used here. This figure seemed reasonable on the basis of data given by Wiegel (3), Johansson (4) and others. Actually a small variation in C_{MP} does not greatly affect the calculation of velocities, as seen in Fig. 9, 12 and 15 where a value of 0,75 has been used for comparison.

In the tests of ref. (1) and (2) the characteristic linear dimension, k, of the block was defined by assuming the average volume of the blocks to be $0{,}5\ k^3$. As a slightly smoother breakwater front had to be used in the present tests, a some-

what reduced value, k = 4 cm was used in the calculations. Again, a change in k does not much affect the calculated velocity. Changing k from 4 to 3 cm causes a change of v about as great as that caused by reducing C_{MP} from 1,0 to 0,75.

For want of something better, the ordinary Prandtl equation for frictional boundary resistance was used in ref. (1), although the roughness of a rubble mound breakwater front certainly is very different from the "sand roughness" of Nikuradse. In ref. (2), however, the figure 14,8 in the last parenthesis of Eq. (5) was changed from 14,8 to 5, based on a note given in ref. (5). The same figure is used here.

The parameters β and z, important in Eq. (1) to (5), define the shape of the individual waves. How to determine appropriate figures for these parameters must depend on the objective aimed at. As the objective of Calculation 1 is to probe the possible merits of our mathematical model by comparison with specific tests, the values of β and z have been taken as nearly as possible representative of the particular waves in which velocities were measured.

Consequently, values of β and z were taken off curves like those in Fig. 5, 6 and 7 and used in CALCULATION 1. Individual values of β and z rarely deviated more than 10 per cent from the curves, corresponding to a deviation in calculated velocity of the order of 5 per cent.

With the parameter values discussed above, velocities in downrush have been calculated from Eq. (2), (4) and (5) and the resulting curves entered in the v - t - diagrams for each of the 17 waves tested (Fig. 9 to 17). On the whole the curves seem to agree fairly well with the plotted test data. Only for the three waves 10,15 and 16 do the measured velocities near the end of downrush exceed the calculated ones by some 25 to 50 per cent.

CALCULATION 2.

Velocities calculated with β- and z-values derived from general relationships.

Practical use of our mathematical model should permit estimating the order of magnitude of the velocity in downrush of a known wave on a known rubble mound breakwater slope within the range of slope steepness considered here. In such a case the appropriate β- and z-values are not known from specific tests, as in Calculation 1, but must be derived from general relationships.

The data plotted in Fig. 5 of ref. (2) indicated the following relationship between β, α and wave steepness H/L . $\beta = \alpha - \delta$, and $\delta = 6{,}56$ H/L. Similar data from the present tests are plotted in Fig. 18. They show considerably more scatter than the former. The line $\delta = 7{,}67$ H/L seems to give about the best fit. If the previous data are taken into account, an overall average value of $\delta = 7{,}0$ H/L may cover the field fairly well. However, in the present calculation $\delta = 7{,}67$ H/L has been used.

With β known, the z of any slice (Fig. 3) is given by $z = u \tan \beta$, and the z of the first slice to pass the SWL at the start of downrush is

$$z = l_{uo} \tan\beta = \frac{R}{\sin \alpha} \tan \beta$$

The uprush, R, is generally considered as being roughly proportional to the wave height, although it is surely influenced also by factors like steepness and roughness of the slope, etc. In the earlier tests, an average value of R was found to be 1,23 H. ((2) p. 980). The R - H relationship found in the present tests is shown in Fig. 19. The scatter is great. The average value, R = 1,36 H, has been used in Calculation 2, corrected for the fact that velocities were measured at the line P - Q, intersecting the slope at a point 4 cm (vertically) below the SWL. The z-value of the first slice to pass the line P - Q at the start of downrush therefore is taken to be:

$$z = \frac{R + 4 \text{ cm}}{\sin \alpha} \tan \beta$$

From these relationships velocities at the P - Q line have been calculated from Eq. (1) to (5) with otherwise the same parameters as used in Calculation 1. As explained in (2), page 981, the calculation must be done by iteration.

The resulting velocity curves have been entered in the v - t - diagrams in Fig. 9 to 17 for comparison with the test data and the curves from Calculation 1. It is seen that Calculation 2 in a number of cases gives somewhat lower velocities than both Calculation 1 and the tests, the difference being most pronounced towards the end of the downrush.

CONCLUSIONS

The comparison between observed and calculated velocities has been summarized in Fig. 20 for Calculation 1, and in Fig. 21 for Calculation 2. It is felt that the former shows about as good agreement between calculation and measurement as can reasonably be expected in this case. Calculation 2 gave velocities somewhat lower than the measured ones, in particular to-

wards the end of the downrush. Probably some adjustment of the R- and δ- relationships would give better agreement.

In total it is concluded that the mathematical model presented in ref. (1) and (2) does provide a means by which velocities in downrush on a rubble mound breakwater slope may be roughly estimated. Discrepancies are hardly avoidable, but Calculation 1 indicates that these may be due, not as much to the mathematical model itself, as to the difficulty of predicting more accurately the values of R and δ in actual cases.

REFERENCES

(1) Anton Brandtzæg: "A Simple Mathematical Model of Wave Motion on a Rubble Mound Breakwater Slope", Proceedings, Eighth Conference on Coastal Engineering, 1963, p. 444 ff.

(2) Anton Brandtzæg and Alf Tørum: "A Simple Mathematical Model of Wave Motion on a Rubble Mound Breakwater Slope", Proceedings of the Tenth Conference on Coastal Engineering, 1966, p. 977 ff.

(3) Robert L. Wiegel. "Oceanographical Engineering" Prentice-Hall International Inc., London, 1965, pp. 269 and 270.

(4) Børje Johansson: "Vågkrafter mot en på havsbottnen liggande cirkulär rörledning", Institutionen för Vattenbyggnad, Kungliga Tekniska Högskolan, Stockholm, 1965.

TABLE I

Scope of tests

cot α = 1,5				cot α = 1,25				cot α = 2,0			
Wave no	H cm	T sec	H/L	Wave no	H cm	T sec	H/L	Wave no	H cm	T sec	H/L
1	15.0	1,5	0,0481	7	15,0	1,5	0,0481	13	15,0	1,5	0,0481
2	18,5	1,5	0,0593	8	18,5	1,5	0,0593	14	18,5	1,5	0,0593
3	14,0	1,9	0,0323	9	14,0	1,9	0,0323	15	14,0	1,9	0,0323
4	19,5	1,9	0,0452	9A	15,0	1,9	0,0347	15A	14,5	1,9	0,0336
5	15,0	2,3	0,0274	10	19,0	1,9	0,0440	15B	15,0	1,9	0,0345
				11	15,5	2,3	0,0283	16	18,5	1,9	0,0429
				12	19,5	2,3	0,0355	17	15,5	2,3	0,0283
				12A	19,5	2,3	0,0355	17A	15,5	2,3	0,0283
								17B	15,5	2,3	0,0283
								18	19,5	2,3	0,0355

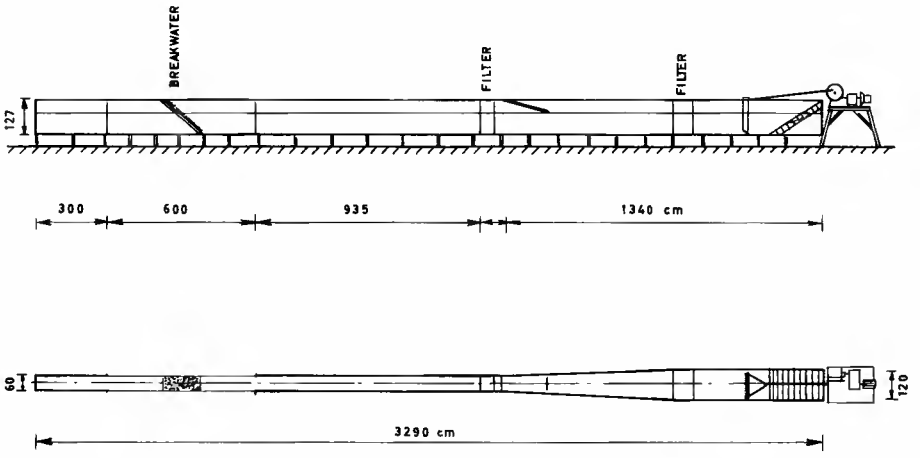
BREAKWATER
FILTER
FILTER
127
300
600
935
1340 cm
60
120
3290 cm

FIG. 1

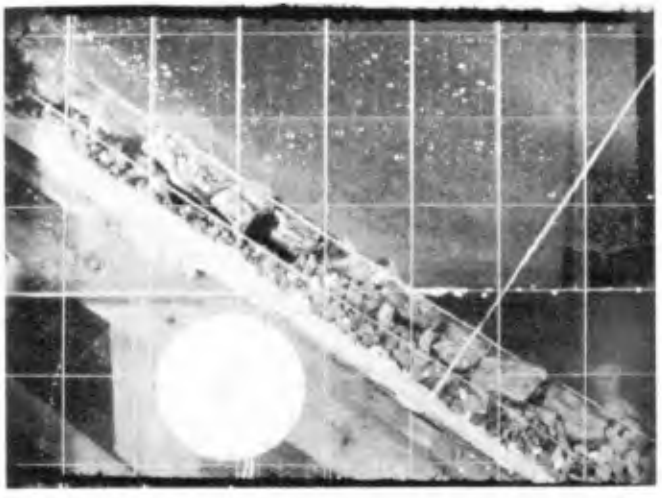

FIG. 2

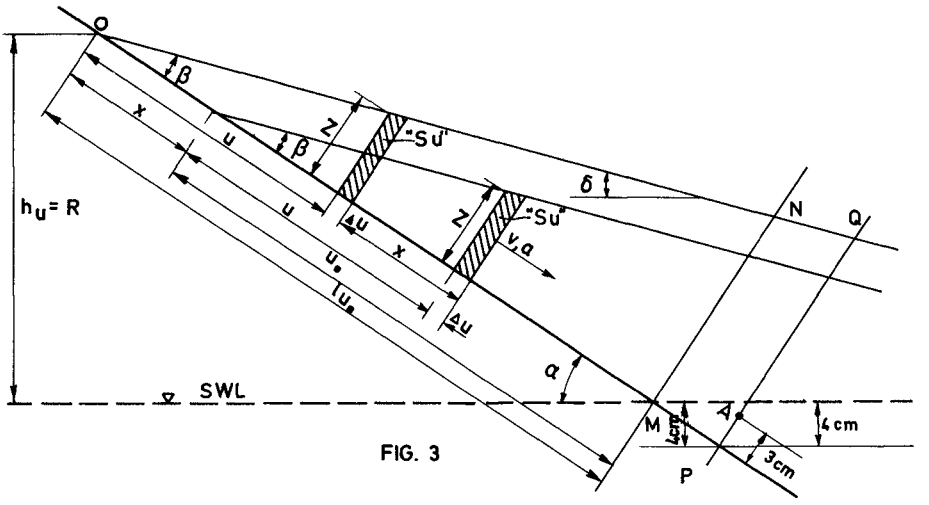

FIG. 3

WAVE 3 H = 14 cm T = 1,9 sec cot α = 1,5

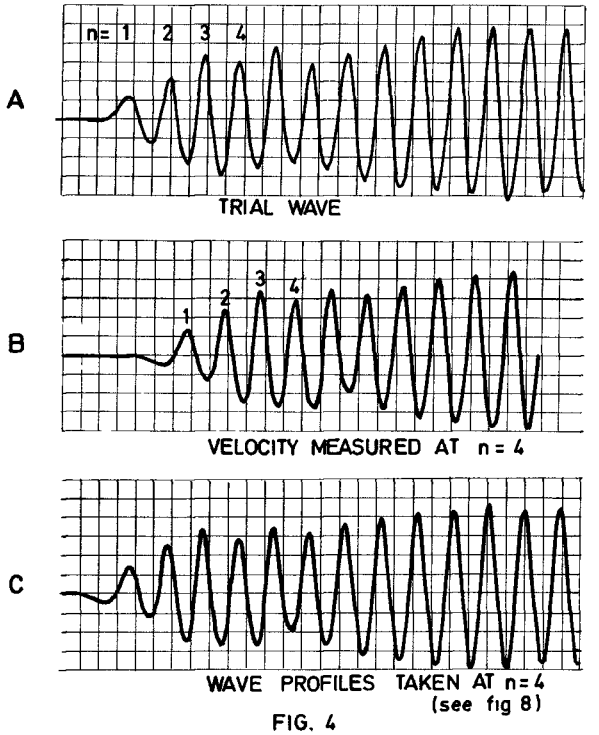

FIG. 4

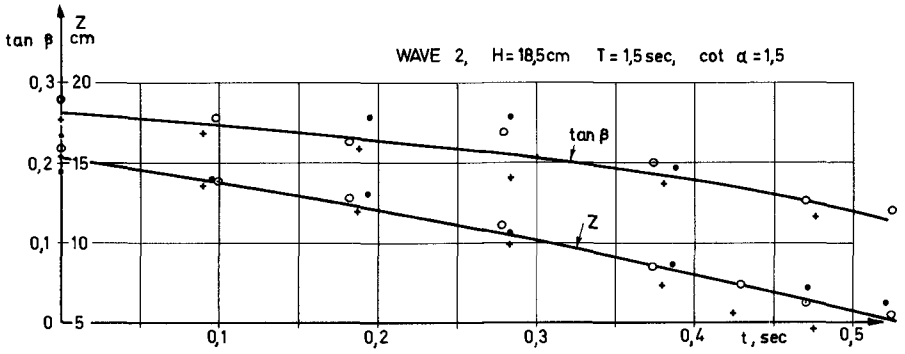
tan β
Z
cm
WAVE 2, H=18,5cm T=1,5 sec, cot α=1,5
0,3
20
0,2
15
0,1
10
0
5
tan β
Z
0,1
0,2
0,3
0,4
t, sec
0,5

FIG 5

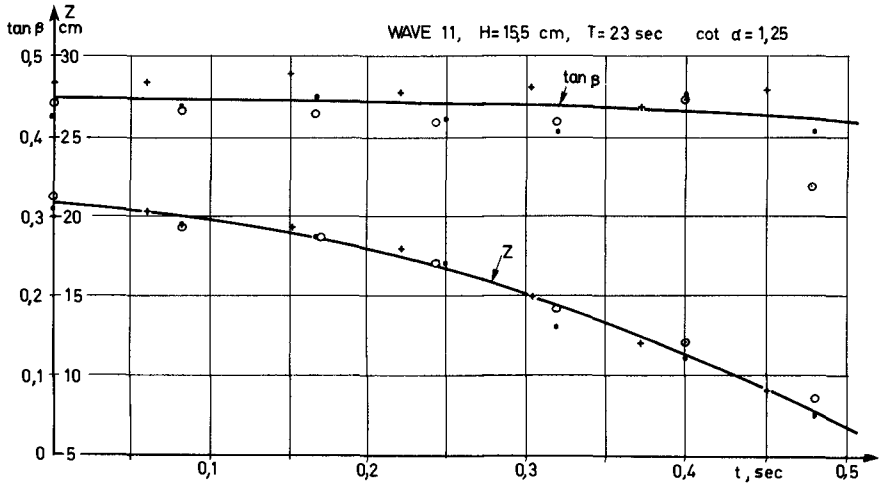
tan β
Z
cm
WAVE 11, H=15,5 cm, T=2,3 sec cot α=1,25
0,5
30
0,4
25
0,3
20
0,2
15
0,1
10
0
5
tan β
Z
0,1
0,2
0,3
0,4
t, sec
0,5

FIG 6

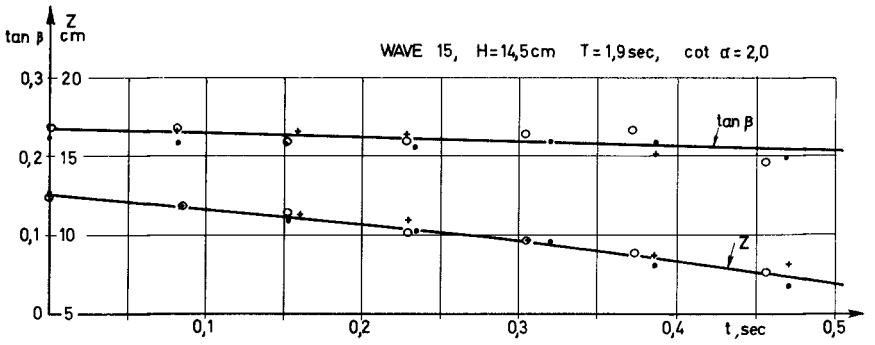

FIG 7

WAVE 5 H = 15 cm T = 2,3 sec cot α =1,5

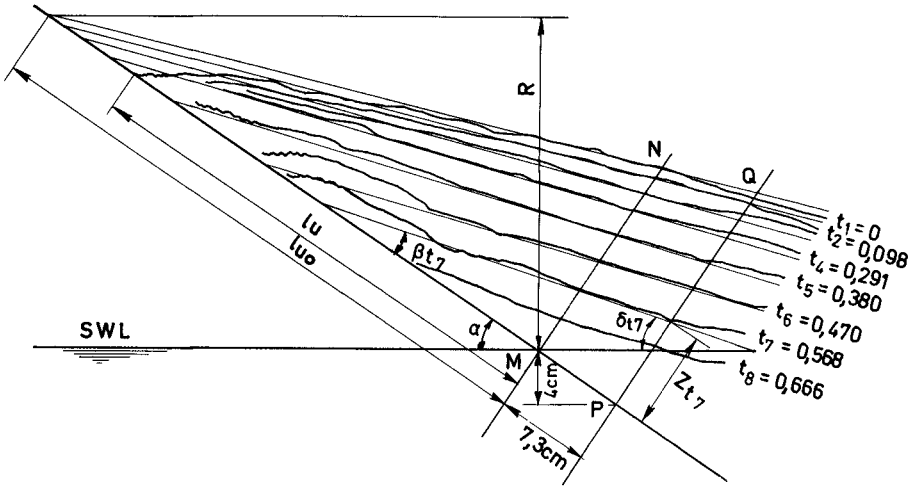

FIG 8

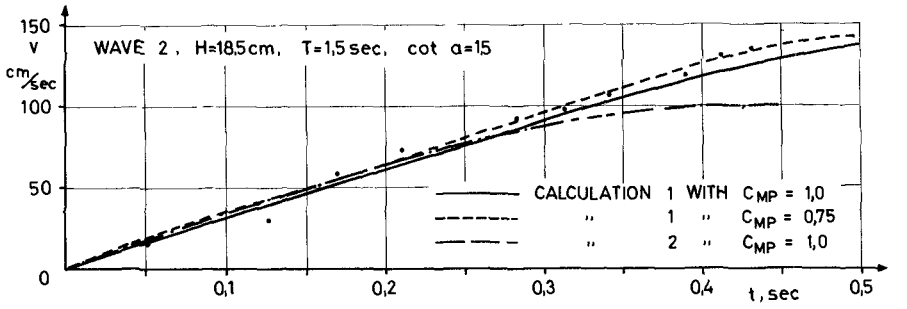

FIG 9

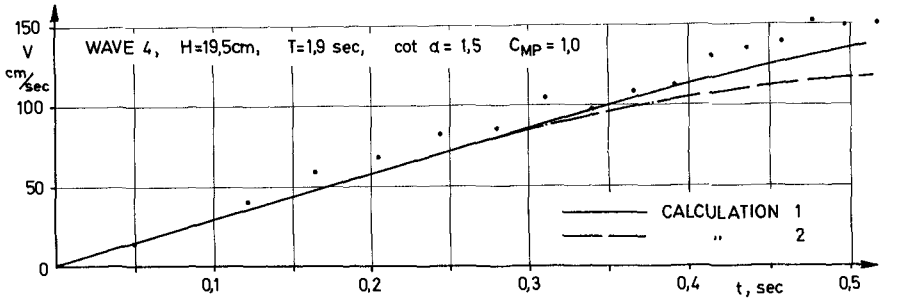

FIG 10

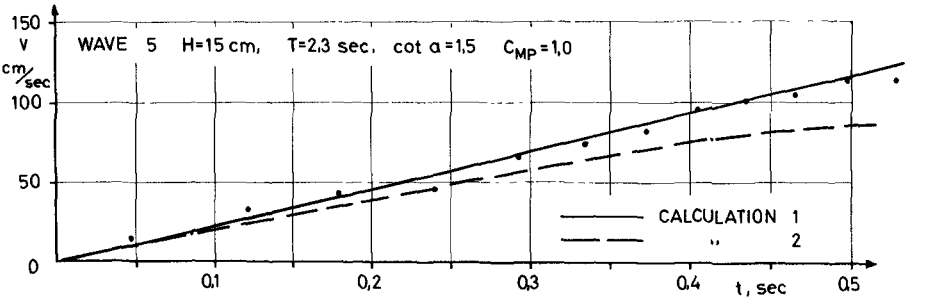

FIG 11

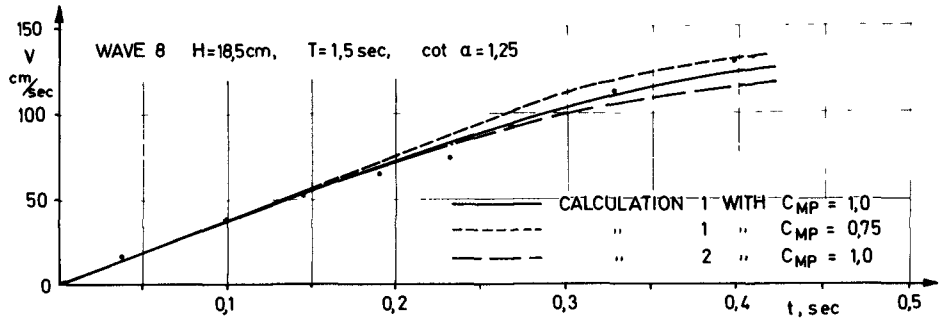

FIG 12

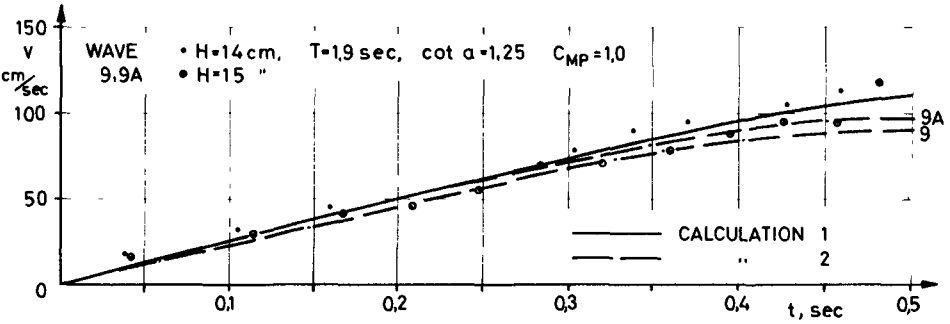

FIG. 13

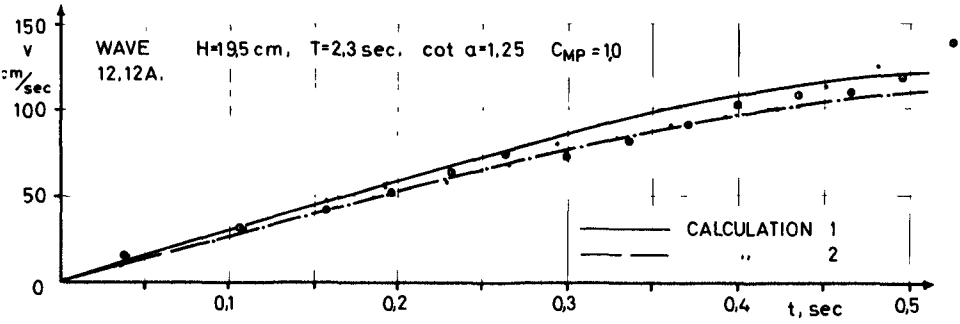

FIG 14

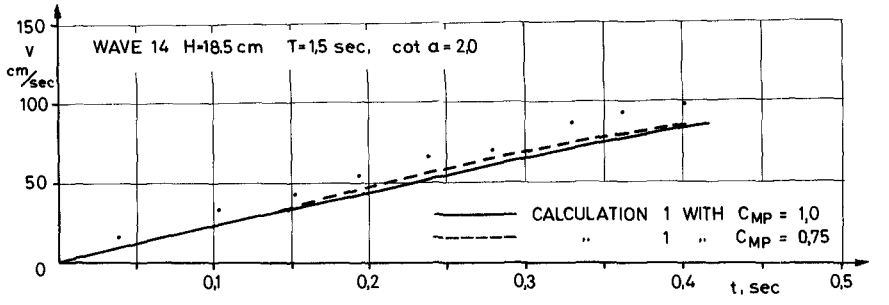

FIG 15

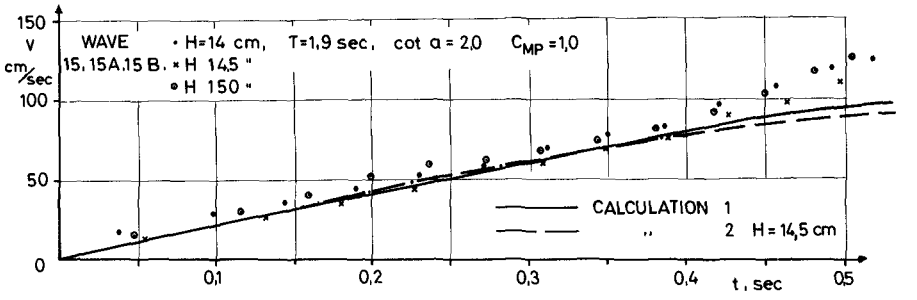

FIG 16.

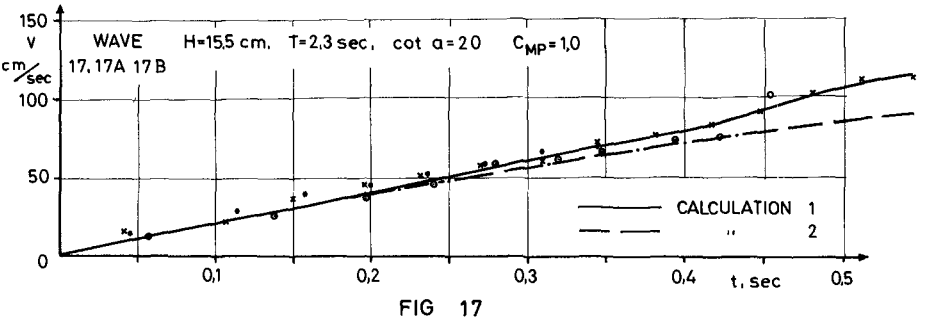

FIG 17

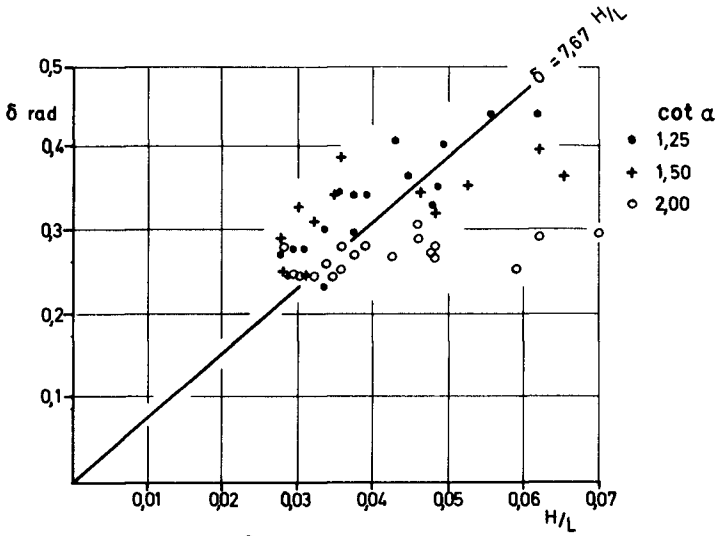

FIG. 18 ANGLE δ AS FUNCTION OF WAVE STEEPNESS

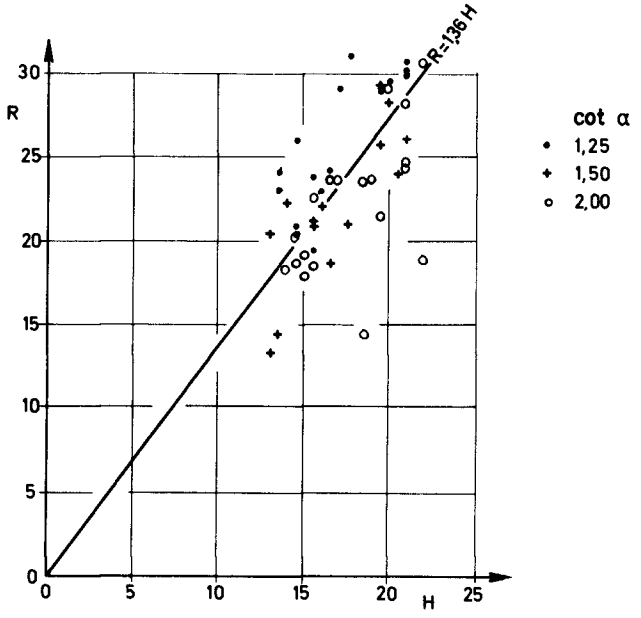

FIG 19 UPRUSH vs WAVE HEIGHT

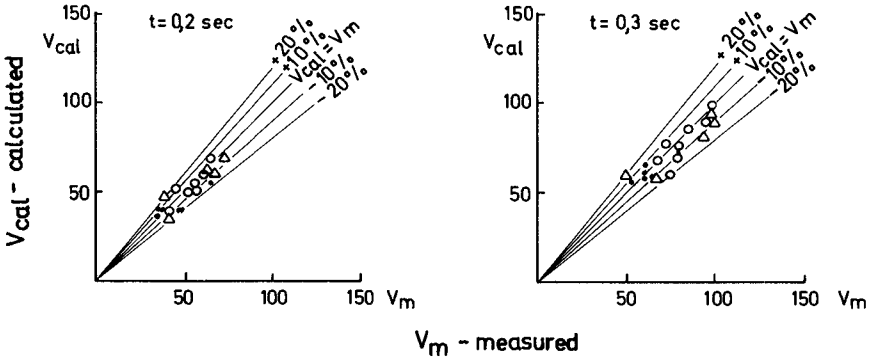

FIG 21 a
SUMMARY OF RESULTS - CALCULATION 2
$\delta = 7{,}67\ H/L, R' = 1{,}36$ H + 4,0 cm $C_{MP} = 1$ k = 4,0 cm

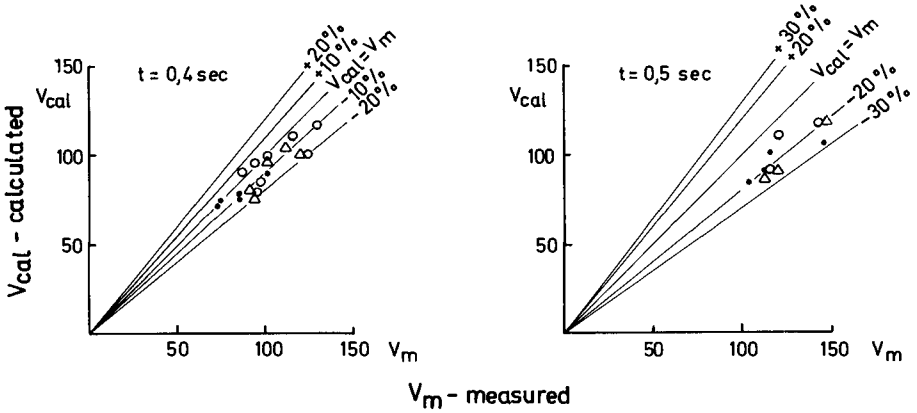

FIG 21 b
CALCULATION 2

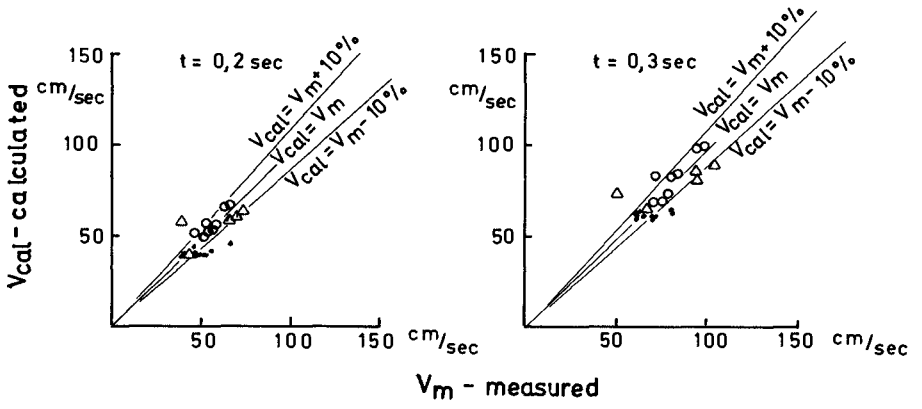

FIG 20 a
SUMMARY OF RESULTS - CALCULATION 1
β-AND Z- VALUES AS OBSERVED, C_{MP} = 1,0 , k = 4,0 cm

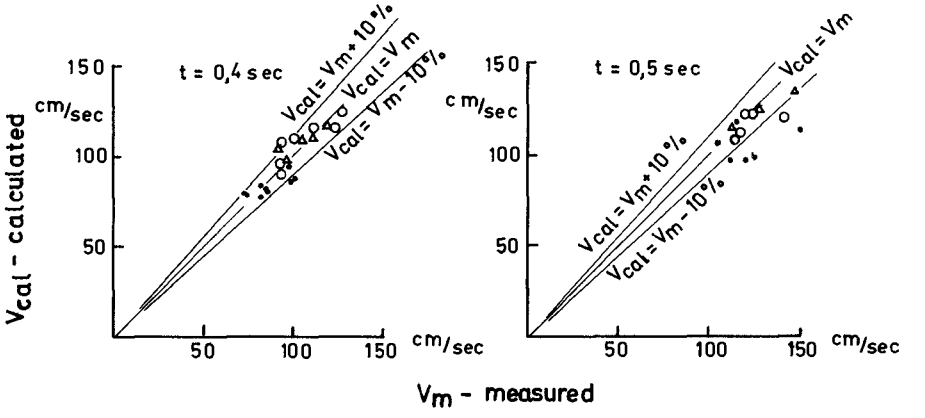

FIG. 20 b
CALCULATION 1

CHAPTER 54

EXPECTED DISCHARGE OF IRREGULAR WAVE OVERTOPPING

Senri Tsuruta, Head

and

Yoshimi Goda

Hydraulics Division, Port and Harbour Research Institute,

Ministry of Transport, Yokosuka, Japan

ABSTRACT

An experiment was carried out on the overtopping of mechanically generated irregular waves over vertical walls. The experimental discharge was almost in agreement with the expected discharge which had been calculated with the wave height histogram and the data of regular wave overtopping based on the principle of linear summation. The expected values of overtopping discharge were calculated for various laboratory data, which had been represented in a unified form of non-dimensional quantities. The calculation has yielded two diagrams of expected overtopping discharge, one for the sea wall of vertical wall type and the other for the sea wall covered with artificial concrete blocks.

INTRODUCTION

The crest height of a sea wall is the critical factor in its planning. With the heightening of the sea wall the degree of protection which it affords increases, but the construction cost also increases. The selection of the sea wall height based on the minimum sum of expected damage and construction cost has been studied and applied to many coastal sites along Japan (Tsuruta et. al. 1964).

The selection of the sea wall height is also made from its hydraulic performance against the design waves. The arguments on the criterion of selection, however, are divided between the maximum run-up height and the allowable quantity of wave overtopping. If a sea wall can be built higher than the maximum run-up of design waves, the sea wall will afford complete protection against the wave action. Such sea wall must be extremely high, however. Even for a regular train of waves, laboratory data indicate the run-up height being from 1.2 H to more than 4 H. For an irregular train of actual waves, the maximum run-up in that wave train will be $2H_{1/3}$ to more than 10 $H_{1/3}$, since the maximum run-up will be realized by the maximum or near-maximum wave, the height of which may exceed twice the significant wave height. With the design wave height of $H_{1/3}$= 4 to 8 m, which is common along the coasts of Japan, the maximum run-up becomes about 10 to 30 m or higher above the design tide level. In addition, even with such an extreme height the sea wall will not guarantee the perfect protection, because the design wave and tide conditions are

not the worst condition possible but only represents an extremely severe condition; we cannot neglect the possibility that the waves and tide surpassing the design conditions may attack the sea wall.

The criterion of allowable discharge of wave overtopping, therefore, becomes the inevitable choice for most case, even though the concept of allowing certain amount of wave overtopping may sound disgraceful for coastal engineers and threatening for people. But the sea wall with appropriate facilities to expel the overtopped water protects well the area behind it even under the attack of the waves and tides surpassing the design condition. The important factor in the planning of a sea wall allowing certain overtopping is the correct estimation of overtopping discharge. This must be done not for regular trains of laboratory wave but for irregular trains of actual waves.

The discharge of overtopping of irregular waves differs from that of regular waves. The difference mainly comes from two sources: the wave height variability and the interference by preceding waves. Some of previous experimental works on irregular wave overtopping have attributed the difference to the interference effect (Paape 1960), or to the general effect of wind including the generation of wave height irregularity (Sibul and Tickner 1956). Although these effects are certainly important, the variability in wave heights distributed from 0 to H_{max} must be the dominating factor, for even the wave interference occurs owning to the presence of wave irregularity. If the effect of wave interference on overtopping is not significant, the overtopping quantity of irregular waves can be estimated as the summation of individual wave overtoppings, the quantities of which are to be determined from the data of regular waves. In order to investigate the applicability of the principle of linear summation for the overtopping of irregular waves, an experiment has been carried out with mechanically generated irregular waves. Supported by the experimental result, the estimation of the expected discharge of irregular wave overtopping has been made for the sea wall of vertical wall type and that covered with artificial concrete blocks as will be described in the following chapters.

EXPERIMENT ON IRREGULAR WAVE OVERTOPPING

WAVE CHANNEL AND IRREGULAR WAVES FOR THE EXPERIMENT

The experiment was carried out in a wave channel of 30 m long, 1.2 m high and 0.5 m wide. The channel was divided into two with a partition wall along the center line which began at 2.5 m away from the wave paddle of piston type. A vertical wall was set in one channel at the distance of 15.5 m from the wave paddle on the slope of 1 to 20, the toe of which was located at 10.5 m from the wave paddle. The water depth was kept at h = 35 cm in front of the vertical wall.

Irregular waves were generated by an oil-pressure pulse motor which is controlled by ten electric oscillators (Tsuruta 1966).

The oscillators with the periods of 0.50, 0.65, 0.83, 1.07, 1.38, 1.77, 2.30, 2.88, 3.84, and 5.00 seconds generate sine waves, the amplitudes of which can be varied with the setting of power adjustment dials. In addition, another power controle dial is provided for the over-all adjustment of composed electric oscillation. By proper combination of ten oscillator amplitudes, power spectra of ocean waves can be simulated. Figure 1 exhibits the power spectrum of one train of test waves with the wave height of $H_{1/3}$ = 10.5 cm. Though the spectrum still exhibits the nature of line spectra, it nevertherless resembles to the spectrum of ocean waves. In the experiment, the dials for the oscillator amplitudes were kept at the pre-determined values and the over-all controls dial was set at one of five different values. By this procedure the magnitude of test waves was varied as shown in Table 1 with out significant change of its statistical property and of shape of power spectra; the ratio of $H_{1/3}/\bar{H}$ varied from 1.4 to 1.5 and $T_{1/3}/\bar{T}$ from 1.0 to 1.1.

Table 1. Characteristics of Irregular Waves Employed

Ident.	Number of waves N	Wave Height $\bar{H}$	Wave Height $H_{1/3}$	Wave Period $\bar{T}$	Wave Period $T_{1/3}$
1	188	5.3 cm	7.5 cm	1.43 sec	1.54 sec
2	180	7.0	10.5	1.51	1.56
3	188	8.4	12.6	1.51	1.60
4	174	10.0	14.8	1.60	1.81
5	170	11.4	16.4	1.58	1.77

The cumulative distribution of wave heights is shown in Fig. 2. The distribution of test waves is narrower than the Rayleigh distribution of

$$P(\eta) = 1 - \exp\left[-(\pi/4)\eta^2\right] \qquad (1)$$

where $\eta = H/\bar{H}$ and P denotes the probability of η lying between 0 and η. For the test waves, an empirical form of $\eta^{2.5}$ instead of η^2 gives a better fit.

The wave records analysed for Table 1 and Fig. 2 are not continuous ones but the accumulations of short runs. The use of short runs has been so required because the measurement of wave overtopping must be stopped before the return of the wave front re-reflected by the wave paddle. Though the very front of wave train travelled with the celerity of $\sqrt{gh}$, its amplitude decreased rapidly. Thus, the end of each measurement was determined as 23.5 seconds after the start of wave generator, based on the travel time of wave front with the phase velocity of waves with T = 1.6 seconds. Also, the initial parts of records before the arrival of main wave group which propagated with the group velocity were discarded, because they only contained the long period components of low amplitudes. Thus, the records from 10.3 till 23.5 seconds after the start of wave generator were utilized for the analysis of incident waves and of wave overtopping.

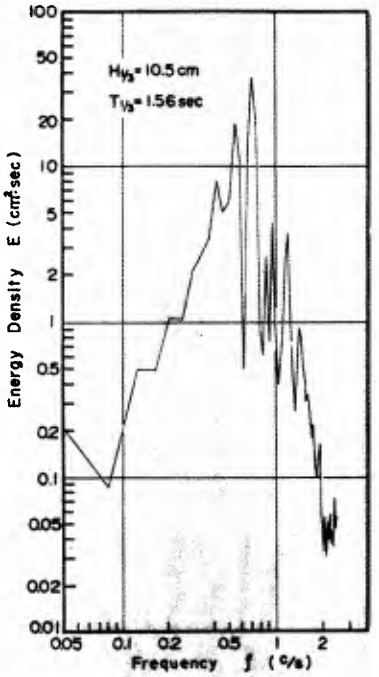

Fig. 1 Power spectrum of one train of test waves

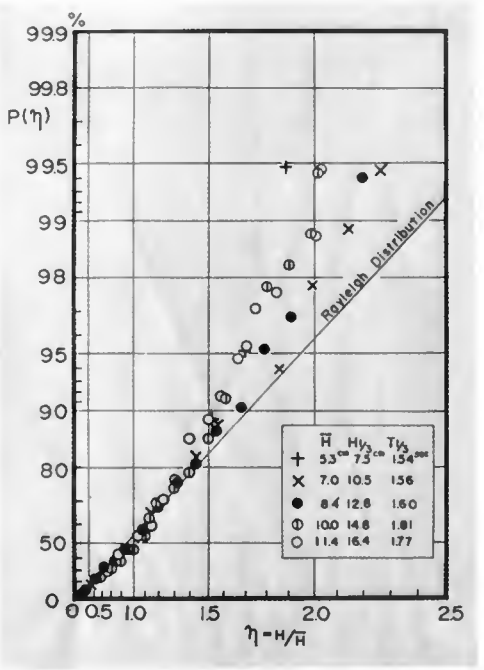

Fig. 2 Cumulative distribution of wave heights of test waves

The tests were repeated twice with and without the model sea wall: the former for the measurement of wave overtopping and the latter for the calibration of incident waves. The records of incident waves were separated into individual waves with the zero-up cross method. The wave height was defined as the distance from a crest to the following trough and the wave period as the time interval between the consecutive zero-up cross points. Each run gave the record of seven to ten waves, depending upon the periods of individual waves, and the test was repeated for twenty runs so that about 180 waves in total could be obtained for both the incident waves and the wave overtopping.

The incident waves was measured with a resistance-wire type wave gauge stationed at the location where the model sea wall was to be set. Another gauge was stationed at the same location in the opposite channel. At the time of overtopping measurement, one gauge was placed at 1 cm away from the vertical wall and the other gauge at the opposite channel. The latter gauge served for the confirmation of the wave overtopping the vertical wall being statistically same with the incident waves which had been analysed before the set of the vertical wall.

MEASUREMENTS OF OVERTOPPING DISCHARGE

The overtopped water was lead into a bucket which was hanged behind a model sea wall as shown in Fig. 3. By means of a movable carriage, the bucket was put into position at the arrival of main wave group and taken away before the return of re-reflected waves. The weight of the bucket with the overtopped water was continuously recorded through a load cell of strain gauge type which was inserted between the bucket and the carriage. When a wave overtopped the vertical wall, the record indicated an increase of the bucket weight about 0.5 second later, which was the time for the water to flow over the deck of model sea wall, as shown in Fig. 4. The difference of weight before and after one wave overtopping gave the amount of the overtopped water produced by that wave.

At the end of a run, the total amount of the overtopped water was measured and divided by the time of measurement period in seconds and the width of the sea wall so as to yield the average discharge of wave overtopping per second per unit width of the sea wall. For regular waves, five runs were repeated and the overtopping discharges of these runs were averaged. For irregular waves, the overtopping amounts of twenty runs were added together and the sum was divided by the total time of measurement periods and the width of the sea wall.

OVERTOPPING DISCHARGE OF REGULAR AND IRREGULAR WAVES

Figure 5 shows the overtopping discharges of regular waves, q ($cm^3/cm.sec$), against the incident wave height, H (cm). Two wave periods of T = 1.38 and 1.77 seconds were applied for the vertical walls of 9.4 and 12.8 cm high above the still water level. Since the height of waves with the period of 1.38 seconds was limited to about 10 cm by the generator performance, the waves with the period

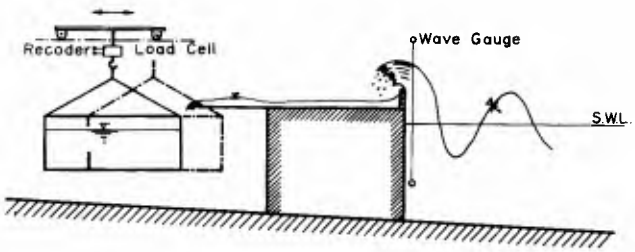

Fig. 3 Experimental set-up for the measurement of wave overtopping

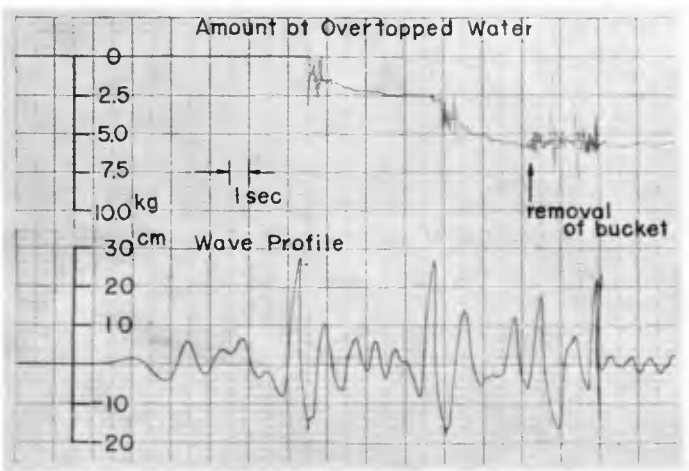

Fig. 4 Sample record of wave overtopping and wave profile

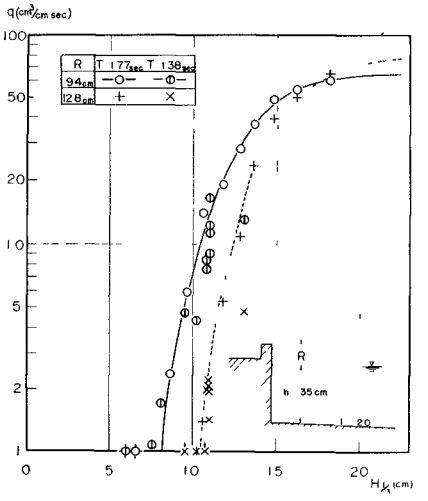

Fig. 5 Overtopping discharge of regular waves on vertical walls

of 1.77 seconds provided the principal source of overtopping data. The overtopping discharge of T = 1.38 seconds was slightly smaller than that of T = 1.77 seconds, but the difference was small. The vertical wall with the crest height of R = 9.4 cm generally produced larger wave overtopping as would be expected. At large wave height, a part of waves having overtopped the vertical wall of R = 9.4 cm flowed back toward the offshore because of the small difference between the top of the wall and the deck; this caused smaller overtopping for R = 9.4 cm than for R = 12.8 cm for the wave height greater than about 17 cm.

The average discharges of irregular wave overtopping were obtained as listed in Table 2. These overtopping discharges of irregular waves were smaller than those of regular waves having the wave

Table 2. Experimental Discharge of Irregular Wave Overtopping

Ident.	Wave Height $H_{1/3}$ (cm)	R = 9.4 cm N	R = 9.4 cm q (cm^3/cm·sec)	R = 12.8 cm N	R = 12.8 cm q (cm^3/cm·sec)
1	7.5	-	-	48	0
2	10.5	-	-	164	1.20
3	12.6	96	5.53	180	5.86
4	14.8	173	10.77	155	7.33
5	16.4	159	16.90	163	12.85

height same with $H_{1/3}$. For example, the overtopping discharge of regular waves with H = 14.8 cm was 37 cm^3/cm·sec for R = 12.8 cm, but the irregular waves with $H_{1/3}$ = 14.8 cm produced the discharge of 7.3 cm^3/cm.sec. The difference between the overtoppings of regular and irregular waves, however, decreases with the decrease of wave height, and the two overtopping discharges become equal at the wave height of $H = H_{1/3}$ = 10.5 cm for R = 12.8 cm. Below this height, the overtopping discharge of irregular waves is estimated to exceed that of regular waves.

The overtopping discharge of individual wave in irregular wave train, on the other hand, does not show much difference with that of regular waves as shown in Fig. 6, where the rate of individual wave overtopping on the vertical wall of R = 12.8 cm is plotted against the wave crest height η_c in front of the vertical wall. Although the data of irregular waves show some scatter, they almost agree with those of regular waves. The scatter is partly due to the difficulty in accurate determination of individual wave overtopping quantity. The interference of preceding waves may have caused additional scatter of the overtopping data, but the tendency of Fig. 6 indicates that the irregular wave overtopping if expressed in terms of wave crest height does not differ much from that of regular waves.

The rise of wave crest of irregular waves in front of the model sea wall was then compared with that of regular waves in Fig. 7. Since the direct comparison was impossible, the wave crest height η_c and the incident wave height H_1 were arranged in order of magnitude

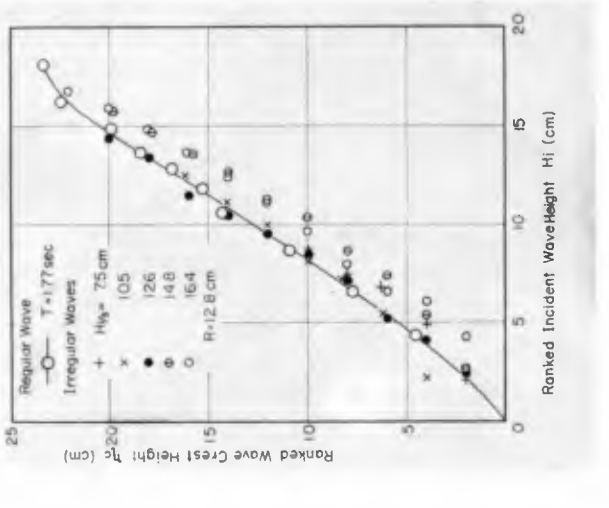

Fig. 7 Ranked wave crest height versus ranked incident wave height of irregular waves

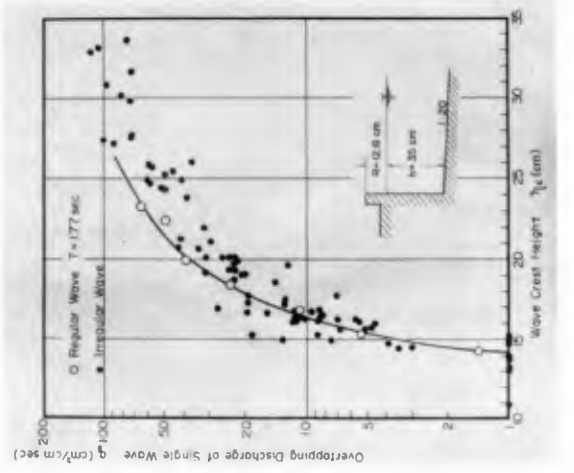

Fig. 6 Overtopping discharge of individual waves in irregular wave train

and these ranked heights were compared. Figure 7 shows that the crest heights of irregular waves in front of the vertical wall were a little lower than those of regular waves; the difference is about 1 to 2 cm in terms of H_1.

CALCULATION OF EXPECTED OVERTOPPING DISCHARGE AND COMPARISON WITH EXPERIMENTAL DATA

The results of Figs. 6 and 7 suggests that the overtopping of irregular waves on a vertical wall can be treated separately for each wave. Therefore, the total amount of wave overtopping is estimated as the sum of individual wave overtopping as

$$Q_{total} = \sum_{i=1}^{N} Q_i(H_i) \tag{2}$$

in which Q_i denotes the overtopping quantity of a regular wave with the height of H_i; for waves under the overtopping limit, $Q_i = 0$. Since we are interested in the rate of overtopping, the above quantity is divided by the total time of wave duration, $N \cdot \overline{T}$. The actual calculation was carried out with the division of wave height $\Delta H = 1$ cm as follows

$$q_{EXP} = \frac{Q_{total}}{N \cdot \overline{T}} = \frac{1}{N} \sum_{J=1}^{M} q_J(H_J) \cdot n_J(H_J) \tag{3}$$

in which q_J is the overtopping discharge of regular waves with the height of H_J, n_J denotes the number of waves with the height between $(H_J - \frac{1}{2}\Delta H)$ and $(H_J + \frac{1}{2}\Delta H)$, and M is the number of divisions for wave height. The variation in wave period, though it affects the overtopping discharge to certain extent, was neglected in order to simplify the calculation. If the total number N is let to become very large and the division of wave height ΔH very small, the above equation is rewritten as

$$q_{EXP} = \int_0^{\infty} q(H)\, p(H)\, dH \tag{4}$$

in which p(H) is the probability density of wave height. Since this is exactly the expression for the calculation of an expected value by definition, the overtopping discharge calculated by Eq. 3 is called the expected discharge of irregular wave overtopping.

With the experimental data of regular wave overtopping shown in Fig. 6 and the histograms of wave height of incident waves, the expected discharge of irregular wave overtopping was calculated for the test conditions of Table 2. The results of calculation are compared with the experimental discharge in Fig. 8 for R = 9.4 cm and in Fig. 9 for R = 12.8 cm. The expected values are generally larger than the experimental ones· about 50 to 80% up for R = 9.4 cm and about 30 to 50% up for R = 12.8 cm. The difference is partly attributed to the effect of interference by preceding waves and to the effect of wave period, but the difficulty in maintaining the same statistical

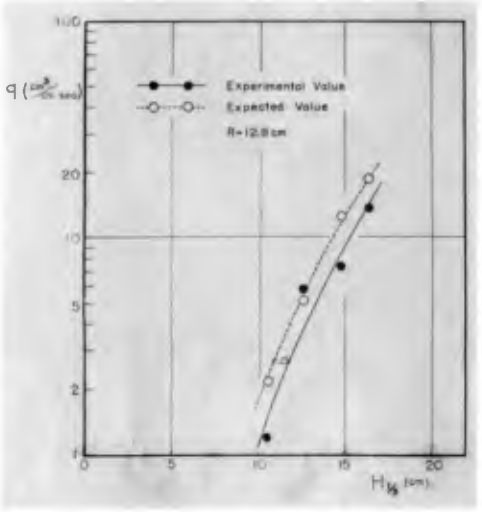

Fig. 8 Comparison of expected and experimental discharges for R=9.4cm

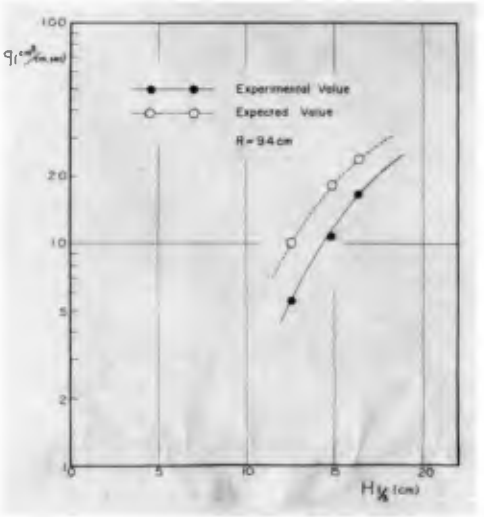

Fig. 9 Comparison of expected and experimental discharges for R=12.8cm

characteristics of irregular waves is another cause of the difference. In spite of these differences, the tendency of expected overtopping discharge agrees with that of experimental data. This agreement supports the applicability of Eq. 3 for the irregular wave overtopping on vertical walls.

ESTIMATION OF EXPECTED DISCHARGE OF IRREGULAR WAVE OVERTOPPING

Non-dimensional representation of wave overtopping data

The expected discharge of irregular wave overtopping can be estimated if the wave height distribution and the q-H curve of regular waves are known. For a specifice structure, the estimation will be done based on the result of model tests. For a general planning of coast protection works, however, an over-all information on the expected overtopping discharge is often needed. The information can be obtained if the q-H curves are generalized so as to cover various laboratory data.

The general q-H curves must be in non-dimensional forms. Among various forms of non-dimensional representation, the one by Kikkawa et. al. (1967) of the following seems to be the most reasonable:

$$\frac{q}{\sqrt{2gH^3}} = \phi\left(\frac{R}{kH}\right) = \frac{1}{5} m k^{3/2} \left(1 - \frac{R}{kH}\right)^{5/2} \qquad (5)$$

in which k represents the ratio of wave crest height at the time of overtopping to the incident wave height and m is the discharge coefficient of overflow on the sea wall. Since this representation is based on the similarity of wave overtopping with overflowing on a weir, this will be most applicable to the sea wall of vertical wall type.

Equation 5 is rewritten as in the following for the convenience of calculating the expected overtopping discharge·

$$\frac{q}{\sqrt{2gh^3}} = \phi\left(\frac{H}{h} ; \frac{R}{h}, \frac{h}{L_o}, i\right) \qquad (6)$$

where i denotes the slope of sea bottom. The parameter of h/L_o represents the effect of wave period. Various laboratory data on the overtopping of regular waves on vertical walls were then re-analysed in the form of Eq. 6. The major sources of data were those by Beach Erosion Board (Saville and Caldwell 1953, and Saville 1955), University of Kyoto (Ishihara et. al. 1960 and Iwagaki et. al. 1963), and Shiraishi and Endo (1963). The bottom slope ranged from 1/10 to 1/30. The data were arranged into groups according to the value of R/h, and those with the same group were plotted against H_o/h, where H_o denotes the deep water wave height. By this procedure, experimental curves for various values of R/h could be drawn as shown in Fig. 10.

The critical wave height $(H_o)_c$ under which no overtopping occurrs was estimated from the data of crest height of standing waves calculated

by the fourth order theory (Goda and Kakizaki 1966) and of the increase of wave height in the shoaling of finite amplitude waves (Iwagaki and Sakai 1967). The result of estimation is as follows:

$R/h = 0.2 \quad (H_0/h)_c = 0.18 \sim 0.19$
$R/h = 0.4 \quad (H_0/h)_c = 0.28 \sim 0.33$
$R/h = 0.7 \quad (H_0/h)_c = 0.35 \sim 0.47$
$R/h = 1.0 \quad (H_0/h)_c = 0.42 \sim 0.58$

In the above estimation, the deep water wave steepness was takes as in the range of $H_0/L_0 = 0.01 \sim 0.03$, which corresponds to the wave height of $3.5 \sim 10.5$ m for the wave period of 15 seconds. The lower figures of the above correspond to the wave steepness of $H_0/L_0 = 0.01$.

In Fig. 10, the parameter of h/L_0 is not expressed. In general, the wave period causes certain effect on wave overtopping; the data of Tp = 15 seconds with low wave heights in Beach Erosion Board experiments shows a large overtopping discharge, much different from the data of other smaller periods. With the limitation of $H_0/L_0 > 0.01$, however, the effect of wave period becomes insignificant in comparison with the scatter of experimental data. This can be seen in Fig. 10 where the data with $R/h = 1.0$ are shown with classification according to the range of h/L_0. Also, the effect of bottom slope is not visible under the scatter of the data. The curves shown in Fig. 10 are inclusive of these factors, being drawn through the center of these data. Thus, specific data may deviate from the corresponding curve of Fig. 10 to the extent to settle around the adjacent curve, but the curves as a whole are considered to represent the tendency of wave overtopping.

NON-DIMENSIONAL OVERTOPPING DISCHARGE ON SEA WALLS OF BLOCK MOUND TYPE

Along the coasts of Japan where the available land is very limited, sea walls covered with artificial concrete blocks are often constructed, because they afford greater protection with lower crests than the sea walls of vertical wall type. Various laboratory data of model tests on wave overtopping were surveyed and re-analysed in the manner described in the previous section. The non-dimensional overtopping curves thus obtained are shown in Fig. 11. These data are of the model tests of the sea walls for the Yui Coast (Iwagaki et. al. 1963), Wakayama Port (Nagai and Takada 1964), the reclaimed area of Oita-Tsurusaki (Tatsumi 1964), the reclaimed area of Nishi-Kobe (Port and Harbour Research Institute 1965), and the Momotori Coast (Tominaga and Sakuma 1966). The data of generalized experiments by Shiraishi and Endo (1963), Nagai et. al. (1967), and Takada (1967) were also analysed. The height of block mounds above the still water level R' in these data was greater than one half of the heights of parapet walls R · i.e. $R > 0.5R'$. The experimental data of the Shonai Coast (Iwasaki and Numata 1967), though the mound heights were low, served to give information on the over-all shape of the q-H curves.

The critical wave height $(H_0)_c$ for the block mound type sea walls was estimated from the wave run-up data by Furuya et. al. (1961), Shiraishi and Endo (1963), Morihira and Yarimizu (1967). Consideration was also given to the fact that for the range of small value of H_0/h

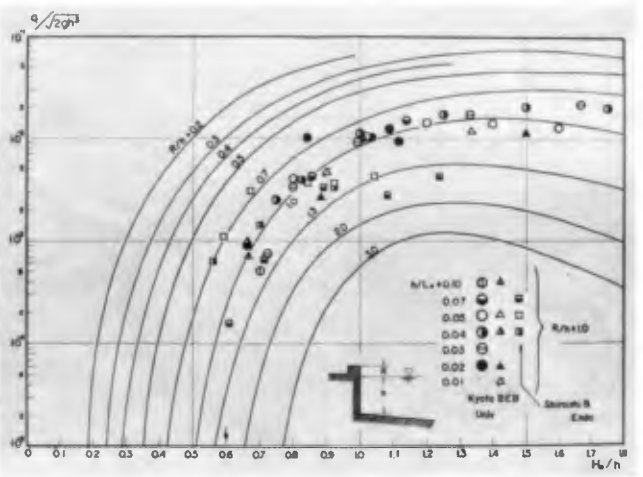

Fig. 10 Non-dimensional overtopping discharge of regular waves on vertical walls.

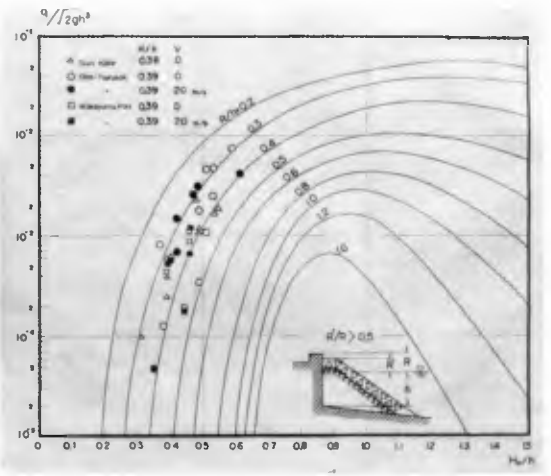

Fig. 11 Non-dimensional overtopping discharge of regular waves on sea walls covered with concrete blocks

the critical wave height is almost equal for the sea walls of vertical wall type and block mound type.

The wave overtopping data on block mound generally show larger scatter than the data on vertical wall. This is due to the fact that a slight modification in the height and width of block mound crest, or in the shape of mound especially around the too often produces significant change in the quantity of wave overtopping. The data shown in Fig. 11 for the relative parapet height of $R/h = 0.38 \sim 0.39$ exhibit rather small scatter. At larger value of R/h, the scatter of overtopping data becomes great, since the data are in the verge of wave run-up on block mound, which is about $(1.0 \sim 1.9)H_o$ depending upon the characteristics of incident waves. Under the scatter of experimental data, the effect of wind upon overtopping waves cannot be recognized clearly. Some of the data for $R/h = 0.38 \sim 0.39$ shown in Fig. 11 have been obtained under the action of winds with the prototype velocity of about 20 m/sec, but they do not show marked increase over the data without the wind action. Thus, Fig. 11 represents a gross estimation of wave overtopping discharge on the sea wall covered with artificial concrete blocks. Though individual laboratory data may differ from the result of Fig. 11, the over-all tendency will be in agreement with that of Fig. 11.

CALCULATION OF EXPECTED OVERTOPPING DISCHARGE

Now the q-H curves of wave overtopping having been determined as in Figs. 10 and 11, the next step in the calculation of q_{EXP} is the estimation of wave height distribution. For the ocean waves, the Rayleigh distribution of Eq. 1 by Longuet-Higgins (1952) is accepted to be applicable. Since the effect of wave period on overtopping is not significant as indicated in Fig. 10, the marginal distribution of wave height and period such as proposed by Bretschneider (1959) has not been considered in the present calculation.

The non-dimensional calculation of expected overtopping discharge has been carried out for predetermined values of $R/(H_{1/3})_o$. Along one q-H curve with the parameter of R/h, $q_{EXP}/\sqrt{2gh^3}$ was calculated by Eq. 3. The result was converted into the form of $q_{EXP}/\sqrt{2g(H_{1/3})_o^3}$ with the ratio of $(H_{1/3})_o/h$, which is obtained by dividing R/h with $R/(H_{1/3})_o$. For the asymptotic case of $(H_{1/3})_o/h \to 0$, Eq. 5 by Kikkawa et. al.(1967) was utilized after rewriting it as follows.

$$\frac{q}{\sqrt{2g(H_{1/3})_o^3}} = 0.1\beta^{3/2}\eta^{3/2}\left[1 - \beta\frac{R}{(H_{1/3})_o}\cdot\frac{1}{\eta}\right]^{5/2} \qquad (7)$$

with $\beta = (H_{1/3})_o/H = 1.60$ and $\eta = H/\bar{H}$.

The parameter k for η_c/H was taken as 1 since at the limit of $(H_{1/3})_o/h \to 0$ the sinusoidal wave gives a good approximation to the wave profile. Also the discharge coefficient, m, was given a little over-estimated value of 0.5 in order to cover the difference between the sinusoidal wave and triangular wave profiles, the latter having been employed in the derivation of Eq. 5.

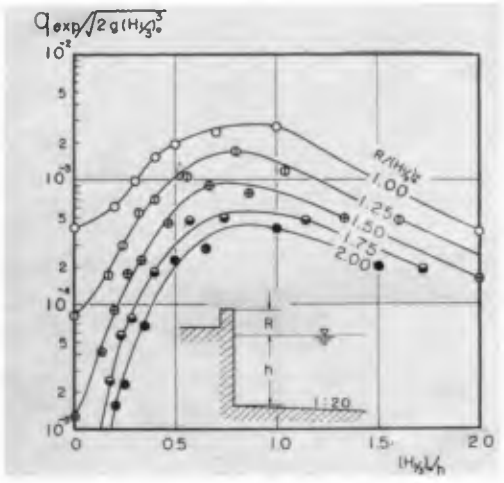

Fig. 12 Expected overtopping discharge on vertical wall

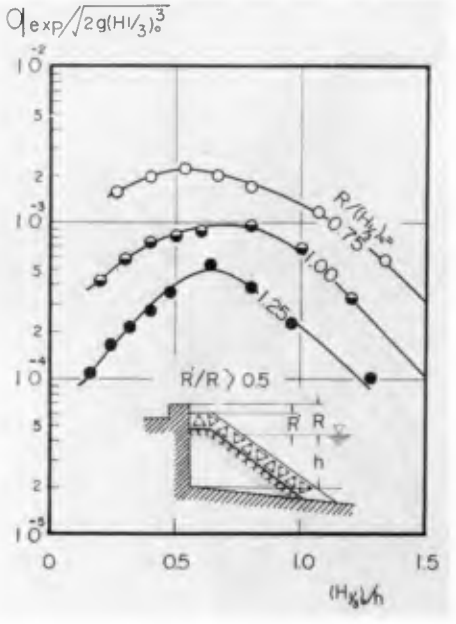

Fig. 13 Expected overtopping discharge on sea walls covered with concrete blocks.

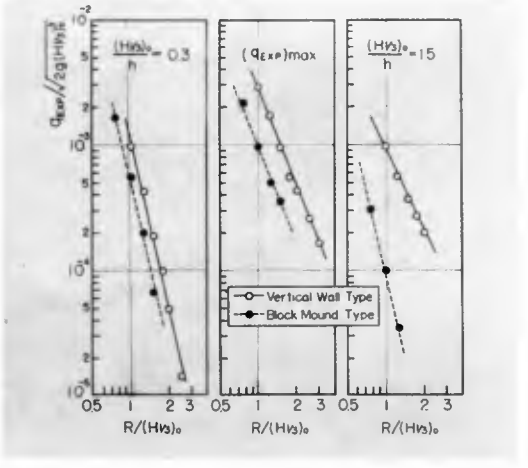

Fig. 14 Sea wall height for a given discharge of irregular wave overtopping

The result of calculation are combined in Fig. 12 for vertical walls and in Fig. 13 for block mound type sea walls. These figures reveal several characteristics of expected overtopping discharge. First, it does not respond sharply to the variation of $(H_{1/3})_o/h$. This is clearly observed for the small value of $R/(H_{1/3})_o$. Second, even with a high parapet of $R/(H_{1/3})_o = 2.0$, the average discharge of overtopping may amount to $0.0004\sqrt{2g(H_{1/3})_o^3}$ for vertical walls. The figure yields the discharge of 0.02 m^3/sec per every one meter of the sea wall for the wave height of $(H_{1/3})_o = 5$ m. If a pumping station for drainage is constructed for every thousand meters of the sea wall, the station must have the capacity greater than 20 ton/sec. Third, the maximum overtopping discharge appears at relatively low wave height i.e., $(H_{1/3})_o/h \fallingdotseq 0.8$ for vertical walls and $(H_{1/3})_o/h = 0.6$ for block mounds. The shift of peak position toward smaller height for block mounds is explained as the result of the promotion of wave breaking by presence of block mounds and of the absorption of after-breaking waves.

The height of sea wall for a given discharge of irregular wave overtopping can be read on Fig. 14 for the non-breaking wave condition of $(H_{1/3})_o/h = 0.3$, the maximum ovetopping condition, and the after-breaking condition of $(H_{1/3})_o/h = 1.5$. Figure 14 indicates that the covering of a sea wall with artificial concrete blocks for the reduction of wave overtopping is most effective for the after-breaking condition and least for the non-breaking condition. The height of block mound type sea wall for a given discharge of allowable wave overtopping can be less than 50% of the vertical wall for the after-breaking condition, but the parapet height of block mound must be about 65% of the vertical wall for the maximum overtopping condition and about 85% for the non-breaking condition.

All the results of expected overtopping discharge do not give suggestions for the amount of wave overtopping which is regarded allowable. The allowable wave overtopping is to be given a priori from the technological, economical and sociological conditions. Once the allowable quantity of wave overtopping is decided, the results of Figs. 12 to 14 will provide basic information for the sea wall height necessary to keep the wave overtopping under the allowable quantity.

CONCLUSIONS

1) The overtopping of irregular waves on a vertical wall can be treated as the linear summation of individual wave overtopping.
2) The effect of wave period on the overtopping discharge is not significant for the deep water wave steepness H_o/L_o greater than 0.01.
3) The expected discharges of irregular wave overtopping on vertical walls calculated from the overtopping data of regular waves and wave height histograms were a little larger than the experimental discharges, but the general tendency was in agreement.
4) Various laboratory data on overtopping of regular waves on sea walls of vertical wall type and block mound type can be represented in a unified form with the non-dimensionarization of $q/\sqrt{2gh^3}$ versus H/h with the parameter of R/h, as shown in Figs. 10 and 11.

5) With the assumption of the Rayleigh distribution for the wave height variability, the expected discharge of irregular wave overtopping has been calculated as shown in Fig. 12 for the sea wall of vertical wall type and in Fig. 13 for the sea wall of block mound type. The result of calculation will provide engineers with basic information for the selection of crest height and the estimation of overtopping quantity in the planning of the sea wall.

ACKNOWLEDGEMENTS

The authors sincerely wish to express their appreciation to Messrs. Hideaki Takeda, Yoshiki Abe, and Toshio Fukumori of the Hydraulics Division of the Port and Harbour Research Institute, who carried out the experiment and data analysis. The author's appreciation is also extended to Assistant Professor Atsushi Numata of Tohoku University, Assistant Professor Hiroshi Mitsui of Tokushima University, Assistant Professor Akira Takada of Chubu Institute of Technology, and Mr. Taiji Endo of Japan Tetrapod Company, who kindly provided the authors with their laboratory data.

REFERENCES*

Bretschneider, C.L. (1959)· Wave variability and wave spectra for wind-generated gravity waves, Beach Erosion Board Tech. Memo., No.118.

Furuya, K., Kogami, Y., and Kondo, Y. (1961)· Experimental study on tetrapod mound breakwaters, Proc. 8th Conf. on Coastal Eng. in Japan, pp.91-96 (in Japanese).

Goda, Y. and Kakizaki, S. (1966) Study on finite amplitude standing waves and their pressures upon a vertical wall. Report of Port and Harbour Research Institute, Vol. 5, No.10, p.35 (in Japanese).

Ishihara, T., Iwagaki, Y., and Mitsui, H. (1960); Wave overtopping on sea walls, Coastal Engineering in Japan, JSCE, Vol. 3, pp.53-62.

Iwagaki, Y., Tsuchiya, Y, and Inoue, M. (1963). Model experiments on wave overtopping on the sea wall at the Yui Coast, Proc. 10th Conf. on Coastal Eng. in Japan, pp.132-137 (in Japanese).

Iwagaki, Y. and Sakai, T. (1967) On the shoaling of finite amplitude waves, Proc. 14th Conf. on Coastal Eng. in Japan, pp. 1-7. (in Japanese).

Kikkawa, H., Shiigai, H. and Kono, F. (1967)· Basic study on wave overtopping on sea wall (1), Proc. 14th Conf. on Coastal Eng. in Japan, pp.118-122 (in Japanese).

---

* The titles and names of publications of papers in Japanese were tentatively translated into English by the authors.

Longuet-Higgins, M S (1952)· On the statistical distribution of the heights of sea waves, Jour. Marine Research, Vol. XI, No.3 pp. 245-265.

Morihira, M. and Yarimizu, Y. 1967: Experiments on wave run-up on sea walls covered with artificial concrete blocks, Hydraulics Division, Port and Harbour Research Institute (unpublished).

Nagai, S. and Takada, A. (1964): Effect of wave absorbing mound on wave overtopping on sea walls, Proc. 11th Conf. on Coastal Eng. in Japan, pp. 279-286 (in Japanese).

Nagai, S., Otsubo, T. and Endo, M. (1967)· Study on sea walls of block mound type in relatively deep water, Proc. 14th Conf. on Coastal Eng. in Japan, pp.182-187 (in Japanese).

Paape, A. (1960): Experimental data on the overtopping of sea walls by waves, Proc. 7th Conf. Coastal Eng., the Hague, pp.674-681.

Port and Harbour Research Institute, Hydraulics Division (1966)· Model tests on the sea wall at Nishi-Kobe District of Kobe City, 59pp (in Japanese).

Saville, T. Jr., and Caldwell, J.M. (1953): Experimental study of wave overtopping on shore structures, Proc. Minnesota Int. Hydr. Conv., pp.261-269.

Saville, T. Jr. (1955): Laboratory data on wave run-up and overtopping on shore structures, Beach Erosion Board, Tech. Memo. No. 64. 32pp.

Shiraishi, N. and Endo, T. (1963): On several problems of wave absorbing mounds, Proc. 10th Conf. on Coastal Eng. in Japan, pp.138-143 (in Japanese).

Sibul, O.G. and Tickner, E.G. (1956): Model study of wind-generated waves on levees with slopes of 1:3 and 1:6, Beach Erosion Board, Tech. Memo. No. 80, 27pp.

Takada, A. (1967): On the effects of the shape of impermeable wall and of the void of permeable slope upon the overtopping quantities, Proc. 14th Conf. on Coastal Eng. in Japan, pp.129-138 (in Japanese).

Tatsumi, H. (1964): On the design of the sea wall of block mound type at the reclaimed area in the Oita Seaside Industrial District, Proc. 11th Conf. on Coastal Eng. in Japan, pp.239-246 (in Japanese).

Tominaga, Y. and Sakuma, N. (1966)· On wave absorbing mounds to prevent wave overtopping, Proc. 13th Conf. on Coastal Eng. in Japan, pp.183-190 (in Japanese).

Tsuruta, S. (1966): A tentative design of an irregular wave generator, Modern Trends in Hydraulic Engineering Research, Central Water and Power Research Station, Poona, Vol. 2, pp.55-59.

Tsuruta, S., Nagao, Y. and Ijima, T. (1964). The economical heights of sea walls for coast protection in Japan, Proc. 9th Conf. Coastal Eng., Lisbon, pp. 518-531

CHAPTER 55

ON THE EFFECT OF ARMOUR BLOCK FACING ON THE QUANTITY OF WAVE OVERTOPPING

Naofumi Shiraishi*, Atsushi Numata**

and Taiji Endo***

INTRODUCTION

Japan, surrounded by sea, is constantly threatened by storm surges and beach erosions, for which protection works are being vigorously undertaken. As a measure for protection, facings of various armour blocks have come to be used for the seawalls and embankments. This is a skillful utilization of characteristic functions of armour blocks to dissipate and absorb wave energy effectively. However, systematic experiments and studies on this subject have been conducted only in very few cases.

This paper treats of the effect of the facing of armour blocks on wave overtopping by comparison of the quantity of waves topped over the vertical seawall with facing and that of without facing. Furthermore, this paper attempts to compare the results of the field observation and the experiments on the quantity of wave overtopping. Based on these data, the authors present a design criterion of the crown height of seawall with armour block facing.

EXPERIMENTAL PROCEDURE

* Dr. Eng., Managing Director, NIPPON TETRAPOD Co., Ltd.
** Assist. Prof. of Civil Eng., Tohoku University, Sendai, Japan.
*** Eng. Dept., NIPPON TETRAPOD Co., Ltd.

The experiments have been conducted by using a wave channel, 46 meters long, 1.5 meters high, and 1 meter wide. The various types of test wave were generated by a flap type wave generator. The blower of wind tunnel has a propeller fan, 1000 millimeters in diameter and a damper to adjust the wind discharge in three steps.

The beach slope was set at 1 on 10 in order to compare the present experiment with the ones conducted at University of Tokyo and others. The beach bed was made of mortal on which the seawall was erected. The model scale was selected to be 1/25 based on the Froude's Similarity Law. The cross sections of seawall used for the experiments are shown in Figs. 1 through 5 which show the respective experimental results. As for armour blocks of model, tetrapods of 240 grams in weight were used. These model blocks corresponded to the 4 tons type tetrapods in field. The wave heights were measured by a parallel wire resistance gauge and recorded by a pen-recorder. The gauge was located in the part of the channel with uniform depth. The water which topped over the seawall was gathered into the collecting tank behind the seawall and its volume was measured.

The waves used for the experiments were regular ones. The prototype wave conditions were 6 sec., 7 sec., and 9 sec. in periods, and 3.0 meters in the equivalent deep water wave height. The steepness of the wave in deep water was in the range of 0.02 and 0.05, which was commonly observed in field.

RESULTS AND DISCUSSION

The symbols used in this paper are as follows :

- T : wave period (second)
- Ho : equivalent deep water wave height (meter)
- Lo : deep water wave length (meter)
- h : water depth at the toe of seawall (meter)
- $\frac{HoLo}{2\pi}$: quantity of water moving onshore per wave and per unit width in deep water
- Q : quantity of wave overtopping per wave and per unit

width of the seawall

$\frac{2\pi Q}{(HoLo)}$: dimensionless quantity of wave overtopping

hc : crown height of the seawall from the still water level (meter)

ht : crown height of the armour block facing from the still water level (meter)

Figures 1 through 5 show the relation between the relative crown height hc/Ho and the dimensionless quantity of wave overtopping $2\pi Q/(HoLo)$. In each case the quantity of wave overtopping decreases as hc/Ho increases, however its tendency is stronger in case of the seawalls with facings than in the case of the vertical walls. Especially, in case of the relative water depth h/Ho = 1.0, it is evident that the seawall with facing provides a stronger tendency of decrease of quantity of wave overtopping (see Figs. 3-a and b). This shows that the effect of the facing on dissipation of wave energy is remarkable.

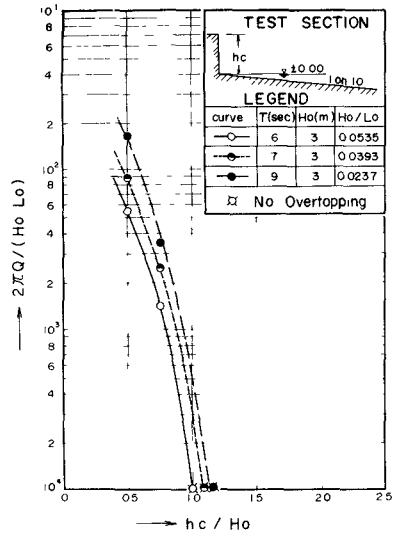

Fig. 1-a, h/Ho = 0

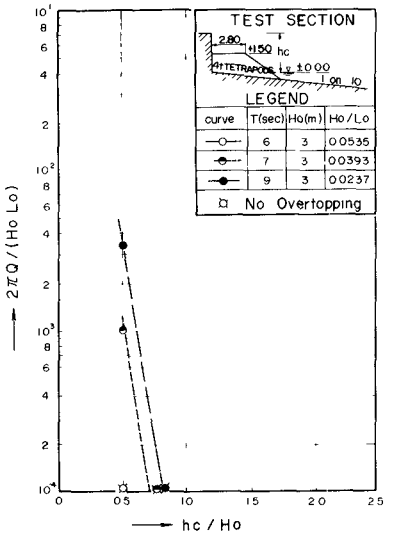

Fig. 1-b, h/Ho = 0

Relation between $2\pi Q/(HoLo)$ and hc/Ho with a parameter of Ho/Lo

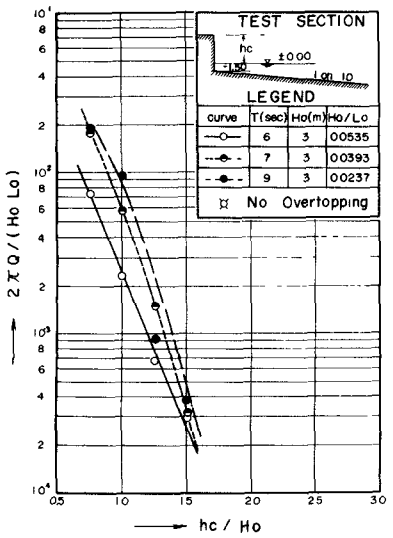

Fig. 2-a, h/Ho = 0.5

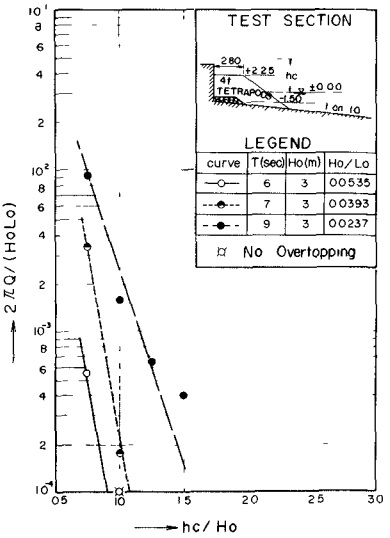

Fig. 2-b, h/Ho = 0.5

Relation between $2\pi Q/(HoLo)$ and hc/Ho with a parameter of Ho/Lo

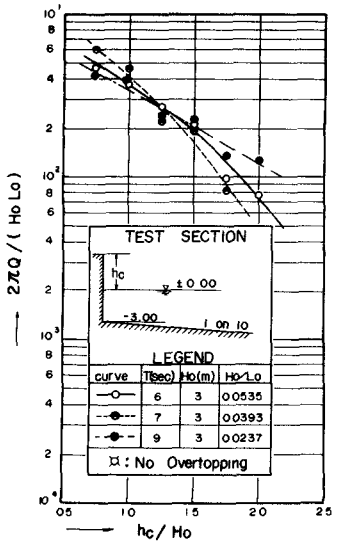

Fig. 3-a, h/Ho = 1

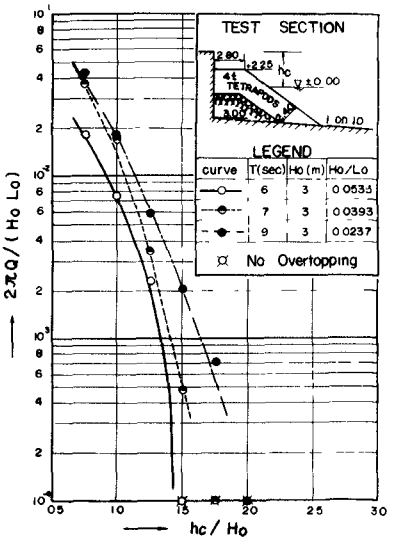

Fig. 3-b, h/Ho = 1

Relation between $2\pi Q/(HoLo)$ and hc/Ho with a parameter of Ho/Lo

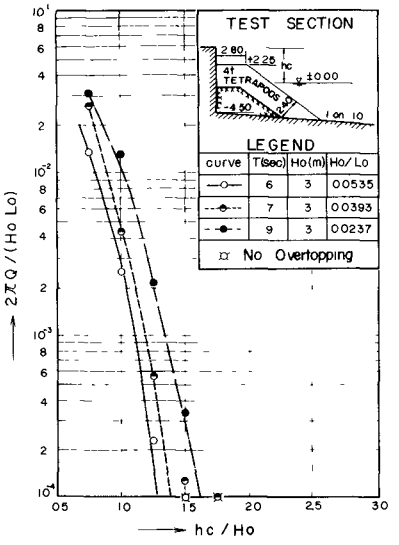

Fig. 4-a, h/Ho = 1.5

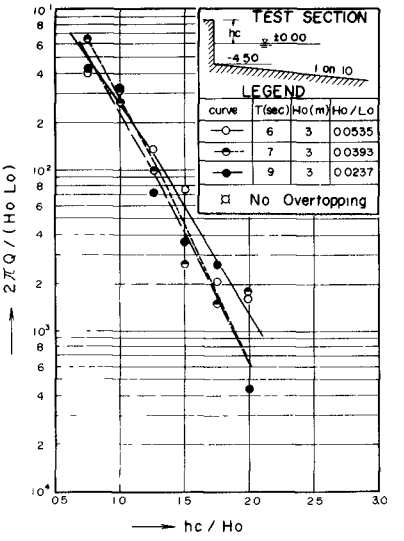

Fig. 4-b, h/Ho = 1.5

Relation between $2\pi Q/(HoLo)$ and hc/Ho with a parameter of Ho/Lo

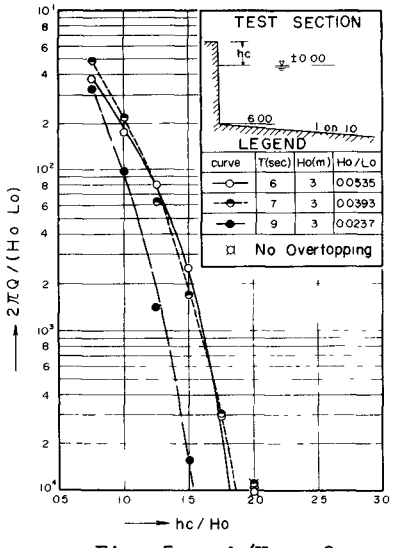

Fig. 5-a, h/Ho = 2

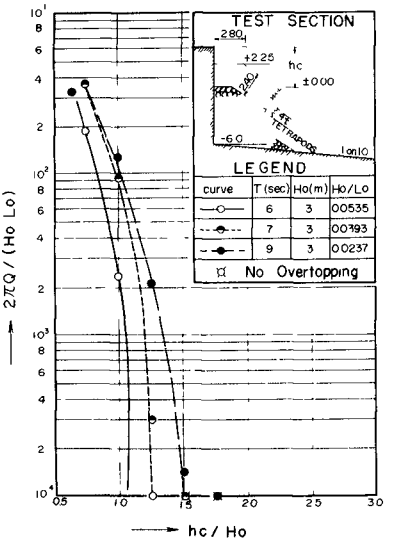

Fig. 5-b, h/Ho = 2

Relation between $2\pi Q/(HoLo)$ and hc/Ho with a parameter of Ho/Lo

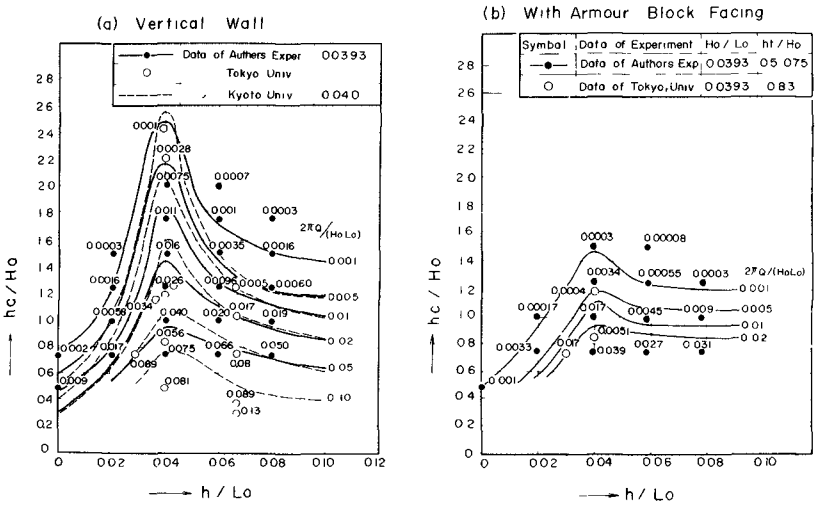

Fig. 6-a Fig. 6-b
Relation between hc/Ho and h/Lo with a parameter of $2\pi Q/(HoLo)$

Figures 6 show the relation between hc/Ho and the relative water depth h/Lo with a parameter of $2\pi Q/(HoLo)$. For the purpose of comparison, the results of experiment at Universities of Tokyo and Kyoto are also shown. In these figures, the results of wave overtopping ($2\pi Q/(HoLo)$) obtained in the present experiments are shown with solid lines, while the results of experiments at Kyoto University with dotted lines. Comparing the solid and dotted lines, it is shown that they nearly correspond except in the vicinity of h/Lo = 0.04.

Figures 7 and 8 show the relation between $2\pi Q/(HoLo)$ and h/Ho with a parameter of hc/Ho. From these figures it is evident that whether it is a vertical wall or a wall with facing, the quantity of wave overtopping reaches a maximum near the wave breaking point. Figure 7 also shows that the quantity of wave overtopping does not decrease much as the crown height increases at the wave breaking point.

Figure 9 shows the variations of the quantity of wave overtopping according to the change of crown height of facing. But

the crown width of facing is kept constant. Figure 9 may be regarded as a useful data to design an economical crown height of seawall and of armour block facing in order to prevent wave overtopping effectively.

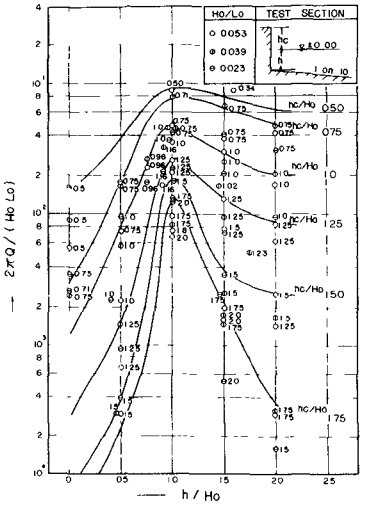

Fig. 7

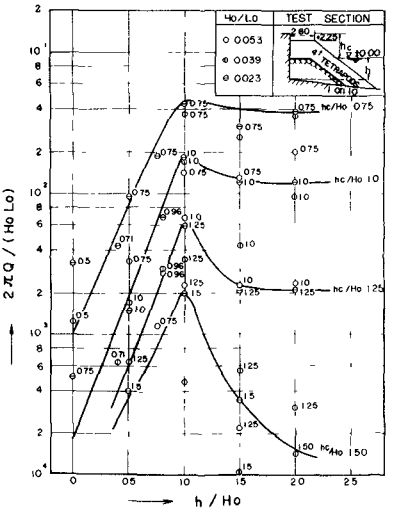

Fig. 8

Figures 7 and 8 Relation between $2\pi Q/(HoLo)$ and h/Ho with a parameter of hc/Ho.

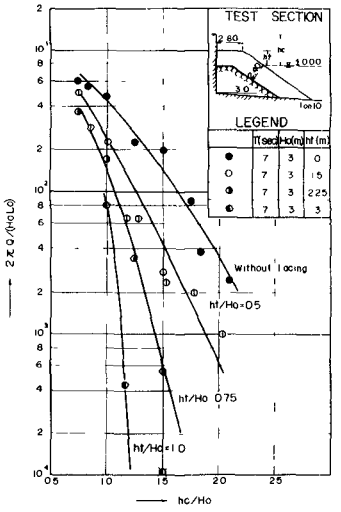

Fig. 9 Rate of wave overtopping by the variation of crown height of armour block facing.

Fig. 9

FIELD OBSERVATION

1) FIELD OBSERVATION AT SAKATA COAST

When the results of experiments are applied to the field, the similarity of the model test to the field is important. To ascertain this, one of the authors has compared the results of field observation conducted by the Ministry of Construction at Sakata Coast with the results of experiments by using regular waves (model scale is 1/20).

Sakata Coast faces on Japan Sea and is constantly attacked by violent waves caused by monsoon in winter (see Fig. 10). Observation of offshore waves was accomplished by the use of a wave recorder of underwater pressure type, while the measurements of the quantity of wave overtopping and the height of wave run-up were performed by the facilities shown in Fig. 11 and Photo. 1. Water topped over the seawall striked against the plate for reception 10 meters in width, and was gathered into the collecting tank through the guideway. Observations were conducted twice at 9 a.m. and 3 p.m. The quantity of wave overtopping for 10 minutes was measured at each time.

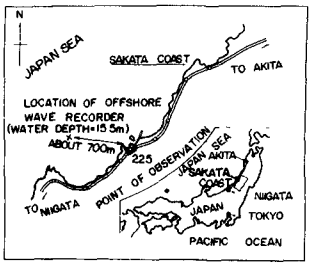

Fig. 10 Location map of Sakata Coast.

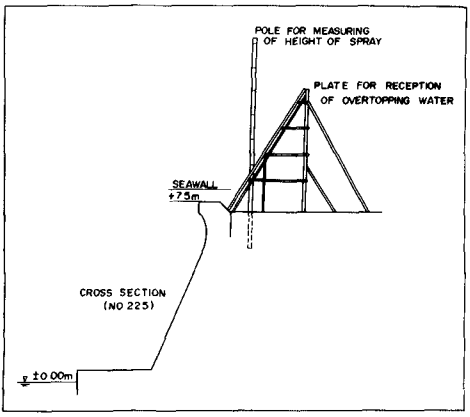

Fig. 11 Facilities of field observation of wave overtopping at Sakata Coast.

The comparison of the values of the field and laboratory observations is shown in Fig. 12. The plotted data of the field observation show the relation between the significant wave heights recorded in 10 minutes and the average quantity of wave overtopping. The solid lines in the figure show the envelopes of the experimental values for wind velocity of zero and 25m/sec. The wind velocity of 25m/sec is the prototype wind velocity which was calculated on the basis of the Froude's Similarity Law. A considerable difference is noted between the experimental values of no wind and wind of 25m/sec. This is due to the fact that the curved-face wall is highly effective in case of no wind and most of jumping waves are bounced back seaward. The observed values are sandwiched in between two envelopes of experimental data of no wind and wind of 25m/sec. Taking into consideration that the wind velocity in field was less than 12m/sec, it is safe to say that the observed values of quantity of wave overtopping in the field are roughly in agreement with the

Photo. 1 Facilities of fiels observation of wave overtopping at Sakata Coast.

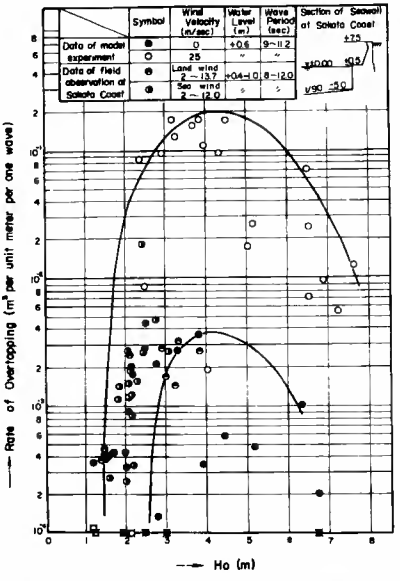

Fig. 12 Comparison between field and experimental data on the quantity of wave overtopping.

experimental values obtained by using regular waves with wind.

2) FIELD OBSERVATION AT OITA AND BEPPU COAST

Table 1 is the records of the water level and waves when Typhoon No. 9 (6309) attacked Oita Coast (see Fig. 13) on August 9, 1963. The conditions of wave overtopping over the seawall at Oita Coast during the typhoon is shown in Photo. 2.

Table 1 Records of the water level and waves when Typhoon No. 9 attacked Oita Coast.

Time	Wind velocity	Water level	H1/3	T1/3	H1/10	T1/10	Hmax	Tmax
13:30	21.7m/sec	+2.18m	3.27 m	7.0 sec	3.86 m	7.0 sec	4.10 m	7.0 sec

Ho1/3 = 3.55m (equivalent significant wave height in deep water)

Photo. 2 Conditions of wave overtopping at Oita Coast.

The 8 mm cine-films and photographs taken at that time show the overtopping of spray. Waves come forth along the seawall and topped over it. The reclaimed land behind the seawall was extremely inundated. The experimental results for the same seawall

are shown in Fig. 14. The cross section of the seawall is also shown in the same figure. The following is the results of estimation of the wave overtopping based on the water level and observed values of waves given in Table 1 :

Ho = 3.55 m, Water level = +2.18 m,
Crown height of the seawall = +5.5 m,
Therefore, hc = 5.5 - 2.18 = 3.3 m,
hc/Ho = 3.3/3.55 = 0.94
From Fig. 14, $2\pi Q/(HoLo) = 1 \sim 2 \times 10^{-2}$
Consequently, dimensionless quantity of wave overtopping at that time can be estimated to be $1 \sim 2 \times 10^{-2}$.

Furthermore, at Beppu Coast adjacent to Oita Coast (see Fig. 13), a great deal of damage due to the wave overtopping was reported at about the same time. The cross section of seawall is shown in Fig. 15. From Photo. 3 which shows the conditions of wave overtopping at that time, we can see that the spray jumped up expremely, and the substantial part of wave overtopped violently. We can also see that water streamed down at the backwash. At that time, the wide area of hinterland was inundated at $0.5 \sim 1.0$ meter in depth on the average.

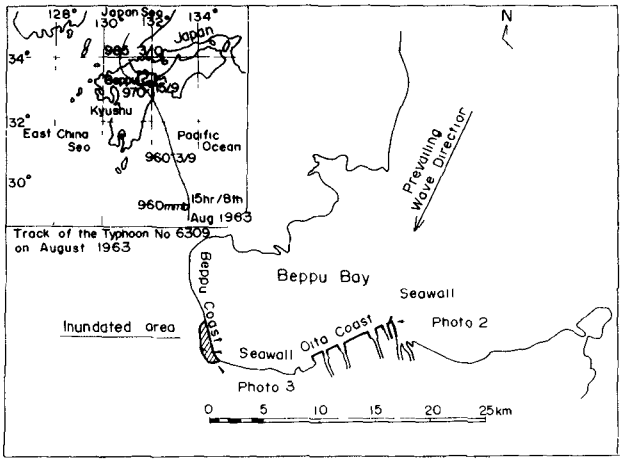

Fig. 13 Location map of Oita Coast.

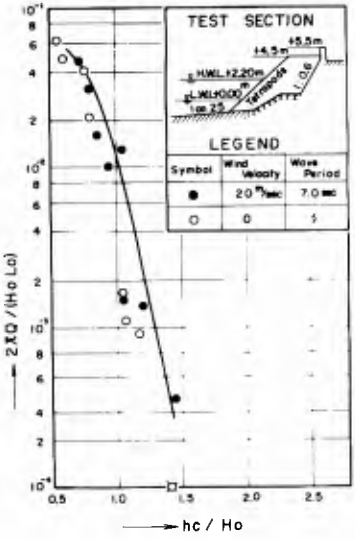

Fig. 14 Experimental results of wave overtopping at Oita Coast.

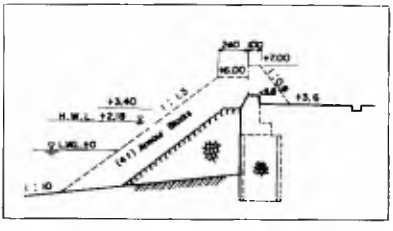

Fig. 15 Cross section of seawall at Beppu Coast. Dotted line is the section of plan to prevent the wave overtopping after the damage at Typhoon No.9.

Photo. 3 Conditions of wave overtopping at Beppu Coast.

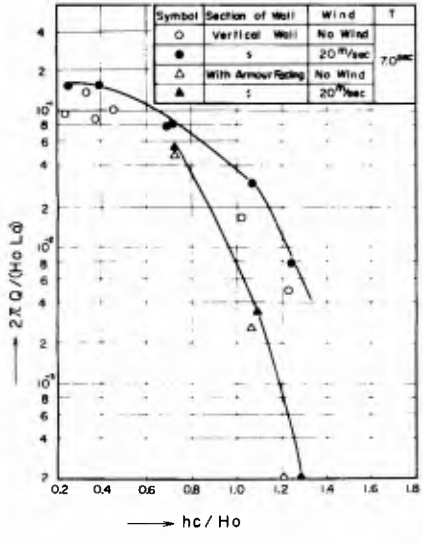

Fig. 16 Experimental results of wave overtopping at Beppu Coast.

The experimental results of wave overtopping for the same cross section is given in Fig. 16. The following is the results of estimation of the wave overtopping based on the water level and observed values of waves given in Table 1. However, the offshore wave height at Beppu Coast is 3.0 meters.

Ho = 3.0 m, T = 7.0 sec, Water level = +2.18 m,
Crown height of the seawall = +4.6 m,
hc/Ho = 2.4/3.0 = 0.8
From Fig. 16, $2\pi Q/(HoLo) = 6.0 \times 10^{-2}$

ALLOWABLE QUANTITY OF WAVE OVERTOPPING

The allowable quantity of wave overtopping is determined by the relationship among the conditions of wave overtopping, the importance of structure in the hinterland, the conditions of drainage facilities, the duration of waves and others. Table 2 was made with reference to the results of experiment conducted by using regular waves with wind and to the results of field observation mentioned previously.

Table 2 Rate of wave overtopping and its wave conditions

Condition of wave overtopping	Rate of wave overtopping $2\pi Q/(HoLo)$
Spray slightly overtops.	$0 \sim 1 \times 10^{-3}$
Considerable spray overtops or substantial part of wave overtops slightly.	$1 \times 10^{-3} \sim 5 \times 10^{-3}$
Spray overtops violently and substantial part of wave overtops considerably.	$5 \times 10^{-3} \sim 1 \times 10^{-2}$
Substantial part of wave overtops considerably.	$1 \times 10^{-2} \sim 10^{-1}$

If we take the crown height to such as extent that no spray will overtop, the seawall must be extremely high and uneconomical. On the other hand, if the crown height is as low as to permit the overtopping of the substantial part of wave, the functions of the seawall to prevent the wave overtopping get worse.

Two of the authors did a survey of the drain of the seawalls used in Japan and found that most of them have the cross section of 0.1 ~ 0.5 square meter. They trially calculated the draining capacity of such a cross section by Manning's formula and obtained the results as shown in Fig. 17. In this case, it seems that the maximum draining capacity is $2\pi Q/(HoLo) = 1 \sim 5 \times 10^{-3}$, under the conditions of T = 6 ~ 8 seconds and Ho = 3.0 m.

From these conditions, it would be supposed that the allowable quantity of wave overtopping to design the crown height of seawall can be generally determined in the range of $2\pi Q/(HoLo) = 1 \sim 5 \times 10^{-3}$.

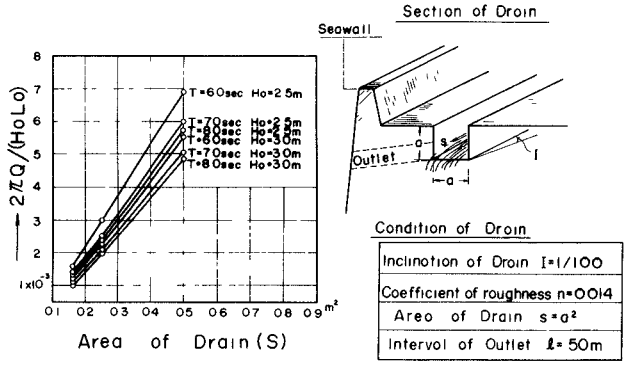

Fig. 17 Relation between wave overtopping and the capacity of drain.

DESIGN OF CROWN HEIGHT

Arranging the data mentioned in the previous chapter, we would like to propose here one convenient criterion to design the crown height of seawall with armour block facing.

Figure 18 shows the required crown height of seawall with armour block facing to keep the condition of $2\pi Q/(HoLo) = 5 \times 10^{-3}$ as the allowable quantity of wave overtopping, corresponding to various water depths where the structure is built. In addition to this, the crown height of vertical wall is shown with dotted line for the reference. In the above discussion the crown height of armour block facing, ht/Ho is $0.5 \sim 0.75$. Generally speaking from Fig. 18, it seems sufficient to take the crown height of seawall with armour block facing 1.3 times as high as offshore wave heights. Besides near the wave breaking point, if we take the crown height of armour block facing being equal to wave height in deep water, the quantity of wave overtopping reduces abruptly as shown in Fig. 9. Therefore, we can reduce the values of hc/Ho as shown in Fig. 18 by 20%.

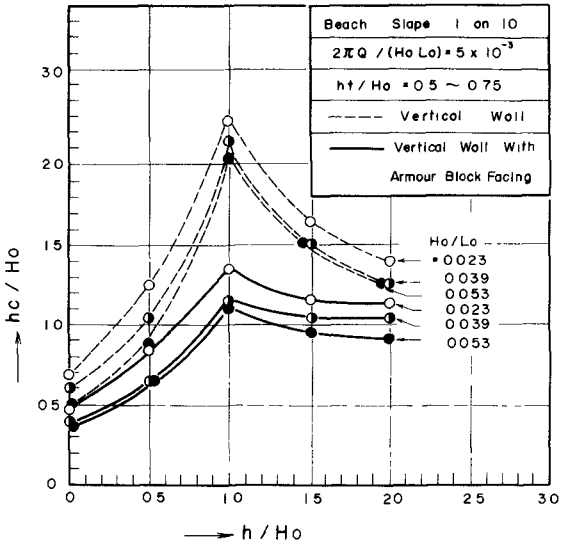

Fig. 18
Relation between hc/Ho and h/Ho.

CONCLUSION

1) As shown in Figs. 1 through 5, armour block facing is very effective for the prevention of wave overtopping. Especially the preventive function of armour block facing is remarkable at the site near the wave breaking point.

2) The observed values in field which are arranged by significant wave heights are roughly in agreement with experimental values obtained by using regular waves.

3) So far as we observed in field, it seems sufficient that we design the crown height of seawall considering the results of hydraulic experiments with regular waves with wind.

4) It would be supposed that the maximum allowable quantity of wave overtopping is : $2\pi Q/(HoLo) = 1 \sim 5 \times 10^{-3}$.

5) The crown height of seawall with armour block facing can be determined easily by using Fig. 18, in which the allowable quantity of wave overtopping is assumed to be $2\pi Q/(HoLo) = 5 \times 10^{-3}$.

6) Further investigations are required to get more accurate data in order to ascertain the above conclusions.

ACKNOWLEDGMENT

The authors extend appreciation to Prof. Toshio Iwasaki of Tohoku University, Prof. Kiyoshi Horikawa of University of Tokyo and Messrs. J.P. Gamot and Y. Mahé of Sotramer, France, for making guidance in completing this paper. Furthermore, they extend appreciation to Messrs. Kenji Izawa and Takao Akagi, former and present heads of Sakata Construction Office of the Ministry of Construction, Messrs. Yoshinori Araki and Kenichi Saito, former and present chiefs of research section of the same office for their enforcement of field observation and advice for model experiment, and Prof. Akira Miura of Nihon University (former

Assist. Prof. of Tohoku University) for his guidance of experiment and analysis of data. Finally appreciation is extended to Mr. Naoki Hase, Assistant of Tohoku University who is in charge of model experiment.

REFERENCES

(1) Hom-ma, M. and K. Horikawa : Hydraulic Experimental Report of The Maritime Industrial Zone of Oita Prefecture. Vol. 1, 1966.

(2) Iwasaki, T. and A. Numata : Scale Effect of Model Experiment on Wave Overtopping on Seawall, J.S.C.E., 22th. Annual Convention, 1967.

(3) U.S.Army Engineer Beach Erosion Board : "Shore Protection Planning and Design", Technical Report Number 4, Beach Erosion Board, Washington D.C., 1961.

(4) Pappe, A. : Experimental Data of the Overtopping of Seawalls by Waves, Proc. of 7th. Conference on Coastal Engineering, Vol. 2, pp. 674～681, 1961.

(5) Saville, T., Jr. : Laboratory Data on Wave Run-up and Overtopping on Shore Structures, Beach Erosion Board, Tech. Memo. No. 64, 1955.

(6) Iwagaki, Y., A. Shima and M. Inoue : Effect of Wave Height and Sea Water Level on Wave Overtopping and Wave Run-up, Coastal Engineering in Japan., Vol. 8, pp. 141～151., 1965.

(7) Sibul, O. J. and E. G. Tickner : Model Study of Overtopping of Wind-Generated Waves on Levees with Slopes of 1 : 3 and 1 : 6, Beach Erosion Board, Tech. Memo. No. 80, pp. 1～27, 1956.

CHAPTER 56

A MODEL STUDY OF THE DISTRIBUTION OF RUN-UP OF WIND-GENERATED WAVES ON SLOPING SEA WALLS

Norman B. Webber
Department of Civil Engineering, University of Southampton
Southampton, Gt. Britain
and
Geoffrey N. Bullock
Hydraulics Division, Central Laboratory, George Wimpey and Co. Ltd.
London, Gt. Britain

ABSTRACT

The behaviour of wind-generated waves on impermeable slopes of 1:2, 1:4 and 1:10 was investigated in a 40 ft long laboratory wind-wave flume. Apparatus for measuring instantaneous values of the run-up was devised. Wind velocities of up to 44 ft/sec were applied, producing wave heights of up to 2.5 in.

Distributions were obtained for the wave and run-up characteristics. The empirical results were compared with theoretical statistical relationships. A comparison was made with the run-ups in paddle-wave experiments.

The relationship between the waves and their run-ups was further investigated by a comparison of simultaneous recordings, using the methods of spectral analysis.

INTRODUCTION

An understanding of the run-up behaviour of waves on sloping faces is of importance both in relation to sea walls and beaches. The subject has been studied for paddle-generated waves (Granthem 1953, Saville 1956) and for wind waves (Sibul and Tickner 1955, 1956; Paape 1960), principally from the point of view of the overtopping characteristics.

For design purposes, the procedure is often adopted whereby the run-up corresponding to the 'significant' wave height is determined from empirical data, such as that in the Coastal Engineering Research Centre Technical Report No. 4 (1966). It may then be quite reasonably inferred that only a small proportion of the run-ups would exceed this value. Saville (1952) has introduced an interesting refinement by developing an approximate distribution, based on the joint distribution of wave height and period proposed by Bretschneider (1959) and utilising the above run-up data, but still assuming each run-up as being the product of an individual wave.

The aim of the present investigation, undertaken with a wind-wave flume, was to examine the run-up behaviour on impermeable slopes of three different inclinations and to establish the relationship with the incident deep-water waves.

EXPERIMENTAL EQUIPMENT

The wind-wave flume was 40 ft long, 1 ft wide, and 3 ft deep, with a constant speed fan at the downstream end. Air flow was controlled by means of a hand-operated butterfly damper, and the wind velocities associated with various damper settings were measured by a pitot-static tube appropriately positioned. A sheet of perspex, with inclination of 1:10, 1:4, or 1:2 constituted the sloping face. Fig. 1 illustrates the working end of the flume and the assemblage of electronic measuring equipment. A hinged paddle-type generator was located at the windward end, so that an alternative means of generating waves was available.

Initially, the variation of the water surface elevation was measured by a wave-recorder of the twin-wire resistance type, but unsatisfactory calibration drift was experienced owing to contamination of the probes. The capacitance type of recorder proved to be much more stable and two such devices were employed.

Measurement of the run-ups proved difficult, because of the small size of the waves and the relatively high wind velocities. Various methods were investigated, including the suspension of wires of the wave recorder type just above and parallel to the sloping surface, so that the run-up covered a varying proportion of the wire. But this arrangement was found to be depth sensitive as well as being affected by clinging droplets. The type of run-up gauge finally evolved was a bank of 40 pairs of thin wire probes, arranged in parallel lines 0.5 in. apart and suspended with their tips 0.05 in. above the surface. The longitudinal spacing of the probes was made appropriate to the run-up range for each of the slopes. Fig. 2 shows the comb-like measuring head, comprising a perspex frame and wire inserts.

By means of an appropriate circuit, the output of the wave run-up gauge was transmitted in staircase voltage wave form proportional to the number of pairs of probes in contact with the water. Calibration was effected by adjusting its position on the slope so that the points of a known number of probes were immersed. The purpose of the pair of probes was to obviate, so far as possible, the errors caused by foam and droplets coming into contact with probes above the leading edge. A voltage change was only produced if the tips of a pair of probes became immersed. The leading edge during wave run-up was thus defined as the highest point at which the depth of water was sufficient to maintain contact.

The recording equipment included a single-channel high-speed pen recorder and a four-speed four-channel F.M. tape recorder. The former provided a visual record of the waves and run-ups, whilst the latter allowed of simultaneous recordings of waves and run-ups, and facilitated a subsequent analysis by analog or digital means.

EXPERIMENTAL PROCEDURE

The flume was filled to a still-water depth of 10 in. An examination of the wave spectra showed that this depth was sufficient to establish 'deep-water' conditions in the flume, with only a small error of about 8 per cent at the maximum wave lengths.

For a reference location, the wave recorder was sited above the toe of the 1:2 and 1:4 slopes, and 4 ft leeward of the toe of the 1:10 slope, the last position being chosen because of the need for comparable fetches. In order to assess the effect of wave reflections from the sloping faces, wave recordings were taken with and without an absorbent covering on the 1:2 slope. It was found that the average reduction in the standard deviation of the water surface elevation was about 5.3% for various wind speeds. This was considered acceptable, especially in view of the fact that the average error for the 1:4 and 1:10 slopes would have been rather less.

Experiments were undertaken at wind speeds of 26, 30, 35, 40 and 45 ft/sec, the characteristic velocity being that at 10 in. above S.W.L. However, it was found that, if satisfactory conditions were to be maintained on a particular slope, the wind velocity could be varied only within a limited range. Below the lower limit of this range the length of the run-up zone was insufficient for accurate measurements, while above the upper limit the quantity of foam and droplets of water on the slope became excessive.

In order to ensure that conditions within the flume had become stabilised, a steady wind was applied for at least half an hour in each test run before the outputs of the gauges were recorded. Calibrations were made before and after each run. In the case of tape recordings, the wave and run-up processes were recorded simultaneously for a period of 80 minutes at a tape speed of 1⅞in./sec.

ANALYSIS OF CHART RECORDINGS

Waves:

Forty wave records, each with one hundred consecutive waves, were analysed for apparent wave height $\tilde{H}$ and apparent period $\tilde{T}$, using a conventional procedure. Values of $\tilde{L}$ were defined as $\tilde{L} = \tilde{T}^2$. The mean water level was also established.

In order that results with different absolute magnitudes could be compared, the set of values obtained for a given wave characteristic in a particular test was normalised by the mean values. Thus

$$H_n = \tilde{H}/\bar{H},\quad T_n = \tilde{T}/\bar{T},\quad L_n = \tilde{L}/\bar{L}$$

A typical set of probability distributions of H_n for different wind velocities with a 35 ft fetch is shown in Fig. 3. For the range available, it was found that the fetch had little effect upon the distribution, but an increase in wind

velocity caused an increase in standard deviation (S_{H_n}) of H_n.

Now, Longuet-Higgins (1952), with some support from observational data, has postulated that a prototype 'sea state' is statistically described by a Rayleigh distribution. On this basis, the probability distribution of H_n is given by

$$P(H_n) = 1 - e^{-\pi H_n^2/4}$$

Theoretical relationships can thus be established between $\bar{H}$ and H_p, where H_p is the average value of the highest p per cent of the waves, also between $\bar{H}$ and the standard deviation σ_H, skewness α_{3H}, and kurtosis α_{4H}.

From a comparison of these theoretical relationships and the experimental data it was evident that the Rayleigh distribution was not a good model for the variability of H for laboratory wind waves of the present scale. For example, in Fig. 3, the Rayleigh curve diverges from the plotted points in the upper and lower quartiles. The graphs for H_{max}, H_{10}, H_{33} ('significant' wave), H_{50}, σ_H, α_{3H}, and α_{4H} further confirmed the discrepancy.

As indicated in Fig. 3, a much better degree of conformity resulted from a Gaussian distribution with mean $\mu = 1.0$, and standard deviation $\sigma = 0.35$.

Run-ups:

The apparent wave run-up height $\tilde{R}$ was defined as the difference in elevation between the mean water level above the toe of the slope and a run-up crest. A definition of this type was necessary because it was impossible either to attribute each run-up crest to an individual wave or to measure a run-up height for each wave.

A more suitable datum for a study of the run-up distribution was the elevation of the mean run-up height $\bar{R}$. When this had been standardised $[(R_m)_s = R_m / S_{\tilde{R}}$, where $R_m = \tilde{R} - \bar{R}]$, it was found that a Gaussian distribution with $\mu = 0$, $\sigma = 1.0$ was in good agreement with the experimental results for all three slopes (Fig. 4).

Wave and Run-Up Relationship:

In view of the apparent Gaussian distribution for the run-ups, and the fact that such a distribution is completely defined when the mean and the standard deviation are known, the experimental data for $\bar{R}$ and $\bar{H}$ and for $S_{\tilde{R}}$ and $S_{\tilde{H}}$ were compared. Linear relationships were obtained by the method of least squares, and it is seen (Fig. 5) that they were reasonably appropriate, except possibly for the 1:10 slope, where a very liberal interpretation has been made, the results being of limited range and probably influenced by wind set-up. It was deduced, in general, that the statistical error of the data was unlikely to exceed 10 per cent.

The average values of the ratio mean wave period / mean run-up period were 0.68, 1.00 and 1.05 for the 1:10, 1:4 and 1:2 slopes, respectively.

Although the exact value of this ratio depended upon the definition of $\tilde{R}$, nevertheless it qualitatively indicated the actual run-up behaviour. For example, it was observed, particularly for the 1:10 slope, that waves tended to combine or be absorbed by the backwash of a previous wave. For a very steep slope, the waves quite often created two run-up crests, the first crest being generated by the leading elements of a plunging breaker, whilst the second crest constituted the body of the wave.

The run-up curves of the Coastal Engineering Research Centre (1966), referred to earlier, served as a useful basis for comparison. These curves, for deep-water uniform waves and for the three relevant slopes, are shown in Fig. 6. Corresponding values were deduced from the experimental wind-wave data, although the possible range of comparison was very limited. As will be seen, there was a fair measure of agreement between the plotted points and the curves, although in the case of the 1:10 slope a breaking depth datum (i.e. M.W.L. at location where mean depth was breaking depth, $\frac{4}{3}H$) resulted in a slightly better fit than the normal convention.

The run-up of equivalent paddle-generated waves in the flume was also investigated and the results were found to be below the relevant curves in Fig. 6. The discrepancy could have been due to the effects of reflected waves, wall friction, gauge error, and smallness of scale; indeed a scale effect correction (additive from model to prototype) is recommended in the C.E.R.C. Report. It was also noteworthy that the chart recordings showed the existence of a double run-up crest of the type mentioned earlier.

SPECTRAL ANALYSIS

A greater understanding of the nature of a non-deterministic phenomenon may be gained from an analysis of the process as a whole. This was the purpose of the F.M. tape recordings described previously.

Because equipment suitable for digitising the tape-recorded signals was not available, much of the analysis of the wave elevation $\eta(t)$ and run-up elevation $\lambda(t)$ was carried out in analog form. From preliminary tests it was found that the energy in both processes occurred at frequencies below 4 cycles/sec, with maximum energy as low as 0.25 cycles/sec for the run-up on the 1:10 slope. Therefore, in order to bring these frequencies up to an acceptable level for analog equipment, it was necessary to replay the recorded signals at an increased speed. In this way, a replay time of 19 seconds for 80 minutes recording time applied.

The voltage corresponding to the mean value of $\lambda(t)$ was measured by means of a mirror galvanometer with a suitable time constant. A random noise r.m.s. voltmeter was used to measure the standard deviations of $\eta(t)$ and $\lambda(t)$. For a given slope, approximately linear relationships were found to exist between S_η and $\bar{\lambda}$ and between S_η and S_λ (Fig. 7).

Probability density functions for $\eta(t)$ and $\lambda(t)$ were obtained by measuring

the proportion of the sample length during which the voltage of the analogous signal was below a known value. In Fig. 8, showing the results for the standardised functions $p(\eta_s)$ and $p(\lambda_s)$, a Gaussian distribution has been superimposed for purposes of comparison. In the case of $p(\eta_s)$, the divergence may be accounted for by the unsymmetrical nature of the wave profiles - short steep crests and long flat troughs. Although the data for $p(\lambda_s)$ exhibited a considerable degree of scatter, the distributions for the steeper slopes showed a tendency to conform to the pattern of $p(\eta_s)$.

The auto-correlation coefficients $\rho_\eta(\tau)$ and $\rho_\lambda(\tau)$ were determined by means of an analog correlator, developed for high frequency analysis. This equipment accepted samples of 10 seconds duration, equivalent in the present case to approximately 43 minutes of experimental time. Whilst ignoring the mean level of the signal, it gave a digital output from which the value of the auto-correlation coefficient could be calculated for the successive time lags τ, the latter being increased from zero by increments of 0.0256 seconds experimental time. From the relevant graphs it was evident that there was considerable difference between the form of $\rho_\eta(\tau)$ and $\rho_\lambda(\tau)$, particularly in respect of the 1:10 slope.

When the signals for $\eta(t)$ and $\lambda(t)$, recorded in the same test run, were fed into the correlator simultaneously, values for the cross-correlation coefficient $\rho_{\eta\lambda}(\tau)$ were obtained, the relevant curves being shown in Fig. 9. It will be observed that there was very little correlation between the waves and the run-ups for the 1:10 slope, but that correlation improved with increasing steepness. It was interesting to note that for the 1:1 and 1:2 slopes the largest peaks in $\rho_{\eta\lambda}(t)$ were negative. This was thought to be due to the unsymmetrical nature of $\eta(t)$ and $\lambda(t)$.

The energy spectra $\left[E_\eta(f)\right.$ and $\left.E_\lambda(f)\right.$ versus $\left.f\right]$ are shown in Figs. 10 and 11 for the three slopes. The maxima of each of the run-up energy spectra obtained for the 1:10 slope (Fig. 10) were found to occur at about 0.33 cycles/sec - a lower frequency than the band containing the wave energy. Also, for this slope, there was little or no response at frequencies corresponding to the peaks of the wave energy spectra. Thus it is not surprising that the mean apparent run-up period was found to be greater than $\bar{T}$. Only in the case of the 1:2 slope was the maximum run-up energy found to be at the same frequency as the maximum wave energy, and, even so, $E_\lambda(f)$ registered half its maximum value in a secondary peak at 0.35 cycles/sec.

CONCLUSIONS

For the waves, a Gaussian distribution ($\mu = 1$, $\sigma = 0.35$) for H_n was found to be reasonably appropriate. For the three slopes that were investigated, a Gaussian distribution ($\mu = 0$, $\sigma = 1$) was a good approximation to the distribution of $(R_M)_s$. Also, linear relationships appeared to exist between $\bar{H}$ and $\bar{R}$, and between $S_{\bar{H}}$ and $S_{\bar{R}}$ for a given slope. If this were found to be true of the prototype then it would be possible to make accurate run-up predictions from a knowledge of the wave conditions.

The visual observations, trace records, and spectral analysis all showed

that it was not possible to establish direct correspondence between individual waves and their run-ups. Indeed, in the case of the 1:10 slope, there were over 30 per cent fewer run-up crests than waves approaching the slope. Thus any method which predicts the distribution of apparent run-up heights on the basis of an individual run-up for each wave must be inaccurate unless the previous waves are taken into account.

Unlike the statistical conditions generally assumed to apply in nature, the laboratory wind waves were not in accordance with a Rayleigh distribution. This must obviously suggest caution when considering the practical application of the results. There is clearly a need for further investigation at a larger scale, and preferably in the prototype.

ACKNOWLEDGEMENTS

The investigation was undertaken at the University of Southampton. The authors are grateful to the University for the use of experimental and computational facilities, and to Dr. K. R. McLachlan, in particular, for advice on electronic instrumentation.

REFERENCES

Bretschneider, C. L. (1959). Wave variability and wave spectra for wind-generated gravity waves : U.S. Army Beach Erosion Board, Tech. Memo. No. 118.

Granthem, K. N. (1953). Wave run-up on sloping structures . Trans. Am. Geophys. Union, vol. 34, pp. 720-724.

Longuet-Higgins, M. S. (1952). On the statistical distribution of the heights of sea waves : J. Marine Res., vol. 11, pp. 245-266.

Paape, A. (1960). Experimental data on the overtopping of seawalls by waves : Hydraulics Laboratory Delft, Pub. No. 23.

Saville, T. (1956). Wave run-up on shore structures : J. Waterways Harbors Divn., Proc. Am. Soc. C.E., vol. 82.

(1962). An approximation of wave run-up frequency distribution : Proc. 8th Conf. Coastal Eng., Council Wave Res., Berkeley, Calif. 1963, pp. 48-59.

Sibul, O. J. and Tickner, E. G. (1955). A model study of the run-up of wind-generated waves on levees with slopes of 1:3 and 1:6 : U.S. Army Beach Erosion Board, Tech. Memo. 67.

(1956). Model study of overtopping of wind-generated waves on levees with slopes of 1:3 and 1:6 : U.S. Army Beach Erosion Board, Tech. Memo. No. 80.

U. S. Army Coastal Engineering Research Center (1966). Shore protection, planning and design : Tech. Rpt. No. 4. pp. 183-195.

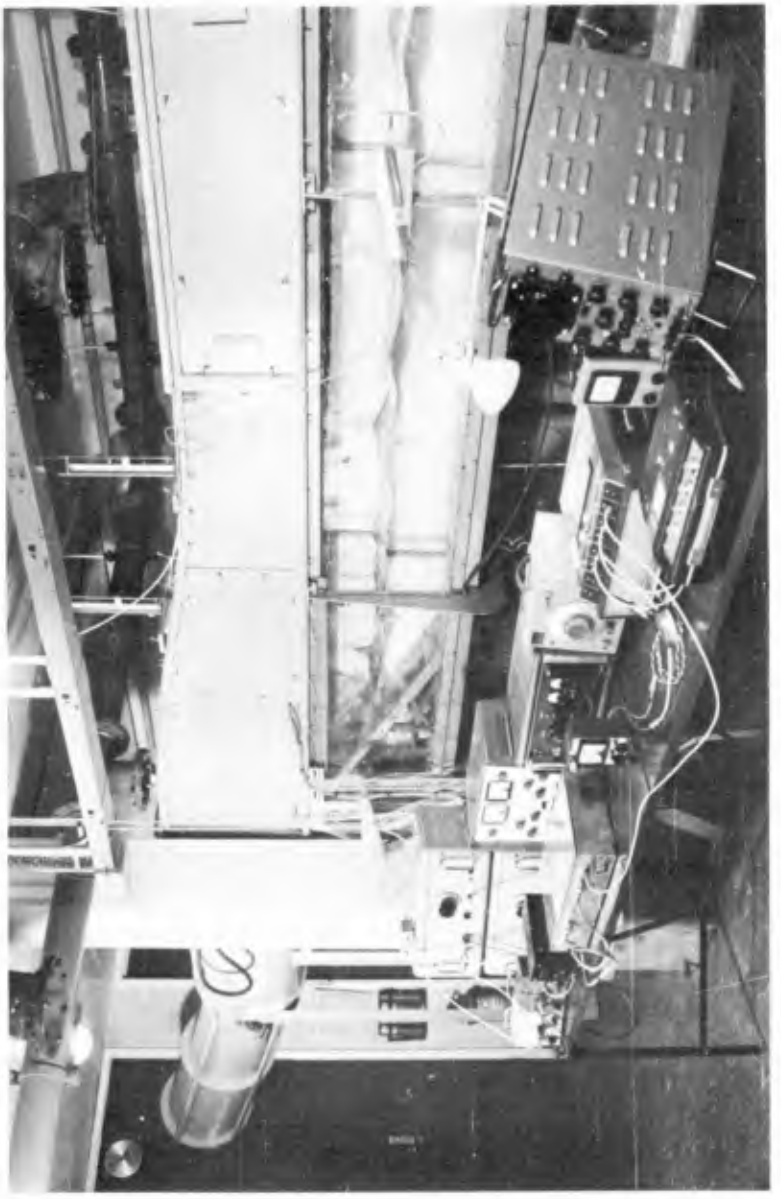

LEEWARD END OF THE WIND-WAVE FLUME WITH THE ELECTRONIC EQUIPMENT

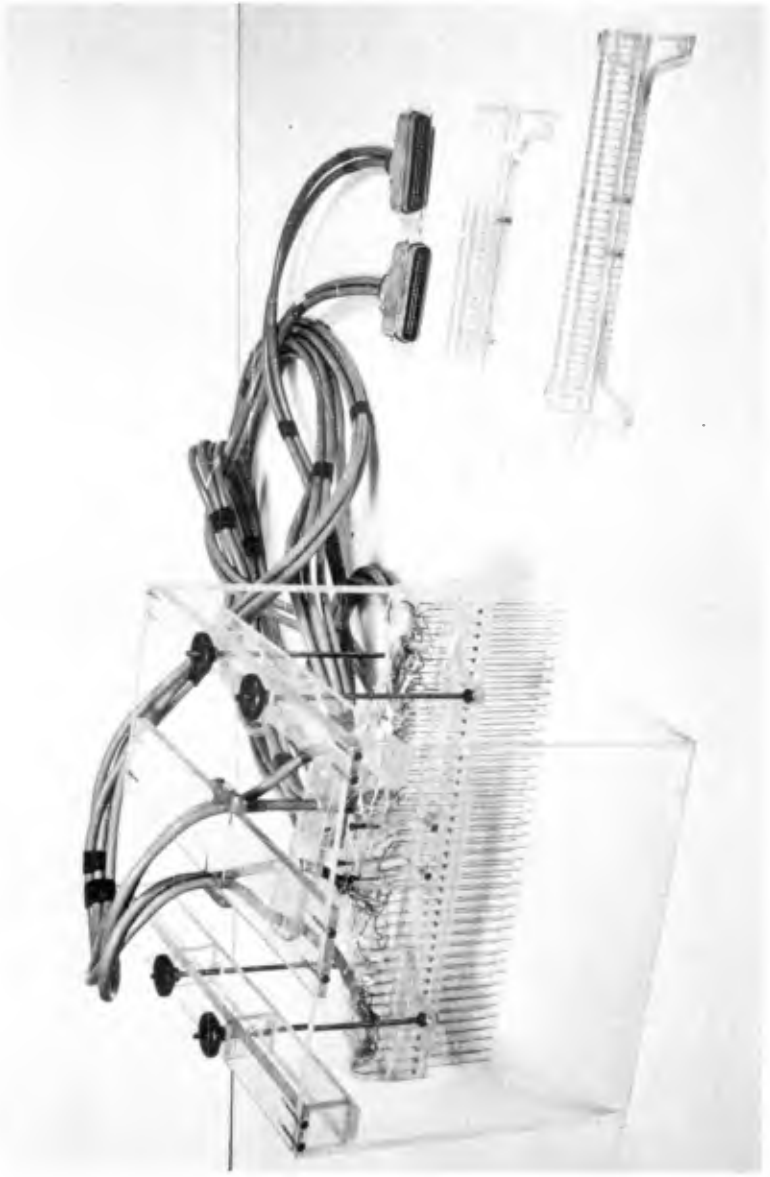

FIGURE 2
MEASURING HEAD OF THE RUN-UP GAUGE

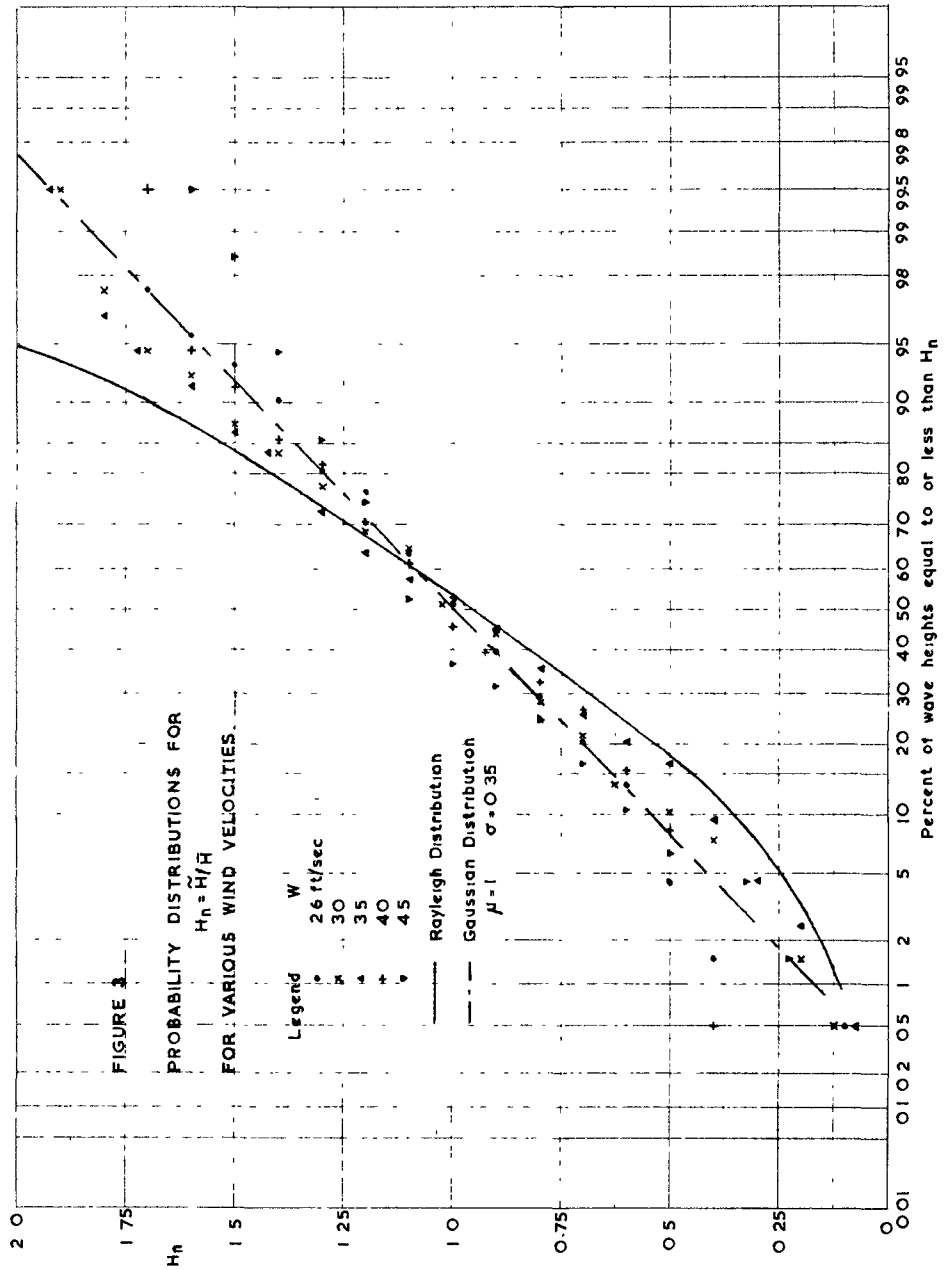
FIGURE 3
PROBABILITY DISTRIBUTIONS FOR
$H_n = H/\bar{H}$
FOR VARIOUS WIND VELOCITIES.
Legend
W'
26 ft/sec
30
35
40
45
Rayleigh Distribution
Gaussian Distribution
$\mu = 1$ $\sigma = 0.35$
H_n
2.0
1.75
1.5
1.25
1.0
0.75
0.5
0.25
0
0.001 0.01 0.02 0.05 0.1 0.2 0.5 1 2 5 10 20 30 40 50 60 70 80 90 95 98 99 99.5 99.8 99.95
Percent of wave heights equal to or less than H_n

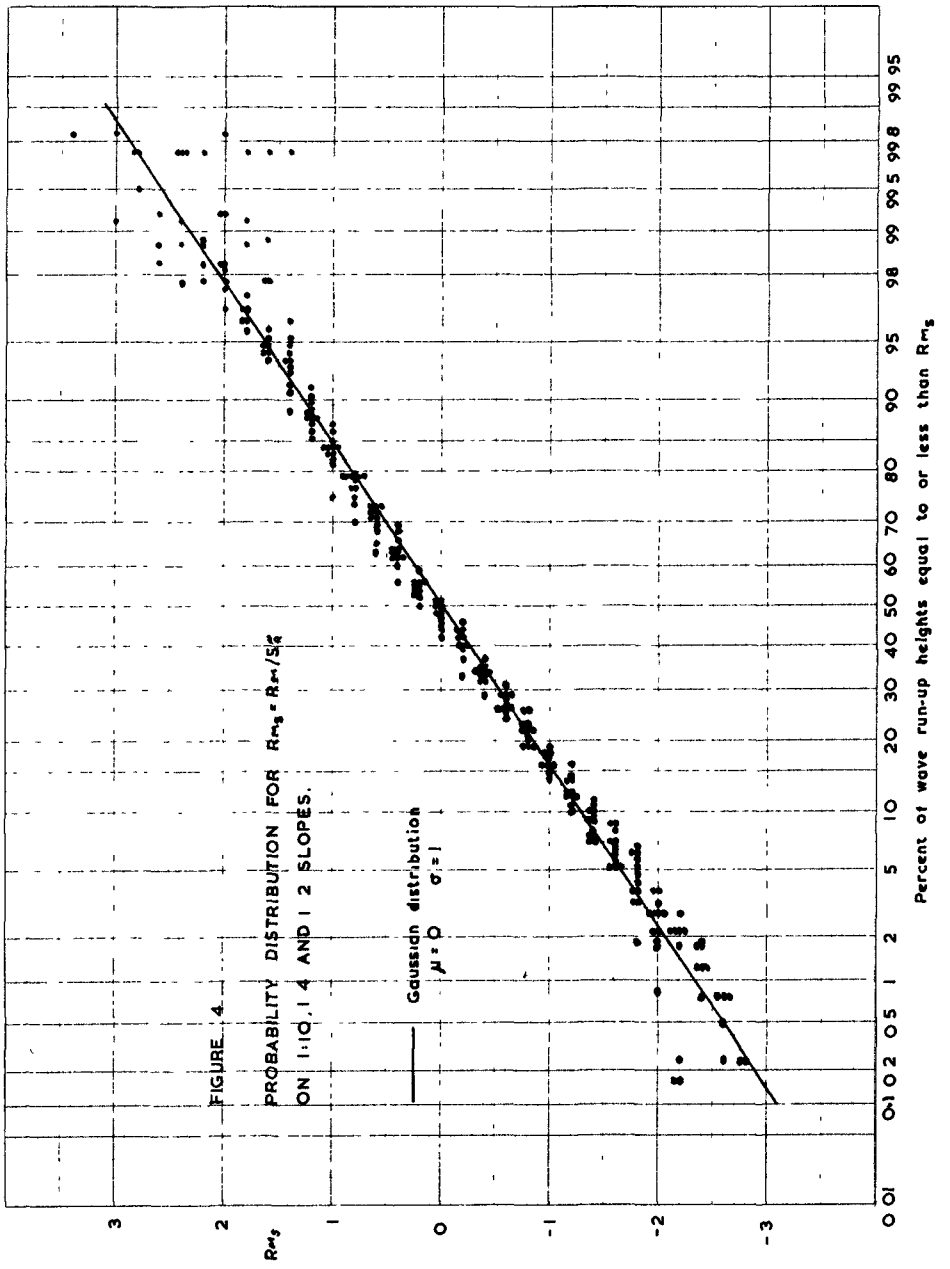

FIGURE 4. PROBABILITY DISTRIBUTION FOR $R_{ms} = R_{s-}/S_{s}$ ON 1:10, 1:4 AND 1:2 SLOPES.

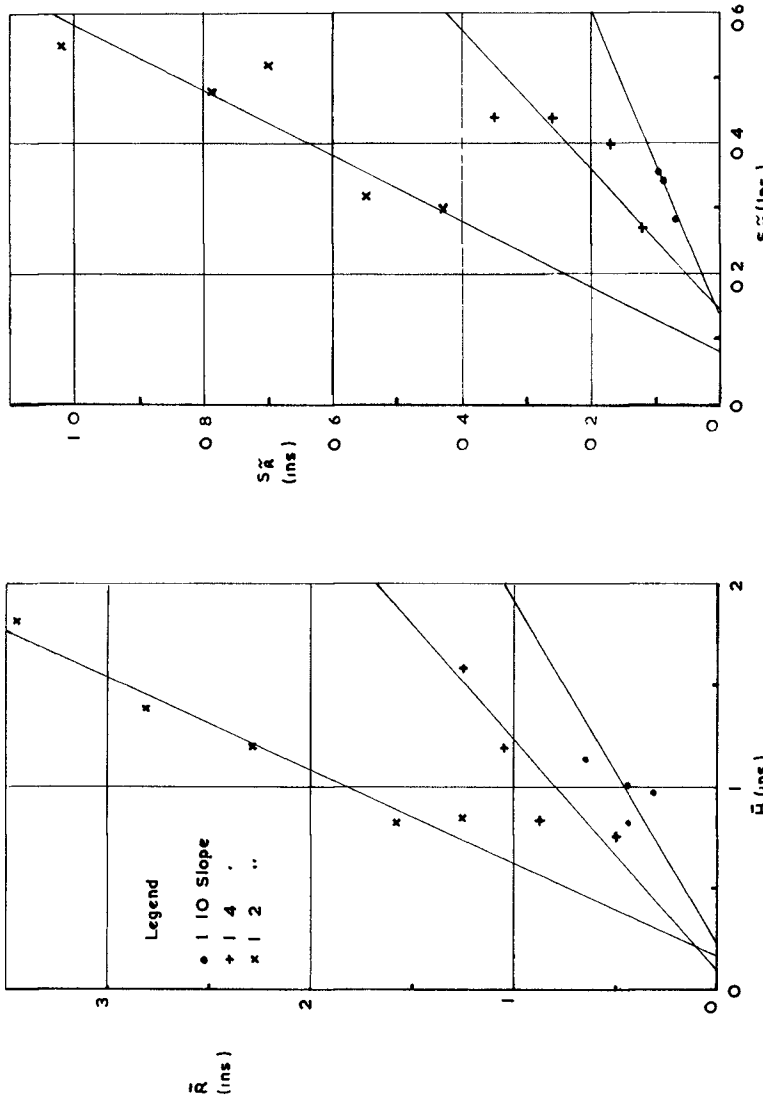

FIGURE 5 VARIATION OF MEAN RUN-UP HEIGHT WITH MEAN WAVE HEIGHT, AND RUN-UP HEIGHT STANDARD DEVIATION WITH WAVE HEIGHT STANDARD DEVIATION

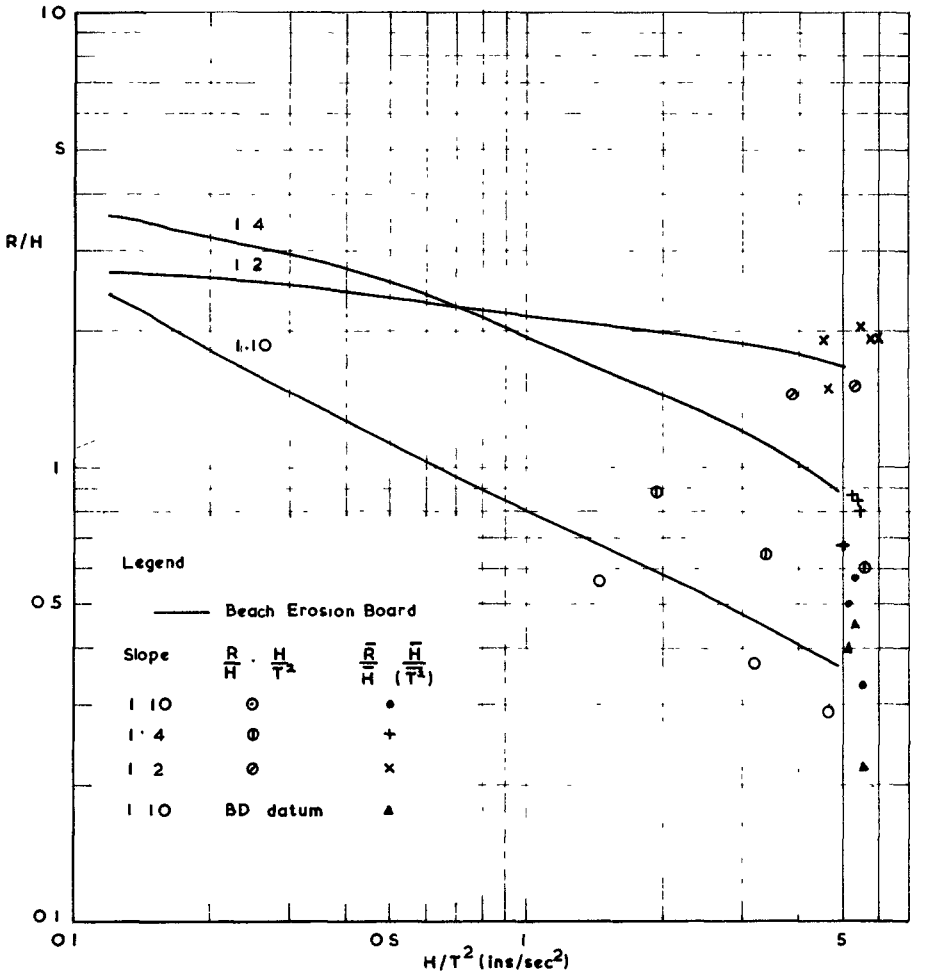

FIGURE 6 THE VARIATION OF RELATIVE RUN-UP WITH WAVE STEEPNESS FOR 1·10, 1 4, AND 1 2 SLOPES

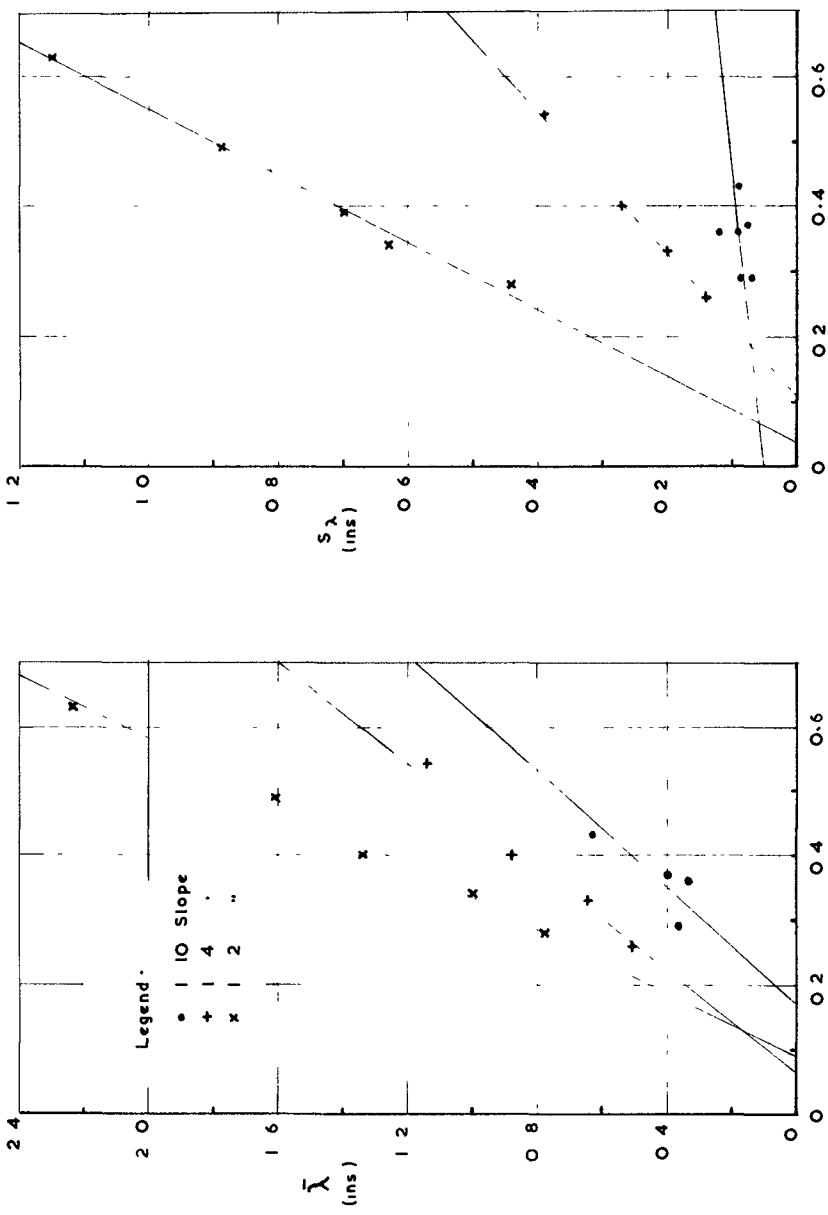

FIGURE 7 VARIATION OF RUN-UP MEAN LEVEL AND STANDARD DEVIATION WITH WAVE STANDARD DEVIATION.

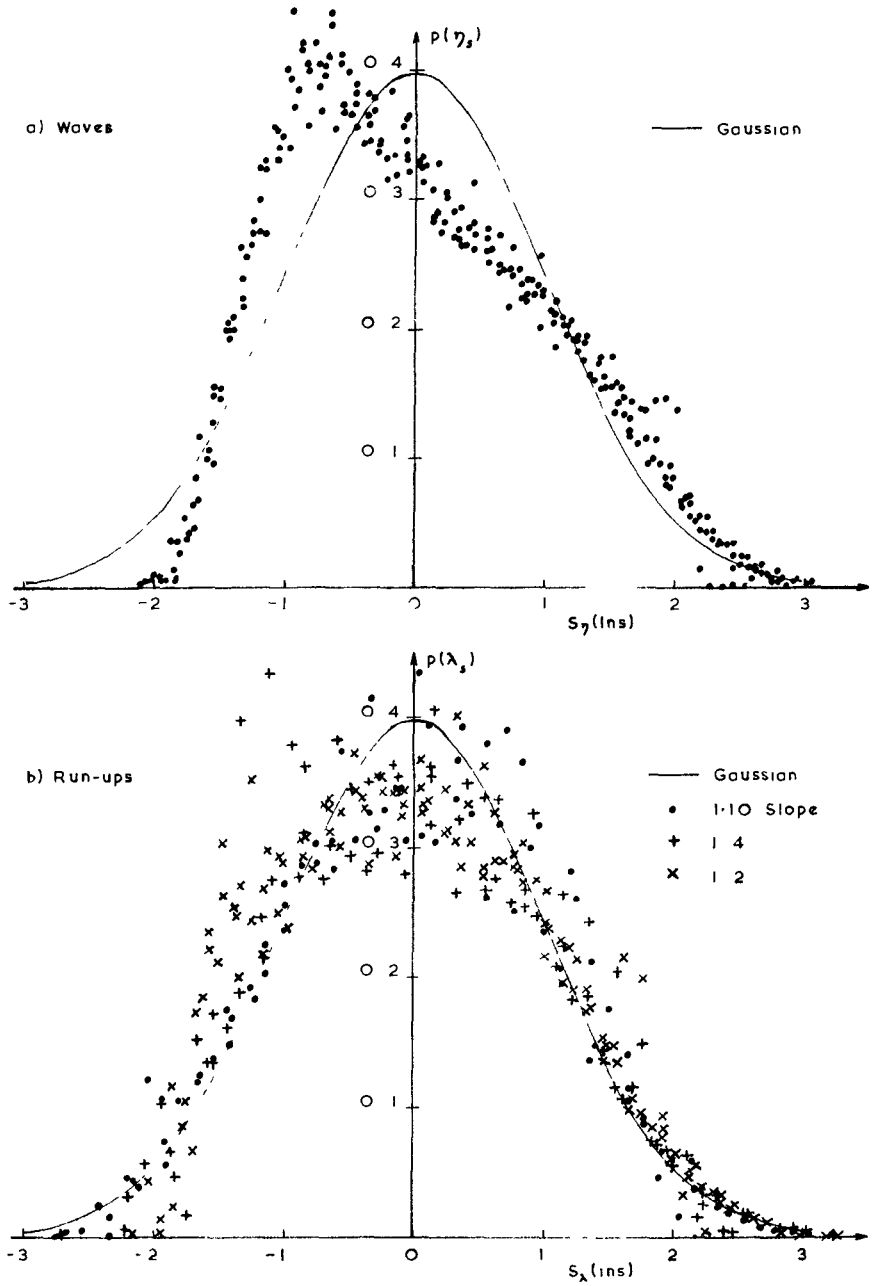

FIGURE 8 PROBABILITY DENSITY FUNCTIONS FOR WATER SURFACE ELEVATIONS IN WAVES AND RUN-UPS

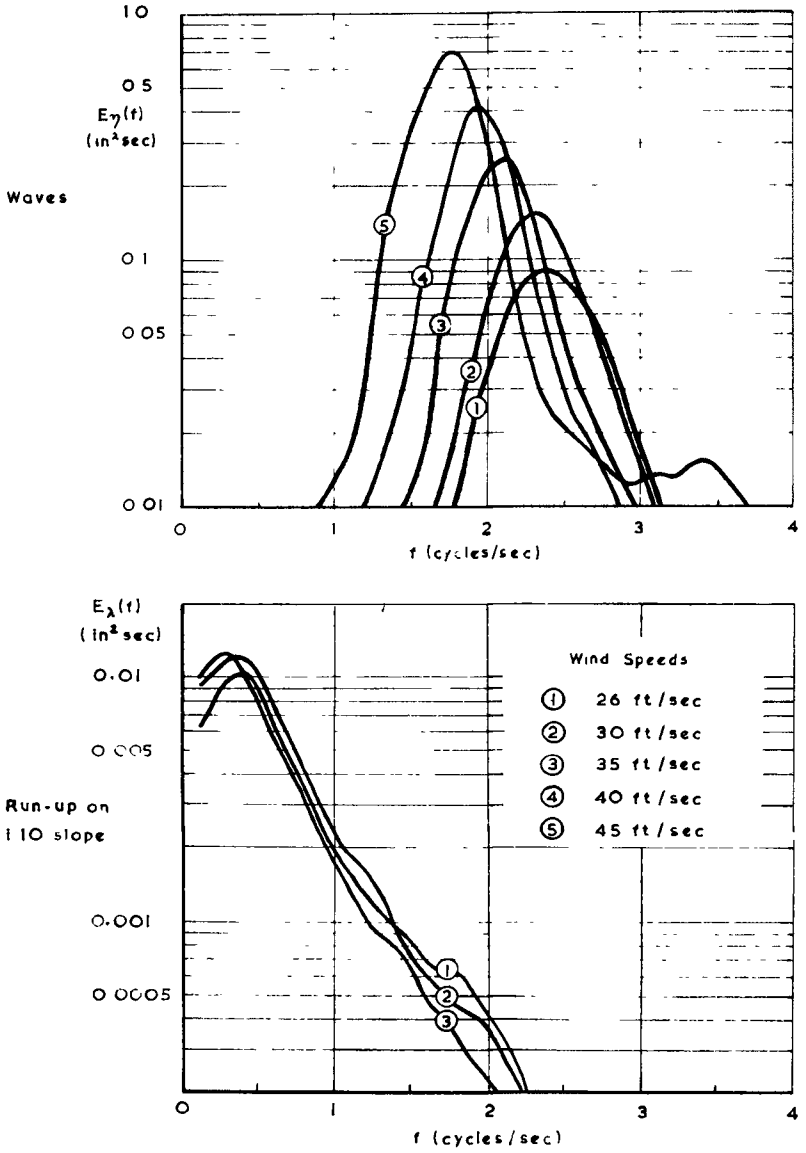

FIGURE 9 ENERGY SPECTRA FOR WAVES AND THEIR RUN-UPS ON A 1 10 SLOPE

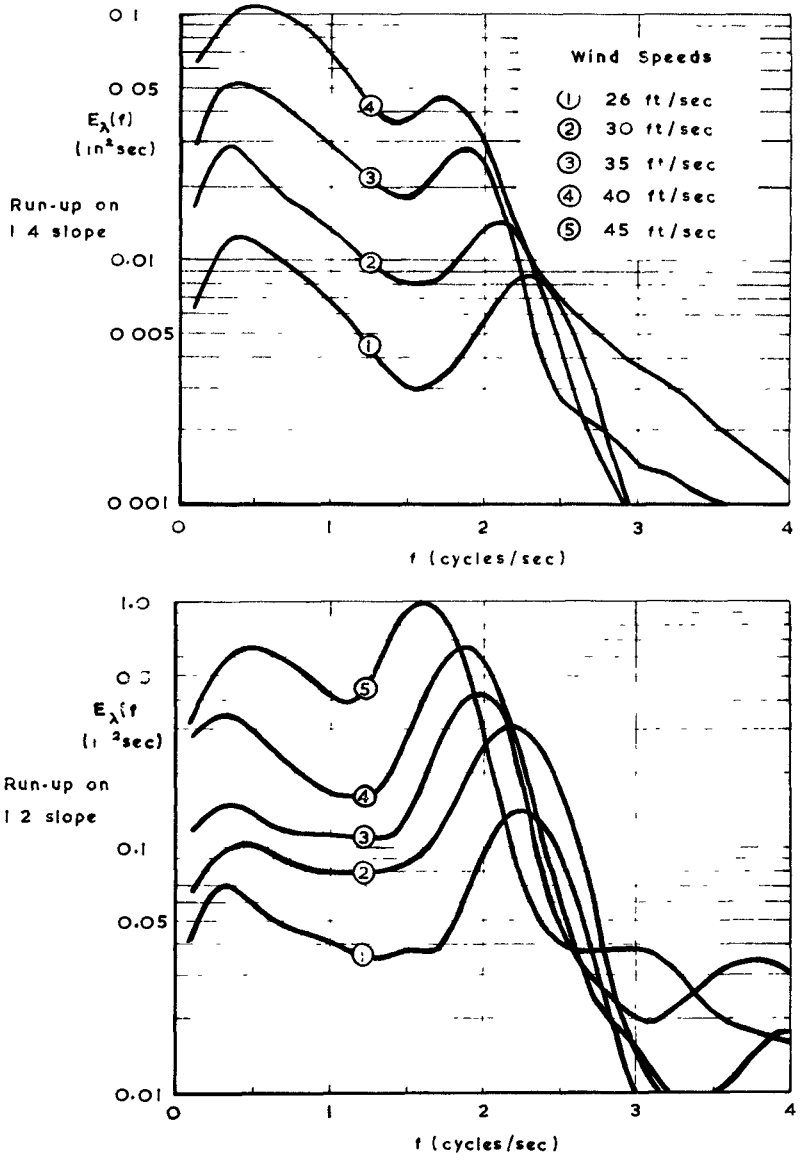

FIGURE 10 ENERGY SPECTRA FOR WAVE RUN-UPS ON 1 4 AND 1 2 SLOPES

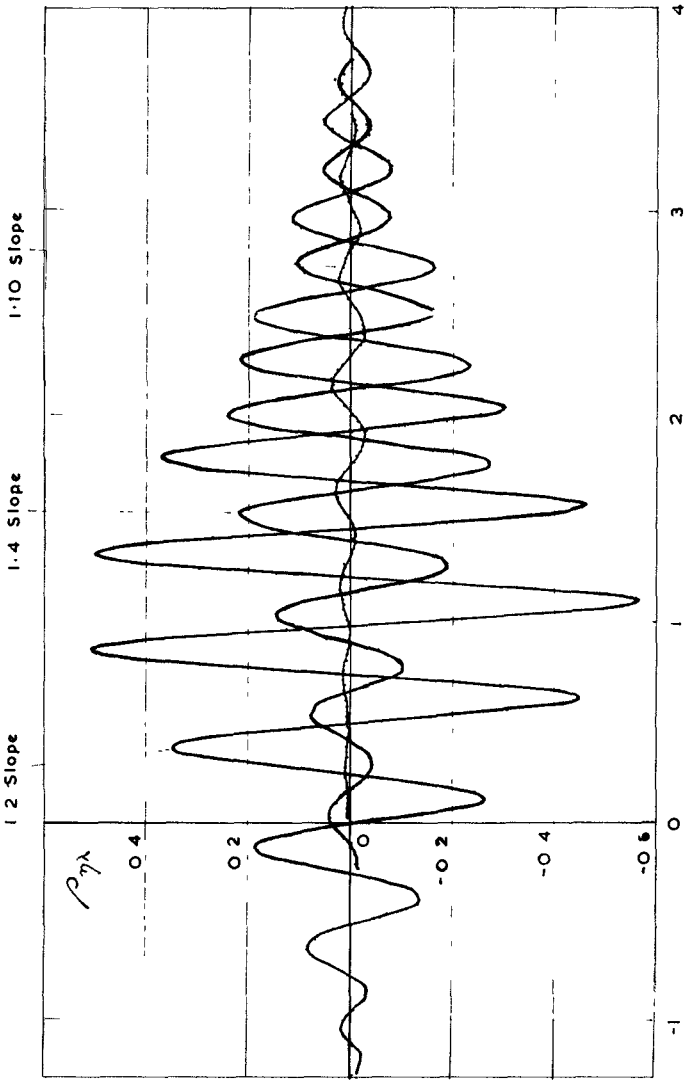

FIGURE 11 CROSS-CORRELATION COEFFICIENT FOR WAVES AND THEIR RUN-UP ON VARIOUS SLOPES AT A WIND VELOCITY OF 35 FT/SEC

CHAPTER 57

THE EFFECT OF WAVE ENERGY SPECTRA ON WAVE RUN-UP

J.H. van Oorschot and K d'Angremond
Delft Hydraulics Laboratory, Delft, Netherlands.

1. ABSTRACT

Previous investigations carried out by the Delft Hydraulics laboratory have shown the necessity of applying irregular waves in studies on wave run-up. The installation of a wave generator driven by hydraulic actuators has created the possibility of producing irregular waves with arbitrary wave spectra.

Investigations performed with this type of wave generator show the influence of the shape of the energy spectrum on the wave run-up on smooth straight slopes of 1:4 and 1:6. The results are compared with run-up figures derived from experiments with wind generated waves and with monochromatic waves.

2. INTRODUCTION

A seawall is generally designed to withstand certain wave conditions. Depending upon the circumstances the conditions may be a storm surge, attack by waves or a combination thereof. The present study is restricted to one aspect of the attack by waves only, i.e. the determination of the crest height above the still water level. An accurate assessment of the required crest level is important as the cross-sectional area of the dyke increases approximately proportional to the square of the crest height.

To determine the crest level on the basis of experiments suitable criteria have to be established with respect to run-up or overtopping. The criteria shall define either the crest level relative to a level of wave run-up under design condictions or an acceptable amount of overtopping. Little is known at present about the mechanism that underlies the damage caused by wave attack on dykes. The assumption seems justified however, that overtopping is one of the major factors causing damage to the inner (grass grown) slopes. It is therefore generally accepted nowadays in the Netherlands that no overtopping is allowed under design conditions. This means that the crest level should be at least at the level of wave run-up.

The prevailing windwaves are unfortunately of a statistical nature with respect to their height and period. Consequently the wave run-up is of a statistical nature too and a distinct maximum cannot be defined. The design level for wave run-up is now adopted in the Netherlands as the level which is exceeded by 2% of the uprushing waves under design con-

ditions. If it is expected that the inner slope of a particular dyke is more or less vulnerable to overtopping this percentage can be adapted accordingly. Paape(Ref. 1) has shown already in 1960 that the amount of overtopping water is a parameter which is in principle more relevant to damage at the inner slope than the run-up. However, it is still a point of investigation and discussion which amount of overtopping will initiate damage to the inner slopes. As long as the proper relationship between damage (onset and extent) and overtopping or run-up is not known neither of these parameters are preferable to each other.

In view of the simplicity of measuring technique, in the present study the run-up is selected as a parameter.

3. PREVIOUS INVESTIGATIONS

In the past extensive model investigations were carried out in several Institutes to determine the wave run-up on smooth and rough, straight and composite slopes. A majority of these tests have been carried out applying monochromatic waves. Though the applicability of these investigations was limited, their great value lies in the insight that was obtained regarding the influence of wave steepness and waterdepth on the relative run-up. (Ref. 2 and 3).

On the basis of the abovementioned data Saville calculated a statistical distribution of run-up assuming a joint distribution of wave heights and periods as described by Bretschneider for the case of fully developed sea.

Apart from the investigations with regular waves, tests have been carried out applying wind waves, generated in a wind flume. (Ref. 1). Due to the limited fetch available, the wind speeds had to be exaggerated in order to generate waves of appreciable height. This resulted in waves with a great steepness and consequently a low relative run-up.

Recently the wind flume of the Delft Hydraulics Laboratory has been equipped with new wave generating facilities and it was decided to extend the investigations of wave run-up applying irregular waves with variable wave spectra, in order to study the influence of the spectral form and the applicability of previous investigations and calculations.

4. RECENT INVESTIGATIONS

4.1 Arrangemen of the model

The experiments have been performed in the wind-wave flume of the Laboratory at Delft. The flume is 4 m wide and 1 m high, and has an effective length of 55 m. The models consisting of plywood, had straight impermeable slopes of 1:4 and 1:6 respectively, with sufficient height to prevent overtopping. The waterdepth in front of the model was 0,40 m. The models had a width of 1 m each and were placed in the flume as shown on Figure 1.

During the tests the wave motion was recorded in between the models. A continuous sampling of these records was fitted into an analogue spectrum analyser for an on-line calculation of the energy spectrum of the waves. Also the frequency distribution of wave heights was measured directly. Apart from the on-line process, all records have been digitized and analysed afterwards on a digital computer, in order to obtain the wave energy spectrum and from it the spectral width parameter.

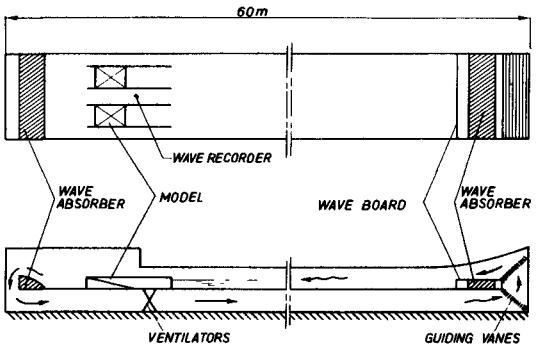

FIG 1 SITUATION OF MODELS

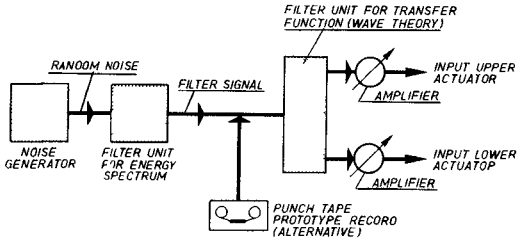

FIG 2 FORMING INPUT SIGNAL FOR THE WAVE GENERATOR

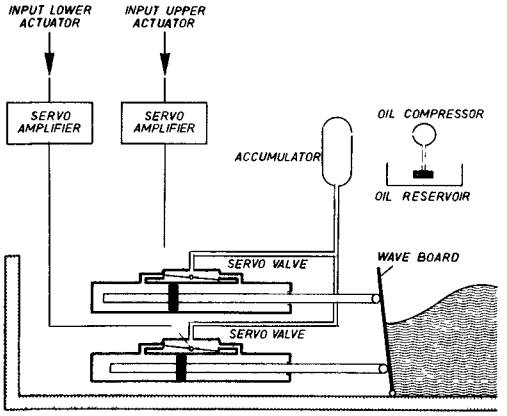

FIG 3 PRINCIPLE OF WAVE GENERATOR

The statistical distribution of the run-up was measured by means of an electronic multi-point gauge, which was fitted just above the slope.

4.2. Generation of waves

Waves were generated by a wave board. The board is driven by two servo-controlled hydraulic actuators to produce waves which have the same statistical properties as the waves in nature.

Via a set of variable analogue filters the signal of a random-noise generator is shaped conform to the required energy spectrum. This signal is filtered again in such a way that the horizontal movements of upper and lower actuator are obtained. This transfer process is based on second order wave theory.

In addition to the artificially generated wave profiles two punchtape records of prototype conditions in the North Sea, made available by the Hydraulics Division of Rijkswaterstaat, were used as an input signal for the wave board. A schematic sketch of the wave generator and a block diagram of the control procedure is given in Fig. 2 and 3.

The adaption of the details of the shape of the waves is obtained by an air stream running over the full length of the flume.

5. WAVE CHARACTERISTICS

The present investigation was directed mainly on the determination of the influence of the spectral form. Therefore a variation of the spectral form was required with other variables kept constant. However, to extend the range of applicability of the experiments, the wave steepness and relative waterdepth, expressed in the dimensionless terms Hs/gT^2 and $D/g\hat{T}^2$ have been varied too. The variation in wave heights and periods was limited by the required accuracy of the measurements and by the capacity of the wave generating facilities.

TABLE I

Test	$\hat{T}$* (sec)	Hs (cm)	$\varepsilon_{5\%}$	$Hs/g\hat{T}^2$ - 10^{-3}	$D/g\hat{T}^2$ x10^{-3}	Wave generation by:
T 1	0,97	3,7	0,38	4,0	43,4	random noise
T 2	1,04	4,2	0,44	4,0	38,1	"
T 3	0,95	3,7	0,50	4,2	45,1	"
T 4	0,97	5,6	0,38	6,1	43,4	"
T 5	0,95	5,6	0,50	6,3	45,1	"
T 6	1,54	10,2	0,34	4,3	17,0	"
T 7	1,54	10,0	0,45	4,3	17,2	"
T 8	1,47	10,2	0,57	4,8	19,0	"
T 6 repeated	1,54	9,3	0,34	4,0	17,0	"
T 8 repeated	1,47	9,7	0,57	4,6	19,0	"
T 9	1,64	13,6	0,38	5,2	15,3	"
T 10	1,55	13,5	0,55	5,7	16,9	"
T 11	1,58	13,5	0,59	5,5	16,3	
T 12	1,44	8,7	0,42	4,3	19,8	punch tape
T 13	1,40	7,4	0,52	3,9	21,1	"
T 14	0,71	6,0	0,22	12,2	81,4	wind only

* $\hat{T}$ is the period in the spectrum with maximum energy density

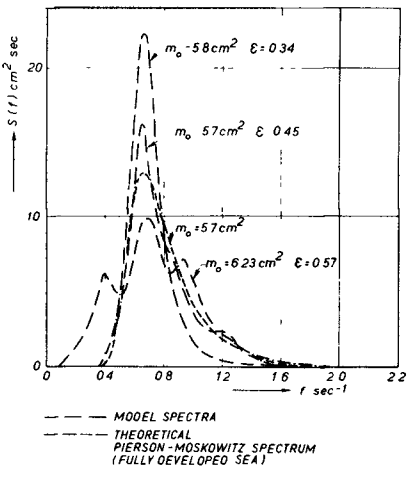

FIG 4 EXAMPLE OF APPLIED WAVE ENERGY SPECTRA

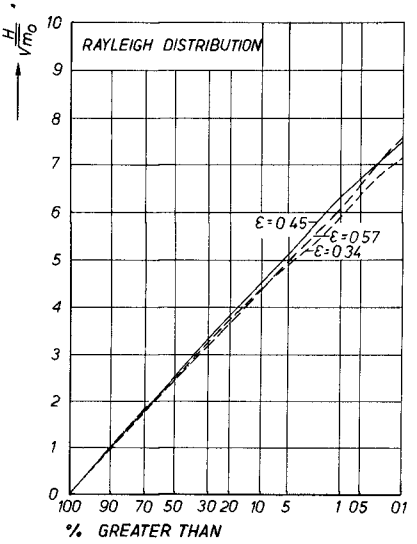

FIG 5 FREQUENCY DISTRIBUTION OF WAVE HEIGHTS

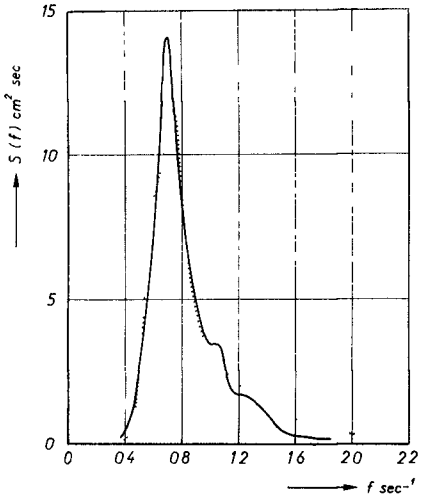

FIG 6 WAVE ENERGY SPECTRUM USING PUNCH TAPE PROTOTYPE RECORD

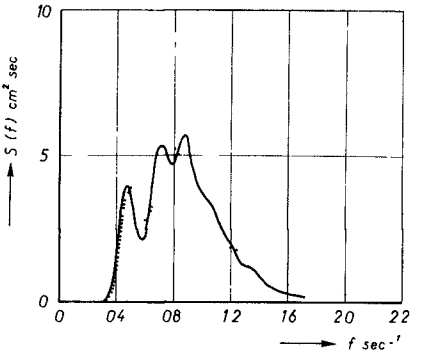

FIG 7 WAVE ENERGY SPECTRUM USING PUNCH TAPE PROTOTYPE RECORD

The relationship between wind speed and energy spectrum of the waves as described by Pierson and Moskowitz for a fully developed sea (Ref. 5) has been used as a reference for the actually applied spectral forms and wave steepnesses. Figure 4 shows such a spectrum type for a particular wave period (wind speed). As the requirements for a state of full development however are restricted to a few cases only, wave spectra and wave steepnesses with appreciable deviations may occur.

By varying the relative waterdepth $D/g\hat{T}^2$ from 15.3×10^{-3} to 45.1×10^{-3}, conditions were accomplished for almost shallow water waves to almost deep water waves.

The spectral form is expressed in the relative width parameter ε. defined as follows (Ref. 6):

$$\varepsilon^2 = \frac{m_0 m_4 - m_2^2}{m_0 m_4} \quad \text{in which} \quad m_n = \int_0^\infty s_{(\omega)} . \omega .^n \, d\omega$$

The calculation of the spectrum and ε has been carried out on a digital computer using the digitized wave records. The Nyquist frequency was 3.2 cps. The frequency interval between adjacent estimates of the spectral density 0.0533 cps. The correlation function was passed through a triangular screen filter. Inherent to the definition of ε, the higher frequencies have an unproportional large influence on the calculated value of ε, whereas both the accuracy and the practical interest of this frequency range is small. Therefore the calculation of m_n is carried out for that part of the spectrum for which the energy density S (ω) at $\omega > \hat{\omega}$ is greater than 5% of the maximum energy density $s(\hat{\omega})$. The consequences of this cut-off procedure for one special case (T13) are shown in Table II.

TABLE II

limitation at	0%	1%	2%	3%	4%	5%
ε	0.648	0.599	0.550	0.533	0.523	0.518

From the two test runs in which the input signal consisted of a prototype wave record from the North Sea a comparison has been made between the wave spectra and wave height distributions from the prototype and those from the wave flume. Figures 6 and 7 show the wave spectra, Figures 8 and 9 the wave height distributions

6. RESULTS

The frequency distribution curves of the run-up of all tests have been plotted on Gaussian distribution paper, like Fig. 10. Comparing sets of distribution curves, each set for wave conditions with the same significant wave height (Hs) and period (T) but different ε values, shows that there is an influence of ε in that way that the "steepness" of the run-up distribution is greater for higher ε values (Fig. 10).

Though only a few tests have been performed in which the waterdepth and the wave steepness have been varied independently it appeared that neither a variation in waterdepth nor a variation in wave steepness has a significant influence on the "steepness" of the run-up distribution curve, so all curves can adequately be characterized by the run-up at

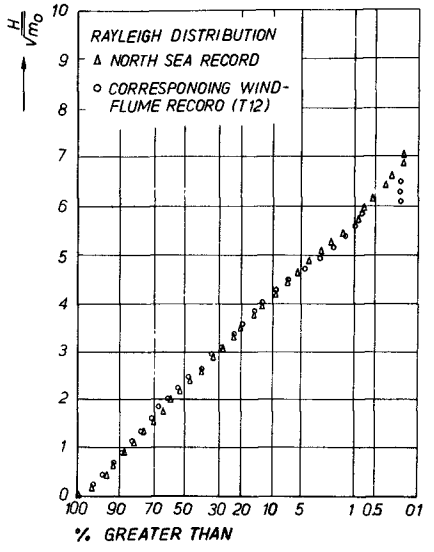

FIG 8 FREQUENCY DISTRIBUTION OF WAVE HEIGHTS USING PUNCH TAPE PROTOTYPE RECORD

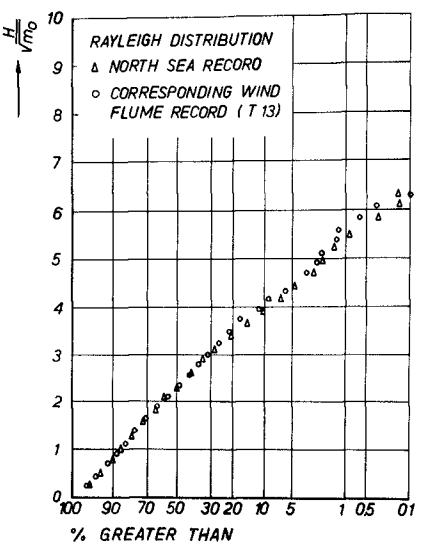

FIG 9 FREQUENCY DISTRIBUTION OF WAVE HEIGHTS USING PUNCH TAPE PROTOTYPE RECORD

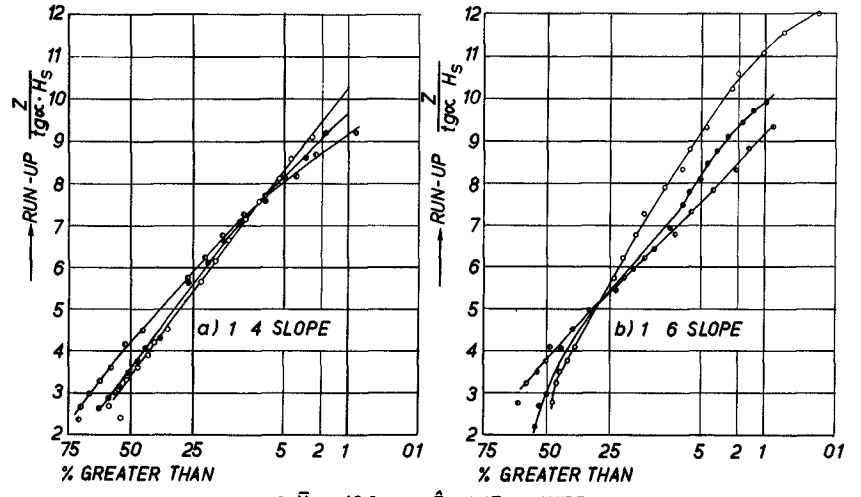

FIG 10 FREQUENCY OF RUN-UP

one specific exceedance percentage.

The run-up distribution curve is characterized by the level of run-up surpassed by 2% of the waves (Z_2) for reasons explained in the Introduction.

In the case of monochromatic waves it is known that for $D < 3H$ the influence of the waterdepth is perceptible. One may expect therefore that the same holds for irregular waves, with a comparatively small D/H ratio. Such a situation has not been investigated so far.

Hunt (Ref. 3) developed an empirical formula for the wave run-up on smooth impermeable slopes, based on tests with monochromatic waves:

$$\frac{Z}{H} = \frac{C \ tg \ \alpha}{\sqrt{H/L_o}} \tag{1}$$

The experiments indicate that also in the case of irregular waves the influence of the slope is well expressed by this formula as far as the differences between the slopes 1:6 and 1:4 are concerned.

Substituting the irregular wave characteristics in (1) the following expression is obtained:

$$Z_n = \frac{C_n(\varepsilon).Hs.tg \ \alpha}{\sqrt{Hs/L}} \tag{2}$$

or

$$Z_n = \frac{C_n(\varepsilon).Hs.tg \ \alpha}{\sqrt{Hs/g\hat{T}^2}} \tag{3}$$

The subscript n denotes the frequency of exceedence. The unknown factor C_n which is directly proportional to the wave run-up is not a constant as for monochromatic waves but a function of ε. In Fig. 11 the C_2 values of all tests have been collected and expressed as a function of ε. Notwithstanding the scatter in the C_2 values, it is evident that ε is an important parameter in the run-up phenomenon in that way that a wave motion with a wider spectrum produces considerable higher run-up for the smaller exceedance frequencies than a wave motion with a narrow spectrum. The C values are separated for both slopes because the influence of ε in the case of 1:6 slope is slightly larger than for the 1:4 slope. The scatter is fairly small if one considers that the calculation of C_2 is based on an empirical formula derived from tests with monochromatic waves. Consequently it seems justified to assume that the influence of the wave characteristics H_s and $\hat{T}$ is well expressed in formula (3). However it should be stressed that this is valid only within the range of conditions tested.

As mentioned before two tests have been conducted with waves generated by making use of wave records from the North Sea (T 12 and T 13) The wave run-up obtained in this way, expressed in the C_2 values of formula (3), is in good agreement with the run-up values obtained by making use of filtered noise (fig. 2) as an input signal for the wave generator. See Fig. 11.

Wind blowing over a water surface in a wind flume has been for many years the only possibility of simulating wind generated ocean waves in the Delft Hydraulics Laboratory, and this method is still used in many other laboratories. At the D.H.L. many tests have been performed with

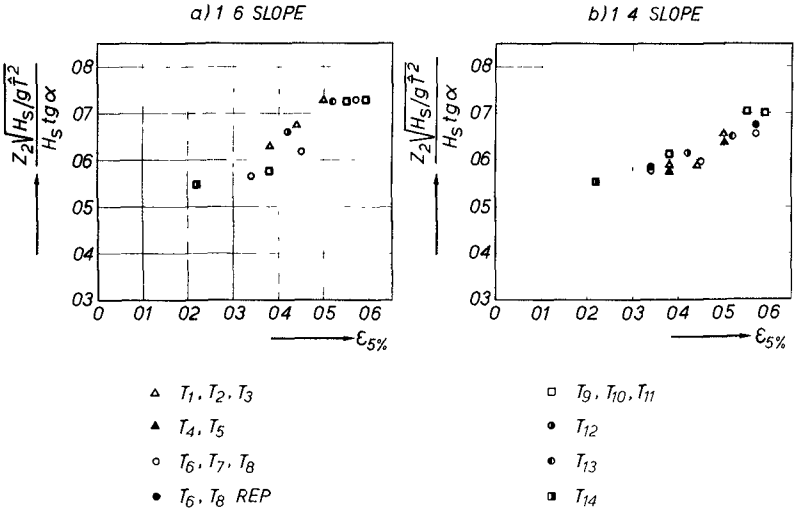

FIG 11 RELATIVE WAVE RUN-UP AS A FUNCTION OF THE SPECTRAL WIDTH $\varepsilon_{5\%}$

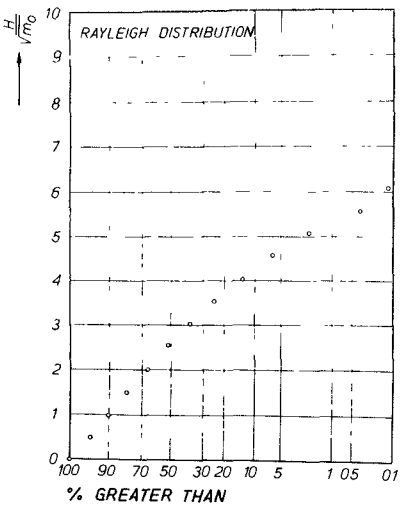

FIG 12 FREQUENCY DISTRIBUTION OF WAVE HEIGHTS FOR WIND GENERATED WAVES

this type of wave generation (Ref. 1). However, since the fetches are mostly relatively short, the wind speed has to be exaggerated to obtain waves of sufficient height and consequently also the wave steepnesses are exaggerated. In view of this, one test has been carried out using wind generated waves instead of mechanically generated waves. (See T 14) of Table I).

The wind speed was such that a comparative wave height was obtained in relation to former experiments. The resulting large wave steepness ($Hs/g\hat{T}^2 = 12.2 \times 10^{-3}$) was primarily the reason for a relatively low run-up on the two slopes, as the run-up decreases at increasing wave steepness. Moreover the wave spectrum was extremely narrow, as may appear from the ε-value of only 0.22, and the wave height distribution was quite different from the Rayleigh distribution as opposed to all other tests. Compare Figure 5 and 12. In spite of the deviating wave characteristics however the location of the corresponding C_2-values (T 14) in Figure 11 indicates that formula (3) is still applicable.

7. ANALYSIS OF RESULTS

To permit an estimation of the variability in irregular wave run-up without the use of facilities for irregular wave generation, Saville has proposed the following calculation of a statistical distribution of wave run-up (Ref. 4), using standard (monochromatic) wave run-up curves.

The probability of a combination of a particular wave height and wave period may be given as:

$$p(H,T) = p(H).p(T), \qquad (4)$$

consequently assuming a zero-correlation between wave height and wave period. The probability distributions used were those proposed by Bretschneider (Ref. 7) for fully developed sea.

With the expression (4) one can obtain a joint distribution of wave steepness $p(H/g\hat{T}^2)$ and wave height, and subsequently

using standard run-up curves giving the relation between relative run-up and wave steepness (Ref. 2), a distribution of individual relative run-up $p(\frac{Z}{H})$. Multiplication of a particular run-up $\frac{Z}{H}$ with the associated wave height from the assumed joint distribution of wave heights and periods for a particular wave condition, results in a distribution of run-up $p(z)$.

To check the applicability of this calculation and to get more insight in the influence of the spectral shape on the wave run-up a calculation as described is performed for two wave conditions (a wide and narrow spectrum) for which run-up distributions have been measured (T 6 and T 8 of Table I). Instead of assuming a zero-correlation between wave heights and periods however actual wave records of the two wave conditions have been used for the determination of the joint distribution $p(H,T)$. The records were analysed by hand, taking 300 successive waves into consideration. The result is shown on Figure 13 in which every point represents a wave with both height and period within a certain class. Following the method of Saville a distribution of run-up of 300 individual waves is obtained for two different spectra and 2 different corresponding H/T correlations. The solid lines on Figure 14 show the result of the calculation. Although this calculation is rather simplified it appears that,

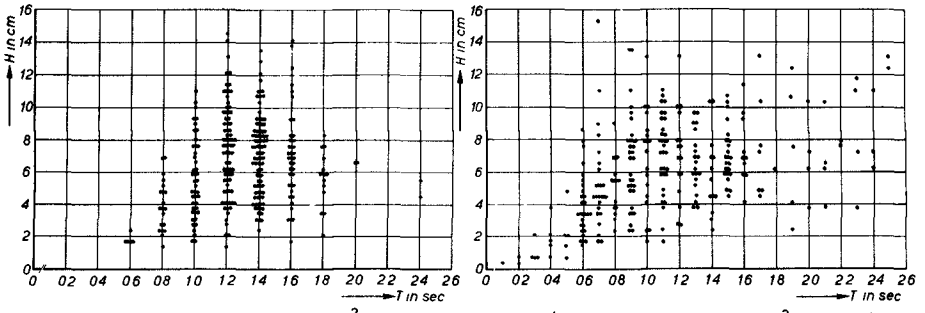

a) NARROW SPECTRUM ($m_0 = 58\,cm^2$ $\varepsilon = 0.34$) b) WIDE SPECTRUM ($m_0 = 6.23\,cm^2$ $\varepsilon = 0.57$)

FIG 13 JOINT DISTRIBUTION OF WAVE HEIGHT AND PERIOD

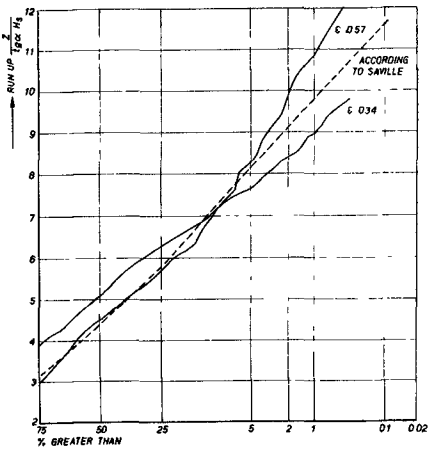

FIG 14 FREQUENCY OF RUN-UP CALCULATED

thanks to the fact that a large amount of waves is considered, the obtained result is in remarkable good agreement with the recorded wave run-up for the same wave condition. Compare Figure 10 and Figure 14.

The calculation shows in addition that the difference in the higher part of the run-up curve for the two wave conditions considered was caused by the few long, low waves present in the case of a wide spectrum only (Fig. 13). This was also confirmed by visual observation. These waves with extreme low steepness hardly break on the slope and consequently cause an unproportional high run-up. The assumption of a zero-correlation between wave height and period according to Saville's method results in a run-up distribution (the dotted line on Figure 14) which corresponds with the measured run-up distribution for the middle one of the three spectra in Figure 4 (the Pierson Moskowitz spectrum for fully developed sea).

Calculated and measured distribution curves diverge at higher exceedance percentages as a result of the applied measuring technique.

8. CONCLUSIONS

- The statistical run-up distribution curves diverge at the smaller exceedance percentages for different spectral forms. Wider spectra are accompanied by higher run-up.
- Increase in wave run-up for wider spectra is caused by differences in the joint distribution of wave heights and periods. The distributions of wave heights only are the same for the different spectra.
- The relationship $Z_n = \frac{C_n(\varepsilon).Hs.tg\ \alpha}{\sqrt{Hs/gT^2}}$ gives a good approximation of the influence of wave height, wave period and slope for the conditions investigated.
- Wind waves generated in the laboratory applying exaggerated wind speed, produce wave run-up which is generally to low due to the extreme narrow wave spectrum.
- The calculation of a statistical wave run-up distribution curve assuming a zero-correlation between wave height and period as described by Saville agrees fairly well with the measured one for a state of fully developed sea. Taking into consideration variations in the joint distribution of wave heights and periods for spectra different from the spectrum of fully developed sea, a higher run-up is obtained for wider spectra; conversely lower run-up goes with narrower spectra.

9. REFERENCES

1. Paape, A., Experimental Data on the Overtopping of Seawalls by Waves; Proc. of the Seventh Conf. on Coastal Eng., 1960.
2. U.S. Army Coastal Engineering Research Center; Shore Protection Planning and Design; Technical Report no. 4, 1966.
3. Hunt, I.A. Jr.; Design of Seawalls and Breakwaters; Proc. of the Am. Soc. of Civ. Eng., Journ. of the Waterw. and Harb. Div.; 85, 1959, no. ww 3, part I, paper 2172.
4. Saville, Th., Jr.; An Approximation of the wave Run-up Frequency Distribution; Proc. of the Eighth Conf. on Coastal Eng., Nov. 1962.
5. Pierson, J.W., Jr.; and Moskowitz, L.; A Proposed Spectral Form for Fully Developed Wind Seas Based on the Similarity Theory of S.A. Kitaigorodskii; Journ. of Geoph. Res., 1964, Vol. 69, no. 24; Dec.
6. Kinsman, B.; Wind Waves; New Jersey, 1965.
7. Bretschneider, Ch.L.; Wave Variability and Wave Spectra for Wind-Generated Gravity Waves; Technical Memorandum No. 118; U.S. Army Coastal Engineering Research Center, 1959.

CHAPTER 58

ON THE OVERLAND FLOW OF TSUNAMI AND EFFECTIVENESS OF WALL AS A COUNTER MEASURE

Toshio Iwasaki
Professor of Tohoku University
and
Hiroyoshi Togashi
Assistant of Tohoku University

Tohoku University
Sendai, Japan

SYNOPSIS

When a tsunami of large magnitude strikes a coast line, various kinds of disaster such as loss of lives, properties or public investments are caused by inundation of tsunami over nearly horizontal area. Although tsunami runup has been investigated for the sloping beach, these populated area is bordered on sea by a vertical wall such as a quaywall or a highway revetment. In this paper, transformation of tsunami waves at a vertical quaywall is analysed using U-C characteristics and overland flow is treated. Effectiveness of a vertical land dike aiming to stop running water is investigated also. Theoretical results are verified by experiments.

INTRODUCTION

Tsunami is caused by a mid-ocean earthquake of large magnitude, having very flat steepness, very long wavelength of several hundred kilometers and wave period of several ten minutes in the ocean. When it approaches to a coast, wave height is increased by effect of shallowness as understood easily by the Green's theorem. Moreover tsunami is amplified by diffraction and reflection owing to favorable nearshore topography and also by harbour resonance. As a result, several or several ten meters of wave height is not unusual which results catastrophic disaster.

In Japan, 101 tsunamis have been recorded since 687, in which 18 tsunamis caused catastrophe. Sanriku Coast is situated in northern part of Honshu, the main island of Japan and faced to the Pacific seismic belt, so this coast has been attacked by tsunamis most frequently in Japan. As this coast is a rias type, there are various kinds of bays in their scale and shape, which depth is usually over 10 or 20 meters at their mouth and have vertical cliffs on most of coastline leaving scarce flat land at the innermost part, where fishery ports and harbours are located with populated area behind it. Stepping over quaywalls of ports and harbours or highway revetments, tsunami waves cause overland flow. Although tsunami runup on a sloping beach has been investigated extensively by various authors, overland flow of this type seems a problem to be solved still now.

This paper deals with mechanism of transformation of tsunami wave at a quaywall and that of overland flow and effectiveness of a land dike as a counter measure.

U-C CHARACTERISTICS OF LONG WAVES OF FINITE AMPLITUDE

As long waves of finite amplitude, following relationships hold also for tsunami waves,

for C+ characteristics $P=c_*2(C-1)+U$ (1)

for C- characteristics $Q=c_*2(C-1)-U$ (2)

in which analysis is confined to one dimensional and the slope of the sea bottom is assumed horizontal. c_* is $\sqrt{gh}$, $C=(1+\eta/h)^{1/2}$ and $U=u/c_*$ where h is the depth, g is the acceleration of the gravity and u is the horizontal velocity. (Lamb 1932)

Eq. (1) implies a U-C characteristics in a U-C plane corresponding to a C+ characteristics in a X-T plane has negative slope of 1/2 which intersects the horizontal axis at a point $(P/c_*, 0)$ which is shown in fig.1. Also by eq. (2), a U-C characteristics corresponding to a C- characteristics has positive slope of 1/2 which intersects the horizontal axis at a point $(-Q/c_*, 0)$

In the progressive wave, Q=0. Hence $U_1=2(C_1-1)$, $P/c_*=4(C_1-1)$ and this is expressed by a point A, namely A_1, A_2, A_3 or A_p corresponding to their value of P/c_* or $4(C_1-1)$ which can be determined by η or surface elevation of each wave element, where suffix 1 refers to values of incident waves and suffix p refers to values at the peak. When these wave elements are stopped at the vertical quaywall, U=0. So, point A moves to point B, namely B_1, B_2, B_3 or B_p which shows U-C characteristics of a perfect clapotis. Then,

$$Cc-1=2(C_1-1) \tag{3}$$

where $Cc=(1+\frac{\eta_c}{h})^{1/2}$ and $C_1=(1+\frac{\eta_1}{h})^{1/2}$ in which suffix c refers to a clopotis.

The reflected wave elements can be expressed by points C_1, C_2, C_3 and C_p as these characteristics must pass points B and $U_r=-2(C_r-1)$ since P=0, where suffix r refers to a reflected wave.

When C_1-1 is larger than $1/2(C_w-1)$, overruning flow takes place, where $C_w=(1+\frac{H_w}{h})^{1/2}$ in which H_w is the quaywall height above still water. Then the clapotis at the quaywall is imperfect. Assumption is made for these reflected wave elements that the velocity is same with incident wave elements, but the surface elevation cannot be higher than $h+H_w$, or $C_r-1=1/2\cdot(C_w-1)$.

Then Cc-1 can be given by two characteristics through C_1 and C_r as shown in fig.2. So,

$$C_c-1=\frac{3}{2}(C_1-1)+\frac{1}{4}(C_w-1) \tag{4}$$

$$U_c=(C_1-1)-\frac{1}{2}(C_w-1) \tag{5}$$

Where C_w-1 is smaller than $2(C_1-1)$. That is,

$$C_w-1 < 2(C_1-1) \tag{6}$$

It may seem interest that when water level is equal to the height of the quaywall, reflection is took place only as time sequence of the velocity without wave configuration as shown in fig.3. In this case,

$$C_c-1 = 3/2(C_1-1) \tag{7}$$

and

$$U_c=C_1-1 \tag{8}$$

as $C_w-1=0$. And since U_c and C_c-1 are positive, these wave elements invade into land causing overland flow.

OVERLAND FLOW OF TSUNAMI

Experiments shew that when overland flow was occured, water depth decreased abruptly at the brink of the quaywall as shown in fig.4 and flow was assumed being transformed from subcritical to supercritical.

For overland flow no-dimensional wave celerity is defined as

$$C'=\sqrt{\frac{\eta'}{h}} \tag{9}$$

Where η' is measured from the horizontal bed.
Then since

$$\eta_c' = \eta_c-H_w \tag{10}$$

$$C_c'=\sqrt{\frac{\eta_c-H_w}{h}} =\sqrt{C_c^2-C_w^2} \tag{11}$$

As $U_c'=U_c$, the following relation can be obtained.

$$C_c'^2-U_c'^2=5/16\ J^2+3/2\ JC_w \tag{12}$$

in which

$$J = 2C_1-C_w-1 \tag{13}$$

Since J is positive when overrunning is occured, the right hand side of eq.(12) is positive which means C_c' is larger than U_c', or flow is subcritical at the brink of the quaywall.

Then a critical flow section A is assumed established at some distance from the brink followed by supercritical flow. As this distance has not been decided yet, an assumption is made here that this distance is infinitely small and the section of critical flow is situated just next to the brink of the quaywall.

For calculation of overrunning flow, the origin of x-axis is taken at the brink of the quaywall. C_+ characteristics emerging from t-axis are expressed by

$$\frac{dx}{dt} = U_c' + C_c' \tag{14}$$

and on which

$$U_c' + 2C_c' = U_A' + 2C_A' \tag{15}$$

As mentioned above,

$$U_A' = C_A' \tag{16}$$

Then from (15) and (16)

$$U_A' = C_A' = 1/3(U_c' + 2C_c') \tag{17}$$

, in which $U_c' = U_c$ and C_c' are given already. As the distance between O and A is infinitely small, the two points are coincided practically and are considered to give a boundary condition.

C- characteristics emerging from A-axis are given by,

$$\frac{dx}{dt} = U_A' - C_A' = 0 \tag{18}$$

, which shows C- characteristics are parallel with t-axis and range of influence is limited to the right half of x-t plane as accepted in practice.

Overrunning flow is resembled with flow after the breaking of a dam in which various assumptions has been presented for the front condition. According to the theory originally proposed by St. Venant, the front depth is zero and so C_+ and C_- characteristics coincide with each other to compose the characteristic envelope. However a more general relation is

$$C_f' = aU_f' \tag{19}$$

for the front condition, in which a is a constant and a reciprocal of the Froude number and suffix f refers to the front. (Abbot, 1961) (Méhauté, 1964) Then the characteristic equation for the leading wave element is,

$$d(U' + 2C') = -f\left(\frac{U'}{C'}\right)^2 \frac{dx}{U' + C'} \tag{20}$$

in which f is a friction coefficient and X=x/h. From eq. (20),

$$\frac{U'^2}{2} = \frac{U_A'^2}{2} - \frac{f}{a^2} \cdot \frac{X - X_A}{(1+a)(1+2a)} \tag{21}$$

for the horizontal bed after Freeman and Méhauté. The front is the envolope of the leading wave element given by

$$\frac{dX}{dT} = U' \tag{22}$$

Eliminating U' from eq. (21) and (22), the leading front characteristics are given.

As shown in fig.5, the succeeding C_+ characteristics emerging from a point F takes over the leading front emerging from a point E. Then on the C_+characteristics,

$$U_f'+2C_f'=U_F'+2C_F'-f(\frac{U_F'}{C_F'})^2\cdot \Delta T_{FG} \tag{23}$$

and on the leading front

$$C_f' = aU_f' \tag{24}$$

Then from eq. (23) and (24)

$$C_f' = \frac{a}{1+2a}\cdot[U_F'+2C_F'-f(\frac{U_F'}{C_F'})^2\cdot \Delta T_{FG}] \tag{25}$$

and also

$$U_f' = \frac{1}{1+2a}[U_F'+2C_F'-f(\frac{U_F'}{C_F'})^2\cdot \Delta T_{FG}] \tag{26}$$

After this intersection G, velocities are changed in accordance with eq. (21) until a next C_+ characteristics takes over.

Internal zone bounded by the t-axis and the characteristic envelope of the leading front can be analysed by two sets of characteristics as usual.

Froude number of the leading front or 1/a is normally assumed as 2 from works by Keulegan, Abbott,Méhauté and others.

REFLECTION AND OVERFLOW AT THE LAND DIKE

Along the Sanriku coast, many land dikes have been constructed to protect resident quarters as one of counter measures for running water of tsunami. Although their height was designed in accordance with the highest trace of inundation, its reliability has not been checked until tsunamis struck these areas by chile earthquake in 1960 which stimulated us beginning this research.

Fig.6 shows schematically reflection and overflow of running tsunami at a land dike. As the Froude number of the leading front is assumed as 2, the incident flow is supercritical in section I. So a bore is occured by reflection, behind which flow is subcritical. If the height of a land dike is lower than that of the reflected bore, overflow takes place as shown in fig.6.

Between section I and II, a shock condition exists as

$$h_1(u_1-\omega)-h_2(u_2-\omega)=0 \tag{27}$$

$$u_1h_1(u_1-\omega)-u_2h_2(u_2-\omega)=\frac{g}{2}\cdot(h_2^2-h_1^2) \tag{28}$$

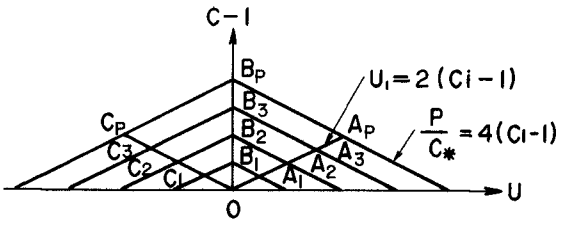

Fig 1 U-C characteristics of a long wave of finite amplitude.

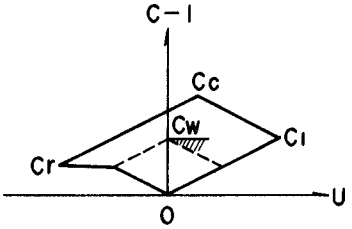

Fig.2 Partial clapotis in U-C plane

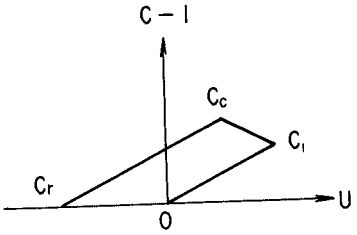

Fig.3 Partial clapotis in U-C plane when $C_w = 1$

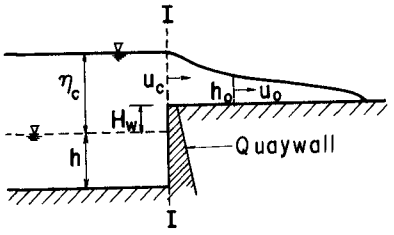

Fig. 4 Tsunami transformation at the quaywall

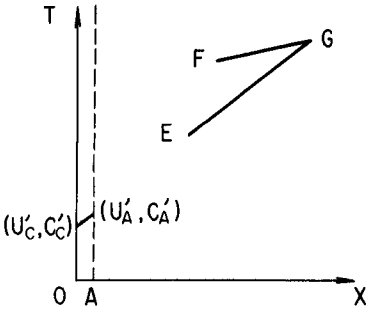

Fig.5 Characteristics at the brink of the quaywall and that of a leading front

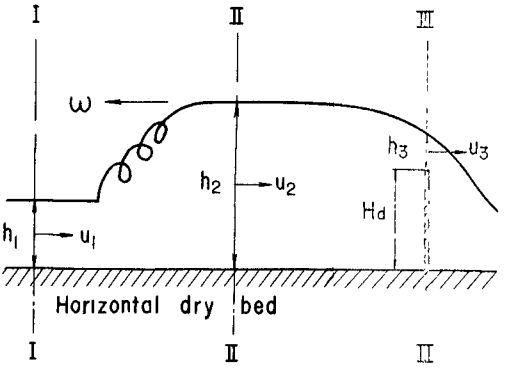

Fig.6 Reflection and overflow at a land dike

where ω is the speed of propagation of the bore front and suffix 1 and 2 refers to values in section I and II respectively.

Between section II and III, an energy equation holds as,

$$h_2+\frac{u_2^2}{2g}=h_3+\frac{u_3^2}{2g}+H_d \tag{29}$$

and

$$u_2h_2=u_3h_3 \tag{30}$$

, in which H_d is the height of the land dike and suffix 3 refers to values in section III. In section III, a critical condition is assumed as,

$$h_3=\sqrt[3]{\frac{(u_3h_3)^2}{g}} \tag{31}$$

From (27) and (28),

$$\omega=u_1=\sqrt{\frac{gh_2}{2h_1}\cdot(h_1+h_2)} \tag{32}$$

as ω is negative.
Putting eq. (32) into eq. (27), we get

$$u_2=(1-\frac{Y}{F_1})u_1=\frac{y}{F_1}u_1 \tag{33}$$

, where

$$Y=(x_2-1)\sqrt{1/2(1+\frac{1}{x_2})}\quad,\quad x_2=\frac{h_2}{h_1}\ . \tag{34}$$

and

$$F_1=\frac{u_1}{\sqrt{gh_1}}\quad,\quad y=F_1-Y \tag{35}$$

From (30) and (33)

$$x_3=x_2^{2/3}\ .\ (F_1-Y)^{2/3}=(x_2y)^{2/3} \tag{36}$$

, where $x_3=h_3/h_1$

Putting (33) and (36) into (29), we get

$$z=x_2+1/2\ y^2-3/2\ (x_2y)^{2/3} \tag{37}$$

, where

$$z=\frac{H_d}{h_1} \tag{38}$$

Fig.7 shows the relationship between x_2 and F_1 with a parameter z and between z and F_1 with a parameter x_2. The height of reflected bore is nearly proportional to the Froude number of the incident flow. Also to keep x_2 constant, z must be lowered when F_1 is increased. From eq. (33), overflow takes place when F_1 is larger than Y, which gives the lower limit of x_2 as the latter is proportional to x. This limit is designated as $x_2(L)$ and is equal to the wall height z as shown in eq. (37).

From eq. (32), the bore must be stopped resulting a hydraulic jump when $\omega = o$, or

$$F_1 = x_2\sqrt{\frac{1}{2}(1 + \frac{1}{x^2})} \tag{39}$$

, which gives the higher limit of x_2 or $x_2(U)$ since the bore is flushed away when o. In this case the wall is no longer useful for a counter measure of the tsunami running flow. From (37),

$$z = z(U) = x_2(U) + \frac{1}{2}\left(\frac{F_1}{x_2(U)}\right)^2 - \frac{3}{2}(F_1)^{2/3} \tag{40}$$

in which z(U) means the wall height ratio for this limit case.

Eliminating x_2 from eq. (36) and (37), the relationship between x_3 and F_1 is given taking z as a parameter which is shown in fig.8. It is found that x_3 is almost linearly proportional to F_1.

As shown in fig.9, flow runs still after overflowing the dike. Between section III and IV, following relations are hold, if energy loss is neglected.

$$h_3 + \frac{u_3^2}{2g} + H_d = h_4 + \frac{u_4^2}{2g} \tag{41}$$

$$u_3 h_3 = u_4 h_4 \tag{42}$$

From eq. (41) and (42), the following equations is given together with eq. (31).

$$x_4^3 - (2 + \frac{3}{2}x_3)x_4^2 + \frac{1}{2}x_3^3 = o \tag{43}$$

in which $x_4 = h_4/h_1$. And

$$F_4 = \frac{u_4}{\sqrt{gh_4}} = \left(\frac{h_3}{h_4}\right)^{3/2} = \left(\frac{x_3}{x_4}\right)^{3/2} \tag{44}$$

However it is convenient that x_4 is expressed as a function of F_1 taken z as a parameter, which is given in fig.10. It is shown that as z is higher, x_4 becomes smaller. Since at the front Froude number is between 1 and 2, height of land dikes is acceptable when it is designed by $0.4 < z < 2.2$.

By difinition,

$$\frac{u_4}{u_1} = \frac{F_4}{F_1} \cdot x_4^{1/2} \tag{45}$$

$$\frac{q_4}{q_1} = \frac{F_4}{F_1} \cdot x_4^{3/2} \tag{46}$$

These are related to F_1 taking z as a parameter, in fig.11. As expected normally, invading flow decreases when the hight of a land dike increases. However velocity ratio increases causing stronger tractive force.

EXPERIMENTAL PROCEDURE

Experiments were conducted in a wave basin 23m long, 0.5m wide and 0.5m high. A pneumatic wave generator was installed at one end of the basin which dimension was 2.5m long, 1.5m wide and 1.5m high and was capable to produce a very long solitary wave. At the other end a horizontal dry bed model 10m long was installed which had a vertical quaywall of the height 0.312m.

Resistance type wave gauges were set 6m and 1m off the quaywall respectively. Fig.12 shows an example of recorded waves. Photographs of running water on the horizontal bed were taken by a motor driven camera and a 16mm movie camera at the rate of 3 frames and 24 frames per second respectively. Scales were marked on the bed and the wall, by which depth of wave front and water sheet were taken their co-ordinates using a profile-projector. Fig.13 and fig.14 show an example of wave fronts just after the quaywall and of waves overflowing the land dike respectively.

The depth of still water was set among 20 and 30cm. As a solitary wave, an incident wave element is expressed by

$$\eta_1 = H_1 \operatorname{sech}^2\left(\frac{x}{h}\sqrt{\frac{3}{4}\frac{H_1}{h}}\right) \tag{47}$$

, where H_1 is the wave height of the solitary wave, in which 98% of total wave volume is included between ± 3.8 of x/h where the x origin is taken at the summit. So, for numerical calculation $_1$ is measured from the elevation at $x/h = \pm 5$. Then H_1 was chosen among 5 and 15cm. Also the period T is taken for the part of $x/h = \pm 5$ in a wave, which was set among 4.7 and 28.5 sec. The height of land dikes was chosen between 3 and 12.5cm and these are located among 50 and 500cm from the quaywall.

Total 426 runs were tested and several runs were compared with results of theoretical calculation.

CALCULATION AND EXPERIMENTAL VERIFICATION

Using one of test conditions, following numerals are used for calculation.

$$h = 28.1\text{cm}, \quad H_1 = 7.7\text{cm}$$

The distance of a land dike from the quaywall L_d is 120 cm and its height

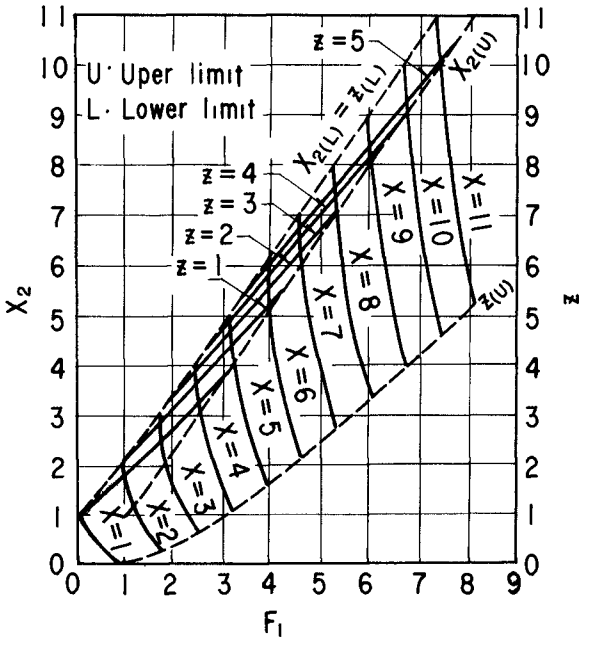

Fig.7 Relationship between x_2, z and F_1.

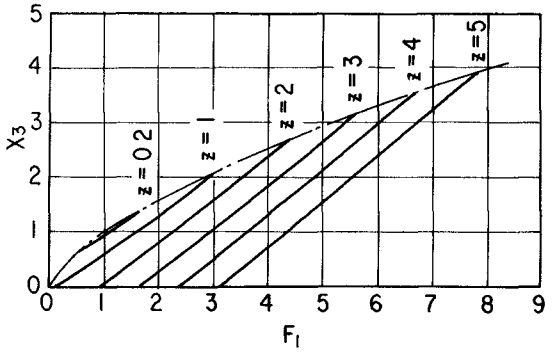

Fig.8 Relationship between x_3 and F_1 with a parameter z.

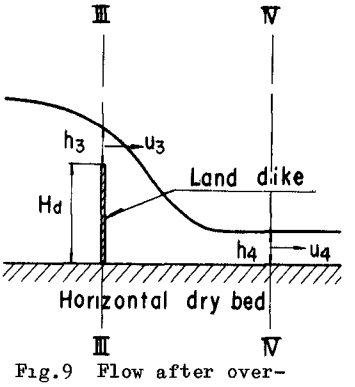

Fig.9 Flow after overflowing the dike.

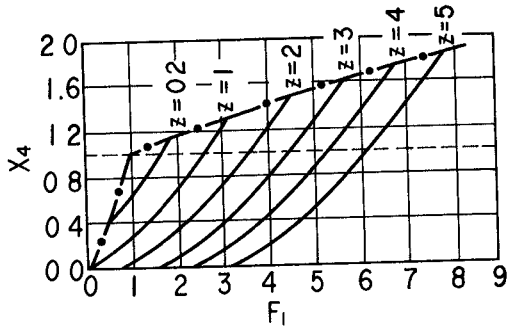

Fig.10 Relationship between x_4 and F_1 with a parameter z.

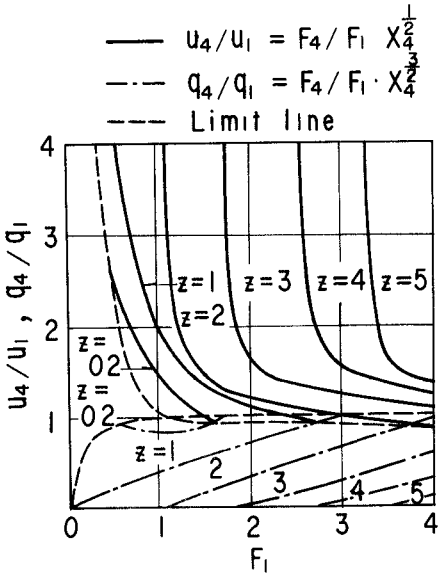

Fig.11 Relationship between u_4/u_1, q_4/q_1 and F_1 with a parameter z.

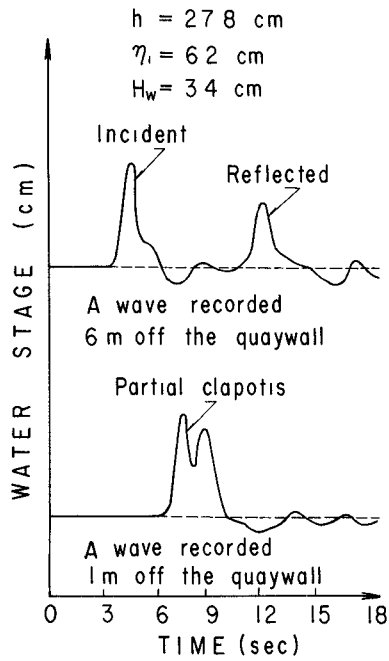

Fig.12 An example of recorded waves

Fig.13 A wave front just after the quaywall.

Fig.14 A wave over the land dike.

H_d is 3.0 cm. Then from eq. (47)

$$\eta_1 = 7.7 \ \mathrm{sech}^2(0.453\ x) \qquad (48)$$

, where X=x/h. In table 1, some specific values are given for points equally spaced on X-axis.

The height of a quaywall is taken as H_w=3.1cm. U-C characteristics give values of the reflecting wave in table 2 following to the theory proposed. X-T and U-C characteristics are given in fig.15 and fig.16 respectively.

Table 1

Calculated point	(5)	(4),(6)	(3),(7)	(2),(8)	(1),(9)	(0),(10)
X	0	1	2	3	4	5
η_1	7.7	6.314	3.717	1.789	0.782	0
$M_1=\eta_1/h$	0.274	0.225	0.132	0.064	0.028	0
$C_1=\sqrt{1+M_1}$	1.129	1.107	1.064	1.031	1.014	1
$U_1=2(C_1-1)$	0.257	0.213	0.128	0.063	0.028	0
$(dX/dT)_+=U_1+C_1$	1.386	1.320	1.192	1.094	1.041	1

Table 2

Calculated point	(5)'	(4)';(6)'	(3)';(7)'	(2)';(8)'	(1)';(9)'	(0)';(10)'
η_r (X=0)	1.532	1.532	1.532	1.532	0.783	0
$M_r=\eta_r/h$	0.055	0.055	0.055	0.055	0.028	0
$C_r=\sqrt{1+M_r}$	1.027	1.027	1.027	1.027	1.014	1
$U_r=-U_1$	-0.257	-0.213	-0.128	-0.063	-0.028	0
$(dX/dT)_-=U_r-C_r$	-1.284	-1.240	-1.155	-1.090	-1.042	-1

Then values of surface elevation are given in table 3 and also are plotted in the left half of fig.17. It is cleary shown that the incident wave is transformed to the partial clapotis and is reflected at the quaywall.

Values of U and C at the quaywall just derived are converted to U' and C' by eq. (16) and $U_c'=U_c$. Then from eq. (17) U_A' and C_A' are calculated which gave boundary conditions for the overland flow. As shown in fig.16, the moment which the clapotis just touches the crest of the quaywall, is not coincided with an intersection of characteristics issuing from points given in table 1 and 2. So, assumption is made this moment is given by a fraction of time increment which is equal to that of U-C segment.

Then the first wave element emerges from (X=0, T=1.27 sec) on the X-T plane, from which a line of C_f characteristic is drawn by $dx/dt=U_A'+C_A'=2U_A'$ since $U_A'=C_A'$ as shown in eq.17. Moreover a line of front

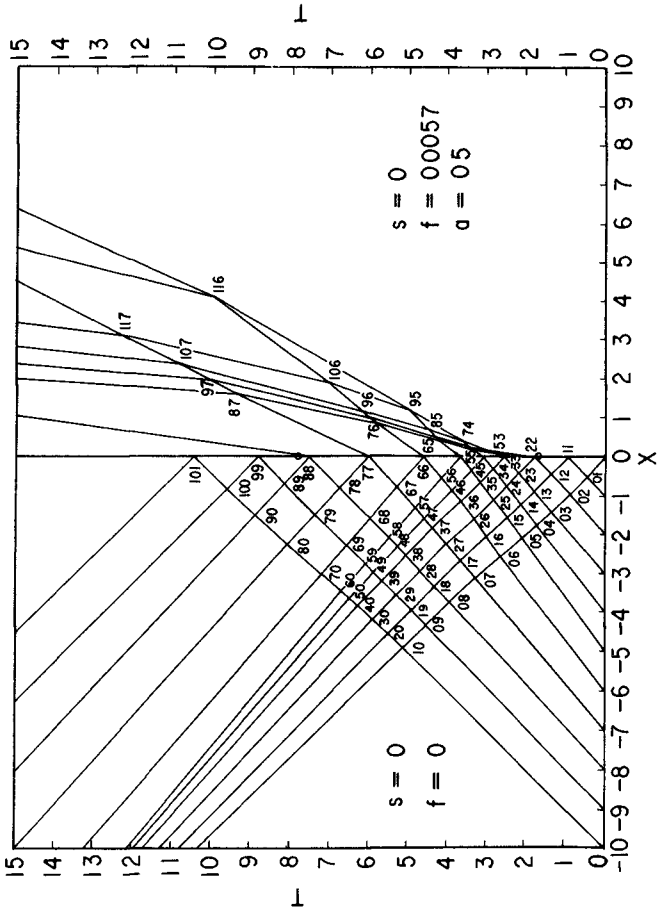

Fig. 15 X-T characteristics

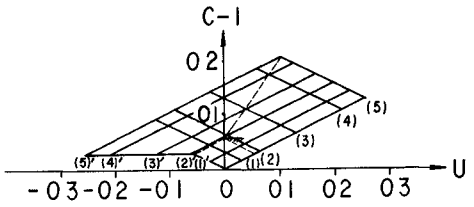

Fig.16 U-C characteristics

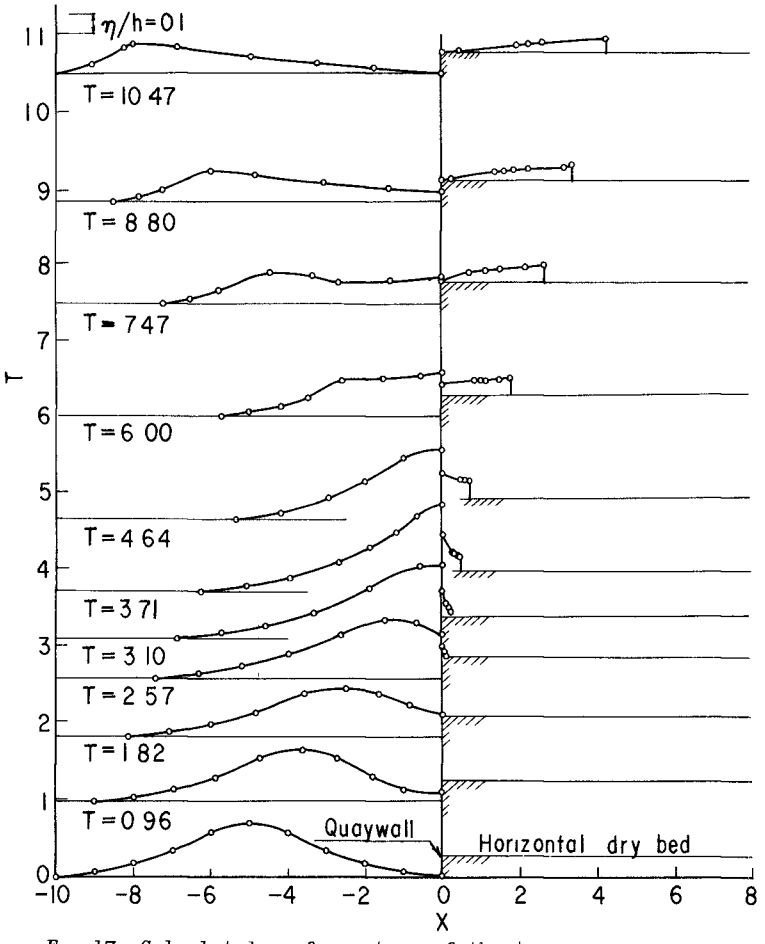

Fig.17 Calculated configuration of the tsunami overrunning the vertical quaywall.

Table 3

T= 0	X	0	-1	-2	-3	-4	-5	-6	-7	-8	-9
	η/h	0	0.028	0.064	0.132	0.225	0.274	0.225	0.132	0.064	0.028
T= 0.96	X	0	-1	-1.80	-2.74	-3.65	-4.73	-5.88	-6.97	-8	-9.03
	η/h	0.053	0.064	0.132	0.225	0.274	0.225	0.132	0.064	0.028	0
T= 1.82	X	0	-0.83	-1.64	-2.50	-3.59	-4.83	-6.00	-7.08	-8.16	
	η/h	0.124	0.164	0.228	0.274	0.225	0.132	0.064	0.028	0	
T= 2.57	X	0	-0.67	-1.50	-2.62	-3.98	-5.20	-6.33	-7.45		
	η/h	0.231	0.295	0.309	0.225	0.132	0.064	0.028	0		
T= 3.10	X	0	-0.58	-1.90	-3.32	-4.62	-5.75	-6.90			
	η/h	0.374	0.371	0.263	0.132	0.064	0.028	0			
T= 3.71	X	0	-0.65	-1.20	-1.87	-2.68	-3.95	-5.11	-6.27		
	η/h	0.454	0.395	0.313	0.234	0.153	0.064	0.028	0		
T= 4.64	X	0	-1.03	-2.03	-2.03	-2.95	-4.20	-5.39			
	η/h	0.374	0.329	0.199	0.115	0.030	0				
T= 6.00	X	0	-1.53	-2.60	-3.50	-4.21	-5.00	-5.76			
	η/h	0.231	0.201	0.193	0.103	0.055	0.026	0			
T= 7.47	X	0	-1.35	-2.70	-3.37	-4.47	-5.82	-6.55	-7.25		
	η/h	0.124	0.115	0.111	0.136	0.160	0.055	0.026	0		
T= 8.80	X	0	-1.40	-3.07	-4.86	-6.00	-7.25	-7.90	-8.53		
	η/h	0.053	0.061	0.092	0.136	-0160	-0055	0.026	0		
T= 10.47	X	0	-1.78	-3.22	-4.95	-6.82	-8.00	-8.26	-9.08	-10.15	
	η/h	0	0.026	0.057	0.092	0.136	0.160	0.136	0.055	0	

characteristics is drawn also by

$$\frac{dX}{dT} = \sqrt{U_A'^2 - \frac{2f}{a^2} \cdot \frac{X-X_a}{(1+a)(1+2a)}} \qquad (49)$$

in which a and f are given as 1/2 and 0.0057 respectively. In the right half of fig.15, X-T characteristics are obtained and in table 4 values of η/h are given. Also in the right half of fig.17, calculated values of surface elevation are plotted. Fig.18 shows the heighest traces of incident, reflected and run-up waves. Agreement between results of experiment and of calculation is fine. Fig.19 shows the relationship between

$\frac{C_c-1}{C_w-1}$ and $\frac{C_1-1}{C_w-1}$, where a full line shows the relationship given by eq. (4)

Table 4

T=2.57	X	0	0.03	0.05	0.08				
	η/h	0.059	0.034	0.029	0.003				
T=3.10	X	0	0.09	0.16	0.21				
	η/h	0.136	0.070	0.053	0.032				
T=3.71	X	0	0.23	0.30	0.42	0.45			
	η/h	0.181	0.098	0.092	0.077	0.074			
T=4.64	X	0	0.47	0.58	0.69	0.98			
	η/h	0.136	0.102	0.097	0.099				
T=6.00	X	0	0.82	1.00	1.11	1.48	1.77		
	η/h	0.059	0.081	0.080	0.081	0.086	0.097		
T=7.47	X	0	0.70	1.13	1.50	2.15	2.65		
	η/h	0.006	0.050	0.059	0.068	0.074	0.093		
T=8.80	X	0	0.21	1.35	1.60	1.83	2.25	3.18	3.37
	η/h	0	0.006	0.044	0.048	0.053	0.062	0.067	0.088
T=10.47	X	0	0.45	1.98	2.23	2.61	4.27		
	η/h	0	0.006	0.037	0.041	0.051	0.067		

and white circles show experimental results. Agreement is also very fine which proves the assumption for the formation of imperfect clapotis. In fig.20, the front characteristics in X-T plane is presented to compare test results and theoretical ones, which were obtained by assuming f as 0.0057 and 0.01. It is concluded that a frictional coefficient must be taken much larger than that ordinary expected.

The Froude number of the wave front was calculated for nearly 80 runs and was found among 0.5 and 2.5 which might correspond to 1.0 and 2.0 given by Abbott and Méhauté.

Finally, test results of x_3 and $F_4=u_4/\sqrt{gh_4}$ are compared with theretical ones in fig.21 and fig.22 respectively, which also show good agreement with each other.

CONCLUSION

U-C characteristics are utilized to analyse perfect and imperfect reflection at the quaywall. Condition of occurance of imperfect clapotis is presented. No dimensional wave celerity and velocity are given by eq. (4) and (5).

Overland flow is calculated assuming that critical flow takes place at the quaywall and Froude number $F_1=U'_f/C'_f=1/a$ on the leading wave front is 2. However whenever this front is took over by the succeeding elements, abrupt change is occured in U' and C'.

Reflection and overflow of running tsunami at a land dike which is designed to prevent the intrusion of tsunami are analysed using shock

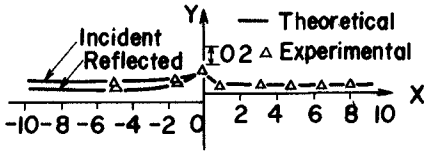

Fig.18 Max. traces of incident, reflected and inundated waves.

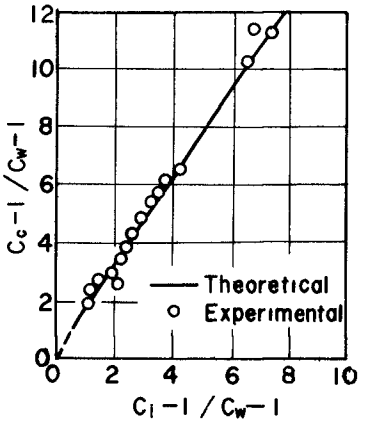

Fig.19 Relationship between C_c-1/C_w-1 and C_1-1/C_w-1.

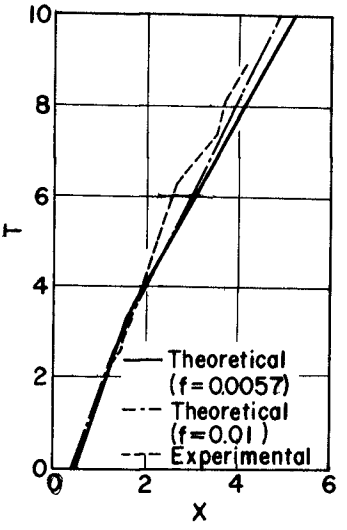

Fig.20 X-T characteristics of the tsunami front on the land.

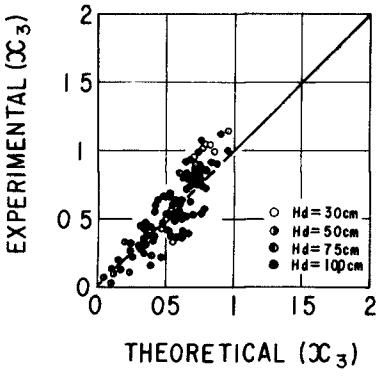

Fig.21 Comparison between theoretical and experimental values of x_3.

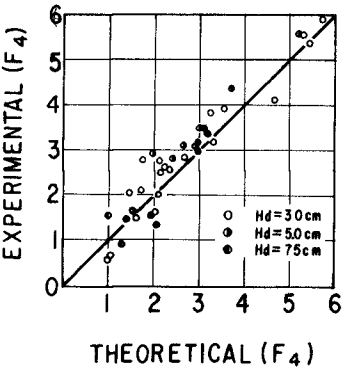

Fig.22 Comparison between theoretical and experimental values of F_4.

condition and an energy equation, in which also the critical depth is assumed to occure at the summit of the dike.

Conditions of perfect reflection and of jet impact are given. Also depth, velocity and discharge behind the dike after overflow are presented. It is found that as the height of a dike increases, overflow discharge decreases as expected ordinary, but velocity increases which necessitates careful inspection on safety of the land behind the dike.

Finally theories are examined by experiments of 426 runs and are verified by comparison of test results and theoretical calculations.

ACKNOWLEDGEMENTS

Authors wish to express their thanks to Messrs. W. Taniguchi, S. Noji, K. Hashimoto and T. Murayama of undergraduate students of Tohoku University for their excellent achievement on experiments and calculations.

REFERENCES

1) M.B. Abbott: On the Spreading of One Fluid over Another.
La Houille Blanche, Decembre 1961 N 6, pp 827-836
2) J.C. Freeman and LeMéhauté B.L.: Wave Brakers on a Beach and Surges on a Dry Bed.
Proc. ASCE. Vol. 90 No.HY2 1964, pp 187-216
3) Lamb, H: Hydrodynamics, 6th edition Cambridge 1932. p.279

CHAPTER 59

FRESSURES BY BREAKING WAVES ON COMPOSITE-TYPE BREAKWATERS

S. Nagai

Professor of Hydraulics,

and

T. Otsubo

Assistant,

Department of Civil Engineering,
Faculty of Engineering,
Osaka City University,
Osaka, Japan.

INTRODUCTION

The intensity and vertical distribution of pressures exerted by water waves on the vertical walls of composite-type breakwaters vary in a very wide range from those of high shock pressures exerted by severe breaking waves to those of low pressures similar to hydrostatic pressure due to standing waves, depending upon the shape of the composite-type breakwaters, the characteristics of incoming waves, and the depths of water where the breakwater are located. In this paper are presented the intensity and vertical distribution of pressures exerted by various kinds of breaking waves on the vertical walls of composite-type breakwaters with low and large base-rubble-mounds constructed in comparaticely deep water.

COMPOSITE-TYPE BREAKWATERS WITH HIGH RUBBLE-MOUNDS

Shock pressures exerted by perfect and partial breaking waves on the vertical walls of composite-type breakwaters with high base rubble-mounds were studied in our laboratory from April of 1953 to March of 1959, and the results were published in June, 1960[1]. Those studies were concerned with the intensities of the shock pressures and their vertical distributions on the vertical walls of composite-type breakwaters, which had as high base-rubble-mounds as h_1/h_2=0 to 0.50, in which h_1 defined a water depth above the top of the rubble-mounds, and h_2 was a water depth at the toe of the harbour-side slope of the rubble-mounds. The top widths of the base-rubble-mounds, B, were so narrow as zero to two meters, and

water depths in front of the vertical walls, h_1, were mostly smaller than 1.3 times the heights of incoming waves, H.

When breaking waves strike on composite-breakwaters, peak pressures at various elevations of the vertical wall of the breakwater do not occur at the same time. In general, there are slight retardations of occurrence in turn towards the wave crest from the bottom of the wall. Therefore the maximum wave pressure inducing the sliding and overturning of the vertical wall is not equal to the resultant of the peak pressures, but equal to the resultant of the simultaneous wave pressures exerting at the same instant as the occurrence of the maximum peak pressure, p_{max}, on the wall. This was proved by numerous experiments(2).

The vertical distributions of the maximum simultaneous pressures exerted by breaking waves on the vertical walls of composite-type breakwaters with high rubble-mounds are divided into three types which were referred to as A, B, and C-types(1).

A-type distribution. The maximum peak pressure on the wall, p_{max}, occurs at or in the vicinity of still water surface, and the pressures acting simultaneously with p_{max} above and below the still water surface decrease quickly in accordance with the following equation

$$p = p_{max} \left(1 - \frac{2y}{H} \right)^2 , \qquad (1)$$

in which p_y defines the intensity of the maximum simultaneous pressure at a distance y above and below the still water surface. The resultant, P, of the A-type distribution is

$$P = 2 \int_0^{H/2} p_y \cdot dy = \frac{1}{3} p_{max} \cdot H . \qquad (2)$$

B-type distribution. p_{max} occurs at the bottom of the vertical wall and the simultaneous pressures above the bottom decrease with increasing elevation in accordance with the following equation

$$p_y = p_{max} \left(1 - \frac{y}{H} \right)^2 , \qquad (3)$$

in which p_y denotes the intensity of the maximum simultaneous pressures at an elevation y from the bottom of the wall. The resultant is

$$P = \int_0^H p_y \cdot dy = \frac{1}{3} p_{max} \cdot H . \qquad (4)$$

C-type distribution. p_{max} occurs at the bottom of the vertical wall, but the run-up along the wall is larger than that of B-type, in accordance with

$$p_y = p_{max} \left(1 - \frac{y}{1.5H} \right)^2 , \qquad (5)$$

therefore the resultant is

$$P = \int_0^{1.5H} p_y \, dy = \frac{1}{2} p_{max} \cdot H . \qquad (6)$$

COMPOSITE-TYPE BREAKWATERS WITH LOW AND LARGE RUBBLE-MOUNDS

1. EXPERIMENTAL EQUIPMENT AND PROCEDURES

Since several years ago in Japan large composite-type breakwaters which have very large and low base rubble-mounds with wide top-widths, B=10 to 20m or more in front of vertical walls have been constructed in seas about 10 to 12m deep. The values of h_1/H in those breakwaters during typhoons are from 1 to 1.8.

Numerous experiments on pressures exerted on the vertical walls of such composite-type breakwaters with low and large base rubble-mounds have been conducted on a model-to-prototype scale of 1:20 since two years ago by the use of a wave channel equipped with a wind blower, 50m long, 1.0m wide, and 1.5m deep, as shown in Fig. 1. The conditions used in the experiments were as follows:

(a) Water depth at the horizontal bottom of the wave channel, h=51 to 81cm, in prototype h_p=10.2 to 16.2m; (the bottom slope of the channel from the toe of the outer slope of a rubble-mound to a 10m-distance is 1/100);

(b) Shape of breakwaters; h_2=20 to 65cm, in prototype h_{2p}=4 to 13m; h_1=10 to 50cm, h_{1p}=2 to 10m; the height of rubble-mounds, h_M=10, 15, 25, and 35cm, in prototype h_{Mp}=2, 3, 5, and 7m; B=0, 12.5, 25, 50, 75 and 100cm, in prototype B_p=0, 2.5, 5, 10, 15 and 20m; h_1/h_2=0.22 to 0.80, and B/h_2=0 to 2.5: Outer slope of the base rubble-mound was constant to be 1:3 in all breakwaters tested.

(c) Characteristics of waves; period T=1.17 to 3.05sec, in prototype T_p=5.2 to 13.6sec; wave height H=5 to 38cm, H_p=1 to 7.6m; wave length L=201 to 801cm, L_p=40 to 162m; h/L=0.08 to 0.37, and h_2/H=1.3 to 6.2.

The range of the experiments are summerized in Table 1.

TABLE 1.- CHARACTERISTICS OF WAVES AND DIMENSIONS OF BREAKWATERS TESTED

		Model	Prototype
Water depth at the horizontal bottom : h		h_m=51 to 81cm	h_p=10.2 to 16.2m
Wave	Period : T	T_m=1.17 to 3.05sec	T_p=5.2 to 13.6sec
	Height : H	H_m=5 to 38cm	H_p=1.0 to 7.6m
	Length : L	L_m=201 to 801cm	L_p=40.2 to 162m
Breakwater	Water depth at the toe of rubble-mound : h_2	h_{2m}=20 to 65cm	h_{2p}=4.0 to 13.0m
	Water depth on the top of rubble-mound : h_1	h_{1m}=10 to 50cm	h_{1p}2.0 to 10.0m
	Height of rubble-mound : h_M	h_{Mm}=10, 15, 25, 35cm	h_{Mp}=2.0, 3.0, 5.0, 7.0m
	Width of the top of rubble-mound : B	B_m=0, 12.5, 25, 50, 75, 100cm	B_p=0, 2.5, 5.0, 10.0, 15.0, 20.0m
Relation between wave and water depth		h/L=0.08 to 0.37, h_2/H=1.3 to 6.2	
Relation between breakwater and water depth		h_1/h_2=0.22 to 0.80, B/h_2=0.0 to 2.5	

The right column in Table 1 shows numerals in prototype which is on a 1:20-model-to-prototype scale.

The experiments were conducted at an each shape of the composite-type breakwaters, as shown in Table 1, to generate from strong breaking waves to standing waves by varying the depth of water and the characteristics of wave for a given value of relative water depth at the horizontal bottom, such as h/L=0,10, 0.15, 0.20, and 0.28, respectively. The bottom-slope of the wave channel at the toe of the outer slope of base-rubble-mound was 1/100 when $h_2/H \geqq 1.80$, and that was 1/40 when $h_2/H < 1.80$. Since it was necessary to know the ranges of adaptability of the equations to obtain the pressures exerted by breaking waves on the vertical walls of composite-type breakwaters with high as well as low and large rubble-mounds, and by standing waves on vertical-wall breakwaters, respectively, comprehensive experiments were performed over a wide

range from composite-type breakwaters with high rubble-mounds to those with extremely low and large mounds similar to a vertical-wall breakwater. In all the experiments six pressure-gages were used simultaneously to measure the maximum simultaneous pressures on the walls, and they were of a same type which have been used in the experiments concerning the pressures of breaking and standing waves. The characteristics of the pressure-gages are shown in Table 2.

TABLE 2.- CHARACTERISTICS OF PRESSURE-GAGES USED

Pressure plate		Phosphor-bronze; 0.2mm thick	
Number of bellows Pitch of bellows		4 to 5 4mm	
Thickness of acrylic plate attached with strain-gages		For the measurement of standing wave pressure	For the measurement of breaking wave
		0.8mm	2.0mm
Frequency of free oscillation	In air	f=140 to 160c/s	f=210 to 160c/s
	In water	f=100 to 110c/s	f=150 to 160c/s
Damping factor		0.02 to 0.03	0.02

2. EXPERIMENTAL RESULTS

(1) When the base-rubble-mounds of a composite-type breakwaters are so low that $h_1/h_2 \geqq 0.75$, and $h_2/H \geqq 1.80$, standing waves are always formed in front of the breakwaters regardless of the top-width of the base-rubble-mound, B. The pressures exerted by perfect or partial standing waves on vertical walls can be obtained with sufficient accuracy for practical design by the use of formulas[3],[4].

(2) When $0.40 \leqq h_1/h_2 < 0.75$, waves formed in front of the vertical walls of composite-type breakwaters vary over a wide range from a perfect breaking wave to a standing wave, depending upon the ratioes of h_1/h_2, B/h_2, h/L, and h_2/H. The ranges of the breaking and standing waves are shown in Figs. 2 to 5.

Generally speaking, as the value of h_1/h_2 becomes smaller towards 0.40, that is, as the height of a base rubble-mound becomes larger, waves become to break severely in front of the breakwater, while when the value of h_1/h_2 approaches to 0.75, there are formed non-breaking waves similar to a standing wave in front of the breakwater. Therefore the intensities of wave pressures vary over a wide range, but p_{max} occurs at or in the vicinity of the still

water surface in almost of the cases when $0.40 \leqq h_1/h_2 < 0.75$.
(3) The value of $\alpha = p_{max}/w_o H$, in which w_o denotes the unit weight of water, varies, depending upon the values of h_1/h_2, B/h_2, and h_2/H, as shown in Figs. 6 to 10.
(4) The vertical distributions of the maximum simultaneous pressures occurring simultaneously with the p_{max}, exerted by breaking or nonbreaking waves on the vertical wall are obtained as follows:

(a) Below the still water surface

The pressure intensity at the point of -z below the still water surface, p_z, is obtained by

$$p_z = p_{max} \frac{\cosh \beta \left(1 + \frac{z}{h_1}\right)}{\cosh \beta} , \tag{7}$$

in which β is a function of α only, being independent of a relative water depth h/L, and is given by

$$\beta = \sqrt{6.0\alpha + 26.0} - 5.0 , \tag{8}$$

in which $1.0 \leqq \alpha \leqq 5.0$. The relation between β and α is shown in Fig. 11.

(b) Above the still water surface

The height of a wave crest above the still water surface, $H_c = \gamma H$, on the vertical wall of a composite-type breakwater with high base-rubble-mound is 0.5H for the A-type distribution given in Eq. 1, and that is (1.0 to 1.3)H for a standing wave[3]. Therefore, the value of $\gamma = H_c/H$ for a composite-type breakwater with low base-rubble-mound is considered to vary from 0.5 to 1.3, depending upon the values of α and h/L. The values of γ for various values of α and h/L obtained by the experiments are shown in Fig. 12, and as the upper values of these experimental ones, available for practical design purposes, were decided as shown in Table 3.

From numerous experiments the distribution of the pressures above the still water surface can approximately be assumed triangular such as

$p_{max} = \alpha w_o H$ at the still water surface,

and

$p_z = 0$ at $H_c = \gamma H$ above the S.W.L.

The values of γ varies shown in Table 3.

TABLE 3.- VALUES OF γ

$h/L < 0.135$		$0.135 \leqq h/L < 0.35$	
$\alpha \leqq 1.3$	$\gamma = 1.3$	$\alpha < 1.0$	$\gamma = 1.0$
$1.3 < \alpha \leqq 1.5$	$\gamma = -2.13\alpha + 4.06$	$1.0 < \alpha \leqq 3.0$	$\gamma = -0.25\alpha + 1.25$
$1.5 < \alpha \leqq 3.0$	$\gamma = -0.25\alpha + 1.25$	$3.0 < \alpha$	$\gamma = 0.50$
$3.0 < \alpha$	$\gamma = 0.50$		

(c) The resultant of the maximum simultaneous pressurea is

$$P = \int_{-h_1}^{0} p_z \cdot d_z + \frac{1}{2} p_{max} \cdot H_c$$

$$= \alpha w_o H \left(h_1 \frac{\tanh \beta}{\beta} + \frac{1}{2} \gamma H \right) . \qquad (9)$$

3. COMPARISONS BETWEEN PRESSURES OBTAINED IN THE EXPERIMENTS AND MEASURED IN PROTOTYPE AND THOSE CALCULATED BY THE EQUATIONS

(1) Comparisons between the Experimental and Calculated Values.

Comparisona of the pressures calculated by Eqs. 7, 8, and 9 with those obtained by the experimente are shown in Figa. 13 to 16 (a), (b), and (c). Figures (a) in these figures show pressures very cloae to those of atanding waves, and figures (b) and (c) pressurea of breaking waves.

According to Figs. 13 to 16, it is known that the values calculated by the equations are in a fairly good agreement with the pressures obtained by the experiments, and the ratioes of the reaultant of pressurea in the experimenta, P_e, and that computed by Eq. 9, P_{cal}, that ia P_e/P_{cal}, are 0.81 to 1.07. In the other numerous comparisons the value of P_e/P_{cal} was moatly 0.85 to 1.0, with very rare cases of $P_e/P_{cal} > 1.0$.

(2) Comparisons between the Measured and Calculated Values.

The only one report on the field measurement of wave pressurea exerted on a composite-type breakwater which the writer could have for recent fifteen years is the field meaaurement which the Hokkaido Development Bureau made in 1957 and 1958 at the Harbor of Haboro in the Japan Sea(5). Fig. 17 shows the cross-section of the breakwater at the Harbor of Haboro and the location of three pressure-gages used for the measurement. The three pressures indicated by a black circle are measured values which would

approximately be considered as the maximum simultaneous pressures during the measurement. The three double-circle marks in Fig. 17 denote the pressures calculated by Eqs. 7 and 8, which were obtained by the following calculation;

The heights and periods of waves during the measurements were $H_{max}\fallingdotseq 2$ to 4.5m and $T\fallingdotseq 7$ to 8sec. The period of wave was assumed T= 7.3sec when the pressure gage located at the still water surface recorded $p_{max}=11\ t/m^2$, but the mean sea level when $p_{max}=11t/m^2$was not reported. Since the tidal range of the Japan Sea is within 0.5 to 0.6, the calculations of pressures were made for two cases of the mean sea level, D.L. +0m and +0.60m.

(i) For the case of D.L. ±0m sea level

The average depth of water at sea (4 to 6) L (wave length) offshore the breakwater is approximately assumed h=7.0m. Therefore L=55m for T=7.3sec, and $h/L\fallingdotseq 0.13$. Since $h_1/h_2=3.5/6.0=0.58$, the breakwater is defined as a composite breakwater with a low base-rubble-mound, and $B/h_2=3.0/6.0=0.50$. If H is assumed 4.0m, $h_2/H=1.5$.

(ii) For the case of D.L.+0.60m sea level

The average depth of water h=7.6m, and L=57m, therefore $h/L=0.133$. If the maximum wave height is assumed $H_{max}=4.5$m, $h_2/H=6.6/4.5=1.46\fallingdotseq 1.5$. $h_1/h_2=0.62$ and $B/h_2=0.46$. Since $h_2/H\fallingdotseq 1.5$ for the both cases, waves are assumed to break in front of the breakwater. From Fig.6, $\alpha=3.0$ for the both cases, then $\beta=1.63$ by Eq.8, and $\gamma=0.50$ from Table 3. The full line shown in Fig. 17 is the curve of vertical distribution of the maximum simultaneous pressures calculated by Eq. 7 by using the values of α, β, and γ. The calculated values show to be comparatively close to the measured. The calculated values of p_{max} are $12.4t/m^2$ for H=4.0m, and $13.9t/m^2$ for H=4.5m, while the design engineers of the breakwater were assumed $p_{max}=14$ to $15t/m^2$. It may be stated that this assumption of p_{max} (presumably made from their experiences) was quitely adequate.

4. EFFECTS OF OVERTOPPING AND WIND ON WAVE PRESSURE

(1) Effect of Wave Overtopping.

According to the results which have been obtained until now in the experiments of composite-type breakwaters with low and large rubble-mounds, it may be stated in general that as the volume of wave overtopping increases, the intensities of the maximum simultaneous pressures would decrease from the top to the bottom of the vertical wall of the breakwater, and when the difference of height between the top of the vertical wall and the still water level is very small, the intensities of the maximum simultaneous pressures would distribute approximately uniformly, as these trends were seen in the results of experiments of breaking waves on composite-type breakwaters with high rubble-mounds and partial standing waves on vertical walls(4).

(2) Effect of Strong Winds.

It is seen that if strong winds with velocities over about 20m per sec blow over waves, the pressure intensities of breaking waves also increase slightly from the top to the bottom of the vertical

wall of composite-type breakwater with low rubble-mound. The studies on the effects of wave overtopping and strong winds are now under way. The detailed report is scheduled to be written in near future.

CONCLUSIONS

From the study on the wave pressures exerted on the vertical walls of composite-type breakwaters with low and large rubble-mounds the followings are concluded.

1. When the base-rubble-mounds of composite-type breakwaters are very low and $h_1/h_2 \geqq 0.75$, and $h_2/H \leqq 1.80$, standing waves are always formed in front of the breakwaters, regardless of the top-width of the rubble-mound, and the pressures exerted by all kinds of standing waves on vertical walls can be obtained by using formulas(3),(4).
2. When $0.40 \leqq h_1/h_2 < 0.75$, breaking waves or standing waves are formed in front of the vertical walls of the composite-type breakwaters, depending upon the values of h_1/h_2, B/h_2, h/L, and h_2/H. The ranges of breaking waves and standing waves are shown in Figs. 2 to 5.

It may be stated that the maximum peak pressure on the vertical walls of the composite breakwaters with low and large rubble-mounds, p_{max}, is always located on the still water surface or on its vicinity, and the value of $\alpha = p_{max}/w_o H$ increases as the value of h_1/h_2 approaches to 0.40, while α decreases as h_1/h_2 approaches to 0.75, being $1 \leqq \alpha \leqq 1.3$ for standing waves.

3. When waves break in front of the vertical wall, the value of α varies, depending upon the values of h_1/h_2, B/h_2, and h_2/H, as shown in Figs. 6 to 10. The vertical distributions of the maximum simultaneous pressures exerted by breaking waves are determined by Eq. 7, and the resultant pressures are obtained by Eq. 9.
4. When the difference of height from the still water surface (or mean sea level during storms) to the top of the vertical wall is so small that there is a large volume of wave overtopping, the intensities of wave pressures on the wall decrease from the top to the bottom, as the volume of wave overtopping increases. The strong winds over waves lead to a slight increase in the intensities of wave pressures on the wall. But since the study on the effects of wave overtopping and strong winds on the pressures of breaking waves on the composite breakwaters is now under way, the detailed report will be written in near future.

REFERENCES

(1) Nagai, S. ; "Shock Pressures exerted by Breaking Waves on Breakwaters", Journal of the Waterways and Harbors Div., ASCE., June, 1960.
(2) Nagai, S. ; "Sliding of Composite-Type Breakwaters by Breaking Waves", Journal of the Waterways and Harbors Div. ASCE., Feb., 1963.

(3) Nagai, S. ; "Pressures of Standing Waves on a Vertical Wall", Journal of the Waterways and Harbors Div., ASCE.(to be published).
(4) Nagai, S. ; "Pressures of Partial Standing Waves", Journal of the Waterways and Harbors Div., ASCE, Aug., 1968.
(5) Kuribayashi, Muraki, and Others ; "On the Pressures exerted on a Breakwater", Proc. of the Fifth Coastal Engineering Conference (Japan), 1958.

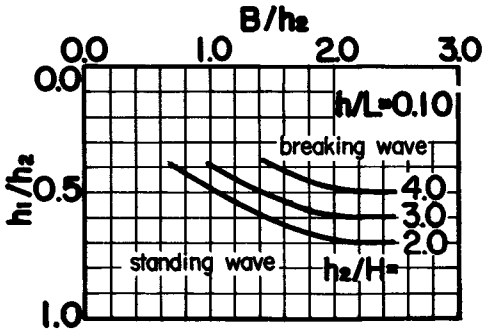

FIG. 2.

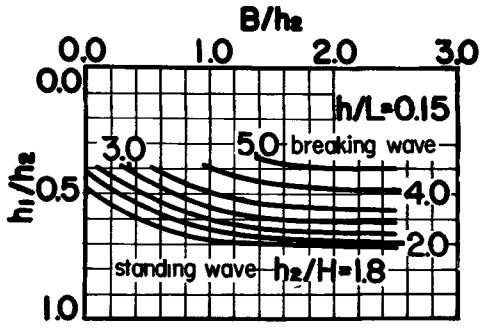

FIG. 3.

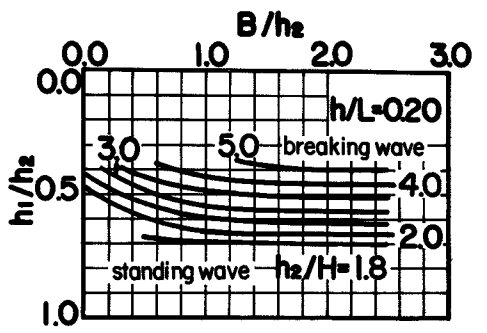

FIG. 4.

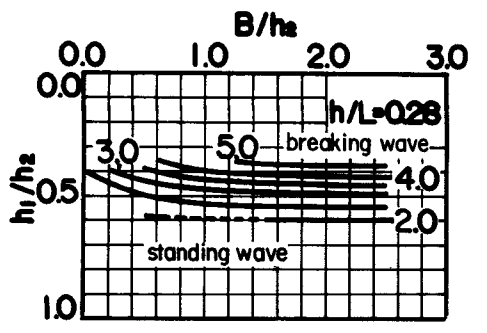

FIG. 5.

FIGS. 2 to 5.- RANGES OF BREAKING AND STANDING WAVES. THE UPPER PART OF THE LINE SHOWS THE RANGE OF BREAKING WAVES AND THE LOWER PART BELOW THE LINE THE RANGE OF STANDING WAVES

FIG. 1.- WAVE CHANNEL WITH WIND BLOWER

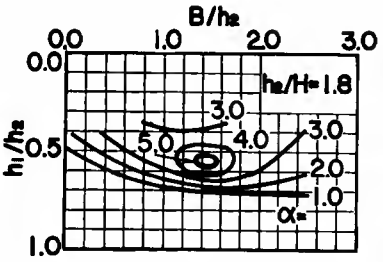

FIG. 7.

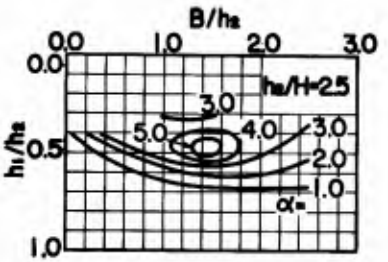

FIG. 9.

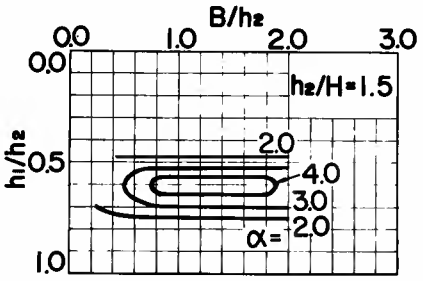

FIG. 6.

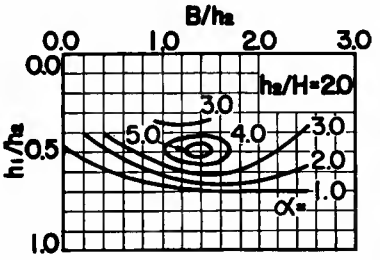

FIG. 8.

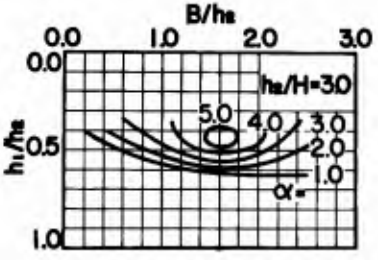

FIG. 10.

FIGS. 6 to 10.- VALUE OF $\alpha = p_{max}/w_o H$

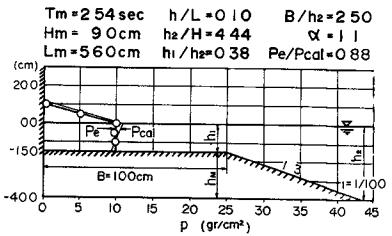

FIG. 13 (a).

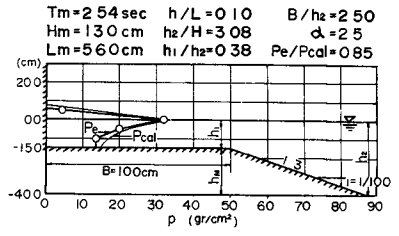

(b).

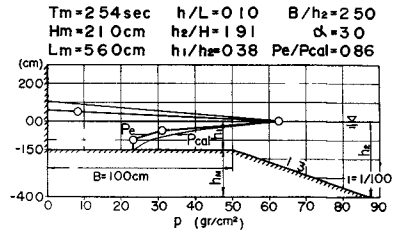

FIG. 13 (c).

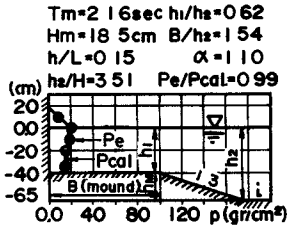

FIG. 14 (a).

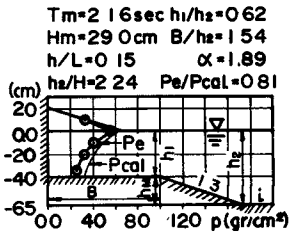

(b).

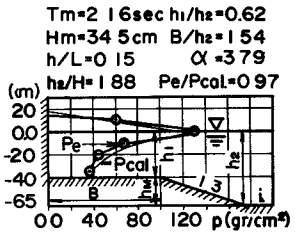

FIG. 14 (c).

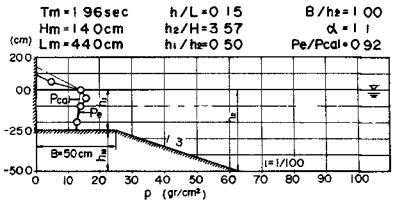

FIG. 15 (a).

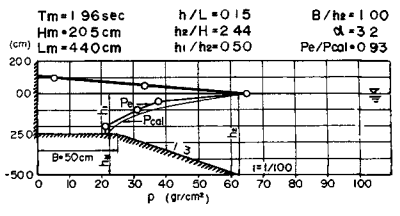

(b).

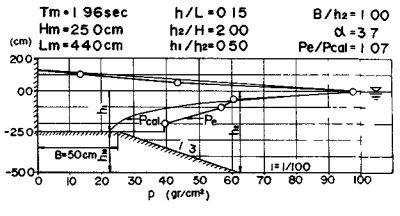

FIG. 15 (c).

FIGS. 13 to 16.- COMPARISONS BETWEEN EXPERIMENTAL AND CALCULATED PRESSURES

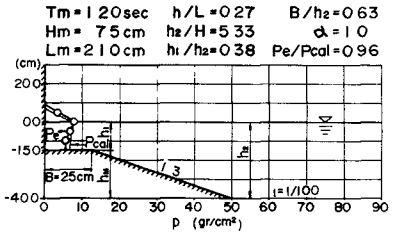

FIG. 16 (a).

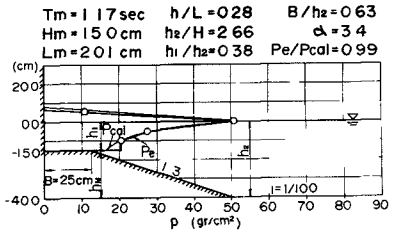

(b).

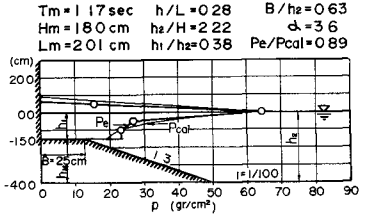

FIG. 16 (c).

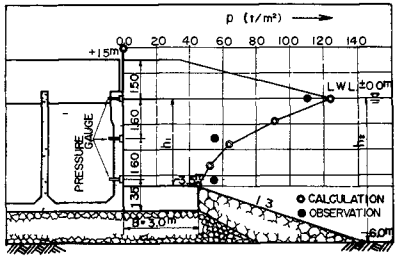

FIG. 17.- CROSS-SECTION OF THE BREAKWATER AT THE HARBOR OF HABORO AND COMPARISON BETWEEN MEASURED AND CALCULATED PRESSURES

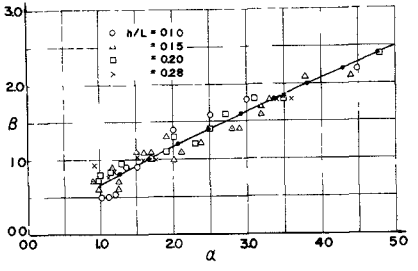

FIG. 11.- RELATION BETWEEN α AND β

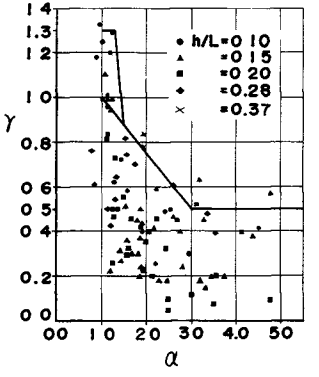

FIG. 12.-RELATION BETWEEN α AND γ

CHAPTER 60

THE EFFECT OF WAVE CRESTS ON WAVE FORCES

A. Trætteberg
Research Engineer, River and Harbour Laboratory at the Technical University of Norway, Trondheim, Norway.

ABSTRACT

This paper deals with wave forces from short crested waves as compared with two dimensional waves. The investigation comprised measurements of wind wave forces on fixed pontoons in a model, and a comparison of wave crest characteristics of wind waves in model and prototype. The model tests showed that the wave crests have a marked influence on the wave forces. The investigation of model and prototype wave data showed that the crest characteristics of the model waves compared well with that of prototype sea.

INTRODUCTION

As known, wind waves are three-dimensional and short crested. When a structure, e.g. a pontoon, is exposed to short crested waves the total force at any moment is determined by the instantaneous water level along the entire length of the structure. If the structure is of approx. the same length as the wave crest, the resultant force will differ considerably from that of the two dimensional case.

The paper deals with an investigation conducted at the River and Harbour Laboratory at the Technical University of Norway to give some information of the effect of wave crests on wave forces as compared with two dimensional waves.

The investigation comprised measurements of wind wave forces on fixed pontoons in a model and a comparison of wave crest characteristics of wind waves in model and prototype.

MODEL TESTS

Model tests have been conducted in a channel with wind generated waves, and horizontal forces on a fixed pontoon were measured. The test arrangement is shown schematically in Fig. 1.

Four pontoons with different lengths (λ = 50-150-200 and 350 cm) in the crest direction were used. The resultant horizontal force was measured by use of strain gauges as indi-

cated in Fig. 1. Practically no wave energy was transmitted to the lee-side of the pontoon, and pressures on the front wall in regular waves with periods in the range of periods of the wind wave spectrum, was found to be equal to the pressures on a vertical wall extended to the bottom.

Fig. 2 shows the energy spectrum and wave height distribution of the incident waves at the location of the front wall of the pontoon. The waves were generated over a fetch of 46 metres with a wind velocity of approximately 8 m/sec. The water depth of 108 cm was "deep water" for all waves present in the wave spectrum.

Fig. 3 shows the distribution of horizontal forces per unit length in the direction of the wave propagation for the four pontoons. The distribution is calculated on the basis of 200 successive force peaks.

The diagram, Fig. 4, shows the maximum force per unit length as a function of a relative pontoon length λ/L_o. L_o designates a characteristic wave length of the wave spectrum; the length of a sinusoidal wave with a frequency equal to the peak frequency of the wave spectrum. F_o is the interpolated maximum force for a relative pontoon length $\lambda/L_o = 1.0$.

As shown in Fig. 3 and 4, the crests of the wind waves in the model had a marked influence on the resultant forces on the pontoon.

COMPARISON OF WIND WAVES IN MODEL AND PROTOTYPE

In connection with the tests a comparison of wind waves in model and prototype has been made. The prototype data have been taken from the SWOP project (1) where stereo photographs of the water surface were obtained and maps of the instantaneous water surface were prepared. In the present investigation profiles of the water surface in the crest direction have been drawn on basis of these maps.

In the model profiles in the crest direction were obtained by photographing the waves as they passed through a finely meshed screen suspended across the channel in the crest direction.

The crest data have been treated as illustrated in Fig. 5. The moving average of the surface level along the crest profiles over a series of lengths, λ', has been calculated. In this manner, one gets the data in a form similar to the test results; λ' corresponding to the pontoon length, λ, and the mean water level, $\bar{\eta}$, corresponding to the resultant force per unit length.

The total length of crest profile used for the analysis was 100 L_o, and the moving average water level has been calculated for a range of λ' from 0,1 L_o to 10,1 L_o.

The results of the crest analysis are shown in Fig. 6, where the maximum values of $\bar{\eta}$ are plotted against the relative length λ'/L_o. The $\bar{\eta}_o$ is the maximum water level above still water level for λ'/L_o = 1.0.

In the model, the crest profiles have been investigated for two fetch lengths, 34 and 46 metres. In order to indicate the scatter for a profile length of 100 L_o, two sets of profiles for the fetch length of 46 metres has been treated.

COMMENTS

The results of the crest investigation as shown in Fig. 6 indicate that the wave crest distribution of the three dimensional SWOP sea is rather similar to that of the model sea. However, the prototype data used for the comparison are very limited and the results apply to deep water conditions only. While the test results must be used with reservation for prototype design, the test results demonstrate that the wave crest represents an important feature of wind waves in relation to the design of certain types of structures.

REFERENCE

Cote et.al.: The Directional Spectrum of Wind Generated Sea as observed from Data obtained by Stereo Wave Observation Project.
Meteorological Papers, Vol. 2, No. 6, New York University.

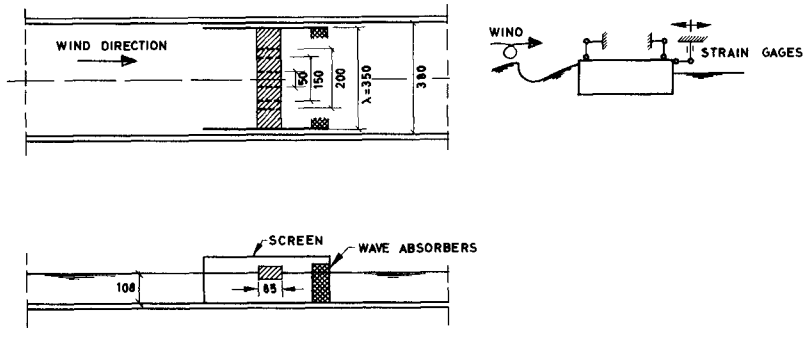

FIG 1 TEST ARRANGEMENT

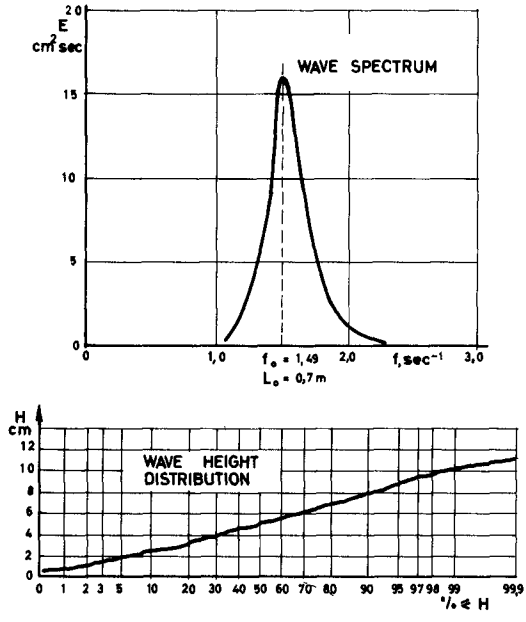

FIG 2 WAVE DATA FROM MODEL

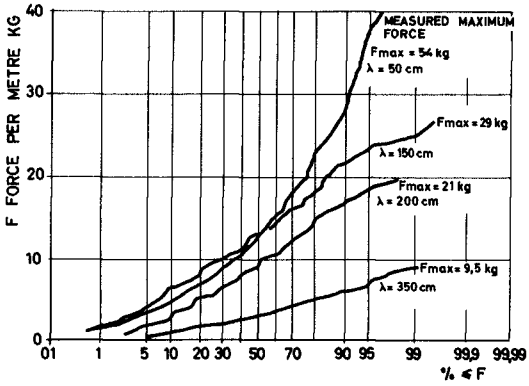

FIG 3 DISTRIBUTION OF RECORDED FORCE PEAKS DIRECTED INWARDS

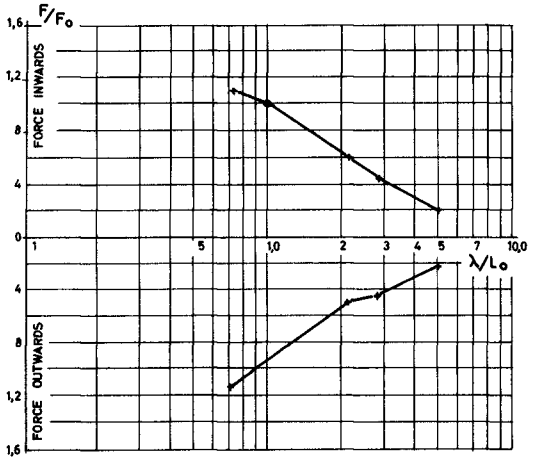

FIG 4 MAXIMUM FORCE PER UNIT LENGTH VS VALL LENGTH

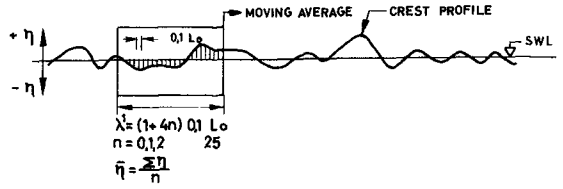

FIG 5 CALCULATION OF MEAN WATER SURFACE LEVEL DISTRIBUTION

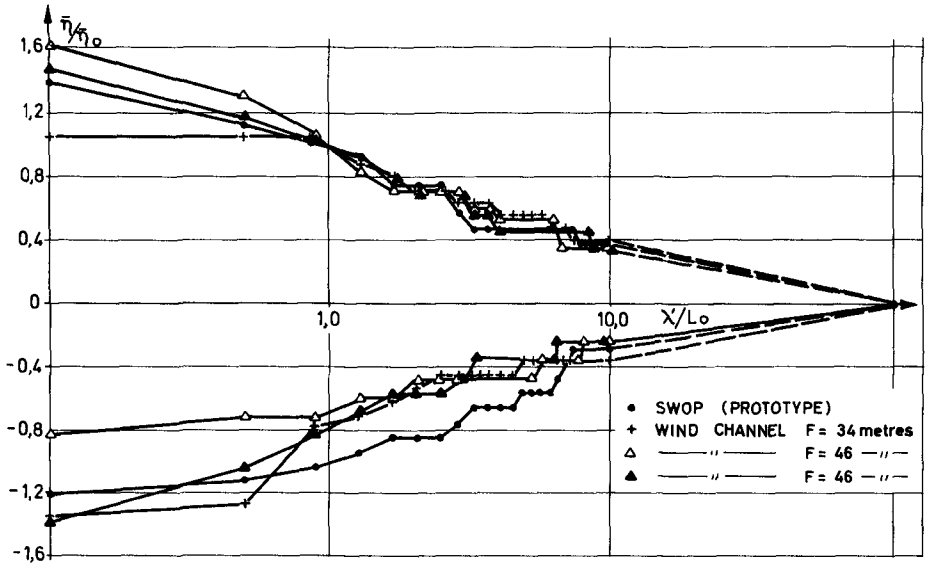

FIG 6 MAXIMUM MEAN SURFACE LEVEL IN CREST DIRECTION

CHAPTER 61

WAVE FORCES ON PILES IN RELATION TO WAVE ENERGY SPECTRA

by

A. Paape
Delft Hydraulics Laboratory, Delft, Netherlands

ABSTRACT

The determination of wave forces on piles is for an important part based upon data obtained with regular laboratory waves. Nonlinearities in the mechanism that underlies these forces may lead to deviations when applying the data to predict forces exerted by irregular waves.

Experiments have been performed with irregular waves to investigate wave forces, more particularly to study the influenoe of the energy density spectrum of the waves.

Within the range of conditions in the experiments, the wave motion is sufficiently characterized by its energy and the frequency (or wave period) at which the energy density is maximum to determine the probability distribution of wave forces.

INTRODUCTION

Wave forces on piles are mainly determined at present either by computation or by performing experiments in regular laboratory waves. The latter also provided information on coefficients of drag (C_D) and inertia (C_M) to be applied in the methods of computation. A wide scatter in these coefficients was often found. This is partially due to the fact that the influence of the flow pattern around the piles on the forces exerted is not adequately characterized by coefficients C_D and C_M which are supposed to be a function of the geometrioal shape of the pile only. Various authors have shown the influence of of the time history of flow on the forces exerted on submerged bodies [1], [2]. This implies that the phenomenon of forces in oscillating flow is in principle non-linear. even if inertia forces are predominant.

In engineering praotice one is mainly interested in forces exerted by irregular waves. In consequenoe of the problems outlined above it is doubtful whether the results of regular-wave experiments can be used to predict forces by irregular waves. Moreover the description of irregular waves in a way that suits this procedure is rather oomplicated.

Experiments have been performed in irregular waves in order to study the effeot of non-linearities and to establish a method for predicting the statistical distribution of wave foroes suitable for

deeign purposes. Some results of theee experiments are preeented in thie paper. The aim of the study wae to get eome insight rather than establishing a set of data for design purposes. The range of variablee was very limited, up till now. It is streesed that the concluеions which have been drawn are not necessarily valid beyond the range of conditions applied in the experiments.

REVIEW OF SOME METHODS

The etarting point for the computation of wave forcee ie generally the deecription of the force as given by Morrison's equation:

$$F(t) = \tfrac{1}{2} \cdot C_D \cdot \rho D \int_{-d}^{\eta} u/u/dy + C_M \cdot \rho \frac{\pi}{4} \cdot D^2 \int_{-d}^{\eta} \frac{du}{dt}\, dy$$

For regular waves the integrals have been expressed in terms of wave height H, wave period T and water depth d. Various methods have been applied to derive the probability distribution of wave forces by irregular waves starting from Morrison's equation, A first method has been propoeed by Borgman[3] for the caee of a narrow-band speotrum. In thie method the wave energy ie eupposed to be concentrated at a fixed frequenoy (hence the wave period ie a constant). Consequently the wave height H ie the only statietioal parameter in the wave motion. By computing the forces for varioue values of H, the probability dietribution of wave forcee can be derived from the probability distribution of H. When considering actual wave energy spectra it is obvious that the aeeumption of constant period is a rather orude one, which has always been reoognized by Borgman himeelf.

Pierson and Holmes [4] and Borgman [5] have derived the probability densitiee of velocitiee u and aoceleratione $\frac{du}{dt}$ and applied in Morrison's equation. In thie way the probability distributions of drag forcee and inertia forces can be determined from which the probability dietribution of peak forces ie derived. An objection to this method is that u and $\frac{du}{dt}$ are coneidered to be independent stochastic variablee. In natural waves with a given energy spectrum the high wavee most often have high valuee of both u and $\frac{du}{dt}$, especially if the spectrum is rather narrow. This hae been overcome by Borgman [5] by computing the time functions of u and $\frac{du}{dt}$ from a sea surface simulation on a computer and applying these functions in an approximation of the Morrison formula. This method ie probably the most advanced one in computatione of irregular wave forces. It is obvious, however, that it ie eubjeot to the reetrictione to be made when applying wave theoriee to irregular waves. Moreover the aesumption of constant C_D and C_M has to be made.

The considerations given above ehow the need of having data from experiments in irregular waves. It will then be interesting to investigate the influence of the energy deneity spectrum of the waves on the forces and to consider the tranefer functions converting wave epectra into force speotra. A eimple expression for thie transfer function ie found in case of small amplitude waves and inertia forces being predominant. Some experiments have been performed by Jen [6] for thie caee which showed good agreement with theory.

EXPERIMENTS

ARRANGEMENT OF THE EXPERIMENTS

The experiments were performed with circular and square piles in vertical position and extending from the bottom of the flume up to a level above the highest crest level of the waves. The piles were attached to force transducers in such a way that the overall horizontal force was measured as well as the moment with respect to a fixed level in order to determine the point of application of the force. No information is presented in this paper, however. on the point of application.

The water depth was kept constant in the experiments at d = 0.45 m. The pile diameters D were:

circular piles: $\emptyset$ 0.125, 0.063 m
square piles : $\square$ 0.12 , 0.06, 0.03 m

The experiments were carried out in a windwave flume, 55 m long and 4 m wide. In this flume irregular waves were generated by means of a wave board driven by servo-controlled hydraulic actuators. The input signals for the hydraulic servo mechanism were obtained by filtering a random noise signal such that the required wave energy spectra were obtained. See also ref.[7]. The wave energy spectra were determined on-line by means of a special analogue computer. Simultaneous wave and force records were set on punched tape for elaboration on a digital computer.

The wave motion was measured by making continuous records of the sea-surface elevation $\eta(t)$ with respect to still water level in a fixed point beside the piles. As a first characteristic of the wave motion the energy density spectrum $S_{\eta\eta}$ has been determined. In the computations of $S_{\eta\eta}$ the autocorrelation function was determined first. using samples of $\eta(t)$ at time intervals of 0.125 sec. From the autocorrelation function 60 points were used to compute $S_{\eta\eta}$, applying a triangular screen filter. The total energy of the wave motion is also used as a parameter. This energy is characterized by $M_{o\eta}$ which is equal to the area enclosed by $S_{\eta\eta}$ and the frequency axis. Some examples of spectra are given in figure 1. For an easy comparison of the shape of the various spectra the relative energy density $S_{\eta\eta}/M_{o\eta}$ has been plotted along the vertioal axis. Hence the area enclosed by the curves and the f-axis is equal to unity in all cases.

The energy spectrum is furthermore characterized by the frequency or period at maximum energy density, $\hat{f}$ or $\hat{T}$ respectively, and a parameter for the width of the spectrum. For the latter the relative width as defined by Cartwright and Longuet-Higgins (see also [7]) has not been used in this case as it presents some problems in practical computations. As a simple parameter for denoting the relative width, the ratio of the maximum energy density $S_{\eta\eta max}$, to the total energy $M_{o\eta}$ has been chosen. It is recognized that $S_{\eta\eta max}/M_{o\eta}$ has not the advantage of being dimensionless. Besides the characteristics of the spectra also the probability distributions of wave heights have been determined. Examples are given in figure 3.

As has been stated above only the overall forces on the piles are considered in this paper. Continuous records of the forces versus time were made, F(t). From these records the spectra of the force S_{FF} were determined in the same way as described for the wave motion. Similarly M_{OF} was computed. When determining the probability distributions of wave forces it is useful to consider separately the distributions of maximum forces exerted by individual waves in the direction of wave propagation and the distributions of maximum forces in the direction opposite to the direction of wave propagation. Only the forces in the direction of wave propagation are considered here. Examples are given in figure 4.

PRESENTATION OF RESULTS

The examples shown in figure 1 give an indication about the variation of the width of the wave-energy spectra applied in the experiments. For reasons of comparison a Pierson-Moskowitz spectrum for fully developed sea has been plotted. For $\hat{f} = 0.8$ ($\hat{T} = 1.25$ sec) the value of $S_{\eta\eta\,max}/M_{o\eta}$ is equal to 1.95 sec. for the Pierson - Moskowitz spectrum. In the experiments values between 1.27 and 3.1 sec. were used for $S_{\eta\eta\,max}/M_{o\eta}$. For $\hat{f} = 0.6$ ($\hat{T} = 1.67$ sec.) the Pierson - Moskowitz value of $S_{\eta\eta\,max}/M_{o\eta}$ is 2.25 sec. whereas values in the experiments ranged from 1.14 to 4.1 sec. Consequently it may be expected that the experiments covered reasonably well the variation in spectrum width which occurs in nature.

The probability distributions of wave heights are close to the Rayleigh distribution in all cases. Examples are given in figure 3. Apparently the width of the energy spectrum did not affect the properties of the wave-height distribution.

As a starting point for the description of the wave forces, the wave-force spectra and the probability distributions of forces in the direction of wave propagation have been used. Examples are given in figure 2 and 4 respectively. For many design purposes this way of describing the forces to be expected under natural wave conditions is the most adequate one. From a set of probability distributions of forces corresponding to various storm-wave conditions a design load can be selected taking into account the probabilities of occurrence of the various storm conditions. The wave force spectra may be important when considering the response of structures to the dynamic loads.

When comparing the wave and force spectra of figure 1 and 2 it appears that there is a considerable shift of the energy to the higher frequencies in the force spectra. This is quite reasonable as in the situation of these examples the wave steepness is moderate, whereas the pile diameter is such that inertia forces are predominant. For the conditions of small amplitude waves and inertia forces being predominant there exists, theoretically, a transfer function converting wave spectra into force spectra which is a function of wave frequency only (Notice that the water depth was constant in the experiments). This holds only, however, if the coefficient C_M is a constant for the particular shape of the pile. A suitable way to define such a transfer function T(f) is:

$$S_{FF} = \left[\rho g \frac{\pi}{4} D^2\right]^2 . T(f) . S_{\eta\eta}$$

in which:

ρ = density of water in kg/m^3

g = acceleration of gravity in m/sec^2

According to linear wave theory T(f) is equal to:

$$T(f) = \left[C_M \cdot \frac{\omega^2}{gk}\right]^2$$

in which:

$\omega = 2\pi f = \frac{2\pi}{T}$

$k = \frac{2}{L}$

T = wave period

L = wave length

The theoretical values of T(f) together with data obtained from the experimental spectra have been plotted in figure 5 and 6. A discussion will be given later on.

The examples of probability distributions of wave forces F, given in figure 4 appears to be rather close to the Rayleigh distribution. Only slight deviations occur for the higher forces. For the approximation of a narrow band spectrum by a single constant frequency as introduced by Borgman in ref. [3] and inertia forces being predominant, the probability distribution of wave forces is of the same nature as the probability distribution of wave heights, hence a Rayleigh distribution. Again this holds only in case C_M is a constant. In all other cases the probability distribution of forces is in principle affected by the wave-energy spectrum and the diameter of the pile compared to the magnitude of the wave heights and cannot be described by a standard distribution law. In order to get an idea about the variability of these distributions some simple parameters are introduced:
Let Fn be the wave force exceeded by n% of a series of peak forces in the direction of wave propagation. The parameters $\frac{F_{50}}{F_{13.5}}$ and $\frac{F_1}{F_{13.5}}$ will be used to have some indication on the variability of the distributions.
Note: In a Rayleigh distribution $F_{13.5}$ is in its meaning comparable to the significant wave height $H_s = H_{13.5}$ in a wave height distribution. If the forces would satisfy the Rayleigh distribution, then:

$$\frac{F_{50}}{F_{13.5}} = 0.62 \quad \text{and} \quad \frac{F_1}{F_{13.5}} = 1.5$$

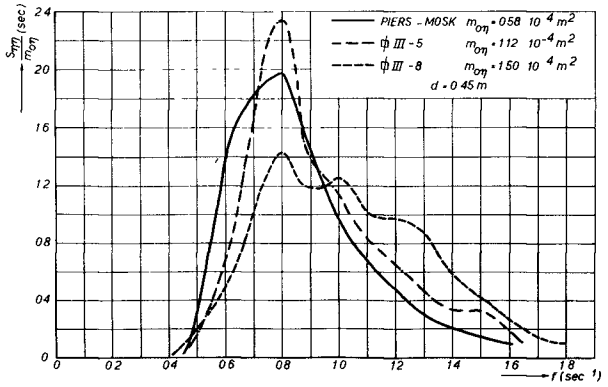

FIG. 1

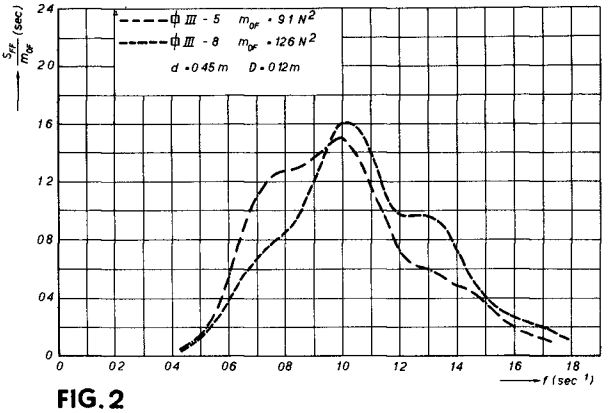

FIG. 2

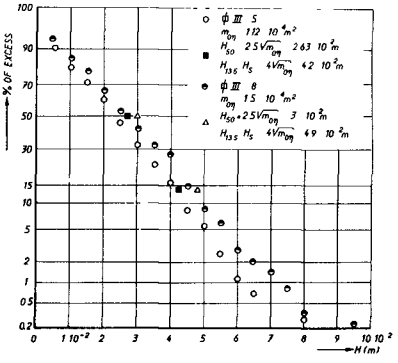

FIG. 3

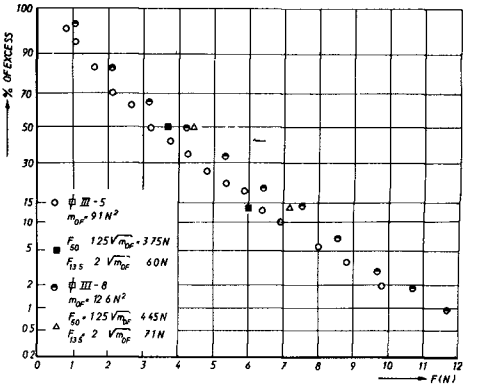

FIG. 4

Applying $F_{13.5}$ as a characteristic force in the probability distribution of forces one may try to relate this force to the parameters selected for the description of the wave conditions and the pile diameter, hence to:

$$\hat{T},\ M_{o_7},\ \frac{S_{77\,max}}{M_{o_7}},\ D.$$

Instead of $F_{13.5}$ the parameter $\dfrac{F_{13.5}}{(\rho g \frac{\pi}{4} D^2)\sqrt{M_{o_7}}}$ has been used.

The results of the experiments expressed in these parameters have been listed in table I.

DISCUSSION OF RESULTS

The values of T(f) obtained from a number of experiments with circular and square piles of 0.125 m and 0.12 m diameter respectively have been plotted in figure 5. In these cases the inertia forces are predominant. The curves give T(f) according to linear wave theory for the values of C_M indicated in the figure. The experimental results show some scatter, especially in the extreme high and low frequency ranges. The energy densities in these parts of the spectra are rather small, however, and consequently the values of T(f) obtained by dividing wave and force spectral densities are relatively inaccurate. It may be said that on the whole reasonably uniform transfer funotions were obtained. No distinct influence of M_{o_7} can be observed, hence no appreciable effect of non-linearity is apparent. It is remarkable that both for the circular and square piles T(f) has a maximum at $f \approx 1.1$ sec^{-1}. The results of Jen [6] slightly indicate a similar effeot. There is also an appreciable difference between the experimental and theoretical values of T(f). The application of higher order wave theories does not lead in this case to a better agreement with the experimental data. An explanation for the deviations cannot be given. It might be that a more or less periodic development of eddies around the piles introduces the effect of a filter, but no further evidence is available so far to support this hypothesis. In evaluating the importance of the irregularities in T(f) and the scatter in results it should be kept in mind that T(f) as defined here is proportional to the square of the forces.

The results presented in figure 5 furthermore indioate that C_M is close to 2 and 3 for the circular and square pile respectively.

For a smaller circular pile the transfer function T(f) has been plotted in figure 6. In this case the contribution of drag forces is no longer negligible. Consequently there should be a nonlinear effect resulting in higher values of T(f) with increasing M_{o_7}. Moreover the values of T(f) should be higher for the smaller pile diameters. (This is a result of the definition of T(f)).

It is understood that if non-linearities occur the description of forces in terms of spectra is in fact not very meaningful.

The dotted line in figure 6 gives the mean values of T(f) for the bigger pile with D = 0.125 m. Examination of the results reveals

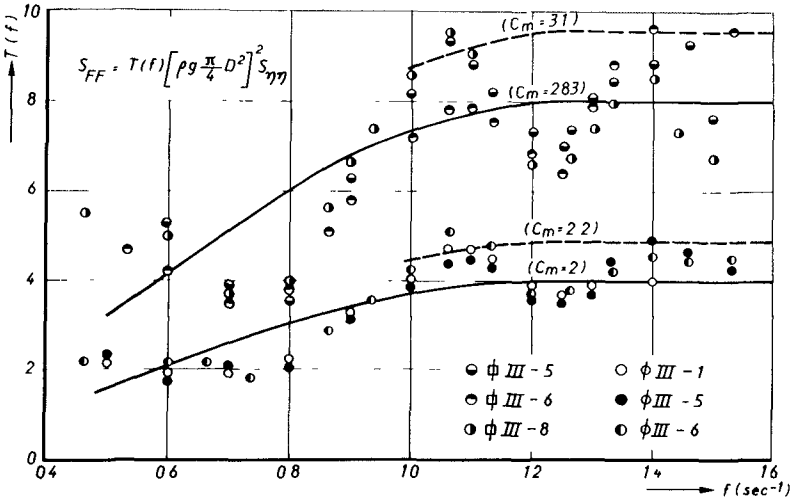
$S_{FF} = T(f)\left[\rho g \frac{\pi}{4} D^2\right]^2 S_{\eta\eta}$
(Cm = 3 1)
(Cm = 2 83)
(Cm = 2 2)
(Cm = 2)
φ III - 5
φ III - 6
φ III - 8
φ III - 1
φ III - 5
φ III - 6
T (f)
f (sec⁻¹)

FIG. 5

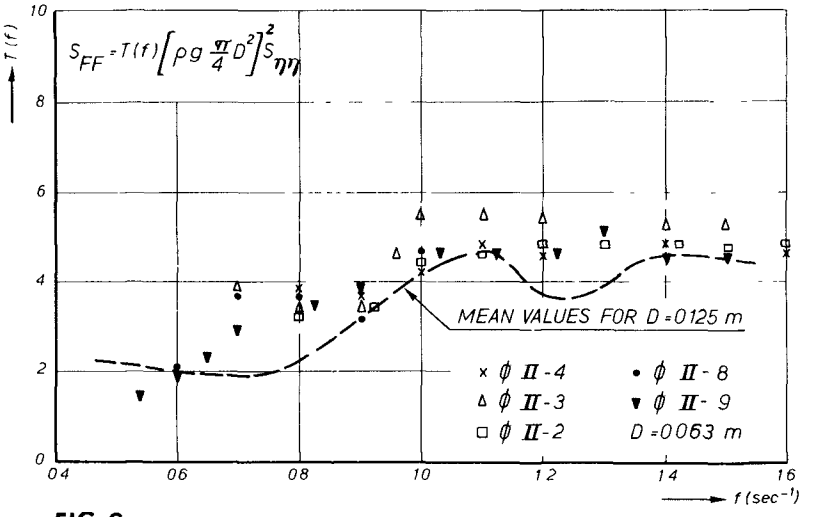
$S_{FF} = T(f)\left[\rho g \frac{\pi}{4} D^2\right]^2 S_{\eta\eta}$
MEAN VALUES FOR D = 0125 m
φ II - 4
φ II - 3
φ II - 2
φ II - 8
φ II - 9
D = 0063 m
T (f)
f (sec⁻¹)

FIG. 6

some typical aspects. It is obvious that the mean values of T(f) are higher for the smaller pile diameter as could be expected, the explanation being the increased contribution of drag forces. This should also lead, however, to increasing values of T(f) with increasing wave heights, hence increasing M_{op}. Such a tendency does not appear as can be seen by comparing the various series using the information listed in table I. Furthermore a distinct maximum as observed in figure 5 does not occur in this case.

Again no reasonable explanation can be given and it is obvious that further experiments are necessary to arrive at reliable conclusions. For the time being it can only be said that it is doubtful whether a simple superposition of drag and inertia forces can be applied in predicting irregular wave forces.

Still nowadays a method which is often applied to determine the design load on piles consists of selecting a design-wave height and period and subsequently computing the wave force using Morrison's equation and data obtained from experiments with regular waves. In this respect it may be interesting to consider a number of waves in an irregular wave train and to compare actual forces with those computed according to Morrison's equation. In the irregular wave train the wave period was defined as the time interval between two downward zero-crossings and the wave height as the vertical distance between the wave crest and the preceding wave trough. The wave force considered is the peak force in the direction of wave propagation. In the computations the integrated orbital velocities and accelerations were determined using the results of Reid and Bretschneider[8]. C_D and C_M values were selected in such a way that on the average the computed wave forces correspond as good as possible with the forces actually recorded. Figures 7 and 8 show actual and computed forces for both a square and a circular pile of such a diameter that the inertia forces are predominant. The C_M values applied are 3.1 and 2 respectively. Figure 9 shows the results for a smaller square pile (D = 0.06) in which case there is an appreciable contribution of drag forces for the higher waves. The coefficients applied in the computations were: $C_D = 2$ and $C_M = 2.83$. From these figures it appears that the actual forces may deviate considerably from the computed forces. One of the reasons is of course that the wave profile in the irregular wave train is a superposition of components with different frequencies. It is felt, however, that also the time history of the flow around the piles has an influence. To illustrate this, an example of simultaneous wave and force records has been given in figure 10. Apparently the wave following the maximum wave in this example produces a relatively small force. Such phenomena were observed several times in the records. It might be that the higher preceding wave generates strong persistent eddies which hamper the development of the flow pattern. The considerable scatter of results from irregular waves compared to results of computations has been observed before. In the author's opinion this leads to the following recommendation:

If a design load has to be determined on the basis of an acceptable probability of occurrence, it shall preferably be derived from probability distributions of forces, rather than

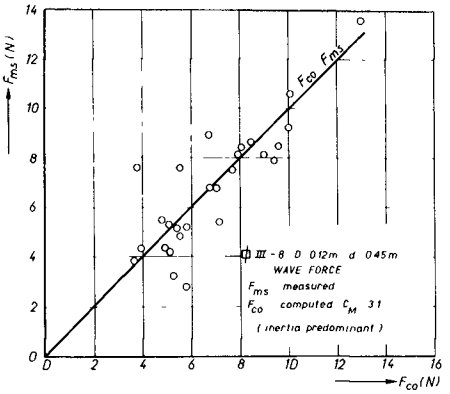

FIG. 7

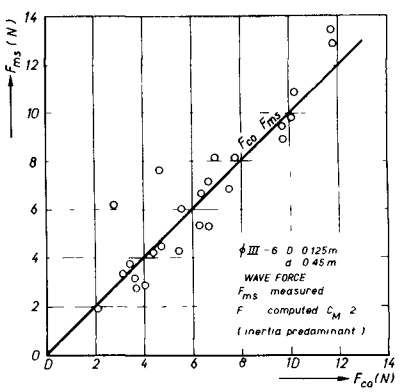

FIG. 8

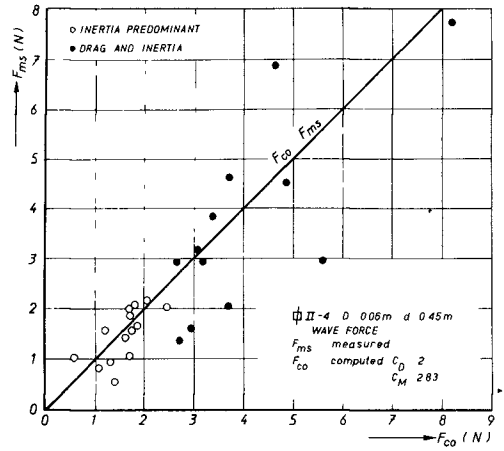

FIG. 9

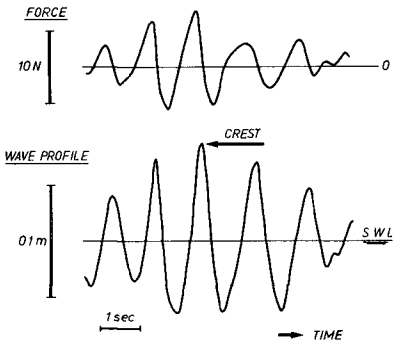

FIG. 10

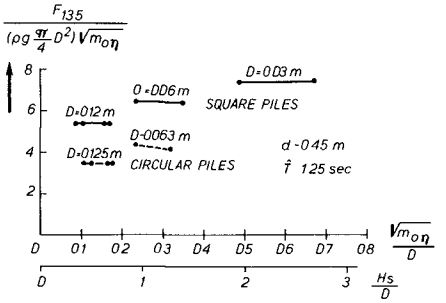

FIG. 11

selecting a design wave which has the accepted probability and computing the force which is expected to be exerted by this wave. For each wave condition the probability distribution of wave forces must then be known.

As has been outlined before the probability distributions will for the time being be characterized by

$$\frac{F_{13.5}}{(\rho g \frac{\pi}{4} D^2)\sqrt{M_{o\eta}}} \quad , \quad \frac{F_{50}}{F_{13.5}} \quad \text{and} \quad \frac{F_1}{F_{13.5}}$$

The results of a number of experiments expressed in these parameters have been listed in table I, together with the data on wave conditions.

When considering the ratio $\frac{F_{13.5}}{(\rho g \frac{\pi}{4} D^2)\sqrt{M_{o\eta}}}$ it appears that there is first of all an influence of the pile diameter. The ratio increases with decreasing pile diameter. This is in agreement with the results obtained for T(f) and it would be reasonable to say that this is due to the increased contribution of drag forces. For the same reason there should be an increase with increasing $M_{o\eta}$. However, as could be seen already from the results of T(f), such a tendency does not appear. It must be kept in mind that the range of variables was rather limited. Nevertheless there is a rather significant indication that the influences of pile diameter and wave height are different from those established in methods of computation.

From the transfer functions given in the figures 5 and 6 one might expect that there is an influence of the width of the spectrum, especially if the spectrum has the maximum energy density at $\hat{f} = 0.8$ sec^{-1}. From table 1, however, one may conclude that in practice the influence of the width, expressed in

$\frac{S_{\eta\eta\,max}}{M_{o\eta}}$, is negligible. In this respect it must be stated

oncemore that T(f) is proportional to the square of the wave forces. Hence there is not such a strong influence of the wave frequency on the forces as suggested by the path of T(f).

In order to illustrate the various problems mentioned above, the results obtained from the experiments with $\hat{T} = 1.25$ sec have been summarized in figure 11. According to theories there should be a gradual increase of

$\frac{F_{13.5}}{(\rho g \frac{\pi}{4} D^2)\sqrt{M_{o\eta}}}$ with increasing $\frac{\sqrt{M_{o\eta}}}{D}$. It is clear from

figure 11 that there is an influence of the pile diameter which is not adequately incorporated in present theories.

The values of $\frac{F_{50}}{F_{13.5}}$ and $\frac{F_1}{F_{13.5}}$ show a variability in the probability distributions of forces. There is a scatter in the results

TABLE I

Results of experiments. Water depth d = 0.45 m

series D=0.12m	$M_{o\eta}.10^4$ (m^2)	$\hat{T}$ (sec)	$\frac{S_{\eta\eta\,max}}{M_{o\eta}}$	$\frac{F_{13.5}}{(\rho g \frac{\pi}{4} D^2)\sqrt{M_{o\eta}}}$	$\frac{F_{50}}{F_{13.5}}$	$\frac{F_1}{F_{13.5}}$	remarks
□ III-1	5.47	1.36	1.8	4.5	0.56	1.57	
III-2	2.39	1.36	2.12	4.6	0.54	1.6	
III-5	1.13	1.25	2.26	5.4	0.5	1.7	
III-6	4.31	1.25	2	5.4	0.57	1.57	
III-7	3.98	1.25	1.7	5.4	0.54	*	
III-8	1.50	1.25	1.38	5.4	0.58	1.54	
D=0.125m							
○ III-1	6.25	1.5	2.16	3.4	0.59	1.54	
III-2	3.5	1.5	2.08	3.3	0.57	1.54	
III-3	4.94	1.25	2.54	3.5	0.57	1.57	
III-4	2.43	1.25	2.34	3.5	0.55	*	
III-5	4.47	1.25	1.66	3.5	0.5	1.74	
III-6	1.76	1.25	1.42	3.5	0.56	1.6	
D=0.06m							
□ II-1	1.75	1.16	1.6	6.2	0.6	1.71	
II-2	4.45	(1.1)	*	6.4	0.54	1.73	1)
II-3	1.97	1.25	2.94	6.5	0.62	1.63	
II-4	4.35	1.25	2.7	6.4	0.54	1.92*	
II-5	2.38	(1.19)	*	6.0	0.6	1.56	2)
II-7	2.33	1.67	4	5.9	0.58	1.72	
II-8	4.7	1.67	3.6	6.3	0.57	1.74	
II-9	5.51	1.68	1.2	6.3	0.54	1.74	
D=0.063m							
○ II-1	2.33	(1.14)	*	3.8	0.59	1.6	3)
II-2	3.85	1.20	1.27	4.1	0.59	1.59	
II-3	2.14	1.25	3.1	4.4	0.63	1.60	
II-4	4.03	1.25	3.02	4.2	0.61	1.71	
II-7	1.98	1.65	4.1	3.5	0.61	1.5	
II-8	4.03	1.63	3.6	3.5	0.61	1.59	
II-9	3.66	1.66	1.14	3.9	0.62	1.62	
D=0.03m							
□ I-1	1.81	1.6	1.65	7.5	0.64	1.58	
I-2	3.89	(1.65)	1.65	7.3	0.57	1.73	4)
I-3	2.12	1.4	3	7.4	0.63	1.63	
I-4	3.92	1.3	3	7.5	0.57	2.0	

* not reliable

1) maxima in $S_{\eta\eta}$ at T = 1.1 and T = 1.38 sec
2) " " " " T = 1.19 " T = 1.74 "
3) " " " " T = 1.14 " T = 1.59 "
4) " " " " T = 1.4 " T = 1.65 "

which makes it somewhat difficult to draw reliable conclusions. Still the following tendencies can be observed:

- The distributions deviate from the Rayleigh distribution. For the smaller probabilities of occurrence the forces are higher than predicted by a Rayleigh distribution ($\frac{F_1}{F_{13.5}} > 1.5$).
- The deviations from the Rayleigh distribution increase with decreasing pile diameters. A relation between $\frac{F_1}{F_{13.5}}$ and $\frac{\sqrt{M_{o7}}}{D}$ could not yet been established.
- The tendencies mentioned above are in agreement with the influence of non-linear drag forces.
- It may be expected that a set of standard distributions can be established which are sufficiently accurate for design purposes.

It is obvious that the information presented in this paper is by no means sufficient to get a reasonable insight into the problems related to irregular-wave forces on piles. Some typical features have been found which could not yet be explained. There exists non-linearities in the mechanism that underlies the forces exerted by irregular waves whioh may lead to deviations between actual forces and the forces derived from data obtained with regular waves or predicted by computations. It is felt that further investigations are necessary to establish a reliable method for the prediction of wave forces which is based on the statistical properties of irregular wave motion.

CONCLUSIONS

The prediction of irregular-wave forces from theories and regular-wave force data reveals many problems. The phenomenon of wave forces is non-linear and the magnitude of the forces is affected by the time-history of flow. The information presented in this paper does not provide sufficient insight into these problems.

The results obtained so far with irregular waves indicate that with respect to forces on piles the wave motion is sufficiently characterized by $\hat{T}$ and M_{o7}, hence that for design purposes the width of the energy spectrum is of minor importance. The results moreover suggest that a set of standard probability distributions of forces can be established in which the water depth, the pile diameter, the period of maximum wave energy and the total energy of the wave motion appear as parameters.

Any tendency or conclusion derived in this paper may not be applied for the time being beyond the range of variables covered by the experiments.

REFERENCES

1. Keulegan, G.H. and Carpenter, L.H.: "Forces on cylinders and plates in an oscillating fluid".
Journ. Res. Nat. Bur. Stand. 60 (5), 1958.

2. Paape, A. and Breusers, H.N.C.: "The influence of pile dimension on forces exerted by waves".
Proc. Xth Conf. on Coast. Eng. Tokyo, 1966.

3. Borgman, L.E.: "Wave forces on piling for narrow-band spectra".
Proc. A.S.C.E. Vol. 91 no. WW3 Part 1, Aug. 1965.

4. Pierson, W.J. and Holmes, P.: "Irregular wave forces on a pile"
Proc. A.S.C.E. Vol. 91, no. WW4 Part 1, Nov. 1965.

5. Borgman, L.E.: "Ocean wave simulation for engineering design".
Proc. A.S.C.E. Conf. on Civ. Eng. in the Oceans. San Francisco, Sept. 1967.

6. Jen, Y.: "Laboratory study of inertia forces on a pile".
Proc. A.S.C.E. Vol. 94, no. WW1, Febr. 1968.

7. d'Angremond, K. and van Oorschot, J.H.: "The effect of wave energy speotra on wave run-up".
Proc. XIth Conf. on Coast. Eng., London, 1968.

8. Reid, R.O. and Bretschneider, C.L.: "Surface Waves and Offshore Structures: Forces on vertical piles and large submerged objects"
Texas A. and M. Res. Found., Oct. 1958.

CHAPTER 62

EXPERIMENTAL INVESTIGATION OF SHOCK PRESSURES AGAINST BREAKWATERS

Gustaf Richert
Tech.lic., Division of Hydraulics
Royal Institute of Technology, Stockholm
Sweden

ABSTRACT

This paper describes an experimental investigation of shock pressures against breakwaters caused by breaking waves. The study only considers shocks of a compressive type, which occur if the wave front is formed in such a way that an air cushion is entrapped between the wave and the wall. In this case the compression and expansion of the air cushion plays an important rôle in the pressure variation.

Only waves preceded by non-breaking waves were used. For different combinations of bottom geometry and water depth the occurrence of shock pressures of different magnitudes was studied varying the wave height and the wave period. For some interesting combinations of bottom geometry and wave dimensions a series of tests were made to investigate the distribution over the wall of shock pressure and of shock impulse. The results, presented in diagrams and tables, have been commented on and analysed with special respect to the chosen test procedure.

INTRODUCTION

The previous research presents a very scattered view on the shock pressure problem. Different bottom slopes from 1:50 (MITSUYASU) to 1:2 (NAGAI) have been tested. Different test procedures have also been used: Solitary waves (e.g. BAGNOLD, DENNY, HAYASHI-HATTORI) and consecutive breaking waves (e.g. RUNDGREN, MITSUYASU) have been studied. The pressures have been measured using different methods, and sometimes the equipment, often insufficiently described in the reports, have, in view of later investigations, been of a too low natural frequency. The results are often contradictory and have been presented in different ways. This regards the characterisation of the waves as well as of the pressure, its duration and distribution and the pressure impulse. Thus, it is extremely difficult to compare the results of different authors or to formulate distinct tendencies for the relations between the shock pressure characteristics, the wave characteristics and the boundary geometries.

For the designing engineers, there are still several deficiencies of knowledge. - In spite of the work by CARR (1954), very little is known about the occurence of shock pressures. Which combinations of wave period and wave height are, for different combinations of bottom slope and water depth, expected to give shock and which are not. - Apart from a few tests by ROSS (1955) breaking

waves preceded by nonbreaking waves have not been systematically investigated. Since such waves are likely to occur in nature and since solitary waves usually give higher pressures than corresponding consecutive breaking waves, this type of wave - the breaking wave preceeded by nonbreaking waves - should be of interest.

Not much is known about the probable and possible horizontal distribution of shock pressures. In spite of the systematic work of NAGAI (1960) more information is needed on the simultaneous vertical pressure distribution against a wall. Contradictory results have been published on this subject.

The main purpose of this investigation has been to fill in some of these deficiencies of knowledge.

TEST INSTALLATIONS

The tests were carried out in a flume which is 1.2 m wide, 0.8 m deep and which has a total length of 19 m, 13.5 m of which a horizontal bottom, see Fig. 1. A flap-type wave generator was hinged at the bottom of the deeper part

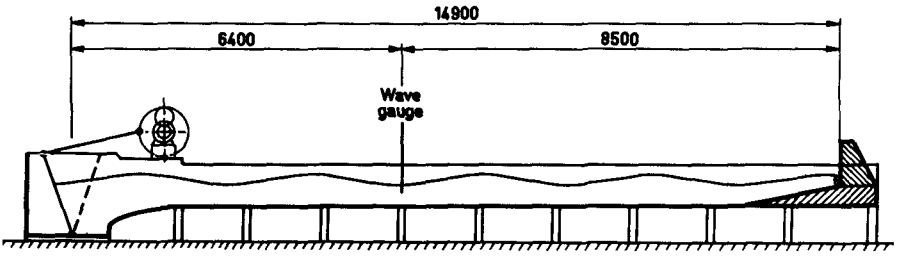

Fig. 1. Test Installations

of the flume. This wave generator can produce regular waves of different periods and amplitudes, the maximum period being about 1.67 s.

At the opposite end of the flume, 14.9 m from the wave generator, a plane test wall was placed on a built-in bottom. This wall consisted of a 15 mm thick steel plate, which was screwed onto a system of 10 vertical buttresses made of concrete and with flanges of steel. The test wall could oppose the waves with its front vertical or sloping 30° to the vertical. Two of the buttresses were designed in such a way that the pressure gauges could be installed between them. 100 x 100 x 15 mm mounting plates into which the pressure gauges were fitted, could be screwed onto the flanges of the buttresses with their surfaces flush with the front plate. The centerline of the vertical row of gauges situated 122 mm to the right of the center line of the flume. Since the pressure gauges could not be placed closer than with their centers 100 mm apart it was made possible to place the set of three gauges at different levels. Thus the vertical pressure distribution could be studied more in detail by repeating

the test runs for the different levels of the pressure gauge set. During the investigation the set of gauges was placed at levels with the center of the lowest gauge 2.2 cm, 4.0 cm, 5.7 cm and 9.0 cm above the bottom of the wall.

In a similar way it was made possible to investigate the horizontal pressure distribution on an arbitrary level. On this level pressure gauges could, besides the one placed 122 mm to the right of the centerline of the flume, be placed 143 mm and 388 mm or alternatively 266 mm and 511 mm to the left of the centerline of the flume.

The gauges were mounted so that the sensitive membranes were flush with the wall. The fissures around the gauge mountings were carefully tightened with plastic material in order to prevent compressed air of the entrapped air cushion to escape that way.

The buttresses, their flanges and the mounting plates for the gauges were calculated to have natural frequencies of at least 10^4 Hz. Any disturbances resulting from oscillations of the test wall or from shock waves reflected within the construction elements were not observed.

The built-in bottoms on which the test wall was placed were of different types. The ones with the slope 1:3 were designed to correspond to the rubble mound of an average composite-type breakwater. In the previous research regarding composite-type breakwaters (e.g. NAGAI, 1960), usually the horizontal width of the top of the mound in front of the wall, a, equals the water depth in front of the wall d_1. Thus, to facilitate comparisons, the width was chosen a 15.0 cm, the same as the most used water depth. In order to get results for values of the ratio d_1/a larger than 1, tests were also made on a mound with a horizontal width a of 7.5 cm. In that way attempts could be made to reproduce the larger tests with a linear scale of 1:2. The mound with a = 15.0 cm had a height of 36.9 cm above the bottom of the flume while the one with a = 7.5 cm had a height of 39.1 cm.

Tests were also made with the wall standing on bottoms with slopes corresponding to natural ones and without horizontal planes on the top. It was first intended to use only the slope 1:10 but, since the results showed important differences to the results for the slope 1:3 tests were also made with bottom slopes of 1:6 and 1:25. The built-in bottoms with natural slopes had a height of 37.2 cm above the bottom of the flume, which is nearly the same as the heights of the rubble mound mentioned above.

RECORDING EQUIPMENT

Wave dimensions. - The heights and the periods of the waves were measured by a resistive water level gauge placed 8.5 m from the test wall. The resistance variations were recorded with the help of an ABEM coil galvanometer recorder which had a paper speed of 2.5 or 5.0 cm/s.

Behaviour of waves. - The action of the waves immediately in front of the wall could be photographed through the glass wall of the flume. The camera was a Paillard Bolex 16 mm Movie Camera, used with a speed of 64 pictures/s. 5 test runs were photographed for each combination of wave height, period and boundary geometry for which the pressure distribution was investigated. All other waves were watched through the glass wall of the flume and their behaviour was noted.

Wave pressures. – The pressure gauges used were of the capacitive type, specially designed for shock pressures by TBR, Delft. A gauge of this type consists of a membrane with 20 mm diameter, which forms one of the electrodes in a capacitor, see Fig. 2. A capacitive displacement meter which fed the gauges with a constant carrier frequency of 1050 kHz also translated the capacitance variations caused by membrane deflections into signals which were recorded by the galvanometer recorder and by an oscilloscope. Since the capacitive displacement meter had only three channels, pressures could be measured at only three points simultaneously. The natural frequency of the pressure gauges was 5500 Hz when they were submerged in water and 8800 Hz in air.

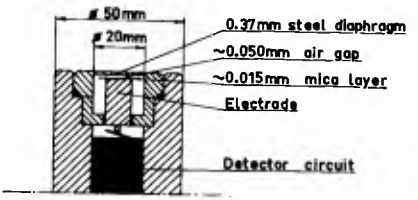

Fig. 2. Pressure gauge.

By means of coil galvanometers with a natural frequency of 8000 Hz, the pressure variations could be recorded on the same paper as the corresponding wave form. In spite of the fact that the paper moved very slowly and the sensitivity of the very fast galvanometers was low, this arrangement proved very useful. The wave which had caused the shock pressure recorded by the oscilloscope could be identified and the order of magnitude of the pressure registration could be checked.

An oscilloscope of a very suitable type, Tectronix 564, was used to study the pressure variations in detail. This oscilloscope is equipped with a storage system, which stores the trace of the sweep on the screen for some time. This made it possible to study the pressure variation and to decide whether it was worth photographing or not. The trace of the sweep could be photographed with a special oscilloscope polaroid camera, a typical photo of which is shown in Fig. 3.

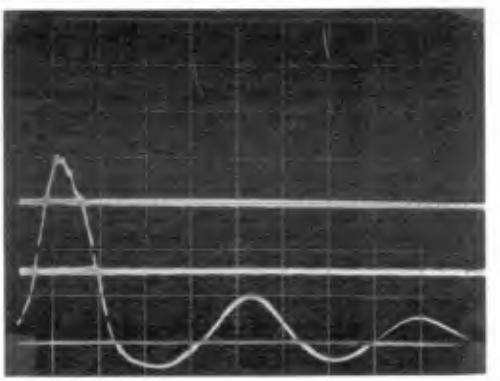

Fig. 3. Oscilloscope photo.

The oscilloscope sweep was started by a trigger mechanism when the pressure reached a certain height.

The pressure recording equipment was calibrated statically with compressed air pressures, after about 200 test runs or when the electrical conditions were changed significantly. The pressure of the air was measured with a mercury manometer. The calibration diagrams showed very small variations from one calibration to another.

TEST PROCEDURE

When a breaking wave hits a vertical wall spray is thrown upwards into the air and the water in front of the wall is mixed with air bubbles. The disturbances caused by the downfall of the spray and by bubbles from the preceding wave are not reproduced in a correct way in model tests. Furthermore, these disturbances would soften the shock pressure. Consequently is was found more interesting and necessary to study the shock pressures caused by breaking waves preceded by non-breaking waves. Such a combination is likely to occur in a prototype.

Thus, the following procedure for the tests was chosen. Before each test run, the wave generator was put in a certain position. The test run was not started until the water surface in the flume was calm. When the wave generator started the beginning of a wave train travelled towards the test wall. As a rule, the 4th wave of this wave train was studied, but occasionally, especially when the wave period was short, it proved necessary to study the 5th, the 6th or even the 9th wave. In a few cases, for the shoal with a = 7.5 cm, the 3rd wave was studied.

For each combination of bottom geometry, water depth and wave period different values of the wave generator amplitude were tested. This amplitude was decreased until the studied wave became so small that it could not break against the test wall but only produced clapotis. On the other side, the amplitude could not be increased too much owing to three reasons:

1. The studied wave became so high that it broke too far from the test wall to produce any shock pressure.
2. The wave preceding the studied wave broke or otherwise produced too much disturbance.
3. The top of the studied wave broke when passing the wave gauge.

In the case of 2 and 3 no upper limit for the occurrence of shock pressures could be determind.

For the 1:25 shoal some tests were carried out with a series of consecutive breaking waves.

TEST PROGRAM

The influence of wave height and wave period on the occurence and magnitude of shock pressures was investigated using several combinations of bottom geometry and water depth. The combinations which have been studied are indicated in

Table 1. The geometry characteristics are defined in Fig. 4.

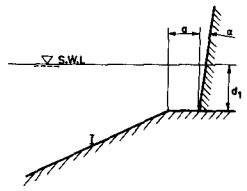

Fig. 4. Definitions of geometry characteristics.

During these investigations, the center of the lowest pressure gauge was normally situated 5.7 cm above the bottom of the wall. It was attemted to make model scale studies at a scale difference of 1:2 by studying tests with a = = 15.0 cm, d_1 = 15.0 cm and a = 7.5 cm, d_1 = = 7.5 cm respectively. Thus, in the tests with a = 7.5 cm the gauges were moved to more comparable positions, with the center of the lowest gauge 2.2 cm above the bottom of the wall.

I	a cm	α °	d, cm			
			5.0	7.5	11.0	15.0
1:3	15	0			x	x
1:3	7,5	0		x		x
1:6	0	0		x	x	x
1:10	0	0		x	x	x
1:25	0	0	x	x	x	x
1:3	15	30			x	x

Table 1. Investigations of occurrence of shock pressures.

Some dangerous or otherwise interesting combinations of wave period and wave height were selected, see Table 2. For each of these combinations 25 tests

Series	I	a cm	α °	d_1 cm	T s	H cm
A	1:3	15	0	15.0	1.40	19.40
B	1:3	15	0	15.0	1 40	20.30
C	1:3	15	0	15.0	1.64	13.30
D	1:3	15	0	11.0	1.30	16.60
E	1:3	7,5	0	15.0	1.50	20.50
F	1:10	0	0	11.0	1.50	11.80
G	1:3	15	30	15.0	1.40	19.90
H	1:3	15	30	15.0	1.40	21.00

Table 2. Investigations of pressure and impulse distributions.

with identical conditions were made for each position of the gauges and the pressure and impulse distributions were evaluated statistically. Since, in the tests with the nonvertical wall, the dispersion of the results was comparatively small, it was decided upon to make 10 runs only for each gauge position.

The extent of the test program was worked out continuously with regard to the results.

INTERPRETATION OF RESULTS.

Wave dimensions. - The wave form registered on the galvanometer recorder paper made it possible to measure wave heights and wave periods. The wave lengths were calculated with the formula

$$L = \frac{gT^2}{2\pi} \tanh \frac{2\pi d}{L} \qquad (1)$$

Fig. 5 shows how the height (H) and period (T) of a particular wave were defined and measured on the registration.

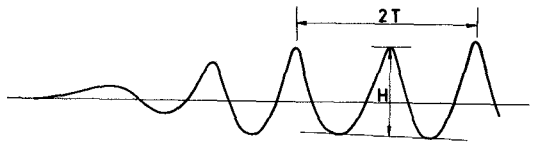

Fig. 5. Definitions of wave characteristics.

The wave dimensions at the point where the wave gauge was situated have been recalculated to dimensions valid for points of interest for a designing engineer. For the tests with bottom slopes of 1:6, 1:10 and 1:25 the wave heights given in this paper represent the dimensions of the studied wave when it passed over the point of the bottom where $d = 0.1L_o$. It is assumed that Stokes theory for finite amplitude waves is valid for $d \geq 0.1L_o$. ($L_o = gT^2/2\pi = 1.56T^2$)

For the tests with the bottom slope 1:3, on the other hand, the waves are valid for the depth of water between the water surface and the bottom of the flume. Assuming this depth being constant in the flume, the recorded wave dimensions have been recalculated as described below to the section of the flume where, during the tests, the water depth was $d = 0.1\ L_o$ over the built-in sloping bottom. Thus, the wave dimensions given in the paper represent what the waves would have been in that section of the flume if the composite-type breakwater construction had not existed.

A theory given by SVERDRUP-MUNK, 1947, was used for the recalculation of the wave dimensions. It assumes that the potential energy of a wave is transmitted with the wave velocity while the kinetical energy is stationary. The potential energy can be calculated from the formula

$$\frac{E_{pot}}{E_{tot}} = n = \frac{1}{2} \cdot \sqrt{1 + \frac{\frac{4\pi d}{L}}{\sinh \frac{4\pi d}{L}}} \qquad (2)$$

The distance (b) between the wave gauge and the point of interest as

described above was different for each combination of bottom geometry and wave period. For each combination the energy transport was calculated with significant mean values of water depth (d), wave length (L) and energy ratio (n). The total energy of the nth wave at the gauge and at the actual point of interest could be determined as the energy of the nth wave n + 6.40/L periods and n + (6.40 + b)/L periods after the start of the wave generator respectively. Thus, the ratio E/Egauge between the total energy of an arbitrary wave at the point of interest and the total energy of the same wave at the wave gauge could be determined.

In the expression for the wave energy

$$E = \frac{\gamma L H^2}{8} \cdot \left(1 - \frac{\pi^2 H^2}{2L^2 \cdot \tanh^2 \frac{2\pi d}{L}}\right) \qquad (3)$$

the second term in the brackets is, for the waves in the test program, small compared to 1. Thus, Eq. (3) can, with good approximation, be simplified to

$$E = \text{const} \cdot L \cdot H^2 \qquad (4)$$

A series of special tests were run in order to investigate the propagation of waves in the beginning of a wave train. These tests were made in a flume with constant depth and 20.5 cm width. The number of tests was 40 and the water depth and the wave dimensions were half of those ueed in the main tests. Wave gauges were installed at points corresponding to the wave gauge and to the test wall in the main tests. Behind the wave gauge corresponding to the test wall there was placed a wave absorber. The investigation showed that the wave period and hence the length of the studied wave corresponded at the two gauges with a maximum error of 4.2 o/o.

Thus Eq. (4) can be transformed into

$$\frac{H}{H_{gauge}} = \sqrt{\frac{E}{E_{gauge}}} \qquad (5)$$

This expression was used for the calculation of the wave heights at the points of interest defined above.

The fact that the wave gauge was situated somewhat too near the wave generator affected the measured values of the wave dimensions in a manner which needs further comments. When the generated wave was very steep it lost its top and foam was created on the wave front before the wave passed the wave gauge. If the amplitude of the generator movement was decreased no such phenomenon occurred and the wave passed the wave gauge with unbroken top. Thus, although the generating energy in the second case was smaller, the recorded wave height could be somewhat larger due to differences in the wave form.

One example of this phenomenon was the relation between series A and B, see Table 2, for which the shock pressure distribution was investigated. In this case the generating energy of the studied wave was 8 o/o higher for the series A, while the measured wave height was 4 o/o higher for the series B. On the other hand the potential energy at the gauge was 2 o/o higher for the series A. Further-

more, the waves in series A behaved as if they were larger immediately in front of the breakwater. Hence, the wave height is not sufficient as characteristic of the wave in cases when the wave steepness is large. Anyhow, since the error was relatively small and since alternative wave characteristics are much more complicated to evaluate from large series of recordings, the wave height has, together with the wave period, been used as main characteristic of the wave form.

Occurrence of shock pressures. - The occurrence and magnitude of the shock pressures registered during this investigation are presented in Figs. 6 to 14. It must be observed that, as mentioned above, the pressure gauges during the studies regarding the occurrence of shock pressures were kept in a constant position. Thus, the pressure magnitudes do not represent maximum pressure peaks. (Compare the distribution diagrams.)

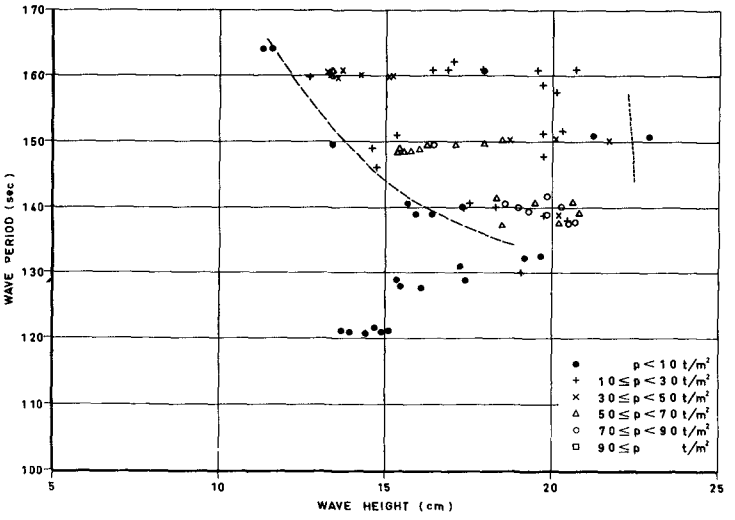

Fig. 6. Shock occurrence diagram. (I=1:3, a=15 cm, d_1= 15 cm)

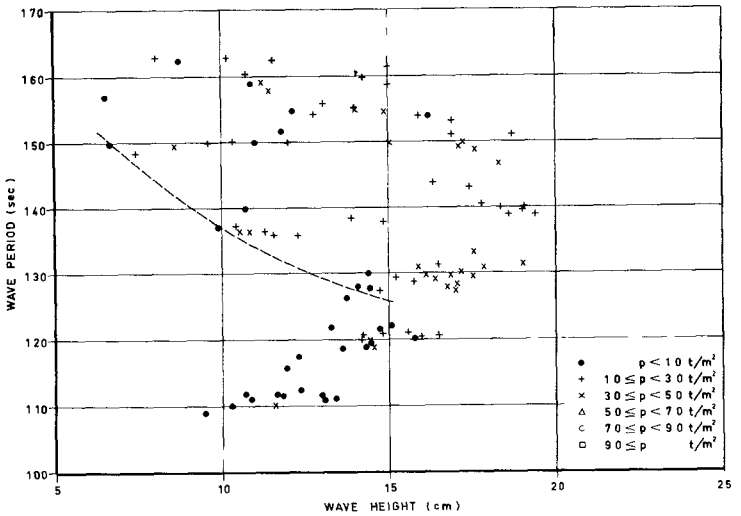

Fig. 7. Shock occurrence diagram. (I=1:3, a=15 cm, d_1= 11 cm)

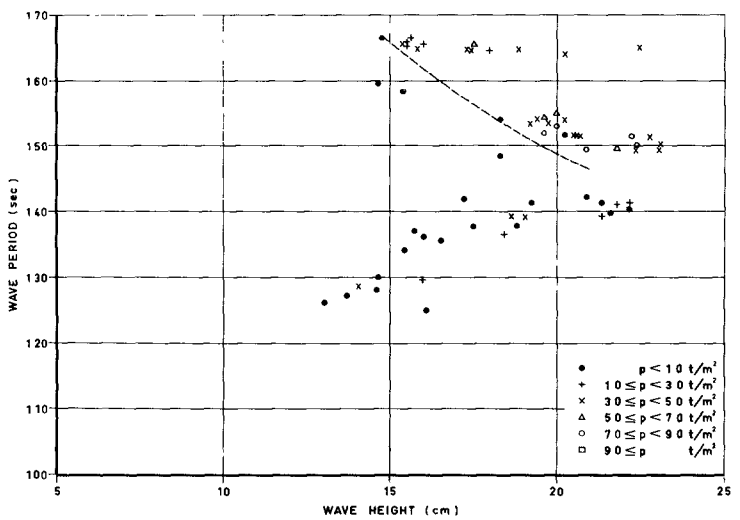

Fig. 8. Shock occurrence diagram. (I=1:3, a=7.5 cm, d_1=15 cm)

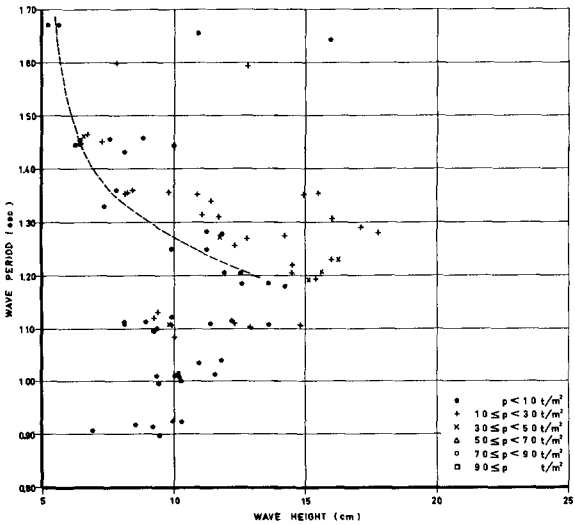

Fig. 9. Shock occurrence diagram. (I=1:3, a=7.5 cm, d_1=7.5 cm)

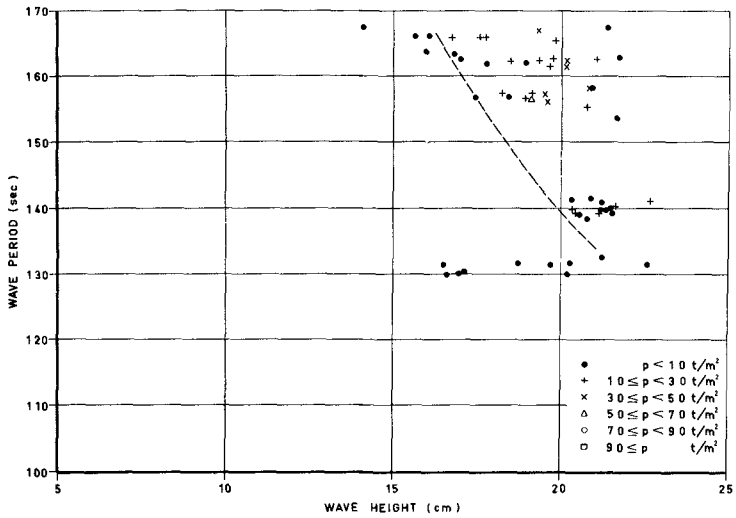

Fig. 10. Shock occurrence diagram (I=1:6, d_1=15 cm)

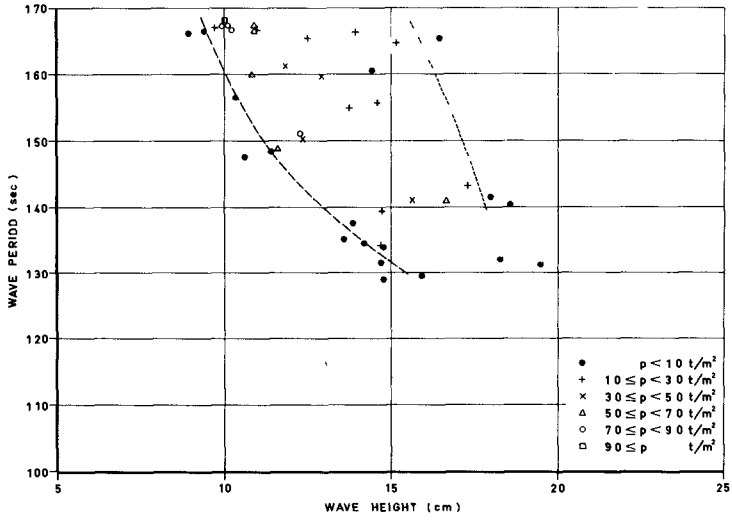

Fig. 11. Shock occurrence diagram. (I=1:6, d_1=11 cm)

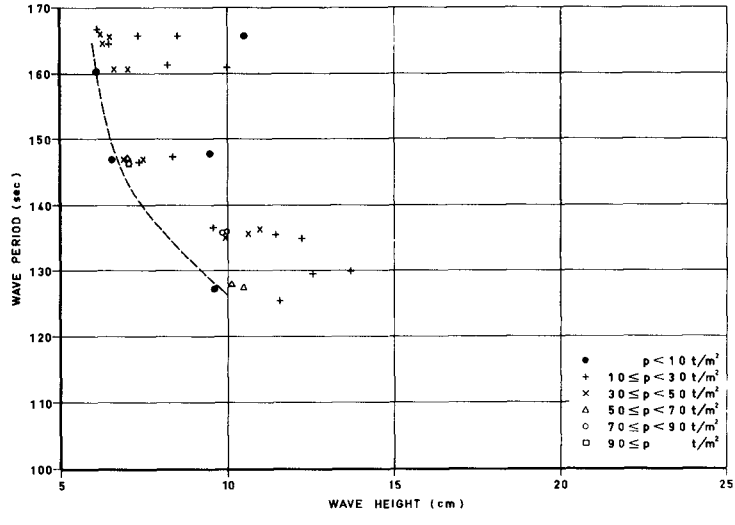

Fig. 12. Shock occurrence diagram. (I=1:6, d_1=7.5 cm)

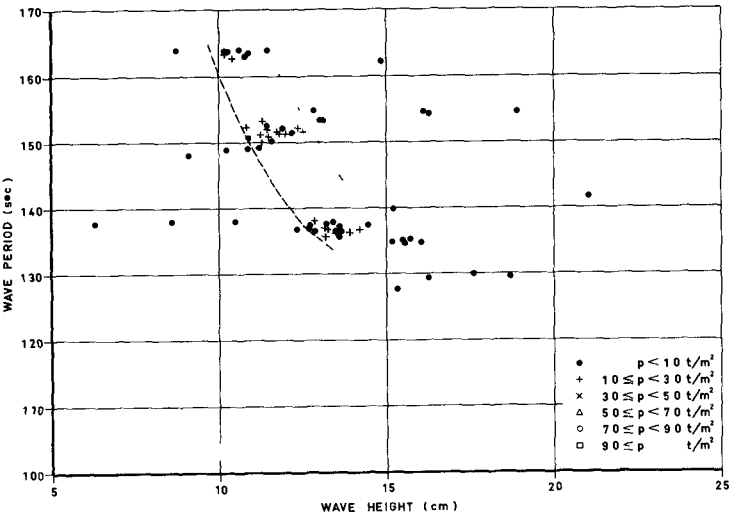

Fig. 13. Shock occurrence diagram. (I=1:10, d_1=11 cm)

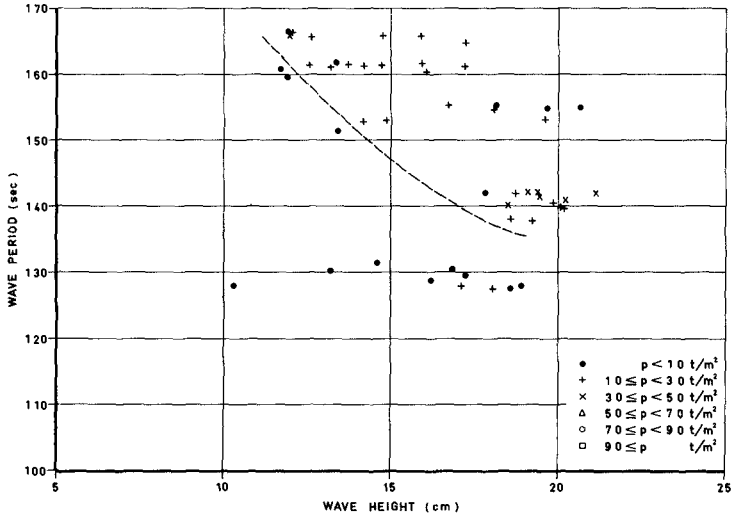

Fig. 14. Shock occurrence diagram. (I=1:3, a=15 cm, $\alpha=30^{\circ}$, d_1=15 cm)

The occurrence and magnitude of the shock pressures were directly dependent on the behaviour of the waves immediately in front of the wall. For a certain period, small waves did not break at all but only produced clapotis in front of the wall. These waves caused pressures against the wall, which were not large enough to start the oscilloscope sweep. Increasing the wave height, a certain, rather distinct value was reached, at which a thin air cushion was entrapped between the wave and the wall. A more distinct and sharp shock was heard and a short but very high shock pressure was recorded. After the first pressure peak the pressure decreased to below zero and then increased again continuing in a quickly damped oscillation. This oscillation can be explained as an adiabatic compression and expansion of the entrapped air cushion. The shortest recorded oscillation period was about 1.5 msec while the rise-time of the first peak corresponded to a somewhat shorter period. This rise-time was, however, very difficult to measure adequately since the time scale was limited by the capacity of the oscilloscope.

A further increase in wave height made the wave break in such a way that the air cushion grew thicker and hence the pressure became smaller but lasted for a longer time causing a longer oscillation period. Finally the wave became so high that it collapsed before it reached the wall. In these cases only very low shock pressures could be recorded if the oscilloscope sweep started at all. The upper limit of the occurrence of shock pressures was not so distinct as the lower limit.

The conditions described above could be observed for long wave periods. For short periods the waves needed a larger wave height to produce shock. However, for reasons given above, it was not possible to produce waves which had a large steepness at the test wall. Thus, it was usually impossible to establish the upper occurrence limit for shorter periods.

The behaviour of the waves in front of the breakwater was particularly affected by reflection phenomena in the test with the steepest bottoms and with short periods. Occasionally, waves which were too small to cause shock pressure against the wall met reflected preceding waves in such a way that parts of the wave were thrown against the wall. In that way shock pressures, although usually not very large, could be created by waves with short periods and lower wave heights than the normal lower shock occurrence limit. Such shock pressures have been recorded for all the tested relative water depths over shoals having a slope of 1:3, see Figs. 6 to 9 and 14.

As seen in Table 1, bottoms having slopes of 1:3, 1:6, 1:10 and 1:25 were tested. A comparison between the results confirms the observation by CARR (1954) that for a fixed wave period the range of wave heights creating shocks is narrower the flatter the slope of the bottom. It was also observed that, with the chosen test procedure, it was impossible to create violent shocks on the flatter slopes. The greatest shock pressure recorded at the shoal slope of 1:10 was 4.4 t/m^2. Using the actual test procedure, no shock at all was recorded for the slope 1:25. However, some shocks, though rather weak, were recorded during tests having many consecutive waves in a wave train.

It was attempted to carry out different tests which were model tests to each other. Tests having a slope of 1:6 and depths of d_1 = 7.5 cm, 11.0 cm and 15.0 cm could be considered to be corresponding scale models. At a slope of 1:3 only tests having a = d_1 = 7.5 cm and a = d_1 = 15.0 cm were scale models to each other.

If the occurrence diagrams of the test series which were corresponding scale

models were put in a dimensionless form they would coincide. For this purpose the wave heights have been recalculated to points with the depth $d = 3\ d_1$. The adapted lower occurence limit curves of the interesting tests have been represented in Fig. 15. The agreement between the curves is not perfect. This seems to be

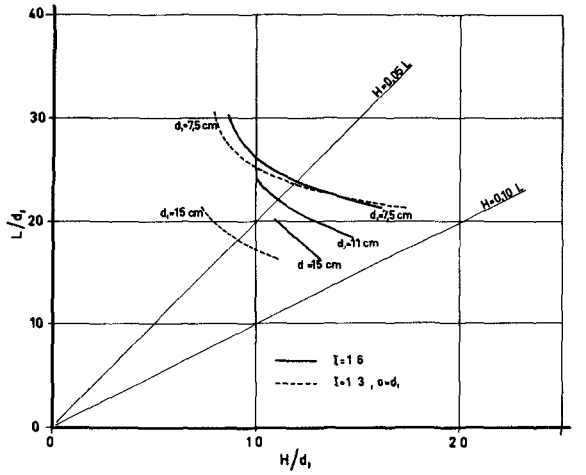

Fig. 15. Lower shock occurrence limits.

mainly due to the fact that even though the wave height H of the waves causing the shock pressures is in scale the preceding wave is not necessarily in the same scale. At smaller periods, the 5th, 6th, or even the 9th wave of the wave trains were studied. In these cases, the preceding waves were only slightly smaller than the studied ones, while on the other hand, the usually studied 4th wave was preceded by a considerably smaller 3rd wave. For shorter periods the studied wave was usually so disturbed by the preceding wave that it, in a sort of clapotis movement, lost parts of its top and hence lost energy before it reached the wall. Thus, for shorter periods, wave breaks and shock pressures were received only from waves having larger relative wave heights. Obviously, the simple notations of the period and height of one studied wave do not give a complete information about the behaviour of this wave. The mechanism of the breaking of a wave strongly depends on both the form of the actual wave and the behaviour of the preceding wave. This must be taken into account both in the planning of model tests for particular projects and in the interpretation of the results.

The influence of the horizontal width a of the top of the mound with slope 1:3 was easily noted by comparison between tests having $d_1 = 15.0$ cm and $a = 7.5$ cm, see Fig. 7. Apparently, much larger waves were needed to produce shock pressures when the width a of the mound was small. The practical use of this information is so important that it should be specially observed.

A comparison between the tests with a vertical test wall and those with a

wall sloping 30° to the vertical gave two interesting results. First, it could be noted that at a water depth of d_1 = 15.0 cm curves representing the lower occurrence limit were almost identical. Secondly, it was not possible to create very large shock pressures against the sloping wall. Tests with a water depth of d_1 = 11.0 cm gave such small pressures and so insecure recordings that a shock occurrence diagram would have no meaning. These results seem to be logical as a breaking wave is not likely to have a water front with a hang-over sloping 30° without losing its top or otherwise showing the irregularities of the required late stage of breaking. Thus, no thin air cushion can be entrapped.

Pressure distribution. - The pressure distribution over the test wall was studied in 8 different cases, see Table 2. The results are represented in Figs. 15 to 23 where, for the different pressure gauge levels, the maximum, average and minimum values of the recorded pressures have been connected to form pressure distribution curves.

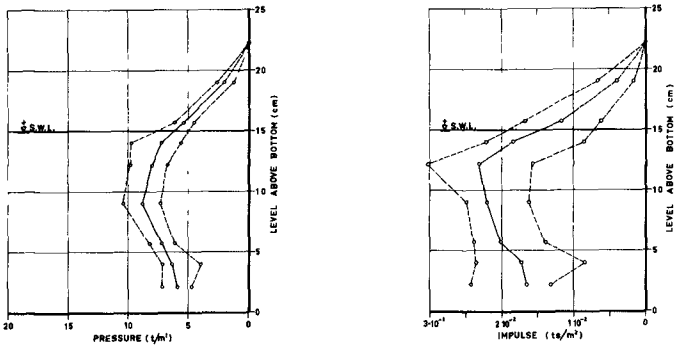

Fig. 16. Distribution diagrams. (I=1:3, a=15 cm, d_1=15.0 cm, T=1.40 s, H=19.4 cm)

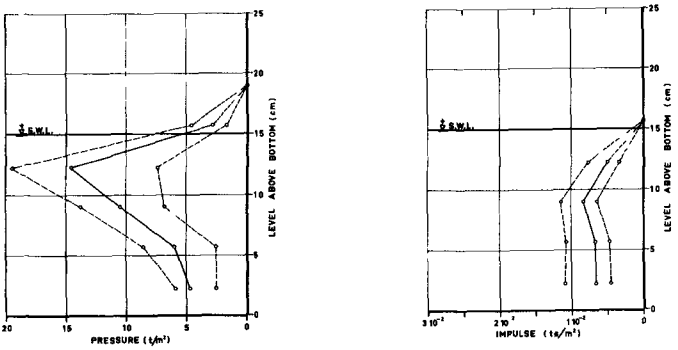

Fig. 17. Distribution diagrams. (I=1:3, a=15 cm, d_1=15.0 cm, T=1.40 s, H=20.3 cm)

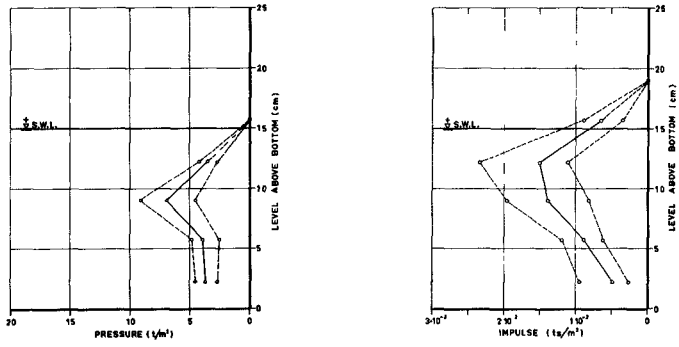

Fig. 18. Distribution diagrams. (I=1:3, a=15 cm, d_1= 15.0 cm, T=1.64 s, H=13.3 cm)

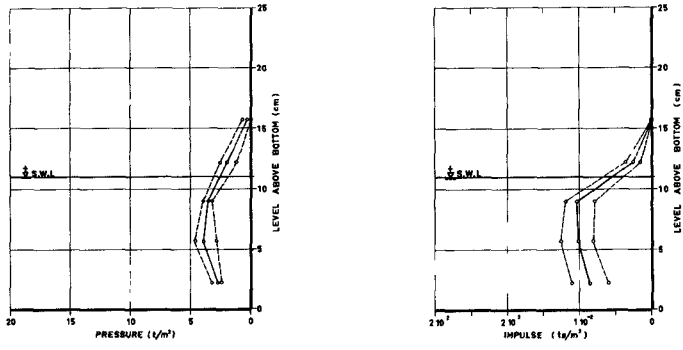

Fig. 19. Distribution diagram. (I=1:3, a=15 cm, d_1=11.0 cm, T=1.30 s, H=16.6 cm)

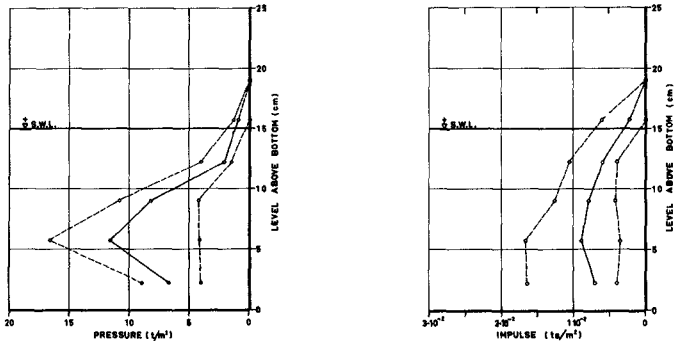

Fig. 20. Distribution diagram. (I=1:3, a=7.5 cm, d_1=15.0 cm, T=1.50 s, H=20.5 cm)

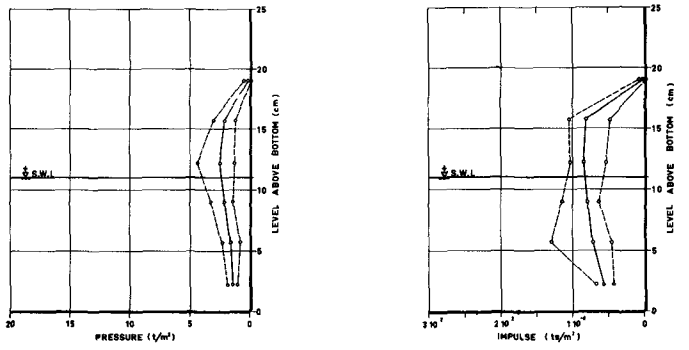

Fig. 21. Distribution diagram. (I=1:10, d_1=11.0 cm, T=1.50 s, H=11.8 cm)

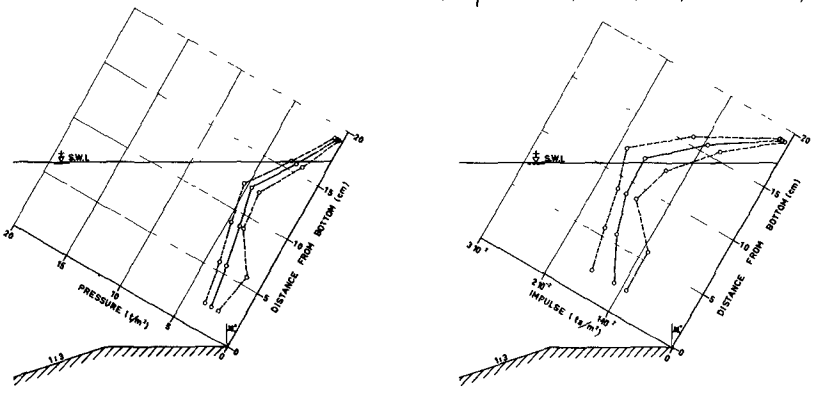

Fig. 22. Distribution diagram. (I=1:3, a=15.0 cm, α=30°, d=15.0 cm, T=1.40 s, H=19.9 cm)

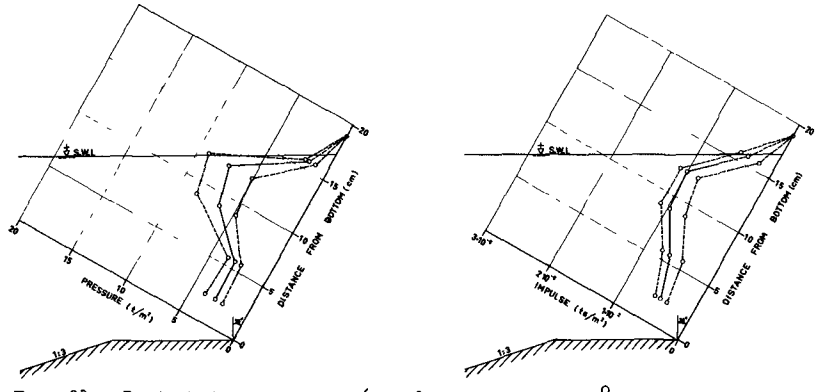

Fig. 23. Distribution diagram. (I=1:3, a=15.0 cm, α=30°, d_1=15.0 cm, T=1.40 s, H=21.0 cm)

A series of 25 tests was run (in the series with the sloping wall only 10 tests)for every level of pressure gauge recording the waves as well as the pressures. The wave height did not in any series deviate more than 7.5 o/o from the mean value. The corresponding maximum deviation for the wave period is only 1.8 o/o. The wave dimensions given in Table 2 are averages of the mean values for the different series. The mean wave height of the series never deviated more than 2.6 o/o from the average mean value given in the Table. The deviation of the mean wave period is quite negligible. These relatively low figures should be compared with the dispersion of the shock pressure magnitude as seen in the diagrams. Since, within each series, no correlation between the wave dimensions and the shock pressure could be discovered, this dispersion seems to be mainly due to occasional small disturbances of the wave front in the different tests. Such disturbances were impossible to detect since the movie films only showed the wave action just at the glass wall and not in the plane where the pressure gauges were placed.

Beside each pressure distribution diagram the corresponding impulse distribution diagram has been represented. The impulse (the surface under the pressure--time curve)has been calculated with a reasonable correction accounting for the first low part of the curve which has not been traced by the oscilloscope sweep. Since the period of oscillation was approximately the same at different levels, the pressure and impulse distributions are fairly congruent.

The maximum pressures occur simultaneously below a level corresponding to roughly 1.25 times the height above the bottom of the point where the convex part of the wave front first hit the wall. The higher regions of the average distribution curves where the shock pressure occurred later than below have been dashed. The comparison between the films and the distribution diagrams also gives the information that the largest pressure always occurred where the entrapped air cushion was initially situated.

A study of the different distribution diagrams can give extensive information on different aspects of the shock pressure phenomenon but in the following only some interesting features will be pointed out.

The largest pressures occur much lower in the tests with the bottom slope 1:3 than in those with the slope 1:10. This tendency is clearly confirmed by the movie films, which also indicate that the pressure distributions for the bottom slope 1:6 will be rather like the ones derived for 1:10. Thus, the resultant force was situated at 40-65 o/o of the still water depth above the bottom for the slope 1:3, while it was at 90 o/o above the bottom for the slope 1:10.

This observation, as well as the fact that the shock pressure against the test wall in no case decreased to zero at the bottom, differs from what has mostly been stated by other authors. This can be explained by the difference in test procedure and hence in the way in which the wave broke against the structures.

The movie films show that in the series A, the air cushion was not only thicker but also larger in the vertical direction than it was in the series B. This corresponds well to the general view of the pressure distribution which shows that in the series B there were higher but more local shock pressures. Thus, the resultant force was nearly the same in the two series while, on the other hand, the shock impulse in the series B was approximately half of the impulse in the series A. This is also in contrast to the statement by e.g. DENNY (1951) that a constant fraction of the forward wave momentum is fransferred into shock impulse.

The tests regarding the horizontal distribution of the shock pressures gave

no special tendency. Sometimes the peak pressures occurred simultaneously over the whole width of the flume and sometimes not.

CONCLUSION

The present investigation gives results from tests with breaking waves preceded by non-breaking waves. These waves caused pressures which could be relatively high ($p_{max} \approx 20$ t/m^2 for a wave with H≈20 cm) and also could have a short duration ($\approx$ 1 msec). The maximum pressures always occurred below the still water surface level and the shock pressures never decreased to zero at the bottom. This paper also presents shock occurrence diagrams which show the conditions for pressures of certain magnitudes to occur when different bottom geometrice are used.

The present investigation only gives results for waves preceded by considerably lower waves. Such waves can cause comparatively high shock pressures for which the adiabatic compression of an entrapped air cushion plays a predominant role. This must be kept in mind when such tests are planned and when the results are converted to prototype scale.

ACKNOWLEDGEMENTS

The present investigation was carried out in the Laboratory of the Division of Hydraulics at the Royal Institute of Technology, Stockholm, Sweden. The author wishes to express his gratitude to Professor E. Reinius, Head of the Division, for his eminent leadership. The author also thanks the Swedish Board for Technical Development for supporting the investigation.

REFERENCES

BAGNOLD, R.A. Interim Report on Wave Pressure Research. J. of the Inst. of Civ.Eng., June 1939.

CARR, J.H. Breaking Wave Forces on Plane Barriers. Calif. Inst. of Tech., Hydr. Struct. Div., Rep. E-11.3., Nov. 1954.

DENNY, D.F. Further Experiments on Wave Pressures. J. of the Inst. of Civ.Eng., June 1951.

HAYASHI, T. and HATTORI, M. Pressure of the Breaker against a Vertical Wall. Coastal Eng. in Japan, 1958.

MITSUYUASU, H. Experimental Study on Wave Force against a Wall. Coastal Eng. in Japan, 1962.

MITSUYASU, H. Shock Pressure of Breaking Waves (I). Coastal Eng. in Japan, 1966.

NAGAI, S. Shock Pressure Exerted by Breaking Waves on Breakwaters. A.S.C.E., Vol. 86, No. WW2, June 1960.

ROSS, C.W. Laboratory Study of Shock Pressures of Breaking Waves. Beach Erosion Board, Tech. Memo No. 59, 1955.

RUNDGREN, L. Water Wave Forces. Royal Inst. of Tech., Div. of Hydraulics, Bull. No. 54, 1958.

SVERDRUP, H.U. and MUNK, W.H. Wind, Sea and Swell. U.S.Navy Department., Hydr.Off.Publ. No. 601, 1947.

CHAPTER 63

EFFECTS OF BLAST LOADING ON A PIER

Young C. Kim
Associate Professor of Civil Engineering
California State College at Los Angeles
Los Angeles, California, U.S.A.

Thorbjorn Karlsson
Senior Research Engineer, Science Engineering Associates
San Marino, California, U.S.A.

William L. Ko
Senior Research Engineer, Southwest Research Institute
San Antonio, Texas, U.S.A.

ABSTRACT

The effects of nuclear explosions on a pier have been investigated to study the interaction phenomena between the blast loading, induced surface waves, the beach geometry, and the depth of coastal region for purpose of damage assessment and protective design of a coastal structure.

For the theoretical analysis, the diffraction pattern predicted by Whitham's theory was used. The characteristic solution for shock diffraction showed the shock front shapes, shock-shock shapes, and flow rays in the pier and beach geometry. A pier model was tested in a six foot diameter horizontal shock tube under four different test situations simulating pier on a beach with water, pier on a dry beach in a Mach reflection region, pier in deep water, and a pier on a dry beach in a region of regular reflection. The model was subjected to various shock overpressures in each of the four test situations.

Transient pressure distribution on the pier was investigated and comparison between the characteristic solution and the test results was made.

INTRODUCTION

The study of loads encountered by coastal structures, such as piers and docks, has in the past been concerned mainly with the action of waves on such structures. There are, however, other types of loads, which may be of concern in certain locations and their effects upon these structures need to be investigated. Among those are loads caused by air blasts and explosions. It is entirely conceivable that uplift forces on a pier deck caused by trapped air underneath or by blast induced water waves can cause heavy damage on those structures.

This paper describes an experimental program which was undertaken in order to obtain a better understanding of the effects of air blast on a pier. An objective of the investigation was to compare the test results with those predicted by existing theories and to make recommendations

pertaining to the use of the experimental results for design and damage assessment.

The experiments were conducted in a six foot diameter shock tube in which a metal pier model was mounted. The paper describes the experimental investigation and presents the test results. These results are compared with theoretical results obtained graphically by the method of characteristics based upon Whitham's theory of shock-shock diffraction.

THEORY OF DIFFRACTION OF A STRONG SHOCK BY AN OBSTACLE

When a strong shock wave impinges on an obstacle it is reflected. Since the reflected shock wave always travels through air which has been heated and compressed by the passage of the incident wave, it travels faster than the incident shock wave and may eventually overtake the incident shock wave front. As a result, the two waves are fused together and form a simple front, the so-called "Mach stem" (or Mach shock) (Ref. 1). Such a reflection is therefore called the Mach reflection in contrast to the regular reflection where the two shocks do not merge. The gas swept up by the Mach stem will flow alongside gas which has passed through both the incident and reflected shocks. Thus a contact discontinuity should pass through the so-called "triple point" where the incident front, the reflected front and the Mach stem intersect.

Whitham's Theory (Refs. 2 to 7) predicts the shape and location of the diffracted shock (Mach shock) at any time. The theory does not predict the shape or location of reflected shocks. As part of the description of the Mach shock the locus of successive positions of the Mach triple point can be found. Whitham calls this locus a "shock-shock," since it represents a Mach shock moving along the incident shock. The basic equations given by Whitham (Refs. 3, 8) for Mach diffractions are

1. Relationship between the ray area A and the Mach number M

$$A = k\, f(M) \tag{1}$$

where

k is an arbitrary constant
f(M) is given by

$$f(M) = \exp\{-[\log\frac{M^2-1}{M} + \frac{1}{\gamma}\log(M^2 - \frac{\gamma-1}{2\gamma}) + \log\frac{1-\mu}{1+\mu}$$

$$+ (\frac{\gamma-1}{2\gamma})^{\frac{1}{2}}\log(\mu + (\frac{2\gamma}{\gamma-1})^{\frac{1}{2}}) - (\frac{\gamma-1}{2\gamma})^{\frac{1}{2}}\log(\mu - (\frac{2\gamma}{\gamma-1})^{\frac{1}{2}})$$

$$+ (\frac{2}{\gamma(\gamma-1)})^{\frac{1}{2}}\log((M^2 + \frac{2}{\gamma-1})^{\frac{1}{2}} + (M^2 - \frac{\gamma-1}{2\gamma})^{\frac{1}{2}})$$

$$+ (\frac{1}{2(\gamma-1)})^{\frac{1}{2}}\tan^{-1}(\frac{(4\gamma - (\gamma-1)^2)M^2 - 4(\gamma-1)}{4\gamma^{\frac{1}{2}}(\gamma-1)(M^2+2/(\gamma-1))^{\frac{1}{2}}(M^2-(\gamma-1)/2\gamma)^{\frac{1}{2}}})]\} \tag{2}$$

where

$$\mu^2 = \frac{(\gamma-1)M^2 + 2}{2\gamma M^2 - (\gamma-1)} \tag{3}$$

and γ is the ratio of specific heats for the gas.

2. Relationship between the characteristic angle m and the Mach number M

$$m = \tan^{-1}\left[\frac{(M^2-1)K(M)}{2M^2}\right] \tag{4}$$

where

$$K(M) = 2\left[\left(1 + \frac{2}{\gamma+1}\frac{1-\mu^2}{\mu}\right)\left(2\mu + 1 + \frac{1}{M^2}\right)\right]^{-1} \tag{5}$$

3. The integral ω corresponding to the Prandtl-Meyer function in supersonic flow is given by

$$\omega = \int_1^M \left[\frac{2}{(M^2-1)\,K(M)}\right]^{\frac{1}{2}} dM \tag{6}$$

Therefore for two-dimensional Mach diffraction the characteristics of Whitham's diffraction equations (Ref. 3) are given by

$$\theta \pm \omega = \text{constant} \tag{7}$$

along curves of slope

$$\frac{dy}{dx} = \tan(\theta \pm m) \tag{8}$$

4. The shock-shock jump conditions for oblique shock-shock are given by

$$\tan(\chi-\theta_o) = \frac{A_o}{M_o}\left(\frac{M_1^2-M_o^2}{A_o^2-A_1^2}\right)^{\frac{1}{2}} \tag{9}$$

and

$$\tan(\theta_1-\theta_o) = \frac{(M_1^2 - M_o^2)^{\frac{1}{2}}\,(A_o^2 - A_1^2)^{\frac{1}{2}}}{A_1M_1 + A_oM_o} \tag{10}$$

where the subscript o refers to the flow before, the subscript 1 to the flow behind the shock-shock, θ_1 is the angle between the ray direction and the x-axis (see Fig. 1), and χ is the angle between the shock-shock and x-axis.

Figs. 2a, b show the full characteristic field, the constructed shock front shapes, shock-shock shapes, and flow rays in the test section of the shock tube for a dry beach. Peak overpressures of 23.3 psi and of 70 psi were chosen for analysis. The procedure for constructing Fig. 2a is described briefly below.

For the case of Fig. 2a the Mach number of the undisturbed shock is $M_o = 1.65$ and the corresponding characteristic angle and the Prandtl-Meyer integral, respectively, are $m_o = 20.295^o$, $\omega_o = 2.249$ rad. (Ref. 8). The characteristic corresponding to $m_o = 20.295^o$ deg. is labeled by 0 - 0. At

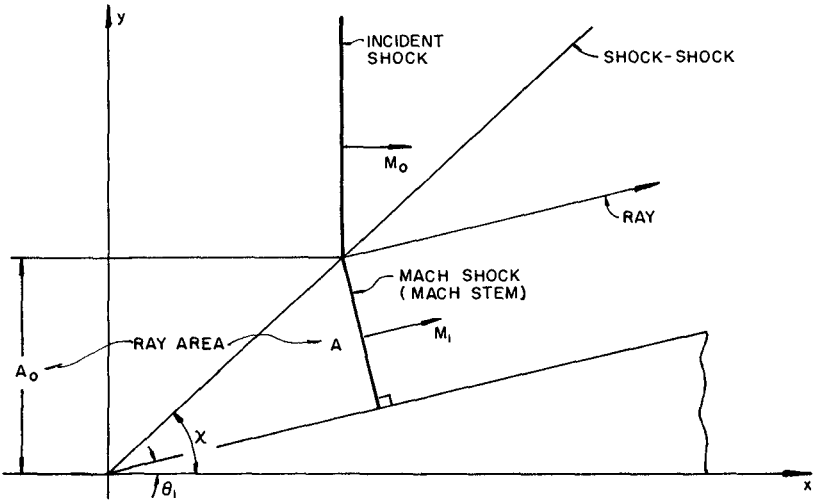

FIGURE 1 MACH DIFFRACTION BY A WEDGE

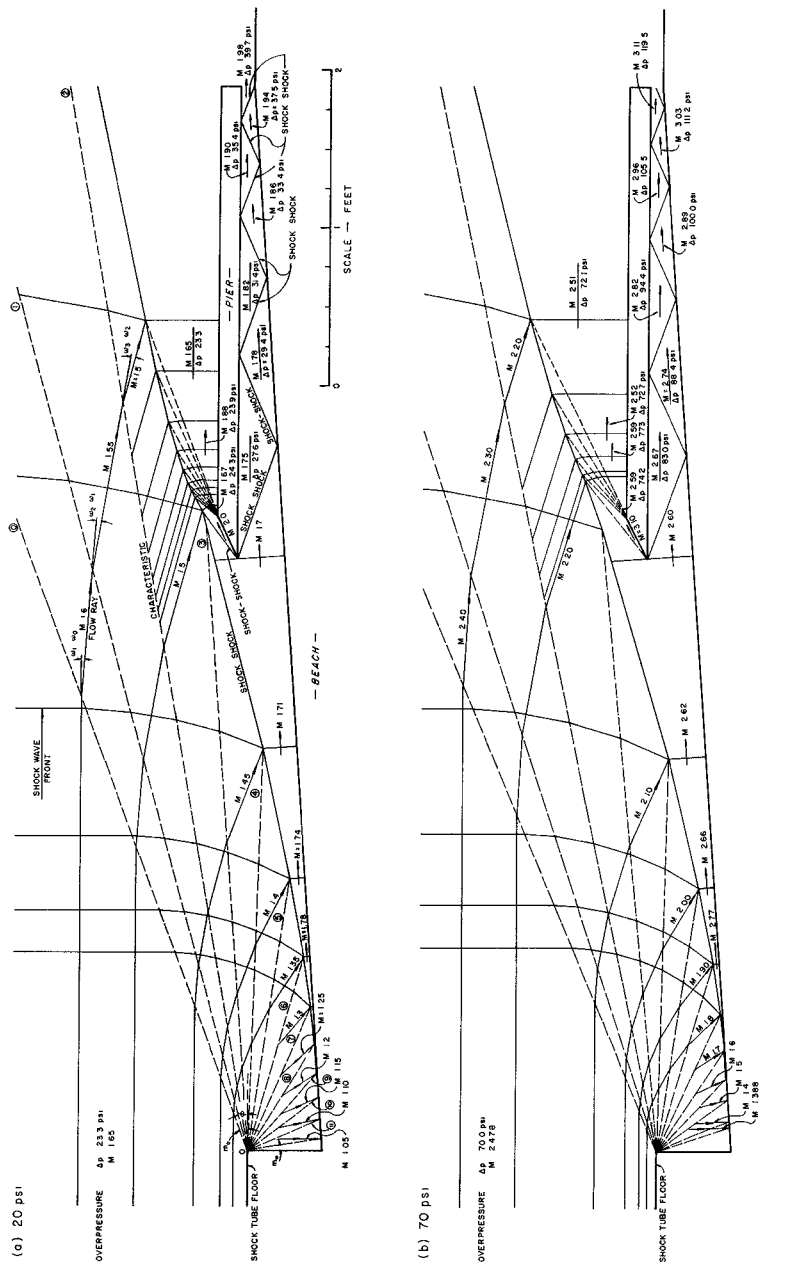

FIGURE 2 CHARACTERISTIC SOLUTION FOR SHOCK DIFFRACTIONS (BEACH SLOPE 1:14.25)

the convex corner θ_1 jumps from zero to negative 90^o and the solution is a centered simple wave. Neglecting reflection of the characteristics from the shock-shock, the characteristics are straight lines along which all flow properties are constant. After 90^o expansion the Prandtl-Meyer integral is given by

$$\omega_w = \omega_o - \pi/2 = 2.249 - 1.57 = 0.679 \text{ radians}$$

where Eq. (7) is used. The Mach number and characteristic angle corresponding to this number are found to be

$$M_w = 1.059$$

$$m_w = 9.056^o$$

where the subscript w signifies flow along the vertical wall. Between M_o = 1.65 and M_w = 1.059, one may choose a series of different Mach numbers (eleven for the present example) and draw the characteristic fans as shown in Fig. 2. The flow field can be made as smooth as desired by increasing the number of characteristics running out from point 0. The inclination of each characteristic line with respect to the horizontal line is calculated as follows. Consider the characteristic 0 - 1 corresponding to M - 1.6. One finds $m_1 = 19.983^o$, $\omega_1 = 2.165$ rad. The angle of inclination ϕ_1 is then

$$\phi_1 = m_1 + (\omega_1 - \omega_o) \times 57.4^o = 15.163^o$$

and the angle of deflection of flow ray is

$$(\omega_o - \omega_1) \times 57.4^o = 4.82^o$$

This process is repeated for all Mach numbers.

When a flow ray is deflected by the beach wall Mach reflection takes place. The angles of flow deflection at point 11 (M = 1.1) and 10 (M = 1.15) are greater than 70^o and the shock-shock is found to be attached to the wall. At point 9 (M = 1.2) the flow deflection angle is $\theta_1 = 60^o$ and the shock-shock angle is found to be $\chi - \theta_1 \approx 0.2^o$ and the shock-shock between points 10 and 9 can be drawn. This process is repeated for constructing the entire shock-shock. When the Mach stem impinges on the pier a secondary shock-shock is formed The Mach number for any location of the Mach stem can be easily obtained for a given angle of deflection and an incident Mach number. Overpressure at a point is obtained from the pressure jump condition

$$\frac{\Delta p}{p_a} = \frac{p-p_a}{p_a} = \frac{2\gamma}{\gamma+1} (M^2 - 1) \qquad (11)$$

where p_a is the ambient pressure ahead of the shock front, p is pressure behind the shock front traveling at Mach number M based on the speed of sound ahead of the shock front, and γ is the ratio of specific heats of the gas. It is seen from Fig. 2 that due to the continuous deflection of the flow ray, the pressure on the lower side of the pier increases in the direction of flow.

It is to be kept in mind that the above characteristic solution is based on the following assumptions:

1. The flow is two-dimensional.
2. The incident shock front is plane.
3. Pier legs and obstacles on the pier surfaces are neglected.
4. Reflection of the characteristics from the shock-shock is neglected.

EXPERIMENTAL INVESTIGATION

The model tests were conducted in a six foot horizontal shock tube at the E. H. Wang Civil Engineering Research Facility (WCERF) of the University of New Mexico and the U. S. Air Force Weapons Laboratory at Albuquerque, New Mexico. The tube is made of steel, 6 feet in diameter and 246 feet long with one end closed. It is made up of 21 sections varying in length from 5 to 20 feet with heavy flanges at either end, which permit the various sections to be bolted together. The tube has a constant circular cross section for a distance of 144 feet downstream from the compression chamber door (closed end) at which point it changes to a partially circular cross section for the remaining length of the tube. The far end of the tube is left open. The blast wave in the shock tube is generated by the detonation of primacord which can produce overpressure ranging from 0 to 100 psi. The primacord consists of a flexible plastic tubing with a PETN (pentaery-thritoltetranitrate, $C_5H_8(NO_3)_4$) core wrapped in a cotton cloth.

The model pier deck was 36.0" long by 6" wide by 1.5" thick and was made up of two steel plates, 3/4" thick each. The deck was supported by six cylindrical steel legs, 1" OD x 36" long. A steel plate (6'9" x 3'9" x 7/16") was located underneath the pier model with a slope of 1 to 14.25 to simulate a beach in a coastal region. The beach could be removed leaving the underside of the pier 13-1/2" above a level bottom to simulate deep water conditions. The pier model was located in a specially designed closure device on an adjustable base at a point approximately 180 feet from the blast. The closure device was rolled under the test section and raised into place to close the tube opening.

Pressure measurements in the shock tube and on the pier model were made with piezoelectric type transducers. The piezoelectric transducer essentially converts a pressure variation into a corresponding electric charge variation. The relationship is linear over a limited pressure and temperature range. The tranducers used were of the "ST" gage series manufactured by the Susquehanna Instrument Company. This gage series utilizes lead zirconate sensing elements. The model used was the ST-2 (1/2" diameter housing x 5/8" long) which is used primarily for pressure measurements of shock waves in air since it is capable of measuring fast-rise phenomena without ringing. This gage has a charge sensitivity of 20 picocoulombs per psi, a natural frequency of 250 kc, and a rise time of the order of 5-10 μ sec. A total of eleven ST-2 gages were used. Four of those were placed in the test section in the vicinity of the pier model for measuring the free field pressure. The pier model was instrumented with seven pressure gages with three facing upward and four facing downward. In addition to the above gages, one strain gage type transducer, the Schaevitz-Bytrex Model No. HFG-2000, was used in the free field.

Each day before starting tests every transducer was calibrated individually for output, pulse response characteristics, and linearity according to the procedure described in Ref. 9. A check on the pressure measurements was obtained by measuring the velocity of the shock wave as it passed through the test section. The shock velocity, U, is easily found since the distances between the gages are known. The shock overpressure is evaluated by using the one-dimensional relationship between pressure and Mach number

$$\frac{\Delta p}{p_a} = \frac{p - p_a}{p_a} = \frac{2\gamma}{\gamma+1}(M^2-1)$$

where p_a is the ambient pressure, γ is the ratio of specific heats for air, and M is the Mach number. The pressure-time variations measured by the various gages during the tests were recorded on magnetic tape as well as photographed from oscilloscope screens. The data recording equipment in use at the WCERF is described in Ref 9.

The pier model was tested in the following four situations:

(a) Pier located above a beach with a slope of 1 to 14.25 and with clearance of 1" between the underside of the shore end of the pier deck and still water level. This situation was intended to represent a pier in shallow water on a sloping beach (Fig. 3a).

(b) Pier located as in (a) but without water. This situation represents a pier on a dry beach in a Mach-reflection region (Fig.3b).

(c) The beach was removed so that the underside of the pier was located 13-1/2" above a level bottom and 1" above the still water surface. This situation represents a pier or platform in deep water (Fig. 3c).

(d) Pier located above beach with 1 to 14.25 slope without water and with clearance of 1" between the underside of the shore end of the pier deck and the beach as shown in Fig. 3d. This situation was intended to represent a pier on a dry beach in a regular reflection region.

In each of the four different situations, the pier model was subjected to five different shock overpressures. The five different overpressures and other shock characteristics were intended to be as follows:

Test No.	Peak Overpressure psi	Duration of Positive Pulse msec	Shock Velocity fps
1	5	70	1400
2	10	85	1500
3	20	100	1700
4	40	120	2100
5	70	135	2700

Three test runs were made at each pressure level. A total of 3 x 4 x 5 = 60

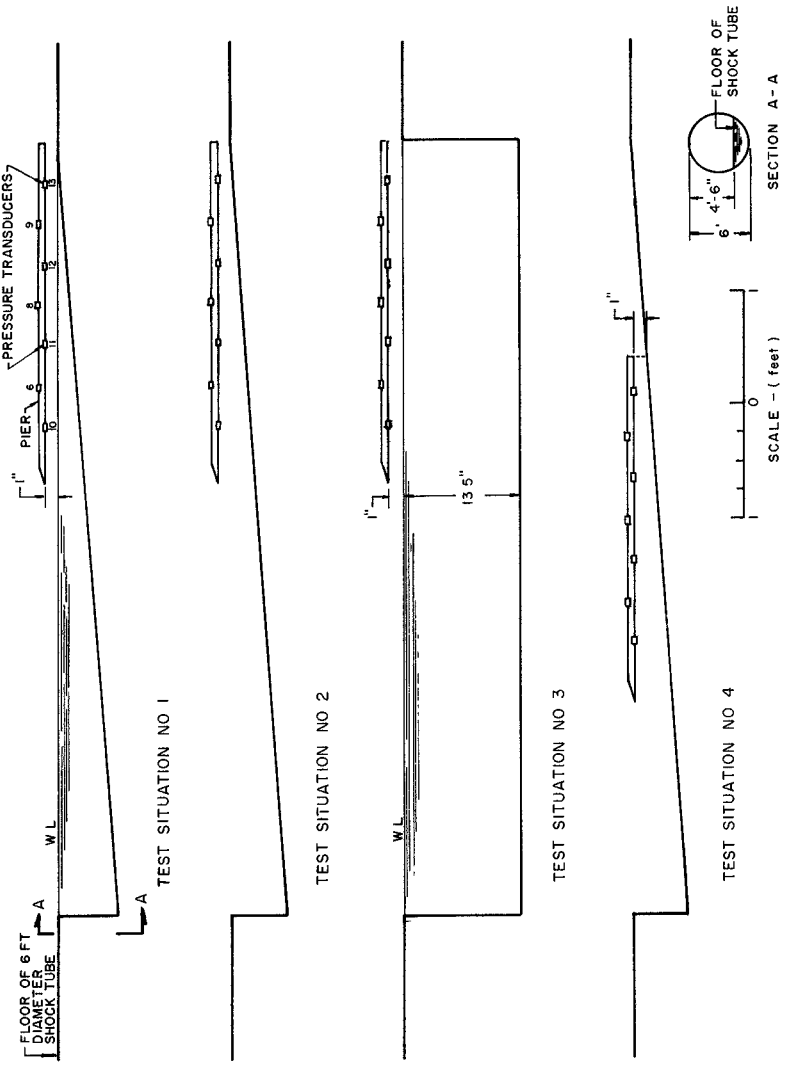

FIGURE 3 TEST SITUATIONS (BEACH SLOPE 1:14.25)

test runs were therefore performed.

ANALYSIS AND DISCUSSION OF RESULTS

The test results were obtained both in the form of magnetic tape recordings and photographic pressure-time diagrams. The photographic records were used to obtain the peak overpressure, impulse strength, and pulse duration at each gage location. In order to obtain a better basis for comparison between the various test situations these values have been normalized to the corresponding free field overpressure. In most instances the means are obtained from two out of the three runs, using the two in closest agreement. In a few cases the three runs gave almost identical values and were therefore all used to obtain the means. In one case (situation 2, 5 psi) only one run was used, since it was the only one close to the desired pressure level.

The reason for normalizing the peak overpressures may need some clarification. Each of the four test situations is tested at five different incident pressure levels. For obvious reasons, however, the intended pressure level is never obtained exactly. For example, the mean free field overpressure levels for the 20 psi overpressure runs were as follows:

Test situation no.	1	2	3	4
Mean free field overpressure, psi	21.1	19.3	20.4	20.5

It is clear that a meaningful comparison between the different test situations is not obtained directly from the pressure readings. While the pressure at any point on the pier is not likely to be a linear function of the free field pressure it seems reasonable to assume that in a narrow region of free field pressure the variation can be approximated by a straight line. On this basis all pressure readings have been normalized to the corresponding free field pressure and the result treated as the normalized pressure for the corresponding nominal pressure level.

A peculiarity is observed in the records from the lowest pressure tests, i.e., where the shock overpressure was less than 5 psi. The records show a double peaked pressure-time relationship at all channels. These two peaks are present in the intended 5 psi tests for test situations 1, 3, and 4, where the peak overpressure is around 3 psi. The very first run of test situation 2, where the shock overpressure is of the order of 2 psi, also shows double pressure peak at all channels. In subsequent runs of test situation 2 when the overpressure is 6-7 psi and higher, the second peak is no longer present. This is also the case for all other test situations until the highest pressure levels of 40-70 psi are reached. At those pressures multiple peaks are observed for test situations 1 and 3 (i.e., with water) at some of the gages located on the pier, whereas all the free field gages show a single peak. The double peak phenomenon at low pressure levels is probably caused by the reflected shock wave from the closed compression chamber end. The reflected shock, moving through air heated and compressed by the direct wave, travels faster than the direct wave and will eventually overtake it. At very low pressures the difference between the two wave

speeds is small so that the reflected wave has not yet caught up with the direct wave as it reaches the test section, resulting in the double-peaked pressure-time record.

As noted above, the multiple pressure peaks at the highest pressure levels are observed only in test situations 1 and 3, i.e., where water is present. The first peak observed is most likely caused by the shock wave whereas subsequent peaks are seemingly due to water splashing on the pier model. These effects, however, could not be observed, since the test section of the shock tube was completely closed. It would be desirable in future tests to use high speed photography to find out what happens in the test section.

The values of normalized net peak pressures on the pier for 40 psi normal overpressure are shown graphically on Fig. 4. This is found as the difference between top and bottom pressures, assuming linear variation between gages. These represent essentially the peak loading on the pier model caused by the blast. The shock wave travels at a speed ranging from 1300 to 2800 fps which means that its travel time over the length of the pier model ranges from 2.3 to 1.1 milliseconds. The pulse duration on the pier is found to vary between 40-120 milliseconds. Thus the travel time of the wave over the length of the pier model is at most approximately 5% of the pulse duration indicating that no appreciable reduction in pressure has taken place at the front end of the pier when the wave arrives at the back end. The effect of water splashing on the pier which was discussed above is not included in Fig. 4. Since the relative wave arrival time at the various gages was not recorded, there is no way to assess the net pressure on the pier caused by the water impact. It should be kept in mind, however, that this effect could conceivably result in much higher uplift pressures than observed during the passage of the shock wave front.

The general trend for all test situations seems to be that the relative net uplift pressure increases very rapidly as the free field pressure is increased, especially at the front end of the pier. However, it is rather difficult to determine any definite trends for the different test situations. A better view is offered in Figs. 5-8 where the normalized pier pressures at each gage have been plotted against the free field pressure. Figs. 5-8, showing the peak pressure at the gages located on the top of the pier, reveal a similar behavior of each gage for all four test situations indicating that these peak pressures are not appreciably affected by the configuration in front of and underneath the pier, with the possible exception of situation #2 (Fig. 6a). This is really not surprising since these are pressures at the shock wave front and any effects of the bottom configuration are not likely to be felt until somewhat later. Fig. 6a shows the effects of the Mach reflection (Fig. 2), resulting in lower peak pressures on the pier top.

Figs. 5b - 8b, showing the peak pressures at the gages located on the underside of the pier, indicate a marked difference between the various test situations. Fig. 6b, showing the situation for a pier on a dry beach, indicates a very sharp relative pressure rise as the free field shock pressure increases, especially at the front end of the pier. The presence of water tends to reduce this pressure appreciably as Fig. 5b shows. Fig. 7b shows the results for a pier in deep water. When compared with Fig. 5b (pier on a beach with water) the difference between the two is negligible at low

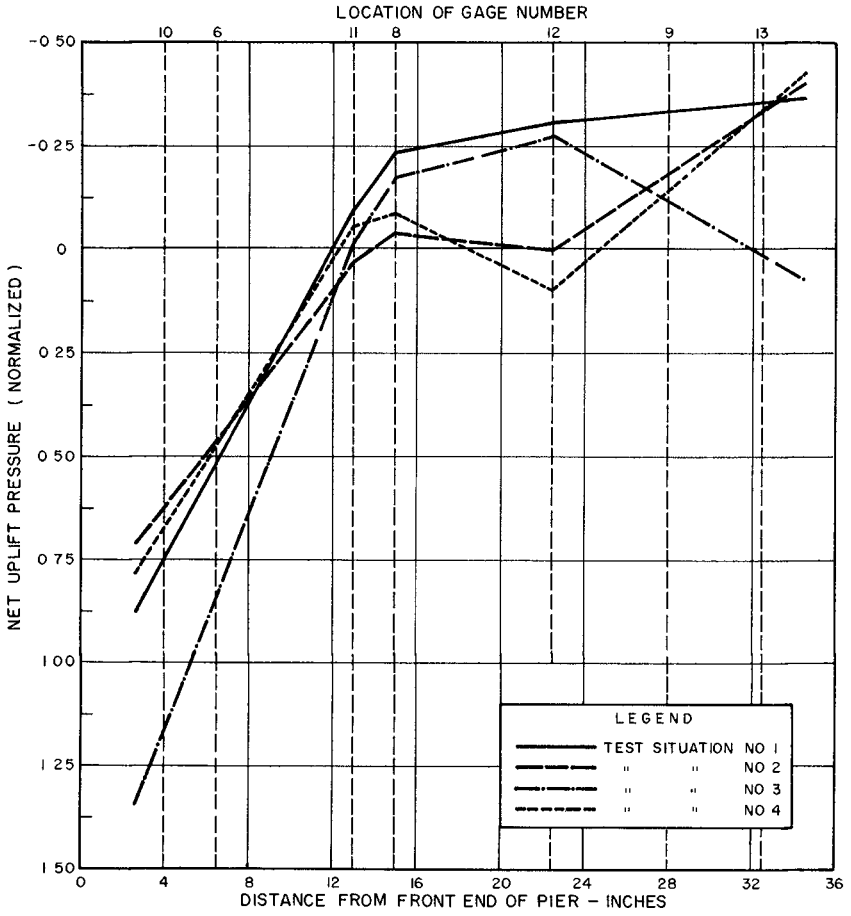

FIGURE 4 DISTRIBUTION OF NORMALIZED PEAK UPLIFT PRESSURE - 40 PSI NOMINAL OVERPRESSURE

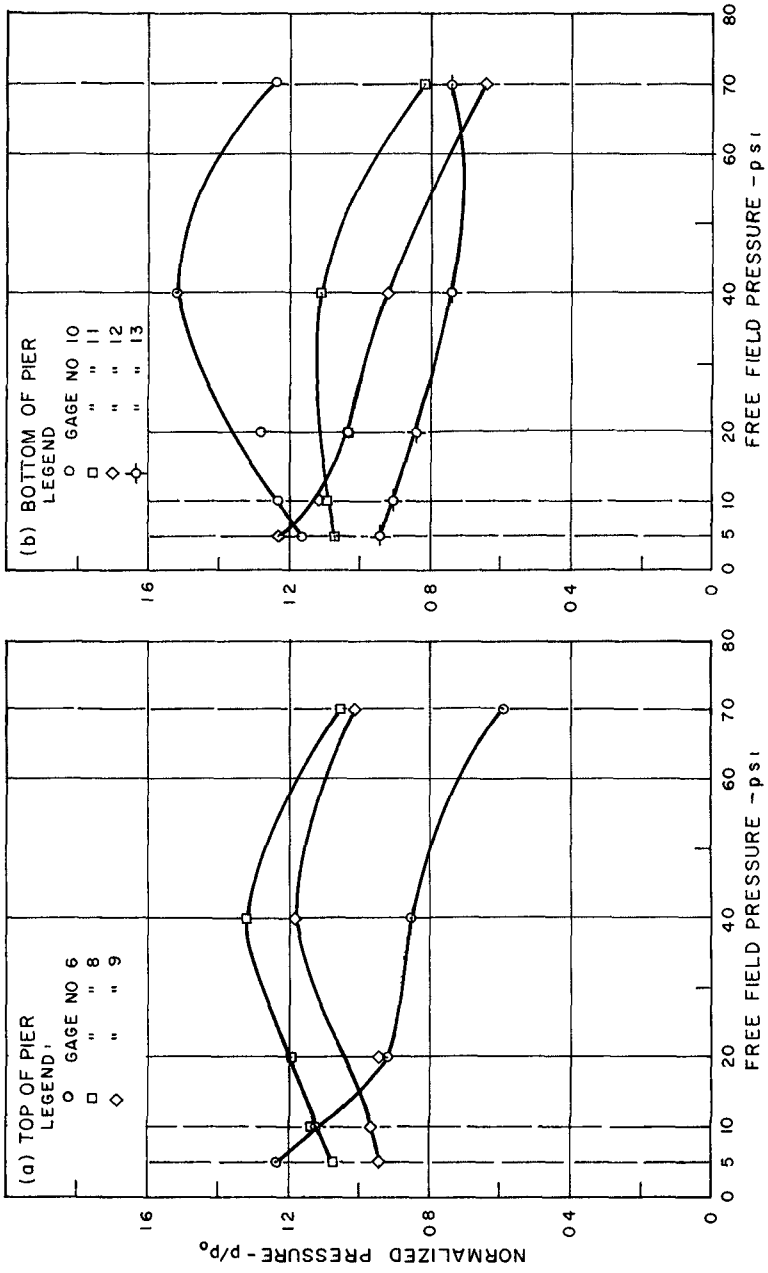

FIGURE 5 NORMALIZED PIER PRESSURE VARIATION WITH FREE FIELD PRESSURE
TEST SITUATION #1

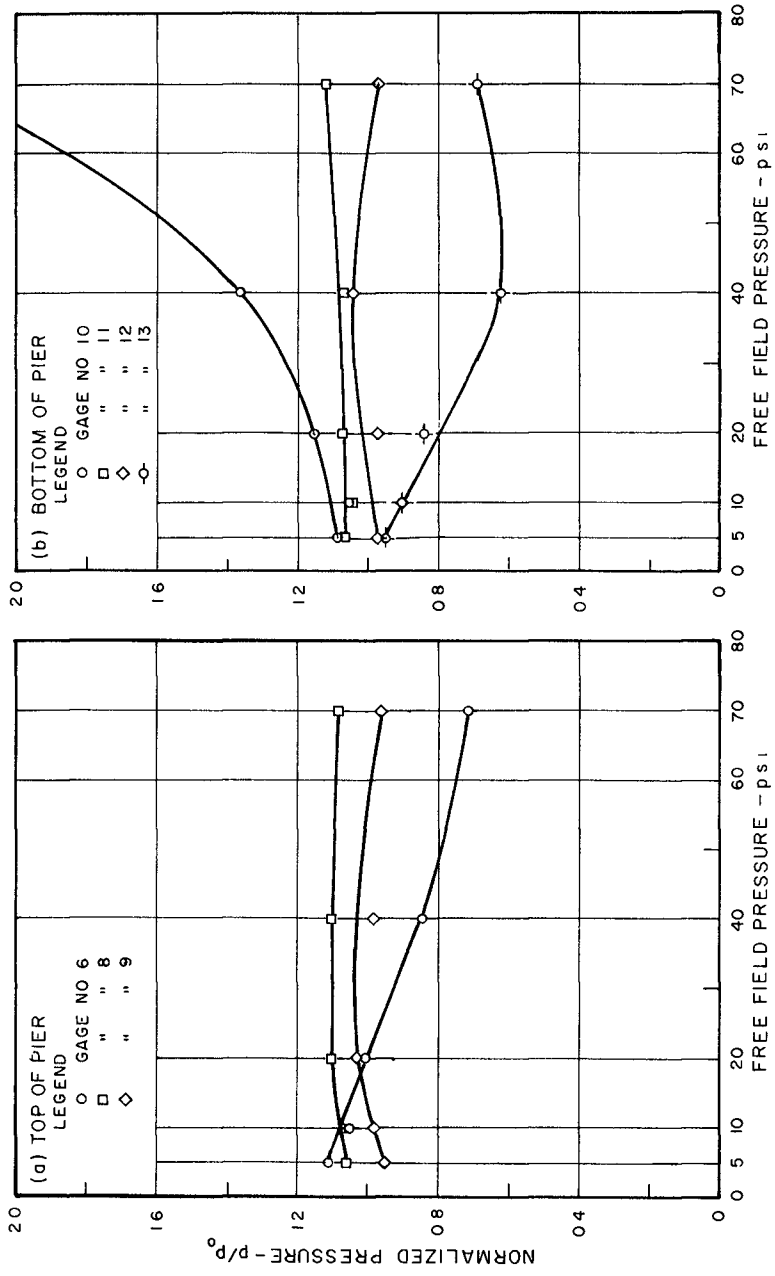

FIGURE 6 NORMALIZED PIER PRESSURE VARIATION WITH FREE FIELD PRESSURE
TEST SITUATION #2

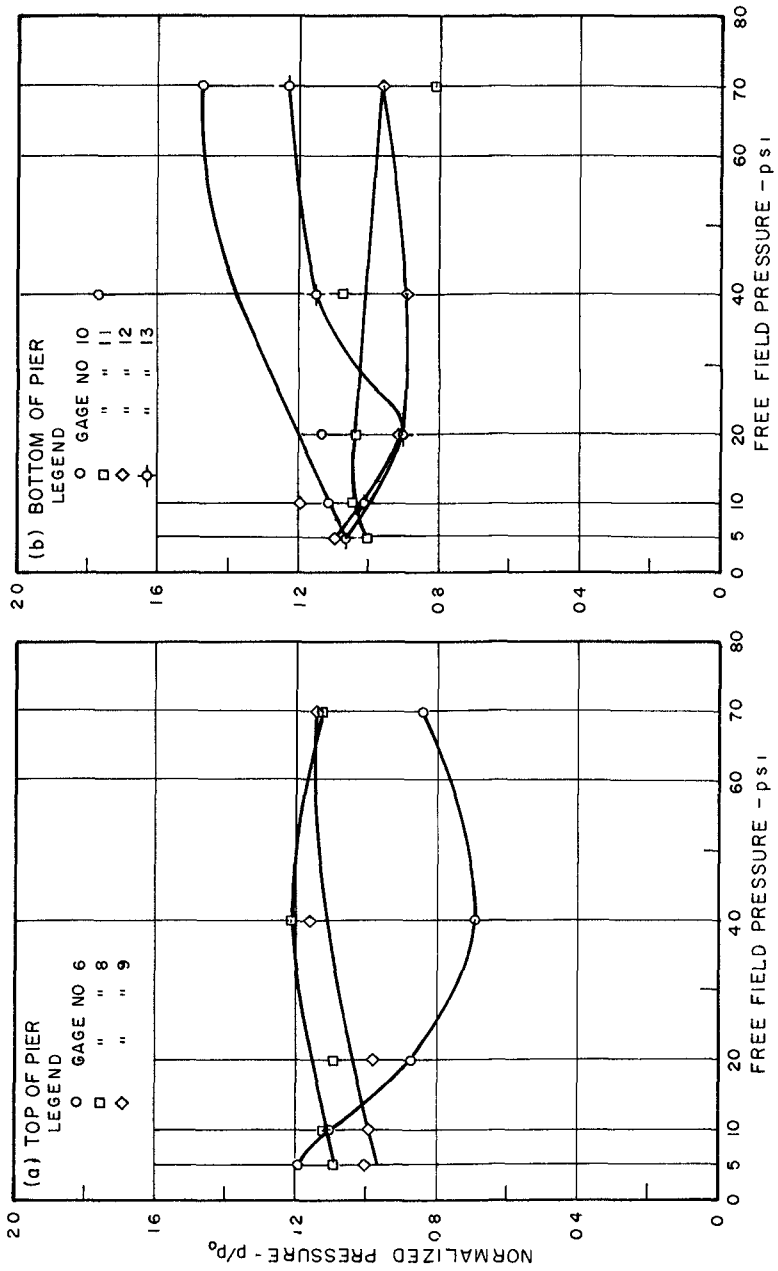

FIGURE 7 NORMALIZED PIER PRESSURE VARIATION WITH FREE FIELD PRESSURE
TEST SITUATION #3

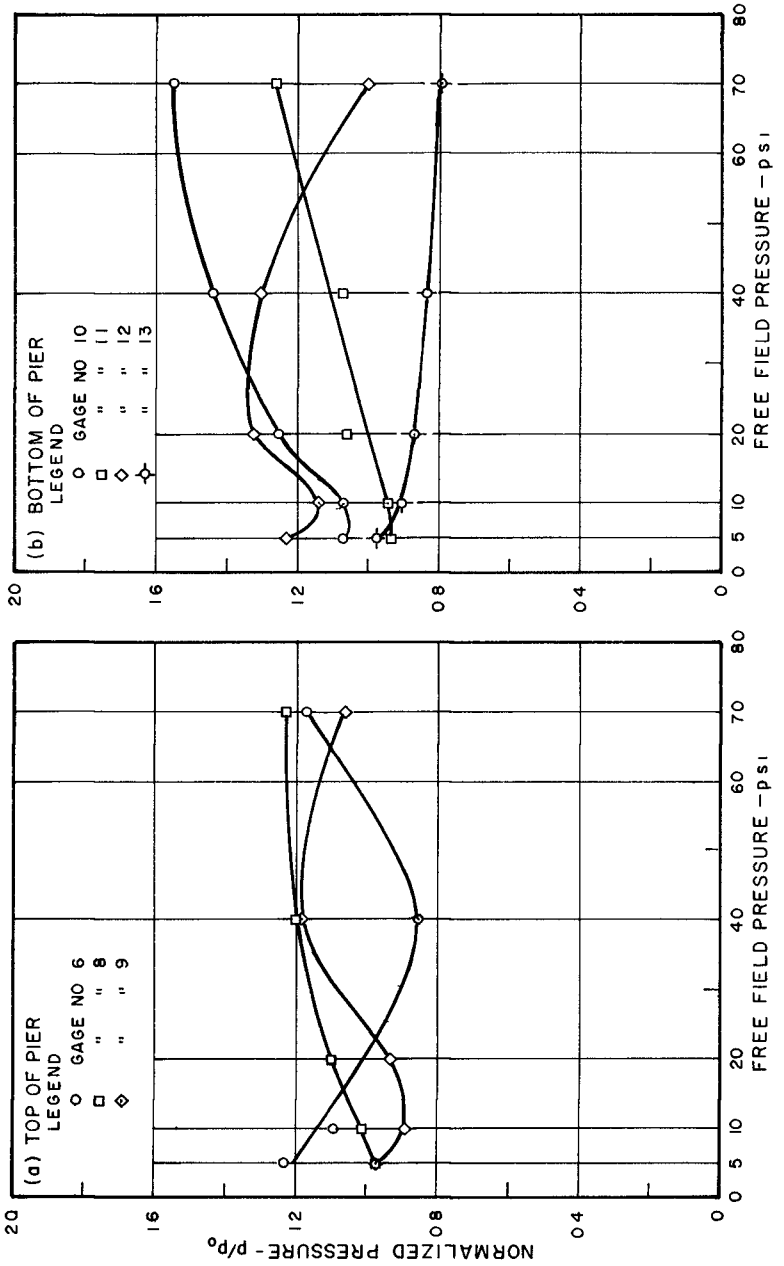

FIGURE 8 NORMALIZED PIER PRESSURE VARIATION WITH FREE FIELD PRESSURE
TEST SITUATION #4

pressure levels, but high shock pressures seem to result in appreciably higher loads on the deep water pier, possibly due to water wave impact. Fig. 8b shows the pressure on a pier in a regular reflection region. Here the loading on the front end of the pier is considerably lower at high shock loads than that experienced in the Mach reflection region (Fig. 6b). Otherwise the two regions do not give appreciably different results.

The theory discussed in a previous section of the paper has been applied to obtain graphically the solution for test situation No. 2 (pier on a dry beach), at free field overpressures of approximately 20 psi and 70 psi. These solutions are shown in Fig. 2a, b. For comparison the results are plotted in Fig. 9a, b, together with experimentally obtained values under similar conditions.

Fig. 9a, showing conditions of 20 psi, shows that the graphical solution results in maximum uplift pressure higher than maximum measured pressure. The distribution of uplift pressure over the length of the pier is quite different for the two cases. The experimental results show that the net uplift pressure decreases in the direction of the shock flow in contrast to the results predicted by the characteristic solution. Fig. 9b, which represents conditions at 70 psi, shows the same general features, although the very high uplift pressure measured at the front end of the pier exceeds the maximum uplift pressure obtained by the characteristic solution. These discrepancies between predicted and observed results indicate that the theoretical model should be modified to represent more closely actual conditions on the pier. Schlieren photographs would be of great value here and this technique should definitely be included in future test of this type. Until such results are available, the following factors can be listed as possible causes of discrepancy:

a. Since the pier model has a very low aspect ratio and a complicated geometry, the flow is three-dimensional. Thus the two-dimensional characteristic solution may not be appropriate to predict the actual flow properties.

b. All transducers except Nos. 6 and 10 are located in a region of shock expansion created by the supporting structure of the pier model which consists of cylindrical legs underneath and hexagonal units on top. The presence of these, which is not taken into account in the theoretical solution, definitely affects the flow field. It can be shown that their effect is to decrease the downstream pressure as observed in contrast with the theoretical results predicting increasing pressure when the cylindrical obstructions are neglected.

c. The shock front generated in the shock tube may not be plane as assumed.

Overpressure peaks on the pier caused by splashing water have been discussed in a previous section. It is possible that the water impact on the underside of the pier can result in much higher net uplift pressures than are caused by the passing shock wave. However, since relative wave arrival

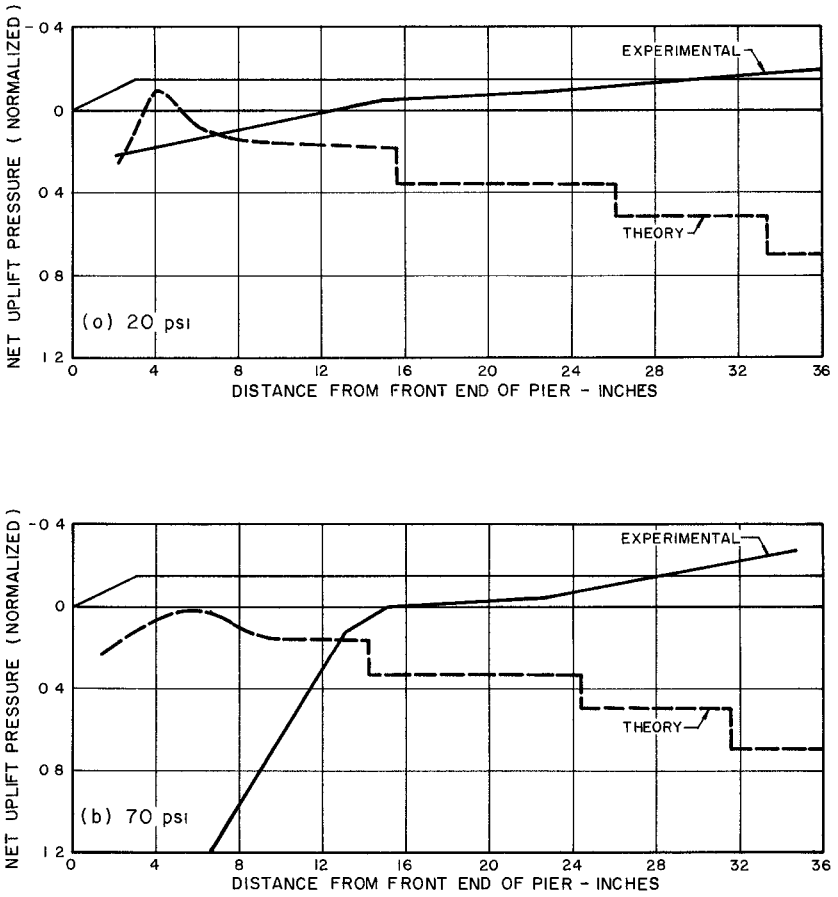

FIGURE 9 NET UPLIFT PRESSURE - THEORETICAL AND EXPERIMENTAL RESULTS FOR PIER ON DRY BEACH

times at each gage were not measured, the severity of the water impact effect cannot be evaluated. Future tests of this type should, therefore, be provided with equipment to measure these relative arrival times at each gage.

CONCLUSIONS

The findings of the study reported here may be summarized as follows:

1. Air shock loading on a pier on a dry sloping beach results in more severe uplift pressure than is experienced for the same configuration in the presence of water (test situation No. 1 vs. No. 2).

2. Air shock loading on a pier in water appears to be more severe in deep water than in shallow water (test situation No. 1 vs. No. 3). This is possibly due to water wave impact.

3. Air shock loading on a pier on a dry beach appears to be more severe when the pier is wholly located in the Mach reflection region than it is when the pier is partly in the regular reflection region (test situation No. 2 vs. No. 4).

4. It can be concluded from 1-3 above that test situation No. 2 - pier on a dry beach in a region of Mach reflection - will result in the most severe uplift pressures on the pier deck caused by the passing air blast wave.

5. Water waves caused by the air blast which splash against the underside of the pier may result in uplift pressures more severe than those caused by the air shock. Further tests are required to assess this effect.

6. Graphical solution for a pier in a region of Mach reflections (test situation No. 2), based on Whitham's diffraction theory, results in conservative estimates of the net uplift pressure at low incident pressures, but appears to underestimate this effect at high pressures. Further studies are required to make the theoretical model more realistic as well as to extend the technique, so that it may be applied to a pier in a region of regular reflection.

ACKNOWLEDGMENTS

The authors wish to express their gratitude to Mr. J. T. O'Brien of the Naval Civil Engineering Laboratory, Port Hueneme, California, for the many useful discussions throughout the course of this study. This investigation was supported by the U.S. Naval Civil Engineering Laboratory under Contract No. N62399-67-C-0049, and was sponsored by the Defense Atomic Support Agency, Washington, D. C. 20305.

REFERENCES

1. Glasstone, S., "The Effects of Nuclear Weapons," United States Atomic Energy Commission, April 1962.

2. Whitham, G. B., "On the Propagation of Shock Waves Through Regions of Non-Uniform Area of Flow," J. Fluid Mech., Vol. 4, pp. 337-360, 1958.

3. Whitham, G. B., "A New Approach to Problems of Shock Dynamics, Part I, Two-Dimensional Problems," J. Fluid Mech., Vol. 2, pp. 145-171, 1957.

4. Pack, D. C., "The Reflexion and Diffraction of Shock Waves," J. Fluid Mech., Vol. 18, pp. 549-576, 1964.

5. Lick, W., "The Shock-Expansion Method and Whitham's Rule," J. Fluid Mech., Vol. 25, pp. 179-184, 1966.

6. Chisnell, R. F., "A Note on Whitham's Rule," J. Fluid Mech., Vol. 22, pp. 103-104, 1965.

7. Miles, J. W., "A Note on Shock-Shock Diffraction," J. Fluid Mech., Vol. 22, pp. 95-102, 1965.

8. Bryson, A. E., Gross, R. W. F., "Diffraction of Strong Shocks by Cones, Cylinders, and Spheres," J. Fluid Mech., Vol. 10, pp. 1-16, 1961.

9. Holt, R. E. and Crist, R. A., "Calibration of a Six-Foot and a Two-Foot Diameter Shock Tube," AFSWC-TDR-63-5, Project No. 1080, Task No. 108005, Air Force Shock Tube Facility, Albuquerque, New Mexico, April, 1963.

CHAPTER 64

THE THEORY AND DESIGN OF BUBBLE BREAKWATERS

by

P.S.Bulson, Ph.D.,B.Sc.(Eng).,M.I.Struct.E.,M.I.Mech.E.

Military Engineering Experimental Establishment and
Southampton University, Great Britain

ABSTRACT

This paper sets down basic information on the behaviour of bubble breakwaters, drawn from analytical and experimental studies carried out by the author and others in recent years. Design formulae are given for surface velocity and thickness of the horizontal current produced by a bubble curtain, and for the quantity of free air required to suppress waves of known length and height. The effect of an intermittent air supply is examined. It is concluded that the quantity of air required is astronomical and the practical difficulties immense.

1. INTRODUCTION

If a surface current of sufficient strength is propagated in opposition to oncoming waves, their length is reduced and their height increased until instability occurs, and they break over the current in the manner of waves breaking on a beach. This well known action occurs naturally when wind formed waves meet an opposing tidal current in an estuary. One method of artificially producing an opposing surface current is by means of a bubble curtain, which can be obtained by releasing air from a line of jets on the sea bed. As the bubbles rise water is entrained in the form of a vertical current, and this spreads into opposing horizontal currents at the surface.

In recent history this concept was first employed by Brasher[1] of New York to protect civil engineering works in 1907. He patented his design, which consisted basically of a perforated pipe on the sea bed fed by air from shore based compressors, and it was used by the Standard Oil Company in 1915 at El Segundo, California. Other projects seem to have been undertaken, but the results were not promising and interest diminished. Research continued spasmodically, however, and in 1936 Professor Thysse of Deft showed that the surface currents produced by the bubbles were the main mechanism of the system, until then there had been considerable speculation about the precise way a bubble breakwater worked.

During the 1939-1945 war, fundamental research was carried out by Professor White[2] and Sir Geoffrey Taylor[3] in England, because the method was seen to have potential as a transportable breamwater for military purposes. As a result of their work it became possible for the first time to predict the quantity of air required to produce a given surface current, and the speed of current required to kill waves of known length. Taylors theory, however, assumed waves of infinitessimal amplitude and sinusoidal form and did not take account of wave height or the possibility of partial wave damping. This fundamental work and the experiments associated with it showed that for the suppression of storm waves characteristic of N.W.Europe, the quantity of air required per foot run of breakwater would be astronomical.

After the war, inventors and scientists from a number of countries searched for methods of increasing the efficiency of the bubble curtain. It is inappropriate to give a complete survey here, and the reader is directed to a summary by the author[4] published a few years ago. Evans[5] carried out a number of illuminating experiments, and it was clear to him and others that large scale tests were desirable to ascertain whether large current horse-powers could be effectively produced in deep water, and whether a measure of wave damping could be obtained in a full scale installation. These tests were carried out by Bulson[6,7] in the early 1960's and later the effect of an intermittent air supply was investigated[8].

From all these experimental and analytical studies it is possible to build up a design theory for bubble breakwaters. This falls into two sections, the first dealing with the magnitude and distribution of surface currents obtainable from a given air supply, the second with the action of a given surface current against waves of known height and length.

2. THE BUBBLE CURTAIN

Taylor[3], drawing an analogy between the vertical current produced in water by releasing bubbles, and in air by releasing heat, quoted the work of Schmidt[9] in showing that

$$V_m^3 = kgQ, \qquad \ldots\ldots(1)$$

where V_m is the surface velocity of the current, see Fig 1,

K is a constant,

Q is the quantity of air emerging per second from the orifices of the submerged pipe, per foot of pipe.

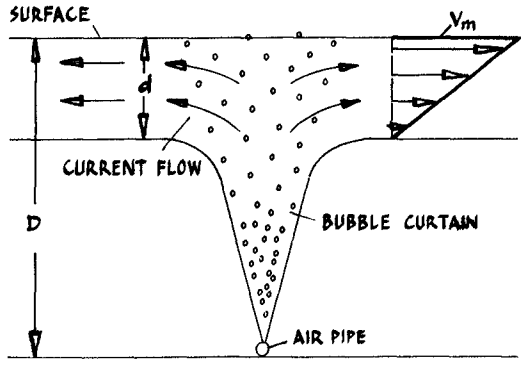
SURFACE
Vm
d
CURRENT FLOW
D
BUBBLE CURTAIN
AIR PIPE

FIG. 1

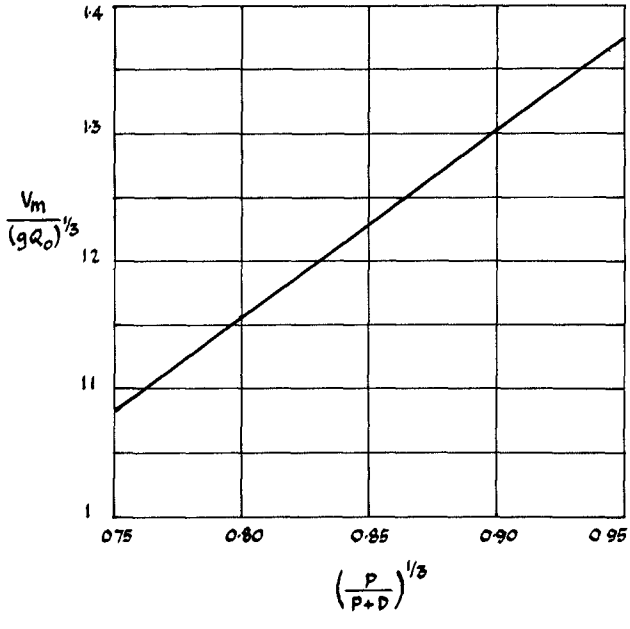
1·4
1·3
1·2
1·1
1
Vm / (gQo)^1/3
0·75
0·80
0·85
0·90
0·95
(P/(P+D))^1/3

FIG 2

The practical engineer is interested in Q_o, the quantity of free air delivered by the compressors per second per foot, and this is linked with Q by a relationship governed by the depth of the manifold (D), and the atmospheric pressure expressed as a head of water (P). Bulson[6] showed that Eq.(1) can be set in the form

$$V_m = 1{\cdot}46 \left(\frac{g Q_o P}{P + D} \right)^{1/3} \text{ feet/sec,} \qquad \ldots\ldots(2)$$

where $1{\cdot}46$ is the value of $K^{1/3}$ found by large scale experiment (Fig 2).

The current velocity, V, diminishes approximately linearly with depth, until it equals zero at a depth d below the surface. Bulson gives the following expression for d,

$$d = 0{\cdot}32\ P \log_e \left(\frac{P + D}{P} \right) \text{ feet,} \qquad \ldots\ldots(3)$$

as shown in Fig 3.

When the same quantity of air is passed through a variety of orifice diameters and spacings there is no significant difference in V_m, further, results for a single manifold at depth D are not noticeably different from those when two or more adjacent manifolds are delivering the same total quantity of air.

When D = 34 ft., the vertical velocity at the centre of the curtain when Q_o = 1 ft^3/sec/ft was found to be about three quarters of the horizontal surface velocity V_m. A typical curve of decay in surface current velocity with distance from the centre of the manifold is shown in Fig 4.

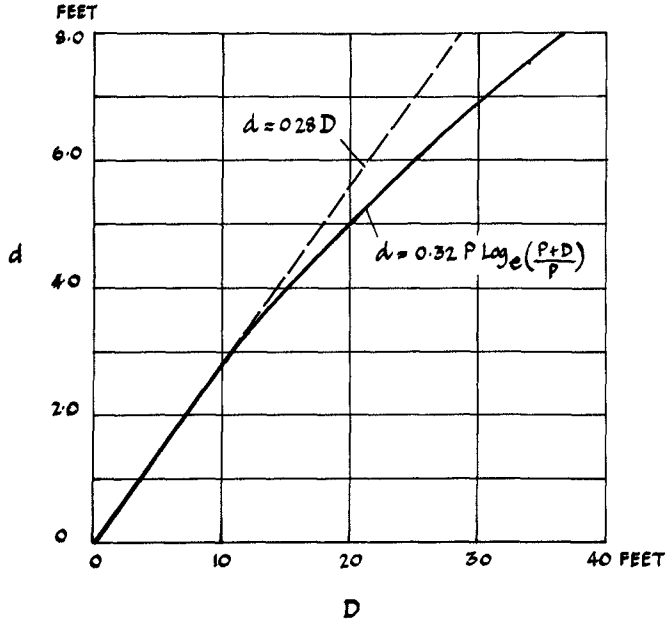
FEET
8·0
6·0
4·0
2·0
0
d
d = 0·28 D
d = 0·32 P Log e (P+D/P)
0
10
20
30
40 FEET
D

FIG. 3

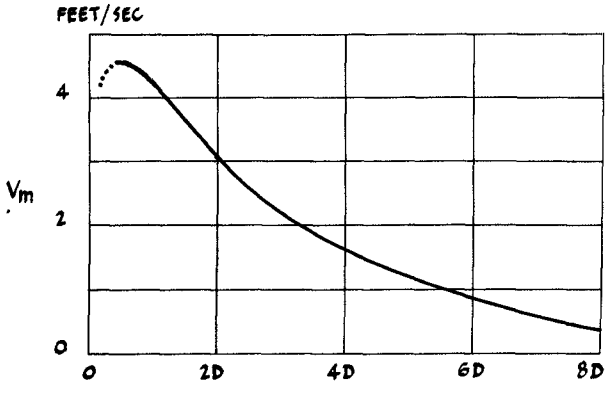
FEET/SEC
4
2
0
Vm
0
2D
4D
6D
8D

FIG. 4

3. COMPLETE WAVE SUPPRESSION

Unna[10], in 1942, discussed the action of a tidal stream on wind formed waves. For deep water waves having a length λ, the velocity of travel, c, is given by

$$c = \left(\frac{\lambda g}{2\pi}\right)^{1/2}, \qquad \ldots\ldots(4)$$

and Unna showed that the critical stream velocity, $\bar{V}$, is equal to $-\frac{c}{4}$. Taylor[3] investigated the general condition when the water cannot be considered deep, and the counter current speed decreases uniformly with depth. The current velocity at the surface to completely suppress the waves, $\bar{V}_m$ was shown to be given by

$$\bar{V}_m = +\frac{1}{\alpha_m}\left[\frac{\lambda g}{2\pi}\right]^{1/2}, \qquad \ldots\ldots(5)$$

where

$$\frac{\alpha_m^2}{Z} = \frac{\lambda}{2\pi d}, \qquad \ldots\ldots(6)$$

$$Z = \frac{dg}{\bar{V}_m^2}, \qquad \ldots\ldots(7)$$

and

α_m is the minimum value of α, where $\alpha = \frac{g}{\bar{V}_m \sigma}$.

(σ is the speed of the orbital motion in radians/sec).

Taylor gives a curve relating $\frac{\alpha_m^2}{Z}$ and α_m, which is reproduced in Fig 5. In very deep water, $\frac{\lambda}{d} \to 0$, and from Eq.6 $\frac{\alpha_m^2}{Z} \to 0$; then, from Fig 5,

$\alpha_m \to 4$, the value given by Unna.

If the quantity of free air to produce $\bar{V}_m$ is Q_{cr}, by combining Eq.2 and 5 we find that

$$Q_{cr} = \left(\frac{P+D}{Pg}\right)\left(\frac{g\lambda}{2\pi}\right)^{3/2}\left(\frac{1}{1.46\,\alpha_m}\right)^3. \qquad \ldots\ldots(8)$$

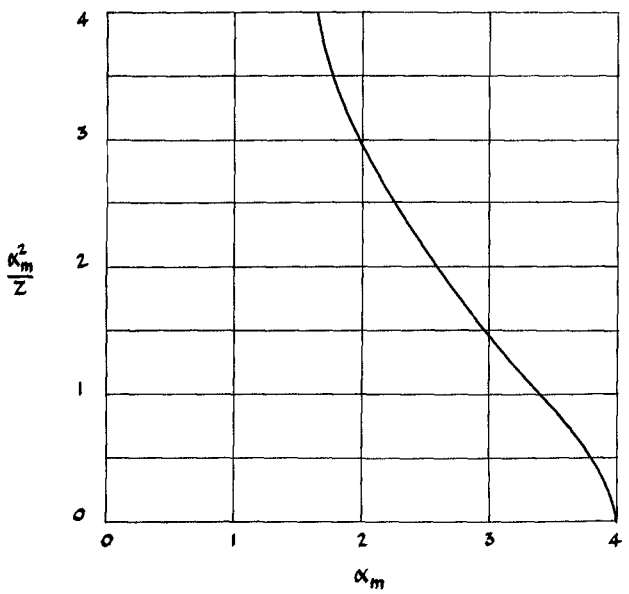

FIG. 5

For a known water depth, D, the current thickness d can be found from Eq.3. For a known wavelength, λ, the value of $\frac{\alpha_m^2}{Z}$ can then be calculated from Eq.6, and Fig 5 used to find α_m. This is substituted into Eq.8 to find the air supply Q_{cr}. The value of Q_{cr} is plotted for a selection of values of D and λ in Fig 6, which graphically illustrates the advantage of setting the air pipe in a depth of water of at least half the wavelength. Q_{cr} rises very steeply when the depth is small.

According to Eq.8, Q_{cr} is independent of wave height, but experiments show that when waves are neither truly sinusoidal nor of infinitessimal height the quantity to produce complete damping can exceed Q_{cr}. If we denote this quantity by Q_{max}, Bulson suggests a linear relationship between $\frac{Q_{max}}{Q_{cr}}$ and the wave steepness $\frac{H}{\lambda}$, as shown in Fig 7.

As an example, supppose we wish to investigate the quantity of air required to suppress sea waves 100 ft long, 4 ft. high, in a water depth of 50 ft. Now, from Eq.3,

$$d = 0{\cdot}32.33 \log_e \frac{83}{33} = 9{\cdot}63 \text{ ft.} \quad (P = 33 \text{ ft. for sea water})$$

Then,

$$\frac{\alpha_m^2}{Z} = \frac{100}{2\pi\ 963} = 1{\cdot}66,$$

and from Fig. 5

$$\alpha_m = 2{\cdot}82.$$

Substitution in Eq.8 gives

$$Q_{cr} = 13{\cdot}3 \text{ cusecs per ft.}$$

Also, $\frac{H}{\lambda} = \frac{4}{100} = 0{\cdot}04$, and from Fig. 7, $\frac{Q_{max}}{Q_{cr}} = 1{\cdot}4$,

therefore the quantity of free air required, $Q_{max} = 1{\cdot}4 \times 13{\cdot}3 = 18{\cdot}6$ cusecs per ft This represents an air power at the pipe of 64 HP per foot.

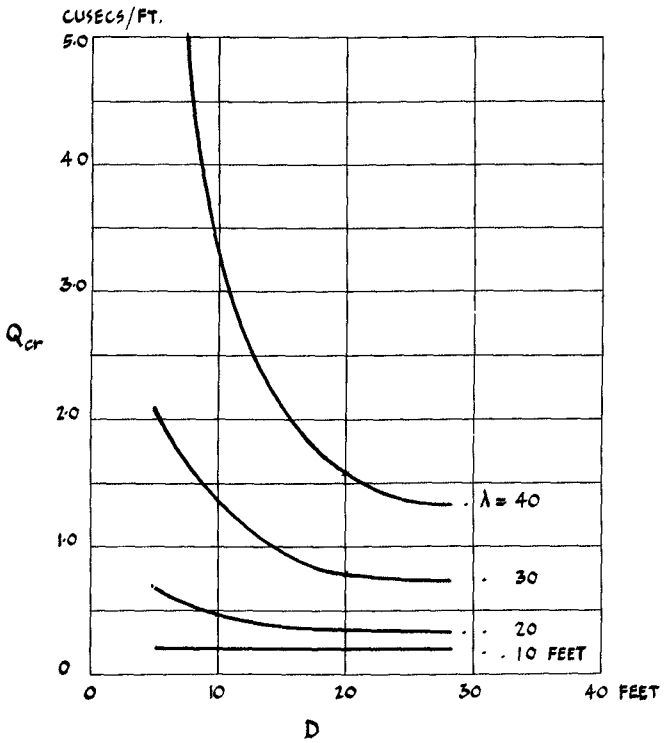

FIG 6

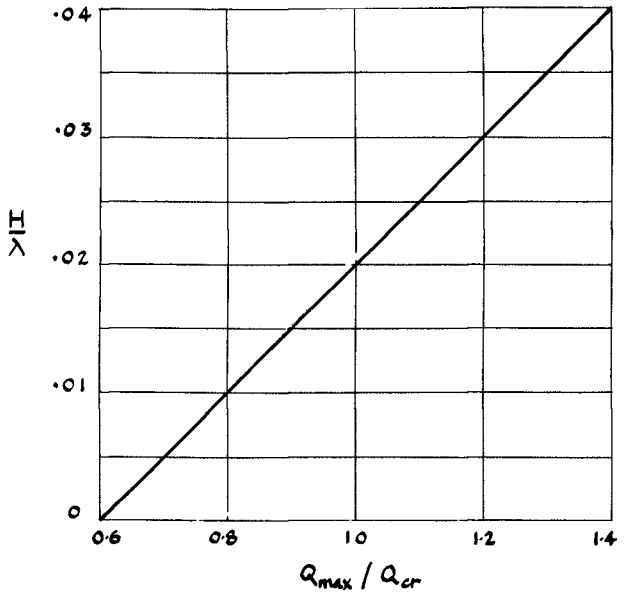

FIG 7

4. PARTIAL WAVE SUPPRESSION

If less than the quantity of air required for complete suppression is supplied, there is some damping of the incident wave. Bulson[7] proposed an empirical relationship between the height of the transmitted wave (h), the height of the incident wave (H), the quantity of air supplied (Q_o), and the quantity to completely kill the waves (Q_{max}), of the form

$$\frac{15}{16}\left(\frac{h}{H}\right)^{\frac{2\lambda}{P}} + \left(\frac{Q_o}{Q_{max}}\right)^2 = 1, \left(\frac{Q_o}{Q_{max}} > 0.25\right). \qquad \ldots\ldots(9)$$

Fig 8 shows a plot of this function for various values of $\frac{2\lambda}{P}$. Note that the amount of damping falls as the wavelength increases, and that for waves greater than 100 ft. in length there is very little reduction in wave height until the quantity of air approaches to within a few per cent of Q_{max}.

5. INTERMITTENT AIR SUPPLY

Bulson[8] showed from model tests that for complete wave suppression an intermittent air pulse offers no advantage over a steady supply; the total quantity of air supplied during a given period must be the same. For partial damping, however, an intermittent supply can be advantageous.

The degree of intermittency is measured by the ratios $\frac{P}{T}$ and n, where

$$\frac{P}{T} = \frac{\text{Time air valve is open}}{\text{wave period}},$$

$$n = \frac{\text{Time air valve is closed}}{\text{Time air valve is open}}, \qquad \ldots\ldots(10)$$

and Fig 9 shows the relationship between $\frac{h}{H}$ and n for various value of $\frac{P}{T}$. The graph illustrates that it is best to use as low a value for $\frac{P}{T}$ as possible, when $\frac{h}{H} = 0{\cdot}75$, the intermittent supply with $\frac{P}{T} = 1$ required 50% of the total air of a continuous supply, and the supply $\frac{P}{T} = 2$ required 66%. Fig 10 shows the comparison of total air flows.

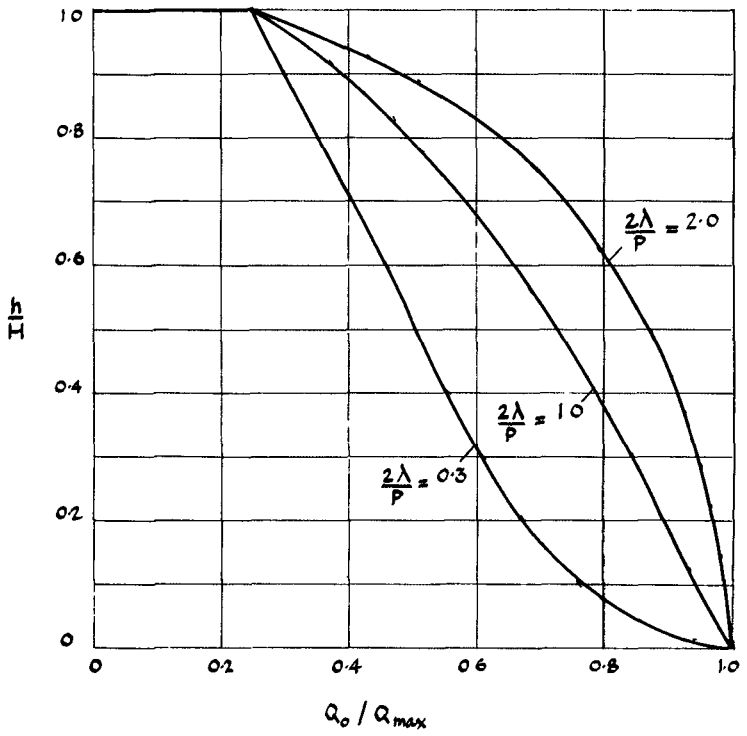

FIG 8

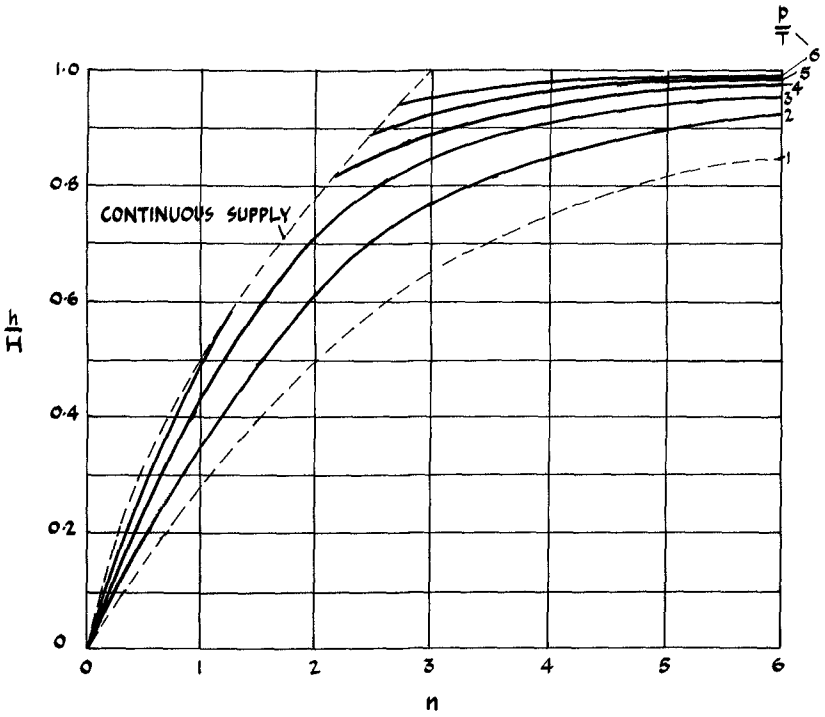

FIG. 9

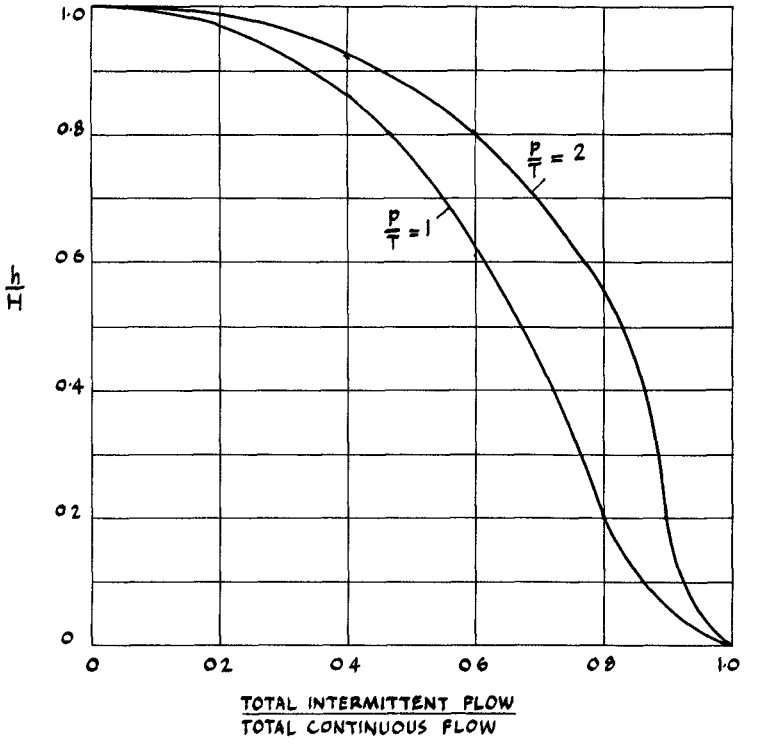
1·0
0·8
0·6
0·4
0·2
0
H/h
p/T = 2
p/T = 1
0
0·2
0·4
0·6
0·8
1·0
TOTAL INTERMITTENT FLOW
TOTAL CONTINUOUS FLOW

FIG 10

6. TYPICAL DESIGN CALCULATION

Suppose we wish to examine the feasibility of using a bubble breakwater in deep water to reduce a range of incident wave heights to a transmitted height of 3 feet. Three feet is assumed to be the maximum height that unloading and berthing operations can take place within the breakwater. By 'deep water' we mean that the air pipe on the sea bed is at least $\frac{\lambda}{2}$ below the surface. Then, taking an incident wave height of 10 feet for the first calculation, and atmospheric pressure, P, as 33 feet of sea water, Eq.9 gives

$$\frac{15}{16}\left(\frac{3}{10}\right)^{\frac{2\lambda}{33}} + \left(\frac{Q_o}{Q_{max}}\right)^2 = 1 . \qquad \ldots .(11)$$

If a wave steepness ratio of 0·03 is assumed, $\lambda = \frac{10}{0{\cdot}03} \simeq 340$ feet, and substituting this value in Eq.11 gives

$$\frac{Q_o}{Q_{max}} \simeq 1 . \qquad .....(12)$$

As indicated earlier, at these long wavelengths the quantity of air for partial suppression is virtually equal to the quantity for complete suppression, Q_{max}.

The next step is to calculate Q_{cr} from Eq.8, and use this value to find Q_{max} from Fig 7. This part of the calculation follows closely the method given in section 3. From Eq.3,

$$d = 0{\cdot}32.33 \log_e \frac{170 + 33}{33} = 19{\cdot}2 \text{ ft.}$$

Then,

$$\frac{\alpha_m^2}{2} = \frac{340}{2\pi \times 25{\cdot}7} = 2{\cdot}82,$$

and from Fig.5 $\alpha_m = 2{\cdot}1$.

Substituting in Eq.8 gives Q_{cr} = 476 cusecs per ft.

Also, $\frac{H}{\lambda} = \frac{10}{340} = 0{\cdot}03$, and from Fig.7 $\frac{Q_{max}}{Q_{cr}} = 1{\cdot}2$, so that the air quantity for complete suppression, Q_{max} = 571 cusecs per ft.

Then, from Eq.12,

Q_o = 34,260 c.f.m per foot of breakwater.

The quantity of air required is seen to be very large. If the breakwater is operating against the same incident waves, but in only 50 feet of water, the quantity is almost doubled. For this condition Eq.3 gives

$$d = 0{\cdot}32.33 \log_e \frac{50 \times 33}{33} = 9{\cdot}63 \text{ ft.},$$

and $\frac{\alpha_m^2}{Z} = \frac{340}{2\pi \times 9{\cdot}63} = 5{\cdot}62.$

From Fig.5 $\alpha_m \doteq 1{\cdot}3$, and substituting in Eq.8 gives

Q_{cr} = 830 cusecs per ft.

$\frac{H}{\lambda}$ = 0·03, as before, and from Fig.7 $\frac{Q_{max}}{Q_{cr}} = 1{\cdot}2$,
so that the air required for complete suppression, Q_{max} = 996 cusecs per ft., and, from Eq.12,

Q_o = 59,700 c.f.m. per foot.

Similar calculations for continuous and intermittent supply produce the curves shown in Fig 11 , which apply to an air pipe set in 50 feet of water.

7. PRACTICAL CONSIDERATIONS

a. Wave height outside breakwater

When the breakwater is operating successfully there is a marked build-up in the height of the incident waves just before they break over the counter current. Judging by the results of trials with 30 ft. wavelengths, an increase in wave height of up to 4 times could be expected, combined with a length decrease of 30%. This means that for an incident wave train 10 ft in height, wave heights immediately offshore of the breakwater might be 40 ft, and wave lengths reduced, for example, from 340 ft to 240 ft. These figures check with the accepted steepness ratio for unstable waves of 0·14 (since $\frac{40}{240}$ = 0·16).

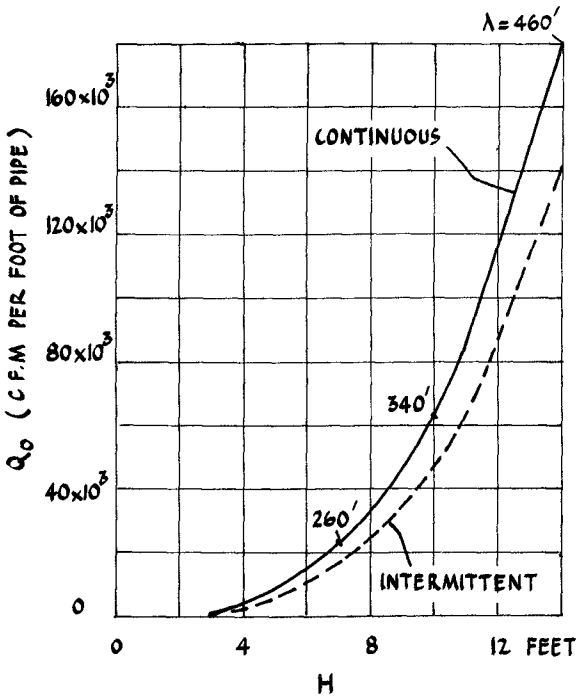
λ = 460′
160×10³
120×10³
80×10³
40×10³
0
Q₀ (C.F.M. PER FOOT OF PIPE)
CONTINUOUS
340′
260′
INTERMITTENT
0
4
8
12 FEET
H

FIG 11

In these conditions it would be difficult for a small vessel to approach the breakwater from the seaward quarter. It would be necessary to sail around and approach from leeward. Similarly, a lighter or small craft leaving the breakwater could not sail out across the bubble curtain without considerable hazard.

b Surface currents within the breakwater

There would be a considerable conflux of surface currents within the breakwater. In the range of breakwater designs considered in section 7, these currents would be at least 12 knots, and might cause difficulty in mooring and controlling small craft.

c. Air supply

It was demonstrated above that to reduce waves 10 feet high, 340 feet long to a height of 3 feet requires a continuous air supply of 34,260 c.f.m. per foot of breakwater. This is under ideal conditions when the depth of water is 170 feet (In 50 ft. of water a supply of 59,700 c.f.m per foot is needed). At best then, the output of 57 large commercial compressors is required for every foot of breakwater, alternatively there are very large engine driven centrifugal compressors available commercially with a capacity of 30-40,000 c.f.m., but these weigh over 20 tons and consume 215 gallons per hour of fuel. On this basis a 500 yard long breakwater would cost about £100,000 per day in fuel and involve a capital expenditure for air supply of £20m.

d. Intermittent supply

An intermittent supply can save air, but the engineering problems in providing one could be difficult to solve. Interrupting the supply from the compressors seems a less likely solution than directing the air along lengths of pipe alternately by means of a valve system. Care would be needed to ensure that the air feed lines to these valves were clear of the hull of any vessel within the breakwater.

8. CONCLUSION

The experimental and theoretical studies during the past 25 years have made it possible for a reasonably accurate estimate to be made of the air quantity required to operate a bubble breakwater. The quantity is astronomical and costly to supply. The practical difficulties of operating a full scale system are immense. It is doubtful whether any novel ideas of bubble formation and size can produce economies, and high cost is bound to be the basic feature of any apparatus of this type which is designed to combat the energy of the sea.

References

1. Brasher, P., Compressed Air Magazine, vol.20, 1915, p.752.
2. White, C.M., Admiralty Report ATR/MSIC/1685, 1943.
3. Taylor, Sir Geoffrey, Proc.Roy.Soc.A., vol.231,1955, p 466.
4. Bulson, P.S., Dock and Harbour Authority, vol.XLVIII, No.560, June 1967, p.41.
5. Evans, J.T., Proc.Roy.Soc.A., vol.231, 1955, p.457.
6. Bulson, P.S., Dock and Harbour Authority, vol.XLII, No.487, May 1961, p.15.
7. Bulson, P.S., Dock and Harbour Authority, vol.XLIV, No.516, Oct 1963, p.191.
8. Bulson, P.S., Dock and Harbour Authority, vol.XLIV, No.514, Aug 1963, p.129.
9. Schmidt, W., 2 Aug. Math.Mech., vol.21, 1941, p.265.
10. Unna, P.J.H., Nature, vol.149, 1942, p.219.

Notation

c velocity of travel of waves
d thickness of current
h height of transmitted wave
k coefficient in formula for current velocity
n ratio of time air valve is closed to time it is open
p time air valve is open
v_m surface velocity of current
$\bar{V}$ critical stream velocity
$\bar{V}_m$ surface current velocity to completely suppress waves

D depth of manifold below surface
H height of incident wave
P atmospheric pressure expressed as head of water
Q quantity of air emerging from orifices, per foot of pipe
Q_o quantity of free air delivered by compressors, per foot of pipe
Q_{cr} quantity of free air to produce $\bar{V}_m$, per foot of pipe
Q_{max} quantity of free air to completely suppress waves of finite height, per foot of pipe
Q_I quantity of free air supplied intermittently per foot of pipe
T wave period
Z $dg/\bar{V}_m^2$.

α $g/\bar{V}_m\sigma$
α_m minimum value of α
λ wavelength
σ speed of orbital motion in radians/sec

CHAPTER 65

ANALYSIS OF THE FLOW INDUCED BY AIR-BUBBLE SYSTEMS

by
Helmut E. Kobus, Ph.D.
Research Engineer,
Versuchsanstalt für Wasserbau und Schiffbau
Berlin, Germany

ABSTRACT

The pattern of vertical velocities induced by an orifice discharging air into water can be represented by Gaussian distribution curves with a linear spread in the vertical except for the regions near the orifice and close to the free surface. An analytical treatment considering the momentum-flux increase due to the buoyancy of the air together with experimental information about the spread of the velocity profiles and the mean rising speed of the air bubble stream, which has been obtained from velocity and density measurements over a wide range of conditions, leads to a complete description of the flow field. The ratio of the water volume flux to the air discharge rate, which has been proposed as an efficiency criterion, is now at hand as a function of depth and air supply for both single orifices and rows. The experimental evidence supports the analysis well and suggests that extrapolation to larger water depths and air supplies should be permissible, which would allow approximate predictions of the volume flux for any air-bubble system.

INTRODUCTION

In recent years, air-bubble systems have been applied successfully as breakwaters and barriers against spreading of oil, salt water intrusion and ice formation. However, all attempts to correlate results from model tests and from field investigations have failed, because no analytical framework is at hand which suits both model and prototype. In a first attempt to close this gap, the vertical velocity field of the air-water mixture above an orifice has been measured and analyzed. The flow pattern produced by an air jet entering vertically into sideways unlimited water shows certain similarities to a submerged water jet [1] which suggest a similar analytical treatment with proper consideration of the momentum-flux increase with height due to the buoyancy of the air [2].

ANALYSIS

The air bubble stream

Consider an air jet discharging vertically upward at depth h below the water surface through a nozzle of diameter d_o at a mass discharge rate Q_o, pressure p_o and density ρ_a^o. If $\forall_o$ is defined to be the volume flux corresponding to Q_o at atmospheric pressure, then the momentum flux is given by

$$M_o = \frac{(\rho_a^{atm} \forall_o)^2}{\rho_a^o \pi d_o^2/4} = \rho_a^{atm} \left(\frac{p_{atm}}{p_o}\right) \frac{\forall_o^2}{\pi d_o^2/4} \qquad (1)$$

or, in terms of a theoretical (loss-free) exit velocity U_o and a discharge coefficient c_D, by

$$M_o = c_D U_o \rho_a^{atm} \forall_o \qquad (2)$$

The continuous air stream discharging through the orifice quickly expands according to the sudden pressure drop across the nozzle and breaks up into bubbles of discrete size. It has been shown [5] that the bubble size distribution depends solely upon the discharge rate and varies neither with the fluid properties nor with the orifice diameter for all practical cases.

The speed of rise of the bubble stream rapidly approaches some terminal mean velocity $\bar{u}_b$. Fig.2 gives an indication of the extent of the "initial region", in which the local conditions at the orifice influence the flow pattern. Beyond this region, the bubble stream rises with a mean velocity $\bar{u}_b$ determined by the bubble size distribution and concentration, which are both functions of the discharge rate $\forall_o$ only. Therefore, $\bar{u}_b$ should be a unique function of $\forall_o$ independent of the local orifice conditions, which is confirmed by the experiments.

Extensive measurements on single bubbles so far have shown no evidence that the speed of rise varies considerably with the depth of submergence, although the change in bubble volume with depth or pressure would suggest so. But, except for very small bubbles, the speed of rise changes only gradually with the bubble diameter, which in turn changes only with the third root of the bubble volume or the local pressure. It is therefore considered a satisfactory approximation to assume the average rate of rise $\bar{u}_b$ of the bubble stream to be independent of height.

The increment in buoyant force exerted upon the water by the air bubbles contained in a horizontal slice of thickness dx is given by the product of the air volume contained and the difference in specific weight. With

$$h^* = h + p_{atm}/\gamma_w \qquad (3)$$

the air density at cross section x can be expressed as

$$\rho_a^x = \frac{\rho_a^{atm}}{p_{atm}} \gamma_w (h^* - x)$$

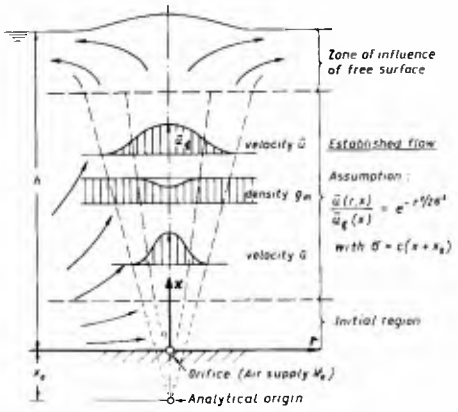

Fig.1 Definition Sketch

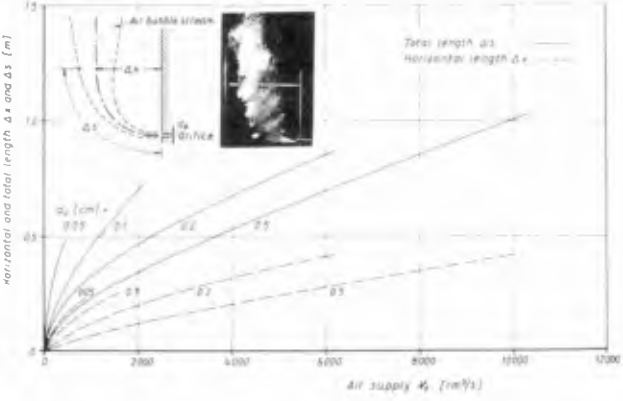

Fig.2 Initial Region

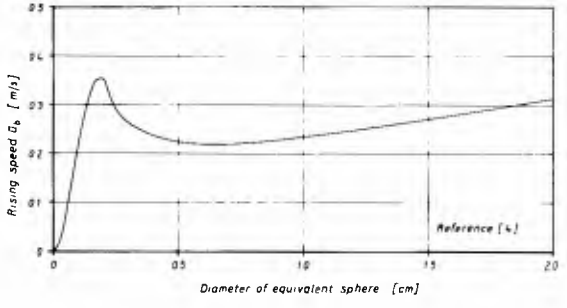

Fig.3 Rising Speed of Single Bubbles

and the increment in buoyant force is given by

$$dF(x) = \frac{Q_o\, dx}{\rho_a^x\, \bar{u}_b}(\gamma_w - \gamma_a) = \frac{P_{atm}\, \forall_o}{\bar{u}_b (h^* - x)} \frac{(\gamma_w - \gamma_a)}{\gamma_w} dx$$

The buoyant force acting between the orifice and cross section x is then (with $\gamma_w - \gamma_a \approx \gamma_w$)

$$F(x) = \frac{P_{atm}\, \forall_o}{\bar{u}_b} \int_0^x \frac{dx}{h^* - x} = -\frac{P_{atm}\, \forall_o}{\bar{u}_b} \ln(1 - x/h^*)$$

and the total momentum flux at cross section x is now given by the sum of initial momentum flux and buoyant force,

$$M(x) = \rho_a^{atm}\, C_D\, U_o\, \forall_o - \frac{P_{atm}\, \forall_o}{\bar{u}_b} \ln(1 - x/h^*) \qquad (4)$$

It is seen that the buoyancy term grows rapidly with distance x from the orifice while the contribution due to the initial momentum soon becomes negligible. The term M_o can be neglected, if

$$\frac{\rho_a^{atm}\, C_D\, U_o\, \forall_o}{-\frac{P_{atm}\, \forall_o}{\bar{u}_b} \ln(1 - x/h^*)} \approx \left(\frac{\rho_a^{atm}}{P_{atm}}\right) \frac{C_D\, U_o\, \bar{u}_b}{x/h^*} \ll 1$$

Since, from the ideal gas law,

$$P_{atm} / \rho_a^{atm} = g\,RT \approx 90\,000\ [m^2/s^2]$$

and since U_o cannot exceed the speed of sound (333 m/s), c_D is roughly 2/3, and $\bar{u}_b$ is of the order of magnitude of 1 m/s, this condition results in

$$\frac{h^*}{500\, x} \ll 1 \qquad \text{or} \qquad x \gg \frac{h^*}{500} \qquad (5)$$

So, for instance, for M_o to be less than 2 % of M(x), x must be larger than $h^*/10$, which is a limit usually within the initial region. Beyond this lower limit, the momentum flux can be approximated by

$$M(x) = -\frac{P_{atm}\, \forall_o}{\bar{u}_b} \ln(1 - x/h^*) \qquad (6)$$

Single orifice (axisymmetric case)

The analysis is based on two assumptions about the form of the velocity profiles : firstly, that the velocity profile at any horizontal section can be described by a Gaussian distribution curve,

$$u(r,x) = u_{\ell}(x)\, e^{-r^2/2\sigma^2}$$

and secondly, that these profiles are similar with respect to an "analytical origin" located at x_o,

$$\frac{u(r,x)}{u_{\ell}(x)} = f\left(\frac{r}{x+x_o}\right)$$

The "analytical origin" results from an analytical extension of the established-flow pattern into and beyond the limits of the initial region. This origin does not necessarily coincide with the location of the orifice because of the markedly different conditions in the initial region; in fact, it may be expected always to lie below the orifice because of the faster expansion rate in the zone of flow establishment.

The similarity criterion requires a linear spread of the Gaussian profiles with distance from the analytical origin,

$$\sigma = c(x+x_o) \tag{7}$$

and hence

$$\frac{u(r,x)}{u_{\ell}(x)} = e^{-r^2/2c^2(x+x_o)^2} \tag{8}$$

If the density defect due to the air bubbles is also described by a Gaussian distribution curve similar with respect to the analytical origin

$$\Delta\rho(r,x) = \Delta\rho_{\ell}(x)\, e^{-r^2/2\alpha^2c^2(x+x_o)^2}$$

(the rate of spread of the bubble stream and of the mixture velocity profiles being proportional to each other) there results

$$\frac{\rho_m(r,x)}{\rho_w} = \frac{\rho_w - \Delta\rho(r,x)}{\rho_w} = 1 - \frac{\Delta\rho_{\ell}(x)}{\rho_w}\, e^{-r^2/2\alpha^2c^2(x+x_o)^2} \tag{9}$$

From the equation of continuity for the air bubble stream

$$\frac{Q_o}{\bar{u}_b} = \int_0^{\infty} \Delta\rho(r,x)\, 2\pi r\, dr = 2\pi\alpha^2c^2(x+x_o)^2\, \Delta\rho_{\ell}(x)$$

follows that

$$\frac{\Delta\rho_{\ell}(x)}{\rho_w} = \left(\frac{\rho_a^{atm}}{\rho_w}\right)\frac{\forall_o}{2\pi\alpha^2c^2\bar{u}_b(x+x_o)^2} \approx \frac{1}{50}\,\frac{\forall_o}{\bar{u}_b(x+x_o)^2}$$

since the density ratio is about 800 and the rate of spread (αc) of the bubble stream is of the order of magnitude of 0.1. From this expression and eq.(9) it is therefore seen that the mixture density can only differ considerably from the water density for air supply rates $\forall_o$ much larger than the product

$\bar{u}_b (x + x_o)^2$. However, $\bar{u}_b$ is of the order of magnitude of 1 m/s, and outside the initial region $(x + x_o)$ is usually larger than 1 m. Hence significant density variations are to be expected only for air supply rates much in excess of 1 m^3/s, which is far beyond any practicable limit. Outside the initial region the variations in density can therefore be safely neglected.

The assumed velocity profiles can now be integrated to yield the mass flux

$$\left.\begin{aligned} Q(x) &= \int_0^\infty \rho_m(r,x)\, u(r,x)\, 2\pi r\, dr = 2\pi \rho_w\, u_\ell(x) \int_0^\infty e^{-r^2/2c^2(x+x_o)^2}\, r\, dr \\ Q(x) &= 2\pi \rho_w\, u_\ell(x)\, c^2 (x+x_o)^2 \end{aligned}\right\} \quad (10)$$

and the momentum flux

$$M(x) = \int_0^\infty \rho_m(r,x)\, u^2(r,x)\, 2\pi r\, dr = \pi \rho_w\, u_\ell^2(x)\, c^2 (x+x_o)^2 \quad (11)$$

Comparison of the expressions for the momentum flux in eqs.(6) and (11), based upon the assumption of negligible pressure differences in the zone of established flow, leads to an expression for the centerline velocity

$$u_\ell(x) = \frac{1}{c(x+x_o)} \sqrt{\frac{-P_{atm}\, \forall_o}{\pi \rho_w\, \bar{u}_b} \ln(1 - x/h^*)} \quad (12)$$

and substitution of eq.(12) into eq.(10) gives the volume flux ratio

$$\frac{Q(x)/\rho_w}{\forall_o} = 2\pi c(x+x_o) \sqrt{\frac{-P_{atm}}{\pi \rho_w\, \bar{u}_b\, \forall_o} \ln(1 - x/h^*)} \quad (13)$$

with the mass flux ratio being about 800 times as large. The momentum flux ratio is given by

$$\frac{M(x)}{M_o} = -\left(\frac{P_o}{P_{atm}}\right) \frac{g R T \pi d_o^2/4}{\bar{u}_b\, \forall_o} \ln(1 - x/h^*) \quad (14)$$

Row of orifices (two-dimensional case)

A two-dimensional slot of width b_o, representing the limiting case for a row of orifices, can be treated in an analog manner. If the mass flux per unit length is Q_o' and the corresponding atmospheric volume flux $\forall_o'$, then the initial momentum is given by

$$M_o' = \rho_a^{atm} \left(\frac{P_{atm}}{P_o}\right) \frac{\forall_o'^2}{b_o} = c_D'\, U_o\, \rho_a^{atm}\, \forall_o' \quad (15)$$

and the buoyant force by

$$F'(x) = -\frac{p_{atm} \forall_o'}{\bar{u}_b} \ln(1 - x/h^*)$$

The total momentum flux is now

$$M'(x) = c_D' U_o \rho_a^{atm} \forall_o' - \frac{p_{atm} \forall_o'}{\bar{u}_b} \ln(1 - x/h^*) \qquad (16)$$

where the contribution due to the initial momentum flux can again be neglected within the same limits as before.

The assumption of Gaussian velocity profiles similar with respect to the analytical origin x_o' yields

$$\frac{u'(y,x)}{u_\ell'(x)} = e^{-y^2/2c'^2(x+x_o')^2} \qquad (17)$$

and similarly the density defect is given by

$$\Delta\rho'(y,x) = \Delta\rho_\ell'(x) e^{-y^2/2\alpha'^2 c'^2 (x+x_o')^2}$$

From the equation of continuity for the air bubble stream

$$\frac{Q_o'}{\bar{u}_b} = 2\int_o^\infty \Delta\rho'(y,x)\, dy = \sqrt{2\pi}\, \Delta\rho_\ell'(x)\, \alpha' c' (x+x_o')$$

there results, with the density ratio being 800 and the rate of spread ($\alpha' c'$) in the order of magnitude of 0.1,

$$\frac{\Delta\rho_\ell'(x)}{\rho_w} = \left(\frac{\rho_a^{atm}}{\rho_w}\right) \frac{\forall_o'}{\sqrt{2\pi}\, \alpha' c' \bar{u}_b (x+x_o')} \approx \frac{1}{200} \frac{\forall_o'}{\bar{u}_b (x+x_o')}$$

and hence

$$\frac{\rho_m'(y,x)}{\rho_w} = 1 - \frac{\Delta\rho_\ell'(x)}{\rho_w} e^{-y^2/2\alpha'^2 c'^2 (x+x_o')^2} \approx 1 - \frac{1}{200} \frac{\forall_o'}{\bar{u}_b (x+x_o')} e^{-y^2/2\alpha'^2 c'^2 (x+x_o')^2}$$

Since the discharge rate $\forall_o'$ will never reach values much larger than $\bar{u}_b \cdot (x + x_o')$, which is of the order of magnitude of 1 m^2/s outside the initial region, it is seen that the variation in density can again be safely neglected.

Integration over the assumed velocity profiles gives the mass flux

$$\left.\begin{aligned} Q'(x) &= 2\int_o^\infty \rho_m'(y,x)\, u'(y,x)\, dx = 2\rho_w u_\ell'(x) \int_o^\infty e^{-y^2/2c'^2(x+x_o')^2} dy \\ Q'(x) &= \sqrt{2\pi}\, \rho_w\, u_\ell'(x)\, c'(x+x_o') \end{aligned}\right\} \qquad (18)$$

and the momentum flux

$$M'(x) = 2\int_0^\infty \rho_m'(y,x)\, u'^2(y,x)\, dx = \sqrt{\pi}\, \rho_w\, u_t'^2(x)\, c'(x+x_o') \tag{19}$$

For negligible pressure differences, the expressions for the momentum flux in eqs. (16) and (19) yield the centerline velocity

$$u_t'(x) = \sqrt{\frac{-P_{atm}\, \forall_o' \ln(1-x/h^*)}{\sqrt{\pi}\, \rho_w\, \bar{u}_b\, c'(x+x_o')}} \tag{20}$$

which leads to the volume flux ratio

$$\frac{Q'(x)/\rho_w}{\forall_o'} = \sqrt{\frac{-2\sqrt{\pi}\, P_{atm}\, c'(x+x_o')}{\rho_w\, \bar{u}_b\, \forall_o'} \ln(1-x/h^*)} \tag{21}$$

and the momentum flux ratio

$$\frac{M'(x)}{M_o'} = -\left(\frac{P_o}{P_{atm}}\right) \frac{g R T b_o}{\bar{u}_b\, \forall_o'} \ln(1-x/h^*) \tag{22}$$

The assumption of similar Gaussian velocity profiles has thus led to expressions describing the flow in which only the rate of spread c of the profiles, the location x_o of the analytical origin and the average rate of rise $\bar{u}_b$ of the bubble stream are yet to be determined by experiment.

EXPERIMENTS

In a basin of 8 x 280 x 4.70 m, vertical velocities above single orifices were measured by Ott current meters. The orifice was located at a depth of 4.50 m and hence 0.20 m above the basin floor in most tests, but some measurements have also been made with an 0.2 cm orifice at a depth of 2 m (elevation above floor = 2.70 m) and again at 4.50 m with a false floor around the orifice (zero elevation above floor). Orifices from 0.05 to 0.5 cm in diameter were tested at air discharges up to 6 200 cm^3/s. Since the flow is subject to considerable fluctuations, it was found necessary to measure over a period of 5 min at each point. Profiles have been taken along the jet axis (for an example, see Fig.4) and in normal planes at various heights (Fig.6).

In the same basin, a row of 0.1 cm orifices spaced 7.5 cm apart was tested. The air pipe with a total length of 4.50 m was located 4.30 m below the surface. The velocities were measured at midsection. In addition, a row of 0.1 cm orifices spaced 10 cm apart has been investigated in a basin of 1 x 10 x 2 m with the air pipe (total length 1 m) located 2 m below the

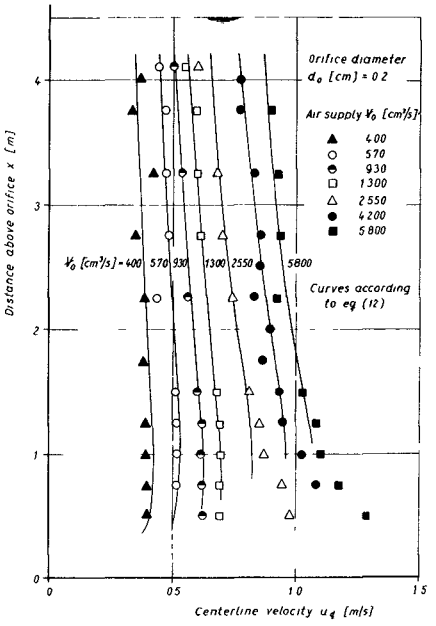

Fig.4 Centerline Velocities above a Single Orifice

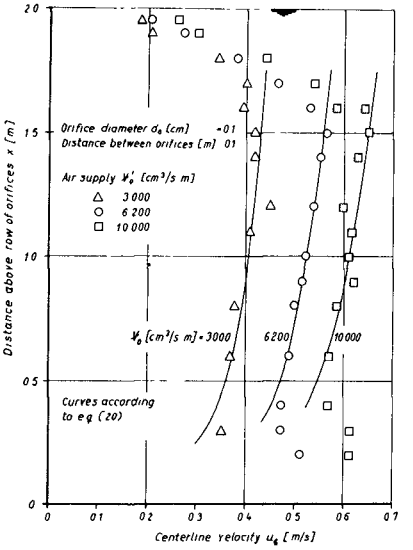

Fig.5 Centerline Velocities above a Row of Orifices

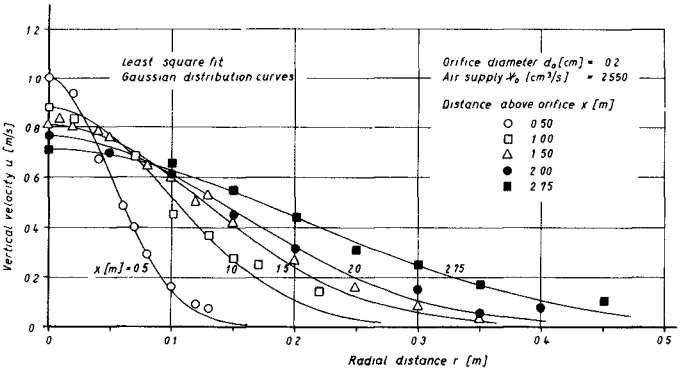

Fig.6 Velocity Profiles above a Single Orifice

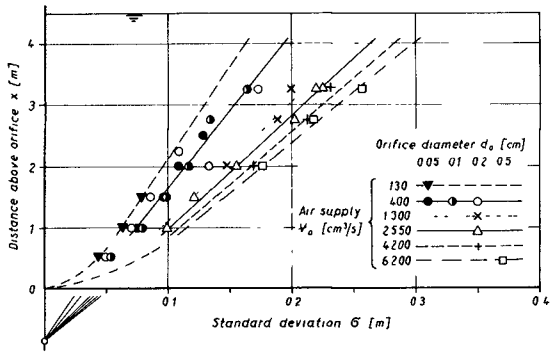

Fig.7 Standard Deviation of Gaussian Velocity Profiles for a Single Orifice

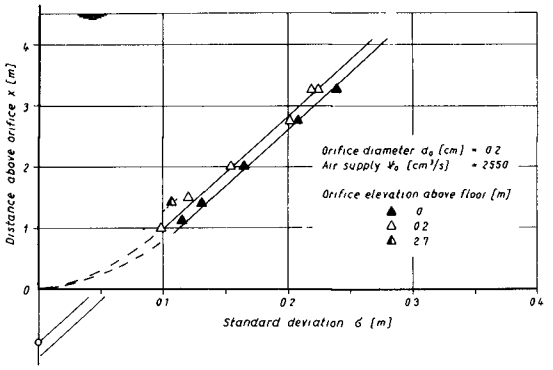

Fig.8 Influence of Orifice Location above the Floor

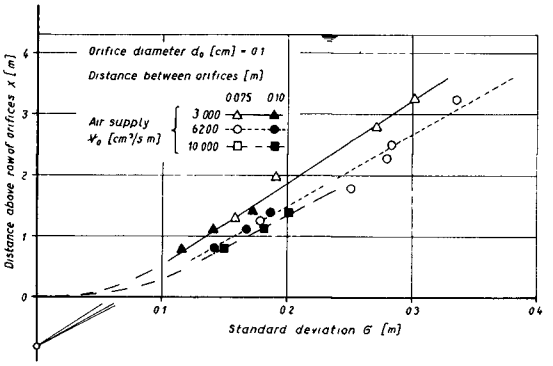

Fig.9 Standard Deviation of Gaussian Velocity Profiles for a Row of Orifices

surface at the basin floor. Fig.5 shows velocity profiles along the jet axis for discharge rates up to 10 000 $cm^2/s \cdot m$.

The average rate of rise $\bar{u}_b$ of the bubble stream in sideways unlimited water was evaluated from density measurements by means of radioisotopes. If a flat, horizontal volume is chosen such that all bubbles have to pass through it, then $\bar{u}_b$ can be determined from the mean density, the dimensions of the volume and the known air supply rate. Figs.11 and 12 show the mean rising speed of bubble streams from various orifices as functions of the air supply for single orifices and rows, respectively. At small air supply rates, for which density measurements become unsatisfactory, but visual observation is possible, time-length measurements have been made.

DISCUSSION OF RESULTS

Gaussian distribution curves are seen (Fig.6) to fit the experimental data well. The standard deviation of the least-square fits increases linearly with height for both single orifices (Fig.7) and rows (Fig.9), which justifies the assumption of similar Gaussian velocity profiles.

From the variation of the standard deviation with height as shown in Figs.7, 8 and 9, the location x_o of the "analytical origin" results from an extension beyond the initial region. Since x_o is an artificial aid to compensate for the untraceable conditions in the initial region, it can be expected to depend upon the local orifice geometry and especially to vary with the orifice elevation above the floor (Fig.8). For the normal test arrangement, x_o was found to be about 0.8 m, independent of the air supply rate. The value of x_o seems to increase slightly with water depth; however, the measurements allow only an estimate with possible variations of several tenths of a meter. Nevertheless this information is sufficient, since x_o appears only in the combination $(x + x_o)$ with x always larger than the extent of the initial region, and therefore small variations in x_o are of little influence upon the results.

The rate of spread c of the velocity profiles, which is determined by the conditions in the region of established flow, is seen to vary with the air supply rate (Fig.10). The parallel shift of the straight lines in Fig.8 shows that it is independent of the local orifice geometry, and Fig.10 indicates independence of orifice size and spacing. The rate of spread increases for both single orifices and rows approximately with the air supply rate to the 0.15 power.

The mean rising speed $\bar{u}_b$ of the bubble stream is shown in Figs.11 and 12. In spite of considerable scatter the results give an indication of the magnitude of $\bar{u}_b$ at least for higher air supply rates. Independent of orifice size, $\bar{u}_b$ increases with the air supply to about the 0.15 power for both single orifices and rows.

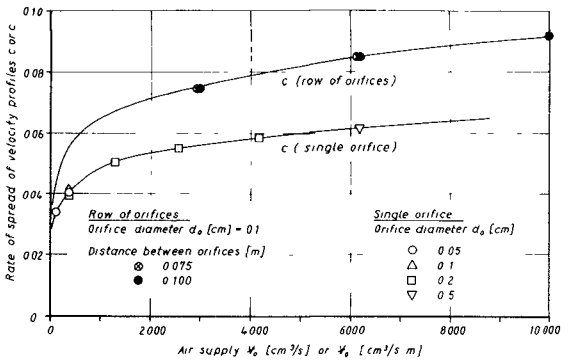

Fig.10 Rate of Spread of the Velocity Profiles

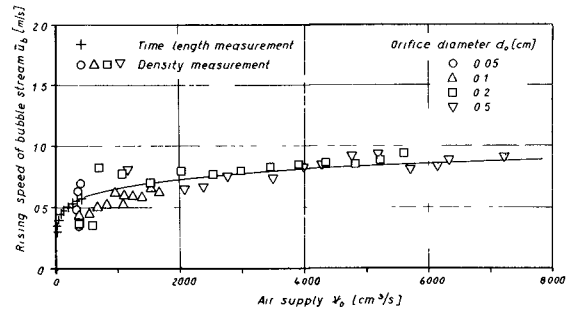

Fig.11 Average Rising Speed of the Bubble Stream from a Single Orifice

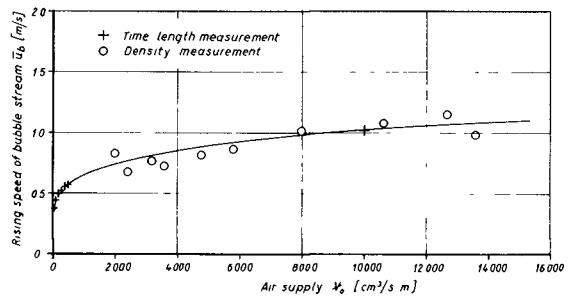

Fig.12 Average Rising Speed of the Bubble Stream from a Row of Orifices

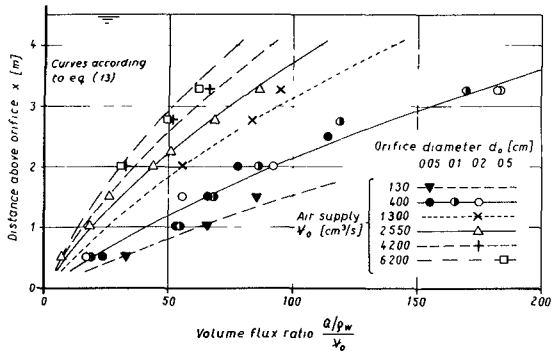

Fig.13 Volume Flux Ratio for a Single Orifice

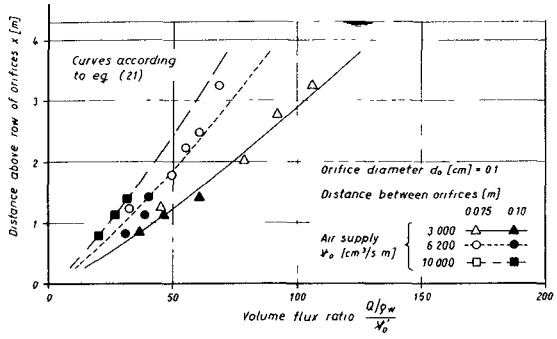

Fig.14 Volume Flux Ratio for a Row of Orifices

With the experimental information about x_0, c and $\bar{u}_b$ at hand, the analysis gives expressions for the centerline velocities and the volume flux ratios which can now be compared with the direct experimental results.

For a single orifice, the centerline velocity varies with the air supply rate to the 1/4 power and shows, after a rapid initial growth, a slight decrease with distance from the orifice (Fig.4). The volume flux ratio (Fig.13) increases more than linearly with height and shows a decrease with the air supply rate to the -0.4 power.

The centerline velocity for a row of orifices increases with distance from the orifice at an ever decreasing rate (Fig.5)

and grows with the air supply to the 1/3 power, which is in agreement with the heat-flow analogy by Taylor [6] and experimental findings of others [3,7]. The volume flux ratio (Fig.14) shows a slightly less than linear increase with height and varies with the air supply to the -1/2 power.

In both cases, the measured velocities deviate from the analytical profiles in the initial region and near the free surface, as was to be expected, but in the region of established flow experimental points and analytical curves show good agreement (Figs.4 and 5). Also, the volume flux ratios as determined from integration of the measured velocity profiles and predicted by the analysis show a fair fit for both single orifices (Fig.13) and rows (Fig.14) even close to the orifice.

CONCLUSIONS

Measurements of vertical velocities in the flow field above an orifice discharging air into water show that profiles in horizontal planes can be represented by Gaussian distribution curves with a linear spread in the vertical. This permits an analytical treatment of similar Gaussian velocity distribution curves with proper consideration of the increase in momentum flux with height due to the buoyancy of the air bubble stream, which leads to a description of the flow pattern except for the regions near the orifice and near the free surface. It contains three experimental parameters: the location x_o of the analytical origin below the orifice, the linear rate of spread c of the velocity profiles, and the mean rising speed $\bar{u}_b$ of the air bubble stream.

While the location x_o of the analytical origin was found to be 0.8 m independent of the air supply rate, but with possible variations of several 1/10 of a meter due to depth of submergence and local orifice geometry (mainly orifice elevation above the floor), the rate of spread c of the profiles is independent of orifice size, spacing and geometry. Both the two-dimensional and the axisymmetric rate of spread increase with the air supply to about the 0.15 power. The mean rising speed $\bar{u}_b$ of the bubble stream seems to grow also with the 0.15 power of the air supply independent of orifice size.

With the experimental information about the parameters x_o, c and $\bar{u}_b$ available, the analysis describes the flow pattern completely and yields in particular the volume flux ratio, which is a criterion for the efficiency of an air-bubble system, in terms of location, water depth and air supply rate. For both single orifices and rows the measured vertical velocities and the volume flux ratios obtained therefrom by integration agree well with the analytical predictions, and it is supposed that

extrapolation to larger water depths and air supplies is permissible. In first approximation this analysis should allow predictions of the volume flux for any air-bubble system, and as a first step towards an analytical framework it may ultimately contribute towards providing a means of correlating model tests and field investigations on air-bubble flows.

ACKNOWLEDGMENTS

The experiments described in this paper have been performed in the towing tank of the Versuchsanstalt fur Wasserbau und Schiffbau Berlin by Mr. P.Fischer in the course of a research program on the use of air-bubble systems for reducing silt intrusion into estuaries, conducted for the Wasser- und Schiffahrtsdirektion Kiel.

SYMBOLS

Subscript "o" refers to conditions at the orifice.
Primed symbols refer to the two-dimensional case.

d_o (b_o)	orifice diameter (slot width)
c	rate of spread of velocity profiles
c_D	discharge coefficient
h	water depth
h^*	$h + p_{atm}/\gamma_w$
p	pressure
$r(y)$	radial (sideward) distance from orifice
$u(u_\ell)$	vertical (centerline) velocity
$\bar{u}_b$	mean rising speed of air bubble stream
x	vertical distance above orifice
x_o	location of analytical origin
F	buoyant force
M	momentum flux
Q	mass flux
R	gas constant for air
T	absolute temperature
U_o	theoretical exit velocity
Ψ	volume flux
α	ratio of expansion rates for air bubble stream and water jet

$\gamma_w (\gamma_a^{atm})$	specific weight of water (air at atmospheric pressure)
$\rho_w (\rho_a^{atm})$	density of water (air at atmospheric pressure)
$\Delta\rho_\ell$	density defect at centerline
σ	standard deviation of Gaussian distribution curve

REFERENCES

[1] Rouse, H., Editor. "Advanced Mechanics of Fluids", John Wiley and Sons, Inc., New York 1959

[2] Baines, W.D.: "The Principles of Operation of Bubbling Systems", Proc., Symposium on Air Bubbling, Ottawa 1961

[3] Bulson, P.S.: "Currents Produced by an Air Curtain in Deep Water", The Dock and Harbour Authority, May 1961

[4] Siemes: "Gasblasen in Flussigkeiten", Chemie-Ingenieur-Technik 26 (1954)

[5] Silberman,E. "Production of bubbles by the disintegration of gas jets in liquid", Proc., 5th Midwestern Conference on Fluid Mechanics, U of Mich., 1957

[6] Taylor, Sir G.: "The action of a surface current used as a breakwater", Proc.Royal Society A, Vol.231, 1955

[7] Kurihara, M: "On the Study of a Pneumatic Breakwater in Japan", Coastal Engineering in Japan, Japan S.C.E., Vol.VIII, 1965

[8] Murota, A. and Muraoka, K: "Turbulent Diffusion of the Vertically Upward Jet", Proc., 12th IAHR Congress, Fort Collins 1967

CHAPTER 66

DISSIPATION OF DEEP WATER WAVES BY HYDRAULIC BREAKWATERS

by

R. E. Nece,[1] E. P. Richey,[2] and V. Seetharama Rao[3]

ABSTRACT

Experimental results are presented for a laboratory study of the effectiveness of hydraulic breakwaters in dissipating deep water waves. Test data are reported for a range of wave steepnesses for wave length: water depth ratios ranging from 0.375 to 1.343.

It is shown that the effectiveness of hydraulic breakwaters depends upon the steepness of the incident wave and upon the ratio of the momentum of the opposing surface current created by the breakwater to the momentum of the incident waves. Results also are compared with the theoretical predictions of Taylor which are appropriate to deep water waves.

Data are presented in a form allowing the determination of hydraulic breakwater manifold discharge characteristics in order to achieve specified attenuation for a particular incident wave. It is concluded that while the hydraulic breakwater is better adapted to deep water waves than to shallow water waves upon which prior studies of the device have concentrated, it is generally inefficient for most practical cases because of excess power requirements. Some possible field applications are indicated.

INTRODUCTION

The hydraulic breakwater is a device which uses a series of horizontal water jets to generate a surface current opposed to the direction of propogation of incident waves; the surface current produces attenuation and/or breaking of the waves. Hydraulic breakwaters have been studied rather extensively by means of laboratory experiments. Quite logically, experimental data have emphasized the behavior of these devices in intermediate-depth water waves ($2 < L/d < 20$), because it has been considered that this type of wave attenuating device would be most useful in installations near the coast. Representative laboratory studies of hydraulic breakwaters have been reported by Evans (1955), Straub et al (1958), and Williams (1960); while some data for deep water waves ($L/d < 2$) are included, these are very limited. The above listing is not a complete

1. Professor of Civil Engineering, University of Washington, Seattle, Washington.
2. Associate Professor of Civil Engineering, University of Washington, Seattle, Washington.
3. Hydraulic Engineer, Lewis-Redford-Engineers, Bellevue, Washington.

one, and is restricted to two-dimensional wave tank studies. Williams and Wiegel (1963) examined the effect of a surface located hydraulic breakwater on wind generated waves, and found that shorter, steeper wave components were attenuated to a greater degree than were the longer wave components.

Growing interest in such structures as floating bridges and pontoon-type marinas which might be located close to shore but which are still in a deep water environment so far as surface waves are concerned has prompted further consideration of the possibility of using hydraulic breakwaters for attenuation of deep water waves. The structures mentioned commonly have plane vertical sidewalls of finite depth which can cause reflection of the incident waves. A suggested application of the hydraulic breakwater is to attach it outboard of such structures in order to attenuate the incident waves before they reach the structure and hence minimize wave reflections which may be undesirable. Currents created by the hydraulic breakwater are confined to a thin zone near the water surface, and for deep water waves the wave energy likewise is concentrated near the surface. It has been agreed generally that hydraulic breakwaters should be expected to provide their best performance in deep water; for shallow water waves, the device has been found relatively inefficient.

The actual physical mechanism by which the breakwater's opposing surface current modifies a wave still is not fully understood. If the incident wave is originally steep and if the current is strong, varying degrees of wave breaking may occur. On the other hand, waves may be damped without breaking taking place. Guidance for the predicted effectiveness of hydraulic breakwaters in deep water is given in the theoretical solution of Taylor (1955). The solution, which is based upon linear wave theory and therefore does not consider the effect of wave height, predicts the longest wave length that may be propogated against a surface current having a finite thickness and a velocity varying linearly from a maximum at the surface to zero at the bottom edge of the current.

Because Taylor's theory considers only the complete stopping of waves and therefore does not consider less than complete wave attenuation, and because previous experimental data were very limited for deep water waves, an experimental program was conducted to study the effectiveness of hydraulic breakwaters in deep water waves.

EXPERIMENTAL APPARATUS AND PROCEDURE

Wave Tank - A schematic drawing of the wave tank used is shown in Figure 1. Pertinent dimensions were: length (excluding forebay), 35 ft. 5 in.; width, 24 inches; depth, 35 inches. The effective length of tank measured from wave generator to absorber beach was 27 ft. 3 in. The tank was a laboratory flume which was converted to a wave tank for the breakwater study. Because the tank was relatively short for wave studies it was equipped with an absorber beach consisting of aluminum turnings loosely packed in wire mesh baskets, with the baskets on the sloping portion of the beach located on an impervious plane support. This type of arrangement has been discussed by Hsu (1965). The reflection coefficient of the beach was approximately 5 percent.

Generator - The flap type generator, made from 1/2-inch aluminum plate, was hinged to the bottom of the wave channel. Both the frequency and the stroke amplitude could be changed in discrete steps. For the experiments presented in this paper the water depth was maintained constant at 32 in. (2.67 ft.), and waves of only four periods were tested, each with a number of discrete wave heights (therefore, steepnesses). The properties of the waves tested are given in the following table; the measurements were made with the manifold removed from the tank.

Period, T (Sec.)	Length, L (ft.)	L/d	Height, H (ft.)	Steepness H/L
0.45	1.00	0.375	0.046	0.046
			.074	.074
			.095	.095
0.53	1.42	0.532	0.049	0.035
			.078	.055
			.100	.071
			.152	.107
0.67	2.33	0.875	0.050	0.021
			.077	.033
			.102	.044
			.146	.063
			.180	.077
0.84	3.58	1.343	0.044	0.012
			.072	.020
			.094	.026
			.139	.039
			.178	.050

Breakwater - The cylindrical manifold completely spanned the wave tank. The manifold was constructed of 1-1/4 in. O.D. plastic tubing with a 1/8-in. wall thickness, and contained 93 circular orifices of 0.04-in. diameter at 1/4-in. spacing. The breakwater discharge was supplied to the manifold by a single inlet pipe at mid-channel. The large number of discharge ports was selected in order to develop a two-dimensional current as close as possible to the manifold. For all runs reported the submergence depth y_o (Figure 2) of the manifold centerline was 0.1-ft., sufficient to have the jets discharging submerged for all waves tested; jet discharge was horizontal.

Discrete flow rates q, in terms of cfs/ft of tank width, were: 0, 0.002, 0.004, 0.005, 0.006, 0.00725. Discharges were measured with a calibrated orifice located in the recirculating loop.

Wave Height Measurements - Wave heights were measured by resistance-type wire gages, the outputs being obtained on a recording oscillograph. Accuracy of measured wave heights was $\pm$ 0.002-ft.

Because of the relative shortness of the wave tank the following procedures were adopted for wave height measurements. All waves were

measured at the gage location shown in Figure 1. As indicated above, values of the incident wave height (Figure 2) were determined with the manifold removed from the channel. For the case of the manifold in place but not discharging (q = 0), as with the determination of H, the heights of a number of waves were averaged soon after regular waves were sensed at the gage. For the transmitted waves H_t with the manifold discharging, the finite size of the tank necessitated the following procedure. The breakwater discharge was started, and then the wave generator. The average of the first three or four waves was taken immediately after recorded wave heights at the gage had reached their maximum and when the heights of successive waves were approximately the same. Tests were repeated to check for reproducibility, but all data points are presented as separate values and not as averages of a number of runs. As noted by previous investigators, the value of H_t never reached a constant value; part of this could be due to randomness associated with the interaction between incident waves and turbulent surface currents, and part to recirculation patterns resulting in the finite-sized tank. Further, for the longest wave tested the gage was less than two wave lengths behind the generator, which could put it in the area in which the waves reforming after passing the manifold still might be regaining amplitude.

Measurement of Breakwater Current Velocities - Currents were measured in the absence of waves. A 1/8-in. O.D. Prandtl tube mounted so as move longitudinally and vertically was used as the sensor. Data reported were taken on the channel centerline, but separate checks indicated the flow patterns to be satisfactorily two-dimensional. The Prandtl tube was used in conjunction with a differential pressure transducer and an X-Y plotter for recording data; the static calibration corresponded to a range of velocities from 5 to 28 in. per second. Velocity values reported were time-averaged values existing approximately 1 - 1-1/2 minutes after the breakwater current had been started in initially still water; this time coincided with that during which the values of H_t were measured in the attenuation runs.

EXPERIMENTAL RESULTS AND ANALYSIS

Breakwater Currents - Some results of the velocity measurements in the surface currents created by the breakwater manifold are given in Figures 3 - 6. These results are discussed briefly.

Figure 3, which applies for the largest manifold flow tested, illustrates the variation in velocity profile with distance from the manifold. The vertical location of the maximum velocity is seen to rise with increasing x, so that at x = 12 in. (x/D = 12/1.25 = 10) the maximum velocity occurs at the surface; this behavior, for an initially submerged jet, has been documented by Mross (1960). For x > 12 in., the velocity profiles do become quite linear.

Figure 4 incorporates data in the "fully developed" region for three discharge rates; all data have been put in non-dimensional form and compared to the normal distribution equation,

$$\frac{v}{v_{max}} = e^{-y/2S^2} \qquad (1)$$

where S is defined as the depth y below the free surface at which the velocity is equal to 0.605 v_{max}, with v_{max} occurring at the free surface. Thus, the current is seen to have a typical turbulent jet mixing profile following the relationship (Eq. 1) used by Albertson et al (1950). It is seen also that the velocity profile could indeed be closely approximated by the linear velocity distribution incorporated in the theory of Taylor.

Figure 5 illustrates, again for three discharges, the growth of the nominal current thickness h with distance. The rate of growth of h with x in the fully developed region is 1:8, which is nearly the same as that measured by Williams for a manifold discharging at (not below) the free surface and containing relatively fewer and much larger discharge ports. The 1:8 spread ratio is also consistent with values for the vertical spread of single neutrally buoyant jets reported by Jen et al (1966).

Finally, Figure 6 indicates that horizontal momentum is indeed conserved in the surface current created by the jets discharging from the manifold, at least for x - distances within which the current's effect on the incident waves was observed. Again, results are compared with those of Williams. The value of the momentum flux per foot of width in the jets leaving the manifold was calculated by:

$$M_o = q\rho\frac{q}{a_o} = \frac{q^2\rho}{a_o} \qquad (2)$$

where for the experiments described $a_o = 4.05 \times 10^{-4}$ ft^2/ft, the total area of orifices per foot of width. Because the orifice diameter was only 0.04-in., compared to the 0.125-in. wall thickness, the orifices could be treated as tubes flowing full at exit. Values of the current momentum M_c at the various stations were obtained by integration of the velocity profiles.

Momentum Correlation of Attenuation Results - The foregoing results have been reviewed as justification and background for correlating the wave attenuation data on a momentum basis. Various manifold geometries could produce the same momentum flux magnitude at the same x - distance from the manifold; consequently, initial energy and power inputs to identical surface currents created by the hydraulic breakwaters could vary. Currents created by manifolds of different geometries have been seen to be comparable and well-behaved from a momentum standpoint. The momentum of the jets leaving the manifold usually may be estimated readily.

Accordingly, the initial jet momentum M_o has been selected as one of the independent parameters. (It might be noted that Taylor implies the wave stopping ability of a surface current to be dependent upon its "flow of inertia" - i.e., momentum flux).

Lamb (1932, Section 250) has shown that surface waves of finite amplitude possess momentum which is directed parallel to the direction of wave propogation. For deep water waves in still water the following expression is given:

$$\text{Mom/wave length/unit width} = \pi\rho a^2 c \tag{3}$$

where a is the wave amplitude and c is the celerity. If Eq. 3 is multiplied by (wave length/unit time) in order to express results in terms of average momentum/unit time/unit width, the result is

$$M_w = \pi\rho a^2 c \left(\frac{c}{L}\right) = \frac{\pi\rho a^2 c^2}{L}$$

For deep water waves, where $c = \sqrt{gL/2\pi}$ substitution gives

$$M_w = \frac{\rho g a^2}{2} = \frac{\rho g H^2}{8} \tag{4}$$

where a is assumed to be one-half the wave height, H.

It is noted in passing that M_w as given in Eq. 4 is equal to the total energy density computed from small-amplitude wave theory and is twice the "radiation stress" defined by Longuet-Higgins and Stewart (1964) as the excess flow of momentum due to the presence of small amplitude waves.

Without proceeding through a formal dimensional analysis, for a given manifold configuration (i.e., size, submergence, and initial direction of discharge) the wave attenuation can be expressed as

$$\eta = \eta\left(\frac{M_o}{M_w}, \frac{H}{L}, \frac{L}{d}\right) \tag{5}$$

where: $\eta = \frac{H-H_t}{H}$, the wave attenuation

$\frac{H}{L}$ = wave steepness

$\frac{M_o}{M_w}$ = relative momenta of current and waves

$$= \frac{g^2 \rho}{\lambda \omega^4}$$

$$\frac{\rho g H^2}{8}$$

For deep water waves it might be anticipated that

$$\eta = \eta\left(\frac{M_o}{M_w}, \frac{H}{L}\right) \tag{6}$$

only, as L/d should no longer be significant. This hypothesis must be examined in light of the test data.

Typical experimental data for one particular value of L/d (here, 0.375) are shown in Figure 7. These results show the effects of variation in manifold discharge (hence, current momentum) for different amplitude waves of the same wave length. Trends in the data are different at low discharges from those at higher flows. Finite attenuation occurs at zero discharge, due to the finite-sized circular manifold submerged just below the free surface. This result differs from the potential flow solution of Dean (1948), which predicted no difference in amplitude between incident and transmitted waves at great distances on either side of a submerged circular cylinder. As noted, the wave gage was not "far" from the manifold. However, at zero discharge the greatest attenuation took place for the shorter waves which in turn would have had a relatively longer distance in terms of wave length in which to reform after passing the manifold. At zero discharge and at the lower manifold discharges there is relatively greater attenuation for the larger (steeper) waves. When the manifold was discharging, distinct reduction in wave heights occurred upstream from the manifold, so for $q>0$ the entire attenuation is credited to the action of the surface currents. Phase shifts occurred as the waves reformed on the lee side of the manifold; as previously noted, the gage may have been too close to the manifold for the longer wave lengths so at the larger L/d values tested the experimental values of η could be somewhat large. For the higher discharges, greater attenuation is obtained with the waves of smaller amplitude; wave steepness no longer appears to be as significant as wave amplitude. For a particular L/d, as typified by the data of Figure 7, no consistent trend of attenuation with respect to wave steepness is apparent.

Results for all the wave attenuation tests are given in Figure 8, in which η is plotted against the relative momenta, M', defined as

$$M' = \frac{M_o}{M_w} = \frac{8q^2}{g\, a_o H^2} \tag{7}$$

Within reasonable limits and for significant non-zero values of M', η is dependent upon wave steepness but independent of L/d. The hypothesis of Eq. 6 is justified. For a given M', the steeper the wave the greater the degree of attenuation. Or, for complete "stopping" (i.e., $\eta = 1.0$), waves of decreasing steepness require relatively greater values of momentum in the surface current.

The overlapping results for small values of both M' and η can be attributed to experimental error and to the presence of the manifold cylinder. In light of the possible sources of experimental error, the greatest validity is attributed to the data showing the larger values of η. Further, these larger attenuation values are the ones of practical interest in possible applications of the hydraulic breakwater. For these significant values of η, which also can be attributed entirely to the surface current without consideration of the size of the manifold obstruction, the dependency of η upon H/L is shown further in Figure 9.

Figure 9 is a replot of the curves of Figure 8, with consideration limited to $\eta > 0.3$. The curve for $\eta = 1.0$ is shown as a dashed line to indicate that it is an approximation obtained by extrapolation of the curves of Figure 8 to $\eta = 1.0$; these extrapolations shown on Figure 8 are used and not the test values for which $\eta = 1.0$ because runs were made at particular discrete values of q and flows were not adjusted in an attempt to find the lowest manifold discharge which produced complete wave attenuation.

As H/L approaches the 0.142 value which is the theoretical steepness at which breaking occurs for deep water waves of finite amplitude, the values of M' do indeed decrease to small values for the 0.3-1.0 range of η shown. For decreasing wave steepnesses there is a monotonic increase in M' required for the same degree of attenuation. Also, for smaller H/L values, the range of M' required to achieve the 0.3-1.0 range of η is much greater than for the steeper waves.

Comparison with Prior Theory - The results of Taylor's theory for the complete stopping of waves by an opposing surface current of finite thickness and linearly varying velocity can be summarized in terms of the critical relationship between two parameters, α_2 and Z_2, defined as

$$\alpha_2 = \frac{gT}{2\pi v_{max}} = \frac{1}{v_{max}}\sqrt{\frac{gL}{2\pi}} = \frac{c}{v_{max}} \qquad (8)$$

for deep water waves

and $$Z_2 = \frac{gh}{v_{max}^2} . \qquad (9)$$

If α_{2m} is defined as the value of α_2 for the case where deep water waves are completely stopped by the opposing current, a plot of α_{2m} vs. Z_2 as prepared from Taylor's results divides the $\alpha_{2m} - Z_2$ plane into two regions, the region below the curve where waves are completely stopped by a surface current described by Z_2 and the region above the curve where the opposing current does not stop the waves. Figure 10 shows the results of the theory.

Some experimental data for the present study are shown on Figure 10; these data were obtained for runs during which complete wave attenuation ("stopping") occurred. Results are subjective, because the criterion used for selecting the station at which the critical stopping current was present was to select by visual observation that station closest to the breakwater beyond which a particular wave would not advance. Because both Z_2 and α_{2m} were evaluated from measured current velocities in still water at the $\bar{x}$- distance so selected, the test points plotted in Figure 10 must be looked on as subjective.

The limited test data do not match the theoretical prediction. In addition, the present deep water results deviate further from Taylor's theory than do the results of Williams which are shown also on Figure 10, and the smaller the value of L/d the greater the deviation from the theory. The inference to be drawn from the values shown on Figure 10 is that the maximum wave length that can be stopped by a given current is, based on experiment, considerably shorter than predicted by Taylor's theory. However, because the theory neglects the wave height (which has been shown to be significant and is incorporated in both M' and H/L) it must be considered as an initial guide only as it predicts performance which is considerably better than the experiments indicate to be possible with hydraulic breakwaters.

CONCLUSIONS, CONSIDERATION OF POSSIBLE FIELD APPLICATIONS

The significant quantitative findings of this study are shown in Figures 8 and 9. The wave attenuation performance of hydraulic breakwaters has been correlated on the basis of the relative momenta of the breakwater's surface current and of the incident waves. Previous investigators (Straub et al, Williams) have demonstrated that the Froude scaling law may be applied to experiments on hydraulic breakwaters. Further, the results of Figure 9 can be used in initial design calculations in which the feasibility of using hydraulic breakwaters under specified wave conditions can be considered. An illustration is given below.

The example selected is based on a particular prototype situation which suggested the study; physical characteristics of the site have been detailed by Richey (1968). A floating highway bridge spanning a lake was observed to cause undesirable reflected waves, and a hydraulic breakwater attached outboard of the bridge was considered briefly as one possible method of reducing the amplitude of the waves reflected from the structure. A typical wave encountered on the 200-foot deep lake has a length of 20 feet, corresponding to a wave period of approximately 2 seconds; a wave height which could be considered a significant wave is a value of H = 2 feet, although infrequent waves of greater height do occur at the location in question. The wave steepness is H/L = 2/20 = 0.10. Two degrees of attenuation ($\eta = 1.0$, $\eta = 0.5$) will be considered. Less than complete attenuation should be considered because the decay with travel upwind of the reflected waves may reduce them to more acceptable heights. The calculations tabulated below assume nozzles of the diameters specified spaced at 1-foot centers.

From Eq. 4, for the 2-foot wave, M_w = 31.2 lb/ft for the fresh water situation. Then, using the results of Figure 9:

$$\eta = 1.0,\ M' = 2.0,\ M_o = 62.5 \text{ lb/ft}$$
$$\eta = 0.5,\ M' = 0.8,\ M_o = 25.0 \text{ lb/ft}$$

Considering the nozzles to discharge full-sized streams with no contraction, the following figures result:

η	D_o - in	a_o - ft^2/ft	q - cfs/ft	v_o - fps	HP/ft
1.0	1	0.00545	0.42	77.0	4.38
	2	.0218	0.84	38.5	2.19
	3	.0492	1.26	25.6	1.46
	4	.0872	1.68	19.2	1.10
0.5	1	.00545	0.27	48.6	1.10
	2	.0218	0.53	24.3	0.55
	3	.0492	0.80	16.2	0.37
	4	.0872	1.06	12.1	0.27

The complete attenuation requirement for the specified wave leads to large power requirements, but the η = 0.5 case gives requirements which are more reasonable. In this regard it must be noted that losses in the piping system necessary to supply the breakwater manifold have not been included.

On the other hand, the "2-second" wave considered above is much shorter than the maximum wave lengths observed at the site in question. Waves of period T = 3 seconds are not uncommon and will be considered here, again for the 2-foot wave height H. For H/L = 2/46 = 0.0435, the following are obtained from Figure 9: if η = 1.0, M' = 9.5; if η = 0.5, M' = 5.5 Assuming 4-inch nozzles at 12-inch spacing (a_o = .0872 ft^2/ft) and a wave attenuation of η = 0.5, the following values result: q = 2.77 cfs/ft, v_o = 31.8 fps, jet power = 4.94 HP/ft. The power requirement is unrealistically high. Further, it may be noted that the M' = 0.8 value which provided η = 0.5 for the 2-second wave is virtually useless and insignificant for the 3-second wave.

It has been demonstrated that counter current producing breakwaters (if it may be assumed that essentially comparable results apply for the pneumatic as well as for the hydraulic devices) follow the general trend of other breakwaters, i.e., being most effective for shorter, steeper waves. Used as a breakwater in the conventional sense, the hydraulic breakwater appears too inefficient and costly for deep water as well as for shallow water waves. However, if reflected waves which lead to cross-wave patterns which in turn may be very undesirable and can be considered a form of water pollution, then as with other types of water pollution the costs inferred from the foregoing sample calculations might be acceptable if there is sufficient demand to eliminate the "pollution." One possibility would be the installation of hydraulic breakwaters around entrances to pontoon-type marinas for which fixed wave attenuators or energy absorbers might not be feasible and where elimination of reflected waves is desired in order to increase the safety and maneuverability of small boats operating in the near vicinity; in such a situation, intermittent operation of relatively short hydraulic breakwaters might be justified.

REFERENCES

Albertson, M. L., Dai, Y. B., Jensen, R. A. and Rouse, H., "Diffusion of Submerged Jets", Transactions ASCE, Vol. 115, 1950, pp. 639-664.

Dean, W. R., "On the Reflexion of Surface Waves by a Submerged Circular Cylinder", Proceedings of the Cambridge Philosophical Society, Vol. 44, 1948, pp. 483-491.

Evans, J. T., "Pneumatic and Similar Breakwaters", Proceedings of the Royal Society, A, Vol. 231, 1955, pp. 457-466.

Hsu, E. Y., "A Wind, Water-Wave Research Facility", Tech. Report No. 57, Department of Civil Engineering, Stanford University, Oct. 1965.

Jen, Y., Wiegel, R. L. and Mobarek, I., "Surface Discharge of Horizontal Warm-Water Jet", Proceedings ASCE, Vol. 92, No. PO 2, April, 1966, pp. 1-30.

Lamb, H., "Hydrodynamics", 6th Edition, Dover Publications, New York, 1945.

Longuet-Higgins, M. S. and Stewart, R. W., "Radiation Stresses in Water Waves: a Physical Discussion, with Applications", Deep-Sea Research, Vol. 11, 1964, pp. 529-562.

Mross, J. J., "The Effect of a Free Surface Upon the Velocity Distribution of a Submerged Jet", M. S. Thesis, State University of Iowa, 1960, (unpublished)

Richey, E. P., "Upwind Travel of Reflected Waves", Proceedings of the Eleventh Conference on Coastal Engineering.

Straub, L. G., Herbich, J. B., and Bowers, C. E., "An Experimental Study of Hydraulic Breakwaters", Proceedings of the Sixth Conference on Coastal Engineering, Council on Wave Research, 1958, pp. 715-728.

Taylor, G. I., "The Action of a Surface Current Used as a Breakwater", Proceedings of the Royal Society, A, Vol. 231, 1955, pp. 466-478.

Williams, J. A., "Verification of the Froude Modeling Law for Hydraulic Breakwaters", Tech. Report No. 104-11, Institute of Engineering Research, University of California, Berkeley, Aug. 1960.

Williams, J. A. and Wiegel, R. L., "Attenuation of Wind Waves by a Hydraulic Breakwater", Proceedings of the Eighth Conference on Coastal Engineering, Council on Wave Research, 1963, pp. 500-520.

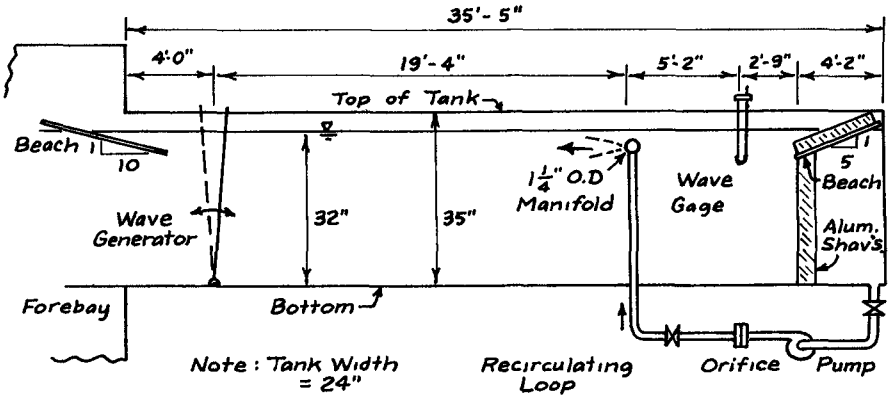

Fig. 1. Schematic Diagram of Laboratory Facility.

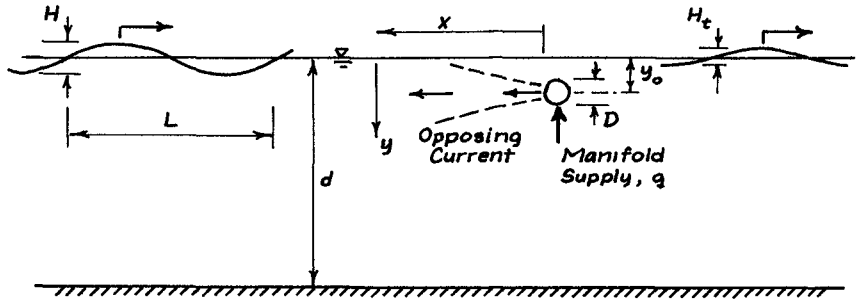

Fig. 2. Definition and Notation Sketch.

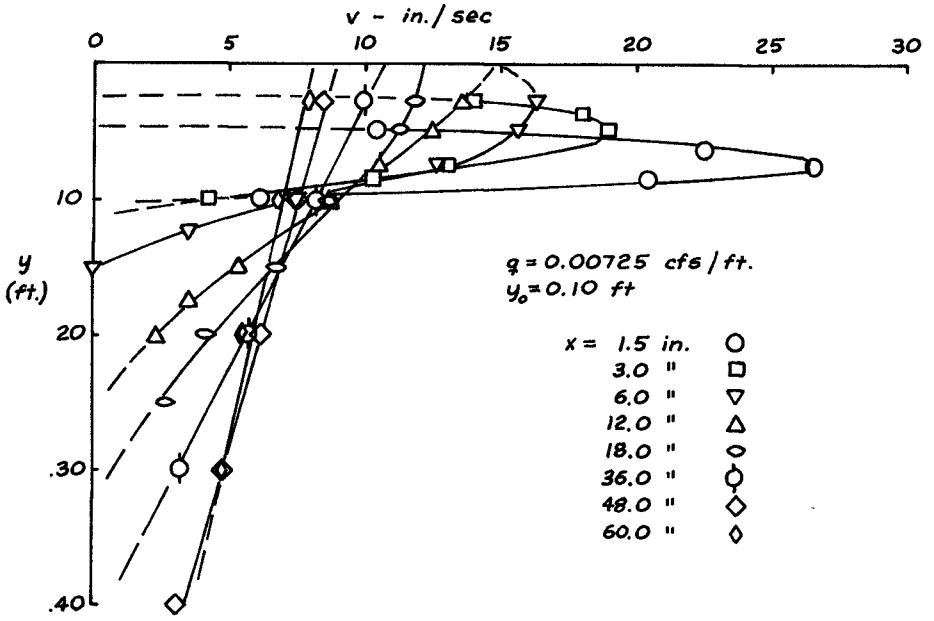

Fig. 3. Variation in Surface Current Velocity Profiles with Distance from Manifold.

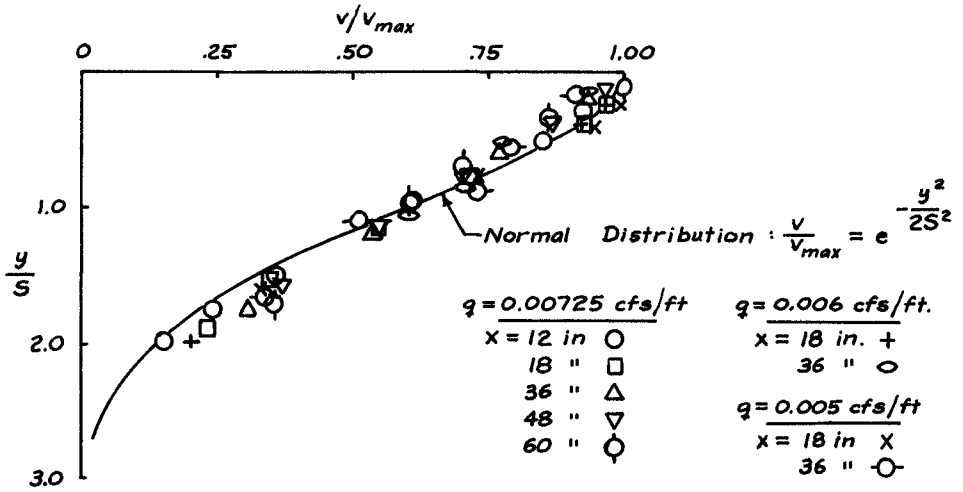

Fig. 4. Comparison of Velocity Profiles with Normal Distribution.

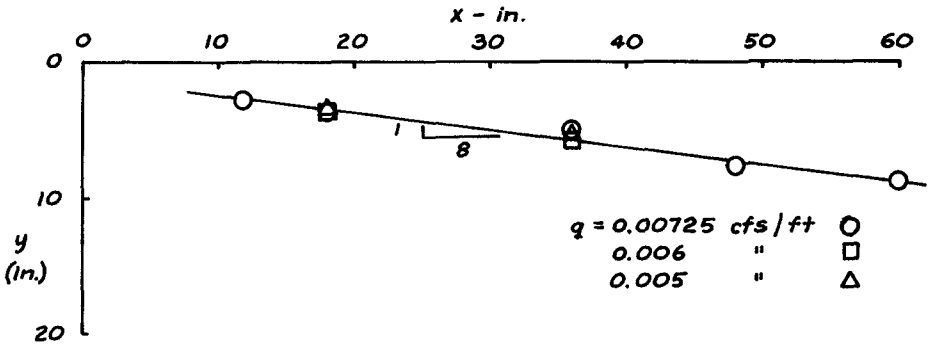

Fig. 5. Growth of Surface Current Thickness.

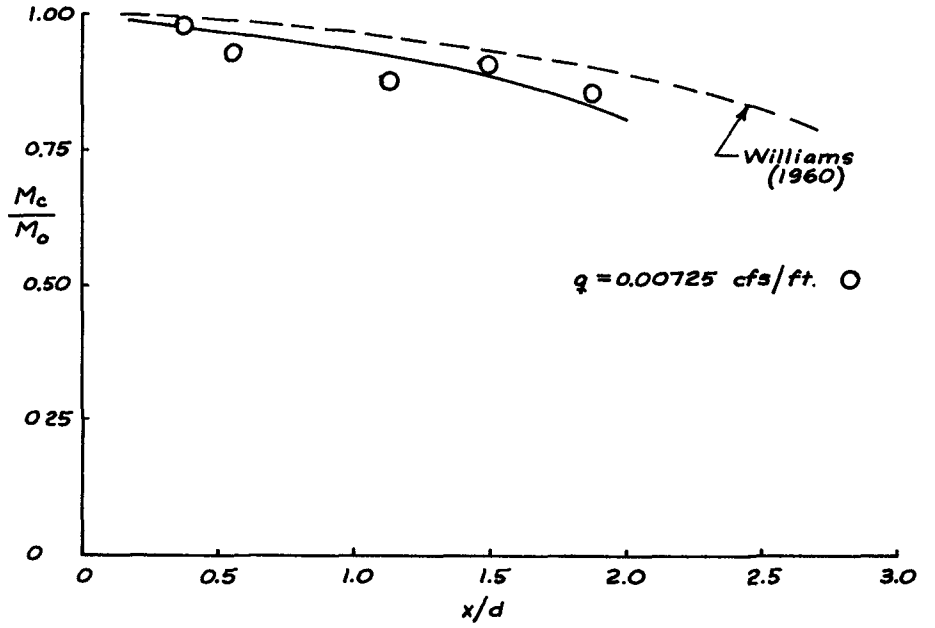

Fig. 6. Variation of Surface Current Momentum Flux with Distance from Manifold.

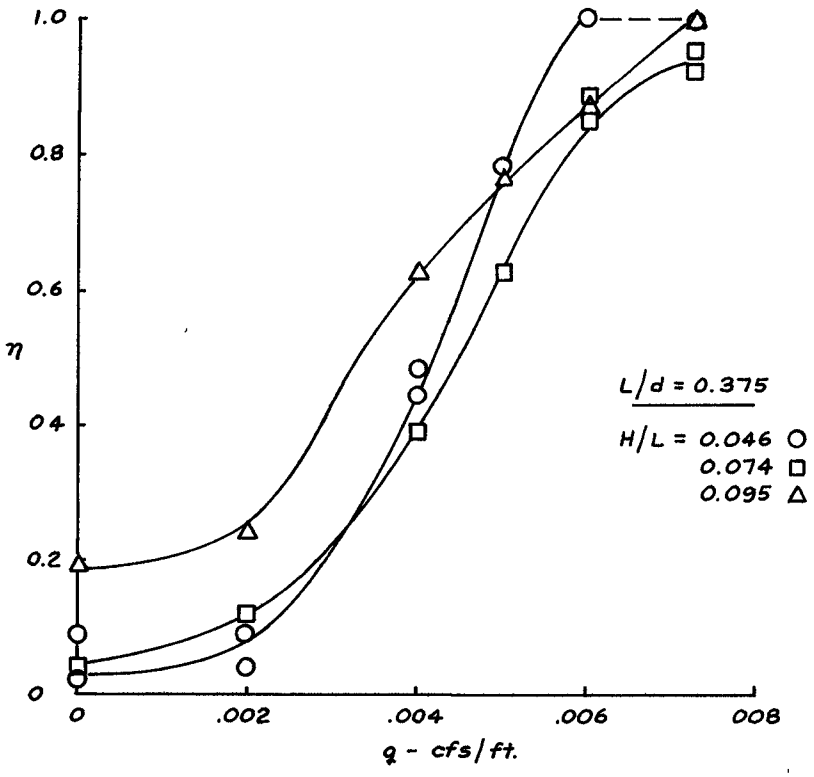

Fig. 7. Typical Wave Attenuation Data for L/d = Constant, H/L Varying.

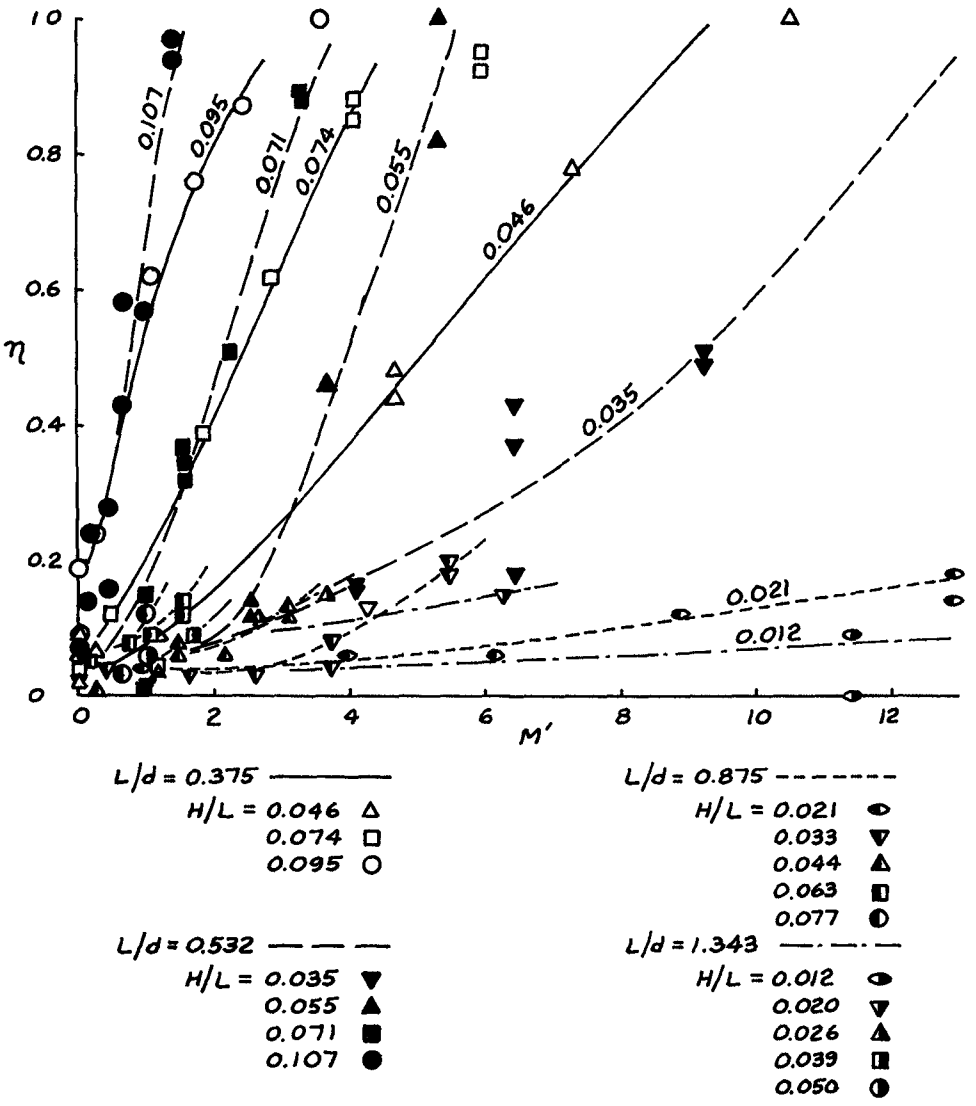

Fig. 8. Summary of Experimental Results, Wave Attenuation vs. Momentum Ratio.

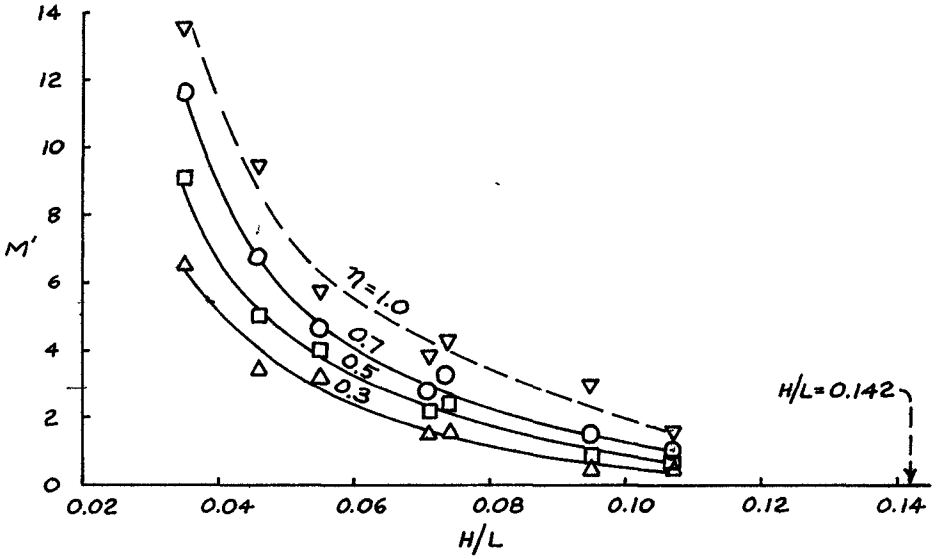

Fig. 9. Effect of Wave Steepness on Momentum Ratio Required for Specified Attenuation.

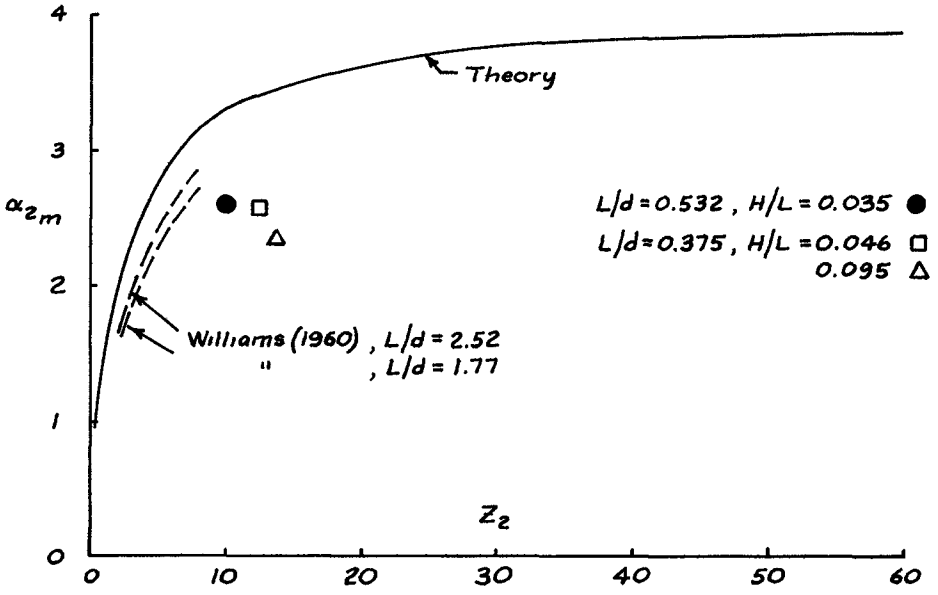

Fig. 10. Comparison with Theory of Taylor.

CHAPTER 67

A FLOATING BREAKWATER

A. J. HARRIS Senior Partner, Harris & Sutherland, London, Great Britain

N. B. WEBBER Lecturer, Civil Engineering Department, University of Southampton, Great Britain

The breakwater consists of a floating slab of breadth comparable to the length of the wave to be obstructed. Performance is improved by various arrangements of slots and mass-damping. The breakwater acts primarily by inhibiting the vertical component of orbital motion; there is a secondary action of energy dissipation by wave-breaking and eddy-making; there is also a degree of reflection. Mooring forces are small; it seems that on an exposed ocean coast, forces of the order of 0.5^{T} per ft. lin. should be catered for. The following series of tests have been carried out; the basic measurements being of wave reduction and mooring force; typical results are shown in diagrams.

1) On models of lengths 3'-4' in the Southampton University tank using wind generated waves.

2) Do. Do. Using paddle generated waves of lengths up to 8'. Series (1) and (2) comprised observations on some forty different configurations.

3) In the National Physical Laboratory tank using a model 42' x 30' overall and waves of lengths up to 35'. Bending strains and vertical displacements were measured.

4) A model has been installed in Queen Mary Reservoir, Staines of 100' x 47' overall; gale force winds are awaited which are expected to produce waves of the order of 40' l.

5) A 1/100 scale model has been installed in a harbour model at the Franzius Institute, Hanover, where the effect of the breakwater in a scaled-down natural site has been investigated.

6) Tests in development of (1) and (2) above are being carried out at the laboratories of Messrs. Taylor Woodrow Ltd. at Southall, London.

MODEL UNDER CONSTRUCTION FOR TESTING AT N.P.L.

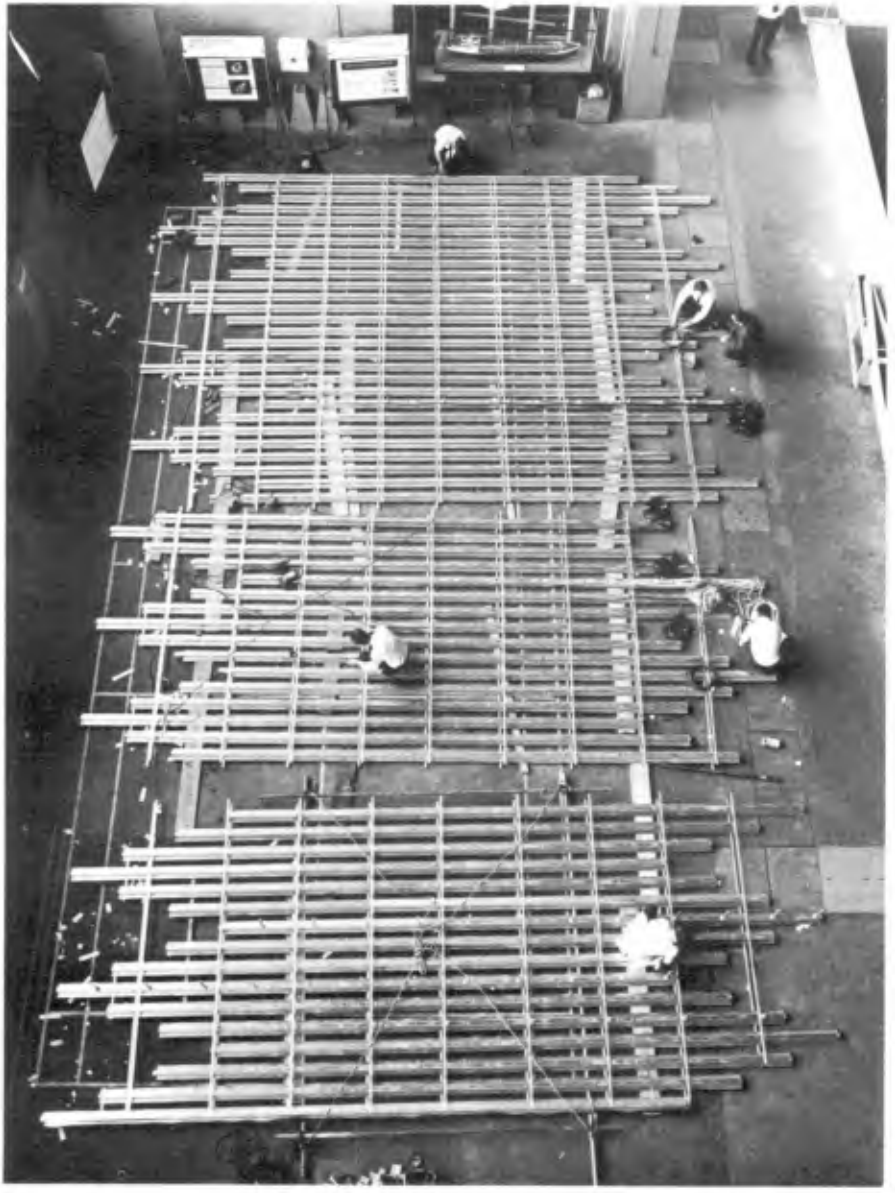

WIND GENERATED WAVE TEST AT SOUTHAMPTON UNIVERSITY

The following conclusions have been drawn.

a) Performance is most sensitive to the area of solid slab per foot length of breakwater, but is sensitive to a lesser degree to overall breadth i.e. with a given area performance is improved if it be expanded over a larger breadth. The area per foot length has in consequence been chosen as the principal parameter; moreover, this value is closely related to cost. It will be referred to as solid breadth.

b) Proportional reduction of wave height is independent of wave height.

c) Mass damping either by structural mass or by enclosed or entrained water improves performance.

d) Mooring forces are at their maximum in the range wavelength/solid breadth = 1.0 - 2.0. The upper limit of the design range is likely to fall within these values. Beyond 2.0, the forces diminish abruptly; on certain models a tendency to move to seaward has been detected. This aspect is important from the point of view of security.

e) Mooring forces are impulsive and the force at a real anchor will result from the interplay of energy of wave, location and magnitude of vertical surfaces, mass of breakwater, length and flexibility of mooring cables, etc. Cables in all tests were effectively inextensible and weightless.

f) Mooring forces are affected primarily by the sum of vertical surfaces facing the waves.

g) Performance is not affected by variation in the stiffness of the mooring system.

h) Performance is not greatly affected by stiffness of structure. A drop in proportional stiffness from 1000 (effectively inflexible) to 1 (very flexible) gave a reduction in performance of approximately 50%.

i) The indications are that bending stresses do not increase with waves longer than the solid breadth but tend rather to diminish.

j) Performance is also improved by a high value of the ratio of depth of flotation to height of freeboard.

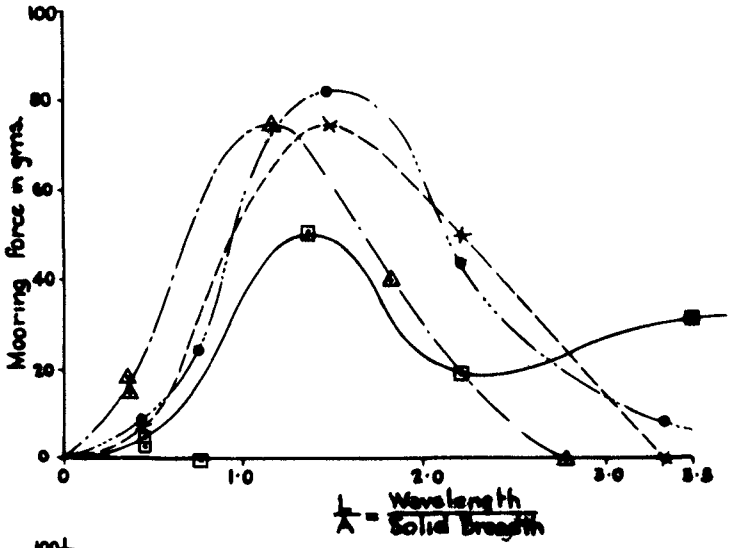

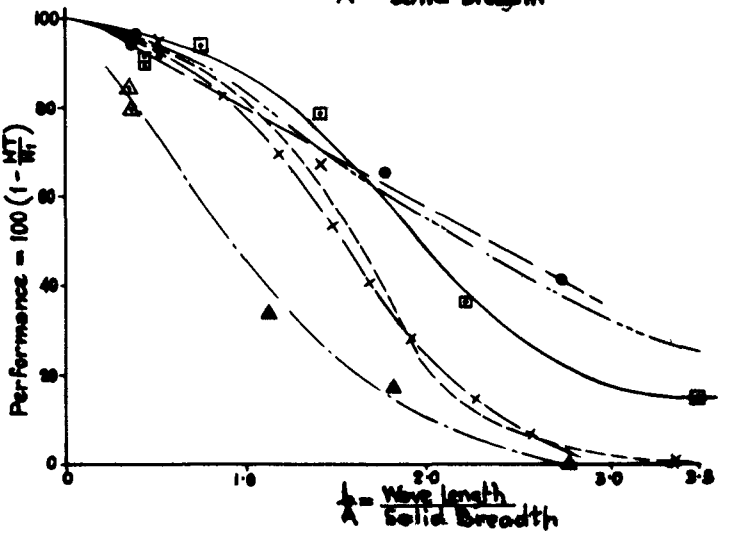

NOTATION :-

	DIMENSIONS	SOLID B
—— —— —— Solid slab, FIXED	36"ℓ x 12"b.	36"
—·—·—·— Solid slab, FREE	36"ℓ x 12"b	36"
— — — — Folded duckboard, FREE	36"ℓ, 4 No. x 2½" slats	30"
——— Closed folded duckboard, FREE	36"ℓ, 2 No. x 5" slats	30"
—··— ·· Duckboard damped at rear	36"ℓ, 4 No. x 2½" slats	30"
—+—+— Mean curve of N.P.L. results		

GRAPHS OF PERFORMANCE & MOORING FORCE

The following matters are now under investigation:

i) Closer estimate of mooring forces.

ii) Optimisation of slot shapes.

iii) Optimisation of structure for various employments e.g. temporary protection for contractor's works; incorporation in permanent harbour works; transportable protection for mineral extraction, etc.

iv) Closer examination of effect of mass damping on performance, mooring forces and structural bending.

Patent protection has been applied for.

CHAPTER 68

FLOATING BREAKWATERS

by

A. Brebner
Professor and Head, Department of Civil Engineering

and

A.O. Ofuya
Research Assistant, Department of Civil Engineering
Queen's University at Kingston, Canada.

ABSTRACT

The general objective of this investigation is to determine the wave damping characteristics of model floating breakwaters designed to reduce incident wave heights by processes of wave reflection, wave interference, forced instability of incident waves and turbulence action. Of most interest is the attempt to determine the method and the extent to which the requirement of large mass may be usefully replaced by large moment of inertia of mass in the development of floating breakwaters. Experiments are conducted in a two-dimensional wave channel. Reflection coefficients, transmission coefficients, breakwater motions and mooring forces are determined by experiments. It is found that the range of effectiveness in wave attenuation of floating breakwaters depends on several factors including breakwater design, incident wave properties, depth of water and the motion characteristics of the structures. It is remarkable that the 'A' Frame Breakwater exemplifies that the range of effectiveness of a floating breakwater can be increased by a large increase of its radius of gyration involving only a slight increase of its mass. The mooring forces are of reasonable magnitude. Experimental measurements and observations indicate that the 'A' Frame Breakwater

is stable throughout the range of model tests.

INTRODUCTION

Floating breakwaters offer numerous advantages as compared to fixed structures such as the rubble-mound and caisson breakwaters in certain engineering applications involving the provisions of temporary harbours for seasonal or transient marine activities, the development of marinas for recreational purposes, and in the protection of reclaimed lands. Marinas built in certain inland bodies of water may require breakwaters which can be installed during the summer months but are removed during the winter months due to ice formation. The important features of floating breakwaters include mobility, short erection time, freedom from silting, scour and foundation problems, and comparatively small initial and maintenance costs, especially for deep water locations. The development of floating breakwaters by investigators has been influenced by certain features including large masses and hence long natural periods of oscillation, small amplitudes of oscillations of massive structures subjected to waves of small periodicities and large damping. A summary of previous investigations on transportable breakwaters is given by Bulson (1). Results of laboratory tests on floating rigid breakwaters can be found in Marks (2), Hom-ma et al (3) and Kato et al (4).

Description of Floating Breakwaters

Fig. (1) shows the basic unit of the 'A' Frame breakwater developed by the Department of Public Works of Canada, and Figs. (2a) and (2b) show variations of the basic unit. The 'A' Frame consists

essentially of a central rigid curtain of wood, and two aluminum cylinders symmetrically located and rigidly connected to the curtain at intervals. The mass radius of gyration of the structure about a lateral axis through its centre of gravity (axis parallel to wave crest) may be varied by altering the cylinder spacing. The lower cylinders in Figs. (2a) and (2b) are 50% porous. In Fig. (2a) the upper and lower cylinders are connected by a series of chains. In Fig. (2b) the cylinders are welded. The 'A' Frame Breakwaters are shown in Plate (1). The Pontoon, Fig. (3) is a massive unit of rectangular cross-section. The Double Module breakwater shown in Fig (4) consists essentially of two massive units of Prismatic cross-sections. The depths of submergence of the Double Module and Pontoon depend on their masses. The properties of the breakwaters are shown in Tables 1 and 2.

Dimensional Considerations

The physical factors which influence the transmission coefficient, reflection coefficient and the horizontal components of the mooring forces of the 'A' Frame breakwater are considered. The analysis refers to the 'A' Frame shown in Fig. (1).

The transmission coefficient H_{t/H_i} is expressed as

$$K_t = H_{t/H_i} = f(H_i, L, L_i, h_i, h_3, d, \gamma_b, \gamma_w, \gamma_s) \quad \ldots\ldots (1a)$$

Hence $$K_t = f_1\left(\frac{H_i}{L}, \frac{L}{L_i}, \frac{h_i}{L}, \frac{d}{L}, \frac{h_3}{L}, \frac{\gamma_w}{\gamma_b}, \frac{\gamma_s}{\gamma_w}\right) \quad \ldots\ldots (1b)$$

The condition for no wave breaking over the structure is expressed as

$$h_3 > \Delta h + \left|\eta_i + \eta_r\right|_{max} \quad \ldots\ldots (2)$$

d_2/d_1	Wt. lbs.	Radius of Gyration K_2 ft.	Metacentric height GM ft.	Natural Period of Heaving T_h Secs.	Natural Period of Rolling T_r Secs,	T_h/T_r
PONTOON						
0.45	45	.475	1.023	.52	.52	1.0
.58	58	.47	0.814	0.591	0.579	1.022
0.92	92	0.468	0.556	0.744	0.696	1.068
DOUBLE MODULE						
.32	19.6	.539	1.6	.441	.472	.935
.44	27.0	.53	1.182	.518	.540	.96
.48	29.4	.528	1.073	.542	.565	.96

TABLE I Properties of Pontoon and Double Module

Half-Cylinder Spacing L_1 (ft.)	Wt. of Breakwater W_1 (lbs.)	Radius of Gyration K_2 (ft.)	Meta-centric Height $\overline{GM}$ (ft.)	Angle of Heel (degree)	Natural Period of Rolling Motion T_r (sec.)
1.17	16.4	1.01	2.92	2.5	0.655
			1.87	5.0	0.82
1.92	17.08	1.58	7.65	1.5	0.63
			5.06	3.0	0.778
1.41	16.64	1.19			
0.54	15.9	0.53			
h_1 = 1.17 ft.					

TABLE (2) Properties of the 'A' Frame Breakwater

where η_i and η_r are the instantaneous elevations of the incident and reflected waves, respectively above still water level and Δh is the rise in still water level given to first order approximation by

$$\Delta h = \frac{H_i^2}{L} \text{ Coth } Kd$$

For a given breakwater system $\frac{\gamma_w}{\gamma_b}$ and $\frac{\gamma_s}{\gamma_w}$ are constant, and if the condition expressed in Eq. (2) obtains, expression (1b) can be simplified by combining h_1/L and d/L to give

$$K_t = f_2 \left(\frac{H_1}{L}, L/L_1, \frac{h_1}{d}\right) \quad \ldots\ (3)$$

Since $\frac{T_n}{T} = f_0\left(L/L_1\right)$,

$$K_t = f_3 \left(\frac{H_1}{L}, \frac{T_n}{T}, \frac{h_1}{d}\right) \quad \ldots\ (4)$$

For deep water waves ($d \geq L/2$) and for values of $h_1 \simeq L/2$,

$$K_t = f_4 \left(\frac{H_1}{L}, \frac{L}{L_1}\right) = f_5 \left(\frac{H_1}{L}, T_n/T\right) \quad \ldots\ (5)$$

Similarly the reflection coefficient $\frac{H_r}{H_1}$ is expressed as

$$K_r = H_r/H_i = f_6 \left(\frac{H_1}{L}, \frac{L}{L}, \frac{h_1}{d}\right) \quad \ldots\ (6)$$

and may be simplified to give

$$K_r = f_7 \left(\frac{H_I}{L}, \frac{L}{L_I}\right)$$

$$= f_8 \left(\frac{H_I}{L}, \frac{T_n}{T}\right) \qquad \ldots\ldots (7)$$

The horizontal component of the mooring force is expressed as

$$F = \phi (H_I, H_r, L, L_I, h_I, d, \gamma_w, \gamma_b, \gamma_s) \qquad \ldots\ldots(8a)$$

Hence $$\frac{F.h_I}{\gamma_w H_I^2 L} = \phi_1 \left(\frac{H_I}{L}, \frac{H_r}{H_I}, \frac{L}{L_I}, \frac{\gamma_w}{\gamma_b}, \frac{\gamma_s}{\gamma_w}, \frac{h_I}{d}\right) \qquad \ldots\ldots(8b)$$

For deep water waves and for values of $h_I \simeq L/2$

$$\frac{F.h_I}{\gamma_w H_I^2 L} = \phi_2 \left(\frac{H_I}{L}, \frac{H_r}{H_I}, L/L_I\right) \qquad \ldots\ldots(9)$$

The left hand term of expression (9) is termed the mooring force function and its denominator is proportional to the wave energy per unit width per wave length of the incident waves. The wave energy dissipated $\left(\frac{H_d}{H_I}\right)^2$ by wave breaking and other sources may be obtained from the equation of conservation of energy,

$$\left(\frac{H_d}{H_I}\right)^2 = 1 - \left(\frac{H_t}{H_I}\right)^2 - \left(\frac{H_r}{H_I}\right)^2$$

$$= f_9 \left(\frac{H_I}{L}, L/L_I, \frac{h_I}{d}\right) \qquad \ldots\ldots(10)$$

Experiments

The experiments were performed in a two-dimensional wave channel 100 ft. long x 2 ft. wide x 4' deep. Near one end of the channel is located a hinged type wave maker with suitable adjustments for varying its pitch. An efficient, mildly sloping, low reflection beach is located

at the end of the channel distant from the wave maker. A filter located about 15 ft. from the wave generator is required to smooth the waves by reducing the irregularities which may arise due to the motion of the wave paddle. The available space for experiment is about 65 ft. between the filter and the beach.

Two wave probes containing the active electrical elements through which the wave profiles are measured are mounted on carriages, one of which can roll along two rails fixed on the top of the channel. Outputs from the electrode system are fed through a bridge circuit into a Sanborn D.C. Amplifier Recorder where the wave profiles are recorded.

The mooring cable of the breakwater is a 1/16 inch diameter steel cable which passes under a fixed frictionless pulley and is attached to a calibrated linear compression spring connected to a rack which can actuate a spur gear controlling the slider of the potentiometer in a bridge circuit. The motion of the breakwater causes a displacement of the slider from its null position and the resulting voltage changes are recorded by a Sanborn Recorder. A schematic representation of the experimental set up is shown in Fig. (5). Plate (2) shows the force meter and Plate (3) shows a sample record of the transmitted waves and mooring forces.

Procedure

The wave length of the incident waves was computed from the relationship

$$L = \frac{gT^2}{2\pi} \tanh kd \qquad \ldots\ (11)$$

The metacentric height ($\overline{GM}$) of the 'A' Frame breakwater was determined by experiment in still water. The natural period of rolling is obtained from the expression

$$T_n = \frac{2\pi K_2}{\sqrt{g\,(\overline{GM})}} \qquad \ldots\ (12)$$

where T_n = natural period of rolling in still water

K_2 = radius of gyration of breakwater

g = acceleration due to gravity

The incident and reflected wave heights were obtained from the measured wave height envelop of the wave form seaward of the breakwater.

That is,

$$H_I = \frac{\left|\eta_I + \eta_r\right|_{max} + \left|\eta_I + \eta_r\right|_{min}}{2}$$

$$H_T = \frac{\left|\eta_I + \eta_r\right|_{max} - \left|\eta_I + \eta_r\right|_{min}}{2} \qquad \ldots\ (13)$$

Due to wave breaking, the incident wave heights given by expression (13) sometimes differed from those obtained by measurement without the breakwater in the wave channel. The latter values were used in the evaluation of the reflection and transmission coefficients and mooring forces.

Scales

The model waves and breakwaters were designed in accordance with Froude's principle. The scales were. 'A' Frame, 1:11; Double Module, 1:12; and Pontoon, 1·14. The breakwaters were 23½ inches wide.

RESULTS AND DISCUSSION

Double Module and Pontoon

Both breakwaters depend mainly on the criterion of large mass for their effectiveness. The double module possesses the additional feature of large radius of gyration for a given mass as compared to the pontoon. The wave damping characteristics of the module and pontoon are shown in Figs. (6) and (7) respectively. Harmonic components in the response characteristics and interference effects seem to increase the wave energy transmission at certain frequencies. These breakwaters may be useful in practical applications where breakwaters may also serve as floating piers.

'A' Frame Breakwater

Effect of Wave Steepness

Fig. (8) and (9) show the effects of wave steepness on transmission coefficients as a function of the ratio of wave length to cylinder spacing, L/L_1. Fig. (10) and (11) concern the reflection coefficients. A simple relationship does not seem to relate either K_t or K_r and L/L_1, as a function H_1/L. But generally steep waves appear to experience greater attenuation than those of smaller steepnesses. Figs. (9) and (11) show the influence of frequency, as expressed in L/L_1, on K_t and K_r.

Depths of Vertical Curtain

The 'A' Frame breakwaters in this series have equal masses and approximately equal radii of gyration. Fig. (12) shows that the

effect of the depths of the vertical curtain is slight for deep water waves, provided $\frac{h_1}{d}$ is about 0.25. The influence of depths would be significant for shallow water waves.

Effect of Moment of Inertia

Fig.(13) and (14) show plots of K_t against $L/_d$ for various values of $L_{l/_d}$ and for two different depths of water. The ratio $L_{l/_d}$, kept constant for each of the curves, specifies the spacing of the cylinders and the radius of gyration of the structure as shown in Table 2. The similarity of trends of the behaviour of the 'A' Frame breakwater for different depths of water is evident. Minimum K_t seems to exist at certain values of $L/_d$ and increases with increasing values of $L_{l/_d}$. If a value of K_t = 50% is arbitrarily defined as cut-off of wave transmission, the range of effectiveness of the 'A' Frame is increased by a factor of about 1.7 for a threefold increase of the radius of gyration. It is of interest that the masses of the breakwaters differ by only about 7%.

Fig. (15) shows the wave attenuation characteristics of the "4" Cylinder 'A' Frames. Better efficiency is achieved by the welded cylinders. Wave generation by the lower cylinders of the chain-connected unit impairs its performance.

Energy Balance

Fig. (16) shows an energy blance curve, Eq. (10). The figure shows the importance of energy dissipation through the various sources including wave breaking and damping as compared to the

reflected wave energy.

Mooring Forces

Figs. (17), (18) and (19) show plots of $\frac{Fh_1}{\gamma_w H_1^2 L}$ against L/L_1 for different 'A' Frame breakwaters. The influence of water depth on peak mooring forces is shown in Figs (19). Fig (20) concerns the forces involved in mooring the double module. A typical frequency distribution of the mooring forces of an 'A' Frame breakwater is shown in Fig.(21). From a design standpoint, the peak forces are of most interest, but the average horizontal force component, which refers here to the mode of a force record of at least seventy cycles of loading, is important from considerations of the fatigue characteristics of the mooring rope.The plots of Figs.(17) to (20) show definite trends.The scatter in the results may be partly attributed to the influence of wave steepness, relative depth of water and the response characteristics of the moored breakwaters to the wave forces.

Effect of Elasticity of Mooring Line

Table (3) shows the effect of the elasticity of the mooring line on both the coefficient of transmission and the mooring forces. Springs of different spring constants were incorporated in the mooring lines as shown in columns (4) and (5). Larger mooring forces are obtained in the system with a stiffer spring. The transmission coefficients vary only slightly except in the welded 'A' Frame, probably caused by wave generation and interference effects on the harbour side of the breakwater.

TABLE (3) Effect of Elasticity of Mooring Cable on Mooring Forces

'A' FRAME $L_1 \simeq 1.17'$									
(1) Wave length L (ft.)	(2) Wave Height H_1 (ft.)	(3) L/L_1	(4) F_1 (lbs.) K_1=21.5lbs /in.	(5) F_2(lbs.) K_3=57lbs /in.	(6) $(K_t)_1$	(7) $(K_t)_2$	(8) $\frac{F_2}{F_1}$	(9) $\frac{(K_t)_2}{(K_t)_1}$	(10) $\frac{F_1' h_1}{\gamma H_1^2 L}$
6.5	.39	5.55	10.4	11.6	.77	.77	1.08	1	0.093
6 5	.43	5.55	11.7	14.9	.77	77	1.27	1	0.0855
6.5	.54	5.55	14.3	17.0	.71	.73	1.19	1.03	0.067
5.1	.40	4.36	10.40	13.2	57	.625	1.27	1.1	0.113
'4' CYLINDER WELDED 'A' FRAME L_1 = 1.41'									
6.5	.40	4.6	13	14.4	.58	.68	1.11	1.17	0.106
5.1	.38	3.62	11	12.1	.41	.475	1.1	1.16	0.127

LEGEND

$(K_t)_1$ = Transmission Coefficient, Mooring Condition, Column (4)

$(K_t)_2$ = Transmission Coefficient Mooring Condition, Column (5)

F_1, F_2 = Total force on mooring cable

F_1' = Horizontal force on cable per ft. width of breakwater.

Observations and Measurements of Motions: 'A' Frame

The effects of resonance were neither apparent from the force records, measurements of motions nor from observations of the motions of the 'A' Frame breakwater.

Fig. (22) shows a plot of the maximum displacement, X_{m/H_I}, in sway motion against the maximum displacement in heave motion, F_{m/H_I}, of the centre of mass of the 'A' Frame. The trends of the relationship between X_{m/H_I} and F_{m/H_I} depends on L/L_I but no simple description is evident.

For short incident waves regular pulsating motions of the breakwater were observed The breakwater would oscillate for a short time, then halt and again commence its oscillations. The angles of heel and the mooring forces during these oscillations were small. Since the metacentric height is found to depend on the angle of heel, it seems difficult to define a unique natural period of oscillation. The influence of added mass, added moment of inertia and damping increases the complexity of the problem.

Conclusions

1. The damping of water waves by the Double Module and Pontoon Breakwaters depends largely on the criteria of large mass. They may be useful in situations where transportable breakwaters may be required to serve as floating piers.

2. The 'A' Frame breakwater exemplifies that an effective floating breakwater system can be developed in which large moment of inertia of mass is the dominant factor rather than the mass.

The reduction of wave heights is effected through the processes of wave reflection, dissipation and wave interference.

3. The reflection and transmission coefficient of the breakwater system are influenced by incident wave steepness, but no simple relationships are apparent.

4. For deep water waves the effect of the depth of the vertical curtain on transmission coefficient is small provided h_1/d is about 0.25.

5. A definite trend is indicated by the plot of the horizontal force function $\frac{F.h_1}{\gamma_w H_1^2 L}$ against L/L_1. The scatter in the result may be due partly to the influence of reflection coefficient, wave steepness and the response characteristics of the breakwater.

6. The peak forces are about 1.5 to 2 times the average forces.

NOMENCLATURE

d	Depth of water
F	Horizontal component of mooring force per foot width of breakwater
h_1	Draft of 'A' Frame Breakwater
h_3	Height of vertical curtain above still water level
H_I	Incident wave height
H_d	Dissipate wave height
H_t	Transmitted wave height
H_r	Reflected wave height
K	Wave number, $\frac{2\pi}{L}$
K_1, K_3	Spring constants
K_2	Radius of gyration
K_r	Reflection coefficient
K_t	Transmission coefficient
L	Wave length
L_1	Distance of cylinder from vertical curtain
L_2	Distance between cylinder centres
T	Period of incident waves
T_n	Natural period of oscillation of breakwater
X_m	Maximum displacement in sway-motion
Z_m	Maximum displacement in heaving motion

γ_b Unit weight of breakwater

γ_s Submerged unit of weight structure

γ_w Unit weight of water

REFERENCES

(1) Bulson, P.S., *"Transportable Breakwaters"*, Dock and Harbour Authority, Vol. 48, No. 560, June 1967, pp 41-46

(2) Marks, Wilbur, *"A Perforated Mobile Breakwater for Fixed and Floating Application"*, Proceedings of the Tenth Conference on Coastal Engineering, Vol. 2, Japan, 1966, pp. 1079-1129

(3) Hom-ma, M., Horikawa, K and Mochizuki, H, *"An Experimental Study on Floating Breakwater"*, Coastal Engineering in Japan, Vol. 7, 1964 pp 85 - 94

(4) Kato, J., Hagino, S. and Uekita, Y., *"Damping Effect of Floating Breakwater to which Anti-Rolling System is Applied"*, Proceedings of the Tenth Conference on Coastal Engineering, Vol. 2, Japan, Sept. 1966, pp 1068 - 1078

PLATE (1)

'A' FRAME BREAKWATER

PLATE (2)

MOORING FORCE METER

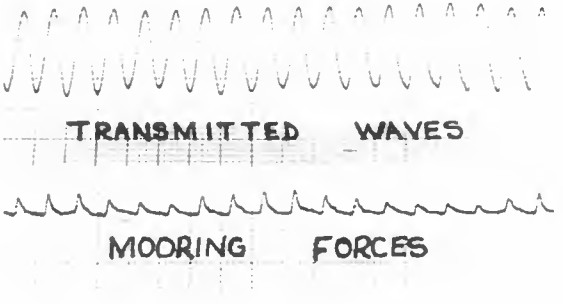

PLATE (3)

SAMPLE RECORD

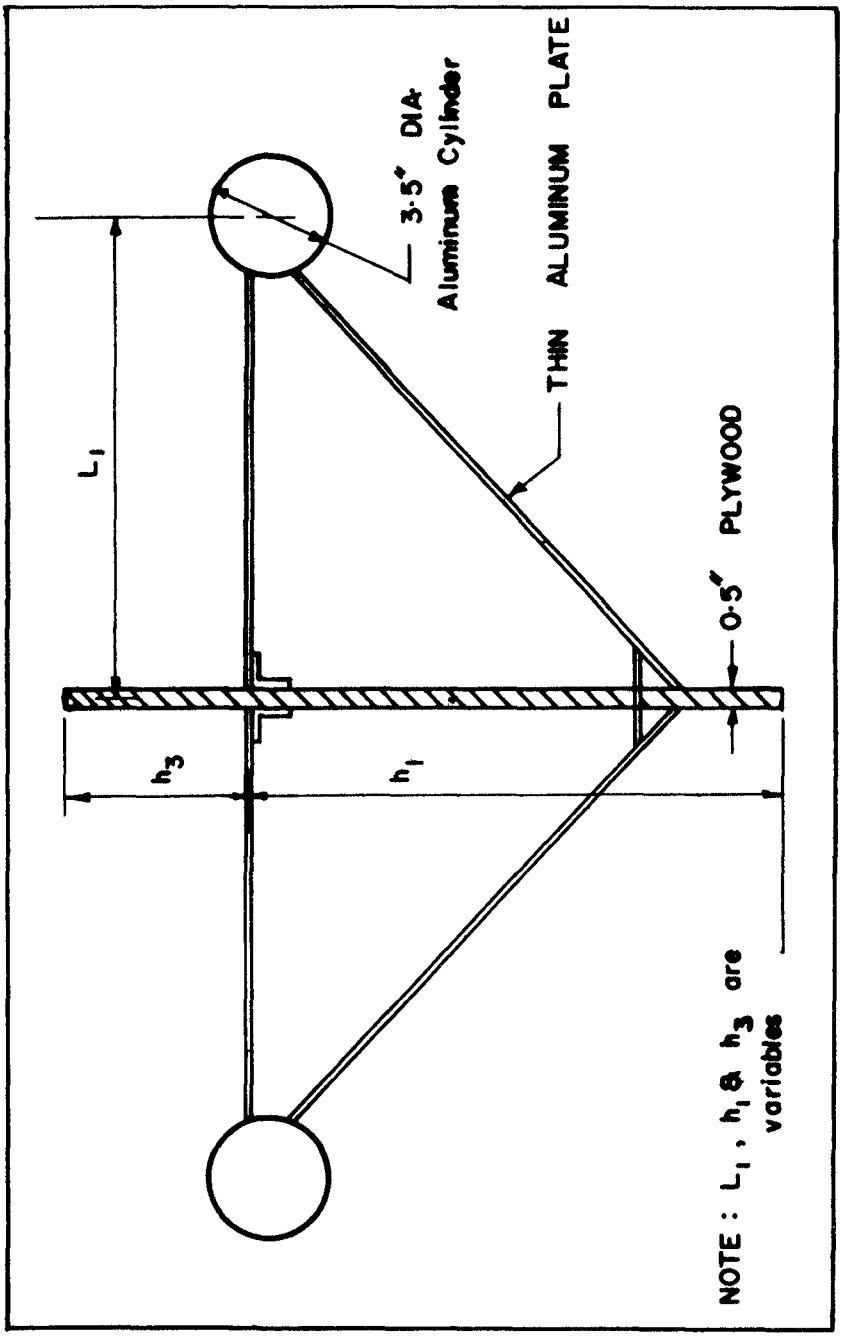

FIG·(1) 'A' FRAME BREAKWATER

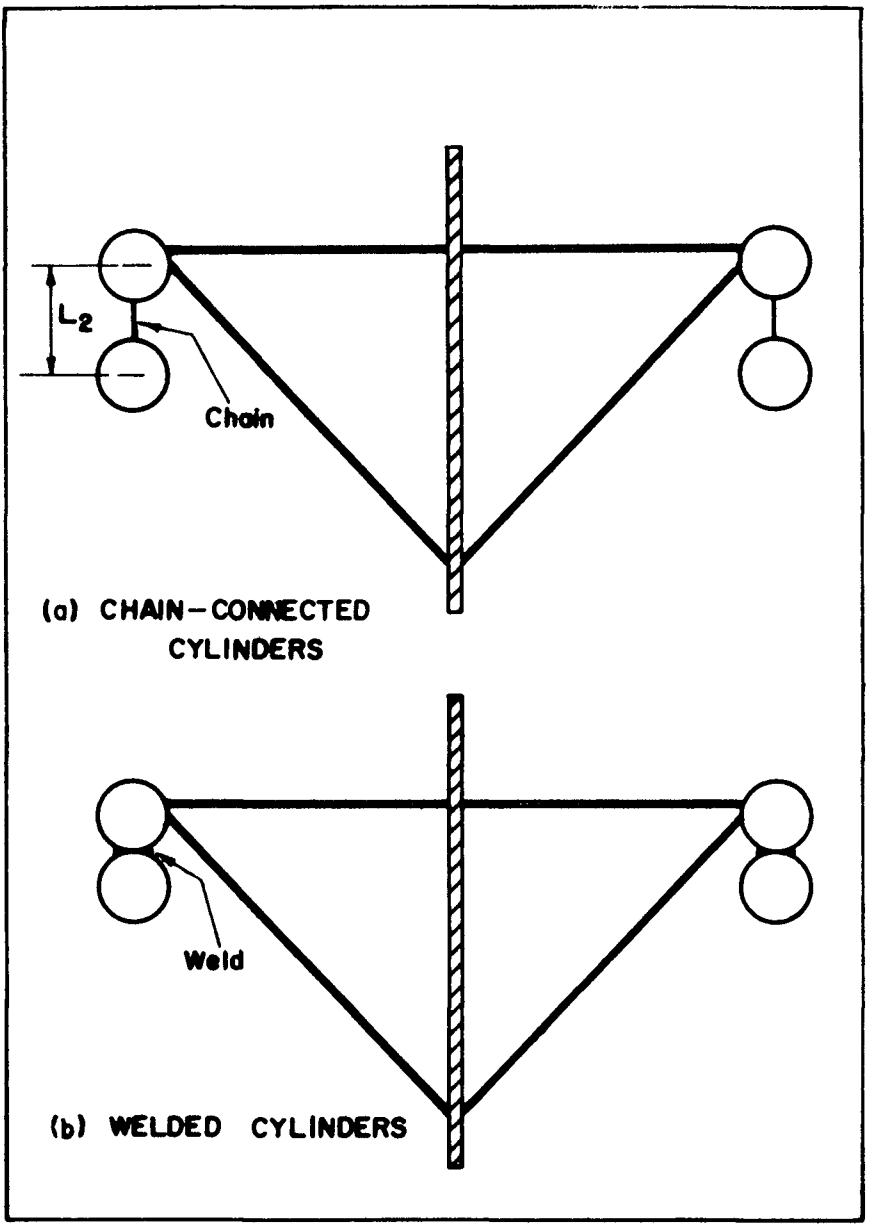

FIG(2) "'4' CYLINDER 'A' FRAME"

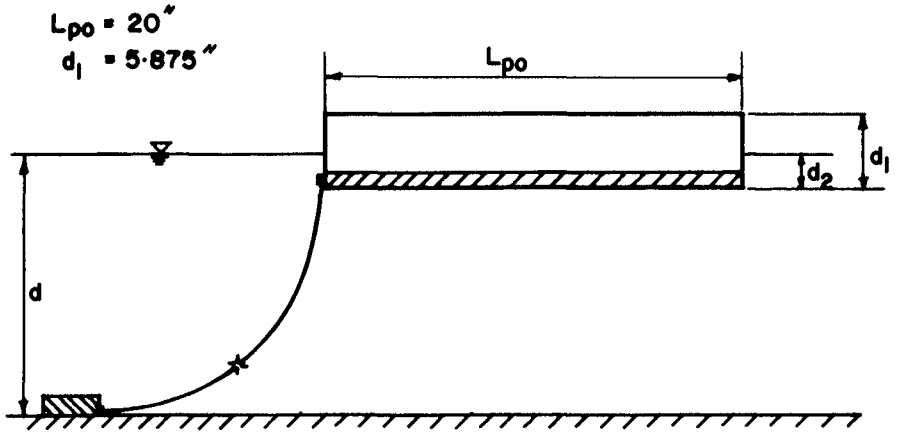

FIG·(3) PONTOON BREAKWATER

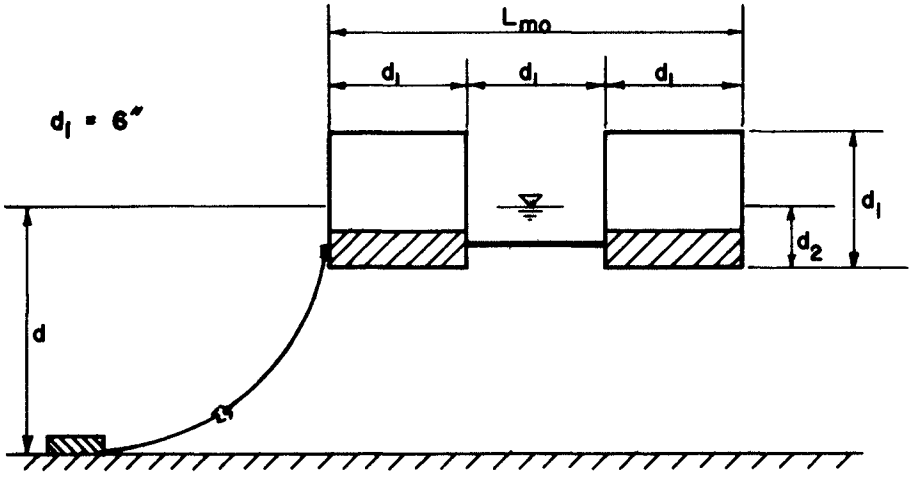

FIG·(4) DOUBLE MODULE BREAKWATER

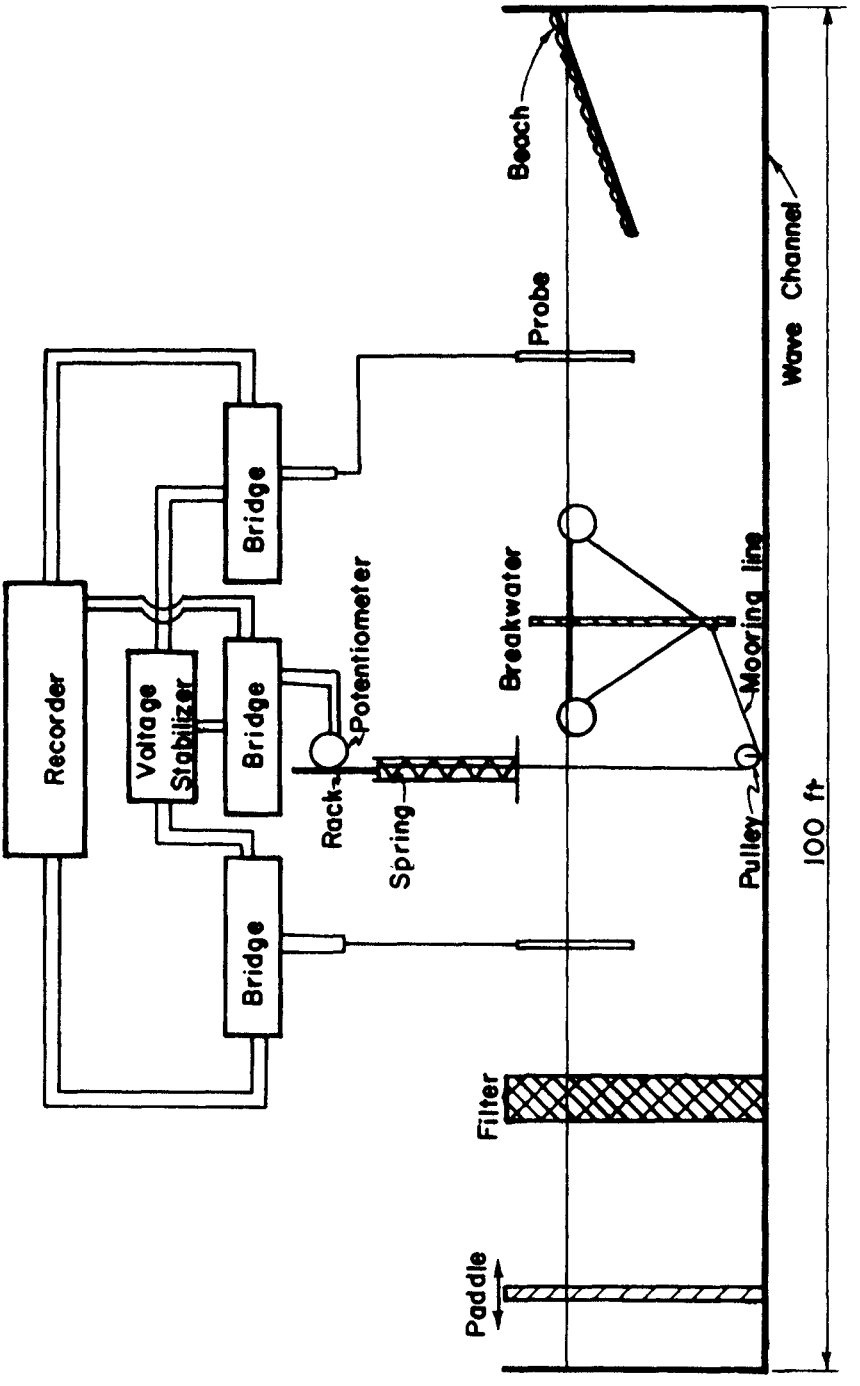

FIG(5) FUNCTIONAL ARRANGEMENT OF EQUIPMENT

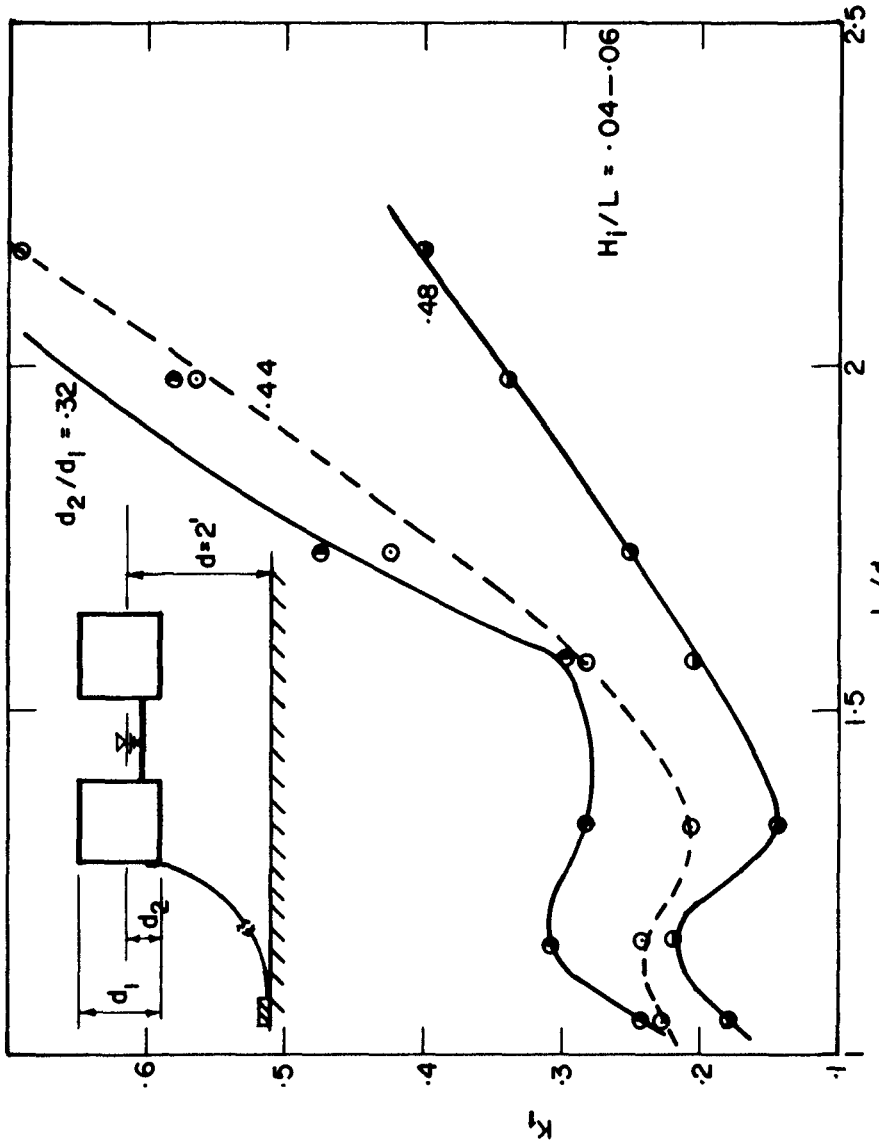

FIG(6) DOUBLE MODULE : WAVE DAMPING CHARACTERISTICS

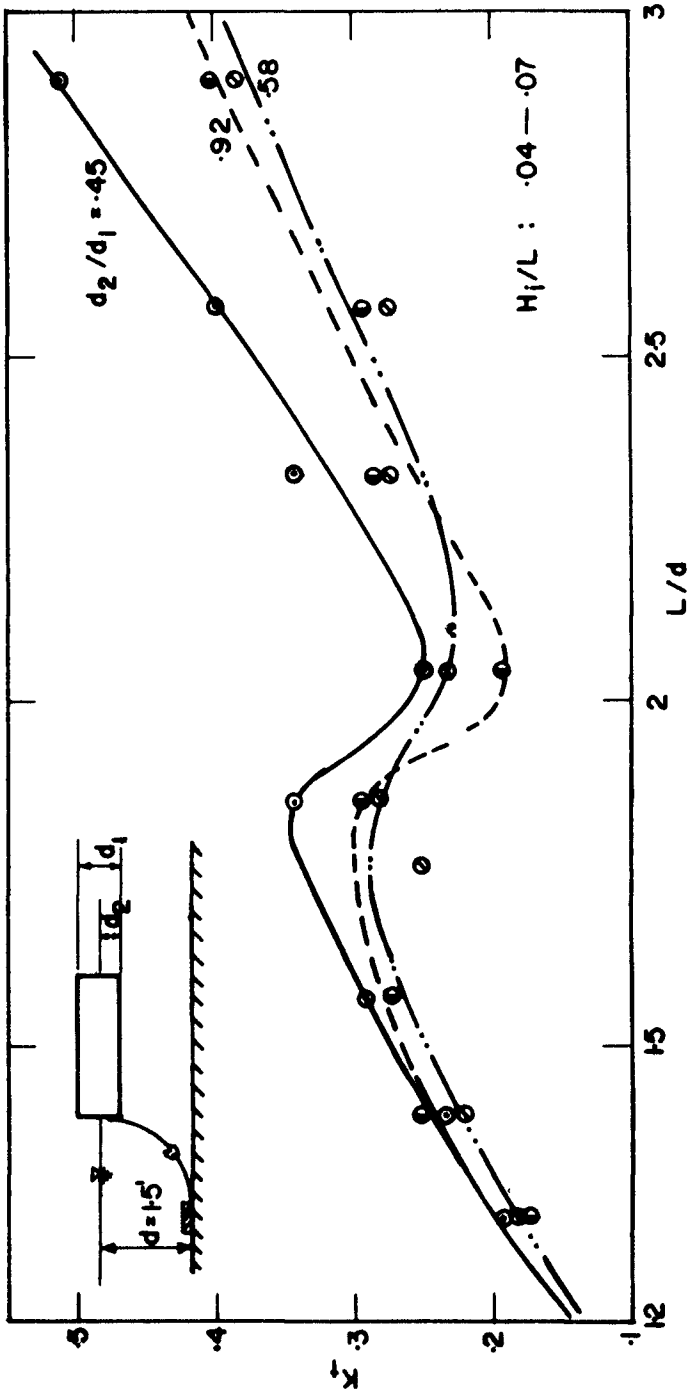

FIG·(7) PONTOON BREAKWATER : WAVE DAMPING CHARACTERISTICS

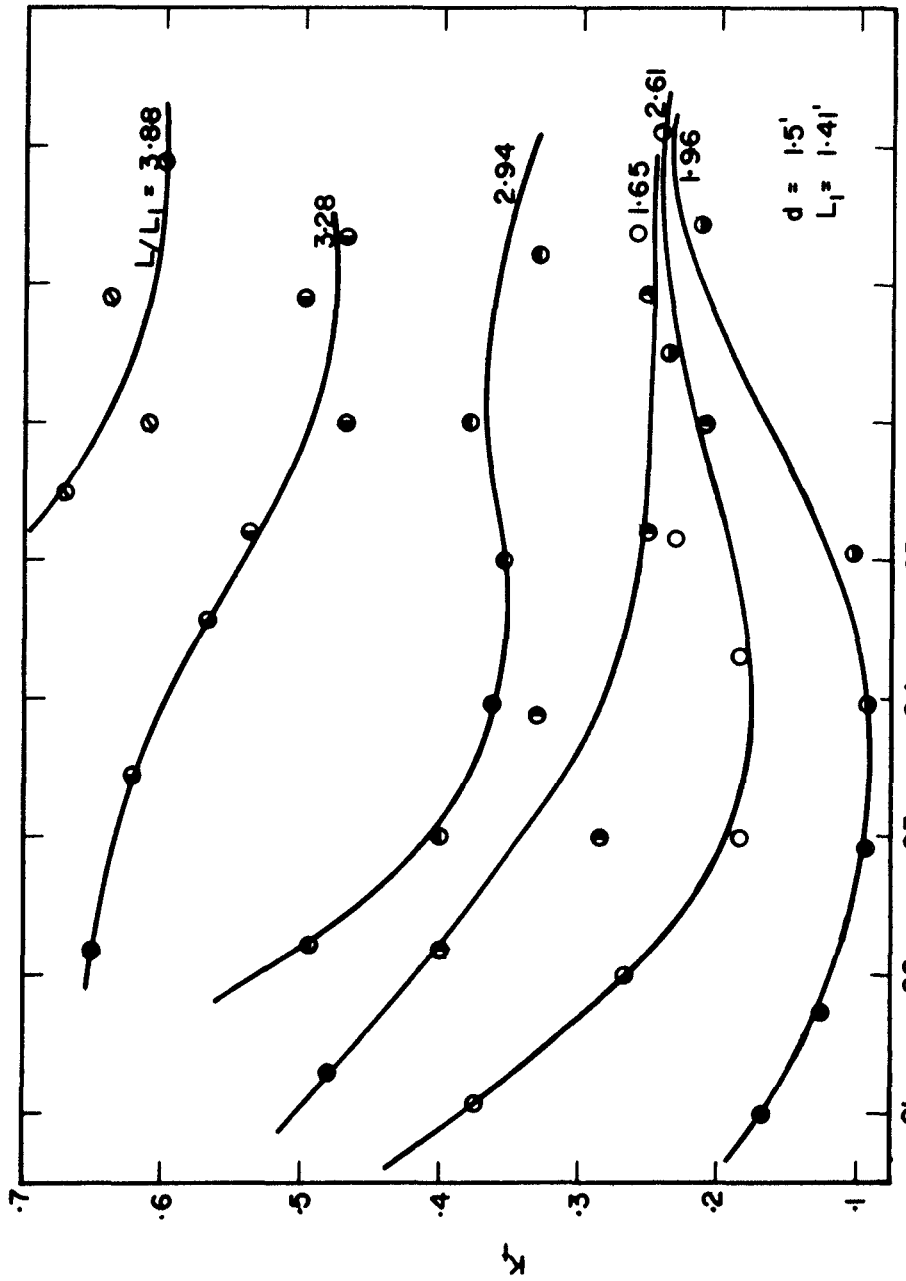

FIG(8) 'A' FRAME BREAKWATER : EFFECT OF WAVE STEEPNESS

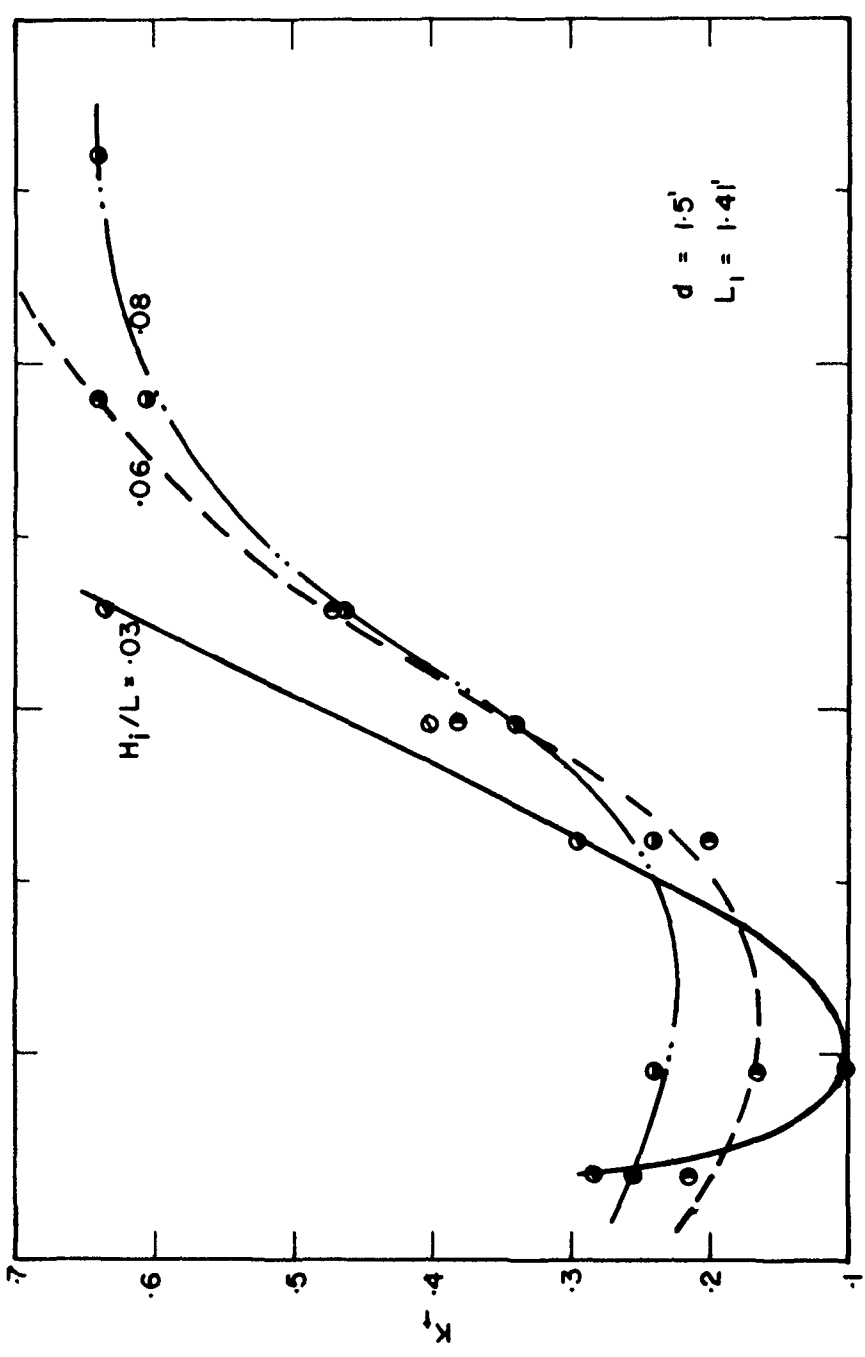

FIG(9) 'A' FRAME : INFLUENCE OF FREQUENCY

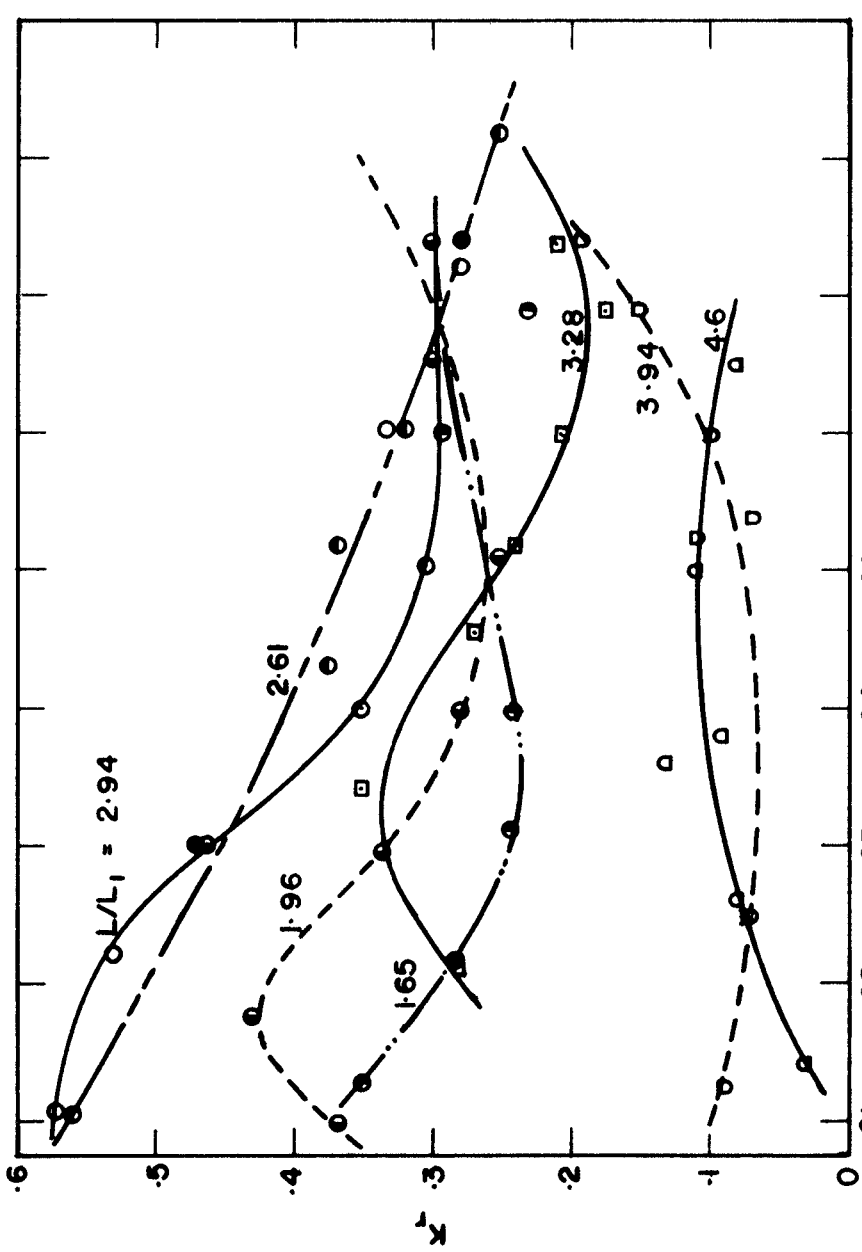

FIG-(10) REFLECTION COEFFICIENT : EFFECT OF WAVE STEEPNESS

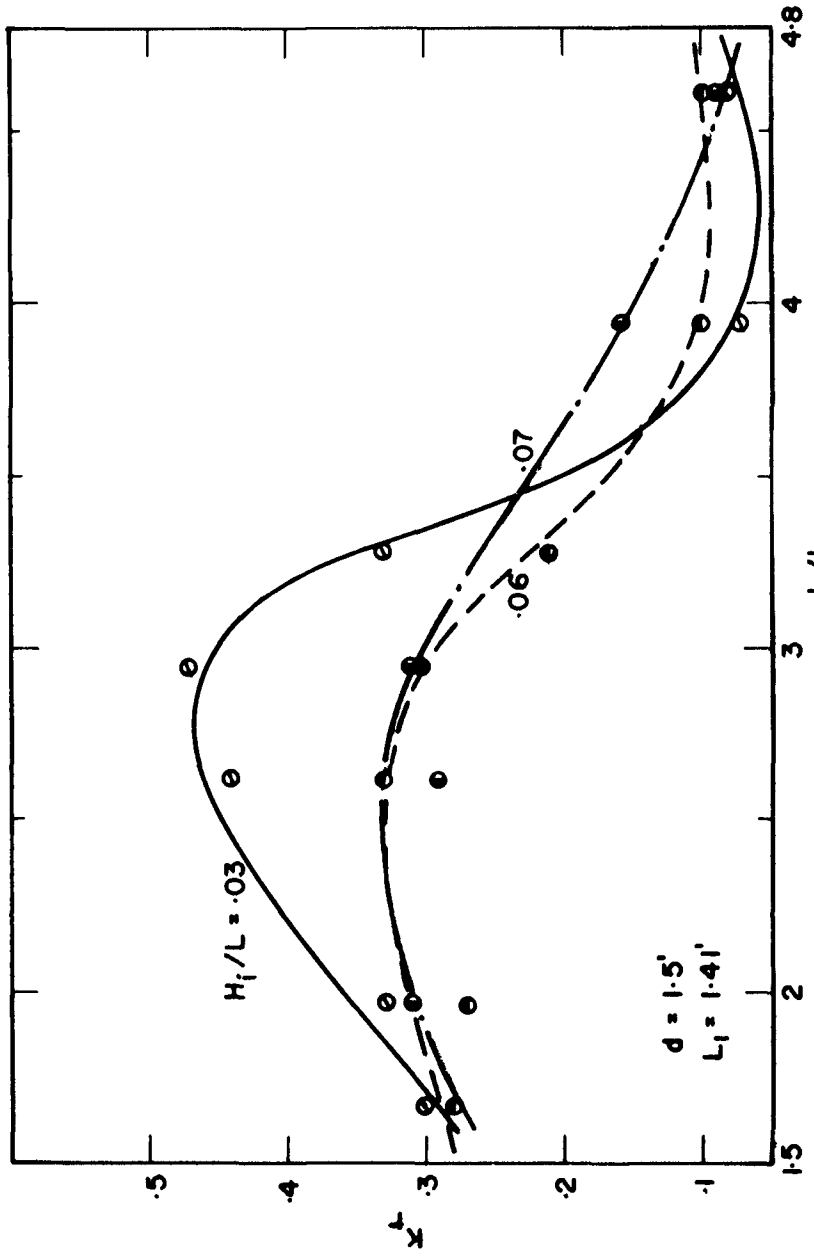

FIG(11) REFLECTION COEFFICIENT : EFFECT OF FREQUENCY

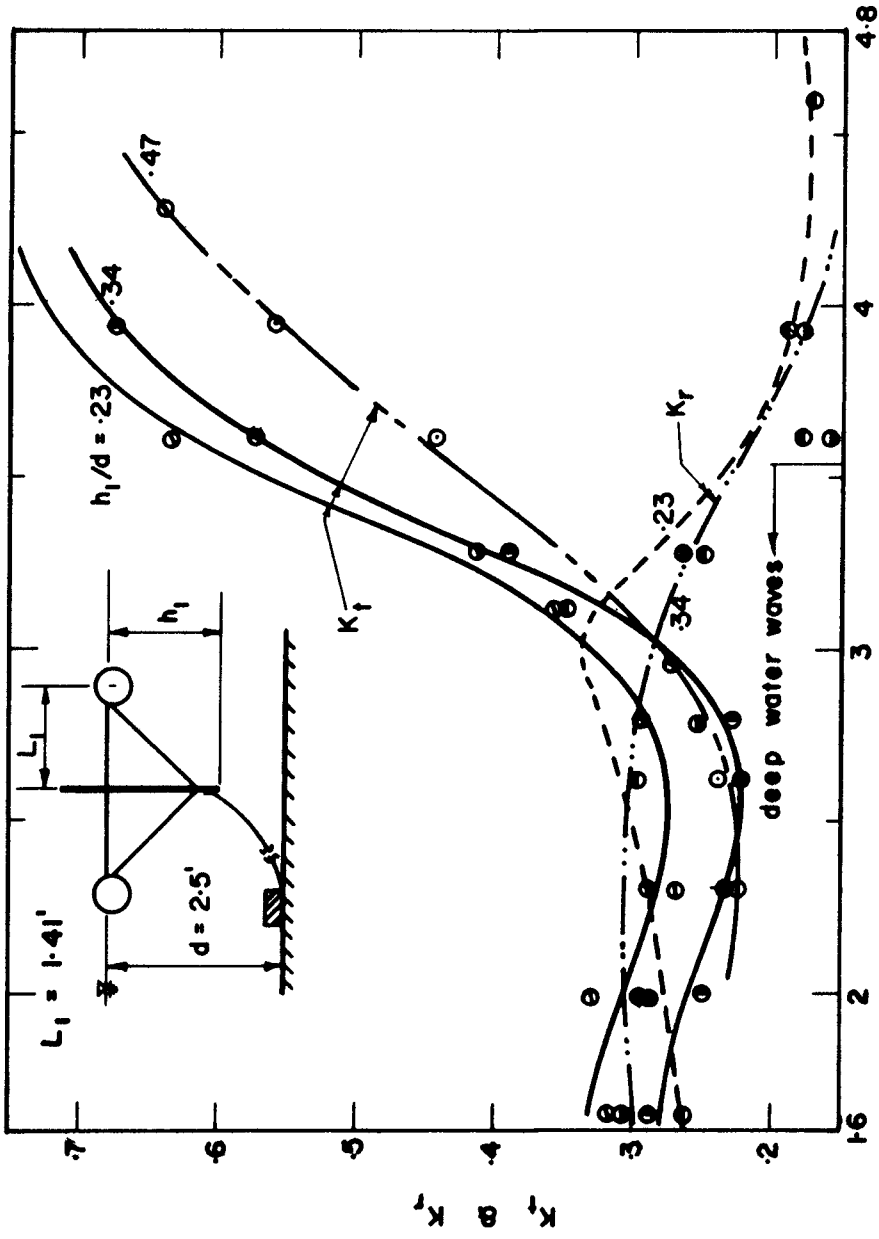

FIG.(12) EFFECT OF DEPTH OF VERTICAL CURTAIN

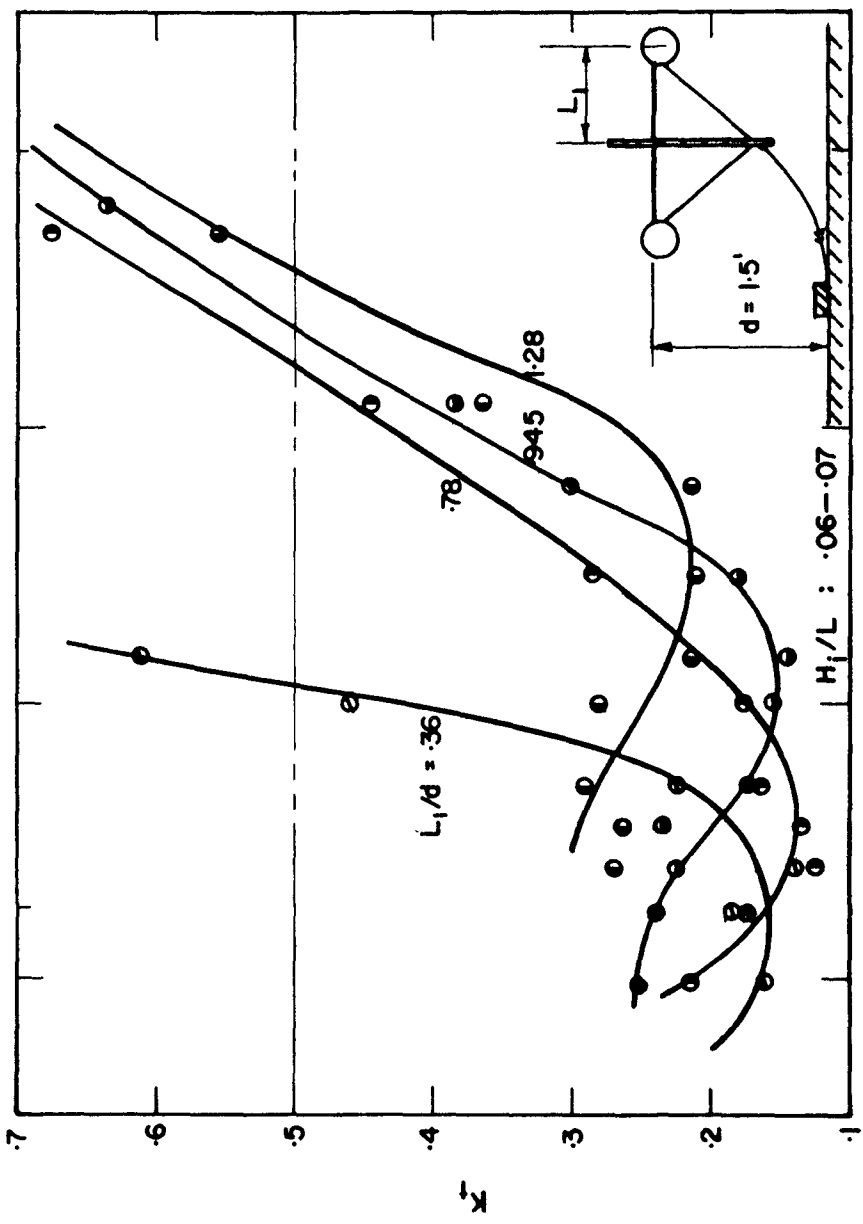

FIG(13) EFFECT OF MOMENT OF INERTIA (d = 1·5')

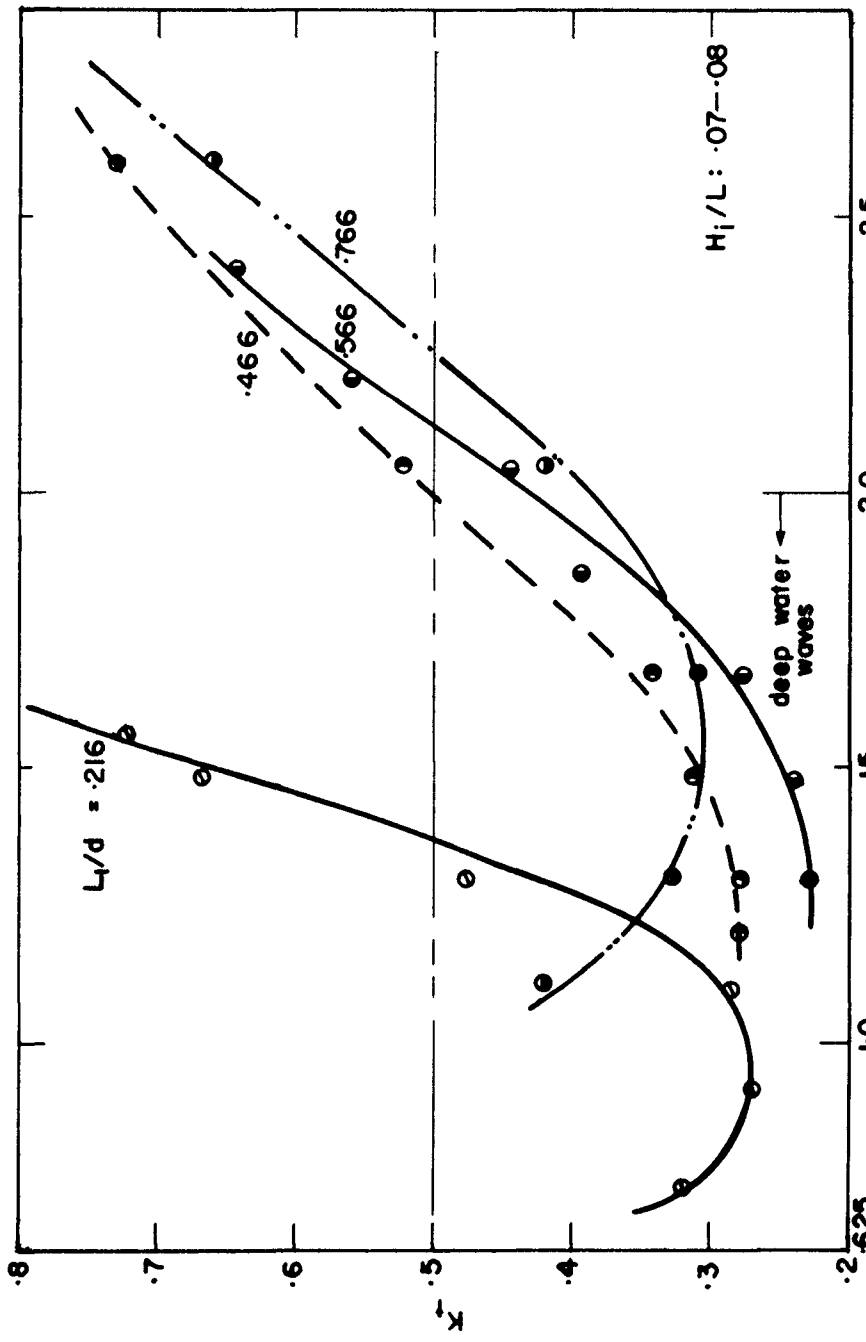

FIG(14) EFFECT OF MOMENT OF INERTIA (d=2·5')

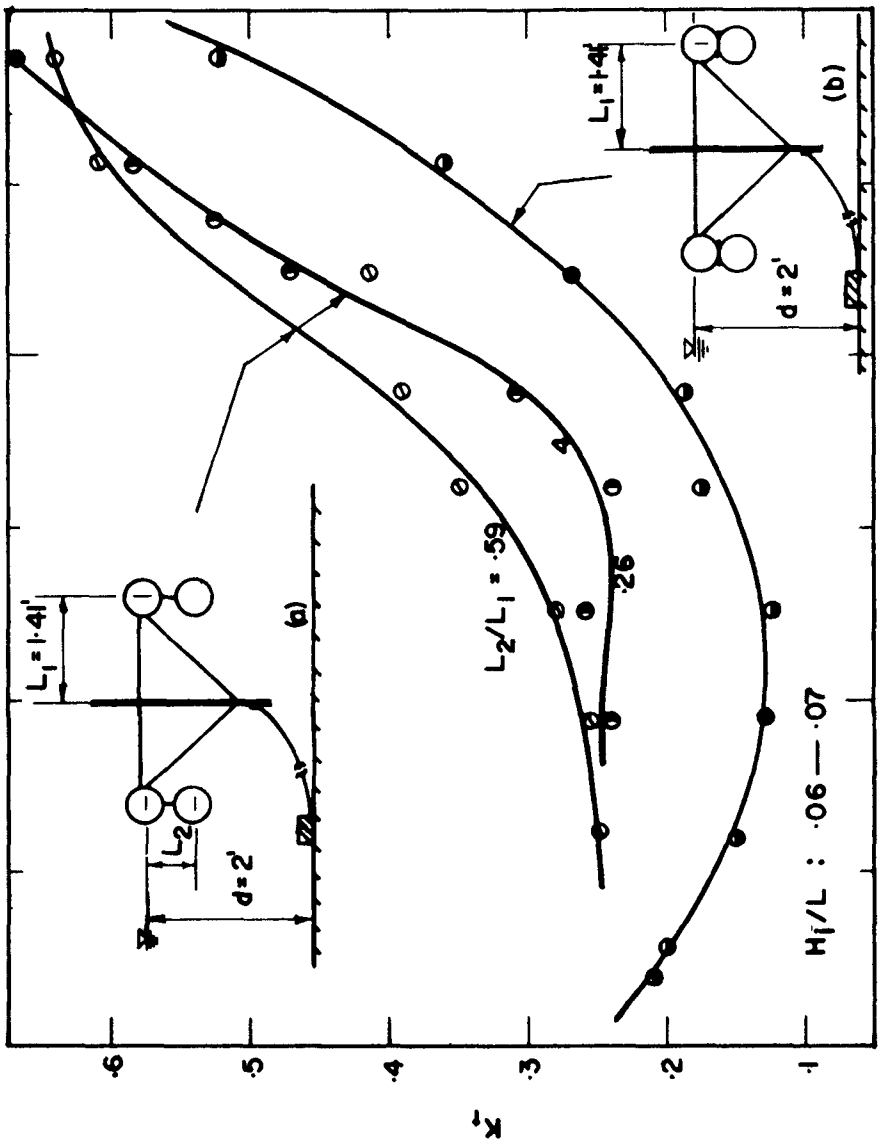

FIG(15) " '4' CYLINDER 'A' FRAME": WAVE DAMPING CHARACTERISTICS

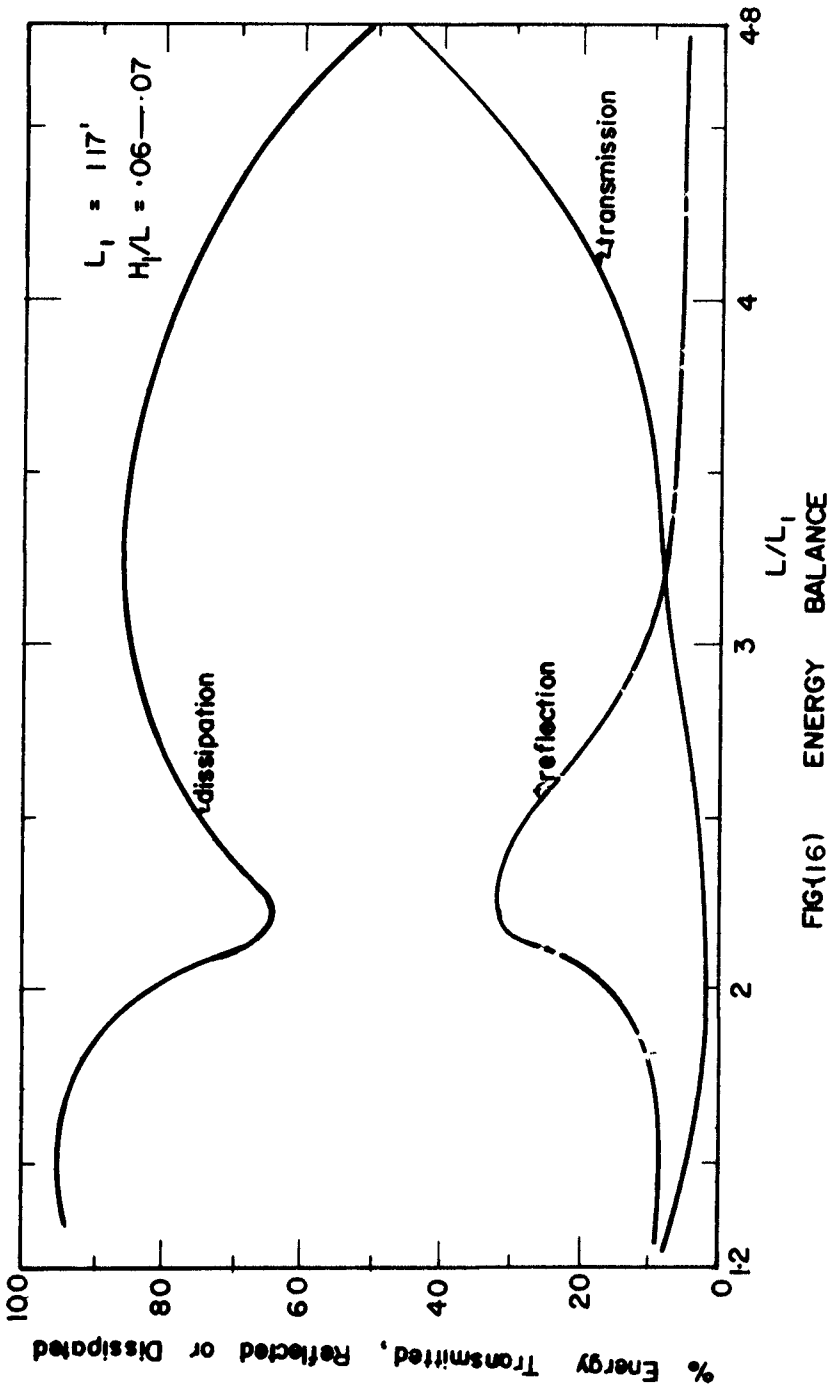

FIG(16) ENERGY BALANCE

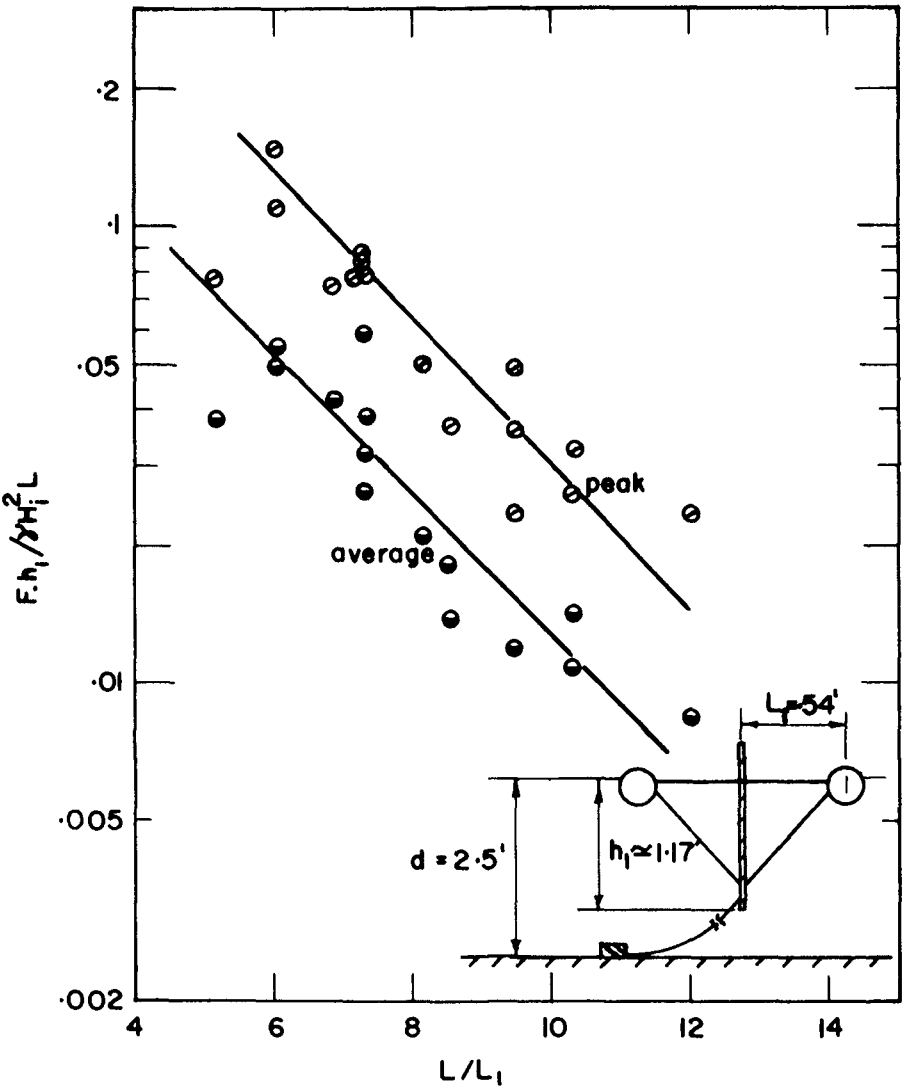

FIG(17) 'A' FRAME : PEAK & AVERAGE MOORING FORCES

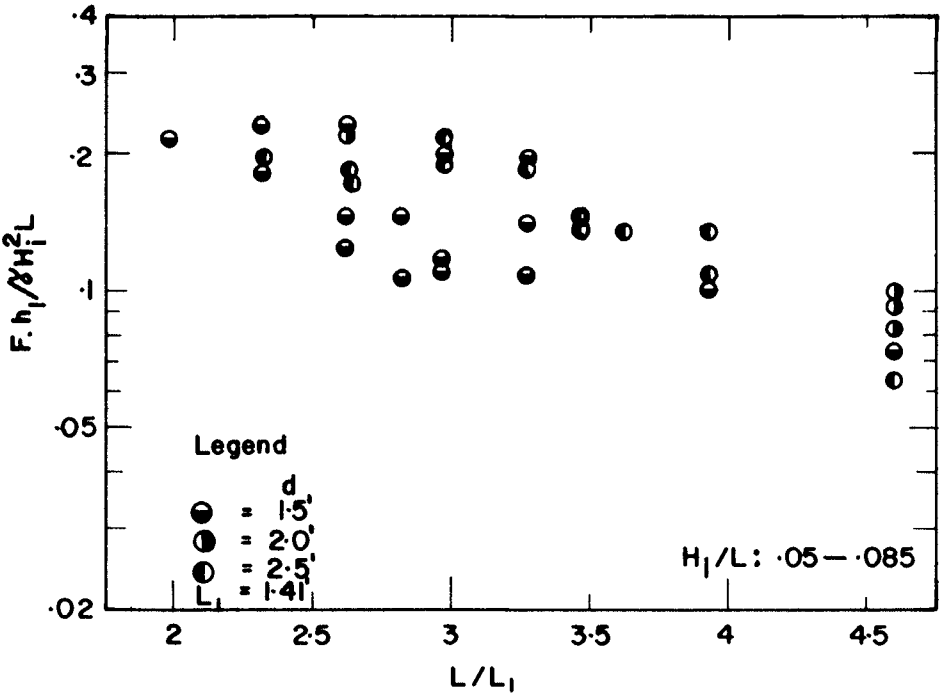

FIG(18) EFFECT OF DEPTH OF WATER ON PEAK MOORING FORCES

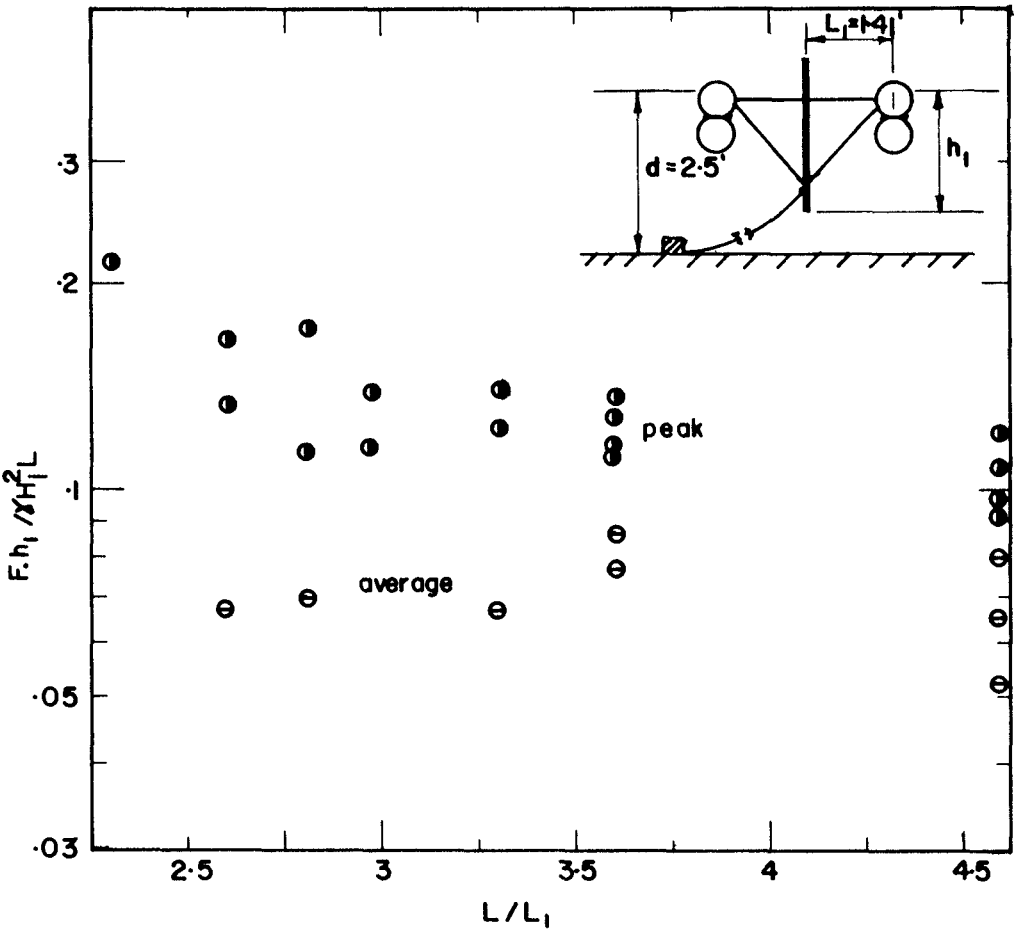

FIG·(19) " '4' CYLINDER 'A' FRAME "
MOORING FORCES

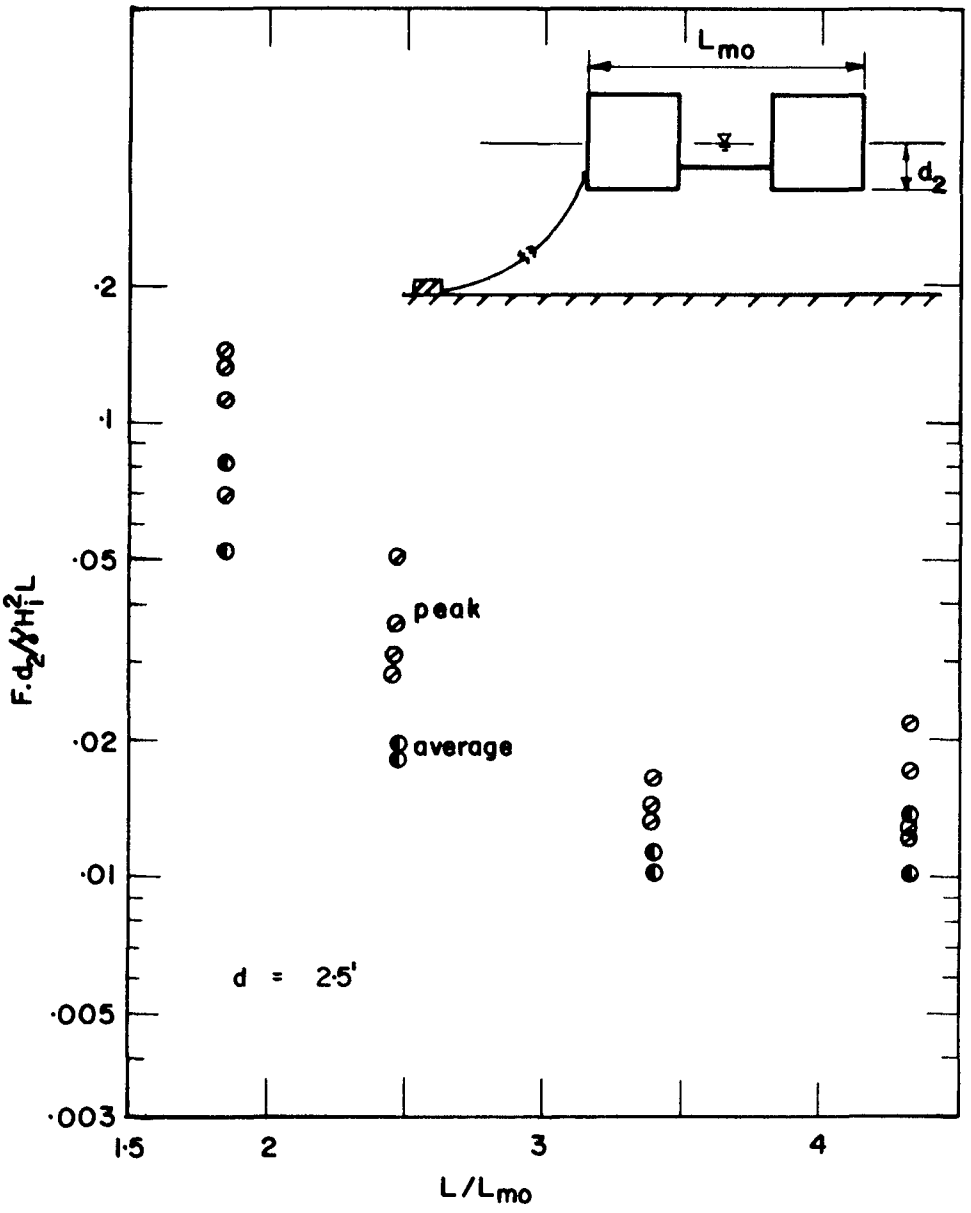

FIG·(20) DOUBLE MODULE : PEAK & AVERAGE MOORING FORCES

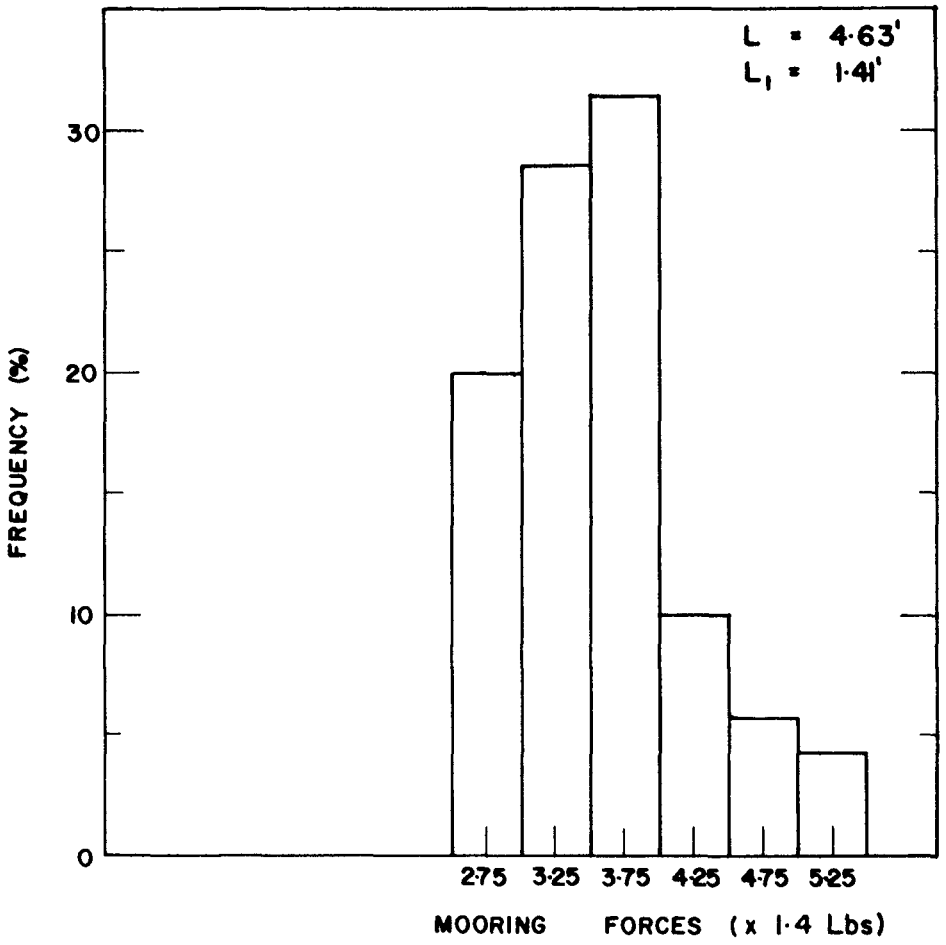

FIG·(21) 'A' FRAME : TYPICAL FREQUENCY DISTRIBUTION OF MOORING FORCES

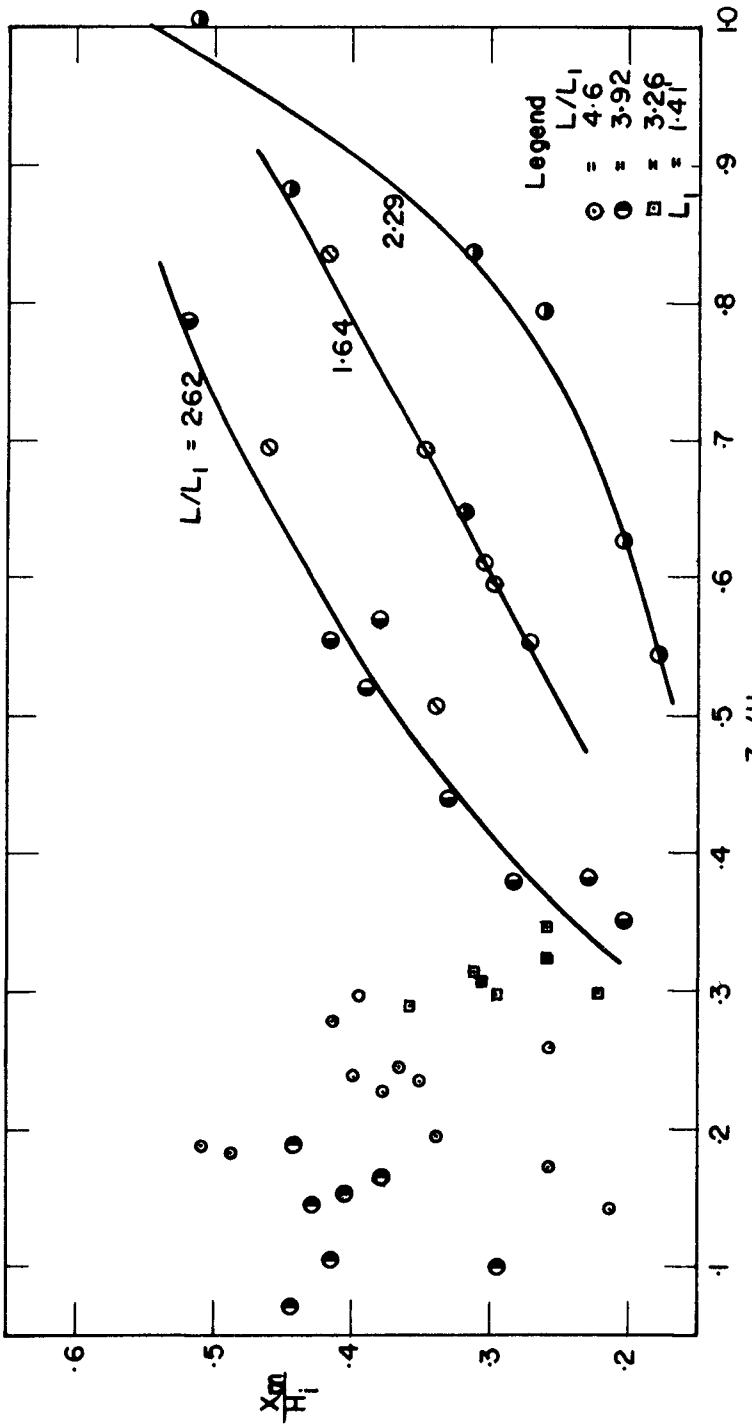

FIG (22) HEAVING & SWAYING MOTIONS OF AN 'A' FRAME BREAKWATER

CHAPTER 69

FLEXIBLE POROUS FLOATING BREAKWATERS

by

R.J. Kennedy
Professor of Civil Engineering

and

J. Marsalek
Postdoctoral Fellow

Queen's University at Kingston, Ontario

ABSTRACT

Observation of the effect of towed rafts of pulpwood on lake and ocean waves led to a systematic investigation at model scale. An empirical equation compatible with wave theory was devised and lines representing this equation together with points representing experimental results are shown for different conditions. An example of the application of the equation to prototype wave action is given. Four box booms with porous fronts, arranged in series, were substituted for the model pulpwood jam and proved to be effective in damping waves.

INTRODUCTION

Towed rafts of loose pulpwood, in which the logs are often two or more layers deep, effectively damp lake and ocean waves. Observation of this process led to consideration of the use of a mass of logs, confined between boom sticks, as a floating breakwater. A series of experiments by Farrell (ref. 1) using model logs in a wave basin, Figure 1, demonstrated that log jam breakwaters do cause significant attenuation over a wide range of conditions.

Notation The meaning of the symbols employed is illustrated in Figure 2. The only designation not in common use is d, the depth from the water surface to

the mean boundary of the bottom of the mass of logs.

EXPERIMENTS WITH MODEL BREAKWATERS

Most of Farrell's experiments were carried out in a 50 feet by 50 feet subdivision of the large University wave basin in 21.25 inches of water. Tests in differing depths of water indicated that the coefficient of transmission was not significantly affected by variations within the range of .3d to .7d, although the forces on the moorings increased at smaller depths. His data were regular and repeatable but in some instances difficult to explain. Later analysis of these data on a somewhat different basis led to revised relationships which gave a strong indication of a resonance effect when x/λ, the length of the jam divided by the wave length, was an integer. Since it seemed possible that some of Farrell's measurements had been affected by multiple reflections it was decided to conduct additional experiments.

The large wave basin being unavailable, the writers carried out a series of two-dimensional tests in a 3 feet by 60 feet flume in 16 inches of water. The relationship between period and length of wave was checked photographically and found to depart very little from first order deep water theory. The beach was made of layers of fibre matting according to Farrell's design and had a coefficient of reflection of about .07. Wave heights were measured by two resistance probes and traced out by a multiple pen recorder.

The data from these experiments are shown as points in Figures 4, 5 and 6. The resonance effect mentioned above seems to be confirmed by the points in Figure 5, although slightly masked by the scatter in one of the series. The increase in the value of C_T, the coefficient of transmission for waves of small height was unexpected but definitely confirmed by several series of tests of which two are shown in Figure 6.

The coefficient of reflection, C_r, taken as the ratio at a position in front of the breakwater, of the wave height with the breakwater in place to that with no breakwater present, was small, seldom exceeding .10. There was no evidence of substantial change in C_r with change in the wave steepness, H/λ, but some indication of larger values when x/λ had a value in the vicinity of .5, 1.5 etc.

be designed into the breakwater system, if it is to meet the stringent requirements given in the Introduction

It is evident that the mooring arrangement influences the "rolling" motion and hence the waves generated behind the breakwater Consequently, an optimum mooring arrangement must be devised whereby motion is minimized without sacrifice of minimum mooring-line force Figure 32 shows several mooring arrangements that might be considered The top system has already been tested The others show promise of restraining motion They should be studied as physical systems subjected to oscillatory force inputs to determine which is likely to produce the least rolling motion The best of these should be tested in the two-dimensional tank to determine the most effective mooring arrangement

The next step in evaluation is to determine the effectiveness of the bottom of the breakwater in reducing motion The two-dimensional experiments at Webb were made without a bottom while the CERC study included both a perforated and solid bottom The solid bottom appeared to reduce the waves more, but eyes are not to be trusted A study of different bottoms (for the best mooring arrangement) should reveal another aspect of motion and wave reduction that will influence the final design

The last phase of design optimization for the floating breakwater involves perforating the back wall (as in the case of the fixed breakwater) to further reduce rolling This will be associated with the best conditions achieved in the preceding tests The net result will be a final basic design for the unit breakwater that hopefully combines achievement of wave reduction, as specified, with a substantial force reduction in the mooring lines as compared with the solid breakwater It goes without saying that two-dimensional tests should be made to verify the expected performance

Once the optimum design for the breakwater unit is determined, it is essential to evaluate its performance as an operational entity This means testing of 5 unit breakwaters in a three-dimensional tank, such as at Stevens Institute of Technology This would include a variety of wave conditions, and, if physically possible, at least one variation in direction of incident waves. In particular, a series of irregular wave forms corresponding to different states of sea, should be used From this data, spectral analysis will reveal the nature of structural and wave damping effectiveness in moderate and storm conditions, without regard to the nonlinearity of the system

If such a program is successful, it will culminate in a final basic design for the complete breakwater system (fixed and floating) including all aspects of breakwater geometry and mooring arrangement

It was assumed that the kinetic energy dissipation would be related to x/λ also and that in addition it would be proportional to the fraction of the total kinetic energy present in a top layer of water which could be affected by the jam. The fraction of the kinetic energy present in a top layer of specified thickness, z, for a wave of given dimensions was designated R(KE) and eventually the equation

$$KE = 1.47\ R(KE)\ (x/\lambda)^{.5}$$

was evolved. For numerical evaluation of R(KE), the following expression (ref. 2) was employed.

$$R(KE) = \left[1 - \frac{\sinh 2kS}{\sinh 2kh}\right] \times 100\%$$

where h is total depth

and $S = h - z - d$

Evaluation of this expression was carried out by computer for a range of values of h/λ, and is shown on Figure 10.

Of course a means of evaluating S for given physical conditions is necessary. Assuming that z is at least related to the thickness of the boundary layer, and that the thickness of the oscillating boundary layer below the extremely rough lower surface of the jam is proportional to the thickness of the turbulent boundary layer formed next to a smooth plate, the following relationship was postulated.

$z \propto (\nu/U)^{1/5} \times^{4/5}$ where

$U \propto \pi H/T \propto \pi H/\sqrt{\lambda}$, and

$x \propto \pi H$

Thus $z \propto H^{.6}\ \lambda^{.1}$ and, choosing a constant on the basis of fit, $z = .025\ H^{.6}\ \lambda^{.1}$.

C_T, as predicted from the equation, is shown by the lines on Figures 4, 5 and 6.

PROTOTYPE PERFORMANCE

The one set of field measurements obtained showed that

waves of length 31 feet and height 1.8 feet had a transmission coefficient of .17 through a jam about .8 feet deep and 300 feet long. The equation indicates a value of .173 for these circumstances but the test is not within the range of practical interest ($x = 10\lambda$) and, while reassuring, should be regarded as inconclusive.

Using the equation it may be predicted that in deep water a wave of length 75 feet and height 3 feet would have a transmission coefficient of .589 through a log breakwater 200 feet wide and 1.5 feet deep. Such a breakwater would contain 200 cords of wood for each 100 feet of length and the transmitted wave would have a height of $(.589)^2\ 3.0 = 1.05$ feet. If the breakwater were 300 feet wide the transmission coefficient would be .468 and the height of the transmitted wave .66 feet.

NEW DESIGN

Since a porous floating breakwater of logs is effective in damping waves and is relatively easy to anchor because of its low reflection characteristics and the fact that it acts on both sides of the wave crest at once, it is worthwhile to consider other methods of constructing such a device.

As a beginning tests were carried out using box booms .2 feet deep with open top and one porous side as shown in Figure 8. The booms were more effective and also had lower coefficients of reflection when the porous side faced the approaching waves. During testing the outer booms of the group were anchored in position using chains of length equal to 5 times the depth of the water. The group was effective in damping the waves only when the tension in these anchor lines was sufficient to maintain the centre to centre spacing. The action of a group of 4 box booms in series is shown in Figure 8, while the coefficients of transmission recorded for the same booms are set forth on Figure 7. It appears that such a wave damping device is most effective when the centre to centre spacing of the booms is equal to one half wave length.

CONCLUSION

A flexible porous floating breakwater extending over 2 or more wave lengths can greatly attenuate waves of moderate length. Such a device has two important advantages over most other breakwaters; its action is

concentrated near the surface where most of the wave energy exists and it tends to dissipate the energy of each wave over a time and space interval, thus avoiding the creation of large shock forces.

It seems probable that breakwaters designed on this principle could be used to create economical temporary harbours for many purposes, including defence, short term commercial operations and summer recreational facilities.

REFERENCES

1. Farrell, J.C: The Attenuation of Water Waves by Hovering Breakwaters, M.Sc. Thesis, Queen's University, Sept. 1965.

2. Ippen, A.T: Estuary and Coastline Hydrodynamics, McGraw-Hill, 1966.

FIGURE 1. Farell's Apparatus

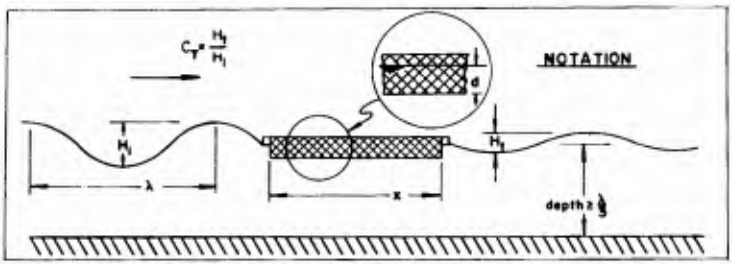

FIGURE 2. Notation Sketch

FIGURE 3. Wave Damping by Log Jam

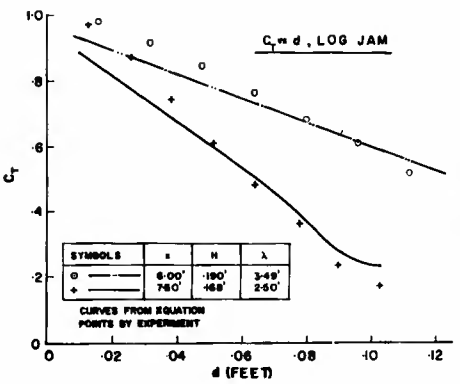

FIGURE 4. C_T vs d, Log Jam

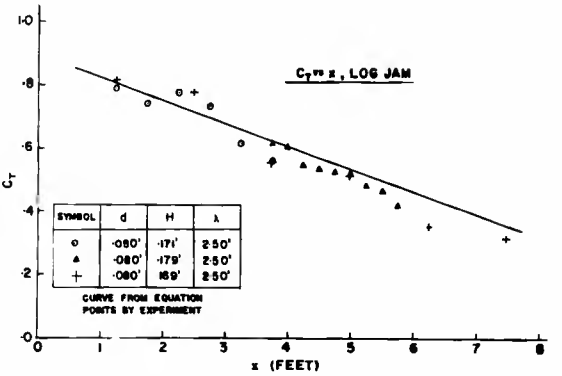

FIGURE 5. C_T vs x, Log Jam

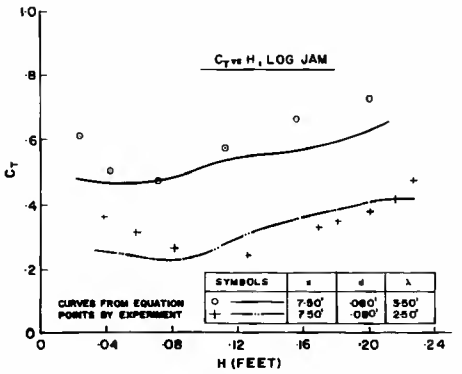

FIGURE 6. C_T vs H_i, Log Jam

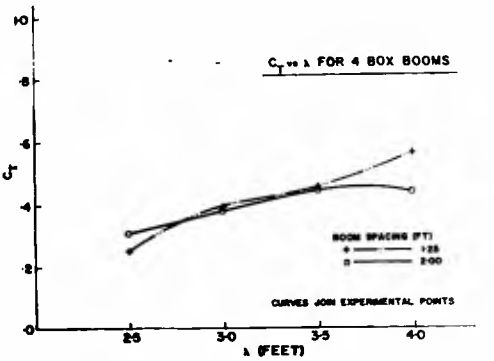

FIGURE 7. C_T vs λ For Box Booms

FIGURE 8. Box Boom

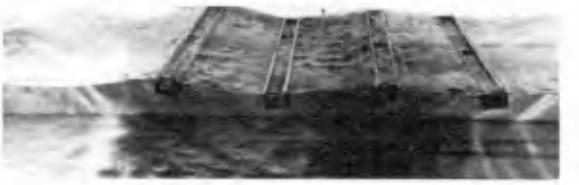

FIGURE 9. Action of Box Boom

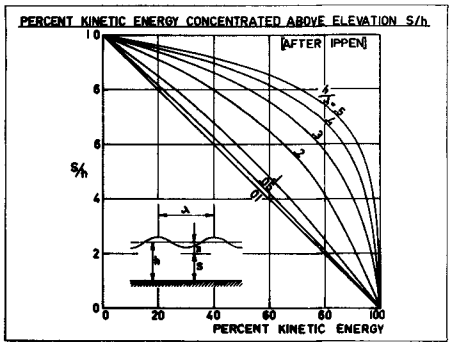

FIGURE 10. Vertical Distribution of Kinetic Energy (After Ippen)

CHAPTER 70

MODEL STUDIES OF A PERFORATED BREAKWATER

by

F.L. Terrett[1], J.D.C. Osorio[2] and G.H. Lean[3]

ABSTRACT

The breakwater proposed for a yacht harbour on the Sussex coast of England comprises a solid base up to the level of low water and a cellular structure, having a perforated front wall and solid backwall, above low water level.

A model of the breakwater (scale 1:48) was tested in a flume at the Hydraulics Research Station, Wallingford, and measurements were made of wave reflections and wave forces.

For comparison force measurements were also made on a solid faced breakwater.

The reflection tests were carried out with waves of normal incidence and at 45° to the breakwater for waves (prototype) in the range 4 to 15 seconds and up to 15 ft. in height. The results are presented in graphical form and a simplified analysis is put forward to explain them.

The force measurements were made for 7 and 10 second waves (prototype) up to 22 ft. in height. The results are presented as a non-dimensional plot with envelope curves of maximum force.

The results are also given of stability tests on a rock mound against the solid base of the breakwater.

INTRODUCTION

In some situations where armour stone is not readily available rubble mound breakwaters may turn out to be expensive; vertical breakwaters although more economical in materials reflect a large proportion of the incident wave energy. An alternative solution is the perforated breakwater, originally suggested by Jarlan (ref.1), an example of which has been built at Baie Comeau, Quebec. Nevertheless, design information is still rather scanty and further model tests have been made to investigate the performance of a particular type of perforated breakwater for a yacht marina.

---

1. Partner) Lewis and Duvivier,
2. Associate) Consulting Engineers, London, England.
3. Principal Scientific Officer, Hydraulics Research Station, Wallingford, England.

Basically the perforated breakwater consists of a screen with openings, which may be a series of slots or holes, placed in front of a solid vertical face. Waves incident on the screen are partly reflected and partly transmitted, energy being lost mainly due to eddying at the perforations. The transmitted wave is reflected from the back face, again suffering energy loss and reflection in its passage through the screen. The superposition of these waves results in standing waves being set up in the chamber between the screen and back face and also outside, the amplitudes of the waves being dependent on the losses in the screen and the distance (L) between the screen and back face. If the reflection coefficient (R) is defined as the ratio of the reflected wave height (H_R) to the incident wave height (H_I), the maximum height of the standing waves outside is $(1 + R)H_I$. Reduction of R will therefore reduce wave activity and navigation risks for craft in the immediate harbour approaches.

The maximum energy loss (R minimum) will occur when the velocity induced by the standing wave system is a maximum at the screen. It may be conjectured that this will occur when $L = \lambda_2/4$ approximately (λ_2 = wave-length in the chamber) or an odd multiple of this distance. On the other hand when the system is such that it induces zero velocity at the screen, the energy loss is zero, the screen is inoperative and reflection occurs from the back face essentially as though the screen were absent. This occurs for waves such that $L = \lambda_2/2$ or an even multiple of $\lambda_2/4$. Thus with a fixed length of chamber the performance of the breakwater in suppressing reflections will be sensitive to wave-length (or period) of the incident waves.

Clearly the reflection will also depend on the resistance of the screen; if the screen is very resistive the transmitted wave will be weak and the incident wave will be nearly wholly reflected from the screen. Conversely if the screen is very open nearly complete reflection will occur from the back face. There is evidently an optimum porosity of the screen for minimum reflection. Also, since the resistance of the screen is proportional to the square of the velocity through the openings whilst the orbit velocity is proportional to the wave height it is easy to see that the optimum porosity depends on the height of the incident wave (H_I). Boivin in tests on a horizontal slotted screen found the optimum porosity was about one-third and for this ratio the reflection decreased almost linearly with wave steepness for $0.01 < H_I/\lambda_1 < 0.05$ (λ_1 being the length of the incident wave) (ref.2).

WAVE REFLECTION

(1) Experimental Work

A section (scale 1:48) of the proposed design of breakwater (Fig.1 and Plate I) of porosity 31% above low water level was tested in a flume 10 ft. wide. The results have been analysed on the basis of Froude's Law, but the important turbulent energy loss at the perforations in the screen clearly depend upon Reynold's Number (R_e), which, for the flow through the screen in the model, was about 5000 and consequently should have been sufficient to develop fully turbulent conditions.

In the first test all the cells of the breakwater were of the same size, the distance from the front face of the screen to the backwall being $34\frac{1}{2}$ ft. (proto.). Wave heights varied from 1 to 5 ft. and periods from 4 to 14 seconds (proto.). The reflection coefficients were derived from the amplitude of the waves at the node (b) and antinode (a) of the standing wave pattern seaward of the breakwater by means of the formula $R = (a-b)/(a+b)$. The height of the incident wave was taken as $(a+b)/2$. These expressions are strictly only valid for sinusoidal waves. Difficulty was experienced in producing stable conditions in the flume due to the re-reflection of waves reflected from the breakwater and with steep waves repeatable results were not obtained.

The reflection coefficients derived from these tests showed a marked sensitivity to wave period, especially for the lower waves, with a minimum at $7\frac{1}{2}$ seconds and a maximum at 4 seconds wave periods (Fig.1.).

One of the objects of the tests was to develop a design which would not give reflections across the harbour entrance in moderate weather conditions when waves of 4 to 6 second periods are dominant. The breakwater was therefore modified by reducing the depth of alternate cells to 20 ft. measured from the face of the perforated screen to the backwall. This was done by inserting a secondary backwall in every second cell. This modification reduced the reflection of the lower and shorter waves at the expense of some loss in performance with higher and longer waves. (Fig.2.).

Since the wave crests in nature will not normally be parallel to the breakwater and the performance of the breakwater with waves approaching from an angle was in doubt reflection coefficients were measured with the breakwater at 45° to the wave crests. The model was installed across the corner at the end of the flume with an opening in the opposite wall so that most of the reflected waves escaped into a large basin adjacent to the flume. This arrangement involved some loss of incident wave energy through the gap and also resulted in a small transverse wave in the flume. For these and other reasons the wave heights varied along the face of the breakwater.

Consequently the results of the experiment are subject to a greater degree of error than those with normal incident waves but nevertheless are considered to give a reasonable indication of the performance of the breakwater with oblique waves.

The wave heights were measured along a traverse at 90^{o} to the face of the breakwater. The results (Fig.3.) show that reflection is generally less than for normal incident waves with a minimum coefficient for waves of about 6 seconds.

(2) Theoretical Treatment

For comparison with the experimental results discussed above the reflection coefficients shown in Figs 2 & 3. have been calculated by means of an analysis which is given in the Appendix and assumes that the incident waves are low and long enough for the approximations of the linear theory of long waves to be applicable. The only energy loss considered is that due to resistance of the screen which is proportional to the (water particle velocity)^{2}. This has been approximated by a fictitious resistance term which is proportional to the velocity, the constant of proportionality being chosen to give the same energy loss per wave period. The acceleration through the screen also introduces a "virtual mass" effect or a head difference across the screen which is in phase with the particle acceleration. This effectively increases the length of the chamber and hence the wave period with which the chamber will resonate. The linear theory while giving generally similar coefficients near resonance clearly predicts greater reflection for the higher and longer waves. At an incidence of 45^{o} the discrepancies are more marked even for low waves.

HORIZONTAL FORCE MEASUREMENTS

Preliminary structural analysis of the breakwater indicated that the governing factor in the design would be sliding on the foundations or shear in the material immediately below the foundation rather than overturning or crushing of the foundation strata. Only horizontal forces were therefore measured, no attempt being made to record either vertical forces or the height of the thrust line above foundation level.

Two central bays of the model were fixed together and suspended from a stiff parallel motion spring system with strain gauges attached and of high enough natural frequency to enable the force variation to be followed.

Measurements were made with waves of 7 and 10 second period (proto.) both on the breakwater with the perforated front wall and with the perforations covered over with a plain solid face extending up to parapet level. For the larger waves, which broke in front of the breakwater, the resulting variable reflections caused the wave heights in the flume to vary, and a range of observations of wave height and

force was therefore obtained from any one setting of the wave generator. In each run a continuous record of forces (F_c and F_t - Fig.3.) and wave height at the wall (H_w) for 50 or more waves allowed the highest forces relative to the wave height to be measured.

For low waves the forces on the breakwater were regular and only slightly higher than that induced by the hydrostatic pressure variation.

For larger waves considerable variation of peak force occurred between one wave and the next, and the highest waves frequently did not produce the largest forces. The force coefficient curves in Fig. 4 are the envelopes of numerous points derived from the records.

The maximum force coefficients in the record increased up to a wave height of about 12 to 15 ft. when the waves started to break and the face of the breakwater began to be overtopped. For further increase in wave height although the force coefficients diminish the maximum force remained sensibly constant up to the maximum waves (22 ft. proto.) that were recorded. Similar experiments with a plain face showed that for 7 second waves the peak positive force coefficients (in the direction of incident wave propagation) were about double those on the perforated breakwater. For 10 second waves the coefficients were similar for the perforated breakwater and the plain face, the maximum forces in this case being of the order of $1\frac{1}{2}$ tons per sq. ft. These results confirm the measurements of Marks which showed that generally the largest horizontal force reductions were to be expected for the lower period waves (ref.3).

STABILITY OF TOE MOUND

Although the perforated face of the proposed breakwater will not extend below low water level and will have a solid base below, scouring of the hard chalk on which it is to be founded is not expected. It is proposed, however, to place a low rock mound against the base near the harbour entrance to reduce wave reflection at low tide. Tests showed that with the most destructive waves that could be generated in the flume, which broke on the toe mound, armour stone of $4\frac{3}{4}$ tons average weight (proto.) was stable at a slope of 1 vertical to $1\frac{1}{2}$ horizontal. $2\frac{1}{2}$ ton stone at this slope was drawn down and the slope flattened to about 1 in $2\frac{1}{2}$.

CONCLUSIONS

The design criteria established by the investigation are:-

1. The length of the wave chamber should not be more than about one third the wave length of the shortest dominant wave to be catered for. With a porosity of 30%, provided the longest wave of significant height is not more than twelve times the chamber depth a maximum coefficient of reflection of 0.5 may be assumed.

2. Lower force coefficients were obtained with the perforated face than with a plain face for 7 second waves, but were little changed with 10 second waves. However some reduction in the forces is obtained at both wave periods due to the fact that the height of the waves at the wall is reduced as shown by the reflection tests.

It is evident from these two conclusions that the requirements for reduction in wave reflections and reduction in wave forces tend to conflict. While the 7 second period wave, which is about 7 times as long as the depth of the breakwater cells gives acceptable force coefficients, the 10 second period wave (length about 11½ times the cell depth) tends to fill the cells and the breakwater then behaves like a solid structure. In practice it would seem that waves of length between 3 and 8 times the cell depth can be absorbed by a sturcture of the type tested; if longer waves of significant height ($H_w/h > 0.2$) are expected then a wider breakwater is necessary, in order to incorporate a greater cell depth, if the structure is not to be subjected to forces nearly as great as those which would be imposed on a solid breakwater.

REFERENCES

1. Jarlan, G.E. Application of acoustic theory to the reflective properties of coastal engineering structures, Quart Bull 1965, Nat. Res. Coun. Canada (1) 1965, 23-63.

2. Boivin, R. Comments on vertical breakwaters with low coefficients of reflection, Dock & Harbour Authority June 1964, 45 56-61.

3. Marks, N. A perforated mobile breakwater for fixed and floating application, Proc. 10th Conf. Coastal Eng. 66, Tokyo II 1079-1129.

Appendix

Analysis

(i) Normal Incidence

We suppose that waves are incident normally on the screen at $x = 1$, the back face being situated at $x = 0$ (Fig. 5). In front of the screen the depth is constant (h_1) and the particle velocity u, wave elevation η; behind the screen the depth is h_2 and the particle velocity u^1, wave elevation η^1

The linearised equations of motion for the flow are

$$\frac{\partial \eta}{\partial t} + h_1 \frac{\partial u}{\partial x} = 0 \qquad (1)$$

$$\frac{\partial u}{\partial t} + g \frac{\partial \eta^1}{\partial x} = 0, \text{ for } x > 1; \qquad (2)$$

and

$$\frac{\partial \eta^1}{\partial t} + h_2 \frac{\partial u^1}{\partial x} = 0 \qquad (3)$$

$$\frac{\partial u^1}{\partial t} + g \frac{\partial \eta^1}{\partial x} = 0, \text{ for } 0 < x < 1 \qquad (4)$$

It is convenient to assume that η, u etc. are proportional to $\exp(i\sigma t)$ in which we will eventually reject the imaginary part, σ being the angular velocity of the waves $2\pi/T$, T being the wave period.

Equations 1-4 are satisfied by

$$\eta = A \exp ik_1 x + B \exp -ik_1 x \qquad (5)$$

$$u = -\frac{\sigma}{k_1 h_1} \left[A \exp ik_1 x - B \exp -ik_1 x \right], \; x > 1 \qquad (6)$$

and

$$\eta^1 = A^1 \exp ik_2 x + B^1 \exp -ik_2 x \qquad (7)$$

$$u^1 = -\frac{\sigma}{k_2 h_2} \left[A^1 \exp ik_2 x - B^1 \exp -ik_2 x \right], 0 < x < 1 \qquad (8)$$

with $$\sigma^2/k_1^2 = gh_1 = C_1^2 \qquad (9)$$

and $$\sigma^2/k_2^2 = gh_2 = C_2^2 \qquad (10)$$

$$\text{and} \quad k_1 = 2\pi/L_1, \; k_2 = 2\pi/L_2 \tag{11}$$

L_1, L_2 being the wave length in front of and behind the screen. A, B are constants representing the amplitudes of the incident and reflected waves in front of the screen and A^1, B^1 represent the transmitted wave and its reflection from the back face.

To determine the constants we have the boundary conditions that at the back face $x = 0$, $u^1 = 0$ and hence

$$A^1 = B^1 \tag{12}$$

and at the screen $x = 1$, we have from continuity and from the momentum balance

$$h_1 u = h_2 u^1 \tag{13}$$

$$\text{and} \quad g(\eta-\eta^1) + k_* u^1 |u^1| + a^1 \frac{\partial u^1}{\partial t} = 0 \tag{14}$$

where $a^1 \rho h_2$ is the effective virtual mass introduced by the screen, ρ being the water density, and k_* is the drag coefficient of the screen.

In order to proceed we have linearised the friction term in (14) by the usual Lorentz approximation to give

$$g(\eta-\eta^1) + (f + a^1 i\sigma)u^1 = 0 \tag{15}$$

$$\text{where} \quad f = 8k_* \tilde{u}^1/3\pi \tag{16}$$

in which $\tilde{u}^1$ is the amplitude of the particle velocity at the screen ($x = 1$).

We may now substitute for η, η^1, u, u^1 from equations (5)-(8) in (15)and (16) to determine the constants and after some manipulation we find the reflection coefficient $R = |B|/|A|$ as

$$R^2 = N_1/D_1 \tag{17}$$

where

$$N_1 = \left[\cos k_2 l - a^1 k_2 \sin k_2 l\right]^2 + \left(\frac{f}{c_2} - \frac{k_1}{k_2}\right)^2 \sin^2 k_2 l$$

and

$$D_1 = \left[\cos k_2 l - a^1 k_2 \sin k_2 l\right]^2 + \left(\frac{f}{c_2} + \frac{k_1}{k_2}\right)^2 \sin^2 k_2 l$$

with

$$\frac{f}{c_2} = \frac{8}{3\pi} k_* \frac{A}{h_2} \; 2\sin k_2 l/D_1 \qquad (18)$$

The latter being an implicit equation to determine f/c_2 in terms of the incident wave height.

We note that R = 1 when $k_2 l = 0, \pi$ .. etc. or the length l is a multiple of half the wave length. Also if we assume for the moment that f is constant, minimum values of R occur at

$$\cot k_2 l = a^1 k_2 \qquad (19)$$

and

$$R^2_{min} = \left[(f/c_2 - k_1/k_2)/(f/c_2 + k_1/k_2) \right]^2 \qquad (20)$$

with $R_{min} = 0$ when $f/c_2 = k_1/k_2$.

To estimate the reflection coefficient we need to estimate the drag coefficient of the screen k_* and the virtual mass coefficient a^1. For the former it has been assumed that a vena contracta is formed at the perforations of area 0.6 times the area of the openings and that the velocity head through the vena contracta is lost.

Thus if s is the area of the openings and S is the area on the downstream side of the screen up to high water, the head loss across the screen is given by

$$g(\eta^1 - \eta) = \left(\frac{u^1}{2}\right)^2 \left[\left(\frac{S}{0.6s} \right)^2 - 1 \right] \qquad (21)$$

$$\text{so that} \quad k_* = \frac{1}{2} \left[\left(\frac{S}{0.6s} \right)^2 - 1 \right] \qquad (22)$$

In the present case s/S = 0.37 and hence $k_* = 9.5$.

There is little guide from theory for the effective value of a^1. Trial calculations were made of the wave periods to give minimum reflection coefficients with different values of a^1 and a value selected (a^1 = 6 ft) which gave agreement with experiment for a uniform chamber length l = 34.5 ft. This value was used in the calculations of R for the smaller length, 27¼ ft.

(ii) Oblique incidence

For waves incident on the screen at an angle θ between the normal to the wave front and the normal to the screen, the equations of motion outside the screen ($x > 1$) are satisfied by

$$\eta = A \exp i(k_1 \cos\theta x + k_1 \sin\theta . y) + B \exp i(-k_1 \cos\theta x + k_1 \sin\theta y) \quad (23)$$

$$u = -\frac{\sigma \cos\theta}{k_1 h_1} \cdot \left[A \exp i(k_1 \cos\theta x + k_1 \sin\theta y) - B \exp i(-k_1 \cos\theta x + k_1 \sin\theta y) \right] \quad (24)$$

$$v = -\frac{\sigma \sin\theta}{k_1 h_1} \cdot \left[A \exp i(k_1 \cos\theta x + k_1 \sin\theta y) + B \exp i(-k_1 \cos\theta x + k_1 \sin\theta y) \right] \quad (25)$$

In which η is the surface elevation and u, v are the velocity components normal and tangential to the screen Ox.

and $\sigma/k_1 = c_1$ as before.

In these equations B is the amplitude of the reflected wave and it has been assumed that the angle of incidence and reflection are equal.

Behind the screen ($0 < x < 1$) the elevation (η^1) and the normal velocity (u^1) are again given by (7), (8) and (12) and to satisfy continuity and friction loss across the screen we again suppose equations (13) and (15) to apply. Substituting for u, η from (23) and (24) in these equations gives after some manipulation

$$R^2 = N_2/D_2 \quad (26)$$

where

$$N_2 = \left[\cos k_2 l - a^1 k_2 \sin k_2 l \right]^2 + \left(\frac{f}{c_2} - \frac{k_1}{k_2 \cos\theta} \right)^2 \sin^2 k_2 l$$

$$D_2 = \left[\cos k_2 l - a^1 k_2 \sin k_2 l \right]^2 + \left(\frac{f}{c_2} + \frac{k_1}{k_2 \cos\theta} \right)^2 \sin^2 k_2 l$$

which is similar to equation (17) but with $k_1/k_2 \cos\theta$ substituted for k_1/k_2. If f is taken constant to a first approximation, we note that R is a minimum when $\cot k_2 l = a^1 k_2$ as for the case of normal incidence, so that the angle of incidence has no effect on

the selectivity of the breakwater to wave period. This is in agreement with the experimental results.

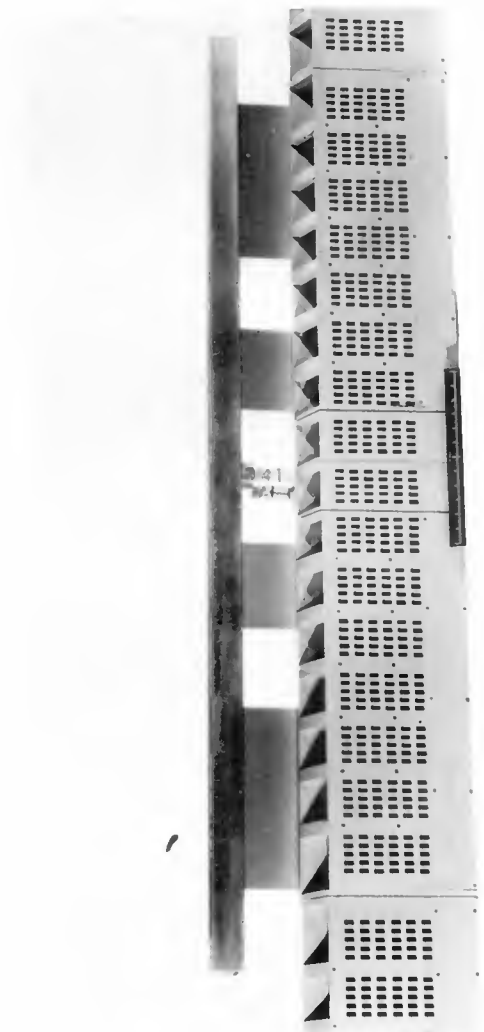

PLATE 1. MODEL BREAKWATER SHOWING PARALLEL CANTILEVER SUSPENSION OF CENTRE SECTION FOR FORCE MEASUREMENT

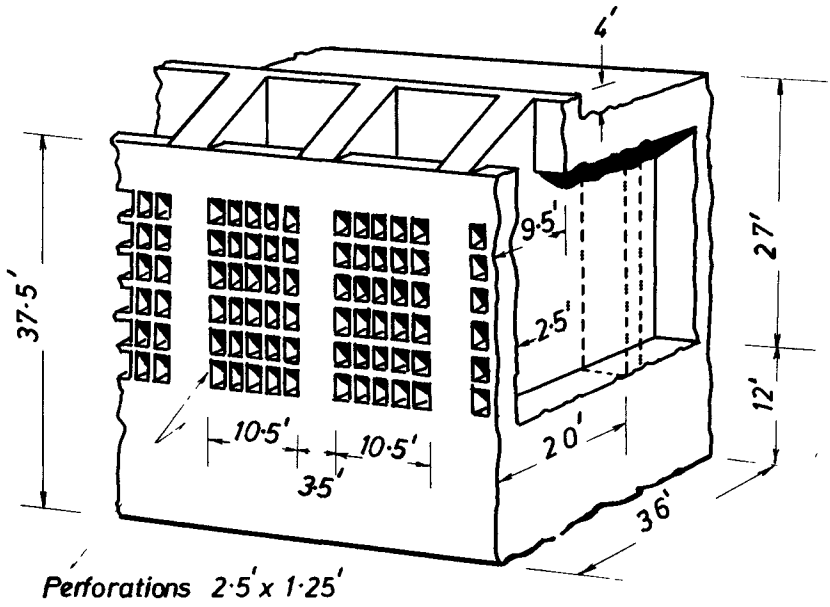

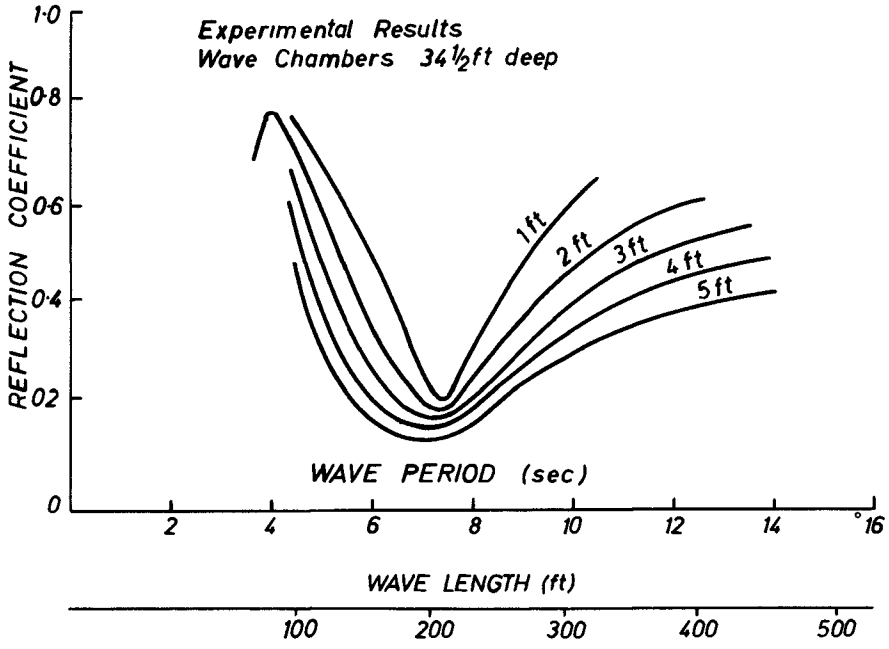

FIG 1 REFLECTION COEFFICIENT - NORMAL INCIDENCE

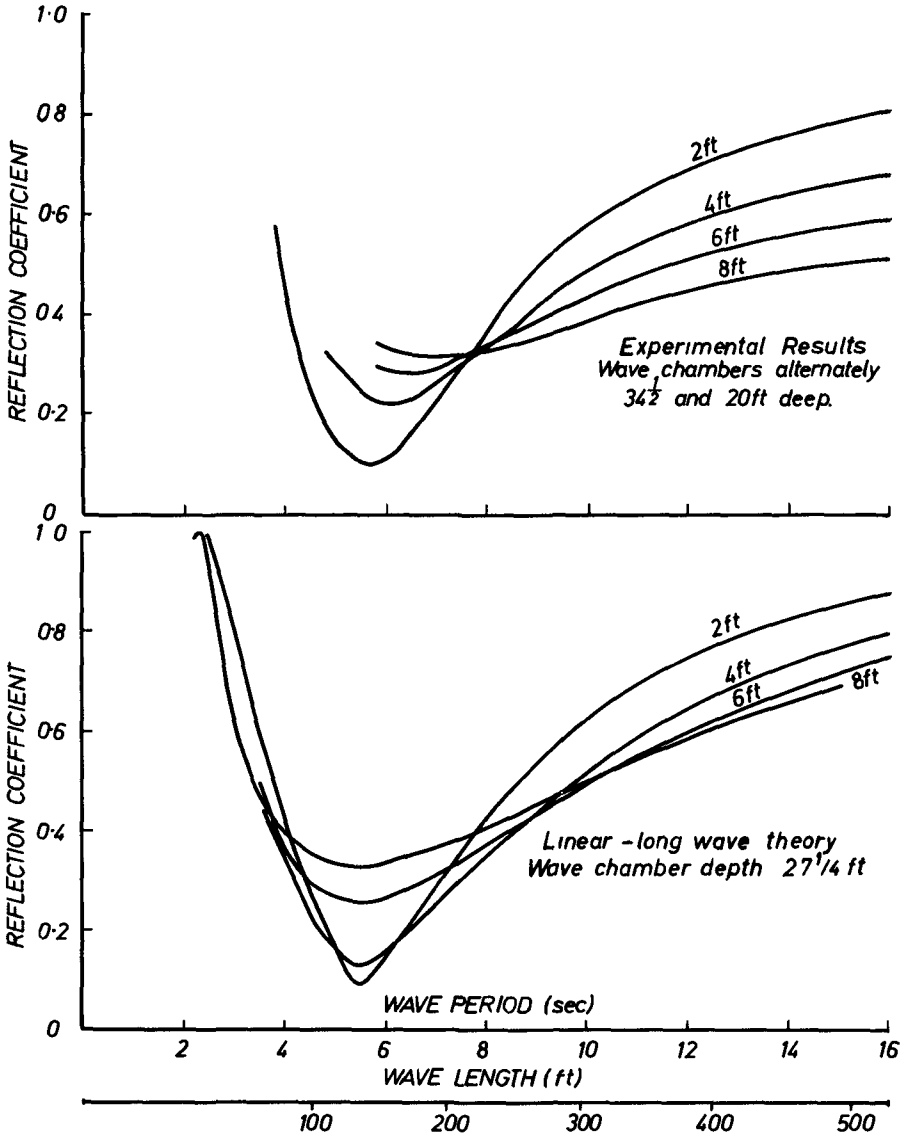

FIG 2. COMPARISON OF EXPERIMENTAL AND THEORETRICAL REFLECTION COEFFICIENTS-NORMAL INCIDENCE.

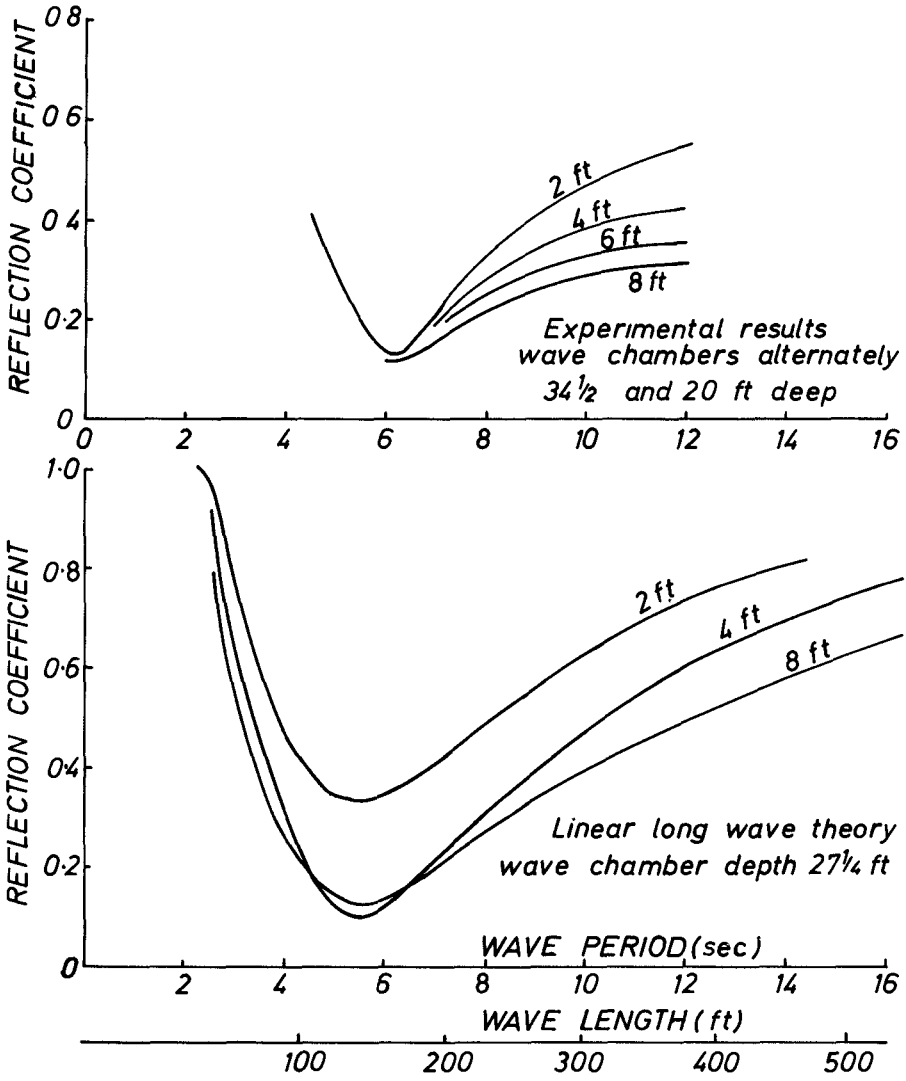

FIG 3 COMPARISON OF EXPERIMENTAL AND THEORETICAL REFLECTION COEFFICIENTS -45° INCIDENCE

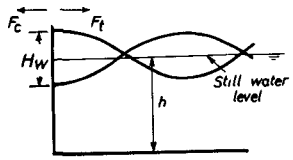

A = area of face of breakwater below still water
γ = specific weight of water

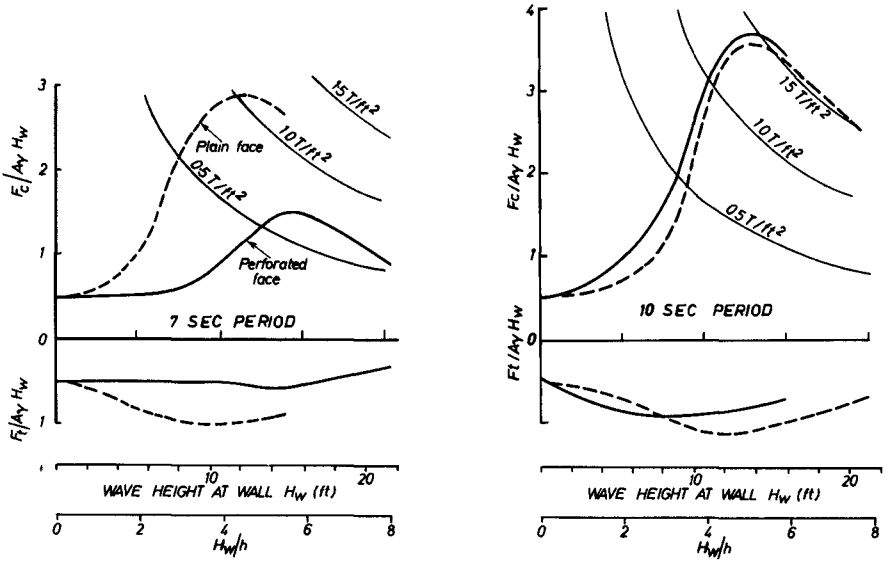

ENVELOPE OF PEAK HORIZONTAL FORCE

FIG 4

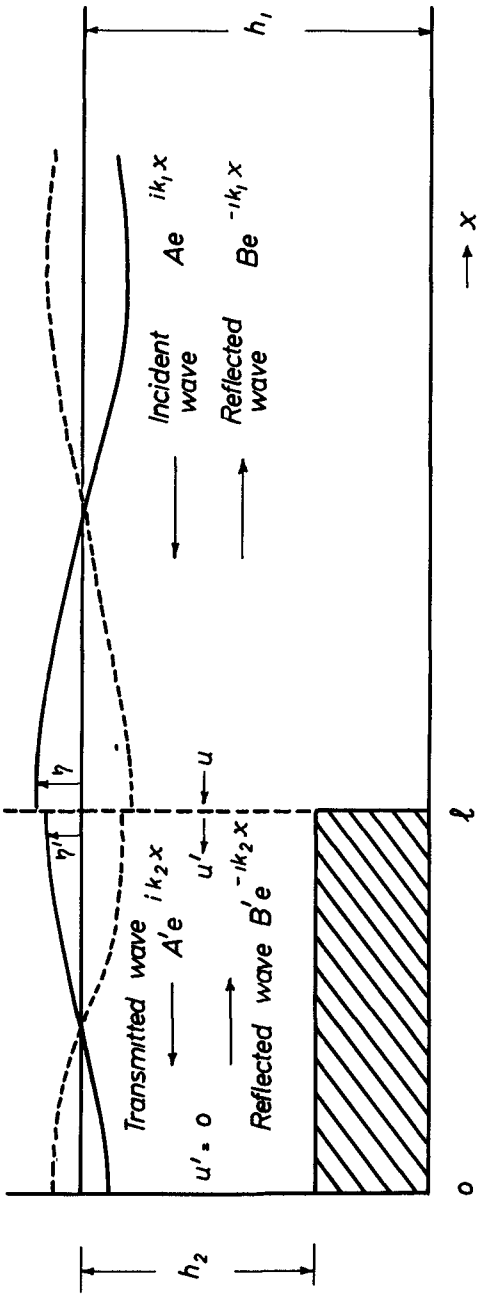

FIG 5 REFLECTION OF WAVE FROM PERFORATED FACE

CHAPTER 71

EXPERIMENTAL STUDIES ON A FIXED PERFORATED BREAKWATER

Wilbur Marks
Executive Vice-President, Oceanics, Inc.
Technical Industrial Park, Plainview, N. Y.

Gerard E. Jarlan
Associate Principal Scientist, Oceanics, Inc.
Technical Industrial Park, Plainview, N. Y.

ABSTRACT

Model tests on a perforated breakwater system were carried out to evaluate effectiveness in different states of sea. Force measurements were made in three long-crested irregular wave systems and, by spectral analysis, the full-scale statistical characteristics of force were obtained. The effect of perforating the back wall was studied to determine the extent of further reduction of force on the structure. An interior perforated wall was also added for force reduction but was not as effective as the perforated back wall. The system was mounted on piles and imbedded in sand for a quasi-quantitative study of scouring in regular waves. In this case, the elevation of the breakwater walls above the sandy bottom was varied. Both the perforations and the elevation contributed to significant reduction in observed scour. The end result of these experiments is to provide information on the kind of improved performance that might be expected as each variation is introduced which, in turn provides input to design for particular applications.

INTRODUCTION

OCEANICS, Inc. has been engaged in development and evaluation of a design concept for a portable breakwater that comprises a perforated front wall with a solid back wall. As a floating system, the chief virtue that is claimed for the perforated breakwater is that it affects a considerable reduction in the height of the incoming waves without paying a penalty in excessive forces on the mooring lines. When the perforated breakwater is fixed to the bottom, it is purported to dissipate sufficient wave energy to cause it to be structurally sound for long periods of time. Furthermore, it is believed that the front wall porosity is an important factor in maintaining stability of bottom sediment such that scouring is minimized and the probability of structural damage and overturning is greatly reduced.

The first phase in the evaluation of the perforated breakwater was aimed at determining whether it was generally more satisfactory than a caisson of the same dimensions for fixed and/or floating operation. That is, do the perforations result in less force on the structure than a solid wall, when the structure is fixed to the bottom? And, when floating, does the perforated breakwater reduce the waves more and still experience appreciably less force? If the perforated breakwater is superior, what is its optimum geometry?

In general, the Phase I study reported by Marks (1966) revealed the following:

1. The fixed perforated breakwater experiences less force overall than the solid breakwater. Greater effectiveness was usually found at lower wave periods except for the very important upward vertical force where the solid breakwater experienced forces greater than 11 times that of the perforated breakwater, at the design wave (13 seconds, 15 feet).

2. The breakwater geometry specifying: 4-foot diameter holes, 4-foot wall thickness, and 40 feet between front and back wall was found to be most effective, as predicted by theory.

3. For the floating case, the perforated breakwater experienced less force in the 4 mooring lines. Again, the degree varied being just slightly less in one instance and one-tenth of the force in the mooring line of the solid breakwater in another. At the design wave, the mooring lines in the perforated breakwater experienced less force by about a factor of 2.

4. The motion of the breakwaters as measured by horizontal and vertical accelerations showed no clear superiority and this was reflected in wave reduction behind the breakwaters.

5. The excessive vertical forces on the face of the solid fixed breakwater caused a layer of sand 3 inches high and one foot in extent to be completely cleared away from the foot of the breakwater. The perforated breakwater produced little or no scouring.

On the basis of the results achieved in the first phase of the study, it was considered to be more practical to pursue the development of the more promising fixed perforated breakwater. Thus, the essence of the work reported here deals with examination of certain variations in breakwater design that are aimed at further reduction of force on the system (fixed to the bottom) without vitiating its wave reduction prowess. The force on the basic structure is developed theoretically and then measurements at model scale are described. Additional measurements were made with such variations as perforating the back wall and

inserting a perforated interior wall. The effect of scour at the base was also examined and is reported here. There is evidence that the perforated breakwater is admirably suited for amphibious operations.

PHYSICAL CHARACTERISTICS OF BREAKWATER

The basic purpose of any breakwater system is to present an obstacle to the oncoming waves that will cause the wave height (hence energy) to be substantially reduced on the shoreward side, without compromising the functional efficiency of the breakwater system during the required time of operation. The perforated breakwater has been specifically designed for such a mission. The original concept of a perforated breakwater was developed by Jarlan (1965).

The dynamic processes that result from the incidence of waves on the perforated breakwater can best be visualized by considering that as the wave impinges on the porous front wall, part of its energy is reflected and the remainder passes through the perforations. The potential energy in the wave is converted to kinetic energy in the form of a jet, upon passage through the perforation, which then tends to be partially dissipated by viscosity in the channel and partially by turbulence in the fluid chamber behind the perforated wall. As the water in the fluid chamber flows back out of the holes, it encounters the next oncoming wave and partial energy destruction is accomplished even before that wave reaches the breakwater. If the walls were not perforated (e.g. a caisson), total reflection would occur on the face of the wall with resultant high impact forces and scouring at the base, if it is fixed to the bottom. If the breakwater were floating and anchored, part of the incident wave force would be transmitted to the mooring cables and part would be directed to oscillating the breakwater thus inducing it to make waves on the shoreward side. In the case of the perforated breakwater, that part of the incident wave energy which is dissipated internally in the form of heat and eddies is not available for such deleterious activity.

To understand more fully what happens when a wave is incident upon a breakwater, consider the following development. The forces exerted by wind-induced gravity waves on a vertical obstacle extending from above the surface to the sea bottom, at a given depth d, are:

1. The weight of the obstacle,

2. The hydrostatic under pressure,

3. The hydrostatic pressures exerted on both vertical sides (horizontal pressures),

4. The dynamic uplift pressure.

Assume that the breakwater is a caisson-like structure of concrete block resting on a stone foundation placed at the bottom and is subject to oscillatory forces. Although the base of the structure may be in contact with the foundation over about 50% of its surface, it is generally assumed that an apparent weight must be accounted for and that the hydrostatic pressure exerted on the base of the breakwater affects its entire area.

Since the surface of the clapotis (standing wave due to reflection from vertical wall) is alternately above and below still water, the accompanying pressure changes due to this vertical motion will increase or decrease the hydrostatic pressure by an amount

$$P = g\rho_w \frac{H}{\cosh \frac{2\pi d}{L}} \qquad (1)$$

where ρ_w = specific gravity of water (slugs), H = amplitude of the clapotis, and L = wave length at depth d (in feet).

As the wave crest reaches the wall (Figure 1), the pressure at the toe on the sea side is greater than on the shore side by an amount equivalent to AB. Since the pressure is transmitted under the structure at approximately the velocity of sound, an uplift pressure will develop under the breakwater according to a triangular distribution. It is assumed that the head losses in the stone mound on which the breakwater is resting are linear.

A similar phenomenon applies in the opposite direction when the trough of the wave is present on the sea side. It must be mentioned that these uplift pressures act in the same direction as the forces exerted on the vertical wall, thereby increasing the overturning moment. It is possible to calculate the moment generated by the forces involved and from this to deduce the stabilizing moment due to weight. With a triangular distribution of the uplift force the resultant cuts the base at the edge of the middle third.

To determine the resistance against sliding, it is necessary to multiply the effective downward force on the structure by a coefficient of static friction. This result is then divided by the horizontal wave pressure, assuming a friction coefficient of about 0.5. The factor of safety should not be less than 2.

The foregoing is a brief review of the procedure generally followed when designing an ordinary vertical wall breakwater. The resultant of the forces per unit length of wall (R) and the moment (M) about the base are given by the formulae

$$R = \frac{1}{2}(d+H+h_o)(\rho d+P) - \rho\frac{d^2}{2} \qquad (2)$$

$$M = \frac{1}{6}(d+H+h_o)(\rho d+P) - \rho\frac{d^3}{6} \qquad (3)$$

where P = pressure due to wave, $\rho = 62.5$ lb.ft.$^{-3}$, h_o is the wave set-up (calculated by the relationship $h_o = \frac{\pi H^2}{L}\coth\frac{2\pi d}{L}$, where L = wave length). The existence of this set-up results from the fact that a pile-up of water, due to orbital motion and mass transport, occurs at the wall, raising the mean sea level by an amount h_o which is a function of $\frac{d}{L}$ and $\frac{H^2}{L}$; h_o defines the mean level of the clapotis.

In the case of the perforated breakwater, two phenomena modify the situation encountered in the case of a plain-wall breakwater. Firstly, the porosity of the system reduces the reflection, thereby diminishing the amplitude of the clapotis which then becomes a partial clapotis. Secondly, the dissipation of the energy is such that about 65% of the incoming wave energy is dissipated through jet diffusion in the back chamber. The energy transferred to the system is thus about 35% of the total energy. Assuming this energy to correspond to a given wave height, the following relationship holds.

$$\left(\frac{H_2}{H_1}\right)^2 \simeq 0.35 \qquad (4)$$

Hence, $H_2 \simeq 0.6H_1$ (equivalent wave height of the non-dissipated energy). For the design wave, H_1 = 15 feet and H_2 = 9 feet.

On the other hand, one may assume a reflection coefficient of about 30% yielding for the amplitude of the clapotis a value H = 9 feet. The total height of the partial clapotis is then 18 feet while the full clapotis would have a height of 30 feet. Under these conditions, when H = 15 feet, T = 13 seconds, d = (40 + 10) feet (height of the breakwater 50 feet) a value of the resultant of R = 25,000 lb. is obtained by substitution in Equation (4). In the case of the perforated breakwater, $h_o \simeq 1$ ft. for the considered initial conditions corresponding to a partial clapotis of 18 feet. The moment is then from Equation (3) M = 589,000 ft.-lb. If for stability against overturning, it is required that the resultant of wave pressure and weight must fall within the middle third of the base, then assuming uplift (triangular distribution) the width of the caisson is found to be about 46 feet and the weight per linear foot is 49,000 lb.

From these simplified calculations, it is seen that the design wave can produce very large forces which are diminished considerably by the perforations. The width of the breakwater is commensurate with the design width required for maximum efficiency and the calculated weight is reduced by supporting the breakwater on piles driven into the bottom. The experiments described here are aimed at further reducing the force on the breakwater by inducing additional energy dissipation through a perforated back wall and through insertion of an inner perforated wall.

The efficiency of energy dissipation, in the breakwater principle proposed here, depends on the geometry of the system which in turn is determined by the nature of the design wave conditions. From the laws of fluid motion in the chamber, the following design criteria are obtained:

1. Ratio of chamber width to wave length.
2. Ratio of wall thickness (channel length) to hole diameter.
3. Ratio of perforated to unperforated areas (solidity ratio).

The theoretical development leading to the establishment of the above criteria, for particular wave inputs, was presented by Jarlan (1965) and Jarlan and Marks (1965).

MODEL EXPERIMENTS

The model experiments were two-dimensional and were carried out in the ship model towing tank (100 ft. x 10 ft. x 5-feet deep) at Webb Institute of Naval Architecture. As in the previous tests reported by Marks (1966) the tank was modified to simulate shallow water by installation of a flume with sloping beach 1:16 (Figure 2). The models were mounted in the shallow end of the flume so that at a scale of 1:45, the models are essentially in 45 feet of water.

The tests were conducted in long-crested irregular waves to simulate, as near as possible, actual conditions. There were three sets of waves employed corresponding to low, moderate and high waves. The wave spectra are shown in Figure 3 and the statistical characteristics for each are given in Table I.

Table I. Statistical Characteristics of Irregular Waves Used in Model Tests.

Wave Spectrum	$\bar{H}$ (ft.)	$\bar{H}$ (1/3)	$\bar{H}$ (1/10)
Low (I)	4.5	7.1	9.0
Moderate (II)	6.9	11.1	14.1
High (III)	8.6	13.8	17.5

In Table I, $\overline{H}$ is the average wave height (in feet); $\overline{H}$ (1/3) is the average of the one-third highest waves (significant height) and $\overline{H}$ (1/10) is the average of the one-tenth highest waves. All of the numbers in the table correspond to full-scale conditions.

For each of the breakwater variations tested, the force on the structure (vertical and horizontal) was measured as well as the irregular wave pattern. The breakwater models were mounted so that the back wall was rigidly fixed to a force transmitting bar that extended across the flume. The front wall was fastened to the back wall by 6 rods and both walls were free of the bottom and sides (by very small clearances) and extended above the design height so that all of the force on the structure would be communicated to the bar without loss. The force transmitting bar passed through the steel side walls of the flume and was fixed rigidly at both ends to the force-measuring strain-gage systems. The strain gages (horizontal and vertical) were mounted rigidly to the steel side walls. Thus, the deflection of the bar relative to the rigid steel sidewalls is a measure of the force exerted on the breakwater by the waves.

DISCUSSION OF RESULTS

The model tests produced a number of records of vertical and horizontal force. These records were converted to appropriate force spectra (Figures 4 and 5) and from these outputs total force calculations were made.

Forces on Prototype Breakwater

The first set of force measurements was made on the basic perforated breakwater. The results are shown in Table II where $\overline{F}$ is the average force and the other symbols correspond to the definitions given in Table I.

Table II. Statistics of Total Force (pounds per foot) on Perforated Breakwater.

Wave Spectrum	$\overline{F}$	$\overline{F}$ (1/3)	$\overline{F}$ (1/10)
I	200	320	407
II	240	384	288
III	282	450	572

Table III shows the same force statistics when the breakwater is not perforated.

Table III. Statistics of Total Force (pounds per foot) of Solid-Wall Breakwater.

Wave Spectrum	$\overline{F}$	$\overline{F}$ (1/3)	$\overline{F}$ (1/10)
I	444	710	903
II	510	814	1035
III	604	965	1230

It is seen by comparison of Table II with Table III that the perforations reduce substantially the force on the breakwater. In this case, the reduction is more than 50% which is in line with theoretical prediction.

Perforated Interior Wall

A perforated wall was placed halfway between the front and back wall in an effort to induce further internal energy dissipation. The results are given in Table IV.

Table IV. Statistics of Total Force (pounds per foot) of Perforated Breakwater with 10% Perforated Interior Wall.

Wave Spectrum	$\bar{F}$	$\bar{F}$ (1/3)	$\bar{F}$ (1/10)
I	425	680	842
II	497	795	1020
III	575	920	1170

Comparison of the statistics in Table IV with those in Tables II and III indicate that the interior perforated wall is relatively ineffective in dissipating wave energy. Moreover, it appears to substantially decrease the effectiveness of the outer perforated wall. There is no evidence that optimizing the geometry of the interior wall will improve performance materially.

Perforated Back Wall

A perforated back wall was installed to further reduce wave force. However, in this case, it was necessary to observe wave formation on the shoreward side of the breakwater and to ascertain that the outpouring did not exceed 10 feet which is assumed to be the maximum stand-off distance for a ship, when the breakwater is used as a pier. It was impossible to make precise measurements, so visual observations had to suffice. Tables V and VI show the results of a perforated back wall. In the case shown in Table V the back wall was 20% perforated; regular and irregular waves were used.

Table V. Observed Outpouring from 20% Perforated Back Wall.

Regular Waves

Period (sec.)	Height (ft.)	Distance (ft.)
7	10.2	1.87
10	11.2	0.94
13	4.3	0.94
13	10.2	1.87
16	7.0	1.87

Irregular Waves

	Average Distance	Maximum Distance
Low	1.98	5.63
Moderate	2.25	6.75
High	2.82	6.75

It appears that the stand-off distance of 10 feet is relatively safe under the conditions tested here. Furthermore, for the design wave period (10 seconds) at an incident wave height of 10.2 feet, the waves on the shoreward side of the breakwater were only about 1/5 the height on the seaward side.

A second experiment was carried out by inserting an interior wall with 10% perforations. The results are shown in Table VI.

Table VI. Observed Outpouring from 20% Perforated Back Wall with 10% Perforated Interior Wall.

Regular Waves

Period (sec.)	Height (ft.)	Distance (ft.)
7	10.2	0.47
10	11.2	1.87
13	4.3	0.94
13	10.2	3.75
16	7.0	1.98

Irregular Waves

	Average Distance	Maximum Distance
Low	0.94	2.34
Moderate	0.94	2.34
High	1.98	3.75

Here the stand-off distance is in no danger of being violated and the waves on the shoreward side are again only about 1/5 the height of those on the seaward side. The interior wall appears to have an overall beneficial effect for this application.

Scour at Base of Structure

Modeling erosion problems is quite complex if precise quantitative measurements are required. In this case, however, it was desired first to establish that perforations reduce scour and then to determine generally how the scour was effected by varying the distance between the bottom of the breakwater and the sand bottom in which it was installed.

Figure 6 shows a schematic drawing of the general scour experiments. A sloping bed of fine sand (dashed lines) was spread under the model which was supported on piles resting on "bedrock". The incident waves were regular with periods of 7, 10, 13 and 16 seconds. The wavemaker was stopped, after the sand deformation appeared to reach a state of equilibrium. Measurements were made of prominent mound locations and depths, as indicated in Figure 6, and from these measurements, the profile of deformation was reconstructed, for each case. In addition, notes were taken on the condition at the base of the piles. Figures 7-9 show some of the results of the scour experiments.

Figure 7 deals with a caisson-type breakwater (solid front and back wall) in which the bottom of the breakwater is on the sand bed. It is seen that the solid-wall breakwater resting on the sand bed is very vulnerable to erosion; the effect increases with wave period, as expected. At 13 and 16 seconds, the erosion under the walls is down to bedrock and would probably have extended deeper if there was more room. When the breakwater is raised off the sand bed (not shown) the effect of scouring diminishes, but is still somewhat pronounced even when the breakwater is 13 feet from the bottom. Equally significant is the observation that the base of the piles was considerably eroded even when the distance to the bottom was a maximum.

When the front wall was perforated (Figure 8), the situation was altered significantly. That is, the front wall sustained very little erosion, while the back wall suffered considerably. Again, the scouring increased with period, but in this case there was no significant difference.

In the final test, both front and back wall were perforated (Figure 9), but only the case of the breakwater resting on the sand bed was treated. As expected, the erosion effects were least, of all the cases tested, and at no time was "bedrock" reached for any wave condition. It is likely that raising the breakwater off the sand bed would have produced still better results as was evidenced in the prior cases.

CONCLUSIONS AND RECOMMENDATIONS

As a result of the experiments reported here and the supporting analytical work, the following conclusions are drawn:

1. There is a substantial force reduction achieved by perforating the front wall of a vertical-wall breakwater. For design purposes, it is likely that a force of 1000 lb./ft. may be adopted with relative safety under most environmental conditions (Tables II and III).

2. The use of an interior perforated wall shows little evidence of being effective in reducing overall force on the structure and is not recommended for such an application.

3. The perforated back wall serves a useful function. Although force measurements were not made, it is obvious that relief of pressure on the back wall must be beneficial. It is important to note that the perforated back wall does not interfere with using the breakwater as a pier. Nor does it permit waves of any appreciable height to form on the shoreward side.

4. Scouring at the base of the breakwater can be a severe problem. The perforations on front and back wall have an astonishing effect on stabilizing sediment transport and reducing erosion, even at the base of piles. It is likely that a relatively small distance between the bottom of the breakwater and the sea-bed will be even more useful in preventing erosion.

There is now adequate evidence that the perforated breakwater can perform a service that is sorely needed. If further evidence is required, it is recommended that a 1/4 scale model be erected and installed at a suitable locale (Chesapeake Bay, Long Island Sound) where it can be instrumented and observed for one winter season. Adequate data could thereby be collected to justify construction of needed systems.

ACKNOWLEDGMENTS

The authors wish to extend their appreciation to the following people for invaluable assistance at various stages of the program. Bob Romandetto participated in the experiments; Bert Kieffer also participated in the experiments and, in addition constructed the models and drafted all the figures; Al Raff assisted in the data analysis; Lois Savastano typed the manuscript.

REFERENCES

Marks, W. (Sept. 1966). A Perforated Mobile Breakwater for Fixed and Floating Application: Proceedings Tenth Conference on Coastal Engineering, Vol. II, Ch. 64, Published ASCE.

Jarlan, G. E. (April 1965). The Application of Acoustic Theory to the Reflective Properties of Coastal Engineering Structures: DME/NAE Quarterly Bulletin No. 1965(1), National Research Council of Canada.

Jarlan, G. E. and Marks, W. (March 1965). Optimum Hydrodynamic Characteristics of a Stable Ocean Platform for Deep-Sea Operations: OCEANICS, Inc. Tech. Note No. 65-07.

Longuet-Higgins, M. S. (March 1953). Mass Transport in Water Waves: Philosophical Transactions, Vol. 245A.

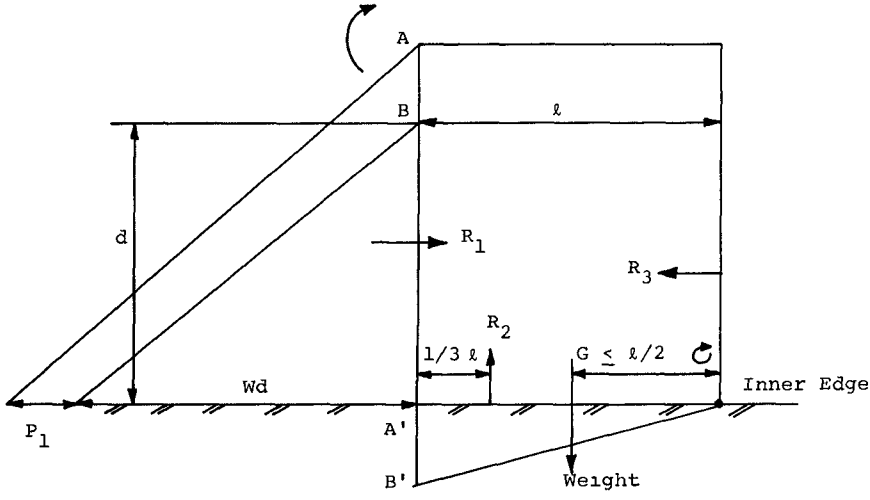

R_1 is the resultant of the horizontal pressure (hydrostatic and dynamic)

R_2 is the uplift pressure

R_3 is the resultant of the initial pressure (hydrostatic)

Figure 1 Wave forces on vertical-wall structure.

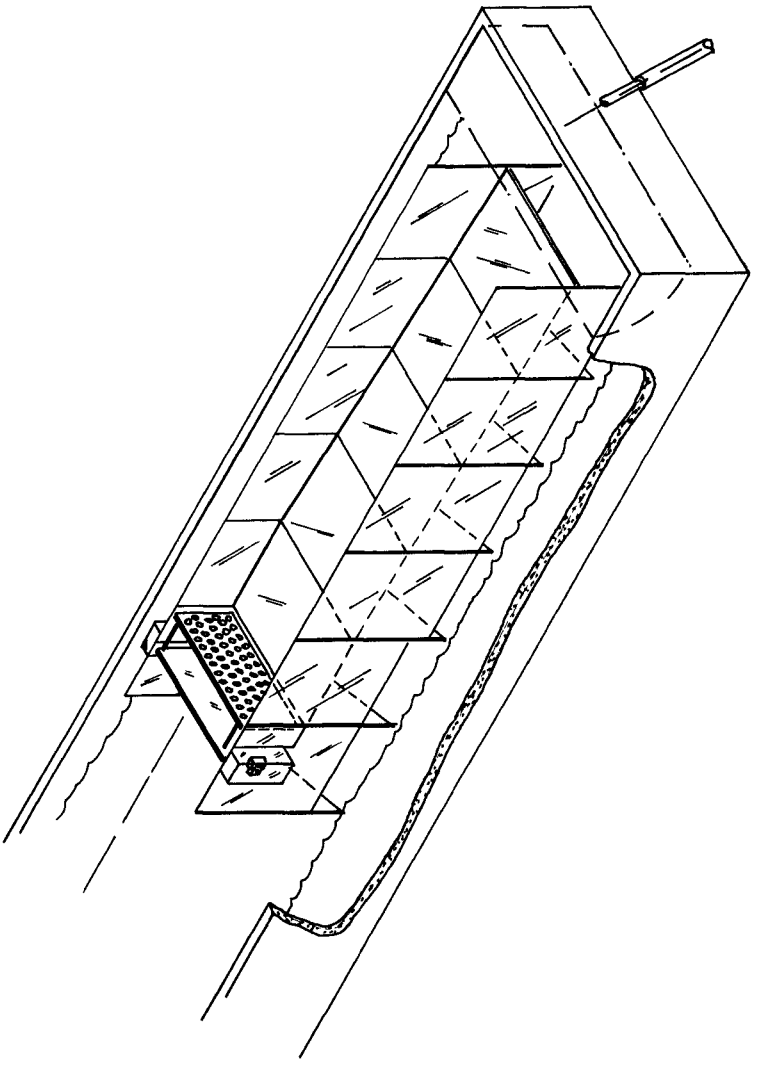

Figure 2 Sketch of OCEANICS shallow-water flume in wave tank.

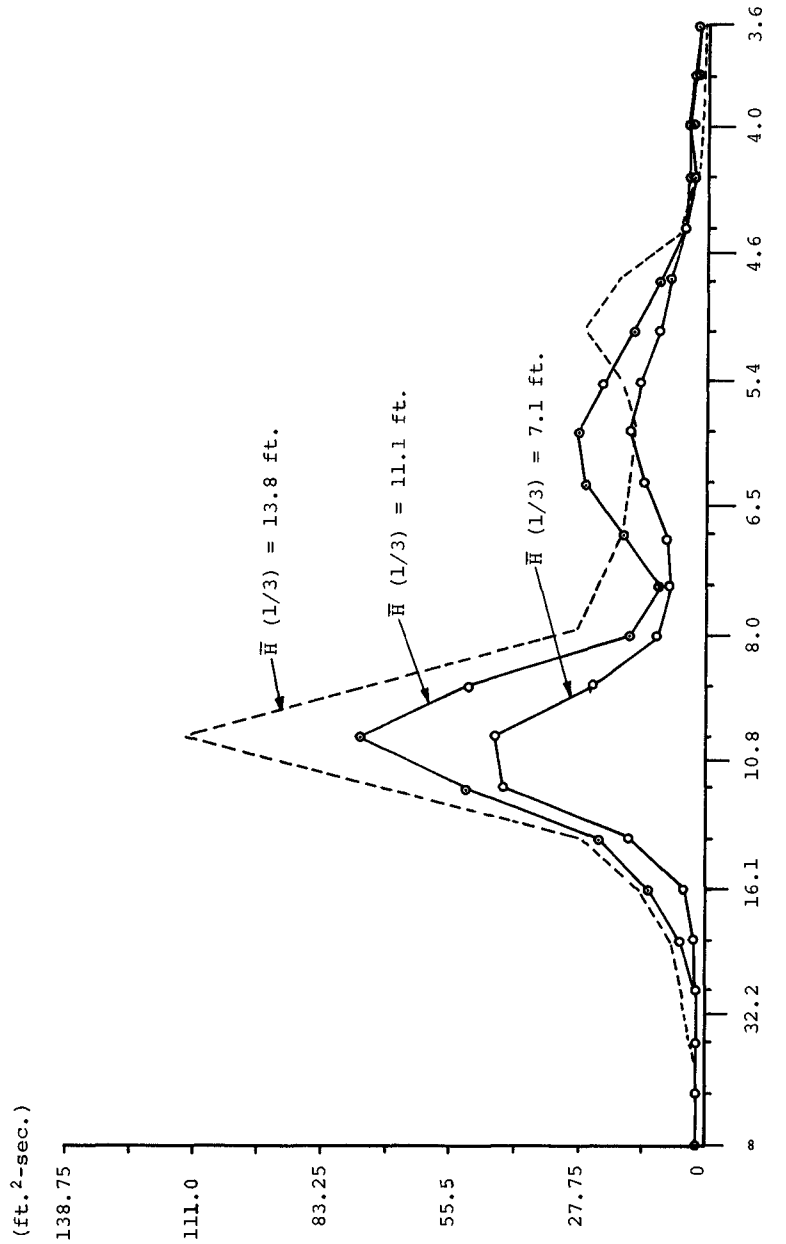

Figure 3 Samples of wave spectra used in model tests.

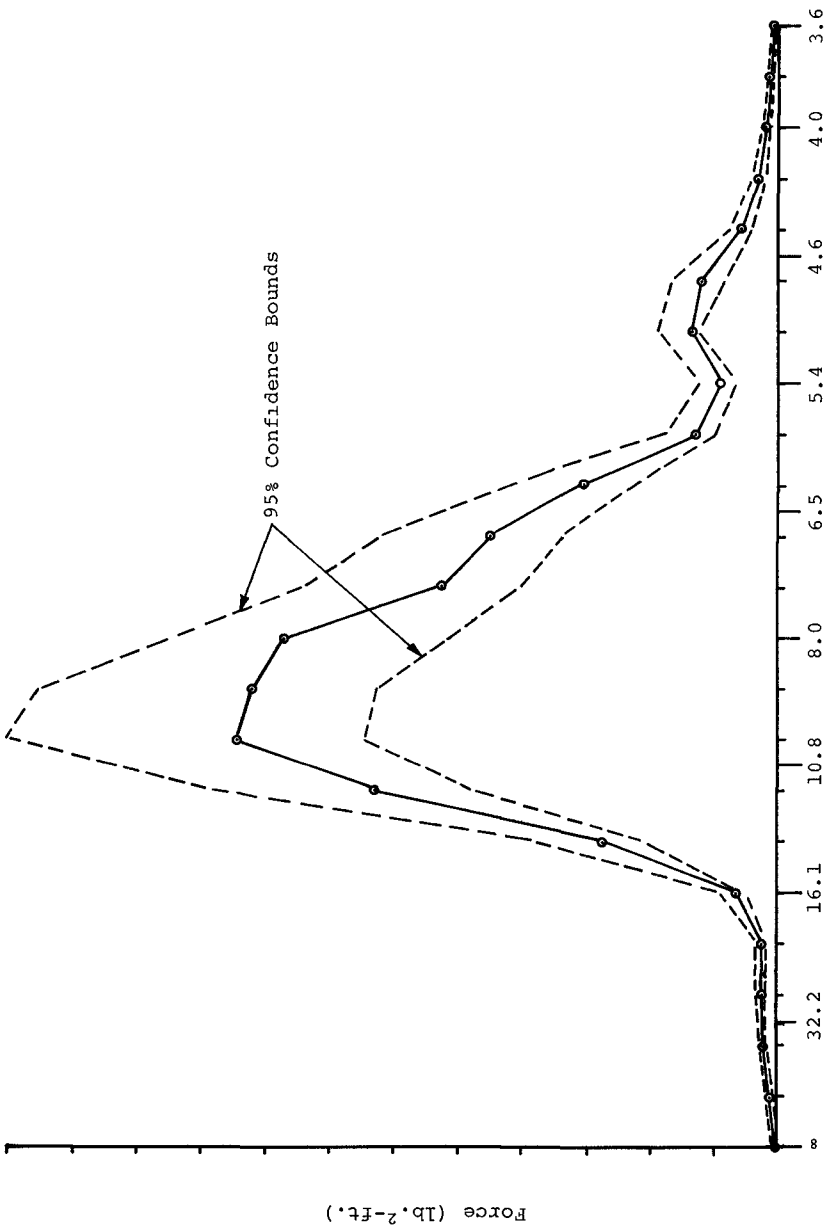

Figure 4 Sample of horizontal force spectrum.

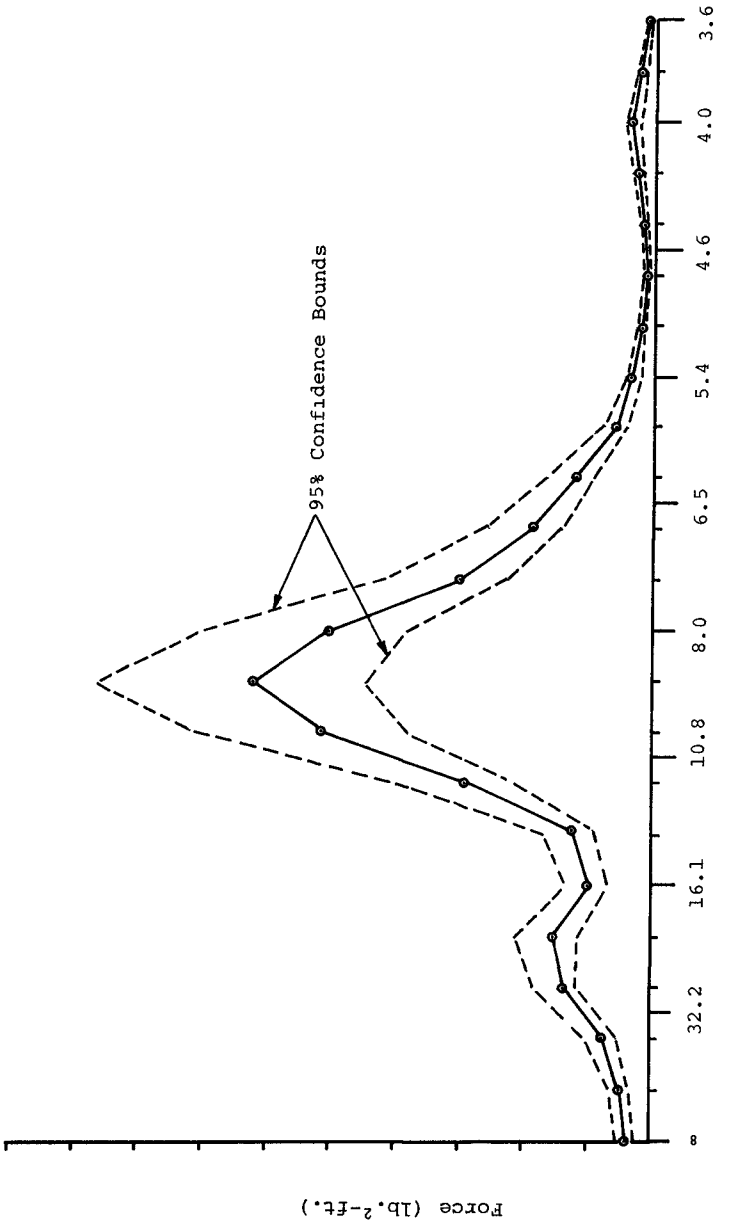

Figure 5 Sample of vertical force spectrum.

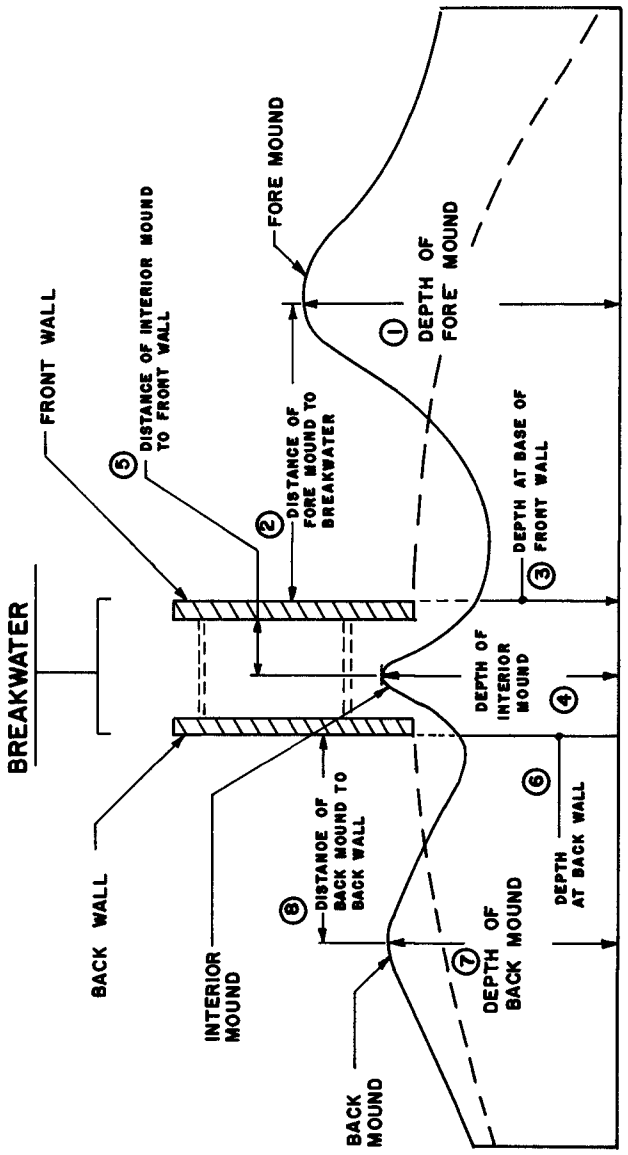

Figure 6 Schematic drawing of scour experiments.

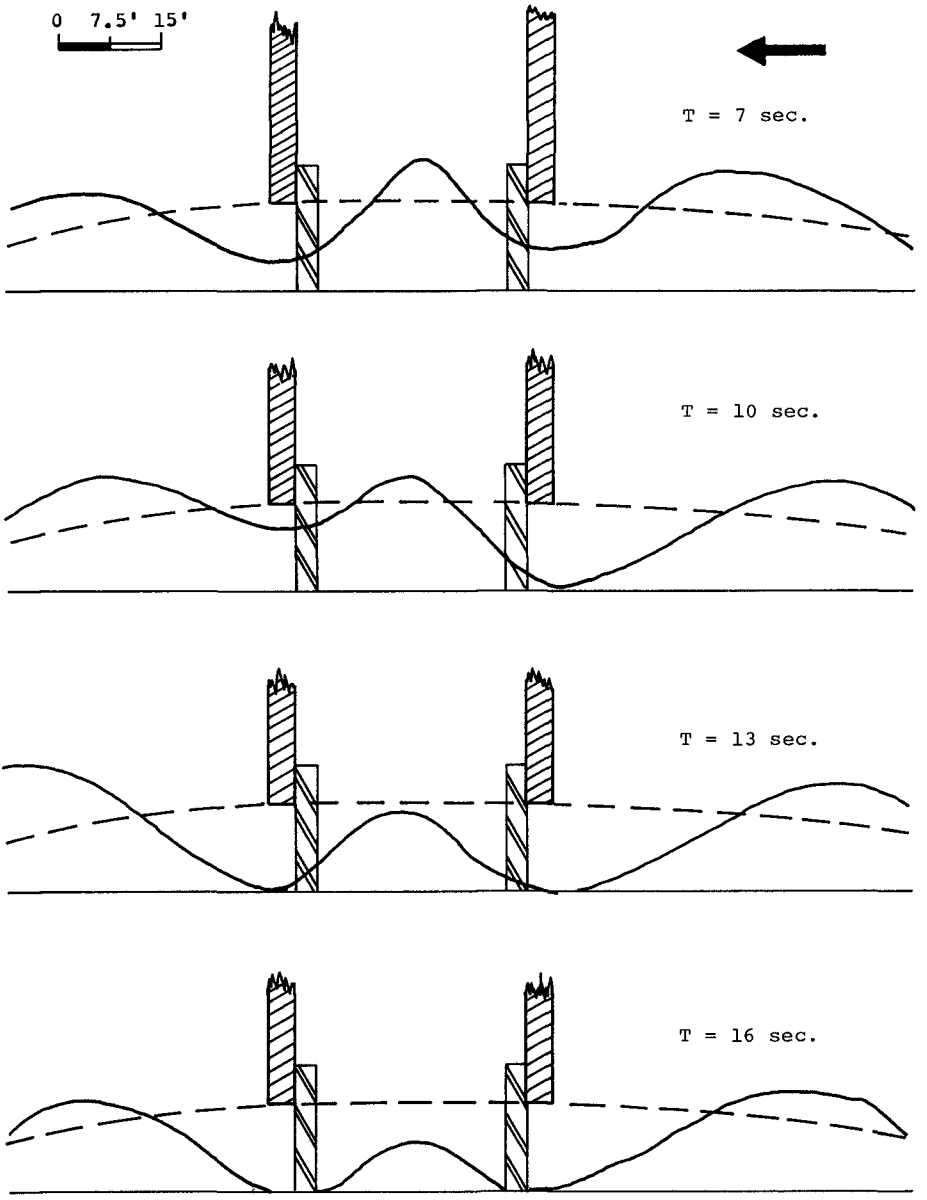

Figure 7 Scour at base of solid-wall breakwater resting initially on sand bed.

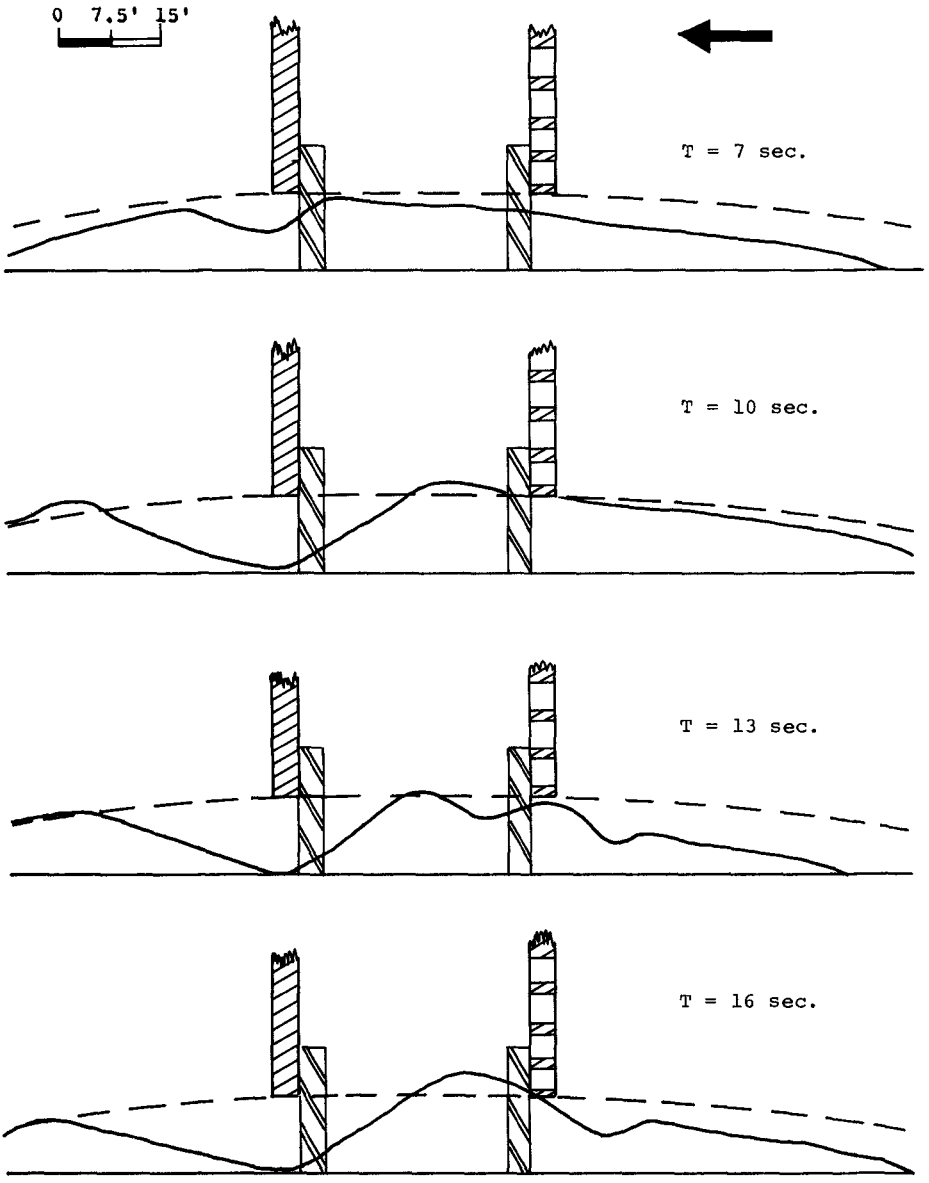

Figure 8 Scour at base of perforated breakwater resting initially on sand bed.

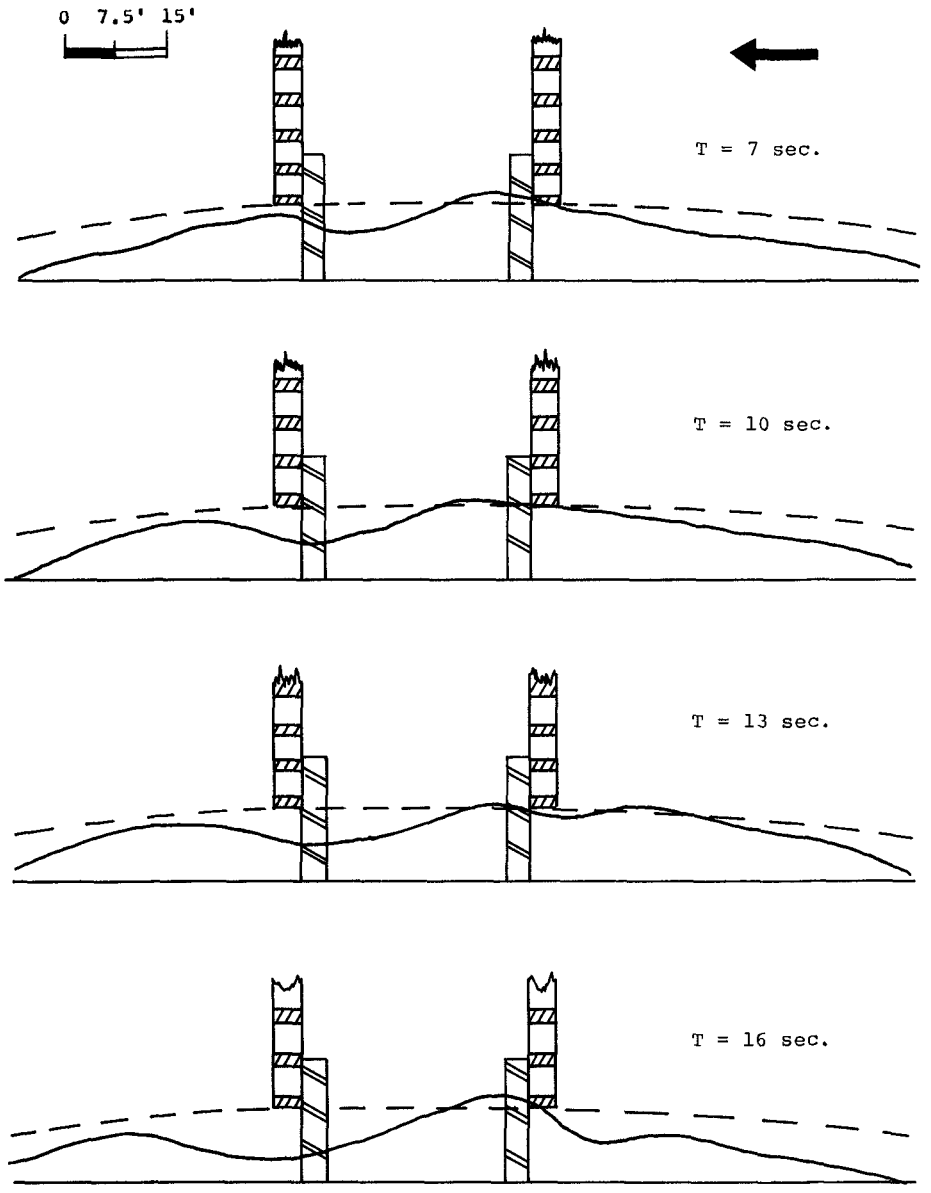

Figure 9 Scour at base of breakwater with perforated front and back walls resting on sand bed.

CHAPTER 72

SOLID AND PERMEABLE SUBMERGED BREAKWATERS

T. Milne Dick
Assoc. Res Officer
National Research Council
Ottawa, Canada

A Brebner
Head, Dept. of Civil Engineering
Queen's University
Kingston, Canada

ABSTRACT The behaviour of thin and rectangular solid submerged breakwaters is re-examined. Dean's theory is found to be correct for a thin barrier in infinitely deep water. An empirical and theoretical relationship for the reflection coefficient of a thin breakwater across the wave number spectrum is proposed. Rectangular solid breakwaters have a maximum reflection when the incident wave has the same period as a standing wave on top of the breakwater and with a wave length equal to the crest width. A submerged permeable breakwater for depths of submergence greater than 5% of the total depth transmits less wave energy than the solid over a certain frequency range. The minimum is transmitted when the criterion above for solid breakwaters is also met. Both permeable and solid rectangular breakwaters cause a substantial loss in wave energy and at least 50% of the incident energy is lost to turbulence. A substantial proportion, 30 to 60% of the energy transmitted is transferred to higher frequencies than the incident wave.

INTRODUCTION

In many locations, submerged breakwaters offer a potentially economic solution to coastal engineering problems. Complete protection from waves is often neither necessary nor desirable and it is in these situations a submerged breakwater becomes feasible. Submerged breakwaters have been used to protect harbour entrances, to control wave action at inshore fishing grounds and to reduce the rate of littoral drift Most applications have been designed on the basis of ad hoc experiments since there is no substantiated body of theoretical or experimental work to permit reliable or safe design

NOTATION

The notation on Fig 1 is largely self-explanatory. H_1 and H_3 are the incident and reflected wave heights respectively The transmitted wave in theory is denoted by H_2 and refers to the height of a sinusoidal wave. In the tests however, except for the thin breakwater, the transmitted wave was not simple but the resultant of a basic carrier wave with the same frequency as the incident wave and waves of higher frequencies. It is believed that the latter were usually harmonics of the incident wave The total transmitted wave energy was therefore represented by a wave having the same frequency

as the incident wave and a wave height defined by

$$H_{eq} = \frac{2\sqrt{2}}{T} \int_0^T \eta^2(t)\, dt \qquad (1)$$

where

T is the incident wave period (secs)
η is the displacement of the water surface from the mean water level (ft)
t the time coordinate.

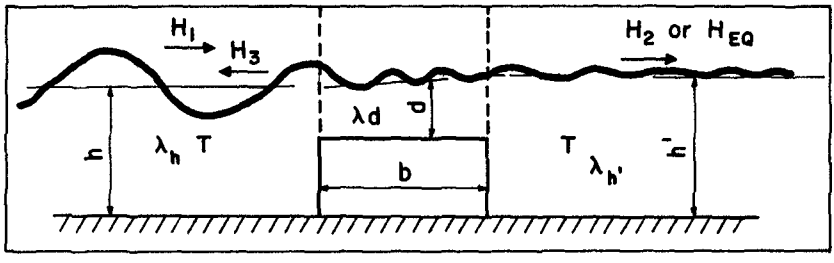

Fig. 1. Notation for Breakwater

The imaginary sinusoidal wave of height H_{eq} is called the equivalent wave and contains the same energy as the actual transmitted irregular wave. A useful idea adopted by most authors is the transmission and reflection coefficients defined by

$$C_T = H_2/H_1 \text{ or } H_{eq}/H_1 \qquad C_R = H_3/H_1$$

Wave energy losses occur at the breakwater and if these losses are made equivalent to a wave of height H_L of the same period as the incident wave and the depth of water is h then it is readily shown by the conservation of wave energy flux that

$$C_T^2 + C_R^2 + C_L^2 = 1 \qquad (2)$$

where $C_L = H_L/H_1$.

SOLID BREAKWATERS

Thin Breakwater. Dean (1945) developed a theoretical expression from linear wave theory for C_T and C_R for a thin lamina extending from infinite depth to some distance d ft below the still water surface. Later Ogilvie (1960) obtained a solution for very long waves in depth h. Solutions for waves occurring in the intermediate zone between shallow water waves and deep water waves are non-existent and recourse must be taken to empirical studies. These two theories cited indicate that the important parameters for the thin breakwater are the relative depth of submergence d/h and the ratio $2\pi d/\lambda_h$.

Rectangular Breakwater An expression for C_T was obtained by Jefferys (1944) for the case of shallow water waves A deep water solution was found by Newman (1965) provided the width of the barrier was great compared with the wave length. Takano (1960) obtained a series solution for a rectangular barrier embracing all wave lengths and widths but unfortunately the solution did not converge rapidly and since 19 simultaneous equations must be solved to obtain the 1st three terms the solution was very cumbersome. However the theories show that d/h and λ_h/b or $\lambda d/b$ are important parameters.

An engineering approach to the problem considered the flux of wave energy and assumed that energy being propagated above the crest level passes over the breakwater and reappears as a wave on the lee side This approach was proposed by Johnson et alii (1951) and in that paper is attributed to Fuchs. Their equation is

$$C_T = \left[1 - \frac{2k(h-d) + \text{SINH } 2k(h-d)}{2kh \quad + \text{SINH } 2kh} \right]^{1/2}$$

where $k = 2\pi/\lambda_h$
h = depth of water in front of breakwater
d = depth of water over breakwater crest
λ_h = wave length in depth h.

Apparatus. The tests were run in a wave tank which was 3 ft wide and contained 2 ft of water. Waves were absorbed by a permeable beach which had a coefficient of reflection of the order of 5% The test breakwater was located 110 ft from the wave machine and 35 ft from the beach. Waves were measured in front of the breakwater by a movable probe which was not moved more than 17 ft from the breakwater. Transmitted waves were measured by a probe fixed at a distance of 25 ft from the breakwater face. The wave probes were the capacitive type and employed #22 gauge teflon covered wire.

Test Procedure In nature, a wave striking a submerged barrier will result in some of its energy being reflected offshore where it is ultimately dissipated by wind and internal stresses. In the laboratory flume the reflected wave strikes the wave paddle and is almost totally reflected. In turn the reflected wave is again partially reflected at the submerged barrier and so on. The net result is a wave system which differs considerably from the simple model in nature, that is assuming monoperiodic waves could occur in nature. In the tests done for this study the wave machine paddle was set in motion very quickly producing a reasonably short wave front. After the primary reflection of the full sized wave had passed the movable probe in the negative direction, the latter was moved to pick up the wave envelope. The waves a short distance in front of the barrier are the sum of the incident and reflected wave trains. Where the waves were exactly in phase then the measured wave height was $H_{MAX} = H_1+H_3$ and where exactly out of phase by π^c then the wave height was $H_{MIN} = H_1-H_3$. Once H_{MAX} and H_{MIN} were measured then H_1 and H_3 were easily calculated. The transmitted

wave H_2 or H_{eq} was derived from the fixed wave probe record.

RESULTS

Thin Breakwater-Deep Water Case: The coefficients of reflection and transmission were obtained for wave lengths of 2 and 4 feet which complied with the deep water condition In these experiments the transmitted wave height was measured directly as H_2 and not by equation 1, since there was little distortion of the sinusoidal wave This was only true if the trough of the waves in front of the breakwater did not fall below the crest level When this occurred irregularities and harmonics were superimposed on the transmitted wave. Tests were run for depths of submergence d = 0.10, 0.15, 0 20, 0.30, 0.40 and 0.60 feet. Varying wave steepnesses were employed All the test results have been plotted on Fig. 2 on which has also been drawn curves calculated from Dean's theory. When Dean published his results he evaluated C_T and C_R only to $2\pi d/\lambda_o \leq 0.25$ because approximate methods were valid up to that point. We have however extended the numerical solution with an electronic computer. Our measurements of C_T and C_R contain the effect of viscous wave attenuation but we have made a correction only to C_T as shown in Fig. 2. Manifestly, the theory and experiments are in good agreement and one can conclude that Dean's theory for a thin breakwater in infinitely deep water is sensibly correct

Thin Breakwater-General Case As for the deep water case values of C_T and C_R were obtained for incident wave lengths of 6, 8, 10 and 12 feet. All the results for λ_h = 2 to 12 were plotted using as parameters λ_h/h and d/h. In Fig. 3 is shown a typical plot[1] of the test measurements upon which has been superimposed Dean's, Ogilvie's and Fuchs' theories. The experimental points have fairly well defined trends and average curves for C_T and C_R were sketched in carefully as indicated by the dotted lines in Fig. 3. All these trend lines have been assembled in Fig. 4 which indicates a theoretical and experimental relationship for C_R, d/h and $2\pi d/\lambda_h$ across the wave number spectrum. For $k_h h > 3$ 14 Dean's theory is assumed to hold and it has been replotted here in another form. For very small wave numbers, i.e. $k_h h < 0.35$ Ogilvie's theory has been drawn in by interpolation from his published solution. In the intermediate zone for $1.0 < k_h h < 3.4$ the experimental trend lines are shown dashed. We have also indicated by a dashed-dot line a possible correction to the present empirical trend lines. The remaining gap for $0.35 < k_h h < 1.0$ remains unknown but we have hazarded that it may be of the form indicated.

At the top of Fig. 4 are plotted the theoretical values of C_T but it was found that the experimental results, because of losses

---

[1] There is insufficient space here to show all the experimental data This can be found in detail in "Solid and Permeable Submerged Breakwaters", T.M. Dick, Civil Engineering Research Report, 1968, Queen's University, Kingston, Ontario.

at the breakwater did not accord with the theory. Consequently, the empirical curves for C_T have been plotted in Fig. 5. We have indicated a dashed line as a correction for d/h = 0.10 to make it comply with the other experiments. The transmitted wave heights as measured deviate from forecasts made by the theory. It seems that because of energy losses at the breakwater the most reliable method for estimating transmitted wave heights will be from empirical graphs.

Rectangular Breakwater-General Case A rectangular breakwater was constructed which had a crest width of 2 feet and three depths of submergence, namely, 0.1, 0.2, and 0.4 feet. Wave lengths of 2 to 12 feet with varying wave heights were employed. The transmitted wave height was generally not a simple wave but was distorted by varying degrees. Hence the transmitted wave energy was evaluated from equation 1. The reflected wave height was obtained in the usual way. A typical test result[1] is shown in Fig. 6 with the trend line sketched through the points. In order to compare the variations caused by the depth of crest submergence, the trend lines have been gathered together in Fig. 7 and 8. It is readily seen that C_R undulates with λ_h/b but the same tendency is not so evident in C_T. We believe that when the reflection is small, the higher wave which tries to pass over the breakwater is eradicated by turbulence and breaking on the crest. In turn when the reflection is high the lower wave which is transmitted tends to pass over the breakwater with less breaking and relatively more energy is transferred. The net result is that C_T is smoothed out. The loss coefficient C_L was calculated from equation 2. The major role played by the wave breaking and turbulence in destroying the incident wave energy is quite evident and was one of the rather unexpected results in the investigation. In the solid case the losses account for greater than 50% of the incident wave energy.

Examination of the maxima exhibited by C_R in Fig. 7 enabled Table 1 to be drawn up.

TABLE 1. Parameters at Maximum Reflection

	d/h	
	0.20	0.10
C_R(MAX)	.40	.60
λ_h/b	3.4	4.9
λ_d/b	2.1	1.9

From Table 1, it seems that the maximum reflection occurs when the length of the wave on the breakwater crest equals twice the crest width. Or, restating, the maximum reflection occurs when the period of a standing wave of length b on top of the breakwater has the same period as the incident wave. A substantial proportion of the transmitted energy is found at frequencies higher than the input frequency. The fundamental wave height H_F was abstracted by obtaining the amplitudes of the Fourier coefficients corresponding to the frequency $2\pi/T$ from the same portion of record

used to establish H_{eq}. Defining $C_F = H_F/H_I$ the experimental trend lines[1] are shown in Fig. 8. As would be expected the value of C_F is always less than C_T but remarkably the ratio C_F/C_T does not vary greatly with d/h for constant λ_h/h. The ratio C_F/C_T has also been plotted on Fig. 8 and lies in the range $0.6 < C_F/C_T < 0.8$. This means that between 36 to 64% of the transmitted energy is being transferred to waves with a greater frequency than the incident wave In nature one might expect these higher frequencies to be less of a problem than the incident swell or significant storm wave. Consequently, the useful attenuation in the wave height may be somewhat greater than that indicated by the equivalent wave height method of calculation.

PERMEABLE BREAKWATER

The possibility of improving the effectiveness of a submerged breakwater by increasing turbulence and wave interference seemed interesting. It was decided to construct a permeable rectangular structure, composed of nested tubes which had their axes parallel to the incident wave direction. A rigid horizontal flat plate was placed on top of the tubes. This arrangement had several objectives. Firstly, the waves passing over the breakwater would continue to lose energy by breaking. Secondly, turbulence and friction would tend to reduce the effect of the pulse passing through the breakwater and lastly, the wave passing over the breakwater could be out of phase with waves caused by the pulse through the tubes. If the latter could be achieved and the phase difference was π then the waves would tend to cancel In addition since the component wave periods would be the same, the beat phenomenon would not occur. The effect of the permeable breakwater on the reflected wave energy was not known but it seemed likely that reflection would be less. Reflected energy was considered to be controlled by the amount of solid surface constituting the forward face of the breakwater. This factor was defined by the porosity (p) given by,

$$p = \frac{\text{Area of apertures within selected zone}}{\text{Total area of selected zone}}$$

We are also assuming that the porosity is uniformly distributed over the forward face of the breakwater.

TEST RESULTS

The model breakwater which had a porosity of 0.72 was composed of nested 1" D aluminum tubes which had the intertubular instertices plugged with plasticene. Other porosities of .18, 0.40 were obtained by placing a 1/8 plate perforated on the same centres as the nested tubes with 1/2" and 3/4" D holes respectively. In order to take matters to the limit, a number of tests were run by removing the tubes entirely, leaving only the top plate in place so that the porosity = 1.0. Tests were run as for the solid rectangular breakwater. A typical result[1] is shown in Fig. 9. A trend line has been carefully sketched through the experimental points

obtained for C_T, C_R and C_L so that equation 2 was satisfied. In Figs. 10, 11, 12 all the trend lines have been gathered together for varying porosities and the results for the solid breakwater p = 0 added for comparison. It can be concluded from Figs. 10, 11 and 12 that the permeable breakwater behaves differently from the solid and that all the permeable breakwaters have sensibly the same behaviour. In Fig. 10 the permeable breakwater transmits slightly greater waves and as the wave length increases the solid type is consistently better Concomitantly the waves reflected from the permeable type are less than the reflection from the solid structure. Losses at the permeable breakwater are slightly larger.

However in Figs. 11 and 12, the behaviour changes and one finds that over a certain wave length range that the permeable breakwater provides a substantial improvement in attenuation over the solid structure This is especially marked in Fig. 12 It is also quite evident that the value of C_R fluctuates in value with the variable λ_h/b and that C_T passes through a minimum when C_R is a maximum. In order to study the influence of the crest width a series of tests were run using only the submerged plate as representative of the permeable type. Crest widths of 1.25 and 3 00 feet were selected.

It was found that the minimum C_T gradually increased with crest width and that the breakwater behaviour was very similar. However the minimum C_T or maximum C_R occurred at various values of λ_h/b. These maxima or minima were picked off from the plotted results[1] and the parameter $\beta = 2\pi b/\lambda_d$ calculated. The results are tabulated below in Table 2.

TABLE 2. Lag Angle β for Horizontal Plate in π Radians

b	d/h .05	.10	.20
	C_T MINIMA		
1.25	1.2	.9	.8
2.00	1.6	1.1	.9
3.00	-	-	1.1
	C_T MAXIMA		
3 00	-	2.1	1.75

The parameter β is a lag angle which represents the time taken for a wave to transit the crest of the breakwater. In the table minimum transmission occurs when $\beta \simeq \pi^c$ and maximum transmission when $\beta \simeq 2\pi^c$. It can be shown from physical reasoning that these results are compatible and confirm one another. Hence for minimum energy transmission

$$\frac{2\pi b}{\lambda_d} \simeq \pi \quad \text{or} \quad \lambda_d \simeq 2b$$

In the same way as for the solid case, the height of the fundamental wave was abstracted from the Fourier series which was equivalent to the analogue wave trace. The results[1] were sensibly the same as for the solid breakwater.

CONCLUSIONS

1. Dean's theory for the transmission and reflection of waves at a thin barrier in infinitely deep water has been confirmed provided the trough of the incident wave system does not fall below the crest level.

2. A relationship across the wave energy spectrum for the reflection coefficient at a thin solid submerged breakwater has been proposed in Fig. 4.

3. In both breakwaters a major portion of the wave attenuation results from energy losses caused by turbulence and breaking at the breakwater.

4. Of the energy transmitted between 36 to 64% has been transferred to frequencies higher than the incident wave. Both breakwaters have about the same characteristics in this regard.

5. The transmission coefficient for the permeable breakwater passes through a minimum and over a certain range transmits a smaller wave than the solid breakwater with the same dimensions. At very shallow depths of submergence both breakwaters are similar in behaviour.

6. The maximum reflection coefficient for the permeable and solid breakwaters occurs when the incident wave has the same period as a standing wave on top of the breakwater. The solid breakwater has no well defined minimum transmission coefficient because turbulence and breaking eradicate fluctuations. However, the permeable breakwater has a well defined minimum coefficient of transmission.

ACKNOWLEDGEMENTS

The experimental work was performed at the Hydraulic Laboratory of the National Research Council by kind permission of the Council and D.C. MacPhail, Director of Mechanical Engineering. Thanks are also due to Dr. S Ince, Head of the Hydraulics Laboratory for his support and encouragement.

REFERENCES

Dean, W.R. (1945) "On the reflection of surface waves by a submerged plane barrier", Proc. Cambridge Phil. Soc. 41, Part 3, pp 231-36

Jeffreys, H. (1944) "Note on the offshore bar problems and reflection from a bar", Gt. Brit. Ministry of Supply Wave Report #3.

Johnson, J.W., Fuchs, R.A , Morison, J.R. (1951), "The damping action of submerged breakwaters", Trans. Amer Geophys Union 32.5, pp 704-718.

Newman, J N. (1965), "Propagation of waves over an obstacle in water of finite depth", Univ of California, Institute of Engineering Research, Berkeley, Calif. Series No 82.

Ogilvie, T F. (1960), "Propagation of waves over an obstacle in water of finite depth", Univ. of California, Institute of Engineering Research, Berkeley, Calif Series No 82.

Takano, K. (1960), "Effets d'un obstacle parallélépipèdique sur la propagation de la houle", La Houille Blanche, No 3, pp 247-267.

Dick, T.M. (1968), "Solid and Permeable Submerged Breakwaters", Civil Engineering Research Report, Queen's University, Kingston, Ontario

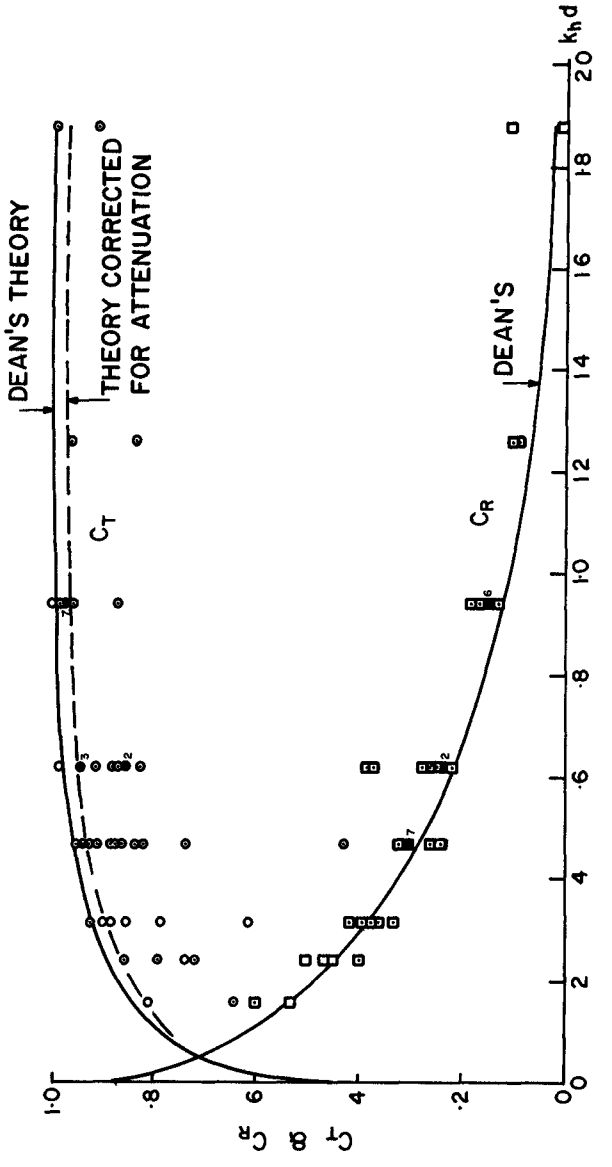

FIG. 2 COMPARISON OF THEORY AND EXPERIMENT FOR THIN BREAKWATER IN INFINITELY DEEP WATER

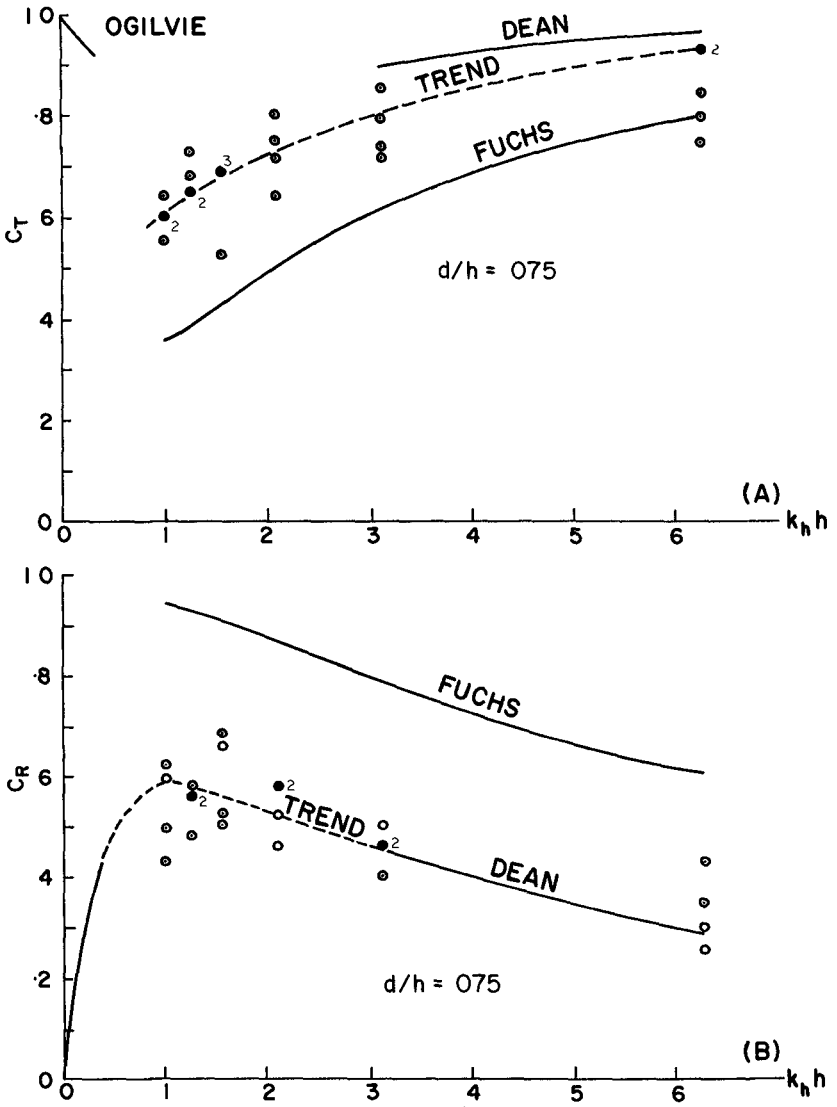

FIG. 3 TYPICAL THIN BREAKWATER TEST WITH AVAILABLE THEORY

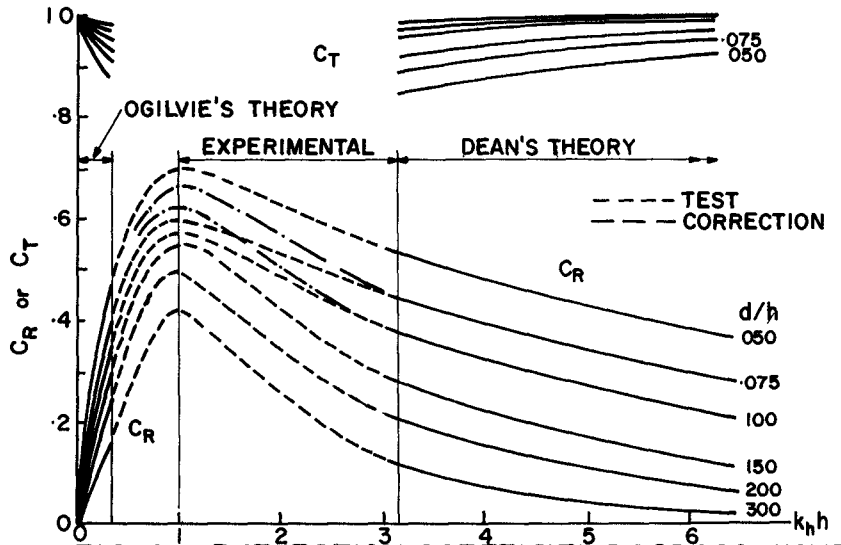

FIG. 4 REFLECTION COEFFICIENT ACROSS WAVE NUMBER SPECTRUM

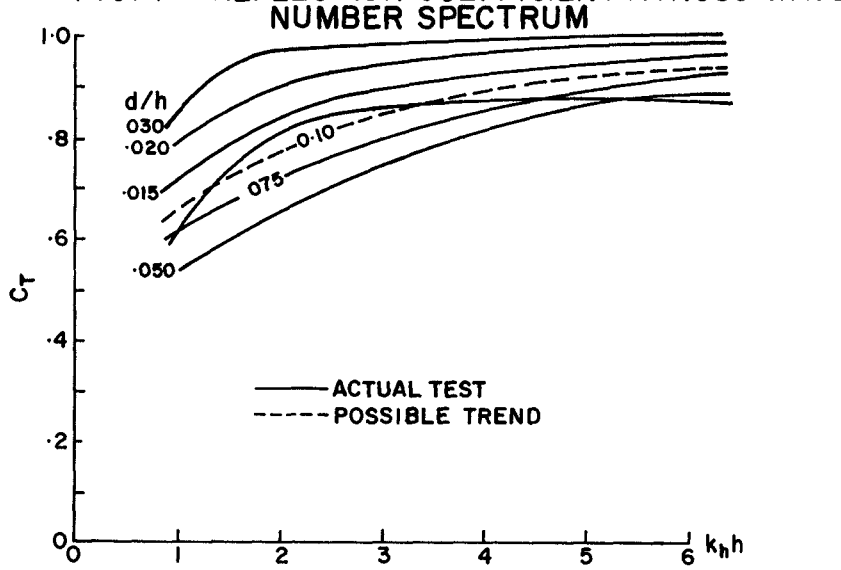

FIG. 5 EMPIRICAL TRANSMISSION COEFFICIENT ACROSS WAVE NUMBER SPECTRUM

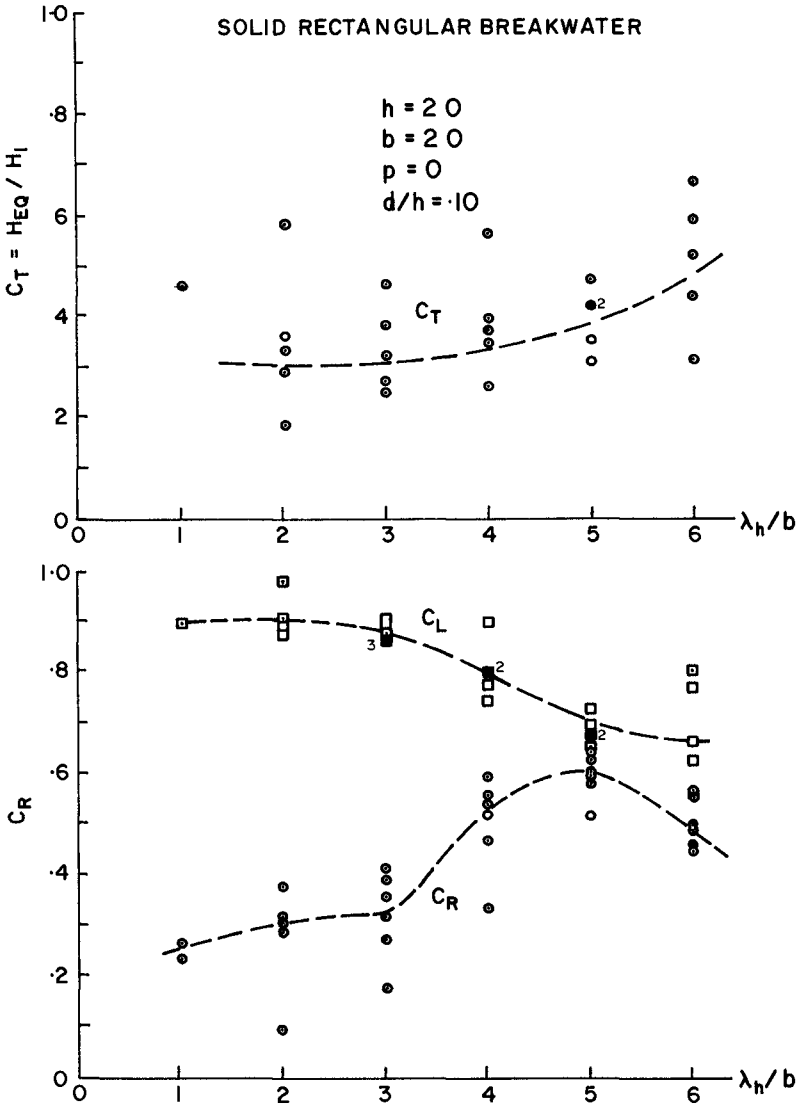

FIG. 6 TYPICAL TEST RESULT

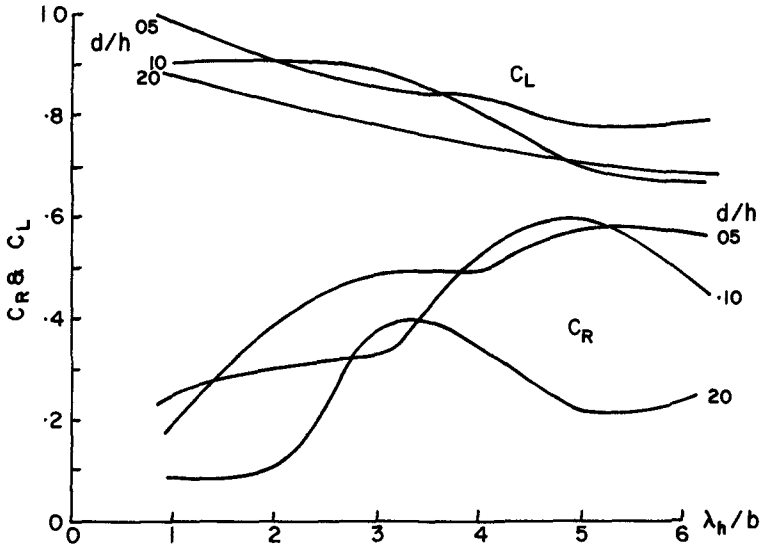

FIG. 7 VARIATION OF C_R WITH d/h

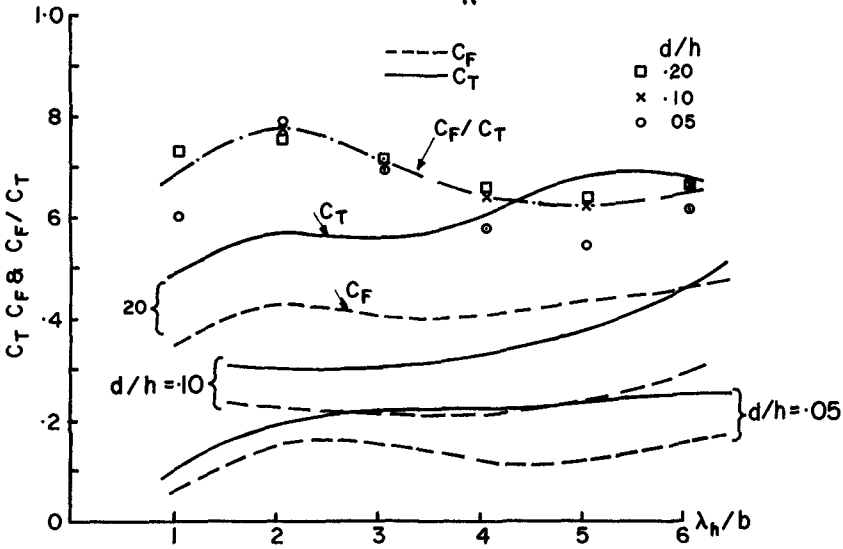

FIG. 8 AVERAGE TRENDS FOR C_F & C_T

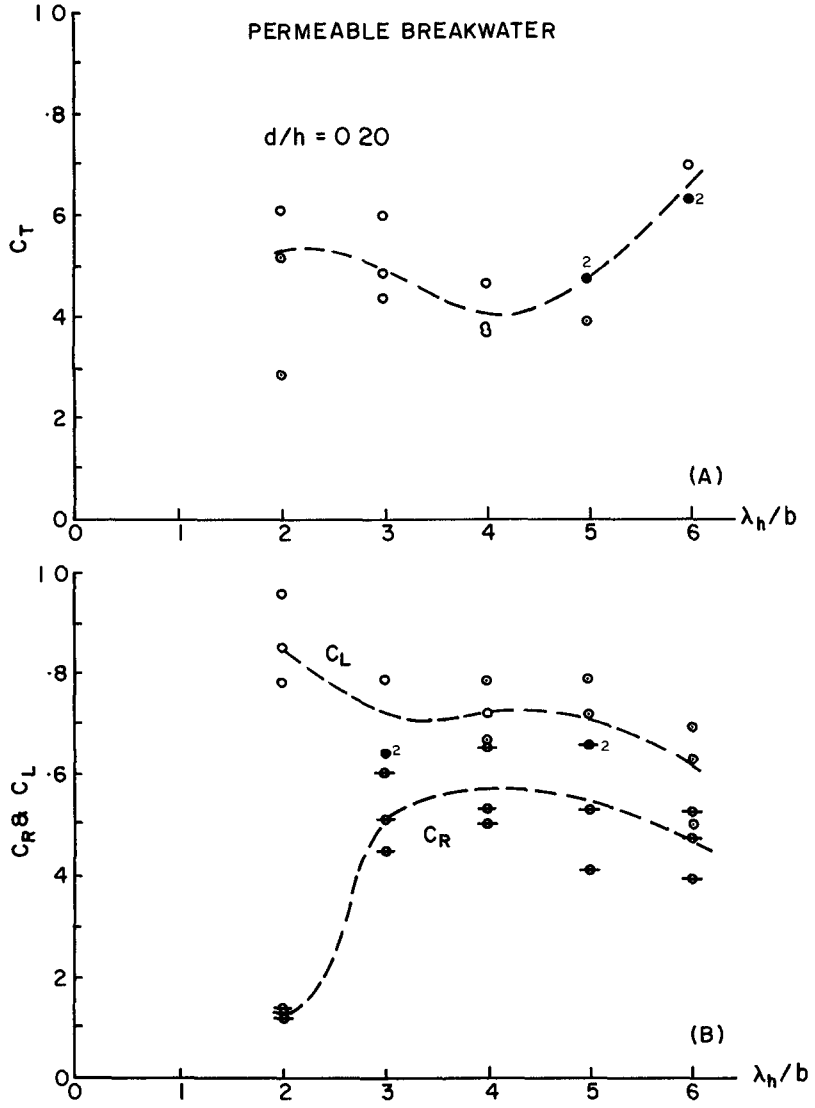

FIG. 9 TYPICAL TEST RESULTS POROSITY = 0·40

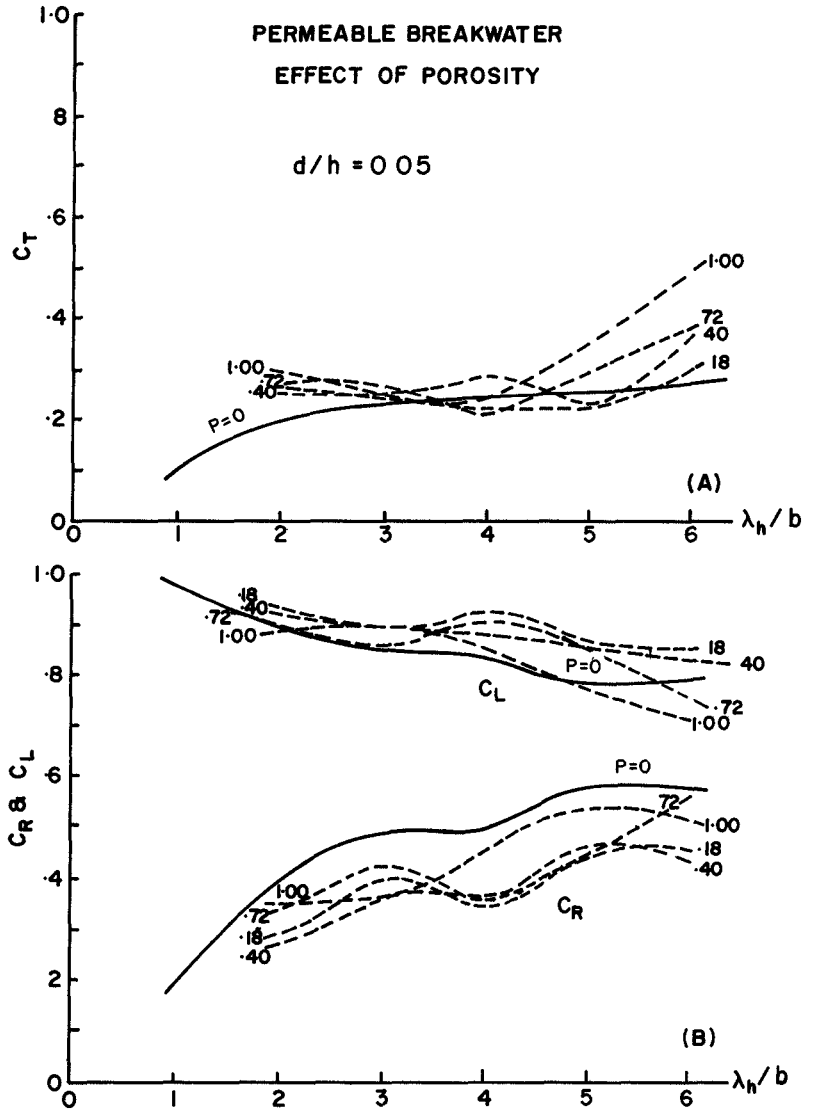

FIG.10 AVERAGE TEST RESULTS d/h = 0·05

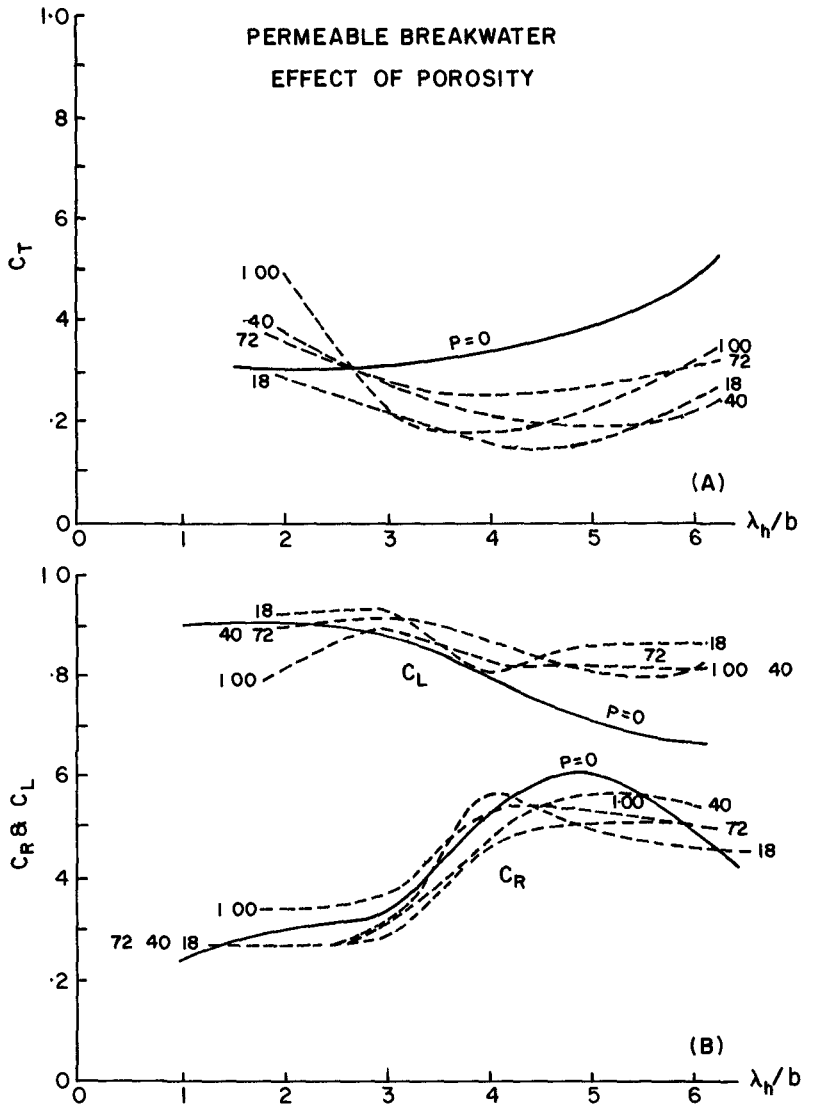

FIG.11 AVERAGE TEST RESULTS d/h = 0·10

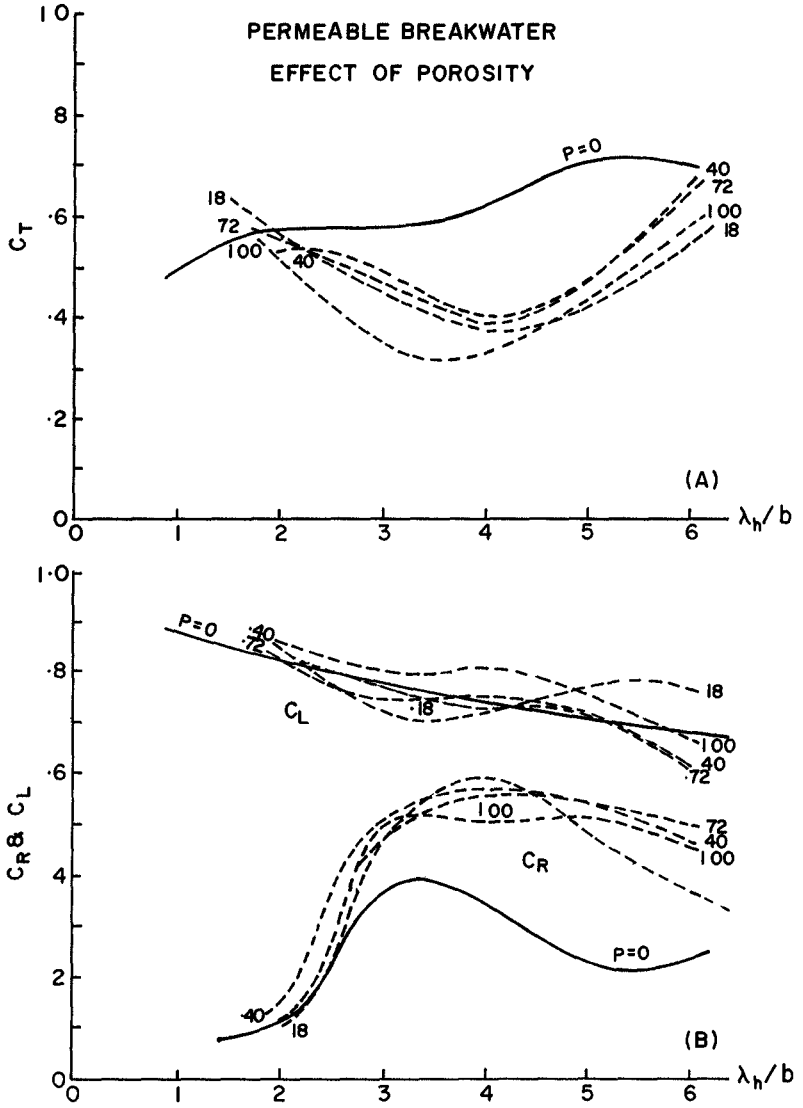

FIG.12 AVERAGE TEST RESULTS d/h = 0·20

CHAPTER 73

DESIGN CRITERIA RECOMMENDED FOR MARINE FENDER SYSTEMS

by

Theodore T Lee*
Associate Researcher
Look Laboratory of Oceanographic Engineering
University of Hawaii
Honolulu, Hawaii
U S A

A B S T R A C T

This paper summarizes the world-wide effectiveness of marine-fender systems A design criteria is recommended as a result of an extensive research and development program executed at the U S Naval Civil Engineering Laboratory, Port Hueneme, California, under the sponsorship of Naval Facilities Engineering Command

Pertinent information includes analytical treatment and experimental investigation of the effects of berthing impact on the design of berthing structures, definition, function, and types of fender systems, advantages and disadvantages of various fender systems, cost-effectiveness and design procedures for different marine environment and exposure conditions. The energy absorption characteristics, berthing velocity, and virtual mass of ship are discussed in detail Energy capacity requirements for marine fender systems are illustrated in both graph and monograph forms. This paper is intended to provide guidelines to coastal engineers who may be involved in design of fender systems for waterfront and offshore structures

INTRODUCTION

As the trend prevails toward the design and construction of offshore structures to serve large vessels and construction barges in exposed seas, it is considered necessary to assess and update the design criteria for marine fender systems

A marine fender system is a protective installation designed to prevent direct contact between ship and dock so that mechanical damage caused by impact and abrasion can be reduced to a minimum. An ideal fender system offers a sensitive response that increases proportionally to the excitations induced by a berthing or moored ship. Such a system absorbs high energy with low load transmission at reasonable construction and maintenance costs Cost-effectiveness is an important criteria to be considered, including the expected loss of effectiveness because of physical and biological deterioration

*Formerly Research Hydraulic Engineer, U S Naval Civil Engineering Laboratory, Port Hueneme, California

This paper summarizes the world-wide effective fender systems, investigated at the Naval Civil Engineering Laboratory, Port Hueneme, California, including the studies by contract (Lee, 1965a, b, 1966a, b, 1967, Risselada and van Lookeren Compagne, 1964; Thorn and Wilson, 1966)

Based on the method of construction, the fender systems can be categorized into three classes defined as follows

1 A fender system attached to a dock is a system designed for directly protecting ship and dock by absorbing impact energy, thus reducing lateral ship thrusts (Figure 1a).

2. A fender system detached from a dock is a system for indirectly protecting a dock by absorbing lateral ship thrusts, tending to permit a lighter dock design (Figure 1b).

3. A breasting-platform fender system is a series of independent breasting dolphins (pile clusters) or platforms independent of a dock and is a variant of the detached fender system (Figure 1c).

ANALYTICAL TREATMENT AND EXPERIMENTAL INVESTIGATION

The mathematical treatment of berthing ships was not systematically presented until Prof Vasco Costa published his paper in the Journal of Dock and Harbor Authority on "Berthing of Ships" in July 1964, and further discussed at the NATO Study Institution held in Lisbon in July, 1965, the Analytical Treatment of Problems of Berthing and Mooring Ships. Pertinent recommendations based on simplified analytical treatment have been made on how to maneuver a large ship to reduce berthing impact (Vasco Costa, 1968)

The complex nature of the berthing and mooring of ships can be well illustrated diagrammatically in the docking process of a ship (Figure 2). During the initial stage, the skills of the captain and pilot, together with the assistance given by the tugs and crew in mooring lines, all influence the berthing maneuvers.

Vasco Costa (1964, 1968) derived the dynamic equations based on the principles of conservation of angular momentum with respect to the point of contact, and of conservation of kinetic energy. The first principle permits the evaluation of the angular velocity (ω) with which the berthing ship will rotate about the point of contact The energy equation will determine the effective kinetic energy to be absorbed by the fender system

Conservation of angular momentum of kinetic moment with respect to point of contact (See Figure 3.)

$$M'U_o a \sin\beta + M'k^2\omega_o = M'(k^2+a^2)\,\omega \tag{1}$$

$$\omega = \frac{U_o a \sin\beta + k^2\,\omega_o}{k^2+a^2} \tag{2}$$

Conservation of kinetic energy.

$$E_{eff} = \frac{1}{2}M'U_o^2 + \frac{1}{2}M'k^2\omega_o^2 - \frac{1}{2}M'(k^2+a^2)\,\omega^2 \tag{3}$$

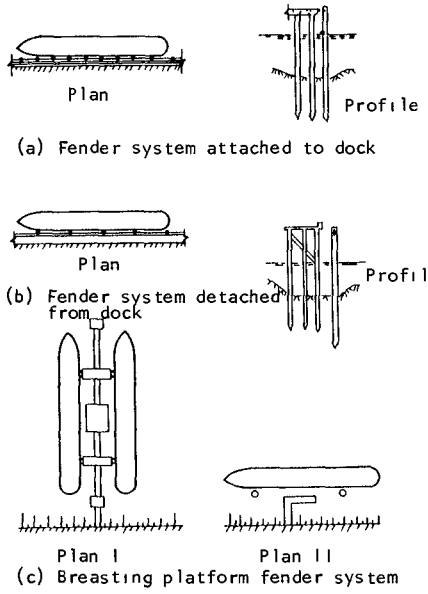

Fig 1 Definitions of fender systems from dock

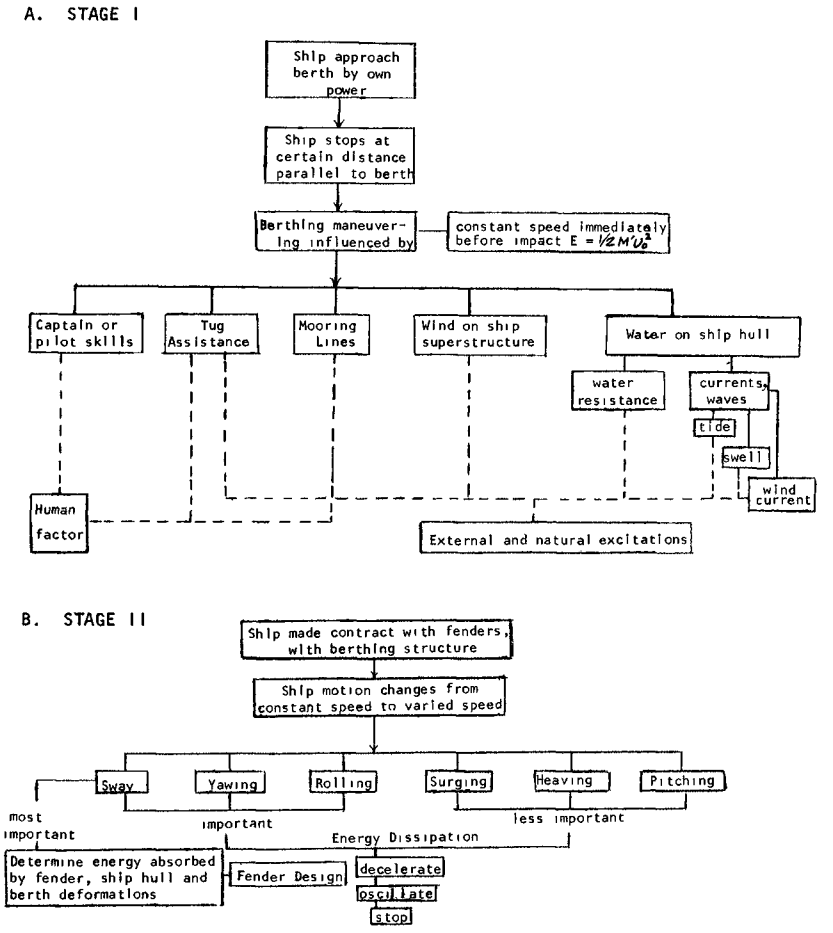

Fig. 2 Berthing Process

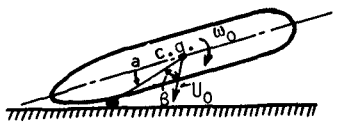

(a) time at initial contact

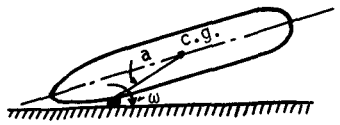

(b) time after initial contact

Fig. 3 Berthing impact instants

By substituting the value given in equation (2) into (3), we obtain

$$E_{ff} = \frac{1}{2}M'U_o^2\left(\frac{k^2+a^2\,\mathrm{Cos}^2\beta}{k^2+a^2}\right) + \frac{1}{2}M'\omega_o^2\,\frac{k^2a^2}{k^2+a^2} - M'U_o\omega_o\,\frac{ak^2\,\mathrm{Sin}\,\beta}{k^2+a^2} \qquad (4)$$

The general equation (4) is the energy absorbed by the fender system which is dependent on (a) virtual mass in sway motion, M', (b) ship velocity in translation motion, U_o, (c) direction of velocity of translation, β, (d) ship velocity in rotational motion, ω_o, (e) radius of gyration of berthing ship, k, (f) point of impact relative to center gravity of ship, a. The above equations do not take into account the energy consumed in resisting ship motions by mooring lines between land and ship or between tugs and ship, if any. Furthermore, the above analytical treatment is based on two degrees of freedom motion - sway and yaw. Other motions such as surge, roll, heave, and pitch are ignored. Therefore, the energy absorbed by the fender so determined is on the conservative side Assumption is made that virtual mass of ship remains unchanged for sway motion and for rotational motion about the center of gravity or about the point on impact, respectively

Soon after the ship makes contact with the fender, the ship may move in a simple mode of motion, i.e , the two limited cases (a) translation without rotation, and (b) rotation without translation

Special Case 1. Ship Motion with Translation Only (without rotation)

$$E_{eff} = \frac{1}{2}M'U_o^2\,\frac{k^2+a^2\,\mathrm{Cos}^2\beta}{k^2+a^2} \qquad (5)$$

When $\beta = 90^o$, $E_{eff} = \frac{1}{2}M'U_o^2\,\frac{k^2}{k^2+a^2}$ (6)

where $\frac{k^2}{k^2+a^2}$ is an eccentricity coefficient

Special Case 2. Ship Motion with Rotation Only (without translation)

$$E_{eff} = \frac{1}{2}M'\omega_o^2 \frac{k^2a^2}{k^2+a^2} \tag{7}$$

In this case, the energy to be absorbed by fender can be expressed as a function of the velocity at the point of contact, which is

$$V_o = \omega_o a \tag{8}$$

$$E_{eff} = \frac{1}{2} M'V_o^2 \frac{k^2}{k^2+a^2} \tag{9}$$

The motion of a berthing ship has been treated as a dynamic problem of three degrees of freedom by Hayashi and Shirai (1963) sway, yaw, and roll The kinetic energy of the berthing ship is absorbed by the following modes (a) elastic deformation of fender system, berthing structure, and ship hull due to sway motion, (b) swing of ship due to yawing motion, and (c) heeling of ship due to rolling motion The dynamic equations are

Sway $$y + \left(\frac{a}{M'}\right) y + a\theta + h\phi = 0 \tag{10}$$

Yaw $$\ddot{\theta} - \left(\frac{k_e a}{M'K^2}\right) y = 0 \tag{11}$$

Roll $$\phi + \left(\frac{Wh_m}{M'K^2}\right) \phi - \left(\frac{k_e h}{I_{M'K^2}}\right) y = 0 \tag{12}$$

By solving the above equations with given initial conditions, one can obtain the maximum overall deformation (y_{max}) of fender system, berting structure, and of ship hull at the point of contact Then the effective energy to be absorbed by the fender systems can be determined The overall effective spring constant, k_e, consists of elastic characteristics of fender system, berthing structure, and ship hull. The values of θ and ϕ represent angle of yaw and angle of roll, respectively. The values of h and h_m represent the vertical distance from center of gravity of ship to point of contact between fender and ship, and the height of metacenter of the ship, respectively Ship displacement is W The value of a is the distance between point of contact and center of gravity of ship along the longitudinal axis. K is the radius of gyration of the ship

Water wave effect on berthing ship was studied by Wilson (1958) Wave effect would be minimum if berthing operation is made on a head sea, but the force will be considerable if berthing is in beam sea The type of berthing structure is particularly important For an open-type structure, waves will be transmitted without sensitive reflection but for a closed-type structure, a standing wave system will be formed to effect the berthing ship. Wilson derived formulas for berthing ship under wave action on impact with both open and closed type structures when impact is at the center of gravity of ship, during which sway motion is only concerned.

Open-type structure $$E_{ff} = \frac{1}{2} M' \left[U_o + \frac{Ag}{\sigma D} \frac{\text{Sinh } kd - \text{Sinh } ks}{\text{Cosh } kd} \frac{\text{Sin } kB/2}{kB/2} \right]^2 \quad (13)$$

Closed-type structure $$E_{ff} = \frac{1}{2} M' \left[U_o + \frac{2Ag}{\sigma D} \frac{\text{Sinh } kt - \text{Sinh } ks}{\text{Cosh } kd} \frac{\text{Sin}^2 kB/2}{kB/2} \right]^2 \quad (14)$$

where A = wave amplitude, l = wave length, $k = \frac{2\pi}{l}$ wave number. d = water depth. S = wave slope, B = ship beam, D = ship draft, $\sigma = \frac{2\pi}{T}$; T = wave period, g = gravitational acceleration Unfortunately, yawing and rolling motions are not considered However, this can easily be taken into account based on Vasco Costa's formulas.

The mathematical treatments of the berthing ships described above are quite complicated for practicing engineers Major difficulties are due to the fact that the dynamic equations involve several undefined parameters such as hydrodynamic masses, wave forces, vertical moments of inertia of ship, and ship velocity in translation and rotational motions When the fender system is having non-linear elastic characteristics and the effects of natural excitations from winds, waves, and currents are taken into account, the situation becomes worse, if not hopeless, for mathematical solutions Keeping these factors in mind, and being realistic in dealing with berthing problems involving human factors also, it is considered feasible to design fender systems by a semi-theoretical and semi-empirical approach which will be discussed in this paper In view of the fact that semi-empirical approach seems satisfactory only when proper engineering judgement is achieved, pertinent information is furnished in this paper on the relative merits of different fender types, the choice of design berthing velocity, hydrodynamic mass, cost-effectiveness, and other factors as related to local marine environment and navigation conditions

Model experiments and full-scale observations or measurements have been used to supplement the mathematical treatment. Statistical approach has also been used for the purpose of finding ways to improve berthing operations In Great Britain, the British Petroleum Company (Saurin, 1963 and 1965) and the Hydraulic Research Station, Wallingford (1961, 1962) are the major contributors, berthing forces of large tankers are assessed to establish a realistic design criteria based on semi-empirical approach In France, the Port of LeHare conducted model experiments on the berthing energy of ships with both translation and rotation motion of ship due to wind effects (Giraudet, 1966) In the U S , this author conducted full-scale investigations of berthing impacts and evaluations of a Hydraulic-pneumatic floating fender (Lee, 1966a) In Norway, field measurements were made of berthing forces of a ferry boat (Tryde, 1965) In Japan, Shiraishi (1962) conducted field tests from which an approximate solution of berthing impact force was recommended

GENERAL TYPES OF FENDER SYSTEMS

Standard pile-fender systems This type of fender system employs piles driven into the ocean bottom along a wharf face Impact energy is absorbed by deflection and limited compression of the pile Energy absorption capacity is dependent on size, length, penetration, and material of the pile It is

determined on internal strain-energy characteristics (Figure 4) The energy absorption capacity is very limited; it declines rapidly as a result of biodeterioration and mechanical damage (Figure 5). Steel piles are occasionally used for fendering in water depth greater than 40 feet or for locations where very high strength is desirable. Regular reinforced concrete piles are unsatisfactory. In some cases, prestressed concrete piles with rubber buffers at deck level have been used with success.

Retractable fender systems· This type of fender retracts under impact, thereby absorbing energy by action of gravity and friction. Energy absorption depends on (a) effective weights, (b) the maximum amount of retraction of the system, and (c) the angle of inclination of the supporting brackets.

The use of composite inclined planes of supporting brackets and proper selection of the maximum retraction are the most feasible means for attaining design energy-absorption capacity (See Figure 6) Deterioration of timber frames does not materially reduce energy-absorption capacity, nor is capacity dependent on internal strain energy as with timber piles.

Rubber fender systems: Rubber fender systems consist of rubber-in compression, rubber-in-shear, and rubber-in-bending buffers These resilient units are normally installed behind standard fender piles so as to increase the energy absorption capacity.

Energy absorption of the rubber-in-compression system is achieved by a compression of the rubber tubes or solid blocks in axial or radial directions The capacity may be increased by using multiple layers; thus also keeping the resistance force to dock or ship at a reasonably low level.

The rubber-in-shear system consists of a series of rubber pads bonded between steel plates to form a series of "sandwiches" which are mounted firmly as buffers between a pile-fender system and a pier The improved version of the so-called "Raykin" buffers have been designed to have a 100 percent overload capacity. This type of fender is most suitable for berths designed for servicing large tankers because of its high energy absorption capabilities. It is capable of resisting direct and glancing impacts. Because of its stiffness and lack of suitable responsiveness to widely varying amounts of impact, it is unfit for servicing vessels varying widely in size at a berth

The rubber-in-bending system, so-called "Lord" flexible fender, consists of an arch-shaped rubber block bonded between two steel plates Impact energy is absorbed by bending and compression of an arch-shaped rubber column When an impact force is applied, it will build up a relatively high load with small deflection, buckle at a further small deflection, and maintain a virtually constant load over the range of buckling deflection (Fig 7).

Rubber-in-torsion fender is a rubber-and-steel combination fabricated in a cone-shaped compact bumper form, molded into a specially-cast steel frame and bonded to the steel. It absorbs energy by torsion, compression, shear, and tension. However, most energy is absorbed by compression (Lee, 1965a)

Gravity type fender systems. Gravity fenders are normally made of concrete blocks suspended from a heavily constructed wharf deck Impact energy is absorbed by moving and lifting the heavy concrete blocks High energy

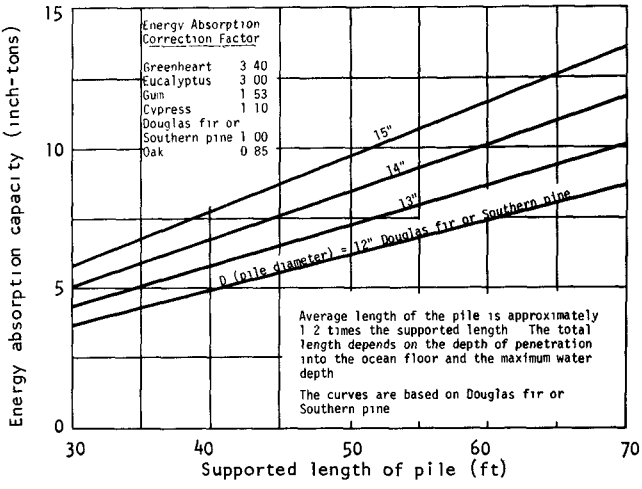

Fig. 4 Energy-absorption of timber fender piles

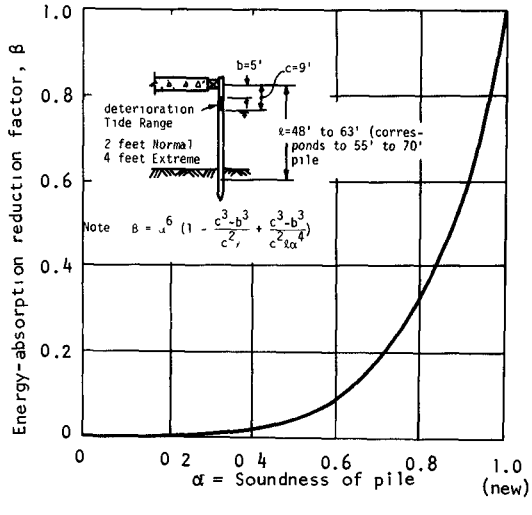

Fig. 5 Energy-absorption reduction due to bio-deterioration

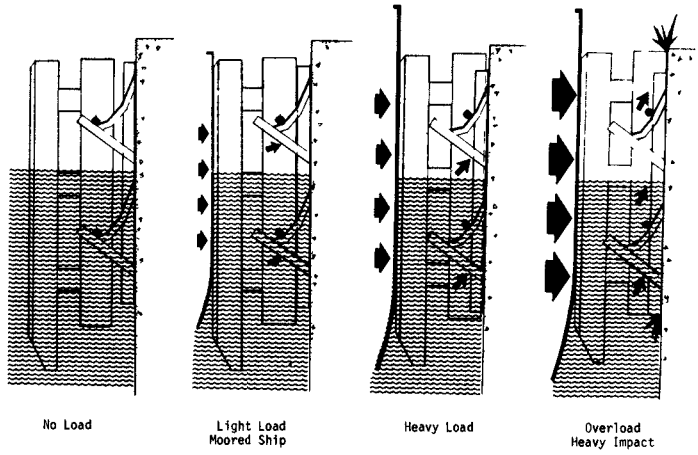

Fig. 6 Operation of modified retractable fender system

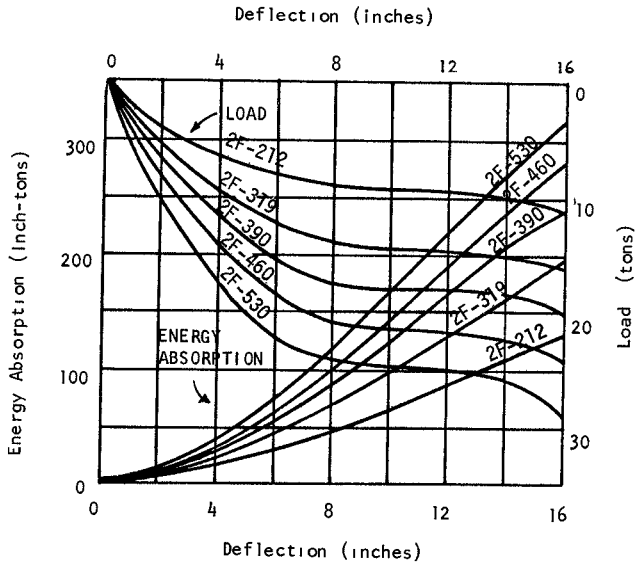

NOTE The part number 2F-212 is defined as a "Lord" rubber fender having an energy-absorption capacity of 21,200 foot-pounds at full deflection of 16 inches.

Fig 7 Load-deflection and energy-absorption characteristics of Lord flexible fender

absorption is achieved through long travel of the weights The movements may be accomplished by (1) a system of cables and sheaves, (2) a pendulum, (3) trunnions, or (4) an inclined plane The type of gravity fender suited to a given situation depends on tidal conditions, energy-absorption requirements, and other load environmental factors such as exposures to wind, waves, and currents For example, heavy vertically-suspended gravity fenders are commonly used in exposed locations with large tidal ranges

Pneumatic fender systems Pneumatic fenders are pressurized and airtight rubber devices designed to absorb impact energy by compression of air inside a rubber envelope These pneumatic fenders are not applicable to fixed dock-fender systems but are feasible for use as ship fenders or shock absorbers on floating fender systems A proven fender of this type is the pneumatic tire-wheel fender This system consists of pneumatic tires and wheels capable of rotating freely around a fixed or floating axis Energy-absorption capacity and resistance load depend on the size and number of tires used and on initial air pressure when inflated

Hydraulic and hydraulic-pneumatic fender systems. This system consists of a cylinder full of oil or other fluid so arranged that when a plunger is depressed by impact, the fluid is displaced through an invariable or variable orifice into a reservoir located at a higher elevation When the ship impact is released, the high pressure inside the cylinder forces the plunger back to its original position, and the fluid flows back into the cylinder by gravity The system is non-floating Its most common use is in locations of severe wind, wave, swell, and current conditions

Hydraulic-pneumatic floating fender system This system consists of a floating rubber envelope filled with water, or with water and air, which absorbs energy by viscous resistance and/or by compression of air This fender seems to meet certain requirements of the ideal fender but is considered expensive in combined first and maintenance costs

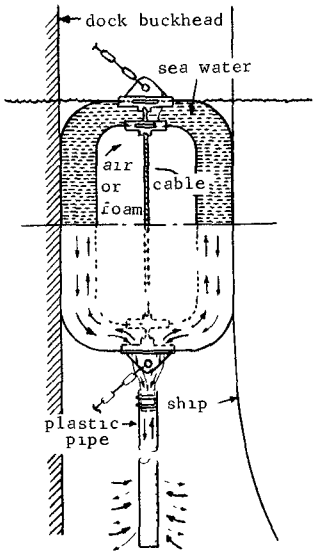

Fig 8 A new concept of hydraulic - pneumatic fender

A new patented (Figure 8) concept has been developed by this writer to overcome the existing deficiencies of both pneumatic and hydraulic fenders by combining the pneumatic and hydraulic principles within a single marine fender As shown in Figure 8, the system employs a pair of inflatable rubber bags, one being an exterior bag and the other being a smaller interior bag which is located within the exterior bag The interior bag which is sealed when in use, may contain air or foam cushion and is sufficiently smaller than the exterior bag so as to define a chamber therebetween for containing water A conduit means may be connected to the exterior bag so as to communicate the water chamber with the exterior body water The marine fender will absorb high impact loading without bursting because of pressure relief caused by the escaping water through the conduit means After berthing, the fender will provide even improved cushioning over the pneumatic type fenders since the water discharge effect will minimize the high

-11-

rebounding effect of the pneumatic bag It is expected that the new fender is particularly feasible for use as separators between ships or small crafts It is sensitive to both berthing and moored vessels.

Torsion fender system. This is a new concept developed by Mr. Turner and Prof. Baker of the Cambridge University Engineering Laboratories. The so-called "Cambridge" finder has been tested with success in both laboratory and field installations It employs the principles of energy absorption by plastic deformation of metals The system consists of a plastically deformable torsion and a mechanism transforming the berthing impact into the shock absorber

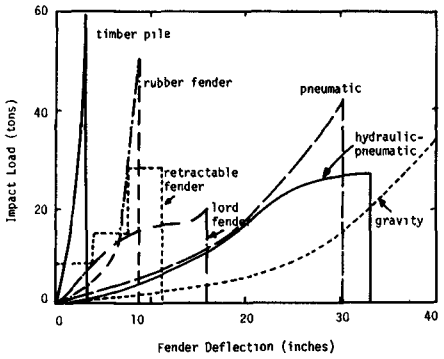

Fig 9 Load-deflection characteristics of various fender systems

To assist the practicing engineers in the selection of the desirable type of fender system, Table 1 is prepared summarizing major advantages and disadvantages of various fender systems described above. Load-deflection characteristics are compared in Figure 9

For case histories and detailed comments on each system, see U S Naval Civil Engineering Laboratory's technical reports (a) "A Study of Effective Fender Systems for Navy Piers and Wharves," R-312, March 1965, and (b) "Review of 'Report on the Effective Fender Systems in European Countries' by Risselada and van Lookeren Campagne," R-376, October 1965 (Lee, 1965 a, b)

DESIGN CRITERIA RECOMMENDED FOR MARINE FENDER SYSTEMS

General. A variety of factors affect the proper selection of a fender system. These include local marine environment, exposure of harbor basins, class and configuration of ships, speed and direction of approach of ship when berthing, available docking assistance, type of berths, and even skills of pilots or ship captains. It is considered impractical to standardize fender designs since local conditions are rarely identical. Previous local experience in the application of satisfactory fender systems should be considered, particularly cost-effectiveness characteristics.

Table 1. Comparison of Various Types of Fender Systems

Fender System	Advantages	Disadvantages
Standard Pile, timber	1. Low initial cost 2. Timber piles are abundant in U S and most world regions	1. Energy absorption capacity is limited It declines as result of biodeterioration 2 Susceptible to mechanical damage and biological deterioration. 3. High maintenance cost if damage and deterioration is significant
Standard Pile, steel	1. High strength 2. Feasible for difficult seafloor conditions.	1 Vulnerability to corrosion 2 High cost
Standard Pile, reinforced concrete	1. Insignificant effects of biodeterioration	1 Energy-absorption capacity is very limited. 2. Corrosion of steel reinforcement through cracks
Standard Pile, prestressed concrete	1 Resistance to natural and biological deterioration 2. Better energy-absorption characteristics than reinforced concrete piles.	1 Limited strain-energy capacity, if rubber buffers are not provided.
Timber Hung System	1. Very low initial cost 2 Less biodeterioration hazard	1 Low energy-absorption capacity 2. Unsuitability for locations with significant tide and current effects

Table 1. Comparison of Various Types of Fender Systems (Continued)

Fender System	Advantages	Disadvantages
Retractable Fender System	1. Effects of biological deterioration on energy absorption-capacity are negligible. 2. No heavy equipment is required for fabrication and replacement 3 Low maintenance cost, minimum time loss during replacement	1. Loss of effectiveness due to corrosion and/or damage to supporting brackets. 2 High initial cost for use at open-type piers.
Rubber Fender Systems Rubber-in-compression	1. Simplicity and adaptability. 2. Effectiveness at reasonable cost.	1. High concentrated loading may result, frictional force may be developed if rubber fenders contact ship hull directly 2 Higher initial cost than standard pile system without resilient units.
Rubber Fender Systems Rubber-in-shear	1. Capable of cushioning berthing impact from lateral, longitudinal, and vertical directions. 2. Most suitable for dock-corner protection. 3 High energy-absorbing capacity for serving large ships of relatively uniform size. 4. Favorable initial cost for very heavy duty piers.	1. "Raykin" buffers tend to be too stiff for small vessels and for moored ships subject to wave and surge action. 2 Steel plates are subject to corrosion 3 Bond between steel plate and rubber is a problem. 4. High initial cost for general cargo berths.

Table 1 Comparison of Various types of Fender Systems (Continued)

Fender System	Advantages	Disadvantages
Rubber Fender Systems Lord Flexible Fender	1 High energy-absorption and low terminal-load characteristics	1 Possible destruction of bond between steel plates and rubber 2 Possible fatigue problems
Rubber Fender Systems Rubber-in-torsion	1 Capable of resisting impact load from all directions	1 Possible destruction of the bond between steel casting and rubber 2 Possible fatigue problems.
Gravity-Type Fender Systems	1 Smooth resistance to impacts induced by moored ships under severe wave and swell action 2 High energy absorption and low terminal load can be achieved through long travel for locations where excessive distance between ship and dock is not a problem	1 Heavy berthing structure is required 2 Heavy equipment is required for installation and replacement 3 High initial and maintenance costs 4 Excessive distance between dock and ship caused by the gravity fender is undesirable for generalcargo piers and wharves
Pneumatic Fender System	1 Suitable for both berthing and moored ships. 2. Fixed tire-wheel type is feasible for pier-corner protection.	1 Use in fixed dock-fendering is limited to bulkhead-type structures. 2 High maintenance cost
Hydraulic and Hydraulic-pneumatic Fender	1. Favorable energy-absorption characteristics for both berthing and moored ships	1 High initial and maintenance cost.

Design Procedures

1. Examine local marine environment and exposure conditions Local natural environment and the degree of protection of harbor basins are important factors in fender system selection A classification of marine environments and navigation conditions is shown in Table 2 Designers may determine local navigation conditions based on local marine environment.

2 Determine the displacement tonnage of ship The fender capacity for any ship depends not only on its size, but also on its frequency of arrival Average size of ships using the berth (i.e , one-half to two-thirds the maximum) should be selected for design. Displacement tonnage is used in measuring the size of ship For design of general-cargo piers and wharves, 20,000 long-tons may be considered as design displacement.

3 Determine the berthing velocity, V. Berthing velocity is determined with due consideration of (a) the size of the vessel, (b) the berthing method (broadside, approach with angle to dock face, with or without tug assistance, (c) navigation condition, and (d) type of dock Figure 10 shows the range of berthing velocity which may be selected for design ships up to 200,000 long-tons displacement

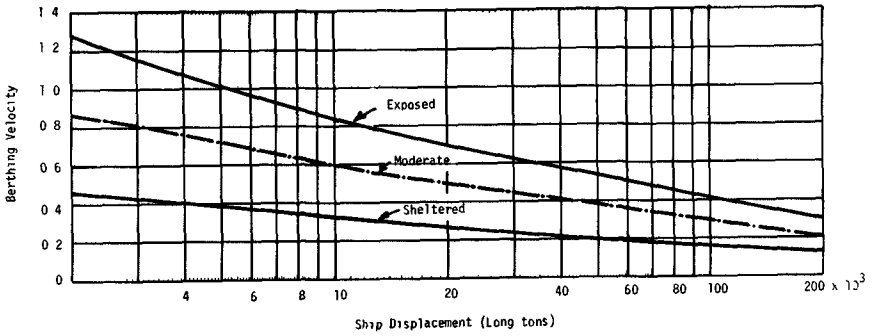

1/ Berthing velocity normal to dock

Fig. 10 Berthing velocity vs. ship displacement.

Table 2. Classification of Marine Environments and Navigation Conditions
(Based on Risselada and van Lookeren Campagne, 1964)

Navigation Condition	Marine Environment		Example of Harbor Tidal/Current Conditions
	Harbor Basin	Description	
1	Sheltered	No or little current up to 0.31 ft/sec Tide range up to 3 ft. No strong winds	Mediterranean ports
2	Sheltered	Some current up to 0.31 ft/sec Tide range. 1 ft (normal), 10 ft (maximum). No strong winds	Baltic ports
3	Moderately sheltered	No or little current up to 0 31 ft/sec Tide range up to 3 ft Fresh gale winds up to 40 knots	Mediterranean ports
4	Moderately sheltered	Moderate current up to 0 7 ft/sec. Tide range 10 ft (normal), 20 ft (maximum) Strong gale winds up to 47 knots	Rotterdam Lisbon N W Germany
5a	Moderately sheltered	Considerable current up to 0 8 ft/sec Tide range 16 ft(normal), 27 ft(maximum) Strong gale winds up to 47 knots	Le Havre
5b	Slightly sheltered	Moderate current up to 0.7 ft/sec Tide range 10 ft (normal), 20 ft (maximum) Strong gale winds up to 47 knots	Rotterdam Lisbon N W. Germany
5c	Exposed	No or little current up to 0 3 ft/sec. Tide range 1 ft (normal), 10 ft (maximum). Strong gale winds up to 47 knots	Baltic ports
6a	Slightly sheltered	Great Current up to 1 0 ft/sec. Tide range 20 ft (normal), 33 ft (maximum) Strong gale winds up to 47 knots	British Atlantic ports
6b	Exposed	Considerable current up to 0 8 ft/sec Tide range 16 ft (normal). Strong gale winds up to 47 knots	Le Havre
7	Exposed	Great current up to 1 2 ft/sec Tide range 20 ft (normal), 33 ft (maximum) Storm winds up to 63 knots. Waves up to 3 feet.	British Atlantic ports
8	Very exposed	Great current up to 1.3 ft/sec Tide range 20 ft (normal), 33 ft (maximum) Storm winds up to 63 knots. Waves 3 ft or greater	British Atlantic ports

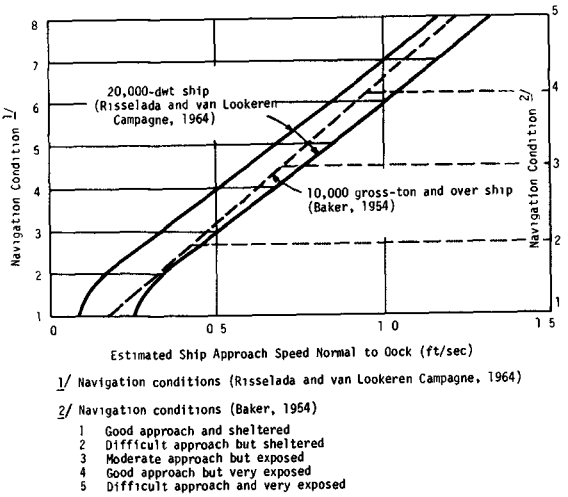

1/ Navigation conditions (Risselada and van Lookeren Campagne, 1964)

2/ Navigation conditions (Baker, 1954)

1 Good approach and sheltered
2 Difficult approach but sheltered
3 Moderate approach but exposed
4 Good approach but very exposed
5 Difficult approach and very exposed

Fig 11 Ship approach speeds recommended

If the fender system is designed for ships of 20,000 long-ton displacement, berthing speed recommended is shown in Figure 11

4. Determine the effective mass or virtual mass of a vessel When a ship approaches a dock, the berthing impact is induced not only by the mass of moving ship, but also by the water mass moving along with the ship The latter is generally called the "hydrodynamic" or "added" mass In determining the kinetic energy of a berthing ship, the effective or virtual mass (a sum of ship mass and hydrodynamic mass) should be used The hydrodynamic mass does not necessarily vary with the mass of the ship but is closely related to the projected area of the ship at right angles to the direction of motion Other factors such as the form of ship, the water depth, the berthing velocity, the acceleration and deceleration of the ship would have some effect on the hydrodynamic mass. Taking into account both model and prototype experiments, the hydrodynamic mass can be estimated as

$$M_h = C_h M = 2 (D/B) M \tag{15}$$

Thus, the virtual mass

$$M' = M + M_h = (1 + 2 D/B) M = C_m M \tag{16}$$

where

M_h = hydrodynamic mass

M' = virtual mass or effective mass

C_h = hydrodynamic coefficient

C_m = virtual mass coefficient

M = ship mass

D = draft of ship

B = beam of ship

Adopting Vasco Costa's formula, a graph (Figure 12) of C_m versus vessel size (long tons) has been plotted, using dimensions of some 70 U S Naval vessels in the 2,000-20,000 long-tons class The virtual mass coefficient as predicted by Vasco Costa's formula is adequate for ships berthing at moderate to high speed Caution should be exerted when design speed is low (Lee, 1966a)

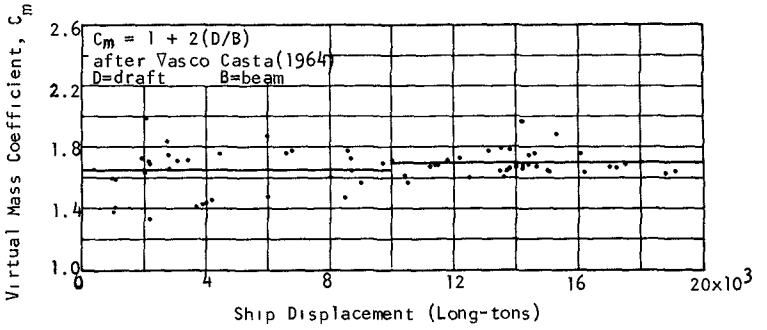

Fig 12 Virtual Mass Coefficient versus Displacement (Thron, 1966)

5 Determine the kinetic energy (E) of berthing ship

$$E = \frac{M' V^2}{2} \quad \text{or} \quad E = 0\ 209\ C_m W V^2 \qquad (17)$$

where

E = kinetic energy of berthing ship in inch-tons

W = ship displacement in long-tons

V = berthing velocity normal to dock in feet per second.

6 Determine effective berthing energy of ship to be absorbed by fender system

$$E'_{eff} = CE = 0.209\ C\ C_m\ WV^2$$

$$C = C_e\ C_g\ C_d\ C_c \qquad (18)$$

where

E'_{eff} = kinetic energy to be absorbed by fender system in inch-tons

C = berthing coefficient

C_e = eccentricity coefficient

C_g = ship geometric coefficient

C_d = ship deformation coefficient

C_c = berth configuration coefficient

Eccentricity coefficient, C_e, is expressed as $C_e = \frac{k^2}{a^2 + k^2}$

where a = distance between the point of impact and the center of gravity of the ship

k = ship radius of gyration about the axis - frequently 0 20 to 0.29 times the ship length

The value of C_e varies from 0 14 to 1 0

Geometric coefficient, C_g, depends upon the geometric configuration of the ship at the point of impact It varies from 0 85 for an increasing convex curvature to 1 25 for concave curvature Generally, 0 95 is recommended for the impact point at or beyond the quarter points of the ship and 1 0 for broadside berthing in which contact is made along the straight side

Deformation coefficient, C_d, corrects the energy reduction effects due to local deformation of the ship's hull and deflection of the whole ship along its longitudinal axis The energy absorbed by the ship depends on the relative stiffness of the ship and the obstruction. The deformation coefficient varies from 0.5 for a nonresilient fender to nearly 1 0 for a very flexible fender

Berth configuration coefficient, C_c, provides for the water cushion effect between pier and ship. It is recommended that 0 8 be used for a closed wharf, 0.9 for a semi-closed type, and 1 0 for an open pier

The berthing coefficient, C, is frequently assumed to be 0 5 where insufficient information is available to allow evaluation of individual coefficients A higher coefficient must be used if broadside berthing is always involved

7 Nomograph. A published nomograph (Fig 13) is reproduced on the following page to facilitate the determination of the energy-absorption requirement of a fender system

8. Compare the energy-absorption capacity requirements determined from (7.) above or with Figure 14 on the following page if the fender system is designed for ships up to 20,000 long-ton displacement for a specific navigational condition

9 Select the final energy-absorption capacity of the fender system, taking into account frequency of berthings, probability of accidents, and expenses that may be involved in the construction, repair or replacement of the main berthing structure, the fender system, and the ships. Cost-effectiveness should be studied in order to determine the feasibility of selecting a high-energy absorption fender system, particularly as compared with existing systems An example is given in Appendix A

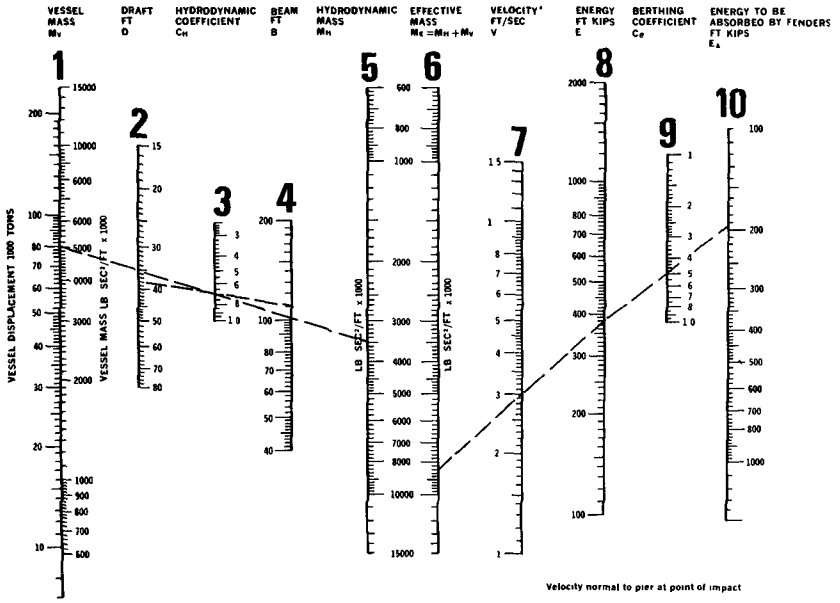

Fig. 13 Nomograph - Energy absorption requirements for marine fender systems (Courtesy of Lord Mfg Co.)

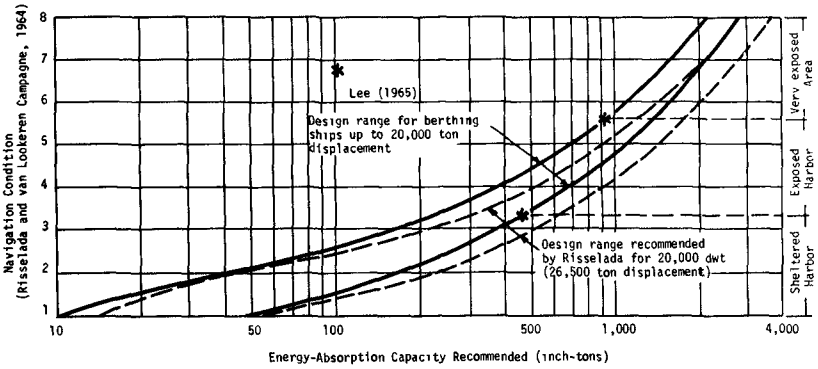

Fig. 14 Energy-absorption capacities recommended for fender design

OTHER RECOMMENDATIONS PERTINENT TO FENDER TYPE SELECTION

Selection of a fender system for a given installation is based on the following factors. Pertinent recommendations are given as follows:

1 Exposure conditions In exposed locations or in areas subject to seiche, a resilient system such as a rubber fender system, should be used. In sheltered basins, a standard timber-pile system, a hung system, or a retractable system is generally used.

2 Berthing ship versus moored ship

(a) For locations where berthing operations are hazardous, stiff fender systems with high energy-absorption characteristics are advisable.

(b) For locations where the behavior of the already moored ship is the governing factor, soft fenders with soft mooring ropes are feasible in minimizing mooring forces and ship motion.

(c) Where berthing operations and the behavior of moored ships seem to pose problems of equal importance, it is best to choose a fender of intermediate type that can act stiffly during berthing and softly when the ship is moored Hydraulic-pneumatic fender systems meet such requirements

3. Acceptable lateral load to docks At berths for vessels up to 20,000 long-ton displacement, the acceptable lateral loading to dock should be kept within 3,000 to 3,500 pounds per linear foot of berth. Special tanker berth may be acceptable for higher lateral loading

4. Acceptable hull loads. For vessels from 15,000 to 20,000 tons, hull pressure of 35 psi is acceptable in general, with overloads of up to 50 psi as an upper limit.

5 Maximum allowable distance between moored ships and dock face The maximum limit is 4 to 5 feet for general cargo berth No problem exists if the fender system is for a tanker berth involving fuel supply only.

6. Pier type as related to fender system selection

(a) Open pier. Any type of fender system may be applicable.

(b) Solid pier This type has little resilience. Consider use of resilient or retractable fenders to minimize vessel damage.

7. Miscellaneous factors related to fender system selection

(a) Resistance to tangential forces

(b) Reliability in operation.

(c) Cost of maintenance.

(d) Evaluation of systems that have given satisfactory service at or near the proposed installation.

(e) Resistance to longitudinal component of berthing force

(f) Ease and economy of replacement

(g) Available docking assistance

(h) Skills of pilots and captains during docking

ACKNOWLEDGEMENTS

Permission by the U S. Naval Civil Engineering Laboratory to publish this paper is acknowledged Contributions by Messrs T J Risselada and J.P A Van Lookeren Campagne of the Netherlands for their contract study of European fender systems are appreciated Contributions by Dr. Basil Wilson, Dr B J Thorn, and Mr. A Torum of Science Engineering Associates for their contract study of engineering and economic evaluation of floating fender concepts are also appreciated. Acknowledgement is made to Lord Mfg Co. for Fig 13

REFERENCES

1 Lee, T T. (1966), "Full-Scale Investigation of Berthing Impacts and Evaluation of a Hydraulic-pneumatic Floating Fender," ASCE Proceedings 10th Conference on Coastal Engineering, Chap 65, p p 1130-1156, 1967.

2 Lee, T T. (1965), "A Study of Effective Fender Systems for Navy Piers and Wharves," TR-312, U S. Naval Civil Eng Lab , (NCEL) Port Hueneme, Calif , March 1965, pp 114.

3 Lee, T T (1965), "Review of 'Report on the Effective Fender Systems in European Countries' by Risselada and van Lookeren Campagne," TR-376, NCEL, Oct 1965, 66pp

4 Lee, T T (1966), "Effects of Biological and Physical Deterioration on the Effectiveness of Timber Fender Systems," Workshop on Protection of Waterfront Structures at NCEL, Sept 1966 (unpublished manuscript).

5. Lee, T T (1967), "Design Manual-Waterfront Operational Facilities Chapter 1 Piers, Section 5· Appurtenance, Part 2 Fender System," NCEL, Aug 17, 1967 (unpublished manuscript)

6 Risselada, T J. & J P A van Lookeren Campagne (1964), "Report on the Effective Fender Systems in European Countries," Contract Report, NCEL May 1964 (unpublished manuscript)

7 Thorn, B J (1966), "An Engineering and Economic Evaluation of Floating Fender Concepts," Contract report, Science Engineering Assoc., Calif , for NCEL, June 1966, 158 pp

8 Giraudet, P (1966), "Recherches Experimentals Sur L'energie D'Accostage des Navires" (Experimental Research on the Berthing Energy of Ships), Port of LeHavre, France, 1966.

9 Great Britain, Hydraulic Research Station (1961), "A Model Investigation to Determine Impact Forces on Fenders Caused by the Berthing of Tankers," Report No. Ex-143, Wallingford, England, August 1962.

10. Great Britain, Hydraulic Research Station (1962), "Further Model Tests to Determine Impact Forces on Fenders During the Berthing of Tankers," Report No Ex-181, Wallingford, England, August 1962.

11 Hayashi, T , and M Shirai (1963), "Force of Impact at the Moving Collision of a Ship With the Mooring Construction," Coastal Engineering in Japan, Vol. 6, 1963.

12. Saurin, B F (1963), "Berthing Forces of Large Tankers," Proceedings of 6th World Petroleum Conference, Frankfurt am Main, Germany, June 1963, Section VII, Paper 10.

13 Saurin, B.F. (1965), "Full-Scale Observation of Berthing Impacts--Their Interpretation and Role of Virtual Mass Concept," lectures presented at the NATO Advanced Study Institute on Analytical Treatment of Problems of Berthing and Mooring Ships, Lisbon, Portugal, July 19-30, 1965

14. Shiraishi, T (1962), "Berth Touching Impact Force of Train Ferry," Railway Technical Research Institute Quarterly Report Vol. 3, No. 2, June 1962, Tokyo, Japan.

15. Tryde, P (1965), "Discussion of Saurin (1965) Lecture on Measurement of Berthing Forces Preliminary Note on Measurement of Impact Energies in Danish Oil Berth," NATO Advanced Study Institute, Lisbon, Portugal, July 19-30, 1965.

16. Vasco, Costa, F (1968), "Berthing Manoeuvres of Large Ships," The Dock and Harbor Authority, Vol. XLVIII, No. 569, March 1968

17 Vasco, Costa, F (1964), "The Berthing Ship--The Effect of Impact on the Design of Fenders and Berthing Structures," The Dock and Harbor Authority, Vol. XLV, Nos 523, 524, 525, May, June and July 1964

APPENDIX A

EFFECTS OF BIOLOGICAL DETERIORATION AND PHYSICAL DAMAGE ON THE EFFECTIVENESS OF TIMBER FENDER SYSTEMS

Biological deterioration and mechanical damage by berthing and moored ships have significant effects on energy-absorption capabilities of conventional timber piles The fender effectiveness depreciates hyperbolically as the treated and untreated piles are attacked by molluscan and crustacean borers such as Teredo, Bankia, and Limnoria Therefore, most timber fender systems in existence are weakened, having a lower energy-absorption capacity than originally designed. Considerable efforts and money would have to be expended to maintain the existing systems to an acceptable level in order to meet their performance requirements. In some cases, annual cost or capitalized cost seems considerably higher than generally realized. To evaluate the cost-effectiveness characteristics, Lee (1966b) conducted on-site investigations and subsequent technical and economical analyses of existing timber fender systems at 10 representative United States Naval stations and shipyards, covering a total of approximately 200,000 linear feet of berth. Discussions included cost-effectiveness aspects, relative merits of creosoted versus untreated fender piles of Douglas fir, Southern pine, oak, gum, cypress, and eucalyptus, extent, cause, and possible solution of fender problems, distribution of fender damage by biological deterioration and ship damage to sound or weakened piles, and physical factors such as marine environment, birth usage, and other navigation conditions as related to above

Cost Effectiveness Analysis Criteria In formulating criteria to evaluate cost-effectiveness of an existing fender system in a particular environment, effectiveness and cost must be considered on a long-term basis Therefore, the initial values are not necessarily the control factor. The most effective fender system must meet not only service requirements initially, but also maintain its effectiveness during a substantial life. The most economical fender system must offer the lowest combined initial and maintenance costs over an extended period. An ideal fender is a system which is most effective and most economical over its lifetime A fender's effectiveness is measured by (a) system serviceability, (b) system reliability, and (c) system availability. Lack of proper record would prevent a meaningful evaluation of the serviceability and availability of existing fender systems. Therefore, reliability may be the yardstick in evaluation of the effectiveness of the existing fender systems. Reliability is determined from energy-absorption capacities with the consideration of the biological deterioration and physical damage to piles. Comparative economics of pile fender systems is determined by annual cost and/or capitalized cost methods involving an assess of the related factors such as initial construction costs, maintenance and replacement costs, and physical life of the system. Indirect costs such as demurrage costs resulting from repairing accidental damage to berthing ships or dock, and obsolescence costs are not normally considered due to unavailability of such data. The method of economic analysis is described elsewhere (Garbaccio et al, 1966, Lee, 1966 b)

Energy-absorption capacity of a fender system is determined from the summation of the total initial strain energy of the total fender piles in action over a 150-foot berth length which represents the normal contact

length of a 20,000-ton cargo transport Effectiveness can be reduced to as much as 28% and as low as 99% of the original capacity, depending on the efforts exercised in fender maintenance and replacement (Fig 15) The fender effectiveness can be determined from a well-kept pile deterioration and replacement record. The annual cost can be computed from cost data collected over an extended period. The life of existing fender systems should be determined from actual pile replacement records As shown in Fig 15, it seems apparent that the fender life is closely related to berth usage and to the extent of mechanical damage by ships

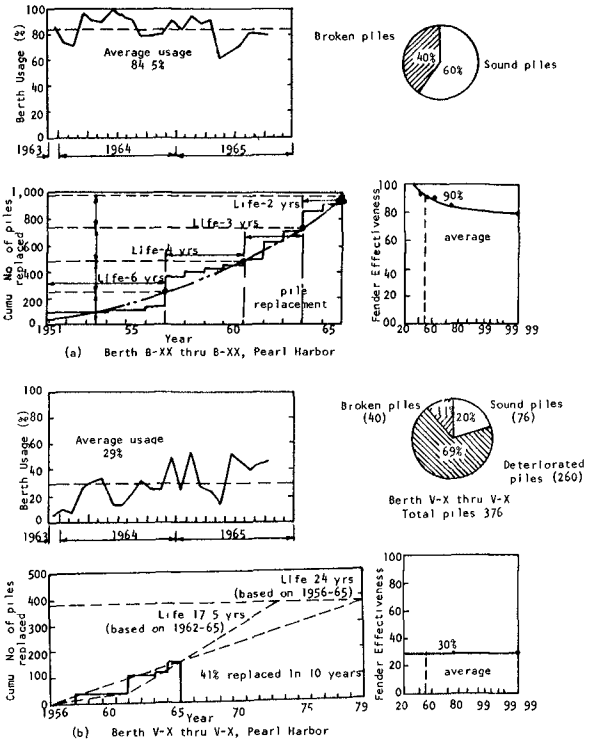

Fig 15 Cost-effectiveness of fender systems at Pearl Harbor

CHAPTER 74

HI-DRO CUSHION CAMEL-a new floating fender concept

by D B Ford, P. E., Research and Design Engineer
B O Young, P E , Research and Design Engineer
G W Walker, P E., Chief Engineer

John Rich Enterprises, Inc , Sacramento, California, U.S A.

ABSTRACT

A new floating fender devise designed to absorb berthing energies of ships against piers or harbor structures is described The principles governing the design and operation of the Hi-Dro Cushion Camel are reviewed The materials used in construction and the results of testing on the prototype are also explained and illustrated. Cost data and other information are given to permit evaluation and economic comparison with other systems. The Hi-Dro Cushion Camel consists of rectangularly arranged thin-walled plastic cylinders grouped in clusters in a sandwich between two structural diaphragms The cylinders are submerged in water and are completely enclosed except for an air vent hole and pressure regulating orifice The orifice controls the pressure build up and water release as the tube walls are pushed together at varying velocities. The ability of the device to adapt to variations in vessel displacement, pier flexibility and berthing velocities, is also discussed

HISTORY OF DEVELOPMENT

In November and December, 1967, a new floating fender system called a Hi-Dro Cushion Camel was constructed and tested at Treasure Island U.S Naval Station in San Francisco Bay. Encouragement for development of this new device came from officers at Treasure Island after witnessing the effectiveness of the Hi-Dro Cushion cells (see Figure No 1) attached in a single row on 12-inch centers to a small-boat marina pier. The cells effectively cushioned a five-ton liberty boat being berthed at speeds which normally are unsafe, without causing damage to the boat or pier Previous to the Treasure Island Boat Marina demonstration, reviews and studies of literature on berthing and mooring forces of ships (3,4,5) available to the writers and coupled with experience obtained in highway safety experiments on this new system (1,2) confirmed that a heavy marine application of the Hi-Dro Cushion cell system was feasible both structurally and economically Adding to this the interest of U.S Naval officers, a prototype was developed which is shown in Photo No 1. The prototype diaphragms were constructed from available timber pilings bolted together at the centerline position of the clusters. To these bolts, 3/8-inch diameter wire cables were strung in a diagonal lacing pattern to resist the longitudinal stresses that would be transmitted from

the ship to the pier. The Hi-Dro Cushion Camel prototype contained eighty-four (84) 36-inch long cells grouped in four clusters. No provisions were made in this camel to overcome the bouyancy so as to completely submerge the cell cluster chambers; however, allowances were made in the orifice design for air voids in the cells. Ideally for most efficient use of the cells, they should be completely submerged without air voids. The prototype was designed to absorb the energy of a 100 ton vessel berthing at a velocity of 6 feet per second or a 1,000 ton vessel berthing at 2 feet per second. Tests on the Hi-Dro Cushion Camel revealed that this objective was reached.

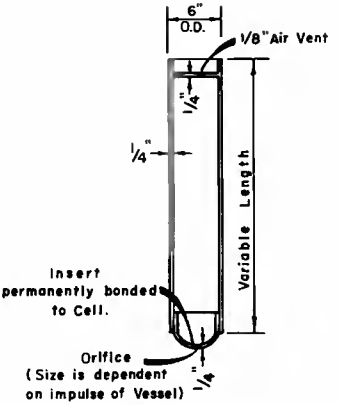

Figure 1 - HI-DRO CUSHION CELL DETAIL

THE WATER-FILLED PLASTIC CELL

The use of a plastic cell filled with water and containing orifices to absorb energy was originally developed under patent by John W. Rich of Sacramento, California for use on automobiles. The automobile water bumper is essentially a horizontally mounted Hi-Dro Cushion cell mounted at front and rear of a car to provide energy absorbing protection. The effectiveness of this system to reduce damage and injuries in automobile collisions is presently becoming more clearly established.

The plastic material makes an ideal container in that it can be molded or extruded in various shapes and sizes. The six-inch diameter cylinder was found to be well suited for use in clusters formed to protect rigid highway hazards such as lighting poles, bridge piers and abutments. The wall thickness and

Photo No. 1.-Hi-Dro Cushion Camel Prototype.

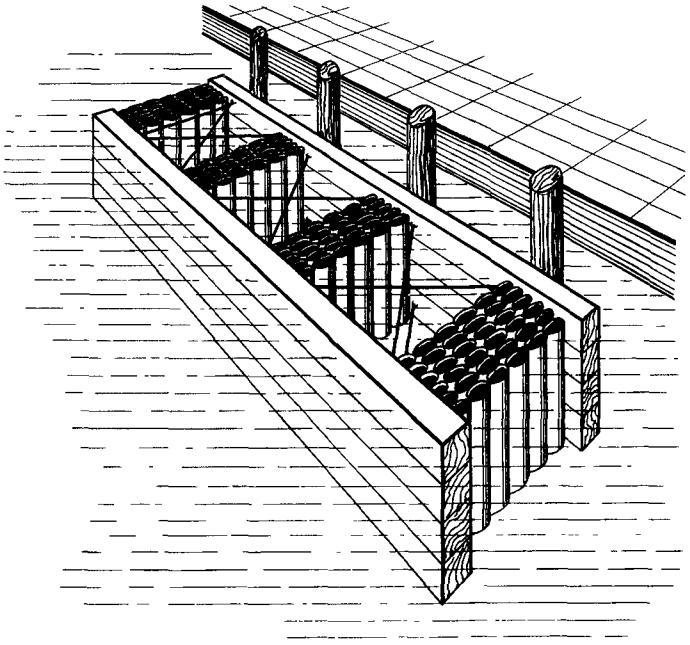

Figure No. 2.- The Hi-Dro Cushion Floating Fender system.

diameter can be varied to suit the stress capability of the plastic material for a specified dynamic pressure The plastic material used in the prototype camel is made from high quality vinyl resins of a high-molecular weight homopolymer combined with totally primary plasticizing systems This plastic possesses the ability to remain plastic at low temperatures and resist distortion at high temperatures The plastic contains stabilizers that inhibit ultra-violet hardening and permit long life under exposed atmospheric conditions. The plastic resists barnacle attachment and attack of marine organisms.

The vinyl plastic has demonstrated its capability to withstand numerous impacts without suffering damage. If failure does occur, however, additional energy is absorbed and the plastic cell is inexpensive to replace. The six-inch diameter cells tested and designed for highway applications are capable of sustaining short-duration (300 millisecond) pressure peaks over 200 psi. In marine uses, however, the impulse periods are longer (4 to 10 seconds). Because the plastic is quite strain-rate sensitive, the ultimate strength of the plastic reduces with increasing load time. This requires the exercise of judgement in assigning allowable design pressures in marine applications

The testing on the prototype demonstrated the distinct capability of the plastic cell clusters to restore to their original shape The reforming force of the cells refilled the clusters within a five to seven second time period after the collapsing load was released

THEORETICAL CONSIDERATIONS

Figure No. 2 is a drawing of a Hi-Dro Cushion Camel that incorporates one major improvement over the prototype. The diaphragms provide a flat surface to bear against the cell clusters. This inhibits the buildup of uneven pressures in the cell ranks and makes the stresses more uniform. Because the cells are constructed with a given size orifice, the pressure impulse of the clusters will vary with the berthing velocity of the ship. The impulse equals the product of internal cell pressure times the area of the cell clusters in contact with the diaphragm times the change in time or.

$$\text{Impulse} = T/g \int_{V_1}^{V_2} dV = \int_{t_1}^{t_2} pA\ dt$$

Where T is the displacement weight of the vessel, dV is the change in velocity of the vessel, g is the gravitational constant, p is the pressure, A is the area of contact between the cells and diaphragm and dt is the change of time. The kinetic energy formulas can also be used to make analysis for a given set of conditions. Further simplifications are possible by assuming constant accelerations and applying an impact or dynamic factor to account for the force-time variations in the equation. The dynamic factors can be verified through experimentation.

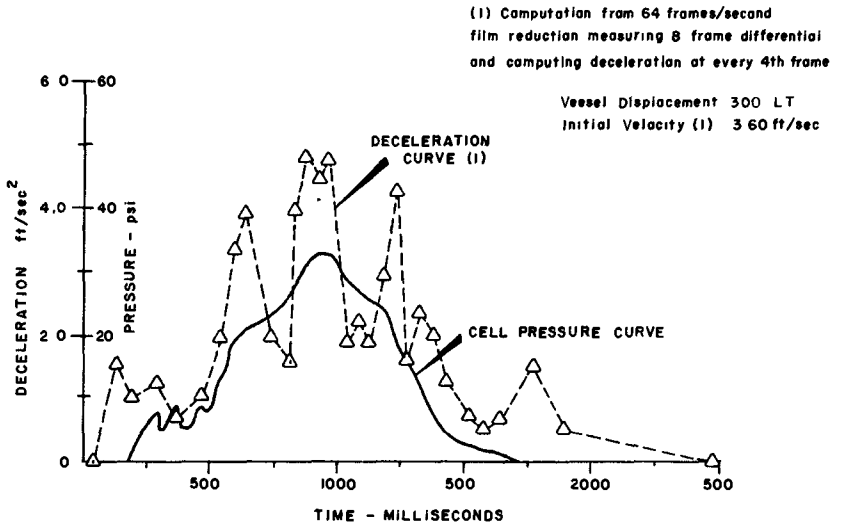

Figure No. 3.- Test No. 9-Hi-Dro Cushion Camel
April 19, 1968- Treasure Island.

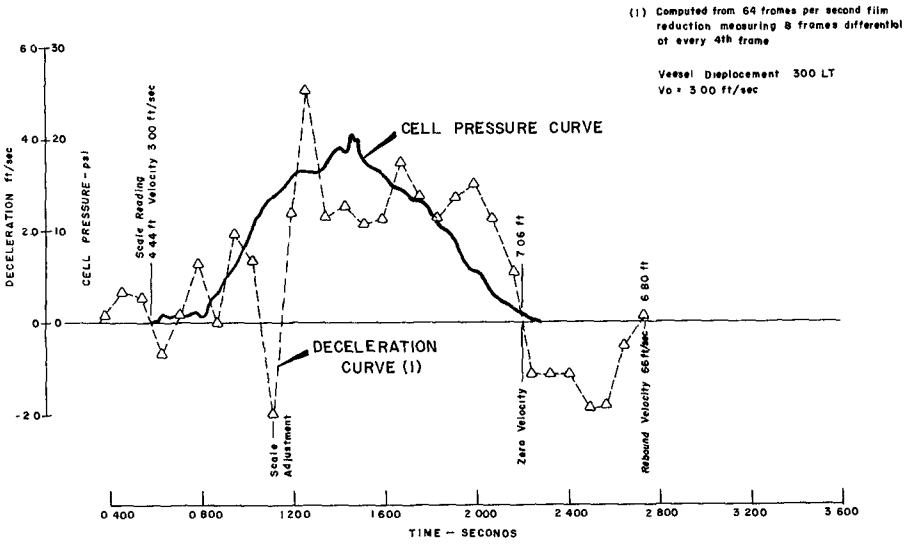

Figure No. 4.- Test No. 8- Hi-Dro Cushion Camel.

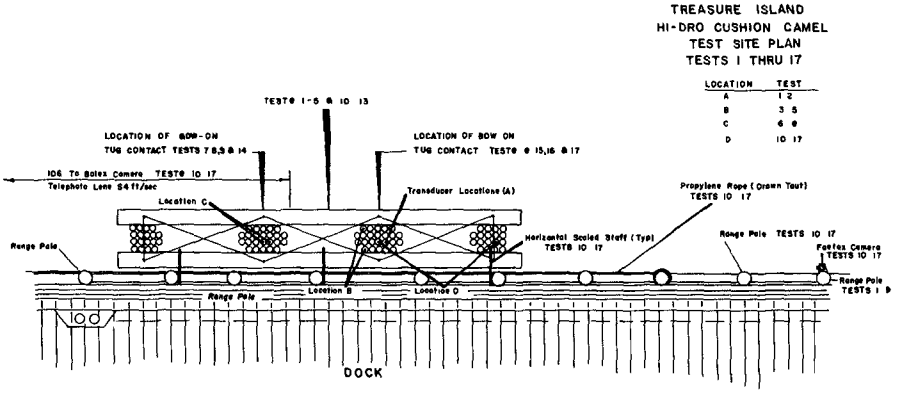

Figure No. 5.- Test Site plan.

HI-DRO CUSHION CAMEL TESTS

Figure No. 5 illustrates the layout of the pier section at Treasure Island Station where two series of tests were conducted on the Hi-Dro Cushion Camel. Photo No. 1 shows pier construction which is identical to the test site.

Tests 1 thru 9 were run on April 19 1968 using a 300 long-ton vessel impacting bow-on into the camel. Velocities into the camel varied between 1.5 and 3.6 feet per second. Acceleration data were measured and computed from 16 m.m. film shot with a Bolex Camera operating at 64 frames per second. Pressure measurements in the cell clusters were recorded on Polaroid film using a C-30 camera mounted to the face of a Tektronic Oscilloscope (2 channels) Type 422 manufactured by Tektronic, Inc. of Portland, Oregon. The pressure transducers were Teleflight Series 185 manufactured by Taber Instrument Corp. of North Tonawanda, New York. The transducers were located in the same cluster and in adjacent cells (See Figure No. 5). Although the cell clusters contained two sizes orifices, nearly identical pressures were recorded in the cells. The orifice sizes were distributed in a checkerboard pattern.

Tests 10 thru 17 conducted on May 13, 1968 used a 400 long-ton displacement vessel. Velocities at impact varied between 1.6 and 3.2 feet per second. Acceleration and pressure measurements were recorded similar to the previous series. Additional Fastax film data was recorded on several hits to measure the fender pile deflections. Transducers were installed in separate units to determine the magnitude of dampening from cluster to cluster due to flexing of the diaphragms.

The fender pilings were 12-inch nominal diameter and extended 30 feet from the deck to the mudline. The water depth was about 18 feet for the first series of tests and about 22 feet for the second series.

In both series of tests the bows of each vessel had smooth receding curvatures that would cause the camel to sink under the bow except at the slower velocities. The override occurred, however, only after the camel had taken most of the energy out of the impact. The tug operator during test 1 thru 6 had difficulties in controlling the ship due to wind conditions. The quartering winds tended to cause the tug at times to hit off-center from the intended target. Tests 7 thru 9 were made on target (See figure No. 5 which shows the locations that the vessel bow initiated contact with the camel). In the second series, the tug was under good control; however, separation of transducer connections at the cells, caused some failures in pressure readings.

TEST RESULTS

Figure No. 3 shows the graphic results of Test No 9. The tug impacted the Camel at an initial velocity of 3 60 feet per second. The computed deceleration curve exhibited some noise or oscillations which are also characteristic to film reduced decelaration data obtained by Warner in Brigham Young University experiments (2). Warner suggests that the noise can be filtered by applying a regression analysis. The deceleration curve plotted in Figure No. 7 (a) did recognize that a computed negative peak did occur even though the magnitude was insignificant. No attempt was made to make special curve fits for the computed deceleration curves. It was interesting to observe that the area under the Deceleration-Time curve of 3.63 fps compared closely to the initial velocity of the tug measured from the film data. In analyzing the curves shown in this paper, please note that the pressure and deceleration curves are shown together for convenience. The time correlation of the two

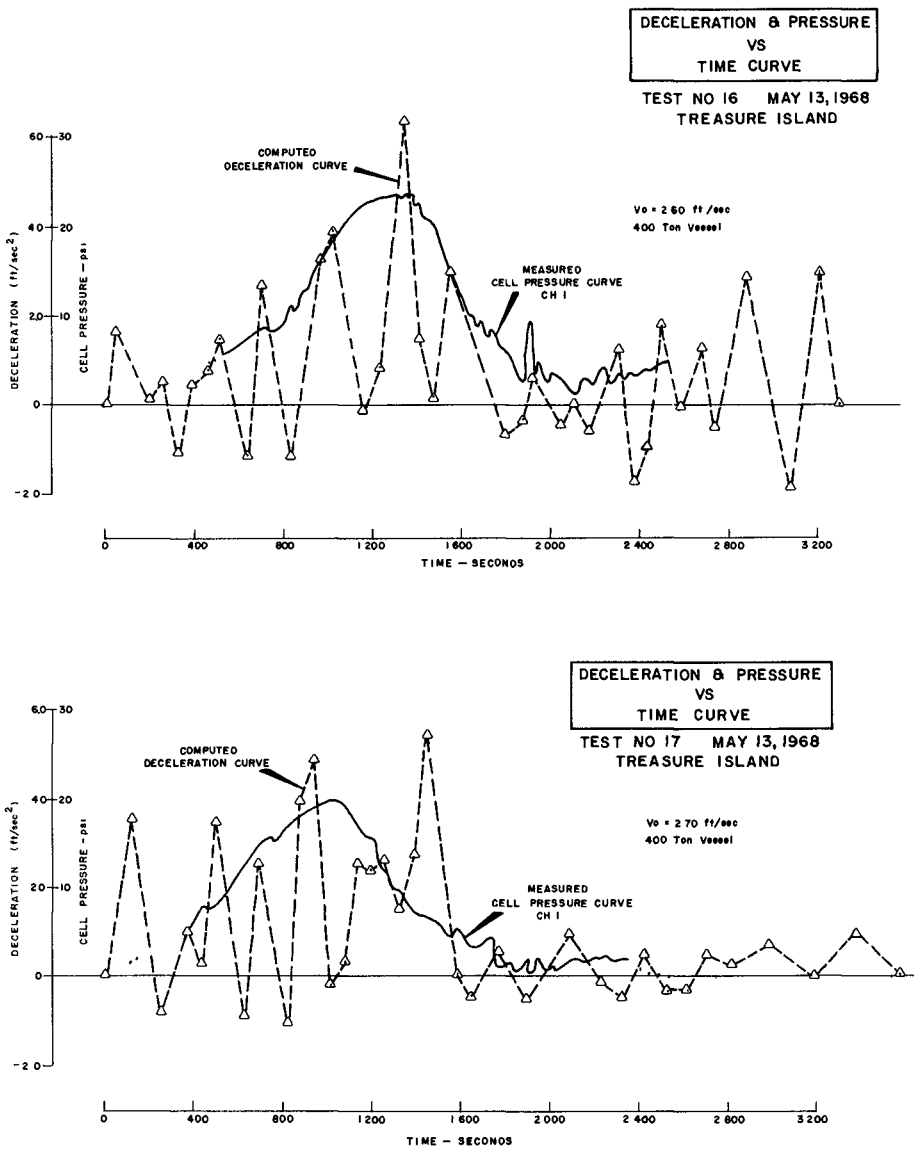

Figure No. 6 - Tests No 16 and 17- Hi-Dro Cushion Camel

curves is not exact, however, it does permit a comparison of the shapes and lengths of the curves.

Figure No. 4 shows a similar set of curves for Test No 8. At a time 1.100 seconds in the event an extreme negative deceleration is shown followed by an almost equally excessive positive peak which indicate how parallax adjustments of the operator in measuring the film data affected the curve It is noted that the pressure wave on the oscilloscope ends near the point of maximum penetration of the tug against the pier Beyond this point in time the tug accelerated away from the pier. The acceleration was caused by stored energy in the pier, and the vessel reached a maximum rebound velocity of 0.66 feet per second. The percentage of stored energy is equal to 100 times the squared ratio of rebound velocity to initial velocity. For Test No. 8, the percentage of rebound was about 5 percent of the total energy. This ratio, however, ignores the influences of hydrodynamic mass. It is characteristic that a slight mass-inertia effect takes place in the early stages of the pressure readings as the camel is suddenly accelerated by the vessel and brought to bear against the pier. The magnitude of the force is small because of the large mass of the tug compared to the mass of the camel However, in other tests where the mass of the cushion system equals the weight of the moving mass, the mass-inertia considerations influence in a large measure, the magnitude of the forces that stop the vehicle. In the marine application, the pressure-resistance effects of the Hi-Dro Cushion Cells are primary.

The deceleration and pressure time curves in Figure No. 6 (Tests No 16 and 17) are similar to those obtained in Tests No 8 and 9. There was, however, a delay in the oscilloscope trace after triggering, before pressure readings showed itself on the scope. This resulted in a loss of measurements of the mass-inertia wave mentioned previously. In these tests, only channel 1 was recorded due to failure in the transducer connection to Channel 2. The curves do correlate in location in time of the recorded peaks. The oscillations of the deceleration curves after pressure effects are over can be explained largely by the sinking of the camel as the bow of the tug rides over the camel and penetrates closer to the pier face. This condition will not exist when most ships are being berthed along a pier. Most ships have sides nearly vertical at the waterline where the loads are taken. The loads will normally be uniformly distributed in a horizontal direction and without a significant vertical component.

Comparisons can be obtained in Figure No 7 in the plot of deceleration and pressure vs time or distance. The oscilloscope pressure readings and acceleration measurements were assumed to correlate on the time base curve and this correlation was platted on the distance base recorded on the film data. The areas under the time based curves are a measure of the change in momentum while the areas under the distance-based curves are a measure of the energy. It can be noted that most of the energy is absorbed before the pressure in the cells is zero. The area under the deceleration-distance curve between 0.25 and 3.50 feet is 6.12 ft.^{2} per sec.^{2} which is 95 percent of the theoretical area. This area can be computed from the measured velocity of impact, i e. $A = \frac{1}{2} V^2$ or $\frac{1}{2} (3.6)^2 = 6.50$ ft.^{2} per sec.^{2} The assumption that the remaining energy would be absorbed in the pier agrees with the comparison made above in Test No. 8.

Test No. 15 shown on Figure No. 8 provided some very interesting data about the flexibility of the round timber diaphragms. This was the only test in this series in which both pressure readings were recorded without a connection failure. Figure No. 5 shows the location of the "bow-on" impact relative to the location of the transducers. The bow of the tug struck the camel at the unit where the Channel 2 transducer was placed and the pressure in this transducer

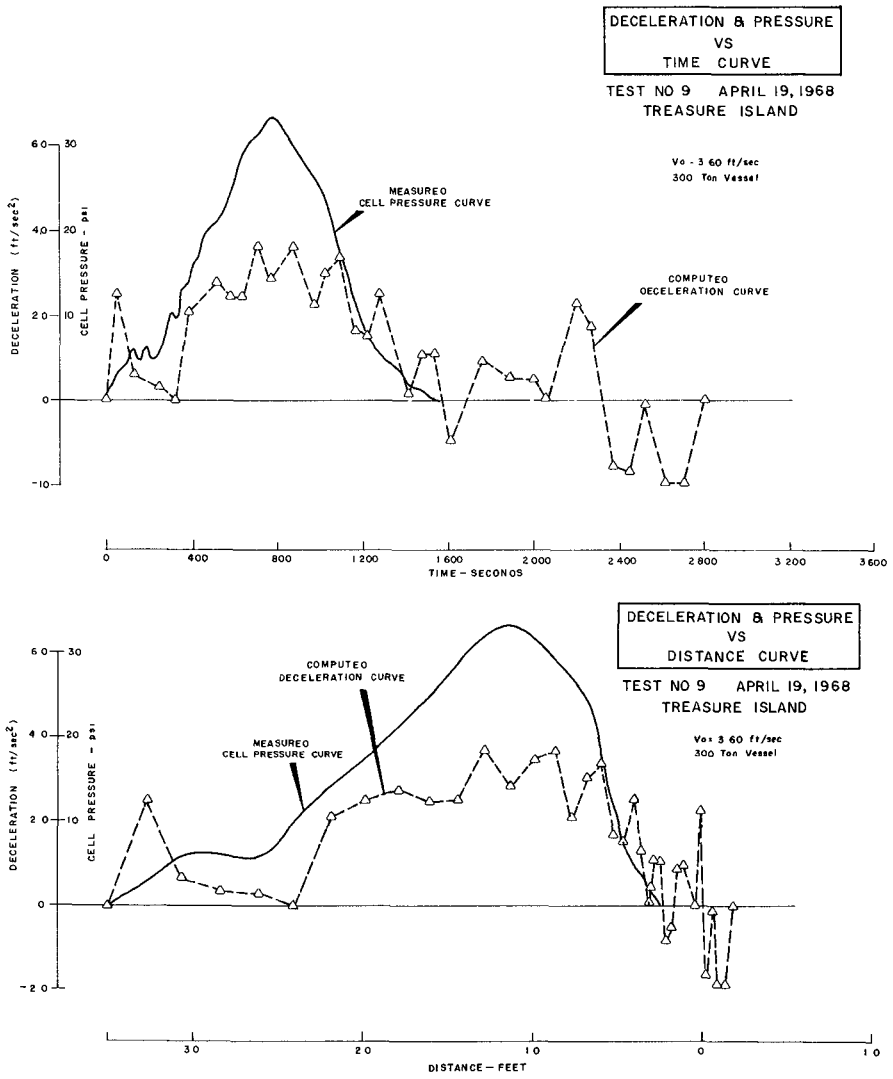

Figure No 7 - A comparison of time and distance curves for Test No 9- Hi-Dro Cushion Camel.

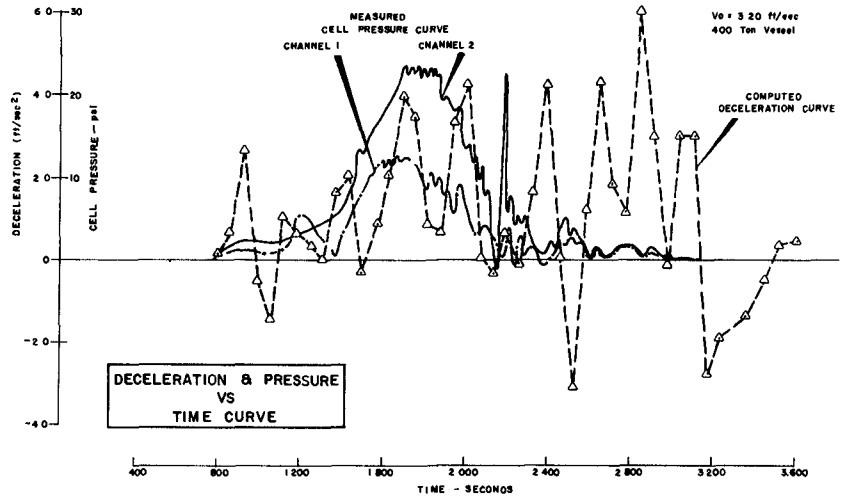

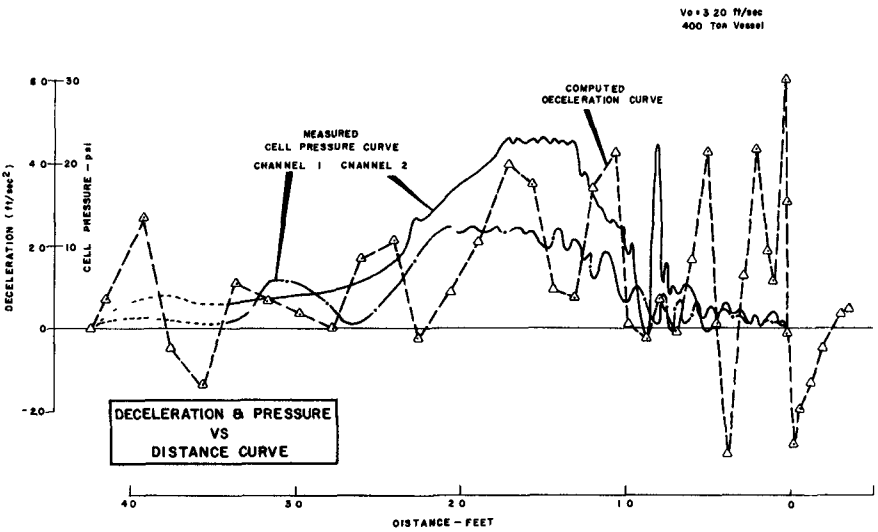

Figure No. 8- Test No 15, May 13, 1968, Treasure Island. Comparison of pressure distribution between adjacent clusters

was measured at 23 psi The impulse pressure recorded on Channel 1 was about 60 percent of the value obtained in the Channel 2 cluster The clusters were spaced uniformly on the camel.

UNIT COSTS

Based upon experience and data gained from installation of the Hi-Dro Cushion Camel tested at Treasure Island, a 45 foot camel, as shown in Figure 2 has been designed with an energy absorbing capability of 3,455 inch-tons The total cost of this camel is estimated at $4,500.00 installed. The cost in place then equals $1 30 per inch-ton per lineal foot The plastic cell clusters comprise 49% of this total cost.

OTHER APPLICATIONS

Figures No 9 and 10 show what can be done to use existing fender material, reconfigured and assembled, to overcome a present fendering problem for a carrier breasted out away from the pier. Figures No 11 and 12 also show how an existing submarine camel can be adapted to receive the increased protection provided by Hi-Dro Cushion Cells. A solution for a breasting or turning dolphin is shown in Figures No 13 and 14

Extensive use in Europe of retractable fender systems has been noted in the literature and many otner types of fender devices are being developed or have been tested (7,8,9.). Some of the disadvantages of these systems can be overcome by using the Hi-Dro Cushion system. Energy absorbing capabilities of some devices can be complimented by adding Hi-Dro Cushion Cells to make the existing fendering system less sensitive to varying ship displacements.

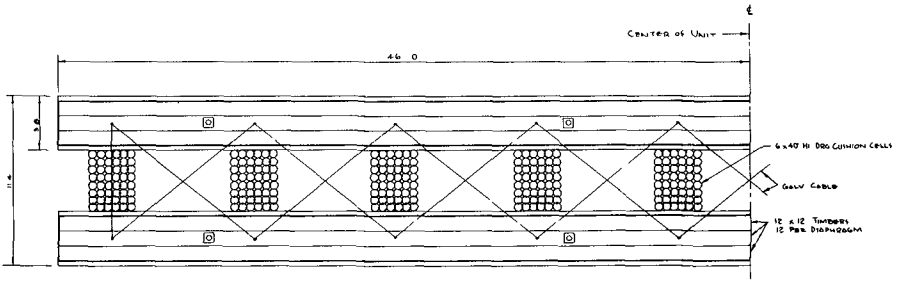

PLAN VIEW
OF
HI-DRO CUSHION CAMEL FOR AIRCRAFT CARRIER

Figure No. 9- Hi-Dro Cushion Camel Layout- Half Plan
(See Fig No. 10 for side view)

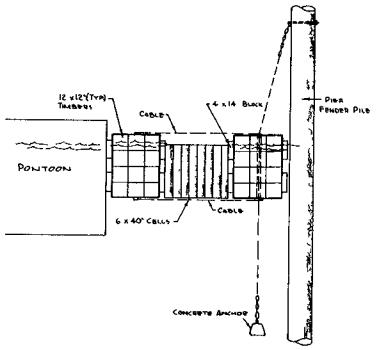

SIDE VIEW
OF
HI-DRO CUSHION CAMEL FOR AIRCRAFT CARRIER

Figure No 10- Aircraft camel detail

AREAS OF INVESTIGATION

The promise of this new floating fender system has opened areas of research that are important from an economic standpoint. Plastics are relatively new materials. Many plastic materials and systems with varying strength properties are being investigated for use in marine applications. There are many plastics that can be produced less expensively than the plastic materials used in the Camel at Treasure Island, however some are prone to harden and stiffen by ultraviolet deterioation when exposed to sunlight. If the cells can be kept submerged and removed from the sunlight, the use of less expensive materials is possible

Research is now in progress on strength and durability of the various plastic materials, especially the fatigue characteristics. It is known that plastics can endure many short duration high peaks without damage. These limits are now being investigated at Brigham Young University

CONCLUSIONS

The tests indicate that the impulse period is lengthened and the forces are reduced during impact on flexible fenders protected by the Hi-Dro Cushion Camel. The benefical effects of the system become apparent. The plastic celled system has a high degree of adaptability to velocity variations and changing masses. This is a distinct advantage when considering piers with multiple use requirements. The Hi-Dro Cushion Camel is economical to construct Maintenance is not expected to be costly.

Development of high strength plastics will also prove to be advantageous. As design pressures can be increased, costs will decrease also.

The construction of larger vessels makes it necessary to develop economical fendering systems. The Hi-Dro Cushion Camel system will most certainly fulfill some of these needs. Harbor structures constructed without fender systems that are adequate to prevent damage to ships, can now be inexpensively

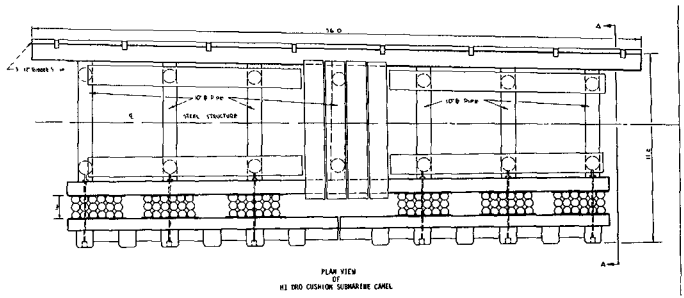

Figure No. 11,- Submarine Camel

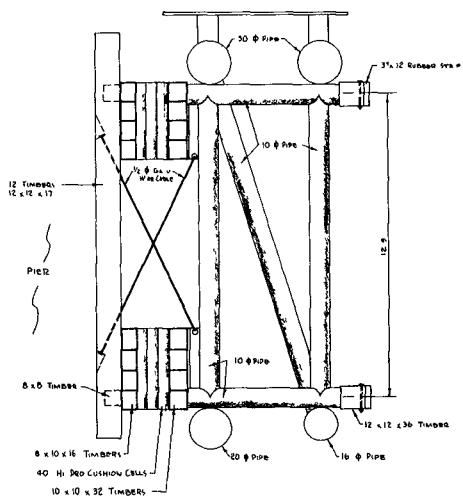

SECTION VIEW
OF
HI-DRO CUSHION SUBMARINE CAMEL

Figure No. 12 - Submarine Camel

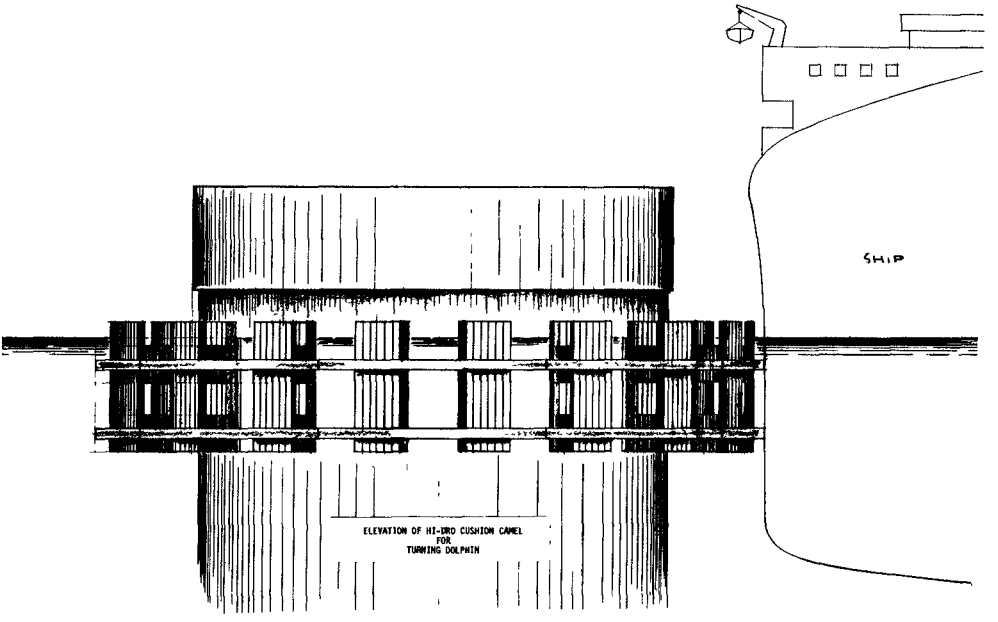

Figure No 13- Turning dolphin details.

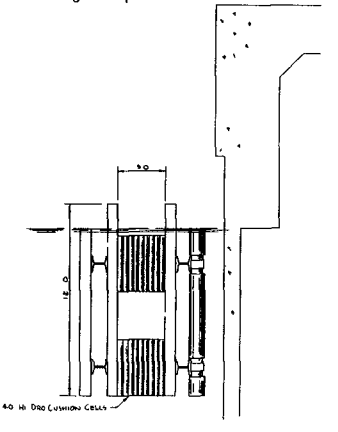

Figure No 14- Turning dolphin details.

and effectively protected This effect alone can reduce shipping rates by inviting commerce from shipping interests that avoid hazardous ports

REFERENCES

1 Warner, C Y., "Engineering Evaluation of Water Filled Plastic Cells In Fixed Barrier Automobile Impacts", Report No RSCB-2, Brigham Young University, Provo, Utah January, 1968

2 Warner, C Y , "Performance of Water-Filled Plastic Bumpers in Full-Scale Automobile Collisions", Dept of Mechanical Engineering, Brigham Young University, Provo, Utah December, 1968

3 Woodruff, G B , "Berthing and Mooring Forces", Transactions ASCE, Vol. 128, 1963 Part IV, Paper No 3504

4 Reeves, N W., "Marine Oil Terminal For Rio De Janeiro, Brazil", Paper No 3410, Transactions, ASCE Vol. 128, 1963, Part IV

5. Chellis, R D , "Pile Foundations", 2d Ed., McGraw Hill Book Co , New York, 1961, pg 191-205

6 Leendertse, J J , "Design Criteria For Camels of Floating Fenders", TR-174 U S. Naval Civil Engineering Laboratory (NCEL), January, 1962

7 Lee, T T , "Review of Report on the Effective Fender Systems in European Countries", By Riselda and Van Lookeren Campagne", TR-376, NCEL, October, 1965

8. Lee, T. T , "A study of Effective Fender Systems for Navy Piers and Wharves", TR-312, NCEL, March, 1965

9 Thorn, B J , "An Engineering and Economic Evaluation of Floating Fender Concepts", CR-66 008, Sience Engineering Assoc for NCEL, June, 1966

CHAPTER 75

DURABILITY OF CONCRETE IN COAST PROTECTION WORKS

by

R.T.L. Allen[1] and F.L. Terrett[2]

ABSTRACT

Frost action and biological attack are not important causes of damage to concrete in coast protection works in the British Isles and no cases of alkali-aggregate reaction have been positively identified. Chemical attack is usually confined to structures containing concrete of indifferent quality. Damage to exposed concrete structures due to abrasion by wave driven shingle is, however, extensive at many sites in the United Kingdom and gives rise to a considerable maintenance problem. A series of experimental panels was laid in the apron of a sea wall at Fleetwood in 1961 in order to compare the performance of different concrete mixes when exposed to attack by the sea. Some provisional conclusions have been drawn from a study of the results of this experiment, and a survey of coast defence works in England and Wales has provided additional information. Suggestions are made for further research into factors affecting the durability of concrete in coast protection works.

SCOPE OF PAPER

The deterioration of concrete structures as a result of chemical attack, repeated freezing and thawing, and alkali-aggregate reaction has been extensively documented, but relatively little information has been published about the effects of abrasion on concrete structures in marine environments. This paper deals in some detail with this problem as well as considering other, better known, causes of deterioration of concrete structures in the coastal waters of the British Isles. It also touches briefly on some aspects of design and construction that have a bearing on durability of marine structures and makes some suggestions for further research.

---

1. Area Engineer for the South West,
   Cement and Concrete Association, Cardiff, South Wales.

2. Partner,
   Lewis & Duvivier, Consulting Engineers, London, England.

CAUSES OF DETERIORATION

The main causes of deterioration of concrete in marine conditions are: repeated freezing and thawing; chemical attack; biological attack; mechanical damage, including abrasion; crystal growth; corrosion of reinforcement.

FREEZING AND THAWING

Severe frost is rare in the coastal waters of the British Isles and freezing and thawing is therefore not an important cause of damage to concrete in marine structures. It may be a contributory factor in the deterioration of any concrete that is of indifferent quality, especially in places such as river estuaries where the salinity of the water is reduced.

CHEMICAL ATTACK

Most marine structures on the coast of Great Britain have been built with concrete containing ordinary or rapid-hardening Portland cement complying with BS 12. These cements correspond approximately to ASTM Types I and III cements, but the alkali and magnesia contents of British Portland cements are usually rather lower than the corresponding American products, the maximum weight of magnesia being limited by the Standard to 4%. In a few cases, sulphate-resisting Portland cement has been used. This is approximately equivalent to ASTM Type V cement; the content of tricalcium aluminate is limited to a maximum of 3.5% and magnesia to 4%.

Experimental work has indicated that in some circumstances special cements may be preferable to ordinary Portland cement in marine structures, particularly where they are subjected to alternate wetting and drying but, in spite of this, numerous structures built with ordinary Portland cement have given satisfactory service. The only cases that the authors have observed in which chemical attack has clearly been a major factor in the deterioration of concrete in sea-water have been structures in which the concrete was of indifferent quality: sometimes the cement content was inadequate and usually the concrete had not been properly compacted with the result that sea-water had permeated the full thickness of the concrete. Some engineers consider that concrete made with sulphate-resisting Portland cement is more resistant to abrasion than concrete made with ordinary Portland cement, but it is possible that some instances of deterioration of ordinary Portland cement concrete which at first sight appear to be due to abrasion may have been aggravated by sulphate attack affecting the surface of the concrete and rendering it more vulnerable to damage by the action of waves and shingle. The additional cost of sulphate-resisting Portland cement is low (currently 32s.6d. per ton), and its use may be a worth-while insurance where satisfactory repairs would be difficult or impossible.

Alkali-aggregate reaction is not considered in this paper because very few reactive aggregates are known to occur in the British Isles.

BIOLOGICAL ATTACK

Biological attack is not likely to occur in marine structures as stagnant conditions are generally required for the growth of the microbes. It is possible however that microbes may contribute to chemical attack on porous or honeycombed concrete where the conditions necessary for their growth may obtain in the pores of the concrete. Chemical secretions from the growth of seaweed on concrete structures may also contribute to surface deterioration (Plate I).

ABRASION

At many places on the coast of Great Britain, abrasion of sea walls and revetments by wave-driven shingle gives rise to a considerable maintenance problem. A particular case is Fleetwood in Lancashire where the foundations of the sea walls along the west shore are protected by sloping aprons with wearing faces of granite blocks and concrete which require continual repair.

In order to compare the performance of different materials a series of experimental panels was constructed in 1961 (Plate II) and records have been kept of the rate of loss by abrasion. Twenty eight concrete panels each 15 ft. x $6\frac{1}{2}$ ft. x 6 in. thick were constructed over a 200 ft. length of apron, the mix designs being all based on the same water/cement ratio and workability.

A control panel using rapid hardening Portland cement, with aggregate/cement ratio 6.6, and $1\frac{1}{2}$ in. and $\frac{3}{4}$ in. single size Shap granite aggregate and beach sand, was included in each day's work so that account could be taken of variations in conditions from day to day during construction and differences in beach level from one end of the experimental length to the other. Interpretation of the results is complicated since each deliberate change involved other variations. The average wear suffered by the six control panels has varied with position from $\frac{1}{2}$ in. in 7 years at one end of the length to $1\frac{3}{4}$ in. at the other. This difference has been taken into account by adjusting all quoted figures so as to be comparable with the most severely abraded control panel.

The loss sustained by the six panels with different cements, which otherwise were of the same proportions and contained the same aggregates as the controls, has varied between $\frac{1}{2}$ in. of wear on average for high alumina cement concrete to $3\frac{1}{2}$ in. for super-sulphated cement concrete. The high alumina cement concrete has decayed in patches, forming isolated cavities several inches deep; this may be due to "conversion", or to alkali attack from Portland cement concrete below the panels. It seems that neither of these panels will have a life much in excess of ten years. Of

the other panels, sulphate-resisting cement concrete appears so far to be the most durable (average wear $1\frac{1}{2}$ in.) followed by ordinary Portland and rapid hardening Portland cement concrete (average wear $1\frac{3}{4}$ in.) and extra rapid hardening Portland cement concrete which has lost $2\frac{1}{2}$ in. on average. Extra rapid hardening cement contains calcium chloride which is incorporated during manufacture and its relative performance as shown by these results is confirmed by one of the control panels in which an admixture containing calcium chloride was used.

The results obtained from changes in grading and type of aggregate are more difficult to compare since changes in aggregate/cement ratio were required in order to maintain the same water/cement ratio and workability. With the same aggregates as used in the panels already discussed, but aggregate/cement ratios (a/c) from 6.2 to 7.0 and sand contents from 30% to 38%, the average loss in 7 years has varied from 2 in. to $2\frac{3}{4}$ in. At a/c = 7.0 a reduction in sand content from 38% to 32% gave no improvement in performance (average wear $2\frac{1}{2}$ in.) but with a/c = 6.2 the amount of wear has been slightly less on concrete with 30% of sand than on that with 36% (2 in. and $2\frac{1}{4}$ in. respectively). The control panel concrete with a/c = 6.6 is apparently more durable than the best of this group and it may be concluded that with $1\frac{1}{2}$ in. maximum size angular aggregate little advantage is to be gained by using mixes richer than about $6\frac{1}{2}$ to 1. A better performance was obtained by the substitution of a crushed granite fine aggregate for the beach sand, but this required a richer mix to maintain workability (a/c = 6.0; wear in 7 years - 1 in. average).

Three panels were cast using a continuously graded coarse aggregate ($1\frac{1}{2}$ in. to 3/16 in.) and a panel was made with $\frac{3}{4}$ in. single size granite aggregate which performed marginally better than the $1\frac{1}{2}$ in. and $\frac{3}{4}$ in. single size or $1\frac{1}{2}$ in. to 3/16 in. graded aggregates but required a richer mix (a/c = 5.8). The differences between these and corresponding panels using $1\frac{1}{2}$ in. and $\frac{3}{4}$ in. single size aggregates are too small for conclusions to be drawn at this stage.

Several different types of aggregates were included in the experiment and from observation to date they may be arranged in the following order from most to least durable: (1) Flint gravel (2) Fine-grained granite (3) Coarse-grained granite (4) Hard blue limestone (5) Limestone (6) Pit gravel containing mainly sandstone (millstone grit) but also some limestone and igneous rock.

In addition to the usual laboratory tests on the concrete and concrete materials, a series of abrasion tests was carried out by sand-blasting 12 in. cubes of some of the concretes used on site. In these tests, the super-sulphated cement concrete and rapid hardening cement concrete with high sand content (38%) were significantly less resistant, and two specimens of flint aggregate concrete significantly more resistant, than the others. Apart from these four cases, no correlation has been found between the abrasion test results and the properties of the concrete, such as strength and density, or the performance in the field.

A full-scale experiment, but more limited than the trials at Fleetwood, is being carried out by the Kent River Authority at Dymchurch, where a sloping apron was reconstructed in 1963. The work consists mainly of panels of precast concrete blocks surrounded by ribs of in-situ concrete, but some panels of granite blocks have been included for purposes of comparison (Plate III). In order to compare the performance of different types of concrete, some of the precast concrete blocks were made with gap-graded aggregate and some with continuously graded aggregate. Flint coarse aggregate of $1\frac{1}{2}$ in. maximum size was used and in the gap-graded concrete was single size. The aggregate/cement ratio was 5 and the cement ordinary Portland. Concrete test cubes made during the course of the work had crushing strengths of about 6,000 lb./in.^{2} at 7 days and 7,300 lb./in.^{2} at 28 days. So far there has not been enough abrasion for any significant differences to be seen between the granite and the various concretes.

Parts of another apron at Littlestone were reconstructed by the Kent River Authority in 1960 and 1966 with ragstone slabs set in fine concrete. The fine concrete jointing material used had an aggregate/cement ratio of $2\frac{1}{2}$ using flint aggregate from Dungeness graded from $\frac{1}{2}$ in. down to no. 100 BS sieve, in accordance with the requirements for all-in aggregates of BS 1201. Sulphate-resisting Portland cement was used with 4% entrained air, and 2% calcium chloride was added as an accelerator. This jointing material appears to be very resistant to abrasion and the ragstone slabs in the 1960 work are showing signs of greater wear than the jointing concrete.

An interesting example of a concrete sea wall exposed to very severe abrasive conditions is at Sheringham on the coast of Norfolk. The beach material consists of a very hard flint shingle and the exposure is severe. The sea wall was built in the summer of 1967 using concrete containing a coarse aggregate consisting of irregular flint gravel ($1\frac{1}{2}$ in. maximum) similar to the beach material and sand from the same source. The proportion of sand in the total aggregate was 34% and the aggregate/cement ratio of the concrete was 7.1 with ordinary Portland cement. Precast reinforced concrete retaining wall units that were part of a manufacturer's standard range were used as permanent formwork. These units were not designed to withstand such severe exposure and in places they have almost completely disappeared (Plate IV). The concrete in the main structure is showing some signs of abrasion but is wearing more slowly.

Coast protection works at a number of places on the coasts of Wales and the West of England where concrete has suffered from abrasion have been examined. Plate V showing a sea wall at Porthcawl in Glamorgan is a typical example. In most cases the work was constructed fifteen or more years ago, and in much of it concrete having nominal mix proportions 1:2:4 by volume was used and the concrete was compacted by hand. Although the performance of structures in different situations cannot be compared, owing to differences in exposure, a general inspection does suggest that the older structures, in which the concrete was probably not very well compacted and in which little quality control was exercised, have not proved as durable as more modern structures incorporating carefully designed concrete mixes with better standards of quality control and compaction.

CRYSTAL GROWTH

Salt crystals growing in cracks in concrete structures may exert enough pressure to cause spalling of the concrete. This is particularly likely near high water level and in the splash zone. It has been suggested to the authors that sodium sulphate formed through the double decomposition of sodium chloride and gypsum is more likely to cause this trouble than crystals of sodium chloride. One of the authors has seen some concrete sea walls in Lincolnshire on the east coast of England in which spalling of concrete has started from fine shrinkage cracks (Plate VI) and this may well have been due to crystal growth.

CORROSION OF REINFORCEMENT

It is considered that there should be at least 2 in. (5 cm.) of dense concrete cover to all reinforcement in marine structures in order to prevent corrosion, and an additional allowance should be made for abrasion when the necessary concrete cover is assessed.

In the past structures have been built at a number of coastal sites in which inadequate compaction of the concrete surrounding the reinforcement has led to corrosion of the steel and cracking of the concrete. Many of these structures were built before mechanical vibrators came into general use, and in some cases the trouble had been aggravated by detailing of reinforcement that made compaction of the concrete difficult. This applies particularly near the lower edges of heavily reinforced beams.

JOINTS

A really satisfactory method of sealing expansion joints does not appear to have been developed. Both hot-poured and cold-poured sealants are often dislodged by wave action and the authors have seen a number of sea walls in which the expansion joints are inoperative because the sealant has been torn out and stones have become wedged in the joints (Plate VII). Extruded plastics sections cast into the concrete have given promising results and

it is suggested that ribbed neoprene strips of the type sometimes used in sealing joints in concrete roads might be tried for this purpose. Atmospheric humidity near the sea varies relatively little and the annual temperature range is considerably less in coastal areas than it is inland, so that movements of joints should be relatively small; it appears that an unnecessary number of expansion joints are often provided. Since coast protection works usually involve fairly massive structures, it is difficult to provide enough reinforcement to control cracking and fairly frequent contraction joints are therefore necessary.

CONSTRUCTION

A problem in the execution of coast protection works is to prevent the sea from washing out the surface of freshly placed concrete. Formed surfaces are protected if the formwork is watertight and rigidly fixed in position, but protection of the upper surface of a lift of concrete or a sloping apron often presents difficulties. Some of the experimental panels at Fleetwood, for instance, suffered superficial damage by the sea during the first few hours after placing, and subsequently had to be cut out and re-cast. In parts of the work carried out by the Kent River Authority at Dymchurch, the precast concrete blocks have proved more durable than the in-situ concrete surrounding them. This may be due to better compaction of the precast concrete, but it is also possible that the surface layers of the in-situ concrete may have been affected by the sea soon after placing.

FURTHER RESEARCH

The most useful information will be gained from full-scale trials in which different materials and structures are exposed to similar conditions for a number of years. Owing to differences in exposure conditions at various places round the coast, it is not possible to draw detailed comparisons between the behaviour of different materials and structures at different places, so that full-scale trials such as those at Fleetwood are the most valuable source of information. The trials at Fleetwood are the most elaborate of which the authors are aware, but it is hoped that other authorities will undertake similar work since definite conclusions cannot be drawn from one set of results. It has been established practice for a number of years in various parts of the world to carry out full-scale trials in connexion with highway design and construction, and the authors hope that similar trials will be carried out for coast protection works.

It would be useful to develop an accelerated wear test for use under laboratory conditions, preferably using larger particles of abrasive material than those used in sand-blasting. The 'rattler test' for abrasion resistance of precast concrete paving flags, described in BS 368 might be suitable for development for this purpose. The apparatus used in this test consists basically of a

steel box measuring about 1 x 1 x 2 ft. A paving flag is fixed to the inside of each 1 x 2 ft. side and 1,000 steel balls $\frac{1}{2}$ in. in diameter are placed in the box. The ends of the box are sealed and it is rotated at 60 revolutions per minute about the long axis for 48 hours. The loss in weight of each paving flag is measured after this period.

In view of the unsatisfactory performance of many types of joint sealing material, there is also a need for experimental work on this subject. The performance of a number of poured sealants is very susceptible to inadequate preparation of the surface of the joint and, because of the difficulty of obtaining clean dry joint surfaces in concrete structures between tide levels, a sealant material that would adhere satisfactorily to a damp surface would be very valuable. Apart from this, the authors would like to see some trials carried out with plastics or neoprene sections as suggested above.

Plate I - Surface deterioration possibly due to seaweed growth

Plate II - Experimental wearing panels at Fleetwood

Plate III - Aprons at Dymchurch with granite and concrete blocks as wearing surfaces

Plate IV - Sea Wall at Sheringham constructed with precast concrete retaining wall units as permanent formwork

Plate V
Abrasion at base of sea wall at Porthcawl

Plate VI
Spalling of stepped concrete apron possibly initiated by crystal growth in hair cracks

Plate VII
Stones wedged in expansion joint from which sealant has been torn out

PART 4

COASTAL AND ESTUARINE PROBLEMS

CHAPTER 76

FIELD INVESTIGATION PRACTICES OF COASTAL STUDIES IN JAPAN

Masashi Hom-ma
Professor Emeritus, University of Tokyo
Tokyo, Japan

ABSTRACT

This paper is a brief reveiw of the publications on the field studies carried out in Japanese coasts. Japan has many projects of coastal works in relation with the development of industrial area, the protection of coastal land from disaster and some other purposes. Before the execution of these projects, the agencies in charge of them make field investigations for their necessary items. The results of investigations in detail are reported in their official publications and sometimes the abstracts of them are reported at the annual meeting of coastal engineering held by the Japan Society of Civil Engineers. As the official publications of the governmental organizations are distributed in strictly limited circles, they are not well known by scientists and engineers outside these organizations. The author intended to collect some of these official reports and selected some additional reports on field study from the proceedings of annual meetings of coastal engineering, and tried to make a classification of the contents and to give a brief review of them.

Art. 1

Japanese engineers have devoted their great efforts to solve numerous coastal problems in order to promote the nation-wide coastal development and to extend the coastal protection works against waves and coastal erosion. It is needless to say that the primarily important practice for attacking the practical problems is to obtain the knowledges on the general features of coastal phenomena qualitatively and quantitatively as much as possible. From this point of view the field investigation techniques have been developed worldwidely by engineers and scientists during the last decade in many aspects. The aim of this paper is to review and summerize the important practices actually applied in the Japanese coast and to contribute to find the future directions of the coastal investigation.

In this country the results of such field investigations are sometimes published in an abstract at the annual meetings on coastal engineering which were held by the Japan Society of Civil Engineers. However the obtained results described in detail are generally available only for strictly limited circles. Beside it, considering the fact that almost all of those publications are written in Japanese language, the author intends

to give a brief review of them and to make clear the agencies where the correspondences are possible about those reports.

The purpose of a coastal investigation for an engineering project is in most cases to study the stability of coastal structures against waves and littoral drift or to predict the effect of the structures on wave action and the stability of coastline. Therefore waves and sediment movement can be said to have the largest importance in many coastal studies. The coastal phenomena, especially beach erosion or sand deposition, are investigated in two aspects; they are macroscopic aspect and detailed (or microscopic) aspect. The former is, for example, to investigate the morphological changes over a wide area for many years, sometimes for hundreds or thousands years. The latter is the studies in detail. They are; the grain analysis of sediment, tracing the movement of sediment and other dynamical problems. The literatures listed at the end of this paper contain the reports of these sorts of investigations applied in the Japanese coasts. From the contents of those literatures the author made a rough classification of the field practices in the following;

1. Geographical and morphological studies of the district which covers the coastal area to be investigated.
2. Mineral analysis and grain size analysis of beach sediment.
3. Observations of wind and waves. Survey of littoral current.
4. Tracing the movement of bed materials using tracer. Observation of suspended sediment in wave and measurement of wind drift sand.
5. Establishing hydrographic survey periodically in order to make the maps of sea bottom topography. Examination of coastal morphology by aerial photogrametry.

Art. 2

Discussion on the shore process of present topography helps the investigation on the future process of the coast. In the literatures 1-3 and E-1 Dr. Shiraishi describes the process of development of Tomakomai coast in Hokkaido during the past four thousands years and makes an estimation of the volume of deposited sand. The coasts of Niigata and Ishikawa are well known for its receding character. In 2-1 and 2-8 there are descriptions about the historical development of coastal dunes which are now being eroded. It is also suggested that relative rise of sea level took place during a period not so long and it caused beach erosion in these coasts.

There is an example of a sudden crast movement which destroyed the equilibrium in shore process. In the case of Kanto big earthquake in 1923, there took place ground rise of approximately one meter along the coast of Sagami Bay (Fig. 1). After this accident the beach is being eroded under the wave action and by very gradual subsidence of ground (3-5, E-3).

Sometimes the cause of beach erosion is attributed to river improvement works. In Japan many kinds of river works have been carried out over the whole land for about seventy years. As the result the amount of debris carried by flood flow took a decreasing tendency which accelerated the recession of sand beach. A notable example is seen at Niigata coast (Fig. 2). Since the floodway of Shinano River was completed about fifty years ago, there appeared a wide deposit of sand at the mouth of floodway. At the same time beach erosion was remarkably accelerated at the west coast of Niigata city which is located at the mouth of Shinano River.

Art. 3

Petrographic studies have been carried out in many coasts by geologists. The examples are found in the literatures 2-7 for Niigata, in 2-9 for Ishikawa, in 3-7 for Tokai coast and in 3-5 for Sagami Bay. The practices applied to these coasts are not proper in Japan. However many beaches in Japan are nourished by debris poured out with flood flow from rivers and the petrographic studies are generally very useful ways to investigate the source of sediment supply. The common items of the investigation are as follows;

1. Grain diameter analysis (the biggest gravel diameter, median of diameter, uniformity and skewness of diameter distribution, etc.).
2. Size analysis of gravel (flatness, etc.).
3. Rock composition of sediment.
4. Mineral composition of sediment; content of heavy mineral in 3-7, and content of magnetic mineral in 2-9.

A part of the literature 2-9 was published by Prof. Aramaki at the 10th Conference on Coastal Engineering in 1966 (E-6).

Art. 4

The wave gauge commonly used in Japan is that of water pressure type developed at the Ministry of Transportation. Step-resistance wave gauge was also applied at some coasts in Japan. A more simple system for the observation of wave height was developed by Mr. Utai (1-1). In this system a transit with special attachment is used to trace and record the movement of buoy set at a proper location in the sea. The results of observations by these systems are found in 1-15, 2-1, 3-1 and 3-3. The literature 1-2 shows an example of wave observation by stereophotography.

Concerning the measurement of wave direction, an adequate method must be chosen according to the site and purpose of observation. The literature 1-9 shows a direct measurement of water motion using electro-magnetic current meter, while 1-14 gives the record of wave direction estimated from the simultaneous data of some wave gauges. 2-6 shows the results of observation used a rador system which makes possible the routine observations of wave direction at fixed places off the shore.

There are two sorts of method for the measurement of littoral current. One is to set a current meter at the site (to set on the bottom or to suspend from a moored ship), and the other is to trace the floating buoy which is transported by the current. In the Niigata coast a current meter was set in a frame fixed on the sea bottom and buoys were trajected from the shore by a special trajector (2-3).

Art. 5

In order to examine the local movement of bed sand, radioisotope or fluorescene are often used as tracers. A compiled description on the application of tracers in Japan is found in the Proceedings of the Symposium "Radioisotope in Hydrology", 1963. The results of recent observations by these tracers are found in the literatures 1-5, 1-11, 2-3, 2-4, 2-5, 3-10, 3-11 and E-5. To estimate the sand movement near the shoreline, test barriers or test groins are sometimes constructed. The literature 3-12 shows the estimation of littoral drift along Kashima coast from the observed data obtained at the test barrier. The maximum scoured depth during a storm was measured using a simple apparatus (Fig. 3) at Niigata coast (2-4).

Concerning the field observation of suspended sediment in sea water, it is required in many cases to know the average condensation over a ceraain extent of time. For such a purpose Professor Fukushima developed a simple sampler made of bamboo. The results of its application are found in 1-4, 3-4, 3-7 and 3-12. The reports on the field study of wind drift are in the literatures 2-7 and 3-4.

Art. 6

Repeating of sounding survey carried out over a certain area with a definite interval of time is very useful to know quantitatively the change of sea bottom. In Japan the contour map of the sea bottom is made approximately every six months over the area where a project is in progress. Comparison of two contour maps of succeeding times makes us known the change of sea bottom which took place during one typhoon season or one winter storm season. In Niigata west coast the comparison of bottom profile of present time with that of about fifty years ago shows that the bottom was eroded over the area of water depth less than 35m (2-2). An example of the seasonal change of bottom profiles at Tokai coast is found in 3-7, (Fig. 4).

The literatures 1-16 and E-7 are the reports of the study on the recession of coastal cliff by means of aerial photography. The use of aerial photogrametry will be developed for wide applications in the future coastal studies.

Art. 7

Literatures from the Proceedings of Annual Meetings on

Coastal Engineering, Japan Society of Civil Engineers.
(Published in Japanese)

1-1 G. Utai: Measuremtnt of wave height using a transit, 1955.
1-2 T. Ijima & others: Wave characteristics in surf zone observed by stereophotography, 1956.
1-3 N. Shiraishi: Observation of littoral drift for the works of harbour construction, 1957.
1-4 H. Fukushima & M. Kashiwamura: Sand drift and its observation, 1959.
1-5 T. Ijima, S. Sato & others: The characteristics of wave and littoral drift on the coast of Fukue, 1960.
1-6 N. Sakamoto, T. Ijima & S. Kimura: Characteristics of wave along the Pacific Coast due to typhoon and their estimation, 1961.
1-7 F. Kakinuma: Size distribution of beach sand along Ozu coast in Atsumi Bay, 1961.
1-8 H. Fukushima & others: Study on littoral drift along Hidaka coast, (1), 1962; (2), 1963.
1-9 Y. Nagata: Observation of wave direction by electro-magnetic current meter, 1963.
1-10 H. Fukushima & others: Study of Ishikari River mouth, 1964.
1-11 T. Ijima & others: Study on the littoral drift along Kashima coast, 1964.
1-12 Y. Iwagaki & others: Investigation of the coefficient of bottom friction at an actual beach, 1965.
1-13 T. Arata & R. Koh: Morphological study of Iwafune Harbour, 1965.
1-14 T. Ijima & others: Observation of wave direction by using wave gauges, 1966.
1-15 J. Itao & others: Wave characteristics in the coast of Japan Sea, (1), 1966; (2), 1967.
1-16 K. Horikawa & T. Sunamura: A study on beach-cliff recession by using aerophotography, 1967.

Literatures from governmental and other agencies.
(Published in Japanese)

a. Reports for the coast of Japan Sea.
2-1 Beach erosion at Niigata coast, 1960.
2-2 " " " " " , (Continued), 1964.
Civil Engineering Section, Niigata Prefectural Government; Gakkomachi, 1-602, Niigata.
2-3 Report of the investigation of Niigata coast, (4), 1966.
2-4 " " " " " " " , (5), 1967.
2-5 " " " " " Sakata Harbour, (4), 1966.
2-6 " " " " " Kanazawa Harbour, (5), 1967.
2-7 Report of the study on beach sediment in Niigata coast, 1962.
The First Harbour Construction Bureau, Ministry of Transportation; Hakusanura 1-332, Niigata.
2-8 Report of the wind drift at the Niigata East Harbour, 1964.
Niigata Harbour Work Office, Ministry of Transportation; Irifunecho 4-3778, Niigata.

2-9 Report on the mouth of Shimbori Outlet, 1962.
Kaga-Sanko Reclamation Office, Hokuriku Agricultural Bureau, Ministry of Agriculture and Forestry; Hirosaka 2-2-60, Kanazawa.

b. Reports for the Pacific Coast.
3-1 Observation of wave by wave gauges, (Report Vol. 4), 1954.
3-2 Investigation of littoral drift by radioisotope, (Tech. Memo. No. 5), 1963.
Port and Harbour Research Institute, Ministry of Transportation; Nagase 3-1-1, Yokosuka.
3-3 Observations of wave at Onahama Harbour, 1967.
The Second Harbour Construction Bureau, Ministry of Transportation; Takashima 1-2-5, Nishi-ku, Yokohama.
3-4 Report on the sand movement by wind and wave at the estuary of Tone River, 1964.
The Lower Tone River Work Office, Ministry of Construction; Sawara 1-4149, Sawara, Chiba Prefecture.
3-5 Report on the investigation for the protection of Katase-Kamakura Beach, 1958.
3-6 Report on the investigation of Sagami River Mouth, 1961.
Civil Engineering Section, Kanagawa Prefectural Government; Nihon Ohdori 1, Naka-ku, Yokohama.
3-7 Report of the investigation of Tokai coast, 1962 (JAP Memo. 1).
3-8 Investigation on the distribution of suspended sediment at Tokai coast, 1963, (JAP Memo. 4).
Japan Atomic Power Co. Ltd.; Ohtemachi Blg., Ohtemachi 1, Chiyoda-ku, Tokyo.
3-9 Report of the investigation of Tomakomai Harbour, 1960.
The First Scientific Research Laboratory, Hokkaido Univ.; N. 12, W. 8, Sapporo.
3-10 An investigation on littoral drift, relating harbour construction, 1963.
Port and Harbour Research Institute, Ministry of Transportation; Nagase 3-1-1, Yokosuka.
3-11 On the natural features of Kashima coast, Vol. 2, 1962.
3-12 On the natural features of Kashima coast--on the littoral drift, 1964.
The Second Harbour Construction Bureau, Ministry of Transportation; Takashima 1-2-5, Nishi-ku, Yokohama.

c. Reports published in English.
E-1 N. Shiraishi: The measurement of littoral drift at shoreline harbours, Coastal Engineering in Japan, Vol. 2, 1959.
E-2 H. Fukushima & M. Kashiwamura: Field investigation of suspended sediment by the use of bamboo samplers, Coastal Engineering in Japan, Vol. 2, 1959.
E-3 M. Hom-ma, K. Horikawa & C. Sonu: A study on beach erosion at the sheltered beaches of Katase and Kamakura, Japan, Coastal Engineering in Japan, Vol. 3, 1960.

E-4 T. Furuhata: New electric ocean wave recorder, MR-MARK III--for the coastal station, Coastal Engineering in Japan.
E-5 S. Sato: Sand movement at Fukue coast in Atsumi Bay and its observation by radioactive glass sand, Coastal Engineering in Japan, Vol. 5, 1962.
E-6 M. Aramaki: A petrographic study on littoral drift in the Ishikawa coast, Proceedings of 10th Conference on Coastal Engineering, 1966.
E-7 K. Horikawa & T. Sunamura: A study on the erosion of coastal cliff by using aerial photographs, Coastal Engineering in Japan, Vol. X, 1967.

Fig. 1 Sites of coastal observation appeared in the report.

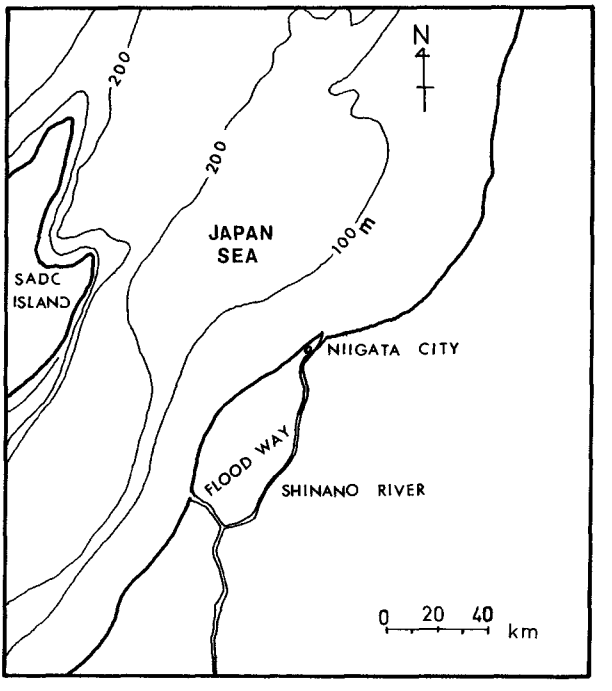

Fig. 2 Niigata coast and Shinano river.

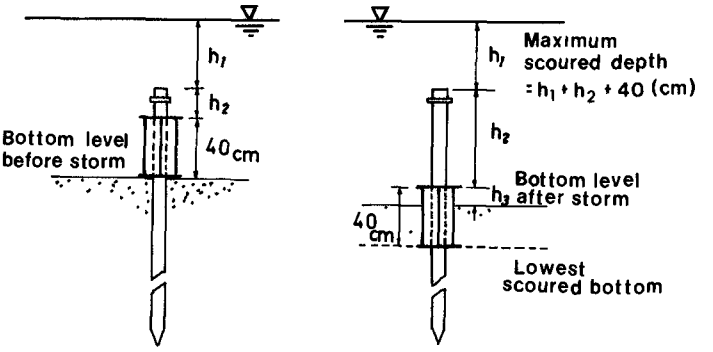

Fig. 3 Apparatus for the measurement of maximum scoured depth.

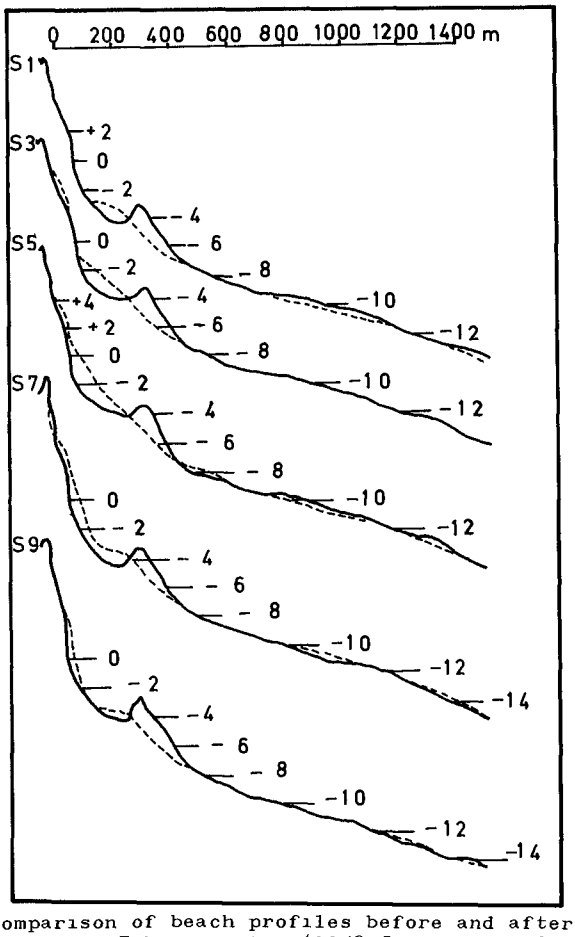

Fig. 4 Comparison of beach profiles before and after a typhoon season in Tokai coast. (1958 July and 1958 Nov.)

CHAPTER 77

THE ATLANTIC COAST OF LONG ISLAND

Frank L. Panuzio, Chief, Engineering Division
Department of the Army, New York District
Corps of Engineers and Fellow ASCE.

SUMMARY

The south shore of Long Island, located on the northeast coast of the United States, consists of 120 miles of headlands and barrier beach which is breached by inlets that interconnect the coastal bays with the Atlantic Ocean. The shore is subject to severe changes due to constant attack of the ocean, rising level of the ocean and severe storms. The predominant, east to west littoral drift moves from 300,000 to 600,000 cubic yards of sand along the shore annually. The affected area encompasses a million people and is valued at $2.5 billions. Improvements have been authorized for 110 miles of shore, and involve sandfill, feeder beaches, groins, jetties, sand bypassing, and inlet barriers The estimated cost for the entire shore improvement is $188 million. The annual charges are about $10 million. The annual benefits are $16 million. The implementation of the authorized work includes the design and model testing of several sections and the completed work in several sections, such as sandfill, feeder beaches, and groins. The completed work shows considerable effect on shore processes. Overall evaluation must await completion of the total improvement in an integral section of the shore.

GENERAL

Location. Long Island is a long, narrow island at a significant indentation of the northeastern coast of the United States, and is bounded on the south and east by the Atlantic Ocean and on the north and west by the mainland, Figure 1.

Objective is to present the history, the problems, the constructive actions and current results dealing with the critical condition of shore recession and erosion, unstable inlets, and coastal inundation.

GEOMORPHOLOGY

The island is part of the Atlantic Coastal Plain province. Glaciation and the attendant effects of ice cover and ice movement mask the original topography. The island consists of glaciated deposits of sand and gravel to depths of over 100 feet. These deposits rest on the remnants of an old, submerged coastal plain. The glacial outwash plain slopes southward from an altitude of about 200 feet above mean sea level at the north shore of Long Island and occupies the entire width of the island, Figure 2. Rising above the plain are two belts of terminal moraine deposits of a later glacial stage. The southernmost, the Ronkonkoma moraine, located in the middle of the island, forms the crest of the southern peninsula, and terminates in the cliffs of Montauk Point. Southward of this moraine and superimposed on the basal outwash plain is a second outwash plain of the same age as the Ronkonkoma moraine. This plain consists of a thin sheet of sand and gravel and slopes to the south. Originally, the south shore of the mainland of Long Island was determined by the intersection of this gently sloping outwash plain with the ocean.

The submerged extension of the coastal plain forms the continental shelf with a width of 80 to 100 miles and with a gentle slope that dips to the southwest, Figure 3. The shelf surface shows characteristic features of underwater erosion, wave formed shores and coarse grain material, as are found close to low water shorelines. Crossing the continental shelf to the southwest is the submarine valley of the Hudson River and Hudson Canyon and to the southeast is the Block Canyon.

PHYSIOGRAPHY

Significant sections. The south shore of Long Island is divided into two

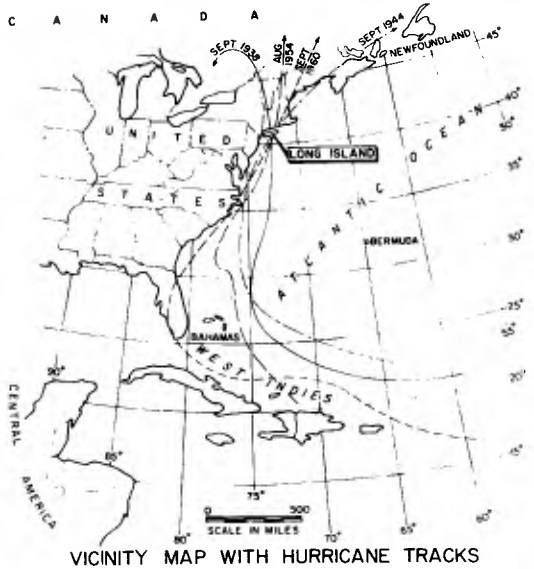

VICINITY MAP WITH HURRICANE TRACKS

OBLIQUE LOOKING GENERALLY EASTWARD

FIG. 1 LONG ISLAND, NEW YORK, U.S.A.

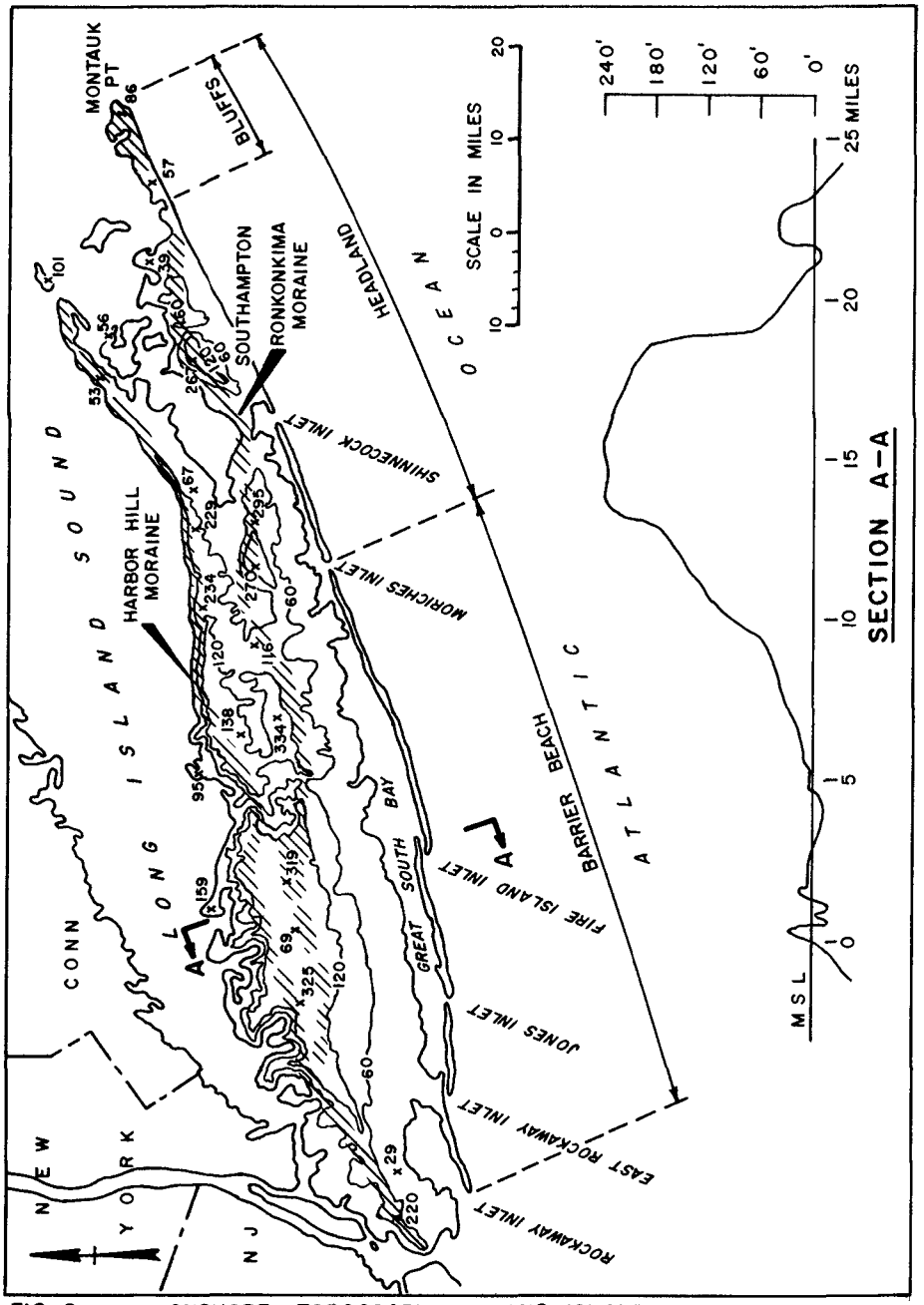

FIG. 2 ONSHORE TOPOGRAPHY — LONG ISLAND, NEW YORK

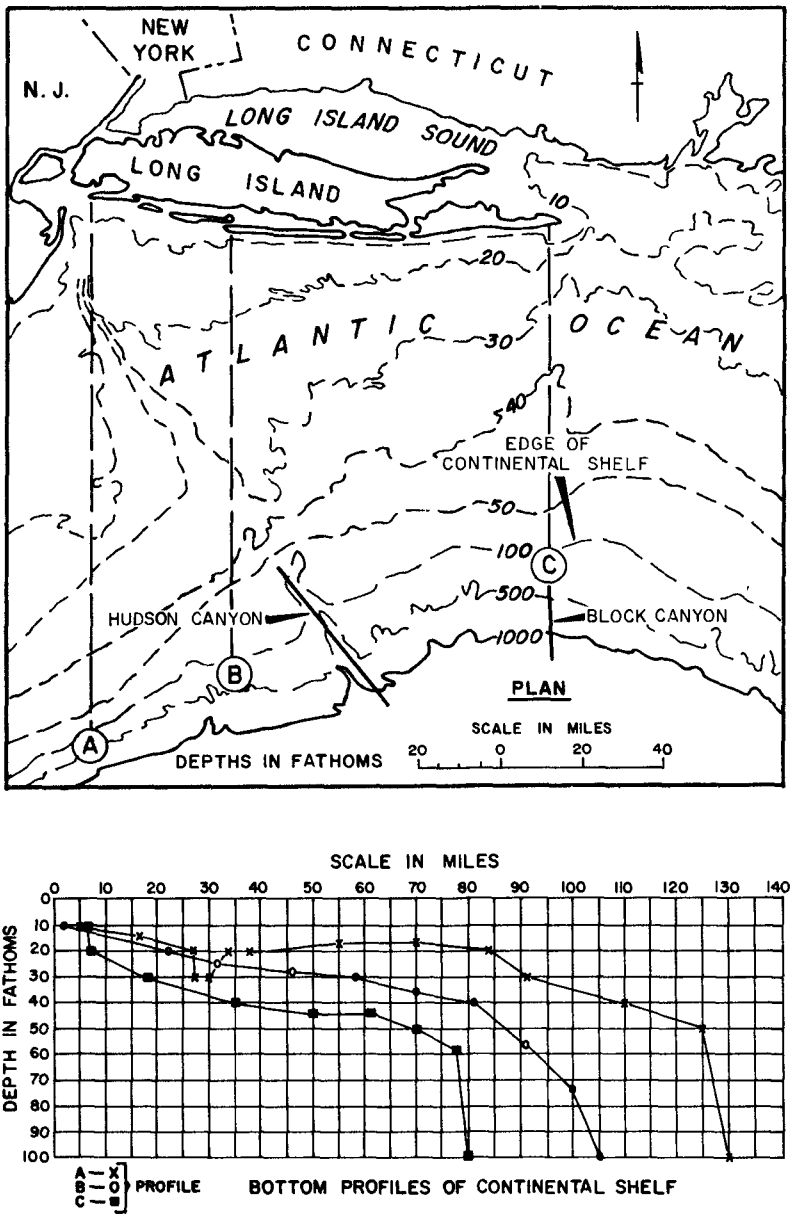

FIG 3 OFFSHORE HYDROGRAPHY – LONG ISLAND, NEW YORK

sections, Figure 2. The headland section extends 33 miles from Montauk Point, the most easterly point of Long Island, to Southampton. The barrier beach section covers the remaining 87 miles from the main island at Southampton to Rockaway Inlet, the most westerly point of Long Island.

Headland section. Submarine shoals lying about two miles off Montauk Point indicate that the land may have extended farther eastward. Westward from Montauk Point, ten miles of bluff lands, formed by the erosion of the southerly face of the Ronkonkoma moraine, rise abruptly from scanty beaches of coarse sand and gravel to 60 feet or more above mean sea level. From this point westward to Southampton, there are four miles of low, narrow sandy beach, often awash under hurricane tides and waves, and 19 miles of sandy beach with abutting continuous dunes reaching to over 20 feet above mean sea level. Included in this section are several small ponds and bays which have been cut off from the ocean by littoral drift material moving westward and forming barrier beaches.

Barrier Beach section consists of four islands, two peninsulas, and six inlets, and separates the shallow interconnected tidal bays to the north from the Atlantic Ocean. These bays vary from a few hundred feet to five miles in width and are separated from each other by promontories except for Jamaica Bay which is not joined to the bays to the east. The long and narrow barrier islands and peninsulas were probably formed as westward growing spits and as wave built barrier bars rising above the submerged portion of the gently sloping outwash plain. These barrier bars and peninsulas are paralleled by a submerged offshore bar.

The barrier islands and peninsulas with widths from one quarter of a mile to more than a mile, are breached by six inlets. The ocean beaches with an average width of 100 to 200 feet, vary in width from none at the eastern end of Long Island to over 500 feet in localized areas. On the landside of the beach from Southampton to Fire Island Inlet is an interrupted belt of eroded dunes with crests up to 30 feet above mean sea level. Westward to Rockaway Inlet the natural dune physiography has been greatly altered by extensive recreational, commercial, and residential developments.

Inlets. The inlets from east to west, Figures 1 and 2, are Shinnecock, Moriches, Fire Island, Jones, East Rockaway, and Rockaway. The latter four inlets predate the earliest available surveys of 1825 and 1835, Table 2. The remaining two inlets were recently formed. All inlets migrated until arrested by jetties and revetments and by navigation dredging, Table 2. The jetties offered temporary relief in stabilizing the inlet until the compartments updrift of the jetties became filled. Then, drift bypassed the jetties and built up within the inlets so as to affect not only navigability of the channel but also downdrift feeding of the shore.

LITTORAL FORCES

Waves. Along the south shore of Long Island from the south-southwest through the east quadrants, fetches of great length would permit the development of large deep water waves. A statistical study of deep water wave height, frequency of occurrence and direction of approach for a station off the entrance to New York Harbor, based on hindcasting technique and use of synoptic weather charts for the period of 1948-1950, showed that about 72 percent of all deep water waves approach from the directions east-northeast through south-southeast. The largest computed waves were between 25 and 30 feet in height.

In general, wave height is lessened as the water shoals across the continental shelf and the offshore. Study of the hydrographic charts of the shore and continental shelf, indicates that the refraction coefficients for a given deep water wave period and direction should generally be about the same for any point along the shore from Rockaway Inlet to Montauk Point. Hence, the wave action will be generally the same for the entire south shore of Long Island, although local conditions may be expected to introduce differences at particular points.

The important factor for the design of shore protection structures is the size of the maximum wave height that can occur within a certain time period. Calculations

TABLE 1 - VARIATION OF LITTORAL MATERIALS AT MID-TIDE FOR SOUTH SHORE OF LONG ISLAND

Values	M_d		S_o		S_k	
	Individual	Cluster	Individual	Cluster	Individual	Cluster
			MONTAUK POINT TO SHINNECOCK INLET			
High	2.00	1.79	1.99	1.77	4.30	1.26
Low	0.33	0.38	1.17	1.19	0.90	0.90
Mean	0 54	0.59	1.32	1.30	1.43	1.02
			SHINNECOCK INLET TO MORICHES INLET			
High	1.22	0.53	1.51	1.43	1.24	0.99
Low	0.41	0.35	1.13	1.27	0.95	0.91
Mean	0.68	0.47	1.35	1.37	1.10	0.95
			MORICHES INLET TO FIRE ISLAND INLET			
High	0.78	0.53	1.68	1.59	1.21	1.24
Low	0.32	0.29	1.12	1.21	0.82	0.87
Mean	0.42	0.41	1.30	1.35	1 00	1.06
			FIRE ISLAND INLET TO JONES INLET			
High	0.30	0.48	1.26	1.59	1.01	1.28
Low	0.30	0.21	1.26	1.14	1.01	0.95
Mean	0.30	0.33	1.26	1.32	1.01	1.05
			JONES INLET TO EAST ROCKAWAY INLET			
High	0.26	0.28	1.50	1.28	1.25	1 04
Low	0.13	0.26	1.25	1.25	0.50	0.99
Mean	0 20	0.27	1.36	1.27	0.94	1.02
			EAST ROCKAWAY INLET TO ROCKAWAY INLET			
High	-	0.62	-	2.21	-	1.62
Low	-	0.28	-	1.25	-	0.83
Mean	-	0.42	-	1.68	-	1.12

M_d = Median diameter is 50 percent point by weight on accumulative size distribution curve.

$S_o = (Q_1/Q_3)^{\frac{1}{2}}$ = Sorting coefficient.

$S_k = \left[Q_1Q_3/(M_d)^2\right]^{\frac{1}{2}}$ = Skewness coefficient.

where: Q_1 = first quartile diameter equal to 25 percent point by weight on accumulative size distribution curve.

Q_3 third quartile diameter equal to 75 percent point by weight on accumulate size distribution curve.

TABLE 2 - WESTERLY MIGRATION OF THE EASTERN SIDES OF INLETS, LONG ISLAND, NEW YORK

Shinnecock Inlet	1829-1839 Inlet Open	1839-1850 Inlet Closed	1850-1890 Inlet Open	1890-1938 Inlet Closed	1938-1951(a) 60 feet	1951-1955 -130 feet	1955-1968 -
	Total Migration West		Littoral Drift			Jetties Built	
	feet	years	feet/yr.	cubic yards/yr.			1952-1954
	60	13	4.6	300,000			
Moriches Inlet	1829-1839 Inlet Open	1839-1931 Inlet Closed	1931-1933(b) 220 feet	1933-1949 3880 feet	1949-1955 150 feet	1955-1968	
	Total Migration West		Littoral Drift		Jetties Built		
	feet	years	feet/yr.	cubic yards/yr.			1952-1954
	4250	24	177	350,000			
Fire Island Inlet	1825-1834 3050 feet	1834-1873 5625 feet	1873-1909 5175 feet	1909-1924 6775 feet	1924-1934 2030 feet	1934-1940 1670 feet	1940-1968 -
	Total Migration West		Littoral Drift			Jetty Built	
	feet	years	feet/yr.	cubic yards/yr.			1939-1944
	24325	115	212	600,000			
Jones Inlet	1835-1879 -2880 feet	1879-1909 3390 feet	1909-1926 2900 feet	1926-1934 1540 feet	1934-1953 2500 feet	1953-1968 -	
	Total Migration West		Littoral Drift			Jetty Built	
	feet	years	feet/yr.	cubic yards/yr.			1953-1959
	10720	74	135	550,000			
East Rockaway Inlet	1835-1879 7920 feet	1879-1909 5130 feet	1909-1926 3620 feet	1926-1934 400 feet	1934-1968 -		
	Total Migration West		Littoral Drift	Jetty Built			
	feet	years	feet/yr.	cubic yards/yr.			1933-1934
	17070	99	172	400,000			
Rockaway Inlet	1835-1877 10030 feet	1877-1902 5190 feet	1902-1928 2740 feet	1928-1934 2450 feet	1934-1968 -		
	Total Migration West		Littoral Drift	Jetty Built			
	feet	years	feet/yr.	cubic yards/yr.			1931-1933
	20410	99	206	400,000			

(a) Break through barrier peninsula during storm of 12 September 1938.
(b) Break through barrier peninsula during storm of 31 March 1931.
Minus indicates easterly migration.

involving sand movement and littoral drift are best correlated with the amount of potential energy transmitted forward and onto the beach by the wave. Calculations of this energy for the station at the entrance to New York Harbor indicate that 50 percent of the energy comes from waves from the east-northeast, 25 percent from the east and the remainder from the quadrant between east and south.

Wave height observation from underwater pressure gages which operated intermittently from 1950-1954 between Fire Island and Jones Inlets, showed a mean wave height of 1.2 feet, a maximum height of 13.4 feet, and an occurrence of 2 feet or greater waves for 20 percent of the time and of 10 feet or more for 1 percent of the time. Visual observations at Jones Inlet from 1954 to 1957, showed that the predominant wave direction was from the southern quadrants with 99 percent of the surf wave height below 6 feet. The maximum observed surf wave height was less than 10 feet even though waves as high as 20 feet were reported in the deeper water offshore. This demonstrates that as storm waves approach the shore, the characteristics are modified by friction along bottom, change in water depth, and local hydrographic conditions.

Tides are semi-diurnal and vary with a mean range of 4.7 feet at Rockaway Inlet, the westerly end of the island, 4.1 feet at East Rockaway Inlet, 4.2 feet at Jones and Fire Island Inlets, and 2.0 feet at Montauk Point, the easterly end of the island. The tide in the interconnected bayshave a range of 1.0 to 2.0 feet except Jamaica Bay where the range is 4.9 to 5.4 feet.

Sea level changes. The relative position of land to sea level in this area since the retreat of the last glacier, about 10,000 years ago, shows that the level of the sea has risen about 25 feet or 0.25 feet per century. However, since the early 1930's, the rate of rise in the sea level has been at the average rate of 2 feet per century.

Winds. The prevailing winds along the south shore are from the northwest to the southwest quadrants. At sea, the winds from the westerly quadrants prevail. Wind velocities, approaching 100 miles per hour, have been reported at points along the island with gust winds reported to 135 miles per hour.

Storms. The south shore of Long Island lies in the Atlantic Ocean storm belt, Figure 1. The most severe storms are hurricanes originating in the equatorial calms during the months of August, September, and October. In most cases tropical storms have moderated considerably before reaching the south shore of Long Island with a few notable exceptions. Records show that about 239 storms of all types have affected the area since 1635. Of these storms, five storms were unusually severe, 19 storms were severe, 50 storms were moderate and 64 storms threatened the area. On this basis the frequency of the unusually severe storm is 3 per 100 year, the severe storms is 22 per 100 year, moderate storms is 81 per 100 year and storms threatening the area is 103 per 100 year.

LITTORAL MOVEMENTS

Shore effects. High water shoreline changes in recent years indicate a fairly stable shore east of East Hampton, a shore eroding from 6 to 10 feet per year from East Hampton to Fire Island Inlet and about 3.5 feet per year from Fire Island Inlet to Jones Inlet, a transition shore from Jones Inlet to East Rockaway Inlet with accretion adjacent to the inlets and erosion in-between up to 7 feet per year, and a shore accreting at a rate of about 10 feet per year from East Rockaway Inlet to Rockaway Inlet. The shore movement west of Jones Inlet has been modified by groins, breakwaters and sandfill. Profile slopes from mean low water in the foreshore vary from 1 on 8 to 1 on 35 and in the offshore from 1 on 25 to 1 on 600.

Littoral drift varies with seasons of the year but is predominantly from east to west. This predominance is evident from the impoundment of littoral material on the east side of groins and jetties, westward migration of spits and inlets, the dominant westerly alongshore components of wave energy as developed by refraction studies and the progressive decrease in grain size and mineral content of sediments from east to west. The computed annual littoral drift to the west in cubic yards increases from 300,000 up to as high as 600,000, Table 2.

Littoral sediments. Along the entire south shore, the littoral sediments are generally coarse to fine sand with varying mineral content. These sediments are subject to variations of particle size distribution laterally along the shore and onshore and offshore as measured by the descriptive parameters of median diameter, the coefficient of sorting and skewness. The median diameter (M_d) identifies the middle size of cumulative particle sizes. The coefficient of sorting (S_o) is a measure of the dispersion of the particle sizes. The skewness (S_k) describes the symmetry of the cumulative particle size distribution with respect to the median diameter. The variation in size of littoral sediment laterally along the shore is demonstrated by the tabulation in Table 1 of these comparative parameters for samples taken at midtide.

Inlet migration. The general position, size, and number of inlets have remained constant since 1834, although for a long period of time, the two most easterly inlets were closed. There is a pattern to inlet migration downdrift along an offshore bar or barrier island. Not all of the littoral drift is deposited on the updrift side of the barrier bar. Some of the drift is drawn through the inlet and forms the inner bar or shoal and is thus removed from the littoral flow. Another portion of the drift forms the outer inlet bar or shoal. The remainder of the drift finds its way across the inlet by transport across the outer bar or by gradual transfer from updrift to downdrift side of the inlet by tidal action. During storms, sudden updrift shift in position of channel through the outer bar transfers a large volume of sediment across the inlet. Such a drift regime results in the growth of the updrift side in a downdrift direction and a retreat of the downdrift side in the same direction.

If the volume of sediment feeding the updrift side is sufficiently great and the tidal exchange small, so that the updrift side grows more rapidly than the downdrift side retreats, the inlet will close naturally. Shinnecock, Moriches and Jones Inlets are representative of this regime, Figure 4. The more complex inlet migration involves the continued growth of the updrift side until it overlaps the downdrift side while the inlet remains open and forces the tidal exchange to flow parallel to the barrier beach before entering the ocean. Fire Island, East Rockaway and Rockaway Inlets are examples of this regime, Figure 4. In this type of inlet the migration is complicated by the size of tidal prism through the inlet, volume of littoral drift at the inlet, and natural bypassing of littoral sediments. A history of the migration at each inlet are given in Table 2.

ECONOMIC CONSIDERATIONS

Development on the barrier beaches and mainland vary from heavy to scarce settlement for residential to recreational use. The ownership of the shore is 37 percent private, 45 percent non-Federal, and 18 percent Federal. The people affected by shore erosion and inundation are estimated at up to two million The real value of the affected property is estimated at about $2\frac{1}{2}$ billions. Damages for the largest flood levels experienced in either the hurricane of September 1938 or the hurricane of September 1960 amount to over $175 million with an average annual damage of about $10 million.

PROTECTIVE MEASURES

Involvement by the Federal Government in beach erosion protection started with the Congressional Act of 1930, and in hurricane protection with the Congressional Act of 1955 Under these authorities, the 120 mile ocean coastline of Long Island was Federally studied Beach erosion and hurricane projects have been approved for 95 miles of the shore from Fire Island Inlet to Montauk Point and from East Rockaway Inlet to Rockaway Inlet; and a beach erosion project for 15 miles of shore from Fire Island Inlet to Jones Inlet. A beach erosion and hurricane study is underway for the 10 miles of shore from Jones Inlet to East Rockaway Inlet

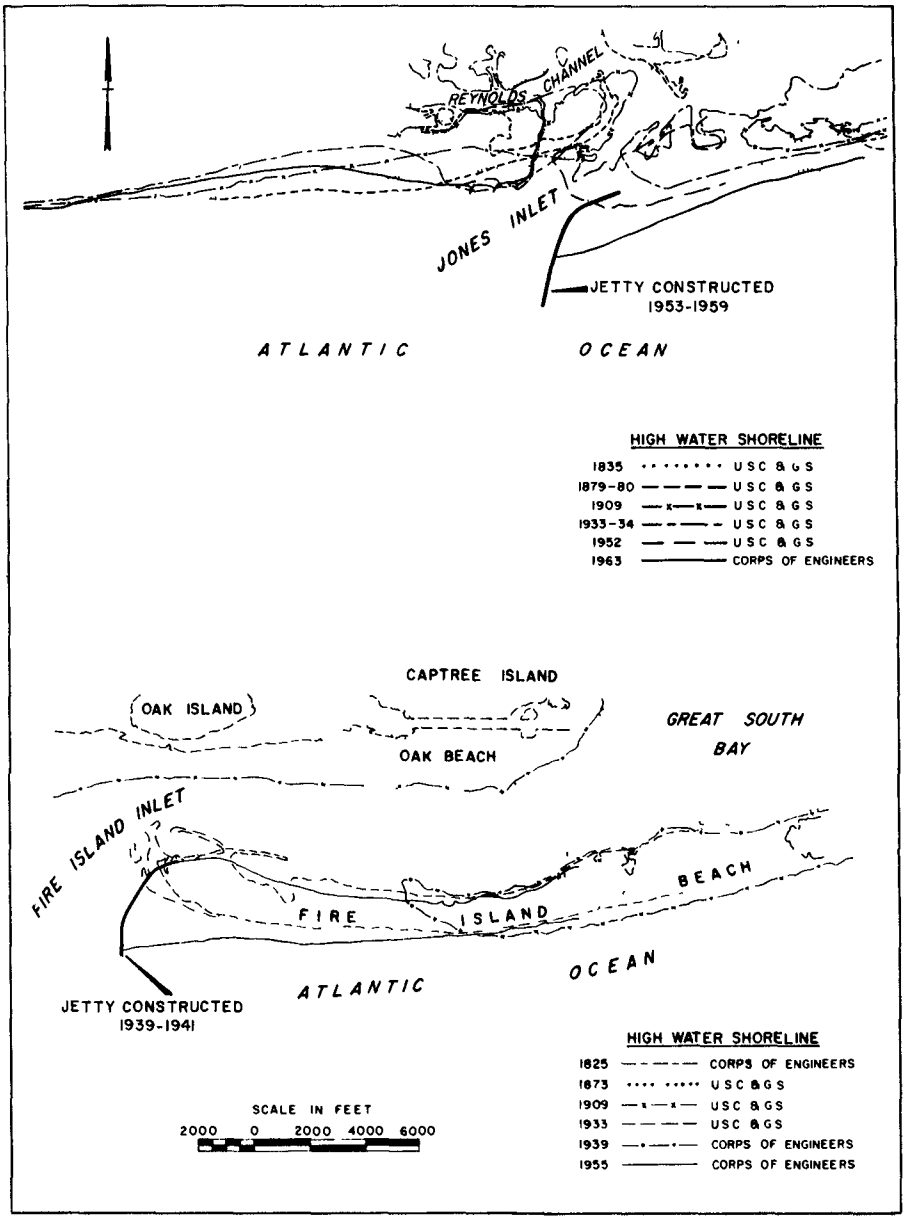

FIG 4 TYPICAL MIGRATION OF INLETS – LONG ISLAND, NEW YORK

Description. The authorized projects consist of sandfill and dunes, feeder beaches, groins, levees, jetties, sand bypassing, and barriers across inlets, Figure 5. The projects as currently estimated will cost about $188 million of which $110 million is Federal cost and $78 million is non-Federal cost. The allocation of costs to Federal and non-Federal interests is based on separable costs between beach erosion and hurricane and equitable division of the joint costs in accordance with the benefits The apportionment of cost is based on Federal law and policy governing beach erosion and hurricane protection. The projects would have annual charges of about $10 million and would return annual benefits of about $16 million.

DESIGN CRITERIA

Hurricane surge is built up as the hurricane passes over the open water of the ocean not only by the force of the wind and the forward movement of the storm wind field but also by differences in atmospheric pressure accompanying the storm. The storm surge is further increased by a gradually shoaling ocean bottom and by the counterclockwise spiraling of the hurricane winds.

Storm levels were computed based on transposition of the highest energy hurricanes having occurred in the area to critical paths with critical wind speed, central pressures, radius of storm and forward speed. The September 1944 hurricane so transposed with a maximum wind speed of 116 miles per hour, with a central pressure range from 27.55 to 27.95 inches of mercury, with a normal pressure of 30.12 inches, with a radius to maximum winds of 30 nautical miles, and with a forward speed of 40 knots per hour, produced a standard project hurricane surge of 12.3 feet for the westerly half of Long Island and 13.1 feet for the easterly half of Long Island.

Based on similar parameters except for a wind of 135 miles per hour and central pressure variation of 27.0 to 27.45 inches of mercury, a maximum probable hurricane surge was computed as 15.3 feet for the entire south shore. Transposition of the September 1938 storm to a critical path produced a surge of 8.9 feet. The maximum surge recorded in the westerly half of Long Island was 8.2 feet for the extra-tropical storm of November 1950.

Design elevations. The optimum practical design level for ocean protective structures was taken as the maximum surge of a standard project hurricane of 12.3 feet on mean sea level plus a wave runup of 5.2 feet for a total of 17.5 feet rounded to 18.0 feet above mean sea level for the shore west of Fire Island Inlet. For the shore, east of Fire Island Inlet, the standard project surge for ocean protective structures was taken as 13.1 feet on a mean high tide of 1.6 feet above mean sea level plus a wave runup of 5.3 feet for a total of 20 feet above mean sea level.

Beach Erosion and Hurricane Section. The need for a protective beach has been demonstrated during severe storms along the south shore of Long Island. In location where dunes were of sufficient height but the beach was of insufficient width, breaks occurred in the dunes because scour at the base of the dunes caused their collapse. In a series of experiments in a wave tank, it was developed that a minimum wave and wave runup occurred at the dune when the beach section had a foreshore slope of 1 on 20, a beach berm height above mean sea level equal to the design surge and a beach berm width of 100 feet at the base of dune having a 1 on 5 slope. With a beach berm at 14 feet above mean sea level, a surge of 14 feet produced waves of only one foot in height at the base of the dune with a runup of only five feet on the dune. This design was used along the easterly section from Fire Island Inlet to Montauk Point, Figure 5. Similar analysis was used in developing the design sections for the westerly section from Fire Island Inlet to Rockaway Inlet, Figure 5.

Barrier design. The height of the barrier was made equal to the height of coastal dunes and walls. The barrier openings were sized to produce no significant effect on tidal prism of the bays during normal times. The barrier openings were gated to

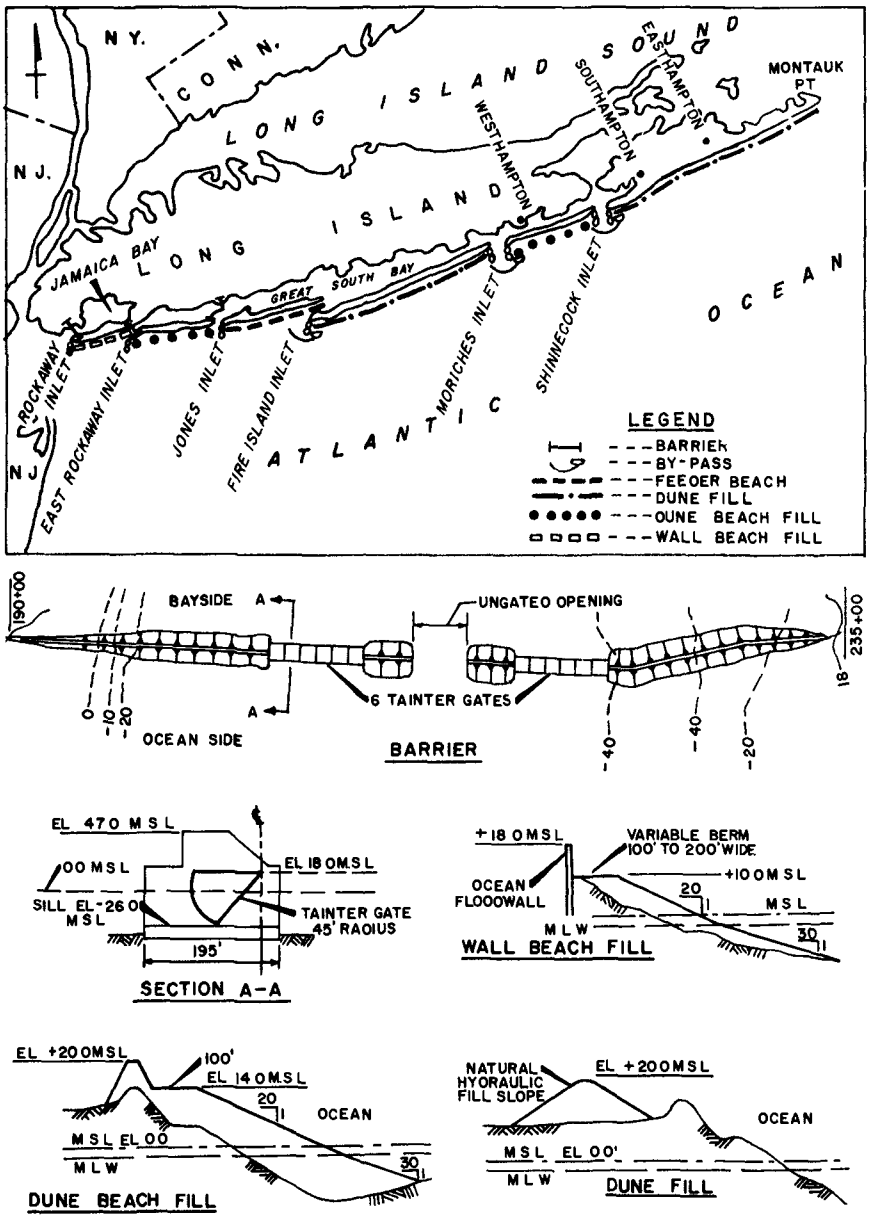

FIG. 5 PROJECTED SHORE IMPROVEMENTS, LONG ISLAND, NEW YORK

permit closing during storms so as to dampen storm surges into the bay area to the degree required to produce no significant damage to developments along the bay's shores, Figure 5.

PROJECT IMPLEMENTATIONS

Model tests are underway to develop the design for a stable navigation channel and a sand bypass system using commercial plant for Fire Island Inlet and Moriches Inlet. Model tests are underway on the barrier to be placed across Rockaway Inlet, Figure 5, to determine the widths of the fixed and gated openings so as to produce no changes in tidal prism of Jamaica Bay during normal operations and the desired changes in storm surges during storm operations.

Groins. The initial work for the beach erosion and hurricane project from Fire Island Inlet to Montauk Point was the construction of 11 groins at a critical reach of the barrier island at Westhampton, Figure 5. This reach between Moriches and Shinnecock Inlets has been frequently breached by storm action. Similarly, two groins were constructed at East Hampton between Shinnecock Inlet and Montauk Point where the dune section was being heavily eroded. From March 1965 to October 1966 the groins about 550 feet long were constructed at about 1,200 to 1,500 feet on centers along the critical sections of the shore to determine if a satisfactory beach and dune section could be developed without the need of placing the dune and beach fill.

Sand dike. To relieve pressure and heavy erosion on the north side of Fire Island Inlet, a sand dike spit was constructed in 1959 as a part of the feeder beach operation west of Fire Island Inlet, Figure 6. This dike was placed to divert the erosive inlet currents from the erodible shore on the north side of the inlet.

Beach nourishment. Beach nourishment was accomplished in 1959 and in 1964 for Fire Island Inlet to Jones Inlet reach as a beach erosion measure to offset the trapping of the littoral drift by Fire Island Inlet, Figure 6. Each time, about two million cubic yards of sand was placed on the feeder beach which was located downdrift of the nodal point of littoral drift movement. The sand was dredged from the shoal material in Fire Island Inlet and pumped about 15,000 feet to the feeder beach.

Sand inventory. The source of sand to construct the initial phases of the projects is the inlet shoals and inner bays. Because of the conflict with fish and wildlife interest, consideration must be given to obtaining future sources from the ocean. The current projects require 65 million cubic yards initially, and about two million cubic yards annually. Therefore, geophysical sonic surveys and core borings are being made of the offshore area along the entire south shore of Long Island to develop the availability of sand.

RESULTS TO DATE

Groin field. The shore conditions at the groin field areas were significantly affected by construction of the groins. The accretion and erosion, the advance and recession of the high and low water shorelines and the minus 12-foot contour are graphically shown on Figure 7 for Westhampton. Interesting observations are evident.

For the two years before the groin construction, the 300,000 cubic yards of littoral drift material moving predominantly from east to west showed an accreting and advancing shore except from mean low water to the minus 12-foot contour in the vicinity of what is now the location of groins 10 and 11. In the following two years including the construction period, the high water and low water shorelines became realigned so as to build up on the updrift side and to erode on the downdrift side with no advance of the average low and high water lines within the groin field because littoral drift material was being cut off at the updrift groins. But from the low water shoreline to minus 12-foot contour there was accretion and advancement due to material being diverted seaward by the groins so as to move in

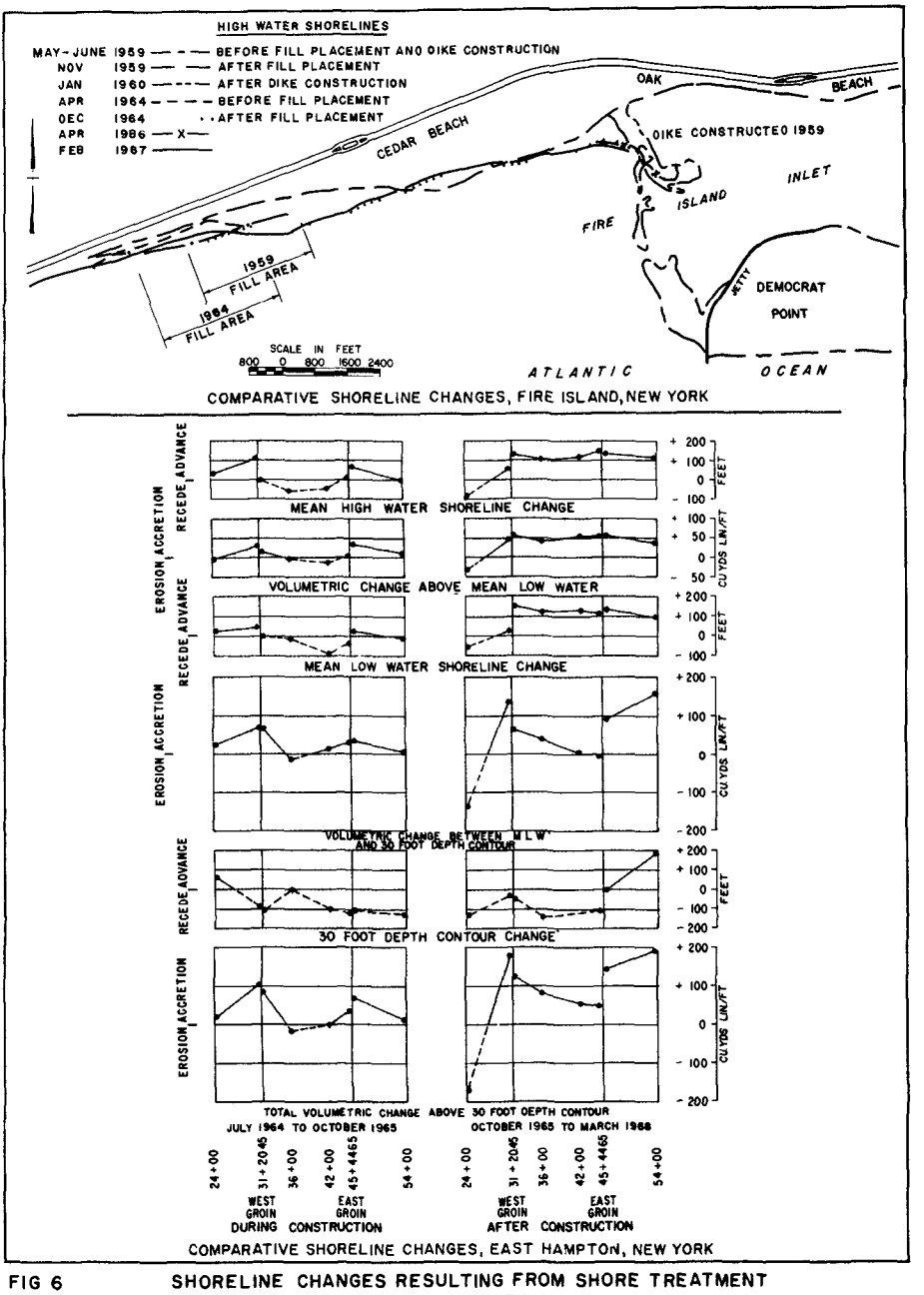

FIG 6 SHORELINE CHANGES RESULTING FROM SHORE TREATMENT LONG ISLAND, NEW YORK

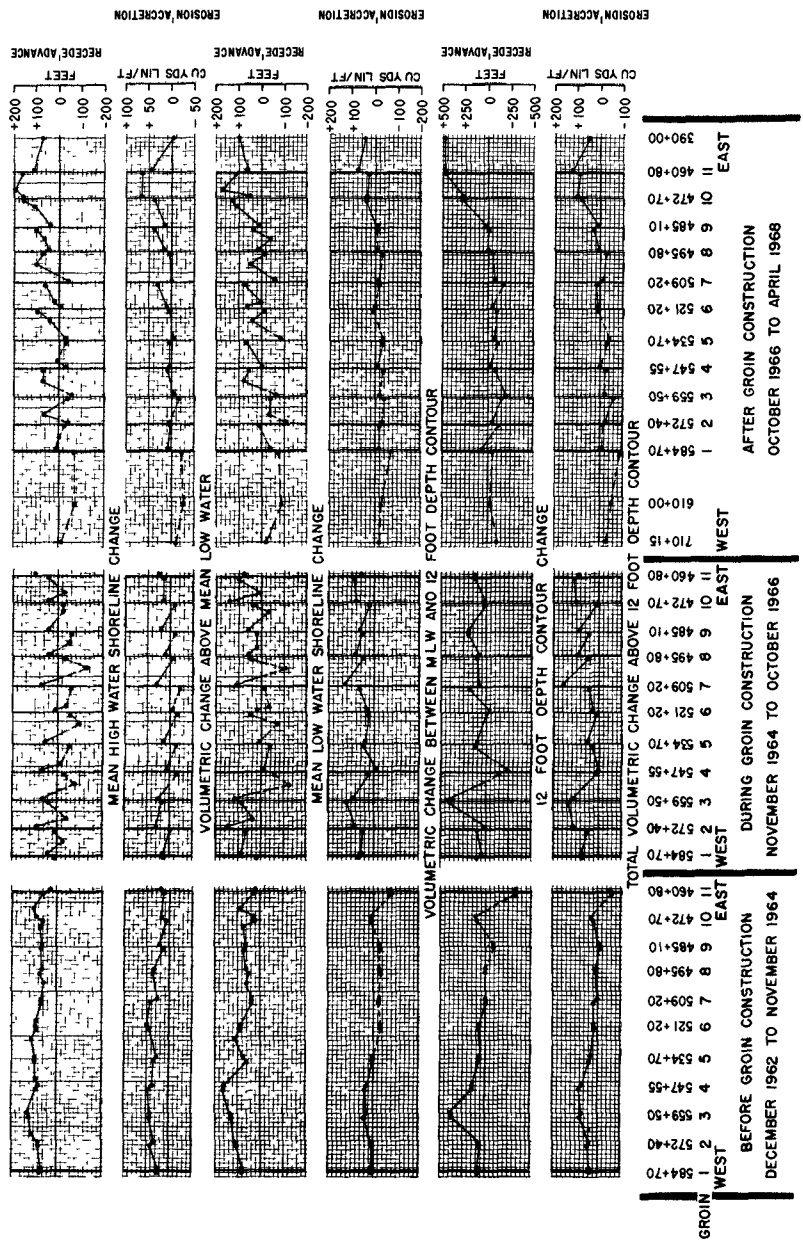

FIG 7 COMPARATIVE SHORELINE CHANGES AT WESTHAMPTON BEACH, LONG ISLAND, NEW YORK

this zone. The total effect above the minus 12-foot contour was accretion.

For the period of 18 months after the completion of the groin field, the pattern was one of erosion and recession west of groin 8 and accretion and advance east of groin 8. The recession and erosion is most significant west of groin 1 because of the trapping of the drift by the updrift groins, Photos 1 and 2. The compartments east of groin 11 and between groins 10 and 11 are filled to capacity. The littoral drift spilling over and bypassing these compartments is moving westward and has reached as far as the compartment between groins 6 and 7.

It is apparent that the filling of all compartments and reestablishing of the east to west littoral drift is several years away and that the downdrift shores will continue to erode and recede unless protected and nourished. Within the downdrift section of the groin field, there is a reversal in the direction of the littoral drift due to trapping and filling at the updrift groins. Intermediate measurements taken since completion, show the drift to be from west to east from May through August and from east to west from September through April as shown by the comparative photographs on Photo 1.

Similar studies were made for the two groins at East Hampton, Figure 6 and Photo 1. The groin field has resulted in accretion and advancement of the shoreline. The predominance of the east to west littoral drift is small here so that the buildup on both sides of the groins is fairly equal. The downdrift erosion and shore recession is evident, but compartments between groins and east of the east groin are almost filled so that downdrift feeding west of the groins is being reestablished.

Severe changes in shorelines will occur in and adjacent to a large groin field until all compartments are filled and the predominant littoral drift is reestablished so as to feed downdrift beaches. To minimize these shoreline changes, the compartments between and updrift of the groin field should be filled as soon as construction of groins allows, thus permitting an earlier reestablishment of downdrift movement. As an interim measure a large feeder beach could he placed downdrift of the groin field to minimize the shore changes in the downdrift shore. The severe shoreline changes could also be prevented if the shore was first restored with sandfill and then groins constructed within the sandfill if found necessary.

Beach nourishment. Sand dike has been successful in diverting the erosion currents from the north shore of the Fire Island Inlet. The construction of the dike modified the drift pattern on the westerly side of the inlet so that the feeding action to west from the first placement of feeder beach was not fully effective. To compensate for this, second placement of feeder beach material was moved about 2,000 feet west of the first feeder beach placement. However, periodic surveys have shown that the nodal point of the westerly drift movement is still farther west and that the feeder beach material is moving both east and west. The feeding material moving to the west is still insufficient to restore the eroding shore.

Placement of fill at spot locations along the shore and in breaks in the offshore bar have been used to try to stabilize weak spots in the shore. Future feeder beach placement is planned farther to the west. Of the material placed in the feeder beach about 25 percent moved in the first six months. About eight years after the initial placement, about 55 percent of the sand is still in place with about 50 percent above and 50 percent below mean low water.

Current observations indicate that the feeder beach must be located farther to the west to produce positive and strong downdrift movement if nourishment is to be effective. Badly eroded shores should be restored by direct sandfill placement prior to nourishment. Nourishment should be designed to maintain a sufficient flow of material downdrift so as to offset loss from shore due to littoral movement.

30 OCTOBER 1967

22 AUGUST 1968

LOOKING EAST FROM GROIN NO. I

30 OCTOBER 1967

22 AUGUST 1968

LOOKING WEST FROM GROIN NO. II

WESTHAMPTON – LONG ISLAND – NEW YORK
SHORELINE CHANGES RESULTING FROM LITTORAL DRIFT REVERSAL
IN FIELD OF ELEVEN GROINS

PHOTO I

LOOKING NORTH
AT ABOUT 1,850 FEET WEST OF GROIN NO. 1

LOOKING NORTHEAST
AT ABOUT 3,300 FEET WEST OF GROIN NO. 1

WESTHAMPTON – LONG ISLAND – NEW YORK
FIELD OF ELEVEN GROINS CONSTRUCTED MARCH 1965 TO OCTOBER 1966
DATE: 20 JULY 1967 – 1:35 P.M. – ONE HOUR AFTER LOW WATER
LITTORAL DRIFT – EAST TO WEST

LOOKING EASTWARD FROM WEST GROIN

LOOKING WESTWARD FROM EAST GROIN

EAST HAMPTON – LONG ISLAND – NEW YORK
FIELD OF TWO GROINS CONSTRUCTED MARCH 1965 TO OCTOBER 1966
DATE: 22 AUGUST 1968 – LITTORAL DRIFT – WEST TO EAST

SHORELINE CHANGES DUE TO GROIN CONSTRUCTION

PHOTO 2

EVALUATION

Findings. It is too early in the project to evaluate completely the overall behavior of the treatment of a significant section of the Atlantic Ocean shoreline of the United States.

REFERENCES

1. Berg, Dennis. Factors Affecting Beach Nourishment Requirements at Presque Isle Peninsula, Erie, Pennsylvania: Reprint 3-66, U.S. Army Coastal Engineering Research Center, Washington, D.C., 1966.

2. Darling, John M., and Dumm, Demetrius G. The Wave Record Program at CERC. Misc. Paper 1-67, U.S. Army Coastal Engineering Research Center, Washington, D.C., 1967.

3. Fairchild, John C. Correlation of Littoral Transport with Wave Energy Along Shores of New York and New Jersey Technical Memorandum No. 18, U.S. Army Coastal Engineering Research Center, Washington, D.C., 1966.

4. Harrison, Wyman, and Wagner, Kenneth A. Beach Changes at Virginia Beach, Virginia: Misc. Paper 6-64, U.S. Army Coastal Engineering Research Center, Washington, D.C., 1964.

5. Helle, James R. Surf Statistics for the Coasts of the United States· Technical Memorandum No. 108, Beach Erosion Board, U.S. Army Corps of Engineers, Washington, D.C.,1958.

6. Saville, Thorndike, Jr. North Atlantic Coast Wave Statistics Hindcast by Bretschneider-Revised Sverdrup-Munk Method: Technical Memorandum No. 55, Beach Erosion Board, U.S. Army Corps of Engineers, Washington, D.C., 1954.

7. Taney, Norman E. Geomorphology of the South Shore of Long Island, New York: Technical Memorandum No. 128, Beach Erosion Board, U.S. Army Corps of Engineers, Washington, D.C., 1961.

8. Taney, Norman E. Littoral Materials of the South Shore of Long Island, New York· Technical Memorandum No. 129, Beach Erosion Board, U.S. Army Corps of Engineers, Washington, D.C., 1961.

9. Report on Cooperative Beach Erosion Control and Interim Hurricane Study of the Atlantic Coast of Long Island, New York, Fire Island Inlet to Montauk Point (1958), New York District, Corps of Engineers: printed as House Document No. 425, 86th Congress, 2nd Session, 1960.

10. Beach Erosion Control Report on Cooperative Study of Atlantic Coast of Long Island, Fire Island Inlet and Shore Westerly to Jones Inlet, New York (1955), New York District, Corps of Engineers: printed as House Document No. 411, 84th Congress, 2nd Session, 1957.

11. Review Report on Beach Erosion Control Cooperative Study of Atlantic Coast of Long Island, N.Y., Fire Island Inlet and the Shore Westerly to Jones Inlet (1963), New York District, Corps of Engineers: printed as House Document No. 115, 89th Congress, 1st Session, 1965.

12. Cooperative Beach Erosion Control and Hurricane Study of the Atlantic Coast of New York City from East Rockaway Inlet to Rockaway Inlet and Jamaica Bay, New York (Interim Survey Report), (1964), New York District, Corps of Engineers: printed as House Document No. 215, 89th Congress, 1st Session, 1965.

13. Interim Hurricane Study of the Atlantic Coast of Long Island, New York, Jones Inlet to Montauk Point (Remaining Areas), (1965), New York District, Corps of Engineers.

14. Shore Protection, Planning and Design: Technical Report No. 4, 3rd edition, U.S. Army Coastal Engineering Research Center, Washington, D.C., 1966.

15. Report on Beach Erosion Control and Interim Hurricane Study of the Atlantic Coast of Long Island, N.Y., Jones Inlet to East Rockaway Inlet (1966), New York District, Corps of Engineers, (Draft).

CHAPTER 78

DESIGN OF A SMALL TIDAL INLET

Morrough P. O'Brien* and Leonardo Zeevaert**

ABSTRACT

Estero Punta Banda on the Pacific Coast of Baja California was to be improved and stabilized as a small boat harbor by the construction of twin jetties. The throat area-tidal prism relationship at this entrance agreed with that of other inlets on sandy coasts in equilibrium. This throat area was retained in the jetty spacing. The major question to be resolved was whether to retain the entrance in its present position at the north end of the lagoon or to cut a new entrance at the south end. The former position was chosen.

- - - - -

Estero Punta Banda is a small tidal lagoon located along the shore of the Bay of Todos Santos on the west Coast of Baja California, about sixty miles south of the Mexico-United States border and seven miles south of the Port of Ensenada. This lagoon is formed by a sand spit (Punta Estero) which extends northward from the headland (Punta Banda) which forms the south boundary of Bahia Todos Santos. Fig. 1 is taken from the survey of the U. S. Ranger, made in 1886. Fig. 2 is an aerial photograph of the lagoon and adjacent beaches. Fig. 3 shows the existing entrance channel and the sand spit to the south.

The generally good weather and warm waters of Southern California are favorable to all-year boating, and the boat population has grown rapidly in recent years. The number of small boats based south of Santa Barbara is estimated to be more than a quarter of a million. Berths for small boats are scarce; most of the land adjacent to the small boat harbors has been subdivided and developed as building lots. Attractive overnight, cruising opportunities are limited, by weather and sea conditions and by the availability of harbors, to the shore and offshore islands between San Diego and Point Conception. Extension of the convenient and safe boating area southward along the coast of Baja California, ultimately as far as La Paz, is a development which would benefit both Mexico and the United States. Estero Punta Banda is within small boat day-cruising range of Southern California.

The Port of Ensenada has been developed primarily for fishing and general cargo. A breakwater gives full protection of the anchorage area and wharves against waves from north through west. Protection against waves

*Professor of Engineering Emeritus, College of Engineering, University of California, Berkeley.
**Professor of Civil Engineering, University of Mexico.

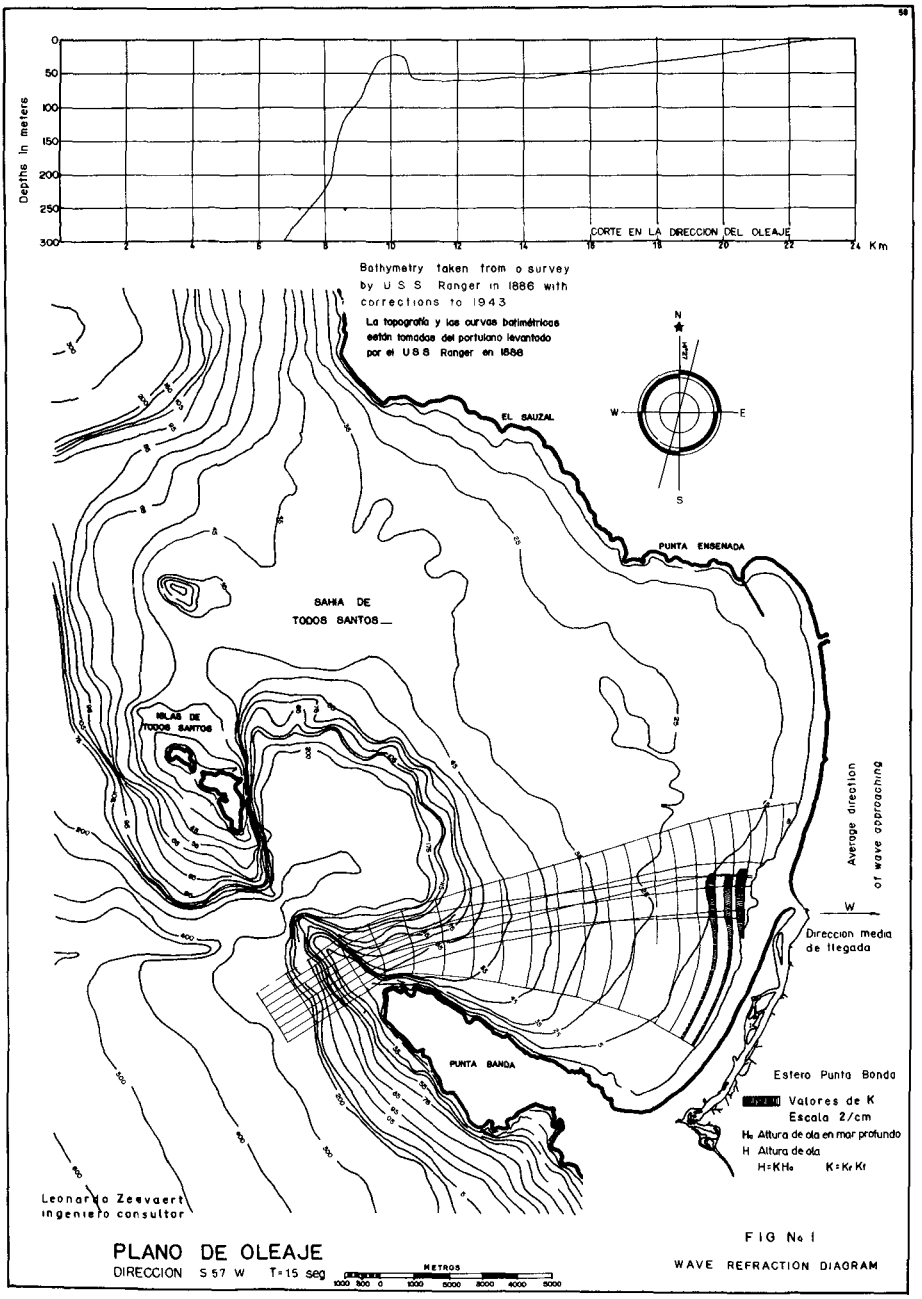

FIG No 1

WAVE REFRACTION DIAGRAM

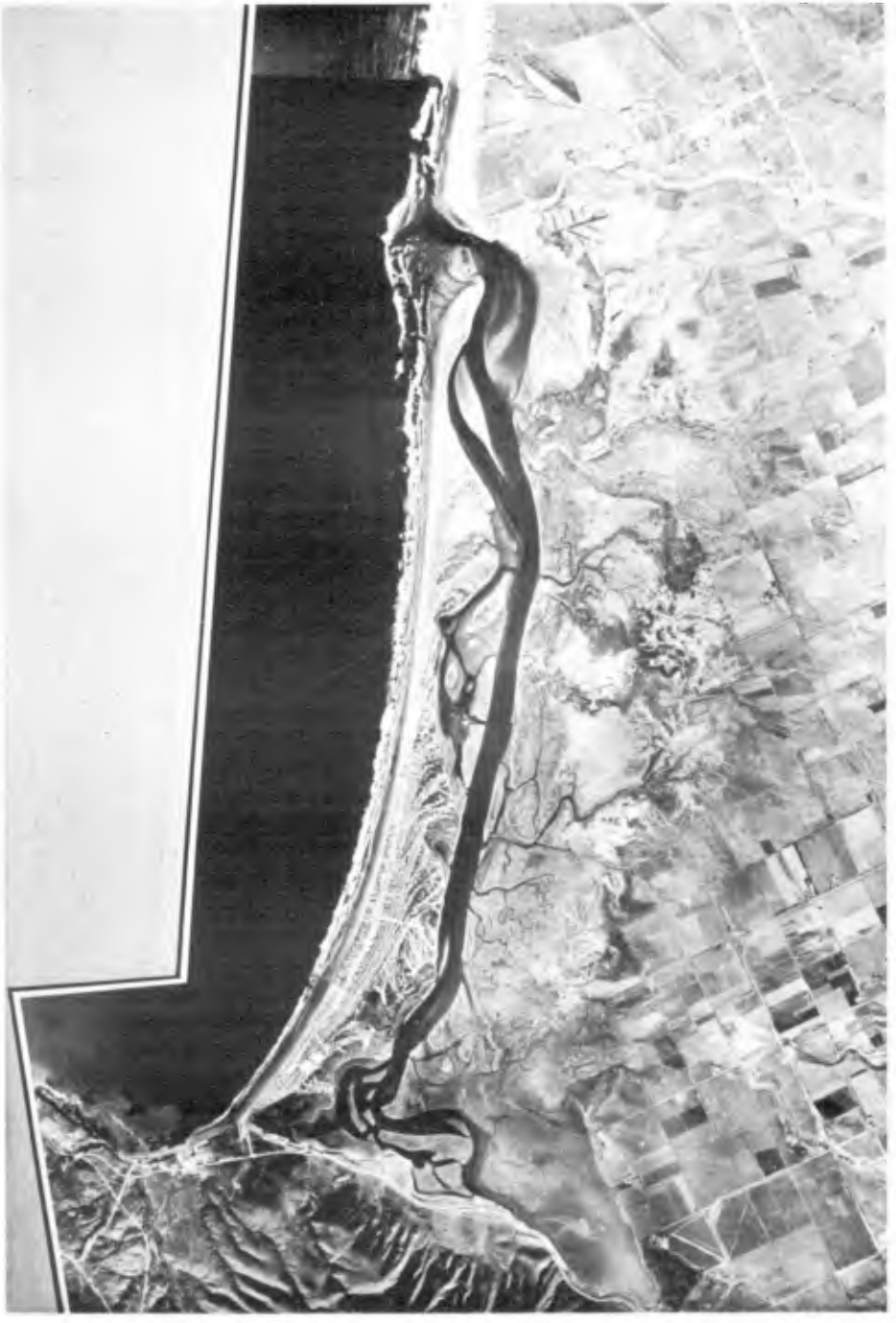

FIG. No. 2

Page 4 - Fig. 3 ENTRANCE CHANNEL

from the south-westerly quarter is adequate for large vessels but not for small pleasure craft. The area available for anchoring or berthing small boats is limited; the commercial harbor may be enlarged in the near future to accommodate the increasing traffic and tonnage of cargo ships and this will further decrease the area available for pleasure craft.

Estero Punta Banda is the first inlet south of the International Border suitable for development as a small boat harbor. The entrance channel, which has not been improved, is used infrequently because the bar channel shifts position and the controlling depth is inadequate. A small resort hotel at the north end, a gun club near the south end, and farms along the mainland side of the bay are the only developments of consequence in the adjacent area. The proposed development, of which the improvement and stabilization of the inlet channel is an essential feature, included a yacht anchorage and marina, a 288 room resort hotel, and a subdivision of waterside building lots. Fig. 4 is the immediate plan for the development of the bay.

The objective of this study was to develop a design which would improve and stabilize the entrance channel into Estero Punta Banda, preserve the existing interior channels which are in good condition, and avoid both erosion of the shoreface of the sand spit, Punta Estero, and wave damage to the developed property at the north end of the lagoon. The shores of the lagoon are almost completely undeveloped and a coordinated plan of development could both increase the low water area and the tidal prism and could also increase the usable upland; the proportions of the entrance channel should be such as to provide a navigable depth of 4 m below MLLW with the present tidal prism and later to accommodate an increased tidal prism. Circumstances of financing and jurisdiction make it desirable to design the channels and structures so as to require a minimum of maintenance.

Estero Punta Banda lies at the seaward edge of the Maneadero Valley which was formed by submergence of a block lying between the rocky peninsula of Punta Banda and the upland north of the inlet. Scarps still mark the location of the two fault lines. The valley was once a deep embayment which has been filled in an earlier geological era by sediments from the San Carlos and San Miguelito water-sheds. These streams rise in forested, mountainous areas, where the run-off is substantial, but their flows are almost completely absorbed by strata of fissured and permeable extrusive igneous rocks in their lower reaches. There is no evidence of substantial flow into the bay in recent years and consequently, no provision has been made in the plan to divert flood flows and sediment, as has been found necessary in similar inlet developments in Southern California.

Punta Estero, the sand spit enclosing the bay, has grown northward from Punta Banda during recent geological times. Evidence of this growth is discernible in Fig. 2 which shows dune lines and vegetation marking earlier positions of the inlet. The north end of the sand spit is pressing the inlet channel against the consolidated upland on its north side, which is formed by the cliff of the northern fault line of the Valley of Maneadero. The shoreface of the spit, Punta Estero, appears to have reached an equilibrium position, but historical surveys are not available to substantiate this conclusion.

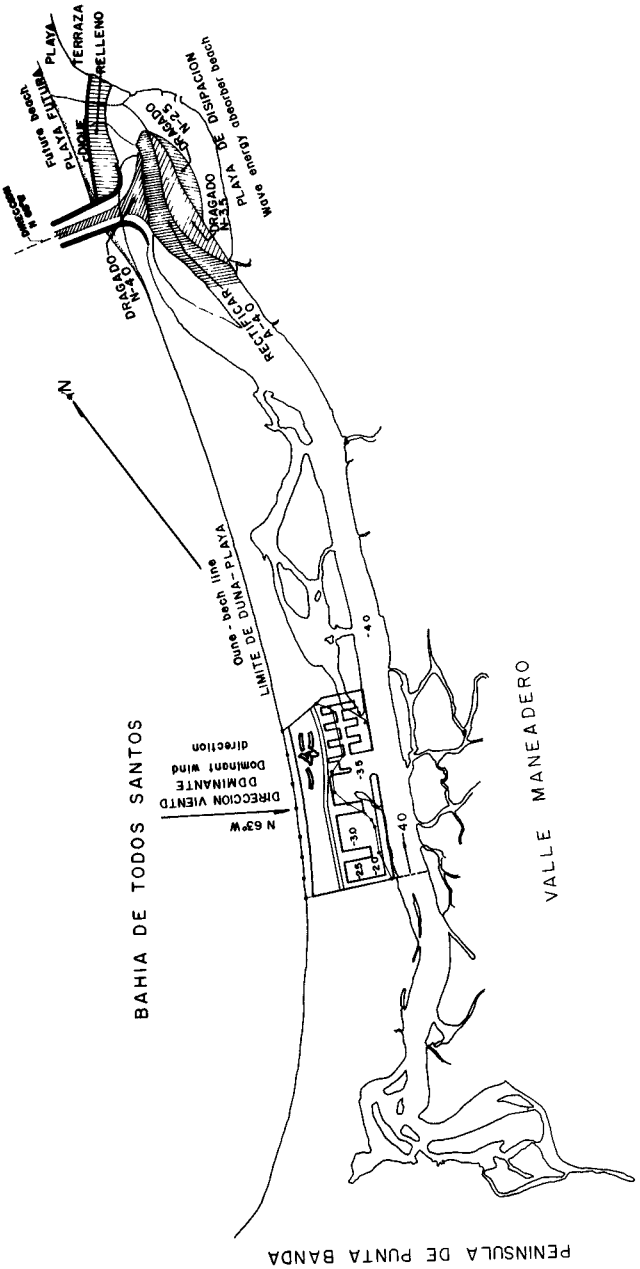

Fig. 4 - PROPOSED ENTRANCE AND IMMEDIATE DEVELOPMENT

The north face of the headland Punta Banda, extending seaward perpendicular to the base of the sand spit Punta Estero, is being eroded and is supplying boulders, coarse gravel, and fine sand to the base of the spit. Fig. 5 shows the shoreface of the spit at its junction with the headline. Fig. 6 shows the size of the beach surface material as a function of position along the beach. A study of the most frequent diameter with very little variations on either side of the entrance channel. However, a slight reduction in diameter of the surface material occurs at the sharp bend of the sand spit beach close to Punta Banda Peninsula at points 3, 4 and 5, Fig. 6. At these locations gravel and boulders are evident on the beach surface, Fig. 5. The wave refraction diagrams show that wave acti' is considerably less active in this area (see Fig. 1).

The configuration of Todos Santos Bay is such that the Punta Banda inlet is exposed to waves between N 55° W and S 57° W. Refraction diagrams were drawn for waves approaching in this sector for wave periods of 15, 10, 8 and 5 seconds. From these diagrams the directions of the waves at the inlet were determined for each assumed sea and swell wave direction. It was found that the bottom contours around Todos Santos Island would cause some focusing and intensification of waves. In order to select the direction of the jetties to stabilize and protect the entrance to the lagoon, the available data[1] were reviewed. Wave directions considered in this study were:

a).	Extraordinary strong wave action	N 73° W
b).	Medium and strong seas	N 61° W
c).	Medium and strong swells	N 65° W
d).	All wave action	N 62° W

This study yielded N 68 ± 5° W as the best alignment for small-boat operation of the jetties at the entrance channel to the lagoon. This direction coincided with the direction of the dominant wind and it is very nearly perpendicular to the general alignment of the sand spit.

There is no natural trap or other means of measuring the annual volume of littoral material reaching the base of the sand spit, Punta Estero. The headland is eroding slowly and must be contributing some material to the beach, but the rate of loss has not been established quantitatively. In addition to the wave data on the Sea and Swell Charts there were available wave hindcasts for an ocean station NW of Point Conception (Lat 35° 30' N, Long 122° W), about 400 miles distant from Estero Punta Banda. Using these data and the refraction diagrams, the northward and southward components of littoral transport were computed for points on the shore at the inlet and at the base of the sand spit[2]. The results were as follows:

---

[1] Atlas of Sea and Swell Charts Northeastern Pacific Ocean. Published by the U.S. Navy Hydrographic Office under the Authority of the Navy. H. O. Publ. No. 799-D.

"Wave Statistics for Seven Deep Water Stations Along the California Coast." Scripps Institute of Oceanography, La Jolla, California.

[2] Caldwell, Joseph M. "Wave Action and Sand Movement near Anaheim Bay, California." U.S. Army, Corps of Engineers, Beach Erosion Board, Tec. Memo. No. 68, February 1956.

Page 8 - Fig. 5 BEACH MATERIAL AT SOUTH END OF SAND SPIT

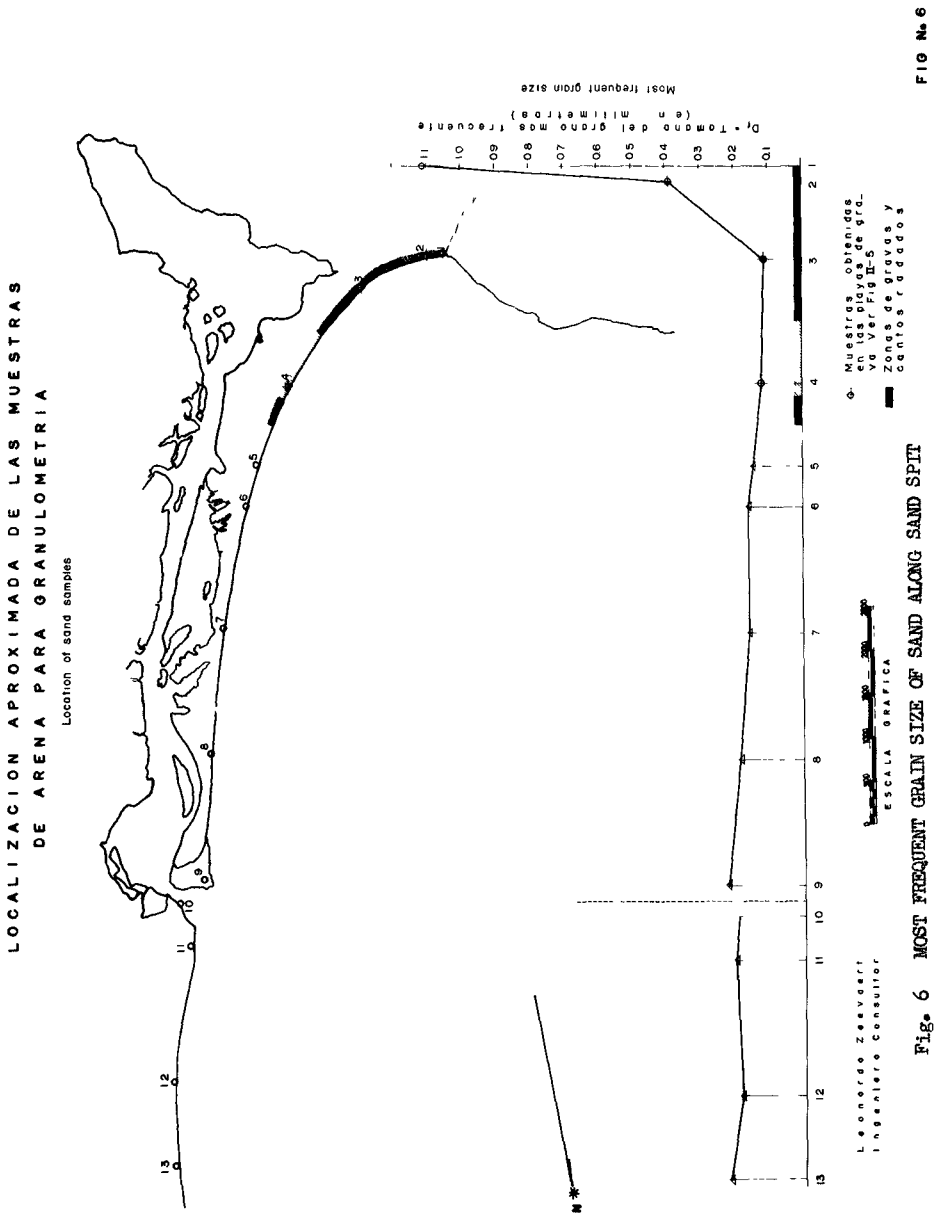

Fig. 6 MOST FREQUENT GRAIN SIZE OF SAND ALONG SAND SPIT

Computed Littoral Transport (m^3/ year)

Location	Northward	Southward	Net Annual
South end of sand spit	273,000	40,000	233,000 North
Estuary entrance	273,000	247,000	26,000 North

These results are approximations because the relationship between wave energy and littoral transport is not known precisely and the probable error is large, the wave data available pertained to a distant station, and the refraction effect of Todos Santos Islands is considerable. However, two conclusions do seem to be justified, namely:

1) Sand movement northward along the sand spit at its junction with Punta Banda is not negligible, and this conclusion agrees with the evidence from materials on the beach and from the erosion of the headland.

2) Net annual northward movement at the location of the existing entrance is small.

Local wind data were not sufficiently detailed to permit calculation of the movement of sand from the beach into the lagoon. Winds are generally light, but even a light wind moves sand wherever vegetation has been removed. As an indication of the magnitude of wind drift, a wind of 16 mph at 5 m above the beach blowing 1 hour per day would transport 14,000 cu mts per year across the length of the sand spit. The actual net drift into the lagoon may be several times this figure.

The area of the lagoon is 2.6 Km^2 at mean lower low water; 10.7Km^2 at mean higher high water. The maximum dimension of the lagoon is 11.5 kilometers. The average diurnal range of tide in the ocean is 1.6 m; the minimum range, 0.7 m; the maximum range 2.6 m. Tide staffs along the channel in the lagoon, reading maximum and minimum levels on each tide, showed the ratio of the tide range in the lagoon to that in the ocean to be 1.03. The computed lag in tide between the mouth and the upper end of the lagoon, using $C = \sqrt{g \times d_{av}}$ is 46 minutes at MLLW. The observed lag of low water, between gages near the mouth and near the upper end was 43 minutes. These facts about the ratio of ranges and the velocity of advance show that the tide proceeds through the lagoon as a solitary wave with little reflection from the upper end and little effect of either friction or storage.

Surging or seiche action is a problem at many small-boat marinas. At Estero Punta Banda, there are no continuous tide gage records which would show the existence of absence of surging. The survey party which made the hydrographic surveys and observed the tide staffs in the months of June and July 1964, saw no indications of surging. The basic period of oscillation along the long axis of the lagoon is approximately 103 minutes at MSL. Transverse periods of oscillation range from 19 seconds near the entrance to 281 seconds at the pond at the upper end. Thus, some part of the lagoon might be in resonance with a wide range of exciting frequencies.

The tidal prism of the lagoon, the volume between MHHW and MLLW is 8.45×10^6 m^3. At the gorge, the area of the existing minimum flow cross-section below MSL is 520 m^2; the width at this section is 95 m at MLLW and 370 m at MHHW; the maximum depth at the gorge is 7.5 m below MLLW.

An important feature of the configuration of the estuary is that a preponderance of the surface area is located at the south end, especially at low stages. The tidal prism of this area must traverse most of the length of the channel during each tide, and this fact accounts for this very good natural channel and its maintenance.

Current velocities were measured at the gorge section by means of floats to determine the maximum surface velocity and to compare this velocity with the mean velocity across this section at the tide range and flow areas existing at the time of measurement. On a diurnal range of tide, the maximum surface velocity at the gorge is on the order of 1.14 m/sec and the mean velocity, 0.70 m/sec.

Hydraulic Design. Experience in similar situations in Southern California indicated that twin jetties would be required to stabilize the entrance channel to Estero Punta Banda.

There are two feasible locations for the entrance, one at the north end of the lagoon near the existing inlet channel and another, at the south end, adjacent to the headland Punta Banda. A choice between these two locations depends primarily on the magnitude and direction of the littoral transport of sand and the consequent condition of the shoreline after the jetties were in place, but other factors were considered. The advantages and disadvantages of the two locations were:

South End: Closing the entrance at the north end would permit access to the sand spit, Punta Estero, by road directly south from Ensenada without circling the bay. The refraction diagrams showed wave action to be lighter at the south end than at the existing entrance. Dredging the inlet channel would be more costly here because it would be longer and be dug in gravel and cobbles; more dredging would be required to create an adequate anchorage near the entrance. Although the rate of littoral transport from Punta Banda is probably small, the storage area south of the south jetty would also be small and would soon be filled, permitting whatever sand movement there is to enter the entrance. Furthermore interruption of sand movement by jetties at the south end would disturb in some degree the equilibrium of the sand spit. The tidal regimen of the interior channels would be altered drastically.

North End: Locating the improved channel at the north end, in substantially the natural location, would bring the least disturbances of the regimen lagoon and inlet. The improved channel must be moved a short distance south from the present location to protect the developed shore on the north side. Erosion either of the spit south or of the upland north is not likely, but if there is a greater littoral transport than expected, the adverse effect on the shoreline would be least with the entrance located here. This location is

closer to the quarry for jetty stone if a trestle is built across the inlet. Somewhat greater intensity of wave action will occur here. Access to the spit by road around the lagoon is a disadvantage.

The choice was made to locate the entrance channel at the north end of the lagoon on the basis that this location involved a lesser change in the existing regimen of shore and lagoon.

The specifications underlying the hydraulic design were:

1) A stable, safe entrance channel with a controlling depth of 4 mts of MLLW.

2) Tidal currents should preserve the outlet channel between the jetties and the bar with little maintenance dredging; the interior channels already in satisfactory condition should require only minor maintenance.

3) The stabilized inlet should permit an increase of depth at a later date, if the tidal prism is increased as recommended.

4) Waves entering between the jetties should be dissipated by an absorbing beach to minimize local wave action inside the jetties and to limit surging in the bay. Adequate space must be provided for a wave-absorbing beach.

5) The sharp turn in the navigation channel near the gorge should be increased in curvature.

6) The developed water front north of the entrance should not be exposed to waves entering the inlet.

At a location approximately 650 mts south of the present channel (see Fig. 7) the inlet channel could be connected to the estuary bay channels by a gradual transition. This location has the disadvantage that the existing channel must be closed after the jetties are built and the channel between them dredged, but this choice of location best meets the design specifications enumerated and justified the added cost as compared to improving the channel in its present location.

The flow area of the gorge of the existing inlet fits almost exactly on the curve of tidal prism versus flow area which has been found to be generally applicable to tidal inlets on sandy coasts[3]. The tidal prism of 8.45×10^6 m^3 could be expected to maintain a channel flow area of 575 m^2 below MSL at the minimum point. The desired depth of the navigable channel below MLLW is 4 mts; the centerlines of the jetties were made almost parallel and 160 mts apart. Fig. 7 shows a cross-section of the jetties at their outer ends and the entrance channel between. The actual channel will probably have a somewhat greater maximum depth and the best channel will probably lie north of the centerline.

---

[3] O'Brien, M. P., "Equilibrium Flow Areas of Tidal Inlets on Sandy Coasts." Proceedings of Xth Conference on Coastal Engineering, Tokyo, Japan, Sept. 1966. Vol. 1, p. 676.

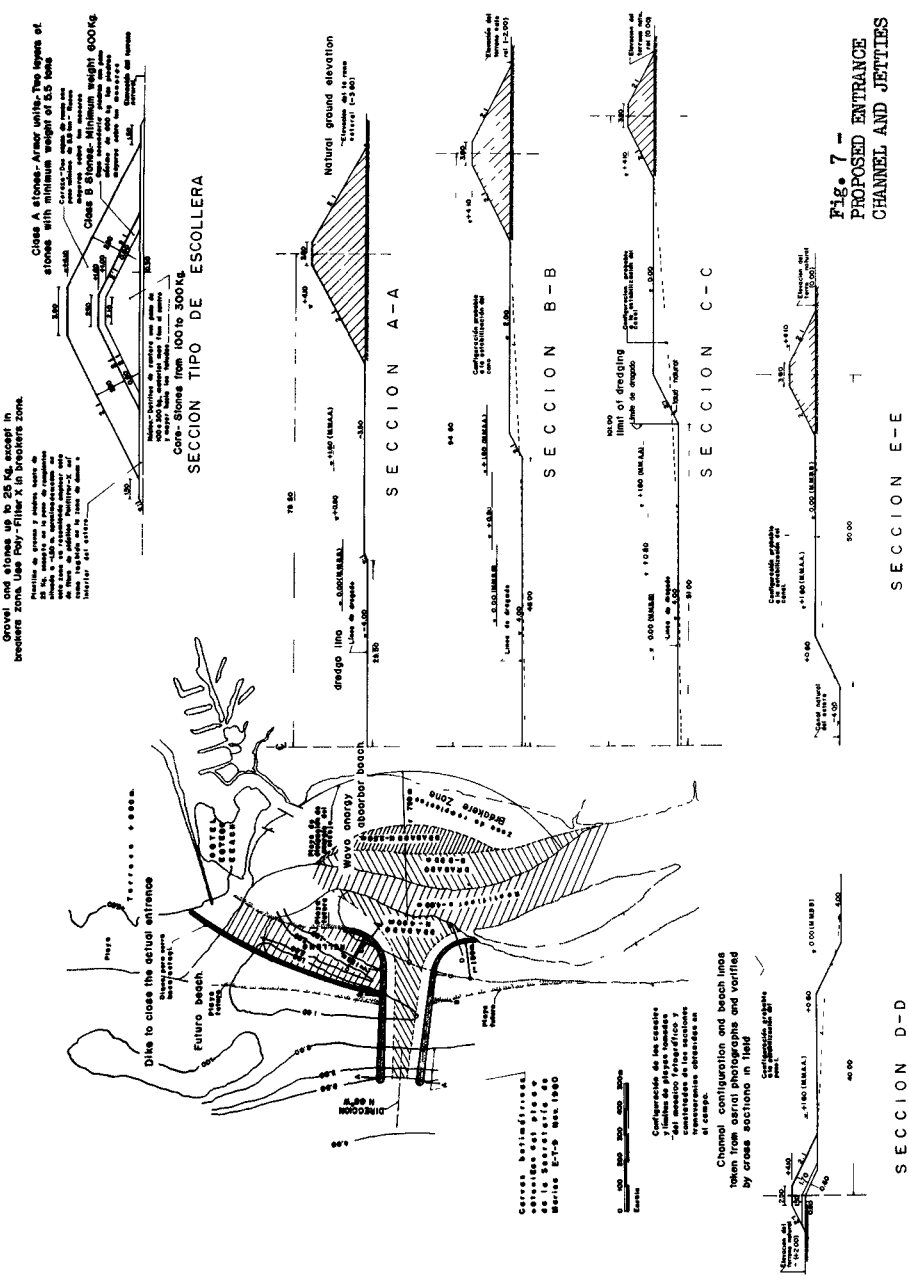

Fig. 7 - PROPOSED ENTRANCE CHANNEL AND JETTIES

The interior shores of the lagoon are almost devoid of improvements which would interfere with a coordinated plan of improvement which could both increase the tidal prism and also the usable upland area. It was recommended that a bulkhead line be established approximately along the position of the HW line and that dredging in the inter-tidal zone be used to fill landward of the bulkhead line. If this plan were followed, the tidal prism could be increased to 12 x 10^6 m^3 and the minimum flow area at the entrance channel would be increased to 780 m^2. To match this increase in cross-section area, the channel would deepen to about 6 m; the jetties should be extended about 500 mts to stabilize this greater depth. Dredging of the interior channels to 5.5 m near the entrance and 4.5 m at the southern end would be desirable to make these depths consistent with the deeper entrance channel; once deepened by dredging these deepened channels should require little maintenance.

Storm waves will enter the channel; bottom friction, diffraction and refraction against the jetties will reduce their heights but the largest wave will retain appreciable amplitude at the inner end of the jetties. Nevertheless, the high spreading of the waves crests after passing the jetties will permit interior navigation even in medium large swells, Fig. 7. A wave absorbing beach, Fig. 7, will be located on an arc centered on the entrance and will be graded to a flat slope to cause breaking and full dissipation.

Structural Design: Exposure to wave action at Estero Punta Banda is similar to that of the coast of Southern California, where many tidal inlets have been improved and stabilized by means of twin jetties. The design of the jetties at Estero Punta Banda follows the same practices as have proved to be adequate in California.

Studies were made from the economical point of view, of various types of armor for the jetties. The elements studied were concrete cubes, tetrapods, tribars, quadripods, akmon and some other armor units. The most economical solution was found to be the use of igneous rocks found in the area. The criteria used to determine the weight of the stones for the armor units of the jetties was Hudson's investigations[4], using a wave height corresponding to the highest possible breaking wave in front of the jetties. The seaward ends of the jetties were designed for 0% damage and the adjacent section along the sides of the jetties for 10% damage. The weight of the stones was reduced gradually to one half of this weight at the beach. The inside slopes of the jetties were protected with lighter stones, as shown in the design drawing, Fig. 7.

The choice among possible construction methods and sequences will be made by the owners and the contractor and will be determined by costs. Under any construction plan adopted, it is important that the inlet be kept under control during the construction and that the old channel be closed as soon as the new one is opened. Fig. 8 shows the ultimate configuration of the jetties and channels. One feasible sequence of operations is to build a trestle across the existing channel to transport stone from the quarry,

---

[4] Hudson, Robert Y., "Laboratory Investigation of Rubble-Mound Breakwaters." U. S. Army Engineer. Waterways Experiment Station, Vicksburg, Mississippi.

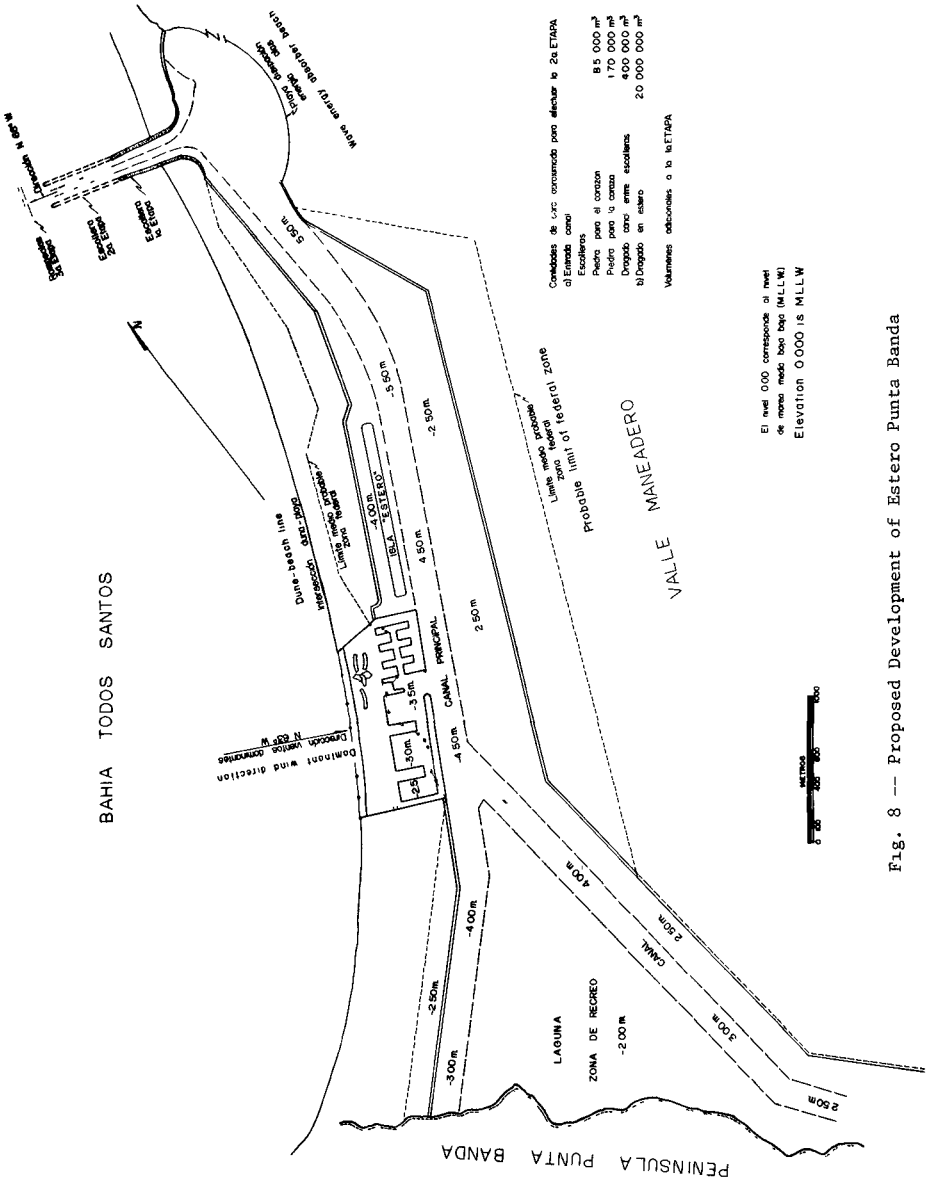

Fig. 8 -- Proposed Development of Estero Punta Banda

build the two jetties to full ultimate sections across the beach, dredge between the jetties and, as this cut nears completion, begin closure of the old channel by dumping stone from the trestle and by depositing dredged material on the north side of the north jetty. In this matter, the flow would be diverted to the new channel. Most of the dredging in the lagoon and the construction of the wave absorbing beach would be deferred until the new flow regime had been established.

The authors wish to acknowledge the collaboration of Ing. Arturo Bello M. who made the field studies and who was responsible for the calculations and the figures presented in this paper. The study was sponsored by Programa Nacional Fronterizo, Mexico.

DUBAI CREEK ENTRANCE

H.Ridehalgh, F.I.C.E.
Partner,Sir William Halcrow and Partners
Consulting Engineers
Newcombe House, 45 Notting Hill Gate, London W.11

INTRODUCTION

The paper describes the works carried out to improve and stabilise the entrance to the Creek at Dubai. The Creek which is about eight miles long discharges through a heavily charged littoral zone in which large volumes of sand are transported across the entrance from west to east.

The works were required urgently and this coupled with financial restrictions prevented a study of the problem on an hydraulic model or the collection of comprehensive site information before construction of the work commenced.

In the event the works were carried out in stages - succeeding stages being planned and designed after the effects of the previous stages on the regime had been established.

The paper presents the results which were achieved using the prototype as a model and traces the effect of each stage on the Creek and littoral regimes from the commencement of the works.

GEOGRAPHICAL LOCATION

Dubai is situated on the south eastern shores of the Arabian Gulf and on the north western coast of the Musandam peninsular at approximately parallel 25° north. Fig.1. indicates the geographical location of Dubai.

HISTORICAL

The State of Dubai is one of the seven Trucial States so called after the truce with Britain in 1820. A thriving entrepot trade has been built up over the years based on the Creek, and the desire to improve the entrance to the Creek was manifested in 1955, in order to facilitate further expansion of the State's trade. The improvement works required were essentially to deepen and stabilise the entrance to the Creek so that unrestricted access at all stages of the tide and during most weather conditions would be possible. The works were commenced in 1959 and completed in 1961/62.

WEATHER

The weather can be divided into the two seasons - winter and summer. The winter is characterised by temperate conditions with light winds mainly from the N.W. Squalls of short high intensity, with wind strengths up to force 7 and sometimes greater are experienced. In the summer, high temperatures persist with fairly strong constant winds from the N.W. In the afternoon this wind is normally about force 3 or 4 on 70% of the days. The wave front conforms with the prevailing wind. What little rainfall there is usually falls in the winter, otherwise arid desert conditions prevail.

PHYSICAL FEATURES

Fig.1. shows the general boundaries of the Creek which is about eight miles long. The southern shores are generally steep sided and ringed with soft sand or sand dunee, whilst the northern shores are generally gently shelving and almost devoid of soft sand, indicating that the Creek traps most of the wind borne sand.

The bed of the Creek varies from hard layers of cemented sand and shells to deposits of fine grey sand. In general the hard layers are only a few inches thick and exist at various levels in the Creek, overlain by sand where accretion is taking place and exposed where erosion is dominant. The hard layer effectively prevents further erosion.

Fig.2. indicates the configuration of the entrance at about the time when the Author first became involved. At that time the ebb flowed away eastwards through several small unstable channels in a shallow coastal zone with the velocity of about half a knot.

The sea bed outside the Creek consists of sand, cemented sand and small areas of live coral, although the area immediately outside the old entrance was predominantly mobile sand.

The coastline is generally flat and sandy with a coastal barrier of sand dunes penetrated by a number of inlets connecting to lagoons behind the barrier.

The inlets are all unstable and appear to evolve cyclically; the entrance to Dubai being one such inlet. The coast is generally low lying and extensive areas of salt flats exist in aseociation with the lagoons behind the barrier of sand dunes.

The direction of littoral drift is from west to east and longshore currents of up to one knot have been recorded off the entrance.

The tidal range in the open sea is of the order of five feet and that within the Creek was about three feet before the works were constructed, high water and low water generally lagging behind those of the open sea; low water lagging approximately twice as much as high water.

THE WORKS AND THEIR PERFORMANCE

The first phase works consisted of dredging a channel some 3,000 feet long and down to six feet below low water through the sand spit as far as the one fathom (six feet) contour in the open sea and the closing of the 1954 and 1957 channels by the construction of a training wall some 1,000 feet long aligned to encourage both ebb and flow to follow the same path. At the same time a groyne was constructed with the intention of protecting the entrance and encouraging accretion on the eroding Shindagah foreshore, as well as to prevent bar formation across the entrance. Fig.3. indicates these proposals. The dredgings were used to raise the level of the low lying area behind Shindagah.

The dredging was limited to six feet below low water by reason of the presence of a hard layer of cemented sand just below this level, the cost of removal of which would have been out of proportion to the benefit received.

It was decided at that time that the quickest and most economic form of construction in these conditions for the groyne and the training wall would be a steel sheet piling and this has remained the case up to the present day.

Even though Creek discharge velocity increased to about three feet per second, these works were only partially successful, and Fig. 4. illustrates the conditions existing at their conclusion, from which it will be seen that further works were necessary.

The bar across the entrance was formed largely as a result of bed and bank erosion within the Creek itself. In particular, large quantities of sand were eroded from the bank at Ras Daira due to the realignment of the entrance and the increased current velocities. The littoral drift naturally contributed to the bar formation, but probably more to the shape than to the size of the bar. At this stage the Shindagah foreshore some distance upstream was beginning to erode due to the influence of the groyne.

Conditions at the entrance which remained navigable for about nine months deteriorated suddenly as a result of a prolonged storm during which the bar was supplemented overnight by an accretion of approximately 100,000 cubic yards, and it became imperative to supplement the works already completed.

It was decided, therefore, to extend the groyne seawards into deeper water in an attempt to reduce the effect of the drift and further protect the entrance. At the same time the training wall was extended inland to encompass the eroding bank at Daira, and so prevent the transport of material from this particular bank to the entrance and, at the same time, it was extended seawards to direct the discharge further out into the littoral drift. By this means discharge velocity was increased to about five feet per second. Fig. 5. shows the Phase II proposals which, in the event, proved most successful and the conditions at the entrance after completion of the work are shown on Fig.6.

The groyne was successful in arresting the drift, and this may well have been fundamental to the success of the scheme in that shelter from the weather and littoral drift facilitated the completion of the rest of the works and enabled the transport of sediment from the Creek to take place under relatively stable conditions without conflict with the littoral stream.

The entrance condition as it stands today is quite stable. The velocity has been improved to a maximum of about five knots and the shoal shown on Fig.6. has moved further east improving access to the entrance. The groyne is now full and material is passing across the entrance to the shoal on the eastern side of the entrance.

SIDE EFFECTS

The Phase II works having been completed and a permanent feature of the coastline having been formed, several side effects appeared.

The principal effect was the erosion of both the Shindagah foreshore and that of Ras Daira.

Whilst the main groyne was able to halt erosion immediately adjacent to it severe erosion took place some distance upstream along the beach. Four concrete groynes were erected which effectively controlled the loss and eventually sufficient accretion was encouraged to replace the beach previously lost.

Eventually it was found necessary to increase the number of groynes to cover a distance of approximately one mile westwards along the beach, i.e. sufficiently far to be outside the effect of the new entrance.

Erosion on the beach further downstream did not manifest itself until some time after the Phase II works were complete. Erosion of the beaches much further east of Dubai has been going on for many years and will eventually become a problem, although at the present time this area of the coast is uninhabited. The beach in this area is subjected to waves from a more northerly direction, due to the influence of the entrance and refraction by the beach contours. The submerged offshore bar comprising the cut-off remains of the old sand spit effectively prevented erosion until the bar itself was eroded, whereupon shore erosion became progressively worse. Four groynes have been erected as an interim measure which have, to a large extent relieved the situation.

The increased discharge velocity of the Creek undoubtedly contributes substantially to the freedom from shoaling at the entrance but, in addition, it is thought that the very high salinity in the upper Creek induces a reversal of normal estuarine flow conditions which also contributes to the absence of bar formation.

It is thought also that the orientation of the end section of the groyne in relation to the normal wave front is such as to produce a small inshore current which tends to hold back the drift. Further west along the coast where the effect of this current is no longer felt, there appears to be some accretion of the beach which might well be the beginning of a new sand spit.

GENERAL

The stage development followed, when using the prototype as a model has, in fact, produced a result of the classical style resulting when a discharge takes place into or through a littoral stream. Accretion and some denudation has taken place on the upstream side and erosion has become evident on the downstream side. There are signs also that some of the accretion on the upstream side is now beginning to find its way into the entrance, although the discharge velocity is still able to maintain a channel free from shoaling.

It could well be argued that the works have made no contribution to the solution of the problem, and that further extensions seawards of both groyne and training wall will be necessary.

This may be true but should be considered in relation to the economic advantages gained by building the entrance in its present form. Trade into the Port has increased four-fold as a result of the new entrance, and has produced a very substantial revenue. Further, considerable sums of money have been derived from the sale of reclaimed areas within the Creek, and it could be said that the scheme has already proved its economic viability. In addition there has been a financial and time saving due to using the prototype as a model.

The income derived as a result of the new entrance, together with newly acquired oil revenues, have resulted in a decision to build a new deep water artificial port, approximately two miles upstream of the original entrance. An hydraulic model has now been built to determine the effects this new port will have on the coastal regime, and consideration will be given during these investigations to the desirability or otherwise of maintaining the present entrance and protecting the adjoining coastal areas.

It is hoped that it will eventually be possible to discharge the Creek through the new Port, in which case any coast protection works built now to safeguard the position resulting from the construction of the present entrance would either be redundant or inappropriate.

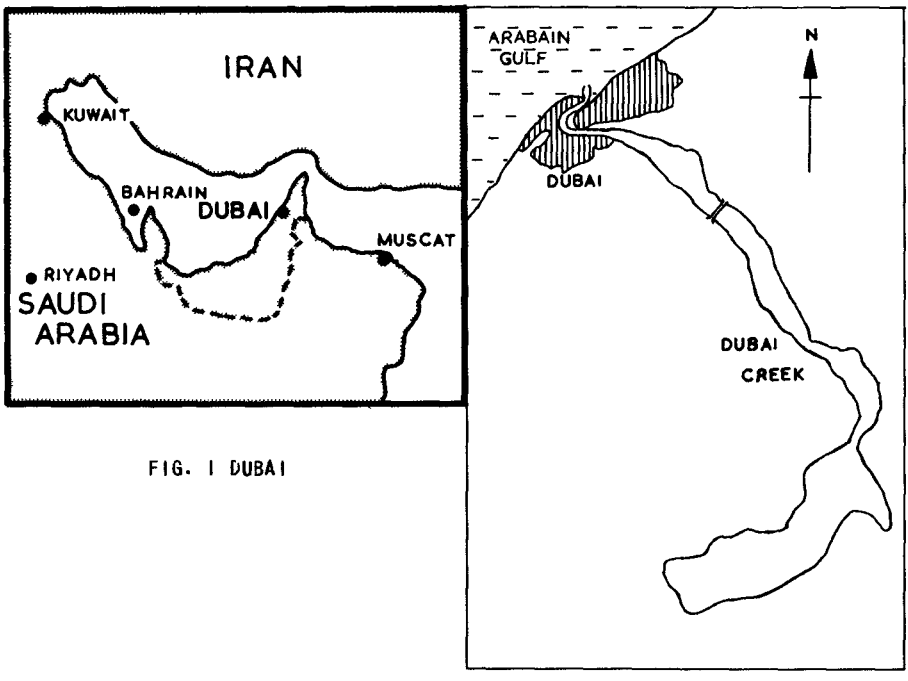
IRAN
KUWAIT
BAHRAIN
DUBAI
MUSCAT
RIYADH
SAUDI
ARABIA
ARABIAN
GULF
N
DUBAI
DUBAI
CREEK

FIG. 1 DUBAI

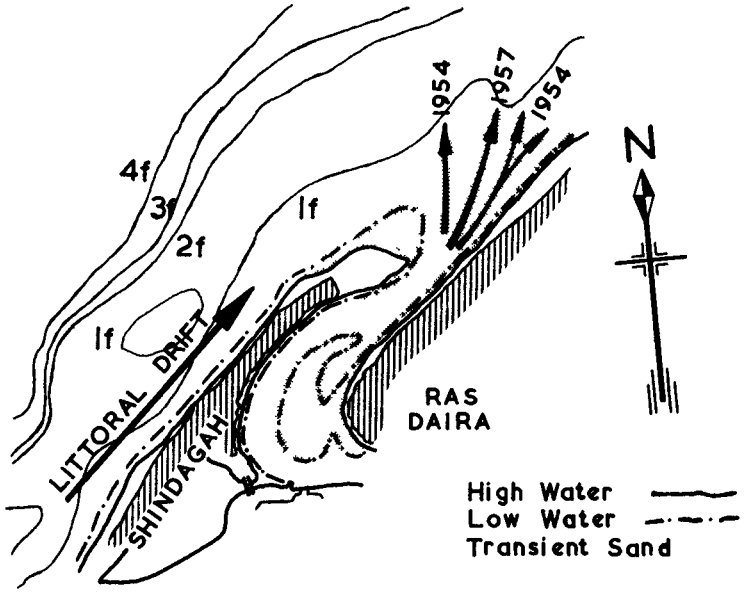

FIG. 2 DUBAI ENTRANCE BEFORE COMMENCEMENT OF WORKS

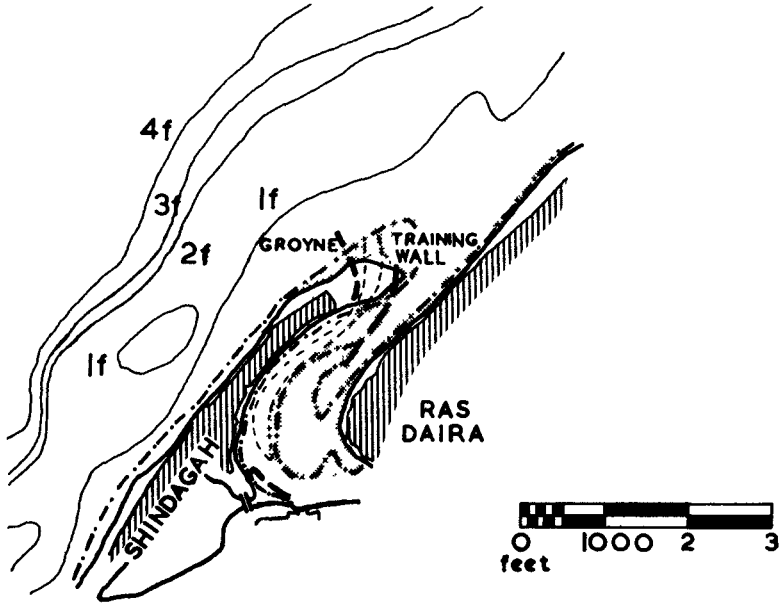

FIG. 3 DUBAI CREEK ENTRANCE PHASE I PROPOSALS

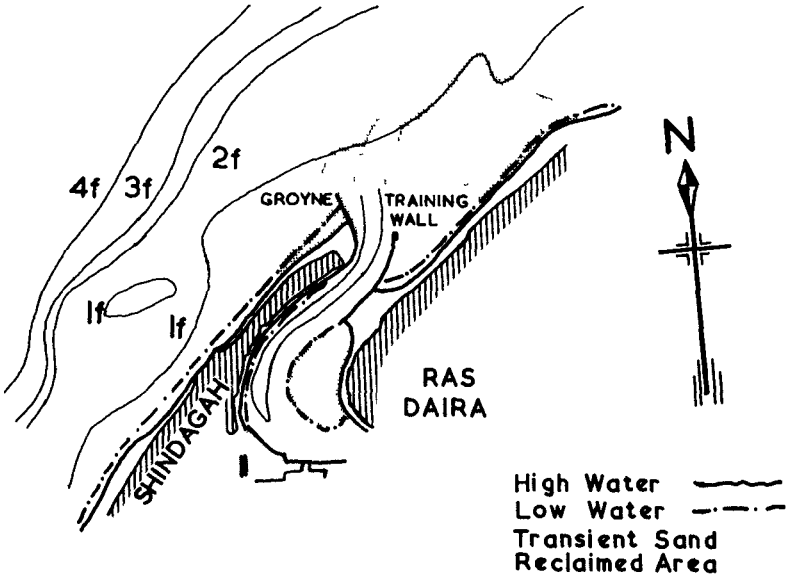

FIG. 4 DUBAI CREEK ENTRANCE AFTER COMPLETION OF PHASE I WORKS

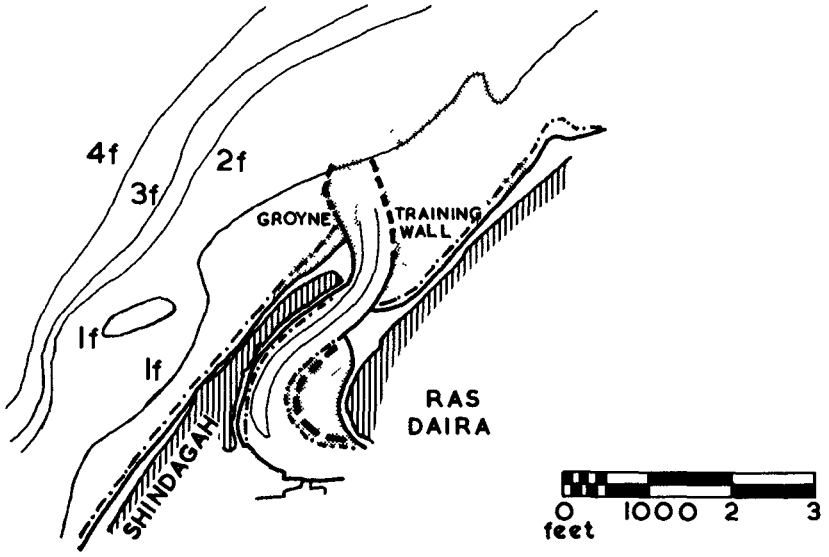

FIG. 5 DUBAI CREEK ENTRANCE PHASE II PROPOSALS

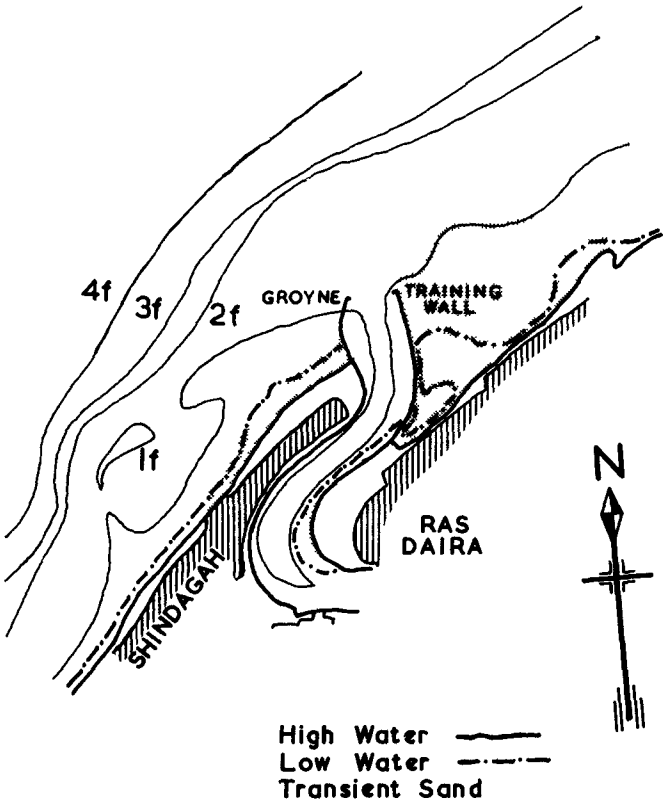

FIG. 6 DUBAI CREEK ENTRANCE AFTER COMPLETION OF PHASE II WORKS

CHAPTER 80

RIVER MOUTH TRAINING IN NEW SOUTH WALES, AUST.

BY

C. D. FLOYD,

Inspecting Engineer Investigation,

Harbours and Rivers Branch, Public Works Department

of New South Wales.

ABSTRACT.

A summary is given of the results of training sixteen rivers in an endeavour to increase bar depths for navigation. The bars are of simple crescent formation fed by littoral drift.

Whilst the training works have improved conditions for navigation they have not resulted in any appreciable increase in bar depths.

Despite the complex mechanisms involved in bar formation a consistent simple correlation is found to exist between channel and bar depths. This correlation seems to apply to all rivers and inlets with simple bar systems and extends over a range from a bar depth of two feet to 60 feet. The correlation holds for rivers elsewhere and with varying climates of exposure

RIVER MOUTH TRAINING IN NEW SOUTH WALES, AUSTRALIA.

INTRODUCTION.

1.1 New South Wales has a coastline running roughly north and south from latitude 28°10'S to latitude 37°30'S a distance of about 650 nautical miles. It faces the South Pacific Ocean and Tasman Sea. Numerous rivers and coastal lakes enter the ocean through sand beaches.

1.2 Sixteen river mouths have been trained to some degree for navigation. These vary in size but all have extremely variable fresh water flow. This variation in the case of the largest, the Clarence River, is from zero to 600,000 cusecs (170,000 cu. meters/sec) and for the greater part of the year the flow is less than 1,000 cusecs (28.3 cu. meter/sec). Tidal flow through the entrance however is about 88,000 cusecs (2,500 cu. meter/sec) at mean spring range (4.4 feet (1.3m) ocean). Other rivers have similar characteristics on a smaller scale and the mouths and lower reaches are in tidal regime. When floods do occure the loss of flow to storage on the flood plain is such that very few floods result in a flow through the mouth much above maximum tidal flow for extreme spring tides.

TRAINING WORKS.

2.1 The rivers became centres of communication early in the history of the State's development as the most convenient and rapid means of transport was by water. Starting with the Hunter River in 1810 training works were constructed to provide safe navigation. The majority of the work was carried out in the period 1880 to 1910 with minor changes and additions to some schemes in the period 1910 to 1930. Commencing in the 1950's a major training scheme was started on the Clarence River and also a programme of development of small river entrances for fishing craft.

2.2 Prior to development all river entrances was unstable and changed with changing weather conditions. In all cases the location of the saddle across the ring bar was variable and often difficult to find or such that a vessel would have to cross a shallower area. The positions of some river mouths also moved up and down the coast over limited distances.

2.3 Training works to improve navigation are conventional and fall into two categories, internal training walls and entrance training jetties. Both types are in all cases of tipped quarry stone or stone and concrete blocks.

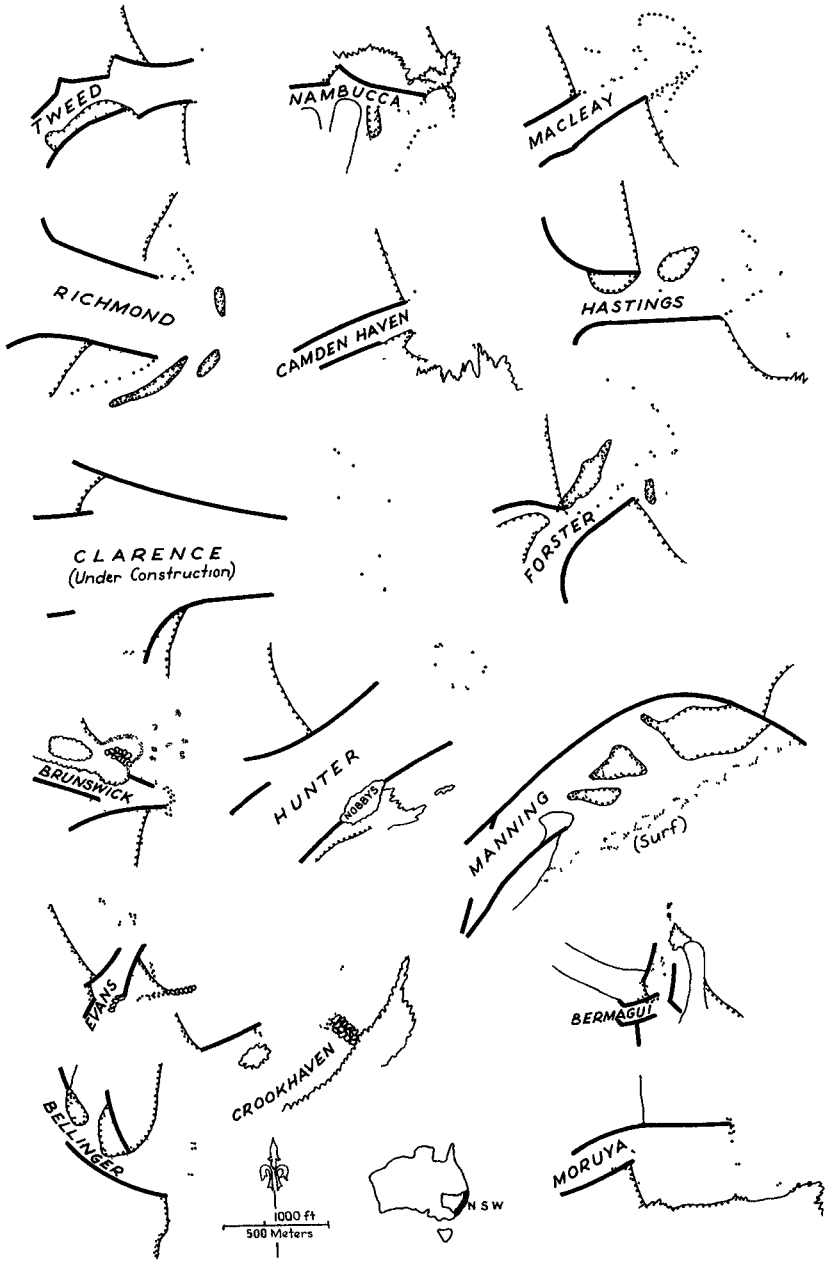

TRAINED RIVER ENTRANCES
IN N.S.W.

FIG. 1

2.4 The internal training walls served two functions; the improvement of channel alignments and depths and the fixing of the point of entry into the ocean. The training jetties at the entrance were constructed to serve three functions; to improve the alignment of the entrance, stabilise the bar location and increase depths across the bar.

TRAINING JETTY GEOMETRY.

2.5 The geometry of all trained river entrances is shown in figure 1. Most are approximately at right angles to the general coastline adjacent to them and facing about due east. Of these four have two jetties of approximately equal length and six have two jetties of unequal length. Those having unequal length jetties are again divided into two with projecting jetties on the northern side and four on the southern side. Another three have single jetties only, two of them are on the northern side and one on the southern.

2.6 Four entrances are aligned in a north easterly direction, two have two training jetties and two have one only with a reef in effect acting as a second.

LITTORAL DRIFT.

3.1 With the exception of Newcastle no measurements have been made of littoral drift past any of the entrances. The drift rate at this location is estimated to be about 100,000 cu. yds. per year with between 10,000 and 30,000 cu. yds passing through what would normally be the bar area.

3.2 Prevailing ocean swell is from the south east and coastal features all indicate a littoral drift from south to north.

3.3 There are no known permanent ocean currents past any of the entrances.

3.4 Sand grain sizes are generally in the range 0.2 to 0.3 m.m. median.

3.5 Although no quantitative data are available the indications are that the volume of littoral drift increases from south to north.

RESULTS OF WORKS.

4.1 The results obtained in attempting to stabilise and deepen the river entrances have been satisfactory to a limited degree. With a few exceptions the aim of providing a static entrance has been achieved. Navigable depths on lines of access over the bars have in most cases been improved but in only a few has the depth of water over the bar "saddle" been increased or the bar removed. The improvement gained has generally taken the form of inducing the "saddle" to remain approximately in line with the trained entrance channel. Where a greater bar depth has been obtained it has been accompanied by a deeper entrance channel resulting from narrowing or improved flow characteristics.

SINGLE TRAINING JETTIES.

4.2 Single jetties have proved almost worthless except for two cases which cannot be regarded as typical. At Nambucca and Manning single jetties on the down drift side of the entrance cannot be said to serve any useful purpose. The entrances are unstable and so far as can be seen from old records no better than when untouched. Port Macquarie (Hasting River) at one stage in its development had a single jetty on the up-drift side and under these conditions it also had an unstable entrance. The two successful single jetty entrances will be discussed later in para. 4.10.

TWO TRAINING JETTIES - perpendicular to shore.

a) Equal Projection.

4.3 The effects of two equal length jetties has been to move the bar seaward and improve navigation by causing the bar saddle to align approximately with the channel. Where the depth over the saddle has increased it seems to be related to an increase in channel depth resulting from decreasing the width of the channel. The position of the saddle moves with changes in weather conditions resulting in a decrease in navigable depth and occasional dredging is required.

b) Unequal Projection.

4.4 Where the up-drift jetty projects a large shoal area forms in its lee and the channel is unstable at the outer end fluctuating in direction over an arc which may be as much as 90°. At times more than one channel may form and the ruling bar depth then decreases. A direct approach across the bar and into the channel is only possible for short periods.

4.5 Usually the flood tide tends to concentrate around the end of the shorter jetty. Breaking waves on the shoal area seem to provide a larger volume of sand for inward transport than would be available for an entrance with equal length walls (this has not been checked by measurement).

4.6 Where the down-drift jetty is the longer the channel is stable in location and the bar behaves much as it would with two equal lengths jetties. The depth over the bar seems to be much the same as can be expected for equal length jetties.

4.7 The main disadvantages seem to be the lack of shelter in the outer channel and an apparent increase in sand feed into the entrance channel.

Entrance angled down-drift.

4.8 Four entrances are angled down drift. Three of them have no bars and the fourth a deeper bar than would normally be expected.

4.9 At Newcastle (Hunter River) training works were started prior to 1810 and completed in 1913. Detail surveys of early conditions are not available but it seems that a bar did exist. The bar was removed early in the training process and the entrance has remained bar free. There is however a mound shoal on the line of the northern jetty. Depths over this mound are only a little less than in the channel between the jetties. Although not certain it seems that the original bar was fed mainly by a local inshore reversal of sand drift in the lee of Nobby's Island and reef. There is only a small sand feed past the end of the present jetties, the majority of the littoral drift being apparently deflected by the reef. (ref. 3.) Channel depth between the ends of the jetties was 32ft. below I. S. L. W. but has recently been increased to 36ft. by dredging. The shoal varies between 30 and 32ft.

4.10 Crookhaven and Bermagui are somewhat similarly located but at Crookhaven a headland and at Bermagui a reef takes the place of a training jetty. As in the case of Newcastle the original bars seem to have been fed by a local inshore reversal of littoral drift. Since construction of the training walls no bar has formed at either entrance. Crookhaven has been like this for over 60 years and Bermagui for 10 years. There is however, a rock bar near the outer end of the entrance channel which perhaps could take the place of a sand bar at Crookhaven.

4.11 The other entrance facing away from prevailing wave ac Evans Head. In this case, however, there is no adjacent reef and two are used, the up-drift one projecting slightly. Since completion in 19(bar has existed although at a greater depth than would be expected for existing channel depths. Recently, there were signs that the bar was becoming unstable and tending to become more shallow. This however lasted only for a few months.

Comparison of Results.

4.12 The data in Table I indicates that there is a relationship between bar depth and channel depth. Sufficiently detailed surveys are available in all cases to obtain an accurate cross section and calculate mean channel depth. For ease of comparison therefore, the maximum d the entrance channel has been taken. The location at which this depth i measured is shown in figure 2. In some cases greater depths occur ups caused by geometry and irregular flow patterns, these have been ignori

4.13 In some cases flow through the entrance channel is not symmetrically distributed and an eccentric cross section occurs. This in a greater maximum channel depth than for symmetrically distributed f Comparison of available detailed cross sections indicates that for unifor distributed flow the following approximations hold.

$$D_{Max} = 1.3\ D_{Mean} = 1.3\ \frac{A}{W} \qquad (1)$$

and for eccentric flow

$$D_{Max} = 1.65\ D_{Mean} \qquad (2)$$

A is cross sectional area of inlet char in sq. ft.

where D is the depth below mean tide l

and W is width at mean tide level.

4.14 When an eccentric cross section exists it has been assume it is equivalent to a section with uniformly distributed flow having a depth 0.8 of that existing.

A natural plot of bar depth against maximum channel depth is in figure 3. Although there is an appreciable scatter there appears to be a simple relationship between bar depth and channel depth despite the complex associations involved. The relationship seems to be the same for trained and natural inlets.

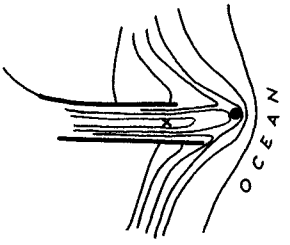

TRAINED INLET

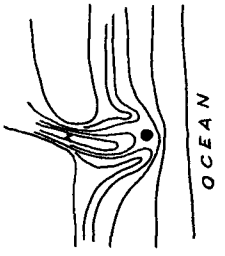

UNTRAINED INLET

FIG. 2

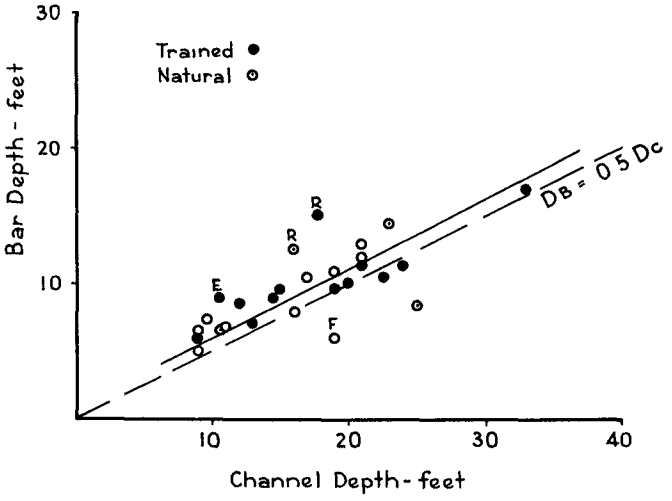

PLOT OF BAR DEPTH V CHANNEL DEPTH
(Depths below Mean Tide Level)
N S W Inlets

FIG. 3

4.15 Some comment on the points showing the greatest departure from the general trend is possible. Points labelled (R) are for the Richmond River. The bar here is notoriously unstable and the survey from which the data is taken for the trained condition records a period of good depths. A depth of 11 feet is not uncommon. Possibly the untrained river survey was also taken at a good period as it also was reported to be very unstable. Point (E) represents conditions at Evans River some four years after construction; there have been signs of instability and a tendency to a reduction in depth, although the present depth is as shown. Point (F) is for untrained conditions at Forster. The survey is rather sketchy and these may have been two outlets across the bar.

4.16 A second plot of distance from the start of channel expansion to the crest of the bar is in figure 4. Although the scatter is greater there is a visible trend.

4.17 The rather remarkable correspondence between channel and bar depth might be thought to result from similar conditions along a relatively short length of coastline. To check this such data as could be obtained from published charts was collected for other Australian rivers. These were also found to follow the same pattern. A number of river entrances throughout the world and taken from such charts were available were also added. These are listed in Table II, and plotted in figure 5. There will be some error in the assumption made that depth at mean tide level represents regime depth. For depths considered the percentage error would be small.

Conclusions.

5.1 Despite the complex inter-relationships of wave climate, tidal currents and littoral drift involved there seems to be a simple correlation between channel depth and bar depths for an inlet which is in tidal regime.

5.2 As has been shown by Bruun & Gerritsen (Ref. 1) and O'Brien (Ref. 2) the cross sectional area of an inlet channel is related to tidal flow.

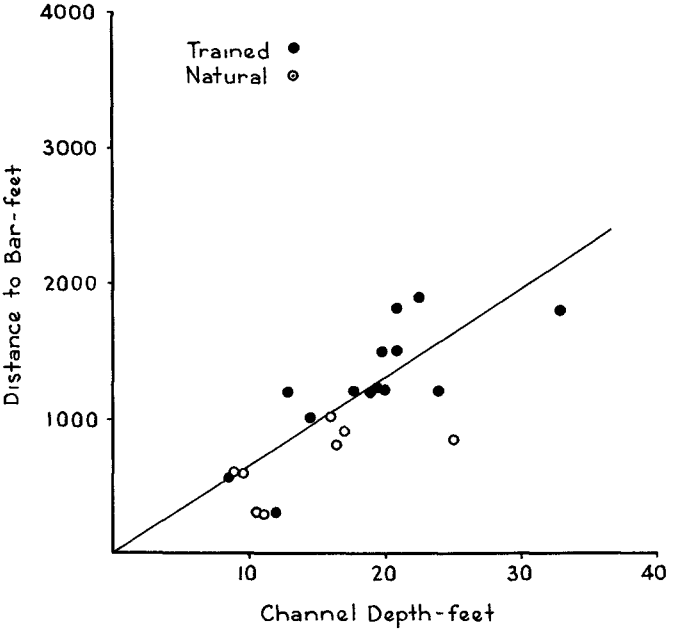

PLOT OF BAR DISTANCE V CHANNEL DEPTH
FIG. 4

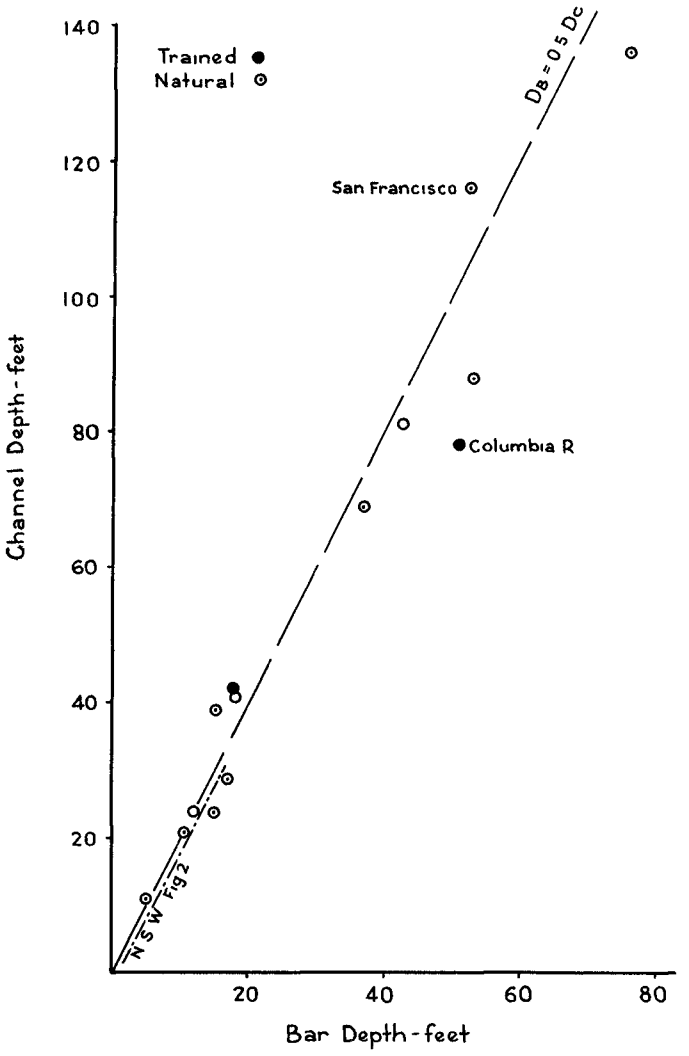

PLOT OF BAR DEPTH V CHANNEL DEPTH
PORTS OTHER THAN N.S.W.
FIG. 5

Approximately

$$A = \frac{Qm}{3} \qquad (3)$$

where A = cross sectional area of inlet channel in sq. feet.

Qm = maximum discharge in cusecs for a tide of mean spring range.

from figure 3 or figure 5 the minimum bar depth to be expected would be given by

$$D_C = 1.3 \frac{A}{W} = 2 D_B \qquad (4)$$

where D_C = maximum channel depth below the surface when Qm occurs.

D_B = depth over bar saddle at the same time
(both in feet)

or

$$D_B = 0.21 \frac{Qm}{W} \qquad (5)$$

5.3 It also seems that other than in exceptional circumstances it is not possible to remove a bar by training jetties and that the best depth across the bar can only be increased to the same degree as it may be practicable to increase the depth in the channel. This of course applies only to the conditions examined which are that littoral drift depends only on waves and wave induced currents, no appreciable ocean currents are present, and off shore contours are regular and entrance alignment is approximately perpendicular to the coastline.

5.4 There is perhaps an indication that bar depths would be less with training jetties angled down drift. This needs more examination.

5.5 As the effect of jetties is to in effect bodily move the bar formation to another location there is perhaps an inference that littoral drift is only temporarily interupted unless permanent dredging of the bar is involved.

5.6 Detailed examination of littoral drift behaviour in the areas adjacent to the entrances where bars have been removed would probably reveal some interesting information.

TABLE II - INLETS ELSEWHERE THAN N. S. W.

INLET		CHANNEL DEPTH at M. T. L. feet	BAR DEPTH at M. T. L. feet
TASMANIA			
Port Dalrymple	(Natural)	136	76
Macquarie Hbr	(Part - trained)	42	18
George Bay	(Natural)	21.5	10.5
QUEENSLAND			
Urangan	(Natural)	29	17
Morton Bay Boat Chl.	(Natural)	11	5
NEW ZEALAND			
Otago	(Trained)	69	37
Whangerei Hbr.	(Natural)	88	53
Paterson Inlet	(Natural)	81	43
Aotea Hbr.	(Natural)	24	12
Waikato Hbr.	(Natural)	24	15
MISCELLANEOUS			
San Francisco	(Natural)	117	53 dredged (2nd saddle 39)
Columbia River	(Trained)	78	51 some dredging
Cuama (Mozambique)	(Natural)	39	15
Porto de Quelimane	(Natural)	41	18 (2nd saddle 17)

TABLE I - N. S. W. INLETS

RIVER		CHANNEL		BAR		
		Width	Max. Depth	Dist. from chl. throat	Depth at Saddle	Original Navigable Depth
		feet	feet	feet	feet	feet
Tweed	(Trained)	300	14.5	1000	9	
	(Natural)	360	21		13	6
Brunswick	(Tr)	200	12	300	8.5	-
	(Na)	250	9	600	6.5	5
Richmond	(Tr)	1200	17.75	1200	15	
	(Na)		16	1000	12.5	10
Clarence	(Tr)	1200	33	1800	17	
	(Na)	Not available	-	-	-	-
Evans	(Tr)	200	10.5	300	9	
	(Na)	180	9.75	600	7.25	5 to 7
Bellinger	(Tr)	300	9		6.25	
	(Na)					6
Nambucca	(Tr)	300	13	1200	7	
	(Na)		*			7
Macleay	(Tr)	650	24(19.2)	1200	11.25	
	(Na)	1000	21	1500	12	8
Hastings	(Tr)	400	19(15.2)	1200	9.75	
	(Na)		18		7(2 saddles)	7
Camden Haven	(Tr)	400	21	1800	11.5	
	(Na)		17	900	10.5	7.5
Forster	(Tr)	440	22.75	1900	10.5	
	(Na)		19	1200	6	5.5
Manning	(Na)		19	1200	11	
Hunter	(Tr)	1200	39	no bar		15
Sussex Inlet	(Na)	300	9	600	5	
Crookhaven	(Tr)		31		16.75(rock)	
	(Na)		23		14.5	14
Moruya	(Tr)	480	20	1500	10	
	(Na)		25.5	850	8.5	9
Wagonga	(Na)	250	16.5	1000	8	
Bermagui	(Tr)	200	11	no bar	-	
		190	10.75	300	7.5	5 to 7
Merimbula	(Na)	200	11	300	7.75	-

Note: Depths are measured below mean tide level as being approximately the level of maximum ebb discharge.

* Figures in brackets are corrected for eccentricity.

CHAPTER 81

DEPARTMENT OF PUBLIC WORKS OF CANADA
DESIGN DIRECTORATE

EXPERIENCE WITH SELF-DREDGING HARBOUR ENTRANCES

by
P. DONNELLY
HEAD, MARINE STRUCTURES SECTION
and
I. MacINNIS
ATLANTIC REGIONAL COASTAL ENGINEER

EXPERIENCE WITH SELF-DREDGING HARBOUR ENTRANCES

by

P. Donnelly, Head, Marine Structures Section, Department of Public Works

and

I. MacInnis, Atlantic Region Coastal Engineer, Department of Public Works

ABSTRACT

About 7 years ago, the Department of Public Works of Canada requested the assistance of the National Research Council to devise a means of reducing sediment deposition in the entrance to a small harbour at Dingwall, Nova Scotia. Siltation of this harbour entrance, which opens to the Atlantic, was so severe that on occasions it was completely blocked by sand at low tides.

The desired objective was to devise a layout of structures which would maintain an entrance depth of 12 feet at low tide. Model studies were carried out and a breakwater configuration was evolved which appeared to have some "self-dredging" characteristics. The recommended structures were built in 1962 and to date have been successful in maintaining minimum depths of 5 feet at low tide which is adequate for the fishing fleet using the harbour. While falling somewhat short of the original objective this performance has been very satisfactory when compared with the conditions which existed before construction.

Similar installations have since been built at two other locations in Nova Scotia Which are on the Gulf of St. Lawrence. Indications so far are that similarly satisfactory results have been obtained.

This paper describes the installations, makes some tentative suggestions concerning the mechanisms involved in their operation and provides data on their performance.

PURPOSE AND SCOPE

Designers of harbour entrances in areas where littoral drift is a problem are constantly searching for solutions which they hope will minimize maintenance dredging problems. The Department of Public Works has, during the past six years, completed three installations of a harbour entrance configuration which was developed for the department by G.E. Jarlan at the National Research Council of Canada and which appears to give promise of a certain measure of success in combatting harbour entrance siltation All three installations have been at small fishing harbours in the Atlantic Province of Nova Scotia. The purpose of this paper is simply to give a very brief description of the design of the entrance and of the results which have been obtained since this concept could perhaps be used to advantage at other locations.

TYPICAL SITE CONDITIONS

The typical site conditions for these installations are

(a) entrance exposed to moderately heavy ocean, or sea, wave climate,

(b) entrance provides access from open sea to inner harbour or lagoon through a sand bar or beach,

(c) depths required at low tide are about 5 to 6 feet to accommodate small fishing vessels,

(d) littoral drift heavy enough to make necessary almost continuous maintenance dredging

DESCRIPTION OF HARBOUR ENTRANCE

The concept of the entrance configuration is illustrated diagrammatically in Fig 1

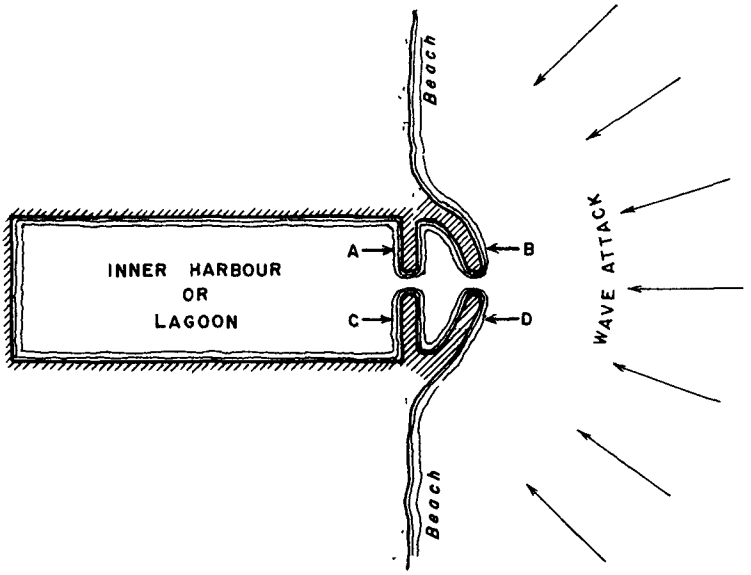

FIG. 1 SPECIAL ENTRANCE CONFIGURATION

Rubble mound breakwater construction has been used for structures A, B, C and D Typical lengths of these structures are

Structures A and C – 240 ft
Structures B and D – 325 ft

The entrance width is approximately 100 feet

The design was developed from model studies about 1960 at the National Research Council of Canada, for the fishing harbour at Dingwall, Nova Scotia, shown in Fig 2 Shoaling of the entrance of this harbour was so severe that it was often possible to walk across the harbour entrance in rubber boots within a few months of completion of dredging to a depth of 13 feet

Prior to the studies which resulted in the design described herein, an attempt had been made to reduce the siltation problem by connecting the harbour with the "North Pond" (See Fig 2) to channel a larger tidal prism through the harbour entrance This, however, failed to solve the problem

The model studies, which did not include tidal effects, showed that the entrance configuration, depicted in Fig. 3, produced a self-flushing action under wave attack Although interesting theoretical explanations of this phenomenon have been proposed (Ref 1), subsequent attempts which were made (Ref 2) to reproduce this self-flushing effect in a laboratory experiment were not very successful The effectiveness and performance of the design can best be judged by consideration of the results of a prototype installation over a period of 6 years

EXPERIENCE TO DATE WITH PROTOTYPE INSTALLATIONS

Harbour entrances based on this design have been installed at Dingwall, Inverness and Pleasant Bay in Nova Scotia Their location is shown in Fig 4. Some of the physical conditions prevailing at these sites are summarized in Table I.

TABLE I – PHYSICAL CONDITIONS

Location	Spring Tidal Range	Area of Lagoon	Area Harbour Entrance at High Spring Tide	Tidal Prism	Annual Dredging Prior to Improvement	Typical Sand Size
	(Ft.)	(Sq. ft.)	(Sq. ft.)	(Cu ft.)	(Cu. yds.)	
Dingwall	4.6	1,700,000	1725	7,820,000	50,000*	Fine sand
Inverness	4.5	1,300,000	1250	5,850,000	5,000	Very fine sand
Pleasant Bay	4.0	243,000	1575	972,000	New location, no data	Shingle beach. Particle size up to 3"

* This was for a dredged depth of approx. 24'.

FIG. 2 AERIAL PHOTOGRAPH OF DINGWALL, N.S.

The installation at Dingwall was completed in 1962, and the entrance between the heads of the breakwaters was dredged to a depth of 12 feet. The design has been successful in maintaining an entrance channel for a minimum depth of 5 feet at low tide which is satisfactory for the fishing fleet using the harbour. No dredging has been required since 1962. Future periodic dredging will be required but this was anticipated.

An indication of developments at the harbour entrance is given in Fig. 5 which compares surveys made in 1959 (before construction), 1963 and 1967. Profiles through the centre line of the harbour entrance for 1961, '62, '63, '64, '65 and '67 are shown in Fig. 6.

It is evident that the action of the structures has enabled an undetermined combination of wave action and tidal currents to bypass the littoral drift on a bar in front of the entrance while maintaining a minimum depth of 5 feet as compared to almost complete blockage before the structures were constructed. The tendency of the bar to advance into the harbour entrance (Fig. 6) is anticipated to be controllable with a very moderate amount of dredging.

FIG. 3 PHOTOGRAPH OF HYDRAULIC MODEL SHOWING GENERAL LAYOUT OF STRUCTURES

The conditions recently prevailing at Inverness which was built in 1965 are shown in Fig. 7. The shoal areas in the channel (min. depth 3 feet) are in all probability derived from "caving-in" of the steep sloped banks of the channel. Dredging to remove these shoals has recently been completed.

Construction of the third prototype installation at Pleasant Bay was completed in 1967 and no performance data is yet available.

THE SELF-FLUSHING ACTION

While tidal currents undoubtedly play a part, it seems that this entrance configuration serves to harness the mass transport aspect of wave motion to produce a periodic seaward directed current through the entrance. The incident waves, entering through the gap between the outer breakwaters, transport a certain mass of water into the harbour. As the bulk of the incident wave energy which enters the harbour is spent on the two inner breakwaters and in the shallow areas to each side of the central channel, a hydraulic head is built up within the breakwater system and the consequent return flow is directed seaward in the form of a periodic flushing current through the gap in the outer break waters. This effect is illustrated diagrammatically in Fig. 8.

The existence of a seiche either in the harbour or within the breakwater system, brought about by the disturbing force of the incident waves impinging on the harbour entrance, has not been proven. If such a seiche does exist it could be a factor contributing to the flushing effect.

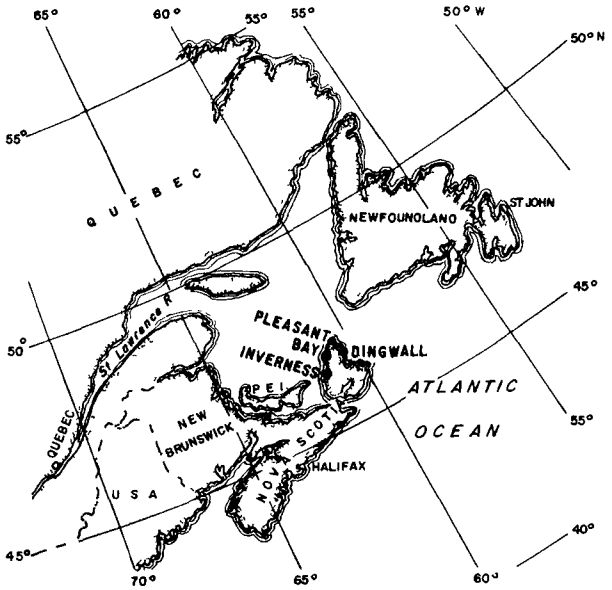

FIG. 4 LOCATION OF PROTOTYPE INSTALLATIONS

NAVIGATION CONSIDERATIONS

This type of entrance has good navigational characteristics because it allows vessels to make a direct entry with no exposure to beam seas. It also is highly effective in reducing wave agitation in the inner harbour

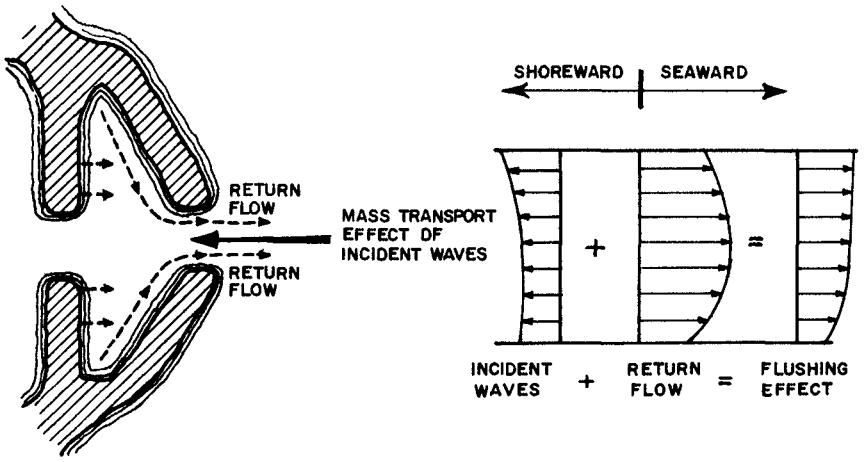

FIG. 8 TENTATIVE ILLUSTRATION OF SELF-FLUSHING ACTION

CONCLUSIONS

While the benefits of these installations could not in any sense be considered spectacular, they have made it feasible to maintain these small fishing harbours in existence without the need for practically continuous dredging in entrance channels exposed to heavy wave action, which presents obvious difficulties The concept may offer a solution in other comparable situations

REFERENCES

1 G E Jarlan, "Remarks on Dingwall Harbour (Nova Scotia)" National Research Council Laboratory Memorandum HY-62. Nov. 1965 (not published)

2 White, I.R P , Investigation of a Self-Dredging Harbour Entrance, Unpublished Thesis, Civil Engineering Dept., Queen's University at Kingston, Canada, April, 1964

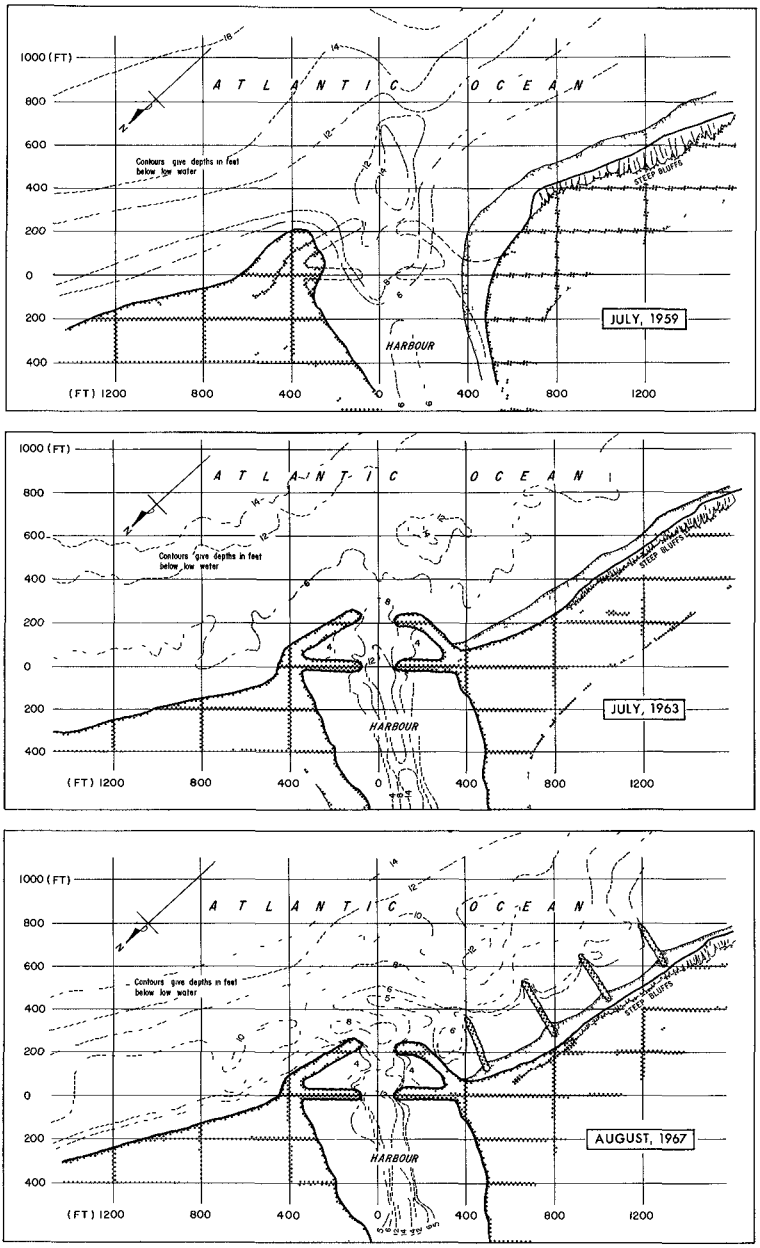

FIG. 5 CONTOUR CHANGES AT HARBOUR ENTRANCE DINGWALL, NOVA SCOTIA 1959–1967

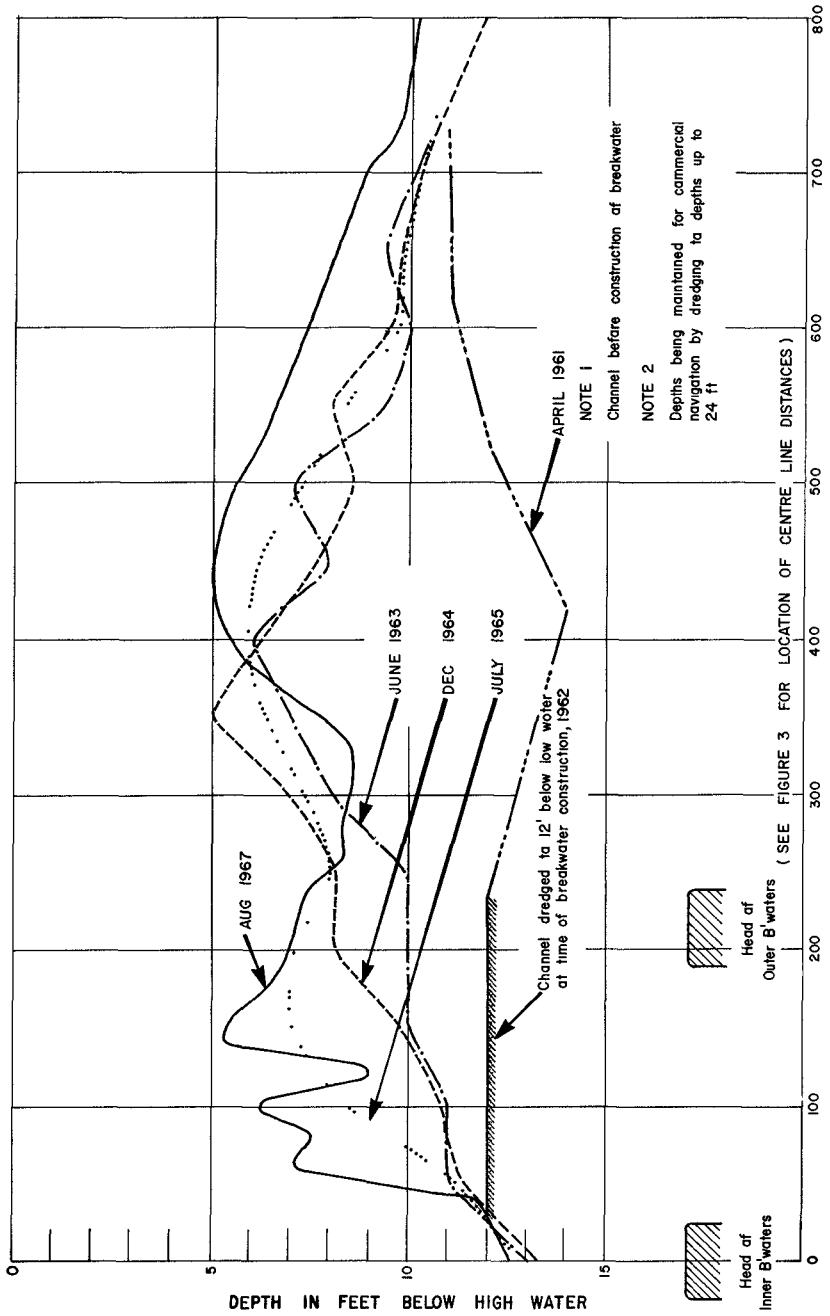

FIG 6 PROFILES ALONG CENTRE LINE OF HARBOUR ENTRANCE

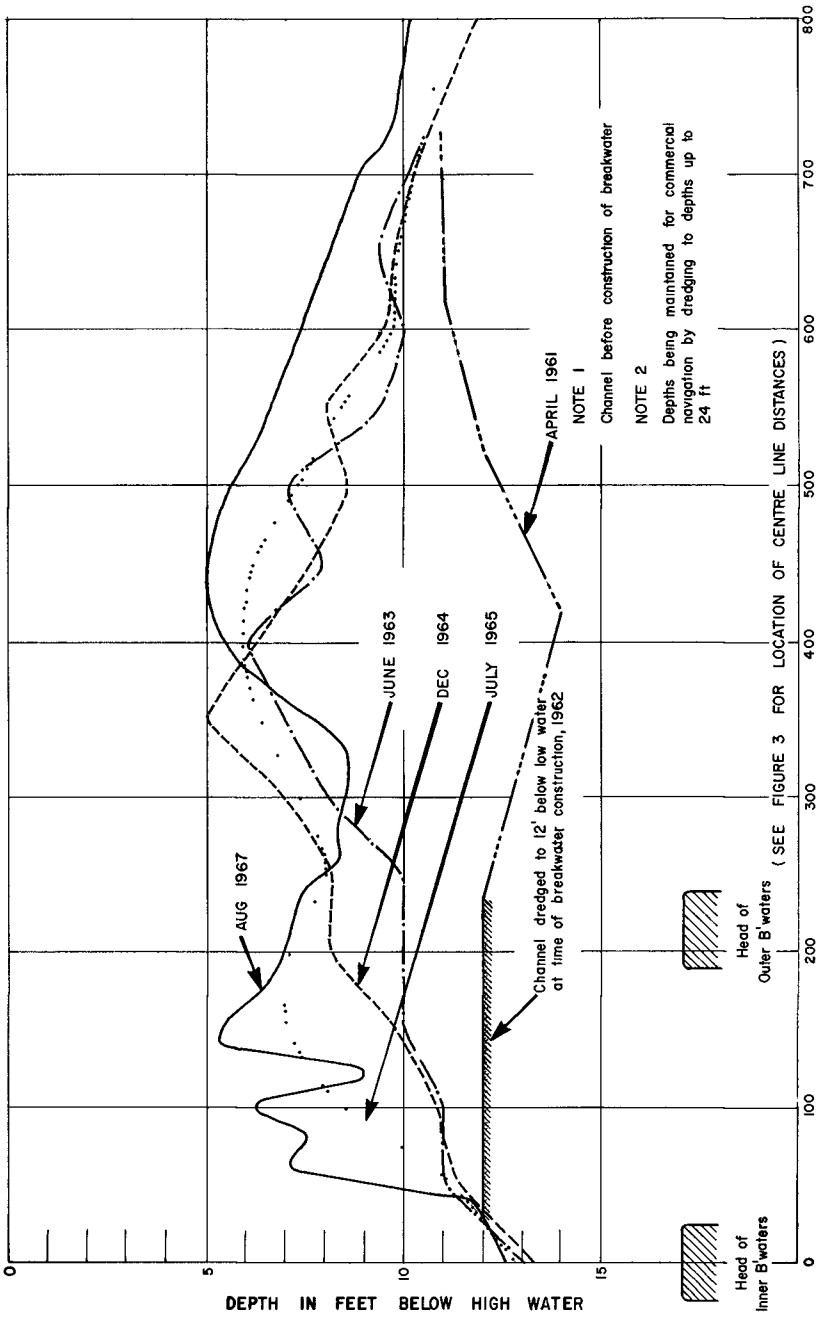

FIG 6 PROFILES ALONG CENTRE LINE OF HARBOUR ENTRANCE

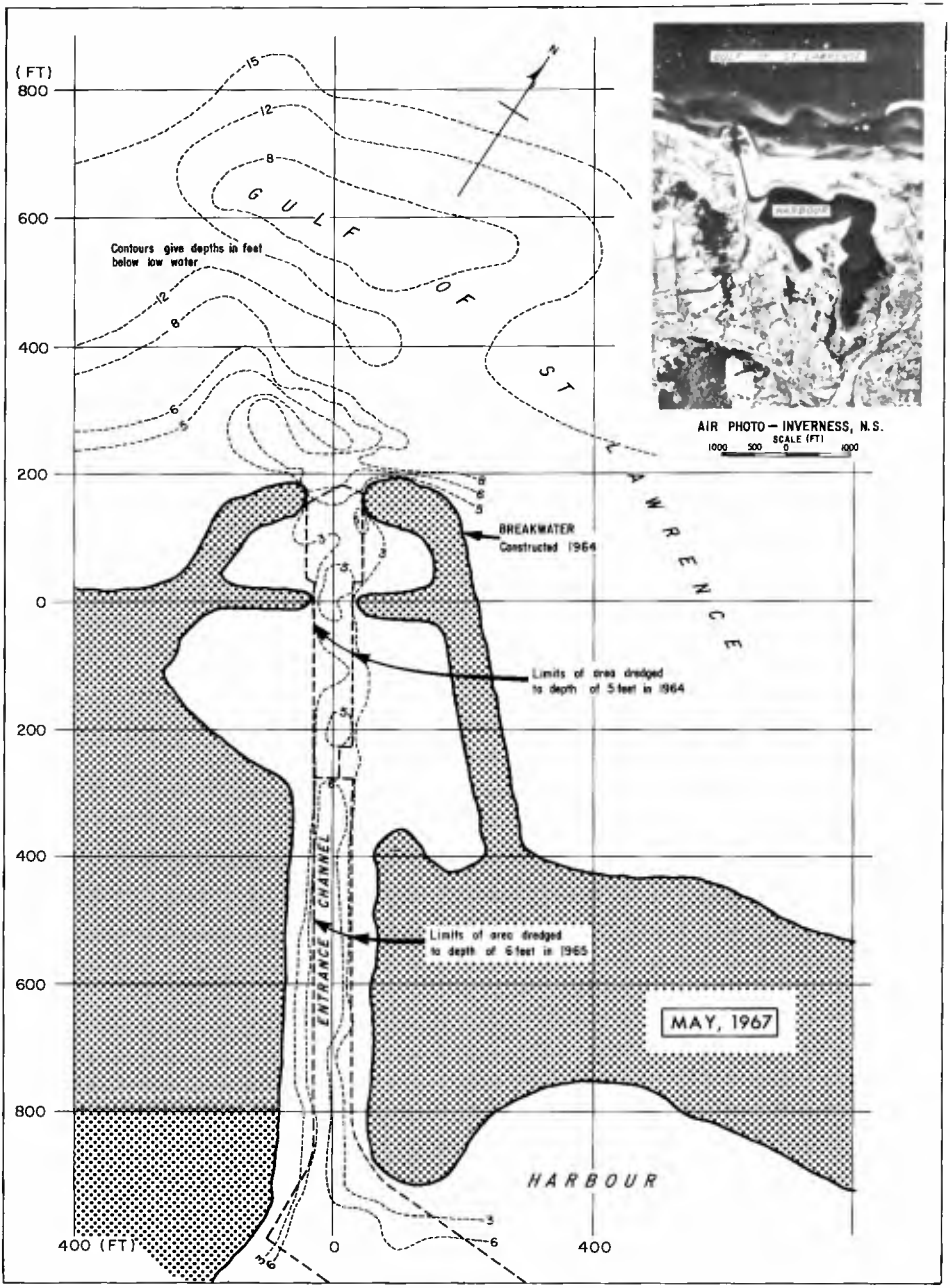

FIG. 7 CONTOUR CHANGES AT HARBOUR ENTRANCE INVERNESS, N. S. 1964 – 1967

CHAPTER 82

CASE HISTORIES OF TWO ESTUARIES

by

C.H. Dobbie, B.Sc., C.Eng., F.I.C.E., M.I.W.E., F.G.S.
Senior Partner, C.H. Dobbie & Partners

ABSTRACT

The coast of Great Britain has many interesting examples of the interaction between tidal estuaries of rivers and the littoral drift of the coast. These have been described with historical detail mainly by geographers (ref.1). Two cases coming to the author's firm for action have interest for coastal engineers. For the River Spey in the Moray Firth of Scotland, a famous and vigorous river, unusual works have been undertaken with success. For Dawlish Warren, a sand spit in the Exe Estuary of Devon in South West England, a scheme of works is being prepared which has novelty in regard to British practices.

THE RIVER SPEY

The River Spey, famous for its whisky distilleries and for its reputably piratical capture of the headwaters of other rivers, is a vigorous, rejuvenated river. As a young river it cannot, of course, have a fixed bed in the valley floor and locally this is recognised together with the biological analogy by a saying: "The Spey is like a bad woman who winna' keep to her own bed".

At its junction with the Moray Firth, a large inlet from the North Sea, it meets a littoral drift of sand and shingle of intensive movement preponderantly in the one direction westwards. The combination produces an extensive shingle spit resting on sand below. This spit has the common cyclic history of such circumstances and this has been traced back to 1724. The westward growth of the spit diverts the river mouth westwards until the hydraulic resis-

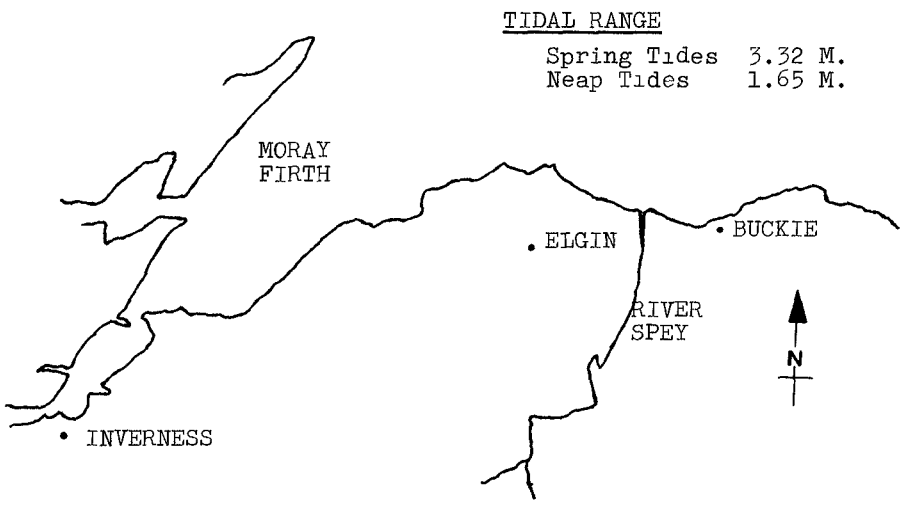

Fig.1: Location Plan

tance of the prolonged passage builds up sufficiently in river spate to cause a burst through the eastern end of the spit. In the last century the owner of the land and of the salmon fishery caused new channels to be cut at intervals to protect his interests.

The chronological order of events is:

1650 - Charles II landed from Holland and was carried ashore (hence the name Kingston)

1724 - Mouth 1555 metres west of Tugnet.

1829 - Year of famous Moray floods.

1860 - New cut brings mouth 232 metres west of Tugnet; old mouth 1555 metres west.

1870 - Mouth is 104 metres east of Tugnet.

1885 - New cut made.

1897 - New cut made 232 metres west of Tugnet.

1903 - Cut still in position of 1897.

1905 - Mouth 457 metres west of Tugnet.

1928 - Mouth 674 metres west of Tugnet.

1933- New cut 232 metres west of Tugnet.

1960- Mouth is 1311 metres west of Tugnet.

In 1961 the Moray County Council became involved as the Coast Protection Authority. The lands that had flooded were in numerous ownership and the valuable salmon fishery had passed to the Crown. A further complication was that extensive commercial abstractions of shingle had been made to the westward of the spit. Two cottages in the village of Kingston had been washed away and more buildings were threatened. Direct protection of the village was rejected by the consultants and a recommendation was made for a new cut. This was accepted and the consultants had a scheme carried out to induce the River Spey to do most of the work itself. The design procedure has been described in considerable mathematical detail related to Lacey's and other formulae for river regime (ref.2).

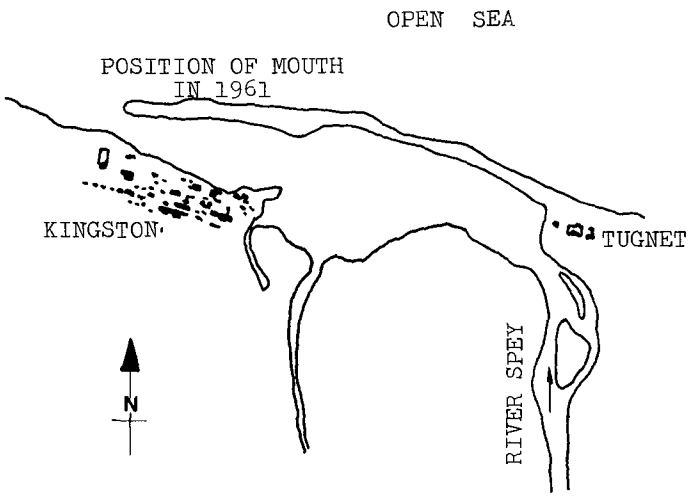

Fig.2: Estuary in 1961

The works included a gabion groyne, various excavations and fillings along the banks and a row of gabions through the spit at the selected site of the new mouth.

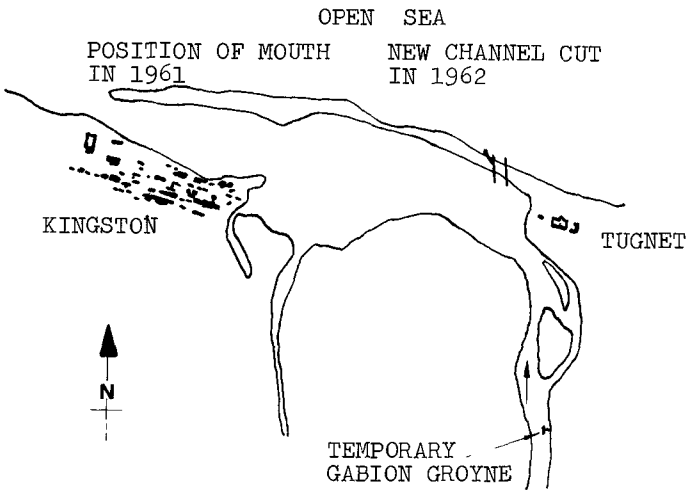

Fig.3: Works to induce new cut.

In July 1962 a flood of 424 cumets did in fact excavate 91,750 cubic metres of shingle and took the selected route out to sea. The old mouth did seal up again in 1965 and the new mouth has started off again on its migration westwards. By 1967, after 5 years, it has moved at an average rate of 92 metres per year and at this rate no further action will be needed for 15 years. Surveys of the spit are available for various years as are oblique aerial photographs illustrating the general problem.

A comment has been offered that the flood of 1962 would have taken the designed course regardless of the prepared works, and that the elaborate design procedure and exercises in fluvial coastal hydraulics were illusionary. To the consulting engineers who had responsibilities, the answer is that the flood would more likely have entered the gravel workings west of Kingston and have caused a great deal of damage generally.

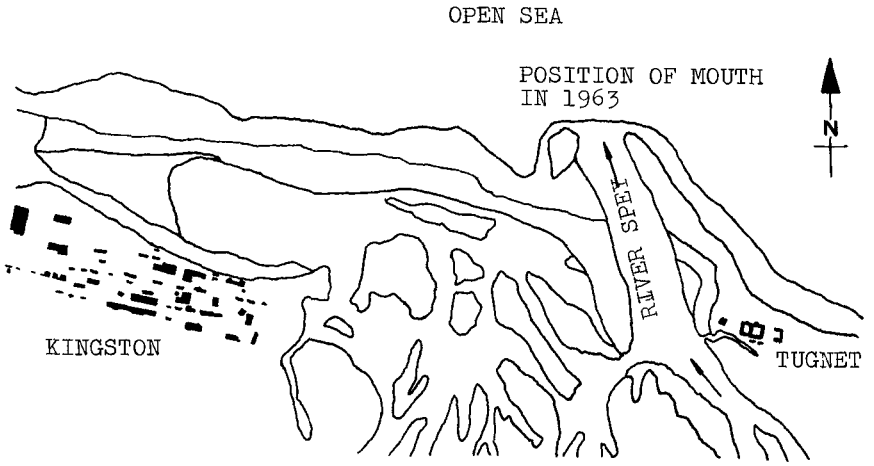

Fig. 4: Estuary 1963.

DAWLISH WARREN

Dawlish Warren is a double sand spit across the mouth of the estuary of the River Exe. The outer spit has been suffering erosion for some time and has been studied since 1872 (ref.3). The Great Western Railway, which runs along the perimeter of the Estuary and along the sea shore, did in the past carry out protective works on the landward root of the spit, but little work has been carried out on the Warren itself.

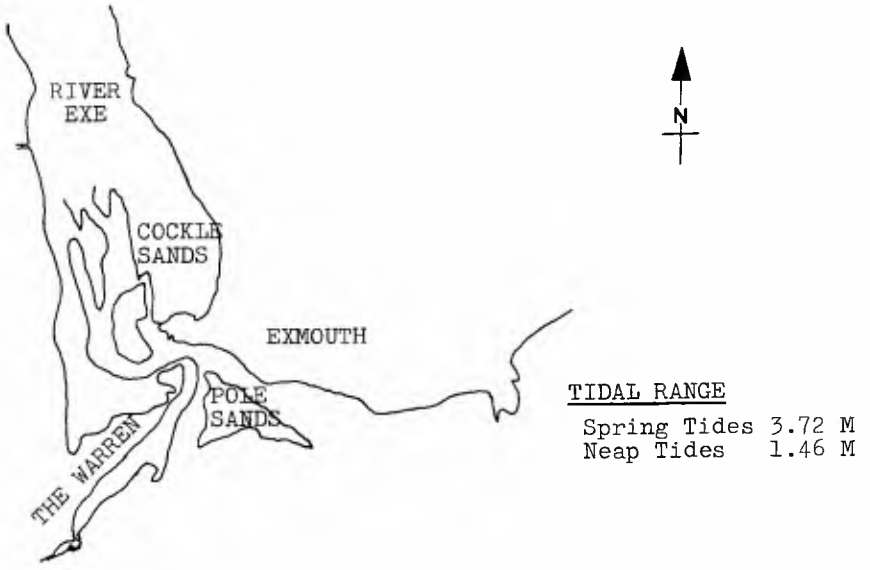

Fig. 5: The Estuary of the River Exe.

The photograph of a model shows the various surveys made since 1787. Some of the surveys were for the south eastern frontage only, hence the esturial frontage of the model are for these surveys shown by a series of semi-circles.

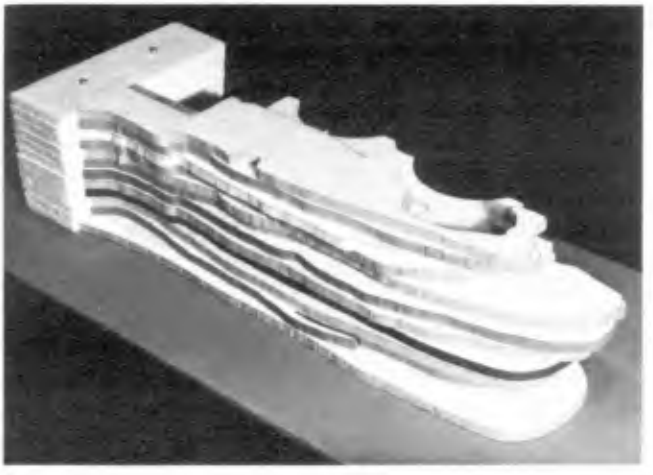

Fig: 6 Model showing the Warren from 1787-1962.

In July 1965 the Devon River Authority obtained a report on the Warren by the Hydraulics Research Station, and in 1966 the author's firm was asked to write a feasibility report on carrying out the works recommended in the report. The consultants reported that the Warren was in danger of disappearing thus losing a valuable amenity area much used by holiday makers. Esturial conditions would change to the detriment of land protection, of fresh water flooding and navigation.

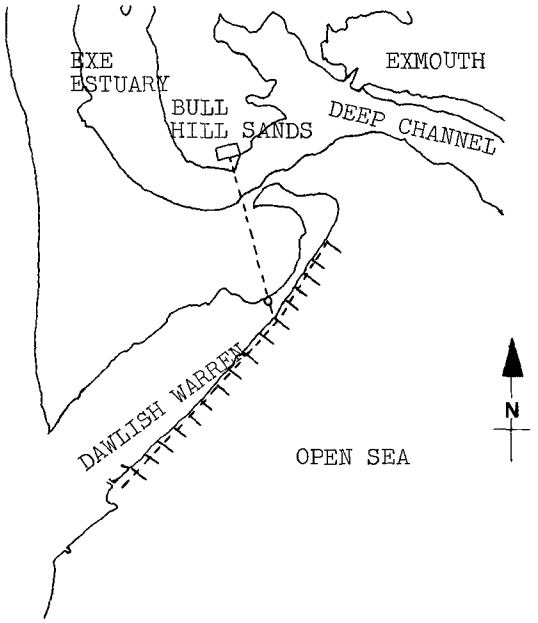

Fig. 7: Dawlish Warren 1962.

The Hydraulic Research Station proposed a large groyne at the distal end of the spit together with other groynes, extensive beach replenishment by pumping from offshore and longitudinal works. The consultants produced a modified Hydraulics Research Station Scheme with more conventional groynes and leaving out the controversial large groyne.

Administrative difficulties having been overcome, the author's firm is now instructed to prepare the scheme in more detail. The scheme now being prepared is for groyning the frontage and protecting the weakest length of beach crest by longitudinal works. A second stage is for beach nourishment. The whole of the Exe seaward estuary is a

massive sand complex as can well be seen on a sunny day at time of low water. The Hydraulics Research Station's idea was to pump sand from the Pole Sands, but the consultants preferred to pump from the Bull Hill Sands which are much more protected from sea action, and this was the basis of their first report. This involved a permanent pipe line underneath the navigation channel and a booster station for distribution on the Warren frontage. Subsequent thought is that it may be possible to obtain supplies from the estuary closer to the Warren without crossing the navigation channel.

The consulting engineers were asked to give an assessment of beach nourishment and reported: "It is, indeed, a difficult task to give a reasonable assessment of the average annual addition needed to keep the beach in good condition. From a geomorphological viewpoint the whole structure is ephemeral, but in the context of everyday coastal engineering to keep the Warren in existence it is necessary to make the best estimate possible of periodical volumes of beach nourishment so that financial provision can be made. Even if the average volume of nourishment is assessed reasonably accurately the annual variations due to weather conditions must be very great.

"Some guidance can be found in the past history of the Warren and Kidson in his paper to the Geological Society in 1964 (Vol.75, part 2) gave the following tables of sand loss above H.W.O.S.T. on the Warren:-

Period	Volume (cubic metres)	Annual rate (cubic metres)
1949-59	100,157	10,015
1959-62	63,458	21,140
1949-62	163,615	12,577

"This gives a loss of 12,577 cubic metres per annum above H.W.O.S.T. It is reasonable to assume on an ordinary sand beach profile that the loss above H.W.O.S.T. is equal to the loss between H.W.O.S.T. and L.W.O.S.T. so that the annual volume lost above L.W.O.S.T. was approximately 25,230 cubic metres per annum.

"To restore the status quo then an average of 25,230 cubic metres should be pumped onto the landward end of the Warren Beach. This is further complicated, as under the modified Hydraulics Research Station Scheme the frontage is to be groyned and the rate of littoral drift will be reduced. The reduction is again a matter of great difficulty with little data. A figure is necessary and perhaps 25,230 cubic metres could be reduced to 19,114 cubic metres.

"Unfortunately, it is well-known that on any frontage pockets of erosion develop without any obvious cause or, over the years, without any obvious pattern. These should be filled with sand when pumping the basic replenishment. If the volume is taken as 3,823 cubic metres the total becomes 22,937 cubic metres and this is the figure taken."

REFERENCES:

1. Steers, J.A. The Coastline of England and Wales, Second edition, C.U.P. 1964. Pps. 627-629.

2. Prus-Chacinski, T.M. Cutting a New Mouth for the River Spey. Details of the Design Procedure. Dock & Harbour Authority, Vol. XLIV, No. 512, June 1963. Pps. 41-47.

3. Kidson, C. Dawlish Warren; A Study of the Evolution of Sand Spits across the Mouth of the River Exe in Devon. Transactions and Papers, Inst. of British Geographers, Paper 16, 1950. Pps. 67-80.

CHAPTER 83

THE BRISTOL CHANNEL BARRAGE PROJECT

by

Eric Montgomery Wilson, Reader in Civil Engineering, University of Salford, England.

Brian Severn, Chief Engineer, Tidal Power Consultants Ltd, Montreal, Canada.

Martin Carson Swales) Postgraduate research students at
Donald Henery) University of Sheffield, England.

Abstract: The paper outlines a proposal to barrage the Bristol channel between Cardiff and Weston-supermare. The benefits from energy generation and to road communications are assessed in detail and in monetary terms. Benefits to navigation and drainage are discussed but not assessed. The effect of the barrage on tidal range, siltation and sediment movement is considered and a suggestion, previously made by others, for a larger international airport on land reclaimed from the enclosed area, is developed.

Cost estimates for the proposal are made and it is shown that the benefit/cost ratio is greater than unity even when only energy and traffic are considered.

1. Introduction

The Severn Estuary and the Bristol channel together form a deep cleft in the western coast of England and Wales extending about 125 miles (200 km) from the Irish Sea in a generally N.E. direction towards the Midland region of England.

The tides of the Irish Sea are accentuated as they move up the channel, partly by resonance and partly by the convergence of the estuary sides, so that the mean tidal range in the upper part of the inlet is about 30.5ft (10 m).

This exceptional tidal range made possible the development of Bristol, Cardiff and Newport as ports since large, deep-draught ships were able to penetrate far up the channel. It has had disadvantages in making bridge building difficult and keeping large amounts of silt and sand in suspension, which foul the waters and silt up the navigation channels.

The estuary* has grown in importance over the last 20 years. The new Severn Bridge, linking S.W. England with Wales and cutting 81 miles (130 km) from the journey between Bristol and Cardiff, was opened two years ago. Three nuclear and three fossil-fuel power stations have been built on its shores. Large steel and chemical plants are to be found on

---

* The term 'estuary' is used to describe both the Bristol channel and the River Severn estuary.

both sides of the channel. Yet its disadvantages are at the same time more evident than before. With the advent of really big ships, its narrow navigation channels and swift currents make it less attractive to bulk carriers and oil tankers. New port developments are proposed but they are on a smaller scale than their neighbouring Continental developments at Le Havre, Dunkerque and Europort.

The regional area which includes the estuary has excellent communications by rail and road with S.E. England and the Midlands but is relatively lightly populated and capable of substantial further development.

The large tidal range has prompted proposals for the generation of tidal energy in the past, notably in 1933[1] and 1945[2] on government initiative and by several private investigators. None of these schemes has proceeded beyond the report stage, primarily because, with the exception of the 1933 scheme, they were not considered as multi-purpose developments and the entire project costs were levied against energy production.

It is now proposed to build a barrage across the estuary on the line shown in Fig 1 from Lavernock Point on the Welsh shore, through the island of Flat Holm to Sand Point on the English shore, a length of 9 miles (14.6 km) excluding the island. This barrage equipped with navigation locks, roadways and turbogenerators would provide benefits in the form of improved communications, improved shipping access to ports and large amounts of electrical energy.

2. Geology and Hydrography

There is little information available about the geology of the sea bed. Donovan[3] suggests that considerable areas have been swept clear of superficial deposits, though there is such cover to the underlying New Red Sandstone and Jurrasic formations on both flanks. There is at present a regular removal of sand from the barrage line near Flat Holm by suction dredgers. The quantity being removed annually is of the order of $4\frac{1}{2}$ million tons.

There are large working quarries in Carboniferous Limestone near the barrage on both sides of the Channel and in the Blue Lias (yielding limestone and shales) at Lavernock Point. There seems to be no shortage of suitable rockfill and armourstone within economic transport distance of the proposed line.

There is no present evidence of soft muds or silts in the areas proposed for embankment and foundation structures but further survey and investigation on this point is needed.

The amplitude of the principal tidal constituents varies widely from the Irish Sea along the Bristol Channel and into the River Severn. The mean tidal range is 20.5 ft (6.2 m) at Swansea, 27.8 ft (8.5 m) at Cardiff and 30.5 ft (9.3 m) at Avonmouth (Port of Bristol). At Cardiff, which is the nearest observation point, the flood takes an hour less than the ebb on spring tides, the two being nearly equal at neaps. At Avonmouth this disparity is more marked and during spring tides the flood

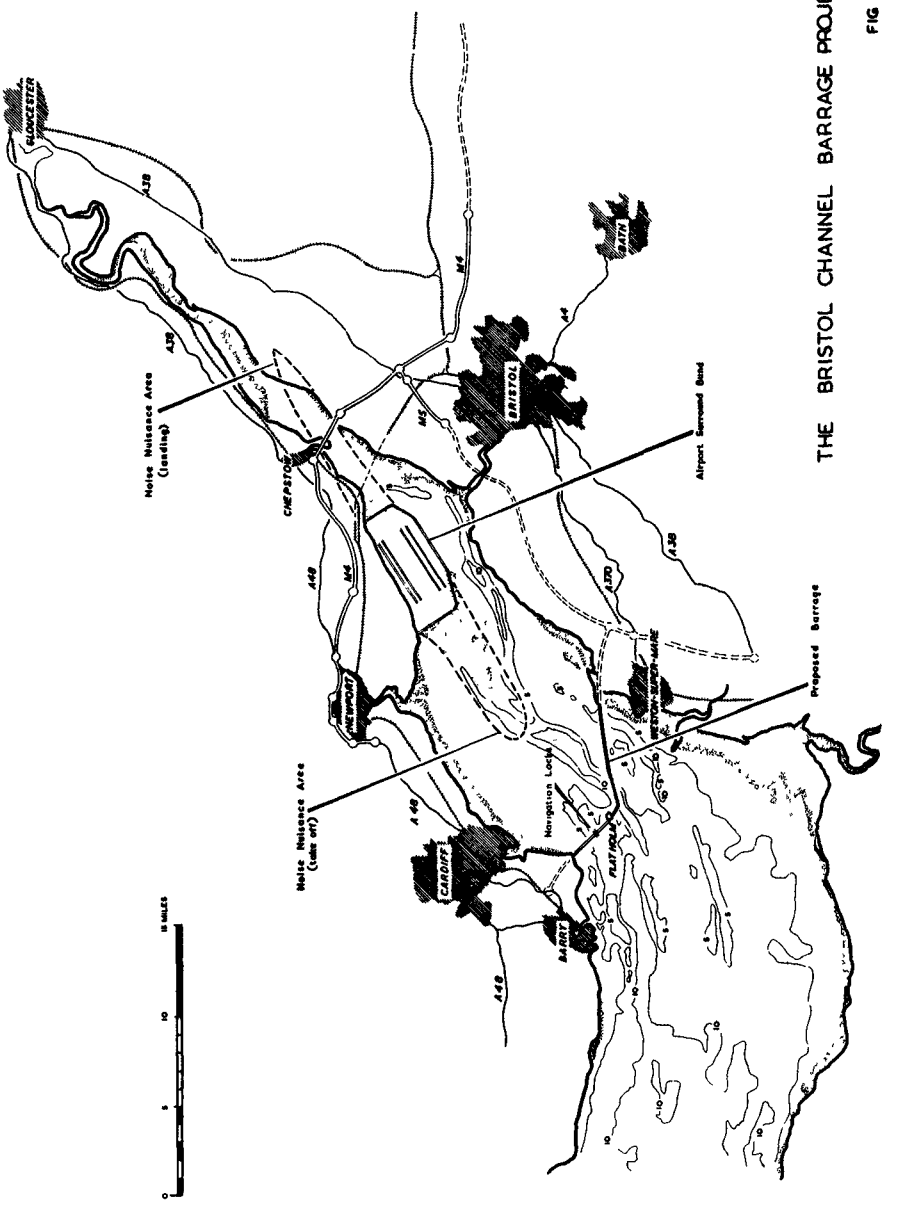

THE BRISTOL CHANNEL BARRAGE PROJECT

FIG 1

is nearly 2 hours shorter than the ebb. The effect of the barrage and its operating regime on the tides and siltation in the estuary is discussed in section 7.

3. Description of the Barrage

The principal components of the barrage are the power station, the refill sluices and the dam sections and typical cross-sections through these components are shown in Figs 2, 3 and 4 respectively.

The powerhouse portion of the barrage consists of cellular caissons of composite prestressed - and reinforced-concrete construction. The substructure of each caisson houses four horizontally-mounted axial-flow turbine-generator units, side by side in individual venturi-shaped water passages.

The barrage above the turbine water-passages is formed by vertical-lift sliding gates, set in sluiceways (referred to here as "oversluices") between piers. The piers are set midway between turbines: two in each caisson are larger, and accommodate access wells serving a turbine-generator unit on each side. Travelling cranes for servicing or dismantling purposes can also be lowered through these wells, on to tracks commanding all four machines in a caisson. The access wells, the oversluice gates, and all stoplog or gate slots, are commanded by gantry cranes travelling on the bridges supported by the piers.

The caissons are to be founded on a prepared bed of rock fill which in no case would exceed 20 ft in depth, so that settlement is unlikely to be appreciable. The alignment and levelling requirements for the machines seems unlikely to be very severe and precise levelling of each caisson would not be required. After sinking of the caissons the void compartments would be ballasted with sand and lean concrete. Scour protection of the rockfill foundation is to be by asphaltic concrete placed underwater. Total length of the power station would be 6,750 ft (2060 m) with 120 straight flow turbines of 30 ft (9.15 m) runner diameter, housed in 30 caissons.

The venturi sluice caissons will each contain four 40 ft square gates which will normally operate fully submerged. A discharge coefficient of 1.6 has been adopted for these waterways based on the laboratory tests of similar sluices proposed for Passamaquoddy[4]. The overall dimensions of the sluice caissons are 123 ft long by 205 ft wide by 112 ft high. There are to be 30 such caissons with an overall length of 6150 ft. The principle of pre-fabrication, flotation, sinking and ballasting on a prepared rock rubble foundation has also been assumed for these units.

The remaining length of the barrage will consist of a sand and rockfill structure constructed by bottom dumping from barges, hydraulic sand-pumping and with scour and wave protection by armour stones or asphaltic concrete, or both. In this length a navigation lock system will be installed. This will probably have two locks, the larger of which will be 1500 ft long by 150 ft wide with sill level at - 55 O.D. The operational research study into the optimum locking system is not completed so £8 million has been allowed in the estimates for the two locks. The locks will be equipped with 2 lifting bridges each so that road traffic can always pass.

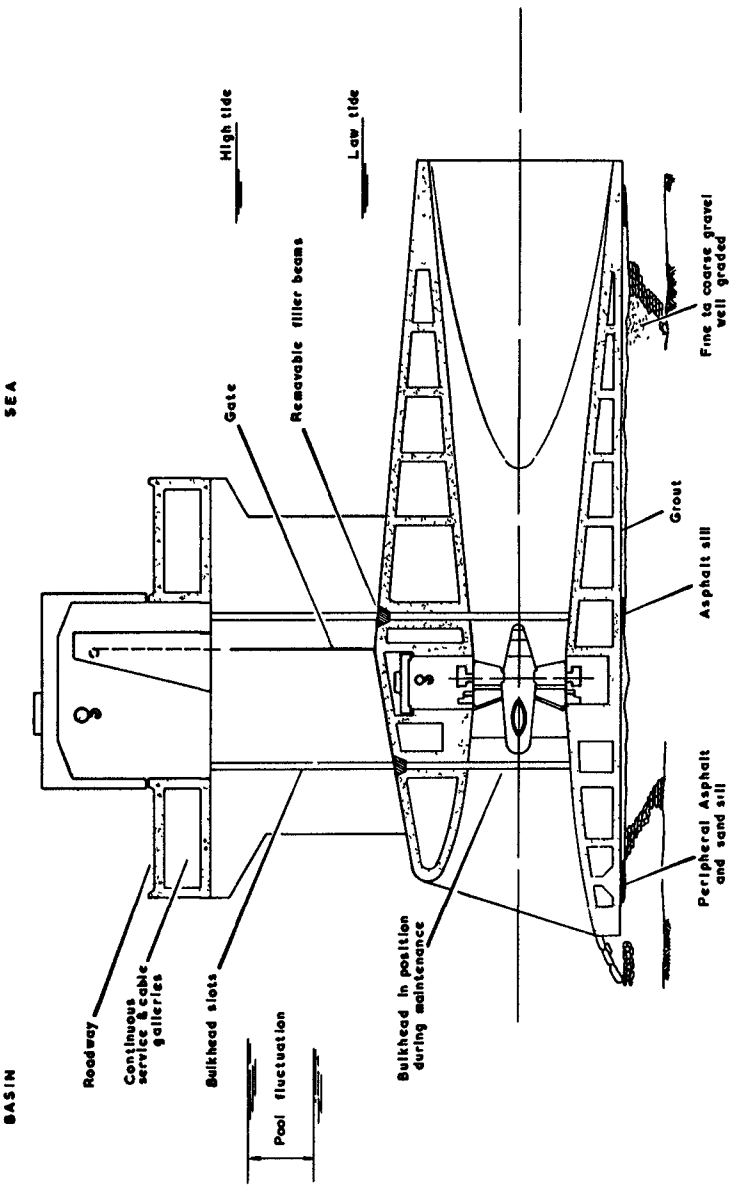

LONGITUDINAL SECTION THROUGH TURBO-GENERATOR CAISSON

FIG 2

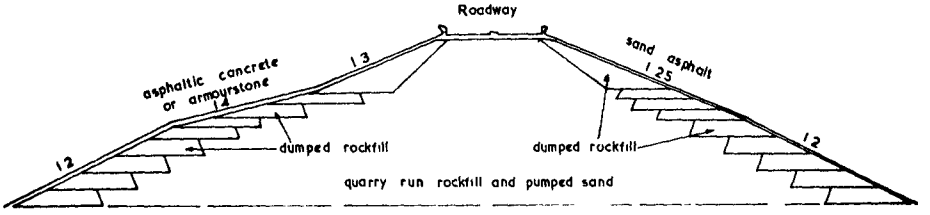

FIG 4 TYPICAL EMBANKMENT SECTION

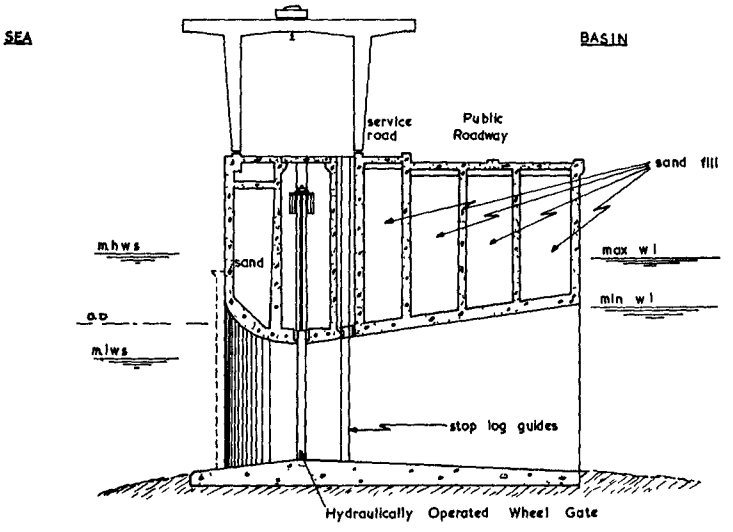

FIG 3 PROPOSED REFILL SLUICE SECTION

Both power station and sluice caissons carry dual-carriageway roads for public traffic as well as service roads. The public roads across the barrage will be continuous over all elemente of the structure with alternate routes at the locks to prevent traffic interruption. As designed, they consist of two 26 ft wide, two-lane carriageways and inter-connection to the trunk road system on the Welsh side, and to M5 motorway on the English side is proposed. Railways are not proposed on the barrage. A plan of the proposed structure is shown in Fig 5.

4. Energy and power

The annual output of energy from the barrage will be 10,432 GWh, generated at powers between 1200 and 4560 MW. The output was computed using the single tide optimisation method[5] on an ICT 1907. Sixteen basic combinatione of numbers of turbines and venturi sluice areas were studied initially and, following a primary economic optimisation, six further combinations were chosen. The annual outputs for all these combinations are shown in Fig 6. The number of turbines and venturi sluice areas were selected using the economic optimisation method[5] and the resulting optimum combination is 120 turbines coupled with generators having a rated capacity of 38 MW and 120 submerged venturi sluices each 40 feet square. The generator rating was chosen by comparing the energy outputs of different ratings and equating them with total project cost to find the lowest cost of energy. The energy outputs for this analysis were taken from the annual power duration curve of Fig 7.

The maximum generator rating required to utilise all the power developed would be 54 MW and the energy loss by installing generators of 38 MW capacity is only 4.3%. This figure may be obtained by measuring the area beneath the power duration curve above the 38 MW power level.

During the energy computations, time allowances were made for the turbines to start up and the generators to synchronise. The turbines are grouped in fours and it was assumed that two groups of four would be started up each minute with all the turbines discharging after 15 minutes. The generators were assumed to be synchronised four minutes after the turbines began discharging.

The refilling sluices were assumed to be fully discharging 15 minutes after the levels of the tide and reservoir become equal. This figure was applied to both the fully submerged venturi sluice and the oversluices which are installed in the same caissons as the turbines. Fifteen minutes was chosen as a compromise between expensive machinery to lift the gatee rapidly and allowing excessive differential head to develop on the gates while being raised.

The introduction of tidal energy into an existing electrical system requires the availability of pumped storage capacity. The relative merits of the different ways of achieving this have been extensively disoussed in the literature[6]. For the British system which will have 1000 MW of pumped storage capacity interconnected by 1975, ebb-flow generation ie likely to be most advantageous. However, the annual production of 10,432 GWh of tidal energy will require further pumped storage capacity to increase the total to around 4000 MW. This will alter the load factors of all existing plant and alter the building priorities of new

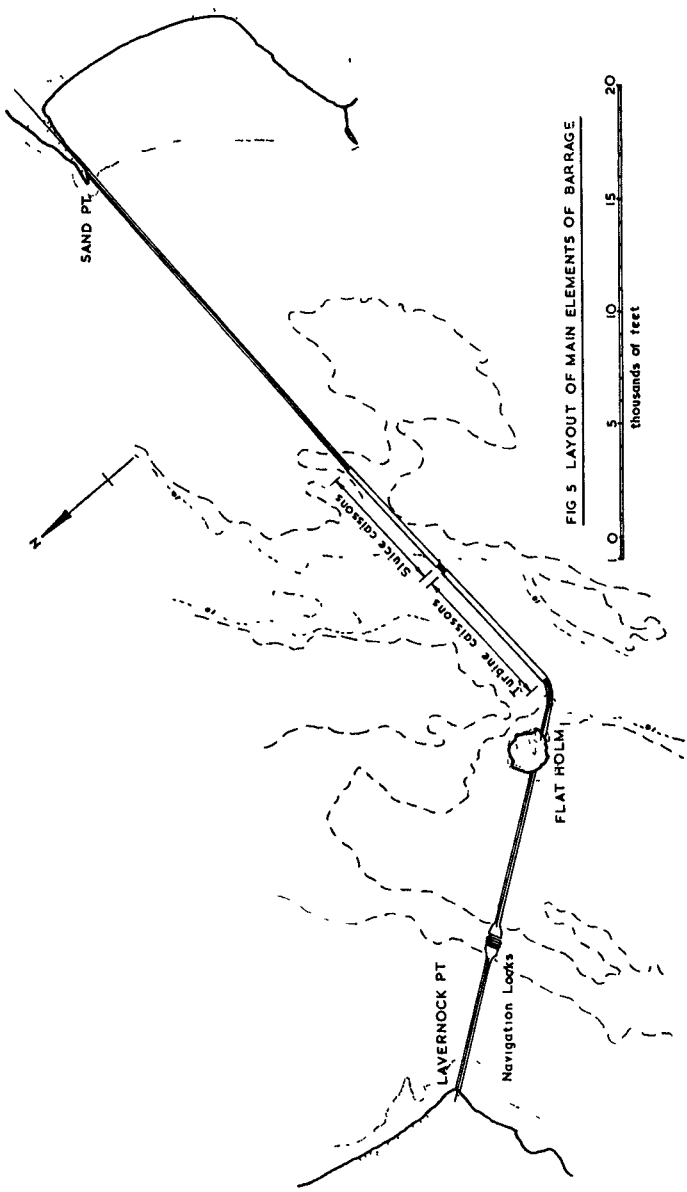

FIG 5 LAYOUT OF MAIN ELEMENTS OF BARRAGE

stations so that the actual value of the tidal energy to the system can only be assessed by comparing the whole system cost with and without it, over a period of about 20 years.

Since it is not practicable for the authors to undertake an investigation of this complexity requiring large amounts of data available only to the C.E.G.B. an estimate has been made of the value of the energy based on published, generation incremental-fuel costs for the early 1970's[7]. The value of the energy only as replacement for incremental fuel undervalues the contribution of tidal energy for the reasons given above and because some 35% of it occurs at peak generation periods and it is entirely predictable in time and quantity.

Fig 8 shows the Authors' estimate of power levels in 1975 and the likely generation incremental fuel cost then, derived from Berrie and Betts. The position of the winter and summer minima for base loads are shown and so weighted values for various blocks of Bristol Channel energy have been derived and are listed in Table 1 below.

%	Winter		Summer	
	GWh	Av value d/kwh	GWh	Av value d/kwh
35	1826	0.6	1826	0.42
65	3390	0.41	3390	0.38

Table 1. Incremental value of Bristol Channel energy.
Mean average value per unit = 0.435 d/kwh. The annual value of the years output is therefore $10{,}432 \times 10^6 \times 0.435^d$ = £18.92 m.

If this value is discounted back at 6% p.a. to 1975 the present worth of the electricity over the assumed economic life of the machinery (taken at 30 years) amounts to £276 million.

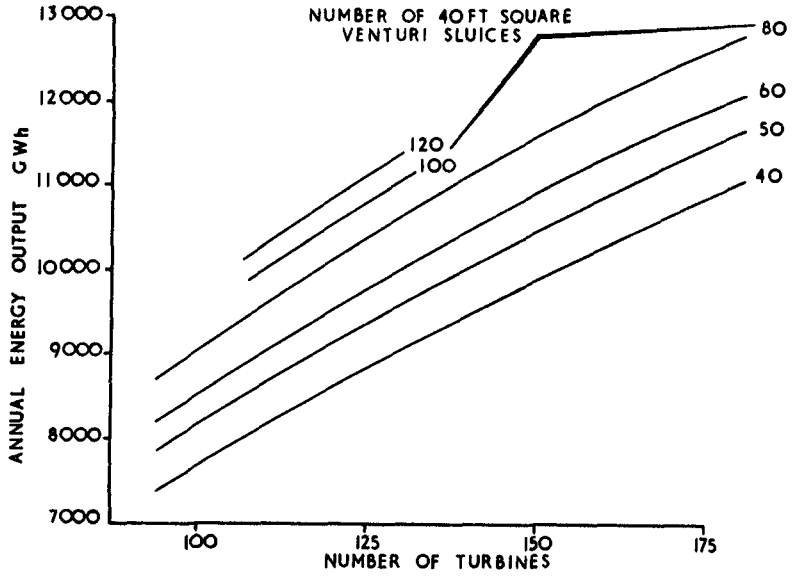

ANNUAL ENERGY OUTPUT FOR COMBINATIONS OF TURBINES AND VENTURI SLUICES

FIG 6

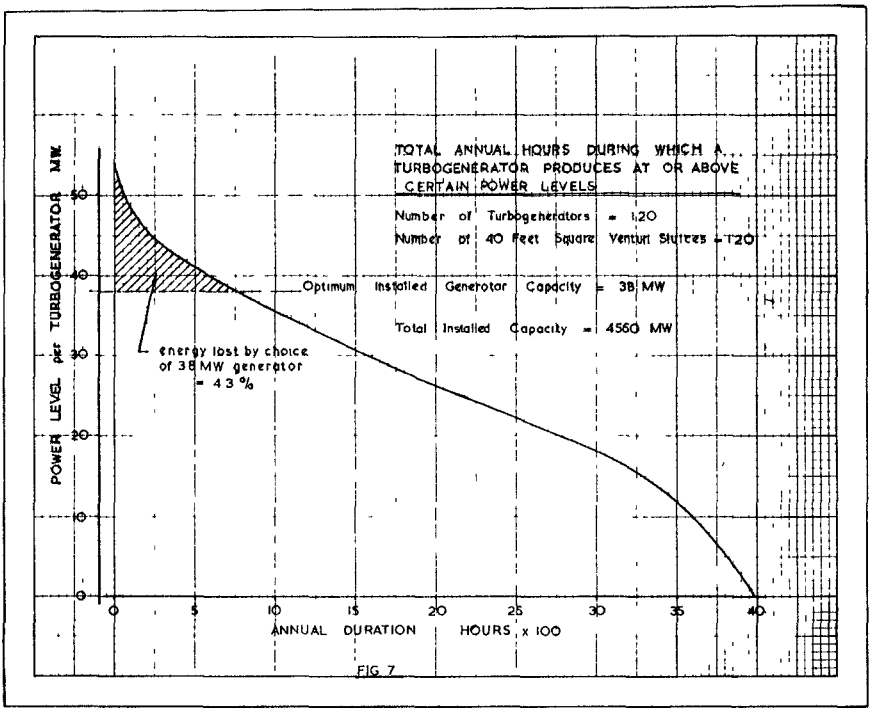

FIG 7

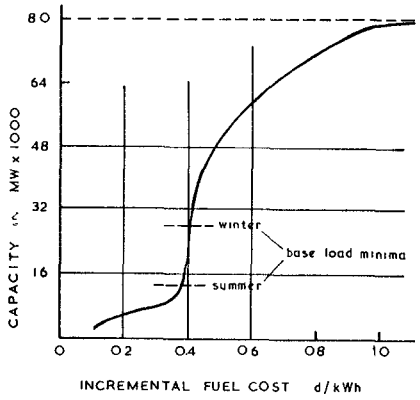

FIG 8
(after Berrie and Betts)

5. Communications

The Severn road bridge opened to traffic in October 1966 and provided a much-needed link between Wales and the west and south-west counties of England. In its first full year of operation (1967) the bridge carried 5.7 million vehicles and was showing a steady increase on this rate in the first half of 1968.

It was estimated by the Ministry of Transport before the bridge opened that the bridge traffic would increase in time as shown in the lower curve of Fig 10, with full capacity reached in 1988 with 17.5 million vehicles per annum. The data to date is shown on the same figure as the two points for 1967 and 1968 (4 months data only) and the upper curve has been drawn as a conservative revised estimate of traffic growth.

In the latter half of 1967, origin and destination surveys of traffic crossing the bridge were made by the Severn Bridge Research Project team for 'light' and 'heavy' traffic. The results of these surveys are given in the Interim Report published in July '68 and full use of the tables therein has been made. The percentage of total light traffic moving on an August 1967 Saturday in both directions was calculated from the o. and d. surveys quoted. Light traffic was considered as all cars and vans plus half the motorcycles. Heavy traffic was taken as all lorries and coaches. It had been separately sampled on a Tuesday (eastbound only) in the same month. The data was analysed as follows:-

1. All traffic using the bridge was assumed to be moving between two of the 18 point/areas shown in Fig 9, and the percentage moving between each possible pair calculated.

2. Of the 153 possible pairs 28 were considered likely to be given a shorter alternative route if the barrage crossing existed.

3. For each of these 28 journeys an arbitrary split was made of 'barrage' and 'bridge' traffic depending on the mileage saved and the road types, conurbations etc to be traversed.

4. This 'split' was applied to the 28 percentages affected, previously calculated under 1.above, and a new 'barrage' percentage only obtained.

5. For each shorter route-alternative journey, the mileage saved was computed from road maps. It was assumed that there was no motorway westward of Newport and that the Weston - M4 spur motorway existed.

6. Arbitrary overall journey speeds were assessed of 35 m.p.h. and 30 m.p.h. for light and heavy vehicles respectively and the journey time saved for the 'barrage' traffic was found for each class of vehicle in percentage terms.

7. Costs of running vehicles were taken from previously published data, updated by applying annual percentage increases. The costs adopted were £1.67 per hr and £2.33 per hr for light and heavy vehicles respectively.

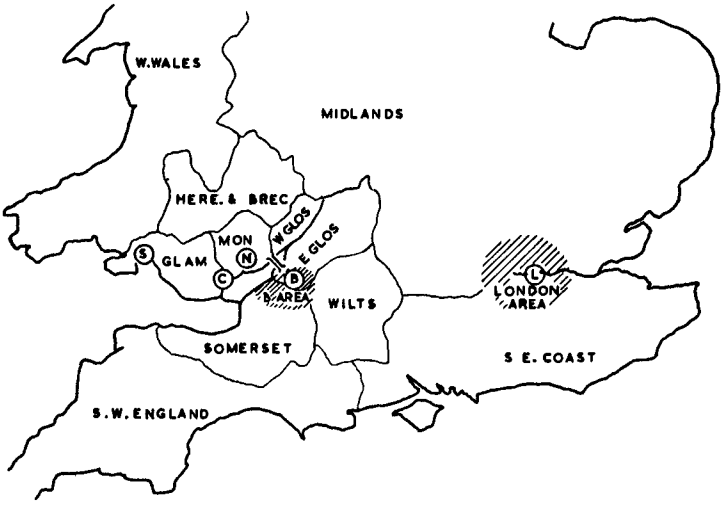

ORIGIN & DESTINATION AREAS USED IN TRAFFIC ANALYSIS

FIG 9

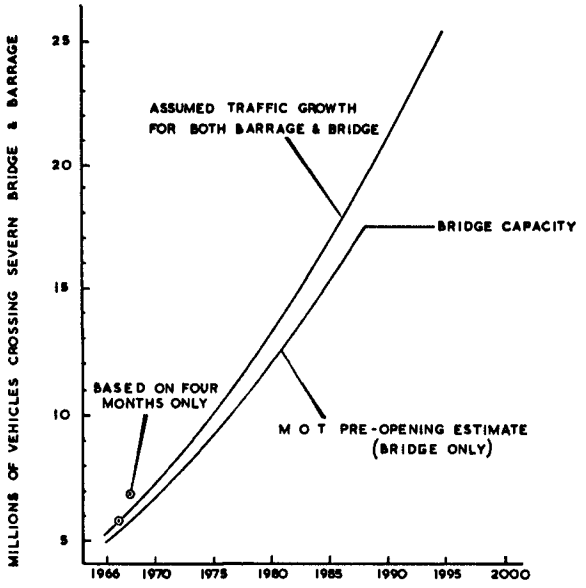

FIG 10

8. The appropriate figures from 6 and 7 were multiplied and the product applied to the future estimated vehicular traffic of the upper curve of Fig 10 (now extrapolated beyond 1985 because of the barrage addition to the road crossings) for each vehicle class. To do this it was necessary to assume a percentage of total vehicles for each class. Since the Severn Bridge traffic has so far shown a high proportion of heavy lorries and coach traffic (about 24% in its first year) and the trend is increasing in the current year, the same proportion has been assumed throughout the 30 year period commencing in 1975.

9. The value of time saving on the forecast traffic was computed for each of the years 1975-2004 and 'discounted back' to 1975 which is the earliest date the barrage could be operative. The results are shown in the following table for the first 5 years of operation and for the year 2000.

Year	Total number of vehicles/yr in millions	Benefit value in millions £ (1968 prices)	Benefit discounted to 1975 in millions £ at 6% p.a.
1975	10.1	3.74	3.74
76	10.7	3.97	3.75
77	11.35	4.20	3.74
78	12.0	4.45	3.74
79	12.7	4.71	3.73
2000	30.4	11.28	2.63
	1975-2004 Cumulative totals		£95.5

It will be seen that in 2000, the traffic benefit will be over £11 million. However by this time both bridge and barrage routes will be at saturation and no further increase in traffic or benefit is expected. Accordingly the discounted benefit falls off more steeply thereafter.

6. Navigation

The major ports upstream of the barrage are Cardiff, Newport and Bristol. Smaller ports exist at Penarth, Sharpness and Lydney. Fig 13 shows the mean arrival rate of ships and gives histograms of arrivals and net registered tonnages at these ports for 1966. Fig 11 shows the correlation between n.r.t. and deadweight tonnage. Table 2 shows relevant statistics for goods handled there in 1965 or 1966.

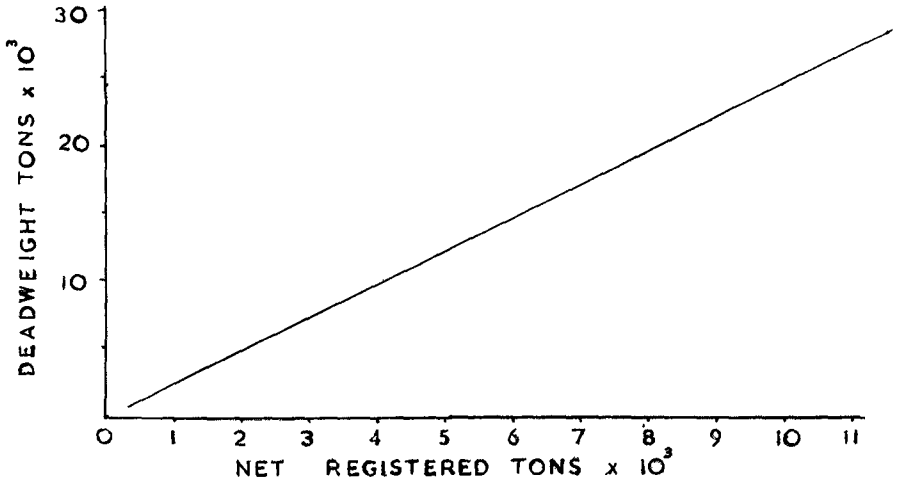

FIG. 11

Port	Imports Tons	Exports Tons	Principal Goods Handled
Cardiff (1965)	2,504,000	140,000	Iron ore, Petroleum, Building materials.
Newport (1965)	3,033,000	889,000	As for Cardiff.
Bristol (1966)	7,563,000	1,049,000	Petroleum, Grain, Animal foodstuffs.
Sharpness (1965) Lidney (1965) Penarth (1965)	1,002,000	None	-

Table 2

Fig 12 indicates navigational movements in the estuary before and after barraging. The tidal range behind the barrage after closure will not exceed 12 feet. Due to this reduction in range and the modified tidal cycle due to power generation, there should be a time saving to shipping on entering and leaving the estuary. However, the possibility of queuing at the barrage locks might reduce the savings due to more favourable water levels.

It had been hoped to present the results of an operational research study into these aspects, based on the regime of Fig 12 and the mean arrival and departure rates of 1966 shipping at the estuary ports shown in Fig 13. This study[8] which should be completed shortly will assess the benefit to existing shipping in terms of time saving for ships and cargo.

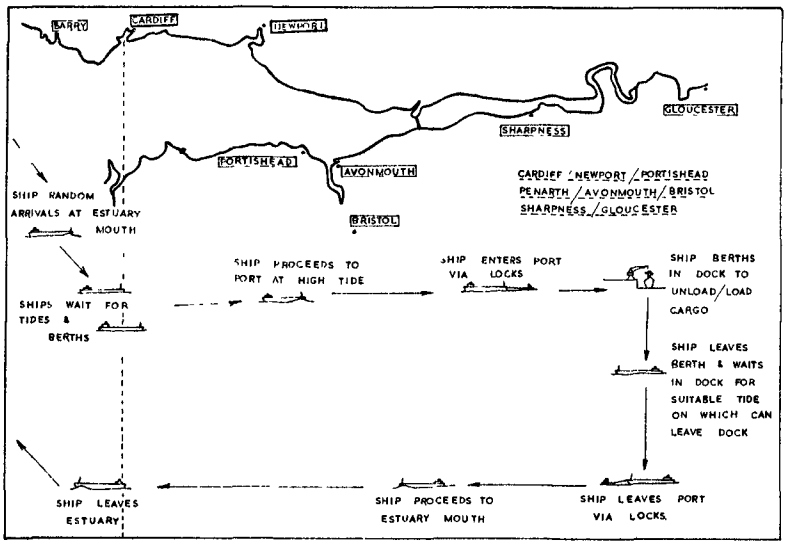

EXISTING REGIME

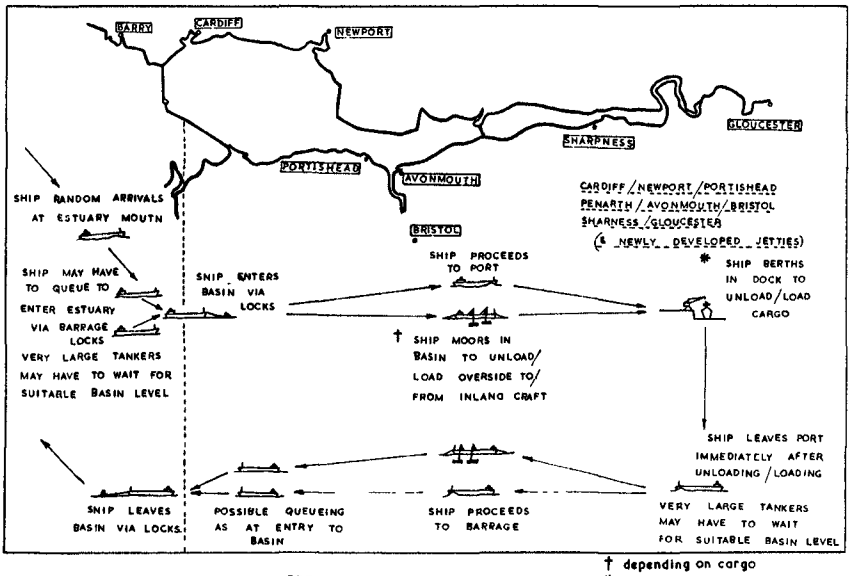

PROPOSED REGIME

† depending on cargo

* existing locks at dock entrances are not shown though they may be retained

FIG 12 THE EFFECT OF BARRAGING ON NAVIGATION

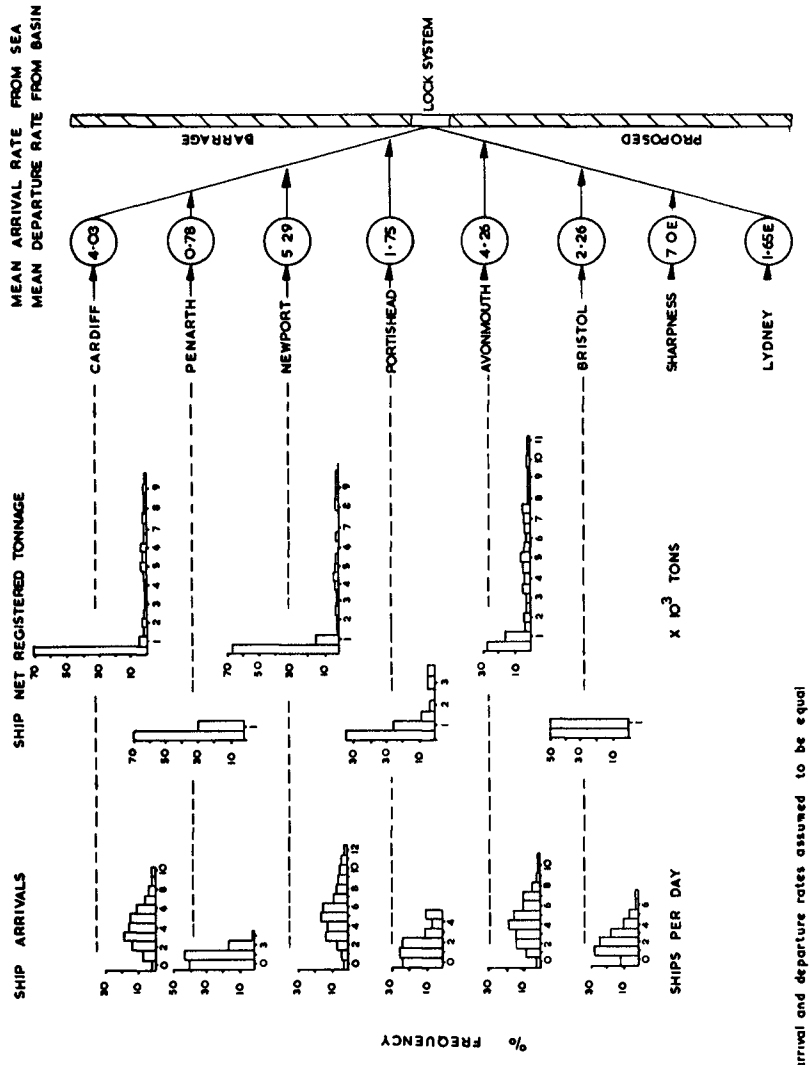

STATISTICAL DISTRIBUTION OF PRESENT NAVIGATION

FIG 13

Mean arrival and departure rates assumed to be equal
Net registered tonnage histograms for arrivals and departures will be equal
Net registered tonnage of ships to Lydney and Sharpness are below 500 tons
E = estimated arrival rate, given total number of arrivals per year

The presencs of a subtantially altered water level in the estuary will radically change any planned expansions for the existing ports. New ports and tidal jetties could be developed in the estuary utilising the deeper water and mors stable sea-bed conditions. New navigation channels could be dredged and existing channels modifisd to accommodats larger vsssels. Lock gates at some of the existing docks could bs removed, permitting shipe to entsr and leave on any water level in the estuary. This would necessitate the dredging of such docks to a greater depth than at present, and in many cases it would be simpler and more economical to operate the existing dock lsvels for an extended access time, while developing new facilities without locks.

The guiding principle behind the expansion of general cargo berths and facilities at modern European ports is to provide the port user with space to expand his activities rather than trying to rebuild old-fashioned layouts. The idea is to give space not only for new quays, but also for transport, handling and storage facilities. Dutch ports reclaim this land from the sea, and it is this kind of space that many British ports do not have and cannot get. The Bristol Channel, as yet relatively under-developed, has great potential in this way for development as a unit, rather than by piecemeal port expansion.

The barrage proposed in this paper would present completely new opportunities to the estuary ports in a protected basin of low tidal range.

7. The sffect of the barrage on tidal range and estuary contours

It must be admittsd that this is both the most important topic, and at the sams time the most imponderable, of the whole proposal. Any major intsrference with the existing natural regime suoh as would be provided by a barrage will have an effect on the tidal range. Heaps[9] has shown the effects of barraging the estuary at various places along its length in terms of the amplitude of the M_2 constituent. The present proposal corresponds approximately with Heap's section 10, where he showed the amplitude of ths M_2 constituent to be reduced by 1.25 ft. The other principle semi-diurnal oonstituent, the S_2, would probably have a pro-rata reduction giving a spring tide range of about 3.2' lsss than the present and a neap tide range of about 1.6' less.

The present proposal however is rather far removed from oomplete closure and involvss a phase-shift of about 2 hours in ths discharge. Published results of such a regims are not availabls but investigations on this point are currently proceeding in France and Britain. The authors havs based their energy analysis on an arbitrary assumption that their regime will cause a range rsduction of 2.5 ft at a 36 ft range and 1.5 ft on an 18 ft range. The histogram of actual tides was altered to account for this during the computation.

There is less information available about the effect of the barrage on sediment dispersal and movement. Like most estuaries with large tidal ranges the Bristol Channel has a fairly heavy silt load. This is to a large extent due to the current velocities produced by a large volume of water being relsased into or drained from the estuary every six hours. Fine matsrial that in estuaries of lesser volumetric exchange would settle out is kept almost permansntly in suspension in a captive,

oscillatory state. The coarser sediments, fine and medium sands, form wide flat and relatively static sand banks in certain areas while a considerable expanse of the sea floor is swept clear[3].

The configuration of the barrage shown in Fig 5 would lead to a change in the tidal current pattern and velocities. Generally the current velocities would reduce somewhat since there would be a reduction in tidal range and in volumetric exchange due to the imposed regime of the tidal power station. Accordingly the trend would be to greater sand bank stability and a reduction of the captive, silt load. Locally at the barrage, current velocities might increase near the turbine and sluice sections while decreasing on the embankment flanks. Here the tendency would be to remould the loose boundary to conform to the new pattern, obviously giving rise to both accretion and erosion.

It will be seen from Fig 5 that the fastest (turbine) currents will be in the deepest clear-swept channel and the slackest water is likely along the N.W. embankment between Lavernock Point and Flat Holm. It is from this area that sand-suction recovery vessels currently remove about 4 m tons per annum for use as building material.

The amount of sediment entering the estuary has also to be considered. Gibson estimated that the Severn and Wye rivers together brought down about 650,000 tons per annum. This is fine sediment and may be the principal source of the captive silt in suspension. Most of this material would continue to be kept in suspension under the new regime though there might be areas of slack water where silt accretion would increase. If it were all to settle out evenly over the basin area it would form a layer about 1 mm thick per annum. Accordingly, if Gibson's estimate is correct the input of silt is not a problem, only its distribution.

The only practicable way to find answers to the questions raised by the redistribution of the estuary sediment is to build loose boundary hydraulic models of the estuary and Channel. The indications seem to be that the overall picture will be better rather than worse though local accretion might be troublesome.

8. Other considerations

(a) Drainage and coastal protection: The low-lying land bordering the estuary upstream of the barrage at present is drained into deep drainage channels which discharge through tidal flaps at low tide. Since the barrage would retain a pool with a 12 ft fluctuation in the upper half of the present tidal range, pumped drainage of this land would become necessary. Estimates previously made[10] for this work indicate annual costs less than £50,000 and no account was then taken of the betterment to the land through a controlled phreatic surface.

The maintenance of the sea walls and embankments which now protect this land is more difficult to assess. The barrage would effectively prevent basin levels rising above about 20 O.D. while occasional tides in the past have risen to 28 O.D. and the top embankment levels are generally above 30 O.D., some being as high as 35 O.D. while the fetch

length to some of the more critical places is reduced by the barrage, it still may be as much as 25 miles and eo waves of 7 feet are quite possible. The Authors believe that the maintenance of sea defences will be made eimpler and in the long run, lese costly than it ie now, but it is fair to point out that some of thoee moet concerned, who have written[11] about the problems which will arise, do not agree with this view.

(b) Fieheries: The Severn and Wye are important fiehing rivers, though not on a commercial scale. The paesage of descending salmon smolts and ascending adult epawning fish might be adversely affected by an alteration in the natural cycle of the estuary. Marine biologists who have been consulted by the authors are reluctant to do more than speculate. However experience in Scottish rivers and power echemes have shown that fish may safely pass through smaller and faster running turbines at higher heads than those proposed here and it is tentatively concluded that there ehould be little, if any, effect on the passage of existing fish populatione.

(c) Airport location: A modern international airport, if it is to cater for foreseable air transport requirements will need an unobstructed flat land area about 6 miles long by 3 miles wide, with four 4000 yd long runways in two pairs 2500 yde apart. The width of the noise swathe will extend a mile beyond the outer runways on each side, 10 miles along the approach paths and 8 miles along the take-off paths. Since the prevailing winds in S. England are S.W., a strip of air space 24 miles long by 4 milee wide on a S.W. - N.E. axis, is required with the actual airport nearly central.

To find a requirement like this in S.E. England, free from urban concentrations is virtually impoesible and the only proepect of achieving it is in the suggested Foulness site where the airport must be built on land reclaimed from the eea with a retaining bund some 12 miles long subject to North Sea wave action and surge. The Foulness site would require the construction of road and rail links, is 50 miles from central London and would serve virtually nowhere else.

If the eearch is shifted from S.E. England to the Brietol region a possible site is immediately apparent in the area contained by the barrage[12]. The propoeed eite is on the land known as the Welsh Grounds and ie the required eize. The take-off noise area ie absolutely clear of habitation and so power reetriction would not be required during take-off. The landing approach noise-area is also almost completely clear, as may be eeen from Fig 1. The axie of the entire area as delineated lies 10^{0} from true N.E. - S.W. at 35^{0}. To eurround the airport area would require a bund about 11 miles long but now protected from surges, high epring tides and all except minor waves. The main S. Wales - London railway line and the M4 motorway touch the N.W. corner of the airport site, which ie therefore already eerved by fast rail and road links to London, S. Wales, the Midlands and S.W. England. Distance to central London ie 120 m, to Brimingham 72m, Cardiff 24m and Bristol 14m. An Advanced Passenger Train, already designed by the Advanced Projects Group of Britieh Rail has been scheduled in recent performance studies to cover the dietance between Severn Tunnel Junction, on the northern extremity of the site, and Paddington in 70 min (including contingency time). Apart from the freedom from noiee and excellent communicatione, the project has the great advantage of requiring no land.

9. Project cost summary

Detailed cost estimates for the barrage have been made and a summary is given below.

	£
Civil	
Foundations, preparation and earthworks	30 770 000
Powerhouse caissons (30 no 4 machine units)	62 880 000
Sluice caissons (30 no 4 gate units)	36 156 000
Miscellaneous works	900 000
Lock system	8 000 000
Mechanical	
Gates and assoc. equip. in powerhouse	16 100 000
Gates and assoc. equip. for refill sluices	16 700 000
Miscellaneous mechanical equipment	1 962 000
Electrical	
Turbo-generator units	90 000 000
Powerhouse equipment	14 950 000
Sub-station equipment	3 730 000
Total construction cost	282 148 000
Contingencies (10%)	28 214 800
Sub-total	310 362 800
Engineering and Administration (6½%)	20 173 200
Gross construction cost	330 536 000
Interest during construction @ 5% p.a. for 4½ yrs say 11¼% =	37 200 000
Total project cost	£367,700,000

Annual costs

Amortisation over 50 years @ 8%	643 000
Maintenance £0.25/kw	1 114 000
Interest on capital @ 8%	29 440 000
	£ 31,197,000

Benefits discounted for 30 years to 1975 @ 6%

1.	Electricity (on incremental fuel cost basis)	= £276 million
2.	Traffic (on basis of text and Fig 10)	= 95
3.	Navigation (a) shipping and cargo time	=
	(b) port expansion	=
4.	Riparian site values for industry and power	=
5.	Agricultural land betterment	=
6.	Amenity (a) prevention of thermal & atmospheric pollution	=
	(b) recreation	
	(c) international airport site	=
	Total (1) and (2)	= £371

Benefit/cost ratio > 1.

Many of the items listed above are difficult to evaluate though the authors hope shortly to publish values for 3(a). Other indirect benefits are not listed. These are concerned with wider political issues of new centres of population, energy from fuel paid for in foreign currencies, the preservation of a tolerable environment for urban populations and so on.

10. Further investigation and research required

This paper represents the results of a detailed desk study and inevitably it raises questions as well as giving answers. These can only be answered by further studies on the following points.

(a) The quantity and extent of siltation. An estuary hydraulic model is needed to investigate the affect of the barrage on current and flow patterns; on sediment transport and on the siting of locks, turbines and sluices; also for the siting and alignment of new port works.

(b) The modification of natural tides due to the barrage. A programme of computations will be required to assess the effect of the barrage on the tides. If the reduction assumed in Section 4 did not occur, electricity production could be increased by nearly 30% at marginal extra cost. (44MW generators instead of 38MW). Initial work on these lines is currently proceeding at Liverpool.

(c) Estuary bed surveys. A programme of bed surveys needs to be initiated (geophysical profiling, sampling and boring) to establish permeability, cohesiveness, consolidation, gradings, shear strengths etc to enable foundation analysis and settlement calculations to be made.

(d) Turbo-generator research. The present programme of the English Electric Co Ltd, supported by the Ministry of Technology, covers the machinery stipulated in the paper. It would possibly require extension to consider stability under large wave conditions and corrosion in sea water.

(e) Communications. More precise traffic surveys and market research in shipping agencies to assess the potential of a unified estuary port.

References

1. Report of the Severn Barrage Committee. HMSO (1933).

2. Report on the Severn Barrage Scheme. Min. of Fuel and Power. HMSO (1945).

3. Donovan D.T. et al "Geology of the Floor of the Bristol Channel" Nature vol 189, No 4758. 7 Jan 1961.

4. International Passamaquoddy Engineering Board, Report to the International Joint Commission on Investigation of International Passamaquoddy Tidal Power Project. Ottawa and Washington, Oct 1959.

5. Swales M.C. and Wilson E.M. "Optimisation in Tidal Power Generation" Water Power, 20.pp 109-114. March 1968.

6. Handbook of Applied Hydraulics (Ed. Calvin Davis) 3rd Ed. McGraw Hill. New York. 1968. Chap 42. Tidal Energy Development by E.M. Wilson.

7. Berrie T.W. and Betts P.E. "Assessment of Costs of Alternative Plant Proposals on the C.E.G.B. System". Paper 3, Symposium on International Extrapolation and Comparison of Nuclear Power Costs. Int. Atomic Energy Agency. London. Oct 1967.

8. Henery D. Studies in barraging the Humber. PhD Thesis. Sheffield University. 1968. Unpublished.

9. Heaps N.S. "Estimated effects of a barrage on tides in the Bristol Channel" Proc. Inst. Civil Engineers. 40. pp 495-509. Aug 1968.

10. Wilson E.M. A multi purpose barrage on the Bristol Channel. Water Power. 18. pp 135-142. April 1966.

11. Rowbotham F.W. Report on the drainage of the lowland areas of south Gloucestershire with special reference to the proposed Severn barrage. 20 July 1945. Unpublished.

12. W.S. Atkins & Partners. A preliminary study of the future port requirements of the Severn estuary. Private report. Oct 1964.

CHAPTER 84

APPLICATION OF RISK CRITERIA IN COASTAL ENGINEERING

ASIT K. BISWAS

Resources Research Centre, Policy & Planning Branch, Department of Energy, Mines & Resources, and Visiting Professor of Civil Engineering, University of Ottawa, Ottawa, Canada

INTRODUCTION: A design of any engineering structure may be said to be optimum when it can meet all the necessary requirements at a minimum possible cost. In all cases there is a probability, however slight (sometimes even incalculable because of lack of data), that the design load can be exceeded and, thus, damages could occur. Obviously, lower the design load, higher would be the cost of anticipated damages and vice versa. Thus, from economical standpoint alone, the ideal solution would be when the total cost of construction and anticipated damages is at its minimum. Very often, however, other factors like social, political, etc., have to be considered, and this makes the whole process a complex decision making problem - sometimes completely out of the jurisdiction of the engineers.

GENERAL CONSIDERATIONS: Risk is inherent in any structure, and those in coastal engineering are no exception. But very often this simple fact is overlooked. With our present state of knowledge (1968) it is impossible to determine the upper limit of any natural phenomenon, and design wave is no exception (for general discussion on the subject see refs. 1, 2, 3). If this concept is not accepted, one has to seriously consider the possibility that a wave height of x ft is possible (a maximum height) but a height of $x + 0.001$ ft is physically impossible. If the physical upper limit concept is abrogated, as is advocated by the author, then it becomes evident, as a corollary, that any design value of wave height, however high, is associated with some probability of occurrence, however small, and thus some degree of risk, however slight. This does not mean that risk in such a design is automatically increased; all it means is that if the probability of occurrence of a design wave x is P, then a higher value of $x + dx$ reduces the corresponding probability to $P - dP$.

RISK CRITERIA: It is not politically much expedient to use the word risk which, at least to the layman, immediately brings unfortunate connotations to mind. An attempt would be made herein to suggest two simple procedures for evaluating risk for design waves by using (i) return periods, and (ii) 'damage' functions.

RETURN PERIOD: If a series of n Bernoulli trials are considered, each of which culminate in either a success or a failure having p and q as their respective probabilities, then the interval between the successes (or failures) may be defined as "recurrence interval", "return period", or "waiting time", and:

$$p + q = 1 \qquad \ldots\ldots\ldots (1)$$

Let the hazard event have an intensity X (a random variable) with a cumulative probability function F(x). The failure of a future event may be said to have occurred when X has a value equal to or less than x, i.e.,

$$F(x) = P(X \leq x) = q = 1 - p \qquad \ldots\ldots\ldots\ldots (2)$$

Let T(x) be the random variable which expresses the time interval between two successive 'exceedence' events (higher than x). The return period of a success in years is defined by (ref. 4):

$$\bar{T}(x) = 1/p = 1/\left[1-F(x)\right] \qquad \ldots\ldots\ldots\ldots (3)$$

Now if exceedance occurs for the first time at the ith trial, it means that it must have failed in the previous (i-1) trials. Hence, the probability P(i) is given by:

$$P(i) = p.q^{i-1} \qquad \ldots\ldots\ldots\ldots (4)$$

As the variable takes only integral values, the left limit will be given by $i > 1$, but it will obviously be unlimited to the right as the event need not occur. It can be easily shown that the distribution function of T in the present discrete case is geometric (it is exponential in the continuous case); and hence the cumulative probability $P(t \leq i)$ that the event occurs before or at the ith trial is given by:

$$P(T \leq i) = p(1+o+q^2+ \ldots\ldots +q^{i-1}) = 1-q^i \qquad \ldots\ldots\ldots\ldots (5)$$

Hence, $$P(i) = 1 - \left[1-1/\bar{T}(x)\right]^i \qquad \ldots\ldots\ldots\ldots (6)$$

If encounter probability E is defined as the probability of occurrence of an event of higher magnitude than x within the designed life of the structure of L years, then:

$$E = 1 - \left[F(x)\right]^L = 1 - \left[1-1/\bar{T}(x)\right]^L \qquad \ldots\ldots\ldots\ldots (7)$$

Equation (7) shows the relationship between return period, encounter probability, and the life of the structure. Figure 1 shows the relationship between the return period and the designed life period for various fixed risk criteria.

DAMAGE FUNCTIONS: In certain cases the above procedure may not be advisable as it gives no information about damages. If it is assumed that (i) the process is stochastic with stationary independent increments and has time-independent average, (ii) 2 or more events cannot occur simultaneously, and (iii) damages are restored to the original level after the hazardous events, then the process becomes a compound Poisson one (ref. 5), that is:

$$L(t) = \sum_{n=1}^{N(t)} D_n, \text{ for } t \geq 0 \qquad \ldots\ldots\ldots\ldots (8)$$

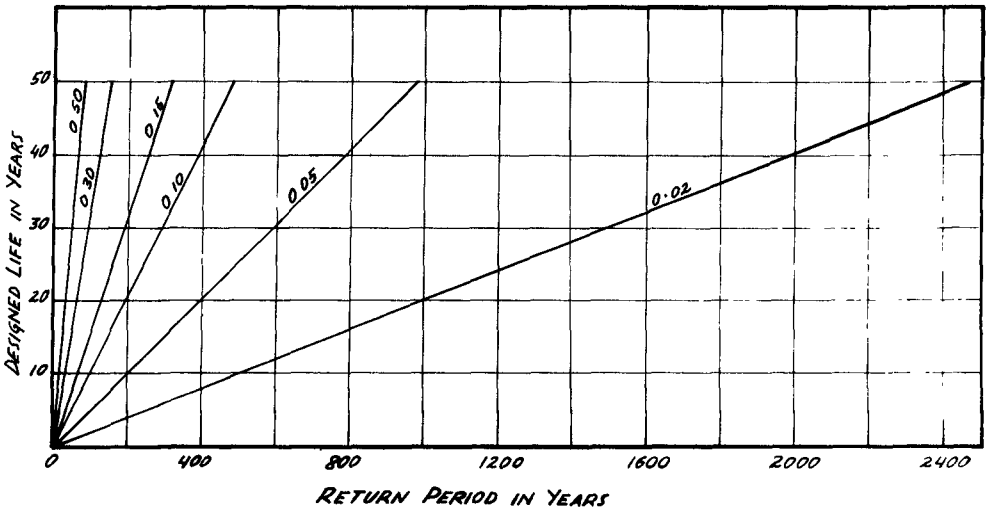

Figure 1. Relation between return period and life of structure for various risk criteria

where, $\{N(t),\ t \geq 0\}$ = a Poisson counting process (number of hazardous events of unspecified magnitudes occurring during the interval o to t)

$\{L(t),\ t \geq 0\}$ = stochastic process of accumulated damage from time o to t

$\{D_n, n=1,2, \ldots N(t)\}$ = family of independent random variables identically distributed as a random variable D, and

n = number of waves exceeding the intensity x_o within the time interval.

From the properties of a compound Poisson process $\{L(t),\ t \geq 0$ the first and second moment functions will be as follows:

Mean : $E[L(t)] = \nu t\ E[D]$ ..... (9)

Variance : $\mathrm{Var}[L(t)] = \nu t\ E[D^2]$ ..... (10)

Covariance : $\mathrm{Cov}[L(s), L(t)] = \nu E[D^2] \min\{s,t\}$ ... (11)

where, $E[.]$ = mathematical expectation,
ν = intensity of the process, and $t > s > 0$.

The relation between variance, mean, and $E[D^2]$ is given by:

$$\mathrm{Var}[D] = E[D^2] - E^2[D] \quad \ldots\ldots\ldots (12)$$

Equations (9) and (10) may give sufficient information about the loss at any time by its mean and variance, and it may not be necessary to estimate entire distribution of damage.

CONCLUSION: For economical as well as practical reasons it is not possible to design a structure which can withstand all the critical conditions acting on it at the same time. Thus, if a risk is necessarily being taken, it is essential that the designer should know the extent of the risk, and if possible, it should be kept consistent from one place to another (other things being equal) in keeping with sound engineering practice. Unfortunately very little research has been done in this highly complex field of risk criteria which sometimes includes the process of decision taking. It is high time to start intensive research programs in this important direction.

ACKNOWLEDGMENT: Preparation of this paper was supported by the National Research Council of Canada's research grant No. A-4359.

REFERENCES

1. Gumbel, E.J. "The Calculated Risk in Flood Control" Scientific Research, Section A, Vol. 5, 1955, pp. 273-280

2. Biswas, Asit K. "Risk Criteria And Flood Estimation" Hydrology Lecture Note No. 1, Queen's University, Kingston, 1967

3. Biswas, Asit K. "The Philosophy of Estimating Spillway Design Flood" 82nd Annual Meeting, Engineering Institute of Canada, Halifax, May, 1968

4. Gumbel, E.J. "Statistics of Extremes" Columbia University Press, New York, 1958, p. 22

5. Parzen, E. "Stochastic Processes" Holden-Day, Inc., San Francisco, 1962, pp. 128-131

CHAPTER 85

A SYSTEMS APPROACH TO PETROLEUM PORT SITE SELECTION

William S. Gaither
Associate Professor of Civil Engineering
University of Delaware, Newark, Delaware (Ref. 1)

and

J. Patrick Sides
Engineer, Collen Brothers Ltd., East Wall
Dublin, Ireland (Ref. 2)

ABSTRACT

Petroleum port site selection is examined in the broad context of the total transportation system from production to consumption area. Basic systems engineering approaches are applied to the problem to formulate a mathematical model which permits all transportation system variables, including capital and operating costs, to be put in quantitative form. An example of the computer solution is given, along with a discussion of the principal calculations involved. Unit transportation cost is selected as the measure of effectiveness of candidate systems. The port site associated with the system yielding the lowest unit transportation cost for the entire range of throughputs is selected.

INTRODUCTION

Oil and many other natural resources are found in areas of the world far from the centers of consumption. Many alternate routes exist between the points of production and consumption; however, only one route, with the optimum mix of vehicles, permits the lowest cost transportation of the commodity.

The great tankers of today often cannot use the sheltered ports frequented by general cargo vessels, and must be moored on an exposed coast where depth and maneuvering room are adequate. Thus oil port site selection no longer represents a choice between a few natural harbors, but rather is a matter of identifying an optimum transportation system and adapting a point on the coast to permit ship loading or discharging. The basic question confronting an engineer-economist responsible for port site selection is how to locate that site, or family of sites, through which petroleum can be transported at the lowest cost.

The systems approach enforces orderly thought and is adaptable to any level of study effort, ranging from a cursory review, to the precise economic comparison of several fully designed systems. Of particular significance is that the systems approach requires that the engineer recognize and examine the entire petroleum transportation system of which the port site is only one part.

This paper examines in successive steps: (1) the basic systems engineering approach, (2) the elements of petroleum transportation systems, (3) systems engineering applied to petroleum port site selection, and (4) a mathematical model for choosing one port site from among several candidates.

BASIC SYSTEMS ENGINEERING APPROACH

A commercial need, such as moving crude oil from a producing field to a refinery and then to the consumer, results in the conception of a system which will satisfy the need both technically and economically. This system may be defined in terms of specific objectives which must be met and also specific constraints which must be observed. Both the objectives and the constraints can be distilled into what can be termed system requirements which become the inputs to various alternate schemes.

Following the determination of system requirements, alternate approaches are developed to satisfy the requirements. In other words how to attain the stated objectives while respecting the limitations of the constraints.

Next a trade-off study, or economic comparison, is conducted to choose the most promising approaches from among all of those proposed. A simple mathematical model is used which accounts for system cost and performance. In some cases only one approach is technically feasible while in other cases many approaches, with nearly equal merit, may be identified. Each scheme which shows technical and economic promise is carried through a preliminary design phase so that all of its parameters may be put in quantitative form. This reqires that both capital costs and operating costs be defined by the system design.

The evaluation of these candidate systems is made on the basis of a measure of effectiveness. This measure of effectiveness is the independent variable of an economic function, or mathematical model, which permits all other system parameters to be expressed as dependent variables. It is essential that this type of study recognize and account for all performance and cost effects of a system design alternative. On this basis the most effective of the candidate systems is selected, resulting in a choice which may be defended both economically and technically.

THE ELEMENTS OF PETROLEUM TRANSPORTATION

The systems engineering approach requires consideration of all parts of the total transportation system which change with different harbor sites and requires understanding of both the technical and economic aspects of various modes of petroleum transportation and their interrelationships.

TRANSPORTATION MODES

Generally, petroleum is moved from the producing field to the consumer by a series of transportation modes. These modes are selected on the basis of economy and are normally pipelines on land and large tankers at sea. Since pipelines provide a continuous flow and ships operate as batch carriers, it is necessary to provide a surge, or storage, capability between these two modes to achieve maximum economy in the system. The size of this storage facility, or tank farm, is determined by the number of products handled, by the method of product segregation, and the regularity with which tankers arrive and depart.

A second important difference between these two widely used modes of crude oil transport is that with an increase in throughput, tankers can be added on an individual basis as required, but that a pipeline of specific diameter and wall thickness must be installed initially.

Each transportation mode and its intervening surge facility may be thought of as a series of separate, but interdependent, links which make up the total petroleum transportation system.

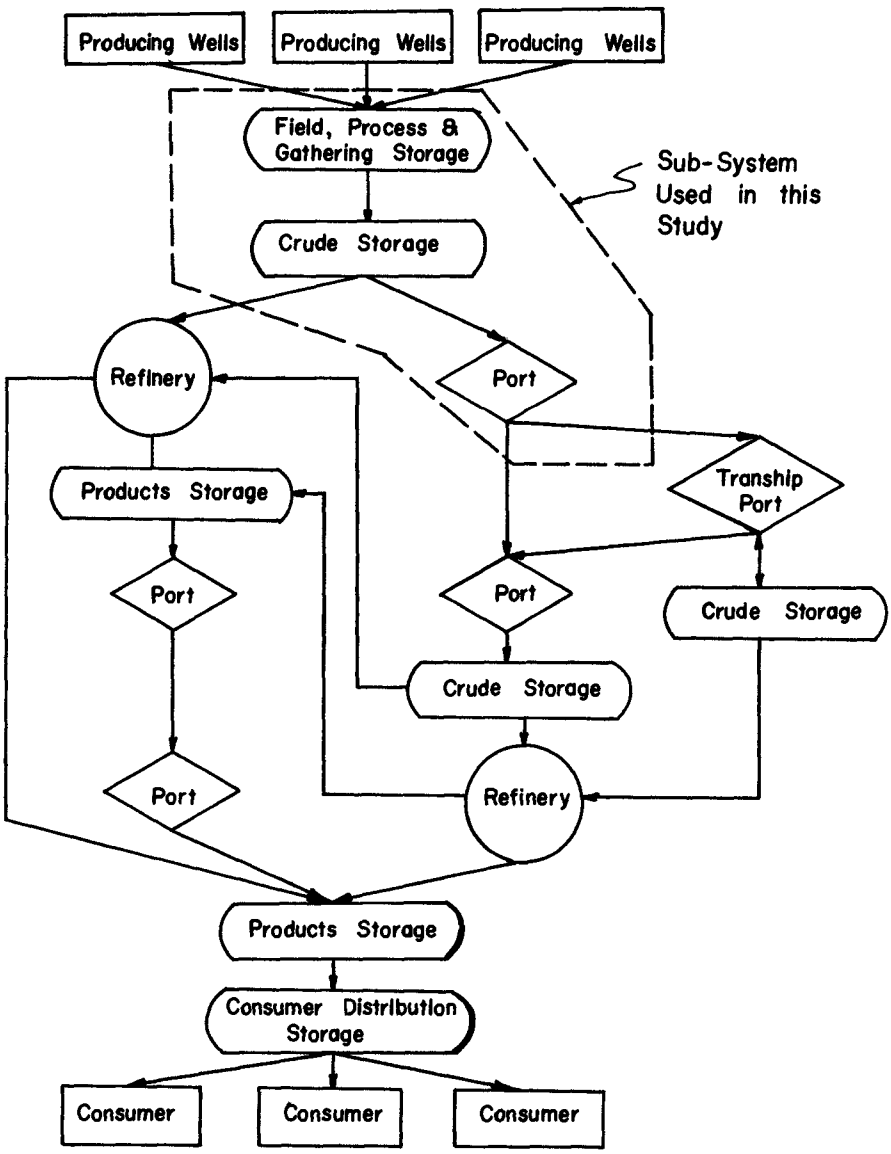

Figure 1
GENERALIZED OIL TRANSPORTATION SYSTEM

THE GENERALIZED SYSTEM

A generalized oil transportation system is shown schematically in Figure 1, from well head to the consumption point, indicating transportation modes and interfaces. The interfaces are either points where one form of transport is exchanged for another or where there is an interruption in flow. Ports, storage tanks and refineries are all interfaces. A port is an example of a change in transportation mode, while field gathering storage is an interruption in the flow along a pipeline.

Crude is pumped from well head to field gathering storage, where gas may be separated from the crude or different crudes mixed together before being transported further. The crude then moves on to an intermediate storage facility before being pumped to a port for shipment by tanker or being piped to a refinery for processing. If oil tankers are used, the oil is unloaded at the port of destination to a tank farm before being pumped to a refinery. With the advent of the very large tankers, which are limited to a few very deep ports, the use of the trans-shipment port has become more prevalent. At a trans-shipment port the oil is off-loaded from the large tanker into smaller tankers and the excess pumped to storage; or if no smaller tankers are present, all the oil is pumped to storage to await their arrival. Alternatively, some of this crude can continue its journey to a refinery by pipeline or other forms of transport. From the refinery the product goes into product storage from which it is distributed, by any of the transportation modes, to the various consumption points.

Figure 1 can thus be used to identify the oil transportation system for any given situation. In a transportation system in which oil tankers are used, the choice of different routes is based mainly on consideration of possible port sites and on possible land transportation routes. Sea routes have also to be considered but they are much more flexible than land routes. If it is required to select a particular facility within a transportation system, such as a port site, it is probably not necessary to analyze the entire transportation system, but only part, or sub-system. The sub-system study described as an example in this paper is indicated on Figure 1.

SYSTEMS ENGINEERING APPLIED TO PETROLEUM PORT SITE SELECTION

The fundamental problem to be solved is how best to move oil from the area of production to the area of consumption. The systems approach provides a logical step by step process whereby the most efficient and economical method of oil transportation can be found. The port which is chosen after such a study may not require the least initial investment or be the least expensive to operate of the candidate port sites, but the transportation system of which it is a part will provide the most economical method of oil transportation from producer to consumer. Figure 2 is a flow diagram showing the steps by which a systems study of this type is carried out.

OBJECTIVES AND CONSTRAINTS

The oil port, like all other parts of the system, must be designed to meet the objectives of the entire system. These objectives normally include a definition of (a) the origin and destination of the petroleum, (b) initial and ultimate throughputs of the system, (c) anticipated rates of system growth, (d) the time scale for construction and start up, and (e) the useful life of the system.

Various types of constraints must also be recognized at the outset of

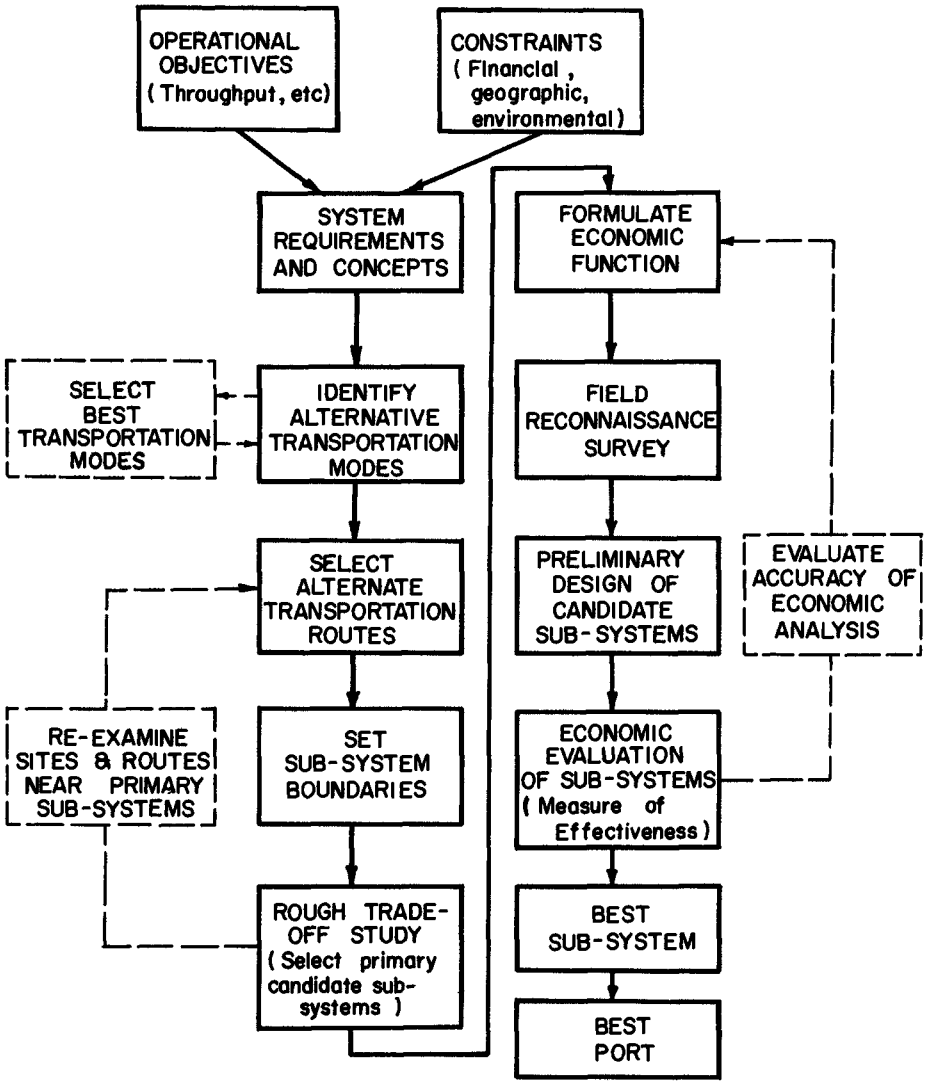

Figure 2
FLOW DIAGRAM FOR SYSTEMS APPROACH TO HARBOR SITE SELECTION

the study. These constraints may be thought of in the broader context of the system "environment". The environment can be broken down into technical, economic, and social environments. The technical environment covers existing oil transportation systems and their technical obsolescence, the present state of technology as it applies to oil transportation, and expected or possible developments in oil transportation. This would, for example, include a study of very large tankers in the 200,000 to 1,000,000 DWT range and methods of mooring, loading and unloading their oil.

The economic environment is concerned with costs of existing and projected systems, unit costs of material and labor, and changing customers and markets. Since the transportation system chosen must operate for a number of years, it must be designed with the flexibility to accomodate possible changes in throughput and consumption areas.

Within the social environment are considered the possible effects of changing political climates on the operation of the system, and the advantages of operating in one country rather than another.

SYSTEM REQUIREMENTS

Under the heading of system requirements all objectives and constraints are distilled into a compatible performance criteria for each part of the system. In this step the scope of the total system is established and the general type of route from origin to destination is identified.

ALTERNATIVE TRANSPORTATION MODES

There will be a number of transportation modes (i.e. tankers, pipelines, railcars, etc.) which may be used to move the oil. These modes are now considered and alternative combinations which satisfy the system requirements are chosen. In this case, one of these modes will be a form of ocean transport requiring a port. The alternative modes are then assessed by making a rough cut trade-off study based on the applicability of the transportation mode to the terrain and its use cost. In the case used in this paper, the modes are pipelines and ocean going tankers.

TRANSPORTATION ROUTES

There are theoretically an infinite number of different routes between the production and consumption areas. Practically, however, only those routes which appear technically feasible are chosen. This choice will normally be made by experienced people using available topographic maps and hydrographic charts. Each port site may be served by several sea routes and also by several pipelines routes. Every different combination, even though passing through the same port site, represents a separate transportation route.

SUB-SYSTEMS

For the purpose of port site selection it may only be necessary to consider part of the total transportation system. It is probable that geographic or national boundaries have placed several constraints on the candidate systems and that all systems pass some common (or nodal) point such as a strait, pass, canal, or cape which may, for study purposes, be regarded as the terminal point of a sub-transportation system. If such sub-systems are in fact independent of the total transportation system they may be used for the optimization study and as a consequence permit a substanital reduction in field investigation, preliminary design, and economic analysis efforts.

Figure 3 shows the transportation sub-system discussed in this paper, and which is shown schematically in Figure 1. The sub-system used as a basis for this optimization study has as its upstream nodal point the field gathering facilities. Proceeding downstream, the sub-system contains the following

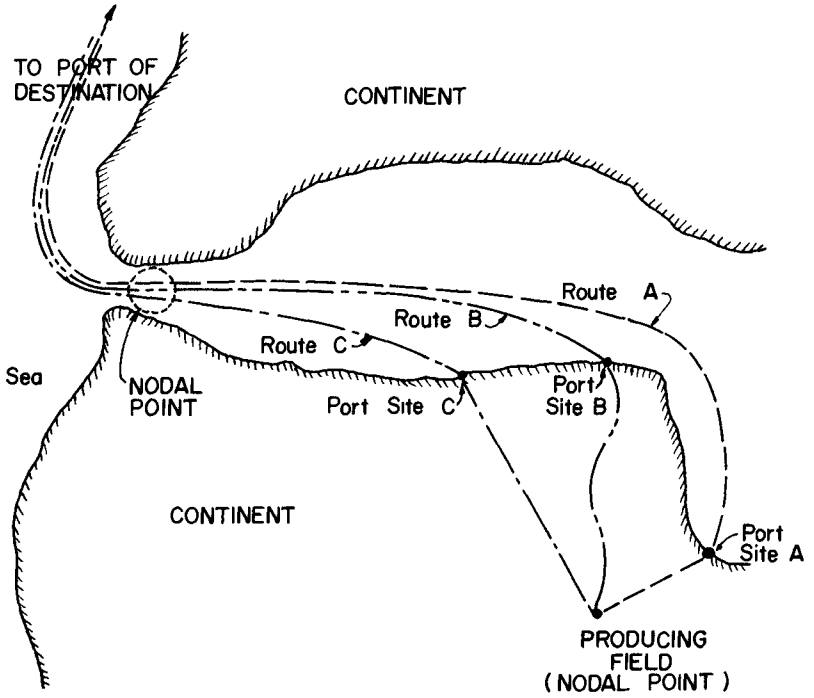

Figure 3
ALTERNATE PETROLEUM TRANSPORTATION ROUTES

links: (1) pipeline, (2) tank farm at the marine terminal, (3) high capacity ship loading lines, (4) the harbor and ship loading berths, and (5) a sea voyage to the downstream nodal point. This nodal point is designated as the nearest point to the candidate harbor sites which all ships pass.

The accuracy required in setting the boundaries, or nodal points, of the sub-systems depends on the accuracy required of the study. In the case of oil port site selection, the transportation route is analyzed both upstream and downstream from the port site until those points are identified which are common to all sub-systems and such that the consideration of any candidate port site has no effect on those portions of the transportation system outside the sub-system boundaries.

ROUGH TRADE-OFF STUDY

Once the candidate sub-systems have been identified a rough trade-off study can be used to eliminate those which are grossly non-competitive. Sub-systems considered in this paper are compared in Figure 4. Each sub-system has been assigned five cost variables which represent the links in the sub-system including: (a) pipeline (b) tank farm, (c) harbor, (d) sea voyage, and (e) unusual operating costs. The last item is used to convert any unique annual costs not common to all sub-systems into a capital cost.

PRELIMINARY EVALUATION OF CANDIDATE SUB-SYSTEMS
(CAPITAL COST BASIS IN MILLIONS OF DOLLARS)
(FOR ANTICIPATED MEDIAN THROUGHPUT)

SUB-SYSTEM	PIPELINE	TANK FARM	HARBOR	SEA VOYAGE	UNUSUAL OPERATING COSTS	SUB-SYSTEM COST	SELECTED PRIMARY CANDIDATES
A	50	9	6	2	—	67	Yes
B	120	10	6	2	1	139	No
C	150	8	7	2	2	169	No
D	55	10	7	3	—	75	Yes
E	70	9	5	3	1	88	Yes
ETC							ETC

Figure 4
ROUGH TRADE-OFF STUDY MATRIX

This simple comparison of the candidate sub-systems shows that due to high pipeline costs for systems B and C neither could be competitive with A, D, and E even though the assigned costs are only approximate. Those sub-systems with the lowest costs are selected as primary candidates for more detailed economic comparison.

THE ECONOMIC FUNCTION

At this point in the study it is desirable to formulate the economic function which will be used in a more precise trade-off study for the comparison of the primary candidate sub-systems. This method of selection requires a mathematical model, though it may be quite simple, which reflects the influence of two types of quantifiable parameters -- one related to system performance, and the other related to system cost. The accuracy of the study rests in the degree to which all parameters are quantifiable, although it is occasionally necessary to use quasi-quantifiable inputs.

The purpose of this procedure is to set forth systematically the parameters which affect the rational selection of a port site under the present, and foreseeable, conditions of system operation. A key part of the trade-off study is the selection of a Measure of Effectiveness (MOE) of all the system design alternatives. The Unit Transportation Cost (UTC), expressed in say dollars per ton, is a measure of effectiveness which permits all other

variables in a petroleum transportation system, or sub-system, to be expressed as dependent variables in a single economic function. It is essential that this type of study recognize and account for all performance and cost effects of a design alternative.

The economic function

$$\text{Unit Transportation Cost} = \sum_{j=0}^{j=n} C_{j(\text{capital})} + \sum_{k=0}^{k=m} C_{k(\text{annual})} \qquad \text{Eqn(1)}$$

contains (n) capital cost terms (C_j) and (m) annual cost terms (C_k), each representing a quantifiable feature of a candidate sub-system. This economic function should be established before undertaking the design of the candidate sub-systems since it identifies the significant cost parameters. The economic importance of each term should be determined early in the study so that the field investigation and design effort can be devoted to the items which have the greatest inpact on the UTC.

Accuracy of the Economic Function

At this stage in the study it is also possible to examine each term of the economic function and make a preliminary estimate of the accuracy with which each can be evaluated. From this the potential range of inaccuracy, or error, of the UTC can be established and in turn the required accuracy of all terms of the economic function can be set.

Comparitive vs Absolute Economic Studies

It should also be decided whether the UTC is to represent the absolute costs of a sub-system or whether its purpose is only to compare similar systems. If absolute UTC's are desired all cost items of each system must be represented by a cost term in the economic function. If comparative UTC's are required, as is the case if port site selection is the only objective, all equal cost terms common to each candidate sub-system may be omitted from the economic function. The omission of these common terms will reduce the amount of effort required to complete the study.

It should be noted that Equation (1) represents a steady-state condition for a given increment of system expansion. Its formulation should not be confused with a dynamic analysis which examines the state of the transportation system at uniform increments of time or at each event.

FIELD RECONNAISSANCE SURVEY

A field reconnaissance survey is normally necessary before beginning the preliminary sub-system design phase, particularly when the candidate routes and sites are located in an unfamiliar part of the world. The first step is to conduct a rough trade-off study as shown in Figure 4, so that only the several most promising sub-systems are retained for further investigation. The second step is to formulate the economic function to identify all significant cost items associated with the sub-systems being compared. The field reconnaissance survey can then be planned to concentrate on those features of the candidate sub-systems which represent the items of greatest cost and about which the least is known.

Typical reconnaissance surveys involve continuous seismic profiling at harbor sites to determine marine soil conditions, estimates of quantities of littoral drift, scattered borings in the tank farm area to appraise foundation conditions, and low level flying of the pipeline routes to determine elevations and assess the types of material to be excavated in pipeline burial. Data is also collected on local costs and availability of material and labor, duties, taxes, etc.

DESIGN OF PRIMARY CANDIDATE SUB-SYSTEMS

Each candidate sub-system, with its attendant port site, must be carried through a preliminary design phase in sufficient detail to permit all major cost items to be quantified.

Criteria

The first step in the preliminary design phase consists of establishing specific engineering criteria for both design and operation. This is contrasted to the general system performance criteria formulated at the beginning of the study.

ENGINEERING DESIGN CRITERIA

Candidate sub-systems were selected on the basis of rough order-of-magnitude estimates of the physical size of the harbor and tank farm area needed to accomodate the ultimate throughput of the system. As a supplement to this selection criteria it is necessary to establish further engineering criteria so that alternate preliminary designs can be prepared for each port site. Typical items for which criteria will be required are average ship size, maximum ship size, water depths, ship turning radii, typical pier configuration, typical breakwater cross-sections, storage tank sizes, and ship loading rates. Since several types of loading facilities (i.e. fixed piers, sea berths and mono-moorings) may be considered for each candidate site, it is necessary to establish comparable sets of criteria for each.

OPERATIONAL CRITERIA

Each alternate route and port site must be studies to determine what environmental characteristics will affect its performance uniquely. Overland and sea transportation routes will be affected by temperature extremes and storms. Port sites are particularly sensitive to wind and wave conditions which delay docking or require ships to leave a berth during loading or unloading operations. For each type of harbor development considered, separate criteria must be established for maximum permissible wave height and wind velocity. In comparing the effects of weather conditions on alternate port sites, a quantifiable parameter is that of port closure.

A ship turnaround time must be established which is compatible with demurrage-free time in port and with ship loading rates. Deballasting time and loading equipment capacity must also be selected to be compatible with ship turnaround.

Harbor Design

Crude oil and petroleum products are normally loaded or discharged across a fixed pier or through hoses to the ship in a sea mooring. Fixed piers may either be in a moderately exposed location or in a horbor sheltered by a breakwater. Sea berths are of either the spread mooring type where the ship rides to the center of a set of fixed lines, or the mono-mooring type where the ship "weather vanes" behind a single point bow attachment. All of these types of

berth designs have different operational requirements and thus will show economic differences at each candidate port site.

In general it can be said that a pier and breakwater design will show a high initial UTC since the first cost of a breakwater is great in relation to the throughput of the port. This assumes that the ultimate harbor area is enclosed initially. As the throughput increases with system expansion to the UTC will drop due to both the greater volume of petroleum shipped and also the minimal weather delays affecting a shelter harbor.

The sea berth and mono-mooring harbors will be closed by storms more often than a sheltered harbor, however their UTC's may be lower due to their installation cost. Also, sea berths and mono-moorings can be installed as needed in the course of system expansion instead of requiring a high early investment as in the case of a harbor sheltered by a breakwater. A small craft harbor to accomodate tugs and line running launches is needed in any event.

Port closure criteria assigned to these three types of harbor installation will normally take the following form:

Type of Harbor	Max. Wave	Max. Wind
Piers with Breakwater	15 feet	40 knots
Sea Berths	5 feet	20 knots
Mono-moorings	5 feet	30 knots

Thus piers sheltered behind a breakwater can be expected to operate under more severe conditions. The sea berth, on the other hand, is hampered

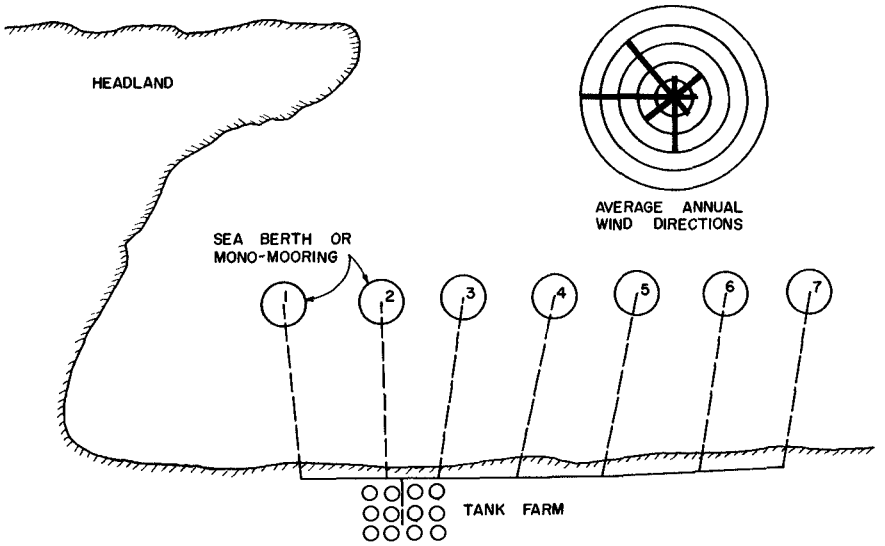

Figure 5
TYPICAL HARBOR EXPANSION PLAN

by small waves due to the inability of line running launches to work in heavy seas and high winds; beam winds particularly may force the ship to leave the berth. The mono-mooring is also hampered by small waves since it must be served by line running launches but it can remain in the berth longer in high winds due to its ability to "weather vane" behind the mooring buoy.

Figure 5 shows a typical harbor expansion plan for sea berths or mono-moorings. If we assume that this port site is exposed to local fetches and thus the wind and wave directions are approximately identical, it can be seen that substantial protection is afforded berth No.1 by protruding headland and that protection decreases along the coast through berth No.7. This then means that berth No.1 will be closed least because wind or waves exceeded the operational limit and that berth No.7 will be closed the most.

Pipeline Design

A pipeline is a part of a petroleum transportation system which represents a high initial investment and which is relatively inflexible once installed. The sub-system used for the study described in this paper includes a pipeline which delivers crude oil to the port. Thus pipeline design is an integral part of the system design.

Pipeline size is normally determined by the anticipated ultimate throughput of the system. Figure 6 shows a typical ground surface profile and hy-

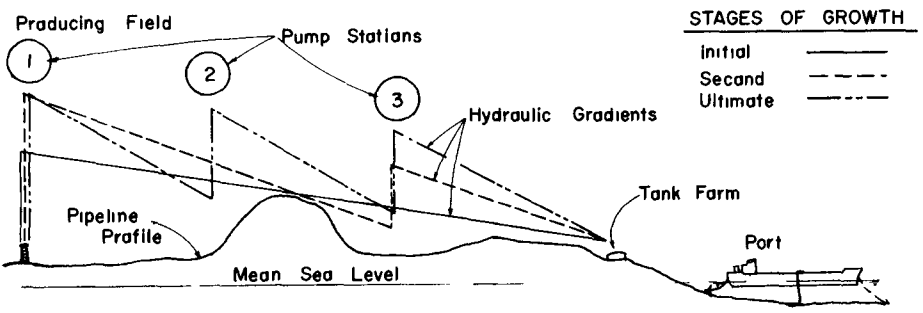

Figure 6
SCHEMATIC OVERLAND PIPELINE PROFILE

draulic gradients at several increments of system expansion. The initial system consists of the pipeline, Pump Station No.1 at the producing field, and a tank farm at the marine terminal. The hydraulic gradient decreases uniformly from Pump Station No. 1 at the producing field to the tank farm. Normally, the hydraulic gradient is kept above the ground surface thus maintaining a positive pressure in the line at all points.

The second stage of growth requires that Pump Station No.3 be installed and that additional horsepower be installed at Station No.1. The hydraulic gradient steepens between stations due to velocity head losses. Ultimate expansion is shown in the third state with the addition of Pump Station No.2 and increasing horsepower in Station No.3.

INCREMENTAL EXPANSION OF SYSTEM

Oil transportation systems are seldom constructed to handle their ultimate capacity initially but rather to be expanded in several increments. The engineering design of each candidate system must be based on incremental expansion of the system, recognizing that failing reserves or marketing considerations could curtail expansion at any intermediate stage.

An oil harbor can be enlarged by adding more berths, a tank farm by adding more storage tanks, and pipeline capacity by adding more pump stations. On the other hand, some parts of the system must be built initially to accommodate the ultimate throughput of the system. Typical of such parts would be pipeline diameter and wall thickness.

All engineering design for study purposes should be carried out on the basis of incremental expansion. Engineering quantities can then be associated with a given throughput of the system.

Tank Farm and Loading Lines

Designs in detail similar to those carried out for the harbor and pipeline portion of the sub-system must also be completed for the tank farms and loading lines. Factors which must be considered are land cost, number of different crudes to be handled, tanker loading rates, pumping requirements, and the availability of labor and local utilities.

Review of the Economic Function

Sub-system design may reveal significant features which were not properly represented in the economic function. Upon completion of the design phase, the mathematical model should be reviewed to be certain that all items are adequately described. This can be readily accomplished by completing the material quantity take off for each increment of sub-system expansion since each quantity must be represented by a term in the economic function.

A MATHEMATICAL MODEL FOR CHOOSING BETWEEN ALTERNATE PORT SITES

The economic function of Equation (1) is the mathematical model which is used to select the "best" sub-system and its attendant port site. While it is not mandatory that the economic function be programmed for a digital computer, investigation of incremental growth and design alternates makes its use quite desirable in all but the most elementary cases. This paper assumes that the iterative capabilities of a digital computer will be employed in the illustrative example which follows.

ORGANIZATION OF ANALYSIS

Figure 7 shows a descriptive computer flow diagram which is designed to analyze the type of sub-system discussed in this paper (i.e. pipeline, tank farm, loading lines, and harbor). It requires as inputs the general data applicable to all systems, quantity data for each sub-system on an incremental basis, unit cost data for both capital and annual costs, and the initial and ultimate system throughputs.

The program then computes the unit transportation cost for each designated increment (usually 1/10 or 1/20 of range between initial and ultimate) of throughput for each candidate sub-system. The output may be either printed or plotted as graphs.

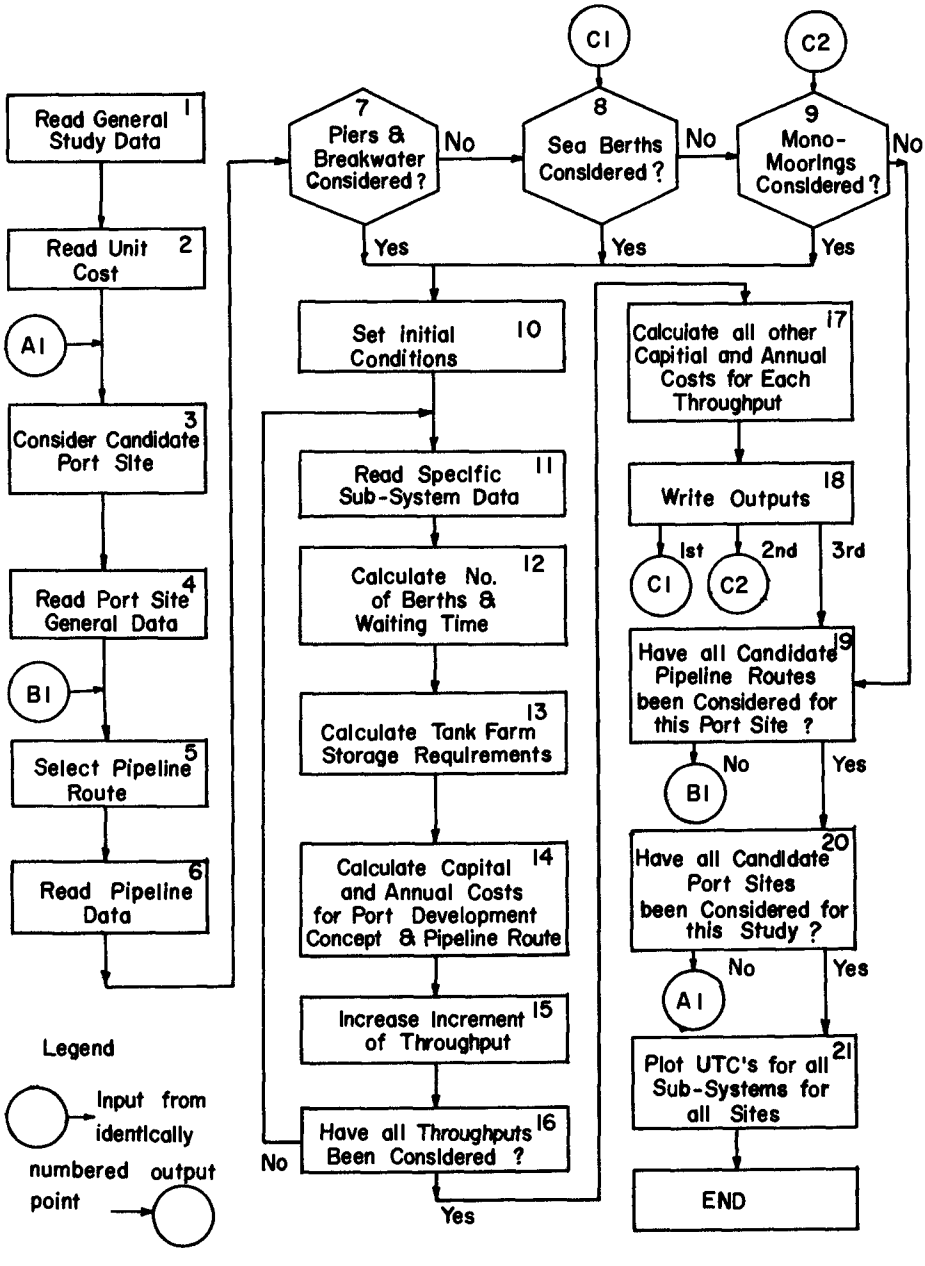

Figure 7
DESCRIPTIVE COMPUTER FLOW DIAGRAM

The following sections describe the principal features of the programmed mathematical model and the basis of important computations.

GENERAL INPUTS

Step 1 in the program is to establish general study data which will typically consist of the following items:

1. Throughput range to be considered.
2. Throughput increment for analysis.
3. Crude oil specific gravity.
4. Ship turnaround time.
5. Storage tank size.
6. Financial costs.
7. Escallation costs.
8. Duties & taxes.
9. Indirect costs.
10. Load factor of system.
11. Contingency allowance.
12. Study currency.

Any other items which will remain constant for all sub-systems may be included in general study data.

Step 2 consists of listing the basic unit cost items which are required to establish both capital and annual costs of all sub-systems. Such items as dredging cost per cubic yard, and pier maintenance cost per year are included in this section. Assignment of unit costs can be simplified by relating all cost units of the same general type of material to a single basic unit. An example would be that of breakwater armor stone cost based on core rock cost times a multiplier. All unit costs are established to represent actual on-site prices.

PORT SITE

Step 3 requires that a port site be chosen that is associated with one of the candidate primary sub-systems for which quantity information has been supplied as data.

The general port site data of Step 4 concerns input items such as cost of land at the port site, cost of access, cost of utilities, and other similar items peculiar to the geographical location of the candidate site.

It is possible that several tank farm sites may be considered at each port site. It is probable however that an independent hand calculation will permit a single tank farm site to be selected for a given port without expanding the sub-system analysis. One of the most significant data items associated with the storage tanks will be earth-moving and foundation preparation.

PIPELINE

To each port site will come several pipeline routes. Step 5 requires that one of these candidate pipeline routes be selected while Step 6 reads the quantity items such as pipeline length, miles of ditching in rock, and pumping horsepower at existing stations or by the addition of new stations along the line.

SPECIFIC HARBOR DEVELOPMENT CONCEPTS

At this point in the analysis a single port site on the coast is under consideration, as is one of several pipelines leading from the producing field to the port. At each port site several harbor development concepts have been carried through the preliminary design phase. For this study three

harbor development schemes are considered for each candidate site, fixed piers with breakwater, sea berths, and mono-moorings. Due however to available area or peculiar bathymetric conditions, some sites may not be adaptable to all three designs.

If the piers and breakwater scheme of Step 7 is to be considered, the throughput is initialized in Step 10 and then specific sub-system data is read in Step 11. Specific data consists of weather delay days or hours which result in port closure (this varies with natural protection at the site as noted in Figure 5 and with the operational limits of the mooring equipment included in the scheme), length and size of loading lines, pumping horsepower, and items such as dredging or removal of wrecks.

Calculate Number of Berths

The number of berths in a port must be such that the throughput can be loaded into tankers in the most economical manner. This calculation depends primarily on tanker size, loading rate, throughput, and weather delay. Observations at several ports have indicated that ship arrivals and queuing can be accurately described by a Poisson distribution (References 3,4, and 5). Two methods may be used to determine what queuing delay is acceptable.

(1) The first method is to assume a maximum congestion figure of say, 5%. This means that 5% of the time there are tankers waiting for a berth. This figure is based on experience with tankers, however, it is rather unsatisfactory as it makes no allowance for variation in demurrage and berth costs.

(2) The alternative, and better, method is to make a benefit-cost analysis by comparing demurrage costs with the capital and annual costs of a new berth. Figure 8 shows the results of such an analysis. Here The Berth Unit Transportation Cost (BUTC, which is the unit cost of moving oil from the tank farm into the tanker) is plotted against throughput. For each number of berths there is optimum throughput giving a minimum BUTC shown by the vertical dotted line in Figure 8. If the throughput is less than this optimum value, the BUTC rises since the berths are not being used at their optimum occupancy. If the throughput is greater, the BUTC again rises due to demurrage costs on waiting tankers, until the curve intersects the downward curve of the next higher number of berths. At this point the BUTC falls again and for this throughput a new berth should be added to the port. As the number of berths increases the BUTC for the optimum throughput decreases due to an increase in berth occupancy for the same delay time.

TANK STORAGE CAPACITY

The necessary volume of tank storage capacity in Step 13 is determined by the uncertainty of tanker arrivals and of discontinuities in pipeline delivery. The Poisson distribution calculation in Step 12 gives the probability of a given number of tankers arriving on a single day and the probability of consecutive days this number will arrive. If no tankers arrive for a number of days, then oil from the pipeline must be stored. If a large number of tankers arrive for several days, for example just after a storm, then there must be sufficient oil in storage to load these tankers even if flow through the pipeline has ceased. For a single crude it is usual to allow three-and-a-half days of storage for pipeline stoppages. The extreme

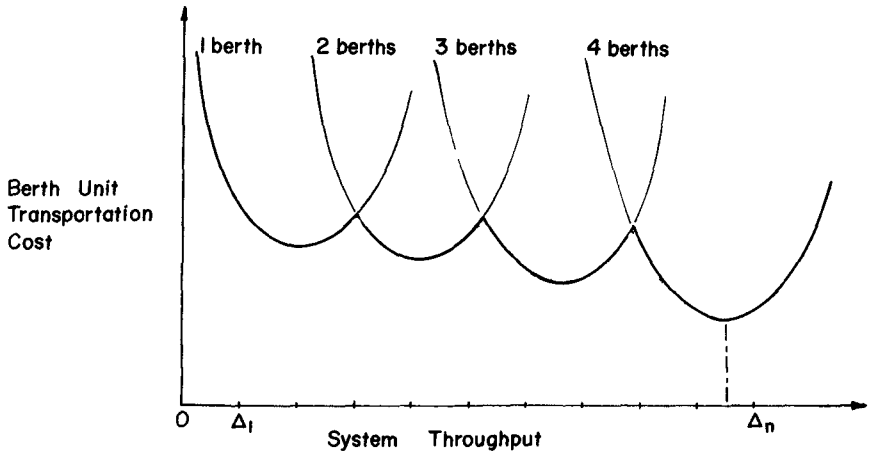

Figure 8
BERTH UNIT TRANSPORTATION COST AGAINST SYSTEM THROUGHPUT

storage requirement which is normally chosen is such that on one or two days a year the storage capacity is inadequate.

After determination of the storage capacity and selection of a tank size, the tank farm area is computed. The tank size and height and slope of dikes is general input data read in Step 1. The program also computes the amount of earth moving required to construct the dikes.

CAPITAL AND ANNUAL COSTS

After the number of berths and tank farm size has been determined in Steps 12 and 13, the program then returns to the input quantities associated with that particular increment of growth. Capital and annual costs are computed on the basis of the unit cost input data for the individual sub-system under consideration. These costs are then stored and the next increment of throughput is considered.

The program completes the analysis of each combination of pipeline and port development concept in Steps 17 through 23.

SELECTION OF PORT SITE

After the computation of unit transportation costs for each increment of throughput, curves are plotted for each sub-system associated with a particular candidate port site. Figure 9 shows curves which typically result from the analysis of three alternate harbor concepts associated with a single candidate pipeline route. Since these curves are plotted from the UTC's computed only at the designed increments of throughput, they may be smoothed by decreasing the increment and thereby plotting a greater number of points.

The high initial UTC associated with the piers and breakwater design can be attributed largely to the high first cost of the breakwater. As throughput

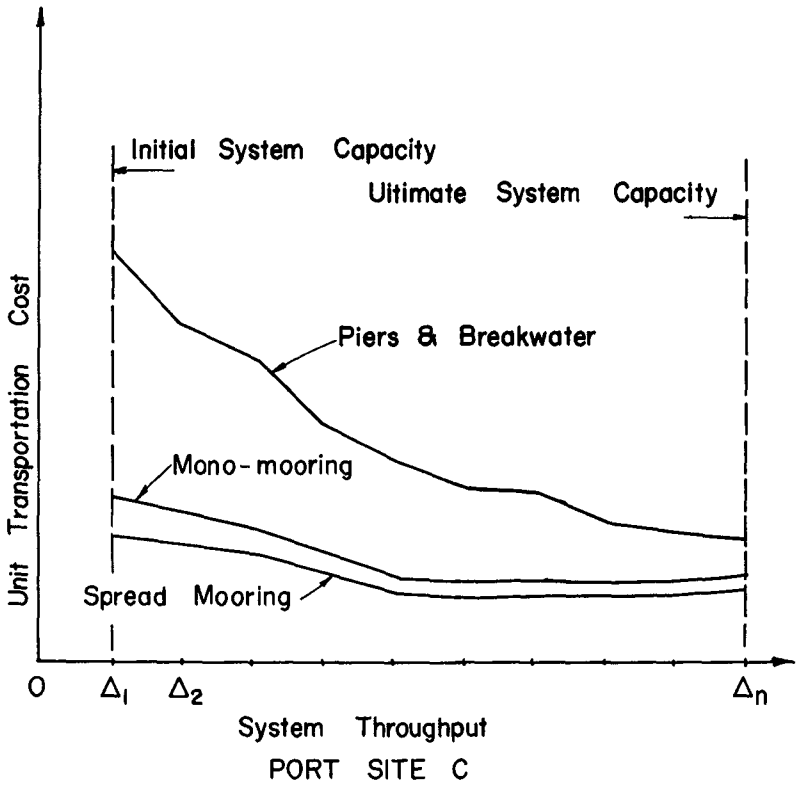

Figure 9
ECONOMIC COMPARISON OF SITE DEVELOPMENT CONCEPTS

increases, the UTC decreases reflecting the fewer weather delays and higher loading rates at fixed piers. Mono-moorings and spread moorings on the other hand show a lower initial UTC due to the fact that the only first cost associated with this type of port, other than the berth equipment, is the small craft harbor. The UTC for these two types of designs remains nearly constant, or increases slightly, with increased throughput. The increased UTC results from longer loading lines to distant berths coupled with larger line sizes and increased loading pump horsepower. The shapes of these curves, however, reflect the local design, construction, and operational pecularities of the candidate port site.

Following the selection of a "best" development concept for each port

site, a composite or summary graph may be plotted as shown in Figure 10. This graph shows only the lowest UTC sub-system for each port site considered. The lowest UTC curve represents the selected site or sites and the associated harbor development concept.

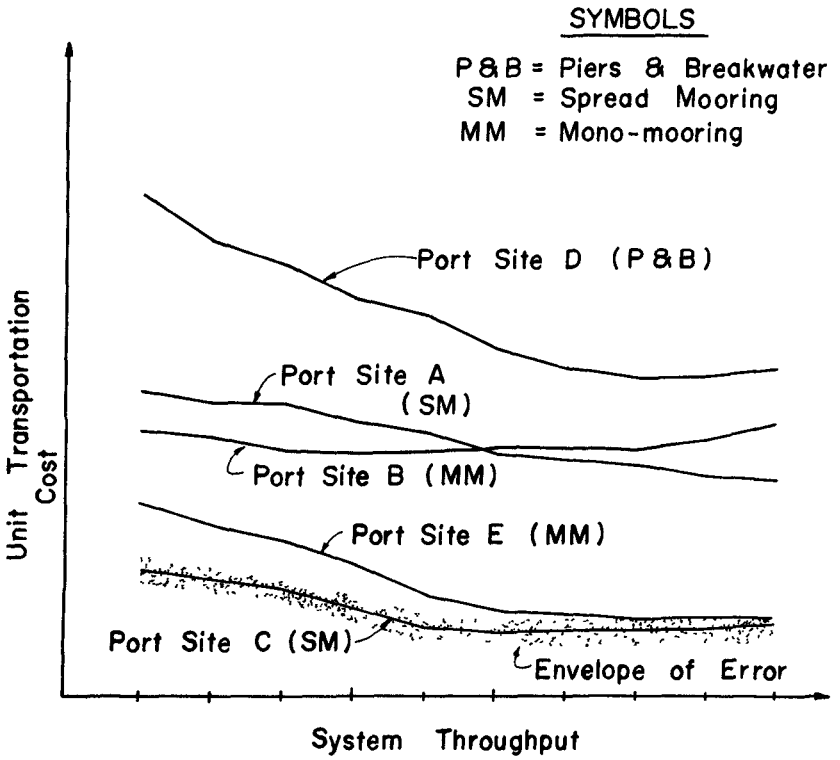

Figure 10
ECONOMIC COMPARISON OF ALTERNATE PORT SITES

ACCURACY OF ANALYSIS

Early in the study the required accuracy of the economic analysis was established. That accuracy can be represented as an absolute or percentage error for each UTC. If that plus or minus error is plotted as an envelope on the lowest curve in Figure 10, it may enclose one or more other curves above it. All curves which fall within this envelope must be considered to represent "best" sub-systems. In Figure 10 the Port Site E employing mono-moorings must be considered to be equal to the Port Site C at higher throughputs. At this

time economic, political, or social factors not expressed in the economic function may determine the port site. In the absence of such factors, an analysis of the type described in this paper, but performed on the basis of more thorough definition of all variables may permit a rational decision to be reached.

When the difference in unit transportation costs times the maximum annual throughput represents a capital cost less than the normal difference in construction bids, further refinement of the analysis is academic.

Occasionally two port sites, or alternate development concepts at one site, will change relative position as throughput is increased. This is shown in Figure 10 for Port Sites A and B. In such a case additional economic factors must be considered to arrive at a rational decision.

CONCLUSIONS

(1) The systems approach to petroleum port site selection requires the engineer to recognize that port site selection is not an independent problem, but is intimately related to adjacent parts of a total transportation system.

(2) The systems approach represents a method of accounting for all variables which affect the economics of shipping through a particular port site and results in economically defensible decisions.

(3) By the systems approach it is possible to determine the accuracy with which unit transportation cost is computed by means of the economic function so that excessive accuracy is not unjustifiably presumed.

ACKNOWLEDGEMENT

The authors wish to acknowledge the contributions of P. M. Girardot and Nancy Jubien of Bechtel Corporation to the formulation of the digital computer adaptation of the method described herein. Permission by Bechtel Corporation to publish this material is appreciated.

REFERENCES

1. Formerly Chief Engineer for Port and Coastal Development, Marine Department, Pipeline Division, Bechtel Corporation, San Francisco, California.

2. Formerly Engineer, Marine Department, Pipeline Division, Bechtel Corporation, San Francisco, California.

3. Fratar, T.J., A.S. Goodman, A.E. Brant. Prediction of maximum practical berth occupancy. Proceedings of the American Society of Civil Engineers, Journal of the Waterways and Harbors Division, V.86, WW 2, June 1960: pp. 69-78.

4. Plumlee, C.H. Optimum size seaport. Proceedings of the American Society of Civil Engineers, Journal of the Waterways and Harbors Division, V.92, WW 3, August 1966: pp. 1-24.

5. Mettam, J.D. Forecasting delays to ships in port. The Dock and Harbor Authority, London, V. XLVII, No. 558, April 1967: pp.380-382.

CHAPTER 86

CONSTITUENT TRANSPORT IN ESTUARIES

Bard Glenne, Asst Professor, Civil Engineering Department, Oregon State University, Corvallis, Oregon, U S A.

During the last two decades considerable progress has been made in analyzing the diffusion process in estuaries. Unfortunately, certain difficulties (e g prediction of diffusion coefficients) still prevent common application of the diffusion method An old technique, related to the diffusion concept, can however, frequently give useful information regarding constituent mixing and transport velocities in natural estuaries

RESIDENCE TIME

Conventionally the residence or detention time refers to the arithmetic mean time spent by all water particles within a certain length of a channel. The residence time of constituent particles in an estuary can be defined as the average length of time the constituent particles will remain within a certain region or reach of the estuary The constituent residence times will change with the location of the constituent sources and sinks and thus generally differ from the conventional residence times.

In the case of a one-dimensional estuary the constituent residence time may be defined as the mean time a constituent will spend traversing a specified section of the estuary For a steady state system the mean time must be

$$dT = \frac{\text{mass of constituent in a section of infinitesimal length (dx)}}{\text{avg mass rate of constituent transport through the section}}$$

where T = mean constituent residence time This expression can also be written

$$dT = \frac{A\bar{c}dx}{A\overline{uc}} \qquad \ldots . \ (1)$$

where A = local cross sectional area, u = local advective ("fresh water") velocity, c = constituent concentration, and the bar denotes the mean values of the parameters taken over a finite interval of time. The axioms of turbulent stresses as proposed by Reynolds (reference 1) can be used to reduce the term $A\overline{uc}$

$$A\overline{uc} = A\,\overline{u}\,\overline{c} + A(\overline{u'c'}) \qquad \ldots.(2)$$

where u' and c' are the instantaneous deviations from the mean values In equation (2) the total constituent transport is expressed as the sum of an advective and a diffusive constituent transport The equation for molecular diffusion further states that the rate of diffusive transport is proportional to the mean constituent gradient This is known as Fick's First Law and can in one-dimension be written

$$\overline{u'c'} = - E\frac{\partial \overline{c}}{\partial x} \qquad \ldots. (3)$$

where E = variable, overall longitudinal diffusion coefficient (ft^2/sec). The applicability of equation (3) in well-mixed estuarine situations is now generally accepted.

When the equations (2) and (3) are substituted in equation (1) the equation for constituent residence time per unit length of estuary results

$$\frac{dT}{dx} = \frac{\overline{c}}{\overline{u}\,\overline{c} - E\,\frac{\partial \overline{c}}{\partial x}} \qquad \ldots (4)$$

When the advective transport overshadows the diffusive transport, equation (4) reduces to the usual detention time equation for plug flow.

To avoid using a diffusion coefficient it is convenient to introduce an integrated form of the steady state, one-dimensional continuity equation for conservative constituents in estuaries (references 2, 3 and 4)

$$AE \frac{\partial \bar{c}}{\partial x} = A \bar{u} \bar{c} - \sum_{o}^{x} S_s \qquad \ldots . (5)$$

where $\sum_{o}^{x} S_s$ is the summation of sinks and sources of the constituent landward of the point x. Eliminating E between equations (4) and (5)

$$\frac{dT}{dx} = \frac{A \bar{c}}{\sum_{o}^{x} S_s} \qquad \ldots (6)$$

A useful observation can be made regarding constituent residence times in natural estuaries. The linearity of equation (5) implies that, for steady conditions, the constituent concentration throughout the estuary is directly proportional to the source strength Thus equation (6) demonstrates that the constituent residence time is independent of the source strength

In Figure 1 are plotted the approximate maximum and minimum integrated residence times for silica and advective flow for the 1961-62 water year in Northern San Francisco Bay. In general, silica can be said to represent a typical landward source constituent in Northern San Francisco Bay. Since silica and "fresh water" essentially have identical source locations the differences in their transport velocities and residence times therefore represent the diffusive transport of silica.

TRANSPORT VELOCITY

When the expression dT/dx is inverted it gives the constituent transport velocity. Inverting equation (4)

$$\frac{dx}{dT} = u - \frac{E}{\bar{c}} \frac{\partial \bar{c}}{\partial x} \qquad \ldots . (7)$$

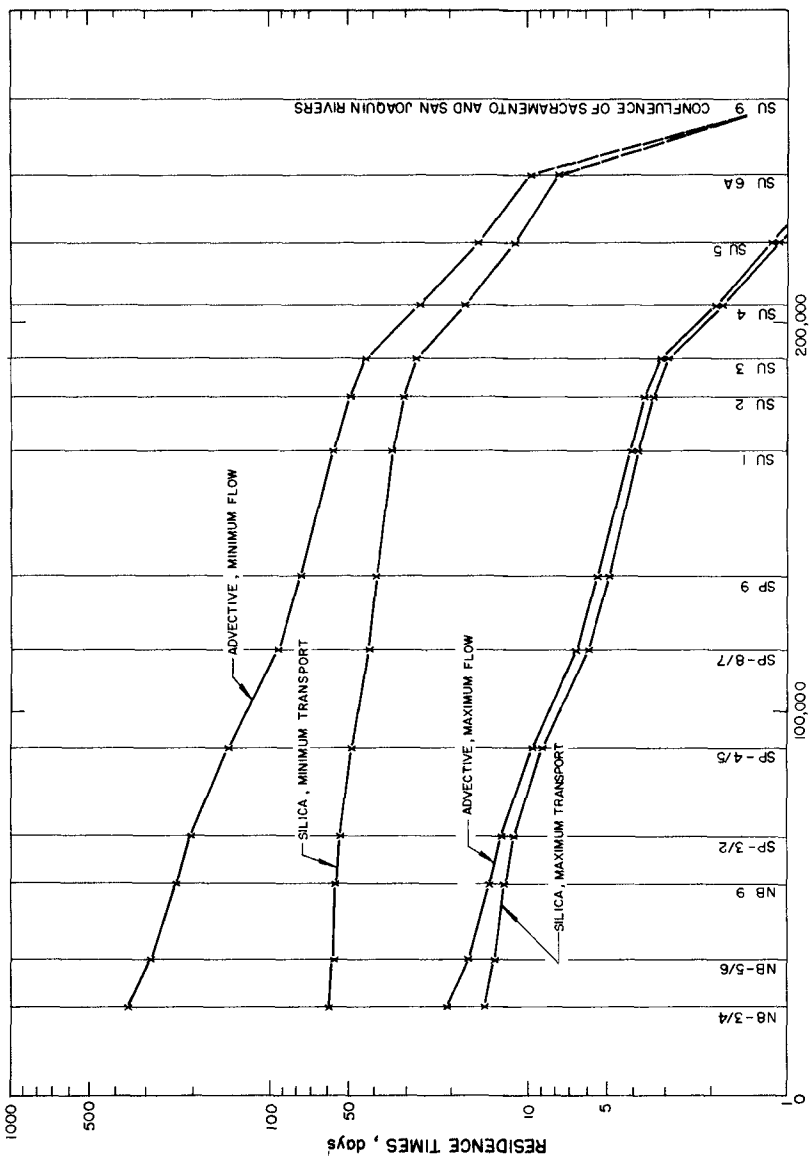

FIGURE 1 RESIDENCE TIMES IN NORTHERN SAN FRANCISCO BAY FOR THE 1961-62 WATER YEAR

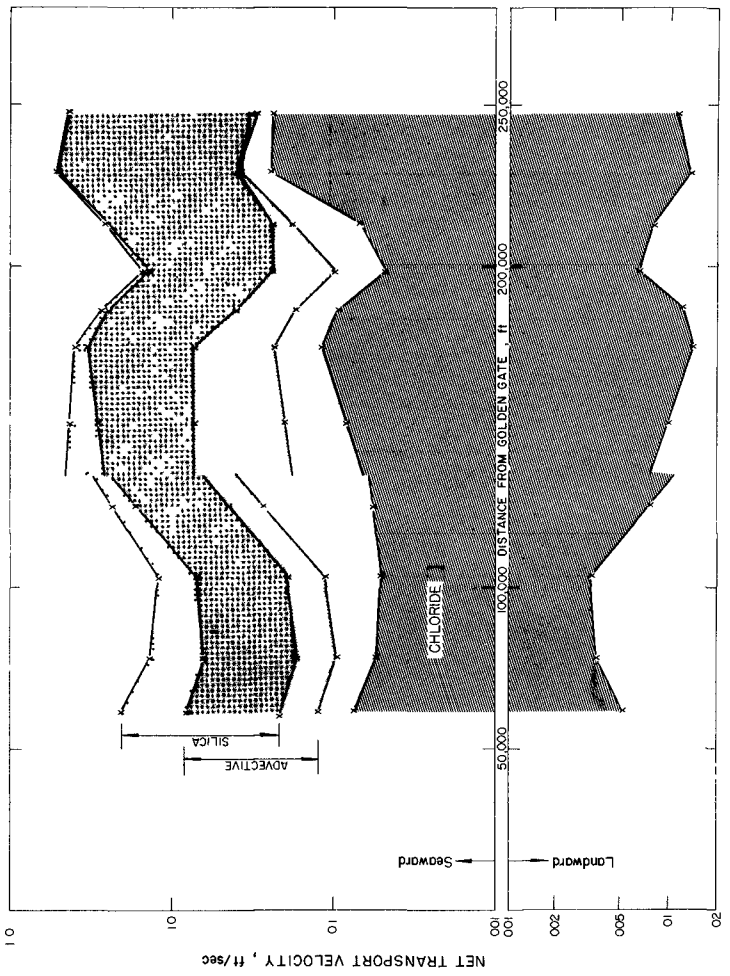

FIGURE 2. RANGE OF NET TRANSPORT VELOCITIES IN NORTHERN SAN FRANCISCO BAY FOR THE 1961-62 WATER YEAR

When the constituent concentration gradient is zero the expression reduces to the advective velocity The significance of the diffusive transport term can be calculated from equation (7). To obtain an expression, void of E, for the local constituent transport velocity equation (6) is inverted

$$\frac{dx}{dT} = \frac{1}{A\,\bar{c}} \sum_{o}^{x} S_s \qquad \ldots\ (8)$$

With a minimum of data available equation (8) can be used to evaluate steady state, one-dimensional constituent transport in an estuary Since the constituent transport in most natural estuaries is not strictly one-dimensional it is usually advisable to divide the estuary into several sections and to stepwise perform the computations (see Figures 1 and 2)

In Figure 2 is plotted the range of transport velocities for silica, chloride, and "fresh water" for the 1961-62 water year in Northern San Francisco Bay A discontinuity in the data is present between San Pablo Bay and Carquinez Strait owing to differences in observation periods.

CONCLUSION

The linear characteristic of the one-dimensional mass continuity equation for constituents (conservative or first order decay) in estuaries shows that the constituent residence times or transport velocities are independent of the constituent source strength This fact permits computation of representative constituent transport velocities using artificial or natural tracers with typical discharge locations

The evaluation procedure outlined above requires a minimum of data and labor; e g no knowledge of diffusion coefficients In estuaries and bays with predominantly one-dimensional constituent transport the procedure gives practical information regarding the mixing and exchange mechanism.

In Northern and Southern San Francisco Bay dissolved silica (SiO_2) was found to be a good representative tracer naturally discharged by rivers and streams.

ACKNOWLEDGMENT

This investigation was part of a study sponsored by the State Water Quality Control Board, Sacramento, Calif , under Standard Agreement No. 12-24, dated July 1, 1960, with the Regents of the University of California, and by the Research Grants Division (WP-649) of the National Institutes of Health of the U.S. Department of Health, Education, and Welfare

The writer wishes to thank Professors Robert L Wiegel and Robert E Selleck of the University of California for valuable advice and help given during the study.

REFERENCES

1 Schlichting, H. Boundary Layer Theory New York: McGraw-Hill Book Co., Inc 1955

2. Ippen, A.T (editor). Estuary and Coastline Hydrodynamics New York: McGraw-Hill Book Co. Inc , 1966.

3. Glenne, B. Diffusive Processes in Estuaries, SERL Report No. 66-6 Sanit. Eng Res Lab , University of California, Berkeley, California, 1966

4 Cederwall, K. Hydraulics of Marine Waste Water Disposal. Report No 42: Hydraulics Division, Chalmers Inst of Technology, Gothenburg, Sweden, 1968

CHAPTER 87

HYDRAULIC MODEL EXPERIMENT ON THE DIFFUSION DUE TO THE COASTAL CURRENT

Haruo Higuchi

Assistant Professor of Physical Oceanography
Disaster Prevention Research Institute
Kyoto University, Kyoto, Japan

and

Yuichi Iwagaki

Professor of Coastal Engineering
Department of Civil Engineering
Kyoto University, Kyoto, Japan

ABSTRACT

The diffusion phenomena due to the tidal current and the longshore current inside and outside a harbor are studied in a hydraulic model experiment, for which the Kashima Harbor area is used as the prototype. The tidal current, the longshore current and the effect of density are taken into account, but the direct effects of wind and waves are not considered.

A model of Kashima Harbor, with horizontal and vertical scales of 1/500 and 1/63 respectively, was constructed, and a semidiurnal tide generated by an automatically controlled pneumatic tide generator and longshore current by a water circulating system were provided for it. The water level at 4 stations and current pattern were measured. The diffusion of dyed water from instantaneous point sources and a continuous point source was investigated by the photographic method and dye concentration analysis.

INTRODUCTION

After the completion of new coastal industrial zones, which are now under construction or in the planning stage, it is expected that various kinds of industrial waste water will be discharged into the sea so that water pollution may become an important problem. In order to execute such a plan rationally it is essential to forecast its probable after-effects and the hydraulic model experiment is one of the most useful means of doing so[1].

Generally there are many factors controlling the diffusion phenomena in the sea, for example the ocean current, the tidal current, the longshore current, density stratification, waves, the wind and so on. In this study, however, the tidal current, the longshore current, and the effect of density are taken into account.

Kashima Harbor, which faces directly to the Pacific Ocean, was used as the prototype.

PROTOTYPE

The Kashima Nada Coast is a monotonously straight coast 70 km long as shown in Fig. 1. The bottom slope in this area is about 1/150 to a depth of 20 m and less than 1/500 from 20 to 40 m as shown in Fig. 2. The contour lines are almost parallel to the coastal line. Kashima Harbor, an artificial harbor for 100,000 ton ships, is now under construction in this area. The water depth in the harbor is 16 m at the entrance and 10 m in the inner part of the harbor. The southern breakwater is 2.8 km long and the northern one 1.4 km. The bottom material in this area is fine sand with a median diameter of 0.13 to 0.17 mm as shown in Fig. 2[2].

There are three major ocean currents in this area as shown in Fig. 3, that is, the Kuroshio, Tsushima Current, and Oyashio. The former two are warm currents and the latter is a cold current. The current pattern in this area is very complex and the relation between such ocean currents and the longshore current in front of Kashima Harbor is not so clear. The longshore current often flows northwards in summer and southwards in winter, which corresponds with the main direction of the winds.

The tidal constants in this area are shown in Table 1. The spring tidal range is about 94 cm and the neap range 35 cm at Choshi, 25 km away from Kashima Harbor. The monthly mean sea level is highest in October and lowest in April as shown in Table 2. The difference between them is about 25 cm.

Table 1 Tidal constant in the prototype

Constituent / Station	M_2		S_2		K_1		O_1	
	H(cm)	κ(°)	H(cm)	κ(°)	H(cm)	κ(°)	H(cm)	κ(°)
Onahama	30.2	127.2	13.9	161.2	22.4	172.6	17.3	159.3
Choshi	32.2	130.7	14.6	163.4	23.0	175.8	18.6	159.6
Mera	35.6	141.3	16.3	171.9	21.6	175.3	16.7	158.5

The current ellipses obtained at a point 16 m deep are shown in Fig. 4. In this figure the length written on the right of the figure shows the value above the bottom. The diurnal tidal current flows almost parallel to the coastline (NNW-SSE) and the semidiurnal rather normal to that (NE-SW).

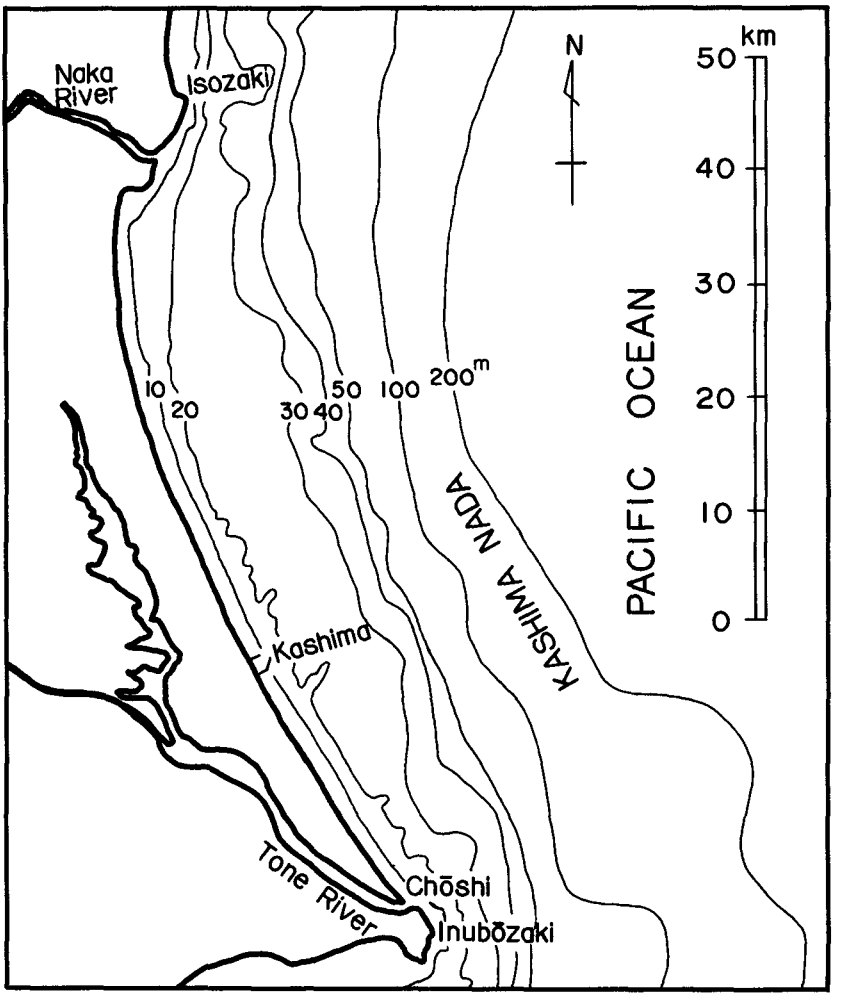

Fig. 1 Bathymetric chart of the Kashima Nada

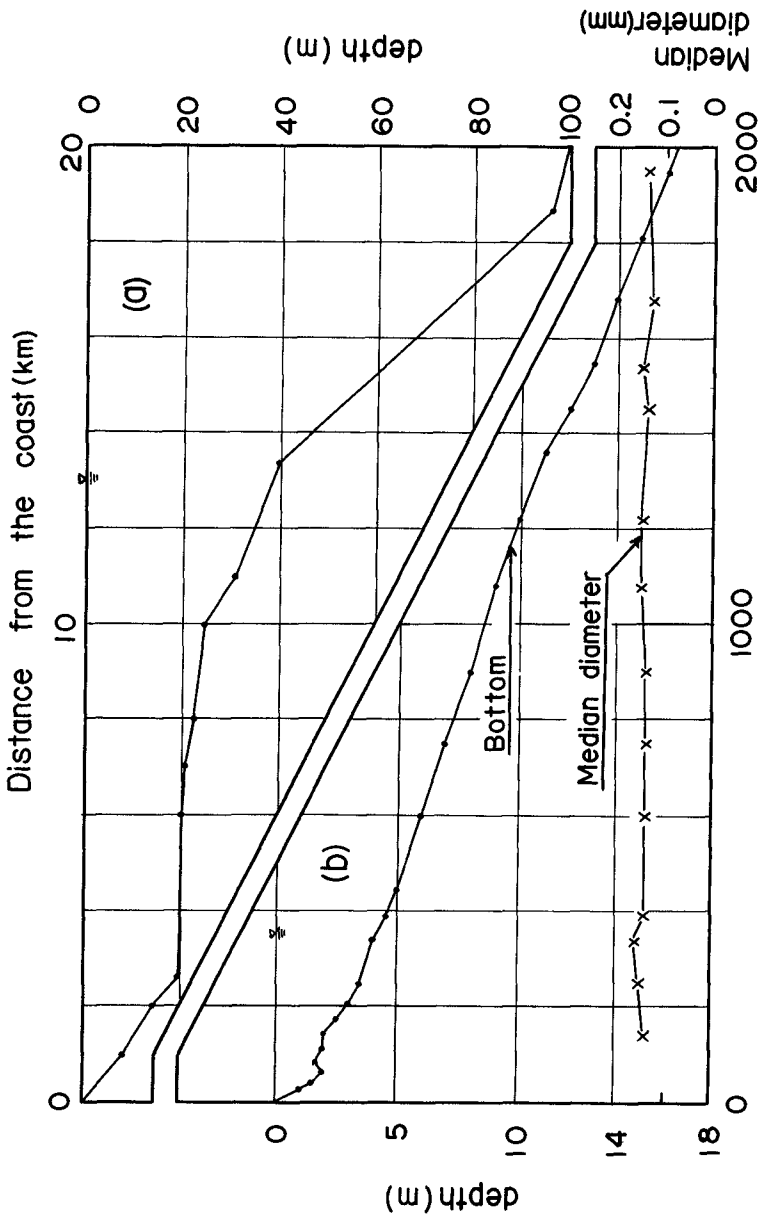

Fig. 2 Bottom profile near the coast (a) and median diameter of bottom material (b)

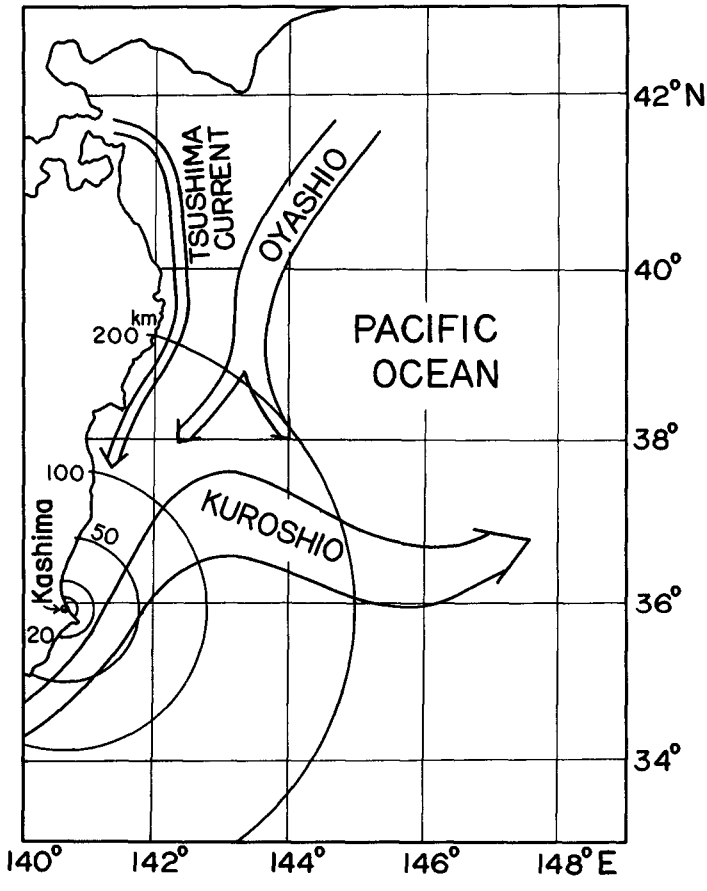

Fig. 3 Ocean currents near the Kashima Nada

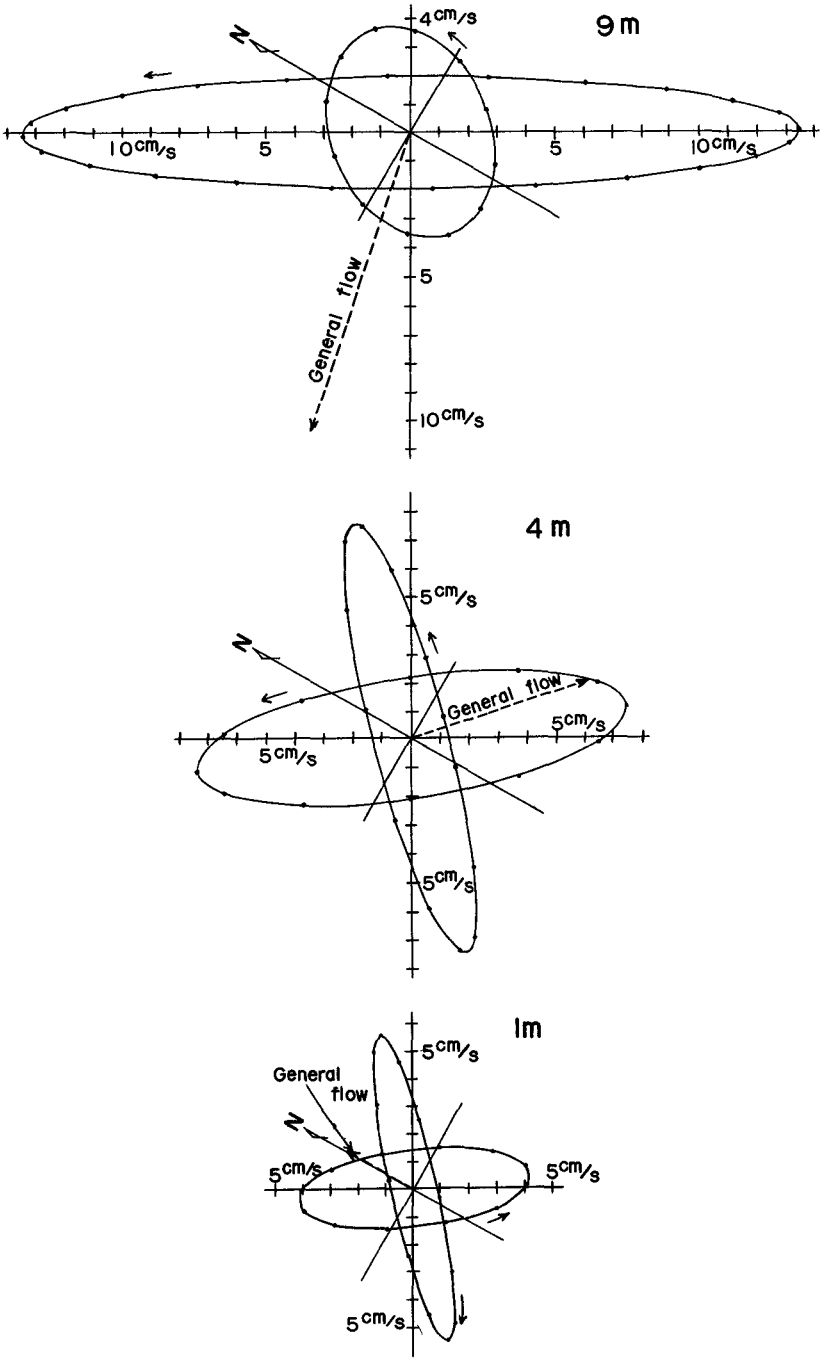

Fig. 4 Tidal ellipse at Kashima at 1, 4, and 9 m above the bottom

Table 2 Monthly mean sea level at Choshi (1955~1965)

Month	1	2	3	4	5	6	
Sea level (cm)	107.9	98.5	94.3	90.0	91.8	101.6	
	7	8	9	10	11	12	Mean
	106.8	111.4	114.6	115.1	107.2	107.6	103.9

When industrial waste water is discharged into the sea, it is supposed that the diffusing area consists of two regions[3] ; the first region, in which vertical mixing mainly occurs due to the upwards intrusion of sea water into the waste water, and the second region, in which horizontal mixing mainly occurs due to the horizontal eddy diffusion. As to Kashima Harbor, it is to be expected that the inner part of the harbor will belong to the first region and the outer part to the second region. Since the harbor has not yet been constructed, a field observation for the diffusivity was carried out only in the outer part of the harbor. This was made by taking aerophotographs of dye patches. A sketch of the movement of the dye patches is shown in Fig. 5. The time change of the area of the dye patches is shown in Fig. 6. In this figure the letters A,B, etc. show the locations in Fig. 5.

The concentration of the dye at time t in the dye patch, which had the symmetrical distribution $C = C_o \exp(-r^2/a^2)$ initially, was obtained as follows.

$$C = \frac{C_o}{1 + 4Kt/a^2} \exp\left\{\frac{-r^2}{a^2\,(1 + 4Kt/a^2)}\right\} \tag{1}$$

from

$$\frac{\partial C}{\partial t} = K\left(\frac{\partial^2 C}{\partial r^2} + \frac{1}{r}\,\frac{\partial C}{\partial r}\right) \tag{2}$$

Supposing the same concentration at the rim of the patch the concentrations at t_{i-1} and t_i are written as follows,

$$\frac{C_o}{1+4Kt_i/a^2} \exp\left\{\frac{-r_i^2}{a^2(1+4Kt_i/a^2)}\right\} = \frac{C_o}{1+4Kt_{i-1}/a^2} \exp\left\{\frac{-r^2_{i-1}}{a^2(1+4Kt_{i-1}/a^2)}\right\}$$

Assuming

$$\frac{1}{1 + 4Kt_i/a^2} \sim \frac{1}{1 + 4Kt_{i-1}/a^2}$$

and

$$\exp\left\{\frac{-r^2}{a^2(1 + 4Kt/a^2)}\right\} \sim 1 - \frac{r^2}{a^2(1 + 4Kt/a^2)}$$

the diffusivity is written as follows,

$$K \sim \frac{r_i^2 - r^2{}_{i-1}}{4(t_i - t_{i-1})} \tag{3}$$

or

$$K \sim \frac{\Delta S_i}{4\pi \Delta t_i} \tag{4}$$

where $S = \pi r^2$, $S_i - S_{i-1} = \Delta S_i$ and $t_i - t_{i-1} = \Delta t_i$.
The relation between the diffusivity Kp evaluated by this equation and the equivalent radius of the patch r is shown in Fig. 7. The slope of the straight line in the figure is 4/3.

SIMILITUDE

In the hydraulic model experiment for the coastal current it is necessary for the following equations to be valid in order to hold a dynamic similitude between the prototype and the model

$$t_r = x_r h_r^{-1/2} \tag{5}$$

and

$$n_r = x_r^{-1/2} h_r^{2/3} \tag{6}$$

where x is the horizontal length, h the vertical length, t the time, n Manning's roughness coefficient, and the suffix r shows the ratio of the quantity in the prototype to that in the model.

When the flow in the model belongs to the turbulent regime the 4/3 power law, $K = \epsilon^{1/3} L^{4/3}$, must be valid, where ϵ is the rate of energy dissipation. On the other hand, the ratio of the diffusivity K_r is expressed by $K_r = x_r^2 t_r^{-1}$ from the consideration of the dimension. Equating both diffusivities under the condition $L_r = x_r$, we get

$$u_r = \epsilon^{1/3} x_r^{1/3} \tag{7}$$

Assuming $\epsilon_r = 1$, the following equations are obtained from equations (5), (6), and (7).

$$h_r = t_r = x_r^{2/3} \tag{8}$$

$$n_r = x_r^{-1/18} \tag{9}$$

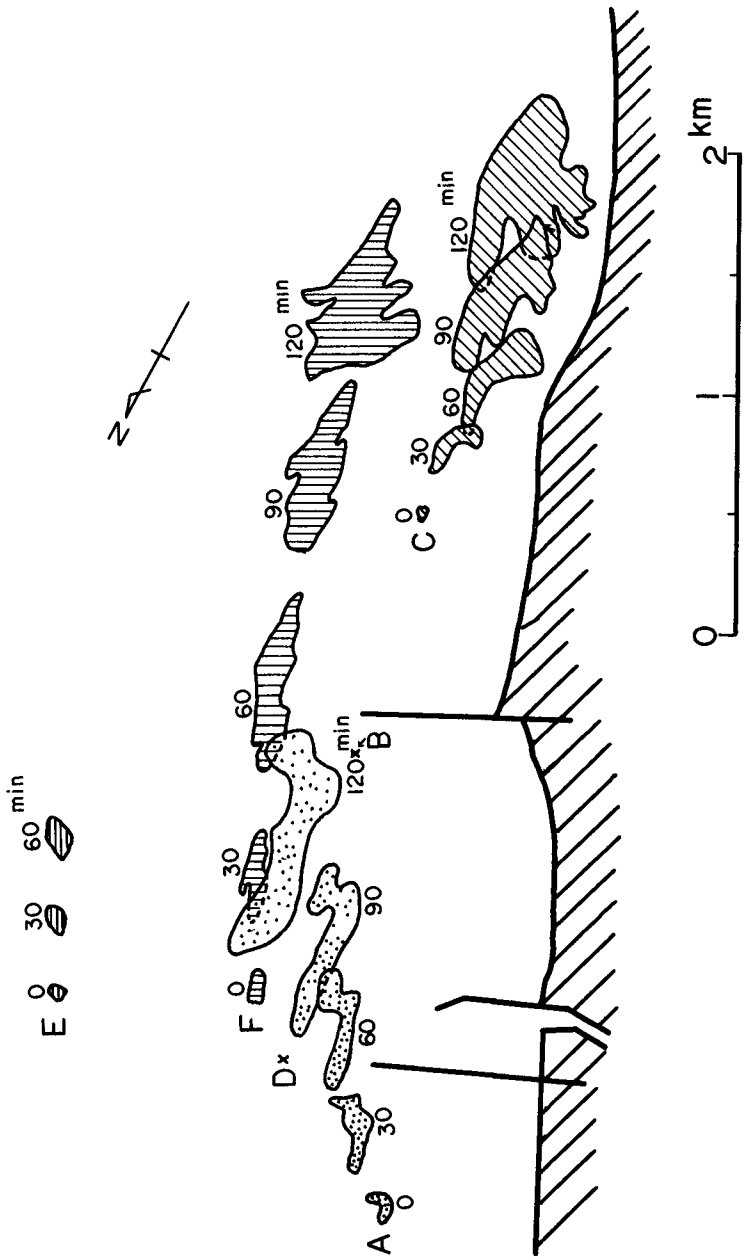

Fig. 5 Sketch of change in the area of dye patches from instantaneous point sources (prototype)

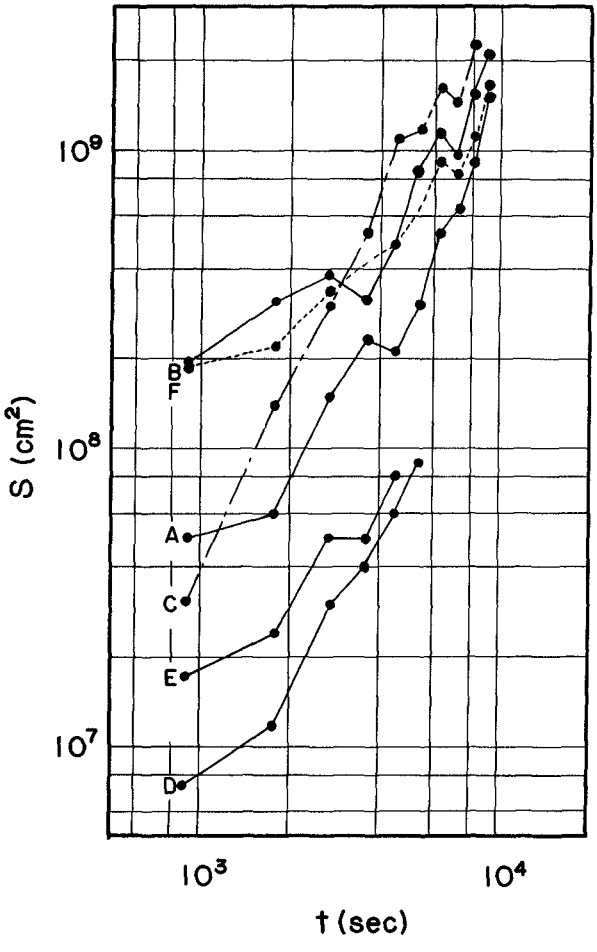

Fig. 6 Change of area with time of dye patches from instantaneous point sources (prototype)

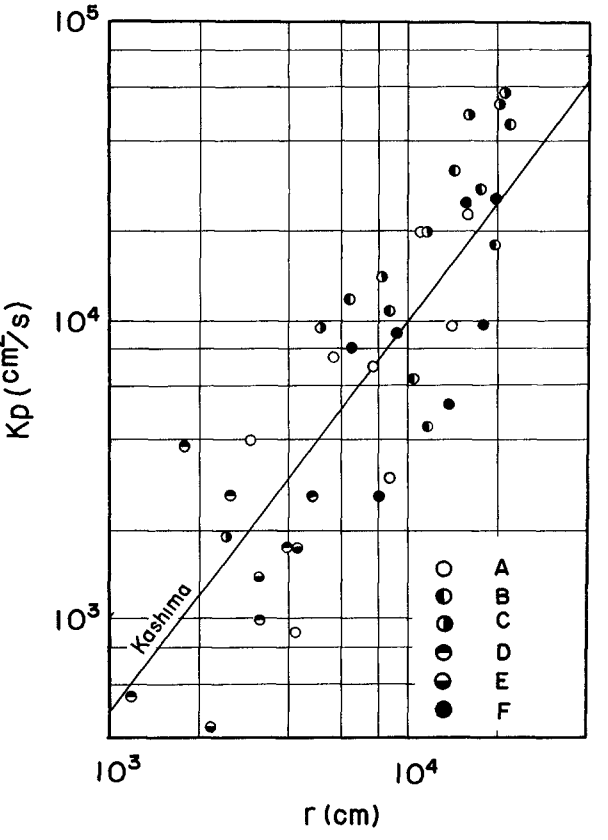

Fig. 7 Diffusivity K_p and equivalent radius r (prototype)

As to the horizontal diffusivity, we get

$$K_r = x_r^{4/3} \tag{10}$$

When $x_r = 500$, other scale ratios become as follows; $h_r = 63$, $t_r = 63$, and $n_r = 0.7$.

The Reynolds number in the area changes according to the tidal phase and the strength of the longshore current. The maximum value in the model is expected to be 3200 at the entrance of the harbor assuming the current velocity to be 10 cm/sec in the prototype. Therefore it can be regarded as an experiment in the turbulent regime.

The hydraulic factors in the model are shown in Table 3.

Table 3 Hydraulic factors in the prototype and the model

Factors	Scale	Prototype	Model
Distance	1/500	4 km	8 m
Water depth	1/63	16 m	25 cm
Tidal range	1/63	126 cm	2 cm
Tidal period	1/63	12 hr 25 m	11 m 50 s
Current velocity	1/8	10 cm/s	1.3 cm/s
Discharge	$1/2.5 \times 10^5$	$9 \times 10^5 m^3$/day	42 cm^3/s
Diffusivity	$1/4 \times 10^3$	4×10^3 cm^2/s	1 cm^2/s

EXPERIMENT

The experiment was carried out at Ujigawa Hydraulic Laboratory, Disaster Prevention Research Institute, Kyoto University.

A model of Kashima Harbor, as shown in Fig. 8 with horizontal and vertical scales of 1/500 and 1/63 respectively, was made of concrete. The bottom roughness in the model was fixed at n = 0.015 by use of sand of 3 mm in median diameter. In this study the model of the harbor in the temporary stage was used, that is, the harbor was closed along the broken lines in Fig. 8. The semidiurnal tide and the longshore current were provided by an automatically controlled pneumatic tide generator and by a water circulating system, respectively. The water level at 4 stations is measured by wave meters of the electric resistance type. The flow pattern was obtained by intermittently photographing many floats scattered on the water surface with 35 mm cameras. The vertical distribution of the current velocity was measured by photographing the colored line drawn by a dye particle in the water. The diffusion from instantaneous point sources and a continuous point source was investigated mainly by the photographic method and dye concentration analysis. Warm water colored by 'methylen blue' dye was used in place of waste water. The difference of the density between sea water and waste water in the model is usually controlled so as to be 1.4×10^{-3}.

The time change of the visual area of dye patches was

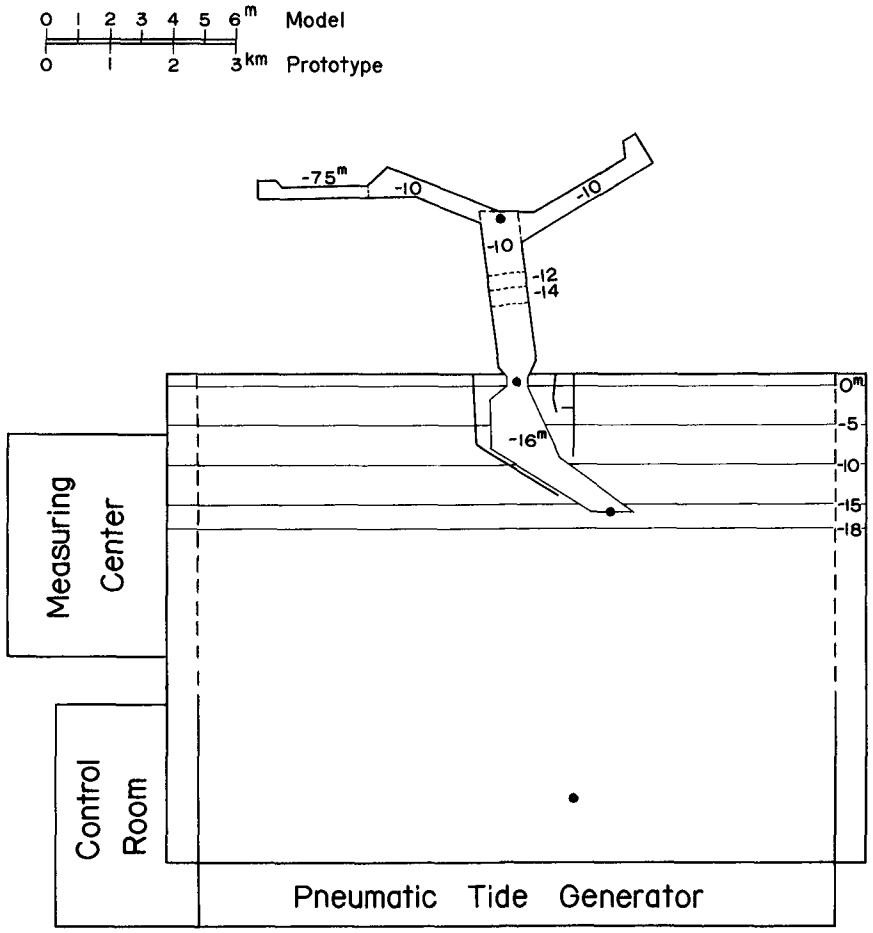

Fig. 8 Model of Kashima Harbor

observed in the same way as in the prototype. When only the semidiurnal tide is provided the diffusivity in and out of the harbor in the model reduced by $K = \Delta S/4\Delta t$, by using warm colored water, is shown in Fig. 9 against the equivalent radius of the patch r. The straight line indicates the value obtained in front of the harbor in the prototype (Fig. 7). The diffusivity in the model is smaller than that in the prototype. This may be caused by the different conditions in the prototype and in the model, that is, there was a southerly longshore current of 20 to 30 cm/sec in the prototype but only the semidiurnal tide was provided in the model.

The diffusivity in the harbor is shown in Fig. 10 when both the semidiurnal tide and the discharge of fresh water of 4.5 x $10^5 m^3$/day from the innermost part of the harbor were provided. The diffusivity is about twice that of the preceding result (Fig. 9). It is considered that the discharged water stimulates the turbulence in the harbor. This figure shows that the diffusivity is about $10^4 cm^2$/sec for the dye patch of 100 m in equivalent radius.

As to the diffusion out of the harbor in presence of both the semidiurnal tide and the longshore current of about 25 cm/sec, the diffusivity has been reduced by $K = \Delta W^2/32\Delta t$ for the plume discharged from a continuous point source, where W is the width of the plume. The result is shown in Fig. 11. In this figure N means the result for northerly current and S for southerly current. Although the methods of analysis are different from each other, the experimental value agrees well with the one observed (Fig. 7).

The front of the dyed water continuously discharged from the innermost part of the harbor is shown in Fig. 12. The full line indicates that in the case without tide and the broken line that with tide. When a discharge of 9 x $10^5 m^3$/day is provided the front comes to the harbor entrance after 2 days, and it goes out to the open sea as a potential flow. The presence of the tide accelerates the diffusion. When the front passes through the harbor entrance in presence of the tide it is pushed into the harbor at high tide and pulled out of it at low tide.

The concentration of the dye near the surface and the sketch of the vertical section along the center line of the harbor is shown in Fig. 13. Entry mixing occurs in the region of the first 1 to 1.5 km and then mixing is weak until a little outside the narrow part (st. 7) and it becomes strong again in the sea area. The length of the region where entry mixing occurs depends on the rate of discharge, that is, the larger the discharge provided is, the longer the length of the region appears.

When both the tide and the longshore current are provided the dyed water pulled out of the harbor at low tide flows discontinuously like a mass of cloud downstream with the longshore current and diffuses horizontally in the early stage. In the later stage, that is, after a few days, the dyed water flows continuously out of the harbor like smoke from a chimney.

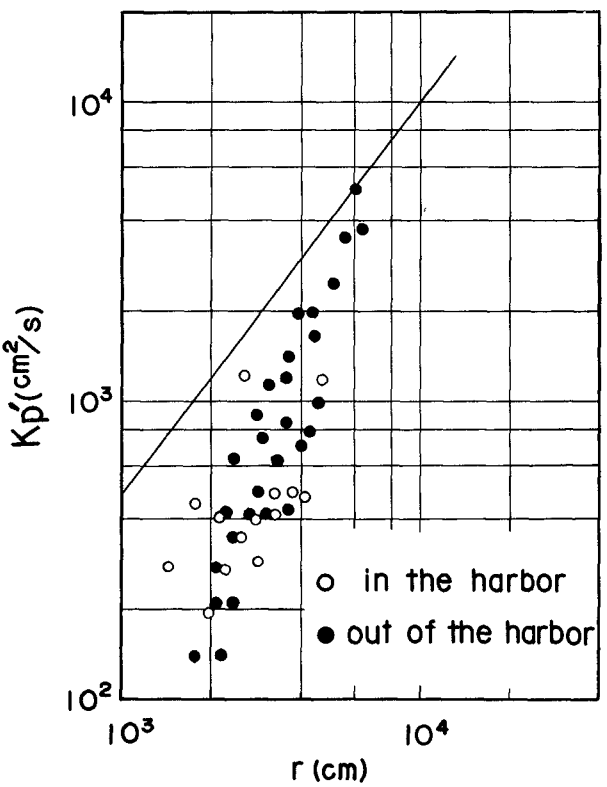

Fig. 9 Diffusivity K_p' and equivalent radius r in presence of the tide (model)

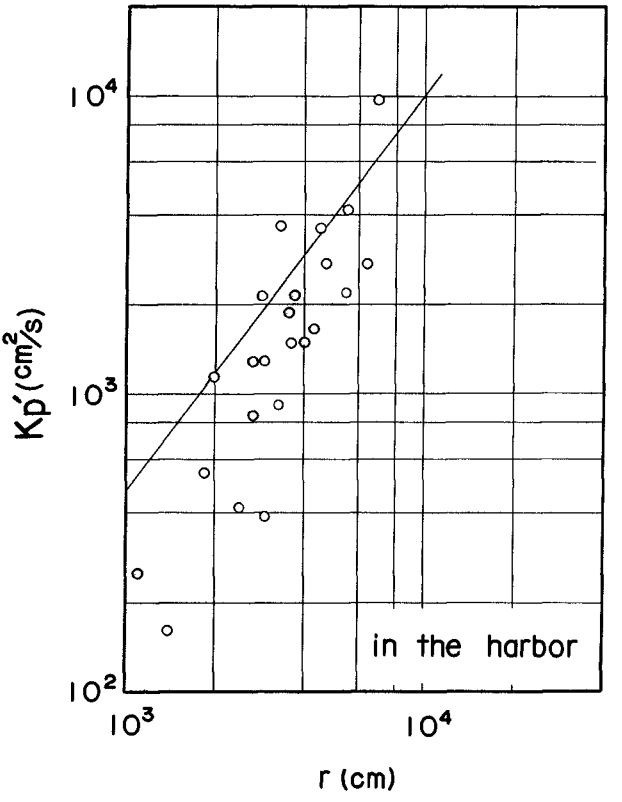

Fig. 10 Diffusivity K_p' and equivalent radius r in presence of both tide and discharge (4.5×10^5 m^3/day) (model)

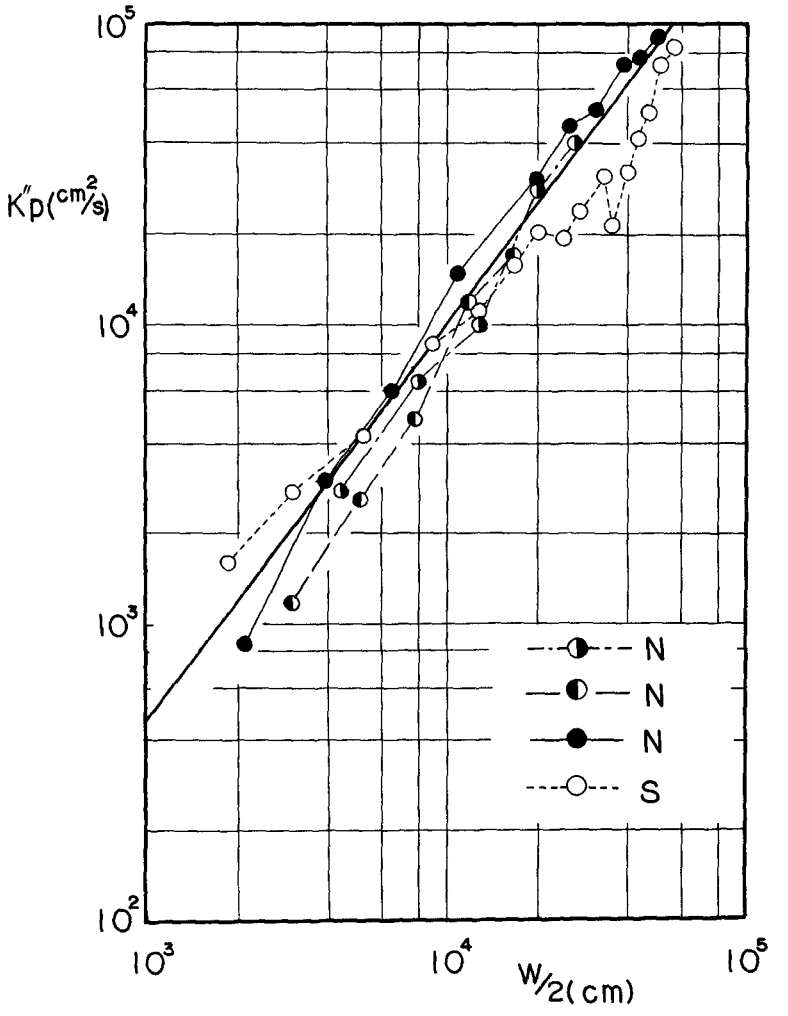

Fig. 11 Diffusivity K_p'' and a half of the width of the plume W/2 in presence of both tide and longshore current (model)

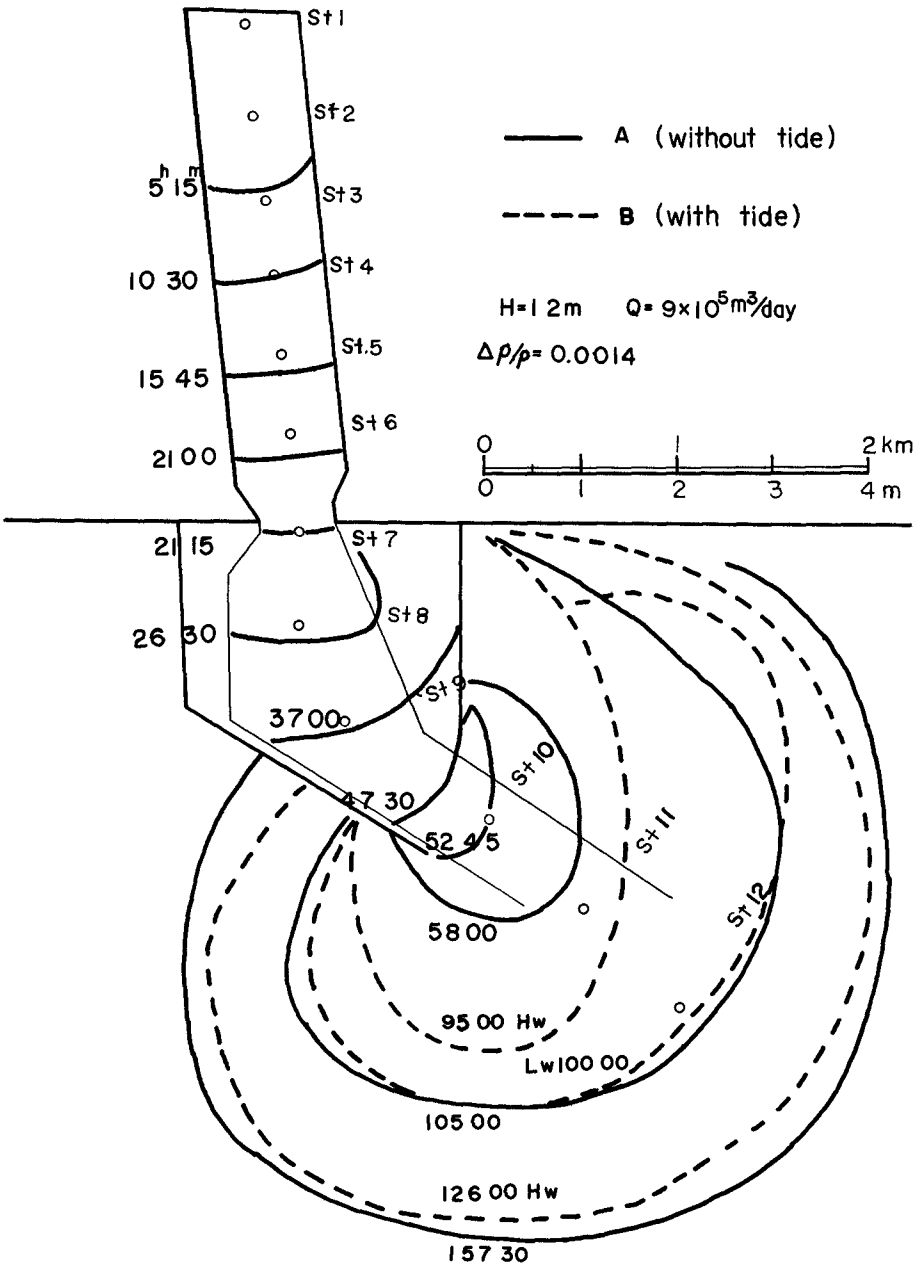

Fig. 12 Change of area with time of dyed water from a continuous point source (model)

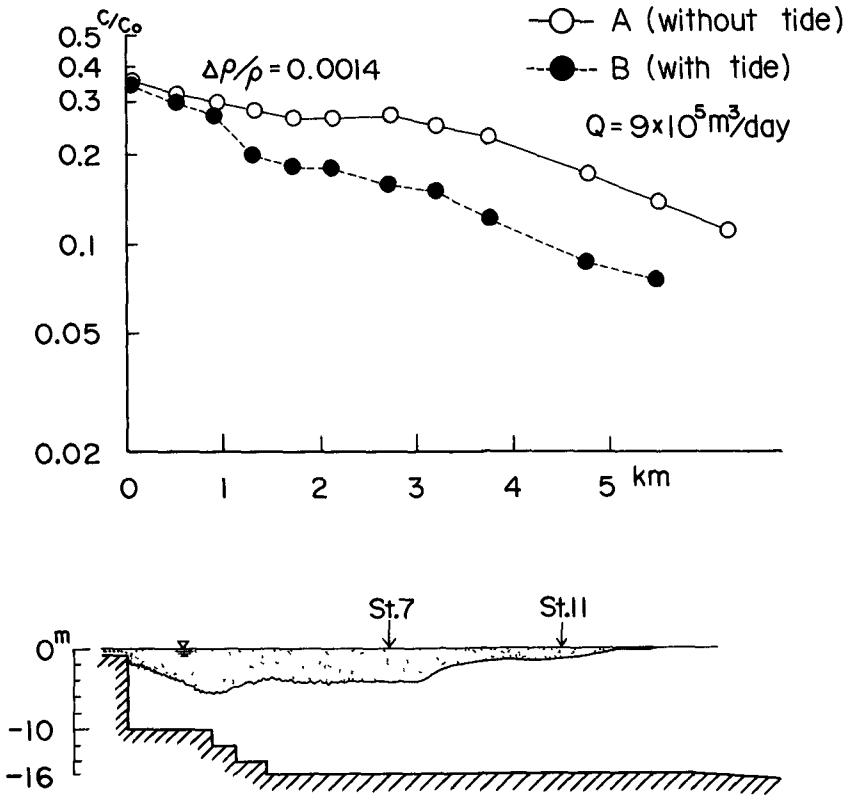

Fig. 13 Horizontal distribution of the relative concentration near the surface (upper)and a sketch of the vertical section (lower) (model)

CONCLUSION

By the present hydraulic model experiment, where the model used to represent the semidiurnal tide and the longshore current had a horizontal scale of 1/500 and a vertical scale of 1/63 and where the direct effect of wind and waves were disregarded, it is established that the diffusion phenomena out of the harbor are almost reproduced in the model. Since the tidal current and also the diffusion are considered to be reproduced in the harbor, the diffusion of waste water in the prototype is expected to be almost the same as in the model.

ACKNOWLEDGEMENTS

The authors wish to thank Professor H. Kunishi, Geophysical Institute, Kyoto University, for his kind advice. Many thanks are also due to Mr. Y. Kitagawa for his assistance in the experiment.

This study was partly sponsored by the Ministry of International Trade and Industry.

REFERENCES

[1] Higuchi, H., and T. Sugimoto (1967): On the hydraulic model experiment on the diffusion due to the tidal current, Disaster Prevention Research Institute Annuals, Kyoto University, No. 10-B, pp. 343-363 (in Japanese)

[2] Ministry of Transportation and Ibaragi Prefecture (1962-1964): On the natural Condition at Kashima Industrial Harbor, Vol. 1, 2, 3, and 4. (in Japanese)

[3] Hirano, T (1966): On the dilution area of effluent in the sea, Special contribution of the Geophysical Institute, Kyoto University, No. 6, pp. 107-112.

CHAPTER 88

SHEAR VELOCITY IN A TIDAL ESTUARY

by

A. Roy Halliwell
Lecturer, Dept. of Civil Eng., Liverpool University, England

and

Brian A. O'Connor
Research Fellow, Dept. of Civil Eng., Liverpool University, England

ABSTRACT

A study involving the determination of the bed shear stress and thence shear velocity in the Narrows of the River Mersey (a well mixed tidal estuary) is described. The two dimensional equation of motion is examined and it is concluded that in order to determine the energy slope (S) (and thence the shear stress and shear velocity) it is essential to evaluate density, inertia and kinetic energy terms as well as surface slopes. Although the density term is much smaller than the other terms it is important at periods of low slack-water.

Measurements of the various terms are described and attention is drawn to the difficulties arising in the case of the surface slopes. Comparison is then made between the values of the shear velocity as predicted from the energy slope and those obtained using velocity traverses throughout the depth and with measurements of velocity at three fixed positions near to the bed. Finally consideration is given to the relationship between the cross-sectional mean velocity ($\bar{\bar{U}}$), the depth-mean velocity ($\bar{U}$) and velocity at 3ft. above the bed (U_3) and the shear velocity obtained from the energy slope. It is concluded that there is good linear correlation of each of these velocities ($\bar{\bar{U}}$, $\bar{U}$ and U_3) with the shear velocity throughout the tidal cycle except for the period around low slack-water.

INTRODUCTION

The shear velocity (u_*) is one of the basic parameters which govern the vertical distribution of sediment in uni-directional flow. It is to be expected that u_* will be as important in the case of tidal flow. However, in this case the variation of the shear velocity with time can be quite rapid; this added complication implies that the problem is essentially more complicated for tidal flow than for the uni-directional case.

Recent research by the junior author has shown that the distribution of sediment in a tidal flow can be described by equations similar to those of the uni-directional flow, e.g. the equation as used by Rouse, Vanoni, Einstein, (ref. 1, 2 and 3) provided the suspension exponent $z = W/\beta K u_*$ is adjusted for the temporal variation of u_* (W is the fall velocity of the sediment particles, K is Von-Karman's constant and β is a numerical constant). The determination of u_* for the case of tidal flows is therefore important for the description of sediment distribution which, in turn, is required if a quantitative analysis of the sediment transport within a tidal area is to be made.

ANALYSIS

The longitudinal equation of motion in two dimensions can be written for an estuary (after Agnew[4]) as:

$$\frac{d}{dt}(\rho U) + \frac{\partial p}{\partial x} - \frac{\partial \tau}{\partial y} = 0 \qquad (1)$$

where ρ : density of water.
τ : shear stress,
y : position on the vertical above the estuary bed,
U : velocity in the x direction (positive seaward)
and p : pressure.

If the vertical density gradient and the velocity in the y direction are ignored and atmospheric pressure is assumed constant then the pressure gradient along the estuary can be written:

$$\frac{\partial p}{\partial x} = -\rho g I + g(H-y)\frac{\partial \rho}{\partial x} \qquad (2)$$

where I : water surface slope (positive ebb direction)
and H : water depth.

Substituting equation (2) into equation (1) and expanding the first term (ignoring variations of density with time) gives

$$\frac{\partial U}{\partial t} + U\frac{\partial U}{\partial x} + \frac{U^2}{\rho}\frac{\partial \rho}{\partial x} - gI + \frac{g}{\rho}(H-y)\frac{\partial \rho}{\partial x} - \frac{1}{\rho}\frac{\partial \tau}{\partial y} = 0 \qquad (3)$$

or

$$\frac{1}{g}\frac{\partial U}{\partial t} + \frac{\partial}{\partial x}\left(\frac{U^2}{2g}\right) + 2D\left[1 - \frac{y}{H} + \frac{U^2}{gH}\right] - \frac{1}{\rho g}\frac{\partial \tau}{\partial y} = I \qquad (4)$$

where D : density slope $= \frac{H}{2\rho}\frac{\partial \rho}{\partial x}$

Substituting $\eta = y/H$ and assuming U^2/gH is very much less than unity, equation (4) can be written:

$$A + F + 2D(1-\eta) - \frac{1}{\rho g H}\frac{\partial \tau}{\partial \eta} = I \qquad (5)$$

Integrating equation (5) throughout the depth (i.e. from $\eta = 0$ to $\eta = 1.0$) and assuming the shear stress at the surface is zero gives

$$\frac{\tau_b}{\rho g H} = S = I - D + A_1 + F_1 \qquad (6)$$

where

$A_1 = -\int_{\eta=0}^{\eta=1.0} A\,d\eta$ = inertia slope,

$F_1 = -\int_{\eta=0}^{\eta=1.0} F\,d\eta$ = kinetic energy slope,

and τ_b = shear stress at the bed.

Now the shear velocity

$$u_* = (\tau_b/\rho)^{\frac{1}{2}} \qquad (7)$$

so equations (6) and (7) show that the shear stress at the bed and the shear velocity are dependent upon density (D), inertia (A_1) and kinetic energy (F_1) terms as well as surface slope (I). In order to determine the variation of u_* throughout a tidal cycle it is therefore necessary (a) to measure the water surface slope along the estuary, (b) to determine the variations of velocity both along the estuary and with time in order to calculate the inertia and

kinetic energy slopes, and (c) to measure the longitudinal variation of density.

In order to determine the inertia and kinetic energy terms A_1 and F_1 the variation throughout the depth of each of the terms A and F is required. It is convenient to consider A and F to increase linearly from zero at the bed to some values A_b and F_b at some small distance above the bed given by $\eta = \eta_1$, and then to increase to surface values of A_s and F_s respectively according to some chosen mathematical relationship. This arrangement is indicated in Fig. 1.

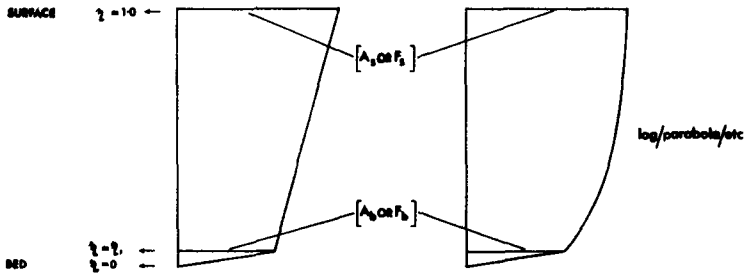

Fig. 1. Assumed variation of inertia and kinetic terms with depth

The simplest relationship to be assumed between $\eta = \eta_1$ and $\eta = 1.0$ is a linear one (Fig. 1a) and the integration of the terms A and F throughout the depth then give:

$$A_1 = -A_b(1 - \tfrac{1}{2}\eta_1) - \tfrac{1}{2}(A_s - A_b)(1 - \eta_1) \qquad (8)$$

and

$$F_1 = -F_b(1 - \tfrac{1}{2}\eta_1) - \tfrac{1}{2}(F_s - F_b)(1 - \eta_1) \qquad (9)$$

The special case of uniform velocity distribution from bed to surface is easily obtained from equations (8) and (9) with $\eta_1 = 0$, $A_s = A_b = A_m$ and $F_s = F_b = F_m$ as

$$A_1 = -\tfrac{1}{2}(A_s + A_b) = -A_m \tag{10}$$

and $$F_1 = -\tfrac{1}{2}(F_s + F_b) = -F_m \tag{11}$$

It is of interest to compute the values of inertia and kinetic energy terms when various distributions throughout the depth are assumed and to compare these values with the linear case given by equations (8) and (9). For this purpose a number of cases are presented below and because the same relationships are true for A_1 and for F_1 only the formulae for F_1 are given.

Log curve with 2 points known

If the value of F near the bed and at the surface are known and the distribution of F is assumed to be logarithmic the expression for F_1 is found to be

$$F_1 = -F_b(1 - \tfrac{1}{2}\eta_1) - \frac{(F_s - F_b)}{\ln(1/\eta_1)} \left[\ln\left(\frac{1}{\eta_1}\right) - 1 + \eta_1 \right] \tag{12}$$

Log curve with 3 points known

In this case it is assumed that a third value of F is known F_1 at η_1 as well as F_b at η_1 and F_s at $\eta = 1.0$. If the distribution is assumed to be linear between the bed and F_b and then two logarithmic curves between F_b and F_1 and F_1 and F_s then the expression for F_1 becomes

$$F_1 = F_b\frac{\eta_1}{2} - F_b\eta_1 - \frac{(F_1 - F_b)}{\ln(\eta_1/\eta_1)} \left[\eta_1 \ln\left(\frac{\eta_1}{\eta_1}\right) - \eta_1 + \eta_1 \right]$$

$$- F_1(1 - \eta_1) + \frac{(F_1 - F_s)}{\ln(1/\eta_1)} \left[\ln\left(\frac{1}{\eta_1}\right) - 1 + \eta_1 \right] \tag{13}$$

Parabolic with 1 point known

The surface value is F_s and the distribution is assumed to be parabolic between the bed and the surface.

$$F_1 = -\tfrac{2}{3} F_s \tag{14}$$

Parabolic with 2 points known

In this case values of F_s and F_b are assumed to be known at $\eta = 1.0$ and η_1 respectively. The distribution of F is assumed to be linear from the bed to $\eta = \eta_1$ and then parabolic to the surface with the requirement that the parabola is tangential to the linear distribution at $\eta = \eta_1$ i.e. no discontinuity in slope at $\eta = \eta_1$. Then

$$F_1 = -\tfrac{1}{2}F_b\,\eta_1 - F_o(1 - \eta_1) - \frac{\tfrac{2}{3}(F_s - F_o)}{\sqrt{1 - \eta_o}}\left[(1 - \eta_o)^{3/2} - (\eta_1 - \eta_o)^{3/2}\right] \qquad (15)$$

where F_o and η_o are given by the equations

$$(F_b - F_o)^2 = \frac{(F_s - F_o)^2}{(1 - \eta_o)}\,(\eta_1 - \eta_o) \qquad (16)$$

and

$$(1 - \eta_o) = \frac{(F_s - F_o)^2}{2F_b(F_b - F_o)} \qquad (17)$$

For consideration of the differences between the various relationships considered it was decided to use typical (maximum) values of the velocities in the estuary reach under study and compute the various values of F_1 obtained using equations (9), (11), (12), (13), (14) and (15).

The surface velocity at either end of the reach under consideration was taken to be 3.0 and 5.0 ft./sec. The variation of velocity with depth was taken as logarithmic and the shear velocity was taken as constant along the reach and equal to 0.24 ft./sec. The velocity near the estuary bed (i.e. $\eta = \eta_1 = 0.05$) was then calculated from the logarithmic velocity distributions and yielded values of 1.21 and 3.19 ft./sec. The mean value of the velocity over the vertical at either end of the reach was also calculated at 2.4 and 4.4 ft./sec. From these figures it is seen that F_s is proportional to $(5^2 - 3^2)$ i.e. 16 while F_b is proportional to $(3.19^2 - 1.21^2)$ i.e. 8.7. If F is determined from the depth-mean velocity, then F is proportional to $(4.4^2 - 2.4^2)$ i.e. 13.6.

The differences between the various assumed vertical profiles for F can now be compared by using the values of F_s and F_b quoted above. The linear distribution (equation (9)) gives F_1 proportional to 12.57 while the simple parabolic case (equation (14)) gives F_1 proportional to 10.7. The more complicated parabolic distribution (equation (15)) gives F_1 proportional to 13.06 whilst the single log curve (equation (12)) gives F_1 proportional to 13.48.

If the value of F is calculated for various elevations above the estuary bed from the two velocity profiles as measured throughout the depth, then the depth-mean value of F is found to be proportional to 13.5. Thus, as expected the single log curve agrees most closely with the depth-mean value of F. The simple linear form is, however, only about 7% less than the much more complicated log expression. The one point parabolic curve shows the worst agreement. The use of the depth-mean velocity to calculate F shows excellent agreement with the depth-mean value of F. Thus the use of the depth-mean velocity to calculate the F_1 term would appear justifiable.

If the velocity profile does not increase regularly from the bed to the surface (e.g. in certain flood profiles in stratified estuaries the surface velocity is lower than at mid-depth) then the value of F_1 will be given by equation (13) with $F_1 > F_s$. In order to examine this type of distribution, the surface velocity at either end of the reach was reduced from 3.0 and 5.0 ft./sec. to 1.8 and 3.0 ft./sec. respectively. The velocity profile is assumed to reduce logarithmically from the surface to mid-depth, the latter has the same value as previously i.e. 2.59 and 4.58 ft./sec. and the distribution below mid-depth is as before. Therefore F_s is now proportional to 5.75 while F_1 in equation (13) is proportional to 14.3 with η_1 equal to 0.50 and $\eta_1 = 0.05$. With these values, F_1 is found to be proportional to 10.64, while the value of F computed from the depth-mean velocity is found to be 10.5. The depth-mean value of F computed at various elevations above the bed from the assumed log velocity profiles is found to be 10.6.

Thus again the value of F_1 computed from the assumed log distribution of F gives excellent agreement with the depth-mean value of F from the velocity profiles. This could be expected since a log curve was chosen for the depth variation both of velocity and of F. There is again close agreement between F computed from the depth-mean velocity and the depth-mean value of F. The depth-mean velocity will therefore be used to compute values of the F_1 term in equation (6).

Consideration of the vertical velocity term in the equation of motion

In deriving equation (6) it was assumed that the vertical velocity could be ignored. For a similar study Sato, Kikkawa and Kishi[5] included this term and found it to be of importance at certain stations of the River Tone. In the case of the Narrows of the River Mersey it was found that this term is relatively small and unimportant. It is possible that at its maximum value it is of the same order as the value of D, however it is only large when the value of S is large and is in general less than 10% of the value of S. The value of D on the other hand is constant throughout the tidal cycle and is therefore important when the value of S is small, around the periods of slack water.

MEASUREMENTS

The previous analysis indicates that four basic quantities, I, A_1, F_1, and D, have to be determined from field observations in order to calculate the bed shear. The necessary field work has formed part of a much larger research programme (which is still in progress) for the investigation of the water and sediment circulation patterns of the Mersey Estuary. This research is sponsored by the Mersey Docks and Harbour Board.

The field observations of velocity, density etc. from which the four basic quantities are determined have been made in an area of the Mersey known as the Narrows. The estuary here runs a straight course for several miles (cross-flow is thus a minimum) and is narrow enough to be unaffected by coriollis forces. It is however, wide enough to be considered two dimensional. The reach is also free of rapid changes in cross-section and the estuary is well mixed so that the vertical salinity distribution in the Narrows is almost uniform (i.e. less than 2% difference between surface and bed). The measurement of I, A_1, F_1 and D in this research are now considered separately.

(1) Water Surface Slope (I)

In the absence of cross-flow, Corriollis and wind forces, the term I can be taken as constant across the width of the estuary. Its magnitude was found initially by an examination of the automatic tide recordings at Gladstone Dock and Princes Pier. These gauges are both situated on the East side of the river at the ends of the reach under consideration. A preliminary examination of water surface slope from the tide gauge records indicated some very odd results e.g. large flood slopes in the middle of the ebb tide.

Each tidewell was then critically examined. At Princes stage it was found that the tidewell (an 8" O.D. pipe) was situated in a fairly fast flowing stream. Research work by Perry [6 & 7] indicated that this particular tide gauge was subject to an error which caused the water surface level inside the well to be greater than that outside and this error depended on the magnitude of the flow velocity past the tide gauge orifice. Meanwhile Lennon[8] had demonstrated that both Princes and Gladstone tide gauges were subject to a salinity stratification i.e. the density of water in the well at high water decreased from the low water salinity value at the surface to the high water salinity value in the region of the orifice. Thus at high water the level inside the tidewell was greater than in the tideway. A further difference of level between the tidewell and tideway can also be caused by the presence of silt which enters the well from the tideway on the flood tide. In the limit the silt completely blocks the tidewell orifice and the water is unable to escape. Further errors can also result from the automatic recording equipment itself e.g. eccentric timing mechanisms and badly aligned pen carriages. Because of all the above mentioned difficulties the water surface slope was determined independently of the automatic tide gauge equipment and of the Princes tidewell.

A self-aligning engineers level was mounted on a floating pontoon attached to Princes Stage (a floating landing stage) at approximately 6-8ft. from a tide staff. The latter could be read to $\pm \frac{1}{4}$". Readings on the tide staff were taken continuously for a period of 30 seconds every 15 minutes. The height of collimation of the level was determined at slack water and checked during the course of the experiment. The water level was also read directly from the tide staff as a cross-check.

The level at Gladstone was determined by using an electronic probe device which indicated the water level relative to the top of the well of the tide-gauge. Basically this instrument consists of a pointer attached to a surveyor's tape through which a current is passed, the other electrode usually being the well itself. As the pointer touches the water surface the circuit is completed and this is registered as a frequency-change in an audio-signal transmitted from the instrument. This instrument could be read to $\pm 1/16$ in. The salinity of the water in the well was measured at slack high and low water as also was the salinity in the tide-way at the orifice level. Errors due to silt were eliminated by cleaning the well, the day previous to the tests. There is little velocity past this well except when ships are entering Gladstone Dock, the level in the tideway is therefore assumed to be equal to that in the well, less the salinity error.

The tide curves at each station were then plotted and smoothed(particularly the Gladstone curve near high water when the passage of ships into the Dock caused the levels to be slightly reduced). The water level at Gladstone was then corrected for the salinity error using the mean value of the salinity (i.e. density) inside and outside the well. The difference at any instant of time between this curve and that observed at Princes is then the water surface slope along the reach (I)

(ii) Inertia Slope (A_1)

In three-dimensional flow this term will not be a constant across the estuary since the lateral distribution of velocity (U) is not constant. In the two-dimensional case the variation of A_1 across the estuary is ignored and the variations of the mean velocity are considered. Thus for the present calculation A_1 will be determined from the cross-sectional mean velocities at the surface and near the bed.

Several days field observations of the water velocity near the estuary bed and at the surface were available for a position in the centre of the river, midway between Princes Pier and Gladstone Dock. These observations were collected as part of the general research work in progress in the Mersey estuary. The velocities were measured using a Kelvin Hughes Direct Reading Current Meter. These field results were plotted out against time and the surface and near-bed velocities taken off the resulting graphs at half-hourly intervals. These velocities were then plotted against high water level (similar to the effect of range in the Mersey) so that a set of velocities could be obtained at half-hourly intervals for a tide of approximately 27.5 ft. H.W. (L.B.D.).

From the work of Burke[9] it is possible to relate the depth-mean velocity ($\bar{U}$) at the position under consideration to the cross-sectional mean velocity ($\bar{\bar{U}}$) i.e. $\bar{U} = a\bar{\bar{U}}$ where a is a constant. Thus it is possible by using this relationship to reduce the half-hourly surface and near bed velocities to the equivalent cross-sectional mean velocity.

Values of A_b and A_s, every half hour were then calculated from the reduced (cross-sectional mean) velocities. A_1 at each time interval then follows from equation (8) with $\eta_1 = 0.05$.

(iii) Kinetic Energy Slope (F_1)

This quantity will also vary across the width of the estuary, depending on the velocity distribution across the width. For the case of two dimensional flow the cross-sectional mean velocity ($\bar{\bar{U}}$) will again be used to compute F_1. In the case of a real estuary the value of $F_1 = \frac{\partial}{\partial x}\left(\bar{\bar{U}}^2/2g\right)$, will not be equal to the mean value of F_1, for the cross-section and a factor (α) must be used

to account for this discrepancy. The constant (α) can vary from 1.0-2.0 depending on cross-sectional shape. In the case of the Mersey, in the area of the Narrows, the constant will be of the order of 1.1 and because of this, the correction will not be applied (i.e. α is taken as 1.0). In order to compare the two dimensional equation with river observations, a position was chosen at which the mean depth is close to the cross-sectional mean-depth. Cross-sectional effects should therefore be a minimum.

The calculation of F using F_b and F_s has not been possible since this requires velocity measurements opposite Princes Pier, which is the centre of ship passenger traffic for Liverpool, Birkenhead, North Wales and the Isle of Man. Use has therefore been made of the cross-sectional mean velocity ($\bar{U}$) in order to calculate F. The value of $\bar{U}$ every half hour throughout a tidal cycle at various cross-sections along the river, including Gladstone and Princes, have been computed by Burke[9] using the continuity equation. The value of F_1 at half-hourly intervals through a tidal cycle can thus be calculated as the difference between ($\bar{U}^2/2g$) at Princes and Gladstone. Adjustments to $\bar{U}$ for different tidal ranges are also possible since the variation of $\bar{U}$ with high water level (or range) is linear in this reach of the Mersey. In the present computations F_1 has been calculated for a high water level of just over 27ft. i.e. similar to the tides for which the surface slope was measured.

(iv) Density Slope (D)

This term indicates the presence of a longitudinal density gradient in the Mersey which is always present due to the mixing of fresh and saline water. Its order of magnitude in the case of the Mersey is small but it can be significant when the terms I, A and F are small (e.g. slack low water).

In order to indicate the relative magnitude of all the terms (I, A_1 and F_1) these have been expressed in terms of D (Fig. 2). Thus on large Spring Tides the total energy slope can be the order of twenty times the density effect, but on Neap Tides with a large freshwater flow this could be reduced to less than ten times the density effect. For the purposes of the present calculation, the density term is taken as solely due to the variation of salinity along the estuary (i.e. depth variation is ignored) and to be a constant throughout the tide.

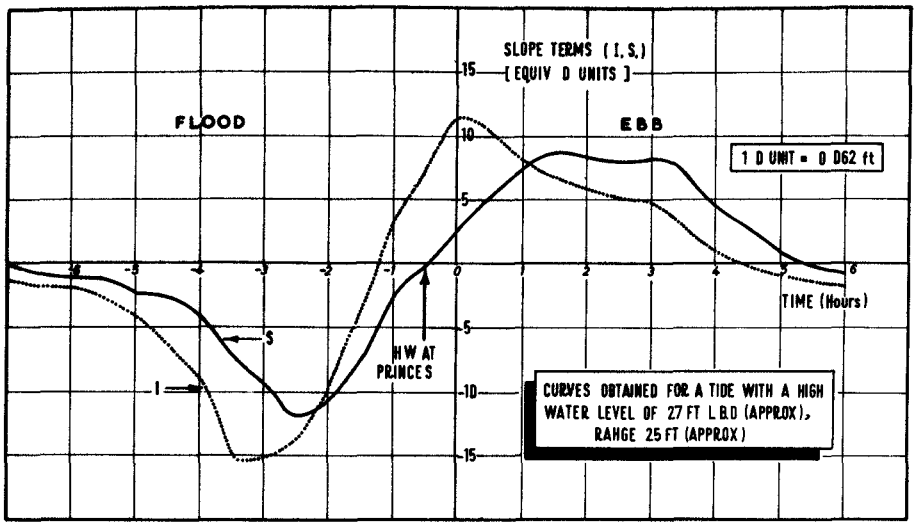

Fig. 2. Variation of Water Surface and Energy Slopes Throughout the Tidal Cycle

Longitudinal salinity data obtained by Wallingford[10] for a model of the Mersey Estuary was examined and a longitudinal profile of mean salinity produced. From this, a mean longitudinal salinity gradient was produced. This was then combined with the centre-line mean-depth of the reach to produce an overall mean figure for the density term D. This amounted to a head difference over the Princes to Gladstone Reach of 0.062 ft. in the horizontal distance of 16,000 ft.

The energy slope (S) can now be calculated from equation (6) using the components I, A_1, F_1 and D and this is shown in Fig. 2. Once S is known, the shear on the bed (τ_b) can be calculated as also can $u_* = (\tau_b/\rho)^{\frac{1}{2}}$ as shown in Fig. 3.

Shear velocity using velocity profiles

The value of u_* thus obtained can also be compared with measurements taken in the field. A position on the cross-section midway between Gladstone and Princes was selected such that the depth at mean tide level was approximately equal to the mean cross-sectional depth at mean tide level. Measurements of the water velocities were made on a vertical from the surface to approximately 3ft. above the estuary bed. This was done using the direct reading current meter. These velocity transverses were made at approximately half-hourly intervals. The velocities in the region 6in. -3ft. above the bed were measured using three Ott Mark V Arkansas Current Meters mounted on a vertical freely pivoting rod which was held within a triangular framework. The Ott Meters were connected to a control unit which enabled the three meters to be read simultaneously. The length of time for which the velocities were recorded could be varied to any time interval.

In the case of the present observations a time interval of 10 seconds was used which appears to have been too low since the included results for u_* show a large scatter. Some of this scatter has been reduced by averaging all the results taken within each fifteen minute time interval. The shear velocity is obtained from the results by making a semi-log plot of the velocities against height above the bed, as was done by Lesser[11]. The same technique was used with the vertical profiles obtained with the D. R. C. M. except that the semi-log plots were confined to below mid-depth so that any wind, ship effects etc. were avoided. The comparison between the river results and those from equation (7) are shown in Fig. 3.

Bowden[12] has suggested that u_* can be related to the depth-mean velocity in a linear fashion i. e. $u_* = k\bar{U}$. In order to examine the relationship between velocity and u_*, the velocity at 3ft. above the estuary bed (U_3), the depth-mean velocity and the cross-sectional mean velocity were plotted against time. Three values of k were determined from these plots such that the sum of the squares of the errors in prediction was a minimum i. e. $\sum(kU-u_*)^2$ was a minimum (with U equal to U_3, $\bar{U}$ and $\bar{\bar{U}}$ in turn). The three values found were $k_1 = 0.077$, $k_2 = 0.052$, $k_3 = 0.054$, for the velocity at 3ft. above the bed, the depth mean and the cross-sectional mean respectively. A measure of the best relationship of the three is provided by the term $\sum(kU-u_*)^2$, it was found that the cross-section mean velocity provided the best fit. The comparison of the three values of u_* using the values of U_3, $\bar{U}$ and $\bar{\bar{U}}$ with that value of u_* calculated from the energy slope method is shown in Fig. 4.

DISCUSSION OF RESULTS

The comparison between u_* computed from the energy slope method and from the tripod results (Fig. 3) is seen to be reasonable. It is felt that much of the scatter on the tripod results is due to two main causes. Firstly, the timing interval for the Ott current meters was too low. This enabled large velocity fluctuations, and thus fluctuations in shear to be recorded. Secondly the two calculations of u_* from the velocities at 6" and 12" and the velocities at 12" and 27" indicate that the top Ott meter (27") may have

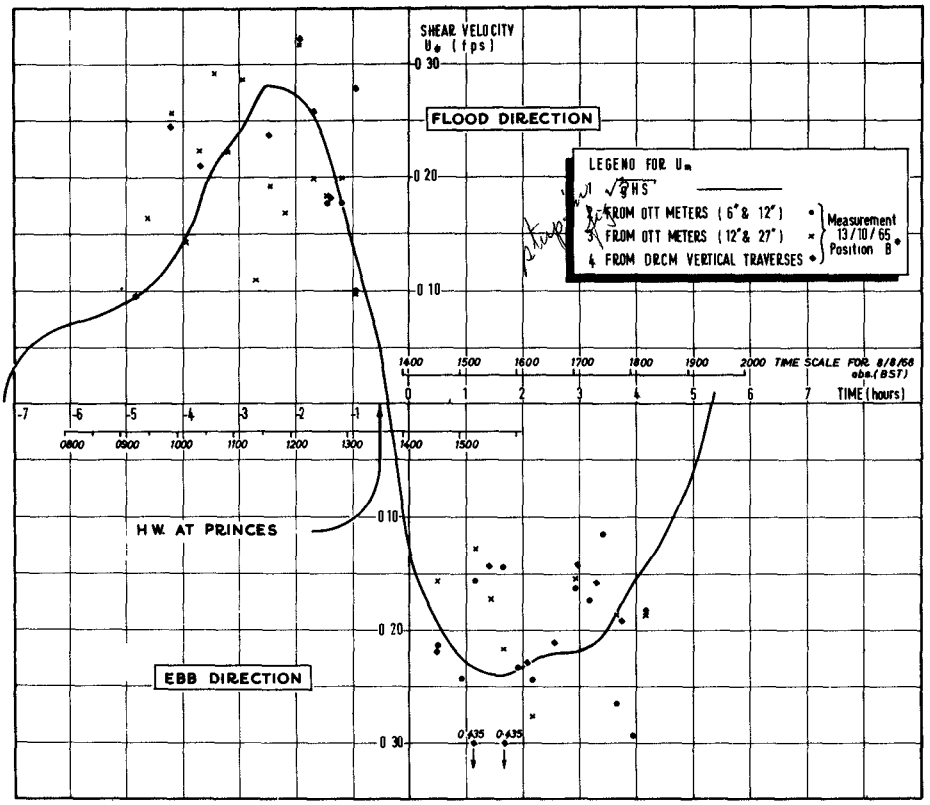

Fig. 3. Comparison between measured values of shear velocity with those obtained from the energy slope

been affected by the supporting framework of the tripod rig. If this is so some re-design of the framework will be necessary. The question of velocity fluctuation can be overcome by a longer timing interval. Another possible reason for the values of u_* obtained from the meters at 12" and 27" generally being too small may be that the meter at 27" had a different blade pitch than the other two meters and this may cause it to react differently to any turbulence.

The shape of the u_* curve (from the energy slope) is seen to closely follow the shape of the velocity distribution near the bed. However, the water surface slope is seen to be out of phase with both the u_* and the velocity curves, particularly on the ebb tide.

If the velocity is used to determine u_* by assuming a linear relationship ($u_* = kU$) i.e. bed roughness is assumed constant, then the cross-sectional mean velocity, rather than the velocity near the bed, is found to be a better fit for u_* as calculated from the energy slope. Thereason for this is probably the uncertainty of the position of the D. R. C.M. near the estuary bed; the averaging over the vertical etc. for the mean velocities tending to reduce these sort of effects. The reasonable fit of the cross-sectional mean velocity to the u_* curve (except at low water) does however mean that the mean velocity could be used to determine the shear velocity in those areas remote from land (e.g. Liverpool Bay) where it is not possible to measure the water surface slope etc. and where density effects are small. These velocities could be obtained by field measurements or even by computation if an accurate mathematical model is available.

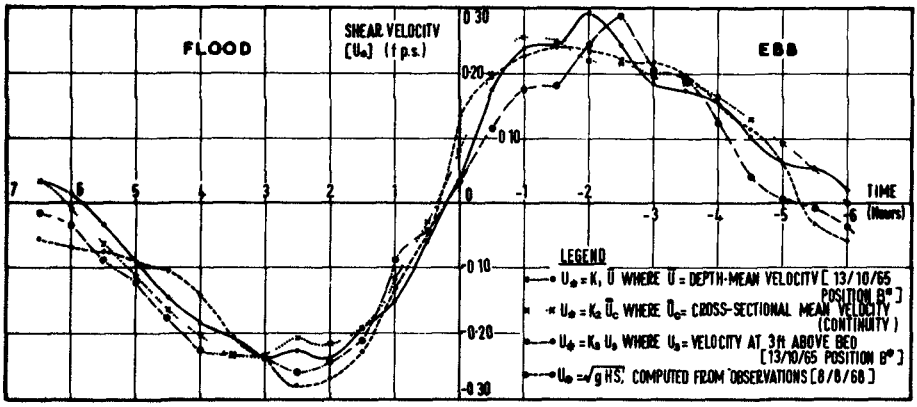

Fig. 4. Comparison between shear velocity obtained from velocity near the bed, depth-mean velocity and cross-sectional mean velocity

The results also indicate that u_* can be found for an estuary without taking many field observations. The water surface slope and density terms can be measured at the shore, while the kinetic and inertia effects could be obtained using velocities computed by applying the continuity equation to the estuary. This would produce the cross-sectional mean velocity ($\bar{U}$) from which the A and F terms could be found.

ACKNOWLEDGMENTS

The work described is part of a general investigation sponsored by the Mersey Docks and Harbour Board. The authors are therefore pleased to acknowledge the help of the Board, in providing vessels and personnel, and the help of members of the University Civil Engineering Department. Thanks are especially due to Messrs. J. A. Nickson, C. Hewitt and M. O'Dell for their help with the field observations.

NOTATION

A : inertia term

D : density slope

F : kinetic energy term

H : water depth

I : surface slope (positive when sloping downwards from land to sea)

U : velocity in the x direction (seawards)

$u_* = (\tau_b/\rho)^{\frac{1}{2}}$: shear velocity

x : distance measured along the estuary, seawards

y : distance vertically above the bed

α : coefficient

$\eta = y/H$: percentage depth

ρ : density

τ : shear stress

Subscripts -

b : near the bed

s : surface

1 : intermediate position

m : mean value

1 : when used with A and F implies integrated values throughout the depth.

REFERENCES

1. Rouse, H. "Modern conceptions of the mechanics of fluid turbulence" Trans. A. S. C. E. Vol. 102, 1937, Fig. 30 p. 536.

2. Vanoni, V. A. "Transportation of suspended sediment by water" Trans. A. S. C. E. Vol. 1946, pp. 67-102.

3. Einstein, H. A. "The bed load function for sediment transportation in open channel flows". United States Dept. of Agric. Tech. Bull. No. 1026, Sept. 1950.

4. Agnew, R. "Estuarine currents and tidal streams" Proc. 8th Coastal Eng. Conf. 1960, Chapter 28, pp. 510-535.

5. Sato, S., Kikkawa, H. and Kishi, T. "On the hydraulic characteristics of the tidal reach of the Tone River" Paper A6, Proc. I. A. H. R., The Hague, 1955.

6. Perry, J. G. "Hydrodynamic Studies on tide gauges" University of Liverpool, M. Eng. Thesis 1967.

7. Halliwell, A. R., and Perry, J. G. "Errors in tide gauges" Dock and Harbour Authority, Vol. XLVIII, February 1968, pp. 305-308.

8. Lennon, G. W. "The behaviour of a stilling well in the presence of periodic density variations" University of Liverpool, Tidal Institute, Internal Report No. 7.

9. Burke, C. "Velocities in tidal flows" M. Eng. Thesis, Liverpool University, August 1966.

10. D. S. I. R. Hydraulic Research Station, 2nd Internal Report on the Mersey Investigation, June 1959.

11. Lesser, R. M. "Some observations of the velocity profile near the sea floor". Trans. A. G. U. Vol. 32, No. 2, April 1951, pp. 207-211.

12. Bowden, K. F. "The mixing processes in a tidal estuary". Int. J. Air Wat. Poll. Pergamon Press 1963, Vol. 7, pp. 343-356.

CHAPTER 89

BUOYANCY SPREAD OF WASTE WATER IN COASTAL REGIONS

IAN LARSEN, Research Engineer
Vattenbyggnadsbyrån (VBB) Ltd, Stockholm, Sweden
TORBEN SÖRENSEN, Director
Danish Institute of Applied Hydraulics, Copenhagen, Denmark

ABSTRACT

Waste water may due to buoyancy effects spread horizontally on top of the recipient. The spreading is chiefly determined by the buoyancy flux and to a large extent unaffected by dilution and diffusion. This phenomenon is of great practical importance for larger outfalls of waste or cooling water in coastal regions.

INTRODUCTION

The discharge of sewage water or cooling water into a recipient normally represents a buoyancy flux: The product of the discharge and the density difference between the receiving water and the waste water due to differences in salinity or temperature. In a homogeneous recipient this product is obviously indifferent to dilution.

The rising of the waste water to the surface if discharged below surface has been described in literature and will not be treated here.

The object of this paper is to describe what may be expected to happen when the diluted waste water at the rate of Q arrives at the water surface - or is trapped at an intermediate level - with almost the same horizontal velocity, U_o, as the main current. Due to the relative difference in density, Δ , the diluted waste water will try to spread in all directions.

BUOYANCY SPREAD WITHOUT VERTICAL TURBULENT DIFFUSION

The sheet of waste water formed on top of the main current is supposed to have a uniform thickness, h, in the direction perpendicular to the main current. According to ABBOTT (ref. 1) a density

front, h in thickness, will advance with a velocity $v = \sqrt{\Delta g h}$ relative to the main current, g being the acceleration of gravity. With the notations of fig. 1 the front condition states

$$U_o \sin\theta = \sqrt{\Delta g h} \qquad (1)$$

When turbulent diffusion is neglected, the continuity equation is

$$2 B h U_o = Q \qquad (2)$$

Integration yields

$$\frac{B}{B_o} = 1.31 \left\{\frac{x}{B_o}\right\}^{2/3} + 1 \qquad (3)$$

where B_o is the initial half width of the sewage field, chosen so that the front velocity at this section equals the velocity of the main current:

$$B_o = \frac{\Delta g Q}{2 U_o^3} \qquad (4)$$

Only the product of Δ and Q, being equivalent to the buoyancy flux appears in Eq (3) and (4). For a homogeneous recipient the spread is evidently not dependent on the initial dilution at x = o.

Normally B_o is larger than the diameter of the rising jet of waste water or the width of the outlet of cooling water. If not the equation of spreading, Eq (3), will have to be modified but the dependence of the buoyancy flux will remain.

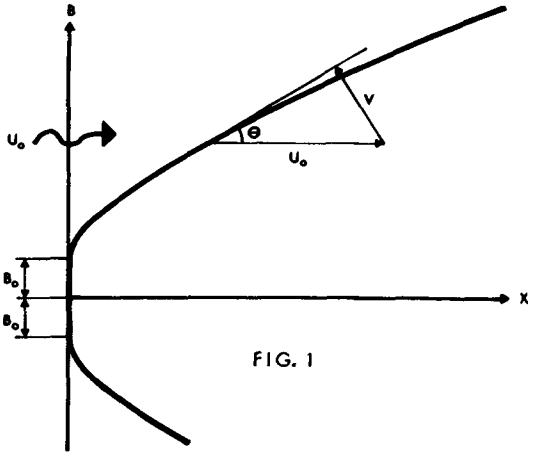

FIG. 1

TURBULENT DIFFUSION

Turbulent diffusion between two layers of slightly different density has been discussed by LARSEN (ref. 2). When turbulence is produced mainly outside the transition region it was by dimensional reasoning found that the velocity of exchange, W_e, between the layers could be expressed by

$$\frac{W_e}{\sqrt[4]{\nu\, w}} = f\left\{\frac{\rho\, w}{\Delta' \rho\, g\, \sqrt[4]{\nu\, w}}\right\} \tag{5}$$

where Δ' is the relative difference in density, ν is the kinematic viscosity, ρ the density of water and w the dissipation of energy into heat per unit mass of water. The function $f\{-\}$ would depend on the ratio between the rates of dissipation in the two layers assuming homogeneous turbulence. When the respective values of w in the two layers are equal, W_e represents the transfer in both directions but in case the level of turbulence in one layer is much lower than in the other the transfer expressed by W_e will only be from that layer to the other. It was estimated that the function $f\{-\}$ in both cases would be rather linear, the coefficient of proportionality, α, being of the order of magnitude 0.2 in agreement with experiments reported by ELLISON and TURNER (ref. 3). The dissipation of energy in the surface layer of a uniform current with a velocity U_o and a depth d is of the order of magnitude

$$w \sim \frac{U_o^3}{1000\, d} \tag{6}$$

and the rate of diffusion may then be estimated by

$$W_e \cdot \Delta' \cdot g \sim \frac{\alpha\, U_o^3}{1000\, d} \tag{7}$$

BUOYANCY SPREAD WITH DIFFUSION

The equation of continuity is

$$\frac{d}{dx}\left\{\Delta' B \cdot h \cdot U_o\right\} = - W_e \cdot \Delta' \cdot B \tag{8}$$

as well in the case of one sided vertical diffusion from the top layer to the underflowing recipient as in the case of symmetrical turbulent exchange between these layers. According to Eq (7) the right hand side of Eq (8) varies only with B. If $\Delta' \cdot h$ and B are considered as the dependent variables, the solutions to Eq (8) and Eq (1) are common for the two cases considered. In the former case Δ' is constant, Δ, and h varies with x. In the latter both Δ' and h vary with x but the total flow $2B \cdot h \cdot U_o$ is constant. (h is here an equivalent thickness of the surface layer).

A parameter of diffusion may be defined according to

$$M = \frac{W_e \cdot \Delta' \cdot g \cdot B_o}{U_o^3} = \frac{a\, B_o}{1000\, d} \qquad (9)$$

The result of integration of Eq (8) and Eq (1) as shown in fig. (2) indicates that the variation of B with x is rather unaffected by

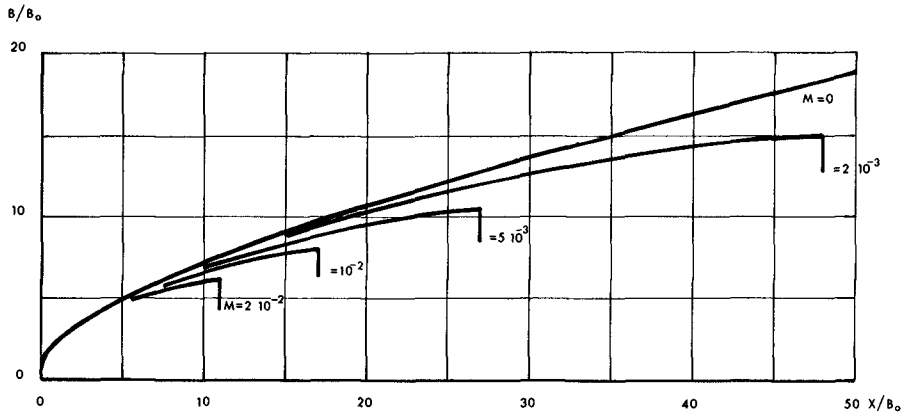

FIG. 2

the rate of turbulent diffusion expressed by the value of M as long as the surface layer exists. The width, B, of the sewage field may therefore be calculated according to Eq (3).

An evaluation of the distance x_m over which the waste water is able to spread due to density effects, may now be obtained by integration of Eq (8) using Eq (3). The result is shown graphically in Fig. 3.

In case of symmetrical turbulent exchange the dilution, S, of the waste water will be determined by

$$\frac{1}{S} = 1 - \frac{Mx}{B_o} \left\{ 0.78 \left(\frac{x}{B_o}\right)^{2/3} + 1 \right\} \qquad (10)$$

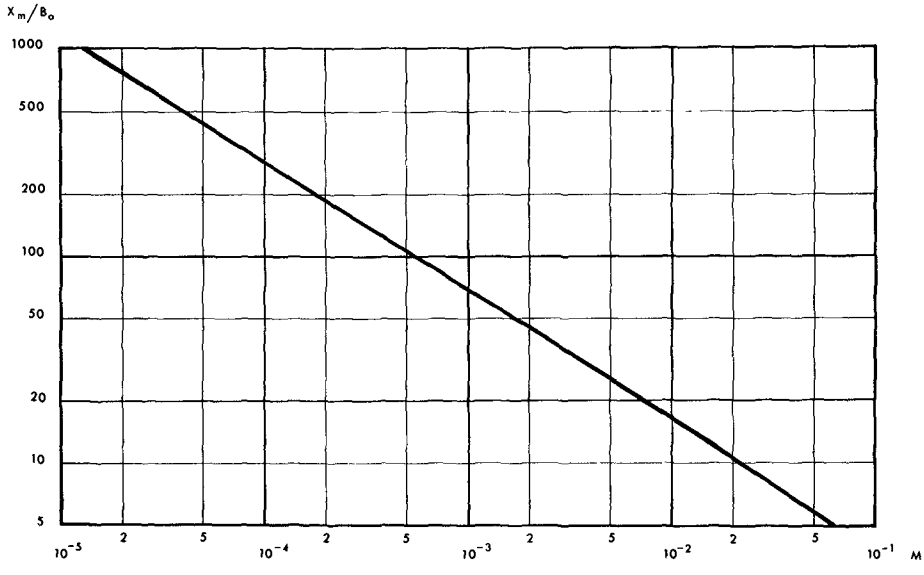

FIG. 3

NUMERICAL EXAMPLE

Waste water is discharged into a homogeneous recipient at the rate of $q = 10\ m^3/sec$. The relative difference in density between the undiluted waste water and the recipient is $\Delta_o = 25\ 10^{-3}$. The depth of the recipient is 10 m. One sided transport is considered and a is taken as 0.2. The dilution at the point of discharge is irrelevant, the buoyancy flux corresponds to $\Delta Q = \Delta_o\ q = 0.25\ m^3/sec$.

According to Eqs (3), (4) and Fig. 3.

U_o	m/sec	0.10	0.20	0.40
B_o	m	1250	156	19.5
M	-	0.025	0.0031	0.00039
x_m/B_o	-	9	35	120
x_m	m	11300	5500	2340
B_m/B_o	-	7	15	31
B_m	m	8700	2340	600

For smaller values of U_o the level of turbulence may no longer be determined by the bottom shear alone. This corresponds to larger values of M and the numerical results may be somewhat doubtful.

CONCLUSION

The theory presented above taking into account the vertical turbulent diffusion shows that the spreading of waste water due to density differences is determined chiefly by the buoyancy flux and to a large extent unaffected by dilution and diffusion. The theory is incorrect in many details but may be expected to give results of the correct order of magnitude. Calculations for outfalls from larger cities will show that places normally considered sheltered from the outfall zone by a region of considerable turbulent diffusion may in some cases be polluted by poorly diluted waste water. The influence of wind may add significantly to this effect.

REFERENCES

1. M.B. ABBOTT: On the spreading of one fluid over another, La Houille Blanche No 5-6 Dec 1961.

2. Ian LARSEN: On turbulent diffusion in the presence of a density gradient. Publication No 1968:3, Institution of Sanitary Engineering, Technical university of Stockholm, Sweden.

3. ELLISON and TURNER : Mixing of dense fluid in a turbulent pipe flow. Journal of Fluid Mechanics Volume 8, 1960.

CHAPTER 90

USE OF A COMPUTATIONAL MODEL FOR TWO-DIMENSIONAL TIDAL FLOW

Jan J. Leendertse*
The RAND Corporation
Santa Monica, California

INTRODUCTION

The numerical solution of tidal hydraulic problems has been greatly facilitated in the last decade by the development of high-speed large-memory computers. Problems which only could be studied by use of hydraulic models can now readily be studied with mathematical models if the computational techniques for solutions are developed.

Unfortunately the difficulties in formulating usable methods for these complicated problems in fluid dynamics are formidable, particularly if the problems are multidimensional in space. As a result the numerical solution approach to these hydraulic problems has generally been limited and has not kept pace with the incressed capabilities of the presently available computers.

In this paper a new approach is given to the solution of two-dimensional tidal flow in shallow water.

THE DIFFERENTIAL EQUATIONS REPRESENTING TIDAL FLOW

The basis of the computational model for tidal flow is the long-period water-wave equations (ref. 1):

$$\frac{\partial U}{\partial t} + U\frac{\partial U}{\partial x} + V\frac{\partial U}{\partial y} - fV + g\frac{\partial \zeta}{\partial x} + g\frac{U(U^2+V^2)^{\frac{1}{2}}}{C^2(h+\zeta)} = 0 \qquad (1)$$

$$\frac{\partial V}{\partial t} + U\frac{\partial V}{\partial x} + V\frac{\partial V}{\partial y} + fU + g\frac{\partial \zeta}{\partial y} + g\frac{V(U^2+V^2)^{\frac{1}{2}}}{C^2(h+\zeta)} = 0 \qquad (2)$$

$$\frac{\partial \zeta}{\partial t} + \frac{\partial[(h+\zeta)U]}{\partial x} + \frac{\partial[(h+\zeta)V]}{\partial y} = 0 \qquad (3)$$

Symbols are defined as follows:

- U, V : vertically integrated velocity components in the x and y direction respectively
- ζ : elevation of the free surface over the undisturbed level
- h : depth
- g : acceleration due to gravity
- f : Coriolis parameter
- C : Chezy coefficient

*This research is sponsored by the United States Air Force under Project RAND. This is an abridgment of RAND Memorandum RM-5294-PR. The views, conclusions, and recommendations expressed herein do not necessarily reflect the official views or policies of the United States Air Force.

THE SYSTEM OF THE FINITE-DIFFERENCE EQUATIONS IN TWO DIMENSIONS

The following notation is used in the approximation of the differential equations:

$$u^{(n)}_{j,k} \equiv U(j\Delta x,\ k\Delta y,\ n\Delta t); \quad \Delta x = \Delta y = \Delta s \tag{4}$$

where

$(x,y) = (j\Delta x,\ k\Delta y)$ and is a spatial grid point

$j,k = 0,\ \pm\tfrac{1}{2},\ \pm 1,\ \pm 3/2,\ \ldots$

$n = 0,\ \tfrac{1}{2},\ 1,\ 3/2,\ 2$

Furthermore, the following notation of averages and differences shown here for ζ, is introduced:

$$\overline{\zeta}^{x}_{j,k} \equiv \tfrac{1}{2}\,(\zeta_{j+\frac{1}{2},k} + \zeta_{j-\frac{1}{2},k}) \tag{5}$$

$$\zeta_{x} \equiv (\zeta_{j+\frac{1}{2},k} - \zeta_{j-\frac{1}{2},k}) \tag{6}$$

$$\overline{\zeta}^{y}_{j,k} \equiv \tfrac{1}{2}\,(\zeta_{j,k+\frac{1}{2}} + \zeta_{j,k-\frac{1}{2}}) \tag{7}$$

$$\zeta_{y} \equiv (\zeta_{j,k+\frac{1}{2}} - \zeta_{j,k-\frac{1}{2}}) \tag{8}$$

$$\overline{\zeta}_{j,k} \equiv \tfrac{1}{4}\,(\zeta_{j-\frac{1}{2},k-\frac{1}{2}} + \zeta_{j-\frac{1}{2},k+\frac{1}{2}} + \zeta_{j+\frac{1}{2},\,k-\frac{1}{2}} + \zeta_{j+\frac{1}{2},k+\frac{1}{2}}) \tag{9}$$

A space-staggered scheme is used where velocities, water levels, and depth are described at different grid points (see Fig. 1). This scheme has the advantage that for the variable operated upon in time, there is a centrally located spatial derivative.

In time, a multistep operation is used in such a manner that the terms containing space derivatives and the Coriolis force are generally taken alternating forward and backward.

The individual operations each have two time levels. The first operation is taken from time n to time n+½, and the second operation is taken from time n+½ to time n+1. Values of the fields of ζ, u, and v at time n+½ are obtained from the fields of ζ, u, and v at time n by an operation which is implicit in ζ and u and explicit in v. Then the fields of ζ, u, and v at time n+1 are computed from the fields of ζ, u, and v at time n+½ by an operation which is implicit in ζ and v and explicit in u. The two sets of difference equations of this multioperation method are now written with the equation of continuity aa the second equation of each set (Eqs. 11, 14), using an integer value for j and k and maintaining the velocity gradients in the convective-inertia terms in differential form within angle brackets < >. The effects of bottom roughness are indicated by a function R. Thus, for the first operation the equations are:

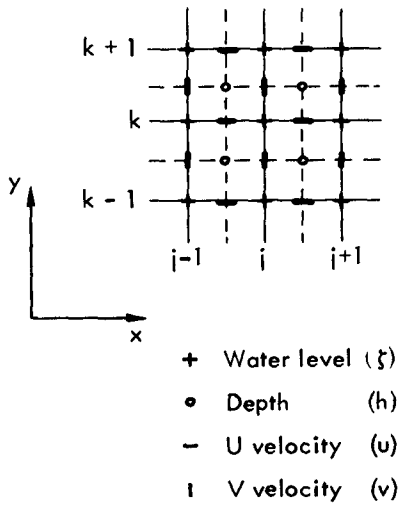

Fig. 1—Space-staggered scheme

$$u^{(n+\frac{1}{2})} = u(n) + \tfrac{1}{2}\Delta t\, f\bar{\bar{v}}^{(n)} - \tfrac{1}{2}\Delta t\, u^{(n+\frac{1}{2})} \langle\frac{\partial u}{\partial x}\rangle^{(n)} - \tfrac{1}{2}\Delta t\, \bar{\bar{v}}^{(n)} \langle\frac{\partial u}{\partial y}\rangle^{(n)}$$

$$- \tfrac{1}{2}\frac{\Delta t}{\Delta s} g\zeta_x^{(n+\frac{1}{2})} - R(x)^{(n)} \qquad \text{at } j+\tfrac{1}{2},\ k \qquad (10)$$

$$\zeta^{(n+\frac{1}{2})} = \zeta^{(n)} - \tfrac{1}{2}\frac{\Delta t}{\Delta s}\left[(\bar{h}^y + \zeta^x)^* u\right]_x^{(n+\frac{1}{2})} - \tfrac{1}{2}\frac{\Delta t}{\Delta s}\left[(\bar{h}^x + \zeta^y) v\right]_y^{(n)}$$

$$\text{at } j,\ k \qquad (11)$$

$$v^{(n+\frac{1}{2})} = v^{(n)} - \tfrac{1}{2}\Delta t\, f\bar{\bar{u}}^{(n+\frac{1}{2})} - \tfrac{1}{2}\Delta t\, \bar{\bar{u}}^{(n+\frac{1}{2})} \langle\frac{\partial v}{\partial x}\rangle^{(n)}$$

$$-\tfrac{1}{2}\Delta t v^{(n+\frac{1}{2})} \langle\frac{\partial v}{\partial x}\rangle^{(n)} - \tfrac{1}{2}\frac{\Delta t}{\Delta s} g\zeta_y^{(n)} - R(y)^{(n+\frac{1}{2})}{}_{j,k+\frac{1}{2}} \qquad (12)$$

For the second operation, the equations are:

$$u^{(n+1)} = u^{(n+\frac{1}{2})} + \tfrac{1}{2}\Delta t\, f\bar{\bar{v}}^{(n+1)} - \tfrac{1}{2}\Delta t\, u^{(n+1)} \langle\frac{\partial u}{\partial x}\rangle^{(n+\frac{1}{2})}$$

$$- \tfrac{1}{2}\Delta t\, \bar{\bar{v}}^{(n+1)} \langle\frac{\partial u}{\partial y}\rangle^{(n+\frac{1}{2})} - \tfrac{1}{2}\frac{\Delta t}{\Delta s} g\zeta_x^{(n+\frac{1}{2})} - R(x)^{(n+1)}$$

$$\text{at } j+\tfrac{1}{2},\ k \qquad (13)$$

$$\zeta^{(n+1)} = \zeta^{(n+\frac{1}{2})} - \tfrac{1}{2}\frac{\Delta t}{\Delta s}\left[(\bar{h}^y + \zeta^x) u\right]_x^{(n+\frac{1}{2})} - \tfrac{1}{2}\frac{\Delta t}{\Delta s}\left[(\bar{h}^x + \zeta^y)^* v\right]_y^{(n+1)}$$

$$\text{at } j,k \qquad (14)$$

$$v^{(n+1)} = v^{(n+\frac{1}{2})} - \tfrac{1}{2}\Delta t\, f\bar{\bar{u}}^{(n+\frac{1}{2})} - \tfrac{1}{2}\Delta t\, \bar{\bar{u}}^{(n+\frac{1}{2})} \langle\frac{\partial v}{\partial x}\rangle^{(n+\frac{1}{2})}$$

$$- \tfrac{1}{2}\Delta t\, v^{(n+1)} \langle\frac{\partial v}{\partial y}\rangle^{(n+\frac{1}{2})} - \tfrac{1}{2}\frac{\Delta t}{\Delta s} g\zeta_y^{(n+1)} - R(y)^{(n+\frac{1}{2})}$$

$$\text{at } j,\ k+\tfrac{1}{2} \qquad (15)$$

where

$$\langle\frac{\partial u}{\partial x}\rangle_{j+\frac{1}{2},k} = \frac{1}{2\Delta s}\left(u_{j+\frac{3}{2},k} - u_{j-\frac{1}{2},k}\right) \qquad (16)$$

$$\langle\frac{\partial u}{\partial y}\rangle_{j+\frac{1}{2},k} = \frac{1}{2\Delta s}\left(u_{j+\frac{1}{2},k+1} - u_{j+\frac{1}{2},k-1}\right) \qquad (17)$$

$$\langle\frac{\partial v}{\partial x}\rangle_{j,k+\frac{1}{2}} = \frac{1}{2\Delta s}\left(v_{j+1,k+\frac{1}{2}} - v_{j-1,k+\frac{1}{2}}\right) \qquad (18)$$

$$\langle\frac{\partial v}{\partial y}\rangle_{j,k+\frac{1}{2}} = \frac{1}{2\Delta s}\left(v_{j,k+\frac{3}{2}} - v_{j,k-\frac{1}{2}}\right) \qquad (19)$$

$$R(x)^{(n)} = \frac{1}{2}\,\Delta t\, g u^{(n)} \frac{\sqrt{(u^{(n)})^2 + (\bar{\bar{v}}^{(n)})^2}}{(\bar{h}^y + \zeta^{x(n)})(C^x)^2} \qquad \text{at } j + \tfrac{1}{2},\ k \tag{20}$$

$$R(y)^{(n+\frac{1}{2})} = \frac{1}{2}\,\Delta t\, g v^{(n+\frac{1}{2})} \frac{\sqrt{(\bar{\bar{u}}^{(n+\frac{1}{2})})^2 + (v^{(n)})^2}}{(\bar{h}^x + \zeta^{y(n+\frac{1}{2})})(C^y)^2} \qquad \text{at } j,\ k + \tfrac{1}{2} \tag{21}$$

$$R(x)^{(n+1)} = \frac{1}{2}\,\Delta t\, g u^{(n+1)} \frac{\sqrt{(u^{(n+\frac{1}{2})})^2 + (\bar{\bar{v}}^{(n+1)})^2}}{(\bar{h}^y + \zeta^{x(n+1)})(C^x)^2} \qquad \text{at } j + \tfrac{1}{2},\ k \tag{22}$$

$$R(y)^{(n+\frac{1}{2})} = \frac{1}{2}\,\Delta t\, g v^{(n+\frac{1}{2})} \frac{\sqrt{(\bar{\bar{u}}^{(n+\frac{1}{2})})^2 + (v^{(n+\frac{1}{2})})^2}}{(\bar{h}^x + \zeta^{y(n+\frac{1}{2})})(C^y)^2} \qquad \text{at } j,\ k + \tfrac{1}{2} \tag{23}$$

A special, additional technique will be employed for the computation of the nonlinear terms marked with an asterisk.

Solutions of the Equations (10-15) are found by direct computation or by solving systems of equations which relate water levels and velocities on lines.

In each of Eqs. (10) and (11) there are three values at the time level $(n + \frac{1}{2})$, which are all situated at the line k and have to be computed. Writing the continuity equation first and omitting the subscript k, we can write Eqs. (10) and (11) in the following form:

$$-\frac{1}{2}\frac{\Delta t}{\Delta s}\left[(\bar{h}^y + \zeta^x)^* u\right]_{j-\frac{1}{2}}^{(n+\frac{1}{2})} = \zeta_j^{(n+\frac{1}{2})} + \frac{1}{2}\frac{\Delta t}{\Delta s}\left[(\bar{h}^y + \zeta^x)^* u\right]_{j+\frac{1}{2}}^{(n+\frac{1}{2})} = A_j^{(n)} \tag{24}$$

$$-\frac{1}{2}\frac{\Delta t}{\Delta s}\, g\zeta_j^{(n+\frac{1}{2})} + \left(1 + \frac{1}{4}\frac{\Delta t}{\Delta s}\left(u_{j+\frac{1}{2}}^{(n)} - u_{j-\frac{1}{2}}^{(n)}\right)\right) u_{j+\frac{1}{2}}^{(n+\frac{1}{2})} + \frac{1}{2}\frac{\Delta t}{\Delta s}\, g\zeta_{j+1}^{(n+\frac{1}{2})} = B_{j+\frac{1}{2}}^{(n)} \tag{25}$$

where

$$A_j^{(n)} = \zeta^{(n)} - \frac{1}{2}\frac{\Delta t}{\Delta s}\left[(\bar{h}^x + \zeta^y)v\right]_y^n \qquad \text{at } j,\ k \tag{26}$$

$$B_{j+\frac{1}{2}}^{(n)} = u^{(n)} + \frac{1}{2}\left[\Delta t\, f - \frac{\Delta t}{2\Delta s}\left(u_{j+\frac{1}{2},k+1}^{(n)} - u_{j+\frac{1}{2},k-1}^{(n)}\right)\right]\bar{\bar{v}}^{(n)}$$

$$- \frac{1}{2}\,\Delta t\, g u^{(n)} \frac{\sqrt{(u^{(n)})^2 + (\bar{\bar{v}}^{(n)})^2}}{(\bar{h}^y + \zeta^{x(n)})(C^x)^2} \qquad \text{at } j + \tfrac{1}{2},\ k \tag{27}$$

Thus, one equation with three unknowns exists for each velocity field point $(u_{j+\frac{1}{2}})$ and each water level field point (ζ_j) on a line k. If a row of N water level points is on the line and velocities are given at the boundaries outside of the water levels concerned, N water levels and N - 1 velocities at time $(n + \frac{1}{2})$ must be solved from 2N - 1 equations.

We now introduce

$$r_{j-\frac{1}{2}} = \frac{1}{2}\frac{\Delta t}{\Delta s}\,(\bar{h}^{y} + \zeta^{x})^{*}_{j-\frac{1}{2}};\quad r_{j+\frac{1}{2}} = \frac{1}{2}\frac{\Delta t}{\Delta s}\,(\bar{h}^{y} + \zeta^{x})^{*}_{j+\frac{1}{2}},\ \ldots \tag{28}$$

$$r_{j} = \frac{1}{2}\frac{\Delta t}{\Delta s}\,g;\quad r_{j+1} = \frac{1}{2}\frac{\Delta t}{\Delta s}\,g;\ \ldots \tag{29}$$

Equations (24) and (25) can be written in matrix form for a line k, assuming that $u_{J-\frac{1}{2}}$ is a given velocity at the lower boundary and $u^{(n+\frac{1}{2})}_{I+\frac{1}{2}}$ is a given velocity at the upper boundary:

$$\begin{bmatrix} 1 & r_{J+\frac{1}{2}} & 0 & 0 & \cdot & 0 \\ -r_{J} & a_{J+\frac{1}{2}} & r_{J+1} & 0 & \cdot & 0 \\ 0 & -r_{J+\frac{1}{2}} & 1 & r_{J+\frac{3}{2}} & \cdot & 0 \\ \cdot & \cdot & \cdot & \cdot & \cdot & \cdot \\ \cdot & \cdot & \cdot & \cdot & \cdot & \cdot \\ \cdot & \cdot & \cdot & \cdot & \cdot & \cdot \\ 0 & 0 & 0 & \ldots & -r_{I-\frac{1}{2}} & 1 \end{bmatrix} \begin{bmatrix} \zeta_{J} \\ u_{J+\frac{1}{2}} \\ \zeta_{J+1} \\ \cdot \\ \cdot \\ \cdot \\ \zeta_{I} \end{bmatrix}^{(n+\frac{1}{2})} = \begin{bmatrix} A_{J} \\ B_{J+\frac{1}{2}} \\ A_{J+1} \\ \cdot \\ \cdot \\ \cdot \\ A_{I} \end{bmatrix}^{(n)} + \begin{bmatrix} r_{J-\frac{1}{2}}\,u_{J-\frac{1}{2}} \\ 0 \\ 0 \\ 0 \\ \cdot \\ \cdot \\ r_{I+\frac{1}{2}}\,u_{I+\frac{1}{2}} \end{bmatrix}^{(n+\frac{1}{2})} \tag{30}$$

where

$$a_{J+\frac{1}{2}} = 1 + \frac{1}{4}\frac{\Delta t}{\Delta s}\left(u^{(n)}_{J+\frac{3}{2}} - u^{(n)}_{J-\frac{1}{2}}\right) \tag{31}$$

The values of the vector $(\zeta_{J},\ u_{J+\frac{1}{2}},\ \zeta_{J+1},\ \ldots,\ \zeta_{I})$ at the $n + \frac{1}{2}$ time level can be solved with a limited number of operations by a process of elimination of unknowns. Starting with the first equation, the water level $\zeta^{n+\frac{1}{2}}_{J}$ is expressed as a function of the unknown velocity $u_{J+\frac{1}{2}}$:

$$\zeta^{(n+\frac{1}{2})}_{J} = -P_{J}u^{(n+\frac{1}{2})}_{J+\frac{1}{2}} + Q_{J} \tag{32}$$

where

$$P_{J} = r_{J+\frac{1}{2}} \tag{33}$$

$$Q_{J} = A^{(n)}_{J} + r_{J-\frac{1}{2}}\,u^{(n+\frac{1}{2})}_{J-\frac{1}{2}} \tag{34}$$

Substitution of Eq. (32) into the second equation of (30) gives

$$-r_{J}(-P_{J}u^{(n+\frac{1}{2})}_{J+\frac{1}{2}} + Q_{J}) + \left(1 + \frac{1}{4}\frac{\Delta t}{\Delta s}(u^{(n)}_{J+\frac{3}{2}} - u^{(n)}_{J-\frac{1}{2}})\right)u^{(n+\frac{1}{2})}_{J+\frac{1}{2}} + r^{(n+\frac{1}{2})}_{J+1}\,\zeta^{(n+\frac{1}{2})}_{J+1} = B^{(n)}_{J+\frac{1}{2}} \tag{35}$$

or expressing $u^{(n+\frac{1}{2})}_{J+\frac{1}{2}}$ as a function of $\zeta^{(n+\frac{1}{2})}_{J+1}$ gives

$$u_{J+\frac{1}{2}}^{(n+\frac{1}{2})} = -R_J \zeta_{J+1}^{(n+\frac{1}{2})} + S_J \tag{36}$$

where

$$R_J = \frac{r_{J+1}}{\left[1 + r_J P_J + \frac{1}{4}\frac{\Delta t}{\Delta s}\left(u_{J+\frac{3}{2}}^{(n)} - u_{J-\frac{1}{2}}^{(n)}\right)\right]} \tag{37}$$

$$S_J = \frac{B_{J+\frac{1}{2}}^{(n)} + r_J Q_J}{\left[1 + r_J P_J + \frac{1}{4}\frac{\Delta t}{\Delta s}\left(u_{J+\frac{3}{2}}^{(n)} - u_{J-\frac{1}{2}}^{(n)}\right)\right]} \tag{38}$$

Again, the water level can be expressed as a function of the next velocity:

$$\zeta_{J+1} = -P_{J+1} u_{J+\frac{3}{2}}^{n+\frac{1}{2}} + Q_{J+1} \tag{39}$$

where

$$P_{J+1} = \frac{r_{J+\frac{3}{2}}}{1 + r_{J+\frac{1}{2}} R_J} \tag{40}$$

$$Q_{J+1} = \frac{A_{j+1}^{(n)} + r_{J+\frac{1}{2}} S_J}{1 + r_{J+\frac{1}{2}} R_J} \tag{41}$$

Generally, the following recursion formulas can be written

$$\zeta_j^{(n+\frac{1}{2})} = -P_j u_{j+\frac{1}{2}}^{(n+\frac{1}{2})} + Q_j \tag{42}$$

$$u_j^{(n+\frac{1}{2})} = -R_{j-1} \zeta_j^{(n+\frac{1}{2})} + S_{j-1} \tag{43}$$

where

$$P_j = r_{j+\frac{1}{2}} / (1 + r_{j-\frac{1}{2}} R_{j-1}) \tag{44}$$

$$Q_j = (A_j^{(n)} + r_{j-\frac{1}{2}} S_{j-1}) / (1 + r_{j-\frac{1}{2}} R_{j-1}) \tag{45}$$

$$R_j = r_{j+1} / \left[1 + r_j P_j + \frac{1}{4}\frac{\Delta t}{\Delta s}\left(u_{j+\frac{3}{2}}^{(n)} - u_{j-\frac{1}{2}}^{(n)}\right)\right] \tag{46}$$

$$S_j = (B_{j+\frac{1}{2}}^{(n)} + r_j Q_j) / \left[1 + r_j P_j + \frac{1}{4}\frac{\Delta t}{\Delta s}\left(u_{j+\frac{3}{2}}^{(n)} - u_{j-\frac{1}{2}}^{(n)}\right)\right] \tag{47}$$

The recursion factors P, Q, R, and S can be computed in succession until the other bound is reached. If $u_{I+\frac{1}{2}}^{(n+\frac{1}{2})}$ is a given velocity, the last two factors computed are P_I and Q_I. Since Eq. (42) expresses ζ_I as a known function of the velocity $u_{I+\frac{1}{2}}^{(n+\frac{1}{2})}$, ζ_I can be computed, and all water levels and velocities can be found in descending order by use of Eqs. (42) and (43).

The nonlinear terms in the continuity equation which are marked with an asterisk can be computed on their proper time level by an iteration procedure. The first estimate of $\zeta^{(n+\frac{1}{2})}$ is made by the implicit procedure of taking the nonlinear term at the time level n. Next, the value $\zeta^{(n+\frac{1}{2})}$ thus computed is used in Eq. (11) for the actual computation. This iteration can be repeated several times. Use of the mathematical model, however, indicated that no gain in accuracy is obtained.

The velocity in the other direction at the time level $n + \frac{1}{2}$ can be found explicitly from Eq. (12), since the velocity $u^{(n+\frac{1}{2})}$ in the Coriolis term is already known. Eq. (12) can then be written:

$$v^{(n+\frac{1}{2})} = \frac{\left\{v^{(n)} - \frac{1}{2}\left[\Delta t\, f + \frac{1}{2}\frac{\Delta t}{\Delta s}\left(v^{(n)}_{j+1,k+\frac{1}{2}} - v^{(n)}_{j-1,k+\frac{1}{2}}\right)\bar{\bar{u}}^{(n+\frac{1}{2})}\right] - \frac{1}{2}\frac{\Delta t}{\Delta s}\, g\zeta^{(n)}_y\right\}}{\left[1 + \frac{1}{2}\Delta t\, g\frac{\sqrt{(\bar{\bar{u}}^{(n+\frac{1}{2})})^2 + (v^{(n)})^2}}{(\bar{n}^{x} + \bar{\zeta}^{y(n+\frac{1}{2})})(\bar{C}^{y})^2} + \frac{1}{4}\frac{\Delta t}{\Delta s}\left(v^{(n)}_{j,k+\frac{3}{2}} - v^{(n)}_{j,k-\frac{1}{2}}\right)\right]}$$

at j, k + ½ (48)

For the second operation, going from the time level $n + \frac{1}{2}$ to n + 1, Eqs. (14) and (15) are solved implicitly in the same manner as described for Eq. (10) and (11). Finally, the velocity in the x-direction can be computed explicitly from Eq. (13). It can be seen that no more than two successive fields have to be stored in the computer memory, as only the latest information available is necessary to compute the next step.

The coefficients for the recursion formulas in the y-direction are

$$P_k = r_{k+\frac{1}{2}}/(1 + r_{k-\frac{1}{2}}R_{k-1}) \tag{49}$$

$$Q_k = (A_k^{(n+\frac{1}{2})} + r_{k-\frac{1}{2}}S_{k-1})/(1 + r_{k-\frac{1}{2}}R_{k-1}) \tag{50}$$

$$R_k = r_{k+1}/\left[1 + r_kP_k + \frac{1}{4}\frac{\Delta t}{\Delta s}\left(v^{(n+\frac{1}{2})}_{k+\frac{3}{2}} - v^{(n+\frac{1}{2})}_{k-\frac{1}{2}}\right)\right] \tag{51}$$

$$S_k = (B^{(n+\frac{1}{2})}_{k+\frac{1}{2}} + r_kQ_k)/\left[1 + r_kP_k + \frac{1}{4}\frac{\Delta t}{\Delta s}\left(v^{(n+\frac{1}{2})}_{k+\frac{3}{2}} - v^{(n+\frac{1}{2})}_{k-\frac{1}{2}}\right)\right] \tag{52}$$

where

$$A_k^{(n+\frac{1}{2})} = \zeta^{(n+\frac{1}{2})} - \frac{1}{2}\frac{\Delta t}{\Delta s}\left[(\bar{n}^{y} + \bar{\zeta}^{x})u\right]_x^{n+\frac{1}{2}} \quad \text{at j, k} \tag{53}$$

$$B_{k+\frac{1}{2}}^{(n+\frac{1}{2})} = v^{(n+\frac{1}{2})} - \frac{1}{2}\left[\Delta t\, f + \frac{1}{2}\frac{\Delta t}{\Delta s}\left(v_{j+1,k+\frac{1}{2}}^{(n+\frac{1}{2})} - v_{j-1,k+\frac{1}{2}}^{(n+\frac{1}{2})}\right)\right]\bar{u}^{(n+\frac{1}{2})}$$

$$- \frac{1}{2}\Delta t\, g v^{(n+\frac{1}{2})}\frac{\sqrt{\left(\bar{u}^{(n+\frac{1}{2})}\right)^2 + \left(v^{(n+\frac{1}{2})}\right)^2}}{\left(\bar{h}^{x} + \bar{\zeta}^{y(n+\frac{1}{2})}\right)\left(C^{y}\right)^2} \qquad \text{at } j,\ k+\frac{1}{2} \tag{54}$$

The recursion formulas in the y-direction are

$$\zeta_k^{(n+1)} = -P_k v_{k+\frac{1}{2}}^{(n+1)} + Q_k \tag{55}$$

$$v_{k-\frac{1}{2}}^{(n+1)} = -R_{k-1}\zeta_k^{(n+1)} + S_{k-1} \tag{56}$$

The explicit operation for the u velocity becomes

$$u^{(n+1)} =$$

$$\frac{\left\{u^{(n+\frac{1}{2})} + \frac{1}{2}\left[\Delta t\, f - \frac{1}{2}\frac{\Delta t}{\Delta s}\left(u_{j+\frac{1}{2},k+1}^{(n+\frac{1}{2})} - u_{j+\frac{1}{2},k-1}^{(n+\frac{1}{2})}\right)\right]\bar{v}^{(n+1)} - \frac{1}{2}\frac{\Delta t}{\Delta s} g\zeta_x^{(n+\frac{1}{2})}\right\}}{\left[1 + \frac{1}{2}\Delta t\, g\frac{\sqrt{\left(u^{(n+\frac{1}{2})}\right)^2 + \left(\bar{v}^{(n+1)}\right)^2}}{\left(\bar{h}^{y} + \bar{\zeta}^{x(n+1)}\right)\left(C^{x}\right)^2} + \frac{1}{4}\frac{\Delta t}{\Delta s}\left(u_{j+\frac{3}{2},k}^{(n+\frac{1}{2})} - u_{j-\frac{1}{2},k}^{(n+\frac{1}{2})}\right)\right]} \tag{57}$$

The formulas developed above cannot be used directly in this form for electronic computation. Coding in FORTRAN presents problems, as coordinate description of the variables can be made only on integers, and integer-and-one-half values do appear in the formulas developed. Multiplication of all coordinate descriptions of the points by a factor of two would eliminate this problem; however, such a lattice system is uneconomical from the point of view of memory use of the computer because not all locations of an array u, v, ζ and h would be used.

It is possible to give each of the variables u, v, ζ and h a separate coordinate system, which would result in a good use of memory and would also allow coordinate description on integers. The computational formulas for these special coordinate systems and the computation program are presented in Ref. 2.

STABILITY, DISSIPATION AND DISPERSION

One of the requirements of the numerical solutions of the equations is that the obtained solutions converge to the solutions of differential equations. Also, the solutions should be stable. This can be investigated by following a Fourier expansion of a line of errors as time progresses. If this line of errors (error wave) grows with time, the computation

becomes unstable and dominates the solution. If, on the other hand, error waves will be damped heavily if computation progresses, then, components of the waves which we try to represent by the numerical procedures will be damped also and possibly in a degree which is not in agreement with the solutions of the differential equations. Such a numerical scheme is dissipative. An investigation[2] of simplified sets of difference equations (10) through (15), indicates that the multioperation method is unconditionally stable and not dissipative.

Numerical procedures however, have influence on the phase speed of the wave. This effect is called dispersive. The discreetness of the representation of the waves in time and in two spatial dimensions, influences this effect. Fig. 2 shows the computed wave velocity versus the wave velocity of the partial differential equations as function of spatial representation for a given ratio of time and spatial gridsize. The direction of the wave compared to the grid influences this ratio. If more than thirty points are used to represent one wavelength on the spatial grid, then the difference between computed wave velocity and the wave velocity of solutions of the partial differential equations are less than 1%.

NUMERICAL EXPERIMENTS

The model was tested by comparing measurements with computational data. The mouth of the Haringvliet in The Netherlands was used (Fig. 3) since detailed measurement of tidal levels and currents were available, by The Netherlands Rijkswaterstaat, and in addition this area had large variations in depth over short distances. A grid size of 400 m with a computational array of 31 by 55 points was chosen. As an aid in the evaluation of the results, a plot program was developed for the display of currents and water levels at certain times of the computation (Fig. 4). The values of the Chezy coefficients were then adjusted until a good agreement was found between measured and computed velocities and water levels (Fig. 5). A detailed description of these experiments can be found elsewhere[2].

As a final check of the general computational procedures developed during the experiments with the Haringvliet area, a tidal computation was made of the southern North Sea (see Fig. 3). The gridsize used is 5600 m.

The northern boundary of the model was described at four locations as a time function of the water levels. Other points of this boundary were computed by linear interpolation or extrapolation (Fig. 6). The southern boundary in the English Channel was described at the coasts as a time function of the water levels, and the intermediate points were computed by interpolation.

In the southwestern part of The Netherlands, currents in the different parts of the estuaries of the Rhine and Schelde were used for the boundary. Tidal data for the period from 0.00 hr (Middle European Time), September 13, 1958, were used for computation. Some adjustments were made at the beginning and end of this period in order to make all tidal curves a complete cycle over this period. The half time step of each operation was taken at 5 min. The C values were computed every half hour (real time) on the location of the water level as a function of the average depth at that moment.

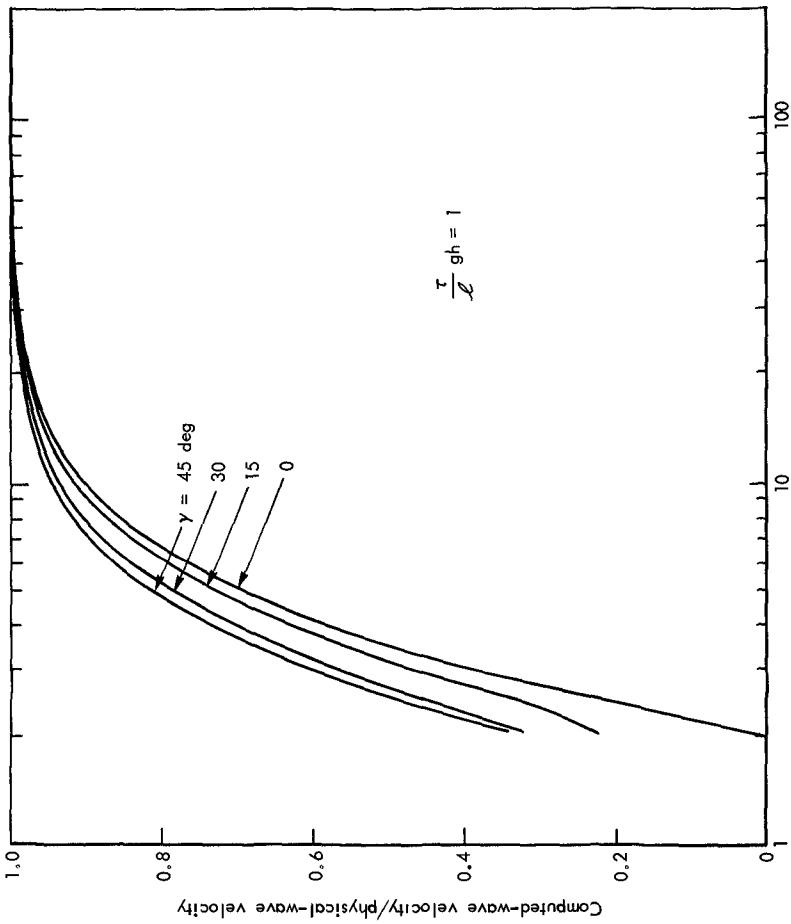

Fig. 2—Ratio of computed-wave velocity and physical-wave velocity as a function of discreetness

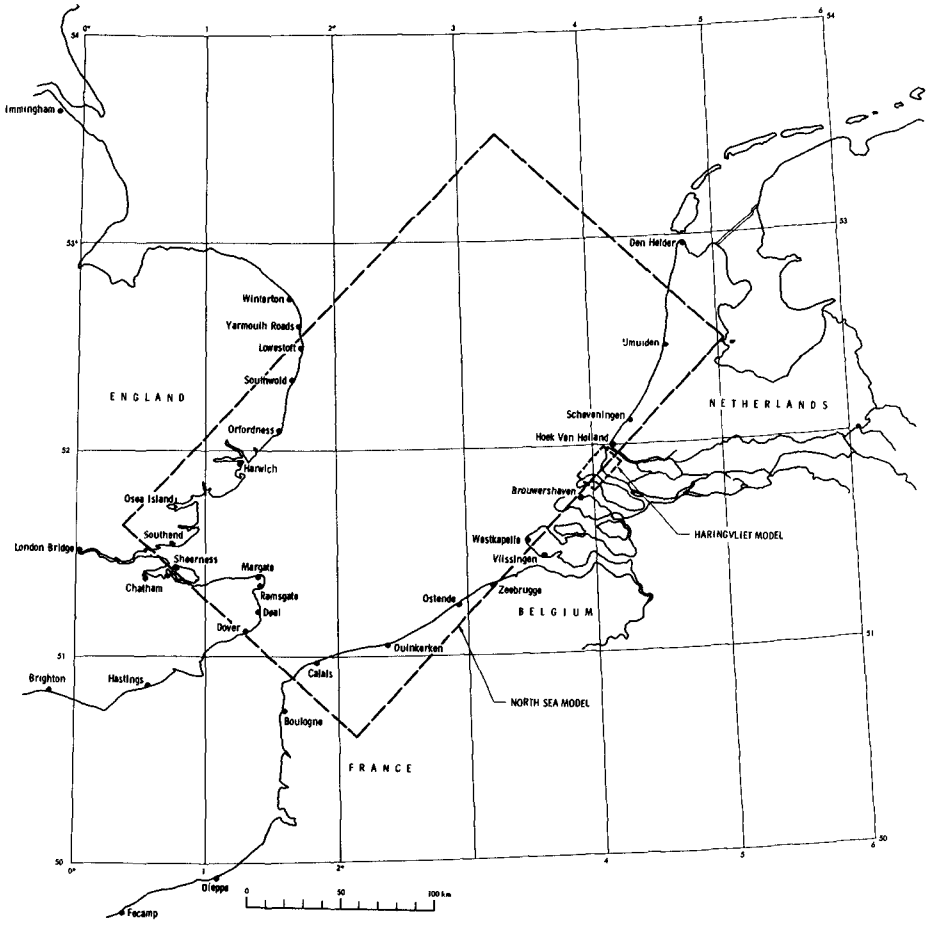

Fig. 3—Location of Haringvliet and North Sea computational models

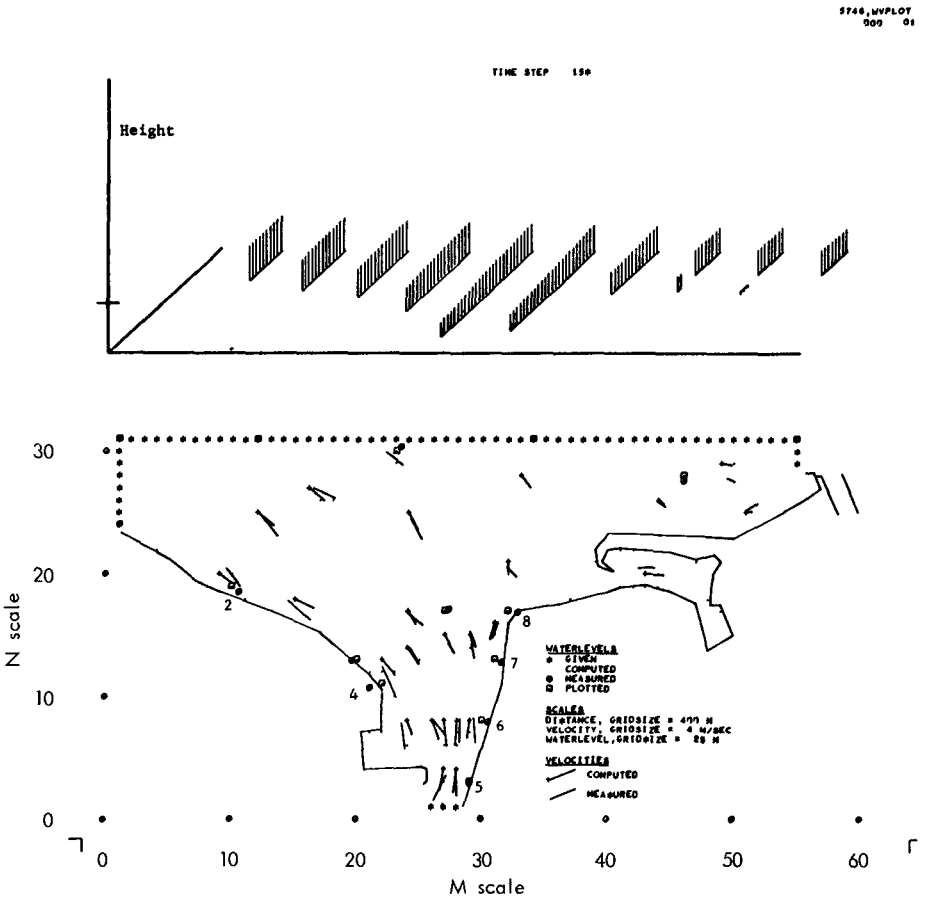

Fig. 4—Haringvliet (estuary of the Rhine) Situation 15.6 hr (real time) after start of computation

Bottom Field of the computotion ond comparison between meosured velocities ond computed velocities. The meosured velocities ore overoge velocities of similar tidol cycles at o porticulor location, while the computed velocities ore the overage velocity in an 800-by-800-m orea of o particular tidal cycle.

Top Isometric sections representing computed water levels on every fifth line of the bottom graph.

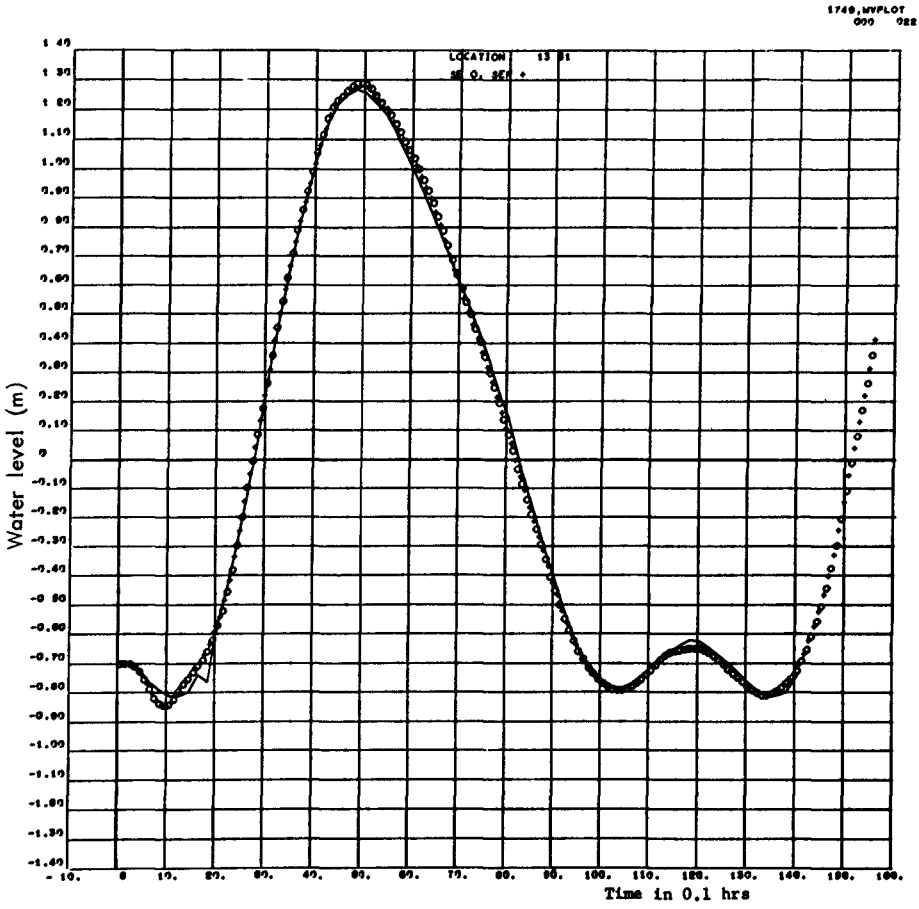

Fig. 5—Typical plot of a water-level history

Gage No. 7 Comparison between measured data (−) and computation (+0+)

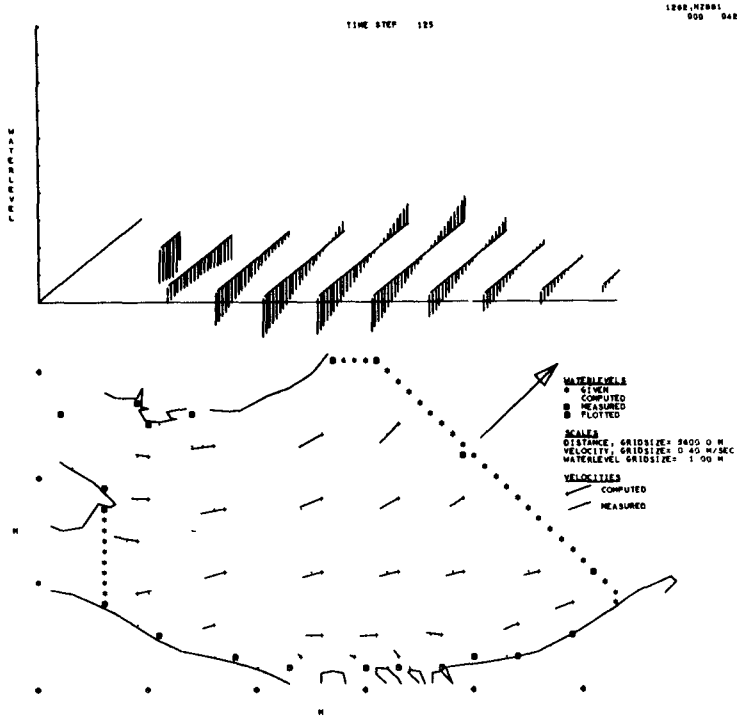

Fig. 6—North Sea computed water-levels and currents on September 12, 1958 at 20.00 hr

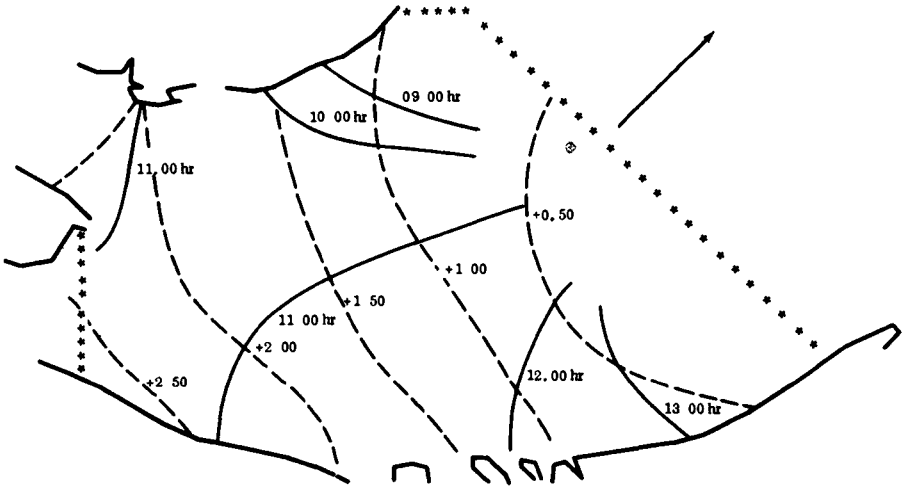

Fig. 7—Iso high-tide levels and times on September 12, 1958

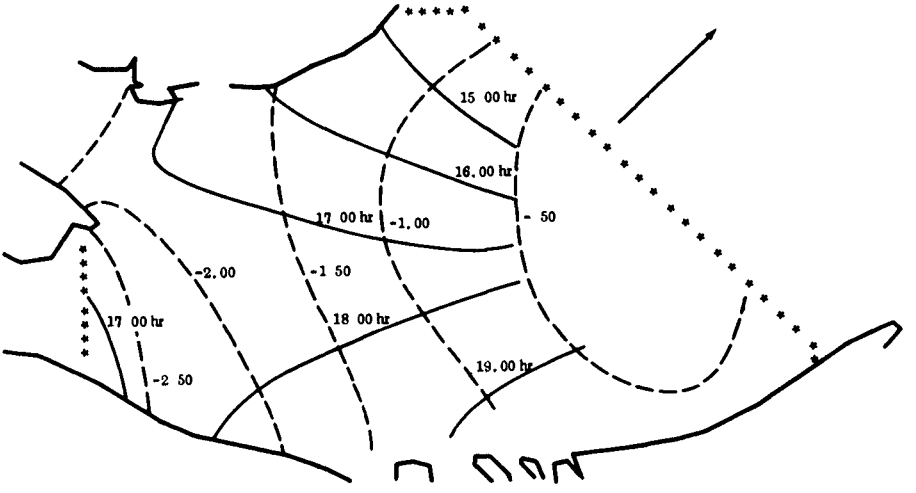

Fig. 8—Iso low-tide levels and times on September 12, 1958

Computations were started with all water levels and velocities taken at zero. The water levels and currents at the open boundaries were increased from zero with five steps into the given tidal curve. The starting disturbance disappeared after approximately 14 hr.

The locations of equal high-tide levels (co-range lines) obtained from the results of this computation are shown in Fig. 7, together with the arrival times of the highest water levels (co-tidal lines). Figure 8 shows the same for the low tides. In these two figures a counterclockwise rotation of the vertical tide may be seen. The water level information shown in Figs. 7 and 8 concurs with tidal information presented by Defant[3] as to phases and amplitudes of the tides.

The maximum magnitude of the computed currents such as shown in Fig 6 agrees with information given on tidal charts, but no detailed analysis has been made of the phase and amplitude of these currents with respect to such information. Water levels and currents along the coast are not accurate as the grid size is too large for a good representation, and also more accurate input data is needed for these computations.

CONCLUDING REMARKS

It has been shown that the propagation of long waves in coastal waters can be studied successfully by use of a numerical integration method. The multioperation method developed is characteristic of implicit methods; namely, there is no upper limit on the time step for stability reasons, as is the case with explicit methods. The multioperation method allows a direct and rapid solution of all velocities and water levels on each time level.

The multioperation method described is particularly suitable for long-wave computation in coastal waters, where water movements are introduced by changes in the water level (or currents) along the sides of the model and where the effect of bottom friction is larger than the effects of lateral eddy viscosity, which is neglected.

The contribution of the convective-inertia terms in the equation of motion is assumed to be small compared to that of other terms. These terms are represented with a lower order of accuracy.

The detailed description of computational procedures[2] permits an expedient introduction of geographic features such as water depth, boundaries, and characteristics of bottom roughness for the modeling of wave propagation in hydraulic engineering research.

Generally, information concerning the magnitude of the effect of bottom roughness is inadequate. In some cases, like the Haringvliet model, the water movements are influenced by bottom roughness to a considerable extent. In such a case, the parameter C has to be found in an iterative manner by comparing computed results with actual field measurements. The rate at which the model can be adjusted to resemble the prototype depends on the extent of available field data and on the experience of the engineer making the investigation and his insight into the physics of the wave problem and into the behavior of the method of numerical solution.

REFERENCES

1. Dronkers, J. J., (1964). Tidal Computations in Rivers and Coastal Waters, John Wiley & Sons, Inc., New York.

2. Leendertse, J. J., (1967). Aspects of a Computational Model for Long-Period Water-Wave Propagation, The RAND Corporation, Santa Monica, California, RM-5294-PR.

3. Defant, Albert, Physical Oceanography, Vol. III, The Macmillan Company, New York, 1961

CHAPTER 91

COMPREHENSIVE TIDAL STUDY OF THE ST. LAWRENCE RIVER

J. Ploeg, Assoc. Research Officer, National Research Council, Ottawa, Canada.

J.W. Kamphuis, Asst. Research Officer, National Research Council, Ottawa, Canada.*

ABSTRACT

The St. Lawrence River is a major waterway connecting the Port of Montreal to the Atlantic Ocean. As is the case with so many natural rivers, extensive dredging has been necessary to provide adequate navigation conditions. About 100 years ago the Ship Channel of the St. Lawrence River was at several places only 10 ft deep and 150 ft wide; presently it has a minimum depth of 35 ft and a minimum width of 800 ft. However, further improvements are necessary, to meet present and future navigation requirements.

The Hydraulics Section of the National Research Council is studying improvement schemes by means of a hydraulic and a mathematical model of the St. Lawrence River from Montreal to Father Point, a distance of about 350 miles. The hydraulic model has been built to a horizontal scale of 1:2000 and a vertical scale of 1·120. The mathematical study uses a finite-difference approach, employing both explicit and implicit computational schemes.

This paper describes the two studies and deals briefly with the merits of operating a mathematical and hydraulic model simultaneously.

1.0 Introduction

The St. Lawrence River (Fig. 1) is the largest river in Eastern Canada. Its drainage basin above Quebec City amounts to some 400,000 square miles, which is comparable to the areas of Great Britain, France and West Germany combined. The Great Lakes on the border between Canada and the United States are part of the St. Lawrence River System. They provide large natural storage areas and, together with the extensive hydro-electric developments, tend to regulate the river flow. The mean fresh water flow at Quebec City is 320,000 cfs, the

---

*)Now Asst. Professor, Queen's University, Kingston, Canada.

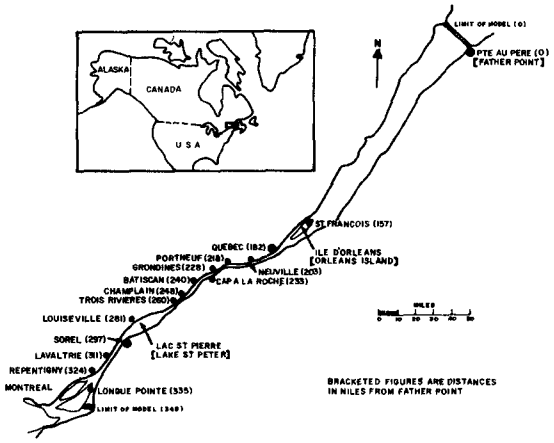

Fig. 1 St. Lawrence River

minimum recorded discharge is 190,000 cfs and the maximum flow is about 500,000 cfs, giving a ratio of 2.6 between the two extremes. Compared to other rivers, this ratio is very low; the ratio between the minimum and maximum flow of the Rhine for instance, is around 20.

The tide propagates up the St. Lawrence River as far as Lake St. Peter, 750 miles inland from the ocean. Because of the large changes in the geometry of the river bed (Fig. 2), the tidal propagation is of a complicated nature. The mean tidal range at Father Point is 10 ft, at Quebec City 15 ft, and at Three Rivers 1 ft. The horizontal tide at Father Point has an average peak flow of 70 million cfs, which is reduced at Quebec City to about 1.5 million cfs.

The St. Lawrence forms the navigation route between the Atlantic Ocean and the Port of Montreal, which together with the smaller ports of Three Rivers and Quebec City, handles approximately 36 million tons of cargo and 400 million bushels of grain annually. In spite of the size of the St. Lawrence River, extensive dredging has been necessary at many places to provide an adequate navigation channel. To meet the requirements of modern navigation, further improvements are necessary.

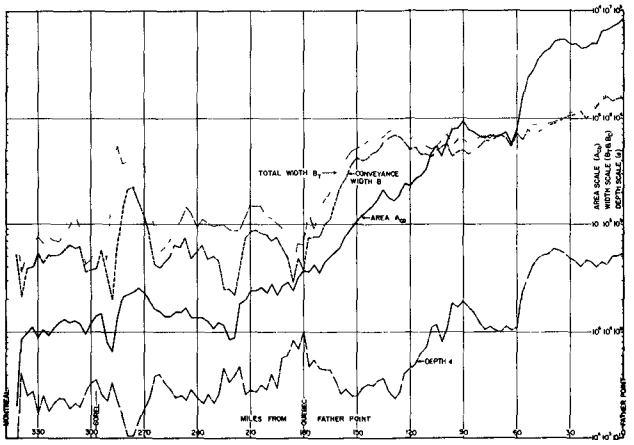

Fig. 2 Representative River Dimensions

The Department of Transport of the Canadian Government is responsible for the maintenance and improvement of the St. Lawrence Ship Channel. This must be accomplished without adversely affecting the water levels in Montreal Harbour or any other region. The Hydraulics Section of the National Research Council was asked to undertake a comprehensive study of the tidal propagation on the St. Lawrence River and to investigate the effect of proposed improvement schemes on the tide and water levels throughout the river system. Because of the importance of the problem, it was decided to conduct simultaneously, studies on a hydraulic and a mathematical model.

2.0 The Hydraulic Model

The Hydraulic Model of the St. Lawrence River at present comprises only the section from Montreal to Quebec City, a distance of 160 miles. Because of the size of the St. Lawrence River, the existing laboratory space was not sufficiently large to accommodate the entire model. While an extension to the building was under construction the

first half of the model was completed and a temporary tidal control mechanism installed at Quebec City. This allowed the calibration of the first stage of the model and also some preliminary testing.

The model has a horizontal scale of 1:2000 and a vertical scale of 1:120. In addition to the practical considerations of available floor space and required accuracy of measurements, a number of other reasons dictated the choice of these scales. For example the Lake St. Peter area is extremely shallow with low current velocities and to obtain turbulent flow in the model in this region, a high distortion is desirable. However, at other locations, the cross-sectional area and shape of the river bed changes quite abruptly; one such area is just upstream of Quebec City. With too high a distortion, it may become impossible to calibrate the model in regions of strongly varying cross sections, since the flow pattern in the model would be drastically different from that of the prototype.

The distortion of about 17, resulting from the choice of the horizontal and vertical scale of the St. Lawrence model, turned out to be close to the optimum. A smaller distortion would certainly have resulted in laminar flow conditions in Lake St. Peter, while a larger distortion would indeed have caused difficulties in the calibration of the model around Quebec City.

The first phase of the model construction was completed by the end of 1967.

The calibration of this section of the model took approximately 6 months. Two sets of boundary conditions were used. In the first case, a mean discharge was used with a spring tide, while in the second case, a nearly mean discharge was combined with a neap tide. A more complete calibration will be carried out next year, when the final section of the model from Quebec City to Father Point is completed. Calibration was achieved mainly by varying the density of the artificial roughness pattern. The roughness elements consist of thin, 3/4" wide aluminum strips. Figure 3 shows some results of the final calibration tests. At all places the water elevations in the model are within 0.10 ft of the recorded prototype water levels.

3.0 The Mathematical Model

During the course of the study several finite-difference mathematical models, both explicit and implicit, were developed to simulate the propagation of the astronomical tides on the St. Lawrence River. Of these only one will be described in this paper and for further details the reader is referred to previous publications by one of the authors (Refs. 1 and 2).

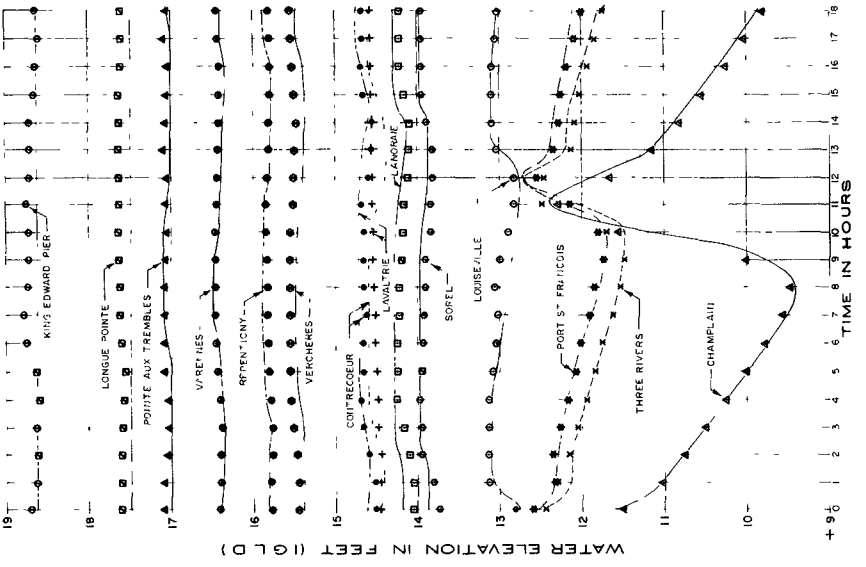

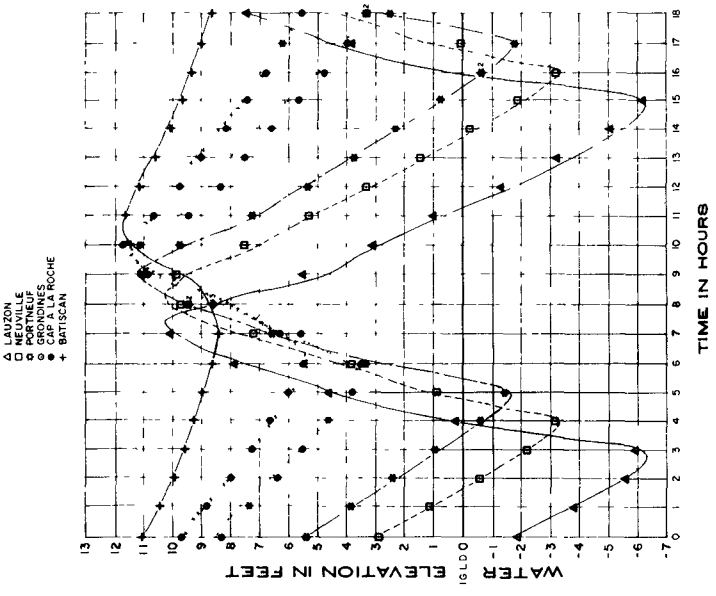

Fig. 3 Comparison of Prototype and Model Observations

The model described here is an implicit finite-difference scheme with only one island taken into account. This is a reasonable simulation since the dimensions of the other islands are small compared with the river dimensions. The model limits are Father Point and Montreal as in the hydraulic study. The river is divided into 204 longitudinal sections. Some of these sections are three miles long, while others, in regions where the river geometry varies considerably, are one mile long. The numbering scheme around Orleans Island is shown in Fig. 4; the section numbers have been circled and 52, 62 and 72 are skipped in the numbering system. The remainder of the numbering scheme is self evident. Section 1 is at Father Point, Section 207 at Montreal.

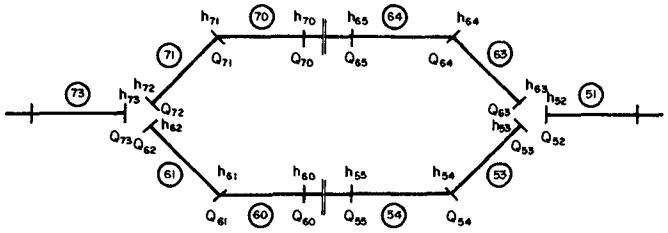

Fig. 4 Nomenclature at Orleans Island

3.1 Equations. The equations considered in this study are the equations of continuity and of motion for one-dimensional unsteady flow in open channels. These may be written respectively as:

$$\frac{\partial Q}{\partial x} + B_S \frac{\partial h}{\partial t} - \frac{Q_T}{dx} = 0 \qquad (1)$$

$$\frac{\theta_1}{gA}\frac{\partial Q}{\partial t} - \left(\theta_1 \frac{\partial A}{\partial h} + \theta_2 B_S\right)\frac{Q}{gA^2}\frac{\partial h}{\partial t} - \frac{\theta_2 Q^2}{gA^3}\frac{\partial A}{\partial x} = -\frac{\partial h}{\partial x} - \frac{Q|Q|}{C^2 A^2 d} \tag{2}$$

where Q is the river discharge, h the water level with respect to a certain datum (IGLD-1955), Q_T the tributary inflow, B_S the surface or storage width, θ_1 and θ_2 the momentum and energy coefficients of velocity distribution, A the conveyance area, g the acceleration due to gravity, C the Chezy friction factor and d the appropriate depth. It is evident that some simplifying assumptions have been made in the derivation of these equations.

These differential equations may be written as difference equations for each section:

$$-h'_m + \beta_m Q'_m + h'_{m+1} + \alpha_m Q'_{m+1} = \gamma_m \tag{3}$$

$$\delta_m h'_m - Q'_m + \delta_m h'_{m+1} + Q'_{m+1} = \varepsilon_m \tag{4}$$

where the dash refers to the values of h and Q at the new time level $t = t + \tau$, τ being the time step chosen and where α, β, γ, δ, and ε are coefficients which are functions of the known tidal conditions at time $t = t$ and of the section dimensions resulting from the schematization process.

When these equations are written for each section and combined with usual conditions at the junction points and with the boundary conditions, $f_1(t)$ and $f_2(t)$, the water level variation at Father Point and the upland flow at Montreal respectively, a set of simultaneous equations resulting in a matrix as shown in Fig. 5 may be set up.

3.2 Schematization: In a finite-difference scheme as described here, the river has to be schematized into a number of sections each with its own constant dimensions. From the charts and from available dredging records it was possible to discern two distinct levels, the chart datum level and the level above which the ground is never inundated (Fig. 6). The river widths at these two levels were determined, B_{CD} is the width at chart datum, and B_T the total width. A third width, B_C, was also taken at the 6 foot depth contour, the width of the conveyance channel. These widths were obtained by planimetering the appropriate surface area for each section. In addition to these widths, the correct mileage from the reference point (Father Point), the cross-sectional area below chart datum (total river volume in the

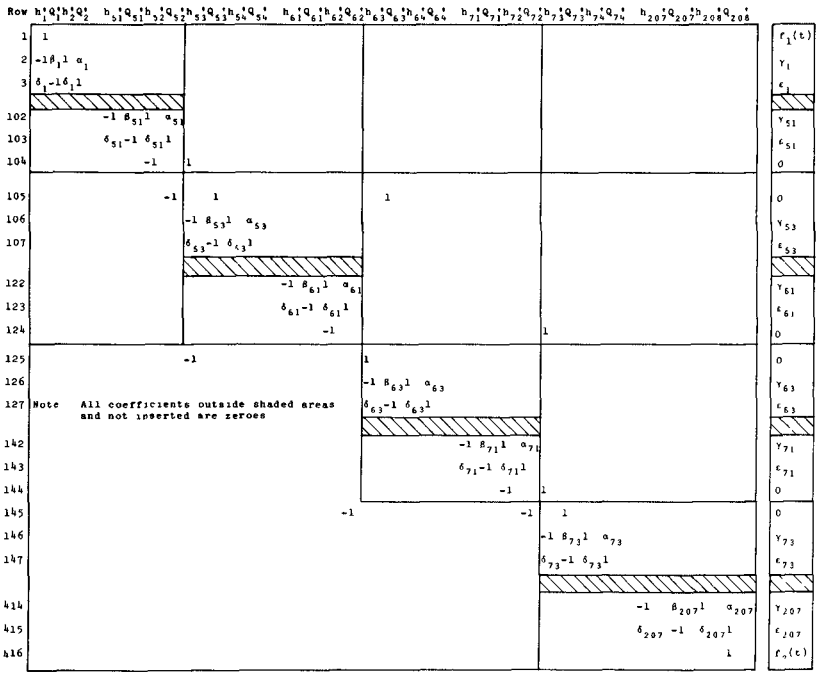

Fig. 5 Matrix Resulting from the Equations

section divided by the section length), the elevation of the chart datum with respect to IGLD, the maximum level of the shallow areas and the tributary discharge into the section were also obtained. Each river cross section was then simplified and represented in the model as shown in Fig. 7.

3.3 Solution: The crux of an acceptable method of solution is the efficient evaluation of the large matrix in Fig. 5 which must be solved at every time step. The procedure followed has been outlined in detail in Refs. 1 and 2, and is somewhat as presented by Dronkers in Ref. 3. In essence, the matrix is reduced to upper triangular form and subsequently the solution proceeds by back-substitution.

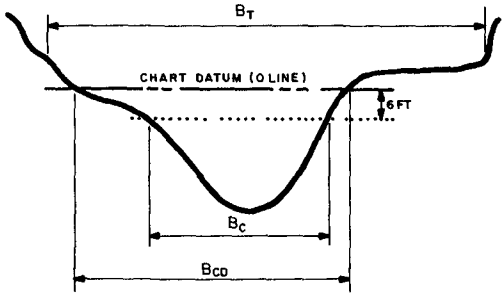

Fig. 6 Definition of Widths

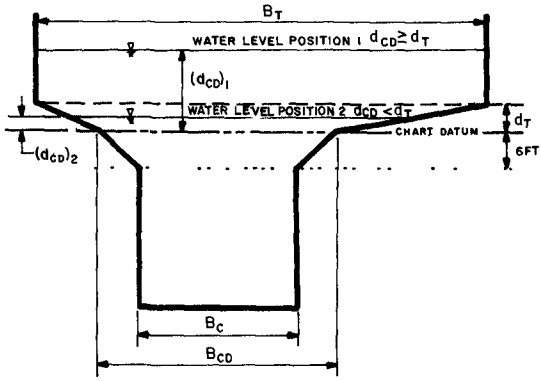

Fig. 7 Adopted Schematization

In the areas away from the island, all values in the matrix of Fig. 5 appear along the major diagonal. In this case it is possible to reduce Eqs. (3) and (4) to

$$Q'_m + q_m h'_{m+1} + t_m Q'_{m+1} = s_m \tag{5}$$

$$h'_{m+1} + p_{m+1} Q'_{m+1} = r_{m+1} \tag{6}$$

where:

$$q_m = \frac{1}{\beta_m + p_m} \quad , \quad t_m = \frac{\alpha_m}{\beta_m + p_m} \quad , \quad s_m = \frac{\gamma_m + r_m}{\beta_m + p_m} \tag{7}$$

$$p_{m+1} = \frac{1 + \zeta_m t_m}{\delta_m + \zeta_m q_m} \quad , \quad r_{m+1} = \frac{\varepsilon_m - \delta_m r_m + \zeta_m s_m}{\delta_m + \zeta_m q_m} \tag{8}$$

and where

$$\zeta_m = 1 + \delta_m p_m \tag{9}$$

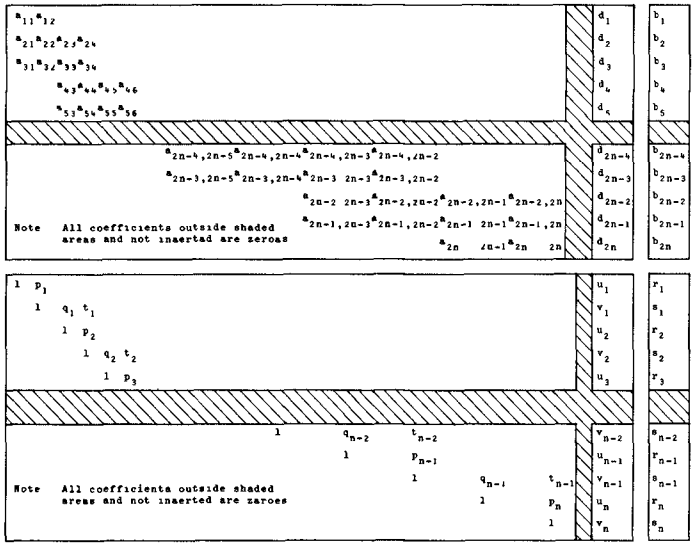

Fig. 8 Triangularization of a Matrix with an Additional Column

In the areas with junctions, the problem of triangularization is more complex since some values appear quite a distance away from the major diagonal. For the case where a value appears to the right and

above the diagonal it is possible to extend the method developed above. Referring to Fig. 8, the top matrix with an additional column denoted by d_n, may be reduced to the lower matrix using the relationships:

$$q_i = \frac{a_{2i,2i+1}}{a_{2i,2i}-a_{2i,2i-1}p_i} \; ; \; t_i = \frac{a_{2i,2i+2}}{a_{2i,2i}-a_{2i,2i-1}p_i}$$

$$s_i = \frac{b_{2i}-a_{2i,2i-1}r_i}{a_{2i,2i}-a_{2i,2i-1}p_i} \; , \; v_i = \frac{d_{2i}-a_{2i,2i-1}u_i}{a_{2i,2i}-a_{2i,2i-1}p_i}$$

$$p_{i+1} = \frac{a_{2i+1,2i+2}+\zeta_i t_i}{a_{2i+1,2i+1}+\zeta_i q_i} \; ; \; r_{i+1} = \frac{b_{2i+1}-a_{2i+1,2i-1}r_i+\zeta_i s_i}{a_{2i+1,2i+1}+\zeta_i q_i} \qquad (10)$$

$$u_{i+1} = \frac{d_{2i+1}-a_{2i+1,2i-1}u_i+\zeta_i v_i}{a_{2i+1,2i+1}+\zeta_i q_i}$$

$$\zeta_i = -a_{2i+1,2i}+a_{2i+1,2i-1}p_i$$

$$p_1 = \frac{a_{12}}{a_{11}} \; , \; r_1 = \frac{b_1}{a_{11}} \text{ and } u_1 = \frac{d_1}{a_{11}}$$

When values of an additional row appear below the band, the matrix is first triangularized and these values subsequently eliminated as in Fig. 9, using the relationships:

$$c = C_{2n-1}+(-1)^n q_{n-1}L_{n-1}$$

$$e = C_{2n} \; +(-1)^n t_{n-1}L_{n-1}$$

$$f = (-1)^n v_{n-1}L_{n-1}+\sum_{i=1}^{n-1}(-1)^i W_i$$

$$g = (-1)^n s_{n-1}L_{n-1}+\sum_{i=1}^{n-1}(-1)^i P_i \; , \qquad (11)$$

where

$$L_{i+1}=(-1)^{i+1}(C_{2i+2}-C_{2i+1}p_{i+1}) + (t_i-q_i p_{i+1})L_i$$

$$P_{i+1}=(-1)^{i+1} C_{2i+1}r_{i+1}+(s_i-q_i r_{i+1})L_i$$

$$W_{i+1}=(-1)^{i+1}\, C_{2i+1}u_{i+1}+(v_i-q_i u_{i+1})L_i$$

$$L_1 = c_1p_1-c_2$$

$$P_1 = c_1r_1-b_{2n+1}$$

$$W_1 = c_1u_1-d_{2n+1} \qquad (11)$$

With these basic tools it is possible to solve the matrix in Fig. 5 and for illustration the successive steps will be given.

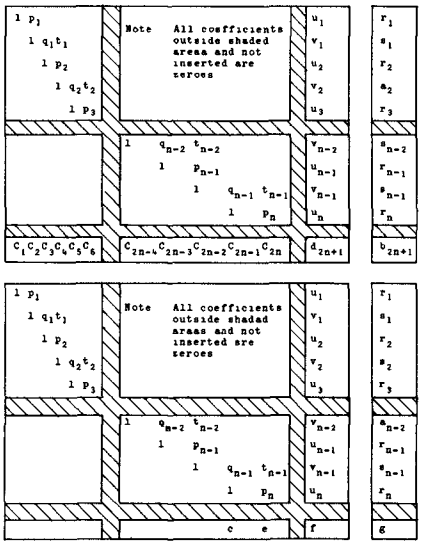

Fig. 9 Triangularization of a Matrix With an Additional Row

Triangularize to row 103 of Fig. 5 using Eqs. (5) and (6). The values slightly off the band in rows 104 and

105 may be easily eliminated. Using Eqs. (10), row 105 to 123 may be triangularized and again the h'_{62} term in row 124 may be eliminated. Eliminate the h'_{53} term in row 125 using (11) and then eliminate the ch_{62} and eQ_{62} terms. Similarly using (10) rows 125 to 143 may be triangularized, and the Q_{62} term in row 145 may be eliminated using (11). The remainder of the matrix is again a single channel and may be reduced to upper triangular form using (5) and (6). The result is the matrix in Fig. 10.

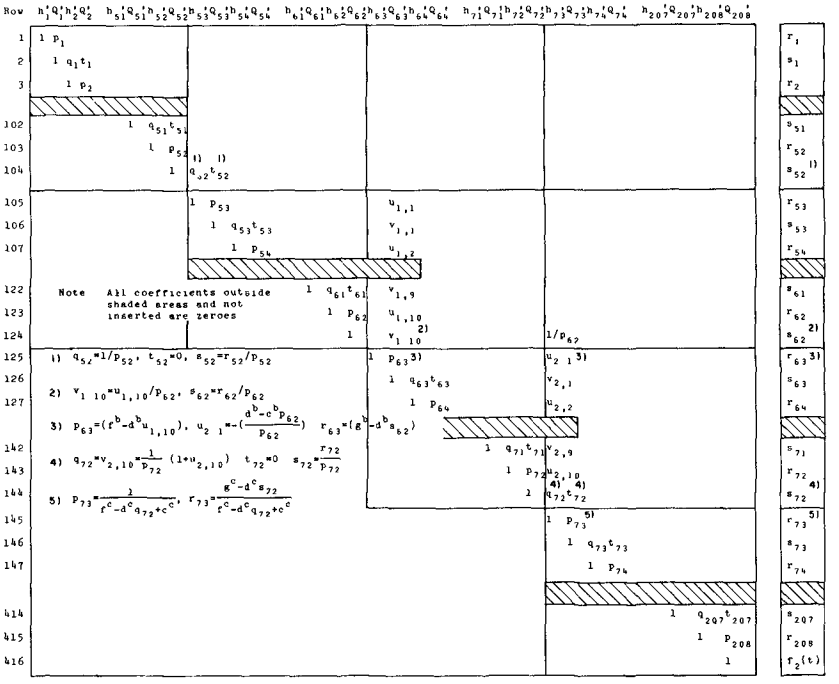

Fig. 10 Triangularized Matrix

The final step in the solution is one of back substitution. Since there is only one unknown in each row, all unknowns may be calculated beginning with Q_{208}.

This method of solution is unconditionally stable, although in the elimination process, where it proceeds through the equations in numerical order, without due regard to the absolute value of the points used to eliminate each column, a type of mathematical instability could occur. In

this particular problem, the growth of errors was not of a magnitude as to cause this type of instability.

The time required for a typical solution was 12 minutes on an IBM 360 model 50 computer. This includes rather lengthy plotting routines.

Some results as they compare with observed prototype data are shown in Figs. 11, 12 and 13, and here it may be seen that the model results correspond quite closely to the field results, the water levels being within 0.1 ft and the time within 15 minutes. Water levels only could be compared since field current observations are at present not available.

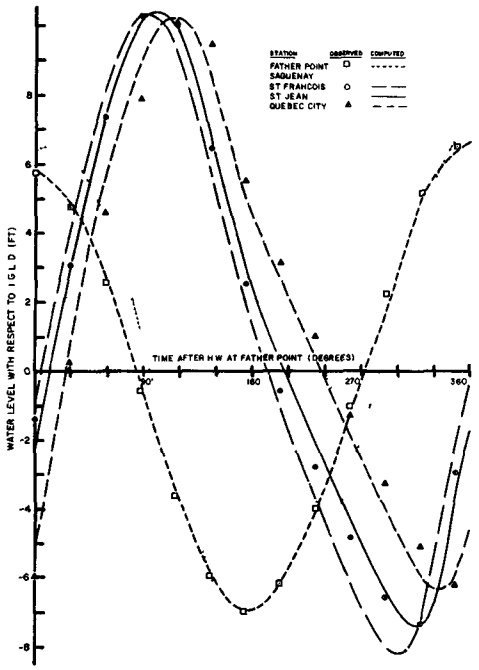

Fig.11 Comparison of Observed and Computed Water Levels

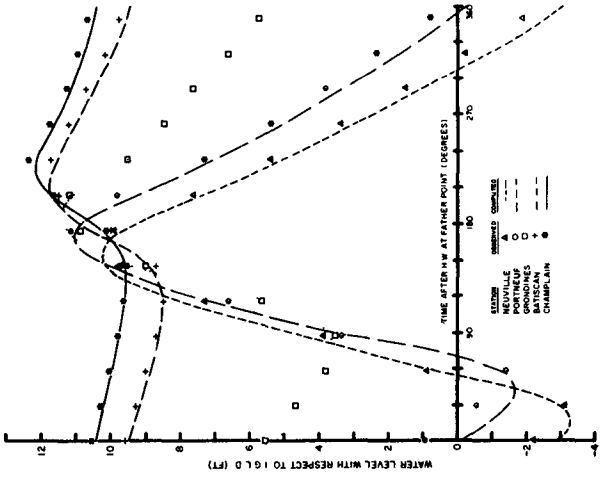

Fig. 12

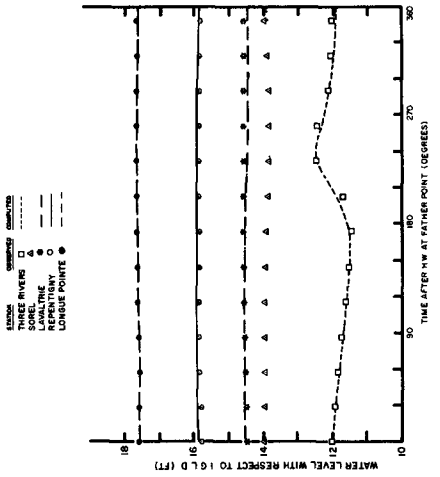

Fig. 13

Comparison of Computed and Observed Water Levels

4.0 Testing Procedures and Results

After the calibrations of the hydraulic and the mathematical model were completed, a series of tests was carried out to study the effect of some of the navigation improvement schemes. First of all, the mathematical model had shown that the change in the tidal conditions at Quebec City as a result of most of the proposed plans was nil or very small. Only the major improvement schemes, involving extensive modifications to the existing river conditions, affected the tidal propagation throughout the system. In such cases the present hydraulic model can no longer be used without changing the downstream boundary conditions. The mathematical model was used to supply the new boundary conditions for the hydraulic model.

Another demonstration of the way in which the two models complement each other involves the generation of the tide at Quebec City in the hydraulic model. The basic input to the hydraulic model is the horizontal tide at Quebec City. This is accomplished with a variable inflow, which either supplies or withdraws the tidal discharge of up to 1.5 cfs. Since no actual discharge measurements are available for the calibration condition, the mathematical model supplies this input to the control circuit of the hydraulic model. A 10 ft wide weir controlled by a feedback circuit connected to the vertical tide, acts as the final trimming device to give the exact tidal profile.

The first improvement schemes which were studied on both models, were the so-called Lake St. Peter plans. One of the plans under consideration, calls for the construction of dykes along the navigation channel through the lake. Lake St. Peter is a large shallow body of water, which now acts as an effective filter influencing the conditions upstream as well as downstream of the lake. In addition, the conditions in winter time on the St. Lawrence are very adversely affected by this shallow lake.

The first series of tests included only the construction of dykes, without changing any of the other conditions. Obviously, this is mainly of academic interest since the new cross sectional area is only 1/5 of the original area and therefore the current velocities in the new channel will be unacceptably high. However, the tests show clearly the importance of Lake St. Peter in regard to its effect on the tidal propagation in the river. Figure 14 shows the envelopes of the high and low water elevations as observed on the hydraulic model and computed on the mathematical model for a spring tide with average upland flow, with and without dykes in Lake St. Peter. The water levels

upstream of the lake have risen as much as 4 ft at Sorel and about 2.5 ft at Montreal, while just downstream of the lake the tidal range has increased considerably. The slight differences between the results of the hydraulic and the mathematical model are caused by the schematization of the delta at the upstream side of Lake St. Peter.

The second series of tests included not only the dykes along the channel, but also control structures which allow a certain amount of the flow to bypass the navigation channel over the north and south banks of the lake. The percentage of water to be diverted is governed by the maximum velocity allowed in the channel, which is in the order of 4 ft/sec. The dotted line in Fig. 14 shows the water levels resulting from a test which included this diversion of flow.

The St. Lawrence Tidal Study has shown encouraging results so far. Having the two models operating simultaneously has indeed proven to be a great advantage and will certainly continue to be of assistance when the section of the St. Lawrence River from Quebec City to Father Point is included in the hydraulic model.

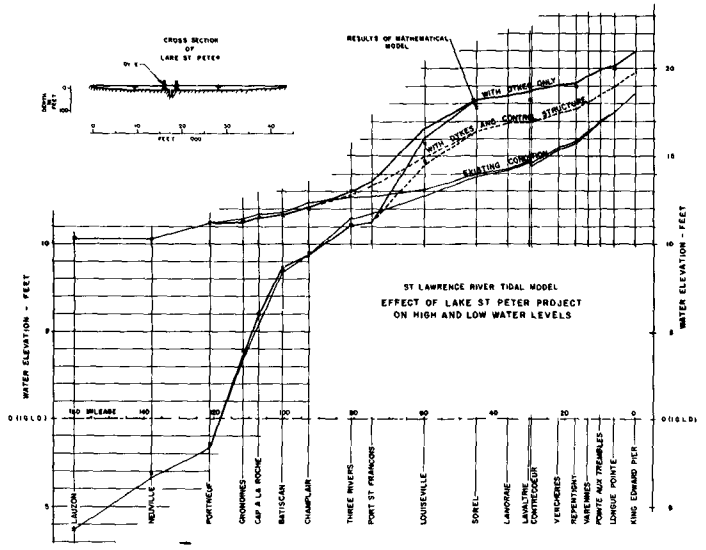

Fig. 14 Effect of Lake St. Peter Project on High and Low Water Elevations

5.0 Acknowledgments

This study is sponsored by the Marine Hydraulics Branch of the Department of Transport.

The authors wish to express their appreciation for the excellent cooperation received from the Departments of Transport and Energy, Mines and Resources in the gathering of the required field data.

Also the cooperation of the Computation Centre and of the Instrument Laboratory of the National Research Council is gratefully acknowledged.

6.0 Bibliography

1. J.W. Kamphuis, 'Mathematical Model Study of the Propagation of Tides in the St. Lawrence River and Estuary', Publication of the National Research Council MH-105 (to be published).

2. J.W. Kamphuis, 'Mathematical Model Study of the St. Lawrence River', presented at the ASCE Hydraulics Division Specialty Conference, M.I.T., Boston, Aug. 1968 (to be published).

3. J.J. Dronkers, "Progress in Tidal Computations for Rivers, Coastal Areas and Seas', presented at the New York Conference of the ASCE, Nov. 67 (to be published).

CHAPTER 92

EFFECT OF CHANNEL DEEPENING ON SALINITY IN THE JAMES ESTUARY

Maynard M. Nichols

Virginia Institute of Marine Science
Gloucester Point, Virginia, USA

SUMMARY

The effect of a 10-foot channel deepening on the salinity distribution and net flow were studied in the James Estuary to predict estuarine-wide changes that might disturb the natural conditions favorable to oyster production. A hydraulic model was employed to determine the physical changes; then the potential biological consequences were evaluated by integrating the model data with corollary field and laboratory observations.

THE ESTUARY AND MODEL

The James is relatively shallow, averaging less than 11.5 ft. Estensive shoals have formed between the shore and central channel and, in the middle estuary, oyster bars grow on these shoals in the salinity range of about 5 to 15 °/oo. Mean range of the tide is 2.5 ft. and estuary water varies from partly-mixed to well-mixed. The proposed channel which would run 87 miles inland for a width of 300 feet. This is part of series of deepenings that have proceeded with development of the estuary.

The "580-foot" long model reproduced to scales of 1:1000 horizontally and 1:100 vertically, the entire tidal James. To accommodate variable salinities in lower Chesapeake Bay, the model was extended seaward 34 miles from the estuary mouth to nearly constant salinity in the ocean. By varying freshwater inflow and sump salinity like that in the natural estuary, successive roughness adjustments were made to reproduce the mean salinity over a tidal cycle (at 1:1) with time as well as over a range of river inflow. Verification showed that the mean salinity difference between model and prototype was less than + 0.9 and - 1.8 °/oo.

EFFECTS OF DEEPENING

Tests were run before and after deepening at several levels of steady freshwater inflow, 11,500, 3,200, and 1,000 cfs at Richmond, and at relatively stable salinity. These conditions were selected because they are critical to control of oyster predation and disease.

The salinity change, though small, was most pronounced in the middle estuary where the major cut was performed (Rocklanding Shoal, Fig. 1). Deepening produced a slight freshening of near-surface water, mainly over the shoals, and an increase of salinity in near-bottom water of the channel. With greater stratification, vertical mixing between upper and lower estuarine layers was reduced. Of the three inflows tested the salinity change was grestest (up to 1.2 °/oo locally) and most widespread at conditions of intermediate flow (3,200 cfs). However, changes were not of sufficient magnitude to cause a significant change in oyster production.

Velocity measurements made with a miniature Price meter in the model over a tidal cycle displayed so much variation within a single cross section and from test to test, they were not satisfactory to calculate changes in the net volume transport produced by deepening. Instead, salt balance equations of Pritchard (1965) were used. Results showed a trend of reduced net trend of reduced net transport in both upper and lower layers reaching 20% in the cross section of the major channel cut.

DISCUSSION

Depth is one of the important parameters - in addition to width, tidal velocity and river inflow - that control estuarine circulation. When other parameters are held constant, the effect of increasing depth is to increase the cross-sectional area of flow, particularly below the level of no-net-motion. Consequently, the same tidal velocities will flush a smaller volume through the section. With greater stratification produced by deepening, tidal forces are less effective in mixing water between the two estuarine layers and consequently net volume transport (up and downstream) is reduced. The overall effect of increasing depth is to shift the salinity regime and circulation pattern from a well-mixed toward a partly-stratified type.

As the need for deeper channels may be expected to continue in the future, it is pertinent to ask: How deep can we go in an estuary before a marked change takes place? Is there a critical or threshold depth beyond which salinity will greatly increase? Further, what optimum river inflow produces the greatest change? These are among the questions formulated for future study in the James, as well as in a new model proposed for all of Chesapeake Bay.

Conference discussion of this and related papers pointed up a need to demonstrate the accuracy and confidence of model results. Hydraulic changes studied by comparing "before and after" conditions demand rigid control of model operation. For example, the ability of a model to establish the same stable salinity conditions over a certain time should be repeated. Then too, what scale is most effective for analyzing salinity regimes in a model? Essential details of the James Estuary model study (1964-1966) as summarized above will be reported in a forthcoming publication. An evaluation of model operation and accuracy is underway.

REFERENCES

Pritchard, D.W., (1965). Dispension of flushing of pollutants. In Evaluation, present state of knowledge of factors affecting tidal hydraulics and related phenomena, C.F. Wicker, editor, Comm. on Tidal Hydraulics. Rept. 3, Chapt. VIII, p. 33-34.

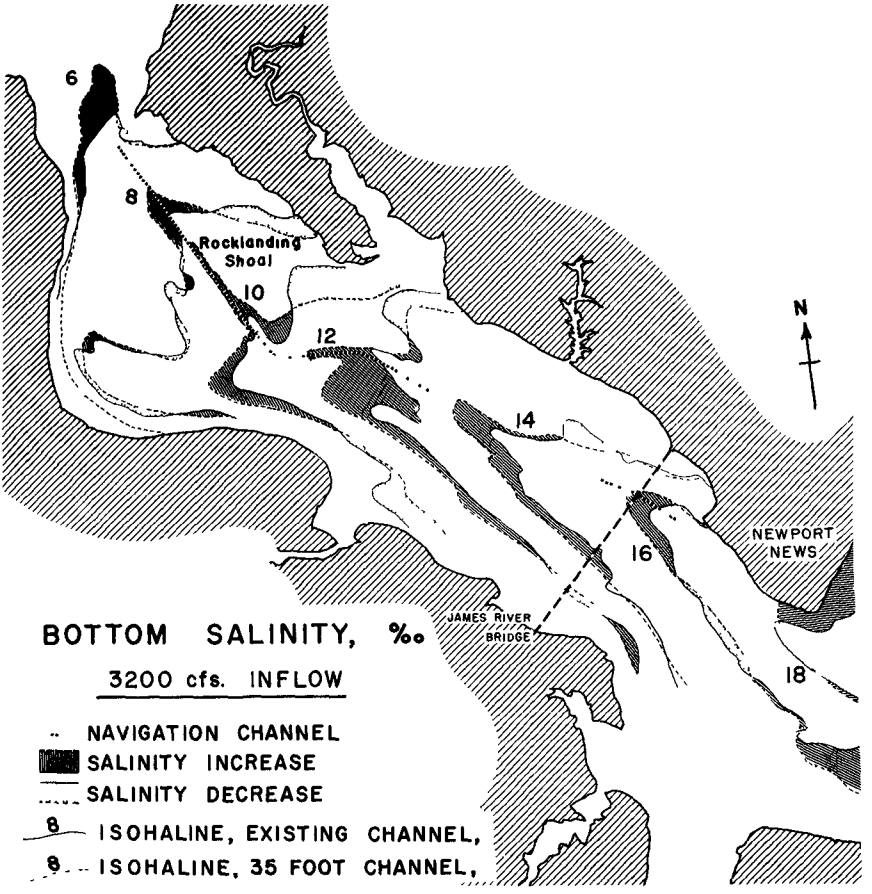

Fig. 1. Distribution of bottom isolines in the model before and after the 10-foot channel deepening.

CHAPTER 93

SOME CONSIDERATIONS ON HYDRAULIC DESIGN OF BOTTOM WATER INTAKE

Shin-ichi Senshu
Supervisor, Coastal Hydraulic Division, Hydraulics Department, Technical Laboratory, Central Research Institute of Electric Power Industry, Tokyo, Japan

ABSTRACT

The selective withdrawal characteristics of bottom water intake placed on the sea bed for the condenser cooling system of steam power station are presented and several design methods are proposed The results of field observations are also shown.

INTRODUCTION

Recently in Japan, the most intake structures for condenser cooling system of thermal (or nuclear) power stations sited on a seashore are designed as bottom water intake in order to withdraw a large quantity of clean water of low temperature from the deep layer of thermally stratified sea basin. The following types have been used for such intake structures: (a) skimmer-wall type, (b) horizontal inlet of intake pipe, and (c) vertical inlet of intake pipe. (shown in Fig. 1) The characteristics of skimmer-wall type intake were previously studied by the author and the bottom water intake of this type has been constructed at several power stations

In this paper, the characteristics of horizontal type inlet of bottom water intake pipe are presented on the basis of fundamental experiments conducted at the Hydraulics Laboratory of CRIEPI and some design methods are proposed. The results of field observations are also shown which were carried out to examine the effect of bottom water withdrawal by such structures

CHARACTERISTICS OF HORIZONTAL TYPE INLET

The withdrawal characteristics of horizontal type inlet depend on the following values; (see Fig. I (b))

- b width of rectangular opening of inlet,
- h_o height of opening,
- Δ · depth from interface of stratification to top of opening,
- z_o rise from sea bed to bottom of opening,
- L · topographical clearance behind opening (horizontal distance from opening to bank),
- L' length of visor horizontally projecting at the top of opening,
- ρ density of lower layer water,
- $\Delta\rho$ difference in density of two layers water,
- Q_c maximum discharge under critical condition, which can be taken from the lower layer water without drawdown of interface,
- u_o mean velocity at the opening under critical condition, $u_o = Q_c / bh_o$

Considering the effect of three-dimensional flow approaching the inlet, the critical withdrawal condition for the horizontal type inlet with rectangular opening can be obtained from the energy equation as follows

$$F_{i_0} = c\left(\Delta h / h_0\right)^{3/2} \quad \cdots \quad (1)$$

where

$$F_{i_0} = \frac{u_0}{\sqrt{g(\Delta\rho/\rho)h_0}}$$

In Eq. 1, c denotes the coefficient depending on the velocity distribution of approaching flow and should be determined experimentally as the function $i = L/h_0$, $m = z_0/h_0$, $n = b/h_0$ and $i' = L'/h_0$.

The value of c is shown in Fig. 2 (a) and (b), which is obtained from the experiment of three-dimensional. These figures correspond to the opening of rectangular section whose ratio of width to height is 4·1 ($n = 4$) However, the results of the experiment show that the effect of the opening geometry (ratio of width to height, n) on the withdrawal characteristics is not dominant for the r range of $n = 2 \sim 4$. For the considerably larger value of n, the value of c has a tendency to become smaller, since the effect of the three-dimensional inflow from the both sides of the opening declines and the two-dimensional inflow prevail prevails. It is found from Fig. 2 (b) that the visor installed at the top of the opening is effectual on increasing the maximum discharge under the critical condition.

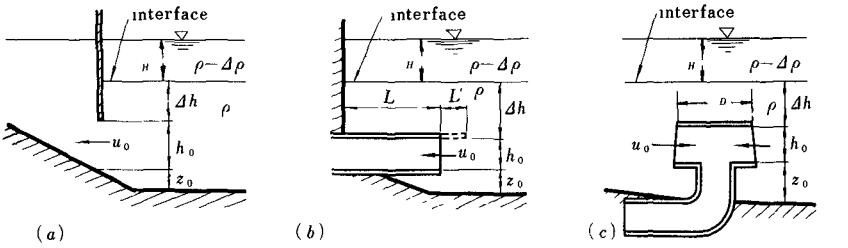

(a) (b) (c)

SKIMMER WALL TYPE HORIZONTAL TYPE INLET VERTICAL TYPE INLET

Fig. 1 Type of bottom water intake

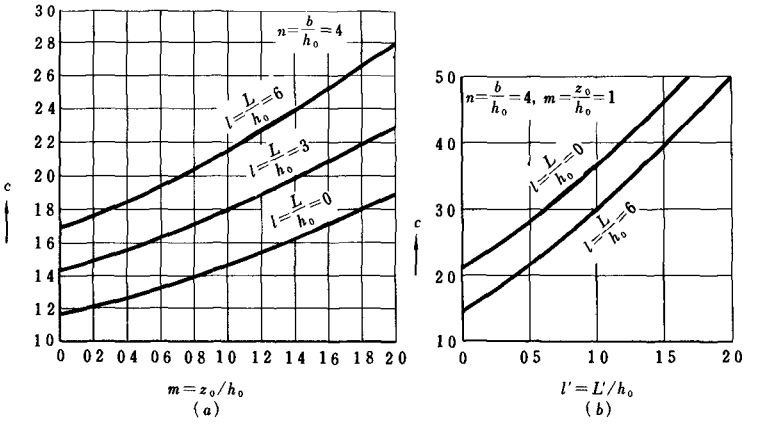

Fig 2. Value of coefficient, c, in Eq. 1.

HYDRAULIC DESIGN OF BOTTOM WATER INTAKE

1. Method of economical design to minimize the total depth

This method is based on the idea that the most economical size of the intake is given by the opening height h_o so as to minimize the total depth below the interface, $z_o + h_o + \Delta h$, for a given discharge under the critical condition. The economical opening height h_o in this manner is obtained from Eq 1 for horizontal type inlet, by differentiating $z_o + h_o + \Delta h$ with respect to h_o and equating to zero, that is

$$h_o = \left\{\frac{2}{3(1+m)}\right\}^{2/5} \left(\frac{Q}{nc\sqrt{g\frac{\Delta\rho}{\rho}}}\right)^{2/5} \quad \cdots \quad (2)$$

and the corresponding depth Δh is

$$\Delta h = \left(\frac{Q}{nc\sqrt{g\frac{\Delta\rho}{\rho}}}\right)^{2/3} \frac{1}{h_o^{2/3}} \quad \cdots \quad (3)$$

The economical opening height, h_o , for skimmer-wall type intake can be obtained in the same manner from the critical withdrawal condition, $F_{to} = 0.9(\Delta h/h_o)$, based on the result of the two-dimenstional experiment presented in the author's previous study, as follows.

$$h_o = \left(\frac{q}{2\times 0.9\sqrt{g\frac{\Delta\rho}{\rho}}}\right)^{2/3} \quad \cdots \quad (4)$$

and the corresponding depth Δh is

$$\Delta h = \frac{q}{0.9\sqrt{g\frac{\Delta\rho}{\rho}h_o}} \quad \cdots \quad (5)$$

where, q is maximum discharge per unit width of skimmer-wall under the critical condition

Several examples of bottom water intake of horizontal type inlet designed by this method are shown in Table-1 In these examples, maximum intake discharge is $Q = 11\ m^3/sec$, depth of upper layer H = 4 m, and relative density difference $\Delta\rho/\rho = 0.0017$ (corresponding to temperature difference between upper and lower layer water, $\Delta T = 5\ ^oC$).

Table-1. Horizontal type inlet designed by the method to minimize total depth (n = 4).

No.	Design condition	Δh (m)	h_o (m)	z_o (m)	Total depth $H+\Delta h+h_o+z_o$ (m)	u_o (m/s)
1	ℓ =6, m=0, ℓ'=0	3.23	2 16	0	9.39	0.590
2	ℓ =6, m=1, ℓ'=0	3.88	1.30	1.30	10.48	1.627
3	ℓ =6, m=1.5, ℓ'=0	4.04	1.08	1.62	10.74	2.360
4	ℓ =6, m=0.5, ℓ'=1	2.88	1.28	0.64	8.80	1.678

2. Method of providing the inlet velocity so as to keep stability of the interface

The design method described above is apt to give rather large magnitude of inlet velocity, which promotes occurrence of turbulent mixing at the interface and results in simultaneous inflow from the upper layer. It would be the practical method, therefore, to determine the value of h_o and Δh under the critical condition, by providing first the inlet velocity u_o with the magnitude to keep stability of the interface.

For horizontal type inlet of rectangular opening ($b = nh_o$),

$$h_o = \sqrt{\frac{Q}{nu_o}} \qquad (6)$$

and

$$\Delta h = \left(\frac{u_o h_o}{c\sqrt{g\frac{\Delta\rho}{\rho}}} \right)^{2/3} \qquad (7)$$

It is adequately recommended that the magnitude of u_o should be taken as 0.10 ~ 0.20 m/sec, on the basis of stability condition of interface of two-layer stratification.

Figure 3 is the design diagram of horizontal type inlet by this method based on Eqs. 6 and 7 for the condition $\Delta\rho/\rho = 0.0017$ ($\Delta T = 5$ °C), n = 4, and c = 1.17 ($l = 0$, $m = 0$).

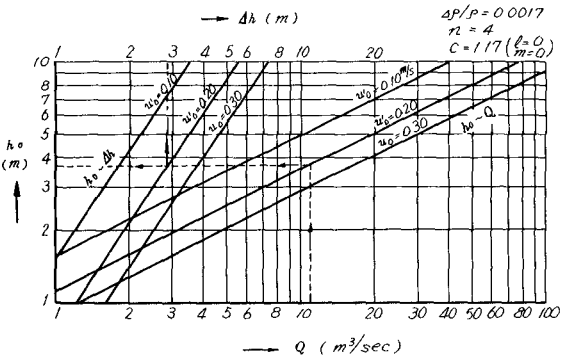

Fig. 3. Design diagram for horizontal type inlet by method of providing the inlet velocity.

For skimmer-wall type bottom water intake, the values of h_o and corresponding Δh for the given inlet velocity u_o are determined by

$$h_o = q/u_o \qquad (8)$$

and

$$\Delta h = \left(\frac{u_o}{0.9 \sqrt{g \frac{\Delta \rho}{\rho}}} \right) h_o^{\frac{1}{2}} \quad \cdots\cdots\cdots\cdots\cdots\cdots\cdots (9)$$

Several examples of bottom water intake of horizontal type inlet designed by this method are shown in Table-2 In these examples, the values of Q, H and $\Delta\rho/\rho$ are same as the ones for the above examples in Table-1

Table 2 Horizontal type and skimmer-wall type inlet designed by the method so as to keep stability of interface (inlet velocity, u_o, is given first).

No	Design condition	Δh (m)	h_o (m)	z_o (m)	Total depth $B+\Delta h+h_s+z_o$ (m)	b (m)	Given inlet velocity u_o (m/sec)
a-1	horizontal type inlet, n = 4 $l = 0$, m = 0, $l' = 0$	2.88	3.70	0	10.58	14.8	0.20
a-2	$l = 0$, m = 0 $l' = 0$	3.30	3.00	0	10.30	12.0	0.30
a-3	$l = 6$, m = 1, $l' = 0$	1.92	3.70	3.70	13.32	14.8	0.20
a-4	$l = 6$, m = 0.3, $l' = 0.4$	1.82	3.70	1.11	10.63	14.8	0.20
b	Skimmer-wall type inlet (two-dimensional case of a-1)	3.32	3.72	0	11.04	14.8	0.20

3. Hydraulic design of vertical type inlet

The vertical type inlet with cover plate and bottom guide plate as shown in Fig. 1 (c), can be designed in the same manner by applying the above-mentioned methods for the horizontal type inlet to each divided portion around the opening

Divide the cylindrical opening formed between the upper cover plate and the lower glude plate of diameter D' into α portions (for each divided portion, $n = (\pi D'/2)/h_o$), and apply the design formular to each portion of β among α, assuming that the remaining part $(\alpha - \beta)$ is ineffectual for withdrawing water due to the surrounding obstruction.

For a given discharge Q and inlet velocity u_o, the opening height h_o is obtained from

$$h_o = \sqrt{\frac{Q}{n\beta u_o}} \quad \cdots\cdots\cdots\cdots\cdots\cdots\cdots (10)$$

then, the corresponding depth Δh can be calculated by Eq. 7, in which the value of coefficient c should be taken for the case of $l = 0$.

On the other hand, in the economical design to minimize the total depth at the inlet, the calculating formulas are as follows:

$$D=\left\{\frac{2n\alpha}{3\pi(1+m)}\right\}^{3/5}\left(\frac{Q}{c\pi\frac{\beta}{\alpha}\sqrt{g\frac{\Delta\rho}{\rho}}}\right)^{2/5} \quad . \quad . \quad (11)$$

$$h_o=\frac{\pi D'}{n\alpha} \quad . \quad . \quad .. \quad .. \quad ..(12)$$

$$u_o=\frac{Q}{\pi D'^2\frac{\beta}{\alpha}h_o} \quad . \quad . \quad (13)$$

For a given discharge Q, the diameter of the cylindrical opening, D', is obtained from Eq 11, then successively h_o from Eq 12, u_o from Eq 13 and Δh from Eq. 7.

Two design examples of bottom water intake of vertical type inlet for the same value of Q, H and $\Delta\rho/\rho$ as in examples above described, are shown in Table-3

Table-3. Vertical type inlet for the given inlet velocity, u_o = 0.20 m/sec

No	Design condition	D' (m)	Δh (m)	h_o (m)	z_o (m)	Total depth $H+\Delta h+h_o+z_o$ (m)
c - 1	ℓ=0, m=0.5, ℓ'=0.4, n=4, α=4, β=3,	10.90	1.48	2.14	1.07	8.69
c - 2	ℓ=0, m=0 3, ℓ'=0.4, n=2, α=4, β=3,	7.72	1.90	3.03	0.91	9.85

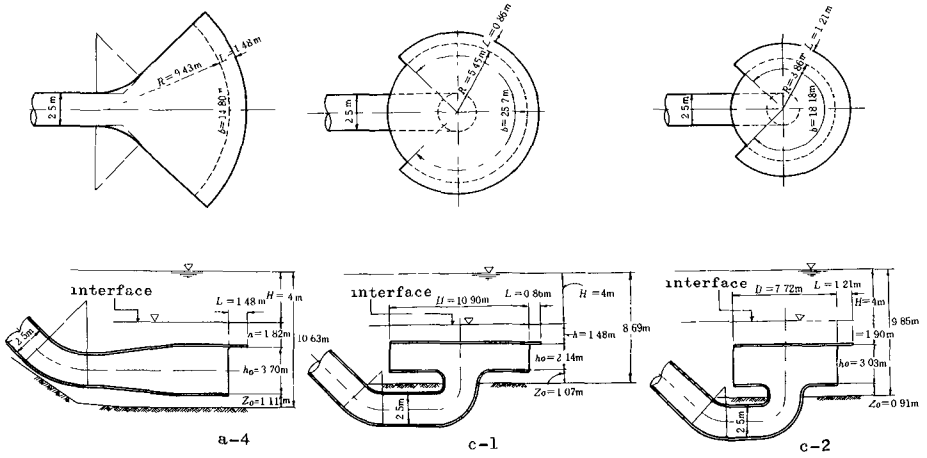

Fig. 4. Design examples of horizontal type and vertical type bottom water intake.

These two vertical type bottom water intakes are sketched in Fig. 4, together with one example of horizontal type intake (a-4 in Table-2) Comparing c-1 with c-2, c-2 for n=2 is rather economical than c-1 for n=4, because the volume of the whole structure for the former is 2/3 of the one for the latter.

4 Method of permitting to entrain the surface layer water of high temperature beyond the critical condition

Above mentioned are the design methods to take the colder bottom water from the thermally stratified basin and to prevent the warmer surface water from withdrawing into the cooling system. However, when the flow rate increases and exceeds the maximum discharge under the critical condition, the interface is drawn down below the top of the opening and simultaneous inflow from the upper layer may develop.

To permit the entrainment of warmer water from the upper layer to some extent brings the design method to obtain more economical intake structures than designed under critical condition. In case of such a design method, the required depth Δh for horizontal type inlet is estimated by the following equation for a given entrainment factor λ ;

$$\Delta h = \Delta h_c (1-\lambda)^{2/3} - \lambda h_o \qquad \cdots\cdots\cdots\cdots \quad (14)$$

in which, Δh_c is the depth for the critical design given by Eq 7, and entrainment factor λ is the ratio of inflow from the upper layer to total discharge withdrawn through the opening. Mean water temperature of cooling water, T_o, when warmer surface water is entrained, is estimated by

$$T_o = \lambda T_1 + (1-\lambda) T_2 \qquad \cdots\cdots\cdots\cdots \quad (15)$$

where T_1 and T_2 is water temperature in upper and lower layer, respectively

For two-dimensional skimmer-wall type intake, the following relation should be used, instead of Eq 14;

$$\Delta h = \Delta h_c (1-\lambda)^{\frac{1}{2}} - \lambda h_o \qquad \cdots\cdots\cdots \quad (16)$$

Equation 15 or Eq 16 can also be used to estimate the entrainment factor λ for the existing intake structures

FIELD OBSERVATIONS

To examine the effect of bottom water intake structures designed by the author's method, field observations have been carried out at several thermal power stations

Figure 5 shows an example of the observed vertical distributions outside and inside of the skimmer-wall type bottom water intake at SAKAI-KO Thermal Power Station sited in Osaka Bay The intake structure was completed in July of 1967. The maximum discharge of cooling water is 100 m^3/sec for the output of 2000 MW in its final project. The opening height below the skimmer-wall, h_o, is 4.8 m, and the designing mean velocity at the opening, u_o, is 0 16 m/sec.

As seen in Fig. 5, the conspicuous stratification due to water temperature difference develops in the basin in front of the intake in August, and this bottom water intake is of great advantage to withdraw colder clean water. The average temperature of cooling water measured at the pumping pit was 24 ^{o}C in spite of the water temperature of 30.5 ^{o}C in surface layer outside of the skimmer-wall.

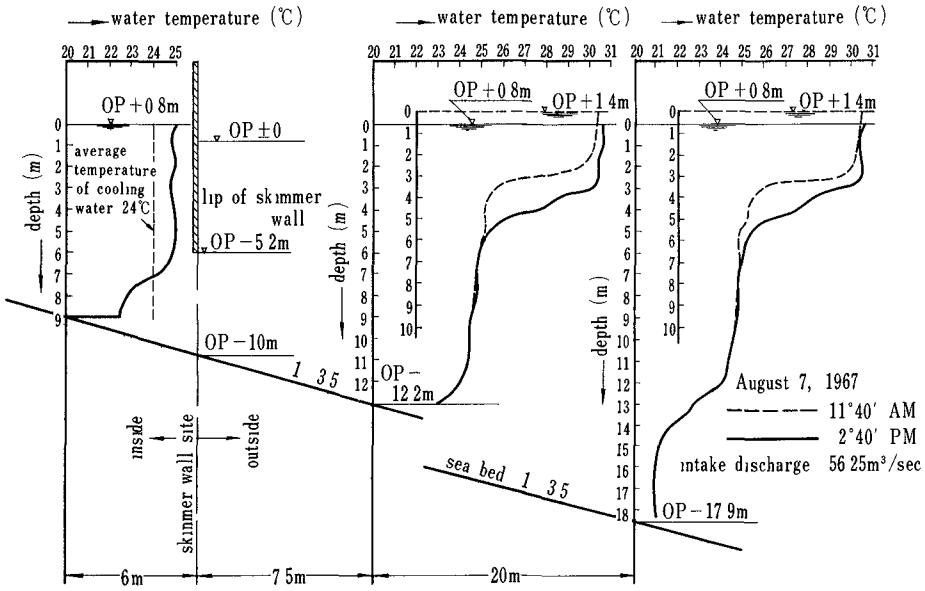

Fig. 5. Observed water temperature distribution at bottom water intake of cooling system for Sakai-ko Thermal Power Station

Figure 6 shows another example of vertical temperature distributions outside of the skimmer-wall type bottom water intake observed at SHIN-SHIMIZU Thermal Power Station sited in Shimizu Port. The maximum discharge of cooling water is 11.7 m^3/sec for the total output of 306 MW, h_0 = 4.12 m and u_0 is 0.07 m/sec. The cooling water discharge during the testing period was 6.15 m^3/sec.

Assuming the discontinuous temperature distribution outside of the skimmer-wall shown by dotted line in Fig. 6, the average temperature of cooling water is calculated by the author's method as 25.85 °C (λ = 6 %) in ebb tide and 26.1 °C (λ = 0) in flood tide. These values are in quite agreement with the observed water temperature at pumping pit.

Figure 7 shows the water temperature distribution in front of the horizontal type bottom water intake with visor observed at ICHIHARA Thermal Power Station in Tokyo Bay Assuming that T_1 = 26.5 °C for upper layer, T_2 = 21 5 °C for lower layer, depth of surface layer H = 3.5 m from the observed temperature distribution on August 15, the average temperature of cooling water is estimated as 21.7 °C (λ = 4.5%).

Figure 8 shows the water temperature distribution around the vertical type inlet of bottom water intake pipe for SAKAI PLANT of UBE KOSAN Industrical Company in Osaka Bay. It is seen that the conspicuous density stratification is formed near the intake. Assuming that T_1 = 27.5 °C, T_2 = 24.3 °C and H = 3.6 m from the observed data, calculation gives λ = 0. Therefore, water temperature of cooling water results in the assumed lower layer temperature, 24.3 °C, which coincides with the average temperature measured at the pumping pit.

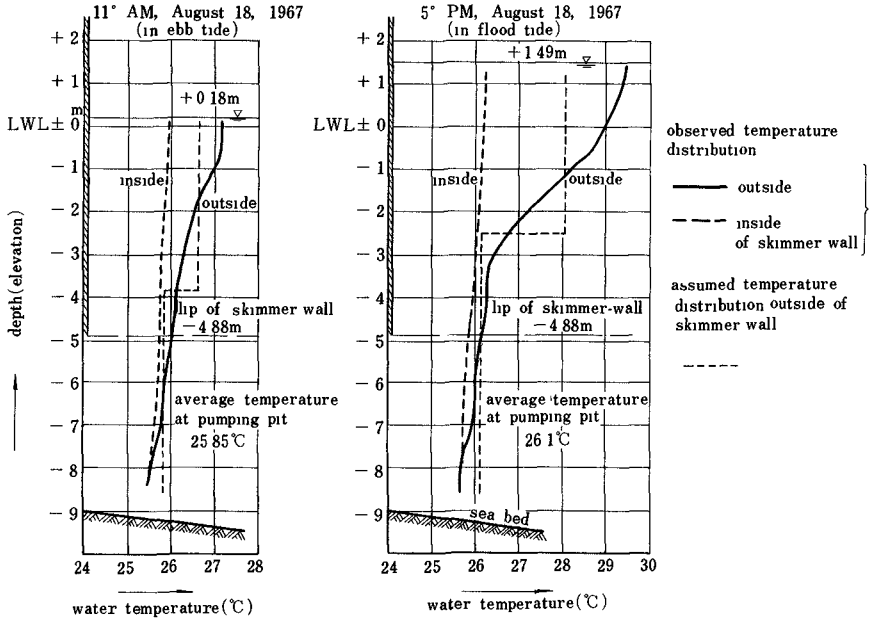

Fig. 6. Observed water temperature distribution at bottom water intake for SHIN-SHIMIZU Thermal Power Station.

Studies are further continued to make clear the characteristics of selective withdrawal in the field of continuous density distribution which is generally more actual condition in sea basin.

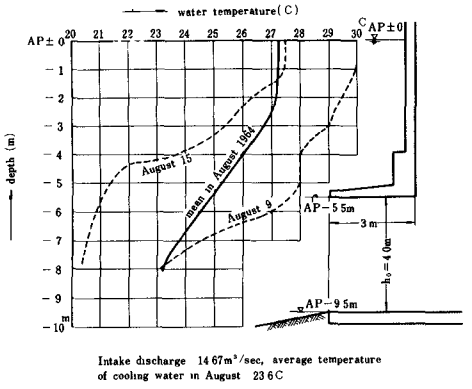

Fig. 7 An example of water temperature distribution observed in front of bottom water intake for ICHIHARA Thermal Power Station.

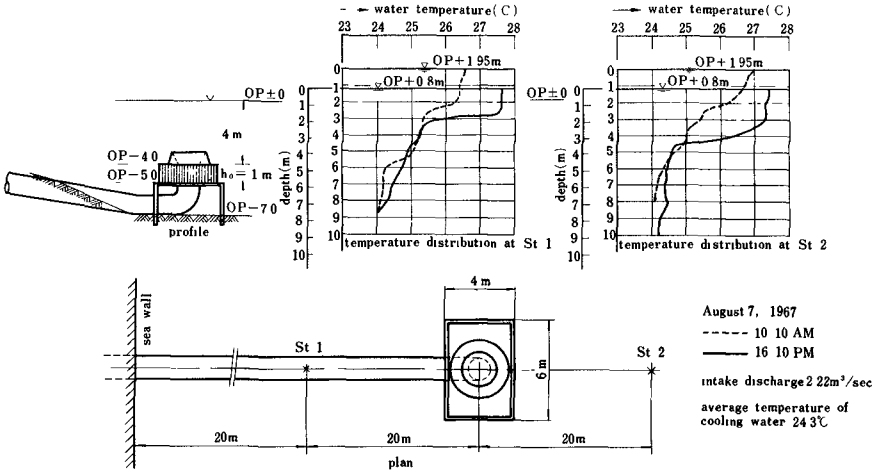

Fig. 8. Water temperature distribution observed at vertical type inlet of intake pipe for SAKAI PLANT of UBE KOSAN INDUSTRIAL COMPANY.

ACKNOWLEDGEMENT

The author wishes to express his gratitude to Dr A. Wada for his advices and to Mr. T. Fujimoto for his assistance in performing all experiments.

REFERENCE

S. Senshu and A. Wada "Study on bottom water intake for condenser cooling system of power stations", Proceedings of the 10th Conference on Coastal Engineering, 1966 (Tokyo).

CHAPTER 94

STUDIES OF PREDICTION OF RECIRCULATION OF COOLING WATER IN A BAY

By Akira Wada, Dr Eng

Technical Laboratory
Central Research Institute of Electric Power Industry
Tokyo, Japan

ABSTRACT

In the present report, a few factors of great importance in the determination of the degree of recirculation of cooling water for power station are chosen for theoretical analysis

First, the problem of flow and thermal diffusion in the sea caused by outfall of warmed cooling water is considered. Numerical solution of the equation of thermal diffusion with a complete set of Eulerian equations in which the values of the eddy coefficient of diffusion and viscosity depend upon the relation to the velocity shear and vertical density gradient is presented The Boussinesq approximation is used throughout The mechanism of development of upwelling phenomenon is discussed from the numberical experiment taking into account of the interaction between the flow and the thermal distribution. From the result of field survey, the occurrence of the return flow in the bottom layer of the coastal region is confirmed The numerical solutions give a good representation of all features of flow and thermal profiles.

Next, study on cold water intake from bottom layer is presented The numerical experiment of the stratified fluid with a continuous density gradient flowing into the submerged intake is conducted to gain additional insight into the mechanism of density flow in the field of the continuously stratified fluid. The results lead to the conclusion that the flow in the field of the continuous distribution of density differs from that for a two-layer system

I INTRODUCTION

In a previous paper[1], the effect of some dominant factors on the recirculation of cooling water was discussed. A practical theory was also presented from which quantitative prediction of water temperature and velocity fields due to discharge of warmed cooling water may be obtained for a bay characterized by a meteorological condition.

By the development of the technique of this numerical model test, the next problems can be solved They are the followings, (a) presumption of approaching velocity to intake entrance, (b) discrimination of thermocline stability caused by the appearance of locally high velocity, (c) influence of outfall of warmed cooling water on a vessel navigation and (d) estimation of influenced range of water temperature rise in the sea in relation to compensation for coastal fishery.

On the basis of these studies, the design criteria of intake and outlet structures can be determined By the application of the developed method of computation to the real planning site, the hydraulic design of the intake and the outlet at Tsuruga Nuclear Power Station, Mizushima Thermal Power Station, Shimane Nuclear Power Station and Oita Thermal Power Station was done

To know the aspect of the thermal diffusion caused by the outfall of warmed cooling water, we can not but rely on the method such as the field survey, the hydraulic model test and the numerical experiment by an electronic computer The positive field survey is especially important for the research work of recirculation of cooling water It is because there is a fundamental defect in the method verifying its result however rich the products of theoretical analysis may get It is necessary to collect the data of field survey as many as possible and to deal with it correctly and then to make efforts approaching the essence of the problem inductively.

There are some methods to solve the problem of recirculation of cooling water But some questions arise. That is, the method by the hydraulic model test comes into question in the point of similarity of real phenomena It is because the flow in the sea is very small, as the discharged water from the outlet has a low velocity and heat exchange between the sea surface and the atmosphere must also be considered. In the present study, the method of numerical experiment is used throughout from this point of view.

In the present report, two factors of great importance in the determination of the recirculation degree of cooling water for power stations are chosen for theoretical analysis. In the first place, the problem of flow and thermal diffusion in the sea caused by the outfall of warmed cooling water is considered. Secondly, study on cold water intake from the bottom layer is presented.

In this report, we present some results of a theoretical investigation of turbulent thermal diffusion in a compressible fluid by means of direct numerical solution of a complete set of dynamic equations. The application of numerical experimentation to physical theory is generally justificable only when more concise analytic methods have been unproductive or have reached apparent limits of usefulness, but these conditions seem to prevail in the field of turbulent fluid mechanics. Although it would be possible to formulate and numerically integrate sets of differential equations, initial and boundary values, appropriate to a broad range of fluid dyanmics phenomena, this method would have little merit in the cases where general analytic solutions are available. One should always keep in mind, however, that the results of numerical experiment are purely logical consequences of the various theoretical approximations and simplifications initially assumed, difficult though it may be to trace through the effects of particular assumption.

An accelerated Liebman method using finite difference in this report is developed for obtaining the distributions of flow and water temperature. In the model to be discribed, a coupled set of simultaneous nonlinear partial differential equations is transformed into difference equation system, which is solved numerically with the aid of electronic computer IBM SYSTEM 360. The Eulerian grid-point representation at points evenly spaced in a rectangular net was chosen principally because of its relatively straightforward program coding and the relatively large fund of knowledge available, pertaining to its characteristic behavior.

II. FORMULATION OF THE PROBLEM

In order to obtain the distributions of flow and thermal diffusion in the sea basin off the outlet, it is necessary to consider both dynamic movement of released water and thermal diffusion of water temperature. As shown in Fig. 1, take the Cartesian coordinates in three dimensional space, the origin of which is taken as the center of outlet The direction of three axis of the coordinates are as seen in the definition sketch (see Fig. 1) Let us assume that the outlet has a rectangular section, 2B in breadth and H in height, from which the cooling water with an initial constant temperature T_0 is released into the sea in the direction perpendicular to the coast

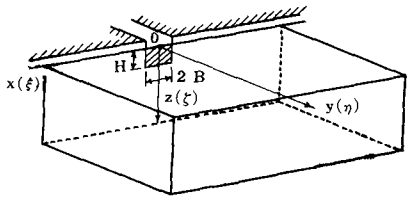

Fig. 1. Definition sketch for thermal spread.

In general, a velocity caused by discharged water in the bay has to be kept small. Because the small relative velocity between an upper and a lower layers keep the stability of the stratification in the bay. Therefore, the eddy viscosities are predominant in a field of the flow in the bay, and the field of flow are strongly subject to the influence of the coastal boundaries near the outlet. In this respect, it differs from the general phenomena of jet flow.

The equations of motion in the i direction and the equation of continuity can be written as

$$\frac{\partial}{\partial x_j}\left(A_j \frac{\partial u_i}{\partial x_j}\right) = u_j \frac{\partial u_i}{\partial x_j} + \frac{\partial p}{\partial x_i} - \rho g \lambda_k \qquad (1)$$

and

$$\frac{\partial(\rho u_i)}{\partial x_i} = 0 \qquad (2)$$

where $j = 1, 2, 3$ corresponds to the x, y, z direction respectively λ_k is the unit vector along the z axis $u_i (i = 1, 2, 3)$ are the velocity components along the x, y, z direction and the eddy viscosities corresponding to those directions are A_x, A_y, A_z respectively p the pressure, ρ the density.

On the other hand, the equation for the thermal diffusion is

$$u_j \frac{\partial T}{\partial x_j} = \frac{\partial}{\partial x_j}\left(\frac{K_j}{\rho} \frac{\partial T}{\partial x_j}\right) + \frac{Q_o}{\rho_w C_w H_w} \qquad (3)$$

where K_j are eddy thermal diffusivities, Q_o represents the heat gain or loss for the surface layer of sea basin, C_w is the specific heat of water and H_w is the thickness of layer between the sea surface and the atmosphere, across which process of momentum and heat transfer occur.

An approximate relation between density and water temperature is

$$\rho = \rho_0 (1 - \alpha T) \qquad (4)$$

where the density, ρ_0, is the standard density of the fluid The main process for the heat balance in any part of the coastal region is shown in the following list (see Fig 2)

Table - 1

Process of heating the sea basin	Process of cooling the sea basin
1 Absorption of radiation from the sun and the sky, $Q_s = Q'_s (1 - \bar{r})$	1 Back radiation from the sea surface, $Q_b = \sigma(T+273)\{1 - a - b\sqrt{e(T_a)}\}\ (1 - K\ n)$
2 Convection of sensible heat from atmosphere, Q_h	2 Convection of sensible heat to atmosphere, $Q_h = h_a (T_a - T)$
3 Condensation of vapor, Q_e	3 Evaporation, $Q_e = k\{e(T_a) - e(T)\}$
4 Addition of waste heat from power plant, $Q_c = (\frac{Q}{A})\ \{(1-r) T_b + T_c - (1-r) T\}$	

The following symbols are adopted for use in Table-1.

- Q_s radiation energy from the sun and the sky.
- $\bar{r}$ average reflectance over the integration period
- T water temperature in the surface layer.
- σ Stefan-Boltzman's constant for black-body radiation
- a, b constants.
- $e(T_a)$ the saturation vapour pressure at the sea surface in mbs

K coefficient depending on the cloud height

n cloudiness on the scale 1 to 10.

T_a : atmospheric temperature.

$e(T)$ saturation pressure for water temperature.

h_a heat transfer coefficient (= 2.77×10^{-4} (0.48 + 0.272V))

k · mass transfer coefficient ($k \simeq 2h$).

Q · intake discharge of cooling water

A · surface area of bay.

r mixing ratio from the upper layer.

T_c rise of water temperature added by condenser of power plant.

T_b · water temperature in the bottom layer.

The net-exchange rate across the sea surface to the above processes is then represented by the linear combination,

$$Q_0 = Q_s - Q_b + Q_h + Q_e = Q_1 - Q_2 T \quad .. \quad (5)$$

The solution of this problem is divided naturally into two parts, one of which corresponds to the radiation effect and diffusion effect, and the other effect of internal diffusion mechanism which results from nonuniform temperature distribution in the water.

Boundary conditions on the velocity are taken to be on the free surface, flow parallel to the surface; at the fixed boundaries, velocity equal to zero The thermal flux must be zero in normal direction to the boundaries except the sea surface or at the mouth of bay. The thermal gradient on the sea surface or at the mouth of bay should be remain constant

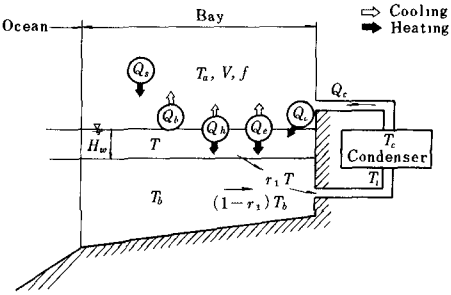

Fig 2. Schematic diagram of main processes for heat balance

In the fundamental equations which govern phenomena of flow and thermal diffusion, the density enters explicitly. It might therefore be expected that variations of density in a vertical direction would modify the results, but the variations of the density in the sea are too small to be of importance in this respect. If the variations of the density are related to the gravitational effect, the product term of ρg , would play an important role in the interaction between the flow and thermal diffusion. And therefore, it should be taken into account in the equations of motion. From this assumption, the equations of continuity can be replaced by the Boussinesq approximation.*

---

* Most studies of fluids with density gradients use the Boussinesq approximation (Boussinesq, 1903), which neglects density variations in the inertial terms of the equations of motion The general meaning is that the density difference $\Delta\rho$ occurs in the acceleration terms as

$$\left(1 - \frac{\Delta\rho}{\rho}\right)\frac{dV}{dt}$$

where $\bar{\rho}$ is the mean density, and therefore, if $\Delta\rho/\bar{\rho} \ll 1$ the acceleration term may be simplified to dV/dt. But, the term $g\,\Delta\rho/\rho$ in the vertical equation of motion should not be neglected because g is large.

The problem now is to solve this nonlinear set of equations subject to the boundary conditions. Since the set is not tractable by any analytical methods known at present, it is necessary to resort to approximate methods for the finite difference solution.

III NUMERICAL CALCULATION OF HEAT BUDGET IN A BAY

There would be two major modes of elimination of heat from power plants, one is the dissipation of heat to the atmosphere through radiation and the other is a gradual movement of warm surface water out to the open sea. The relative losses between each other would depend on meteorological and tidal conditions. The determination of the sea surface temperature not only provides a means of predicting the amount of recirculation for intake and outfall conditions, but also plays a definite and specific role in the determination of the effect of intake and outlet design on the amount of recirculation In this case, it is very important for the effective utilization of the cooling water to investigate the water temperature distribution in the bay and its change as time goes

The technique with the aid of an analogue computer for estimating the distribution of water temperature in the bay has been developed to provide a reasonably accurate procedure which requires only available meteorological data. The heat balance of the water in the bay is calculated by integrating the equation of heat-conduction over the entire water masses of the bay The heat transfer in the atmosphere and the bay water are then calculated under the following assumptions

1) The bay is divided into some blocks for mathematical development Thermal diffusion and tidal effect would be taken into consideration in executing numerical simulation.

2) During summer, there exists a remarkable layer of thermocline at $3 \sim 4$ m below the sea surface in the bay. This interface is stable in spite of tidal changes and wind.

3) The warmed cooling water would spread from the outlet in the form of a thin layer on the surface of the bay, and therefore high temperature content of discharged cooling water is not diffused into the lower layer through the layer of thermocline with large stability.

4) The tidal change is simulated by the sinusoidal curve due to the field survey.

5) The water temperature at the open sea is equal to normal temperature not influenced by the discharged warm water.

In the above case of treating the problem of time history of water temperature in the calculation of heat budget, the meteorological data such as the radiation, atmospheric temperature, need the records with the variation of a day. Such calculations give only a rough estimate these phenomena, but they serve to give an approximately quantitative idea of the interplay between the bay water and the atmosphere. From these calculated values the general features of the daily change of the heat loss or gain from the sea surface can at least be grasped.

Wada, A. and N. Katano[2] have applied this technique to some bays in which the recirculation of cooling water comes into question, and obtained the balancing water temperature in the surface layer and intake water temperature against parameters such as the dimensions of bay, meteorological condition, the tidal flow, and the cooling water flow.

Take, for instance, the case of J. Power Station. This station is planned to be located on the innermost of T. Bay. T. Bay is similar to a rift valley in shape The width of the bay at the innermost is about 300 m with a depth of about 15 m The width and depth increase gradually toward the mouth and the widest section is about 700 m at the mouth of the bay, while the depth increases to about 25 m Its length is about 1,700 m. From the result of the field survey, it is clear that the waters of the inner bay and the outer sea are interchanging, and that the tempera-

ture of the bottom water below the interface between two layers in the bay about 25 °C

The cooling water intake will be located at the innermost of the bay of 13 m deep, and the warmed water is returned to the same bay through the outlet about 200 m distant from the intake The water in the bay has a pronounced temperature stratification. One should intend to use the bottom layer water which has a more suitable temperature for the cooling condenser with a view to achieving a higher efficiency and reducing the trouble associated with impurities in the water.

From the above-mentioned assumptions, the rate of temperature rise dT/dt in each block, taking the effects of tidal current and thermal diffusion into account, is given by

$$\left.\begin{aligned}
\frac{dT_1}{dt} &= \frac{1}{C_w\rho(H_w+\eta_1)}\left\{(Q_{ps}-Q-Q_{r1})+\frac{1}{A_1}(Q_{c_0}-Q_{t1}-Q_{k1}+Q_{k_1}+Q_{c_1})\right\} \quad \text{for No 1 Block}\\
\frac{dT_2}{dt} &= \frac{1}{C_w\rho(H_w+\eta_2)}\left\{(Q_{ps}-Q_a-Q_{r2})+\frac{1}{A_2}(Q_{c_1}-Q_{c_2}+Q_{k_2}-Q_{k_1}+Q_{t1}+Q_{t2})\right\} \quad \text{for No 2 Block}\\
\frac{dT_3}{dt} &= \frac{1}{C_w\rho(H_w+\eta)}\left\{(Q_{ps}+Q-Q_{r3})+\frac{1}{A_3}(Q_{c_2}-Q_{c_3}+Q_k-Q_{k_3}-Q_{t_3}+Q_{t3})\right\} \quad \text{for No 3 Block}
\end{aligned}\right\} \qquad (6)$$

in water column of cross section 1 cm² and thermocline depth of $H_w+\eta$ (see Fig. 3) Figure 4 represents schematic diagram of flow and heat advection in T bay. Energy losses from the sea surface to the air by contact with cooler air and that due to evaporation are dealt with as negatives. The sign in the equation (6) represents a positive one for incoming heat energies into blocks. In the above equation (6), the definitions are as follows

Q_{ps} the net radiation $(=Q_s-Q_b)$

$Q_a=$ $aT_a+\beta$ $(a=h(2fm+1),\ \beta=2hn(1-f))$

$Q_r=$ $rT(r=h(2m+1))$

$\eta(t)$ tidal change,

A_i surface area for each block,

Q_{ci} heat energy in each block by the discharge of warm water,

Q_i heat energy transferred by the mixing from upper layer,

Q_{ki} heat energy advected by the tidal current.

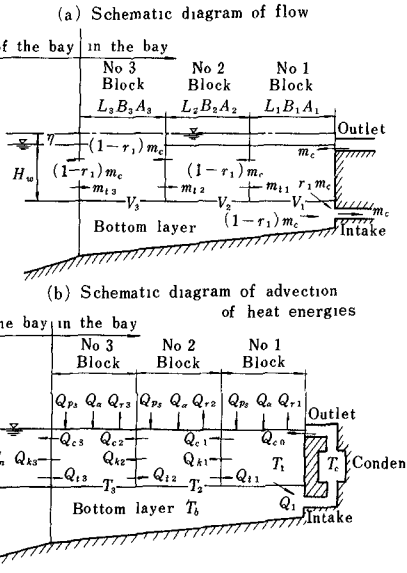

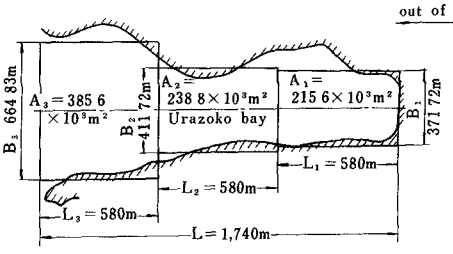

Fig 3. Choice of block

Fig. 4. Schematic diagram of flow and heat advection in T. Bay

In the following numerical calculations, the undermentioned values were used for the various factors in the heat budget, according to the meteorological data observed in the summertime at T bay over the period of twenty years

Average air temperature 28.5 °C

Average wind velocity V = 3 3 m/sec

Relative humidity · 79 %

Cloud amount · n = 6 3

Coefficient depending on cloud height K = 0.083

The above-mentioned records represent the values of average state However, in the case of treating the problem of time history of water temperature in the calculation of heat budget, the meteorological data such as the radiation, atmospheric temperature, need the records with the variation of a day These data were chosen from the records taken in site Figures 5 and 6 represent the daily variations of the radiation and the atmospheric temperature From the process of convergence of the water temperature in the surface layer at natural condition, the

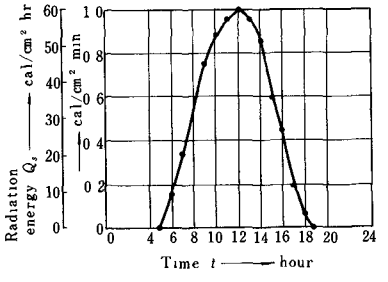

Fig 5 Daily variation of radiation at the T. site (July-August, 1964)

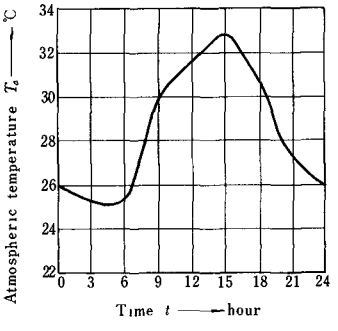

Fig. 6 Daily variation of atmospheric variation at T. site (July - August, 1964)

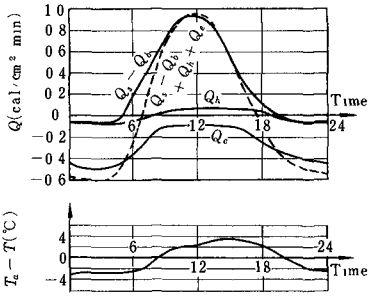

Fig 7 Heat budget in the surface layer (Natural condition).

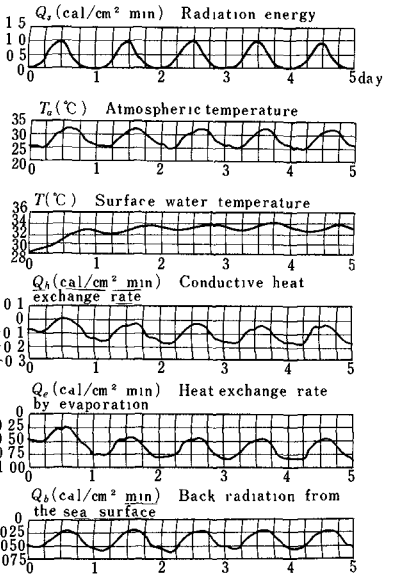

Fig 8 Process of convergence of water temperature in the surface layer affected by discharged warm water

daily variation of heat budget was obtained as shown in Fig 7. Figure 8 shows the process of convergence of the water temperature in the surface layer effected by the discharged warm water. Based on heat-budget concepts, graphs have been developed to permit the estimation of the water temperaure of sea surface, taking into consideration of the addition of heat by plant to bay (see Fig. 9)

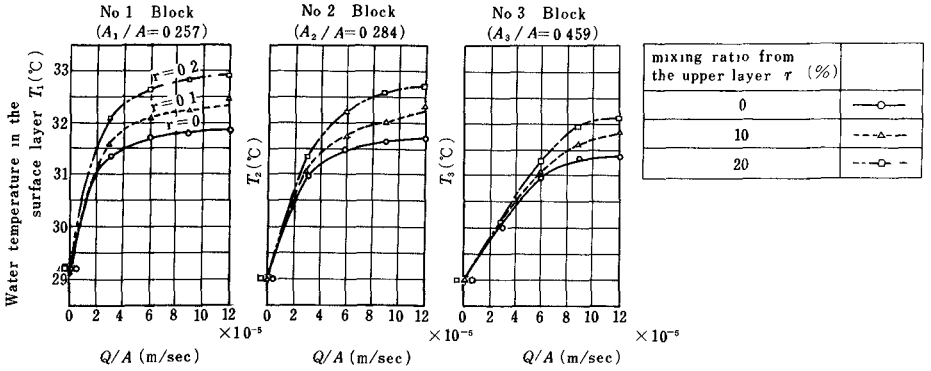

Fig. 9 Relation between water temperature in the surface layer and Q/A for mixing ratio r

IV. INTERACTION BETWEEN FLOW AND THERMAL DISTRIBUTION

4.1 Preface

Generally speaking, phenomena of flow and thermal diffusion caused by the outfall of warmed cooling water seem to be composed of complex processes. The field of flow would change that of water temperature distribution in the vertical section. The diffusion process of warmed water would also change the field of flow. Thus, these processes of two phenomena can not be considered independently each other, but must be taken into account of the interaction between these two phenomena.

In order to confirm the realization of the above mentioned matter, it is necessary to conduct the numerical experiments on the thermal diffusion in the vertical section taking into account of the thermal diffusion-velocity correlation.

4.2 Actual state of thermal diffusion of cooling water and stability of stratified distribution in density

The following points were made clear as the result of the discussion carried out to make clear possibility of intake and outfall of cooling water in the same basin of bay, in confirmation of preparatory investigation data for water temperature of the sea around the Mizushima Bay and other research data

1) The thermocline is stable in spite of tidal change. The eddy viscosity near the boundary is very small (about 0 05 c.g.s.) and the stratification of density is not destroyed by mixing caused by the prevailing winds of 5 ~ 8 m/sec.

2) Based on the data of the field survey, the thermal diffusion coefficients are calculated. It is found that the horizontal thermal diffusivity is at least 50 times greater than the vertical, the order of which seems to be about 0.01 m²/sec. Accordingly, it is concluded that the decrease of the temperature observed in the field tests should be due to the horizontal

mixing with the surrounding waters of lower temperature, with addition to the process of cooling the sea surface and the process of entrainment of the lower colder water to the upper layer current

Generally, the warmed cooling water discharged from the outlet flows as an upper layer current partly because of its inertial momentum and partly because of its lower density. The upper layer current thus exerts the tangential stress on the lower layer which favours the compensation current along the sea bottom That is, the water temperature in the lower layer is almost unchanged, but there is a slow movement of lower layer upstream from the open sea to compensate for the water lost by entrainment. It seems that the surface outfall of cooling water gives rise to upwelling motion near the outlet.

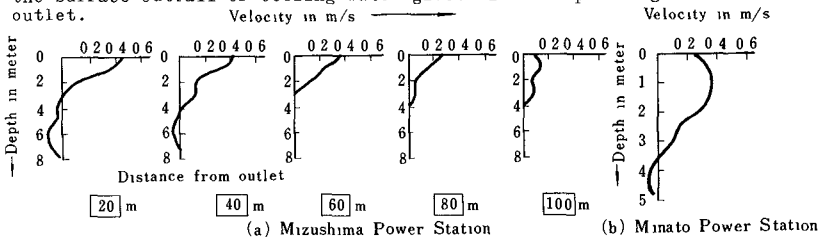

(a) Mizushima Power Station (b) Minato Power Station

Fig 10. Vertical variation of velocity off the outlet

Until recently the investigation of upwelling motion was not enough to afford any insight into the inner mechanism of this phenomenon. Detailed systematic field surveies of the upwelling phenomena have been made at power plants located on the Mizushima Bay and the Miike Port. The results indicate the occurrence of the return flow in the bottom layer due to the outfall of cooling water Figure 10 represents the state of occurrence of the return flow in the bottom layer of the coastal region off the outlet by the outfall of cooling water at the Mizushima and the Miike Thermal Power Plants. The upwelling motion may be also understood by the vertical structure on the thermal diffusion of Fig. 11, in which the uniform rise of the isothermal line towards coast is a particularly marked feature of the thermocline structure of the upwelling region.

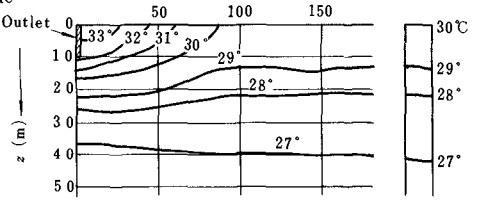

Fig 11 Vertical distribution of water temperature along the y-axis perpendicular to the shore in M Bay

This compensation current phenomenon probably occurs at the sea region off shore the outlet. The upwelling brings water of greater density and also leads to change in the distribution of mass, and exercises therefore a widespread influence upon the sea conditions off coasts where the process take place.

V DIFFUSION IN THE DENSITY STRATIFIED SEA

In the theory of locally isotropic turbulence, it was found originally by Kolmogoroff that the eddy viscosity and eddy diffusivity increase with the scale of the phenomena concerned. The basic idea is that a wide spectrum of turbulent motions, or eddies, exists with scales varying from less than a centimeter up to the dimensions of the body of water itself. There exists an intermediate range of eddies which are in energy equilibrium. It is shown that in this range $K \propto L^{\frac{4}{3}}$, where L is a linear dimension representative of the scale of diffusion being

studied. A number of authors have suggested that this law should be applicable to horizontal diffusion in the sea. In a stratified sea the application is complicated by the effect of density currents and the shear effect It would seen unwise to assume that the 4/3 power law applies in a given stratified condition unless an independent experiment there has indicated that it does so.

The process of turbulent exchange in the stable stratified sea is different from that in the homogeneous sea region The existence of the density gradient may introduce into the energy spectrum a new equilibrium range —the "buoyancy subrange"— situated in a range of lower wave numbers than the inertial subrange, as suggested by Bolgiano (1959)[3] As for the vertical diffusivity K_z, on the contrary, the 4/3 power law will not be useful as much as for the horizontal diffusivity, not only because of a fact that the integral scale of turbulence is comparable or even smaller than the scale of phenomena in the vertical direction, but also because of a strong dependence of K_z on the stratification is still lacking

An application of the transfer theory or the mixing length theory has been extensively accepted, as a useful approximation, to practical problems of turbulent diffusion in the sea. Various empirical formulas have been proposed to represent the variation of K_z, or the mixing length associated with it, with R_i Taylor (1931)[4] examined on turbulent phenomena of very small scale and pointed out that the influence on the vertical exchange and the diffusion of momentum were of many kind and that the process of exchange was isotropic. A semi-empirical study based on the mixing length theory was first developed by Rosshy and Montgomery (1935)[5] by introducing certain stratification parameter —Richardson number— into the expression for the mixing length Thus, the application of their idea to the coefficient of diffusion results in

$$K_z = \ell_z^2 \left|\frac{d\bar{u}}{dz}\right| = \ell_0^2 \left|\frac{d\bar{u}}{dz}\right| (1+\beta R_i)^{-1} = K_z^0 (1+\beta R_i)^{-1} \qquad (7)$$

where ℓ_z and ℓ_0 denote the mixing length for the stable stratified and the nonstratified sea, respectively, and R_i represents the Richardson number given by

$$R_i = (g\ \partial\rho/\partial z)/\rho(\partial\rho/\partial z)^2$$

Different considerations of the exchange mechanism in the stratified sea produce different expressions for the coefficient of diffusion on the degree of stability

The influence of stability on the vertical mixing process due to turbulence has also been treated by Mamayev (1958)[6], who considered that the appropriate forms for A_z and K_z were

$$K_z = K_0\, e^{-n R_i}, \quad A_z = A_0\, e^{-m R_i} \qquad (8)$$

where $n - m > 0$ From Jacobsen's data it was deduced that n = 0.8, m = 0.4

The effect of the density stratification in the vertical section on the horizontal exchange of turbulence was first investigated by Parr (1936)[7] and Bowden (1965)[8] The results show that the turbulent exchange in the stable stratified sea is very nonisotropic and that the effective coefficient of horizontal diffusion is inversely proportional to the coefficients of the vertical eddy diffusion. The occurrence of a stable gradient of density therefore increases the effective horizontal mixing very considerably. This conclusion is inconsistent with that led by Taylor previously mentioned. But, Taylor's theory concerns with the exchange process of very small scale The above conclusion is applicable only to phenomena with long duration. R.V. Ozmidov (1965)[9] proposed a new model of turbulent exchange in the stable stratified sea. From the theory of locally isotropic turbulence, the mean velocity gradient of the turbulent eddies is given by the following equation

$$\frac{du}{d\ell} = c\varepsilon^{\frac{1}{3}}\ \ell^{-\frac{2}{3}} \qquad (9)$$

where c is a universal dimensionless constant, ε is the energy dissipation rate and ℓ is the distance The critical scale ℓ_{cr} that the turbulent field loses its nonisotropy may be obtained by taking ℓ_{cr} as ℓ when R_i approaches a finite value, a

The effect of shear existing in the Richardson number R_i may be replaced with equation (9) The critical scale ℓ_{cr} depends on energy dissipation rate ε and on parameter $\beta=(g/\rho)(\partial\rho/\partial z)$ In this case ℓ_{cr} is given by

$$\ell_{cr}=\left(\frac{a\nu^2\rho^{\frac{2}{3}}}{g(\partial\rho/\partial z)}\right)^{\frac{3}{4}}=a\varepsilon^{\frac{1}{2}}\beta^{-\frac{3}{4}} \quad . \qquad (10)$$

where a is a dimensionless constant

The values of the vertical and horizontal turbulent exchange coefficient K_z and K_h also depend parameters ε and β . Within scales varing from the critical scale ℓ_{cr} up to the "Kolmogorov micro scale", $\ell_0=(\nu^3/\varepsilon)^{\frac{1}{4}}$, where is ν is the kinematic viscosity, the turbulent fields have the isotropy even in the stratified sea For eddies with $\ell>\ell_{cr}$, large turbulent eddies have only vertical axis. That is, we have $K_h>K_z$ for large scale exchange because the diffusion velocity has its upper limit even if the spot of diffusion becomes large

The maximum value of K_z can be estimated on the basis of the 4/3 power law from the theory of locally isotropic turbulence. That is

$$K_{z\,max}=c_1\varepsilon^{\frac{1}{3}}\ell_{cr}^{\frac{4}{3}}=\frac{a\nu^2c_1\rho\varepsilon}{g(\partial\rho/\partial z)} \quad . \qquad (11)$$

where c_1 is an universal constant

The proposed turbulent model in the stable stratified sea is summarized as follows (see Fig. 12). For small scale turbulent exchange there is a three dimensional turbulence, that is $K_h=K_z$ But for exchange phenomena larger than ℓ_c we have $K_h>K_z$ Then, the value of K_h is controlled by the 4/3 power law in the horizontal space As the dimension of the scale becomes large, scale of turbulence amounts to the maximum eddy with ℓ_1 in the horizontal direction This dimension corresponds to several kilometers in the ocean

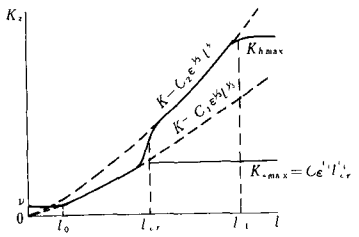

Fig 12 Relation between scale of phenomena and K_h, K_z in the stable stratified sea

VI METHODS OF SOLVING FUNDAMENTAL EQUATIONS

The distributions of flow and water temperature in the continuously stratified sea caused by outfall and intake of cooling water must be obtained by taking account of the interaction between flow velocity and thermal distribution In order to obtain the velocity and the density fields, the numerical experiments is conducted in the vertical section. In the fundamental equations which govern phenomena of flow and thermal diffusion, the density enters explicitly In this report, the Boussinesq approximation is used throughout, which neglects density variations in the inertial terms of the equations of motion From this assumption, the equation of continuity can be replaced by this approximation. And therefore we can introduce a stream function P into the fundamental equations Replacing the equations (1)~(4) by a Laplacian equation of the stream function, an equation satisfying the vorticity, and an equation for the thermal diffusion, we obtain the following equations (12)~(14) To obtain the equation for the transfer of vorticity, the pressure p is eliminated between equations in the x- and z-directions of equation (1) by cross-differentiation and subtraction Solution of the equation

of thermal diffusion with a complete set of Eulerian equations may be obtained numerically.

$$\xi=-\frac{1}{2}\left(\frac{\partial^2 P}{\partial x^2}+\frac{\partial^2 P}{\partial z^2}\right) \qquad (12)$$

$$2\left(\frac{\partial P}{\partial z}\frac{\partial \xi}{\partial x}-\frac{\partial P}{\partial x}\frac{\partial \xi}{\partial z}\right)=-g\alpha\rho_0\frac{\partial T}{\partial x}+2\left(A_h\frac{\partial^2\xi}{\partial x^2}+A_z\frac{\partial^2\xi}{\partial z^2}\right)$$
$$+\frac{\partial}{\partial x}\left(\frac{\partial A_z}{\partial z}\frac{\partial w}{\partial z}\right)-\frac{\partial}{\partial z}\left(\frac{\partial A_z}{\partial z}\frac{\partial u}{\partial z}\right)+\frac{\partial A_z}{\partial x}\frac{\partial^2 w}{\partial z^2}-\frac{\partial A_z}{\partial z}\frac{\partial^2 u}{\partial z^2} \qquad (13)$$

$$\frac{\partial P}{\partial z}\frac{\partial T}{\partial x}-\frac{\partial P}{\partial x}\frac{\partial T}{\partial z}=\frac{\partial}{\partial x}\left(\frac{K_z}{\rho_w}\frac{\partial T}{\partial x}\right)+\frac{\partial}{\partial z}\left(\frac{K_z}{\rho_w}\frac{\partial T}{\partial z}\right) \qquad (14)$$

The term of thermal horizontal gradient is contained in the first term of the righthand side of equation (13). And this term could probably be interpreted as one having power of binding the flow associated with addition of the warmed cooling water.

The effect of thermal gradient is omitted, in the first order approximation, to simplify the mathematical development. Solutions of the first order approximation are applicable only to bay having negligible stratification or gravitational convection. A more general solution is obtained by the combination of equations (12), (13) and (14), by applying these first order values obtained above. If the processes are repeated, the required solution will be obtained finally Solutions thus obtained give the values which are influenced, to some extent, by the thermal distribution-velocity interaction.

In the experimental treatments of the previous paper[1], the coefficients of eddy diffusivity and eddy viscosity were assumed to be constant despite the fact that the magnitude of the coefficient depends strongly on the local turbulence The existence of thermal activity and buoyancy effects add great complexity to the exchange problem. Generally speaking, the effect of a thermal stratification on the state of turbulence is described by means of the local Richardson number.

It is, in fact, doubtful that a universal equilibrium theory can be established to relate turbulent transfers to mean gradients, regardless of scale and for the entire range of the Richardson number. The assumption we will make essentially imply above mentioned theory. Thus we must apply a considerable amount of empiricism, and can not expect the resulting expressions to be necessarily valid for all physical frameworks.

In this treatment, the eddy coefficients of viscosity and diffusivity are assumed to be of form proposed by Mamayev This formulation must have a finite value as $R_i\to\infty$. And therefore, the following relations are adopted

$$A_z=(A_1+A_0\,e^{-mR_i}) \qquad (15)$$

$$K_z=(K_1+K_0\,e^{-nR_i}) \qquad (16)$$

where A_1 , A_0 , K_1 and K_0 are constants.

VII NUMERICAL EXPERIMENTS OF THERMAL DIFFUSION

In this report, the most basic contributions to the velocity fields in the sea are the net outseaward flow required for disposal of the warmed cooling water, and the gravitational convection due to the density difference between warmed water and lower water Numerical solutions have been obtained for the coupled system of partial differential equations describing the flow circulation and the water temperature distribution for a given sea condition with meteorological data. These solutions provide new insight into the interaction of the water temperature and velocity fields as a control mechanism in coastal dynamics. The mechanism of development of upwelling motion could also be confirmed by numerical experiment. Figures 13 and 14 represent respectively the vertical profiles of water temperature and velocity along the longitudinal section obtained by the calculation.

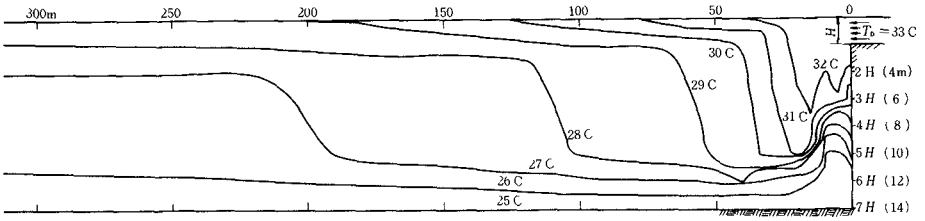

Fig 13. Water temperature distribution along a longitudinal section.

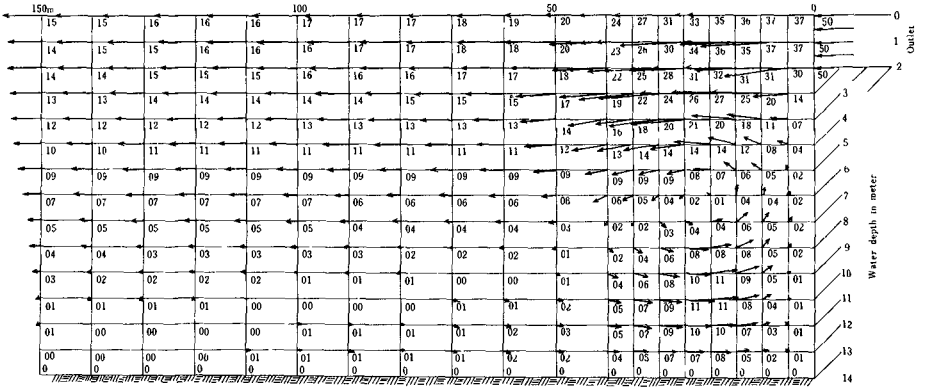

Fig. 14. Velocity distribution along a longitudinal section.

The general feature of the velocity solution is shown in Fig. 15, where the value, $A_z/A_x = 0.1$, has been used This figure utilizes only the first and the fourth order velocity. These curves show a surface outflow and a deeper inflow of water. Higher order approximation, taking into account of interaction, has a considerable effect on the shape of the vertical profiles of water temperature and velocity.

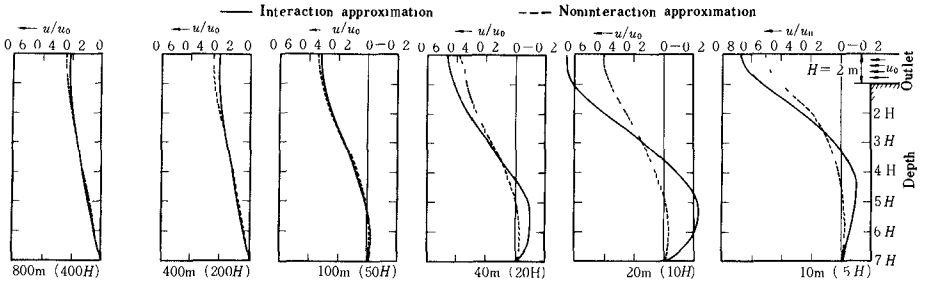

Fig 15. Variation of velocity profile.

An interaction solution in the vicinity of the outlet gives the velocity larger or smaller than that give by the first order solution at the surface or at the bottom. However, off the outlet, differential advection between two layers will tend to develop a density instability in these layers, giving a much increased vertical coefficient of diffusivity The motion of water particles near the outlet can be grasped from velocity distribution along a longitudinal section shown in Fig. 14. From these series of experiments, it can be seen that colder water in the lower layer is sucked into the upper layer along the vertical wall, and that the temperature of released water in the upper layer is decreased, to some extent, by entrainment and its volume also increases as it moves offshore. This upwelling action will also change the vertical profile of the water temperature This can be understood by the process of formation of the thermocline shown in Fig. 15 The upper movement of isothermal lines near the outlet would be probably determined from the relation between the turbulent intensity of cooling water flow and upwelling motion In this case, it seems that the upwelling phenomenon is excelled in the fluid motion near the outlet Figure 13 is similar to the vertical structure on the thermal profile of the field survey shown in Fig. 11, in which the uniform rise of the isothermal lines toward the coast is a particularly marked feature of the thermocline structure of the upwelling region. The numerical solutions give a good representation of all features of flow and thermal profiles. From the velocity profile at the site 80 m (or 40 H, where H is the height of outlet) shown in Fig. 15, the difference between the first and the higher order approximations can't be almost found.

The process of the formation of water temperature distribution is different from that of velocity fields. As the solution goes to a higher order approximation the heat energy caused by the outfall of warmed cooling water has a tendency to accumulate in the form of wedge shaped in the surface layer (see Fig. 16)

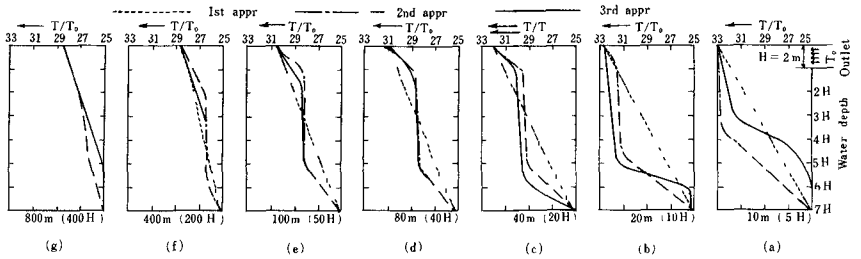

Fig. 16 Profile of water temperature distribution
$K_z = K_1 + K_0\, e^{-n\,Ri}$, $A_z = A_1 + A_0\, e^{-m\,Ri}$.

This phenomena can also be understood by the distribution of water temperature at the site far off the outlet. The results do suggest that the mixing process resulting in the entrainment into the upper layer predominates over that by the eddy diffusion near the outlet Therefore, refinement of the influenced range of flow and water temperature rise by the surface outfall is obtained by taking the supply of the lower water into account. The subject of future research would be the theoretical description of upwelling in a stratified, two-layer sea This point is being investigated.

VIII CONSIDERATION OF COLD WATER INTAKE FROM A STRATIFIED FLUID

Finally, problem on the colder water intake from the bottom layer in the sea with relation to design of the intake structure of cooling water is considered.

Up to present, the study on the selective withdrawal intaking colder water of lower layer has been carried out on the assumption that the sea water has a two-layer system with a discrete interface across which the density changes abruptly In the field, however, such a well-defined interface does not usually occr The vertical distribution of the density presents continuous profile by development of the intermediate layer when the mixing between two layers is promoted by the wind action. However, an equivallent interface has been assumed to exist at the place in the depth at which the vertical gradient of temperature or density is a maximum

It appears desirable to extend the theory and experiment to systems with continuous density stratification Namely, paying attention to the dynamic interactions between the density (or temperature) and the velocity distributions, intake equipments to promote the efficiency of cooling water intake should be designed.

Because of the inherent difficulty in making steady experiments with continuously stratified flows, the results are not very conclusive. For a given intake geometry, the maximum colder water discharge that can be withdrawn without inducing appreciable withdrawal from the upper layer in the sea with two-layers was only determined. It is interesting to investigate the selective withdrawal problem of a fluid with known density from a stably stratified fluid in the sea because little work has been done in the field of continuously stratified flow

Theoretical studies of incompressible, steady, viscous flow towards a sink in a stably stratified fluid were made by W R Debler (1959)[10] , Yih, O'Dill and Debler (1962)[11] , Robert C.Y. Koh (1966)[12] , and Onishi and Hino (1967)[3] In these studies, it is assumed that the density increases linearly from the sea surface to the bottom and that the intake opening is taken as a line sink

In the present report, the numerical experiments of the stratified fluid with a continuous density gradient flowing into the submerged intake with a finite opening is undertaken to gain additional insight into the mechanism of density flow in the field of the continuously stratified fluid In this section, some calculations are made to obtain the distributions of flow and water temperature at varying velocities

The intake structure is in the form of submerged curtain wall with a finite opening. The height of opening is 3 m.

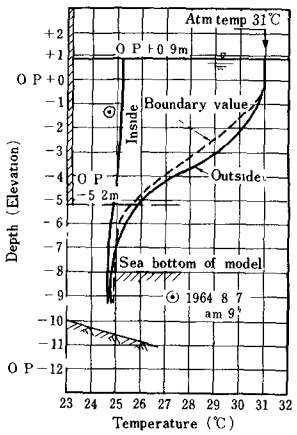

Fig 17 An example of field survey and setting up of boundary value.

The numerical model contains the dimensions of 9 m in water depth, 390 m far off the intake structure in longitudinal section This model corresponds to the intake type of curtain-wall structures at Sakai-Port Thermal Power Station. Figure 17 shows the cross section of curtain-wall type for this Power Station. An example of the result of temperature measurements for bottom water intake is shown in this figure The conditions of calculation is setting up on the basis of the result of the field survey at the Sakai-Port site

The boundary conditions of numerical calculation are given as follows.

(i) T = 31 °C at the sea surface, T = 25 °C at the sea bottom,

(ii) The water temperature for the sea infinitely far off is set up by solving the diffusion equation $\frac{d}{dz}\left(\frac{K_z}{\rho}\frac{dT}{dz}\right) = 0$ with the model of diffusivity, $K_z = K_0 + K_1 e^{-mR_1}$

Its result is shown in Fig. 17 with the dotted line. The general features of the velocity solution by numerical experiments is shown by Fig. 18. In this case, the values, A_z/A_x = 0.1, K_z/K_x = 0.1, $K_1 = A_1$ = 0.01 m²/sec and $K_0 = A_0$ = 0.1 m²/sec have been used. The values of intake velocity as a parameter are u_0 = 0.2 m/sec, 0.5 m/sec. This figure gives the first and the fifth order velocity. Figure 19 represents a result of the vertical profiles of water temperature accompanied by bottom water intake (u_0 = 0.5 m/sec) Higher order approximation has a considerable influence on the vertical profiles of the velocity and the water temperature in the sea region The interaction solutions in the vicinity

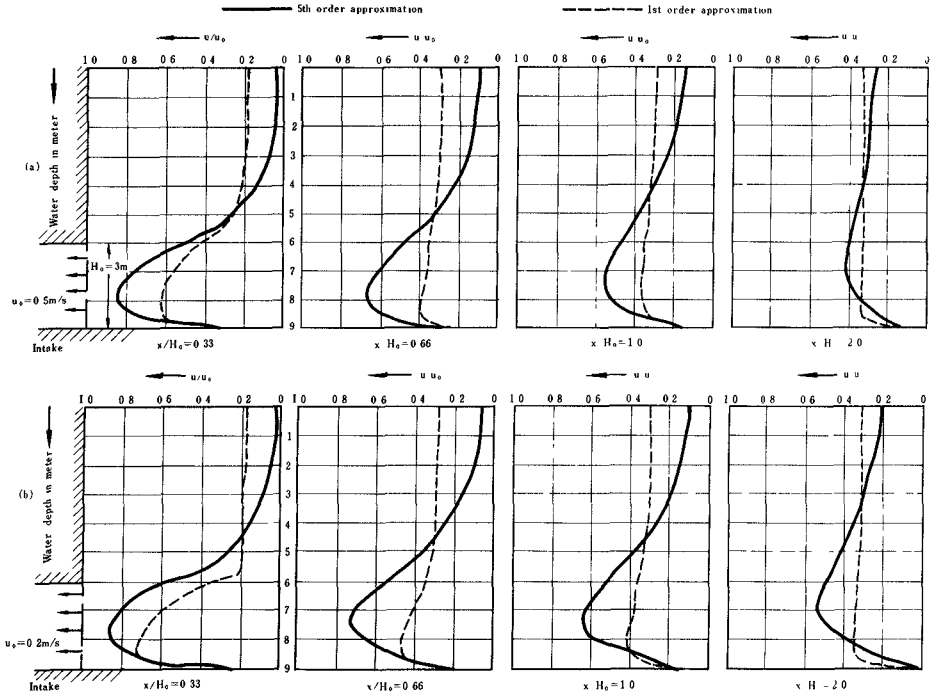

Fig. 18. Variation of velocity profile.

of the inlet give larger than that give by the first order solution especially at the bottom layer. From Figs. 18 (a) and 18 (b), the characteristics of the intake for the different values of intake velocity may be understood. If one makes the intake velocity small, it can be seen from Fig. 18 that we can expect effectiveness of intake

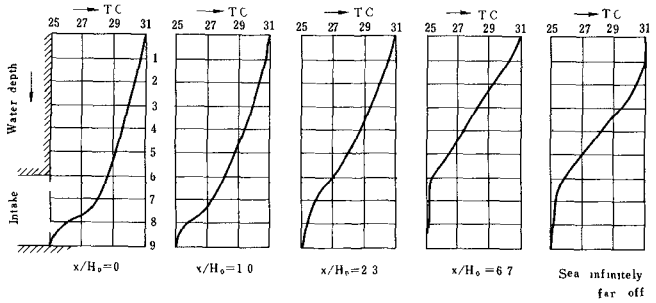

Fig. 19 Profile of water temperature

Figure 20 shows the distribution of the water temperature near the inlet for the two values of intake velocity. The full lines means the case of u_0 = 0.2 m/sec. From Figs. 19 and 20, it can be seen that the vertical profile of water temperature in the sea is not subject to the influence of the intake for the section far off $x/H_0 = 5 \sim 6$ (H_0 is the intake opening, x is the distance from the inlet) from the intake structure.

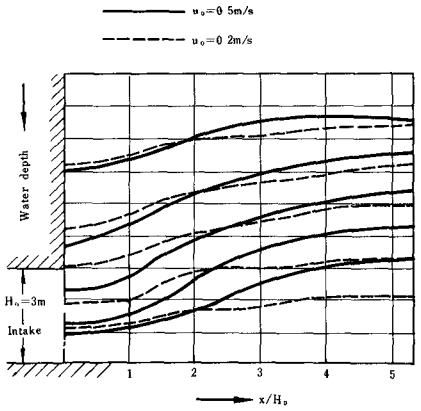

Fig. 20 Water temperature near outlet.

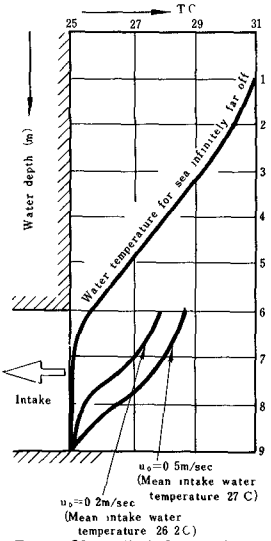

Fig 21 Intake water temperature.

The result of calculation of the intake water temperature from the continuously stratified field is shown in Fig. 21 for the two values of intake velocity. The water temperature of intake, T_i, is 27 °C at the intake velocity of u_0 = 0.5 m/sec, T_i = 26.4 °C at u_0 = 0.2 m/sec. There is less change in the value of the water temperature of intake than it was expected. In the continuously stratified field, there exist a flow which has only a small velocity in the surface layer This flow toward the coast in the surface layer changes into the flow towards vertical down in the neighborhood of vertical wall upper the intake opening.

The results lead to the conclusion that tbe flow in the field of the continuous distribution of density differs slightly from that for a two layer system having a discrete interface. However, these results seem support the view that the application of a two-layer system to the design of the practical intake structure is possible. Further studies in this respect must be the subject of future research.

CONCLUSIONS

The following points were made clear as the results of the field surveys and the numerical experiments. Those were carried out to make clear the possibility of the intake and the outfall of cooling water in the same basin.

1) Numerical solution of the equation of thermal diffusion with a complete set of Eulerian equations in which the values of the eddy coefficients of diffusion and viscosity depend upon the relation to the velocity shear and vertical density gradient was presented. Our efforts to develop a numerical model capable of simulating density flow problems have evidently been partially successful. Results of the computation are in reasonable agreement with the observed features. It also seems that the eddy exchange terms in the vertical section partially satisfy a real physical requirement.

2) The mechanism of development of upwelling phenomenon was made clear from the numerical experiment, taking into account of the interaction between the flow and the thermal distribution. It was made clear that the colder water in the lower layer was sucked into the upper layer along the vertical wall of the coast. And therefore, the mixing process resulting in the entrainment into the upper layer predominates over that by the eddy diffusion near the outlet. These phenomena were also confirmed by the field surveys with respect to the velocity and the water temperature off the outlet.

3) The numerical experiments of the stratified fluid with a continuous density gradient flowing into the submerged intake opening were conducted. The results lead to the conclusion that the flow in the field of the continuous distribution of density differs slightly from that for a two layer-system having a discrete interface. However, these results seem support the view that the application of a two-layer system to the design of the practical intake structure is possible.

ACKNOWLEDGEMENTS

The author wishes to express his gratitude to Dr. Senshu, Chief of Coastal Hydraulics Section, for his encouragement. The fields observations were conducted under the auspices of Civil Engineering Departments of the Chugoku Electric Power Company, the Kansai Electric Power Company, and Construction Department of the Japan Atomic Power Company in Japan.

REFERENCES

1) Wada, A. (1966): A study on phenomena of flow and thermal diffusion caused by outfall of cooling water, Proceedings of the Tenth Conference on Coastal Engineering, Tokyo.

2) Wada, A. and Katano, N (1967). Numerical calculation of heat budget in a bay by outfall of warmed cooling water, Technical Report of Central Research Institute of Electric Power Industry.

3) Bolgiano (1959)· Turbulent spectra in a stable stratified atmosphere, J Geophys. Res., 64, No 12

4) Taylor, G C. (1931) Internal waves and turbulence in a fluid of variable density, Conseil Perm Intern l'exp. Mer. 76

5) Rossby, C G. & R.B. Montgomery (1935). The layer of fricitional influence in wind and ocean currents, Papers in Phys. Oceanogr. Meteorol., 3, No. 3

6) Mamayev, O.1 (1958) The influence of stratification on vertical turbulent mixing in the sea, Izv. Acad. Nauk USSR, Geofiz , No 7

7) Parr, A E. (1936): On the probable relationship between vertical stability and lateral mixing processes, Conseil Perm. Intern. pour l'exploration de la Mer., J. du Conseil, 11, No 3.

8) Bowden, K.F. (1965) Horizontal mixing in the sea due to a shearing current, Jour. of Fluid Mechanics, Vol. 21, Part 2.

9) Ozmidov (1965) On the turbulent diffusion in the stable stratified sea, Izv Acad. Nauk USSR, Fizika Atmofery i Okena No. 8.

10) Debler, W.R. (1959). Stratified flow into a line sink, Trans. A.S.C.E , No. 3101, 491-504

11) Yih, C S., O'Dill, W. & Debler, W.R. (1962) Prevention of stagnation zones in flows of stratified or a rotating fluid, Proc. 4th U.S. Natl. Congr. App. Mech. 1441-1453.

12) Rober C Y. Koh (1966) Viscous stratified flow towards a sink, Jour. of Fluid Mechanics, Vol. 24, 555-575.

13) Onishi, S. & M. Hino (1967). Considerations on a stratified flow towards bottom water intake, Proceedings of the 14th Conference on Coastal Engineering in Japan (in Japanese).

CHAPTER 95

SHIP WAVES IN NAVIGABLE WATERWAYS

DUNCAN HAY, M.S.

REGIONAL COASTAL ENGINEER

DEPARTMENT OF PUBLIC WORKS OF CANADA

VANCOUVER, B.C.

ABSTRACT

Model tests were conducted at the University of California, Berkeley, on six ship models to determine the heights of the waves produced by ships. Measurements were made at various distances from the sailing line with the models moving at various speeds in various water depths. The results of the tests are presented in graphical form, as prototype values.

INTRODUCTION

There has been considerable theoretical and experimental work conducted on the pattern of ship waves and the resistance offered to the ship by the waves it produces. Most of the previous work was conducted in order to understand the mechanism of wave generation, the wave pattern, and the squat of the ships. There are, however, very little data available on the height of waves at various distances from the sailing line, produced by ships of various hull configurations, moving at various speeds.

This report presents the results of model studies carried out at the University of California, Berkeley, on six model ships. The maximum height of the generated waves at various distances from the sailing line, and various water depths, is related to the ship's speed. The results will provide data for the design of harbour and channel revetments which are subject to attack by ship waves. On waterways where public safety is a factor or control of erosion is necessary, the results give an indication of the maximum allowable speed of a ship in the waterway.

TESTING PROCEDURE

The types and dimensions of the six models tested are tabulated in Table 1. These models were chosen to represent a wide range of hull configurations. Bow views of the models are shown in Figures 12 and 13.

TABLE I

MODEL	TYPE	SCALE	PROTOTYPE DIMENSIONS			MODEL
			Overall Length Ft.	Beam Ft.	Draft Ft.	Displacement for Tests Lbs.
A	Mariner Class Cargo Ship	1:96	566	74	24	37.32
B	David Taylor Series 60	1:96	505	64	24	30.45
C	Moore Dry Dock Tanker	1:96	504	66	28	45.48
D	Auxiliary Supply Vessel	1:32	156	36.3	9	61.00
E	Barge	1:48	263.5	54.5	14	97.80
F	Tug	1:32	152.7	34.3	14	66.50

The models were towed by a taut nylon line which was connected to the model fore and aft. Suspended weights connected to a sheave provided the driving force. When the weights were released and the velocity was constant, the time required for a given number of revolutions of the sheave of known diameter was recorded and the velocity of the model was calculated. The waves produced by the models were measured by wave gauges positioned at distances from the sailing line of 0.5, 1.5, 2.5, and 3.5 times the model ship's length. The waves were recorded on a four-channel Sanborn recorder. For a given model, four series of tests were run for water depth to draft ratios of 1.375, 2.0, 2.5 and 3.5. These four ratios were chosen to cover the range of water depths normally encountered in navigation channels. For each run the still water depth was the same at all gauges.

RESULTS

The height of the largest wave in the wave group, measured from the preceding trough to the crest, is designated H_{max}. Figures 1 to 9 present prototype values of some of the test results. In these plots, X is the distance from the sailing line at which H_{max} was measured, L is the overall length of the ship, D is the ship's draft in feet, and d is the still water depth, in feet.

From the graphs presented it is possible to obtain cross-plots such as Figure 10. In this manner it is possible to show the decay of H_{max} from the sailing line or the effect of water depth on H_{max}. In Figure 10, F_r is defined, as usual, as dimensionless $v/\sqrt{gd}$.

DISCUSSION

The results of the tests show that in protected waterways ships may produce waves of significant magnitude relative to wind generated waves. The graphs presented will provide data for harbour and coastal engineers, or port authorities, to determine necessary protective measures or limiting speeds of vessels in navigable waterways. It is noted that smaller vessels such as the tug of Figure 9, may produce waves comparable in height to the waves produced by a large vessel, but at a lesser speed.

The test results show that for a given ship, speed and distance from the sailing line, the value of H_{max} increases with decreasing water depth. The increased wave heights in shallow water are related to the increased resistance and squat a vessel experiences in shallow water. When a vessel enters shallow water the return velocity of the water alongside the ship increases. By Bernoulli's equation it is possible to show that an increase in wave height and squat must accompany this increased velocity. The connection between the ship's squat and the heights of the waves produced is evident by the similar asymptotic character of the curves presented in this report and the curves presented by Schijf for squat. (Ref. 1.)

During the model tests the wave gauges were arbitrarily positioned at fixed locations as determined by the overall length of the ship. Therefore, the results show the maximum wave heights at the point of the wave gauges which is not necessarily the maximum wave heights in the wave pattern. A ship produces diverging and transverse waves (ref. 2). The highest waves in the wave pattern are where the diverging and transverse waves intersect and superimpose. These locations are termed cusps. It is evident that the position of the wave gauges was not necessarily in line with the location of the cusps. This may explain the apparent irregularities of some of the curves. Also, a cross-plot taken from the data, such as figure 10, is only correct at the points X/L equal to 0.5, 1.5, 2.5 and 3.5. A curve drawn through these points is only indicative of the wave decay and does not take into account the possibility that the location of a cusp may be at an intermediate value of X/L. However, for practical purposes, the error in drawing a smooth curve on the cross-plot is not appreciable.

As mentioned previously, the water depth and the ship's speed are important factors with respect to the heights of ship produced waves. Another factor is the fineness or configuration of the vessel's hull. Brebner defined a fineness ratio as, $L^{\prime\prime}/\sqrt{A}$. (ref. 3) $L^{\prime\prime}$ is the length of the curved part of the bow, at the waterline, measured in the horizontal plane, and A is the cross-sectional area of the parallel middle-body, below the waterline.

The effect of the fineness of the bow is shown in the cross-plot of figure 10. It was not the purpose of the tests to explicitly study the effect of the bow fineness; therefore, the data does not lend itself to the isolation of this factor. The factors of wave decay and velocity are not totally excluded in Figure 10, therefore all the curves do not lie in order. Generally, figure 10 does confirm intuition and observation by showing that the wave producing capacity of a ship decreases with increasing fineness.

A comparison between models A and B and the results obtained by Brebner for the 650 foot Empress of Canada is shown on Figure 11. The fineness ratio of the Empress of Canada is 4.04. The results are in reasonable agreement.

SUMMARY

Ships travelling in waterways may produce damaging waves. The graphs presented in this paper give an indication of the magnitude of the waves which may be expected for various vessels. It should be noted that the results are for vessels travelling in water of constant depth. Further tests were conducted on ship waves in shoaling water. The results of these additional tests will be presented by Professor J.W. Johnson, Department of Civil Engineering, University of California, Berkeley.

ACKNOWLEDGMENTS

The research for this paper was sponsored by the U.S. Army Coastal Engineering Center, Washington, D.C. The advice of Professor J.W. Johnson was appreciated.

BIBLIOGRAPHY

1. Schijf, M.J.B., Section 1, Communication 2, XVII Congress, Permanent International Association of Navigation Congresses, 1949; also Section 1, Communication 1, XVIII Congress.

2. Johnson, J.W., 'Ship Waves in Navigation Channels'. Proc. Conf. on Coastal Engr., 1958, Chap. 40, pps. 666-690.

3. Brebner, A., Helwig, P.C., and Carruthers, J. 'Waves Produced by Ocean-Going Vessels: A Laboratory and Field Study'. Proc. Tenth Conf. on Coastal Engr., 1966, Chap. 28, pps. 445-459.

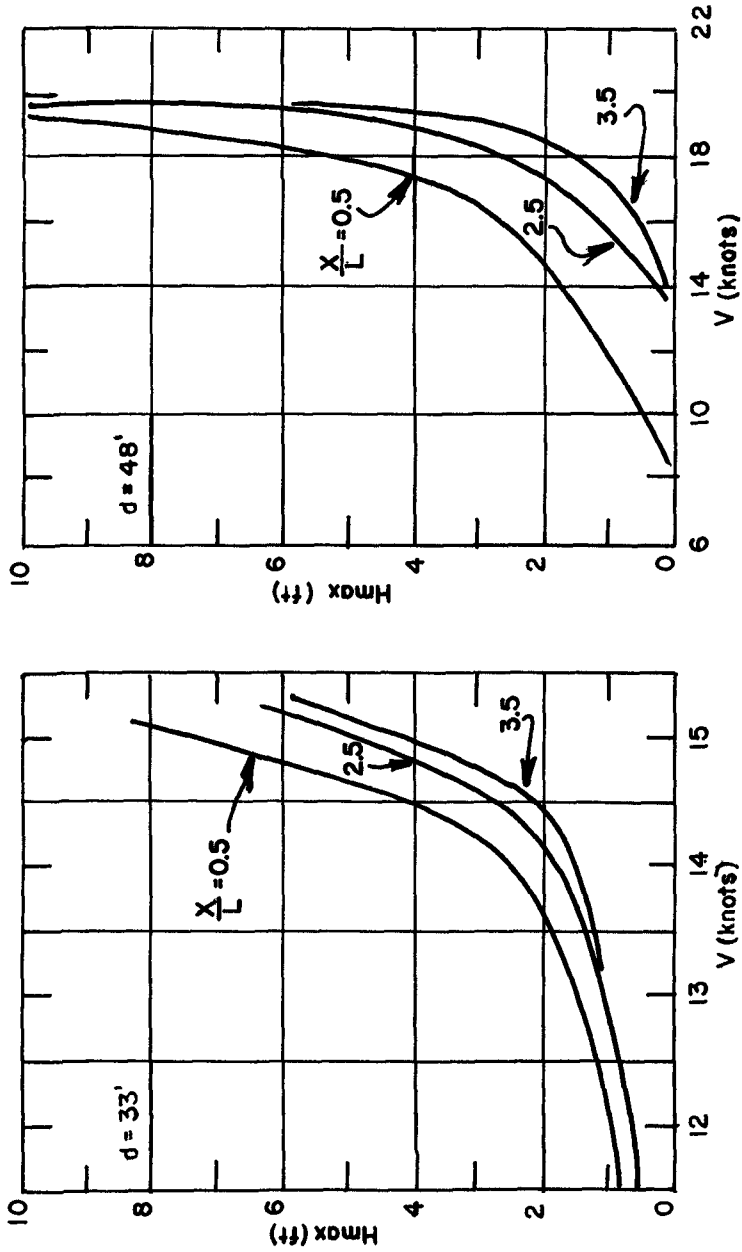

FIG 1. MARINER CLASS CARGO SHIP. L=566' D=24'

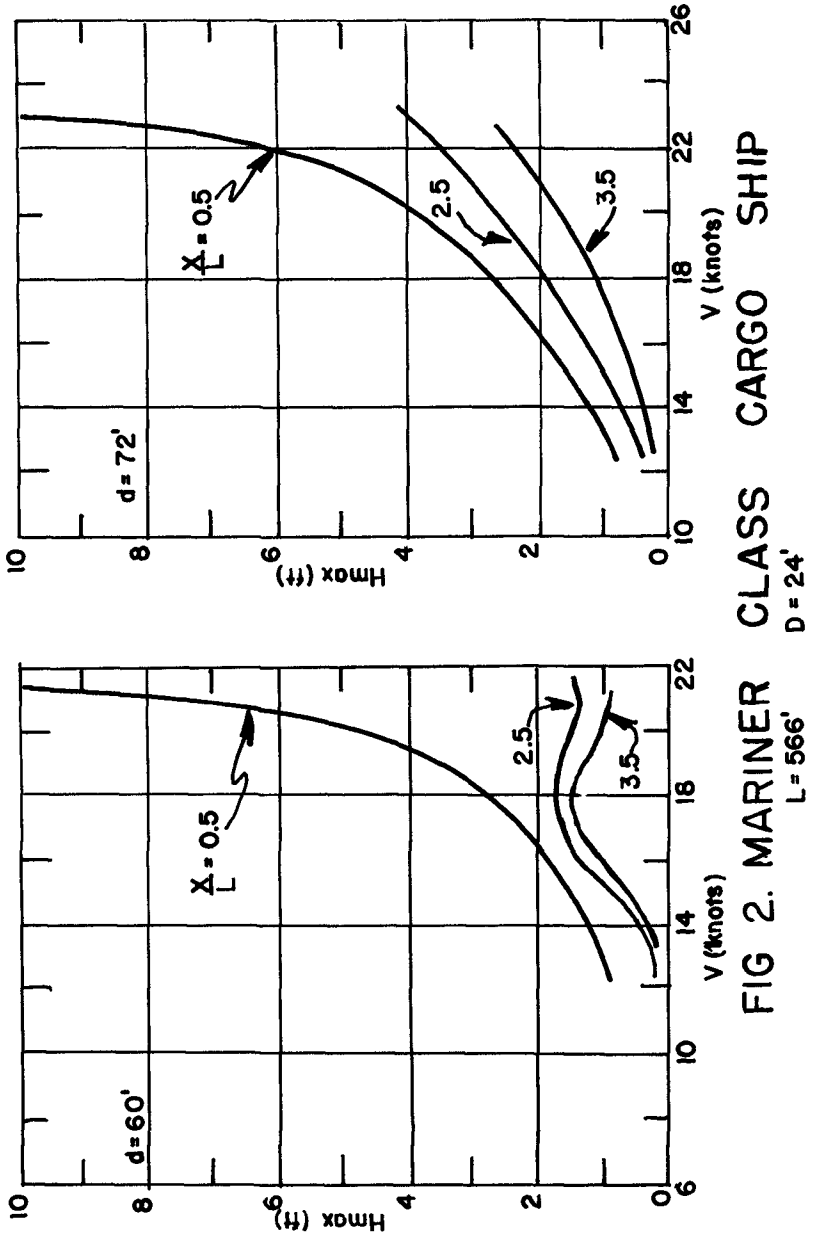

FIG 2. MARINER CLASS CARGO SHIP
L = 566' D = 24'

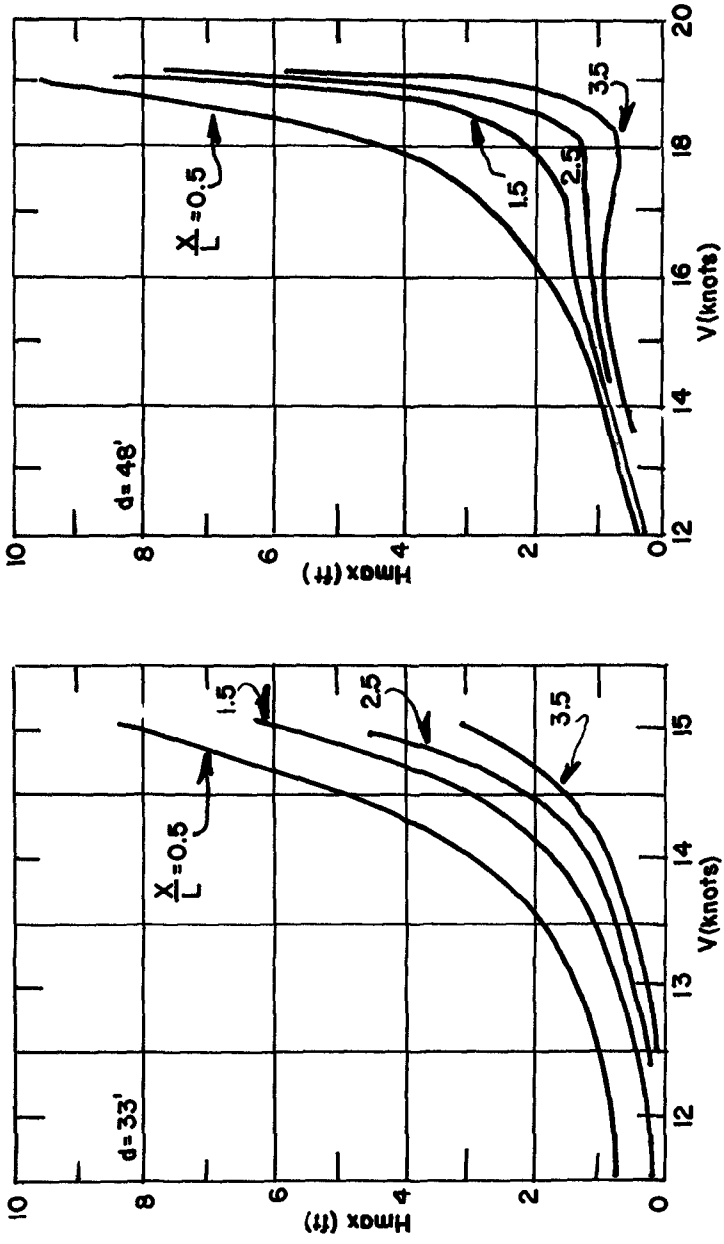

FIG 3. DAVID TAYLOR SERIES 60
L=505' D=24'

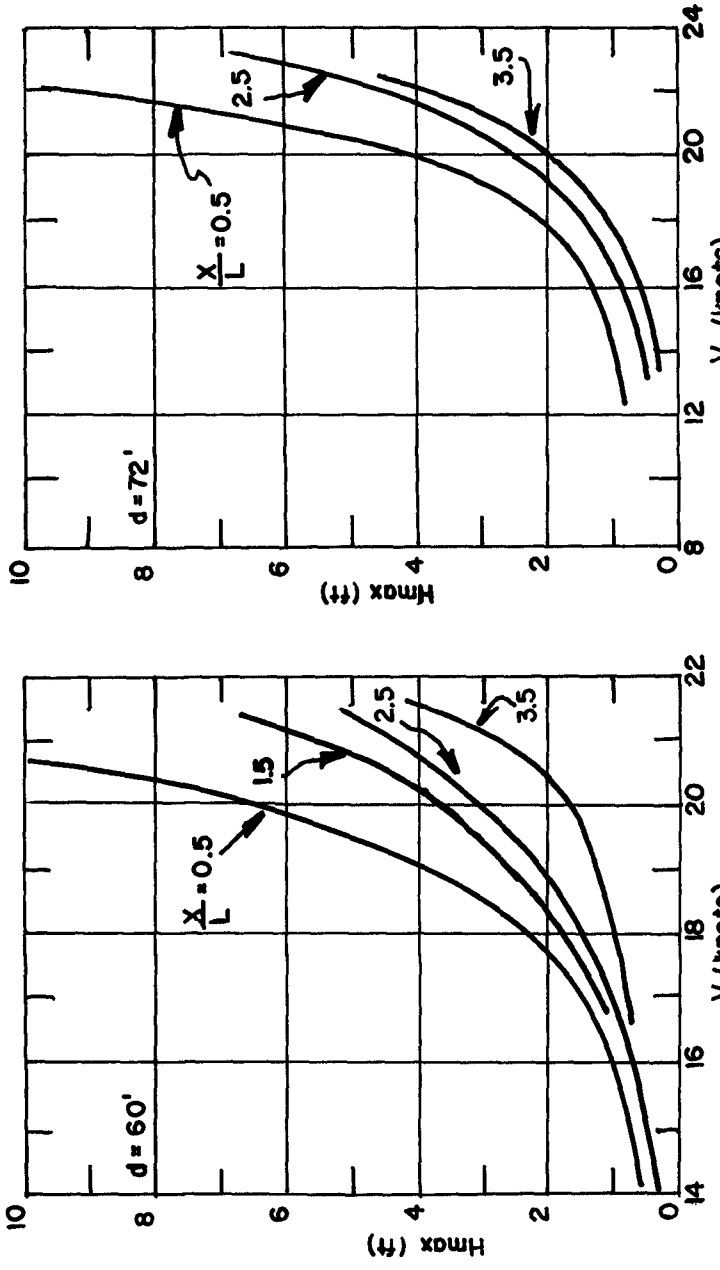

FIG 4. DAVID TAYLOR SERIES 60. L = 505' D = 24'

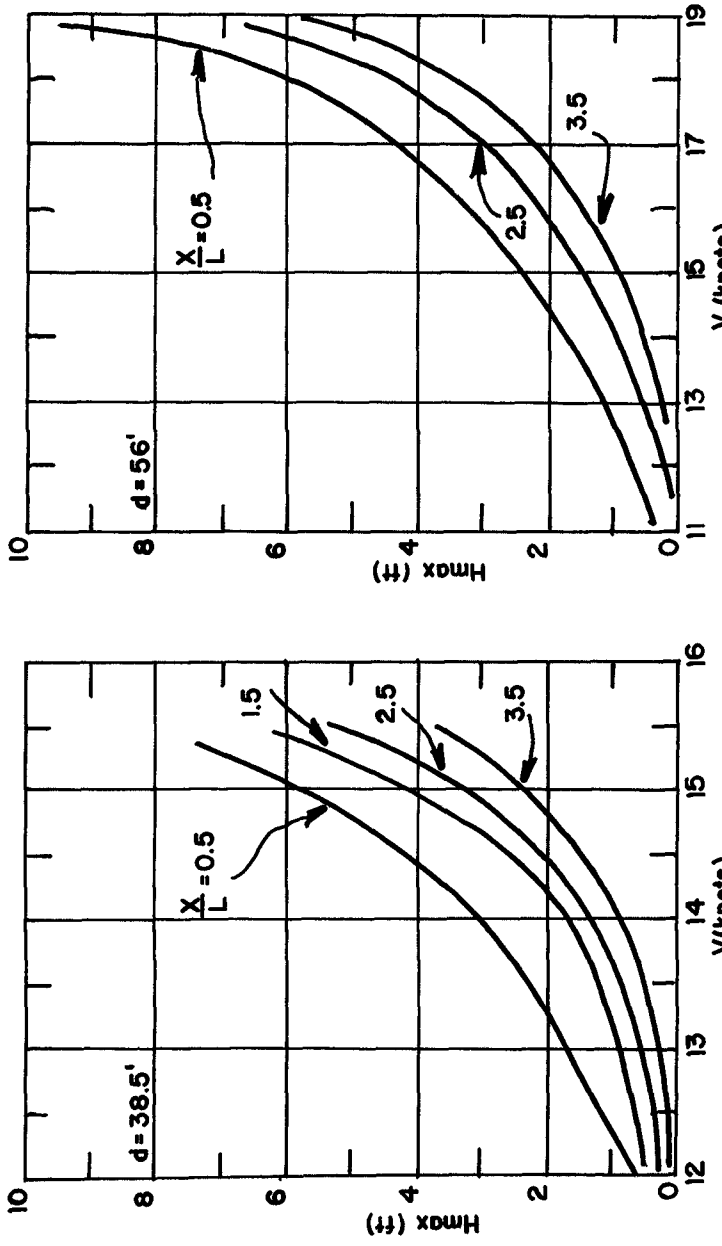

FIG 5. MOORE DRY DOCK – TANKER. L = 504' D = 28'

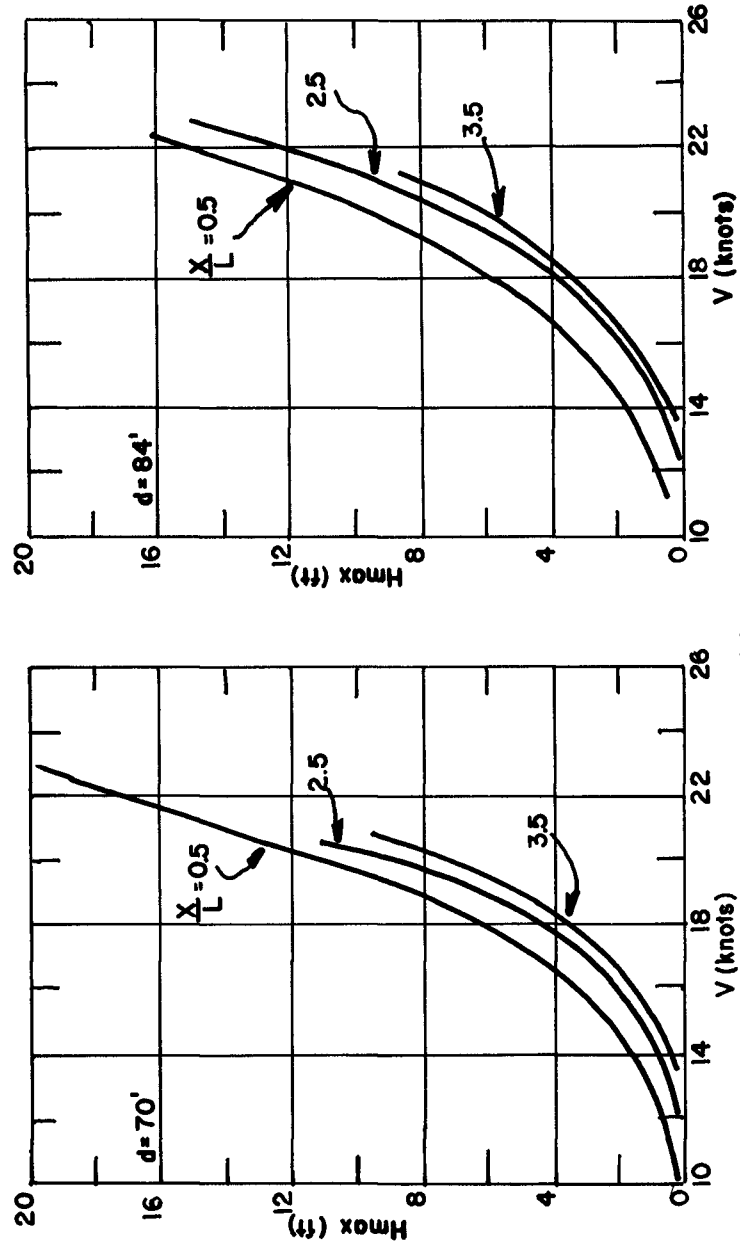

FIG 6. MOORE DRY DOCK - TANKER. L=504' D=28'

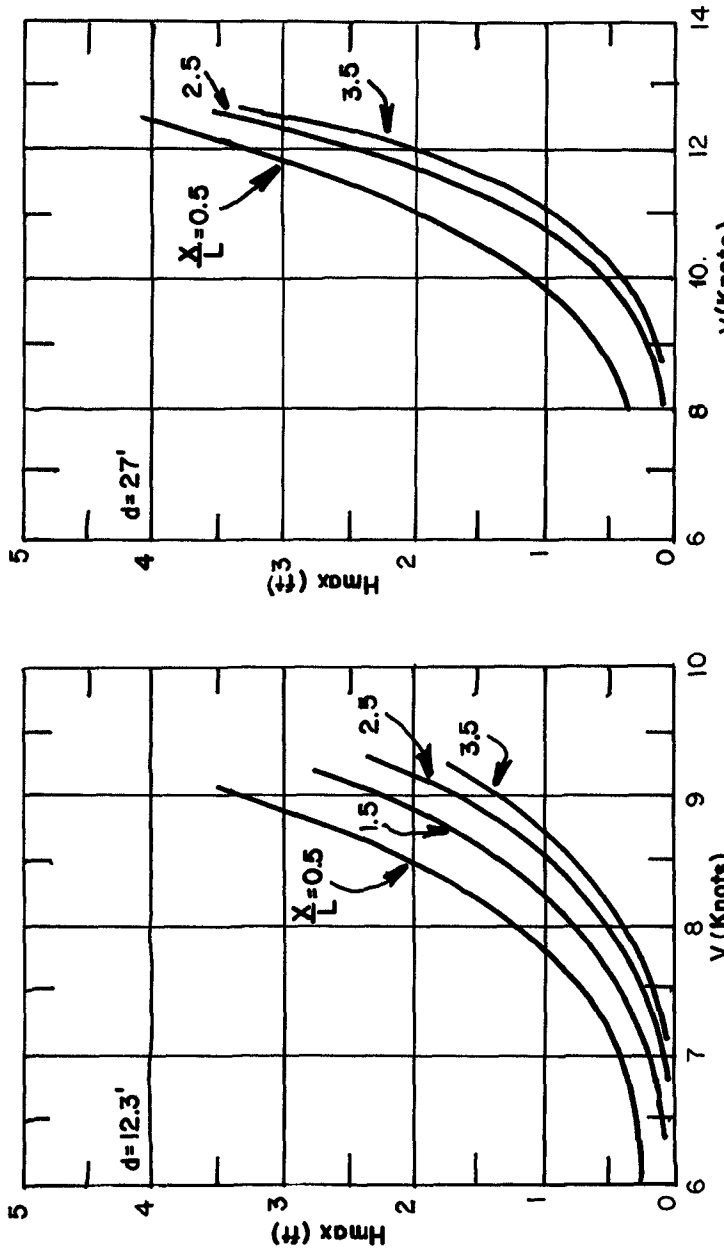

FIG 7. AUXILIARY SUPPLY VESSEL. L=156' D=9'

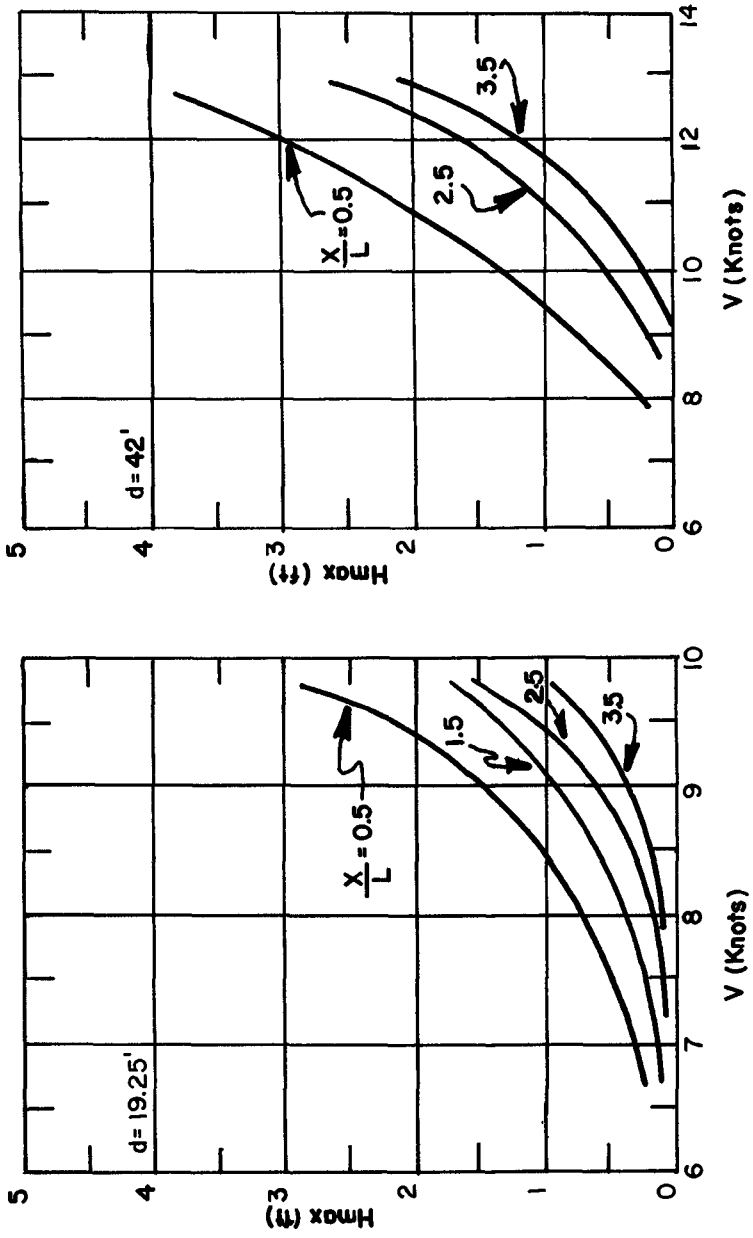

FIG 8. BARGE.
L= 263.5' D=14'

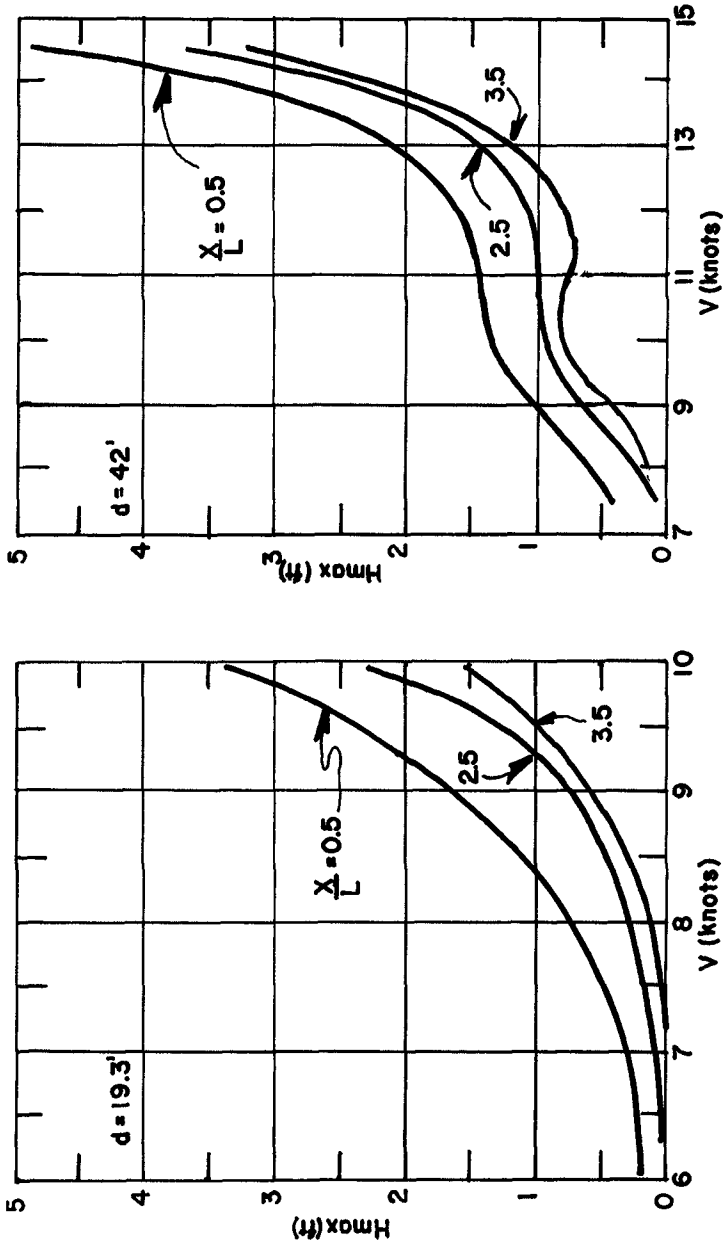

FIG 9. TUG
L = 153', D = 14'.

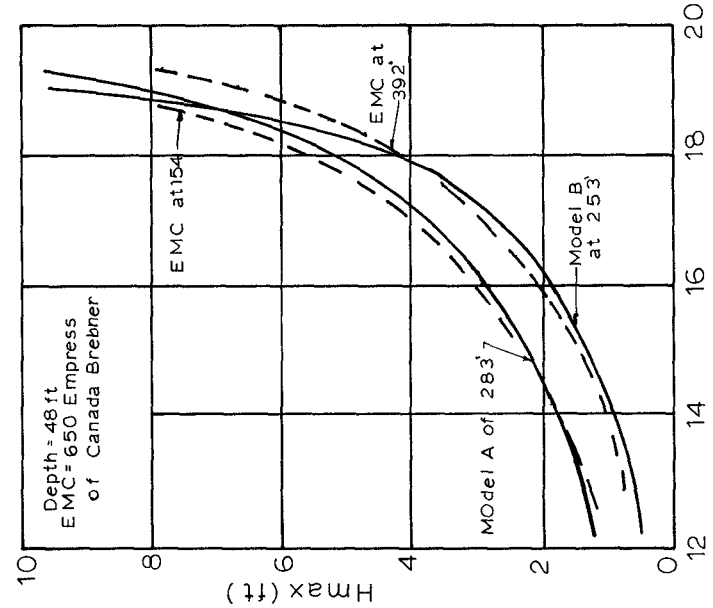

FIG 11 COMPARISON OF MODELS A & B WITH TESTS ON EMPRESS OF CANADA

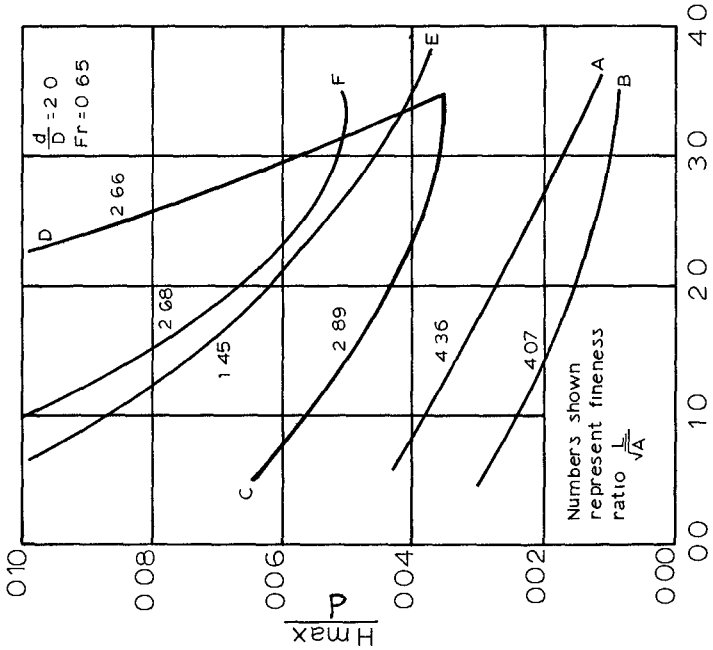

FIG 10 CROSS-PLOT OF $\frac{H_{max}}{d}$ VS $\frac{X}{L}$

FIG. 12 MODELS

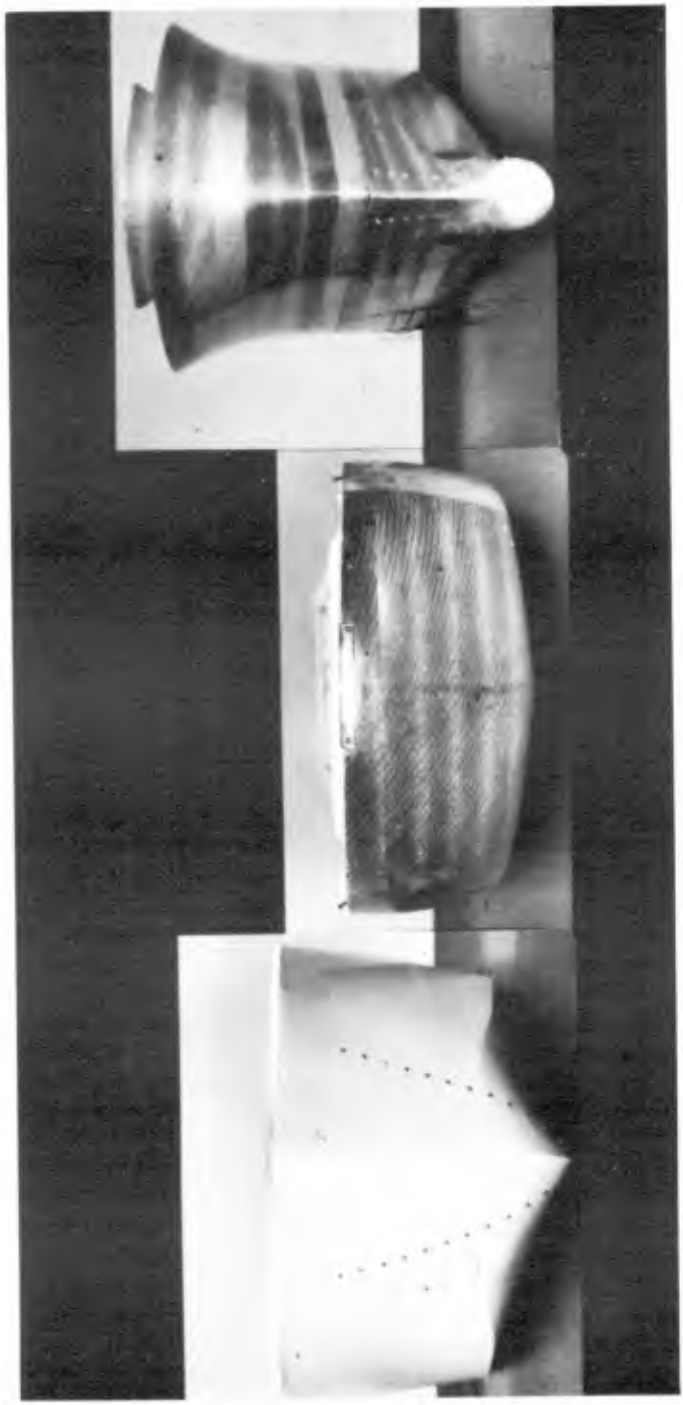

FIG. 13 MODELS

CHAPTER 96

SHIP WAVES IN SHOALING WATERS

J. W. Johnson
University of California
Berkeley

ABSTRACT

Models of two types of vessels were towed at various speeds in water of uniform depth. On one side of the sailing line the ship waves were allowed to move over beaches of various slopes. The wave heights were measured and compared at two points equidistant from the sailing line--patterns were determined by photographs.

INTRODUCTION

Several studies have been made at the University of California to determine the characteristics of waves generated by moving ships. The initial studies by Johnson (1)* were concerned with model tests in the laboratory as well as some field tests with a power boat. More recently Sorensen (2,3) measured the waves generated by five different types of ships moving in the Oakland Estuary in California. Sorensen (3,4) and Moffitt (5) also determined the surface contours of a ship-wave system by stereophotography of a ship model moving at various speeds through water of constant depth. To extend the work of Sorensen (2,3), Duncan Hay has determined by model studies the wave characteristics of several large commercial type ships, barges, tugs, etc., moving at various speeds in shallow water of various uniform depths. Hay's data are presented in the foregoing chapter of this publication.

A typical ship-wave pattern consists of diverging waves and transverse waves. These waves form a constant pattern and meet to form a locus of cusps with an angle to the sailing line. In deep water this angle is about 19° 28' and becomes greater in shallow water. The maximum wave height occurs when the locus of cusps passes a measuring point. It has been customary to refer to the maximum wave height H_{max}, as the maximum vertical distance between any given wave trough and the following crest. The magnitude of the maximum wave for a given ship is a function of the ship speed, the water depth, and the distance from the sailing line. Some information on maximum wave heights for several types of ships, as determined by both laboratory and field studies, are presented below.

*See References

SHIP WAVE MEASUREMENTS

An indication of the general order of magnitude of the height and period of the maximum wave generated by boats from 3 to 343 tons is given in Table 1. These data are derived from the measurements of Sorensen (1) in the Oakland Estuary in which a depth of approximately 35 ft. existed. The maximum wave height and half period is given at distances of 100 and 500 ft. from the sailing line with the boats moving at 10 knots. The length, beam, and draft of each vessel is also presented. It is to be noted that the difference in wave height between the extremes of size of vessel is relatively small for the depth of water existing in the tests. As discussed elsewhere (1) the critical factor governing the maximum wave height is the ratio of draft to depth, a factor which is not readily apparent in the comparisons shown in Table 1.

The data presented in Table 1 pertain to ship waves in water of uniform depth. To obtain information on the transformation of such waves as they move into shoaling water, a series of laboratory measurements were made with models of the Mariner Class cargo ship and a barge similar to that used by Hay but to a 1:96 scale. The characteristics of these models are described in Table 2. Cross sections of the sloping beaches used in the tests are shown in Fig. 1. The models were towed at various

TABLE 1. WAVES GENERATED BY VARIOUS BOATS OPERATING AT 10 KNOTS IN THE OAKLAND ESTUARY (depth = approx. 35')

Boat	Length (ft)	Beam (ft)	Draft (ft)	Displacement (tons)	Distance from sailing line			
					100 ft		500 ft	
					H_{max} ft	T/2 sec	H_{max} ft	T/2 sec
Cabin Cruiser	23	8.25	1.66	3	1 1	-	0.8	-
Coast Guard Cutter	40	10	3.5	10	1.6	1.0	1.0	1.0
Tugboat	45	13	6	29	1.6	1.2	0.9	1.2
Fishing Boat	64	12.8	3	35	1.8	1 0	0.7	1.0
Fireboat	100	28	9-12	343	1.6	1.3	1.0	1.3

TABLE 2. SHIP CHARACTERISTICS

Type	Prototype Dimensions				Model Length Scale
	Displacement (tons	Length (ft)	Beam (ft)	Draft (ft)	
Mariner Class Cargo	16,500	566	74	24	1 96
Barge	5,400	263	55	14	1·96

TABLE 3. TEST CONDITIONS FOR WAVES ON SLOPING BEACHES (PROTOTYPE DIMENSIONS)

Model	Bench Slope								
	1 10			1 5			Composite		
	d_1 (ft)	d_6 (ft)	x (ft)	d_1 (ft)	d_6 (ft)	x (ft)	d_1 (ft)	d_6 (ft)	x (ft)
Cargo Ship	60	5	1006	60	15	725	56	8	932
Barge	42	3.5	882	42	10.5	665	56	8	932

speeds in water of various depths, and the wave heights were recorded at equi-distances on the two sides of the sailing line. On one side (sta. 1) the water was of uniform depth, and on the other side (sta. 6) the waves were allowed to pass over beaches of three different slopes. The water depths at stations 1 and 6 and the distances of these stations from the sailing line are summarized in Table 3. The results of the various wave measurements with the two models are presented in Figures 2 and 3. It is evident from Fig. 2 that at the lower speeds the waves from the cargo ship appear to be less on the 1:5 and 1:10 slopes than in water of uniform depth--apparently as a result of refraction effects. At the highest speeds the waves are as high or greater on the sloping beaches than in water of uniform depth. Because of the relatively low maximum speed of the barge, the wave heights on the sloping beach are always less than in water of uniform depth. In all instances it should be noted that, even though the waves on the beaches may be lower than in the deeper water on the opposite side of the sailing line, the waves will peak up and break on the shoreline.

Some indication of the character of the wave pattern in the nearshore area is illustrated by Fig. 4 which shows contours of the wave surfaces resulting from the passage of the Mariner Class ship model. These contours were obtained by stereophotogrammetric analysis from stereophotographs taken as the ship waves moved from water of uniform depth onto a 1:10 beach. The dimensions shown in Fig. 4 are model values. In prototype terms, this figure shows that a Mariner Class cargo ship of 16,500 tons displacement moving at 19 knots in water 48 ft. deep along a sailing course parallel to and 890 ft. from the waters edge will give the pattern shown in Fig. 4 as the waves move over a 1:10 beach. The ship's stern is approximately 960 ft. ahead of point A (Fig. 4), and the height of the breaking wave crest at point B is 10 ft. above the still-water level. The length of shoreline covered in Fig. 4 is approximately 500 ft.

To supplement the wave patterns obtained by stereophotogrammetry, illustrated by Fig. 4, ripple-tank photographs obtained by towing a 1:576 scale model of the Mariner Class ship at various speeds were obtained in the ripple tank at the University of California and are shown in Figs. 5 and 6. The technique of obtaining these photographs is described elsewhere by Laitone (6). These photographs show the waves as they move from water of uniform depth onto beaches with slopes of 1:5 (Fig. 5) and 1:10 (Fig. 6). Two views of the waves are presented for each ship speed to permit a detailed evaluation of the entire wave system. The wave patterns are shown for four different values of the parameter,

$$\lambda = C/C_o$$

where C is the speed of the ship and C_o is the velocity of a wave in shallow water; i.e., $C_o = \sqrt{gd}$, where g is the acceleration of gravity, and d is the water depth. Examination of the various photographs shows the obvious change in wave height and geometry of the wave pattern with ship speed. Also of interest is the large bow waves that exist when the critical speed of $\lambda = 1$ is exceeded. The nature of the refraction and reflection of this bow wave, as well as the following smaller waves, from the sloping sides also is of interest.

SUMMARY

The above data provide some measure of the heights of waves resulting from the passage of typical ships moving at various speeds near sloping shorelines. The magnitude of such waves when ships travel at relatively high speeds obviously may create hazardous conditions to unobserving users of the shoreline. Floating equipment and docks along a shoreline also are subject to damage.

ACKNOWLEDGMENT

The model experiments described herein were conducted on a project sponsored by the U. S. Army Coastal Engineering Research Center, Washington, D. C.

REFERENCES

1. Johnson, J. W., "Ship Waves in Navigation Channels," *Proc. Sixth Conference on Coastal Engineering,* 1958, pp. 666-690.

2. Sorensen, Robert M., "Investigation of Ship-Generated Waves," *Journal of the Waterways and Harbors Division,* A.S.C.E., February 1967, pp. 85-99.

3. Sorensen, Robert M., "Waves Generated by a Moving Ship," *Shore and Beach,* Vol. 35, No. 1, April 1967, pp. 21-25.

4. Sorensen, Robert M., "Stereophotogrammetric Analysis of Wave Surfaces," *Journal of the Hydraulics Division,* A.S.C.E., January 1968, pp. 181-194.

5. Moffitt, F. H., "Wave Surface Configuration," *Photogrammetric Engineering,* February 1968, pp. 179-188.

6. Laitone, E. V., "A Study of Transonic Gas Dynamics by the Hydraulic Analogy," *Journal of the Aeronautical Sciences,* Vol. 19, No. 4, April, 1952, pp. 265-272.

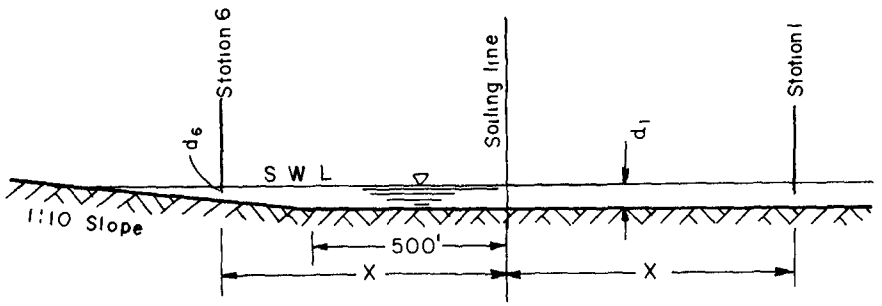

(a) CHANNEL CROSS-SECTION, BEACH SLOPE 1:10

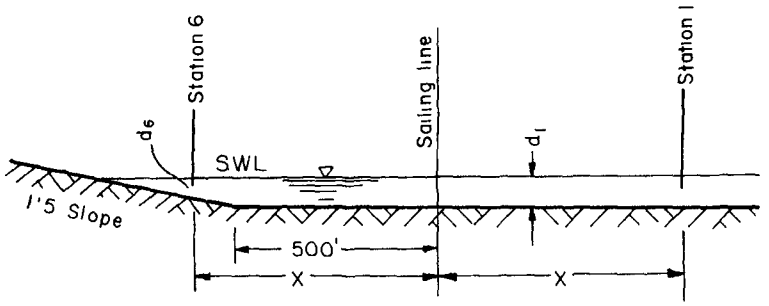

(b) CHANNEL CROSS-SECTION, BEACH SLOPE 1:5

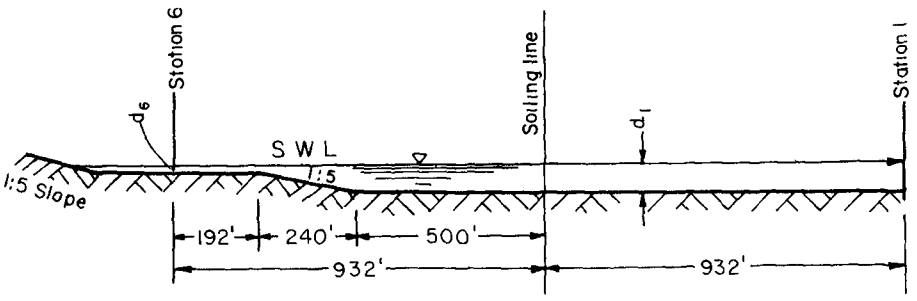

(c) CHANNEL CROSS-SECTION, COMPOSITE SLOPE

Fig. 1 - Channel cross sections used in model investigations of ship waves on sloping beaches (prototype dimensions).

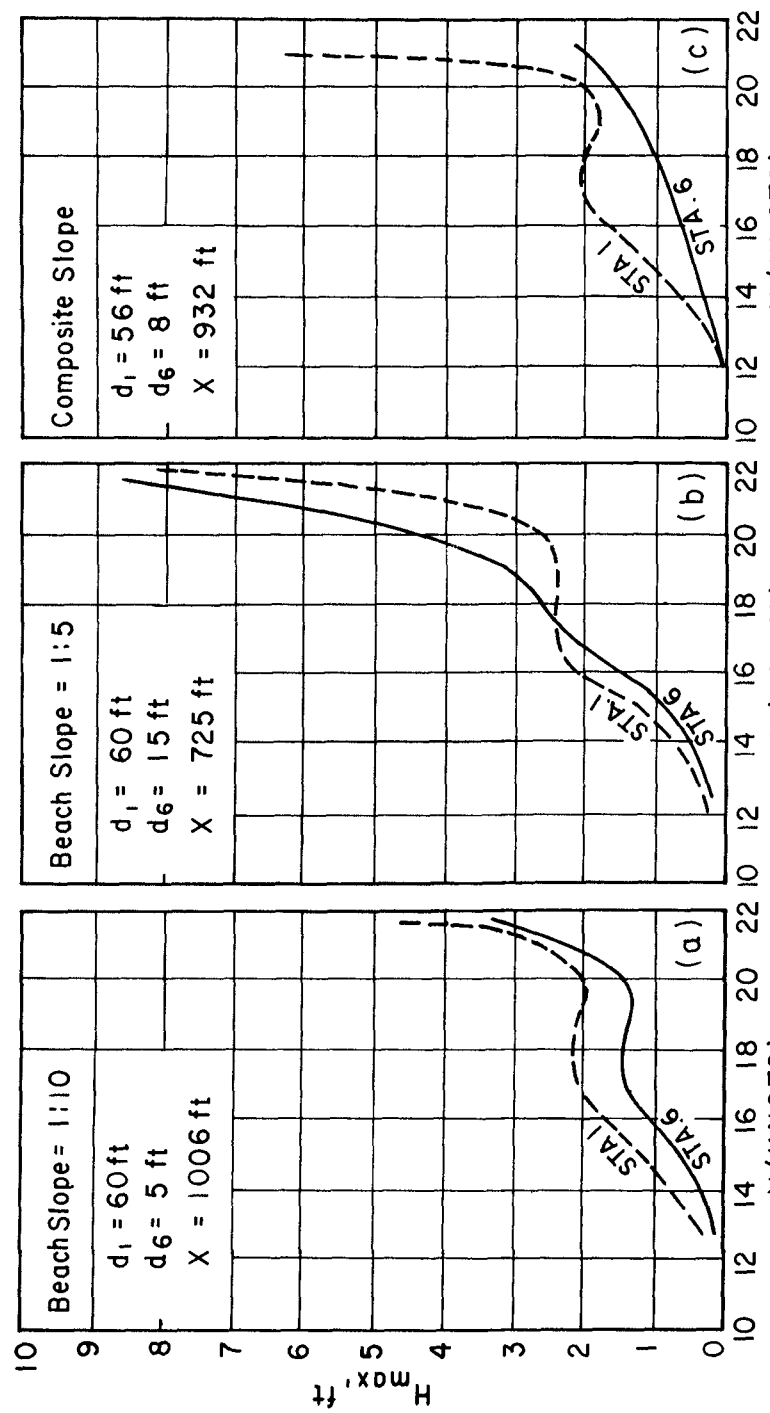

Fig. 2 - Maximum wave heights generated by a Mariner Class Cargo ship. Ship waves measured in water of uniform depth (sta. 1) and over a sloping beach (sta. 6).

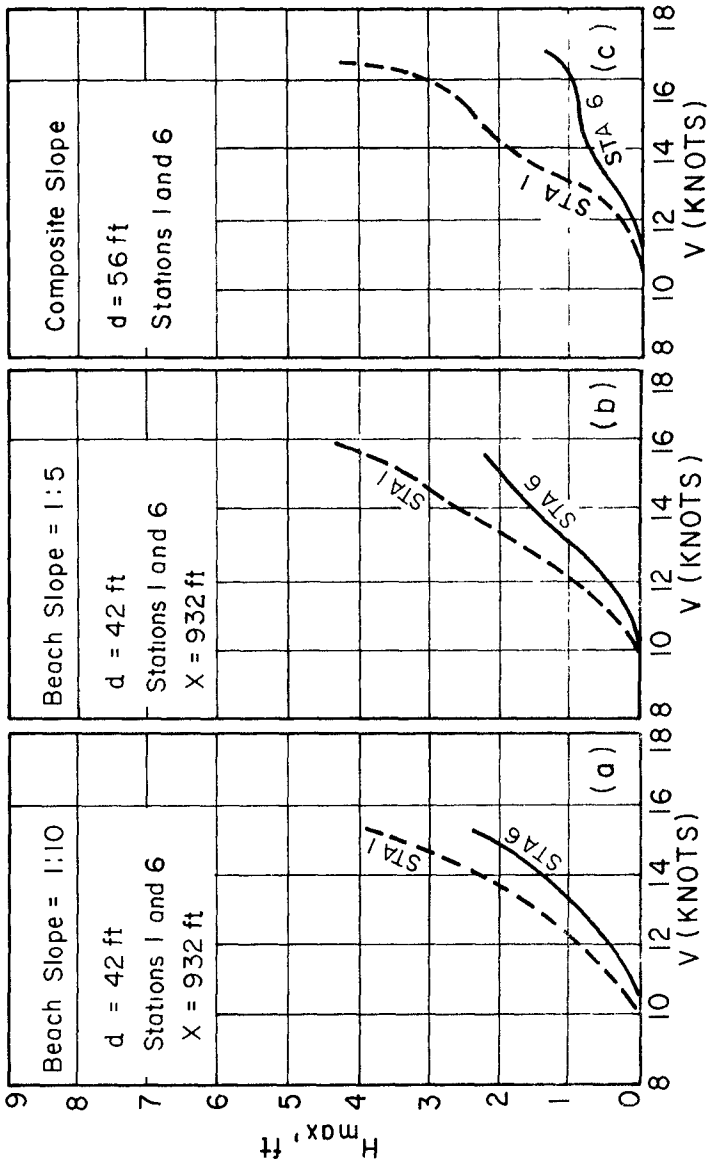

Fig. 3 - Maximum wave heights generated by a Barge. Ship waves measured in water of uniform depth (sta. 1) and over a sloping beach (sta. 6).

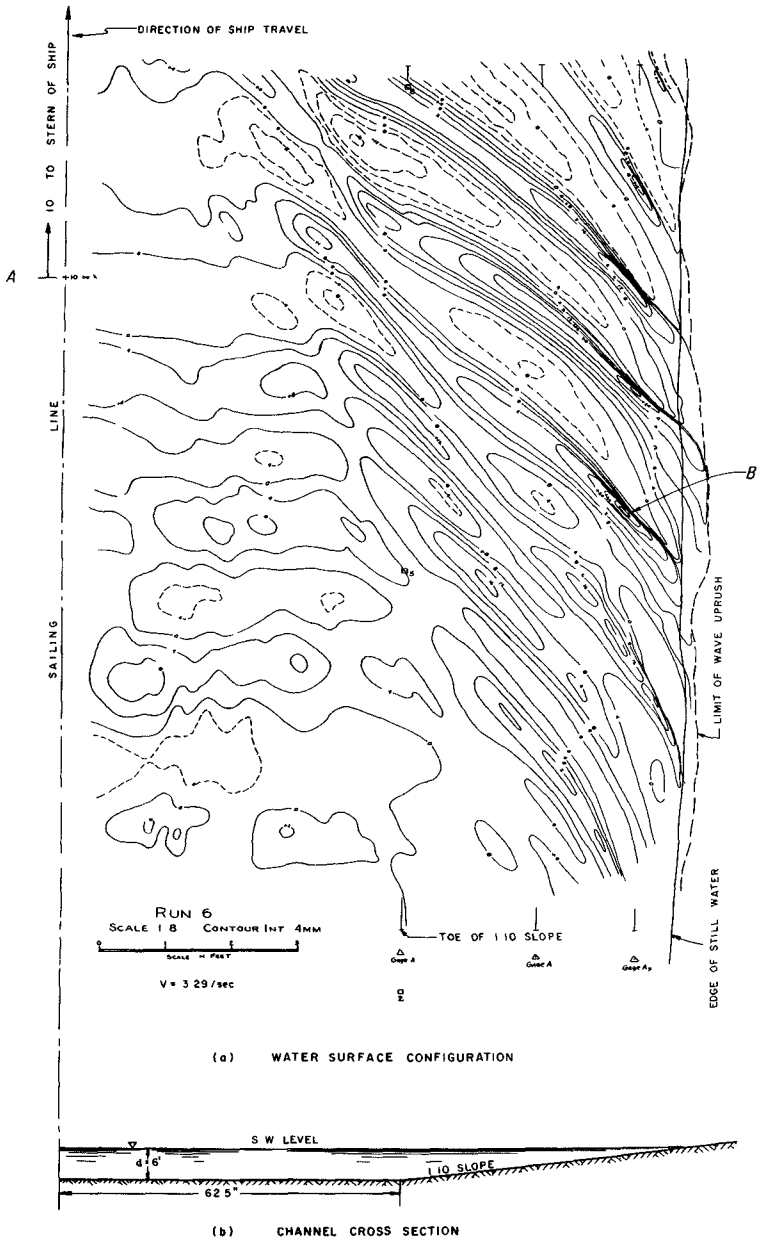

Fig. 4 - Surface contours of waves generated by a Mariner Class cargo ship moving at 19 knots in 48 feet of water 890 feet from the shore which has a 1:10 beach slope.

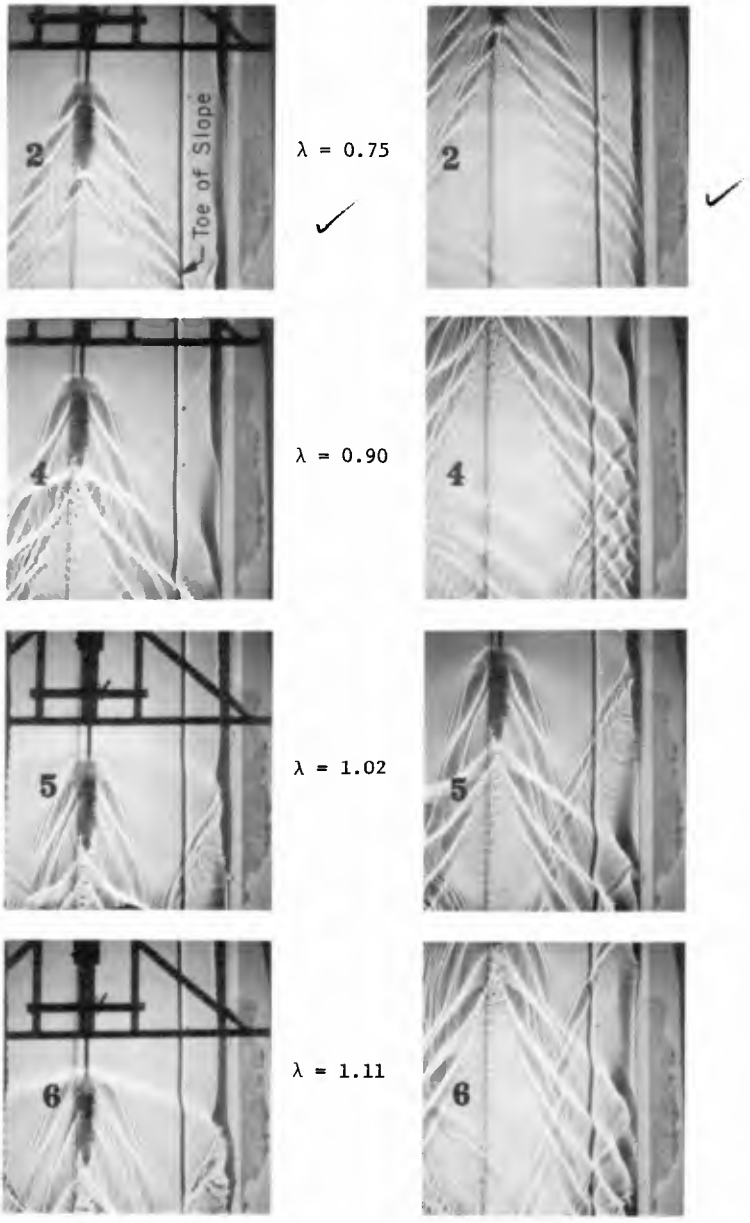

Fig. 5. Ripple tank photographs of ship waves moving onto a beach with a 1:5 slope.

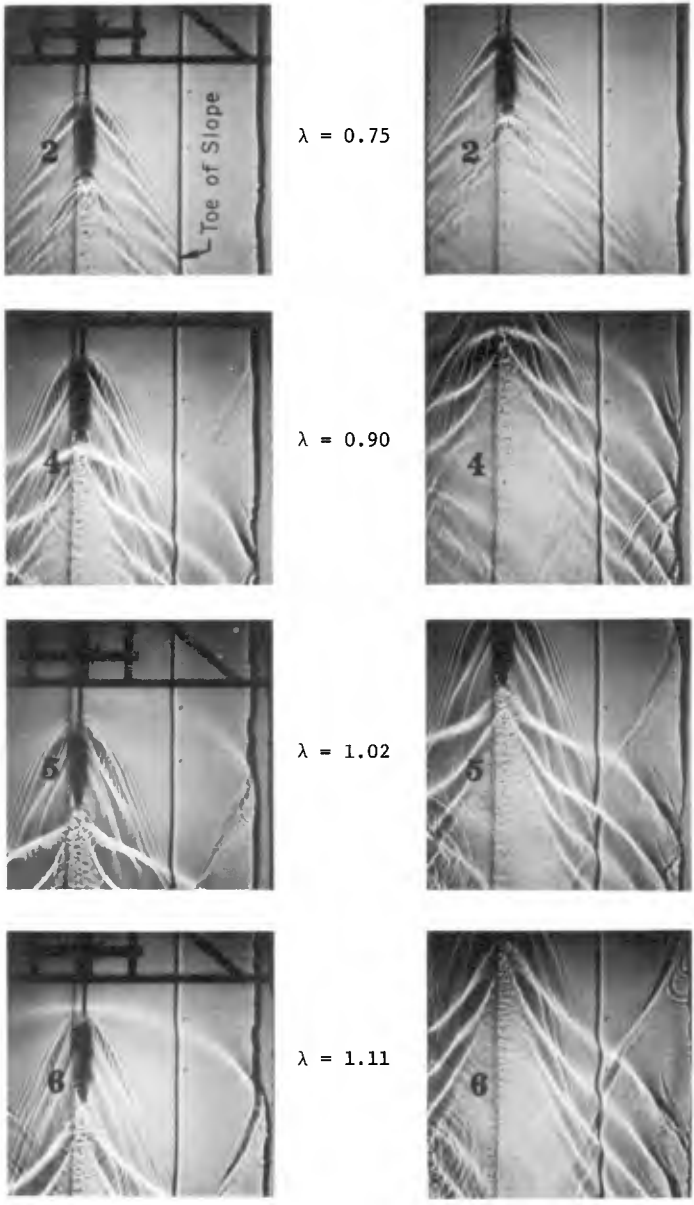

Fig. 6. Ripple tank photographs of ship waves moving onto a beach with a 1:10 slope.

CHAPTER 97

MEASURING OF SQUAT IN THE FAIRWAY TO THE PORT OF LULEÅ, NORTH SWEDEN

Carl G Carlström, Chief Engineer Harbour Projects
Luossavaara-Kiirunavaara AB, Stockholm, Sweden.

ABSTRACT

The importance of knowledge of squat and expected underkeel clearance for ships passing a fairway is essential to the navigational safety and the economy of a harbour.

In order to check the squat of ships in the fairway to the port of Luleå a photographic measuring method has been evolved and used in measurements on three different ships. Determining of squat is made by levelling the position of vessels in relation to water level at the berth before sailing and en route at measuring points along the fairway.

The accuracy of measurements was determined by observations on reference staffs. The order of standard deviation is 1/2 inch. at 2,400 feet distance. Observations indicate squat ranging from 1 foot 5 inches at speeds of 9 knots to 2 inches at 3½ knots.

The measured squat corresponds rather good to theoretically calculated values according to Woltiger and Shell/Sogreah.

The measuring method used has reduced the field work. The greatest advantage is that adequate values of squat will be directly recorded with only a few corrections including irregular factors such as turbulent flow, hull deformations and variable channel sections.

A condition is however sheltered water and possibilities of solid foundation for instrument arrangement.

INTRODUCTION

The importance of knowledge of squat and expected underkeel clearance for ships passing a fairway is essential to the navigational safety and the economy of a harbour

In order to check the squat of ships in the fairway to the port of Luleå, a photographic measuring method has been evolved and used in measurements on three different ships Determining of squat is made by levelling the position of vessels in relation to water level at the berth before sailing and en route at measuring points along the fairway.

The accuracy of measurements was determined by observations on reference staffs The order of standard deviation is 1/2 inch. at 2400 feet distance. Observations indicate squat ranging from 1 foot 5 inches at speeds of 9 knots to 2 inches at 3 1/2 knots

The measured squat corresponds rather good to theoretically calculated values according to Woeltiger and Shell/Sogreah

The measuring method used has reduced the field work The greatest advantage is that adequate values of squat will be directly recorded with only a few corrections including irregular factors such as turbulent flow, hull deformations and variable channel sections.

A condition is however sheltered water and possibilities of solid foundation for instrument arrangement.

THE FAIRWAY

A new ore loading terminal and a new fairway were built in 1962-65 at Luleå, North Sweden, by the Swedish mining company LKAB and taken into full operation in the summer of 1965. Shipping season is normally 7 months from May to December.

The total length of the fairway is 7 nautical miles, $5\frac{1}{2}$ miles of which have been dredged; removed volumes totalling $7\frac{1}{2}$ mill. cu.yds. consist of clay, gravel, sand (Fig. 1). Some 100,000 cu yds. was blasted rocks. The minimum depth at mean water level is mainly 40 feet. The blasted sections hold 45 feet and an excavated part with full channel cross section has 42 feet minimum depth. (Fig. 2).

The min. bottom width on one nautical mile stretch is 250 feet, in the remaining parts 330 feet.

There is no tide, but irregular variations in water level by currents and winds occur. Normal deviations from mean water are ± 1 foot (93 % duration). Lowest recorded water is about 3 feet below mean water level

Size of ships

At present the underkeel clearance recommended is 3 feet permitting a draught of 37 feet which corresponds to vessels of about 40,000 tons dw fully laden at mean water level The reckord load of about 45,300 tons in a 50,000 tons dw ship was shipped in August 1968 The current draught was 36' - 5" at abt. 8" low water.

NEED OF INFORMATION ON SQUAT

It is a well- known fact that a ship in motion changes the margin between the keel and the bed compared to the value when the ship is at rest. The change of this underkeel margin resulting from change of the ship's trim and sinkage of the water level due to motion is usually combined under the term squat

Ships'officers and pilots have in general only their own experience to make themselves an idea of the required underkeel clearance. This often leads to overrating of the safety factor by adding considerable margins for squat. Seen from the point of safety this is inviolable but from the freight economy less satisfactorily. It is quite clear, that without underrating the safety, one should not base decisions of underkeel margin on thumb-rules but on real knowledge for an optimal utilization of investments made in harbours and approach channels

In 1960-1961, when the period of planning was in progress, much discussion occured about the dimensions of the channel and the order of underkeel clearance to be stipulated. Differences of opinion particularly among the pilots has forced to measurements in order to determine squat and evaluate underkeel clearance with ships in motion.

MEASURING METHODS

Already in 1904 observations on squat were made by US Army Engineers in the Ambrose Channel at the entrance to New York. These observations showed that big vessels needed large margins at high speeds. A few years ago model scale tests were made by Shell with experimented work executed by the Sogreah Laboratory, Grenoble A continuation of these investigations in full scale have been carried out by Shell in the deep channel to Maracaibo in Venezuela with echo sounding The method has given interesting results and has led to a pratical method for determining of squat.

Photographic measuring method

At the request of LKAB the Swedish consulting firm Skandiaconsult has evolved a method which seems to give rather thorough statements of vessels' squat. A condition is however that there is sheltered water and possibilities

for solid positioning of the levelling instruments near the fairway. The method is suitable for inland waterways in semi-open water.

Principally the sinkage of ships is photographically registered by means of levelling instrument combined with camera equipment. (Fig. 3). This method has the advantage of making the levelling operation possible after the field work, thus eliminating misreadings on the levelling staffs and preserving the basic measurement material. The measuring distance with equipment now used can under good visibility conditions reach up to about $\frac{1}{2}$ nautical mile with an accuracy of about $\pm \frac{1}{2}$ inch. (12.7 mm).

Determining of squat is made by levelling the position of the vessel in relation to the water level in the trimming position at the berth before the sailing and en route at measuring points along the channel. The difference between the values of ship in motion and at rest makes the sinkage demanded, which practically includes squat and hull deformations, appearing with ships in motion.

Equipment and arrangements

For determining the position of the vessel in relation to the water level, graded levelling staffs are put up midship and near the bow and stern. (Fig. 4) Listing of the ship is found with a pendulum 30 - 50 feet in length attached to the sky-light of the engine room. The positions are determined by observations of the light buoys passed and the speed by timing between the buoys.

Water table fluctuations are observed by means of a water level indicator. The current stationary water level on the actual occassion of measuring is used as reference level. The heights over the water level of the instrument are decided with stationary levelling staffs put up at the measuring stations along the fairway. The collimation errors of the instruments can easily be corrected by a number of measurements between the stationary staffs.

The measuring equipment consists of a combination of a standard model self-aligning level instrument (Zeiss, Ni2, 30 X Magn.) and reflex cameras with a picture size of 24 x 36 mm of good optical quality, (type Canon 1:2 and Minolta 1:1.2. Film: Kodak Plus X, exposure 1/30 - 1/60 sec.).

Registration of the height positions of the vessel related to the stationary water level is made by photographing the levelling staffs, when the vessel is passing the observation lines from the measuring stations. (Fig. 5).

Assessment of the registrations is made from the photos by means of a micrometer with a reading accuracy of 0,01 mm. The ship's sinkage can be determined in relation to the reproduced cross hairs which represents the stationary water level in the observation line. On calculation of the reference water level and the squat, corrections for earth curvature, refraction and the listing of ship must be made. Corrections for variations in water density were unnecessary.

OBSERVATIONS

Measurements on ships' sinkage and determinations of squat have been carried out for three different vessels carrying 23,300, 37,200 and 35,700 tons of load respectively.

Dimensions of the ships:

No.	DW	Length, PP	Breadth moulded	Depth moulded	Draught, SFB
1.	23,420 tons	560'- 0"	74'- 6"	44'- 3"	32'- 11½"
2.	38,270 tons	abt. 700'	88'- 2"		35'- 3½"
3.	36,200 tons	630'- 2"	88'- 6"	52'- 0"	35'- 11½"

The 36,200 tons ships traversed the fairway three times under similar conditions at different speeds. Observations were made from stations positioned on two light-houses and one point on the canal embankment. Distances ranged from 300 metres (1,000 feet) to 900 metres (3,000 feet) in three or four lines from each station to the centre line of the fairway. (Fig. 1).

Accuracy of measurements was determined by a great number of observations on the reference staffs. The order of the standard deviation ranges from ± 4.2 mm (± 0.065 inches) to ± 13 4 mm (± 0.53 inches) at a distance of 800 metres (2,600 feet). The values stated indicate the accuracy of the measurements, including the error in reading the photos. A previous series of 20 measurements in a known precision levelling net has showed a mean deviation of 11- 14 mm (0.43 - 0.55 inches) at a distance of 740 metres (2,400 feet).

Results of observations indicate that speed of the ship has great influence on the squat. The order of squat measured was maximum 370 - 430 mm (1'- 2½" to 1'- 5") for the 4 knots for the 36,200 tons ship.

Squat diagram for the 36,200 tons ship (Fig. 6) inward bound show moderate squat values of 3½ - 4½ inches at a speed of 4 - 4½ knots and 5 - 7 inches at 5 - 5½ knots. (Corrections are made for counter-current of 0,2 - 0.4 knots).

The listing due to trimming or sheering is at most 60 mm (2½ inches) converted to required extra margin at a speed of 8 knots, negligible at 4 - 5 knots Change of listing was observed at the curves.

All the ships was changing the trim slightly by the bow, maximum about 2 inches at speed of 7 - 9 knots, when passing the constricted cross section of the channel In the other parts of the fairway with incomplete cross sections and semi-open water, no observable change of trim could be stated. In the trimming position at the berth, all the ships had a trimming to the stern between 8 inches and 1 foot. The change of trim when they passed the channel was less than 2 inches.

Evaluation of the underkeel clearance

The minimum depth stated is regularly being controlled by bar-sweeping along the total bottom area of the fairway with help of a measuring frame suspended on a catamaran driven by two out-board motors and operated by 2 - 3 men. (Fig. 7). According to the observations and calculations on squat, there was a minimum underkeel clearance of fully 3 feet at the current high water level of 6 to 8 inches on the occasion of measurements.

SQUAT CALCULATIONS

Measured squat based on the photographic levelling method have given some results which might be of interest especially in comparison with calculated squat based on theoretical methods.

Two methods of calculation have been tested against the measured squat values. The calculations, referring to the three passages of the 36,200 tons ship at different speeds, have been carried out for observation line No. 2 (semi-open water, incomplete cross section) and line No. 9 (full cross section, calculated area 3640 sq.metres). The speed of the ship ranged from $3\frac{1}{2}$ to 5 knots in line No. 2 and 4 to 6 knots in line No. 9.

The graphs show that in this particular case the measured squat corresponds rather good to a somewhat modified method according to Wöltiger at low speeds and in semi-open water, while a method developed by Shell and Sogreah is nearer to the measured values at full cross section and higher speeds. (Fig. 8 and Table 1). The graphs even indicate the well-known fact, that the speed of the ship has great influence on the order of squat.

CONCLUSIONS

Though the measurements of squat at present should be regarded as preliminary, some conclusions for practical purpose can be drawn on the results. One is that the ships observed seemed to be trimmed to the stern $\frac{1}{2}$ to 1 foot more than necessary for the passage of the fairway. A trimming to an even keel could probably help to improve the underkeel margin or alternatively increase the load, in case of underkeel clearance sufficient to the navigational safety.

Another conclusion is that the ships were changing the trim slightly by the bow, when they passed the full cross sectional area of the channel. The change of trim was max. 2 inches at speeds of 7-9 knots. In other parts of the fairway with incomplete cross sections and semi-open water minor change of trim could be observed.

Bibliography:

Captain A F Dickson. "Navigation of Tankers through Channels", paper submitted by Shell Tankers Ltd, on behalf of the Royal Dutch Shell Group of Companies

Captain A F Dickson: "Underkeel Clearance" Journal of The Institute of Navigation, October 1967 No 4

Studien zu Bau- und Verkehrsproblemen der Wasserstrassen, Offenbach am Main 1949.19. O Wöltiger

Helm, K Mochel W, Woltiger O.

"Ueber die gegenseitige Beeinflussung von Schiffen und Kanalen." Mitt. Hannoverschen Versuchanstalt für Grundbau und Wasserbau 1953 nr 36/39 90 årg. 12 sept. 1953

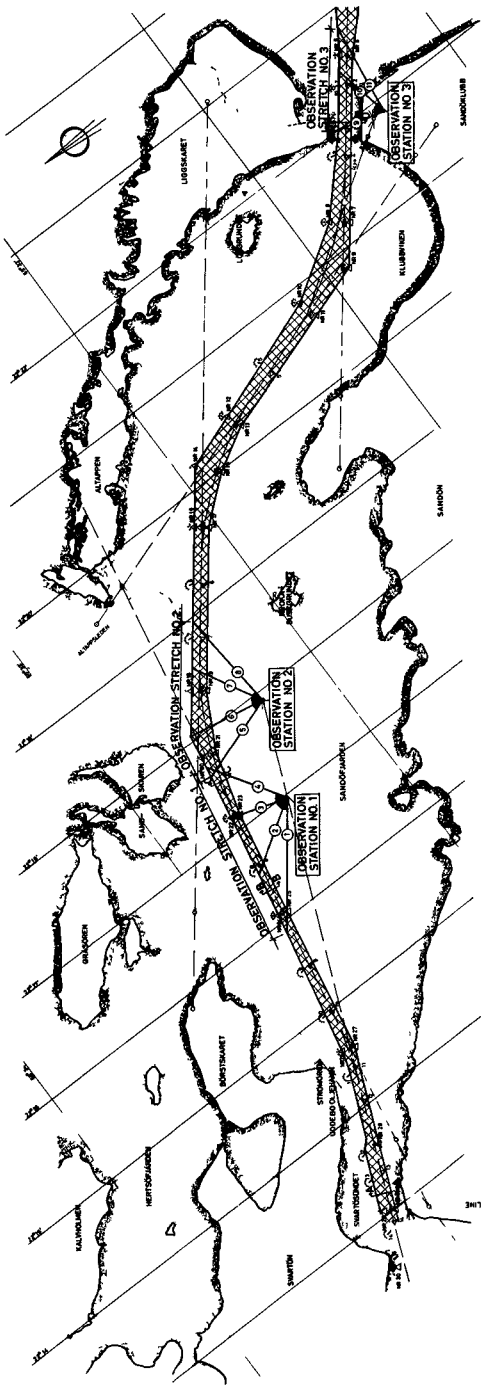

FIG. 1

THE SANDO CHANNEL, LULEÅ
SQUAT MEASUREMENTS
GENERAL PLAN

Section No	Speed over ground	Direction	Current velocity	Relative speed	Measured squat			Calculated squat according to	
					F	M	S	Shell	Wöltjer
1	4.4	O	0.2	4.2	5	6	5	17.0	8.4
	4.5	I	0.2	4.7	12	7	8	21.1	10.2
	3.8	O	0.2	3.6	5	5	1	13.6	5.9
2	4.4	O	0.2	4.2	6	6	3	14.4	6.4
	4.5	I	0.2	4.7	8	8	8	17.2	7.9
	3.6	O	0.2	3.4	2	2	3	11.3	3.9
3	4.6	O	0.2	4.4	6	6	3	16.0	9.2
	4.5	I	0.2	4.7	9	8	7	17.8	10.8
	3.6	O	0.2	3.4	5	3	2	10.6	5.3
4	4.8	O	0.2	4.6	4	5	6	13.7	8.0
	4.6	I	0.2	4.8	8	8	7	14.3	9.2
	3.8	O	0.2	3.6	5	5	5	9.5	5.1
5	4.8	O	0.2	4.6	6	3	4	13.7	8.0
	4.5	I	0.2	4.7	11	8	8	13.7	8.3
	3.9	O	0.2	3.7	4	3	3	10.1	5.1
6	4.8	O	0.2	4.6	5	2	4	15.2	6.8
	4.5	I	0.2	4.7	9	12	11	15.7	7.3
	3.8	O	0.2	3.6	4	6	4	1.0	4.5
7	4.8	O	0.2	4.6	6	5	5	18.6	7.7
	4.4	I	0.2	4.6	9	10	9	18.6	7.7
	3.8	O	0.2	3.6	6	5	5	13.4	5.0
9	4.5	O	0.4	4.1	7	5	4.5	13.4	6.1
	5.0	I	0.4	5.4	17	13	12	21.2	11.7
	6.0	O	0.4	5.6	21	14	14	22.4	12.6
10	4.5	O	0.3	4.2	5	1	1	11.8	7.1
	5.1	I	0.3	5.4	15	10	12	17.5	12.8
	6.7	O	0.3	6.4	22	17	12	24.4	16.8
11	4.6	O	0.2	4.4	6	6	4	12.7	7.3
	5.3	I	0.2	5.5	13	9	12	18.8	11.7
	7.0	O	0.2	6.8	20	21	18	27.1	18.6

TABLE 1: SUMMARY OF MEASURED AND CALCULATED SQUAT

NOTATIONS

Speed over ground)
Current velocity) expressed in knots
Relative speed)

Measured squat)
Calculated squat) expressed in centimetres

F - Fore
M - Midship
S - Stern
O - Outgoing
I - Incoming

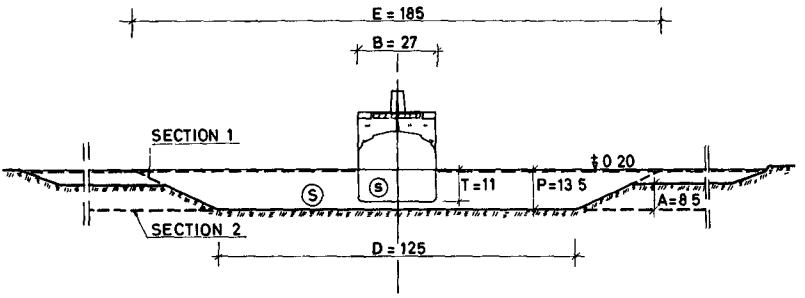

NOTE

THE DATA OF THE BOTTOM PROFILE ARE AFTER FINAL DREDGING AND DO NOT CORRESPOND TO THE DATA ON THE GENERAL PLAN
S = CROSS SECTIONAL AREA
s = MIDSHIP AREA = 0.98 x B x T

FIG. 2

CROSS SECTION AT LINE 9 (OBSERVATION STATION NO 3, SEE GENERAL PLAN,

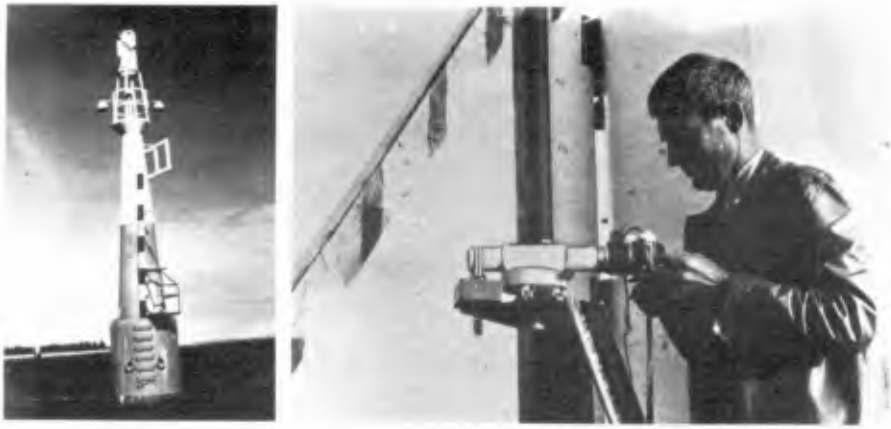

FIG. 3 OBSERVATION STATION AT LIGHTHOUSE
LEVELLING INSTRUMENT AND ATTACHED CAMERA

FIG. 4 LEVELLING STAFFS ATTACHED TO SHIP

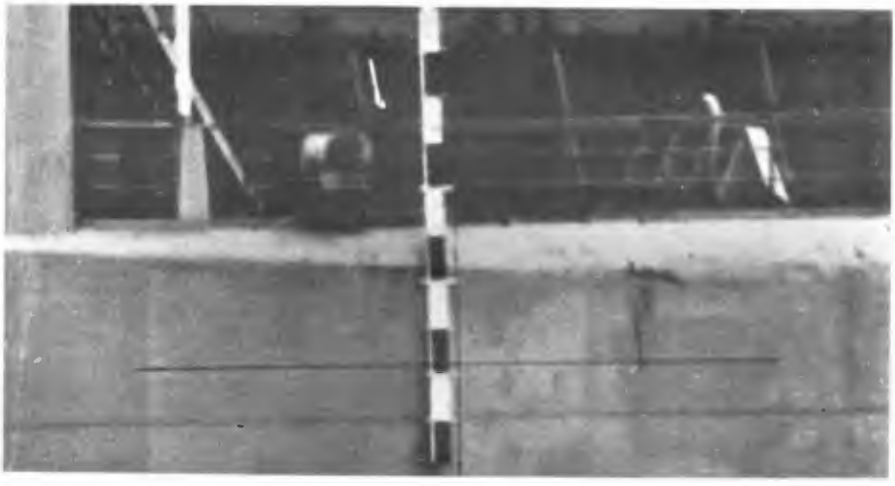

FIG. 5 OBSERVATION PHOTO OF LEVELLING STAFF AND CROSS-HAIRS

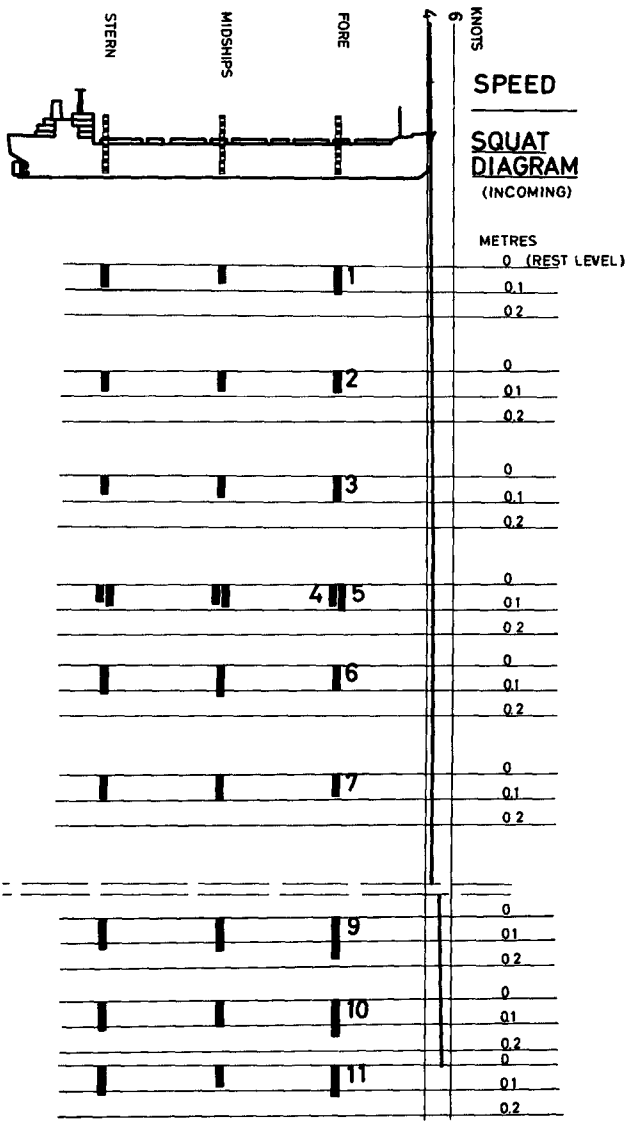

FIG. 6 SQUAT MEASUREMENTS, AUGUST 20, 1967
SQUAT DIAGRAM FOR MS "LAPONIA"

FIG. 7 BAR-SWEEPING CONTROL EQUIPMENT

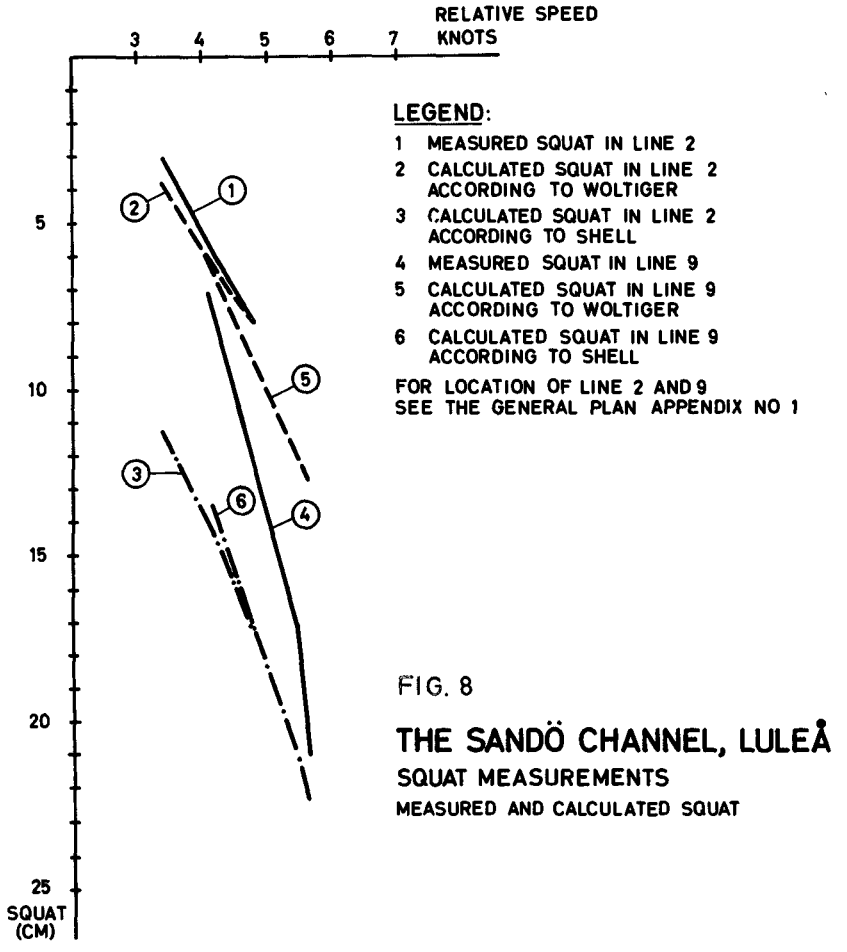

FIG. 8

THE SANDÖ CHANNEL, LULEÅ

SQUAT MEASUREMENTS

MEASURED AND CALCULATED SQUAT

CHAPTER 98

RECTANGULAR RESONATORS FOR HARBOUR ENTRANCES

by

William James*

ABSTRACT

A complete theoretical analysis of the behaviour of resonators built into the breakwaters of a harbour entrance would be extremely difficult. This paper describes an approximate development for extreme values of resonator geometry and shows how a combination of these cases explains certain observed phenomena for intermediate shapes.

The paper also describes comprehensive laboratory tests on resonators and draws attention to certain significant discrepancies from present design practice. In particular, the paper indicates the extent to which optimum resonator geometry depends upon the harbour entrance width and demonstrates that such resonators can be designed to prevent any penetration of waves into harbours, without restricting shipping.

INTRODUCTION

A resonator is taken to be a short rectangular branch canal, completely closed on three sides, built orthogonally on to the entrance breakwaters of a harbour (see Fig.1). Only the action of such resonators in parallel straight breakwaters has been investigated and this geometry is identical to that studied by Valembois in 1953 (ref.1). In this present paper the effect of distributed reflections from the harbour is not considered; this study pertains only to the geometry of such resonators and their action on waves entering harbours.

The dimensions of the resonator should be optimized such that a mass of water contained within the resonator and that part of the entrance channel contiguous with the resonator mouth (here termed the "junction element" as shown in Fig.1), has a resonance frequency equal to that of the harmful incident wave that should be totally reflected back into the ocean. For the purposes of this paper the lowest frequency eigenvalue is used; for batteries of resonators tuned to cover a wide frequency band, resonance will also occur at higher harmonics.

Limiting the treatment to semi-infinite oceans and harbours results in simpler mathematics but introduces complications in the experiments, since the wave generator channel and harbour must be completely decoupled. Further simplifications in the mathematical treatment result from the use of first order linear wave theory and the assumption of irrotational motion. Such development will accord closely with the tsunami-type waves likely to excite range action in real harbours but experimental waves are necessarily Stokian and, for accuracy, non-linear effects must be accounted for. Consequently, in this study, wave measurement was effected by micrometers and corrections were applied to render the readings correct to the nearest 0.005 inch.

* Lecturer, University of Natal.

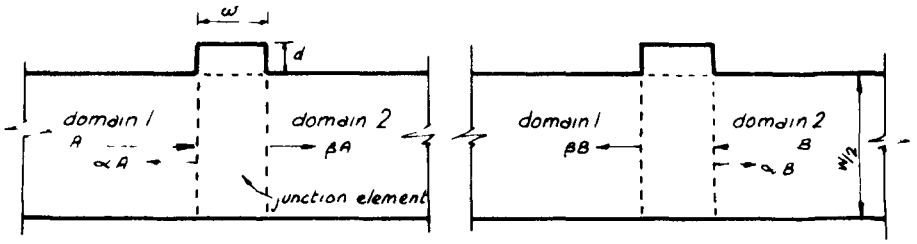

Fig.1 Wave components

MATHEMATICAL TREATMENT

Evidently the zone of protection provided by a resonator in the downstream direction, at resonance, is limited to a width of one half the incident wavelength (ref.2). Hence wave energy transmitted into the downstream domain will increase directly with increase in channel width above one wavelength, for the case where resonators are placed on both sides of the entrance channel. It follows that a resonator investigation of this type may be limited to one-dimensional propagation. Note that, though the assumption of plane waves is invalid near the junction element, two-dimensional motion becomes one-dimensional at distances of the order of twice the depth from the discontinuity, for these channel widths. Moreover, researchers have found that this limitation is not at all serious, provided that no transverse resonance occurs (ref.3). Transverse resonance is likely to occur when the basin width is close to an integral number of half-wavelengths.

The resonator geometry may be intermediate in shape between extremes that are either long and narrow, when the motion is in a direction normal to that of the waves in the entrance channel, or short and wide, when the motion is parallel to that of the entrance channel. These cases are denoted mode I and mode II respectively (see Fig.2). It is assumed that the complicated motion for intermediate geometries can be approximated by superposition of these unidirectional components. Each mode is considered in turn and then a combination is shown to accord with observations for an intermediate case. The effect of turbulent dissipation is also discussed.

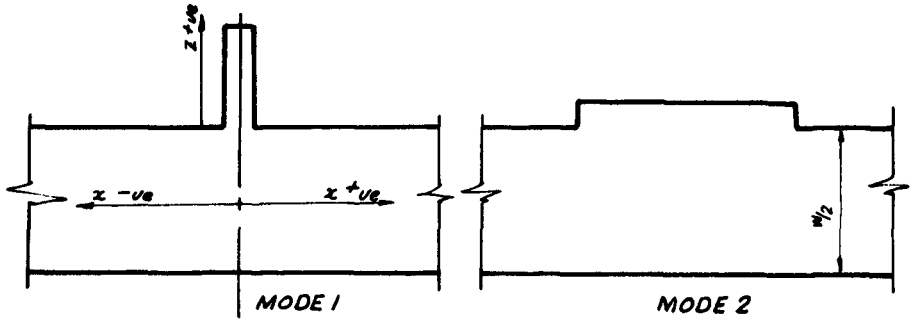

Fig. 2 Extreme cases.

Mode I

Notation is defined at the end of this paper.

For mode I,

$$wW << \lambda^2$$

Hence: (a) the water surface of the junction element remains approximately horizontal and (b) the origins for the resonators and the channel may be assumed to coincide.

Using complex representation, the reflected wave is written:

$$\eta = \bar{\alpha}\, a e^{j(kx+\sigma t)}$$

The water surface for the original incident wave, the reflected wave, the partial clapotis in the resonators and the transmitted wave may be matched for each contiguity:

$$\bar{\imath} + \bar{\alpha} = \bar{\beta} = (1+\bar{R})\bar{\theta} \tag{1}$$

The equation of continuity for the junction element is:

$$\sum_{1,2,R} \left\{ \int_{-h}^{0} \left(-\frac{\partial \phi}{\partial x}\right)_{x=0} dy \right\} = \omega W \frac{\partial \eta}{\partial t}$$

or:

$$k\omega W \bar{\beta} = -j\left\{ W(\bar{\imath} - \bar{\alpha} - \bar{\beta}) - 2\omega\bar{\theta}(1-\bar{R}) \right\} \tag{2}$$

for equal depths throughout.

Equations (1) and (2) can be solved for $|\alpha|, |\beta|, |\theta|, \hat{\alpha}, \hat{\beta}, \hat{\theta}$ in terms of $|R|$, $\hat{R}$, and, in this study, an Elliot 803 computer was used to tabulate the results. All results were checked against the expression for the conservation of energy developed below.

Mode II

In this case the $\bar{\theta}$ and $\bar{\theta}\bar{R}$ waves are parallel to the main channel. The waves are matched for discharge and surface continuity again at each channel discontinuity as follows:

$$\bar{\imath} + \bar{\alpha} = \bar{\theta}(1+\bar{R})$$
$$\bar{\beta} = \bar{\theta}\left(1 + \bar{R} e^{2jkw}\right)$$
$$W(\bar{\imath} - \bar{\alpha}) = \bar{\theta}(1-\bar{R})(W+2d)$$
$$W\bar{\beta} = \bar{\theta}(W+2d)(1-\bar{R}e^{2jkw})$$

These equations were solved, checked against energy conservation and tabulated using an I.B.M. 1620 computer.

Energy conservation

The energy of the reflected and transmitted waves is equal to that of the original incident wave less the energy dissipated in the resonators and junction element.

Proceeding from $$E = \frac{1}{2}\rho \iint g\eta^2 dx\, dz + \frac{1}{2}\rho \iint \left(\phi \frac{\partial \phi}{\partial y}\right)_{y=0} dx\, dz \tag{3}$$

we get, for no dissipation, $$|\alpha|^2 + |\beta|^2 = 1$$

For tsunamis and the experimental waves, viscous attenuation is negligible in the resonators. However, turbulence at the upstream edge is considerable and a lumped head loss can be postulated at this point:

$$H_L = a\left(|\theta| - |\theta||R|\right) = K\frac{u|u|}{2g}$$

Equation (3) then leads to:

$$|\alpha|^2 + |\beta|^2 + |\theta|^2(1-|R|^2)\frac{2w}{W} = 1$$

This allows H_L to be computed from observations of $|\alpha|$, $|\beta|$ and $|\theta|$.

U should include allowances for:
(a) local high velocities at the upstream re-entrant,
(b) the overall flow pattern in the junction element,
(c) the vertical velocity distribution.

The problem can be simplified by considering a steady-state flow pattern applicable to resonant conditions only and ignoring the local effects of surface deformations. Thus the transverse velocity profile along an equipotential emanating from the upstream edge of the resonator provides a good basis. Extreme velocities close to the edge can be reduced to manageable proportions by ignoring velocities within a nominal boundary layer and the vertical velocity distribution can be assumed to be the same as that given by Airy theory under a node in a standing wave. Using Schwarzian transforms for the upper half-plane the co-ordinates for given incremental values of ψ can be computed along the equipotential starting from the sharp edge. The velocity $\bar{q}$ is given by these differences and K can be calculated from

$$\int_{-h}^{0}\int_{0}^{l} \bar{q}|\bar{q}|\,ds\,dy = \frac{1}{K}\,2ga(|\theta| - |\theta||R|)$$

Intermediate geometry.

Any general combination of the type

$$(\alpha,\beta)_{total} = (\alpha,\beta)_{I} f_1(w,d) + (\alpha,\beta)_{II} f_2(w,d)$$

where the subscripts refer to the results obtained from computations for modes I and II and $f_i(w,d)$ denotes a simple function of the type $d/(w+d)$ and $w/(w+d)$ respectively, would reveal that:
(a) $\beta_{minimum} \neq 0$ and $\alpha_{max} \neq 1$ generally.
(b) for large w, there is an increasing tendency for the resonant value of d/λ to exceed a value of 0.25.
(c) for large w, there is a second type of resonance.
(d) resonant values of d/λ depend upon both w and W.

PRELIMINARY VERIFICATION.

A suitable experimental programme could not be devised without preliminary pilot studies. The results of these tests are now described and refer to an isolated single resonator.

Apparatus. The narrow "perspex" flume and timber housing for opposed adjustable rectangular resonators is shown in fig.3.

The rear wall of each resonator cantilevered vertically downwards from a system of clamps, which traversed along both side walls for the full length of the resonator. Hence any variation of resonator width, which was effected by means of a false (upstream) side wall, necessitated a change in width of the rear wall. This was achieved by means of twin thin overlapping galvanised iron sheet lips. An intermediate perspex wall was used to reduce the width of the entrance channel. For such tests filters were arranged at the upstream sharp edge of the

intermediate wall and on the seaward side an efficient wave absorber was built.

Where the theoretical domain is semi-infinite, it is axiomatic that wave re-flections off the paddle are NOT allowed and wave filters were used for such decoupling devices. These filters were not effective at low wave steepnesses. Nevertheless, results were frequently obtained under stop/start conditions, i.e. before the initial waves would re-reflect and hence were of some value.

The desideratum that domain 2 be semi-infinite caused difficulty, because of insufficient space (in which to absorb all the energy of the transmitted wave.) Of necessity the writer adopted an absorber similar to that developed by Hamill (ref.4).

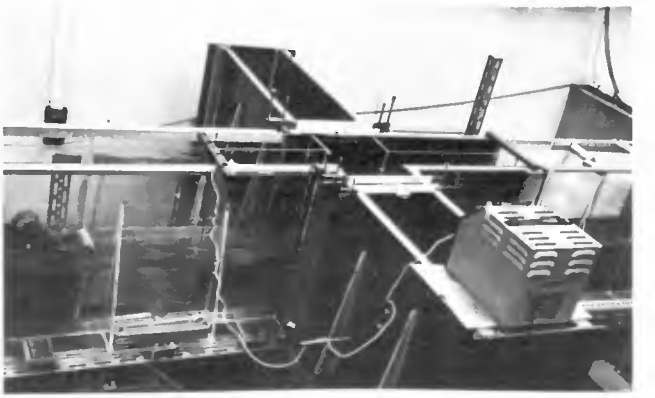

Fig.3 Preliminary apparatus.

Procedure. Envelope heights were directly measured to 0.01" by means of a simple steel pointed probe of 0.10" diameter, detected with the aid of a standard CRO, the time base adjusted to give a stationary signal. The actual reading recorded was such that only 5 signals were obtained in any 10 consecutive waves.

Envelope heights were measured for each value of 'd', the length of the resonator. 'd' was varied up to 8 times per value of resonator width, which was varied up to 7 times for each value of width of entrance channel. In all, four different entrance channel widths were tested. The wavelength was generally held constant. Wave periods were measured by timing 100 consecutive waves and wavelengths were then calculated by substitution into the first-order equations.

Every experimental "run" commenced from still water conditions and measurements were conducted as soon as the partial clapotis in each domain had stabilised. Wave periods were measured both at the start and the end of the run.

Results.

All experimental readings were plotted. Nodes and loops were measured off these plots and the coefficients of reflection and transmission

were computed. In this pilot study no allowance was made for attenuation, non-linear effects, or experimental error.

The coefficients were then all plotted against the dimensionless tuning parameter d/λ together with relevant results from theory (see Fig.4).

A number of photographs were taken of the entrance conditions at the resonator.

Discussion.

The photographs indicated extreme turbulence throughout the resonator and junction element. Velocities of this nature will occur very seldom indeed in any full-scale structure but the photographs provided an obvious warning of the navigational hazards resulting from an irrational design.

An obvious result is the discrepancy of the resonating values of the tuning parameter from that predicted by theory, not only for the fundamental mode but also for higher harmonics. Similar experimental results have in fact been obtained in analogous systems and have led to the formulation of "end corrections." The results of tests on resonators with curved entrances revealed further reductions in both the tuning parameter and the distance of the domain 1 partial clapotis from the resonator at resonance. This, of course, was to be expected.

FURTHER EXPERIMENTS

Introduction.

The pilot study provided reasonable agreement with the theoretical development, with the reservation that the "end correction" for the tuning parameter be evaluated empirically. However, the results obtained for large resonator widths were inconclusive and it was apparent that the main objectives in the final programme should necessarily include:

(a) a substantial reduction of non-linear effects,
(b) improved measurement technique, with regard to both accuracy and speed,
(c) vastly improved decoupling devices,
(d) a study of the effect of entrance channel width,
(e) a study of the effect of large resonator widths.

Perhaps the most important object of this second programme was to check whether a single resonator behaved as a single-degree-of-freedom oscillator, or, if not, to delineate the conditions under which this postulate did hold. Another important aim was to ascertain the validity of the linear theory used.

Apparatus. Experiments were carried out in the narrow flume, shown in Fig.5. It was hoped to shorten the upstream domain considerably in order to provide sufficient space for efficient measurement and absorbtion in the downstream domain. Eventually, however, a compromise was reached by the construction of the bend seen in Fig.5.

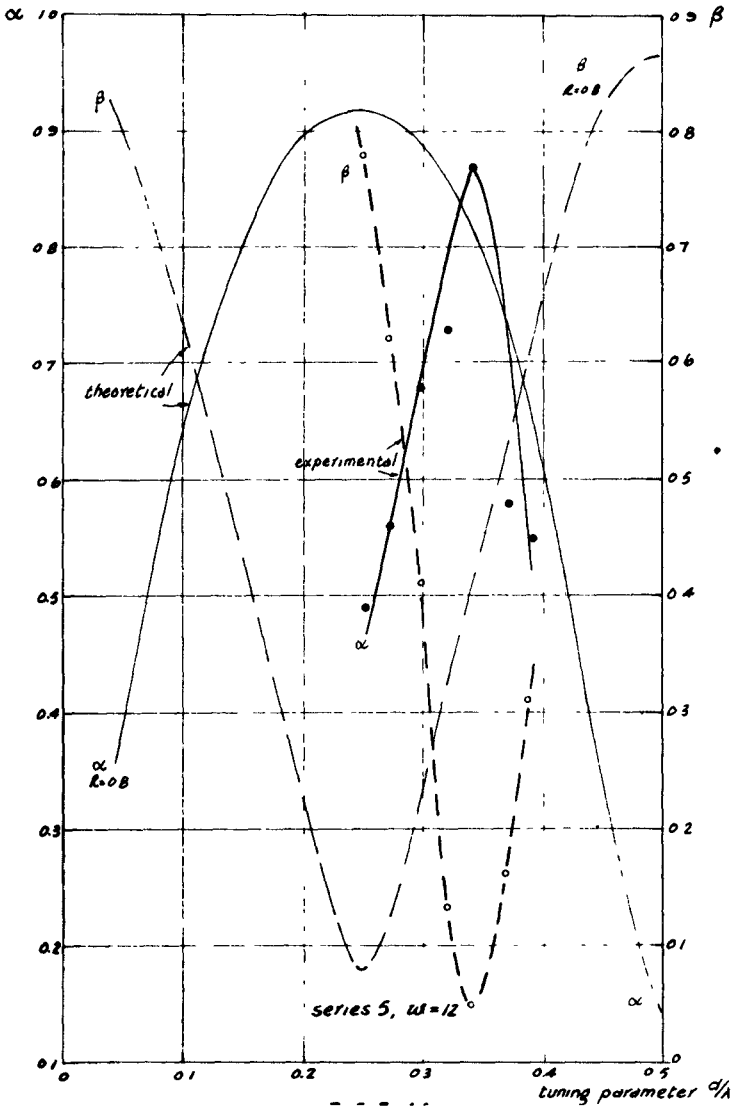

Fig. 4. Typical Preliminary Results.

Transverse oscillations were avoided by prohibiting such troublesome frequencies. No low frequency vibrations greater than 0.0001" were detected. Nevertheless a special instrument was attached, in case parasitic oscillations developed from other sources(see p.10).

Despite the smoothness of the perspex walls, side effects were easily visible under suitable low-level lighting. Disturbances radiated from the loops of the partial clapotis. Other sources of similar pseudorandom surface undulations were the filters, inconsistencies along the boundaries, vibrations inherent in the generator mechanism, and external vibrations, especially due to laboratory pumps and turbines and passing vehicular traffic. Surface tension was generally minimal, because of dispersive agents used in the measuring procedure, and consequently the "noise" resulting from meniscus inversion was probably of the order of 0.001" in amplitude.

Fig. 5 Final Apparatus.

The incident wave periods and still water depths were chosen such that consistent waves were delivered at the resonators. For $T<0.45$ secs. waves became too unstable and it was found that the standard deviation of wave heights varied inversely with still water depth. For reasonably shallow depths, this instability rendered wave measurement exceedingly difficult. Shallow still water depths also necessitated long probes which increased measuring errors and consequently the smallest depth tested was 5".

Standard deviations were measured by means of a "dekatron" counting unit and the probes described below. The count recorded the "number of crests greater than" (or "number of troughs less than") for each micrometer setting. Such a count was taken for batches of 100 consecutive waves at setting increments of 0.0005" throughout the range.

Histograms were plotted from the differences in the counts for sequential settings, of which a sample is given in Fig.6. and these revealed symmetrical relative-frequency distributions. The computed standard deviations were of the order of 0.0015" for a = 0.25" and under the conditions obtaining. The coefficient of variation was less than 1%. This compares very favourably with standard deviations quoted by other workers.

The symmetrical bell-shape shown in Fig. 6. greatly facilitated measurement; the mean reading is given by approximately half the number of a fairly large sample of waves, say 20.

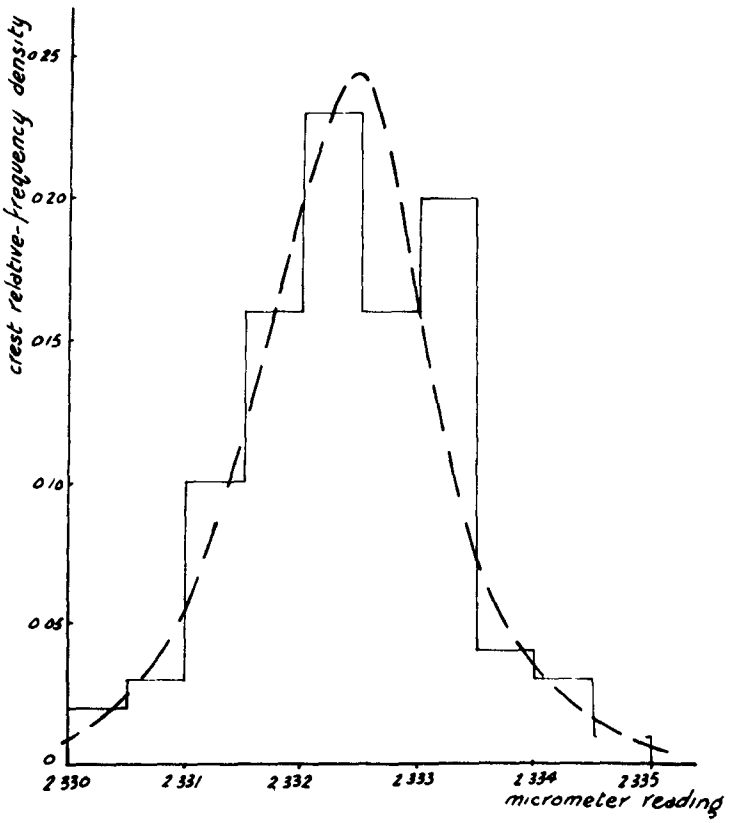

Fig. 6. Wave measurement histogram.

The writer did not investigate the reflection/transmission characteristics of the bend alone; the overall effect of the absorber downstream, the filters at each end of the bend, as well as the bend itself was examined. The filters were constructed of perforated zinc plate, 16 gauge (similar to those shown in Fig.7), 36" long, at 0.5" pitch, extending throughout the depth of water and measured coefficients of transmission were of the order of 0.4 - 0.6, depending upon wave length.

At least two filters were arranged in each domain, whence the total "decoupling coefficient" for each domain was at worst 0.06, assuming total reflection off the paddle and absorber.

Fig. 7. Wave filters.

The reflectivity of the absorber used in the pilot study was found to be about 0.1. Although this is considerably better than rubble-mound absorbers - for which the value would have been about 0.3, a desirable value would be $\alpha \nearrow 0.02$. The requirements of linear theory dictate that wave steepnesses be kept minimal and this in turn demands a highly efficient absorber.

Constructed in perspex, the final absorber was 6'0" x 9" and the perforations were 1" dia. at 2" centres. When fixed in position downstream of the bend, the overall gradient was less than 0.007. The reflectivity of the entire domain 2 set-up was measured and the readings adjusted for experimental errors and non-linearity. The results demonstrated two points:

(a) decreasing transmission (from domain 1 to domain 2) with decreasing wavelength, due entirely to the dissipative forces.

(b) increasing reflectivity with increasing wavelength.

In an effort to detect long period fluctuations in water level, a 3 l. separating flask was attached to the end of the flume. A column of water was positioned in a short horizontal section of capillary tube attached to a large diameter rubber bung and the lower end of the flask was connected to the flume through large diameter glass tubing. A change of water level in both the flume and the flask of 0.001" would therefore displace the column of water several inches. The indicator had to be replaced regularly, as evaporation in the main flume caused sufficient reduction in water level. Short period fluctuations were ineffective because of the overall impedance of the arrangement. Within limits, the impedance could be adjusted by stop-cocks. The instrument was attached to the flume behind the absorber, downstream of the bend.

Major sources of error are surface tension effects. When these effects are reduced, e.g. by using very fine probes and limiting instantaneous contact to a depression of the crest surface rather than actually puncturing it, it is usually impossible to see any meniscus effect. Probes were fashioned out of fine stainless steel sewing needles, nominal diameter about 0.015". The needles were coated with a thin layer of a P.V.C. akraline non-wetting paint, to ensure that no column of water drained down off the probe as it emerged from a crest. Probably because of galvanic corrosion, it was necessary to maintain the sharp points by careful abrasion.

Probes were attached to micrometer heads, capable of being read to 0.0001". The micrometer heads were securely mounted on heavy cross-bars, clamped to the flume and the signal relayed to the cathode ray tube. A newer improved instrument uses a dial gauge, as shown in Fig.8. Another possible source of error is the sum of

(a) the depth to which the crest is actually depressed before a signal is obtained
(b) the height to which the surface of the crest is raised before contact is broken.

A dispersive agent was added continuously to reduce this and numerous very careful measurements were made on still water. The maximum correction was found to be 0.007". The extent of dynamic effects was not established.

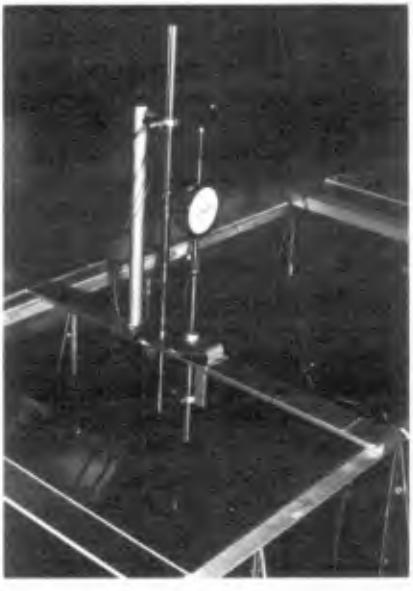

Fig. 8. Wave measurement.

General Procedure.

Wave periods (for at least 100 consecutive waves) were measured both at the outset and at the conclusion of the experiment. Both transverse oscillations and seiches were successfully avoided, so that the generator was stopped only at the conclusion of each experimental "run" when the resonator geometry was adjusted. Experiments were controlled in the laboratory by simultaneous curve-plotting. In this way the parameters were chosen to yield the family of curves plotted in Fig.13.

Usual methods for evaluating the two primary components of the partial clapotis in both domains have two basic assumptions in common:

1. The fundamental waves have harmonic wave-form.
2. Only two such constituents are present.

Consequently, disregarding measuring errors, the accuracy of both methods increases with decrease in both amplitude and wavelength of the incident wave (because of reflectivity). It was found that values of α calculated by the 3-point method were usually unreliable and the method was soon discarded in favour of the loop-and-node method. This enabled on-the-spot plotting of characteristics and thus greater flexibility and control of each experiment, a most important consideration.

On the other hand accurate scanning demands between 8 and 20 measurements of envelope height for each experiment, a somewhat protracted and tedious labour.

Data Processing. Resonator antinodes and loops and nodes for both domains were punched-up and a program was then written to correct for the measuring errors described above and to compute, inter alia, α and β.
These results were plotted as shown in Figs. 9 and 10.
The effect of attenuation and non-linearity is immediately apparent, from the fact that the plots do not tend to 1.0 or 0, as the case may be, as $d/\lambda \rightarrow 0$.

Discussion.

In assessing the accuracy of the results, the errors have been evaluated as follows:

(a) Systematic errors, due to attenuation and non-linearity. These errors do not affect the derivation of the geometry for resonance but are of paramount importance in establishing absolute values of reflectivity and transmissivity. Corrections for both these errors can be applied easily:

(i) Attenuation. All values of α and β should be corrected by multiplication by the reciprocal of β_o, the transmissivity at $d/\lambda = 0$.

This operation yields even larger values of α_0. The effect of domain 2 reflectivity at resonance is very small, i.e. usually $< 0.01A$ in amplitude in domain 1. It is incorporated in the random errors discussed below.

(ii) Non-linearity. The analysis of real partial clapotis produces low values of α, and negligible effect on β, when α is not very small. Corrections for this can be applied easily.

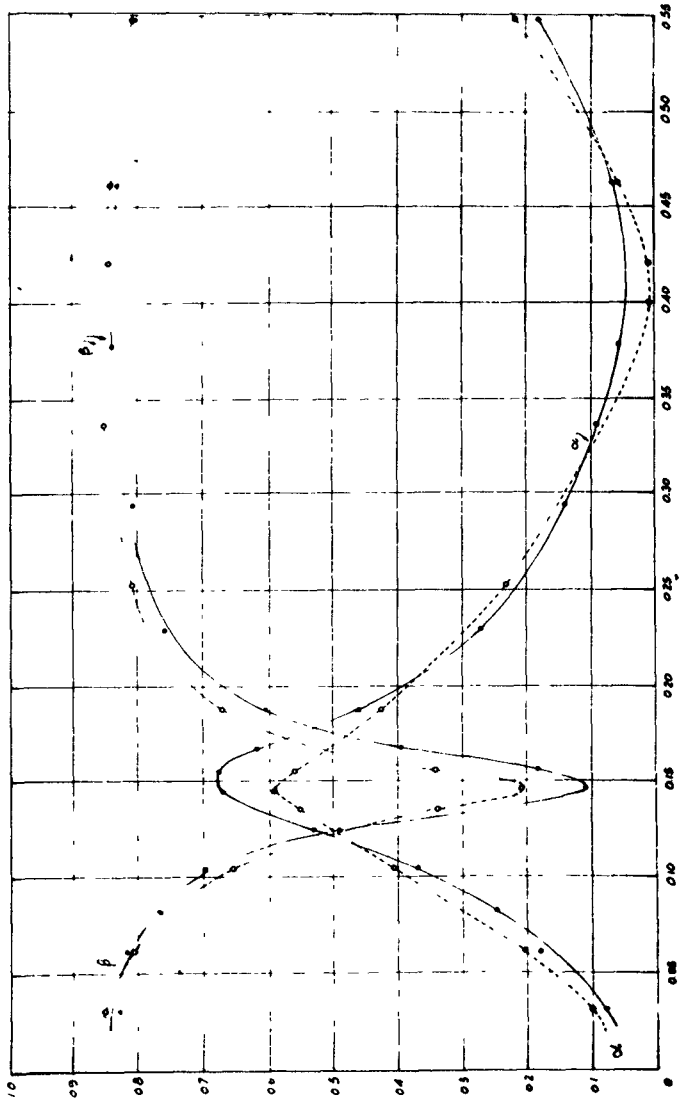

Fig. 9. Single Resonator Results, 1st mode.

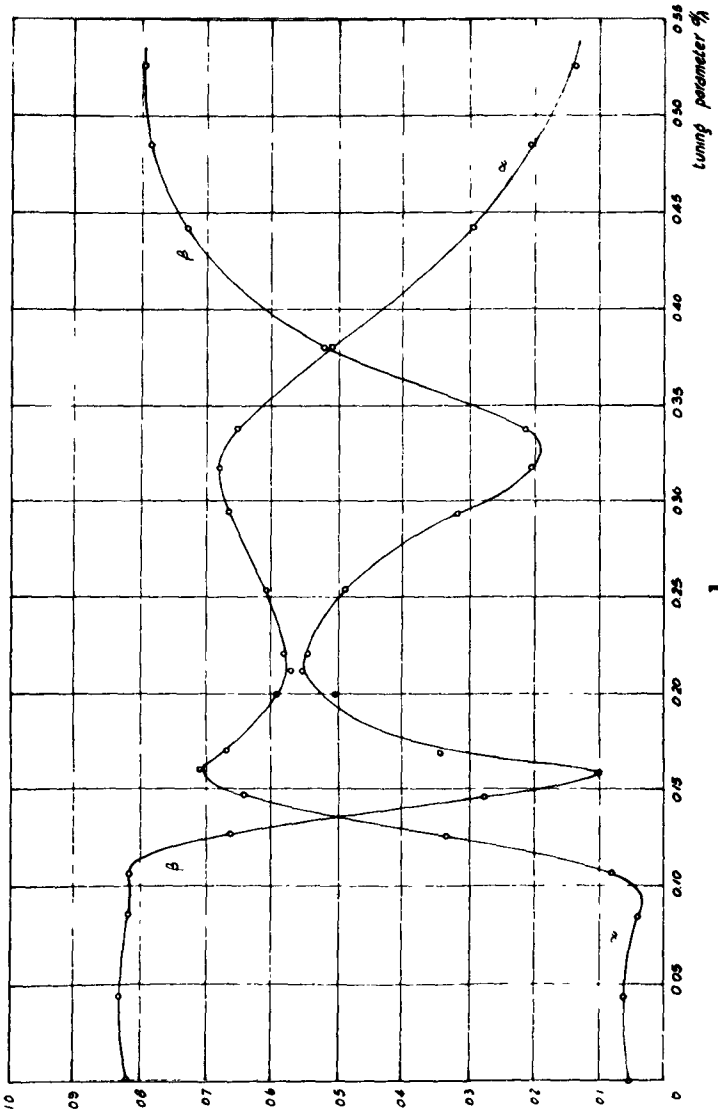

Fig. 10. Single Resonator Results, 2nd mode.

(b) Pseudo-random errors, attributable to generator instability, surface "noise", negative waves from domain 2 and the errors in the processes from measurement to plotting.

The writer did not attempt to assess individually such imponderable errors, as these are best calculated from the scatter obtaining in the graphs.

In error analyses, only graphs with a relatively high density of experimental results are admissible. As little scatter was found during the laboratory control of the experiments, the number of experiments was reduced to a minimum and, ipso facto, most of the curves plotted are unsuitable for error evaluation. However, certain curves were analysed and the probable error on the plot having the largest scatter of all the tests performed in the final programme was found to be 0.0146. The writer therefore submits that the random error was not much more than 1%.

The parameters of resonator geometry were rounded off to the second decimal place. The calculation of wavelength to this order of accuracy required an accuracy of measurement of wave period of 0.001 secs. and of still water depth of 0.05".

Figures 9 and 10, clearly indicate that the combined resonator and junction element acts as a two-degrees-of-freedom oscillator, under certain conditions. An appraisal of the α and β curves reveals a gradual transition from the single-degree system to the two-degrees system and an eventual preponderance of the second mode of resonance as w/λ increases beyond a value of 0.5. Further appraisal reveals that this "critical" w/λ increases with increase in W/λ .

The modes of oscillation are illustrated in figs. 11 and 12 respectively.

Note that the water surface sketched is exaggerated in the vertical scale; amplitudes were small and consequently the nodal lines sketched are inaccurate. Nonetheless, the sketches elucidate the mechanisms at resonance and illustrate the transition between these states.

Results for the first resonant mode were finally combined in Fig.13.

GENERAL CONCLUSIONS.

For the sake of simplicity, only the points of primary importance are enumerated below:

1. Resonators can be applied in harbour engineering for the elimination of waves causing short period agitation, influx of sea sediments and/or range action.
2. The results corroborate the results of the analytic theory developed and verify that the response of a short rectangular branch canal to periodical plane gravity waves propagated across the mouth is analogous to that of a single degree of freedom oscillator within certain limits:

For small values of W/λ and when $w/\lambda > 0.5$, the resonator becomes a two degrees of freedom oscillator. For larger values of W/λ this limiting value of w/λ increases.

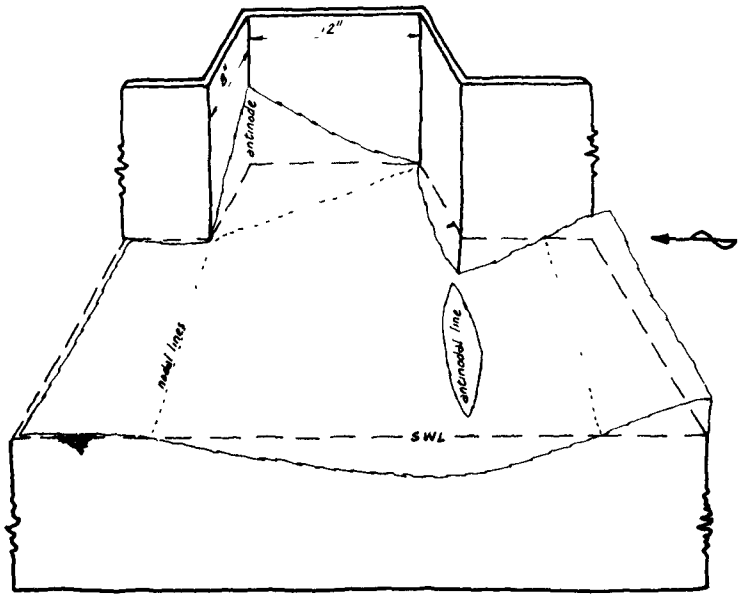

Fig.11. First mode of resonance.

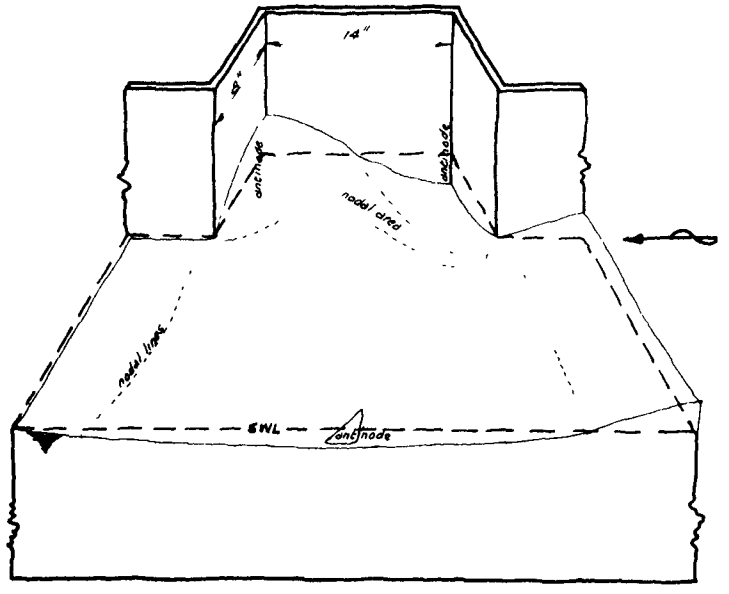

Fig.12. Second mode of resonance.

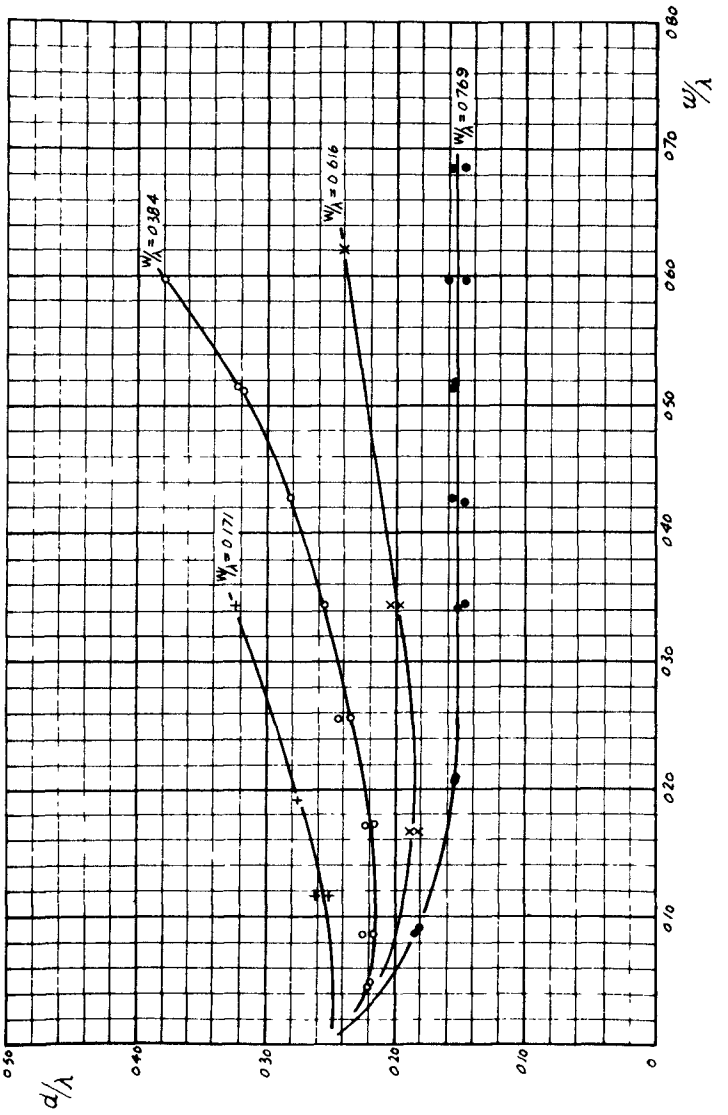

Fig. 13. First Resonant Mode.

Waves of the characteristic resonance frequency are not transmitted past the resonator but are reflected upstream as negative waves.

3. The zone of protection provided by a resonator is limited to a width of $\lambda/2$ in the downstream domain. Consequently, the benefits of resonators vanish as W increases beyond λ .

4. Resonant amplitudes of vertical oscillation in a resonator are finite, irrespective of viscous dissipation.

5. The cardinal point established in this investigation, is that resonator geometry for resonance differs greatly from earlier recommendations. Of utmost significance is the width of the entrance channel. Harbour entrance geometry at resonance is accurately related to incident wavelengths by the family of curves in Fig.13, which has immediate application in design.

6. The frequency band width for which β is less than any prescribed value is a function of w/λ (and increases directly with increase in w/λ) as well as a function of W/λ .
The dependence of the tuning parameter d/λ on w/λ at resonance is such that a minimum exists at $w/\lambda < 0.2$. Generally, however, the tuning parameter increases with increase in w/λ .
These two points indicate a compromise in the selection of w and d.

7. Optimum resonator performance is related to the energy dissipated in the resonator. At resonance, $\alpha = 1 - \beta$ approximately. Optimum performance appears to be relatively sensitive and further experiments, in which viscosity is carefully controlled, may be useful to fix absolute values. (In these tests there was no temperature control and changes of viscosity of up to 20% were involved.)

8. Finite wave heights reduce the effectiveness of the resonator. The effect appears to be small, however. Wave height has no influence on resonator geometry for resonance.

9. Small values of w/λ are accompanied by both decreased efficiency and high resonant velocities. Such velocities could prove a serious navigational hazard.

10. Where there is partial reflection in domain 2 the resonator should be located at $l = n\lambda/2 (n = 1, 3, 5 \ldots)$, or at the position of a loop if reflections are distributed. Ad hoc model tests would then be advisable.

11. Still water depth is of little or no consequence in the resonator geometry for resonance.

12. Non-uniform depths effectively reduce performance. However, the tuning parameter could be substantially reduced in the case of long waves and considerable savings in financial outlay could then accrue.

13. Current techniques used for the reduction of finite partial clapotis incur unreasonable errors, because of the trochoidal waveform. Suitable corrections can be applied easily. Current wave-flume measuring

techniques also incur systematic errors through viscous attenuation and menisci effects. Corrections for these can be easily applied. The random error encountered in similar investigations need not exceed 1% if a similar measuring procedure and experimental apparatus is adopted.

ACKNOWLEDGEMENTS

Guidance from Prof. J. Allen and financial assistance from the S. African C.S.I.R. and the University of Natal is gratefully acknowledged.

NOTATION

w	resonator width	l	length of an equipotential
W	channel width	$\|R\|$	transmissivity for resonator
λ	wavelength	$\|\Theta\|$	reflectivity in resonator
η	surface ordinate	y	vertical ordinate
a	semi-amplitude	h	still water depth
$\bar{\alpha}$	complex vector	ϕ	velocity potential
$\|\alpha\|$	reflectivity	E	total energy
j	$\sqrt{-1}$	ρ	mass density
$\hat{\alpha}$	phase angle	g	gravitational acceleration
k	wave number	z	transverse co-ordinate
x	horizontal abscissae	H_L	equivalent head loss
σ	circular frequency	U	a generalised velocity
t	time	K	dimensionless coefficient
$\bar{i}$	unit vector in x direction	$\underline{d}$	length of resonator
$\|\beta\|$	transmissivity	$\underline{q}$	velocity vector
c	a constant	s	distance along an equipotential.
ψ	stream function		

Subscripts 1, 2, R, refer to semi-infinite ocean, downstream domain and resonators respectively.

Subscripts I,II refer to mode I and mode II respectively.

REFERENCES

1. Valembois, J. "Etude de 1'Action d'Ouvrages Resonants sur la Propagation de la Houle", Proc. Minnesota Int. Hyds. Conf., Minneapolis,1953, pp 193-200.

2. Penny, W.G., and Price, A.T. "The diffraction theory of sea waves and the shelter afforded by breakwaters", Phil. Trans. Roy.Soc., series A, Vol.244, No.882, March 1952, pp 236-253.

3. Le Mehaute, B. "Theory of wave agitation in a harbour", Jour.ASCE, HY9, March 1961, paper 2765, pp 31-50.

4. Hamill, P.A., "Experimental development of a perforated wave absorber of simple construction and minimum length", Mech. Eng. Report MB-252, N.R.C. No.7472, Ottawa, Canada, May 1963.

CHAPTER 99

THE MOTIONS OF SMALL BOATS IN STANDING WAVES

by Fredric Raichlen, Assoc. Professor of Civil Engr.,
W. M. Keck Lab of Hydraulics and Water Resources,
Calif. Inst. of Tech., Pasadena, Calif., USA

ABSTRACT

Some dynamical aspects of the surge motions of small boats moored asymmetrically with elastic non-linear restraints are discussed herein. In connection with the theoretical analysis of mooring dynamics, experiments were conducted to determine the periods of the free oscillations of a 26-ft boat moored in various ways in a floating slip. These results are in reasonable agreement with those predicted theoretically. An analytical study of the mooring dynamics of seven small boats indicated that the periods of free oscillation were less than about 10 sec., hence, for these boats the important wave periods for forced oscillations would be in the range of those of storm waves.

INTRODUCTION

An important question which is raised in the design of harbors for small boats of the size usually used for pleasure is the range of wave periods which could be expected to cause damage to these moored boats If these periods can be predicted then the problem of minimizing wave-induced oscillations in a small-boat harbor may be simplified, because it would be sufficient to investigate the response of a harbor to waves only over the limited range of wave periods which affects small craft. The objective of the study reported herein was to develop a method of predicting this range of wave periods for surge motions of a small boat given the dimensions and characteristics of the boat and its mooring system.

It is first important to consider some of the major differences between small and large boats which relate to their dynamics. The most obvious difference between the two cases is size, in the case of small pleasure boats the vessels which are of interest are less than approximately 60 ft long and the displaced weights are less than approximately 10 tons as compared to large vessels whose length may be 300 ft to 700 ft with displaced weights ranging from 9,000 to 50,000 tons. However, it is not the displaced weight alone which is of importance in defining the response of the vessel to waves, but the important parameter is the ratio of the restoring force associated with the mooring system to the inertial force (which depends on the displaced weight of the vessel).

With respect to this ratio, the nature of the restoring force for large ships can be quite different from that for small boats. Wilson (1967a) has described the mooring systems used by a number of large vessels. In general those systems consisted of a large number of lines extending from the bow, the stern, and the midship of the vessel to the dock which restrict motion both in the fore and aft direction as well as in the direction perpendicular to the dock. Even though the elastic characteristics of the individual mooring lines may be quite different from one another, on the average the restoring force for motion in the fore and aft direction for similar displacements would be approximately the same. (It should be noted, however, that

for motions of a large vessel in sway, i.e., in a direction perpendicular to the dock, the restoring forces would be highly asymmetrical.) In addition to these features, usually the mooring lines for large ships have slack to allow for motions due to changes in the tide.

In contrast, generally small boats are moored with only a few lines, e.g., in mooring in a "U-shaped" slip usually only two bow lines and two stern lines are used. Under these conditions, it is evident that the restoring force for motion in one direction may be quite different from the restoring force for similar displacements in the opposite direction. This asymmetry can have a significant effect upon the motion of the boat and potential boat damage. For instance, if a boat is moored in the slip with little clearance between the bow of the boat and the front of the slip, impact damage to the bow may be possible due to the asymmetrical restoring forces. This type of damage possibly would be eliminated by using a stiffer more symmetrical mooring system.

Although only two examples of the differences have been presented, through these it is evident that attention must be given to the details of mooring for small boats which could perhaps be neglected for large vessels.

THEORETICAL CONSIDERATIONS

An analysis is presented in this section which describes the motions of a moored body in surge when exposed to a standing wave system. The mooring system used in the analytical model can result in non-linear asymmetrical restoring forces which resist the wave-induced motions. Only surge motions (boat displacements either toward the bow or toward the stern) are considered, and the boat is treated as a block body with no attempt being made to fully describe in detail the shape of the vessel. The innovation in this development concerns incorporating a non-linear asymmetrical restoring force in the equation of motion of the analytical model. For a more complete development of the basic equation of motion the interested reader is referred to Wilson (1958), Kilner (1960), and Raichlen (1965).

The block body is a rectangular parallelepiped of length 2L, beam B, and draft D moored in a way such that the only allowable motions are in surge. The standing wave is formed in water of a constant depth d by a progressive wave which is reflected from a perfectly reflecting surface located a distance b from the center of the moored body. The x-coordinate is measured from the center of the body in the at-rest-position and denotes the movement of the center in surge motion. (A schematic diagram of this body moored in a standing wave system is shown in Fig. 1.)

The equation of motion in surge of the moored body is

$$M\ddot{x} = F_p + F_i + F_d + F_r \qquad (1)$$

where $\ddot{x}$ is the acceleration of the body, (d^2x/dt^2), M is the mass of the body and F_p = net pressure force acting on the ends of the body, F_i = inertial force due to the unsteady motion of the body and the fluid, F_d = force due to viscous effects, F_r = restoring force due to the mooring system.

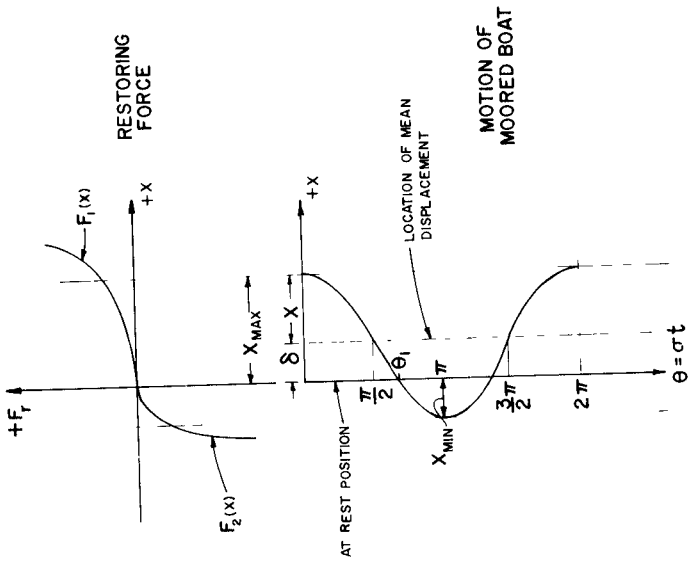

Fig 2 Schematic Diagram of Non-Linear Asymmetrical Restoring Force and Assumed Resultant Boat Motion

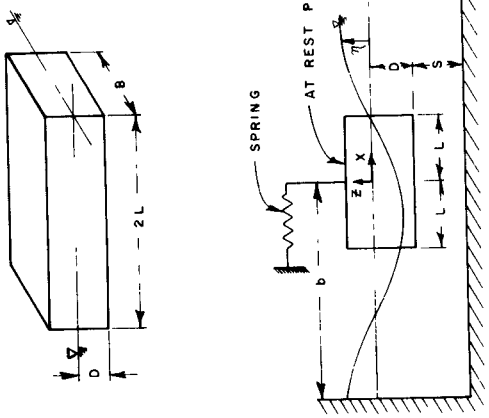

Fig 1 Schematic Diagram of Block Body

Considering small amplitude standing waves and certain assumptions relating to the water particle accelerations it can be shown (see Wilson (1958)) that, neglecting viscous effects, Eq. 1 becomes

$$\ddot{x} + (F_r/C_M M) = \dot{U} \tag{2}$$

where $C_M M = M + M_x'$ (M_x' is the added hydrodynamic mass) and

$$\dot{U} = \zeta \sigma \cos \sigma t \tag{3a}$$

$$\zeta = Ag\,[\sinh kd - \sinh ks]\,\sin k L \sin kb/(LD\sigma k \cosh kd) \tag{3b}$$

The forcing function $\dot{U}$ is the average over the displaced volume of the block body of the water particle accelerations in the standing wave. It is introduced as a simplification in describing the pressure force and the inertial force in Eq. 1 (see Wilson (1958) and Raichlen (1965)).

The problems in solving Eq. 2 arise primarily due to the form of the restoring force, F_r. Although the variation of the virtual mass coefficient, C_M, with boat shape and other conditions is not well known, the effect of this quantity on the dynamic response of a small moored boat in most cases is not as important as the effect of the restoring force if a reasonable estimate of C_M is made initially.

Consider the following general expression for the restoring force

$$F_r(x) = F_1(x) \text{ for } x > 0 \tag{4a}$$

$$F_r(x) = F_2(x) \text{ for } x < 0 \tag{4b}$$

where x is defined as positive for motion toward the bow and negative for motion toward the stern. (The functions of Eqs. 4 may take any form linear or non-linear, symmetrical or asymmetrical, free travel or no free travel.)

For simplicity, the equation of motion (Eq. 2) is rewritten so that the phase relation between the forcing function and the body response is incorporated in the forcing function

$$\ddot{x} + (F_r/C_M M) = \zeta \sigma \cos (\theta - \varphi) \tag{5}$$

where $\theta = \sigma t$ and φ is the phase angle and Eq. 4 describes the variation of F_r.

If the restoring forces $F_1(x)$ and $F_2(x)$ are different then it is reasonable to assume that the mean position of motion of the vessel will be different from the at-rest-position of the vessel. Therefore, the general solution to Eq. 5 is taken as

$$x = \delta + X \cos \theta \tag{6}$$

Eq. 6 is an approximate solution which neglects the effect of higher harmonics; however, it has been shown in most mooring problems (see Kilner (1960)) that this is justified. The motion described by Eq. 6 is shown in a schematic manner in Fig. 2 along with assumed restoring forces described by Eq. 4.

By setting x = 0, Eq. 6 describes the degree of asymmetry of the restoring force, that is

$$\delta = -X \cos \theta_1 \tag{7}$$

and for $\theta_1 = \pi/2$ the displacement of the mean position from the at-rest-position, δ, becomes equal to zero. It is noted from Fig. 2 that $\theta_1 = \pi/2$ implies that $F_1(x) = -F_2(x)$, hence, the restoring forces and the resultant motion for that case are symmetric about the at-rest-position of the boat. If, on the other hand, $\theta_1 = \pi$ the boat motion is highly asymmetrical and in accordance with Eqs. 6 and 7 there would be no motion of the vessel in the minus x-direction, i.e., for a given displacement $F_2(x) >> F_1(x)$.

Klotter (1951) has described the solution of an equation such as Eq. 5 with non-linear restoring forces based on the averaging method of W. Ritz. Rewriting Eq. 5 as

$$E(x) = \ddot{x} - \zeta \sigma \cos (\theta - \varphi) + (F_r / C_M M) \tag{8}$$

the averaging method furnishes the following two conditions

$$\int_0^{2\pi} E(x) \cos \theta \, d\theta = 0 \tag{9a}$$

$$\int_0^{2\pi} E(x) \sin \theta \, d\theta = 0 \tag{9b}$$

Assuming the form of the displacement described by Eq. 7, the first two terms of Eq. 8 can be integrated directly in accordance with Eq. 9a (or Eq. 9b). The integral in Eq. 9a which is comprised in part of the third term in Eq. 8, referring to Fig. 2, can be integrated over three intervals, hence·

$$\int_0^{2\pi} \frac{F_r}{C_M M} \cos \theta \, d\theta = \int_0^{\theta_1} \frac{F_1(x)}{C_M M} \cos \theta \, d\theta + \int_{\theta_1}^{2\pi-\theta_1} \frac{F_2(x)}{C_M M} \cos \theta \, d\theta$$

$$+ \int_{2\pi-\theta_1}^{2\pi} \frac{F_1(x)}{C_M M} \cos \theta \, d\theta \tag{10}$$

In order to solve Eq. 10 so that the solution to Eq. 9a can be obtained it is necessary to evaluate the restoring forces $F_1(x)$ and $F_2(x)$ for a particular mooring system. To carry out the indicated integrations it is assumed that the functions $F_1(x)$ and $F_2(x)$ can be represented reasonably well over the range of displacements which are of interest by polynomials consisting of odd powers of x, that is to say

$$F_1(x) = a_1 x + a_2 x^3 + a_3 x^5 \tag{11a}$$

$$F_2(x) = r_1 x + r_2 x^3 + r_3 x^5 \tag{11b}$$

Eq. 6 is substituted into Eqs. 11a and 11b and the resulting expressions are then substituted into Eq. 10. Although the integrations indicated in Eq. 10 are straightforward, the result consists of numerous terms in powers of

sines and cosines of θ_1 and other system parameters and for the sake of brevity will not be given explicitly in this discussion (see Raichlen (1968)). In order to evaluate θ_1 the equation of motion (Eq. 8) is averaged over one wave period. When this is done only one term remains

$$\int_o^{2\pi} \frac{F_r}{C_M M} d\theta = 0 \tag{12}$$

Eq. 12 can be integrated over the same intervals as used in Eq. 10 and a solution can be obtained for the variation of θ_1 with X (see Raichlen (1968) for details of this analysis).

Solving Eq. 9b in a similar way it can be shown that $\varphi = 0, \pi$, which is as it should be for the forced oscillations of an undamped dynamic system.

Using this approach the following general equation is obtained which describes the response in surge of the arbitrarily moored body in terms of its maximum displacement in the positive x-direction from the at-rest-position

$$\sigma^2 + \frac{\zeta(1 - \cos\theta_1)}{X_{max}} \sigma - \frac{(1 - \cos\theta_1)}{\pi X_{max} C_M M} \int_o^{2\pi} F_r \cos\theta \, d\theta = 0 \tag{13}$$

where $X_{max} = \delta + X = X(1 - \cos\theta_1)$

The integral in Eq. 13 is evaluated from Eq. 10 with the variation of θ_1 with X determined from Eq. 12. It should be noted, the most direct solution to Eq. 13 is to solve for σ given values of ζ, X, and θ_1. Since the maximum displacement in the negative x-direction, X_{min}, can be obtained from the relation $X_{min} = (2\delta - X_{max})$, the response curve is fully defined.

To demonstrate some of the general features of the solution the problem is reduced to one with linear restoring forces by letting $a_2 = a_3 = r_2 = r_3 = 0$. It can be shown that Eq. 13 reduces to:

$$\sigma^2 + \frac{\zeta(1 - \cos\theta_1)}{X_{max}} \sigma - \frac{S}{C_M M} = 0 \tag{14a}$$

where $S = (a_1 - r_1)\left[\frac{\theta_1}{\pi} - 1 - \frac{\sin 2\theta_1}{2\pi}\right] + a_1$ (14b)

and θ_1 is given by $\tan\theta_1 = \left[r_1 \pi + (a_1 - r_1)\theta_1\right]/(a_1 - r_1)$ (14c)

For $a_1 \neq r_1$ this case corresponds to a bi-linear asymmetrical restoring force and for $r_1 >> a_1$, θ_1 tends to π which indicates highly asymmetrical motions. When $a_1 = r_1$, Eq. 14a becomes the equation of motion for a linear spring system and Eq. 14c shows that θ_1 equals $\pi/2$, the condition of symmetry as seen in Fig. 2.

In an actual mooring problem neither of these two cases is likely to occur and the problem must be treated as indicated by Eqs. 10 and 13 after fitting Eqs. 11a and 11b to the predicted (or measured) restoring forces. In order to develop a method of predicting these restoring forces, consider first the schematic diagram of Fig. 3 which shows a block body (representing the small boat) moored with four lines to a dock. Initially the lines are slack by some arbitrary amount $\Delta\ell$. Upon movement of the body in the positive x-direction this slack becomes zero after the boat moves through a distance Δ_f denoted as the free travel. Until the vessel has moved this distance the restoring force is considered to be zero. This is because the lines usually have a small unit weight and the restoring force is assumed to develop only due to the elastic characteristics of the lines Therefore, when $x = \Delta_f$ the line tension is zero ($T^* = 0$), and T^* becomes greater than zero for $x > \Delta_f$.

The restoring force F_r shown in the plan view in Fig. 3 is equal to the sum of the x-components of the line tensions, T^*, for all lines acting to restrain the boat's motion in a given direction. Hence

$$F_r = \sum_{n=1}^{N} T^*_{x_n} \tag{15}$$

where from the geometry of Fig. 3

$$T^*_{x_n} = T^*_n \cos \beta_n \cos \alpha_n \tag{16}$$

The elastic characteristics of the mooring line can be represented as

$$T^*/T^*_{Brk.} = R\, \epsilon^m \tag{17}$$

where $T^*_{Brk.}$ is the average breaking strength of the particular line, ϵ is the strain (total elongation divided by length), and R and m are constants.

Consider the definition sketch of a typical line shown in Fig 4 where the line goes from a cleat on the dock to a cleat on the boat passing through a guide at its point of first contact with the boat. Therefore, the line is divided into two sections the first section going from dock to boat with a length $\ell' = \ell + \Delta\ell$, and the second section on the boat with a length ℓ_1.

For small elongations and considering the geometry shown in Fig. 4 the x-component of the line tension can be expressed as

$$T^*_{x_n} \cong K_1 \left[\frac{f + \Delta_f}{\ell'(\ell' + \ell_1)}\right]^m \frac{\left[1 - (\frac{y_o}{\ell'})^2\right]^{1/2}}{\left[1 - (\frac{z_o}{\ell'})^2\right]^{(m - 1/2)}} [x - \Delta_f]^m \tag{18}$$

where $K_1 = RT^*_{Brk.}$ (see Raichlen (1968)).

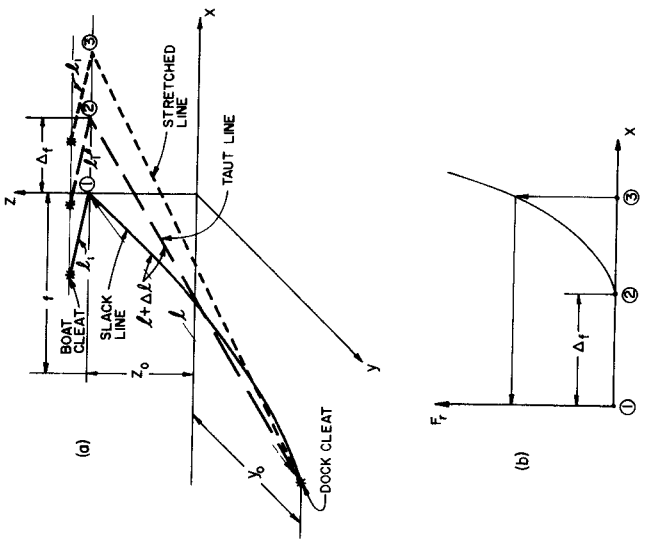

Fig 4 a) Geometry of Typical Mooring Line
b) Schematic Diagram of Non-Linear Restoring Force with Free Travel

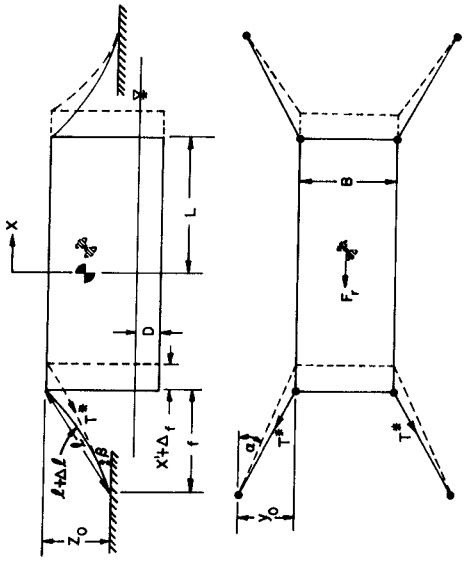

Fig 3 Schematic Diagram of Four-Point Mooring System

The method of approach used in determining the variation of the restoring force with the displacement of the boat in the direction of either the bow or the stern follows directly from Eqs. 17 and 18. For a given displacement the component tensions, $T^*_{x_n}$, computed from Eq. 18 and the corresponding elastic characteristics K_1 and m, are summed in accordance with Eq. 15, repeating this procedure until the restoring force vs. displacement curve is constructed.

In order to determine the coefficients R and m in Eq. 17 the elastic characteristics of various materials used for mooring have been obtained from various manufacturers. In addition to these data, tensile tests were conducted in the laboratory using a short section of 5/8-inch diameter manila rope. Based on the available information the values used in this study are: R = 18, m = 1.48 for manila and R = 2.54, m = 1.65 for nylon. The breaking strength of ropes composed of various materials, $T^*_{Brk.}$, were obtained from the manufacturer's data or from Wilson (1967b).

RESULTS AND DISCUSSION OF RESULTS

A series of tests were conducted at a small craft harbor near Los Angeles, California, (Marina del Rey) to determine the periods of free oscillation of a 26 ft boat (referred to herein as Harbor Boat No. 3) moored with a system of four 5/8 in. diameter manila lines (two bow and two stern lines) to a "U" shaped floating slip. The boat had a length of 26 ft, a beam of 9 ft 2 in., a maximum draft of 2 ft 4 in., and a loaded displacement of approximately 7,000 lbs. The hull in cross section was a modified Vee shape and for this reason the block body approximation used for the shape is perhaps not as good as when applying this to larger vessels, such as tankers. The dimensions of the mooring system are presented in Table 1 using the nomenclature of Fig. 4.

Table 1. Dimensions of Mooring Lines of Harbor Boat No. 3

	Bow Lines		Stern Lines	
	Port	Starboard	Port	Starboard
z_o	27.5*	29.	18.	16.
y_o	27.	32.	33.	36.
f	60.	57.	76.	80.
ℓ	71.	72.	85.	89.
ℓ_1	36.	36.	0.	0.
	*Note all dimensions in inches			

These dimensions show that although an attempt was made to moor the boat in the center of the slip, this objective was not achieved exactly. The length of the mooring line, ℓ, shown in Table 1 is for the case of all lines taut, in the test two other cases were examined· 4 in. and 8 in. of slack in all lines.

In these tests the boat was displaced in either the direction of the bow or the stern with known applied forces and the displacement relative to the dock was recorded photographically by means of a time-lapse movie camera. A photograph of the boat and its mooring system is presented in Fig. 5, which also shows the experimental arrangement for the tests. A scale is fixed to the boat along with an electric stop clock to facilitate measurements of the displacement and of the period of the free oscillation. The vessel was displaced using rigging that went either from the bow or the stern of the boat to piling located nearby. After the force vs. displacement characteristics of the mooring system were determined the boat was displaced either in the positive or the negative x-direction with an applied force of 200 lbs or 500 lbs and then suddenly released. Although it would have been desirable to use an applied force greater than 500 lbs this was not considered possible due to the condition of the pilings. The motions of the boat after it was released were recorded using a time-lapse camera and the displacement-time history of the boat's motion as well as the period of free oscillation were determined from a frame-by-frame analysis of the film. Such experiments were conducted for the condition of taut lines, 4 in. slack in all lines, and 8 in. slack in all lines, with the initial force applied first to the bow and then to the stern.

The variation of the restoring force with displacement for Harbor Boat No. 3 moored with taut 5/8-in. manila lines is presented in Fig. 6. In addition to these data, predicted restoring force curves are presented in Fig. 6 which were obtained from Eqs. 15 and 18 using the elastic characteristics presented along with the breaking strength of this rope (4400 lbs). The agreement between measurements and theory in Fig. 6 is relatively good, one of the main reasons for disagreement is the fact that the point of application on the boat of the applied load was above the center of gravity of the boat. Therefore, some pitching of the boat was introduced, contrary to the conditions of the analysis.

Predicted force displacement curves are presented in Fig. 7 for the three conditions which were tested. Curves are shown for the bow lines (resisting motion in the negative x-direction) and the stern lines (resisting motion in the positive x-direction) for the four-point mooring system which is shown in the inset in Fig. 7. The effect of the addition of even a small amount of slack between approximately 5% and 10% of the line length) is seen in Fig. 7, for these cases the force displacement curves approach a constant displacement for small applied forces corresponding to the free displacement of the vessel. The measured data for the two cases of slack lines are not included in this figure, the agreement between the experiment and the theory was good with respect to the slope of these curves but it was poor with respect to the prediction of the free displacement of the vessel. The primary reason for this is attributed to difficulties in measuring the at-rest-position of the vessel for the case of slack lines.

Typical examples of the free oscillations of the small boat are presented in Figs. 8a and 8b for the case of all lines taut and 8 in. slack in all lines. The periods of free oscillation were determined from such displacement-time histories for all cases tested.

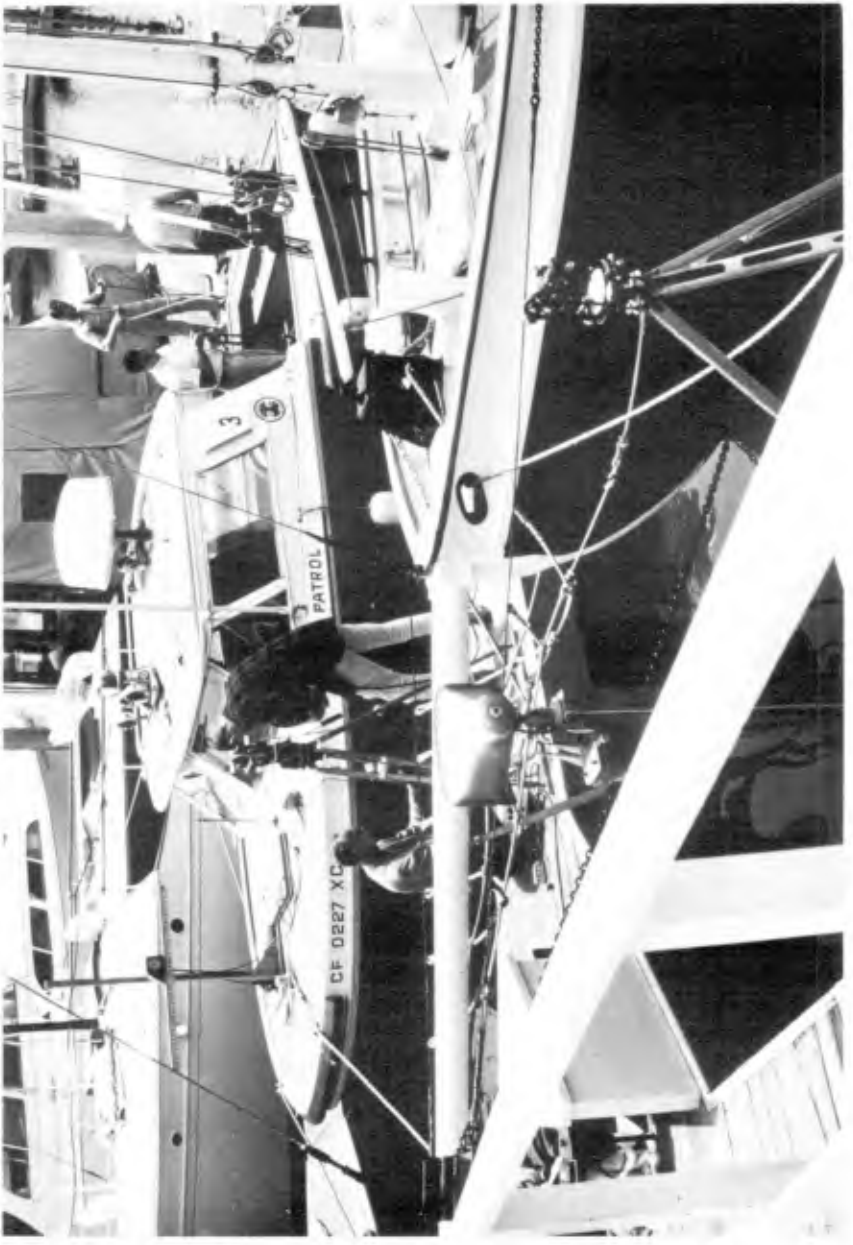

Fig. 5 Photograph of Harbor Boat No. 3 and Experimental Equipment

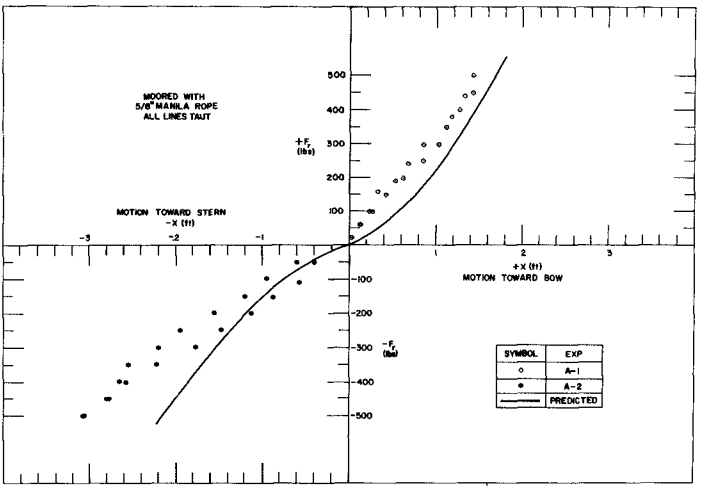

Fig 6 Measured and Predicted Restoring Force vs Displacement Harbor Boat No 3, All Lines Taut

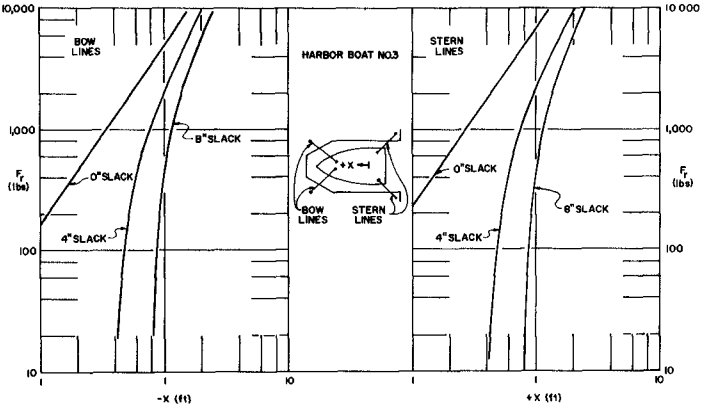

Fig 7 Predicted Restoring Force vs Displacement Harbor Boat No 3, All Lines. Taut, 4 inches Slack, 8 inches Slack

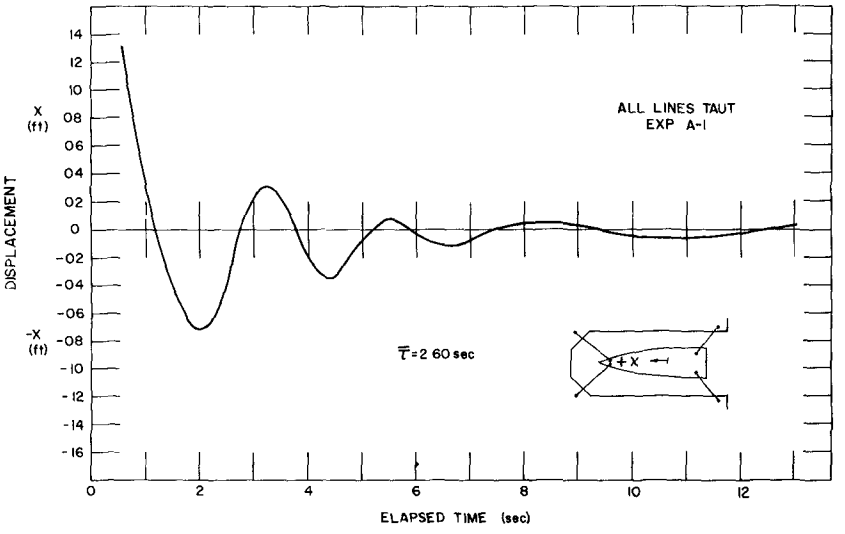

Fig 8a Free Oscillations, Harbor Boat No 3, Taut Lines, 500 lbs Force Applied to Bow

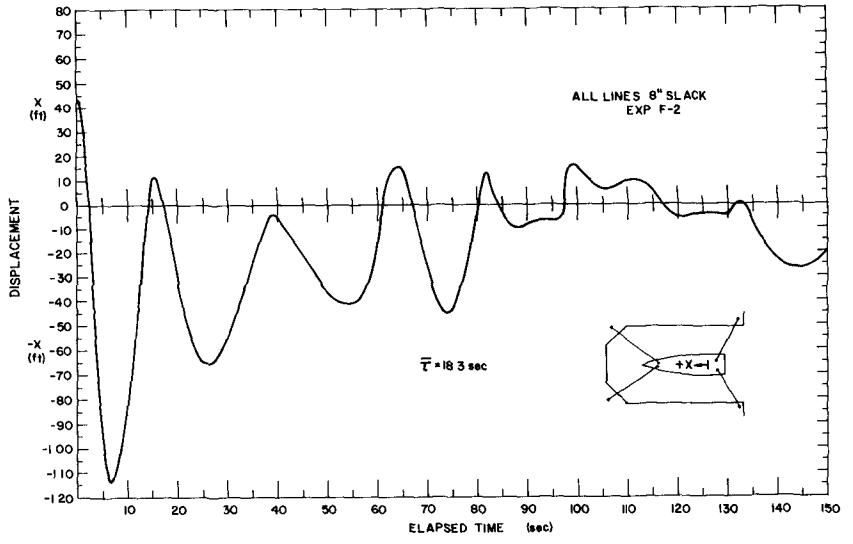

Fig 8b Free Oscillations, Harbor Boat No 3· 8 inches Slack, 500 lbs Force Applied to Bow

The results of these experiments are compared to the results of the theoretical analysis in Fig. 9. The equation of motion for the case of free oscillations is given by Eq. 5 with the right-hand side set equal to zero. A value of the virtual mass coefficient of $C_M = 1.2$ has been used in Eq. 5 for Harbor Boat No. 3 in accordance with data from Wilson (1958) for a floating body with a similar beam-to-length ratio. The curves which result are presented in Fig. 9 for the three cases investigated taut lines, 4 in. slack in all lines, and 8 in. slack in all lines. Measured data, similar to that obtained from figures such as 8a and 8b are included in Fig. 9 for two different definitions of the initial displacement. One set of data is based on initial displacements which were determined experimentally and the second set of data is for initial displacements which were theoretically determined for the given applied force, the former is labeled Meas. Init Displ and the latter is labeled Pred. Init. Displ. in Fig. 9. It is seen that both sets of experimental data show reasonable agreement with the theory except for the case of 4 in. slack and the case for taut lines with a force of 500 lbs applied in the negative x-direction. For small values of displacement the theoretical curve of free oscillations for the case of taut lines tends to a constant value of the period of oscillation because of the approximation to the force which was used (Eqs. 11) and not due to the nature of the mooring system. For displacements less than the free travel, for the cases with slack, motion is undefined since the restoring force is zero.

The undamped non-linear response curves for Harbor Boat No. 3 moored under the three different line conditions are presented in Figs. 10, 11 and 12. These response curves, obtained from Eq. 13, are plotted as the variation of the maximum displacement of the boat in surge from the at-rest-position (X_{max} or X_{min}) with the wave period, T, for various values of the forcing function ζ. It has been seen from Eq. 3b that the parameter ζ is the maximum with respect to time of the water particle velocity averaged over the displaced volume of the moored body. Since this is a function of the standing wave amplitude as well as certain parameters of the system, in general the interpretation of ζ is not simple and its value must be determined for given system parameters and wave amplitudes as a function of the wave period. The "backbone" curves, $\zeta = 0$, correspond to the case of free oscillation and are the same as those shown in Fig. 9.

These examples demonstrate that simple changes in the mooring system can have a profound effect upon the dynamics of the moored boat. For instance, the motions induced by storm waves (8 sec. to 12 sec. periods) for the boats moored with 8 in. of slack in the lines are approximately five to six times greater than those for the boat moored with taut lines. Where one mooring arrangement may be considered safe, the other may be potentially dangerous. In addition, damage to the boat moored with taut lines may be due to the failure of the lines or fittings, however, for the case with slack lines impact of the boat with the dock due to excessive motion may be the probable source of damage. It is interesting that for the three cases which are considered resonance occurs well below the periods associated with storm waves, viscous effects would not tend to alter this significantly.

Consider the variation of the forcing function ζ, with the wave period. A specific case is presented in Fig. 13 where the variation of the ratio of the forcing function to the wave amplitude, ζ/A, with wave period is shown for a block body whose center is located 120 ft from a reflecting surface

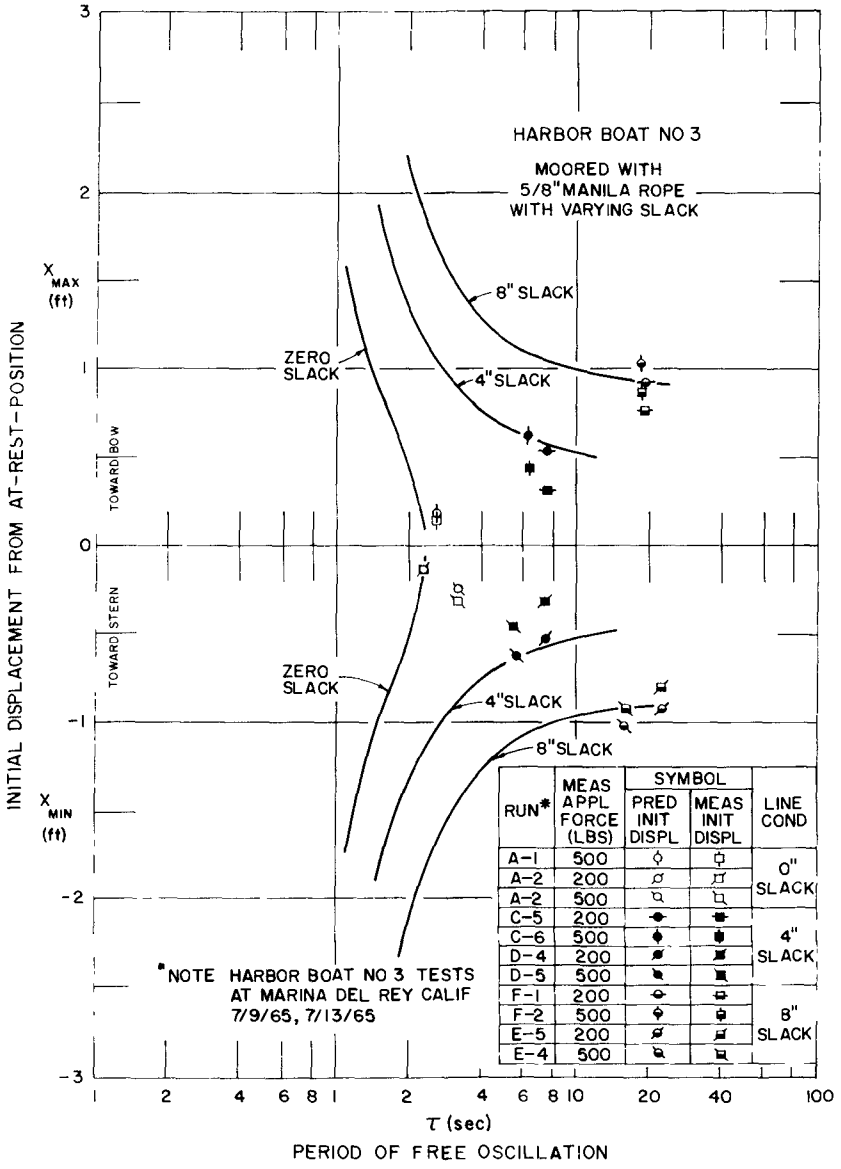

Fig 9 Measured and Predicted Periods of Free Oscillation Harbor Boat No 3

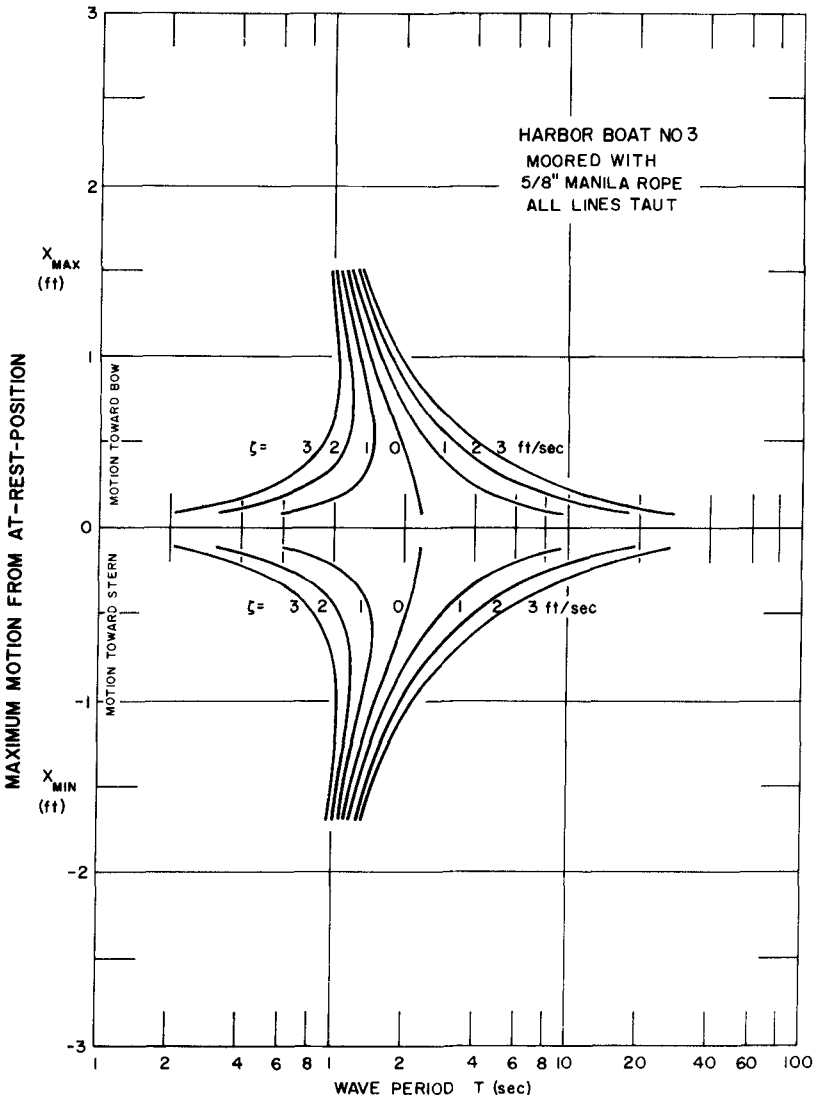

Fig 10 Response Curve Harbor Boat No 3, Taut Lines

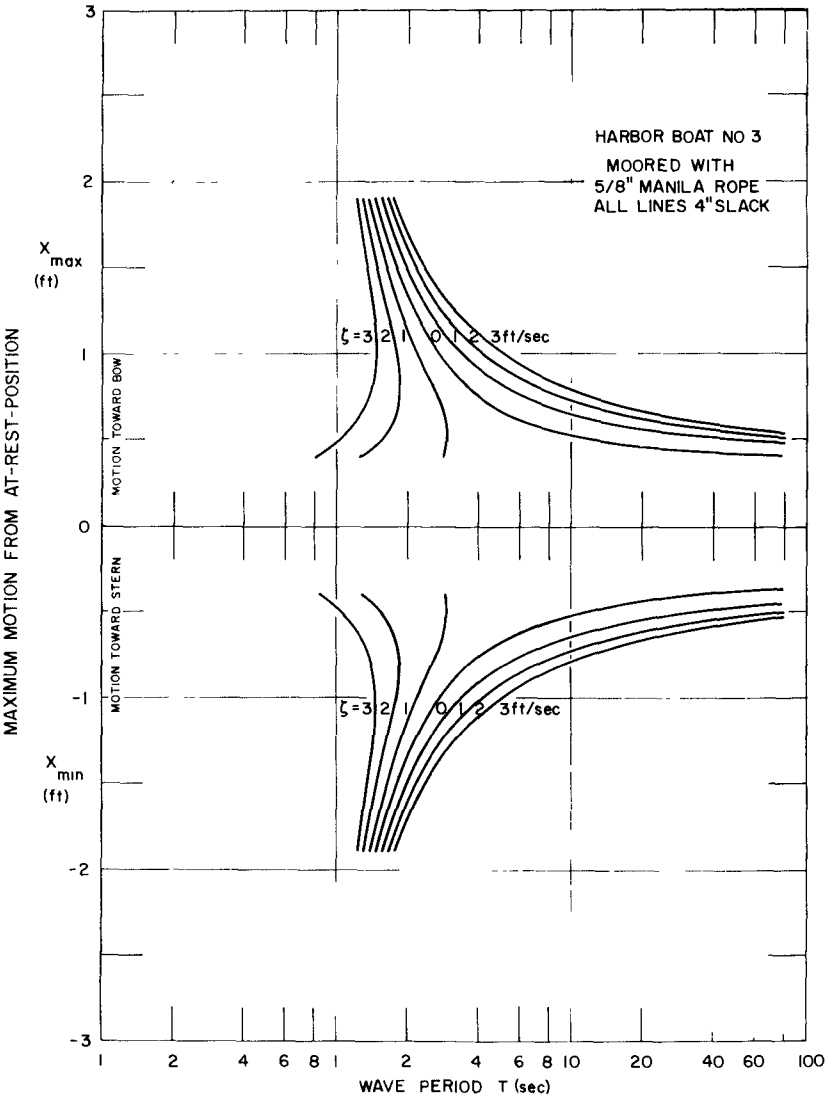

Fig 11 Response Curve Harbor Boat No 3
4 inches Slack in All Lines

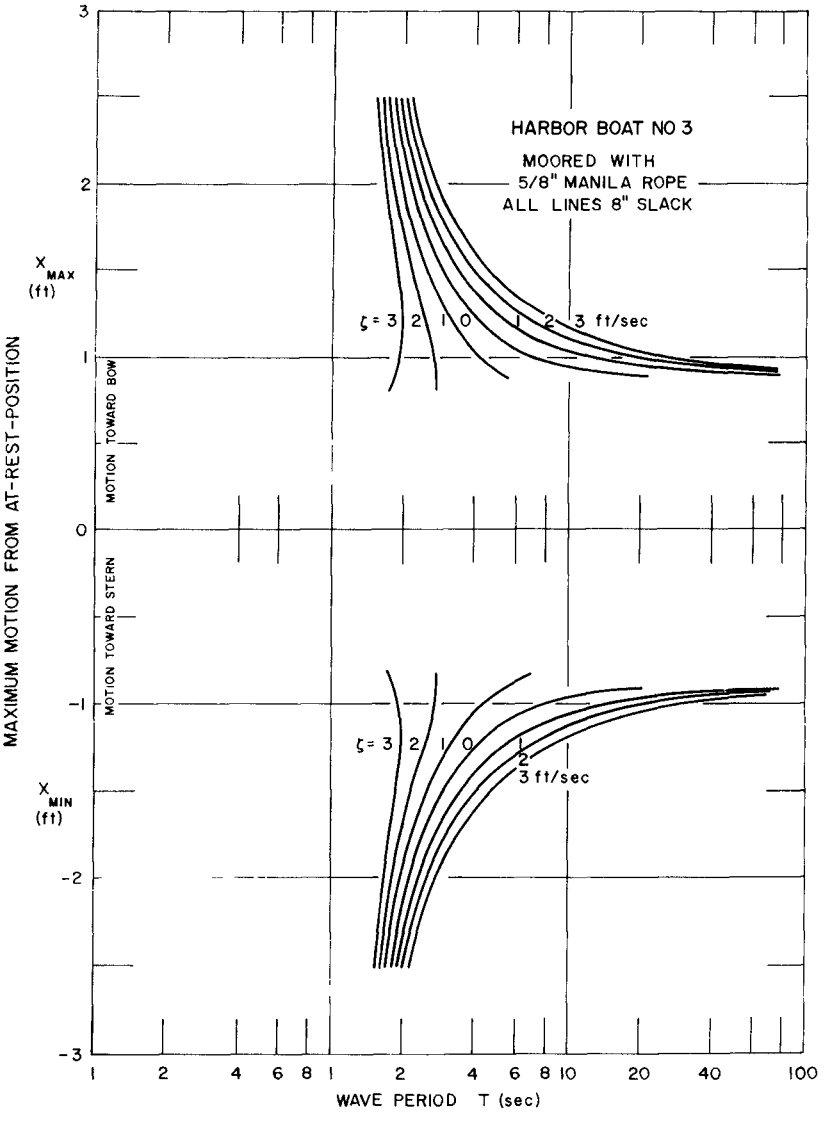

Fig 12 Response Curve Harbor Boat No 3
8 inches Slack in All Lines

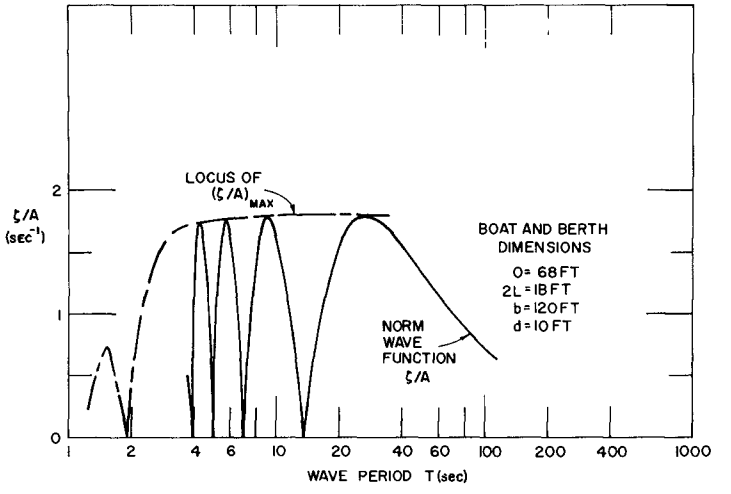

Fig 13 Variation of Normalized Forcing Function, ζ/A as a Function of Wave Period, T

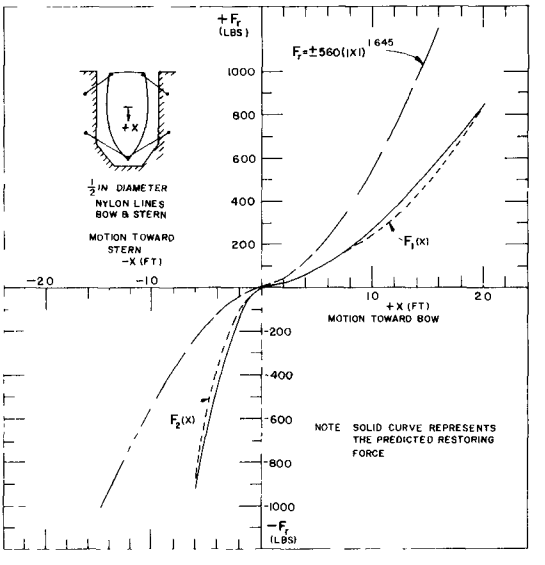

Fig 14 Predicted Restoring Forces vs Displacement, 25 ft moored Boat, Calif Reg No , CF 0394 CV

(b = 120 ft), the depth of water at the mooring site chosen for this example is 10 ft (d = 10 ft). These dimensions were chosen to demonstrate some of the features of the forcing function and only in a general way do they represent conditions at the berth at Marina del Rey. However, Fig. 13 demonstrates the periodic nature of the variation of the quantity ζ/A with wave period, at certain intervals this function and the locus of the maxima of this function become zero. This occurs when the crest of the standing wave is located at the center of the body and there is no net force acting, conversely at maxima nodes occur at the center of the body. Therefore, in general it is not sufficient to view the response curves for a particular boat simply as curves of constant ζ since the variation of the forcing function ζ with wave period is also important in completely describing the dynamic motion of the boat. However, to investigate potential damage it is possible to use a relation such as that shown in Fig. 13 to determine the maximum value of the forcing function, ζ_{max}, which would be realized for a particular wave amplitude and then to view the response curves (such as Figs. 10, 11 and 12) which correspond to that maximum value.

A consequence of neglecting the asymmetric nature of the mooring systems for small boats is illustrated by the response curve of another boat whose in situ mooring dimensions were obtained at Marina del Rey. The boat is approximately the same size as Harbor Boat No. 3 a length of 25 ft., a maximum beam of 9 ft. and a maximum draft of approximately 2.5 ft. The estimated displaced weight of this boat is 5200 lbs. The variation of the restoring force with displacement predicted for this boat using Eqs. 15 and 18 is presented in Fig. 14. The solid curve corresponds to the predicted force-displacement relation and the curve with short-dashed lines corresponds to Eqs. 11a and 11b fitted to this relation. It is seen that due to the dimensions of the mooring system the restoring force for motion in the negative x-direction is greater than the force which results from similar displacements in the positive x-direction.

One set of response curves for ζ = 2 ft/sec. is presented in Fig. 15a based on the restoring forces labeled as $F_1(x)$ and $F_2(x)$ in Fig. 14 showing the asymmetrical nature of the response of this boat to a periodic forcing function. Included in Fig. 15a is the variation of δ (the distance from the average position to the at-rest-position) with wave period which also shows that the motion is not symmetrical about the at-rest-position but it is symmetrical about a mean position a distance δ away.

Since large vessels are usually treated as symmetrically moored systems (see Wilson, 1967a) it is of interest to treat the mooring system of this boat in a similar fashion to investigate the resulting response curves. A symmetrical restoring force was obtained by first plotting the predicted curves shown in Fig. 14 in the positive F_r vs. x-quadrant and then computing the average displacement for a given applied force. The expression which best describes the resulting average curve is shown in Fig. 14 with long-dashed lines. The response curves for ζ = 2 ft/sec. based on the "averaged" restoring force are presented in Fig. 15b for motions only in the positive x-direction, the curves which correspond to motions in the negative x-direction would be mirror images. A comparison of Fig. 15a and Fig. 15b shows the problems which may arise in assuming symmetry where the mooring system is highly asymmetrical. For example, if the clearance between the bow of the boat and the slip had been small it would be possible

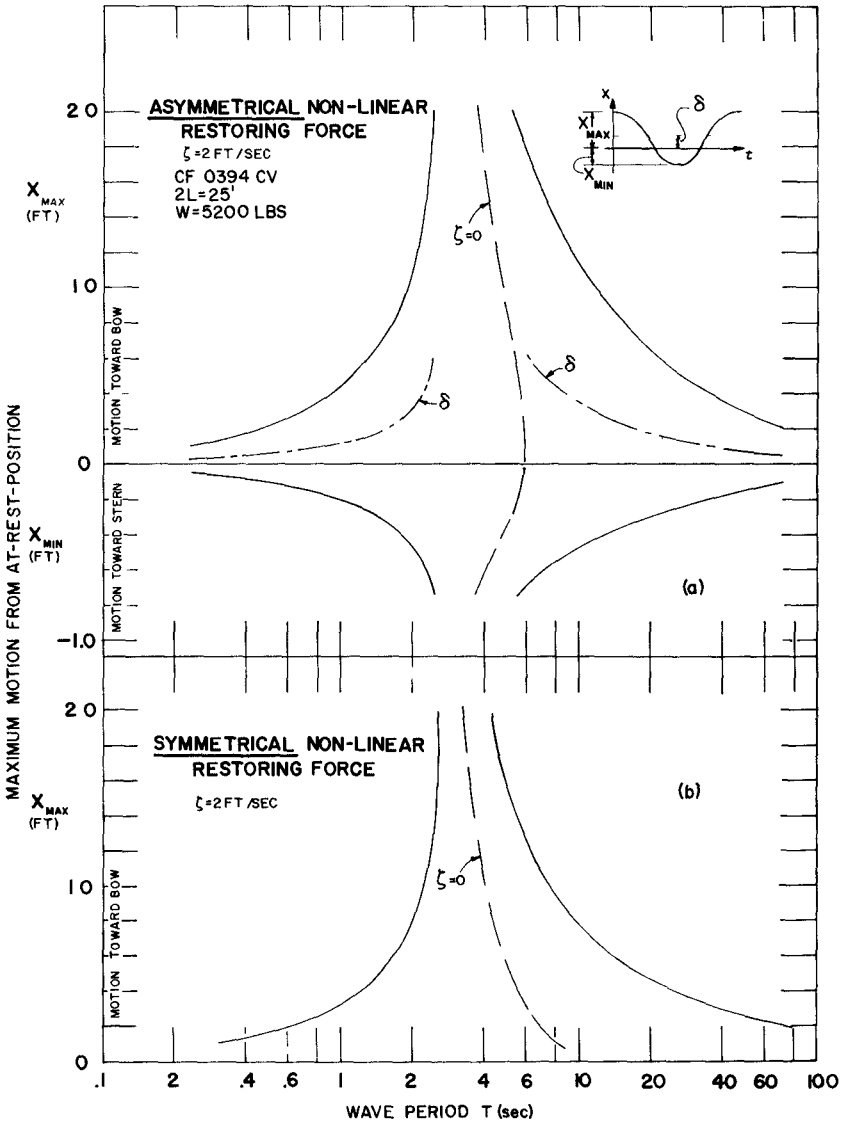

Fig 15 (a) Response Curve, 25 ft Moored Boat with Predicted Restoring Force

(b) Response Curve, 25 ft Moored Boat with Averaged Restoring Force

to conclude, using an average restoring force system, that no damage would be expected due to waves of certain heights and periods whereas using the predicted restoring forces a distinct possibility could exist that the boat would actually strike the dock.

In a similar manner the response curves were obtained for six other small boats moored at Marina del Rey. The force-displacement relations were determined from the elastic characteristics of manila and nylon described previously and in situ measurements of the mooring dimensions. The lengths and estimated displaced weights of the boats are presented in Table 2, for more details of the mooring systems the interested reader is referred to Raichlen (1968).

Table 2. Measured Lengths and Estimated Weights of a Sample of Small Boats

State of California Registration Number	Length (Ft-In.)	Estimated Weight (Lbs)
CF 6141 CB	22'-5"	3,700
CF 0675 CJ	24'-8"	5,200
CF 0394 CV	25'	5,200
CF 0310 CV	25'	5,200
CF 7651 CL	29'-3"	8,200
CF 7198 CJ	33'	11,500
CF 1756 CW	38'	17,000

The important range of wave periods for these small boats is shown in Fig 16 where the variation of the period of free oscillation is plotted as a function of the ratio of the displaced weight of the boat to the restoring force which corresponds to a given boat displacement in either the positive or the negative x-direction. Fig. 16 shows that for the range of restoring forces (or displacements) considered the periods of free oscillation of the boats varied from approximately 2 sec to 10 sec. In the region of large line stresses, $10 > W/F_r > 1$, the periods generally were less than 6 sec. It is interesting to note that the smallest boat had associated periods which were about twice as large as the periods associated with the largest boat investigated. This was due to the characteristics of the mooring systems, demonstrating that it is possible without mooring restrictions in a small boat harbor for the range of the important periods of oscillation of small pleasure boats to be close to the periods of storm waves. However, Fig. 16 also indicates the incidehce of small boat damage due to waves in a harbor may be reduced by adopting restrictions on the elastic characteristics of lines and the mooring geometry which are permitted for certain size boats.

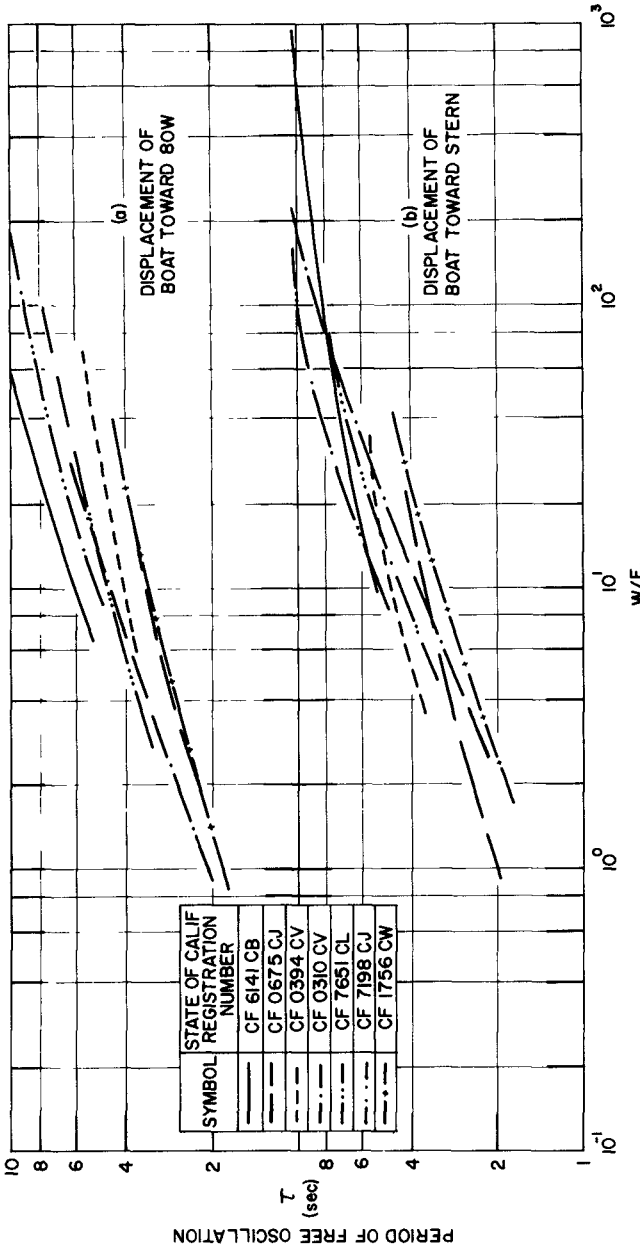

Fig 16 Variation of Period of Free Oscillation with W/F_r
a) Initial Displacement of Boat Toward Bow
b) Initial Displacement of Boat Toward Stern

CONCLUSIONS

The following major conclusions may be drawn from this study

1. The theory which is developed to treat the surge motions of small boats which are moored asymmetrically with elastic non-linear restraints appears adequate when the results are compared to experimental results of the free oscillations of a small moored boat.

2. A major difference between the mooring systems of small boats and large ships is the restoring forces which oppose surge motions, for small boats these forces will probably be asymmetrical whereas relatively symmetrical restoring forces are expected for large moored ships.

3. An analytical study of the mooring dynamics of seven small boats has indicated that the nature of the restoring force may be more important in defining the periods of oscillation of these boats than the displaced weight of the boat.

4. For the seven small boats studied the periods of free oscillation were less than about 10 sec. For forced oscillations of a small boat in surge the important wave periods would be increased by an amount dependent upon the magnitude of the forcing function and the permitted motion of the boat, but they would still probably remain in the range of those of storm waves.

ACKNOWLEDGMENT

This study was supported by the U. S. Army Corps of Engineers under Contract DA-22-079-CIVENG-64-11.

LIST OF REFERENCES

Kilner, F. A., "Model Tests on the Motion of Moored Ships Placed in Long Waves", Proc. of 7th Conf. on Coastal Engr., The Hague, 1960.

Klotter, K., "Non-Linear Vibration Problems Treated by the Averaging Method of W. Ritz", Proc. of 1st U. S. Nat. Cong. of Appl. Mech., Chicago, Ill., 1951.

Raichlen, F., "Wave-Induced Oscillations of Small Moored Vessels", Report KH-R-10, W. M. Keck Lab. of Hydraulics and Water Resources, Calif. Inst. of Tech., Pasadena, Calif., Oct. 1965.

Raichlen, F., "Motions of Small Boats Moored in Standing Waves", Report KH-R-17, W. M. Keck Lab. of Hydraulics and Water Resources, Calif. Inst. of Tech., Pasadena, Calif., Aug. 1968.

Wilson, B. W., "The Energy Problem in the Mooring of Ships Exposed to Waves", Proc. of Princeton Conf. on Berthing and Cargo Handling in Exposed Locations, Princeton Univ., New Jersey, Oct. 1958.

Wilson, B. W., "The Threshold of Surge Damage for Moored Ships", Proc. Inst. Civ. Engrs., 38, Sept. 1967 (a).

Wilson, B. W., "Elastic Characteristics of Moorings", Jour. of Waterways and Harbors Div., ASCE, Nov. 1967 (b).

CHAPTER 100

TSUNAMI HEIGHT, OAHU, HAWAII: MODEL AND NATURE

by

Jan Malan Jordaan, Jr.*, Associate Professor of Civil Engineering, University of Delaware, Newark, Delaware

and

William Mansfield Adams, Professor of Geosciences and Director of Tsunami Research, Hawaii Institute of Geophysics, University of Hawaii, Honolulu,Hawaii.

Abstract

A 1 20,000 scale model was built of the island of Oahu and neighboring topography. The model was undistorted and rotatable so that an incoming tsunami from any direction could be easily incorporated by turning the 12' x 12' model to face the wave generator from the desired angle. The wave basin was 30' wide and 40' long; with a 1:10 wave absorbing beach situated at the opposite end from the wave generator. The waves were modeled to a vertical scale of 1:2000.

The model was supplemented by a small-scale (1:247,500) model, also undistorted, in a transparent 6' x 12' ripple tank. This model represented the eight principal islands of the island chain and their surrounding topography.

Nature data of runup height for four different tsunamis around Oahu show a strong *local* amplification effect, varying more with respect to fixed positions around the island (prominent features, points, bays, reefs, etc.) rather than with respect to variations in deep sea direction.

A less pronounced local effect was obtained in the model tests and direct point-to-point correlation of model and nature data was not very meaningful beyond a general trend agreement. The orientation effect was similar on the model as in prototype.

---

*Formerly Associate Professor of Civil Engineering, University of Hawaii, Honolulu, Hawaii.

Introduction

The general nature of tsunami waves can best be illustrated by Fig. 1, tide gage records of tsunamis at Johnston Island, 700 miles west-southwest of Oahu (Ref. 3). Tsumami records for Oahu show furthermore, considerable variation in the maximum extent of run-up. It was attempted here to obtain in the model records similar to Fig. 1 for the tsumami run-up around the perimeter of the scale model. Suitable regular wave sequences to approximate the more complicated tsunami record were arrived at by successful trials.

Pilot Tests

Preliminary tests were run while the instrumentation was developed and the performance of the model was determined. The following tests in Table IA were used as a guide to the later series of tests and served to optimize the wave generation, measurement and control of ambient test conditions in the model. This data is superseded by the tests as in Table 2 which were made under optimum conditions.

Table IA

Pilot Model Tests

Origin	Direction, θ	Large Model Test wave period	Small Model Test wave period and direction
Aleutians	354°	1 to 4,5,8	-
Chile	124°	8,10,12 sec.	2 sec. (145°, 167½°, 180°)

Prototype Data

Information on wave run-up around the shore of Oahu was obtained from the available records published by MacDonald, Cox and others (Ref. 1, 2) for the following tsunamis.

Table I

Tsunami Records Examined

Date	Origin	Direction, θ
1 April 1946	Aleutians	354°
5 Nov. 1952	Kamchatka	310°
23 May 1960	Chile	124°
27 March 1964	Alaska	6°

The prototype data were plotted on polar coordinate graphs centered on the island center, with values at 10° intervals determined by interpolation for comparison with the model data taken at 10° intervals around Oahu. The data were replotted after being normalized (divided by the average of the 36 values) for each individual tsunami record. These data showed a similar trend for each tsunami, in that, independent of the direction of origin, θ, the normalized run-up values showed a consistent increase or decrease relative to the position azimuth angle β. Further analysis showed that the principal augmentative effect was associated with certain sections of the coast, hence offshore topography, rather than the azimuth of the tsunami origin.

Model Data

The model data were obtained by sensing the water surface fluctuation at 10° intervals around the island by means of immersed floats attached to strain gages. Readings with 2% accuracy were obtained for water waves 0.3 mm in height and 5m in wavelength. The amplification factor at the 50m (nature) depth contour was determined by dividing the wave height here by that in deep water (4000m). The phase lag of wave arrival around the island was also obtained from the record and used as a control on the reliability of the model performance. The phase lag in the model correlated with arrival times of waves around the island obtained from wave refraction diagrams (MacDonald, Shepard, Cox, and Cox and Mink).

Model-Prototype Correlation
1946 and 1952 Tsunamis

These tsunamis arrived on Oahu from the north to northwest and were not materially influenced by the neighboring islands. The model tests showed firstly a rather marginal correlation with the prototype values, about a 0.4 correlation. When normalized, the model tests for

three wave periods (8, 10, 12 seconds model) showed a consistent agreement with the hypothesis above that the principal augmentative effect is due to the submarine topography and hence varies with the location angle β more strongly than with the wave original direction angle θ. Examination of the areas of poor and even negative correlation between the model and prototype showed that these were where low values in nature were associated with medium-high values in the model. The apparent reason was the presence of coral barrier reefs in nature, which were too near the coastline or too shallow to be minutely scalable in the model.

1960 Tsunami

The Chilean tsunami was simulated lastly on the model because of the inherent complication caused by the presence of four islands in line with the origin of the wave. In an effort to determine the incident wave directions to be used near Oahu for the simulation, a series of tests was made on the small scale model of all the islands, Table 2. Its wave generator was set up in three separate test runs to generate waves from the south, southeast and SSE directions in turn. Wave heights were recorded near the Oahu island perimeter at 12 locations, using the same gages as used on the large model. The normalized data was plotted on a polar graph, and found to agree with the azimuthal distribution of the 1946, 1952 tsunamis on the large model. The local wave crest orientation, however, was not readily determinable.

A wave refraction diagram was thereupon prepared to determine local wave direction input using the available transpacific wave refraction diagram presented by MacDonald *et al* (Ref. 1) for obtaining the incident direction of 135° southeast of Hawaii Island. The local wave refraction and diffraction by the wave front method was carried out by A. Fallon and the wave crests and orthogonals determined. It was found that the incident wave near Oahu is an interrupted tsunami wave-front, refracted to an average approach direction of 124°, with the two branches diffracting on each side around the four islands - Hawaii, Maui, Lanai, and Molokai, in turn, to approach Oahu from two angles of 80° and 190°, reaching the shores on either side almost simultaneously.

The wave was simulated by aligning the model island's north at -124° to the line normal towards the wave generator, and interrupting a length of 10 ft. in front of the central portion of the wave generator by an impervious wave absorbing barrier (Fig. 3). This resulted in two diffracted as well as refracted wave systems sweeping in from the end portions of the wave generator and approximately representing the desired condition in nature.

The model tests were completed in July 1968 with the running of a series of tests with the above simulated tsunami origin from the south-east to determine the shoreline wave distribution for the 1960 Chilean tsunami event.

The data for three parallel cases were then rigorously analyzed, namely, the following three cases:

Table 2

Final Model Test Data Series

Series	Direction from North, θ	Source and data of simulated tsunami	Wave periods in model
A	354°	Aleutians, 1946	8,10,12 sec.
B	310°	Kamchatka, 1952	8,10,12 sec.
C	124°	Chile, 1960	8,10,12 sec.

Description of Test Procedure

For each test case, A, B, or C, there were altogether 36 wave measuring points, spaced 10° apart around the 50 meter (nature) deep perimeter of the island. At each point, as well as at a deep water location, wave probes were placed and records obtained for each of a series of four waves of 8, 10, 12 seconds, respectively. The wave generator was oriented relative to the model to generate a wave from the required direction. To accomplish this orientation, the model was rotated on its turntable and the offshore slopes adjusted to conform approximately to the underwater ridge connecting the islands. The wave period was then set, for 8, 10, and 12 seconds in turn and the generator run for four cycles in each case, creating four wave crests and starting with a crest. The record obtained contained the time-trace of the wave in deep water near the wave generator, and at the successive shoreline positions with 10° increments where the other gage was located. Since the two gages were nominally identical and were calibrated to prove this identical linear response, the shoreline amplification of the wave was obtainable directly by reading the trough to crest values from the two traces and dividing the shallow water value by the deep water or

"reference value". This was done for two selected waves out of the sequence of four successive crests; namely (a) the first crest, measured from undisturbed level, (b) the third crest measured from the preceding trough level. These were called (a) "First arrival", (b) "third wave", respectively.

Analysis of Data

With three wave origin direction conditions and three periods at each direction, there were thus nine distributions of wave amplification of the "first arrival" and the "third wave" around the island. In order to abstract any existent general trend, first the distributions for 8, 10, 12 seconds were added together for each direction, giving a set of three distributions (for the three directions: A, B, C) for "first arrival" amplification around the island, and a corresponding set of three distributions for the "third wave" amplification around the island.

Trends of Model Data Analyzed

Upon inspection of these six distributions it was found that two clear trends emerged.

1. The "first arrival" amplification showed a strong correlation with original wave approach direction, the amplification being a maximum approximately at the azimuth position around the island which faces the incoming wave system, and declining towards minimum at points $\pm$ 120° away from that maximum position (with a smaller secondary maximum at the position diametrically opposite).

2. The "third wave" amplification, showed a strong correlation with individual features around the island periphery such as bays and points of land. The correlation with features appeared to be ascribable to resonant conditions being excited in some of the larger bays and bights and around headlands. This resonance was reached by the time of "third wave", but not the first, and persisted as a gradually diminishing surge after the sequence of four waves from the generator was over.

Data Presentation

The trends for 8, 10, 12 second period (model times)*

---

*Nature time is 141 x model time

waves were constant with each other and, although there were minor variations, the amplification distribution patterns were sufficiently similar that it is concluded that there were no sudden trend reversals likely with a slight period increase or decrease, and that an average of the data for the three periods was a well-enough representation of a typical tsunami case.

The final data presentation is therefore in the following form·

1. Distribution of "first arrival" amplification with respect to angle between shoreline position and original wave direction for each of three cases (Fig. 4).

2. Distribution of (1) above for the three cases combined (Fig. 5).

3. Distribution of "third wave" amplification with respect to angle of shoreline position with true north for each of three cases of tsunami origin (Fig. 6).

4. Distribution of (3) above for the three cases combined (Fig. 7).

This model data is then comparable to prototype tsunami data from run-up records published (Refs. 1, 2).

Prototype Data

Data for the three cases, A,B, C, (Table 2) were obtained from published tables and were plotted and digitized by 10° intervals around the island periphery to facilitate model to prototype correlations (Fig. 8, typ). Since there was no information on the "deep water wave height" in the prototype, and since the three cases A, B, C in the prototype had most likely different deep water wave heights, it was decided to remove a possible bias when comparing these to model data where A, B, C all had the same deep water wave height as follows

The thirty-six digitized values of shoreline run-up height in nature for each case (A, B, or C) were added and an average value obtained. The individual values were then divided by this average. It was assumed this average would be proportional to the non- available "deep water wave value", (Fig. 9).

Prototype Trends

The data when so processed revealed a trend which agreed for all three cases, namely, a correlation of high values of relative shoreline run-up amplification with position around the island. For instance, the shoreline run-up would be high at a certain location compared to the average around the island, regardless of whether the tsunami originated from north, northwest or southeast. A fourth case, 1957 tsunami, was also compared with this trend and found to agree as well.

Model/Prototype Correlations

Comparison of an individual model test with the prototype run-up distribution generally was not very encouraging (Fig. 10). It would agree in certain respects but not in others. Another test at a different period would give conflicting trends (Fig. 11). It was realized that to attempt correlations by eye would be likely to introduce personal bias, as to whether the model/prototype correlation was good, bad, or indifferent.

A rigorous correlation study was made for selected model test distributions for the 4 sec. period and Aleutian 1946 tsunami condition which formed part of the priliminary series of verification tests. The correlation study revealed fairly weak correlations at first, and after a major improvement in the offshore topography in the island model was made, the correlation was improved to 0.4 (1.0 being ideal, and 0 being no correlation).

It was concluded that two factors contributed to an apparent lack of strong model to prototype data correlation.

1. Selectivity of model test conditions, which do not cover all possibilities of wave period and resonant interaction that might all contribute to the highest water mark in nature.

2. Scale-effect, which influences the ultimate behavior of the water's edge. In nature the wave might break and reach pretentious heights against cliffs, in the model the topography is considerably generalized and surface tension prevents breaking of the very modest wave oscillations. Furthermore, the model data is taken for practical purposes at some distance from the actual shoreline (-50 meter contour· about 3 to 6 inches out from the water's edge in the model) whereas the nature data is taken from the debris line left by the actual water line excursion inland.

To avoid arriving at spurious correlations in some instances and none at others, the only comparison of model and prototype finally presented consists of comparing with each other (I) the distribution of "third-wave heights" around the model, (which showed a strong correspondence with position around perimeter) and (II) the distribution of "maximum relative run-up" around the prototype island in nature (which likewise showed a strong correspondence with position around the perimeter). Comparing (I) with (II), the result is not a perfect match, and in fact is a rather poor agreement, although somewhat better in certain places than in others (Fig. 12).

Causes for Lack of Positive Model/Prototype Agreement are.

1. The effects of nearshore submerged features, coral reefs, basalt outcrops,are not reproduced in the model due to the large scale-reduction of 1.20,000. This is best seen in Kaneohe Bay and Kaena Point. The model data for each of these locations gives essentially one value respectively. MacDonald, Shepard and Cox in their paper on the 1946 Aleutian tsunami (Ref. 1) show how the tsunami run-up varied near Kaena Point, and ascribe this due to coral reef outcrops. In the model the reefs are not reproducible and the water depth is of the same magnitude as the wave height. At Kaneohe Bay the reported surge is about 4 ft. maximum. The use of a 10 x greater scale for wave height in the model is perhaps the cause of questionable behavior in very shallow areas like Kaneohe Bay, where reef outcrops could not be represented on model scale.

2. The effect of the model basin boundaries, and partial reflection and return of wave energy from the wave absorber beach in the basin.

   In nature the interaction of a "monochromatic" train of waves and an island of arbitrary shape leads to a scattering in radiating fashion of all the wave reflection that takes place off the island perimeter. Apart from some multiple reflections between adjacent shorelines, this reflected energy radiates outwards eventually to be lost from the system. In the model, however, it is practically impossible to avoid some return of scattered energy from the confining side walls of the basin. The waves passing the model are intended to be perfectly absorbed by a sloping beach covered with rubberized hair Tests showed that about 60% of the wave amplitude is absorbed and 40% returns to form a partial standing wave system with the incoming waves. The reflected waves eventually reflect once more off the wave generator end and decay eventually as standing waves having several nodal systems.

General Discussion on Use of a Sequence of Waves

For the reason above of partial reflection by the basin boundaries, testing with a continuous train of waves would not be valid as some of the basin nodal lines would intersect the island perimeter and give spurious values of zero amplification, whereas the basin antinodal lines would give exaggerated amplification values.

The use of a short sequence of several waves (in this case 4) does permit data to be obtained before the reflected waves return from the beach and sidewall to interact with the amplification of the traveling wave system. The purest information will be obtained with a single crest or trough, since the return signal will be identifiable as a separate single wave of smaller amplitude occurring later in the record. Use of a single or solitary wave would give essentially the same data as the leading wave of a short sequence, but since the solitary waves does not have a definite period, no information on resonance behavior of adjacent shorelines would be obtained. The use of a sequence of four waves was then decided upon by observation of the optimum behavior of traces obtained with 1, 2, 3, 4, and more wave sequences (Fig. 13).

Evaluation of Reliability of Model Data

The model results are quantitative but are not to be interpreted as quantitative *predictions* of prototype behavior; because:

1. Prototype wave height input is unknown, hence model wave height input is an arbitrary choice.

2. Prototype waves are spectral, whereas model waves are monochromatic. Absolute predictability comes nearest in the first crest, and here the model results agree markedly well with theoretical prediction for an idealized conical island.

3. The ultimate run-up in the prototype is greatly dependent on non-modelable features, e.g., cliffs, reefs, perimeter roads and roadside features, canefields, tropical vegetation, houses and streets, buildings, yards and lands.

Apart from the above limitations the model data are subject to certain artificially-imposed restrictions:

1. Subjectivity in selection of wave period and origin, especially in a complicated case like the 1960 Chile tsunami which is prior-refracted by four other islands.

2. Reflection and partial standing waves caused by side and end walls and beach in model basin.

3. The model data are more reliable for the first arrival than for the later waves.

4. The model data are considered more reliable on the exposed shore than on the lee shore with reference to the wave origin because the lee shore receives in addition to the refracted incoming wave, also the unrealistic partial reflection from the absorbing beach.

5. The data from the model for the Barber's Point-Pearl Harbor-Diamond Head-Koko Head area appear to give higher wave amplification than experienced in nature For two of the three test cases this is the lee-side with respect to incoming waves, and therefore subject to a back reflection from the model basin beach. For the *third* case (Chile 1960) the pre-conditioning of the incoming wave, to strike the south and east shores in a fashion in accordance with the theoretical wave refraction pattern (produced by the ridge to the south east forming the four islands south of Oahu) was not fully achieved. There is, therefore, some uncertainty in the data for this 1960 Chile wave condition which is more so on the exposed south shores.

6. The data obtained served to illustrate partially the type of general behavior that the tsunami wave system undergoes in its interaction with the nearshore island topography.

Conclusions

The model study of tsunami wave amplification around Oahu yielded quantitative data which correlate to a certain extent with field data. It yielded qualitative understanding of the phenomena involved in the process of interpreting the results obtained and increasing the precision of measurement and control of test procedure.

Although the model data in itself do not show sufficiently strong correlations with observed data to permit detail prediction of inundation levels given a certain wave height, period and orientation, nevertheless a qualitative generalized behavior pattern is

evident, as has been stated in Trends of Model Data Analyzed. The prototype data trends also found in the course of this study are remarkably consistent. It is hoped that tsunami forecasting could make use of these two trends in arriving at a decision to call a tsunami alert, or to determine the area to be evacuated.

References

1. MacDonald, G., Shepard, F.P., and Cox, D.C., The Tsunami of April 1946 in the Hawaiian Islands; Pacific Science, January 1947. Scripps Institute of Oceanography, Bull. 5, 6, 1960, pp. 391-528.

2. Cox, D.C. and Mink, J.F., The Tsunami of 23 May 1960, in the Hawaiian Islands, Bull. Seism. Soc. of Am., Vol. 53, No. 6, pp. 1101-1209, December 1963.

3. Wennekens, P.M., Office of Naval Research report, "Tsunami vs. Johnston Island", and Hawaii Institute of Geophysics Records.

4. Havelock, T.H., "The Pressure of Water Waves Upon a Fixed Obstacle", Proc. Roy. Soc. (Lond.), Vol. 175A, 18 July 1940, pp. 409-415.

Acknowledgments

This research was sponsored by the National Science Foundation under Grant No. GK 1374, and was performed at the Look Laboratory of Oceanographic Engineering, University of Hawaii. The principal research assistance was provided by Mr T.D. Krishna Kartha and Mr A.R. Fallon, Research Associates. The assistance of Mr. G. Pararas-Carayannis and of the secretarial staff of the Tsunami Group, Hawaii Institute of Geophysics, and of the Civil Engineering Department staff, University of Delaware is gratefully acknowledged.

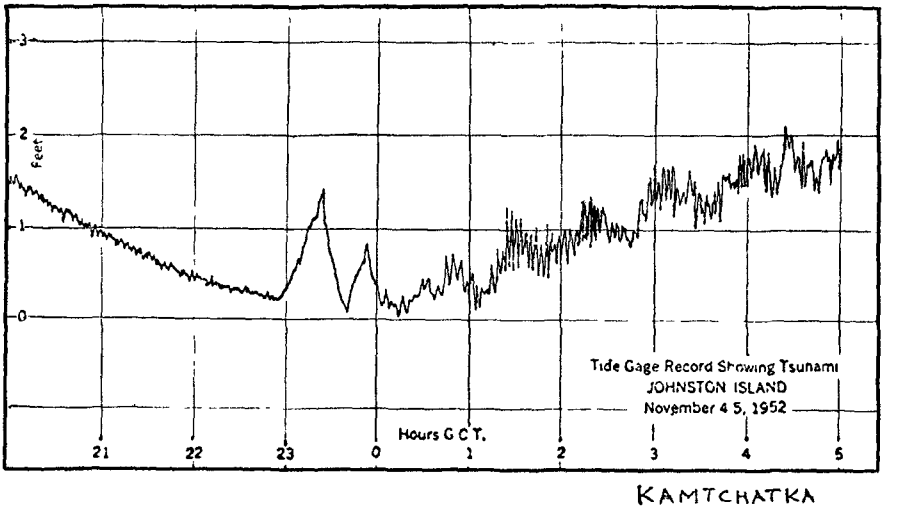

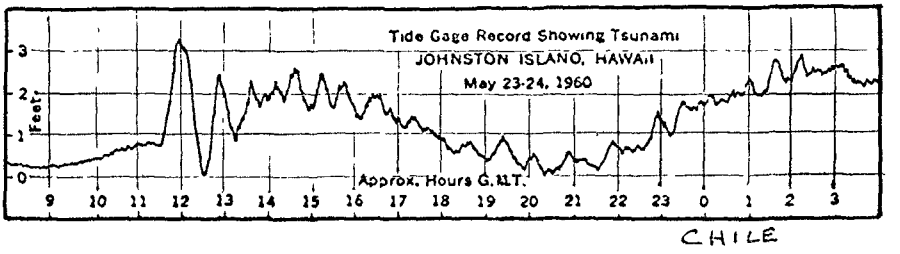

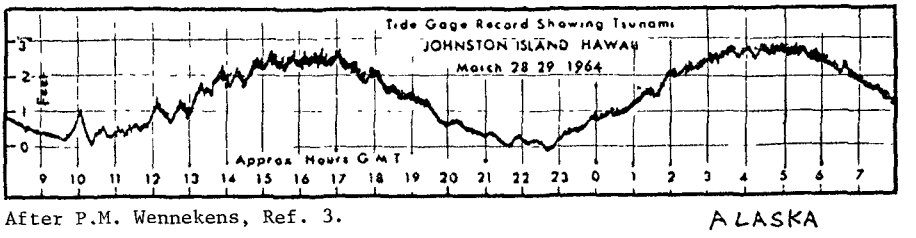

After P.M. Wennekens, Ref. 3.

Figure 1. Tide Gage Records Showing Tsunamis at Johnston Island, Pacific Ocean Lat. N. 16° 45', Long. W. 169° 31'.

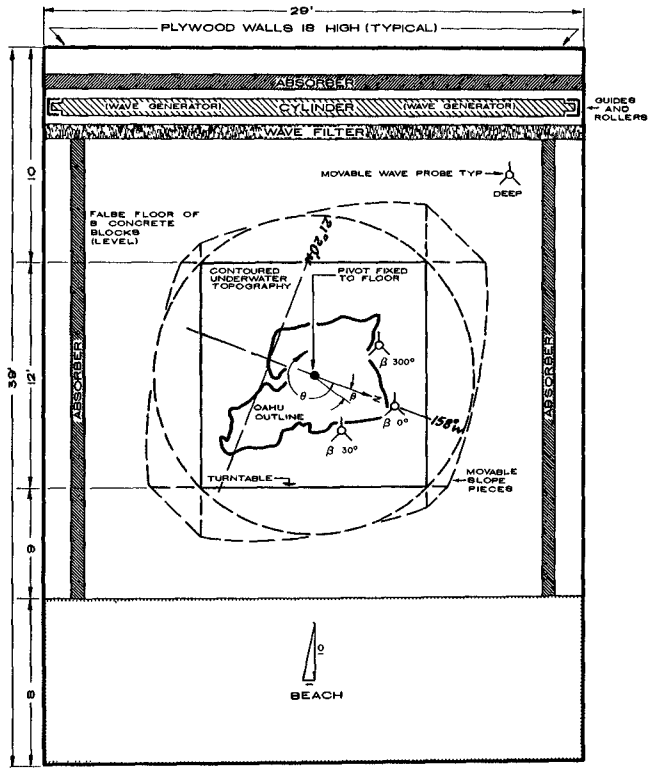

FIGURE 2 OAHU TSUNAMI RUN-UP MODEL

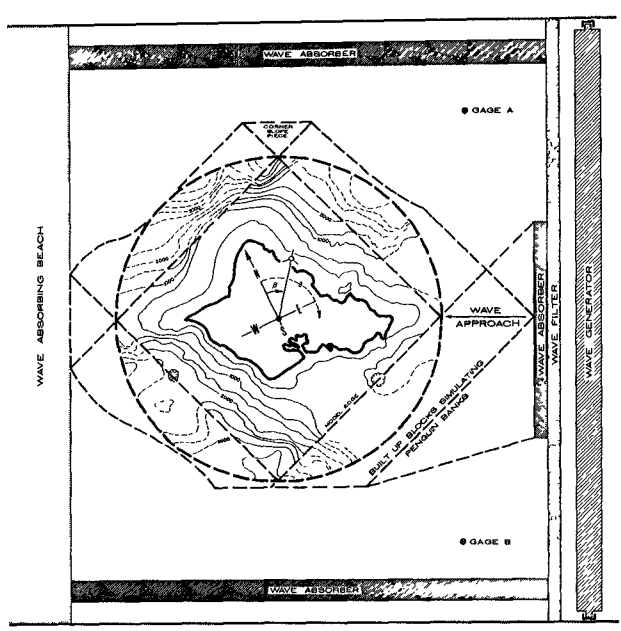

FIGURE 3 TSUNAMI RUNUP MODEL, OAHU SHOWN FOR 1960 CHILE

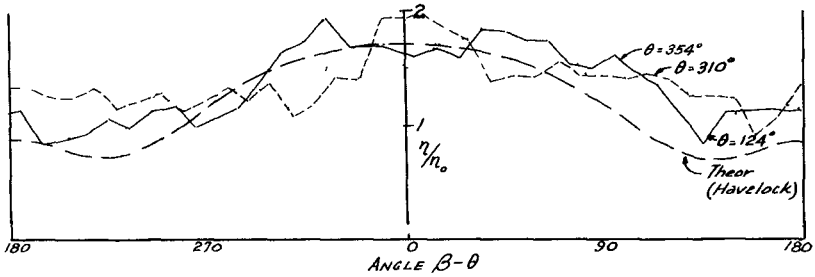

Figure 4. Model data, initial crest amplification.

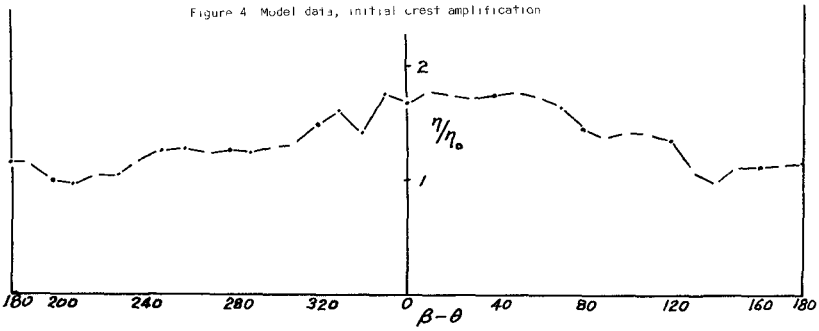

Figure 5. Average of three cases, initial crest amplification.

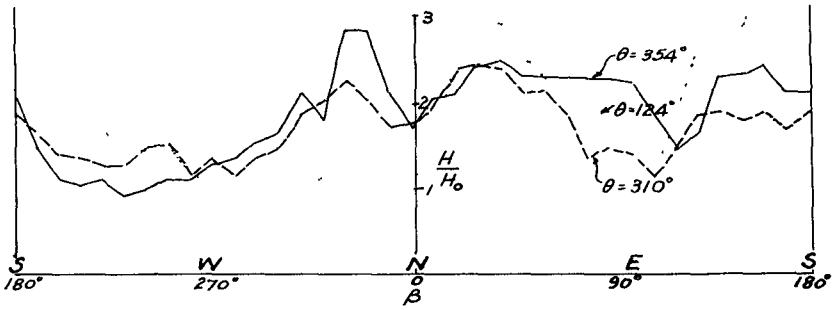

Figure 6. Model data, third wave amplification

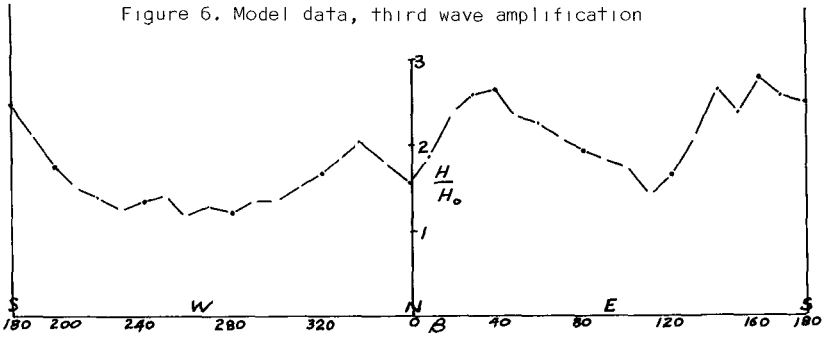

Figure 7. Average of three cases, third wave amplification.

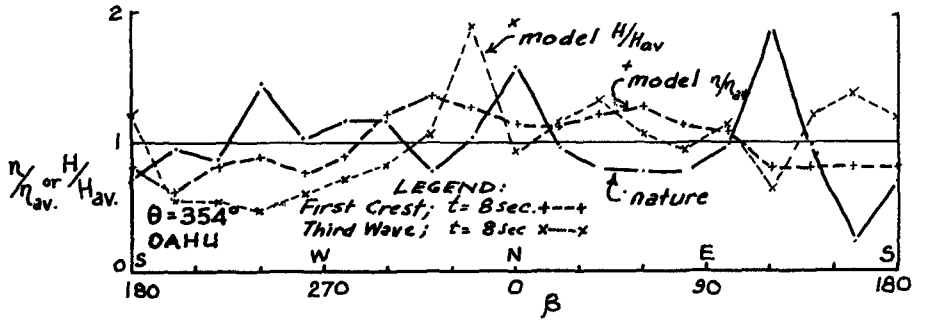

Figure 8. Typical model-prototype correlation of data.

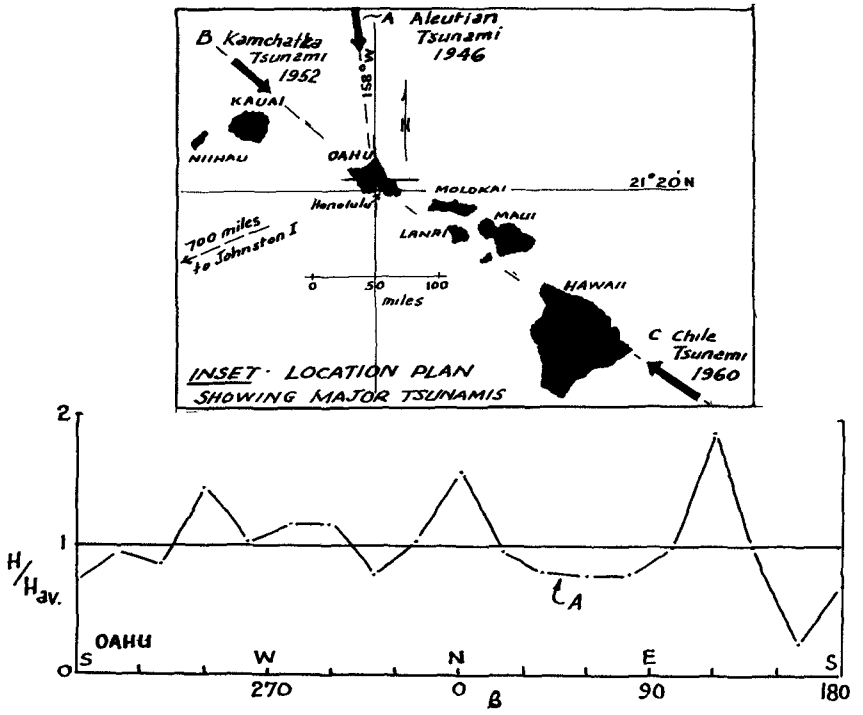

Figure 9. Average of prototype distribution of tsunami relative heights for three tsunamis.

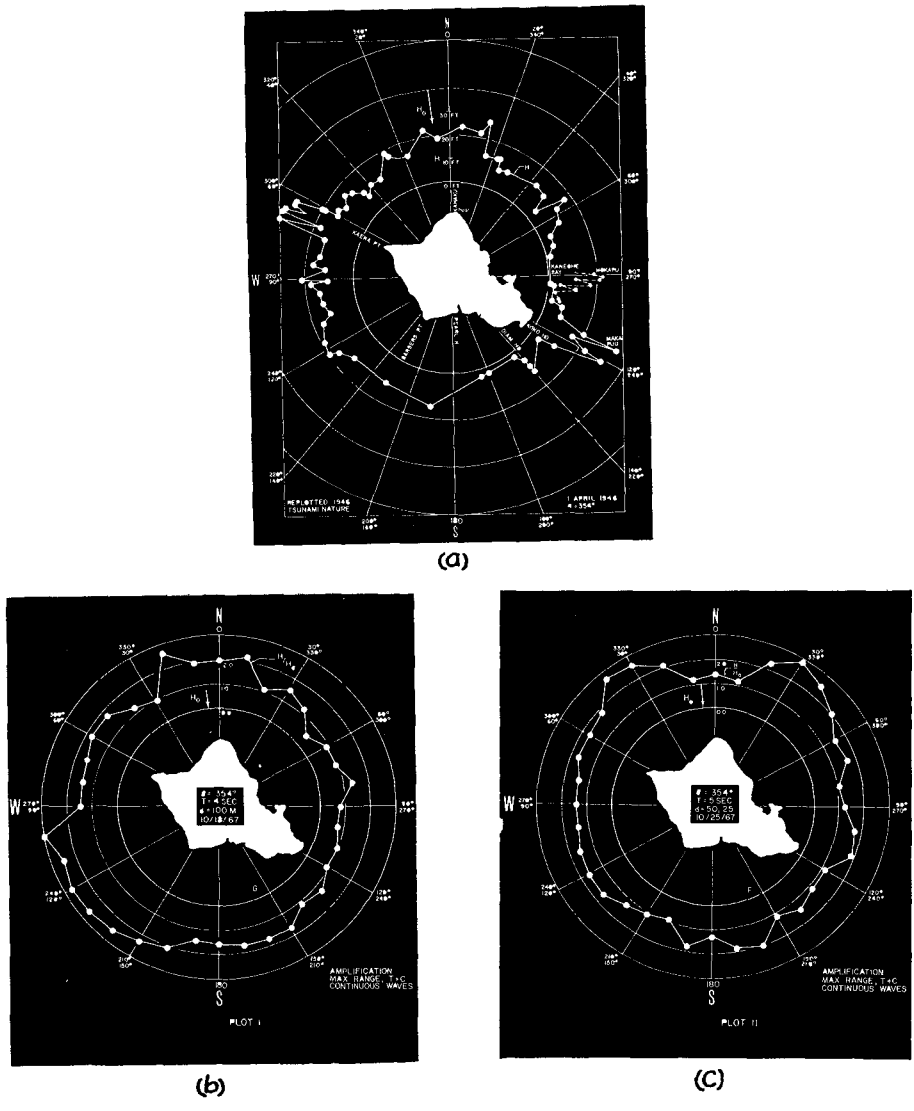

Figure 10. Prototype and Model Data for two periods, θ=354°, Aleutian Tsunami.
(a) Prototype (nature)
(b) Model 4 - second period, continuous waves
(c) Model 5 - second period, continuous waves

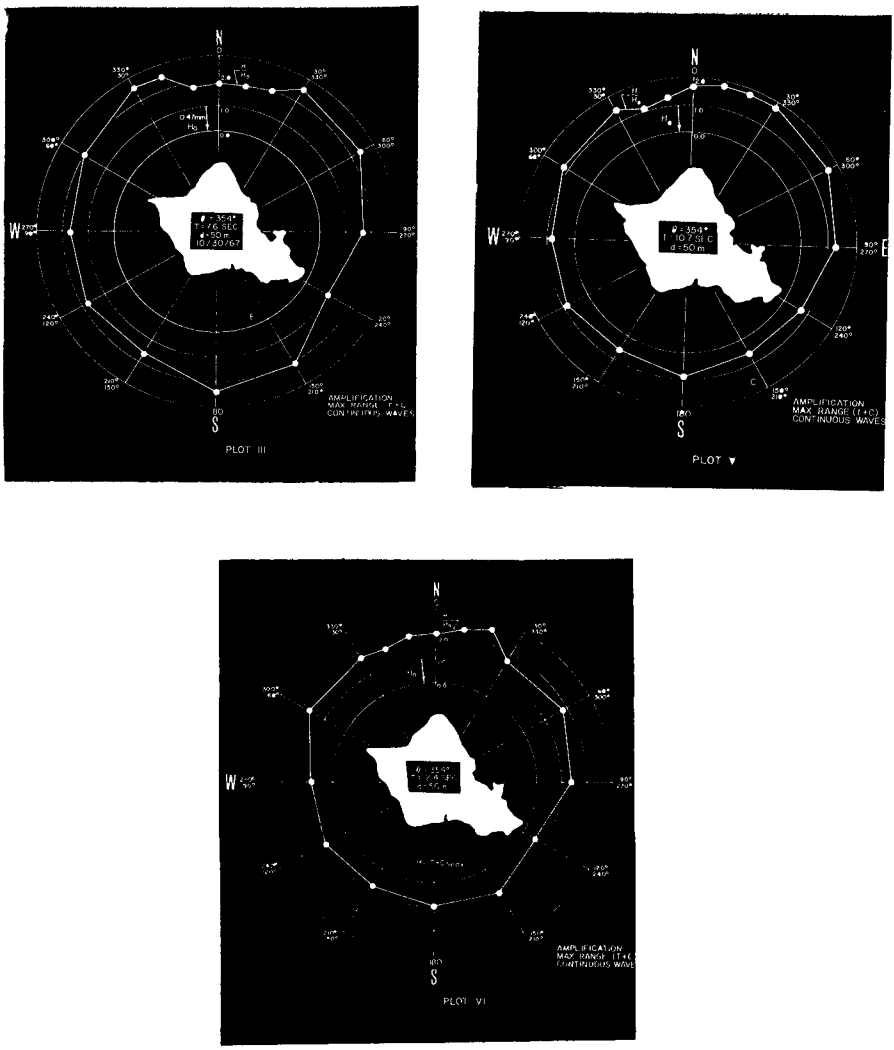

Figure 11. Model data, showing effect of further variation of period, 7.6 sec., 10.7 sec., and 12.4 sec., respectively.

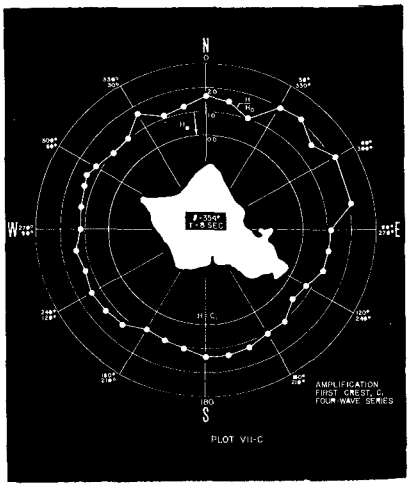

(a)

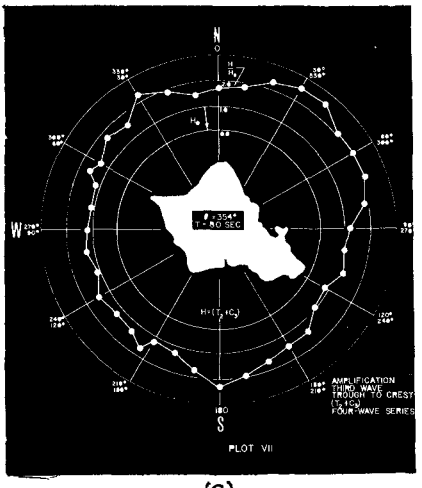

(c)

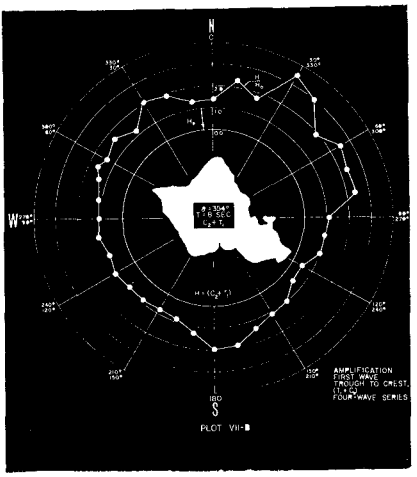

(b)

Figure 12. Comparison of distribution of (a) amplitude of initial crest, (b) height of wave first trough to second crest, (c) height of third wave (second trough to third crest), for an 8 sec. period, four wave sequence, as in Fig. 13.

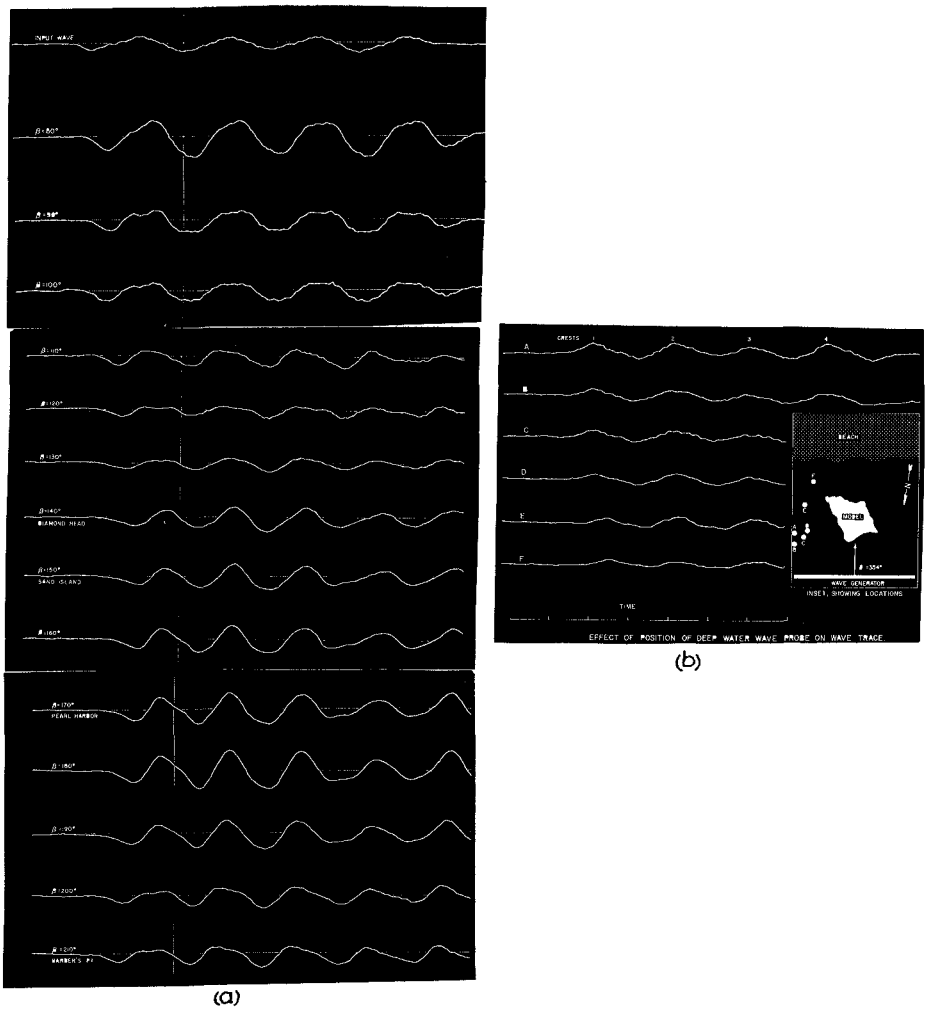

Figure 13. (a) Typical data sequence, 8 sec. period, four waves (traces shown inverted). Plot of data in Fig. 12-c (Plot VII-B).
(b) Comparison of same wave sequence at six different positions in Test Basin (traces shown right way up).

CHAPTER 101

THE INVESTIGATION OF THE WAVES AT THE BAY ON THE MODELS WITH FIXED BED AND THE ESTIMATION OF THE SCALE EFFECT

by

M.E.Plakida - The Wave Laboratory Chief at Moscow Branch of the Leningrad Institute of Water Transport (M.B.L.I.W.T.)

and

N.T.Perepetch - Engineer of the Wave Laboratory, M.B.L.I.W.T.

Moscow, U.S.S.R.

SUMMARY

The wave model regime, in the given bay of the arbitrary outline, have been studing at the three scales 1:150, 1:300 and 1:450. The models had the fixed bed. The model of the scale 1:150 had been conditionally admited as the prototype at the investigation.

As a result of the study the scale effect for the present case have been found. The correction scale factors depend on the relative water depth.

The largest correction scale factors are $n = 1.5$ for the model scale 1:300 and $n = 2.1$ for the model scale 1:450. At these cases the relative water depth is less than $\frac{H}{\lambda} < 0.20$.

The correction scale factor is $n = 1$ for the model scale 1:300 and 1:450, if the relative water depth is more than $\frac{H}{\lambda} > 0.30 - 0.35$.

LIST OF SYMBOLS

h - wave height;

λ - wave length,

τ - wave period;

H – depth of water measured from SWL;

h_i – wave height at the point i;

λ – wave length at the point i;

$k_i = \frac{h_i}{h}$ – coefficient of the remaining wave height at the point i;

$n = \frac{K_{150}}{K_s}$ – correction scale factor (where S = 300 and 450)

INTRODUCTION

The determination of the model scale is one of the principal question at the study the port protection from waves. It is well known, that the model scales are applied from 1:40 up to 1:500 for such investigations in the practice of the hydraulic laboratories.

The relationship between the laboratory model figures and the same figures of the prototype is calculated by the Froud's law at any scale of the model. However, the loss of the wave energy is more at the models of the small scale than at the ones of the large scale. As a result we can have the underestimation of the wave heights. To avoid the underestimation of the wave heights some investigators (1,2) had proposed to introduce the correction scale for the wave heights at the port study on the models of the small scales. For example, T.Blu (3) takes notice that the relative wave heights at the model scale 1:400 are twice less than the ones at the model scale 1:100. We can find a lot of articles and research work (4–7) concerning to the dissipation of the wave energy at the model investigation.

The great interest to this problem is explained by natural desire to get reliable results at the least expenses and without wasting much time.

Indeed, at present time one can get the most reliable results for the estimation of the wave regime only with the help of the model study, as the analytical methods remain till now rather imperfect.

MODEL

The study of the wave regime had been carried out on the fixed bay model of the arbitrary relief. The general scheme of the bay model is presented in Fig.1. The situation of the wave generator and the points in which wave gauges were installed are also shown in the same Fig.1 and here you can see the direction of the wave fetch by the arrow, at which we have results presented in this paper.

The model of the bay was disposed on the concrete floor in the hangar. The bay isobaths had been drawn by the chalk on the concrete floor and according to the sheet iron strips of the appropriate size were placed. The space between the strips was filled up by sand, which had been moistened by water and had been rammed. The cement solution of 1,5 cm covered the sand model. After three-four days the model of the bay was prepared for the wave study. All models of the scale 1:150, 1:300 and 1:450 had been built in this way.

EQUIPMENT AND METHODS

The waves were generated by a flatter-type machine, driven by 10 kw- the direct current motor. The electric wave gauges

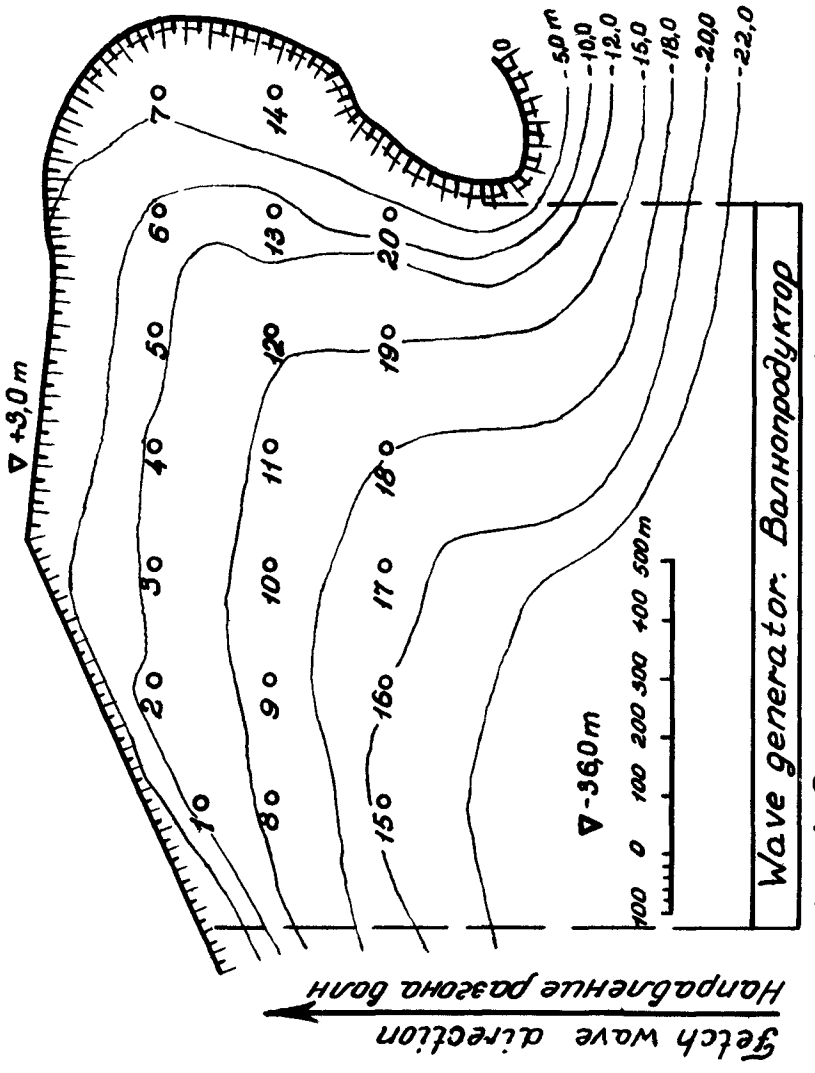

Fig. 1. Scheme of the bay
Рис.1. Схема бухты

of the ohm resistance were used to measure the wave heights.

The wave trains consisted up to 30 waves by 3 times and they were continiously recorded by the oscillograph on the photopaper belt.

We calculated the mean wave heights from $\frac{1}{3}$ of the largest wave height for any point. The relation of the mean wave height calculated by the above method, to the height of the initial wave, measured at the open sea, determined the coefficient of the remaining wave height at the given point $k_i = \frac{h_i}{h}$. If one knows the coefficient of the remaining wave height at every point it is possible to plot the isolines of the coefficients of the remaining wave height.

ANALYSIS OF RESULTS

The wave regime is shown for the three scale models in Table 1.

Table 1

NN	Name		Unit of measur.	Scale of model		
				1:150	1:300	1:450
1	Wave height	h	cm.	4.2	2.2	2.0
2	Wave length	λ	cm.	66	25	20
3	Wave period	τ	sec.	0,65	0,40	0,31
4	Wave depth in the open sea	H	cm.	24	12	8
5	Wave slopness	$\frac{\lambda}{h}$		15,6	11,2	10,0
6	Relative water depth	$\frac{H}{\lambda}$		0,36	0,48	0,40
7	Mean water depth in the bay	H_1	cm.	12	6	4,5

As shown in Table 1 the waves were of considerable steepness and they were generated at rather great water depth. According to the Froud's law the wave characterizations of the prototype are following: $h = 4{,}5$ m, $\lambda = 70$ m and $\tau = 7$ sec.

The estimation of the automodelity of mean wave regime in the bay for the all three scale models was made by Reynolds' number according to Mich's and Ofitzerov's formulas

$$R_m = \frac{U_g H_1}{\nu} \qquad (1)$$

where $U_g = \dfrac{\pi h}{\sqrt{\dfrac{\pi\lambda}{g}\, sh \dfrac{4\pi H_1}{\lambda}}}$ – bottom velocity

$\nu = 0.011$ ($t = 15^{\circ}C$) kinematik viscosity of water

$$R_o = \frac{U_n h}{\nu} \qquad (2)$$

where $U_n = h\sqrt{\dfrac{\pi g}{2\lambda}\, cth \dfrac{2\pi H_1}{\lambda}}$ – orbital velocity

Table 2 schows the Reynolds' numbers for the all three models

Table 2

	1:150	1:300	1:450
R_m	14200	4200	3500
R_o	8500	3620	3450

In Table 2 on can see that the Reynolds' numbers for all the models appeared to be more than 2000.

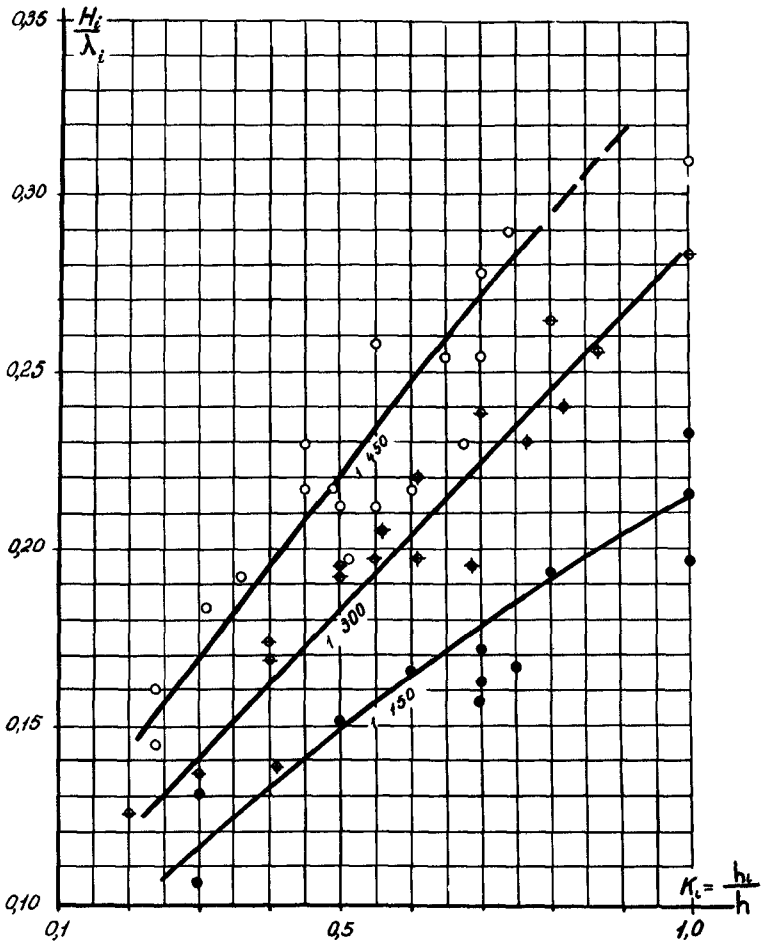

Fig.2 Relationship between Kana $\frac{H_i}{\lambda_i}$ to three model scales
Рис.2. Зависимость коэффициента остаточной высоты волны от относительной глубины воды

It allows to believe that the wave regimes in all our models are within the limits of the same automodel zone.

The values of the coefficient of the remaining wave height and the relative water depth to any point were calculated. The values were then marked on the paper and by them one drew the three curves (Fig.2). The curves are in entire confirmity to each other.

The less the scale of the model - the more the curve steepness and therefore, for the same relation of the water depth to the wave length $\frac{H_i}{\lambda_i}$ the coefficient of the remaining wave height K_i is appeared to reduce with the decreasing of the model scale.

The dissipation of the wave energy results from the turbulent viscosity of the water and the bottom friction. The less the relative water depth $\frac{H_i}{\lambda_i}$ the more the loss of the wave energy because of the bottom friction.

I.Stepanov (8) notes in his work, that the imformation about the influence of the turbulent viscosity upon the decreasing of the wave height is very contradictory.

The dependency between the relation of the coefficients of the remaining wave heights of the studied models $n = \frac{K_{150}}{K_s}$ and the relative water depths $\frac{H_i}{\lambda_i}$ are given in Fig.3 The Fig.3 is based on Fig.2.

In Fig.3 one can see that the correction scale factor $n = 1$ for the models with the scale 1:300 and 1:450 when the relative water depths are $\frac{H_i}{\lambda_i} \geqslant 0.30 - 0.35$, but when the relative water depths are $\frac{H_i}{\lambda_i} < 0.20$ we have $n = 1.5$ for the scale 1:300 and $n = 2.1$ for the scale 1:450.

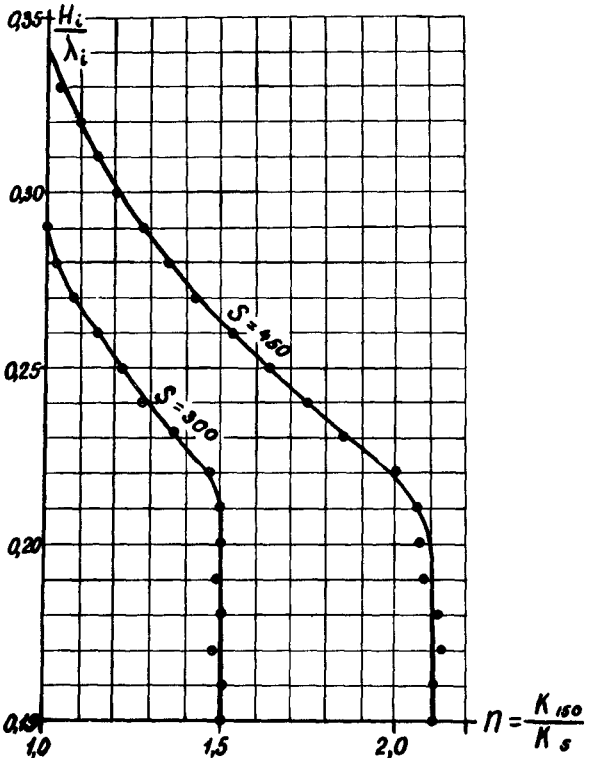

Fig. 3 Relationship between $n=\frac{K_{150}}{K_s}$ *and* $\frac{H_i}{\lambda_i}$ *(where S=300 and 450)*

Рис. 3. Зависимость отношения $n=\frac{K_{150}}{K_s}$ *от относительной глубины воды (где S=300 и 450)*

As the relative water depth $\frac{H_i}{\lambda_i}$ decreases from 0,30 up to 0.20 the correction scale factor increases.

CONCLUSION

The investigation carried out can not claim to establishment the correction scale factors in all possible cases. However, these investigations display great importance of the problem, which can be solved more completely by the investigation of the scale series including wave research in field conditions.

REFERENCES

1. Офицеров А.С. Вопросы методики лабораторных волновых исследований и линейные потери энергии волнения. Изд. ВНИИ ВОДГЕО, 1958
Ofitserov A.S. The method questions of the wave laboratory study and the loss of the wave energy. VNII, VODGEO, 1958

2. Вайсфельд И.А. Выбор масштаба и масштабные поправки при моделировании портов. Волновые исследования гидросооружений. ВОДГЕО, 1961
Vaisfeld I.A. Determination of the scale and scale correction at port modelling. Wave investigation of the hydraulic engineering. VODGEO, 1961

3. Johnson J.W. Influence of the scale at the wave laboratory investigation. The Transactions of the American Geophysical Union N 4-5, 1949

4. Mich R. Amortissement des houles dans le domaine de l'eau peu profonde. La Houille Blanche N 5, 1956

5. Mich R. Sur quelques résultats d'amortissement des houles de laboratoire et leur interprétation. La Houille Blanche N 1, 1958

6. Valembois J. Quelques consideration sur la similitude dans les essais de houle sur modèles. Compte rendu des IV-es Journées de l'hydraulique. Paris, 1956

7. Biésel F. et Carry C. A propos de l'amortissement des houles dans le domaine de l'eau peu profonde. La Houille Blanche N 6, 1956

8. Степанов И.А. Поправки систематических искажений волн на моделях. Труды ЛИВТ"а вып.88. Водные пути и гидросооружения. Ленинград, 1967

Stepanov I.A. Systematic corrections of the wave distortion on the models. The Transactions of L.I.W.T. Vol.88 "Water Ways and Engineering" Leningrad, 1967.